

Analysis of prostaglandins in SD rats by capillary zone electrophoresis with indirect UV detection

He Jin-Lan ^{a,*}, Li Hui-Ping ^b, Li Xiao-Ge ^a

^a Department of Chemistry, Zhanjiang Normal College, Zhanjiang 524048, People's Republic of China

^b Respiratory Diseases Research Laboratory in Affiliated Hospital of Guangdong Medical College, Zhanjiang 524001, People's Republic of China

Received 22 January 1997; received in revised form 3 July 1997; accepted 8 July 1997

Abstract

This paper reports an investigation on optimal separation and detection for animal prostaglandins, i.e. prostaglandin E₂(PGE₂) and thromboxane B₂(TXB₂) by capillary zone electrophoresis with indirect detection at 254 nm. It was found that the addition of 3 mmol l⁻¹ phosphomolybdic acid in 5 mmol l⁻¹ chromate buffer can lower the detection limits of PGE₂ and TXB₂, i.e. the calculated detection limits ($k = 3$) with phosphomolybdic acid is 0.05 μg ml⁻¹, only a 1/5-fold improvement compared to that without phosphomolybdic acid. Also adding phosphomolybdic acid, the mechanism for improving detection limits was explained properly. The separation and detection of PGE₂ and TXB₂ can be completed in 4 min. The linear ranges for PGE₂ and TXB₂ were the same, i.e. 5 ~ 80 μg ml⁻¹, analytical precision ($n = 8$) was 1.2 ~ 1.4% and 3.5% for the measurement of migration times and determination of peak height, respectively. The approach was demonstrated in the lung tissue of SD rats, the measurement results were in good agreement with previous investigations. © 1998 Elsevier Science B.V. All rights reserved.

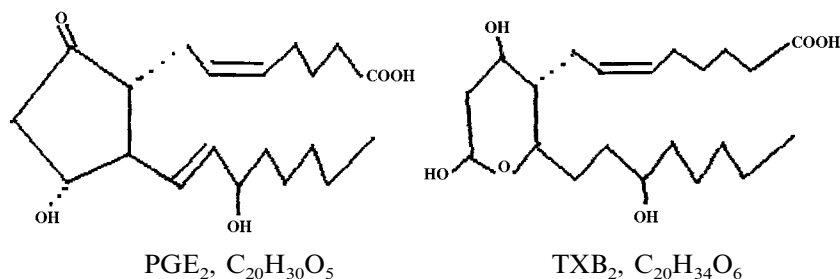
Keywords: Capillary zone electrophoresis; Indirect UV detection; Prostaglandins

1. Introduction

Prostaglandins (PGs) are one type of important bioactive material in human and animal

bodies. Their synthesis from arachidonic acid is mediated through the cyclooxygenase pathway in vivo. Prostaglandins E₂(PGE₂) and thromboxane B₂(TXB₂) are two of the more important kinds of metabolic products in the body. Their physiological effects are different, but their molecular structure is similar. Their molecular formula is as follows:

* Corresponding author.



Capillary zone electrophoresis (CZE) is a type of separation technique characterized by high efficiency and small sample volume, great progress has been made in instrumentation and application in the last several years. In principle, CZE has been considered particularly suitable for bioseparation. Most capillary electrophoretic separations are performed using UV detection. However, many biomolecules such as the platelet activating factor (PAF), TXB_2 and PGE_2 , lack chromophores at useful wavelengths and cannot be detected with UV methods.

Indirect detection can be used as a universal detection scheme, without the need for time-consuming precolumn derivatization or experimentally complicated postcolumn derivatization procedures. Indirect UV detection in capillary electrophoresis (CE) has been applied to the detection of various compounds such as organic acids [1,2] inorganic ions [3,4] and the biomolecules PAF [5].

The goal of this work was to investigate the separation of PGE_2 and TXB_2 in animal bodies by CZE with indirect UV detection at 254 nm. Modification of the indirect detection sensitivity and separation selectivity of CZE as a relation of components in the background electrolyte was investigated. As a result of this work, we found that the presence of phosphomolybdic acid in chromate system can improve the detection and separation of PGE_2 and TXB_2 .

2. Experimental

2.1. Apparatus

All electropherograms were generated using a Mode 1229 capillary electrophoresis system with

254 nm UV detector (New Technology Application institute of Beijing). The uncoated fused-silica capillary (Hebei Yongnian Light Fiber Factory) was 50 μm i.d. \times 374 μm o.d. with an effective length of 50 cm long and the total length was 65 cm. The signals were transmitted to a X-Y recorder (Sichuan Meter Factory). All experiments were carried out at ambient temperature (ca. 24–26°C). UV spectra were measured with a Shimadzu UV-2100 scanning spectrophotometer, using quartz cuvettes with an optical path 0.5 cm.

2.2. Chemicals

PGE_2 and TXB_2 were obtained from Sigma. All other reagent came from China and were analytical-reagent grade. All the solutions were prepared by subboiling distilled water.

2.3. Disposal of SD rat lung samples

Fifteen rats were divided into three groups, five in the normal group, five in the hypoxic group and five in the drug group, 15 ml of methanol was added to 0.50 g of broken SD rat lung and mixed immediately on a vortex vibrator, then centrifuged (4000 rpm \times 15 min). The supernatant was drawn out, the protein and other impurities were removed, 7 ml of water and 7 ml chloroform were added into the supernatant and mixed until two layers were seen clearly. The chloroform phase was taken out and dried with N_2 , then stored at -4°C waiting for measurement.

2.4. Procedures

The capillary was initially washed with 1 M KOH for 10 min, then with water for 10 min and

running buffer for 30 min. When the buffer solution in the capillary was changed, the capillary was purged for 3 min with the new buffer solution. In order to make sure the precision of migration time, the capillary was purged for 1 min with the running buffer before each injection.

Stock solutions of potassium chromate, potassium hydrogen phthalate and sodium benzoate (0.1 mol l^{-1} each) and 0.15 mol l^{-1} phosphomolybdic acid were prepared by dissolving the chemicals in subboiling water. Lower concentration solutions were obtained by dilution and filtered through a $0.3 \mu\text{m}$ membrane before going into the capillary separating column.

PGE₂ and TXB₂ standard solutions in methanol (1 mg ml^{-1} each) were adjusted to the required pH value by 0.1 mol l^{-1} KOH or 0.1 mol l^{-1} HCl solution in order to keep the sample pH close to the test buffer pH value, then diluted to the desired concentration with buffer and the indicated concentration was that after dilution with buffer.

3. Results and discussion

3.1. Selection of the indirect absorption probe ions

Because PGE₂ and TXB₂ lack chromophores at 254 nm, indirect absorption detection must be employed. In indirect detection, a detectable ion is chosen as one of the components of the background electrolyte, thus creating a large background signal. When a non-detectable sample ion passes the detection window, there will be a decrease in the background signal. The detectable ion has UV absorption properties and is called an indirect absorption probe ion. The technique results in a negative peak as a sample component displaces a chromophoric ion. Because indirect UV detection relies on the displacement of a chromophore, the probe ion should have a large molar absorption to maximize the decrease in signal resulting from its displacement. Additionally, the matching of electrophoretic mobility of a

probe ion with a sample ion would give a high-resolution separation.

At pH 8.0, 10 mmol l^{-1} potassium chromate, 20 mmol l^{-1} potassium hydrogen phthalate and 20 mmol l^{-1} sodium benzoate were chosen respectively and each of these act both as a kind of probe ion and as a running buffer system. Fig. 1 shows the results of separation and detection of PGE₂ and TXB₂ ($40 \mu\text{g ml}^{-1}$ on buffer solution each). From Fig. 1 we can see, from sensitivity, peak shapes, background noise and resolution, that the chromate system is superior to potassium hydrogen phthalate and sodium benzoate system. However, the resolving power is not enough for separating PGE₂ and TXB₂, and the detected sensitivity is very poor.

3.2. Effect of phosphomolybdic acid

3.2.1. Improving detection limits

Phosphomolybdic acid is always used as a visualizing agent for the analysis of PGE₂ and TXB₂ in chromatography [6]. The investigators found that when 3 mmol l^{-1} of phosphomolybdic acid was added to the chromate buffer system, the absorption of chromate at 254 nm increased rapidly, and the optimized concentration of chromate was decreased from 10 mmol l^{-1} to 5 mmol l^{-1} , in the case of hydrogen phthalate and benzoate buffer system, there was no promotive effect. As can be seen in Fig. 1(a) and Fig. 3, the detected signals of PGE₂ and TXB₂ are much larger with phosphomolybdic acid than without.

In indirect UV detection, the key factors determining the detection limit have been reported to be the concentration of the visualization agent, C_p ; the dynamic reserve, D_r (i.e. the ratio of the background absorbance to the noise) and the displacement ratio, R , (i.e., the number of visualization agent molecules transferred by one sample molecule). The detectable concentration C_D can be estimated as follows [7,8].

$$C_D = C_p / R \cdot D_r$$

It can be seen that, decreasing C_p or increasing D_r will reduce the detection limit.

Phosphomolybdic acid is a visualization agent which has a stronger complex capability, and was

used to complex with PGE₂ and TXB₂ at 80 ~ 90°C [6]. Here, perhaps there is some complex effect between chromate and phosphomolybdic acid. Mixing them can form a kind of complex compound which has stronger molar absorption at 254 nm. The UV-absorption spectrogram (Fig. 2) confirmed our speculation. Fig. 2 presents three UV-absorption spectrograms, Fig. 2(a) obtained from 3 mmol l⁻¹ phosphomolybdic acid (pH 8.0), Fig. 2(b) from 10 mmol l⁻¹ phosphomolybdic acid (pH 8.0) and Fig. 2(c) from the mixed solution of 5 mmol l⁻¹ chromate and 3 mmol l⁻¹ phosphomolybdic acid (pH 8.0). Obviously, the complex compound between chromate and phosphomolybdic acid has been formed and it has stronger molar absorption at 254 nm.

The indirect absorption detection limits of PGE₂ and TXB₂ were decreased from 0.25 µg ml⁻¹ to 0.05 µg ml⁻¹ ($k = 3$) by adding 3 mmol l⁻¹ phosphomolybdic acid in 5 mmol l⁻¹ chro-

mate buffer system at pH 8.0. The experiments confirmed that the detection limit would be improved by lowering C_p or increasing the molar absorption of the visualization agent in the presence of phosphomolybdic acid. A phenomenon observed in Fig. 3 is that the noise was obviously increased. This degradation of signal-to-noise ratio is amplified by the increase of noise at high absorbency values occurring in most photometers [2].

3.2.2. Effect on the separation

In order to further investigate the effect of phosphomolybdic acid on the separation of PGE₂ from TXB₂, the migration times of electroosmotic flow (methanol), PGE₂ and TXB₂ were measured under different phosphomolybdic acid concentrations in the 5 mmol l⁻¹ K₂CrO₄ system (pH 8.0) (Fig. 4). Fig. 4 suggests that the migration times

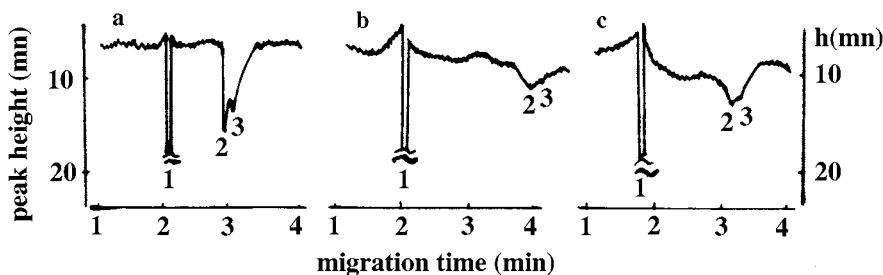


Fig. 1. The detected sensitivity and separation for PGE₂ and TXB₂ in different probe ion systems. Peak 1, methanol; Peak 2, PGE₂; Peak 3, TXB₂. Running buffer (pH 8.0 each): (a) 10 mmol l⁻¹ potassium chromate (28 kV, 18 µA), (b) 20 mmol l⁻¹ sodium benzoate (28 kV, 15 µA), (c) 20 mmol l⁻¹ potassium hydrogen phthalate (28 kV, 28 µA).

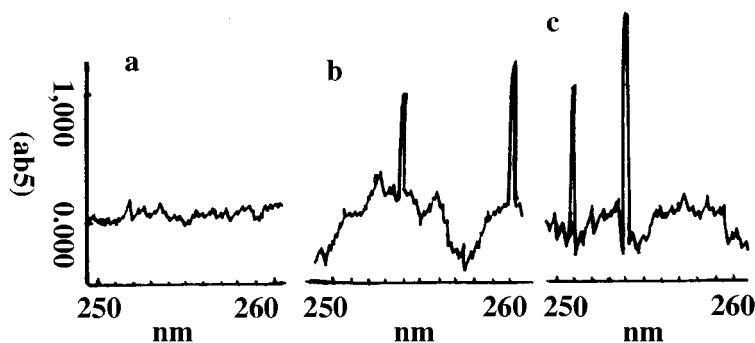


Fig. 2. The UV-absorption spectrogram, (a) 3 mmol l⁻¹ phosphomolybdic acid (pH 8.0), (b) 10 mmol l⁻¹ chromate (pH 8.0), (c) 3 mmol l⁻¹ phosphomolybdic acid and 5 mmol l⁻¹ chromate (pH 8.0).

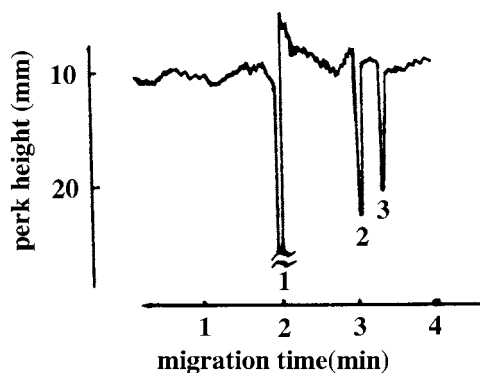


Fig. 3. Effect of phosphomolybdic acid on the detection sensitivity and the separation of PGE₂ and TXB₂. Buffer, 5 mmol l⁻¹ potassium chromate and 3 mmol l⁻¹ phosphomolybdic acid (pH 8.0). Applied voltage, 25 kV. Sample concentration, 40 μg ml⁻¹ each. Peak 1, methanol; Peak 2, PGE₂; Peak 3, TXB₂.

of methanol PGE₂ and TXB₂ will be shortened by increasing the concentration of phosphomolybdic acid. A main cause was that the ion strength in the buffer solution was increased, thus leading to a higher separation current and larger electroosmotic flow. However, the migration time of PGE₂ was reduced dramatically. So the concentration of phosphomolybdic acid did not exceed 5 mmol l⁻¹, otherwise, the PGE₂ peak would be eluted with electroosmotic flow. The separation efficiencies for PGE₂ and TXB₂ are the highest when the concentration of phosphomolybdic acid is between 3 and 4 mmol l⁻¹. If the concentration of phosphomolybdic acid was below 3 mmol l⁻¹, the retention times of components are increased, resulting in badly tailing peaks and poor resolution. So, in this work, a 3 mmol l⁻¹ concentration of phosphomolybdic acid was chosen, and the highest plate numbers, between 5×10^5 and 6.2×10^5 , were obtained. The improvement of resolution further confirmed that the effective mobility of PGE₂ and TXB₂ would be closely matched to those probe ions, due to the complex formed between phosphomolybdic acid and chromate, resulting in sharper peak shape and leading to higher separation efficiency.

3.2.3. Effect of pH

The pH of the running buffer solution controls the mobility of weak acids. The PGE₂ and TXB₂ are all typical weak acids. The pH of the electrolyte solution used in our work can have a large effect on the separation of PGE₂ and TXB₂. The changes in electroosmotic flow and the retention time of the components as the pH changes in the buffer system were described in Fig. 5. Fig. 5 showed that as the pH value increased, the electroosmotic flow enlarged, i.e. the retention time of methanol was shorter. The dramatic change occurred at pH 5~8. The tendency of the retention times to change for PGE₂ and TXB₂ were the same with methanol. At lower pH, both PGE₂ and TXB₂ will become easily protonated and a decrease in their electrophoretic mobility is observed, resulting in a tailing peak. As the pH is increased, the electroosmotic flow is increased, which leads to an increase in the effective mobility and sharpens the separation peak of PGE₂ and TXB₂. But, if the pH is over 9, the separation current is increased dramatically. The experiments show that the highest efficiency separation of PGE₂ from TXB₂ is at pH 7~8.

3.2.4. Correction curve and sample analysis

The optimum buffer solution for the separation of PGE₂ and TXB₂ contained 5 mmol l⁻¹ potassium chromate and 3 mmol l⁻¹ phosphomolybdic acid at pH 8.0, which combines complete resolution with a shear analyses. When

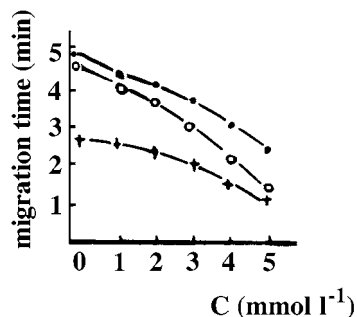


Fig. 4. Effect of phosphomolybdic acid concentration on the migration time of electroosmotic flow (×). PGE₂ (○), TXB₂ (●). Other conditions as in Fig. 3.

Table 1

The characteristic parameters of the correction curve for PGE₂ and TXB₂ in CZE

Component	Detection limit ($\mu\text{g ml}^{-1}$) ($k = 3$)	Linear range ($\mu\text{g ml}^{-1}$)	Linear regression coefficient	R.S.D.% ($n = 8$)	
				tr. ^a	h ^b
PGE ₂	0.05	5~80	0.9971	1.2	3.5
TXB ₂	0.05	5~80	0.9956	1.4	3.5

^a tr., retention time.^b h, peak height.

the applied voltage was 25 kV, the retention times for PGE₂ and TXB₂ were 3 min 5 s and 3 min 32 s, respectively (Fig. 3). The correction curve was described by the separation peak height against component concentration. The characteristic parameters of correction curve were shown on Table 1.

The standard curve method was used for analysis of PGE₂ and TXB₂ in the lung samples of SD rats. First, the lung sample diluted with 25 μl methanol was used for the determination of PGE₂, then 75 μl of methanol was added for the determination of TXB₂. In order to measure the recovery, five normal lung samples were taken, then every sample was divided described by the

separation peak height against component concentration. The characteristic parameters of correction curve were shown on Table 1.

The standard curve method was used for analysis of PGE₂ and TXB₂ in the lung samples of SD rats. First, the lung sample diluted with 25 μl methanol was used for the determination of PGE₂, then 75 μl of methanol was added for the determination of TXB₂. In order to measure the recovery, five normal lung samples were taken, then every sample was divided into two aequators and 2 μg standards of PGE₂ and 8 μg TXB₂ were added into one of the aequators. The disposal process of the sample recovery test was the same as mentioned previously in Section 2. The analysis results for PGE₂ and TXB₂ of rat lung in each group and recovery in this work were shown in Table 2.

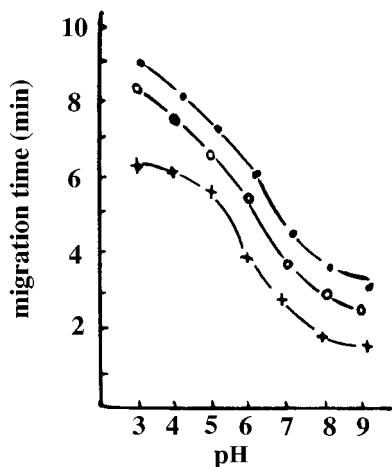


Fig. 5. Effect of pH on the electroosmotic flow time (\times) and the migration times of PGE₂ (\circ) and TXB₂ (\bullet). Other conditions as in Fig. 3.

4. Conclusions

In this work, the analysis of components in an organism by CZE was studied. The following conclusions have been drawn:

1. Capillary electrophoresis is an efficient method for analysis of trace components in a complicated matrix because the matrix influence can be easily removed.
2. For the separation of trace components, the optimum buffer system should insure that the separating time is as short as possible, which would decrease peak broadening due to diffusion of molecule.

Table 2
The analysis results for PGE₂ and TXB₂ in various SD rat lungs ($\mu\text{g ml}^{-1}$)

Group	<i>n</i>	PGE ₂		TXB ₂		Recovery (%)
		Mean value	Range	Mean value	Range	
Normal	5	0.62	0.38~0.82	11.7	9.6~14.5	85
Hypoxia	5	0.71	0.58~1.02	12.5	9.6~16.3	—
Drug	5	0.57	0.28~0.83	9.54	8.2~12.7	—

- Since many biological compounds lack chromophores at useful wavelengths, the indirect absorption detection is a kind of universal and simple detection method. We found that the probe ion, which has high molar absorption and mobility matched to the sample ion, must be selected so as to obtain high detection sensitivity and resolution.
- A complex formed between chromate and phosphomolybdic acid has high molar absorption, which could improve the detection sensitivity for PGE₂ and TXB₂. So, the complex should be used for the detection of the other compounds.

References

- [1] T. Wang, R.A. Hartwick, *J. Chromatogr.* 589 (1992) 307.
- [2] G.J.M. Bruin, A.C.V. Asten, X. Xu, H. Poppe, *J. Chromatogr.* 608 (1992) 97.
- [3] F. Foret, S. Fanali, A. Nardi, P. Bocek, *Electrophoresis* 11 (1990) 780.
- [4] P. Jandik, W.R. Jones, A. Weston, P.R. Brown, *LC-GC* 9 (1991) 634.
- [5] J.L. He, H.P. Li, L. Chen, W.Z. Chen, *Chem. J. Chin. Univ.* 17 (1996) 1198.
- [6] T.L. Yue, L. Dong, X.S. Chen, K. Mai, *J. Second Military Med. Univ.* 9 (1988) 365.
- [7] T. Wang, R.A. Hartwick, *J. Chromatogr.* 607 (1992) 119.
- [8] Y.Z. Deng, J.L. He, *High Performance Capillary Electrophoresis*, 1st ed., Science Press, Beijing, 1996, p. 257.

Extraction-spectrophotometric determination of phenytoin in capsules and plasma using potassium permanganate/dicyclohexano-24-crown-8

Mohamed A. Korany *, Mona M. Bedair, Rim S. Haggag

Department of Pharmaceutical Analytical Chemistry, Faculty of Pharmacy, University of Alexandria, 21521 Alexandria, Egypt

Received 25 October 1996; received in revised form 8 July 1997; accepted 25 July 1997

Abstract

An extraction-spectrophotometric method for the determination of phenytoin in capsules and plasma is presented. The method is based upon oxidation of phenytoin using alkaline potassium permanganate solubilized in chloroform/cyclohexane (1:1) after crowning with dicyclohexano-24-crown-8 (DC-24-C-8). The formed benzophenone being soluble in the oxidation reaction medium was directly measured at 238 nm. The optimum conditions for the reaction were studied and the detection limit was found to equal 1.2 mg/100 ml. The developed method was applied to the determination of the drug in capsules and plasma. The method is simple, accurate and avoids laborious multistep extraction procedures. © 1998 Elsevier Science B.V. All rights reserved.

Keywords: Phenytoin; Extraction-spectrophotometry; Potassium permanganate; Crown ethers

1. Introduction

Phenytoin, 5,5-diphenylimidazolidine-2,4-dione, is one of the most frequently prescribed anticonvulsants. It is considered as the drug of choice in treating all forms of epilepsy except absence seizures. It is also used to treat various psychoses, trigeminal and related neuralgias and various cardiac arrhythmias [1]. Phenytoin is extensively metabolized in the liver to 5-(*p*-hydroxyphenyl)-5-phenylhydantoin (PHPPH) and between 60 and 70% of the administered dose is excreted as free or as a glucuronide conjugate of PHPPH.

Minor metabolites include 5-(3-hydroxyphenyl)-5-phenylhydantoin, 3,4-dihydro-3,4-dihydroxyphenytoin, catechol and 3-*O*-methylcatechol. The plasma half-life varies considerably within the approximate range of 7–60 h and is dose-dependent [2].

Phenytoin is a weakly absorbing compound ($A_1^{1\%} = 27$ at 258 nm), moreover, the lack of a well defined UV absorption spectrum makes its determination in low concentrations by direct UV spectrophotometry difficult, and this problem is more aggravated if it is needed to be estimated in biological fluids.

Phenytoin has been determined spectrophotometrically by a variety of methods ranging from a

* Corresponding author.

simple procedure based on measuring the absorbance at 235 nm [3] to more complicated ones that involve chemical derivatization. Wallace et al. [4] described a method for determining phenytoin in blood based on hydrolysis of the hydantoin ring in strong alkali followed by a Hofmann degradation of the resulting amide with bromine to yield benzophenone which was steam-distilled and measured at 257 nm. At a later stage, Wallace [5] published a method for the assay of phenytoin in biological specimens consisting of hydrolysis of the hydantoin ring in strong alkali, then permanganate oxidation to benzophenone which was extracted into n-heptane after reflux for 30 min and measured at 247 nm. A more recent method [6,7] for the determination of phenytoin in plasma was based on extracting the sample with 1,2-dichloroethane, followed by back extraction from the organic layer into alkali and oxidation by potassium permanganate with heating on a steam bath. The oxidation product was extracted into 2,2,4-trimethylpentane and measured at 247 nm. Other methods for the estimation of phenytoin in pharmaceutical preparations and/or biological fluids include: colorimetry [8], spectrophotometry using orthogonal functions [9], titrimetry [10], fluorimetry [11], thin layer chromatography (TLC) [12], gas liquid chromatography (GLC) [13] and high performance liquid chromatography (HPLC) [14].

The previously published spectrophotometric methods used for the assay of phenytoin are time consuming, laborious (they need multistep extractions and reflux) and require fairly large plasma samples. GLC methods are often complicated for routine clinical situations and usually demand a time interval exceeding that required for a spectrophotometric scan. Additionally, hydantoins may be liable to thermal degradation at the injection temperature [15]. HPLC methods, although sensitive, are expensive and require sophisticated instrumentation which might not be available in many modest quality control laboratories.

Extraction analysis has been practiced for more than a century, but the use of macrocyclic compounds for this purpose is of recent date. Frensdorff and Pedersen [16,17] carried out pioneer work on extraction with crown ethers, however

their use in chemical analysis is still limited because the stability constants between metal ions and crown ethers are low. Potassium permanganate dissolved in benzene by dicyclohexyl-18-crown-6 was used for oxidising alkenes under mild conditions [18]. Also, quantitative oxidations of stilbene to adipate and of benzyl alcohol to benzoate have been demonstrated. The scope of these oxidations is still being developed since this reagent could be particularly useful where water solubility is a major limitation and where mild conditions are necessary.

In the present work, dicyclohexano-24-crown-8 (DC-24-C-8) has been used to solubilize potassium permanganate in cyclohexane/chloroform mixture (1:1). The metal complex anion formed could be used efficiently for the quantitative oxidation of phenytoin to benzophenone which, being soluble in the reaction medium, could be measured spectrophotometrically.

2. Experimental

2.1. Apparatus

A Perkin Elmer spectrophotometer Model 550 S and a laboratory centrifuge with maximum speed (4000 rpm) were used.

2.2. Materials

Phenytoin and phenytoin sodium (pharmaceutical grade) were kindly provided by Alex for pharmaceutical and chemical industries, Alexandria, Egypt. 'Epanutin' capsules containing 100 mg phenytoin sodium per capsule (Parke-Davis), DC-24-C-8, 97% containing <2% dibenzo-24 crown-8 (Aldrich), potassium permanganate AR, formalin solution 40% w/v (BDH), chloroform AR and cyclohexane AR were used.

2.3. Reagents

2.3.1. Potassium permanganate/DC-24-C-8

Weigh and transfer 0.06 g of DC-24-C-8 to a 50 ml volumetric flask using a chloroform/cyclohexane mixture (1:1). Add 600 mg of potassium

permanganate and shake the flask mechanically for 10 min. Complete the volume to the mark with the same solvent mixture. This solution was always freshly prepared.

2.3.2. Sodium hydroxide/DC-24-C-8

Weigh and transfer 0.03 g of DC-24-C-8 to a 25 ml volumetric flask by means of chloroform/cyclohexane mixture (1:1). Add 2 g of NaOH and shake the flask mechanically for 30 min. Complete to the mark with the same solvent mixture and filter the solution.

2.4. Standard phenytoin sodium solution

Accurately weigh 25 mg of phenytoin sodium and transfer it to a 120 ml separatory funnel. Add 10 ml of 1 M sulphuric acid followed by two 25 ml portions of chloroform and shake to extract phenytoin. Combine the extract in a 100 ml volumetric flask and adjust the volume.

2.5. Sample preparation

Accurately weigh and transfer an amount of the mixed contents of 20 capsules corresponding to 25 mg of phenytoin sodium to a 120 ml separatory funnel. Add 10 ml of 1 M sulphuric acid followed by 50 ml of chloroform. Shake vigorously to extract phenytoin. Combine the extract in a 100 ml volumetric flask and adjust the volume.

2.6. Procedure

2.6.1. Calibration graph

Accurately transfer volumes of 0.3–1.3 ml (in 0.2 ml steps) of standard phenytoin sodium solution to 10 ml volumetric flasks. Continue as described under assay procedure.

2.6.2. Assay

Transfer 1 ml of each of the test and standard solutions to 10 ml volumetric flasks. Add to each flask 4 ml of the prepared $\text{KMnO}_4/\text{DC-24-C-8}$ reagent and 1 ml of NaOH/DC-24-C-8 solution. Leave the flasks for 10 min for reaction time, add 1 drop of formalin solution and shake for 1 min. Complete the volume to the mark using chloro-

form and cyclohexane so that their final concentration is 50% v/v. Centrifuge the solutions at 4000 rpm for 15 min filter (to ensure the complete elimination of the formed MnO_2) and finally measure the absorbance at 238 nm against a reagent blank similarly prepared side by side using the same reagents but without drug solutions.

2.7. In vitro assay of phenytoin sodium in plasma

To 10 ml plasma contained in a 60 ml separatory funnel add 1 ml of phenytoin sodium standard solution prepared in distilled water (0.2 mg ml^{-1}) and 5 ml of 1 M sulphuric acid. Extract with three 10 ml portions of chloroform. After separation, collect the chloroformic extracts into a graduated measuring cylinder and evaporate in a water bath until the volume is reduced to 2 ml. Continue as described under assay procedure starting from 'add to each flask 4 ml of the prepared $\text{KMnO}_4/\text{DC-24-C-8}$...'. Calculate the concentration of recovered drug from a calibration graph.

3. Results and discussion

Fig. 1(a) shows the UV absorption spectrum of phenytoin in chloroform. It is obvious that the lack of well defined peaks with reasonable specific intensity renders its direct determination by UV spectrophotometry a fairly hard task especially when good sensitivity is a prerequisite. In the present study, alkaline potassium permanganate oxidation was conducted in organic solvent (cyclohexane/chloroform 1:1) where both the drug and its oxidation product are soluble. Solubilization of KMnO_4 and NaOH in this organic mixture was made possible through the use of a macrocyclic polyether 'DC-24-C-8' which has the useful property of solubilizing inorganic compounds in aprotic solvents including aromatic hydrocarbons. The formed benzophenone (Scheme 1) was consequently measured directly at 238 nm against a blank (Fig. 1(b)). The shift of λ_{max} towards a shorter wavelength (238 nm) may be due to the high polarity of the medium contributed by chloroform and the crown ether [19].

DC-24-C-8 does not absorb significantly above 220 nm. The absorption spectrum of KMnO_4 /DC-24-C-8 in chloroform/cyclohexane (1:1) is very similar to that of aqueous permanganate ion in 0.1 M sulphuric acid (Fig. 2(a) and (b)), thus proving its solubilization in organic solvents by using the crown ether as ligand.

3.1. Optimization of the reaction conditions

3.1.1. Choice of the cyclic polyether

The cyclic polyether was chosen in such a way to give a stable complex with potassium. Thus, DC-24-C-8 was used in the present study for the following reasons.

1. Having a hole diameter of approximately 4 Å, it can accommodate potassium ions with ionic diameter of 2.66 Å which provides a comfortable fitting condition for them.

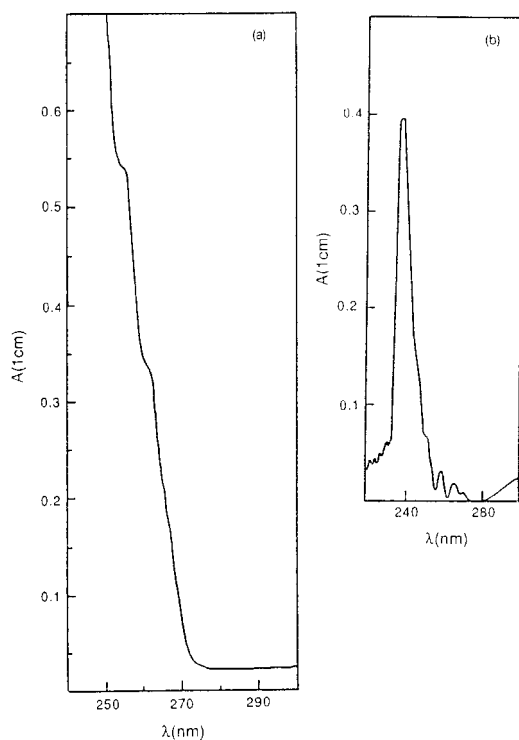
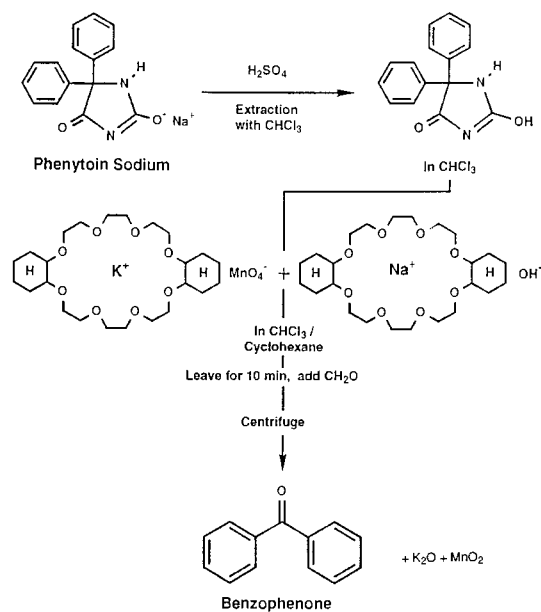


Fig. 1. (a) Absorption spectra of 18.4 mg/100 ml of phenytoin in chloroform and (b) benzophenone in 10 ml of cyclohexane/chloroform mixture 1:1 corresponding to 3 mg/100 ml of phenytoin sodium after oxidation with potassium permanganate/DC-24-C-8 reagent.



Scheme 1.

2. It possesses eight oxygen atoms which can form ion dipoles with potassium ion. Moreover, these oxygen atoms are arranged in a cylindrical symmetrical configuration which permits the formation of stable salt complexes [20].

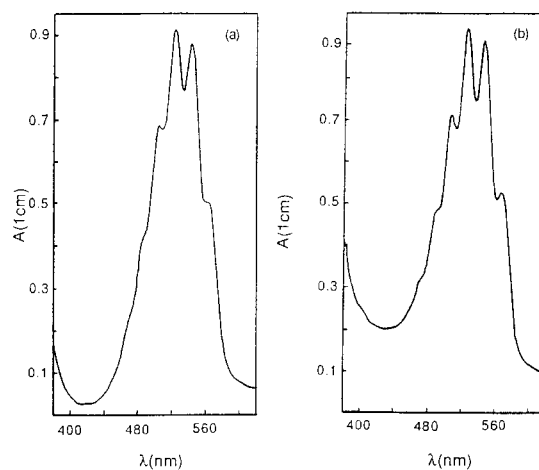


Fig. 2. (a) Absorption spectra of 3.045 mg potassium permanganate in 50 ml of 0.1 M sulphuric acid and (b) 47.90 mg of potassium permanganate in 10 ml of cyclohexane/chloroform mixture 1:1 containing 0.0049 of DC-24-C-8.

- It has two cyclohexyl groups rather than two benzo groups which firstly increases the basicity of oxygens leading to higher stability of the formed complex, secondly, the transparency in the UV region and thirdly, the flexibility of the macrocyclic ligand to wrap itself around the cation (i.e. steric hindrance produced by the benzo groups results in a weaker cation–ligand interaction).

3.1.2. Choice of the solvent

The solvent or reaction medium was chosen on the basis of three factors: (1) the solubility of phenytoin and benzophenone; (2) the UV cutoff of the solvent; and (3) the extractability of $\text{KMnO}_4/\text{DC-24-C-8}$. In general, the common solvents in extraction with crown ethers are chloroform, 1,2-dichloroethane, benzene and nitrobenzene. In order to fulfill all the above requirements, a 1:1 mixture of chloroform and cyclohexane was found to be the most suitable.

3.1.3. Effect of $\text{KMnO}_4/\text{DC-24-C-8}$ and $\text{NaOH}/\text{DC-24-C-8}$ concentrations

The effect of changes in $\text{KMnO}_4/\text{DC-24-C-8}$ concentration was studied by measuring the absorbance of benzophenone at 238 nm, for solutions containing a fixed concentration of phenytoin and different volumes of $\text{KMnO}_4/\text{DC-24-C-8}$ reagent. It was found that 4–6 ml of the reagent gave maximum absorption. On the other hand, it was previously demonstrated that within wide limits the molarity of NaOH is not critical for the oxidation of phenytoin [15].

3.1.4. Effect of oxidation time

The effect of oxidation time was studied by using a fixed concentration of phenytoin and the optimum reagent concentration. The optimum time was selected as 10 min.

3.1.5. Elimination of excess potassium permanganate

An excess of KMnO_4 was used to oxidise phenytoin. The remaining unconsumed oxidant was eliminated. Several reducing agents were tried where formalin solution was found to be the most convenient.

3.2. Calibration graph construction

Using the previously described optimum experimental conditions, it was found that the graph obtained by plotting the absorbance at 238 nm versus concentration of phenytoin sodium showed a linear relationship over the range of 0.87–3 mg/100 ml. The linear regression equation was found to be: $A = 0.008 + 0.126C$, where C is the concentration in mg/100 ml. The correlation coefficient was 0.9994 and the detection limit was found to equal 1.2 mg/100 ml.

4. Applications

The proposed method was applied to the determination of phenytoin sodium in capsules and the results obtained are presented in Table 1. The presence of interferences in commercial capsules can not be overlooked, therefore the results obtained using the proposed method were compared to those of an HPLC method [21] (Table 1) using t - and F -tests. The calculated values did not exceed the corresponding theoretical ones, thus indicating the insignificant difference between the compared methods.

Monitoring of phenytoin plasma level is of great importance in clinical studies because of its non-linear elimination pharmacokinetics [21] and the possibility of toxicity or inadequacy of the dosage after long treatment. The ability of the proposed method to determine phenytoin in plasma has been appraised through spiking plasma samples with the drug at different concentration levels. It was found that phenytoin sodium could be estimated with good recoveries (Table 2) at the levels of 16–22 $\mu\text{m l}^{-1}$ in plasma (provided that 6–10 ml specimens are used), thus indicating that there is no interference from endogenous constituents. Also, the primary metabolite (PHPPH) does not interfere [5]. The alkaline nature of the permanganate solution and the polarity of the hydroxyl group make the phenolic metabolites insoluble in the organic phase.

Table 1

Assay results of phenytoin sodium in capsules by the proposed spectrophotometric method and the comparative HPLC method

Exp. no.	Spectrophotometry (proposed method)		HPLC (comparative method)	
	Label claim (mg/100 ml)	Found (%)	Label claim (mg/100 ml)	Found (%)
1	1.24	99.7	2.02	97.6
2	2.24	99.4	2.42	98.6
3	2.48	98.5	2.42	99.4
4	2.48	98.3	3.23	98.5
5	2.48	100.2	3.64	99.4
6	2.48	99.0	4.04	99.2
7	2.98	97.4	4.04	98.5
Mean		98.9		98.7
S.D.		0.9		0.6
C.V. (%)		0.9		0.6
t^*	0.46			
F^{**}	2.12			

* Theoretical = 2.18 at $P = 0.05$ and $\theta = 12$.** Theoretical = 4.28 at $P = 0.05$ and $\theta_1 = \theta_2 = 6$.

Table 2

Recovery of phenytoin sodium added to human plasma after oxidation and extraction using potassium permanganate/DC-24-C-8

Concentration of phenytoin sodium ($\mu\text{g ml}^{-1}$)	Recovery ($\mu\text{g ml}^{-1}$)	% Recovery
22.60	21.96	97.2
22.60	20.90	92.5
19.20	18.49	96.3
17.70	16.94	95.7
15.80	15.09	95.5
Mean \pm S.D.		95.4 \pm 1.8
C.V. (%)		1.9

5. Conclusion

The proposed method is suitable for the determination of phenytoin in capsules and in plasma. It is specific, rapid and simple as no tedious extraction steps or pH adjustments are required.

References

- [1] A.G. Gilman, T.W. Rall, A.S. Nies, P. Taylor, The Pharmacological Basis of Therapeutics, 8th ed., Pergamon, Oxford, 1991.
- [2] A.C. Moffat, J.V. Jackson, M.S. Moss, B. Widdop, E.S.

Greenfield, Clarke's Isolation and Identification of Drugs, 2nd ed., The Pharmaceutical Press, London, 1986.

- [3] V.G. Belikov, E.V. Kompantseva, A.S. Saushkina, *Zavod. Lab.* 40 (1974) 265.
- [4] J.E. Wallace, J.D. Biggs, E.V. Dahl, *Anal. Chem.* 37 (1965) 410.
- [5] J.E. Wallace, *Anal. Chem.* 40 (1968) 978.
- [6] S.N. Ahmed, B.L. Jaikhani, N.F. Jaffery, *J. Indian Med. Res.* 74 (1981) 600.
- [7] S.N. Ahmed, B.L. Jaikhani, N.F. Jaffery, *J. Pharmacol. Methods* 9 (1983) 33.
- [8] G.R. Rao, S.S.N. Murty, *Indian Drugs* 19 (1981) 22.
- [9] M.M. Amer, A.K.S. Ahmed, S.M. Hassan, *J. Pharm. Pharmacol.* 29 (1977) 291.
- [10] N.A. Tret'yakov, *Farmatsiya* 31 (1982) 67.
- [11] G.N. Meier, D.S. Kuhn, F.O. Pierart, *Rev. Med. Chile* 107 (1979) 583.
- [12] H.Y. Aboul Enein, V. Serignese, *Anal. Lett.* 27 (1994) 723.
- [13] L. Erdey, Y.M. Dessouky, L. Kaplar, J. Takacs, *Acta Pharm. Hung.* 40 (1970) 102.
- [14] M.T. Maya, A.R. Farinha, A.M. Lucas, J.A. Morais, *J. Pharm. Biomed. Anal.* 10 (1992) 1001.
- [15] J.E. Wallace, H.E. HamiHon, *J. Pharm. Sci.* 63 (1974) 1795.
- [16] I.M. Kolthoff, *Anal. Chem.* 51 (1979) 1R.
- [17] M. Yoshio, H. Noguchi, *Anal. Lett.* 15 (1982) 1197.
- [18] D.J. Sam, H.F. Simmons, *J. Am. Chem. Soc.* 94 (1972) 4024.
- [19] S. Walker, H. Straw, *Spectroscopy*, vol. 2, Science Paperbacks, Chapman and Hall, London, 1967, p. 240.
- [20] J.J. Christensen, J.D. Hill, R.M. Izatt, *Science* 174 (1971) 459.
- [21] J.E. Slonek, G.W. Peng, W.L. Chiou, *J. Pharm. Sci.* 67 (1978) 1462.



ELSEVIER

Talanta 46 (1998) 15–21

Talanta

Fabrication of a multilayer film electrode containing porphyrin and its application as a potentiometric sensor of iodide ion

Changqing Sun ^{a,*}, Jinghong Zhao ^a, Hongding Xu ^a, Yipeng Sun ^b, Xi Zhang ^b, Jiacong Shen ^b

^a Department of Chemistry, Jilin University, Changchun 130023, People's Republic of China

^b Key Lab of Supramolecular Spectra and Structure, Jilin University, Changchun 130023, People's Republic of China

Received 7 April 1997; received in revised form 24 July 1997; accepted 28 July 1997

Abstract

A novel iodide ion-selective electrode has been produced based on a molecular deposition technique in which water-soluble porphyrin was alternatively deposited with water-soluble polypyrrole on a 2-aminoethanethiol modified silver electrode. The potentiometric response is independent of pH of the solution between pH 1 and 7, while it is dependent on the nature of the medium. The electrode has a linear dynamic range between 1.6×10^{-6} and 0.1 M with a Nernstian slope of 59 mV/decade and a detection limit of 1.0×10^{-6} M in acetate buffer (0.1 M, pH 4.6). The electrode has the advantages of low resistance, short conditioning time and fast response. © 1998 Elsevier Science B.V. All rights reserved.

Keywords: Multilayer films; Sensor; Potentiometry; Iodide ion; Porphyrin

1. Introduction

The fabrication of an electrode surface with functional multilayer films has been attracting much interest because of its potential application [1,2]. Recently, Decher and coworkers developed the preparation of multilayer ultrathin films by alternating deposition of bipolar cationic and anionic compounds (or polyelectrolytes) [3–5]. This new technique is an extension of self-assembly developed by Sagiv [6] and is a rapid and experimentally very simple way to produce complex layered structures with precise control of layer

composition and thickness. We developed this concept further and achieved molecular deposition (MD) films containing polyelectrolytes [7], porphyrin, phthalocyanine [8], enzyme [9], superfine particles [10] and so on. In addition, assembling alternate dye-polyion molecular films by electrostatic layer-by-layer adsorption was reported by Ariga et al. [11].

In this paper, this new technique was applied to fabricate a new kind of chemically-modified electrode (CME) by alternating deposition of water-soluble porphyrin and polypyrrole on the surface of a 2-aminoethanethiol-modified silver electrode. The CME was shown to exhibit excellent potentiometric response toward iodide ion. In this

* Corresponding author. Fax: +86 431 9823907.

work, our primary interest was focused on devising a new kind of CME which could be used as a potentiometric sensor for iodide ion and would also possess quite a few features, such as simple fabrication, fast response, independence of electrode size and topology, good mechanical and chemical stability, and so on.

2. Experimental

2.1. Reagents

The molecular structures of the porphyrin and polypyrrole used to fabricate the multilayer film electrode are shown in Fig. 1. 2-Aminoethanethiol and tetraphenylporphinetetrasulfonic acid (tppS₄) were obtained from Aldrich. Pyrrole obtained from Aldrich was distilled and stored under a nitrogen atmosphere before use. Water-soluble polypyrrole solutions were prepared following the literature [12]. In short, pyrrole monomer was

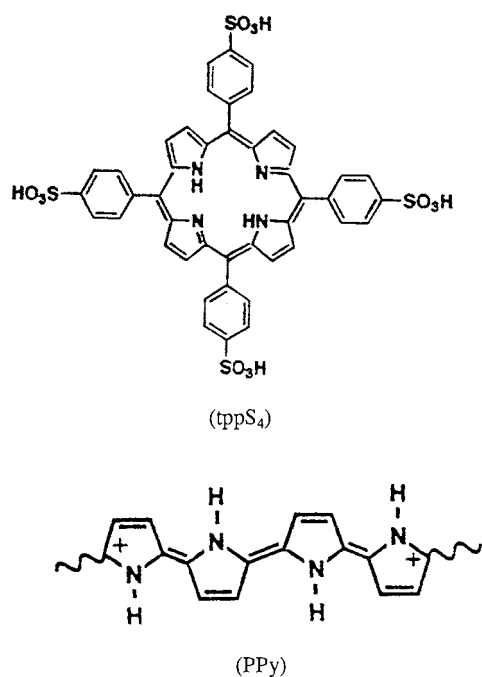


Fig. 1. Molecular structures of the porphyrin and polypyrrole used to fabricate the multilayer film electrode.

added to an aqueous ferric chloride solution whose pH had been adjusted to the desired level using concentrated HCl (typically pH 1.0). The solution was aged for 15 min and filtered prior to use. Typical solutions were composed of 0.02 M pyrrole monomer and 0.006 M FeCl₃. To ensure controlled deposition, the solutions were typically used for only 2–3 h. All other chemicals were of analytical grade and all the solutions were prepared with doubly distilled water.

2.2. Apparatus

UV–Vis spectra were obtained using a Shimadzu 3100 UV-Vis-near-IR recording spectrophotometer. Potential measurements were made with a Model pHx-215 Ionalyzer (Shanghai Second Analytical Instrument Plant, China). The electrochemical cell used can be represented by: Ag|MD film | acetate buffer (0.1 M, pH 4.6)|| KCl(sat.), Hg₂Cl₂|Hg

The electrode potential was measured in 50 ml of a 0.1 M acetate buffer solution (pH 4.6) with stirring at 25°C. The electrodes were preconditioned in stirred water for 5–10 min until a steady potential was obtained before use. Cyclic voltammetric experiments were performed on a Model DH-2 potentiostat/galvanostat (Jilin Longjing Analytical Instrument Plant, China). A three-electrode cell was used with silver electrode modified with MD film or bare silver electrode as the working electrode, saturated calomel as the reference electrode and platinum wire as the auxiliary electrode. 2:1(v/v) phosphate buffer solution (0.1 M, pH 5.0)/acetonitrile were used as cyclic voltammetric experiments and deoxygenated for 10 min before use.

2.3. Fabrication of multilayer film electrode

Fabrication of multilayer films on quartz slides is similar to that of tppS₄/PyC₆BPC₆Py system [8] by substituting PyC₆BPC₆Py with water-soluble polypyrrole. Fabrication of multilayer films on a silver electrode was as follows: a silver electrode (1.5 mm diameter) was polished with emery paper followed by alumina (1.0, 0.5 and 0.3 μm). The

resulting electrode was thoroughly washed with water, sonicated in ethanol, washed again with water and ethanol and finally dried in air. A clean silver electrode was first immersed for 24 h at room temperature in an ethanolic solution that consisted of 0.01 M 2-aminoethanethiol to give one monolayer of self-assembled film. After rinsing with ethanol, the electrode was transferred into 0.1 M HCl to obtain a positively charged surface followed by immersion in a solution containing 1 mg tppS₄ in 10 ml H₂O for 30 min. In this way the surface of the electrode was covered with one layer and its surface charge was reversed. After rinsing with water, the electrode was transferred into the in situ polymerized polypyrrole solution for 10 min, thus adding a second layer and restoring the original surface charge. A multilayer tppS₄ film can be obtained by repeating these two steps in a cyclic fashion. In the present experiments, a silver electrode deposited with six layers of tppS₄ was used throughout. Between measurements, the electrode was stored in a dry state at room temperature.

3. Results and discussion

3.1. Fabrication of the multilayer film electrode

Self-assembly of a monolayer of alkanethiols on a silver surface has been reported [13–15]. In this study, a clean silver electrode was first incubated in an ethanolic solution of aminoethanethiol to get a self-assembled monolayer film. Afterwards, the modified substrate was dipped into 0.1 M HCl solution to obtain a positively charged surface. The multilayer tppS₄ anions can be obtained by alternating deposition of tppS₄ with water-soluble polypyrrole based on electrostatic interaction. The deposition process was followed by UV–Vis absorption spectra using a quartz slide as substrate (Fig. 2). An obvious absorption peak was found at 422 nm, which corresponds to the Soret band of the porphyrin. The linear increase in the optical density of the films with number of layers indicates a process of uniform deposition. The broad visible

absorption confirms the existence of highly conductive polypyrrole. Fig. 3 shows cyclic voltammograms of a bare silver electrode and a silver electrode modified with six layers of porphyrin in 2:1(v/v) phosphate buffer (0.1 M, pH 5.0)/acetonitrile, respectively. It can be seen that no response was obtained with the bare silver electrode; however on the modified silver electrode, one coupled redox peak appeared which is assigned to the contribution of the porphyrin. These results show that multilayer films containing porphyrin can be fabricated on the surface of the silver electrode by means of the molecular deposition technique.

3.2. The pH dependence of the multilayer film electrode response to iodide ion

Fig. 4 shows the pH dependence of the observed potentials of the electrode in different pH values of H₃PO₄ and NaH₂PO₄ buffer solutions in the presence of 1×10^{-3} M iodide ion. From Fig. 4 it can be seen that stable response potentials were obtained in a pH range of 1–7. This result shows that in the pH range of 1–7, the pH value of the solutions had no effect on the response behavior of the electrode.

3.3. Effects of media on the multilayer film electrode response

Fig. 5 shows the effects of different buffer media at the same concentration [0.1 M] and different pH on the response behavior of the electrode. As indicated in Fig. 5, the electrode had the largest dynamic range in acetate buffer (pH 4.6) and phosphate buffer (pH 4.0). The response slopes were 59 and 55 mV/decade, respectively. The linear ranges were between 1.6×10^{-6} and 0.1 M and 2.0×10^{-6} and 0.1 M, respectively. In pH 2.0 and 6.0 phosphate buffer, the responses of the electrode were good, but their linear ranges were narrow (6.3×10^{-6} and 0.1 M for pH 2.0 and 4.0×10^{-6} and 0.1 M for pH 6.0). Because the acetate buffer solution is the buffer system usually used, it was chosen for the following experiments.

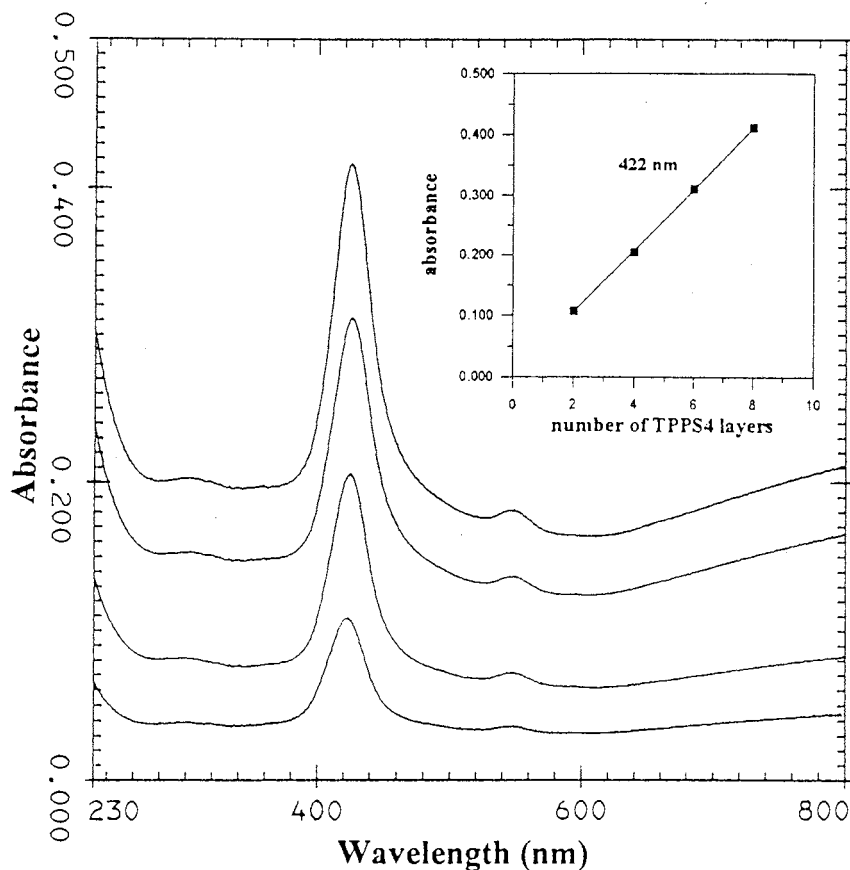


Fig. 2. UV-Vis absorption spectra of alternating film deposition of tppS₄ and water-soluble polypyrrole. From the lower to upper curves, the number of tppS₄ layers is 2, 4, 6, 8. The insert shows the absorption at 422 nm as a function of the number of layers deposited.

3.4. Performance of the multilayer film electrode

A typical calibration graph for the electrode is shown in Fig. 6. The electrode has a linear response over the range of 1.6×10^{-6} to 0.1 M with a Nernstian response slope of 59 mV/decade and a detection limit (extrapolation of linear graph) of 1.0×10^{-6} M. The typical dynamic response time of the electrode (t_{95}) was less than 15 s under stirred conditions for 1×10^{-5} to 1×10^{-4} M iodide ion. The steady state potential response after addition of iodide ion remained constant for 30–60 s, then slowly increased in the negative direction and reached a final steady potential value.

The potential response of the electrode towards iodide ion has good repeatability. The relative standard deviation (R.S.D.) is 1.7% for ten determinations of 1×10^{-3} M iodide ion at pH 4.6, 0.1 M acetate buffer.

3.5. Studies of interference

The selective coefficients of the electrode were determined by the method involving a fixed interfering ion concentration of 0.1 M, in 0.1 M acetate buffer (pH 4.6) [16]. In the calculations, activities were replaced by the corresponding concentrations. Table 1 lists the selectivity coefficients (average of three determinations). From Table 1 it

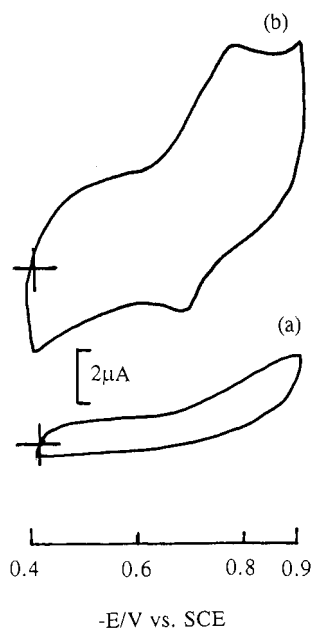


Fig. 3. Cyclic voltammograms of the bare silver electrode (a) and silver electrode modified with six layers of porphyrin (b) in 2:1(v/v) phosphate buffer (0.1 M, pH 5.0)/acetonitrile. Scan rate, 50 mV.

can be seen that for the common anions the electrode has good selectivity compared with poly[tetrakis(*p*-aminophenyl)porphyrin] film-modified electrode [17].

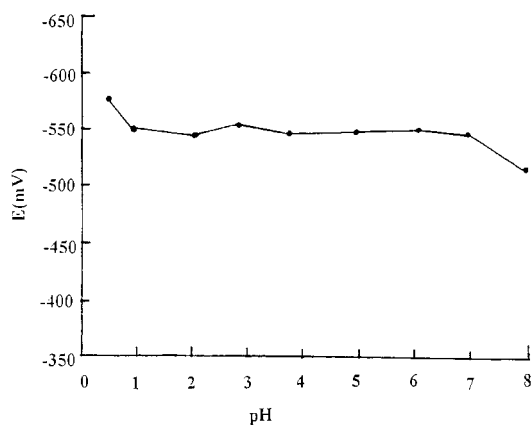


Fig. 4. pH dependence profile of the multilayer film electrode containing tppS₄. The solutions contain H₃PO₄-NaH₂PO₄ and 1×10^{-3} M iodide ion.

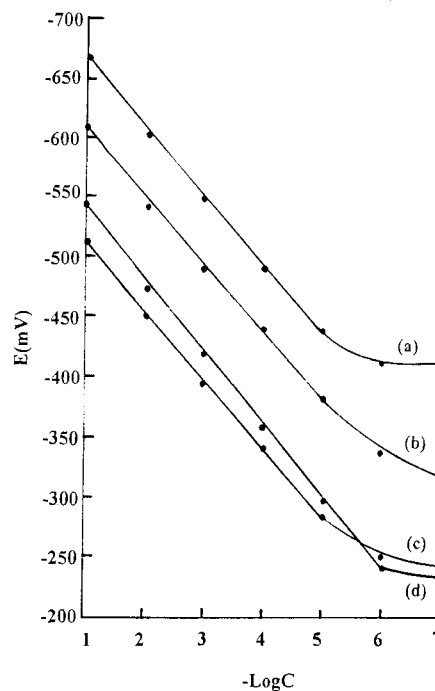


Fig. 5. Effects of different buffer media on the response of the electrode to iodide ion.

1. (a): 0.1 M H₃PO₄-NaH₂PO₄ (pH 2.0)
2. (b): 0.1 M Na₂HPO₄-NaH₂PO₄ (pH 4.0)
3. (c): 0.1 M Na₂HPO₄-NaH₂PO₄ (pH 6.0)
4. (d): 0.1 M HAC-NaAC (pH 4.6).

3.6. Stability of the multilayer film electrode

In the experiments, we found that the number of tppS₄ layers deposited has a marked influence on the response and stability of the multilayer film electrode, an optimum number of layer existing for the best response and stability. When the electrode consisted of six layers of tppS₄ in our case, the best response and stability were obtained. For example, for 60 days after the sensor has been fabricated, a calibration graph was obtained every 2 days, and its slope did not change.

3.7. Analytical application

A suitable amount of dry edible seaweed was weighed into a china crucible, 2 ml no-iodine water and 2 ml 2 M KOH solution added and

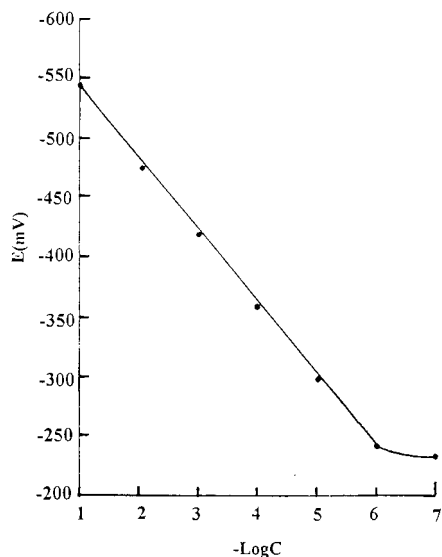


Fig. 6. A typical calibration graph for the electrode (acetate buffer: 0.1 M, pH 4.6).

stirred until a paste formed. Then it was transferred into an oven for 1–2 h at 80–100°C, then into a high temperature oven for 4–6 h at 550–600°C. After charcoal formed, it was washed with hot no-iodine water, filtered into a 50-ml calibrated flask and adjusted to pH 7 with concentrated H_2SO_4 solution then diluted to the mark with no-iodine water. An appropriate volume of the solution was added to the cell and tested according to the above procedure. The results obtained were compared with a spectrophotometric method [18] and were shown to be in agreement: for sample 1, 10.0 mg/kg for the proposed method and 9.8 mg/kg for the spectrophotometric

Table 1
Selectivity coefficients for the electrode

Anion	Log K_{ij}^{pot}
Cl^-	-4.9
Br^-	-3.9
NO_3^-	-5.0
SO_4^{2-}	-5.5
SCN^-	-3.7
SO_3^{2-}	-4.5
NO_2^-	-4.0
ClO_4^-	-3.7

method; for sample 2, values are 12.5 and 12.0; for sample 3, 11.5 and 11.7 mg/kg, respectively.

4. Conclusion

An iodide ion-selective electrode fabricated by the molecular deposition technique has a stable and selective potential response toward iodide ion in 0.1 M acetate buffer solution with a detection limit of 1.0×10^{-6} M and a slope of 59 mV/decade. The electrode has a fast response, low resistance and good reproducibility.

Acknowledgements

The authors are grateful for the support of the Electroanalytical Open Laboratory of Changchun Institute of Applied Chemistry, and the Chinese Academy of Sciences.

References

- [1] I. Willnor, A. Riklin, B. Shoham, D. Rivenzon, E. Katz, Development of novel biosensor enzyme electrodes: glucose oxidase multilayer arrays immobilized onto self-assembled monolayers on electrodes, *Adv. Mater.* 5 (1993) 912.
- [2] D. Ingersoll, P.J. Kulesza, L.R. Faulkner, Polyoxometalate-based layered composite film on electrodes: preparation through alternate immersion in modification solution, *J. Electrochem. Soc.* 141 (1994) 140.
- [3] G. Decher, J.D. Hong, Buildup of ultrathin multilayer films by a self-assembly process: 1. Consecutive adsorption of anionic and cationic bipolar amphiphiles, *Macromol. Chem., Macromol. Symp.* 46 (1991) 321.
- [4] Y. Lvov, G. Decher, H. Mohwald, Structural characterization, and thermal behavior of layer-by-layer deposited ultrathin films of poly(vinyl sulfate) and poly(allylamine), *Langmuir* 9 (1993) 481.
- [5] G. Decher, Y. Lvov, J. Schmitt, Proof of multilayer structural organization in self-assembled polycation-polyanion molecular films, *Thin Solid Films* 244 (1994) 772.
- [6] J. Sagiv, Organized monolayers by adsorption. 1. Formation and structure of oleophobic mixed monolayers on solid surfaces, *J. Am. Chem. Soc.* 102 (1980) 92.
- [7] M. Gao, X. Kong, X. Zhang, J. Shen, Build-up of molecular deposition films bearing mesogenic groups, *Thin Solid Films* 244 (1994) 815.

- [8] X. Zhang, M. Gao, X. Kong, Y. Sun, J. Shen, Build-up of a new type of ultrathin film porphyrin and phthalocyanine based on cationic and anionic electrostatic attraction, *J. Chem. Soc., Chem. Commun.* (1994) 1055.
- [9] W. Kong, X. Zhang, M. Gao, H. Zhou, W. Li, J. Shen, A new kind of immobilized enzyme multilayer based on cationic and anionic interaction, *Macromol. Rapid Commun.* 15 (1994) 405.
- [10] M. Gao, X. Zhang, Y. Yang, B. Yang, J. Shen, A monolayer of PbI_2 nanoparticles adsorbed on MD-LB film, *J. Chem. Soc. Chem. Commun* (1994) 2229.
- [11] K. Ariga, Y. Lvov, T. Kunitake, Assembling alternate dye-polyion molecular films by electrostatic layer-by-layer adsorption, *J. Am. Chem. Soc.* 119 (1997) 2224.
- [12] J.H. Cheung, A.F. Fou, M.F. Rubner, Molecular self-assembly of conducting polymers, *Thin Solid Films* 244 (1994) 985.
- [13] P.E. Laibinis, G.M. Whitesides, D.L. Allara, Y.-T. Tao, A.N. Parikh, R.G. Nuzzo, Comparison of the structures and wetting properties of self-assembled monolayers on n-alkanethiols on the coinage metal surfaces, Cu, Ag, Au¹, *J. Am. Chem. Soc.* 113 (1991) 7152.
- [14] P.E. Laibinis, C.D. Bain, G.M. Whitesides, Attenuation of photoelectrons in monolayers of n-alkanethiols adsorbed on copper, silver, and gold, *J. Phys. Chem.* 95 (1991) 7017.
- [15] J.Y. Gui, D.A. Stern, D.G. Frank, F. Lu, D.C. Zapien, A.T. Hubbard, Adsorption and surface structural chemistry of thiophenol, benzyl mercaptan, and alkyl mercaptans, *Langmuir* 7 (1991) 955.
- [16] X. Gao, *Introduction to Electroanalytical Chemistry*, Academic Publishing House, Beijing, 1986, p. 133.
- [17] Y. Yan, Y.C. Cai, Y.C. Yu, Chemically modified electrode sensitive to iodide based on electropolymerized porphyrin derivative, *Chim. Sinica Acta* 52 (1994) 192.
- [18] F.L. Liu, J.X. Dai, *Physical and Chemical Methods of Foods*, Light Industry Publishing House, Beijing, 1987, p. 355.



ELSEVIER

Talanta 46 (1998) 23–38

Talanta

Quantitative analysis of chromium(V) by EPR spectroscopy

John Chappell, Barry Chiswell *, Arran Canning

Department of Chemistry, The University of Queensland, Brisbane QLD 4072, Australia

Received 13 May 1997; received in revised form 24 July 1997; accepted 28 July 1997

Abstract

A procedure to accurately quantitate chromium(V) in environmental and medicinal chemistry samples was developed using electron paramagnetic resonance spectroscopy (EPRS) as the method of detection. It was found to have an error in the order of $\pm 10\%$ and a detection limit of 0.010 mM (0.5 mg l^{-1}) chromium(V). The method has been used to quantitate the formation of chromium(V) in the interaction of chromium(VI) with fulvic acid and a simple model of this acid, viz, 1,2-dihydroxybenzene. Analysis of solutions obtained from the reaction of 1,2-dihydroxybenzene with chromium(VI) demonstrated that even when the organic substrate was present in a 182-fold excess, the maximum chromium(V) concentration attained represented just 1.44% of the initial chromium(VI). Reactions between chromium(VI) and fulvic acid yielded similar results. It was therefore concluded that at background environmental concentrations of chromium and fulvic acid, the production of chromium(V) is insignificant, however, its possible importance in contaminated systems cannot be disregarded on this basis alone. The method for quantitative analysis reported in this paper should be an invaluable tool for investigations into the significance of chromium(V) in the toxicological mechanism of chromium(VI) and its role as a mutagenic agent. © 1998 Elsevier Science B.V. All rights reserved.

Keywords: Chromium(V); Quantitative analysis; Electron paramagnetic spectroscopy; Fulvic acid; Environment

1. Introduction

Speciation of chromium in environmental samples has generally been a 2-fold process. Typically, the total chromium concentration is determined by techniques such as atomic absorption spectroscopy, while the hexavalent chromium is analysed by a variety of procedures including the diphenyl carbazide method [1–3] and ion chromatography [4]. The underlying assumption in this methodology is that all chromium present will

be inorganic and in either the hexavalent or the trivalent form [5–8]. Therefore, by obtaining the concentration of one species [Cr(VI)] and knowing the total chromium concentration, the concentration of the other species [Cr(III)] can be obtained by difference. Some researchers have suggested that such assumptions are simplistic and result in mis-leading conclusions because they do not take into consideration the possibility of organically or colloiddally bound chromium being present in the system. In an effort to overcome such problems, these researchers have developed methods using ion chromatography and high per-

* Corresponding author.

Table 1
EPR parameters for the analysis of chromium(V) formed from the dihydroxybenzene/chromium reactions

Vol. Cr(VI) (ml)	Vol. diol (ml)	Vol. water (ml)	Mole Cr(VI) (ml)	Mole diol (ml)	Molar ratio diol:Cr(VI)
10.0	10.0	0.0	0.0002	0.00182	9.1:1
10.0	6.0	4.0	0.0002	0.00109	5.5:1
10.0	2.0	8.0	0.0002	0.00036	1.8:1

formance liquid chromatography to account for these other forms of chromium [9–12].

Most previous work has ignored the possible presence of chromium compounds in oxidation states other than (VI) and (III), and until the advent of EPRS studies, the formation of chromium(V) was an unproven hypothesis in the chromium(VI) reduction cycle due to its high reactivity and low kinetic stability [13]. Detection of both inorganically [14] and organically bound chromium(V) with ligands containing both oxygen and sulfur donor atoms such as diols and glycols [15–17], phenols [18] and thiols [19–21] has been achieved, although quantitation has been unsuccessful. Chromium(V) production has also been reported with compounds of biological and biochemical interest, including D-glucose, D-fructose and other saccharides and their derivatives [22,23], ascorbate [24], L-rhamnose and D-mannose [25] and adenosine [26].

Although chromium(III) is probably the ultimate form of the metal bound in the cell, there is evidence accumulating that the oxidation states +4 and +5 maybe important in the reaction sequence leading to the adverse biological behaviour of chromium [27]. For instance, chromium(IV) and chromium(V), both exchange ligands more readily than chromium(III), leading to these species being proposed to be the active genotoxic forms of chromium [28]. In 1982, Wetterhahn [29] was the first to report a stable intermediate chromium(V) compound formed from the metabolism of inorganic chromate by rat liver microsomes in the presence of NADH. The chromium(V) was detected by EPRS and persisted for approximately 80 min after initiation of the reaction. The suggested formation of the chromium(V) was by a one-

electron transfer by the microsomal electron transport P-450 system to chromate [29]. Since then there has been a vast amount of work undertaken in determining what leads to the production of chromium(V) in the cells, and relatively long-lived chromium(V) species have been produced by the following methods: the action of glutathione on chromate [21,27]; the reaction of riboflavin (vitamin B₂) with chromium(VI) [30]; and chromate reactions with ribonucleotides. These reactions have all been studied in vitro due to the limitations of EPRS, but recently the detection of chromium(V), from chromium(VI) reduction, has been found to be possible using low frequency EPRS [31]. Recent studies have shown also that chromium(V) intermediates are definitely capable of producing damage to DNA [29].

It has been suggested from the results of EPRS studies that stable, water-soluble chromium(V) compounds can form from the reaction of humic substances with hexavalent chromium [32–34]. While the evidence for these reactions is sound, the concentrations of reactants used in the relevant studies were unrealistically high with respect to likely concentrations of chromium to be found environmentally. It was the aim of this research to verify the production of stable, water-soluble chromium(V) complexes with fulvic acid and to quantify the amounts of chromium(V) formed using electron paramagnetic resonance (EPR) spectroscopy as a detection method. The method of analysis developed was also applied to the determination of chromium(V) produced from the interaction of chromium(VI) with 1,2-dihydroxybenzene, which can be considered to be a very simple model molecule of fulvic acid.

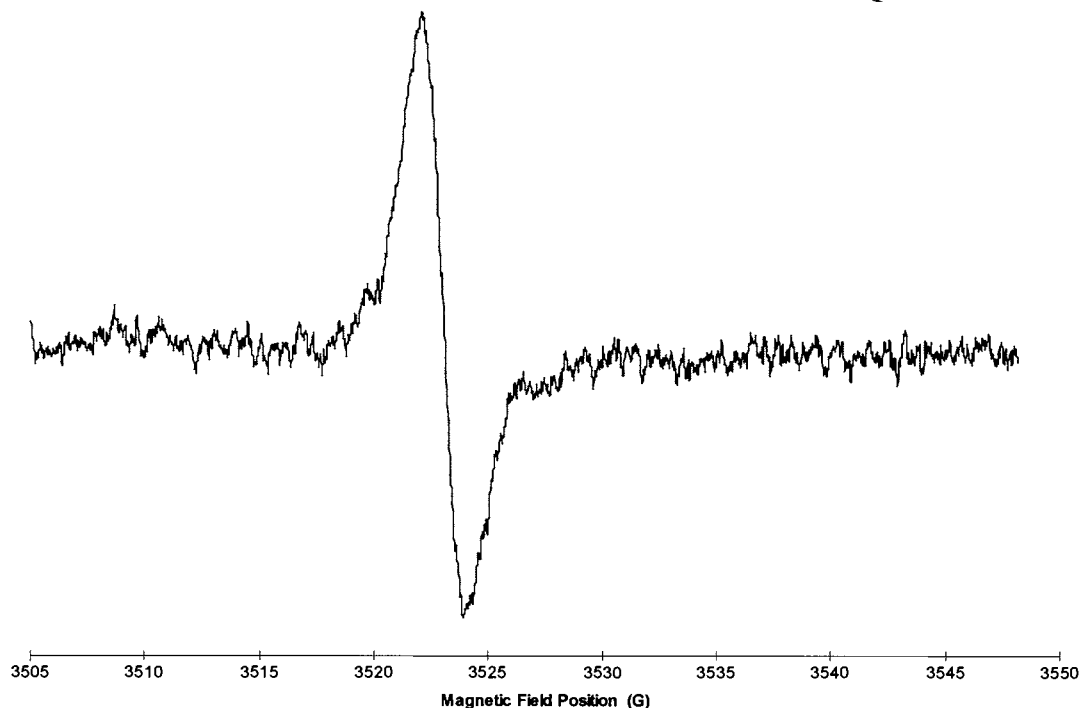


Fig. 1. EPR spectrum of the chromium(V) formed from the reaction of equal volumes of 0.14% (w/v) fulvic-L and 0.020 M potassium chromate in aqueous solution at pH 4.2. EPR parameters: microwave power = 126 mW; receiver gain = 3.20×10^5 ; modulation amplitude = 1.6 G.

2. Experimental

2.1. Reagents and glassware

A stock solution of 0.020 M chromium(VI) was prepared from potassium chromate (K_2CrO_4 , 99.5%, BDH Chemicals Ltd.). Fulvic acid solutions were prepared on the day of use from solid fulvic acid extracted from lucerne compost by a method outlined previously [35]. Solutions of 1,2-dihydroxybenzene ($\text{C}_6\text{H}_6\text{O}_2$, 99.0%, Riedel-deHaen) were prepared on the day of use and stored away from light to minimise decay. Commercially available 2-ethyl-2-hydroxybutyric acid ($\text{C}_6\text{H}_{12}\text{O}_3$, Aldrich Chemical Company Inc., 99%) was used without further purification. Anhydrous sodium dichromate was obtained from the dihydrate ($\text{Na}_2\text{Cr}_2\text{O}_7$, 99.5%, BDH Chemicals Ltd.) by drying in vacuo at 100°C for at least 10 h to constant weight. Ace-

tone and doubly distilled hexane were dried over molecular sieves (Ajax Chemicals, type 4A). All other chemicals were of analytical grade and dilutions were performed with distilled water.

All glassware was soaked for at least 12 h in 4 M nitric acid after cleaning with distilled water. Final rinsing was performed with milli-Q water.

2.2. Preparation of phosphate buffers

A phosphate buffer was prepared from potassium dihydrogen orthophosphate (KH_2PO_4 , 99.5%, BDH Chemicals Ltd.) and disodium hydrogen orthophosphate (Na_2HPO_4 , 99.0%, BDH Chemicals Ltd.). A pH of 7.4 was attained by mixing 6.54 ml of 0.02 M KH_2PO_4 with 28.97 ml of 0.02 M Na_2HPO_4 and adjusting the final volume to 100 ml with distilled water.

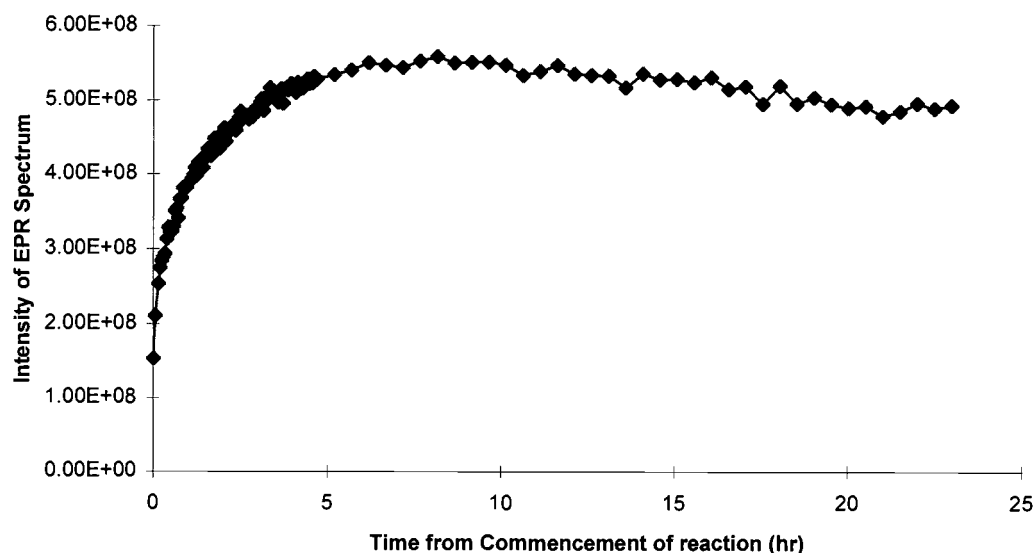


Fig. 2. Formation and decay of chromium(V) formed from the interaction of equal volumes of 0.14% (w/v) fulvic-L and 0.020 M potassium chromate at pH 4.2.

2.3. Electron paramagnetic resonance spectroscopy

Electron paramagnetic resonance analysis was performed in the X-band region with a Bruker ESP300E spectrometer using a 1 mm i.d. quartz flow-through cell. The instrument was programmed to record and store spectra at pre-determined time intervals. Analysis of the spectra was performed using WinEPR and X-EPR, computer software packages developed by Bruker.

Simulations of experimental spectra were obtained using SOPHE, a computer program developed by the Centre for Magnetic Resonance, The University of Queensland, Australia.

2.4. Synthesis of

sodium(2-ethyl-2-hydroxybutyrate)

oxochromate(V) monohydrate

The synthesis and characterisation of sodium(2-ethyl-2-hydroxybutyrate)oxochromate(V) monohydrate was performed according to the method reported by Krumpolc and Rocek in 1979 [36].

2.5. Preparation of standard solutions for EPR analysis

Solutions of sodium(2-ethyl-2-hydroxybutyrate)oxochromate(V) monohydrate were prepared in 0.01 M 2-ethyl-2-hydroxybutyric acid.

Solutions of 2,2,6,6-tetramethylpiperidine-1-oxyl ($C_9H_{18}NO$, 98.0%, Aldrich Chemical Company, Inc.), otherwise known as TEMPO, were prepared by dissolution in distilled water.

2.6. Fulvic acid/chromium(VI) reactions

Equal volumes of 0.020 M potassium chromate and 0.14% (w/v) fulvic acid were mixed and the pH adjusted to between 4 and 5 with 5 M hydrochloric acid.

Table 2
Carbon and hydrogen microanalysis for
 $Na[CrO(HEBA)_2] \cdot H_2O$

	%C	%H
Calculated	39.03	6.01
Experimental	38.42	6.00
Literature [17]	39.42	6.00

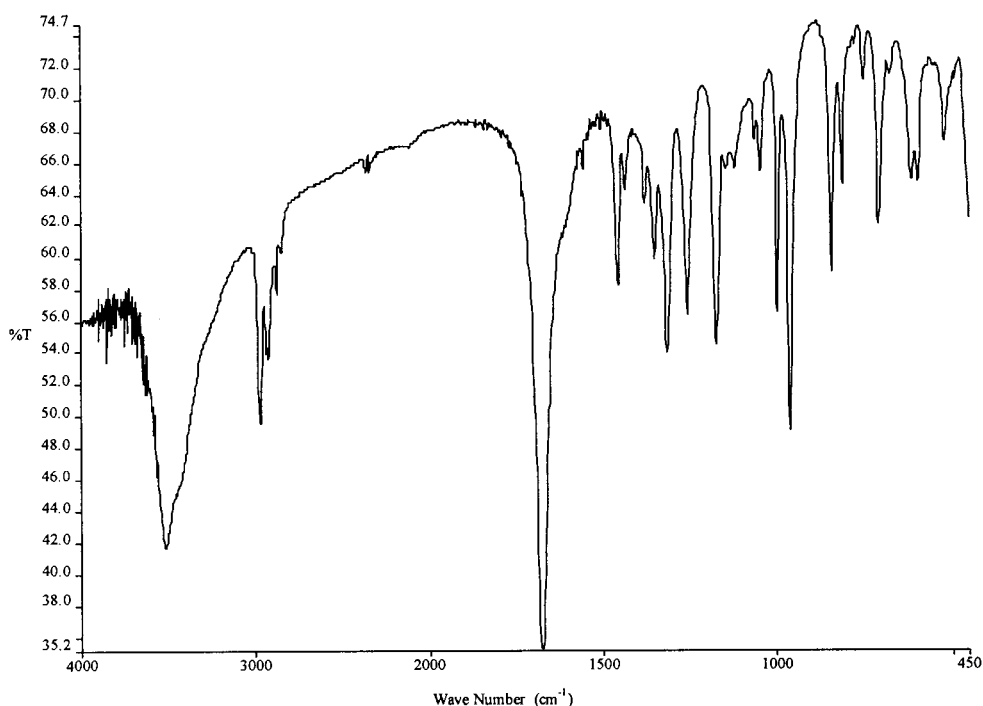


Fig. 3. Infrared spectrum of sodium bis(2-ethyl-2-hydroxybutyrate) oxochromate(V) monohydrate (KBr pellet).

2.7. 1,2-Dihydroxybenzene/chromium(VI) reactions

Solutions of 0.020 M potassium dichromate and 0.182 M 1,2-dihydroxybenzene were prepared in a phosphate buffer (pH 7.40) and mixed as

Table 3
Infrared signals for $\text{Na}[\text{CrO}(\text{HEBA})_2] \cdot \text{H}_2\text{O}$

Experimental	Literature [17]
3508.6 (m, br)	3510 (m, br)
1676.5 (s, br)	1680 (s, br)
1314.5 (m)	1312 (m)
1258.4 (m)	1257 (m)
1176.3 (m)	1177 (m)
1047.1 (w)	1045 (w)
998.5 (m)	998 (m)
961.6 (s)	961 (s)
	888 (w)
845.3 (w)	845 (w)
814.4 (w)	815 (w)
707.8 (m)	712 (m)

Abbreviations: m, medium; br, broad; s, strong; w, weak.

outlined in Table 1. The initial pH for each reaction mixture was adjusted to 7.36 ± 0.03 by addition of small amounts of 1 M hydrochloric acid.

To achieve a molar ratio of 182:1, equal volumes of 1.82 M 1,2-dihydroxybenzene and 0.010 M potassium chromate were mixed. The initial pH of the reaction mixture was adjusted to 7.36 ± 0.03 with 5 M hydrochloric acid.

3. Results and discussion

Reaction of chromium(VI) with fulvic acid produced a chromium(V) complex whose EPR spectrum had $g = 1.9784$ and a line width of 1.80 G (Fig. 1). The reaction occurred in the pH range of 4–8 with increased rates of formation and decay at lower pH values. The concentration of chromium(V) increased to a maximum before slowly decreasing. When conducted at pH 4.2, the maximum chromium(V) concentration was attained approximately 8 h after the reaction was com-

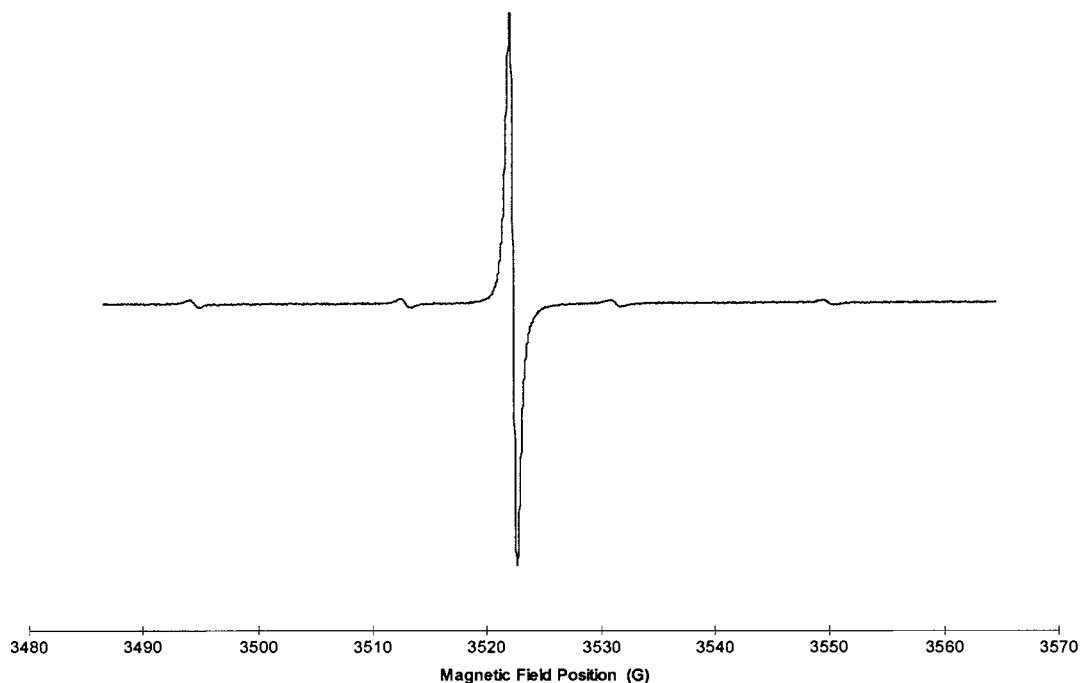


Fig. 4. EPR spectrum of 0.002 M sodium bis(2-ethyl-2-hydroxybutyrate) oxochromate(V) monohydrate in 0.010 M 2-ethyl-2-hydroxybutyric acid. EPR parameters: microwave power = 2 mW; receiver gain = 1.25×10^4 ; modulation amplitude = 0.184 G.

menced (Fig. 2) and the signal was still detectable 1 week later. At pH values below 3.5, a precipitate was formed, and EPR analysis of the supernatant yielded a broad signal in the $g = 2$ region, which is indicative of the presence of chromium(III). Chromium(V) was not observed at $\text{pH} > 8$. These results are consistent with the findings reported by Boyko and Goodgame [32], although the chromium(V) production was reported over a greater pH range in their work.

As with any instrumental method of analysis, quantitative determination by EPR spectroscopy requires the use of a reference material for calibration purposes. As a matter of convenience, it is useful if the reference material has the same electron spin multiplicity as the unknown. Two such materials are sodium(2-ethyl-2-hydroxybutyrate) oxochromate(V) monohydrate and 2,2,6,6-tetramethylpiperidine-1-oxyl (TEMPO).

The synthesis of sodium(2-ethyl-2-hydroxybutyrate)oxochromate(V) monohydrate, a chromium(V) compound that is relatively stable in

aqueous solution was first reported by Krumpolc and Rocek in 1979 [36]. It was later found that dissolution of the complex in an excess of the hydroxy acid ligand, resulted in the chromium(V) being highly stable in solution for periods of about 1 h [37].

After synthesis, the chromate(V) complex was tested for impurities by microanalysis, iodometric analysis and infrared spectroscopy. The experimental results for carbon and hydrogen microanalysis agree well with both the calculated results and those reported by Krumpolc and Rocek (Table 2). The infrared spectrum of $\text{Na}[\text{CrO}(\text{HEBA})_2] \cdot \text{H}_2\text{O}$ obtained in this work is shown in Fig. 3, together with previously reported values (Table 3). The agreement between the experimental and literature values is excellent.

The possible presence of chromium(VI) in the chromium(V) complex was determined spectrophotometrically using an iodometric method of analysis [36]; no chromium(VI) was detected. In addition, the iodometric procedure allowed the

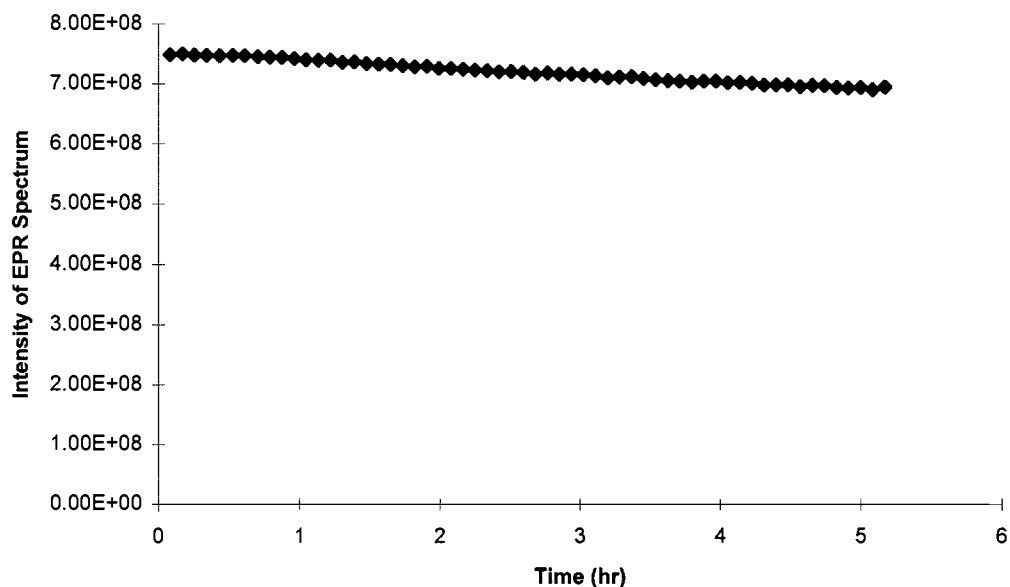


Fig. 5. Decay of 0.002 M sodium bis(2-ethyl-2-hydroxybutyrate) oxochromate(V) monohydrate in 0.010 M 2-ethyl-2-hydroxybutyric acid with time.

calculation of the chromium concentration in solution; this was 14.05%, and compared very well with the calculated value of 14.08%. EPR spectroscopy of a portion of $\text{Na}[\text{CrO}(\text{HEBA})_2] \cdot \text{H}_2\text{O}$ solid did not yield any indication of the presence of chromium(III). Likewise, UV/Vis spectroscopy of an aqueous solution of the chromium(V) complex indicated that the tri- and hexavalent chromium species are not present.

On the basis of the microanalysis and the iodometric method, the sodium bis(2-ethyl-2-hydroxybutyrate)oxochromate(V) monohydrate is approximately 99% pure and is suitable for use as a standard chromium(V) material. However, the material does not fulfil the requirements of a primary standard and requires standardisation before use.

The EPR spectrum of an aqueous solution of 0.002 M $\text{Na}[\text{CrO}(\text{HEBA})_2] \cdot \text{H}_2\text{O}$ prepared in 0.01 M 2-ethyl-2-hydroxybutyric acid contains a signal with $g = 1.9786$. The hyperfine coupling constant and line width are 17.06 and 1.30 G respectively (Fig. 4).

The stability of the chromium(V) solution was established by recording the EPR spectrum every

5 min for approximately 5 h (Fig. 5). At the conclusion of the experiment, the chromium(V) had decreased 8.15% relative to the initial concentration. However, no significant decrease in concentration was observed for the first 30 min of the experiment; after 40 min, the concentration had decreased by 0.40% and at 1 h, 1.20%. Therefore, it was concluded that if the standard solution could be prepared and analysed within 30 min, it would be stable enough to be used as a standard for quantitative EPR spectroscopy.

2,2,6,6-Tetramethylpiperidine-1-oxyl, otherwise known as TEMPO, is a commercially available organic radical. Its stability is well known and it has been used extensively as a radical scavenger and as a standard material for quantitative EPR analysis [38–40]. Solid TEMPO is unstable at room temperature and must be stored in a refrigerator; therefore, it is only useful as a reference material if it can be standardised. Fortunately, the extinction molar coefficients for the compound in various organic solvents are well known, allowing the determination of TEMPO concentration in those solvents by UV/Vis spectroscopy [41]. However, a thorough search of the literature failed to

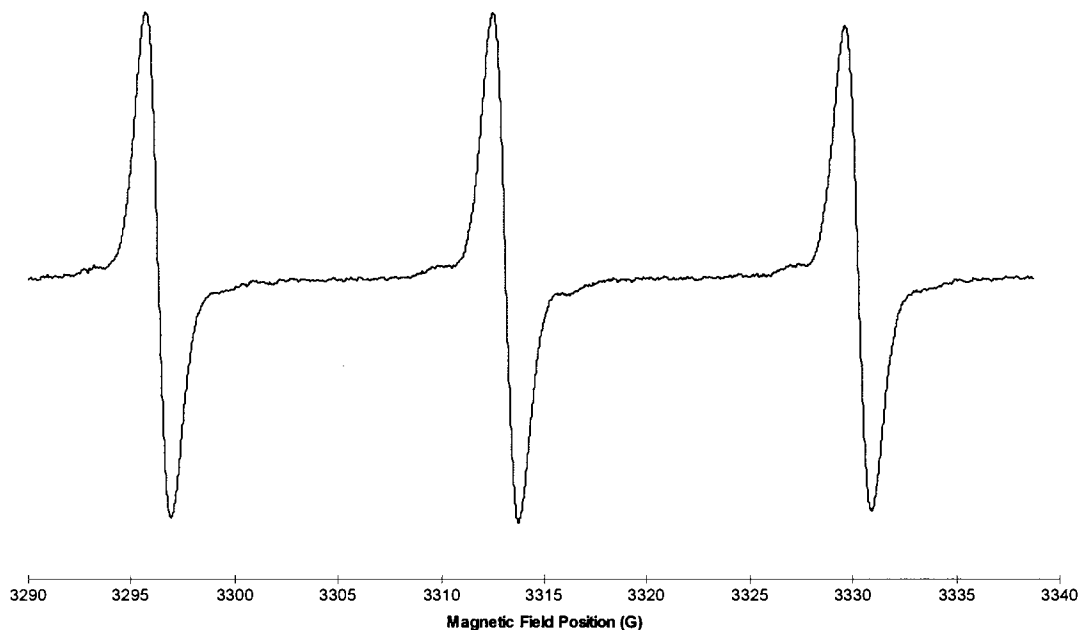


Fig. 6. EPR spectrum of 0.002 M 2,2,6,6-tetramethylpiperidine-1-oxyl. EPR parameters: microwave power = 2 mW; receiver gain = 1.25×10^4 ; modulation amplitude = 0.184 G.

find any molar extinction coefficient values for TEMPO in aqueous solution. Therefore, TEMPO was standardised by weighing two 0.03127 ± 0.00002 -g samples; these are identical weights within experimental error. One sample was dissolved in water and used for EPR experiments, the other was dissolved in methanol and the concentration of solution determined using its quoted molar extinction coefficient and UV/Vis spectroscopy ($\epsilon_{\lambda=450 \text{ nm, methanol}} = 10.4 \text{ M}^{-1} \text{ cm}^{-1}$) [41].

The methanol solution with a calculated concentration of 2.0013 mM was determined by visible spectroscopy to have an actual concentration of 1.9471 mM. Therefore, the TEMPO solid can be taken to be 97.3% pure; the main source of impurity is most likely to be absorbed water. The concentration of aqueous solutions of TEMPO used in EPR experiments was adjusted accordingly.

The EPR spectrum of an aqueous solution of 0.002 M TEMPO is centred about $g = 2.0051$ and exhibits a hyperfine coupling between the electron

and ^{14}N ($I = 1$, 99.63% abundant) of 15.85 G (Fig. 6). Weak signals can also be observed for the hyperfine coupling between the electron and ^{15}N ($I = 1/2$, 0.37% abundant), and to a lesser extent, with ^{17}O ($I = 5/2$, 0.037% abundant).

The double integral of an EPR spectrum yields the number of electron spins within the sample cavity. By comparison of an unknown sample with a reference material, the number of spins can be converted to a sample concentration. It is often the case that the reference material will have quite a different paramagnetic centre from the unknown material, and in order to determine the concentration of the unknown compound, one must consider the difference in transition probabilities for the materials [42].

The difference in transition probabilities was first considered by Aasa and Vanngard with respect to anisotropic powder spectra [43]. It was demonstrated that the difference could be corrected for if the double integral of the first derivative EPR signal was divided by the average g value (g^{av}) given by the formula,

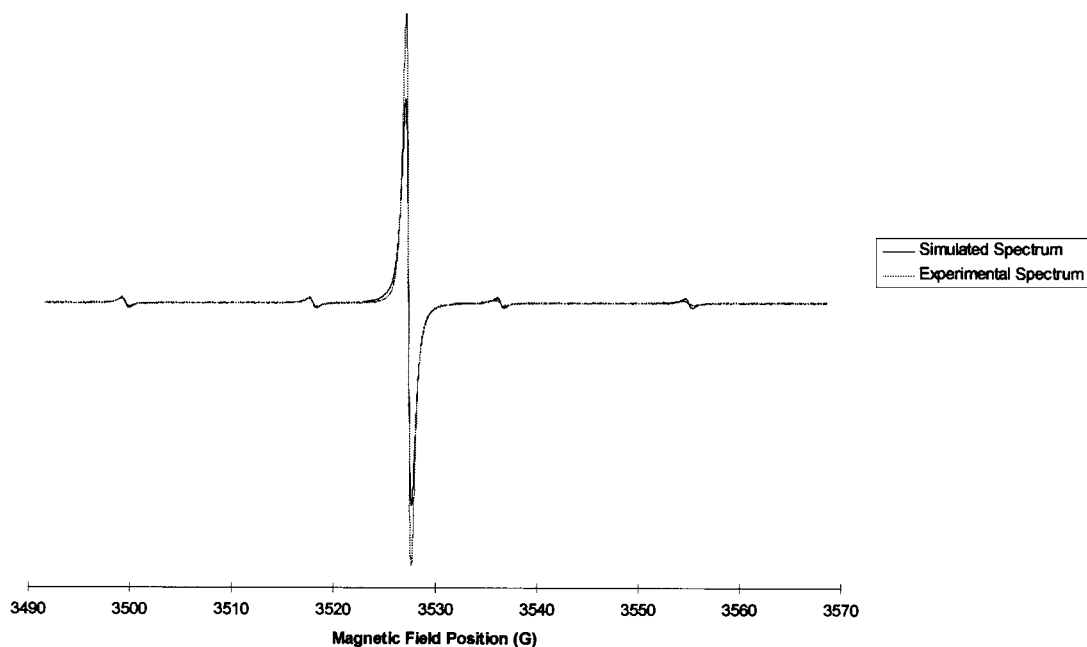


Fig. 7. Comparison of EPR spectrum of 0.002 M Na[CrO(HEBA)₂]·H₂O with its simulation. EPR parameters: microwave power = 2 mW; receiver gain = 1.25 × 10⁴; modulation amplitude = 0.184 G.

$$g^{av} \cong \frac{2}{3} \sqrt{\frac{g_x^2 + g_y^2 + g_z^2}{3}} + \frac{1}{3}(g_x + g_y + g_z). \quad (1)$$

In the isotropic system g_x , g_y , and g_z are equal and by Eq. (1), g^{av} equals the experimental value of g . Therefore, in the isotropic system, the differences in transition probabilities are accounted for by dividing the double integral by the relevant experimental g value.

Another method for correction of differences in transition probabilities relies on simulations of the experimental spectra and the following formulae¹ [44]:

$$N_{Ou} = N_{Or} \frac{I(\text{Exp})_u}{C'_u I(\text{Sim})_u} \times \frac{C'_r I(\text{Sim})_r}{I(\text{Exp})_r} \quad (2)$$

¹ The normalisation constant, C' , reported in the literature is the inverse of that described here. During the course of this research, it was found that the formulae in the literature contained an error. The finding was confirmed by one of the authors of the original work, G.R. Hanson. The formulae presented in this research paper are correct.

where

$$C' = \frac{S(S+1)(RG)(MA)P^{1/2}}{T}$$

and $I(\text{Exp})$ = double integral of the experimental spectrum; $I(\text{Sim})$ = double integral of the simulated spectrum; C' = normalisation constant; (RG) = receiver gain; (MA) = modulation amplitude; P = microwave power; T = temperature; S = electron spin, and the subscripts u and r refer to the unknown and reference samples, respectively.

An EPR spectrum of an aqueous solution of 0.002 M Na[CrO(HEBA)₂]·H₂O and its simulation are presented in Fig. 7. It is evident that the simulated and experimental spectra have different intensities. However, the intensity difference is even more significant for the EPR spectrum of aqueous TEMPO and its simulation (Figs. 8 and 9).

Simulations of spectra obtained from low concentrations of chromium(V) are more difficult to achieve. For instance, a 4 × 10⁻⁵ M Na[CrO(HEBA)₂]·H₂O solution requires the use of high microwave power and receiver gain. To increase

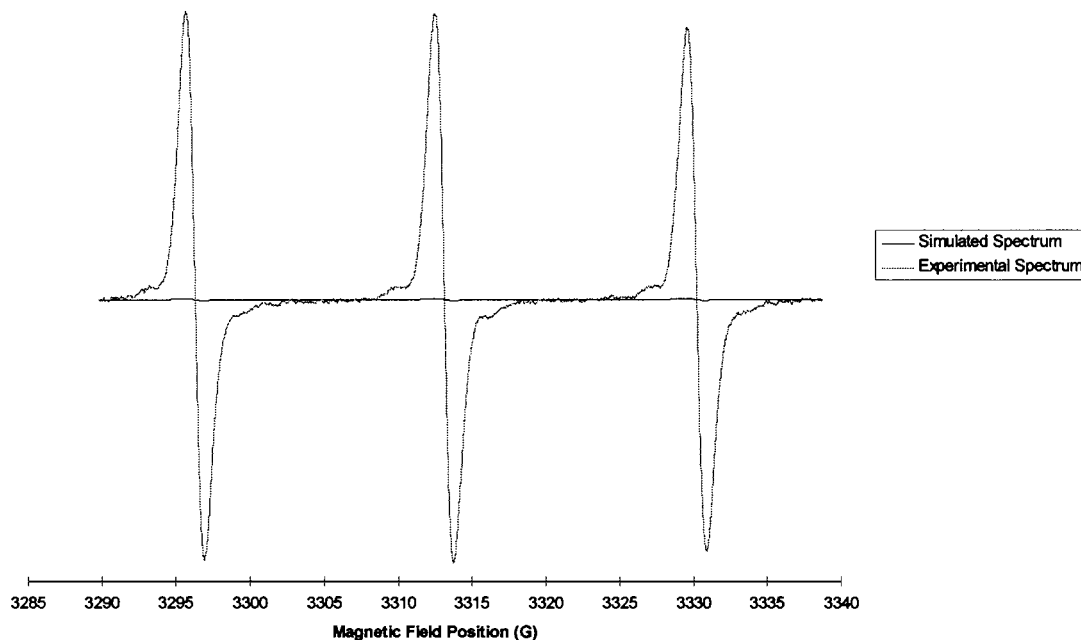


Fig. 8. Comparison of EPR spectrum of 0.002 M TEMPO with its simulation. EPR parameters: microwave power = 2 mW; receiver gain = 1.25×10^4 ; modulation amplitude = 0.184 G.

the signal to noise ratio, the modulation amplitude is increased, leading to changes in the line shape of the EPR signal. The resulting spectrum cannot be accurately simulated with either Gaussian or Lorentzian line shape models (Fig. 10). A similar problem, although not as significant, exists for the simulation of spectra obtained from solutions of low TEMPO concentration. One of the limitations of the software used for simulations was the inability to use line shape models other than Gaussian or Lorentzian. It is expected that poor simulations of experimental spectra will introduce significant error into the procedure.

Experimental data for standard solutions of chromium(V) and TEMPO are presented in Table 4. The intensity of the experimental spectrum, $I(\text{Exp})$, is recorded as the mean of at least five experimental results. Parameters which effect the spectral intensity are also presented.

Using a TEMPO solution with a standardised concentration of 1.9968 mM, a $\text{Na}[\text{CrO}(\text{HEBA})_2] \cdot \text{H}_2\text{O}$ solution with a calculated concentration of 1.7825 mM was determined to be

1.7616 mM by substitution of the relevant data (Table 4) into Eq. (2). This corresponds to a purity of greater than 98.8% for the $\text{Na}[\text{CrO}(\text{HEBA})_2] \cdot \text{H}_2\text{O}$ standard.

Because the simulated spectra did not fit the experimental spectra very well for solutions with low concentrations of $\text{Na}[\text{CrO}(\text{HEBA})_2] \cdot \text{H}_2\text{O}$, the spectral simulation method was tested by calculating concentrations of dilute TEMPO solutions from dilute $\text{Na}[\text{CrO}(\text{HEBA})_2] \cdot \text{H}_2\text{O}$ solutions. The examples presented (Table 5) clearly demonstrate that poor simulation of an experimental spectrum will lead to erroneous results.

For this particular application, the spectral simulation procedure is useful for the standardisation of $\text{Na}[\text{CrO}(\text{HEBA})_2] \cdot \text{H}_2\text{O}$, but not for the routine analysis of low concentration solutions. For this task, the average g method must be employed.

The determination of unknowns is performed using the $\text{Na}[\text{CrO}(\text{HEBA})_2] \cdot \text{H}_2\text{O}$ standard solutions. Similar results could also be obtained from the TEMPO solutions, but an additional calculation step is necessary. The hyperfine coupling of

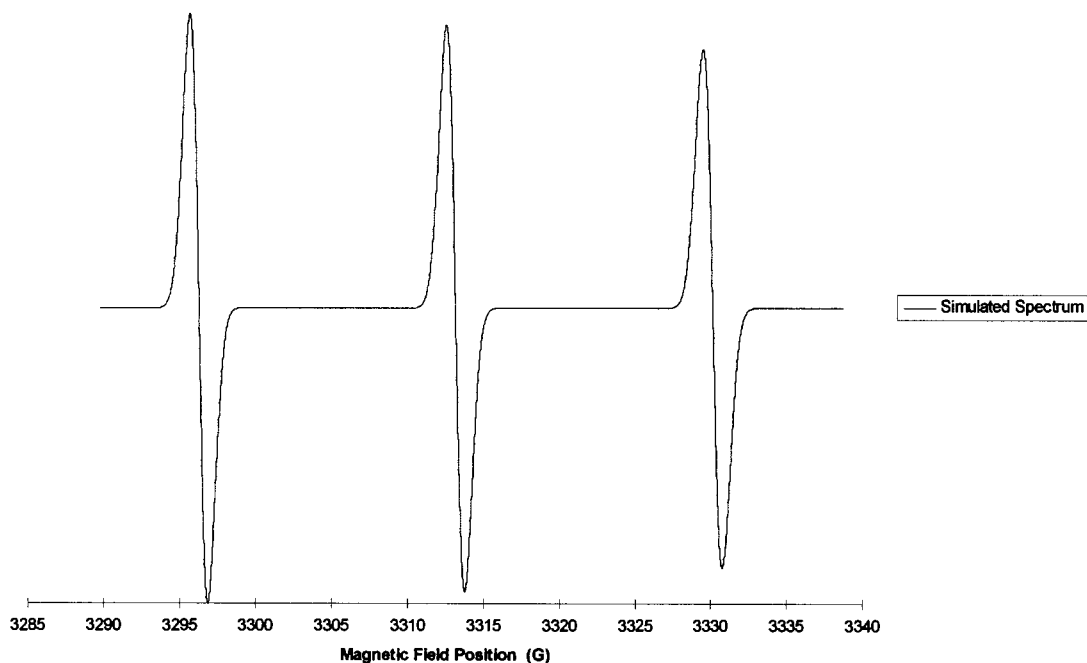


Fig. 9. Simulated EPR spectrum for TEMPO.

the electron with ^{53}Cr ($I = 3/2$, natural abundance = 9.55%) was generally not observed for low concentration chromium(V) solutions. Therefore, the experiments were focused on the centre signal, attributed to the one unpaired electron. However, the double integral of that signal represents only 90.45% of the total number of spins within the spectrometer's cavity. The hyperfine coupling for TEMPO is observed in all cases. If comparing the area of the centre signal of a chromium(V) spectrum with the area of a TEMPO spectrum, the resulting chromium(V) concentration will only account for 90.45% of the actual concentration. It is more convenient to use $\text{Na}[\text{CrO}(\text{HEBA})_2] \cdot \text{H}_2\text{O}$ as the reference material and compare the centre signals for both reference and unknown.

A calibration curve is constructed by plotting the double integrals of the EPR spectra against concentration. However, to compensate for differences in transition probability between the reference and unknown, the areas of the spectra must be divided by the g value. Before a concentration can be determined from the calibration curve, the

double integral of the unknown must also be divided by the corresponding g value.

The calibration data for chromium(V) standards within the concentration range of the unknown materials is shown in Table 6. The blank value was obtained from 0.01 M 2-ethyl-2-hydroxybutyric acid. The resulting correlation coefficient is 0.9998, indicating excellent linearity.

If spectra have been recorded using different instrument parameters, the data must be normalised. EPR spectra of the chromium(V) product of the reaction between 1,2-dihydroxybenzene and chromium(VI) were recorded with modulation amplitude = 10.11 G, microwave power = 126 mW, and receiver gain = 1.250×10^4 . These parameters differ from those of the $\text{Na}[\text{CrO}(\text{HEBA})_2] \cdot \text{H}_2\text{O}$ standard solutions. Therefore, the double integrals must be normalised to the parameters used to record the reference solutions (Table 7).

It was found that when the 1,2-dihydroxybenzene and chromium(VI) were reacted at a ratio of 182:1, the maximum concentration of chromium(V) produced was 0.144 mM (Table 7). Since

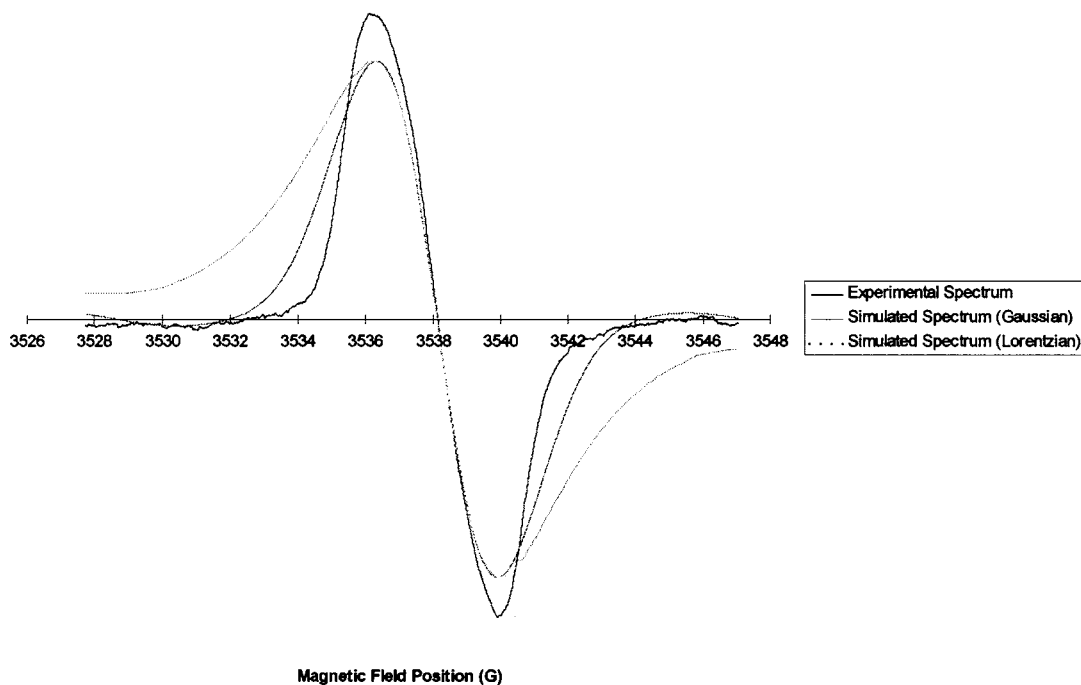


Fig. 10. Comparison of the EPR spectrum of 4×10^{-5} M $\text{Na}[\text{CrO}(\text{HEBA})_2] \cdot \text{H}_2\text{O}$ with simulations based on Gaussian and Lorentzian line shapes. The intensities of the simulated spectra are multiplied by 60 to aid comparison. EPR parameters: microwave power = 126 mW; receiver gain = 1.25×10^4 ; modulation amplitude = 5.15 G.

the initial concentration of chromium(VI) was 0.020 M, or 20 mM, the maximum chromium(V) concentration represents only 0.71% of the total amount of chromium in the system. The reactions conducted at lower molar ratios produced less chromium(V) (Table 7). A relationship was not found between the molar ratio and the maximum concentration of chromium(V).

The interaction between chromium(VI) and fulvic acid was studied with modulation amplitude = 10.11 G, microwave power = 126 mW and receiver gain = 1.250×10^5 . Again, these parameters differ from those used for the chromium(V) reference solutions, necessitating a normalisation process (Table 8). The maximum chromium(V) concentration was found to be only 0.014 mM.

The main source of error associated with analysis by the spectral simulation procedure is due to the EPR spectrometer. Based on the standard deviation of 10 spectral intensities of 0.2 mM TEMPO, the error associated with the EPR spec-

trometer may be taken as $\pm 9.3\%$ (assuming that the error is equivalent to two standard deviations). Consideration of the other errors associated with the procedure (analytical balance and volumetric glassware) lead one to propose an overall error of $\pm 10\%$.

Determination of error and detection limit for analyses performed by division of spectral intensities by the relevant g value is achieved from the linear regression analysis. If the detection limit is taken as 0.010 mM chromium(V) (0.5 mg l^{-1}), the error does not exceed $\pm 10\%$.

Normally the development of a new analytical procedure is accompanied by a validation of the results. This is usually achieved by either analysing some internationally recognised standard reference material (SRM) and comparing the experimental and accepted results, or by employing a standard additions procedure. In the standard additions procedure, samples of the unknown are spiked with known amounts of ana-

Table 4
Experimental data for standard aqueous solutions of chromium(V) and TEMPO

Material	Conc. ^a (mM)	MA ^a (G)	Power ^a (mW)	RG ^a	<i>I</i> (Exp) ^a	<i>I</i> (Sim) ^a
Na[CrO(HEBA) ₂]·H ₂ O ^b	1.7825	0.18	2	1.250e3	1.1e4	4.3e3
	0.0355	5.15	126	1.125e4	3.1e6	6.3e4
	0.0178	5.15	126	1.125e4	1.5e6	6.3e4
	0.0071	5.15	126	1.125e4	6.3e5	6.3e4
	0.0036	5.15	126	1.125e4	3.0e5	6.3e4
TEMPO ^c	1.9968	0.18	2	1.250e4	1.3e6	4.4e4
	0.1997	2.05	20	1.250e4	4.3e6	4.4e4
	0.0799	2.05	20	1.250e4	1.6e6	4.4e4
	0.0399	2.05	126	1.250e4	1.7e6	4.4e4
	0.0200	2.05	126	1.250e4	8.3e5	4.4e4
	0.0079	2.05	126	1.250e4	3.2e5	4.4e4

^a Conc., concentration; MA, modulation amplitude; Power, microwave power; RG, receiver gain; *I*(Exp), double integral of experimental spectrum; *I*(Sim), double integral of simulated spectrum.

^b Concentration of Na[CrO(HEBA)₂]·H₂O solutions are non-standardised.

^c TEMPO concentrations have been standardised by UV/Vis spectroscopy.

Table 5

Determination of TEMPO concentration using low concentration aqueous solutions of Na[CrO(HEBA)₂]·H₂O as reference

Reference concentration (mM)	Expected TEMPO concentration (mM)	Determined TEMPO concentration (mM)
0.0351	0.0399	0.0623
	0.0200	0.0306
0.0176	0.0399	0.0650
	0.0200	0.0320

lyte. If analysis yields results consistent with the spiked additions, the procedure is deemed valid [45]. Unfortunately, neither of these procedures are suitable for the systems studied in this project. The first option is not possible because there are

Table 6

Calibration data for a chromium(V) standard series (Na[CrO(HEBA)₂]·H₂O)

Na[CrO(HEBA) ₂]·H ₂ O concentration (mM)	Double integral	Adjusted double integral ^a
0.0000	0.0e0	0.0e0
0.0036	3.0e5	1.5e5
0.0070	6.3e5	3.2e5
0.0176	1.5e6	7.4e5
0.0351	3.0e6	1.5e6
0.0705	6.0e6	3.0e6
0.0881	7.4e6	3.7e6
0.1762	1.5e7	7.8e6
0.3523	2.9e7	1.5e7

^a Double integral divided by the *g* value (1.9786).

no SRMs available for chromium(V) in aqueous solution. The latter procedure is not possible since, with the exception of sodium bis(2-ethyl-2-hydroxybutyrate) oxochromate(V) monohydrate prepared in excess 2-ethyl-2-hydroxybutyric acid, aqueous chromium(V) exhibits poor stability. In the reaction mixtures studied, the chromium(V) concentration increases to a maximum value before slowly decreasing. The literature suggests that the concentration of chromium(V) is dependant on the ratio of concentrations of chromium(VI), the organic substrate and other reaction products [46]. Addition of a known excess of chromium(V) would almost definitely alter the quasi-equilibrium state, thereby changing the expected concentration of chromium(V).

The calibration curve for the standards proved to have an excellent linear fit and the standardisation of Na[CrO(HEBA)₂]·H₂O with TEMPO, a recognised reference material for quantitative EPR analysis, gave good results. However, in the

Table 7

Maximum chromium(V) concentration obtained from the reaction of chromium(VI) and 1,2-dihydroxybenzene at varying molar ratios

Molar ratio ^a	<i>I</i> (Exp)	Normalised <i>I</i> (Exp) ^b	Adjusted <i>I</i> (Exp) ^c	[Cr(V)] (mM)
182.0:1	2.7e7	1.2e7	6.2e6	0.144
9.1: 1	1.3e7	6.0e6	3.1e6	0.072
5.4: 1	1.0e6	4.6e6	2.4e6	0.056
1.8: 1	4.6e6	2.1e6	1.1e6	0.025

^a 1,2-Dihydroxybenzene:chromium(VI).

^b Experimental double integral normalised to MA = 5.15 G, power = 126 mW, RG = 1.125 × 10⁴.

^c Normalised double integral divided by the *g* value (1.9716).

absence of a suitable validation technique for this particular method, it must be conceded that any results obtained should be treated with caution.

The detection limit of the developed procedure is 0.01 mM, or 0.5 mg l⁻¹. While this is comparable with techniques such as atomic absorption spectroscopy (AAS), it is not low enough for determination of chromium(V) at background environmental concentrations. In non-contaminated conditions the concentration of chromium(VI) in the natural water rarely exceeds 1 µg l⁻¹ [47]. Therefore, without a pre-concentration step, EPR analysis is not a useful technique for the determination of background chromium(V) concentrations in the natural environment, particularly with respect to aqueous samples. However, the technique still has great potential for use within the laboratory situation for in vitro investigations of the interactions of chromium(VI) with biologically significant compounds such as glutathione and ascorbate.

The development of a pre-concentration step for the analysis of chromium(V) would be

Table 8

Maximum chromium(V) concentration obtained from the reactions of chromium(VI) with fulvic acid

<i>I</i> (Exp)	Normalised <i>I</i> (Exp) ^a	Adjusted <i>I</i> (Exp) ^b	[Cr(V)] (mM)
2.6e7	1.2e6	6.1e5	0.014

^a Experimental double integral normalised to MA = 5.15 G, power = 126 mW, RG = 1.125 × 10⁴.

^b Normalised double integral divided by the relevant *g* value (1.9784).

difficult. Because of the instability of the species in aqueous solution, there is high risk that the usage of common pre-concentration techniques, such as column chromatography and solvent extractions, might alter the oxidation state of the metal. Furthermore, chromium(V) often exists in a quasi-equilibrium state, dependant on the ratio of reactants. A pre-concentration step might alter the concentrations of reactants, and hence the amount of chromium(V) produced, thus leading to results that are not consistent with the original sample.

If using 'real' samples such as dam water or cell tissue, it is possible that the presence of other paramagnetic species might obscure the chromium(V) signal, making quantitative analysis impossible. For instance, a dam water sample might contain manganese(II), copper(II) or iron(III), all of which give EPR signals in the *g* = 1.9–2.0 region. It should be possible to overcome this problem by subtracting a background spectrum from the analytical spectrum. If, for example, manganese(II) and copper(II) were interfering with a chromium(V) signal, then the unknown sample could be analysed by AAS to determine the concentrations of manganese and copper. A background solution containing the interfering metals at the determined concentrations could then be prepared. Subtraction of the background EPR spectrum from that of the unknown sample would result in an unobscured chromium(V) signal. It would also be necessary to know the relevant salt or chelating agent for any interfering metal, since these can have an effect on the EPR spectrum [48].

In the reaction between chromium(VI) and 1,2-dihydroxybenzene, where the organic compound is present in a 182-fold excess, the amount of chromium(V) produced represents only 1.44% of the total chromium in the system. Because all chromium(VI) must proceed through the chromium(V) intermediate, it is most likely that the reduction of chromium(V) to chromium(III) occurs at a rapid rate, yet slowly enough to allow detection.

The amount of chromium(V) produced from the interaction of chromium(VI) with fulvic acid is also quite small in relation to the total chromium in the system. The maximum concentration of chromium(V) produced from the reaction of equal volumes of 0.020 M chromium(VI) and 0.14% (w/v) fulvic acid was 0.014 mM. This value is about half that obtained for the interaction of 1,2-dihydroxybenzene with chromium(VI) at a molar ratio of 1.8: 1 (Table 7). However, the results do not indicate that all interactions between chromium(VI) and suitable organic compounds will produce only a small percentage of chromium(V).

The analytical procedure reported in this paper can now be used to obtain quantitative data for the chromium(V) producing reactions between the chromium(VI) and various organic compounds of biological and environmental significance.

References

- [1] R.J. Bartlett, J.M. Kimble, *J. Environ. Qual.* 5 (1976) 379–383.
- [2] B.R. James, R.J. Bartlett, *J. Environ. Qual.* 12 (1983) 173–176.
- [3] Standard Methods: For the Examination of Water and Wastewater, 16 ed., APHA, AWWA, WPCF, New York, 201 (1985).
- [4] M. Sperling, X. Yin, B. Welz, *Analyst* 117 (1992) 629–635.
- [5] E. Orvini, T. Zerlia, M. Gallorini, M. Speziali, *Radiochem. Radioanal. Lett.* 43 (1980) 173–184.
- [6] Dionex, Technical Note 26, May 1990, pp. 1–7.
- [7] J. Jen, G. Ou-Yang, C. Chen, S. Yang, *Analyst* 118 (1993) 1281–1284.
- [8] C. Archundia, P.S. Bonato, J.F. Lugo Rivera, L.C. Mascioli, K.E. Collins, C.H. Collins, *Sci. Total Environ.* 130/131 (1993) 231–236.
- [9] E. Nakayama, H. Tokoro, T. Kuwamoto, T. Fujinaga, *Nature* 290 (1981) 768–770.
- [10] K.E. Collins, P.S. Bonato, C. Archundia, M.E.L.R. de Queiroz, C.H. Collins, *Chromatographia* 26 (1988) 160–162.
- [11] M. Hiraide, A. Mizuike, *Fresenius Z. Anal. Chem.* 335 (1989) 924–926.
- [12] C.A. Johnson, *Anal. Chim. Acta* 238 (1990) 273–278.
- [13] F.H. Westheimer, *Chem. Rev.* 45 (1949) 419.
- [14] M. Mitewa, P.R. Bontchev, *Coord. Chem. Rev.* 61 (1985) 241.
- [15] W. DeBoer, *Nucl. Instrum. Methods* 107 (1973) 99.
- [16] P.R. Bontchev, M. Mitewa, K. Kabassanov, A. Malinowski, *Inorg. Nucl. Chem. Lett.* 11 (1975) 799.
- [17] P.F. Brammar, T. Lund, J.B. Raynor, C.J. Williw, *J. Chem. Soc. Dalton Trans.* (1975) 45.
- [18] M. Mitewa, P.R. Bontchev, V. Bojinov, *Inorg. Nucl. Chem. Lett.* 8 (1972) 51.
- [19] E.I. Steifel, R. Eisenberg, R.C. Rosenberg, H.B. Gray, *J. Am. Chem. Soc.* 88 (1966) 2956.
- [20] S. Kitagawa, H. Seki, F. Kametani, H. Sakurai, *Inorg. Chim. Acta* 152 (1988) 251.
- [21] P. O'Brian, J. Pratt, F.J. Swanson, P. Thorton, G. Wang, *Inorg. Chim. Acta* 169 (1990) 265.
- [22] C.P. Rao, S.P. Kaiwar, *Carbohydr. Res.* 237 (1992) 195.
- [23] S.P. Kaiwar, M.S. Srinivasa, C.P. Rao, *Carbohydr. Res.* 256 (1994) 29.
- [24] D.M.L. Goodgame, A.M. Joy, *Inorg. Chim. Acta* 135 (1987) 115.
- [25] L.F. Sala, S.R. Signorella, M. Rizzotto, M.I. Frascaroli, F. Gandolfo, *Can. J. Chem.* 70 (1992) 2046.
- [26] M. Quiros, D.M.L. Goodgame, *Polyhedron* 11 (1992) 1.
- [27] D.M.L. Goodgame, A.M. Joy, *Inorg. Biochem.* 26 (1986) 219.
- [28] P.H. Connett, K.E. Wetterhahn, *Struct. Bonding* 54 (1983) 93.
- [29] J. Wetterhahn, *Am. Chem. Soc.* 104 (1982) 874.
- [30] M. Sugiyama, K. Tsuzuki, X. Lin, M. Costa, *Mut. Res.* 283 (1992) 211.
- [31] K.J. Liu, J. Jiang, H.M. Swartz, X. Shi, *Arch. Biochem. Biophys.* 313 (1984) 248.
- [32] S.L. Boyko, D.M.L. Goodgame, *Inorg. Chim. Acta* 123 (1986) 189–191.
- [33] D.M.L. Goodgame, P.B. Hayman, D.E. Hathway, *Inorg. Chim. Acta* 91 (1984) 113–115.
- [34] X. Lu, J. Hook, R.F. Howe, W.D. Johnson, Abstract, Third Conference Environmental Chemistry Division RACI, Perth, 1993.
- [35] S.M. Harper, D.G. Edwards, G.L. Kerven, C.J. Asher, in: R.A. Date, N.J. Grundon, G.E. Raymont, M.E. Probert (Eds.), *Plant Soil Interactions at Low pH*, Kluwer Academic Publishers, Dordrecht, 1995, pp. 585–588.
- [36] M. Krumpolc, J. Rocek, *J. Am. Chem. Soc.* 101 (1979) 3206–3209.
- [37] M. Krumpolc, J. Rocek, *Inorg. Chem.* 24 (1985) 617–621.

- [38] S. Ohkoshi, Y. Ohba, M. Iwaizumi, S. Yamauchi, M. Ohkoshi-Ohtani, K. Tokuhisa, M. Kaitani, T. Akiyama, A. Sugimori, *Inorg. Chem.* 35 (1996) 4569.
- [39] S. Mishra, *Indian J. Biochem. Biophys.* 32 (1995) 254.
- [40] E.E. Voest, E. van Faassen, J.J.M. Marx, *Free Radic. Biol. Med.* 15 (1993) 589.
- [41] R. Briere, H. Lemaire, A. Rassat, *Bull. Soc. Chim. France* (1965) 3273.
- [42] D. Siebert, J. Dahlem, V. Nagy, *Anal. Chem.* 66 (1994) 2640.
- [43] R. Aasa, T. Vanngard, *J. Mag. Res.* 19 (1975) 308.
- [44] J.R. Pilbrow, G.R. Hanson, *Methods Enzymol.* 227 (1993) 330.
- [45] W. Holak, J.J. Specchio, *Atomic Spectrosc.* 12 (1991) 105.
- [46] J. Rocek, A.E. Radkowsky, *J. Am. Chem. Soc.* 90 (1968) 2986.
- [47] C.R. Parker, *Water Analysis by Atomic Absorption Spectroscopy*, Varian Techtron, Springvale, 1972, p. 46.
- [48] H.M. Swartz, J.R. Bolton, D.C. Borg, *Biological Applications of Electron Spin Resonance*, John Wiley & Sons, Inc., New York, 1972, pp. 129–134.



ELSEVIER

Talanta 46 (1998) 39–44

Talanta

Spectrophotometric methods for the determination of certain catecholamine derivatives in pharmaceutical preparations

P. Nagaraja ^{a,*}, K.C. Srinivasa Murthy ^b, K.S. Rangappa ^a, N.M. Made Gowda ^c

^a Department of Studies in Chemistry, Mysore University, Manasagangotri, Mysore 570006, India

^b Cipla Limited, Virgonagar, Bangalore 560 049, India

^c Department of Chemistry, Western Illinois University, Macomb, IL 61455, USA

Received 28 April 1997; received in revised form 24 July 1997; accepted 29 July 1997

Abstract

Two simple, rapid and sensitive spectrophotometric methods for the determination of catecholamine derivatives (pyrocatechol, dopamine, levodopa and methyl dopa) are developed. The first method involves the oxidation of *o*-dihydroxybenzene derivatives by *N*-bromosuccinimide followed by oxidative coupling with isoniazid leading to the formation of a red-coloured products of maximum absorbance ($\lambda_{\max} = 480\text{--}490\text{ nm}$). The second method is based on the formation of green to blue complex ($\lambda_{\max} = 635\text{--}660\text{ nm}$) between *o*-dihydroxybenzene derivatives and sodium nitroprusside in the presence of hydroxylamine hydrochloride. All measurements of the two procedures are carried out in an alkaline medium at room temperature. The two methods are successfully applied for the determination of dopamine hydrochloride, levodopa and methyl dopa in injections and tablets of pharmaceutical preparation. The common excipients used as additives in pharmaceuticals do not interfere in the proposed methods. The reliability of these methods are established by parallel determination with the reported and official methods. © 1998 Elsevier Science B.V. All rights reserved.

Keywords: Pyrocatechol; Dopamine hydrochloride; Levodopa; Methyl dopa; Isoniazid; Hydroxylamine hydrochloride; Sodium nitroprusside; *N*-Bromosuccinimide; Spectrophotometry; Pharmaceuticals

1. Introduction

Catecholamine drugs are aromatic vic-diols in which either the 3- or 4-position is unsubstituted and these positions are not sterically blocked. These drugs are now widely used in the treatment of bronchial asthma, hypertension, Parkinson's disease, myocardial infarction and cardiac

surgery. Dopamine, a neurotransmitter, is one of the naturally occurring catecholamines, and its hydrochloride salt is being used in the treatment of acute congestive failure and renal failure [1]. This has stimulated many investigators to work out compendial methods for the determination of catecholamine in authentic and dosage forms. Various methods like spectrofluorimetry [2,3], spectrophotometry [4], ion-exchange column chromatography [5], gas chromatography [6,7]

* Corresponding author.

Table 1
Experimental conditions and optical characteristics

Parameters	Method					
	A				B	
	PCL	DPH	LDP	MDP	PCL	DPH
Colour	Red	Red	Red	Red	Blue	Green
λ_{max} (nm)	485	490	480	480	660	635
Stability (h)	24	48	10	8	10	3
Beer's law ($\mu\text{g ml}^{-1}$)	0.8–5.85	2.8–14.0	2.4–12.0	5.0–16.0	1.5–10.0	2.4–17.0
Molar absorptivity ($\text{l mol}^{-1} \text{cm}^{-1}$)	1.27×10^4	6.47×10^3	8.38×10^3	3.96×10^3	7.59×10^3	7.4×10^3
Sandell's sensitivity ($\mu\text{g cm}^{-2}$)	0.0086	0.0293	0.0235	0.0533	0.0145	0.0257
Regression equation ^a						
Slope (<i>a</i>)	0.1109	0.0390	0.0410	0.0200	0.0663	0.0388
Intercept (<i>b</i>)	0.037	−0.032	−0.003	−0.050	−0.001	0.011
Correlation coefficient	0.9980	1.0101	0.9958	0.9994	0.9977	0.9999

^a $y = ax + b$, where *x* is the concentration of PCL, DPH, LDP or MDP in $\mu\text{g ml}^{-1}$.

Table 2
Experimental conditions

Method	Volume of NBS (0.05%) or HAH (0.07%) in ml	Volume of INH (0.02%) or SNP (0.3%) in ml	Volume of NaOH (0.01 M) or Na ₂ CO ₃ (5%) in ml
A	1.5 ^a (1.25–2.0) ^b	4.0 ^a (2.0–6.0) ^b	1.5 ^a (1.0–2.5) ^b
B	0.5 (0.25–1.0)	2.5 (1.0–4.0)	2.5 (1.0–3.5)

^aUsed in the proposed procedure.

^bRange for maximum absorbance and stability.

and radioimmunoassay [8,9] have been described in the literature for the determination of dopamine and dopa from the various biological samples and pharmaceutical preparation. The present work describes the two simple sensitive and accurate spectrophotometric methods for the determination of catecholamine derivatives (pyrocatechol, levodopa, methyl dopa and dopamine hydrochloride) using isoniazid (INH) in the presence of *N*-bromosuccinimide (NBS). The other method determines the pyrocatechol and dopamine hydrochloride using sodium nitroprusside (SNP) in the presence of hydroxylamine hydrochloride (HAH). The methods are adopted for the assay of three catecholamine drugs in pure and pharmaceutical formulations. These three drugs are officially listed in USP [10] which describes a nonaqueous titration for the assay of dopamine hydrochloride in raw material and an

HPLC technique for injection solutions. A visual titration and UV spectrophotometric methods at 280 nm are prescribed for levodopa and methyl dopa, respectively.

2. Experimental

2.1. Apparatus

A Jasco Model UVIDEDEC-610 UV-VIS spectrophotometer with 1.0-cm matched cells was used for the electronic spectral measurements.

2.2. Reagents

Dopamine hydrochloride (Sigma, USA), levodopa (SD Fine, India), methyl dopa (SD Fine, India), Pyrocatechol (CDH, India), Isoniazid

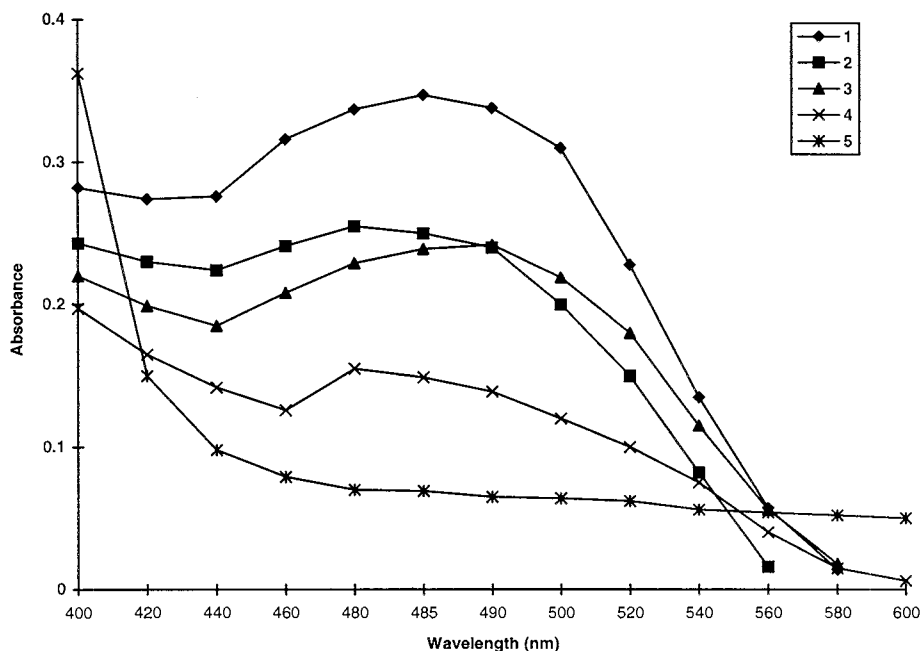


Fig. 1. Absorption spectra of: (1) PCL ($3 \mu\text{g ml}^{-1}$) + NBS + INH product; (2) LDP ($6 \mu\text{g ml}^{-1}$) + NBS + INH product; (3) DPH ($7 \mu\text{g ml}^{-1}$) + NBS + INH product; (4) MDP ($8 \mu\text{g ml}^{-1}$) + NBS + INH product; (5) NBS + INH reagent blank.

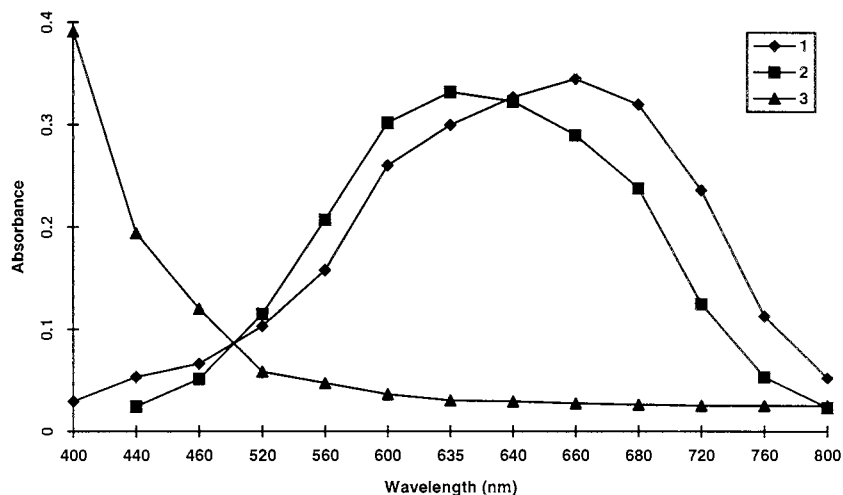


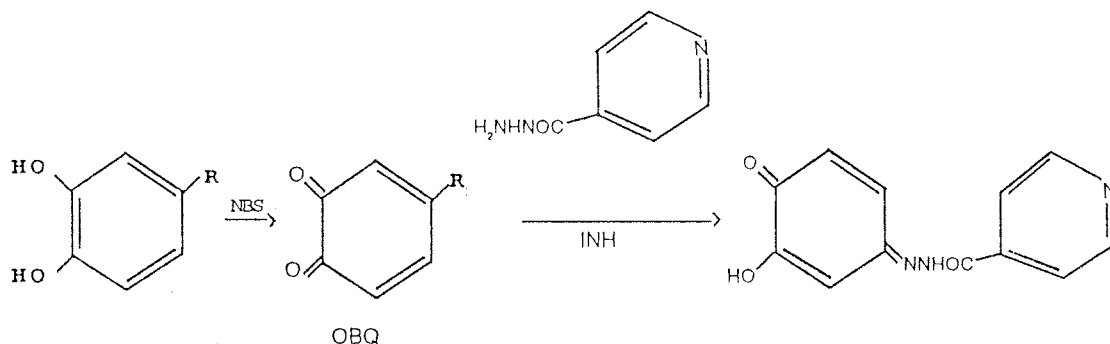
Fig. 2. Absorption spectra of: (1) PCL ($5 \mu\text{g ml}^{-1}$) + HAH + SNP product; (2) DPH ($8.5 \mu\text{g ml}^{-1}$) + HAH + SNP product; (3) HAH + SNP reagent blank.

(BDH, Poole, UK), sodium nitroprusside (E-Merck, Germany) were used.

All other chemicals used were of analytical reagent grade. Deionised water was used to prepare all solutions and in all experiments.

2.3. Solutions

Freshly prepared aqueous solutions of the pure drugs and pyrocatechol (PCL) (protected from sun light) ($50 \mu\text{g ml}^{-1}$) were used as the standard



solution for analytical purposes. Dopamine hydrochloride (DPH), levodopa (LDP), and methyl-dopa (MDP) were standardised by the reported method [11]. Solutions of 0.2% aqueous isoniazid, 0.07% aqueous hydroxylamine hydrochloride, 0.3% aqueous sodium nitroprusside, 0.05% *N*-bromosuccinimide, 5% sodium carbonate and 0.01 M sodium hydroxide were used.

2.4. General procedure

2.4.1. Method A

Aliquots of standard solutions of PCL (20–146 μg), DPH (70–350 μg), LDP (60–300 μg) or MDP (125–400 μg) were transferred to a 25-ml calibrated flask, to which 0.05% NBS, 0.02% INH and 0.01 M sodium hydroxide were added to the catecholamine solution, and the mixture was set aside for 5 min. The contents were diluted to the mark and mixed well. The absorbance at λ_{max} was measured against a reagent blank.

2.4.2. Method B

Aliquots of standard solutions of PCL (37–250 μg) or DPH (60–425 μg) were transferred to a 25-ml calibrated flask, to which 0.3% SNP, 0.07% HAH and 5% sodium carbonate solution were added, and the mixture was set aside for 5 min. The contents were diluted to the mark and mixed well. The absorbance at λ_{max} was measured against a reagent blank.

Details of the experimental conditions of the two methods are given in Tables 1 and 2.

2.5. Procedure for the assay of catecholamines in pharmaceutical preparation

2.5.1. Tablets

Twenty tablets were weighed and finely powdered. A weighed amount of the powder containing 50 mg of LDP or MDP was dissolved in water and filtered. The filtrate was made up to 100 ml and an aliquot of this solution was treated as described above for the determination of LDP or MDP.

2.5.2. Injection

DPH injection solutions were appropriately diluted with water to get the required concentration of the drug, and then the general procedure was followed. The amount of DPH was calculated from a calibration graph.

3. Results and discussion

3.1. Absorption spectra

A red-coloured oxidating coupling product with an absorption maximum at 480–490 nm is formed when PCL, DPH, LDP or MDP were allowed to react with NBS in the presence of INH in a sodium hydroxide medium. Green to blue products with absorption maxima at 635–660 nm were formed, when PCL or DPH are allowed to react with SNP in the presence of HAH in a sodium carbonate medium. The absorption spectra of

Table 3
Determination of catecholamines in pharmaceutical preparations

Drug	Label claim (mg)	DPH content per 5 ml of injection or LDP and MDP content per tablet (mg) % recovery ^a ± RSD			
		BP method	Reported method	Proposed method	
				A	B
DPH					
Injection ^b	200/5 ml	98.85 ± 1.21	99.04 ± 1.10	100.07 ± 1.03	99.82 ± 0.75
Injecion ^c	200/5 ml	99.2 ± 0.82	100.09 ± 0.99	100.2 ± 0.51	99.94 ± 0.63
Tablets					
LDP ^d	500	98.78 ± 1.10	97.83 ± 0.96	99.01 ± 0.74	—
MDP ^e	250	99.5 ± 0.86	—	99.95 ± 0.90	—

^aAverage of six determinations.

^bMarketed by TTK Pharma.

^cMarketed by TRIOKA Parenterals.

^dMarketed by Wallace.

^eMarketed by Merind Limited.

both red, green and blue products and the reagent blanks are shown in Figs. 1 and 2.

The details of optical characteristics are summarised in Table 2.

3.2. Reaction sequence

Vicinal dihydroxybenzene derivatives were readily oxidised to *o*-benzoquinone by NBS. INH, by virtue of its strong electron-donating group, couples with *o*-benzoquinone in alkaline medium leading to the formation of oxidative coupled products as given in the reaction in Scheme 1 [12,13]. Other oxidising agents such as $\text{Cr}_2\text{O}_7^{2-}$, H_2O_2 , chloramine-T and MnO_4^- were tried instead of NBS and found to be less effective. However, in acidic medium dichromate and MnO_4^- oxidising agents does not form any colour under the experimental conditions.

A characteristic green to blue-coloured product is formed when DPH or PCL is allowed to react with SNP in the presence of HAH in an alkaline medium. Use of this method was unsuccessful for the identification of the product in solid form. However, Gupta and co-workers [14] and Nagaraja et al. [15] have proposed the formation of

indophenol blue or a coordination complex with a charge transfer absorption using SNP as a reagent for the analysis of phenol. This indicates that the formation of the green to blue colour by the proposed method B may be due to either the formation of indophenol blue or a coordination complex of CT type.

3.3. Stability

The resultant products of the proposed methods were studied at different temperatures. The results indicate that the absorbance values remain constant in the temperature range 5–70°C. At higher temperatures the absorbance values decrease, indicating the dissociation of the products on prolonged heating. The coloured products were stable for 3–48 h at room temperature.

3.4. Interference

An antioxidant, sodium metabisulphate, and sodium chloride that is commonly present in the DPH injection, and also commonly used excipients such as starch, talc, glucose, lactose, dextrose

and magnesium stearate, did not interfere, while vitamin C, adrenaline and noradrenaline were found to have interfered. In method B, the results of interference shows that a 2-fold excess of LDP and MDP do not interfere.

3.5. Application

The applicability of the method to assay of pharmaceutical preparations was examined. The results obtained (Table 3) compared favourably to those reported by El-Kommos et al. [13] and the official method [11].

4. Conclusions

The proposed methods are simple, rapid, precise, sensitive and economical. The two methods can be successfully applied as an alternative to the existing methods.

Acknowledgements

One of the authors (K.C.S.M.) thanks the Mysore University for the support of this research work.

References

- [1] B.K. George, in: L.S. Goodman, A. Gilman (Eds.), *The Pharmacological Basis of Therapeutics*, 3rd ed., The Macmillan Company, NY, 1965, p. 427.
- [2] C.E. Bell, A.R. Somerville, *Biochem. J.* 98 (1966) 1C.
- [3] Imai, Kazuhizo, *J. Chromatogr.* 105 (1975) 135.
- [4] R.T. Sane, P.M. Deshpande, C.L. Sawant, S.M. Dolas, V.G. Nayak, S.S. Zarakar, *Indian Drugs (and references cited)* 24 (1987) 199.
- [5] Seki, Tokaichizo, Wada, Hiroshi, *J. Chromatogr.* 114 (1975) 227.
- [6] P.J. Murphy, T.L. William, D.L. Kau, *J. Pharmacol. Exp. Ther.* 199 (1976) 423.
- [7] K. Satoshi, T. Zenzo, *Chem. Pharm. Bull. Tokyo* 16 (1968) 1091.
- [8] B.F. Erlanger, *Pharmacol. Rev.* 25 (1973) 271.
- [9] L.J. Ricebery, H.V. Vunakis, L. Levin, *Anal. Biochem.* 60 (1974) 551.
- [10] *US Pharmacopoeia XXI*, United Pharmacopoeial Convention, Inc., 12601, Twinbrook Parkway, Rockville, MD 20852, 1985, pp. 348, 353.
- [11] *British Pharmacopoeia*, London, SIN 85 NQ, 1993, pp. 239, 380 and 424.
- [12] C.S.P. Sastry, V. Gurucharana Das, K. Ekambareswara Rao, *Analyst* 110 (1985) 395.
- [13] M.E. EL-Kommos, F.A. Mohamed, A.S. Khedr, *J. Assoc. Off. Anal. Chem.* 73 (1990) 516.
- [14] S. Amlathe, S. Upadhyay, V.K. Guptha, *Analyst* 112 (1987) 1463.
- [15] P. Nagaraja, J.M. Bhandari, B.N. Achar, *Indian J. Chem.* 32A (1993) 641.

Gas chromatographic characteristics and application studies of the stationary phase of CH-B-15-C-5

Qing Xiaotian ^{a,*}, Zhou Zaide ^b, Xie Minggui ^b, Zeng Yongchang ^b, Tang Ying ^c

^a Department of Chemistry, North Sichuan Medical College, Nanchong 637000, People's Republic of China

^b Department of Chemistry, Sichuan University, Chengdu 610064, People's Republic of China

^c Department of Chemistry, Chongqing Teachers' College, Yongchuan 632168, People's Republic of China

Received 4 October 1996; received in revised form 28 July 1997; accepted 29 July 1997

Abstract

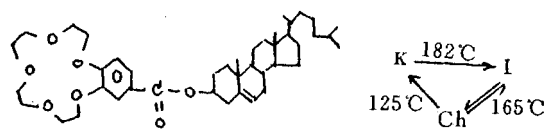
In this paper, separations of organic compounds, such as, *n*-alkanes, alcohols, ethyl esters of C₁–C₈ carboxylic acid, halogen derivatives, position-isomers of the replacement aromatic hydrocarbon, optical isomers of ethyl lactate and isoamyl alcohol, etc. were studied using 4'-cholestenoxycarbonyl-benzo-15-crown-5 liquid crystal crown ether (CH-B-15-C-5) as stationary phase in gas-solid chromatography (GSC), general gas-liquid chromatography (GLC) and crown ether liquid crystal gas-liquid chromatography (CL-GLC). Also, the chromatographic characteristics, such as the chemical stability, thermal stability, selectivity, polarity and operating temperature range, of the CH-B-15-C-5 as stationary phase for GSC, GLC and CL-GLC systems were studied. The results showed that the polarity of this chromatographic column is mean-weak; the chemical and thermal stabilities and the selectivity are good and the operating temperature range is wide. The results of separations of organic compounds are satisfactory. © 1998 Elsevier Science B.V. All rights reserved.

Keywords: Gas chromatography; Application studies; Stationary phase; CH-B-15-C-5

1. Introduction

Recently, much attention has been paid to chromatographic characteristics and applications of crown ether stationary phase [1–5]. Cholesteric liquid crystal crown ether CH-B-15-C-5 has different phase states under a range of different temperatures, and a large variety of physical properties under different operating conditions in the same temperature range. The constitutional

formula and phase transition temperatures of CH-B-15-C-5 are described in the following.



When the temperature is decreased from 182 to 165°C, the compound forms cholesteric liquid crystal. If it is decreased to 125°C, it remains anisotropic liquid crystal; then if the temperature

* Corresponding author.

decreases below 125°C it forms anisotropic solid crystal. But, in the course of heating from below 125 to 182°C it cannot form cholesteric liquid crystal. Therefore, the stationary phases of CH-B-15-C-5 have three gas chromatographic functions: gas-solid chromatography (GSC), general gas-liquid chromatography (GLC) and crown ether liquid crystal gas-liquid chromatography (CL-GLC). We separated organic compounds, such as, *n*-alkanes, alcohols, ethyl esters of C_1 – C_8 carboxylic acid, halogen derivatives, etc., and position-isomers of the replacement aromatic hydrocarbons, such as the *o,m,p*-xylenes, -dichlorobenzenes, -nitrochlorobenzenes, and 1,3,5- and 1,2,4-trimethylbenzene, etc. Good separation results were achieved using crown ether liquid crystal stationary phase under the different chromatographic conditions. We have explored the chiral resolutions of optical isomers of ethyl lactate and isoamyl alcohol in gas chromatography (GC) with a new cholesteric liquid crystal crown ether (CH-B-15-C-5) stationary phase.

We have not seen any other reports on this type of study up to now.

2. Experimental

2.1. Apparatus and reagents

An SC-6 Gas Chromatograph, with a hydrogen flame ionization detector, was used. Chromatographic column: stainless steel column, 2 m \times 3 mm I.D.; stationary phase, Chromosorb W (60–80 mesh) on the column packed with 10% CH-B-15-C-5.

CH-B-15-C-5 liquid crystal crown ether was prepared by Prof. Xie Mingguo, and was determined by IR, NMR, MS and elemental analysis [6,7]. Ethyl lactate and isoamyl alcohol were chromatographic pure reagents. *R*(–)-Ethyl lactate and *S*(–)-2-methyl-1-butanol were optically pure (Fluka, USA). Other reagents were analytically pure.

2.2. Procedure

In the GSC method, column temperature was raised from room temperature to 182°C at a rate of 10°C min⁻¹, kept there for 30 min, then lowered to 165°C at a rate of 2°C min⁻¹ and kept there for 30 min, then lowered to below 125°C to the necessary temperature and separation of organic compounds was carried out.

In the GLC method, the temperature was raised to 130–190°C and organic compounds were separated.

In the CL-GLC method, the column temperature was raised to 182°C at a rate of 10°C min⁻¹, kept there for 30 min, then lowered to 165°C at a rate of 2°C min⁻¹, and kept there for 30 min, then lowered at a rate of 2°C min⁻¹ to the necessary temperature and organic compounds were separated.

3. Results and discussion

3.1. Separations of ethyl esters of C_1 – C_8 carboxylic acid, C_5 – C_{12} *n*-alkanes, C_1 – C_8 alcohols and some organic mixtures

In the GSC method, ethyl esters of C_1 – C_8 carboxylic acid, C_5 – C_{12} *n*-alkanes, C_1 – C_8 alcohols and some organic compounds mixtures were separated, at a column temperature of 120°C. Carrier gas was nitrogen. Hydrogen and air flow-rates were 30 and 60 cm³ min⁻¹, respectively (for results see Fig. 1).

The results show that the homologues of alkane and ethyl esters of carboxylic acid abide by carbon number law (see Fig. 1A Fig. 1B), but in the *n*-alcohol homologous series, methanol deviates considerably from carbon number law. A comparison of the size of the methanol molecule and CH-B-15-C-5 demonstrates the cause: methanol molecules enter the crown ether cavity, but higher alcohols can not.

It is evident from Fig. 1D that aromatics are retained for a larger time in the GSC method than with cyclohexane and cyclohexene. The most likely cause of this behaviour is the similarity of aromatics to the aromatic nucleus in the CH-B-15-C-5 cavity [8].

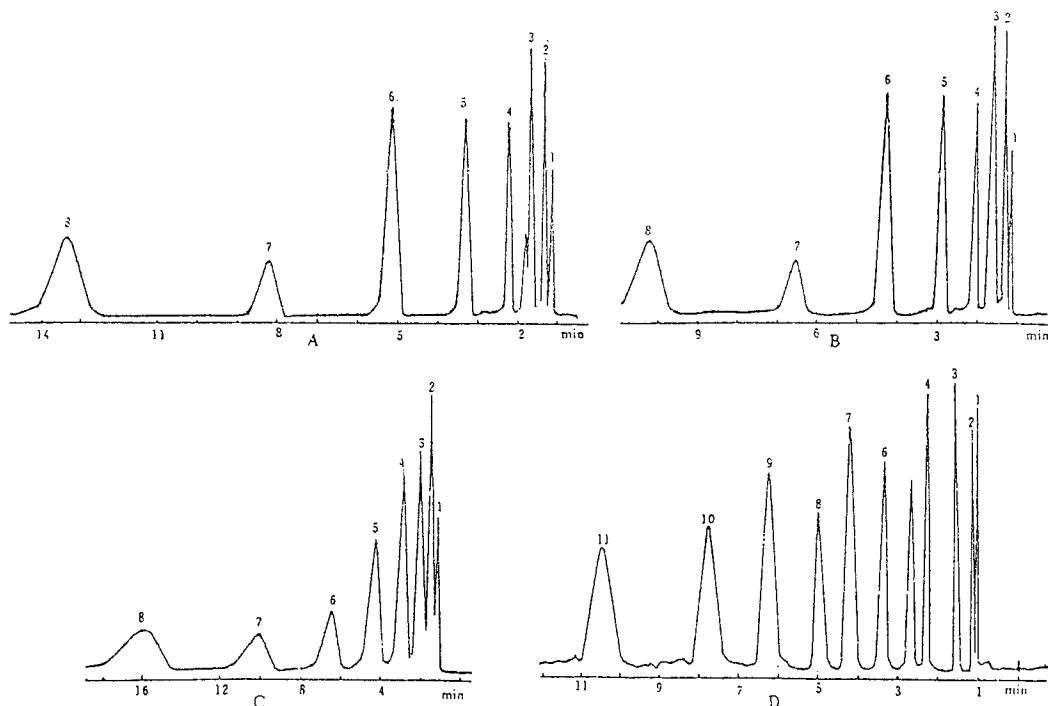


Fig. 1. GSC of homologous series of ethyl esters of carboxylic acids, *n*-alkanes, alcohols, and organic mixtures at a column temperature of 120°C. (A) The GSC of ethyl esters of C₁–C₈ carboxylic acid (carrier gas flow-rate was 20 cm³ min⁻¹). (1) Ethyl ester of formic acid; (2) ethyl ester of acetic acid; (3) ethyl ester of *n*-propionic acid; (4) ethyl ester of *n*-butyric acid; (5) ethyl ester of *n*-valeric acid; (6) ethyl ester of *n*-caproic acid; (7) ethyl ester of *n*-enanthic acid; and (8) ethyl ester of *n*-caprylic acid. (B) The GSC of C₅–C₁₂ *n*-alkanes (carrier gas flow-rate was 15 cm³ min⁻¹). (1) *n*-Pentane; (2) *n*-hexane; (3) *n*-heptane; (4) *n*-octane; (5) *n*-nonane; (6) *n*-decane; (7) *n*-undecane; and (8) dodecane. (C) The GSC of alcohols (carrier gas flow-rate was 20 cm³ min⁻¹). (1) Methanol; (2) ethanol; (3) *n*-propanol; (4) *n*-butanol; (5) *n*-pentanol; (6) *n*-hexanol; (7) *n*-enanthol; and (8) *n*-octanol. (D) The GSC of aromatics and other organic mixtures (carrier gas flow-rate was 30 cm³ min⁻¹). (1) Cyclohexane; (2) methylcyclohexane; (3) cyclohexene; (4) benzene; (5) toluene; (6) *m*-xylene; (7) isopropylbenzene; (8) butylbenzene; (9) *o*-ethyltoluene; (10) 1,3,5-trimethylbenzene; and (11) *p*-cymene.

3.2. Separations of position-isomers for replacement aromatic hydrocarbons

Carrier gas flow-rate was 20 cm³ min⁻¹. Hydrogen and air flow-rates were 25 and 50 cm³ min⁻¹, respectively. *o,m,p*-Xylenes, -dichlorobenzenes, -nitrochlorobenzenes, and 1,3,5- and 1,2,4-trimethylbenzene were separated at a column temperature of 110°C by the GSC method (for results see Fig. 2).

Carrier gas flow-rate was 20 cm³ min⁻¹. Hydrogen and air flow-rates were 25 and 50 cm³ min⁻¹, respectively. *o,m,p*-Xylenes, -dichlorobenzenes, -nitrochlorobenzenes, and 1,3,5- and 1,2,4-

trimethylbenzene were separated at a column temperature of 130°C by the GLC method (for results see Fig. 3).

Carrier gas flow-rate was 20 cm³ min⁻¹. Hydrogen and air flow-rates were 25 and 50 cm³ min⁻¹, respectively. *o,m,p*-Dichlorobenzenes, -nitrochlorobenzenes, and 1,3,5- and 1,2,4-trimethylbenzene were separated at a column temperature of 130°C by the CL-GLC method (for results see Fig. 4).

In the GSC and GLC methods, retention behaviour of the position-isomers on the CH-B-15-C-5 column accorded with the retention law of the crown ether stationary phase [9]. That is, on the

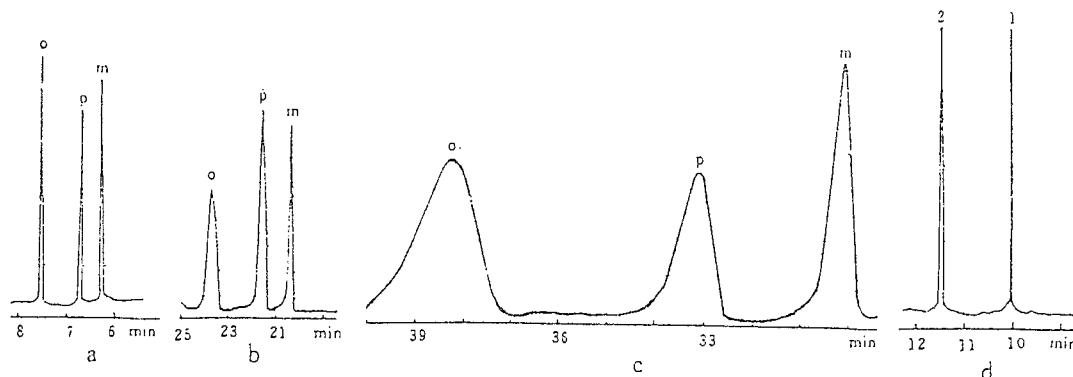


Fig. 2. GSC of position-isomers of replacement aromatic hydrocarbons at a column temperature of 110°C. (a) Xylenes; (b) dichlorobenzenes; (c) nitrochlorobenzenes; (d) 1,3,5-trimethylbenzene (peak 1) and 1,2,4-trimethylbenzene (peak 2).

crown ether column, retention times of substances depended on polarity, hydrogen bond and crown ether cavity, etc. In the separation of xylenes, dichlorobenzenes and nitrochlorobenzenes, molecular polarity order was $o \rightarrow m \rightarrow p$ -, but peak order was $m \rightarrow p \rightarrow o$ - (see Figs. 2 and 3) because the p -isomer molecular shape was columnar, which could accord with the cavity of crown ether [10].

In the CL-GLC method, because of the orderly arrangement of crown ether liquid crystal molecules and the increase of orientation effect of these molecule and the columnar molecule of p -isomer, the order of chromatographic peaks was $m \rightarrow o \rightarrow p$ - (see Fig. 4).

3.3. Separations of optical isomers of ethyl lactate and isoamyl alcohol

Carrier gas flow-rate was $25 \text{ cm}^3 \text{ min}^{-1}$. Hydrogen and air flow-rates were 25 and $60 \text{ cm}^3 \text{ min}^{-1}$, respectively. In a column temperature operating range of 75–125°C, ethyl lactate and isoamyl alcohol were separated using the CH-B-15-C-5 GSC stationary phase (for results see Table 1).

Carrier gas flow-rate was $30 \text{ cm}^3 \text{ min}^{-1}$. Hydrogen and air flow-rates were 25 and $50 \text{ cm}^3 \text{ min}^{-1}$, respectively. In a column temperature operating range of 130–190°C ethyl lactate and isoamyl alcohol were separated with the CH-B-15-C-5 GLC stationary phase (for results see Table 2).

Carrier gas flow-rate was $30 \text{ cm}^3 \text{ min}^{-1}$, hydrogen and air flow-rates were 25 and $50 \text{ cm}^3 \text{ min}^{-1}$, respectively. In a column temperature operating range of 130–175°C, ethyl lactate and isoamyl alcohol were separated with the CH-B-15-C-5 CL-GLC stationary phase (for results see Table 3).

From experiments of chiral resolution for optical isomers in the GSC, GLC and CL-GLC systems we found that the separations of ethyl lactate and isoamyl alcohol could be obtained by this stationary phase, and the resolutions were almost as good as those on the GSC, GLC [11] and CL-GLC systems. But, relatively, with the GLC method chiral resolution able was lower than that with the GSC and CL-GLC methods, especially in the high-temperature column, resolution R values were evidently lower than in the GSC and CL-GLC systems.

3.4. Polarities and stabilities of the columns

Polarities of CH-B-15-C-5 were determined by the determination of the McReynolds phase constants. The results showed that the polarity of the column in the GSC system was stronger than that of SE-30 column, but weaker than that of the PEG-20M and B-15-C-5 columns [12], and in the GLC and the CL-GLC systems the polarities of this crown ether liquid crystal column were weaker than that in the GSC system. Thus, the polarity of the CH-B-15-C-5 column was mean-weak (see Table 4).

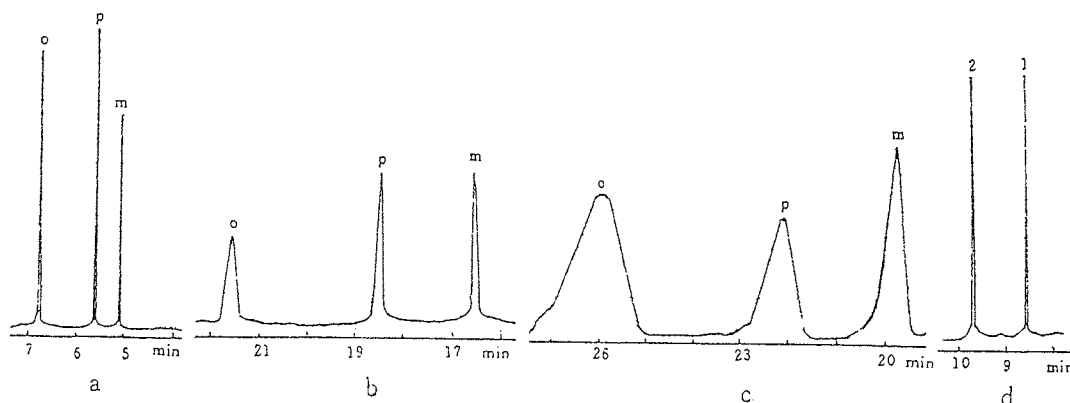


Fig. 3. GLC of position-isomers of replacement aromatic hydrocarbons at a column temperature 130°C. (a) Xylenes; (b) dichlorobenzenes; (c) nitrochlorobenzenes; (d) 1,3,5-trimethylbenzene (peak 1) and 1,2,4-trimethylbenzene (peak 2).

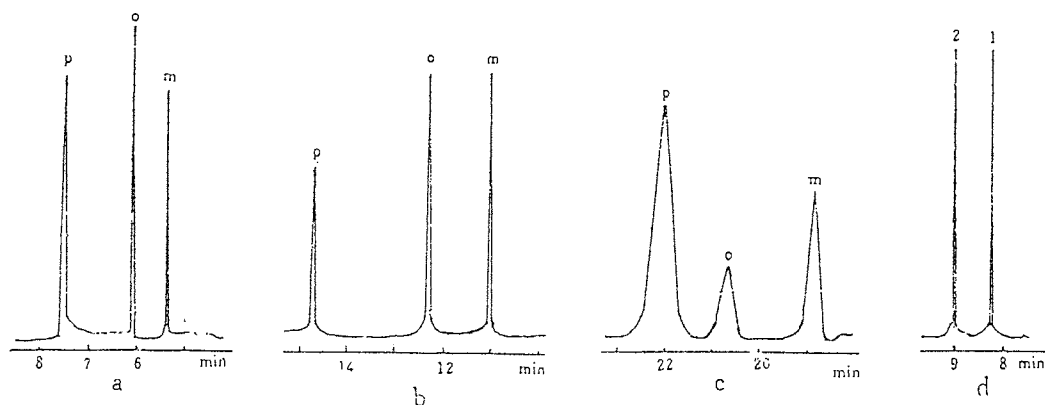


Fig. 4. CL-GLC of position-isomers of replacement aromatic hydrocarbons at a column temperature of 130°C. (a) Xylenes; (b) dichlorobenzenes; (c) nitrochlorobenzenes; (d) 1,3,5-trimethylbenzene (peak 1) and 1,2,4-trimethylbenzene (peak 2).

The chemical stability and thermal stability of CH-B-15-C-5 were very good as results determined by this column were satisfactory. Also, the chemical properties of this liquid crystal crown ether compound were stable for a long time at a temperature of 200°C [13] and the possible operating temperature range was wide.

3.5. Shape of chromatographic peaks

The chromatographic peak shapes were good. Basic GLC theory could explain the symmetrical chromatographic peaks in the GLC [14] and the CL-GLC systems (e.g. Figs. 3 and 4), but basic GSC theory could not explain the symmetrical

chromatographic peak in the GSC system of this crown ether column (e.g. Figs. 1 and 2). We presume that, besides adsorption theory, in the GSC stationary phase the molecular steric arrangement is of great importance for the retention behaviour of organic compounds.

In the CH-B-15-C-5 GSC stationary phase, after the crown ether compound was kept at a temperature of 182°C for 30 min, solid crystal was orderly arranged at temperatures lower than 125°C. Under the above conditions of GSC, it is beneficial to obtain symmetrical chromatographic peaks, in the GSC system, of organic homologous series compounds, position-isomers of replacement aromatic hydrocarbons [15], and optical isomers of ethyl lactate and isoamyl alcohol.

Table 1

Retention times t_R (min) and resolutions (R) of chiral separations for optical isomers of ethyl lactate and isoamyl alcohol using CH-B-15-C-5 stationary phase in the GSC system

Temp. (°C)	Ethyl lactate			Isoamyl alcohol		
	$t_{S(+)}$	$t_{R(-)}$	R	$t_{R(+)}$	$t_{S(-)}$	R
75	11.5	12.7	3.41	23.5	25.0	3.80
85	10.6	11.7	3.10	16.5	18.4	3.60
95	9.6	10.6	2.90	6.5	8.1	3.46
105	8.5	9.6	2.61	3.1	4.2	3.05
115	7.0	8.2	2.30	2.1	3.0	2.50
125	6.6	7.5	1.85	1.8	2.5	2.12

3.6. Selectivity of the column

CH-B-15-C-5 is a low-molecular crown ether liquid crystal compound that has non-polar carbon-carbon bonds, polar carbon-oxygen bonds and aromatic rings, etc., therefore, it can act with many organic compounds, for example, alkane and alkene homologues, alcohols, ethers, aromatics, position-isomers, etc. This crown ether compound also has chiral carbon atoms which possess chiral recognition for the optical isomers, for example, ethyl lactate, isoamyl alcohol, etc.

The resolving power of the GSC, GLC and CL-GLC systems was compared using resolution R values.

CH-B-15-C-5 are orderly arranged solid crystals in the GSC and crown ether liquid crystals have an orderly arrangement in the CL-GLC system. Compound molecular chiral carbon atoms were orderly arranged because the crown

Table 2

Retention times t_R (min) and resolutions (R) of chiral separations for optical isomers of ethyl lactate and isoamyl alcohol using CH-B-15-C-5 stationary phase in the GLC system

Temp. (°C)	Ethyl lactate			Isoamyl alcohol		
	$t_{S(+)}$	$t_{R(-)}$	R	$t_{R(+)}$	$t_{S(-)}$	R
130	6.2	7.7	1.80	1.7	2.1	1.77
145	4.6	5.0	1.50	1.2	1.4	1.65
160	3.4	4.0	1.08	0.8	1.1	1.40
175	2.4	2.7	0.95	0.6	0.8	1.00
190	1.5	1.5	—	0.4	0.4	—

Table 3

Retention times t_R (min) and resolutions (R) of chiral separations for optical isomers of ethyl lactate and isoamyl alcohol using CH-B-15-C-5 stationary phase in the CL-GLC system

Temp. (°C)	Ethyl lactate			Isoamyl alcohol		
	$t_{S(+)}$	$t_{R(-)}$	R	$t_{R(+)}$	$t_{S(-)}$	R
130	6.0	7.4	2.00	1.9	2.6	1.95
145	4.5	5.6	1.85	1.5	2.0	1.86
160	3.1	3.9	1.50	1.2	1.7	1.60
175	2.0	2.7	0.60	1.0	1.4	1.51

ether molecules were orderly arranged. But, in the GLC system, CH-B-15-C-5 could not form liquid crystal, thus the compound molecular chiral carbon atomic arrangement was disorderly.

The orderly arrangement state was useful for chiral molecular orientation [16]. The chiral resolving power of orderly arranged CH-B-15-C-5 molecules was stronger than that of the disordered orientation state. Therefore, the R value of the CL-GLC system was higher than that of the GLC system under the same experimental conditions, e.g., carrier gas flow-rates, hydrogen and air flow-rates, and column temperature, etc. (see Tables 2 and 3). On the other hand, chiral carbon atomic disordering effect increased with increase of molecular thermal motion. As the CH-B-15-C-5 molecular chiral resolving power was lower, the resolution R value decreased with the increase of temperature in the GLC system (see Table 2).

To sum up, separations can be obtained of organic homologues, organic mixtures, position-isomers of replacement aromatic hydrocarbon, optical isomers of ethyl lactate and isoamyl alcohol, etc., using CH-B-15-C-5 as a stationary phase in GC. Satisfactory results can be obtained in the column temperature range of 75–140°C, and

Table 4

Comparison of polarities of chromatographic columns

Temp. (°C)	SE-30	PEG-20M	B-15-C-5	CH-B-15-C-5
120	43	548	275	167
130	41	539	268	148

column temperature can be increased if using the CL-GLC method to separate substances of high boiling point.

References

- [1] A.M. Stalcup, S.C. Chang, *J. Chromatogr.* 531 (1990) 181.
- [2] T. Shinbo, T. Yamaguchi, H. Yanagishita, D. Kitamoto, K. Sakaki, M. Sugiura, *J. Chromatogr.* 625 (1992) 101.
- [3] A. Kohoutova, E. Smolkova-Keulemansova, L. Feltl, *J. Chromatogr.* 471 (1989) 139.
- [4] R. Kuhn, C. Steinmetz, T. Bereuter, P. Haas, F. Erni, *J. Chromatogr.* 666 (1994) 367.
- [5] B. Sellergren, M. Lepisto, K. Mosbach, *J. Am. Chem. Soc.* 110 (1988) 5853.
- [6] M. Xie, J. Qin, *Mol. Cryst. Liq. Cryst.* 209 (1991) 155.
- [7] M. Xie, *Synthetic Commun.* 22 (1992) 2253.
- [8] P. Mnuk, E. Smolkova-Keulemansova, L. Feltl, *J. Chromatogr.* 623 (1992) 297.
- [9] J.D. Lamb, R.G. Smith, *Talanta* 39 (1992) 923.
- [10] W. Chaiping, *J. Chromatogr.* 5 (13) (1995) 339.
- [11] R. Kuhn, R. Erni, T. Bereuter, J. Hausier, *Anal. Chem.* 64 (1992) 2815.
- [12] Z. Zaide, *J. Sichuan Univ. (Nat. Sci. Ed.)* 1 (1995) 74.
- [13] W.H. Delphin, E.P. Horwitz, *Anal. Chem.* 50 (7) (1978) 843.
- [14] N.R. Ayyangar, A.S. Tambe, S.S. Biswas, *J. Chromatogr.* 543 (1991) 179.
- [15] N. Thuaud, B. Scbille, A. Deretaini, G. Ielievere, *J. Chromatogr.* 555 (1991) 53.
- [16] S. Fanali, *J. Chromatogr.* 274 (1989) 441.

Binary and ternary complexes of inosine

M.M. Khalil *, A.M. Radalla

Department of Chemistry, Faculty of Science, Cairo University, Beni-Suef Branch, Beni-Suef, Egypt

Received 14 May 1997; received in revised form 29 July 1997; accepted 30 July 1997

Abstract

Formation of binary and ternary complexes of Cu(II) and Ni(II) metal ions with inosine as a primary ligand and some biologically important aliphatic and aromatic carboxylic acids (succinic, oxalic, malic, maleic, malonic, tartaric, 5-sulfosalicylic, salicylic and phthalic acids) as secondary ligands was studied by the potentiometric technique at 25°C and 0.10 M (NaNO₃) ionic strength. The ternary complex formation was found to take place in a stepwise manner. The stability constants of these binary and ternary systems were calculated. The lower stability of 1:2 complexes of inosine compared to the corresponding 1:1 systems is in accord with statistical considerations. The values of $\Delta \log K$ for the ternary complexes studied have been evaluated and discussed. The mode of chelation of ternary complexes was ascertained by conductivity measurements. © 1998 Elsevier Science B.V. All rights reserved.

Keywords: Binary and ternary complexes; Inosine; Potentiometric and conductometric studies

1. Introduction

Interaction of nucleosides and nucleotides with metal ions has been a subject of much recent interest. Because of the role of bivalent metal ions in many biochemical processes [1–7], considerable research is being undertaken to understand the nature of metal ion interaction with vital molecules like DNA and RNA. Ternary complexes of nucleosides and nucleotides have attracted the attention of many workers [8–21]. This is mainly because they provide models for metalloenzyme reactions in biological systems [22–24]. They also explain to some extent the specific and selective interactions that take place

in many biological systems. As a continuation of our research program to study the binary and ternary complexes of biological importance [25–28], the present work traces the formation and characterization of binary and ternary complexes involving Cu(II) and Ni(II) metal ions, inosine and some biologically important aliphatic and aromatic carboxylic acids.

2. Experimental

2.1. Materials and solutions

Chromatographically pure inosine was purchased from Sigma. A fresh sample was weighed and a solution was prepared for each titration to

* Corresponding author. Fax +20 823 14606.

exclude loss by hydrolysis or photochemical decomposition. The metal salts were provided by BDH as nitrates. All solutions of Cu(II) and Ni(II) metal ions were prepared and standardized complexometrically by EDTA using suitable indicators [29]. Carbonate-free sodium hydroxide (titrant, prepared in 0.1 M NaNO₃ solution) was standardized potentiometrically with KH-phthalate solution (Merck AG). Aliphatic and aromatic carboxylic acids, nitric acid and sodium hydroxide were from Merck p.a.

2.2. Apparatus

Potentiometric pH measurements were carried out on solutions in a double-walled glass vessel at 25 ± 0.1°C using a Griffin pH J-300-101G digital pH meter. The temperature was controlled by circulating water through the jacket, from a constant temperature bath. The cell was equipped with a magnetic stirrer and a tightly fitting rubber stopper, through which an Amel 882 delivery dispenser, readable to 1 µl, and electrode system were inserted. The electrode system was calibrated in terms of hydrogen-ion concentrations instead of activities. Thus, all constants determined in this work are concentration constants.

Conductance of solutions was measured with a SUNTEX, conductivity meter SC-170.

2.3. Procedure and measuring techniques

The following solutions were prepared and titrated potentiometrically against standard carbonate-free NaOH (0.10 M) solution:

1. (a) 0.032 M HNO₃ (5 cm³) + 0.50 M NaNO₃ (10 cm³)
2. (b) (a) + 0.01 M carboxylic acid (5 cm³)
3. (c) (b) + 0.01 M metal ion (2 cm³)
4. (d) (a) + 0.01 M inosine (5 cm³)
5. (e) (d) + 0.01 M metal ion (2 cm³)
6. (f) (a) + 0.01 M metal ion (5 cm³) + 0.01 M carboxylic acid (5 cm³) + 0.01 M inosine (5 cm³)

The total volume was adjusted to 50 cm³ by adding double-distilled water in each case. All pH-metric titrations were performed at 25°C and µ = 0.1 M (NaNO₃). An Irving and Rossotti pH

Table 1

Stability constants of 1:1 and 1:2 metal–inosine complexes and Δ log K values for these systems at 25 ± 0.1°C, µ = 0.1 M (NaNO₃)^a

Metal ion	log K _{ML} ^M	log K _{ML₂} ^{ML}	Δ log K
Cu(II)	5.00 ± 0.06	3.64 ± 0.05	−1.36
Ni(II)	4.40 ± 0.08	3.92 ± 0.05	−0.48

^aFor inosine: pK_a = 8.65 ± 0.09.

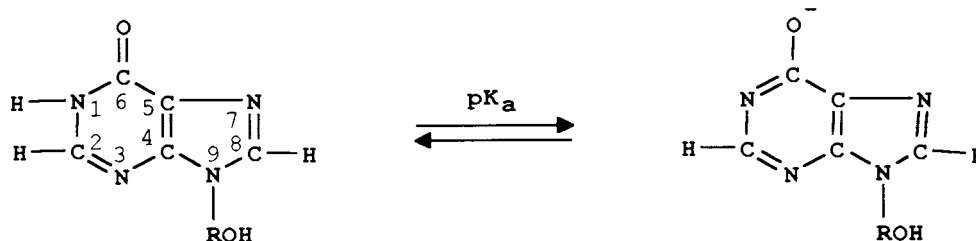
titration technique [30] with modifications [31,32] was used to determine the protonation constants of the ligands and formation constants of the metal complexes. Multiple titrations have been performed for each system. All our calculations of stability constants have been determined successfully in the low pH region. Therefore, the formation of hydroxy complexes or mixed ligand complexes with hydroxy groups could be neglected.

The mixture (g) was titrated conductometrically against 0.10 M NaOH solution: g, 0.01 M Cu^{II} (10 cm³) + 0.01 M salicylic acid (10 cm³) + 0.01 M inosine (10 cm³).

3. Results and discussion

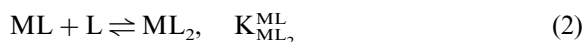
The dissociation constant of cationic inosine, H₃L⁺, could not be calculated potentiometrically, because of the highly acidic nature of the associated proton (pK_a = 1.2) [33]. The first proton association constant of neutral inosine, H₂L, was determined potentiometrically in aqueous solutions, under the experimental conditions (t = 25°C, µ = 0.1 M NaNO₃). Proton ionization was assigned to the N₁H group with the oxygen at the 6 position assuming the negative charge. The value obtained (8.65) agreed quite well with that previously reported by Simpson using the spectrophotometric technique [33]. The second dissociation of the proton from the ribose OH group of inosine takes place at higher buffer region (pH > 12) and hence the corresponding dissociation constant could not be calculated by this method.

The proton-dissociation step involved in the titration of inosine can be represented as follows:



R = Ribose

The equilibria involved in the formation of 1:1 and 1:2 metal–inosine binary complexes may be represented as follows:



The stability constants of 1:1 and 1:2 binary complexes of inosine with Cu(II) and Ni(II) metal ions have been determined (Table 1). The constant determined by us for Cu (inosine) 1:1 complex agrees well with that given previously by Albert [34]. However, our stability constant for the Ni (inosine) 1:1 complex is somewhat higher than the value given by the same author. It was also found that the stability constants determined in this work for normal 1:1 metal complexes of inosine are higher than those determined recently by Reddy and Reddy

[21]. The disagreement found may be attributed to the different methods, temperature and ionic strength used for determination.

It is of great interest to compare the stability constants of 1:1 metal–inosine complexes with those of hypoxanthine species [34]. Both hypoxanthine and inosine (purine and its corresponding nucleoside, respectively) form metal complexes with the same binding site (N₇ of the imidazole moiety). The weak basicity of inosine is reflected in the lower stability of its metal complexes than that of hypoxanthine.

The stability constants of the 1:2 metal–inosine complexes are lower than those of the corresponding 1:1 systems, as expected from statistical considerations. The $\Delta \log K$ ($\log K_{ML_2}^{ML} - \log K_{ML}^M$) values for the inosine complexes are negative (Table 1). This is the

Table 2

Acidity constants of carboxylic acids and stability constants of their 1:1 and 1:2 binary complexes at $25 \pm 0.1^\circ\text{C}$, $\mu = 0.1 \text{ M}$ (NaNO_3)

Carboxylic acid (A)	pK_a	pK_{2a}	$\log K_{CuA}^{Cu}$	$\log K_{CuA_2}^{CuA}$	$\log K_{NiA}^{Ni}$	$\log K_{NiA_2}^{NiA}$
Succinic acid	4.20 ± 0.05	5.65 ± 0.07	3.20 ± 0.05	—	3.12 ± 0.09	—
Oxalic acid	1.40*	4.25 ± 0.08	4.60 ± 0.06	4.10 ± 0.08	3.46 ± 0.08	2.96 ± 0.05
Malic acid	3.40 ± 0.07	5.20 ± 0.06	6.80 ± 0.09	—	4.60 ± 0.07	—
Malonic acid	2.90 ± 0.07	5.65 ± 0.06	4.82 ± 0.05	3.37 ± 0.06	3.92 ± 0.07	2.92 ± 0.06
Maleic acid	1.80*	6.22 ± 0.06	4.07 ± 0.08	2.89 ± 0.07	3.70 ± 0.06	2.82 ± 0.08
Tartaric acid	3.00 ± 0.05	4.35 ± 0.05	6.96 ± 0.07	5.70 ± 0.07	4.68 ± 0.07	4.36 ± 0.05
Phthalic acid	2.95 ± 0.04	5.35 ± 0.06	3.48 ± 0.07	2.52 ± 0.08	3.26 ± 0.07	1.92 ± 0.05
Salicylic acid	2.88 ± 0.05	13.60*	10.62 ± 0.05	8.46 ± 0.05	8.65 ± 0.05	4.65 ± 0.09
5-Sulfosalicylic acid	2.50 ± 0.06	11.60*	9.42 ± 0.09	6.98 ± 0.07	6.35 ± 0.05	3.82 ± 0.06

*From ref. [35].

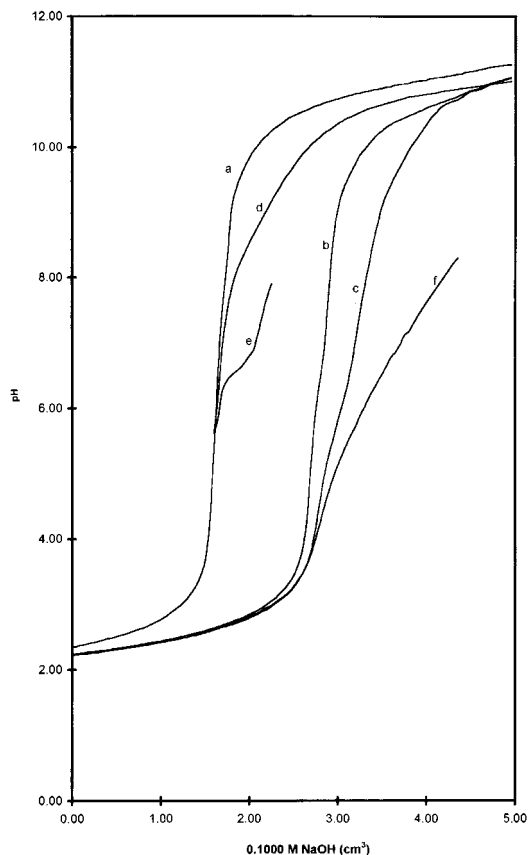


Fig. 1. Potentiometric titration curves for the Cu^{II} -5-sulfosalicylic acid-inosine system.

normal trend in neutral ligands where the enthalpy is more favourable for a 1:1 species (exothermic) as compared to a 1:2 species.

The acidity constants of carboxylic acids and the stability constants of their $\text{Cu}(\text{II})$ and $\text{Ni}(\text{II})$ complexes have been determined (Table 2) under the same experimental conditions.

The stability constants of binary $\text{Cu}(\text{II})$ complexes with the ligands studied are found to be higher than those of $\text{Ni}(\text{II})$ complexes (Tables 1 and 2), which is in accordance with Irving-William's order [36].

In Figs. 1–6, representative sets of experimental titration curves obtained according to the sequence described in the experimental part for the

different mixed-ligand systems are displaced. The formation of a ternary complex is ascertained by comparison of the mixed-ligand titration curve with the composite curve obtained by graphical addition of the inosine titration data to that of the (1:1) M^{II} -carboxylic acid titration curve. The Ni^{II} -salicylic acid-inosine system is taken as representative, as shown in Fig. 7. The mixed-ligand system was found to deviate considerably from the resultant composite curve indicating the formation of a ternary complex.

Therefore, it is assumed that in the presence of both ligands, the carboxylic acid is ligated to the metal ion, then followed by ligation of inosine, i.e. the ternary complex formation could be considered in stepwise equilibria (Eqs. (3) and (4)):

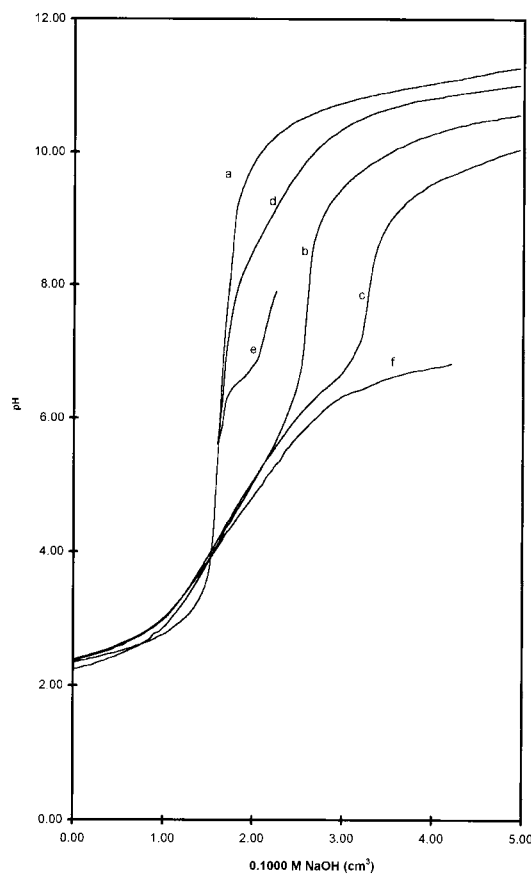


Fig. 2. Potentiometric titration curves for the Cu^{II} -succinic acid-inosine system.

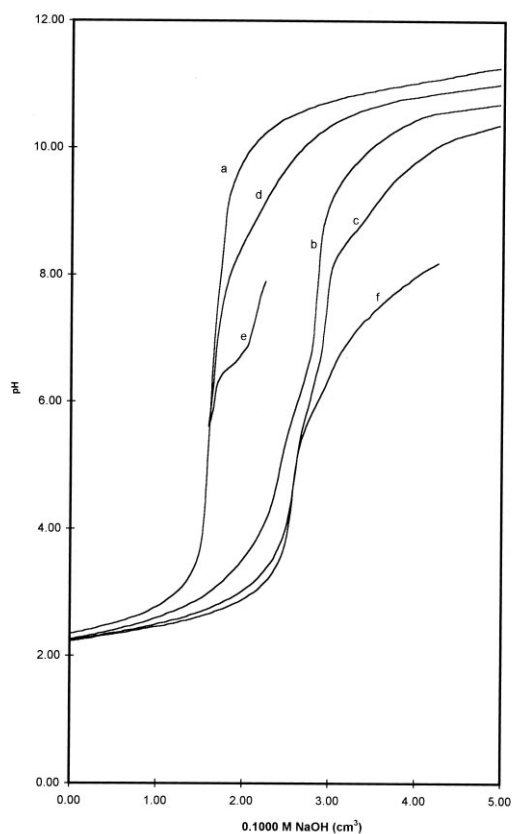


Fig. 3. Potentiometric titration curves for the Cu^{II} -oxalic acid-inosine system.



$$K_{\text{MAL}}^{\text{MA}} = \frac{[\text{MAL}]}{[\text{MA}][\text{L}]} \quad (5)$$

The overall stability constant $\beta_{\text{MAL}}^{\text{M}}$ may be represented by Eq. (6):



$$\begin{aligned} \beta_{\text{MAL}}^{\text{M}} &= \frac{[\text{MAL}]}{[\text{M}][\text{A}][\text{L}]} \\ &= K_{\text{MAL}}^{\text{MA}} \times K_{\text{MA}}^{\text{M}} \end{aligned} \quad (7)$$

where A = carboxylic acid and L = neutral ligand inosine.

The relative stability of the ternary complexes,

as compared to that of the corresponding binary complexes, can be quantitatively expressed in different ways. A review of those methods [37] has shown that, for a variety of reasons, the most suitable comparison is in terms of $\Delta \log K$. Table 3 demonstrates the difference in stabilities of the binary and ternary complexes in terms of $\Delta \log K$ as defined by Eq. (8)

$$\Delta \log K = \log K_{\text{MAL}}^{\text{MA}} - \log K_{\text{ML}}^{\text{M}} \quad (8)$$

In the ternary systems studied, the values of $K_{\text{MAL}}^{\text{MA}}$ were found to lie in the sequence: phthalic > salicylic > 5-sulfosalicylic > succinic > malic > malonic > maleic > tartaric > oxalic acid.

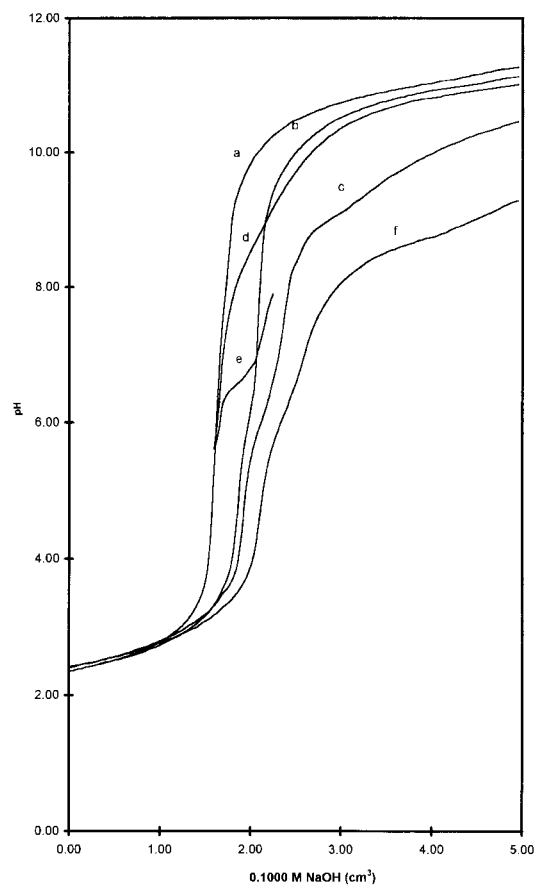


Fig. 4. Potentiometric titration curves for the Ni^{II} -salicylic acid-inosine system.

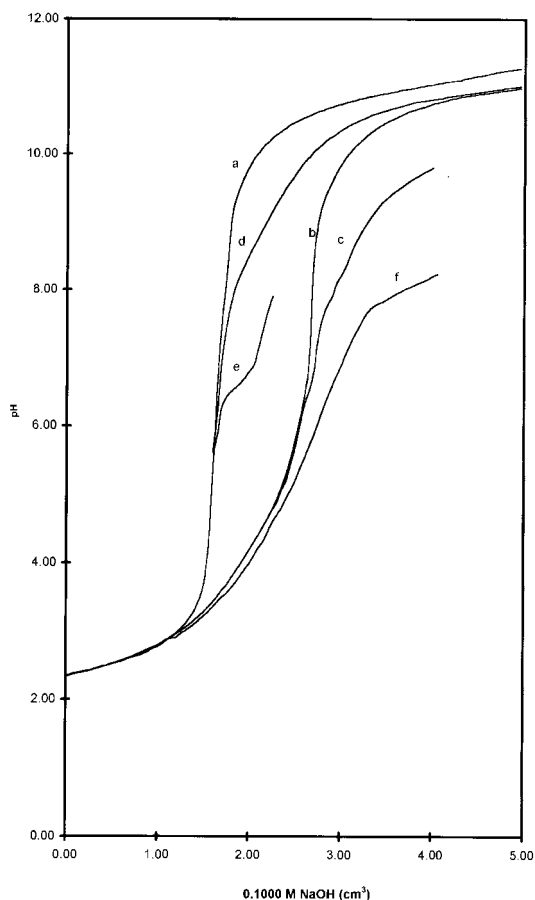


Fig. 5. Potentiometric titration curves for the Ni^{II} -malic acid-inosine system.

The higher stability of phthalic acid complex than salicylic acid may be explained [38] as follows: since the carboxylate oxygen is not directly bound to the benzene nucleus, it therefore adjusts stereochemically more easily than the phenolate oxygen which is directly attached to the benzene nucleus. The coulombic repulsion between the end oxygens will be more when both O,O donor atoms are phenolic oxygens than when they are carboxylic oxygens. Thus the $\Delta \log K$ should be higher when the ligand coordinates through the two carboxylate oxygens (phthalic acid) than when it is salicylic acid, which contains one carboxylate and one phenolate oxygen.

The relative stabilities of the ternary complexes of salicylic acid and 5-sulfosalicylic acid follow their relative basicities.

With respect to aliphatic acids, the order of stabilities of their mixed-ligand complexes is in accord with the basicities ($\text{p}K_{\text{a}} + \text{p}K_{2\text{a}}$) of the ligands. It is well known that the increase in basicity of a ligand increases the stability of its metal complexes.

The higher values of $\Delta \log K$ with aromatic acids than aliphatic acids may be attributed to the presence of an aromatic ring [39,40] which alters the bonding properties of these carboxylic acids.

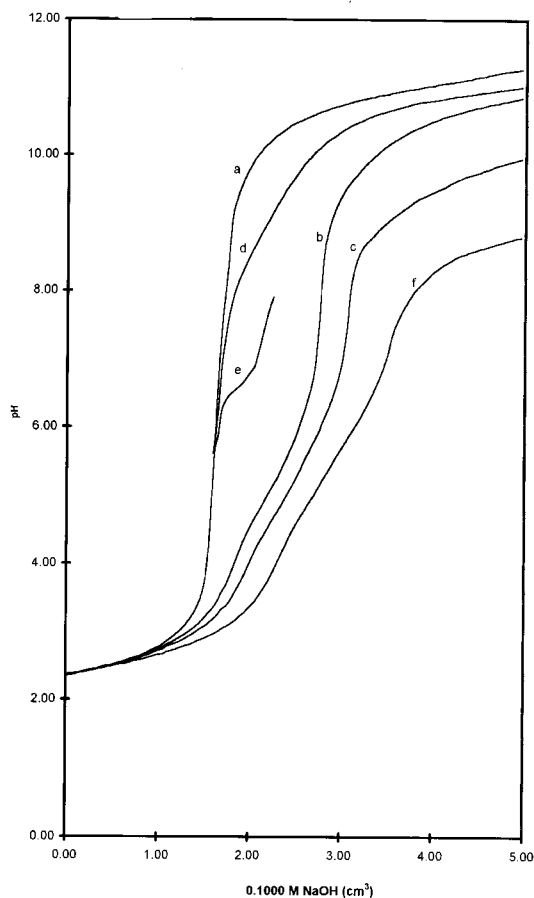


Fig. 6. Potentiometric titration curves for the Ni^{II} -phthalic acid-inosine system.

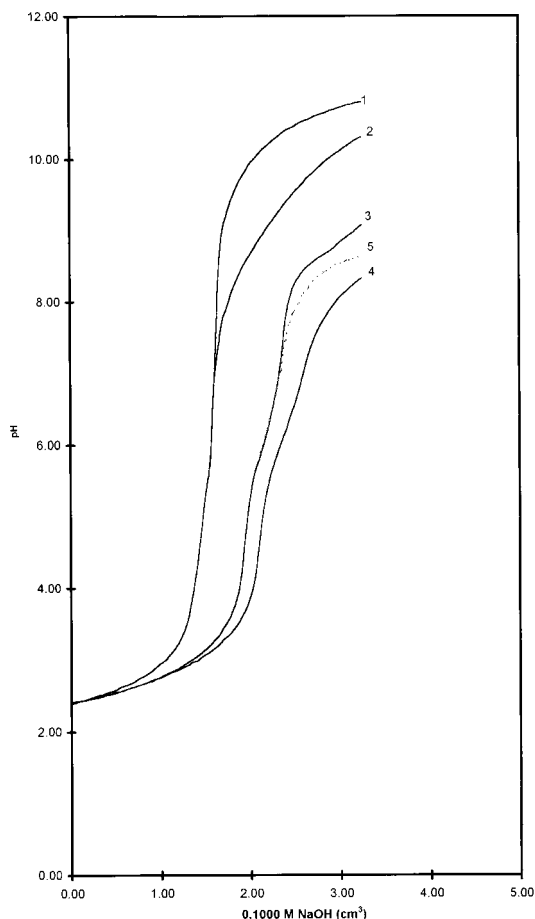


Fig. 7. Ni^{II}-salicylic acid-inosine system. (1) HNO₃; (2) Inosine; (3) Ni^{II}-salicylic acid (1:1); (4) Ni^{II}-salicylic acid-inosine; (5) Composite curve.

Another parameter, percent Relative Stabilisation (% R.S.) to quantify the stability of a ternary complex may be defined [41] as

$$\% \text{ R.S.} = [(\log K_{\text{MAL}}^{\text{MA}} - \log K_{\text{ML}}^{\text{M}}) / \log K_{\text{ML}}^{\text{M}}] \times 100$$

The values of % R.S. have been calculated (Table 3).

For some systems, the parameter % R.S. is negative. This may be attributed to the higher stability of binary M^{II}-inosine complexes than those corresponding to the ternary systems involving carboxylic acids. Negative values of % R.S. agree with the $\Delta \log K_{\text{M}}$ values, as shown in columns 6 and 7 in Table 3.

In Fig. 8, a representative conductometric titration curve for the ternary complex of copper(II) with salicylic acid and inosine is displaced. The titration curve shows an initial decrease and an inflection at $a = 2$. This probably corresponds to the neutralization of H⁺ ions resulting from the formation of the Cu(II)-salicylic acid binary complex.

Between $2 < a < 3$, the conductance increases slightly due to the formation of the ternary complex and is associated with the release of a proton from inosine. Beyond $a = 3$, the conductance increases more uniformly due to the presence of an excess of NaOH.

Evidence for the structure of isolated solid ternary complexes needs further study (e.g. X-ray crystal structure determination), which must be considered in the future.

Table 3

Stability constants for ternary metal complexes of inosine with carboxylic acids at $25 \pm 0.1^\circ\text{C}$, $\mu = 0.1 \text{ M}$ (NaNO₃)

Carboxylic acid (A)	$\log K_{\text{CuAL}}^{\text{CuA}}$	$\log K_{\text{NiAL}}^{\text{NiA}}$	$\log \beta_{\text{CuAL}}^{\text{Cu}}$	$\log \beta_{\text{NiAL}}^{\text{Ni}}$	$\Delta \log K_{\text{Cu}}$	$\Delta \log K_{\text{Ni}}$	R.S.(%) M = Cu(II)	R.S.(%) M = Ni(II)
Succinic acid	5.18 ± 0.05	4.92 ± 0.06	8.38	8.04	0.18	0.52	3.60	10.40
Oxalic acid	4.33 ± 0.07	3.70 ± 0.08	8.93	7.16	-0.67	-0.70	-13.40	-14.00
Malic acid	5.07 ± 0.07	4.83 ± 0.05	11.87	9.43	0.07	0.43	1.40	8.60
Malonic acid	4.86 ± 0.05	4.55 ± 0.04	9.68	8.47	-0.14	0.15	-2.80	3.00
Maleic acid	4.82 ± 0.09	3.84 ± 0.06	8.89	7.54	-0.18	-0.56	-3.60	-11.20
Tartaric acid	4.78 ± 0.08	3.77 ± 0.07	11.74	8.45	-0.22	-0.63	-4.40	-12.60
Phthalic acid	5.79 ± 0.06	5.38 ± 0.07	9.27	8.64	0.79	0.98	15.80	19.60
Salicylic acid	5.54 ± 0.04	5.10 ± 0.03	16.16	13.75	0.54	0.70	10.80	14.00
5-Sulfosalicylic acid	5.37 ± 0.06	4.98 ± 0.09	14.79	11.33	0.37	0.58	7.40	11.60

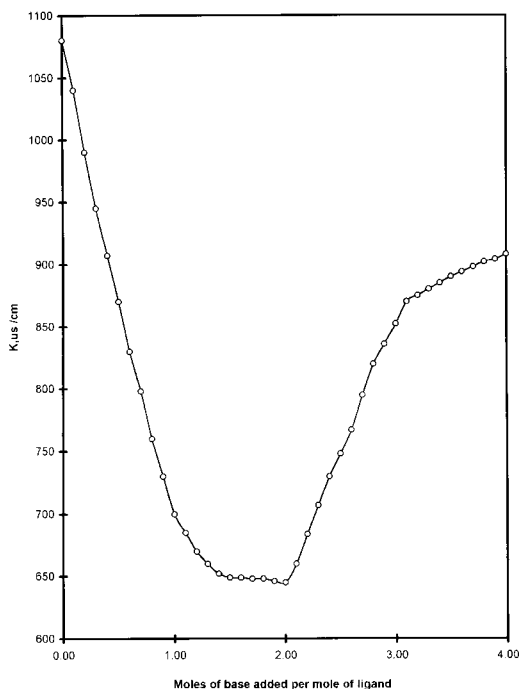


Fig. 8. Conductometric titration curve for the Cu^{II} -salicylic acid-inosine system.

References

- [1] J.P. Slatter, I. Tamir, L.A. Loeb, A.S. Mildman, Mechanism of *Escherichia Coli* deoxyribonucleic acid polymerase. Magnetic resonance and kinetic studies of the role of metals, *J. Biol. Chem.* 247 (1972) 6784.
- [2] C.C. Widnell, R.J. Tata, Isolation and enzyme activity of rate-liver nuclei, *Biochem. J.* 92 (1964) 313.
- [3] M. Tal, On the role of Zn^{2+} and Ni^{2+} in ribosome structure, *Biochim. Biophys. Acta* 169 (1968) 564.
- [4] P. Ballard, H.G. Nathans-Ashman, *Nature (Lond.)* 203 (1964) 150.
- [5] S. Hiai, Effects of cupric ions on thermal denaturation of nucleic acids, *J. Mol. Biol.* 11 (1965) 672.
- [6] G.L. Eichorn (Ed.), *Inorganic Biochemistry*, Vol. 2, Elsevier, Amsterdam, 1973, p. 210.
- [7] T.A.L. Walters, G.A.T. Van, Manganese binding to Yeast ribosomes, *Biopolymers* 10 (1971) 11.
- [8] H. Sigel (Ed.), in: *Metal Ions in Biological Systems*, Vol. 2, Marcel Dekker, New York, 1973.
- [9] B.T. Khan, G.N. Goud, S.V. Kumari, Interaction of platinum(II) amino acid complexes with nucleosides, *Inorg. Chim. Acta* 80 (1983) 145.
- [10] L.G. Marzilli, B. de Castro, C. Solorzano, Nucleoside complexing: A ^{13}C NMR spectroscopic study of binding of metal ions to guanosine and related nucleosides in solution, *J. Am. Chem. Soc.* 104 (1982) 461.
- [11] R.B. Martin, Y.H. Mariam, in: H. Sigel (Ed.), *Metal Ions in Biological Systems*, Ch. 2, Marcel Dekker, New York, 1979.
- [12] L. Pellerito, G. Ruisi, M.T. Logudice, J.D. Donaldson, S.M. Grimes, 6-Thiopurine complexes of organotin (IV) moieties. Synthesis and structural characterization by infrared and Maessbauer spectroscopy, *Inorg. Chim. Acta* 58 (1982) 21.
- [13] P. Chaudhri, H. Sigel, Ternary complexes in solution. 26.¹ Stacking interaction in the mixed-ligand complexes formed by adenosine or inosine5-triphosphate, 2,2-bipyridyl, and cobalt(II), nickel(II), copper(II) or zinc(II). Evidence for phosphate-protonated complexes, *J. Am. Chem. Soc.* 99 (1977) 3142.
- [14] M.S. Mohan, M.M.T. Khan, Novel seven and eight coordinate complexes of ruthenium(II) with monotertiary-phosphines and arsines, *J. Coord. Chem.* 8 (1979) 207.
- [15] N.K. Davidenko, P.A. Manorik, Mixed-ligand complexes of copper(II) and nickel(II) with nucleotides and glycine, *Zh. Neorg. Khim.* 25 (2) (1980) 437.
- [16] E.R. Werner, B.M. Rode, Complex formation of copper(II) with ATP and aliphatic dipeptides in aqueous solution, *Inorg. Chim. Acta* 91 (1984) 217.
- [17] N. Saha, H. Sigel, Comparison of the coordination complexes of Mn(II), Co(II), Ni(II), Cu(II), Zn(II) or Cd(II) and uridine5'-triphosphate or adenosine5'-triphosphate, *J. Am. Chem. Soc.* 104 (15) (1982) 4100.
- [18] P.R. Reddy, V.B.M. Rao, Role of secondary ligands in the structure and stability of metal-cytidine complexes in solution, *Polyhedron* 4 (9) (1985) 1603.
- [19] H.A. Azab, A.M. El-Nady, S.A. El-Korashy, M.M.A. Hamed, Ternary complexes of Co(II) with adenosine 5'-mono, 5'-di-, and 5'-triphosphates as primary ligands and some biologically important zwitterionic buffers as secondary ligands, *J. Chem. Eng. Data* 40 (1) (1995) 83.
- [20] K. Ramalingam, C.R. Krishnamoorthy, Primary amide hydrogen exchange in model amino acids: asparagine, glutamine and glycine amides, *Inorg. Chim. Acta* 67 (1982) 167.
- [21] P.R. Reddy, M.R.P. Reddy, Quantitative study of hydrophobic interactions in ternary complexes involving nucleosides and amino acids, *Indian J. Chem.* 30 (A) (1991) 1028.
- [22] H. Sigel, in: I. Bertini, L. Lunazzi, A. Dei (Eds.), *Advances in Solution Chemistry*, Plenum, New York, 1981, p. 149.
- [23] C. Helene, J.L. Dimicoli, F. Brun, Reflectance and luminescence of molecular complex formation between tryptophan and nucleic acid components in frozen aqueous solutions, *Biochemistry* 10 (1971) 3802.
- [24] C. Helene, Interaction of aromatic amino acids with nucleic acids. Structure of complexes and conformation of changes, *Nucleic Acids Res.* 2 (1975) 961.

- [25] M.M. Khalil, S.A. Mohamed, A.M. Radalla, Potentiometric and conductometric studies on the binary and mixed-ligand complexes in solution: M^{II} -dipicolinic acid-glycine systems, *Talanta* 44 (1997) 1365.
- [26] M.M. Khalil, A.H.H. Elghandour, M. Mostafa, M.M. Shoukry, Metal chelates of some 1-substituted-3-thiazole-2-ylthiourea, *Polyhedron* 13 (1994) 3295.
- [27] E.M. Shoukry, M.M. Khalil, A.H.H. Elghandour, M.M. Shoukry, Binary and ternary complexes of sulphamethoxazole, *Monatshefte für Chemie* 126 (1995) 241.
- [28] M.M. Shoukry, W.M. Hosny, M.M. Khalil, Equilibrium and hydrolysis of α -amino acid esters in mixed-ligand complexes with *N*-(acetamido)-iminodiacetate copper(II), *Transition Met. Chem.* 20 (1995) 252.
- [29] F.J. Welcher, *The Analytical Uses of Ethylenediaminetetra-acetic acid*, Van Nostrand, Princeton, 1965.
- [30] H.M. Irving, H.S. Rossotti, Methods for computing successive stability constants from experimental formation curves, *J. Chem. Soc.* (1953) 3397.
- [31] H.M. Irving, H.S. Rossotti, Calculation of formation curves in metal complexes from pH titration curves in mixed-solvents, *J. Chem. Soc.* (1954) 2904.
- [32] M.V. Chidambaram, P.K. Bhattacharya, Studies in amino-amino acids mixed-ligand chelates-1, *J. Inorg. Nucl. Chem.* 32 (1970) 3271.
- [33] R.B. Simpson, Association constants of methylmercuric and mercuric ions with nucleosides, *J. Am. Chem. Soc.* 86 (1964) 2059.
- [34] A. Albert, Quantitative studies of the avidity of naturally occurring substances for trace metals. 3. Pteridine, riboflavin and purines, *Biochem. J.* 54 (1953) 646.
- [35] J. Inczedy, Determination of equilibrium constants. In: *Analytical Applications of Complex Equilibria*, Ellis Horwood, Chichester, UK, 1976.
- [36] H. Irving, R.P. Williams, Reversion: a new procedure in absorptiometry, *Nature (Lond.)* 162 (1948) 746.
- [37] R.B. Martin, R.J. Prados, Some factors influencing mixed complex formation, *J. Inorg. Nucl. Chem.* 36 (1974) 1665.
- [38] G. Venkatnarayana, S.J. Swamy, P. Lingaiah, Synthesis and spectral studies of complexes of cobalt(II), nickel(II), copper(II), zinc(II), ruthenium(II), palladium(II) and platinum(II) with 2,3-disubstituted quinazolin-(3H)-4-ones, *Indian J. Chem.* 27 (A) (1988) 613.
- [39] J.B. Clayton, S.D. McClure, The ultraviolet transitions of benzoic acid. 1. Interpretation of the singlet absorption spectrum, *J. Am. Chem. Soc.* 101 (1979) 2335.
- [40] J.B. Clayton, S.D. McClure, The ultraviolet transitions of benzoic acid. 2. Hydrogen bonding in the ground and excited states, *J. Am. Chem. Soc.* 101 (1979) 2430.
- [41] S.N. Limaye, M.C. Saxena, Polarographic study of mixed ligand (thioglycolate-glutamate) complexes of cadmium(2+), lead(2+) and thallium(2+), *J. Indian Chem. Soc.* 61 (1984) 842.

The hexacyanomanganate(IV)–hydrogen peroxide reaction. Kinetic determination of vanadium

R. Angulo^a, G. López-Cueto^b, C. Ubide^{a,*}

^a *Departamento de Química Aplicada, Facultad de Química, Universidad del País Vasco, Apdo. 1072, 20080 San Sebastián, Spain*

^b *Departamento de Química Analítica, Facultad de Ciencias, Universidad de Alicante, Apdo. 99, 03080 Alicante, Spain*

Received 18 March 1997; accepted 31 July 1997

Abstract

The reaction between hexacyanomanganate(IV) and hydrogen peroxide in acidic medium is strongly catalysed by vanadium. The stoichiometry has been proved to be $\Delta[\text{Mn(IV)}]/\Delta[\text{H}_2\text{O}_2] = 1$. S-shaped absorbance–time curves are obtained for a wide range of conditions, which seems to be due to the transient formation of hydroperoxyl radicals, $\text{HO}_2\cdot$; therefore, the reaction is autoinduced. The reaction kinetics is first order on the hexacyanomanganate(IV) concentration. Complex dependence of the initial rate on the H_2O_2 as well as H^+ concentrations are observed both for the uncatalysed and for the catalysed reactions, but the rate laws are given and reaction mechanisms are proposed. The catalytic effect of vanadium has been used to determine traces of vanadium (the (IV) and (V) oxidation states are determined together). By applying the initial rate method a detection limit of 0.9 ng ml^{-1} (18 nM), and a linear range up to 50 ng ml^{-1} were found. The relative standard deviations for the 4 and 25.5 ng ml^{-1} levels were 5.2 and 2.5% respectively. Positive kinetic interferences from Cr(VI), Hg(I) and Ag(I) have been observed; other interferences are less severe and Cr(III), Fe(II) and Fe(III), among many others, do not interfere. The Mn(IV) solution must be prepared daily and its conservation needs some care (0°C) but the proposed method has been applied to the determination of vanadium in a phosphate rock (reference material, BCR No. 32) without previous separations. Recovery experiments have also been performed; excellent results were obtained in both cases. © 1998 Elsevier Science B.V. All rights reserved.

Keywords: Hexacyanomanganate(IV); Hydrogen peroxide; Vanadium catalytic determination; Kinetics

1. Introduction

Hexacyanomanganate(IV), Mn(CN)_6^{2-} , is a relatively strong oxidizing agent. From the halfwave potential of its reversible voltammetric reduction at a rotating platinum-disk electrode, a formal

potential of about 0.85 V (vs. SCE) in acidic medium can be estimated [1]. Hexacyanomanganate(IV) cannot be easily isolated [2] but it can be yielded in acidic solution by fast disproportionation of hexacyanomanganate(III) [1,3] (Mn(II) and $(\text{CN})_2$ are also produced). The hexacyanomanganate(IV) solution is not stable and it slowly decomposes to yield Mn(II) , $(\text{CN})_2$ and HCN [3], but the reaction is fairly slow at room

* Corresponding author. Fax: +34 43 212236; e-mail: qa-pubsec@sq.ehu.es

temperature and it can be used for oxidizing purposes for a period of time. For instance, hexacyanomanganate(IV) has been used, in the reaction $\text{Mn}(\text{CN})_6^{2-}$ –As(III) [4], as the indicator reagent for the kinetic determination of iodide [5]. We observed that the hydrogen peroxide oxidation by hexacyanomanganate(IV) is slow and it is strongly catalysed by vanadium. This could well be the basis of a catalytic method for the determination of vanadium.

Vanadium has a well-known industrial relevance (steels, pigments, inks, paints, etc.) [6] or; it is also important in biochemistry as it seems to be an essential element [7]. It can also be considered a path finder for original type of crude oil [8], for uranium deposits [9] or for human industrial activities (in waters, air, soils, etc.). Methods for the determination of vanadium were reviewed some years ago [10]. In the following years the number of publications dealing with the determination of vanadium has continually grown and a new review has appeared [11]. Catalytic methods for vanadium are among those with high sensitivities and low detection limits (the counterpart is the need for time measurements) and they usually include reactions in which vanadium catalyses organic substrate oxidations by bromate, chlorate or peroxydisulphate [12]. In the last few years more papers dealing with the catalytic determination of vanadium have appeared [13,14] and most of them have been applied to the determination of vanadium in steels [15–18], petroleum products [18–20], water [16,21–26], aerosols [27,28] and atmospheric particulate matter and human serum [29]. These methods usually have limits of detection at the parts per billion (ppb) level. The initial rate method is frequently used.

On the other hand, the reactions between manganese in high oxidation states and species such as O_2 , O_2^- and H_2O_2 seem to have a great importance in biological processes, though not much is known about them [30]. These kinds of reactions have a number of interesting features. For instance the Mn(III)– H_2O_2 reaction has been found to be autocatalytic [31] and the MnO_4^- – H_2O_2 reaction has been found to be oscillatory [32]. This behaviour is not strange in oxidations by permanganate ion. The MnO_4^- –mandelic acid re-

action [33] and the MnO_4^- – N_2H_4 reaction [34] are autocatalytic and the MnO_4^- – $\text{C}_2\text{O}_4^{2-}$ reaction is autocatalytic in closed (batch) conditions [35] and bistable in open (flow) conditions [36]. Owing to these characteristics all these reactions could serve, at least theoretically, as the basis of chemical oscillators [37], but this would need detailed kinetics and mechanistic information. We thought that the title reaction might have common aspects with some of the aforementioned reactions. Hence we decided to study the kinetics of the $\text{Mn}(\text{CN})_6^{2-}$ – H_2O_2 reaction.

Modern approaches to kinetic determinations include the use of multivariate calibration methods. The most used algorithm is probably partial least squares calibration (PLSR) [38,39] but some others such as principal components regression (PCR) and artificial neural networks (ANN) [40,41] have also been used. These methods are finding increasing use in analytical work because they do not need previous knowledge of the kinetic model, rate constants, etc. Some of them can be applied not only to linear but also to non-linear systems. They have been applied specially in the simultaneous determination of multiple components of interest and a review on the subject has recently appeared [42]. Though PLSR has begun to be used for individual kinetic determinations [43], the interest for the study of the reaction kinetics has driven us to use the classical approach.

The present work has clearly two different aims: to study some interesting kinetic aspects of the indicator reaction hexacyanomanganate(IV)–hydrogen peroxide and to develop a method for the catalytic determination of vanadium.

2. Experimental

2.1. Reagents

All chemicals were of analytical-reagent grade and doubly-distilled water was used throughout. Potassium hexacyanomanganate(III) was prepared according to the method of Lower and Fernelius [44]. Spectrophotometric assays by the methods previously reported [45] indicated a con-

tent of at least 95%. The solid is indefinitely stable if kept in the dark.

Hexacyanomanganate(IV) solution (2.7×10^{-3} M) was prepared by dissolving 0.0443 g of $\text{K}_3\text{Mn}(\text{CN})_6$ (whenever $\text{K}_3\text{Mn}(\text{CN})_6$ is taken into acidic solution HCN is produced, so care should be taken) in a dark 25 ml standard flask containing 1 g of sodium perchlorate and some 0.1 M perchloric acid previously cooled to 0°C (probably owing to kinetic effects the sodium perchlorate prevents precipitation of manganese(IV) oxide by hydrolysis and lowers the freezing point of the solution). The solution is diluted to volume with 0.1 M perchloric acid. Before use the solution must be kept at $\approx 0^\circ\text{C}$ for about 1 h to allow the Mn(III) disproportionation to proceed to completion. The Mn(IV) solution thus obtained can be used for a period of 6–8 h if kept at $\approx 0^\circ\text{C}$. Other solutions with different Mn(IV) concentrations were obtained by the same procedure if required.

Hydrogen peroxide (30%), perchloric acid (70%) and solid sodium perchlorate (Fluka all of them) were used as received. Hydrogen peroxide was assayed from time to time with permanganate [46] and its content was always according to specifications. Perchloric acid was standardized with Na_2CO_3 (methyl red as indicator). A 10^{-2} M vanadium(V) solution was prepared by dissolving 0.610 g of NaVO_3 (Merck) in 500 ml of water; it was standardized with ferrous sulphate solution [47] and stored in a polyethylene bottle in the refrigerator.

2.2. Apparatus

A Shimadzu UV-260 spectrophotometer with 1 cm path-length fused-silica cells, and constant-temperature cell-holders was used. The temperature in the cells was continuously monitored by means of a small Pt 100 temperature probe, installed just before the water entrance in the cell-holder, and kept constant ($\pm 0.2^\circ\text{C}$) by circulating water from a Haake F3 K thermostat controlled by the probe. A microcomputer HP Vectra ES/12, coupled to the spectrophotometer, controlled it, acquired the data and allowed to process them through laboratory written programs.

Volumes less than 1 ml were added with micropipettes (Eppendorf or Brand).

2.3. Procedures

2.3.1. Stoichiometry measurements

When $\text{Mn}(\text{CN})_6^{2-}$ was in excess the following spectrophotometric procedure was used. In a 10 ml standard flask, 2.76 g of $\text{NaClO}_4 \cdot \text{H}_2\text{O}$ (ionic strength control), 0.4 ml of 2.5 M HClO_4 and a measured amount of H_2O_2 were added; the volume was finally adjusted to 10 ml with water. A 2.5 ml portion was accurately measured into a thermostated cuvette of the spectrophotometer and the thermal equilibrium was allowed to be reached (5–10 min). Then $100 \mu\text{l}$ of 2.7×10^{-4} M V(V) as catalyst and $100 \mu\text{l}$ of $\text{Mn}(\text{CN})_6^{2-}$ of the required concentration were added. The cell was shaken (zero time) and the reaction was followed at 387 nm (where the $\text{Mn}(\text{CN})_6^{2-}$ species shows an absorption maximum [45]), with water as reference. The remaining Mn(IV) was determined by extrapolating to zero time the final straight line of the $\ln A$ vs. time plot ($A_\infty = 0$) (a linear regression program was used). The method is similar to the logarithmic extrapolation method for the resolution of mixtures by differential reaction rate methods [48]. Each run was repeated once and the final result was the mean of the two runs.

Under conditions where an excess of H_2O_2 was present the stoichiometry was determined by the following titrimetric procedure. In a 50 ml standard flask, 19 g of $\text{NaClO}_4 \cdot \text{H}_2\text{O}$ (ionic strength control), 2 ml of 2.5 M HClO_4 and a measured amount of H_2O_2 were added; the volume was adjusted to 50 ml with water. To a 10 ml aliquot, 0.15 ml of 10^{-3} M V(V), as catalyst, and 5 ml of $\text{Mn}(\text{CN})_6^{2-}$ of the required concentration were added. After the reaction had proceeded to completion (and no colour was detected) 5 ml of 2.5 M H_2SO_4 were added and the remaining peroxide was determined by titration with 0.02 M KMnO_4 standard solution. In all cases the result was the mean of three replicates.

2.3.2. Kinetic measurements

A 2.5 ml volume of a solution containing the required amounts of H_2O_2 , $\text{NaClO}_4 \cdot \text{H}_2\text{O}$ (ionic

strength control) and HClO_4 were placed in a 1 cm cuvette. After the thermal equilibrium was reached 100 μl of a vanadium solution and, finally, 100 μl of a $\text{Mn}(\text{CN})_6^{2-}$ solution were added. The cell was shaken (zero time) and the absorbance–time data (387 nm) were obtained at least for three half-lives. The initial rate was determined by using the first straight part of the run (usually the 3–5% of the reaction) and linear regression analysis was applied. The temperature was varied between 15 and 45°C, the ionic strength between 0.1 and 3, the acidity between 0.001 and 2 M, the added Mn(II) concentration between 0 and 0.05 M, the H_2O_2 concentration between 0 and 0.2 M, the initial $\text{Mn}(\text{CN})_6^{2-}$ concentration between 0.25×10^{-4} and 2.25×10^{-4} M and the vanadium concentration between 0 and 10^{-6} M. With the exception of the variable studied the initial conditions were: $\text{Mn}(\text{CN})_6^{2-}$, 2×10^{-4} M; H_2O_2 , 0.1 M; H^+ , 0.1 M; T, 25°C; μ , 2 and V(V), 5×10^{-7} M (only for the catalysed reaction). Each kinetic run was usually repeated once, with the replicate measurement agreeing to within $\pm 5\%$ for 95% of the cases, and the initial rate was taken as the mean of the two runs.

2.3.3. Vanadium determination

In a 25 ml standard flask, 11.5 g of $\text{NaClO}_4 \cdot \text{H}_2\text{O}$, 1.7 ml of 2.5 M HClO_4 and 1 ml of 30% H_2O_2 are added. The solution is taken to volume with water. A 1.5 ml portion is accurately measured into the cuvette and left to stand for 10 min in the controlled temperature cell-holder of the spectrophotometer. One millilitre of the sample solution ($\leq 0.13 \mu\text{g V}$) and 100 μl of 2.7×10^{-3} M $\text{Mn}(\text{CN})_6^{2-}$ are added carefully to avoid mixing, the lid is put on and the cell inverted two or three times (this point was taken as zero time). The absorbance is followed just enough time to determine the initial rate (less than a 5% decrease in absorbance is sufficient, and this is attained in a 10–30 s time, depending on the vanadium content). The measured initial rate is used to read the vanadium concentration from a calibration plot prepared in the same way. Each determination was repeated once and the final result was taken as the mean of the two determinations.

2.3.4. Vanadium determination in phosphate rock samples

Homogeneous and dried (2 h at 105°C) phosphate rock are accurately weighted (0.1 g), dissolved in some few ml of a HCl and HNO_3 mixture (3:1) and taken practically to dryness on a sand bath. The residue is dissolved in water and diluted to volume in a 250 ml standard flask with some more water. A 1 ml portion is treated as for determination of vanadium.

3. Results and discussion

3.1. Stoichiometry

A reaction time short enough to allow reliable data was attained with 10^{-5} M vanadium(V) as catalyst. When $\text{Mn}(\text{CN})_6^{2-}$ was in excess, a mean of 1.04 ($s = 0.04$, $n = 9$) was found for the $\Delta[\text{Mn}(\text{IV})]/\Delta[\text{H}_2\text{O}_2]$ ratio, this value being significantly higher than 1 (t -test, $P = 0.05$), probably owing to the $\text{Mn}(\text{CN})_6^{2-}$ decomposition (Fig. 1). On the other hand, when H_2O_2 was in excess this value does not differ significantly from unity. Taking into account all the results ($[\text{Mn}(\text{IV})]_0/[\text{H}_2\text{O}_2]_0$ ranging from 0.1 to 5), the stoichiometry will be 1:1; that is, $\text{Mn}(\text{CN})_6^{2-}$ acts as a two-electron oxidizing species, in the same way of some precedence [4], its reaction product being some colour-

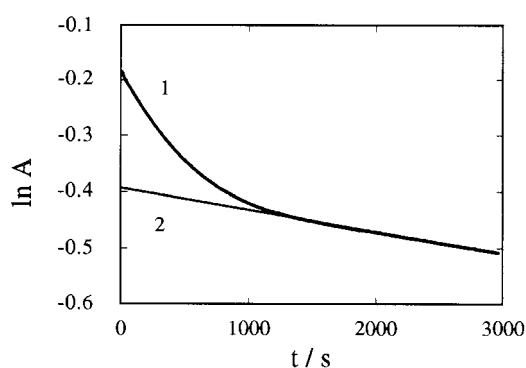
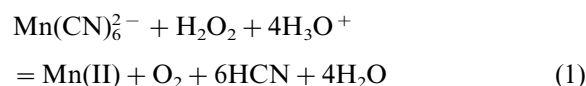


Fig. 1. Stoichiometry with excess $\text{Mn}(\text{CN})_6^{2-}$. (1) kinetic run; (2) extrapolation. Conditions: $[\text{Mn}(\text{IV})]_0$, 2×10^{-4} M; $[\text{H}_2\text{O}_2]_0$, 4×10^{-5} M; $[\text{H}^+]$, 0.1 M; $[\text{V}(\text{V})]$, 10^{-5} M; T, 25°C; μ , 2; λ , 387 nm.

less Mn(II) species because a flat visible spectrum is obtained in the final solution. A high evolution of bubbles indicates that oxygen is another reaction product. Therefore, the reaction can most probably be represented by the equation:



3.2. General aspects of the overall reaction kinetics

Ultraviolet light decomposes hexacyanomanganate(IV) [49] but the rate of the reaction $\text{Mn(CN)}_6^{2-} - \text{H}_2\text{O}_2$ was photochemically insensitive at light levels present in the spectrophotometer, since the reaction proceeded to the same extent both in the spectrophotometric cell and in the dark.

The $\text{Mn(CN)}_6^{2-} - \text{H}_2\text{O}_2$ reaction displays kinetic curves that under certain conditions exhibit S-shaped profiles (Fig. 2A). Consequently, tests on the kinetic behaviour show that first-order plots are not linear, but they show in all cases a (negative) continuously increasing slope (Fig. 2B). However, the initial slope of these plots seems to be independent of the Mn(CN)_6^{2-} concentration. This kind of behaviour seems to indicate that, after first-order kinetics in the early stages of the reaction, an autoacceleration effect takes place, perhaps due to an autocatalytic or chain process. The well-known permanganate–hydrogen peroxide and permanganate–oxalate reactions [35,50] are autocatalytic, the Mn(II) species produced being responsible for the catalysis. It could be thought that the $\text{Mn(CN)}_6^{2-} - \text{H}_2\text{O}_2$ reaction behaves in a similar way. In order to test this possibility a series of five runs was made by adding successively new amounts of Mn(CN)_6^{2-} to the reaction mixture once the reaction had gone to completion. The successive curves obtained practically reproduced the first kinetic run. This indicates that the accumulated Mn(II) does not exert any significant effect on the kinetics, at least at the concentration levels produced in the reaction mixture. Nevertheless, when a Mn(II) salt is initially added in a great excess (10^{-3} M or higher) the reaction is faster but the shape of the

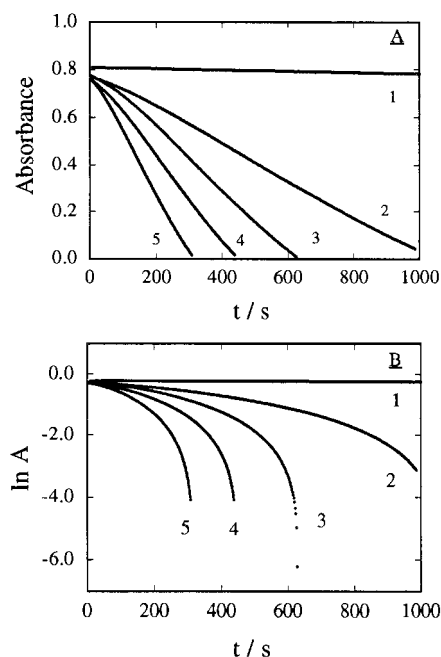
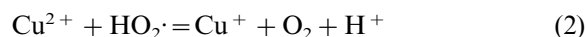


Fig. 2. (A), typical kinetic runs and (B), pseudo-first order plots. $[\text{Mn(IV)}]_0$, 2×10^{-4} M; $[\text{H}^+]$, 0.1 M; T, 25°C; μ , 2; λ , 387 nm; $[\text{H}_2\text{O}_2]$, (1) 0, (2)–(5) 0.1 M; $[\text{Mn(II)}]_{\text{added}}$, (1) (2) (4) (5) 0, (3) 10^{-3} M; $[\text{V(V)}]$, (1)–(3) 0, (4) 2×10^{-7} M, (5) 5×10^{-7} M.

reaction profile does not change (Fig. 2A, curve 3). That is to say, Mn(II) added at high concentrations actually catalyses but some other species, instead of Mn(II), must be responsible for the autoacceleration effect, most probably some highly reactive intermediate. In the oxidation of H_2O_2 by either Mn(III), Ce(IV) or Co(III) compounds the hydroperoxyl radical, $\text{HO}_2\cdot$, has been proposed as an intermediate [31]. This radical is highly reactive and usually leads to chain mechanisms which are responsible for autoacceleration kinetics. The presence of the radical $\text{HO}_2\cdot$ can be detected by adding Cu^{2+} that acts as scavenger for it [51]. In the presence of Cu^{2+} the following reaction takes place at close to diffusion-controlled rates:



the Cu^+ produced will be rapidly oxidized to Cu^{2+} in the reaction mixture. The effect of Cu^{2+}

on the $\text{Mn}(\text{CN})_6^{2-} - \text{H}_2\text{O}_2$ reaction was tested and the results are illustrated in Fig. 3. In the presence of Cu^{2+} at concentrations higher than 10^{-4} M the autoaccelerating effect significantly diminishes and the reaction kinetics approaches to the kinetic curve in the absence of H_2O_2 (Fig. 3, curve 1) (concentrations of Cu^{2+} higher than 5×10^{-3} M could not be used since it precipitates with $\text{Mn}(\text{CN})_6^{2-}$). Therefore, it can be concluded that the hydroperoxyl radical, $\text{HO}_2\cdot$, is an intermediate in the H_2O_2 oxidation by $\text{Mn}(\text{CN})_6^{2-}$ and it is the responsible species for the autoacceleration. Since $\text{HO}_2\cdot$ does not remain as a reaction product but it has a transient nature, the autoacceleration process should not be properly termed autocatalysis. A chain mechanism (autoinduction) could probably explain the observed results better. It should be here emphasized that the initial rate is not affected by Cu^{2+} because it only influences the propagation steps (Fig. 3).

Attempts to fit the entire absorbance–time curves to the usual kinetic models for autocatalytic reactions [52,53] were unsuccessful. The methods of Guggenheim and Kezdy-Swinbourne [54], for cases in which a slow secondary reaction sets in, were also unsatisfactory. Therefore, only the kinetics of the early stages of the reaction (before the autoacceleration effect becomes appreciable) has been quantitatively studied. Initial rate measurements were made.

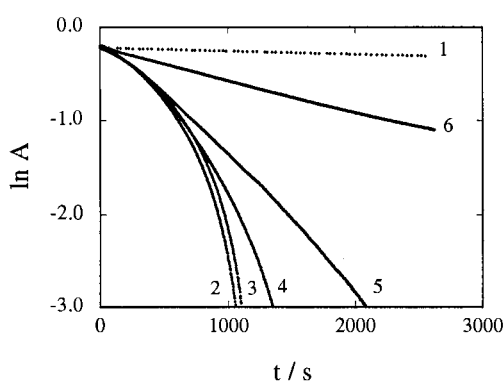


Fig. 3. Effect of Cu^{2+} addition. $[\text{Mn}(\text{IV})]_0$, 2×10^{-4} M; $[\text{H}^+]$, 0.1 M; T, 25°C ; μ , 2; λ , 387 nm; $[\text{H}_2\text{O}_2]$, (1) 0, (2)–(6) 0.1 M; $[\text{Cu}^{2+}]$, (1) (2) 0, (3) 10^{-4} M, (4) 5×10^{-4} M, (5) 10^{-3} M, (6) 5×10^{-3} M.

3.3. Effect of variables on the initial rate

Plots of the initial rate vs. the $\text{Mn}(\text{CN})_6^{2-}$ initial concentration are linear both in the absence and in the presence of vanadium(V) as catalyst. This means that the reaction shows a first order dependence on the hexacyanomanganate(IV) concentration in the initial stages; afterwards, the pseudo-first order is disrupted by the autoinduced process.

The initial rate increases with the vanadium(V) concentration (Fig. 2, curves 2,4,5) according to a linear dependence. When vanadium(IV) was added instead, exactly the same results were obtained. This could be due to the oxidation of V(IV) by Mn(IV); in fact a standard potential of about 1.09 V (vs. HNE) can be estimated for the $\text{Mn}(\text{CN})_6^{2-}/\text{Mn}(\text{CN})_6^{3-}$ couple from the reversible halfwave potential in acidic medium [1]; this is a somewhat higher value than 1 V, the standard potential of the $\text{VO}_2^+/\text{VO}^{2+}$ couple in acidic medium [55], so that the $\text{Mn}(\text{CN})_6^{2-} - \text{V}(\text{IV})$ reaction is thermodynamically favourable in this medium. The responsibility for the catalytic path should actually be some V(V)/V(IV) cycle through which the electron transfer from H_2O_2 to $\text{Mn}(\text{CN})_6^{2-}$ takes place in an easier way. On the other hand, the catalytic activity of vanadium has been found to be lowered through time if it is previously mixed with the hydrogen peroxide solution, so some vanadium–hydrogen peroxide interaction appears to be produced. Most probably slow formation of vanadium(V) peroxocomplexes with a lower, if any, catalytic activity is involved [56]. This is the reason why hydrogen peroxide and vanadium must be mixed just before starting the reaction (see Section 2).

As it was mentioned above, aquomanganese(II) acts also as a catalyst. A plot of the initial rate vs. $[\text{Mn}(\text{II})]_{\text{added}}$ (in the absence of vanadium) gives a straight line with positive intercept, at least in the range $10^{-3} - 10^{-1}$ M. In the presence of vanadium a parallel straight line with a higher intercept is obtained. This indicates that the catalytic effects of vanadium and manganese are independent, which suggests the existence of two parallel catalytic pathways in addition to the non-catalytic one. The non-catalytic pathway actually consists

of two reactions, the $\text{Mn}(\text{CN})_6^{2-}$ decomposition [3] and the uncatalysed reaction. According to these results, the observed initial rate, v_0 , can be satisfactorily described by the following equation

$$v_0 = -\frac{d[\text{Mn}(\text{IV})]}{dt} = k_{\text{obs}}[\text{Mn}(\text{IV})] \\ = (k_d + k_u + k_{c,\text{Mn}}[\text{Mn}(\text{II})]_{\text{added}} + k_{c,\text{V}}[\text{V}(\text{V})]) \\ [\text{Mn}(\text{IV})] \quad (3)$$

where k_{obs} , the pseudo-first-order constant, includes the decomposition reaction of $\text{Mn}(\text{IV})$ (k_d) [3], the uncatalysed reaction (k_u) and the reactions catalysed by manganese ($k_{c,\text{Mn}}[\text{Mn}(\text{II})]_{\text{added}}$) and vanadium ($k_{c,\text{V}}[\text{V}(\text{V})]$) respectively.

The value of k_d is known from previous work [3], and so k_u can be evaluated from the slope of the plot v_0 vs. $[\text{Mn}(\text{IV})]$ in the absence of catalysts. For $[\text{H}_2\text{O}_2]$, 0.1 M; $[\text{H}^+]$, 0.1 M; μ , 2 and T, 25°C; $k_{\text{obs}} = (7.6 \pm 0.4) \times 10^{-4} \text{ s}^{-1}$ ($n = 8$). In these conditions $k_d = 4.6 \times 10^{-5} \text{ s}^{-1}$, and from here:

$$k_u = (7.1 \pm 0.4) \times 10^{-4} \text{ s}^{-1} \quad (n = 8)$$

For the same conditions the value of $k_{c,\text{V}}$ can be evaluated from a plot of v_0 vs. $[\text{V}(\text{V})]$, and it was found to be:

$$k_{c,\text{V}} = (2.3 \pm 0.1) \times 10^3 \text{ s}^{-1} \text{ M}^{-1} \quad (n = 5)$$

Finally, the value of $k_{c,\text{Mn}}$ can be calculated both in the presence and in the absence of vanadium from a plot of v_0 vs. $[\text{Mn}(\text{II})]$ provided all other constants are known. In the above conditions:

$$k_{c,\text{Mn}} = (0.24 \pm 0.02) \text{ s}^{-1} \text{ M}^{-1} \quad (n = 12)$$

(all the errors are given as standard errors estimated from the regression analysis).

An increase in the concentration of H_2O_2 increases the initial rate, in the absence as well as in the presence of vanadium as shown in Fig. 4. This behaviour suggests an inner-sphere mechanism in which the charge transfer step is preceded by some $\text{Mn}(\text{IV})\text{-H}_2\text{O}_2$ interaction. A similar $\text{Mn}(\text{IV})\text{-substrate}$ interaction was proposed for the reaction $\text{Mn}(\text{CN})_6^{2-}\text{-As}(\text{III})$ [4]. Taking into account such a precedent, a similar mechanism can be proposed for the uncatalysed reaction

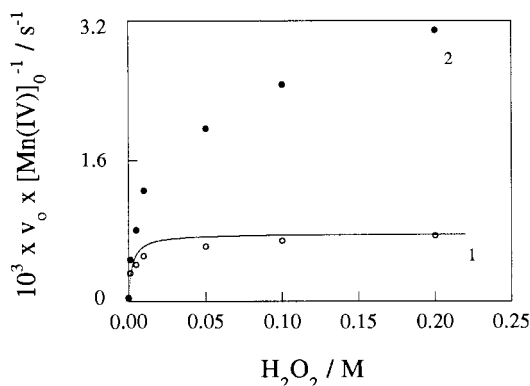
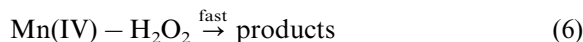
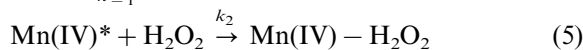


Fig. 4. Effect of H_2O_2 concentration. $[\text{Mn}(\text{IV})]_0$, $2 \times 10^{-4} \text{ M}$; $[\text{H}^+]$, 0.1 M; μ , 2; T, 25°C, λ , 387 nm; $[\text{V}(\text{V})]$, (1) 0, (2) $5 \times 10^{-7} \text{ M}$. The solid line curve represents the simulated dependence profile for the uncatalysed reaction.



The kinetics depends on reactions (4) and (5) because reaction (6) is fast and does not exert influence on the rate law. In the same way than for the $\text{Mn}(\text{CN})_6^{2-}\text{-As}(\text{III})$ reaction [4] the species $\text{Mn}(\text{IV})^*$ would be a very reactive intermediate and the species $\text{Mn}(\text{IV})\text{-H}_2\text{O}_2$ an adduct in which the charge transfer from H_2O_2 to $\text{Mn}(\text{IV})$ would not have completely taken place.

From the proposed mechanism, and by applying the steady-state assumption to the $\text{Mn}(\text{IV})^*$ species, the following rate law for the reaction in the absence of vanadium is derived:

$$v_0 = \left(k_d + \frac{k_1 k_2 [\text{H}_2\text{O}_2]}{k_{-1} + k_2 [\text{H}_2\text{O}_2]} \right) [\text{Mn}(\text{IV})] \quad (7)$$

Eq. (7) can take two limiting forms depending on the H_2O_2 concentration:

(i) At high $[\text{H}_2\text{O}_2]$

$$v_0 = (k_d + k_1) [\text{Mn}(\text{IV})] \quad (8)$$

(ii) At low $[\text{H}_2\text{O}_2]$

$$v_0 = \left(k_d + \frac{k_1 k_2}{k_{-1}} [\text{H}_2\text{O}_2] \right) [\text{Mn}(\text{IV})] \quad (9)$$

That is to say, a plot of $v_0/[\text{Mn(IV)}]$ vs. $[\text{H}_2\text{O}_2]$ should be straight for low $[\text{H}_2\text{O}_2]$ approaching a constant value for high $[\text{H}_2\text{O}_2]$. Fig. 4 shows such a plot; from it a value of $8 \times 10^{-4} \text{ s}^{-1}$ and $0.29 \text{ s}^{-1} \text{ M}^{-1}$ can be estimated for the limiting value of $v_0/[\text{Mn(IV)}]$ and for the initial slope respectively. Taking into account the value of k_d it results:

$$k_1 = 7 \times 10^{-4} \text{ s}^{-1}$$

and

$$k_2/k_{-1} = 3.9 \times 10^2 \text{ M}^{-1}$$

Using these values the effect of $[\text{H}_2\text{O}_2]$ can be simulated and compared with the experimental results (Fig. 4). The result obtained can be considered satisfactory. The reaction in the presence of vanadium shows a similar behaviour (Fig. 4), but the limiting value of $v_0/[\text{Mn(IV)}]$ (if it exists) has not been attained experimentally and so the rate constant values can not be calculated and the simulation is not possible.

The effect of the acidity is quite complex. When the acidity effects for the uncatalysed and the catalysed reactions are compared (Fig. 5) three pH regions can be distinguished. Only in the central region (pH from 0 to 2 approximately) the reaction rate is clearly increased by the presence of vanadium. This can be explained by considering three Mn(IV) species with different protonation grades (probably Mn(CN)_6^{2-} ,

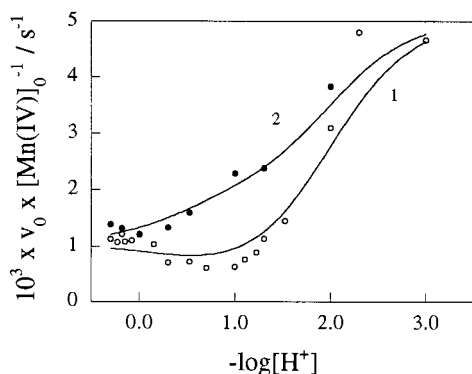


Fig. 5. Effect of acidity. $[\text{Mn(IV)}]_0$, $2 \times 10^{-4} \text{ M}$; $[\text{H}_2\text{O}_2]$, 0.1 M ; μ , 2; T, 25°C , λ , 387 nm ; $[\text{V(V)}]$, (1) 0, (2) $5 \times 10^{-7} \text{ M}$. Solid line curves represent simulated dependence profiles.

$\text{Mn(CN)}_5(\text{CNH})^-$ and $\text{Mn(CN)}_4(\text{CNH})_2$ agreeing with previous evidence [1]). If all the three species react, three parallel pathways should be expected. However, only the reaction of the monoprotonated complex (the predominant species at pH 0–2 [1]) seems to be catalyzed by vanadium.

Considering the uncatalysed reaction, the effect of acidity was studied for $0.1 \text{ M H}_2\text{O}_2$ and so Eq. (8) can be applied; if $k_{1(0)}$, $k_{1(1)}$ and $k_{1(2)}$ are the rate constants for the three Mn(IV) species with different protonation degrees, the rate law will depend on $[\text{H}^+]$ in the following way:

$$v_0 = \left(k_d + \frac{k_{1(0)}[\text{H}^+]^2 + k_{1(1)}K_1[\text{H}^+] + k_{1(2)}K_1K_2}{[\text{H}^+]^2 + K_1[\text{H}^+] + K_1K_2} \right) [\text{Mn(IV)}] \quad (10)$$

where K_1 and K_2 are the successive dissociation constants of the diprotonated species $\text{Mn(CN)}_4(\text{CNH})_2$. A plot of $v_0/[\text{Mn(IV)}]$ vs. $-\log[\text{H}^+]$ can be seen in Fig. 5. From such a plot the following values can be roughly estimated [57]:

$k_{1(0)} = 1 \times 10^{-3} \text{ s}^{-1}$ (the value of the ordinate for $-\log[\text{H}^+]$ values low enough).

$k_{1(1)} < 6 \times 10^{-4} \text{ s}^{-1}$ (the value of the ordinate for $-\log[\text{H}^+]$ values neither too low nor too high. Because K_1 and K_2 are not distant enough, the value of this constant can only be tentative).

$k_{1(2)} = 5 \times 10^{-3} \text{ s}^{-1}$ (the value of the ordinate for $-\log[\text{H}^+]$ values high enough).

$K_1 = 0.4$ (the inflection point for $-\log[\text{H}^+]$ low values).

$K_2 = 3 \times 10^{-2}$ (the inflection point for $-\log[\text{H}^+]$ high values) and from these values Eq. (10) has been calculated and plotted in Fig. 5 (for simulation purposes a value of $k_{1(1)} = 5 \times 10^{-4} \text{ s}^{-1}$ has been tentatively used).

The rate constants for the catalysed reaction can be obtained by difference between the overall and the uncatalysed reactions. If, as it has been stated above, only the reaction of the monoprotonated species is catalysed by vanadium, the Eq. (3) will take the form:

$$v_0 = \left(k_d + k_u + \frac{k_{1(1),v}K_1[\text{H}^+]}{[\text{H}^+]^2 + K_1[\text{H}^+] + K_1K_2} [\text{V(V)}] \right) [\text{Mn(IV)}] \quad (11)$$

By using the K_1 and K_2 values previously obtained and the concentration of vanadium added (5×10^{-7} M), a value of

$$k_{1(1),V} = 3 \times 10^3 \text{ s}^{-1} \text{ M}^{-1}$$

can be estimated. The constant $k_{1(1),V}$ is similar to $k_{1(1)}$ but for the catalysed reaction. Eq. (11) has been plotted in Fig. 5. Both for the catalysed and uncatalysed reactions the agreement between experimental points and simulated dependences can be considered satisfactory, even if sometimes the simulated curves do not perfectly fit the experimental data points, pointing out the possibility of some extra complexity.

Ionic strength exerts opposite effects on the reaction kinetics in the presence and in the absence of vanadium. Thus, when ionic strength increases from 0.1 to 3 a slight increase in the initial reaction rate is produced when vanadium is present, whereas a slight decrease is produced when it is absent.

From the effect of temperature (15–45°C), on the initial reaction rates, apparent activation energies of 78 ± 2 and 62 ± 7 kJ mol⁻¹ were found for the uncatalysed and the catalysed reactions respectively ($n = 7$ in both cases).

3.4. Optimization

In any instrumental method the conditions selected should achieve the maximum signal/background ratio. In a catalytic method the signal and background values are obtained from the overall and uncatalysed reactions respectively. In our case the parameter to be optimized was the ratio of reaction rates overall/uncatalysed [58]. The effect of the variables affecting the initial rate was studied by the univariate method.

Taking into account the effect of each variable on the initial reaction rate, the following optimum conditions were chosen:

- The Mn(IV) concentration does not seem to affect the initial rates ratio. A value of 10^{-4} M [Mn(IV)] was chosen in order to get suitable initial absorbance values.
- Low Mn(II) concentrations increase the reaction rates ratio and so, no Mn(II) was initially added for vanadium determination.

- The effect of H₂O₂ on the reaction rates ratio is similar to the effect on the kinetics: for low [H₂O₂] values the rates ratio rapidly increases with [H₂O₂] and it tends to level off for values of [H₂O₂] higher than 0.2 M. A value of 0.2 M [H₂O₂] was selected.
- The reaction rates ratio has a very sharp maximum value for 0.1 M [H⁺] and so it was selected as optimum for vanadium determination.
- High ionic strengths and low temperatures increase the reaction rates ratio; because of it, values of 3 for ionic strength and 25°C were chosen as optimum.

3.5. Calibration

Owing to the reaction kinetics (autoinduction) the rate constant method (integral) cannot be used. The fixed time and the fixed concentration methods were tried but unsatisfactory (non-linear) plots resulted regardless of the time and concentration chosen. It was previously stated that the title reaction is first order on the V(V) concentration; so plots of the initial rate, v_0 , vs. [vanadium] were straight and they can be used as calibration plots.

Under the optimum conditions the calibration plot was linear up to 50 ng ml⁻¹ vanadium and the equation of the regression line was found to be:

$$\begin{aligned} v_0(\text{A.U.} \times \text{s}^{-1}) \\ = (2.4 \pm 0.1)10^{-4} + (2.80 \pm 0.05)10^{-5} \\ \times C_V(\text{ng ml}^{-1}) \quad (r = 0.9989; n = 10) \end{aligned}$$

where the errors in both the intercept and the slope are given as standard errors estimated from the regression analysis.

From the standard deviation of the background signal, the detection limit [59] was estimated to be 0.9 ng ml⁻¹ (18 nM). The relative standard deviation calculated at the 4 and 25.5 ng ml⁻¹ levels were 5.2 and 2.5% respectively (10 replicates).

Table 1
Interferences in the determination of 25 ng ml⁻¹ vanadium (5.0 × 10⁻⁷ M)

Tolerated concentrations of interferent species (M)	Mole ratio, [ion]/[V(V)]	Species
10 ⁻¹ ^a	200 000	NO ₃ ⁻ , SO ₄ ²⁻ , PO ₄ ³⁻ , acetate
10 ⁻²	20 000	Cl ⁻ , F ⁻ , SiO ₃ ²⁻ , citrate
10 ⁻³	2000	Tartrate, BrO ₃ ⁻ , As(V)
10 ⁻⁴ ^b	200	NO ₂ ⁻ , EDTA, As(III), Sb(III), Mo(VI), Bi(III), Pb(II), Fe(II), Fe(III), Zn(II), Os(VIII), Tl(III), W(VI), Cu(II), Cd(II), Al(III), Ni(II), Co(II), Sn(II), Cr(III)
10 ⁻⁵	20	Br ⁻ , SCN ⁻ , Mg(II), Hg(II), Ti(IV)
10 ⁻⁶	2	I ⁻ , SO ₃ ²⁻ , C ₂ O ₄ ²⁻ , S ₂ O ₃ ²⁻ , Cr(VI), Hg(I)
10 ⁻⁷	0.2	IO ₃ ⁻ , Ag(I)

^a Maximum level tested for anions.

^b Maximum level tested for cations.

3.6. Effect of foreign ions

The study of interferent ions is summarized in Table 1. A species was considered to interfere when the vanadium concentration found differed from the expected one more than twice the standard deviation at that level of concentration. Some comments may be made on the data in Table 1. The metal ions which most seriously interfere are Ag(I), Hg(I) and Cr(VI), which also seem to exert some catalytic effect. The presence of Hg(II), Ti(IV) and Mg(II) is tolerated up to 20-fold the molar concentration of vanadium. No significant effect has been observed from any other metal ions. Although Fe(II), Sn(II) and As(III) reduce hexacyanomanganate(IV) they do not interfere, even at concentrations higher than those specified, because they are previously oxidized by hydrogen peroxide in the recommended procedure. Among anions, iodate interferes at concentrations higher than 10⁻⁷ M, and at a concentration of 10⁻⁴ M it completely changes the shape of the kinetic curves; this behaviour cannot be easily explained but it could be related to the very complex iodate–hydrogen peroxide reaction, which has been studied previously [60] and can be oscillatory [61]. Other anionic species such as iodide, thiosulphate, thiocyanate, oxalate and bromide slowly reduce hexacyanomanganate(IV), whereas sulphite does it faster. Less important effects are produced by nitrite, tartrate and bromate. Chloride, fluoride, silicate and citrate only interfere at levels higher

than 10⁻² M. The presence of EDTA (> 10⁻⁴ M) significantly modifies the reaction kinetics.

3.7. Application

The proposed method has been applied to the determination of vanadium in a natural Moroccan phosphate rock (phosphorite) (certified reference material, BCR No 32) without previous separations and with excellent results. The results of the vanadium determination and the data from some recovery studies are summarized in Table 2. The mean per cent of vanadium found in the reference material was 99.7% ($s = 2\%$; $n = 10$) and the mean per cent found in the recovery studies was 101.2% ($s = 3.2\%$; $n = 12$). In both cases the mean values do not differ significantly from 100% (t -test, $P = 0.05$) and the standard deviations do not differ significantly from each other (F -test, $P = 0.05$).

4. Conclusions

The catalytic effect of vanadium on the reaction Mn(CN)₆²⁻–H₂O₂ can be used for the determination of vanadium at the ppb level. The indicator reaction seems to be a chain reaction induced by the HO₂· radical. Though the integral methods are precluded, tentative mechanisms for the effects of H₂O₂ and acidity are proposed. The initial rate

Table 2

Determination of vanadium in a Moroccan phosphorite (reference material, BCR No 32)^a; two replicates

Sample (No)	Pure reference material		Spiked reference material			
	V ($\mu\text{g g}^{-1}$) found	Recovery (%)	Added	V ($\mu\text{g g}^{-1}$) total found	Recovered	Recovery (%)
1	153	100.0				
2	153	100.1	78.8 ^b	234.2	81.2	103.0
3	152	99.6	78.8 ^b	232.7	79.7	101.2
4	153	99.8	76.4 ^b	233.5	80.5	105.4
			137.5 ^b	289.7	136.7	99.4
5	151	98.8	76.4 ^b	227.0	74.0	96.8
			137.5 ^b	292.3	139.3	101.3
6			78.8 ^c	232.9	79.9	101.4
7			78.8 ^c	229.8	76.8	97.4

^a Certified values: (ng g⁻¹): Hg, 55. ($\mu\text{g g}^{-1}$): As, 9.5; B, 22.6; Cd, 20.8; Cr, 257; Co, 0.59; Cu, 33.7; Mn, 18.8; Ni, 34.6; Ti, 171; V, 153; Zn, 253. (mg g⁻¹): Ca as CaO, 517.6; total P as P₂O₅, 329.8; carbonate as CO₂, 51.0; F, 40.4, Si as SiO₂, 20.9; total S as SO₃, 18.4; Al as Al₂O₃, 5.5; Mg as MgO, 4.0; Fe as Fe₂O₃, 2.3.

^b Vanadium added after acid treatment.

^c Vanadium added before acid treatment.

method has been used. This allows us to take the data along a short period of time if compared with other catalytic methods. Though some other catalytic methods have been reported to have lower detection limits, the proposed method is among those with low detection limits, good reproducibility and wide dynamic range. All this, together with a relatively low number of interferences has allowed the determination of vanadium in phosphate rocks without needing previous separation.

Acknowledgements

The authors acknowledge financial support from the Universidad del Pais Vasco (Proyecto UPV 221-215-014489) and from the Diputacion Foral de Guipúzcoa.

References

- [1] G. López-Cueto, C. Ubide, *Can. J. Chem.* 69 (1991) 2112.
- [2] G. Trageser, H.H. Eysel, *Z. Anorg. Allg. Chem.* 420 (1976) 273.
- [3] G. López-Cueto, C. Ubide, *Can. J. Chem.* 64 (1986) 2301.
- [4] G. López-Cueto, C. Ubide, *Can. J. Chem.* 66 (1988) 2855.
- [5] G. López-Cueto, C. Ubide, *Talanta* 37 (1990) 849.
- [6] J.D. Lee, *Concise Inorganic Chemistry*, 4th ed., Chapman and Hall, London, 1991, p. 698.
- [7] F.A. Cotton, G. Wilkinson, *Advanced Inorganic Chemistry*, 5th ed., Wiley, New York, 1988, p. 1375.
- [8] B.P. Tissot, D.H. Welte, *Petroleum Formation and Occurrence*, Springer Verlag, Berlin, 1984, p. 474.
- [9] R.W. Boyle, *Geochemical Prospecting for Thorium and Uranium Deposits*, Elsevier, Amsterdam, 1982, p. 498.
- [10] G. Svehla, G. Tolg, *Talanta* 23 (1976) 755.
- [11] M.J.C. Taylor, J.F. van Staden, *Analyst* 119 (1994) 1263.
- [12] D. Pérez-Bendito, M. Silva, *Kinetic Methods in Analytical Chemistry*, Horwood, Chichester, 1988, p. 52.
- [13] S.B. Jonnalagadda, P. Sawunyama, *Fresenius' Z. Anal. Chem.* 340 (1991) 173.
- [14] L. Darbha, J. Arunachalam, *Talanta* 40 (1993) 135.
- [15] R. Forteza, V. Cerda, *Anal. Chem.* 58 (1986) 453.
- [16] A.Ch. Zotou, C.G. Papadopoulos, *Analyst* 115 (1990) 323.
- [17] R. Forteza, J.M. Estela, V. Cerda, *Analyst* 116 (1991) 1171.
- [18] A.A. Ensafi, A. Kazamzadeh, *Anal. Chim. Acta* 298 (1994) 27.
- [19] R.M. Marcé, M. Calull, J. Torres, F. Borrull, *Analyst* 113 (1988) 505.
- [20] R. Forteza, M.T. Oms, J. Cárdenas, V. Cerdá, *Analisis* 18 (1990) 491.
- [21] C. Qihua, G. Bo, Z. Yuyong, *Talanta* 36 (1989) 665.
- [22] M. Sugiyama, T. Hori, *Anal. Chim. Acta* 261 (1992) 189.
- [23] S. Kawakubo, B. Liang, M. Iwatsuki, T. Fukasawa, *Analyst* 119 (1994) 1391.
- [24] S. Kawakubo, Y. Tsuchiya, M. Iwatsuki, *Anal. Chim. Acta* 310 (1995) 501.
- [25] A.A. Mohamed, M. Iwatsuki, T. Fukasawa, M.F. El-Shahat, *Analyst* 120 (1995) 2281.

- [26] S. Kawakubo, K. Ogihara, M. Iwatsuki, *Analyst* 120 (1995) 2719.
- [27] J. Mateu, R. Forteza, V. Cerdá, M. Colom-Altés, *Analyst* 119 (1994) 1077.
- [28] J. Mateu, R. Forteza, V. Cerdá, *Thermochim. Acta* 247 (1994) 457.
- [29] M. León Camacho, M. Ternero Rodríguez, M. Callejón Mochón, A. Guiraúm Pérez, *Anal. Chim. Acta* 244 (1991) 89.
- [30] K.S. Yamaguchi, D.T. Sawyer, *Isr. J. Chem.* 25 (1985) 164.
- [31] G. Davies, L.J. Kirschenbaum, K. Kustin, *Inorg. Chem.* 7 (1968) 146.
- [32] A. Nagy, L. Treindl, *Nature* 320 (1986) 344.
- [33] T.J. Kemp, in: C.H. Bamford, C.F.H. Tipper (Eds.), *Comprehensive Chemical Kinetics*, vol. 7, Elsevier, Amsterdam, 1972, p. 325.
- [34] T.G. Costner, N. Ganapathisubramanian, *Inorg. Chem.* 28 (1989) 3620.
- [35] J.W. Ladbury, C.F. Cullis, *Chem. Rev.* 58 (1958) 403.
- [36] J.S. Reckley, K. Showalter, *J. Am. Chem. Soc.* 103 (1981) 7012.
- [37] N. Ganapathisubramanian, K. Showalter, *J. Chem. Phys.* 80 (1984) 4177.
- [38] J.M. García, A.I. Jiménez, J.J. Arias, K.D. Khalaf, A. Morales Rubio, M. de la Guardia, *Analyst* 120 (1995) 313.
- [39] G. López-Cueto, S. Maspoch, J.F. Rodríguez-Medina, C. Ubide, *Analyst* 121 (1996) 407.
- [40] S. Ventura, M. Silva, D. Pérez-Bendito, C. Hervás, *Anal. Chem.* 67 (1995) 4458.
- [41] M. Blanco, J. Coello, H. Iturriaga, S. Maspoch, M. Redón, *Anal. Chem.* 67 (1995) 4477.
- [42] T.F. Cullen, S.R. Crouch, *Mikrochim. Acta* 126 (1997) 1.
- [43] G. López-Cueto, J.F. Rodríguez-Medina, C. Ubide, *Analyst* 122 (1997) 519.
- [44] J.A. Lower, W.C. Fernelius, *Inorg. Synth.* 2 (1946) 213.
- [45] G. López-Cueto, A. Alonso-Mateos, C. Ubide, G. del Campo Martínez, *Talanta* 35 (1988) 795.
- [46] D.J. Bucknell (Ed.), 'Analar' Standards for Laboratory Chemicals, BDH, Dorset, 1984, p. 373.
- [47] G.H. Walden, L.P. Hammett, S.M. Edwards, *J. Am. Chem. Soc.* 56 (1934) 57.
- [48] H.A. Mottola, *Kinetic Aspects of Analytical Chemistry*, Wiley, New York, 1988, p. 124.
- [49] G. López-Cueto, J.F. Rodríguez-Medina, C. Ubide, *Talanta* 43 (1996) 2101.
- [50] R.H. Simoyi, P. De Kepper, I.R. Epstein, K. Kustin, *Inorg. Chem.* 25 (1986) 538.
- [51] A. Bakac, J.H. Espenson, I.I. Creaser, A.M. Sargeson, *J. Am. Chem. Soc.* 105 (1983) 7624.
- [52] F.J. Andrés Ordax, A. Arrizabalaga, *An. Quim.* 81 (1985) 431.
- [53] F. Mata-Pérez, J.F. Pérez-Benito, *J. Chem. Educ.* 64 (1987) 925.
- [54] J.H. Espenson, *Chemical Kinetics and Reaction Mechanism*, McGraw-Hill, New York, 1981, p. 25.
- [55] Y. Israel, L. Meites, in: A.J. Bard, R. Parsons, J. Jordan (Eds.), *Standard Potentials in Aqueous Solution*, Marcel Dekker, New York, 1985, p. 520.
- [56] M. Orhanovic, R.G. Wilkins, *J. Am. Chem. Soc.* 89 (1967) 278.
- [57] P. Zuman, R. Patel, *Techniques in Organic Reaction Kinetics*, Wiley, New York, 1984, pp. 158–162.
- [58] G. López-Cueto, C. Ubide, *Anal. Proc. Including Anal. Commun.* 32 (1995) 235.
- [59] ACS Committee on Environmental Improvement, *Anal. Chem.* 52 (1980) 2242.
- [60] I.R. Wilson, in: C.H. Bamford, C.F.H. Tipper (Eds.), *Comprehensive Chemical Kinetics*, vol. 6, Elsevier, Amsterdam, 1972, p. 386.
- [61] S.D. Furrow, in: R.J. Field, M. Burger (Eds.), *Oscillatory and Traveling Waves in Chemical Systems*, Wiley, New York, 1985, p. 171.



ELSEVIER

Talanta 46 (1998) 75–82

Talanta

Application of principal component regression to the determination of Captopril by differential pulse polarography with no prior removal of dissolved oxygen

J.M.G. Fraga, A.I.J. Abizanda, F.J. Moreno, J.J.A. León *

Departamento de Química Analítica, Nutrición y Bromatología, Universidad de La Laguna, La Laguna, 38071 Tenerife, Spain

Received 3 February 1997; received in revised form 8 July 1997; accepted 1 August 1997

Abstract

As shown in this paper, multivariate calibration in general and principal component regression (PCR) in particular allow the determination of Captopril by differential pulse polarography (DPP) in the presence of oxygen despite the overlap between their polarographic bands. Electrochemical parameters (pulse amplitude, pulse delay and drop time) are optimized from response surfaces using PCR to determine the relationship between the variables to be optimized and the relative square error of prediction (RSEP), which was adopted as the parameter to be minimized. The proposed method is quite fast and inexpensive as a result of the decreased analysis times and sparing use of the inert gas. It was applied to the determination of Captopril in synthetic samples and a commercially available pharmaceutical preparation, with relative errors and confidence intervals < 2.5% and 2.0%, respectively. It should be noted that the sample can be analysed directly following dissolution in water without the need to remove the excipients. © 1998 Elsevier Science B.V. All rights reserved.

Keywords: Captopril; Polarography; Principal component regression

1. Introduction

One of the main reasons for the relatively scant use of polarography in routine analyses is the need to remove oxygen from the sample before any polarograms are recorded in order to avoid side reactions and/or overlap between the analytical signal and that for oxygen. If oxygen removal could be dispensed with, then analytical costs

would be substantially reduced and the throughput increased.

Oxygen is easily reduced at a dropping mercury electrode (DME) in two steps. In the first wave hydrogen peroxide is formed and in the second, more negative wave, the peroxide is reduced to water. In acid and neutral media, the reduction of oxygen to hydrogen peroxide is an irreversible electrode process, above pH 10, it becomes reversible. On the other hand, hydrogen peroxide is oxidized with a high overvoltage in both acid and alkaline media.

* Corresponding author. Fax: +34 22 635602; e-mail: jjar-ias@ull.es

Dissolved air must usually be removed from the analytical solution in order to avoid interactions of oxygen with the target analyte or side reactions between the analyte and oxygen (or the hydrogen peroxide resulting from its reduction). Usually, air is removed by bubbling an inert gas through the solution, after which the gas stream is passed over the solution surface while the polarogram is being recorded. The time required for effective removal of the oxygen varies with the gas flow-rate, solution volume and geometry of the polarographic cell, but is usually 10–15 min. Avoiding the need to remove oxygen and hence decrease analysis times and use of inert gas is therefore a desirable objective.

This paper shows that multivariate calibration and, specifically, principal component regression (PCR), enables the differential pulse polarographic (DPP) determination of analytes whose bands are fully overlapped with that of oxygen, even if this is not removed from the solution. In order to check the method developed, Captopril, a potent antihypertensive agent used in the treatment of both renovascular and essential hypertension, was determined. This drug has so far been determined in both biological samples and pharmaceutical preparations by use of chromatographic [1], spectrofluorometric [2] and radioassay methods [3], in addition to various electrochemical techniques including cyclic voltammetry [4] and DPP [5], where Captopril gives a wave that is fully overlapped with the first wave for oxygen at the maximum sensitivity.

Developing an effective analytical method entails optimizing every single variable that influences its performance. Electrochemical methods are usually optimized by altering each variable in turn while keeping all others constant. This involves time-consuming preliminary experiments and, frequently, the obtainment of inappropriate optimal parameter values that can lead to spurious results through disregard of potential interactions between variables.

In this work, surface response methodology was used to optimize the experimental model for the determination of Captopril by DPP in the presence of oxygen.

2. Experimental

2.1. Apparatus and software

The measurements were performed with an IN-ELECSA Electrochemical System consisting of a PDC1212 Potentiostat and a CTG drop time controller, interfaced to an ACER 550 computer. A DME was used as the working electrode, an Ag/AgCl saturated electrode and a Pt electrode as reference and auxiliary electrodes, respectively.

Calculations were made at a 486DX4/AT personal computer.

PCR and optimization process were carried out with the program UNSCAMBLER, version 5.00 [6].

2.2. Solutions and reagents

200 $\mu\text{g ml}^{-1}$ solutions of Captopril was prepared from the corresponding hydrochloride (Sigma).

Analytical grade reagents were used throughout and all solutions were prepared from double-distilled water.

2.3. Procedure

Several 25-ml flasks were filled with 10 ml of 0.25 M HCl, an appropriate volume of Captopril solution and double-distilled water to the mark. The solutions were then used to record differential pulse polarograms. The Captopril concentrations in these synthetic samples were obtained from polarograms recorded at 3 mV intervals over the range -73 to -130 mV, using a pulse amplitude of -50 mV, a pulse delay of 20 ms and a drop time of 3 s. The drug concentration was calculated by applying PCR to the data obtained from -82 to -121 mV, using a single principal component (PC).

For the determination of Captopril in pharmaceutical formulations, 10 tablets were placed in a 250-ml flask, made to volume with double-distilled water and ultrasonicated for 3 min. An aliquot of 0.2 ml of the resulting solution was transferred into a 25-ml flask that was then filled with 10 ml of 0.25 M HCl and made to the mark

with double-distilled water. This solution was used to record a differential pulse polarogram under the same conditions as for the synthetic samples and the polarogram was processed as described in the previous paragraph.

3. Results and discussion

Below pH 3, Captopril [(2S)-1-(3-Mercapto-2-methyl-propionyl)-L-proline] exhibits a single, anodic polarographic peak resulting from the reaction of its thiol group with the mercury electrode according to the following, well-known scheme for the thiol function:



The peak is diffusion-controlled and its current is linearly dependent on the concentration over a wide range of the latter. Above pH 3, a new peak (specifically, an adsorption pre-peak) appears that is related to the COOH group of Captopril (pK_a 3.52 and 2.86 for the *trans* and *cis* forms, respectively).

Fig. 1 shows the DPP obtained for a solution containing $16 \mu\text{g ml}^{-1}$ Captopril in 0.1 M HCl, with bubbling of argon for a variable time. As can be seen, in the absence of bubbling, a peak at -25 mV

due to dissolved oxygen and a small shoulder due to Captopril and fully overlapped with the previous one were obtained. As bubbling was extended and oxygen gradually removed as a result, the Captopril wave became increasingly more defined.

The reduction of oxygen at -25 mV involves the formation of hydrogen peroxide, which can also react with Captopril, thereby reducing its concentration and diminishing its wave. In order to confirm this assumption, two solutions containing the same Captopril concentration in 0.1 M HCl but H_2O_2 concentrations differing by a factor of 10 were prepared. After 10 min, both solutions were deoxygenated by bubbling argon through them and their polarograms recorded. A comparison of the waves obtained confirmed that the presence of hydrogen peroxide had no effect on the Captopril wave.

3.1. Influence of electrochemical variables

The effect of the different electrochemical variables potentially affecting the DPP for Captopril (viz. pulse amplitude, pulse delay and drop time) was studied. For this purpose, a non-deoxygenated $10 \mu\text{g ml}^{-1}$ solution of Captopril was used to record polarograms at variable values of one parameter and constant values of the other two. Fig. 2a illustrates the influence of pulse amplitude between -90 and -10 mV . As can be seen, the less negative pulse amplitude produce a decrease of the background current and the peak is shifted to more negative potentials and noise increased. In addition, the less negative pulse amplitudes increased the definition of the Captopril shoulder as a result of the distance between the maxima for oxygen and the drug being increased. This is more clearly reflected in the contour map (Fig. 2b): line B (Captopril maximum) departs from line A (oxygen maximum) as the pulse amplitude becomes less negative. Therefore, the condition of maximum signal (-90 mV) coincide with maximum overlap between the oxygen and Captopril peaks and minimum overlap (-10 mV) coincides with maximum noise and band broadening and minimum signal. A compromise must thus be made for optimal performance.

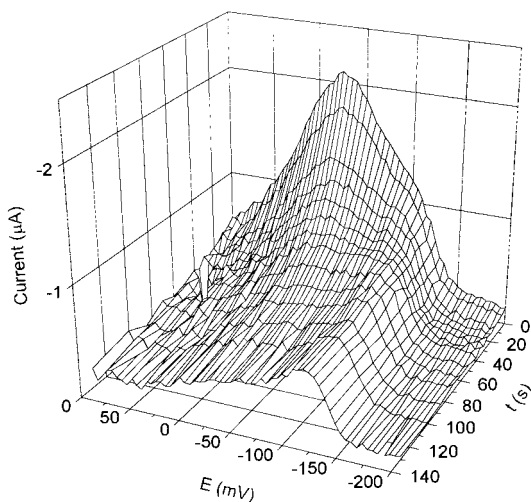


Fig. 1. Influence of the gas bubbling time on the DPP for a solution containing $16 \mu\text{g ml}^{-1}$ Captopril in 0.1 M HCl. Pulse amplitude, -40 mV ; pulse delay, 40 ms; drop time, 3 s.

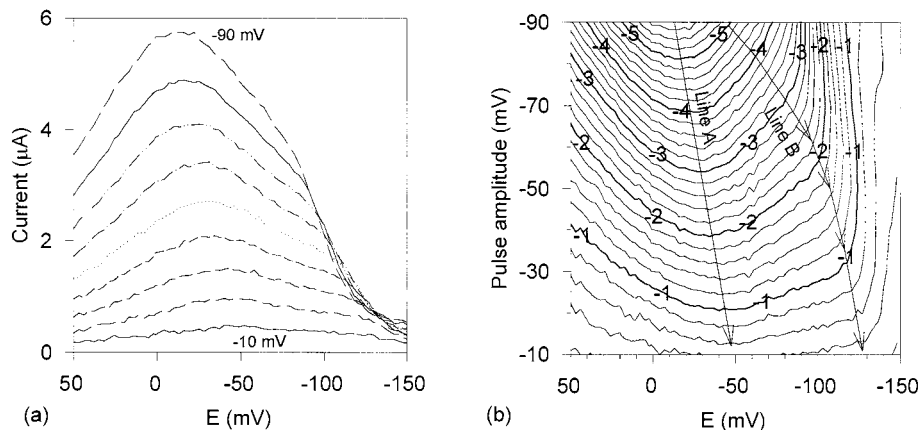


Fig. 2. (a) Effect of pulse amplitude on the DPP for a solution containing $16 \mu\text{g ml}^{-1}$ Captopril in 0.1 M HCl (pulse delay, 20 ms; drop time, 3 s). (b) Contour map.

On the other hand, changes in pulse delay only affected the peak height, as can be expected and decreasing the delay (Fig. 3) increased the signal, with no change in the background current. Finally, increasing the drop time increased the signal as a result of the increased electrode area (Fig. 4).

3.2. Response surface

Faced with the difficulty of choosing the most appropriate pulse amplitude, pulse delay and drop time, we used response surface methodology, which comprises various mathematical and statistical techniques of assistance in modelling and analysing problems where the response of interest is influenced by several variables simultaneously.

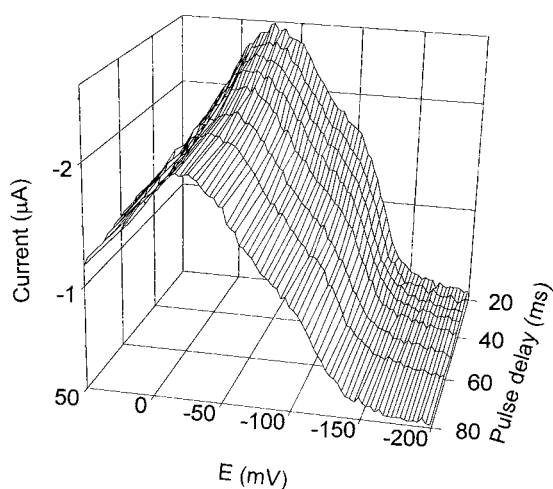


Fig. 3. Effect of pulse delay on the DPP for a solution containing $16 \mu\text{g ml}^{-1}$ Captopril in 0.1 M HCl (pulse amplitude, -50 mV ; drop time, 3 s).

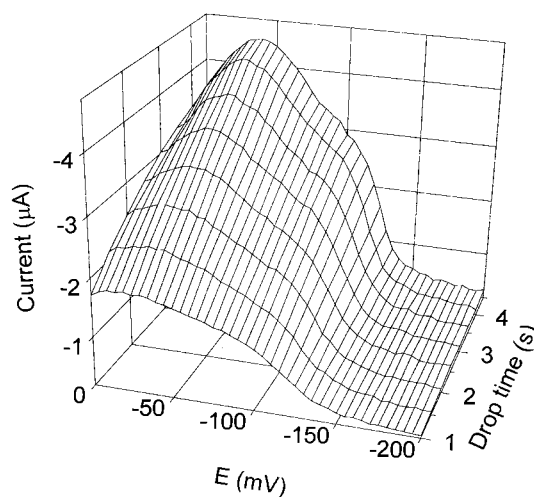


Fig. 4. Effect of drop time on the DPP for a solution containing $16 \mu\text{g ml}^{-1}$ Captopril in 0.1 M HCl (pulse amplitude, -50 mV ; pulse delay, 20 ms).

The relation between the response and the independent variables is unknown in most cases, so the first step in the process involves an approximation to the actual relation between the response and the set of independent variables. As a rule, such a relation is approximated via polynomial functions. In this work, we used PCR to construct the surface response.

The first problem encountered was determining which variable or quantity should be used as the response. While most available methods for this purpose seek to maximize the signal, these conditions (a large pulse amplitude) were previously found to result in maximum overlap between the oxygen and Captopril bands and because the final goal was the quantitative determination of Captopril, the most appropriate response variable was thought to be that allowing the calibration and prediction errors to be quantified. To this end, the relative standard error (RSE) [7] defined as

$$\text{RSE} = 100 \times \sqrt{\frac{\sum (c_{\text{found}} - c_{\text{added}})^2}{\sum (c_{\text{added}})^2}}$$

was chosen, which is known as RSEC or relative square error of prediction (RSEP) according to that the concentration values are referred to the calibration or prediction process.

Variables were optimized by using the programme Unscrambler [6,9] and a Box Behnen factor design [8] at three levels (using middle points instead of corner points), with the following high and low values: pulse amplitude, -30 to -60 mV; pulse delay, 20–50 ms; drop time, 2–4 s.

The program constructs an optimization matrix from 15 experiments where, in addition to the variables to be optimized (A pulse amplitude, B pulse delay and C drop time), interaction effects (AA , BB , CC , AB , AC and BC) are included. In order to obtain RSEC and RSEP, a calibration set consisting of four solutions containing 3, 7, 12 and $16 \mu\text{g ml}^{-1}$ Captopril in 0.1 M HCl and a prediction set comprising three solutions containing 5, 9.5 and $14 \mu\text{g ml}^{-1}$ Captopril, also in 0.1 M HCl, were prepared and their differential pulse polarograms recorded from -65 to -145 mV

under each of the 15 different conditions. The calibration set was subjected to PCR [9] under each condition considered, using a single PC because the variance of the concentration matrix accounted for in the validation (cross-validation) process always exceeded 97%. As the Captopril peak changed with pulse amplitude, various intervals (-95 to -135 , -85 to -125 and -75 to -115 mV) were used at the pulse amplitudes -30 , -45 and -60 mV, respectively. After the models were constructed, the calibration and prediction sets were predicted and RSEC and RSEP, respectively, calculated.

The next step involved finding the models that relate the obtained values of RSE and the variables (A , B , C , AA , BB , CC , AB , AC and BC) using PCR. The established models were checked in order to find the possible existence of non-significant effects. So, for this purpose, a normal probability plot of effect and values of the estimated effects was made. Finally, the models were recalculated by giving a zero weight to those variables subject to no significant effects. In this way, models with normally distributed residuals (and hence correct fitting between the variables to be optimized and RSEC or RSEP) were obtained.

Fig. 5a shows the response surface (RSEC) obtained at the intermediate drop time tested (3 s), which was that resulting in the lowest RSEC. As can be seen, RSEC decreased with decreasing delay pulse (i.e. the peak height increased). On the other hand, increasing the pulse amplitude decreased RSEC through decreased overlap between the Captopril and oxygen peaks. The maximum RSEC was obtained at long pulse delays and more negative pulse amplitudes, whereas the minimum RSEC corresponded to short pulse delays (maximum signal). These optimum conditions, while broad, were restricted as a result of the study of the response surface for RSEP (Fig. 5b). As can be seen, in the zones of minimum RSEC values (short pulse delays) for the calibration process, RSEP values depended on pulse amplitude. At less negative pulse amplitude, RSEP decreased as a result of the decreased overlap and reached a minimum at -50 mV, beyond which it increased as a result of the increased noise in the polarograms. Under these conditions of pulse am-

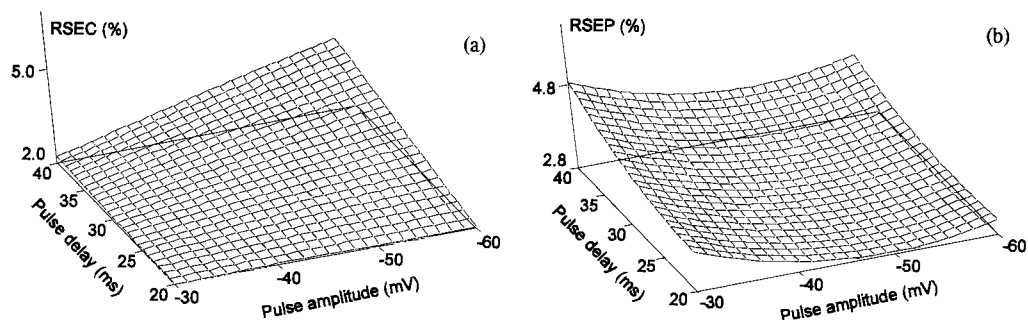


Fig. 5. Response surface for (a) RSEC and (b) RSEP.

plitude, noise associated was more important than the decreased overlap (relative maximum at about -50 mV in Fig. 2b). As regards pulse delay, the effect was the same as for RSEC: a decrease in the delay decreased RSEP through decreased height peak.

The conditions that minimized RSEP and hence those used to determine Captopril in the presence of oxygen were thus a pulse amplitude of -50 mV, a pulse delay of 20 ms and a drop time of 3 s.

3.3. Calibration

After the optimum conditions for the determination of Captopril were established, a new calibration was performed by using a larger number of solutions. Thus, nine solutions containing Captopril concentrations between 3.2 and $16.0 \mu\text{g ml}^{-1}$ at $1.6 \mu\text{g ml}^{-1}$ intervals were used to record differential pulse polarograms under the same optimum conditions, in duplicate (in order to ensure that the calibration matrix included noise as a source of variability). The data obtained from the 18 polarograms recorded from -79 to -139 mV (the maximum for Captopril lay at -109 mV, the mid-point of the range), at 3 mV intervals, were used for PCR calibration using the program Unscrambler [6–9] and the cross-validation method with as many segments as objects existed. The model thus obtained, Model 1 (from -79 to -139 mV), accounted for 99.6% of the variance of the concentration matrix with a single PC, as well as for 97.4% of the variance of the current matrix—both in the validation process.

More exhaustive selection of the variables used to construct the model increased both variance values. Fig. 6 shows the initial variance of the current matrix as a function of the different variables, as well as the residual variance obtained with a single PC. As can be seen, the last corresponded largely to variables above -121 mV. On the other hand, the variation of the current residuals against the leverage for each variable (Fig. 7) reveals that some variables had high residuals and/or low leverages and might thus be distorting the model. Such variables corresponded to the range from -124 to -139 mV.

For both reasons, variables below -121 mV were excluded and the system was recalibrated

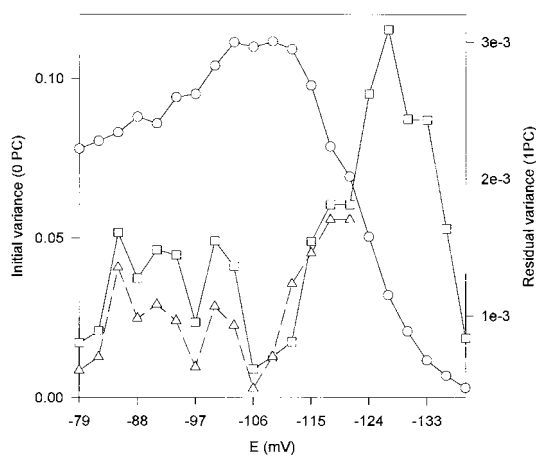


Fig. 6. Plot of variance vs. potential: (○) Initial variance; Residual variance obtained with a single PC. [(□) Model 1, (△) Model 2].

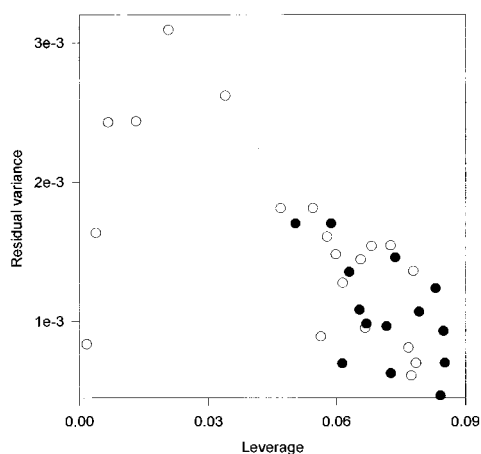


Fig. 7. Plot of residual variance vs. leverage. (●) Model 1, (○) Model 2.

using the same validation procedure. The new model, Model 2 (from -79 to -121 mV), accounted for 99.8 and 98.5% of the variance of the concentration and current matrix, respec-

tively, reduced the variance not explained by a single PC (Fig. 6) and, as a rule, decreased residuals and increased variable leverages (Fig. 7). RSEC was 2.03% for Model 1 and this value was reduced to 1.45% for Model 2.

The variance of the current matrix not accounted for by the model using the first factor was ascribed to noise in the polarograms, as reflected in most of the figures shown in this work. The decrease in the signal increased noise and hence led to noisier variables. Consequently, excluding the currents at more negative potentials from Model 2 increased the variance it accounted for. The noise cannot be attributed to the presence of oxygen because it was also observed in its absence, rather, it originated from the potentiostat itself. The difference between the concentrations found for each measurement made on each calibration solution was $<1.5\%$ in every case but one, where the variation was 3.1%.

Table 1

Results obtained in the determination of Captopril in synthetic samples, each one was measured twice

Added amount (mg ml ⁻¹)	Found amount \pm confidence interval (mg ml ⁻¹)	Relative error (%)	Found amount ^a \pm S.D. (μ g ml ⁻¹)	Relative error (%)
5.61	5.51 \pm 0.10 5.56 \pm 0.06	-1.78 -0.87	5.54 \pm 0.04	-1.25
8.82	9.09 \pm 0.13 8.79 \pm 0.11	3.09 -0.34	8.94 \pm 0.21	1.34
12.02	12.19 \pm 0.09 12.02 \pm 0.11	1.37 -0.01	12.12 \pm 0.12	0.83
15.23	15.49 \pm 0.09 15.41 \pm 0.08	1.68 1.17	15.45 \pm 0.06	1.44

^a Average of two measurements of the same sample.

Table 2

Results obtained in the determination of Captopril in a pharmaceutical preparation (Cesplón)

Declared amount (mg)	Found amount \pm confidence interval (mg)	Recovery (%)	Found amount ^a \pm S.D. (mg)	Recovery (%)
25.00	25.41 \pm 0.33	101.64	—	—
25.00	24.88 \pm 0.38	99.52	25.19 \pm 0.28	100.76
25.00	25.28 \pm 0.44	101.12	—	—

^a Average of three determinations.

3.4. Determination of Captopril in synthetic samples

The predictive capacity of the proposed model was checked by quantifying the amount of Captopril present in solutions of known concentration. Recordings were obtained under the same conditions as those for the calibration solutions and predictions were calculated by the programme Unscrambler.

Table 1 shows the results. The relative S.D. of the predicted values for a given solution was always $\pm 1.0\%$. Also, there was close agreement between the amounts added and found: relative errors were all $< 2.5\%$ and the confidence intervals $< 2\%$ of the amounts predicted.

3.5. Determination of Captopril in a commercially available pharmaceutical preparation

The proposed method was used to quantify the analyte in a commercially available formulation: Cesplón. As can be seen from Table 2, the percent recoveries and confidence intervals obtained were quite good.

4. Conclusions

The use of PCR for calibration allows Captopril to be determined in the presence of oxygen, where the differential pulse polarograms for the two are fully overlapped. Use of response surface methodology allows the optimum values for the

electrochemical variables (pulse amplitude, pulse delay and drop time) to be established in order to minimize errors.

The proposed method expedites analyses as it avoids the need to bubble an inert gas to remove oxygen and allows the determination of Captopril in real samples (pharmaceutical preparations) with no excipient separation pretreatment.

Acknowledgements

The authors wish to acknowledge the financial support of this work by the Canary Autonomous Government, Grant No. 93/042.

References

- [1] C.M. Pereira, Y.K. Tam, R.L. Collins-Nakai, J. Chromatogr. 425 (1988) 208.
- [2] E. Ivashkiv, J. Pharm. Sci. 73 (1984) 1427.
- [3] J. Tu, E. Lin, E.L. Nickoloff, Ther. Drug Monit. 6 (1984) 59.
- [4] P. Passamonti, S. Ferraro, V. Bartucci, F. Pucciarelli, Electroanalysis 3 (1991) 847.
- [5] J.A. Squella, I. Lemus, Y. Borges, L. Nuñez-Vergara, J. Bol. Soc. Chil. Quím. 37 (1992) 259.
- [6] Unscambler-Ex (version 5.0), Computer-Aided Modelling A/S, Thondheim, Norway, 1993.
- [7] G. López-Cueto, S. Maspoch, J.F. Rodríguez-Medina, C. Ubide, Analyst 121 (1996) 407.
- [8] Douglas C. Montgomery, Diseño y Análisis de Experimentos, in: P. Nicolás Grepe (Ed.), Grupo Editorial Iberoamérica, Mexico, 1991, p. 490.
- [9] H. Martens, T. Næs, in: Multivariate Calibration, Wiley, Chichester, 1991.

Differential pulse polarographic determination of ofloxacin in pharmaceuticals and biological fluids

M. Rizk, F. Belal *, F.A. Aly, N.M. El-Enany

Department of Analytical Chemistry, Faculty of Pharmacy, University of Mansoura, Mansoura 35516, Egypt

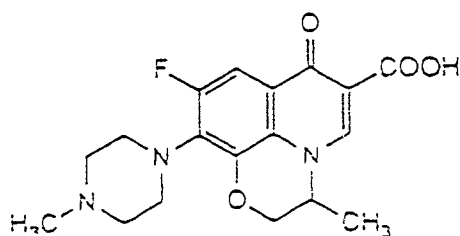
Received 8 October 1996; received in revised form 23 July 1997; accepted 4 August 1997

Abstract

A sensitive method is described for the determination of ofloxacin in its pure form, dosage forms and biological fluids. The proposed method depends upon the polarographic activity of ofloxacin in Britton Robinson buffers, whereby a well-defined cathodic wave is produced over the pH range 4.1–10.3. The wave was characterized as being irreversible, diffusion-controlled with limited adsorption properties. The current-concentration relationship was found to be rectilinear over the range 5×10^{-5} – 5×10^{-4} M and 1×10^{-5} – 5×10^{-4} M using the DC_t and DPP modes respectively, with a minimum detectability (S/N = 3) of 3×10^{-7} M. The proposed method was successfully applied to the determination of ofloxacin in tablets and biological fluids. The results obtained were found to be in agreement with those obtained by a reference method. © 1998 Elsevier Science B.V. All rights reserved.

Keywords: Ofloxacin; Polarography; Pharmaceutical analysis; Biological fluids

1. Introduction



Ofloxacin is a synthetic fluorinated quinolone

derivative having activity against both gram negative and gram positive bacteria through inhibition of their DNA gyrase [1]. It is widely used in the treatment of respiratory tract and urinary tract infections [2]. Various techniques have been utilized for the determination of ofloxacin either per SE or in dosage forms. These techniques include: potentiometric titration [3], spectrophotometry [4–7], spectrofluorometry [5,6], HPLC [8–17], microbiology [18] and adsorptive stripping voltammetry [19].

During the preparation of this manuscript, a paper dealing with the polarographic determination of ofloxacin appeared [20]. Astonishingly, the authors used BRb of pH 4 for their determination, at that medium, the wave was very poorly

* Corresponding author.

defined. The wave was found to be substantially improved as the pH value of the medium was increased up to pH 8.36 (the one we used) whereby well-defined wave was obtained. Meanwhile the authors [20] had limited their method to the use of DC_T mode, therefore we attempted the Differential Pulse Polarography (DPP) mode which allowed better working range and lower detection limit.

2. Experimental

2.1. Materials

Ofloxacin was kindly provided by Hoechst Oriented Pharmaceutical Company (Cairo, Egypt) and was used as received. Tablets (each containing 200 mg of ofloxacin) were obtained from commercial sources.

Reagents

- Britton Robinson buffers (0.08 M) [21], covering the pH range 2.7–10.3.
- Methanol: AR grade (Aldrich).
- A stock solution (2.5×10^{-3} M) of ofloxacin was prepared in methanol, and was further diluted with the same solvent to give the appropriate concentrations.

The methanol concentration in the polarographic cell was kept always at 20%. The solutions were purged with pure nitrogen for 5 min, then polarographed at ambient temperature.

2.2. Apparatus

The polarographic study and DPP measurements were carried out using the Polarecord E 506 Metrohm (Herisau, Switzerland). The drop time (1 s) was electronically controlled using a 663 VA Stand from the same company. The polarograms were recorded using a potential scan of 10 mV s^{-1} . A three-electrode system composed of a Dropping Mercury Electrode (DME), $Ag^0/AgCl$ reference electrode, and a graphite rod as the auxiliary electrode, was used. Phase-selective AC_T polarograms were recorded using the same instrument; the superimposed alternating voltage being 15 mV at a frequency of 75 Hz and a phase angle of 90° .

The effect of mercury height was studied using Sargent-Welch Polarograph Voltametric Analyzer equipped with $Ag^0/AgCl$ reference electrode and a platinum wire as the auxiliary electrode.

The cyclic voltametry apparatus consisted of a Wenking LB 75 potentiostat, a Wenking VSG 72 function generator, a Goldstar DM 6135 digital multimeter and a Philips PM 8271 xyt recorder, a three-electrode system composed of a graphite working electrode, $Ag^0/AgCl$ reference electrode, and a platinum auxiliary electrode was used.

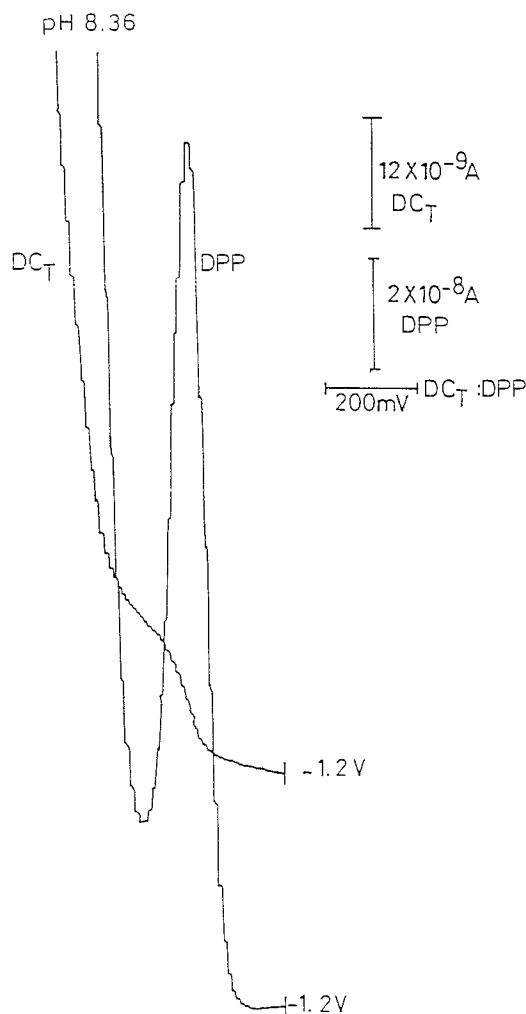


Fig. 1. Typical polarogram of ofloxacin (1×10^{-4} M) in BRb pH 8.36 containing 20% methanol.

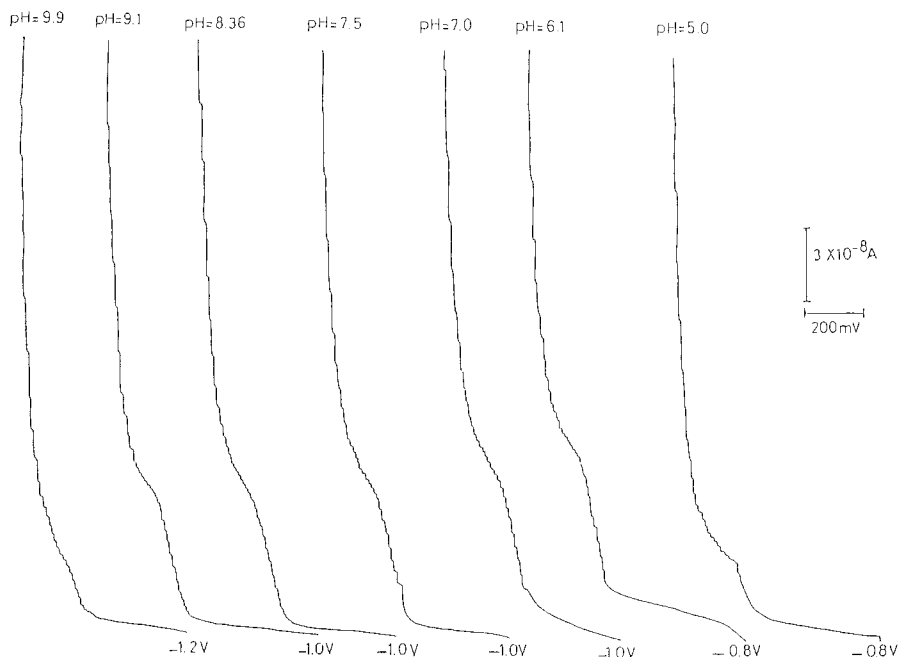


Fig. 2. Effect of pH on the development of the polarographic waves of ofloxacin (5×10^{-4} M).

The voltammogram of 5×10^{-4} M solution were recorded at different scan rates of 20, 50, 100, 200 and 500 mV s^{-1} .

2.3. Procedure for tablets

Weigh and pulverize 10 tablets. Transfer a weighed quantity of the powder equivalent to 20 mg of ofloxacin. Dissolve in 100 ml of methanol then filter. Transfer 2 ml of the filtrate into 25 ml volumetric flask and complete to the mark with BRb of pH 8.36. Pour the contents of the flask into the polarographic cell. Record the DC_t and DPP polarograms. Calculate the nominal content of the tablet using previously plotted calibration graph or the corresponding regression equation.

2.4. Procedure for spiked urine

Add a quantity of ofloxacin to the urine to obtain a final concentration of $0.5 \text{ mg} \cdot \text{ml}^{-1}$ then add 2 ml of phosphate buffer (pH = 7.0). Stir the mixture, extract with 3×10 ml of dichloromethane–isopropyl alcohol mixture

(90:10 V/V). Allow the extract to dry under nitrogen gas at room temperature. Dissolve the residue in methanol and filter into 50 ml volumetric flask. Complete to the mark with methanol, proceed as described above.

3. Results and discussion

Fig. 1 shows a typical (DC_t and DPP) polarogram of ofloxacin in BRb of pH 8.36 containing 20% methanol. Methanol was added as a solubilizer for ofloxacin, meanwhile it decreased adsorption interferences. Reduction of ofloxacin at the DME was found to be pH dependent. The $E_{1/2}$ was shifted to more negative values upon increasing the pH as shown in Fig. 2. A plot of $E_{1/2}$ versus pH gave two straight lines with a break at pH 6.1 (Fig. 3) which corresponds to the second pK_a value of ofloxacin (the first one at 0.9 did not appear on the curve because the pH range over which reduction occurs began from 4.1) by analogy to the second pK_a value of nalidixic acid which has almost the same function group [26].

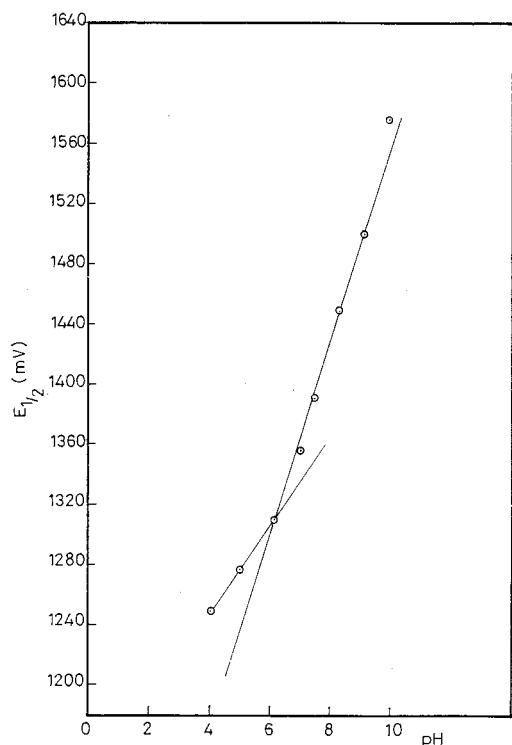


Fig. 3. Effect of pH on the $E_{1/2}$ (mV) values of ofloxacin (5×10^{-4} M) in BRb containing 20% methanol.

The relation between $E_{1/2}$ and pH for the wave is expressed by the following equations:

$$E_{1/2} = -0.9622 - 0.0577 \text{ pH} \quad (R = 0.99560) \quad (1)$$

Over the pH range of 2.6–7.0 and

Table 1
Effect of pH on the development of the polarographic waves of ofloxacin

pH $E_{1/2}$ (V)	$E_{1/2}/\text{pH}$ (mV)	Half-peak width ($W_{1/2}$) (mV)	Number of protons (Z)	αn_a
4.10--1.250	-28	13	0.34	0.9
5.00--1.270	-36	12	0.63	1.03
6.10--1.310	-51	12	1.01	1.08
7.00--1.360	-60	12	1.12	1.10
7.50--1.390	-68	14	1.27	1.10
8.36--1.450	-57	11	1.13	1.17
9.10--1.490	-106	14	1.94	1.08
9.90--1.575	-112	—	1.99	1.05
10.30--1.620	—	—	—	0.93

$$E_{1/2} = -0.4994 - 0.1089 \text{ pH} \quad (R = 0.99959) \quad (2)$$

Over the pH range of 7.5–10.3.

Logarithmic analysis of the reduction waves obtained in BRb of different pH values resulted in straight lines. Assuming that the rate determining step involves the transfer of two electrons (a free radical, one electron-transfer is not likely to occur), the values of the slopes suggest that the reduction process is irreversible in nature. The αn_a values were calculated using the treatment of Meites and Israel [22] and were listed in Table 1.

It is noticed that, the degree of reversibility increased as the pH is raised up to pH 8.36 then it began to decrease. This character was further confirmed by CV measurements. The cyclic voltammograms of ofloxacin (5×10^{-4} M solution) in BRb of pH values 4.0, 7.0 and 10.0 show one cathodic peak using different scan rates (10 – 500 mV s^{-1}). The peak potentials of the wave display a cathodic shift on increasing the scan rate, thus revealing the irreversible nature of the reduction process [23].

The number of protons, Z , consumed in the electrode reaction is given by the following equation [24]:

$$E_{1/2}/\text{pH} = -\frac{0.059Z}{\alpha n_a}$$

where is the transfer coefficient. The value of αn_a was calculated from the following equation:

$$E = E_{1/2} - (0.0559/n_a)\log[(i/i_d) - i]$$

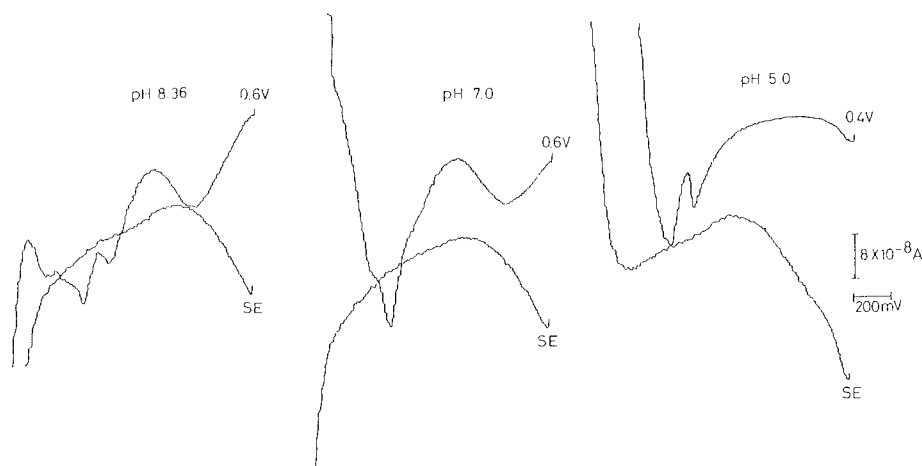


Fig. 4. Alternating current behavior of ofloxacin (5×10^{-4} M) in BRb of different pH values. Superimposed alternating voltage: 15 mV; frequency: 75 Hz; phase angle: 90° (SE: supporting electrolyte).

Where i_d is the limiting current. At pH 8.36 Z was found to be 1.13, i.e. two protons are probably consumed in the electrode reaction.

3.1. Study of the wave characteristics

Increasing the mercury height (h) resulted in a corresponding increase in the waveheight (w); a plot of \sqrt{h} vs. the waveheight gave a straight line. A plot of $\log w$ gave a straight line, the slope of which was 0.49. Changing the buffer concentration over the range 0.006 to 0.06 M resulted in a negligible decrease in the waveheight. These two characters point out to the diffusion-controlled nature of the wave.

The alternating current behavior (AC_t) of ofloxacin was studied using a phase-selective angle of 90° . In BRb of pH 5.0, 7.0 and 8.36, the summit potentials (Es) were shifted to more negative values of 119, 99.27 and 90.625 mV respectively. Fig. 4 demonstrates that a pH values of 7.0 and 8.36, adsorption of the reduction product of the depolarizer may occur.

The diffusion coefficient (D) was calculated using the Ilkovic equation [25] and was found to be 2.72×10^{-7} cm². S⁻¹ in BRb of pH 8.36 (Table 2).

Solutions of ofloxacin in BRb of pH 8.36 containing 20% methanol were found to be stable for about 2 h, after which the waveheight began to decrease slowly.

The relation between the limiting current i_d (μ A) and the concentration, C (mM), was found to be rectilinear over the concentration range 5×10^{-5} – 5×10^{-4} M and 1×10^{-5} – 5×10^{-4} M in the DC_t and DPP modes, respectively.

$$C = 0.0002 + 0.838i_d \quad (r = 0.99998)$$

using DC_t mode, and

$$C = -0.0002 + 0.774i_d \quad (r = 0.99999)$$

using DPP mode respectively, with a minimum detectability of 3×10^{-7} M (S/N = 3).

The diffusion current constant [$I_d = i_d/C$ m^{2/3} t^{1/6}] was calculated at 25° and found to be 0.63 ± 0.01 .

3.2. Number of electrons involved in the electrode reaction

The number of electrons consumed during the reduction was accomplished through comparison of the waveheight of ofloxacin with that obtained from an equimolar solution of a closely related compound, i.e. nalidixic acid [26]. In BRb of pH

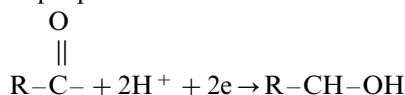
Table 2
Correlation between concentration and limiting current in the DC_t mode

No.	Concentration (mM)	Current (μA)	i_d/C (μA mM ⁻¹)	$I_d i_d/cm^{2/3} t^{1/6}$
1	5×10^{-2}	0.060	1.20	0.65
2	0.10	0.119	1.190	0.856
3	0.20	0.237	1.185	0.853
4	0.30	0.359	1.197	0.861
5	0.40	0.475	1.188	0.855
6	0.50	0.597	1.194	0.859
\bar{x}			1.192	0.858
±SD			0.005	0.004

NB: The results are the average of 18 separate determinations.

8.36 both compounds gave one peak of the same height pointing out to a two electron transfer process.

Based on these facts, the following mechanism is proposed.



3.3. Analytical application

Polarogram of ofloxacin in BRb of pH 8.36 exhibits cathodic wave. The current is diffusion-controlled and proportional to the concentration over a convenient range of concentration. Both DC_t and DPP modes were successfully applied to the assay of ofloxacin in commercial tablets (200 mg-tablet) and the results obtained are shown in Table 3. The percentage recoveries based on the average of nine separate determinations were 98.5 ± 0.4 and 99.01 ± 0.3 , respectively. The results obtained were favourably compared with a

reference [5] was 98 ± 0.5 based on measuring the native fluorescence of ofloxacin in 1 M sulphuric acid at 512 nm after excitation at 298 nm. Statistical analysis [27] of the results obtained by both methods using the Student *t*-test and Variance Ratio *F*-test, shows no significant difference between the performance of the two methods regards the accuracy and precision, respectively (Table 3).

Ofloxacin is given by mouth in doses of 200–400 mg daily. It is metabolized to desmethyl and *N*-oxide metabolites. It is eliminated mainly by the kidneys. Excretion is affected by tubular secretion and glomerular filtration, and 75–80% of the dose is excreted unchanged in the urine over 24–48 h, resulting in high urinary concentration [28] (Table 4).

The DPP mode could be successfully applied to the determination of ofloxacin in urine over the concentration range of 4–180 μg ml⁻¹. Thus the proposed study could be applied to the determination of ofloxacin in spiked urine. The results are

Table 3
Statistical analysis of the results obtained by the proposed and reference method for pure sample of ofloxacin

Method	DC _t	Reference method [29]	DPP mode
(1) Number of experiments	6	3	8
(2) Mean found (%)	100.09	100.03	99.90
(3) Variance	0.32	0.08	0.30
(4) Students <i>t</i> -value		0.17 (2.365)	0.38 (2.262)
(5) Variance ratio <i>F</i> -test		4.0 (5.79)	3.75 (4.74)

NB: Figures in parentheses are the tabulated *t*- and *F*-values, respectively, at *P* = 0.05 [27].

Table 4
Assay of ofloxacin in commercial tablets using the proposed and a reference method

No.	DC _t	DPP	Reference method [5]
1	98.89	99.28	
2	98.15	99.0	
3	98.50	98.75	
<i>x</i>	98.5	99.01	98.60
±SD	0.40	0.30	0.40
	<i>t</i> = 0.28	<i>t</i> = 1.48	<i>t</i> = (2.78)
	<i>F</i> = 1.14	<i>F</i> = 2.29	<i>F</i> = (19.00)

*Tarivid tablets (ofloxacin, 200 mg/tablets), product of Hoechst Orient Pharm., Cairo, Egypt.

NB: Figures in parentheses are the tabulated *t* and *F* values, respectively, at *P* = 0.05 [27].

abridged in Table 5. It can also be adopted for the pharmacokinetic studies of ofloxacin.

The within-day precision was evaluated through replicate analysis of urine samples spiked with ofloxacin at certain concentration level. The percentage recoveries based on the average of four separate determinations were 97.36 ± 0.73 , the corresponding RSD% was 0.75 indicating high precision of the method. The between-day precision was also evaluated as proceeding above. The percentage recoveries based on the average of four separate determinations were 96.25 ± 1.62 , the corresponding RSD% was 1.68 indicating also the high precision of the method.

Table 5
Polarographic determination of ofloxacin in spiked urine using DPP mode

Concentration (mM)*	% found	
mM (taken)	mM (found)	Proposed method
0.05	0.0484	96.80
0.08	0.0769	96.13
0.10	0.0966	96.60
0.20	0.1943	97.15
<i>x</i>		96.67
±SD		±0.43

*Average of at least three triplicate determinations.

References

- [1] K. Sato, U. Matura, M. Inone, T. Ueno, Y. Osada, H. Ogawa, M. Mitshuhashi, *Antimicrob. Agents Chemother.* 22 (1982) 548.
- [2] N. Ichihara, H. Tachizawa, M. Tsumura, T. Une, K. Sato, *Chemotherapy*, Tokyo 32 (1984) 118.
- [3] D.S. Lee, H.J. Han, K. Kim, W.B. Park, J.K. Cho, J.H. Kim, *J. Pharm. Biomed. Anal.* 12 (1994) 157.
- [4] G. Garlucci, P. Mazzeo, T. Fantozzi, *Anal. Lett.* 26 (1993) 2193.
- [5] F.A. Elyazbi, *Spectros. Lett.* 25 (1992) 279.
- [6] Y. Fujitta, I. Mori, K. Fujitta, Y. Nakahashi, T. Tanaka, *Chem. Pharm. Bull.* 35 (1987) 5004.
- [7] S.C. Mathur, Y. Kumar, N. Murugesau, Y.K.S. Rathore, P.D. Sethi, *Indian Drugs* 29 (1992) 376.
- [8] A. Mizuno, T. Uematsu, M. Nakashima, *J. Chromatogr.* 653 (1994) 187.
- [9] R. Jain, C.L. Jain, *Liq. Chromatogr.–Gas Chromatogr.* 10 (1992) 707.
- [10] D.K. Xu, A.Z. Ding, Y.S. Yuan, Y. Diao, *Yaouxue. Xuebao* 27 (1992) 462; *A.A. Thro* 55 8G (1993) 112.
- [11] A. Le Cogenic, R. Bidault, R. Farinotti, A. Dauphin, *J. Chromatogr.* 434 (1988) 320.
- [12] K. Matsu Bayashi, T. Une, Y. Osada, *J. Chromatogr.* 495 (1989) 354.
- [13] D.J. Griggs, R. Wise, *J. Antimicrob. Chemother.* 24 (1989) 437.
- [14] T. Ohkubo, T. Nambara, *J. Chromatogr.* 527 (1990) 441.
- [15] O. Oka Zaki, H. Aoki, H. Hakus, *J. Chromatogr.* 563 (1991) 31.
- [16] T. Ohkubo, M. Kudo, K. Sugawara, *Anal. Sci.* 7 (1991) 741.
- [17] T. Ohkubo, M. Kudo, K. Sugawara, *J. Chromatogr.* 573 (1992) 289.
- [18] M.R. Lockley, R. Wise, J. Dent, *J. Antimicrob. Chemother.* 14 (1984) 647.
- [19] A. Tamer, *Anal. Chim. Acta.* 231 (1990) 129.
- [20] G. Zhou, J. Pan, *Anal. Chim. Acta.* 307 (1995) 49.
- [21] J. Heyrovsky, P. Zuman, in: *Practical Polarography*, Academic Press, New York, 1968, pp. 163, 179.
- [22] L. Meites, Y. Israel, *J. Am. Chem. Soc.* 83 (1961) 4903.
- [23] P. Delahy, in: *New Instrumental Methods in Electrochemistry*, Interscience, New York, 1953.
- [24] J. Prosz, V. Cielezky, K. Gyorburo, in: *Polarographie Text Book*, Akademia Kiado, Budapest, 1987, p. 385.
- [25] J. Heyrovsky, J. Kuta, in: *Principles of Polarography*, Czechoslovak Academy of Science, Prague, 1965, p. 82.
- [26] W.J. Vaoort, R.H.A. Sorel, D. Brusse, S.G. Schulman, P. Zuman, *J. Denhartigh, Anal. Chem. Acta.* 149 (1983) 175.
- [27] J.D. Hichen, *Practical Statistics for Research*, Methuen, London, 1969.
- [28] J.G.F. Reynolds (Ed), Martindale, *The Extra-Pharmacopeia*, 30th ed., The Pharmaceutical Press, London, 1993.
- [29] *The United States Pharmacopeia XXII*, National Formulary XVII, Rockville, USA Convention, 1990, pp. 912, 963.

Taurine as a ligand. An investigation of Ag(I)– and Cd(II)–taurine complex equilibria by direct and competitive techniques, and use of the Ag(I)–taurine complex electrode to assess taurine in solution

Emilio Bottari *, Maria Rosa Festa

Dipartimento di Chimica, Università 'La Sapienza', P. le A. Moro 5, 00185 Roma, Italy

Received 5 May 1997; accepted 4 August 1997

Abstract

The behaviour of taurine as a ligand (L) towards silver(I) and cadmium(II) was studied at 25°C and in 1 mol dm⁻³ NaClO₄, as a constant ionic medium. Experimental data, obtained for both cations from electromotive force measurements performed by using silver and cadmium amalgam and glass electrodes, were explained by assuming the formation of the AgL, AgL₂, CdL, and CdL₂ complexes. The taurine protonation constant and stability constants of the above complexes were determined. The cadmium(II)–taurine system was investigated by determining the free concentration of taurine from the Ag electrode potential and the knowledge of equilibria existing between silver(I) and taurine. Experimental data obtained from this approach were explained by assuming the presence of the above species with very close stability constant values. The success of this method supports the possibility of using the Ag/Ag–taurine, taurine electrode to measure the free concentration of taurine in its solutions. © 1998 Elsevier Science B.V. All rights reserved.

Keywords: Silver electrode; Silver(I)–taurine complexes; Cadmium(II)–taurine complexes; Free concentration taurine measurement

1. Introduction

Generally, aminoacids develop their basic and acid function through the –NH₂ and carboxylic groups, respectively. On the contrary, taurine contains an aminic and a –SO₃⁻ group. However, its ligand properties depend on the presence of the

aminic nitrogen atom so that it acts as a monodentate ligand.

In the human body taurine is conjugated with bile cholic acids and forms taurodeoxycholic and taurocholic acids with deoxycholic and cholic acids, respectively. Micellar aggregates of the former bile cholic salts have been previously investigated [1,2].

Although taurine is a simple compound, only few studies can be found in the literature on its

* Corresponding author. Tel.: +39 6 49913643; fax: +39 6 490631; e-mail: BOTTARI@AXRMA.UNIROMA1.IT

behaviour as a ligand towards cations. This is probably due to the poor stability of its complexes. Only five papers deal with stability constants of taurine complexes [3,4].

Albert [5] studied the complex formation of taurine with cobalt(II) and copper(II) at 20°C. In 1959, Datta et al. [6] investigated the complex formation between silver(I) and taurine at 25°C. Both groups performed electromotive force (e.m.f.) measurements in solutions at low ionic strength (about 0.01 mol dm⁻³) in order to determine the taurine protonation and complex formation constants. In 1972, van Poucke et al. [7] studied equilibria occurring between silver(I) and taurine at 25°C and in 0.5 mol dm⁻³ KNO₃. They explained their glass electrode e.m.f. measurements assuming the presence of two complexes, 1:1 and 1:2, with logarithm of stability constants 2.97 and 6.15, respectively.

More recently, equilibria between taurine (L) and both calcium(II) and nickel(II) were investigated. For calcium(II), the formation of CaL (log β = 0.217) and CaHL (log β = 8.426) was assumed to explain nuclear magnetic resonance (NMR) and electron spin resonance (ESR) data [8]. In the case of nickel(II) [9], e.m.f. measurements carried out with a glass electrode at 25°C in 0.1 mol dm⁻³ NaClO₄ or LiClO₄, were explained by assuming the existence of the only species, NiL, with stability constant log β = 3.62.

The aim of this research is to investigate the properties of taurine as a ligand with several cations in a wide range of concentration of the reagents. To this purpose, we decided to adopt the constant ionic medium method proposed by Biedermann and Sillén [10] to minimise the activity coefficient variations due to the change of the concentrations of the reagents. The conditions are 25°C and 1 mol dm⁻³ NaClO₄, as an ionic medium.

Complex formation between silver(I) and taurine was studied for several purposes. Only two reports are present in the literature and they do not agree with each other. Moreover, they were not performed at 25°C and 1 M NaClO₄, one was carried out at a very dilute ionic strength. Furthermore, the high redox potential of the Ag⁺/Ag couple allows the use of this electrode to investi-

gate the behaviour of taurine as a ligand towards other cations. This can be very useful when the free concentration of the cation cannot be measured at equilibrium, using an amalgam electrode.

The protonation of taurine (L⁻ = C₂H₆NO₃S⁻) and equilibria taking place between silver(I) and taurine were characterized together with the relative stability constants. From the knowledge of the silver(I)–taurine system, a silver electrode in a silver(I)–taurine solution provides the free concentration of taurine, *c_L*. The possibility of such an electrode to work as an indicator of taurine was verified. To this purpose the cadmium(II)–taurine system was studied following two independent procedures. First, cadmium amalgam and glass electrodes were employed. The same system was then investigated by using glass and Ag/Ag–taurine, taurine electrodes. Comparison of the results obtained with both procedures supports the reliability of the response of the taurine electrode.

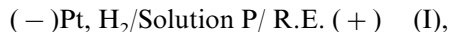
2. Experimental

2.1. Method

The behaviour of taurine as a ligand was studied using different approaches. The first step of the analysis involved the determination of the taurine protonation and of the silver(I)–taurine complex constants. The second step was the characterization of the cadmium(II)–taurine system using both a direct (cadmium amalgam) and competitive (silver–taurine electrode) technique.

2.1.1. Protonation of taurine (L⁻)

Knowledge of the taurine protonation is necessary to study the complex formation of taurine with silver(I) and cadmium(II). The protonation of taurine was studied at 25°C by measuring the e.m.f. of the following cell:



where Pt, H₂ is a H₂ electrode, R.E. is the reference electrode previously described [11], and the e.m.f. is measured as a function of $0 \leq C_L \leq 0.05$ mol dm⁻³, $0.00 \leq C_H \leq 0.1$ mol dm⁻³ and $12 \geq -\log c_H \geq 2$.

Solution P has the following general composition: C_H M in H^+ , C_L M in taurine, $(1.00 - C_H)$ M in Na^+ and 1 M in ClO_4^- .

The analytical excess of hydrogen ions is indicated with C_H . Capital and small C_x indicate the total and free concentration of the x species, respectively.

2.1.2. The silver(I)–taurine system

In order to investigate equilibria taking place between silver(I) and taurine, the e.m.f. of the following galvanic cells was measured:



where Ag E. and G.E. are silver and glass electrodes, respectively and R.E. is the reference electrode. Solutions S were prepared in a constant ionic medium, 1 mol dm^{-3} $NaClO_4$, with the following general composition: C_{Ag} M in Ag^+ , C_H M in H^+ , C_L M in taurine, $(1 - C_{Ag} - C_H)$ M in Na^+ , 1 M in ClO_4^- .

According to Biedermann and Sillén [10], in a constant ionic medium, it is possible to substitute concentrations per activities, so that the e.m.f. of cell (II) and (III) at 25°C and in mV units, can be written as follows:

$$E_{II} = E_{II}^{\circ} + 59.16 \log c_{Ag} + E_j; \quad (1)$$

$$E_{III} = E_{III}^{\circ} + 59.16 \log c_H + E_j. \quad (2)$$

C_{Ag} , C_H and c_{Ag} and c_H indicate the total and free silver and hydrogen ion concentrations, respectively. In Eqs. 1 and 2, E_{II}° and E_{III}° are related to the activity coefficients γ through the relations:

$$E_{II}^{\circ} = E'_{II} + 59.16 \log \gamma \text{ and}$$

$$E_{III}^{\circ} = E'_{III} + 59.16 \log \gamma.$$

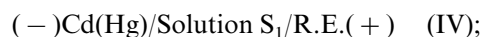
The activity coefficients are held constant by the presence of an ionic medium. E_{II}° and E_{III}° which are constant and E_j , which represents the liquid junction potential, were first determined in the absence of the ligand, when $C_{Ag} = c_{Ag}$ and $C_H = c_H$. E_j depends only on c_H in acid solutions. In the investigated experimental conditions, $E_j = -60 c_H$. Then C_{Ag} and C_H were kept constant while the total concentration of the ligand, C_L ,

was gradually increased and E_{II} and E_{III} were measured for each point.

The experimental data obtained from this approach were the analytical concentration of silver(I), hydrogen ions, and taurine, C_{Ag} , C_H and C_L respectively, and the free concentration of silver(I) and hydrogen ions, c_{Ag} and c_H , obtained directly by measuring the e.m.f.

2.1.3. The cadmium(II)–taurine system (cadmium amalgam)

Equilibria taking place between cadmium(II) and taurine were studied at 25°C in 1 mol dm^{-3} $NaClO_4$ by measuring the e.m.f. of the following galvanic cells:



where Cd(Hg) is a cadmium amalgam electrode and the other symbols have the same meaning as above. Solutions S_1 has the following general composition: C_{Cd} M in Cd^{2+} , C_H M in H^+ , C_L M in taurine, $(1 - 2C_{Cd} - C_H)$ M in Na^+ , 1 M in ClO_4^- .

According to Biedermann and Sillén [10] the e.m.f. of cell (IV) and (V), at 25°C and in mV units, can be written as follows:

$$E_{IV} = E_{IV}^{\circ} - 29.58 \log c_{Cd} - E_j;$$

$$E_V = E_V^{\circ} + 59.16 \log c_H + E_j.$$

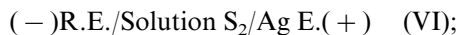
The procedure followed to obtain E_{IV}° , E_V° , c_{Cd} and c_H was similar to that described in Section 2.1.2.

The experimental data obtained through this approach were the analytical concentrations of cadmium and hydrogen ions, C_{Cd} and C_H , respectively, and the free concentrations of cadmium(II) and hydrogen ions, c_{Cd} and c_H , respectively.

2.1.4. The cadmium(II)–taurine system (silver–taurine electrode)

The hypothesis was formulated that a silver electrode dipped in a taurine solution can work as a taurine electrode. From the knowledge of the silver(I)–taurine system, studied above, and from the potential of the silver electrode it should be possible to obtain the free concentration of taurine.

To verify this hypothesis the cadmium(II)–taurine system previously studied using glass and cadmium amalgam electrodes, was further investigated with the glass and the silver(I)–taurine electrodes. Comparison of the results obtained by these two procedures supported the validity of the hypothesis. To this purpose the e.m.f. of the following cells was measured:



The symbols indicate the same electrodes as above, but solution S_2 had the following general composition: C_{Ag} M in Ag^+ , C_{Cd} M in Cd^{2+} , C_{H} M in H^+ , C_{L} M in taurine, $(1 - C_{\text{Ag}} - 2C_{\text{Cd}} - C_{\text{H}})$ M in Na^+ , 1 M in ClO_4^- .

The e.m.f. can be expressed at 25°C and in mV units, by equations similar to (Eq. (1)) and (Eq. (2)). E_{VI}° , E_{VII}° and E_j were determined in the first part of each measurement in the absence of taurine, but in the presence of cadmium(II). From several preliminary e.m.f. measurements it was deduced that appreciable concentrations of other cations such as cadmium(II), copper(II), nickel(II), cobalt(II) (cation/silver concentration ratio up to 10), did not interfere with the response of the silver electrode. E_{VI}° and E_{VII}° values did not change in the presence of the above cations.

Table 1 shows an example of the trend of E_{VI}° of the silver electrode, in the presence of increasing concentrations of copper(II). Even increasing the $C_{\text{Cu}}/C_{\text{Ag}}$ ratio up to 10, the E_{VI}° values are constant within ± 0.03 mV.

After the determination of E_{VI}° , E_{VII}° and E_j , an

Table 1

The response of the silver electrode in the presence of increasing concentration of copper(II)

E_{Ag} (mV)	C_{Ag} (mol dm ⁻³) $\times 10^3$	C_{Cu} (mol dm ⁻³) $\times 10^3$	E_{Ag}° (mV)
231.93	0.414	2.86	254.59
244.61	0.678	5.46	254.58
250.97	0.867	7.83	254.63
254.85	1.009	10.0	254.63

Average value, $E_{\text{Ag}}^\circ = 254.61 \pm 0.03$.

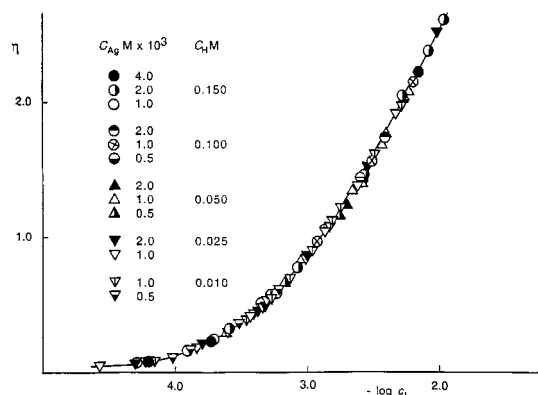


Fig. 1. Complex formation between taurine and silver(I). The curve is calculated with the constants of Table 2.

alkaline solution containing taurine was added to reach the selected values of C_{L} and $-\log c_{\text{H}}$, by keeping constant C_{Ag} . The e.m.f. of the cells was measured by keeping C_{L} , C_{Ag} and $-\log c_{\text{H}}$ constant and by increasing gradually C_{Cd} until a slight cloudiness was observed. The values of C_{H} were calculated for each point.

The experimental data obtained from this procedure were the C_{L} , C_{Ag} , C_{Cd} and C_{H} analytical values, and the c_{H} , and c_{Ag} measured directly by means of cell (VI) and (VII).

2.2. Materials and analysis

Silver(I) perchlorate was prepared by dissolving Ag_2O in a slight excess of dilute HClO_4 . Silver oxide was prepared by adding a slight excess of carbonate free NaOH to a dilute solution of AgNO_3 , BDH p.a., recrystallized from water. The oxide obtained was washed with bidistilled water at least 25 times, until neutrality.

The standard solution was filtered through a gooch (G3) and kept in dark glass, away from the light.

The total silver(I) concentration, C_{Ag} , was determined volumetrically and potentiometrically against NaCl . The results of several determinations agreed better than $\pm 0.1\%$. The analytical excess of hydrogen ions, C_{H} , was determined potentiometrically, according to Gran [12].

NaClO_4 , HClO_4 , NaOH and $\text{Cd}(\text{ClO}_4)_2$ were prepared and analysed as described before [13,14].

2.3. Details on the e.m.f. measurements

Cadmium amalgam (0.01%) was prepared as previously described [14]. Silver electrodes were prepared coulometrically by covering a Pt wire used as a cathode, with electrolytic silver, flowing a 0.1 mA current for about 10 h through a 1% $\text{KAg}(\text{CN})_2$ solution. Electrodes of different lengths (between 1.0 and 2.5 cm), gave responses in good agreement. Potential values measured from two different silver electrodes dipped in the same solution agreed within ± 0.05 mV.

The other experimental apparatus included an electronic voltmeter Keithley mod. 199, pHM 65 Radiometer and mod. 654 Metrohm equipped with hydrogen and glass electrodes, respectively. Salt bridge, reference electrode and all the other details of the e.m.f. measurements are similar to those described earlier [11].

All measurements were performed at 25°C. All solutions containing silver ions were kept away from the light. Their analysis was carried out in red light to avoid the photochemical decomposition of silver ions. In these conditions, the e.m.f. values of the cell containing silver ions were constant within 30 min after each new addition and remained stable (within ± 0.10 mV) for several hours, even at low C_{Ag} concentration ($\geq 0.1 \times 10^{-3}$ M). In white light, the e.m.f. values never reached stable values, but a slow drift of 0.02 mV per 1–2 min was observed. After each series of e.m.f. measurements, the Ag electrodes were thoroughly washed with NH_3 and kept in bidistilled water overnight. Electrodes prepared as previously described gave correct responses even after a few months from their preparation, if washed and kept correctly.

A stream of nitrogen (99.999%) was bubbled through the solutions throughout the measurements to prevent the absorption of CO_2 .

The response of the glass electrodes was checked against that of a H_2 electrode, assumed to be correct. Both measured values agreed within ± 0.1 mV up to $-\log c_{\text{H}} \leq 9$, while beyond this c_{H} , the glass electrode showed remarkable deviations. In order to study the protonation of taurine a H_2 electrode was used. H_2 (99.999%) was supplied by cylinders.

3. Results

The results of the present investigation will be given after the style of Section 2.1

3.1. Protonation of taurine

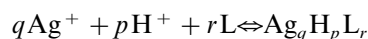
Taurine shows two possible protonation steps, the first corresponding to the $-\text{NH}_2$ and the second to the $-\text{SO}_3^-$ group. In the range of concentrations studied we were able to appreciate only the protonation of the aminic group.

As the protonation function is independent of the total taurine concentration, no appreciable evidence of polynuclear species was found, as expected. The experimental data were explained by assuming the presence of HL with protonation constant $\log K_1 = 9.01 \pm 0.02$, where $K_1 = c_{\text{HL}} / (c_{\text{H}} c_{\text{L}})^{-1}$.

No reliable values were obtained for K_2 , as solutions with a sufficient fraction of H_2L^+ , can be obtained only at very high C_{H} values. At such C_{H} it was hard to assume that the activity coefficients were constant, as the composition of the ionic medium changed markedly. This did not involve any loss of accuracy, because only $\log K_1$ was used in further calculations.

3.2. The silver(I)–taurine system

Several series of measurements were carried out at $C_{\text{H}} = 0.01, 0.025, 0.05, 0.1$ and 0.15 mol dm^{-3} and $C_{\text{Ag}} = 0.5, 1, 2, 4 \times 10^{-3} \text{ mol dm}^{-3}$. Without a preliminary hypothesis, it can be assumed that the reagents participate to the general equilibrium:



with the stability constant $\beta_{q,p,r}$, where $q \geq 1, p \leq 0, \geq 0, r \geq 1$.

Experimental data were elaborated to determine the q, p, r prevailing values and the relative equilibrium constants. From the mass balance of silver ion, taking into account the mass action law, the following equation can be written:

Table 2
Species formed by taurine with silver(I) and cadmium(II)

Cation		Species ML		Species ML ₂	
Ag ⁺		3.53 ± 0.07	Graphic	6.47 ± 0.05	Graphic
		3.53 ± 0.05	BSTAC	6.48 ± 0.01	BSTAC
		3.53 ± 0.05	Proposed value	6.48 ± 0.05	Proposed value
Cd ²⁺	Cd amalgam	2.05 ± 0.10	Graphic	3.74 ± 0.08	Graphic
		2.01 ± 0.08	BSTAC	3.78 ± 0.03	BSTAC
		2.01 ± 0.08	Proposed value	3.78 ± 0.05	Proposed value
Cd ²⁺	Ag/Ag(I)–taurine	2.00 ± 0.10	Graphic	3.78 ± 0.10	Graphic
		2.1 ± 0.12	BSTAC	3.8 ± 0.1	BSTAC

The stability constant values are expressed as $\log \beta_{1,0,r}$. Protonation constant $\log K_1 = 9.01 \pm 0.02$

The error limits relative to the constants obtained by the graphic method correspond to the maximum difference possible with a still acceptable agreement between experimental and calculated data. The SD is reported in the other cases.

$$\eta = \log(C_{Ag}/c_{Ag})$$

$$= \log(1 + \sum \sum \sum q\beta_{q,p,r} c_{Ag}^{q-1} c_H^p c_L^r) \quad (3)$$

For the analysis of the experimental data it was necessary to calculate the ligand free concentration c_L , which was obtained from the mass balance of C_H , taking into account the mass action law:

$$C_H = c_H + K_1 c_H c_L + \sum \sum \sum p\beta_{q,p,r} c_{Ag}^q c_H^p c_L^r \quad (4)$$

In Eqs. 3 and 4 hydrolytic species of silver were considered negligible on the basis of the previous results [15,16]. As a first approximation the hypothesis was formulated that the presence of complexes involving protons was negligible. As a consequence, the last term of Eq. (4) could be neglected for the calculation of c_L . The validity of this hypothesis was demonstrated a posteriori.

The function η versus $-\log c_L$ is plotted for each experimental point in Fig. 1. Note that independently of C_{Ag} and C_H , all the points fall on the same curve. Therefore, the presence of polynuclear and mixed complexes involving protons can be discarded, i.e. $q = 1$ and $p = 0$. The trend of the experimental points can be explained by assuming the presence of the AgL and AgL_2 species, and the above formulated hypothesis can be assumed to be true.

By applying the normalized curve method [17] the values of the relative constants $\beta_{1,0,1}$ and $\beta_{1,0,2}$ were obtained. The equilibrium constant values were also obtained by analysing the experimental data with the BSTAC program [18]. In Table 2 the values obtained by graphical methods and those calculated by computer are collected and they are in good agreement. The constants of Table 2 were used to calculate the theoretical curve of Fig. 1. The agreement between experimental points and calculated curve is satisfactory.

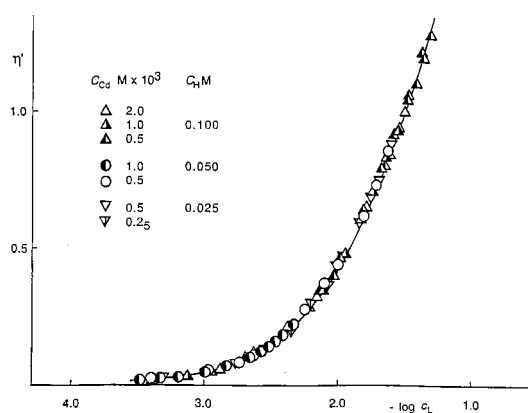


Fig. 2. Complex formation between cadmium(II) and taurine. The curve is calculated with the constants of Table 2. The points were obtained by using the cadmium amalgam electrode.

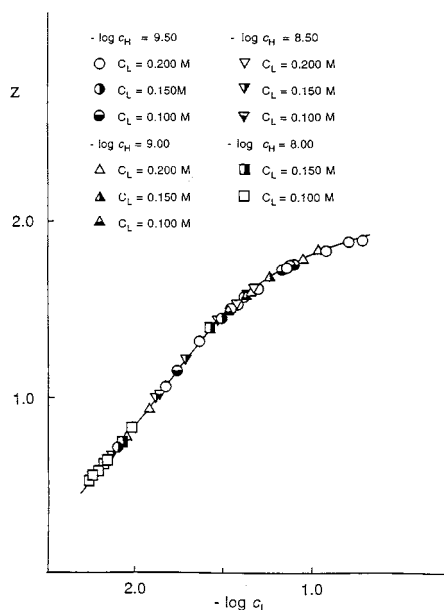


Fig. 3. Most of the points obtained by using Ag/Ag(I)–taurine, taurine electrode to study the cadmium(II)–taurine system. The curve is calculated by using the constants of Table 2.

3.3. The cadmium(II)–taurine system (cadmium amalgam)

Similarly to the above section, several series of experimental data were obtained at different $C_H = 0.025, 0.05, 0.1 \text{ mol dm}^{-3}$ and $C_{Cd} = 0.25, 0.5, 1$ and $2 \times 10^{-3} \text{ mol dm}^{-3}$.

Experimental data were elaborated by applying a treatment similar to the one explained before, but in this case mass balances of cadmium, C_{Cd} and hydrogen ion, C_H were considered.

In Fig. 2 the η' function ($\eta' = \log C_{Cd}/c_{Cd}$) is plotted as a function of $-\log c_L$. Also in this case, all the experimental points fall on the same curve independently of C_{Cd} and C_H . Polynuclear and mixed complexes involving protons are not present in appreciable concentrations.

Equilibria taking place between cadmium(II) and taurine can be accounted for by assuming the presence of the CdL and CdL_2 species.

In Table 2 the values of stability constants obtained by graphical and computer methods are reported. Also in this case the values are in good agreement. The curve in Fig. 2 was calculated

with the constant values of Table 2. The calculated curve and the experimental points are in satisfactory agreement, supporting the validity of the procedure adopted.

3.4. The cadmium(II)–taurine system (silver–taurine electrode)

Several series of e.m.f. measurements of cell (VI) and (VII) were carried out at $-\log c_H = 8, 8.5, 9$ and 9.5 and $C_L = 0.1, 0.15, 0.2 \text{ mol dm}^{-3}$. C_{Ag} was kept constant for each series and the cadmium(II) concentration was gradually increased until a slight colloidal precipitate was observed by the Tyndall effect.

These results were used to obtain prevailing species and relative constants to verify if the silver electrode dipped in a taurine solution works reversibly to give the free concentration of taurine, c_L .

From the C_{Ag} and c_{Ag} experimental data and from the knowledge of the silver(I)–taurine system, it was possible to calculate c_L , by using the mass balance equations relative to silver ions:

$$C_{Ag} = c_{Ag} + \beta_{1,0,1} c_{Ag} c_L + \beta_{1,0,2} c_{Ag} c_L^2 \quad (5)$$

On the other hand, by taking into account the range of C_H and c_H investigated, Eq. (4) could be written for all the points measured, as follows:

$$C_H = c_H + K_1 c_H c_L \sim K_1 c_H c_L \quad (6)$$

From the analytical concentrations of taurine and cadmium(II), the mass balance equation of taurine could be written, by taking into account the mass action law:

$$C_L = c_L + \beta_{1,0,1} c_{Ag} c_L + 2\beta_{1,0,2} c_{Ag} c_L^2 + C_H + ZC_{Cd} \quad (7)$$

In Eq. (7) all symbols are already explained. Z indicates the formation function, defined as the average number of ligands per central group, in this case cadmium(II). In the same equation, hydrolytic species of cadmium(II) were neglected on the basis of the results obtained by Biedermann and Ciavatta [19].

The experimental data in the form $Z(-\log c_L)$ plotted in Fig. 3 show that all the points fall on

Table 3

Stability constants ($\log \beta_{1,p,r}$) of complexes formed by cadmium(II) with taurine, ammonia [23] and glycine [22] at 25°C and in 1 mol dm⁻³ ClO₄⁻

		CdHL	CdL	CdL ₂	CdL ₃	CdL ₄
Taurine	(This work)	—	2.01	3.78	—	—
NH ₃	[23]	—	2.54	4.78	6.08	7.26
Glycine	[22]	10.52	4.36	7.99	10.13	—

the same curve independently of C_L , C_H , C_{Cd} and the ratio C_{Cd}/C_{Ag} . Polynuclear, mixed silver(I)–cadmium(II)–taurine complexes and complexes involving hydrogen ions can be excluded. Points at low Z could not be obtained as at $C_{Cd} \geq 3.5 \times 10^{-3}$ mol dm⁻³ a colloidal precipitate was detected. As $Z_{max} = 2$, two taurine molecules can be bound per cadmium(II), as expected from the approach carried out using the cadmium amalgam electrode. As only two species CdL and CdL₂ were formed, the formation function can be written as follows:

$$Z = (c_{CdL} + 2c_{CdL_2})/C_{Cd}$$

or

$$Z = (\beta_{1,0,1} c_L + 2\beta_{1,0,2} c_L^2)/(1 + \beta_{1,0,1} c_L + \beta_{1,0,2} c_L^2) \quad (10)$$

By applying the graphical method of normalized curves proposed by Sillén [17] the stability constants for the CdL and CdL₂ species could be obtained. On the other hand, experimental data introduced in the BSTAC [18] computer program, gave very close values. Both graphical and computed results are collected in Table 2. The values agree well with each other and the calculated curve obtained by using the constants of Table 2 fits well with the experimental data (Fig. 3).

4. Discussion

Different considerations can be formulated on the basis of the results of this paper. The first one refers to the behaviour of taurine as a ligand towards silver(I) and cadmium(II). No data were available from the literature at 25°C and in 1 mol dm⁻³ NaClO₄ as an ionic medium.

As taurine is a monodentate ligand, it cannot form chelate complexes, hence species with poor stability

are expected. The study of the complex formation of taurine and cations performed using only the glass electrode causes many difficulties, as it involves the competition between proton and cation for taurine. This competition takes place in the range $8 \leq -\log c_H \leq 10$, where taurine is partially deprotonated, but every cation can easily hydrolyse or even precipitate as hydroxide. For example, Leden [20] and Froneaus [21] used the ratio between total and free metal as a function of the ligand concentration to study complex formation by measuring the free concentration of the cation.

This paper shows that it is advantageous to measure directly the free concentration of the cation (with silver or cadmium amalgam electrodes, respectively) or that of the ligand (with the silver electrode).

Table 2 of this paper gives the stability constants of the AgL, AgL₂, CdL, and CdL₂ species.

The values of the stability constants for the CdL and CdL₂ species, obtained with cadmium amalgam and silver electrodes agree very well together. This result supports the validity of our procedure and allows the silver, silver(I)–taurine, taurine electrode to be used to perform direct measurements of the ligand free concentration. The high potential value of the Ag/Ag⁺ couple suggests that this procedure can be applied to many other cases. The presence of several cations, such as copper(II), cadmium(II), lead(II), nickel(II), and cobalt(II), does not interfere with the response of the silver electrode (see Table 1). This is advantageous if cations like calcium(II) and magnesium(II) are to be studied. We are applying this method to the investigation of the behaviour of taurine as a ligand towards such cations and this will be the subject of a next study.

A difficulty of this method is the low stability of silver(I) solutions when exposed to light. Otherwise, silver electrodes can be prepared very easily and can be used for a long time.

We were not able to find quantitative data in the literature on the complex formation between cadmium(II) and taurine.

Protonation constant of taurine was determined at very low ionic strength [5]. Our value, by taking into account the different experimental conditions, agrees with that of the literature (9.01 and 9.08, respectively). Also for silver(I), literature values were determined at ionic strengths 0.01 and 0.5 mol dm⁻³ KNO₃. The values proposed in this study are higher than those of the literature [6,7], but the latter disagree with each other. Only the value of log $\beta_{1,0,2}$ proposed for AgL₂ agrees with that proposed by Datta et al. [6], if the different experimental conditions are considered.

The behaviour of taurine can be compared with glycine and ammonia.

In Table 3 the values of this work and those of the constants of the complexes of cadmium(II) with glycine [22] and ammonia [23] obtained in the same experimental conditions, are collected and compared.

Only glycine is able to form complexes involving protons. There is no evidence of polynuclear complexes.

Ammonia forms four complexes, glycine three, and taurine only two. The values of $\beta_{1,0,1}$ and $\beta_{1,0,2}$ of taurine and NH₃ are of the same order of magnitude, while the complexes formed by glycine are far more stable. NH₃ can never be able to form chelates because it is an unidentate ligand. From values of the constants of species formed by taurine, it is confirmed that taurine is also not able to form chelates. This is in agreement with Ahrlund et al. [24] who asserted that the -SO₃⁻ group has few possibilities to be an electron donor and therefore the formation of chelate because of its presence it is very improbable.

The high capability of NH₃ to form complexes with respect to taurine can be explained by a probable bigger steric hindrance of the latter molecule.

5. Conclusion

This paper contributes to the knowledge of the behaviour of taurine as a ligand towards proton, silver(I), and cadmium(II).

Two independent procedures were used to study the cadmium(II)–taurine system and the agreement between these two approaches has proved the reliability of this method. For this reason it can be used to obtain the free concentration of taurine when it is not possible to measure the free concentration of the cation or when difficulties arise using the glass electrode.

Acknowledgements

This work was supported by Consiglio Nazionale delle Ricerche (CNR) and by Ministero dell'Università e della Ricerca Scientifica e Tecnologica (MURST) of Italy.

References

- [1] E. Bottari, M.R. Festa, *Analyst* 119 (1994) 469.
- [2] E. Bottari, M.R. Festa, *Langmuir* 12 (1997) 1777.
- [3] A.E. Martell, L.G. Sillén, *Stability Constants*, Special Publications no. 17, 25, The Chemical Society, London 1964, 1971.
- [4] L.D. Pettit, H.K. Powell, IUPAC, *Stability Constants: Database*, Academic Software, Timble, Otley, Yorks, UK, 1993.
- [5] A. Albert, *Biochem. J.* 47 (1950) 531.
- [6] S.P. Datta, A.K. Grzybowski, *J. Chem. Soc.*, 1091 (1959).
- [7] L. van Poucke, G. Thiers, Z. Eeckhaut, *Bull. Soc. Chim. Belge* 81 (1972) 357.
- [8] C.S. Irving, B.E. Hammer, S.S. Danyluk, P.D. Klein, *J. Inorg. Biochem.* 13 (1980) 137.
- [9] J. Maslowska, L. Chruscinski, *Polyhedron* 3 (1984) 1329.
- [10] G. Biedermann, L.G. Sillén, *Ark. Kem.* 5 (1953) 425.
- [11] E. Bottari, M.R. Festa, *Ann. Chim. (Rome)* 80 (1990) 217.
- [12] G. Gran, *Analyst* 77 (1952) 661.
- [13] E. Bottari, *Ann. Chim. (Rome)* 66 (1976) 139.
- [14] E. Bottari, *Mh. Chemie* 106 (1975) 451.
- [15] P.J. Antikainen, D. Dyrssen, *Acta Chem. Scand.* 14 (1960) 95.
- [16] S. Hietanen, L.G. Sillén, *Ark. Kem.* 32 (1970) 111.
- [17] L.G. Sillén, *Acta Chem. Scand.* 10 (1956) 186.
- [18] C. De Stefano, P. Mineo, C. Rigano, S. Sammartano, *Ann. Chim. (Rome)* 83 (1993) 243.
- [19] G. Biedermann, L.G. Ciavatta, *Acta Chem. Scand.* 16 (1962) 2221.
- [20] I. Leden, *Sven. Kem. Tidskr.* 56 (1944) 31.
- [21] S. Froneaus, *Acta Chem. Scand.* 4 (1950) 72.
- [22] E. Bottari, *Ann. Chim. (Rome)* 66 (1976) 677.
- [23] I. Leden, *Diss. Lund* 1943, p. 112.
- [24] S. Ahrlund, J. Chatt, N.R. Davies, A.A. Williams, *J. Chem. Soc.*, 264 (1954).

Degradation of ampicillin in the presence of cadmium (II) ions

Ana Márquez García^b, Pilar Gutiérrez Navarro^{a,*}, Pedro J. Martínez de las Parras^a

^a Department of Physical Chemistry, Faculty of Pharmacy, University of Granada, E-18071 Granada, Spain

^b Department of Physical and Analytical Chemistry, University of Jaen, Jaen, Spain

Received 28 January 1997; received in revised form 28 July 1997; accepted 5 August 1997

Abstract

Cadmium (II) ion-catalyzed degradation of ampicillin in methanol at 20°C has been studied. It has been observed that the rate values tend to saturate when the concentration of ampicillin or the metal ion is increased. The results obtained in the present study suggest that ampicillin degradation occurs through the formation of a 1:1 (SM) and 2:1 (S₂M) ampicillin–metal complexes. These complexes decompose giving a single product (absorption maximum at 285 nm; $\epsilon_p = 1.82 \times 10^4 \text{ l mol}^{-1} \text{ cm}^{-1}$) that has been isolated and identified $(\text{Cd}^{\text{II}} (\text{L}^{2-})_2 (\text{H}_2\text{O})_4 \text{ Na}_2)$. The appearance of this product reflects a first order reaction with respect to the 1:1 complex, with a rate constant of $3.87 \times 10^{-2} \text{ min}^{-1}$ and the existence of an equilibrium between the 1:1 and 2:1 initial complexes. The equilibrium constant value, calculated from kinetic data, is $1.7 \times 10^3 \text{ l mol}^{-1}$. © 1998 Elsevier Science B.V. All rights reserved.

Keywords: β -lactam; Ampicillin; Kinetics; Cadmium

1. Introduction

The opening of the β -lactam ring by a serine hydroxy group is thought to be the first chemical step in the reaction of penicillins and cephalosporins with transpeptidase and β -lactamase enzymes [1]. The first of these bacterial enzymes is the primary killing site for the lethal action of β -lactam antibiotics [2]. The second is the primary method of defence used by bacteria to resist these bactericides [3]. Both reactions are interpreted as hydroxylic addition across the β -lactamic bond to give a penicilloyl enzyme intermediate, an ester of penicilloic acid. The

β -lactamic bond is broken and the hydroxylic hydrogen atom migrates to the nitrogen atom of β -lactam amide. Because of the importance of the alcoholysis reaction with β -lactamic antibiotics quite a lot of theoretical and experimental research has been reported [4–6].

In the present study we describe the decomposition of ampicillin [I] in methanol medium catalyzed by Cd^{2+} , the latter, having a large ionic radius, is presumed to have a great catalytic effect. In order to obtain a kinetic scheme for the reaction, degradation kinetic data were used. The reaction occurs initially with the formation of two complexes of intact ampicillin and cadmium with stoichiometric values of 1:1 and 2:1 (ampicillin/cadmium), respectively. The complexes decompose due to the nucleophilic attack of the

* Corresponding author. Tel.: +34 58 243827; fax: +34 58 244090; e-mail: mpgn@platon.ugr.es

methanol molecule so that at the end of the reaction a single final product is obtained. The analytical results show that this compound is a complex formed by the binding of two molecules of penamaldate derivative of ampicillin (which precedes from antibiotic degradation) to a Cd^{2+} ion.

2. Experimental

Sodium ampicillin [I] (99% pure) was obtained from Aldrich. Methanol, CdCl_2 and $\text{Cd}(\text{NO}_3)_2 \cdot 4\text{H}_2\text{O}$ were from Merck. All other reagents used were of analytical grade.

2.1. Stoichiometric determination

The stoichiometry of the single reaction product of ampicillin degradation catalyzed by Cd^{2+} ions was determined using the continuous variation method on a long-term basis (24 h).

2.2. Long-term agreement with Beer's law and application of Coleman's test

Compliance with Beer's law was verified at 285 nm in two series of solutions in which the mole ratio between ampicillin and metal was kept constant at 2:1 and 2.3:1, respectively, while reagent concentration was varied. Absorbance measurements at 285 nm were carried out on a Spectronic 2000 spectrophotometer equipped with a Selecta thermostat ($\pm 0.1^\circ\text{C}$) 24 h after the preparation of these solutions, sufficient time for the kinetic reaction to end. Coleman's matrix method [7] was applied in graphic form to the absorbance data (A_{ij}) measured using a wide range of wavelengths. In this way, we determined the number of absorbent species at the end of the reaction. A_{ij} denotes the absorbance value of a particular solution j at a specific wavelength i . The entire set of absorbance data for each series of spectra was displayed as the matrix A_{ij} .

2.3. Kinetic measurements

The kinetic measurements were made by monitoring the appearance of a reaction product of ampicillin degradation at 285 nm on a Perkin Elmer Lambda 5 spectrophotometer equipped with a thermostatic cell holder.

The reaction was carried out using a series of methanolic solutions containing different excesses of ampicillin (ranging from 10 to 500×10^{-4} M), constant metal concentration (1×10^{-4} M), and also in ampicillin solutions of constant concentration (1×10^{-4} M) and different metal ion concentration (ranging from 2×10^{-5} to 2×10^{-3} M). The measurements were taken vs. methanol in 1 cm path length spectrophotometric cells.

In each kinetic experiment the reaction rate was calculated from the slope of the straight line obtained when the initial absorbance values were plotted vs. time, dA/dt , and from the molar absorptivity of degradation product, which is equal to $1.82 \times 10^4 \text{ l mol}^{-1} \text{ cm}^{-1}$. In the kinetic mixture which contained excess antibiotic (2000:1), a zero order rate constant was obtained from the 285 nm absorbance increase.

2.4. Isolation and analysis of the degradation product

A solution with 0.7427 g of sodium ampicillin and 0.3084 g of $\text{Cd}(\text{NO}_3)_2 \cdot 4\text{H}_2\text{O}$ in 50 ml of methanol (mole ratio 2:1) was kept at room temperature for 24 h. After the completion of the reaction, the solution was then evaporated in vacuum at room temperature and cooled to around 4°C obtaining a yellowish white precipitate. The solid was filtered, washed with methanol, ether and acetone, air-dried, and finally, dried in a vacuum desiccator with P_2O_5 .

Infrared spectra were recorded between 4000 and 400 cm^{-1} on a Nicolet 20SXB using potassium bromide pellets. $^1\text{H-NMR}$ and $^{13}\text{C-NMR}$ spectra were recorded at 300 MHz on a Bruker AM-300 spectrometer. The powdered sample was dissolved in DMSO-d_6 using TMS as reference. Chemical analysis was performed on Perkin Elmer 2380 atomic absorption equipment. An electron impact mass spectrum was carried out on

a Hewlett Packard HP-5988-A, with DIP: ramp of 25°C until 280°C (The electronic ionization was at 70 eV) and a LSIMS/FAB⁻ spectrum by bombardment with Cs⁺ ions in glycerol was carried on a mass spectrometer Micromass model AutoSpecEQ.

The results obtained were: C, 41.12; H, 4.95; N, 8.47; S, 6.49; Na, 4.60 and Cd, 11.40. δ_{H} , 1.35(6H, CH₃) 3.4(3H, OCH₃) 7.25 (5H, C₆H₅); δ_{C}^{13} : 30.58, 56.55, 57.41, 127.63, 127.97, 170.01, 203.50; ν_{max} (KBr/cm⁻¹) 1672, 1603 and 1385.

3. Results and discussion

Fig. 1 shows the spectra, of a methanol solution of ampicillin with Cd(II) ion at equimolar concentrations at different periods of time. The spectrum presents a steady rise in absorption, reaching a peak at 285 nm. The changes observed in the spectrum could be attributed either to the decomposition reaction kinetics of ampicillin or to a kinetic process in which a complex 1:1 was transformed with time to another complex 2:1, both formed by intact ampicillin coordinated with the

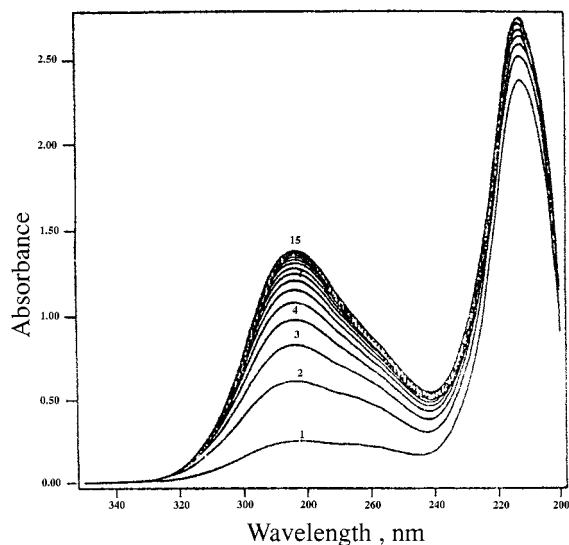


Fig. 1. Absorption spectra of sodium ampicillin (1.25×10^{-4} M) and cadmium chloride (1.25×10^{-4} M) in methanol (20°C). The curves are labelled at times 0, 5, 10, 15, 20, 25, 30, 35, 40, 45, 50, 55, 60 and 70 min of reaction.

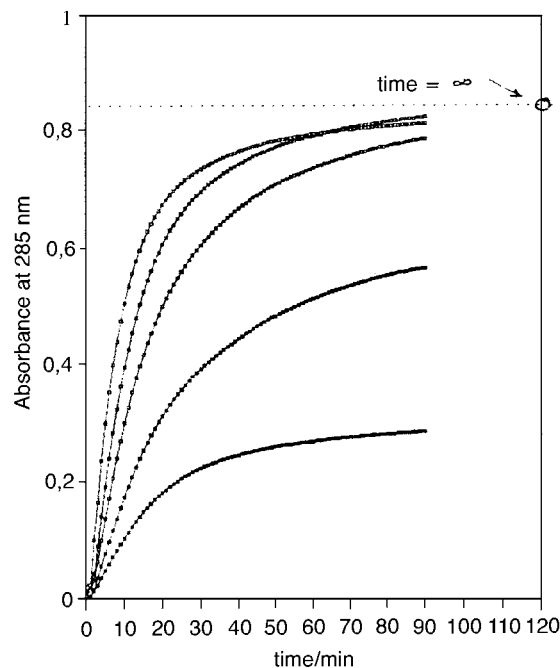


Fig. 2. Absorbance change vs. reaction time in the Cd²⁺ promoted methanolysis of ampicillin (1×10^{-4} mol dm⁻³) at 20°C: Cd²⁺ concentration (mol dm⁻³) 2×10^{-3} , 3×10^{-4} , 1×10^{-4} , 4×10^{-4} , 2×10^{-5} . Infinity time = 24 h.

Cd(II) ion. However, the second possibility can be ruled out, since it is known that metal ions catalyze the degradation of β -lactam compounds [6], in both methanolic and aqueous media.

The absorbance at 285 nm tends towards a constant value with time as can be seen in Fig. 2 where the spectrum at infinity was recorded. These absorbance values obtained at the end of the reaction are related to the initial concentrations of ampicillin and metal ion. Fig. 3 shows the absorbance values at infinity of kinetic mixtures with different mole ratio. We can see that the break point appears at a mole fraction value of ampicillin equal to 0.67. This value corresponds to a theoretical value for a 2:1 mole ratio. It suggests that at the end of the reaction a product, P with peak absorption at 285 nm, was formed by the binding of two molecules of an assumed ligand, produced as a result of ampicillin decomposition, to the Cd(II) ion(2:1). The shape of the plot in Fig. 3 also demonstrates that the forma-

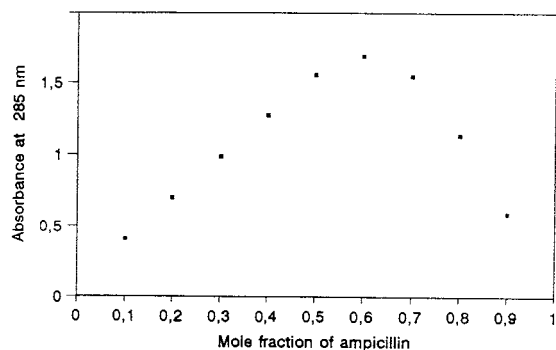


Fig. 3. Job's plot using absorbance values measured at the end of the reaction (24 h) at 20°C. The sum of the reactants was 2.5×10^{-4} M.

tion of the product occurs in a complete reaction, showing that the absorbance values are proportional to the reagent which is not present in excess.

At the end of the reaction, under the experimental conditions used, only the above mentioned 2:1 compound was formed. This fact was confirmed by Coleman's graphic test which was positive for a single absorbent species (Fig. 4). Thus, we applied the test to the spectrophotometric data

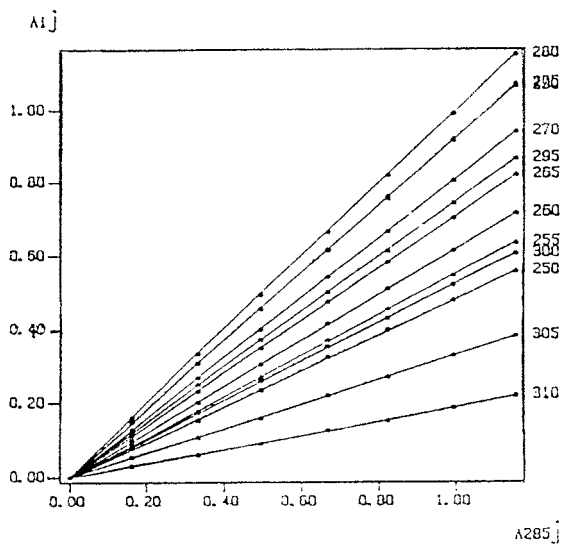
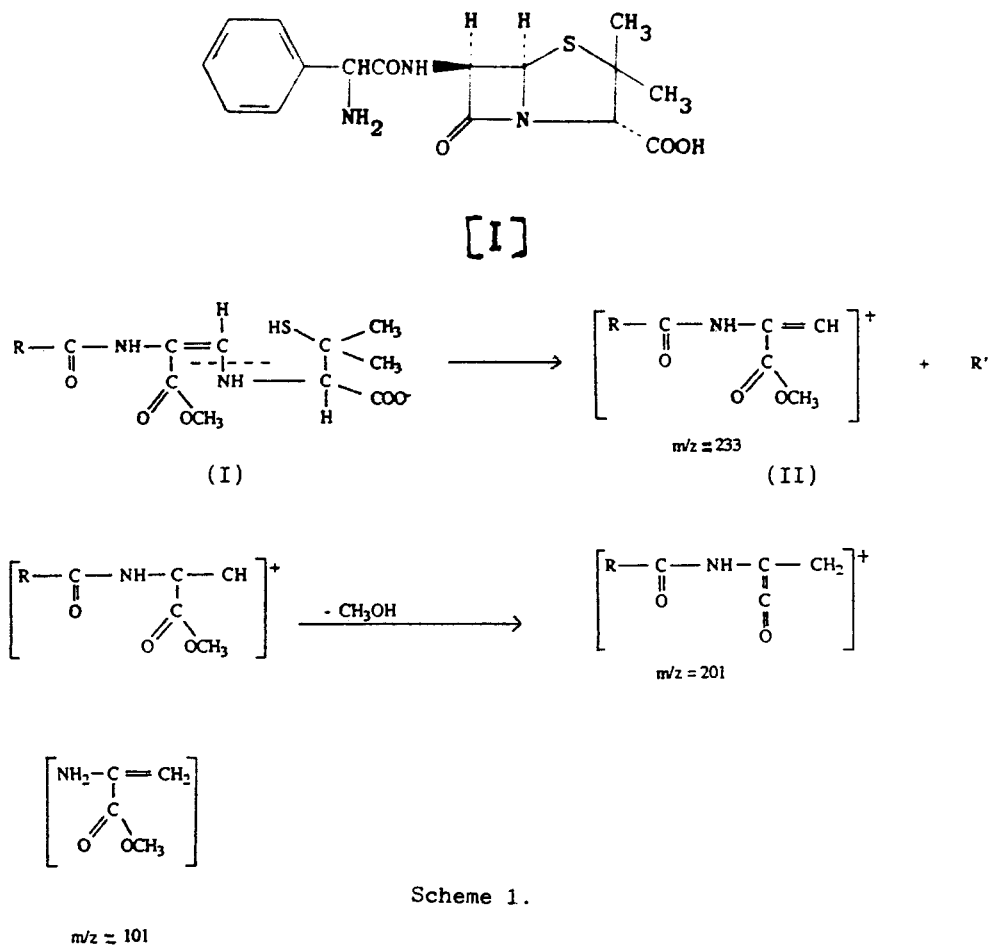


Fig. 4. Computer-assisted test for one species in the cadmium-ampicillin system, based on the absorbance data taken after 24 h of reaction, infinity time. (A_{ij} is the absorbance value of a solution j at a wavelength i).

corresponding to two series of methanolic solutions with varied concentration of reagents and constant mole ratios (ampicillin: Cd) at 2:1 and 2.3:1, respectively. We obtained a family of lines radiating from the origin when A_{ij} values were plotted vs. A_{285j} , as can be seen in Fig. 4. This group of lines agrees with Beer's law throughout the entire range of ultraviolet wavelengths, and gives evidence that at the end of the reaction a single reaction product is formed. Taking this fact into account and that absorbance due to excess ampicillin is negligible at the wavelength used. We can suppose that absorbance at infinity time is produced exclusively by the reaction product, P. Thus, the molar absorption coefficient, ϵ_p , was determined from the absorbance values at infinity time of kinetic solutions in the presence of excess ampicillin (from 4:1 to 16:1). The concentration of the product, P, was assumed to be equal to that of the Cd(II) ion, i.e. the reagent available in lower amounts in all kinetics experiments. The average value obtained for ϵ_p was $18\,162 \pm 276$ l mol⁻¹ cm⁻¹. The wavelength of maximum absorption (at 285 nm) and the value of the molar absorption coefficient can be associated with the formation of the penamaldate derivative of ampicillin [9–11] (formula 1 in Scheme 1).

This result is according to stoichiometry, L₂Cd(II), obtained by analyzing the isolated solid. The elemental analysis results of the compound obtained are consistent with the empirical formula: Cd^{II} (L²⁻)₂ (H₂O)₄, 989.30 g mol⁻¹. The two atoms of sodium probably form a salt through the carboxylate group. In addition, the spectrum UV as well as the molar absorption coefficient at 285 nm (1.9×10^4 l mol⁻¹ cm⁻¹) were the expected values according to the study made in solution.

The IR bands are consistent with the proposed structure. The characteristic band of the carboxylic group is observed at 1603 cm⁻¹ (ν_{as} COO⁻) and at 1385 cm⁻¹ (ν_s COO⁻). Moreover, the distance between the two bands, 218 cm⁻¹, is similar to that observed in the IR spectrum of the sodium salt of ampicillin. This fact justifies the presence of the sodium ion in the molecule of reaction product. The C=O (β -lactam) absorption is not observed near 1780 cm⁻¹.



Scheme 1. Fragmentation of the degradation product.

Nonetheless, a band appears at 1672 cm^{-1} , which can be attributed to an ester group. It indicates that the $\text{C}=\text{O}$ β -lactam is esterified in the ampicillin degradation product. The presence of the ester group is also confirmed from the $^1\text{H-NMR}$ spectrum, in which absorption at 3.4 ppm can be assigned to the protons of the methoxyl group [8]. In the $^{13}\text{C-NMR}$ spectrum a signal at 170.1 ppm can be observed. This signal relates to the carbon from the β -lactamic carbonyl group, which appears in ampicillin at 175.5 ppm [14]. This implies the breaking of the ampicillin molecule.

Fig. 5a shows the electron impact mass spectrum of the isolated solid at the end of the reaction. The proposed fragmentation mechanism for the forma-

tion of ion fragments with higher stability (m/z 233, 201 and 101) is depicted in Scheme 1. Aside from the above fragments, it is possible that the peak at m/z ratio 465 is probably due to the binding of two fragments (m/z 233) with the loss of a proton. This is not surprising if we take into account the high stability of fragment m/z 233. Ion fragments of m/z 261 would result from the loss of a $\text{R}-\text{C}=\text{O}$ group by the ligand molecule. Finally, the peak at m/z 344 can be attributed to a fragment of m/z 261 which remains linked to Cd(II) ion, losing a methoxyl group. The m/z values of the ion fragments are in agreement with the proposed formula for both the reaction product, P, and the ligand, L, the latter arising from ampicillin methanolysis.

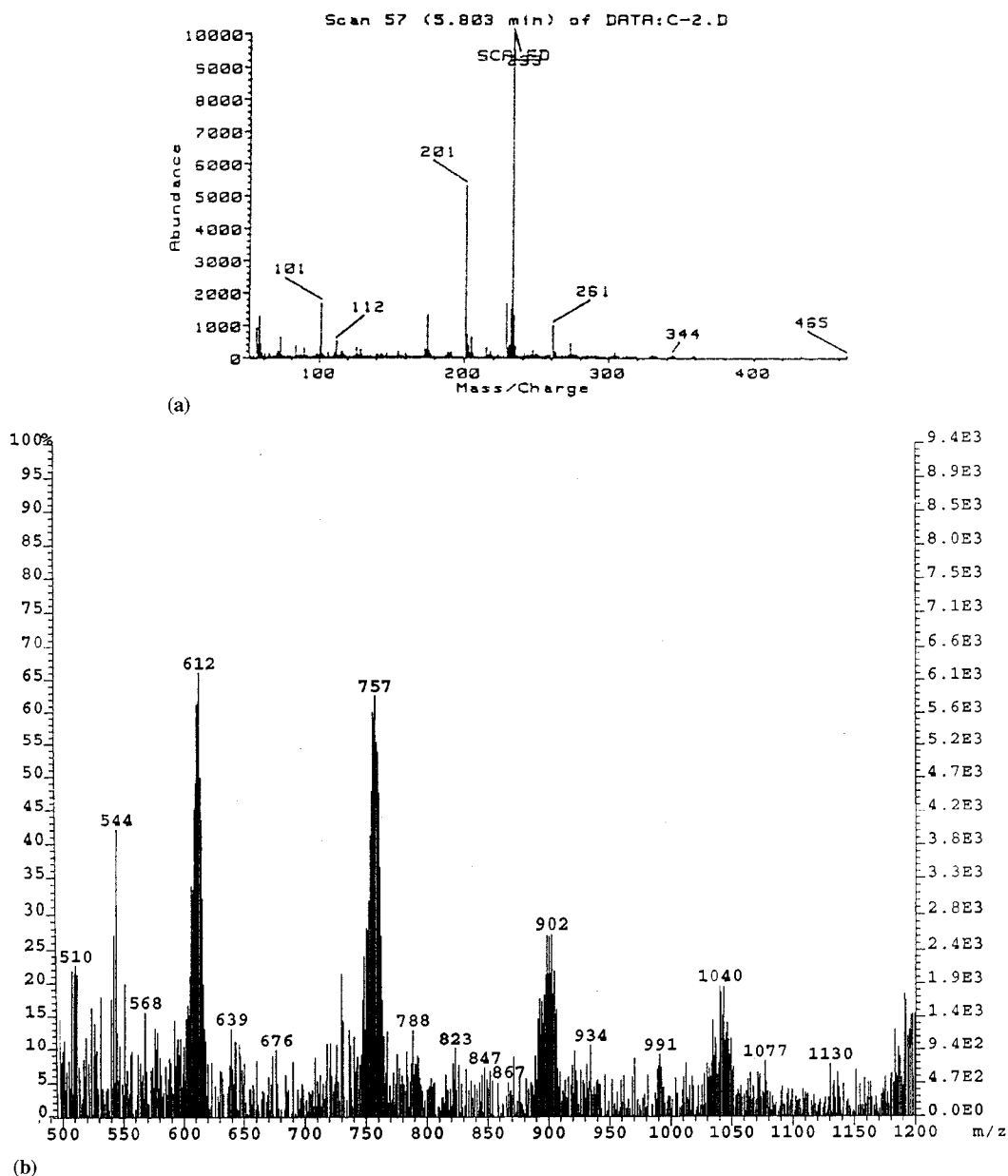


Fig. 5. (a) Mass spectrum (electron impact) of degradation product of ampicillin. (b) Mass spectrum (LSIMS) of the solid in glycerol.

Spectrum FAB⁻ (Fig. 5b) presents a series of signals with a distribution of isotopic peaks which are the expected for the proposed formula. Cd isotopes contribute in an essential way to such distribution. If we take into account that the most

abundant Cd isotope has a mass of 114, the peak at a value m/z 991 can be related to a molecular ion from the isolated compound with a molecular weight of 989.3 g/mol, as mentioned previously. The highest spectrum peak at m/z 612 could

Table 1
The kinetics of ampicillin decomposition in methanol in the presence of cadmium (II) ions at 20°C

[Ampicillin] × 10 ⁴ (mol dm ⁻³)	(dA/dt) × 10 ²	v _{obs} × 10 ⁶ (mol · dm ⁻³ min ⁻¹)	r ²
10	4.753	2.617	0.999
12	3.663	2.017	0.999
16	2.313	1.274	0.998
25	1.856	1.022	1.000
50	0.7477	0.4117	0.998
100	0.6286	0.3461	0.998
150	0.5237	0.2878	0.999
200	0.4414	0.2430	1.000
250	0.4244	0.2332	0.999
500	0.3414	0.1880	0.995

Initial Cd(II) concentration: 1 · 10⁻⁴ M.

correspond to the ion fragment resulting from the loss of a ligand molecule (with a mass of 379.4) by the molecular ion. The peak at 757 can be related to a complex molecule which has lost a fragment of m/z 233 (formula II in Scheme 1) plus a proton. The fragment of m/z 233 is the most stable when the molecule is ionized by electron bombardment. Therefore, the LSIMS spectrum provides additional information to that obtained from the electron impact spectrum, both are in accordance with the proposed formula for product P.

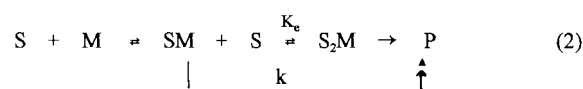
Once the empirical formula and the molar absorption coefficient at maximum absorption (285 nm) for the single reaction product of ampicillin in presence of cadmium ions was determined, we studied the kinetic formation of the product P. In order to do so, we measured the absorbance (285 nm) of methanolic mixtures of ampicillin and metal at different times. The initial rate values (v_{obs}) of the kinetic process were calculated for each experiment giving the following equation:

$$v_{\text{obs}} = \frac{dA}{dt} \frac{1}{\epsilon_p} \quad (1)$$

where dA/dt is the slope of the linear plot of the initial absorbance data vs. time, and ε_p, as noted above, equals 1.82 × 10⁴ l mol⁻¹ cm⁻¹. The values of v_{obs}, dA/dt, and the linear determination coefficient, r², were calculated by fitting the absorbance–time plots, (Table 1).

The v_{obs} values were related to the initial concentration of ampicillin, as shown in Fig. 6a. It indicates that the initial rate of the process decreases when antibiotic concentration increases, at high concentrations of ampicillin, the rate tends to become constant. This saturation effect is also observed with respect to the metal ion as shown in Fig. 6b. Under conditions of excess ampicillin (> 1000 times), a constant rate was observed. Thus, in this case a linear plot of absorbance vs. time is obtained for all the reaction time. This plot has not been included due to its simplicity.

To explain the saturation curves (Fig. 6) we propose a scheme for the reaction where it is assumed that the formation of two complexes of ampicillin, S, and cadmium ion, M. The proposed scheme is described in Eq. 2:



where P is the reaction product. The appearance rate of this product can be written as:

$$\frac{d[P]}{dt} = k_0 + k[SM] \quad (3)$$

The values of k (the first order constant with respect to SM) and of K_c (the formation constant for the 2:1 complex (S₂M) from the 1:1 complex (SM)) were calculated following the kinetic scheme given above, where k₀ is the lower rate for

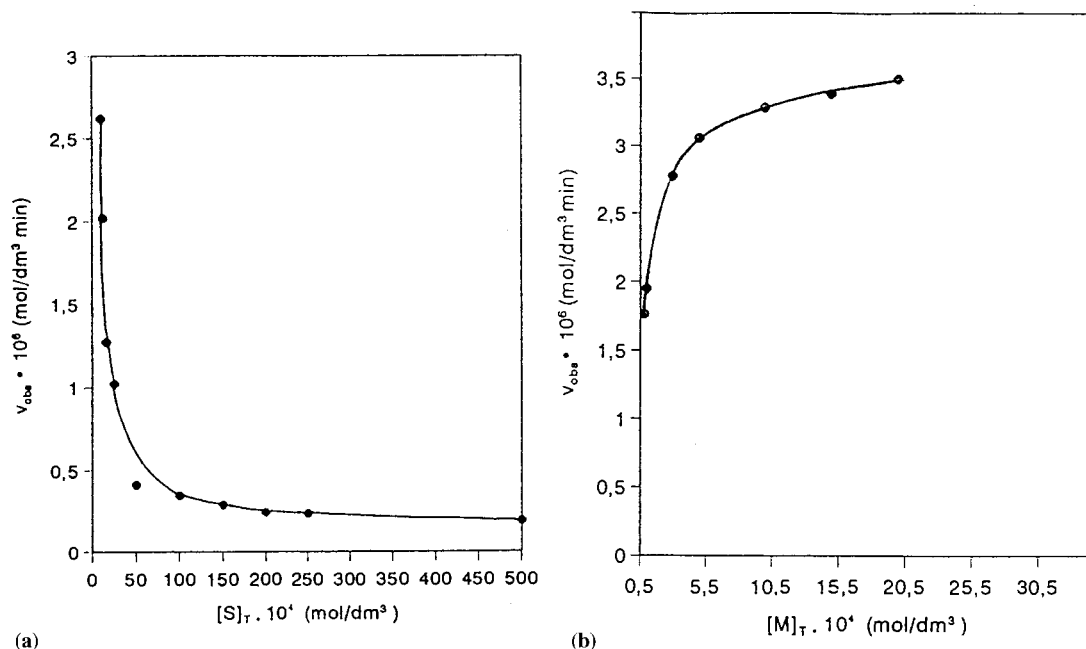


Fig. 6. (a) Plot of v_{obs} vs. substrate concentration. $[M] = 1 \times 10^{-4} \text{ mol dm}^{-3}$. (b) Plots of v_{obs} vs. metal ion concentration: $[\text{Ampicillin}] = 1 \times 10^{-4} \text{ mol dm}^{-3}$. Temperature = 20°C .

ampicillin degradation and can be associated to the non-catalyzed reaction rate and/or to antibiotic degradation coordinated to metal complex 2:1 (S_2M). Its value, which corresponds to the rate asymptotic value of the curve in Fig. 6a, has been obtained in a separated kinetic experiment with a large excess of ampicillin (2000 times). Under these conditions, the rate was constant $1.41 \times 10^{-7} \text{ mol l}^{-1} \text{ min}^{-1}$.

Formation of compounds SM was assumed to be faster than their decomposition; ampicillin concentration, which was much higher than cadmium ion concentration, remained virtually constant. The equilibrium constant was therefore written as:

$$K_c = \frac{[\text{S}_2\text{M}]}{[\text{SM}][\text{S}]_T} \quad (4)$$

The concentration of SM was expressed as:

$$[\text{SM}] = \frac{[\text{M}]_T - [\text{P}]}{1 + K_c[\text{S}]_T + \frac{1}{K_1[\text{S}]_T}} \quad (5)$$

where $[\text{M}]_T$ is the initial cadmium concentration.

In practice, the concentration of the product $[\text{P}]$ and the concentration of free cadmium ion were very small at the beginning of the reaction, and, as such, could be neglected in the calculations. Thus, the initial rate of appearance of the product, v_{obs} , could be expressed as:

$$\frac{1}{v_{\text{obs}} - k_o} = \frac{1}{k[\text{M}]_T} + \frac{K_c}{k[\text{M}]_T} [\text{S}]_T \quad (6)$$

Taking these equations into account, the first order rate constant for formation of product k , and the association constant K_c , were obtained from the kinetic data of solutions in which the concentration of Cd(II), $[\text{M}]_T$, was kept constant as the concentration of ampicillin was varied (provided that $[\text{S}]_T$ was much greater than $[\text{M}]_T$).

Fig. 7 shows the kinetic data plotted according to Eq. (6). The curve was fitted using the least squares method. The value of the linear determination coefficient (r^2) was equal to 0.994. The first order rate constant (k), calculated from the intercept (2.583×10^5) in Fig. 7, was 3.87×10^{-2}

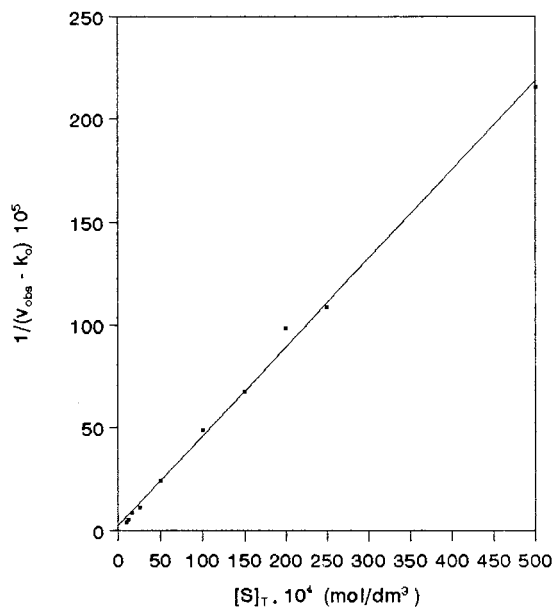


Fig. 7. Plot of $1/v_{\text{obs}} - k_o$ vs. antibiotic concentration, $[S]_T$.

min^{-1} at 20°C . Considering the first order rate constant and the slope, we calculated the association constant (K_o), which was $10^{3.23} \text{ l mol}^{-1}$.

On the other hand, the methanol in the medium may be involved in nucleophilic attack on the ampicillin molecule by the β -lactam carbonyl group. Such a step would be favored considering the arrangement of the cadmium ion to the ampicillin molecule. The methanol, due to its marked basicity ($\text{p}K_a > 9$), would act as a nucleophilic catalyzer, leading to the formation of the corresponding unstable penicilloic ester [13]. The breakdown of this intermediate ester would be expected to be slower than the rate of formation, since the $\text{p}K_a$ of methanol is higher than 14 [12].

In addition, this ester (intermediate derivative) appears to disrupt the thiol ring, an event that would lead to the formation of the α -methyl penamaldic derivative [12], a compound compatible with peak absorption at around 280 nm.

Much remains to be clarified as to the chemical mechanism of metal ion catalysis in the reaction of ampicillin degradation. Nevertheless, we can submit that the catalytic effect in methanolysis of β -lactam catalysed by the metal ion appears to be closely related to the different arrangement of the metal ion.

References

- [1] M.I. Page, Adv. Phys. Org. Chem. 23 (1987) 165.
- [2] J.M. Frère, B. Joris, CRC Crit. Rev. Microbiol. 11 (1985) 299
- [3] J.M. Hamilton-Miller, J.T. Smith, (Eds.), B-Lactamases, Academic Press, New York, 1979.
- [4] W. Cabri, I. Candiani, A. Bedeschi, Tetrahedron Lett. 33 (1992) 4783.
- [5] S. Wolfe, C.K. Kin, K. Yang, Can. J. Chem. 72 (1994) 1033.
- [6] M. Company, M.J. Benitez, J.S. Jiménez, Int. J. Biol. Macromol. 13 (1991) 225.
- [7] J.S. Coleman, L.P. Varga, S.H. Martin, Inorg. Chem. 9 (1970) 1095.
- [8] A. Skoog, D.M. West, Análisis Instrumental, Edit. Mc Graw-Hill/Interamericana de México, 1990.
- [9] P. Joseph, J.W. Poole, J. Pharm. Sci. 58 (1969) 447.
- [10] M.A. Schwartz, A.J. Delduce, J. Pharm. Sci. 58 (1969) 1137.
- [11] M. Davis, M.I. Page, J. Chem. Soc., Chem. Commun. (1985) 1702.
- [12] J.C. Stenberg, H.S. Stille, R.H. Shwendeman, Anal. Chem. 32 (1960) 84.
- [13] A.H. Cook, Q. Rev. Chem. London 2 (1948) 429.
- [14] N.J. Clayden, C.M. Dobson, L. Lian, J.M. Twyman, J. Chem. Soc. Perkin Trans. 2 (1986) 1933.

Charge-transfer complexes of barbiturates and phenytoin

Gamal A. Saleh

Pharmaceutical Analytical Chemistry Department, Faculty of Pharmacy, Assiut University, Assiut 71526, Egypt

Received 3 April 1997; received in revised form 30 July 1997; accepted 5 August 1997

Abstract

Simple and sensitive spectrophotometric methods are described, for the first time, for the determination of sodium salts of phenobarbital (1), thiopental (2), methohexital (3) and phenytoin (4). The methods are based on the reaction of these drugs as n -electron donors with the σ -acceptor iodine and various π -acceptors: 7,7,8,8-tetracyanoquinodimethane; 2,3-dichloro-5,6-dicyano-1,4-benzoquinone; 2,3,5,6-tetrachloro-1,4-benzoquinone; 2,3,5,6-tetrafluoro-1,4-benzoquinone; 2,5-dichloro-3,6-dihydroxy-1,4-benzoquinone; tetracyanoethylene and 2,4,7-trinitro-9-fluorenon. Depending on the solvent polarity, different coloured charge-transfer complexes and radicals were developed. Different variables and parameters affecting the reactions were studied and optimized. The formed complexes were examined by UV/VIS, infrared and $^1\text{H-NMR}$. Due to the rapid development of colours at ambient temperature, the obtained results were used on thin layer chromatograms for the detection of the investigated compounds. Beer's plots were obeyed in a general concentration range of 1–400 $\mu\text{g ml}^{-1}$ for the investigated compounds with different acceptors. Interference from some co-formulated drugs was also studied. No interference was observed due to additives commonly present in the pharmaceutical preparations. The proposed methods could be applied successfully to the determination of the investigated compounds in pure and pharmaceutical dosage forms with good accuracy and precision, the recoveries ranged from 98.7 ± 0.5 to $101.1 \pm 0.5\%$. The results were compared favourably with the official methods. © 1997 Elsevier Science B.V.

Keywords: Spectrophotometry; Charge-transfer complexes; Barbiturates and phenytoin; Pharmaceutical analysis

1. Introduction

Barbiturates are widely used as sedative hypnotic drugs in a wide variety of conditions and are also employed to produce anesthesia [1]. Phenytoin is one of the cyclic ureides which related in structure to the barbiturates. It was reported to be the least hypnotic, most strongly anticonvulsant and most effective against grand mal [1].

Different methods for the determination of the sodium salts of barbiturates and phenytoin have been reviewed [2–5]. Few direct spectropho-

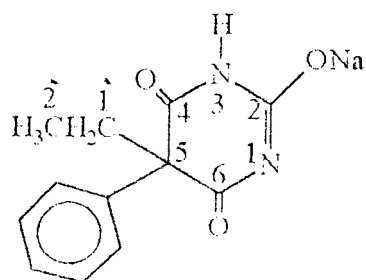
metric methods have been reported for the determination of the investigated compounds [6–9]. Other reported methods involve, titrimetry [10–13], gravimetry [13,14], stripping voltametry [15] and chromatography [9,16–18]. Quantification of phenytoin sodium in combination with either phenobarbital free acid or phenobarbital free acid, caffeine citrate and atropine sulphate (anti-sacer compositum tablets) cannot be achieved by adopting the B P 1993 method as these substances will interfere through co-extraction. In addition, the analysis of phenytoin sodium tablets is not specified by USP 23 NF 18.

With the exception of HPLC methods, most procedures suffer from some drawbacks. The British Pharmacopeia titrimetric and gravimetric methods are time consuming and depend upon measuring fairly concentrated solutions. They lack simplicity, sensitivity and selectivity. In addition, they could not be used for the determination of the dosage forms containing barbiturate free acids in conjunction with those of sodium salts. Therefore, it was considered worthwhile to develop rapid and selective procedures suitable for their routine quality control analysis. Moreover, the existing spectrophotometric methods cannot be used to distinguish between the sodium salts and the corresponding free acid derivatives. There is a need for selective spectrophotometric methods which could be utilized in detecting and distinguishing between the sodium salts and the free acids without the need for any pretreatment or prior separation.

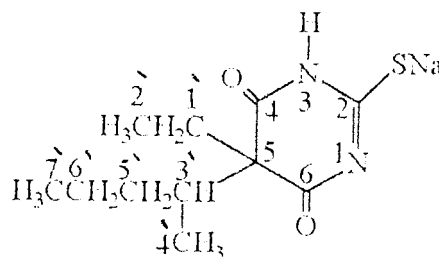
The molecular interactions between electron donors and acceptors are generally associated with

the formation of intensely coloured charge-transfer complexes [19], which absorb radiation in the visible region. A variety of electron donors [19–22] were reported to yield charge-transfer complexes with various acceptors. Rapid formation of the complexes makes their utility in photometric analysis simple and convenient. Barbiturates and phenytoin sodium salts have not yet been investigated as n -electron donors to form charge-transfer complexes and radical ions with iodine and different π -acceptors.

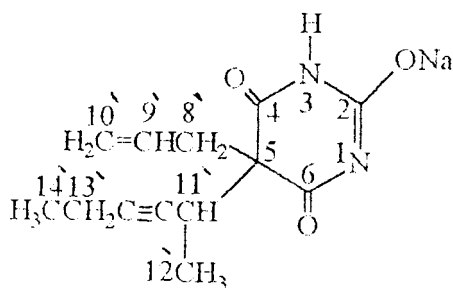
This paper describes, for the first time, the application of iodine, tetracyanoquinodimethane, tetracyanoethylene and dichlorodicyanobenzoquinone, which were selected according to their high electron affinities, to the spectrophotometric determination of the sodium salts of phenobarbital, thiopental, methohexital and phenytoin in pure samples and in dosage forms. Interference from commonly encountered substances was also studied. The structures of the compounds studied are given in scheme 1.



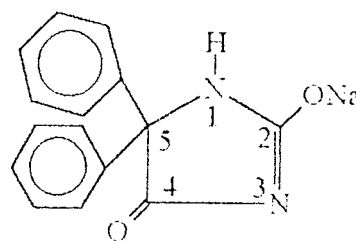
Phenobarbital Sodium (1)



Thiopental Sodium (2)



Methohexital Sodium (3)



Phenytoin Sodium (4)

Scheme 1.

2. Experimental

2.1. Apparatus

A Perkin-Elmer 3B UV/VIS, Norwalk, CT and a Uvidec-320, Tokyo, Japan. Spectrophotometers with 1-cm matched quartz cuvettes. Infrared Spectrometer IR-470, Shimadzu, Japan. $^1\text{H-NMR}$ Spectrometer, EM-360, 60 M Hz NMR Spectrometer, Varian Instrument Division, Palo Alto, CA. The geometries of phenobarbital anion, TCNE and both together in all possible spatial positions were fully optimized at the full self-consistent field (SCF) level by using MNDO/3, a general molecular orbital package implemented with molecular mechanics software MMX-PC [23].

2.2. Materials and reagents

All solvents used were of analytical reagent-grade. Phenobarbital sodium: El-Nasr for Pharmaceutical Chemicals, Cairo, Egypt; thiopental sodium: Egyptian International Pharmaceutical Industries, Cairo, Egypt; methohexital sodium: Lilly Research Center, Windlesham, Germany; phenytoin sodium: The Nile Company for Pharmaceuticals and Chemical Industries, Cairo, Egypt. Iodine: resublimed, Riedel De-Haen AG, Germany, 8.5 mg ml^{-1} in 1,2-dichloroethane, the solution was found to be stable for at least one week at 4°C . 7,7,8,8-Tetracyanoquinodimethane (TCNQ): Aldrich Chemical, Milwaukee, WI, 1 mg ml^{-1} in acetonitrile, the solution was found to be stable for at least one week at 4°C . Tetracyanoethylene (TCNE): Nacalai Tesque, Kyoto, Japan, 1 mg ml^{-1} in acetonitrile, prepared fresh daily. 2,3-Dichloro-5,6-dicyano-1,4-benzoquinone (DDQ): Merck-Schuchardt, Munich, Germany, 2 mg ml^{-1} in methanol, the solution was prepared fresh daily. 2,3,5,6-Tetrachloro-1,4-benzoquinone (Chloranil), Prolabo, Rhone-Poulenc, France. 2,3,5,6-Tetrafluoro-1,4-benzoquinone (Fluoranil): Aldrich-Europe (Beerse, Belgium). 2,5-Dichloro-3,6-dihydroxy-1,4-benzoquinone (Chloranilic acid), BDH Chemicals, Poole, UK. 2,4,7-Trinitro-9-fluorenon (TNF), Fluka, Switzerland. Fluoranil,

chloranil, chloranilic acid and TNF, each 5 mg ml^{-1} in acetonitrile, were prepared fresh daily.

2.3. Pharmaceutical formulations

The following commercial dosage forms were subjected to the analytical procedures: (1) sominaletta ampoules (The Alexandria Company for Pharmaceuticals and Chemical Industries, Alexandria, Egypt), labelled to contain phenobarbital sodium 40 mg per 1 ml ampoule; (2) thiopental sodium vials (Egyptian International Pharmaceutical Industries, Cairo, Egypt), labelled to contain 500 mg thiopental sodium per vial; (3) brietal vials (Lilly Research Center, Windlesham, Germany), labelled to contain 500 mg methohexital sodium per vial; (4) epanutin capsules (The Nile Company for Pharmaceuticals and Chemical Industries, Cairo, Egypt), under license from Parke-Davis, Detroit, MI), labelled to contain phenytoin sodium 100 mg per capsule; (5) epanutin with phenobarbital capsules (The Nile Company for Pharmaceuticals and Chemical Industries, Cairo, Egypt, under license from Parke-Davis, Detroit, MI), labelled to contain phenytoin sodium 100 mg and phenobarbital free acid 50 mg per capsule; and (6) antisacer compositum children tablets (Swiss Pharma, Cairo, Egypt, under license from Wander, S.A., Berne, Switzerland), labelled to contain phenytoin sodium 50 mg , phenobarbital free acid 25 mg , potassium bromide 200 mg , caffeine citrate 10 mg and atropine sulphate 0.2 mg per tablet.

2.4. Procedures

2.4.1. Preparation of standard stock solutions

Into a 50-ml calibrated flask, $100\text{--}200 \text{ mg}$ of the drug was weighed accurately and dissolved in 2 ml methanol, completed to volume with the same solvent (in case of DDQ), with 1,2-dichloroethane (in case of iodine) and with acetonitrile (in case of other acceptors) and diluted quantitatively to obtain the suitable final concentration listed in Table 1.

Table 1

Linear calibration limits and molar absorptivity values for the reaction of the investigated compounds with various acceptors

Acceptor/donor	Linear limits $\mu\text{g ml}^{-1}$, $\epsilon/10^3 \text{ dm}^3 \text{ mol}^{-1} \text{ cm}^{-1}$			
	Phenobarbital	Thiopental	Methohexital	Phenytoin
Iodine	25–150, 1.32	25–100, 1.63	25–150, 1.36	25–200, 0.73
TCNQ	5–20, 11.40	1–10, 25.20	5–250, 14.10	5–20, 14.00
TCNE	10–75, 2.72	5–50, 4.80	10–75, 2.66	10–75, 3.76
DDQ	10–100, 1.76	10–100, 2.21	10–100, 1.85	10–100, 2.09
TNF	10–150, 1.07	10–150, 1.34	10–150, 1.12	10–150, 1.27
Chloranil	50–400, 0.44	50–400, 0.55	50–400, 0.45	50–400, 0.32
Fluoranil	25–300, 0.71	50–400, 0.37	10–100, 2.15	25–200, 3.21
Chloranilic acid	25–150, 0.98	25–150, 1.19	25–150, 1.03	25–150, 1.17

The solvents used were 1,2-dichloroethane for iodine, methanol for DDQ and acetonitrile for other acceptors and the drugs were as their sodium salts.

2.4.2. General procedure

Aliquot volumes of standard stock solutions, containing 10–4000 μg drug was transferred to 10-ml calibrated flasks. One millilitre of the reagent was added and diluted to volume with the same solvent (in case of DDQ), with 1,2-dichloroethane (in case of iodine) and with acetonitrile (in case of other acceptors). The absorbances of the resulting solutions were measured at the wavelength of maximum absorption after the appropriate times, listed in Table 2, at $25 \pm 5^\circ\text{C}$ against reagent blanks treated similarly.

2.4.3. Analysis of tablets and capsules

The contents of 20 tablets or capsules of each drug were weighed and powdered or evacuated and a quantity of the powder $\equiv 100 \text{ mg}$ was transferred into a 50-ml calibrated flask, dissolved in 2 ml of methanol, swirled and sonicated for 2 min, completed to volume with the corresponding solvent (as in standard solution), shaken well for 15 min and filtered, rejecting the first portion of the filtrate and then proceeded as in Section 2.4.2.

2.4.4. Analysis of ampoules

A volume of the mixed 10 ampoules containing about 50 mg drug was transferred into a 50-ml calibrated flask and proceeded as directed in Section 2.4.3.

2.4.5. Analysis of vials

Into a 50-ml calibrated flask, 50 mg of the drug was accurately weighed and then proceeded as in Section 2.4.3.

2.4.6. Preparation of the complexes for infrared measurements

To 2 ml of 0.05 M drug in methanol, 2 ml of 0.05 M of each acceptor in the appropriate solvent (methanol for DDQ, 1,2-dichloroethane for iodine and acetonitrile for other acceptors), was added in a round bottom flask containing $\approx 30 \text{ ml}$ of the appropriate solvent and stirred for 30 min. The solvent evaporated under reduced pressure and the resulting oily residues were dried over calcium chloride.

2.4.7. Solutions for $^1\text{H-NMR}$ measurements

30 mg of each drug, scheme 1, were dissolved in 1 ml $\text{d}_6\text{-DMSO}$ and 1 ml containing an equimolar amount of the acceptors in the same solvent was added and used directly for $^1\text{H-NMR}$ measurements.

3. Results and discussion

3.1. Reaction with iodine

1,2-Dichloroethane was found to be an ideal solvent for the formation of tri-iodide ion pair (inner complex). Methylene chloride, chloroform

Table 2
The reaction time, peak position and intensity in polar and non-polar solvents

Acceptor	Reaction time, (min)	1,2-dichloroethane ^a		Acetonitrile ^a	
		λ_{\max} (nm)	ϵ_{\max}	λ_{\max} (nm)	ϵ_{\max}
Iodine	5	293, 363	1320, 671	— ^b	— ^b
TCNQ	20	605	1258	842	11400
TCNE	15	420	288	414	2720
DDQ	12	388	2008	460 ^c	1760 ^c
TNF	30	412	178	485	1070
Chloranil	5	440	258	430	440
Fluoranil	5	312	487	400	712
Chloranilic acid	5	435	376	525	980

^a Using phenobarbital sodium as donor.

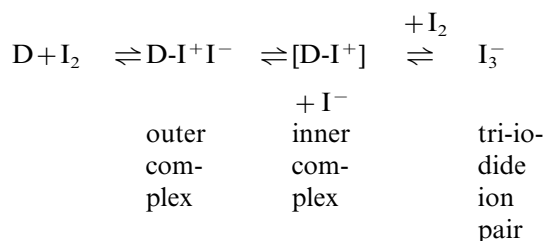
^b High blank readings.

^c The same readings were obtained with methanol.

and carbon tetrachloride produced lower absorbance readings. Polar solvents were found to be unsuitable as their blanks with iodine gave high absorbances.

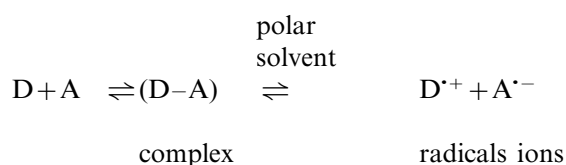
The violet colour of iodine in 1,2-dichloroethane (λ_{\max} at 240 and 515 nm) immediately changed into lemon yellow (λ_{\max} at 293 and 363 nm) upon the addition of any of the investigated compounds typical for charge-transfer complexes (Fig. 1). The consistency of these two bands, in spite of the structural variations among the different studied compounds, is probably due to the common origin of the transition in n-electron transfer from the sodium salts of barbiturates and phenytoin to the σ -acceptor iodine. The high intensity of the charge-transfer bands are common to complexes of n-donors with iodine [19]. The appearance of absorption peaks at 293 and 363 nm was attributed to the formation of a charge transfer complex between the investigated drugs and iodine having an ionized structure $DI^+ \dots I_3^-$, taking into account that the spectrum of I_3^- in 1,2-dichloroethane shows two absorption maxima at 293 and 363 nm ($\epsilon = 45\,800$ and $25\,000 \text{ dm}^3 \text{ mol}^{-1} \text{ cm}^{-1}$, respectively). This complex should originate from an early intermediate outer complex $D \dots I_2$. From the investigated compounds and iodine, only thiopental sodium absorbs at 293 nm, other compounds have no absorption at 293 and 363 nm. Therefore, measurements are carried out at 363 nm for thiopental sodium due to interfer-

ence from its native uv absorption and at 293 nm for other compounds.



3.2. Reaction with π -acceptors

The interaction of the investigated compounds with certain polyhalo and polycyanoquinones π -acceptors in non-polar solvents (such as 1,2-dichloroethane), Table 2 was found to produce coloured charge-transfer complexes with low molar absorptivity values. In polar solvents, such as acetonitrile, (Table 2 and Fig. 2), complete electron transfer from the donor to the acceptor moiety takes place with the formation of intensely coloured radical ions with high molar absorptivity values, according to the following scheme:



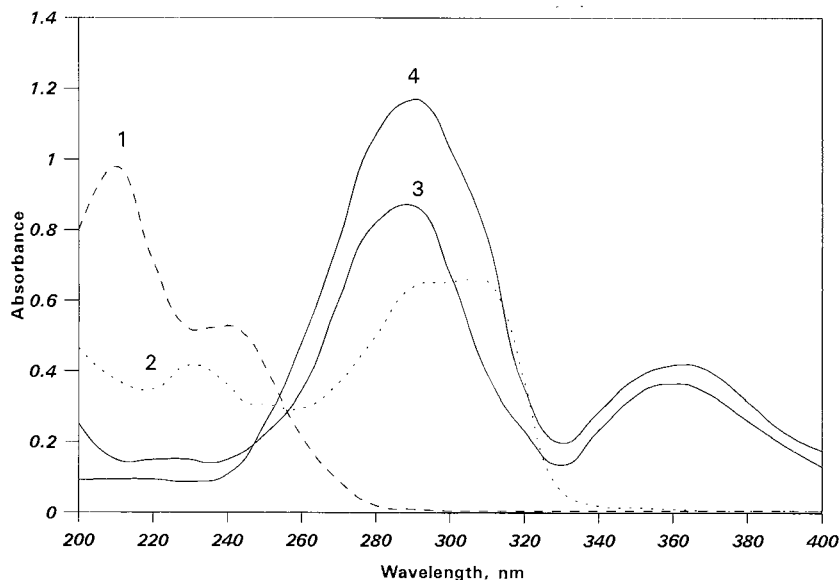


Fig. 1. Absorption spectra of: phenobarbital sodium (1); thiopental sodium (2) and their reaction products with iodine (3,4), using 25, 10, 175 and 70 $\mu\text{g ml}^{-1}$ respectively, all in 1,2-dichloroethane.

The dissociation of the (D–A) complex is promoted by the high ionizing power of the solvent acetonitrile [24].

The resulting bands of the named compounds with π -acceptors are similar to the maxima of radical anions of the acceptors obtained by iodide reduction method and coincide with the values reported in the literature [24].

The predominant chromogen with TCNQ in acetonitrile is the bluish-green coloured radical anion which exhibits strong absorption maxima at 842, 825, 762, and 742 nm. These bands may be attributed to the formation of the radical anion $\text{TCNQ}^{\cdot-}$, which was probably formed by the dissociation of an original donor–acceptor (D–A) complex with the investigated compounds in acetonitrile. With TCNE, the characteristic shaped absorption band of TCNE radical anion with reported maximum in acetonitrile at 432 nm was not formed. Instead, droplet at 394 and 414 nm was formed which corresponds to 1,1,2,3,3-pentacyano propenide (PCNP) anion. From the quantitative point of view, PCNP anion is preferable to TCNE anion in having high molar absorptivity [24].

The formation of radical anions were possible in methanol, ethanol, propan-1-ol, propan-2-ol or dimethylsulphoxide. However, non-linear response compared with acetonitrile was observed. The latter was considered as an ideal solvent as it also afforded maximum sensitivity due to its high dielectric constant which promotes maximum yield of radical anions in addition to its high solvating power of the reagents. Methanol gave maximum sensitivity in case of DDQ, inspite chloroform and carbon tetrachloride could also be used.

The relative sensitivity of the seven acceptors in analytical work may be compared by their ϵ -values. TCNQ, TCNE, DDQ and iodine, exhibiting the highest ϵ -values related to their high electron affinities were selected for further quantitative work. The weak and small values in cases of TNF, chloranil and fluoranil may be explained on the basis of insufficient ionization of these relatively weak π -acceptors which possess lower electron affinities [19].

The application of the Job's method [25] of continuous variation indicated 1:1 ratio for all the investigated compounds with all acceptors stud-

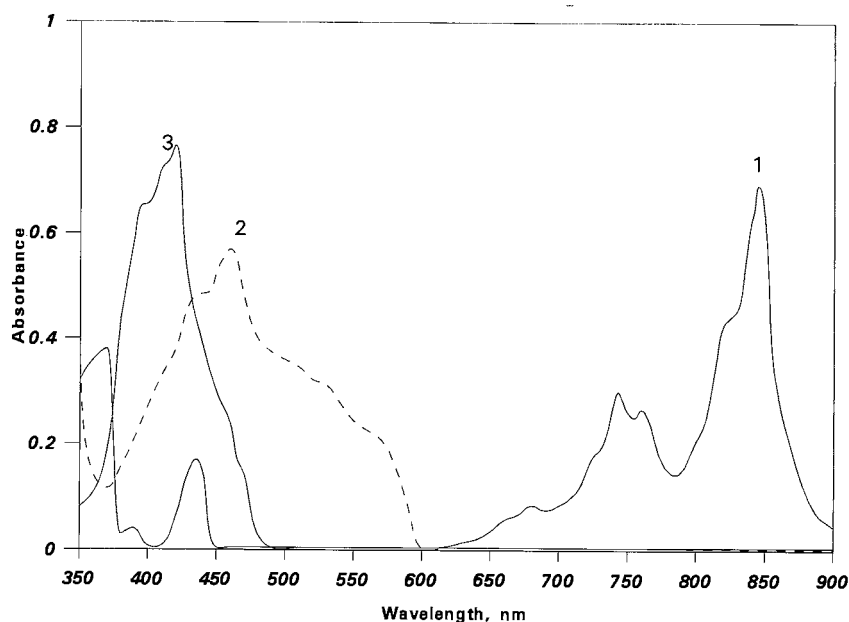


Fig. 2. Absorption spectra of the reaction products of phenobarbital sodium (15 , 83 and $67 \mu\text{g ml}^{-1}$) with each of TCNQ (1), DDQ (2), TCNE (3) respectively, (2) in methanol, (1 and 3) in acetonitrile.

ied. This indicates that only one center is responsible for the complex formation. These findings are supported by the reaction of the sodium salts with hydrochloric acid where they were found to be titrated as monobases.

3.3. Reagent concentration

The results for variation of reagent concentration indicated that 1 ml of either 0.05% iodine, 0.1% TCNQ or TCNE, 0.2% chloranilic acid, 0.4% DDQ 0.5% chloranil or fluoranil, 1% TNF are suitable. The higher concentrations used of the reagents may be useful for rapidly reaching equilibrium, thus minimizing the time required to attain maximum absorbance readings at the corresponding maxima.

3.4. Reaction time

The optimum reaction time was determined by following the colour development at ambient temperature ($25 \pm 5^\circ\text{C}$). Complete colour development was attained instantaneously or after 5 – 30

min with all compounds investigated (Table 2). The colours remain stable for at least a further 30 min.

3.5. Infrared and $^1\text{H-NMR}$ studies

The formation of donor–acceptor complexes was confirmed by both IR and $^1\text{H-NMR}$ techniques.

The majority of infrared measurements on such complexes have been concerned with shifts in the vibrational frequencies in donor or acceptor (or both). Decreases in the vibration frequency of a particular band have been used as evidence for a particular site of a charge-transfer interaction [19]. The infrared spectra of the complexes show some differences compared with the sum of the spectra of the two components. This was used to distinguish between weak charge-transfer complexes and the products of electron transfer or proton-transfer reactions [19].

The IR bands of the C–O or the C–S in the complexed molecules are shifted $\approx 20 \text{ cm}^{-1}$ lower than the absorption of the free compounds.

This indicates a decrease in the stretching force constant and favours coordination to the oxygen or sulphur atom. Moreover, the absorption frequencies assigned to the C–N stretches are shifted $\approx 20 \text{ cm}^{-1}$ to higher frequencies. These shifts are expected if the oxygen or sulphur atoms are the donor centers. Similar changes in the IR spectra of the donor upon complexation have been reported for several carbonyl compounds [26]. Dimethylacetamide and thioamides were reported to bind the iodine by oxygen or sulphur respectively [27].

In $^1\text{H-NMR}$, generally, the protons of the donor are shifted to a lower field (paramagnetic shift). The $^1\text{H-NMR}$ spectra of the complexes of the investigated compounds, with different acceptors were recorded in d_6 -DMSO together with the spectra of the free compounds.

The aromatic protons of the complexed phenobarbital sodium are shifted to a lower field ($\Delta\delta = 0.15 \text{ ppm}$) and the methyl and methylene protons are shifted (from 0.1 to 0.2 ppm). In the complexed thiopental sodium, 4- CH_3 , 1- CH_2 and 3- CH are shifted to a lower field ($\Delta\delta = 0.15 \text{ ppm}$). In the complexed methohexital sodium, 8- CH_2 and 11- CH are shifted to a lower field ($\Delta\delta = 0.2 \text{ ppm}$), while the other protons remain unchanged. In the complexed phenytoin sodium, the aromatic protons are shifted ($\Delta\delta = 0.07 \text{ ppm}$). Hence, as stated in similar reports [21,22], it could be deduced that the charge-transfer may proceed from the anion formed from the dissociation of ONa or SNa of barbiturates or phenytoin.

3.6. Molecular modelling, molecular mechanics and proposed interaction mechanism

To study the sites of interactions between the donor and the acceptor, the donor and the acceptor were minimized alone and together by computation. In this work, molecular modelling and mechanics for phenobarbital sodium and TCNE as examples for donors and acceptors respectively led to the following:

(1) In the case of electroneutral fully optimized molecules, phenobarbital sodium attacks TCNE at the area of C=C. Phenobarbital sodium has two

possible donating entities (O^- and the N–1 by its lone pair of electrons). It is acceptable that the electrostatic surface area of two molecules, such as phenobarbital sodium and TCNE, can be the mathematical sum of their individual total surface areas (S_T). By this calculation, the hypothetical sum will be 231 \AA^2 (S_T of phenobarbital anion) + 145 \AA^2 (S_T of TCNE) = 376 \AA^2 . Strong electrostatic attraction at the mentioned centers between the two molecules when minimized together was found to result in an actual total surface area of 351 \AA^2 , i.e. 25 \AA^2 less than the hypothetical sum.

(2) The distance between the O^- of phenobarbital anion and each of the two carbons of TCNE (C=C) equals 2.83 and 3.14 Å.

(3) The distance between the N–1 of phenobarbital anion and each of the two carbons of TCNE (C=C) equals 2.92 and 3.26 Å.

From these studies it could be concluded that there is a strong interaction between phenobarbital anion, the donor with TCNE and the acceptor, guided by the reduced electrostatic surface (25 \AA^2). Again, the source of electron donation can be better from the O^- than the N–1 of phenobarbital anion mediated by the distance between each of these atoms and the acceptor.

3.7. Quantification

Under the specified reaction conditions, the molar absorptivity at the λ_{max} was found to be a function of concentration of the investigated drugs. In all cases studied, Beer's law plots ($n = 10$) were linear with very small intercepts (-0.0276 to $+0.0257$), slopes ranged from 0.009 to 0.097 in the concentration ranges given in Table 1. The correlation coefficients ranged from 0.9950 to 0.9998. The confidence intervals for slopes and intercepts were calculated. The intervals for intercepts were tested at 95% confidence limits and 8 df and the results show that there were no significant difference between zero and intercepts.

The mean of eight replicate analyses of solutions of the studied compounds at the concentration limits listed in Table 1 gave relative S.D. values up to 1.8%. This level of precision of the

Table 3
Analysis of phenobarbital and phenytoin sodium salts in the presence of some co-formulated ingredients

Ingredients	Amount (mg)	Recovery %, \pm S.D. ^a			
		Iodine	TCNQ	TCNE	DDQ
Phenobarbital sodium (10 mg):					
Paracetamol	200	99.0 \pm 0.9	99.5 \pm 1.1	99.4 \pm 0.5	99.6 \pm 1.1
Ergotamine tartarate	1	100.7 \pm 0.6	98.7 \pm 0.2	100.2 \pm 1.1	99.7 \pm 1.2
Mebroamate	150	100.99 \pm 1.2	99.5 \pm 0.9	100.3 \pm 0.9	99.8 \pm 1.3
Chlorpheniramine maleate	1	108.9 \pm 1.1	108.7 \pm 0.9	108.6 \pm 0.8	108.4 \pm 0.5
Phenytoin sodium (50 mg):					
Thiocol	150	101.0 \pm 0.2	100.0 \pm 0.8	99.4 \pm 0.6	99.6 \pm 1.1
Caffeine citrate	50	100.3 \pm 1.3	99.0 \pm 0.5	100.1 \pm 1.1	100.1 \pm 1.4
Phenobarbital	50	99.9 \pm 1.2	99.9 \pm 0.6	100.1 \pm 0.2	99.7 \pm 1.2
Atropine sulphate	0.2	99.4 \pm 1.0	99.4 \pm 1.3	99.3 \pm 1.1	100.1 \pm 1.2
Methylphenobarbital	100	99.8 \pm 1.0	99.4 \pm 1.0	99.6 \pm 1.1	99.7 \pm 0.9
Potassium bromide	200	100.3 \pm 1.2	99.2 \pm 1.2	99.4 \pm 0.9	100.3 \pm 0.8

^a Average of three determinations.

method is adequate for the quality control analysis of the studied drugs.

3.8. Specificity and interference

The proposed procedures have the advantage that most of the assays are performed in the visible region away from uv-absorbing interferents that might be co-extracted from dosage forms. Owing to the basic character of the investigated compounds, they can act as strong n-electron donors ($pK_a = 11-12$), the reactions were found to be specific for the sodium salts derivatives in the presence of the structurally related barbituric, thiobarbituric, phenobarbital and methylphenobarbital free acids ($pK_a = 6-8$).

Interference studies were carried out in order to investigate the effect of commonly encountered compounds that present in barbiturate dosage forms. No interference was observed from phenobarbital, methylphenobarbital free acids, paracetamol, atropine sulphate, thiocol, potassium bromide, ergotamine tartarate, meprobamate and caffeine citrate. On the other hand, chlorpheniramine maleate being basic enough ($pK_a = 9.2$) was found to interfere with the assay procedures, Table 3.

3.9. Analysis of pharmaceutical formulations

The obtained high intensity absorption bands and the very low reagent backgrounds make these procedures suitable for the routine quality control analysis of the investigated compounds with minimum interference. The proposed and official methods were applied to the determination of tablets, capsules, ampoules and vials. The obtained mean values (\pm S.D.) of the labelled amounts ranged from 98.7 ± 0.5 to 101.1 ± 0.5 , Table 4. In the 't' and 'F' tests, no significant differences were found between the calculated and theoretical values (95% confidence) of both the proposed and official methods. This indicates similar precision and accuracy.

3.10. Identification on thin-layer chromatograms

The different colours developed from the interaction of the investigated compounds with the different acceptors could be used on thin layer chromatograms for detection and differentiation of these compounds (from their R_f values), Table 5. So spraying with iodine solution colours all the spots yellow while with TCNQ spray reagent, bluish-green radical anions spots are observed. The colours obtained for other spray reagents are given in Table 5. In general, the order of de-creas-

Table 4
Determination of the investigated compounds in dosage forms

Dosage forms ^a	Claimed (mg/unit)	Recovery %, \pm S.D. ^b				
		Iodine	TCNQ	TCNE	DDQ	Official
Sominaletta ampoules	40	98.7 \pm 0.5 t: 1.52 F: 2.71	100.5 \pm 0.7 t: 2.42 F: 1.14	101.1 \pm 0.5 t: 1.96 F: 2.71	98.8 \pm 0.5 t: 1.21 F: 2.40	99.3 \pm 0.8 ^c
Thiopental sodium vials	500	100.0 \pm 0.7 t: 0.33 F: 4.56	99.5 \pm 0.9 t: 0.32 F: 2.64	99.1 \pm 0.8 t: 0.85 F: 2.90	99.0 \pm 0.8 t: 1.02 F: 2.97	99.7 \pm 1.4 ^d
Brietal vials	500	99.2 \pm 1.0 t: 0.89 F: 3.11	99.4 \pm 1.0 t: 0.76 F: 2.93	99.6 \pm 1.1 t: 0.52 F: 2.72	99.1 \pm 0.8 t: 1.14 F: 4.71	100.1 \pm 1.8 ^d
Epanutin capsules	100	99.9 \pm 1.0 t: 0.34 F: 3.14	99.4 \pm 1.2 t: 0.12 F: 2.12	99.7 \pm 1.0 t: 0.18 F: 3.41	99.4 \pm 0.9 t: 0.16 F: 4.33	99.5 \pm 1.8 ^d
Epanutin with phenobarbital capsules	100	100.7 \pm 0.5 t: 1.29 F: 3.69	99.5 \pm 1.0 t: 0.10 F: 3.05	99.8 \pm 0.7 t: 0.28 F: 5.96	99.8 \pm 1.0 t: 0.26 F: 3.24	99.5 \pm 1.7 ^e
Antisacer compositum children tablets	50	99.8 \pm 1.0	99.3 \pm 1.2	99.4 \pm 1.0	100.4 \pm 0.8	

Theoretical values for t: 2.78 and for F: 6.39 (at $p = 0.05$).

^a For detailed composition, see Section 2.

^b Average of five determinations.

^c B P 1993 (titrimetric).

^d B P 1993 (gravimetric).

^e USP 23 NF 18 (HPLC).

ing sensitivity is: TCNQ, TCNE, DDQ, iodine, fluoranil, chloranil chloranilic acid, bromanil and TNF. The detection limits with TCNQ (the most sensitive reagent) ranged from 0.5 to 5 μg per 50 mm^2 for the studied compounds. The rapid development of colours at room temperature with non-corrosive reagents, the variation of colour shades, the sensitivity and stability of colours suggest obvious use of these acceptor reagents to supplement existing methods for the detection of the sodium salts of barbiturates and phenytoin on chromatograms.

4. Conclusions

The proposed spectrophotometric methods are simpler, time saving and more sensitive than the

British Pharmacopeia gravimetric and titrimetric methods. In addition, they can be applied to the quality control analysis of the sodium salts of phenobarbital, thiopental, methohexital and phenytoin pure or in combination with other drugs. TCNQ exhibiting the highest ϵ values with all the studied compounds could be considered the most suitable one for further work.

Moreover, the proposed methods could be considered superior to the British Pharmacopeia 1993 as they could be used successfully for the analysis of phenytoin sodium in the presence of phenobarbital free acid (epanutin with phenobarbital capsules and antisacer compositum tablets). In addition to ultraviolet-visible spectrophotometry, infrared and ¹H-NMR spectroscopy could also be used to study the possible site of interaction between the donor and acceptor.

Table 5
Colours of TLC spots of the investigated compounds after spraying with different acceptor solutions

Acceptors	Phenobarbital sodium	Thiopental sodium	Methohexital sodium	Phenytoin sodium
Iodine	Yellow	Yellow	Yellow	Yellow
TCNQ	Blue	Brown	Bluish-green	Bluish-green
TCNE	Yellow	White	White	Red
DDQ	Red	Red	Red	Red
Chloranil	Brown	Violet	Brown	Brown
Fluoranil	Violet	Brown-violet	Violet	Orange-yellow
Bromanil	Violet	Brown-violet	Violet	Orange-yellow
Chloranilic acid	Violet	Violet	Violet	Violet
TNF	Brown	White	Brown	Brown

Adsorbent: silica gel G254 precoated plates; Solvent system: benzene:chloroform:ether:methanol (22:22:4:2); R_f : 0.33, 0.82, 0.76 and 0.18 for phenobarbital, thiopental, methohexital and phenytoin sodium salts, respectively.

Acknowledgements

The author wishes to express his thanks to Dr Abdel-Nasser El-Shorbagi, Associate Professor of Pharmaceutical Organic Chemistry, Faculty of Pharmacy, Assiut University, for the molecular orbital calculations.

References

- [1] J.N. Delgado, W.A. Remers, Wilson and Gisvold's Textbook of Organic Medicinal and Pharmaceutical Chemistry, 9th ed., J.B. Lippincott, Philadelphia, 1991, p. 39, 341, 376.
- [2] M.K.C. Chao, K.S. Albert, S.A. Fusari, in: K. Florey (ed.), Analytical Profiles of Drug Substances, vol. 7, Academic Press, New York, 1978, p. 359.
- [3] M.J. Mcleish, in: K. Florey (ed.), Analytical Profiles of Drug Substances, vol. 21, Academic Press, New York, 1992, p. 535.
- [4] J. Philip, I.J. Holcomb, S.A. Fusari, in: K. Florey, (ed.), Analytical Profiles of Drug Substances, vol. 13, Academic Press, New York, 1984, p. 417.
- [5] S. Ebel, Handbuch der Arzneimittel-Analytik, Verlag Chemie, Weinheim/Bergstr., 1977, p. 234.
- [6] S. Liu, R. Li, P. Guo, Y. Yang, Yaowu Fenxi Zazhi, 10 (1990) 100; through Anal. Abstr. 53 (1991) 4 G30.
- [7] C.S.P. Sastry, P. Satyanarayana, A.R.M. Rao, N.R.P. Singh, Indian Drugs 26 (1980) 84.
- [8] M. Sharf El-Din, F. Belal, S. Hassan, Zentralbl. Pharm. Pharmakother. Laboratoriumsdiagn. 127 (1988) 133.
- [9] The United States Pharmacopeia 23, National Formulary 18, US Pharmacopeial Convention, Rockville, MD, 1995.
- [10] S.F. Chen, C.H. Yang, H.B. Duan, Yaowu Fenxi Zazhi 14 (1994) 60; through Anal. Abstr. 56 (1994) 10 G71.
- [11] S.A. Soliman, Y.A. Beltagy, I.M. Roushidy, J. Pharm. Pharmacol. 21 (1969) S44.
- [12] P.C. Markunas, J.A. Riddick, Anal. Chem. 23 (1951) 337.
- [13] British Pharmacopeia, HMSO, London, 1993.
- [14] L. Nu, X. Zhang, S. Yao, Mikrochem. Acta 1 (1990) 287.
- [15] O.M. Zakharova, V.V. Rnev, Zh. Anal. Khim. 46 (1991) 1019; through Anal. Abstr. 54 (1992) 6 G180.
- [16] V.M. Okudzhava, B.G. Chankvetadze, M.D. Rukhadze, Khim.-Farm. Zh. 24 (1990) 79; through Anal. Abstr. 53 (1991) 7 G10.
- [17] R.H. Liu, A.M. Mckeeham, B.A. Cinnamon, G. Foster, W.D. Bensley, J.G. Langner, A.S. Walia, J. Forensic Sci. 39 (1994) 1504.
- [18] T.I. Maksimenko, Farm. Zh. (1988) 79; through Anal. Abstr. 50 (1988) 7 D85.
- [19] R. Foster, Organic Charge-Transfer Complexes, Academic Press, London, 1969, p. 51, 387.
- [20] A.M. Taha, C.S. Gomaa, J. Pharm. Sci. 65 (1976) 986.
- [21] K.-A. Kovar, M. Abdel-Hameed, Arch. Pharm. 317 (1984) 246.
- [22] G. Saleh, N. Omar, N. El-Rabbat, M. Neugebauer, G. Rücker, Arch. Pharm. 322 (1989) 953.
- [23] QCMP Program Catalogue Computational Chemistry Software for IBM-PC and Compatible Computers, QCPE, Indiana University, Bloomington, IN, 1992.
- [24] A. Taha, G. Rücker, Arch. Pharm. 310 (1977) 485.
- [25] P. Job, Ann. Chem. 16 (1936) 97; through Advanced Physicochemical Experiments, 2nd ed., Oliver and Boyd, Edinburgh, 1964, p. 54.
- [26] G.D.I. Glusker, H.W. Thompson, R.S. Mulliken, J. Chem. Phys. 21 (1953) 1407.
- [27] C.D. Schmulbach, R.S. Drago, J. Am. Chem. Soc. 82 (1960) 4484.



ELSEVIER

Talanta 46 (1998) 123–128

Talanta

Preconcentration of trace uranium from seawater with solid phase extraction followed by differential pulse polarographic determination in chloroform eluate

Dj. Dojozan, M.H. Pournaghi-Azar *, J. Toutouchi-Asr

Department of Analytical Chemistry, Faculty of Chemistry, University of Tabriz, Tabriz, Iran

Received 7 April 1997; received in revised form 30 July 1997; accepted 5 August 1997

Abstract

In the present study, an effective method is presented for the separation and preconcentration of uranium (VI) by solid phase extraction (SPE). For this purpose, U(VI) oxinate is formed by the reaction of U(VI) with 8-hydroxyquinoline and adsorbed onto the octylsilane (C-8) SPE cartridge. The analyte is completely eluted with chloroform and determined by differential pulse polarography. The SPE conditions were optimized by evaluating the effective factors such as pH, oxine concentration, type and concentration of buffer and masking agent. By the proposed method a preconcentration factor more than 100 was achieved. The average recovery of uranium (VI) oxinate (0.1 mg l^{-1}) was 99.8%. The relative standard deviation was 1.6% for seven replicate determinations of uranyl ion in the solution with a concentration $20 \text{ } \mu\text{g l}^{-1}$. Some concomitant ions such as Ca^{+2} , Mg^{+2} and Fe^{+3} which interfere in extraction or determination process of uranium were masked with EDTA in aqueous phase during the extraction process. The proposed method was successfully used for the determination of uranium in Caspian Sea and Persian Gulf water samples. © 1998 Elsevier Science B.V. All rights reserved.

Keywords: Uranium; Seawater; Solid phase extraction; Oxine; Chloroform; Trace analysis; Differential pulse polarography

1. Introduction

Considerable interest has developed in the determination of trace uranium in environmental sites as well as in facilities of the nuclear industry. Electroanalytical techniques have frequently been used for this purpose. In particular, adsorptive stripping voltammetry (ADSV) is becoming a widely accepted tool for ultra-trace measurement

of uranium [1–9]. While characterized by detection limit in the subnanomolar range, such procedure often suffer from interferences due to overlapping stripping peaks (from some co-existing metals). However, recently a direct and selective ADSV has been described [10,11]. A chemical separation of the trace uranium prior to analysis serves the dual purpose of:

- increasing its concentration to levels at which it can be reliably determined by differential pulse polarography.

* Corresponding author.

- removing it from the seawater matrices to enhance the polarographic selectivity.

One of the most popular separation and preconcentration methods in trace metal analysis involves the liquid–liquid extraction of the analytes. We have successfully used this technique followed by adsorptive differential pulse polarography for the determination of uranium in mineral ores [12]. Concentration factors of this technique are insufficient for ultra-trace analysis even using sensitive methods as well as differential pulse polarography. In an attempt to overcome these limitations a method which involves complexation of the metal ions with chelating agents followed by adsorption on octadecylsilane chemically bonded silica gel (ODS) [13] or activated carbon have been reported [14]. Although ODS has been used for the preconcentration of some trace metals from seawater [15,16]. This technique has never been used for the separation and preconcentration of uranium from seawater. The application of ODS solid phase cartridge to the separation and concentration of U(VI) from seawater and its differential pulse polarographic determination after elution from the solid phase with chloroform is reported here.

2. Experimental

2.1. Chemicals and reagents

Chloroform, tri-butylamine, perchloric acid, and 8-hydroxyquinoline (oxine) were from E. Merck p.a. grade. The supporting electrolytes used were tri-butylammonium perchlorate (tri-BAP) and tetrabutylammonium perchlorate (TBAP). Tri-BAP was prepared by gradual neutralization of tri-butylamine with perchloric acid while cooling the solution in iced water. Tri-BAP formed in slightly acid solution was filtered, then washed several times with double distilled water and dried in vacuum. The dried crystals were washed by normal hexane and evaporated the solvent. 400 mg solid phase extraction cartridges were from E. Merck.

Standard uranium solutions: A 10^{-3} M aqueous solution of $\text{UO}_2(\text{NO}_3)_2 \cdot 6\text{H}_2\text{O}$ from E. Merck was prepared as a stock solution. The standard solutions were prepared by successive dilution of this stock solution.

2.2. Apparatus

All voltammograms were recorded with a three electrode system. A polarograph E506 was used with an E505 VA Stand including a dropping mercury electrode from Metrohm (Switzerland) to plot the DP polarograms. Solid phase extractions were performed using vacuum waste collect adsorbex, SPU, E. Merck (Germany).

2.3. Electrodes

The reference electrode Ag/AgCl (sat.), TBACl (sat.) and TBAP 0.5 M in chloroform in separated compartment was directly immersed in the reaction cell. The working electrode were DME and the auxiliary electrode was a platinum wire.

2.4. Preconcentration procedure

(1) Evaluation of alkaline earth cations concentration in seawater: To a 25 ml portion of seawater were added 10 ml ammonia buffer, pH 10, and a few amounts of Erio chrom black T and titrated by a standard solution of $\text{Na}_2\text{H}_2\text{Y}$.

(2) Sample pre-treatment: Seawater samples were filtered through 25–50 and 4–5.5 μm sintered glass respectively. To 100–500 ml filtered seawater or standard solution of uranium (0.4 mg l^{-1}), were added 0.025 M plus a required excess amount (depending on the alkaline earth cations concentration) of $\text{Na}_2\text{H}_2\text{Y}$ and oxine up to 2×10^{-3} M. After 1 min stirring the pH was adjusted to 5.5 with HCl or NaOH (solution A).

(3) Solid phase extraction step: SPE cartridges were first conditioned by successive washing by 1 ml acetonitrile and 1 ml water. A 10 ml portion of oxine solution passed through over conditioned cartridges, hence the columns were saturated with oxine. The solution A was passed from SPE cartridge at about $2.5\text{--}3 \text{ ml min}^{-1}$. The cartridges were washed with 2 ml of the solution containing $\text{Na}_2\text{H}_2\text{Y}$, pH 5.5. The analyte was then eluted with 5 ml of chloroform and the eluate was collected in a 5 ml volumetric flask containing 2×10^{-4} M supporting electrolyte and 0.1 M oxine. The resulting solution was transferred into a polarographic cell for recording of the polarograms.

2.5. Polarography of uranium (VI) oxinate in chloroform

Polarographic characteristics of U(VI) in chloroform were described with detail in our previous work [12]. On the basis of the results obtained (calibration graph was linear over the range 0.5–80 μM with correlation coefficient of 0.998 and L.O.D. of 0.4 μM), the differential pulse polarographic measurement of U(VI)-oxinate in chloroform eluate may be done as follows:

Add 0.25 g of tri-BAP as supporting electrolyte to 5 ml chloroform eluate, bubble nitrogen presaturated with chloroform through the solution for 20 min, record the DP polarogram by sweeping the potential from 0.200 to -0.500 vs. reference electrode with scan rate of 5 mV s^{-1} , construct the standard addition calibration graph to determine uranium.

3. Results and discussion

3.1. Optimization of experimental conditions

Using 100 ml aqueous solution of 0.1 mg l^{-1} UO_2^{+2} , several experimental variables involve: type and quantity of solid phase, loading rate, concentration of oxine (HOX) in liquid phase as well as on SPE cartridge, pH of sample, type and concentration of buffer, type and volume of conditioning, washing and elution solutions were optimized.

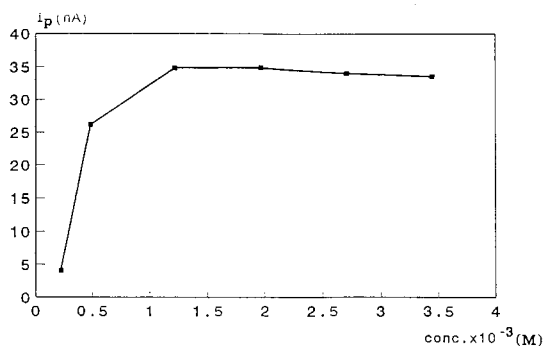


Fig. 1. Effect of aqueous oxine concentration on the extraction efficiency from 100 ml of 0.1 mg l^{-1} of uranium.

3.2. Choice of solid phase cartridge

One of the reasonable ways for quantitative adsorption of the metal ions on the solid phase is the complexation of the metal ions with chelating agents and retention of the produced hydrophobic compounds on the non-polar solid phase. For this purpose we have chosen oxine as chelating agent and we have examined the efficiency of various columns such as octylsilane (C-8), octadecylsilane (C-18), phenyl bonded silica, and unmodified silica. The results obtained showed that C-8 (100–400 mg) cartridge has the most satisfactory behavior. Therefore in further experiments, we have used this type of solid phase cartridge.

3.3. Conditioning of solid phase

For this purpose, the cartridges were usually washed by methanol and water successively. The preliminary experiments in this work showed that successive washing by 1 ml acetonitrile and 1 ml water represent better results.

3.4. Choice of chelating agent

For solid phase extraction of U(VI), the use of a chelating agent is required. For this purpose we have chosen oxine and reasons are as follows.

(1) The uranium (VI) oxinate can be eluted from solid phase with organic solvents such as chloroform and dichloromethane.

(2) The uranium (VI) oxinate eluted, can be determined directly in chloroform by differential pulse polarographic method which has been previously developed by present authors [12].

3.5. Loading step

The preliminary experiment showed also that for quantitative extraction of uranium oxinate on a single column C-8 (400 mg), the concentration of the analyte must not be exceeded from 3 mg l^{-1} . In the light of extremely minute amount of uranium in seawater, and relatively great adsorptive capacity of the C-8 (400) column, no overloading problem is made, even for the processing of several liters of sample. The optimum loading rate was found 2.5–

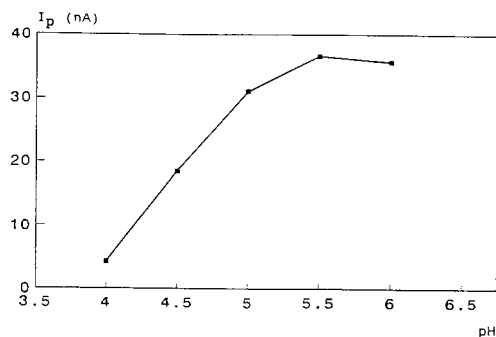


Fig. 2. Effect of pH on uranium extraction efficiency from 100 ml of 0.1 mg l^{-1} of model solution. Oxine (HOX), $1.96 \times 10^{-3} \text{ M}$ and EDTA 0.025 M .

3 ml min^{-1} and had a little influence on the results. On the other hand we have investigated the optimum conditions for quantitative adsorption of the uranium oxinate on the solid phase.

Influence of oxine concentration: The presence of oxine on the solid and liquid phase and its abundance is an effective parameter on the extraction efficiency of U(VI). From the results obtained the most satisfactory and reproducible results were obtained when the solid phase was presaturated with oxine and over $2 \times 10^{-3} \text{ M}$ oxine was dissolved in sample solution (Fig. 1).

Influence of pH and type of buffer: Since the solid phase used in SPE may be distracted at high and low pH, therefore the pH range 2–8 often offered as operation conditions. We have investigated the effect of pH on the efficiency of $\text{UO}_2(\text{OX})_2$ extraction. The results obtained showed that the pH 5.5 was suitable (Fig. 2). Since EDTA was used as an effective masking agent for the selective extraction of analyte in the presence of some concomitant elements, we have examined the suitability of $\text{Na}_2\text{H}_2\text{Y}$ for buffering of sample solution at 5.5. We have demonstrated that a 0.025 M disodium salt of EDTA for the present SPE was convenient. Note that in the absence of EDTA, uranium oxinate precipitated on the solid phase at the same pH. It seems that the presence of EDTA in the solution is desirable, probably due to the formation of some soluble aggregates between $\text{UO}_2(\text{OX})_2$ and EDTA.

Washing step: For the elimination of any concomitant ions or compounds, the cartridge washed

with 2 ml of solution containing $\text{Na}_2\text{H}_2\text{Y}$, pH 5.5. The waste solution was analysed and no significant uranium content was observed.

Elution: Due to excellent solubility of uranium oxinate in chloroform and good electrochemical behaviors of this compound in chloroform [12], we have chosen this solvent as the eluant to benefit from very sensitive electrochemical method as well as differential pulse polarography for the previous analysis. The adsorbed uranium oxinate was eluted by three successive 5 ml portions of chloroform. The analysis of the elutes showed that in the optimum conditions, the average recovery of uranium oxinate in the first eluate was over than 99.8% and is sufficient for quantitative analysis.

3.6. Extraction efficiency and concentration factor

The results obtained for the various portions of 0.1 mg l^{-1} model solution of uranium showed that, the recovery of uranium from 100 to 500 ml of the solutions was 98–101% and concentration factor exceeded than 100-fold. A typical pulse polarogram recorded for chloroform eluate, corresponding to 100 and 500 ml of uranium model solution is shown in Fig. 3.

3.7. Interference study

Interfering ions in seawater may be divided into two groups:

(a) The elements with major amounts such as Ca and Mg which their oxinates formed in the extraction conditions of $\text{UO}_2(\text{OX})_2$, fixed on the SPE column and prevent the complete extraction of analyte. However, their presence in the chloroform eluate do not interfere with the pulse polarographic determination of $\text{UO}_2(\text{OX})_2$.

(b) The ions with minor amounts such as Cu and Fe which are extractable by SPE and their presence in chloroform eluate, may interfere with the pulse polarography of uranium. Each of the two groups may be masked by EDTA in aqueous media. We have demonstrated that in the presence of suitable EDTA concentration (0.02 M , plus a required excess, depending on the alkaline earth cations concentration) there was no interference from concomitant ions mentioned above.

Table 1
Results of recoveries from model uranium solutions

Volume of solution (ml)	Recovery (R%)			$\bar{R}\%$	RSD%
	1	2	3		
100 (0.1 $\mu\text{g ml}^{-1}$)	101.9	98.7	98.8	99.2	1.9
500 (0.2 $\mu\text{g ml}^{-1}$)	98.2	98.5	102.5	99.7	2.4

3.8. Recovery and precision

Before attending analysis of seawater, a series of experiments were performed to assess the recovery of uranium at the concentration ten times higher than normal concentration in seawater in the experimental conditions optimized. Uranium spiked bidistilled water (0.1 mg l^{-1}) was analysed by proposed methods, using standard addition procedures in polarographic cells.

The results obtained are given in Table 1. As seen from this table, the recovery of uranium was 99.8% and the relative standard deviation for five replicate determinations was 1.9–2.4%. On the other hand, the relative standard deviation for seven replicate determinations of 500 ml model water sample containing 20 $\mu\text{g l}^{-1}$ uranyl ion, was about 1.6%.

3.9. Seawater analysis

Results for the analysis of two seawater samples (Caspian Sea and Persian Gulf) are given in Table 2. All samples were analysed in triplicate.

Table 2
Uranium contents of seawater samples

No. of samples	Uranium Contents ($\mu\text{g l}^{-1}$)	
	Persian Gulf	Caspian Sea
1	2.25	2.85
2	2.30	2.75
3	2.28	2.80
	C = 2.28	C = 2.80
	RSD% = 1.2	RSD% = 1.8

Since a standard method for the determination of uranium in seawater has not been reported in literatures and inductively coupled plasma mass spectrometry (ICP-MS) as accepted independent method is not available, the accuracy of the method was examined by recovery study of the spiked samples. The recovery of the spikes added to seawater samples is given in Table 3. The quantitative recovery of the uranium spikes and relative standard deviation of 2.5% confirm the good precision and accuracy of the proposed method for the determination of uranium which can be converted to U(VI) oxinate at SPE conditions.

4. Conclusions

Solid phase extraction of $\text{UO}_2(\text{OX})_2$ combined with its pulse polarographic determination in chloroform eluate, provide an accurate, precise and reliable technique for the separation, concentration and determination of trace uranium from 500 ml of sea-water. Due to the accessible high concentration factor (100-fold), this method is very sensitive.

Table 3
Recovery of 2.5 μg of uranium spiked in 500 ml of seawater

No. of sample	Persian Gulf (%)	Caspian Sea (%)
1	99.2	99.7
2	99.5	98.6
3	98.1	99.3
	RSD% = 1.8	RSD% = 2.1

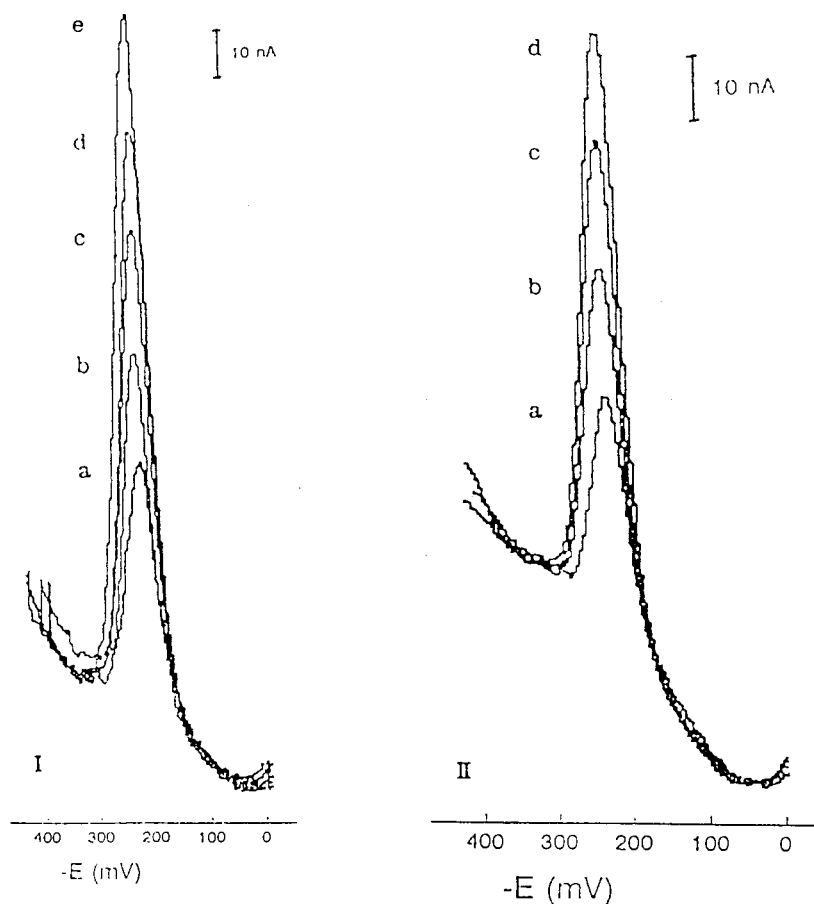


Fig. 3. Differential pulse polarograms of (a) 5 ml chloroform eluate obtained from SPE in optimized conditions, (b)–(e) successive addition of 5 μg of uranium as $\text{UO}_2(\text{OX})_2$ to (a). Supporting electrolyte 0.2 M tri-BAP + 0.01 M Oxine, pulse amplitude, 50 mV. Scan rate 2 mV s^{-1} , polarogram I for 100 ml of solution containing 0.1 mg l^{-1} of UO_2^{+2} , polarogram II for 500 ml of solution containing 0.02 mg l^{-1} of UO_2^{+2} .

References

- [1] J. Wang, R. Setiadji, *Anal. Chim. Acta* 264 (1992) 205.
- [2] P. Ugo, B. Ballarian, S. Daniele, G.A. Mazzocchim, *J. Electroanal. Chem.* 324 (1992) 145.
- [3] P.A.M. Farias, A.K. Ohara, *Feresenius, J. Anal. Chem.* 342 (1992) 87.
- [4] C.M.G. Van den Berg, *Analyst* 114 (1989) 1527.
- [5] R. Kalvoda, M. Kopanica, *Pure Appl. Chem.* 61 (1989) 97.
- [6] C.M.G. Van den Berg, Z.Q. Huang, *Anal. Chim. Acta* 164 (1984) 209.
- [7] J. Wang, J.M. Zadji, *Talanta* 34 (1987) 247.
- [8] C.M.G. Van den Berg, M. Nimmo, *Anal. Chem.* 59 (1987) 924.
- [9] N.K. Lam, R. Kalvoda, M. Kopanica, *Anal. Chim. Acta* 154 (1983) 79.
- [10] S. Sander, G. Henze, *Fresenius, J. Anal. Chem.* 349 (1994) 654.
- [11] S. Sander, W. Wagner, G. Henze, *Analytica Chim. Acta* 305 (1995) 154.
- [12] M.H. Pournaghi-Azar, R. Zargharian, *Anal. Chim. Acta* 328 (1996) 33.
- [13] P.C. Uden, D.M. Parees, F.H. Walters, *Anal. Lett.* 8 (1975) 795.
- [14] B.M. Vanderborcht, R.E. Van Grieken, *Anal. Chem.* 49 (1977) 311.
- [15] R.E. Sturgeon, S.S. Berman, S.N. Willie, J.A.H. Desaulniers, *Anal. Chem.* 53 (1981) 2337.
- [16] H. Watanabe, K. Goto, S. Taguchi, J.W. McLaren, S.S. Berman, D.S. Russel, *Anal. Chem.* 53 (1981) 738.

Modelling the background current with partial least squares regression and transference of the calibration models in the simultaneous determination of Tl and Pb by stripping voltammetry

Ana Herrero *, M. Cruz Ortiz

Dpto. Química, Fac. de CyTA y C. Químicas, Universidad de Burgos, Pza. Misael Bañuelos s/n, 09001 Burgos, Spain

Received 14 May 1997; received in revised form 24 July 1997; accepted 5 August 1997

Abstract

With the aim of carrying out a calibration transfer for routine analysis, partial least squares (PLS) regression was successfully applied to simultaneously determine thallium and lead by stripping voltammetry when an interfering background current is present. The presence of a significant blank signal that overlaps the thallium peak, together with the overlapping thallium and lead signals were both suitably modelled by this multivariate regression technique. Moreover, once the PLS models are built, the piecewise direct standardization (PDS) method can be used to transfer these models over time in such a way that the number of calibration samples that will be needed in future determinations is reduced from 25 to 9, without a loss of quality in the analyses. The mean of the relative errors (in absolute values) obtained for thallium and lead is below 4.94% and 3.19%, respectively. © 1998 Elsevier Science B.V. All rights reserved.

Keywords: Calibration transfer; Partial least squares regression; Background current; Overlapping signals; Multianalyte determination; Stripping voltammetry

1. Introduction

The simultaneous determination of thallium and lead is commonly performed by stripping voltammetry, where the current recorded during the stripping step is given by the sum of both the current corresponding to the metal of interest and the background current, unrelated to the reaction of interest. The latter can also be divided into the

charging current and the background component related to redox reactions of impurities, supporting electrolytes, solvents or reactions of the electrode itself.

The accuracy of the stripping voltammetric determinations depends on the discrimination that can be achieved against the different contributions to the total current, i.e. on the uncertainty in measuring the current of the reaction of interest. Effective approaches for compensating the charging current have been developed, perhaps the

* Corresponding author.

most widely used being the differential pulse stripping voltammetry [1] which in addition, gives a gain in the overall signal-to-background ratio.

However, it should be noted that the differential pulse mode discriminates only against the nonfaradaic charging current whereas it does not correct the various faradaic components of the background current. To also discriminate this latter contribution some subtractive procedures have been developed with the aim of measuring the background current and subtracting it from the recorded current. Among these, the subtractive stripping voltammetry [1] presents the disadvantage of needing two identical electrodes (with the same surface area, morphology, etc.), which implies that, since two electrode surfaces are not perfectly matched, the background current is not always completely compensated.

The present-day electrochemical instrumentation and Chemometrics [2] provide wide information about a system under study and useful mathematical tools respectively, that allows one to approach the background current problem from a different point of view. The use of multivariate regression techniques [3], such as the partial least squares (PLS) regression [4,5], implies the extraction of the most relevant information related to the analyte of interest and possibly a way to discriminate the background current, from the whole voltammetric signal (not only from the peak current).

In this paper, PLS regression has been used to simultaneously determine thallium and lead by differential pulse anodic stripping voltammetry (DPASV) when the experimental blank also gives a voltammetric peak that seriously interferes with the thallium peak. The determination of these two metals in most electrolytes is difficult because of the similar potentials at which both are oxidized, which results in the overlapping of their voltammetric peaks and, hence, in an analytical error. In fact, several chemical and mathematical approaches have been proposed to solve these two overlapping peaks that include the use of extraction techniques [6], suitable electrolytes [7,8] or surfactants [9], medium-exchange [10,11], and others such as: derived voltammetry [12], Kalman filter [13,14], PLS [15] or continuum regressions [16], etc.

Once the PLS models had been built, a calibration transfer procedure was carried out to reduce the experimental effort that would be needed in similar analyses in the future carried out in a routine way. Among the several standardization procedures [17–20] that have been developed, the piecewise direct standardization (PDS) method [17,21] has provided very successful results when it has been used with NIR spectroscopic data, but it can also be applied to polarographic [22] and voltammetric data [23]. This method is based on calculating a matrix, the transformation matrix F , which relates a subset of signals measured for instance on a specific instrument or a set day to other signals measured on another instrument or a different day. Then, the PLS model built with the whole primary calibration set can be applied to the signals of the new situation corrected by means of the transformation matrix, in such a way that only a small subset of calibration samples has been measured in the new situation.

In this way, the number of samples needed for simultaneously determining thallium and lead in future analyses by means of the PLS regression has been reduced from 25 to 9, without a loss of quality in the determinations.

2. Experimental

2.1. Apparatus

The voltammetric measurements were carried out using a Metrohm 646 VA processor with a 647 VA stand in conjunction with a Metrohm multimode electrode (MME) used in the hanging mercury drop electrode (HMDE) mode. The three-electrode system was completed by means of a platinum auxiliary electrode and an $\text{Ag}|\text{AgCl}|\text{KCl}$ (3 mol dm^{-3}) reference electrode. A Crison micro pH-2002 pH-meter was used for pH measurements. The analysis of data was done with PARVUS [24] and MATLAB [25].

2.2. Reagents

Analytical-reagent grade (Merck) chemicals were used without further purification. All the

solutions were prepared with deionised water obtained in a Barnstead NANO Pure II system. The voltammetric measurements were carried out in an oxalic acid (0.1 mol dm^{-3}) and hydrochloric acid (0.1 mol dm^{-3}) supporting electrolyte medium ($\text{pH} = 1.037$). Nitrogen (99.997%) was used to remove dissolved oxygen.

2.3. Procedure

The solution was placed in the voltammetric cell and purged with nitrogen for 10 min. Once the solution had been deoxygenated, a deposition potential of -0.600 V was applied to the

Table 1
Experimental design used in calibrates A and B

Sample	Experimental design level		Concentration ($\text{M} \times 10^7$)	
	Thallium	Lead	Thallium	Lead
1	1	1	3.2659	2.2909
t1	1	1.5	3.2594	3.4295
2	1	2	3.2530	4.5636
3	1	3	3.2402	6.8185
4	1	4	3.2275	9.0557
5	1	5	3.2148	11.2754
6	2	5	6.4047	11.2315
7	2	1	6.5059	2.2818
8	2	2	6.4803	4.5457
9	2	3	6.4549	6.7918
10	2	4	6.4297	9.0203
t3	2.5	4	8.0214	9.0027
11	3	1	9.7205	2.2728
12	3	2	9.6824	4.5278
13	3	3	9.6445	6.7652
14	3	4	9.6070	8.9852
15	3	5	9.5698	11.1880
16	4	1	12.9098	2.2639
17	4	2	12.8594	4.5102
t2	4	2.5	12.8343	5.6267
18	4	3	12.8093	6.7389
19	4	4	12.7597	8.9504
20	4	5	12.7104	11.1448
t4	4.5	5	14.2717	11.1233
21	5	1	16.0742	2.2551
22	5	2	16.0117	4.4926
23	5	3	15.9496	6.7128
24	5	4	15.8880	8.9158
25	5	5	15.8269	11.1019

t1 to t4 are the test set samples.

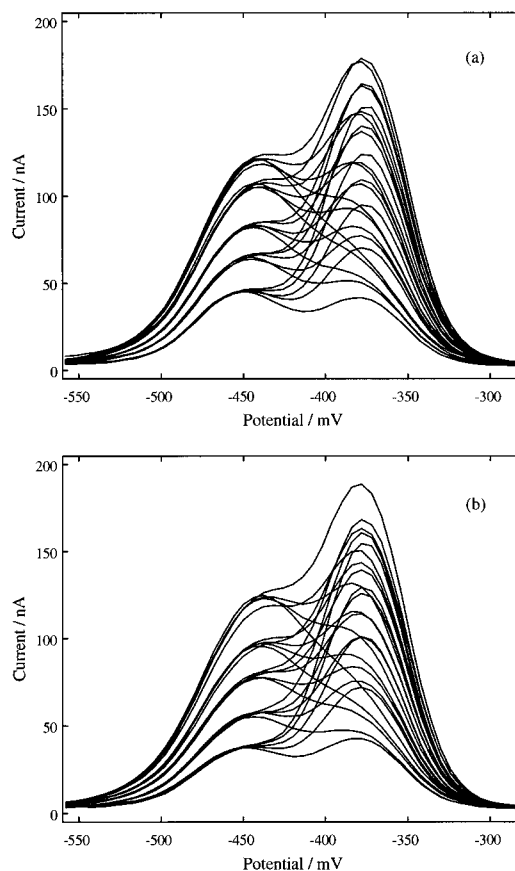


Fig. 1. Stripping voltammograms recorded for calibrates A (a) and B (b). The peaks correspond to thallium (left) and lead (right).

mercury electrode during 30 s. Next, the stirrer was switched off and, after 30 s of rest period, an anodic potential scan was initiated from -0.558 V to -0.282 V in the differential pulse mode. Other instrumental parameters were: modulation amplitude, 50 mV ; pulse repetition time, 0.6 s ; nominal area, 0.40 mm^2 ; scan rate, 10 mV s^{-1} ; stirring rate, $1290 \text{ rev. min}^{-1}$. The solution was stirred and deoxygenated for 15 s after each addition.

3. Results and discussion

The major overlap of thallium and lead peaks is the most significant obstacle found in the

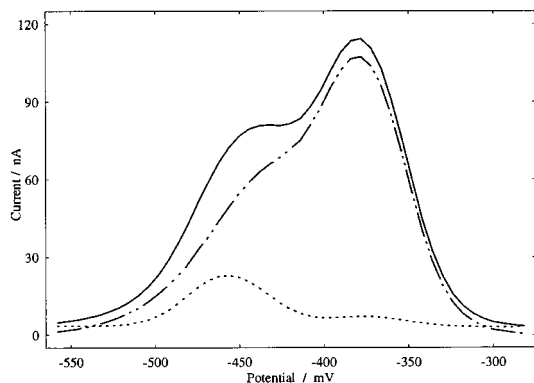


Fig. 2. Stripping voltammograms corresponding to the experimental blank (dotted line) and to sample 33 of calibrate A with (dash-dot line) and without (solid line) subtracting the blank signal.

simultaneous determination of both metals by stripping voltammetry. Previous analyses demonstrate that this interference is so important that if an insufficient experimental design is used (eight training samples distributed in a central composite design), then the information provided to the PLS model is too limited and, consequently, the regression model built becomes useless (explained variance below 96%). Therefore, the experimental design showed in Table 1 has been used, which exhaustively covers the considered concentration ranges; the training set is formed of 25 calibration samples whereas the test set is composed of four samples.

A whole calibration set was recorded by applying the experimental procedure to the samples of the experimental design, the corresponding voltammograms being shown in Fig. 1a, that henceforth will be denoted as calibrate A. As expected, the presence of two overlapping voltammetric peaks, that can be analysed by means of multivariate techniques [15,16], is observed; the first (left) assigned to thallium and the second (right) to lead.

However, the supporting electrolyte used in this paper also gives a voltammetric peak which, as can be seen in Fig. 2, overlaps the thallium peak. This signal, considered background current, leads to a significant increase in the recorded signal (solid line) with regard to the net signal (dash-dot line) obtained when the blank signal is subtracted. Likewise, a shifting of the thallium peak (the left peak) is observed since the blank signal and the thallium peak potential do not coincide exactly, which is more evident by comparing the voltammograms in Fig. 2. In Fig. 1a the thallium peak is being shifted to more positive potentials when the concentration of thallium is increased, i.e. when the thallium contribution to the peak is greater. Whereas in Fig. 2, when the blank signal has been subtracted, the peak potential is about -0.435 V in all the voltammograms recorded for the different levels of thallium considered.

Usually, if a blank gives a voltammetric signal in the potential range where the peaks of the metals to be determined appear, this signal is

Table 2

Explained and cross-validated variance of the PLS models built for calibrate A

L. V.	Thallium			Lead		
	Y block		X block	Y block		X block
	Explained variance	Cross-validated variance	Explained variance	Explained variance	Cross-validated variance	Explained variance
1	47.15	48.93	81.00	54.43	55.71	81.00
2	94.31	94.62	98.10	99.28	99.32	98.10
3	99.68	99.65	99.33	99.36	99.40	99.27
4	99.71	99.67	99.52	99.58	99.57	99.57
5	99.72	99.64	99.72	99.58	99.52	99.75
6	99.72	99.53	99.86	99.59	99.49	99.86

L.V. is the number of the considered latent variables.

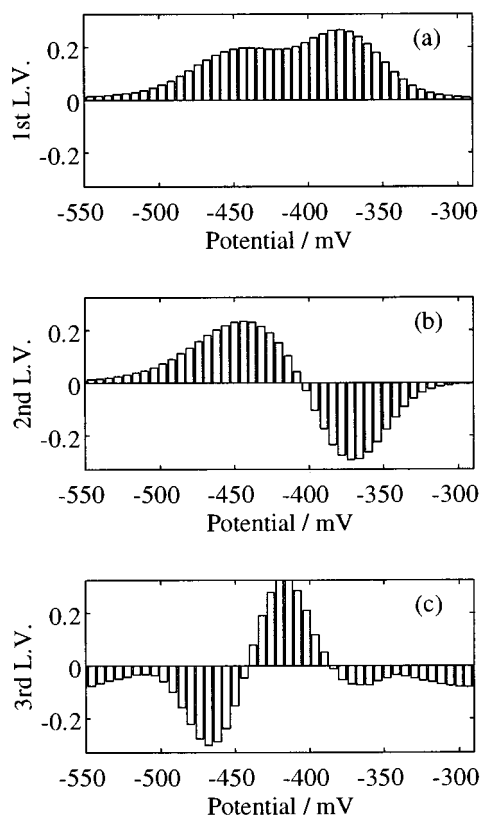


Fig. 3. Loadings for the 1st (a), 2nd (b) and 3rd (d) latent variables corresponding to the PLS model built for thallium (calibrate A).

subtracted from the calibration and test set voltammograms alike to avoid undesirable analytical errors. But, it is not always possible to have the experimental blank signal and so, a method able to model this interference would be of great interest. So, to evaluate the ability of the PLS regression to model this kind of interference, which in this case is added to the above indicated strong overlap of thallium and lead peaks, the original signal has been used in the analysis, i.e. the voltammograms showed in Fig. 1 where the blank signal has not been subtracted.

3.1. Multivariate regression models

A PLS model has been built independently for both thallium and lead, taking the current

recorded at 47 potential values as predictor variables for each sample, the concentration of metal being the response variable in each case. The data have not been autoscaled. The full cross-validation method [26,27] has been used with the aim of evaluating the stability and prediction ability of the PLS models built.

The high explained and cross-validated variance values, showed in Table 2, indicate that the interference due to the blank signal has been suitably modelled by the PLS regression, despite the significance of the phenomenon, principally on the thallium calibration. The models built for both metals consist of four latent variables, whose

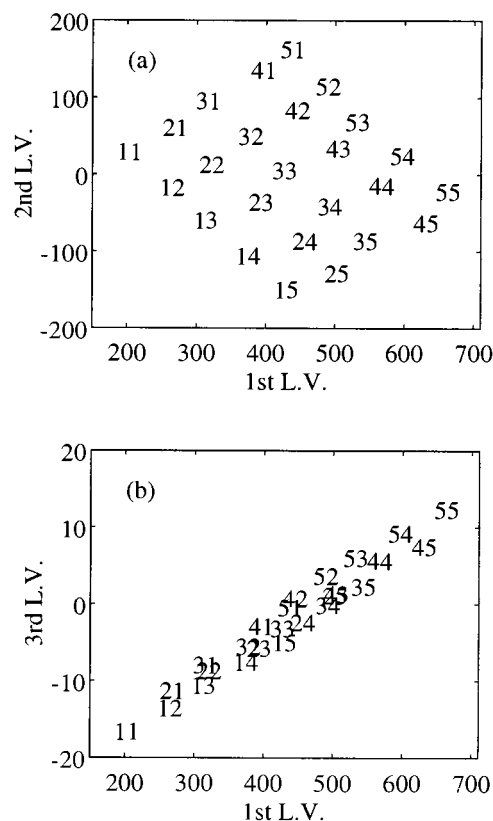


Fig. 4. Scores for the 1st–2nd (a) and 1st–3rd (b) latent variables corresponding to the PLS model built for thallium (calibrate A). The first digit indicates the concentration level of thallium, the second is the level of lead.

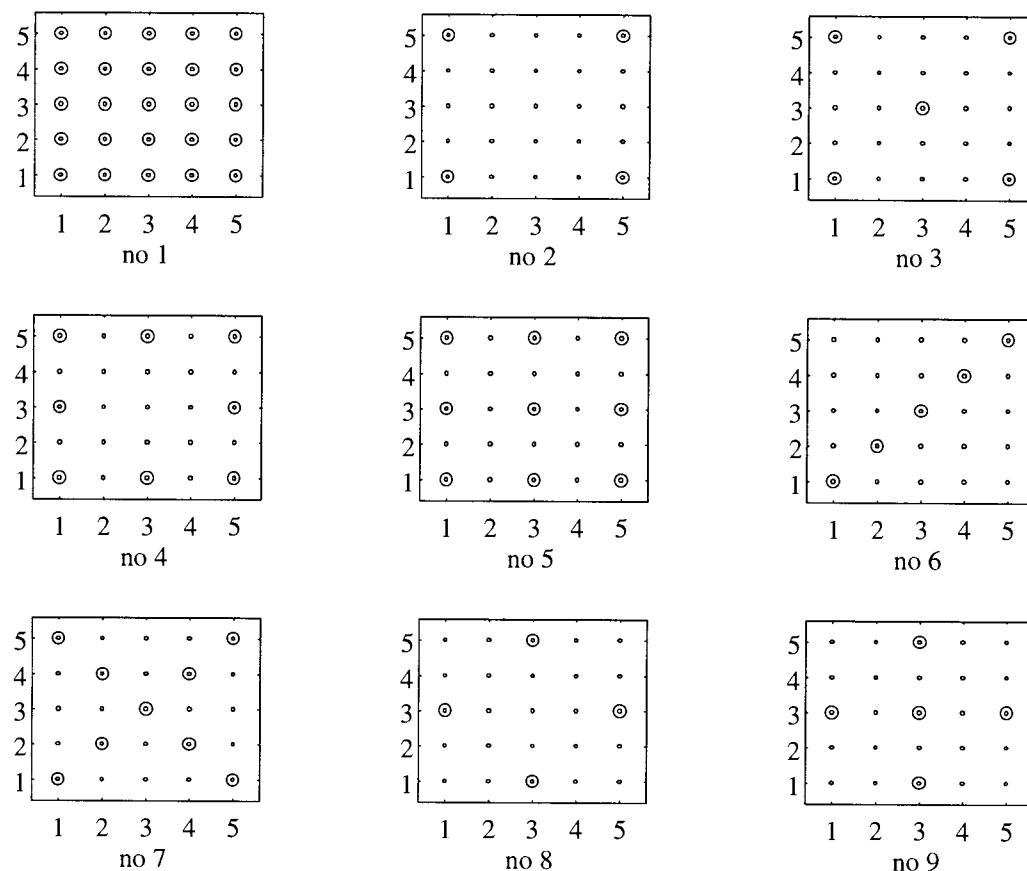


Fig. 5. Standardization subsets (samples signalled with a circle) used in the calibration transfer procedures. On ordinates the level of thallium and on abscissae that of lead.

chemical interpretation has been analysed through the corresponding loadings and scores, Fig. 3 and Fig. 4, respectively.

The shape of the loadings calculated for the first latent variable, showed in Fig. 3a for thallium, corresponds to a 'mean voltammogram', which indicates that it is a size factor, as was expected. However, the loadings corresponding to the second latent variable, Fig. 3b, establish a difference between the two 'evident' overlapping peaks of the signal, extracting that information related to the metal of interest in each case and adequately correcting the interference due to the other overlapping peak. Thus, those potentials related to the metal of interest have positive val-

ues, whereas the contribution of the rest to the signal is subtracted through the negative sign of the corresponding loadings. In fact, the distribution of the scores in the plane formed by these first two latent variables reproduces the experimental design used (Fig. 4a) where the samples are arranged along the abscissae axis in increasing concentration order (from sample 11 to 55). The models built with both latent variables have high explained and cross-validated variance (Table 2) but the need for more variables in the PLS models is evident, especially for thallium since the interference of the blank signal is critical in this case.

On the other hand, the loadings obtained for the third latent variable in the model built for

Table 3

Effect of modelling the blank interference on the concentration calculated with the PLS models for the test set samples of calibrate A. True values are found in Table 1

Sample	Concentration ($M \times 10^7$) calculated with the two latent variables PLS models (without modelling interferences)		Concentration ($M \times 10^7$) calculated with the four latent variables in PLS model (modelling interferences)	
	Thallium	Lead	Thallium	Lead
<i>t1</i>	5.3312	3.3714	3.2613	3.5082
<i>t2</i>	13.1027	5.8917	13.3710	5.7825
<i>t3</i>	8.5162	10.0103	8.0696	9.4880
<i>t4</i>	12.9128	11.6537	14.0989	11.0425

thallium (Fig. 3c) are related principally to the left side of the voltammogram, establishing the difference between those potentials related to the thal-

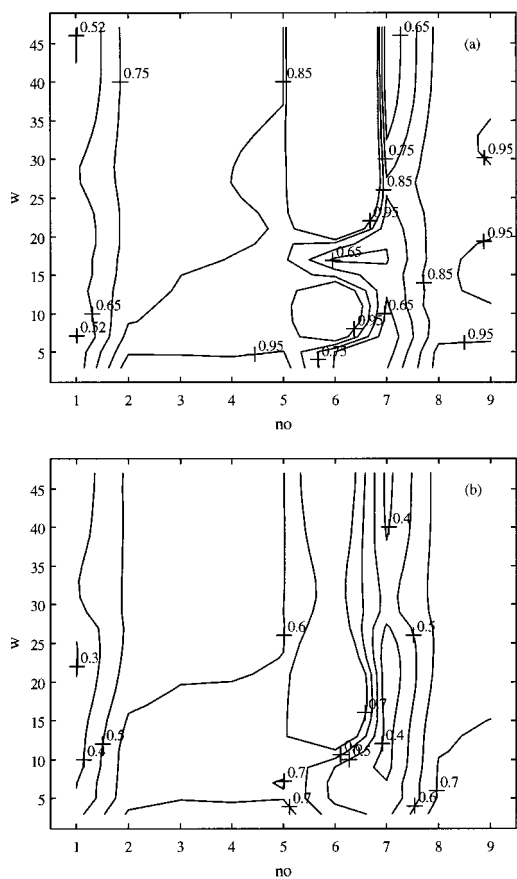


Fig. 6. SEP contour lines of the response surfaces corresponding to thallium (a) and lead (b).

lium peak and those corresponding to the blank signal, which is subtracted. Moreover, the linear relation that exists between the scores of the first (size factor) and third latent variables (Fig. 5b) indicates that the phenomenon modelled by the third latent variable is intimately related to the predictor variables themselves, i.e. to something referred to the global signal and not to the concentration of the metals. This was confirmed since another two PLS models built by subtracting the blank signal to the training set voltammograms had similar explained and cross-validated variance values, but no latent variable presented this characteristic structure (the scores in Fig. 4b seem to 'put in order' the samples in the plane of the 1st and 3rd latent variables taking into account the sum of the concentrations or levels of both analytes).

With regard to the fourth latent variable, which is included in the models of both metals, it seems to be related rather to specific samples or objects than to more general phenomena.

Table 4

Relative errors (%) for the test set samples of calibrate B calculated without and with calibration transfer

Sample	With the full calibration matrix B		Using calibration transfer	
	Thallium	Lead	Thallium	Lead
<i>t1</i>	7.01	7.17	5.07	0.71
<i>t2</i>	-2.39	-2.79	-3.13	-2.95
<i>t3</i>	-2.20	-4.47	-4.72	-5.24
<i>t4</i>	-2.85	-3.40	-6.77	-3.38

The parameters used in the calibration transfer were: $no = 7$ and $w = 47$ for thallium and $no = 7$ and $w = 21$ for lead.

The third and four latent variables are then related to the interference and some irregularities so, if one does not consider these two latent variables, it is possible to evaluate the error due to the interference. In the training set, considering only two latent variables, the mean relative error (in absolute value) is 3.11% versus 2.24% when the concentration of lead is calculated with four latent variables. In the case of thallium the effect is much more important, 14.48% versus 1.51% with two and four latent variables, respectively. This high discrepancy is due to the fact that the interference shows an overlapping signal in the range of potentials where the thallium peak appears. Detailed errors for test samples are shown in Table 3. Mean errors obtained are 5.59% versus 2.80% for lead and 20.34% versus 1.51% for thallium.

The loadings and scores shown in Fig. 3 and Fig. 4 for thallium were similar to those obtained in the PLS model built for lead, so a parallel analysis was made.

3.2. Calibration transfer

As the PLS regression technique has proved to be useful in the determination carried out, a calibration transfer procedure, the PDS method, has been applied for minimizing the experimental effort that would be necessary in later routine analyses. For this purpose, a new calibration set, henceforth named calibrate B, was recorded some days later following the above experimental design. This new training set (Fig. 1b) is very similar to the former, corresponding to the calibrate A showed in Fig. 1a, but they are not identical.

The PDS method [17,21] consists of relating the voltammograms measured in two different situations, in this case on different days, through a transformation matrix \mathbf{F} which is calculated from a small subset (standardization subset) of voltammograms recorded in both situations ($\bar{\mathbf{X}}_A$ and $\bar{\mathbf{X}}_B$ for calibrates A and B, respectively).

$$\bar{\mathbf{X}}_A = \bar{\mathbf{X}}_B \mathbf{F}$$

The standardization subset should be large enough in such a way that predictor variables sufficiently cover the whole experimental range. In

this way, each predictor variable (x_i) from the first day is related to a moving window (\mathbf{Z}_i) of variables measured on the second day by means of a local multivariate regression, the corresponding regression vectors being arranged along the main diagonal of the transformation matrix and the rest of the elements being zero, so the size of \mathbf{F} is $p \times p$, p being the number of predictor variables measured.

$$\mathbf{Z}_i = [x_{B,i-j}, x_{B,i-j+1}, \dots, x_{B,i+k-1}, x_{B,i+k}]$$

$$x_{A,i} = \mathbf{Z}_i \mathbf{b}_i$$

Then, \mathbf{F} can be used to correct any voltammogram measured on the second day to the format which would have been obtained if it had been measured on the first day. In this way, the previously built and analysed PLS models can be applied, through their corresponding closed forms [28], to the corrected signals for determining the concentration of thallium and lead in the samples measured on the second day.

The m-function *pdsgen*, implemented in the PLS Toolbox by Wise [29], has been used to calculate the transformation matrix \mathbf{F} . The input parameters for this function are the two training sets (\mathbf{X}_A and \mathbf{X}_B), the window size and the standardization subset. With the aim of optimizing the standardization procedure, several values have been used for the last two parameters. The window size (w) has taken the following values: 3, 5, 7, ..., 47; i.e. 23 different values in all, whereas the different standardization subsets (no) used are those shown in Fig. 5.

The standard error of prediction (SEP), calculated from the test set samples, has been used to evaluate the quality of the calibration transfer procedures carried out, although those errors related to the training set samples have also been taken into account. SEP is given by the square root of

$$s^2 = \frac{\sum_j (y_j - \hat{y}_{B,j})^2}{J}$$

where y_j and $\hat{y}_{B,j}$ are the true concentrations and those computed by the PLS model built for calibrate B respectively, and J is the number of

objects in the test set. Fig. 6 shows, through the contour lines of the response surfaces, the values of SEP obtained for both metals as a function of the different values of w and no used in the calibration transfer (a total of 207 independent calibration transfers have been done). As can be seen, the best results are related to the standardization subsets 1 and 7; whereas the worst were obtained with the standardization subset 6, whose samples correspond to one of the diagonals of the design (Fig. 6) and for this reason, this subset provides highly correlated voltammograms that lead to a significant structural defect in this standardization subset [30].

Since $no = 1$ implies all the training set samples in the standardization procedure, i.e. it corresponds to a full recalibration (25 training set samples), and $no = 7$ requires only the measurement of nine standardization samples in the new situation, it is evident that the latter is the optimum standardization subset for simultaneously determining thallium and lead by DPASV through the calibration transfer procedure proposed. The use of only one standardization subset for both metals is a desirable feature of the calibration transfer because, in this way, no additional experimental effort is necessary to determine one of the metals.

The influence of the different window sizes used on the SEP values is less than that of the standardization subsets. For $no = 7$, the minimum SEP corresponds to $w = 47$ for thallium and $w = 21$ for lead. The larger window size for thallium is due to the fact that the blank signal seriously interferes with the thallium peak, which makes necessary the use of some potentials where this interference does not exist to adequately carry out the calibration transfer. So, the interference of the background current is also detected in the calibration transfer step.

The relative errors corresponding to test set samples of calibrate B calculated by means of the calibration transfer and the PLS models built with the full recalibration are shown in Table 4. The errors obtained with the calibration transfer for both test and training sets are similar to those corresponding to the full recalibration, i.e. to those calculated by the PLS models built with all

the calibration samples of calibrate B, which indicates the success of the standardization approach. To confirm the ability of the instrumental standardization to predict the concentrations of thallium and lead, the procedure has been applied to the 16 samples of calibrate B which do not belong to transfer set $no = 7$; these samples are independent of the standardization procedure and their concentrations are known. The mean of the relative errors (in absolute values) obtained for thallium and lead is 4.94% and 3.19% respectively. These errors are in the range expected when this stripping technique is used, but the number of standard calibration samples that will be needed in later routine determinations of both metals has been reduced to 64%.

Acknowledgements

This work has been partially supported by Consejería de Educación y Cultura de la Junta de Castilla y León under Project BU22/96.

References

- [1] J. Wang, Stripping Analysis: Principles, Instrumentation and Applications, VCH Publishers, Derfield Beach, 1985.
- [2] S.D. Brown, R.S. Bear, Crit. Rev. Anal. Chem. 24 (1993) 99.
- [3] H. Martens, T. Næs, Multivariate Calibration, 2nd edn., Wiley, New York, 1992.
- [4] R.G. Brereton, Chemometrics, Applications of Mathematics and Statistics to Laboratory Systems, Ellis Horwood, Chichester, UK, 1990.
- [5] M. Meloun, J. Militký, M. Forina, Chemometrics for Analytical Chemistry, Vol. 2, Ellis Horwood, New York, 1994.
- [6] Y.A. Karbainov, A.G. Stromberg, Izv. Tomsk. Politekh. Inst. 151 (1966) 7.
- [7] M.A. Allus, R.G. Brereton, Analyst 117 (1992) 1075.
- [8] Z. Lukaszewski, W. Zembruski, A. Piela, Anal. Chim. Acta 318 (1996) 159.
- [9] Z. Lukaszewski, M.K. Pawlak, A. Cizewski, Talanta 27 (1980) 181.
- [10] L. Anderson, D. Jagner, M. Josefson, Anal. Chem. 54 (1982) 1371.
- [11] R. Neeb, I.Z. Kiehnast, Fresenius Z. Anal. Chem. 226 (1967) 153.
- [12] J.J. Berzas, J. Rodríguez, Fresenius Z. Anal. Chem. 342 (1992) 273.

- [13] D.P. Binkley, R.E. Dessy, *Anal. Chem.* 52 (1980) 1335.
- [14] C.A. Scolari, S.D. Brown, *Anal. Chim. Acta* 166 (1984) 253.
- [15] A. Henrion, R. Henrion, G. Henrion, F. Scholz, *Electroanalysis* 2 (1990) 309.
- [16] M.C. Ortiz, M.J. Arcos, L.A. Sarabia, *Chemometr. Intell. Lab. Syst.* 34 (1996) 245.
- [17] Y. Wang, D.J. Veltkamp, B.R. Kowalski, *Anal. Chem.* 63 (1991) 2750.
- [18] O.E. de Noord, *Chemometr. Intell. Lab. Syst.* 25 (1994) 85.
- [19] M. Forina, G. Drava, C. Armanino, R. Boggia, S. Lanteri, R. Leardi, P. Corti, P. Conti, R. Giangiacomo, C. Galliena, R. Bigoni, I. Quartari, C. Serra, D. Ferri, O. Leoni, L. Lazzeri, *Chemometr. Intell. Lab. Syst.* 27 (1995) 189.
- [20] B. Walczak, E. Bouveresse, D.L. Massart, *Chemometr. Intell. Lab. Syst.* 36 (1997) 41.
- [21] Y. Wang, M.J. Lysaght, B.R. Kowalski, *Anal. Chem.* 64 (1992) 562.
- [22] A. Herrero, M.C. Ortiz, *Anal. Chim. Acta*, in press.
- [23] A. Herrero, *Análisis Multivariante y Transferencia de Calibrado en Voltamperometría*. Ph.D. thesis, University of Burgos, 1996.
- [24] M. Forina, R. Leardi, C. Armanino, S. Lanteri, *PARVUS: An Extendable Package of Programs for Data Exploration, Classification and Correlation*, Ver. 1.1, Elsevier Scientific Software, 1990.
- [25] Matlab, The MathWorks, Natick, Mass., 1992.
- [26] M. Stone, *J. R. Stat. Soc. Ser. B* 36 (1974) 111.
- [27] S. Lanteri, *Chemometr. Intell. Lab. Syst.* 15 (1992) 159.
- [28] E. Marengo, R. Todeschini, *Chemometr. Intell. Lab. Syst.* 12 (1991) 117.
- [29] B.M. Wise, *PLS Toolbox for use with MATLAB*, ver. 1.3, available from the author.
- [30] J.H. Kalivas, P.M. Lang, *Mathematical Analysis of Spectral Orthogonality*, in: *Practical Spectroscopy series*, Vol. 17, Marcel Dekker, New York, 1994.



ELSEVIER

Talanta 46 (1998) 139–143

Talanta

Determination of rhodium in waters by Mg–W cell-electrodeposition and electrothermal atomic absorption spectrometry

Satoshi Kaneco *, Jiniti Ogawa, Kiyohisa Ohta, Syn-ichi Itoh, Takayuki Mizuno

Department of Chemistry for Materials, Faculty of Engineering, Mie University, Tsu, Mie 514, Japan

Received 28 May 1997; received in revised form 4 August 1997; accepted 5 August 1997

Abstract

A new concentration method of rhodium using Mg–W cell-electrodeposition has been developed. The method was combined with electrothermal atomic absorption spectrometry (ETAAS) with a tungsten tube atomizer. The optimal immersing time was 120 s. The most suitable pH for rhodium electrodeposition was 1.0. Under optimal conditions, the detection limit of rhodium by the ETAAS with the preconcentration was 13 ng ml^{-1} (3S/N). The severe interferences on the AAS signal of rhodium by large amounts of Ca, Cu, Fe, K, Na, Pb and Zn were eliminated by the Mg–W cell-electrodeposition method. The method was applied to the determination of rhodium in river and sea water. The recovery of rhodium spiked environmental samples was in the range of 95.6–109%. The present Mg–W cell-electrodeposition method can be utilized in in-situ sampling of trace elements in environmental samples (water). Furthermore, after sampling, it is easy to carry and store the W-sheet without contamination for a long time. © 1998 Elsevier Science B.V. All rights reserved.

Keywords: Preconcentration; Electrodeposition; Mg–W cell; Electrothermal atomic absorption spectrometry; Rhodium; Water

1. Introduction

Until now, ion-exchange chromatography, liquid chromatography, plane, chromatography, gel-filtration chromatography, liquid–liquid extraction, coprecipitation ($\text{Fe}(\text{OH})_3$, $\text{La}(\text{OH})_3$, $\text{Zr}(\text{OH})_4$, etc.), electrolytic deposition (electrodeposition, stripping voltammetry), electrophoretic

separation, evaporation, flotation, freezing (cold-trap), sorption and adsorption (activated carbon, alumina, glass beads, silica gel, tungsten wire, etc.) and ultrafiltration have been reported as preconcentration (collection) and separation methods of trace metals in various samples [1–13]. These preconcentration methods combined with instrumental analysis have frequently been used for the determination of ultra-trace analytes in complex matrix samples. Most of them are complicated and time-consuming, except for ad-

* Corresponding author. Tel.: +81 59 2319427; fax: +81 59 2319442; e-mail: kaneco@chem.mie-u.ac.jp

sorption methods, which are simple and convenient. The electrolytic deposition method needs a power supply (electric source) like a potentiostat but metal ions are collected efficiently. A preconcentration method having the advantage of both is the new electrodeposition method, reported here.

Recently, rhodium has been widely used as a catalytic converter for the control of automotive emission and as a raw material of plating in electronic instruments [14]. As a result, rhodium has been widely spread in the environment. ETAAS with a metal tube, a conventional method for the determination of trace elements [15–17], is useful for the determination of rhodium in biological samples [18].

In this work, a novel, simple and convenient electrodeposition method is presented and applied to the determination of trace rhodium in environmental samples such as seawater and river water by ETAAS with a tungsten tube atomizer.

2. Experimental

2.1. Apparatus

The galvanic electrodeposition cell (Mg–W cell), used here for the preconcentration of rhodium, was reported in previous papers [19,20]. As cathode, a tungsten sheet (2.5 × 2.5 mm, 0.05 mm thick, 99.95% purity, Rembar) and, as anode, a magnesium sheet (8 × 8 mm, 0.10 mm thick, 99.9% purity, Niraco), were used. Both were connected with a copper lead wire having clips at both ends.

The ETAAS optical system employed for the rhodium determination was described in detail elsewhere [18]. A tungsten tube atomizer (20 mm long × 2.0 mm i.d.) made of tungsten foil (0.05 mm thick, 99.95% purity, Rembar) was used for the ETAAS measurements. The atomizer had a slit (0.08 × 2.7 mm) at the mid-point of the tube to insert the W-sheet. The analytical line was 343.5 nm Rh (hollow cathode lamp, Hamamatsu Photonics).

2.2. Reagents

Solutions of the matrix elements for the interference study were prepared as chlorides in 0.1–6 M

hydrochloric acid. A standard stock solution (1 mg ml⁻¹, 1 M HCl solution) of rhodium was obtained from Kishida Chemistry, Osaka, Japan. All of the chemicals used here were of analytical grade purity.

2.3. Procedures

Mg and W sheets used as electrodes were de-fatted with acetone and washed with 0.1 M HCl prior to electrodeposition. Sample solution (3 ml) was put into the cell and the pH adjusted to 1.0 with HNO₃. Mg–W sheets with a copper wire dipped into the solution and the solution was stirred for 120 s. The W-sheet put out was washed with demineralized-water and then perpendicularly inserted from a slit on the tungsten tube atomizer into the atomizer. An upper part of the W-sheet was exposed from the atomizer. The W-sheet was dried at 80°C for 10 s, pyrolyzed at 590°C for 10 s and atomized at 2230°C (using a heating rate of 5.5°C ms⁻¹) for 3 s in Ar 480 ml min⁻¹ + H₂ 20 ml min⁻¹ purge gas.

3. Results and discussion

When two metals (magnesium and tungsten) are combined and then dipped in acidified solution, a spontaneous redox reaction begins in the solution. Since this is a galvanic cell, the cell can provide a voltage and an electron flow through an electrical circuit. The voltage and the electrons can be used for the deposition of metal ions in the solution. Thus, a Mg–W cell was proposed for the preconcentration of rhodium in sample solutions. Since tungsten metal is relatively inert in dilute acids, the redox half-reactions [21] in the cell are as follows:



Therefore, the reaction proceeds from left to right. Based on the Nernst equation it could be calculated that when the Mg^{2+} concentration becomes 0.01 M, then Rh^{3+} is completely electrodeposited because its theoretical concentration becomes 7.0×10^{-163} M. Thus the Mg–W cell is suitable for the preconcentration of rhodium on a W-sheet.

It has been reported in a previous paper [18] that the optimal purge gas on ETAAS with a tungsten tube atomizer was $\text{Ar } 480 \text{ ml min}^{-1} + \text{H}_2 \text{ } 20 \text{ ml min}^{-1}$, the optimal atomization temperature was 2230°C and the pyrolysis temperature 590°C , to obtain the maximum absorbance of rhodium and protect the metal atomizer from oxidation by residual traces of oxygen in the atomizer chamber. Therefore, the subsequent experiments with the preconcentration of the electrodeposition were performed under these experimental conditions.

3.1. Effects of pH and immersing time on the electrodeposition of rhodium

It has been found that electrolytic deposition, sorption and adsorption methods are frequently affected by pH and immersing time [1–4]. Therefore, the effects of pH and immersing time on the electrodeposition of rhodium in a Mg–W cell were investigated. The results are illustrated in Figs. 1 and 2. The effect of pH was evaluated at immersing times of 120 s. Above pH 2, the amount of electrodeposition of rhodium decreased with pH. In 1.5 M of HNO_3 , it was observed that the consumption of the Mg-sheet was very high. Consequently, 1.0 was recommended as optimum pH for the Rh electrodeposition.

The absorbance of rhodium increased with immersing time up to 120 s and then reached a plateau. Subsequently, an immersing time of 120 s was selected.

3.2. Effect of electrodeposition on interferences

Chemical interferences by some matrix elements in the determination of rhodium by ETAAS have been observed [18]. Therefore, the electrodeposi-

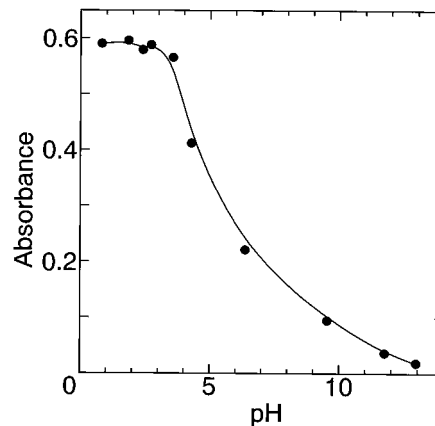


Fig. 1. Effect of pH of electrolyte on absorbance of rhodium. Rh 500 ng ml^{-1} , Immersing time 120 s; Purge gas, $480 \text{ ml Ar min}^{-1} + 20 \text{ ml H}_2 \text{ min}^{-1}$; Pyrolysis temperature, 590°C ; Atomization temperature; 2230°C .

tion of rhodium on the W sheet in the presence of matrix elements such as Ca, Cu, Fe, K, Na, Pb and Zn (1000–10 000 folds) was investigated. The rhodium AA signal was measured in terms of both peak height and peak area. The results are summarized in Table 1. Most of the matrix elements did not interfere with the rhodium

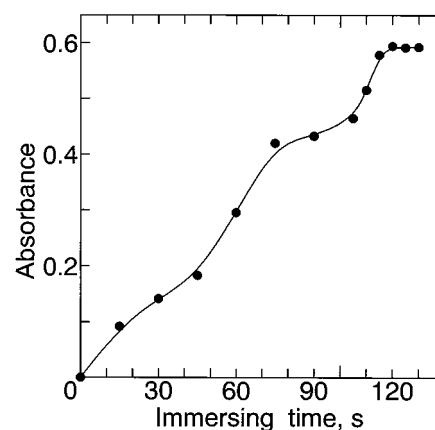


Fig. 2. Effect of electrodeposition time on absorbance of rhodium. Rh 500 ng ml^{-1} , pH 1.0; Purge gas, $480 \text{ ml Ar min}^{-1} + 20 \text{ ml H}_2 \text{ min}^{-1}$; Pyrolysis temperature; 590°C ; Atomization temperature; 2230°C .

Table 1
Effect of Mg–W cell electrodeposition on the interferences

Interfering element (amount)	Peak height	Peak area
	Abs.	Abs. *t
Rh (250 ng ml ⁻¹)	0.298 ± 0.073	0.309 ± 0.055
Ca (250 µg ml ⁻¹)	0.294 ± 0.026	0.283 ± 0.043
(2.5 mg ml ⁻¹)	0.296 ± 0.026	0.293 ± 0.051
Cu (250 µg ml ⁻¹)	0.319 ± 0.053	0.303 ± 0.028
Fe (250 µg ml ⁻¹)	0.305 ± 0.072	0.296 ± 0.048
K (250 µg ml ⁻¹)	0.300 ± 0.021	0.292 ± 0.060
(2.5 mg ml ⁻¹)	0.292 ± 0.026	0.283 ± 0.063
Na (250 µg ml ⁻¹)	0.316 ± 0.060	0.306 ± 0.015
(2.5 mg ml ⁻¹)	0.313 ± 0.024	0.300 ± 0.024
Pb (250 µg ml ⁻¹)	0.296 ± 0.001	0.291 ± 0.070
Zn (250 µg ml ⁻¹)	0.312 ± 0.025	0.301 ± 0.053

The number of measurement > 3.

absorbance. The standard potentials of major co-existing ions [21] are as following.

$$E^\circ = 0.342 \text{ V (Cu}^{2+}\text{)}$$

$$E^\circ = -0.037 \text{ V (Fe}^{3+}\text{)}$$

$$E^\circ = -0.126 \text{ V (Pb}^{2+}\text{)}$$

$$E^\circ = -0.762 \text{ V (Zn}^{2+}\text{)}$$

From these values, it can be understood that, except for copper, rhodium is preferentially electrodeposited in the Mg–W cell. Therefore, it is reasonable that the coexisting metals investigated did not interfere with the rhodium signal, by considering this interference study.

Since this electrodeposition method seems relatively interference-free, the Mg–W cell electrodeposition method was used to determine rhodium in environmental samples.

3.3. Detection limit and reproducibility

The detection limit of rhodium by the ETAAS combined with the electrodeposition method was 13 ng ml⁻¹ (3S/N). The value was approximately the same as the detection limit obtained with graphite atomizers [22] and better than those obtained with ICP-AES (30 ng ml⁻¹ [23]). The reproducibility for the ETAAS with preconcentra-

tion of the electrodeposition was investigated. The relative S.D. for 500 ng ml⁻¹ of rhodium was 4.1% for 10 measurements.

3.4. Determination of rhodium in river and sea waters

Environmental samples spiked with 100–250 ng Rh ml⁻¹ were analyzed by ETAAS with the tungsten tube atomizer after the Mg–W cell-electrodeposition method under optimal conditions. The calibration curve constructed from standard solutions of rhodium was lined up to 350 ng ml⁻¹. Table 2 shows the results obtained for the environmental samples. The recovery from rhodium-spiked river and sea water was in the range of 95.6–109%. The relative S.D. for the determination of rhodium in the environmental samples by the proposed method were better than 10% at > 3 replicate analyses.

The preconcentration method developed is simple, rapid and relatively free from interferences caused by matrix elements. By the combination of ETAAS using a tungsten tube atomizer and the Mg–W cell electrodeposition method, many ultra trace metals in heavily contaminated samples can be determined rapidly and accurately, immediately after the dip of the Mg–W electrodes into

Table 2
Determination of rhodium in sea and river water

Sample	Amount of rhodium, ng ml ⁻¹		
	Added	Found	Recovery, (%)
Sea water			
Ise bay	—	nd	—
	100	107 ± 11	107
	250	266 ± 10	106
River water			
Iwata river	—	nd	—
	100	109 ± 10	109
	250	248 ± 7	99.2
Shitomo river	—	nd	—
	100	102 ± 8	102
	250	239 ± 8	95.6

The number of analysis > 3.

nd, not detected.

acidified sample solutions. The preconcentration method can be most suitable to in-site sampling of environmental samples like seawater. Furthermore, after sampling, it is easy to carry and store the W-sheet without contamination for a long time.

Acknowledgements

This work was supported financially by the Ministry of Education, Science, Sports and Culture of Japan.

References

- [1] Yu. A. Zolotov, N.M. Kuz'min, *Preconcentration of Trace Elements*, Elsevier, Amsterdam, Oxford, New York, 1990.
- [2] Z.B. Alfassi, C.M. Wai, *Preconcentration Techniques for Trace Elements*, CRC Press, Boca Raton, FL, 1992.
- [3] C. Kantipuly, S. Katragadda, A. Chow, H.D. Gesser, *Talanta* 37 (1990) 491.
- [4] K. Terada, *Anal. Sci.* 7 (1991) 187.
- [5] H.B. Evans, C.A.A. Bloomquist, J.P. Hughes, *Anal. Chem.* 34 (1962) 1692.
- [6] A. Diamantatos, A.A. Verbeek, *Anal. Chim. Acta* 91 (1977) 287.
- [7] Z. Marczenko, E. Kowalczyk, *Anal. Chim. Acta* 108 (1979) 261.
- [8] E.W. Berg, D.M. Downey, *Anal. Chim. Acta* 121 (1980) 239.
- [9] S.J. Al-Bazi, A. Chow, *Anal. Chem.* 53 (1981) 1073.
- [10] K. Brajter, K. Slonawska, J.A. Cox, *Anal. Chem.* 57 (1985) 2405.
- [11] B.J. Mueller, R.J. Lovett, *Anal. Chem.* 57 (1985) 2693.
- [12] H. Niskavaara, E. Kontas, *Anal. Chim. Acta* 231 (1990) 273.
- [13] R. Boisvert, M. Bergeron, J. Turcotte, *Anal. Chim. Acta* 246 (1991) 365.
- [14] R. Gaita, S.J. Al-Bazi, *Talanta* 42 (1995) 249.
- [15] K. Ohta, S. Itoh, S. Kaneco, T. Mizuno, *Anal. Sci.* 8 (1992) 423.
- [16] K. Ohta, S. Kaneco, S. Itoh, T. Mizuno, *Anal. Chim. Acta.* 267 (1992) 131.
- [17] K. Ohta, M. Yokoyama, S. Itoh, S. Kaneco, T. Mizuno, *Anal. Chim. Acta.* 291 (1994) 115.
- [18] K. Ohta, J. Ogawa, T. Mizuno, *Anal. Lett.* 30 (4) (1997) 787.
- [19] K. Ohta, J. Ogawa, T. Mizuno, *Analysis* 25 (1997) 1.
- [20] K. Ohta, J. Ogawa, T. Mizuno, *Fresenius' Anal. Chem.* 357 (1997) 995.
- [21] D.R. Lide (Ed.), *Handbook of Chemistry and Physics*, 72nd ed., CRC Press, Boca Raton, FL, 1991, pp. 8–20.
- [22] Z. Aneva, S. Arpadjan, I. Kalaidjieva, *Anal. Chim. Acta* 236 (1990) 385.
- [23] L.H.J. Lajunen, *Spectrochemical Analysis by Atomic Absorption and Emission*, Royal Society of Chemistry, Cambridge, UK, 1992, pp. 230–231.



ELSEVIER

Talanta 46 (1998) 145–148

Talanta

A useful UV spectroscopic method for the determination of the concentration of diethylenetriamine (DETA) in aqueous mineral flotation solutions

Heather J. Gass^a, Ian S. Butler^{a,*}, S. Ram Rao^b, Zhenghe Xu^b, James A. Finch^b

^a Department of Chemistry, McGill University, Montreal, Quebec, Canada

^b Department of Mining and Metallurgical Engineering, McGill University, Montreal, Quebec, Canada

Received 22 April 1997; received in revised form 4 August 1997; accepted 6 August 1997

Abstract

An alternative method for the determination of the concentration of diethylenetriamine (DETA) in aqueous mineral flotation solutions is described. This method is based on the formation of a DETA-Ni(II)-sulphite complex, which shows a UV absorption maximum at 285 nm that varies linearly with the concentration of DETA throughout the 0–50 mg l⁻¹ DETA range. A high concentration of Ni(II) is used to offset the effect of any Cu(II) or Ni(II) ions that may already be present in the industrial plant solutions under analysis. The intensity of the absorbance maximum is dependent on the sulphite ion concentration, but this problem is overcome by measuring the absorbances when the test solutions are spiked with different concentrations of DETA and then extrapolating the absorbance versus DETA concentration plot to zero absorbance to obtain the original concentration of DETA in the test solutions. © 1998 Elsevier Science B.V. All rights reserved.

Keywords: Diethylenetriamine; Concentration; Aqueous

1. Introduction

Diethylenetriamine [*N*-(2-aminoethyl)-1,2-diaminoethane, HN(CH₂CH₂NH₂)₂, DETA] has been suggested as a reagent for the depression of pyrrhotite (FeS) in industrial flotation circuits [1,2]. It can be analyzed by means of a UV spectroscopic method in which the absorption maximum at 386 nm for the complex formed

between DETA and fluram (4-phenylspiro[furan-2(3H),1'-phthalan]3,3'-dione) is monitored [3]. The absorbance of the DETA-fluram complex at this wavelength varies linearly as a function of the concentration of DETA. The method is only accurate and reliable provided the plant solutions being tested do not contain any interfering species. In our experience, however, the results obtained by this method are subject to significant variations if the plant solutions contain any ionic species that can interact with DETA. In the presence of Ni(II) ions, we have found that the absorbances recorded are significantly lower than

* Corresponding author. Fax: +1 514 3983797.

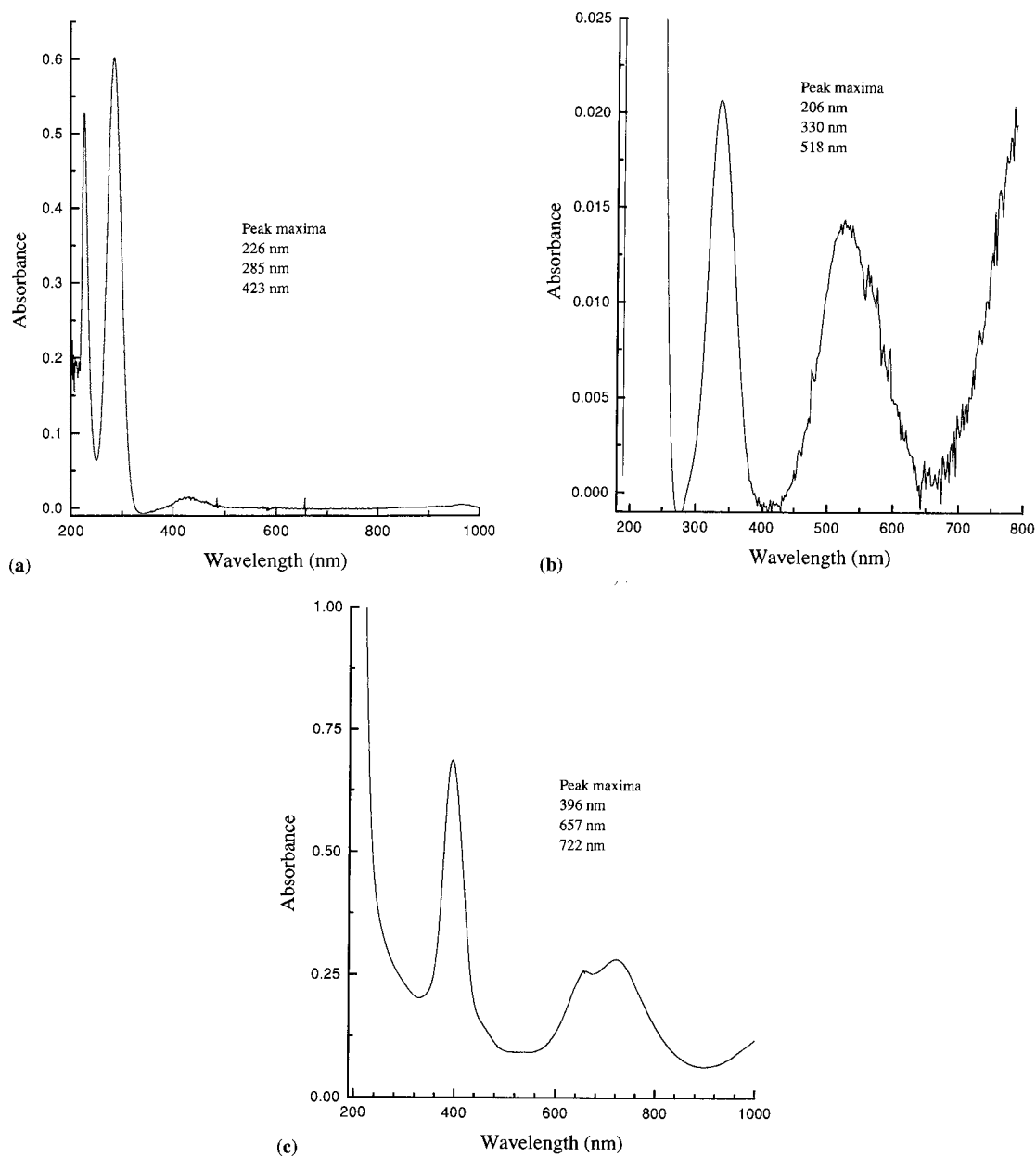


Fig. 1. UV absorbance spectra of: (a) Ni/DETA/Metabisulfite; (b) [Ni(DETA)₂]Br₂; (c) [Ni(H₂O)₆]SO₄.

those in the absence of Ni(II) ions. These absorbance differences are attributable to the formation of Ni(II)-DETA coordination complexes and can be compensated for by using reference blanks having the same Ni(II) concentrations as the test

solutions. In routine industrial operations, however, this is not an easy procedure. While it is relatively simple to determine the concentration of Ni(II) by atomic absorption spectroscopy, the chemical state of the Ni(II) ions depends on which

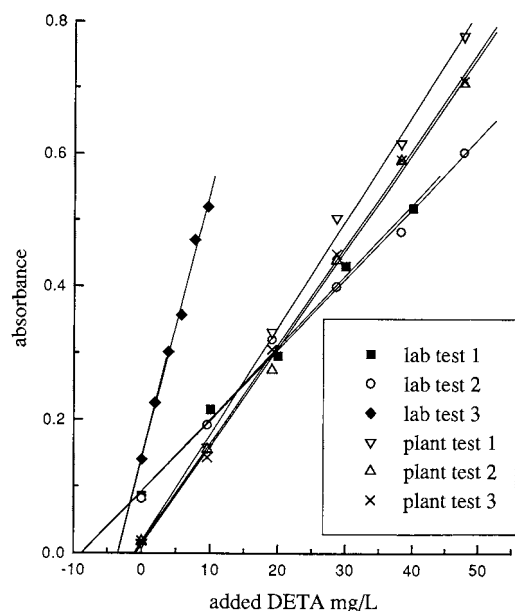


Fig. 2. Variation of absorbance (285 nm) with added DETA concentration mg l^{-1} (all correlations have r values of 0.933 or better). Laboratory test trials use an artificial unknown DETA sample, plant test trials are the simulated flotation circuit samples.

other ionic species are present in the solution. For example, in the presence of sulphite or metabisulphite ions, Ni(II) forms a Ni(II)-DETA-sulphite complex, which shows significantly different absorbances in its UV spectrum (Fig. 1a) than those for Ni(II)-DETA mixtures in the absence of sulphite or metabisulphite ions, e.g. $[\text{Ni}(\text{DETA})_2] \cdot \text{Br}_2 \cdot \text{H}_2\text{O}$ (Fig. 1b) or from $[\text{Ni}(\text{H}_2\text{O})_6]^{2+}$ itself (Fig. 1c).

We have now developed an alternative method for the quantitative determination of DETA in aqueous mineral flotation solutions by UV spectroscopy. The analysis is based on monitoring the variation of the absorbance of the UV maximum at 285 nm of the complex formed when DETA interacts with Ni(II) in the presence of sulphite ion at alkaline pH 8.5–9.5. The presence of varying amounts of Ni(II) ions in solution is overcome by having a large excess of Ni(II) (by addition a soluble nickel salt) in the test solutions. This alternative procedure has also been designed to offset the effect of sulphite ions on the measured

absorbance values. As with any standard addition procedure, it is best that the additions be comparable to those expected in the test solutions. If the range is too large, the relationship is no longer linear, too small and the results are not relevant.

2. Experimental

The following stock solutions were prepared: $\text{NiSO}_4 \cdot 7\text{H}_2\text{O}$, 5 g $\text{Ni}(\text{II}) \text{ l}^{-1}$; simulated industrial plant DETA solutions containing 1 g l^{-1} sodium metabisulphite and set to pH 9.0–9.5 by adding lime; reference blank solution containing 1 g l^{-1} sodium metabisulphite and set to pH 9.0–9.5 by adding lime; standard DETA solution, 0.955 g l^{-1} DETA.

2.1. Procedure

Nickel sulphate solution (10 ml) and the reference blank solution (85 ml) were mixed together in a 100-ml volumetric flask. The volume was then made up to the 100-ml mark with distilled water. The mixture was centrifuged on an International Micro-Centrifuge for 6 min and a sample of the resulting green solution was decanted into a 1.00-cm quartz cuvette and the background UV absorbance at 285 nm was determined. The time between mixing the solutions and recording the UV spectrum was set at 10 min in each case, as the absorbance does decrease with time. The same procedure was repeated for 85 ml samples of the industrial plant test solutions by adding known quantities of the standard DETA solution to the mixtures before making up to the 100-ml mark with distilled water. The concentration of the DETA added was in the 0–50 mg l^{-1} range. The absorbances measured at 285 nm for the different solutions were plotted as a function of the concentration. The concentration of the DETA in the plant test solutions was determined by extrapolating the graph to zero absorbance and dividing the

¹ This concentration is about ten-fold in excess of that required in order to minimize the effect of any Cu(II) or Ni(II) ions already present in the industrial solutions under analysis.

Table 1
Concentrations of DETA from the Ni(II)-DETA-sulphite absorbance measurements

Actual DETA concentration (mg l ⁻¹)	DETA concentration from our method (mg l ⁻¹)	Range of added DETA used in trial (mg l ⁻¹)
10.0	10.1 ^a	0–48.0
1.20	1.14 ^a	0–48.0
3.87	4.18	0–10.0
1.22 ^b	1.02	0–40.0

^a Average of three replicate trials.

^b Value determined by fluram method.

value of the *x*-axis intercept by 0.85 (to account for the volume dilution from 85 to 100 ml).

3. Results and discussion

The UV spectrum of the Ni(II)-DETA-sulphite complex is shown in Fig. 1a. The 285-nm absorption band is clearly characteristic of the complex and increases proportionately with increasing concentration of DETA. Fig. 2 is a typical plot of the results obtained for an initially unknown concentration of DETA. The concentration of DETA measured by this method compares well with that determined by the fluram method. The results given in Table 1 show that our alternative UV spectroscopic procedure is reliable over the tested

range of 1–50 mg l⁻¹ DETA, which is the range normally expected in flotation plant solutions and effluents. Moreover, it will probably prove to be the method of choice for industrial situations where varying concentrations of Ni(II) ions are already known to be present in the pulp solutions.

References

- [1] M.A. Marticorena, G. Hill, A.N. Kerr, D. Liechti, D.A. Pelland, INCO develops new pyrrhotite depressant, in: T. Yalcin (Ed.), *Innovations in Mineral Processing*, Laurentian University, Sudbury, Ontario, Canada, 1995, pp. 15–33.
- [2] S. Kelebek, S.O. Fekete, P.F. Wells, *Proceedings of the Fourteenth International Mineral Processing Congress*, SME, New York, 1995, pp. 181–187.
- [3] S. Udenfriend, *Science* 178 (1972) 871.

Determination of the solubility product of $\text{Ba}(\text{IO}_3)_2$ by flow injection with amperometric detection

Bianca Mendes Martins, Mauro Bertotti *

Instituto de Química, Universidade de São Paulo, São Paulo, 05508-900, Brazil

Received 1 July 1997; accepted 6 August 1997

Abstract

The solubility of $\text{Ba}(\text{IO}_3)_2$ has been determined in solutions containing a supporting electrolyte (KCl) to maintain the ionic strength in the 0–0.5 M range. The approach envisaged was based in the amperometric determination of iodine (or triiodide) generated in the reaction involving iodate in equilibrium in the saturated solutions and iodide contained in the solution carrier using a flow injection procedure, the electrode potential being maintained at +0.2 V in a wall-jet cell. The effect of the supporting electrolyte on the solubility of barium iodate was demonstrated and a good approximation of the value for the thermodynamic solubility constant of the precipitate was found by an appropriate correction of the solubility data using mean activity coefficients of barium iodate. The mean activity coefficients were estimated at each ionic strength by using the Debye–Hückel equation and the corrected solubility constant determined at 27°C was found to be $2.7 \times 10^{-9} \text{ mol}^3 \text{ l}^{-3}$. © 1998 Elsevier Science B.V. All rights reserved.

Keywords: Solubility product; $\text{Ba}(\text{IO}_3)_2$; Flow injection; Amperometric detection

1. Introduction

The determination of the solubility of a slightly soluble compound in a specific solvent requires measurements of the equilibrium concentration of one or both species in a saturated solution at a fixed temperature. Owing to the influence of the ionic strength in the solubility of ionic precipitates, it is very important to take into account that the measurements can be influenced by the ions of the compound itself (when the solubility is not negligible) or by ions of an inert electrolyte deliberately added to the solution. If side reac-

tions (hydrolysis of metal ions or protonation of anions derived from weak acids) are not of importance, thermodynamic solubility products can be achieved after consideration of the activity coefficients of the ions, which are dependent on the ionic strength of the solution. Hence, the relationship between the concentration solubility product (K_s) and the thermodynamic solubility product (K_s^0) for an A^+B^- compound is expressed by the following equation [1]:

$$K_s^0 = K_s f_{\text{A}^+} f_{\text{B}^-} \quad (1)$$

where f_{A^+} and f_{B^-} are defined as the activity coefficients for both ions, which can be theoretically calculated by using the Debye–Hückel equation [2].

* Corresponding author. Fax: +55 11 8155579.

In this paper we have carried out some studies on the determination of the solubility of barium iodate at various values of ionic strength maintained with KCl. A very common procedure to determine the solubility of iodate compounds consists of a titration of the iodine generated after addition of iodide to the filtered saturated solutions [3]. In a similar way, the iodine quantitatively formed can also be quantified spectrophotometrically at a fixed wavelength [4] and this procedure is best suitable for iodate precipitates which have solubility values low enough to restrict titrimetric methods. In this end, we have developed an alternative method based on the generation of iodine (or triiodide) with further amperometric detection at a suitable potential. This indirect amperometric determination with chemically generated iodine has already been reported in the development of analytical methods for nitrite [5,6]. Methods for determination of sulphite have also been used with this principle in mind, but in these cases the quantification of the analyte was based on the decrease of the amperometric signal for iodine [7,8]. In order to avoid time consuming procedures and to achieve a higher sample throughput, we have proposed a flow injection analysis method with amperometric detection for the determination of the equilibrium iodate concentration in the saturated solutions, the analytical signal being compared with those ones of standard iodate solutions. We will show that this approach (electrochemical detection associated with flow injection analysis) allows the determination of the equilibrium iodate concentration to be performed with excellent sensitivity, high reproducibility, high sampling rates and low volume of samples.

2. Experimental

2.1. Materials

All solutions were prepared from reagents of analytical grade. Iodate stock solutions were prepared from the primary standard potassium salt dissolving 0.1070 g in to a 50 ml calibrated volumetric flask to give a 10 mM solution. Iodide

solutions were prepared just after each experiment in order to avoid the formation of iodine in sulphuric medium. Saturated barium iodate solutions were prepared by addition of a sufficient quantity of the compound to each of a series of 25 ml volumetric flasks containing potassium chloride solutions, ranging in the concentration from zero (i.e. pure water) to 0.5 M. The barium iodate solutions were shaken vigorously during 1 h and laid down for a week in order to achieve a complete saturation. The excess solid barium iodate was removed by a filtering process, so that the solutions could be analyzed without interference from any suspended solid particle. Experiments were carried out at 27°C.

2.2. Apparatus

Voltammetric experiments were performed with an EG and G Model 273A potentiostat interfaced to an IBM 486 PC, the electrodes being a glassy carbon electrode (area = 3 mm²), Ag/AgCl as reference (3 M NaCl) and a platinum wire as auxiliary. Before experiments, the bare glassy carbon electrode was polished with alumina (1 μm). Voltammetric experiments involving the use of microelectrodes were carried out in a two electrode cell, the reference electrode being a Ag/AgCl electrode. Platinum microelectrodes were fabricated by sealing microwires ($r = 12.5 \mu\text{m}$)

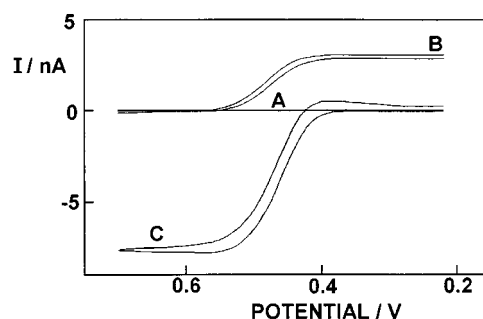


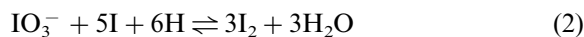
Fig. 1. Steady state voltammograms for a platinum microelectrode ($r = 12.5 \mu\text{m}$) in a solution containing 0.1 M H_2SO_4 (A), 0.1 M H_2SO_4 + 0.4 mM iodine (B) and 0.1 M H_2SO_4 + 1 mM iodide (C). Potential scan rate = 20 mV s^{-1} .

into glass pipettes and polishing the resulting microdiscs with moist alumina powder (0.05 μm) on a polishing cloth. The flow cell was a wall-jet type, where the stream flows from a nozzle perpendicularly onto the working electrode surface. The body of the cell was made of glass, the reference electrode being a silver wire covered by silver chloride immersed in a plastic tube containing KCl. The auxiliary electrode was a steel wire. The diagrams were recorded in an HP 7090 A plotting and measurement system connected to the 273A potentiostat output. The carrier flow was delivered by gravity, the characteristic parameters being as follow: flow rate = 2 ml min^{-1} , injection loop = 100 μl and tube dimension = 1 mm inner diameter (polyethylene).

3. Results and discussion

3.1. Analytical determination of iodate

The proposed method for monitoring the equilibrium concentration of iodate in the series of solutions containing different amounts of supporting electrolyte involved the measurement of iodine (or triiodide) resulting from the reaction between the analyte and iodide in excess in acidic medium, according to the following equation:



The measurement of the current for the reduction of iodine provides a convenient and reproducible way to monitor the concentration of iodate assuming that reaction Eq. (2) is carried out quantitatively to the formation of products. This can be accomplished working with excess of iodide and protons, so all experiments were performed in a 0.1 M sulphuric acid + 40 mM iodide solution, taking in account that the expected value for the solubility of barium iodate is around a few mM. The potential for monitoring the iodine concentration was selected with base in steady state voltammetric curves recorded for iodine and iodide using a 12.5 μm platinum microelectrode. As it is shown in Fig. 1, iodide is oxidized at potentials more positive than +0.4 V. Fig. 1 also shows that at less positive potentials iodine can be

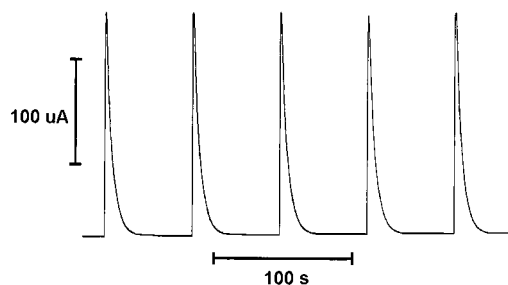


Fig. 2. Amperometric signals recorded at a glassy carbon electrode (area = 3 mm^2 , $E = +0.2$ V) after sequential injections of 100 μl of 2.0 mM potassium iodate to a carrier solution containing 40 mM iodide + 0.1 M H_2SO_4 .

detected at the microdisc due to an electrochemical reaction that involves its reduction to iodide according to the following equation:



Therefore, the cathodic current at +0.2 V was used to monitor the concentration of iodine and hence the iodate level in the solutions without interference from the components of the carrier solution or even from dissolved oxygen, since the signal for its reduction at +0.2 V is negligible if a comparison is made with the iodine signal after injection of saturated iodate solutions. Limiting currents data for the anodic and cathodic processes shown in Fig. 1 are in excellent agreement with the steady state currents calculated using the equation that describes the limiting current for a disc microelectrode [9], which is a function of the concentration of the electroactive species, radius of the microelectrode, number of electrons involved in the electrochemical reaction and the diffusion coefficient ($1.6 \times 10^{-5} \text{ cm}^2 \text{ s}^{-1}$ and $0.83 \times 10^{-5} \text{ cm}^2 \text{ s}^{-1}$ for iodide and iodine respectively [6,10]).

Fig. 2 shows some consecutive diagrams recorded after injection of aliquots of 2.0 mM potassium iodate to the carrier solution (sodium iodide in sulphuric medium). As the reaction involving iodate and iodide takes place in the flowing solution, electroactive iodine is generated giving rise to a peak when it reaches the electrode surface maintained at +0.2 V. The reproducibility of the peaks shown in Fig. 2 was very good

(standard deviation = 0.9% for $n = 5$) and after all injections the current dropped to its background value. For a 0–3 mM iodate range the peak currents were plotted as a function of the analyte concentration, a very nice straight line being obtained which can be represented by the equation

$$I(\mu\text{A}) = 107.0C_{\text{iodate}}(\text{mM}) + 3.0 \quad (4)$$

with a regression coefficient, $r^2 = 0.9992$.

3.2. Determination of iodate in the barium iodate solutions

The effect of both barium ions and the supporting electrolyte on the recorded current at +0.2 V was checked by addition of solutions of barium chloride (3 mM) and potassium chloride (0.5 M) to the flowing solution (iodide + sulphuric acid). No signal was observed after addition of these species, what means that the response obtained after injection of barium iodate samples to the carrier solution is exclusively dependent on the amount of iodate. A test was also carried out to verify the eventual influence of the ionic strength on the measured signal but the peak current had

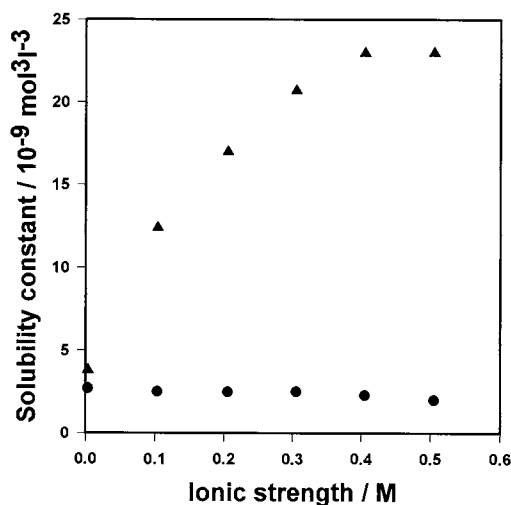


Fig. 3. Plot of the solubility product for barium iodate as a function of the ionic strength maintained with potassium chloride (triangles). Circles represent the same values after correction using the appropriate activity coefficients for barium iodate.

Table 1
Corrected solubility product of barium iodate at various ionic strength values calculated by using Eq. (6)

Ionic strength (M)	Ba(IO ₃) ₂ activity coefficient	Corrected solubility product ($10^{-9} \text{ mol}^3 \text{ l}^{-3}$)
0.003	0.890	2.7
0.104	0.602	2.5
0.205	0.531	2.5
0.305	0.491	2.5
0.405	0.463	2.3
0.505	0.443	2.0

The activity coefficients for barium iodate were determined according to Eq. (7).

the same value whatever a solution containing 1 mM potassium iodate or 1 mM potassium iodate + 0.5 M KCl was injected. Hence, the iodate quantification in the solutions containing potassium chloride was performed by comparing the resulting peaks with an analytical curve ranging from 0 to 5 mM potassium iodate dissolved in pure water. Three injections were made for each one of the set of barium iodate solutions containing KCl and the average value was used to calculate the equilibrium concentration of iodate, standard deviations of the peak currents not being larger than 1%. The concentration equilibrium constant, i.e. the equilibrium constant using molar concentrations (K_s), was calculated for which one of the six barium iodate solutions containing potassium chloride (0–0.5 M) by multiplying the ionic concentrations of both ions and taking in consideration that $[\text{Ba}^{2+}]$ was half of $[\text{IO}_3^-]$ in the saturated solutions. Fig. 3 shows a plot of K_s as a function of the ionic strength (μ) of the solutions calculated according to the following equation [1]:

$$\mu = \frac{1}{2} \sum C_i z_i^2 \quad (5)$$

which can be rearranged taking in account that the barium iodate is a 2:1 electrolyte to give

$$\mu = C_{\text{KCl}} + 3C_{\text{Ba}(\text{IO}_3)_2} \quad (6)$$

where C means the molar concentration of potassium chloride and the solubility of the barium iodate solutions respectively.

The increase in K_s values and in solubility as shown in Fig. 3 is due in part to the electrostatic attraction between the inert electrolyte ions and the ions in the crystal lattice of the solid. This effect can be corrected taking into account the mean activity coefficients of barium iodate at each of the solutions to convert the K_s values to a set of corrected solubility constants using the relationship expressed by Eq. (1). The activity coefficients for $\text{Ba}(\text{IO}_3)_2$ in the solutions containing potassium chloride at different concentrations were calculated by using the Debye–Hückel equation [2], which follows:

$$\log f_{\pm} = -\frac{0.511|Z_A+Z_B+\sqrt{\mu}}{1+0.329a\sqrt{\mu}} \quad (7)$$

where f_{\pm} is defined as the geometric mean of the single-ion activity coefficients and it is preferable to be used since it is inherently impossible to measure activity coefficients for individual ions. Values for barium iodate mean activity coefficients were calculated according to Eq. (7) using Kielland's values of \bar{a} [11]. For barium iodate $\bar{a} = 4.5 \text{ \AA}$, which resulted in the set of f_{\pm} values for each ionic strength shown in Table 1. Corrected solubility products for barium iodate were then calculated by using Eq. (1) taking into account the relationship between single-ion activity coefficients and mean activity coefficient expressed by Eq. (8):

$$f_{\pm} = (f_{\text{Ba}^{2+}} \cdot f_{\text{IO}_3^{-2}})^{1/3} \quad (8)$$

Solubility products data for the compound after the correction using the mean activity coefficients would all be the same if the Debye–Hückel equation were perfect and the slight deviation is likely to be related with the increasing error in the equation as the ionic strength increases. Therefore, the value obtained from the solution containing no KCl (ionic strength = 0.003 M) was adopted as a more reliable determination of the $\text{Ba}(\text{IO}_3)_2$ solubility product and this result is in a good agreement with other value reported in the literature ($1.6 \times 10^{-9} \text{ mol}^3 \text{ l}^{-3}$ at 25°C [12]).

4. Conclusions

The proposed flow injection procedure was found to be a very reliable way to determine the equilibrium concentration of iodate in solutions saturated with barium iodate. The indirect amperometric detection with iodine allows very low concentrations of iodate to be quantified, so even more insoluble iodate precipitates like $\text{Hg}(\text{IO}_3)_2$ ($K_s = 2.0 \times 10^{-19} \text{ mol}^3 \text{ l}^{-3}$) would have its solubility successfully determined. The simplicity, reproducibility of the results and low volume of saturated solutions (typically a few hundred microliters) are also of importance and make the method very advantageous for solubility studies involving other iodate compounds.

The solubility product of barium iodate was determined after the needed corrections using the activity coefficients in the potassium chloride medium were performed. The Debye–Hückel equation was used for this end and the determined solubility constant is to be found as a good approximation of the thermodynamic solubility product of barium iodate since this system is immune to problems associated with side reactions involving Ba^{2+} or iodate at the working pH (~ 6) [13,14]. On the other hand, some errors may be expected owing to the dependence of activity coefficients upon the specific chemical properties of the ions instead of upon just the charge and radius. Another aspect to concern refers to the formation of soluble ion pairs which would involve both ions in a side equilibrium. This is particularly likely to occur for a 1:2 electrolyte and many examples are to be seen like AgSO_4^+ or $\text{HgCl}_2(\text{aq})$ [15].

Acknowledgements

The authors are grateful for financial support from CNPq (Conselho Nacional de Desenvolvimento Científico e Tecnológico) and FAPESP (Fundação de Amparo à Pesquisa do Estado de São Paulo).

References

- [1] M. Dole, *Principles of Experimental and Theoretical Electrochemistry*, McGraw Hill, New York, 1935.
- [2] P. Debye, E. Hückel, *Physik. Z.* 24 (1923) 185.
- [3] R.M. Ramette, *Chemical Equilibrium and Analysis*, Addison Wesley, Reading, 1981.
- [4] B.G. Osborne, *Analyst* 112 (1987) 137.
- [5] M. Trojanowicz, W. Matuszewski, B. Szostek, J. Michalowski, *Anal. Chim. Acta* 294 (1994) 251.
- [6] M. Bertotti, D. Pletcher, *Anal. Chim. Acta* 337 (1997) 49.
- [7] X. Huang, W.T. Kok, *J. Liquid. Chromatogr.* 14 (1991) 2207.
- [8] N.T.K. Thanh, L.G. Decnop-Weever, W.T. Kok, *Frese-nius J. Anal. Chem.* 349 (1994) 469.
- [9] M. Wightman, D.O. Wipf, *Electroanal. Chem.* 15 (1989) 267.
- [10] S. Swathirajan, S. Bruckenstein, *J. Electroanal. Chem.* 112 (1980) 25.
- [11] J. Kielland, *J. Am. Chem. Soc.* 59 (1937) 1675.
- [12] L.G. Sillén, *Stability Constants of Metal-ions Complexes, Part I, Inorganic Ligands*, The Chemical Society, London, 1997.
- [13] J.H. Carpenter, *J. Chem. Educ.* 66 (1989) 184.
- [14] G.D. Gillispie, *J. Chem. Educ.* 67 (1990) 143.
- [15] L. Meites, J.S.F. Pode, H.C. Thomas, *J. Chem. Educ.* 43 (1966) 667.

A supercoiled DNA-modified mercury electrode-based biosensor for the detection of DNA strand cleaving agents

Miroslav Fojta^a, Veronika Staňková^a, Emil Paleček^{a,*}, Pavel Koscielniak^b,
Josef Mitáš^b

^a *Institute of Biophysics, Academy of Sciences of the Czech Republic, Královopolská 135, 612 65 Brno, Czech Republic*

^b *DIAMO (State Enterprise), Division GEAM, 592 51 Dolní Rožinka, Czech Republic*

Received 26 May 1997; received in revised form 8 August 1997; accepted 11 August 1997

Abstract

DNA-damaging agents in the environment represent a serious danger to human health. We use a supercoiled DNA-modified mercury electrode as a fast-response biosensor for the detection of DNA strand cleaving agents. The sensor is based on a strong difference between the a.c. voltammetric responses of covalently closed circular (supercoiled) and of open circular (nicked) plasmid DNA. We show that the sensor can detect hydroxyl radicals in laboratory-prepared solutions and in various natural and industrial water samples. The sensor is also capable of detecting unknown DNA-damaging agents in industrial waters. © 1998 Elsevier Science B.V. All rights reserved.

Keywords: Supercoiled DNA; DNA-modified electrode; Electrochemical biosensor; ·OH radicals; DNA damage; Environmental analysis

1. Introduction

In recent years, a number of nucleic acid-based electrochemical biosensors were developed. Most of these biosensors [1–6] were constructed for DNA sequence-specific recognition based on nucleic acid [1–3,6,7] or peptide nucleic acid [4] probe immobilization at the electrode surface followed by hybridization with the target DNA and an electrochemical [1–5,7] or electrogenerated chemiluminescence [6] signal transduction. Several papers have dealt with electrochemical DNA

biosensors for the detection of substances, such as drugs and pollutants, that selectively interact with the probe DNA (e.g. by intercalation [8]) or that damage the DNA by chemical modification of base residues (e.g. hydrazines [9] or dimethyl sulfate [10]).

Damage to DNA usually results in serious disturbances in the life of the cell (e.g. mutations, malignant transformation, apoptosis [11]) and may endanger human health. Thus, monitoring of DNA-damaging agents in the environment is very significant. Many kinds of DNA damage result in the formation of DNA strand breaks (i.e. cleavage of the DNA sugar-phosphate backbone). Recently, we have found that transition of covalently

* Corresponding author. Tel.: +42 05 41517177; fax: +42 05 41211293; e-mail: palecek@ibp.cz

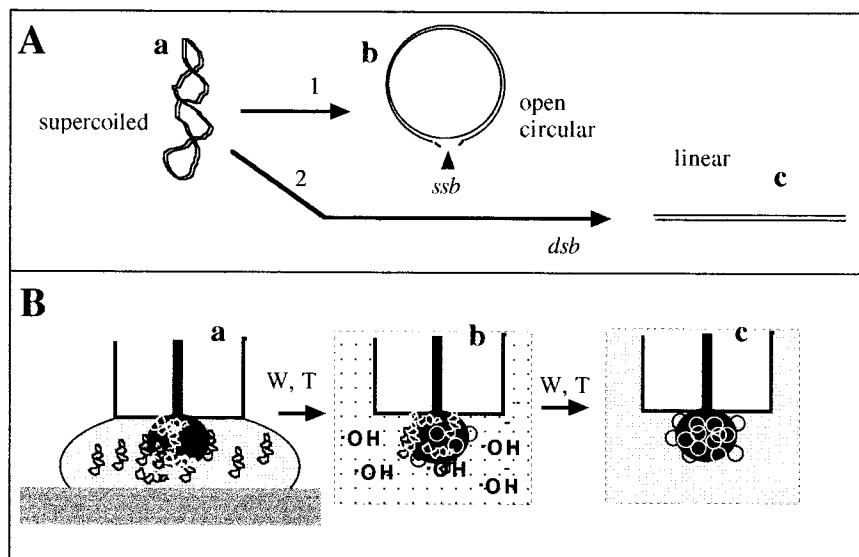


Fig. 1. (A) Scheme of supercoiled DNA (a) and the formation of open circular (b) or linear (c) DNAs as the result of interruption of one DNA strand (1, single-strand break (ssb); e.g. by ionizing radiation) or both strand in the same site (2, double-strand break (dsb); e.g. by a restriction endonuclease or by high doses of radiation); in the latter case, the molecule of linDNA contains a number of single strand breaks. (B) Scheme of the sensor for DNA strand cleavage based on scDNA-modified HMDE. The sensor electrode is prepared by immersing of HMDE into solution containing scDNA which is adsorbed at the electrode surface (a). After washing (W), the scDNA-modified electrode is transferred (T) into the sample tested (b). If the sample contains hydroxyl radical for example, surface-attached scDNA is nicked, thus producing oc (or linear) DNA. After washing, the sensor electrode is transferred into blank background electrolyte (c) followed by voltammetric signal transduction.

closed circular, supercoiled (sc) DNA to open circular (oc) DNA (by introduction of a single-strand break into the scDNA molecule) or to linear DNA (by scission of both DNA strands at the same site) (Fig. 1) results in the appearance of an a.c. voltammetric peak 3 [12] (Fig. 2). It has been shown that the latter peak (a non-faradaic peak observed in weakly alkaline solutions), characteristic of single-stranded DNA [13,14], is also produced by oc and linear double-stranded DNAs. These DNA molecules have free strand ends of one or both DNA strands and they can be partially unwound at the electrode. Supercoiled DNA, both strands of which are covalently closed circles, cannot be unwound and consequently, scDNA does not yield peak 3 [12,14]. Under certain conditions, one DNA strand break can be detected using a.c. voltammetry among several hundred thousand phos-

phodiesteric bonds [12]. Compared to gel electrophoresis (currently applied for this purpose), the voltammetric assay is substantially faster (it takes a few minutes, in contrast to the hours necessary to run gel electrophoresis) and offers easier quantitation of data.

Intact scDNA can be anchored at the mercury electrode surface by adsorption forces [12,14–16]. If the scDNA-modified electrode is dipped into a solution containing DNA cleaving agent (e.g. chemical [12] or natural nucleases), strand breaks are introduced into the probe DNA immobilized at the electrode surface (Fig. 1), which are subsequently detected by means of a.c. voltammetry [12]. In this paper, we demonstrate the possible use of this sensor for detection of DNA strand cleaving agents in several natural samples, including mine and technological water obtained from the uranium industry.

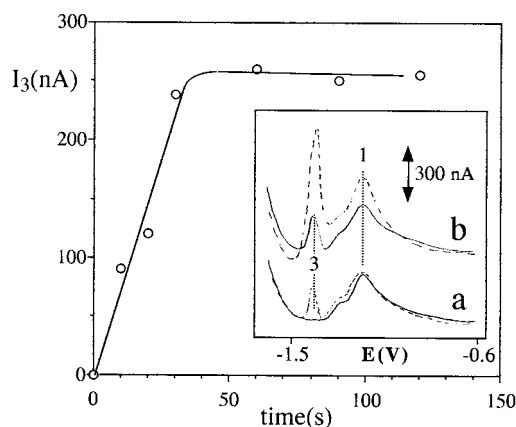


Fig. 2. The dependence of peak 3 height on time for which the sensor was exposed to 50 μM Fe/EDTA reagent (see Section 2) in 50 mM sodium phosphate, pH 8.5. The reaction was started by addition of hydrogen peroxide into a stirred solution of other components with dipped sensor electrode. Inset (a), blank sensor response for scDNA (solid) and for ocDNA control (oc DNA was prepared by DNase I-treatment of scDNA in solution and subsequently adsorbed at HMDE, dashed); (b) sensor response for 60 s incubation of scDNA-modified electrode in 50 μM Fe/EDTA reagent in 50 mM sodium phosphate pH 8.5 (solid) and for 120 s incubation in the same mixture with an addition of fresh hydrogen peroxide and ascorbate after the first 60 s. For other conditions, see Section 2.

2. Experimental

2.1. Material

Supercoiled plasmid pUC19 DNA was isolated by lysozyme/SDS/EDTA lysis followed by CsCl-gradient centrifugation as described [12]. Control oc DNA was prepared by treatment of scDNA with 0.02 U of deoxyribonuclease I (Sigma) in 6

mM MgCl_2 , 2 mM CaCl_2 and 40 mM Tris-HCl pH 7.4 at 0°C for 90 min followed by extraction with phenol and chloroform, then ethanol precipitation [17].

2.2. Fenton reaction

The reaction mixture contained FeSO_4 , EDTA and sodium ascorbate at the ratio 1:2:20; the starting H_2O_2 concentration was always 0.03% (about 9 mM) [18] (for example, '50 μM Fe/EDTA reagent' contained 50 μM FeSO_4 , 0.1 mM EDTA, 1 mM sodium ascorbate and 9 mM H_2O_2). The sensor electrode was immersed in a solution containing the reaction components except H_2O_2 followed by hydrogen peroxide addition (with intensive stirring).

2.3. Mine and technological water samples

Water samples obtained from the uranium industry (from a flooded mine, from a water purification plant and a sample of free circulating technological water from a chemical uranium ore-dressing plant) were used for testing the usability of the sensor in water (environmental) analysis. The content of some substances in the samples is displayed in Table 1.

2.4. Sensor procedure

DNA was adsorbed at the electrode surface from 5 μl drops of solution containing 100 $\mu\text{g ml}^{-1}$ scDNA (or 50 $\mu\text{g ml}^{-1}$ ocDNA for control measurements), 0.2 M NaCl and 10 mM Tris-HCl (pH 7.4) for 60 s. The DNA-modified elec-

Table 1

Characterization of mine and technological water samples: approximate contents of some substances

Sample	U (mg l^{-1})	Fe (mg l^{-1})	Mn (mg l^{-1})	SS (mg l^{-1})	IS (mg l^{-1})	Radioactivity (Bq l^{-1})	pH
VK3 ^a	10	19	6	2839	14	1.7	7
HVP ^b	0.02	4	5	2725	5	0.02	6.9
VCA II ^c	0.3	1.1	0.5	7909	18	—	9.5

SS, soluble substances; IS, insoluble substances.

^a Water from a flooded uranium mine taken at the input of the water purification plant.

^b Water taken at the output of the water purification plant.

^c Free circulating technological water from the chemical uranium ore-dressing plant.

trode was washed with distilled water and transferred into the solution of the tested sample for 60 s, if not stated otherwise. The electrode was then washed with water, followed by a background electrolyte solution and transferred into deaerated blank background electrolyte, which was then bubbled with argon for 60 s. The initial potential $E_i = -0.6$ V was applied at the electrode for 15 s (quiescent period) prior to the voltage scan.

2.5. Voltammetric signal transduction

Alternating current voltammetric measurements were performed with an EG and G PAR 174A Polarographic Analyzer connected to a 174/50 AC Polarographic Interface, a 5208 Two Phase Lock-in Amplifier and a Philips PM 8134 $X_t Y_1 Y_2$ Recorder. The following parameters were chosen: frequency 230 Hz, amplitude 10 mV, scan rate 20 mV s^{-1} . The phase-in component was measured due to better resolution of the DNA signals as compared to the out of phase component. Linear sweep and square wave voltammetry were performed with an AUTOLAB (EcoChemie, Utrecht, The Netherlands; for settings, see legend to Fig. 3). A Metrohm 647 VA-Stand electrode in HMDE mode controlled by a 646 VA-Processor was used. All measurements were performed with a saturated calomel reference electrode (SCE) and a platinum wire counter electrode. 0.3 M NaCl , $50 \text{ mM sodium phosphate}$, pH 8.5 was used as a background electrolyte.

3. Results and discussion

3.1. Nicking of scDNA at the mercury electrode surface by hydroxyl radicals or by deoxyribonuclease I

We showed previously [12] that peak 3 appears (Fig. 2, inset) as a result of submerging the scDNA-modified HMDE in a solution containing free radicals prior to the a.c. voltammetric measurement (Fig. 1B). In this study, we use this system for testing natural and industrial samples.

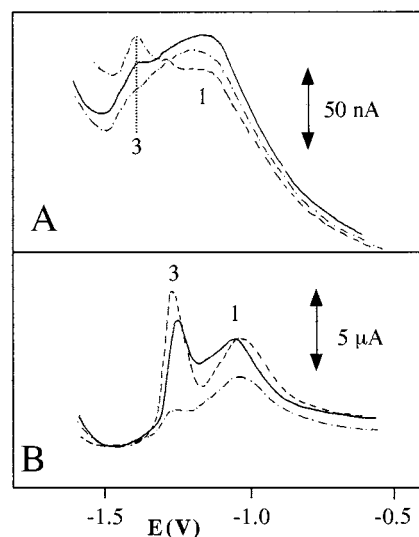


Fig. 3. Linear sweep (A) and square-wave (B) response of the sensor. (---), control ocDNA (see Fig. 2); (-·-·-), blank scDNA response; (—), sensor response for $50 \mu\text{M} [\text{Fe}(\text{EDTA})]^{2-}$, $1 \text{ mM sodium ascorbate}$, $0.03\% \text{ H}_2\text{O}_2$ in $50 \text{ mM sodium phosphate}$ pH 8.5. LSV, scan rate 1 V s^{-1} ; SWV, frequency 2 kHz , step potential 3.05 mV , amplitude 100 mV . For other details, see Fig. 2.

We tested the influence of individual components of the Fenton reaction mixture (in which hydrogen peroxide is reduced to hydroxide anion and hydroxyl radical by $[\text{Fe}(\text{EDTA})]^{2-}$; the ferrous ion is then regenerated by reaction with ascorbate [18]) on the immobilized scDNA. No cleavage was observed in the absence of H_2O_2 (in a solution of $50 \mu\text{M Fe}^{2+}$). However, in solutions free of the ferrous complex or ascorbate (but containing hydrogen peroxide), a small peak 3 was obtained (Table 2). For this reason, in all further experiments the reaction was started by addition of hydrogen peroxide into stirred solution with an immersed sensor electrode. Fig. 2 displays the temporal increase of peak 3 in a stirred solution of $50 \mu\text{M Fe/EDTA}$ reagent; under these conditions, the peak 3 height rapidly increased up to about 1 min and then leveled off, probably due to decomposition of a substantial portion of the H_2O_2 and/or ascorbate added. Deeper DNA cleavage (resulting in a further increase of peak 3 as more strand breaks occur) can be achieved by increasing the starting concentra-

tion of hydrogen peroxide and ascorbate or by a second addition of these compounds after the first minute (see inset in Fig. 2). Similar results were obtained when the ferrous/ferric redox pair was replaced by the cuprous/cupric pair (Table 2). In another experiment, the sensor was immersed in a solution containing 20 U ml⁻¹ deoxyribonuclease I, an enzyme that introduces single-strand breaks in DNA. Again, an incubation time-dependent increase of peak 3 was observed (Table 2). More details about the enzyme interaction with immobilized DNA will be published elsewhere.

3.2. Testing of natural and industrial samples

The possibility of detecting damage to immobilized scDNA by hydroxyl radicals generated through the Fenton reaction in various media was investigated. In addition, the influence of the sample by itself (with no additions) on the sensor response was tested. Results are shown in Table 3. In natural ground water samples, as well as in technological waters, the additions of the reagents yielded qualitatively similar results as the laboratory-prepared solutions, suggesting that the sensor is applicable in environmental analysis. Satisfactory results were obtained with beverages such as

Table 2
DNA cleavage at the HMDE surface

Agent	Peak height ^a (%)
None ^b	0
Fe(EDTA) + ascorbate + H ₂ O ₂ ^c	95
Fe(EDTA) + H ₂ O ₂ ^c	14
ascorbate + H ₂ O ₂ ^c	10
Fe(EDTA) + ascorbate ^c	0
Cu ^d	0
Cu + ascorbate + H ₂ O ₂	105
DNase I ^e , 1 min	35
DNase I ^e , 2 min	60

^a The height of peak 3 yielded by ocDNA control (see Fig. 2) was taken as 100%.

^b 50 mM sodium phosphate pH 8.5.

^c Complete 50 mM Fe/EDTA reagent in 50 mM sodium phosphate pH 8.5, stirred.

^d 50 μM CuSO₄, 1 mM sodium ascorbate, 0.03% H₂O₂ in 50 mM sodium phosphate pH 8.5, stirred.

^e 20 U ml⁻¹ deoxyribonuclease I in 6 mM MgCl₂, 2 mM CaCl₂, 40 mM Tris-HCl pH 7.4, unstirred.

Table 3
Testing of various samples by the sensor

Peak 3 height	No additions I ₃ (%) ^b	Complete ^a I ₃ (%) ^b
Water from puddle	5	203
River water	8	212
VK3 ^c	125	—
HVP ^c	3	220
VCA II ^c	0	110
Wine	9	22
Wine, diluted ^d	9	47
Tangerine juice ^e	45	47
Tangerine juice, boiled ^f	0	17

^a Complete 100 μM Fe/EDTA reagent.

^b Height of peak 3 yielded by ocDNA control (see Fig. 2) was taken as 100%.

^c See Table 1.

^d 10-fold diluted by distilled water.

^e Juice squeezed from fresh tangerine, centrifuged and 10-fold diluted with distilled water.

^f Juice squeezed from fresh tangerine, centrifuged, 10-fold diluted with distilled water and heated in a boiling water bath for 5 min.

wine or tangerine juice (especially if diluted 10-fold, Table 3). With tangerine juice, significant DNA nicking activity was detected in the pure (centrifuged and diluted) natural sample; however, after 5 min of boiling, no DNA damage was observed. When the complete Fenton reaction mixture was added to the boiled sample, nicking of the probe DNA was observed again, suggesting that the original nicking was due to the activity of a thermolabile nuclease.

Strong damage to the immobilized scDNA was observed in the water sample obtained from a flooded uranium mine (sample VK3 with no additions, Tables 1 and 3). In contrast, the water sample taken at the output of the water purification plant (HVP) and from the open catchpit (VCA II) provided no sensor response unless the Fenton reaction mixture was added. This result demonstrates the capability of the sensor to monitor the contamination of technological waters and to detect unknown DNA damaging agents. (As shown in Table 1, the 'input' sample displays a higher content of iron, uranium and insoluble substances as compared to the 'output' sample.

Redox active metal-induced damage to DNA by non-Fenton mechanisms under aerobic conditions has been published by others [19–21]). The low (or zero) sensor responses for the HVP and VCA II samples (without addition of the Fe/EDTA reagent, Table 3), not exceeding the response of, for example water from a puddle, also suggest the good efficiency of the decontamination process and relative safety of the uranium technology.

It may be expected that biological samples with high protein contents (blood) will require deproteination to prevent protein interferences [12,22,23].

3.3. Linear sweep (LS) and square-wave (SW) voltammetry

The best resolution of DNA peak 3 is reached using phase-sensitive alternating current voltammetry (phase-in component). This technique, however, is not included in most moderately priced instruments and will hardly be widely applied in biochemical and molecular–biological laboratories. For this reason, we tested more common fast-scan voltammetric techniques (included in the software of many modern voltammetric analyzers) for their ability to differentiate between sc and oc DNA-modified mercury electrodes and to give the sensor response for 50 μM Fe/EDTA reagent after 1 min. Fig. 3 shows, in LSV, only a poorly developed peak (inflex) 3 was obtained as a result of the cleavage reaction (although the control ocDNA-modified electrode yielded a quite well-developed peak). On the other hand, square wave voltammetry provided much better sensitivity, yielding a well-developed peak 3 under the same conditions. In SWV, peak 3 is even relatively higher (as compared to the less negative peak 1, yielded by both sc and ocDNA) than in a.c. voltammetry. However, the peak resolution is somewhat worse. In any case, SWV seems to be a valuable technique for electrochemical transduction of the sensor response. Our preliminary results further suggest that damage to scDNA can also be sensitively detected using constant current derivative chronopotentiometry in neutral ammonium formate [24,25]. HMDE may represent a relative disadvantage of this biosensor. Our at-

tempts to utilize carbon electrodes for the same purpose were however, not successful, as the response of lin (oc) DNA and scDNA did not substantially differ [26]. Further experiments will be performed to find and to optimize the electrochemical technique that provides the best sensitivity and selectivity.

In conclusion, our results show that a scDNA-modified HMDE that sensitively reflects DNA strand breaks can be applied as an electrochemical biosensor for the analysis of DNA damage-inducing agents in natural and industrial waters. This biosensor is capable not only to detect the presence of an unspecified DNA-nicking agent, as shown in this paper, but also to provide information about the nature of this agent. Our preliminary results show that by combining electrochemical and biochemical approaches, information about the nature of the metal involved in Fenton chemistry as well as about the base damage preceding the strand interruption can be obtained. More details will be published elsewhere.

Acknowledgements

This work was supported by grants from the Grant Agency of the Czech Republic Reg. No. 204/97/K084.

References

- [1] M. Maeda, Y. Mitsunashi, K. Nakano, M. Takagi, *Anal. Sci.* 8 (1992) 83.
- [2] S. Mikkelsen, *Electroanalysis* 8 (1996) 12.
- [3] K.M. Millan, S.R. Mikkelsen, *Anal. Biochem.* 65 (1993) 2317.
- [4] J. Wang, G. Rivas, X. Cai, E. Paleček, H. Shiraishi, N. Dontha, D. Luo, P.A.M. Farias, *J. Am. Chem. Soc.* 118 (1996) 7667.
- [5] J. Wang, X. Cai, G. Rivas, H. Shiraishi, *Anal. Chim. Acta* 326 (1996) 141.
- [6] X.-H. Xu, A.J. Bard, *J. Am. Chem. Soc.* 117 (1995) 2927.
- [7] K. Hashimoto, K. Ito, Y. Ishimori, *Anal. Chim. Acta* 286 (1994) 219.
- [8] P.C. Pandey, H.H. Weetall, *Anal. Chem.* 66 (1994) 1236.
- [9] J. Wang, M. Chicharro, G. Rivas, X. Cai, N. Dontha, P.A.M. Farias, H. Shiraishi, *Anal. Chem.* 68 (1996) 2251.

- [10] F. Jelen, M. Tomschik, E. Paleček, J. Electroanal. Chem. 423 (1997) 141.
- [11] S.S. Wallace, B. van Houten, Y.W. Kow, DNA damage. Effects on DNA structure and protein recognition, The New York Academy of Sciences, New York, 1994.
- [12] M. Fojta, E. Paleček, Anal. Chim. Acta 342 (1996) 1.
- [13] E. Paleček, Modern polarographic (voltammetric) methods in biochemistry and molecular biology. Part II. Analysis of macromolecules, in: G. Milazzo (Ed.), Topics in Bioelectrochemistry and Bioenergetics, Wiley, London, 1983, pp. 65.
- [14] E. Paleček, Electroanalysis 8 (1996) 7.
- [15] E. Paleček, I. Postbieglová, J. Electroanal. Chem. 214 (1986) 359.
- [16] E. Paleček, F. Jelen, C. Teijeiro, V. Fučík, T.M. Jovin, Anal. Chim. Acta 273 (1993) 175.
- [17] J. Sambrook, E.F. Frisch, T. Maniatis, Molecular Cloning, Cold Spring Harbor Laboratory Press, New York, 1989.
- [18] M.A. Price, T.D. Tullius, Using hydroxyl radical to probe DNA structure, in: D.M.J. Lilley, J.E. Dahlberg (Eds.), Methods in Enzymology, Academic Press, New York, 1992, pp. 194.
- [19] Y. Takehara, K. Yamaoka, E.F. Sato, T. Yoshioka, K. Utsumi, Physiol. Chem. Phys. Med. NMR 26 (1994) 215.
- [20] K. Ito, K. Yamamoto, S. Kawanishi, Biochemistry 31 (1992) 11606.
- [21] S. Oikawa, S. Kawanishi, Biochemistry 35 (1996) 4584.
- [22] E. Paleček, M. Fojta, Anal. Chem. 66 (1994) 1566.
- [23] C. Teijeiro, K. Nejedlý, E. Paleček, J. Biomol. Struct. Dyn. 11 (1993) 313.
- [24] E. Paleček, M. Tomschik, V. Staňková, L. Havran, Electroanalysis, in press.
- [25] M. Fojta, L. Havran, E. Paleček, Electroanalysis, in press.
- [26] X. Cai, G. Rivas, P.A.M. Farias, H. Shiraishi, J. Wang, M. Fojta, E. Paleček, Bioelectrochem. Bioenerg. 40 (1996) 41.

Liquid–liquid extraction of palladium(II) with *N-n*-octylaniline from hydrochloric acid media

T.N. Lokhande, M.A. Anuse, M.B. Chavan *

Department of Chemistry, Shivaji University, Kolhapur-416004, India

Received 25 November 1996; received in revised form 5 August 1997; accepted 11 August 1997

Abstract

N-n-Octylaniline in xylene is used for the extractive separation of palladium(II) from hydrochloric acid medium. Palladium(II) was extracted quantitatively with 10 ml of 2% reagent in xylene from 0.5–2 M hydrochloric acid medium. It was stripped from the organic phase with 1:1 ammonia and estimated spectrophotometrically with pyrimidine-2-thiol at 420 nm. The effects of metal ion, acids, reagent concentration and of various foreign ions have been investigated. The method affords binary separation of palladium(II) from iron(III), cobalt(II), nickel(II) and copper(II) and is applicable to the analysis of synthetic mixtures and alloys. The method is fast, accurate and precise. © 1997 Elsevier Science B.V.

Keywords: Palladium; *N-n*-Octylaniline; Solvent extraction

1. Introduction

The abundance of palladium in the earth's crust is $8.5 \times 10^{-13}\%$. Palladium and its alloys have a wide range of applications both in the chemical industry and in instrument making. As a catalyst it is principally used in various organic reactions.

Solvent extraction has been widely used for separation of the platinum metals [1–3]. This technique of separation uses the differences in their kinetic behaviour for the formation of extractable species as well as the strength of electrostatic interaction of their chloro-complexes with liquid anion exchangers. The inertness of the chloro-complex of palladium(II) towards aqua-

tion plays an important role in its extraction from acidic solution by an anion exchange mechanism with organic bases such as amines [4–7].

High molecular weight amines (HMWA) popularly known as liquid anion exchangers, uniquely combine some of the advantages of liquid–liquid extraction and ion exchange. Further, Smith and Page [8] observed that the acid binding property of HMWA depends on the fact that the acid salts of these bases are essentially insoluble in water but readily soluble in hydrocarbon solvent.

The use of *n*-octylaniline in the extraction of the noble metals has been described [7,9–12]. Palladium(II) was extracted with 1 M *n*-octylaniline in chloroform from 3 M hydrochloric acid but this method requires several extraction stages for quantitative recovery of metal ion (2×15

* Corresponding author. Fax: +91 231 656133.

min) [7] and the effectiveness of *n*-octylaniline in these extractions depends on its method of preparation [13]. Tri-iso-octylamine [14] has been used as a group extractant for the noble metals from 1 M hydrochloric acid medium with 2 min shaking. Palladium(II) was completely extracted from 11.5 M hydrochloric acid as a chloro-complex in the presence of tin(II) chloride by tri-*n*-octylamine (TOA) [15] in benzene and measured at 410 nm. Other extractants reported for palladium(II) are triphenylphosphine [16], di-octyl sulphoxide [17], tri-isobutyl phosphine sulphide [18] and sulphide podand 1,12-di-2-thienyl-2,5,8,11-tetra-thiadodecane (TTD) [19].

N-n-Octylaniline has been employed successfully in this laboratory for extractive separation of In(III), Tl(III), Zn(II), Bi(III) and Ga(III) [20–22]. Owing to generally greater solubility, primary amines are used less frequently than secondary amines. In addition, in *N-n*-octylaniline, the presence of an octyl group attached to the amino group in aniline renders this amine less soluble in water. Here, the use of *N-n*-octylaniline as an extractant for palladium(II) from hydrochloric acid is reported.

Because the determination of small amounts of noble metals in minerals containing large amounts of base metals is difficult, the effectiveness of *N-n*-octylaniline was evaluated as an extractant

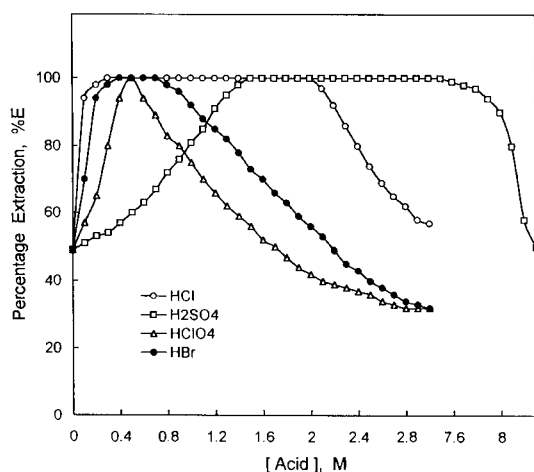


Fig. 1. Extraction of Pd(II) with 2% *N-n*-octylaniline in xylene as a function of acid concentration. Pd(II) = 100 μ g.

Table 1
Extraction behaviour of palladium(II) as a function of *N-n*-octylaniline concentration

[HCl] (M)	<i>N-n</i> -Octylaniline (% v/v)	% E	D
0.5 M	0.2	35	1.35
	0.5	50	2.50
	1.0	78	8.86
	2–7	100	∞
1 M	0.2	75	7.50
	0.5	94	39.00
	1–7	100	∞
2 M	0.2–7	100	∞
3 M	0.2	26.0	0.88
	0.5	32.0	1.18
	1.0	42.0	1.80
	2.0	57.0	3.31
	3.0	71.6	6.30
	5.0	95.0	47.50
	7.0	100	∞
	4 M	0.2	14.0
5 M	0.5	18.0	0.55
	1.0	23.8	0.78
	2.0	44.0	1.96
	3.0	68.6	5.46
	5.0	83.6	12.74
	7.0	91.7	27.62
	0.2	9.0	0.25
5 M	0.5	11.0	0.30
	1.0	18.0	0.55
	2.0	40.0	1.66
	3.0	46.3	2.16
	5.0	59.7	3.70
	7.0	74.6	7.34

Pd(II) = 100 μ g; Aq/Org = 25:10.

for palladium(II) from a variety of palladium-bearing materials and process solutions. The method proposed here offers extraction separation and determination of palladium(II) from associated elements as a function of hydrochloric acid media.

2. Experimental

2.1. Apparatus

An Elico digital spectrophotometer model CL-27 with 1-cm quartz cells was used for absorbance measurements.

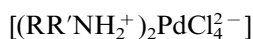
2.2. Reagents

A stock solution of palladium(II) was prepared by dissolving 1 g of palladium chloride hydrate (Johnson Matthey, UK) in dilute analar hydrochloric acid (1 M) and diluting to 100 ml with distilled water and standardised [23]. A working solution of 100 µg/ml was made from it by diluting the stock solution with distilled water.

Other standard solutions of different metals used to study the effect of diverse ions were prepared by dissolving weighed quantities of their salts in distilled water or dilute hydrochloric acid. Solutions of anions were prepared by dissolving the respective alkali metal salts in water. All the chemicals used were of AR grade. Distilled water was used throughout. *N-n*-Octylaniline was prepared by the method of Gardlund et al. [24] and its solutions (% v/v) were prepared in xylene.

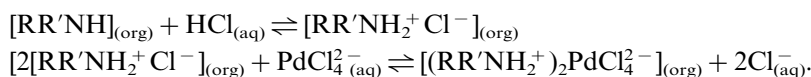
2.3. Procedure

To an aliquot of solution containing 100 µg palladium(II) in a 125-ml separatory funnel, enough hydrochloric acid and water were added to give a final concentration of 1 M with respect to hydrochloric acid in a total volume of 25 ml. The aqueous phase was equilibrated once with 10 ml of 2% *N-n*-octylaniline solution in xylene for 1 min. The phases were allowed to separate and the metal from the organic phase was back-stripped with two 5-ml portions of 1:1 ammonia solution. The extracts were evaporated to moist



where R = $-C_6H_5$, R' = $-CH_2(CH_2)_6CH_3$.

The extraction mechanism can be explained as follows:



dryness and leached with dilute hydrochloric acid to form the solution. Palladium(II) was estimated spectrophotometrically with pyrimidine-2-thiol [25,26].

3. Results and discussion

3.1. Effect of acidity

The extraction of 100 µg of palladium(II) was carried out from different acid media with 2% *N-n*-octylaniline in xylene keeping the aqueous to organic volume ratio 2.5:1. The extraction was found to be quantitative from hydrochloric, sulphuric, perchloric and hydrobromic acid (Fig. 1) but was incomplete in nitric acid due to emulsion formation. Although the extraction is quantitative in sulphuric acid media over a wide range, it needs a higher concentration while in perchloric acid and hydrobromic acid media, a narrow range of acidity is required and the equilibration time is greater. Hence the use of hydrochloric acid is recommended for further studies.

3.2. Effect of reagent concentration and nature of the extracted species

The concentration of *N-n*-octylaniline in xylene was varied from 0.2 to 7% over the acid range 0.2–10 M hydrochloric acid. It was found that 2% reagent in xylene was needed for quantitative extraction of metal ion from 1 M hydrochloric acid (Table 1).

Log–log plots of the distribution ratio versus *N-n*-octylaniline concentration (Fig. 2) at 4.0 and 5.0 M hydrochloric acid yield slopes of 1.8 and 1.5, respectively indicating that the metal to amine ratio in the extracted species is 1:2. The probable extracted species is,

Variation of equilibration period from 5 s to 30 min showed that shaking for 30 s each for hydrochloric and sulphuric acid, 10 min for perchloric acid, 5 min for hydrobromic acid is

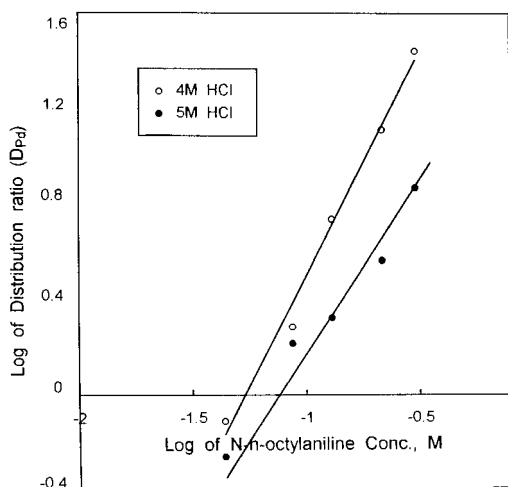


Fig. 2. Log–log plot of distribution ratio (D_{Pd}) versus N - n -octylaniline concentration at 4 M and 5 M HCl.

needed for complete extraction of palladium(II). Prolonged shaking up to 30 min had no adverse effect on the extraction.

The extraction of palladium(II) was quantitative when aqueous to organic volume ratio was 100:10. The aqueous to organic volume ratio in the recommended procedure was 2.5:1.

The loading capacity of 10 ml of 2% N - n -octylaniline was found to be 7.5 mg of palladium(II).

3.3. Effect of diluents

The extractions were performed from 1 M hydrochloric acid medium using 2% N - n -octylaniline in various solvents as diluents. The extraction was incomplete with n -butyl alcohol, 4-methyl-2-pentanol, chloroform and amyl alcohol as diluents for amine. The extraction becomes quantitative with amine solution in benzene, toluene, xylene, isobutyl methyl ketone, carbon tetrachloride and amyl acetate. Xylene is recommended for further extraction procedures.

Table 2

Effect of diverse ions on the extractive determination of Pd(II)

Diverse ion added	Amount tolerated (mg)	Diverse ion added	Amount tolerated (mg)
Mn(II)	15	Os(VIII)	1
Cd(II)	20	Au(III)	1
Mg(II)	20	Ag(I)	5
Fe(II)	5	Cr(VI) ^a	5
Fe(III)	20	Se(IV)	20
Pb(II)	10	Te(IV)	15
Hg(II)	5	Rh(III)	0.5
V(V)	10	Ru(III)	1
U(VI)	15	Pt(IV)	1
Ni(II)	10	Mn(VII)	20
Bi(III)	10	Sr(II)	20
Tl(III)	15	Sb(III)	5
Co(II)	20	Ir(III)	0.5
Ce(IV)	20	Tartrate	200
Sn(II)	5	Fluoride	200
Zn(II)	20	Citrate	200
Be(II)	15	Ascorbate	Interfere
Ca(II)	20	Oxalate	200
Ba(II)	20	Acetate	200
Mo(VI)	15	EDTA	20
Cu(II)	20		

Pd(II) = 100 μ g; aqueous phase = 1 M HCl; Aq/Org = 25:10; extractant = 2% N - n -octylaniline in xylene.

^a Masked with tartrate.

Table 3

Binary separation of palladium(II) from iron(III), cobalt(II), nickel(II) and copper(II)

Composition of metal ion, μg	Recovery of palladium(II) ^a (%)	Relative standard deviation (%)	Recovery of added metal ion ^a (%)	Relative standard deviation (%)
Pd, 200; Fe(III), 5000	99.7	0.07	99.5	0.19
Pd, 200; Co(II), 5000	99.6	0.13	99.4	0.15
Pd, 200; Ni(II), 5000	99.8	0.13	99.6	0.25
Pd, 200; Cu(II), 5000	99.6	0.11	99.5	0.16

^a Average of six determinations.

3.4. Effect of diverse ions

Palladium(II) was extracted in the presence of a large number of diverse ions. The tolerance limit was set at the amount of foreign ions caus-

ing an error of less than $\pm 2\%$ in the recovery of palladium(II) (Table 2). It is observed that the method is free from interference from a large number of transition, non-transition metal ions and anions.

Table 4

Analysis of synthetic mixtures

Composition (μg)	Palladium found ^a (μg)	Recovery(%)	Relative standard deviation (%)
Pd, 200; Au, 1000	199.6	99.8	0.05
Pd, 200; Os, 1000	199.8	99.9	0.07
Pd, 200; Pt, 1000	199.4	99.7	0.07
Pd, 200; Ru, 1000	199.6	99.8	0.05
Pd, 200; Rh, 500	199.4	99.7	0.07
Pd, 200; Ir, 500	199.2	99.6	0.06
Pd, 200; Pt, 500; Ru, 500	199.0	99.5	0.07
Pd, 200; Pt, 500; Rh, 500	199.4	99.7	0.07
Pd, 200; Pt, 500; Ir, 500	199.2	99.6	0.06
Pd, 200; Ru, 500; Os, 500	199.4	99.7	0.07
Pd, 200; Ru, 500; Ir, 500	199.4	99.7	0.07
Pd, 200; Os, 500; Ir, 500	199.6	99.8	0.05
Pd, 200; Ru, 500; Rh, 500	199.8	99.9	0.07
Pd, 200; Rh, 500; Ir, 500	199.6	99.8	0.05
Pd, 200; Rh, 500; Os, 500	199.2	99.6	0.06
Pd, 200; Pt, 500; Os, 500	199.0	99.5	0.07
Pd, 200; Pt, 200; Ru, 200; Rh, 200; Os, 200; Ir, 200	198.8	99.4	0.05
Pd, 200; Pt, 200; Ru, 200; Rh, 200; Os, 200; Ir, 200; Au, 200	199.0	99.5	0.07
Pd, 200; Fe, 2000; Co, 2000; Ni, 2000; Cu, 2000	199.4	99.3	0.07
Pd, 200; Pt, 200; Ru, 200; Rh, 200; Os, 200; Ir, 200; Au, 200; Fe, 2000; Co, 2000; Ni, 2000; Cu, 2000	199.4	99.6	0.07
Pd, 200; Ni, 1200; V, 200	199.2	99.6	0.06
Pd, 200; Pt, 200; Ni, 600; V, 95	199.6	99.8	0.05

^a Average of six determinations.

Table 5
Analysis of alloys

Alloy	Composition (%)	Palladium taken (μg)	Palladium found ^a (μg)	Recovery (%)	Relative standard deviation (%)
Dental alloy	Pd, 25; Pt, 15; Au, 17; Ag, 38; Cu, 4; Zn, 1	250	248.5	99.4	0.06
Low melting dental alloy	Pd, 34; Au, 10; Co, 22; Ni, 34	170	169.15	99.5	0.09
Stibio palladinite mineral	Pd, 75; Sb, 25	150	149.4	99.6	0.08
Jewellery alloy (Pd–Ru alloy)	Pd, 95.5; Ru, 4.5	191	190.61	99.8	0.05
Jewellery alloy (Pd–Au alloy)	Pd, 50; Au, 50	100	99.7	99.7	0.11
Solder alloy	Pd, 30; Pt, 10; Au, 60	150	149.7	99.8	0.08
Oakay alloy	Pd, 10.5; Pt, 20; Ni, 60; V, 9.5	105	104.48	99.5	0.13
	Pd, 18.2; Pt, 18.2; Ni, 54.2; V, 9.1	182	181.64	99.8	0.07
Pd–Cu alloy	Pd, 60; Cu, 40	120	119.64	99.7	0.12
Pd–Ag alloy	Pd, 60; Ag, 40	120	119.52	99.6	0.11
Golden coloured silver alloy resistant to transhing	Pd, 25.5; In, 21; Cu, 18; Ag, 35	102	101.49	99.5	0.10

^a Average of six determinations.

3.5. Binary separation of palladium(II) from iron(III), cobalt(II), nickel(II) and copper(II)

The method permits separation and determination of palladium(II) from a binary mixture containing either iron(III), cobalt(II), nickel(II) and copper(II).

Palladium is separated from iron(III), cobalt(II), nickel(II) and copper(II) by its extraction with 2% *N-n*-octylaniline in xylene from 1 M hydrochloric acid. Under these conditions all the base metals remain quantitatively in the aqueous phase where these are determined spectrophotometrically with thiocyanate [23], 1-nitroso-2-naphthol [23], DMG [23] and pyrimidine-2-thiol [27], respectively. Palladium is stripped from the organic phase with two 5-ml portions of 1:1 ammonia solution. The extracts were evaporated to moist dryness and leached with 1 M hydrochloric acid to form the solution. Palladium(II) was estimated spectrophotometrically with pyrimidine-2-thiol. The recovery of palladium(II) and that of the added ions was 99.4% and the results are reported in Table 3.

3.6. Separation and determination of palladium(II) in a synthetic mixture

Naturally occurring palladium(II) is always associated with the other platinum group and base metals, hence its separation from these metals is of great importance. Under the optimum extraction conditions for palladium(II), there is a quantitative extraction of Au(III), Pt(IV), Os(VIII) and incomplete extraction of Ru(III), Rh(III) and Ir(III). But the coextracted metal ions cannot be backstripped by 1:1 ammonia solution. Thus the reagent (*N-n*-octylaniline) is made selective towards palladium(II) by taking advantage of the stripant used. The proposed method allows the separation and determination of palladium(II) from many metal ions and the results of analyses are shown in Table 4.

3.7. Analysis of alloys

The proposed method is applicable for the analysis of various alloys for palladium content. If the sample is available, the dissolution is carried out

according to the earlier procedures [25,26,28]. This brings the elements present into the proper oxidation states for extraction of palladium(II) with *N-n*-octylaniline. However, the samples were not available at the working place, which forced us to use synthetic mixtures. These were prepared corresponding to the composition of the alloys. The results of the analysis are reported in Table 5. The average recovery of palladium(II) was 99.6%.

4. Conclusion

The important features of the method described here are that: (i) it permits selective separation of Palladium(II) from other platinum group and base metals which are generally associated with it; (ii) it is free from interference from a large number of diverse ions which are associated with palladium(II) in its natural occurrence; (iii) low reagent concentration is required; (iv) time required for equilibration is very short (30 s); (v) the method is applicable to the analysis of palladium(II) in synthetic mixtures with composition corresponding to alloys; (vi) the method appears to enable a higher ratio of sample to reagent solution to be used which can be of advantage when dealing with trace amounts of palladium(II), as in refinery process streams; and (vii) it is very simple, selective, reproducible and rapid requiring only half an hour for separation and determination.

Acknowledgements

One of the authors (TNL) is grateful to the University Grants Commission, New Delhi for providing financial assistance.

References

[1] F.E. Beamish, *The Analytical Chemistry of the Noble Metals*, Pergamon, Oxford, 1966.

[2] F.E. Beamish, J.C. Van Loon, *Recent Advances in the Analytical Chemistry of the Noble Metals*, Pergamon, Oxford, 1972.

[3] F.E. Beamish, J.C. Van Loon, *Analysis of Noble Metals: Overview and Selected Methods*, Academic Press, London, 1977.

[4] S.N. Invanova, L.M. Gindin, L.Y. Mironova, *Chem. Abstr.* 62 (1965) 4682b.

[5] L.M. Gindin, P.I. Bobikov, E.F. Kouba, *Chem. Abstr.* 56 (1962) 9779C.

[6] M.A. Khattak, R.J. Magee, *Anal. Chim. Acta* 45 (1969) 297.

[7] C. Pohlandt, *Natl. Inst. Metall. Republ. South Africa*, Project No. 03276, 28 March 1977.

[8] E.L. Smith, E.J. Page, *J. Soc. Chem. Ind.* 67 (1948) 48.

[9] A.A. Vasilyeva, I.G. Yudelevich, L.M. Gindin, T.V. Lantina, R.S. Shulman, I.L. Kotlarevsky, V.N. Andrievsky, *Talanta* 22 (1975) 745.

[10] C. Pohlandt, *Natl. Inst. Metall. Republ. South Africa*, Report No. 1881, 1977.

[11] C. Pohlandt, M. Hegetschweiler, *Natl. Inst. Metall. Republ. South Africa*, Report No. 1940, 1978.

[12] C. Pohlandt, *Talanta* 26 (1979) 199.

[13] R.N. Gedye, J. Bozic, P.M. Durbano, B. Williamson, *Talanta* 36 (1989) 1055.

[14] M.Y. Mirza, *Talanta* 27 (1980) 101.

[15] M.A. Khattak, R.J. Magee, *Anal. Chim. Acta* 35 (1966) 17.

[16] M. Mojski, *Talanta* 27 (1980) 7.

[17] G.H. Rizvi, P.R. Natarajan, *Fresenius Z. Anal. Chem.* 336 (1990) 498.

[18] M. Hidaigo, A. Masana, V. Salvado, *Talanta* 38 (1991) 483.

[19] E. Lachowicz, M. Czpiuk, *Talanta* 37 (1990) 1011.

[20] G.N. Mulik, S.R. Kuchekar, M.B. Chavan, *Indian J. Chem.* 25A (1986) 1073.

[21] G.N. Mulik, S.R. Kuchekar, M.B. Chavan, *J. Indian Chem. Soc.* LXIV (1987) 68.

[22] N.B. Kadam-Patil, S.S. Sawant, G.N. Mulik, M.B. Chavan, *Bull. Bismuth Inst.* 64 (1992) 5.

[23] A.I. Vogel, *A Text Book of Quantitative Inorganic Analysis*, 4th edn., ELBS, London, 1978, pp. 474, 739, 741, 747.

[24] Z.G. Gardlund, R.J. Curtis, G.W. Smith, *Liq. Crystals Ordered Fluids* 2 (1973) 541.

[25] M.A. Anuse, N.A. Mote, M.B. Chavan, *Talanta* 30 (1983) 323.

[26] M.A. Anuse, M.B. Chavan, *Chem. Anal. (Warsaw)* 29 (1984) 409.

[27] S.R. Kuchekar, M.A. Anuse, M.B. Chavan, *Indian J. Chem.* 25A (1986) 1041.

[28] M.A. Anuse, S.R. Kuchekar, N.A. Mote, M.B. Chavan, *Talanta* 32 (1985) 1008.

Bovine serum albumin as a means to immobilize DNA on a silver-plated bulk acoustic wave DNA biosensor

Hong Zhang, Ronghui Wang, Huwei Tan, Lihua Nie, Shouzhuo Yao *

New Material Research Institute, Chemistry and Chemical Engineering College, Hunan University, Changsha, 410082, People's Republic of China

Received 4 April 1997; received in revised form 6 August 1997; accepted 11 August 1997

Abstract

A simple, inexpensive, on-line bulk acoustic wave (BAW) DNA biosensor is proposed by using an Ag-plated surface rather than the conventional Au surface. Bovine serum albumin (BSA) is used as an active coating for DNA immobilization. Impedance analysis reveals that the film composed of didodecyl dithiono-oxamide (DDDTO) and BSA can dramatically enhance the amount of immobilized DNA. Detection of dissociation and hybridization of immobilized DNA is demonstrated as an example of the potential application of this type of acoustic wave DNA biosensor in clinical practice. © 1998 Elsevier Science B.V. All rights reserved.

Keywords: Bovine serum albumin; DNA biosensor; Silver surface; Bulk acoustic wave; Immobilization

1. Introduction

For many years, researchers have made great efforts to develop a good method for DNA sensing, and DNA hybridization is most often used. Radioactive probe (usually labeled with ^{32}P) techniques dominated the field of hybridization assay for more than two decades and provided extremely high sensitivities. However, the short shelf life, the health hazard, the cost and the long exposure times (many hours to days) have limited its development in the clinical laboratory. Therefore, new methods, which eliminate the time-consuming labeling procedures and the problem of

fluctuations, are necessary to make it safer and more convenient for DNA molecular diagnostics.

Among those methods tried, an optical sensor with a detection limit of 86 ng/ml was reported [1]. As another approach, nano or subnanogram quantities of the complementary DNA were detected by using electrochemical techniques, such as voltammetric DNA sensors [2,3], carbon-paste/PSA method [4], and FIA [5]. Hashimoto et al. [6] even reported a 0.1 pg/ml detection limit for a 4.4-kb target sequence. These sensors have the ability to respond to the structure/formation changes of DNA duplex. But they have the limitation of requiring the use of redox-active DNA intercalators or groove-binders as label, which are often sequence-dependent. A similar situation is also faced by optical DNA sensors. Strictly, these

* Corresponding author. Fax: +86 731 8824525; e-mail: szyao@hunu.edu.cn

two kinds of DNA sensor cannot provide real response signals, i.e. they measure other substances rather than the DNA molecule itself.

On the other hand, the bulk acoustic wave (BAW) DNA biosensor, because of its simplicity, capability of offering in-situ information and possibility for miniaturization and incorporation in a microchip array, has attracted much attention. This so-called DNA biosensor is a bulk acoustic wave device with single stranded (ss-)DNA immobilized on the sensing areas of the device. The ss-DNA complementary to target DNA are then hybridized with a sample solution containing the target DNA, and the bulk acoustic wave signals are recorded. Compared with the existing techniques, it does not need an extra indicator and reflects the real reaction responses. It has the advantages of low sensitivity to nonspecific DNA and high sensitivity to the target molecule. Moreover, it has the ability to record a real-time plot of each step of the DNA reaction and thus provides an approach to the dynamic and mechanism study. A key step in developing such sensors is to immobilize probe DNA molecules effectively onto the surface of the bulk acoustic wave devices.

Most bulk acoustic wave DNA biosensors are made with gold-plated quartz crystals. Fawcett et al. [7] first reported such a sensor in 1988. They took an AT-cut gold-plated quartz crystal and had the single-stranded nucleic acid immobilized onto it through covalent binding to a styrene-acrylic acid copolymer. The real in-situ liquid-phase measurement was carried out by Okahata et al. [8] who bound the modified ss-DNA having an -SH group at the 5'-phosphate end onto a BAW device with Au electrodes on both sides through self-assembled chemisorption, which was developed by Ito et al. [9]. They also developed a cast film of a DNA-lipid complex deposited on a quartz-crystal microbalance to study intercalation behavior of dyes in DNAs [10]. Su et al. [11] undertook a study to elucidate the immobilization of nucleic acids on PdO deposited on Au-plated quartz crystals with a view to study the DNA biosensor through the network analysis method. In addition to these, LB-membrane and other

methods have also been developed [12,13].

However, to our knowledge, few investigations have been undertaken to evaluate the immobilization behavior of DNA on the surface of Ag-electrode quartz crystals of the bulk acoustic wave (BAW) sensor — these are more easily available and have the advantages of much lower cost than the Au-plated ones. In this paper, we proposed a BAW biosensor with probe DNA covalently immobilized on the didodecyl dithiono-oxamide (DDDTO)-bovine serum albumin (BSA) modified Ag surface.

Bovine serum albumin, as an important modifying material in clinical laboratories, has attracted much interest. Due to the presence of amino groups in its structure, it has been widely used in enzyme sensors to assist the immobilization of enzyme molecules [14,15]. Results have shown that BSA can hardly be desorbed from the surface of the self-assembly thiol monolayer [16]. Thus, the BSA method combined with the self-assembly technique in more recent years has improved its stability and widened its application in the study of biological phenomena. The reports from those early researchers have confirmed that sulfide and/or disulfide compounds can be strongly adsorbed on Ag surfaces, as well as Au and Cu surfaces, forming a very stable monolayer [17]. Hence, the combination of BSA method and self-assembly technique can be used for immobilizing DNA on Ag-plated BAW sensors.

In our preliminary work, the possibility of immobilizing DNA on an Ag-plated BAW device is investigated. Impedance analysis has been used to study the surface modification procedures and the DNA immobilization processes. The experiment results show that DNA can be successfully immobilized on the less costly BAW sensor with an Ag surface which gives a good result in terms of immobilizing capacity and stability. The dissociation and hybridization experiments reveal that the proposed Ag-plated BAW DNA biosensor can be reused and can give as good results as those from Au-plated ones.

2. Experimental

2.1. Apparatus

The experimental setup was the same as that described previously [18]. An AT-cut 9 MHz quartz crystal (Model JA-5, Peking Factory No. 707) with silver electrodes on both sides (area: $0.28 \text{ cm}^2 \times 2$) was used as the BAW resonator. A home-made oscillator [19] was used to drive the crystal at its resonant frequency in aqueous solutions. The frequency output from the oscillator was measured by a universal counter (Model SC-7201, Iwatsu Co., Tokyo) and was recorded by an IBM compatible personal computer via an HPIB bus and an HP-IB interface plugged in the computer (Hewlett-Packard). An HP 4192A-LF impedance analyzer was employed to perform admittance measurements of the BAW crystal. The temperature was controlled by a water jacket and a model WMZK-1 Temperature Controller (Medical Equipment Co. Shanghai) at $15 \pm 0.1^\circ\text{C}$ except where otherwise stated.

2.2. Materials

Double-stranded salmon sperm DNA (ds-DNA, Shanghai Biochemical Products Institute) and bovine serum albumin (MW 66 000, $A_{415 \text{ nm}}^{0.1\%} < 0.06$, Shanghai Bo'ao Biotechnical Co.) were used as received. Denatured single-stranded DNA was obtained by heating the native dsDNA in a water bath at 100°C for ca. 5 min followed by rapid cooling in an ice bath. $2 \times \text{SSC}$ buffer solution was prepared by mixing 300 mmol l^{-1} sodium chloride with 30 mmol l^{-1} sodium citrate, and its pH value was adjusted to pH 7.4. Didodecyl dithiono-oxamide (DDDTO) of chemical-reagent grade was used. HOAc–NaOAc buffer solution (pH 5.0) was deoxygenated before each experiment. All chemicals used were of analytical-reagent grade. Double distilled water was used for the reagent preparation and throughout the procedure.

2.3. Surface modification

The surface modification processes were monitored through impedance measurements. The measurements were made in-situ with one surface of the BAW resonator in contact with solutions, except where otherwise stated. Before the experiments, 30 min were needed to stabilize the whole setup including the impedance analyzer, the frequency counter and the power supply.

1. *Cleaning procedure.* The BAW resonator was mechanically polished to a mirror finish using 50-nm alumina to avoid the effects of surface roughness on frequency response. After being rinsed with distilled water, the resonator was dipped for 30 min in 1.0 mol l^{-1} NaOH and rinsed again with distilled water. Then 1.0 mol l^{-1} HCl was applied to the surface for another 30 min, followed by rinsing with water, alcohol, water and air-dried. With this cleaning, a clean crystal surface was formed on each sensor to give better repetition.
2. *DDDTO–BSA modification.* The cleaned BAW resonator was dipped in a ca. 1.2% solution of DDDTO in acetone for 1.5 h, then air-dried and washed with acetone and water three times. After this, the sensing surface was treated with $20 \mu\text{l}$ 4.5% (wt.) of BSA solution for 2 h.
3. *DNA immobilization.* After rinsing thoroughly with water and then HOAc–NaOAc buffer solution, $20 \mu\text{l}$ ds-DNA solution ($0.5 \mu\text{g } \mu\text{l}^{-1}$) was added into the detector cell and left for 1.5 h. Then the crystal was washed with HOAc–NaOAc buffer and water.

3. Results and discussion

3.1. Modified Ag-plated BAW sensor with DDDTO and BSA

It is well known that a bulk acoustic wave sensor is an electromechanical transducer which converts electrical energy to mechanical energy, and vice versa. Its electrical equivalent circuit was shown previously [20]. For this equivalent circuit, the admittance Y (reciprocal of impedance Z) is:

$$Y = 1/Z = G + jB$$

where G is conductance and B , susceptance, which are the real part and the imaginary part of admittance Y , respectively. From the impedance analysis, the four circuit elements, i.e. R_m , the motional resistance, L_m , the motional inductance, C_m , the motional capacitance and C_0 , the static capacitance, can be related to the loss of mechanical energy dissipated to the surrounding medium, the mass and the mechanical elasticity of the vibrating body, and the geometry of the quartz crystal electrode [20], respectively. They can be extracted from G and B frequency spectra obtained through impedance measurements (Fig. 1) by fitting admittance data using a nonlinear least square technique, the Levenberg–Marquardt method [21,22], to minimize the sum of the squares of the differences between measured and computed admittance data.

The modification of DDDTO and BSA onto the Ag surface was monitored by the BAW device through impedance measurements. Fig. 2(a) shows a typical profile of the frequency of maximum conductance (f_o , $f_o = 1/2\pi(L_m C_m)^{1/2}$) responses of the sensor upon the introduction of DDDTO solution onto the Ag surface. As can be seen from Fig. 2(a), f_o decreases rapidly during the first 10 min for up to 33 Hz, and then slows down. As DDDTO is self-assembled onto the Ag

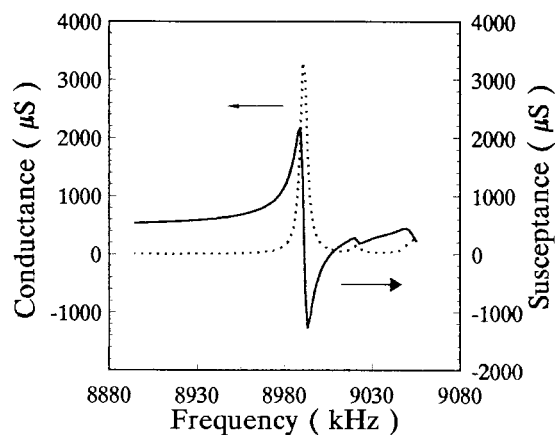


Fig. 1. Typical plots of the conductance (G) and susceptance (B) spectra of a 9-MHz BAW resonator.

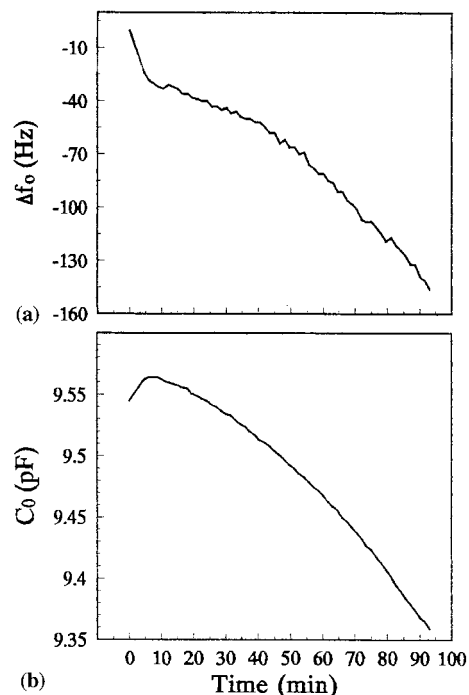


Fig. 2. Responses of the resonant frequency (Δf_o , a) and static capacitance (C_0 , b) of the 9-MHz BAW device with silver-plated electrodes upon DDDTO loading.

surface, we can assume that initially the binding sites on the surface were sufficient enough to let DDDTO molecules be easily adsorbed onto the Ag surface when its solution was applied to the bare Ag electrode and caused a rapid decrease in f_o . With time, the adsorbed monolayer began the procedure of assembling towards a highly ordered structure [17,23–25], as well as the procedure of adsorbing onto the Ag surface. Accordingly, the rearrangement of the DDDTO molecules made the mass loading not so significant as during the first 10 min.

Additional information, such as the static capacitance C_0 , can be obtained from the equivalent circuit parameters measurements. C_0 is predominantly determined by the dielectric properties of the quartz crystal. Yet, in a conductive solution, it is directly affected by the structure of the electrified interface, i.e. the capacity of the electrical double layer at the charged interface [26]. As shown in Fig. 2(b), the initial adsorption results in

an increase in C_0 and further adsorption leads to a significant decrease. The DDDTO molecules approach the surface in its native state with most of the polarizable groups located on the outer surface, which causes an increase in the polarity and hence the charge density at the inner Helmholtz plane and thus a rise in the double-layer capacitance. As the adsorbed monolayer forms a self-assembly structure, the declination in surface polarity due to the redistribution of those groups occurs, leading to a decrease in the double-layer capacitance and thus in C_0 [27].

The BSA modification step was subsequently carried out. From the experiment, we noted that the DDDTO-coated BAW sensor exhibited a rather hydrophobic surface, which gave a good background for BSA adsorption because BSA molecules tend to be adsorbed strongly to a hydrophobic surface [28]. The pH was pH 5.0 which was around the isoelectric point of the BSA molecule and thus enhanced its hydrophobicity by loss of its net electric charge.

In impedance analysis, L_m is the quantity reflecting the mass of the vibrating body. Yet, because L_m and C_m are always correlated, the corrected L' is used [29]. The real-time plots of changes in L' during the procedure of BSA adsorption are given in Fig. 3. The overall L' shift is 60.44 μH corresponding to a frequency shift of 120 Hz.

It is known that the width of the half-height of the conductance maximum of the crystal should broaden if the viscoelastic properties of the film affect the resonant frequency. In this stage, no significant difference was found between the bare crystal and the DDDTO–BSA coated one. Therefore the film behaved as a quasi-rigid layer under the experimental conditions. Assuming that BSA is an ellipsoidal molecule with rough dimension of $4 \times 4 \times 14$ nm [30], monolayer coverage of BSA should be approximately 550 ng cm^{-2} for head-on type adsorption and 140 ng cm^{-2} for side-on type arrangement calculated from the molecular mass of 66 000 as two extreme cases. These correspond to frequency changes of ca. 140 Hz and 36 Hz for our 9-MHz AT-cut quartz crystal, respectively, based on the Sauerbrey's equation [31]. The frequency shift obtained in our experiment shows

BSA loading is between the two extreme cases, suggesting that the arrangement of BSA molecules under the experiment conditions was not exactly like the two extreme cases. The above discussion does not take into account the possible denaturing and unfolding of BSA on the electrode surface. It should be emphasized that this discussion is not strictly enough, however this theoretical calculation can provide a rough estimate of the upper and lower limits of the amount of adsorption.

3.2. Immobilization of DNA

Covalent immobilization of DNA on the DDDTO–BSA modified Ag surface was observed (Fig. 4). The in-situ frequency responses of the control experiments are also shown in Fig. 4.

The frequency shift Δf_0 of the first curve (bare electrode surface) is -140 Hz, while the third curve (DDDTO–BSA modified crystal) gives Δf_0 of -482 Hz, confirming the successful immobilization of DNA on the Ag-plated BAW device.

Owing to the presence of amino groups in the BSA structure, the BSA-coated quartz crystal becomes protonated and attracts the negative charge of the nucleic acid's 5'-phosphate groups, forming a phosphoramidate bond.

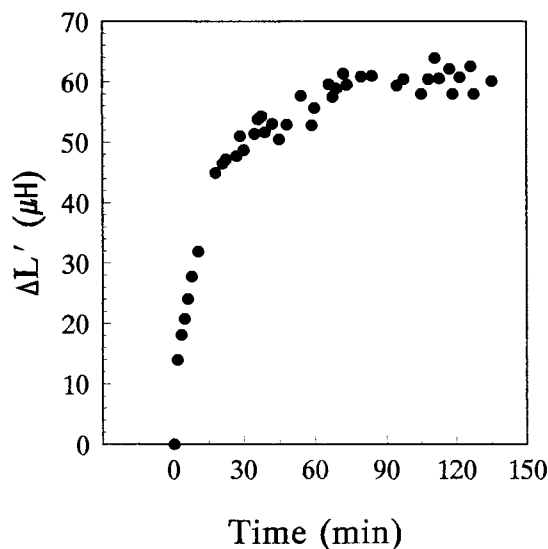


Fig. 3. Inductance changes of the silver-plated BAW sensor with time upon BSA adsorption.

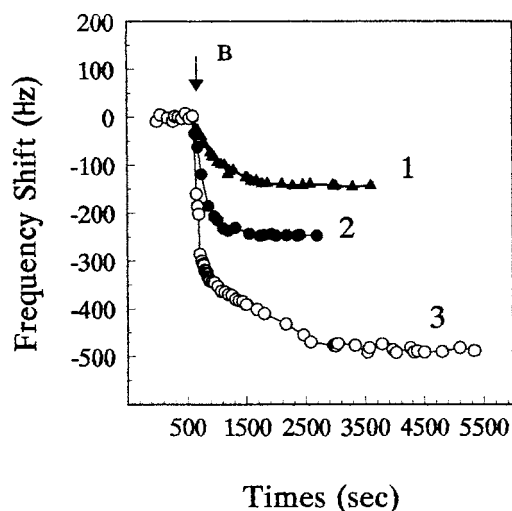


Fig. 4. Comparison of frequency changes of the silver-plated BAW DNA biosensor with time after addition of DNA solution (at point B) under different surface modification conditions: (1) Bare electrode; (2) Single DDDTO modified electrode; (3) DDDTO-BSA modified electrode.

It is known that the isoelectric point of the DNA molecule is in the range of pH 4.0 ~ 4.5. When pH > 4.0, the DNA molecule exhibits a highly polycationic state. On the other hand, as the stability of hydrogen bond formed between the base pairs depends on the pH value, the pH of the solution is often kept at less than 11 for the sake of stability [32]. Thus, the medium pH in this experiment is chosen to be within the range of 5.0 ~ 7.4, which makes the DNA molecule more readily bind the amino groups of the BSA molecule.

Conductance spectra of the BAW resonator in solutions are shown in Fig. 5, the G_{\max} decreases during the DNA immobilization and the width of the half-height of the conductance maximum broadens, suggesting that the adsorbed DNA film is more viscous than that of the sublayers and hence the amount of the adsorbed DNA cannot be determined exactly using the Sauerbrey's equation. Further study on the relationship between the frequency response of the proposed BAW DNA biosensor and the mass of adsorbed DNA is being undertaken. The initial DNA contact (curve b) causes the decrease in G_{\max} (or an

increase in R_m) while the f_o remains unchanged (which implies no significant mass loading or elasticity change takes place), suggesting an increase in loss of mechanical energy dissipated to the surroundings, i.e. addition of DNA causes an increase in $\rho\eta$ of the solution. On the other hand, the final f_o of the DNA solution shifts towards a lower frequency (curve c), reflecting an increase in L_m . The above observation reflects the adsorption of DNA onto the surface of the silver-plated electrode.

3.3. Comparison of immobilizing capacity

Because of its amido groups, DDDTO can attract the nucleic acid's 5'-phosphate groups, too. However, due to the steric hindrance effect caused by the two long alkyl chains in its structure, it might not provide many active binding sites for immobilizing DNA which itself is a huge molecule. To compare the value of the frequency shift corresponding to DNA immobilization on different surfaces, a series of experiments were carried out (Fig. 4). The frequency changes of the BAW device were monitored under the same conditions.

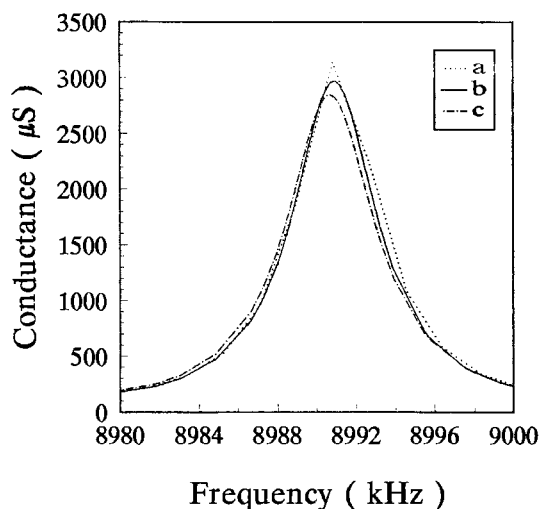


Fig. 5. Conductance spectra of the silver-plated BAW DNA biosensor in solution observed in the course of DNA immobilization. (a) DDDTO-BSA coated crystal; (b) Initial contact of the crystal with DNA; (c) The sensor with immobilized DNA.

Compared with the bare crystal and the single DDDTO coated one, the film consisting of DDDTO and BSA layers dramatically enhanced the amount of immobilized DNA. Thus we may deduce that the BSA coated on the DDDTO sublayer possesses a large surface area and provides a rich active site for immobilizing DNA.

In order to test the stability of the modified DNA layer, the unreacted BSA was blocked with 0.1 M glycine solution (pH 7.4). Then, the crystal was immersed in HOAc–NaOAc buffer, and the frequency was monitored. Results showed that the frequency of the BAW DNA biosensor slightly increased (perhaps resulting from the removal of nonspecific adsorption), only in the initial 10 min, and then stabilized with a frequency variation of ± 8 Hz for an observation interval of 1 h.

3.4. Dissociation and hybridization of DNA on the BAW DNA biosensor

The dissociation and hybridization processes of the immobilized DNA were monitored as an example of the potential application of this BAW DNA biosensor. An HOAc–NaOAc solution containing 1 mg ml⁻¹ DNA was applied to the DDDTO–BSA treated Ag surface. It was then allowed to incubate overnight. Immobilized DNA was dissociated by treating with 95 ~ 90°C 2 × SSC buffer solution (pH 7.4) for 5 min to get single-stranded (ss-)DNA. Then it was hybridized again with ss-DNA. In order to get a highest ratio of hybridization, the condition was controlled at 65°C in a 2 × SSC hybridization buffer solution (pH 7.4) [33]. The series resonate frequency was measured before and after each step and the results are listed in Table 1. Apparently, the longer the incubation time, the more the amount of immobilized DNA, provided that the saturation point was not reached.

The overall Δf_0 corresponding to DNA immobilization is 658 Hz, confirming the successful immobilization of DNA on the Ag-plated BAW sensor. The dissociation step caused an increase in f_0 for about 335 Hz. Somehow it is a bit higher than that expected for the loss of all complementary single strands (329 Hz). Partial removal of nonspecific adsorption during the washing step

Table 1
Frequency responses of the BAW DNA sensor under different conditions

BAW DNA sensor	Δf_0 , Hz
Coated with DDDTO–BSA ^a	0
Modified with ds-DNA (1 h)	-119 ± 2
Modified with ds-DNA (overnight)	-658 ± 2
Dissociated	-323 ± 2
Hybridized	-651 ± 2

The values are the average of five experiments.

^aThe frequency responses to DDDTO and BSA coatings are controlled at about 160 Hz and 120 Hz, respectively.

might account for this observation. However, the difference is not very significant and is around the range of experimental error. In the hybridization procedure, the 328-Hz decrease is in accordance with the expected value, suggesting a possible way to make the sensor reusable. Compared with the results given by the Au-plated DNA sensors [13], it can be said that our Ag-plated BAW DNA biosensor can provide as good results as those from Au-plated ones.

4. Conclusions

The possibility of immobilizing DNA on Ag rather than an Au-plated BAW device has been investigated. The results demonstrated that on the basis of DDDTO–BSA coating, DNA can be immobilized on the Ag surfaces. Successful DNA immobilization in our experiment makes the proposed silver-plated BAW DNA biosensor a promising tool in clinical applications. The standard deviation of background signals during the measurement of series resonant frequency is in the region of ± 2 Hz. Accordingly, the limit of detection for on-surface DNA under the currently unoptimized experimental conditions is about 2 ng. Since this method is uncomplicated, rapid, conceptually simple, and economically feasible, it will become a competitive method over presently existing techniques. Further exciting possibilities for the future lie in the development of a rapid response method combined with this BAW DNA biosensor. The specificity could be raised by im-

mobilizing a highly specific genetic fragment as the probe.

Acknowledgements

We are grateful to the financial support from the National Natural Science Foundation and Education Commission Fund of China. We also thank Dr J.H. Chen of the Chemistry and Chemical Engineering College of Hunan University for helpful discussion.

References

- [1] P.A.E. Piunno, U.J. Krull, R.H.E. Hudson, M.J. Damha, H. Cohen, *Anal. Chem.* 67 (1995) 2635.
- [2] K.M. Millan, S.R. Mikkelsen, *Anal. Chem.* 65 (1993) 2317.
- [3] K.M. Millan, A. Saraullo, S.R. Mikkelsen, *Anal. Chem.* 66 (1994) 2943.
- [4] J. Wang, X. Cai, G. Rivas, H. Shiraishi, *Anal. Chim. Acta* 326 (1996) 141.
- [5] J. Wang, L. Chen, M. Chicharro, *Anal. Chim. Acta* 319 (1996) 347.
- [6] K. Hashimoto, K. Ito, Y. Ishimori, *Anal. Chem.* 66 (1994) 3830.
- [7] N.C. Fawcett, J.A. Evans, L.C. Chien, N. Flowers, *Anal. Lett.* 21 (1988) 1099.
- [8] Y. Okahata, Y. Matsunobu, K. Ijio, M. Mukae, A. Murakami, K. Makino, *J. Am. Chem. Soc.* 114 (1992) 8299.
- [9] K. Ito, K. Hashimoto, Y. Ishimori, *Anal. Chim. Acta* 327 (1996) 29.
- [10] Y. Okahata, Y. Matsuzaki, K. Ijio, *Sensors and Actuators B* 13-14 (1993) 380.
- [11] H.B. Su, M.S. Yang, K.M.R. Kallury, M. Thompson, *Analyst* 113 (1993) 309.
- [12] M.A. Karymov, A.A. Kruchini, Y.A. Balova, L.A. Remisova, N.G. Sukhodolov, A.I. Yanklovich, A.M. Yorkin, *Sensors and Actuators B* 6 (1992) 208.
- [13] S. Yamaguchi, T. Shimomura, T. Tsuma, N. Oyama, *Anal. Chem.* 65 (1993) 1925.
- [14] S. Nakamoto, N. Ito, T. Kuriyama, J. Kimura, *Sensors and Actuators* 13 (1988) 165.
- [15] J. Kondoh, Y. Matsui, S. Shiokawa, W.B. Wlodarski, *Sensors and Actuators B* 20 (1994) 199.
- [16] J. Anzai, B. Guo, T. Osa, *Bioelectrochem. Bioenerg.* 40 (1996) 35.
- [17] M.A. Bryant, J.E. Pemberton, *J. Am. Chem. Soc.* 113 (1991) 3629.
- [18] K. Chen, D. Le, H. Zhang, L.H. Nie, S.Z. Yao, *Anal. Chim. Acta* 329 (1996) 83.
- [19] S.Z. Yao, Z.H. Mo, *Anal. Chim. Acta* 193 (1987) 97.
- [20] T.A. Zhou, L.H. Nie, S.Z. Yao, *J. Electroanal. Chem.* 293 (1990) 1.
- [21] D. Marquardt, *J. Soc. Ind. Appl. Math.* 11 (1963) 431.
- [22] H.W. Tan, D. Le, L.H. Nie, S.Z. Yao, *Analyst*, 122 (1997) 179.
- [23] R.G. Nuzzo, L.H. Dubois, D.L. Allara, *J. Am. Chem. Soc.* 109 (1987) 2358.
- [24] H.O. Finklea, S. Avery, M. Lynch, *Langmuir* 3 (1987) 409.
- [25] T.H. Joo, K. Kim, M.S. Kim, *J. Phys. Chem.* 90 (1986) 5816.
- [26] M.S. Yang, M. Thompson, *Anal. Chem.* 65 (1993) 3591.
- [27] J.H. Chen, Ph.D. thesis, Hunan University, 1997.
- [28] P. Van Dulm, W. Norde, *J. Colloid Interface Sci.* 91 (1983) 248.
- [29] M.A.M. Noel, P.A. Topart, *Anal. Chem.* 66 (1994) 484.
- [30] A.K. Wright, M.R. Thompson, *Biophys. J.* 15 (1975) 137.
- [31] G. Sauerbrey, *Z. Phys.* 155 (1959) 206.
- [32] H.Y. Zhang, *Courses of Biochemistry*, Sichuan University Press, Chendu, 1988, p. 135 (in Chinese).
- [33] R.F. Schleif, P.C. Wensink, in: R.F. Schleif, P.C. Wensink (Eds.), *Practical Methods in Molecular Biology*, Chapter 6, Springer, New York, 1984 (in Chinese).

Chemiluminescence (CL) emission generated during oxidation of pyrogallol and its application in analytical chemistry. I. Effect of oxidant compound

Nicholaos P. Evmiridis *, Nicholaos K. Thanasoulas, Athanasios G. Vlessidis

University of Ioannina, Department of Chemistry, Laboratory of Analytical Chemistry, 45110 Ioannina, Greece

Received 28 April 1997; received in revised form 8 August 1997; accepted 11 August 1997

Abstract

An investigation of chemiluminescence (CL)-emission generated by the oxidation of pyrogallol using various inorganic oxidant compounds is reported in this F.I.A.-merging zone application. The oxidant compounds that showed measurable CL-emission were permanganate, periodate, hypochlorite anions, cerium(IV) and hydrogen peroxide. The different oxidant compounds showed CL-emissions at different pH-ranges. The CL-emission was limited by the inner filter effect and this was more intense for oxidants of selective oxidation. Kinetic effects were also found in the case of oxidation by permanganate. Plots of CL-emission against pH give evidence of speciation and or deactivation mechanism effects. The analytical parameters for the determination of the oxidants are given. Sensitivities of 895 600, 19 500, 33 723, 10 680 and 56 703 mV M⁻¹ were found for the determination of permanganate, cerium(IV), periodate, hypochlorite and hydrogen peroxide, respectively. The calibration curves of the oxidant determination were generally S-shaped; the S-shaped calibration curve of periodate was closer to a straight line relationship while that of hypochlorite was almost a straight line; detection limits in the range of 10⁻⁴ M oxidant concentration were found for nearly all oxidants. The analytical parameters for determination of pyrogallol by the CL-emission generated through oxidation by the different oxidants at optimum conditions were 1.16 × 10⁶ mV M⁻¹ for permanganate; 0.086 × 10⁶ mV M⁻¹ for cerium(IV); 0.91 × 10⁶ mV M⁻¹ for periodate; 0.012 × 10⁶ mV M⁻¹ for hypochlorite; and 0.25 × 10⁶ mV M⁻¹ for hydrogen peroxide. The detection limit was 1.0 × 10⁻⁴ M. The nearly straight-line relationship (initial part of the plot) for CL-emission with oxidant concentration gives an indication that the CL-reaction of pyrogallol oxidation by hypochlorite proceeds through a process that involves energy transfer while the pronounced S-shaped curve produced by permanganate gives the indication that the reaction proceeds through a process that does not involve energy transfer according to the mathematical model of CL-emission that controls the F.I.A.-merging zone technique of the flow apparatus used in this work. The sequence of completeness of the oxidation process by each oxidant was MnO₄⁻ > H₂O₂ > IO₄⁻ > OCl⁻; the stoichiometric quantity of the oxidant per pyrogallol molecule for the rapid part of the overall oxidation by each different oxidant was attempted; this is an index-value of the oxidation state of the fluorescent excited molecule. Finally, the impact of the above findings for further analytical applications is discussed. © 1998 Elsevier Science B.V. All rights reserved.

Keywords: Chemiluminescence (CL)-emission; Pyrogallol oxidation; Oxidants; pH-selectivity; Prospects for analytical applications

* Corresponding author.

1. Introduction

Chemiluminescence (CL)-reactions are becoming increasingly popular for trace analysis, because of their high sensitivity, rapidity, simplicity and low cost of instrumentation [1–3]. Some CL-reactions are extremely sensitive to concentration changes while recent developments in increasing sensitivity and reliability of photomultipliers have given extra interest in CL-reactions. In addition the implementation of the CL-reaction analytical system with a F.I.A. manifold gives an extra element of simplicity, reproducibility, rapidity, convenience and above all provides a degree of automation to the analytical procedure.

The CL-emission generated during pyrogallol oxidation by H_2O_2 has not met the proper attention by researchers because other CL-systems were far more sensitive. However, the CL-emission that accompanies the oxidation of pyrogallol by H_2O_2 [4] is also observed with oxidation by other oxidants i.e. by permanganate [5,22], by periodate [6–8], and is observed with other pyrogallol substituted compounds (i.e. gallic acid, tannins, etc.). The CL-emission intensity can be enhanced by catalytic or sensitizing effects [4,6,22]. Finally, and more important the CL-emission is pH-range selective to the oxidants and the pyrogallol-compounds.

The above properties of the pyrogallol CL-system are very important in analytical chemistry and further investigation of the system may lead to useful applications in the determination of organic compounds in samples like drugs, pharmaceuticals, food products, biological fluids, etc. The generation of CL-emission by a number of oxidant reagents that show pH-range specificity may become a tool for the determination of such oxidants in different fields of science, i.e. in environmental chemistry (determination of OCl^-), clinical chemistry (determination of H_2O_2) and in organic analytical chemistry (determination of IO_4^-). The selective determination of oxidative anions may also be of benefit to ion-chromatography with post column detection of these anions. Finally, the phenomenon is important in instrumental analysis using enzyme immobilization on particles of high specific surface area and packing

them in the optical cell. Many such applications are being investigated in our laboratory.

The present study reports the investigation of the CL-emission generated during pyrogallol oxidation by different oxidant compounds. Each pyrogallol-oxidant system is investigated for the effects of the pH, and of concentrations of pyrogallol and oxidant.

2. Experimental

2.1. Reagents

All chemicals were of analytical reagent grade unless otherwise specified and distilled water was used throughout.

Buffer solutions of $\text{HClO}_4/\text{NaClO}_4$, $\text{H}_3\text{PO}_4/\text{H}_2\text{PO}_4^-$, $\text{CH}_3\text{COOH}/\text{CH}_3\text{COO}^-$, $\text{H}_2\text{PO}_4^-/\text{HPO}_4^{2-}$, $\text{H}_2\text{CO}_3/\text{HCO}_3^-$ and $\text{HCO}_3^-/\text{CO}_3^{2-}$ were prepared by dissolving a tenth of the formula weight of the corresponding salt in water and diluting to 900 ml, adjusting to the desired pH by the addition of 70–72% w/w HClO_4 (Merck) or 1 M NaOH titrisol solution (Fluka) and making up to 1 l with distilled water.

Oxidant stock solutions (0.01 M) of potassium permanganate (Baker), cerium sulfate tetrahydrate (Merck), and potassium periodate (Fluka), were prepared by dissolving one hundredth of the specific formula weight of the oxidant compound in the desired buffer solution and further diluting with the buffer solution to 1 l. The oxidant solutions were stored in reagent bottles or when necessary in dark brown glass bottles to avoid photochemical decomposition.

Oxidant 0.01 M stock solution of hydrogen peroxide was prepared by diluting the proper volume of 30% w/v H_2O_2 (Merck) to 1 l with the proper buffer solution.

Oxidant 0.1 N standard solution of hypochlorite was prepared by standardising a commercial sodium hypochlorite solution by iodometric titration and then diluting a certain volume of the commercial solution to the appropriate volume with the proper buffer solution.

Pyrogallol working solutions were freshly prepared by dissolving the appropriate weight of

pyrogallol (Merck) in the desired buffer solution and making up to the proper volume of the volumetric flask with the same buffer solution. Volumes of 100.0 ml were prepared each time and special care was taken to avoid long exposure to light and air.

2.2. Apparatus

An F.I.A. manifold equipped with flow-cell CL-detector was used (Fig. 1). The red sensitive photomultiplier (EMI 9865 B) combined with power supply at 1600 V was used for detecting the emission of light. A pH-meter (Crison Micro pH 2000) equipped with pH-electrode (Ingold) and temperature measuring element was used for adjusting the pH of buffer solutions.

2.3. F.I.A. method

The method of merging zone was used to mix the stream of oxidant with the stream of pyrogallol (Pg) solution just before entering the flow cell of the detector.

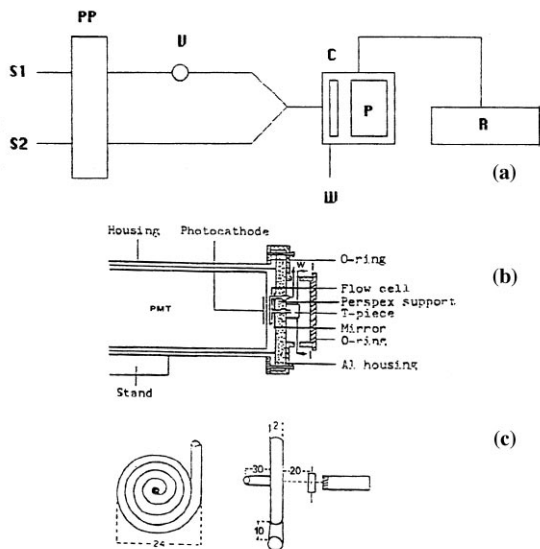
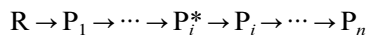


Fig. 1. (a) F.I.A. manifold: (PP) peristaltic pump; (C) optical cell; (P) photomultiplier; (R) recorder; (V) injection valve; (W) waste bottle; (S1, S2) flow streams for the buffered solution of pyrogallol and oxidant, respectively. (b) Details of the cell compartment. (c) Details of the design of the optical cell (dimensions in mm).

2.4. Mathematical expression of CL-emission under the operating conditions of this apparatus

For a CL-reaction (Scheme A)



$$+ \\ *h\nu$$

in a batch-type reactor, the general equation for CL-emission is given by Eq. (1)

$$I(t) = f \cdot h\nu \cdot n_{P^*}(t) \quad (1)$$

where $h\nu$ = quantum of light emitted from the electronic transition of a single P^* -species; $n_{P^*}(t)$ = the number of P^* -species that are present at time, t , in the CL-solution; f = the quantum efficiency of P^* -species to relax through the emission of light.

Because the P^* -species formed are transient species of negligibly short life, the $n_{P^*}(t)$ will be given by the rate of formation of P^* -species at time t and therefore Eq. (1) is modified to

$$I(t) = C \cdot f'(t) \quad (2)$$

where $f'(t) = d(n_{P^*}(t))/dt$, and $C = f \cdot h\nu$

Under the regime of integral reactor, the operational mode of F.I.A./merging zone, and the design of the tubular snail-shaped optical-cell, the CL-emission intensity, $I(\text{CL})$, observed is given by Eq. (3)

$$I(\text{CL}) = \int_0^{t_{\text{eq}}} I(t) dt \quad (3)$$

where t_{eq} is the time needed for the reaction to reach equilibrium (i.e. $P_i^* = 0$).

However, dealing with a flow system, the time variable is given by

$$t = s/F \quad (4)$$

where s = the distance of the position of the front of the CL-solution from the start of the optical-cell; and F = the flow rate of the pumped CL-solution.

Therefore, from Eqs. (2) and (3)

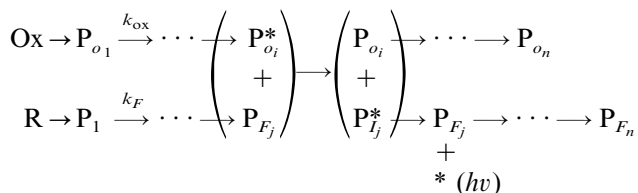
$$I(\text{CL}) = C \cdot \int_0^{t_{\text{eq}}} f'(t) dt \quad (5)$$

and if we modify for the independent variable of s

$$I(\text{CL}) = C' \cdot \int_0^{S_{\text{eq}}} f'(s) ds = C' \cdot [f(s)]_0^{S_{\text{eq}}} = C' \cdot (n_{\text{P}^*})_{\text{eq}} \quad (6)$$

where $(n_{\text{P}^*})_{\text{eq}}$ is the total number of P_i^* -species formed until the reaction has reached equilibrium.

For CL-reaction with energy transfer i.e. (Scheme B);



For reasons similar to those mentioned above, the CL-emission in a batch type reactor is given by Eq. (7)

$$I(t) = f \cdot h\nu \cdot n_{\text{P}^*_{oi}}(t) \cdot n_{\text{P}_F}(t) = C' \cdot f'(t) \cdot g(t) \quad (7)$$

where $f'(t) = d(n_{\text{P}^*_{oi}})/dt$ i.e. the rate of formation of P^*_{oi} species at time t ; and $g(t) = \int_0^t (d(n_{\text{P}_F})/dt) dt = \int_0^t g'(t) dt$ (i.e. the number of P_{Fj} -species formed from $t = 0$ to time t) and for the integral reactor regime

$$I(\text{CL}) = C'' \cdot \int_0^{S_n} f'(s) \cdot g(s) ds \quad (8)$$

where at each infinitesimally small CL-solution volume ds_s , the $f'(s)$ is the rate of formation of P^*_{oi} and $g(s)$ the number of P_{Fj} species present, and S_n is the length of the cell-reactor where the front of the CL-solution stops to emit CL-light.

2.5. Investigation of the mathematical expression of the CL-emission

Eq. (8) suggests that the CL-emission is proportional to the common area defined by the $f'(s)$ and $g(s)$ curves in their plot against the independent variable s from $s = 0$ to $s = S_n$ as shown in Fig. 2.

The total length of CL-solution, S_n , emits CL-light from every infinitesimally small volume, $\pi r^2 ds$ in the tubular cell which is proportional to the height of the shaded area at each s_i in Fig. 2.

The light-dark shaded area corresponds to the CL-light that comes from the range of s where the P^*_{oi} -species are dominant while the heavy-dark shaded area corresponds to the CL-light that comes from the range where the P_{Fj} -species are dominant. The shaded area is the integral

$$\int_0^{S_{\text{max}}} g(s) ds + \int_{S_{\text{max}}}^{S_n} f'(s) ds$$

and the CL-emission measured is proportional to this area. Therefore the CL-light that is generated is given by the summation of the two definite integrals

$$I(\text{CL}) = \kappa \cdot \left(\int_0^{S_{\text{max}}} g(s) ds + \int_{S_{\text{max}}}^{S_n} f'(s) ds \right) \quad (9)$$

According to Eq. (9), if there is no energy transfer, the two integrals combine into one and we end up with Eq. (6) since in this particular case $g(s) \equiv f'(s)$ and $S_n = S_{\text{eq}}$.

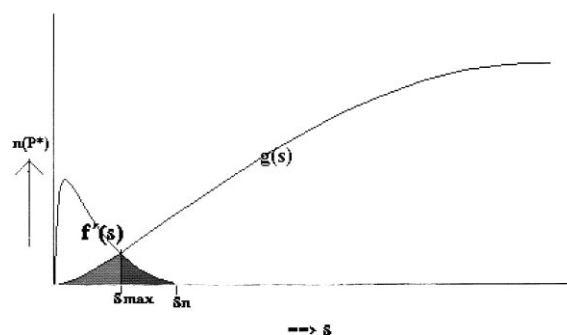


Fig. 2. The ideal number of fluorescent excited molecules (under energy transfer CL-reaction scheme) at each distance s from the start of the cell, and the total length of the solution that emits light in reference to Eq. (9).

Further investigation of Eq. (9) is made by suggesting limiting cases of equilibrium and kinetic parameters of Scheme B CL-processes. The assumptions lead to the derivation of the limiting equations in Table 1.

3. Results and discussion

3.1. Determination of oxidants by CL-emission generated by oxidation of pyrogallol

In this investigation we scanned a large number of inorganic oxidants. The most effective ones are given below.

3.1.1. Optimization of the pumping tubes diameter

For the investigation of the CL-emission generated during oxidation of pyrogallol, the flow-through manifold was optimized for best performance. The grey/grey tubes were chosen because they gave a reproducible signal although the larger diameter ones gave relatively higher CL-signals.

3.1.2. Effect and optimization of pH and the concentrations of pyrogallol and the oxidant

The different oxidants showed a different behavior in the CL-emission generated by the oxida-

tion of pyrogallol as shown by the different effects of factors like the pH and concentrations on CL-emission described below:

3.1.2.1. $KMnO_4$ oxidant. The CL-emission produced with this oxidant is relatively high (range of 10 V) and generates CL-emissions in the pH range of 0–5.

CL-emission versus pH. There is a profound effect of pH on CL-emission (Fig. 3a). Initially, the CL-emission increases and goes through a maximum in the pH-range of 0.6–0.8, then drops steeply and at pH = 5 it is almost zero. The oxidation of permanganate at low pH values proceeds via the reaction



However, the oxidation reaction at higher pH values proceeds with the following reaction



The increase of pH increases the extent of the oxidation reaction (Eq. (R2)) and produces more MnO_2 which coats the glass walls of the optical cell. Therefore the measurements at relatively high pH were made after previously cleaning the cell with a solution of hot oxalate at pH = 0. Apart from this fouling effect which was taken care of by cleaning the optical cell after each CL-measurement, the drop in CL-emission with pH increase is justified by the slow-down of the Eq. (R1) in favor of Eq. (R2).

CL-emission versus concentration of pyrogallol, [Pg]. The effect of [Pg] on the CL-emission at pH = 0.65 and $[MnO_4^-] = 1 \times 10^{-2}$ M is shown in Fig. 3b. The CL-emission increases gradually at low concentrations but increases more rapidly at higher concentrations until it reaches $[Pg] = 5 \times 10^{-3}$ M and then starts falling again. The appearance of the maximum reveals the competition of two processes. The cause of the CL-emission increase is due to the increase of the CL-species in the reacting mixture; the drop of CL-emission with [Pg] increase is related to the inner filter effect which is quite common in all luminescence processes.

CL-emission versus concentration of permanganate, $[MnO_4^-]$. The effect of $[MnO_4^-]$ on the

Table 1
Mathematical expression of CL-emission for limiting conditions of energy transfer CL-reactions (Scheme B)

Parameter		CL-emission intensity
Kinetic	Equilibrium	
$k_{ex} \gg k_F$	All cases	$I(CL) = \kappa \int_0^{S_{max}} g(s) ds \quad (10)$
		with $S_{max} \rightarrow 0$
$k_{ex} \ll k_F$	$[P_F]_{eq}$	$I(CL) = \kappa \cdot f(s) = [P_{oi}^*]_{eq} \quad (11)$
	$\gg (f'(s))_{max} \cdot \delta s$	
$k_{ex} \ll k_F$	$[P_F]_{eq}$	$I(CL) = \kappa \cdot [P_F]_{eq} \quad (12)$
	$\ll (f'(s))_{max} \cdot \delta s$	

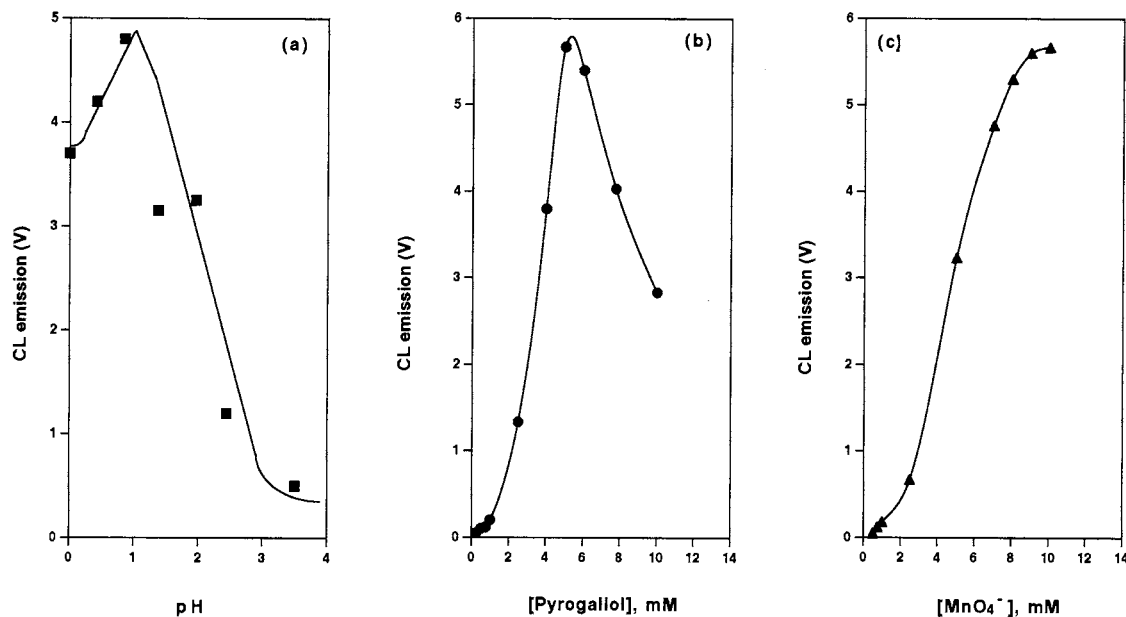


Fig. 3. CL-emission vs (a) pH at $[Pg] = 5 \times 10^{-4}$ M and $[MnO_4^-] = 1 \times 10^{-2}$ M; (b) $[Pg]$ at pH = 0.65 and $[MnO_4^-] = 1 \times 10^{-2}$ M; and (c) $[MnO_4^-]$ at pH = 0.65 and $[Pg] = 5 \times 10^{-3}$ M, for permanganate oxidant.

CL-emission at pH = 0.65 and $[Pg] = 5 \times 10^{-3}$ M is shown in Fig. 3c. The profile of the curve obtained is S-shaped. The plateau of the CL-emission increase with $[MnO_4^-]$ is reached at the value of $[MnO_4^-] = 8.0 \times 10^{-3}$ M which gives a ratio of $[MnO_4^-]/[Pg]$ around 1.6. The effect of $[MnO_4^-]$ on the CL-emission at pH = 0.65 and at various different pyrogallol concentrations was also investigated. The maximum CL-emission was very close to $[MnO_4^-]/[Pg] = 2$; but with the increase of $[Pg]$ this ratio drops gradually. The change of the maximum with $[Pg]$ -level is related to the inner filter effect. However, the maximum observed in the CL-emission vs $[MnO_4^-]$ at relatively low $[Pg]$ -range is due to the kinetic effect on the overall oxidation process. The value of 2 for the ratio suggests that the number of electrons used to oxidize completely each pyrogallol molecule is approximately 10, if the K -value of the oxidation process is large enough to guarantee complete conversion.

3.1.2.2. Ce(IV) oxidant. The CL-emission generated by the use of this oxidant is relatively low

(range of 100 mV) and generates CL-emission in the pH-range of 2–6.

CL-emission versus pH. There is a profound effect of pH on CL-emission (Fig. 4a). There is an abrupt increase of CL-emission from 2.5 to 3.2 and then a sudden drop until pH = 6 where it reaches the value of zero. The drop of the CL-emission goes along with the solubility of the hydrolysis Ce-species formed at different pH values. Therefore we justify this drop on the formation of insoluble Ce-hydroxide species. The precipitation is pronounced at high concentrations of Ce^{4+} -solutions at these pH-values.

CL-emission versus concentration of pyrogallol, $[Pg]$. The effect of $[Pg]$ on the CL-emission at pH = 3.5 and $[Ce(IV)] = 1 \times 10^{-2}$ M is shown in Fig. 4b. The profile of the curve shows a maximum at $[Pg] = 5 \times 10^{-4}$ M. The maximum here is related to the inner filter effect of pyrogallol species formed during the oxidation process.

CL-emission versus concentration of ceric(IV), $[Ce^{4+}]$. The profile curve of the effect of ceric(IV) on the CL-emission at pH = 3.5 and $[Pg] = 5 \times 10^{-4}$ M is shown in Fig. 4c. The curve shows a

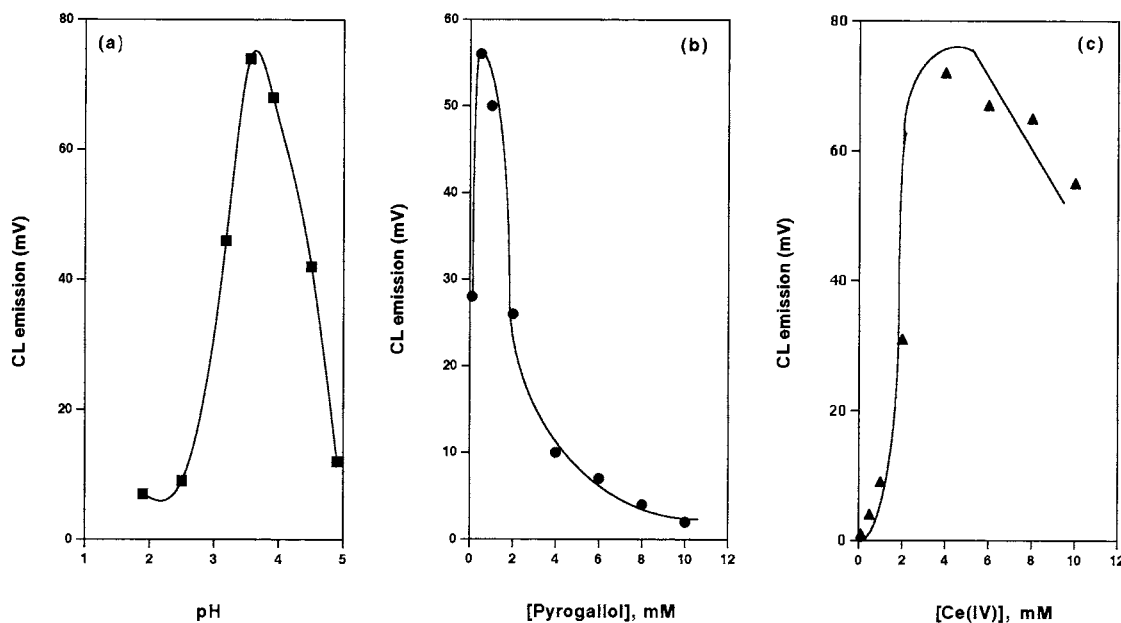


Fig. 4. CL-emission vs (a) pH at $[Pg] = 5 \times 10^{-4}$ M and $[Ce(IV)] = 1 \times 10^{-2}$ M; (b) $[Pg]$ at pH = 3.5 and $[Ce(IV)] = 1 \times 10^{-2}$ M; and (c) $[Ce(IV)]$ at pH = 3.5 and $[Pg] = 5 \times 10^{-4}$ M, for Ce(IV) oxidant.

maximum at 4×10^{-3} M; this value is almost ten times higher than the $[Pg]$. The maximum is, at least, partly justified from the increasing amount of precipitate with increasing concentration of the oxidant thus producing larger amounts of precipitate that gives denser turbidity to the solution in the optical cell.

3.1.2.3. KIO_4 oxidant. The CL-emission generated by the use of this oxidant is moderately high (range of 1000 mV) and generates CL-emission in the pH range of 4–13.

CL-emission versus pH. There is a continuous increase of CL-emission by the increase of pH from the value of 4 to the value of 7.2 which stays approximately the same up to pH = 7.8 and then drops to a relatively low value at pH = 9 and stays almost constant up to pH = 12 and then drops to zero at pH > 13 (Fig. 5a). The CL-emission in the optimum pH-range of 7.2–7.8 is assigned to the pyrogallol species that are liable to fluorescence with relatively high quantum efficiency. However, the pH-range of lower CL-emission intensity may be related to

species of lower quantum efficiencies perhaps products of pyrogallol condensation. It is already known that pyrogallic compounds of different substitution show the maximum at higher pH values with significantly lower CL-intensities.

CL-emission versus concentration of pyrogallol, $[Pg]$. The effect of $[Pg]$ on the CL-emission at pH = 8 is shown in Fig. 5b. The profile curve shows a maximum at $[Pg] = 7.0 \times 10^{-4}$ M. The maximum is related to the inner filter effect due to pyrogallol or pyrogallol-species formed during the oxidation process; these species show an intense inner filter effect evidenced by the steep drop of CL-emission with increase of $[Pg]$.

CL-emission versus concentration of periodate, $[IO_4^-]$. The effect of $[IO_4^-]$ on the CL-emission at pH = 8 and $[Pg] = 7.0 \times 10^{-4}$ M is shown in Fig. 5c. The profile curve shows a gradual increase with an S-shaped appearance. Unfortunately, it is not possible to increase the concentration of periodate beyond the value of 10^{-2} M since the potassium periodate has limited solubility in water.

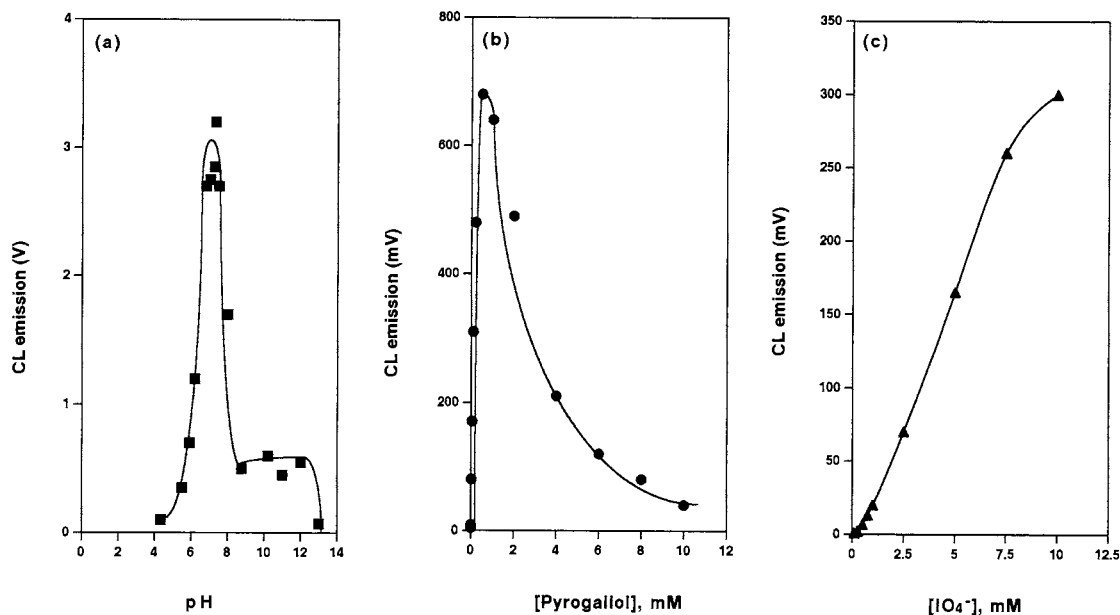


Fig. 5. CL-emission vs (a) pH at $[Pg] = 5 \times 10^{-4}$ M and $[IO_4^-] = 1 \times 10^{-2}$ M; (b) $[Pg]$ at pH = 8.0 and $[IO_4^-] = 1 \times 10^{-2}$ M; and (c) $[IO_4^-]$ at pH = 8.0 and $[Pg] = 7 \times 10^{-4}$ M for periodate oxidant.

3.1.2.4. NaOCl oxidant. The CL-emission generated by the use of this oxidant is relatively low (limited to a maximum of 250 mV) and generates CL-emission in the pH-range of 6–13.

CL-emission versus pH. There is a curve of CL-emission with increasing pH which shows two maxima, one at pH = 8.0 and the other at pH-range between 10.7 and 11.5; the CL-emission in the pH-range of 8.0–10.7 shows a shallow valley; there is an increase of CL-emission at the pH-range of 6.0–8.0 and a gradual decrease beyond pH = 11.5 up to 13 (Fig. 6a). The range of pH in which chemiluminescence is observed is definitely related to the particular oxidant since this oxidant is well known that works in alkaline media. However, the two maxima may be due to the different CL-species involved. A further investigation was held to examine the CL-emission vs pH at different levels of $[Pg]$; the results show that the two maxima increase in CL-emission with the increase of $[Pg]$; however the increase of the maximum at pH-range of 10.7–11.5 is rather pronounced while that around pH = 8 only slight with the $[Pg]$ in-

crease; finally when the $[Pg]$ is further increased, a peak at pH = 9.7 appears that is much larger while the other two start dropping. The two maxima at low $[Pg]$ indicate two kinds of pyrogallolic CL-species with different inner filter effects; the high pH maximum shows a less pronounced inner filter effect; the more intense maximum at pH = 9.7 generated at relatively high pyrogallol concentration is probably due to the chemical interaction of the two CL-species and the formation of a more efficient one.

CL-emission versus concentration of pyrogallol, $[Pg]$. The effect of $[Pg]$ on CL-emission at pH = 9 and $[OCl^-] = 1 \times 10^{-2}$ M is shown in Fig. 6b. The profile of the curve shows an abrupt increase with $[Pg]$ and then a gradual decrease. The maximum is found around $[Pg] = 5 \times 10^{-3}$ M ($[OCl^-]/[Pg] = 2$). The maximum is due to the antagonism between the inner filter effect and the net formation of CL-species. Since the CL-emission at pH = 9 is influenced largely by the CL-species of intense inner filter effect, the curve shows the characteristics of a relatively intense inner filter effect.

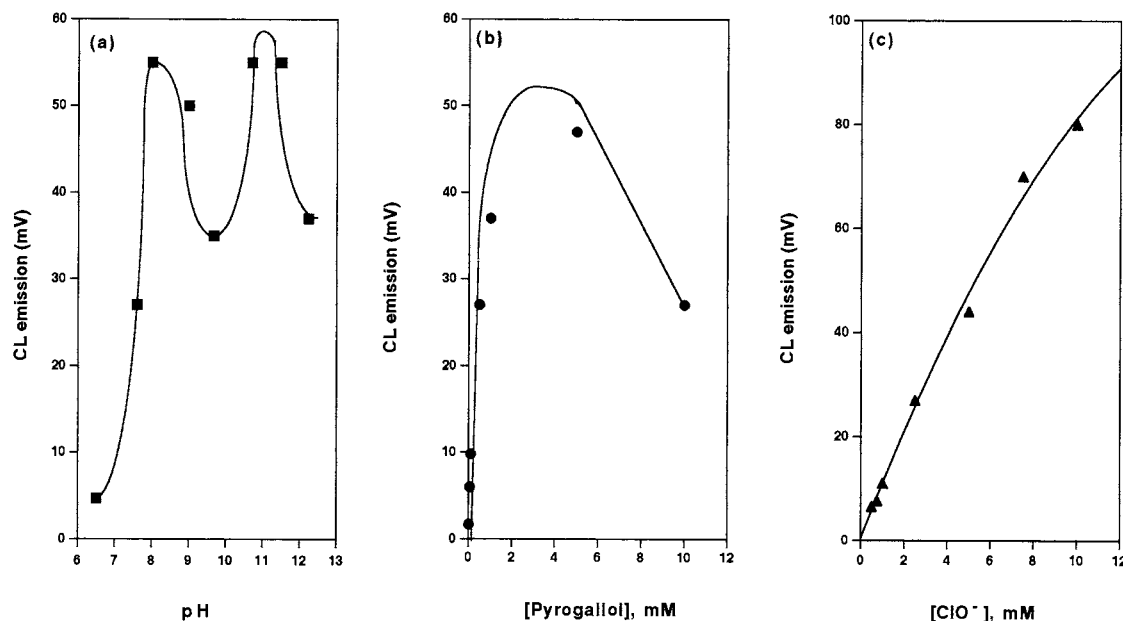


Fig. 6. CL-emission vs (a) pH at $[Pg] = 5 \times 10^{-4}$ M and $[OCl^-] = 1 \times 10^{-2}$ M; (b) $[Pg]$ at pH = 9.0 and $[OCl^-] = 1 \times 10^{-2}$ M; and (c) $[OCl^-]$ at pH = 9.0 and $[Pg] = 5 \times 10^{-3}$ M for hypochlorite oxidant.

CL-emission versus concentration of hypochlorite, $[ClO^-]$. The effect of the $[ClO^-]$ on the CL-emission at pH = 9 and $[Pg] = 5 \times 10^{-3}$ M is shown in Fig. 6c. The profile curve is obtained of almost straight-line form or slightly convex at the initial part of the smooth profile curve.

3.1.2.5. H_2O_2 oxidant. The CL-emission generated by the use of this oxidant is relatively low (limited to maximum 350 mV) and generates CL-emission in the pH-range of 8–13. The hydrogen peroxide is, however, decomposed in alkaline solutions and the decomposition becomes more intense as the pH is increased. The decomposition of H_2O_2 at pH = 11 is quite rapid at relatively high concentrations. Therefore, to avoid bubble formation in the FIA Teflon-tubing, the tubing was kept short and the concentration low ($\leq 1.0 \times 10^{-2}$ M).

CL-emission versus pH. There is a continuous increase of CL-emission with the increase of pH from the value of 8 up to 11 and then a continuous drop up to 13 (Fig. 7a). This is probably a combined contribution of the oxidant and the

pyrogallol originated CL-species in the oxidation process. It is already known that quinonoic compounds are chemiluminescent at pH = 11.

CL-emission versus concentration of pyrogallol, $[Pg]$. The effect of $[Pg]$ on the CL-emission at pH = 11 and $[H_2O_2] = 1.0 \times 10^{-2}$ M is given in Fig. 7b. The profile of the curve shows an initial steep increase and then a steep decrease; the maximum is obtained at $[Pg] = 1 \times 10^{-3}$ M. The maximum here is due to the competition between the increase of CL-emission by the increase of CL-pyrogallol derived species and the inner filter effect of increased number of fluorescent pyrogallol derived species; these species show an intense inner filter effect as indicated from the steep drop of the CL-emission with $[Pg]$ at the relatively high $[Pg]$ -range.

CL-emission versus concentration of hydrogen peroxide, $[H_2O_2]$. The effect of $[H_2O_2]$ on the CL-emission at pH = 11 and $[Pg] = 1 \times 10^{-3}$ M is shown in Fig. 7c. The profile curve shows a gradual increase with increasing concentration of oxidant and is S-shaped in the range of the obtained measurements.

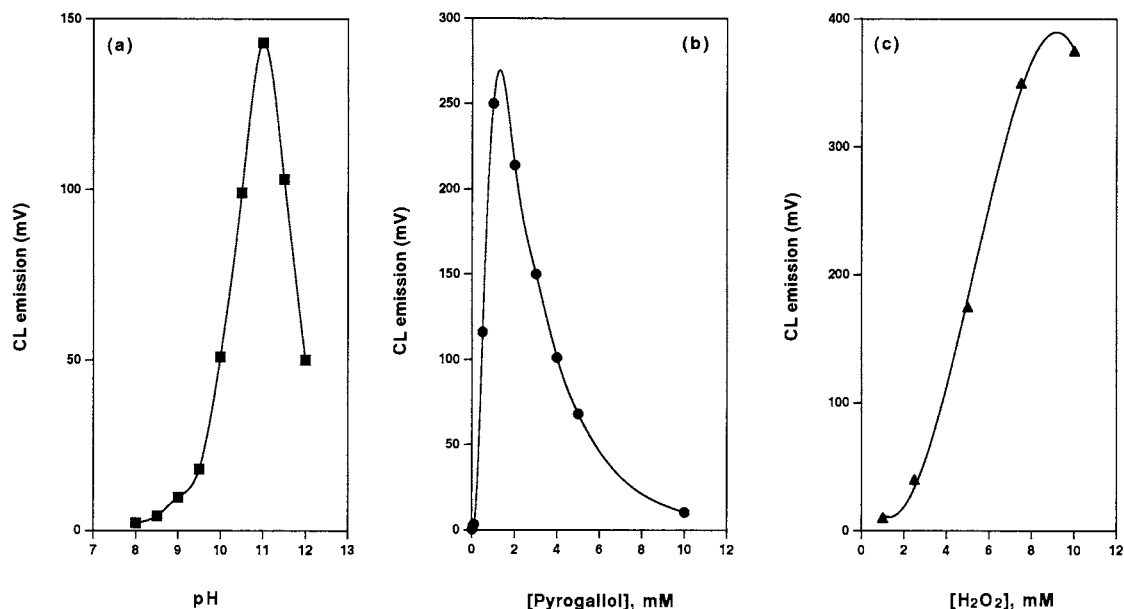


Fig. 7. CL-emission vs (a) pH at $[Pg] = 5 \times 10^{-4}$ M and $[H_2O_2] = 1 \times 10^{-2}$ M; (b) $[Pg]$ at pH = 11.0 and $[H_2O_2] = 1 \times 10^{-2}$ M; and (c) $[H_2O_2]$ at pH = 11.0 and $[Pg] = 1 \times 10^{-3}$ M, for hydrogen peroxide oxidant.

3.1.2.6. *Oxidant calibration curves and analytical parameters.* The data obtained and shown in Figs. 3c, 4c, 5c, 6c and 7c are simulated with an S-shaped model equation (Hill equation)

$$y = \frac{a \cdot x^n}{K + x^n} \quad (13)$$

where y is the CL-emission in volts or millivolts, x is the [oxidant] in M and a and K are constants. These plots give non-straight line calibration curves which are shown in Fig. 8a together with the first-differential plots for the different oxidants Fig. 8b.

However, a linear transform of Hill Eq. (13) is the logarithmic Eq. (14)

$$\log(aY - 1) = n \log X + \log K \quad (14)$$

where $Y = 1/y$ and $X = 1/x$ and the remaining parameters are as above.

The linear regression procedure provides n and K values of the linear transformation equation; these values are different from the optimum parameters calculated by the non-linear simulation and this is reasonable because the weighting

is different for the two procedures. Using the n and K parameter estimates from the linear regression of Eq. (14) and keeping a parameter estimate from the simulation of the data by the Hill equation, the equation traces a curve that shows poor fit for the high x -values while it fits better at the low x -values; this is useful to calculate the detection limits by the a/K standard error. In the present report, the limit of detection is taken from the noise of the photomultiplier/recorder introduced by the pulses of the peristaltic pump which reaches the value of 0.1 mV; this choice was made on simplistic, realistic grounds. The noise value, however, can be improved by using a more expensive pumping system. The sensitivity is determined by the slope of the non-linear calibration curve at each x -value. To obtain a mean value at some range interval of x , the easiest way is to simulate the S-shaped curve by three straight-line parts and quote the average sensitivity at the concentration-range of the steepest straight-line part for each oxidant. This is done with the aid of the first-differential plot of each calibration curve by the following method:

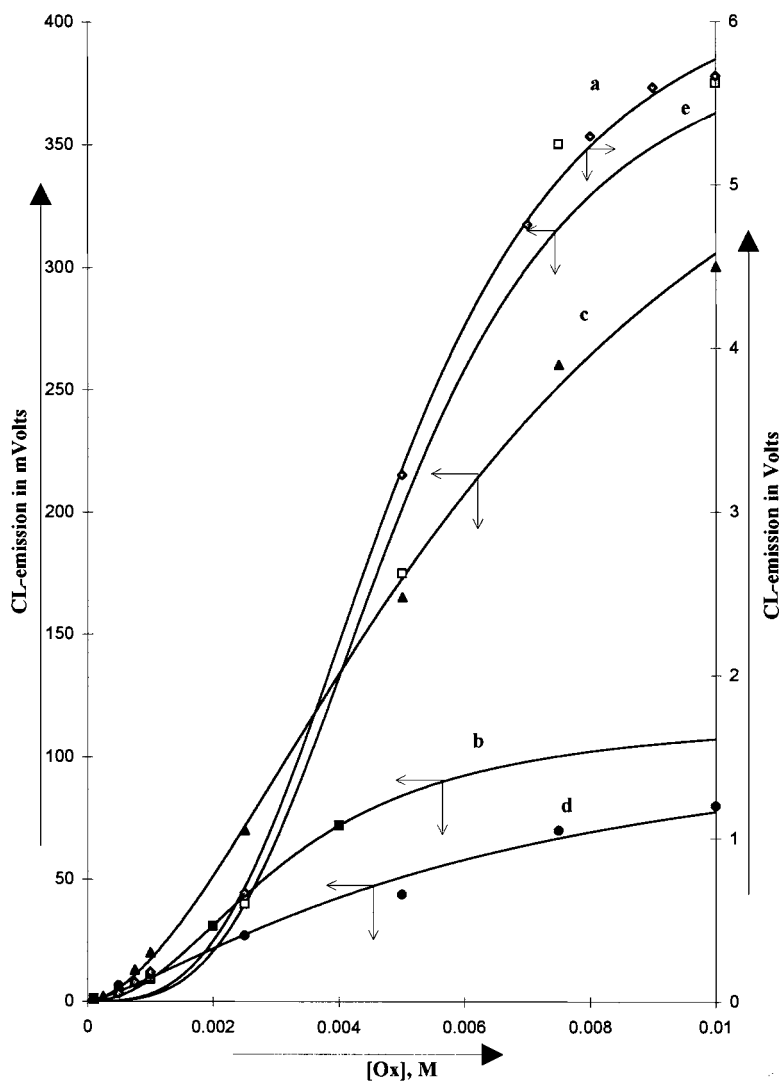


Fig. 8. (a) Calibration curves of oxidant based on fitting Hill model equation to the data points for (a) permanganate, (b) Ce(IV), (c) periodate, (d) hypochlorite, and (e) hydrogen peroxide.

The line at the half-height of each peak in the differential plot is drawn parallel to the x -axis and the points where this line crosses the bell-shaped curve define the concentrations of the oxidant on the steepest part of the calibration curve that the straight line passes through; the slope of this straight line is an approximation of the sensitivity of the determination of the oxidants.

The optimum parameters of the Hill equation and its linear transform for the data of the calibration curve of each oxidant are given in Table 2 together with their standard errors. The analytical parameters of sensitivity, valid range and detection limits are estimated as mentioned above and are given in Table 3.

Model equations for the calibration curves with a better fit to experimental data are necessary for

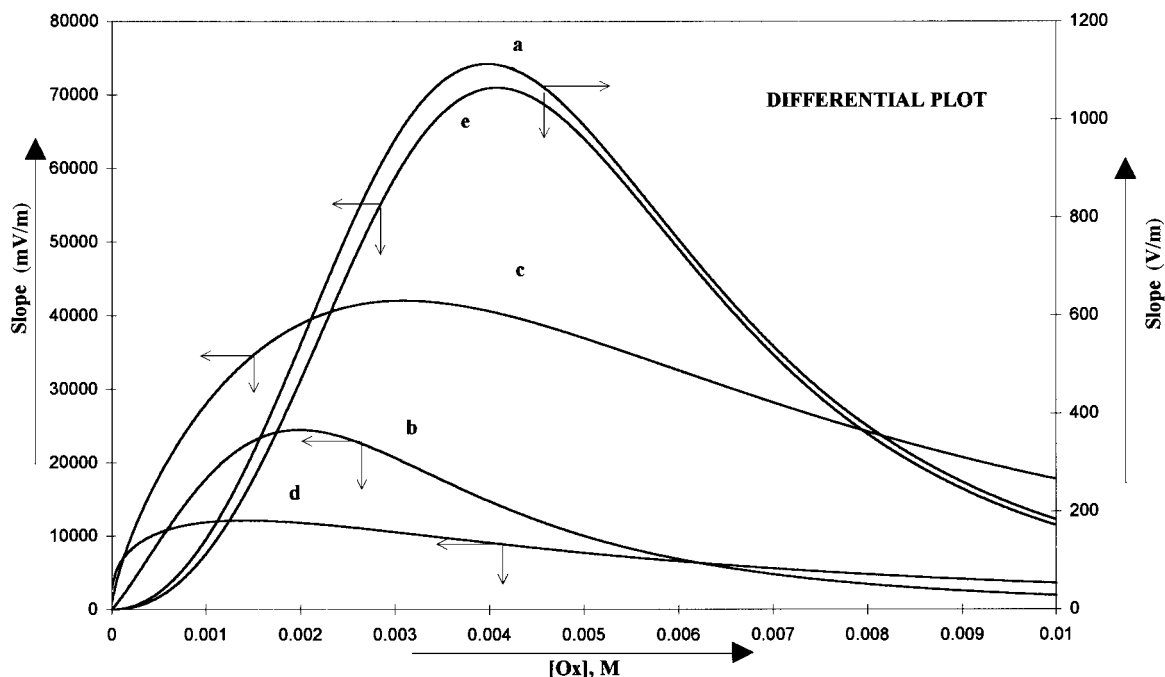


Fig. 8(b). The first-differential plots of the calibration curves of Fig. 8a.

the determination of oxidants which are sigmoidal. However, there is software available [19,21] and a design for experiments to obtain the sigmoidal curve from just three experimental points [20] and this is very convenient for routine analysis.

3.1.2.7. Analytical parameters of pyrogallol determination. The optimized conditions for obtaining the highest CL-emission signal are shown in Table 4 together with the CL-emission in millivolts. The data show a sensitivity for pyrogallol determination of: 1.16×10^6 mV M⁻¹ for permanganate; 0.086×10^6 mV M⁻¹ for Ce(IV); 0.91×10^6 mV M⁻¹ for periodate; 0.012×10^6 mV M⁻¹ for hypochlorite; and 0.25×10^6 mV M⁻¹ for hydrogen peroxide. These values correspond at optimum conditions and it can be seen that maximum sensitivity is obtained for oxidation by periodate and by permanganate. But in the case of oxidation by periodate, the sensitivity is very high for low concentrations while that by permanganate for relatively large concentrations. Detection lim-

its for pyrogallol of the range of 10^{-4} M have been obtained with most oxidants and in some cases even lower. Furthermore, there is always the possibility to increase the sensitivity by using sensitizers or catalysts and enable trace analysis for pyrogallol compounds. The reproducibility of the signal is less than 5% for pyrogallol concentrations in the middle of the valid range for oxidation with most of the oxidants. However, special care should be taken with permanganate because MnO₂ may be accumulated in the optical cell if the pH is not carefully controlled either during the analytical procedure or during the washings. Also, there is always a possibility to have precipitation of cerium hydroxide when the cerium concentration is increased or the pH is increased above the optimum.

3.2. Effect of chemistry and oxidation mechanism on pyrogallol CL-emission

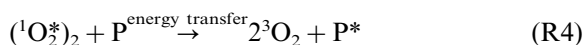
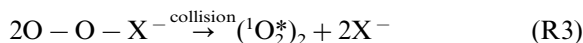
It is generally accepted today that the CL-emission during oxidation of pyrogallol by H₂O₂ is

Table 2

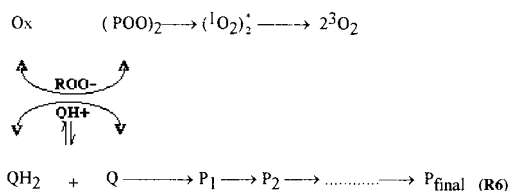
Optimum parameters and standard errors for the Hill equation and its linear transformation for each oxidant

Oxidant	a (mV)	S.E. (mV)	K ($\times 10^{-6}$)	S.E. ($\times 10^{-6}$)	n	S.E.	log K	S.E.	n	S.E.
KMnO ₄	6411	134	0.069	0.05	3.1	0.12	-5.27	0.15	2.26	0.15
Ce(IV)	135.3	13.5	19.2	12.3	1.94	0.09	-3.33	0.6	1.4	0.191
KIO ₄	461.8	50.6	195	192	1.71	0.14	-3.364	0.11	1.564	0.037
NaOCl	117.6	7.3	1118	1435	1.333	0.2	-2.7	0.18	1.22	0.18
H ₂ O ₂	402.4	22	0.046	0.026	3.19	0.10	-6.62	0.86	2.81	0.35

due to the formation of (O₂^{*})₂ excimers which then transfer their energy to species coming from the oxidation of pyrogallol according to the following reaction equations [9–11]



The excimer is formed through the collision of two peroxide species and is released from the transition state collision complex. The energy transfer may be intramolecular from the peroxide collision locus of the transition state complex to a distant part or may be intermolecular energy transfer. Eq. (R4) suggests an intermolecular transfer. For the intermolecular energy transfer, the overall oxidation mechanism will involve the two major reaction steps which are necessary for CL-emission i.e. the step of excimer formation and the step of formation of pyrogallol-oxidation species with high quantum efficiency that will enable, through energy transfer, the CL-emission of the excimer oxygen-species. The oxidation process of phenolic compounds proceeds through an autoxidation mechanism [15] and forms a sequence of oxidation products [16–18] in a number of steps as follows,



where QH₂ = phenolic compound, Q = quinonoid compound, P_i = oxidation products. In addition, it is well known that the oxidation path of pyro-

gallol by H₂O₂ goes through an oxidative condensation with purpurogallin as intermediate product (a highly fluorescent compound).

However, the different oxidants may act as reagents either of 'soft' oxidation in the sense that proceed through relatively stable intermediates, like the periodate and the hydrogen peroxide, or of 'deep' oxidation in the sense that convert the compound completely to the final product like permanganate. In the latter, the intermediate products are transient products of very short life, but significantly greater than the life of the excited species. But, it is not known, yet, clearly whether the CL-reaction is of Scheme A or B for all the oxidants or the choice depends on the oxidant. However, it was shown that the CL-emission under Scheme A is given by Eq. (6) while under Scheme B for the various limiting conditions by Eqs. (10)–(12). Eq. (10) is the most likely in this system because the CL-emission duration under stopped flow regime is extremely short. Therefore, by Eq. (6), the CL-emission is controlled by the equilibrium status of the overall reaction while by Eq. (10), it is controlled by the initial rate of pyrogallol oxidation. Furthermore, it is possible to discriminate the two processes by following the CL-emission versus the concentration of the oxidant. To check the choice we must examine the relationship of CL-emission with the oxidant concentration. Therefore, we plot the CL-emission versus [Ox]/[Pg] in Fig. 9.

From Fig. 9, it is seen that the CL-emission increases with the concentration of the oxidant. The shape of the curve for this relationship is not the same for all oxidants but it is generally an ascending curve that reaches a plateau. The start of the plateau is an important point because if the

Table 3
Analytical parameters for the determination of each oxidant

Oxidant	Non-linear range ^a (M)	Linear range ^b (M)	Sensitivity (mV M ⁻¹)	Detection limit (M)
KMnO ₄	$1.5 \times 10^{-3} - 1 \times 10^{-2}$	$2.0 \times 10^{-3} - 7.0 \times 10^{-3}$	895 600	3.0×10^{-4}
Ce(IV)	$1.75 \times 10^{-3} - 1 \times 10^{-2}$	$6.6 \times 10^{-4} - 4.5 \times 10^{-3}$	19 471	3.5×10^{-4}
KIO ₄	$1.15 \times 10^{-3} - 1 \times 10^{-2}$	$6.3 \times 10^{-4} - 1 \times 10^{-2}$	33 723	2.3×10^{-4}
NaOCl	$3.5 \times 10^{-3} - 1 \times 10^{-2}$	$8.1 \times 10^{-5} - 6.5 \times 10^{-3}$	10 680	6.1×10^{-4}
H ₂ O ₂	$2.25 \times 10^{-3} - 1 \times 10^{-2}$	$2.1 \times 10^{-3} - 7.0 \times 10^{-3}$	56 703	4.5×10^{-4}

^a The lower value is determined by multiplying the detection limit by 10; the maximum value is the maximum concentration of the oxidant in these experiments; for most oxidants (KMnO₄, Ce(IV), KIO₄, H₂O₂) this is the real maximum because of restrictions; for the oxidant NaOCl the real maximum is higher, about 0.1 M.

^b The linear range is defined from terminal values of the line-width of the first-differential plot.

reaction is complete (*K*-value high), it designates the stoichiometric quantity of the specific oxidant for the initial pyrogallol concentration in the CL-solution. The start of the plateau is not evident in some of the curves. The most evident point is the point of highest slope of the smooth curve and it is found by plotting the first differential of the curves in Fig. 9. This point gives the value of half of the oxidant molecules that are necessary to reduce one pyrogallol molecule. However, from the plots of Fig. 9b this is not so simple because the bell-shaped curves are not always symmetric to guarantee that the maximum is a contribution from measurements at equilibrium of the overall process (there may be contributions from measurements of kinetic regime of later steps of the overall reaction involved in total value). The symmetric bell-shaped curves give the indication that the measurements are made at the equilibrium region of the total reaction profile; a tailing of the symmetric bell-shaped curve may indicate measurements at the equilibrium region for the major part of the reaction system plus measurements at the kinetic region for a residual part that reacts slowly in a multi-equilibrium system. On the other hand, asymmetric bell-shaped curves may suggest measurements of multi-equilibria systems made at the equilibrium region for some steps and a significant contribution from measurements at the kinetic regime for some other steps of the whole process. But the height of the bell-shaped curve gives an indication of the size of the *K*-value of the relatively rapid part of the oxidation process. Furthermore the line-width of the bell-shaped

curve gives an indication of the number of the equilibrium-steps involved in the overall oxidation when the measurements are made at the equilibrium region of the overall process; however, the line-width largely increases if the measurements made involve reaction steps that are relatively slow. Table 5 gives the shape of the first-differential plots in Fig. 9b and their characteristics as described above.

From Table 5 and the conclusions that are implied by the shape parameters therein for the rapid part of pyrogallol oxidation process it is found that the oxidation process is relatively complete (highest *K*-value) for permanganate; less complete for hydrogen peroxide, periodate and cerium(IV); and much less-complete for hypochlorite oxidant. From the height of the bell-shaped curves shown in Table 5, a sequence for the size of the equilibrium constant is obtained as follows:



In addition, the size of line-width in combination with the symmetry and the height indicates that: (a) a slow step of oxidation accompanies the rapid oxidation process by periodate in accordance with the findings of Feifer et al. [17]; (b) another reaction is involved in the rapid oxidation process by Ce(IV) which infers an increase of precipitation that occurs with the increase of [Ce(IV)] at optimum pH; [3] another relatively slower reaction accompanies the oxidation by hydrogen peroxide which is in agreement with reported oxidation mechanism [12–14].

Table 4
Optimized conditions and maximum CL-emission for different oxidant compounds

Oxidant compound	Optimized pH	Pyrogallol conc. ($\times 10^4$ mol l ⁻¹)	CL-emission (mV)	Rel. CL-emission (%)
Permanganate	0.8	50	5800	100
Cerium(IV)	3.5	7	60	1
Periodate	7.8	7	640	11
Hypochlorite	9.0	50	60	1
Hydrogen peroxide	11.0	10	248	4

The number of electrons moved during the oxidation of the pyrogallol gives the extent of oxidation that this molecule suffers by different oxidants; this is possible if the measurements are done at equilibrium for all concentrations of the oxidant and the oxidation reaction is complete. This is approximately true for the oxidation of pyrogallol by KMnO_4 . The consumption of nearly 10 electrons per pyrogallol molecule suggests the rupture of the aromatic ring and the formation of one oxalate ion. In the case of periodate there is a large degree of uncertainty since part of the CL-emission is a contribution from CL-emission measurements of variable size in the kinetic regime. In the case of Ce(IV), it is possible that the oxidant acts like permanganate but this is not clearly seen from the results since the CL-emission is definitely affected by the extent of precipitation of Ce(IV) hydrolysis-species. Finally in the case of NaOCl, the CL-emission is of the kinetic regime and there is no guarantee that the start point of the plateau reveals the stoichiometric quantity of oxidant required to oxidize one molecule of pyrogallol.

The linear initial part of the CL-emission vs $[\text{NaOCl}]/[\text{Pg}]$ is in agreement with Eq. (10) and demonstrates a CL-process that proceeds via energy transfer (Scheme B). On the other hand, the bell-shaped symmetric first-differential plot of the corresponding curve for permanganate in Fig. 9a suggests a CL-emission that proceeds without energy transfer (Scheme A). The data for hydrogen peroxide, however, are somewhat misleading. They give a symmetric bell-shaped first-differential plot of the curve in Fig. 9a which is similar to permanganate and suggest a CL-emission without energy transfer which is

contrary to the literature; however, the degradation of hydrogen peroxide in alkaline solutions (pH = 11) forms bubbles in the tube manifold of the FIA system which increase as the concentration is increased producing less accurate measurements; the lower accuracy of the data may, partly, contribute to the disagreement. In the remaining cases i.e. periodate and Ce(IV), the curves of CL-emission vs $[\text{Ox}]/[\text{Pg}]$ seem to move towards a straight-line relationship as shown by the parameter n of fitting the experimental data to Hill equation which in the different oxidants takes the values: around 3.1 (S.E. 0.2) for permanganate; around 1.9 (S.E. 0.2) for Ce(IV); around 1.7 (S.E. 0.15) for periodate; around 1.1 (S.E. 0.17) for hypochlorite; and around 3.25 (S.E. 0.88) for hydrogen peroxide. The standard error for the case of hydrogen peroxide reveals the poor fit to the Hill equation. Furthermore, the disagreement between the data in this work and the reported literature for the hydrogen peroxide case may, also, suggest that this particular case is definitely not a limiting case for Scheme B and therefore the limiting condition Eqs. (10)–(12) are not valid.

Based on the estimates of the equivalents found for the case of permanganate which provides the stoichiometry of the relatively rapid oxidation part, the maximum in Fig. 3b should appear at a corresponding value of pyrogallol concentration that is in agreement with the stoichiometry obtained. However, the maximum found in Fig. 3b does not match the stoichiometry value obtained, in fact this is 20% lower, suggesting the existence of an inner filter effect from the pyrogallol or pyrogallol oxidation products. The inner filter effect is found for oxidations by other oxidants as

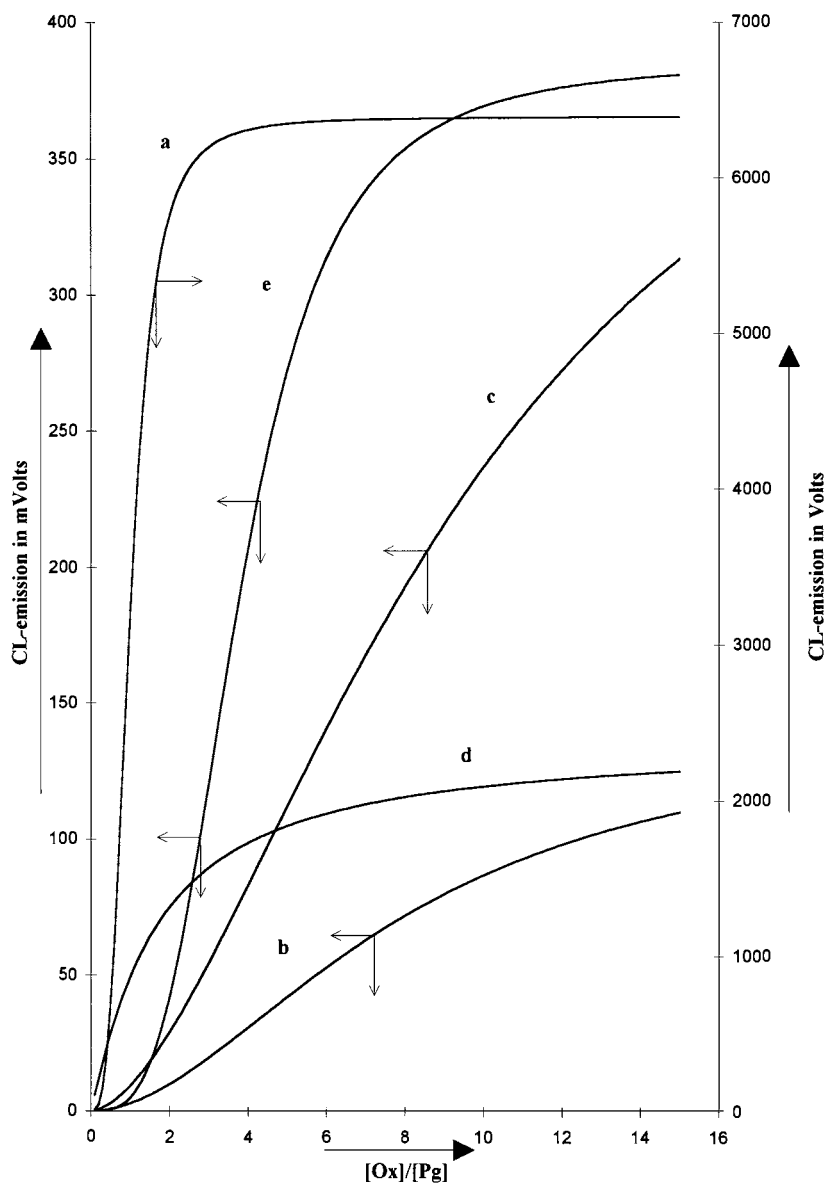


Fig. 9. (a) CL-emission vs $[Ox]/[Pg]$ simulated by Hill equation curves for (a) permanganate; (b) Ce(IV), (c) periodate, (d) hypochlorite and (e) hydrogen peroxide.

well and the size of the effect can be estimated roughly from the steepness of the drop of CL-emission in Figs. 4b, 5b, 6b and 7b. The trend is that oxidation by periodate shows the most intense inner filter effect followed by hydrogen peroxide; this trend suggests that the size of inner

filter effect is related to the mechanism that each oxidant follows i.e. in the oxidation by permanganate that attacks the double bonds, it is low while in selective oxidation by periodate that breaks polyhydroxy compounds, it is relatively high. This implies that either the consecutive

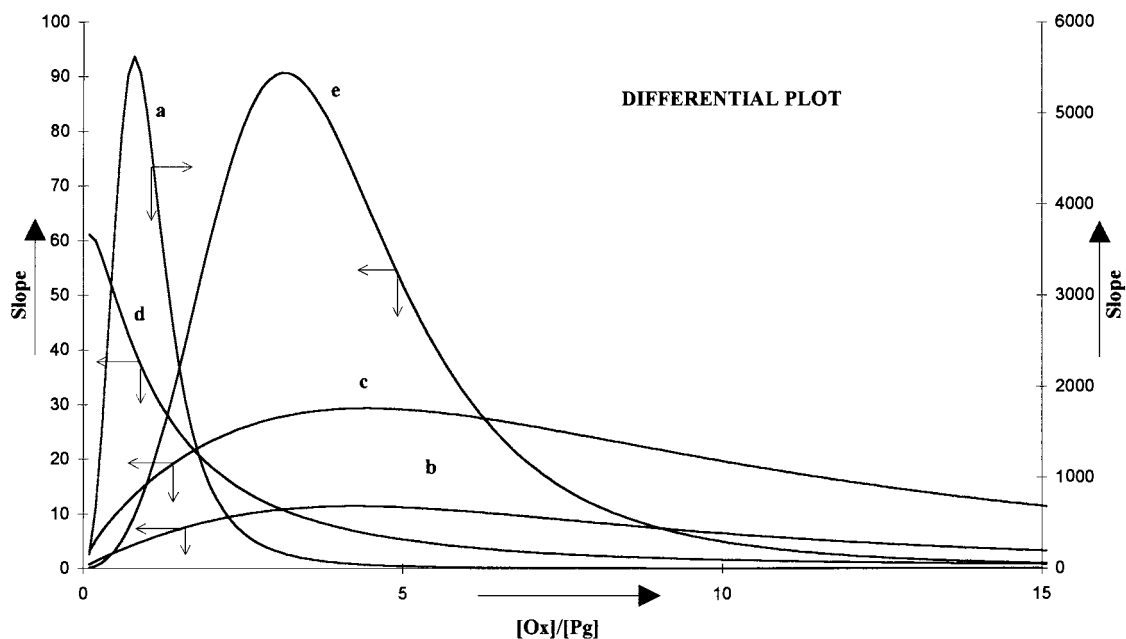


Fig. 9(b). The first-differential plots of curves of Fig. 9a.

products of selective oxidation of pyrogallol are capable of a more effective inner filter effect, or that the concentration of the highly fluorescent product is much lower in a non-selective oxidation process; the latter is more reasonable in cases where the fluorescent product is not the final product of the rapid oxidation part (Scheme A), since the concentration of the transient intermediate products in a consecutive reaction is very much lower.

Since under both schemes of CL-reactions, the CL-emission is related to the number of excited molecules with high quantum efficiency, it is

clear that the pH dependence of CL-emission suggests that either the number of such species varies with pH or that the quantum efficiency of these species is altered by changes in pH; the latter is a well known phenomenon in the field of fluorescent compounds. However, changes of the number of such fluorescent species with pH is of great importance since it is well known that the kinetics of many reactions are affected by pH changes. In addition, we have to point out that independent of the change of CL-emission with pH, we also observed a distinct pH-range where the CL-emission is observed and

Table 5
Characteristics of first-differential curves of the CL-emission vs $[Ox]/[Pg]$

Oxidant	Shape	Symmetry	Maximum	Height (mV)	Line-width
KMnO ₄	Bell	Symmetric	0.8	1 113 000	0.9
Ce(IV)	Bell	Asymmetric	4.3	24 422	9.8
KIO ₄	Bell	Asymmetric	4.4	42 012	11.8
NaOCl	Linear concave	Dropping	0.1	12 090	—
H ₂ O ₂	Bell	Tail-symmetric	3.1	70 980	3.6

this range coincides with the pH-range where the specific oxidant has its maximum oxidation rate.

3.3. Analytical impact to other applications

The system is ideal for being implemented with F.I.A. manifold and a photomultiplier or a fiber optic CCD detector to provide a convenient, rapid and inexpensive analytical set up which can be further automated and linked to an instrument for various determinations based on the oxidation of organic molecules or for the detection of anions in a post column ion chromatography analysis. In cases where lower sensitivity of the CL-signal is necessary, it can be adjusted appropriately by changing the pyrogallol concentration or by changing the power supply voltage to the photomultiplier. The property of pH-selectivity among the oxidative anions enables the detection and determination of permanganate in the presence of periodate and hypochlorite anions or the reverse. Such an application may be interesting in biological or medical fields when more than one oxidant is involved in the same system. The intensity variations with pH for a specific oxidant may lead to a pH-meter based on CL-emission. The CL-emission can also be used as an external indicator for indirect titrations where the oxidant is in excess if the titration apparatus is implemented with an F.I.A. manifold.

References

- [1] S. Pantel, H. Weisz, *Anal. Chim. Acta* 74 (1975) 275.
- [2] W.R. Seitz, M.P. Neary, in: D.N. Hercules, G.M. Hieftje, L.R. Snyder, M.A. Evenson (Eds.), *Contemporary Topics in Analytical and Clinical Chemistry*, London, 1977, pp. 49–125.
- [3] D.B. Paul, *Talanta* 25 (1978) 377.
- [4] D. Balcerowitz, K. Balcerowitz, D. Slawinska, J. Slawinski, *Chem. Anal.* 15 (1970) 479.
- [5] D.F. Marino Jr., J.D. Ingle, *Anal. Chim. Acta* 124 (1981) 23.
- [6] N.P. Evmiridis, *Analyst* 112 (1987) 825.
- [7] N.P. Evmiridis, *Analyst* 113 (1988) 1051.
- [8] N.P. Evmiridis, *Talanta* 36 (3) (1989) 357.
- [9] U.A. Khan, M. Kasha, *J. Chem. Phys.* 39 (8) (1963) 2105.
- [10] U.A. Khan, M. Kasha, *Nature* 204 (1964) 241.
- [11] U.A. Khan, M. Kasha, *J. Am. Chem. Soc.* 88 (7) (1966) 1574.
- [12] D. Slawinska, J. Slawinski, *Anal. Chem.* 47 (1975) 2101.
- [13] M.G. Evans, H. Eyring, J.F. Kincaid, *J. Chem. Phys.* 6 (1938) 349.
- [14] E.J. Bowen, R.I. Lloyd, *Proc. Roy. Soc. Ser. A* 275 (1963) 465.
- [15] G. Pannetier, P. Souchay, *Chemical Kinetics*, Elsevier, Amsterdam, 1967, p. 288.
- [16] E. Adler, R. Magnusson, B. Berggren, H. Thomelius, *Acta Chim. Scand.* 14 (1960) 515.
- [17] J.P. Feifer, M.A. Smith, B.R. Willeford, *J. Org. Chem.* 24 (1959) 90.
- [18] B. Sklarz, *Q. Rev.* 21 (1967) 3.
- [19] E.M. Papamichael, N.P. Evmiridis, *Trends Anal. Chem.* 7 (10) (1988) 366.
- [20] E.M. Papamichael, N.P. Evmiridis, N. Thanasoulis, D. Stefanou, *Chemometr. Intell. Lab. Syst.* 30 (1995) 227.
- [21] N.P. Evmiridis, E.M. Papamichael, *Chemometr. Intell. Lab. Syst.* 12 (1991) 39.
- [22] D. Balcerowitz, K. Balcerowitz, D. Slawinska, J. Slawinski, *Anal. Abstr.* 20 (1971) 4188.

Determination of stability constants of Fe(II), Co(II) and Cu(II)–nitrilotriacetate–penicillamine mixed complexes by electrophoresis

V.K. Gupta ^{a,*}, Imran Ali ^b

^a *Department of Chemistry, University of Roorkee, Roorkee 247667, India*

^b *National Institute of Hydrology, Roorkee 247667, India*

Received 22 May 1997; received in revised form 7 August 1997; accepted 12 August 1997

Abstract

The stability constants of Fe(II), Co(II) and Cu(II)–NTA–penicillamine were determined by paper electrophoresis. The values of these constants were found to be 5.06, 5.16 and 5.28 (log *K* values), respectively at $\mu = 0.1$ and 35°C. © 1998 Elsevier Science B.V. All rights reserved.

Keywords: Electrophoresis; Stability constants; Penicillamine

1. Introduction

Penicillamine has been known as a degradation product of penicillin since 1943 [1]. However, its use in recent years as a drug [2] in treating Wilson's diseases (hepatolenticular degradation), as a protective agent against radiation [3] and as an antidote in metal ion poisoning [4–7] warrant the examination of its metal chelate properties. The properties and most important chemical reactions of naturally occurring penicillamine have already been widely studied [8–11]. The main biochemical aspects have been reviewed by Jocelyn [8]. The biological importance is attributed to the capabilities of the mercapto group to undergo various complex formation processes, primarily in

non-haem iron protein [9] and blue copper protein [10]. Sorensen [11] has demonstrated the anti-inflammatory activity of the copper–penicillamine complex. The complexes of Fe(II), Co(II) and Cu(II) with penicillamine and other sulphur containing amino acids are of great importance because of the interesting biological role of Fe(II), Co(II) and Cu(II) metal ions. The significance of investigations relating to these complexes is further enhanced by the recognition that penicillamine can be used for the treatment of metal ion poisoning [4–7] and for the resolution of racemic mixtures of penicillamine itself and other amino acids [12,13]. A search of literature [14–17] indicates that a few reports are available on Co(II) and Cu(II) binary complexes with penicillamine and no information on ternary (mixed complexes) system is available. It is also reported in literature

* Corresponding author. Fax: +91 1332 73560.

that the modes of coordination in penicillamine are amino, thio and carboxylic groups [18] and in NTA are carboxylic groups [19]. In view of this, attempts were made to determine the stability constants of the metal (M)–penicillamine, M–nitrioltriacetate (NTA) and M–NTA–penicillamine mixed complexes. The present paper describes the electrophoretic determination of the stability constants of these complexes.

2. Experimental

2.1. Apparatus

A Systronic (Naroda, India) Model 604 electrophoresis system was used. It has a built in power supply (a.c.–d.c.) that is fed directly to a paper electrophoresis tank. In order to maintain the temperature constant, two hollow metallic plates coated with thin plastic paper on the outer surface were used for sandwiching paper strips and thermostated water (35°C) was circulated through these plates. pH measurements were made with an Elico (Hyderabad, India) Model L_{1–10} pH meter using a glass electrode.

2.2. Chemicals

Fe(II), Co(II) and Cu(II) perchlorate solutions were prepared by precipitating the corresponding carbonates from solutions of nitrates (A.R. grade) with sodium hydrogencarbonate, washing the precipitates thoroughly with boiling water and treating them with a suitable amount of 1% perchloric acid. The resulting mixtures were heated to boiling on a water bath and then filtered. The solutions were standardized and diluted as required. Metal spots were detected, as violet to red in color, on the paper by spraying a saturated solution of alizarin in ethanol followed by 25% ammonium hydroxide and glacial acetic acid. A saturated aqueous solution (0.9 ml) of silver nitrate was diluted with acetone to 20 ml. Glucose, as a black spot, was detected by spraying with this solution and then with 2% ethanolic sodium hydroxide.

2.3. Background electrolyte

The background electrolytes used in the study of binary complexes were 0.1 M perchloric acid and 0.01 M penicillamine. For the study of ternary system the background electrolytes used were 0.1 M perchloric acid, 0.01 M NTA and various amounts of 0.01 M penicillamine. The ternary system was maintained at pH 8.5 by the addition of sodium hydroxide.

Stock solutions of 9.0 M perchloric acid, 2.0 M sodium hydroxide and 0.5 M penicillamine were prepared from A.R. grade reagents (BDH). A 0.01 M NTA solution was prepared from the compound obtained from Merck.

2.4. Procedure

The hollow base plate in the instrument was levelled and a 150-ml volume of background electrolyte was placed in each tank of the electrophoretic apparatus. Paper strips (Whatman No. 1, 30 × 1 cm) in triplicate were then spotted with metal ion solutions and glucose in the centre with a micropipette and were subsequently placed on the base plate and sandwiched under the upper hollow metallic plate with the end of strips lying in the two sides of the tank solution. A 200-V potential difference was then applied between the tank solution and electrophoresis was carried out for 60 min. The strips were then removed and the spots were detected. The average of the triplicate strips was noted for calculation and the movement of the glucose spot was used as a correction factor. It was found that the variation in the movement was about $\pm 5\%$. The mobilities were calculated by dividing the distance by the potential gradient and are expressed in $\text{cm}^{-2} \text{V}^{-1} \text{min}^{-1}$.

3. Result and discussion

3.1. M(II)–penicillamine binary system

The plot between ionophoretic mobility and pH is given in Fig. 1 which clearly indicates three plateaux. The first corresponds to a region in

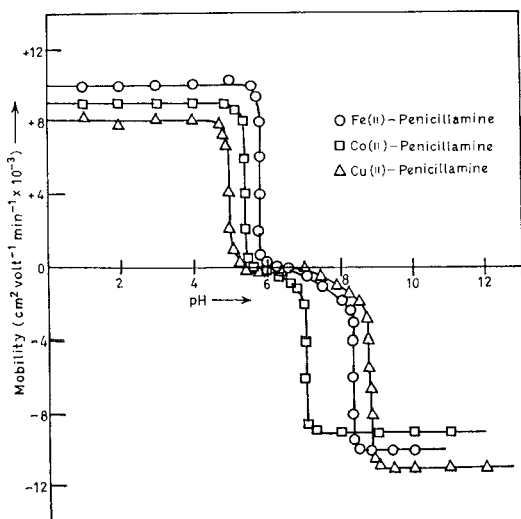
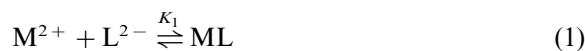


Fig. 1. Mobility curve for M–penicillamine systems.

which metal ions are uncomplexed. The second plateau with zero mobility indicates the formation of 1:1 neutral complexes while the third plateau with negative mobility shows the anionic nature of the metal complexes. The predominant chelating properties of unprotonated anionic species of penicillamine have also been reported ruling out any such property of a zwitterion [20]. In view of these observations, the complexation of the metal ions with the penicillamine anion (L^{2-}) can be represented as



The metal spot on the paper is thus a combination of uncomplexed metal ions, a 1:1 complex and a 1:2 complex. The overall mobility of these is given by

$$U = \frac{u_0 + u_1 K_1 [L^{2-}] + u_2 K_1 K_2 [L^{2-}]^2}{1 + K_1 [L^{2-}] + K_1 K_2 [L^{2-}]^2} \quad (3)$$

where u_0 , u_1 and u_2 are the mobilities of the uncomplexed metal ions, the 1:1 metal complexes and the 1:2 metal complexes, respectively.

The first stability constant (K_1) was calculated by considering the region between the first and second plateaux. The overall mobility (U) will be equal to the arithmetic mean of the mobility of uncomplexed metal ion, u_0 , and that of the first complex, u_1 , at a pH where $K_1 = 1/[L^{2-}]$. The concentration $[L^{2-}]$ of the chelated penicillamine was calculated by the equation

$$[L^{2-}] = \frac{L_T}{1 + [H]/k_3 + [H]^2/k_2 k_3 + [H]^3/k_1 k_2 k_3} \quad (4)$$

where, L_T is the total concentration of the penicillamine and k_1 , k_2 and k_3 are the dissociation constants of penicillamine with $10^{1.90}$, $10^{7.85}$ and $10^{10.55}$ values, respectively.

The second stability constant (K_2) of the second complexes can be calculated by the region between the second and the third plateaux of the

Table 1
Stability constants of binary and ternary mixed complexes of Fe(II), Co(II) and Cu(II)

Metal ion	Stability constant ^a			
	Log $K_1 \frac{M}{ML}$	Log $K_2 \frac{M}{ML_2}$	Log $K_3 \frac{M}{M-NTA}$	Log $K_4 \frac{M}{M-NTA-L}$
Calculated values (this work)				
Fe(II)	8.80	15.10	9.97 ± 1.0	5.06
Co(II)	9.20	18.18	10.60 ± 0.5	5.16
Cu(II)	9.50	16.90	8.41 ± 2.0	5.28
Literature values				
Fe(II)	—	—	8.90 [19]	—
Co(II)	8.90 [21]	—	10.60 [19]	—
Cu(II)	9.70 [21]	16.50 [22]	12.70 [19]	—

Ionic strength, 0.1; Temperature, 35°C; NTA anion, $N(CH_2COO)_3^{3-}$; penicillamine, $(CH_3)_2C(SH)CH(NH_2)COO^-$.

^a $K_1 \frac{M}{ML} = [ML]/[M][L]$; $K_2 \frac{M}{ML_2} = [ML_2]/[ML][L]$; $K_3 \frac{M}{M-NTA} = [M-NTA]/[M][NTA]$; $K_4 \frac{M}{M-NTA-L} = [M-NTA-L]/[M-NTA][L]$; M, metal cation; L, ligand (penicillamine); NTA, nitrilotriacetate.

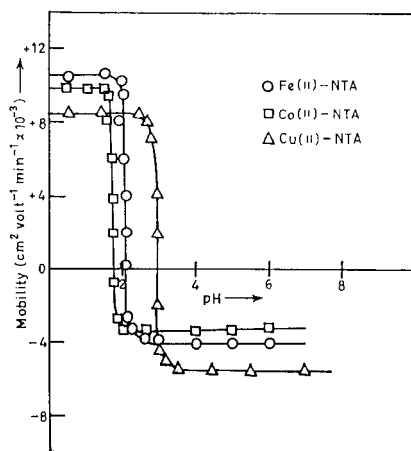
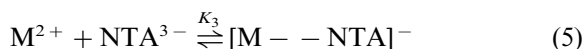


Fig. 2. Mobility curve for M-NTA systems.

curve. The calculated values of K_1 and K_2 are given in Table 1.

3.2. M(II)-NTA binary system

The overall mobilities of the metal spots in the presence of NTA at different pH are given in Fig. 2. There are two plateaux out of which the second plateau is negative indicating the anionic nature of all three metal ion complexes. The stability constants (K_3) of these complexes were calculated using the same method as described for the M(II)-penicillamine binary system and are given in Table 1. The dissociation constants for NTA are k_1 , k_2 and k_3 with $10^{1.66}$, $10^{2.67}$ and $10^{9.49}$ values respectively. The complexation may be represented as



3.3. M-NTA-penicillamine ternary system

It is observed from the binary systems of penicillamine and NTA that the binary complexes are formed at $pH < 8.5$ and the metals do not form hydroxo complexes up to this pH. Therefore, to avoid any side interaction, the conversion of the $[M-NTA]^-$ binary complex into the $[M-NTA-penicillamine]^{3-}$ ternary complex was studied at pH 8.5. The plot of mobility against the logarithm of the concentration of penicillamine added gives

a curve with two plateaux (Fig. 3). It is concluded that the moiety in the last plateau is due to the coordination of penicillamine anion to the $[M-NTA]^-$ moiety (1:1), resulting in the formation of a 1:1:1 $[M-NTA-penicillamine]^{3-}$ mixed complex which can be shown as



where L is the penicillamine.

In this study, the transformation of a simple complex into a mixed complex takes place and hence the overall mobility (U) of this complex is given by

$$U = u_0 \phi_{[M - NTA]} + u_1 \phi_{[M - NTA - L]} \quad (7)$$

where u_0 , u_1 and $\phi_{[M-NTA]}$, $\phi_{[M-NTA-L]}$ are the mobilities and mole fractions of $[M-NTA]^-$ and $[M-NTA-L]^{3-}$ complexes, respectively.

By the addition of the values of the mole fractions, the above equation becomes

$$U = (u_0 + u_1 K_4 [L^{2-}]) / (1 + K_4 [L^{2-}]) \quad (8)$$

where u_0 and u_1 are the mobilities in the region of the two plateaux of the curve.

The concentration of penicillamine anion at pH 8.5 was calculated. K_4 is obviously equal to $1/[L^{2-}]$. The values of K_4 are given in Table 1.

It may be concluded from these studies that penicillamine and NTA may be used to reduce the level of Fe(II), Co(II) and Cu(II) in biological

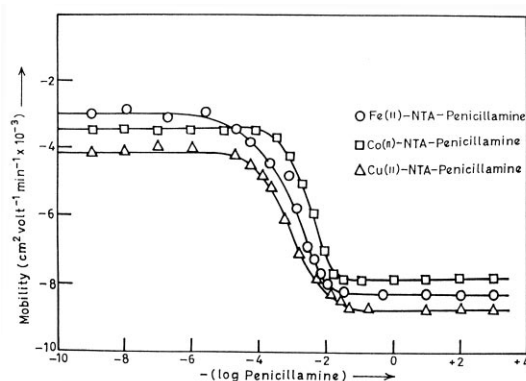


Fig. 3. Mobility curve for M-NTA-penicillamine systems.

systems. In addition, these results may be used for the resolution of racemic mixtures of penicillamine and other amino acids.

Acknowledgements

One of the authors (IA) is grateful to the Council of Scientific and Industrial Research, New Delhi for financial assistance.

References

- [1] E.P. Abraham, E. Chain, W. Baker, P. Robinson, *Nature* 151 (1943) 107.
- [2] J.M. Walsh, *Metal Binding Med., Proc. Symp., Philadelphia* 1959, 1960, p. 263.
- [3] H. Langendorff, M. Langendorff, R. Koch, *Strahlentherapie* 107 (1958) 121.
- [4] H.V. Aposhina, *Metal Binding Med., Proc. Symp., Philadelphia* 1959, 1960, p. 290.
- [5] C.E.C. Harris, *Can. Med. Assoc. J.* 79 (1958) 664.
- [6] W.B. Stavinoha, G.A. Emerson, J.B. Nash, *Toxicol. Appl. Pharmacol.* 1 (1959) 638.
- [7] S.K. Srivastava, V.K. Gupta, B.B. Tiwari, I. Ali, *J. Chromatogr.* 635 (1993) 171.
- [8] C.P. Jocelyn, *Biochemistry of the SH Group*, Academic Press, New York, 1972.
- [9] R.G. Moore, P.J.R. Williams, *Coord. Chem. Rev.* 18 (1976) 125.
- [10] A.J. Fee, *Struct. Bonding (Berlin)* 23 (1975) 11.
- [11] R.J. Sorensen, *J. Med. Chem.* 19 (1976) 135.
- [12] W. Szczepaniak, W. Ciszewska, *Chromatographia* 15 (1982) 38.
- [13] L. Cecchi, P. Malaspina, *Anal. Biochem.* 192 (1991) 219.
- [14] G.R. Lenz, A. Martell, *Biochemistry* 3 (1964) 745.
- [15] Y. Sugiura, H. Tanaka, *Chem. Pharm. Bull.* 18 (1970) 746.
- [16] N. Kojima, Y. Sugiura, H. Tanaka, *Bull. Chem. Soc. Jpn.* 49 (1976) 1294.
- [17] M.T. El-Haty, A.H. Amrallah, R.A. Mahmoud, A.A. Ibrahim, *Talanta* 42 (1995) 1711.
- [18] K.S. Rajan, S. Mainers, J.M. David, *J. Inorg. Nucl. Chem.* 40 (1978) 2089.
- [19] A.E. Martell, *Chemistry of the Metal Chelate Compounds*, Prentice-Hall, Englewood Cliffs, NJ, 1962, p. 534.
- [20] J.R. Blackburn, M.M. Jones, *J. Inorg. Chem.* 35 (1973) 1605.
- [21] B.B. Tewari, *Trans. SAEST* 30 (1995) 76.
- [22] L.G. Sillen, A.E. Martell, *Stability Constants of Metal Ion Complexes (Special Supplement No. 1)*, Chemical Society, London, 1964.

Studies on the extraction and separation of lanthanide ions with a synergistic extraction system combined with 1,4,10,13-tetrathia-7,16-diazacyclooctadecane and lauric acid

Yoshitaka Masuda ^{a,*}, Yawen Zhang ^a, Chunhua Yan ^b, Biaoguo Li ^b

^a Division of Science of Materials, The Graduate School of Science and Technology, Kobe University, Rokkodai Nada-ku, Kobe 657, Japan

^b State Key Laboratory of Rare Earth Materials, Chemistry and Applications, Peking University, Beijing 100871, People's Republic of China

Received 27 January 1997; received in revised form 13 August 1997; accepted 14 August 1997

Abstract

1,4,10,13-Tetrathia-7,16-diazacyclooctadecane (ATCO) and its binary extraction system containing lauric acid were studied extensively as extractants of lanthanide ($M^{3+} = La^{3+}, Ce^{3+}, Pr^{3+}, Nd^{3+}, Sm^{3+}, Eu^{3+}$ and Gd^{3+}) in 1,2-dichloroethane solution. The percentage extraction of Ce^{3+} and Eu^{3+} by ATCO were only measured to be less than 5% during a pH range 5.5–7.0 in NCS^- , ClO_4^- and PF_6^- mediums respectively, which indicates that ATCO alone has very low extractability to lanthanide, due to the bad fit of metal ions in its cavity. However, when lauric acid was added to the ATCO organic phase, because of forming rare earth adduct, the percentage extraction for lanthanide until Gd^{3+} was enhanced in the binary system in comparison with that did not adopt the lauric acid within the pH range 6–7. The extraction species and extraction equilibrium constants $\log K_{ex}$ were found to be $CeLA_3 \cdot 3HA$, -8.5 , $EuLA_3 \cdot HA$, -6.7 , and $GdLA_2NO_3 \cdot 2HA$, -1.8 , respectively. The separation factor between Eu^{3+} and Ce^{3+} was found to be 2.5, however, poor selectivity for lanthanide was observed. From Gd^{3+} to Er^{3+} and Lu^{3+} , the synergistic effect of the binary extraction system decreases with increasing atomic number. For gadolinium, the synergistic effect becomes much weaker than that of Ce^{3+} and Eu^{3+} , no synergistic effect existed for erbium and lutetium. Thermodynamic data for synergistic solvent extraction are also reported in this paper. The order of organic phase stability constants of the extraction species is $Sm (5.8) > Pr (5.7) > Eu (5.6) > Ce (5.3) > La (5.2) > Gd (2.8)$. © 1998 Elsevier Science B.V. All rights reserved.

Keywords: 1,4,10,13-Tetrathia-7,16-diazacyclooctadecane; Lauric acid; Lanthanides; Synergistic extraction; Stability constant

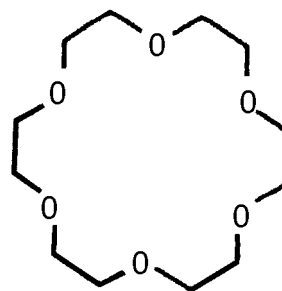
1. Introduction

Separation chemistry and technology of rare earth elements has always been of interest, especially in the latest decades, because of rare earths

* Corresponding author. Fax: +81 78 8030722; e-mail: ymasuda@kobe-u.ac.jp

wide and important applications in the fields of catalysts, glasses, ceramics, magnets, optics and electronics etc. The rapid development of lanthanides applications requires continuous improvement in the separation process for obtaining lanthanide products of high quality and in large amounts. The chemical and physical properties of lanthanides are too similar to be easily separated, to develop fine extractants with high selectivity to rare earths has become a challenging research area. Macrocyclic ligands as host-guest compounds has become a meaningful choice for research on rare earth separation, owing to its metal ion recognition and cavity size-effect fitting ability. Recently, as one branch of lanthanide coordination chemistry—the design and synthesis of macrocyclic ligands and their lanthanides complexation has been the most active and fascinating research area in inorganic and analytical chemistry and many exciting developments, which were reviewed by Alexander [1], have been found. With the expansion of this area, more and more macrocyclic ligands have been used as rare earths extractants. In this class of ligands, the size of the cavity usually determines metal-ion selectivity and specificity. According to this principle, generally, the configuration of 1,4,7,10,13,16-hexaoxocyclooctadecane (18-Crown-6, Scheme 1) is considered to hold the optimum cavity size for lanthanides, so research work has still been focusing on the extraction and separation of lanthanide with it [2,3], using its ternary extraction system with β -diketones [4], and its ionizable derivatives.

In comparison with studies of 18-crown-6 and its derivatives, thia-aza crown ethers, e.g. 1,4,10,13-tetrathia-7,16-diaza-cyclooctadecane (ATCO, Scheme 2), has never been adopted and explored for lanthanide separation, but has only been studied for transition metal element separation until now [5,6], perhaps because of its higher binding affinity and selectivity for transition metal elements rather than rare earth elements. In spite of its lower affinity to rare earth metals, what extent of extractability and selectivity to the metals has it? Can it form synergistic extraction systems combined with other extractant for lanthanide? Furthermore, can it serve as an applicable extractant in lanthanide separation? In order



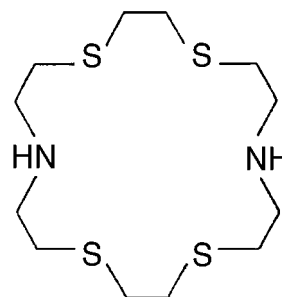
Scheme 1. Configuration of 18-crown-6

to answer these questions—as a representative thia-aza crown ether ligand, ATCO has become our interest, because it holds similar configuration with 18-Crown-6, which is thought to be best fitting for rare earth ions. Thus, this work has a certain meaning and significance in analytical chemistry and separation chemistry of rare earth metals.

2. Experimental

2.1. Apparatus

Extraction procedure was carried out in a TAITEC ML-10 cool bath shaker at $25.0 \pm 0.1^\circ\text{C}$. Ultra-violet and visible absorption spectra of Arsenazo-III method for lanthanide determination were obtained from a Shimadzu self recording spectrophotometer (model 240-UV-Vis) with 10 mm optical path quartz cells. The pH of an aqueous solution was measured with a ORION RESEARCH (Model 701A/digital IONANALYZER). A Kokusan H-200 centrifuge was used



Scheme 2. Configuration of ATCO

for rapid and complete separation of two phases. The FT-IR spectra were taken down by a JASCO FT-IR spectrometer using KBr pellet under the region 400–4000 cm^{-1} .

2.2. Materials

1,4,10,13-Tetrathia-7,16-diazacyclooctadecane (98%) was purchased from Lancaster, and used without any further purification. The other reagents such as lauric acid (99%), 2-(N-Morpholino)ethanesulfonic acid (MES) (G.R.) and 1,2-dichloroethane (G.R.) etc. were bought from Nacalai Tesque. The lanthanide nitrate solutions were prepared according to the method in reference [7].

2.3. Procedures

The organic phase stock solutions of ATCO and lauric acid were prepared by dissolving appropriate amounts of them in 1,2-dichloroethane up to the concentrations 0.001 and 0.025 M, respectively. An aqueous phase solution was prepared by mixing a certain amount of a lanthanide nitrate solution and a required counter-anion solution, under a certain pH 5.0–7.0 adjusted by 0.01 M MES–NaOH buffer solution. The ionic strength was maintained by 0.2 M NaNO_3 . The organic phase containing an appropriate amount of extractant and the aqueous phase containing 5×10^{-5} M or 1×10^{-4} M lanthanide metal ion, were placed in a stoppered 50 ml glass tube at a volume ratio 10:10 ml (organic phase to aqueous phase). Before shaking, the samples were left standing in the water bath for 15 min, in order that the extraction solutions were kept at the same temperature as the water bath. Then, the two phases were mixed by a shaker at 200 strokes min^{-1} at $25.0 \pm 0.1^\circ\text{C}$, the shaking time of 3 h was enough for finishing the extraction equilibrium. After shaking, the two phases were centrifuged for 10 min, which is sufficient for complete separation. Finally, the equilibrium pH was determined using a pH meter, and the concentration of rare earth metal ions in aqueous phase by the means of Arsenazo III photometric method [8]. In all the employed experimental con-

ditions, organic and ionic interference were not found, and the lanthanide could be nearly completely recovered. It seemed that very little hydrolysis of lanthanide developed during the experimental process within the pH region 5.5–7.0 and under the working concentration of metals. Finally, the rare earth concentrations of organic phase could be calculated from the equation $[\text{M}^{3+}]_{(o)} = (C_M - [\text{M}^{3+}]_{(a)})/R$ (R: phase solution volume ratio). By using the slope analysis method, the composition of extraction species and extraction mechanism could be determined.

3. Results and discussions

3.1. ATCO's extractability of Ce^{3+} and Eu^{3+} in aqueous solution containing NCS^- , ClO_4^- and PF_6^- anion

The experimental results of extraction equilibrium depending on shaking time at pH 6.5 showed that no obvious change of extraction percentage occurred within 6 h of shaking, so 3 h was selected as the shaking time, which was considered as adequate for reaching extraction equilibrium. From the percentage extraction variations for Ce^{3+} and Eu^{3+} as a function of pH in NCS^- , ClO_4^- , PF_6^- mediums, it can be seen that the percentage extraction of ATCO for Ce^{3+} and Eu^{3+} are less than 5%, during the pH range 5.7–6.8 in the above extraction system, and the percentage extraction of Ce^{3+} is a little larger than that of Eu^{3+} . As far as we know, ATCO is a weak basic macrocyclic crown ether extractant, which contains two strong donor nitrogen atoms and four soft donor sulfur atoms within its ring linkage. Why does it have poor extractability for Ce^{3+} and Eu^{3+} ? In answering this question, two factors should be considered. Obviously, rare earth ions are hard acid ones, but ATCO is a soft base ligand, according to the theory of hard and soft acids and bases (HSAB), it should be a little difficult for them to combine with each other. On the other hand, because the atomic radii of the sulfur atom in its ring is larger than that of oxygen, the macrocyclic cavity size of 18-crown ether decreases from 2.6 Å of 18-crown-6 [9] to

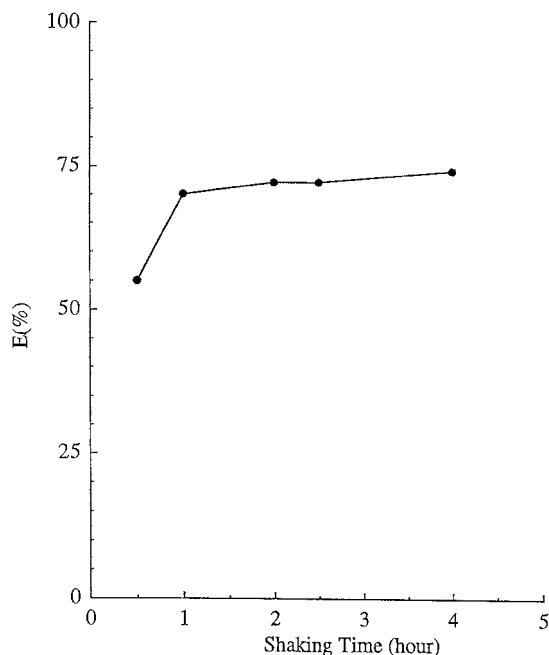


Fig. 1. Percentage extraction of Eu^{3+} as a function of shaking time in ATCO–lauric acid medium. Aqueous phase: 1×10^{-4} M Eu^{3+} , 0.2 M NaNO_3 , and 0.01 M MES–NaOH buffer solution. Organic phase: 1×10^{-4} M ATCO and 1.25×10^{-3} M lauric acid (HA)₂ pH 6.5.

2.2 Å of ATCO (C.P.K. model), which is too small to hold rare earth ions. Therefore, its rare earth extractability must be much smaller than that of 18-crown-6, and it is very effective to soft basic metal ions (Pb^{2+} , Cd^{2+} and Cu^{2+}) rather than lanthanide. However, because Ce^{3+} is a bit softer than Eu^{3+} , the extractability of ATCO for Ce^{3+} ($\approx 4\%$) is a little larger than that for Eu^{3+} ($< 3\%$).

3.2. Synergistic extraction of Ce^{3+} , Eu^{3+} and Gd^{3+} combined with ATCO and lauric acid

Because ATCO is very poor at extracting Ce^{3+} and Eu^{3+} in aqueous solutions containing inorganic counter-ions, many studies have taken on the use of organic counter-ions. In past studies on rare earth extraction using crown ethers, the picrate ion is often taken on as a lipophilic counter anion because of the large solubility of oxacrown ethers in the aqueous phase [10]. However, ATCO

is nearly insoluble in the aqueous phase of the neutral region, so the laurate ion was used in this work instead of picrate ion in order to estimate ATCO's metal-ion selectivity and specificity. Because lauric acid is a weak carboxylic acid, which is very sensitive to pH variation, with a $\text{p}K_a$ 5.3, it should have a certain extractability for lanthanide. Thus, before studying solvent extractability of lanthanide with laurate ion and ATCO, the lanthanide extraction behavior with lauric acid alone should be firstly examined.

3.3. Dependence of extractability on shaking time

The dependence of extractants' extractability of Eu^{3+} on shaking time was studied at pH 6.5. In the absence of ATCO, the percentage extraction of lauric acid for Eu^{3+} does not change after been shaken for 30 min. It means that the extraction can reach equilibrium in less than 30 min. In the presence of ATCO, the percentage extraction plotted in Fig. 1 is unchangeable after shaking for 2 h. It seems that the extraction can reach equilibrium in less than 2 h. In the experiments, 3 h was chosen as the shaking time, which was ample for completely finishing the extraction reaction. With the coexistence of ATCO and lauric acid in the organic phase, the extraction equilibrium time becomes much longer than that of using lauric acid alone as Eu^{3+} extractant. This result suggests that ATCO plays a certain role in the extraction process and the extraction reaction was slowed down.

3.4. Effect of lauric acid on the solvent extraction of Ce^{3+} , Eu^{3+} and Gd^{3+}

3.4.1. Effect of pH on the extraction of Ce^{3+} , Eu^{3+} and Gd^{3+} under constant concentration of lauric acid

Under constant concentration of lauric acid, the effect of pH on the extraction of Ce^{3+} , Eu^{3+} and Gd^{3+} were studied. When $\log D_0$ (the logarithmic distribution ratio for Ce^{3+} , Eu^{3+} and Gd^{3+} extracted by lauric acid alone) vs. pH is plotted three straight lines with slopes about 3.4, 2.6 and 2.0 for Ce^{3+} , Eu^{3+} and Gd^{3+} respectively are obtained in Fig. 2. These slopes indicate

that about three protons for Ce^{3+} and Eu^{3+} , two protons for Gd^{3+} can be released during the extraction process, respectively. On the other hand, lauric acid can only extract lanthanide at $\text{pH} > 6$, which is in agreement with [10], because it is a weak carboxylic acidic extractant.

3.4.2. Effect of lauric acid concentration on the extraction of Ce^{3+} , Eu^{3+} and Gd^{3+} at constant pH

At constant pH, the effect of lauric acid concentration on the extraction for Ce^{3+} , Eu^{3+} and Gd^{3+} was examined. The carboxylic acid extractant in the dilution used is present as a dimer [10]. Thus, in data treatment, lauric acid is considered to be present in 1,2-dichloroethane as a dimer, which can be seen from the FT-IR spectra, due to no vibration frequency for free OH^- at the wave number for about 3500 cm^{-1} . When $\log D_0$

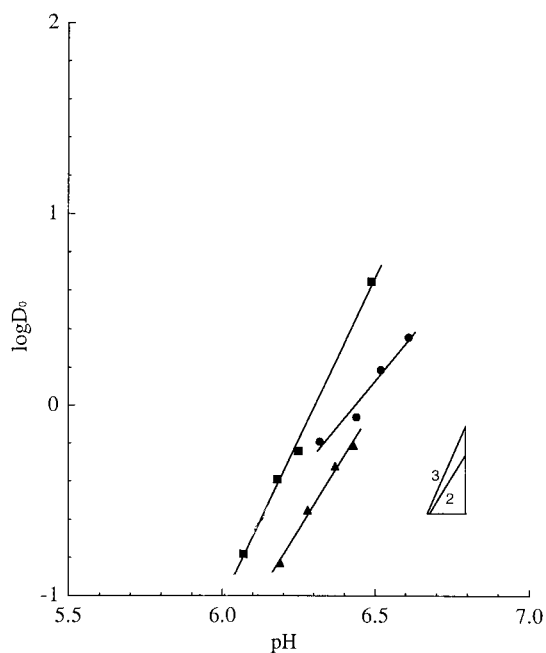


Fig. 2. Plots of logarithmic of distribution ratio for Ce^{3+} (■) and Eu^{3+} (▲) and Gd^{3+} (●) as a function of pH in lauric acid medium. Aqueous phase: 1×10^{-4} M Ce^{3+} (or Eu^{3+} , or Gd^{3+}), 0.2 M NaNO_3 , and 0.01 M MES–NaOH buffer solution. Organic phase: 1.25×10^{-3} M lauric acid (HA)₂ for Ce^{3+} , 6.25×10^{-4} M (HA)₂ for Eu^{3+} and Gd^{3+} , respectively.

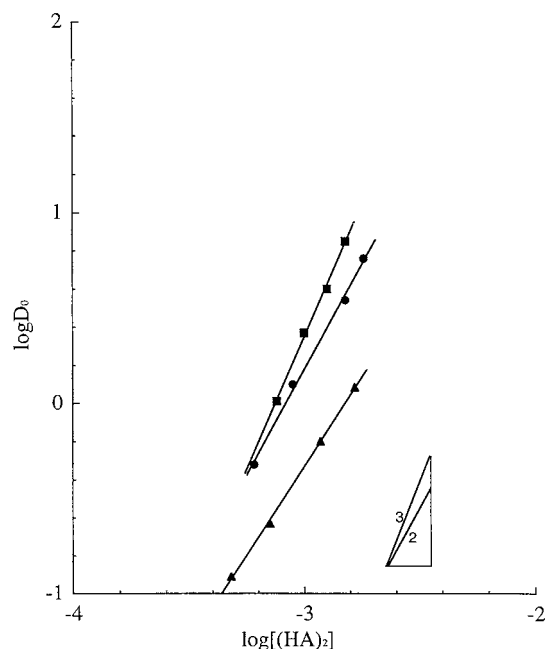
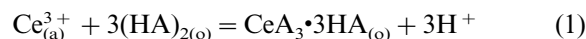


Fig. 3. Plots of logarithmic of distribution ratio for Ce^{3+} (■) and Eu^{3+} (▲) and Gd^{3+} (●) as a function of dimer concentration of lauric acid. Aqueous phase: 1×10^{-4} M Ce^{3+} (or Eu^{3+} , or Gd^{3+}), 0.2 M NaNO_3 , and 0.01 M MES–NaOH buffer solution, pH 6.5 for Ce^{3+} , and pH 6.3 for Eu^{3+} and Gd^{3+} , respectively. Organic phase: 5×10^{-4} – 1.8×10^{-3} M lauric acid (HA)₂.

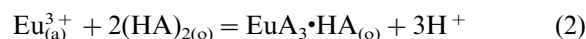
vs. $\log[(\text{HA})_2]$ (logarithmic concentration of free lauric acid) is plotted three straight lines with slopes 2.8, 1.9 and 2.2, respectively, are obtained Fig. 3. These slopes indicate that three (HA)₂ molecules for Ce^{3+} , two (HA)₂ molecules for Eu^{3+} , and two (HA)₂ molecules for Gd^{3+} are involved in the extraction reaction, respectively. The effects of pH and concentration of lauric acid on the extraction of Ce^{3+} , Eu^{3+} and Gd^{3+} suggests that lauric acid can extract lanthanide by the cation exchange mechanism. The extraction species of Ce^{3+} and Eu^{3+} should be $\text{CeA}_3 \cdot 3\text{HA}$ and $\text{EuA}_3 \cdot \text{HA}$, respectively. However, the extraction species of Gd^{3+} is different from the former, it may be combined with one NO_3^- or OH^- . Based on the stability constants of Gd^{3+} with NO_3^- and OH^- respectively, the concentrations of different species of Gd^{3+} in aqueous solution within pH range 6–7 can be calculated. Consequently, the

concentration sequence is $[Gd^{3+}] > [Gd(NO_3)_2^{2+}] \gg [Gd(OH)^{2+}]$. Therefore, the extraction species of Gd^{3+} should be suggested as $GdA_2NO_3 \cdot 2HA$ instead of $GdA_2OH \cdot 2HA$. Accordingly, the extraction equilibrium equations can be written as follows:

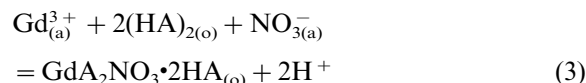
for Ce^{3+}



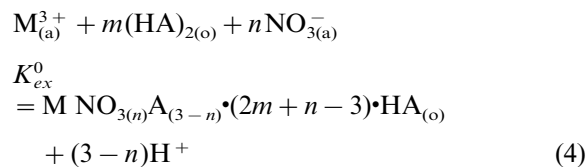
for Eu^{3+}



for Gd^{3+}



Therefore, the general extraction equilibrium equation can be described as



The extraction equilibrium constant K_{ex}^0 when only using lauric acid as extractant, can be expressed as:

$$\log K_{ex}^0 = \log D_0 - n \log [NO_3^-] - m \log [(HA)_2] \\ - (3 - n)pH \quad (5)$$

where, m and n are the number of moles of $(HA)_2$ and NO_3^- , respectively. $[NO_3^-]$ is the equilibrium concentration of NO_3^- . Based on Eq. (5), the extraction equilibrium constants of Ce^{3+} , Eu^{3+} and Gd^{3+} can be calculated, respectively, and the average values of $\log K_{ex}^0$ for

Table 1
Extraction constants $\log K_{ex}^0$, $\log K_{ex}$, thermodynamic data ΔH^0 and ΔS^0 for extraction of Ce^{3+} , Eu^{3+} and Gd^{3+}

	Ce^{3+}	Eu^{3+}	Gd^{3+}
$\log K_{ex}^0$	-13.8	-12.3	-4.6
$\log K_{ex}$	-8.5	-6.7	-1.8
ΔH^0 (kJ mol ⁻¹)	-72.3	-106.1	-51.8
ΔS^0 (kJ mol ⁻¹ deg ⁻¹)	-0.38	-0.48	-0.20

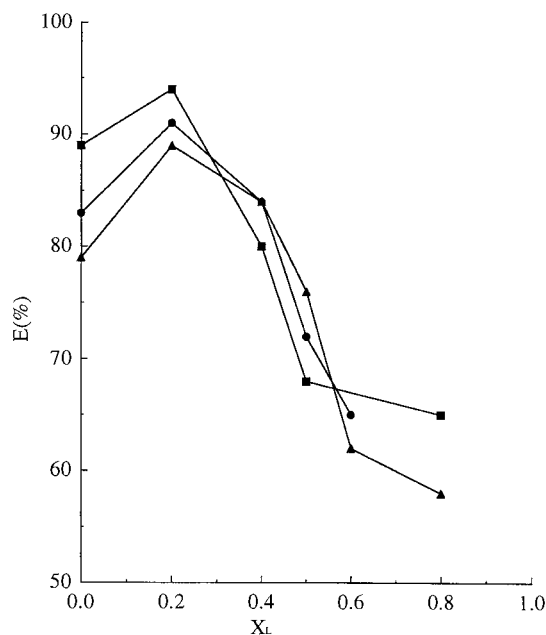


Fig. 4. Plots of percentage extraction for Ce^{3+} (■) and Eu^{3+} (▲) and Gd^{3+} (●) as a function of mole fraction of ATCO in ATCO–lauric acid medium. Aqueous phase: 1×10^{-4} M Ce^{3+} (or Eu^{3+} , or Gd^{3+}), 0.2 M $NaNO_3$, and 0.01 M MES–NaOH buffer solution, pH 6.5. Organic phase: total concentration of ATCO and lauric acid $(HA)_2$ being 0.001 M.

Ce^{3+} , Eu^{3+} and Gd^{3+} are shown in Table 1.
3.5. Metal-ion selectivity of ATCO's extraction of Ce^{3+} , Eu^{3+} and Gd^{3+} in organic solution containing laurate ion

3.5.1. Synergistic extraction effect towards Ce^{3+} and Eu^{3+} and Gd^{3+}

Under constant pH and the total concentration of ATCO and lauric acid, the extractability for Ce^{3+} , Eu^{3+} and Gd^{3+} was studied with continuous variation of the mole fractions of the two ligands. The plots of percentage extraction (%E) vs. molar fraction X_L of ATCO is shown in Fig. 4. It can be found that %E values for Ce^{3+} , Eu^{3+} and Gd^{3+} reach maximum percentage extraction by the molar ratio of about ATCO:A⁻ = 1:3–1:2. It was definitely found that synergistic extraction effect occurred in the extraction process.

3.5.2. Effect of pH on the extraction of Ce^{3+} , Eu^{3+} and Gd^{3+} under constant concentration of lauric acid and ATCO

Under constant concentration of lauric acid and ATCO, the effect of pH on the extraction of Ce^{3+} , Eu^{3+} and Gd^{3+} were studied. When $\log D$ (the logarithmic distribution ratio for Ce^{3+} , Eu^{3+} and Gd^{3+} extracted by ATCO and lauric acid) vs. pH is plotted three straight lines with slopes 3.3, 2.8 and 1.9 for Ce^{3+} , Eu^{3+} and Gd^{3+} , respectively, were obtained (Fig. 5). These slopes indicate that about three protons for Ce^{3+} and Eu^{3+} , and two protons for Gd^{3+} can be released during the extraction process, respectively. Meanwhile, the extraction system can extract Ce^{3+} , Eu^{3+} and Gd^{3+} only at pH > 6, which is the same as the extraction using lauric acid alone.

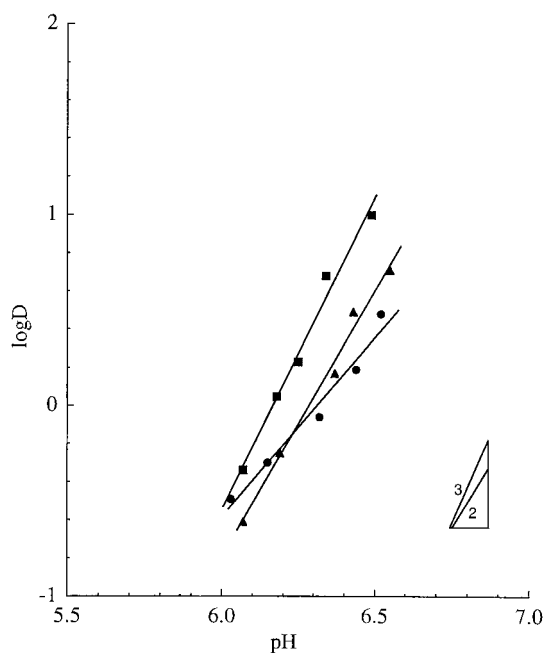


Fig. 5. Plots of logarithmic distribution ratio for Ce^{3+} (■) and Eu^{3+} (▲) and Gd^{3+} (●) as a function of pH in ATCO–lauric acid medium. Aqueous phase: 1×10^{-4} M Ce^{3+} (or Eu^{3+} , or Gd^{3+}), 0.2 M $NaNO_3$, and 0.01 M MES–NaOH buffer solution. Organic phase: 1×10^{-4} M ATCO and 0.00125 M lauric acid $(HA)_2$ for Ce^{3+} , 3×10^{-4} M ATCO and 6.25×10^{-4} M $(HA)_2$ for Eu^{3+} and Gd^{3+} .

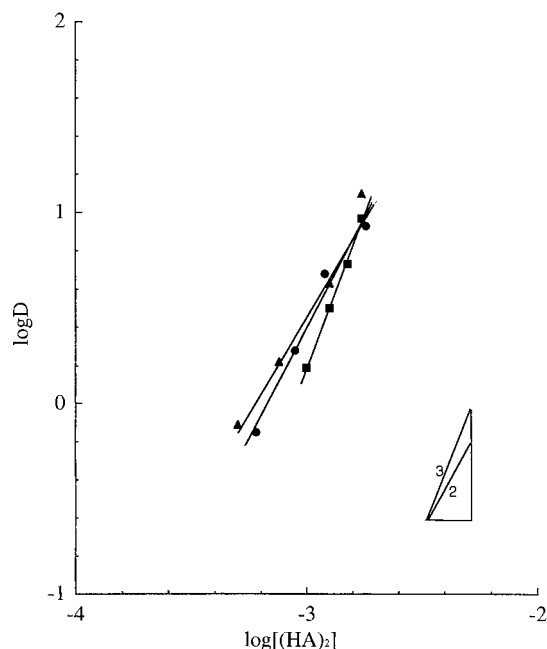


Fig. 6. Plots of logarithmic distribution ratio for Ce^{3+} (■) and Eu^{3+} (▲) and Gd^{3+} (●) as a function of dimer concentration of lauric acid in ATCO–lauric acid medium. Aqueous phase: 1×10^{-4} M Ce^{3+} (Eu^{3+} , or Gd^{3+}), 0.2 M $NaNO_3$, and 0.01 M MES–NaOH buffer solution, pH 6.5 for Ce^{3+} , and pH 6.3 for Eu^{3+} and Gd^{3+} respectively. Organic phase: 3×10^{-4} M ATCO and 5×10^{-4} – 1.8×10^{-3} M lauric acid $(HA)_2$.

3.5.3. Effect of lauric acid concentration on the extraction of Ce^{3+} , Eu^{3+} and Gd^{3+} under constant pH and concentration of ATCO

Under constant pH and concentration of ATCO, the effect of lauric acid concentration on the extraction for Ce^{3+} , Eu^{3+} and Gd^{3+} was studied. When $\log D$ vs. $\log[(HA)_2]$ is plotted three straight lines with slopes of 3.2, 2.0 and 2.3 for Ce^{3+} , Eu^{3+} and Gd^{3+} , respectively, see Fig. 6. These slopes indicate that about three $(HA)_2$ molecules for Ce^{3+} , two $(HA)_2$ molecules for Eu^{3+} and for Gd^{3+} are involved in the extraction reaction, respectively.

3.5.4. Effect of ATCO concentration on the extraction of lanthanide (La^{3+} – Gd^{3+}) under constant pH and concentration of lauric acid

Under constant pH and concentration of lauric acid, the effect of ATCO concentration on the

extraction of La^{3+} , Ce^{3+} , Pr^{3+} , Nd^{3+} , Sm^{3+} , Eu^{3+} , Gd^{3+} , Er^{3+} and Lu^{3+} was examined. According to experimental data in Figs. 7–9, the extraction behavior for the elements studied is classified into three different types: (1) when $\log D/D_0$ vs. $\log [L]$ (logarithmic equilibrium concentration of ATCO) is plotted for La^{3+} , Ce^{3+} , Pr^{3+} , Nd^{3+} , Sm^{3+} , Eu^{3+} , six straight lines with slopes 1.2, 1.2, 1.4, 1.2, 1.4, and 1.4 respectively, are achieved (Fig. 7). However, (2) $\log D/D_0$ values for Gd^{3+} increase with increasing concentration of ATCO from 2×10^{-4} to 5×10^{-4} M, while, at ATCO concentrations larger than 5×10^{-4} M, $\log D/D_0$ begins to decrease with increasing ATCO concentration, having negatively keened slope (Fig. 8), (3) for Er^{3+} and Lu^{3+} , $\log D/D_0$ values are unchanging when the concentration of ATCO is increased from 2×10^{-4} to 7×10^{-4} M (Fig. 9). This means that no synergistic effect takes part in the extraction process for erbium(III) and lutetium(III). The result of slope analysis suggests that ATCO countered by laurate ions can extract Ce^{3+} and Eu^{3+} and Gd^{3+} by the cation exchange

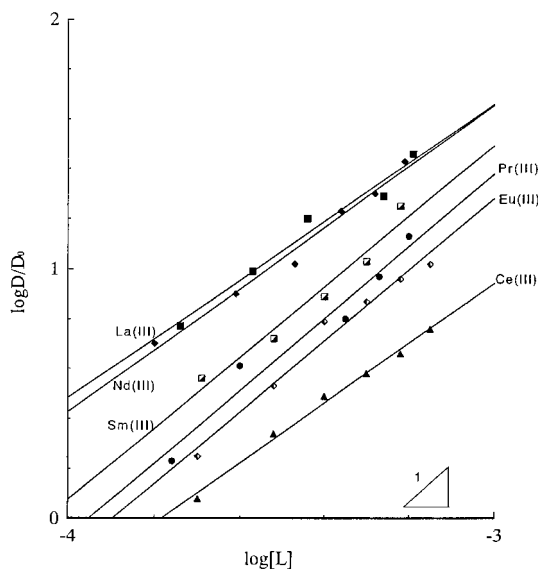


Fig. 7. Plots of $\log D/D_0$ for La^{3+} , Ce^{3+} , Pr^{3+} , Nd^{3+} , Sm^{3+} , and Eu^{3+} as a function of ATCO concentration in ATCO–lauric acid medium. Aqueous phase: 1×10^{-4} M Ln^{3+} , 0.2 M NaNO_3 , and 0.01 M MES–NaOH buffer solution, pH 6.5. Organic phase: 2×10^{-4} – 7×10^{-4} M ATCO and 6.25×10^{-4} M lauric acid $(\text{HA})_2$.

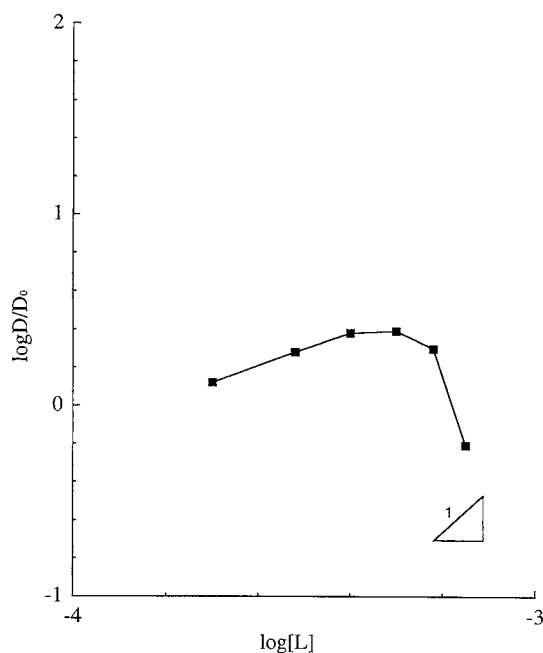
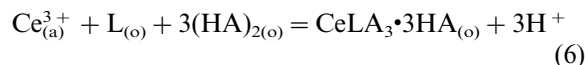
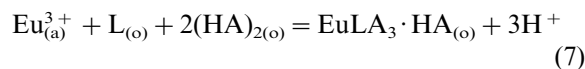


Fig. 8. Plot of $\log D/D_0$ for Gd^{3+} as a function of ATCO concentration in ATCO–lauric acid medium. Aqueous phase: 1×10^{-4} M Gd^{3+} , 0.2 M NaNO_3 , and 0.01 M MES–NaOH buffer solution, pH 6.5. Organic phase: 2×10^{-4} – 7×10^{-4} M ATCO and 6.25×10^{-4} M lauric acid $(\text{HA})_2$.

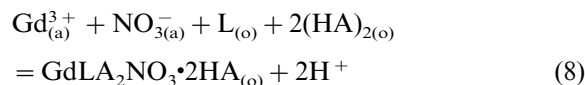
mechanism with the formation of extraction adducts, respectively. The proposed extraction species should be $\text{CeLA}_3 \cdot 3\text{HA}$, $\text{EuLA}_3 \cdot \text{HA}$ and $\text{GdLNO}_3\text{A}_2 \cdot 2\text{HA}$, respectively. And the extraction equilibrium equations can be written as follows: for Ce^{3+}



for Eu^{3+}



for Gd^{3+}



Therefore, the general extraction equilibrium equation can be described as

$$\begin{aligned}
 & M_{(a)}^{3+} + pL_{(o)} + m(HA)_{2(o)} + nNO_{3(a)}^- \\
 & K_{ex} \\
 & = M L_p NO_{3(n)} A_{(3-n)} \cdot (2m + n - 3) HA_{(o)} \\
 & \quad + (3 - n)H^+ \quad (9)
 \end{aligned}$$

The synergistic extraction equilibrium constant K_{ex} can be expressed as:

$$\begin{aligned}
 \log K_{ex} = \log D - m \log [(HA)_2] - n \log [NO_3^-] \\
 - (3 - n)pH - p \log [L] \quad (10)
 \end{aligned}$$

where, $\log D$ is the distribution ratio of the synergistic extraction, when using ATCO and lauric acid as extractants; m , n and p are the number of moles of $(HA)_2$ and NO_3^- and ATCO, respectively. Through Eqs. (5)–(10), we obtain

$$\log D/D_0 = \log K_{ex} - \log K_{ex}^0 + p \log [L] \quad (11)$$

Based on the Eq. (10) and Eq. (11), the synergistic extraction equilibrium constants of Ce^{3+} , Eu^{3+} and

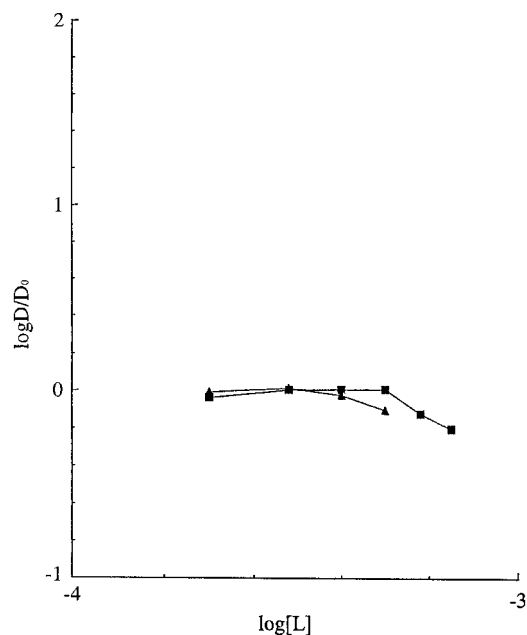


Fig. 9. Plot of $\log D/D_0$ for Er^{3+} (■) and Lu^{3+} (▲) as a function of ATCO concentration in ATCO–lauric acid medium. Aqueous phase: 1×10^{-4} M Er^{3+} (or Lu^{3+}), 0.2 M $NaNO_3$, and 0.01 M MES–NaOH buffer solution, pH 6.5. Organic phase: 2×10^{-4} – 7×10^{-4} M ATCO and 6.25×10^{-4} M lauric acid.

Gd^{3+} can be estimated by determination of the slope and intercept. $\log K_{ex}^0$, and $\log K_{ex}$ values of Ce^{3+} , Eu^{3+} and Gd^{3+} are summarized in Table 1.

From Table 1, it can be seen that the extractability of Ce^{3+} , Eu^{3+} and Gd^{3+} are enhanced by forming the adductive extraction species with laurate ions. The K_{ex} values of Ce^{3+} , Eu^{3+} and Gd^{3+} are improved by the magnitude of $10^{5.3}$, $10^{5.6}$ and $10^{2.8}$, respectively, in the existence of ATCO. Therefore, the synergistic extraction effect played a very important role during the extraction process, which is in complete agreement with the composition of extraction species deduced from the results of the mole fraction variations of ATCO. Moreover, $\log \beta_0$ for Gd^{3+} is so much smaller than that of Ce^{3+} and Eu^{3+} , it seems that both the extraction with lauric acid alone and the extraction with ATCO and lauric acid spontaneously exist in the extraction process of Gd^{3+} . During the low concentration region of ATCO (2×10^{-4} – 5×10^{-4} M), the percentage extraction for Gd^{3+} with lauric acid is larger than that with ATCO and lauric acid, but, within the high concentration region ($> 5 \times 10^{-4}$ M), the percentage extraction with ATCO and lauric acid is larger than that with lauric acid alone. Therefore, increasing the concentration of ATCO, causes the extraction to reach a maximum because of the decrease in free lauric acid concentration $[(HA)_2]$ with the concentration increment of association species between ATCO and lauric acid, which was confirmed by IR spectra of the extractants in CCl_4 . With the existence of ATCO, the frequency of C=O vibration lies in 1710 cm^{-1} , and the frequency of $\nu_{C-O}(\nu_{O-H})$ vibration shifts from 1253 cm^{-1} of $(HA)_2$ to 1255 cm^{-1} of $(HA)_2$ -ATCO, with the frequency difference equal to 2 cm^{-1} . It shows that there is a weak association interaction between ATCO and lauric acid. Due to the coexistence of $GdA_2NO_3 \cdot 2HA$ and $GdLA_2NO_3 \cdot 2HA$ in the extraction procedure, there is a deviation existing in the above deduction for determining the extraction constant of Gd^{3+} .

3.6. Thermodynamic data in the extraction of Ce^{3+} , Eu^{3+} and Gd^{3+} using ATCO and lauric acid

Under constant pH and concentrations of ATCO and lauric acid, the effect of temperature

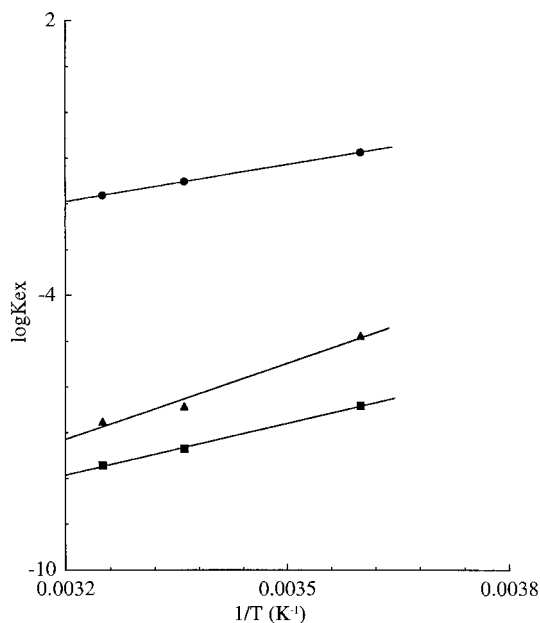


Fig. 10. Plots of logarithmic of extraction constants for Ce^{3+} (■) and Eu^{3+} (▲) and Gd^{3+} (●) as a function of $1/T$ in ATCO–lauric acid medium. Aqueous phase: 1×10^{-4} M Ce^{3+} (Eu^{3+} , or Gd^{3+}), 0.2 M NaNO_3 , and 0.01 M MES–NaOH buffer solution, pH 6.3. Organic phase: 2×10^{-4} M ATCO and 6×10^{-4} M lauric acid (HA_2)

on the extraction of Ce^{3+} , Eu^{3+} and Gd^{3+} was studied. According to the deduced extraction mechanism, $\log K_{\text{ex}}$ at different temperatures can be calculated. Then, based on Vant Hoff's equation $\log K_{\text{ex}} = -\Delta G^0/2.303RT$ and Gibbs–Helmholtz equation $\Delta G^0 = \Delta H^0 - T\Delta S^0$, the equation $\log K_{\text{ex}} = -\Delta H^0/2.303RT + \Delta S^0/2.303R$ can be obtained. Thus, when $\log K_{\text{ex}}$ is plotted against $1/T$, three straight lines are represented in Fig. 10. ΔH^0 and ΔS^0 , which are also given in Table 1, can be determined from the slope and intercept, respectively.

Comparing ΔH^0 of Ce^{3+} , Eu^{3+} and Gd^{3+} with each other in Table 1, it can be seen that the absolute stability sequence of extraction species is $\text{Eu}^{3+} > \text{Ce}^{3+} > \text{Gd}^{3+}$. Ensor et al. [11] reported a synergistic extraction of trivalent actinides and lanthanide using HTTA and 4,13-didecyl-1,7,10,16-tetraoxa-4,13-diazacyclooctadecane (K22DD), which showed no extraction for Ce^{3+}

and Eu^{3+} in this study. The $\log K_{\text{ex}}^0$ of HTTA for Ce^{3+} and Eu^{3+} were -9.95 and -8.58 respectively, and $\log K_{\text{ex}}$ of the synergistic agents K22DD and HTTA for Ce^{3+} and Eu^{3+} were -4.70 and -3.87 respectively, and $\log \beta_0$ for Ce^{3+} and Eu^{3+} were 5.25 and 4.71 respectively. In comparison with results of this work, it appeared very similar on the extraction properties for Ce^{3+} and Eu^{3+} . As to the formation of the extraction species, Ensor et al. also indicated that it correlated with the coordination interaction between the lanthanide and nitrogen atoms in the macrocyclic linkage. Therefore, the synergistic effect of this work is probably mainly related to the interactions between the lanthanide ions and nitrogen atoms of ATCO and oxygen atoms of lauric acid, and to the lowest extent, the interaction between the lanthanide ions and sulfur atoms of ATCO.

3.7. Organic phase stability constants of the extraction species and separation factors

According to the above suggested extraction mechanisms, the formation of synergistic complex can be described as an organic phase reaction represented by the organic phase stability constant β_0 , which can be defined from the following equation and deduction.

$$\begin{aligned} & \text{M NO}_{3(m)}\text{A}_{(3-n)} \cdot (2m+n-3)\text{HA}_{(o)} + p\text{L}_{(o)} \\ & \beta_0 = \frac{\text{M L}_p \text{NO}_{3(m)}\text{A}_{(3-n)} \cdot (2m+n-3)\text{HA}_{(o)}}{[\text{M NO}_{3(m)}\text{A}_{(3-n)}] \cdot (2m+n-3)\text{HA}_{(o)} [\text{L}]^p} \\ & \beta_0 = \frac{[\text{M L}_p \text{NO}_{3(m)}\text{A}_{(3-n)}] \cdot (2m+n-3)\text{HA}_{(o)}}{[\text{M}]_{(a)}} \\ & \beta_0 = \frac{[\text{MNO}_{3(m)}\text{A}_{(3-n)}] \cdot (2m+n-3)\text{HA}_{(o)}}{[\text{M}]} \\ & [\text{L}]^p = D/D_0[\text{L}]^{-p} \end{aligned} \quad (12)$$

Table 2
Organic phase stability constants of the extraction species

	La^{3+}	Ce^{3+}	Pr^{3+}	Nd^{3+}	Sm^{3+}	Eu^{3+}	Gd^{3+}
$\log \beta_0$	5.2	5.3	5.7	5.3	5.8	5.6	2.8

After mathematical treatment of Eq. (12), Eq. (13) can be obtained as:

$$\log D/D_0 = \log \beta_0 + p \log [L] \quad (13)$$

Comparing Eq. (13) with Eq. (11), it can be found $\log \beta_0 = \log K_{\text{ex}} - \log K_{\text{ex}}^0 = \Delta \log K_{\text{ex}}$, $\log \beta_0$ values of La^{3+} , Ce^{3+} , Pr^{3+} , Nd^{3+} , Sm^{3+} , Eu^{3+} , and Gd^{3+} are listed in Table 2.

From Table 2, it can be found that the organic phase stability constants of the extraction species of La^{3+} , Ce^{3+} , Pr^{3+} , Nd^{3+} , Sm^{3+} and Eu^{3+} are nearly the same, but much larger than that of Gd^{3+} . Therefore, the tendency of synergistic extraction reaction for light rare earths La^{3+} , Ce^{3+} , Pr^{3+} and Nd^{3+} , and medium rare earths Sm^{3+} and Eu^{3+} are much similar, but for gadolinium which becomes much more weaker than that of the former ones, and decreases quickly from Gd^{3+} to Er^{3+} and Lu^{3+} with increasing atomic number. For heavier rare earth elements, no synergistic effect can be produced, perhaps owing to the bad fitting between lanthanide and the extraction system. The separation factors (S.F.) between Gd^{3+} and Eu^{3+} (C_L : 2×10^{-4} – 5×10^{-4} M), Eu^{3+} and Ce^{3+} (C_L : 2×10^{-4} – 7×10^{-4} M) were obtained to be 1.4 and 2.5, respectively, where C_L is the initial concentration of ATCO. It is estimated that the best separation between Eu^{3+} and Ce^{3+} can be obtained in this condition.

4. Conclusion

Due to ATCO containing soft donor sulfur atoms within its macrocyclic linkage, its binding capability and smaller cavity size can not be fitted into lanthanide ion. Of course, it alone has very low extractability and selectivity for lanthanide than oxa-crown ethers and aza-crown ethers, thus is unavailable for applicable purpose. However, because it can form a synergistic extraction system in the presence of lauric acid, which tends to

extract light and medium rare earths such as Ce^{3+} and Eu^{3+} by forming rare earth adductant with lauric acid in the neutral range, it can help us to deeply understand its binding and extraction behavior for rare earths from the viewpoint of fundamental chemistry. Unfortunately, in speaking of the real structure of extraction species, it could not be determined exactly from the experiment employed, and is worthy of further study.

Acknowledgements

This research work is part of a project financed by Ministry of Education, Science and Culture, Government of Japan (No. 06241250 and No. 08220246) for the development of new preparation methods of rare earth compounds. The authors are also grateful for the financial aid received from the foreign student center of Kobe University and the scholarship provided by the Hyogo International Association.

References

- [1] V. Alexander, Chem. Rev. 95 (1995) 273.
- [2] T. Shigekaza, M. Masatoshi, K. Yoshinobu, Y. Tadashi, U. Shigeo, S. Takayuki, T.H. Le Quyun, M. Masakazu, Anal. Chem. 67 (1995) 1645.
- [3] R. Frazier, C.M. Wai, Talanta 39 (3) (1992) 211.
- [4] M. Yoshihiro, K. Yoshihiro, K. Takaumi, Y. Zenko, Kidorui 26 (1995) 380.
- [5] H. Sakamoto, J. Ishikawa, M. Otomo, Bull. Chem. Soc. Jpn. 68 (1995) 2831.
- [6] K. Saito, Y. Masuda, E. Seikido, Anal. Chim. Acta 151 (1983) 447.
- [7] Y. Masuda, M.D.H. Zahir, Talanta 42 (1) (1995) 93.
- [8] Z. Marczenko, Spectrophotometric Determination of Elements, Wiley, New York, 1976, p. 441.
- [9] K. Nakagawa, S. Okada, Anal. Chem. 60 (1988) 2527.
- [10] Gmelin Handbook of Inorganic Chemistry (Sc, Y, La-Lu Rare Earth Elements), D6, (1988), 67.
- [11] D.D. Ensor, M. Nicks, D.J. Pruet, Sep. Chem. Technol. 23 (1988) 1345.

Determination of chromium in waste-water and cast iron samples by fluorescence quenching of rhodamine 6G

Nianqin Jie *, Qiang Zhang, Jinghe Yang, Xirong Huang

Department of Chemistry, Shandong University, Jinan, People's Republic of China

Received 20 May 1997; received in revised form 16 August 1997; accepted 16 August 1997

Abstract

A new simple, selective and sensitive fluorescence quenching method was developed to determine chromium with rhodamine 6G. The method is based on the oxidation of rhodamine 6G by chromium(VI) in sulfuric acid solution. The linear calibration graph was obtained in the range 8–80 ng ml⁻¹ chromium(VI). The detection limit is 0.8 ng ml⁻¹. The method was applied successfully to the determination of chromium in waste water and cast iron samples. © 1998 Elsevier Science B.V. All rights reserved.

The chromium content of water is probably increasing steadily as a result of industrial activity in populated areas. Chromium appears frequently as a pollutant in our environment [1]. The hexavalent form is of prime concern because of its high toxicity. Cr(VI) poisoning causes skin disorders and liver damage, and there are some reasons to believe that chromates are carcinogenic. For these reasons, its maximum allowable level in drinking water has been limited to 0.05 mg l⁻¹ hexavalent Cr(VI). On the other hand, the chemistry of chromium is very important in the field of metallurgical industry. The addition of small amounts of chromium to cast iron significantly modified its wear and heat resistance. Therefore, the accurate determination of Cr at trace level is important in the field of environmental science and industry.

Many spectrophotometric methods for the determination of chromium have been developed [2–4]. Electrometric methods are also available [5,6], as well as AAS methods [7,8] and iron chromatography methods [9,10]. These methods have their advantages and their disadvantages respectively. Some of these methods suffer from interferences of other substances, and some require separation or complicated instrumentation.

Fluorometric methods have been reported for the determination of Cr(VI) in water and cast iron samples [11–13], but these methods also suffer from the interferences of Fe(II), Pb(II) and Hg(II), and they have low sensitivity. Fluorescence quenching method for the determination of chromium(VI) is rarely reported [14,15], and these methods are of low sensitivity. So far, there has been no report on the determination of chromium(VI) using rhodamine 6G. In this paper, a fluorescence quenching method for the determina-

* Corresponding author.

tion of Cr(VI) using rhodamine 6G has been described. The method is based on the measurement of decrease in fluorescence intensity at 545 nm of rhodamine 6G in sulfuric acid medium. The method offers several distinct advantages over other fluorometric methods [11–15] for chromium(VI): higher sensitivity, good selectivity and ease of operation. The method has been used to determine trace chromium in waste water and cast iron samples. The results are satisfactory.

1. Experimental

1.1. Apparatus

An RF-540 spectrofluorimeter (Shimadzu, Kyoto) with a plotter unit and a 1 cm quartz cell was used for recording the spectra and making fluorescence measurements.

1.2. Reagents

All chemicals were of analytical–reagent grade. Deionized, distilled water was used throughout.

Chromium(VI) stock solution: 1 mg ml^{-1} . Dissolve 0.2827 g of potassium dichromate in water and dilute to volume in a 100 ml standard flask. The stock solution was diluted to μg of chromium(VI)/ml as working solution.

Rhodamine 6G stock solution: 1.5 mg ml^{-1} . It was diluted to $1 \mu\text{g ml}^{-1}$ as working solution. Sulfuric acid solution: 12.5 mol l^{-1} .

1.3. Analytical procedure

As aliquot of working solution of chromium(VI), 1.5 ml of rhodamine 6G working solution, and 1.0 ml sulfuric acid solution (12.5 mol l^{-1}) were added sequentially to 25 ml standard volumetric flask. The contents of the flask were mixed, then it was placed in a boiling water bath for 5 min, after which it was cooling under tap water and diluted to the mark with water and mixed. The fluorescence intensity was measured at 545 nm (with excitation at 525 nm) against a reagent blank, prepared concurrently.

2. Results and discussion

2.1. Spectra characteristics

As shown in Fig. 1, the excitation and emission spectra of the rhodamine 6G and rhodamine 6G chromium systems are similar. The excitation and emission wavelength were at 525 and 545 nm, respectively. But the fluorescence intensity of rhodamine 6G decreased when the chromium(VI) was added.

2.2. Optimum conditions for fluorescence quenching

The results indicated that a maximum and constant fluorescence quenching was reached in the range 1.0–2.0 ml of rhodamine 6G ($12.5 \mu\text{g ml}^{-1}$) (Fig. 2). In this work, 1.5 ml of rhodamine 6G ($12 \mu\text{g ml}^{-1}$) was chosen. The effect of sulfuric acid concentration on the fluorescence quenching of the system was examined. The maximum fluorescence quenching occurred in the range 0.25–0.75 mol l^{-1} of sulfuric acid. The fluorescence quenching decreased for values outside this range (Fig.

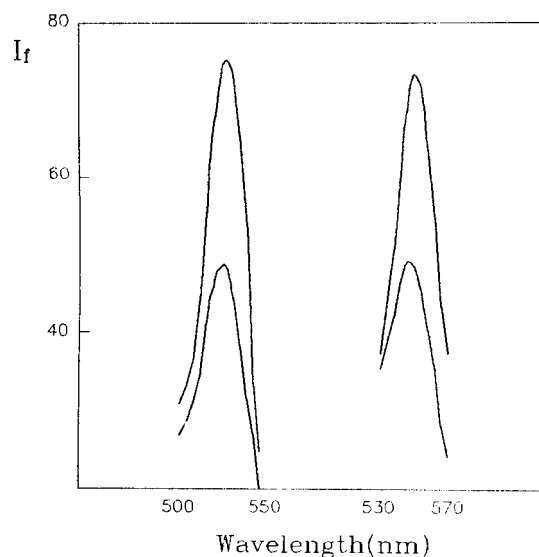


Fig. 1. Fluorescence spectra. (a) Excitation and (b) emission spectra of rhodamine 6G system(1,2) and rhodamine 6G-Cr(VI) system(1',2') condition: 40 ng ml^{-1} Cr; 0.5 mol l^{-1} H_2SO_4 ; and $0.72 \mu\text{g ml}^{-1}$ rhodamine 6G.

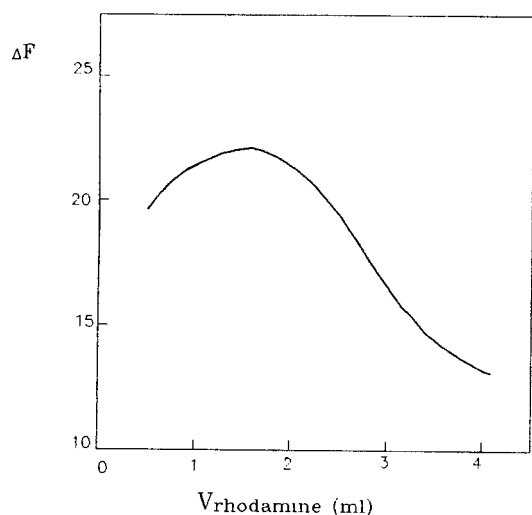


Fig. 2. Effect of rhodamine 6G concentration. Conditions: 40 ng ml⁻¹ Cr, and 0.5 mol l⁻¹ H₂SO₄.

3). A 0.5 mol l⁻¹ of sulfuric acid was selected. The temperature and time on the fluorescence quenching of the system was also investigated. The optimum fluorescence quenching was reached at 100°C for 5 min and remained unaltered for up to 10 h.

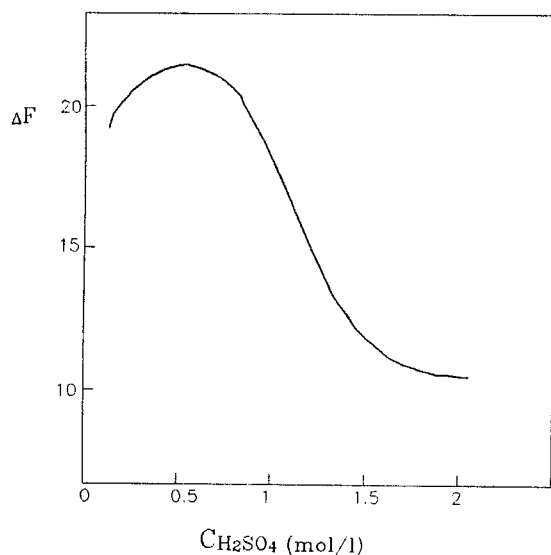


Fig. 3. Effect of sulfuric acid concentration. Condition: 40 ng ml⁻¹ Cr, and 0.72 μg ml⁻¹ rhodamine 6G.

Table 1
Tolerance of foreign ions in the determination of 1 μg Cr(VI)

Ions added	Tolerance ratio (W/W)
As(V)	5000
PO ₄ ³⁻	4000
Co(II)	3000
NO ₃ ⁻ , NH ₄ ⁺	2500
Ni(II), Ca(II)	2000
Mg(II), Zn(II), Be(II)	1500
Al(III), Cd(II), F ⁻	1000
Mn(II), Br ⁻ , Cl ⁻	800
Bi(III), Mo(VI)	500
Ba(II)	200
Hg(II)	80
Pb(II)	40
Fe(III)	20
Cu(II)	4
V(V)	1
Ce(IV)	0.4
NO ₂ ⁻	0.2

2.3. Interferences

The tolerance limits of some ions for the determination of 1 μg Cr by the procedure described were studied, and the results are given in Table 1. The relative error is less than ± 5%. It can be seen that most of ions examined do not interfere, even when present in large excess. However, only Ce(IV), nitrite ions seriously interfere with the determination of Cr(VI). Therefore, the method is of good selectivity.

2.4. Calibration

The calibration graph for the determination of chromium(VI) was constructed under the optimum conditions. The linear calibration graph was obtained in the range 8–80 ng ml⁻¹ Cr(VI). The detection limit, based on three times the standard deviation of the blank, was 0.8 ng ml⁻¹ of chromium(VI). The linear regression equation and the coefficient are: $\Delta F = 19.07C + 1.13$, $r = 0.998$ (the unit of C is μg–25 ml), where ΔF is the fluorescence quenching and C is the Cr(VI) concentration.

Table 2
Determination of chromium in waste water

Sample	Reference value of Cr (mg l ⁻¹) ^a	Found of Cr (mg l ⁻¹) ^b
1	117	120 ± 1.7
2	0.546	0.548 ± 0.002

^aUsing 1,5-diphenylcarbazide as the color reagent.

^bMean ± STD Dev. (*n* = 5).

2.5. Practical application

Determination of Cr(VI) in industrial waste-water samples. The water samples were collected from different sources and were filtered before analysis. The results compare favorable to the spectrophotometric method and are shown in Table 2.

Determination of chromium in cast iron samples. Dissolve the weighed cast iron samples in a minimum volume of hydrochloric acid (12 mol l⁻¹) and heat gently on a hot plate to complete dissolution, then add 10% NaOH until pH is 10. Then add 2 ml of 30% H₂O₂ solution and heat gently to remove the excess of H₂O₂. Filter the solution into a flask and wash the residue on the filter paper repeatedly with hot water. Collect the filtrate and washing into the same flask, add 2.5 mol l⁻¹ of sulfuric acid until the pH is 6. Transfer the solution to a 100 ml calibrated flask, and dilute to the mark with water. Take appropriate amounts of this solution for the determination of Cr(VI) according to the procedure described above. The results are summarized in Table 3 and were compared with the certified value of Cr(VI). The contents of elements in cast iron standard samples are shown in Table 4.

Table 3
Determination of Cr in cast iron

Standard sample ^a	Standard value of Cr (%)	Found of Cr (%) ^b
BH2012	1.10	1.10 ± 0.02
BH2013	0.19	0.19 ± 0.004

^aThe samples were obtained from Jinan Institute of Metallurgy.

^bMean ± STD Dev. (*n* = 5).

Table 4
The contents of elements in cast iron standard samples (%)

Element	BH-2012	BH-2013
Cr	1.10	0.19
V	0.036	0.026
Mo	0.002	0.51
Ni	0.027	0.35
Co	0.014	0.015
Cu	0.123	0.22
Mn	1.07	0.645
Sb	0.004	0.001
Ti	0.094	0.059
As	—	0.008

2.6. Nature of the reaction between Cr(VI) and rhodamine 6G

Rhodamine 6G is a triphenylmethane dye and emits very strong yellow–green fluorescent light. When oxidized by such strong oxidizers as potassium periodate and potassium bromate, its molecular structure is destroyed and the fluorescence disappears [16,17]. In this system, Cr(VI) is strong oxidizer, and rhodamine 6G could be oxidized by Cr(VI). Therefore, the fluorescence intensity of rhodamine 6G decreases after adding Cr(VI) to this system. It is clear that the reaction between Cr(VI) and rhodamine 6G in acidic solution is redox reaction.

3. Conclusion

A fluorometric determination of Cr(VI) with rhodamine 6G was developed in this paper. The nature of the reaction was discussed. The current method was compared with other methods and found to be more sensitive and selective. The procedure can be satisfactorily applied to the determination of Cr(VI) in waste-water and cast iron samples.

References

- [1] C.N. Sawyer, R.L. McArty, Chemistry for Environmental Engineering, McGraw Hill, New York, 1978.
- [2] F.J. Zou, Fenxi Shiyanshi 14 (1995) 29.

- [3] D.T. Burns, M. Harriott, S.A. Barakat, *Anal. Chim. Acta* 259 (1992) 33.
- [4] M. Kamburova, *Talanta* 40 (1993) 713.
- [5] C. Elleouet, F. Quentel, C. Madec, *Anal. Chim. Acta* 257 (1992) 301.
- [6] A.M. Dobney, G.M. Greenway, *Analyst* 119 (1994) 293.
- [7] R. Rubio, A. Sanuquillo, G. Rauret, L. Garcia Beltra, P. Quevallviller, *Anal. Chem. Acta* 283 (1993) 207.
- [8] S. Dyg, T. Anglov, J.M. Christensen, *Anal. Chim. Acta* 286 (1994) 273.
- [9] P. Janos, *Fresenius J. Anal. Chem.* 342 (1992) 195.
- [10] E.J. Arar, J.D. Praff, *J. Chromatogr.* 546 (1991) 335.
- [11] N.Q. Jie, W.G. Yu, *Chin. J. Appl. Chem.* 7 (1990) 71.
- [12] N.Q. Jie, J. Jiang, *Analyst* 116 (1991) 395.
- [13] N.Q. Jie, J.H. Yang, W. Fu, R.X. Zhang, *Fenxi Huaxue* 22 (1994) 864.
- [14] N.Q. Jie, J.H. Yang, J. Guo, *Anal. Lett.* 25 (1992) 1447.
- [15] T.S. Chen, Z.G. Chen, D. Wu, *Fenxi Huaxue* 22 (1994) 129.
- [16] G. Zhang, D.X. Cheng, S.L. Feng, *Talanta* 40 (1993) 1041.
- [17] G.Z. Zhang, H.Q. Zhang, X.W. He, W.L. Yang, H.M. Shi, *Fenxi Huaxue* 22 (1994) 1006.

Simultaneous determination of pseudoephedrine hydrochloride and diphenhydramine hydrochloride in cough syrup by gas chromatography (GC)

S.V. Raj, S.U. Kapadia, A.P. Argekar *

Analytical Laboratory, Department Of Chemistry, The Institute of Science, 15, Madam Cama Road, Mumbai, 400 032, India

Received 30 April 1997; received in revised form 12 August 1997; accepted 18 August 1997

Abstract

A simple, rapid and precise gas chromatographic method has been developed for the simultaneous determination of pseudoephedrine hydrochloride and diphenhydramine hydrochloride in cough syrup, using a SS column of 10% OV 1 on chromosorb W-HP (80–100 mesh) and nitrogen as a carrier gas at a flow rate of 30 ml min⁻¹. The oven temperature was programmed at 135°C for 1 min, with a rise of 10°C min⁻¹ up to 250°C (held for 5 min). The injector and detector port temperatures were maintained at 280°C. Detection was carried out using Flame ionization detector. Guaphenesin was used as an internal standard. Results of assay and recovery studies were statistically evaluated for its accuracy and precision. © 1998 Elsevier Science B.V. All rights reserved.

Keywords: Simultaneous determination; Pseudoephedrine hydrochloride; Diphenhydramine hydrochloride; Cough syrup; Gas chromatography

1. Introduction

Pseudoephedrine Hydrochloride (PSE), is a sympathomimetic agent. It is used for the symptomatic relief of nasal congestion. Diphenhydramine Hydrochloride (DPH), is an antihistamine with antimuscarinic and pronounced sedative properties. It is also used as an antiemetic [1].

Literature survey reveals that both PSE and

DPH are official in U.S.P. [2], B.P. [3] and I.P. [4]. Various Spectrophotometric [5,6] and HPLC [7] methods are reported for the individual determination of PSE and Spectrophotometric [8] and GC [9] methods are reported for the individual determination of DPH from its formulations. HPLC determination of DPH and Ephedrine Hydrochloride in biachuanpeng tablets [10] and HPLC determination of DPH and Ondansetron mixture in 0.9% NaCl injection [11] are also reported. A HPTLC [12] method has been reported for the simultaneous determination of PSE and DPH in combined dosage form. However instru-

* Corresponding author.

Table 1
Results of system suitability

Sr. No.	Typical analytical parameters used in assay validation as per U.S.P. 23	PSE	DPH	As per U.S.P. 23 requirements
1	Accuracy (%)	98.32	98.19	90–110% of labeled amount
2	Precision [R.S.D. (%)]	1.85	1.73	2.00
3	Limit of detection (mg)	0.5	0.4	—
4	Limit of quantification (mg)	2.0	1.5	—
5	Linearity (<i>r</i>)	0.99	0.99	—
6	Range (mg ml ⁻¹)	9	8	—
		1	1	—
		—	—5	—
		10	—	—
7	Theoretical plates	3500	4400	Normally not less than 500
8	Resolution factors	2.1	2.0	Varies from Monograph to Monograph
9	Tailing factor	2.4	2.1	Same as above

mental facility of HPTLC being rare as compared to GC and HPLC and there is no method for the simultaneous determination of PSE and DPH by GC. So a new method for the simultaneous determination of PSE and DPH from cough syrup by GC technique is developed.

2. Experimental

2.1. Instrument

CHEMITO 5210 gas chromatograph equipped with an Oracle 2 integrator and a flame ionization detector was used.

2.2. Carrier gas

Nitrogen was used as a carrier gas at a flow rate of 30 ml min⁻¹.

2.3. Stationary phase

An S.S. column (2.50 m in length and 2 mm id) of 10% OV 1 on Chromosorb W-HP (80–100 Mesh), manufactured by Sky Lab, Thane, Mumbai, was used as a stationary phase.

2.4. Solvents and chemicals

Chromatography grade Chloroform and A.R. Grade Sodium Hydroxide were used.

2.5. Standard stock solution

A combined standard solution of PSE (5 mg ml⁻¹) and DPH (5 mg ml⁻¹) were prepared in water. These Standards were procured from Merind, Mumbai, India and their purities were found to be 98.95 and 99.28% respectively.

2.6. Internal standard

Guaphenesin standard of 98.89% purity, was procured from TATA Pharma, Patalganga, India. A solution of 5 mg ml⁻¹ was prepared in water.

2.7. Procedure for calibration

In a series of separating funnels aliquots of standard drug solution equivalent to 1–10 mg ml⁻¹ for PSE and 1–5.0 mg ml⁻¹ for DPH were taken. 1 ml of internal standard and 20 ml of 1 N NaOH were added and extracted with three quantities, each of 20 ml of chloroform. The chloroform layer was collected in a conical flask and

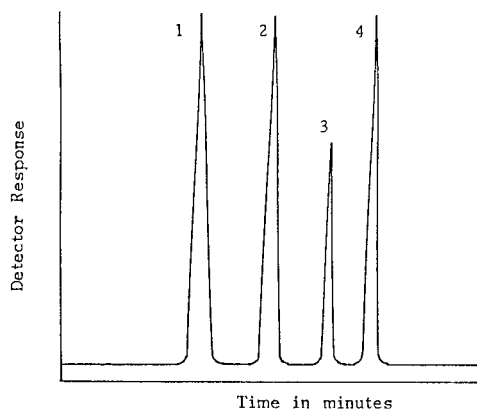


Fig. 1. Typical chromatogram of PSE and DPH.

evaporated till 5 ml solution was left. Further evaporation was done using nitrogen up to dryness. The residue was reconstituted in 2 ml of chloroform. All the operating chromatographic conditions were set and the instrument was stabilized for steady baseline. 2 μ l of the solution were injected into the chromatographic system. The chromatograms were recorded and peak area ratios were computed.

2.8. Procedure for assay

Ten grams of cough syrup was accurately weighed and then transferred into a separating funnel. To this 1 ml of internal standard solution and 20 ml of 1 N NaOH solution were added and proceed as described in the procedure for calibration. The amount of drug present in mg per 5 ml was calculated using the formula:

Amount of drug (mg per 5 ml)

$$= \frac{RA/RI \times C \times D}{RB/RI \times W}$$

where RA = area of sample, RB = area of standard, RI = area of internal standard, C = Concentration of standard in mg ml⁻¹, D = dilution factor, W = weight of sample in mg.

2.9. Procedure for recovery studies

To study the accuracy, reproducibility and precision of the above method, recovery of the added standard was studied at three different levels. Each level was repeated three times. A plot of the amount of the drug found by the proposed method (Y-axis) against the amount of the standard added (X-axis) was drawn. The intercept on the Y-axis indicates the amount of drug present per five ml of cough syrup. From the amount of drug found. Percentage recovery was calculated using the formula:

$$\% \text{Recovery} = \frac{N(\sum XY) - (\sum Y)(\sum X)}{N(\sum X^2) - (\sum X)^2} \times 100$$

where X = amount of standard drug added, Y = amount of drug found by the proposed method, N = number of observations.

3. Results and discussion

3.1. System suitability

To ascertain the resolution and reproducibility of the chromatographic method, system suitability tests were carried out on freshly prepared standard stock solution of PSE and DPH. The Parameters obtained are as shown in Table 1. These results are in concurrence with U.S.P. 23 requirements.

3.2. Chromatography

10% OV1 column gave a good separation of the drugs and the internal standard. Sharp and sym-

Table 2
Results of GC assays from tablets

Sr. No.	PSE (Label claim: 30 mg per 5 ml)	DPH (label claim: 15 mg per 5 ml)
1	28.92	14.30
2	30.19	15.24
3	28.48	13.63
4	29.27	13.85
5	28.54	14.66
Mean	29.34	14.76
R.S.D. (%)	1.85	1.73

Table 3
Results of recovery analysis

Level No.	Amount of drug in mg per 5 ml of syrup	Amount of standard added in mg	Amount of drug recovered in mg per 5 ml of syrup ^a	R.S.D. (%)
Pseudoephedrine hydrochloride				
1	30	0	29.18	1.80
2	30	5	34.32	1.92
3	30	10	39.06	1.88
4	30	15	43.98	1.98
% recovery = 98.32%				
Diphenhydramine hydrochloride				
1	15	0	14.70	1.69
2	15	3	17.84	1.76
3	15	6	20.57	1.89
4	15	9	23.46	1.85
% recovery = 98.19%				

^a Average of three experiments.

metrical peaks were achieved by programming the oven temperature at 135°C for 1 min, with a rise of 10°C min⁻¹ up to 250°C (held for 5 min). The retention times of PSE and DPH were about 4.69 and 10.50 min respectively. Retention time of the internal standard was 8.00 min (Fig. 1).

3.3. Linearity, limit of detection and limit of quantification

A linear relationship was obtained in the concentration range of 1–10 mg ml⁻¹ for PSE and 1–5 mg ml⁻¹ for DPH respectively. The calibration curves could be represented by the linear regression equations:

$$Y_{\text{PSE}} = 8.1980X + 3.9850 \quad (r = 0.999)$$

$$Y_{\text{DPH}} = 5.4006X + 5.2358 \quad (r = 0.998)$$

where Y = area and X = concentration of the drug in mg.

The Limit of Detection (LOD) and the Limit of Quantification (LOQ) of PSE and DPH were calculated on the peak area using the following equations:

$\text{LOD} = 3 \times N/B$ and $\text{LOQ} = 10 \times N/B$ where N , the noise estimate, is the standard deviation of the peak areas ($n = 5$) of the respective drugs and B is the slope of the corresponding calibration curve. LOD and LOQ were 0.5 and 2.0 mg ml⁻¹ for PSE and 0.4 and 1.5 mg ml⁻¹ for DPH respectively.

3.4. Assay

In a replicate analysis ($n = 5$) for the cough syrup (LUPIHIST, Batch No. 6001, date of manufacturing: Feb. 1996, manufactured by Lupin, Chikalthana, Aurangabad, India.), the amounts of PSE and DPH per 5 ml of the cough syrup found by the proposed method were 29.34 mg (R.S.D. = 1.85%) and 14.76 mg (R.S.D. = 1.73%) respectively, as shown in Table 2. The low values of R.S.D. indicate that the method is precise and accurate.

A blank run of the excipients present per 5 ml of cough syrup, such as Sodium Citrate (150 mg), ammonium chloride (150 mg) and menthol (0.01 ml) did not show any interference.

3.5. Accuracy and precision

The percentage recoveries obtained for PSE and DPH were 98.32 and 98.19% respectively, which indicates that the method is precise, accurate and there is no interference due to excipients present in the cough syrup (Table 3).

4. Conclusion

The proposed GC method is accurate, precise and rapid for the simultaneous determination of PSE and DPH from cough syrup. Hence it can be easily and conveniently adopted for the routine quality control analysis.

Acknowledgements

Authors are thankful to M/S Merind Limited, Mumbai, India, for providing the instrumental facilities.

References

- [1] Martindale The Extra Pharmacopoeia, 31st ed. 1588, The Royal Pharmaceutical Society of Great Britain, 1996, p. 442.
- [2] The United States Pharmacopoeia, 534, 23rd ed. The United States Pharmacopoeial Convention, Inc., 1995, p. 532.
- [3] British Pharmacopoeia, 231, 563. HMSO, 1993, p. 147.
- [4] Indian Pharmacopoeia, 641–642. The Controller of Publications, Delhi, 1996, p. 259.
- [5] J.L. Murtha, T.N. Julian, G.W. Radebaugh, *J. Pharm. Sci.* 77 (8) (1988) 715–718.
- [6] H.S.I. Jan, M. Kolmanpunporn, *Anal. Chim. Acta.* 226 (11) (1989) 159–164t.
- [7] Abdel-Moety, O.A. Al-Deeb, N.A. Khattab, *J. Liq. Chromatogr.* 18 (20) (1995) 4127–4134.
- [8] B. Xu, T. Bi, *Yaoxue Xuebao* 24 (5) (1989) 360–365.
- [9] Y. Zhang, C. Yang, *Zhongguo Yaoxue Zazhi (Ch.)* 26 (3) (1991) 163–164.
- [10] Y. Yu, *Yaowu Fenxi Zazhi* 10 (6) (1990) 355–356.
- [11] L. Ye, J.T. Stewart, *J. Liq. Chromatogr. Relat. Tech.* 19 (5) (1996) 711–718.
- [12] J.E. Haky, D.A. Sherwood, S.T. Brenkan, *J. Liq. Chromatogr.* 12 (6) (1989) 907–917.

Possibilities for speciation of Al–citrate and other negatively charged Al complexes by anion-exchange FPLC–ICP–AES

Tjaša Bantan^a, Radmila Milačič^{a,*}, Boris Pihlar^b

^a Department of Environmental Sciences, Jožef Stefan Institute, Jamova 39, 1000 Ljubljana, Slovenia

^b Faculty of Chemistry and Chemical Technology, University of Ljubljana, Aškerčeva 5, 1000 Ljubljana, Slovenia

Received 26 May 1997; received in revised form 19 August 1997; accepted 25 August 1997

Abstract

An anion-exchange fast protein liquid chromatographic–inductively coupled plasma atomic emission spectrometric procedure (FPLC–ICP–AES) was developed for speciation of Al–citrate and other negatively charged Al complexes. FPLC separations were carried out on a Mono Q HR 5/5 strong anion-exchange FPLC column over a pH range from 3.5 to 11.0. An aqueous—NaNO₃ (4 mol dm⁻³) linear gradient elution was applied over 10 min for separation of a particular Al species. The separated Al species were determined in 0.5 cm³ eluate fractions ‘off line’ by ICP–AES. Under optimal analytical procedures Al–citrate was separated from Al–oxalate and Al–EDTA in a neutral pH range. Good reproducibility of the FPLC–ICP–AES procedure was obtained for determination of a particular Al species at optimal measurement conditions (RSD ± 2%). Al³⁺ and neutral Al–citrate species were strongly adsorbed on the column resin and did not interfere with the separation of negatively charged Al complexes. Al(OH)₄⁻ species were separated from Al–citrate in an alkaline pH region, but quantitatively determined only at a pH of 11.0. The distribution of Al species over a pH range from 3.5 to 11.0 agreed with the reported calculated data. The limit of detection (3σ basis) for separated Al species was 0.1 μg cm⁻³. © 1998 Elsevier Science B.V. All rights reserved.

Keywords: Speciation of Al; Separation of Al–citrate; Al–EDTA; Al–oxalate ; Anion-exchange FPLC–ICP–AES

1. Introduction

Interest in Al bioavailability and toxicity resulted in the development of numerous analytical techniques for speciation of Al. These techniques identified and quantified particular groups of Al species. The most frequently used techniques include spectrophotometry [1–6], ion-exchange

chromatography [6,7] and chelating ion-exchange chromatography [8–12] which enable the determination of the sum of positively charged monomeric Al species. In recent years investigations were directed at the development of an analytical method using a single procedure for the simultaneous determination of various Al species in environmental samples [13–18]. For this purpose ion chromatography in combination with post-column derivatization using UV–VIS [13,14] or fluorescence [15,16] detection was employed,

* Corresponding author. Tel.: +386 61 177 3900; fax: +386 61 219 385; e-mail: radmila.milacic@ijs.si

and HPLC cation-exchange chromatography with fluorescence detection [17] or cation-exchange FPLC–ICP–AES [18]. Speciation of Al using capillary zone electrophoresis was employed for simultaneous determination of Al^{3+} , Al–fluoro and Al–oxalato positively charged complexes in synthetic aqueous solutions [19].

Protein complexes and low molecular weight organic complexes of Al play an important role in biological systems. Human serum was the most widely investigated biological fluid [20–23]. Ultrafiltration and microultrafiltration [20] indicated that the majority of Al in serum is bound to serum proteins. Employing a polymeric methacrylate based anion-exchange column with ETAAS detection and gel electrophoresis [21] it was verified that approximately 90% of Al in spiked serum is bound to transferrin. Another peak appeared after separation of Al–transferrin representing the remaining 10% of Al which was presumed to be Al–citrate. Analogous observations were reported by D’Haese et al. [22] who used a similar polymer-based weak anion-exchange column with ETAAS detection for speciation of Al in the serum of dialysis patient. FPLC gel chromatography with ETAAS detection was also employed in speciation studies of Al in serum from a patient with chronic renal failure [23]. The addition of excess citric acid to serum resulted in a chromatographic peak which was assumed to correspond to Al–citrate—significantly increased. Speciation of Al–citrate was also investigated employing the HPLC–ETAAS technique [24]. Various normal, reversed phase and mixed phase (ODS/– NH_2) columns and different mobile phase conditions were used. Promising results for synthetic standard solutions of Al–citrate using a mobile phase containing MeOH:H₂O (1:1; v/v) with 0.1 M TEA and glacial acetic acid (pH 4.0) were obtained when cyclobond and cyanobonded phase columns were employed. Al–citrate recovery were moderate and did not exceed 65%. Investigation of equilibrium reactions of the citrate ion with Al by potentiometry and ¹³C NMR [25] were also reported. Al speciation in serum [26,27], blood plasma and the gastrointestinal tract [28] were investigated by a computer simulation through calculations using known thermodynamic

equilibrium constants. There is no doubt that Al–citrate is a very important low molecular weight species in biological fluids [21–23,26–28]. It is also presumed that it exists in plant leaves and is synthesized in acid forest soils, as well as other aliphatic organic acids, by organic acid-producing microorganisms [29]. Studies on the oral consumption of Al–citrate in rats indicated that it may play a key role in the delivery of Al to tissues by crossing the tissue membranes [30]. Although there are many analytical techniques available for determination of monomeric positively charged Al species [1–19], there is still a lack of reliable and quantitative analytical procedures for determination of low molecular weight Al species which are the most active in terms of Al bioavailability. In addition to computer simulation there is a need to incorporate more detailed speciation data into studies on Al bioavailability and toxicity in biological systems [31,32]. For these purposes reliable analytical procedures for determination of low molecular weight Al complexes should be developed.

The aim of our work was to perform a systematic study of the possibilities for quantitative determination of Al–citrate and other negatively charged low molecular weight Al complexes using FPLC separation on a Mono Q HR 5/5 strong anion-exchange column with ICP–AES detection.

2. Experimental

2.1. Apparatus

A strong anion-exchange FPLC column (Pharmacia, Sweden) of Mono Q HR 5/5 (column dimensions 5 × 50 mm, 10 μm beaded hydrophilic polyether resin substituted with quaternary amine groups, pH stability 2–12) was employed for the separation of Al species. The column was connected to a Varian Star gradient high pressure pump, equipped with a Rheodyne Model 7161 injector (0.5 cm³ loop). Separated Al species were determined on a Perkin–Elmer Plasma 40 emission spectrometer, adjusted to a wavelength of 396.152 nm. The plasma was operated at a power of 1.0 kW and a frequency of 40 MHz, with argon

as the coolant gas at a flow rate of $15 \text{ dm}^3 \text{ min}^{-1}$, and a nebulization flow rate of $1 \text{ dm}^3 \text{ min}^{-1}$. An Iskra MA 5740 pH meter with combined glass electrode was employed to determine the pH of the samples.

2.2. Reagents

Merck suprapur acids and water doubly distilled in quartz were used for the preparation of samples and standard solutions. All other chemicals were of analytical-reagent grade.

2.2.1. Aluminium standards

A standard Al stock solution ($500 \mu\text{g Al cm}^{-3}$) was prepared in a 0.5 dm^3 calibration flask by dissolving 3.4760 g of $\text{Al}(\text{NO}_3)_3 \cdot 9\text{H}_2\text{O}$ (Riedel-de Haën) in water. Al–citrate, Al–oxalate and Al–EDTA complexes were made by mixing a solution of $\text{Al}(\text{NO}_3)_3 \cdot 9\text{H}_2\text{O}$ salt with an appropriate amount of ligand (3:1 ligand to Al ratio) [33]. Stock Al–citrate, Al–oxalate and Al–EDTA solutions ($500 \mu\text{g Al cm}^{-3}$) were prepared weekly in 0.5 dm^3 calibration flasks by dissolving 3.4760 g of $\text{Al}(\text{NO}_3)_3 \cdot 9\text{H}_2\text{O}$ (Riedel-de Haën) in water followed by addition of either 5.8 g of citric acid (Merck), 5.2 g of oxalic acid (Merck) or 10.2 g of EDTA. The Al–EDTA was heated for 24 h at 80°C to assure quantitative formation of the complex [33]. Fresh working standards were prepared each day. The same stock solutions were used either for the preparation of standards for calibration in ICP-AES determinations (dilution with a yttrium solution), or for the preparation of synthetic standard solutions (dilution with buffer) which were used in the investigation of Al speciation on the FPLC column.

2.2.2. Internal standard

A Merck standard yttrium stock solution ($1000 \mu\text{g cm}^{-3}$) was used as the internal standard in inductively coupled plasma-atomic emission (ICP-AES) measurements.

2.2.3. Buffer solutions

Potassium hydrogenphthalate (0.05 mol dm^{-3}) buffer solution (Merck) with the addition of an appropriate amount of nitric acid (0.5 mol dm^{-3})

(Merck) or potassium hydroxide (0.5 mol dm^{-3}) (Merck) was used to adjust pH in the range 3.5–4.5. Imidazole ($\text{C}_3\text{H}_4\text{N}_2$) (0.2 mol dm^{-3}) (Merck) buffer solution with the addition of an appropriate amount of hydrochloric acid (0.1 mol dm^{-3}) (Merck) was used to adjust the pH of samples in the range 5.0–8.0. pH values higher than 8.0 were obtained by the addition of an appropriate amount of potassium hydroxide (0.5 mol dm^{-3}).

2.2.4. Reagents in FPLC separations

Merck sodium nitrate (5 mol dm^{-3}) was prepared by dissolving 424.95 g of NaNO_3 in water and diluting to 1 dm^3 . The reagent was purified before use by a batch procedure. Five grams of chelating ion-exchange resin Chelex 100 (Na^+ form, 100–200 mesh) was added to the reagent, stirred for 24 h and filtered through a $0.45 \mu\text{m}$ filter. Lower concentrations of sodium nitrate were prepared by dilution with water.

2.3. Synthetic solutions of Al complexes

To study the distribution of Al species over a wide pH range the following procedure was applied for preparation of synthetic solutions. Buffer solution was first adjusted to the required pH. Buffer solution (45 cm^3) was then transferred to a 50 cm^3 volumetric flask. An appropriate amount of Al stock solution was added and the flask filled to the mark with buffer solution.

2.4. Recommended procedure

Separations of negatively charged low molecular weight organic complexes of Al were carried out on a Mono Q HR 5/5 strong anion-exchange column. The sample (0.5 cm^3) was injected onto the column. An aqueous—(0–100% 4 mol dm^{-3} NaNO_3) linear gradient elution was applied over 10 min at a flow rate of $1.0 \text{ cm}^3 \text{ min}^{-1}$. After separation, the column was left to regenerate for 5 min with 4 mol dm^{-3} NaNO_3 at a flow rate of $1.0 \text{ cm}^3 \text{ min}^{-1}$ and then equilibrated with water firstly for 20 min at a flow rate of $2.0 \text{ cm}^3 \text{ min}^{-1}$ and in the following 5 min at a flow rate of $1.0 \text{ cm}^3 \text{ min}^{-1}$. The separated Al species were deter-

mined in 0.5 cm³ eluate fractions 'off line' by ICP-AES. Fractions were diluted prior to analysis with 0.5 cm³ of Y standard solution, such that the internal standard concentration was 10.0 µg cm⁻³. The sequential mode of the instrument did not allow measurement of the transient emission signal for Al and Y simultaneously. Therefore, the chromatographic column was not connected 'on line' to the ICP-emission spectrometer.

3. Results and discussion

3.1. Development of the FPLC—ICP-AES procedure

At a neutral pH range Al–citrate exists as a mixture of negatively charged complexes [26–28,34]. Therefore, as a negatively charged species it should be quantitatively separated on an anion-exchange column. Gradient elution with NaCl (4 mol dm⁻³) was efficient in separating negatively charged Al–citrate but disadvantageous owing to corrosion problems with the stainless steel components of the HPLC system. In order to avoid corrosion, NaNO₃ (2–5 mol dm⁻³) was examined. Quantitative separation of Al–citrate and a narrow range of separated Al–citrate peak was obtained when gradient elution with 4 mol dm⁻³ NaNO₃ at a flow rate of 1 cm³ min⁻¹ was applied. The increasing ionic strength of the eluent during the chromatographic run (gradient elution) allowed the separation of negatively charged Al species. After separation the column resin was regenerated with 4 mol dm⁻³ NaNO₃. Washing with water followed to equilibrate the column resin before the next separation. Experimentally, it was found that to obtain reproducible retention times it was very important to ensure quantitative washing of NO₃⁻ (a large ion) from the column resin. Therefore, initial equilibration with water was applied for 20 min at a flow rate of 2.0 cm³ min⁻¹ and for the next 5 min at a flow rate of 1.0 cm³ min⁻¹. To determine the separated Al species, 0.5 cm³ fractions were collected. The high salt content of the eluent af-

fects the nebulization efficiency in ICP-AES measurements. To eliminate this influence, fractions were diluted with 0.5 cm³ of Y solution which acts as an internal standard. The concentration of Y in the diluted fractions and in the standards and blank solution which were used in the calibration procedure was 10 µg cm⁻³. During the chromatographic run the pH of the water–NaNO₃ eluent ranged from 7.0 to 6.0. It was found experimentally that the pH of the eluent did not influence the separation of Al–citrate, nor that of other Al negatively charged complexes investigated. The same retention times and efficiency of separation was obtained when either water–NaNO₃ was employed in gradient elution or when the column was equilibrated with buffer at the pH of the sample analyzed and a buffer solution in combination with buffered NaNO₃ was applied in the separation of the Al species. On the basis of these considerations the procedure was developed as described under Section 2 and was employed in further investigations of Al speciation by anion-exchange FPLC—ICP-AES.

A typical chromatogram for Al–citrate at pH of 7.0, separated on an anion-exchange FPLC Mono Q HR 5/5 column with ICP-AES detection, is presented in Fig. 1. It is evident that

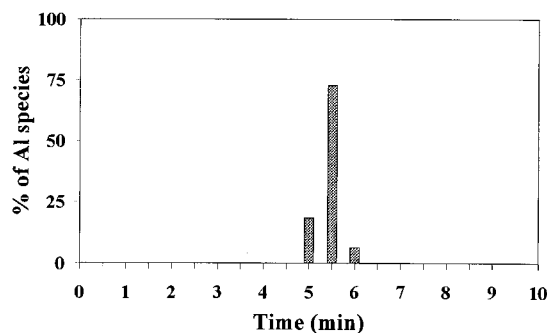


Fig. 1. Typical chromatogram of Al–citrate (3.0 µg Al cm⁻³, 3 M excess of citric acid) at pH 7.0, separated on an anion-exchange FPLC Mono Q HR 5/5 column with ICP-AES detection. Sample volume 0.5 cm³, aqueous-NaNO₃ (4 mol dm⁻³) linear gradient elution, flow rate 1 cm³ min⁻¹, fraction collection 0.5 cm³, *n* = 3.

Table 1
Reproducibility of measurements and the efficiency of Al–citrate separation^a

Synthetic solution of Al–citrate.	Al added ($\mu\text{g cm}^{-3}$)	Anion-exchange FPLC—ICP-AES ($\mu\text{g cm}^{-3}$)					Al found ($\mu\text{g cm}^{-3}$)	Recovery (%)
		t = 4.5 ^b	t = 5.0	t = 5.5	t = 6.0	t = 6.5		
1. Replicate	3.00 ± 0.02	<LOD ^c	0.83 ± 0.02	1.55 ± 0.02	0.62 ± 0.02	<LOD	3.00 ± 0.02	100
2. Replicate	3.00 ± 0.02	<LOD	0.64 ± 0.02	2.02 ± 0.02	0.57 ± 0.02	<LOD	3.05 ± 0.02	102
3. Replicate	3.00 ± 0.02	<LOD	0.68 ± 0.02	1.80 ± 0.02	0.46 ± 0.02	<LOD	2.94 ± 0.02	98
4. Replicate	3.00 ± 0.02	<LOD	0.63 ± 0.02	1.80 ± 0.02	0.52 ± 0.02	<LOD	2.95 ± 0.02	98.3
5. Replicate	3.00 ± 0.02	<LOD	0.48 ± 0.02	2.02 ± 0.02	0.54 ± 0.02	<LOD	3.04 ± 0.02	101
6. Replicate	3.00 ± 0.02	<LOD	0.65 ± 0.02	1.79 ± 0.02	0.45 ± 0.02	<LOD	2.89 ± 0.02	96

^a Al–citrate (3.0 $\mu\text{g Al cm}^{-3}$, 3 M excess of citric acid) at pH 7.0, tested for six consecutive determinations by employing anion-exchange FPLC with ICP-AES detection (fraction collection 0.5 cm^3). Mono Q HR 5/5 column, sample volume 0.5 cm^3 , aqueous- NaNO_3 (4 mol dm^{-3}) linear gradient elution, flow rate 1 $\text{cm}^3 \text{min}^{-1}$

^b t, time (min).

^c LOD, limit of detection (0.1 $\mu\text{g cm}^{-3}$).

$\bar{x} = 2.98 \pm 0.02 \mu\text{g cm}^{-3}$.

RSD = ± 2%.

negatively charged Al–citrate species are quantitatively eluted as a single chromatographic peak at the retention time of 5.5 min.

3.2. Reproducibility of the FPLC—ICP-AES procedure, linearity of measurement, limit of detection

In order to study the reproducibility of the procedure developed, six consecutive determinations of synthetic Al–citrate sample (3.0 $\mu\text{g Al cm}^{-3}$) were performed at pH 7.0. The results are summarized in Table 1. It is evident from the data of Table 1 that Al–citrate elutes reproducibly and quantitatively, between 5 and 6 min with a maximum at the retention time of 5.5 min. The recoveries range from 98 to 102%. It is also evident that good reproducibility of measurement (± 2.0%) is obtained. On the basis of these observations it can be concluded that the analytical procedure developed enables quantitative and reproducible determinations of Al–citrate in the neutral pH range. The calibration graph was found to be linear up to 4.0 $\mu\text{g cm}^{-3}$ of total Al species. The limit of detection (LOD), calculated on a 3σ basis (a value of three times the standard deviation of the blank), for separated Al species was 0.1 $\mu\text{g cm}^{-3}$.

3.3. Influence of pH on the distribution of Al species in synthetic samples of Al–citrate

To investigate the speciation of Al–citrate in the pH range 3.5–11.0, synthetic solutions of Al–citrate (2.5 $\mu\text{g Al cm}^{-3}$) were prepared at various pH values and injected onto the column. The results are presented in Fig. 2. It can be seen from this figure that the retention time for negatively charged Al–citrate complexes is 5.5 min and that the separation is quantitative in the pH range of 6.5–7.4. At pH values lower than 6.0 the percentage of negatively charged species is decreased presumably due to neutral Al–citrate complexes appearing in the solution. At a pH of 3.5 a broad peak is observed for the positively charged Al–citrate complex at an elution time of 1.0–3.0 min, and a small peak occurs indicating a negatively charged Al–citrate complex at 5.5 min. Al species which were not eluted at pH values lower than 6.0 (neutral Al–citrate, Al^{3+}) were strongly adsorbed on the column resin and did not influence the following separations. These species were removed from the column resin at the solvent front (1.0–1.5 min) by washing the column with NaOH (2 mol dm^{-3}), which is recommended by the producer as the cleaning agent.

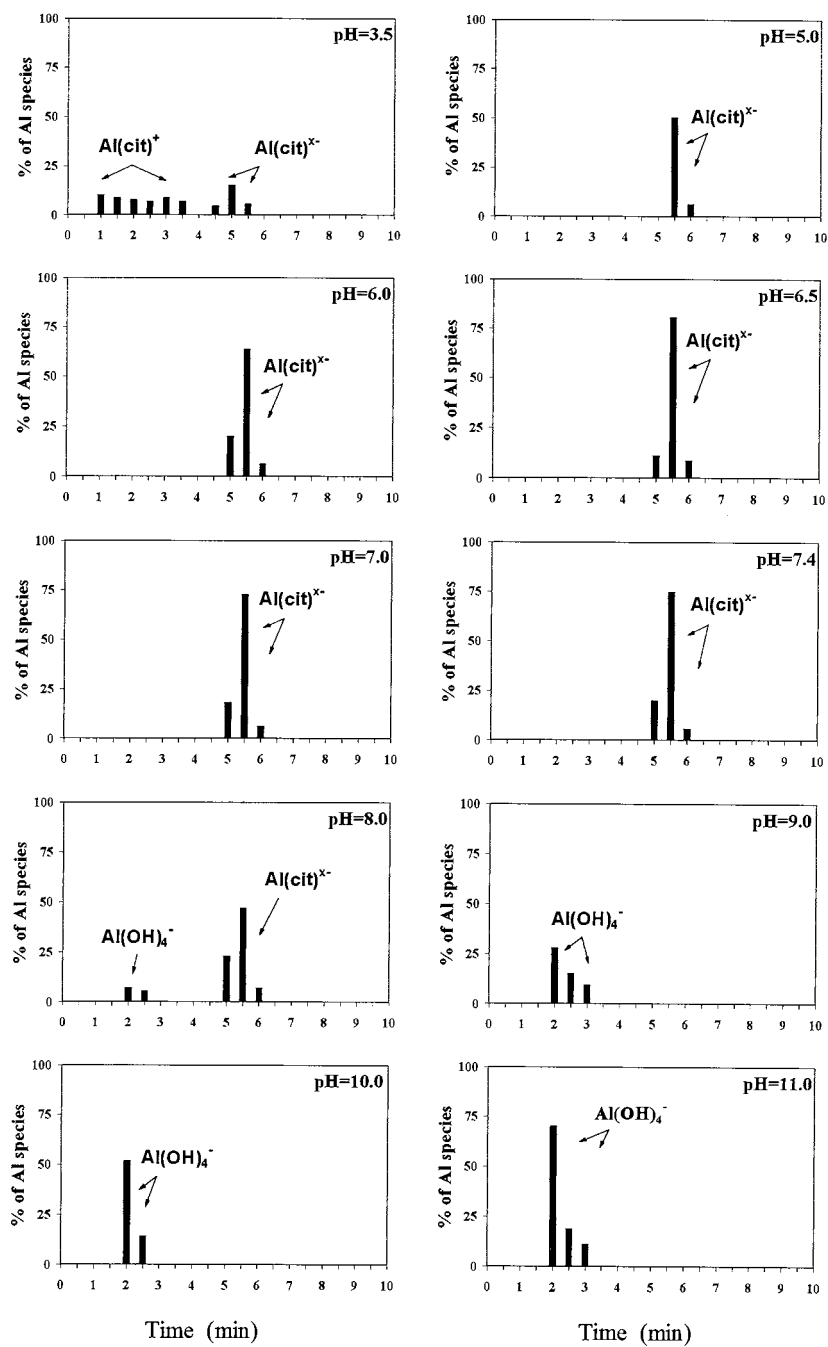


Fig. 2. Influence of pH on the distribution of Al species ($2.5 \mu\text{g Al cm}^{-3}$, 3 M excess of citric acid) employing anion-exchange FPLC with ICP-AES detection (fraction collection 0.5 cm^3). The percentage of monomeric Al species in synthetic samples of Al-citrate. Mono Q HR 5/5 column, sample volume 0.5 cm^3 , aqueous- NaNO_3 (4 mol dm^{-3}) linear gradient elution, flow rate $1 \text{ cm}^3 \text{ min}^{-1}$, $n = 3$.

With increasing pH values, above 7.4 the percentage of negatively charged Al–citrate decreases since the predominant species becomes $\text{Al}(\text{OH})_4^-$. Although $\text{Al}(\text{OH})_4^-$ species separates from negatively charged Al–citrate at the retention time of 2.0 min, its 100% recovery is only achieved at a pH of 11.0. This indicates that with increasing pH Al–citrate complexes are transformed to $\text{Al}(\text{OH})_4^-$ species. In the pH range of 8.0–10.0 the elution of Al is not quantitative due to the presence of an intermediate the hydroxo–citrate species which are strongly adsorbed on the column resin. An additional experiment was initiated by applying 8 mol dm^{-3} NaNO_3 in gradient elution, but the recoveries for $\text{Al}(\text{OH})_4^-$ were not higher. Species which were adsorbed on the column resin at pH values higher than 7.4 did not influence the following separations. These species were removed only when the column was washed with NaOH (2 mol dm^{-3}). The distribution of Al species (Fig. 2) versus pH in the presence of a 3 M excess of citric acid, in general agreed with the calculated data reported by Martin [26,27] Venturini and Berthon [28], although their calculations, based on thermodynamic equilibrium constants, were performed for different Al concentrations and, Al to citrate molar ratios.

3.4. Behaviour of $\text{Al}(\text{NO}_3)_3$ on a mono Q HR 5/5 FPLC column

Synthetic solutions of $\text{Al}(\text{NO}_3)_3$ ($2.5 \mu\text{g Al cm}^{-3}$) were prepared in buffers adjusted to pH values of 3.5, 7.0, 9.0 and 11.0. In aqueous solutions at a pH 3.5 positively charged Al^{3+} prevails, while at alkaline pH values the prevailing species is $\text{Al}(\text{OH})_4^-$ [26,18]. It could be assumed that positively charged Al^{3+} species would elute on an anion-exchange column with the solvent front, while negatively charged $\text{Al}(\text{OH})_4^-$ species should be separated on the column resin. Our experiments indicated that free Al^{3+} at a pH of 3.5 and other complexes (mixed hydroxo species) at pH of 7.0 were strongly adsorbed on the column resin. These adsorbed species did not influence the following separations and were removed only by washing with NaOH (2 mol

dm^{-3}). At pH 9.0 and 11.0 the fraction of $\text{Al}(\text{OH})_4^-$ increased and identical $\text{Al}(\text{OH})_4^-$ behaviour was observed on the column resin as in Fig. 2, where Al–citrate was prepared from $\text{Al}(\text{NO}_3)_3$ in the presence of a 3 M excess of citric acid. From these observations and from the observations in Fig. 2 it can be inferred that positively charged aqua–Al species and negatively charged $\text{Al}(\text{OH})_4^-$ do not influence the separation of negatively charged Al–citrate complexes.

3.5. Separation of Al–EDTA and Al–oxalate on a Mono Q HR 5/5 FPLC column

In order to investigate the possibility of determining other negatively charged Al complexes, Al–EDTA and Al–oxalate were prepared at pH 7.2 and injected separately onto the column. At this pH Al–EDTA exists as a negatively charged complex [34], while Al–oxalate exists partially as a negatively charged complex. This complex is in equilibrium with an intermediate, hydroxo–oxalate Al species since at higher pH the predominant species is $\text{Al}(\text{OH})_4^-$ [35]. Typical chromatograms of these separations in comparison with Al–citrate are presented in Fig. 3.

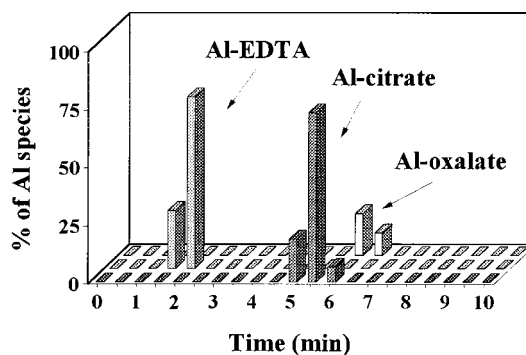


Fig. 3. Typical chromatograms of Al–EDTA, Al–citrate and Al–oxalate ($2.5 \mu\text{g Al cm}^{-3}$, 3 M excess of ligand) at pH 7.2, separated on an anion-exchange FPLC Mono Q HR 5/5 column with ICP-AES detection. Sample volume 0.5 cm^3 , aqueous- NaNO_3 (4 mol dm^{-3}) linear gradient elution, flow rate $1 \text{ cm}^3 \text{ min}^{-1}$, fraction collection 0.5 cm^3 , $n = 3$.

It can be seen that Al–EDTA is quantitatively eluted at a retention time of 2.0 min and therefore completely separated from Al–citrate. Although the retention time of Al–oxalate is 6.0 min and is close to Al–citrate (5.5 min), the peaks are still separate. The recovery of Al–oxalate at this pH is only about 30%. At this pH hydroxo–oxalate Al are the prevailing species in the presence of oxalate [35], and knowing that at pH 7.2 hydroxo–Al species are strongly adsorbed on the column resin, these observations agree with theoretical predictions [35].

3.6. Applicability of the developed FPLC—ICP-AES procedure to real samples

The developed procedure for quantitative determination of Al–citrate in the physiological pH range and the ability to understand the behaviour of other Al complexes on the column resin provides a promising basis for speciation of Al in biological samples. On the basis of the developed speciation procedure the project will start on the study of Al species uptake in plants. Plants will be grown in hydroponics nutrient solutions. Before the experiment they will be transferred to solutions of various pH, containing different concentrations of various Al species. The accumulation of Al in plant xylem and leaves will be followed using various time spans and total Al and Al species determined.

The developed speciation procedure also provides a good facility for Al bioavailability investigations in the gastrointestinal tract. The experiments will be carried out on rats, fed with high concentrations of Al–citrate. The fluid from different compartments of the gastrointestinal tract will be analysed for total Al content and particular Al–citrate species will be examined in order to understand the transport mechanisms of Al from gastrointestinal fluid to body fluids and tissues.

Before applying the developed speciation procedure to biological systems, additional steps must be investigated prior to analysis of Al–citrate, pertaining to sample preparation and the design of the experiments.

4. Conclusions

A technique was developed for speciation of Al–citrate and other negatively charged Al complexes—by separation on a Mono Q HR 5/5 strong anion-exchange FPLC column with ICP-AES detection. Linear aqueous- NaNO_3 (4 mol dm^{-3}) gradient elution enabled quantitative and reproducible determinations of Al–citrate in synthetic solutions at a retention time of 5.5 min. In a neutral pH range the recovery of Al–citrate is 100%, since it is eluted as a negatively charged species. Al^{3+} and neutral Al–citrate species do not interfere with determinations of negatively charged Al–citrate, since they are strongly adsorbed on the column resin. $\text{Al}(\text{OH})_4^-$ species are separated from Al–citrate but quantitatively determined only at a pH of 11.0. The distribution of Al species in the presence of the 3 M excess of citric acid is closely matched with theoretical calculations on the basis of thermodynamic equilibrium constants over a pH range from 3.5 to 11.0.

The completeness and the reproducibility of the developed procedure are its main advantages in comparison with other previously reported analytical procedures.

In a neutral pH range Al–EDTA is quantitatively determined as a negatively charged complex and completely separate from Al–citrate, while Al–oxalate elutes close to the retention time of Al–citrate. The recovery of negatively charged Al–oxalate species (30%) at neutral pH agrees with theoretical predictions.

The developed analytical procedure for quantitative determination of Al–citrate in the physiological pH range provides a promising basis for speciation of Al in biological samples. It will be applied to the complex interdisciplinary studies of Al species uptake in plants and in the investigation of Al bioavailability in the gastrointestinal tract—as a reliable analytical tool for the interpretation of experimental data.

Acknowledgements

The authors would like to thank the Ministry of Science and Technology of Slovenia for financial support.

References

- [1] B.R. James, C.J. Clark, S.J. Riha, *Soil Sci. Soc. Am. J.* 47 (1983) 893.
- [2] J. Luster, A. Yang, G. Sposito, *Soil Sci. Soc. Am. J.* 57 (1993) 976.
- [3] N. Clarke, L.G. Danielsson, A. Sparén, *Int. J. Environ. Anal. Chem.* 48 (1992) 77.
- [4] G.M. Morrison, *Analyst* 115 (1990) 1371.
- [5] M. Achilli, G. Ciceri, R. Ferraroli, G. Culivicchi, S. Pieri, *Water, Air, Soil Pollut.* 57–58 (1991) 139.
- [6] C.T. Driscoll, *Int. J. Environ. Anal. Chem.* 16 (1984) 267.
- [7] B.D. LaZerte, C. Chun, D. Evans, *Environ. Sci. Technol.* 22 (1988) 1106.
- [8] P.G.C. Campbell, R. Bougie, A. Tessier, J.P. Villeneuve, *Verh.- Int. Ver. Limnol.* 22 (1984) 371.
- [9] J.R. Miller, J.B. Andelman, *Water Res.* 21 (1987) 999.
- [10] E. Courtijn, C. Vandecasteele, R. Dams, *Sci. Total Environ.* 90 (1990) 191.
- [11] N. Kožuh, R. Milačič, B. Gorenc, *Ann. Chim.* 86 (1996) 99.
- [12] N. Kožuh, R. Milačič, B. Gorenc, O. Abollino, C. Sarzanini, *Int. J. Environ. Anal. Chem.*, in press.
- [13] P.M. Bertsch, M.A. Anderson, *Anal. Chem.* 61 (1989) 535.
- [14] I.R. Willett, *Soil. Sci. Soc. Am. J.* 53 (1989) 1385.
- [15] J.A.E. Gibson, I.R. Willett, *Commun. Soil. Sci. Plant Anal.* 22 (1991) 1303.
- [16] P. Jones, B. Paull, *Anal. Proc.* 29 (1992) 402.
- [17] S.H. Sutheimer, S.E. Cabaniss, *Anal. Chem.* 67 (1995) 2342.
- [18] B. Mitrovič, R. Milačič, B. Pihlar, *Analyst* 121 (1996) 627.
- [19] N. Wu, W.J. Horvath, P. Sun, C.W. Huie, *J. Chromatogr.* 635 (1993) 307.
- [20] J. Pérez Parajón, E. Blanco González, J.B. Cannata, A. Sanz Medel, *Trace Elem. Med.* 6 (1989) 41.
- [21] K. Wróbel, E.B. Gonzáles, K. Wróbel, A. Sanz-Medel, *Analyst* 120 (1995) 809.
- [22] P.C. D'Haese, G.F. Van Landeghem, L.V. Lamberts, M.E. De Broe, *Mikrochim. Acta* 120 (1995) 83.
- [23] F.Y. Leung, A.E. Niblock, C. Braadley, A.R. Henderson, *Sci. Total Environ.* 71 (1988) 49.
- [24] A.K. Datta, P.J. Wedlund, R.A. Yokel, *J. Trace Elem. Electrolytes Health Dis.* 4 (1990) 107.
- [25] J.E. Gregor, H. Kipton, J. Powell, *Aust. J. Chem.* 39 (1986) 1851.
- [26] R.B. Martin, *Clin. Chem.* 32 (10) (1986) 1797.
- [27] R.B. Martin, *J. Inorg. Biochem.* 28 (1986) 181.
- [28] M. Venturini, G. Berthon, *J. Inorg. Biochem.* 37 (1989) 69.
- [29] G. Sposito, *The Environmental Chemistry of Aluminium*, CRC Press, Boca Raton, Florida, 1989, pp. 125,126.
- [30] B. Quartley, G. Esselmont, A. Taylor, M. Dobrota, *Food Chem. Toxicol.* 31 (1993) 543.
- [31] W.R. Harris, G. Berthon, J.P. Day, C. Exley, T.P. Flaten, W.F. Forbes, T. Kiss, C. Orvig, P.F. Zatta, *J. Toxicol. Environ. Health* 48 (1996) 543.
- [32] A.C. Alfrey, J.D. Birchall, J. Savory, R.A. Yokel, *J. Toxicol. Environ. Health* 48 (1996) 527.
- [33] E.E. Cary, W.H. Allaway, O.E. Olson, *J. Agric. Food Chem.* 23 (1975) 23.
- [34] R.B. Martin, *Bioinorganic chemistry of aluminium*, in: S. Sigel, A. Sigel (Eds.), *Metal Ions in Biological Systems. Aluminium and its Role in Biology*, vol. 24, Marcel Dekker, New York, 1988, pp. 20–31.
- [35] C.T. Driscoll, W.D. Schecher, *Aluminium in the environment*, in: S. Sigel, A. Sigel (Eds.), *Metal Ions in Biological Systems. Aluminium and its Role in Biology*, vol. 24, Marcel Dekker, New York, 1988, pp. 65–69.

Book reviews

Trends in Analytical Chemistry, Reference Edition, volume 14, 1995. Edited by Y. Goshi, J.F.K. Huber and A. Townshend, Elsevier, Amsterdam, 1995. ix + 534 pp. Dfl. 889.00. ISBN 0-444-82388-3.

Most scientists with an interest in analytical chemistry will know this series to be of immense value, both as a teaching aid and as a means of keeping-up-to-date on new developments and applications. The book is in fact a compilation of articles reprinted from regular monthly editions of TrAC, but excludes meeting reports, book reviews and news items. For those who subscribe to the journal this volume is available 'free of charge'. The cost of journal subscription is a good buy being only a little more than the Dfl. 889 for the compilation volume.

This edition has 10 sections (one for each edition) which are sub-divided into 'trends', regional trends, computer corner, internet column and features. There are some fascinating reads in this volume and the editors have done a splendid job in making sure that the articles are readable, relevant and authoritative. The regional trends articles are a recent and welcome development and concentrate (in this volume) on methodology that is useful to third world nations. There are four such articles in this volume which focus on the measurement of environmental pollutants in Malaysia, Bangladesh, Vietnam and the Philippines.

The 'trends' articles concentrate on new developments and applications and include articles on such diverse topics as mobile mass spectrometers, membrane introduction mass spectrometry, optical biosensors, capillary electrophoresis, supercritical fluid extraction, enzyme-based amperometric

biosensors, biosensors for environmental monitoring, laboratory robotics, etc.

In short, this is a superb publication and is a valuable resource for anyone with an interest in analytical chemistry.

B.A. McGraw

PII S0039-9140(97)00267-1

Capillary Electrophoresis Procedures Manual edited by E. Jackson and L.W. Jackim, Elsevier, Amsterdam, 1996. 295 pp. Loose-leaf binder. US\$ 187.50. ISBN 0-444-82535-5. Distributed in the Americas by Applied Science Communications, Peace Dale, RI, USA.

This well designed, well researched, easy to read, loose-leaf manual represents a fund of practical information for the CE or would be CE experimenter. There is no doubt that reference to this manual could obviate the necessity for that time-consuming search for appropriate literature method for your particular analytical problem.

The three pages of 'quick tips' given at the beginning offer both an excellent check-list and comment on commonly encountered practical problems. This is followed by 266 pages of one page abstracts. The abstracts (taken from mainly recent literature and manufacturers' archives) cover in a concise, consistent way the procedural and equipment requirements of a very wide range of CE applications involving a large number of different classes of compound. Most importantly, as an essential guide to the expected results, each abstract includes a reprint of the expected electropherogram. In general, the quality of these reprints is good but a few are too faint or too blurred to be easily readable.

Book reviews

Trends in Analytical Chemistry, Reference Edition, volume 14, 1995. Edited by Y. Goshi, J.F.K. Huber and A. Townshend, Elsevier, Amsterdam, 1995. ix + 534 pp. Dfl. 889.00. ISBN 0-444-82388-3.

Most scientists with an interest in analytical chemistry will know this series to be of immense value, both as a teaching aid and as a means of keeping-up-to-date on new developments and applications. The book is in fact a compilation of articles reprinted from regular monthly editions of TrAC, but excludes meeting reports, book reviews and news items. For those who subscribe to the journal this volume is available 'free of charge'. The cost of journal subscription is a good buy being only a little more than the Dfl. 889 for the compilation volume.

This edition has 10 sections (one for each edition) which are sub-divided into 'trends', regional trends, computer corner, internet column and features. There are some fascinating reads in this volume and the editors have done a splendid job in making sure that the articles are readable, relevant and authoritative. The regional trends articles are a recent and welcome development and concentrate (in this volume) on methodology that is useful to third world nations. There are four such articles in this volume which focus on the measurement of environmental pollutants in Malaysia, Bangladesh, Vietnam and the Philippines.

The 'trends' articles concentrate on new developments and applications and include articles on such diverse topics as mobile mass spectrometers, membrane introduction mass spectrometry, optical biosensors, capillary electrophoresis, supercritical fluid extraction, enzyme-based amperometric

biosensors, biosensors for environmental monitoring, laboratory robotics, etc.

In short, this is a superb publication and is a valuable resource for anyone with an interest in analytical chemistry.

B.A. McGraw

PII S0039-9140(97)00267-1

Capillary Electrophoresis Procedures Manual edited by E. Jackson and L.W. Jackim, Elsevier, Amsterdam, 1996. 295 pp. Loose-leaf binder. US\$ 187.50. ISBN 0-444-82535-5. Distributed in the Americas by Applied Science Communications, Peace Dale, RI, USA.

This well designed, well researched, easy to read, loose-leaf manual represents a fund of practical information for the CE or would be CE experimenter. There is no doubt that reference to this manual could obviate the necessity for that time-consuming search for appropriate literature method for your particular analytical problem.

The three pages of 'quick tips' given at the beginning offer both an excellent check-list and comment on commonly encountered practical problems. This is followed by 266 pages of one page abstracts. The abstracts (taken from mainly recent literature and manufacturers' archives) cover in a concise, consistent way the procedural and equipment requirements of a very wide range of CE applications involving a large number of different classes of compound. Most importantly, as an essential guide to the expected results, each abstract includes a reprint of the expected electropherogram. In general, the quality of these reprints is good but a few are too faint or too blurred to be easily readable.

The section containing information on equipment and materials is very USA orientated. This section also contains, for reference, a decent selection of recent (1992–95) books—this would have been better in a separate literature section.

The manual has a comprehensive index—about 1000 compounds are included. From it the reader can look up the compound of interest then the relevant abstract(s). The authors are to be commended for the amount of effort which has gone into the production of this unique practically orientated CE manual. It is a value for money text which I would have no hesitation in recommending to any CE user.

R.R. Moody

PII S0039-9140(97)00266-X

Capillary Electrophoretic Separations of Drugs edited by A.S. Cohen, S. Terabe and Z. Deyl, Elsevier, Amsterdam, 1996. ix + 450 pp., NLG 450.00, US\$ 281.25. ISBN 0-444-82519-3.

This book represents a collection of review articles (nine) and original research papers (21) reprinted from *Journal of Chromatography A*, volume 735.

The reviews (208 pages) and the research papers (240 pages) bring together many, if not all, of the leading experts in this field from a large number of countries.

The seven reviews represent well-referenced overviews of the important aspects of the development, theory, methodology and applications of CE techniques to, for example, drug assays, analysis of drugs in body fluids, chiral drug separations and the separation of macromolecules. All are consistent in format and of high standard of presentation. The figures are clear, illustrative and free from error. The many comparative tables are informative and well referenced. The extensive reference lists (complete up to 1995) given at the end of each review ensures that the reader can readily gain access to further appropriate reading material.

A range of good quality research papers is given in the research paper section. Advances in techniques, optimization and comparison with chromatography (seven papers), chiral separations

(eight papers) and the analysis of macromolecular drugs (three papers) amply illustrate the main areas of current activity. The last group of six miscellaneous papers collectively serve to illustrate the potential that CE techniques have to solve difficult analytical problems, e.g. the screening for drugs of abuse in biological fluids.

A handy author index to the articles and papers is included at the end of the book. For those with limited library facilities this hard backed edition represents a quality reference source to CE separations of drugs well worth having.

R.R. Moody

PII S0039-9140(97)00265-8

Practical HPLC Method Development, 2nd edition by L.R. Snyder, J.J. Kirkland and J.L. Glajch, Wiley, Chichester, 1997, xxvi + 765 pp. £70.00. ISBN 0-471-00703-X.

This book aims to provide a comprehensive treatment of all aspects of HPLC method development. To accomplish this, its size and scope has been increased considerably since the first edition. The original chapters covering aspects of separation theory, column characteristics, systematic method development, difficult separations, gradient elution, special samples, and computer-assisted method development have essentially been retained and brought up to date to include the large body of literature on HPLC which has appeared in the last 10 years. New chapters are included on detection, sample preparation, biochemical samples, chiral separations, preparative HPLC, quantification, an validation.

The material is mostly dealt with in commendable detail, or the reader is pointed elsewhere by way of extensive lists of references that appear at the end of each chapter. Notes on how to use the book most effectively are given in a helpful preface. This guide is certainly necessary and the authors acknowledge the challenge presented to the reader looking for information relevant to a particular separation or problem. One feels that some of these difficulties could have been avoided if the framework imposed on the book from the first edition had been rejected for a more logical and concise format. This would minimise repeti-

The section containing information on equipment and materials is very USA orientated. This section also contains, for reference, a decent selection of recent (1992–95) books—this would have been better in a separate literature section.

The manual has a comprehensive index—about 1000 compounds are included. From it the reader can look up the compound of interest then the relevant abstract(s). The authors are to be commended for the amount of effort which has gone into the production of this unique practically orientated CE manual. It is a value for money text which I would have no hesitation in recommending to any CE user.

R.R. Moody

PII S0039-9140(97)00266-X

Capillary Electrophoretic Separations of Drugs edited by A.S. Cohen, S. Terabe and Z. Deyl, Elsevier, Amsterdam, 1996. ix + 450 pp., NLG 450.00, US\$ 281.25. ISBN 0-444-82519-3.

This book represents a collection of review articles (nine) and original research papers (21) reprinted from *Journal of Chromatography A*, volume 735.

The reviews (208 pages) and the research papers (240 pages) bring together many, if not all, of the leading experts in this field from a large number of countries.

The seven reviews represent well-referenced overviews of the important aspects of the development, theory, methodology and applications of CE techniques to, for example, drug assays, analysis of drugs in body fluids, chiral drug separations and the separation of macromolecules. All are consistent in format and of high standard of presentation. The figures are clear, illustrative and free from error. The many comparative tables are informative and well referenced. The extensive reference lists (complete up to 1995) given at the end of each review ensures that the reader can readily gain access to further appropriate reading material.

A range of good quality research papers is given in the research paper section. Advances in techniques, optimization and comparison with chromatography (seven papers), chiral separations

(eight papers) and the analysis of macromolecular drugs (three papers) amply illustrate the main areas of current activity. The last group of six miscellaneous papers collectively serve to illustrate the potential that CE techniques have to solve difficult analytical problems, e.g. the screening for drugs of abuse in biological fluids.

A handy author index to the articles and papers is included at the end of the book. For those with limited library facilities this hard backed edition represents a quality reference source to CE separations of drugs well worth having.

R.R. Moody

PII S0039-9140(97)00265-8

Practical HPLC Method Development, 2nd edition by L.R. Snyder, J.J. Kirkland and J.L. Glajch, Wiley, Chichester, 1997, xxvi + 765 pp. £70.00. ISBN 0-471-00703-X.

This book aims to provide a comprehensive treatment of all aspects of HPLC method development. To accomplish this, its size and scope has been increased considerably since the first edition. The original chapters covering aspects of separation theory, column characteristics, systematic method development, difficult separations, gradient elution, special samples, and computer-assisted method development have essentially been retained and brought up to date to include the large body of literature on HPLC which has appeared in the last 10 years. New chapters are included on detection, sample preparation, biochemical samples, chiral separations, preparative HPLC, quantification, an validation.

The material is mostly dealt with in commendable detail, or the reader is pointed elsewhere by way of extensive lists of references that appear at the end of each chapter. Notes on how to use the book most effectively are given in a helpful preface. This guide is certainly necessary and the authors acknowledge the challenge presented to the reader looking for information relevant to a particular separation or problem. One feels that some of these difficulties could have been avoided if the framework imposed on the book from the first edition had been rejected for a more logical and concise format. This would minimise repeti-

The section containing information on equipment and materials is very USA orientated. This section also contains, for reference, a decent selection of recent (1992–95) books—this would have been better in a separate literature section.

The manual has a comprehensive index—about 1000 compounds are included. From it the reader can look up the compound of interest then the relevant abstract(s). The authors are to be commended for the amount of effort which has gone into the production of this unique practically orientated CE manual. It is a value for money text which I would have no hesitation in recommending to any CE user.

R.R. Moody

PII S0039-9140(97)00266-X

Capillary Electrophoretic Separations of Drugs edited by A.S. Cohen, S. Terabe and Z. Deyl, Elsevier, Amsterdam, 1996. ix + 450 pp., NLG 450.00, US\$ 281.25. ISBN 0-444-82519-3.

This book represents a collection of review articles (nine) and original research papers (21) reprinted from *Journal of Chromatography A*, volume 735.

The reviews (208 pages) and the research papers (240 pages) bring together many, if not all, of the leading experts in this field from a large number of countries.

The seven reviews represent well-referenced overviews of the important aspects of the development, theory, methodology and applications of CE techniques to, for example, drug assays, analysis of drugs in body fluids, chiral drug separations and the separation of macromolecules. All are consistent in format and of high standard of presentation. The figures are clear, illustrative and free from error. The many comparative tables are informative and well referenced. The extensive reference lists (complete up to 1995) given at the end of each review ensures that the reader can readily gain access to further appropriate reading material.

A range of good quality research papers is given in the research paper section. Advances in techniques, optimization and comparison with chromatography (seven papers), chiral separations

(eight papers) and the analysis of macromolecular drugs (three papers) amply illustrate the main areas of current activity. The last group of six miscellaneous papers collectively serve to illustrate the potential that CE techniques have to solve difficult analytical problems, e.g. the screening for drugs of abuse in biological fluids.

A handy author index to the articles and papers is included at the end of the book. For those with limited library facilities this hard backed edition represents a quality reference source to CE separations of drugs well worth having.

R.R. Moody

PII S0039-9140(97)00265-8

Practical HPLC Method Development, 2nd edition by L.R. Snyder, J.J. Kirkland and J.L. Glajch, Wiley, Chichester, 1997, xxvi + 765 pp. £70.00. ISBN 0-471-00703-X.

This book aims to provide a comprehensive treatment of all aspects of HPLC method development. To accomplish this, its size and scope has been increased considerably since the first edition. The original chapters covering aspects of separation theory, column characteristics, systematic method development, difficult separations, gradient elution, special samples, and computer-assisted method development have essentially been retained and brought up to date to include the large body of literature on HPLC which has appeared in the last 10 years. New chapters are included on detection, sample preparation, biochemical samples, chiral separations, preparative HPLC, quantification, an validation.

The material is mostly dealt with in commendable detail, or the reader is pointed elsewhere by way of extensive lists of references that appear at the end of each chapter. Notes on how to use the book most effectively are given in a helpful preface. This guide is certainly necessary and the authors acknowledge the challenge presented to the reader looking for information relevant to a particular separation or problem. One feels that some of these difficulties could have been avoided if the framework imposed on the book from the first edition had been rejected for a more logical and concise format. This would minimise repeti-

tion and reduce the need to cross-reference other parts of the book.

The 'enlightened trial-and-error' approach to method optimisation described in the first edition is restated in updated form. It can be recommended as being applicable to a range of sample types without the need for detailed theoretical knowledge of the starting material. The guidelines are illustrated throughout with examples from the literature, although much use is also made of computer-generated simulations. The authors provide a wealth of useful technical information that is often presented in tables alongside the text. It would have been better to collect much of this together in the appendices for easier reference.

As is to be expected from such distinguished HPLC experts, this work is authoritative, contains few errors and is generally well written. Having said that, the authors make a common mistake among analysts by their repeated use of 'quantitation' instead of 'quantification'. This becomes irritating in Chapter 14, a particularly bad example being the expression 'minimum quantifiable amount' (p. 645) which should of course be 'minimum quantifiable amount'. Elsewhere in this

chapter (p. 675) it states that one litre or more of an aqueous sample can be injected into an analytical reversed-phase column to obtain vastly increased sensitivity for trace analysis. Such a procedure can hardly be recommended as being practicable. Chapter 10, on computer-assisted method development, promotes the authors' method-development software, DryLab (LC Resources), and no attempt has been made to research currently available alternatives, for example HPLC Optimization (Alltech) and the Hipac range of software (Phase Separations). The information given on Enhancer, a package previously supplied by ATI Unicam, Cambridge, UK, but withdrawn at least 5 years ago, is long since out of data.

This is undoubtedly valuable work in an already well published field, but one cannot help feeling that an opportunity has been missed to produce a definitive reference source for chromatographers.

D.A. Stead

PII S 0039-9140(97)00268-3

Metallothioneins: historical review and state of knowledge

M. Nordberg *

Institute of Environmental Medicine, Karolinska Institutet, S-171 77 Stockholm, Sweden

Received 21 November 1996; received in revised form 3 March 1997; accepted 4 March 1997

Abstract

The history of metallothionein (MT) research is reviewed. Various methods for isolation, characterisation and quantification are evaluated. The role of MT in metal metabolism and toxicity is explained. Gender differences and polymorphisms are brought to the attention of the reader and the possible relationship with disease is discussed. The review is an evaluation based on data from literature and from own original experimental data. Future aspects on research within the MT field is stressed. © 1998 Elsevier Science B.V. All rights reserved.

Keywords: Metallothionein; Protein; Quantification; Metals; Metabolism; Polymorphism; Gender; Disease

1. Introduction

Scientific research history of metallothionein begins in the 1950s almost 40 years ago. This review of metallothionein (MT) research displays the progress in knowledge as well as a review of biochemical and experimental methods used in such research during the last four decades. Development of MT research include contributions from scientists in the fields of biochemistry, environmental hygiene/medicine, medicine, toxicology, pathology and nutrition and is best illustrated by the number of articles that have been published. A search on medline with 'metallothionein' as the entry revealed that for the interval 1966–1975 there were 34 articles, for 1976–1979: 156 articles, 1980–1985: 691 articles, 1986–1991: 1499 articles and for 1992–April

1996, 1100 articles had been published (Fig. 1).

This means that to date approximately 4000 articles have contributed to the available information about MT. There has been a considerable development of methods in protein research, including isolation and analytical methods for iden-

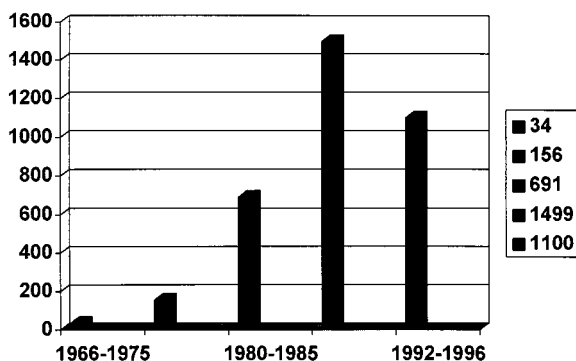


Fig. 1. Search on medline.

* Fax: +46 8 314124; e-mail: monica.nordberg@imm.ki.se

Table 1
History of metallothionein

1960, 1961	Metallothionein	Kägi and Vallee [1,2]
1964	Induction by cadmium	Piscator [3]
1971	Modification of Cd-toxicity	Nordberg et al. [4]
1972	Amino acid composition	Nordberg et al. [5]
1976	Sequence	Kojima et al. [6]
1979	1st international meeting	Kägi and Nordberg [7]
1979	Consensus nomenclature Radioimmunoassay	Vander Mallie and Garvey [8] Goyer et al. [9]
1983	International meeting Metallothionein and nephrotoxicity	
1985	2nd International meeting on metallothionein	Kägi [10]
1992	3rd International meeting on metallothionein	Suzuki et al. [11]
1996	Meeting Geel	

tification during this time. Interest in MT was in the beginning focused mainly on two topics. The main interests were the strict protein chemistry and the toxicological, i.e. the metabolic pathways for metal toxicology particularly with regard to cadmium kinetics. Later on other interests and aspects on MT have expanded the field. In recent years important contributions have been brought in from molecular biology. Consensus and conclusions reached at several scientific meetings on metallothionein based on published data have been published as depicted in Table 1.

2. History of metallothionein

In 1957 data on a cadmium binding protein in equine tissue was published [12]. However this study was initiated by a report in the form of an abstract [13] dealing with cadmium in human organs. Small amounts of cadmium had been shown to be present in tissues and body fluids in several animal species. Hypotheses were postulated to explain this unexpected finding. Either cadmium could be present as bound to a macromolecule and therefore have a natural function in

biological system or cadmium could also be just a contaminant. In 1960 the first report on metallothionein was published [1,2]. This was the first time that the cadmium containing protein, isolated from equine renal tissue, was named 'metalothionein' based on an extremely high content of sulphur of 4.1% g^{-1} dry weight and 2.9% of Cd and 0.6% Zn. Isolation was performed from five frozen horse kidneys with for that time conventional methods. Later studies reported data on physical properties, molecular weight was estimated to be 10000 ± 260 . Specific absorption at 250 nm was explained by cadmium mercaptide bonds. Metallothionein was assumed to lack aromatic amino acids as indicated by absence of absorption at 280 nm. This was later verified by aminoacid analyses [5,14]. The high concentration of sulphur of 8.5% is explained by aminoacid analyses that revealed high content of cysteine. At this time reactive protein mercapto groups were determined by titration with silver ions, CMB and *N*-ethylmaleimide. Aminoacids were determined by two dimensional paper chromatography and ion exchange chromatography. Cysteine residues were determined as cysteic acid after oxidation of metallothionein with performic acid and as derivatives of *N*-ethylmaleimide. Sedimentation constant was determined via Schlierendiagram by use of sedimentation by ultracentrifugation to 1.75 ($S_{0,20w}$). Diffusion constant, partial specific volume and friction ratio was reported. The estimated molecular weight of the protein was still varying from 9790–10500. This was partly explained by various artefacts during preparation. Metal analyses for cadmium and zinc reported 5.2 g atoms mol^{-1} and 5.9% of MT weight for cadmium and for zinc 3.3 g atoms mol^{-1} and 2.2% by weight. Some exchange between zinc and cadmium was obviously taking place. It was suggested that bonding with three SH-groups together with one atom of either cadmium or zinc was formed.

As part of the research on health effects caused by cadmium in the Swedish group a study on rabbits [3] showed that cadmium–metalothionein could be induced by repeated injections of small doses of cadmium. A single high dose of cadmium [4] was found to be more toxic to the organism giving rise to lethality and liver damage, while the

same dose administered as several small doses during a prolonged exposure time gave no similar effects. As a matter of fact, animals with induced metallothionein synthesis by pretreatment with smaller doses of cadmium, developed resistance to the acute toxicity to the liver [4] and the testes [15]. Isolation of cadmium binding protein from the livers of cadmium exposed rabbits showed an increase of MT in relation to administered dose or amount of cadmium [5]. It was demonstrated that in animals protected by pretreatment, cadmium in the target tissues liver and testis, respectively was bound to a low molecular weight protein similar to MT.

New techniques for isolation of the protein was used. After homogenization of the tissues rivanol was used to precipitate high molecular weight proteins and cell fragments. Several steps of precipitation, dialyses and various gel chromatography steps were used. Sephadex gel had recently been introduced into protein chemistry. The first assumptions by Piscator in 1964 [3] were later confirmed in these animal experiments which demonstrated that exposure to cadmium increased concentration of MT in livers. These findings gave further support to the initial ideas of metallothionein induction as a mechanism of making tissue cadmium less toxic. For this group working with toxicity and kinetics of cadmium, it was known that cadmium gave raise to adverse health effects increasing upon exposure particular renal damage. MT research now continued or developed into two tracks—one in protein chemistry and the other one concerning its importance for kinetics and toxicity of cadmium. All studies demanded however pure and well characterized MT and this was prepared with modern techniques. Tissue was homogenized in buffer system mostly Tris–HCl buffer in sodium chloride with a pH of 8.1. This step is followed by ultracentrifugation at 105 000 g and the supernatant is taken for gelchromatography-Sephadex gel G-75. If the absorption ratio of 250 and 280 was low, improvement could be achieved in one step by G-50 for the preparative purpose that showed a protein with high absorption of 280 but no metal content was eluted from e.g mouse livers at the same fractions as MT [16]. For further separation into isoforms, frac-

tions containing MT are either taken for isoelectric focusing or ion exchange chromatography after concentration and desalting by ultrafiltration on UM-2 filters with cut off level for molecular weight of 1000 [5]. Further separation by isoelectric focusing revealed at least three isoforms in rabbit liver with pI 3.9, 4.5 and 6.0. Two of these were identified by aminoacid analyses [5]. In order to be successful with the preparation of MT from tissue it was obvious quite early on that avoidance of oxidation of the protein by a rapid preparation and in cool conditions was crucial. Mercaptoethanol could however restore oxidized MT [17,18] as shown by gelchromatography on Sephadex G-75 where MT showed up in the ordinary place after treatment of mercaptoethanol. An important contribution to tertiary structure was made when [19] two metal clusters, i.e. α and β domains with four and three metals respectively, as part of the structure was described. The α domain constitutes the C-terminal and the β domain the N-terminal of the protein.

The other track expanded into several metals and importance of MT for many metals and in particular for copper [20] and mercury [21–23]. Several pioneer works [15] showed that MT could protect against testicular damage caused by cadmium. Knowledge on MT and its involvement in transport of cadmium and that cadmium partly is present in blood [24] as MT lead to a metabolic model for cadmium toxicity. Further work focused on speciation of cadmium and it was found that cadmium as MT is taken up in the renal tubules and causes renal damage at as low concentrations as 10 ug g^{-1} of cadmium [25].

In the 1970s and early 1980s, there was only a limited number of research groups performing research related to MT. An increasing number of publications in which different nomenclature for MT was used made it clear that an evaluation of the knowledge available at that time would be of importance. A workshop with approximately 25 invited participants who had submitted background manuscripts was arranged and a tentative report [26] was prepared and distributed in advance to each participant. A consensus report was agreed during the meeting held in 1978 [7].

During this first international meeting on MT, held in Zurich consensus was reached about, e.g. nomenclature and methods for preparing the protein. This first meeting has been followed by one more meeting in Zurich 1985 which was more open but still with a workshop consensus. In-between, a meeting was arranged in Aberdeen in 1981. Other meetings have introduced a more limited focus on various areas of interests, e.g. cadmium binding proteins in non-mammalian species was brought to attention in an international meeting [27] and pharmaceutical interests as was the case at the third international meeting held in Japan in 1992 [11].

3. Protein chemistry

Important features of MT are depicted in Table 2 which is compiled from data according to Nordberg and Kojima [26] from the first international meeting on MT and with some important additional findings [28–30].

The structure of MT has two domains consisting of one cluster with three and one with four metal atoms and was first described by Winge and Miklossy [19]. The MT gene is located on chromosomes varying with species. For humans and other primates it is on chromosome 16 [31]. The protein consists of a number of isoforms coded by various alleles. The ratio of mRNA for MT-I and MT-II genes remains constant during induction

Table 2
Characteristics of metallothionein

1.	Molecular weight 6000–7000, 61 amino acids
2.	20 Cysteine (30%), N-acetylmethionine, C-alanine, no aromatics, no histidine
3.	Unique amino acid sequence [6]
4.	Tertiary structure/metal clusters [19]
5.	Metal content; Cd, Zn, Cu, Hg; 5–10% w/w
6.	Absorption 250 nm (Cd), 225 nm (Zn), 275 nm (Cu), 300 nm (Hg)
7.	Induced synthesis by Cd, Zn
8.	No disulfide bonds
9.	Heat stability
10.	Cytoplasmic localization
11.	Isoforms
12.	Localization on chromosome [31]

by metals, e.g. Cd, Cu, and Zn. It was found that there is 1.4 times more MT-I RNA than MT-II RNA indicating that transcription rate is slightly higher for MT-I gene compared to MT-II gene [31]. MT-IA and MT-IIA genes seems to be differentially regulated by metals. Lack of MT gene expression makes the organism sensitive to toxic effects. The MT gene becomes transcriptionally inactive as a consequence of DNA-methylation. Cells with extra copies of MT-genes can be selected by exposure to toxic concentration of cadmium. In metal exposed mammals zinc is the dominating metal ion in MT. One zinc seems always to be present in MT. Various biological factors influence metal ion composition such as tissue of origin, age and stage of development. This means that renal MT is higher in Cd and Cu in exposed animals than liver MT from same organism. For purification of MT various gels have been used during the years. However, Sephadex G-75 and G-50 has been proven, in an evaluation of several gels, to at present still be the most efficient technique. However, sometimes it is necessary to add mercaptoethanol to the samples in order to reduce MT back to non polymerized MT as has been discussed previously [18].

Transgenic mice [32] have been introduced in order to gain new insights on MT and metal toxicity. Experimental laboratory animals, mainly mice, have shown that species differences with regard to sensitivity and resistance to metal toxicity exists [33]. By introduction of transgenic animals the mechanism behind this would be elucidated.

4. Methods for the quantification of MT

Several methods for measuring and quantifying MT are available [33,34] as displayed in Table 3. A review of various methods has also been edited [35]. In addition to the information in Table 3 it should be mentioned that metal binding assays based on binding of metals such as cadmium [36,37], mercury [22] and silver-pulse polarography [38], immunoassay such as radio immunoassay and ELISA based on use of antibody [39] are used. Each of these methods have advan-

Table 3
Methods for quantification of MT

After isolation	
Freeze-drying	Nordberg et al., 1972; Kägi et al., 1974 [5,40])
Calculation aminoacid analyses	Kägi, 1970; Nordberg et al., 1972 [5,14]
Biuret method	Nordberg et al., 1972 [5]
In crude tissue fractions:	
In vitro binding Hg	Piotrowski et al., 1973 [22]
In vitro binding Cd	Onosaka and Cherian, 1981 [36]
Radioimmunoassay	Vander Mallie and Garvey, 1978 [8]
ELISA	Garvey, 1984 [39]

tages and disadvantages. Methods that are dependant on the use of atomic absorption spectrophotometry and especially those dependant on Ag-binding should avoid sodium chloride in samples as this may cause interference with the analyses. The radio immunoassay needs specific antibodies that do not cross react. The immunoassay-ELISA is still under development.

4.1. Immunohistochemical

Most cadmium in the urine of humans occurs bound to MT. Urinary cadmium and MT concentrations correlate well as shown in elderly women exposed to cadmium in the general environment [41,42] and in occupationally exposed male cadmium workers [43,44], who reported values of 2–155 ng MT/g urine and for plasma 2–11 ng g⁻¹ in cadmium exposed workers. The detection limit for MT by RIA in humans is reported in plasma or serum to be 1–16 ug l⁻¹ and in urine to be 5–3000 ug g⁻¹ creatinine [41,42]. In cadmium exposed persons MT in urine is a good indicator of urine concentration of cadmium and can also be assumed to be an index of the burden of cadmium.

Immunohistochemical staining of MT in placental tissue indicated that metallothionein reflects the concentration of copper in this tissue.

The method could be used for pre-and postnatal diagnosis of Menke's disease [45].

A gender difference is observed. Women have higher MT concentration in urine compared to men even at similar cadmium levels [46] as shown with RIA [46,47]. As shown in Table 4 [39], the range of normal concentrations of MT is defined.

Levels of MT reported in various tissues are given in Table 5.

Determination of MT concentration in urine and blood have been found to be related to problems which have not been observed in tissue analyses. This is likely due to techniques for sampling and storage of samples which is most crucial for the results of analyses. Usually urine samples are treated with bactericides in order to prevent bacterial contamination with a reduced pH as result. Since metallothionein loses the metals and free thionein is obtained a change in configuration and instability of the protein follows. This is likely to influence the whole analyses and with fault of the result as has been observed in samples from humans (personal communication) that cadmium concentration in urine and MT concentration sometimes do not follow each other. In experimental studies [50] excretion of MT, cadmium, calcium, and various enzyme markers in urine were followed in male rats exposed to cadmium. MT was determined by ELISA method. Interference with luminal and basolateral membranes and handling of calcium was demonstrated [51,52]. This is in accordance with suggested model that Cd is released from CdMT after it is catabolized in lysosomes and appears in the cytoplasm of renal tubule cells where it may change the electrochemical gradient across the luminal membrane with decreased calcium absorption.

Table 4
Range of normal concentrations of MT

Method	Media	Concentration (ng ml ⁻¹)	Status
RIA	Sera	0.01–1	Normal
RIA	Sera	>2	Abnormal
RIA	Urine	1–10	Normal
RIA	Urine	>10	Abnormal

Table 5
Normal concentration of metallothionein related to method in various tissues and media

18 ug g ⁻¹	Liver	Rat	ELISA	Chan et al., 1993 [48]
30 ug g ⁻¹	Kidney	Rat	ELISA	Chan et al., 1993 [48]
35 ug g ⁻¹	Kidney cortex	Rat	ELISA	Liu et al., 1994 [49]

Detection limit ELISA 100 pg MT [48].

Thus, it is necessary to evaluate and standardize the method for urine and blood. As the body fluids are used for biological monitoring of many metals it would be most valuable to manage to measure as well metallothionein and relate concentration of metals to concentration of MT.

During the COMTOX conference in Vancouver in 1995 which was arranged by IUPAC, methods for estimation and quantification of MT were discussed. It is interesting too see that problems in MT research similar to those identified in the early phase of such research still cause confusion among scientists.

One problem with the estimation of MT in tissues and body fluids is how to manage to express true concentration and relate it to biological events. For long time this has been in the form of ug MT/g wet weight tissue. Due to the fact that the concentration of MT varies with many factors this has to be further expressed in relation to something that is stable, normal or a controlled change in the cell, e.g. MT mRNA or something else. Concentration of MT apart from being age dependent is also dependant on exposure to numerous agents [10]. Several methods for and pitfalls concerning the various methods for MT determination have been summarized recently by contributions from many scientists in MT research [35]. It is urgent to develop a method for MT quantification with high precision, accuracy and specificity. To test specificity a known amount of MT may be added to the samples. To spike the samples, several questions are raised: How should various forms of MT be quantitated? The various forms of MT might reflect various biological functions that are related to both age and to exposure as suggested previously [18]. Isoelectric focusing is a rapid, quick and good method for preparation of the various isoforms of MT. Commercially available MT has to be

checked with regard to purity even if a well recognized method has been used for preparation. It has been noticed that metal concentration in some shippings has been extremely low, indicating a lower purity of the protein.

Commercial antibodies were reported to be available for MT I, II and III. Monoclonal antibodies were believed not to be specific enough to be taken for ELISA. For in vivo measuring of MT concentration in biological samples radioimmunoassay methods with ¹⁰⁹Cd binding seems not to be useful. Dosage of ¹⁰⁹Cd is important as it has to reflect concentration of MT but cadmium might already be present.

Recently methods from molecular biology have developed the possibility to quantitate MT in eucaryotes and procaryotes that are taken for PCR. MT-gene transcription and RT-PCR to measure MT mRNA is possible. It is mentioned that to use a DNA probe for RNA-synthesis and expressed DNA is possible. MT-2 expression in lymphocytes can be performed by PCR techniques.

A question to be answered is how determination and estimation of MT in body fluids and tissues should be performed and how to relate the concentration of MT to effects? A RT-PCR method for MT-mRNA primers and oligoprobes were mentioned to be commercial available.

5. Role in metal metabolism and toxicology

MT plays an important role in the metabolism and kinetics of metals as shown in Table 6.

This has been shown for cadmium [53,54] and later for copper as summarized [55]. Cadmium is known to cause toxicity to the kidney after long-term exposure to inorganic cadmium compounds, i.e. the chemical species Cd²⁺. In animal experi-

ments it has been shown that Cd administered as MT may cause similar renal damage at tissue concentrations of Cd at 10 ug g^{-1} wet weight [25] compared to 200 ug g^{-1} wet weight when administered as Cd-ions.

In addition to the early findings of modifications of cadmium toxicity by metallothionein induction [3,4] mentioned in Section 2, data have been provided concerning the binding of Cd to MT in blood [8,18,25]. The identification of binding forms of Cd in blood-plasma and studies by autoradiography showing that Cd is distributed selectively to the kidney after administration of CdMT, while it is predominantly taken up by the liver after injection of Cd^{2+} or as Cd-albumin, provided a background for a mechanistic model for kinetics of cadmium [25,53,54]. Immediately after uptake in blood, cadmium is bound to albumin in blood plasma and distributed and taken up in the liver. It is speculated that an albumin receptor is present on the surface of liver cells. Once in the liver cadmium binds to already present MT by an exchange of zinc in the MT molecule. Cadmium induces synthesis of metallothionein and the newly synthesized MT is sequestering cadmium from other binding sites, thus protecting liver cells from toxicity. Cadmium as MT is released to the blood stream and is transported to the kidney where it is filtered through the glomerulus and is as well taken up by pinocytosis. MT is catabolized in the lysosomes of the tubules and free cadmium ions induce new synthesis of MT in the cell and cadmium is free to react with sensitive sites. Salts, calcium and low molecular weight proteins are excreted in the urine. Cadmium has a biological half-time of 10–15 years which is regarded as very long. It might be

explained by the possibility to induce synthesis of MT. This model has been further developed by contributing data from [56,57]. CdMT induced kidney damage was shown to decrease uptake and binding of calcium in membrane vesicles isolated from animals injected with CdMT [56]. Rats given combined exposure by injection of CdMT (0.25 mg kg^{-1}) Zn (12.5 mg kg^{-1}) and Cu (6.25 mg kg^{-1}) had considerably increased levels of MT in the renal cortex, i.e. up to 746 ug g^{-1} wet weight. These high concentrations of MT were considered to be of major importance explaining the protection against renal damage from Cd in these animals [49]. Repeated injections of CdMT given within a short time interval gave rise to a considerably prolonged and possibly irreversible calciuria in rats [57]. Increased excretion of magnesium has been found in rats with CdMT induced nephrotoxicity [58]. Possible contribution of endogenous intestinal metallothionein to renal accumulation of cadmium was studied in rats fed with cadmium [59]. To distinguish between exogenous and endogenous MT isoforms from the rat and pig, differences in chromatographic behaviour was used [60]. A similar pathway in the biological system was shown for copper [55].

Another important function for MT is cellular defense mechanism against free radicals where methionin might serve as a free radical scavenger as discussed in many publications, e.g. [53,55]. MT may protect DNA by sequestering copper and preventing its participation in redox reactions and may thus prevent the formation of free radicals and prohibit the reaction as further pointed out by [61].

MT regulates toxicity of various metals and trace elements. The kinetics of cadmium copper and zinc are examples of this. With regard to high-tech metals, e.g. gallium (Ga), germanium (Ge), indium (In), antimony (Sb), Tellurium (Te), Yttrium (Y), Niobium (Nb), Thallium (Tl) and Bismuth (Bi) and some more recently introduced high-tech compounds used in superconductors for instance yttrium–barium–copper–oxide (YBCO) and $\text{Bi}_2\text{Sr}_2\text{Ca}_2\text{Cu}_3\text{O}_{10}$ (BSCCO), their content of Bi and Cu may induce MT and exist as BiMT and CuMT. It can not be excluded that among exposed people MT levels might increase and evalu-

Table 6
Function of metallothionein

1.	Transport of metals
2.	Detoxification of metals
3.	Protection from metal toxicity
4.	Free radical scavenger
5.	Storage of metals
6.	Metabolism of essential metals
7.	Immune response
8.	Genotoxicity and carcinogenicity

Table 7
Metallothionein and DNA

-
1. Genetic polymorphism—several genes for MT on the same chromosome coding specific MT-function?
 2. MT-I, -II, -III, -IV
 3. Age; fetus, new-born, adult, aged
 4. Gender aspects men and women
 5. MT-higher in liver women than in men
 6. Increased Cd in blood women
 7. Increased MT in women
 8. Iron deficiency increases MT-I in bone marrow, MT in liver unchanged, in kidney decreased
 9. Iron status MT–Cd
-

ation in relation to MT is warranted in the electronics industry when handling some semiconductor and superconductor materials [62].

Another aspect of toxicity of MT is exposure via food. MT and MT-like proteins have been described in various foodstuff. This question were recently asked in toxicity and intakes of various forms of metals [63] and as well discussed in a previous review [47].

6. Metallothionein and DNA, genetic polymorphism, gender perspectives

In literature data on MT, genetic polymorphism and gender perspectives are limited. Table 7 summarizes aspects on this matter. MT is regarded as an adduct for cadmium and various metals. There are 14 different genes in the human being. All are located in a gene cluster on chromosome 16 of about 82 kb [64]. Six of these have been identified to be functional and two are not. The remaining six have not been characterized [65]. The genes have been identified on the basis of nucleotide sequence and are more than expressed identified metallothioneins. As several genes coding for MT are present on the same chromosome, this might code for a specific purpose—biological function as was suggested during the first international meeting on metallothionein [7]. An age dependent correlation with metallothionein and metal indicates a specific function. In the fetus no cadmium is found but the concentration of metallothionein is high. Dur-

ing gestation and in the newborn a high concentration of intracellular MT rich in copper and zinc is mainly present in the liver [47,66]. Such copper probably serves as an important function in providing Cu for functions during the first period of life when tissue copper concentration declines to the concentration characteristic of adult life time if no metabolic disorders are present. A similar situation occurs for zinc-metallothionein. Immunohistochemical localization of MT shows MT in nucleus of hepatocytes in neonates for several days and later MT is present as a cytoplasmic protein during postnatal development as studied in rats [67]. That DNA synthesis and cell growth is stimulated by very low concentration of cadmium [68] was shown in cultured mammalian cells. Human brain tissue has been found to be rich in MT-III [69]. A growth inhibitory factor (GIF) from this tissue was identified to be a metallothionein. MT-III shows a tissue specificity and a structure that differs by having six glutamic acid insert near the C-terminal and one additional insert in the N-terminal. Expression of MT-III is not regulated by metals. MT-III is down regulated in Alzheimer's disease. So far this is the only metallothionein that has a function in relation to growth. The GIF gene and MT genes are both located on chromosome 16 in humans. MT in growing tissue and its possible relation to tumors is reported [70]. MT concentration measured by the Cd-saturation method displays a clear age dependence. A decline of MT in kidneys after age 60 is in accordance with findings for cadmium kinetics. It has been postulated [71] that the capacity of renal tissues to produce MT is age dependant and protein synthesis may be less efficient at older biological ages. Epidemiological and experimental studies in laboratory animals show that females are more vulnerable to cadmium toxicity than males [46,48]. Women have higher cadmium concentration in blood, e.g. [72], compared to men even if differences in general for cadmium levels in blood is overwhelmed by smoking habits [72]. Women have higher concentration in liver. Iron status is of importance for cadmium and MT concentration. Low iron status increases the absorption of cadmium [33]. Iron deficiency also increase the concentration of MT-I in the

bone marrow of rats exposed to cadmium, revealing an effect on the bone marrow as also suggested by Piscator [3] in rabbits with hemolytic anemia. Concentration of MT in liver is unchanged but renal concentration was reduced in animals with iron deficiency [73]. However as cadmium concentration seems to be higher in aged women compared to men it is contradictory to that observation that men have higher MT levels than women. A gender perspective is present in MT. Involvement in signal transduction has not been found in the literature. MT-III or IV might however be involved in this. MT-IV is expressed in stratified squamous epithelia differentiating cells.

MT apart from transport of metals such as cadmium and copper in the cell also functions as a free radical scavenger.

7. MT and disease

There are diseases that are linked to metabolic disorders of handling metals genetically transferred from generation to generation and metals that cause adverse health effects upon exposure. This presentation discusses conditions that MT to some extent is related to. As depicted in Table 8, examples of such diseases are Menke's and Wilson's disease. Menke's disease, an inherited X-linked recessive disturbed copper metabolism results in accumulated copper concentration in the liver and also in the placenta. Another inherited disorder with regard to copper accumulation is Wilson's disease. Patients suffering from Wilson's disease fail to excrete excess copper in bile from the liver leading to, e.g. neurological disease.

Table 8
Metallothionein and disease

Agent/metal	Organ	Illness
Cadmium	Kidney	Proteinuria, calciuria, Itai-itai-disease
Copper	Liver	Wilson's disease
Copper	Placenta	Menke's disease
GIF	Brain	Alzheimer's disease
Copper	Liver	Indian liver cirrhosis

Treatment with zinc has been suggested [74] to improve conditions by a mechanism whereby zinc induces synthesis of intestinal and hepatic metallothionein that sequester copper for the structure. To study metabolic disorders related to copper animal models have been introduced. Recently LEC-rats have been introduced and a model for involvement of MT and copper in Wilson's disease. It is proposed that non-MT bound copper is transferred to ceruloplasmin and coppertrithiomolybdate binds specifically to albumin. The toxicity is explained by participation of MT and active oxygen species that are produced upon reactions involving copper [75]. Livers of patients with diabetes mellitus have high concentrations of MT. In humans approximately 600 $\mu\text{g MT g}^{-1}$ and 60 $\mu\text{g Zn g}^{-1}$ have been reported in livers. The susceptibility of spontaneously diabetic mice to CdMT nephrotoxicity was studied [76]. In mice with spontaneous diabetes, CdMT injections gave rise to renal damage at considerably lower doses than in normal mice [76].

8. Discussion—future aspects on MT

At the first meeting on MT in Zurich it was discussed to set up a bank or producer of MT in order to have pure and standardized MT. Discussions dealt with whether interlaboratory exchange and a quality control (QC) programme would solve some difficulties that might occur due to reports on various purity of MT. To gain more information on MT it is necessary to harmonise methods for the quantification of MT. Several methods for estimating and measuring MT concentration in tissues and body fluids have been developed. At present several methods which have proved more or less successful are in use. It is necessary to bear in mind factors that influence MT concentration in tissues and fluids. To use metallothionein as a biomarker would be an advantage. As for all biomarkers MT also has to be related to some other factor. As exposure to many agents of which metals are inducers with high potency and cadmium being the strongest known inducer, it is necessary to be aware of factors influencing the concentration of metallothionein.

Table 9
Future aspects on metallothionein

-
1. Method for isolation
 2. Method for purification
 3. Method for quantification
 4. Techniques for sampling
 5. Reference material
 6. Medical aspects
 7. Metallothionein as a biomarker in tissue samples
 8. Marker of environmental exposure
 9. Normal values
 10. Harmonization
-

Little is known about the biological ageing of the synthesis of metallothionein. Studies on cadmium concentration in renal tissue have shown a decrease after the age of 50–60 years in human beings. It is most controversial to estimate the normal concentration of metallothionein. A method to measure the concentration of metallothionein should be protein specific and should manage to measure changes such as increase or decrease of normal or more precisely basic concentration. Cadmium concentration increases with exposure and particularly with age as the newborn has a low concentration of cadmium since this metal does not pass the placenta barrier. Concentration of metallothionein in the cell is influenced by so many parameters and factors that a method to quantitate concentration of metallothionein has to be standardized with respect to many factors. Just to measure the concentration in relation to exposure to some inducing agent many of the previously mentioned methods are quite acceptable. However in order to tell some ‘normal’ values and to compare obtained concentration requires an in relation factor. Cadmium has been shown to be the strongest inducer that means that lowest present concentration increases mRNA. Thus, future aspects of MT should deal with the same topics as usual. This is depicted in Table 9.

MT is a protein that demands further research and attracts scientists from many fields. A number of aspects have been brought to attention. The state of the present knowledge and seen from the historical point of view indicate that results of future research on MT will contribute to explain many biological effects.

Acknowledgements

Support from the EU-commission and workshop at Geel and Funds from Karolinska Institute are gratefully acknowledged.

References

- [1] J.H.R. Kägi, B.L. Vallee, *Biochemistry* 235 (1960) 3460.
- [2] J.H.R. Kägi, B.L. Vallee, *Biochemistry* 236 (1961) 2435.
- [3] M. Piscator, Om kadmium i normala människornjurur samt redogörelse för isolering av metallothionein ur lever från kadmiumexponerade kaniner (English summary), *Nordisk hygienisk tidskrift* 65 (1964) 76.
- [4] G.F. Nordberg, M. Piscator, B. Lind, *Acta Pharmacol. Toxicol.* 29 (1971) 456.
- [5] G.F. Nordberg, M. Nordberg, M. Piscator, O. Vesterberg, *Biochem. J.* 126 (1972) 491.
- [6] Y. Kojima, C. Berger, B.L. Vallee, J.H.R. Kägi, *Proc. Natl. Acad. Sci. USA* 73 (1976) 3413.
- [7] J.H.R. Kägi, M. Nordberg (Eds.), *Metallothionein*, Birkhauser, Basel, 1979, pp. 1–378.
- [8] R.J. Vandermallie, J.S. Garvey, *J. Biol. Chem.* 254 (1979) 8416.
- [9] R.A. Goyer, B.A. Fowler, G.F. Nordberg, G. Shepard, L. Moustafa (Eds.), *Proceedings of the Metallothionein and Cadmium Nephrotoxicity Conference 1983*, *Environ. Health Perspect.* 54 (1984) 1–295.
- [10] J.H.R. Kägi, Y. Kojima, *Metallothionein II*, Birkhauser, Basel, 1987.
- [11] K.T. Suzuki, M. Imura, M. Kimura, *Metallothionein III Biological Roles and Medical Implications. ALS Advances in Life Sciences*, Birkhauser, Basel, 1993.
- [12] M. Margoshes, B.L. Vallee, A cadmium protein from equine kidney cortex, *J. Am. Chem. Soc.* 79 (1957) 4813.
- [13] D.P. Maliuga, *Doklady Akad. Nauk. USSR* 31 (1941) No 2 145 and *Cadmium and Organismus Chemical Abstracts* 37.1. 894, Translation RJ-296 (1943)
- [14] J.H.R. Kägi 8th Int. Congr. Biochem, Abstract, (1970) 130.
- [15] G.F. Nordberg, *Environ. Physiol.* 1 (1971) 171.
- [16] M. Nordberg, G.F. Nordberg, M. Piscator, *Environ. Physiol. Biochem.* 5 (1975) 396.
- [17] M. Nordberg, *Studies on Metallothionein and Cadmium*, Doctoral thesis. Department of Environmental Hygiene, Karolinska Institute, Stockholm, Sweden, 1977.
- [18] M. Nordberg, *Environ. Res.* 15 (1978) 381.
- [19] D.R. Winge, K.A. Miklossy, *J. Biol. Chem.* 257 (1982) 3471.
- [20] I. Bremner, in: J.H.R. Kägi and M. Nordberg (Eds.), *Factors Influencing the Occurrence of Copper-Thioneins in Tissues*, *Metallothionein*, Birkhauser Verlag, Basel, 1979, pp. 273–280.

- [21] M. Nordberg, B. Trojanowska, G.F. Nordberg, *Environ. Physiol. Biochem.* 4 (1974) 149.
- [22] J.K. Piotrowski, W. Bolanowska, A. Sapota, *Acta Biochim. Pol.* 20 (1973) 207.
- [23] L. Björkman, B. Palm, M. Nylander, M. Nordberg, *Biol. Trace Element Res.* 40 (1994) 255.
- [24] G.F. Nordberg, M. Piscator, M. Nordberg, *Acta Pharmacol. Toxicol.* 29 (1971) 289.
- [25] M. Nordberg, G.F. Nordberg, *Environ. Health Perspect.* 12 (1975) 103.
- [26] M. Nordberg, Y. Kojima, in: J.H.R. Kägi, M. Nordberg (Eds.), *Metallothionein and Other Low Molecular Weight Metal-Binding Proteins* Metallothionein, Birkhauser, Basel, 1979, pp. 41–116.
- [27] B.A. Fowler, *Proceedings of High Affinity Metal-Binding Proteins in Non Mammalian Species*, *Environ. Health Perspect.* 65 (1986) 3–224.
- [28] Nordberg, M., Isoelectric focusing of mammalian metallothioneins, in: J.F. Riordan, B.L. Vallee (Eds.), *Methods in Enzymology*, vol. 205, Academic Press, New York, 1991, pp. 247–252.
- [29] C.G. Elinder, M. Nordberg, *Metallothionein*, in: L. Friberg, C.G. Elinder, T. Kjellström, G.F. Nordberg (Eds.), *Cadmium and Health*, Vol. I, CRC Press, Boca Raton, FL, 1985, pp. 65–79.
- [30] M. Nordberg, *Metallothionein deserves attention*, in: W. Kalow, H.E. Goedde (Eds.), *Ethnic Differences in Reactions to Drugs and Xenobiotics*, Alan R. Liss, New York, 1986, pp. 401–410.
- [31] R. Palmiter, *Metallothionein*, in: J.H.R. Kägi, Y. Kojima (Eds.), *Metallothionein-II*, Birkhauser, Basel, 1987, pp. 63–80.
- [32] Y. Liu, J. Liu, R.D. Palmiter, C.D. Klaassen, *Toxicol. Appl. Pharmacol.* 137 (1996) 307.
- [33] G.F. Nordberg, T. Kjellström, M. Nordberg, *Metabolism and kinetics*, in: L. Friberg, C.G. Elinder, T. Kjellström, G.F. Nordberg (Eds.), *Cadmium and Health*, Vol. I, CRC Press, Boca Raton, FL, 1985, pp. 103–197.
- [34] M. Nordberg, *Environ. Health Perspect.* 54 (1984) 13–20.
- [35] J.F. Riordan, B.L. Vallee, *Methods in Enzymology*, Academic Press, vol. 205, 1991, pp. 247–252.
- [36] S. Onosaka, M.G. Cherian, *Toxicology* 22 (1981) 91.
- [37] D.L. Eaton, B.F. Toal, *Toxicol. Appl. Pharmacol.* 66 (1982) 134–142.
- [38] R.W. Olafson, R.G. Sim, *Anal. Biochem.* 100 (1979) 343.
- [39] J.S. Garvey, *Environ. Health Perspect.* 54 (1984) 117.
- [40] J.H.R. Kägi, S.R. Himmelhoch, P.D. Whanger, J.L. Bethune, B.L. Vallee, *J. Biol. Chem.* 249 (1974) 3537.
- [41] C. Tohyama, Z.A. Shaikh, A. Nogawa, E. Kobayashi, R. Honda, *Toxicology* 22 (1981) 289.
- [42] C. Tohyama, Z.A. Shaikh, K.J. Ellis, S.H. Cohan, *Toxicology* 20 (1981) 81.
- [43] G.F. Nordberg, J.S. Garvey, C.C. Chang, *Environ. Res* 28 (1982) 179.
- [44] H.A. Roels, R.R. Lauwreys, J.P. Buchet, A. Bernard, J.S. Garvey, H.J. Linton, *Int. Arch. Occup. Environ. Health* 52 (1983) 159.
- [45] T. Haerslev, G.K. Jacobsen, N. Horn, E. Damsgaard, *Acta Pathologica, Microbiologica et Immunologica Scandinavia* 103 (7-8) (1995) 568–573.
- [46] WHO/IPCS *Environmental Health Criteria Document 134 Cadmium*, WHO, Geneva, 1992.
- [47] M.G. Cherian, M. Nordberg, *Toxicology* 28 (1983) 1.
- [48] H.M. Chan, L.F. Zhu, R. Zhong, D. Grant, R.A. Goyer, M.G. Cherian, *Toxicol. Appl. Pharmacol.* 123 (1993) 89.
- [49] X. Liu, T. Jin, G.F. Nordberg, M. Sjöström, Y. Zhou, *Toxicol. Appl. Pharmacol.* 126 (1994) 84.
- [50] T. Jin, M. Nordberg, G.F. Nordberg, *Toxicology* 75 (1992) 29.
- [51] G.F. Nordberg, T. Jin, M. Nordberg, *Environ. Health Perspect.* 102 (3) (1994) 191–194.
- [52] T. Jin, K.F. Norrback, M. Nordberg, X. Liu X., G.F. Nordberg, *The role of cadmium and zinc pretreatment on the distribution of cadmium bound to proteins in renal membrane and microsome (Abstract)*, COMTOX, Vancouver, 1995.
- [53] M. Nordberg, G.F. Nordberg, *Biological roles of metallothionein and other high affinity metal binding proteins in regulating cell injury from metals*, in: B.F. Fowler (Ed.), *Mechanisms of Cell Injury: Implications for Human Health*, Dahlem Konferenzen, Wiley, Chichester, 1987, pp. 53–65.
- [54] M. Nordberg, T. Jin, G.F. Nordberg, *Cadmium, metallothionein and renal tubular toxicity*, in: G.F. Nordberg, L. Alessio, R.F.M. Herber (Eds.), *Cadmium in the Human Environment: Toxicity and Carcinogenicity*, 1992, IARC Scientific Publications No. 118, pp. 293–297.
- [55] I. Bremner, in: J.H.R. Kägi, Y. Kojima (Eds.), *Nutritional and Physiological Significance of Metallothionein, Metallothionein II*, Birkhauser, Basel, 1987, pp. 81–107.
- [56] T. Jin, P. Leffler, G.F. Nordberg, *Toxicology* 45 (1987) 307.
- [57] P. Leffler, T. Jin, G.F. Nordberg, *Toxicology* 112 (1996) 151.
- [58] P. Leffler, T. Jin, G.F. Nordberg, *Toxicol. Appl. Pharmacol.* 103 (1990) 180.
- [59] B. Elsenhans, K. Kolb, K. Schumann, W. Forth, *Endogenous intestinal metallothionein possibly contributes to the renal accumulation of cadmium*, in: G.F. Nordberg, L. Alessio, R.F.M. Herber (Eds.), *Cadmium in the Human Environment: Toxicity and Carcinogenicity*, 1992, IARC Scientific Publications No. 118, pp. 225–230.
- [60] J.P. Groten, E. Hissink, P.J. van Bladeren, *Differences in chromatographic behaviour of rat and pig metallothionein isoforms: a possible method of distinguishing between exogenous and endogenous metallothioneins*, in: G.F. Nordberg, L. Alessio, R.F.M. Herber (Eds.), *Cadmium in the Human Environment: Toxicity and Carcinogenicity*, 1992, IARC Scientific Publications No. 118, pp. 219–224.

- [61] L. Cai, J. Koropatnick, M.G. Cherian, *Chem.-Biol. Interact.* 96 (1995) 143–155.
- [62] M. Nordberg, G.F. Nordberg, *Environ. Sci.* 4 (3) (1996) 187.
- [63] M. Nordberg, G.F. Nordberg, Toxicity and intakes of various forms of heavy metals, in: J.T. Kumpulainen, J.T. Salonen (Eds.), *Natural Antioxidants and Food Quality in Atherosclerosis and Cancer Prevention*, The Royal Society of Chemistry, Cambridge, UK pp. 412–416.
- [64] A.K. West, R. Stallings, C.E. Hildebrand, R. Chia, M. Karin, R.J. Richard, *Genomics* 8 (1990) 513.
- [65] B.L. Vallee, W. Maret, The functional potential and potential functions of metallothioneins: a personal perspective, in: K.T. Suzuki, M. Imura, M. Kimura, (Eds.), *Metallothionein III Biological Roles and Medical Implications*, ALS Advances in Life Sciences Birkhauser, Basel, 1993, pp. 1–27.
- [66] B.R. Sonawane, M. Nordberg, G.F. Nordberg, G.W. Lucier, *Environ. Health Perspect.* 12 (1975) 97.
- [67] N.O. Nartey, D. Banerice, M.G. Cherian, *Pathology* 19 (1987) 233.
- [68] T. von Zglinicki, C. Edvall, E. Östlund, B. Lind, M. Nordberg, N.R. Ringertz, J. Wroblewski, *J. Cell Sci.* 103 (1992) 1073.
- [69] Y. Uchida, Growth inhibitory factor in brain, in: K.T. Suzuki, M. Imura, M. Kimura, (Eds.), *Metallothionein III Biological Roles and Medical Implications*, ALS Advances in Life Sciences Birkhauser, Basel, 1993, pp. 315–328.
- [70] M.G. Cherian, *Environ. Health Perspect.* 102 (1994) 131.
- [71] M. Nordberg, *Talanta* (1997).
- [72] C.G. Elinder, Normal values for cadmium in human tissues, blood and urine in different countries, in: L. Friberg, C.G. Elinder, T. Kjellström, G.F. Nordberg (Eds.), *Cadmium and Health*, Vol. 1., CRC Press, Boca Raton, FL, 1985, 82 pp.
- [73] A. Robertson, J.N. Morrison, A.M. Wood, I. Bremner, *J. Nutr.* 119 (1989) 439.
- [74] G.J. Brewer, *Drugs* 50 (2) (1995) 240–249.
- [75] K.T. Suzuki, *Res. Commun. Mol. Pathol. Pharmacol.* 89 (2) (1995) 221–240.
- [76] T. Jin, G.F. Nordberg, O. Sehlin, P. Leffler, J. Wu, *Toxicology* 89 (1994) 81.

Strategies for the qualitative and quantitative analysis of metallothionein isoforms by capillary electrophoresis

John H. Beattie *

Trace Element and Gene Expression Group, Rowett Research Institute, Greenburn Road, Bucksburn, Aberdeen AB21 9SB, Scotland

Received 11 December 1996; accepted 14 March 1997

Abstract

Metallothioneins (MT) are a heterogeneous family of proteins coded from multiple linked genes whose individual expression can be readily determined at the transcriptional level by assay of mRNA using specific DNA probes targeted against the untranslated regions. Analysis of translated protein products is more challenging since sequence variation between MT isoforms can be as little as one in 61 amino acids. Separation of these isoforms therefore requires a high resolution technique which can exploit minor differences in charge or hydrophobicity. The use of capillary electrophoresis (CE) for MT isoform separation is reviewed, including practical information on capillaries and electrolyte conditions which are most suitable for qualitative evaluation of purified MT and also for quantification of isoforms from biological tissues. Methods of sample preparation are discussed, as are methods of characterising the separated components and enhancing sensitivity of their detection. © 1998 Elsevier Science B.V. All rights reserved.

Keywords: Metallothionein; Isoform separation; Capillary electrophoresis; MECC; SPE-CE; MALDI-TOFMS

1. Introduction

Following the initial discovery of a Cd-binding protein in equine renal cortex by Margoshes and Vallee [1], subsequent characterisation of the protein [2,3] suggested the presence of a single polypeptide form with an apparent M_r of about 10 000 by velocity sedimentation and diffusion techniques and the protein was named metallothionein (MT) due to its high metal and cysteine content. Further analysis of horse MT indicated a

true apoprotein M_r of 6000 [4,5] and additional studies on rabbit MT by gel filtration, ion exchange chromatography, polyacrylamide gel electrophoresis and isoelectric focusing, demonstrated its inducibility by metals and the presence of two isoforms [4,6] which were expressed in a coordinate way in response to injection with Zn or Cd. The isoforms were named MT-1 and MT-2 according to their order of elution from an anion exchange column and their difference in charge at neutral or alkaline pH, this was related to the presence or absence of an acidic amino acid at residue 10 or 11 from the N-terminus. Since the location of cysteine residues in MT-1 and MT-2 is

* Tel.: +44 1224 716631; fax: +44 1224 716622; e-mail: J.Beattie@rri.sari.ac.uk

highly conserved and their metal binding complement in a 2-domain structure is identical, early opinion favoured a similar role for both isoforms.

However, when separation techniques based on differences in hydrophobicity, such as reversed phase HPLC, were applied to purified samples of MT, it quickly became apparent that the charge types MT-1 and MT-2 from many, particularly mammalian, species often contain two or more proteins [7–9]. These isoforms code from distinct MT genes [10,11] and screening of DNA libraries with subsequent cloning and sequencing of candidate genes suggested that there was considerable heterogeneity in many mammalian MTs. Nevertheless, little effort has been devoted to the separation and identification of the proteins coding from these genes and, as yet, there is no rational basis for assuming that a charge difference between MT-1 and MT-2 forms, due to substitution of a single acidic amino acid, is any more biologically significant than the influence of substituting other residues. Indeed, this point is illustrated by the discovery of MT-3, the expression of which has been identified in brain [12] and maternal deciduum [13], and whose activity in an *in vitro* culture system [14], can be distinguished from that of MT-1 and MT-2 due to the presence of two proline residues substituting for at least one hydroxyamino acid and an alanine [15] and not due to the insertion and substitution of acidic or basic amino acids. Aside from resolving the historical problems of MT nomenclature, it is important that the potential biological significance of each charge-similar isoform is not neglected simply because the analytical techniques available cannot easily separate them.

In order to monitor the expression of individual MT genes with regard to their function, we believe it is necessary to measure isoform protein in addition to mRNA, since there is growing evidence that MT translation can be regulated independently of transcription [16]. The separation of closely related isoforms requires a high resolution technique which can be optimised without restrictive limitations on the use of separation conditions. CE is ideal for this purpose and many types of capillary can withstand a wide

range of electrolyte composition, including extremes of pH, detergents and solvents. In addition, analysis time is rapid (usually < 15 min.), sample consumed is very small (lower nl) and commercial instruments offer automation of analysis. As a consequence of these distinct advantages and the successful application of CE to the analysis of other metalloproteins and peptides [17], we selected this technique for MT isoform analysis. Excellent introductory booklets on CE are supplied by several CE instrument manufacturers and more detailed information is available in the literature [18].

Suggestions concerning the strategies for successful qualitative evaluation and quantitative measurement of MT isoforms are outlined in this review, along with examples of separations and practical information to help select conditions best suited to a particular application. While the conditions described have worked well in our laboratory for the specified MT species, they may not be optimal for other MTs and should be regarded as a starting point for further optimisation.

2. Qualitative evaluation

Purified MT samples should be analysed for isoform heterogeneity and contamination and CE is a good technique for making this evaluation. Many methods of MT induction and purification have been published and the reader is referred to a comprehensive book describing a variety of techniques [19]. Assuming that sufficient purified material is available (at least 20 μl of a 1–5 mg MT ml^{-1} solution), there are several possible approaches to making a qualitative evaluation of MT isoform composition. The aim is to achieve as high a resolution as possible while taking advantage of electrolyte and capillary conditions which best discriminate between small differences in isoform charge and/or hydrophobicity. This may necessarily involve some compromise in sensitivity or separation time. The choice of electrolyte involves selection of a suitable buffer and, perhaps, a modifying agent such as a solvent or detergent.

2.1. Uncoated capillaries

In uncoated capillaries, highest resolution is achieved by using high ionic strength (IS) electrolytes, which improve resolution and inhibit interaction of proteins with the capillary wall. However, the currents generated by high IS electrolytes can cause excessive Joule heating and consequential loss of resolution. The capillary cooling efficiency of the CE instrument can therefore be critical to maintaining good resolution at high IS. Optimisation is therefore required, although if a higher IS buffer is particularly advantageous, an alternative strategy is to increase the capillary length or reduce the diameter, which increases electrical resistance and heat dissipation efficiency, thereby reducing current flow and Joule heating effects. This results in longer separations and/or reduced sensitivity. On some commercial instrumentation, the maximum capillary cooling capacity is around 0.05 W cm^{-1} which equates to a current of about $100 \mu\text{A}$ at 30 kV in a 57 cm capillary. Heating the capillary externally increases electro-osmotic flow (EOF), shortening MT isoform migration times [20] and modifying their separation [21].

The potential choice of buffers and modifiers is diverse and some form of separation of MT charge-distinct isoforms can be obtained using a wide variety of electrolyte conditions and chemistry. Nevertheless, selection of suitable electrolytes should be influenced by three main factors, namely their UV absorbance, conductivity and buffering pH range. In addition, a few particular conditions offer distinct advantages for MT isoform separation. Sodium phosphate is an appropriate choice because it has very low absorbance at UV wavelengths and several buffering pH ranges, since phosphoric acid can dissociate three protons with pK_a values of 2.12, 7.21 and 12.67. Compared with sodium borate, the resolution obtained with sodium phosphate is superior but the currents generated are much greater, and narrower bore (25 and $50 \mu\text{m}$) or longer (50 – 100 cm) capillaries are recommended at concentrations exceeding 50 mM . Borate buffers, on the other hand, have low conductivity, and resolution can be improved by using higher buffer concen-

trations. Good separations of MT charge forms can be achieved using organic zwitterions such as Tris [22,23] and mixed buffer systems such as Tris–borate have been used to resolve several components in horse and rabbit MT samples [21]. The advantage in using zwitterionic buffers is their low conductivity at or around the pI and therefore low Joule heating. However, if UV detection is used, particularly below 220 – 230 nm , absorbance by some organic buffers is limiting at high concentrations.

Arguably the best separations and resolution that have so far been achieved in uncoated capillaries have been obtained at low pH using high IS phosphate buffers [24,25]. A comparison of rabbit MT separations in organic and inorganic low pH buffers is shown in Fig. 1 and it is clear that the inorganic phosphate buffer gave a better separation than the organic formate buffer. At low pH, Cd and Zn dissociate from MTs and the separations are therefore of apoproteins [25]. Dissociation of these metals results in a diminution of UV absorbance and hence the concentration of MT sample must be sufficiently high for adequate detection. Separations of Cd, ZnMTs within the pH range 3–5 does not appear to be reproducible, probably due to partial metal dissociation (unpublished observations). The rabbit liver MT-1 and MT-2 charge forms which are available commercially (Sigma-Aldrich, Poole, U.K.) and which were used to obtain the electropherograms in Fig. 1, contain appreciable contamination by the other charge form. Hence, one of the major peaks in the MT-1 separations (Fig. 1C and D) corresponds to the major component in the MT-2 electropherograms (Fig. 1E and F). This confirms previous findings from different laboratories [23,26,27]. Being more highly charged, MT-3 migrates rapidly and separates completely from MT-1 and MT-2 by CE at low and neutral pH [28].

An alternative technique for qualitative evaluation of purified MT samples involves addition of an ionic surfactant to the electrolyte. The technique is known as micellar electrokinetic capillary chromatography (MECC) [29] and has been successfully applied to the separation of MT isoforms in several species [30,31]. Of the surfactants screened in our laboratory, sodium dodecyl sul-

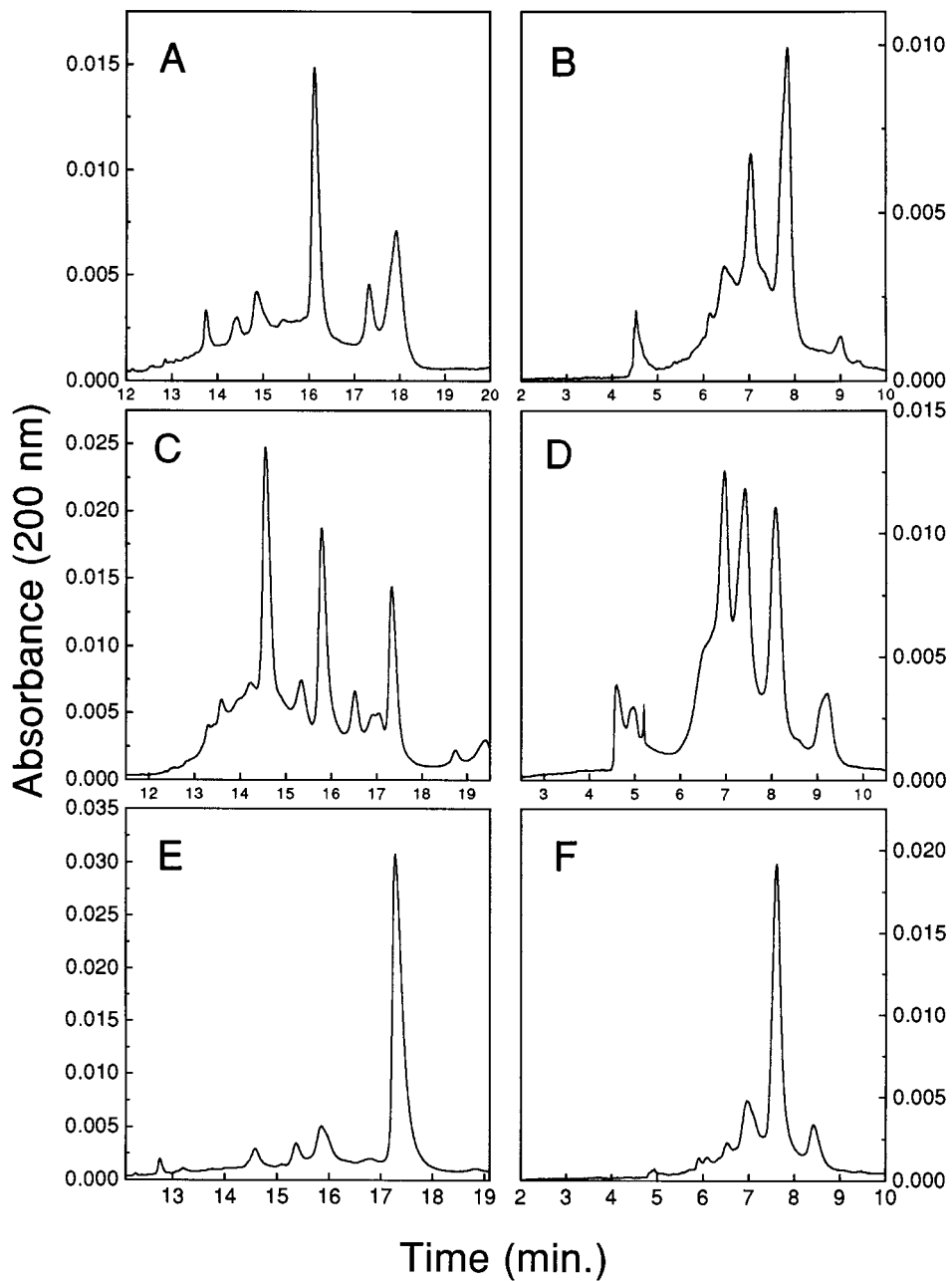


Fig. 1. Comparison of rabbit liver MT (A and B), MT-1 (C and D) and MT-2 (E and F) separations by capillary electrophoresis on a Beckman P/ACE 5000 instrument using an uncoated 57 cm \times 50 μ m fused silica capillary, with a 300 mM sodium phosphate buffer, pH 2.0 (A, C and E), or a 300 mM sodium formate buffer, pH 2.5 (B, D and F). The separation voltages (normal polarity, cathode at outlet) using the phosphate and formate buffers were 20 kV and 30 kV, respectively. MT samples (5 mg ml^{-1} in deionised water) were loaded by pressure injection for 10 s at 0.5 psi and the capillary temperature during all separations was maintained at 25°C.

phate (SDS) has yielded the best separations. The principle of analyte separation in MECC involves their partitioning between the hydrophilic environment of the aqueous electrolyte and the hydrophobic interior of the negatively charged SDS micelles. Hence, separation is made on the basis of differences in hydrophobicity as well as charge. In fact, the M_r cut-off for inclusion into SDS micelles is about 5000 Da and so the principle involved in MT separation may be more influenced by the association of SDS molecules with the protein. The resolution that can be achieved by MECC is generally lower than with other CE techniques but separation efficiency and reproducibility of peak migration time and area are advantageous. For MT isoforms that will not readily separate by changing the pH of phosphate buffers under standard CE conditions (e.g. sheep MT isoforms), MECC can be a robust and useful alternative. As can be seen in Fig. 2, adjusting the MECC separation conditions for sheep and rabbit MTs can yield partial or complete isoform separation. By further manipulation of the buffer and SDS concentrations, complete separation of sheep MT-1 isoforms is readily achieved [31]. When first attempting MECC separations of different MT proteins, use of a 50 cm \times 75 μ m uncoated capillary with a 300 mM borate buffer pH 8.4 containing 85 mM SDS is recommended. In our hands, MECC at 10 kV gives better separations than higher voltages and isoform migration may be considerably modified by varying the pH from 8.4 to 10.4 or the SDS concentration from 60–120 mM.

2.2. Coated capillaries

The internal surface of fused silica capillaries can be modified or coated with a variety of sub-

stances or ligands, thus affecting its surface charge, hydrophobicity or chemistry. At the present time, the most widely available commercial coated capillaries include those with an amine group (+ve charged, reversed EOF), a neutral coating (no charge, no EOF) and various hydrophilic or hydrophobic coatings. The latter capillaries are intended to be used with addition of surfactant or solvent to the electrolyte and the partial blocking of silanol groups reduces wall interaction of some proteins. However, used in the way intended by the manufacturers, these capillaries do not improve separations of purified MT because wall-interactions of this protein do not appear to be a very significant problem.

Neutral capillaries are very suited to protein separations and are very useful for qualitative evaluation of MT isoforms. By changing the polarity appropriately, separation of multiple MT isoforms can be obtained at low and neutral pH [24,25] and a wide range of different electrolyte buffers are compatible with this type of capillary. Both phosphate [24,25] and mixed zwitterionic buffers [27,32] have been used to obtain good separations of MTs from a range of different species.

Because of the positively charged wall, amine capillaries are more suited to the separation of positively charged proteins i.e. at a pH below the protein pI but some types of amine capillary are not suitable for use below pH 3.5. Thus, from a theoretical perspective, MT isoforms, with a pI of 4–4.5 and a charge ranging from over -1 (MT-1 forms) to -13 (MT-3) at neutral pH, should not be ideal candidates for amine capillary separations at neutral or alkaline pH. Nevertheless, good separation and resolution of MTs have been obtained with a pH as high as 8, using a high IS phosphate buffer as electrolyte [33]. Separations

Fig. 2. Comparison of rabbit liver MT (A and B) and sheep liver MT (C and D) separation by capillary zone electrophoresis using a 57 cm \times 50 μ m polyamine coated capillary (A and C) and by micellar electrokinetic capillary chromatography (MECC) using a 57 \times 25 (B) or a 57 \times 75 μ m (D) uncoated fused silica capillary. Separation conditions using the polyamine capillary were as follows: electrolyte of 100 mM sodium phosphate buffer pH 7.0, pressure injection for 5 s at 0.5 psi, separation voltage 30 kV (reversed polarity with anode at outlet). For MECC, the electrolyte was 100 mM sodium borate buffer containing 75 mM SDS, pH 8.4, loading was by pressure injection for 1 s at 0.5 psi and separation was at 10 kV (normal polarity with cathode at outlet). All separations were performed using a Beckman P/ACE 5000 instrument at 25°C and the MT sample concentrations were 1 mg ml⁻¹ in deionised water. Components labeled '1' and '2' correspond to MT-1 and MT-2 charge forms, respectively.

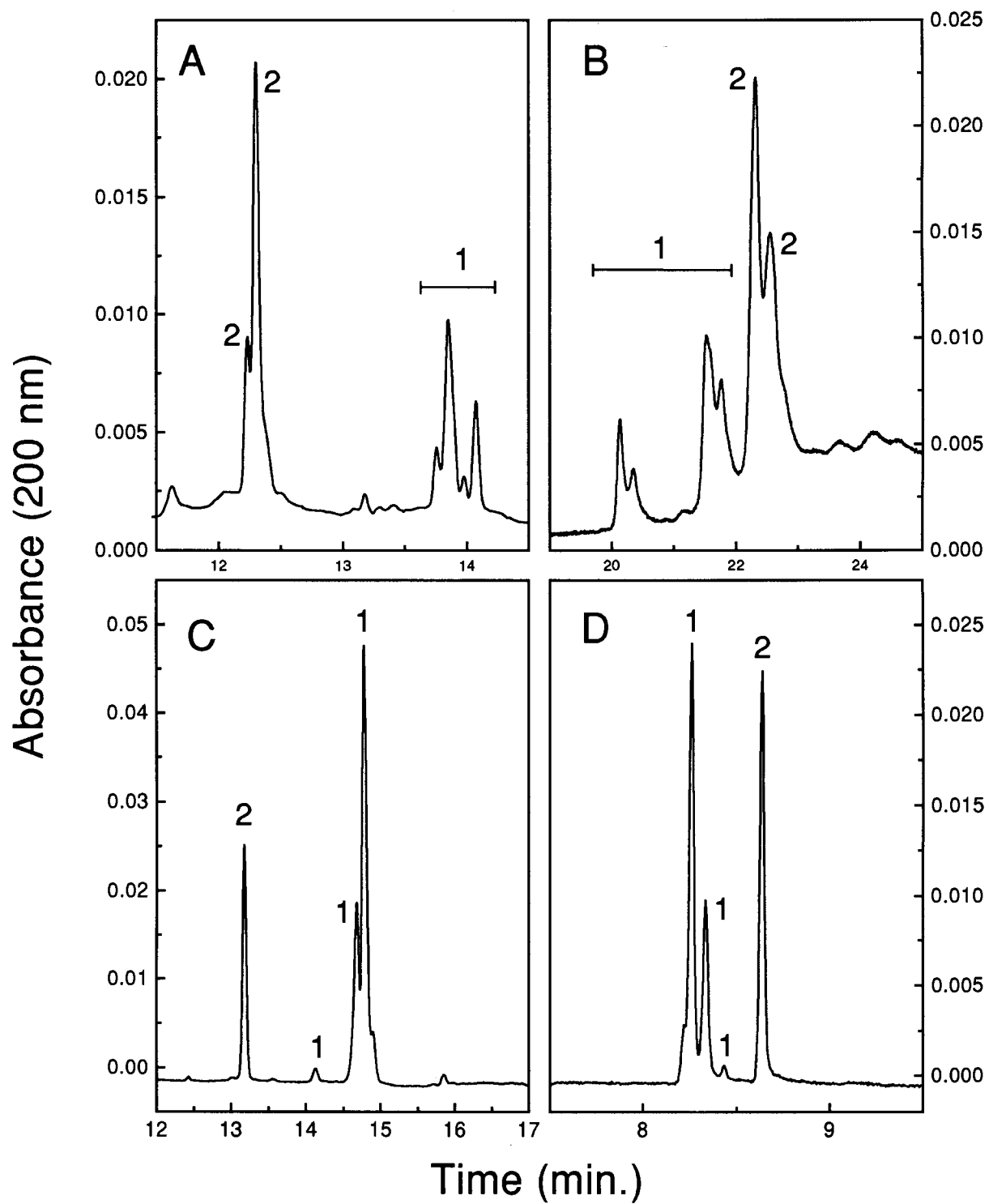


Fig. 2. (Continued)

in an amine capillary can be mirror images of electropherograms obtained by MECC (Fig. 2), which suggests a similar separation principal, possibly involving some unfolding of the MT proteins.

3. Quantitative analysis of MT isoforms

Quantification of MT in biological tissues ideally requires a rapid sample preparation procedure followed by a suitable and compatible analytical technique. In the case of a radioimmunoassay for MT, the analytical technique can be applied directly to diluted tissue cytosols whereas for chromatography or electrophoresis, the MT in samples must initially be completely or semi-purified. Inevitably, more purification steps result in reduced recovery and so there is a need to (a) optimise recovery, (b) optimise precision and (c) find a suitable internal standard and quality control. Recently, the production of an MT standard has been the subject of much debate and, as regards CE, a suitable candidate would be an isoform which shows distinctive migration characteristics and is not expressed in most tissues, such as MT-3.

3.1. Sample preparation

The traditional method of semi-purifying MT from tissue cytosol samples is gel exclusion chromatography [4] using, for example, Sephadex G-75, or more recently, Sephacryl S-100 or Superdex 75 (Pharmacia, Milton Keynes, U.K.). However, for rapid analysis of more than a few samples, this technique is impracticable. CdMT and ZnMT are relatively heat stable and so heat treatment has been used extensively as an initial step in removing contaminating protein. The most commonly quoted protocols describe heat treatment at anything from 60°C for 10 min to 100°C for 1 min and in practice, the temperature–time combination selected should be appropriate for the volume of sample being treated. Unlike many proteins, MTs do not readily denature at low pH and so acidification of tissue extracts has been used for additional deproteinisation of samples

prior to MT analysis [25]. MT is also relatively stable in 50% solutions of water miscible solvents such as ethanol, acetone and acetonitrile whereas many other proteins will precipitate under these conditions. Attempts to analyse 50% solvent extracts directly, reveal a complex variety of contaminating components [30], many of which are low M_r species, since they can be removed by desalting with, for example, Bio-gel P4 or P2 chromatography media (Bio-Rad Laboratories, Hemel Hempstead, U.K.). This procedure results in some sample dilution whereas from an analytical point of view, it is desirable to increase MT concentration. MTs will precipitate, without denaturation, at solvent concentrations of at least 80% and a two-step solvent extraction procedure has been used in the large-scale preparation of MT from animal tissues [34]. Similar 50% and 80–90% two-step solvent techniques have been applied to the rapid deproteinisation of smaller samples and they yield a semi-pure and concentrated extract [35], which is ideal for analysis by CE [31]. Recovery of MT using acetone as the solvent appears to be relatively poor and variable but improved by the addition of 10 mM dithiothreitol to the sample buffer [36]. In our experience, MT recovery using an acetonitrile–ethanol solvent procedure is reproducible and the recovery efficiency can be improved by addition of 0.5 M sodium chloride to the homogenisation buffer of 100 mM Tris–HCL pH 8.0. This sample preparation method has been applied to the analysis by CE of MT-1 and MT-2 levels in developing sheep foetal liver [37].

3.2. Sample analysis

A quantitative method of analysis requires that a predictable relationship is established between concentration of analyte and the signal obtained. In the case of MT analysis by CE, it has been shown, using peak area, that this relationship is linear over a wide concentration range [20,22,33]. However, peak areas of components separated by CE are directly related to their transit rate past the detector, which will decrease with increasing migration time. Peak areas of separated isoforms are therefore not directly comparable until they

are corrected by division with their respective component migration times.

The CE method of choice for quantification of MT isoforms is influenced by the degree of sensitivity and specificity required. In principal, any of the CE techniques described for qualitative evaluation can be applied in a quantitative way but for quantification, sensitivity and reproducibility are critical issues and some methods are therefore more suitable than others. At low pH, metals such as Cd and Zn dissociate from MT and there is a corresponding reduction in UV absorbance, not only at the mercaptide absorbance maxima, but also at lower wavelengths down to 200 nm and below. Therefore, use of low pH is not advisable for quantification. Polyacrylamide-coated neutral capillaries give good separations of isoforms at neutral pH but they have a limited life span and their performance deteriorates at high field strengths. The life span of amine capillaries is also limited and the reproducibility of migration times can be variable when separating complex sample extracts.

When using UV detection with coated or uncoated capillaries, careful thought should be given to the buffer used in the electrolyte. Some organic buffers e.g. HEPES and tricine, will strongly absorb UV light below 230 nm which will limit the use of lower wavelengths for greater detection sensitivity. While this may not be important for qualitative work, it is a distinct disadvantage for quantification. Sodium phosphate and borate do not significantly absorb UV light and are very suitable for quantification work. In addition to low conductivity, SDS also shows low UV absorbance and therefore MECC is a viable alternative to the use of coated capillaries for quantitative analysis. In addition, MECC is a robust technique and sequential separations of tissue sample extracts using borate/SDS electrolytes at alkaline pH show good reproducibility of migration time and peak area. With MT from some species, resolution of all isoforms may be less readily achieved than with neutral capillaries in particular, but on balance, we believe that MECC is best suited for quantitative work.

MECC separations of solvent extracts from the liver of different species are compared in Fig. 3

and the difference in the component migration pattern between species is evident. In the case of sheep and rat samples, MT isoforms were identified by a combination of the techniques described below but the pig isoforms have yet to be confirmed. The migration rate of a major unidentified component partially co-migrating with rat MT-2 was considerably modified by use of a high 2-mercaptoethanol concentration during sample preparation and Fig. 4 shows the resulting separations, using liver from rats injected with different doses of Cd. As might be expected, there was a dose-response effect of Cd injection on both MT-1 and MT-2 levels. The solvent extraction method of sample preparation is particularly effective at removing most non-MT protein but nevertheless, some contaminants remain and can co-migrate with MT isoforms when separated by CE in uncoated capillaries using non-MECC electrolytes at neutral or alkaline pH [38]. Use of SDS in the electrolyte effectively changes the relative mobility of MTs and contaminants so that they no longer co-migrate. In our experience, a two-step solvent extraction procedure followed by MECC separation in 100–300 mM borate/60–120 mM SDS, pH 8.4–10.4 (exact conditions depending on the MT species) is a practical approach to the analysis of MT isoforms in tissues with high basal levels and significant expression of the protein e.g. liver.

4. Identification of putative isoforms

While the separation of multiple putative isoforms in tissue extract and purified MT samples using capillary electrophoresis has proved very successful, identification of the separated components is more problematic due to the limited amount of material that can be collected for subsequent characterisation. It is important to confirm that separated components are MTs and, if possible, identify the isoforms. The first of these tasks is easier to address and the most convenient method of confirmation is to examine the UV spectra of putative isoforms using diode array detection. Characteristically, MTs have no UV absorbance at 280 nm due to the absence of aromatic amino acids. It is also possible to iden-

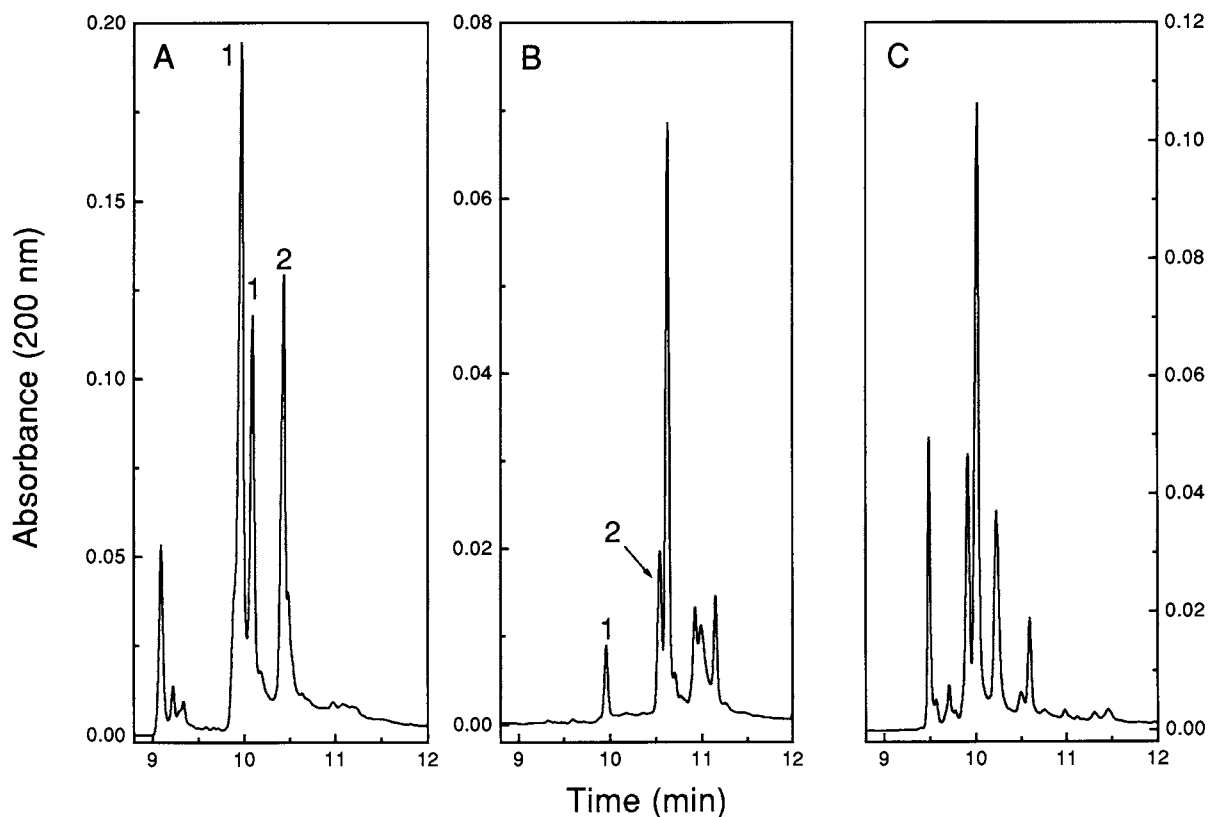


Fig. 3. Separation of liver extracts from Zn-injected sheep (A), Cd-injected rat (B) and Zn injected pig (C). Extracts were prepared using a two-step solvent extraction procedure [31] in which the homogenisation buffer and solvents contained 10 mM 2-mercaptoethanol. Separation was by MECC using a 75 cm \times 57 μ m capillary and conditions specified in the legend of Fig. 2. Components labeled '1' and '2' correspond to MT-1 and MT-2 charge forms, respectively.

tify Zn or CdMT isoforms by an absorbance shoulder at 225 or 250 nm. Examples of the spectral information which can be obtained from diode array detectors is shown in Fig. 5 and comparison of the standard and liver extract spectra strongly support the migration time data which indicate the presence of all the standard isoforms in the extract. Further evidence for this can be obtained by spiking the extract with the purified protein of known isoform identity. Different metalloforms of MT isoforms appear to migrate with identical retention times [30] although addition of metals to the proteins can shift absorbance from MT peaks to a slower-migrating, unidentified component in the case of Hg (unpublished data) and diminish MT isoform absorbance in a concentration dependent manner in the case of Cd [27].

As regards identification of isoforms, or indeed, dimerised or polymerised MT, a more direct approach may be required. Mass spectrometry is one of the few techniques that requires very little sample to obtain spectra and on some CE instrumentation, it is possible to do this off-line by collecting fractions for subsequent analysis. We have used matrix-assisted laser desorption ionisation, time-of-flight mass spectrometry (MALDI-TOF) to verify the purity of MT samples and also the identity of major components from repeated CE separations which are collected, by a brief pressure purge, into a small volume of water (5–10 μ l). A MALDI-TOFMS spectrum of purified sheep MT-1 is shown in Fig. 6 and this information can be obtained rapidly with little experience of mass spectrometry. The major peak

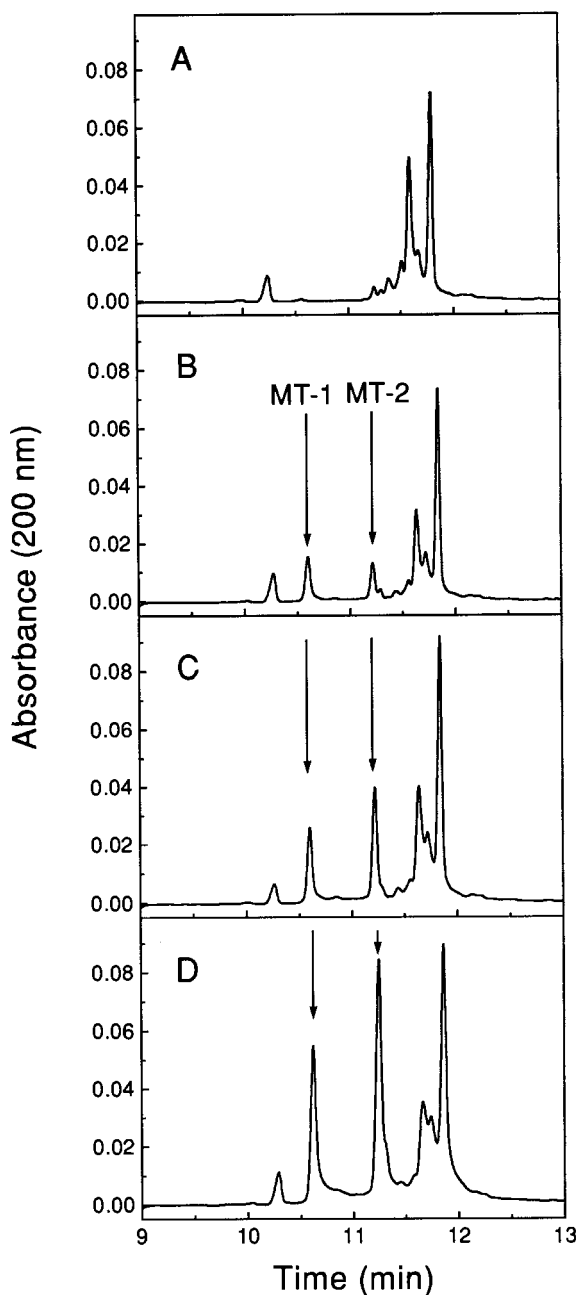


Fig. 4. Separation of liver extracts from rats injected i.p. with saline only (A), 0.1 (B), 0.25 (C) and 0.5 (D) mg Cd kg⁻¹ body weight and killed 24 h after Cd administration. Extracts were prepared using a two-step solvent extraction procedure [31] in which the homogenisation buffer and solvents contained 100 mM 2-mercaptoethanol. Separation was by MECC using a 75 cm × 57 μm capillary and conditions specified in the legend of Fig. 2.

in MT spectra is always composed of apo-protein(s) and low resolution instruments cannot resolve isoforms of similar mass. Nevertheless, partially metallated species can be seen at higher resolution and, in any case, MT spectra have a characteristic 'tailing' on the high mass side of the principal ion, which is caused by the presence of partially metal-saturated isoforms and adduct ions. MTs give much better spectra by high resolution electrospray ionisation mass spectrometry (ESI-MS) [39,40] and we are currently investigating the use of on-line CE-ESI-MS for sequential identification of all separated components. Such equipment is not widely available but new lower resolution bench-top electrospray instruments will make this technique more accessible.

5. Enhancing sensitivity

There are a number of factors that can be optimised before considering the nature of electrolyte and capillary chemistry. UV spectra of MTs show that their maximum absorbance is between 180 and 200 nm (Fig. 5) and the enhancement in sensitivity over absorbance detection at 230 nm is about 4-fold for Zn or Cd proteins and over 10-fold for apoproteins [25]. Light instability increases at lower wavelengths and a monitoring wavelength of 200 nm gives a good signal:noise ratio. While a diode array detector is very useful for characterising components in a separation, the sensitivity achieved by a fixed wavelength UV detector may be superior. Another simple technique for increasing sensitivity is to increase the detector path length, usually by increasing the capillary i.d. Where this is undesirable, the i.d. can be increased only at the point where the UV light passes through the capillary. This is conveniently achieved using extended light path or 'bubble cell' capillaries (Hewlett Packard, Stockport, UK). CE instrument manufacturers offer different sensitivity enhancement features, including methods of focusing the UV light path through the centre of the capillary, or increasing the light path 'window' i.e. the length of capillary through which light passes.

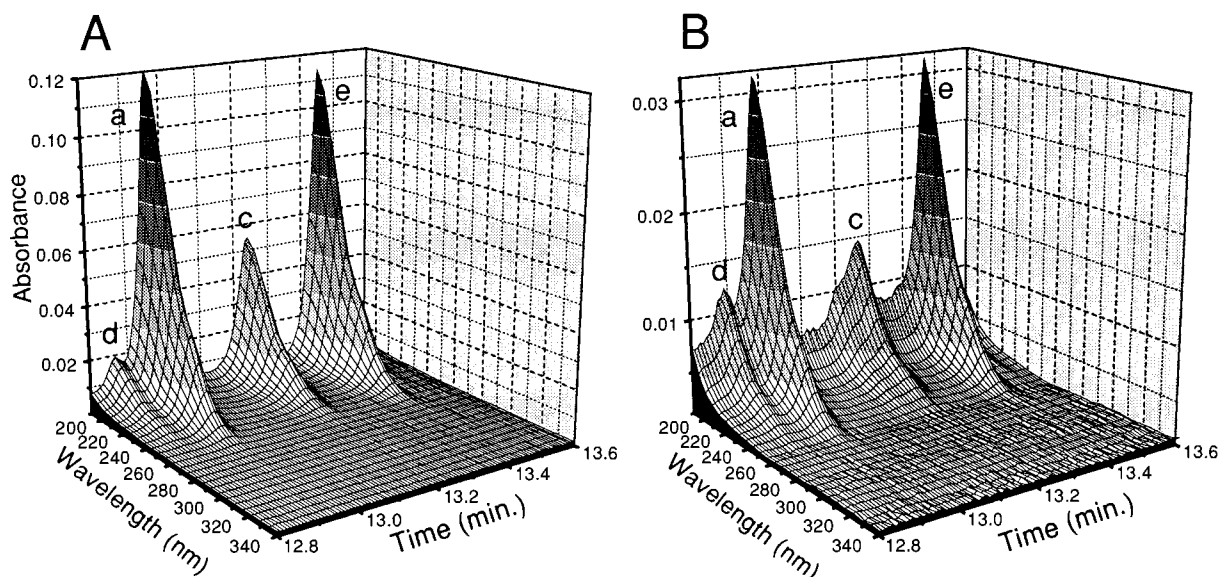


Fig. 5. The utility of diode array detection for characterisation of components separated by capillary electrophoresis. A separation of purified sheep MT (A) is compared with that of a sheep liver extract (B) which was obtained by a two-step solvent extraction procedure [31] without the use of 2-mercaptoethanol. Separation was by MECC using a 75 cm \times 57 μ m capillary and a 300 mM sodium borate buffer containing 85 mM SDS, pH 8.4. All other conditions for MECC are specified in the legend of Fig. 2 and UV scans between 190 and 340 nm were obtained at a rate of 2 Hz. Components labeled a, c and e are isoforms MT-1a, MT-1c and MT-2, respectively and component d is an unidentified MT isoform.

On calculating the quantity of MT in a CE capillary which gives an absorbance peak using a UV monitor at 200 nm, it is clear that femtomole amounts of the protein can be readily detected. Nevertheless, the sample injection volume is very small and it is necessary to use relatively concentrated MT samples to achieve injection of femtomole quantities. Sample loading can be increased by injecting for a longer time, but this will usually adversely affect resolution. Concentration of the sample by reducing its volume is practicable down to about 20 μ l although on many CE instruments, it is possible to inject from as little as 5 μ l. Nevertheless, the physical constraints of the instrumentation and problems such as sample evaporation become significant obstacles with very small volumes.

To an extent, sample concentration can be achieved on-line by processes known as field amplification and 'stacking' [41]. Stacking involves hydrodynamic injection of sample solution which has a lower IS than that of the electrolyte. On

application of an electrical potential across the capillary, a higher electric field is generated within the sample 'plug' than in the electrolyte. The protein molecules therefore migrate at higher velocity within the sample solution and slow down when they reach the interface with the electrolyte. This results in concentration at the interface, which also enhances resolution. However, injection of too much sample will degrade resolution and so investigation of optimal sample injection volume is required. A related way of enhancing sensitivity is to load electrokinetically from a sample of lower IS than the electrolyte. This has been used to advantage in uncoated capillaries but can be even more effective in neutral capillaries which have no EOF. An example of sensitivity enhancement using this method is shown in Fig. 7 but it should be emphasised that electrokinetic injection will result in preferential loading of more highly charged species. This is illustrated in Fig. 7 by the relative increase in the absorbance of the early migrating (more highly charged) of the two princi-

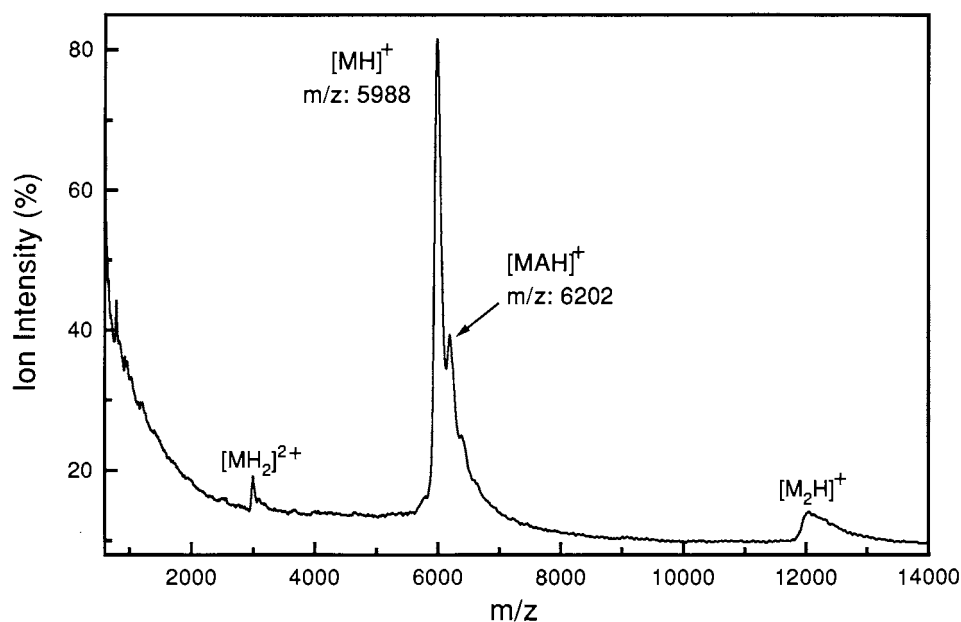


Fig. 6. Analysis of purified sheep MT-1 by matrix-assisted laser desorption–time of flight mass spectrometry (MALDI-TOFMS) using a Finnigan MAT ‘Lasermat’ Mass Analyser instrument. The sample (1 μ l) containing 30 pmol of sheep MT-1 in sinapinic acid (10 mg ml⁻¹), was applied and dried onto the target surface of the metal sample slides. After loading and evacuating the sample chamber, the slide target surface was bombarded with laser light at 30% power and 30 shots were summed to obtain the spectrum. Mass calibration was external using insulin and ubiquitin. $[MH]^+$ is the protonated molecular ion of MT-1 (all isoforms), $[MH_2]^{2+}$ is the double-protonated ion and $[M_2H]^+$ is a protonated MT-1 dimer. $[MAH]^+$ is the putative protonated sinapinic adduct ion of MT-1.

pal peaks following electrokinetic loading as compared with hydrodynamic injection.

Of the on-line pre-concentration techniques, perhaps the most elegant method is isotachopheresis (ITP), since it efficiently enhances both sensitivity and selectivity. However, on-line ITP-CE instruments are not yet commercially available. A less sophisticated but practical method employs on-line solid phase extraction (SPE-CE), which can be adapted to existing instrumentation [42–44] and has been applied to the analysis of MT isoforms [37,38]. Although the solid phase extractors have to be constructed in the laboratory, the procedure is straightforward, taking about 10 min with experience, and the materials are inexpensive and commonly available [37]. With appropriate reversed phase material and loading/separation conditions, the SPE device has been used for at least 100 separations of MT isoforms in tissue extract samples, giving at least a

100-fold sensitivity enhancement for injection times up to 5 min. An example of a SPE-CE separation of rabbit MT (0.1 mg ml⁻¹, 60 s injection) is shown in Fig. 8 and peak areas of the two separated isoforms are almost 40-fold greater than those obtained by a CE separation of the same sample without the SPE device [38].

6. Conclusions

Mammalian MTs often contain multiple isoforms encoded by different genes and various traditional electrophoretic and chromatographic techniques, with the exception of RP-HPLC, have proved inadequate in separating these proteins. Reproducible separations of these isoforms have been demonstrated by a variety of CE techniques, which have the advantages of being rapid (usually under 15 min), requiring very little sample (nl

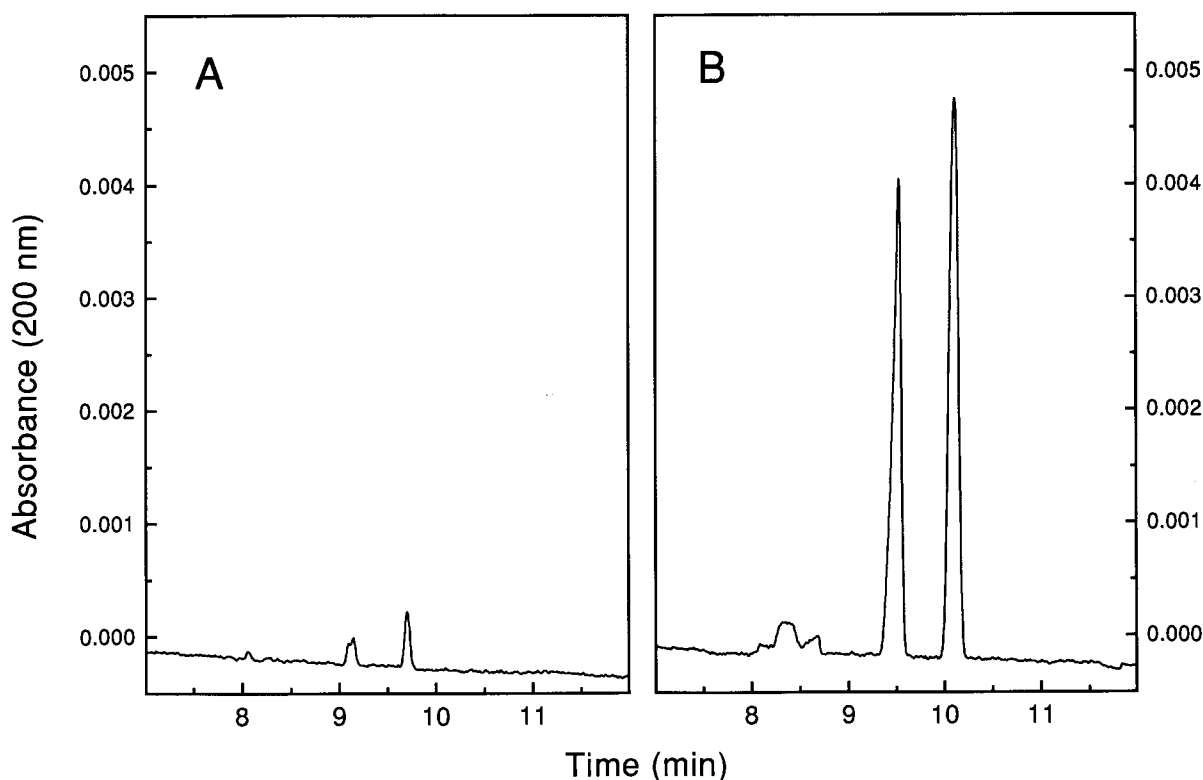


Fig. 7. Sensitivity enhancement using electrokinetic sample loading in combination with a neutral capillary at neutral pH and reversed polarity (anode at outlet). A sample of purified rabbit MT-2 (2 mg ml^{-1} in deionised water) was loaded by pressure injection for 30 s at 0.5 psi (A) or electrokinetically at 5 kV for 30 s (B). A $57 \text{ cm} \times 50 \text{ }\mu\text{m}$ 'Celect-N' stable neutral capillary (Supelco, Poole, UK) was used in combination with a 50 mM sodium phosphate buffer pH 7.0. Electrophoresis was performed at 20 kV and 25°C .

quantities) and having a very high resolution, which in combination with a wide flexibility of electrolyte chemistry and capillary coating, can be utilised to separate proteins of very similar structure. Although many CE techniques can be applied to the qualitative evaluation of isoform composition or their quantitative assay, careful selection of the most appropriate separation conditions and capillaries for the study objective is desirable. Table 1 summarises a variety of separation conditions which have been shown to be advantageous for MT isoform separation. The most appropriate conditions for qualitative evaluation would appear to be low pH phosphate buffers in combination with uncoated capillaries or neutral pH phosphate buffer in combination with a polyacrylamide-coated neutral capillary.

Quantitative work is best attempted using borate–SDS electrolytes at alkaline pH in uncoated capillaries. Samples can be prepared using a rapid two-step solvent extraction method and the identity of separated components can be verified using diode array detection and/or mass spectrometry. Detection sensitivity can be enhanced using a novel on-line solid phase extraction device, whose utility and reproducibility has been recently demonstrated.

Acknowledgements

The author would like to thank Prof. Ian Bremner and Dr Adrian West for their helpful comments on this manuscript and Florian Graedler

Table 1
Summary of conditions demonstrated to be suitable for the analysis of metallothionein isoforms by capillary electrophoresis

Application	MT sample		Electrolyte		Capillary		Injection		Separation		Ref.	
	Species	Conc ^a	Buffer	pH	Additive	L	I.d.	Coating	Type	Time (s)		Temp (°C)
Qualitative	Rabbit/horse	5 mg ml ⁻¹	150 mM Phosphate	2.5	None	57	50	Uncoated	PR 0.5	10	25	30 NP
	Horse	5 mg ml ⁻¹	500 mM Phosphate	2.0	None	27	20	Uncoated	PR 0.5	10	25	15 NP
	Horse	1 mg ml ⁻¹	110 mM Tris-borate	6.9	None	57	50	Uncoated	PR 0.5	10	20	20 NP
	Sheep	1 mg ml ⁻¹	500 mM Borate	8.4	100 mM SDS	57	25	Uncoated	PR 0.5	10	25	10 NP
	Rabbit	1 mg ml ⁻¹	500 mM Borate	10.4	100 mM SDS	57	25	Uncoated	PR 0.5	10	25	10 NP
	Rabbit	1 mg ml ⁻¹	100 mM Phosphate	7.0	None	57	50	Polyamine	PR 0.5	10	25	20 RP
	Rabbit	1 mg ml ⁻¹	50 mM Phosphate	7.0	None	37	50	Polyacrylamide	PR 0.5	3	25	18.5 RP
	Sheep	>20 µg ml ^{-1a}	300 mM Borate	8.4	85 mM SDS	57	75	Uncoated	PR 0.5	1–10	25	10 NP
	Mouse	>30 µg ml ^{-1a}	25 mM HEPES-Tris	7.4	None	33	75	Polyacrylamide	Gravity	3	26	15 RP
	Chicken	>0.3 µg ml ^{-1a}	500 mM Phosphate	2.0	None	27	20	Uncoated	PR 0.5	10	25	15 NP
Sheep	>0.3 µg ml ^{-1a}	20 mM Phosphate	7.0	None	57	75	Uncoated	SPE 0.5	300	25	20 NP	

^a Figures based on detection of MT isoforms in tissue extracts. Detection limit concentrations for purified standards can be up to 10-fold lower.

L, length (cm); I.d., internal diameter (µm); PR, hydrodynamic injection at specified pressure (psi); SPE, on-line solid phase extraction; NP, normal polarity (–ve at outlet); RP, reversed polarity (+ve at outlet).

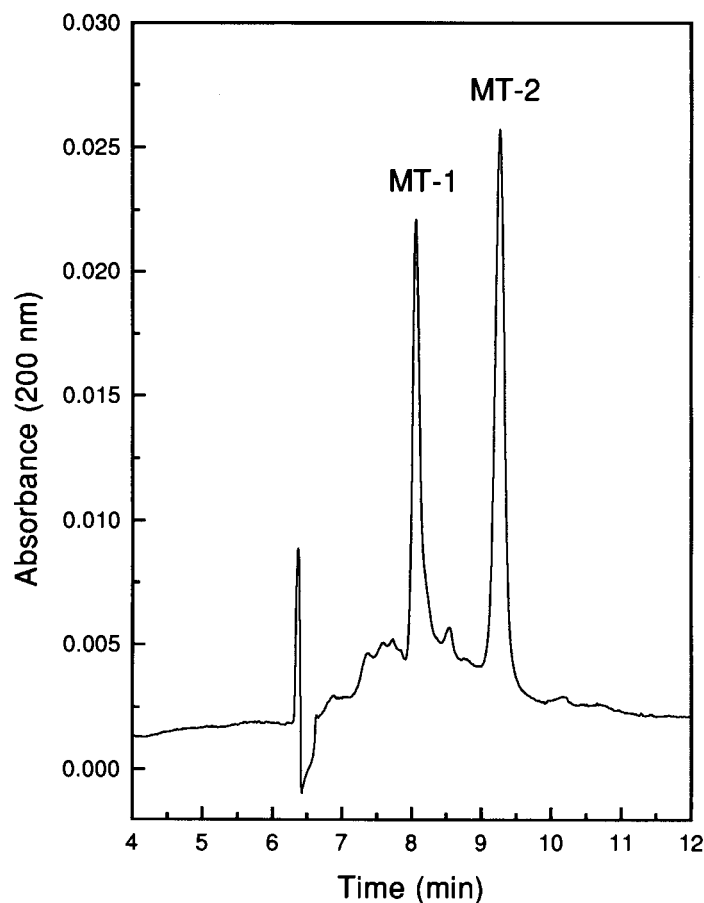


Fig. 8. On-line solid phase extraction for the pre-concentration of MT prior to elution and separation by capillary electrophoresis. Rabbit liver MT (0.1 mg ml^{-1} in deionised water) was injected for 60 s at 0.5 psi and the SPE device washed with electrolyte buffer (30 mM sodium phosphate, pH 7.0) for 1 min. Bound components were eluted by injecting 33% acetonitrile in 15 mM sodium phosphate buffer, pH 2.5, for 9 s at 0.5 psi and electrophoresis was performed in an uncoated $57 \text{ cm} \times 75 \text{ }\mu\text{m}$ capillary at 30 kV and 25°C .

for analysis of sheep MT-1 by MALDI-TOFMS. This work was supported by the Scottish Office Agriculture, Environment and Fisheries Department, U.K.

References

- [1] M. Margoshes, B.L. Vallee, *J. Am. Chem. Soc.* 79 (1957) 4813.
- [2] J.H.R. Kägi, B. Vallee, *J. Biol. Chem.* 235 (1960) 3460.
- [3] J.H.R. Kägi, B.L. Vallee, *J. Biol. Chem.* 236 (1961) 2435.
- [4] G.F. Nordberg, M. Nordberg, M. Piscator, O. Vesterberg, *Biochem. J.* 126 (1972) 491.
- [5] J.H.R. Kägi, S.R. Himmelhoch, P.D. Whanger, J.L. Bethune, B.L. Vallee, *J. Biol. Chem.* 249 (1974) 3537.
- [6] M. Piscator, *Nord. hyg. Tidskr.* 45 (1964) 76.
- [7] M. Kimura, N. Otaki, T. Kakefuda, in: J.H.R. Kägi, M. Nordberg (Eds.), *Metallothionein*, Birkhauser Verlag, Basel, 1979, p. 187.
- [8] P.E. Hunziker, *Methods Enzymol.* 205 (1991) 244.
- [9] P.E. Hunziker, P. Kaur, M. Wan, A. Kanzig, *Biochem. J.* 306 (1995) 265.
- [10] G.K. Andrews, *Prog. Food Nutr. Sci.* 14 (1990) 193.
- [11] A.K. West, R. Stallings, C.E. Hildebrand, R. Chiu, M. Karin, R.I. Richards, *Genomics* 8 (1990) 513.
- [12] Y. Uchida, K. Takio, K. Titani, Y. Ihara, M. Tomonaga, *Neuron* 7 (1991) 337.
- [13] L.C. Liang, K. Fu, D.K. Lee, R.J. Sobieski, T. Dalton, G.K. Andrews, *Mol. Reprod. Dev.* 43 (1996) 25.

- [14] A.K. Sewell, L.T. Jensen, J.C. Erickson, R.D. Palmiter, D.R. Winge, *Biochemistry* 34 (1995) 4740.
- [15] R.D. Palmiter, S.D. Findley, T.E. Whitmore, D.M. Durnam, *Proc. Natl. Acad. Sci. U.S.A.* 89 (1992) 6333.
- [16] M.H. Vasconcelos, S.-C. Tam, J.H. Beattie, J.E. Hesketh, *Biochem. J.* 315 (1996) 665.
- [17] M.P. Richards, J.H. Beattie, *J. Cap. Elec.* 3 (1995) 196.
- [18] S.F.Y. Li, *J. Chromatogr. Sci.* 33 (1995) 669.
- [19] J.F. Riordan, B.L. Vallee (Eds.), *Metallobiochemistry. Part B: Metallothionein and Related Molecules, Methods in Enzymology*, vol. 205, Academic Press, San Diego, 1991.
- [20] G.Q. Liu, W. Wang, X.Q. Shan, *J. Chromatogr. B. Biomed. Appl.* 653 (1994) 41.
- [21] V. Virtanen, G. Bordin, A.R. Rodriguez, *J. Chromatogr. A* 734 (1996) 391.
- [22] J.H. Beattie, M.P. Richards, R. Self, *J. Chromatogr.* 632 (1993) 127.
- [23] M.P. Richards, J.H. Beattie, R. Self, *J. Liq. Chromatogr.* 16 (1993) 2113.
- [24] M.P. Richards, P.J. Aagaard, *J. Cap. Elec.* 1 (1994) 90.
- [25] M.P. Richards, J.H. Beattie, *J. Chromatogr. B. Biomed. Appl.* 669 (1995) 27.
- [26] M.P. Richards, J.H. Beattie, *J. Chromatogr.* 648 (1993) 459.
- [27] T. Minami, H. Matsubara, M. O-higashi, K. Kubo, N. Okabe, Y. Okazaki, *Electrophoresis* 17 (1996) 1602.
- [28] M.P. Richards, G.K. Andrews, D.R. Winge, J.H. Beattie, *J. Chromatogr. B-Bio. Med. Appl.* 675 (1996) 327.
- [29] S. Terabe, K. Otsuka, T. Ando, *Anal. Chem.* 57 (1985) 834.
- [30] J.H. Beattie, M.P. Richards, *J. Chromatogr. A* 664 (1994) 129.
- [31] J.H. Beattie, M.P. Richards, *J. Chromatogr. A* 700 (1995) 95.
- [32] T. Minami, H. Matsubara, M. O-higashi, N. Otaki, M. Kimura, K. Kubo, N. Okabe, Y. Okazaki, *J. Chromatogr. B. Biomed. Appl.* 685 (1996) 353.
- [33] M.P. Richards, *J. Chromatogr. B. Biomed. Appl.* 657 (1994) 345.
- [34] M. Vasak, *Methods Enzymol.* 205 (1991) 39.
- [35] J. Hidalgo, M. Giralt, J.S. Garvey, A. Armario, *Am. J. Physiol.* 254 (1988) E71.
- [36] J.A.J. Thompson, A.E. Sutherland, *Comp. Biochem. Physiol. [B]*, 102 (1992) 769.
- [37] C.B. Knudsen, J.H. Beattie, *J. Chromatogr. A* (1997) in press.
- [38] J.H. Beattie, R. Self, M.P. Richards, *Electrophoresis* 16 (1995) 322.
- [39] X. Yu, M. Wojciechowski, C. Fenselau, *Anal. Chem.* 65 (1993) 1355.
- [40] J.H. Beattie, J. Lomax, M.P. Richards, R. Self, R. Pesch, H. Munster, *Biochem. Soc. Trans.* 24 (1996) 220S.
- [41] R.-L. Chien, D.S. Burgi, *Anal. Chem.* 64 (1992) 489.
- [42] N.A. Guzman, *J. Liq. Chromatogr.* 18 (1995) 3751.
- [43] M.A. Strausbauch, B.J. Madden, P.J. Wettstein, J.P. Landers, *Electrophoresis* 16 (1995) 541.
- [44] A.J. Tomlinson, S. Naylor, *J. Liq. Chromatogr.* 18 (1995) 3591.

Analysis for metallothioneins using coupled techniques

R. Lobinski *, H. Chassaigne, J. Szpunar

LPPM, CNRS URA 348, University of Bordeaux I, 33 405, Talence, France

Received 18 November 1996; accepted 9 December 1996

Abstract

Analytical chemistry of metallothioneins based on the coupling of a high resolution separation technique with an element or species selective detection technique is discussed. The role of size-exclusion chromatography (SEC) with on-line atomic spectrometric detection for the quantification of metallothionein fraction in cell cytosols is evaluated. Particular attention is given to the conditions for the separation of metallated metallothionein isoforms (MT-1, MT-2, MT-3) and sub-isoforms within these classes by anion-exchange and reversed-phase HPLC. Techniques for interfacing chromatography with atomic absorption spectrometry (AAS), inductively coupled plasma atomic emission spectrometry (ICP AES) and ICP mass spectrometry (MS) are assessed. The potential of electrospray (tandem) mass spectrometry for the characterization of metallothionein isoforms with respect to molecular mass and amino acid sequence is highlighted. Perspectives for capillary zone electrophoresis (CZE), microbore and capillary HPLC with ICP MS and electrospray MS(/MS) detection for the probing of metallothioneins are discussed. Applications of hyphenated techniques to the analysis of real-world samples are reviewed. © 1998 Elsevier Science B.V. All rights reserved.

Keywords: Metallothioneins; Coupled techniques; High resolution separation technique

1. Introduction

Metallothioneins (MTs) are a group of non-enzymatic low molecular mass (6–7 kDa), cysteine-rich metal-binding proteins which are resistant to thermocoagulation and acid precipitation [1–3]. The most popular are mammalian MTs that have been isolated from kidney, liver and brain samples; MTs isolated from mussels, plants and fungi

have also been reported. The interest in the determination and characterization of MT-isoforms is a derivative of their role in homeostatic control, metabolism and detoxification of a number of essential (Zn, Cu) and toxic (Cd, Hg) trace metals. Also, being the product of genetic polymorphism characteristic of MT genes in animals and humans, MT-isoforms draw attention to studies on metal-mediated gene expression mechanisms [1–3].

Classical techniques for the determination of MTs include metal-saturation assays [4,5,8,12,13], polarography [6,7,10] and immunological assays, both radioimmunoassay (RIA) [10,11] and en-

* Corresponding author. Present address: CNRS EP132, Hélioparc, 2, av. Pr. Angot, 64000 PAU, France. Tel.: +33 559 806884; fax: +33 559 801292; e-mail: Ryszard.lobinski@univ-pau.fr

zyme-linked immunosorbent assay (ELISA) [5,6,9]. Recent studies on the measurement of metallothionein and its isoforms have been reviewed [14]. Metal saturation assays based on the competitive displacement and the subsequent determination of the initially MT-bound metal (usually Cd and Zn) by a metal with higher affinity to MT (usually Hg and Ag) depend sometimes on speculative assumptions of stoichiometry and lack selectivity with regard to the individual MT-isoforms. Electrochemical techniques based on the quantification of MT-fraction via sulfhydryl groups may suffer from interferences by other redox systems present in the sample and fail to give information both on the initial metal content and on the isoform composition. The unmatched absolute detection limits (down to 1 pg) by immunological assays (RIA or ELISA) are off-set, because of the difficulties encountered in raising high titers of antibodies, by their length, inability to quantify individual MT isoforms in a mixture, and inability to provide information on the original metal composition. The key challenges to the analytical chemistry of metallothioneins include: (1) selectivity with regard to the different MT iso- and sub-isoforms, (2) selectivity with regard to metal, and (3) sensitivity, able to cope with non-induced levels in real-world samples.

The isoform selectivity can be achieved using high performance separation techniques; various modes of high performance liquid chromatography (HPLC) or electrophoresis have become standard [15,16]. The relatively poor sensitivity of quantification based on the UV-signal or on dye-staining does not generally allow the non-induced concentrations of MTs to be determined. More important is that the lack of sufficiently pure calibration standards does not allow for unambiguous identification of MT-isoforms in HPLC and CZE chromatograms whereas the accuracy of molecular mass assessment in SEC leaves a lot to be desired. Additional information totally lost refers to the metal composition of the metallothioneins studied.

In the last decade a universally accepted approach to speciation analysis has been offered using hyphenated (coupled, hybrid) techniques which are undergoing rapid and continuous devel-

opment [17–21]. They are based on a combination of separation techniques (gas chromatography (GC), HPLC, or CZE) with a sensitive and species selective detector (atomic absorption, plasma emission or mass spectrometer). The recent explosion of electrospray ionization MS [22,23], collision induced dissociation (CID) for tandem MS [24], and enhanced fragmentation in the ion-spray source [25] opens new exciting possibilities for the detailed characterization of metallothioneins in terms of molecular mass, amino acid sequence, and metal content, respectively.

The state-of-the-art and opening perspectives for coupled techniques in the field of quantification and characterization of metallothioneins is the topic of this paper.

2. The joy of coupling

There exists various possibilities for on-line coupling between a separation technique and an element (moiety, species) specific detector for the characterization and determination of metallothioneins. They include different modes of HPLC or capillary zone electrophoresis (CZE) on the separation side, and flame AAS, ICP AES, ICP MS or electrospray MS(/MS) on the detection side. The choice of a hyphenated system depends primarily on the research objective. The separation component of the coupling system is favoured when the characterization of the maximum number of iso- or sub-isoforms is of interest, whereas the detector component becomes crucial when a high sensitivity is required.

Various separation mechanisms have been proposed for the separation of metallothionein isoforms. The separation of the MT fraction is usually achieved with SEC, this method, however, is unable to distinguish between the different isoforms. Separation of Cd and Hg-MT-fraction in spiked human urine by affinity chromatography was reported [26]. The characterisation of amino acid microheterogeneities has been achieved by anion-exchange and reversed phase which allowed the definition of the major MT classes (MT-1, MT-2, ...). The resolution of capillary elec-

trophoresis has enabled a further subdivision of the major isoforms into a variety of sub-isoforms.

The presence of a metal bound to MT is a prerequisite when using an “inorganic” atomic spectrometric detector such as atomic absorption, ICP atomic emission or ICP MS spectrometer. The ADLs of several femtograms of the latter often make it possible to detect non-induced metallothioneins in on-line mode (in contrast to immuno assays). The linear range and multielement capability of these detectors make them a rapid alternative to metal-saturation assays. An electrospray mass spectrometer is unmatched when characterising MT isoforms in terms of molecular mass. A CID cell and another mass spectrometer in series are necessary to provide structural information in terms of the amino acid sequence.

An important problem often encountered is the interface between chromatography and spectrometry, as the separation conditions may not be compatible in terms of flow rate and mobile phase composition with those required by the detector. High concentrations of organic solvents in reversed-phase HPLC negatively affect the plasma but enhance the ESI process. On the other hand, the relatively concentrated buffers used in ion-exchange chromatography suppress the signal in electrospray. The nanoliter sample volume and low microliter per minute flow rate makes the dead volume and sensitivity critical in AAS and plasma techniques, whereas they are not far from the optimum nebulization techniques in ESI MS. These considerations make the choice and optimization of the best hyphenated system for a given task difficult and requires some experience.

3. Separation of metallothioneins

Since the complexation equilibria between metallothioneins and metals are strongly pH-dependent, the control of pH on the mobile phase is crucial irrespective of what separation technique is used. Acidic pH is responsible for the depletion of metals leading gradually to apoforms. For instance, Zn is lost at pH 5, at pH 3.0 Cd₄ adducts isoforms are present, at pH 2 copper still

remains attached. Various intermediate forms partially metallated occur at various pH regions. The buffer chosen should therefore ensure that speciation of the analyte be unaltered during its passage through the column.

3.1. Size-exclusion chromatography

Size-exclusion chromatography (SEC) is based on the molecular sieve effect and enables species to be separated according to their size, and to a lesser extent, shape. The average time a substance spends in the pores is determined by its size which for a given shape, can usually be related directly to its molecular weight. The resolution of SEC is insufficient for discrimination of small amino acid heterogeneities, this technique serves in the separation of the MT fraction from samples. Applications of SEC to the quantification of the MT-fraction from biological cytosols are summarized in Table 1.

3.1.1. Packing

Separation by SEC should be independent of the analyte's charge but in practice the stationary phase surface displays charged properties so that a mixed mode separation is observed. This makes the choice of packing critical. The two categories of packing used included silica and organic polymers. At nanogram metal levels, significant silanophilic effects including metal losses in the presence of low ionic strength eluents on silica-based SEC supports were detailed [4,13,38]. A copolymeric styrene-divinylbenzene SEC support which provides a symmetrical peak with negligible losses of Cd during chromatography was proposed [4,13]. The average pore size of the packing used varied from 100 to 1000 Å.

3.1.2. Mobile phase

The optimum eluent should ensure minimum competition between buffer and cytosolic ligands, and between these ligands and the gel. The separation by SEC with H₂O as mobile phase prevented structural changes, denaturation of proteins and destruction of protein–metal complexes [39]. In practice, various aqueous mobile phases of fairly high ionic strength have been used

Table 1
Size-exclusion chromatographic methods for the separation of metallothioneins

Element	Sample	Column	Eluent (flow rate)	Detection	Reference
Cu, Zn	Vegetables	Sephadex G-50 superfine (700 × 30 mm)	20 mM Tris-HCl, pH 8.0 (5°C)	UV (254 nm), off-line GF AAS	[28]
Cu	Mussel tissue (digestive gland)	Progel TSK G3000 SW (30 cm × 7.8 mm)	50 mM K ₂ HPO ₄ -KH ₂ PO ₄ buffer, pH 7.5 (0.7 ml min ⁻¹)	ICP AES	[29] [30]
Cd, Zn	Mussel tissue (digestive gland)	GPC Water ProteinPack 125 Sephadex (100 cm × 1.5 cm) with a 3 cm guard column	50 mM K ₂ HPO ₄ -KH ₂ PO ₄ buffer, pH 7 (0.7 ml min ⁻¹)	UV (254 nm) ICP AES	[31]
Cd, Zn	Cd-induced rat liver	Sephacryl S-100 (120 × 1.6 cm)	10 mM (NH ₄) ₂ CO ₃	AAS	[27,33]
Cd	Pig kidney	Pharmacia Superose-12 (2 cm × 5 mm)	120 mM Tris-HCl, pH 7.5	ICP MS	[33]
Cd	Pig kidney simulated gastro-intestinal digest	Progel-TSK, G 3000PWxL, (30 cm × 7.8 mm)	30 mM Tris-HCl, pH 8.6	AAS, ICP MS	[4], [13]
⁶³ Cu, ⁶⁶ Zn and ¹¹⁴ Cd	Osprey blood, mussels	Progel-TSK G2000 SW (60 cm × 7.5 mm)	100 mM Tris-HCl/100 mM NaCl, pH 7.4/0.02% NaN ₃ (1 ml min ⁻¹)	UV (220 nm), on-line radioactivity	[34]
³⁵ S	³⁵ S-containing hepatoma tissue culture	Asahipak GFA-30F (30 cm × 7.6 mm)	50 mM Tris-HCl pH 7.5 and 200 mM (NH ₄) ₂ SO ₄ /0.1 mM EDTA (0.8 ml min ⁻¹)	ICP MS	[35]
Zn isotope ratios	Chicken meat simulated gastro-intestinal digest	Pharmacia Superose-12 (30 cm × 10mm)	100 mM CH ₃ COONH ₄ 0.1% TFA, pH 6.0	ICP MS	[36]
	Rat liver	Sephadex G-75 column (1 m × 24 mm)	50 mM Tris-HCl pH 6.8 (1 ml min ⁻¹)	UV (254 nm)	[37]
	Freshwater mussels (<i>Anodonta grandis</i>)	TSK SW2000 (30 × 0.75 cm) and a precolumn TSK (7.5 × 0.75cm)	10 mM Tris-HCl-100 mM NaCl-0.03% NaN ₃ (pH 7)(0.5 ml min ⁻¹)	UV (254, 280 nm)	[38]
Cd	Defatted human breast milk	Merck Fracto-TSK-gel SW 55 (6 cm × 4 mm)	H ₂ O (0.5 ml min ⁻¹)	UV (280 nm)	[39]
		TSK gel G3000 SW	Tris-HCl (pH 7.2–8.6) (1 ml min ⁻¹)	UV, AAS	[40]
	Rat kidney	Protein-Pack 125 (30 cm × 7.8 mm)	20 mM HCOONH ₄ buffer of pH 7.65 (1 ml min ⁻¹)	UV (254 nm), off-line radioactivity, liquid scintillation for ²⁰³ Hg	[41]
Cd	<i>M. galloprovincialis</i>	Progel TSK G3000PWxL (30 cm × 7.8 mm)	30 mM Tris-HCl (0.8 ml min ⁻¹)	ICP MS	[42]
⁶³ Cu, ⁶⁸ Zn, ¹¹⁴ Cd	Cyanobacterium	Dupont GF-250 (250 × 9.4 mm)	50 mM Tris-HCl, pH 7.5, 0.2 M (NH ₄) ₂ SO ₄	ICP MS	[43]

to avoid interactions with the packing material. Dilute buffers, in general, may cause adsorption of low molecular weight proteins by the column packing. When silica-based packings cannot be avoided, the addition of a non-complexing salt (e.g. 100 mM NaCl) to the mobile phase was shown to suppress the residual silanol activity of the column packing [38]. Under these conditions no significant exchange of Cd occurred but occasional (for Hg) or appreciable losses (for Zn) were observed for other metals [38].

The addition of EDTA, proposed by some authors to minimize metal ion-gel interactions [43] was found unsuitable by others [33] because of the occasional presence of anomalous Cd peaks in subsequent runs. Polymeric supports suffer from the deposition of excess free Cd^{2+} which interacts with analytes, often causing severe degradation in peak resolution [13]. Because the weak complexing character of Tris is not sufficient to compete with the polymeric support for Cd^{2+} , complexation with β -mercaptoethanol was advised [13].

The wide variety of buffers reported in the literature (Table 2) makes it relatively easy to choose a suitable one for the detection technique. Up to 30 mM Tris-HCl was found to be tolerated in ICP MS whereas 20 mM formate or acetate buffer in 10% methanol was found to be acceptable for ESI. Addition of 0.03% NaN_3 as a retardant of bacterial activity is advised to protect the column from damage resulting from bacterial growth when real-world samples are analysed.

3.1.3. Analysis time

This is a function of column size and flow rate. Even though columns up to 120 cm were used the standard 30×7.6 mm column is a good choice. At a flow rate of 1 ml min^{-1} , the separation requires ca. 20 min to go to completion. Separation of MT-bound and unbound cadmium within 3 min on a 4.0 cm SEC column was reported [42]. The choice of small-bore columns with size-exclusion packings on the market is still limited, such columns enable rapid characterization of various metal-containing molecular weight fractions in unknown cytosols by direct injection nebulization ICP MS or ESI-MS.

3.2. Reversed-phase chromatography (RPC)

The separation of MT-isoforms is most frequently carried out using reversed-phase chromatography between a non-polar stationary phase (usually a covalently bound C_8 or C_{18} linear hydrocarbon), and a relatively polar mobile phase. Reversed-phase HPLC seems to be superior to SEC and ion-exchange, because the packing material for RPC is principally free of ligands for metals [44]. Since hydrophobicity of a polypeptide primarily dictates its retention in RPC, gradual elution of individual MT isoforms of a mixture is achieved by decreasing the polarity of the mobile phase by the addition of methanol or acetonitrile. Isolation of MT-isoforms by RP-HPLC was reviewed [15]. Applications of reversed-phase chromatography to the separation of MT-isoforms is summarized in Table 2.

Wide-bore (4–5 mm) 15–25 cm long columns are the most frequently used. The narrow-bore and microbore columns are expected to gain significance, because of their higher sensitivity and resolution. The presence of a 10–50 mM buffer is necessary. Tris-HCl is the most widely used in the separation of metallated isoforms. Apo-MT-isoforms have been separated using 0.1% trifluoroacetic acid (TFA) [46,48] or sub-percent acetic acid [51]. The resolution of isoforms is affected by pH [47].

Table 2 shows that UV detection has been used so far in most cases. This is because the high content of organic modifier makes the RP HPLC not quite compatible with ICP MS. A set of Pt-cones and the addition of oxygen to the nebulizer gas are highly recommended. Loss in sensitivity is unavoidable. On the other hand, RP separation conditions are close to the ideal for ESI MS detection which is expected to gain popularity in near future.

3.3. Anion-exchange chromatography

MT-1 and MT-2 fractions, which have a negative charge in aqueous solutions can be separated using anion exchange chromatography. High performance liquid chromatography is usually employed but the use of a fast-flow anion-exchange

Table 2
Reversed-phase chromatographic methods for the separation of metallothioneins

Element	Sample	Column	Column	Eluent (flow rate)	Detection	Reference
⁶⁴ Cu	Chicken macrophage and hepatic cytolysis	Pecosphere-3C C ₁₈ (8.3 cm × 4.6 mm × 3 μm)		Gradient elution: 100–90% of aq. 60% CH ₃ CN in 10 mM NaH ₂ PO ₄ in 5 min (1 ml min ⁻¹)	UV (214, 280 nm) (DL 1 μg)	[45]
	⁶⁴ Cu-labelled hepatoma tissue culture incubated for 24 h in a growth medium	μ-Bondapak C ₁₈ Radial Pack (10 cm × 8 mm × 10 μm) with a C ₁₈ precolumn		Gradient elution with 25 mM Tris-HCl buffer of pH 7.4 and 60% CH ₃ CN in the buffer (1.25 ml min ⁻¹)	UV (214 nm), on-line radioactivity detection	[34]
Cd, Cu, Zn	Liver tissue	LiChrospher 100 RP-8 (12.5 cm × 4 mm × 5 μm)		20 min linear gradient from 0.5–30% MeOH in 50 mM Tris-HCl buffer (pH 7.0) (1.5 ml min ⁻¹)	ICP MS	[35]
	<i>Anacystis nidulans</i>	Capcellpak C ₈ (15 cm × 4.5 mm)		CH ₃ CN/50 mM Tris-HCl pH 7.5 (9:91) and 0.1 mM-EDTA (1 ml min ⁻¹)	ICP MS	[35]
	Crab hepatopancreas	Waters C ₁₈		Gradient elution with aq. 0.1% TFA-0.1% TFA in CH ₃ CN (9:1 to 2:3 in 40 min)	UV 254 nm, off-line F AAS, GF AAS	[46]
	Fractions corresponding to the metallothionein peak, were combined and concentrated under N ₂	μ Bondpak C ₁₈ (30 cm × 7.8 mm × 5 μm)		Gradient elution with 100% Tris-HCl (Ph 6.8) (A) and A-CH ₃ CN (2:3, B) from 0–30% B over 30 min (1.25 ml min ⁻¹)	UV (220 nm)	[37]
	Liver, horse kidney and rabbit, human, rat, chicken, pig and sheep liver	Vydac C ₈ (25 cm × 4.6 mm)		Two-step linear gradient elution with CH ₃ CN in 10 mM sodium phosphate buffer of pH 2.5, 7 or 11 (1 ml min ⁻¹)	UV (214 nm)	[47]
Cu, Cd, Zn	Fish tissue (breem)	Merck Purosphere® RP-18 (250 mm × 4 mm × 5 μm)		Gradient elution with 30 mM acetate buffer pH 7 (A) and methanol (B).10–30% B in 15 min. isocratic with 30% B). 0.5 ml min ⁻¹ .	ICP MS	[42]
Cu, Zn	Crab hepatopancreas	Nova-Pak C ₁₈ (30 cm × 3.9 mm × 4 μm)		Gradient elution with 10–60% of 0.1% TFA (II)-CH ₃ CN in 0.1% II- H ₂ O (0.5 ml min ⁻¹)	UV (254 nm)	[48]
	Liver and kidney tissue	μ-Bondapak C ₁₈ (10 cm × 8 mm × 10 μm)		Negative gradient of 10 mM sodium phosphate (pH 7.0) in the same buffer containing 60% of CH ₃ CN (3 ml min ⁻¹)	UV (214 nm)	[49]
Cd, Cu, Zn	Liver or kidney tissues	PLRP-S (15 cm × 4.6 mm × 8 μm)		Gradient elution with 10 mM (NH ₄) ₂ HPO ₄ (pH 8.2)	UV (220 nm), AAS	[50]
	Melphalan-modified peptides released from rabbit liver metallothionein by tryptic digestion	Synchrom C ₁₈ (25 cm × 1 mm × 6.5 μm)		Gradient elution with aq. 0.25% CH ₃ COOH and 0.25% CH ₃ COOH in CH ₃ CN (25 μl min ⁻¹)	UV (206 nm) and ESI MS	[51]

column (40×3 cm) has been reported [32]. Separation efficiency and recovery were the same as the conventional method, but analysis time was reduced to one-third [32]. Usually, metallothioneins before being applied to anion exchange are first pre-separated using SEC. Anion-exchange methods developed for the separation of metallothioneins (summarized in Table 3).

A weak-anion exchanger with diethylaminoethyl functional groups is the only type of the support used. Aqueous buffers are used with a linear concentration gradient. The high potential separation of the MT-1 and MT-2 isoforms by anion exchange is not fully exploited in the coupled systems because the common end-concentration of 0.25 M buffer is not tolerated well by ICP MS and suppresses the electrospray ionization.

3.4. Capillary electrochromatographic techniques

These techniques involve the separation of MT-isoforms in an electrical field [55–57]. Neutral compounds can be trapped in micelles of an ionic surfactant and thus can migrate in an aqueous solution using electrophoresis (micellar electrokinetic chromatography, MEKC) [58]. Application of CE to the separation of metalloproteins and metal binding peptides was reviewed [16]. The rapidity of CZE combined with the high separation efficiency and small sample requirements make this technique useful for the analysis of metallothionein isoforms. A comparison of CZE with reversed-phase HPLC showed these techniques to be complementary and employing both enables maximum information to be acquired [59]. Applications of capillary electrochromatographic techniques to the separation of MT isoform are summarized in Table 4.

The basic parameters that affect the CZE resolution include surface characteristics (untreated or coated capillaries), and the mobile phase composition (the buffer, its pH, concentration, and the presence of zwitterionic reagents, inorganic salts, metal ions, ion-pairing agents and organic solvents). The choice of capillary and running conditions depends on the complexity of the MT-mixture to be resolved. CZE in uncoated silica capillaries provides a rapid analysis of non-

heterogeneous MT-isomers in neutral or alkaline buffers. Most heterogeneous isomers, and those in complex matrices, can be separated using high-ionic strength (0.5 M) buffers [66]. Uncoated capillaries offer high speed analysis and durability but their resolution often leaves a lot to be desired.

Surface-modified capillaries (usually coated with a polyimide, polyamine or a linear polyacrylamide) provide enhanced resolution of MT isoforms [67]. The coating minimizes the interaction of MT with the wall and thus suppresses the electroosmotic flow (EOF), and consequently increases resolution [68]. The numbers of putative isoform peaks resolved from various animal species were human MT-1 (5–6), horse (3–5), pig (4–5), rabbit (3–6), rat (2–3) and sheep (4–5) [59]. The resolution of MT-isoforms is further affected by pH [47]. In neutral or alkaline media, the three basic MT-isoforms classes were well separated at pH 7 in 7 min, with MT-1 migrating the fastest and MT-3 the slowest. The spectra showed differences for the Zn and Cd forms. The order of migration of apoforms (at pH 2) was reversed [69].

Separation of MT-isoforms by MEKC using an SDS-containing borate buffer (pH 8.4) was reported but no advantage over CZE was apparent [63,67].

The basic drawback of electrophoretic techniques is poor sensitivity resulting from very small (a few nanoliters) samples that can be injected onto a capillary. This problem can be overcome by on-line preconcentration prior to the capillary inlet. A C_{18} concentrator was shown to enhance sensitivity (down to 0.1 g ml^{-1}) and specificity of MT isoform separation in sheep liver [70].

4. Interfacing HPLC with atomic spectrometry for probing MT-isoform

LC mobile phases consist typically of some combination of organic solvents, salts of buffer solutions and/or ion-pair reagents. The LC-AS interface should take into account the compatibility of composition and flow-rate of the chromatographic mobile phase with those acceptable by the

Table 3
Anion-exchange chromatographic methods for the separation of metallothioneins

Element	Sample	Column	Eluent (flow rate)	Detection	Reference
Cd, Zn	Cd-induced rat liver	DEAE-Sephacel Flow (40 × 3 cm)	Linear salt gradient (2–1) (limiting buffer, 250 mM Tris-HCl, pH 8.6)	AAS	[32]
⁶⁵ Zn	⁶⁵ Zn-containing hepatoma tissue culture incubated for 24 h in a growth medium	DEAE-5PW (7.5 cm × 7.5 mm) (Waters)	20 mM Tris-HCl of pH 7/0.02% NaN ₃ (A) and 250 mM Tris-HCl (pH 7)/0.02% NaN ₃ (B). 0–5 min: (A), 5–20 min: a linear gradient from (A) to (B) (1 ml min ⁻¹)	UV (220 nm) on-line radioactivity detection	[34]
Cd	Rabbit and mouse liver tissue	DEAE-5PW (Waters)	Gradient elution with 100% 10 mM Tris-HCl (pH 8.6) to 100% 250 mM Tris-HCl (pH 8.6) in 15 min (1 ml min ⁻¹)	UV, off-line AAS (DL 5 µg g ⁻¹)	[52]
Cd, Zn	Rat liver	DEAE-5PW (7.5 cm × 7.5 mm)	Gradient elution with 0–40% of 200 mM Tris-HCl (pH 7.4) in 10 mM Tris-HCl (1 ml min ⁻¹)	UV (214 nm), AAS	[53]
Cd	Kidney and liver	DEAE-5PW (7.5 cm × 7.5 mm) TSK gel DEAE-3SW	Gradient elution with Tris-HCl (10–250 mM, pH 8.6) (1 ml min ⁻¹) Gradient elution with Tris-HCl (pH 7.2–8.6) (1 ml min ⁻¹)	UV (254 nm), off-line GF AAS UV, AAS	[54] [40]
Cu, Zn	Crab hepatopancreas	DEAE-Sephacel	Gradient elution with 10–40 mM NaCl in 20 mM Tris-HCl	UV (254 nm), off-line F AAS, GF AAS	[46] [48]

Table 4
Capillary electrophoresis methods for the separation of metallothioneins

Sample	Injection (time)	Capillary	Electrolyte	Voltage (kV)	Temperature (°C)	Detection (nm)	Detection limit (range)	Reference
Chicken or sheep liver	Pressure (1 s)	Polyimide-coated fused-silica (50 cm × 75 µm)	100 mM-borate buffer of pH 8.4, 775 mM-SDS	10	25	200, 214, 254, 280	0.5–1 mg ml ⁻¹	[60]
Horse kidney, human, rat, chick, pig, rabbit and sheep liver		Fused-silica (57 cm × 75 µm)	10 mM-sodium phosphate buffer of pH 2.5, 7 or 11	30	25	200		[47]
Rabbit kidney		Untreated fused-silica column (70 cm × 50 µm)	20 mM-Na ₂ B ₄ O ₇ -10 mM-Tris, pH 9	10, 15, 20, 25	30	250	10–50 µg ml ⁻¹	[61]
Chicken liver		Polyamine-coated fused-silica (57 cm × 50 µm)	0.1 M-NaH ₂ PO ₄ -Na ₂ HPO ₄ , pH 7	20		200	5 µg ml ⁻¹	[59]
Eukaryotic species	2–4 s	Untreated polyimide-clad fused-silica (94 cm × 75 µm)	50 mM-Tris-HCl (pH 9.1)	30		214		[62]
Sheep liver	Low pressure (3.45 kPa) (10 s)	Untreated fused-silica (57 cm × 25 µm)	300 mM-borate-85 mM-SDS, pH 8.4	10	25	200 or 190-340		[63]
	Low-pressure (3.45 kPa) (2 s) for separation at pH 7, (5 s) for separation at pH 2	Uncoated (57 cm × 50 µm, 50 cm to detector)	50 mM-phosphate buffer of pH 2 or 7	30	25	200 or 190-340		
Rabbit liver, horse kidney (commercial)	Pressure (0.5 psi) (5 and 10 s)	Uncoated fused-silica (57 cm × 75 µm)	110 mM Tris-borate, pH 6.9	11	20	200		[64]
Purified and semi-purified MT samples from animal species			20 mM Tris-HCl (pH 9.1)	30			1 to 10–500 µg ml ⁻¹	[65]

detector. This criterion is often much more difficult to be fulfilled than in the case of the UV detector, where the optical transparency of the mobile phase above 200 nm is the only condition.

The requirements of an HPLC-AS interface vary according to the function of the separation mode and the detector used. Size-exclusion chromatography in general shows good compatibility in terms of the flow rates used ($0.7\text{--}1.0\text{ ml min}^{-1}$) and mobile phase compositions, unless concentrated buffers are used with AAS and ICP techniques. Organic solvents are not a problem in anion-exchange chromatography but the buffers used often exceed 0.1 M which can clog the nebulizers. In RPC the organic solvent must be accommodated, whereas the buffer concentration is seldom a problem. The flow rate depends strongly on the column geometry, varying the column inner diameter from 8 to 0.18 mm allows the flow rate to change from 10 ml min^{-1} to $2\text{ }\mu\text{l min}^{-1}$.

4.1. Atomic absorption spectrometry (AAS)

The metals that preferentially bind to MTs (Cd, Zn, Cu) are among the elements which give the most intensive response in AAS. Off-line analysis of MT-bound metals after HPLC by fraction collection and graphite furnace (GF) AAS analysis has been a common approach [54]. Being less sensitive than GF AAS, flame AAS offers the possibility of an on-line approach. This technique is compatible both with the flow-rates and with the mobile phase composition (including organic solvent) commonly used in HPLC. Taking into account the widespread availability of this technique, it is no wonder that HPLC-AAS was the first hyphenated technique to be used in the determination of MT-isoforms [71].

The basic interface is very simple. The outlet of the UV detector is coupled to the nebulizer of an atomic absorption spectrometer and Cd, Cu and Zn are determined at 228.8, 324.8 and 213.8 nm, respectively. This allows the molar ratios of the metals to be calculated for the major MT-isoforms. Calibration graphs were reported to be rectilinear up to 200 g ml^{-1} of metallothionein and up to 20 g ml^{-1} of metal [44,50].

Several advanced interfaces based on thermospray have been proposed [72–74]. A simple and inexpensive thermospray interface was described that could be connected to a flame AAS system without the need to modify the nebulizer and burner assembly [73]. Detection limits at low nanogram levels were reported [73]. Another design included a silica transfer line attached to the HPLC column end and positioned with a guide tube in a thermospray tube, which was fitted with a heating jacket. The super-heated mobile phase then passed to a pyrolysis chamber fitted with gas inlets for H_2 and O_2 . Calibration graphs were linear over two orders of magnitude from near the detection limits (sub-ng) with aqueous or methanolic mobile phases [72]. A micro-atomization interface (made of quartz tubes) which was fuelled by hydrogen and could operate with 100% aqueous mobile phase used in HPLC was developed [74]. The detection limit obtained for HPLC-AAS of Cd-MTs was over 200-fold lower than that obtained with using a conventional flame AAS detector, and ca. 30-fold lower than that obtained by a thermospray-enhanced flame AAS system [74].

The primary interest in HPLC-AAS lies in its simplicity, wide availability and compatibility with mobile phases used in HPLC. AAS is not truly a multielement technique; nevertheless, with the latest instruments, up to four elements can be measured simultaneously, which is sufficient for practical applications. Despite the fact that detection limits obtained with advanced interfaces almost match those of ICP MS, the primary field of application of HPLC-AAS is the characterization of MT-isoforms after metal saturation protocols.

4.2. Inductively coupled plasma atomic emission spectrometry

Compared with flame AAS, ICP AES offers lower (at the 1 ng ml^{-1} level) detection limits [29,30], but lower solvent compatibility. High organic solvent ($> 10\%$) contents may not be easily tolerated. The unmatched advantage of ICP AES is the possibility of the monitoring sulfur together with metals. A detection limit for S below 10 ng ml^{-1} is common. ICP AES instruments with axial

plasmas, recently commercialized, seem to offer lower detection limits for transition metals. Multi-element capability is an advantage of instruments equipped with a polychromator.

4.3. Inductively coupled plasma mass spectrometry

ICP MS has been enjoying considerable popularity because of its multielement character and low detection limits. A wider expansion of high resolution ICP mass spectrometers (with potentially lower detection limit and larger freedom of interferences) is hampered by the prohibitive cost of the instrumentation and high maintenance costs.

4.3.1. Conventional pneumatic nebulization interface

The interface is straightforward—a piece of narrow-bore tubing that connects the outlet of the LC column with the liquid flow inlet of the nebulizer. Typical LC flow rates of 0.5–2 ml min⁻¹ are within the range usually required for pneumatic nebulization. The limitation is the low (1–5%) transfer efficiency, losses in spray chamber, and thus degraded sensitivity. Aqueous eluents with buffer contents up to 50 mM are tolerated. Organic solvents negatively influence plasma performance because of the increasing instability of the plasma (up to extinction in extreme cases) and deposition of carbon on the sampling cone and torch. The use of a water-cooled spray chamber and an increase in RF power (up to 1.7 kW) can help to reduce the solvent load to the plasma and increase its stability. The addition of oxygen (1–3%) to the nebulizer gas flow can help to minimize carbon deposition and clogging of the sample cone at the expense of the cone's lifetime [35,75]. Salts can cause short-term signal depression or enhancement and cause blockage of the nebulizer and the sampling cone [76]. The potential of LC ICP MS for trace metal speciation was discussed [77]. In general, ICP MS needs more dilute buffers or a lower concentration of solvents than ICP AES. Post-column split and makeup with water to lower the concentration of the organic modifier is a possible remedy, however, at the expense of sensitivity [42].

4.3.2. Direct injection nebulizer interface

The direct injection nebulizer (DIN) is a micro-concentric pneumatic nebulizer with no spray chamber; it nebulizes the liquid sample directly into the central channel of the ICP torch. The low dead volume (< 2 µl) and the absence of a spray chamber in the DIN minimizes post-column peak broadening and facilitates the use of microbore LC columns and liquid flow rates (30–100 µl min⁻¹) [78]. Another advantage is the fast sample washout with minimal memory effects which is especially useful for Hg which shows memory effects when a spray chamber is used.

The carbon deposits on the sampler and skimmer orifices are less important than in the case of pneumatic nebulizer. Adding O₂ to the aerosol gas to prevent clogging by the salts dissolved in the mobile phase was not necessary for SEC [78]. Organic solvents in reversed phase chromatography require, however, the addition of oxygen to keep the plasma stable.

4.3.3. Hydraulic high pressure nebulizer interface

The hydraulic high pressure nebulizer (HHPN) not only enhances the sensitivity by one order of magnitude but also allows an optimum adaptation to the low flow-rate by choosing an optimal nebulization nozzle (10 µm instead of 20 or 15 µm) [35]. The HHPN is also less affected by salt content than the pneumatic nebulizer. A dedicated desolvation unit can cope with methanol concentrations usually used in reversed-phase chromatography.

5. Capillary zone electrophoresis interfaced with ICP MS

The major problem with the application of the CZE-ICP coupling is the small sample volume (typically 10–100 nl) which requires a very sensitive detector to cope with the naturally occurring analyte levels. In addition, the low flow rate (1–5 µl min⁻¹) limits the choice of nebulizer. In terms of the practical applications to the characterisation of MT-isoforms, the high resolution of CZE has thus long been off-set by the lack of a suitable element/species selective detector. The recent in-

strumental developments regarding the CZE-ICP MS and CZE-ESI MS coupling are likely to result in numerous contributions to the field of metallothioneins in the foreseeable future.

Olesik et al. [79] developed an interface in which the CZE capillary terminus, which was coated with silver paint (serving as a conductor to complete the electrophoresis circuit), was fitted into the center tube of a concentric, pneumatic nebulizer with a spray chamber. The latter was responsible for some band broadening. In another interface a glass frit nebulizer was used [80]. One end of the capillary was inserted through stainless-steel tubing, while the grounded buffer solution passed over the capillary in the same tubing along with the ground (earth) electrode. The electrical connection was complete to the point of aerosol formation. The clogging and the fairly complex configuration were expected to be overcome by the use of an ultrasonic nebulizer [80]. In another type of interface, the CE capillary was inserted into the nebulizer central tube and another fused-silica capillary was also inserted coaxially around the capillary. A coaxial liquid sheath of 10 mM NaCl was supplied through the outer capillary and used as the return ground for the CE capillary. The variable position of the CE capillary in the interface allowed a compromise between separation resolution and signal intensity [81]. An elegant interface based on commercially available components was built using the DIN [82]. The CE capillary was placed concentrically inside the fused-silica DIN sample introduction capillary. A makeup liquid was pumped at a flow rate of 15 $\mu\text{l min}^{-1}$ into the fused silica DIN sample transfer capillary via a T-connector. The makeup liquid established continuous and stable electrical contact at the exit (grounding) terminus of the CE capillary.

Some of the above interfaces were tested for characterization of MT-isoforms. The detection limit for ^{114}Cd was 4 fg for 74 nl injections which corresponds to 0.05 ng ml^{-1} in the injected sample [81]. This allows for characterization even of non-induced MT-isoforms.

6. Electrospray-ionization mass spectrometry

Electrospray ionization allows multiply charged molecular ions to be obtained without any fragmentation. The envelope of peaks in a mass spectrum is a manifestation of protons attaching to the species to give the multiple-charging phenomenon which is the basis for the very accurate molecular weight determination of polypeptides.

Despite its enormous potential this technique is just at the start of its use in the characterization of MT-isoforms and its complexes with metals. It was used for the determination of the major rabbit metallothionein isoform II [13]. ESI mass spectra of purified rabbit MT-2 revealed the presence of two isoforms in the sample that differed by 30 mass units, and the characteristic spectra for the apoproteins and metal-saturated proteins at acidic and alkaline pH gave information about the number and the identity of metals bound to the protein [83]. Recent unpublished studies showed an even higher number of putative MT-2 isoforms in a commercial MT-2 standard [84]. ESI is more interesting—the metallated proteins seem to produce stable ions in the gas phase. The method can be used to accurately and rapidly determine how many and what cations are incorporated in each molecule of protein. A single measurement provides information about molar distributions and estimates of relative abundances of various complexes in the sample. The method is faster and more sensitive than AAS coupled with protein analysis.

While measurement of molecular weight is a major step towards the characterization of an isoform, information on the amino acid sequence makes this characterization quasi-complete. Some data is likely to be obtained after dissociation of large multiply charged ions by collision with a neutral target gas in the collision cell. The m/z values of dissociation products are then measured in the second mass analyser [24]. Another potential use of the electrospray technique for MT characterization is enhancing fragmentation down to the elemental ion [25]. The combination of these three modes of data acquisition should enable the exhaustive characterization of the MT-isoforms.

6.1. High-performance liquid chromatography-ESI MS(/MS)

Pneumatically assisted electrospray (ion-spray) produces stable ion currents for a wide range of sample flow rates from less than $1 \mu\text{l min}^{-1}$ to greater than $200 \mu\text{l min}^{-1}$. An in-line splitter is provided to accommodate solvent flows up to 2 ml min^{-1} . The electrospray ionization source is compatible with 0.1% TFA buffers but better sensitivities are obtained with peptides using solvents containing 0.5% acetic acid. The use of concentrated buffers should be avoided since they suppress the signal.

In studies with sheep MT, the four isoforms predicted from gene sequencing information were resolved by acidic RP HPLC-ESI MS and their masses determined to within one mass unit of the predicted apoprotein values [85]. In another recently reported application, melphalan-modified peptides were released from rabbit liver metallothionein by tryptic digestion, and separated by LC on C_{18} column. By comparison with chromatograms from unmodified metallothionein, several alkylated peptides were identified [51].

6.2. Capillary zone electrophoresis-electrospray MS(/MS)

The normal electrospray flow rates between $1\text{--}10 \mu\text{l min}^{-1}$ are not much higher than that used in CZE. Interfacing is relatively straightforward using an adapter kit allowing for a makeup flow. A microionspray interface launched recently by SCIEX appears to offer a higher sensitivity.

7. Analysis of real samples

Sample preparation protocols used for the characterization of metallothionein isoforms in real samples are summarized in Table 5. Washing the cells in a Tris-HCl buffer (pH 8) containing 1 M EDTA to remove metal ions reversibly bound to the cell wall was recommended [35]. In most studies, SEC [32,34,37,41,46,48,50] has been preferred to heat treatment [29–31,33,54] for the isolation of the metallothionein fraction from a

tissue cytosol. Guidelines for the preparation of biological samples prior to quantification of MTs were discussed with particular attention to the care necessary to avoid oxidation [86].

Soluble extracts of tissues and cultured cells are prepared by homogenizing tissue samples in an appropriate buffer. Neutral buffers are necessary for extracting MTs since Zn start to dissociate from protein at pH 5. Cd and Cu are removed at lower pH values. A 10–50 mM Tris-HCl buffer at pH 7.4–9 is the most common choice [4,13,29–31,33,35,41,43,44,54,74]. For cytosols containing Cd-induced MTs dilution factors up to 10 have been used whereas for those with natural MT levels equal amounts of tissue and buffer have been found suitable.

Metallothioneins are prone to oxidation during isolation due to their high cysteine content. During oxidation disulphide bridges are formed and the MTs either copolymerize or combine with other proteins to move into the high molecular weight fraction. Since MTs may be oxidized by, e.g. oxygen, Cu(I) or heme components, the homogenization of tissues and subsequent isolation of MT should be performed in deoxygenated buffers and/or in the presence of a thiolic reducing agent [13]. β -Mercaptoethanol is added as antioxidant which also prevents the formation of dimeric forms of MT [44]. Other components added during homogenation include 0.02% NaN_3 , added as antibacterial agent [74,87] and phenylmethanesulfonylfluoride which is added as a proteases inhibitor [4,13,48,74]. The homogenization step is followed by centrifugation. The use of a refrigerated ultracentrifuge ($100\,000 \text{ g}$) is strongly recommended.

As a result a soluble fraction (cell supernatant, cytosol) and a particulate fraction (cell membranes and organelles) are obtained. Only the supernatant is analysed for metallothioneins. It is recommended that it is stored at -20°C under nitrogen prior to analysis [44]. Extraction efficiency by sucrose-Tris at pH 8 was 30–25% [33]. Other workers using experimental animals (rats and mice) have found that 50–80% Cd can be solubilized using similar extraction procedures [33]. The percentage of metals in the cytosols is typically 50–85% and 30–57% in the case of Zn and Cd, respectively [28,88].

Table 5
Sample preparation methods

Sample	Initial sample preparation	Centrifugation	Coagulation method	Preseparation	Reference
Foodstuffs (vegetables)	Homogenization in 20 mM Tris-HCl (pH 8.0)	20 000 rpm			[28]
Mussel tissue (digestive glands)	Homogenization in 20 mM Tris-HCl (pH 8.6), 0.5 M sucrose, in the presence of NaCl, leupeptin and 50 mM toluene- α -sulphonyl fluoride	20 000 rpm (10 min)	Thermocoagulation (10 min, 70°C)		[29] [30]
Cd-induced rat liver		Centrifugation	Treated with ethanol, the precipitate dissolved in 0.01 M Tris-HCl buffer (pH 8.6)	Sephacryl S-200 (90 \times 3 cm), elution with 0.01 M Tris-HCl buffer of pH 8.6 (2 ml min ⁻¹)	[32]
Chicken or sheep liver	Homogenized by sonication in H ₂ O, CH ₃ CN added to the homogenate	Centrifugation	Dried by centrifugal vacuum evaporation dissolved in 100 mM borate buffer, pH 8.4		[60]
Pig kidney	Homogenization in 20 mM Tris-HCl, 0.25 M sucrose, pH 8.0.	10 000 g (20 min)			[33]
Pig kidney simulated gastric and gastro-intestinal digest	Lipoclean addition Enzymolysis with 1% pepsin in saline pH 1.8 (gastric), 3% paeceatin, 1% α -amylase and bile salts in saline (intestinal)	40 000 rpm (4°C, 0.5–5 h)	Thermocoagulation		[33]
Osprey blood	Hemolysis, dilution with 30 mM Tris-HCl (pH 7.6)	13 000 g			[13]
Mussels	Homogenization in 30 mM Tris-HCl (pH 8.6) with 0.1 mM of phenylmethylsulfonylfluoride (protease inhibitor)	145 000 g			[4] [13]
Rabbit and mouse liver	Homogenization in 5 ml of 50 mM Tris-HCl (pH 7.4) with 250 mM sucrose and 5 mM 2-mercaptoethanol	Centrifugation 100 000 g (70 min, 4°C)			[52] [44]

Table 5 (continued)

Sample	Initial sample preparation	Centrifugation	Coagulation method	Preparation	Reference
<i>Anacystis nidulans</i>	Washed three times in Tris-HCl (pH 8) with 1 M EDTA, homogenization by ultrasonification in 10 mM Tris-HCl (pH 8) with 1 mM dithiothreitol	Centrifugation			[35]
Chicken meat [#] , pig kidney [§]	Enzymolysis (4 h, 37°C) with 1% pepsine in dli. HCl (pH 1.8), adjusting to pH 6 with NaHCO ₃ , enzymolysis (4 h, 37°C) with 3% pancreatin, 1% amylase and 1.5 g l ⁻¹ bile salts	20 000 rpm (3 h, 4°C) [#] 40 000 rpm (4°C, 5 h) [§]			[33] [36]
Liver from rats subjected to subcutaneous injections of CdCl ₂ (2 mg kg ⁻¹) ⁶⁵ Zn, ⁶⁴ Cu, ³⁵ S-labelled hepatoma tissue culture incubated for 24 h	Homogenized at 4°C in 100 mM Tris-HCl (pH 7.4) with 25 mM glucose	170 000 g (1 h)		Sephadex G-75 (1 m × 24 mm) with 50 mM Tris-HCl (pH 6.8) (1 ml min ⁻¹)	[37]
	Washed with cold phosphate-buffered NaCl solution, frozen in liquid N ₂ , thawed in 25 mM Tris-acetate (pH 7.4) with 5 mM of β mercaptoethanol and 0.1% aprotinin	105 000 g		TSK G3000 SWG column (60 cm × 21.5 mm) with 100 mM Tris-HCl with 100 mM NaCl (pH 7.4) and 0.02% NaN ₃ (5 ml min ⁻¹) ^a	[34]
Crab hepatopancreas	Homogenization with Tris-HCl (pH 8.6)	25 000 g (3 h)		Sephadex G-50 with Tris-HCl (pH 8.6) with 0.5 mM dithiothreitol	[46]
Crab hepatopancreas	Homogenization in Tris-HCl with 0.1 mM phenylmethanesulfonyl fluoride	Centrifugation		The cell-containing fractions freeze-dried and desalted by passage through a Sephadex G-25, the supernatant soln, prepared on Sephadex G-50 with Tris-HCl (pH 8.6) with 0.5 mM dithiothreitol	[48]
Liver or kidney tissue	Homogenization in 10 mM (NH ₄) ₂ HPO ₄ (pH 8.2)	Centrifugation		Sepharose CL-6B with 10 mM (NH ₄) ₂ HPO ₄ (pH 8.2)	[50]

Table 5 (continued)

Sample	Initial sample preparation	Centrifugation	Coagulation method	Preseparation	Reference
Rat kidney	Homogenization in 10 mM Tris-HCl (pH 8.6) with 250 mM sucrose and 5 mM 2-mercapto ethanol,	105 000 g (4°C, 90 min)		Sephadex G-75 (70 × 2.6 cm i.d.) with 20 mM HCOONH ₄ (pH 7.65)	[41]
Liver and kidney tissue	Homogenization in 10 mM Tris-HCl (pH 8.6)	Centrifugation			[54]
Rat liver	Homogenized in Tris-HCl, the cytosolic homogenate saturated with Cd, removal of excess of Cd	Centrifugation	Thermocoagulation (60°C, 5 min)		[53]
Cyanobacterium	Homogenization in 10 mM Tris-HCl (pH 8.0) with 1 mM of dithiothreitol	164 000 g	Precipitation with and dissolved in mobile phase 50 mM Tris-HCl buffer pH 7.5 containing 0.2 M (NH ₄) ₂ SO ₄		[43]

^a Preseparation employed before anion-exchange only (not used for subsequent RP and SEC).

A heat-treatment (at 60°C for 15 min) of the cytosol extracts (especially of concentrated ones) is recommended to separate off the high-molecular fraction which coagulated from the supernatant (containing MTs which are heat stable). Such a treatment reduces the protein load on the HPLC column not only improving the separation of MT isoforms but also prolonging the column lifetime. Enzymolysis in simulated gastric and gastrointestinal juice was proposed for meat samples [33,36].

Filtration of the cytosol (0.22 µm filter) before introducing it to the chromatographic column is strongly advised [33,36,44]. A guard column should be inserted to protect the analytical column from the effects of lipids, which otherwise degrade the separation [33]. Any organic species that adhere to the column can also bind inorganic species giving rise to anomalous peaks in subsequent runs [33]. A new guard column was used for each injection to prevent adsorption by ligands with a high affinity for cadmium that would otherwise interfere with subsequent injections [33]. An extensive column clean-up was necessary [33]. To avoid contamination of the analytical column by trace elements, buffers should be passed by Chelex-100 [27,33,36].

8. Conclusions

Hyphenated techniques are an attractive tool for rapid, sensitive and comprehensive characterization and quantitative determination of MT-isoforms in biological samples. Unfortunately, since the pioneering work carried out by Suzuki in 1980 [71] advances in coupled techniques have not been widely transferred to MT research. The progress in ICP MS, electrospray (tandem) mass spectrometry and the increasing speed and efficiency of modern separation techniques, are expected to bring valid alternatives to metal saturation assays, immunoassays and electrochemical techniques in the near future.

There is an urgent need to create an interface between biochemists, whose studies on the role and mechanisms of MTs are still hampered by the tediousness and labour-intensive analytical procedures, and analytical chemists for whom metal-

lothionein is nothing more than a sample to demonstrate the usefulness of their newly developed instrumental techniques. The availability of a certified reference material for MT would enable the validation of hyphenated techniques against immunoassays which would facilitate their entry into biochemical and clinical laboratories.

References

- [1] M.J. Stillman, C.F. Shaw, K.T. Suzuki (Eds.), *Metallothioneins Synthesis, structure and Properties of Metallothioneins, Phytochelatins and Metalthiolate Complexes*, VCH, New York, 1992
- [2] J.F. Riordan, B.L. Valee (Eds.), *Metallobiochemistry part B. Metallothionein and Related Molecules, Methods in Enzymology*, vol. 205, Academic Press, New York, 1991.
- [3] M.J. Stillman, *Coord. Chem. Rev.* 144 (1995) 461.
- [4] K.A. High, J.S. Blais, B.A.J. Methven, J.W. McLaren, *Analyst* 120 (1992) 629.
- [5] M. Bienengraeber, S. Forderkunz, D. Klein, K.H. Summer, *Anal. Biochem.* 228 (1995) 69.
- [6] S. Duquesne, M.A. Janquin, C. Hogstrand, *Fresenius' Z. Anal. Chem.* 352 (1995) 589.
- [7] A. Munoz, A.R. Rodriguez, *Analyst* 120 (1995) 529–532.
- [8] D. Klein, S. Sato, K.H. Summer, *Anal. Biochem.* 221 (1994) 405–409.
- [9] F. Tei, A. Pan, B.G. Ru, W.Q. Wang, Y.H. Hu, *J. Immunol. Methods* 149 (1992) 115–120.
- [10] C. Hogstrand, C. Haux, *Anal. Biochem.* 200 (1992) 388.
- [11] T.P.J. Mulder, A.R. Janssens, H.W. Verspaget, C.B.H.W. Lamers, *J. Immunol. Methods* 130 (1990) 157.
- [12] D. Klein, R. Bartsch, K.H. Summer, *Anal. Biochem.* 189 (1990) 35.
- [13] K.A. High, B.A. Methven, J.W. McLaren, K.W.M. Siu, J. Wang, J.F. Klaverkamp, J.S. Blais, *Fresenius' Z. Anal. Chem.* 351 (1995) 393.
- [14] M. Sato, K. Suzuki, *Biomed. Res. Trace Elem.* 6 (1995) 13.
- [15] M.P. Richards, *Methods Enzymol.* 205 (1991) 217.
- [16] M.P. Richards, J.H. Beattie, *J. Cap. Elec.* 1 (1994) 196.
- [17] S. Caroli, *Microchem. J.* 51 (1995) 64.
- [18] R. Lobinski, in: B. Welz (Ed.), *Colloquium on Analytical Atomic Spectrometry*, BSW Perkin Elmer, Überlingen, 1996.
- [19] R. Lobinski, Z. Marczenko, *Spectrochemical Trace Analysis for Metals and Metalloids*, Elsevier, Amsterdam, 1996.
- [20] J. Szpunar, C. Witte, R. Lobinski, F.C. Adams, *Fresenius' Z. Anal. Chem.* 351 (1995) 351.
- [21] N.P. Vela, L.K. Olson, J.A. Caruso, *Anal. Chem.* 65 (1993) 585A.

- [22] R.D. Smith, J.A. Loo, C.G. Edmonds, C.J. Barinaga, H.R. Udseth, *Anal. Chem.* 62 (1990) 882.
- [23] S.A. Hofstadler, R. Bakhtiar, R.D. Smith, *J. Chem. Educ.* 73 (1996) A82.
- [24] J.R.A. Yates, L. McCormack, A.J. Link, D. Schieltz, J. Eng, L. Hays, *Analyst* 121 (1996) 65R.
- [25] J.J. Corr, *J. Anal. At. Spectrom.* 12 (1997) 537.
- [26] A. Kabzinski, T. Takagi, *Biomed. Chromatogr.* 9 (1995) 123.
- [27] J.R. Dean, S. Munro, L. Ebdon, H.M. Crews, R.C. Massey, *J. Anal. At. Spectrom.* 2 (1987) 607.
- [28] K. Guenther, H. Waldner, *Anal. Chim. Acta* 256 (1992) 165.
- [29] A. Mazzucotelli, A. Viarengo, L. Canesi, F. De Paz, E. Ponzano, P. Rivaro, *Anal. Proc.* 28 (1991) 79.
- [30] A. Mazzucotelli, P. Rivaro, *Microchem. J.* 5 (1995) 231.
- [31] A. Mazzucotelli, A. Viarengo, L. Canesi, E. Ponzano, P. Rivaro, *Analyst* 116 (1991) 605.
- [32] A.H. Pan, F. Tie, B.G. Ru, L.Y. Li, T. Shen, *Biomed. Chromatogr.* 6 (1992) 205.
- [33] H.M. Crews, J.R. Dean, L. Ebdon, R.C. Massey, *Analyst* 114 (1989) 895.
- [34] O.M. Steinebach, H.T. Wolterbeek, *Chromatogr. Biomed. Appl.* 130 (1993) 199.
- [35] K. Takatera, N. Osaki, H. Yamaguchi, T. Watanabe, *Anal. Sci.* 10 (1994) 567–907.
- [36] L.M. Owen, H.M. Crews, R.C. Hutton, A. Walsh, *Analyst* 117 (1992) 649.
- [37] M. Apostolova, P.R. Bontchev, C. Nachev, I. Sirakova, *J. Chromatogr., B, Biomed. Appl.*, 1993, 131 (*J. Chromatogr.*, 620), 191.
- [38] S. Micallef, Y. Couillard, P.G.C. Campbell, A. Tessier, *Talanta* 39 (1992) 1073–1079.
- [39] B. Michalke, P. Schramel, *J. Trace Elem. Electrolytes Health Dis.* 4 (1990) 163.
- [40] K. Suzuki, H. Sunaga, Y. Aoki, M. Yamamura, *J. Chromatogr.* 281 (1983) 159.
- [41] M.A. Morcillo, J. Santamaria, *J. Chromatogr.* 655 (1993) 77.
- [42] J. Szpunar, H. Chasaigne, O. Donard, J. Bettmer, R. Lobinski, in: G. Holland (Ed.), *Applications of Inductively Coupled Plasma Mass Spectrometry*, RSC, Cambridge, 1997.
- [43] K. Takatera, T. Watanabe, *Anal. Sci.* 8 (1992) 469.
- [44] H. Van-Beek, A.J. Baars, *J. Chromatogr.* 442 (1988) 345–352.
- [45] D.E. Laurin, K.C. Klasing, R.L. Baldwin, *BioChromatography* 4 (1989) 254.
- [46] S.G. Ang, V.W.T. Wong, *J. Liq. Chromatogr.* 14 (14) (1991) 2647.
- [47] M.P. Richards, J.H. Beattie, *J. Chromatogr.* 648 (1993) 459.
- [48] S.G. Ang, V.W.T. Wong, *J. Chromatogr.* 599 (1992) 21.
- [49] M.P. Richards, N.C. Steele, *J. Chromatogr.* 402 (1987) 243.
- [50] H. Van-Beek, A.J. Baars, *At. Spectrosc.* 11 (1990) 70.
- [51] I.A. Kaltashov, X. Yu, C. Fenselau, *J. Pharm. Biomed. Anal.* 13 (1995) 279.
- [52] A. Pan, Z. Wang, B. Ru, *Biomed. Chromatogr.* 5 (1991) 193.
- [53] L.D. Lehman, C.D. Klaassen, *Anal. Biochem.* 153 (1986) 305.
- [54] P. Sun, X. Shan, Y. Zheng, L. Jin, W. Xu, *J. Chromatogr. B, Biomed. Appl.* 110 (1991) (*J. Chromatogr.* 572) 73.
- [55] M. Albin, P.D. Grossman, S.E. Moring, *Anal. Chem.* 65 (1993) 489A.
- [56] F. Foret, L. Krivánková, P. Bocek, *Capillary Electrophoresis*, VCH, Weinheim, 1993.
- [57] S.F.Y. Li, *Capillary Electrophoresis*, Elsevier, Amsterdam, 1992.
- [58] J. Vindevogel, P. Sandra, *Introduction to Micellar Electrokinetic Chromatography*, Hüthig, Heidelberg, 1992.
- [59] M.P. Richards, *J. Chromatogr. B, Biomed. Appl.* 657 (1994) 345.
- [60] J.H. Beattie, M.P. Richards, *J. Chromatogr. A* 664 (1994) 129.
- [61] G.Q. Liu, W. Wang, X.Q. Shan, *J. Chromatogr. Biomed. Appl.* 653 (1994) 41.
- [62] M.P. Richards, J.H. Beattie, R. Self, *J. Liq. Chromatogr.* 16 (1993) 2113.
- [63] J.H. Beattie, M.P. Richards, *J. Chromatogr. A* 700 (1995) 95.
- [64] V. Virtanen, G. Bordin, A.R. Rodriguez, *J. Chromatogr. A* 734 (1996) 391.
- [65] J.H. Beattie, M.P. Richards, R. Self, *J. Chromatogr.* 632 (1993) 127.
- [66] T. Minami, H. Matsubara, M. Ohigashi, N. Otaki, M. Kimura, K. Kubo, N. Okabe, Y. Okazaki, *J. Chromatogr., Biomed. Appl.* 685 (1996) 353.
- [67] M.P. Richards, J.H. Beattie, *J. Chromatogr. B, Biomed. Appl.* 669 (1995) 27.
- [68] M.P. Richards, P.J. Aagaard, *J. Cap. Elec.* 1 (1994) 90–95.
- [69] M.P. Richards, G.K. Andrews, D.-R. Winge, J.H. Beattie, *J. Chromatogr. B, Biomed. Appl.* 675 (1996) 327.
- [70] J.H. Beattie, R. Self, M.P. Richards, *Electrophoresis* 16 (1995) 322.
- [71] K. Suzuki, *Anal. Biochem.* 102 (1980) 31.
- [72] Y. Tan, G.M. Momplaisir, W. Jin, W.D. Marshall, *J. Anal. At. Spectrom.* 9 (1994) 1153.
- [73] E.H. Larsen, J.S. Blais, *J. Anal. At. Spectrom.* 8 (4) (1993) 659–664.
- [74] K.A. High, R. Azani, A.F. Fazekas, Z.A. Chee, J.S. Blais, *Anal. Chem.* 64 (1992) 3197.
- [75] H. Suyani, J. Creed, T. Davidson, J. Caruso, *J. Chromatogr. Sci.* 27 (1989) 139.
- [76] D. Heitkemper, J. Creed, J. Caruso, F.L. Fricke, *J. Anal. At. Spectrom.* 4 (1989) 279.
- [77] S.J. Hill, M.J. Bloxham, P.J. Worsfold, *J. Anal. At. Spectrom.* 8 (1993) 499–515.
- [78] S.C.K. Shum, R.S. Houk, *Anal. Chem.* 65 (1993) 2972–2976.

- [79] J.W. Olesik, J.A. Kinzer, S.V. Olesik, *Anal. Chem.* 67 (1995) 1.
- [80] M.J. Tomlinson, L. Lin, J.A. Caruso, *Analyst* 120 (1995) 583.
- [81] Q. Lu, S.M. Bird, R.M. Barnes, *Anal. Chem.* 67 (1995) 2949.
- [82] Y. Liu, V. Lopez-Avila, J.J. Zhu, D.R. Wiederin, W.F. Beckert, *Anal. Chem.* 67 (1995) 2020.
- [83] X. Yu, M. Wojciechowski, C. Fenselau, *Anal. Chem.* 65 (1993) 1355.
- [84] R. Lobinski, H. Chassaigne, *Fresenius' J. Anal. Chem.* (in press).
- [85] J.H. Beattie, J. Lomax, M.P. Richards, R. Self, R. Pesch, H. Münster, *Proceedings of the 42nd ASMS Conference of the American Society for Mass Spectrometry and Applied Topics*, Chicago, 1994, p. 667.
- [86] K.T. Suzuki, M. Sato, *Biomed. Res. Trace Elem.* 6 (1995) 51.
- [87] K. Lange-Hesse, L. Dunemann, G. Schwedt, *Fresenius' J. Anal. Chem.* 339 (1991) 240.
- [88] C.K. Jayawickreme, A. Chatt, *Biol. Trace Elem. Res.* 26-27 (1990) 503.

Metallothionein isoforms from horse, rabbit and rat separated by capillary zone electrophoresis at low pH

Tore W. Wilhelmsen ^a, Pål A. Olsvik ^b, Sverre W. Teigen ^a, Rolf A. Andersen ^{b,*}

^a *Pharmaceutical Department, The Norwegian Medicines Control Authority, Sven Oftedalsvei 6, N-0950 Oslo, Norway*

^b *Department of Zoology, Norwegian University of Science and Technology, N-7055 Trondheim, Norway*

Received 4 November 1996; received in revised form 6 January 1997; accepted 20 February 1997

Abstract

A comparative study of MT isoforms in rat liver and in commercial Sigma MT preparations from rabbit liver and horse kidney was performed using capillary zone electrophoresis (CZE). Electropherograms revealed the co-migration of MT forms from these species. A special form, the a-form (not binding Cd), occurred in various MT samples in different amounts, depending on the method used for MT purification. In the rabbit liver electropherogram a main form appeared (the b-form), which might be a modified MT form. A band of unknown composition, running ahead of the rat liver MT-I and -II forms on polyacrylamide gels, not having Cd binding affinity, probably had its counterpart in a yet unidentified CZE peak. CZE electropherograms of purified MT samples may contain main peaks that do not represent genuine and functional MT isoforms. Results are also presented which indicate that at low pH the MT-II form is more unstable than MT-I. © 1998 Elsevier Science B.V. All rights reserved.

Keywords: Metallothionein isoforms; Anion exchange chromatography; Polyacrylamide gel electrophoresis; Capillary zone electrophoresis

1. Introduction

Recent interest in metallothionein (MT) research, including ecotoxicological aspects has increased tremendously, this protein is used as a biomarker for heavy metal pollution and various types of stress.

The purification of MT from heat treated liver cytosols of cadmium (Cd) treated animals generally involves gel permeation followed by anion exchange chromatography. Our method differs

from other previous procedures [1,2] in that the gel permeation step was run in Tris buffer of the same low ionic strength as the starting buffer used in the gradient system for anion exchange to obtain the final separation [3]. In this way dialysis and lyophilization were omitted in order to prevent oligomerizations and oxidation of the reactive MT protein [4].

A typical elution profile for rat CdMT obtained by anion exchange chromatography monitored at 254 nm includes three peaks [3]. The fractions corresponding to those eluted as the second and third contain high amounts of added ¹⁰⁹Cd, while

* Corresponding author.

those that correspond to the first peak does not contain the isotope, even though they had a relatively high absorbance at 254 nm (see Fig. 1). It is speculated that the second and third peak contain MT-I and -II, respectively. The first eluting peak was designated the a-form.

Samples of material collected from these three peaks were run on capillary zone electrophoresis (CZE). This was done in a sodium phosphate buffer at low pH. The fused silica capillary was linearly coated with acrylamide [5]. One important advantage of using this neutral hydrophilic surface compared with uncoated or positively coated capillaries (e.g. polyamine polymers) is that appropriate buffers can be designed to produce separations either toward the cathode (normal polarity) or to the anode (reversed polarity). This offers additional selectivity without significant peak broadening caused by electroendosmotic flow.

An important factor in using acidic buffer conditions is metal dissociation (below MTs pI 3.8–4.4) causing apothioneins, thereby adding more resolving power to the system than at high pH [6–10]. At neutral or alkaline pH metal containing isoforms may co-migrate because of little differences in the net charge of the two main MT-I and MT-II types [11].

In our MT measurements using the CZE technique the a-form was also found in commercial rabbit and horse MT preparations. In rabbit liver a major form occurred, designated the b-form, most probably a spontaneous modified MT form. The stability of the various MT forms was also tested. The CZE technique, which separates compounds based on their charge to mass ratio, has proven successful for fast, sensitive and reproducible separation of MT isoforms [6–10,12–15].

2. Experimental

2.1. Animal housing and maintenance

Two male rats (*Rattus norvegicus*, Mol: WIST, 200–300 g) were used in the experiments. The animals were kept in macrolon cages and maintained in 12 h light/12 h darkness at 20°C and

55% relative humidity. They were fed ad libitum with an EWOS commercial pelleted diet (EWOS, Södertälje, Sweden). The animals had free access to water.

2.2. Chemicals

The isotope $^{109}\text{CdCl}_2$ (sp.act. 760 mCi mg^{-1} Cd, carrier free) was obtained from DuPont de Nemours, Wilmington, DE. The column materials Sephadex G-75 and DEAE-Sephadex A-50 were obtained from Pharmacia, Uppsala, Sweden. All chemicals were of analytical grade. 3-Amino-9-ethylcarbazole, bovine serum albumin, cadmium sulphate ($3\text{CdSO}_4 \cdot 8\text{H}_2\text{O}$), Coomassie Brilliant Blue R, *N,N'*-dimethylformamide, sodium acetate, Trizma base, Trizma hydrochloride, Trizma pre-set crystals, horse kidney MT (lot 73H9544) and rabbit liver MT (lot 93H9559; new lot 44H9568) were from Sigma, St. Louis, MO. Bromophenol blue, glycerol, glycine buffer substance, methanol, 4-chloro-1-naphthol, perhydrol (30% H_2O_2), ortho-phosphoric acid (99% pure cryst.), potassium chloride, sodium hydroxide pellets and zinc acetate were all from E. Merck, Darmstadt, Germany. Sodium dodecyl sulfate (SDS), *N,N'*-methylene-bis-acrylamide (BIS), acrylamide (99.9% pure), ammonium persulfate, *N,N,N',N'*-tetra-methylethylenediamine (TEMED) and 2-mercaptoethanol were all from Bio-Rad Laboratories, Life Science Group, Richmond, CA. Fluorinert™ liquid (FC-77) came from 3M, Haven, Belgium. The nitrocellulose membrane filter (2 μm) was obtained from Schleicher & Schuell, Dassal, Germany. Peroxidase conjugated IgG fraction of goat anti-rabbit IgG was prepared by Cooper Biomedical, Malvern, PA.

2.3. Metallothionein induction and preparation

Because MT isoforms are labile it was thought necessary to give a rather comprehensive description of the procedure for MT preparation.

Cold $3\text{CdSO}_4 \cdot 8\text{H}_2\text{O}$ was injected intraperitoneally to rats each day for a period of 4 days, 0.35 mg kg^{-1} on day 1, then 1.4 mg kg^{-1} on day 2, 3 and 4. After killing the animals on day 6 the livers were quickly removed and chilled on ice.

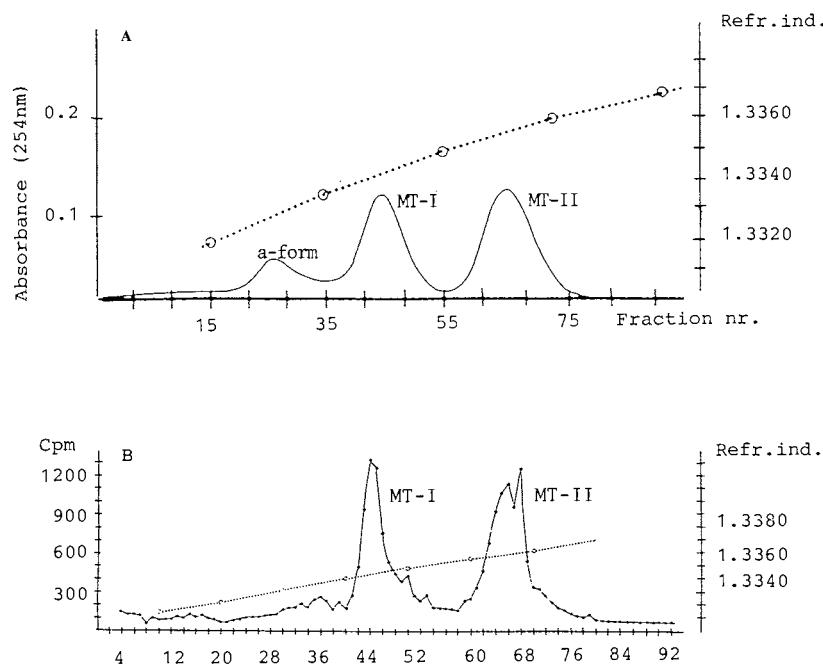


Fig. 1. (A) The major Cd binding fractions from the chromatography of rat liver cytosol on the Sephadex G-75 column pooled and rechromatographed on a DEAE Sephadex A-50 column with a linear Tris buffer gradient from 5 to 500 mM, pH 8.5. Absorbance 254 nm —. Refractive index ······. See text for further details. (B) Individual fractions assayed for added ^{109}Cd marker —•—•—. MT-I is shown to elute at a refractive index of 1.3345, MT-II at 1.3360.

The livers were then homogenized in 5 mM Tris buffer, pH 8.5 (1:4 w/v) using a glass-Teflon homogenizer (Potter-Elvehjem) rotating at 1400 rpm. After centrifugation at 20 300 g for 30 min at 4°C the supernatant was heat treated by equilibrating it on a water bath during temperature elevation from 20 to 80°C. Then the supernatant was kept at this temperature for 2 min, after which it was quickly chilled. The heat treated mixture was centrifuged at 20 300 g for 30 min at 4°C and the supernatant saved.

An aliquot of the heat treated supernatant (6–10 ml) was applied to a Sephadex G-75 column (2.5 × 72.5 cm) and eluted with 5 mM Tris buffer pH 8.5 at a flow rate of 1 ml min⁻¹. Supernatant samples were equilibrated for 5 min with 10 µl of Cd isotope solution, containing 100 000 cpm µl⁻¹ prior to gel permeation. Fractions (each 4.25 ml) were collected and analysed for ^{109}Cd by a Packard Minaxys Auto-gamma counter, model 5550 (Packard Instruments, IL).

The peak radioactivity fractions eluted from the Sephadex G-75 column were pooled and applied directly on a DEAE-Sephadex A-50 anion exchange column (1.5 × 25 cm) equilibrated with 5 mM Tris buffer, pH 8.5. After washing in (100 ml buffer) elution was started with a linear Tris buffer gradient (5–500 mM, pH 8.5, 600 ml). Eluate fractions of 4.25 ml were collected and analysed for UV absorption at 254 nm and for ^{109}Cd . The peak fractions were then pooled and lyophilized to get the final purified MT preparations. Tris salt was not removed.

2.4. Polyacrylamide gel electrophoresis and staining

The Bio-Rad Protean II Slab Cell was used for SDS polyacrylamide electrophoresis using the Laemmli reducing buffer system [16] as well as the native gel system. The stacking gel for the SDS system contained 4% acrylamide (0.35% bis), separation gel 12% (1% bis). The sample buffer con-

sisted of 4.0 ml aq. dest., 1.0 ml 0.5 M Tris–HCl (pH 6.8), 0.8 ml glycerol, 1.6 ml 10% (w/v) SDS, 0.4 ml 2-mercaptoethanol and 0.05% (w/v) bromophenol blue. Protein samples were diluted 1:4 with this buffer and heated to 80°C for 2 min to minimize negative charge differences and disulphide linkages prior to each run.

For native polyacrylamide gel electrophoresis the method by Jovin et al. [17] was used, except for riboflavin being replaced by TEMED and ammonium persulfate for upper gel polymerization. The stacking gel contained 2.5% acrylamide, separation gel 7.5%.

The Protean II slab cell apparatus was run at 40 V (16 h) overnight using the Bio-Rad Power Supply, model 250/2.5. The acrylamide gels were stained with Coomassie Brilliant Blue.

2.5. Electroblooming of MT, identification of Cd binding proteins, Western blotting

The electrotransfer of MT from polyacrylamide gels to nitrocellulose filters was per-

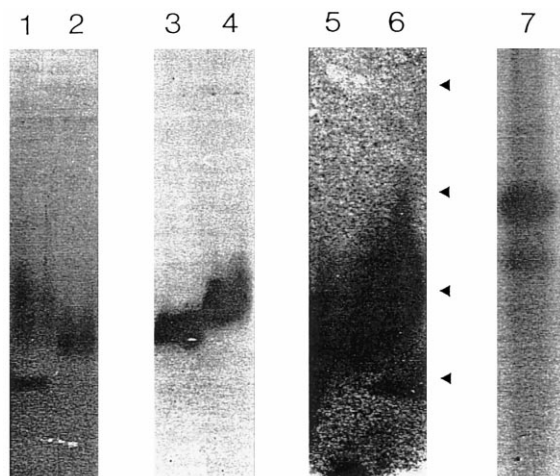


Fig. 2. Polyacrylamide SDS gel electrophoresis, Western blotting, autoradiography and native gel electrophoresis of our purified MT isoforms. In lanes (1), (2) the individual MT-II and MT-I preparations, respectively, Coomassie stained; (3), (4) Western blotting of MT-I and MT-II, respectively; (5), (6) autoradiography. In lane (7) MT-I and MT-II isoforms mixed, subjected to native gel electrophoresis. Arrowheads indicate positions of the SDS molecular weight markers (from top to bottom: ovalbumin, 45 kDa; carbonic anhydrase, 31; soybean trypsin inhibitor, 21.5; lysozyme, 14.4).

formed using the Bio-Rad Trans-Blot Cell according to the method employed by Towbin et al. [18]. The polyacrylamide gels (0.75 mm in thickness) were run as previously described [16]. After electrophoresis the gels were equilibrated in 500 ml Tris–glycine electrotransfer buffer (3.03 g Tris base, 14.4 g glycine, 200 ml methanol, aq. dest. to 1l) for 30 min. Then the electrotransfer was performed for 2 h at 60 V (Bio-Rad Power Supply, model 250/2.5).

To identify Cd binding proteins using autoradiography [19] the filter was equilibrated for 2 h in 400 ml of 10 mM Tris buffer, pH 7.4 at 4°C. The filter was then submerged for 10 min at room temperature in 25 ml of 10 mM Tris buffer, pH 7.4 containing 1 μCi $^{109}\text{CdCl}_2$ ml^{-1} , 0.1 mM zinc acetate and 0.1 M KCl. The filter was then washed twice in aq. dest. at room temperature and completely dried. Autoradiography was performed at -70°C for 38–48 h using Kodak X-Omat AR (XAR-5) film and DuPont Cronex Quanta II intensifying screens. The films were manually processed with Kodak LX 24 developer and AL 4 fixative.

Using nitrocellulose filters prepared as described above, our anti rat MT antibodies (developed in rabbits) were subjected to Western blotting [3,20]. The filters were washed in phosphate buffered saline for 15 min and then kept for 30 min in a solution consisting of 3 g bovine serum albumin to 100 ml phosphate buffered saline. The filter was then treated with antibody (rabbit serum without further purification) at a concentration of 40 μl 10 ml^{-1} blocking solution by gentle shaking overnight. The antibody solution was removed by washing with phosphate buffered saline. The filter was then treated with peroxidase conjugated IgG fraction goat anti-rabbit IgG in the concentration of 10 μl (undiluted) 10 ml^{-1} blocking solution. After shaking for 2 h the filter was developed in a mixture of 2 ml aminoethylcarbazole (AEC, fresh stock), 50 ml sodium acetate buffer, pH 5 and 25 μl hydrogen peroxide. The stock solution consisted of 0.25 g AEC to 25 ml dimethylformamide.

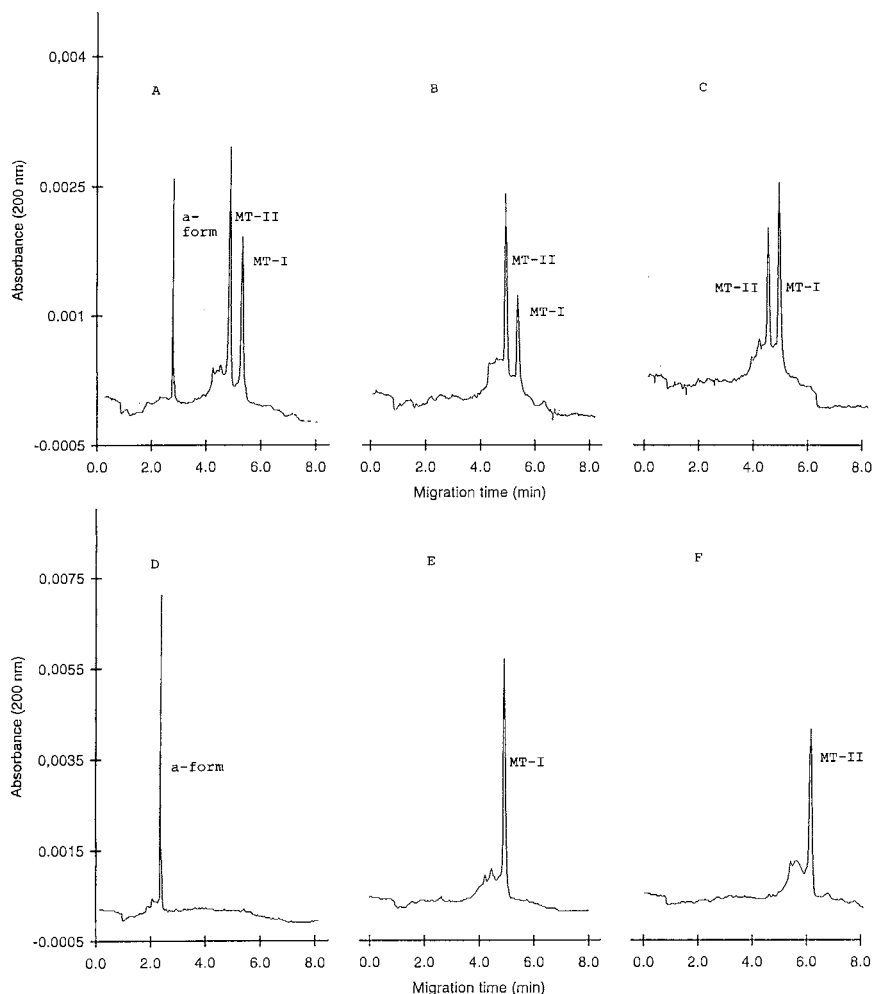


Fig. 3. Mixtures of our rat MT isoforms subjected to capillary zone electrophoresis (CZE) at 200 mM sodium phosphate, pH 2.0. The individual forms were diluted 10 times from stock solutions (see text) and mixed in equal volumes. (A) The a-form ($17 \mu\text{g ml}^{-1}$) + MT-I ($16 \mu\text{g ml}^{-1}$) + MT-II ($29 \mu\text{g ml}^{-1}$), run at 10 kV. (B) MT-I ($25 \mu\text{g ml}^{-1}$) + MT-II ($44 \mu\text{g ml}^{-1}$). (C) MT-I ($37 \mu\text{g ml}^{-1}$) + MT-II ($22 \mu\text{g ml}^{-1}$), volume 3:1. (B) and (C) run at 12 kV. (D–F) the individual a-form ($50 \mu\text{g ml}^{-1}$), MT-I ($49 \mu\text{g ml}^{-1}$), MT-II ($87 \mu\text{g ml}^{-1}$), run at 10 kV. Given concentrations represent end values after mixing.

2.6. Capillary zone electrophoresis of MT samples

The BioFocus™ 3000 Capillary Electrophoresis System with Spectra Software version 3.00, Integration Software version 3.01 and BioFocus Capillary Cartridge, 17 cm \times 25 μm I.D., 375 μm O.D., polyacrylamide coated (12.5 cm to the detector window), from Bio-Rad Laboratories, Life Science Group, Richmond, CA., were used for MT analysis.

The lyophilized a-peak sample prepared in our laboratory was diluted in 200 μl aq. dest., the MT-I sample in 500 μl aq. dest and MT-II in 1 ml (stock solutions). These samples were again diluted 1:9 in aq. dest. before CZE. The commercial Sigma reference samples of rabbit (lot 93H9559, new lot 44H9568) and horse MT (lot 73H9544), claimed to be essentially salt free, were dissolved in 10 mM Trizma pre-set crystal buffer at pH 9.1 to a final concentration of $180 \mu\text{g ml}^{-1}$. Further

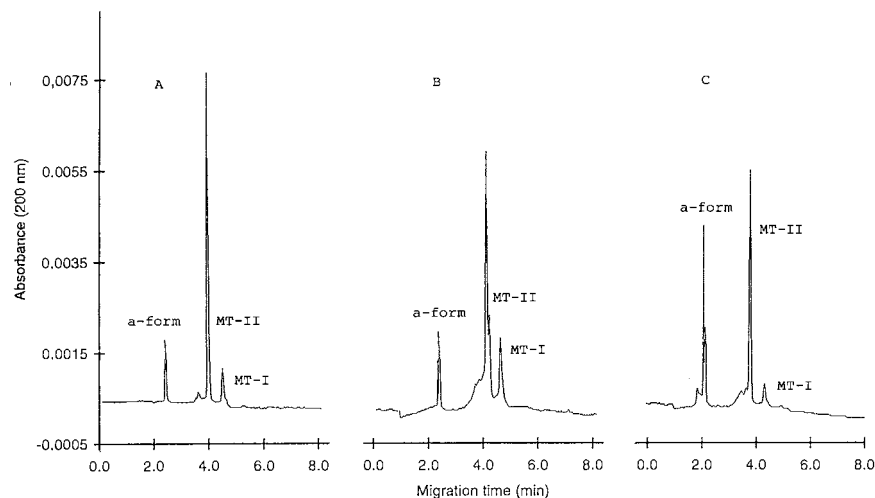


Fig. 4. Separation of mixed samples of horse and rat MT isoforms by CZE in 200 mM sodium phosphate, pH 2.0 at 10 kV. (A) Commercial horse MT preparation alone ($180 \mu\text{g ml}^{-1}$) (rat isoform mixture alone shown in Fig. 3), (B) horse MT ($90 \mu\text{g ml}^{-1}$) + rat MT ($93 \mu\text{g ml}^{-1}$), (C) horse MT ($90 \mu\text{g ml}^{-1}$) + the individual rat a-form ($25 \mu\text{g ml}^{-1}$). Given concentrations represent end values after mixing.

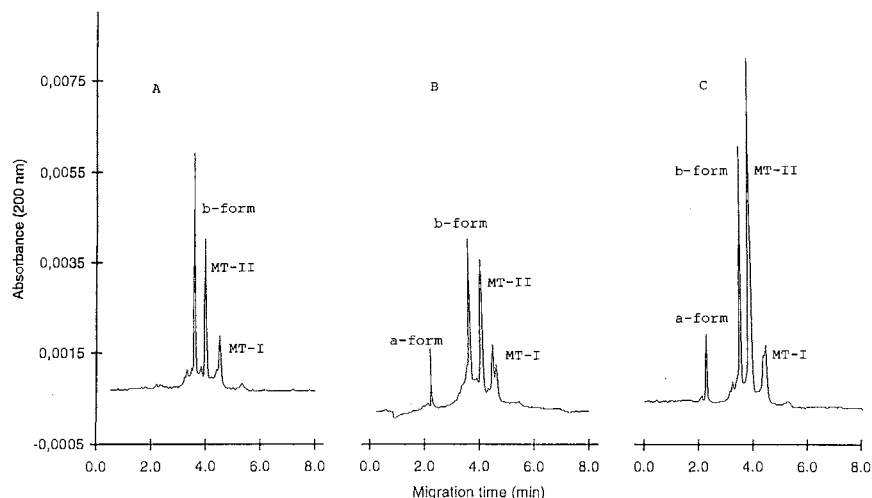


Fig. 5. Separation of mixed samples of rabbit, rat and horse MT isoforms by CZE in 200 mM sodium phosphate, pH 2.0 at 10 kV. (A) Commercial rabbit MT preparation alone (old lot 93H9559) ($180 \mu\text{g ml}^{-1}$), (B) rabbit MT ($90 \mu\text{g ml}^{-1}$) + rat MT ($93 \mu\text{g ml}^{-1}$), (C) rabbit MT ($90 \mu\text{g ml}^{-1}$) + horse MT ($90 \mu\text{g ml}^{-1}$). Given concentrations represent end values after mixing.

dilutions of the samples were done in aq. dest. The MT samples were kept as stock solutions at -70°C . Samples were mixed by volume ratio 1:1, except for rat MT-I and MT-II which were also mixed 3:1 (Fig. 3C).

All CZE measurements were performed in 200 mM sodium phosphate at pH 2.0 ($19.6 \text{ g H}_3\text{PO}_4$ diluted

in aq. dest., titrated by 1 M NaOH to pH 2.0 and then aq. dest. to 11). The experiments were done at constant voltage (10 or 12 kV) giving a maximum current of $55 \mu\text{A}$ in the capillary. Detection was performed at 200 nm. The cartridge and the carousel were thermostated at 20°C by the Peltier thermoelectric cooling system with Fluorinert™ liquid.

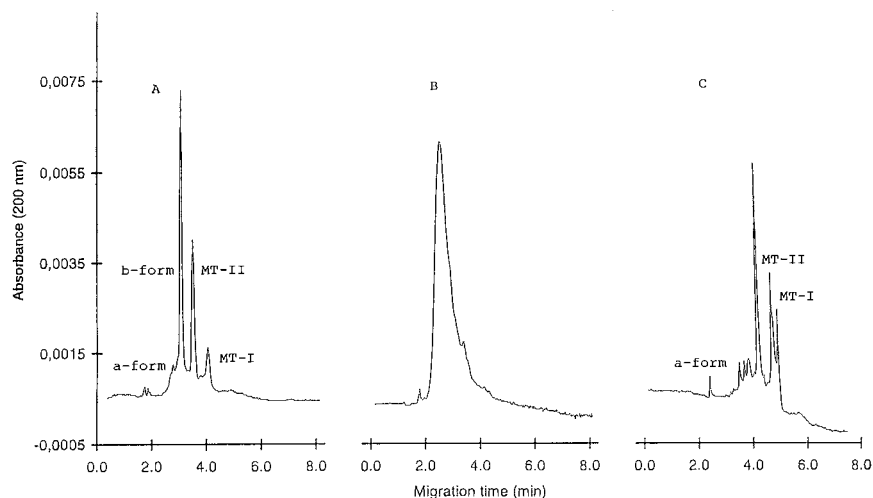


Fig. 6. Stability of the commercial rabbit MT preparations kept under atmospheric conditions, pH 9.1 at room temperature and measured by CZE in 200 mM sodium phosphate, pH 2.0. (A) Old lot (93H9559), 65 h (old lot, 0 h shown in Fig. 5A), (B) old lot, 60 days, (C) new lot (44H9568), 0 h. The b-form is clearly distinguished from the old lot, not in the new lot. In (B) peaks are merged. (A) and (B) run at 12 kV, (C) run at 10 kV.

All samples were applied hydrodynamically under pressure (20 psi \times s) and analysed using polarity from the positive to the negative electrode. The important washing procedure between each single run was as follows: 15 s with 50 mM H_3PO_4 at pH 1.85; 10 s with electrophoresis buffer (see above); 10 s with 0.25 mM NaOH and finally electrophoresis buffer for 15 s.

3. Results and discussion

Fig. 1A shows that freshly purified MT after anion exchange chromatography on the DEAE-Sephadex A-50 column, monitored at 254 nm, elutes as three peaks. When peak material was tested for ^{109}Cd binding affinity (Fig. 1B), it turned out that the second and third eluting peak contained MT-I and MT-II, respectively. The non metal binding material (Fig. 1) eluting at refractive index of 1.3333 in the Tris buffer gradient, thereby appearing in front of the two MT isoforms, was designated the a-form.

Our rat MT preparations gave three individual bands on Coomassie stained SDS polyacrylamide and native gels (Fig. 2). Both gel systems separated the two common MT isoforms with the I

form running ahead of the II form. The faint band appearing in front of these two isoforms may correspond to an unknown protein discovered previously in the MT-II fraction by Beattie et al. [12] and assumed to be hemoglobin. This band may, however, represent a precursor of active metal binding MT [3]. The functional studies represented by Western blotting, the autoradiography data (Fig. 2, lanes 3–6) as well as the ^{109}Cd binding study shown in Fig. 1B, show that MT-I and MT-II isoforms are only functionally capable of metal binding, not the material in the faint band. The metal binding in this band in lane 6 is probably unspecific caused by presence of the Cd isotope in excess.

When MT samples isolated in our experiments on the DEAE-Sephadex A-50 column were pooled and run through the CZE system, three peaks were seen (Fig. 3A). Runs of mixtures of MT forms in different proportions clearly demonstrates that the first eluting peak in the CZE electropherogram at low pH corresponds to the a-form, the second to MT-II and the third peak to the MT-I isoform (Fig. 3A–C). In addition to the running voltage, the positions of the various MT forms in the electropherogram are largely dependent on ionic strength and pH, at acidic pH the

MT-II form is more positively charged than the MT-I form. In separate runs of individual MT forms, as shown in Fig. 3E, F, MT-I migrates faster than MT-II in spite of the higher charge of the latter. This is explained by the higher ionic strength of the MT-II sample, being eluted at a higher salt than MT-I in the anionic exchange gradient (Fig. 1A). When the MT samples are mixed and thereby run under equal conditions, as in Fig. 3A–C, MT-II migrates faster than the MT-I form.

Further experiments to determine the content of the a-peak were not carried out. It is, however, unlikely that it contains low molecular weight sulphhydryls due to improper heat treatment, as is suggested from the work of Olafson and Olsson [21]. Such species are removed when selecting the MT containing fractions from the Sephadex G-75 column prior to further processing on the ion exchange column. In the commercial rabbit MT

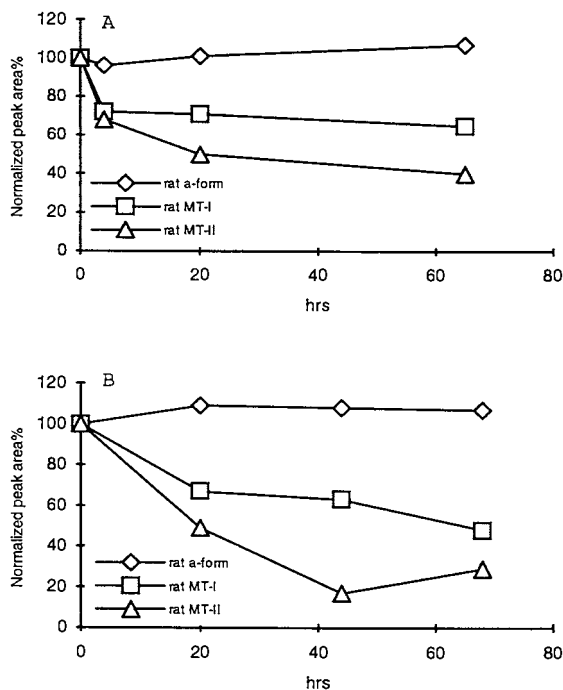


Fig. 7. Stability of the rat MT isoforms kept under atmospheric conditions, pH 9.1 and measured by CZE in 200 mM sodium phosphate, pH 2.0 at 12 kV. (A) Room temperature at 0, 4, 20 and 65 h, (B) refrigerated at 5°C at 0, 20, 44 and 68 h. Each point gives the mean of two or three individual runs.

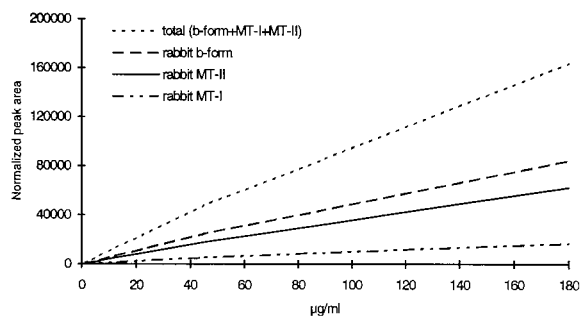


Fig. 8. Regression analysis of individual isoforms for the rabbit MT preparation (old lot 93H9559) under atmospheric conditions, pH 9.1 and room temperature measured by CZE in 200 mM sodium phosphate, pH 2.0 at 10 kV covering the concentration range of 1.4–180 $\mu\text{g ml}^{-1}$. Migration time and area reproducibility of $\pm 2\%$ was observed. Achieved regression of normalized peak areas ($\text{mV} \times \text{s}/\text{migration time}$, see text) was $r^2 = 0.99896$ for the b-form, $r^2 = 0.99931$ for MT-II, $r^2 = 0.99805$ for MT-I and $r^2 = 0.99903$ for total MT. Individual points represent the mean of three separate runs.

preparation used in the present work the a-form could only be seen in the old lot (lot 93H9559) at concentrations above 500 $\mu\text{g ml}^{-1}$ MT. In a recently purchased preparation (new lot 44H9568) this form could be seen at 200 $\mu\text{g ml}^{-1}$. The a-form was also present in MT preparations studied by others [9,10]. We believe that the presence of this form in MT samples depends on the ability of picking only the MT-I and -II containing fractions in the purification procedure. The isoelectric focusing used as the final step in the isolation of the rabbit liver Sigma MT preparation [22] seems to be more effective in achieving this than the anion exchange procedure used for the Sigma horse kidney MT separation [23,24]. A proper interpretation of the CZE electropherograms of MT samples should include the functionality of separated forms.

When the commercial horse MT preparation and our rat MT preparations were pooled prior to CZE, marked co-migration between peaks was observed (Fig. 4A–C), with only minor differences confined to the a-peak and the MT-II peak. Corresponding results for rabbit commercial and rat MTs as well as for commercial rabbit and horse MT preparations, are shown in Fig. 5A–C with minor differences related only to the MT-I

peak. Co-migration at this level therefore seems to be related to mutual factors between isoforms, no further studies were carried out. It can also be seen that the rabbit MT preparation had one dominant form, marked as the b-form in Fig. 5A, which did not concur with any of those present in horse and rat MTs. In Fig. 6A,B it is shown that this form developed gradually with time at pH 9.1 under atmospheric conditions at room temperature. The electropherogram of the new lot of rabbit MT, however, did not show this peak (Fig. 6C), indicating the rabbit b-form develops spontaneously during storage. In recent work on rabbit MT isoforms by Virtanen et al. [6] their major g-peak was characterized as a modified isoform, which probably corresponds to the b-form described in the present work. A corresponding peak is also seen in electropherograms from other workers [8–10] having run rabbit MT preparations using the CZE technique at acidic conditions. When Fig. 3A is compared with Fig. 5B, it is interesting to note that a small indication of the b-form presence was also seen in our rat liver MT preparation as the part ahead of the MT-II peak in Fig. 3A.

By using our CZE technique, stability of the freshly prepared rat MT preparations were tested at pH 8.5 under atmospheric conditions at room temperature and refrigerated at 5°C over a period of 65 and 68 h, respectively. Analysis of aliquots showed that the a-form did not degrade in contrast to MT-I and -II (Fig. 7). Under these conditions the I form was more stable than the II form. Corresponding results (not shown) were found for the rabbit (pH 9.1) and horse MT (pH 9.1) preparations. At tested levels the a-form was not found in rabbit. The observation that the MT-I form is more stable than the MT-II form is surprising [25]. At pH 2.0, however, at which the stability measurements were performed, metal is stripped from the protein resulting in apoprotein (apothionein) formation. Under these conditions the MT-II form may be more vulnerable than the MT-I form. During degradation experiments, new peaks were not observed in our rat MT forms.

The regression analysis of individual MT forms in rabbit covering the range 1.4–180.0 $\mu\text{g ml}^{-1}$ is shown in Fig. 8. The observed detection limit for

MT preparations below 5 $\mu\text{g ml}^{-1}$ corresponds to the sensitivity level found by others [8,12,13,15]. Other MT preparations studied in the present work gave similar results (not shown). The concentration of the individual isoforms in the rat liver MT preparations was determined by measuring the total and relative percentage levels of the individual forms. These values were then related to the measured total level of forms in the horse Sigma preparation, for which the MT concentration was given by the supplier. This preparation contained similar isoform types as found in rat liver (Fig. 4). In the commercial rabbit preparation the a-form was seen only at higher concentrations, and it contained considerable amounts of the b-form.

It is important to keep in mind that when the sample is applied hydrodynamically (pressure) to the CZE capillary as in this work, the separated forms move through the detector window at different speeds. Peak area is a better measure for actual amounts than peak height when using different running conditions, i.e. voltage and unequal salt concentration in the samples. To compare peak areas in stability testing and regression, however, they must be divided by the corresponding migration times to give normalized values (Fig. 8) [26,27].

Acknowledgements

The authors would like to thank Prof. Stellan Hjertén, Department of Biochemistry, BMC, S-751 23 Uppsala, Sweden, for his critical review of the manuscript. We are especially grateful for the gift of coated capillaries from the Bio-Rad Laboratories, Life Science Group, Richmond, CA., and to Director Lars Th. Wold, Bio-Test A/S, N-1580 Rygge, Norway, for the courtesy of free disposal of the BioFocus™ 3000 system.

References

- [1] R.J. Vander Mallie, J.S. Garvey, *Immunochemistry* 15 (1978) 857–868.

- [2] S. Ohi, G. Cardenosa, R. Pine, P.C. Huang, *J. Biol. Chem.* 256 (1981) 2180–2184.
- [3] R.A. Andersen, H.L. Daae, *Comp. Biochem. Physiol.* 90B (1988) 59–67.
- [4] D.T. Minkel, K. Poulsen, S. Wielgus, C.F. Shaw, D.H. Petering, *Biochem. J.* 191 (1980) 475–485.
- [5] S. Hjertén, *J. Chromatogr.* 347 (1985) 191–198.
- [6] V. Virtanen, G. Bordin, A.-R. Rodriguez, *J. Chromatogr. A* 734 (1996) 391–400.
- [7] J.H. Beattie, M.P. Richards, *J. Chromatogr. A* 700 (1995) 95–103.
- [8] M.P. Richards, *J. Chromatogr. B* 657 (1994) 345–355.
- [9] M.P. Richards, J.H. Beattie, *J. Chromatogr.* 648 (1993) 459–468.
- [10] M.P. Richards, P.J. Aagaard, *J. Cap. Elec.* 1 (1994) 90–95.
- [11] J.H.R. Kägi, Y. Kojima: in J.H.R. Kägi, Y. Kojima (Eds.), *Metallothionein II*, Birkhäuser Verlag, Basel, 1987, pp. 25–61.
- [12] J.H. Beattie, M.P. Richards, R. Self, *J. Chromatogr.* 632 (1993) 127–135.
- [13] M.P. Richards, J.H. Beattie, R. Self, *J. Liq. Chromatogr.* 16 (9 and 10) (1993) 2113–2128.
- [14] J.H. Beattie, R. Self, M.P. Richards, *Electrophoresis* 16 (1995) 322–328.
- [15] G.-Q. Liu, W. Wang, X.-Q. Shan, *J. Chromatogr. B* 653 (1994) 41–46.
- [16] U.K. Laemmli, *Nature* 227 (1970) 680–685.
- [17] T. Jovin, A. Chrambach, M.A. Naughton, *Anal. Biochem.* 9 (1964) 351–369.
- [18] H. Towbin, T. Staehelin, J. Gordon, *Proc. Natl. Acad. Sci. U.S.A.* 76 (1979) 4350–4354.
- [19] Y. Aoki, M. Kunitomo, Y. Shibata, K.T. Suzuki, *Anal. Biochem.* 157 (1986) 117–122.
- [20] O.J. Mesna, I.-L. Steffensen, A. Melhuus, H. Hjertholm, H.E. Heier, R.A. Andersen, *Gen. Pharmacol.* 21 (1991) 909–917.
- [21] R.W. Olafson, P.-E. Olsson: in J.F. Riordan, B.L. Vallee (Eds.), *Methods in Enzymology, Metallobiochemistry (Part B), Metallothionein and Related Molecules*, vol., 205, 1991, pp. 205–213.
- [22] G.F. Nordberg, M. Nordberg, M. Piscator, O. Vesterberg, *Biochem. J.* 126 (1972) 491–498.
- [23] J.H.R. Kägi, S.R. Himmelhoch, P.D. Whanger, J.L. Bethune, B.L. Vallee, *J. Biol. Chem.* 249 (1974) 3537–3542.
- [24] Y. Kojima, C. Berger, B.L. Vallee, J.H.R. Kägi, *Proc. Natl. Acad. Sci. U.S.A.* 73 (1976) 3413–3417.
- [25] K.T. Suzuki, M. Sato, *Biomed. Res. Trace Elements* 6 (1995) 51–56.
- [26] S. Hjertén, K. Elenberg, F. Kilar, J.-L. Liao, A.J. Chen, C.J. Siebert, M.-D. Zhu, *J. Chromatogr.* 403 (1987) 47–61.
- [27] K.D. Altria, D.R. Rudd, *Chromatography* 41 (1995) 325–331.

Cadmium and metallothionein turnover in different tissues of the gastropod *Littorina littorea*

M.J. Bebianno ^{a,*}, W.J. Langston ^b

^a *Unidade de Ciência e Tecnologia dos Recursos Aquáticos, Universidade do Algarve, Campus de Gambelas, 8000 Faro, Portugal*

^b *Plymouth Marine Laboratory, Citadel Hill, Plymouth PL1 2PB, UK*

Received 21 November 1996; received in revised form 3 March 1997; accepted 4 March 1997

Abstract

This paper attempts to link the kinetics of Cd and metallothionein turnover in the intertidal marine snail *Littorina littorea*. The results demonstrate that the turnover of metallothionein is tissue dependent. Metallothionein has an estimated half-life of 69 and 160 days in the gills and kidney, respectively. The half-life could not be calculated for metallothionein in the digestive gland and is probably much longer than the other two tissues. Cadmium elimination from the gill and kidney is considerably slower than the respective metallothioneins (half-life in excess of 300 days) indicating closed cycling of the metal in these tissues. In contrast, cadmium levels in the digestive gland continue to increase during the detoxification period reflecting some remobilization from other tissues. Metallothionein turnover is extremely slow in *Littorina* when compared with mammals and other bivalve molluscs: even though metallothionein degradation is measurable in some gastropod tissues, the released cadmium may induce de novo metallothionein synthesis to which cadmium becomes resequenced. The slow metallothionein turnover rates and the lack of significant cadmium excretion testify to the relatively stable nature of the cadmium-metallothionein complex in this invertebrate. © 1998 Elsevier Science B.V. All rights reserved.

Keywords: Metallothionein; Turnover; Molluscs; Cadmium

1. Introduction

Various marine invertebrates, including several species of gastropod molluscs, have been proposed as indicators of metal contamination, due to their ability to reflect the bioavailability of enhanced environmental metal levels [1]. Exposure of these organisms to elevated concentrations of some essential and non-essential metals can

induce the synthesis of low molecular weight, cysteine-rich, metal-binding proteins known as metallothioneins (MT) [2]. Consequently these proteins are regarded as potentially specific biological-response markers for metal pollution and measurement of MT's are included increasingly in biomonitoring programmes. However, it is necessary to identify suitable marine organisms or specific tissue preparations and to validate responses to metal contamination before widespread field application of the assay can be undertaken. It was

* Corresponding author.

demonstrated in earlier studies that there is sometimes a marked interspecific variability in the net production of metallothionein, even among members of the same phylum [3]. Consequently, the properties and functions of these proteins have often yet to be identified and characterised in marine invertebrates.

Of all the properties which influence the expression of MT induction in marine invertebrates exposed to metals, the turnover rates of metallothioneins must be considered vitally important. Therefore, in order to understand the significance of MT in metal metabolism and detoxification, estimates of turnover parameters are desirable, particularly when attempting to use concentrations of the protein as a marker of the biological effects of metal contamination.

The common periwinkle *Littorina littorea* is considered to be a good bioindicator of metal contamination, particularly for non-essential metals such as cadmium, because metal levels in its tissues usually reflect metal levels in the environment [4–8]. Metals are usually localised in particular tissues (e.g. gill, kidney, mantle and digestive gland) and their presence and concentration is largely dependent on the quantity and nature of the ligands available at the cellular level [5]. Intracellular partitioning of cadmium is, therefore, somewhat variable among tissues, nevertheless a significant proportion of cadmium is always present, for all major tissues, in the metallothionein pool [7,9,10]. The presence of metallothionein in different tissues of *L. littorea* has now been reported in a variety of studies, following exposure to a range of cadmium concentrations in the laboratory, or in individuals collected from the field [6,7,9–12].

We have shown previously, by measuring metallothionein concentrations in component tissues of Cd-dosed *L. littorea* using differential pulse polarography, that the induction of metallothionein synthesis is quantitatively tissue dependent [13]. Thus, metallothionein levels increase by 3- and 4-fold respectively in the kidney and gills of *L. littorea* exposed to cadmium ($400 \mu\text{g Cd l}^{-1}$ for 1 month): However, in the digestive gland, net increases in metallothionein concentration cannot be detected even at these high Cd exposure levels,

due to inherently high levels of constitutive metallothionein in this tissue. Clearly, individual tissues from this gastropod possess significantly different capacities to handle the excess of metals, following contamination [9,10].

The digestive gland contains two thirds of the total metallothionein content in *L. littorea* and can store correspondingly large amounts of metals. Intuitively it would seem a prime candidate for biomarker studies but the poor net response to Cd and the presence of interfering high molecular weight thiolic proteins reduce the value of this tissue preparation for the direct determination of metallothionein concentrations [9]. Although some interfering high molecular weight thiolic proteins are also detected in gills, these are easier to eliminate and subsequently the induction of metallothionein in this tissue (up to 4-fold) is found to be proportional to Cd-exposure, suggesting that gill-MT concentrations can be used as a biological response [10]. Metallothionein determinations in the kidney (an important site of Cd accumulation) suffer from few interferences from other heat-stable proteins and can also be used to quantify biological response to sublethal levels of cadmium on a routine basis [10]. Metallothionein concentrations of $3\text{--}4 \text{ mg g}^{-1}$ (measured by differential pulse polarography, using rabbit metallothionein standards) are typical for kidneys of winkles collected from sites free of cadmium contamination. These concentrations reach $10\text{--}12 \text{ mg g}^{-1}$ following Cd-exposure [10].

The absence of significant cadmium excretion in *L. littorea* [7] seems to indicate that the metabolism of the cadmium-metallothionein complex in winkles is similar to that observed for *Mytilus edulis* [14]. However, no information is available on the turnover rates of metallothionein in *Littorina* or any other marine gastropod. Indeed there is very little information on metallothionein turnover in marine invertebrates, generally. The only other available molluscan data concerns bivalves, where half-lives in *M. edulis*, (whole) for example are of the order of 25 and 300 days, for MT and Cd respectively, following exposure to cadmium [14]. Turnover rates of two metallothionein isoforms in gills of Cd-exposed oysters *Crassostrea virginica* are somewhat quicker (half-lives up to 7 days; [15]).

Turnover rates for metallothionein have been measured in liver and kidney of mammals [16–24] and fish [25,26] and generally appear to be more rapid than most invertebrates, although this may depend on the associated metal. The turnover rates of metallothioneins induced by exposure to cadmium are slow by comparison with those induced by copper or zinc.

With a view to improving our interpretation of biological responses in aquatic biota to pollutant metals, this paper attempts to determine metallothionein turnover in the gills, digestive gland and kidney of the gastropod *L. littorea* exposed to Cd. Experiments were devised to determine the half-life of MT and its associated cadmium in the tissues of *Littorina*, in vivo, by following the incorporation of cadmium and [³⁵S]-cysteine into metallothionein, and observing the subsequent loss of both protein and metal.

2. Materials and methods

L. littorea (shell length 20–22 mm) were collected in April 1990 from Jennycliff, south west England, and acclimated in aerated seawater, salinity 34‰, at 15°C for 1 week prior to the experiments. Subsequently, groups of 50 animals were held in 5 l aquaria and exposed to a cadmium concentration of 400 µg l⁻¹. Although this is considerably above the concentrations likely to be encountered at all but the most highly contaminated of field sites, it was chosen, on the basis of earlier experiments, to ensure a sufficient degree of MT induction against which turnover rates could be adequately determined. Control groups of winkles were maintained in clean seawater (37.2 ± 3.6 ng Cd l⁻¹). Water in each tank was changed twice each week. Losses of Cd from seawater were not significant during this period.

Controls and individuals exposed to cadmium for 2 weeks were anaesthetised in a solution of magnesium chloride (75 g l⁻¹) for 1–3 h before injecting 2.5 µCi of L-[³⁵S]-cysteine, directly into the relaxed foot. The winkles were returned to the tanks from which they had been taken and exposure to cadmium (or uncontaminated seawater in the case of controls) was continued. Four days

after injection (the time taken to allow L-[³⁵S]-cysteine to equilibrate in tissues) the cadmium-exposed *L. littorea* were divided into two sub-groups; one was kept in the same (400 µg l⁻¹) cadmium concentration ('exposed' group) and the other was transferred to clean seawater ('detoxified' group).

Controls, cadmium-exposed and 'detoxified' winkles were sampled for analysis 4, 11, 18, 25 and 32 days after injection with ³⁵S-cysteine. Additional samples of 'detoxified' winkles were sampled after 84 and 115 days of injection. Snail shells were removed after careful cracking in the plastic-covered jaws of a small vice and digestive gland, gills and kidney from six animals were dissected out and pooled at each sampling. Each pooled tissue sample was weighed and homogenised in three volumes of ice-cold 0.02 M Tris-HCl (pH 8.6) buffer and 3–5 ml taken for centrifugation at 30 000 × g for 1 h at 4°C. The supernatant cytosol was separated from the pellet for size-exclusion gel chromatography in order to identify and quantify major ³⁵S-cysteine-containing pools (including metallothioneins).

2.1. Measurement of radio-isotope uptake and loss

The total ³⁵S activity in homogenates of the digestive gland, gills and kidney from winkles injected with labelled cysteine was determined by digesting an aliquot of 0.2 mg of the homogenate overnight in 1 ml of tissue solubilizer (Optisolv). Subsequently 14 ml of liquid scintillant (Optiphase 'MP') was added and samples counted in a LKB Wallac 1215 Rackbeta II scintillation counter. Aliquots of the cytosol (0.5–1 ml), described in the previous section, were chromatographed on a Sephadex G-75 column (1.5 × 60 cm) and eluted with 0.02M Tris-HCl (pH 8.6) to separate the major ³⁵S-containing components by virtue of their molecular size. The ³⁵S activity of each column fraction was determined by adding 14 ml of liquid scintillant to 1 ml of each fraction and counting as described above. The ³⁵S activities were expressed as disintegrations per minute (DPM) as a function of the original dry tissue weight (DPM g⁻¹) and were corrected

for quenching, decay and background. Counting efficiency was $98 \pm 3\%$. The coefficient of variation of counting (analytical precision) was $< 5\%$.

2.2. Cadmium analysis

Cadmium analysis was performed on nitric acid-digested subsamples of the homogenate and cytosol of the digestive gland, gills and kidney of *L. littorea*, using atomic absorption spectrophotometry (Varian AA20).

3. Results

3.1. Incorporation of L-[^{35}S]-cysteine into the metallothionein pool of different tissues, and subsequent degradation of MT

Four days after injection of L-[^{35}S]-cysteine into the foot of the winkles most of the ^{35}S activity (60–80%) was found in the cytosol of the gills, kidney and digestive gland of control, cadmium-exposed and cadmium-detoxified winkles.

Following fractionation on a Sephadex G-75 column most of the ^{35}S present in the cytosol of these tissues from control winkles eluted near the void volume of the column (fractions 10–15-mol wt% $> 75\,000$ Da-HMW protein pool-) and around the total volume of the column (fractions 30–45-mol wt% < 3000 Da-VLMW pool, containing amino-acids, including cysteine). This pattern was maintained throughout the experiment and the absence of any inducible cysteine-rich pool of intermediate molecular weight indicates negligible synthesis of metallothionein in uncontaminated individuals.

The ^{35}S elution profiles of the cytosol from tissues of cadmium-‘exposed’ and cadmium-‘detoxified’ winkles are shown in Fig. 1. In contrast to controls, there was an additional pool (eluting between fractions 20–25) with an apparent molecular weight of about 10 000–20 000 Da, which corresponded to the metallothionein-containing pool in cadmium-‘exposed’ and cadmium-‘detoxified’ winkles (MT has molecular weight variants of 10 and 20 KDa in this species, though to represent monomeric and dimeric forms;

[6,27]). The ^{35}S cysteine activity in this pool tended to increase in the gill (Fig. 1A) and kidney (Fig. 1C) of the ‘exposed’ group, largely at the expense of what is assumed to be free ^{35}S cysteine in the VLMW pool which decreases over time. These results are consistent with MT induction in gill and kidney tissue. In contrast, changes in digestive gland were far less pronounced (Fig. 1E,F) signifying only minor incorporation of labelled cysteine into newly synthesised MT in this tissue.

The summed ^{35}S activity in pooled metallothionein-containing fractions (20–25) were calculated for each tissue, in control, cadmium-‘exposed’ and cadmium-‘detoxified’ *Littorina*. These results, plotted against time, are shown in Fig. 2. Following the first 2 weeks of cadmium-treatment, the rapid incorporation of injected ^{35}S -cysteine into gill metallothionein of the ‘exposed’ group clearly demonstrates the speed and scale of MT induction: This is represented by a 6-fold ($P < 0.01$) increase in ^{35}S -labelled MT levels in contaminated gill tissue, relative to controls (Fig. 2A). Although values subsequently fluctuated over time there was little additional increase in gill-MT in Cd-dosed *Littorina* even after a further 32 days exposure (Fig. 2A). The ^{35}S activity in the gills of ‘detoxified’ *Littorina* indicated a net loss of 34% following 32 days in clean seawater ($P < 0.01$). However in view of the scattered nature of the data points over this period some uncertainty should be attached to the estimated half life. Results do however indicate the slow nature of the turnover. No significant change with time was detectable in the (small) metallothionein pool from gills of controls (Fig. 2A).

A similar pattern with a 7-fold increase in MT levels in exposed animals relative to controls ($P < 0.01$) was observed in the kidney (Fig. 2B). Though even greater fluctuations in ^{35}S levels were detected in the metallothionein pool of Cd-treated individuals throughout the experimental period. Nevertheless, the kidney of ‘detoxified’ individuals had lost only 21% of the ^{35}S activity originally associated with metallothionein after 32 days, indicating again slow and somewhat erratic degradation of the protein. A small increase in ^{35}S -labelled metallothionein was observed in the

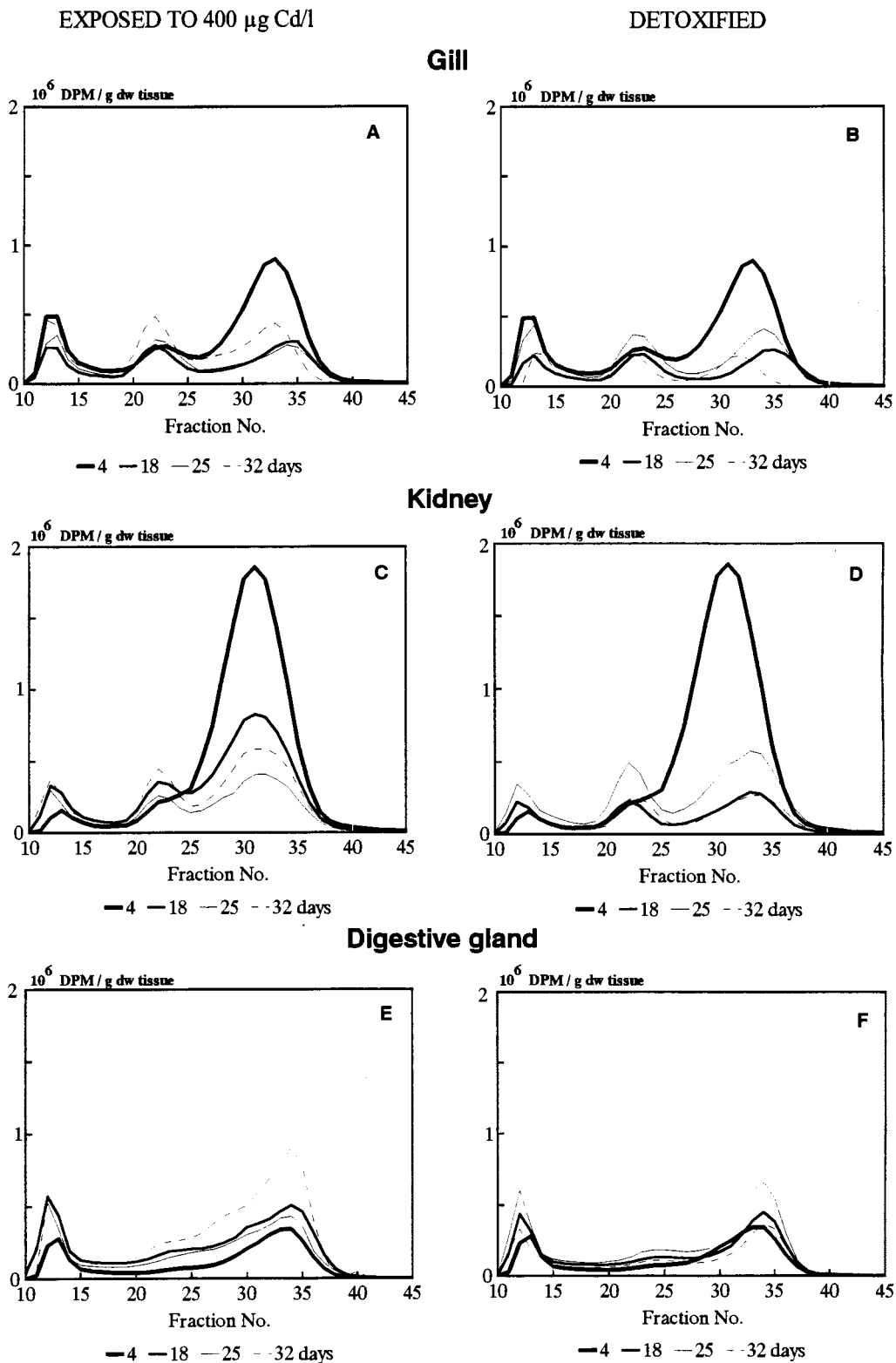


Fig. 1. *L. littorea*. Chromatographic elution profiles of ³⁵S of the cytosol of the gill (A,B), kidney (C,D) and digestive gland (E,F) of exposed and detoxified winkles at different times after injection. Pooled samples of six individuals.

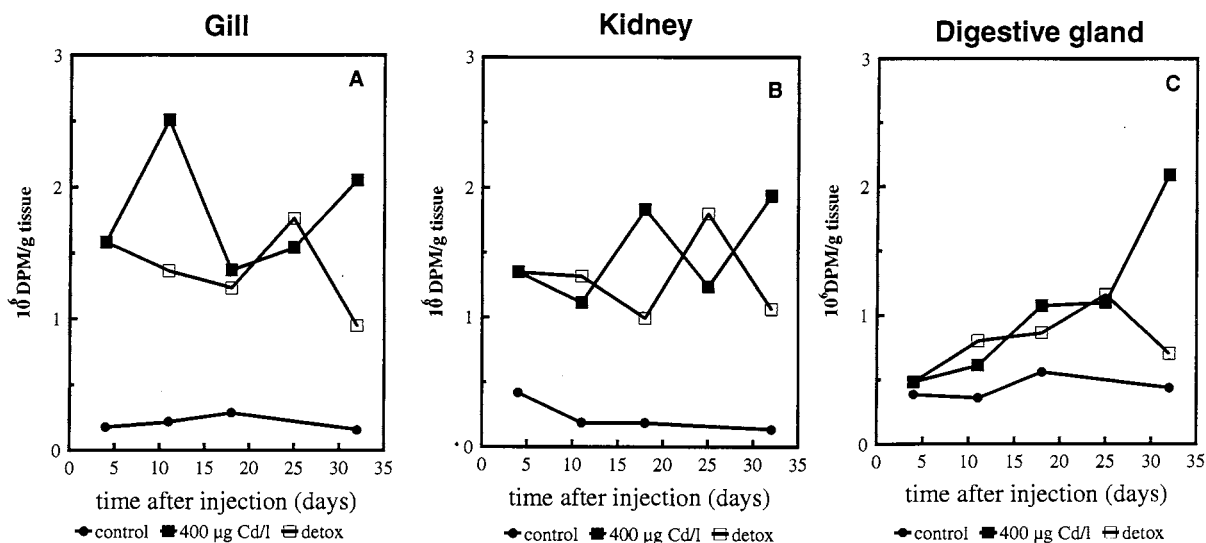


Fig. 2. *L. littorea*. Incorporation of ^{35}S into the metallothionein pool (fraction 20–25 see Fig. 1) of control, Cd-exposed and Cd-detoxified winkles—gills (A), kidney (B) and digestive gland (C)—at different times after injection of the isotope. Tissue pooled from six individuals.

‘exposed’ winkles during this period. No significant changes were detected in controls (Fig. 2B).

As indicated in Fig. 1E,F, the incorporation of L-[^{35}S]-cysteine into the metallothionein fraction of the digestive gland was initially much less pronounced when compared to the gill and the kidney. This is reflected in the relatively small increases ^{35}S -labelled MT in digestive gland of the ‘exposed’ group, relative to controls, following the initial 2 week period of contamination (initial data points in Fig. 2C). Nevertheless activity in this pool continues to increase in the digestive gland of ‘exposed’ individuals ($P < 0.05$), approaching the levels found in the gills and kidney after a further 32 days exposure (Fig. 2C). Interestingly, in the digestive gland of cadmium-‘detoxified’ winkles, there was also a gradual increase in metallothionein ^{35}S activity, until day 25 ($P < 0.05$). Thereafter there are indications that ^{35}S -MT may have been dropping by day 32, although, overall, no net loss was observed when compared with the levels present in the digestive gland at the start of the detoxification period. Again, no significant changes were detected in the activity in the digestive gland of controls (Fig. 2C).

Results depicting degradation of MT in gills, kidney and digestive gland of *Littorina* during longer-term depuration are plotted in Fig. 3 A,B and C, respectively. These semilogarithmic plots of ^{35}S activity in the metallothionein pool of tissues from detoxified winkles have been used to establish the rate of turnover (half-life) of metallothionein which is clearly tissue dependent. Thus, the decrease in the ^{35}S -labelled MT content of both the gills, and, to a lesser extent, kidney, is shown to be statistically significant (ANOVA, $P < 0.05$) following the removal of Cd contamination whilst this was not the case in the digestive gland (ANOVA, $P > 0.05$). The half-lives of metallothionein in the gills and kidney were calculated to be 69 and 160 days, respectively. In contrast the minimal turnover of MT ^{35}S in the digestive gland of cadmium-detoxified winkles prevented the calculation of a protein degradation rate in this tissue. Bearing in mind the variable and limited nature of the data, turnover times of the protein are at best estimates. Nevertheless they represent one of the few attempts at direct quantification in molluscs and testify the nature of the slow turnover in the kidney and gills, and negligible degradation in digestive glands. These

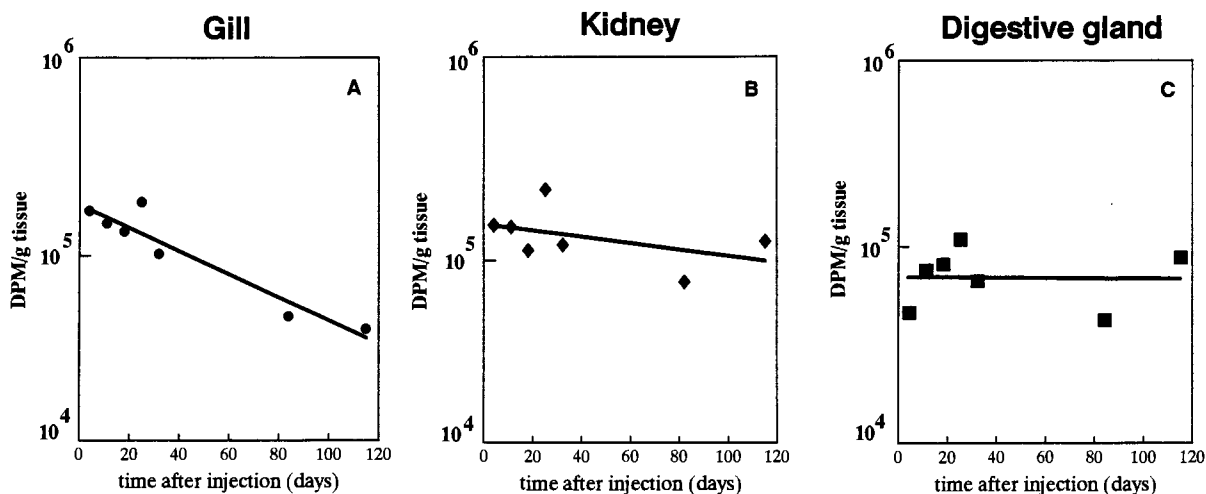


Fig. 3. *L. littorea*. Loss of ³⁵S from the metallothionein containing pool of gills (A), kidney (B) and digestive gland (C) during a 4 month detoxification period. Pooled samples of six individuals.

observations carry important implications for monitoring schemes.

3.2. Accumulation and elimination of cadmium in *L. littorea*

Cadmium concentrations in the gills, kidney and digestive gland of the 'detoxified' group of *Littorina* are shown in Fig. 4, which includes both exposure and depuration phases.

Total, cytosolic and MT-bound cadmium concentrations present in the tissues of *L. littorea* at the end of each phase (after 18 days of exposure and 126 days of depuration), and in controls, are summarised in Table 1. The pattern of total cadmium concentrations in tissues of cadmium-exposed winkles was: kidney > digestive gland > gills. After 126 days of depuration this ranking changed to: digestive gland > kidney > gills (see Table 1). The uptake rates for total and cytosolic cadmium in these tissues, during exposure, are shown in Table 2 and are in agreement with earlier results [7,9].

The variations in total and cytosolic cadmium concentrations in *Littorina* tissues (Fig. 4) contrast somewhat with protein (MT) kinetics. During detoxification/depuration, the loss of cadmium (total and cytosolic) is extremely slow in the gills (Fig. 4A) and the kidney (Fig. 4B) despite

the apparent degradation of MT (described above). In the kidney, large Cd fluctuations of a possible cyclical nature are evident at the end of exposure/beginning of depuration and may signify attempts at Cd homeostasis (Fig. 4B), though this has yet to be confirmed. During the same 126 days depuration period, total and cytosolic cadmium concentrations increased in the digestive gland, by 19 and 24%, respectively (Fig. 4C), suggesting that cadmium which has been lost from other tissues, such as kidney and gills, albeit slowly, may be transported and held here, even after the exposure to cadmium had stopped.

Thus, after 4 months of 'detoxication', following Cd-exposure, winkles still retained much of the original accumulated body burden (95%). The half-life for cadmium in the kidney was calculated to be approximately 300 days. Loss from the gills was not measurable with sufficient accuracy to derive a half-life, whilst in the digestive gland Cd continues to increase slightly, confirming its role as the major storage organ for the metal.

The gel chromatographic profiles of cadmium in the cytosol of the gills, kidney and digestive gland of *L. littorea* revealed that even after 4 months of depuration most of the cadmium was bound to metallothionein in each of these tissues (60, 76 and 54%, respectively; Table 1).

Table 1
L. littorea; cadmium distribution in tissues of winkles exposed to 400 $\mu\text{g Cd l}^{-1}$ for 2 weeks and subsequently depurated for 126 days, together with controls

Tissue	Control			Exposure—day 18			Depuration—day 126					
	Total Cd	Cytosolic Cd	Cd-MT	Total Cd	Cytosolic Cd	Cd-MT	Total Cd	Cytosolic Cd	Cd-MT			
	$\mu\text{g g}^{-1}$	$\mu\text{g g}^{-1}$	(%)	$\mu\text{g g}^{-1}$	$\mu\text{g g}^{-1}$	(%)	$\mu\text{g g}^{-1}$	$\mu\text{g g}^{-1}$	(%)			
Kidney	13.2	9.1	69	4.5	204.1	116.3	57	98.8	155.7	134.9	87	118.3
Gill	2.3	1.5	65	0.7	84.6	54.0	64	47.1	77.2	65.9	85	46.2
Digestive gland	2.2	1.8	82	0.5	196.2	112.7	57	72.5	234.2	139.3	60	126.6

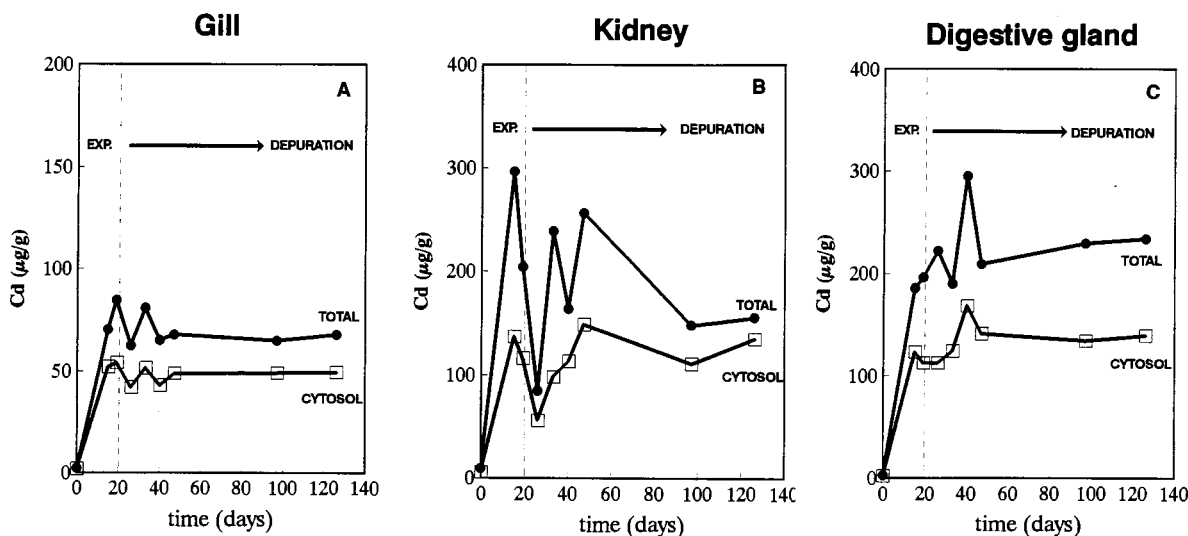


Fig. 4. *L. littorea*. Total and cytosolic cadmium concentrations in the gills (A), kidney (B) and digestive gland (C) following exposure to $400 \mu\text{g Cd l}^{-1}$ for 18 days and subsequent depuration in clean seawater. Pooled samples of six individuals

4. Discussion

The present study confirms that the rates of synthesis and degradation of Cd-induced metallothionein in *L. littorea* are tissue dependent.

The concentrations of metallothionein-incorporated ^{35}S -cysteine in tissues of unexposed *L. littorea* followed the pattern: digestive gland > gill > kidney, with the level of ^{35}S activity in the MT-pool of digestive gland being twice that of the other tissues. Similar, relative concentrations were observed for baseline metallothionein concentrations determined by differential pulse polarography and are indicative of a high level of constitutive MT in the digestive gland, possibly associated with the regulation of metal during

metabolism of the Cu-containing blood pigment haemocyanin [9,10,27].

In the gills and kidney of *L. littorea* the incorporation of the L- ^{35}S -cysteine label into metallothionein increased significantly (6-fold and 3-fold, respectively) when the animals were treated with cadmium, whilst only a small increase (10%) was detected in the digestive gland. Clearly cadmium strongly induces the synthesis of metallothionein in both the gills and kidney. The respective 6- and 3-fold increase in the ^{35}S -MT content in the gills and kidney of cadmium-exposed winkles, relative to controls, is remarkably similar to the increases in metallothionein concentrations, determined by differential pulse polarography [9,10]. The lack of response of the digestive gland is also a consistent feature. These data therefore validate the application of two widely differing techniques in measuring relative induction of metallothionein.

The slow linear increase in the ^{35}S -labelled MT pool in the digestive gland of 'detoxified' winkles, which is maintained for 25 days after Cd exposure is removed, indicates that metallothionein synthesis may continue here as a result of remobilization of cadmium from other tissues of *L. littorea*, and that the Cd-metallothionein complex formed in

Table 2
L. littorea; cadmium accumulation rates in different tissues during exposure of the winkles to $400 \mu\text{g Cd l}^{-1}$ for 18 days

	Cadmium ($\mu\text{g g}^{-1} \text{d}^{-1}$)	
	Total	Cytosolic
Kidney	6.47	4.68
Gill	3.98	2.40
Digestive gland	9.14	6.84

the digestive gland is extremely stable. A similar phenomenon may explain observations by Olafson [22] who reported that, in mice intestine, a tissue where metallothionein induction is very slow, the incorporation of ^{35}S -cysteine continues after exposure to zinc is stopped.

The disappearance of ^{35}S -labelled metallothionein from gills and kidney of detoxified winkles became significant only after animals had been maintained in Cd-free seawater for 25 days, illustrating that the turnover of MT in these tissues, though faster than the digestive gland, is far from rapid. The half-life of metallothionein in the gills and the kidney of *L. littorea* was calculated to be 69 and 160 days, respectively. Breakdown of metallothionein could not be detected in the digestive gland during the 4 month depuration period.

Cd depuration in these molluscs appears to be even slower than MT turnover, at least in gill and kidney tissue, and implies recycling. In kinetic terms the linear nature of cadmium accumulation in *L. littorea* [7–10] as in many other molluscan species such as oysters and mussels [14,28–32,36,37,39–41] is explained by the extremely slow rate of elimination of cadmium. However, Marigomez and Ireland [8] have observed an exponential loss of cadmium from the whole soft tissues of *L. littorea* exposed to 0.5 and 1.25 mg Cd l^{-1} (higher doses than used in the present study) and determined a half-life for the metal of 69 and 115 days, respectively, at these concentrations. Among bivalves, the half-life for cadmium ranges from 300 days in the whole soft tissues of *M. edulis* [14] to 70 days in the clam *Macoma balthica* [27]. The more rapid elimination of Cd in the latter species may be due to a lack of inducible MT, and hence less effective Cd-binding [27].

In the present work cadmium was accumulated in the gills during exposure but was not lost during the depuration period. Similar results were obtained for the gills when *L. littorea* was exposed to 0.5 mg Cd l^{-1} for 27 days and depurated during 74 days [8,33]. However, an exponential decrease in gill Cd was detected by the latter authors following exposure of winkles to 1.25 mg Cd l^{-1} . Rates of cadmium elimination from gill tissues may, therefore, be related to previous ex-

posure concentrations and appear to be significant only at extreme concentrations, perhaps as normal metal binding ligands became saturated. Loss of Cd in these circumstances may again be a reflection of less effective Cd-binding and possible saturation of MT.

The calculated cadmium half-life in the kidney of *L. littorea* determined in the present study is 300 days. This half-life is of similar magnitude to the one calculated for the kidney and whole soft tissues of *M. edulis* (300 days) [14,34]. However, Marigomez [33] and Marigomez and Ireland [8] calculated shorter half-lives of 78 days and 39 days for Cd in the kidney of *L. littorea* exposed to 1.25 and to 0.5 mg Cd l^{-1} respectively, further illustrating the possible significance of exposure levels on elimination rates.

During depuration, the increase in Cd levels in the digestive gland indicates that transport occurs from other tissues of *L. littorea* such as kidney and gills. These data confirm earlier results obtained by Langston and Zhou [7] which showed an increase of 32% in total cadmium in the digestive gland, and a corresponding decrease in Cd burdens in other tissues, after depuration for 7 months.

Storage and retention of cadmium in the digestive gland of *L. littorea* clearly involves binding of the metal to metallothionein, at least in part. However, X-ray microanalytical studies have detected intracellular accumulations of cadmium and sulphur which usually take the form of membrane bound granular structures and suggests a possible link between protein- and granular-based detoxification systems [35]. Furthermore, Marigomez [33] concluded that the metabolic pathway of cadmium accumulation and elimination is related to the lysosomes of the digestive cells. To date however, these lysosomes and the intracellular granules in the basophil cells of the digestive gland are the only sites of accumulation that have been visualised to date. Between these compartments, the turnover of MT and associated metals may be influenced by a variety of physiological and seasonal variables, which may partly explain the differences in elimination rates observed between studies. Metallothionein turnover in the digestive gland of *L. littorea* was unde-

tectable in the current study supporting the view that the complex of cadmium and MT can, under certain circumstances, be extremely stable.

The fact that cadmium levels in the gills of *L. littorea* remained constant during depuration in the present study, whilst ³⁵S-labelled MT was degraded slowly, suggests that further, newly synthesised, metallothionein efficiently retains any excess, re-released Cd which is present in the cytosol. Turnover of metallothionein in the kidney (half-life 160 days) is intermediate between gill and digestive gland. Although cadmium concentrations vary considerably in the tissue following transfer of winkles to clean sea water, cadmium elimination is undoubtedly slow (half-life 300 days) relative to protein (MT) turnover, indicating possible metal re-sequestration by newly synthesised metallothionein, as indicated also in gills.

There have been few comparable studies on protein-metal kinetics in other molluscs. Nevertheless there appears to be some consistency in the reported behaviour of the Cd-MT complex, even in unrelated species. Thus, Chen et al. [16] demonstrated how, in rat liver, the levels of cadmium in the metallothionein fraction remain constant while the protein itself is metabolised. It is suggested that when the protein degrades the released cadmium immediately stimulates further metallothionein synthesis and that any 'free Cd' is quickly re-sequestered: thus Cd does not disappear with the degraded protein moiety and becomes bound to the newly synthesised protein. The same mechanism is observed in the bivalve *M. edulis* [14].

The difference between metallothionein and cadmium half-lives in *Littorina* gills and kidney therefore indicates that while metallothionein breaks down, the released cadmium is closed-cycled within the cytosol by inducing de novo metallothionein synthesis to which the metal becomes re-sequestered. The resistance of the *Littorina* to cadmium toxicity is clearly related to the efficiency with which metallothionein complexes cadmium, though the apparent stability of the Cd-metallothionein complex may result in virtually irreversible loading of tissues under certain conditions.

In conclusion metallothionein acts as a detoxifying ligand for Cd in the gills and kidney and fulfils an efficient storage/detoxification function in the digestive gland of *L. littorea*. The half-life for metallothionein is of the order of 69 and 160 days for the gills and the kidney; considerably longer in the digestive gland. These results, along with similar data obtained for the mussel *M. edulis* [14], imply that metallothionein turnover for molluscs is slow when compared with fish [25] and mammalian species [16,38]. These are important implications for Cd bio-monitoring schemes involving molluscs, since determinations of MT or Cd concentrations in tissues could reflect previous historical inputs during the life span of the individual, rather than conditions at the time of sampling. This need not be a disadvantage if, for example, an integrated picture of the recent contamination history of a site is required. Where the current situation needs to be assessed, the measurement of fluxes of Cd and MT in transplanted individuals might be more appropriate. In this context the use of injected ³⁵S-cysteine has been shown to be a viable technique in molluscs for measuring MT induction in response to Cd.

Acknowledgements

M.J. Bebianno was supported by a grant from the Junta Nacional de Investigação Científica e Tecnológica (JNICT) of Portugal. Support from INVOTAN and NATO (CRG. 920027) is also acknowledged.

References

- [1] D.J.H. Phillips, P.S. Rainbow, *Biomonitoring of Trace Aquatic Contaminants*, Elsevier, Barking, 1993.
- [2] G. Roesijadi, Metallothionein in metal regulation and toxicity in aquatic animals, *Aquatic Toxicol* 22 (1992) 81–114.
- [3] W.J. Langston, M.J. Bebianno, M. Zhou, A comparison of metal-binding proteins and cadmium metabolism in the marine molluscs *Littorina littorea* (Gastropoda), *Mytilus edulis* and *Macoma balthica* (Bivalvia), *Marine Environ. Res.* 28 (1989) 195–200.
- [4] G.W. Bryan, W.J. Langston, L.G. Hummerstone, G.R. Burt, Y.B. Ho, An assessment of the gastropod, *Littorina*

- littorea*, as an indicator of the heavy-metal contamination in United Kingdom estuaries, J. Marine Biol. Assoc. UK 63 (1983) 327–345.
- [5] A.Z. Mason, K. Simkiss, Interactions between metals and their distribution in tissues of *Littorina littorea* (L.) collected from clean and polluted sites, J. Marine Biol. Assoc. UK 63 (1983) 661–672.
- [6] W.J. Langston, M. Zhou, Evaluation of the significance of metal-binding proteins in the gastropod *Littorina littorea*, Marine Biol. 92 (1986) 505–515.
- [7] W.J. Langston, M. Zhou, Cadmium accumulation, distribution and metabolism in the gastropod *Littorina littorea*: the role of metal-binding proteins, J. Marine Biol. Assoc. UK 67 (1987) 585–601.
- [8] J.A. Marigomez, M.P. Ireland, Accumulation, distribution and loss of cadmium in the marine gastropod *Littorina littorea* (L.), Sci. Total Environ. 78 (1989) 1–12.
- [9] M.J. Bebianno, W.J. Langston, K. Simkiss, Metallothionein induction in *Littorina littorea* (Mollusca: Prosobranchia) on exposure to cadmium, J. Marine Biol. Assoc. UK 72 (1992) 329–342.
- [10] M.J. Bebianno, W.J. Langston, Induction of metallothionein synthesis in the gill and kidney of *Littorina littorea* exposed to cadmium, J. Marine Biol. Assoc. UK 75 (1995) 173–186.
- [11] A.G. Howard, G. Nickless, Heavy metal complexation in polluted molluscs. III. Periwinkles (*Littorina littorea*), cockles (*Cardium edule*) and scallops (*Chlamys opercularis*), Chem.-Biol. Interact. 23 (2) (1978) 227–231.
- [12] F. Noel-Lambot, J.M. Bouquegneau, F. Frankenne, A. Disteche, Le role des metallothioneines dans le stockage des metaux lourds chez les animaux marins. Rev. Int. Oceanogr. Medicale XLIX (1978) 13–20.
- [13] M.J. Bebianno, W.J. Langston, Quantification of metallothioneins in marine invertebrates using differential pulse polarography, Port. Electrochim. Acta 7 (1989) 59–64.
- [14] M.J. Bebianno, W.J. Langston, Turnover rate of metallothionein and cadmium in *Mytilus edulis*, Biol. Metals 6 (1993) 239–244.
- [15] G. Roesijadi, M.M. Vestling, C.M. Murphy, P.L. Klerks, C.C. Fenselau, Characterization of two molluscan metallothioneins (MT): structure and rates of synthesis and turnover, in: Proceedings of the 6th International Symposium of Responses of Marine Organisms to Pollutants, Woods Hole Oceanographic Institution, Woods Hole, MA, 1991.
- [16] R.W. Chen, P.D. Whanger, P.H. Weswig, Biological function of metallothionein. I. Synthesis and degradation of rat liver metallothionein, Biochem. Med. 12 (1975) 95–105.
- [17] Z.A. Shaikh, J.C. Smith, The biosynthesis of metallothionein in rat liver and kidney after administration of cadmium, Chem.-Biol. Interact. 15 (1976) 327–336.
- [18] S.L. Feldman, R.J. Cousins, Degradation of hepatic zinc-thionein after parental zinc administration, Biochem. J. 160 (1976) 583–588.
- [19] R.D. Andersen, W.P. Winter, J.J. Maher, I.A. Bernstein, Turnover of metallothionein in rat liver, Biochem. J. 174 (1978) 327–338.
- [20] I. Bremner, W.G. Hoekstra, N.T. Davies, B.W. Young, Effect of zinc status of rats on the synthesis and degradation of copper-induced metallothioneins, Biochem. J. 174 (1978) 883–892.
- [21] S.L. Feldman, K.S. Squibb, R.J. Cousins, Degradation of cadmium-thionein in rat liver and kidney, J. Toxicol. Environ. Health 4 (1978) 805–813.
- [22] R.W. Olafson, Differential pulse polarographic determination of murine metallothionein induction kinetics, J. Biol. Chem. 256 (3) (1981) 1263–1268.
- [23] K. Cain, B.L. Griffiths, A comparison of isometallothionein synthesis in rat liver after partial hepatectomy and parenteral zinc injection, Biochem. J. 217 (1984) 85–92.
- [24] D.D. Held, W.G. Hoekstra, The effects of zinc deficiency on turnover of cadmium-metallothionein in rat liver, J. Nutr. 114 (1984) 2274–2282.
- [25] J. Overnell, R. McIntosh, T.C. Fletcher, The enhanced induction of metallothionein by zinc, its half-life in the marine fish *Pleuronectes platessa*, and the influence of stress factors on metallothionein levels, Experientia 43 (1987) 178–181.
- [26] J.A. McCarter, M. Roch, Chronic exposure of coho salmon to sublethal concentrations—III. Kinetics of metabolism of metallothionein, Comp. Biochem. Physiol. 77C (1984) 83–87.
- [27] W.J. Langston, M. Zhou, Cadmium accumulation, distribution and elimination in the bivalve *Macoma balthica*: neither metallothionein nor metallothionein-like proteins are involved, Marine Environ. Res. 21 (1987) 225–237.
- [28] G.E. Zaroogian, Studies on the depuration of cadmium and copper by american oyster *Crassostrea virginica*, Bull. Environ. Contam. Toxicol. 23 (1979) 117–122.
- [29] J.B. Luten, W. Bouquet, M.M. Burggraaf, A.B. Rauchbaer, J. Rus, Accumulation, elimination and speciation of cadmium and zinc in mussels, *Mytilus edulis* in the natural environment, Bull. Environ. Contam. Toxicol. 37 (1986) 579–586.
- [30] M.J. Bebianno, W.J. Langston, Metallothionein induction in *Mytilus edulis* exposed to cadmium, Marine Biol. 108 (1991) 91–96.
- [31] M.J. Bebianno, W.J. Langston, Metallothionein induction and cadmium binding in *Mytilus galloprovincialis*, Comp. Biochem. Physiol. 103C (1992) 79–85.
- [32] M.J. Bebianno, M.A.P. Serafim, M.F. Rita, Involvement of metallothionein in cadmium accumulation and elimination in the clam *Ruditapes decussata*, Bull. Environ. Contam. Toxicol. 53 (5) (1994) 726–732.
- [33] J.A. Marigomez, Aportaciones cito-histologicas a la evaluacion ecotoxicologica de niveles subletales de cadmio en el medio marino: estudios de laboratorio en el gasteropodo prosobranchio *Littorina littorea* (L.). Ph.D. Thesis, University of the Basque Country, Bilbao, Spain, 1989, 430 pp.

- [34] S.G. George, B.J.S. Pirie, The occurrence of cadmium in sub-cellular particles in the kidney of the marine mussel *Mytilus edulis*, exposed to cadmium: The use of electron microprobe analysis, *Biochim. Biophys. Acta* 580 (1979) 234–244.
- [35] J.A. Nott, W.J. Langston, Cadmium and the phosphate granules in *Littorina littorea*, *J. Marine Biol. Assoc. UK* 69 (1989) 219–227.
- [36] Z.S. Evtushenko, N.N. Belcheva, O.N. Lukyanova, Cadmium accumulation in organs of the scallop *Mizuhopecten yessoensis*-II. Subcellular distribution of the metals and metal-binding proteins, *Comp. Biochem. Physiol.* 83C (2) (1986) 377–383.
- [37] S.G. George, E. Carpena, T.L. Coombs, J. Overnell, A. Youngston, Characterization of cadmium-binding proteins from mussels, *Mytilus edulis* (L.), exposed to cadmium, *Biochim. Biophys. Acta* 580 (1979) 225–233.
- [38] D.H. Hamer, Metallothionein, *Annu. Rev. Biochem.* 55 (1986) 913–951.
- [39] K. Köhler, H.U. Riisgard, Formation of metallothioneins in relation to accumulation of cadmium in the common mussel *Mytilus edulis*, *Marine Biol.* 66 (1982) 53–58.
- [40] W.E. Robinson, D.K. Ryan, Metal interactions within the kidney, gill and digestive gland of the hard clam *Mercenaria mercenaria* following laboratory exposure to cadmium, *Arch. Environ. Contam. Toxicol.* 15 (1986) 23–30.
- [41] A. Viarengo, S. Palmero, G. Zanicchi, R. Capelli, R. Vaissiere, M. Orunesu, Role of metallothioneins in Cu and Cd accumulation and elimination in the gill and digestive gland cells of *Mytilus galloprovincialis* Lam, *Marine Environ. Res.* 16 (1985) 23–36.

Characterisation of human foetal liver Zn-metallothioneins using differential pulse polarography

Oscar Nieto ^a, Godelieve Hellemans ^b, Guy Bordin ^a, Marc De Ley ^b,
Adela Rosa Rodríguez ^{a,*}

^a *European Commission, Joint Research Centre, Institute for Reference Materials and Measurements, Retieseweg, B-2440 Geel, Belgium*

^b *Laboratory for Biochemistry, Katholieke Universiteit Leuven, Celestijnenlaan 200/G, B-3001, Heverlee, Belgium*

Received 4 November 1996; received in revised form 31 January 1997; accepted 3 June 1997

Abstract

A study on electrochemical characterisation of three isoforms of human foetal liver Zn-metallothioneins, labelled MT-0, MT-1 and MT-2, has been performed by using differential pulse polarography (DPP). Two different peaks, attributed to two different Zn complexes with metallothioneins, have been detected. The electrochemical behaviour is similar for the three studied isoforms. Studies on the addition of Cd^{2+} and Zn^{2+} as well as studies as a function of pH have been carried out. The association and dissociation equilibria of metal ions with MTs are reversible in the studied pH range. The behaviour of Zn complexes in human foetal liver Zn-metallothioneins is comparable to the Cd complexes obtained using other mammalian Cd, Zn-metallothioneins, particularly as a function of pH. © 1998 Elsevier Science S.A. All rights reserved.

1. Introduction

Metallothioneins (MT) are ubiquitous low molecular weight proteins (~ 6000 Da). The peptidic structure bears 61 amino acids, 20 of which are cysteinyl residues. MTs are characterised by a pronounced capability of binding metal ions such as Zn, Cd, Cu, Hg, etc. [1–5].

Studies of MT properties, especially the metal complexation properties, have been performed using a wide variety of analytical methods. During the first studies in our group, the acid-base con-

stants and binding constants with metal ions for MTs were evaluated using spectrophotometric methods [6].

Voltammetric and polarographic techniques have been used for qualitative and quantitative determinations of disulphide and thiolate groups in proteins and in peptides as well as in amino acids [7]. The first systematic study on the characterisation of MTs by cyclic voltammetry was carried out by Olafson [8]. In our team, differential pulse polarography (DPP) has been used for elucidation of the electrochemical systems involved in different commercially available mammalian MTs, such as rabbit liver (RL), horse kidney (HK) and human adult kidney and foetal liver

* Corresponding author. Tel.: + 32 14 571200; fax: + 32 14 584273

Cd, Zn MTs. Likewise, the influence of the pH as well as of the additions of Zn and Cd, which are initially contained in MTs, on the polarographic response have been studied [9–12]. Recently, Sestakova et al. [13] have published a work on the electrochemical characterisation of metallothioneins using mercury, glassy carbon and carbon paste electrodes. DPP and voltammetry have been applied for the quantitative determination of MTs contained in different animal tissue [14,15].

The peptidic fragment, Lys-Cys-Thr-Cys-Cys-Ala (56–61) MT I (FT), a molecule intrinsic to the mouse liver MT structure, cluster α , has been taken as a simpler model for the study of complexation and ion exchange properties with cadmium and zinc. The electrochemical behaviour of the peptidic fragment, FT, in the presence of Cd and Zn is very similar to that obtained with Cd, Zn MTs, particularly with respect to the variation of the pH under the same given experimental conditions [16–20]. Likewise, in recently published works, the fact that Zn(II) complexed with FT exhibits two possible forms of co-ordination, like Cd(II) complexes with FT [18,19] has been reported.

In our team, several studies on the characterisation of HK and RL MTs and FT (from Sigma) by HPLC [21,22] and capillary electrophoresis [23] have been performed.

The structure of MTs is intricate and the proposed characteristics determined by several research teams depend on the origin of the animal tissue from which the MTs are isolated. Although several articles have been published about the electrochemical behaviour of MT, most of them describe the protein complexed with Cd or Cd and Zn. In this work, the MT is isolated from human foetal liver, a very important tissue for the developing foetus. The human foetal liver (HFL) MT obtained is not only unique because of its natural origin without any further *in vitro* induction and consequently containing merely Zn, but also because of the occurrence of three isoforms therein. Besides MT-1 and MT-2, the two widespread isoforms, differing from each other in an uncharged amino acid residue at position 11 for MT-1 in comparison to a negatively charged residue for MT-2, a third separable isoform, MT-

0, is present in the human foetal liver [24]. This isoform was previously considered as being a foetal specific isoform because of its presence in foetal liver but not in adult liver. However, MT-mRNA has been found in human adult liver tissue [25] and recently, both at the protein and RNA level, the MT-0 was found in human monocytes after induction with zinc [26]. This MT-0 differs from the other isoforms in having an extra negative charge at amino acid position 8 and a substitution of negatively charged amino acid by a positive one at position 23, a strictly conserved region of the protein. The cysteinyl residues surrounding both substitutions co-ordinate the same metal ion, as shown by X-ray diffraction and ^{113}Cd NMR studies of MT-2 [27], which makes alterations in the strength of the metal binding possible.

In this article a study of complexation properties of HFL MTs by using polarographic techniques is presented for the first time. Comparisons with results previously obtained for HK, RL and human MTs, and the peptidic fragment FT are also made.

2. Experimental

2.1. Apparatus

A potentiostat BAS 100B/W (West Lafayette, IN) coupled to a polarographic stand BAS 'Controlled Growth Mercury Electrode' which is equipped with a static mercury drop electrode, an Ag/AgCl reference electrode and a platinum wire as a counter electrode was used for the polarographic studies.

A potentiostat EG&G PARC model 384B (Princeton, IL) coupled to a polarographic stand EG&G PARC model 303A which is equipped with a static mercury drop electrode, an Ag/AgCl reference electrode, a platinum wire as a counter electrode and a water-jacketed cell was used for the determination of the thiolate groups contained in the MTs.

A flame atomic absorption spectrophotometer Perkin Elmer model 372 (Überlingen, Germany) was used to measure the metal concentration for each MT.

A Shimadzu UV-2100 spectrophotometer (Kyoto, Japan) was used for the UV spectrophotometric measurements.

A pH-meter Orion (Boston, MA) model 920S equipped with a glass combined Ag/AgCl reference electrode from Radiometer Copenhagen (Villeurbanne, France) model XC100 was used for all the experiments.

2.2. Reagents

The human foetal liver Zn–MT isoforms were obtained as described in Section 2.3.

Standard solutions of 5.0×10^{-4} M CdCl₂ and ZnCl₂ were prepared from 1.000 g l⁻¹ Titrisol standard solutions by Merck (Darmstadt, Germany).

Rabbit liver MT 1 from Sigma (St. Louis, MO) Lot 93H9559 containing 3.20 mol Cd(II) and 0.55 mol Zn(II)/mol MT, was used as standard for the determination of thiolate groups contained in the foetal liver MT samples.

All the reagents used were of analytical grade quality and the water was purified by using a Barnstead Nanopure II water deionization in conjunction with a Jencons double distillation still.

2.3. Procedure

The post mortem foetal liver tissues, obtained by autopsy, were immediately frozen in liquid nitrogen and stored at -80°C until use. The MT was isolated by homogenisation of the tissue in 10 mM Tris–HCl, 0.25 M sucrose, pH 7.4 at 4°C (20% w/v) in a Dounce apparatus. After centrifuging at $100\,000 \times g$ for 2 h at 4°C , the homogenate was heated for 2 min at 80°C and centrifuged again at $10\,000 \times g$ for 20 min. The supernatant was eluted on a Sephadex G-75 column (60×6 cm) in 10 mM Tris–HCl, pH 7.4 at a flow rate of 24 ml h^{-1} . The absorbance of the fractions was measured at 218 and 280 nm and the metal content was determined by flame atomic absorption spectrophotometry (FAAS). The zinc containing fractions with a high 218 nm/low 280 nm absorption ratio were pooled, for the purposes of MT concentration and applied on a DEAE-Sephacel anion-exchange column ($17 \times$

2.5 cm). The isoforms were eluted by a linear 10–200 mM Tris–HCl, pH 8.0 gradient and the pooled isoMTs were further concentrated through ultrafiltration.

The concentration of thiolate groups contained in the MTs samples was determined by DPP using the procedure based on the Brdicka method [28]. The experimental conditions are the following: a solution containing 0.78×10^{-3} M hexaminecobalt(III) chloride, 0.20 M ammonium buffer and 1.03% (w/w) of Triton X-100 at pH 9.5 was used as a supporting electrolyte. The scans were carried out from -1.3 to -1.7 V at a scan rate of 2 mV s^{-1} , a drop time of 2 s, a pulse amplitude of 100 mV, a pulse width of 50 ms and a sample width of 17 ms. A water-jacketed cell was used at a temperature of 10°C . The concentration of thiolate groups was determined by standard addition using the RL MT-1 solution as a standard. The total concentration of Zn(II) in the MT samples was determined by FAAS. The values obtained are 6.53, 7.03, and 7.38 mol Zn/mol MT for MT-0, MT-1, and MT-2, respectively. In the three studied MT isoforms studied, the proportion of [Zn]:[MT] is close to saturation, which means [Zn]:[MT] = 7:1.

The solution was purged before the commencement of the experiments with nitrogen for 5 min and the purging time was 2 min between each measurement. A nitrogen stream was passed over the solution during the recording of the polarograms. The supporting electrolyte for all the experiments was 0.01 M phosphate buffer. The polarograms were recorded at room temperature, in the most suitable scan range for the complete development of peaks and the following instrumental conditions were applied: drop time 1.00 s, scan rate 2 mV s^{-1} , pulse amplitude 50 mV, pulse width 50 ms, sample width 17 ms.

The polarographic responses of free cadmium and zinc (Titrisol standard solutions) were determined in the phosphate buffer 0.01 M supporting electrolyte, in the 3–12 pH range.

The study of the variation of the polarographic response with the different ratios of metals with respect to the protein was carried out by adding successive amounts of Cd and Zn to the MT solution.

The study of the variation of the polarographic response with the pH was carried out by addition of suitable amounts of NaOH and HClO₄ to the initial MT solution in order to adjust the pH to a given value.

3. Results and discussion

3.1. Assignment of polarographic peaks

The assignment of the polarographic peaks in this study has been made according to results obtained in previous works [9–12,16–20] using different polarographic and voltammetric techniques. The MTs from HK and RL as well as from human origin and FT alone and in the presence of Cd and/or Zn were used in these works. FT has been widely used for the assignment of polarographic peaks, for the elucidation of electrochemical mechanisms, for the study of diffusion-adsorption process and for assessing the reversibility of each electrochemical system. In fact, this peptide contains three cysteinyl residues which are considered as being the basic structural unit involved in their binding properties [29]. The use of the FT has an advantage over the MT in that it permits the study of the behaviour of free thiol groups and the complexation of each of the cadmium and zinc cations, usually bound to the MT, separately. The studies of FT alone and in the presence of Cd and/or Zn at different ratios metal ion:peptide—effect of concentration, electrocapillary curves, mathematical analysis of I–E waves, effect of adsorption phenomena—using DC and DPP (DME) [16–18] and SWV and CV (HMDE) [19,20] allowed us, on the one hand, to attribute, without any ambiguity, the response due to thiol groups to the reversible oxidation of the mercury electrode and, on the other hand, to establish that the reduction processes in which cadmium and zinc are involved are reversible with the charge rate coefficients being close to $\alpha = 1$. The experimental conditions under which the adsorption phenomena are not prevalent were also determined. It is necessary to point out that results obtained from Cd, Zn metallothioneins are very similar to those found using a mixture of Cd, Zn, FT.

Under our experimental conditions, low concentrations of compounds and the use of a dropping mercury electrode, in a freshly prepared solution of a Cd, Zn–MT at pH 7.5, three polarographic peaks are observed by DPP, which are the following: the MT peak ($E_p = -410$ mV) due to the oxidation of the mercury electrode in the presence of thiol groups; the CdT peak ($E_p = -780$ mV) due to the reduction of Cd(II) bound to MT and the ZnT peak ($E_p = -1100$ mV) due to the reduction of Zn(II) bound to MT. Another peak labelled CdT' ($E_p = -690$ mV) is obtained under particular experimental conditions and is attributed to the reduction of Cd(II) in another complexation form with MTs different to the original CdT. The CdT' peak is detected either after the addition of Cd²⁺ and Zn²⁺ to the MT solution or in the pH range 6.0–10.0 once the MT has previously been at acid pH [10–12].

In Fig. 1, the polarogram of 1.7×10^{-6} M HFL MT-2 in 0.01 M phosphate buffer at pH 8.0

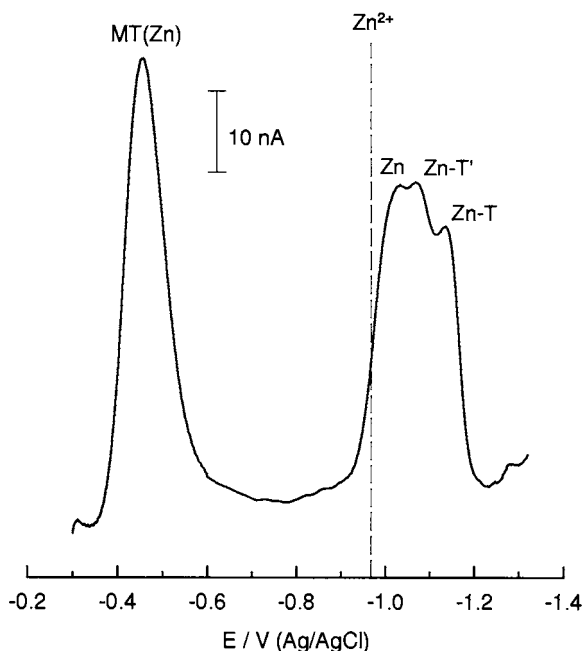


Fig. 1. DPP of 1.7×10^{-6} M HFL MT-2 in 0.01 M phosphate buffer at pH 8.0. Conditions: Scan rate 2 mV s^{-1} , drop time 1 s, pulse amplitude 50 mV, pulse width 50 ms, sample width 17 ms. Dashed line: cathodic peak potential of free Zn²⁺ obtained under the same experimental conditions.

is shown. The dashed line corresponds to the peak potential of free Zn^{2+} under the same conditions. Similar polarograms have been obtained for MT-0 and MT-1. The peak at $E_p = -458$ mV, which is labelled MT(Zn), corresponds to the oxidation of the mercury electrode in the presence of thiol groups of MTs and in the presence of Zn(II). In the potential range between -950 and -1150 mV, three polarographic peaks are observed. Those peaks are not well defined because their peak potentials are very close to each other. The peak at $E_p = -1010$ mV is labelled Zn and is attributed to the reduction of free Zn^{2+} in the solution even if small differences of potential are found between this peak potential and that previously determined for a solution of Zn^{2+} alone under the same experimental conditions. The peak at $E_p = -1066$ mV and the peak at $E_p = -1136$ mV are labelled ZnT' and ZnT respectively. In our previous study of the complexation of Zn with the peptidic fragment FT performed under analogous experimental conditions, two peaks of complexed Zn were found depending on the proportion of Zn with respect to FT [19]; these two signals have been attributed to two different complexes of Zn with FT. By analogy with these results, the possibility of two complexation forms of Zn(II) with MTs, labelled ZnT and ZnT' in accordance with the CdT and CdT' peaks, respectively [10–12], is suggested. The ZnT' and ZnT peaks have never been observed in mammalian HK and RL MTs because of the low concentration of zinc and because of the difficulty distinguishing between the peak potentials of Zn^{2+} and complexed Zn(II). However, in the case of some other MT from human foetal liver and adult kidney, the same kind of response has also been detected [12].

3.2. Variation of the polarographic responses of MT-0, MT-1 and MT-2 with the addition of Zn^{2+} and Cd^{2+}

Additions of Zn^{2+} to these MTs were first carried out since it is the metal ion originally present. This study should allow one to follow the evolution of polarographic peaks which correspond to the reduction of Zn(II) complexed with

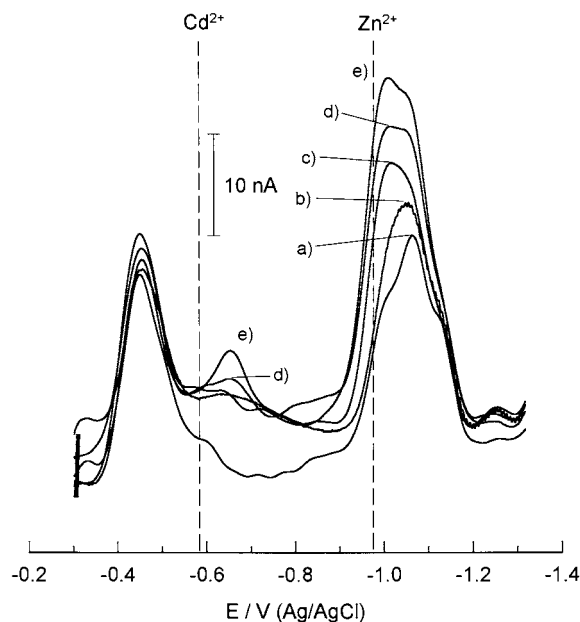


Fig. 2. Polarograms of 4.8×10^{-6} M of HFL MT-0 in 0.01 M phosphate buffer at pH 8.0 with the successive additions of Zn^{2+} and Cd^{2+} . Additions: (a) 0.0; (b) 1.6; (c) 4.0 mol Zn^{2+} /mol MT and (d) 0.2; (e) 0.5 mol of Cd^{2+} /mol MT. Other conditions as in Fig. 1. Dashed lines: cathodic peak potentials of free Cd^{2+} and Zn^{2+} obtained under the same experimental conditions.

the MTs. To 4.8×10^{-6} , 7.9×10^{-6} and 1.7×10^{-6} M solutions of MT-0, MT-1 and MT-2, respectively, successive additions of Zn^{2+} were carried out. The final point of the additions is the corresponding amount for which the current of the Zn peak becomes predominant. In Fig. 2 the polarogram (a) corresponds to the initial solution of MT-0 and the polarograms (b) and (c) correspond to those resulting from successive additions of Zn^{2+} in the range of proportions between 0.8 and 4.0 mol Zn^{2+} /mol protein. On the one hand, no variation in the features of the shoulder at $E_p = -1136$ mV corresponding to the ZnT peak is observed with successive additions of Zn^{2+} , while on the other hand, the ZnT' peak increases with additions of Zn^{2+} . The signal observed as a shoulder for a proportion of 3.2 mol Zn/mol protein and its peak current seems to be the predominant for a proportion of 4.0 mol Zn/mol protein. The evolution of polarographic peaks with the addition of Zn^{2+} is similar for the three

isoforms studied, taking into account that the initial proportions of Zn with respect to the MTs are similar. On adding Cd^{2+} to MT-0 after the additions of Zn^{2+} , in proportions of 0.2 and 0.5 mol/mol protein (Fig. 2(d) and (e) respectively), a peak at $E_p = -656$ mV increasing in current is observed. At this pH, addition of Cd^{2+} provokes, as can be expected [9–12], the appearance of the peak corresponding to the reduction of complexed Cd(II), labelled CdT'. This peak is different to the one found at a potential of $E_p = -0.88$ V, labelled CdT, from a freshly prepared MT solution under the same experimental conditions. The CdT' peak has also been detected after the addition of a given amount of Zn^{2+} to a native RL and HK MT. Therefore, for HFL MTs containing only zinc, the detected peak corresponding to the reduction of complexed Cd(II) is CdT'. The appearance of the CdT' peak does not only depend on the proportion of Cd(II) complexed with the MT but also on the total concentration of metal ions complexed by the MT [11,12]. The same behaviour has also been observed in the other two isoforms, MT-1 and MT-2.

From all these results and others previously obtained, a qualitative attribution of peaks is possible, but the proportion in which Zn(II) is complexed with the MT cannot be quantitatively determined because of the small differences between peak potentials. The two peaks of reduction of Zn(II), ZnT' and ZnT, are attributed to two different complexes of Zn–T which suggests the existence of at least two different complexation forms of Zn with MTs.

3.3. Influence of the pH on the polarographic response of MT-0, MT-1 and MT-2

3.3.1. Influence of the pH on the polarographic response of MT-0, MT-1 and MT-2 in their initial forms

The initial pH 8.0 of MT-0, MT-1 and MT-2 solutions was altered up to pH 10.0 by means of small additions of concentrated solution of NaOH, in order to avoid variations in the MT concentration. Afterwards, the pH was changed back to neutral values by additions of small amounts of HClO_4 .

The polarograms recorded from a solution of MT-2 at different pH values are shown in Fig. 3. The peak potentials of each peak shift towards more cathodic values as can be expected in a complexation equilibrium of metal ions with ligands which have acid-base properties. Moreover, because the shift of ZnT peak potentials with pH is greater than that of ZnT', the peaks are more separated and the ZnT peak is better defined. Likewise, the peak current of each peak decreases when the pH increases. The Zn and ZnT' peaks are not observed at pH 9.5 and pH 10.0, respectively. The variation in the peak current ratio between $i_{p\text{ZnT}'}$ and $i_{p\text{ZnT}}$ versus the pH decreases which indicates that the complexation of Zn(II) is more stable in the Zn–T form than in that of the Zn–T' at more basic pH values.

In Fig. 4, the variation of peak potentials of the three isoforms versus the pH is represented. The same values of peak potentials are found for each MT isoform under the same experimental condi-

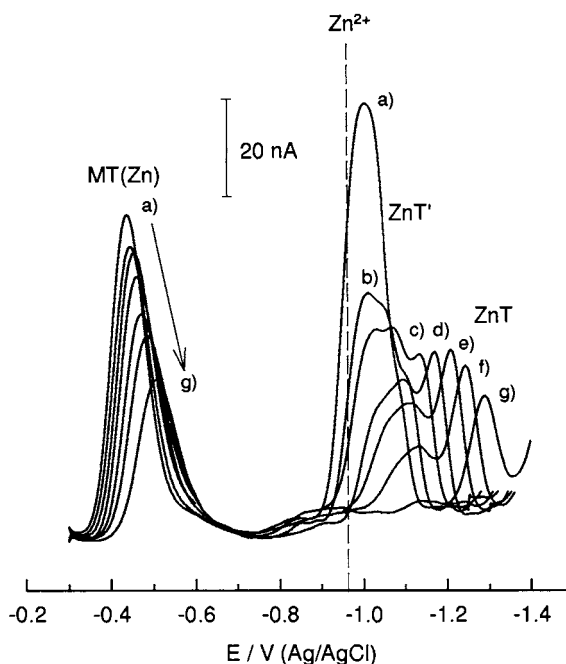


Fig. 3. Polarograms of $1.7 \cdot 10^{-6}$ M HFL MT-2 in 0.01 M phosphate buffer at the following pH values: (a) 7.0; (b) 7.5; (c) 8.0; (d) 8.5; (e) 9.0; (f) 9.5 and (g) 10.0. Other conditions as in Fig. 1. Dashed line: cathodic peak potential of free Zn^{2+} obtained under the same experimental conditions.

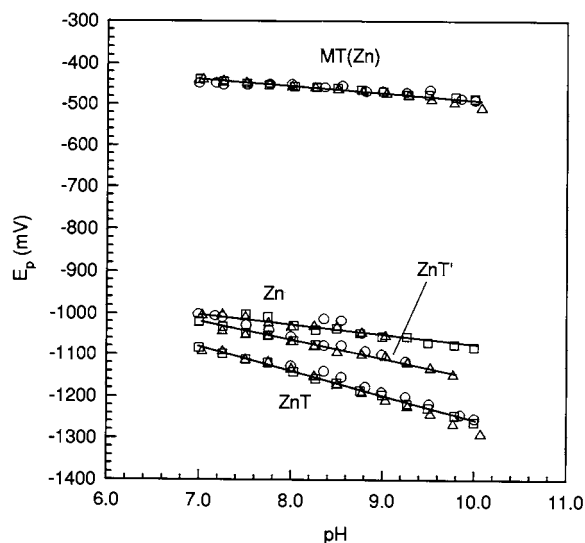


Fig. 4. Variation of E_p from 4.8×10^{-6} M MT-0 (circles), 7.9×10^{-6} M MT-1 (squares) and 1.7×10^{-6} M MT-2 (triangles) in their native form versus the pH.

tions. All studied isoforms behave in a similar way but the predominance of each polarographic peak in the chosen pH range is not identical. The differences in the pH ranges in which the polarographic peaks are observed for the three isoforms are due to the small variations in the proportion of metal ions with respect to MT for each of the studied isoforms.

When the variation of pH is carried out from neutral to basic pH and from basic to neutral pH, the same linear relationships between E_p and pH are obtained as those observed for others MTs [10,12]. Likewise, irrespective of the mode in which the pH was modified, the features of polarographic peaks for HFL MTs at the same value of pH are identical. Therefore, both Zn–T complexes are not modified in the pH range of between 7.0 and 10.0.

Linear relationships are obtained on representing E_p versus pH for all polarographic peaks. A slope of -44 mV per unit of pH was obtained for the ZnT' peak and the ZnT peak potential shifted with the pH giving a slope of -60 mV per unit of pH. In the case of HK and RL MTs [10], the ZnT peak potential shifts with a slope of -90 mV per unit of pH in the pH range of between 6.0

and 10.0 when the pH is modified from neutral to basic and from basic to acid, which does not correspond to the results obtained for HFL MTs. Comparing the results presented in this study with those for HK MT and RL MT 1 in the pH range of between 6.0 and 10.0 and a slope of -60 mV per unit of pH has been found for RL MT 2 and RL MT 1 + 2 in the same pH range. In those cases, the variation of pH was carried out from pH 2.0 to basic pH, to enable the formation of the Cd,ZnMT produced from its depleted form. These values of the slope obtained for the ZnT peak in HK and RL MTs, correspond to one single peak attributed to the reduction of complexed Zn(II).

Depending on the value of the slope, the number of thiolate groups bound to the Zn(II) can be evaluated. In fact, the peak potential shifts with pH according to the equation $E_p(\text{V}) = C + 0.059 \frac{m}{n} \text{pH}$ [30], where C is a constant value, n is the number of electrons transferred and m is the number of protons substituted by Zn(II). The number of protons involved in the electrochemical reaction corresponds to the number of thiolate groups in which a metal ion is replaced by protons.

From the values of the slopes and assuming that the number of electrons transferred is $n = 2$, the ratio between the thiolate groups and the metal ions can be evaluated. The obtained S^-/M ratios are 1.5 and 2.0 for Zn–T' and for ZnT, respectively, which are lower than the results obtained with HK and RL MTs. Furthermore, the S^-/M ratio is equal to 3.0 for the recognised structure of MTs, cluster β , in which the complexed Zn(II) is contained [4]. A ratio of $S^-/M = 2.9$ has been found for Zn(II) complexed with commercial HK and RL MTs with a variation of pH being performed from basic to acid pH [10]. Outwardly, the characteristics of zinc complexes of human foetal MTs are different, especially with respect to the binding with thiolate groups, compared to those observed in HK and RL MTs. Therefore, the Zn(II) complexed with HFL MTs is probably co-ordinated in a different manner than for HK and RL MTs, containing both ions, cadmium and zinc.

3.3.2. Influence of the pH on the polarographic response of MT-0, MT-1 and MT-2 after the addition of $Zn^{2+} + Cd^{2+}$

A study of variation of pH similar to that described in Section 3.3.1 was carried out for the three studied isoforms after additions of Zn^{2+} and Cd^{2+} . Zn^{2+} was added until the Zn peak was predominant with respect to the other two Zn(II) complexes, and additions of Cd^{2+} were made until a well defined CdT' peak was observed. These additions lead to the following proportions of metals with respect to each isoMT: 4.8×10^{-6} M MT-0 + 4.2 mol Zn/mol MT + 0.8 mol Cd/mol MT
 7.9×10^{-6} M MT-1 + 0.5 mol Zn/mol MT + 1.5 mol Cd/mol MT
 1.7×10^{-6} M MT-2 + 1.8 mol Zn/mol MT + 2.2 mol Cd/mol MT
 in which the MT(Zn), CdT', Zn, ZnT' and ZnT peaks are well defined for the given experimental conditions at pH 8.0.

The polarograms obtained for MT-1 in the pH range of 8.0 and 10.0 are shown in Fig. 5. For the three isoforms, the MT(Zn) peak current decreases when the pH increases and the MT(Zn) peak potential is almost maintained constant in the entire pH range which was studied.

The pH-dependent evolution of polarographic peaks attributed to the reduction of complexed Zn(II) is the same as that previously observed without the addition of metal ions (Section 3.3.1). On the one hand, the Zn and ZnT' peak currents decrease when the pH increases until their disappearance at a given value of pH. The pH value at which they disappear is different for each isoform and depends on the concentration of metals which has been added. On the other hand, the ZnT peak current increases with the increase of pH up to pH 9.0 and thereafter it decreases for higher pH values. Therefore, ZnT becomes the predominant peak for pH values higher than 9.0. The evolution of Zn, ZnT' and ZnT peaks indicates that the complexation of Zn(II) with MT is not influenced by the presence of Cd, at the given concentration but, in agreement with results already observed using HK and RL MTs [11], Cd(II) complexed with MT is influenced by the presence of Zn(II).

The potential of the CdT' peak, the only one which corresponds to the reduction of complexed Cd(II) with MTs at the given proportion of metal ions, does not shift with pH in agreement with the behaviour observed in previous studies [9,10]. For pH values higher than 9.5 (polarogram 5 (g)), this peak disappears and another peak at $E_p = -896$ mV at pH 10.0 (polarogram 5 (i)) is observed. This peak is labelled CdT and is the peak obtained from freshly prepared native HK or RL MT solutions. The change from CdT' peak at pH values higher than 9.0 is the typical behaviour of other mammalian MTs [10–12], indicating that the prevalent form of complexation of cadmium is Cd–T at high pH. Whatever the direction of pH variation from neutral to basic or from basic to neutral, the features of the polarographic peaks remain identical at a given pH. Hence, the complexation equilibria are reversible in the studied pH range. The equilibrium between CdT and

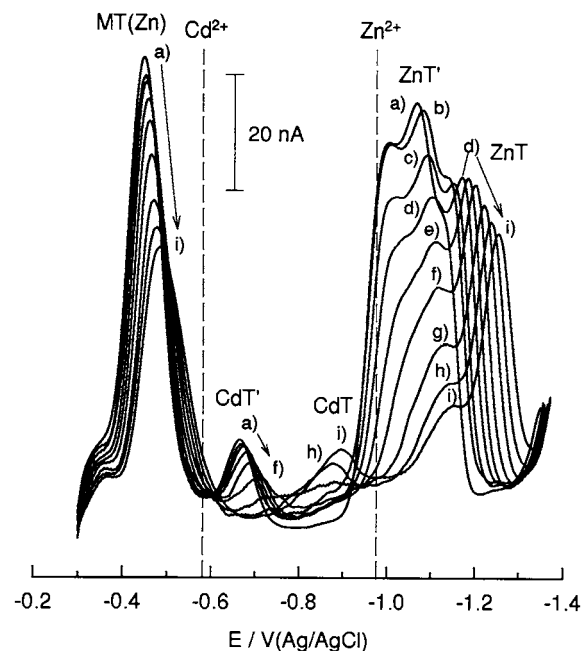


Fig. 5. Polarograms of 7.9×10^{-6} M HFL MT-1 + 0.5 mol Zn/mol MT + 1.5 mol Cd/mol MT in 0.01 M phosphate buffer at the following pH values: (a) 8.00; (b) 8.25; (c) 8.50; (d) 8.75; (e) 9.00; (f) 9.25; (g) 9.50; (h) 9.75; and (i) 10.00. Other conditions as in Fig. 1. Dashed lines: cathodic peak potentials of free Cd^{2+} and Zn^{2+} obtained under the same experimental conditions.

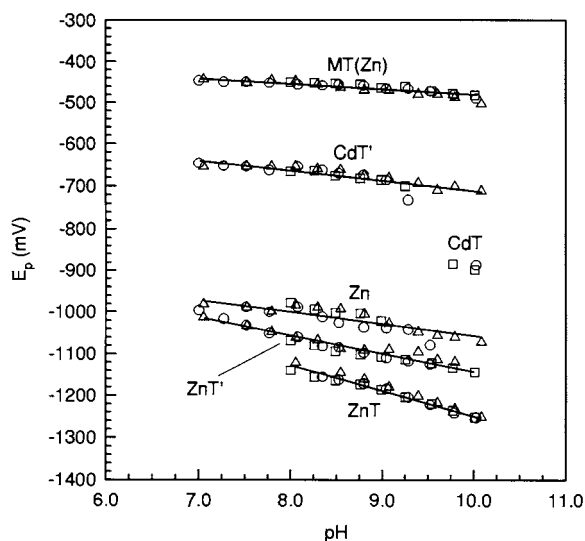


Fig. 6. Variation of E_p from 4.8×10^{-6} M MT-0 + 4.2 mol Zn/mol MT + 0.8 mol Cd/mol MT (circles), 7.9×10^{-6} M MT-1 + 0.5 mol Zn/mol MT + 1.5 mol Cd/mol MT (squares) and 1.7×10^{-6} M MT-2 + 1.8 mol Zn/mol MT + 2.2 mol Cd/mol MT (triangles) versus the pH.

CdT' peaks is also reversible for HFL MTs and each peak can simply be obtained by changing the solution pH.

Fig. 6 shows the variation of peak potentials versus pH. The shift of Zn, ZnT' and ZnT peak potentials with pH is equal to that observed in Section 3.3.1. The pH ranges where those peaks are obtained are different for each studied MT isoform. The $E_{pZnT'}$ and E_{pZnT} peak potentials shift with a slope of -44 mV and -60 mV per unit of pH respectively, for the three isoforms. The variation of $E_{pCdT'}$ is not pronounced enough to consider that the protons of thiolate groups of MTs are involved in the complexation reaction with Cd(II) for the given experimental conditions.

The most stable complexation forms are Cd–T and Zn–T at basic pH values. In this case, the change of ZnT' to ZnT occurs at pH values higher than 9.5, where the ZnT peak becomes predominant. A similar phenomenon was observed in the study of HK and RL Cd–T complexes, in which the equilibrium between CdT and CdT' peaks depends on the solution pH [11].

4. Conclusions

This work constitutes the first study on electrochemical characterisation of human foetal liver MTs. DPP is a simple technique which provides results easy to interpret. In this case, the electroactive species are the free and the complexed metals ions as well as the organic part of the metallothionein throughout the thiol groups. Hence, the use of electroanalytical techniques allows one to study the characteristics of Zn–MTs, especially concerning their complexation of metal ions.

Because the rate to reach the chemical equilibrium is very high, significant modifications in the polarograms are observed after a short period of time (2 min of nitrogen purging between the measurements) on slightly changing the conditions such as pH, metal concentration, etc.

The existence of two peaks ZnT' and ZnT which have been observed here for the first time in this type of MT, could be attributed to two different Zn(II) complexes with MTs. The ZnT peak is better defined at basic pH values and it is suggested that the behaviour of ZnT' and ZnT peaks is similar to that observed for CdT' and CdT peaks for Cd, Zn MTs. Hence, the behaviour of these HFL MTs, after the addition of Cd^{2+} and consequently when both metal ions are complexed with the MT, is comparable to other mammalian Cd, Zn–MTs.

The results presented in this paper are of interest in order to obtain a better interpretation of structural data. Particularly, the fact that two different electrochemical signals for both Cd(II) and Zn(II) complexes have been distinguished and attributed to two different Cd–T and Zn–T complexes. Those complexes possess different characteristics not mentioned in works on MT characterisation using analytical methods other than electroanalysis. Hence the use of electroanalytical methods can be considered as a useful complement for the interpretation of nuclear magnetic resonance and circular dichroism data determined by other authors with native and reconstituted MTs.

Acknowledgements

The authors thank Professor Dr J. Lauwerijns and Professor Dr Ph. Moerman (Department of Biomedical Research, K.U. Leuven) for kindly providing us with the human foetal liver tissues. Dr Oscar Nieto also thanks the European Commission for a post-doctoral grant in the frame of the Human Capital and Mobility Programme.

References

- [1] J.H.R. Kägi, M. Nordberg (Eds.), *Metallothionein*, Birkhäuser, Basel, 1979.
- [2] J.H.R. Kägi, Y. Kojima (Eds.), *Metallothionein*, vol. II, Birkhäuser, Basel, 1987.
- [3] K.T. Suzuki, N. Imura and M. Imura (Eds.), *Metallothionein*, vol. III, Birkhäuser, Basel, 1993.
- [4] M.J. Stillman, C.F. Shawn III, K.T. Suzuki (Eds.), *Metallothioneins: Synthesis, Structure and Properties of Metallothioneins, Phytochelatins and Metal-Thiolate Complexes*, VCH, New York, 1992.
- [5] J.F. Riordan, B.L. Vallee (Eds.), *Methods of Enzymology*, vol 205, Academic Press, London, 1991.
- [6] A. Muñoz, J. Chivot, A.R. Rodríguez, *Quim. Anal.* 14 (1995) 36.
- [7] J.M. Sequaris, Analytical voltammetry of biological molecules, in: M.R. Smyth, J.G. Vos (Eds.), *Analytical Voltammetry*, vol. XXVII, Wilson & Wilson's Comprehensive Analytical Chemistry, Elsevier, Amsterdam, 1992 and references therein.
- [8] R.W. Olafson, *Bioelectrochem. Bioenerg.* 19 (1988) 111.
- [9] A. Muñoz, A.R. Rodríguez, *Electroanalysis* 7 (1995) 674.
- [10] C. Ruiz, J. Medieta, A.R. Rodríguez, *Anal. Chim. Acta* 305 (1995) 285.
- [11] C. Ruiz, A.R. Rodríguez, *Anal. Chim. Acta.* 325 (1996) 43.
- [12] C. Ruiz, A.R. Rodríguez, *Anal. Chim. Acta* 350 (1997) 305.
- [13] I. Sestakova, D. Miholova, H. Vodickova, P. Mader, *Electroanalysis* 7 (1995) 285.
- [14] A. Muñoz, A.R. Rodríguez, *Analyst* 120 (1995) 529.
- [15] B. Raspor, J. Pavicic, *Fresenius J. Anal. Chem.* 354 (1996) 529.
- [16] J. Medieta, J. Chivot, A. Muñoz, A.R. Rodríguez, *Electroanalysis* 7 (1995) 663.
- [17] A. Muñoz, A.R. Rodríguez, *Electroanalysis* 7 (1995) 670.
- [18] J. Medieta, A.R. Rodríguez, *Electroanalysis* 8 (1996) 473.
- [19] O. Nieto, A.R. Rodríguez, *Bioelectrochem. Bioenerg.* 40 (1996) 215.
- [20] C. Harlyk, G. Bordin, O. Nieto, A.R. Rodríguez, *Electroanalysis* 9 (1997) 608.
- [21] G. Bordin, F. Cordeiro Raposo, A.R. Rodríguez, *Can. J. Chem.* 72 (1994) 1238.
- [22] G. Bordin, F. Cordeiro Raposo, A.R. Rodríguez, *J. Liq. Chromatogr.* 19 (1996) 3085.
- [23] V. Virtanen, G. Bordin, A.R. Rodríguez, *J. Chromatogr.* 734 (1996) 391.
- [24] S.R. Clough, R.S. Mitra, A.P. Kulkarni, *Biol. Neonate* 49 (1986) 241.
- [25] A. Soumillion, J. Van Damme, M. De Ley, *Eur. J. Biochem.* 209 (1992) 999.
- [26] M. Pauwels, J. Van Weyenbergh, A. Soumillion, P. Proost, M. De Ley, *Eur. J. Biochem.* 220 (1994) 105.
- [27] A.H. Robbins, D.E. McRee, M. Williamson, S.A. Collet, N.H. Xuong, W.F. Furey, B.C. Wang, C.D. Stout, *J. Mol. Biol.* 221 (1991) 1269.
- [28] E. Palecek, Z. Pecham, *Anal. Biochem.* 42 (1971) 59.
- [29] W.F. Furey, A.H. Robbins, L.L. Clancy, D.R. Wing, B.C. Wang, C.D. Stout, *Science* 231 (1986) 704.
- [30] B. Trémillon, *Electrochimie Analytique et Réactions en Solution*, Tome 2. Masson, Paris, 1993, 248 pp.

New competitive enzyme-linked immunosorbent assay for determination of metallothionein in tissue and sera

Margarita Apostolova ^{a,*}, Choudomir Nachev ^b, Milena Koleva ^c,
Panayot R. Bontchev ^d, Ivan Kehaiov ^e

^a Department of Chemistry and Biochemistry, Medical Academy, 2, Zdrave Strasse, Sofia 1431, Bulgaria

^b Department of Internal Medicine, Clinic of Cardiology, Medical Academy, Sofia 1431, Bulgaria

^c Department of Biochemistry, Faculty of Biology, Sofia University, Sofia 1421, Bulgaria

^d Department of Analytical Chemistry, Faculty of Chemistry, Sofia University, Sofia 1126, Bulgaria

^e Laboratory of Molecular Immunology, Bulgarian Academy of Sciences, Sofia 1113, Bulgaria

Received 4 November 1996; received in revised form 10 June 1997; accepted 12 June 1997

Abstract

Very little information is available concerning the relationship between metallothionein (MT) and diseases in humans. Several methods to measure MT levels exist but many of these assays are not sensitive to measure MT in human sera. A new sensitive competitive ELISA system has been developed using MT labeled with horseradish peroxidase as a conjugate and high-titre polyclonal antibodies obtained from rabbit immunoglobulin G for MT determination in human sera. The cELISA proposed here permits a reliable determination of MT in the range 10–2 000 000 pg ml⁻¹. The method was compared with Cd-hem assay and showed good agreement of results. The recovery of the assay was determined by spiking rat MT into rat and human sera, and comparing it with spiked diluent controls. The overall recoveries of the added MT were 101% for rat sera and 89% for human sera. The variation within-assay and between assay were 3 and 6%, respectively. A significant difference ($P < 0.001$) was found between the MT-level in human sera from patient with essential hypertension (646 ± 223 ng ml⁻¹, $n = 90$) and normotensive subjects (21 ± 18 ng ml⁻¹, $n = 236$). A correlation between arterial hypertension and MT-level seems possible. A very sensitive new cELISA method was presented for determination of MT in sera and tissues. It enables investigation of possible correlations between sera MT-concentration and certain diseases. © 1998 Elsevier Science B.V. All rights reserved.

Keywords: Metallothionein; Hypertension; Competitive ELISA; Western blotting

1. Introduction

Metallothionein (MT) is a low molecular weight protein with a very important role in heavy metal detoxification and metal homeostasis [1,2]. This protein contains 20 cysteine (CYS)

* Corresponding author. Tel.: + 359 2 9515664; fax: + 359 2 517278; e-mail: margo@ns.medfac.acad.bg

residues and no aromatic aminoacids [3]. MT genes are highly conserved and have strong inducible promoters [4]. The synthesis of MT is induced by various metal ions (Cd^{2+} , Zn^{2+} , etc.) [3], glucocorticoids [4], catecholamines, IL-1 and IL-6 and interferons [5–7]. Structural analysis of MT shows two domains, the first one includes the carboxyl-terminal part and binding four bivalent metal ions and the second domain containing three bivalent metal ions. Immunological studies of MT have suggested that the N-terminal region is the most immunogenic domain [8]. An epitope consists of a region of five to seven aminoacids residues [9].

Different methods for quantitative determination of MT have been described [10–12]. MT can be measured indirectly, based on the known binding stoichiometries between metals and MT, by quantifying the number of atoms the Cd- or Hg bound to the protein [13,14]. Radioimmunoassays (RIA) and an enzyme linked-immunoassays (ELISA) have been developed for determination of MT [15–18]. Immunological studies using different antisera against MT showed that the antibodies were crossreactive with various kinds of mammalian MT [19]. These methods have a typical detection limit of about 0.1–1 ng of MT and determination of MT in body fluids is difficult due to low MT concentrations.

In previous studies [20], we have found that the basal MT levels in liver from spontaneously hypertensive rats (SHR) were higher than that in the Wistar–Kyoto rats (WKY). The close similarity of the SHR-model and human hypertension disease makes the investigation of the relation between MT homeostasis and arterial hypertension in humans interesting.

In order to investigate physiological functions and roles of metallothionein in humans, the aim of this study was to develop a new competitive ELISA system for MT determination in human sera with low detection limit.

2. Experimental

2.1. Reagents

Cadmium chloride, Tris-(hydroxymethyl)-

amino-metan, $\text{Na}_2\text{HPO}_4 \cdot 12\text{H}_2\text{O}$, $\text{NaH}_2\text{PO}_4 \cdot 6\text{H}_2\text{O}$ were obtained from Sigma (St. Louis, MO). The acrylamide, bis-acrylamide and sodiumlaurylsulfate (SDS) were acquired from Merck (Darmstadt, Germany). All other reagents were purchased from Aldrich Chemical (Windsor, ON, Canada).

The aqueous solutions were prepared with highly purified water ($< 18 \text{ M}\Omega$) using Milli-Q reagent water system (Millipore, Milford, MA, USA).

2.2. Animals and human sera

Male Wistar rats and guinea pigs were obtained from the animals laboratory (Medical Academy, Sofia, Bulgaria). Rats weighing 170–190 g (10 weeks old) were housed in groups of five per cage in an environmentally controlled room (light 7–19 h, $23 \pm 1.5^\circ\text{C}$).

Four male New Zealand rabbits (3 kg) were received from the laboratory of molecular immunology (Institute of Reproduction, Bulgarian Academy of Sciences, Sofia, Bulgaria). Animals were supplied with water and a commercial laboratory chow, ad libitum.

The human sera from patients with essential hypertension ($n = 90$) and normotensive subjects ($n = 236$) were received from the Department of Internal Medicine II, Clinic of Cardiology (Medical Academy, Sofia, Bulgaria) and National Institute for Blood Collection (Sofia, Bulgaria).

2.3. Purification of MT-antigen

Fresh or frozen liver from rats, in which the MT concentration has been induced by CdCl_2 were cut into small pieces and homogenized in 25% (w/v) of 0.1 M Tris–HCl buffer pH 8.6, containing 0.25 M with Teflon-glass homogenizer ($8\text{--}10 \text{ strokes min}^{-1}$). The homogenate was centrifuged at $10\,000 \times g$ for 10 min. The resulting supernatant was heated for 1 min at 100°C . The precipitate was removed by centrifugation at $100\,000 \times g$ for 30 min and 5 ml from the supernatant were applied into a Sephadex G-75 gel-filtration column (2.6 cm/1 m, Pharmacia,

Uppsala, Sweden). Elution was carried out with 50 mM Tris–HCl buffer, pH 7.4 at a flow rate of 1 ml min⁻¹. The absorbency of elute at 254 and 280 nm was continuously recorded using a flow cell and UV detector (Pharmacia, Uppsala, Sweden). Fractions of 5 ml were collected. All fractions corresponding to MT were combined and concentrated under nitrogen on an Amicon (Danvers, MA) YM 2 membrane. Aliquots of the concentrated solution (300 µl) were used for HPLC separation of MT isoforms (MT1 and MT2). HPLC was performed on a semi-preparative µBondapak C₁₈ column (300 mm/7.8 mm/5 µm) obtained from Waters (Milford, MA). The details concerning the MT separation by HPLC systems have been discussed in previous papers [20,21]. The MT concentration was determined by Bradford assays [22]. We used as a standard MT produced by Sigma (St. Louis, MO, Cat # M7641).

The Zn and Cd contents were determined in all samples by electrothermal atomic absorption spectrometry (Perkin-Elmer Zeeman 5000) with an HGA-500 graphite furnace, AS-40 autosampler and ASDS-10 data station.

2.4. Preparation of antibodies

Fig. 1 shows the homogeneity of MT1 and MT2 used as immunogen. The conjugation of MT with lysozyme (Sigma, St. Louis, MO) was carried out essentially using the method of Reichlin et al. [23]. Rat MT (mixture from MT1 and MT2, 0.5 mg ml⁻¹ for each one) and lysozyme (2 mg ml⁻¹) were dissolved in 500 µl of 0.1 M potassium phosphate buffer, pH 7.0. A total of 250 µl of 1% glutaraldehyde was added dropwise to the protein solution while constantly stirring and the reaction mixture was incubated for 60 min at room temperature. Then 1 ml of physiological saline was added to conjugated MT solution and the mixture was emulsified with 2 ml of Freund's complete or incomplete adjuvant (DIFCO Laboratories, Detroit). Male New Zealand rabbits were injected s.c. with 2 ml from the emulsion 2–6 mg of the conjugates. The first four injections of the antigen emulsified with Complete Freund's adjuvant were given at

2 weeks interval. The amount of MT in the conjugates were 6, 4, 2 and 2 mg per each interval. The final injection, after 2 months, consisted of MT emulsified with mixture from complete and incomplete adjuvants.

Blood was drawn from rabbits before immunization (in order to obtain preimmune serum) and 7 days after each injection to obtain anti-serum. It was kept at 37°C for 1 h and at 4°C for 2 h. After the serum was separated by centrifugation, the immunoglobulin fractions were separated by ammonium sulfate precipitation. The serum was stored at –80°C until ready to use.

2.5. Characterization of the rabbit anti-rat MT antibodies

The antibodies formation was checked by double diffusion with 1% agar on a glass plate at room temperature. The antigenic reactivities of various MT and lysozymes and the potency of

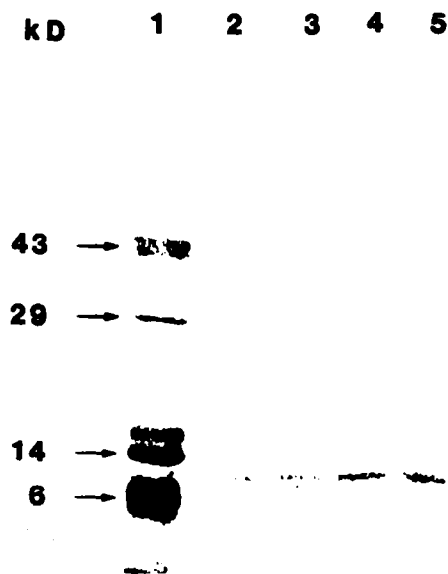


Fig. 1. SDS-PAGE of metallothionein 1 (line 2 and 4) and metallothionein 2 (line 3 and 5). Line 2 and 3 were developed without β -mercaptoethanol in the sample buffer, line 4 and 5 with β -mercaptoethanol.

various rabbit antisera were determined by the direct ELISA systems [17].

2.6. SDS-polyacrylamide gel electrophoresis (SDS-PAGE) and Western blotting

SDS-PAGE was performed by the method of Laemmli [24]. The separating gel containing 15% (w/v) acrylamide was 6×9 cm in size and 1 mm thick. Samples were dissolved in a sample buffer (125 mM Tris-HCl, pH 6.8 containing 15 (w/v) SDS, 10% (w/v) glycerol and 0.01% bromphenol blue with or without β -mercaptoethanol) and incubated in a water bath at 80°C for 5 min. After the electrophoresis, the gel was soaked in a transfer buffer (25 mM Tris/192 mM Glycin/20% (v/v) methanol) and the proteins in the gel were transferred electrophoretically to a nitrocellulose membrane (Bio-Rad, Richmond, CA) using the modified method of Towbin et al. [25].

2.7. Detection of MT on the nitrocellulose membrane

The membrane was soaked in 10 mM PBS (KCl, KH_2PO_4 , NaCl, $\text{Na}_2\text{HPO}_4 \cdot 12\text{H}_2\text{O}$) pH 7.4 containing 10% (v/v) Tween-20 for 1 h. The MT on the membrane were detected immunochemically using rabbit anti-rat MT serum (1:10 000) diluted in TBS for 1 h, at room temperature. After the membrane was washed with TBS (PBS + 0.05% (v/v) Tween-20) buffer, it was incubated in a peroxidase conjugated goat anti-rabbit IgG and the membrane method was developed according to the manufacturer's instructions.

2.8. Conjugation of enzyme (horseradish peroxidase, HRPO) to antigen (MT*)

HPLC-purified rat MT1 and MT2 (4 mg each) were dialyzed against 0.1 M carbonate buffer pH 7.0, overnight at 4°C. A total of 250 μl from 4 mg ml^{-1} HRPO (dissolved in 0.1 M carbonate buffer, pH 8.7) was mixed with 200 μl of freshly prepared 0.1 M NaIO_4 and incubated at room temperature for 20 min in the dark. After that, the mixture was dialyzed against 1 mM acetate buffer, pH 4.4. Immediately after dialysis the pH

was adjusted to 9.0–9.5 with 0.2 M carbonate buffer and MT (mixture from MT1 and MT2, 8 mg) was added. This solution was stirred gently for 2 h at room temperature. Freshly prepared 0.1 ml NaBH_4 (4 mg ml^{-1}) solution was added and incubated for 2 h at 4°C. The excess of unbounded HRPO was separated by gel chromatography (Superose 12™ column, FPLC, Pharmacia, Sweden) gel-chromatography. The HRPO labeled MT (MT*) was mixed with glycerol as a cryoprotector mixed with glycerol and stored at -20°C until ready to use.

2.9. Competitive ELISA system (cELISA)

The 50 μl from MT-antibodies diluted in 10 mM carbonate buffer, pH 9.7 was adsorbed on the flat type microwell plates overnight at 4°C. After 1 h incubation with PBS plus 1% (v/v) Tween-20 (200 μl), the MT* (25 μl , 1:400 dil.) and the samples (25 μl) to be studied were added and incubated for 2 h at 37°C. The reaction was visualized by means of orthophenylenediamine in phosphate citrate buffer, pH 5.5, 0.006% H_2O_2 and stopped with 10% H_2SO_4 . The absorption at 492 nm was measured by ELISA reader (Dynatech, Germany). After each step the plates were washed three times with TBS for 5 min.

2.10. Statistical analysis

The statistical evaluation of the obtained results was performed by regression and ANOVA analysis, $P < 0.001$ (Microcal Origin, version 3.5). The data were expressed as mean \pm SD.

3. Results

3.1. Development and optimization of a sensitive competitive ELISA for human sera

In order to develop a competitive ELISA, rat metallothioneins were coupled to HRPO and different combinations between MT* and Ab were tested in order to obtain an optimal cELISA condition all combination. A highly sensitive ELISA was obtained by the absorption of MT

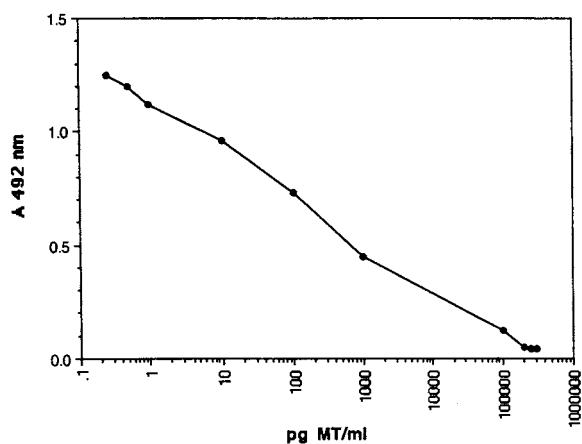


Fig. 2. Competitive ELISA, using absorption of antigen (MT) on the microwell plate and MT* (MT conjugated with horseradish peroxidase) as a conjugate. Rat liver MT was assayed in the range 10–2 000 000 pg ml⁻¹.

antibodies on the microwell plate in combination with the analyzed samples and MT* (see Section 2) as a conjugate. This cELISA permitted determination of MT as low as to 0.5 pg well⁻¹ MT (Fig. 2). MT concentrations of 10–2 000 000 pg ml⁻¹ can produce changes in the percentage binding that are linearly related to the logarithm of the MT concentrations. Metallothionein concen-

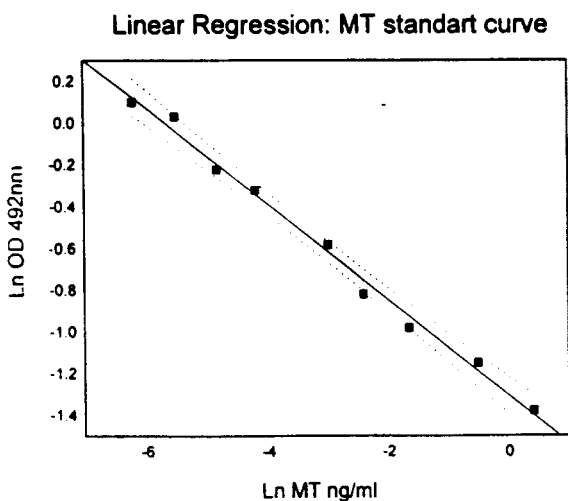


Fig. 3. MT standard curve (linear regression) from competitive ELISA, using absorption of antigen (MT) and MT* conjugated with horseradish peroxidase, as a conjugate.

Table 1
Quantification of MT in different tissue cytosols by cELISA and Cd-hem assay

Type MT	Concentration of MT ($\mu\text{g g}^{-1}$ tissue)	
	Cd-hem ^a	cELISA ^a
Rat liver		
Control	6.6 \pm 1.4	5.2 \pm 1.7
Cd-injected	511 \pm 17	504 \pm 23
Rat kidney		
Control	6.1 \pm 1.3	9.7 \pm 2.3
Cd-injected	174 \pm 11	182 \pm 25
Guinea pig		
Control	6.9 \pm 2.1	8.9 \pm 1.5
Cd-injected	497 \pm 32	475 \pm 14

^a Mean \pm SD of 66 determinations.

trations were determined by linear regression (Fig. 3).

Regression analysis of the total MT concentrations in Table 1 obtained by Cd-hemoglobin assay and cELISA using the MT* show good linear relationship, with the slope of the regression line = 0.843. The sensitivity of the competitive ELISA assay, permitted us to measure MT concentration in human and animal sera with low detection limits.

In order to assess the metal-dependency of the ELISA, single different derivatives, prepared from rat hepatic MT by metal exchange ($\text{Zn}_{6.22}\text{Cu}_{0.52}\text{MT}$, $\text{Cd}_{5.33}\text{Zn}_{1.33}\text{MT}$, $\text{Cd}_{6.54}\text{MT}$, AMT), were compared. As shown in Fig. 4, the Zn-loaded and apometallothionein (AMT) forms yield the highest signal on equal molar ratio.

3.2. Specificity, recovery, reproducibility and sensitivity of the assay

The specificity of the antisera was examined by the Ouchterlony's method. A single precipitation line was observed between the rat hepatic MT and the antiserum (after the antiserum was immunoaffinity purified, data not shown). As shown in Fig. 5 similar competitive inhibition patterns were obtained when the rabbit anti-rat MT serum reacted with MTs from mammalian organs: rat hepatic MT, guinea pig hepatic MT, human

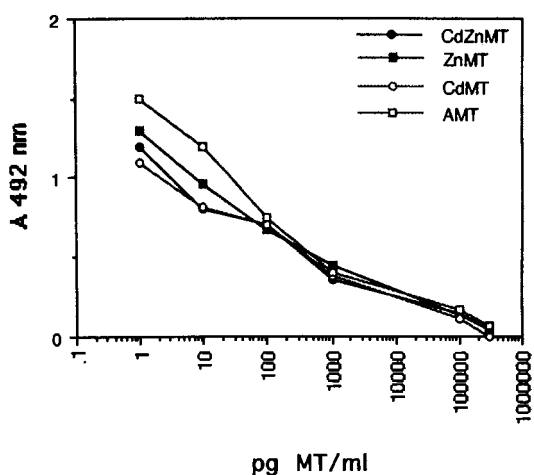


Fig. 4. Metal-dependence of competitive ELISA using MT*, as a conjugate. MTs derivatives (CdMT: Cd_{6,24}MT; ZnMT: Zn_{6,22}Cu_{0,52}MT; CdZnMT: Cd_{5,33}Zn_{1,33}MT, AMT) were obtained from rat liver.

serum MT. Lysozyme solution used for conjugation of MT did not show any cross reactivity (Fig. 5).

The recovery of the assay has been determined by spiking normal rat and human sera with known amounts of rat MT and comparing them with the controls (Table 2). The overall average

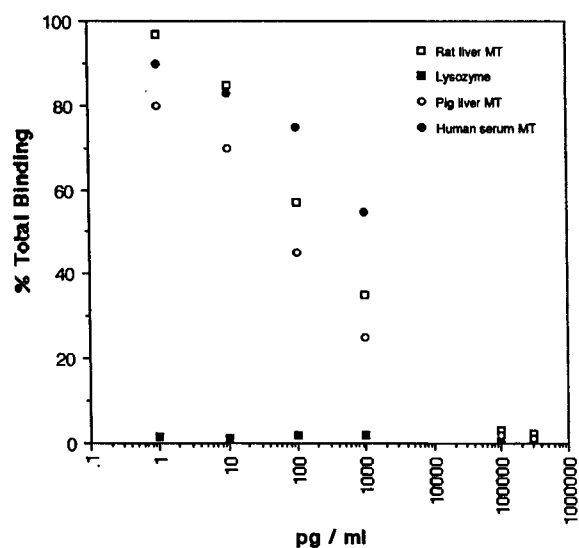


Fig. 5. Binding (%) of different MTs and lysozyme with the rabbit anti-rat MT antiserum by competitive ELISA.

Table 2
Recovery of serum MT by cELISA

MT pg well ⁻¹	Rats ^a	Human ^b
	Recovery (%)	Recovery (%)
1.5	96 ± 5	89 ± 7
2.5	97 ± 7	97 ± 5
5.5	103 ± 4	83 ± 7
25.5	99 ± 6	91 ± 3
50.5	105 ± 5	88 ± 2
75.5	111 ± 12	90 ± 9

The recovery in the cELISA has been determined by spiking rat MT in rat and human sera and comparing with spiked standard diluent controls.

^a, ^b Mean ± SD of 15 experiments.

recoveries of the added MT* were 101% for rat sera and 89% for human sera.

Table 3 summarizes the within-assay and between-assay reproducibility obtained by cELISA system. The assay gave reliable results for analyses of MT in both sera and tissue cytosols. The within-assay coefficient of variation was less than 3% and the between-assay coefficient of variation was less than 6%.

From the standard curves and all the data described above, it appears that reliable results can be obtained for MT in sera and tissue in the range 10–2 000 000 pg ml⁻¹, using the cELISA method described here.

3.3. Detection of MT from rat and guinea pig liver by Western blotting technique

MT was isolated from the liver of several mammals. The MT fraction (10 kDa) from all cytosols

Table 3
Reproducibility of MT in human sera by the cELISA

MT pg well ⁻¹	Within-assay	Between-assay
	Coefficient of variation (%)	Coefficient of variation (%)
10	1.3	5.9
20	2.4	5.7
50	3.3	6.1

n = 30.

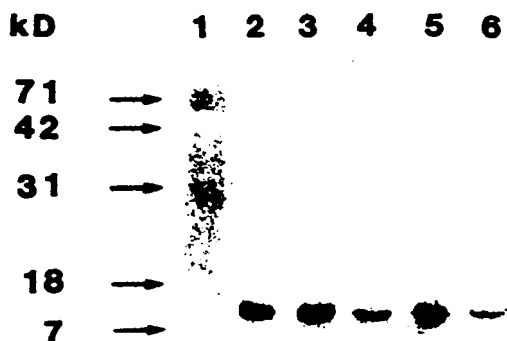


Fig. 6. Detection of different MT forms by Western blotting. Line 1—molecular weight standard markers: 71 kDa, BSA; 42 kDa, carbonic anhydrase; 31 kDa, soybean trypsin inhibitor; 18 kDa, lysozyme; 7 kDa, aprotinin. Lines 2–6, cytosols from: rat liver in which MT synthesis was induced by (2) CdCl₂, (3) ZnCl₂, (4) control. Lines 5–6, cytosol from guinea pig liver, (5) CdCl₂, (6) control

were separated by gel chromatography and investigated by an immunoblotting technique. The results from Fig. 6 indicate that different amounts of MT can be detected by Western blotting. The limit of detection for each MT isoform from the animals studied was 4 ng. The control MT content or MT induced in the rat liver after Cd or Zn administration were detected by the method described above.

3.4. Detection of MT in the sera from patients with essential hypertension and normotensive subjects

The MT concentrations in sera from patients with essential hypertension ($n = 90$) and normotensive subjects ($n = 236$) obtained with this competitive ELISA method showed that, the MT level in human serum from patients with essential hypertension is significantly higher than that in the sera from normotensive subjects (Fig. 7).

4. Discussion

The purpose of this report is to describe the development and usefulness of a simple competitive ELISA, capable of reliable determination of MT concentration in sera and tissues in the range

as low as 0.5 pg well⁻¹ of MT. After optimizing the reagents concentration, the incubation times and temperature, the IgG fraction of our antiserum provided a level of sensitivity better than the lowest range reported up to now—by ELISA [16,26]. The IgG fraction of the antiserum containing antibodies showed greater affinity for rat MT than for human MT because our rabbit antiserum was obtained against rat liver MT1 and MT2. Most of the rabbit or sheep anti-MT antisera obtained against either MT1 or MT2 have been reported to show greater cross reactivity to both isoforms [18,27]. In the present study it is shown that MT from rat liver, guinea pig and human serum exhibit very similar inhibition patterns (Fig. 5). The complete cross reactivity with various mammalian MT is due to similarities in their primary structure and epitope sequence [9]. On the basis of the primary and the tertiary structure of the MT, it seems reasonable to speculate that the epitopes detected by our IgG fraction are not exposed to very essential stereochemical changes. The data also suggests that the conformation changes in the MT after binding with HRPO, at least in the vicinity of the epitopes, are also smaller. This cELISA method demonstrated that the affinity of the IgG fraction against the purified rat Zn_{6,22}Cu_{0,52}MT and Cd_{5,33}Zn_{1,33}MT was similar. The observed increase in the immunological affinity of the antibodies for AMT indicate that the metals which determine the MT conformation are not very important for reaction of the antibody obtained by us with MT. However, this result contrasts with earlier reports, showing that the removal of the metals from MT results in a decrease [18,28] or in a significant difference [26] in its antigenicity.

A highly sensitive cELISA was developed with labeling of the antigen (MT) with HRPO. This assay allowed the detection of 0.5 pg well⁻¹ of human serum MT and exhibited a relatively smaller metal-dependent response for Apo-, Zn- and Cd-MT derived from rat liver. A potential change in MT during the sample preparation was checked by the Western blotting method. It was shown that the MT genes were differently induced by Cd and Zn [4]. The immunoblot results showed good correlation with these data and proved that

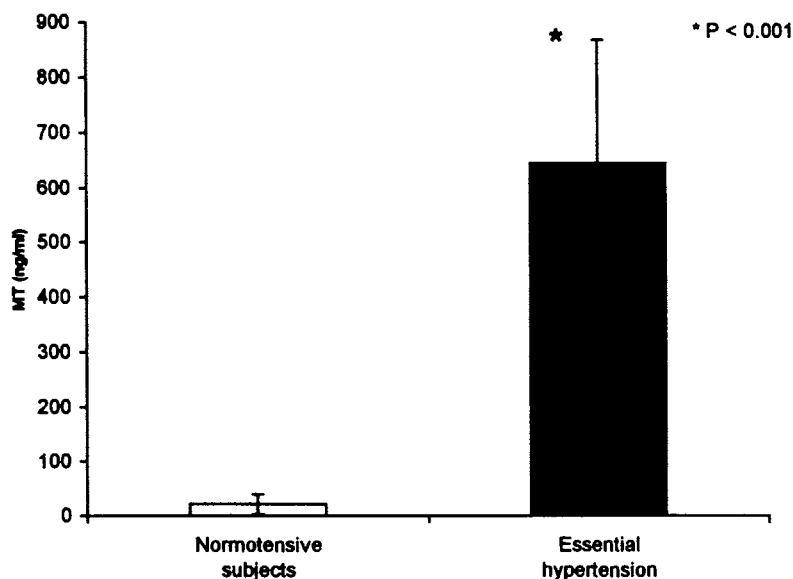


Fig. 7. Metallothionein concentration determined by competitive ELISA in sera from patients with essential hypertension ($n = 90$) and normotensive subjects ($n = 236$).

the anti-MT antiserum is highly sensitive in detecting the basal level of MTs in rat liver.

Several methods for MT determination in biological materials have already been described [10–12]. These procedures rely on rather unspecified parameters such as the total metal content of determination of metals by atomic absorption spectrometry or HPLC analyses. The immunological studies of course, represent an exception in this respect. More specific are RIA [18] and ELISA with monoclonal antibodies [16,29]. They allow the detection of 60 pg well^{-1} MT and are sufficiently sensitive to assess the basal MT level in biological materials. The cELISA method, here proposed, with its detection limit of 0.5 pg well^{-1} , is therefore an alternative to the existing RIA [15,18] and monoclonal ELISA [16,28].

The successful determination of MT in sera from animals and humans in normal and pathological conditions described in the present report show that this cELISA can be applied not only for determination of the basal MT level but also for investigation of minor deviations in MT concentrations. The present studies not only confirm the earlier observations on the appearance of MT

in the body fluids but also provides evidence for an increased of MT level in serum during the development of essential hypertension in humans. The MT concentration in patients with essential hypertension is significantly higher in comparison to the MT levels of the healthy controls. The results for the MT evaluation in human sera suggest that the intracellular MT can be leached out extracellularly and transported by the serum. Several key enzymes and biologically active substances which are connected with regulation of blood pressure are metal-containing and related to the zinc and copper homeostasis (dopamine- β -hydroxylase, tyrosinase, angiotensin converting enzyme). The Zn level also, paralleled the metabolite-to-precursor fatty acid ratios, being constantly higher in hypertensive patients [30,31]. Zn ions have been identified as constitutive cofactors of desaturase activity in human, animal, and in vitro studies [32–35]. The MT level strongly affects Zn and Cu concentration and its very wide distribution, made MT a crucial factor in the metabolism of these metals. The possible causative interrelation between MT and arterial hypertension can not be excluded.

Acknowledgements

The authors are grateful to the American Agency for International Development, which supported this study (USA Grant # EUR-0037-G-00-1083-00, MSCI Project # CVD-YO22-08).

References

- [1] M. Webb, Toxicological significance of metallothionein, in: Jeremias H.R. Kagi, Yutaka Kojima (Eds.), *The Metallothionein II*, Birkhauser, Basel, 1987, p. 109.
- [2] M.G. Cherian, H.M. Chan, Biological functions of metallothionein—A review, in: K.T. Suzuki, N. Imura, M. Kimura (Eds.), *The Metallothionein III*, Birkhauser, Basel, 1993, p. 87.
- [3] J.H.R. Kagi, Y. Kojima, Chemistry and biochemistry of metallothionein, in: Jeremias H.R. Kagi, Yutaka Kojima (Eds.), *The Metallothionein II*, Birkhauser, Basel, 1987, p. 25.
- [4] R.D. Palmiter, Molecular biology of metallothionein gene expression, in: Jeremias H.R. Kagi, Yutaka Kojima (Eds.), *The Metallothionein II*, Birkhauser, Basel, 1987, p. 63.
- [5] J. Liu, Y.P. Liu, L.E. Sendelbach, C.D. Klaassen, *Toxicol. Appl. Pharmacol.* 109 (1991) 235.
- [6] F.O. Brady, B.S. Helvig, A.E. Funk, S.H. Garrett, The involvement of catecholamines and polypeptide hormones in the multihormonal modulation of rat hepatic zinc thionein levels, in: Jeremias H.R. Kagi, Yutaka Kojima (Eds.), *The Metallothionein II*, Birkhauser, Basel, 1987, p. 555.
- [7] J.U. Bell, M.J.P. Lawman, J.M. Lopez, L.E. DesJardin, L.A.D. Applewhite, Effects of type I interferon-inducing agents on hepatic metallothionein, in: Jeremias H.R. Kagi, Yutaka Kojima (Eds.), *The Metallothionein II*, Birkhauser, Basel, 1987, p. 581.
- [8] J.S. Garvey, Antibodies to metallothionein, in: James F. Riordan, Bert L. Vallee (Eds.), *Methods of Enzymology, Metallobiochemistry, Part B*, Academic Press, New York, 1991, p. 141.
- [9] K. Nakajima, K. Suzuki, N. Otaki, M. Kimura, Epitope mapping of metallothionein antibodies, in: James F. Riordan, Bert L. Vallee (Eds.), *Methods of Enzymology, Metallobiochemistry, Part B*, Academic Press, New York, 1991, p. 174.
- [10] H.H. Dieter, L. Muller, J. Abel, K.H. Summer, Metallothionein-determination in biological materials: Interlaboratory comparison of 5 current methods, in: Jeremias H.R. Kagi, Yutaka Kojima (Eds.), *The Metallothionein II*, Birkhauser, Basel, 1987, p. 351.
- [11] R.W. Olafson, Electrochemical quantification and characterization of metallothionein, in: Jeremias H.R. Kagi, Yutaka Kojima (Eds.), *The Metallothionein II*, Birkhauser, Basel, 1987, p. 329.
- [12] C.D. Klaassen, L.D. Lehman-McKeeman, Separation and quantification of isometallothioneins by high-performance liquid chromatography—Atomic absorption spectrometry, in: James F. Riordan, Bert L. Vallee (Eds.), *Methods of Enzymology, Metallobiochemistry*, Academic Press, New York, 1991, p. 190.
- [13] J.K. Piotrowski, W. Bolanowska, A. Sapota, *Acta Biochem. Pol.* 20 (1973) 207.
- [14] D.L. Eaton, M.G. Cherian, Determination of metallothionein in tissues by cadmium-hemoglobin affinity assay, in: James F. Riordan, Bert L. Vallee (Eds.), *Methods of Enzymology, Metallobiochemistry, Part B*, Academic press, New York, 1991, p. 83.
- [15] Z.A. Shaikh, Radioimmunoassay for metallothionein in body fluids and tissues, in: James F. Riordan, Bert L. Vallee (Eds.), *Methods of Enzymology, Metallobiochemistry, Part B*, Academic press, New York, 1991, p. 120.
- [16] K. VanHoudt, I. Nicasi, E. Van Mechelen, B. Veulemans, M. DeLey, *Immunol. Lett.* 32 (1992) 21.
- [17] R.J. Cousins, Measurement of human metallothionein by enzyme-linked immunosorbent assay, in: James F. Riordan, Bert L. Vallee (Eds.), *Methods of Enzymology, Metallobiochemistry, Part B*, Academic press, New York, 1991, p. 131.
- [18] R.K. Mehra, I. Bremner, *Biochem. J.* 213 (1983) 459.
- [19] C. Tohyama, Z.A. Shaikh, *Fundam. Appl. Toxicol* 1 (1981) 1.
- [20] M. Apostolova, P.R. Bontchev, C. Nachev, I. Sirakova, *Jpn. J. Med. Sci. Biol.* 45 (1992) 185.
- [21] M. Apostolova, P.R. Bontchev, C. Nachev, I. Sirakova, *J. Chromatogr. (Biomed. Appl.)* 620 (1993) 191.
- [22] M.M. Bradford, *Anal. Biochem.* 72 (1976) 248.
- [23] M. Reichlin, J.J. Schnure, U.K. Vance, *Proc. Soc. Exp. Biol. Med.* 128 (1968).
- [24] U.K. Laemmli, *Nature (London)* 227 (1970) 680.
- [25] H. Towbin, T. Staehelin, J. Gordon, *Proc. Natl. Acad. Sci.* 76 (1979) 4350.
- [26] H.M. Chan, G.A. Pringle, M.G. Cherian, *J. Biochem. Toxicol.* 7 (4) (1992) 219.
- [27] C. Tohyama, Z.A. Shaikh, *Biochem. Biophys. Res. Commun.* 84 (4) (1978) 907.
- [28] R.J. Vander Mallie, J.S. Garvey, *J. Biol. Chem.* 254 (1979) 8416.
- [29] B.G. Talbot, G. Bilodeau, J-P. Thirion, *Mol. Immunol.* 23 (10) (1986) 1133.
- [30] C. Russo, O. Oliviero, D. Girelli, P. Guarini, R. Pasqualini, M. Azzini, R. Corrocher, *Hypertension* 29 (1997) 1058.
- [31] S.C. Cunnane, *Prog. Lipid Res.* 21 (1982) 73.
- [32] M. Narce, P. Asdrubal, M.C. Delachambre, E. Vericel, M. Lagarde, J.P. Poisson, *Mol. Cell. Biol.* 141 (1994) 9.
- [33] J.A. Simon, J. Fong, J.T. Bernert, *Hypertension* 27 (1996) 303.
- [34] T. Macchia, R. Mancinelli, D. Attard Barbini, F. Taggi, U. Avico, A. Cantafora, *Clin. Chim. Acta* 199 (1991) 59.
- [35] S.C. Cunnane, *Prog. Food Nutr. Sci.* 12 (1988) 151.

The determination of environmental and industrial exposure to heavy metals based on the quantitative isolation of metallothionein from human fluids, with application of covalent affinity chromatography with thiol-disulphide interchange gel as a solid-phase extraction support¹

A.K.M. Kabziński *

University of Łódź, Faculty of Mathematic, Physics and Chemistry, Department of General and Inorganic Chemistry, Chromatography, Biochromatography and Environmental Analysis Laboratory, Narutowicza, 68 str., Poland

Received 04 November 1996; received in revised form 10 April 1997; accepted 07 August 1997

Abstract

The aim of this study was to present a new analytical method for the quantitative determination of metallothionein (MT) proteins in human body fluids and tissues, in order to determine the level of environmental and industrial exposure to heavy metals. For MT isolation, covalent affinity chromatography with thiol-disulphide interchange (CAC-TDI) was applied. Fundamentals of indirect determination of the contents of metallothionein proteins were worked out through estimation of the quantities of metals bound with metallothionein protein and adsorbed on covalent affinity chromatography gel as on solid-phase extraction support during separating process. The (CAC-TDI) gel, specially prepared, was used as a solid phase extraction support (SPE) for preconcentration of Hg–thionein (Hg-Th), Cd–thionein (Cd-Th), Zn–thionein (Zn-Th) and Cu–thionein (Cu-Th) proteins and Hg, Cd, Zn and Cu bonded with MTs from water, human fluids such as: urine, human plasma, breast milk and tissues homogenates. © 1998 Elsevier Science B.V. All rights reserved.

Keywords: Metallothionein; Covalent affinity chromatography; Heavy metal

1. Introduction

Exposure to heavy metals is a big problem in environmental toxicology. Acute intoxication to metals and their compounds is now rather the

exception and the present type of exposure has rather a chronic character. The metals and their compounds are adsorbed through the air passages and alimentary canal with food and drinking water. Most of the heavy metals, especially: Hg, Co, Cd, Bi, Zn, Cu, Ag, Au, Pb, Pt, Sn, Ni, Rb and Tc are very dangerous for a human body. They disturb the economy of endogenous metals and

* Tel.: +48 42 781603; fax: +48 42 783958.

¹ Material presented at the 3rd International Workshop on 'Metallothionein', Gell-Belgium, 30–31 October, 1996.

biochemical equilibrium. They have an etiological effect on hypertension, cancer, decrease the ventilation of the lungs and other lung diseases. Heavy metals are the source of degeneration, reduction of pancreatic efficiency and dysfunction of kidneys [1–3]. Exposure to Cd is the source of Itai–Itai disease which is characterized by acute damage of the kidneys. Poisoning with Hg brings about Minamata disease [4,5]. In both cases intoxication was produced through the alimentary canal by consumption of fish living in waters contaminated with heavy metals. The daily doses of Cd differ from country to country and depend on their industrialization, density of population and the condition of environmental protection. The daily doses reach: 10–20 $\mu\text{g d}^{-1}$ in Sweden, 15–35 $\mu\text{g d}^{-1}$ in England, 20–70 $\mu\text{g d}^{-1}$ in the USA and above 215 $\mu\text{g d}^{-1}$ in Japan [6]. One of the indicators of exposure to Cd and other heavy metals is the measurement of their concentration in urine, blood, liver and kidneys. Another indicator is the content of endogenous metals (Zn, Cd) in these tissues [7–10]. The specificity of these methods was rather low and the results depended on: the type of metals, the type of exposure time from the last doses obtained, etc. The obtained results were difficult to interpret and the determination of correlation coefficients between time of exposure and value of metals deposited was very difficult or sometimes even impossible.

In 1956, for the first time, increased content of amino acids in urine after exposure to Cd was noticed [11]. The presence of the low molecular weight proteins (MW < 40.0 kDa) was observed in urine, resulting from damage of the kidney ducts [12–15]. Among these peptides the most important ones are: β -microglobulin (11.8 kDa), orosomucoid (44.0 kDa), retinol binding protein-RBP (21.4 kDa), β_{2x} -globulin (21.0 kDa), post- γ -protein (10.0 kDa), ribonucleases (13.0; 20.0; 32.0 kDa), lysozyme (14.6 kDa), minialbumin (10.0 kDa), β - and γ -trace free immunoglobulin light chains (30.0 and 10.0 kDa), carbonic anhydrase B (25.0 kDa) and immunoglobulin free light chains (23.0 kDa) [16–19]. Other indicators of exposure to Cd are total content of amino acids and proteins in urine

and plasma. All these proteins have no good correlation coefficients between concentration of these proteins in human fluids and concentration of heavy metals in human tissues and fluids. The correlation coefficient (r) between Cd and other heavy metals concentrations in blood and urine, and the concentrations of these proteins were about 0.1–0.6, which means that they are not good as specific indicators of exposure to Cd, similar to determination of metals concentrations [16,19,20].

Specific protein appearing in urine, plasma and human milk only after exposure to metals is metallothionein (MT). MT was discovered in 1957 by Margoshes and Vallee and characterized by Kagi and Vallee as the low molecular weight protein of about 6.5 kDa. MT is rich in –SH groups, containing about 30% of cysteine in the molecule. It is chelated with: Cd, Zn, Cu, Hg, Au, Ag, Bi, Co which are stimulators of its biosynthesis and all these metals bind to the induced protein [21–25]. The mammalian MTs binding a total seven equivalents of the multivalent ions and have the higher stoichiometries (12 equivalents) with univalent d(10) ions such as: Cu(I), Ag(I) and Au(I). The affinity of the metal ions for the binding sites of mammalian MTs follows the order of the thiolate-metal complexes: Zn(II) < Pb(II) < Cd(II) < Cu(I), Ag(I), Hg(II), Bi(III) [26]. MTs have two domains ($-\alpha$)[31–61] and ($-\beta$)[1–29] of about 15–20 Å diameter, which contain two metallothiolate clusters of different structures and different affinity to individual metals ([A—three-metal cluster, preference Cu, Zn, Cd], [B—four-metal cluster, preference Cd, Zn, Cu]) [27–30]. In physiological states it exists in trace amounts, as confirmed by radio-immunological or latex-immunological methods (RIA or LIA). Metallothionein concentration in plasma and urine was found to be about $2.4 \pm 2.2 \mu\text{g MT protein/g creatinine}$, where 100–200 pg of MT is the detection limit for using analytical methods. After exposure to Cd, metallothionein concentration in urine and plasma ranged from 20.0 to 2500.0 $\mu\text{g/g creatinine}$ [31–38]. The application of this technique allowed determination of quite a satisfactory correlation between the contents of MT

in human fluids and concentration of Cd in the blood, urine, kidney and liver, ranging from 0.74 to 0.95. These correlations are very good indicators of the environmental exposure to these metals [32,36–38].

In experiments using RIA and LIA techniques, the main problem is however obtaining metallothionein antibodies, because the molecular mass of MT is too low as a hapten and there is also need for the long period of immunization of experimental animals. The metallothionein protein before being used must be polymerized, but in this process random aggregation also occurs. The immunological answer of an immunological system is not homogenic and antibodies in RIA or LIA techniques give unspecific reactions with the other proteins present in plasma and urine and the analysis is not quantitative. In order to avoid all these difficulties, investigations on quantitative concentration of metallothioneins the new method was tested. MTs were carried out by covalent affinity chromatography gel as a solid phase extraction (SPE) support, specific for the thiol proteins, gives better results than the classical physico-chemical methods [39–44]. The idea of this method was based on earlier results obtained for separation of different metallothioneins by CAC-TDI method and our proposed mechanism of separation [45–48].

Covalent affinity chromatography with thiol-disulphide interchange (CAC-TDI) is one of the special techniques of separation of affinity chromatography based on the exchange reaction between disulphide bridges (–S–S–) fixed on the insoluble support and thiol groups (–SH) of the proteins being separated [49,50]. CAC-TDI technique was first applied for the separation of MTs from tissues by Squibb, Cousins, Ryden and Deutsch in 1977/78 [51,52]. The yields of separation of different MTs were about 10–50% for applied protein and about 15–80% for metals bonded formerly with MTs and depend on pH of using buffers, type of MTs, length of spacer arm and type of dithiol ligand [52–58](Fig. 1).

2. Experimental

2.1. Preparation of metallothioneins

The prepurified metallothioneins (Hg–thionein (Hg-Th); Cd–thionein (Cd-Th); Zn–thionein (Zn-Th) and Cu–thionein (Cu-Th) and cadmium apothionein (Apo-Th) were obtained from critical tissues (Hg-kidney; Cd, Zn, Cu-liver) of the experimental female white rats (Wistar, 190–210 g of body weight) after exposure to the salts of heavy metals, administered subcutaneously in the form of physiological salt solutions (HgCl₂ 1.0 mg of Hg/kg body weight (b.w.) 3 times per week for 4 weeks; CdCl₂ 1.0 mg of Cd/kg b.w. 3 times per week for 4 weeks; ZnSO₄ 20.0 mg of Zn/kg b.w. 7

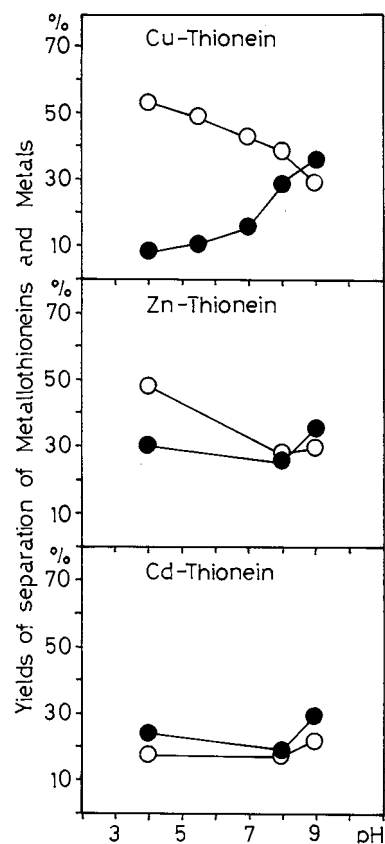


Fig. 1. The relations between yields of separation of different metallothioneins and metals and pH of buffers used for separation by covalent affinity chromatography with thiol-disulphide interchange method on Sepharose-DTNB.

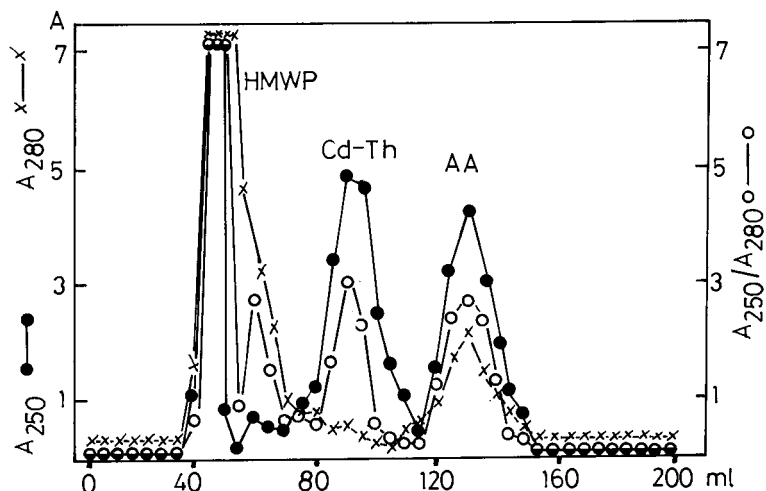


Fig. 2. The chromatogram of postmitochondrial supernatant obtained from the livers of female white Wistar rats after exposure to CdCl_2 , separated by gel permeation chromatography (GPC) method on Sephadex G-75 (column K26/100, Pharmacia, Uppsala, 0.1 mol l^{-1} ammonium-formate buffer, pH = 8.0, ionic strength $\mu = 0.1$, 0.05% NaN_3 , flow rate 20.0 ml h^{-1} , fractions of 5.0 ml were collected).

times per week for 2 weeks, CuSO_4 3.0 mg of Cu/kg b.w. 7 times per week for 2 weeks). The homogenates of tissues [liver 25% (w/v) and kidney 20% (w/v)] in 1.15% KCl were prepared. Homogenates were centrifuged ($3000 \times g$ for 30 min) and after initial dialysis (dialysing bag Serva 20/32 and Aquacide II from Serva), the supernatants (5.0 ml) were separated by low pressure gel permeation chromatography (LPGPC) method on

Sephadex G-75 (column K26/100, Pharmacia, Uppsala, 0.1 mol/l ammonium-formate buffer, pH = 8.0, ionic strength of buffer $\mu = 0.1$, 0.05% NaN_3 , flow rate 20.0 ml h^{-1} , fractions of 5.0 ml). The fractions of MTs were collected and the concentration of protein, thiol groups and metals were determined. The molecular weight and the control of quality of obtained MTs and their physicochemical parameters were measured by

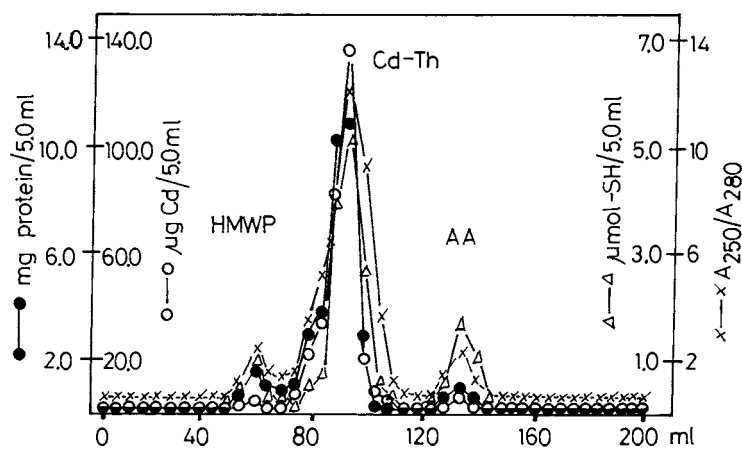


Fig. 3. The chromatogram of postmitochondrial supernatant obtained from the livers of rats after initial preconcentration by dialysis on Serva bag 20/32, separated by gel permeation chromatography (GPC) method on Sephadex G-75 (condition of separation the same as on Fig. 2).

high-pressure gel permeation chromatography method (HPGPC) (HPLC Pump 2248, auto-sampler Model 2157, UV/VIS detector VWM 2141, low pressure mixer, fraction collector Redi-Frac-LKB Pharmacia, control panel Chromatopic C-R5A-Shimadzu, GPC column Superdex 75HR 10/30 with gel of mean particle size 13 μm (Pharmacia, Uppsala), 0.1 mol/l ammonium-formate buffer, pH = 8.0, ionic strength of buffer $\mu = 0.1$, flow rate 1.0 ml min^{-1}). All fractions of metallothioneins were lyophilized and stored [53–58].

2.2. Synthesis of gels for covalent affinity chromatography

The gel for covalent affinity chromatography with thiol-disulphide interchange (CAC-TDI)

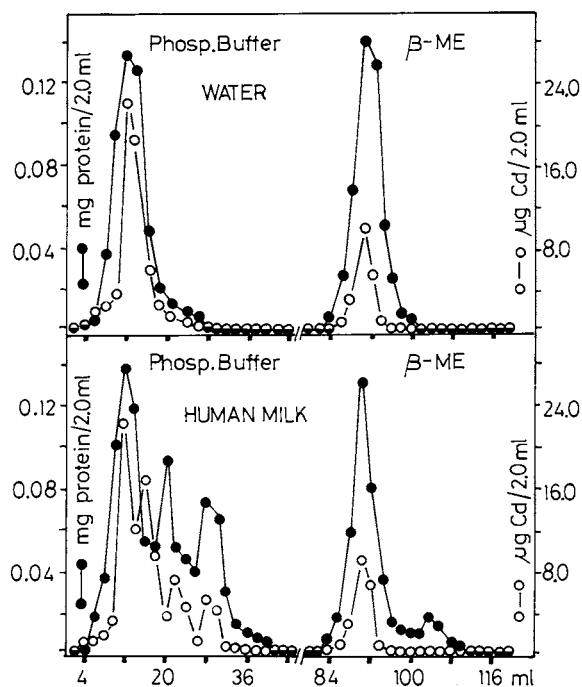


Fig. 4. The separation of Cd-thionein added to the distilled water and human milk by covalent affinity chromatography with thiol-disulphide interchange (CAC-TDI) on Sepharose-DTNB with using two-step elution (column 130 \times 10 mm i.d., $v \sim 10.0$ ml, flow rate 30.0 ml h^{-1} , fractions of 2.0 ml were collected, elution by: (a) 0.05 mol/l phosphate buffer, pH = 8.0, (b) 0.05 mol/l β -mercaptoethanol in phosphate buffer, pH = 8.0).

Table 1

The correlation coefficients (r) between metallothionein concentration added to the different mediums as determined by an indirect method

No.	Correlation	(r) ^a
1.	Hg-Th/water	0.95
2.	Hg-Th/urine	0.87
3.	Hg-Th/plasma	0.73
4.	Cd-Th/water	0.97
5.	Cd-Th/urine	0.84
6.	Cd-Th/plasma	0.81
7.	Cd-Th/human milk	0.72
8.	Cd-Th/homogenate	0.71
9.	Zn-Th/water	0.96
10.	Zn-Th/urine	0.84
11.	Zn-Th/plasma	0.72
12.	Zn-Th/human milk	0.70
13.	Cu-Th/water	0.96
14.	Cu-Th/urine	0.80
15.	Cu-Th/plasma	0.71
16.	Cu-Th/human milk	0.69

^a Correlation coefficients (r) were calculated for $n = 5$ replicated analysis for the same concentration of MT in fluids.

Sepharose-1,6-diaminohexylo-X (where X was 5,5'-dithiobis-(2-nitrobenzoate) [Sepharose-DTNB] or 2,2'-dithiobis-(2-nitropyridine)-[Sepharose-DTNP]) were prepared by own methods [44]. The CH-Sepharose 4B gel (Pharmacia, Uppsala), DTNB (Windsor Laboratories), DTNP (BDH) and *N*-cyclohexyl-*N'*-[2-(*N*-methylmorpholino)ethyl] carbodiimide-*p*-toluene sulphonate (carbodiimide CMC, BDH) were used for covalent affinity chromatography gels synthesis. The degree of substitution was about 0.15–0.18 mmol DTNB or DTNP per gram of Sepharose gel and were similar to these types of the commercial materials.

2.3. Preparation of biological material.

Physiological human urine, plasma and human milk were collected from five people (non-smokers) in a good state of health after clinical control. All samples were collected and pooled. The samples were protected by addition of sodium azide (NaN_3) in final concentration 0.05% (w/v). The concentration of protein, thiol groups and metals (Hg, Cd, Zn and Cu) were measured and physico-

Table 2

The correlation coefficients (r) between metallothionein concentration added to the different mediums and determined by chemical methods

No.	Sample	Correlation coefficients (r) ^a				
		Lowry method	Modified Lowry method	Tannin method	CBB method	BCA method
1.	Hg-Th/water	0.87	0.91	0.92	0.91	0.90
2.	Hg-Th/urine	0.66	0.70	0.75	0.71	0.70
3.	Hg-Th/plasma	0.49	0.59	0.68	0.62	0.61
4.	Cd-Th/urine	0.85	0.87	0.89	0.90	0.89
5.	Cd-Th/urine	0.61	0.64	0.76	0.68	0.69
6.	Cd-Th/plasma	0.48	0.51	0.55	0.53	0.52
7.	Cd-Th/human milk	0.42	0.45	0.53	0.50	0.51
8.	Cd-Th/homogenate	0.40	0.42	0.53	0.47	0.45
9.	Zn-Th/water	0.86	0.88	0.91	0.89	0.90
10.	Zn-Th/urine	0.70	0.75	0.83	0.81	0.80
11.	Zn-Th/plasma	0.58	0.62	0.74	0.63	0.61
12.	Zn-Th/human milk	0.41	0.43	0.59	0.44	0.43
13.	Cu-Th/water	0.87	0.88	0.90	0.90	0.89
14.	Cu-Th/urine	0.69	0.74	0.83	0.77	0.75
15.	Cu-Th/plasma	0.53	0.57	0.72	0.61	0.60
16.	Cu-Th/human milk	0.41	0.44	0.56	0.51	0.50

^a Correlation coefficients (r) were calculated for $n = 5$ replicatd analysis for the same concentration of MT protein in fluids.

chemical parameters of urine, plasma and milk were checked by low- and high-pressure GPC method (Sephadex G-75, Sephadex G-200 and Sephadex G-10, Superdex 75HR-Pharmacia, Uppsala) [39–43,59–61].

2.4. Chromatographic preconcentration of metallothionein samples with application of covalent affinity chromatography gel and quantitation.

Hg-Th, Cd-Th, Zn-Th and Cu-Th were added to triple distilled water, physiological human urine, plasma or human breast milk in different concentrations (1, 5, 10, 25, 50, 100 and 250 $\mu\text{g ml}^{-1}$). Proteins were applied on Sepharose DTNB or Sepharose-DTNP columns (130×10 mm i.d. $v \sim 10$ ml) in volume 5.0 ml and were eluted with: (a) 0.05 mol/l phosphate buffer, pH 8.0; (b) 0.04 mol/l β -mercaptoethanol in phosphate buffer. 2.0 ml fractions were collected at the flow rate 30.0 ml h^{-1} . The CAC-TDI columns were regenerated by DTNB or DTNP in concentration 0.04 mol l^{-1} in phosphate buffer. The concentrations of MTs were calculated from

metals concentrations on CAC-TDI supports, determined by atomic absorption spectrometry (AAS) technique and correlation coefficients between known concentrations and calculated by indirect methods were determined [39–43,59–61].

The concentrations of MTs protein in samples were calculated according to Eq. (1) [39–44]

$$c = (A \times 100\% \times M_{\text{MT}}) / (M_{\text{M}} \times m \times R\%) \quad (1)$$

where: (c) is calculated concentration of MTs in the sample [μg], (A) is content of metals bonded to the CAC-TDI gel [mg], (M_{MT}) is molecular weight of metallothionein protein [g mol^{-1}], (M_{M}) is molecular weight of the determined metals [g mol^{-1}], (m) is the coefficient determined experimentally, characterizing the content of the metals in metallothionein molecule [$\text{mol metal/mol protein}$] and (R) is the mean recovery of adsorption of the metals in the process of metallothionein separation with use of the CAC-TDI method [%], obtained in experiments with separation of MTs on CAC-TDI supports. The added amounts of MT proteins to the samples with different concentration have been compared with the contents as determined by the use of the

Table 3

The mean errors (%) between added amount of metallothionein protein and that determined by chemical and proposed indirect method for the lowest concentration of MT protein ($5.0 \mu\text{g ml}^{-1}$)

No.	Sample	The mean errors in determination of MTs content (%) ^a					
		Lowry method	Modified Lowry method	Tannin method	CBB method	BCA method	Indirect CACTDI method
1.	Hg-Th/water	11.9	9.1	6.5	8.9	8.8	2.0
2.	Hg-Th/urine	12.7	10.2	7.4	10.1	10.1	2.0
3.	Hg-Th/plasma	14.3	12.5	8.1	12.5	12.4	2.1
4.	Cd-Th/water	11.5	9.8	6.3	9.5	9.3	2.8
5.	Cd-Th/urine	12.9	11.3	7.8	11.0	11.2	2.8
6.	Cd-Th/plasma	14.8	13.1	8.9	13.3	13.1	3.1
7.	Cd-Th/milk	16.2	12.5	11.3	12.6	12.5	4.3
8.	Cd-Th/homog.	17.6	13.3	10.9	13.7	13.4	4.2
9.	Zn-Th/water	11.3	8.8	5.6	8.7	8.8	2.1
10.	Zn-Th/urine	11.9	8.8	6.8	8.9	8.9	2.7
11.	Zn-Th/plasma	14.7	10.4	8.9	10.2	10.2	3.4
12.	Zn-Th/milk	15.6	12.2	10.1	12.4	12.1	3.6
13.	Cu-Th/water	11.0	8.7	6.0	8.6	8.5	1.2
14.	Cu-Th/urine	12.1	9.3	7.7	9.1	9.2	2.9
15.	Cu-Th/plasma	15.2	11.8	8.8	12.1	11.9	3.9
16.	Cu-Th/milk	16.7	12.9	9.9	12.7	12.9	4.1

^a The mean errors were calculated for the lowest concentration of MTs protein added to the $n = 5$ samples, the volume of sample $v = 5.0$ ml.

indirect method based on determining of the heavy metals as: Hg, Cd, Zn or Cu contents in biological samples.

2.5. Analytical methods

In the investigations the following determinations were carried out: protein concentration by Lowry method [62–66], tannin method [67], BCA method (Pierce, USA) [68–71], CBB method (Bio-Rad, USA) [72–75], thiol groups concentration [76,77], heavy metals (Hg, Cd, Zn and Cu) concentration by the atomic absorption spectrometry (AAS method) [53,54,56–58].

3. Results and discussion

The typical separation of metallothionein (Cd-thionein, Cd-Th) from postmitochondrial supernatant, obtained from the liver of rats after exposure to CdCl_2 , by gel permeation chromatography on Sephadex G-75 and rechromatography

after preconcentration by dialysis are presented in Figs. 2 and 3. The separation of Cd-Th protein by CAC-TDI method with two-step elution is presented in Fig. 4. The correlations between MT protein concentration added to the different mediums (water, urine, plasma, human milk, homogenate) and determined by indirect method are given in Table 1. The correlation coefficients (r) between MT protein concentration added to the same mediums and determined by chemical methods (Lowry, tannin, BCA and CBB) are given in Table 2. The mean errors between the added amount of MT protein and that determined by chemical method and indirect method for two concentrations (5.0 and $250.0 \mu\text{g ml}^{-1}$) are given in Tables 3 and 4. The mean detection limits for different MTs in different mediums with quantitation by indirect method with CAC-TDI gel as SPE support are given in Table 5.

Previous results showed the mechanism of separation of polythiolmetalloproteins was very complicated and that separated proteins change their native structures [45–48] and yields after protein

Table 4

The mean errors (%) between added amount of metallothionein protein and that determined by chemical and proposed indirect method for the highest concentration of MT protein ($250.0 \mu\text{g ml}^{-1}$)

No.	Sample	The mean errors in determination of MTs content (%) ^a					Indirect CACTDI method
		Lowry method	Modified Lowry method	Tannin method	CBB method	BCA method	
1.	Hg-Th/water	9.2	6.3	4.1	5.8	5.9	0.8
2.	Hg-Th/urine	10.3	6.8	4.5	6.4	6.6	0.9
3.	Hg-Th/plasma	11.9	7.8	4.5	7.5	7.7	1.3
4.	Cd-Th/water	9.1	5.1	3.8	5.0	5.1	1.2
5.	Cd-Th/urine	10.2	6.4	4.4	6.4	6.6	1.4
6.	Cd-Th/plasma	11.7	8.1	4.65	8.3	8.0	1.9
7.	Cd-Th/milk	12.6	10.5	5.7	10.3	10.4	2.2
8.	Cd-Th/homog.	13.7	11.3	6.2	11.3	11.2	2.1
9.	Zn-Th/water	8.9	6.2	3.9	6.3	6.1	1.2
10.	Zn-Th/urine	10.1	7.6	4.6	7.7	7.8	1.5
11.	Zn-Th/plasma	11.8	8.6	4.9	8.5	8.5	1.9
12.	Zn-Th/milk	12.5	10.7	5.6	10.5	10.6	2.3
13.	Cu-Th/water	9.0	6.3	4.0	6.2	6.1	1.1
14.	Cu-Th/urine	10.5	7.8	4.5	7.7	7.5	1.9
15.	Cu-Th/plasma	12.1	8.8	5.1	8.9	8.6	2.0
16.	Cu-Th/milk	13.3	10.8	5.9	10.5	10.4	2.4

^a The mean errors were calculated for the highest concentration of MTs protein added to the $n = 5$ samples, the volume of sample $v = 5.0$ ml.

separation were rather low. Additionally metals formerly bonded with MTs were adsorbed on the CAC-TDI gel not only via immobilized proteins, but also by direct adsorption on the supports and, what is very important, the yields of these reactions are very constant [45–48]. As follows from previous data (Fig. 1)[52–58], the direct concentration of metallothionein protein for analytic purposes is very difficult or even impossible, because of too low yield of binding the MTs protein with CAC-TDI gel, due to the occurrence of reactions, competitive to the binding ones [45–48] and very high detection limit ($0.1\text{--}5.0 \mu\text{g ml}^{-1}$) of chemical methods (Lowry, BCA, tannin and CBB) used for the protein quantitation [62–75]. The binding of 10–50% for different MTs is too low for quantitative isolation, and variations in these values are too big for its theoretical estimation. The situation is not improved even by higher efficiency of binding MT protein in case of its small concentrations in a sample. This fact was observed in synthesis in polysomal cell-free system, where the reaction of intermolecular oxida-

tion of protein –SH groups is much less [51,78–82]. An important fact is the very high and constant content of metals (Hg, Cd, Zn and Cu) in fractions bounded to the CAC-TDI gels. Thus, it is possible to determine the contents of Hg-Th, Cd-Th, Zn-Th and Cu-Th indirectly by the estimation of Hg, Cd, Zn and Cu concentration in the fractions bounded to CAC-TDI gels [39–43,59–61].

The data presented show that the actual contents of protein as well as the ones determined by the indirect method demonstrate a very good correlation in a wide range of concentrations (Table 1). The correlation coefficients ranged between 0.69 and 0.97. The lowest correlation coefficients were for plasma, tissue homogenate and milk while higher correlation were found for urine and water. In comparison, the correlation coefficients (r) between the present concentration of MT and that determined by chemical methods (Lowry, tannin, BCA and CBB methods) ranged from 0.53 to 0.92 for tannin method, 0.40 to 0.91 for the Lowry method, 0.43 to 0.90 for the BCA

Table 5

The mean detection limits for different metallothioneins protein obtained from different mediums with preconcentration by solid phase extraction method on CAC-TDI support

No.	Materials	The detection limits (ng ml ⁻¹)			
		Hg-Th	Cd-Th	Zn-Th	Cu-Th
1.	Water	5.47 ± 0.03	6.67 ± 0.07	6.92 ± 0.06	6.73 ± 0.09
2.	Urine	5.47 ± 0.05	6.74 ± 0.08	7.2 ± 0.1	7.3 ± 0.1
3.	Plasma	6.0 ± 0.2	7.7 ± 0.1	8.6 ± 0.2	8.9 ± 0.2
4.	Milk	—	8.0 ± 0.2	8.9 ± 0.2	9.3 ± 0.3
5.	Homog. ^a	—	8.9 ± 2.2	—	—

^a Homogenates was obtained from liver of rats exposed to CdCl₂.

and 0.44 to 0.91 for CBB but for all physiological fluids were lower than 0.83 for tannin, lower than 0.75 for Lowry, lower than 0.80 for BCA and lower than 0.81 for the CBB method (Table 2). The errors between the actual content of protein in the sample and the concentration as determined by the indirect method consisting in metals analysis of the metals bound with CAC-TDI does not exceed 2.4% for the highest concentration of MT protein added (250 µg ml⁻¹) and 4.3% for the lowest concentration (5 µg ml⁻¹). For the chemical methods the errors ranging between 3.8 and 11.3% for the tannin method, 5.1–13.3% for the modified Lowry method, 5.1–13.4%, for the BCA and 5.0–13.7% for the CBB and were higher than for proposed indirect CAC-TDI method (0.8–4.3%) (Tables 3 and 4). The detection limits for CAC-TDI methods are about 5.47–9.28 ng ml⁻¹ for different types of MTs (Table 5). Thus, the described method may be applied to the indirect determination of metalloproteins in physiological fluids by means of evaluation of the metal contents on the CAC-TDI gel after adding the metalloprotein samples. The process of metal binding itself has a quantitative character unlike binding of thiolproteins where a complex mechanism of interaction CAC-TDI gel-separating protein causes lowering of binding efficiency [45–48]. The yields of adsorption depend on the structure of CAC-TDI gel (length of spacer arms, their modification and type of ligand) and pH of using buffers. Additionally buffer has the influence on the mechanism of adsorption reaction (cationic or anionic) and yields of separation of the thiol-

proteins [44,83–86]. Thus, the described method of indirect evaluation of protein content may be applied in clinical and toxicological analysis. The CAC-TDI gel itself may function as a sorbent for preconcentration of thiol- and metallothiol-proteins at solid phase extraction (SPE) technique allowing us to concentrate proteins. It may also function in a similar way in relation to heavy metals as: Hg, Cd, Co, Cu, Mo, Zn, Au, Ag, etc. acting both on free ions of these metals and those bound with proteins. The metals bound with the CAC-TDI gel with participation of mercaptide bonds of metal-sulphur may be easily washed from it by means of low-molecular thiolcompounds. Ease of adsorption and desorption are among the basic factors qualifying deposits of CAC-TDI types as sorbent in the SPE method. With detection limits for AAS method about 1.0–0.01 ng of metals (Hg, Cd, Zn, Cu) ml⁻¹ [87–99] and with conversion factors of 3–8 mol metal/mol MT protein and with yields of adsorption of heavy metals with 30–40% of applied doses. The detection limit for MT protein at in-direct method can be about 1–10 ng ml⁻¹. This detection limit for presented indirect method is lower than for chemical methods (100–500 ng ml⁻¹) but higher than for immunological method as RIA or LIA (0.1–0.01 ng ml⁻¹). The very important fact is that sensitivity of proposed indirect method with application of CAC-TDI gel has a proper level for clinical analysis.

Urine, plasma, human milk samples and corresponding solutions of tissue must be collected. After addition of MTs to urine, plasma or other

physiological fluids, they play a role in the model of physiological fluids containing MTs, from people after exposure to heavy metals. It seems necessary to carry out pretreatment by the high- or low-pressure GPC method, in order to remove proteins heavier than MT, and also amino acids, oligopeptides and low-molecular metal compounds, mainly Hg ones (Fig. 5). This procedure

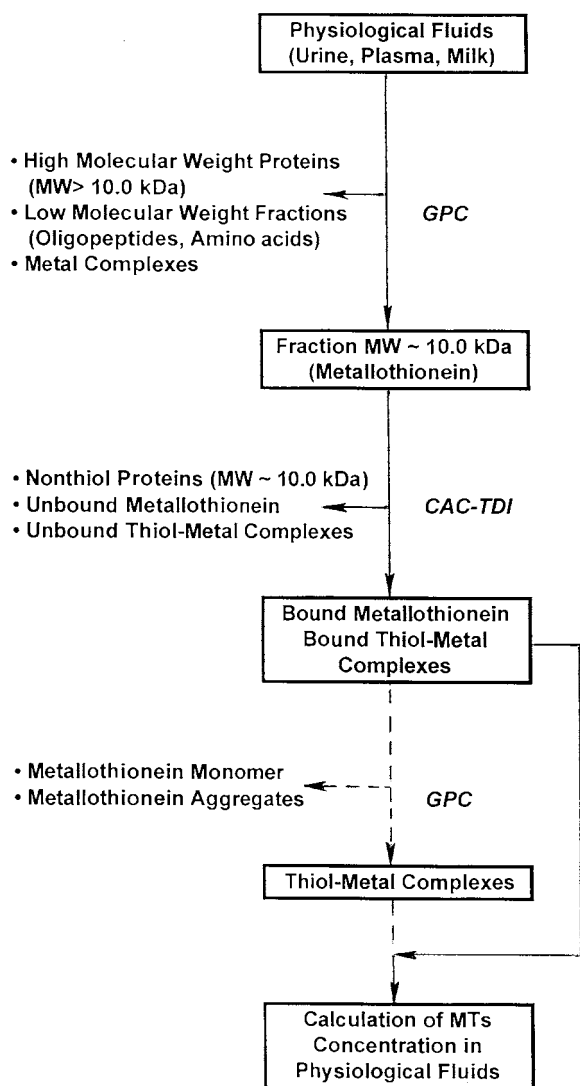


Fig. 5. The scheme of procedure of metallothioneins and metals pre-concentration on covalent affinity chromatography with thiol-disulphide interchange (CAC-TDI) gel as support for solid-phase extraction (SPE) method.

is essential while investigating MTs in the human urine, plasma and milk, which contains small amount of proteins, oligopeptides and amino acids with quite high contents of -SH groups. The other important problem during the investigations is carried out a short time after exposure to heavy metals appearing in the body fluids in the form of low-molecular compounds [100,101]. The preparation obtained in this way can be considered to be the initial fraction. Application of CAC-TDI method at a further stage allows recovery of only about 20–30% of applied MT protein, about 30–40% of Cd, Zn or Cu and about 80% of Hg (Fig. 5). The sample, prepared in this way does not contain any other ballast proteins of 10|000 Da mass, which could contain only a few -SH groups or none at all [102,103]. This method allows us to obtain concentrated preparations, containing Hg, Cd, Zn and Cu mobilized from mercaptide bonds in Hg-Th, Cd-Th, Zn-Th and Cu-Th. The metals can be determined by AAS method already at this stage, in the presence of MTs protein [39–44,59–61].

4. Conclusions

In conclusion we can emphasize that, the supports for covalent affinity chromatography with thiol-disulphide interchange (CAC-TDI) can be used as a solid phase extraction (SPE) gel for pre-concentration of metallothioneins protein and metals bonded to them. The concentration of metallothioneins in human fluids (urine, plasma and milk) can be determined by the indirect method, based on calculation of MTs concentration from content of metals bonded to the covalent affinity chromatography column and the detection limits for these methods are about 5.47–9.28 ng ml⁻¹, a proper level for clinical analysis. The correlation coefficients for the presented indirect method are 0.69–0.97. The presented method can be used in toxicological analysis for the determination of industrial and environmental exposure to heavy metals, and environmental analysis for determining the value of intoxication of the environment by heavy metals.

References

- [1] H. Winter, *J. Appl. Toxicol.* 2 (1982) 61.
- [2] Z.A. Shaikh, C. Tohyama, *Environ. Health Perspect.* 54 (1984) 171.
- [3] Z.A. Shaikh, K.M. Harnett, S.A. Perlin, P.C. Huang, *Experientia* 45 (1989) 146.
- [4] K. Nogawa, A. Ishizaki, S. Kawano, *Environ. Res.* 15 (1978) 135.
- [5] K. Nogawa, Y. Yamada, R. Honda, M. Ishizaki, I. Tsuritani, K. Kawano, T. Kato, *Toxicol. Lett.* 17 (1983) 263.
- [6] C. Travis, E.L. Etnier, *Environ. Res.* 27 (1982) 1.
- [7] M.A. Webb, D.R. Chettle, K. Al-Haddada, S.M.P.J. Downey, T.C. Harvey, *Ann. Occup. Hyg.* 25 (1982) 33.
- [8] E. Hassler, B. Lind, M. Piscator, *Brit. J. Ind. Med.* 40 (1983) 420.
- [9] S. Iwao, K. Tsuchiya, M. Sugita, *Arch. Environ. Health* 38 (1983) 156.
- [10] R. Lauwerys, J.P. Buchet, H. Roels, A. Berlin, J. Smeets, *Clin. Chem.* 21 (1975) 551.
- [11] T.W. Clarkson, J.E. Kench, *Biochem. J.* 62 (1956) 361.
- [12] L. Friberg, *Acta Chem. Scand.* 138 (1950) 1.
- [13] M. Piscator, *Arch. Environ. Health* 4 (1962) 55.
- [14] G.S. Thind, *J. Air Pollut. Control Ass.* 22 (1972) 267.
- [15] A.M. Bernard, R.R. Lauwerys, V. Starace, P.L. Masson, *Biochem. Biophys. Res. Commun.* 93 (1980) 535.
- [16] N.E. Kowal, M. Zirkes, *J. Toxicol. Environ. Health* 11 (1983) 607.
- [17] K. Nomiyama, M. Yotoriyama, H. Nomiyama, *Arch. Environ. Contam. Toxicol.* 12 (1983) 143.
- [18] M. Stewart, E.C. Hughes, *Brit. J. Ind. Med.* 38 (1981) 170.
- [19] A. Bernard, H. Roels, G. Hubermont, J.P. Buchet, P.L. Masson, R.R. Lauwerys, *Int. Arch. Occup. Environ. Health* 38 (1976) 19.
- [20] A.A.E. Wibowo, R.F.M. Herber, W. van Dyeck, R.L. Zielhuis, *Int. Arch. Occup. Environ. Health* 49 (1982) 265.
- [21] M. Margoshes, B.L. Vallee, *J. Am. Chem. Soc.* 79 (1957) 4813.
- [22] J.H.R. Kagi, B.L. Vallee, *J. Biol. Chem.* 235 (1960) 3460.
- [23] J.H.R. Kagi, B.L. Vallee, *J. Biol. Chem.* 236 (1961) 2435.
- [24] J.H.R. Kagi, S.R. Himmelhoch, P.D. Whanger, J.L. Bethune, B.L. Vallee, *J. Biol. Chem.* 249 (1974) 3537.
- [25] Y. Kojima, C. Berger, B.L. Vallee, J.H.R. Kagi, *Proc. Natl. Acad. Sci. USA* 73 (1976) 3413.
- [26] J.H.R. Kagi, Y. Kojima, *Experientia Suppl.* 52 (1987) 25.
- [27] A. Arseniev, P. Schultze, E. Worgotter, W. Braun, G. Wagner, M. Vasak, J.H.R. Kagi, K. Wutrich, *J. Mol. Biol.* 201 (1988) 637.
- [28] W. Braun, W. Wagner, E. Worgotter, M. Vasak, J.H.R. Kagi, K. Wutrich, *J. Mol. Biol.* 187 (1986) 125.
- [29] J.H.R. Kagi, A. Schaffer, *Biochemistry* 27 (1988) 8509.
- [30] J.H.R. Kagi, *Methods Enzymol.* 205 (1991) 613.
- [31] C. Tohyama, Z.A. Shaikh, *Biochem. Biophys. Res. Commun.* 84 (1978) 907.
- [32] C.C. Chang, R.J.V. Mallie, J.S. Garvey, *Toxicol. Appl. Pharmacol.* 55 (1980) 94.
- [33] G.F. Nordberg, J.S. Garvey, C.C. Chang, *Environ. Res.* 28 (1982) 179.
- [34] C. Tohyama, Z.A. Shaikh, K. Nogawa, E. Kobayashi, R. Honda, *Toxicology* 20 (1981) 289.
- [35] F.Y. Falck, L.J. Line, R.G. Smith, J.S. Garvey, A. Schork, B. England, K.D. McClatchey, J. Linton, *Brit. J. Ind. Med.* 40 (1983) 305.
- [36] C. Tohyama, Z.A. Shaikh, K.J. Ellis, S.H. Cohn, *Toxicology* 22 (1981) 181.
- [37] C.C. Chang, R.R. Lauwerys, A. Bernard, H. Roels, J.P. Buchet, J.S. Garvey, *Environ. Res.* 23 (1980) 422.
- [38] H. Roels, R.R. Lauwerys, J.P. Buchet, A. Bernard, J.S. Garvey, H.J. Linton, *Int. Arch. Occup. Environ. Health* 52 (1983) 159.
- [39] A.K.M. Kabzinski, T. Takagi, *Biomed. Chromatogr.* 9 (1995) 123.
- [40] A.K.M. Kabzinski, T. Paryjczak, *Chem. Anal.* 40 (1995) 831.
- [41] A.K.M. Kabzinski, *Chem. Anal.* 40 (1995) 847.
- [42] A.K.M. Kabzinski, T. Takagi, T. Paryjczak, *Eur. J. Clin. Biochem.* 33 (1995) 56.
- [43] A.K.M. Kabzinski, *Pol. J. Environ. Stud.* 5 (1996) 9.
- [44] A.K.M. Kabzinski, *J. Chromatogr. A* 766 (1997) 121.
- [45] A.K.M. Kabzinski, T. Paryjczak, *Chromatographia* 24 (1989) 247.
- [46] A.K.M. Kabzinski, *Chromatographia* 35 (1993) 439.
- [47] A.K.M. Kabzinski, T. Paryjczak, *Acta Chromatogr.* 5 (1995) 34.
- [48] A.K.M. Kabzinski, T. Takagi, *Acta Chromatogr.* 5 (1995) 60.
- [49] K. Brocklehurst, J. Carlsson, M.P.J. Kiersten, E.M. Crook, *Biochem. J.* 133 (1973) 573.
- [50] K. Brocklehurst, J. Carlsson, M.P.J. Kiersten, E.M. Crook, *Methods Enzymol.* 34 (1974) 531.
- [51] K.S. Squibb, R.J. Cousins, *Biochem. Biophys. Res. Commun.* 75 (1977) 806.
- [52] L. Ryden, H.F. Deutsch, *J. Biol. Chem.* 253 (1978) 519.
- [53] A.K.M. Kabzinski, T. Paryjczak, *Chem. Anal.* 36 (1991) 111.
- [54] A.K.M. Kabzinski, T. Paryjczak, *Chem. Anal.* 36 (1991) 123.
- [55] A.K.M. Kabzinski, T. Paryjczak, *Chem. Anal.* 36 (1991) 699.
- [56] A.K.M. Kabzinski, *Zesz. Nauk. P.L.* 43 (1991) 456.
- [57] A.K.M. Kabzinski, *Chem. Anal.* 42 (1997) 11.
- [58] A.K.M. Kabzinski, T. Takagi, K. Tanaka, *Chem. Anal.* (in press).
- [59] A.K.M. Kabzinski, *Biomed. Chromatogr.* (in press).
- [60] A.K.M. Kabzinski, *Biomed. Chromatogr.* (in press).
- [61] A.K.M. Kabzinski, *Chromatographia*, (in press).
- [62] O.H. Lowry, H.J. Rosenbrough, A.L. Farr, R.J. Randal, *J. Biol. Chem.* 193 (1951) 265.

- [63] M. Higuchi, Y. Oshida, *Anal. Biochem.* 77 (1977) 542.
[64] E. Ross, G. Schatz, *Anal. Biochem.* 54 (1973) 304.
[65] P.J. Geiger, S.P. Bessman, *Anal. Biochem.* 49 (1972) 467.
[66] T. Unemoto, Y. Sakakibara, Hayashi, *Anal. Biochem.* 67 (1975) 198.
[67] W. Mejbaum-Katzenellenbogen, *Acta Biochim. Polon.* 11 (1959) 279.
[68] P.K. Smith, R.J. Krohn, G.T. Harmanson, A.K. Mallia, F.H. Gartner, M.D. Provenzano, E.K. Fujimoto, M.M. Goeke, B.J. Olson, D.C. Klenk, *Anal. Biochem.* 150 (1985) 76.
[69] L.C. Davies, G.A. Radke, *Anal. Biochem.* 161 (1987) 152.
[70] H.D. Hill, J.M. Strake, *Anal. Biochem.* 170 (1988) 203.
[71] K.J. Wiechelman, R.D. Brown, J.D. Fitzpatrick, *Anal. Biochem.* 175 (1988) 231.
[72] M. Bradford, *Anal. Biochem.* 72 (1976) 248.
[73] T. Spector, *Anal. Biochem.* 86 (1978) 142.
[74] S.M. Hale, *Anal. Biochem.* 81 (1977) 485.
[75] R.W. Rubin, R.W. Warten, *Anal. Biochem.* 83 (1977) 773.
[76] G.L. Ellman, *Arch. Biochem. Biophys.* 82 (1959) 70.
[77] P.A.W. Butterworth, H. Baum, J.W. Porter, *Arch. Biochem. Biophys.* 118 (1967) 716.
[78] S.G. Shapiro, K.S. Squibb, L.A. Markowitz, R.J. Cousins, *Biochem. J.* 175 (1978) 833.
[79] S.G. Shapiro, L.A. Markowitz, K.S. Squibb, R.J. Cousins, *Fed. Proc.* 37 (1978) 214.
[80] S.G. Shapiro, R.J. Cousins, *Biochem. J.* 190 (1980) 755.
[81] C.C. McCormick, M.P. Menard, R.J. Cousins, *Am. J. Physiol.* 240 (1981) 414.
[82] S.R. Quinones, R.J. Cousins, *Biochem. J.* 219 (1984) 959.
[83] A.K.M. Kabzinski, *Chromatographia* 43 (1996) 513.
[84] A.K.M. Kabzinski, T. Paryjczak, *Przem. Chem.* 71 (1992) 309.
[85] A.K.M. Kabzinski, T. Paryjczak, *Przem. Chem.* 72 (1993) 202.
[86] A.K.M. Kabzinski, T. Paryjczak, *Przem. Chem.* 75 (1996) 338.
[87] A. Starek, Z. Inglot, *Med. Pracy* 25 (1974) 507.
[88] S. Alexandrov, *Fresenius Z. Anal. Chem.* 321 (1985) 578.
[89] L. Ping, F. Kuwa, K. Matsumoto, *Anal. Chim. Acta* 171 (1985) 279.
[90] B.A. Bushaw, *Anal. Chem.* 57 (1985) 2397.
[91] L. Magos, *Analyst* 96 (1971) 847.
[92] L. Magos, T.W. Clarkson, *J. Am. Org. Atom. Control.* 55 (1972) 966.
[93] K.S. Subramanian, J.C. Meranger, J.E. McKeen, *Anal. Chem.* 55 (1983) 1067.
[94] C. Hallam, K.C. Thompson, *Analyst* 110 (1985) 315.
[95] R. Heinrich, J. Angerer, *Fresenius Z. Anal. Chem.* 315 (1983) 528.
[96] E. Pruszkowska, G.R. Carnrick, W. Slawin, *Clin. Chem.* 29 (1983) 477.
[97] W.E. Weira, J.W. Hansen, *Clin. Chem.* 27 (1981) 73.
[98] B. Rocks, R.A. Sherwood, L.M. Bayford, C. Bailey, *Anal. Clin. Biochem.* 19 (1982) 3381.
[99] G.V. Ivanger, *Biol. Trace Elem. Res.* 12 (1987) 263.
[100] M. Jakubowski, J.K. Piotrowski, B. Trojanowska, *Toxicol. Appl. Pharm.* 16 (1970) 743.
[101] J.K. Piotrowski, W. Bolanowska, *Med. Pracy* 21 (1970) 338.
[102] H. Stone, J. Overnell, *Comp. Biochem. Physiol.* 80C (1985) 9.
[103] S.L. Feldman, R.J. Cousins, *Biochem. J.* 160 (1976) 583.

Separation of metallothionein isoforms of mouse liver cytosol by capillary zone electrophoresis

Takeshi Minami *, Chigusa Yoshita, Masaki Tanaka, Kanenobu Kubo, Nobuo Okabe, Yuko Okazaki

Faculty of Pharmaceutical Sciences, Kinki University, 3-4-1 Kowakae, Higashi-Osaka, Osaka 577, Japan

Received 4 November 1996; received in revised form 5 August 1997; accepted 27 September 1997

Abstract

Metallothionein (MT) isoforms of mouse liver cytosol were separated by capillary zone electrophoresis (CZE) using a polyacrylamide-coated tube at neutral pH, samples prepared from non-treated, heat-treated, and ethanol-precipitated specimens were compared. The liver was homogenized in three kinds of media, 0.25 M sucrose containing 100 mM Tris-HCl buffer at pH 7.4 (BS), BS containing 1% ascorbic acid (BS-C), and BS containing 5 mM β -mercaptoethanol (BS-M). Mouse liver was used 24 h after subcutaneous injection of 50 mg Zn kg⁻¹. In the non-treated specimen of the cytosol fraction, the MT-2 isoform was separated in all three media, while the MT-1 isoform was difficult to identify. In the ethanol-precipitated specimen, MT isoforms were separated well using either BS or BS-C. However, when BS-M was used, a small MT-2 peak was obtained the MT-1 peak could not be identified. MT-1 isoform in the heat-treated specimen was difficult to identify. In contrast, MT-2 isoform was separated well in all three kinds of media. In the non-treated specimen of the control liver cytosol, the MT-2 isoform was detected using all three media, the MT-1 peak was undetected. Based on these results, MT isoforms can be detected in the crude cytosol fraction of liver using CZE combined with a polyacrylamide-coated tube at neutral pH. © 1998 Elsevier Science B.V. All rights reserved.

Keywords: Metallothionein; Isoform; Capillary zone electrophoresis; Polyacrylamide-coated tube

1. Introduction

Metallothionein (MT) is a protein induced by various stimuli such as metals, stress, and some chemicals [1,2]. MT is necessary for absorbing

and storing essential metals, and for maintaining both Zn and Cu levels in tissues. Detoxification of heavy metals and scavenging of free radicals are also reported as important actions of MT. However, the essential role of MTs in a variety of tissues is still unknown. MTs in mammalian tissues have two major isoforms, MT-1 and MT-2. In addition, two new isoforms, MT-3 and MT-4, were recently found in brain and tongue, respectively [3–5]. Among these isoforms, it is interest-

* Corresponding author. Present address: Laboratory of Cell Biology, Department of Anatomy, Nara Medical University, 840 Shijo-Cho, Kashihara, Nara 634, Japan. Tel.: +81 744 223051 (Ext. 2229); fax: +81 744 248432; e-mail: minami@nmu-gw.cc.naramed-u.ac.jp

ing to observe the functions of MT-1 and MT-2, as these isoforms have very similar amino acid sequences and are induced in the same organs by the same stimuli.

Capillary zone electrophoresis (CZE) is an effective method for the separation and quantification of various substances, because of high speed, resolution and sensitivity [6]. However, factors affecting electroosmotic flow and nonspecific adsorption to the inner surface of the tube can interfere with the separation of fractions. MT isoforms have also been separated by CZE [7,8]. As suggested by Richards and Beattie [9], optimal separation of MT isoforms can be obtained using the correct choice of capillaries, buffers, and sample separation techniques. We previously reported that a polyacrylamide-coated tube was effective in separating tissue MT isoforms at neutral pH [10], although there have been several reports that used uncoated tubes for MT isoforms separation [11,12]. Polyacrylamide-coated tube has a neutral surface over the whole pH range, up to pH 10, it is independent of pH in the electrophoresis buffer, sample buffer and in the buffer of the coating medium. Therefore, in the present study, we investigated various media and sample preparation methods in order to improve the separation of tissue MT isoforms on CZE using a polyacrylamide-coated tube at neutral pH, and tried to separate MT isoforms from other proteins in crude samples.

2. Materials and Methods

2.1. Materials

Acrylamide, ammonium persulfate, *N,N,N',N'*-tetramethyl ethylene diamine (TEMED), tris (hydroxymethyl) aminomethane (Tris), ascorbic acid, and β -mercaptoethanol were purchased from Wako, (Osaka, Japan). 3-Methacryloxypropyltrimethoxysilane (3MTMS) was purchased from Shin-Etsu, Tokyo, Japan, and *N*-2-hydroxy ethyl piperazine-*N'*-ethanesulfonic acid (HEPES) was purchased from Dojindo, Kumamoto, Japan. The other reagents were purchased from Wako, Osaka, Japan.

2.2. Experimental animals

Male ddY mice (6-weeks old) were obtained from Japan SLC (Shizuoka, Japan). Before experiments were carried out, they were housed for 1 week during which time they were fed standard mouse food (MF, Oriental Yeast, Tokyo, Japan) and were given free access to tap water.

2.3. Coating of the inner surface with polyacrylamide and zone electrophoresis

The polyacrylamide-coated tube was prepared by the modified method of Hjertén [13]. Details are given in a previous report [10,14]. A fused-silica capillary tube (75 μm i.d., Otsuka Electronics, Osaka, Japan) was cut to a length of 50 cm. The capillary tube was flamed to remove polyimide, and a UV detection window was made on the wall of the tube about 16 cm from one end. The capillary tube was flushed with water, 0.1 M sodium hydroxide, 0.1 M hydrochloric acid, acetone, and 1:1 mixture of acetone and 3MTMS, sequentially. The tube was then filled with 3MTMS, and allowed to stand overnight at room temperature. After washing the tube, the tube was filled with a mixture of acrylamide, ammonium persulfate, and TEMED in sodium phosphate (50 mM, pH 7.0), and the mixture was allowed to polymerize overnight. After washing the tube, both ends of the polyacrylamide-coated capillary tube were cut to give a final column length of 42 cm.

The polyacrylamide-coated tube was installed in an Otsuka CAPI-3000 (Otsuka Electronics) capillary electrophoresis system. The running buffer was 25 mM HEPES–Tris buffer (pH 7.4). Samples were loaded onto the column (by gravity) for 10 s. The inlet of the capillary was at the cathode. The analysis was performed at 25 kV and $25 \pm 1^\circ\text{C}$, and peaks of MT isoforms were monitored at 200 nm as suggested by Richards and Beattie [8].

2.4. Drug administration

Mice were subcutaneously injected doses of 50 mg Zn kg^{-1} in the form of zinc sulfate. In the

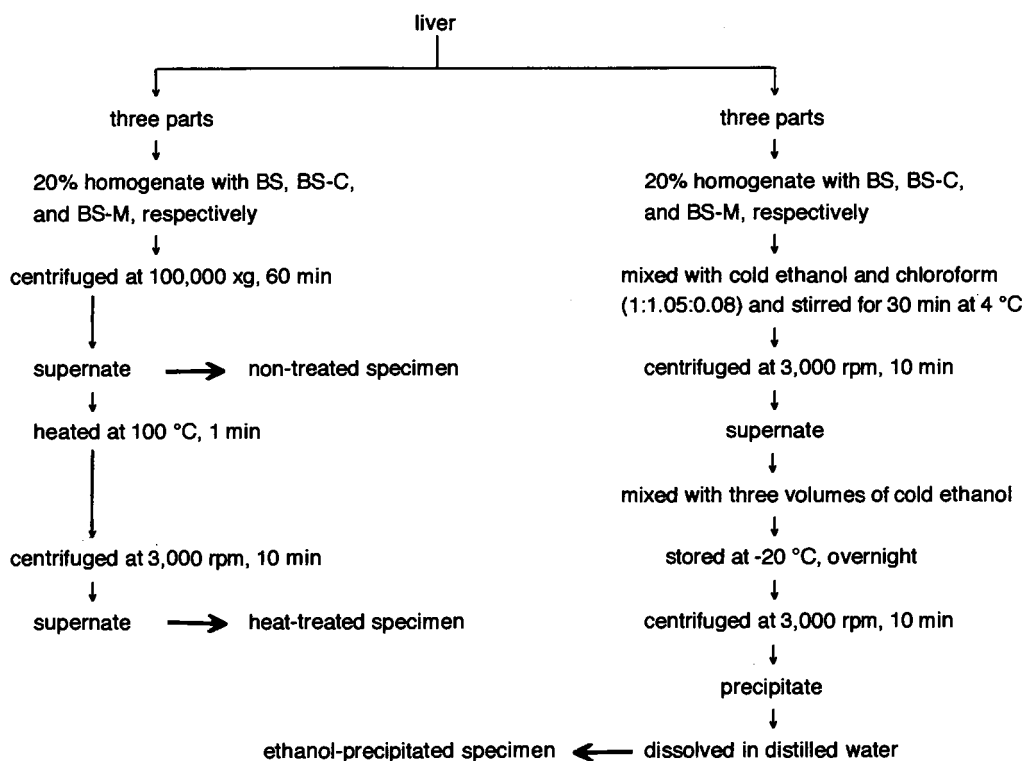


Fig. 1. Scheme of preparation of specimens for MT analysis

control, mice were subcutaneously injected with 10 ml saline kg^{-1} instead of zinc. Zinc-injected mice and saline-injected control mice were decapitated after 24 h, and the livers were removed.

2.5. Preparation of MT samples from mice liver

The liver was divided into six parts, and each part was homogenized to make a 20% homogenate with three kinds of media: 100 mM Tris-HCl, pH 7.4, 0.25 M sucrose (buffered sucrose solution: BS), BS containing 1% ascorbic acid (BS-C), and BS containing 5mM β -mercaptoethanol (BS-M), respectively, with an ultra-speed blender (Phycotron, NITI-ON, Kanagawa, Japan). Non-treated, heat-treated, and ethanol-precipitated specimens were obtained as shown in Fig. 1.

Each specimen was passed through a filter (0.45 μm , Chromatodisk 4A, Kurabo, Osaka, Japan) before CZE analysis. Peaks corresponding to MT-

1 and MT-2 isoforms of the specimens were identified by co-electrophoresis with purified MT-1 and MT-2, which were obtained from the liver of a Cd-administered mouse [10]. Each purified MT-1 and MT-2 appeared as a single peak on the CZE chromatograms, as described in our previous report [10].

3. Results

In the case of CZE analysis, it is difficult to measure the metal contents of the sample for the identification of MT isoforms, because the sample loading volume for analysis is small, and because fractionation after separation is difficult. Therefore, both MT-1 and MT-2 isoforms of the samples were identified by their migration times which coincided with those of standard MT-1 and MT-2 isoforms, and further identified by the addition of standard isoforms to the samples.

MT-1 and MT-2 isoforms were found in the non-treated specimen prepared from the liver of a zinc-injected mouse with BS (Fig. 2a). MT-2 was clearly distinguished from the other peaks, but MT-1 was difficult to identify. The ratio of the peak areas (MT-1/MT-2) was 0.95 ± 0.32 (mean \pm SD, $n = 3$). When BS-C or BS-M was used, the MT-1 and MT-2 peaks were detected as well as they were with BS (Fig. 2b and 2c), and the ratios of MT-1/MT-2 were 1.11 ± 0.55 (BS-C) and 0.24 ± 0.14 (BS-M), respectively.

In the ethanol-precipitated specimen, the MT-1 and MT-2 isoforms were separated with BS (Fig. 3a), and the ratio of MT-1/MT-2 was 1.75 ± 0.95 . MT-1 and MT-2 isoforms prepared with BS-C were also separated clearly (Fig. 3b), and the ratio of MT-1/MT-2 was 3.65 ± 1.38 . However, in the sample prepared with BS-M, a small MT-2 peak was obtained, and MT-1 peak was not identified (Fig. 3c).

In the heat-treated specimen, a small and broad MT-1 peak was detected in the sample prepared with all three media, while MT-2 peak was identified clearly in all three media (Fig. 4).

In the non-treated specimen from the control mice, the MT-2 isoform was detected clearly with all three media. However, no peak corresponding to the MT-1 isoform was found with any of the three media (Fig. 5).

4. Discussion

The MT-1 isoform is related to metal uptake or detoxification of heavy metals, while the MT-2 isoform is related to cell growth or various stresses [15]. However, the different role of these two MT isoforms is still unclear. Several methods have been reported for the separation of the MT

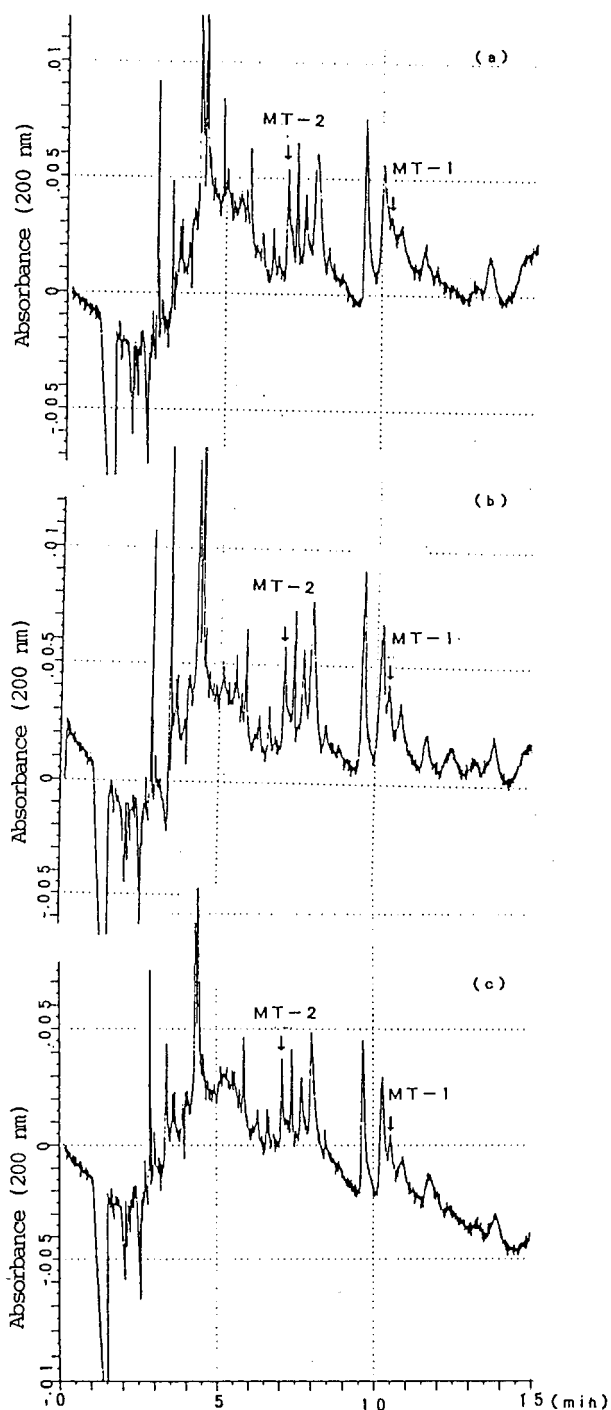


Fig. 2. (Continued)

Fig. 2. Electropherograms of MT isoforms in non-treated specimens of liver from a zinc-injected mouse. The liver was homogenized with three kinds of media: (a) BS; (b) BS-C; (c) BS-M. The non-treated specimen was loaded onto the column by gravity for 10 s at the cathode side, and the analysis was performed at 25 kV and $25 \pm 1^\circ\text{C}$ using 25 mM HEPES–Tris buffer at pH 7.4 as running buffer. Detection of MT isoforms was monitored at 200 nm.

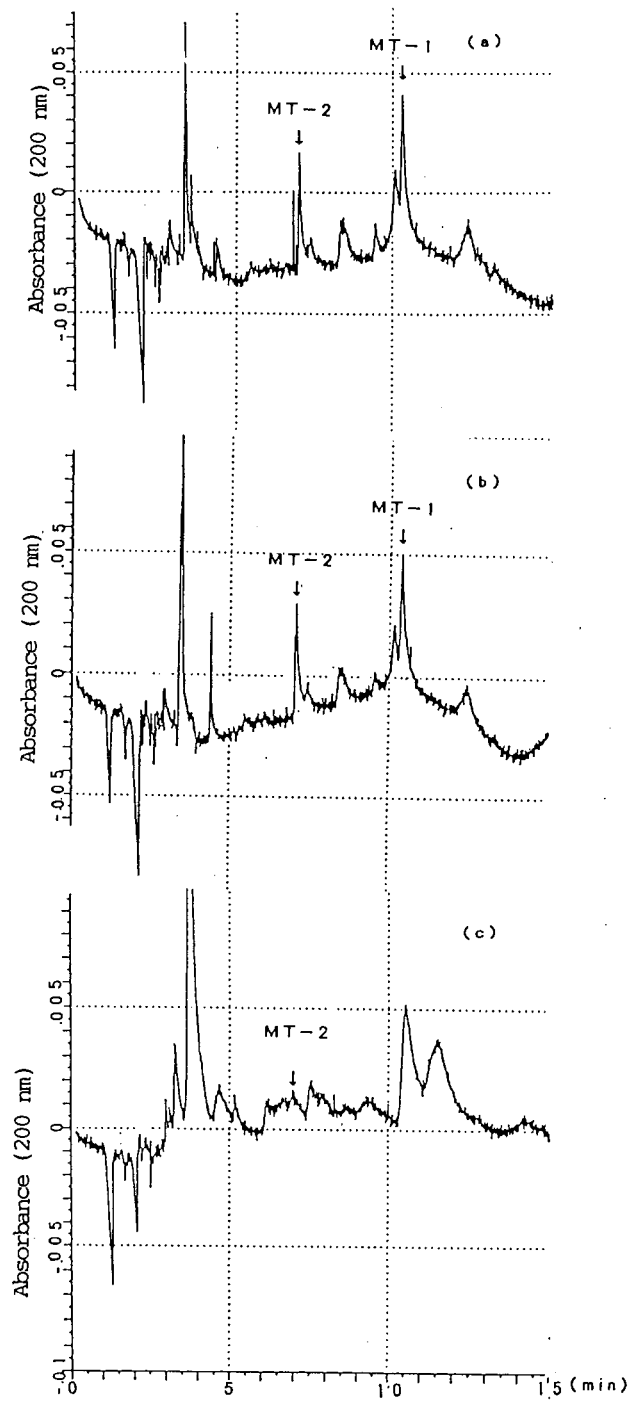


Fig. 3. Electropherograms of MT isoforms in ethanol-precipitated specimens of liver from a zinc-injected mouse: (a) BS; (b) BS-C; (c) BS-M. Ethanol-precipitated specimen was loaded onto the column by gravity for 10 s.

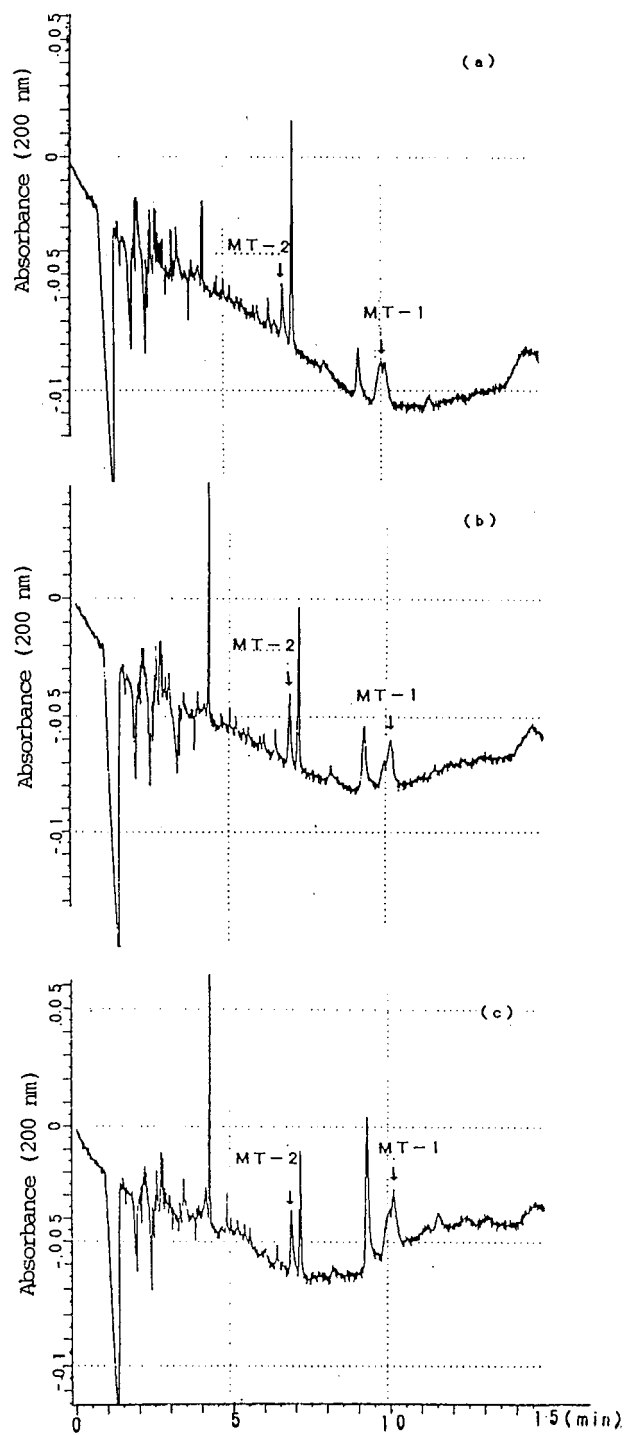


Fig. 4. Electropherograms of MT isoforms in heat-treated specimens of liver from a zinc-injected mouse: (a) BS; (b) BS-C; (c) BS-M. Heat-treated specimen was loaded onto the column by gravity for 10 s.

isoforms, such as anion-exchange chromatography, high performance liquid chromatography (HPLC) and enzyme-linked immunosorbent assay (ELISA) [3]. Recently, CZE analysis was used. We have shown that a polyacrylamide-coated tube is effective for separating tissue MT isoforms at neutral pH with CZE [10]. As MT is stable at heat treatment, heat treatment is usually used for measuring MT contents in the tissue, Cd–heme method [3,16]. In contrast, the ethanol-precipitated method is a well known method for purification of MT [17]. MT isoforms of specimens obtained from non-treated, heat-treated, and ethanol-precipitated methods were separated by CZE at neutral pH, and compared. The present results show that MT isoforms can be identified in the both non-treated and ethanol-precipitated specimens from the livers of zinc-injected mice. In the heat-treated specimen, both MT isoforms were separated, even though a small and broad MT-1 peak was obtained. In the control mice, the MT-1 isoform was not detected in the non-treated liver specimen as shown in Fig. 5. The MT-1 isoform was detected in ethanol-precipitated specimens of livers from control mice, as described in previous reports [10,14]. It was difficult to identify the MT-1 isoform in the control liver from the non-treated specimen.

It is known that each MT isoform has several sub-isoforms [15,18,19]. Indeed, each MT isoform of a commercial standard was shown to have several peaks [10]. Virtanen et al. [12] reported that some sub-isoforms were found in the commercial standard, and that CZE could separate sub-isoforms. However, we could not detect sub-isoforms for each MT isoform in the present study, because using CZE, each purified MT isoform was observed a single peak as shown in our previous report [10]. In addition, as we could not determine the metal contents in those peaks, it was difficult to identify the presence of MT sub-isoforms. Standards used in the present study were Cd-MTs instead of Zn-MTs. In the previous report [14] as the peak of MT-1 decreased significantly following the addition of Cd, it is thought that a change in the MT electric charge occurred. Suzuki and Yamamura [20] also reported that the dimer forms of MT isolated from rabbit liver

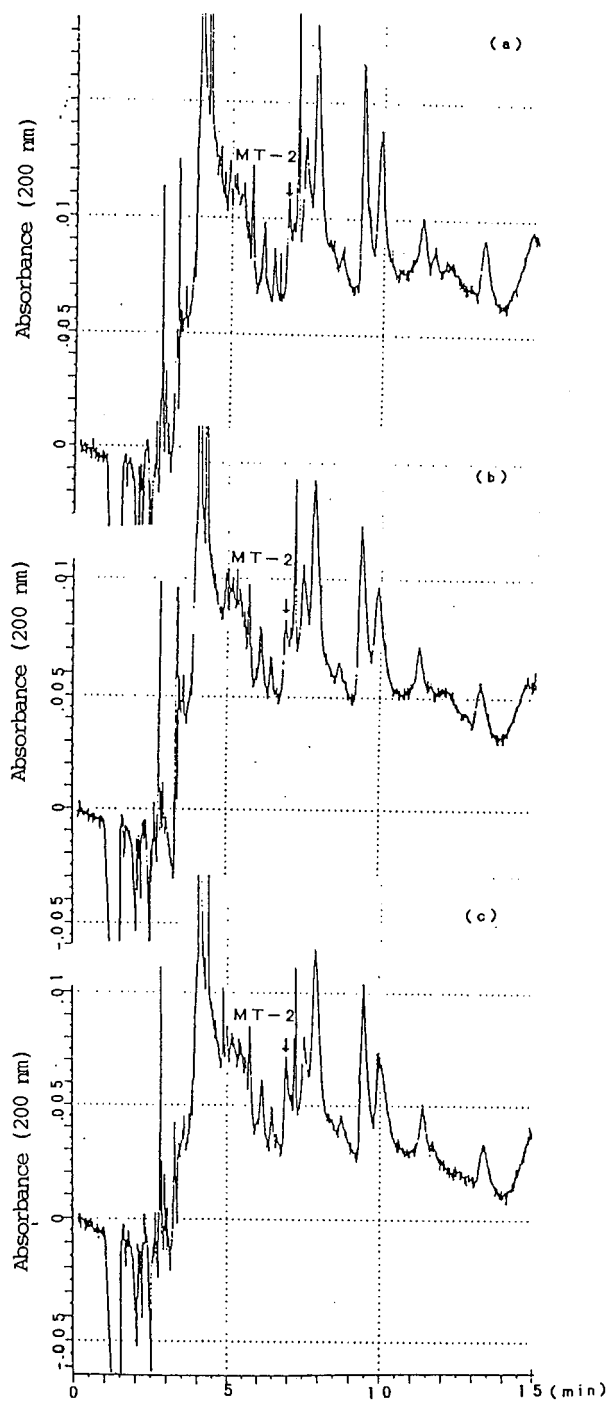


Fig. 5. Electropherograms of MT isoforms in non-treated specimen of control mouse liver: (a) BS; (b) BS-C; (c) BS-M.

accumulated a large quantity of Cd. MT may form dimers and/or polymers easily in the presence of excess Cd, and there is doubt as to whether Cd-MTs are adequate standards, as MT isoforms are identified using both the migration times and co-electrophoresis with purified Cd-MT isoforms. The peak areas identified as MT isoforms increased after zinc injection, the peak ratio of MT-1/MT-2 was similar to that reported previously [15], purified Cd-MT isoforms may be used as standards. In addition, the baseline was not stable during analysis, although we calculated the peak ratio of MT-1/MT-2 from their migration times. It is necessary to obtain a stable baseline for quantification of MT isoforms.

It is known that the MT-1 isoforms in less stable to air-oxidation than the MT-2 isoform and Zn-MT is unstable in comparison with Cd-MT [21]. Therefore, denaturalization by air-oxidation must be considered at each step of MT isoforms preparation. In the present study, as both MT isoforms are well separated with BS-C in comparison with BS and BS-M, BS-C may be useful for preparation of MT.

In conclusion, CZE analysis with a polyacrylamide-coated tube at neutral pH is effective for separating tissue MT isoforms in mouse liver cytosol.

References

- [1] I. Bremner, J.H. Beattie, *Annu. Rev. Nutr.* 10 (1990) 63.
- [2] J.S. Lazo, B.R. Pitt, *Annu. Rev. Pharmacol. Toxicol.* 35 (1995) 635.
- [3] M. Sato, K.T. Suzuki, *Biomed. Res. Trace Elem.* 6 (1995) 13.
- [4] Y. Uchida, *Biol. Signals* 3 (1994) 211.
- [5] C.J. Quaife, S.D. Findley, J.C. Erickson, G.J. Froelick, E.J. Kelly, B.P. Zambrowicz, R.D. Palmiter, *Biochemistry* 33 (1994) 7250.
- [6] Y. Xu, *Anal. Chem.* 67 (1995) 463R.
- [7] J.H. Beattie, M.P. Richards, R. Self, *J. Chromatogr.* 632 (1993) 127.
- [8] M.P. Richards, J.H. Beattie, *J. Chromatogr.* 648 (1993) 459.
- [9] M.P. Richards, J.H. Beattie, *J. Chromatogr. B* 669 (1995) 27.
- [10] T. Minami, H. Matsubara, M. O-higashi, N. Otaki, M. Kimura, K. Kubo, N. Okabe, Y. Okazaki, *J. Chromatogr. B* 685 (1996) 353.
- [11] G.-q. Liu, W. Wang, X.-q. Shan, *J. Chromatogr. B* 653 (1994) 41.
- [12] V. Virtanen, G. Bordin, A.-R. Rodriguez, *J. Chromatogr. A* 734 (1996) 391.
- [13] S. Hjertén, *J. Chromatogr.* 347 (1985) 191.
- [14] T. Minami, H. Matsubara, M. O-higashi, K. Kubo, N. Okabe, Y. Okazaki, *Electrophoresis* 17 (1996) 1602.
- [15] S. Kobayashi, J. Sayato-Suzuki, *Biochem. J.* 251 (1988) 649.
- [16] W.P. Waalkes, in: J.A. Thomas (Ed.), *Endocrine Method*, Academic Press, New York, 1996, p. 371.
- [17] M. Kimura, N. Otaki, M. Imano, in: J.H.R. Kägi, M. Nordberg (Eds.), *Experientia Supplementum* 34, Birkhäuser Verlag, Basel, 1979, p. 163.
- [18] S. Koizumi, N. Otaki, J. Saegusa, F. Otsuka, *Toxicol. Lett.* 66 (1993) 165.
- [19] S. Saito, P.E. Hunziker, *Biochem. Biophys. Acta* 1289 (1996) 65.
- [20] K.T. Suzuki, M. Yamamura, *Biochem. Pharmacol.* 29 (1980) 689.
- [21] K.T. Suzuki, T. Maitani, *Chem. Pharm. Bull.* 31 (1983) 4469.

Zinc sulphate induced metallothionein in pancreatic islets and protected against the diabetogenic toxin streptozotocin

Patricia Ohly^a, Zhiyong Wang^a, Josef Abel^b, Helga Gleichmann^{a,*}

^a *Clinical Experimental Department, Diabetes Research Institute, Medical Institute of Environmental Hygiene, Heinrich-Heine-University Düsseldorf, D-40225 Düsseldorf, Germany*

^b *Division of Toxicology, Medical Institute of Environmental Hygiene, Heinrich-Heine-University Düsseldorf, D-40225 Düsseldorf, Germany*

Received 11 November 1996; received in revised form 19 August 1997; accepted 24 October 1997

Abstract

In mice, autoimmune diabetes can be induced with multiple low doses of streptozotocin (MLD-STZ). Specific T cell-dependent immune reactions and non-specific inflammatory damage induced by reactive oxygen species (ROS) are involved in the pathogenesis of MLD-STZ diabetes. Metallothionein (MT) can be significantly ($P < 0.05$) induced with $ZnSO_4$ in pancreatic islets in vivo and in vitro. In vitro, preincubation of isolated islets with $ZnSO_4$ prevented STZ-induced loss of β -cell-function and in vivo, intraperitoneal pretreatment with $ZnSO_4$ prevented MLD-STZ-induced diabetes. It is proposed that $ZnSO_4$ -induced MT rescued β -cells by scavenging STZ-generated hydroxyl-radicals ($\cdot OH$). © 1998 Elsevier Science B.V. All rights reserved.

Keywords: Metallothionein; Pancreatic islets; Streptozotocin; Diabetes

1. Introduction

Streptozotocin (STZ) is a naturally occurring antibiotic and potent toxin for insulin-producing β -cells in mice, rat, and humans [1]. To induce diabetes in mice by STZ, two experimental protocols that involve different pathogenic pathways are being used. A single injection of a high dose (HD-STZ) exerts direct toxicity on the insulin-producing β -cells, which results in necrosis within 48–72 h and overt hyperglycemia. A form of

autoimmune diabetes can be induced with multiple low doses (MLD-STZ), i.e. intraperitoneal injections of 40 mg STZ kg^{-1} body weight on five consecutive days. STZ is a bipartite molecule that is composed of a glucose moiety and a methylnitrosourea (MNU) moiety. With MLD-STZ, two different effects are being exerted, namely direct β -cell toxicity followed by T cell-dependent inflammatory immune reactions [2,3]. The glucose moiety of STZ specifically directs the agent to the β -cells while toxicity is inflicted on the cells by the MNU moiety [1,4]. It has been suggested that in the HD-STZ diabetes model β -cell damage may be mediated by STZ-generated hydroxyl radicals

* Corresponding author. Tel.: +49 211 33821; fax: +49 211 3382603; e-mail: gleich@dfi.uni-duesseldorf.de

(\cdot OH) [5,6], which are the most toxic of the group of reactive oxygen species (ROS). In the MLD-STZ-induced autoimmune diabetes model ROS are also suspected to be involved in the pathogenesis, namely as non-specific mediators of inflammatory reactions. We studied the possibility that induction of metallothionein (MT) in pancreatic islets may protect against STZ-induced toxicity and loss of β -cell function.

MT are cytosolic proteins, they are present in a wide variety of eukaryotic species, and it is assumed that they have essential biological roles. Although the precise function of MT is still not known, the ability to both bind and be induced by heavy metal ions strongly suggest a central role in metal metabolism and detoxification [7,8]. Other possible functions for MT might be control of intracellular redox potential and scavenging of \cdot OH [9–11]. In order to resolve the function of MT numerous attempts have been made in vitro and in vivo using various experimental protocols. In vitro, e.g. resistance of MT-I-transfected chinese hamster cell line to spontaneous mutagenesis was observed [12] and MT was found to be superior to glutathione (GSH) in inhibiting \cdot OH-generated DNA degradation [10]. Thus, a concentration of 13 μ M MT was equivalent to 10 mM GSH in preventing DNA degradation and for an equivalent protective potential a 38.5 higher thiol content was required for GSH than for MT. In vivo, e.g. significant reduction of nickel-induced mortality by MT induction in mice was reported [13] and significant reduction of STZ-hyperglycemia in rats [14].

Recently, this laboratory was first to report that MT is constitutively expressed in pancreatic islets of mice and that it can be induced significantly by zincsulphate (ZnSO_4) in vivo [15] and in vitro [16]. Here, we present data demonstrating that pre-treatment with ZnSO_4 protected islets from STZ-induced loss of β -cell function in vitro and in vivo.

2. Experimental design and results

C57BL/6 male mice, 5–6 weeks old, were purchased from Bomholtgard (Bomholtvej, Den-

mark). They were kept under specific pathogen-free conditions and received tap water and rodent chow ('Ssniff M', Ssniff, Soest, Germany) ad libitum. They were 7–8 weeks old when used for experimental investigations.

For in vitro studies, islets were isolated by collagenase digestion as described previously [15]. Duplicates of 10 islets each were used for a given experimental protocol. To analyze the effect of ZnSO_4 -induced MT on STZ toxicity four different groups of cultures were set up, two of these were used as experimental and two as control cultures. One culture group containing each of the experimental and control ones was preincubated with 0.05 mM ZnSO_4 (Merck, Darmstadt, Germany) as final concentration for 24 h. Following a washing procedure the experimental cultures were incubated for 30 min with a toxic dose of STZ (Boehringer Mannheim, Mannheim, Germany), i.e. 3 mM STZ as final concentration and the control cultures with the solvent of STZ. After a washing procedure a β -cell function test was performed as described [17]. Then the islets were cultured for another 3 days before repeating the β -cell function test. In this assay basal and glucose-stimulated insulin release are determined and the results are calculated as index of glucose-stimulated insulin release which is the ratio of glucose-stimulated insulin release over that of basal insulin release. Islets were stimulated with 16.7 mM glucose as final concentration. Insulin release was determined as immune reactive insulin levels by RIA kits (Pharmacia Biotech, Freiburg, Germany) according to the manufacturer's instruction. For each analysis the mean values of duplicate cultures were used. To analyze the effect of ZnSO_4 -induced MT in pancreatic islets on MLD-STZ-induced diabetes, groups of ten mice each were injected intra-peritoneally with either MLD-STZ, i.e. 40 mg STZ kg^{-1} body weight on 5 consecutive days or in addition with 10 mg ZnSO_4/kg body weight 24 h before each of the five STZ injections. Blood glucose was determined by the hexokinase method as described previously [3]. Blood glucose concentrations were measured before and at weekly intervals after starting treatment. Mice which had a blood glucose level of ≥ 250 mg dl^{-1} (= 13.88 mM) on 3 consecutive weeks were diagnosed as diabetic.

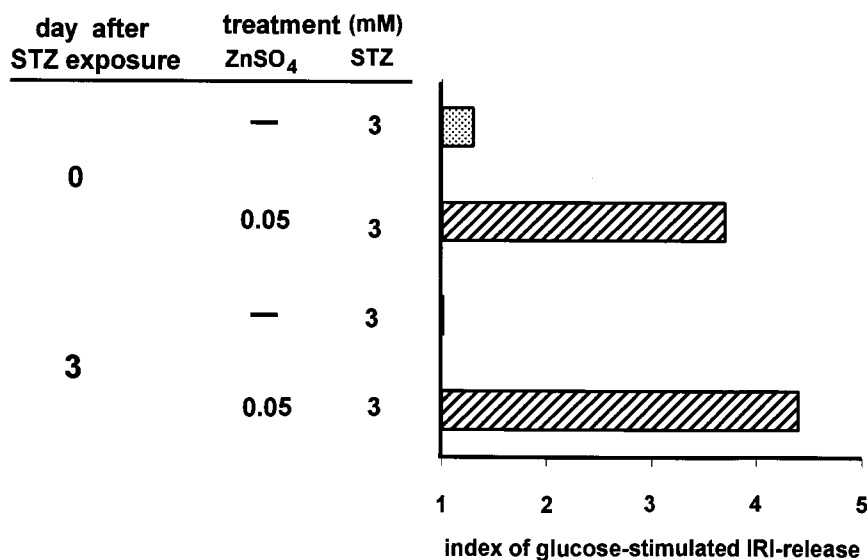


Fig. 1. Index of glucose-stimulated insulin release of pancreatic islets of C57BL/6 mice in vitro. The islets were incubated with either STZ only or preincubated in addition with ZnSO₄. The indices represent the ratio of glucose-stimulated insulin release over that of basal insulin release. The indices were calculated by using the mean values of duplicate cultures.

As shown in Fig. 1, incubation of islets with STZ abolished glucose-stimulated insulin release, whereas pretreatment with 0.05 mM ZnSO₄ rescued the physiological β -cell function as indicated by an index of approximately 4 which is similar to those obtained in control cultures (not shown). This protective effect of MT induction was also observed after pretreatment with 0.1 mM ZnSO₄. Since preincubation of control cultures with ZnSO₄ failed to exert essential effects on glucose-stimulated insulin release the results are not shown.

This laboratory recently reported that MT is constitutively expressed in isolated pancreatic islets of mice and that MT can be induced by intraperitoneal injection with either ZnSO₄ or STZ [15]. MT concentrations were assessed by using both the Cd-hemoglobin saturation assay [18] and the more sensitive Cd-Chelex assay [19]. A significant ($P < 0.001$) and dose-dependent MT induction was obtained by treatment with both ZnSO₄ and STZ. MLD-STZ treatment proved to be the most potent MT inducer with an index of 8.6. In a first series of experiments we analyzed the effect of MT induction in pancreatic islets on MLD-STZ-induced diabetes. As shown in Fig.

2A, pretreatment with ZnSO₄ significantly ($P < 0.05$) prevented MLD-STZ-induced hyperglycemia and resulted in a significantly ($P < 0.05$) higher prevalence of euglycemic recipients, namely 75% compared with only 20% euglycemic mice in the group treated with MLD-STZ only (Fig. 2B).

3. Discussion

Besides being involved in metal metabolism [7,8], MT have been proposed to play a protective role against ROS-mediated cellular damage at sites of inflammation [7,8] and have been found to efficiently scavenge $\cdot\text{OH}$ in vitro [9–11]. Based on the protective role of MT in many in vitro observations, it is necessary, however, to evaluate if there is also an essential role for MT as cellular antioxidant in vivo under physiological conditions and in disease.

Our aim was to analyze if the induction of MT in pancreatic islets of mice by treatment with ZnSO₄ may protect against the β -cell toxin STZ. The present data demonstrate that preincubation of isolated pancreatic islets with ZnSO₄ prevented STZ-induced loss of glucose-stimulated insulin re-

lease in vitro. In vivo pretreatment with ZnSO_4 conferred significant protection toward MLD-STZ-induced diabetes. It is assumed that the protective effects observed are due to MT induced by ZnSO_4 in the β -cells. Similar effects of ZnSO_4 -induced MT on STZ-induced diabetes were reported by Yang and Cherian [14]. Just as we did it with mice, they injected rats also with $10 \text{ mg ZnSO}_4 \text{ kg}^{-1}$ body weight prior to STZ and obtained significant reduction of STZ-induced hyperglycemia. Their rat model, however, differs

from our mouse model because the rats were injected with a single high dose of STZ mediating acute toxicity and subsequent β -cell necrosis which results in immediate hyperglycemia, whereas in the MLD-STZ system diabetes develops more slowly. The underlying mechanism, however, of the protective effects of ZnSO_4 -induced MT might be comparable.

Based on our data it is hypothesized (Fig. 3) that STZ-induced generation of $\cdot\text{OH}$ results in preferential damage of the glucose transporter 2 which is pivotal for β -cells to respond to extracellular glucose concentrations to initiate the signal transduction for adequate insulin secretion. Induction of MT is assumed to scavenge $\cdot\text{OH}$ and thus rescue the β -cells from oxidative damage. The rationale for this working hypothesis is that: (1) STZ-induced H_2O_2 -mediated DNA fragmentation has been reported in pancreatic islets [6], therefore, $\cdot\text{OH}$ can be generated in the presence of adventitious iron (Fe^{++}) due to a Fenton-type reaction [7]; (2) we found MLD-STZ to preferentially and significantly reduce glucose transporter 2 protein and mRNA expression in pancreatic islets ex vivo, whereas MLD-STZ failed to affect mRNA expression of glucokinase, a pivotal enzyme required for glucose metabolism, mRNA expression of proinsulin, a β -cell specific molecule, and mRNA expression of β -actin, a house-keeping gene [20]; and (3) that $\cdot\text{OH}$ have been directly detected in pancreatic islets of untreated donors rats by electron spin resonance spectroscopy [21]. Further aims are to apply this technology to evaluate the role of $\cdot\text{OH}$ generation and MT induction under the pathological conditions in the MLD-STZ diabetes model in mice. These investigations as well as the use of MT-transgenic [22] and MT-knockout mice are expected to contribute to resolve the possible function of MT in induced diabetes.

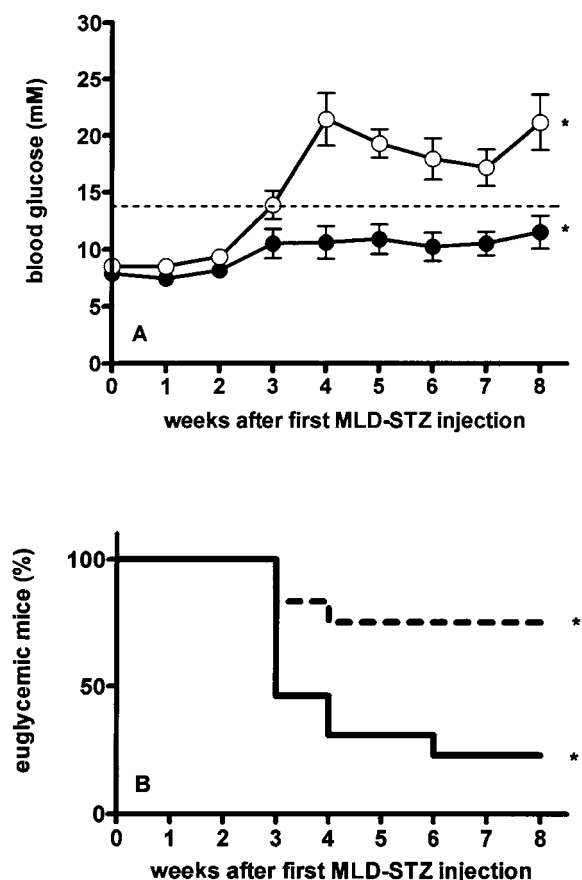


Fig. 2. Effect of treatment with ZnSO_4 on MLD-STZ diabetes in C57Bl/6 male mice. A: Blood glucose values (mean \pm SE) in recipients treated with MLD-STZ (○) and pretreated with ZnSO_4 (●). B: The percentage of euglycemic mice is given in animals treated with MLD-STZ only (—) or in addition with $10 \text{ mg ZnSO}_4 \text{ kg}^{-1}$ body weight 24 h prior to each STZ injection (- - -). * Indicates significant differences with $P < 0.05$.

Acknowledgements

This study was supported by the Deutsche Forschungsgemeinschaft SFB 503 'Molecular and cellular mediators of exogenous noxae', project B5 and by the Bundesministerium für Gesundheit, Bonn, Germany.

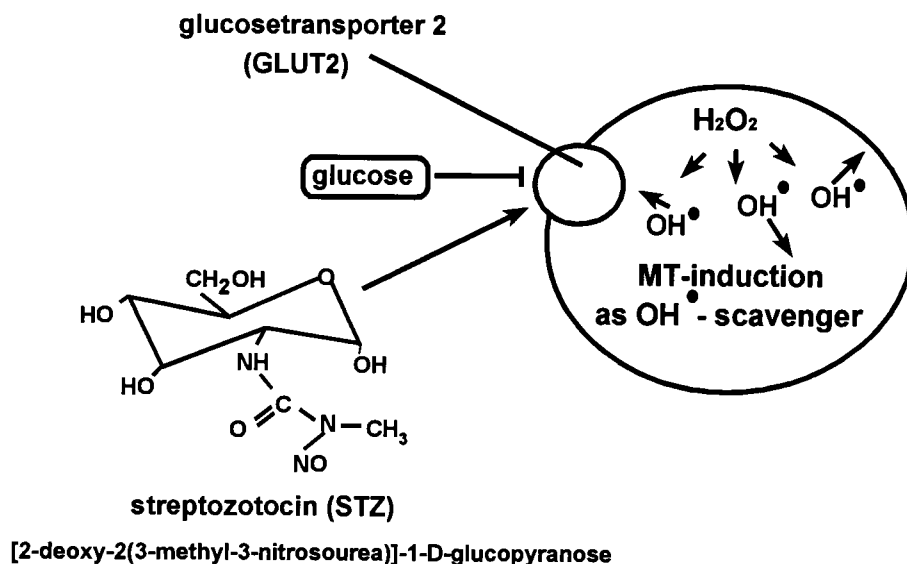


Fig. 3. Hypothesis of STZ-mediated damage on β -cells and the role of MT as cytosolic scavenger of STZ-generated OH^\bullet . The glucose transporter 2 is a crucial target molecule for STZ and its severe reduction or loss abolishes the insulin response to glucose. Induction of MT prior to this diabetogenic insult might prevent OH^\bullet -mediated toxicity on the glucose transporter 2 and rescue β -cell function.

References

- [1] G.L. Wilson, E.H. Leiter, in: T. Dyrberg (Ed.), *Current Topics in Microbiology and Immunology*, Springer Verlag, Berlin, 1990, p. 27.
- [2] C. Klinkhammer, P. Popowa, H. Gleichmann, *Diabetes* 37 (1988) 74.
- [3] Z. Wang, C. Dohle, J. Friemann, B.S. Green, H. Gleichmann, *Diabetes* 42 (1993) 420.
- [4] W.J. Schnedl, S. Ferber, J. Johnson, C.B. Newgard, *Diabetes* 43 (1994) 1326.
- [5] H. Yamamoto, Y. Uchigata, H. Okamoto, *Nature (Lond.)* 294 (1981) 284.
- [6] N. Takasu, I. Komiya, T. Asawa, Y. Nagasawa, T. Yamada, *Diabetes* 40 (1991) 1141.
- [7] M. Sato, I. Bremner, *Free Radic. Biol. Med.* 14 (1993) 325.
- [8] M.A. Dunn, T.L. Blalock, R.J. Cousins, *Proc. Exp. Biol. Med.* 185 (1987) 107.
- [9] P.J. Thornalley, M. Vasak, *Biochim. Biophys. Acta* 827 (1985) 36.
- [10] J. Abel, N. de Ruiter, *Toxicol. Lett.* 64 (1989) 177.
- [11] L.S. Chubatsu, R. Meneghini, *Biochem. J.* 291 (1993) 193.
- [12] E.I. Goncharova, T.B. Rossman, *Cancer Res.* 54 (1994) 5318.
- [13] R.C. Scrivastava, S.K. Hasan, J. Gupta, S. Gupta, *Biochem. Mol. Biol. Int.* 30 (1993) 261.
- [14] J. Yang, M.G. Cherian, *Life Sci.* 55 (1994) 43.
- [15] S. Zimny, F. Gogolin, J. Abel, H. Gleichmann, *Arch. Toxicol.* 67 (1993) 61.
- [16] P. Ohly, H. Gleichmann, *Exp. Clin. Endocrinol.* 103 (1995) 79.
- [17] D.L. Eizirik, E. Strandell, S. Sandler, *Diabetologia* 34 (1991) 6.
- [18] S. Onosaka, M.G. Cherian, *Toxicology* 23 (1982) 11.
- [19] R. Bartsch, D. Klein, K.H. Summer, *Arch. Toxicol.* 64 (1990) 177.
- [20] Z. Wang, H. Gleichmann, *Diabetes* 46 (suppl. 1) (1997) 39A.
- [21] G.M. Pieper, C.C. Felix, B. Kalyanaraman, M. Turk, A.M. Roza, *Free Radic. Biol. Med.* 19 (1995) 219.
- [22] M.B. Iszard, J. Liu, Y. Liu, T. Dalton, G.A. Andrews, R.D. Palmiter, C.D. Klaassen, *Toxicol. Appl. Pharmacol.* 133 (1995) 305.

Development of a quick leaching test for monolithic materials by using factorial design

M. Wahlström^{a,*}, A.-M. Fällman^b, O. Hjelmar^c, K. H. Karstensen^d,
E.L. Sveinsdottir^e, X.-M. Song^a

^a VTT Chemical Technology, P.O. Box 1403, FIN 02044 VTT, Finland

^b Swedish Geotechnical Institute, S-581 93 Linköping, Sweden

^c Water Quality Institute, 11 Agern Allé, DK-2970 Hørsholm, Denmark

^d SINTEF SI, P.O. Box 124 Blindern, N-0314 Oslo, Norway

^e The Icelandic Building Research Institute, Rb-Keldnaholti, IS-112 Reykjavik, Iceland

Received 25 May 1997; accepted 14 October 1997

Abstract

A quick leaching test procedure for monolithic waste materials has been developed by a Nordic expert group using experimental factorial design. The Dutch quick leaching test proposal in which the wetting time of the test specimen is reduced by applying vacuum was chosen as a starting point. The influence of the following parameters were studied: vacuum, stirring, open or closed vessel, water renewal frequency, leachant quality and laboratory or batch differences. The study was performed with test specimens prepared from a cement stabilised soil containing As, Cr and Cu. The test specimens were immersed in water and the water was renewed at certain time intervals. The study clearly showed that the use of vacuum had a strong effect on the release rate and that the open vessel lowered the pH-values of the eluates due to uptake of carbon dioxide in the water. The results also indicate higher emissions when stirring was applied. The following test conditions are recommended: application of vacuum prior to testing, use of closed test vessel, use of stirring, a test time of 3 days with four water renewals after 15 min vacuum steps, and then after e.g. 2 h, 23 h and 3.2 days, use of demineralised water as leachant. The amount of water must be selected according to the size of the test specimen. A liquid to surface (L/A) ratio of 5–10 ml cm⁻² is recommended. All four eluates collected are filtered and analysed. © 1998 Elsevier Science B.V. All rights reserved.

Keywords: Monolithic material; Solidified; Leaching test

1. Introduction

A Nordic expert group was formed in 1994 with the task of developing a Nordic quick leaching test for monolithic materials. In the expert

group the following institutes were represented: VTT (Finland), Swedish Geotechnical Institute (Sweden), Water Quality Institute (Denmark), SINTEF SI (Norway) and Icelandic Building Research Institute (Iceland). The experimental work was set up in the expert group. Each participating laboratory performed a given test series on a

* Corresponding author.

cement stabilised test material. The work was organised by VTT.

The primary mechanism of contaminant release from monolithic materials is through diffusion or dissolution from the surface [1]. Monolithic materials cannot be studied using same test methods as granular materials. The containment of the contaminants is neglected, if the monolithic material is crushed for testing. The leaching behaviour of monolithic or stabilised materials is usually studied by a tank leaching test [1,2]. The amount of contaminants available for leaching can be estimated from crushed material by the Dutch availability test [1] or by the Canadian sequential chemical extraction test [2].

The Dutch tank leaching test for monolithic materials [3] was recommended by the Nordic expert group for studies on the leaching behaviour of monolithic material [4]. In the Dutch tank leaching test a specimen is immersed in water and the water is renewed at certain time intervals. The leaching mechanism, the diffusion coefficient and the release per surface area of the specimen are estimated in the test. The test time in the tank leaching test is long (64 days).

A quick test for monolithic materials is needed especially for screening, quality control and for regulatory purposes. A quick test means shorter testing time and lower testing costs. The requirements for a quick test on monolithic materials were the following:

- easy to perform
- a test time of less than 1 week
- reasonable testing costs (not more than three to four eluates to analyse)
- indication of the leaching mechanism of constituents
- indication of the diffusion coefficients of constituents
- a measure of the release per surface area.

The starting point in the development of a quick test was the Dutch quick test proposal [5]. The initial leaching of stabilised materials occurs from the surface. Leaching governed by diffusion from the inner parts of the specimen can take place first when the outer layers of the specimen are wetted. In a Dutch test proposal the wetting time is minimised by applying vacuum.

2. Experiments

2.1. Test material

Soil samples contaminated with As, Cr and Cu were taken from an old site of a wood preserving plant. The samples contained sand, till and humus. The average concentrations of the contaminants in the soil samples were: As 50 000 mg kg⁻¹ dry matter, Cr 9000 mg kg⁻¹ dry matter, and Cu 14 000 mg kg⁻¹ dry matter. The soil samples were homogenised and the test specimens (cylinder with diameter 10 cm and height 10 cm) were prepared by mixing the soil in batches with cement and water (no additives were used in order to have measurable concentrations in the eluates). The ratio of cement to soil was 1:4.5. The compression strength of the test specimen was 5–6 MPa.

2.2. Test methods and experimental plan

2.2.1. Standardised test methods

The availability of As, Cr, Cu, Ca and Na for leaching was studied using the Dutch availability test [6]. Crushed and milled samples from two batches were studied as duplicates. Finely ground material, 95% < 125 μm, is mixed with water at a liquid to solid ratio 100. The test is carried out in two consecutive leaching steps. In the first step, pH 7 is held constant for 3 h by the addition of nitric acid. The mixture is filtered through a 0.45 μm filter and the eluate is stored. In the second step the filter containing the waste material is mixed with fresh water and the pH of the mixture is kept at pH 4 for 3 h by the addition of nitric acid. The eluate is separated from the mixture by filtration. The eluates from both leaching steps are combined. The metals were analysed using AAS/flame.

The leaching of Na, Ca, As, Cr and Cu from the test specimens was studied using a Dutch full long (64 days) tank leaching test [3]. In the tank leaching test a test specimen with a known surface area is immersed in a weakly acidified water at pH 4 in a closed vessel by a nylon string. At certain time intervals, 0.25, 1, 2.25, 4, 9, 16, 36 and 64 days after start of the test, the water is replaced

by fresh water and analysed for pH and constituents of interest after filtration through 0.45 µm filter. The metals were analysed using AAS/flame or AAS/graphite furnace (low concentrations).

2.3. Experimental plan

The experiments were planned so as to indicate the effects of the relevant parameters. The following parameters were identified:

- application of vacuum prior to testing
- leachant to surface area (L/A) ratio
- frequency of water renewal
- stirring
- leachant medium
- use of open or closed vessel.

The following leaching test was designed for the study: a test specimen was placed in a vacuum tank. Vacuum was applied (alternatively not applied) for 5 min. before the addition of water to the vacuum tank, 10 min after immersing the test specimen in water. The test specimen was removed from the vacuum tank and placed in a test vessel which contained weakly acidified water with an initial pH of 4 (alternatively demineralised water). The amount of water (L, liter) to the surface (A, cm²) of the test specimen was L/A 2.5 (alternatively 5 and 10). The test vessel was closed (alternatively open) during the test. The water in the test vessel was renewed after 0.5, 2, 7, 23, 47 h and 3.2 days (alternatively after 2, 23 h and 3.2 days). All eluates were filtered. The pH and conductivity of the eluates were measured and the eluates were analysed for Na, Cu and Cr. The metals were analysed using AAS/flame or AAS/graphite furnace (low concentrations)

The experimental plan is attached as Appendix A. The design was based on the orthogonal array [7]. The effect of seven parameters (including laboratory and batch differences) can be determined. Moreover, the influence of interactions between these parameters (e.g. L/A and vessel and L/A and stirring) can be studied.

The experimental study with 16 runs was performed in four Nordic countries (with specimens from four batches). The confirmation tests with four runs were performed later after analysis of the results from the 16 runs.

3. Results and discussion

3.1. Influence of selected parameters on leaching

3.1.1. Interpretation of pH values

The pH-values varied from 10.4 to 11.5 in the eluates collected after 3.2 days. The use of open vessel had the strongest influence on pH value at 3.2 days. The pH values was on average about 0.4 higher in an open vessel than in a closed vessel. The influence of pH was not as significant at 23 h. The uptake of carbon dioxide from air with time is the main reason for the lower pH-value in the open vessel. The effects of other parameters were not significant.

The contribution ratio to the variations of pH and conductivity were estimated after 1 day of leaching and at 3.2 days of leaching (Fig. 1).

3.1.2. Interpretation of conductivity

The conductivity varied between 15 and 67 mS m⁻¹ in the eluates collected after 3.2 days. The vessel had the strongest effect on conductivity after 3.2 days. Closed vessel had on average 20 mS m⁻¹ higher values. This means that the leachant composition was different in open vessel due to lower leaching rate or precipitation. A similar effect could also been seen at time 23 h (Fig. 1).

The use of larger L/A decreased the conductivity only in closed vessels. The conductivity was not clearly influenced by the increase of L/A in the open vessel, which indicated a strong influence of air on the leachant composition. The effects of other parameters were not significant.

3.1.3. Interpretation of leached amounts

It was not possible to evaluate the results obtained for chromium. It is also likely that chromium was bound to several compounds with different leaching properties. The concentrations of chromium in the eluates was also lower than the concentration of copper.

The effects of parameters were studied by comparing the cumulative measured release during the test period of 3.2 days. The release included the release from the vacuum or wetting step (which was 2–4% of the total amount for copper and around 4% for sodium).

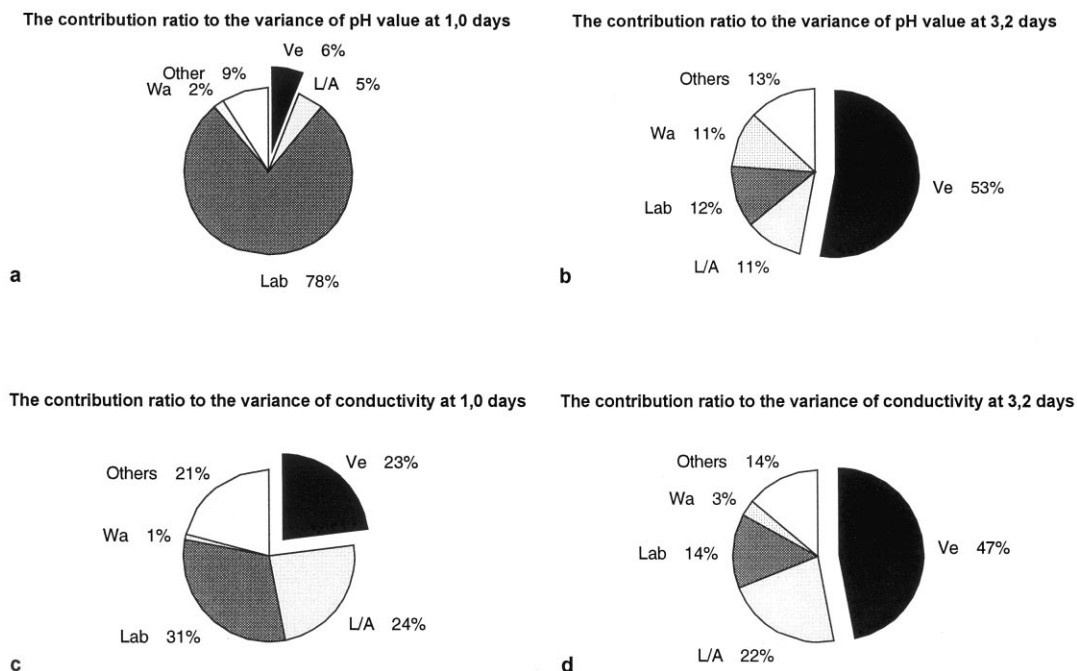


Fig. 1. The contribution ratio to the variations of pH and conductivity at day 1 and 3.2 days of leaching.

The results for copper have been summarised in Fig. 2a. The blocks in the figure indicate the gain in release due to selected test parameters. The use of vacuum had the strongest effect. The release was on average 32 mg m^{-2} days when vacuum was applied and on average 21 mg m^{-2} days with no

vacuum. The increase in release was due to the wetting of the material, which enabled the leaching process to proceed. The effect of stirring increased the result on average by 4.9 mg m^{-2} . The differences in results from different batches or laboratories were high, which is indicated by the blocks in the figures.

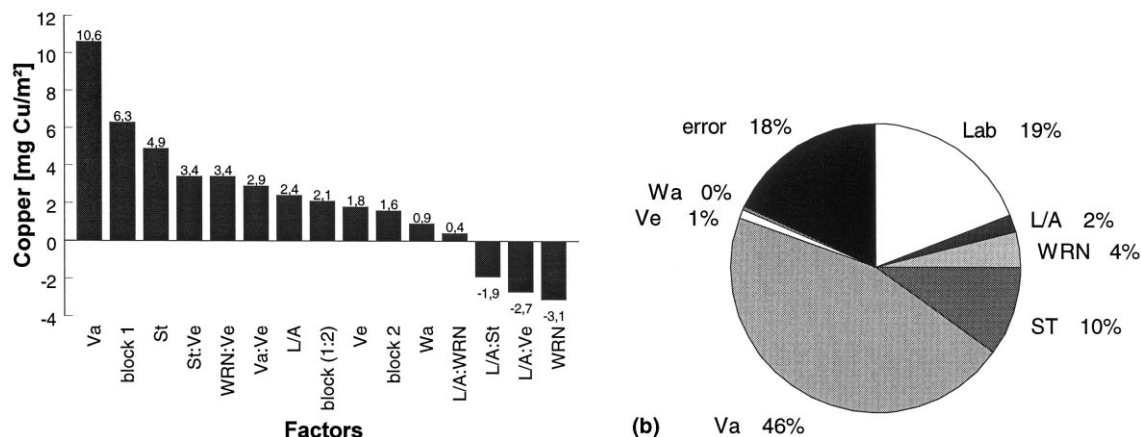


Fig. 2. (a) The gain of changing the levels of parameters on the leaching of copper. (b) The contribution ratio to the variations on the leaching of copper at 3.2 days.

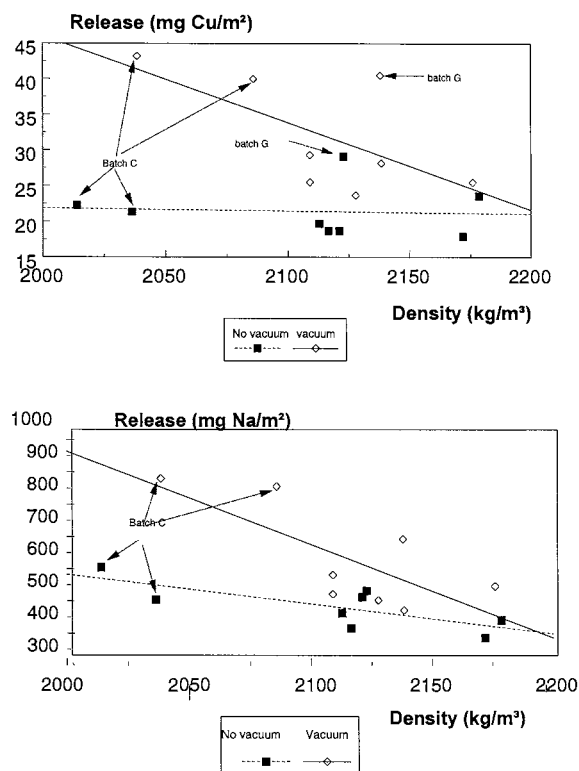


Fig. 3. Correlation of leached amounts to the density of the specimen.

The laboratory and batch strongly influenced the leaching of sodium. The use of vacuum also had a strong effect. The release was on average 640 mg m^{-2} when vacuum was applied and on average 470 mg m^{-2} with no vacuum. The use of stirring increased the results to 70 mg m^{-2} . The

other parameters had very little effect on the results.

3.1.4. Influence of batch and laboratory

There were large batch and laboratory influences on both copper and sodium leaching as indicated by the blocks in the Fig. 2a. The differences in the physical structure of the specimens from different batches can be studied from the density of the specimen. A low density (which indicates a high porosity) was assumed to give larger leaching. In Fig. 3. the leached amounts of copper and sodium are compared with the density of the specimen. Leaching of copper, when applying vacuum, correlated with densities. A low density (batch C) resulted in large leaching. When vacuum was not applied the density did not correlate with the leached amounts. Leaching could in this case have been controlled by surface reactions. The leaching of sodium also indicates a correlation with density.

In this study it was not possible to analyse the influence of batch and laboratory separately due to the design of the experimental plan.

3.1.5. Results from confirmation runs

The effect of vacuum, use of stirring and use of high water renewal effect were checked in the confirmation runs. The results from the confirmation study are summarised in Table 1. The conclusions from the confirmation runs were,

1. Comparison of the results from Conf-4 to Conf-2 confirms the strong effect of vacuum. The effect of vacuum on leaching was estimated for a given set of test conditions in Table 2.

Table 1
Experimental conditions and results in the confirmation tests

Run	WRN ^a	Stirring	Vacuum	Leached amount of copper (mg m^{-2})	Leached amount of sodium (mg m^{-2})
Conf-1	4	Stirring	Vacuum	42.0	622
Conf-2	4	No stirring	Vacuum	27.7	594
Conf-3	7	Stirring	Vacuum	38.1	538
Conf-4	4	No stirring	No vacuum	16.4	435

^a WRN, water renewal frequency

Table 2

Estimations of the effects of vacuum and stirring on the leaching of copper and sodium

	Copper		Sodium	
	In experiments (%)	In confirmation test (%)	In experiments (%)	In confirmation test (%)
Effect of vacuum	25	51	28	31
Effect of stirring	19	41	13	5

Calculated for a given set of test conditions: use of vacuum, L/A 5, WRN 4, use of stirring, closed vessel and pH 4 adjusted water.

- Comparison of results from Conf-2 to Conf-1 confirms the effects of stirring effects. The effect of stirring on leaching was estimated for a given set of test conditions in Table 2. The effect of stirring was also dependent on two other parameters, namely L/A and vessel. Stirring was much more effective with L/A at low level (e.g. for copper: increase 6.8 mg m^{-2}) than with L/A at high level (e.g. for copper: increase only 2.9 mg m^{-2}). Stirring was also more effective with closed vessel (e.g. for copper: increase 8.3 mg m^{-2}) than with open vessel (e.g. for copper: increase 1.46 mg m^{-2}).
- Comparison of the results from Conf-3 to Conf-1 showed no advantage using higher water renewal frequency.
- The test conditions in Conf-3 were expected to give the maximum leaching conditions for sodium. The confirmation experiment does not confirm this. However, the results of confirmation experiments for leaching of sodium are similar to the results of the leaching of copper. This inconsistency to the predicted values may be due to the relatively large differences between batches/laboratories that effects the accuracy of the predictions for sodium.

3.2. Comparison of results from the Nordic quick test to a full long test

The results from the availability test and the tank leaching test are shown in Table 3. An average effective diffusion coefficient has been calculated for all constituents, even if the leaching was not diffusion controlled for all constituents during the whole test time. In the calculations of the diffusion coefficient the average results from the availability test was used. The effective diffusion coefficient pD_e

indicated that Na, Ca, As, Cr and Cu had a low mobility.

The leaching results has been compared with the full long test (Fig. 4). In the figure all the data were collected from experiments performed with the specimen from the same batch in order to eliminate the batch difference in the comparison. The results from other experiments and batches were in accordance with these results.

Comparing these results from the quick tests it must be noticed that the samples were stored at different time periods before testing (the full long tests were performed 2 months after preparation of test specimen and the quick tests 4 months). Storage of specimen often lowers the solubility of several constituents.

A comparison of effective diffusion coefficients from experiments with specimen from the same batch is presented in Table 4. In the full long test the diffusion coefficients was calculated for that period where leaching was diffusion controlled and in the short test it was calculated for the period between 23 h and 3.2 days. The results indicated that the magnitudes of effective diffusion coefficients for the studied constituents were lower for a full long test than for a short test. The tests performed with vacuum naturally gave higher diffusion coefficients.

4. Conclusions and recommendations

The study of the influence of relevant test parameters in a quick leaching test for monolithic materials showed clearly the increase in release, when vacuum was applied, and increase in pH, when closed vessel was used. The leaching results also indicate an increase in release when stirring was used. The other parameters did not have a significant influence and can therefore be chosen

Table 3
Results from the Dutch availability test (four subsamples studied) and from the Dutch tank leaching test (test specimen stored about 2 months before the start of the test).

Element	Availability test		Tank leaching test		ρD_e^a	Average measured release $\text{mg m}^{-2} \text{64 d}$	Standard deviation $\text{mg m}^{-2} \text{64 d}$	Repeatability (%)	Repeatability (%)	(Average effective diffusion coefficient)
	Average mg kg^{-1} dry matter	Standard deviation mg kg^{-1} dry matter	Average mg kg^{-1} dry matter	Standard deviation mg kg^{-1} dry matter						
Na	1230	50	3430	390	4.1	3430	390	4.1	11.3	12.6
Ca	58 900	2100	36 200	2900	3.6	36 200	2900	3.6	8.0	13.6
As	1150	80	195	16	7.0	195	16	7.0	8.3	15.0
Cr	53	10	56	11	18.8	56	11	18.8	20.3	13.4
Cu	970	125	137	18	12.8	137	18	12.8	13.1	15.2

^a An average effective diffusion coefficient ρD_e ($= -\log D_{er} \text{ m}^{-2} \text{ s}^{-1}$) was calculated for all elements for the whole test period even if the leaching was not diffusion controlled according to the Dutch tank leaching test

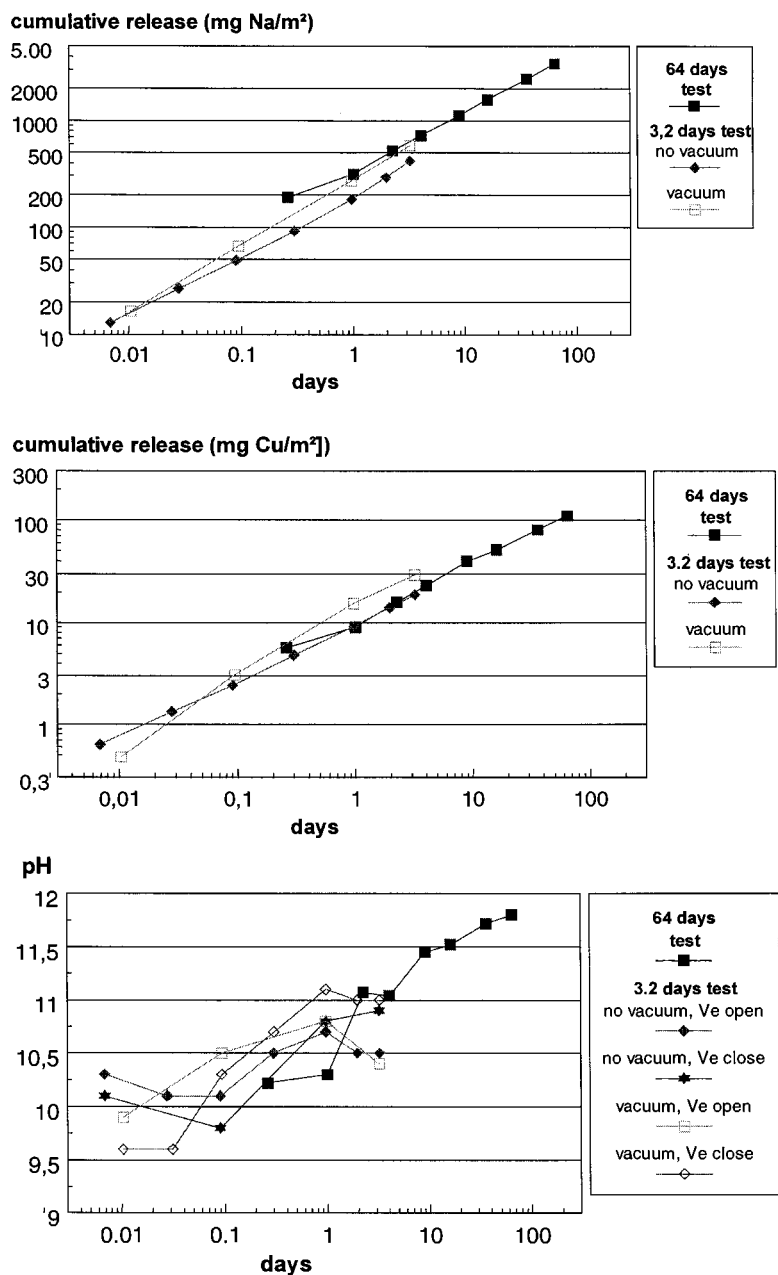


Fig. 4. Comparison of leaching results for Na and Cu in a quick 3.2 days test and a full long test.

based on practical reasons. The recommendations for test conditions in a quick test are summarised in Table 5. This project clearly showed the benefits of using experimental design to systematically study the effects of relevant parameters.

The results from the quick test and from the full long test were comparable for constituents studied here. The quick test gave higher release as was expected due to the wetting before testing. The quick leaching test also gave an indication of the magnitude of diffusion coefficients.

Table 4

Comparison of diffusion coefficients calculated from a short test and a full long test for specimen from same batches.

	Batch D		Batch G	
	$\rho D_{e,Na}$	$\rho D_{e,Cu}$	$\rho D_{e,Na}$	$\rho D_{e,Cu}$
Full long test (64 d)	12.6	15.4	12.6	15.2
Quick test without vacuum (3.2 d)	12.3	14.9	12.2	14.6
Quick test without vacuum (3.2 d)	12.3	14.8	12.3	15.0
Quick test applying vacuum (3.2 d)	12.1	14.6	12.3	14.9
Quick test applying vacuum (3.2 d)	12.2	14.6	12.1	14.3

Table 5

Recommended test conditions in a quick test for monolithic materials.

Operation	Preferred option	Remark
Pretreatment of specimen	Use of vacuum	The vacuum process shortens the water uptake (wetting process)
Amount of water	L/A 5–10	A practical amount of water is dependent on the size of the test specimen. A sufficient amount of water is needed for water immersion of the specimen and to ensure sufficient amount eluates for analysis. On the other hand, too much water leads to very small concentrations in eluates.
Test time	3 days	Practical for a suitable water renewal frequency, which enables calculation of diffusion coefficient, smaller deviations in e.g. pH and conductivity when applying 3 test days
Water renewal frequency	Wetting+three water renewal under 3 days of testing	Practical to perform as a routine testing
Stirring	Use of stirring	Stirring minimises a concentration build up at the surface of the specimen
Vessel	Use of closed vessel	Open vessel leads to uptake of carbon dioxide from air
Leachant	Use of distilled (demineralised) water	The amount of distilled water or weakly acidified water does not strongly influence the result for alkaline waste materials

Appendix A. Experimental design for the study of the influence of some parameters in the development of a quick leaching test for monolithic materials.

- Lab. Laboratory
 L/A. Ratio of leachant to specimen surface
 WRN. Frequency of water renewal
 St. Stirring
 Va. Vacuum option
 Ve: Vessel option (open or closed)
 Wa. Leachant medium

Level/factor	Lab	L/A	WRN	St	Va	Ve	Wa
Level 1	Lab. 1	2.5 (5)	4	No stirring	No Vacuum	Open	pH adj. Water
Level 2	Lab. 2	5 (10)	7	Stirring	Vacuum	Closed	Demineralised water

Level 3	Lab. 3						
Level 4	Lab. 4						
Level 5	Lab. 5						
Test run	Lab.	L/A	WRN	St	Va	Ve	Wa
1	1	5	4	No stirring	No vacuum	Open	pH adj. water
2	1	2.5	7	Stirring	No vacuum	Closed	Demin.water
3	1	5	7	Stirring	Vacuum	Open	pH adj. water
4	1	10	4	No stirring	Vacuum	Closed	Demin.water
5	2	5	7	No stirring	No vacuum	Open	Demin.water
6	2	10	4	Stirring	No vacuum	Closed	pH adj. water
7	2	5	4	Stirring	Vacuum	Open	Demin.water
8	2	2.5	7	No stirring	Vacuum	Closed	pH adj. water
9	3	10	4	Stirring	No vacuum	Open	Demin.water
10	3	5	7	No stirring	No vacuum	Closed	pH adj. water
11	3	2.5	7	No stirring	Vacuum	Open	pH adj. water
12	3	5	4	Stirring	Vacuum	Closed	Demin.water
13	4	2.5	7	Stirring	No vacuum	Open	pH adj. water
14	4	5	4	No stirring	No vacuum	Closed	Demin.water
15	4	10	4	No stirring	Vacuum	Open	pH adj. water
16	4	5	7	Stirring	Vacuum	Closed	Demin.water
17 (confirmation)	5	5	4	Stirring	Vacuum	Closed	pH adj. water
18 (confirmation)	5	5	4	No stirring	Vacuum	Closed	pH adj. water
19 (confirmation)	5	5	7	Stirring	Vacuum	Closed	pH adj. water
20 (confirmation)	5	5	4	No stirring	No vacuum	Closed	pH adj. water

References

- [1] H.A. van der Sloot, *Waste Manag. Res.* 8 (1990) 215.
- [2] J. Stegemann, P. Coté, Summary of an investigation of test methods for solidified waste evaluation, *Waste Manag.* 10 (1990) 41.
- [3] NEN7345: Leaching Characteristics of soil and stony building and waste materials—Leaching tests—Determination of the leaching of inorganic components from building and monolithic waste materials with the diffusion test. NNI, Delft, The Netherlands, 1995.
- [4] M. Wahlström, NT Technical Report 294 Nordtest, Esbo, Finland, 1995.
- [5] H.A. van der Sloot, Compliance test for construction materials and stabilized waste materials, Netherlands Energy Foundation, ECN, Petten, The Netherlands, 1994 (unpublished).
- [6] NEN7341: NEN 7341: Leaching characteristics of building materials and solid waste material—Leaching tests—Determination of leaching characteristics of inorganic components from granular and building waste materials. NNI, Delft, The Netherlands, 1992.
- [7] D.C. Montgomery, *Design and Analysis of Experiments*, 3rd ed., New York Wiley, 1991.

Pollutants leaching behaviour from solidified wastes: a selection of adapted various models.

Pierre Moszkowicz ^{a,*}, Florence Sanchez ^a, Radu Barna ^{a,b}, Jacques Méhu ^b

^a *Laboratoire d'Analyse Environnementale des Procédés et des Systèmes Industriels (LAEPSI), Institut National des Sciences Appliquées de Lyon-INSA Lyon 20, avenue Albert Einstein, F-69621 Villeurbanne Cedex, France*

^b *Polden, INSAVALOR, BP 2132, 69603 Villeurbanne Cedex, France*

Received 25 May 1997; accepted 14 October 1997

Abstract

Leaching tests are essential in the environmental assessment of stabilized wastes. Research programmes were conducted on their interpretation in order to develop tools for the evaluation of long term release of pollutants contained in solidified wastes. Models for the leaching of porous materials are discussed in this paper according to the specificity of the chemical species (i.e. transport model with total dissolution of species-diffusional model; transport model with progressive dissolution of species due to limitation of solubility-shrinking core model; and the model coupling transport and chemical phenomena). The leaching behaviour of pollutants (i.e. lead) solidified in a cement matrix was studied under different chemical conditions. Results have shown that the release of species whose solubilities depend on the physico-chemical conditions, and especially the pH (e.g. amphoteric metals), is governed by the solubility of the species in the pore water at local conditions and by the pH evolution within the matrix. A coupled dissolution/diffusion model was developed to describe the release of chemically complex species contained in a porous medium in contact with water. Leaching tests of cement matrices and artificial porous matrices containing calcium hydroxide and pollutants were conducted in order to validate the coupled dissolution/diffusion model. A good assessment of the retention of some pollutants contained in cement matrices could then be obtained by the association of two tests: solubilization of the pollutants related to the chemical context (pH) under steady state conditions and monolithic long term dynamic leaching tests in order to characterize the evolution of the chemical context (pH) and consequently the release of pollutants. The objective is to integrate this approach in the standardization process (CEN TC 292- WG 6, in progress). © 1998 Elsevier Science B.V. All rights reserved.

Keywords: Pollutant leaching; Solidified wastes; Leaching tests

1. Introduction

The development of stabilization/solidification processes using hydraulic binders is a result of the

increasingly stringent regulations in the field of environmental protection. The new evaluation tools that have resulted from research programs carried out for authorities, producers or waste disposers have reoriented the issue of environmental assessment towards better knowledge and pre-

* Corresponding author.

diction of long term behaviour and eco-compatibility. The evaluation of the long term performance of stabilized processes requires model research, depending on the environmental level of exposure corresponding to the considered scenario according to new standardization in the development of the CEN TC 292- WG 6 framework.

The characterization of the leaching behaviour of stabilized/solidified wastes is crucial in most reuse/disposal scenarios; water plays a multiple role in pollutant transfer from the stabilized/solidified wastes and their dispersion in the environment. Leaching tests are very important tools in this field.

2. Modeling pollutant leaching behaviour from solidified wastes

The objective of leaching tests is to provide an assessment of pollutant release from a solid material (i.e. waste) to the surrounding environment. In the environmental exposure scenario two modes of water contact may occur: percolation through the waste, water flow around the waste or through fractures. This paper deals with scenarios for which the solid block (i.e. a solidified waste) is in contact with static solutions (i.e. there is no convective flow around or through the solid) that are renewed periodically or continuously at a very slow rate. In the laboratory we used serial batch tests where the water is renewed after fixed contact time to avoid approaching saturation of the solution and thus preventing a solubility-control phenomenon in the leachate. An average flux of the constituent species of interest can then be determined by measuring concentrations in each leachant solution.

The overall release of soluble species contained in a porous cement block in contact with water is the result of complex and coupled phenomena.

- Water transfer in the porous medium up to aqueous saturation.
- Dissolution of species in the pore water according to local chemical conditions.
- Change of species solubilities in the pore water (including possible reprecipitation) if the chem-

ical conditions are changed due to the release of species controlling the pH (e.g. portlandite).

- Transport of species from the porous medium to the leaching solution due to the effect of concentration gradients.
- Transport of species in the leaching solution.

Up to now, the interpretation of leaching results has generally not accounted for this coupling of physical and chemical phenomena.

Most researchers in this field consider that mass transfer during leaching can often be globally described by an apparent diffusion mechanism [1]. Whereas certain models only take into account Fick's diffusion law by proposing the 'analytical' solution (semi-infinite solid) or the numerical one (finite solid volume), other models account for a coupling effect (i.e. diffusion and chemical reactions [2] or mass transfer at the interface).

In order to develop tools for the evaluation of long-term release of soluble pollutants contained in cement-based solidified wastes, we have conducted several research programs on the interpretation of leaching tests. From the obtained experimental results [3], two cases may be distinguished: species whose solubilities do not change according to physico-chemical conditions (case of relatively soluble species); and species whose solubilities depend on physico-chemical conditions and especially pH (case of amphoteric metals).

2.1. Case 1: Soluble species whose solubilities do not change with physico-chemical leaching conditions (e.g. Na^+ or Cl^- or Ca^{2+})

In this case, a diffusional model based on Fick's law or a shrinking core model correctly describes the released flux. The diffusional model is essentially based on the assumption that the pollutant is initially present in an homogenous medium and mass transfer is caused by concentration gradients. This model is a good representation of the reality in the case of a completely dissolved pollutant in pore water (e.g. case of sodium). The shrinking core model is more realistic: the pollutant is assumed to be initially present in the matrix in the solid phase.

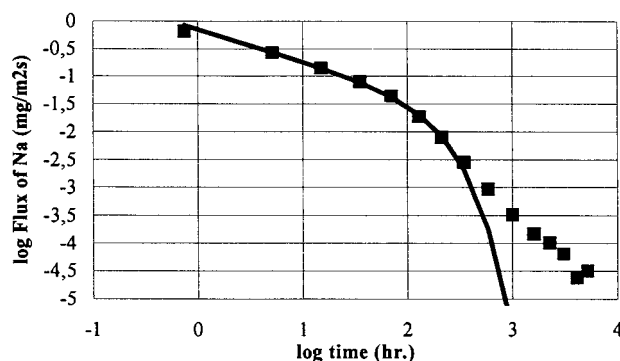


Fig. 1. Comparison of diffusional model prediction and experimental data. The sodium flux during a leaching test with demineralized water is shown.

2.1.1. Diffusional model

Two parameters characterize the intensity and the dynamics of the release: C_0 , the initial leachable concentration (available release potential) and D_e , the effective diffusion coefficient of the species in the porous medium. The model can be resolved in 3D to account for depletion of the species in the solid core [3]. This may occur with highly soluble species incorporated in very porous matrices in permanent contact with water. Long term simulation for any scenario involving contact between the solid and leaching solution is then theoretically possible. The limits of the model are reached when the physical characteristics of the material itself are modified (e.g. increase of porosity or destruction of the porous structure). Fig. 1 shows typical results obtained for sodium. The points represent the average experimental flux; the continuous curve represents the simulation results obtained using the 3D diffusional model.

After 500 h of leaching, a residual flux (which is quantitatively speaking low compared with the original one) can be observed. This flux, greater than the theoretical diffusional one, appears while the quasi-totality of sodium has been removed. A possible explanation of this phenomenon could be a dissolution of the constitutive phases of the matrix itself.

2.1.2. Shrinking core model

Two zones, separated by a dissolution front, can be distinguished in the solid block: a zone, within the solid near the solid–liquid interface, in which the

solid form of the species (S_0 concentration) has been dissolved and in which the species, in the pore water, is transported by diffusion towards the leaching solution (D_e effective diffusion coefficient); a second zone, near the solid core, in which there is no mass transfer (the species concentration in the pore solution is then the saturation concentration). Solubilization is assumed to be instantaneous. This model is well suited to describe the release of calcium without coupling with other species.

From the experimental results obtained during a monolithic leaching test (i.e. species mass released in the leachate), it is not possible to distinguish between the diffusional model and the shrinking core model, as long as the solid ‘remains’ semi-infinite, the mass released is proportional to the square root of time.

A very important difference between the two models exists in the case of portlandite release contained in cement blocks. Shrinking core or diffusional models can describe well the release of calcium hydroxide. Though with the shrinking core model it is possible to calculate the evolution of the pH profile in the pore water and at the solid/liquid interface.

2.2. Case 2: Species whose solubilities depend on the physico-chemical conditions and especially pH (e.g. amphoteric metals)

In this case, our experiments have shown that pollutant release is controlled by the solubility of

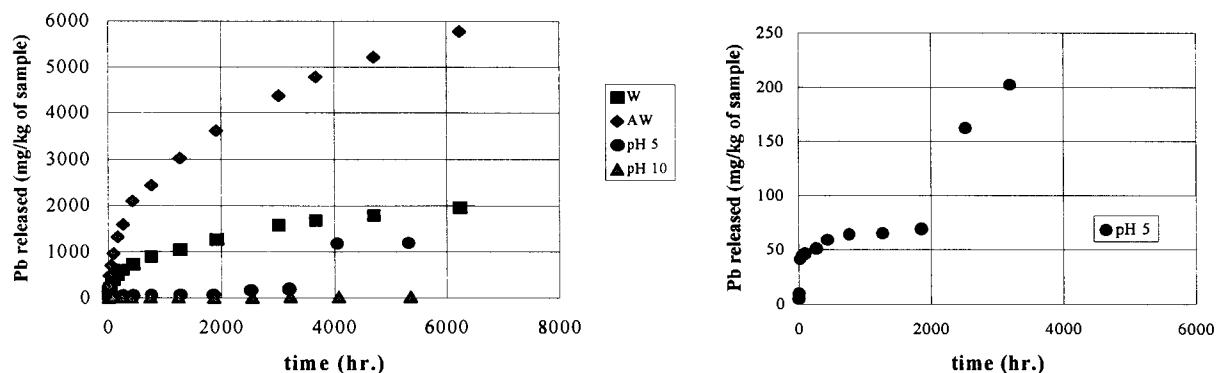


Fig. 2. Leaching of lead under different chemical conditions.

the species in the pore water at the local conditions and by the pH evolution within the solid, especially at the solid–liquid interface [4].

Lead is a typical case of such behaviour. The release of lead from a Portland cement-based matrix under different chemical conditions (demineralized water—W; controlled pH 5 and 10; alkaline water at pH 12.5—AW) is presented in Fig. 2 (i.e. sequential leaching tests of identical samples of the same monolithic material containing PbO). The leaching tests were conducted at a liquid to solid ratio of 10 ml g⁻¹ during 8 months with periodic renewals.

The least aggressive leaching solution (near to the equilibrium with the matrix—AW) results in the highest release of lead due to a high pH maintained at the interface. The amphoteric character of lead at this high pH results in increased solubility and thus the large release.

The most aggressive solution (pH 5) leads to a low release of lead: a pH 5 in the leachant provides within the matrix a pH situated between 5 and the initial pH of the pore water (close to the pH of a solution saturated with calcium hydroxide ~ 12.4), according to the important buffer capacity of cement matrices. However, it is important to note that after 4 months (~ 3000 hours) of leaching under these conditions, the release of lead increases dramatically.

The chemical conditions which change with time inside the monolithic material are the result of successive equilibria between the acid neutral-

ization capacity of the matrix and the surrounding leaching medium. Lead release is sensitive to the chemical conditions of the leaching solution and cannot evidently be interpreted by the simple diffusional model.

A coupled dissolution/diffusion model has been developed to describe the release of chemically complex species contained in a stable porous matrix in contact with water [5]. The model was used to simulate the case of a porous matrix containing only two leachable components: calcium hydroxide and lead hydroxide. Indeed, this is the typical case of an ordinary Portland cement-based solidified waste containing lead and leached with demineralized water. The main assumption of the model is local equilibrium: dissolution is assumed to be instantaneous. The porosity of the medium is also assumed to be constant: this implies that phase dissolution or phase precipitation does not affect the porous structure of the matrix.

The coupled dissolution/diffusional model can be divided into several stages:

- Release of portlandite using a shrinking front model;
- Calculation of the induced pH profile, assuming that the thermodynamic equilibrium takes place in the pore water;
- Determination of local lead solubility (by calculation assuming the main equilibria or from experimental results from ANC type tests, which is proposed for standardization at the European level as ‘influence of pH under

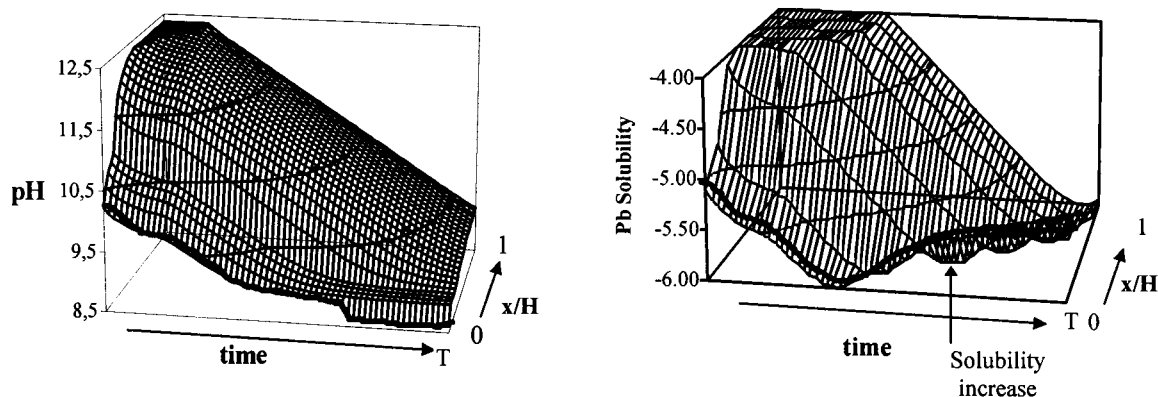


Fig. 3. Simulation of the pH and lead solubility within a leached cement matrix.

steady state conditions'), and; Description and calculation of lead transport by diffusion in the pore water.

In Fig. 3, the influence of a significant release of calcium on the pH evolution of the pore water and its consequences on the lead solubility are presented according to the coupled dissolution/diffusional model. The role of the leaching interface is apparent in the simulations.

3. Validation of the coupled dissolution/diffusion model

In order to validate the coupled dissolution/diffusion model, a specific experimental approach has been developed [4]: it consists of the study of the leaching of an artificial porous matrix. The matrix is obtained by 'sintering' a mixture of glass powder (diameter $< 160 \mu\text{m}$), calcium hydroxide and pollutants and is assumed to be a simplified representation of a cement matrix (i.e. porous medium, alkaline pore water). This approach allows better knowledge and better control of the studied medium. A wider range of pH variation at the leaching interface can be obtained and consequently prediction of the pollutants behaviour tendency can be carried out on a longer term.

3.1. Leaching behaviour of artificial porous matrices—experimental and theoretical solubility tendencies

The leaching behaviour of artificial matrices made of a mixture of glass powder, calcium hydroxide and lead oxide or cadmium oxide was studied. These matrices are supposed to simulate a Portland cement-based solidified waste containing lead or cadmium. Lead and cadmium were chosen because of their different levels of solubility and their different pH values of the lowest solubility: pH 9.3 for lead and pH 11.1 for cadmium (Fig. 4). Leaching tests by using demineralized water were conducted during 3 months with periodic renewals. The average experimental flux of lead and cadmium are pre-

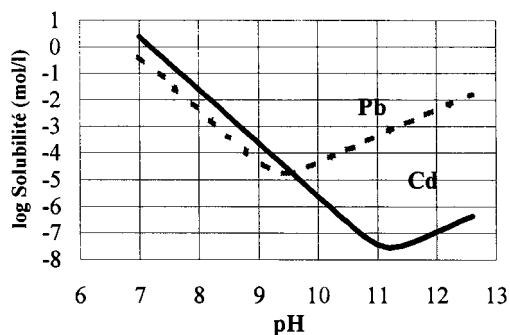


Fig. 4. Comparison of solubility curves for $\text{Pb}(\text{OH})_2$ and $\text{Cd}(\text{OH})_2$ [7].

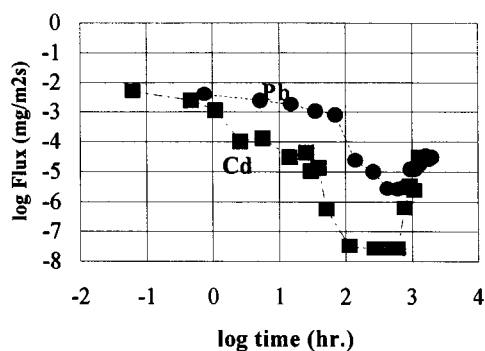


Fig. 5. Comparison of experimental flux of lead and cadmium.

sented in Fig. 5 (i.e. logarithm of released flux [$\text{mg m}^{-2} \text{s}^{-1}$] versus the logarithm of time [h]).

The study of these two heavy metals provides qualitatively an analogous behaviour of the released flux that is shifted in time and two different leaching intensities. These results are in good agreement with the solubility curves.

3.2. Leaching behaviour of artificial porous matrices—modeling

This approach allowed an initial qualitative validation of the model: a good representation of the experimental results with diffusional or shrinking core model for Na^+ , Cl^- or Ca^{++} was obtained. For lead and cadmium, the coupled dissolution/diffusion model allows us to hypothesize the main phenomena involved in mass transfer, on the time scale of laboratory leaching tests (3 months). Simulations have shown that there is no depletion of lead in solid form at the solid–liquid interface (i.e. at the interface between the matrix and the leaching solution). The simulated flux of lead is then the result of a solubilization phenomenon at the solid–liquid interface. Comparisons between experimental and simulated leaching results for calcium and lead are presented in Fig. 6.

A calculation from the percentage of lead released by assumption of a uniform release, allows us to estimate that after 3 months of leaching, only $15 \mu\text{m}$ of porous medium have been affected by the leaching phenomenon. This ‘theoretical depth’ affected by the ‘depletion’ of the solid form

confirms that phenomena take place near the interface. Besides, the presence of lead in solid crystallized form was experimentally observed at the surface of the matrix by using a magnifying glass.

Comparison between the simulation obtained for the flux of calcium and the flux of lead is presented in Fig. 7.

While the decrease of the flux of calcium is due to a depletion of calcium in solid form within the matrix, the decrease of the flux of lead is only due to a decrease of the solubility. Release of calcium and release of lead appear to be governed by two different phenomena: a shrinking core phenomenon for calcium and a solubilization phenomenon at the solid–liquid interface for lead.

4. Application of the coupled model to the leaching of cement matrices

Long term leaching tests using demineralized water were conducted on matrices containing lead (i.e. cement matrices spiked with lead oxide having a cylindrical geometry with a 4 cm diameter and a 2 cm height). The leaching solution was renewed periodically until 8 months (contact time used: 3, 5, 16, 24 h; 2, 3, 4 days; 1, 2, 3, 4 weeks and every month). A liquid-to-solid ratio of 10 ml g^{-1} was used. All the results have been reported elsewhere [4].

The use of the coupled dissolution/diffusion model allows us to represent the experimental results obtained and confirms the interfacial character of lead release. As long as lead is present in solid form in the matrix zone near the leaching surface, its release is controlled by a solubilization phenomenon at the solid–liquid interface. In this case, the leaching model can be simplified. The diffusional transport of lead within the matrix can be neglected and the flux of lead can be expressed in terms of a transfer coefficient of global mass and the difference between the saturation concentration and the concentration of the leaching solution.

Consequently, a model based on the shrinking core model to describe the release of calcium and taking into account pH evolution at the solid–

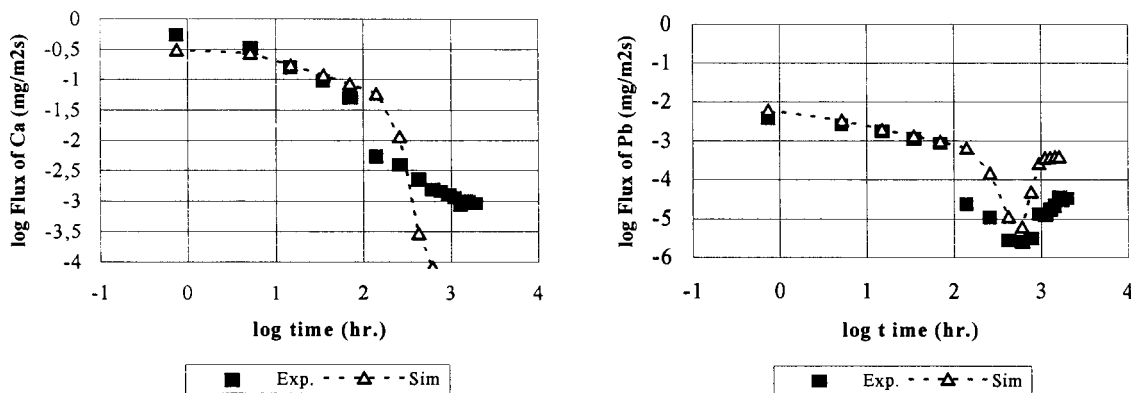


Fig. 6. Comparisons of experimental and simulated flux of calcium and lead using the coupled dissolution/diffusion model for porous artificial matrix.

liquid interface and variable lead solubility according to this pH, well represents the leaching phenomena of lead (Figs. 8–11). Indeed, simulation of the calcium release (Fig. 8) allows us to calculate the pH profile within the matrix and especially at the solid–liquid interface (Fig. 9). The knowledge of the pH at the solid–liquid interface allows us, from the experimental solubility curves (Fig. 10), to assess the saturation concentration of lead at this interface. The amount of lead released (Fig. 11) can then be obtained by using an interfacial transfer coefficient. In Figs. 8–11, the points represent the average experimental flux; the continuous curves represent the simulation results. Discontinuities observed in the simulation of the pH evolution at the solid–liquid interface (Fig. 9) are the result of the sequential

character of the leaching test used (i.e. periodic renewals of the leaching solution).

The experimental curve of the lead solubility was obtained from a leaching test carried out on samples of finely crushed material contacted with nitric acid solutions of different concentrations. This test, based on the Acid Neutralization Capacity test [6] was developed [4] in order to measure the alkalinity of the matrix and to determine the effects of variations in the matrix pore water conditions on the pollutants solubility.

The direct use of the experimental pollutants solubility curves (Fig. 10) in the model to determine the equilibrium concentrations according to the pH appeared to be an interesting approach. This technique allows us to account for the total chemical conditions, which avoids the use of a

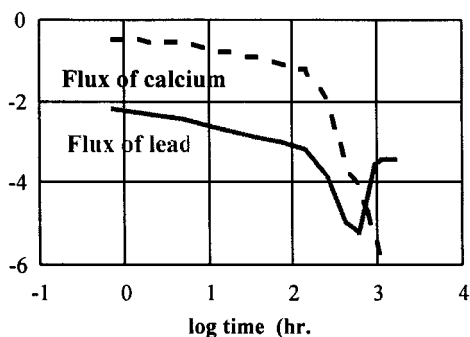


Fig. 7. Comparison of simulated flux of calcium and lead ($\text{mg m}^{-2} \text{s}^{-1}$) using the coupled dissolution/diffusion model for porous artificial matrix.

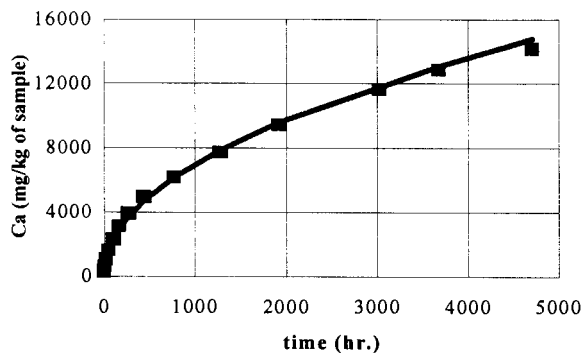


Fig. 8. Simulation of the calcium release.

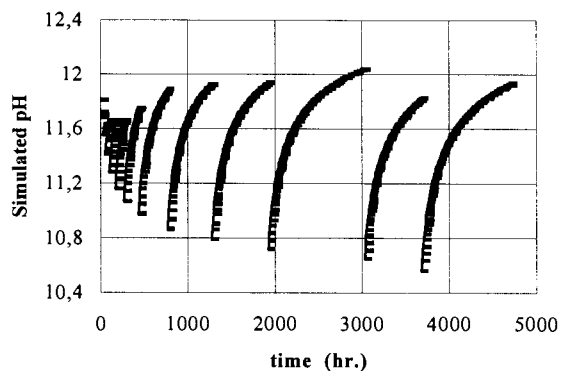


Fig. 9. Simulation of the pH profile at the solid-liquid interface.

simplified representation of the pore water of the cement matrix (i.e. by assuming the main equilibria) that would provide a simplified estimate compared to the whole real phenomena.

5. Conclusions

Simple tests and the diffusional model are generally sufficient to describe the leaching of highly soluble species contained in solidified wastes. For amphoteric metals (e.g. lead), the results obtained demonstrate the importance of chemical interactions and, in particular, the coupling of phenomena concerning solubiliza-

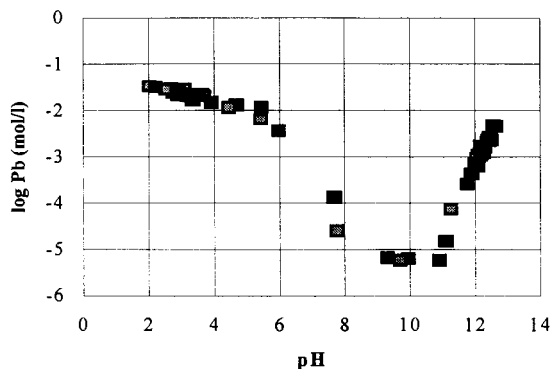


Fig. 10. Experimental lead solubility.

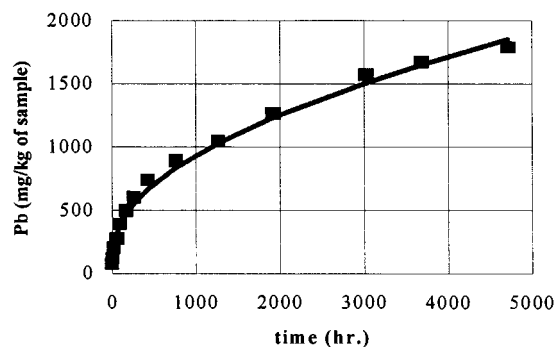


Fig. 11. Comparison of experimental and simulated cumulative release of lead using the coupled dissolution/diffusion model.

tion and diffusional transport during leaching: on the time scale of laboratory leaching tests, the release is governed by solubilization phenomena at the solid-liquid interface which is controlled by the evolution of pH, consequence of the release mainly of portlandite.

In the framework of CEN TC 292 WG 6 'basic characterization of leaching behaviour' a methodology guideline was developed and proposed as a pre-standard. Now a toolbox of several leaching tests is being developed to address different aspects of the behaviour: influence of pH under steady state conditions, percolation through a granular waste mass, dynamic release from monolithic waste,...

The objective of the authors is to valorize the research works conducted in this field to contribute at the French level to help selection and use of the appropriate tests from the complete toolbox and then to interpret the results according to the considered scenario and the relevant behavioural models.

Acknowledgements

This research was largely supported by the Association RE.CO.R.D (French Cooperative Network for Waste Research) in collaboration with the HSMRC (Hazardous Substances Management Research Center—USA).

References

- [1] P. Moszkowicz, R. Barna, J. Mehu, H. van der Sloot, D. Hoede, Environmental aspects of construction with waste materials, in: J.J.M. Goumans, H.A. van der Sloot, T.G. Aalbers (Eds.), Proc. Int. Conf., WASCON'94, 1994.
- [2] M. Hinsenveld, A shrinking core model as a fundamental representation of leaching mechanisms in cement stabilized waste, Ph.D. thesis, University of Cincinnati, OH, 1992.
- [3] R. Barna, Etude de la diffusion des polluants dans les déchets solidifiés par liants hydrauliques, Thèse doctorat, INSA Lyon, 1994, p. 210.
- [4] F. Sanchez, Etude de la lixiviation de milieux poreux contenant des espèces solubles: application au cas de la lixiviation des déchets solidifiés par liants hydrauliques, Thèse doctorat, INSA Lyon, 1996, p. 245.
- [5] P. Moszkowicz, J. Pousin, F. Sanchez, J. Comput. Appl. Math. 66 (1996) 377.
- [6] J.A. Stegemann, C. Shi, R.J. Cadwell, Environmental aspects of construction with waste materials, in: J.J.M. Goumans, H.A. van der Sloot, T.G. Aalbers (Eds.), Proc. Int. Conf., WASCON'94, 1994.
- [7] M. Pourbaix, Atlas des Équilibres Electrochimiques à 25°C, Gauthiers-Villars and Cie, Paris, 1963, p. 553.

Coupling superheated water extraction with enzyme immunoassay for an efficient and fast PAH screening in soil

Sabine Kipp, Harald Peyrer, Wolfgang Kleiböhmer *

Institut für Chemo- und Biosensorik e.V., Mendelstr. 7, D-48149 Münster, Germany

Received 25 May 1997; accepted 14 October 1997

Abstract

The coupling of an enzyme immunoassay with a superheated water extraction is an attractive technique because of the reduced use of hazardous solvents, due to their hostile impact on the environment. This paper describes the use of superheated water extraction and enzyme immunoassay (EIA) for the determination of polycyclic aromatic hydrocarbons (PAHs) in native (not spiked) surface soil and sediment samples. The extraction recoveries with superheated water were comparable to those achieved with conventional Soxhlet techniques. The benefits of superheated water extraction-EIA includes replacement of harmful organic solvents used in extraction, fast extractions (15–30 min.) with an inexpensive extractant, reduced number of steps in the determination of the target compounds, and the application of sensitive and relatively inexpensive assays. Further advantages of the superheated water extraction are higher extraction efficiencies compared with the methanol based extraction kits associated with the EIA and direct measurement of the extracts with EIA. Both techniques can be used as efficient screening methods in the field since the type of equipment used in superheated water extraction and EIA can be loaded into a van and operated on a car battery or a small generator. © 1998 Elsevier Science B.V. All rights reserved.

Keywords: Superheated water extraction; Enzyme immunoassay (EIA); Polycyclic aromatic hydrocarbons (PAHs); Field analysis; Soil

1. Introduction

In the last few years there has been an increase in the demand for rapid and especially reliable field portable methods for the quantification of organic pollutants present at waste sites.

In order to make appropriate decisions regarding site clean-up and remediation, fast and accu-

rate determinations are necessary. In the meantime several methods, like portable gas chromatography (GC) or gas chromatography-mass spectrometry (GC/MS) have become available for field determinations. However, there has been a lack of rugged quantitative extraction methods for field measurements.

Conventional extraction methods based on organic solvents like Soxhlet and sonication are hardly applicable in the field, because of the time needed to achieve quantitative extractions, the

* Corresponding author. Fax: +49 251 9802890; e-mail: kleiboe@uni-muenster.de

fragile, elaborate glassware and the large amounts of organic solvents employed. In the last few years, supercritical fluid extraction (SFE) with CO₂ has been shown to yield good recoveries for a range of organic pollutants from real environmental samples using short extraction times (10–60 min) with a minimum of organic solvents only. Especially for polycyclic aromatic hydrocarbons (PAHs), polychlorinated biphenyls (PCBs), and organochlorine pesticides, various working groups have reported good agreements between SFE and conventional extraction methods [1–4]. In addition, the US-EPA has recently adopted SFE as the official method for the extraction of total petroleum hydrocarbons (TPHs) and PAHs from environmental matrices and is presently in the process of adapting a method for the extraction of PCBs and organochlorine pesticides [5–7].

Consequently, SFE with CO₂ as extractant is a natural choice for field extractions because they can be performed quite efficiently with only a minimum of solvents and equipment required and can yield real time results that facilitate on-site decisions.

Another environmentally friendly solvent like CO₂ is water. However, at ambient temperature and pressure, water has a dielectric constant of $\epsilon \approx 80$ and is therefore extremely polar and thus not a suitable solvent for non-polar organics [8,9]. For water under these conditions the solubility of naphthalene is 32 mg l⁻¹, chrysene is 0.002 mg l⁻¹ and benz[ghi]perylene is 0.0003 mg l⁻¹ [10]. Up until now there have been very few papers dealing with water as an analytical extraction fluid for non polar compounds.

Water has a much lower dielectric constant and higher solubility for non-polar compounds under supercritical conditions ($T > 374^\circ\text{C}$ and $P > 22.1$ MPa). The dielectric constant for supercritical water varies between $\epsilon = 5$ and $\epsilon = 15$ depending on temperature and pressure. Supercritical water is an effective solvent for organic pollutants [8,9,11]. However, supercritical water is not suitable for routine extractions because of the necessary temperature and pressure requirements.

Steven Hawthorne and his group showed that the dielectric constant of water under much milder conditions can be dramatically lowered by increas-

ing the temperature at moderate pressures (5 MPa) up to 250°C [11–13]. Doing this the dielectric constant decreases from $\epsilon = 90$ –130. Hawthorne demonstrated that superheated water at 250°C and 5 MPa is an efficient extraction fluid for the extraction of chlorophenols, PAHs and PCBs from soil and sediment. With optimized conditions quantitative extractions were achieved in less than 15 min, if only pure water was used as extraction solvent [11–13].

In field analysis nearly always wet samples (soil, sediments, sludges) have to be analyzed. However, all common extraction methods (Soxhlet, sonication, SFE and ASE) require dried sample material. The water content of the sample can be determined separately, but drying of all sample material is very time consuming and hardly suitable for fast field analysis. For the extraction with superheated water no drying is necessary. The sample can be extracted almost as it was taken.

As such for several reasons water is the ideal extraction solvent for field and also for laboratory application.

The analysis of SFE extracts by field portable GC methods has proven to be relatively resource-intensive. However, immunoassay technologies, such as the enzyme immunoassay (EIA), has shown a potential for providing rapid, low-cost methods for the determination of environmental pollutants, including PCBs, PAHs, polychlorinated dibenzodioxins (PCDDs). Several EIA-based, semiquantitative or quantitative field methods for the determination of the total amount of PAHs are available. In general, these methods allow the determination of the samples that contain PAHs above or below a decision threshold [14,15].

An important disadvantage of the commercially available EIA is the associated extraction kit. For the extraction of PCBs and PAHs the samples are mixed with an extraction solution (provided with the kit) that consists of 20 ml of methanol containing a soil-dispersing agent, and are shaken vigorously for at least 60 s. The samples are then left to settle, filtrated and diluted with a buffer solution. This procedure is more or less the same for all EIA test kits. Knowing that even Soxhlet extractions of several hours can show incomplete extraction rates or have different analyte and/or

matrix depending extraction efficiencies, it is no surprise that there is a gap between the results obtained with an EIA test kit and those obtained with conventional analytical methods. The study presented here was carried out with the aim of narrowing this gap by coupling superheated water extraction with EIA.

2. Experimental

2.1. Samples and reagents

For the evaluation of our method, native samples were used. The PAH containing soil sample was taken from a polluted industrial site. The sample was freeze-dried and homogenized in an electric mill. The certified reference material is a marine sediment (HS-3 of the National Research Council of Canada) purchased from Promochem (Wesel, Germany). All solvents and reagents were purchased from Merck (Darmstadt, Germany) or Baker (Griesheim, Germany) in the highest purity available. The sample extracts were investigated using HPLC to determine the content of the following PAHs: naphthalene (N), acenaphthene (A), fluorene (Fluo), phenanthrene (Phen), anthracene (Anth), fluoranthene (F), pyrene (Py), benz[a]anthracene (B[a]A), chrysene (Chry), benzo[b]fluoranthene (B[b]F), benzo[k]fluoranthene (B[k]F), benzo[a]pyrene (B[a]P), dibenz[a,h]anthracene (D[a,h]A), benzo[ghi]perylene (B[ghi]P) and indeno[1,2,3-c,d]pyrene (I[c,d]P). The EIA method was used to quantify the total PAH amount in the extracts.

3. Reference method

3.1. Soxhlet extraction

Soxhlet extraction of soil samples was performed according to DIN 38414, part 1 [17]. Soil (5 g) was transferred to a cellulose extraction thimble and extracted for 8 h with 150 ml *n*-hexane/acetone (1:1). The solvent volume was reduced to 50 ml using a rotary evaporator.

A 1 ml aliquot was transferred to a silica-solid phase extraction (SPE) cartridge for clean-up. The column was eluted with 5 ml *n*-hexane/dichloromethane (1:1) and the solvent was removed under a gentle stream of nitrogen. Phthalic acid diethylester (50 μ l) was added to prevent evaporation to dryness. Acetonitrile (950 μ l) was added to the remaining residue and the solution was analysed by HPLC.

3.2. HPLC method for the quantification of PAHs

HPLC separation was performed on a HP 1050 liquid chromatograph equipped with a diode-array detector (DAD) and a fluorescence-detector (FLD). The DAD signal was used to ascertain peak purity and the FLD signal for quantification. A wavelength program was used to detect the different PAHs at optimal absorption and emission wavelengths. Separation was achieved on a Bakerbond PAH 16 Plus 250 \times 3 mm i.d. column with a gradient elution [16].

3.3. Superheated water extraction

The water extractions were performed at 5 MPa and 250°C analogous to the extraction described by Hawthorne et al. [11]. Extraction time was 30 min. For soil extraction 1 g of sample was used, while for extractions of the sediment 50 mg of sample was used. A schematic diagram of the extraction system is shown in Fig. 1. The carefully degassed water was pumped at a flow rate of 1–1.5 ml min⁻¹ in the constant pressure mode (5 MPa) with an ISCO Model 260D syringe pump (Axel Semrau GmbH, Sprockhövel, Germany) through a 2 m stainless steel pre-heating coil to the extraction cell. All extractions were performed in 3.5 ml stainless steel cells (Keystone Scientific, Bellefonte, PA). The pre-heating coil and the extraction cell were placed inside a Carlo Erba Model Series 4160 GC oven. The outlet of the extraction cell was connected by stainless steel transfer line to an ISCO Model variable restrictor (Axel Semrau GmbH, Sprockhövel, Germany).

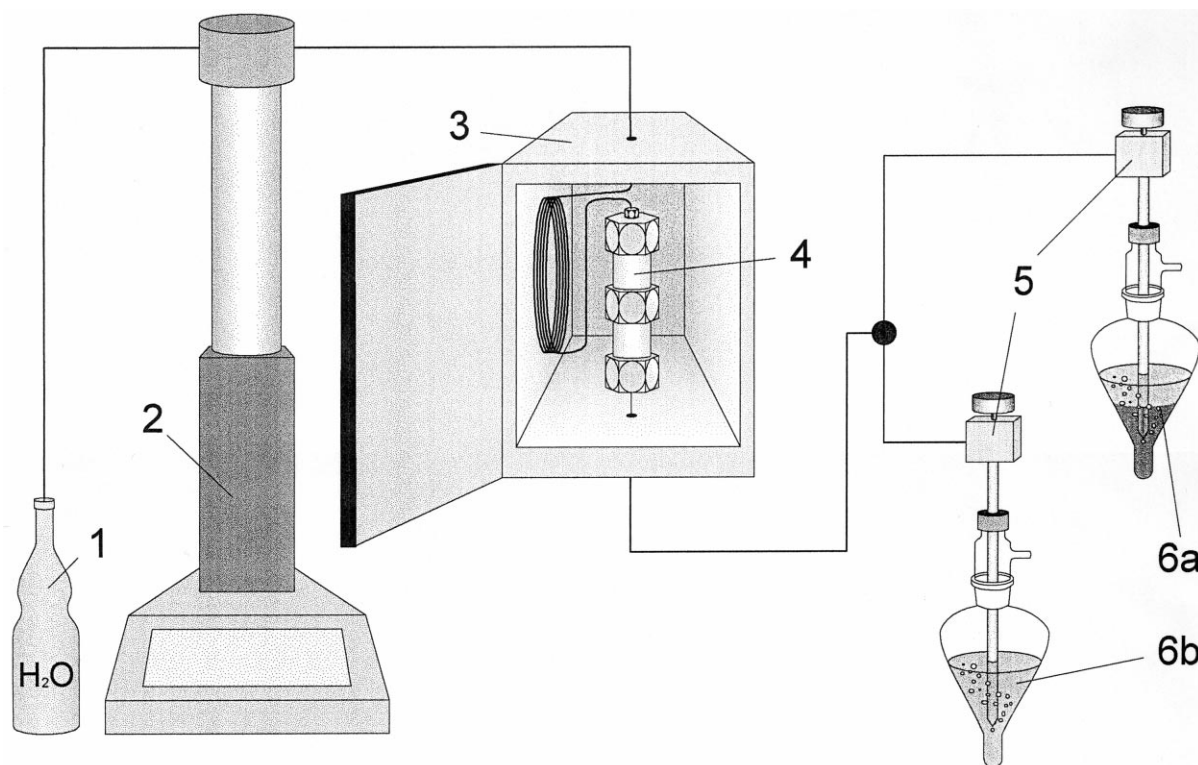


Fig. 1. Basic set up for the superheated water extraction system. (1) Deionised water reservoir; (2) syringe pump; (3) GC-oven; (4) extraction vessel; (5) adjustable restrictor; (6a + 6b) collection devices

For HPLC analysis the extracts were collected at 0°C in 10 ml of *n*-hexane as collection solvent. After the extraction and cooling down of the system the transfer line and the restrictor were rinsed with 3 ml of *n*-hexane into the collection vial. The water extract and the collection solvent were vigorously shaken and the *n*-hexane phase was separated from the water phase. The water phase was again extracted with 10 ml *n*-hexane. The *n*-hexane phases were united and a keeper (50 µl phthalic acid diethylester) was added to the sample prior to the evaporation of the solvent under a gentle stream of nitrogen. 950 µl acetonitrile was added to the remaining residue and the solution was analysed using HPLC.

For the coupling with EIA 10 ml of methanol was used as collection solvent. After extraction, the methanol–water volume was filled up to 100 ml with water and a 1 ml aliquot was used for EIA.

3.4. Enzyme immunoassay

The PAH content of the two investigated samples were measured with a commercial magnetic bead-based EIA. The test kit (PAH RaPID Assay, Ohmicron, Axel Semrau GmbH, Sprockhövel, Germany) employs polyclonal anti-phenanthrene antibodies and shows a general sensitivity to PAHs. The functional description of the immunochemical detection is exemplified in Fig. 2.

The assay procedure was executed following the test kit instructions. Specific amounts of sample extract, enzyme conjugate and analyte specific antibody coated on magnetic particles were added to a test tube and incubated for 30 min at room temperature (Fig. 2A). The calibrant solutions provided with the assay kit were treated similarly.

The tubes were then placed in the magnetic rack. All magnetic particles were pulled and held to the tube wall while excess reagents could be

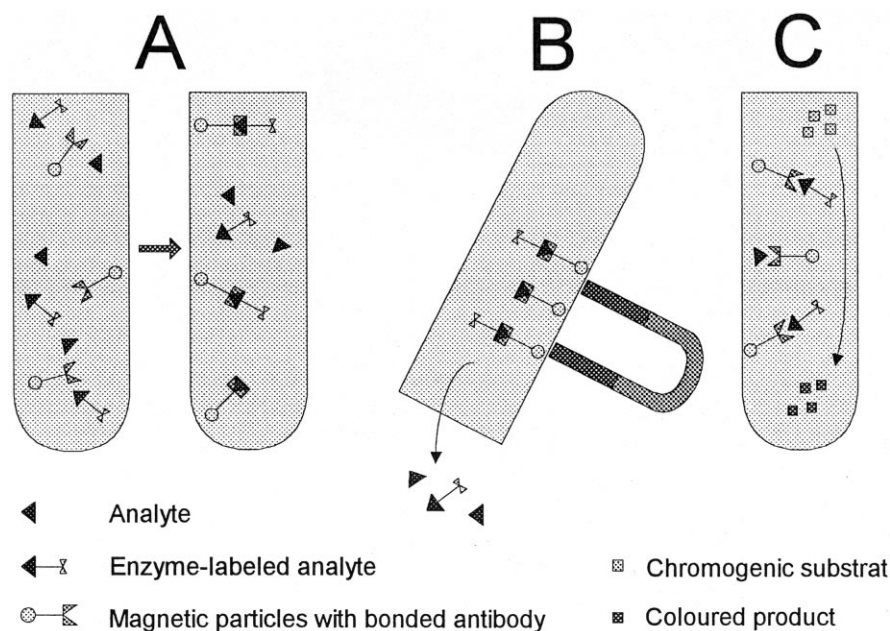


Fig. 2. Detection principle of the magnetic bead-based EIA. (A) Immunological reaction; (B) separation; (C) colour reaction

decanted. The particles were washed twice with a washing solution (Fig. 2B). A mixture of enzyme substrate (hydrogen peroxide) and chromogen (3,3',5,5'-tetramethylbenzidine) was added to the tube and allowed to react for 20–30 min at room temperature (Fig. 2C). After this the colour reaction was stopped by the addition of 2 mol l⁻¹ sulfuric acid. Since the labeled analyte and the analyte in the sample were competing for the antibody sites, colour development is directly dependent on the concentration of the enzyme labeled analyte and indirectly dependent on the concentration of analyte in the sample.

The absorption of the coloured complex was measured with a photometer at 450 nm.

4. Results and discussion

4.1. Superheated water extraction versus Soxhlet extraction

To estimate the efficiency of new extraction methods in most cases the recoveries were compared with those obtained using the Soxhlet ex-

traction or compared with certified values of a reference material. We used Soxhlet extraction, because it is the most standardised method.

Our superheated water extraction investigations were executed using the experimental conditions described by Hawthorne et al. [11]. Critical parameters are the flow rate and temperature, but the selected conditions are within an optimal region. Even with the first extraction, we obtained recoveries comparable with the Soxhlet extraction. In Table 1 the concentrations obtained with superheated water extraction and with Soxhlet extraction for the sediment HS-3 are compared with certified values. The results of our superheated water extraction do not differ significantly from those of the conventional Soxhlet extraction and both results are very close to the certified values or at least within the standard deviations specified on the certificate. The differences between the certified values and the superheated water and Soxhlet extraction are difficult to interpret because no information about the analytical procedure used for the certification of HS-3 was available.

Table 1

Comparison between superheated water extraction ($n = 3$), Soxhlet extraction ($n = 5$) and certified values for the reference material HS-3

	Certified values (mg kg ⁻¹)	Soxhlet (mg kg ⁻¹)	Superheated water (mg kg)
N	9 ± 0.7		6.1 ± 0.6
A	4.5 ± 1.5		3.6 ± 0.4
Fluo	13.6 ± 3.1	6.2 ± 1	6.8 ± 0.4
Phen	85.0 ± 20	79.6 ± 0.5	76.2 ± 4.8
Anth	13.4 ± 0.5	7.9 ± 0.5	8.4 ± 0.8
F	60 ± 9	63 ± 1	61.9 ± 5.9
Py	39 ± 9	47 ± 0.3	35.0 ± 3.1
B[a]A	14.6 ± 2	9.2 ± 0.3	12.6 ± 2.4
Chry	14.1 ± 2	11.6 ± 0.6	10.3 ± 1.4
B[b]F	7.7 ± 1.2	7.9 ± 0.4	1.4 ± 1.5
B[k]F	2.8 ± 2	3.8 ± 0.5	3.7 ± 0.4
B[a]P	7.4 ± 3.6	4.8 ± 0.4	4.8 ± 0.5
D[a,h]A	1.3 ± 0.5	1.4 ± 0.2	0.6 ± 0.1
B[ghi]P	5 ± 2	8.9 ± 0.9	3.4 ± 0.2
I[c,d]P	5.4 ± 1.3	3.8 ± 0.1	8.8 ± 1.1
Sum	282.8 ± 58.4	257.8 ± 6.7	253.5 ± 20.3

In addition to the certified reference material we also investigated a real world soil sample. Fig. 3 shows a HPLC chromatogram of the superheated water extract of this soil sample and in Table 2 the concentrations obtained with this extraction are compared with those of the Soxhlet

Table 2

Comparison between superheated water extraction ($n = 3$) and Soxhlet extraction ($n = 3$) for a real soil sample

	Soxhlet (mg kg ⁻¹)	Superheated water (mg kg ⁻¹)
N		0.1 ± 0.1
A		0.2 ± 0.2
Fluo	0.1 ± 0.02	0.1 ± 0.1
Phen	1.1 ± 0.2	1.3 ± 0.6
Anth	0.3 ± 0.1	0.3 ± 0.1
F	4.7 ± 0.4	4.2 ± 1.4
Py	3.7 ± 0.3	3.1 ± 1.0
B[a]A	3.0 ± 0.2	2.2 ± 0.4
Chry	3.1 ± 0.2	2.2 ± 0.4
B[b]F	6.2 ± 0.3	4.4 ± 0.7
B[k]F	1.7 ± 0.1	1.2 ± 0.2
B[a]P	3.2 ± 0.2	1.5 ± 0.4
D[a,h]A	0.7 ± 0.10	0.3 ± 0.1
B[ghi]P	3.1 ± 0.2	1.9 ± 0.1
I[c,d]P	1.5 ± 0.4	4.4 ± 0.4
Sum	32.4 ± 2.5	27.4 ± 5.2

extraction. We could not quantify naphthalene and acenaphthene in the Soxhlet extract since losses occurred during the solvent reduction steps because of their low vapour pressure. As shown in Table 2, there is no significant difference between the PAH values obtained with superheated water extraction and Soxhlet extraction.

It should be kept in mind that the superheated water extraction method was not optimized, but applied as published by Hawthorne [11]. So further optimization of the trapping system, extraction pressure, temperature and the adaption of some minor technical problems can lead to higher extraction efficiencies and to improved reproducibility.

4.2. Superheated water extraction-enzyme immunoassay

Coupling the extraction with the detection technique is straightforward. Since immunoassays are typically conducted in aqueous media, the extracted material can be collected in a solvent that is already used in the immunoassay. When water is used as extraction solvent, the extracted analytes should be collected in methanol to have sufficient solubility for the PAHs. Methanol is

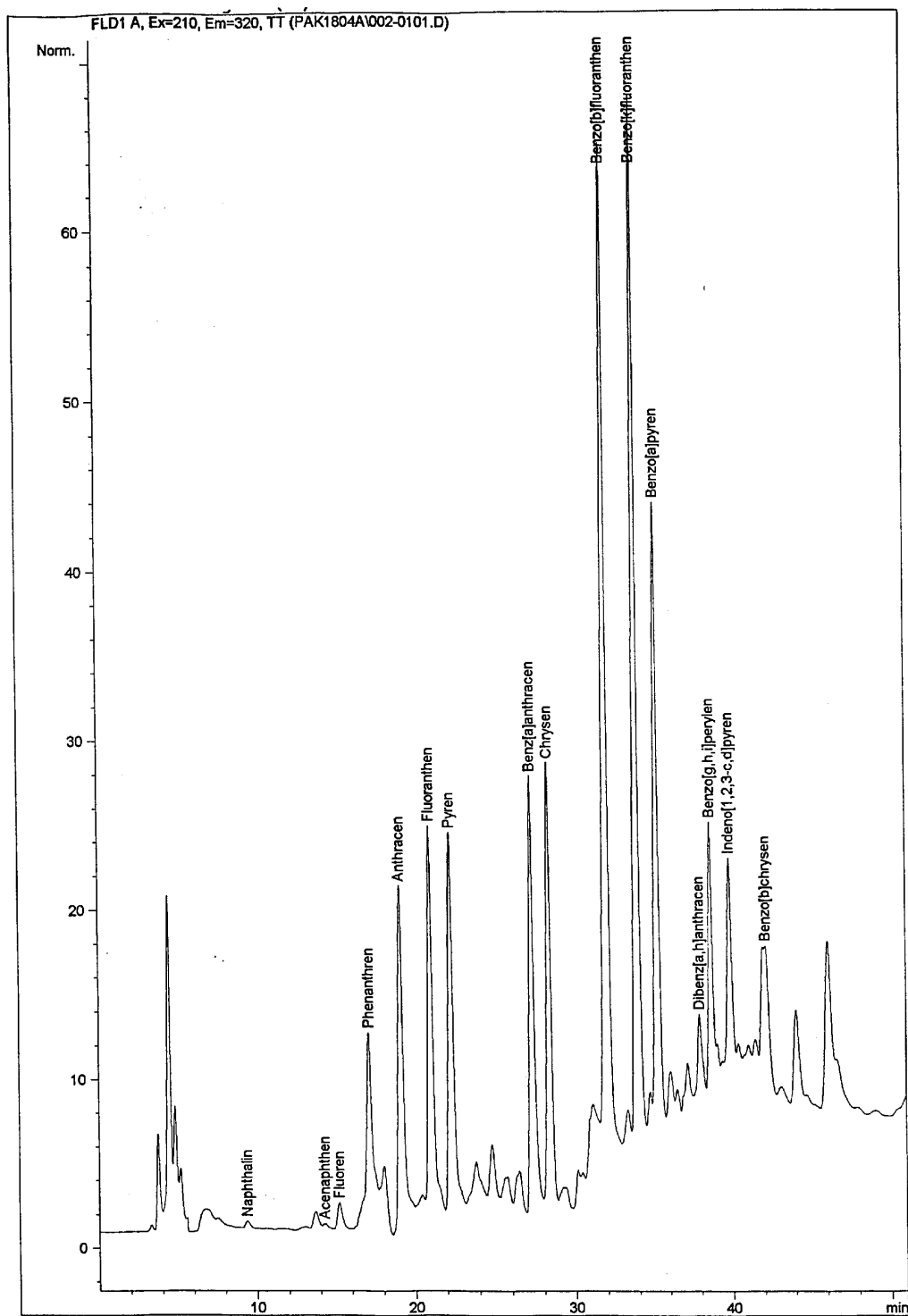


Fig. 3. HPLC-chromatogram of a superheated water extract of the soil sample

Table 3

Comparison of the PAH concentrations quantified by HPLC and by Ohmicron EIA using the supplied phenanthrene calibrant solution

	EIA (mg kg ⁻¹)	HPLC (mg kg ⁻¹)
HS-3	3100	253.5
Soil	477	27.4

already provided as an extractant with the test kit and can easily be diluted with buffer prior to EIA. By this denaturation of the antibodies by an organic solvent can be avoided.

The methanol–water mixtures were analyzed with a PAH specific assay, and the first results obtained for the certified reference material and the soil sample were not very encouraging as can be seen in Table 3. The sum values obtained with the EIA were about a factor 10 higher than the values obtained with HPLC. While the calibration of the HPLC was performed with a certified reference solution (NIST SRM 1647b) the calibration of the EIA was carried out with phenanthrene calibrant solution provided with the test kit. Checking this calibrant solution with HPLC resulted in the discovery that a 50 ~ µg kg⁻¹ labeled phenanthrene solution actually had a concentration of 5 ~ µg kg⁻¹! We assume that with this shift in the calibration curve a low extraction efficiency of the test kit should be compensated. In combination with the efficient extraction method, however this calibration leads to incorrect results.

After correction of EIA results using this factor, the sum values for the PAHs obtained with HPLC and those of the EIA are very similar (HS-3: EIA = 310 mg kg⁻¹, HPLC = 253 mg kg⁻¹; real soil sample: EIA = 47.7 mg kg⁻¹, HPLC = 27.4 mg kg⁻¹). Nevertheless the results for EIA are slightly higher than those for HPLC. We assume that this may be caused by the cross reactivity of the EIA. In the fluorescence chromatogram (Fig. 3) it can be seen that there are much more compounds in the extract than the 15 quantified analytes. These compounds most probably are isomeric or substituted analogues to the 15 quantified PAHs and they can react with the antibody leading to slightly higher results.

Other current research includes the evaluation of other antibodies.

5. Conclusion

Two sets of environmental samples, a certified reference material and a real soil sample, were analyzed using a superheated water extraction method and a quantitative PAH-EIA. The quantitative results were nearly identical with the certified values and with results obtained by conventional Soxhlet extraction and HPLC methods. This suggest that the superheated water extraction-EIA method is an appropriate screening method.

Extraction and analysis using superheated water extraction-EIA results in a greater sample throughput, allowing rapid screening of environmental samples. Furthermore both techniques can be used in the field because no toxic organic chemicals are needed and the type of equipment used can be loaded into a van and operated on a car battery or a small generator. With the superheated water extraction it is possible to extract wet samples directly, thus avoiding the time consuming drying step, as required for SFE or for other extraction methods. Superheated water extraction is a very fast method, it allows quantitative extraction within 15–30 min.

For laboratory use the extraction as well as EIA can be automated for multianalyte analysis and high sample throughput. Because of the high sensitivity of EIA only a very small aliquot of the extract is needed, so that the result can be verified using a different technique (e.g. HPLC) if required.

Acknowledgements

We gratefully acknowledge the Ministerium für Wissenschaft und Forschung des Landes Nordrhein-Westfalens for their financial support. The authors want to thank Axel Semrau GmbH (Sprockhövel) for their generous support donating EIA test kits. This work is part of a doctoral thesis at the Westfälischen Wilhelms-Universität in Münster, Germany.

References

- [1] J.J. Langenfeld, S.B. Hawthorne, D.J. Miller, *Anal. Chem.* 64 (1992) 2263.
- [2] J.J. Langenfeld, S.B. Hawthorne, D.J. Miller, J. Pawliszyn, *Anal. Chem.* 67 (1995) 1727.
- [3] C. Friedrich, K. Cammann, W. Kleiböhmer, *Fresenius Z' Anal. Chem.* 352 (1995) 730.
- [4] T. Paschke, S.B. Hawthorne, D.J. Miller, B. Wenclawiak, *J. Chromatogr.* 609 (1992) 333.
- [5] EPA method 3560, Supercritical fluid extraction of total recoverable petroleum hydrocarbons, SW-846 update 111, Environmental Protection Agency, Washington, DC, 1995.
- [6] EPA method 3561, Supercritical fluid extraction of polynuclear aromatic hydrocarbons, SW-846 update 111, Environmental Protection Agency, Washington, DC, 1995.
- [7] EPA method 3562, Supercritical fluid extraction of polychlorinated biphenyls and organochlorine pesticides, scheduled for future update of SW-846, Environmental Protection Agency, Washington, DC, 1995.
- [8] J. Josephon, *Environ. Sci. Technol.* 16 (1982) 548A
- [9] E.U. Frank, *Pure Appl. Chem.* 24 (1970) 13.
- [10] D. Mackay, W.Y. Shiu, *J. Chem. Eng. Data* 22 (1977) 399.
- [11] S.B. Hawthorne, Y. Yang, D.J. Miller, *Anal. Chem.* 66 (1994) 2912.
- [12] Y. Yang, S. Bowadt, S.B. Hawthorne, D.J. Miller, *Anal. Chem.* 67 (1995) 4571.
- [13] K. J. Hageman, L. Mazeas, C.B. Grabanski, D.J. Miller, S.B. Hawthorne, *Anal. Chem.* 68 (1996) 3892.
- [14] V. Lopez-Avila, C. Charan, *Trends Anal. Chem.* 13 (1994) 118
- [15] J.C. Johnson, J.M. van Emon, *Anal. Chem.* 68 (1996) 162.
- [16] N. Hüsers, W. Kleiböhmer, *J. Chromatogr.* 697 (1995) 107.
- [17] Draft DIN 38414, part 21 (German Industrial Standard), October 1993

Speciation of organotin in environmental sediment samples

M. Ceulemans, S. Slaets, F. Adams *

Department of Chemistry, University of Antwerpen (UIA) B-2610 Wilrijk, Belgium

Received 25 May 1997; accepted 14 October 1997

Abstract

An optimized sample preparation procedure for organotin speciation in sediment samples has been applied to the analysis of sediments collected in the environment. The method is based on tropolone complexation of the ionic organotins, followed by extraction into a hexane–ethylacetate mixture and derivatization by NaBEt₄. The method was applied to the determination of organotin in various harbour, shipyard and dry-dock sediments in Belgium. Butyltin compounds were detected in all samples analyzed, often at high mg kg⁻¹ levels. A limited number of samples showed the presence of phenyltin compounds. Further, the method was adapted to the analysis of river sediments sampled from the vicinity of shipyards. Butyltin concentrations were detected at the µg kg⁻¹ level in the majority of samples. © 1998 Elsevier Science B.V. All rights reserved.

Keywords: Speciation; Organotin; Gas chromatography; Atomic emission spectrometry

1. Introduction

The input levels of organotin compounds in the environment have been considerably restricted in the recent past in most countries due to legislation. Tributyltin (TBT), and to a lesser extent triphenyltin (TPT) used as biocides in anti-fouling paints, nevertheless remain common pollutants of the marine environment, particularly in the sediment matrix. It appears that tri-organotins and the products of their degradation accumulate in the sediment. Attention given to sediment analysis is increasing, considering that the sediment is recognized as the ultimate ‘sink’ for organotin compounds which are released into the aquatic

environment and may create an eco-toxicological risk long after anthropogenic sources are banned from a given area. Therefore, the short residence time of TBT in the water column alone is not an adequate criterion for evaluating its potential environmental hazards. Hence, it is essential that reliable analytical methods are developed for the determination of butyl- and phenyltin compounds in sediments.

In natural waters, TBT has a short residence time, with a half-life in the range of several days to weeks [1,2]. Adsorption of TBT onto suspended particulate matter is thought to be an important removal process. Randall and Weber reported that between 57 and 95% of TBT in the water column is sorbed under simulated estuarine conditions [3]. In this way a significant proportion

* Corresponding author. Fax: +32 3 8202376.

of TBT appears to be deposited, and concentration factors of $\sim 10^3$ relative to the overlying waters are common [4–6]. Slow degradation of TBT in sediments would increase its persistence in the aquatic environment. Studies of TBT degradation in sediment/water mixtures under experimental conditions have been carried out by Maguire et al. [7] and Stang et al. [8] and suggested that TBT has a half-life in sediments of several months. An alternative approach consists in obtaining profiles of TBT concentrations within sediment cores [9], which yields a longer half-life of 1.85 years. Similarly, Quevauviller et al. [10] in a study of sediment cores of Arcachon Bay, France, reported that TBT concentration remains high long after regulation was implemented, hence that this compound is not rapidly degraded in sediment as was previously assumed. Further, TBT has been found to accumulate to concentrations which can probably inhibit biological degradation. The same is valid for TPT compounds which have been shown to have low mobility, low aqueous solubility, and strong binding to soil and sediments in the aquatic environment [11].

Sample preparation procedures for organotin speciation analysis in sediments are generally more complicated than those for water samples. Since organotin compounds are not involved in mineralogical processes and bind onto the surface of the sediment the complete dissolution of the sediment matrix prior to the analysis is not considered necessary. The basic approach to release organotin compounds from the sediment involves, e.g. acid leaching in aqueous or methanolic medium by sonification, stirring or Soxhlet extraction with an organic solvent. Generally, sample preparation procedures for the separation of organotin compounds from sediments are time consuming (several hours). A recent alternative is the use of a low power microwave field which was shown to accelerate the leaching of the organotin species from the sediments considerably and to reduce actual leaching times to a few minutes [12,13].

Data of organotin contents detected in sediments originating from the environment in Belgium are scarce. The only study on TBT contamination, to our knowledge, was carried out

in the frame of a quality survey of dredging sludge originating from some important marine yacht- and fishing harbours [14]. The highest TBT concentrations were found in the harbour of Zeebrugge, as can be seen from Table 1. Further, it was found that locations displaying a high TBT content were also characterized by a strong organic pollution, mainly polycyclic aromatic hydrocarbons. Since TPT compounds strongly adsorb to suspended matter and sediments, they are readily detected in this matrix. During a Belgian survey on the presence of various pesticides in the environment, phenyltin compounds were found in 15% of the sediment samples, with contents ranging from 120 to 190 $\mu\text{g kg}^{-1}$. The highest concentrations were found in the mouth of the Yser river, in the Gaverbeek, a small tributary of the river Scheldt at Harelbeke and in the river Scheldt itself at Doel [15].

This paper presents the application of a sample preparation procedure based on tropolone complexation, liquid–liquid extraction and NaBeT_4 derivatization in a monitoring study to assess the organotin pollution in a number of environmental sediments originating from various waterways in Belgium. The aim was to investigate the impact of dry-docking operations on the contamination of both surficial sediments from shipyard terrains and in river sediments originating from the vicinity of shipyards with regard to their organotin content.

2. Experimental

2.1. Apparatus

GC–AES. Organotin species were separated on an HP-1 capillary column using a Model 5890

Table 1
TBT concentrations detected in marine Belgian harbours [14]

Location	TBT concentration ($\mu\text{g kg}^{-1}$)
Zeebrugge	8–895
Nieuwpoort	15
Oostende	29
Blankenberge	41

Series II gas chromatograph and detected by means of an HP Model 5921 A atomic emission detector (Hewlett–Packard, Avondale, PA). The GC was equipped with a KAS 503 (Gerstel, Mulheim, Germany) programmable temperature vaporization (PTV) injector.

GC–AAS. A Varian Model 3700 gas chromatograph (Varian, Sunnyvale, CA) fitted with a RSL-150 (RSL, Eke, Belgium) megabore column, or an HP Model 5890 Series II gas chromatograph fitted with an HP-1 capillary column were used to separate the analytes prior to the detection by quartz furnace atomic absorption spectrometry (QFAAS); PE Model 2380 (Perkin Elmer, Norwalk, USA). For megabore column GC, samples were introduced on-column through a septum in a wide bore hot on-column liner. Injections on the capillary column were done using PTV as described earlier [16].

Injector, gas chromatograph, interface and detector operating conditions have been described in detail earlier for GC–AAS [17] and GC–AES [18].

2.2. Reagents

Analytical reagent grade chemicals obtained from Merck (Darmstadt, Germany) were used unless otherwise stated. Deionized water, further purified in a Milli-Q system (Millipore, El Paso, TX) system was used throughout. Pentylmagnesiumbromide (2 mol l^{-1} in diethylether) was obtained from Aldrich (Milwaukee, WI). Sodium tetraethylborate was obtained from Strem Chemicals (Bischheim, France). A 0.3% (w/v) aqueous solution was prepared daily. Diethyldithiocarbamic acid was prepared by dissolving 2.25 g of sodium diethyldithiocarbamate (NaDDTC) salt in water. The solution of DDTC in pentane was obtained by shaking the aqueous solution with 20 ml of 0.5 mol l^{-1} of H_2SO_4 and extracting with 10 ml of pentane for 5 min. Acetate buffer (pH 5; 0.1 mol l^{-1}) was prepared by dissolving 13.6 g of sodium acetate trihydrate in 1 l of water, followed by pH adjustment with concentrated acetic acid. A 0.05% tropolone solution was prepared by dissolving the appropriate amount in hexane/ethylac-

etate (1/1). The sources, purity and synthesis of organotin standards have been described earlier [19].

2.3. Procedure

Circa 1 g of sediment was accurately weighed and placed in a centrifugation vessel with glass stopper together with 2 ml of hydrochloric acid (32%) and 8 ml of water; 25 ml of the hexane/ethylacetate mixture (1/1), containing 0.05% tropolone were added and the mixture was sonicated for 1 h, followed by centrifugation at 3000 rpm for 5 min. The organic phase was transferred into an extraction vessel and evaporated to dryness using rotary evaporation. Then, 0.5 ml of hexane, containing Pe_3SnEt as an internal standard, were added and the complexes were derivatized by addition of 1 ml of the NaBEt_4 solution together with 50 ml of acetate buffer solution. The mixture was shaken manually for 5 min and after phase separation the hexane phase was sampled for clean up/analysis. A detailed description and discussion of extract clean-up has been presented previously [20]. A Pasteur pipette was filled with basic alumina to form a plug of 5 cm. The sediment extract was introduced onto the clean-up column. After elution of the original extract volume, an additional volume of 1 ml diethylether was brought onto the clean-up column. The diethylether was evaporated from the combined eluate using a gentle stream of nitrogen.

2.4. Sampling

Sampling of superficial sediments was done using a Peelman drill, or by simple collection by means of a spade. Water-underlying sediments were collected using a Van Veen grab. After removal of stones, leaves and pieces of wood, the sediment was grounded with an agate mortar and pestle. Sediments were either oven-dried at 50°C or freeze-dried and stored at -20°C until analysis, i.e. in agreement with recommendations on sampling and storage procedures for organotin analysis in the marine environment [21,22].

Table 2
Results for the analysis of shipyard and dry-dock sediments

Sample	TBT	DBT	MBT	TPT	DPT	MPT
Concentration \pm 95% confidence interval ($\mu\text{g g}^{-1}$)						
1	35.8 \pm 2.9	13.6 \pm 1.0	6.23 \pm 0.50	1.26 \pm 0.15	0.65 \pm 0.08	1.32 \pm 0.18
3	6.82 \pm 0.42	3.03 \pm 0.16	1.00 \pm 0.09	0.38 \pm 0.07	0.27 \pm 0.05	0.40 \pm 0.06
5	26.4 \pm 1.8	10.0 \pm 0.6	26.4 \pm 1.8	— ^a	—	—
6	141 \pm 10	103 \pm 6	46.2 \pm 3.4	5.55 \pm 0.72	1.55 \pm 22	6.48 \pm 0.91
Concentration \pm 95% confidence interval (ng g^{-1})						
2	390 \pm 35	173 \pm 15	199 \pm 18	—	—	—
4	20.3 \pm 2.2	11.6 \pm 1.0	11.3 \pm 1.4	—	—	—

Mean results for three replicate analyses of each sediment.

^a Concentration below detection limit ($<1 \text{ ng g}^{-1}$).

2.5. Certified reference materials

To evaluate the performance of the plethora of existing sample preparation procedures and instrumental setups used among different laboratories, certified reference materials (CRM's) were prepared by different organizations for the quality control of analytical results. Analysis results of CRM's presented in some reports show that the reliability of sample preparation is often not sufficient and that several limitations still remain. Especially the accurate determination of monobutyltin (MBT) remains doubtful since, according to some reports on certification experiments [23–25], no reliable method for the determination of this compound has been reported up to now. This is apparent from Table 2.

Analysis of CRM's proved that the method presented is able to accurately determine TBT and dibutyltin (DBT) in sediments, while MBT determination in general still remains doubtful due to the absence of reliable, or no or only indicative values for this compound in reference materials. However, the method was shown to be suitable for MBT determination in certain sediments [16].

An attempt to apply the developed procedure to the analysis of phenyltin compounds led to the conclusion that the determination of these species is most favorable in the absence of any tropolone complexing agent and using acetic acid for leaching.

3. Results

3.1. Determination of organotin in harbour and dry-dock sediments

3.1.1. Shipyard located in the Antwerp harbour

Huge point sources such as dry-dock facilities are responsible for the release of the largest fraction of TBT into the aquatic environment. An investigation was carried out to assess the contamination of a shipyard terrain after years of intense dry-docking activities. Further, the influence of these activities on the contamination of the harbour sediment was also investigated.

Fig. 1 shows the location of the sampling sites with the sampling points indicated. A total of five surface samples was taken from the shipyard terrain, three at places where grit blasting activities had taken place, and two samples from other locations at the yard, this in order to assess the background concentration found at the terrain. The investigated ship repair yard was located in the Antwerp harbour, which itself is characterized by intense shipping in an almost enclosed environment with a low flushing rate.

In a previous study on the determination of organotins in waters of the Antwerp harbour, which was carried out over a 4-month period between May and August 1991, two sampling locations (W1, W2) were situated in the vicinity of the shipyard investigated in the present study [26].

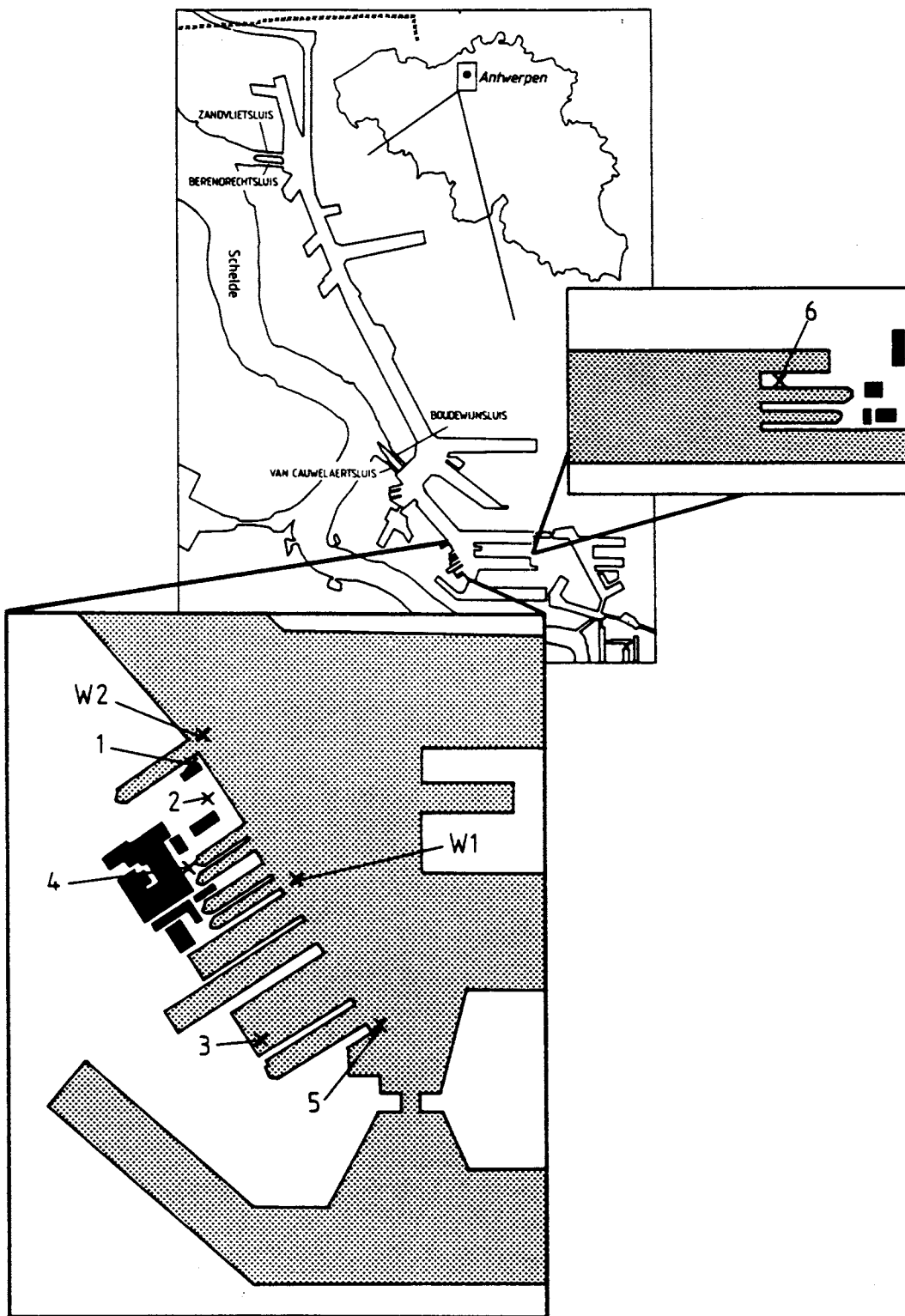


Fig. 1. Sampling locations.

This previous study indicated an overall TBT contamination level in the harbour in the range of 10–45 ng l⁻¹. The concentrations detected at locations W1 and W2 were significantly higher with concentrations ranging between 50 and 440 ng l⁻¹ over the 4-month study period for these two locations. These elevated concentrations found in the water column at these two locations were found due to the discharge of hazardous amounts of TBT in hosing-down water which originates from the washing of ships' hulls, with a high-pressure hosing system before repainting activities. The contaminated water first remains for several days in a sinking-basin and is afterwards released into the poorly flushed harbour dock area. This study already showed the impact of dry-dock activities on the contamination levels in waters of the Antwerp harbour.

In the present study, the impact of dry-docking operations on the contamination of the yard terrain, and harbour sediment was evaluated. The results of the analyses are presented in Table 3. From the results it can be seen that sediments 1, 3 and 6, sampled at locations where grit blasting takes place, generally display very high TBT concentrations at the mg kg⁻¹ level. Comparison with the Environmental Quality Target (EQT) value for TBT in sediments, set at 1–2 µg kg⁻¹ and implemented now in most European countries indicates severe contamination of these surface sediments [27]. Especially the concentration found in sediment 6 (141 mg kg⁻¹), originating from another smaller dry-dock located in the Antwerp harbour, is at extremely high level. Also

DBT and MBT, the intermediate products of TBT degradation to inorganic tin, were found in all the samples. Further, phenyltin compounds were as well detected in these samples, however at much lower concentrations. The presented concentration figures for monophenyltin (MPT) should be considered as indicative values, as extraction and derivatization for this compound was found to be irreproducible as shown earlier [28]. Triphenyltin compounds (mainly TPT fluoride and small amounts of TPT chloride) are used in anti-fouling paints, however to a much lesser extent compared to TBT compounds. About 80% of all anti-fouling paints used contain TBT oxide or TBT metacrylate/methylmetacrylate copolymer, ~12% are TBTF based and ~8% are TBTF based [29,30]. Since TPT compounds are only used in free-association paints, and since there seems to be a general agreement to discontinue the use of this type of paint it is expected that discharges of TPT compounds from anti-fouling paints will decrease in the near future.

The detected contents in samples 2 and 4 taken at places on the yard where no dry-docking operations such as grit blasting, washing, painting, etc. take place display much lower contents at µg kg⁻¹ level. However, the fact that butyltin compounds are detected at these locations may be attributed to an overall contamination of the yard terrain. Sediment 5, collected in the harbour, displays very high TBT concentrations, most probably originating from the hosing-down of TBT waste water in the harbour water and accumulation in the underlying sediments which act as a 'sink' for TBT. A chromatogram for this sediment after sample preparation and GC–AAS measurement is shown in Fig. 2.

The results of this study indicate the need for strict dockyard management to minimize waste generation from dry-docking activities and treatment of contaminated waste waters. Potential waste minimization methods for marine maintenance and repair operations include the minimization of fugitive oversprays of paint (e.g. by changing application methods), the minimization of abrasive blast wastes and of chemical stripping wastes. Apart from high pressure hydro-washing abrasive blasting is often used to remove paint

Table 3
Results for the analysis of dredging sludge samples originating from the Ostend harbour

Sample	Concentration ± 95% confidence interval (µg g ⁻¹)		
	TBT	DBT	MBT
1	1112 ± 120	232 ± 24	80.5 ± 8.1
2	169 ± 14	63.9 ± 6.0	29.2 ± 2.3
3	394 ± 31	181 ± 13	106 ± 8
4	450 ± 32	217 ± 14	123 ± 9

Mean results of three replicate analyses for each sediment.

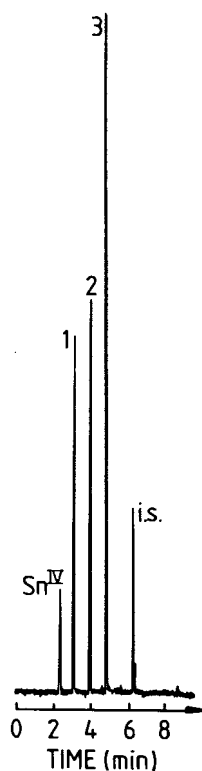


Fig. 2. Chromatogram for a sample of Antwerp harbour sediment: (1) MBT; (2) DBT; (3) TBT; (is) internal standard (Pe_3SnEt).

layers. The most commonly used blasting media are sand or grit together with a large volume of water. The presence of paint chips containing hazardous metallic and/or organometallic biocides makes abrasive blasting wastes potentially hazardous. Blast waste water generally constitutes the largest single waste stream for many yards. For instance, wet abrasive blasting of an average sized naval vessel can generate up to 180 tons of wet abrasive and ca. 2 000 000 l of contaminated water [31]. At the moment research and testing is underway on a number of innovative alternatives to both grit blasting and chemical stripping [32]. Segregation and recycling of blast media is possible because of the difference in density between the grit materials and the waste paint chips. Therefore, in many cases the contaminated grit can be reused several times before becoming too contaminated and requiring off-site disposal. An

approach to prevent fugitive dust emissions would be to enclose the area with plastic sheeting or screening, this confining the waste to the immediate vicinity of the blasting. After blasting has been completed, the waste should be collected and transported to a licensed landfill. Chemical stripping wastes primarily consist of the stripping agent, of which methylenechloride is the most commonly used, and paint sludges. Waste minimization would include the use of less toxic stripping agents such as inorganic strippers consisting of aqueous solutions of caustic soda, and the reuse and recycling of contaminated strippers.

Waste water should be treated in such a way that its TBT contents reduced to a level acceptable for discharge to river or estuarine waters. Equipment for this purpose is commercially available and generally uses a 4-stage process, two concerned with solids (principally paint solids) reduction and two concerned with removing TBT from the water. Briefly, the different stages are as follows: (1) flocculation and settling in which the pH of the raw wash water is adjusted to effect flocculation and agglomeration of the solids present; (2) filtration where the supernatant water from the settling stage is pumped to a 2-stage filtration system, and particles are removed to the sub-micron diameter range to ensure that paint particles which could still release TBT to the surrounding water are not present in the subsequent treatment steps; (3) carbon adsorption where the first stage of dissolved TBT removal is effected by adsorption onto activated carbon; (4) after passing through the carbon bed, the process water passes through a filter, to remove residual carbon particles and then to a device whereby it is irradiated with short-wave UV light. The concentrations of TBT can be effectively reduced to concentrations less than $0.2 \mu\text{g l}^{-1}$ by oxidation reactions induced by the UV light, producing harmless tin oxide. The UV light irradiation step is the final stage in this type of waste water treatment plant. However, the majority of commercial shipyards discharge their effluents directly to the aquatic environment at no direct costs. Any treatment system thus becomes an additional cost burden to their operations. This cost burden will only be acceptable commercially if all yards (in-

side and outside EU) are required to undertake environmental protection measures simultaneously. It is estimated that through the use of waste water treatment plants a reduction of emissions up to 85% could be accomplished.

3.1.2. Dredging sludge from the Ostend harbour

Dredging sludge samples were originating from various locations in the Ostend harbour where dredging activities had taken place. The harbour is characterized by intense shipping activities from pleasure crafts and ferry ships. Samples were analyzed in order to assess the organotin levels present in the Ostend harbour. Further, analyses of these samples would give an idea about the organotin contamination which may be introduced into non-contaminated areas, through dumping of these dredging sludges.

The results of the analyses are presented in Table 4. All samples showed the presence of butyltin compounds at concentrations up to mg kg^{-1} level, indicating contamination of the Ostend harbour due to shipping activities. Further, results suggest that dredging sludges originating from harbours and marinas should be collected and treated with care in order to avoid contamination of other areas through dumping of this sludge. Contaminated soils must be removed and either incinerated in special plants or be deposited at special waste disposal sites according to local or government regulations. Generally, it was found that dredging activities reduce TBT concentrations in harbours and marinas [33]. Dredging removes TBT-contaminated sediments, and because of the sediment-water partitioning, finally results in lower TBT concentrations in the water phase.

3.1.3. Shipyard for pleasure crafts

A surface sediment was taken from a small shipyard located at the Zuidwillemsvaart (Bocholt, Limburg). The yard is mainly used for the maintenance of small vessels and pleasure crafts. Amounts detected were $6.60 \pm 0.08 \text{ mg kg}^{-1}$ for TBT, $1.67 \pm 0.20 \text{ mg kg}^{-1}$ for DBT and $1.15 \pm 0.05 \text{ mg kg}^{-1}$ for MBT. A chromatogram for this sediment, after sample preparation and GC-QFAAS measurement is shown in Fig. 3. The

height of the TBT concentration detected, plus the pattern of the concentrations of the degradation products DBT and MBT, which were found in much lower concentrations, indicate recent dis-

Table 4
Results for the analysis of river sediments originating from the vicinity of shipyards

Shipyards	Concentration \pm 95% confidence interval ($\mu\text{g kg}^{-1}$)		
	TBT	DBT	MBT
Rupelmonde	17.3 ± 2.8	30.5 ± 3.3	19.4 ± 1.6
	30.5 ± 2.8	61.5 ± 5.8	34.3 ± 1.8
	65.8 ± 11.8	97.8 ± 15.3	47.8 ± 10.5
	76.8 ± 4.5	221 ± 11	130 ± 9
	73.3 ± 5.8	169 ± 31	77.0 ± 15.3
	21.2 ± 1.3	41.5 ± 4.3	19.2 ± 3.1
	63.5 ± 5.5	117 ± 6	69.3 ± 4.3
	2.37 ± 1.12^a	2.78 ± 0.80	0.83 ± 0.13
Nieuwe	54.0 ± 6.0	106 ± 8	49.3 ± 5.3
Scheldewerven	55.3 ± 8.5	98.3 ± 8.8	52.3 ± 9.8
	227 ± 24	196 ± 12	111 ± 6
	89.0 ± 6.0	155 ± 11	70.8 ± 5.5
	85.0 ± 4.3	144 ± 9	70.3 ± 5.5
	88.3 ± 3.5	181 ± 15	72.0 ± 6.8
	95.0 ± 11.3	168 ± 9	78.0 ± 4.5
	<DL ^a	5.38 ± 1.20	2.69 ± 0.58
Boelwerf	133 ± 17	166 ± 11	60.0 ± 4.2
	316 ± 30	286 ± 31	108 ± 10
	82.0 ± 10.4	90.6 ± 10.8	32.3 ± 2.3
	43.7 ± 6.1	96.6 ± 11.0	34.9 ± 4.2
	<DL ^a	3.49 ± 1.2	9.65 ± 2.6
	4.49 ± 0.63^a	4.10 ± 0.82	7.75 ± 1.55
Fulton Marine	50.3 ± 4.8	140 ± 14	82.0 ± 10.5
	271 ± 78	1499 ± 173	717 ± 144
	51.2 ± 5.6	194 ± 18	81.0 ± 10.0
	68.2 ± 6.2	260 ± 16	150 ± 15
	4.44 ± 1.00	47.3 ± 5.2	20.4 ± 2.7
	134 ± 9	119 ± 9	47.3 ± 4.4
	9.11 ± 1.40	43.5 ± 4.1	19.9 ± 2.5
	7.71 ± 1.1	58.7 ± 5.2	26.4 ± 2.6
Langerbrugge	105 ± 6	42.4 ± 2.6	15.4 ± 1.1
	34.6 ± 3.8	31.1 ± 2.2	19.3 ± 2.5
	88.5 ± 10.1	22.1 ± 3.5	9.50 ± 1.9
	2.91 ± 0.72^a	<DL	<DL
	<DL ^a	<DL	<DL

<DL, below detection limit ($<1 \mu\text{g kg}^{-1}$).

Mean results of three replicate analyses for each sediment.

^a Sediments taken at larger distances from the yard.

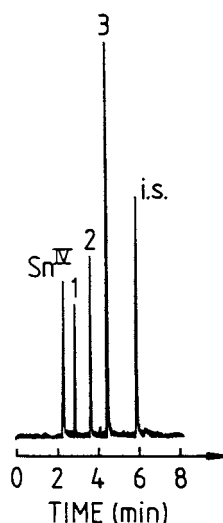


Fig. 3. Chromatogram for a sample of Bocholt shipyard sediment: (1) MBT; (2) DBT; (3) TBT; (is) internal standard (Pe_3SnEt).

charges of TBT, suggesting the illegal usage of TBT-containing anti-fouling paints, since following current legislation the use of these paints is forbidden on ships smaller than 25 m.

3.1.4. Determination of organotin in river sediments

Analyses of sediment samples originating from shipyards and dry-dock terrains revealed the presence of very high concentrations of various organotin compounds. In cooperation with the Flemish Environmental Agency (VMM) a sampling campaign was carried out (Summer '95) in which river sediments were taken from the vicinity of shipyards. The aim of the study was to investigate whether the pollution is restricted to the yard and dock terrains itself or also has a wider effect on the contamination of the adjacent rivers. A total of 35 river sediments, originating from the vicinity of five different yards located in Flanders were analyzed. For a given shipyard sampling was carried at different locations in the river. Further, for each shipyard sediments were also taken at larger distances from the yard, up- and down-stream on the river, in order to assess the polluting impact of shipyard activities over longer distances.

The results of all 35 sediments are presented in Table 4. Generally, butyltin compounds were detected in all river sediments which were sampled in the vicinity of the shipyards. Phenyltin compounds were not detected in any of the samples. The detected levels are, in comparison with contents detected on the yard terrain itself, generally much lower, however in the majority of the samples analyzed they are a multiple of the EQT value for TBT in sediments, set at $1\text{--}2\ \mu\text{g kg}^{-1}$. Concentrations detected in river sediments sampled at larger distances, generally display contents below detection limits or at the low $\mu\text{g kg}^{-1}$ levels indicating the local impact of dry-dock operations on the contamination of adjacent rivers. A chromatogram for a sample of river sediment is shown in Fig. 4.

TBT concentrations detected in the river sediments originating from the vicinity of the Rupelmonde shipyard range between $17\text{--}77\ \mu\text{g kg}^{-1}$ representing an overall contamination level in the seven sediments sampled in the vicinity of the

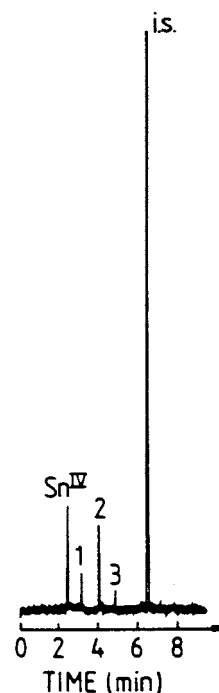


Fig. 4. Chromatogram for a sample of river sediment: (1) MBT; (2) DBT; (3) TBT; (is) internal standard (Pe_3SnEt).

yard. TBT contents detected in the river Scheldt in the vicinity of the Nieuwe Scheldewerven range between 54 and 95 $\mu\text{g kg}^{-1}$ for the seven sediments analyzed, with one peak value of 227 $\mu\text{g kg}^{-1}$. This higher value may be attributed to the fact that this sampling location could have been close to a waste water disposal line of the shipyard. TBT contents detected in Scheldt river sediments taken from the vicinity of the Boelwerf display more varying concentrations ranging between 44 and 316 $\mu\text{g kg}^{-1}$, a concentration level suggesting a high transfer of TBT contaminants from the yard into the river. The concentrations detected in the Wintham–Brussel Canal near the Fulton Marine yard are more variable and range from 4 to 271 $\mu\text{g kg}^{-1}$. The same variability of detected contents occurs in the vicinity of the yard in Langerbrugge with concentrations between 35 and 105 $\mu\text{g kg}^{-1}$. Analysis of water samples taken from the draining system of this particular yard already showed butyltin concentrations up to the $\mu\text{g l}^{-1}$ level.

The results of this study clearly indicated that organotin contamination of the environment through dry-docking activities is not only restricted to the yard terrain itself, but also has wider polluting effects on the adjacent waterways. Further, it was shown that through the analysis of sediments originating from larger distances that the polluting impact is restricted to the immediate vicinity of the yard.

4. Conclusions

This work describes the application of a novel method for the speciation analysis of organotins to a number of environmental sediment samples. Through the analyses of surficial sediments originating from shipyards and dry-docks it was concluded that dry-dock operations may create severe organotin contamination of the yard territories. Further, the results from the analysis of river sediments sampled in the vicinity of dry-docks and shipyards showed the transfer of organotin contaminants from shipyards to the adjacent rivers and show the need for effective dry-dock management and waste water treatment in order

to protect the aquatic environment. TBT was detected in the majority of the samples analyzed, often at concentrations much higher than the Environmental Quality Target for TBT in sediments, indicating that the problem of contamination of the marine environment is far from solved, despite recent alternative anti-foulants, legislation and EU directives towards the use of this compound.

References

- [1] R.F. Lee, A.O. Valkirs, P.F. Seligman, *Environ. Sci. Technol.* 23 (1989) 1515.
- [2] J.E. Thain, M.J. Waldoock, M.E. Waite, *Oceans '87*, 1987, p. 1256.
- [3] L. Randall, J.H. Weber, *Sci. Total Environ.* 57 (1986) 191.
- [4] R.J. Maguire, R.J. Tkacz, Y.K. Chau, G.A. Bengert, P.T.S. Wong, *Chemosphere* 15 (1986) 253.
- [5] V.F. Hodge, S.L. Seidel, E.D. Goldberg, *Anal. Chem.* 51 (1979) 1256.
- [6] C. Stewart, S.J. de Mora, *Environ. Technol.* 11 (1990) 565.
- [7] R.J. Maguire, R.J. Tkacz, *J. Agric. Food Chem.* 33 (1985) 947.
- [8] P.M. Stang, P.F. Seligman, *Oceans '86*, 1986, p. 1256.
- [9] S.J. de Mora, N.G. King, M.C. Miller, *Environ. Technol. Lett.* 10 (1989) 901.
- [10] Ph. Quevauviller, O.F.X. Donard, H. Etcheber, *Environ. Pollut.* 84 (1994) 89.
- [11] S.J. Blunden, L.A. Hobbs, P.J. Smith, in: P.J. Craig (Ed.), *Organometallic Compounds in the Environment*, Longman, Harlow, 1986, p. 111.
- [12] J. Szpunar, M. Ceulemans, V.O. Schmitt, F.C. Adams, R. Lobiński, *Anal. Chim. Acta* 332 (1996) 225.
- [13] O.F.X. Donard, B. Lalère, F.M. Martin, R. Lobiński, *Anal. Chem.* 67 (1995) 4250.
- [14] BMM, *Diensten van de Vlaamse Executieve, Openbare Werken en Verkeer, Bestuur der Waterwegen en van het Zeewezen*, Report, October 1989.
- [15] C. Plasman, M.A. Demeyere, *Rapport sur les Recherches de Pesticides dans les eaux de surface en Belgique, Unité de Gestion du Modèle Mathématique de la Mer du Nord*, Report, July 1993.
- [16] M. Ceulemans, F.C. Adams, *Anal. Chim. Acta* 317 (1995) 161.
- [17] W. M. R. Dirx, R. Lobiński, F.C. Adams, *Anal. Sci.* 9 (1993) 273.
- [18] R. Lobiński, W.M.R. Dirx, M. Ceulemans, F.C. Adams, *Anal. Chem.* 64 (1992) 159.
- [19] M. Ceulemans, R. Lobiński, W.M.R. Dirx, F.C. Adams, *Fres. J. Anal. Chem.* 347 (1993) 256.

- [20] M. Ceulemans, C. Witte, R. Lobiński, F.C. Adams, *Appl. Organomet. Chem.* 8 (1994) 451.
- [21] Ph. Quevauviller, O.F.X. Donard, *Fres. J. Anal. Chem.* 339 (1991) 6.
- [22] Ph. Quevauviller, in: O.F.X. Donard, S. Caroli (Eds.), *Element Speciation in Bioinorganic Chemistry*, vol. 135, Wiley, New York, 1996, p. 331.
- [23] S. Zhang, Y.K. Chau, W.V. Li, A.S.Y. Chau, *Appl. Organomet. Chem.* 5 (1991) 431.
- [24] Ph. Quevauviller, M. Astruc, L. Ebdon, Y. Desauziers, P.M. Sarradin, A. Astruc, G.N. Kramer, B. Griepink, *Appl. Organomet. Chem.* 8 (1994) 629.
- [25] Ph. Quevauviller, M. Astruc, L. Ebdon, G.N. Kramer, B. Griepink, *Appl. Organomet. Chem.* 8 (1994) 639.
- [26] W.M.R. Dirkx, R. Lobiński, M. Ceulemans, F.C. Adams, *Sci. Total Environ.* 136 (1993) 279.
- [27] M. Ceulemans, Development of organometal speciation analysis by GC based hyphenated techniques and environmental applications, PhD thesis, 1996.
- [28] J.A. Stäb, U.A.Th. Brinkman, W.P. Cofino, *Appl. Organomet. Chem.* 8 (1994) 577.
- [29] O.M. Crijns, Watersysteemverkenningen, een analyse van de problematiek in aquatisch milieu, RIZA nota 92014, April 1992.
- [30] P.R. Willemsen, G.M. Ferrari, Emissies van organotin naar Nederlands oppervlaktewater, TNO-Report N C92.1004.
- [31] C.M. Adema, G.D. Smith, Development of cavitating water jet paint removal system, in: *Waste Minimization and Environmental Programs within DoD*, Proc. 15th Environmental Symposium, April 1987, pp. 270–275.
- [32] EPA, Guides to pollution prevention: the marine maintenance and repair industry, US Environmental Protection Agency, Cincinnati, Ohio, OH 45268, EPA/625/7-91/015, October 1991.
- [33] R. Ritsema, *Appl. Organomet. Chem.* 8 (1994) 5.

Macro and microchemistry of trace metals in vitrified domestic wastes by laser ablation ICP-MS and scanning electron microprobe X-ray energy dispersive spectroscopy

M. Motelica-Heino ^{a,*}, P. Le Coustumer ^b, J.H. Thomassin ^b, A. Gauthier ^b,
O.F.X. Donard ^a

^a *Laboratoire de Chimie Bio-Inorganique & Environnement, EP CNRS 132, Helioparc, 6400 Pau, France*

^b *Laboratoire des Matériaux et Géologie Environnementale, ESIP, 40 Av. du recteur Pineau, 86022 Poitiers cedex, France*

Received 25 May 1997; accepted 14 October 1997

Abstract

Management of domestic wastes often relies on incineration, a process that eliminates large amount of wastes but also produces toxic residues that concentrate heavy metals. Those hazardous secondary wastes require specific treatment. Vitrification is seen as a powerful way to stabilise them. However, concern exists about the long term behaviour of these glass wastes and the potential release of toxic species into the environment. The answers will come with further investigation into the physico-chemical evolution of the vitrified wastes and the mobility of hazardous elements within the matrix with appropriate analytical methods. Laser ablation coupled with inductively coupled mass spectrometry (LA-ICP-MS) is a challenging technique for the chemical analysis of trace elements in solid materials. This paper presents an evaluation of the potential of LA- ICP-MS for macro and microanalysis of trace metals in domestic vitrified wastes with regards to other physical analytical techniques of solids such as scanning electronprobe X-ray energy dispersive spectroscopy (SEM-EDXS). Two typical samples, vitreous and crystallised, are used to compare the analytical performances of the two techniques. SEM-EDXS was used for mineralogical characterisation and chemical analysis of the mineralogical phases. Relative micro-analysis and bulk quantitative analysis of 30 major, minor and trace elements was performed by LA-ICP-MS: precision was between 10 and 20% for most elements and quantitative analysis proved possible with an accuracy of 20% and relative detection limits of 0.1 mg kg⁻¹. © 1998 Elsevier Science B.V. All rights reserved.

Keywords: Laser ablation; ICP-MS; Vitrified wastes; Trace metals; Structure and texture

1. Introduction

Management of domestic waste is an important issue for the community in a changing context of

regulations requiring wastes to be treated and recycled. One popular elimination technique is based on the incineration of wastes followed by the treatment of fumes. This process reduces the volume of waste but also generates secondary toxic wastes: ashes and residues of filtration of

* Corresponding author.

fumes (REFIOM in French). REFIOM concentrate metals such as Zn, Cu, Pb, Sn, Cr, Ni coming from batteries, plastic or metallic cans, inks etc. Therefore specific treatment is needed to stabilise these wastes before they can be considered as ultimate wastes. Two methods of stabilisation and neutralisation are investigated i.e. incorporation in a solid matrix (cement or concrete) or vitrification. Investigations of hazardous wastes employing vitrification in a plasma torch at temperatures over 6000°C have been carried [1]. This original process produces glasses from the wastes themselves. Vitrified glasses from ashes collected after the thermal incineration of domestic wastes are ceramic-like glasses. This matrix seems to be an ideal host for toxic elements. However, before classification of these 'ultimate wastes' it is necessary to understand the long term behaviour of their matrix and evaluate the potential release of toxic species to the environment. Risk assessment studies require evaluation methodologies based on experimental predictive models and analytical tools to monitor the evolution of vitrified waste matrix and the fate of hazardous elements trapped in the matrix.

Chemical analysis of solids often requires samples to be dissolved prior to analysis which is often time consuming, difficult to perform and might result in some contamination.

Instrumental techniques that allow direct analysis of solid samples are mostly based on physical techniques: so far non destructive methods such as X-ray fluorescence (XRF), particle induced X-ray excitation (PIXE), electronprobe microanalysis (EPMA) and destructive methods like neutron activation analysis (NAA), ion microprobe (SIMS) have been extensively used for micro, bulk and surface analysis.

Micro-beams coupled with trace element techniques provide new tools for the direct analysis of trace elements in solid samples. LA-ICP-MS is a tandem analytical technique where the laser beam is used as a sampling probe and the ICP-MS as a detector. When targeted to the sample surface the laser beam generates microparticulate material that is brought with an argon stream into the inductively plasma where it is atomised and ionised, ions are then separated and detected within the mass spectrometer.

LA-ICP-MS has been extensively reviewed, for its fundamental aspects [2,3], technology [4] and application to geochemical analysis [5,6]. Although it can be used for bulk analysis its key feature is the ability to spatially resolve chemical analysis at different space scales. LA-ICP-MS can perform micro-analysis with high spatial resolution up to 10 µm as well as lateral profiling, surface mapping and depth gradients. Therefore LA-ICP-MS can deal with heterogeneous samples without losing information.

Little work has been carried out with in-situ characterisation of trace metals in the REFIOM vitrified wastes. SEM-EDXS was used for chemical analysis of mineralogical phases but the analysis is limited to major and minor elements [7]. So far chemical analysis of trace elements in REFIOM relied on the use of conventional ICP-MS after dissolution of the material or were performed on leaching solutions [8]. Therefore no spatial information is available for trace metals distribution in vitrified wastes.

The aim of this work is to perform spatially resolved chemical analysis of trace metals in vitrified wastes using LA-ICP-MS. Two real vitrified waste samples were used as models to investigate the analytical potential of LA-ICP-MS and its performances compared with analytical techniques of solids such as SEM-EDXS.

2. Experimental

2.1. Samples

Two typical samples representative of vitrified domestic wastes generated by plasma techniques were used in the present sets of experiments.

The original material originated from a single melting bath at 1616°C after elaboration by plasma techniques. The material from the melting bath underwent fractionated crystallisation during the cooling process and two phases (vitreous and crystallised) could be distinguished at macroscopic level. The two samples 1C and 1V were extracted respectively from the crystallised and vitreous phase by diamond drilling and then manufactured in the form of pellets (1 cm diameter, 2

mm high). The two samples showed different structure and texture. These wastes have been characterised elsewhere for their mineralogy and chemical composition using conventional ICP-MS [8]. The REFION glass wastes contains vitreous and crystallised phases, mostly sorosilicates and spinels.

2.2. Instrumentation

2.2.1. AAS

The chemical composition of the matrix (major and minor elements) were established with the Perkin Elmer 3110 Atomic Absorption Spectrometer (AAS). Samples were fused into strontium metaborate after grinding into a fine powder that was dissolved with acid prior to analysis using a conventional protocol defined previously [9].

2.2.2. XRD

Each sample was crushed and ground up to a micrometer size powder before analysis. An X-ray diffractometer PHILIPS PW1729 (X-Ray lamp with an Co anticathode at a voltage of 30 kV with an emission current of 40 mA) with a Bragg Goniometer (rotation speed $0.02^\circ \text{ s}^{-1}$ and acquisition time 2 s by step) was used to investigate the structure and the mineralogy of the samples.

2.2.3. SEM-EDXS

The texture of the samples at micrometer scale was studied with a Scanning Electron Microscope (SEM). A JEOL 6400C SEM equipped with an tungsten filament (voltage 15 keV, filament current 200 μA and current emission 10 μA) was used. To access the submicrometric chemistry the SEM was fitted with a Kevex X-ray Energy Dispersive Spectroscopy (X-EDS) detector (Si–Li diode, ultra-thin parylene window). Electron beam size modulation allowed investigation at different space scales, from 1 μm^2 in punctual mode up to 1000 μm^2 in the window mode. Acquisition parameters were the following: 25 mm height, 30° take-off angle, 120 s acquisition time. Each spectrum was treated using the following procedure: background subtraction, gaussian deconvolution and ZAF correction using a standard database [10]. With this configuration a rela-

tive precision of about 5–6% for elements with an atomic number above 10 and a concentration above 10 g kg^{-1} can be expected [11]. Before the analysis samples were polished (optical quality) and metallized by amorphous carbon. SEM-EDXS was used to fingerprint elements within specific locations and to measure concentration variations in a given sample.

2.2.4. LA-ICP-MS

The CETAC LSX 100 laser sampling device has been coupled to the standard Perkin-Elmer ELAN 5000 ICP-MS. The Nd:YAG laser was operated at the fourth harmonic wavelength of 266 nm with a pulse frequency of 1–20 Hz and maximum energy of 4 MJ per pulse in the Q-switched mode. The laser beam was focused 1 mm under the sample surface. The sample was translated to allow analysis of a specific area. The sampling pattern was therefore a straight line. The ICP-MS was tuned while firing the NIST 612 glass standard to produce a continuous signal. B11, La 139 and Th232 were used as tuning elements to maximise sensitivity and limit signal fluctuations to 5% RSD.

Laser and ICP-MS operating conditions are presented in Table 1. Cr^{52} was used to correct for isobaric interference of Fe^{54} . Rastering the sample generated a continuous signal. The blank was subtracted from the raw signals further processing. The time resolved analysis mode allows signals to be on-line normalised to a reference signal. Absolute or relative signals were then averaged over the acquisition. Glass NIST 612 was used for calibration. This certified reference material is a homogenous glass with 61 elements at a nominal concentration of 50 mg kg^{-1} . Thirty elements are certified: SiO_2 (720 g kg^{-1}), CaO (120 g kg^{-1}), Na_2O (140 g kg^{-1}), Al_2O_3 (20 g kg^{-1}), Ba (41 mg kg^{-1}), B (32 mg kg^{-1}), Ce (39 mg kg^{-1}), Co (35.5 mg kg^{-1}), Cu (37.7 mg kg^{-1}), Dy (35 mg kg^{-1}), Er (36 mg kg^{-1}), Eu (36 mg kg^{-1}), Gd (39 mg kg^{-1}), Au (5 mg kg^{-1}), Fe (51 mg kg^{-1}), La (36 mg kg^{-1}), Pb (38.57 mg kg^{-1}), Mn (39.6 mg kg^{-1}), Nd (36 mg kg^{-1}), Ni (38.8 mg kg^{-1}), Rb (31.4 mg kg^{-1}), Sm (39 mg kg^{-1}), Ag (22 mg kg^{-1}), Sr (78.4 mg kg^{-1}), Tl (15.7 mg kg^{-1}), Th (37.79 mg kg^{-1}), Ti (50.1 mg kg^{-1}), U (37.38 mg kg^{-1}).

Table 1
Laser and ICP-MS operating conditions

Laser parameters	
Laser type	Nd:YAG
Wavelength	266 nm
Mode	Q-switched
Energy	4 MJ
Shot repetition rate	20 Hz
Focus	+1 mm
Translation rate	10 $\mu\text{m s}^{-1}$
Plasma conditions	
RF power	1200 W
Plasma gas flow	15.0 l min^{-1}
Auxiliary gas flow	0.85 l min^{-1}
Nebulizer gas flow	1.20 l min^{-1}
Data acquisition parameters	
Scanning mode	Peak hop
Replicate time	200 ms
Dwell time	200 ms
Sweeps/reading	1
Reading/replicate	1
Number of replicates	10
Acquisition time	1 min
Elements scanned	Li ⁷ , B ¹¹ , Mg ²⁶ , Al ²⁷ , Si ²⁹ , P ³¹ , Ti ⁴⁹ , Cr ⁵² , Cr ⁵³ , Fe ⁵⁴ , Mn ⁵⁵ , Co ⁵⁹ , Ni ⁶⁰ , Cu ⁶³ , Zn ⁶⁶ , As ⁷⁵ , Sr ⁸⁸ , Zr ⁹⁰ , Mo ⁹⁸ , Ag ¹⁰⁷ , Cd ¹¹⁴ , Sn ¹²⁰ , Sb ¹²¹ , Cs ¹³³ , Ba ¹³⁷ , La ¹³⁹ , Ce ¹⁴⁰ , Nd ¹⁴⁶ , W ¹⁸⁶ , Pb ²⁰⁸ , Bi ²⁰⁹ , Th ²³² , U ²³⁸

kg^{-1}), Yb (42 mg kg^{-1}). The uncertainty of these certified values are 5% or better.

2.3. Method

The matrix of the vitrified wastes was first characterised for physico-chemical properties such as bulk composition and mineralogy using physical analytical techniques of solids. SEM-EDXS was used to perform chemical analysis of different mineralogical phases. LA-ICP-MS was used to study trace elements at different space scales. The investigation strategy is summarised in the flowchart (Fig. 1).

2.3.1. Physico-chemistry of the matrix

The vitrified wastes were characterised for their matrix properties by physical analytical techniques. Physico-chemical characterisation of the matrix included determination of chemical com-

position, structure and texture. Bulk chemical composition samples 1C and 1V were analysed using AAS. The structure of the two samples was investigated by XRD and the texture was studied using optical microscopy and SEM. Matrix physico-chemical properties are summarised in Table 2.

2.3.1.1. Chemical composition of the matrix.. The average chemical composition of the matrix was similar for the two samples. Vitrified REFION were calco-silico-alumino glasses with Fe, Mg, Ti, P, K, Zn occurring as minor elements ($\sim 10 \text{ g kg}^{-1}$).

2.3.1.2. Structure.. For sample 1V, XRD analysis recorded typical patterns of amorphous materials. For the crystallised sample 1C the presence of Gehlenite and Melilite was noticed together with some amorphous parts.

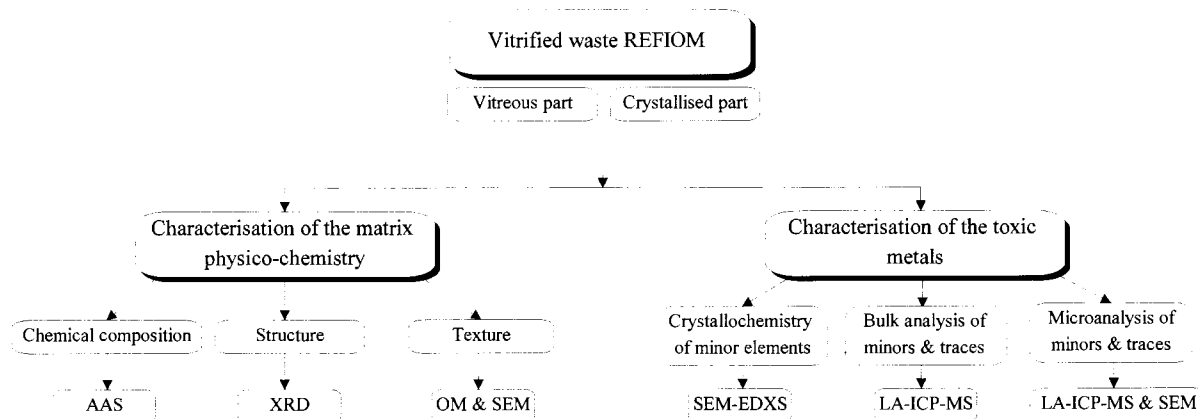


Fig. 1. Characterisation of hazardous elements in vitrified wastes—Methodology

2.3.1.3. Texture. Optical microscopic examination led to distinguishing two textural sets: amorphous dominant (1V) and crystallised dominant (1C). At this scale sample 1V appeared homogeneous (aphanitic texture) with some rare crystallised zones (square crystals with dark extinction in polarised light, typically spinels). SEM observation confirmed the homogeneity of this sample. Sample 1C was heterogeneous at the microscale level. The texture was a microlitic one including large automorphous crystals (10–100 μm size) surrounded by a thin amorphous matrix. At SEM scale cavities of 100 μm size occurred. Some of these cavities contained automorphous micrometric crystals (10–100 μm size) such as spinels (cubic crystals, XY_2O_3) and sorosilicates ($\text{X}_x\text{Y}_y\text{Si}_z\text{O}_7$). The spinel crystals were precipitates of oxides of Fe or Al such as Gahnite (ZnAl_2O_4) and Franklinite (ZnFe_2O_4). The sorosilicates were Melilite ($\text{NaCaAlSi}_2\text{O}_7$) and Gehlenite ($\text{Ca}_2\text{Al}_2\text{SiO}_7$).

2.3.2. Crystallochemistry of the wastes

Chemical characterisation of the mineralogical phases was performed using SEM-EDXS to investigate the partition of metals between the crystallised and the vitreous phase. The metal chemistry of the two REFIOM samples 1V and 1C were compared. SEM-EDXS was used as a relative technique to investigate the variations of major and minor elements between individual

mineralogical phases.

The analysis of one spinel crystal in sample 1C was performed in the punctual mode (1 μm^2 window). A larger window (100 μm^2 window) was used to scan the vitreous phase (sample 1V) and the crystallised sample 1C at two typical locations: one with automorphous crystals and the other with microlitic crystals. SEM-EDXS data for different mineralogical phases are presented in Fig. 2.

The sorosilicates crystals contained more Fe, Zn, Na, Cr, and Mn than the vitreous phase. Zn, Fe and Cr were slightly enriched in the automorphous crystals compared with the microlitic ones. The spinel crystal showed depletion in Si, P, K and Ca together with strong enrichment of Al and Mg and also some enrichment of Fe and Zn compared with the sorosilicates crystals and the vitreous phase.

2.3.3. Chemical analysis of trace metals by LA-ICP-MS

Characterisation of the trace metals trapped in vitrified wastes was based on bulk and also microanalysis by LA-ICP-MS. LA-ICP-MS was used for quantitative bulk analysis of samples 1C and 1V. For microanalysis, LA-ICP-MS was used as a relative technique to study the variations of trace metals between different mineralogical phases in sample 1C.

Table 2
Physico-chemical characterisation of the vitrified waste matrix

Sample	1V	1C
Structure (DRX)	Mainly amorphous Minor crystallised phase	Mainly crystallised Sorosilicates Melilite($\text{NaCaAlSi}_2\text{O}_7$), Gehlinitite ($\text{Ca}_2\text{Al}_2\text{SiO}_7$) Spinel Gahnite(ZnAl_2O_4), Franklinite(ZnFe_2O_4) Minor amorphous phase
Texture (OM&SEM)	Vitreous matrix with micrometric automorphous crystals Homogeneous texture	Auto morphous crystals 10–50 μm (sorosilicates and spinels) and microlitic crystals (sorosilicates) included in a vitreous phase Heterogeneous texture with cavities (100 μm) containing spinels and sorosilicates
Bulk composition (AAS) $\times 10 \text{ g kg}^{-1}$		
1		
SiO_2	31	30
Al_2O_3	21	25
CaO	32	30
Fe_2O_3	3	3
MgO	4	3
TiO_2	3	3
Na_2O	2	2
P_2O_5	2	2
K_2O	0	0
MnO	0	0
Cr_2O_3	0	0
ZnO	1	1

2.3.3.1. *Sampling and analytical strategy.* When defining the sampling scale and the analytical strategy, there is a compromise between the amount of ablated material, the number of elements scanned by the mass spectrometer and the limits of detection expected. With a pulse frequency of 20 Hz, an energy of 4 MJ pulse⁻¹ and 10 $\mu\text{m s}^{-1}$ sampling translation rate, the laser drills 50 μm size pits, thus generating a continuous straight line, width 50 μm . The sampling probe is therefore bigger than the size of the individual components of the sampled matrices. In fact 1V was homogeneous at this scale and 1C was heterogeneous at the micrometric scale. The elemental ablation pattern chosen was a 2 mm long line. With this sampling pattern and the acquisition settings of the ICP-MS, sufficient material can be sampled to allow the acquisition of 30 elements.

The signal dispersion from one acquisition reflected fluctuations in the ablation process. Fluctuations of the ablation conditions were partly caused by variations in the laser parameters such as energy or focus and could be compensated working with relative signals. Fluctuations due to the sample itself were caused by textural variations, that can be partly compensated with relative signals, or by uneven elemental distribution within the mineralogical phases. Therefore elemental signals were on-line normalised to Si^{29} , minor isotope of a matrix element, to limit these variations.

2.3.3.2. *LA-ICP-MS bulk analysis.* LA-ICP-MS analysis was performed at three different locations for samples 1C, 1V and glass NIST 612. Signals were normalised on-line to Si^{29} to allow intercomparison between samples to compensate for varia-

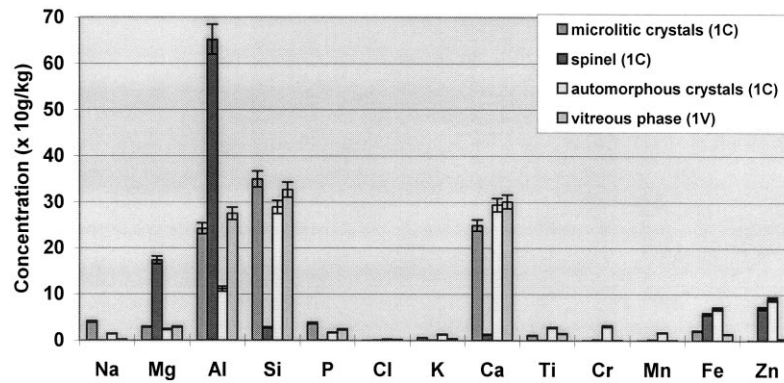


Fig. 2. Microchemistry of different mineralogical phases of vitrified samples by SEM-EDXS

tions in the total amount of sampled material. Each individual acquisition generated averaged relative signals and the mean of the three individual analysis was finally retained.

Bulk composition of samples 1C and 1V were determined using NIST-612 glass for calibration. Composition of sample 1C was also determined using 1V as a calibrant taking the ICP-MS data from Colombel [8] as reference values.

2.3.3.3. Microanalysis by LA-ICP-MS. LA-ICP-MS was used to investigate the distribution of metals within the mineralogical phases of the vitrified wastes. Sample 1V had a globally vitreous matrix whereas sample 1C had a heterogeneous crystallised matrix with a vitreous phase between the crystals.

Analysis was carried out at different locations for samples 1C and 1V. SEM was used to locate and characterise the laser impacts. Fig. 3 shows a laser raster in the vitreous phase (sample 1V). For sample 1C the laser probe was focused on two different locations containing different crystals: the first laser pit was located at a textural set dominated by automorphous crystals included in a vitreous matrix (Fig. 4) and the second one contained microlitic crystals also included in a vitreous matrix (Fig. 5).

LA-ICP-MS signals were normalised to Si to work with relative concentrations. Relative concentrations are then normalised to relative concentrations of the pure vitreous phase (sample 1V) to enhance differences between the crystallised phases and the vitreous matrix.

2.3.4. Characterisation of the laser impacts.

SEM-EDXS was used for in-situ characterisation of the laser impacts. The morphology, location and surface chemistry of the sampled areas were considered. The surface chemistry of the sample 1V was investigated at two different locations by SEM-EDXS: inside the channel drilled by the laser beam and outside the ablated area (scanning window of 250 μm^2). For sample 1C the analysis of a laser raster in the microlitic crystals area was performed using the same operating conditions.

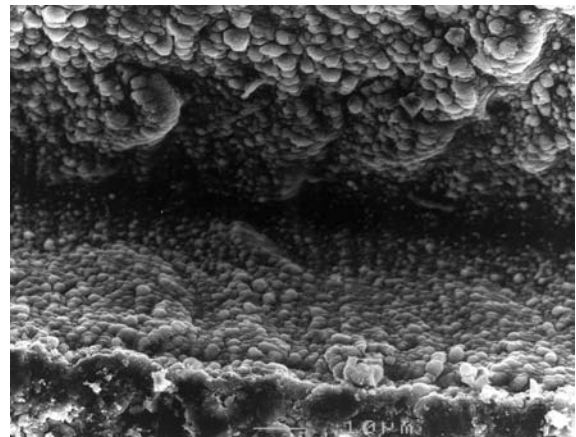


Fig. 3. SEM picture of an ablation raster on sample 1V ($\times 1000$)

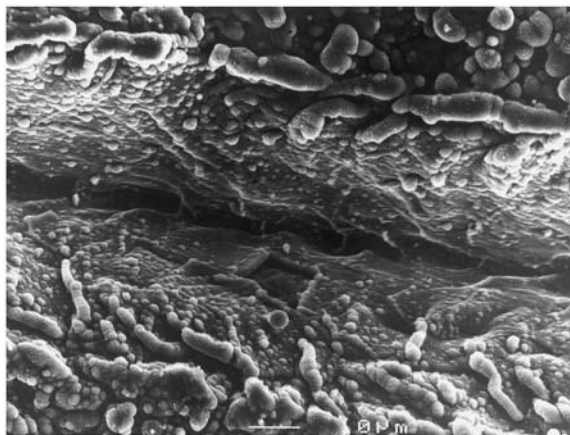


Fig. 4. SEM picture of an ablation raster on sample 1C (microlitic crystals texture) ($\times 1000$)

3. Results and discussion

3.1. Quantitation with LA-ICP-MS

LA-ICP-MS can be used for bulk quantitative analysis of trace metals in solid materials. When using a multi-size sampling tool such as the laser probe, one has to be careful about statistical representativity of the sampled material to assess the significance of the chemical analysis, especially for heterogeneous samples. Depending of the ana-

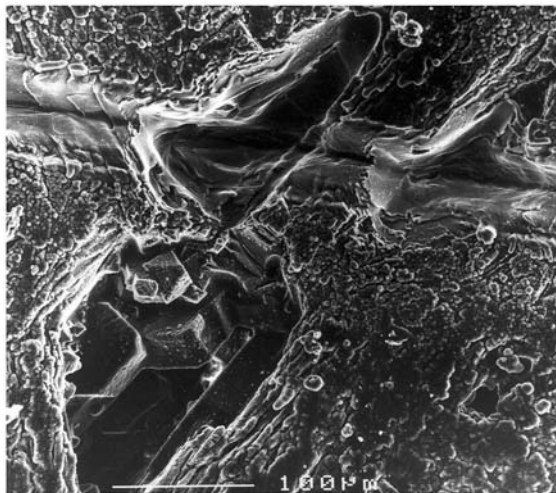


Fig. 5. SEM picture of an ablation raster on sample 1C (automorphous crystals texture) ($\times 250$)

lytical strategy, macro or microanalysis, there must be an adequate relation between the sampling scale and the size of individual components of the sample or the heterogeneity scale of the material. Sampling at different locations and averaging the information was used for bulk analysis. Estimated reproducibility of the LA-ICP-MS bulk analysis was 5% RSD for NIST-612 glass standard and higher for the vitrified waste samples (10% RSD for sample 1V and 10–20% RSD for sample 1V) for elements in the mg kg^{-1} up to the 10 g kg^{-1} concentration range. For bulk analysis of heterogeneous samples the spatial resolution of the analytical technique has to be higher than the homogeneity scale of the sample. The Nd:YAG laser device working at the fourth harmonic at 266 nm can drill 10 μm diameter pits in glasses. For heterogeneous samples the amount of material sampled and analysed has to be increased to be representative of the bulk sample. This can be done by averaging the local chemical information given by LA-ICP-MS by defocusing the laser beam, rastering large areas or performing statistics from individual local analysis. The effects of the sampling scale on bulk analysis of heterogeneous samples by LA-ICP-MS have been investigated by some authors. Scholze analysed heterogeneous powdered soils by LA-ICP-MS and studied the influence of sample inhomogeneity on the precision of analytical results using a correlation function [12]. To achieve reliable information on the bulk composition of heterogeneous samples, the crater size and number have to be increased according to the grain size. For bulk analysis using LA-ICP-MS the heterogeneity of the matrix can therefore limit the level of precision. Quantification is based on external calibration and a solid material is used as a calibrant together with an internal standard (IS). This strategy requires an independent method to determine at least one element, the IS in the unknown sample and in the standard. Si is used as an internal standard. For the vitrified wastes samples, Si concentration comes from AAS data. Concentration of an analyte E in the unknown sample is then given by the relation $C_{\text{un}}(\text{E}) = C_{\text{standard}}(\text{E}) \cdot I_{\text{un}}(\text{E}) / I_{\text{standard}}(\text{E}) \cdot I_{\text{standard}}(\text{IS})$

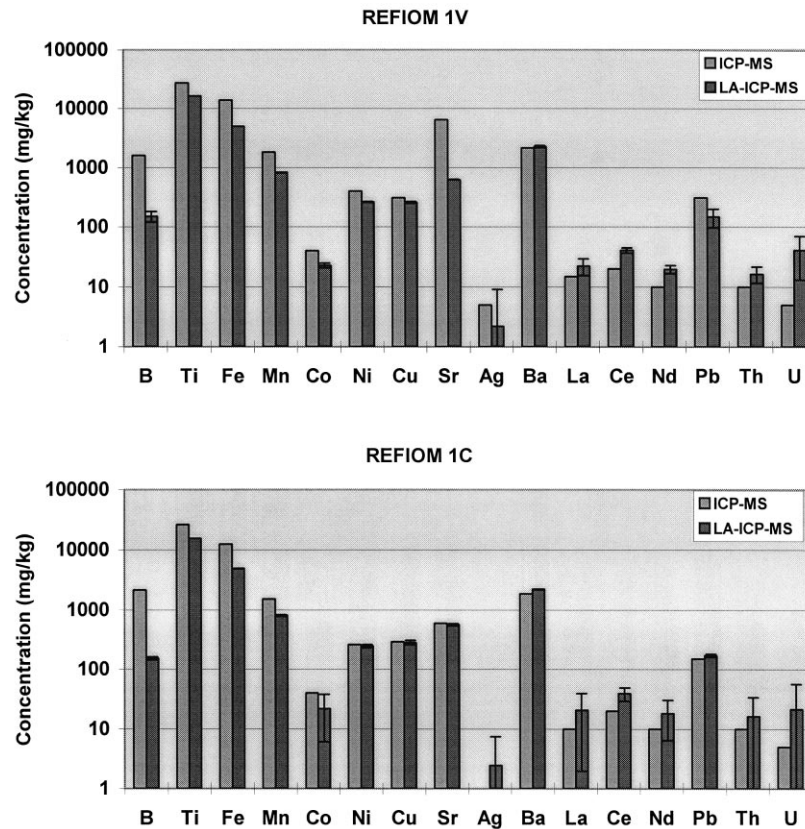


Fig. 6. Bulk quantitative analysis of vitrified wastes by LA-ICP-MS using NIST 612 as a calibrant

$I_{un}(IS) \cdot C_{un}(IS) / C_{standard}(IS)$ where I stands for LA-ICP-MS response and C for concentration. Fig. 6 shows the results of analysis by LA-ICP-MS of vitrified wastes samples 1C and 1V using NIST 612 glass standard for calibration. Results for 16 major, minor and trace elements are presented. LA-ICP-MS data is compared with nebulisation ICP-MS data [8] to check the validity of the analytical technique for quantification. From the ICP-MS data samples 1C and 1V have the same bulk composition for most major, minor and trace elements. An interesting feature is the occurrence of several toxic metals such as Ti, Fe, Zn, Cr, Pb, Sn at high concentration levels (from 1 up to 20 g kg⁻¹). Other metals such as As, Cu, Sb, Co, Ni, W are present at trace levels and up to 400 mg kg⁻¹. Analysis of samples 1V and 1C by LA-ICP-MS with NIST-612 gave globally lower values compared with the ICP-MS data. The LA-

ICP-MS values range within 10 and 50% of the ICP-MS data for most elements. Results from the analysis by LA-ICP-MS of the crystallised waste (sample 1C) using vitreous waste (sample 1V) as a calibrant are presented in Fig. 7. The concentrations obtained range within 10 and 20% of the ICP-MS values for most elements.

Accuracy of quantitative analysis of vitrified wastes depends on the external standard used. LA-ICP-MS analysis with NIST 612 gives lower results than ICP-MS data for vitrified wastes, with concentrations ranging from 10 to 50% from the ICP-MS data for samples 1C and 1V. This maybe due to differences in the concentration range between the wastes and the NIST 612 glass standard that has much lower concentrations for some elements. But the technique could also be slightly matrix-dependant because of specific ablation behaviour of the different glass matrices due

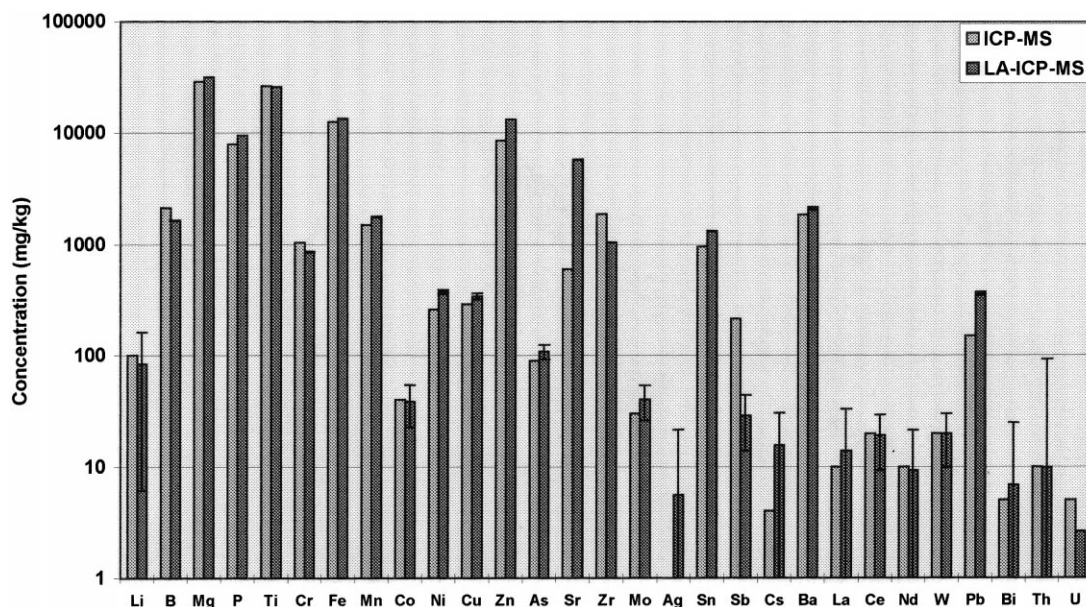


Fig. 7. Analysis of REFION 1C by LA-ICP-MS with REFION 1V as a calibrant

to their particular structural, textural and chemical properties.

Using a REFION calibrant for LA-ICP-MS quantitative analysis gave better results than NIST 612 with respect to ICP-MS data. Using this strategy the LA-IP-MS concentrations are between 10 and 20% of the ICP-MS data. The two samples have close matrix properties and therefore give similar responses to the LA-ICP-MS.

The potential of LA-ICP-MS for quantitative analysis of glass material has been investigated by many authors. Results on domestic vitrified wastes are compared with results of LA-ICP-MS analysis on analogue materials from the literature. The closest materials to the vitrified wastes are synthetic or natural glasses for the vitreous phase and silicates for the crystallised phase. The results on these analogues are presented in Table 3. Moenke-Blankenburg analysed fluorophosphate glasses for seven elements with an IR laser. She demonstrated the ability of LA-ICP-MS to analyse for major elements using liquid solid calibration [13]. The same calibration method was applied by Cromwell for the analysis of synthetic glasses. Cromwell achieved semiquantitative anal-

ysis of nine minor elements with an UV laser [14]. Other authors performed solid calibration using a certified reference glass such as NIST-612. Stix worked with natural glasses such as felsic and mafic glasses. Micro-analysis of trace metals was performed using an UV laser with NIST-612 for calibration [15]. Fedorowich analysed trace elements in silicates. The reference basalt BIR-1 prepared in glass fused beads was analysed using an IR laser and NIST-612 for calibration [16]. Heuzen also analysed trace elements within silicates. Samples were prepared in glass beads and an IR laser was also used. This author achieved more accurate results using synthetic calibration standards prepared from the fusion of oxides in glass silicates [17].

As indicated by Shuttleworth [18], UV laser provides better results in LA-ICP-MS analysis for glass-like material. Whereas much of the previous work on glass material was done with IR lasers, the use of UV laser probes gives better analytical results for trace element analysis in glass materials. More accurate results are obtained when using a matrix-matched calibrant. Therefore quantitation of vitrified wastes should be performed using a reference waste. The vitreous

Table 3
Quantitative analysis of glass-like materials by LA-ICP-MS

Reference	Samples	Elements	Calibration	Sampling	Performances	Laser parameters
Glasses						
[14]	Glass SRM 1834	Li, Ti, B, Fe, Sr, Na, Mg, Zr, Cr, concentration: 100–10000 mg kg ⁻¹	Liquid–solid Fe ⁵⁷ IS	Bulk analysis raster	RSD 2–10% accuracy 10–40%	266 nm 10 Hz, 60 MJ pulse ⁻¹
[13]	Fluorophosphate synthetic glass	Al, La, Ca, Sr, Mg, F, P, concentration: 20–400 g kg ⁻¹	Liquid–solid Sr ⁸⁴ –Sr ⁸⁷ IS	Bulk analysis mean of individual analysis	RSD 5% accuracy 2–5%	1064 nm, 10 Hz, 250 MJ, 1 mm craters
[18]	Waste glass	Li, Mg, Sc, V, Cr, Mn, Co, Ni, Cu, Zn, Ga, Rb, Sr, Y, Zr, Nb, Mo, In, Ba, Ta, W, Pb, Bi, U, REE concentration: ~0.1–100 mg kg ⁻¹	Synthetic glass standard	Bulk analysis	RSD 1–10%	1064 nm, 12 Hz, 30 MJ pulse ⁻¹
[15]	Mafic and felsic glasses	Li, Be, B, Rb, Cs, Sr, Ba, Pb, Co, Cu, Zn, Cr, Sc, Y, Hf, Zr, Th, V, Nb, Ta, U, REE concentration: 0.1–100 mg kg ⁻¹	NIST 612 Sr ²⁹ , Ca ⁴⁴ IS	Bulk analysis	RSD 10% accuracy 10%	266 nm, 4 Hz, 3.6 MJ pulse ⁻¹
[22]	Volcanic glass shards	Ba, Ce, Ga, Rb, Sr, Y, Zr, Nb, Cs, REE concentration: 1–100 mg kg ⁻¹	NIST-612 Ce ¹⁴⁰ IS	Microanalysis	RSD 20% accuracy 15%	1064 nm, 8 Hz, 125 MJ 500 μm crater
Silicates						
[16]	Basalt BIR-1 in fused glass beads	Sc, V, Cr, Co, Ga, Rb, Sr, Y, Zr, Nb, Sa, Cs, Ba, Hf, Ta, Pb, REE, Th, U concentration: 0.5 mg kg ⁻¹ –10 g kg ⁻¹	NIST-612 Al ²⁷ IS	Bulk analysis mean of individual analysis	RSD 5–15% accuracy 20%	1064 nm, <10 Hz, 144 MJ 100 μm crater
[17]	Basalt NBS 688 in fused glass bead	Mg, Al, Sc, Ti, V, Cr, Mn, Fe, Co, Cs, Ba, REE concentration: 0.3 ppm–10 g kg ⁻¹	Metallic oxides in glass Sr ⁸⁴ IS	Bulk analysis raster	RSD 2–4% accuracy 10%	1064 nm, 10 Hz, 200 MJ

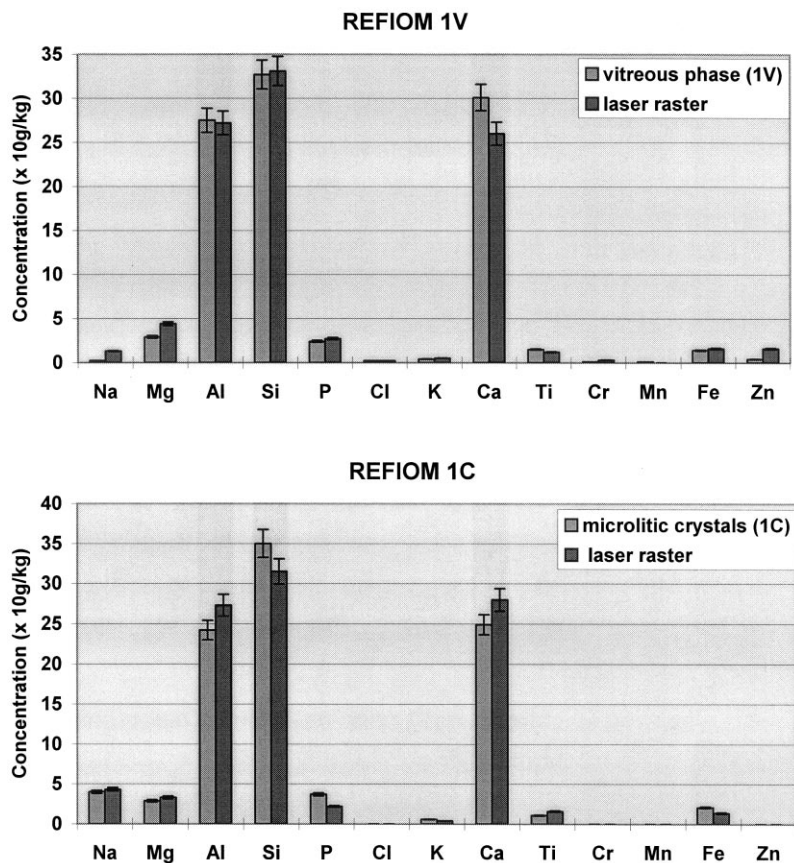


Fig. 8. Microchemistry of laser impacts on vitrified wastes by SEM-EDXS

waste sample seems ideal for this purpose because it is homogeneous material. It can be characterised for its trace metals content using alternate techniques such as digestion ICP-MS.

LA-ICP-MS can be used as a quantitative technique for the bulk analysis of heavy metals occurring in vitrified wastes at trace levels. The relative limits of detection were estimated at 0.1 mg kg^{-1} which is sufficient to investigate toxic trace metals in solid wastes.

3.2. Comparison between chemical analysis based on digestion and LA-ICP-MS

For laser ablation like any other introduction technique it is important to assess to what extent the material analysed by the ICP-MS is truly representative of the original material. Potential

transformation of the material is likely to occur during the ablation process such as physical and chemical fractionation. The interaction of the laser beam with solid material is a complex process controlled by both laser parameters such as wavelength, energy, pulse frequency and the physico-chemical structure of the sample.

Chemical analysis by SEM-EDXS is used to investigate at the microscopic level the chemical fractionation patterns. Fig. 8 shows the SEM-EDXS analysis of two laser rasters in the vitreous (sample 1V) and crystallised phase (sample 1C). Data is presented for major and minor elements. For the vitreous phase there is no significant variation between the bulk matrix and the ablated area in the vitreous phase. The SEM-EDXS data shows no significant variations between the ablated area and the unaltered matrix for the mi-

colitic crystals. Therefore, major and minor element surface chemistry of the vitrified or crystallised matrix is the same before and after sampling by the laser beam. This indicates that with the laser conditions used, i.e. with an energetic UV laser beam, laser ablation should not modify the composition of the sampled material. Fractionation studies can also be done using the ICP-MS as a detector. Shuttleworth investigated fractionation occurring in the ablation of synthetic vitrified glasses containing wastes [18]. The effects of laser fluence on the ICP-MS signal was studied for two Nd:YAG lasers at 1064 nm and 266 nm. Fractionation occurred only with the IR laser.

Characterisation of the laser impact at microscopic level can also bring information about the sampling process and potential fractionation. SEM picture of laser impacts in the vitreous phase and in the crystallised phase are presented in Figs. 3 and 4 respectively. The Nd:YAG UV laser produces well shaped craters free of any deposits. Thermal effects are likely to be limited in the ablation process. SEM was often used to study the morphology of the laser impacts on glass-like material. Fedorowich analysed silicates prepared in a fused glass bead with a Nd:YAG IR laser (1064 nm). The occurrence of solidified droplets of melt ejected around the crater was noticed [16]. Jeffries compared IR and UV Nd:YAG lasers (1064 nm and 266 nm) for the microanalysis of single mineral phases. For some minerals showing specific orientation (cleavage plans) catastrophic ablation patterns were noticed for the IR laser [19]. Bea performed microanalysis of minerals in thin sections using an Excimer laser at 308 nm and made some comparisons with an IR Nd:YAG laser. Laser craters comprised an internal zone where laser matter interaction is stronger and a peripheral halo caused by thermal effect. This halo appeared to be much smaller for the UV laser [20].

With energetic and short pulse (ns) laser beams in the UV, the interaction of laser with solid material is mainly ablation i.e. explosion generating fragmentation of the target and expulsion of micro-particulate material [2]. Therefore chemical fractionation should be limited. UV lasers ap-

peared to be more suitable for the analysis of glass-like material by ICP-MS.

Laser ablation is a sampling tool that allows direct and rapid extraction of material from solid samples. For the analysis of solid samples that are difficult to dissolve such as REFION, LA-ICP-MS is a good alternative to conventional analysis by ICP-MS. Moreover the laser sampling probe allows direct extraction with no modification of the mineralogical phases of the matrix as in methods based on dissolution. The sampled material should then be more representative of the original sample.

3.3. Microanalysis of trace metals by LA-ICP-MS

For microanalysis of trace metals in glass wastes, LA-ICP-MS is used as relative technique to monitor the variation of elemental concentration between the different mineralogical phases. Microanalysis of two different groups of crystals of the crystallised sample 1C (microlitic crystals and automorphous crystals) was performed by LA-ICP-MS. Relative to Si concentrations of crystals normalised to those of pure vitreous phase are presented in Fig. 9. Within an individual sampling area the signal dispersion for trace elements is 10% or less in the vitreous phase (sample 1V) and higher for the crystallised sample 1C (20% or more). This dispersion reflects the local heterogeneity in the elemental or micro-phase distribution.

Li, B, Cs, Nd, As, Ag, Nd, Bi and Mo show higher relative concentrations, from five to 10 times, in the vitreous phase compared with the crystallised phases. These elements seem therefore to be depleted in the crystals. The relative concentration of Ti, Cr, P, Fe, Mn, Ni, Cu, Zn, Sn, Sb, Pb, W, Mg, Co, Ce and Ba is higher, from 20 up to 100%, in the automorphous crystals texture compared with the vitreous phase. The relative concentrations of Cu, Zn, Sn, Sb, W and Pb are also slightly higher in the microlitic crystals texture compared with the vitreous phase.

LA-ICP-MS data show a partition between the vitreous and the crystallised phases. Since major elements such as Ti, Fe and Zn, minor elements

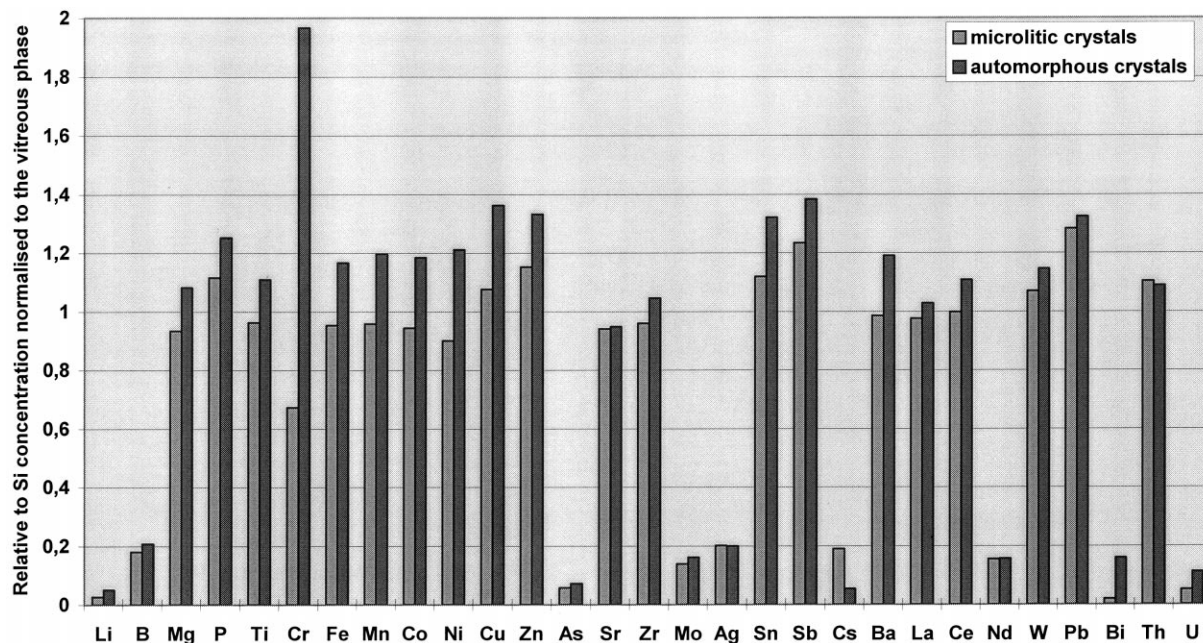


Fig. 9. Microanalysis by LA-ICP-MS of different mineralogical phases of REFIOM IC

like Cr, Sn, Mn, Ba and traces such as Sb, Ni, Cu, Pb show higher concentrations in the automorphous crystals texture compared with the vitreous phase, they are likely to be incorporated in crystals (sorosilicates and spinels).

Estimation of the absolute concentrations of these metals in the crystals are obtained from relative concentrations using Si concentrations of the different mineralogical phases from SEM-EDXS data. Sorosilicates have a bulk composition similar to the vitreous phase. Therefore those crystals should at least incorporate Ti, Fe and Zn in the 10–30 g kg⁻¹ concentration range, Cr, Sn, Mn and Ba from 1 g kg⁻¹ up to 2.5 g kg⁻¹ and Sb, Ni, Cu and Pb in the 20–350 mg kg⁻¹ range. As spinels are depleted in Si compared with the vitreous phase (50 g kg⁻¹ compared with 300 g kg⁻¹), more metals should concentrate. Therefore spinel crystals could at least incorporate Ti, Fe and Zn in the 60–200 g kg⁻¹ concentration range, Cr, Sn, Mn and Ba up to 10 g kg⁻¹ and Sb, Ni, Cu and Pb in the 100–1000 mg kg⁻¹ range.

Clozel studied the crystallochemistry of toxic metals such as Ti, Sr, Cr, Zn and Pb in vitrified

domestic wastes (REFIOM) within individual crystals by SEM-EDXS [7]. He found that Cr, Sn, Ti, Mn and Zn have an affinity for the spinel crystals whereas Zn can also be incorporated in sorosilicates and Pb is trapped in the vitreous phase.

In the vitrified waste, crystals concentrate in toxic metals. These hazardous elements can be part of the crystal matrix as Al and Fe for spinels and Al for sorosilicates. They can also be trapped in crystals (spinels and sorosilicates) like Sn, Ti, Mn, Fe, Cr, Zn but also Ni, Ba, Sb, Cu and W.

LA-ICP-MS adds new information about the chemistry of trace metals in REFIOM.

Despite the fact that it is important to characterise the bulk composition of trace metals in the vitrified wastes, this approach is however not sufficient. In fact, further knowledge of the distribution of trace metals in the waste material is needed. Knowledge of the partition of toxic metals between the mineralogical phase and particularly the partition between the vitreous and the crystallised phase is a fundamental requisite to assess the potential mobility and release of hazardous elements in the environment. Obtaining

Table 4
Comparison of LA-ICP-MS and SEM-EDXS for the characterisation of toxic metals in vitrified wastes

		LA-ICP-MS	SEM-EDXS
Probe	Macro	Bulk analysis	Not applicable
	Micro	10 μm	10 nm
	Spatial resolution specific information	Automorphous crystals group of microlitic crystals	Individual crystals
Analysis	Physical	No information	Structure & texture
	Chemical		
	Sensitivity	Traces	Major&minors
	Detection limits	0.1 mg kg ⁻¹	10 g kg ⁻¹
	Precision	10–20% RSD	5% RSD
Quantitation		Absolute analysis with external calibrant	Relative analysis
	Accuracy	10–20% RSD	

good correlation between trace metal chemistry, structural and textural patterns is the first step toward this objective.

Key-features of LA-ICP-MS and SEM-EDXS for the characterisation of toxic metals in vitrified domestic wastes is presented in Table 4. LA-ICP-MS can monitor local concentrations of trace elements in the mineralogical phases but cannot deal with individual micro-crystals. On the other hand SEM-EDXS can perform chemical analysis on individual microlitic crystals but is limited to minor elements. LA-ICP-MS is more sensitive than the physical analytical techniques of solids such as SEM. However so far SEM-EDXS provides higher spatial resolution than LA-ICP-MS.

Further finer investigation of the affinity of heavy metals to specific mineralogical phases by LA-ICP-MS should be possible with new laser microprobes. Developments of laser technology will generate laser probes with a spatial resolution lower than 10 μm . Investigation of the distribution of trace metals within the microlitic individual crystals in REFION by LA-ICP-MS would then be feasible. As commercial lasers are basically designed for bulk analysis some modifications are necessary to build up the laser micro-probe using compound focusing objectives. Chenery demonstrated the ability of laser ablation microprobes for the analysis of single mineral

grains [21]. Their laser device produces craters of 5 μm or less that are almost comparable to the spatial resolution provided by SEM-EDXS.

4. Conclusion

A trace analytical method for the in-situ characterisation of trace metals in vitrified wastes based on LA-ICP-MS was developed and validated. LA-ICP-MS is an attractive tandem technique that combines sensitive trace multi-elementary analysis and rapid spatially resolved analysis. LA-ICP-MS allows spatially resolved chemical analysis at different space scales from the bulk characterisation to the microanalysis within mineralogical phases.

It can perform precise and accurate analysis of trace metals for both bulk and micro-analysis down to the microscale. LA-ICP-MS can monitor relative concentrations between the mineralogical phases. Quantitative bulk analysis proved to be possible when using a matched-matrix reference material. However the weakness of this technique for absolute quantitative analysis is the need of a well-characterised external standard, with a matrix similar or close to the samples. LA-ICP-MS appears as an efficient in-situ characterisation

technique of trace metals in complex solid matrixes. Performances of this technique for both relative micro-analysis and bulk quantitative analysis was evaluated with regard to SEM-EDXS. With the laser probe the ICP-MS can cope with microscale analysis and therefore compete with physical analytical techniques.

LA-ICP-MS is also more sensitive than physical techniques of analysis such as SEM-EDXS although its spatial resolution is still lower. However LA-ICP-MS is blind to structural or textural variations. This can be a serious problem when analysing heterogeneous samples at the microscale level. Therefore LA-ICP-MS requires a complementary technique. In-situ investigation of vitrified wastes relies on the use of LA-ICP-MS together with SEM-EDXS to correlate chemical and textural information. Complementary to lixiviation studies, LA-ICP-MS together with SEM-EDXS can monitor the evolution of wastes from the point of the altering matrix. This is an interesting combination of physical and chemical analytical tools for studying the long term behaviour of solid wastes and the mobility of hazardous elements. Information about the structure and texture of the wastes is important to understand the behaviour of their matrix. Vitrified wastes will have different evolution during the leaching process under altering conditions, according to their structure and texture. Information about the affinity of heavy metals to specific crystalline phases will give answers to the potential mobility of hazardous elements and therefore predict the release of toxic species into the environment.

References

- [1] R. Meunier, L'arc électrique pour le traitement de RE-FIOM toxiques, Congrès Procédés de solidification et de stabilisation des déchets, Nancy, 28 Nov–1 Déc., 1995 pp. 138–142.
- [2] R. Russo, *Appl. Spectrosc.* 49 (1995) 14A.
- [3] S. Darke, *J. Anal. At. Spectrom.* 8 (1993) 145.
- [4] E. Denoyer, *Anal. Chem.* 63 (1991) 445A.
- [5] C. Neal, US National Report to IUGG 1991–94, *Rev. Geophys.* 33 Suppl. (1995).
- [6] W. Perkins, Mineral microanalysis by laserprobe inductively coupled plasma mass spectrometry, in: P. Potts (Eds.), *Microprobe Techniques in the Earth Sciences*, Chapman and Hall, London, 1995, pp. 291–325.
- [7] B. Clozel, Caractérisation minéralogique et cristalochimique de vitrifiats, Congrès Procédés de solidification et de stabilisation des déchets, Nancy, 28 Nov–1 Déc., 1995 pp. 53–57.
- [8] P. Colombel, Etude du comportement à long terme de vitrifiats de REFIOM, Thesis of University of Poitiers, France, 1996.
- [9] E. Jeanroy, *Analisis* 2 (1974) 703.
- [10] N. J. Zalusec, *Introduction to Analytical Microscopy*, Plenum, New-York, 1979, 121.
- [11] J. L. Pouchou, 'Modeles de corrections pour la micro-analyse X quantitative', *Microanalyse par Sonde Electronique: aspects quantitatifs*, A.N.R.T, Paris, 1989.
- [12] H. Scholze, *Fresenius' Z. Anal. Chem.* 350 (1994) 247.
- [13] L. Moenke-Blankenburg, *JAAS* 7 (1992) 251.
- [14] E. F. Cromwell, *Anal. Chem.* 67 (1995) 131.
- [15] J. Stix, *Can. Mineralogist.* 33 (1995) 435.
- [16] J. S. Fedorowich, *Chem. Geol.* 106 (1993) 229.
- [17] A. A van Heuzen, *Spectrochim. Acta* 46B (1991) 1803.
- [18] S. Shuttleworth, *Appl. Surface Sci.*, 96–98 (1996) 513.
- [19] T.E. Jeffries, *Analyst* 120 (1995) 1365.
- [20] F. Bea, *Chem. Geol.* 133 (1995) 145.
- [21] S. Chenery, *J. Atom. Anal. Chem.* 8 (1993) 299.
- [22] J. Westgate, *Appl. Geochem.* 9 (1994) 323–335.

Methods for chemical analysis of contaminated soil samples—tests of their reproducibility between Nordic laboratories

K.H. Karstensen ^{a,*}, O. Ringstad ^a, I. Rustad ^a, K. Kalevi ^b, K. Jørgensen ^b,
K. Nylund ^c, T. Alsberg ^c, K. Ólafsdóttir ^d, O. Heidenstam ^e, H. Solberg ^f

^a SINTEF, P. O. Box 124, N-0314 Oslo, Norway

^b Finnish Environment Institute, Hakuninmaantie 4-6, FIN-00430 Helsinki, Finland

^c ITM, Stockholm University, S-106 91 Stockholm, Sweden

^d Department of Pharmacology, University of Iceland, P. O. Box 8216, IS-128 Reykjavik, Iceland

^e Swedish Environmental Protection Agency, S-10648 Stockholm, Sweden

^f Norwegian Pollution Control Authority, P. O. Box 8100 Dep., N-0314 Oslo, Norway

Received 25 May 1997; accepted 14 October 1997

Abstract

In an effort to develop common analytical methods for contaminated soil samples the Environmental Authorities of the Nordic countries have, together with Nordtest, published the report Nordic Guidelines for Chemical Analysis of Contaminated Soil Samples. The aim of these guidelines has been to describe analytical methods which could be accepted in all the Nordic countries and in that way contribute to reducing the variation in the analytical results between laboratories. The methods covered, reflects environmental concerns and priorities in the Nordic countries for now, i.e. heavy metals, chlorophenols, creosote, volatile organic compounds, PCB, THC and PAH. The repeatability and reproducibility of the guideline methods were determined in a Nordic inter-laboratory test in 1996, and the results showed some variations. The analytical methods and the results from the inter-laboratory tests are given for heavy metals, chlorophenols, creosote, volatile organic compounds and PCB. © 1998 Elsevier Science B.V. All rights reserved.

Keywords: Contaminated soil; Chemical analysis; Reproducibility; Nordic laboratories; Heavy metals

1. Introduction

Extensive work has been and is being done to identify and remediate landfills and hazardous 'waste' contaminated sites, the so called 'past

sins', in Nordic countries. When facing the large costs for cleaning up contaminated sites, it is necessary that chemical analysis provides a foundation for cleanup efforts to be comparable, reproducible and reliable.

Sample treatment and preparation, along with chemical analysis are often performed differently

* Corresponding author.

at different laboratories and may provide different results, despite the fact that some of these laboratories are accredited. It was therefore a priority to develop complete guidelines that could contribute to make the results comparable and reproducible even when the analyses are performed in different laboratories in Nordic countries. This is especially important when the effects of remedial action need to be verified.

An environmental survey of a site is carried out in order to obtain information about the kind, extent and distribution of contaminants, and if needed, to select the most appropriate cleanup methods. Guidelines for soil investigations have already been developed in Denmark, Finland, Norway and Sweden [1,6,12]. These guidelines give appropriate methods for sampling and are meant to be used for planning, executing and reporting these types of environmental surveys.

Samples from such surveys (soil, groundwater, leachate, air, etc.) are sent to an analytical laboratory for chemical analyses in order to ascertain the composition of the polluting contaminants. The results from the analyses will in turn be used when deciding upon further action. For example, if high concentrations of environmentally hazardous compounds are found, costly cleanup efforts may be initiated, while any further activity could be halted and the site declared acceptable if low concentrations are found. Errors in these results from such analysis can have environmental and economic consequences.

Advanced chemical analyses are complicated to perform and can be fraught with error. These errors can be minimised, however, with adequate routines. Another uncertainty factor which can be eliminated, is the use of different methods or conditions for the same analysis at different laboratories. However, the laboratories should still have the opportunity to use their own or alternative methods, but this should preferably be validated and compared with the proposed method in the guideline, to give an estimate of the performance.

The Nordic Guidelines [5] describes methods for heavy metals, chlorophenols, creosote, volatile organic compounds, PCB, THC and PAH, and covers also quality assurance, sampling strategy

and validation. The analytical methods are first of all based on the already existing national or international standards, i.e. ISO/TC 190 and various CEN standards, and/or on common practice.

The repeatability and reproducibility of the proposed methods in this guideline were determined in a Nordic inter-laboratory test according to ISO 5725-2.

2. Analytical methods

The following paragraphs give a brief description of the analytical methods for the determination of heavy metals, chlorophenols, creosote, volatile organic compounds and PCB.

2.1. Heavy metals: As, Cd, Cr, Cu, Hg, Ni, Pb and Zn

The method for determination of heavy metals is a partial digestion method using air dried (24 h) and sieved (< 2 mm) samples. Approximately 1 g of the dried sub sample is introduced into a 100 ml digestion bottle, made of uncoloured pyrex glass with polypropylene screw caps or suitable closures. Bottles and closures should be temperature resistant up to 120°C and a pressure of 200 kPa. Nitric acid (HNO₃) (20 ml of 7 mol l⁻¹) is added and the mixture is heated in an autoclave at 120°C (200 kPa) for 30 min. The solution is cooled, filtered and transferred to a 100 ml flask, diluted with distilled or deionized water. The solution should be transferred to a plastic bottle prior to instrumental analysis. Blank solutions are prepared in the same way. Alternatively, samples could be digested in polytetrafluoroethylene (PTFE) bombs, heated in a microwave oven. The laboratory is free to choose the instrumental methods for determination of analytes.

2.2. Chlorophenols

Field moist soil samples are extracted with acidic acetone:hexane (1:1) by sonication for 6 × 2 min during 1 h. The clear part of the mixture is further extracted (twice) with NaOH and acidified by HCl. The extract is then extracted twice with

hexane, and the hexane phase further extracted (twice) with K_2CO_3 . The chlorophenols in the alkaline extract are then acetylated by acetic anhydride, after which the acetylated chlorophenols are extracted with hexane. The extract is dried using Na_2SO_4 . Chlorophenols in the hexane phase are determined by gas chromatography using a dual column system and electron capture detection. The calibration is based on peak height and on the response of internal standard, 2,4,6-tribromophenol.

2.3. Creosote

Soil samples are extracted with acetone including internal standard by rotation for 1 h. The supernatant is removed after centrifugation. This procedure is repeated once and the organic phases are combined and evaporated to 2–4 ml with nitrogen. An equal volume of water is added and the extract is extracted twice with 5 ml of *n*-hexane. The hexane phases are combined and evaporated to a volume of 1–2 ml. The target compounds are determined by GC-FID.

The target compounds in the analyses of creosote in soil are the following: PAH: naphthalene, 2-methylnaphthalene, 1-methylnaphthalene, biphenyl, acenaphthene, fluorene, phenanthrene, anthracene, fluoranthene, pyrene, benz(a)anthracene, chrysene, benzo(b)fluoranthene, benzo(k)fluoranthene, benzo(e)pyrene and benzo(a)pyrene. Phenols: *o*-cresol and *p*-cresol. *O*-heterocyclics: dibenzofuran. *N*-heterocyclics: carbazole. *S*-heterocyclics: dibenzothiophene.

2.4. Volatile organic compounds-VOC

The guideline describe two methods, with no preference for one or the other. Method 1 is based on solvent extraction. Internal standards and the extraction solvent (pentane) are introduced through the vial septum. The solvent/soil mixture is shaken manually until a slurry is obtained, then treated for a minimum of 5 min in an ultrasonic bath, and extracted for at least 45 min on a mechanical shaker. The pentane extract is isolated after addition of pH 2 water, and after drying with sodium sulphate, analysed with gas chromatography/mass spectrometry (GC/MS).

2.5. PCB

Dry samples are moistened with water. Prior to extraction recovery standards (PCBs 53, 112, 198; 100–1000 ng depending on the level of contamination) are added and the samples shaken gently to mix. Acetone (3–5 ml g^{-1}) is added, the samples are sonicated for 5 min and then shaken vigorously for 1 h. After repeating the extraction with acetone:hexane (1:3) (3–5 ml g^{-1}) the organic phases are washed with 50 ml of 0.2 mol l^{-1} NaCl 0.1 mol l^{-1} H_3PO_4 . After separation the water phase is washed twice with 10 ml hexan:diethylether (9:1) and the organic phases are combined and evaporated almost to dryness at 60°C in a waterbath. The samples are cleaned with H_2SO_4 (conc.) and/or with TBA to remove sulphur and/or the samples are fractionated by silica gel.

The individual PCB congeners are analysed by GC-MSD or GC-ECD with 60 m capillary columns of two polarities. GC-conditions should be optimised in respective laboratories which could for example be: injector 270°, ECD 290°, MSD interface 290°; oven 85° for 2 min, 30° min^{-1} to 210°, hold 28 min, 2° min^{-1} to 250°, 7° min^{-1} to 280° (DB1701) or 310° (DB5), hold as necessary to elute PCB 209. A long isothermal period early in the temperature program is necessary to separate components like PCB 28 and PCB 31.

Prior to injection, the sample is dissolved in isooctane containing the injection standard (for example tetrachloronaphthalene). The calibration is based on the peak height of individual PCBs/peak height of the injection standard. Detection limits will vary with amount and type of contamination. It should be close to $10 \mu\text{g kg}^{-1}$ for each congener but needs to be determined on a case to case basis.

3. Inter-laboratory tests

All laboratories in the Nordic countries which analyse heavy metals and organic pollutants in contaminated soil, were invited to take part in the inter-laboratory test. The invitation was sent out to more than 90 laboratories.

The inter-laboratory test was arranged as a test of repeatability and reproducibility of a standard measurement method. The statistical treatment was performed according to the international standard ISO 5725-2, First edition 1994-12-15: 'Accuracy (trueness and precision) of measurement methods and results, part 2: basic method for the determination of repeatability and reproducibility of a standard measurement method' [3].

A balanced uniform level experiment was performed. The aim was to test one or two different levels of contamination in soil and one test solution, each with three replicates. Each group of replicate measurements ($n = 3$) belonging to one level should be carried out under repeatable conditions, i.e. within a short interval of time and by the same operator. The statistical program involved the testing of the within-laboratory standard variances by Cochran's test and the testing of the variation of means by Grubb's test after which statistical outliers were excluded from the final calculation of the repeatability and reproducibility of the method. Some datasets contained some extreme values which could be due to the use of incorrect units, dilution errors and lack of analytical performance. These extreme values were rejected from the dataset before calculation. Symbols and abbreviations used in the following tables:

Level j	sample types (described for each parameter)
N	number of laboratories participating (or replicates)
p_j	number of laboratories used for calculation
m_j	mean value (for solid samples mg kg^{-1} , for solutions mg l^{-1})
S_r	standard deviation within laboratory (the repeatability)
S_R	standard deviation for the reproducibility
CV_r	the variation coefficient within laboratory (%)
CV_R	total variation coefficient reproducibility (%)
Ref. value	reference value, for certified reference materials or solutions

3.1. Heavy metals

Two real soil samples (samples A and B), one EPA certified reference real soil sample (sample C: CRM 021-100) and one standard solution (sample D) were tested [11].

The real soil samples were sandy soil obtained from sites of polluted soil in Norway. The two real soil samples were air-dried at room temperature. Coarse material (e.g. stones) was removed manually, after which the material was sieved through a 2 mm sieve, followed by sieving through a 500 μm sieve. The real soil samples were mixed for several days using a tumbler. The homogeneity was checked by randomly taking eight sub-samples prepared as wax pellets and subsequent determination of Cr, Fe, Ni, Cu, Zn and Pb with X-ray fluorescence spectrometry. This homogeneity test revealed that the spread among the test samples for most of the measured elements was less than 5%.

The reference material (C) was used as received, without any further homogenisation. The dry matter content was 98.8, 98.8 and 99.7% for samples A, B and C, respectively. The organic matter content (determined as loss of ignition; 2 h ignition at 550°C) was 5.9, 7 and 2% for samples A, B and C, respectively.

Table 1
 Repeatability results of heavy metals within the producers laboratory

Element	Level <i>j</i>	<i>N</i>	m_j	S_{vj}	CV_r	Ref. value
As	A	10	7.3	0.61	8.3	24.8
	B	10	200	12.3	6.2	
	C	10	39.4	3.1	7.9	
Cd	A	6	2.45	0.13	5.5	1.20
	B	6	2.07	0.18	8.9	
	C	11	1.26	0.10	7.8	
Cr	A	11	29.4	0.83	2.8	10.70
	B	11	37.6	0.71	1.9	
	C	10	10.6	2.4	22.6	
Cu	A	10	136	11.8	8.7	4792.4
	B	11	533	22	4.2	
	C	10	4797	596	12.4	
Hg	A	6	0.36	0.06	16.3	4.7
	B	6	0.49	0.07	13.6	
	C	6	4.5	0.5	11.1	
Ni	A	11	30.3	1.0	3.3	12.6
	B	11	45.7	1.5	3.3	
	C	11	12.7	1.7	13.3	
Pb	A	10	167	10.7	6.4	114 742.4 ^a
	B	11	575	62	10.8	
	C	11	238 882	19 854	8.3	
Zn	A	11	881	42.8	4	546.4
	B	11	156 5	62	10.8	
	C	10	583	64	11.1	

^a indicated value

The soil samples were polluted with an unknown level of heavy metals. The calibrant solution (D) containing As, Cd, Cr, Cu, Hg, Ni, Pb and Zn was prepared in water using 1000 mg l⁻¹ certified solutions of individual elements and diluting the mixture to a final volume of 2.5 l and adjusting the matrix to 5% HNO₃.

Each laboratory received 25 g of sample A and B, 8 g of sample C and 100 ml of sample D. The soil samples were sent out in small plastic bags, tightly closed, and the test solution in a screw-capped plastic bottle. The samples were sent out on May 2, 1996, and the last date of accepted results was June 30.

The samples were also analysed by the producers laboratory according to the guideline method. The relative standard deviation within the laboratory (the coefficient of variation, CV_r) varied between 2

and 10% for soil A and B and between 7 and 22% for soil C (Table 1). The larger spread in sample C could be due to some inhomogeneity in the sample itself, caused by potential settling and stratification in storage, shipping and handling.

Thirty-eight laboratories from Denmark (13), Finland (11), Iceland (2), Norway (7) and Sweden (5) took part in the inter-laboratory test for heavy metals. Two of the laboratories participated only using their own method and five laboratories performed their own method in addition to the guideline method. The majority of participants submitted full datasets with the exception of As and Hg where relatively fewer data were submitted. The results of this test are summarised in Table 2.

The overall performance on the test solution was good with a total coefficient of variation CV_R between 3.73% for Cu to 13.9% for Hg. The

Table 2
Inter-laboratory test results for heavy metals

Element	Level j	N	p_j	m_j	S_{vj}	CV_r	S_{Rj}	CV_R	Ref.value
As	A	29	24	7.2	0.43	5.9	2.2	30.1	
	B	29	26	198	14.5	7.3	32	16.1	
	C	28	21	34.6	2.4	7.1	9.9	28.6	24.8
	Solution	29	21	0.249	0.01	4.4	0.02	9.1	0.25
Cd	A	36	33	2.3	0.16	7.0	0.48	20.7	
	B	36	29	2.0	0.15	7.5	0.45	22.7	
	C	36	30	1.5	0.11	7.6	0.21	14.5	1.20
	Solution	37	27	0.29	0.005	1.8	0.023	7.9	0.30
Cr	A	36	34	29.4	1.7	5.9	5.1	17.3	
	B	36	31	36.5	1.1	2.9	6.0	16.6	
	C	35	30	10.0	0.6	6.3	2.5	24.8	10.70
	Solution	37	28	1.76	0.03	1.6	0.12	6.8	1.75
Cu	A	35	32	13 0	8.6	6.6	14.0	10.8	
	B	35	30	524	23.0	4.4	43.0	8.2	
	C	33	25	4461	294	6.6	556	12.5	4792.4
	Solution	36	23	2.5	0.02	0.77	0.09	3.7	2.50
Hg	A	28	25	0.30	0.017	5.5	0.07	23.6	
	B	28	25	0.46	0.03	7.0	0.11	24.1	
	C	28	19	3.7	0.18	5.0	1.5	40.9	4.7
	Solution	23	15	0.095	0.005	5.1	0.013	13.9	0.100
Ni	A	36	34	30.1	1.2	4.0	3.3	10.8	
	B	36	32	46.0	1.3	2.8	5.3	11.6	
	C	36	29	12.3	1.1	9.2	1.9	15.4	12.6
	Solution	38	27	2.03	0.02	1.0	0.13	6.3	2.00
Pb	A	36	30	170	16.8	9.9	28.4	16.7	
	B	36	30	585	33.9	5.8	58.5	10.0	
	C	36	29	248 889	11 910	4.8	15 845	6.4	114 742 ^a
	Solution	37	27	4.13	0.08	1.9	0.26	6.3	4.30
Zn	A	36	34	885	23.9	2.7	51.3	5.8	
	B	36	32	1555	52	3.3	105	6.8	
	C	36	25	562	57.9	10.3	66.3	11.8	546.4
	Solution	38	28	14.6	0.13	0.09	0.63	4.3	15.00

^a indicated value

laboratories seem to have larger difficulties analysing As and Hg than the other elements, 90% of the laboratories were able to analyse the test solution within 25% of the assigned values for Cd, Cr, Cu, Ni, Pb and Zn and around 80% of the laboratories were able to analyse the test solution for the same elements within 10% of the assigned values. For As and Hg respectively 85 and 80% of the laboratories were able to analyse within 25% and 55% and 40% within 10% of the assigned values.

For the soil samples the coefficient of variation CV_R varied between 6 and 26% for soil A and B, and between 6 and 40% for soil C. Around 85% of the laboratories were able to analyse the soil samples within 25% of the assigned values for all the elements except As and Hg. Around 65% of the laboratories were able to analyse As and Hg within 25% of assigned values. The exception was the level of high content of As in soil B, which was analysed satisfactory by 85% of the participants.

Table 3
Homogeneity of samples used in the inter-laboratory test ($n = 5-10$)

Sample	246-TCP		2346-TeCP		PCP	
	m_j	CV_r	m_j	CV_r	m_j	CV_r
A	0.19	8.2	1.95	9.6	4.9	12.2
B	0.08	18.3	2.8	21.6	1.4	15.8
C	0.74	2.3	208	10.3	1500	6.7
Solution	47.8	4.1	47.6	1.3	171	5.0

Soil C gave a higher coefficient of variation CV_R than soil A and B. This reflects a larger degree of inhomogeneity of soil sample C. The number of outliers were between 1 and 6, indicating systematic errors in some laboratories. Poor performance on the calibrant solutions was often reflected in the results for soil samples.

Five laboratories tested their own method in addition to the guideline method and two laboratories tested their own method only. Three laboratories digested the sample in aqua regia, two used a mixture of HNO_3/H_2O_2 , one used 10% HNO_3 , and one used a 5 g sample in concentrated HNO_3 . Some of these laboratories reported 'out of range' results. In general, however, no significant differences were found between the Nordtest method and their own methods.

3.2. Chlorophenols

Three real soil samples (samples A, B and C) and one calibrant solution (sample D) was used in the inter-laboratory test [4]. The real soil samples were obtained from a sawmill site. They were sieved through an 8 mm sieve. The dry matter content was 80.0, 78.9 and 75.6% for samples A, B and C, respectively. The organic matter content was 5.3, 5.6 and 9.3% for samples A, B and C, respectively. Sample A was of the same batch as sample B, but it was spiked with 2 mg kg^{-1} of 2,4,6 trichlorophenol (TCP), 2 mg kg^{-1} of 2,3,4,6-tetrachlorophenol (TeCP), and 5 mg kg^{-1} of pentachlorophenol (PCP). The soil samples had a natural content of more than 16 different chlorophenol congeners. The samples were homogenised in a tray and then sub-sampled into glass jars. Sample D was prepared in water from

stock solutions of 16 different chlorophenol congeners. The homogeneity of the samples was tested and the coefficient of variation varied between 1.3 and 21.6% (Table 3).

Twenty laboratories from Denmark (4), Finland (10), Norway (1) and Sweden (5) participated in the inter-laboratory test. Several laboratories reported results for up to 16 different chlorophenol congeners, but the majority reported results only for 2,4,6-trichlorophenol, 2,3,4,6-tetrachlorophenol and pentachlorophenol. The amount of data only allowed statistical handling for results of three of these compounds. The results are given in Table 4.

3.3. Creosote

Three samples were sent to the participants [7]. One creosote contaminated soil and two extracts in *n*-hexane from the soil. The soil was collected in Sweden at an old impregnation site. It was dried in a fume hood and then sieved through a 2 mm sieve. The dry matter content was 99.7%. Before sending the soil sample to the participants it was tested for homogeneity. The standard deviation of the determination of the target compounds in 15 sub samples was between 4.5 and 10.8%. The two soil extracts were spiked with compounds which originally were present at low concentrations in the soil. The variation for the solutions was between 1.1 and 6.0%. The concentrations of the target compounds were between n.d. to 51 mg kg^{-1} .

Twelve laboratories reported results, Denmark (4), Finland (2), Norway (1) and Sweden (5). Five laboratories participated using their own methods. One laboratory used its own method only.

Table 4
Inter-laboratory test results for chlorophenols

Compound	Level j	N	p_j	m_j	S_{vj}	CV_r	S_{Rj}	CV_R	Ref. value
2,4,6-TCP	A	18	16	0.253	0.027	10.6	0.081	31.8	60
	B	17	15	0.083	0.014	17.0	0.034	40.8	
	C	16	13	1.98	0.244	12.4	1.40	71.1	
	Solution	17	14	53.4	2.80	5.24	9.26	17.3	
2,3,4,6-TeCP	A	19	17	2.33	0.266	11.4	1.11	47.9	60
	B	19	16	2.22	0.271	12.2	1.06	47.6	
	C	19	17	193	38.4	19.9	110	56.9	
	Solution	16	13	52.8	2.32	4.4	18.0	34.1	
PCP	A	20	19	5.85	0.548	9.4	2.34	40.0	200
	B	20	17	1.36	0.212	15.5	0.443	32.4	
	C	18	15	1418	183	12.9	646	45.6	
	Solution	17	14	158	12.7	8.1	51.9	32.9	

The results are summarised in Table 5. The results clearly show that the sub sampling and/or extraction step is critical, the soil sample (sample A) showing a variation that is approximately a factor of two larger than that of the solutions. The highest variation was seen for the compounds present at the lowest concentrations. The within laboratory variation was quite acceptable, although there is room for improvement especially for the soil sample.

The between laboratory variation was quite large, probably due to a number of reasons. For instance, the 60% variation for naphthalene in the soil sample is likely explained by evaporative losses being controlled to a varying degree among the laboratories. In addition, the high variation for benzo(e)pyrene in sample B and C may be explained by differing chromatographic performance, since imperfections in the chromatographic systems primarily are reflected in high variations for the higher molecular species (and those present at low concentrations). Another plausible reason for high between laboratory variations is the fact that the laboratories used their own calibration solutions.

A comparison between the guideline method and the laboratories own methods, showed that the results were quite similar, with a tendency for the recommended method to give somewhat higher yields (in the order of 10%) for lower molecular weight compounds, which also were

present in higher concentrations. It should be taken into account, however, that the statistical basis for this statement is rather weak.

3.4. VOC

Two soil samples (samples A and B), of two different levels of contamination, and one standard solution in methanol were prepared [10]. The soil samples were sandy soil obtained from sites of polluted soil in Norway. The soil was air dried at room temperature. Coarse material was removed manually. The material was sieved through a 2 mm sieve and ground to an average size $< 500 \mu\text{m}$. The organic content was 5.9 and 7.4% for samples A and B, respectively. No background levels of the target VOC compounds was detected in the blank soils. Aliquots of the soil was transferred to 40 ml vials with an open hole screw cap, and a Teflon coated septum. Water was added to the soil to represent 83% dry weight. The soil was spiked with test solutions containing the target compounds, and conserved with methanol before the vial with its content was sealed. The 11 target compounds included benzene, toluene, ethylbenzene, cumene, *p*-cymene, *n*-butylacetate, chlorobenzene, chloroform, 1,1,1-trichloroethane, trichloroethene, and tetrachlorethene.

Each laboratory received three replicates of

Table 5
The interlaboratory test results for creosote

Compound	Level j	N	p_j^1	m_j	S_r	CV_r	S_R	CV_R
<i>o</i> -Cresol	Soil A	8	1	0.33	0.086	26.4		
	Extract C	8	8	7.8	0.34	4.3	2.2	27.5
<i>p</i> -Cresol	Soil A	8	1	0.49	0.14	28.5		
	Extract C	8	8	7.4	0.46	6.2	1.6	21.5
Naphthalene	Soil A	11	6	0.16	0.034	21.1	0.099	60.7
	Extract B	12	11	12	0.70	5.8	2.9	24.1
	Extract C	12	7	0.35	0.011	3.2	0.096	27.2
2-Methyl-naphthalene	Soil A	11	5	0.062	0.008	13.4	0.022	36.2
	Extract B	11	7	13	0.19	1.5	1.1	8.6
	Extract C	11	5	0.25	0.010	3.9	0.072	28.2
1-Methyl-naphthalene	Soil A	10	5	0.097	0.007	7.6	0.021	21.6
	Extract B	10	8	21	0.32	1.5	4.1	19.8
	Extract C	10	5	0.23	0.011	4.8	0.062	27.2
Biphenyl	Soil A	9	5	0.17	0.007	4.0	0.043	25.3
	Extract B	10	7	0.49	0.027	5.5	0.12	25.6
	Extract C	10	6	0.41	0.016	4.0	0.11	27.6
Acenaphthene	Soil A	11	11	2.5	0.18	7.4	0.54	22.0
	Extract B	12	12	6.2	0.49	8.0	1.0	16.7
	Extract C	12	9	5.5	0.13	2.3	1.0	18.7
Dibenzofuran	Soil A	9	9	2.6	0.20	7.7	0.47	18.3
	Extract B	10	9	6.5	0.59	9.1	1.1	16.6
	Extract C	10	6	6.2	0.16	2.6	0.42	6.8
Fluorene	Soil A	11	11	6.1	0.46	7.5	1.8	29.2
	Extract B	12	9	14	0.19	1.4	2.1	15.3
	Extract C	12	11	13	0.60	4.5	2.6	19.8
Dibenzo-thiophene	Soil A	9	9	2.1	0.20	9.4	0.42	19.6
	Extract B	9	8	4.5	0.18	4.1	0.99	22.2
	Extract C	9	9	4.6	0.18	3.9	1.3	28.0
Phenanthrene	Soil A	11	11	25	1.4	5.4	6.8	26.6
	Extract B	12	10	51	1.5	2.8	8.9	17.3
	Extract C	12	12	49	1.9	3.8	9.1	18.6
Anthracene	Soil A	11	9	4.9	0.65	13.3	1.6	33.5
	Extract B	12	11	17	0.69	4.1	3.1	17.9
	Extract C	12	12	16	0.72	4.6	2.7	16.9
Carbazole	Soil A	9	9	1.1	0.14	12.9	0.28	25.6
	Extract B	10	10	3.5	0.41	11.4	1.0	28.9
	Extract C	10	9	3.6	0.16	4.5	0.74	20.4
Fluoranthene	Soil A	11	11	16	0.83	5.3	4.5	28.5
	Extract B	12	12	31	1.6	5.2	7.9	25.6
	Extract C	12	11	26	0.84	3.2	2.9	11.4
Pyrene	Soil A	11	11	9.5	0.71	7.5	2.4	25.4
	Extract B	12	12	19	0.97	5.2	4.6	24.9
	Extract C	12	12	17	0.63	3.7	3.4	20.0

Table 5 (continued)

Compound	Level <i>j</i>	<i>N</i>	p_j^1	m_j	S_r	CV_r	S_R	CV_R
Benz(a)-anthracene	Soil A	11	11	2.4	0.16	6.6	0.59	25.0
	Extract B	12	12	4.9	0.43	8.7	1.3	26.4
	Extract C	12	11	4.6	0.15	3.2	0.66	14.5
Chrysene	Soil A	11	11	2.2	0.13	5.9	0.46	20.9
	Extract B	12	12	4.8	0.35	7.3	1.2	24.0
	Extract C	12	12	4.4	0.20	4.4	0.74	16.9
Benzo(b)-fluoranthene	Soil A	7	7	0.82	0.077	9.4	0.37	45.1
	Extract B	8	8	13	1.2	9.5	3.3	26.3
	Extract C	8	7	1.7	0.081	4.7	0.68	40.0
Benzo(k)-fluoranthene	Soil A	6	6	0.74	0.079	10.8	0.22	30.5
	Extract B	7	7	8.9	0.60	6.8	2.3	26.2
	Extract C	7	7	1.4	0.074	5.3	0.65	47.3
Benzo(b+k)-fluoranthene	Soil A	10	9	1.6	0.096	6.1	0.41	25.6
	Extract B	11	11	21	1.5	7.0	5.3	25.4
	Extract C	11	9	2.7	0.14	5.0	0.85	31.6
Benzo(e)-pyrene	Soil A	9	7	0.48	0.031	6.4	0.12	24.1
	Extract B	10	10	8.7	0.84	9.7	3.7	41.9
	Extract C	10	9	1.1	0.055	5.2	0.50	47.7
Benzo(a)-pyrene	Soil A	11	10	0.66	0.040	6.1	0.18	27.4
	Extract B	12	12	10	1.1	10.3	3.2	31.1
	Extract C	12	8	1.2	0.064	5.2	0.28	22.5

the calibrant solution on May 1st and had to report their results before July 1st 1996.

Eleven laboratories submitted datasets, Denmark (4), Finland (5), and Sweden (2). No laboratories from Norway or from Iceland participated. Eight of the laboratories used a solvent extraction method, while two of the laboratories used the purge and trap method. One of the laboratories participated with its own method only. The participants submitted full datasets with the exception of cumene, *p*-cymene and *n*-butylacetat, which some of the laboratories did not report.

The nominal concentrations of the VOC target compounds in the calibrant solution were used as assigned values. The grand mean was used as the assigned values for soil A and B. The results of the test are summarised in Table 6.

The test solution was reported with a reproducibility ranging from 15 (1,1,1-trichloroethane) to 40% (*p*-cymene). A similar range was observed for the soil samples. The results indicate that there were no significant differences in the performance of the calibrant solution compared with the soil

samples. On the average 65% of the laboratories reported test results within $\pm 25\%$ of the theoretical value. However, within the dataset, all laboratories had one or several values extending to the $\pm 25\%$ level.

Most laboratories seemed to perform the analysis of nonhalogenated VOCs (benzene and alkylated benzenes) better than the haloforms. However, the number of participating laboratories was low for statistics to be conclusive. Only six of the participating laboratories reported test results for *p*-cymene and *n*-butylacetate, whereas eight laboratories reported test results for cumene. One laboratory did not report results for the calibrant solution and three laboratories reported only single results for the calibrant solution.

The majority of laboratories conducted the analysis within 2 weeks of receiving the sample set. One laboratory conducted the analysis after 7–8 weeks. Most of the reported values from the latter laboratory were within acceptable limits, but contained some extreme values. One laboratory conducted its own method only (static

Table 6
The inter-laboratory test results for VOC

Compound	Level j	N	p_j	m_j	S_r	CV_r	S_R	CV_R	Ref. value
Benzene	1	11	10	3.07	0.30	9.8	0.76	24.9	3.5
	2	11	11	23.79	1.50	6.3	4.79	20.1	2 8.1
	Solution	10	6	7.25	0.20	2.8	2.35	32.4	8.8
Toluene	1	11	10	6.27	0.37	5.8	1.75	27.9	6.9
	2	11	11	22.58	1.42	6.3	5.39	23.9	24.3
	Solution	10	7	7.81	0.34	4.3	1.51	19.2	8.7
Ethylbenzene	1	11	11	5.74	0.36	6.9	1.95	34.0	5.5
	2	11	11	34.08	1.57	4.6	11.52	33.8	34.4
	Solution	10	7	8.49	0.38	4.5	1.68	19.8	8.6
Cumene	1	8	8	5.96	0.37	6.2	2.03	34.1	5.5
	2	0	0						ni
	Solution	7	4	8.03	0.27	3.4	1.29	16.0	8.6
<i>p</i> -Cymene	1	0	0						ni
	2	6	6	16.47	1.58	9.6	1.59	9.6	17.2
	Solution	5	3	10.34	0.72	6.9	4.20	40.7	8.6
<i>n</i> -Butylacetate	1	6	6	3.36	0.27	7.9	0.86	25.5	4.2
	2	6	6	14.5 3	0.48	3.3	3.41	23.5	17.6
	Solution	6	4	7.48	0.14	1.9	1.16	15.5	8.8
Chlorobenzene	1	11	11	3.06	0.18	5.7	0.77	25.0	3.5
	2	11	11	18.74	1.23	6.6	4.34	23.2	22.2
	Solution	10	7	10.08	0.42	4.2	2.11	21.0	11.1
Chloroform	1	11	11	3.65	0.32	8.7	1.42	38.8	4.6
	2	0	0						ni
	Solution	10	6	13.60	0.516	3.8	4.90	36.0	14.6
1,1,1-Trichloro-ethane	1	11	10	5.50	0.57	10.4	2.04	37.1	7.4
	2	11	10	10.52	0.82	7.8	3.07	29.2	13.4
	Solution	10	6	11.63	0.23	2.0	1.78	15.3	13.4
Trichloroethene	1	0	0						ni
	2	11	11	13.99	0.90	6.5	4.73	33.8	17.5
	Solution	10	7	12.68	0.5 9	4.6	3.15	24.8	14.6
Tetrachloro-ethene	1	11	10	1.09	0.18	17.0	0.42	38.4	1.3
	2	11	11	24.85	2.05	8.3	7.71	31.0	32.4
	Solution	10	6	15.21	0.43	2.8	3.97	26.1	16.2

ni, not included

headspace). The reported calibrant solution results from this laboratory were good, but the results from the soil samples were only approximately 50% of the theoretical values. This is consistent with observations made by SINTEF, suggesting that a static headspace technique is not an appropriate method for quantitative analysis of VOC residues in soil.

3.5. PCB

The inter-laboratory test [9] concerned the analysis of nine different PCB congeners (28, 52, 101, 105, 118, 138, 153, 156, 180) in one level of contaminated soil. Every laboratory tested the proposed guideline method in three sub samples of the soil containing 0.3 g of CRM 481 from

Table 7
The inter-laboratory test results for PCB

Congener	Level j	N	p_j	Expected level	m_j	Accuracy (%)	S_r	CV_r	S_R	CV_R
28	A	17	11	0.03	0.032	107	0.007	21	0.022	69
	B	11	7	0.03	0.024	78	0.002	9.4	0.020	83
	Solution	18	18	32.2	47.1	146	2.6	5.5	18.3	39
52	A	20	15	0.29	0.28	97	0.01	5.0	0.10	35
	B	13	11	0.29	0.37	128	0.04	11	0.17	47
	Solution	20	18	29.1	28.5	98	1.9	6.7	6.9	24
101	A	21	21	3.7	3.5	95	0.19	5.6	0.95	27
	B	14	13	3.7	3.5	93	0.25	7.1	1.3	36
	Solution	20	20	45.7	44.8	98	1.9	4.2	9.9	22
105	A	10	7	0.1	0.37	373	0.017	4.6	0.3 8	102
	B	7	4	0.1	0.20	200	0.02	10.0	0.14	71
	Solution	12	10	20.2	20.6	102	0.92	4.5	3.9	19
118	A	20	16	0.94	1.18	126	0.11	9.6	0.80	68
	B	13	10	0.94	0.96	102	0.09	9.7	0.30	36
	Solution	19	17	33.8	29.4	87	0.97	3.3	8.1	28
138	A	21	21	9.2	11.1	121	0.78	7.0	3.8	34
	B	14	14	9.2	11.0	120	1.1	10	4.0	36
	Solution	20	18	131	119	91	3.9	3.3	33.6	28
153	A	21	20	13.7	12.5	91	0.66	5.3	3.9	31
	B	14	14	13.7	11.8	86	1.3	11	3.6	31
	Solution	20	19	71.4	69.0	97	2.3	3.4	19.8	29
156	A	12	10	0.7	0.83	118	0.05	6.4	0.29	36
	B	9	7	0.7	0.71	101	0.06	8.5	0.25	35
	Solution	12	10	62.2	58.6	94	1.9	3.3	4.6	7.9
180	A	21	21	12.4	11.8	95	0.82	6.9	3.7	31
	B	14	14	12.4	11.8	95	0.9	7.6	3.6	31
	Solution	20	16	74.1	70.6	95	1.9	2.7	16.0	23

BCR mixed with 2.7 g of PCB-free soil and if desired their own method on a different set of the same soil. All laboratories were also supposed to analyse a solution that contained all nine PCBs to give an idea of the calibration and chromatographic performance. The analyte solution was made from neat crystals of respective congeners and PCB 31 from Promochem, Germany, and dissolved in isooctane p.a. The soil samples were sent out in screw-capped glass vials and the analyte solution in sealed glass-ampoules.

The samples were sent out on May 7, 1996. The number of laboratories receiving samples were 28 but only 21 returned results. Last date of accepted results was August 31, 1996. The results, which are summarised in Table 7, revealed that

many of the participating laboratories have problems concerning calibration of the individual PCB congeners and can therefore not be expected to give accurate results when analysing soil samples. It is evident that the preparation of calibrants and the method of calibration are a major source of error in the determination of PCBs. One of the 21 labs returning results did not analyse the analyte solution, but of the remaining 20 laboratories only 7–14 laboratories were able to determine the analyte solution within 25% deviation from the expected values.

Generally, higher variability was found with lower level congeners and it has been proposed by CEN to allow 100% variation at levels close to the detection limits of individual PCBs (around

0.01–0.05 mg kg⁻¹ for the soil), 50% variation at a level 10 × higher than that and 25% variation at still higher levels (prEN 1528-1:1996). Many laboratories did not analyse PCBs 105 and 156. These are usually present at low levels but are nevertheless very important congeners toxicologically (mono-*ortho*).

The treatment of PCB 138 was questionable, because it was unclear whether the laboratories were analysing 138 + 163 together, in which case the total amount detected would have been 12.3 instead of 9.2 for only PCB 138. The mean values were in-between these figures, so most laboratories were probably analysing the two together although they did not indicate that in their results and we therefore used 9.2 as the expected value.

Fourteen laboratories tested their own method and in general not much difference was found between the guideline method and their 'own methods'. Seven laboratories reported very good results, indicating that the method is sufficient for the purpose.

4. Discussion

4.1. Heavy metals

The nominal concentration of the metals in the calibrant solution was used as the assigned values. The overall performance on the test solution was good with a total coefficient of variation CV_R between 3.73% for Cu to 13.9% for Hg. The laboratories seem to have larger difficulties analysing As and Hg than other elements. The performance of the calibrant solution was regarded acceptable, although some poor results were reported.

The grand mean were used as the assigned values for soil A and B. For soil samples the coefficient of variation CV_R varied between 6 and 26% for soil A and B, and between 6 and 40% for soil C. At least 75% of the participants were able to analyse the soil samples regarding Cd, Cr, Cu, Ni, Pb and Zn within 25% of the assigned values, but only between 60 and 75% were able to analyse As and Hg within 25% of assigned values, respectively. The testing of homogeneity of the test

samples showed a variation which was less than 5%.

Soil C was certified for all the elements of interest except for Pb. It was revealed during the test that this soil sample was not completely homogeneous and gave a higher coefficient of variation CV_R than soil A and B.

The proposed method for analysing heavy metals in contaminated soil seems to work sufficient for its purpose. All datasets contained extreme values, and indicate that some of the participating laboratories need to improve their quality assurance.

4.2. Chlorophenols

The test material was field moist, obtained from a contaminated site, representing a relevant composition of soil and sawdust. Homogeneity experiments revealed a variation of 2–22%, which was deemed acceptable for this kind of samples. The repeatability variation coefficient, CV_r , which indicates the within-laboratory variation was also satisfactory. It was lower than 8.1% for the test solution and less than 17% for all the soil samples. The results of the inter-laboratory test showed, however, that the reproducibility between the laboratories to analyse the chlorophenol solution was very poor. The coefficient of variation, CV_R , for the solution ranged from 17.3 to 34.1% and for soil samples from 31.8 to 71.1%.

The variation may be due to the fact that the laboratories used the tested method for the first time and thus had problems finding the right level of concentration. However, this problem can be overcome by better validation in separate laboratories. At present there is no commercial reference material available. The reason for the variation in the results for the soil samples, however, was not due to the quality of the test material, but rather due to problems with analytical performance, as was evident from the results of the calibrant solution. The CV_R was highest for soil C, which had a very high concentration. For soils A and B it varied from 31.8 to 47.9%.

4.3. Creosote

The within laboratory variation was quite acceptable, although there is room for improvement especially for the soil sample [8]. The between laboratory variation was quite large, probably due to a number of reasons. For instance, the 60% variation for naphthalene in the soil sample is likely explained by evaporative losses being controlled to a varying degree among the laboratories. The within laboratory variation for the 21 compounds was:

Sample A, between 4.0 (for biphenyl) and 21% (for naphthalene).

Sample B, between 1.4 (for fluorene) and 11% (for carbazole).

Sample C, between 2.3 (for acenaphthene) and 6.2% (for *p*-cresol).

The between laboratory variation was:

Sample A, between 17 (for dibenzofuran) and 60% (for naphthalene).

Sample B, between 8.4 (for 2-methylnaphthalene) and 42% (for benzo(e)pyrene).

Sample C, between 6.13 (for dibenzofuran) and 48% (for benzo(e)pyrene).

The results from the methods evaluation showed that it is a good candidate for recommendation on a Nordic basis. It should however be pointed out that a less contaminated soil probably requires a more specific method, e.g. gas chromatography in combination with mass spectrometry (GC-MS). Also, it should be kept in mind that soil samples of different origin may have substantially different properties, and that the soil used in this investigation should not be regarded as being representative of the majority of contaminated soils. There may very well be other soil types, e.g. with higher humic content that would yield less favourable results as far as the method evaluation is concerned.

4.4. VOC

The overall reproducibility was considered to be acceptable, but there is room for improvement. The results suggest that some of the observed differences are related to factors within the laboratories, and are not related to obvious

weaknesses in the proposed method. A strong indication of this is the fact that the reproducibility results of the test solution were comparable with the results of the soil samples.

The test solution was reported with a reproducibility ranging from 15 (1,1,1-trichloroethane) to 40% (*p*-cymene). A similar range was observed for soil samples. Most laboratories were able to analyse the samples within $\pm 25\%$ of the theoretical values. Some extreme values were observed, but can probably be related to errors in the analytical performance of the laboratory in question rather than to limitations in the proposed method. The proposed guideline method includes some critical steps which, when handled improperly, can give erratic analytical results. One is the proper handling of the VOA vial when extractant solvent is added to the soil/methanol phase.

The soil/methanol phase should be mixed well in the sealed vial prior to the addition of extractant solvent. It is recommended to add the extractant and the internal calibrant solution directly into the sealed vial. Opening of the vial first may result in loss of VOCs. The second critical step is calibration. Calibration solutions should be freshly prepared. Stock calibrant solutions must be controlled and preferably renewed every 3 months. Keeping control of the critical steps above, most VOCs can be quantitatively analysed using the proposed guideline method.

4.5. PCB

After the exclusion of outliers the reproducibility (CV_R) for the analyte solution ranged from 8–29%, except for PCB 28 where the reproducibility was only 39%, most likely because some laboratories were not separating PCBs 28 and 31 adequately. For soil, reproducibility was dependent on the level found, so that when close to the detection limit it was close to 100%, but when levels were higher, the reproducibility improved to about 30% except for PCB 118 with only 68% reproducibility, possibly due to insufficient separation from PCB 149.

5. Conclusion

The most crucial step in attaining a comparable analytical method, apart from the sampling, is pre-treatment (i.e. crushing and sieving), the preparation step (i.e. extraction and digestion) and accurate and careful calibration of the instrument.

It is also important that the test report for organic compounds always contains a copy of the chromatograms from the analysis. In this way it can be seen which compounds are analysed and identified and the number of unidentified peaks. The water content of the sample should always be measured and reported, and the test results should normally be reported as mg kg^{-1} dry matter.

If the sample is sieved before analysis, this should be described in the report, and the mass of the two (or more) particle fractions from the sieving process should be reported. Only in this way is it possible to relate the concentration to the whole sample.

The inter-laboratory tests showed variable repeatability and reproducibility for the different methods, but this is more likely due to the lack of adequate quality routines in the participating laboratories than to the method. In general, the guideline methods had better reproducibility than the laboratories own methods. However, there is also room for improvement for some of the guideline methods.

References

- [1] T. Assmuth, T. Strandberg, A. Joutti, K. Kalevi, Investigation Methods for Chemically Contaminated Soil, Kemiallisesti saastuneen maaperan tutkimusmenetelmät, No. 97, Publications of the Water and Environment Administration-Series A, National Board of Waters and the Environment, ISBN 951/47-5716-5, Helsinki, Finland, 1992.
- [2] EPA Test Methods for Evaluating Solid Waste, vol. 1B: Laboratory Manual Physical/Chemical Methods, Method 8260 'Gas Chromatography/Mass Spectrometry for Volatile Organics', 1986.
- [3] ISO 5725-2, Accuracy (trueness and precision) of measurement methods and results, Part 2: Basic method for the determination of repeatability and reproducibility of a standard measurement method, 1994.
- [4] K. Kalevi, Inter-laboratory test of methods described in the report 'Nordic Guidelines for Chemical analysis of contaminated soil samples'—Analysis of Chlorophenols in Contaminated Soil, Finnish Environment Institute, Helsinki, Finland, 1997.
- [5] K. H. Karstensen, 'Nordic Guidelines for Chemical Analysis of Contaminated Soil Samples', Nordtest project 1143-93/ Technical Report 329, Nordtest, P.O. Box 116, FIN-02151 Espoo, Finland, 1997.
- [6] Norwegian Pollution Control Authority, Management for contaminated land—Preliminary guidelines for executive procedures, SFT Report 97:01, TA-1414/1997, ISBN-82-7655-030-4, P.O. Box 8100, 0032 Oslo, Norway, 1997.
- [7] K. Nylund, L. Asplund, B. Jansson, P. Jonsson, K. Litzén, U. Sellström, Analysis of some polyhalogenated organic pollutants in sediment and sewage sludge, Chemosphere 24 (1992) 1721–1730.
- [8] K. Nylund, Inter-laboratory evaluation of analytical method for creosote in soil, ITM Report 52, ISSN 1103-341X, Institute of Applied Environmental Research, Stockholm University, Stockholm, Sweden, 1996.
- [9] K. Ólafsdóttir, Analysis of PCB in contaminated soil, University of Iceland, Reykjavik, Iceland, 1996.
- [10] O. Ringstad, Inter-laboratory test(s) of methods described in the report 'Nordic Guidelines for Chemical analysis of contaminated soil samples'—Test of the method for Volatile Organic Compounds (VOC), SINTEF Report STF 66 A97509, Oslo, Norway, 1997.
- [11] I. Rustad, Inter-laboratory evaluation of analytical method for the heavy metals As, Cd, Cr, Cu, Ni, Hg, Pb and Zn in contaminated soil, SINTEF Report STF 66 A96550, Oslo, Norway, 1997.
- [12] Swedish Environmental Protection Agency, Site Remediation Action Plan—We're well on the way, S-106 48 Stockholm, Sweden, 1995.

Use of microwave digestion for estimation of heavy metal content of soils in a geochemical survey

D. McGrath

Teagasc, Johnstown Castle Research Centre, Wexford, Ireland

Received 25 May 1997; accepted 14 October 1997

Abstract

A procedure for the rapid and safe analysis of soils with widely differing organic matter contents has been investigated and validated. Surface soils, totalling 295 and sampled on a grid basis, representing 22% of the land-base of the Republic of Ireland, have been analysed for cadmium, chromium, copper, nickel, lead and zinc. Soil concentrations of cadmium, chromium, lead and nickel exhibit patterns of regionalised elevation. Implications of this elevation are considered in relation to sewage sludge application to land, future requirement for baseline surveys and concerns over concentrations in food products. © 1998 Elsevier Science B.V. All rights reserved.

Keywords: Soils; Microwave digestion; Heavy metals

1. Introduction

Trace element content of soil is largely determined by geochemical factors, the nature of the parent material and by soil forming processes, including glaciation. The influence of man is also evident in many areas [1] including Ireland [2]. Elevated concentrations of some elements including Se [3], Mo [4] and Cd [5] have been found. A recent investigation has raised concerns in relation to anthropogenic pollution of soils in urban areas by Pb in particular [2] and of geochemical pollution by Cd [5], which had previously remained undetected, in a rural area. This has led to the initiation of a National Soil Geochemical Survey, similar in many respects to that already conducted in England and Wales [6]. To date almost a quarter of the country has been sampled and

analyses performed for a suite of heavy metals. Soils were collected in 1995 (138 samples) and 1996 (157 samples).

Chemical analysis of heavy metals in soils requires matrix destruction particularly of siliceous material [7]. This can only be ensured by using HF. The procedure followed [8], using microwave digestion, has been most widely used for plants [9] but has also been used for organic soils [10] and for soil major component analysis in particular [11,12].

The heavy metals analysed, Cd, Cr, Cu, Ni, Pb and Zn are those, which in addition to Hg, are listed in the EU Directive on the Use of Sewage Sludge in Agriculture: the latter has taken legal effect in Ireland by SI 183 of 1991 [13]. This legislation is the only such relating to Irish soils and the listed metals, together with concentrations

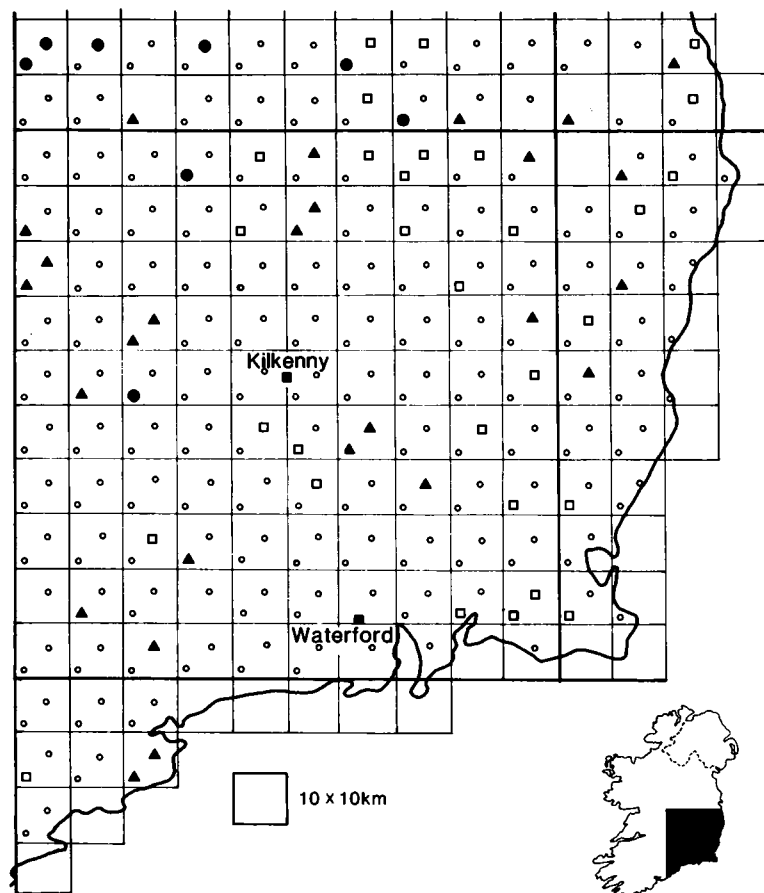


Fig. 1. Land use at sampling points; pasture (○), tillage (□), forest (▲), peat (●).

of each that are tolerated in soil that may legally receive sewage sludge, are the only threshold values available. Results are thus considered against this backdrop.

2. Experimental

2.1. Soil sampling

Sampling locations were determined using Ordnance Survey maps assisted by a Global Positioning System. Samples were taken at fixed points, two from each 10 × 10 km segment of the National Grid. In the event of it not being possible to sample at a particular location a default procedure, similar to that used for the Geochemi-

cal Survey of England and Wales [6], was put in place, subject to a deviation of not more than 400 m. Soil was sampled to a depth of 10 cm, one soil core being obtained at 5 m intervals from each intersection on a grid measuring 20 × 20 m. The combined sample of 25 cores weighed approximately 2 kg. Soil was dried at $t < 30^{\circ}\text{C}$ and sieved to pass a 2 mm mesh. A subsample was ground in a mortar and pestle and sieved to pass a 0.42 mm mesh.

2.2. Sample digestion

The procedure used was that described for digestion of soil in the CEM Digestion Applications Manual [8]. Soil (0.500 g) was placed in a Teflon vessel (100 ml capacity) with water (10 ml), HNO_3

Table 1
Composition of CRM 142R (BCR)

	Heavy metal ($\mu\text{g g}^{-1}$ in CRM)					
	Pb	Ni	Cu	Cr	Zn	Cd
Found	35.2	60.6	69.7	111.8	96.1	0.37
SD	2.6	1.9	1.8	2.8	1.6	0.04
Certified value	40.2	64.5	69.7	113	101	0.34
SD	1.9	2.5	1.3	4	6	0.04

^a Indicative value.

(5 ml), HF (4 ml) and HCl (1 ml). It was then subjected to treatment for 30 min, in a CEM Digestion System Model MDS 2000 (CEM Corporation Matthews, NC.). Each set of 12 digests consisted of 10 treatments, a certified reference material CRM 142 R [14] and a reagent blank. Since power input, maximum 630 W, was interrupted when the pressure within the control vessel reached 0.828 MPa, and since pressure generation within vessels was influenced largely by the organic matter content of soil, it was important on the grounds of safety to place the most labile sample in the control vessel. To facilitate this, samples were attended to in order of decreasing organic matter. Digests were treated with crystalline H_3BO_3 (2 g) to neutralise excess HF, transferred to polythene containers and made up to a weight of 53.95 g (equivalent to 50 ml).

2.3. Analyses

Analysis for Cu, Ni and Zn was performed by flame atomic absorption using a Varian AA-1475. Standards within the range 0–2 $\mu\text{g ml}^{-1}$, were made up in a synthetic digestion mix. Cr was similarly determined using 1% Na_2SO_4 modifier [15]. For accurate quantification of Pb at low concentrations by atomic absorption it was found necessary to extract metals as their chelates with ammonium pyrrolidine carbodithioate into 4-methylpentan-2-one (APCD). Cd was measured by atomic absorption with electrothermal atomisation using a Varian Spectra AA-400 with GFA-96 and Pd–ascorbic acid as modifier. Samples, for which measured values were higher than the threshold value for sewage sludge use [13], were reanalysed for the relevant metal after redigestion.

Table 2
Frequency distribution of heavy metal concentrations ($n = 295$)

	Heavy metal ($\mu\text{g g}^{-1}$ in soil)					
	Pb	Ni	Cu	Cr	Zn	Cd
Mean	30.4	13.5	16.9	49.5	70.3	0.52
SD	15.2	12.5	9.6	26.7	35.6	0.46
Skewness	1.89	4.87	1.32	3.78	0.71	2.75
Curtosis	4.94	47.5	3.77	36.5	1.17	9.84
Transformed log	27.3	9.15	14.2	42.9	59.7	0.39
SD	1.6	2.7	1.9	1.8	1.9	2.17
Skewness	0.04	−0.69	−0.96	−1.44	−1.49	−0.58
Curtosis	2.13	−0.09	1.86	3.79	3.77	3.11
SI 183 treshold value	50	30	50	100	150	1.0
Number of soils exceeding	30	14	2	2	4	30

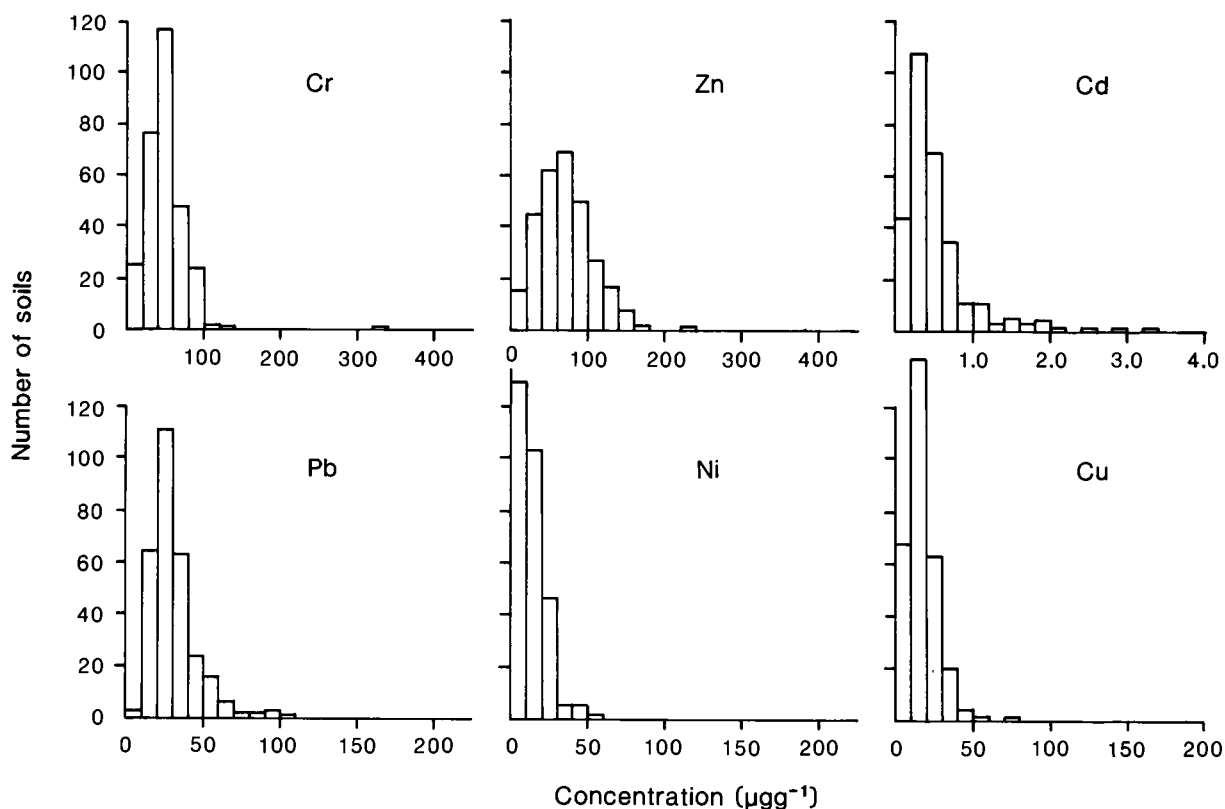


Fig. 2. Frequency distribution of heavy metal concentration ($\mu\text{g g}^{-1}$) in soils

Pb was reanalysed using the electrothermal procedure with NaH_2PO_4 as modifier. Background correction was used in all instances.

Organic carbon in soil was determined by the Walkley Black method [16].

3. Results And Discussion

3.1. Soil selection

The sampled area represented 22% of the land base of Ireland. Because sampling locations were predetermined, sampling bias was eliminated. Collected soils totalled 295 with 10 associated failures, due largely to inaccessibility. Four categories of land use were identified (Fig. 1), namely, permanent pasture ranging in quality from well-managed ryegrass pastures to mountain heath (78.2%), tillage, largely barley production (10.2%),

forest, largely coniferous, (8.8%) and basin peat (2.7%).

3.2. Analysis for heavy metals

Complete digestion of mineral soil matrix was achieved for all samples. Soils with a wide range of organic carbon contents, ranging from less than 2% to more than 44% were digested in the pressure control vessel. Nevertheless no depression in content of any analyte was encountered in the certified reference material, which was digested with each set despite the decreasing energy input. In a separate replicated trial there was no significant decrease in values obtained for a low carbon (12.03 mg g^{-1}) soil when the control vessel contained this soil, the reference soil or a high organic matter (peat) soil.

Values found for the certified reference material were considered satisfactory (Table 1). A problem

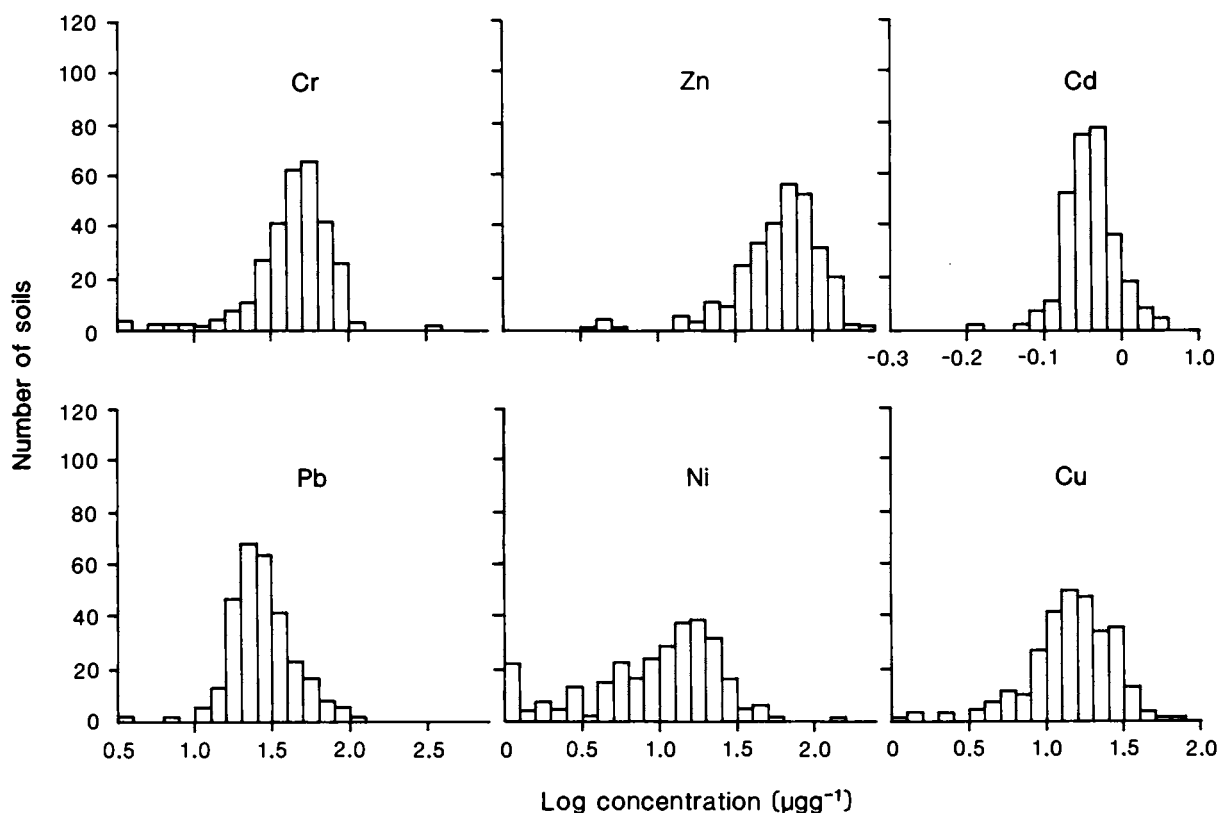


Fig. 3. Frequency distribution of log-transformed heavy metal concentration ($\mu\text{g g}^{-1}$) in soils

was encountered with the quantification of Pb which was not overcome using the method of additions. Solvent extraction of APCD chelates [17] gave accurate results. Results for high value soils were confirmed using electrothermal atomic absorption. Indeed, except for two samples collected at an early date which initially had erroneously high values for Ni and Cr, first measurements were found to be essentially correct.

3.3. Heavy metal levels in Irish soils

Mean concentrations determined for heavy metals (Table 2) were not greatly dissimilar to those reported elsewhere [18–20]. Plotted frequency distributions (Fig. 2) showed departures from normality with severe skewness (asymmetry) and curtosis (influence of peripheral values). These were only partially remedied by the usual

device of employing log-transformation (Fig. 3). Interestingly, high values were best highlighted in untransformed distributions whereas low values were highlighted by transformation.

Low values were not infrequent especially for Cu, Cr, Ni and Zn. Examination in relation to land use (Table 3) showed that concentrations of these metals were low in both forest and peat soils, albeit Cr concentrations were not greatly depressed in forests.

Elevated values (Figs. 2 and 3), those exceeding the threshold fixed by Irish legislation [13], were found for all metals (Table 2). High concentrations were most common for Pb, Cd and to a lesser extent Ni. Some high values were associated with forest soils (Table 3) but not with peat soils as noted by others [21].

Highest mean concentrations of Cd, Cr and Ni were associated with tillage soils. Though it may be tempting to speculate that this may have arisen

Table 3
Heavy metal concentrations by land use

Land use (n)	Carbon (mg g ⁻¹)	Heavy metal (ug g ⁻¹ in soil)					
		Pb	Ni	Cu	Cr	Zn	Cd
Pasture (231)							
Mean	73.1	30.0	13.4	18.0	49.5	73.1	0.52
SD	32.7	14.1	9.2	9.5	19.5	32.7	0.42
Tillage (30)							
Mean	37.0	30.3	23.3	19.1	67.6	88.6	0.76
SD	34.3	14.6	26.6	8.5	52.6	42.4	0.71
Forest (26)							
Mean	152.8	38.1	5.5	8.7	42.5	38.0	0.29
SD	111.1	10.8	5.6	5.9	24.3	25.2	0.29
Peat bog (8)							
Mean	437.7	17.6	4.4	4.9	6.0	26.2	0.35
SD	15.9	11.7	4.2	3.3	2.0	25.2	0.20

as a consequence of anthropogenic activity, perhaps through fertiliser application, as fertilisers are known to contain significant concentrations of all heavy metals [22], the reason may in reality be different as considered later.

Strong associations existed between metals as shown by regression (Table 4). In particular Cr was associated with Ni and Zn with Cu. The significance of these relationships were not greatly weakened by ignoring peat and forest soils.

3.4. Geographic distribution of heavy metals

In order to evaluate regional distribution the strategy adopted was to plot values exceeding the threshold value and also those amounting to 75% of such values. Only two soils had Cu values above the threshold and these were from areas

where there had been mining activity in the past. On the other hand, thirty soils exceeded the threshold value for Cd. Of the affected soils seven were under tillage: the proportion with pH > 7.0 was 40% compared with 10% for all soils. Soils of the main areas affected (Fig. 4) are derived primarily from limestone till [23] and it is known that such soil can show moderate elevations of Cd and other heavy metals [24]. A lesser number of soils with elevated Ni and some with Zn concentrations in excess of 75% of the threshold also fell within the northern section of the Cd affected area.

There appeared (Fig. 5) to be a low (to 75% of threshold), but widespread, enrichment of chromium in soils of the southeast. This was not apparent for Ni despite its association with Cr. It is known [25] that Cr₃ with an ionic radius of

Table 4
Correlation coefficient (*r*) for heavy metals (*n* = 295)

	Carbon	Pb	Ni	Cu	Cr	Zn	Cd
Carbon	—	0.028	-0.146*	0.266***	0.324***	-0.295***	-0.017
Pb		—	0.101	0.386***	0.180 **	0.352***	0.038
Ni			—	0.304***	0.615***	0.464***	0.387***
Cu				—	0.391***	0.632***	0.233***
Cr					—	0.307***	-0.086
Zn						—	0.445***
Cd							—

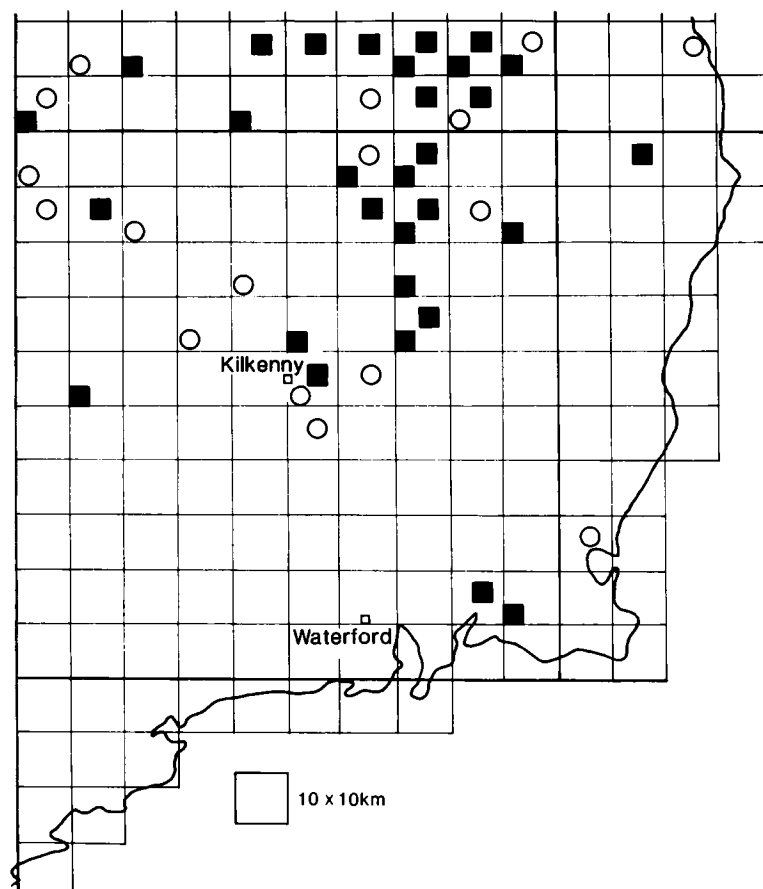


Fig. 4. Locations showing concentrations of Cd exceeding 1.0 (■) and 0.75 (○) $\mu\text{g g}^{-1}$ in soil.

0.064 readily substitutes for Fe with atomic radius of 0.067 nm. Fe content of soils in this area are exceptionally high, generally exceeding 30 mg kg^{-1} . The pattern of enrichment also coincides with mapped [26] extrusions of gabbro and basalt which tend to be enriched in both Cr and Ni [25].

The pattern of enrichment for Pb (Fig. 6) was quite different to that for Cd or Cr. Elevation of Pb in soils to concentrations well above those found in the present investigation is known to occur as a consequence of emissions from petrol fume exhausts in Ireland [2] and elsewhere [27]. It is known that deposition rates fall off rapidly within a short distance from the roadway but that a small proportion of emitted Pb can travel long distances [27]. In the present investigation inspection of site distances from thoroughfares, gener-

ally rural roads, with low traffic density, and associated soil Pb values did not encourage the belief that short-range deposition of Pb was involved. Longer range transportation from the United Kingdom and Continental Europe, as is known to happen with SO_2 [28] remains a possibility but an unlikely one in view of the quantities that would be necessary to cause the elevations mentioned.

3.5. Significance of results

A large number of soils totalling 64 or 22% of soils examined would be disqualified under legislation, S1 183 of 1991, from receiving sewage sludge. This together with the proportion of tilled soils that were affected and their proximity to

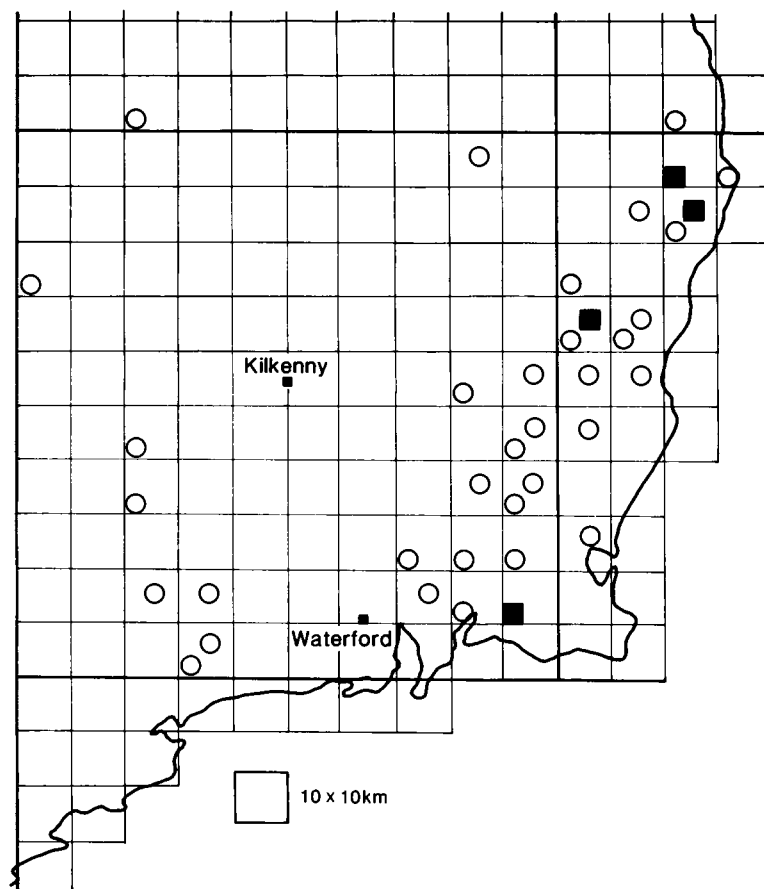


Fig. 5. Locations showing concentrations of Cr exceeding 100 (■) and 75 (○) $\mu\text{g g}^{-1}$ in soil.

high population centres in the east of Ireland has relevance to future plans to expand sludge use in agriculture.

The fact that some metals, including Cd, Ni, Cr and Pb, and also Hg [29] all exhibit strong localised concentration effects, makes it imperative that information be obtained for the rest of country, otherwise baseline surveys, which need to be conducted prior to industrial/mining development, cannot be properly planned or evaluated.

The mildly elevated concentration of Cd, similar in intensity to that already reported for an area in the West of Ireland [5], makes it imperative that follow up investigations be conducted to

ensure that this has no significant impact on plant, animal or human health [24].

Acknowledgements

The author wishes to thank S. McCormack for technical assistance, T. Cowman for electrothermal atomic absorption analysis for Cd and Pb and W.E. Murphy for statistical analysis. Gratitude is also extended to the EU for financial assistance under the Structural Funding Programme.

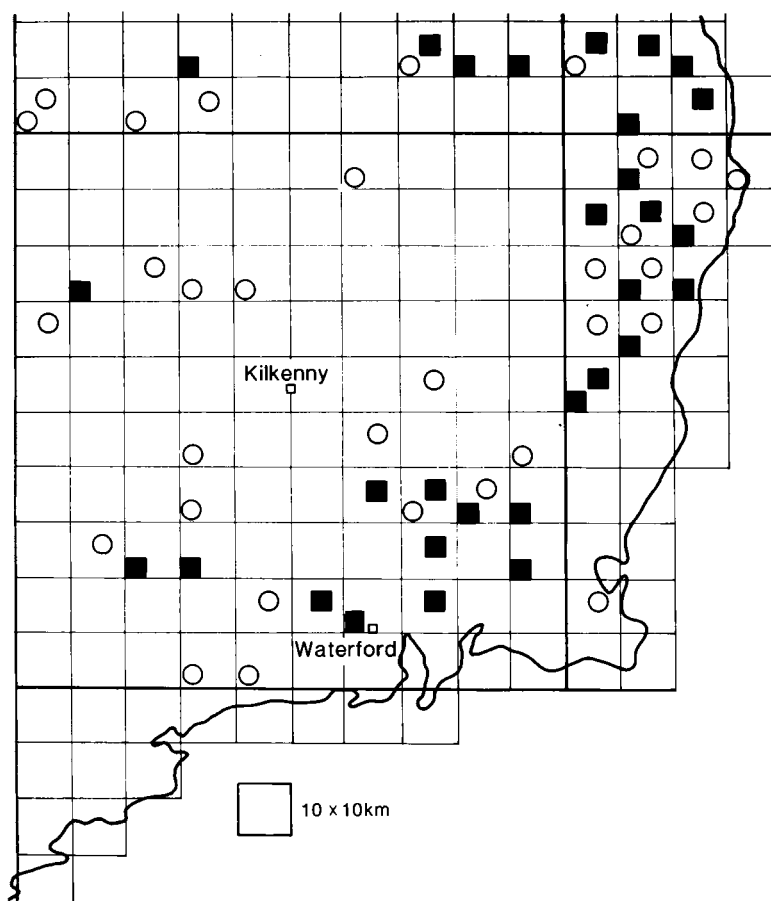


Fig. 6. Locations showing concentrations of Pb exceeding 50 (■) and 37.5 (○) $\mu\text{g g}^{-1}$ in soil.

References

- [1] B.J. Alloway, The origins of heavy metals in soils in: B.J. Alloway (Ed.), *Heavy Metals in Soils*, J. Wiley and Sons, New York, 1990, pp 29–39.
- [2] D. McGrath, *Sci. Total Environ.* 164 (1995) 125.
- [3] T. Walsh, G.A. Fleming, R. O'Connor, A. Sweeney, *Nature (London)* 168 (1951) 881.
- [4] J.C. Brogan, G.A. Fleming, J.E. Byrne, *Ir. J. Agric. Res.* 12 (1973) 71.
- [5] D. McGrath, *Sci. Total Environ.* 178 (1996) 37.
- [6] S.P. McGrath, P.J. Loveland, *The Soil Geochemical Atlas of England and Wales*, Blackie, Glasgow, 1992, 101.
- [7] R.A. Nadkarni, *Anal. Chem.* 56 (1984) 2233.
- [8] Anon, *Microwave Digestion Applications Manual*, CEM, USA, 1994.
- [9] I. Novozamsky, R. van Eck, V.J.G. Houba, J.J. van der Lee, *Commun. Soil Sci. Plant Anal.* 27 (1996) 867.
- [10] C.S.E. Papp, L.E. Fischer, *Analyst* 112 (1987) 337.
- [11] C.J. Warren, B. Xing, M.J. Dudas, *Can. J. Soil Sci.* 70 (1990) 617.
- [12] J.T. Ammons, M.E. Essington, R.J. Lewis, A.O. Gallagher, G.M. Lessman, *Commun. Soil Sci. Plant Anal.* 26 (1995) 831.
- [13] Statutory Instrument No. 183 Department of the Environment., Stationary Office, Dublin, 1991, 14.
- [14] E.A. Maier, B. Griepink, H. Muntau, K. Vercoutere, Certification of the Total Contents (Mass Fractions) of Cd, Co, Cu, Pb, Mn, Hg and Ni and the Aqua Regia Soluble (Mass Fractions) of Cd, Pb, Ni and Zn in a Light Sandy Soil. CRM 142R, BCR, CEC, Brussels. 56 (1994).
- [15] J.A. Hurlbut, C.D. Chriswell, *Anal. Chem.* 43 (1971) 465.
- [16] E. Byrne, *Chemical Analysis of Agricultural Materials*, An Foras Taluntais, Dublin, 1979, 194.

- [17] S.R. Koirtyohann, J.W. Wen, *Anal. Chem.* 45 (1973) 1986.
- [18] H.J.M. Bowen, *Environmental Chemistry*, vol. 2, The Royal Society of Chemistry, London, 1992, 204.
- [19] F.C. Archer, I.H. Hodgson, *J. Soil Sci.* 38 (1987) 421.
- [20] G.G.S. Holmgren, M.W. Meyer, R.L. Chaney, R.B. Daniels, *J. Environ. Qual.* 22 (1993) 335.
- [21] G.A. Reaves, M.L. Berrow, *Geoderma* 32 (1984) 1.
- [22] N. Senesi, M. Polemio, *Fert. Res.*, 1981 (2) 289.
- [23] M.J. Gardiner, T. Radford, *Soil Associations of Ireland and their Land Use Potential 1980*, An Foras Taluntais, Dublin.
- [24] B.J. Alloway, Cadmium, in: B.J. Alloway (Ed.), *Heavy Metals in Soils*. Wiley, New York, 1990, pp 100–124.
- [25] S.P. McGrath, S. Smith, Chromium and Nickel, in: B.J. Alloway (Ed.), *Heavy Metals in Soils*, Wiley, New York, 1990, pp 125–150.
- [26] M.V. O'Brien, *Geological Map of Ireland*, Geological Survey, Dublin 1962.
- [27] K.G. Tiller, L.H. Smith, R.H. Merry, P.M. Clayton, *Aust. J. Soil Res.* 25 (1987) 155.
- [28] J.J. Bowman, M. McGettigan, *Water, AirSoil Pollut.* 75 (1994) 159.
- [29] D. McGrath, Unpublished observation, 1997.

Extraction procedures for the determination of heavy metals in contaminated soil and sediment

Gemma Rauret

Dept. Química Analítica, Universitat de Barcelona, Barcelona, Spain

Received 25 May 1997; accepted 14 October 1997

Abstract

Extraction tests are commonly used to study the mobility of metals in soils and sediments by mimicking different environmental conditions or dramatic changes on them. The results obtained by determining the extractable elements are dependent on the extraction procedure applied. The paper summarises state of the art extraction procedures used for heavy metal determination in contaminated soil and sediments. Two types of extraction are considered: single and sequential. Special attention is paid to the Standard, Measurement and Testing projects from the European Commission which focused on the harmonisation of the extraction procedures and on preparing soil and sediment certified reference materials for extractable heavy metal contents. © 1998 Elsevier Science B.V. All rights reserved.

Keywords: Extraction procedures; Heavy metals; Contaminated soil; Sediment; Certified reference materials

1. Introduction

Trace metals in soils and sediments may exist in different chemical forms or ways of binding. In unpolluted soils or sediments trace metals are mainly bound to silicates and primary minerals forming relatively immobile species, whereas in polluted ones trace metals are generally more mobile and bound to other soil or sediments phases. In environmental studies the determination of the different ways of binding gives more information on trace metal mobility, as well as on their availability or toxicity, in comparison with the total element content. However, the determination of the different ways of binding is difficult and often impossible. Different approaches are used for soil and sediment analysis, many of them

focused on pollutant desorption from the solid phase; others are focused on the pollutant adsorption from a solution by the solid phase. Among those approaches based on desorption, leaching procedures are the most widely accepted and used.

Extraction procedures by means of a single extractant are widely used in soil science. These procedures are designed to dissolve a phase whose element content is correlated with the availability of the element to the plants. This approach is well established for major elements and nutrients and it is commonly applied in studies of fertility and quality of crops, for predicting the uptake of essential elements, for diagnosis of deficiency or excess of one element in a soil, in studies of the physical-chemical behaviour of elements in soils

and for survey purposes. To a lesser extent they are applied to elements considered as pollutants such as heavy metals. The application of extraction procedures to polluted or naturally contaminated soils is mainly focused to ascertain the potential availability and mobility of pollutants which is related to soil-plant transfer of pollutants and to study its migration in a soil profile which is usually connected with groundwater problems [1].

For sediment analysis, extraction is used to assess long term emission potential of pollutants and to study the distribution of pollutants among the geochemical phases. As far as heavy metals are concerned sediments are usually a sink but may also become a source under certain conditions, especially in heavily contaminated areas or in drastically changing environments. Chemical extraction of sediments has proven to be adequate for determining the metal associated with source constituents in sedimentary deposits [2], but the general aim of many studies involving chemical extraction is the determination of element distribution among different phases of a sediment. Single extractants are usually chosen to evaluate a particular release controlling mechanism such as desorption by increasing salinity or complexing by competing organic agents. Generally, fractions can be isolated more specifically by using sequential extraction schemes. For sediments these procedures are frequently used and are designed in relation to the problems arising from disposal of dredged materials.

Extraction tests, either in soils and sediments, are always restricted to a reduced group of elements and as far as soil is concerned they are applied to a particular type of soil; silicious, carbonated or organic. In a regulatory context, two applications for leaching tests can be recognised: the assessment or prediction of the environmental effects of a pollutant concentration in the environment and the promulgation of guidelines or objectives for soil quality as for example for land application of sewage sludge or dredge sediments. The data obtained when applying these tests are used for decision makers in topics such as land use of soil or in countermeasures application.

2. Commonly used extraction procedures in soils

During the last decades several extraction procedures for extractable heavy metals in soils have been developed and modified. In this respect, two groups of tests must be considered: the single reagent extraction test, one extraction solution and one soil sample, and in the sequential extraction procedures, several extraction solutions are used sequentially to the same sample although this last type of extraction is still in development for soils. Both types of extraction are applied using not only different extracting schemes but also different laboratory conditions. This leads to the use of a great deal of extraction procedures. In Table 1 a summary of the most common leaching test are given.

Table 1
Most common single extraction tests

Group	Type and solution strength	Reference
Acid extraction	HNO ₃ 0.43–2 mol l ⁻¹	[3]
	Aqua regia	[4]
	HCl 0.1–1 mol l ⁻¹	[3]
	CH ₃ COOH 0.1 mol l ⁻¹	[5]
	Melich 1:	[6]
	HCl 0.05 mol l ⁻¹ + H ₂ SO ₄ 0.0125 mol l ⁻¹	
Chelating agents	EDTA 0.01–0.05 mols l ⁻¹ at different pH	[3]
	DTPA 0.005 mol l ⁻¹ + TEA 0.1 mol l ⁻¹	[7]
	CaCl ₂ 0.01 mol l ⁻¹	
	Melich 3:	[8]
	CH ₃ COOH 0.02 mol l ⁻¹	
	NH ₄ F 0.015 mol l ⁻¹	
	HNO ₃ 0.013 mol l ⁻¹	
EDTA 0.001 mol l ⁻¹		
Buffered salt solution	NH ₄ -acetate, acetic acid buffer pH = 7; 1 mol l ⁻¹	[9]
	NH ₄ -acetate, acetic acid buffer pH = 4.8; 1 mol l ⁻¹	[3]
Unbuffered salt solution	CaCl ₂ 0.1 mol l ⁻¹	[3]
	CaCl ₂ 0.05 mol l ⁻¹	[3]
	CaCl ₂ 0.01 mol l ⁻¹	[3]
	NaNO ₃ 0.1 mol l ⁻¹	[10]
	NH ₄ NO ₃ 1 mol l ⁻¹	[3]
	AlCl ₃ 0.3 mol l ⁻¹	[11]
BaCl ₂ 0.1 mol l ⁻¹	[12]	

Table 2
Extraction methods proposed for standardisation or standardised in some European countries

Country	Method	Method	Reference
Germany	1 mol l ⁻¹ NH ₄ NO ₃	Mobile trace element determination	[15]
France	0.01 mol l ⁻¹ Na ₂ -EDTA+1 mol l ⁻¹ CH ₃ COONH ₄ at pH = 7 DTPA 0.005 mol l ⁻¹ +TEA 0.1 mol l ⁻¹ + CaCl ₂ 0.01 mol l ⁻¹ at pH = 7.3	Available Cu, Zn and Mn evaluation for fertilisation purposes	[16]
Italy	0.02 mol l ⁻¹ EDTA+0.5 mol l ⁻¹ CH ₃ COONH ₄ at pH = 4.6 DTPA 0.005 mol l ⁻¹ +TEA 0.1 mol l ⁻¹ + CaCl ₂ 0.01 mol l ⁻¹ at pH = 7.3	Available Cu, Zn, Fe and Mn evaluation in acidic soils	[17]
Netherlands	CaCl ₂ 0.1 mol l ⁻¹	Availability and mobility of heavy metals in polluted soils evaluation	[18]
Switzerland	NaNO ₃ 0.1 mol l ⁻¹	Soluble heavy metal (Cu, Zn, Cd, Pb and Ni) determination and ecotoxicity risk evaluation	[19]
United Kingdom	EDTA 0.05 mol l ⁻¹ at pH = 4	Cu availability evaluation	[20]

From Table 1 it can be observed that a single extraction including a large spectra of extractants are used. It ranges from very strong acids, such as aqua regia, nitric acid or hydrochloric acid, to neutral unbuffered salt solutions, mainly CaCl₂ or NaNO₃. Other extractants such as buffered salt solutions or complexing agents are frequently applied, because of their ability to form very stable water soluble complexes with a wide range of cations. Hot water is also used for the extraction of boron. Basic extraction by using sodium hydroxide is used to assess the influence of the dissolved organic carbon in the release of heavy metals from soils. A large number of extractants are reviewed by Pickering [13] and Lebourg [14].

The increasing performance of the analytical techniques used for element determination in an extract, together with the increasing evidence that exchangeable metals better correlate with plant uptake, has lead extraction methods to evolve towards the use of less and less aggressive solutions [10]. These solutions are sometimes called soft extractants and are based on non buffered salt solutions although diluted acids and complexant agents are also included in the group. Neutral salts dissolve mainly the cation exchangeable fraction although in some cases the complexing ability

of the anion can play a certain role. Diluted acids dissolve partially trace elements associated to different fractions such as exchangeable, carbonates, iron and manganese oxides and organic matter. Complexing agents dissolve not only exchangeable element fraction but also the element fraction forming organic matter complexes and the element fraction fixed on the soil hydroxides. Nowadays it is generally accepted that extractants are not selective and that minor variations in analytical procedures have significant effects on the results.

Some leaching procedures for soils have been adopted officially or its adoption is under study in different countries with different objectives [14]. An account of these methods are given on Table 2.

3. Commonly used extraction procedures in sediments

As for soils, exchangeable metal in sediments are selectively displaced by soft extractants. Other extractants used are less selective and they co-extract the exchangeable fraction together with metals bound to different sediment phases more

or less extensively. The phases considered relevant in heavy metals adsorption in sediments are oxides, sulphides and organic matter. Fractionation is usually performed by using sequential extraction schemes. The fractions obtained, when applying these schemes, are related to exchangeable metals, metals mainly bound to carbonates, metals released in reducible conditions such as those bound to hydrous oxides of Fe and Mn, metals bonded to oxidable components such as organic matter and sulphides and residual fraction. The extractants more commonly used in sequential extraction schemes are generally applied according to the following order: unbuffered salts, weak acids, reducing agents, oxidising agents and strong acids.

In Table 3 the extractants most commonly used to isolate each fraction are given [21]. The water soluble fraction may be obtained by two ways, by sampling sediment pore solution using in situ filtration, dialysis tubes or bags, or by a leaching procedure in the laboratory. When this procedure is used the pH may be indeterminate because of

Table 3
Most common extractants used in sequential extraction schemes

Group	Type and solution strength
Water soluble fraction	H ₂ O
Exchangeable and weakly adsorbed fraction	NaNO ₃ 0.1 mol l ⁻¹
	KNO ₃ 0.1 mol l ⁻¹
	MgCl ₂ 1 mol l ⁻¹
	CaCl ₂ 0.05 mol l ⁻¹
	Ca(NO ₃) ₂ 0.1 mol l ⁻¹
Carbonate bound fraction	NH ₄ OAc 1 mol l ⁻¹ pH = 7
	HOAc 0.5 mol l ⁻¹ HOAc/NaOAc 1 mol l ⁻¹ pH = 5
Fractions bound to hydrous oxides of Fe and Mn	NH ₂ OH.HCl 0.04 mol l ⁻¹ in acetic or nitric acid NH ₄ Ox Sodium ditionite, sodium citrate, sodium bicarbonate (DCB)
Organically bound fraction	H ₂ O ₂ NaOCl

the low buffering capacity of the extractant and problems with readsorption occurs. Exchangeable fraction uses an electrolyte such as salts of strong acids and bases or salts of weak acids and bases at pH 7 to prevent oxyhydroxy phases precipitation. The carbonate bound fraction generally uses an acid such as acetic or a buffer solution acetic acid-sodium acetate at pH 5. These reagents are not able to attack all the carbonate content, as for example dolomitic carbonates, neither to attack carbonate selectively as they also remove partially organically bound trace metals. The fraction obtained when a reducing solution is used as extractant is mainly related to metals bound to iron and manganese oxides. Hydroxylamine in acid solution is the reducing agent most widely used to solubilise these oxides although iron oxide is not completely dissolved. Ammonium oxalate seems to be most effective when used in the dark, although some problems in heavy metals oxalate phase precipitation may occur even at low pH. The sodium dithionite/citrate/carbonate reagent dissolves the oxide and hydroxyoxides but can attack iron rich silicates. So reducing extractants are neither selective nor completely effective for iron and manganese oxides. Other group of extractants used sequentially includes oxidising reagents which destroy organic matter and also oxidises sulphides to sulphates. The extractants most widely used in this group are H₂O₂ and NaOCl. Hydrogen peroxide seems to be more efficient if used after the oxide extraction step.

The most widely used extraction scheme is the one proposed by Tessier [22] which has been modified by several authors [23–25]. Many of these modifications make more specific the isolation of the iron and manganese oxide and hydroxide phases. The Tessier procedure is schematised in Table 4 together with the modified procedures of Förstner [26] and of Meguelatti [24].

4. Harmonisation and method validation

Owing to the need of establishing common schemes in Europe for extractable trace metals in soils and sediments the EC Standards, Measurement and Testing Programme, formerly BCR (Bu-

Table 4
Sequential extraction schemes

Method	1	2	3	4	5
Tessier et al.	MgCl ₂ 1 mol l ⁻¹ pH 7 exchangeable	NaOAc 1 mol l ⁻¹ pH 5 carbonate	NH ₂ OH.HCl 0.04 mol l ⁻¹ 25% HOAc Fe/Mn oxides	H ₂ O ₂ 8.8 mol l ⁻¹ HNO ₃ /NH ₄ OAc organic matter + sulphide	HF/HClO ₄ residual silicate phase
Förstner	NaOAc 1 mol l ⁻¹ pH 5 exchan + carb	NH ₂ OH.HCl 0.1 mol l ⁻¹ easily reducible	NH ₄ Ox/HOx 0.1 mol l ⁻¹ pH 3 in dark moderately reducible	H ₂ O ₂ 8.8 mol l ⁻¹ pH 7 NH ₄ OAc organic matter + sulphide	HNO ₃ residual silicate phase
Meguellati	BaCl ₂ 1 mol l ⁻¹ pH 7 exchangeable	H ₂ O ₂ 8.8 mol l ⁻¹ + HNO ₃ organic matter + sulphide	NaOAc 1 mol l ⁻¹ pH 5 carbonate	NH ₂ OH.HCl 0.1 mol l ⁻¹ 25%HOAc Fe/Mn oxides	ashing + HF/HCl residual silicate phase

reau Community of Reference), has sponsored from 1987 several projects focused on single extraction for soils and sequential extraction for soils and sediments. The project started with the intercomparison of existing procedures tested in an interlaboratory exercise [27]. The next step was to adopt common procedures for single extraction of trace metals from mineral soils. The second step was to adopt a common procedure for sequential extraction of sediment. As a conclusion of the first step, single extraction procedures using acetic acid, 0.43 mol l⁻¹, and EDTA, 0.005 mol l⁻¹ for mineral soils and a mixture of DTPA, 0.005 mol l⁻¹ diethylenetriamine pentaacetic acid, 0.01 mol l⁻¹ CaCl₂ and 0.1 mol l⁻¹ triethanolamine for calcareous soils were adopted for extractable Cd, Cr, Cu, Ni, Pb and Zn. In order to improve the quality of the determination of extractable metal content in different types of soil using the procedures previously adopted, the extraction procedures were validated by means of intercomparison exercises [28,29]. Moreover the lack of suitable certified reference materials for this type of studies did not enable the quality of the measurements to be controlled. With the purpose to overcome this problem three certified reference materials: a terra rossa soil, a sewage amended soil and a calcareous soil have been

prepared and their extractable trace metal contents were certified (CRM 483, CRM 484 and CRM 600) [30,31].

The second step of the EC, Standards, Measurement and Testing was focused on a feasibility study on the adoption and validation of a sequential extraction scheme for sediment samples. In a workshop held in 1992 in Sitges (Spain) a sequential extraction scheme was proposed which includes three steps: acetic acid, hydroxylamine hydrochloride or a reducing reagent and hydrogen peroxide or an oxidising reagent. This procedure is schematised in Table 5. Moreover in this workshop the main analytical limitations in sequential extraction of trace metals in sediments were thoroughly discussed and practical recommendations were given [32,33]. These recommendations deal with sampling and sample pre-treatment, practical experiences with reagents and matrices and analytical problems after extraction.

Once the scheme was designed, it was tested through two round robin exercises using two different type of sediment, silicious and calcareous [34]. In these exercises some critical parameters in the protocol were identified such as the type and the speed of the shaking and the need of an optimal separation of the liquid–solid phases after the extraction. It was stated that the sediment

should be continually in suspension during the extraction. In these intercomparison exercises an important decrease was noted on the acceptable set of values for concentration in the extract lower than $10 \mu\text{g l}^{-1}$, which illustrates the difficulties experienced by a number of laboratories in the determination of such concentration levels in these matrices. It was concluded that when electrothermal atomic absorption spectrometry is used for the final determination, the method of standard additions is strongly recommended for calibration. The results obtained in the round robin exercises encouraged to proceed with the organisation of a certification campaign in order to produce a sediment reference material following the sequential extraction scheme adopted. So the next step of the project was the preparation of a sediment certified reference material for the extractable contents of Cd, Cr, Cu, Ni, Pb and Zn, following the three-step sequential extraction procedure. A silicious type sediment with rather high trace metal content was chosen for this purpose. This material has been recently certified for five metals, Cd, Cr, Ni, Pb and Zn in the first step, Cd, Ni and Zn in the second step and Cd, Ni and Pb in the third step [35]. Not all the elements

were certified because the lack of reproducibility attributable to non adherence to the protocol, in the acceptance of too large tolerances in the conditions specified in it or in the existence of critical aspects in the procedure referred mainly to the second step. These aspects were mainly pH, redox conditions and possible losses of sediment in the transfer. The results obtained in the certification exercise recommended to continue the development of the extraction protocol in order to increase reproducibility. Consequently the causes of non reproducibility are now under study in a new SMT project.

5. Conclusions

The advantages of a differential analysis over investigations of total metal contents and about the usefulness of single and sequential chemical extraction for predicting long-term adverse effects of heavy metals from polluted solid material, soils and sediments, is beyond any doubt. The advances in this field, especially to make available soil and sediment certified reference materials for extractable element contents by using harmonised procedures, is going to increase the quality of the results due to the possibility of verifying the analytical quality control.

Nevertheless some problems need to be solved with these procedures for example: (1) reactions are not selective and are influenced by the experimental conditions so it is necessary to identify the main variables which involves a lack of reproducibility when applying a procedure, to write very well defined protocols and to validate them; (2) labile fractions could be transformed during sample preparation and during sequential extraction schemes application so problems encountered when preparing certified reference materials are not representing all the problems to be found when working with environmental samples such as wet sediments, some work in this area is needed; (3) analytical problems due to the low level of metals to be measured in the different fractions especially when using soft extractants; and (4) the procedures need to be optimised and validated for different type of soils, including organic soils and sediments.

Table 5
EC Standard, Measurements and Testing procedure

Step	Conditions
1	0.11 mol l ⁻¹ HOAc, V m ⁻¹ 40 ml g ⁻¹ temp. 20°C, shaking overnight
2	0.1 mol l ⁻¹ NH ₂ OH.HCl (pH = 2 with HNO ₃) V m ⁻¹ 40 ml.g ⁻¹ temp. 20°C shaking overnight
3	8.8 mol l ⁻¹ H ₂ O ₂ (pH = 2–3 with HNO ₃) V m ⁻¹ = 10 ml g ⁻¹ room temperature 1h. New addition 10 ml g ⁻¹ 85°C for 1h. reduce volume to few ml. 1 mol l ⁻¹ NH ₄ Oac (pH = 2 with HNO ₃) V m ⁻¹ = 50 ml g ⁻¹ 20°C shaking overnight

References

- [1] H.A. van der Sloot, L. Heasman, Ph. Quevauviller (Eds.), Harmonization of leaching /extraction test, Chap. 3, 1997, 41–56.
- [2] H.A. van der Sloot, L. Heasman, Ph. Quevauviller (Eds.), Harmonization of leaching /extraction test, Chap. 5, 1997, pp. 75–99.
- [3] I. Novozamski, Th.M. Lexmon, V.J.G. Houba, *Int. J. Environ. Anal. Chem.* 51 (1993) 47–58.
- [4] E. Colinet, H. Gonska, B. Griepink, H. Muntau, EUR Report 8833 EN, 1983, p. 57.
- [5] A.M. Ure, Ph. Quevauviller, H. Muntau, B. Griepink, *Int. J. Environ. Anal. Chem.* 51 (1993) 135–151.
- [6] C.L. Mulchi, C.A. Adamu, P.F. Bell, R.L. Chaney, *Common. Soil Sci. Plant Anal.* 23 (1992) 1053–1059.
- [7] W. L. Lindsay, W.A. Norvell, *Soil Sci. Soc. Am. J.* 42 (1978) 421–428.
- [8] A. Melich, *Common. Soil Sci. Plant Anal.* 15 (1984) 1409–1416.
- [9] A.M. Ure, R. Thomas, D. Litlejohn, *Int. J. Environ. Anal. Chem.* 51 (1993) 65–84.
- [10] S. K. Gupta, C. Aten, *Int. J. Environ. Anal. Chem.* 51 (1993) 25–46.
- [11] J.C. Hughes, A.D. Noble, *Common. Soil Sci. Plant Anal.* 22 (1991) 1753–1766.
- [12] C. Juste, P. Solda, *Agronomie* 8 (1988) 897–904.
- [13] W. P. Pickering, *Ore Geol. Rev.* 1 (1986) 83–146.
- [14] A. Lebourg, T. Sterckeman, H. Cielsielki, N. Proix, *Agronomie* 16 (1996) 201–215.
- [15] DIN (Deutsches Institut für Normung) (Ed.) Bodenbeschaffenheit. Vornorm DIN V 19730, in: *Boden-Chemische Bodenuntersuchungsverfahren*, DIN, Berlin, 1993, p. 4.
- [16] AFNOR (Association Francaise de Normalization), AFNOR, Paris, 1994, p. 250.
- [17] UNICHIM (Ente Nazionale Italiano di Unificazione), UNICHIM, Milan 1991.
- [18] V.J.G. Houba, I. Novozamski, T.X. Lexmon, J.J. van der Lee, *Common. Soil Sci. Plant Anal.* 21 (1990) 2281–2291.
- [19] VSBo (Veordnung über Schadstoffgehalt im Boden) Nr. 814.12, Publ. eidg. Drucksachen und Materialzentrale, Bern, 1986, pp. 1–4.
- [20] MAFF (Ministry of Agriculture, Fisheries and Food), Reference Book 427 MAFF, London 1981.
- [21] A. Ure, Ph. Quevauviller, H. Muntau, B. Griepink, Report EUR 14763 EN, 1993.
- [22] A. Tessier, P.G.X. Campbell, M. Bisson, *Anal. Chem.* 51 (1979) 844.
- [23] W. Salomons, U. Förstner, *Environ. Lett* 1 (1980) 506.
- [24] M. Meguellati, D. Robbe, P. Marchandise, M. Astruc, Proc. Int. Conf. on Heavy Metals in the Environment, Heidelberg, CEP Consultants, Edinburgh, 1983, p. 1090.
- [25] G. Rauret, R. Rubio, J.F. Lopez-Sanchez, *Int. J. Environ. Anal. Chem.* 36 (1989) 69–83.
- [26] U. Förstner, in: R. Lechsber, R.A. Davis, P. L’Hermitte (Eds.), *Chemical Methods for Assessing Bioavailable Metals in Sludges*, Elsevier, London, 1985.
- [27] A. Ure, Ph. Quevauviller, H. Muntau, B. Griepink, *Int. J. Environ. Anal. Chem.* 51 (1993) 135–151.
- [28] Ph. Quevauviller, M. Lachica, E. Barahona, G. Rauret, A. Ure, A. Gomez, H. Muntau, *Sci. Total Environ.* 178 (1996) 127–132.
- [29] Ph. Quevauviller, G. Rauret, A. Ure, R. Rubio, J-F López-Sánchez, H. Fiedler, H. Muntau, *Mikrochim. Acta* 120 (1995) 289–300.
- [30] Ph. Quevauviller, G. Rauret, A. Ure, J. Bacon, H. Muntau, Report EUR 17127 EN, 1997.
- [31] Ph. Quevauviller, M. Lachica, E. Barahona, G. Rauret, A. Ure, A. Gomez, H. Muntau, Report EUR 17555 EN, 1997.
- [32] Ph. Quevauviller, G. Rauret, B. Griepink, *Int. J. Environ. Anal. Chem.* 51 (1993) 231–235.
- [33] B. Griepink, *Int. J. Environ. Anal. Chem.* 51 (1993) 123–128.
- [34] Ph. Quevauviller, G. Rauret, H. Muntau, A.M. Ure, R. Rubio, J-F López-Sánchez, H.D. Fiedler, B. Griepink, *Fres. J. Anal. Chem.* 349 (1994) 808–814.
- [35] Ph. Quevauviller, G. Rauret, J-F. López-Sánchez, R. Rubio, A. Ure, H. Muntau, Report EUR 17554 EN, 1997.

The EC Standards, Measurements and Testing Programme in support of the quality control of waste analysis

Ph. Quevauviller *

European Commission, Standards, Measurements and Testing Programme (M075 3/9), 200 rue de la Loi, B-1049 Brussels, Belgium

Received 25 May 1997; accepted 14 October 1997

Abstract

Projects funded within the EC Standards, Measurements and Testing Programme (SM&T) of the European Commission aim to contribute to the harmonization and improvement of methods and measurements carried out within the European Union and hence to the comparability of data necessary for e.g. trade activities, monitoring of environment, food and health control, etc. This goal may be achieved by e.g. the organization of interlaboratory studies and certifications of reference materials, the development of new methods and pre-normative research. Examples of projects undertaken in support of the quality of waste analysis are given in this paper, covering different aspects, namely interlaboratory study and certification of extractable trace metals in sewage sludge amended soil reference materials, pre-normative research for the characterisation of stabilized waste (interlaboratory study), and development of field-measurement device for the monitoring of waste water quality; this paper gives also an account of a network aimed at harmonising leaching/extraction tests used for environmental risk assessment. Finally, the main topics of the workshop on Standards, Measurements and Testing for Solid Waste Management are given in the annex, along with a list of participants. © 1998 Elsevier Science B.V. All rights reserved.

Keywords: SM&T programme; Quality control; Waste analysis; Interlaboratory studies; Pre-normative research; Method development

1. Introduction

The lack of quality control of analyses, performed in routine, industrial and research laboratories may create strong economic losses due to the possible misuse of inaccurate data. In relation to waste management, this may lead to an incorrect evaluation of environmental risks due to e.g.

leaching of wastes or impossibilities to comply with regulations (standards or directives) which will have an impact on re-use of stabilised wastes (e.g. decisions on use for landfill purposes or dumping). Quality is one of the salient feature of the 1990's and a wide variety of actions have been undertaken in many countries to verify the quality chemical data produced e.g. by control laboratories; these actions included the implementation of accreditation systems, QA guidelines and norms (e.g. ISO 9000 and EN 45 000 series), organization

* Tel.: +32 229 63351; fax: +32 229 58072; e-mail: Philippe.quevauviller@dg12.cec.be

of interlaboratory studies, proficiency testing and production of laboratory and certified reference materials. This paper describes the objectives of the SM&T programme and some examples of RTD projects in support of the quality of waste analysis.

2. Objectives of the SM&T programme

The Standards, Measurements and Testing Programme [1], SM&T, of the European Commission aims to improve the quality of measurements and consequently harmonize the results obtained within the European Union particularly in support of EC regulations (compliance with EC Directives), standardization (pre-normative research) and means of calibration (transfer standards in metrology, CRMs in chemistry). Emphasis is given to the support of Measurements for Quality European Products and Written Standards for Industry (Theme I), Research related to Written Standards and Technical Support to Trade (Theme II) and Measurements related to the Needs of Society (Theme III). Equally to other RTD programmes of the DG XII of the European Commission, the participation in the SM&T programme is open to all legal entities. RTD projects may be submitted in the frame of time-limited calls for proposals. Two calls have been opened on Theme I in 1994 and 1996 [1,2]; two other calls have been concluded in 1995 and 1997 on Themes II and III. In parallel to these calls, dedicated calls in support of Community policies are organised at regular intervals in response to requests from other General Directorates or standardization bodies, e.g. to establish technical basis for the implementation of directives or standards. The SM&T programme also offers the possibility of proposing thematic networks on various topics with the aim being to create links between research organizations and industry. Finally, accompanying measures may be proposed, e.g. organization of scientific workshops or training actions, submission of doctoral or post-doctoral grants (in support of projects selected for funding) etc.

3. Examples of projects in support of the quality of waste analysis

The projects currently selected in the frame of SM&T calls for proposals that deal with four main types of activities, namely (i) interlaboratory studies, (ii) certification of reference materials, (iii) pre-normative research and (iv) development of new methods or instrumentation. The projects described below were selected for funding by the SM&T programme.

3.1. *Interlaboratory study and certification of sewage sludge amended soil*

One of the best ways of assessing the performance of analytical methods is to compare them within the frame of interlaboratory studies [3]. The comparison of different techniques as applied in different laboratories allows the detection of errors due to a particular method, or part of a method (e.g. insufficient extraction, uncontrolled interferences), or due to a lack of quality control within one laboratory. The participation in such interlaboratory studies may then help in establishing the state of the art in a particular field of analysis and to improve the quality of the measurements. These studies are often carried out to remove all sources of error in the application of techniques to be used in certification campaigns or to test the performance of a standard prior to its implementation. The example given below describes an interlaboratory study on extractable trace metal contents in a sewage sludge amended soil, followed by a certification campaign.

Single extraction tests are commonly used to study the eco-toxicity and mobility of metals in soils and sludges, e.g. to assess the bioavailable metal fraction (and thus to estimate the related phyto-toxic and nutritional deficiency effects) and the environmentally accessible trace metals upon disposal of e.g. sediment on to a soil (e.g. contamination of ground waters). However, lack of uniformity in different procedures does not allow the results to be compared worldwide or the validation of procedures. The results obtained are defined by the determination of extractable elements using a given procedure, therefore, their

significance is highly dependent on the given extraction protocol applied. Moreover, the lack of suitable reference materials for this type of study did not, in the past, enable the quality of the measurements to be controlled. Because the pitfalls likely to occur in the use of extraction protocols for soil analysis, the SM&T programme has hence launched a project aiming at harmonizing measurements for extractable trace metal contents in soil. This project followed a stepwise approach (through interlaboratory studies) of which the final aim was to certify soil reference materials for their extractable trace element contents [4,5]. The choice of operationally-defined procedures tested was directed towards single step methods rather than sequential extraction ones; in a first stage, EDTA (ethylene-diamine-tetra-acetic acid) and acetic acid were selected for interlaboratory studies on a sewage sludge amended soil which was followed by the certification of two reference materials for their extractable contents of Cd, Cu, Cr, Ni, Pb and Zn [4]. Another project was launched on a sewage sludge amended calcareous soil for which EDTA and DTPA (diethylene-triamine-pentaacetic acid) were selected as extractants: the organisation of a preliminary study was considered to be essential prior to certification in order to test the extraction procedures and possibly amend them. To do so, a sewage sludge contaminated calcareous soil was selected from the bank of reference materials of the Environment Institute of the Joint Research Centre of Ispra (Italy) in order to present both the characteristics of a calcareous soil (CaCO_3 content of 228 g kg^{-1}) with high heavy metal contents. The most critical steps discussed in the technical scrutiny of the results of the interlaboratory study were the type and speed of shaking, filtration and centrifugation. As a general remark, it was stressed that the use of standard additions for calibration was a prerequisite for electrothermal absorption spectrometry. It was also recalled that the use of an end-over-end shaker was required, therefore, the data obtained using a horizontal shaker was rejected. The DTPA extraction was criticized owing to the high mass/volume ratio which limited the vol-

ume of extract collected after centrifugation. This procedure was not considered to be applicable to Cr determination. On the basis of the results obtained in this exercise, the choice of EDTA and DTPA for certification was discussed. Whereas EDTA was widely accepted, the choice of DTPA was further criticized because of its operational difficulties; the wide use of the latter would, however, justify the certification of DTPA extractable trace element contents, providing that its limitations in comparison with EDTA were clearly identified. Following the interlaboratory study, a candidate CRM was prepared and its homogeneity and long term stability were verified on the basis of the observed variations in EDTA- and DTPA- extractable heavy metal contents. The material was shipped to a group of ca. 20 laboratories which were requested to make a minimum of five independent replicate determinations of each element on at least two different bottles of the CRM on different days, following strictly the EDTA and DTPA extraction protocols previously defined. The techniques of final determination were electrothermal atomic absorption spectrometry (ETAAS), flame atomic absorption spectrometry (FAAS), inductively coupled plasma emission spectrometry (ICPAES) and inductively coupled plasma mass spectrometry (ICPMS). All the results were discussed at a technical evaluation meeting to confirm the accuracy of the methods of analysis. At the technical meeting, it was recalled that strict observance of the extraction protocols would be a criterion for considering the results for discussion. The participants recommended that a tolerance of $\pm 30\%$ be included in the extraction protocols for the shaker speed. Most of the errors detected were due to calibration errors rather than the application of the extraction procedures. The certification of this material (CRM 600) has been accepted by the board of evaluators for BCR-certifications and it is now available on the market.

For additional information, please contact the co-ordinator of the project: Prof. G. Rauret, Universidad de Barcelona, Departamento de Química Analítica, Avda. Diagonal 647, E-08829 Barcelona (e-mail: rauret@zeus.qui.ub.es).

3.2. Pre-normative research for leaching tests applied to stabilized wastes

As mentioned previously, one approach for testing a proposed standard method consists of preparing reference materials to be analysed by a group of expert laboratories and to possibly improve or adopt the method on the basis of the results obtained. The example above shows that CRMs certified for operationally-defined parameters (following a standardized method, e.g. single or sequential extraction) may be prepared for the quality control of the measurements. The SM&T programme may hence provide support to the technical evaluation of proposed standardized methods on which basis official bodies such as CEN, ISO etc. will discuss the adoption of a standard.

In this paper, the pre-normative aspect is exemplified by the results of a study of leaching tests for stabilized wastes [6]. The potential environmental hazards caused by waste materials vary strongly between wastes from different sources. Although elimination and minimization of waste streams have the highest priority, it is obvious that significant waste release remains. These have to be dealt with in an environmentally acceptable manner. Some bulk wastes and treated wastes can be beneficially applied in construction [7]. Several waste streams will require treatments, such as stabilization, before disposal to minimize adverse environmental effects. At present, proper methods to address potential environmental effects from monolithic waste forms are not implemented in regulation. Therefore, proper performance criteria for the evaluation of the effectiveness of the immobilization technologies are lacking. Current regulatory test procedures based on single extraction of crushed material at a fixed liquid to solid ratio are inadequate to assess the environmental impact from these types of solid specimens [8]. The mechanism controlling the release from monolithic specimen is neglected when crushed materials are used. In addition, reference materials are needed in this field for quality control purposes. With respect to the harmonization of standard leaching tests, an interlaboratory study on leaching tests was carried out with 23 labora-

tories from the EU and Associated Member States. After a preliminary study of homogeneity and reproducibility of testing within one laboratory, the intercomparison of leaching tests for monolithic stabilized wastes (samples of cement-based stabilized wastes) was carried out using a tank leaching test procedure as a common method. Other test methods have been applied to put the test results in perspective. A standard leachate was provided to verify between laboratory variability of the analytical methods applied. The results of the interlaboratory study indicated that the agreement was quite good for the elements measured (Ba, Ca, Cd, Cl, K, Na, Pb, SO₄, Sr, Zn) with sufficient analytical precision. Both the within and between laboratory standard deviation was poor for elements present at low concentration levels such as Pb and Zn. In the case of sulphate, between laboratory standard deviation was relatively high in spite of sufficient analytical sensitivity. Changes in the predominant leaching mechanism with aging of the cement-based matrix was the main reason for this effect. The continued hardening of the cementitious matrix after 28 days of curing caused changes in the release rates due to an increase of the tortuosity of the matrix. This aspect of leaching of cementitious matrices needed to be taken into account in evaluating the test results. This intercomparison was carried out when changes in material properties were largely stabilized.

The results of other tests, largely consisting of regulatory tests for granular materials, could be placed in perspective using a pH static leaching procedure. It was shown that the equilibrium pH reached in these tests largely dictates the leached quantity. Based on these observations, the Unified Approach for Leaching as developed for granular materials can be extended to monolithic materials by combining dynamic aspects of leaching from the tank leach test with solubility control of leaching from a pH static leaching test. This allows interpretation of changes in release under different exposure conditions (e.g. carbonation). The tank leach test provides a means of assessing physical and chemical parameters controlling release which is useful in the improvement of stabilization product development. In the discussion of

results with the participants, it was concluded that the tank leach tests are a good characterization tool to assess the release from stabilized wastes for regulatory purposes. Further work in data interpretation is needed to make full use of the information contained in the test. A short version linked closely to the extended test should be developed for quality control purposes. The method has been proposed for standardization to CEN. The preparation of cement stabilized specimen as reference material for leach tests was recommended. The preparation of standard leachates at high and low concentration levels was recommended for quality control in leachate analysis.

For additional information, please contact the co-ordinator of the project: Dr H.A. van der Sloot, Energieonderzoek Centrum Nederland, P.O. Box 1, NL-1755 ZG Petten (e-mail: vanderlsoot@ecn.nl).

3.3. Network to harmonise leaching/extraction tests

The above projects are complemented by the establishment of a network of experts for discussing possible strategies to harmonise leaching and extraction schemes used for environmental risk assessment (analysis of waste, contaminated soil, compost, construction materials, concrete etc.). This network was launched after a workshop held in Maastricht in 1994 [9] where scientists from different fields of expertise discussed various approaches to improve the present situation which does not allow data to be compared from one field to another, and sometimes within a single field, owing to the operational character of the procedures used. The experts recommended in particular the creation of a network and the organisation of interlaboratory studies to test the various existing schemes. These recommendations had two effects (1) creation of a network as a pilot action between 1994 and 1996, which will be followed by a wider action, starting in 1998, and (2) technical work in support of this network.

With respect to the pilot network, expert discussions aimed to harmonize the approaches in existing leaching tests used in the fields of soils, sediments, sludges, waste, stabilized waste and

construction materials, to exchange information among different fields and define the problems in specific fields, to facilitate the development of a generic approach by intensive expert consultations, to form a strong network of experts, and to formulate recommendations for the implementation of more generally applicable approaches and identify research needs. This pilot action was carried out in 1994–1996 and resulted in the production of a comprehensive book [10] which will serve as a basis for the further development of a wider network which was selected for funding by the SM&T programme at the end of 1997.

The basis for this technical work in support of the above described network was based on the growing concern on the environmental impact of waste disposal, re-use of waste, recycling of materials, transport of waste, waste treatment, clean-up of contaminated soil, re-use of cleaned soil and utilization of secondary materials in construction has led to an increased demand for leaching and/or extraction procedures that would be able to assess the environmental consequences of these different activities. As stressed above, these operationally-defined procedures are usually developed within a specific field, without much interaction from outside that field. When the use and development of such procedures are not co-ordinated in a wide context and harmonized, it may result in the multiplication of different tests which may lead to an almost unmanageable situation with respect to drafting regulations and evaluating environmental risks. The overall objective of this work is to provide a technical basis for discussion about harmonization of leaching /extraction tests developed in very diverse fields such as soil, contaminated soil, sediment, sludge, compost, waste, stabilized waste, construction materials, drinking water pipes and impregnated wood, and to provide recommendations for test use, test modification, unified data reporting, presentation, and implementation of tests in the various fields. To meet these objectives a selection of materials from the different fields-soil, contaminated soil, sediment, sludge, compost, waste, stabilized waste, construction materials, drinking water pipes and impregnated wood-will be subjected to different leaching/extraction tests covering different aspects

of leaching. A range of inorganic constituents of environmental concern will be analysed to ensure that general conclusions can be drawn on the validity of the comparisons. Comparisons between test results within one field and between different fields will be feasible using the experimental set-up. Modelling of leaching behaviour will be carried out to allow the prediction of release under different exposure conditions. The information generated will be discussed with representatives from the different fields at expert meetings organised by the Network on Harmonization of Leaching/Extraction Tests, and disseminated through this channel and through regulatory bodies. For additional information, please contact the co-ordinator of the projects: Dr H.A. van der Sloot, Energieonderzoek Centrum Nederland, P.O. Box 1, NL-1755 ZG Petten (e-mail: vandersloot@ecn.nl).

3.4. Waste water monitoring

As mentioned in Section 1, the SM&T programme funds RTD projects aimed at developing new instruments/methods for measurements and testing; this section exemplifies the reasoning for selecting one project.

The European Community decided in 1991 to oblige all EU Member States with wastewater treatment plants for all cities whose wastewater organic load is greater than 15 000 equivalent-inhabitants (before the 31st December 2000) and 2000 equivalent-inhabitants (before the 31st December 2005). The quality of the treated wastewaters must be better than reference values for parameters such as Biological Oxygen Demand (BOD), Chemical Oxygen Demand (COD), Total Suspended Solids (TSS) and even the global nitrogen and total phosphorus. These dispositions are of great importance but unfortunately surveys are not very satisfying since the chosen parameters are not easy to measure without sampling, storage and laboratory analysis. A SM&T project has, therefore, developed a simple wastewater quality monitoring device based on spectrophotometric methods for the measurement of BOD, COD, TSS, global N (sum of nitrate, nitrite and Kjeldahl nitrogen) and total P; other parameters such as nitrate, nitrite, ammonia and orthophosphate were also considered.

The prototype was developed by three universities (France, Greece and Spain) in collaboration with a French SME. The multiparameter monitor was built around a single spectrophotometric detector with modules for the simple pre-treatment of the sample if required (using a simple reagent to obtain a whole absorption spectra). The project initially focused on the optimization of the UV spectrophotometric method proposed by one of the partners for the measurement of COD, BOD and computation of the concentration of nitrate and nitrite and then the development of simple pseudo-FIA (Flow Injection Analysis) methods for the determination of total Kjeldahl nitrogen and total phosphorus (involving a digestion step). The results enabled the design of a simple UV detector for the estimation of global pollution parameters (TOC, BOD, COD, TSS) and the determination of specific compounds (e.g. nitrate and anionic surfactants), and to design a set of Sequential Injection Analysis (SIA) procedures for the determination of non-absorbant species (ammonia, organic nitrogen, orthophosphates and organic phosphorus). These findings served to build a prototype including the UV detector, the SIA system and a simple visible detector which is designed as a portable UV-spectrophotometer to enable field-measurements of wastewater quality to be performed. A full description of the development phase of the prototype is available elsewhere [11]. This project is a good illustration of partnership between universities and SME (Small and Medium Enterprise).

For additional information, please contact the Co-ordinator of the project: Prof. O. Thomas, Ecole des Mines d'Alès, 6 avenue de Clavières, F-30319 Alès Cédex (e-mail: othomas@ensm-ales.fr).

3.5. The workshop on standards, measurements and testing for solid waste management

The new regulations related to industrial waste management have the ambitious objective of stopping the direct release of wastes by the year 2002, implying that wastes from different origins should be treated for possible recycling. The effects of different waste treatment processes should be

accurately determined to ensure a correct waste management and the industry is aware that much effort is required to optimize these treatments for obvious economic reasons. The quality of treatment processes and of final (recycled) products rely upon the availability of standards (such as those prepared by CEN or ISO) and testing methods (e.g. chemical analysis for the assessment of environmental risks or landfill use). There is a clear need to develop (and validate) methods for the control of treatment processes or for the characterization of the end-products in view of their use for in landfill, concrete, construction materials etc. In this respect, the collaboration between industry and research organizations should be strengthened. As a response to this need, the workshop on Standards, Measurements and Testing for Solid Waste Management was held in Pau (France) on 5–7 May; its aim was to stimulate partnership between industry and research, for the identification of possible actions to be undertaken in this field, to discuss the state of the art of solid waste analysis, to define the applicability of current methodologies, to investigate where limitations exist and identify possible progressive developments in this field. The following topics were debated in roundtables during the workshop (see programme in the annex).

- Field measurements and screening tests
- Rapid techniques for physico-chemical characterization
- Elaborated measurement techniques
- Modelling, expert systems and data-bases
- Standards, reference materials and quality control

Each topic was introduced by a plenary lecture, followed by discussions chaired by a selected expert. Minutes of the discussions were taken by a rapporteur. A summary of these discussions has been published in a special issue of *Trends in Analytical Chemistry* [12].

4. Additional information

The programme publishes an information bulletin, the 'Measurements and Testing Newsletter', describing the calls for proposals and including

summaries of on-going and finished projects, which can be obtained free of charge (please contact the author by fax: +32 229 58072 or e-mail: philippe.quevauviller@dg12.cec.be).

CRMs produced by the SM&T programme are available at the Institute for Reference Materials and Measurements (IRMM), Retiesweg, B-2440 Geel (fax: +32 14 590406); they are provided with a certification report describing their preparation, homogeneity and stability studies, and give details on the methods used, all individual results and a summary of the statistical evaluation. The report also contains detailed instructions for use that should be strictly followed when analysing the CRM

References

- [1] Measurements and Testing Newsletter, vol.2, N°1 (1994).
- [2] Measurements and Testing Newsletter, vol.5, N°1 (1997).
- [3] Ph. Quevauviller, E.A. Maier, B. Griepink, (Eds.), *Quality Assurance for Environmental Analysis*, Elsevier, Amsterdam, 1995.
- [4] Ph. Quevauviller, M. Lachica, E. Barahona, G. Rauret, A. Ure, A. Gomez, H. Muntau, *Sci. Total Environ.*, 178 (1996) 127–132
- [5] Ph. Quevauviller, M. Lachica, E. Barahona, A. Gomez, G. Rauret, A. Ure, H. Muntau, *Fresenius' Z. Anal. Chem.*, (in press)
- [6] H.A. van der Sloot, D. Hoede, G.J. de Groot, G.J.L. van der Wegen, Ph. Quevauviller, *Intercomparison of leaching tests for stabilized wastes*, EUR Report, European Commission, Brussels, 16133 EN, 1995, 69.
- [7] WASCON 1994: Environmental aspects of construction with waste materials. J.J.J.M. Goumans, H.A. van der Sloot, Th.G. Aalbers (Eds.), Elsevier, Amsterdam, 1994.
- [8] H.A. van der Sloot, *Leaching behavior of waste and stabilized waste materials; characterization for environmental assessment purposes*. *Waste Manag. Res.*, 8 (1990) 215–228.
- [9] Ph. Quevauviller, H. van der Sloot, A. Ure, H. Muntau, A. Gomez, G. Rauret, *Sci. Total Environ.*, 178 (1996) 133–139.
- [10] H.A. van der Sloot, L. Heasman, Ph. Quevauviller (Eds.), *Harmonization of Leaching/Extraction Tests*, Elsevier, ISBN 0-444-82808-7, 1997.
- [11] O. Thomas, F. Theraulaz, V. Cerda, M.T. Oms, A. Cerda, A. Cladera, D. Constant, J.M. Rigal, N. Evmiridis, Ph. Quevauviller, *Wastewater quality monitor*, EUR Report, European Commission, Brussels, 16914 EN, 1996, 77.
- [12] Ph. Quevauviller, in: special issue of *Trends in Analytical Chemistry*, Standards, measurements and testing for solid waste management, (in press)

Review paper

Sensitivity and selectivity of electrochemical enzyme sensors for inhibitor determination

G.A. Evtugyn *, H.C. Budnikov, E.B. Nikolskaya

Kazan State University, 420008, Kazan, Russia

Received 22 January 1997; received in revised form 16 June 1997; accepted 5 September 1997

Abstract

The performance of electrochemical biosensors developed for the determination of inhibiting species is considered. The role of various factors affecting the analytical characteristics of biosensors, their selectivity toward inhibitors to be tested as well as operational characteristics is discussed. The choice of enzyme-inhibitor system, the influence of enzyme immobilization on the behaviour of a biosensor, the modes of the optimization of working conditions are discussed. Most conclusions are illustrated with the models of the application of biosensors for monitoring environmental pollutants. © 1998 Elsevier Science B.V. All rights reserved.

Keywords: Sensitivity; Selectivity; Electrochemical; Enzyme sensors; Inhibitor determination

1. Introduction

The development of biosensors is most promising in the progress of analysis of biologically active compounds. In the past two decades biosensors had emerged from laboratories and in some cases became conventional devices for routine analysis [1–3] owing to the advantages biosensors possess, such as simple measurement procedure, short response time, sufficient sensitivity and selectivity. This refers to the analysis of

glucose, urea, lactate, cholesterol and of several medications [4–8]. Traditional monitoring methods are often slower and call for expensive equipment which makes them unsuitable for real time control. This makes biosensors more attractive, especially for unqualified users and for field applications.

The commercial production of biosensors is associated with the biomedical analysis of a limited number of metabolites and pharmaceuticals [2–4]. As substrates of appropriate enzymes they can be determined directly in biological fluids with detection limits down to 10^{-6} – 10^{-7} mol l^{-1} . This is more than sufficient for most practical purposes. Substrate biosensors are often considered to be reagentless methods of analysis. Such

* Corresponding author. Tel.: +7 8432 387051; fax: +7 8432 380412; e-mail: Gennady.Evtugyn@ksu.ru

biosensors can be simply introduced in various automatic analyzers with operating efficiency up to 100 samples per hour. Recently, current efforts in the progress of substrate biosensors are devoted to improving the operation features, i.e. long-term response stability, the possibility of sterilization, specific problems of implantable biosensors etc. [9,10]. The selectivity of such biosensors is provided for by the high substrate specificity of the enzymes used and by a limited number of interfering species presented in the fluids analyzed. The selectivity of the electrochemical detection of enzyme response in the presence of some components, e.g. ascorbic acid or bilirubin is attained by lowering the operating potential owing to the application of redox-mediators or the additional protecting films [11–13].

The situation is quite the opposite if biosensors are developed for the determination of inhibitors. This kind of biosensors offers huge possibilities for the determination of a wide range of toxic compounds, some of which being common environmental pollutants [14–16]. In special cases the detection limits down to $n \cdot 10^{-12}$ – $n \cdot 10^{-13}$ mol l⁻¹ can be attained without time-consuming pretreatment of the sample tested (cholinesterase based detection of isopropylmethylphosphonofluoridate and *O*-ethyl-*S*-diisopropylaminoethylmethylphosphonothiate in sea water [17], cholinesterase based determination of 2,4-dichlorophenoxyacetic acid (2,4-D) in aqueous solutions and in milk in the presence of activating additives of calcium ions [18], the determination of Malathion based on carboxylesterase from northern deer [19]). This is lower than the appropriate maximum permissible concentrations of environmental pollutants and than their detection limits typical for traditional analytical techniques, i.e. chromatography or spectrometry, except immuno- and radiochemical methods. For this reason biosensors for the determination of inhibitors seem to be very attractive for environmental monitoring, especially for field applications [14–16].

The unbalance between the prospects and the observed moderate level of R and D activities in the field of inhibitor biosensors is mostly the result of the problems concerning the selectivity of determination. Contrary to the substrates, the

specificity of the enzymes towards inhibitors does not usually allow the determination of separate compounds [20]. Apart from the presence of inhibitors, biosensor response depends on the other species in the sample tested which affect the sensitivity of biosensors towards inhibitors. A high sensitivity of inhibiting effect to the operating parameters (i.e. pH value, buffer capacity of the working solution, the nature and the concentration of the substrate) and sample content is considered to be a weak point of inhibitor biosensors. Hence, as a rule the inhibitor biosensors do not refer to reagentless methods, and the estimation of the content of inhibitors involves a two-step procedure, including the measurement of the initial response of a biosensor and its decay after the contact with the inhibitor solution. This results in the directions for the measurement of inhibition being too complicated. Though the mechanism of the enzyme-inhibitor interaction is usually well-known, the immobilization of the enzyme and the heterogeneous kinetics of the enzymatic reaction affect both the experimental kinetic parameters of inhibition and the optimal conditions of the determination of inhibitors, and the analytical characteristics of inhibitor determination are often far from those obtained with native enzymes.

On the other hand, the high sensitivity of biosensor characteristics opens up new opportunities for purposeful modification of the sensitivity and selectivity of the determination of inhibitors. Careful investigation of the substrate-inhibitor system, both for native and immobilized enzyme, the optimization of the measurement procedure and of the detection system make it possible, not only to elaborate the analytical characteristics of the determination of inhibitors, but also to control the dynamic range and detection limits depending on the particular analytical problem to be solved.

In this review factors concerning analytical and operational characteristics of inhibitor biosensors have been discussed and approaches to their optimization summarized. It is not meant to be an exhaustive description of the reports in the field of development of inhibitor biosensors. The objective is to demonstrate the feasibility of the researches in the optimization of biosensor

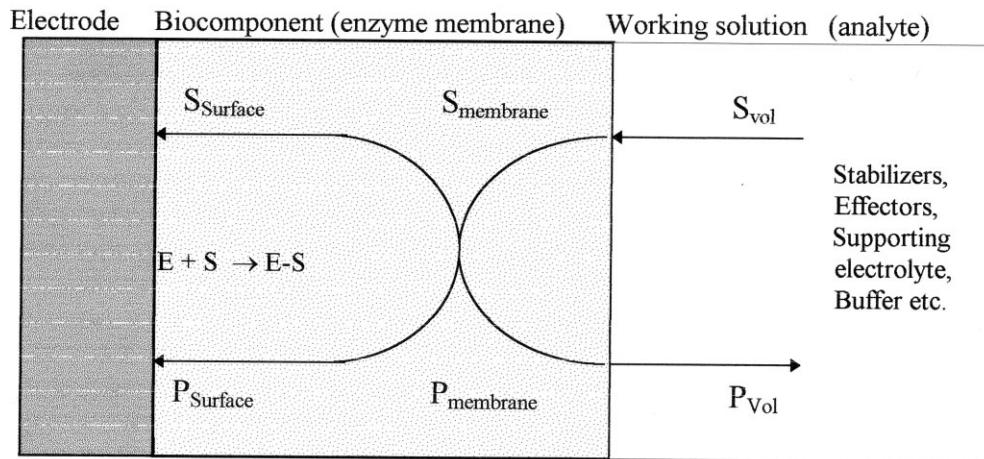


Fig. 1. General scheme of the formation of the response of an enzyme biosensor, S, substrate; P, product of the enzymatic reaction. Electrode biocomponent (enzyme membrane) working solution (analyte).

characteristics and the linkage between the inhibition results obtained for native and immobilized enzymes. The main attention is given to the application of biosensors for monitoring environmental pollutants. Apart from electrochemical biosensors, some principles of biosensor optimization are illustrated with the reports relating to optic biosensors and experiments with native enzymes.

2. General

A biosensor is a measurement system based on a combination of a biochemical and electronic elements which are in close contact with each other and are incorporated in a single unit. A biochemical component (i.e. an enzyme or biological material with the enzyme activity such as microorganisms [21], plant [22] or animal tissues and cells [23], etc.) is chosen for its selectivity toward the substrate or the inhibitor to be determined. The electronic signal-transducing element (e.g. electrode, optical detector, piezo crystal etc.) converts the biochemical response into electric and optic signals which are amplified, measured and decoded by an appropriate electronic unit. Mostly biosensors are based on electrochemical transducers owing to the advantages they possess,

e.g. simple user-friendly design, compatibility with the standard commercial equipment, the possibility of sensor miniaturization and automated measurement and a well-developed theory of the behaviour of electrochemical biosensors [24,25]. For determination of inhibitors, the results obtained with electrochemical sensors can often be extended to some other detection systems if the measurement conditions are similar to each other. A scheme of a typical biosensor is shown in Fig. 1.

The resulting response of a biosensor to the addition of a substrate is determined by the concentration of the product (P) of enzymatic reaction on the sensing surface of the sensor. The latter is controlled by the rates of two conjugated processes, i.e. the enzymatic conversion of the substrate (S) and the diffusion of the product being formed from the body of the membrane to the bulk solution.

In membrane with a high level of enzyme activity, the decrease of a substrate concentration is not compensated in full measure by the transfer from the bulk solution due to the diffusion limitations. Because of this, only a part of the enzyme active centers is involved in the interaction with a substrate. In this case (diffusion control of a response) the sensitivity of immobilized enzyme toward inactivation, be it heating or inhibitor

effect, is lower than that of the native enzyme. The inactivated centers are replaced by the centers remained active in the inner layers of the membrane [26]. The lower the specific activity of immobilized enzyme the higher the sensitivity of a biosensor toward inactivation, including specific inhibition. In an extreme case, each enzyme active center in the membrane is occupied by a substrate molecule, so the response of a biosensor depends on the specific activity of an enzyme but not on the concentration of a substrate (kinetic control of a response). The response of such a biosensor is much lower than that in the case of diffusion control but highly sensitive to the inhibitors. The theoretical evaluation of the influence of diffusion limitation on the sensitivity of immobilized enzyme and biosensor response toward various inactivating factors are supported by numerous experimental results irrespective of the enzyme, membrane material or inhibitor [20,24–26].

The choice between diffusion and kinetic control can be made by enzyme loading and substrate concentration [25]. In practice, the measurement conditions and membrane content are a compromise between the requirements of sensitivity and those of accuracy of response determination, and the substrate concentration is usually no less than $n \cdot 10^{-4} \text{ mol l}^{-1}$.

The inhibiting effect of the chemicals on the response of the biosensor can be expressed as a relative decay of the response value after the contact of the biosensor with the sample tested, e.g. inhibition degree ($I, \%$). In place of the inhibition degree, the absolute value of the response of a biosensor can be used for plotting the calibration curves. This does not change the slope of the curve but hampers the comparison of the results obtained with various enzymatic membranes.

The empirical linear calibration curve can be used for irreversible inhibitors in plots $I, \%$ (or biosensor response) vs. $\lg C_1$ where C_1 is the inhibitor concentration [20]. For reversible inhibitors, calibration is plotted in linear coordinates, i.e. $I, \%$ (respectively, response value)- C_1 .

The sensitivity of a biosensor toward an inhibitor can be defined as a slope of an appropriate calibration curve. A steeper slope does not mean a

lower concentration range of the inhibitor to be determined because the reproducibility of the response may not be as high.

The determination of the inhibiting effect and the inhibitor concentration, respectively, involves at least three stages:

1. Determination of the initial response value. If not specially indicated, this is implied to be performed during the preliminary study of a biosensor performance;
2. The contact of a biosensor with an inhibitor solution (incubation stage). For irreversible inhibitors the inhibition procedure is usually performed with no substrate and the resulting decay of the enzyme activity and of the response of the biosensor increase with the duration of the contact (i.e. with the time of incubation). For reversible inhibitors the sample tested is injected into the working solution together with the substrate solution or later so that the incubation takes place in the presence of the substrate;
3. The repeated determination of a reduced response of the biosensor with the following calculation of the inhibition degree as the relative decrease of the response value.

It follows from the above that the accuracy of the determination of inhibitor concentration should be at least twice lower than that of the substrate determination as it is based on two consecutive determinations of the response value with one and the same biosensor. If the relative standard deviation (R.S.D.) of the response determination for electrochemical biosensors is commonly in the range 1–3%, the detection limit should retain the inhibitor concentration that results in at least 4–6% of the inhibition degree. For commercial biosensor devices developed for the monitoring the environmental contamination, the inhibition degree referring to the minimal detectable level of the pollutant is assumed more than 10% [27,28].

The selectivity of biosensors towards various inhibitors is estimated by comparing the dynamic ranges of concentrations or by the ratio of calibration slopes or the experimental kinetic parameters of the inhibition determined for the immobilized enzyme. The comparison should be

Table 1
Enzyme-inhibitor systems utilized in electrochemical biosensors for inhibitor determination

Enzyme	Inhibitor	Reference
Cholinesterase	Organophosphorus and carbamate pesticides, heavy metal salts, non-ionic surfactants, pharmacuetics (nitrogen containing drugs with anticholinesterase activity, antagonists), fluorides, azides	[17,19,27,28,33–65]
Urease	Fluorides, heavy metal salts	[66–68]
Glucose oxidase	Heavy metal salts	[69,70]
Tyrosinase (phenol oxidases)	Thiourea, ethylenethiourea and other derivatives of thiourea, cyanides, azides, atrazine, benzoic acid, chlorophenols	[71–79]
Alcohol dehydrogenase	Cyanides, heavy metal salts	[80–82]
Amino oxidase	Plant growth regulators, primary and secondary amines	[83–85]
Aldehyde dehydrogenase	Fungicides	[86]
Cytochrome c	Cyanides, sulfur hydrogen	[87–90]
Catalase	Heavy metals	[69,91]
Peroxidase	Cyanides, heavy metal salts, respiration poisons	[92–96]

performed for the same or close concentrations of the substrate used. However, for field applications, the value of these calculations is often restricted by the non-additive combination of certain inhibition effects of the inhibitors in multi-component media.

Three main modes of improvement of performance of inhibitor biosensors and analytical characteristics of inhibitor determination are considered: the choice of enzyme-substrate system, the optimization of the immobilization of the enzyme and the fitting of working conditions.

3. Optimization of the enzyme-inhibitor system

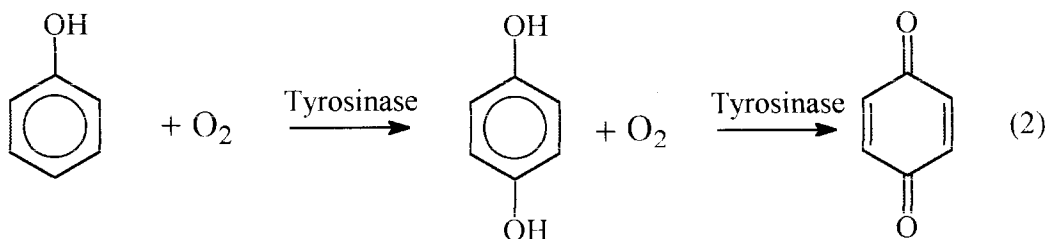
3.1. The choice of an enzyme for inhibitor determination

The choice of an enzyme for the determination of certain chemicals affecting its activity is determined by the mechanism of their toxic effect on living beings. As for common environmental pollutants, their toxicity is usually investigated enough. Thus, the cholinesterase of insects is a target for the commercial preparations of

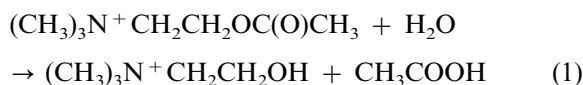
organophosphorus and carbamate insectoacaricides, (e.g. Parathion, Malathion, Zolone etc.) [29], and, therefore, they may be determined with this enzyme. Dithiocarbamate fungicides can be determined with the biosensors based on aldehyde dehydrogenase, which is considered as a target [30]. Herbicides suppress photosynthetic reactions, tyrosinase or peroxidase. Cyanide ions inhibit cytochrome oxidase [31]. Many chemicals, i.e. heavy metal ions, thiourea, fluoride and azide ions exert an inhibiting influence on several enzymes [32]. In this case the availability of commercial enzyme preparations, the stability of the enzyme during storage and application, and the convenience of the detection of the enzymatic reaction are taken into account.

A summary of the enzymes utilized in the electrochemical biosensors described for the inhibitor determination is presented in Table 1.

Cholinesterase is one of the most popular enzymes used for the inhibitor determination. This enzyme provides for the hydrolysis of natural neurotransmitter, acetylcholine Eq. (1), and is common in various living beings, from insects to humans.



Scheme 1.



The application of native or immobilized cholinesterase makes it possible to determine a wide range of pollutants, some of which refer to the common environmental pollutants, i.e. organophosphorus and carbamate pesticides, heavy metal ions, fluorides, cationic surfactants etc. [33].

Recently tyrosinase and peroxidase is often introduced into the biosensor assembly, owing to their high stability and activity in organic solvents. These enzymes promote the oxidation of various phenolic compounds Scheme 1 and are inhibited by heavy metal ions, herbicides, respiration poisons etc.

The measurement of their activity is based on the anodic detection of hydrogen peroxide or cathodic reduction of the quinones formed.

The list of enzymes used in electrochemical biosensors for inhibitor determination does not exhaust the potentialities of the enzyme based determination of inhibitors. Hence, the application of carboxylesterases from various sources has been described for the determination of primary and secondary amines, and organophosphates [18,83,84]. Alkaline phosphatase is effectively inhibited by the traces of ions of beryllium and lead [97–99]. Zinc exhibits either an inhibiting or activating effect on apo-enzyme and active form of alkaline phosphatase in separate concentration ranges [100]. However, these methods are based on spectrometric detection or the immobilized enzyme is separated from the sensor used for the measurement of response.

Even promising enzymes with high sensitivity and/or selectivity towards certain chemicals are often unsuitable for practical application in a biosensor assembly because of their low stability, difficulties of detection of the enzyme activity or problems of isolation from living tissues or cell culture. Hence, the selective determination of tin could be attained with aminolevulinic acid dehydratase (ALAD) [101] while the isolation of a raw enzyme fraction results in a rapid loss in the activity of an enzyme.

In this respect the application of whole living cells or organelles with the essential enzyme activity presents an alternative to the isolated enzymes [102–109]. Hence, microbial sensors have been designed for the monitoring systems of waste water treatment [102–108]. They are based on the quantitative estimation of oxygen consumption of the sludge or of yeast microorganisms in standard conditions of air saturation and in the presence of toxic substances in the waste waters to be tested. The phytotoxicity test based on the response of thylakoids on the presence of herbicides is also described [109].

The choice of enzyme determines the nature of the substrate used and the appropriate detection system for the measurement of a response (i.e. the transducer incorporated into a biosensor assembly). The following optimization might include the variation of the source of the enzyme and the immobilization procedure.

In a number of cases the sensitivity towards an inhibitor can vary even with isoenzymes from one source. Thus, carboxylesterase from northern deer is electrophoretically separated into two fractions, one of which, in gelatin gel, was used for the determination of Malathion with the detection

limit of $10^{-12} \text{ mol l}^{-1}$, whereas, that for the other was 10 000 times higher [19]. The application of potentiometric biosensor involving the acetylcholinesterase from electric eel makes it possible to reach the detection limit for Malathion down to $10^{-10} \text{ mol l}^{-1}$ but after preliminary oxidation of the analyte with bromine water into the more toxic oxygen analog, i.e. Malaoxon [38]. The application of carboxylesterase allows the omission of any pre-treatment of the sample tested. It was proposed and confirmed by kinetic analysis, that Malathion affects the enzyme activity as a specific substrate of carboxylesterase, so the enzymatic conversion of the indophenyl acetate used for the spectrometric detection of the enzyme activity begins only after the full hydrolysis of Malathion. This results in the occurrence of the induction period on the kinetic curve and in the decrease of the biosensor response measured at a fixed time after the substrate addition.

Cholinesterases from insects are more sensitive to insecticides than those from mammals [45,85,110]. However, the isolation of these enzymes and their stabilization are considered to be the weak point in their practical application.

For mitochondrial monoaminoxidase from mouse and rat liver, the sensitivity towards reversible and irreversible inhibitors depends on the nature of the substrate used [83–85]. This is assigned to the presence of two forms of the enzyme in the raw preparations, one of which is more sensitive to serotonin and the other one to benzylamine as substrates. This made it possible to develop high-sensitive and selective methods for the determination of some pharmaceuticals and pesticides with detection limits down to $10^{-9} \text{ mol l}^{-1}$. An appropriate biosensor has been designed as a combination of the monoaminoxidases immobilized in gelatin gel with an NH_3 -sensitive air gap electrode [83].

For peroxidase from horseradish, used in solution or immobilized on chromatography paper, the detection limits of mercury(II), affecting the activity as an irreversible inhibitor, vary from $5 \times 10^{-2} \text{ mg l}^{-1}$ for *o*-phenylenediamine to $1 \times 10^{-5} \text{ mg l}^{-1}$ for tolidine as substrates [111].

The purification of raw enzyme preparations can also give rise to a change in the selectivity of

an enzyme towards inhibitors. Thus, the purification of plant peroxidases results in the increase in the detection limit of mercury(II) and alkylmercury compounds. The stepwise isolation of monoaminoxidase from dog intestine results in the change of both the selectivity towards primary and secondary amines, (e.g. substrates) and towards heterocyclic compounds used as plant growth regulators, (e.g. reversible inhibitors) [112]. The possible reasons for this phenomenon comprise the local concentration of the inhibitor at the inert protein, the change of the isoenzyme ratio in the enzyme preparation, changes in conformation of the active center and its environment and the removal of the natural enzyme stabilizer.

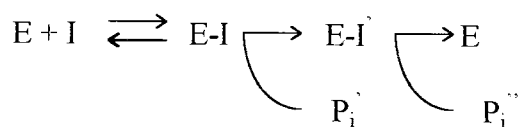
The future progress in the optimization of the enzyme-inhibitor system involves the purposeful modification of the enzyme to attain higher sensitivity and/or selectivity, the search for novel non-traditional sources of enzymes with a higher selectivity, the development of novel methods for isolation and stabilization of enzymes which demonstrate higher sensitivity and selectivity to the inhibitors to be determined.

3.2. Kinetics of enzyme-inhibitor interaction

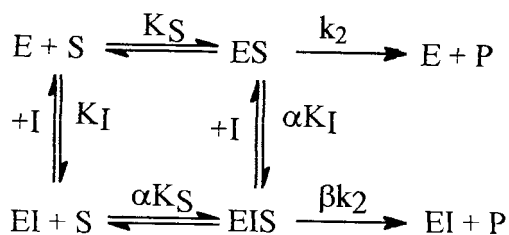
The optimal procedure of the measurement of inhibiting effect depends essentially on the mechanism of enzyme-inhibitor determination.

For irreversible inhibitors, enzyme-inhibitor interaction results in the formation of covalent bond between enzyme active center and the inhibitor.

The term 'irreversible' means that the decomposition of the enzyme-inhibitor complex results in the destruction of the molecule of the inhibitor, e.g. its hydrolysis, oxidation etc. This process proceeds usually stepwise, as for phosphorylated cholinesterase Scheme 2, and can be accelerated by special reagents.



Scheme 2.



Scheme 3.

For irreversible inhibitors the following equation can be used for the determination of either the concentration of the inhibitor C_I or the bimolecular rate constant of the enzyme-inhibitor interaction k_{II}

$$\ln(v_0/v_i) = k_{II} C_I \tau \quad (2)$$

where τ is the incubation time, v_0 and v_i are the initial rates of an enzyme reaction prior to and after the contact of the enzyme with the inhibitor, respectively [113]. This equation is valid for a short incubation period ($\tau < 10\text{--}15$ min) and when the concentration of the inhibitor is much higher than that of the active centers of the enzyme.

The influence of reversible effector (i.e. inhibitor I or activator) on the two-step enzyme reaction can be presented by the general scheme Scheme 3 in assuming that the effector reacts with the enzyme E or enzyme-substrate complex ES in the ratio 1:1, where K_I and K_S are the equilibrium constants of dissociation of enzyme-inhibitor and enzyme-substrate complexes, C_E , C_S and C_I are the initial concentrations of the enzyme, substrate and inhibitor, respectively. It is assumed that C_S , $C_I \gg C_E$.

The initial rate of enzymatic reaction $v_i = 0$ can be expressed by the Eq. (3)

$$v = \frac{k_2 \frac{\alpha K_I + \beta C_I}{\alpha K_I + C_I} C_E C_S}{\alpha K_S \frac{K_I + C_I}{\alpha K_I + C_I} + C_S} \quad (3)$$

Beresin and Martinek [114] have given a full kinetic analysis of the possible cases of both inhibition and activation in accordance with the Eq. (2). Several special cases of prime importance are

often used for the description of experimental results. This refers to the competitive ($\alpha \rightarrow \infty$, non-competitive ($\alpha = 1$, $\beta = 0$), uncompetitive ($\alpha = \beta < 1$) and mixed type ($\alpha \neq 1$, $\beta \neq 1$) inhibition.

Thus, for purely competitive inhibition, the inhibitor binds with enzyme active center but not with enzyme-substrate complex. In this case the Eq. (3) is simplified to the well-known Eq. (4).

$$\begin{aligned}
 v &= \frac{k_2 C_E C_S}{K_S (1 + C_I/K_I) + C_S} \\
 &\approx \frac{K_m C_S}{K_m (1 + C_I/K_I) + C_S} \quad (4)
 \end{aligned}$$

where K_m is the Michaelis constant. The equilibrium constant of reversible inhibition K_I corresponds to the reciprocal value of the inhibitor concentration which involves a 2-fold decrease of the rate of enzyme reaction: $K_I = C_I^{-1}$ at $v_i/v_0 = 0.5$. This concentration value or, more commonly, its logarithm $pI_{50} = -\log C_I$ can be used for the characterization of the sensitivity of the enzyme towards reversible inhibitors. It should be mentioned that the pI_{50} value does not carry any information on the dynamic range of the inhibitor concentration to be determined and the appropriate detection limits could be achieved.

Similar approaches, based on the dependence of the rate of enzymatic reaction or of the experimental values of K_m on the concentrations of the substrate and inhibitor are also developed for other cases of inhibition.

Thus, the generalized kinetic equation Eq. (5) was proposed for the mixed type reversible inhibition.

$$v_0/v_i = \frac{K_m (1 + C_I/K_I) + C_S (1 + C_I/K'_I)}{K_m} \quad (5)$$

where v_0 and v_i are the rates of the enzyme reaction without any inhibitor and in the presence of the inhibitor and K_I and K'_I are equilibrium constants of the competitive and non-competitive inhibition, respectively. The relationship between K_I and K'_I determines the mechanism of inhibition. Thus, for competitive inhibition $C_I/K'_I \ll 1$, for non-competitive inhibition $K_I = K'_I$ etc.

The effectivity of inhibition in this case is characterized with the generalized equilibrium constant Eq. (6) which makes it possible to compare the affect of various inhibitors with different mechanisms of inhibition.

$$\frac{K'_1 + K_1}{K_1 K'_1} = \frac{1}{K_1} \quad (6)$$

The appropriate experimental data are linearized in plots $v_0/v_i - C_1$ and a generalized experimental equilibrium constant of inhibition is calculated from the slope of the curve for various substrate concentrations.

The determination of the kinetic parameters of inhibitors makes it possible to identify inhibitors owing to the investigation of their inhibiting effect on enzymes from different sources.

For irreversible inhibitors this can be evaluated from Eq. (2) for the same incubation time.

$$(k_{11})_1/(k_{11})_2 = \{\ln(v_0/v_i)\}_1/\{\ln(v_0/v_i)\}_2 \quad (7)$$

and for reversible inhibitors, respectively,

$$(K_1)_1/(K_1)_2 = (v_0/v_i)_1/(v_0/v_i)_2 \quad (8)$$

where subscripts 1 and 2 refer to the data obtained with enzymes from different sources and is a generalized equilibrium constant of reversible inhibition. As a practical matter, it is important that Eq. (7) and Eq. (8) do not contain the concentrations of inhibitor, so the identification can be attained for the samples of unknown content. Ideally, when increasing the number of the enzymes with different inhibitor selectivity it is possible to completely rely on the identification of the inhibitor. In fact, this approach is limited by the lack of the necessary kinetic data. For example, the identification of 53 preparations of organophosphates was proposed on the base of the kinetic data of their inhibition by four cholinesterases from various sources [115].

A similar approach was used for the selective determination of various substituted phenols and chlorophenols [76] which affect, as substrates and competitive inhibitors, the response of amperometric biosensor utilizing immobilized polyphe-noloxidase.

On the other hand, the enzyme mixture can be used with the same substrate for the extension of

the number of inhibitors determined with the required sensitivity in a single measurement. This was attained by the co-immobilization of acetyl- and butyrylcholinesterase in one membrane introduced into the assembly of an amperometric biosensor with acetylthiocholine as a substrate [51]. The developed biosensor demonstrates wider abilities for monitoring the contamination of organophosphorus pesticides.

The possibility of the identification of eight pesticides in the presence of heavy metal salts is attained due to the simultaneous determination of the inhibiting effect of the mixture with multi-enzyme biosensing system [116]. The system consists of three pH sensors whose sensitive surfaces are connected with a membrane on which one enzyme (i.e. acetylcholinesterase, alkaline and acid phosphatases) is immobilized at a time. The selectivity results from the optimization of the measurement conditions and from the chemometric analysis of the inhibiting effect on each biosensor.

4. Enzyme immobilization and the role of surface factors

All the kinetic equations (Eqs. (2)–(5) and Scheme 3) mentioned in the previous section are based on the assumption of homogeneous kinetics of the enzyme-substrate and enzyme-inhibitor(s) interactions. The appropriate parameters of inhibition (i.e. k_{11} , K_1 , K'_1 etc.) indicate the potentialities of an enzyme which could be extended or reduced through the immobilization and incorporation of the enzyme into the membrane material.

The immobilization of an enzyme is an indispensable part of the development of biosensors. The multiplicity of application of the enzyme due to immobilization reduces the cost of measurement. The immobilized enzyme is more stable towards extreme working conditions, e.g. high temperature, and can be easily combined with an appropriate sensor in the biosensor assembly.

For inhibitor determination, the economic advantages are not so compelling because the inhibition proper implies the decay of the enzyme activity and therefore a limited number of consecutive measurements with the same batch of immo-

bilized enzyme, be it a membrane or a reactor. Based on this, the practical application of the inhibitor biosensor was stated primarily for reversible inhibitors. More precisely, the initial response of a biosensor devoted to field applications should be recovered after inhibition in a reasonably short period of time. For reversible inhibition the initial response can be recovered with a washing out procedure after contact with inhibitor. For heavy metals, the complexing reagents such as EDTA or cysteine for mercury can be used [17,20,39,47,48]. Much more important is the application of special reactivators for irreversible inhibitors.

The treatment of an inhibited enzyme with special chemicals (i.e. reactivators) makes it possible to accelerate the spontaneous recovery of the enzyme activity to a degree, depending on the nature of the enzyme-inhibitor complex and the period of time from the initial contact with the inhibitor to the reactivation procedure. Reactivation prolongs the lifetime of a biosensor but complicates the whole cycle of the inhibitor determination. Reactivation is specific for a particular inhibitor and an enzyme. In several cases, pharmaceutical medications, i.e. antidotes, are used. 2-Pyridinealldoxime methiodide (2-PAM) or 1,1'-trimethylenebis-4-(hydroxyiminomethyl)

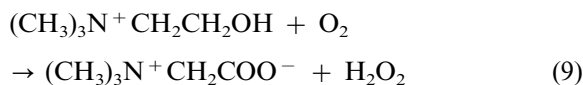
pyridinium bromide (TMB-4) are a well-known example of reactivators used for phosphorylated cholinesterase [20,35,38,45,49,51–54,57,59–63]. The specificity of reactivation in combination with simple kinetic investigations (i.e. the dependence of the inhibiting effect on the presence of the substrate during incubation or on the period of incubation) can provide for the identification of the inhibitor or simplify the choice between several possible inhibitors available in the sample tested [20].

However, the problem of reactivation and the prolonged lifetime of a biosensor is more likely to be related to the economic aspects of the practical applications of inhibitor biosensors. Of a greater significance is that the immobilization procedure very much alters the analytical characteristics of the determination of inhibitors. This might occur owing to the following reasons:

1. The slow transfer of the substrate from the bulk solution into the membrane body (diffusion limitations);
2. The changes in the microenvironment of the active center of the immobilized enzyme;
3. The interaction of the substrate and/or inhibitor with the membrane material (sorption effect).

First of all, the transfer of the consideration of the enzyme-inhibitor interaction from homogeneous kinetics to the heterogeneous conditions of the enzyme membrane calls for an essential study of the role of diffusion. As was briefly shown earlier, if the rates of consumption and of the transport of a substrate in a membrane are comparable, the active centers of the immobilized enzyme are not saturated with the molecules of the substrate. The inactivation of active centers is compensated for by the other free active centers, and the resulting decay of biosensor response is lower than it would be in a homogeneous solution. Mostly reports describe the increase of the detection limits of the inhibitors after immobilization [20,41,42,50,58]. Hence, the inhibition degree of biosensors, based on immobilized acetylcholinesterase and urease in the presence of fluoride ions, decreases with the loading of the enzyme and thickness of the membrane formed, i.e. with the increase of the specific activity of the enzymes. A similar result is attained by varying the time of treatment of the membrane with cross-linking glutaraldehyde [20]. The detection limit of Paraoxon obtained with an amperometric biosensor based on three enzymes (i.e. cholinesterase, choline oxidase and peroxidase immobilized in methacrylate gel), was $0.75 \mu\text{g l}^{-1}$ for native cholinesterase and $125 \mu\text{g l}^{-1}$ when the enzymes are co-immobilised in the membrane [50].

The use of multi-enzyme biosensors is reported for the determination of the inhibitors of cholinesterase [41,42,50,55,56,58]. The introduction of additional enzymes (i.e. choline oxidase) makes it possible to use the standard Clark-type electrode for the determination of biosensor response and techniques developed mainly for the glucose electrodes. The choline formed in the enzymatic hydrolysis of acetylcholine (see Eq. (1)) is oxidized to betaine in the second consecutive reaction promoted by choline oxidase Eq. (9).



The rate of the latter reaction is measured from the decrease of oxygen concentration with a Clark-type amperometric sensor. However, this does not contribute to the improvement of analytical characteristics of the determination of cholinesterase inhibitors.

A 2–10-fold increase in the detection limits of both reversible and irreversible inhibitors was reported for monoamine oxidase, carboxylesterase and cholinesterase followed by their immobilization in gelatin and agar membranes [84,85,112].

The influence of the content of the membrane on the analytical characteristics of the determination of an inhibitor is much more pronounced for thick membranes with a high activity of the enzymes such as gelatin membrane in the latter case. For thin enzyme films, formed directly on the electrode surface, the diffusion limitation is not as high and the results obtained are much more affected by the nature of the enzyme and by the specific enzyme activity. Hence, the detection limits of organophosphorus pesticides obtained with pH-sensitive field effect transistor (FET) covered with an ultra-thin layer of cholinesterase [43], and potentiometric biosensors with a replaceable membrane [63] are similar to each other.

For reversible inhibitors, the experimental value of the inhibition degree must depend on the ratio of the rates of diffusion of a substrate and an inhibitor. Usually, they are assumed equal for low molecular compounds, but for charged substrates and/or inhibitors this ratio in a membrane body can essentially differ from that in a solution. Even if this does not occur, the time necessary for attainment of equilibrium in a membrane body can exceed the duration of the measurement, therefore for a typical reversible inhibitor the experimental value of inhibition degree depends on the period of incubation. The use of isotopes of zinc and thallium showed that the stationary concentration of zinc ions in a gelatin membrane is established only after 40 min after the addition of appropriate salts into a solution contacting with the gelatin membrane [53].

An additional effect is observed, when the inhibitor is non-specifically adsorbed on the membrane material. This diminishes the actual concentration of the inhibitor interacting with the active center of the enzyme and consequently the inhibition degree of the biosensor response. The sorption can be suppressed with the addition of surfactants. This results in an increase of the sensitivity of cholinesterase biosensors to organophosphorus pesticides [60,62].

For biosensors based on potentiometric pH-sensitive ion-selective electrodes or FETs, the consideration of kinetic limitations should be extended to the acid formed in the enzyme reaction. In a weak buffer medium the pH shift to 1–1.5 units can be observed in a membrane body. This involves both the changes in the activity of an enzyme and in the kinetic parameters of inhibition which are also pH sensitive. This phenomenon is more conspicuous for a higher response of the biosensor, i.e. for a higher enzyme activity.

The pH value of the working solution is commonly selected close to the pH maximum of the enzyme activity observed for a native enzyme. Hence, the pH shift in the membrane body results in an additional decrease in the sensitivity of an immobilized enzyme to the inhibitor in comparison with that of a native enzyme in similar working conditions.

Another effect of the excess of H^+ ions in an enzyme membrane is that the response of such biosensors does not reflect only the enzyme activity.

The results of the determination of irreversible inhibitors with a potentiometric cholinesterase biosensor were recalculated from the units of the relative response decay (i.e. inhibition degree I , %) to the ratio of the rates of the cholinesterase reaction before and after the contact with the inhibitor: $v_0/v_i = (100 - I)/I$ [63]. However, the linear curve in plots $\ln(v_0/v_i) - C_1$, predicted in Eq. (2), was obtained only for small inhibiting effects ($I < 20\text{--}25\%$) when the pH shift is considered to be nearly constant. On the contrary, the response of amperometric biosensors to various inhibitors is often considered to be a linear function of the enzyme activity, and the calculations of kinetic

parameters based on this assumption are in a good agreement with the results obtained with traditional measurements of the specific activity of the immobilized enzyme [89,95].

Most enzyme carriers, and the immobilized enzyme proper, possess buffer properties to a certain degree. It follows that the pH dependence of the response differs from that of the activity of the native enzyme. Thus, the immobilization of butyrylcholinesterase on cellulose dinitrate results in a shift of the pH maximum of the enzyme activity from pH 8–9 (native enzyme) to 9.5–10 (immobilized enzyme) [18,37,45]. On the other hand, the dependence of a biosensor response on the pH value of the working solution is relatively lower than that of the native enzyme.

Apart from the pH changes, the immobilization of the enzyme can cause other changes in the local microenvironment of the active center of the enzyme, e.g. variations in ionic strength, electrostatic interactions etc.

Of particular interest are the cases when the decrease of the detection limits of certain inhibitors is observed. Extra low detection limits down to 10^{-11} mol l^{-1} of dimethyl-2,2-dichlorovinyl phosphate (DDVP) and 10^{-12} mol l^{-1} of 2,4-D were reported for the amperometric biosensor based on the silver amalgamated electrode and the butyrylcholinesterase membrane obtained by the combination of two techniques: the cross-linking with glutaraldehyde and the microcapsulation of the enzyme aqueous solution into the cellulose nitrate matrix [18]. This is much more surprising as 2,4-D does not affect the native enzyme in the same working conditions and the minimal detectable concentration of DDVP in experiments with the native enzyme is 10 000 times higher. Undoubtedly, this calls for additional factors amplifying the actual decay of the enzyme activity. They can involve the sorption of the inhibitor on the hydrophobic membrane material resulting in a pre-concentration of the inhibitor, as in solid-phase extraction. In this case, the interaction of the inhibitor with calcium ions in a working solution can promote the transfer of the inhibitor in the form of salt from water solution into the body of the membrane. This biosensor is the only one with the cathodic detection of

the cholinesterase reaction. This prevents the accumulation of the H^+ ions in a membrane and the shift of local pH value from its optimum for the enzyme reaction. A similar increase of sensitivity toward inhibitors has been demonstrated for other biosensors when the enzyme is immobilized on commercial membranes of cellulose nitrate (Sartorius, Amersham) or disposable films of cellulose trinitrate formed directly on the active surface of a sensor, but not on a very large scale [45,61–63].

The response of the potentiometric biosensor based on a glass pH electrode covered with a cellulose trinitrate film with immobilized butyrylcholinesterase is sensitive to 2,4-dinitrophenol and Dieldrin which do not affect the native enzyme [117]. Unfortunately, the immobilization of cholinesterase on such hydrophobic materials is followed by the loss of 80–95% of the initial activity of the enzyme and the lifetime of the biosensor is not as high [63].

As to other membrane materials, the biggest changes in the analytical characteristics of the determination of the inhibitors are observed for rather thick membranes of gelatin, agar and methacrylate polymers swelling in aqueous solutions. The results obtained for thin non-swollen membranes are much closer to each other, irrespective of the transducer used [61,62].

The sensitivity toward inhibitors is moderately higher if the enzyme is immobilized directly on the surface of the transducer, be it a standard ion-selective electrode or a FET than if replaceable membranes of the same material are used for the same transducers. This might be the result of the inflow of the working solution in between the transducer and the membrane, followed by smoothing the response.

A special case is when the enzyme is incorporated into the material of the electrode, usually carbon paste [49,89,118]. In this case, only a very thin layer of the enzyme in contact with the working solution provides for the response observed. After inhibition, the mechanical polishing and removal of the outer layer of the electrode makes it possible to recover the initial response. Due to the bulk modification of the carbon paste a high reproducibility of the response is achieved

(R.S.D. < 1%). For oxidoreductases, such as peroxidase or cytochrome c oxidase, the electric contact and electron transfer between the enzyme and the electrode are simplified and, consequently, the working potential is lower. Other compounds required for the activity of enzyme or the response detection can be introduced into the carbon paste, i.e. lipids, mediators of electron transfer etc. Thus, 7,7,8,8-tetracyanoquinodimethane (TCNQ) was introduced together with cholinesterases from electric eel, horse serum or bovine erythrocytes into carbon-epoxy resin composition to reduce the working potential from 0.7 V vs. Ag/AgCl to 0.3 V [119]. Such carbon-paste biosensors are free from many drawbacks characteristic of membrane covered electrodes, i.e. diffusion limitations, high ohmic resistance, and contact of the membrane with the sensor. The same is true for screen-printed planar electrodes covered with ultra-thin enzyme layers [55,56]. The manufacture of such disposable biosensors maintains a high accuracy of the response determination (R.S.D. down to 0.7–1.3%) and a low background signal. This makes it possible to decrease the working concentration of the substrate and the detection limits of competitive inhibitors, respectively. Furthermore, the decrease of the working concentration of the substrate makes it possible to simplify the procedure of measurement, when the irreversible inhibiting effect is determined in the presence of the substrate. Generally, this results in the decrease of the appropriate detection limit of the irreversible inhibitor owing to the so called ‘protecting effect’ of a substrate [45,46]. The less the concentration of a substrate, the lower the shift of sensitivity of inhibitor determination. However, for such a biosensor the improvement of operation conditions is not, as yet, followed by notable changes of the sensitivity of the determination of an inhibitor, as compared with traditional membrane biosensors.

5. Working conditions

The determination of the response of a biosensor is usually performed in weakly buffered media containing a supporting electrolyte, stabilizers of

enzyme, cofactors, (e.g. NADH, ATP, etc.), an organic solvent, etc. Apart from their target function they can alter the analytical characteristics of the determination of inhibitors.

5.1. pH value of working solution

The pH value of the working solution is usually regarded as a most important factor determining the performance of the biosensor and its sensitivity toward inhibitors. As a rule, the pH maximum of the enzyme activity is evaluated as most appropriate, both for the substrate and inhibitor determination. Indeed, the pH-dependence of the observed inhibiting effect often corresponds to that of the response of a biosensor. Thus, enzyme sensors utilizing various esterases are most sensitive to organophosphates at the pH 8–9 when the response of a biosensor is maximal.

Carbon paste electrode, modified by cytochrome c and cytochrome oxidase, demonstrates the peak of sensitivity toward cyanide at pH 6.3, and the equilibrium constant of inhibition K_i remains approximately the same in the range pH 5.5–7.5 [89].

Urease is proposed for the determination of heavy metal ions at pH 8–10 [19,26,67,120], whereas glucose oxidase or catalase are sensitive to heavy metal ions at pH 5–8 [69,70,91]. As mentioned earlier, enzyme immobilization can shift the pH optimum to a higher value relative to the measurements with a native enzyme owing to the accumulation of H^+ ions in the membrane body.

Certain inhibitors are converted to the active form only in aqueous solution in the reaction of reversible protonation or hydrolysis. In this case the pH optimum of inhibition can be sufficiently shifted from the optimum for the enzyme-substrate interaction. This is typical for secondary amines which inhibit carboxylesterase and cholinesterase after preliminary protonation and the maximum of inhibition is observed in weakly acidic media (pH 6.0–7.0) [45,84,85]. If the reaction of the formation of an active form of the inhibitor (i.e. protonation) is hindered, the pH shift can be higher. Hence, intermolecular binding diminishes the basicity of the nitrogen atom in

α -aminophosphonates. As a result, they exhibit an inhibiting effect on native microbial carboxylesterase at pH 3–4.5 [121]. The activity of cholinesterase in this pH range is too slow, this retards quantitative measurement of the inhibiting effect of this compounds. Incidentally, the immobilization of cholinesterase on a paper membrane makes it possible to detect these compounds with the pH maximum of the inhibition at pH 6–6.5. Similar results were obtained for hydrazones of benzaldehyde and cinnamaldehyde.

For multicharged ions, the inhibiting effect on cholinesterase is preceded by their partial hydrolysis and the formation of hydroxy ions MeOH^+ . Hence, the pH maximum of inhibition depends on the appropriate equilibrium constants of hydrolysis.

Apart from the pH value of the working solution, the actual pH shift in a membrane body during the formation of the response of a biosensor is determined by the nature of the buffer solution. The change in the inhibition degree with the buffer used can result from the change of the capacity of the buffer or the ion strength. Some of the buffer solutions (e.g. borate buffer for cholinesterase) demonstrate a weak inhibiting effect of the enzyme. In this respect the basicity of the working solution is commonly not as high, even for amperometric biosensors which do not measure the pH shift, and do not exceed $10^{-2} \text{ mol l}^{-1}$.

For biosensors exploiting two enzymes, co-immobilised in the same membrane or separated in different compartments of a biosensing device (e.g. membrane and solution), the pH value of the working solution is usually chosen according to the pH optimum of the key enzyme determining the response of a biosensor. Hence, for a two-enzyme biosensor, utilizing cholinesterase and choline oxidase, the determination of cholinesterase inhibitors was performed at pH 7.0, referring to the optimum of activity of choline oxidase [41,42]. Such an approach is rewarding if it contributed to the performance of a biosensor and the pH sensitivity of inhibition is not as high. In other cases this can result in the decline of the analytical characteristics of inhibitor determination.

The shift of the pH value from the optimum for the enzyme-substrate or enzyme-inhibitor interaction can arise to meet the needs of detecting the enzyme reaction or the stability of a sensor. Hence, electrodes based on the composition of epoxy resin and carbon are unstable in basic media. Therefore, when this composition containing cholinesterase is used for inhibitor determination, all the measurements are performed at pH 7.0 [49].

For irreversible inhibitors, the incubation procedure is performed before the substrate is added. The conditions of inhibition and of the following determination of reduced response can differ, and some of the limitations can be avoided. The incubation of a cholinesterase biosensor in non-buffered media at pH 7–7.5 with the following determination of the response in standard conditions for this enzyme (pH 8.0, phosphate buffer) makes it possible to detect both heavy metal ions and organophosphorus pesticides [45]. The incubation in a phosphate buffer at pH 8.0 with the same conditions of response measurement results in the selective determination of organophosphates in the presence of heavy metal ions. For determination of organophosphorus pesticides, the incubation can be conducted immediately in organic solvents used for extraction. Following washing eliminates the interfering influence of the organic solvent on the response of the biosensor in standard buffer solution [52].

The concentration of supporting electrolyte is not so important for biosensor response as the pH value of the working solution. Most measurements are performed at constant ion strength which rarely exceeds 0.1 mol l^{-1} . The increase of electrolyte concentration contributes to the reproducibility of biosensor response together with the decay of the response value and the lifetime of the immobilized enzyme. This can be followed by the decrease of the sensitivity of the enzyme toward reversible and irreversible inhibitors, i.e. the increase of the pI_{50} and K_i values and the minimal detectable concentration of the inhibitor [27,89]. As a result, most procedures for the determination of the inhibitor specify the highest permissible content of the salts both in the working solution and the sample tested [27,28].

5.2. Measurements in organic media

In several reports, the influence of organic solvents on the response and sensitivity of biosensors for the determination of inhibitors has been described [52,77–79,94,122–127]. The measurements in non-aqueous media are very attractive because they offer new opportunities for the application of such biosensors, as in-line control of industrial processes or the detectors for HPLC. The employing enzymes in organic media allows the increase in the solubility of non-polar substrates and/or inhibitors and to shift the sensitivity of the enzymes toward various substrates and effectors [127].

Only a few enzymes retain their activity when the content of water does not exceed several percent. Tyrosinase and peroxidase based biosensors are the most investigated ones for the determination of various substrates and inhibitors in organic solvents containing various amounts of water, i.e. acetonitrile, alcohols, 1,4-dioxane, acetone, chloroform, etc.

The measurement in organic solvents places more stringent requirements upon the immobilization of the enzyme. The appropriate carrier must neither dissolve nor swell in organic media and the immobilized enzyme must retain its activity in the working conditions. The application of photocrosslinkable polymer, PVASbQ (Toyo Gosei Corp., Tokyo) [52], cellulose derivatives [79], conducting PVC-copolymers [78], Eastman AQ-55D [124,125] has been described for this purpose. The physical sorption of the enzyme on the graphite surface [126] or dialyze membrane [77] was also found appropriate for water-immiscible solvents and emulsions.

The response of the tyrosinase biosensor increases with water content to the limit, determined by the concentration of the substrate used. The minimal amount of water required for the measurements of the response depends on the polarity of the solvent and the substrate. When phenol was used as a substrate of tyrosinase, the detectable amounts of water consist of 0.01–0.005% v/v [125].

The measurements in non-aqueous media makes it possible to determine the compounds,

the solubility of which in water is insufficient. This refers to the derivatives of thiourea, inhibiting tyrosinase [77]. The determination was performed in n-hexane saturated with phosphate buffer. The presence of a water phase is used for establishing electric conductivity, which is necessary for electrochemical measurements. For non-polar solvents two-phase solutions can be also used, in which the organic phase forms reversed micelles with a low amount of aqueous buffer solution maintaining both the enzyme activity and the electric conductivity. Described cases of enzyme catalysis in dehydrated solvents (cholesterol oxidase, cholesterol esterase and others) [128] have not, as yet, been definitely applied for the determination of inhibitors.

Most enzymes reduce their activity in the presence of water-miscible solvents. Their addition pursues the same goals as the use for the measurements of organic media: the increase of solubility of the inhibitors to be determined, the possibility of direct analysis of extracts from plants or soil without the evaporation of the extract, etc. The maximum part of solvents to be used in the working solution depends on the nature of the enzyme and the membrane material. The immobilization decreases the sensitivity of the enzyme toward organic solvents. Thus, for acetyl- and butyrylcholinesterase immobilized in agar films and on tracing paper the tolerable content of ethanol and acetone is reported up to 20% [45], whereas 20% ethanol is used to stop the Ellman reaction in the standard technique of the determination of activity of native cholinesterase [129]. The immobilized enzymes retain their activity during at least 30 min after the addition of the solvent. For horseradish peroxidase the increasing hydrophilicity of the solvent (i.e. methanol > acetonitrile > acetone) results in a decrease of sensitivity of the biosensor toward thiourea and ethylenethiourea [94].

An alternative method of overcoming limitations of organic solvents (i.e. insufficient electric conductivity, low enzyme stability) is to perform the incubation in organic media and the biosensor response measurement in aqueous standard solution. Thus, 30-min incubation in pure alkanes C₆–C₁₂, benzene, butyl acetate, ethyl ether, ace-

tonitrile does not significantly alter the activity of acetylcholinesterase whereas alcohols, DMSO, chloroform diminish the enzyme activity by 50–100% [52]. The stability of immobilized was higher than that of free acetylcholinesterase. This was explained by the hydrophilic properties of the enzyme carrier PVA-SbQ which stabilizes the essential water layer around the enzyme. The influence of the solvent on the enzyme activity was characterized with the parameter $\log P$, defined as the logarithm of the partition coefficient in a standard octanol-water two-phase system ($P = (C_{\text{solvent}})_{\text{octanol}} / (C_{\text{solvent}})_{\text{water}}$). The highest enzyme activities (up to 120% for free enzyme and up to 115% for immobilized cholinesterase) were obtained after the incubation in hydrophobic solvents ($\log P > 4$ for free and > 2 for immobilized enzyme).

As to inhibitory effect, the role of organic solvents is ambiguous. For reversible inhibition, it may depend on the hydrophilic/hydrophobic properties of the substrate and inhibitor. Thus, for cholinesterase immobilized in a gelatin membrane the addition of ethanol results in the decrease of the reversible inhibiting effect of certain amines when butyrylcholine iodide is used as a substrate. An opposite effect is reported for the same inhibitors and working conditions, when indophenyl acetate is used as a substrate [130]. The altering effect of organic solvents on the Michaelis constants and apparent equilibrium constants is described for peroxidase biosensors with thiourea and ethylenethiourea as reversible inhibitors. For irreversible inhibitors, the influence of organic solvents on the inhibiting effect is considered to be lower than that for reversible inhibitors.

The addition of small amounts of methylcellulose to the buffer solution was also described [28] for automated alarm systems for the detection of traces of anticholinesterase pesticides in air and fresh waters based on cholinesterase immobilized in pad reactors and galvanostatic detection. For the same purpose 1% of acetonitrile was added to the buffer solution for the determination of anticholinesterase pesticides with screen printed choline biosensor and native acetylcholinesterase [131]. Acetone, tetrahydro-

furan and ethyl acetate were found inappropriate, due to their inhibiting affect on the response of the biosensor.

5.3. The use of enzyme effectors

The working solution can involve stabilizers and effectors of the enzyme incorporated in the biosensor assembly. This is a most promising and a less investigated direction of the progress in the development of biosensors for the determination of inhibitors. Thus, the detection limits of mercury(II), which inhibit peroxidase from horse serum, can decrease by a factor of 1000, when the enzyme is preliminary incubated in diluted solution of thiourea [111]. Moreover, this treatment prevents the interfering effect of the other heavy metals. With the choice of appropriate substrates, this approach resulted in the development of high selective methods of mercury determination with the detection limits down to 10^{-6} mg l⁻¹ if native enzyme is used. The immobilization of peroxidase on paper or cellulose derivatives decreases the sensitizing effect of thiourea. As thiourea exhibits a general denaturing effect on peptides, its influence is observed for small concentrations and the limited duration of the contact with the enzyme, during which the decay of initial enzyme activity does not exceed 40%.

The activating effect of calcium and some other doubly charged cations is described on the response of amperometric biosensor utilizing butyrylcholinesterase immobilized in cellulose dinitrate and its sensitivity toward irreversible inhibitors [18]. The sensitizing effect is observed within narrow limits of experimental conditions, i.e. at pH 9–10 and low concentration of supporting electrolyte. The more the concentration of supporting electrolyte, the less influence of effectors on response and sensitivity of biosensor toward inhibitors. Similar measurements with cholinesterase immobilized at paper membrane in Tris buffer (pH 6–8) containing 0.1 mol l⁻¹ of NaCl do not demonstrate any changes of analytical characteristics of inhibitor determination in the presence of such effectors.

Aluminum ions in the concentration range from 10^{-4} – 10^{-3} mol l^{-1} increase the activity of native butyrylcholinesterase by 15–20%. Moreover, the sensitivity of native enzyme to Paraoxon is increased in the presence of this amount of aluminum by 10–15%. Meanwhile, the response of cholinesterase biosensor utilizing the enzyme immobilized on paper membrane diminishes by 20–25%, and the decay of the response of biosensor after incubation in the solution of Paraoxon containing 10^{-4} mol l^{-1} of aluminum ions is lower than that observed without any additives as if aluminum exhibit typical ‘protecting effect’ [45,46]. One of the possible reasons of differ influence of activators on native and immobilized enzyme assumes the sorption of ions effecting enzyme activity on the polar hydrophilic material of membrane. Sorption and possible partial hydrolysis of aluminum salts hinders the access of a substrate and/or inhibitor in membrane body followed by the decrease of apparent inhibition degree.

This is borne out by the results of joint action of reversible effectors (both activating or inhibiting enzyme) and surfactants on the response of biosensor and its sensitivity toward irreversible inhibitors [62]. The addition of 10⁻³% w/v of non-ionic surfactants not only diminishes the reversible inhibiting effect of traditional inhibitors, i.e. fluoride and copper(II) ions, but also suppress ‘protecting effect’ of such reversible inhibitors on the determination of irreversible inhibitors: the slope of appropriate calibration curves of Paraoxon or Diazinon decreases when effectors are added to the working solution but returns to the initial value in the presence of surface active compounds, i.e. PEG-10 000, Triton-X-100 or Tween-20. In the concentration range 10^{-1} – 10^{-3} % the above compounds diminish the response of the biosensor as reversible inhibitors.

This may be important for the possible application of membrane biosensors for direct monitoring of environmental pollution. Indeed, some components of environment, i.e. water-soluble peptides, humic and fulvic acids, biogenic polyphenols, clays exhibit in variable degrees surface-active features and can alter the actual

inhibition caused by the contamination of the sample tested.

6. Future prospects of biosensors for inhibitor determination

Although practical application of inhibitor biosensors seems currently much more complicated than that of substrate biosensors, their potentialities are far from being exhausted. First of all this refers to the application of biosensors for environmental monitoring. Contrary to the conventional techniques and analytical equipment, inhibitor biosensors make it possible to detect directly dangerous pollutants (i.e. heavy metal ions, pesticides, cyanides, respiration poisons, etc.) without any preconcentration or sample treatment. The achieved detection limits in most cases refer to the maximum permissible levels of pollution in environmental objects. Simple procedure or response measurement as well user-friendly design make such biosensors very attractive for preliminary estimation of pollution especially in field conditions.

However the realization of these advantages calls for the solution of several problems, i.e. the selectivity of response, the calibration of biosensors in multi-component media, the influence of natural enzyme effectors and last but not least—the directional regulation of biosensor performance depending on particular analytical problems. Recently, various results of the biosensor based testing of the real samples (fruits, vegetables, wastewaters, river sediments) have been described [131–133].

The interpretation of biosensor response in multi-component media, i.e. waste and natural waters, extracts etc. is based commonly on the presentation of cumulative inhibiting effect of all pollutants presented in the sample in the units of concentration of a standard inhibitor, i.e. DDVP [28] or Paraoxon [59]. This approach does not account for non-additive combination of partial effects as takes part for reversible and irreversible inhibitors due to the ‘protecting effect’. On the other hand, the variety of the factors effecting biosensor response (i.e. sorption of

surface-active compounds and hydrolyzing salts, presence of natural enzyme effectors, etc.) offers novel possibilities to use inhibitor biosensors as indicators of general pollution or toxicity of the samples tested. In this case for calibration the estimation of acute toxicity of sample on hydrobionts (e.g. *Daphnia* or *Infusoria*) can be used for the calibration of the response of the biosensor. The combination of several enzymes or joint interpreting the results of biosensor based measurements and biotesting extend the potentialities of the application of biosensors [132].

Recently, modes for the further improvement of biosensors based on well-known enzymes, i.e. cholinesterases, peroxidase, tyrosinase, must be related to the development of novel sensors-transducers providing for better operation conditions (response time, lifetime of enzymatic membrane, etc.). The improvement of sensitivity can be afforded by the optimization of working conditions, including the incorporating enzyme activators into membrane or electrode material as well as in working solution.

The expansion of the list of species to be detected can also be attained by using enzyme process for indication of the changes in the membrane body or on the surface of the sensor, which are not connected directly with enzyme, as such. Thus, the determination of benzoic acid based on mediated tyrosinase biosensor is described [74]. Competitive inhibition observed arises from the interaction of benzoic acid with the active form of mediator, generated through enzymatic process. Similarly, sorptional membrane effects described earlier [62] are detected with cholinesterase reaction.

New opportunities are considered with the application of novel enzymes or enzyme sources as well as biocomponents with necessary enzyme activity. Besides the improvement of sensitivity or selectivity of the determination of traditional pollutants, this biosensors can serve as models of toxic effects of appropriate compounds or their mixtures on living cells and living being. Combined with traditional biosensors and test kits this biosensing devices can be applied as alarm monitors of environmental pollution.

References

- [1] L.J. Blum, P.R. Coulet, *Biosensor Principles and Applications*, Marcel Dekker, New York, 1992.
- [2] A.P.F. Turner, *Advances in Biosensors*, JAC Press, London, 1991.
- [3] D.L. Wise, *Bioinstrumentation and Biosensors*, Marcel Dekker, New York, 1991.
- [4] M. Mascini, G. Palleshi, *Selective Electrode Rev.* 11 (1989) 191.
- [5] S.L. Brooks, I.J. Higgins, J.D. Newman, A.P.F. Turner, *Enzyme Microbiol. Technol.* 13 (1991) 946.
- [6] R.P. Buck, W.E. Hatfield, M. Umana, E.F. Bowden, *Biosensor Technology*, Marcel Dekker, New York, 1990.
- [7] J.J. Carr, J.M. Brown, *Introduction to Biomedical Equipment Technology*, 2nd Ed., John Wiley and Sons, New York, 1993.
- [8] G.G. Guilbault, R.D. Schmid, *Biotechnol. Appl. Biochem.* 14 (1991) 133.
- [9] D.A. De Marre and D. Michaels, *Bioelectronic measurements*, Prentice-Hall, New Jersey, 1983.
- [10] S.J. Alcock, B. Danielsson, A.P.F. Turner, *Biosensors Bioelectron.* 7 (1992) 243.
- [11] C.A. Groom, J.H.T. Luong, *Anal. Lett.* 26 (1993) 1383.
- [12] S.A. Emr, A.M. Yacynych, *Electroanalysis* 7 (1995) 913.
- [13] A.S. Jdanova, S. Poyard, A.P. Soldatkin, N. Jaffrezic-Renault, C. Martelet, *Anal. Chim. Acta* 321 (1996) 35.
- [14] M.J. Dennison, A.P.F. Turner, *Biotechnol. Adv.* 13 (1995) 1.
- [15] M.P. Marco, D. Barcelo, *Measurement Sci. Technol.* 7 (1996) 1547.
- [16] K.R. Rogers, L.R. Williams, *Trends Anal. Chem.* 14 (1995) 289.
- [17] H.O. Michel, E.C. Gordon, J. Epstein, *J. Environ. Sci. Technol.* 7 (1973) 1045.
- [18] H.C. Budnikov, E.P. Medyantseva, S.S. Babkina, *J. Electroanal. Chem.* 310 (1991) 49.
- [19] E.B. Nikolskaya, L.I. Kugusheva, V.P. Nesterov, *Abstracts of the Third International Scientific Workshop 'Biosensing Materials and Biosensors'*, Suzdal, Russia, 1995, 28.
- [20] C. Tran-Minh, *Ion-Select. Electrode Rev.* 7 (1985) 41.
- [21] I. Karube, Y. Nomura, Y. Arikawa, *Trends Anal. Chem.* 14 (1995) 295.
- [22] J. Gardea-Torresdey, D. Darnall, J. Wang, *Anal. Chem.* 60 (1988) 72.
- [23] I. Karube, K. Hiramoto, M. Kawarai, K. Sode, *Membrane* 14 (1989) 311.
- [24] S.O. Ogundiran, S. Varanasi, E. Ruckenstein, *Biotechnol. Bioeng.* 37 (1991) 160.
- [25] Kulys J., *Analytical Systems Based on Immobilized Enzymes*, Mokslas, Vilnius, 1981 (Russia).
- [26] M.D. Trevan, *Immobilized Enzymes. An Introduction and Applications in Biotechnology*, J. Wiley and Sons, Chichester, 1980.
- [27] H. El-Yamani, C. Tran-Minh, M.A. Abdul, D. Chavanne, *Sensors Actuators* 15 (1988) 193.

- [28] L.H. Goodson, W.B. Jacobs, *Methods Enzymol.* 44 (1976) 647.
- [29] E. Usden, *Anticholinesterase agents*, Pergamon Press, London, 1970.
- [30] M. Wiegand-Rosinus, K. Haberer, U. Obst, A. Wild, *Z. Wasser Abwasser Forsch.* 23 (1990) 98.
- [31] V. Berka, T. Vygodina, A. Musatov, P. Nicholls, A.A. Konstantinov, *FEBS Lett.* 315 (1993) 237.
- [32] L. Webb, *Enzyme inhibitors and metabolism*. Mir, Moscow, 1966.
- [33] L.H. Goodson, W.B. Jacobs, A.W. Davis, *Anal. Biochem.* 51 (1973) 362.
- [34] V.J. Razumas, J.J. Kulys, A.A. Malinauskas, *Environ. Sci. Technol.* 15 (1981) 360.
- [35] P. Durand, D. Thomas, *J. Environ. Pathol. Toxicol.* 5–4 (1984) 51.
- [36] R. Gruss, F. Scheller, M.J. Shao, C.C. Liu, *Anal. Lett.* 22 (1989) 1159.
- [37] H.C. Budnikov, E.P. Medyantseva, S.S. Babkina, A.V. Volkov, *Zh. Anal. Khim. (Russian)* 44 (1989) 2253.
- [38] C. Tran-Minh, P.C. Pandey, S. Kumaran, *Biosensors* 5 (1990) 461.
- [39] P. Skladal, *Anal. Chim. Acta* 252 (1991) 11.
- [40] K.R. Rogers, M. Foley, S. Alters, P. Kogaz, M. Eldefrawi, *Anal. Lett.* 24 (1991) 191.
- [41] L. Campanella, M. Achilli, M.P. Sammartino, M. Tomassetti, *Bioelectrochem. Bioenerg.* 26 (1991) 237.
- [42] M. Bernabei, C. Cremisini, M. Mascini, G. Palleschi, *Anal. Lett.* 24 (1991) 1317.
- [43] C. Dumshat, H. Muller, K. Stein, G. Schwedt, *Anal. Chim. Acta* 252 (1991) 7.
- [44] P. Skladal, M. Mascini, *Biosensors Bioelectron.* 7 (1992) 335.
- [45] E.B. Nikolskaya, G.A. Evtugyn, *Zh. Anal. Khim. (Russian)* 47 (1992) 1358.
- [46] M.S. Dehlawi, A.T. Eldefrawi, M.E. Eldefrawi, N.A. Anis, J.J. Valdes, *J. Biochem. Toxicol.* 9 (1994) 261.
- [47] M. Stoycheva, *Anal. Lett.* 27 (1994) 3065.
- [48] M. Stoycheva, *Bull. Soc. Chim. Belg.* 103 (1994) 147.
- [49] D. Martorell, F. Cespedes, E. Martinez-Fabregas, S. Alegret, *Anal. Chim. Acta* 290 (1994) 343.
- [50] A. Roda, P. Rauch, E. Ferri, S. Girotti, S. Ghini, G. Carrea, R. Bovara, *Anal. Chim. Acta* 204 (1994) 35.
- [51] P. Skladal, M. Pavlik, M. Fiala, *Anal. Lett.* 27 (1994) 29.
- [52] N. Mionetto, J.-L. Marty, I. Karube, *Biosensors Bioelectron.* 9 (1994) 463.
- [53] E.P. Medyantseva, M.G. Vertlib, H.C. Budnikov, E.B. Nikolskaya, *Zh. Anal. Khim. (Russian)* 49 (1994) 1220.
- [54] T. Imato, N. Ishibashi, *Biosensors Bioelectron.* 10 (1995) 435.
- [55] A. Cagnini, I. Palchetti, M. Mascini, A.P.F. Turner, *Mikrochim. Acta* 121 (1995) 155.
- [56] A. Cagnini, I. Palchetti, I. Lioni, M. Mascini, A.P.F. Turner, *Sensors and Actuators B* 24–25 (1995) 85.
- [57] S. Kumaran, M. Morita, *Talanta* 42 (1995) 649.
- [58] C. Cremisini, S. Di Sario, J. Mela, R. Pilloton, G. Palleschi, *Anal. Chim. Acta* 311 (1995) 273.
- [59] J.L. Marty, N. Mionetto, S. Lacorte, D. Barcelo, *Anal. Chim. Acta* 311 (1995) 265.
- [60] G.A. Evtugyn, H.C. Budnikov, D.F. Achmetzjanova, *Proc. 10th European Conference on Solid-State Transducers. Eurosensors X.*, Leuven, Belgium, September 8–11, 1996. Vol.3, 1996, 937.
- [61] E.B. Nikolskaya, G.A. Evtugyn, R.R. Iskanderov, V.Z. Latypova, *Zh. Anal. Khim.* 51 (1996) 561.
- [62] G.A. Evtugyn, H.C. Budnikov, E.B. Nikolskaya, *Analyst* 121 (1996) 1911.
- [63] H.C. Budnikov, G.A. Evtugyn, *Electroanalysis* 8 (1996) 817.
- [64] A.L. Ghindilis, T.G. Morzunova, A.V. Barmin, I.N. Kurochkin, *Biosensors Bioelectron.* 11 (1996) 873.
- [65] P. Skladal, *Food Technol. Biotechnol.* 34 (1996) 43.
- [66] C. Tran-Minh, J. Beaux, *Anal. Chem.* 51 (1979) 91.
- [67] H. Sakai, N. Kaneki, T. Hoze, K. Shimada, H. Tanaka, H. Hara, *Denki Kagaku Oyobi Koguo Butsuri Kagaku* 57 (1989) 440–441.
- [68] G.A. Zhylyak, S.V. Dzyadevich, Y.I. Kopran, A.P. Soldatkin, A.V. El'skaya, *Sensors Actuators B* 24–25 (1995) 145.
- [69] C.C. Liu, F.M. Fryburg, A.K. Chen, *Bioelectrochem. Bioenerg.* 8 (1981) 703.
- [70] F. Winquist, K. Lindstrom, B. Danielsson, *Anal. Lett.* 21 (1988) 1801.
- [71] A.M. Donlan, G.J. Moody, J.D.R. Thomas, *Anal. Lett.* 22 (1989) 1873.
- [72] M.H. Smit, G.A. Rechnitz, *Anal. Chem.* 62 (1990) 2429.
- [73] F.A. MacArdle, C. Persaud, *Analyst* 118 (1993) 419.
- [74] M.H. Smit, G.A. Rechnitz, *Anal. Chem.* 5 (1993) 747.
- [75] J.L. Besombes, S. Cosnier, P. Labbe, G. Reverdy, *Anal. Chim. Acta* 311 (1995) 255.
- [76] J.L. Besombes, S. Cosnier, P. Labbe, G. Reverdy, *Anal. Lett.* 28 (1995) 405.
- [77] L. Stancik, L. Macholan, F. Scheller, *Electroanalysis* 7 (1995) 649.
- [78] G. Robinson, D. Leech, M.R. Smyth, *Electroanalysis* 7 (1995) 952.
- [79] Q. Deng, S. Dong, *Analyst* 121 (1996) 1979.
- [80] M. Parra, J. Almendral, M.A. Alonso, M.C. De Garcia, R.G. Leonor, *Analyst* 117 (1992) 921.
- [81] C.A. Groom, J.H.T. Luong, *J. Biotechnol.* 21 (1991) 161.
- [82] P.P. Glagyshev, Ju.V. Shapovalov, B.E. Novikov, *Vestnik of Acad. Sci. of Kazakhstan (Russian)* 3 (1988) 21.
- [83] E.B. Nikolskaya, O.V. Jagodina, V.M. Kostrova, *Biokhimiya (Russian)* 47 (1982) 290.
- [84] L.P. Kuznetsova, L.I. Kugusheva, E.B. Nikolskaya, O.V. Jagodina, *Zh. Anal. Khim. (Russian)* 45 (1990) 1426.
- [85] L.I. Kugusheva, L.P. Kuznetsova, E.B. Nikolskaya, O.V. Jagodina, *Zh. Anal. Khim. (Russian)* 47 (1992) 1478.
- [86] J.L. Marty, T. Noguier, *Analisis* 21 (1993) 231.

- [87] W.J. Albery, A.E. Cass, J.A.M. Hubbard, Z. Shu, *Biochem. Soc. Trans.* 14 (1986) 1212.
- [88] W.J. Albery, A.E. Cass, Z. Shu, *Biosensors Bioelectron.* 5 (1990) 397.
- [89] A. Amine, M. Alafandy, J.-M. Kauffmann, M.N. Pekli, *Anal. Chem.* 67 (1995) 2822.
- [90] W.J. Albery, P.N. Bartlett, *J. Electroanal. Chem.* 194 (1985) 223.
- [91] K. Stein, J.-U. Hain, *Microchim. Acta* 121 (1995) 93.
- [92] M.H. Smit, A.E.G. Cass, *Anal. Chem.* 62 (1990) 2429.
- [93] V.A. Bogdanovskaya, V.A. Fridman, M.R. Tarasevich, F. Scheller, *Anal. Lett.* 27 (1994) 2823.
- [94] O. Adeyou, E.I. Iwuoha, M.R. Smyth, *Anal. Chim. Acta* 305 (1995) 57.
- [95] O. Adeyoju, E.I. Iwuoha, M.R. Smyth, *Electroanalysis* 7 (1995) 924.
- [96] U. Wollenberger, B. Neumann, K. Riedel, F.W. Scheller, *Fresenius J. Anal. Chem.* 348 (1994) 563.
- [97] R.S. Grier, M.B. Hood, M.B. Hoagland, *J. Biol. Chem.* 180 (1949) 289.
- [98] T.N. Shekhovtsova, I.F. Dolmanova, V.V. Kutcherayeva, *Zh. Anal. Khim. (Russian)* 40 (1985) 1810.
- [99] I.F. Dolmanova, T.N. Shekhovtsova, V.V. Kutcherayeva, *Talanta* 34 (1987) 201.
- [100] T.N. Shekhovtsova, I.F. Dolmanova, A.A. Baykov, *Biochem. Biotechnol.* 1 (1991) 72.
- [101] M.C. Fossi, C. Leonzio, D. Peakall, in: *Nondestructive Biomarkers in Vertebrates, International workshop, Siena, Italy, 25–27 May, 1992.* p.3.
- [102] P.A. Vanrolleghem, D. Dries, W. Westraete, *Proc. 5th European Congress on Biotechnology, Copenhagen, Denmark, 8–13 July 1990, Vol. 1, 1990,* 161.
- [103] F.M. Van Hoof, E.G. De Jonghe, M.G. Briers, P.D. Hansen, H.J. Pluta, D.M. Rawson, A.J. Wilmer, *Int. J. Environ. Toxicol. Water Qual.* 7 (1992) 19.
- [104] Z. Kong, P.A. Vanrolleghem, W. Westraete, *Biosensors Bioelectron.* 8 (1993) 49.
- [105] P.A. Vanrolleghem, Z. Kong, G. Rompouts, W. Verstraete, *J. Chem. Tech. Biotechnol.* 59 (1994) 321.
- [106] F. Li, T.C. Tan, *Biosensors Bioelectron.* 9 (1994) 445.
- [107] L. Campanella, G. Favero, M. Tomassetti, *Sci. Total Environ.* 171 (1995) 227.
- [108] L. Campanella, G. Favero, D. Mastrofini, M. Tomassetti, *Proc. 10th European Conference on Solid-State Transducers Eurosensors X, Leuven, Belgium, 8–11 September 1996, Vol. 2, 1996,* 417.
- [109] M. Purcell, R. Carpentier, *Water. Poll. Res. J. Can.* 25 (1990) 175–185.
- [110] M.H. Sadar, S.S. Kuan, G.G. Guilbault, *Anal. Chem.* 42 (1970) 1770.
- [111] T.N. Shekhovtsova, C.V. Chernetskaya, *Anal. Lett.* 49 (1994) 1317.
- [112] E.B. Nikolskaya, L.I. Kugusheva, O.V. Jagodina, M.M. Dianova, G.A. Evtugyn, R.R. Iskanderov, V.Z. Latypova, *Proc. Intern. Congress. Sensor-Techno-93, St-Petersburg, 22–23 June 1993, Vol. 2,* 68.
- [113] V.A. Jakovlev, *Kinetics of Enzymatic Catalysis, Nauka, Moscow, 1965.*
- [114] I.V. Beresin, K. Martinek, *Mol. Biol. (Russian)* 5 (1971) 347.
- [115] S. Moralev, E.B. Nikolskaya, *Zh. Evolucion. Physiol., in press (Russian).*
- [116] T. Danzer, G. Schwedt, *Anal. Chim. Acta* 318 (1996) 275.
- [117] S.S. Sokolova, R.R. Iskanderov, A.I. Startseva, G.A. Evtugyn, V.U. Smirnova, Ju.V. Rydvansky, Ju.S. Kotov, S.A. Patin, *Influence of anthropogenic factors of lake ecosystems, GosNIORCh Works, Moscow* 312 (1990) 122.
- [118] S. Alegret, *Analyst* 121 (1996) 1751.
- [119] D. Martorell, F. Cespedes, E. Martinez-Fabregas, S. Alegret, *Anal. Chim. Acta* 337 (1997) 305.
- [120] W.H.R. Shaw, D.N. Raval, *J. Am. Chem. Soc.* 83 (1961) 3184.
- [121] G.A. Evtugyn, E.E. Stoikova, H.C. Budnikov, and E.B. Nikolskaya, *Proc. 5th Intern. Symp. on Kinetics in Analytical Chemistry, Moscow, 25–28 September 1995,* 45.
- [122] M. Lutz, E. Burestedt, J. Emneus, H. Liden, S. Gobhadi, L. Gorton, G. Marko-Varga, *Anal. Chim. Acta* 3005 (1995) 8.
- [123] J. Wang, G. Rivas, J. Liu, *Anal. Lett.* 28 (1995) 2287.
- [124] J. Wang, E. Dempsey, A. Eremenko, M.R. Smyth, *Anal. Chim. Acta* 279 (1993) 203.
- [125] J. Wang, A.J. Reviejo, *Anal. Chem.* 65 (1993) 845.
- [126] A.J. Reviejo, F. Liu, J.M. Pingarron, J. Wang, *J. Electroanal. Chem.* 374 (1994) 133.
- [127] L. Stancik, *Chemicke Listy* 91 (1997) 30.
- [128] R.Z. Karandjian, J.S. Dordick, A.M. Klivanov, *Biotechnol. Bioeng.* 28 (1986) 417.
- [129] G.L. Ellman, K.D. Courtney, V. Andres, R.M. Featherstone, *Biochem. Pharmacol.* 7 (1961) 88.
- [130] A.P. Brestkin, L.P. Kuznetsova, E.B. Nikolskaya, *Ukr. Biokhim. Zh.* 63 (1991) 51.
- [131] I. Palchetti, A. Cagnini, M. Delcarlo, C. Coppi, M. Mascini, A.P.F. Turner, *Anal. Chim. Acta* 337 (1997) 315.
- [132] G.A. Evtugyn, E.P. Rizaeva, E.E. Stoikova, V.Z. Latypova, H.C. Budnikov, *Electroanalysis, 1997,* submitted.
- [133] P. Scladal, M. Fiala, J. Krejci, *Intern. J. Environ. Chem.* 65 (1996) 139.

Liquid chromatographic determination of cobalt(II), copper(II) and iron(II) using 2-thiophenyaldehyde-4-phenyl-3-thiosemicarbazone as derivatizing reagent

M.Y. Khuhawar *, S.N. Lanjwani

Institute of Chemistry, University of Sindh, Jamshoro, SindhPakistan

Received 28 October 1996; received in revised form 2 July 1997; accepted 7 July 1997

Abstract

The complexing reagent 2-thiophenyaldehyde-4-phenyl-3-thiosemicarbazone (TAPT) was examined for high performance liquid chromatographic (HPLC) separations of cobalt(II), copper(II) and iron(II) or cobalt(II), nickel(II), iron(II), copper(II) and mercury(II) as metal chelates on a Microsorb C-18, 5- μm column (150 \times 4.6 mm i.d.) (Rainin Instruments Woburn, MA, USA). The complexes were eluted isocratically with methanol:acetonitrile:water containing sodium acetate and tetrabutyl ammonium bromide (TBA). UV detection was at 254 nm. The solvent extraction procedure was developed for simultaneous determination of the metals, with detection limits within 0.5–2.5 $\mu\text{g ml}^{-1}$ in the final solution. The method was applied for the determination of copper, cobalt and iron in pharmaceutical preparation. © 1998 Elsevier Science B.V. All rights reserved.

Keywords: Chromatographic determination; Complexing reagent; Solvent extraction

1. Introduction

A number of complexing reagents have been used for high performance liquid chromatographic (HPLC) determination of cobalt, copper and iron, including 8-hydroxyquinoline [1,2], 6-hydroxy-5-nitrosonaphthalene-2-sulphonic acid [3], acetylacetone [4], diethyldithiocarbamate [5] and various azo derivatives [6–10].

Thiosemicarbazones and phenylthiosemicarbazones are interesting complexing reagents, because they form highly stable and intensely coloured complexes immediately, by bonding through the sulphur and hydrazino nitrogen atoms, which are ideally suited for spectrophotometric detection. Different thiosemicarbazones and phenylthiosemicarbazones have been reported as spectrophotometric [11–14] and spectrofluorimetric [15] reagents for metal ions. They have also been investigated as indicators for

* Corresponding author. Tel.: +92 771 328.

complexometric titrations [16,17]. Some of useful HPLC separations have been reported using these ligands [18–23]. Uehara et al. [20] have reported picolinaldehyde-4-phenyl-3-thiosemicarbazone for the separation of bismuth(III), cadmium(II), cobalt(II), copper(II), nickel(II) and iron(III) from an ODS column by including pyridine in the mobile phase. 2-Acetylpyridine-4-phenyl-3-thiosemicarbazone [21] has been used for the separation and determination of copper(II), iron(II) and cobalt(II) from reversed phase HPLC columns. Biacetyl bis-(4-dimethylaminophenyl)-3-thiosemicarbazone [23] has been used for the separation of bismuth(III), copper(II), nickel(II) and palladium(II) from RP-80 polymeric resin as well as for separation of indium(III), copper(II) and mercury(II) from a C-18 silica column. The reagents glyoxal dithiosemicarbazone, glyoxal bis(4-phenyl-3-thiosemicarbazone) and dimethylglyoxal bis(4-phenyl-3-thiosemicarbazone) coated on Amberlite XAD resin have been used for preconcentration of mercury(II), copper(II), zinc(II), cadmium(II), lead(II) and palladium(II) [23], followed by reversed phase HPLC separation of palladium, copper, mercury or cadmium, lead and copper. Uehara et al. [24] have compared several hydrazone derivatives for reversed phase HPLC. They have reported 2-thiophenylaldehyde-4-phenyl-3-thiosemicarbazone (TAPT) Fig. 1 for HPLC detection of iron(II) and nickel(II). In the present paper, TAPT has been assessed for the HPLC separation of cobalt(II), copper(II), iron(II), mercury(II) and nickel(II) and for the determination of copper(II), cobalt(II) and iron(II).

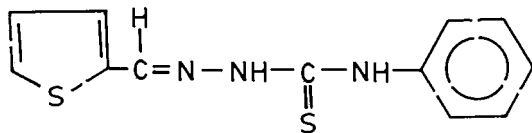


Fig. 1. Structural diagram of 2-thiophenylaldehyde-4-phenyl-3-thiosemicarbazone.

2. Experimental

2.1. Preparation of 2-thiophenylaldehyde-4-phenyl-3-thiosemicarbazone (TAPT)

4-Phenyl-3-thiosemicarbazide (1.67 g) dissolved in 20 ml methanol:water (1:1) was added to 1 ml of 2-thiophenylaldehyde in 10 ml of methanol. To the mixture was added 0.5 ml glacial acetic acid and it was then refluxed for 30 min. The mixture was cooled and the precipitate obtained was recrystallized from methanol m.p. 212°C. $C_{22}H_{22}N_3S_2$ required (%): C = 55.17, H = 4.21, N = 16.09; found (%): C = 55.29, H = 3.92, N = 16.0.

2.2. Analytical procedures

2.2.1. Aqueous methanolic solutions

A solution (1–5 ml) containing cobalt(II), copper(II) and iron(II) (0–200 μ g) was transferred to a 10-ml volumetric flask and the volume was adjusted to 5 ml. Reagent solution (2 ml, 7.7 mM in methanol) was added and the contents were mixed well. This was followed by 2 ml sodium bicarbonate buffer pH 9 and the volume was adjusted with methanol. The solution (5 μ l) was injected onto a Microsorb C-18 5- μ m column (Rainin Instruments Woburn, MA, USA) and the complexes eluted with methanol:acetonitrile: water:sodium acetate (1 mM):tetrabutyl ammonium bromide (TBA) (1 mM) (70:18:10:1:1 v/v/v/v) using a flow rate of 1 ml min⁻¹. Detection by UV was at 254 nm.

2.2.2. Solvent extraction of metals

A solution (1–20 ml) containing cobalt(II), copper(II), iron(II), mercury(II) and nickel(II) (0–100 μ g each) was transferred to well-stoppered test tubes and 2 ml reagent solution was added (7.7 mM in methanol) as well as 2 ml sodium acetate–acetic acid buffer pH 6 (1 M). Chloroform (2 ml) was added and the layers were mixed well. The organic layer was separated and to the aqueous layer was added 0.5 ml reagent solution (7.7 mM in methanol) and 2 ml of sodium bicarbonate–sodium carbonate buffer pH 9. Extraction was repeated with 2 ml chloroform. Exactly 2 ml of chloroform from the combined extract was

transferred to a sample vial and the solvent was evaporated. The residue was dissolved in 1 ml methanol and 5 μ l of the solution was injected onto a Microsorb C-18, 5- μ m column. The complexes were eluted with methanol:acetonitrile:water:sodium acetate (1 mM):TBA (1 mM) (78:10:10:1:1 v/v/v/v) using a flow rate of 1.0 ml min⁻¹. Detection by UV was at 254 nm.

2.2.3. Recovery (%) of metals on solvent extraction

Extraction was carried out on a 20-ml solution containing copper, iron, nickel and cobalt (50 or 100 μ g of each) and reagents as described in Section 2.2.2. The aqueous phase was collected, 2 ml nitric acid (65%) was added and it was heated to near dryness. The residue was dissolved in water and the volume was adjusted to 25 ml. The metal ion contents were determined using an air-acetylene flame atomic absorption spectrophotometer. The amounts of metal ions remaining in the aqueous phase were evaluated using a standard calibration curve for each element.

2.2.4. Analyses of copper, iron and cobalt in a pharmaceutical preparation

To a 1.3991-g Centrum tablet (Lederle Laboratories Division, Cyanamide Pak, Karachi) was added 0.5 g potassium bisulphate dissolved in 2 ml of water, 10 ml hydrochloric acid (37%) and 5 ml nitric acid (65%) spiked with 20 μ g cobalt(II). To this was added 2–3 mg solid ascorbic acid, 2 ml reagent solution (7.8 mM in methanol), 2 ml sodium carbonate buffer pH 9 and 2 ml chloroform. The contents were mixed well, the organic layer was collected and extraction was repeated with 2 ml chloroform. After the addition of 0.5 ml reagent solution (7.7 mM in methanol), the procedure was continued as described in Section 2.2.2.

Elemental micro-analysis of TAPT was carried out at the HEJ Research Institute of Chemistry, University of Karachi. Spectrophotometric studies were carried out using a Hitachi 220 spectrophotometer. A Hitachi 655A liquid chromatograph connected to a variable wavelength UV monitor, Rheodyne 7125 injector and Hitachi D2500 chromato-integrator was also used, in addition to a Microsorb C-18, 5- μ m

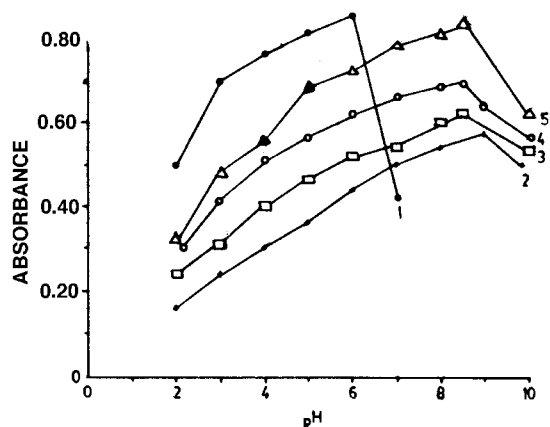


Fig. 2. Effect of variation in pH on the formation of (1) mercury(II); (2) iron(II); (3) cobalt(II); (4) copper(II); and (5) nickel(II) as complexes of TAPT against reagent blanks. Final concentration 10, 2, 1, 1 and 1 μ g ml⁻¹, respectively.

column (150 \times 4.6 mm i.d.) and a YMC Pack ODS (150 \times 4.6 mm i.d.) (YMC, Japan). A Varian Spectr AA 20 atomic absorption spectrometer with air-acetylene flame atomization was used according to the manufacturer's instructions.

Phenylthiosemicarbazide, 2-thiophenylaldehyde, tetrabutyl ammonium-bromide (Fluka), G.R. Grade acetonitrile, methanol, sodium acetate and hydrochloric acid (Merck) were used. Freshly prepared double distilled water was used for HPLC studies.

3. Results and discussion

The reagent reacts with copper(II), nickel(II), cobalt(II) and mercury(II) in aqueous methanolic solution to develop colour immediately in pH range 3–10, but for iron, the pH must be adjusted to within pH 5–10 after addition of the reagent. Mercury(II) developed turbidity in aqueous methanolic solution, but when extracted in chloroform, a clear solution was obtained. The colours of the complexes are highly stable both in aqueous methanolic solution and in chloroform and no change in absorbance was observed for up to 8 h. The maximum colour development of mercury(II) occurs at pH 6, cobalt(II), nickel(II), copper(II) at pH 8.5 and iron(II) at pH 9 (Fig. 2).

Table 1
% Recovery of the metals using solvent extraction (% C.V)

Metal ions	Single extraction	Double extraction
Iron	85.25 (1.1)	93.5 (1.2)
Copper	75.00 (1.7)	92.5 (1.6)
Cobalt	82.00 (1.6)	96.2 (1.8)
Nickel	92.00 (1.4)	98.0 (1.3)

The transfer of metals from the aqueous to the organic phase was examined. Recovery % of copper, iron, nickel and cobalt, based on the metals remaining in aqueous phase was 75–92% using single extraction and 92.5–98% using double extraction (Table 1).

The composition of metal chelates was investigated by changing the metal:ligand mole ratio spectrophotometrically. The absorbances of nickel(II), cobalt(II), copper(II) and iron(II) were measured at 393, 398, 390 and 388 nm in aqueous methanolic solution. Mercury(II) was monitored at 397 nm after extraction in chloroform. The results, shown in Fig. 3, suggest that nickel(II), cobalt(II), copper(II) and iron(II) form a 1:2 complex but mercury has a 1:3 composition.

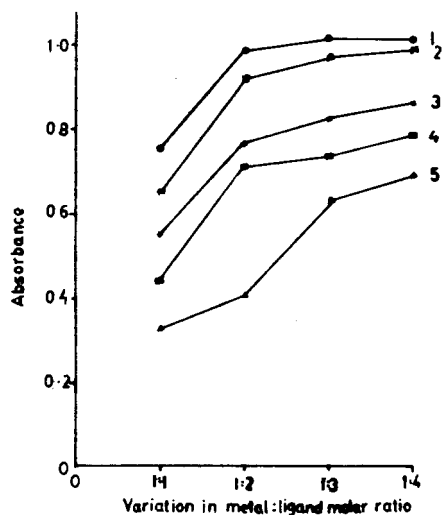


Fig. 3. Effect of variation in molar ratio of metal (4×10^{-5} M) and ligand TAPT (4×10^{-5} – 16×10^{-5} M) for the formation of maximum metal complexes: (1) nickel; (2) cobalt; (3) copper; (4) iron(II); (5) mercury.

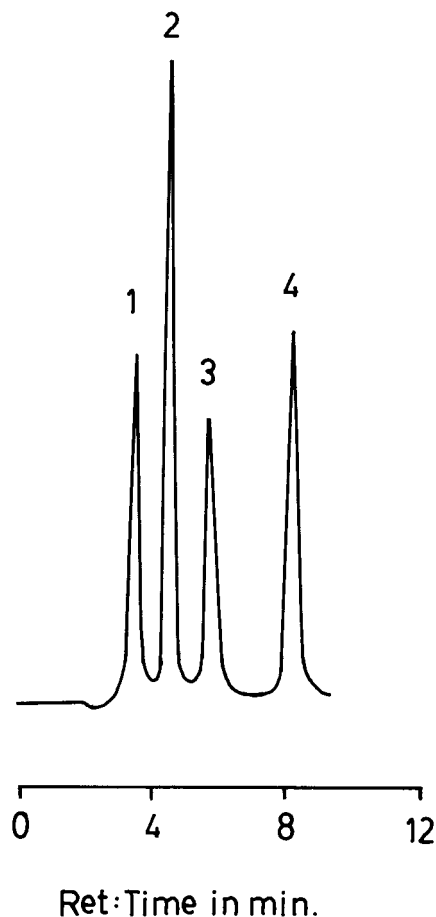


Fig. 4. HPLC separation of (1) TAPT; (2) cobalt(II); (3) iron(II); and (4) copper(II) complexes. Conditions as described in Section 2.2.1.

Copper(II), iron(II) and cobalt(II) form water soluble complexes. Their solutions were injected on a Microsorb C-18 column and complexes were eluted with acetonitrile–water or methanol–acetonitrile–water containing sodium acetate and tetrabutyl ammonium bromide, as reported for the separation of related metal chelates [21,22]. An optimal separation was obtained when eluted isocratically with a mixture of methanol–acetonitrile–water containing sodium acetate and TBA, using a flow rate of 1 ml min^{-1} , with UV detection at 254 nm (Fig. 4). The metals could also be extracted as metal chelate compounds in chloroform with a preconcentration factor of at least

ten. A mixture of cobalt(II), nickel(II), iron(II), copper(II) and mercury(II) on a Microsorb C-18 column completely separated when eluted with a mixture of methanol:acetonitrile:water:sodium acetate (1 mM):TBA (1 mM) (78:10:10:1:1 v/v/v/v/v) with a flow rate of 1 ml min⁻¹. UV detection was at 254 nm. Excess reagent added for derivatization eluted before metal chelates and did not interfere with the determinations. The resolution factor (R_s) between two adjacent peaks was > 1.66 (Fig. 5).

Additions of sodium acetate and TBA had a significant effect on the elution and separation of metal chelates. When sodium acetate was added in the eluent, cobalt and mercury eluted as symmetrical peaks, but copper(II), nickel(II) and iron(II) chelates were retained for longer, with elution time > 15 min. However, when TBA was included in the mobile phase, the retention times of nickel(II), iron(II) and copper(II) were reduced to 5.88, 7.26 and 8.10 min, respectively (Fig. 5). The effect of TBA concentration on the elution, retention time and capacity factor (K') of TAPT, cobalt(II), nickel(II), iron(II), copper(II) and mercury(II) was investigated. The concentration of TBA in the eluent was varied between 1.25 to 25 μ M. It was observed that K' decreased in TBA concentrations from 1.25 to 15 μ M. However, further increases in the concentration of TBA up to 25 μ M resulted in an increase of K' and an increase in the back pressure of the column (Fig. 6). Therefore, the concentration of TBA was fixed at 10 μ M for this study.

Thiosemicarbazones are reported [22] to form water soluble cationic complexes. Also, it is possible that acetate and bromide ions present in the eluent form ion pairs, thus influencing the elution and separation of metal chelates. Qian and Fritz [22] have observed a decrease in the retention time of metal chelates of thiosemicarbazones by including cation generating ions (TBA) in the mobile phase. They have attributed the reduction in retention times to the adsorption of bulky, positively charged groups on the surface of stationary phase and the repulsive force to the cationic metal chelates.

Linear calibration curves, calculated by measuring average peak height ($n = 3$), were within 0–50

μ g ml⁻¹ of each metal ion with correlation coefficient (r) 0.994, 0.984, 0.988 and 0.996, for cobalt(II), mercury(II), copper(II) and iron(II), respectively. Detection limits, measured as three times the background level for simultaneous detection, were 2.5 μ g ml⁻¹ mercury and 0.5 μ g ml⁻¹ cobalt, copper, nickel and iron, corresponding to 12.5 ng mercury and 2.5 ng cobalt, copper, nickel and iron per 5- μ l injection.

Finally, a pharmaceutical product (Centrum tablet) was analysed for cobalt, copper and iron content using the HPLC method. Cobalt content

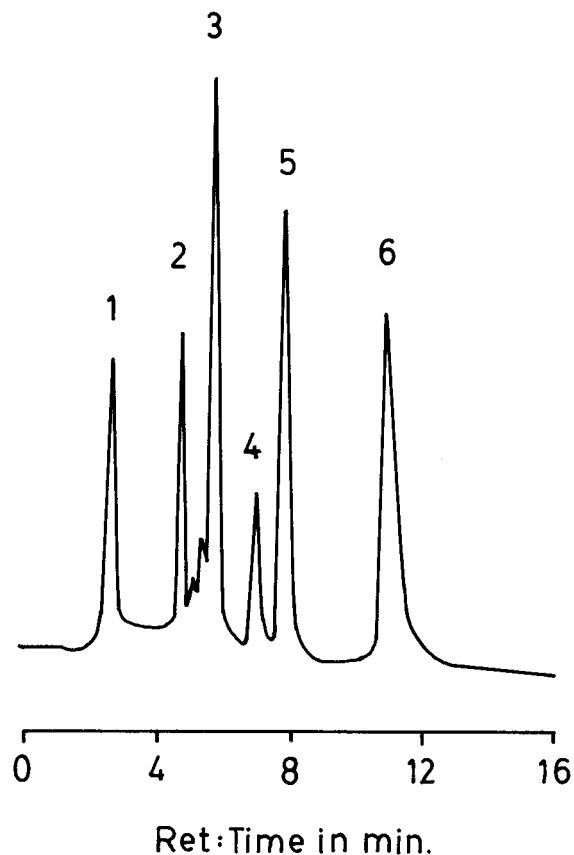


Fig. 5. HPLC separation of (1) TAPT; (2) cobalt(II); (3) iron(II); (4) nickel(II); (5) copper(II); and (6) mercury(II) complexes on a Microsorb C-18 5- μ m column (150 \times 4.6 mm id) using elution with methanol:acetonitrile:water containing sodium acetate (1 mM): tetrabutylammonium bromide (1 mM) (78:10:10:1:1 v/v/v/v/v), at a flow rate of 1.0 ml min⁻¹ and with UV detection at 254 nm.

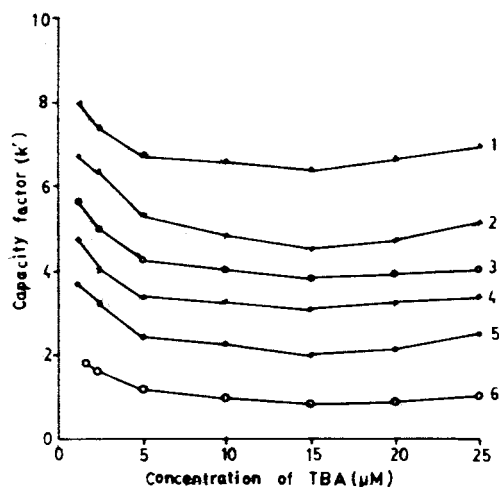


Fig. 6. Variation in capacity factor (K') with concentration of TBA. (1) mercury; (2) copper; (3) iron; (4) nickel; (5) cobalt; and (6) TAPT. Conditions: YMC pack ODS 5- μm (150×4.6 mm id) column. The eluent is methanol:acetonitrile:water:sodium acetate (1 mM):TBA (0.125–2.5 mM) (78:10:10:1:1 v/v/v/v/v), with a flow rate of 1 ml min^{-1} and UV detection at 254 nm.

of the tablet was determined by standard addition technique, after spiking the sample with $20 \mu\text{g}$ of cobalt. Copper and iron content was evaluated from a calibration curve. The amounts of cobalt, copper and iron found were $43 \mu\text{g}$, 2.66 and 8.50 mg/tablet respectively, with RSD 3.6, 5.2 and 4.8%, respectively. The tablet was also analysed using air-acetylene flame atomic absorption and the results were $39 \mu\text{g}$, 2.79 and 8.7 mg/tablet cobalt, copper and iron respectively, with RSD 4.4, 1.8 and 1.1%, respectively.

4. Conclusion

A good yield of the reagent TAPT can be easily prepared from inexpensive chemicals ($> 80\%$) and reacts immediately with a limited number of metal ions to form stable coloured complexes. Reverse phase liquid chromatographic method has been developed for the separation of cop-

per(II), nickel(II), cobalt(II), iron(II) and mercury(II) using TAPT. The detection limits are obtained at 2.5–12.5 ng/injection. This method is applied for the determination of copper, iron and cobalt in a pharmaceutical preparation with RSD within 3.6–5.2%.

References

- [1] C. Baiocchi, G. Saini, P. Bertolo, G.P. Castoni, G. Pettiti, *Analyst* 113 (1988) 805.
- [2] T. Yasui, A. Yuchi, H. Wada, G. Nakagawa, *J. Chromatogr.* 596 (1992) 73.
- [3] H. Siren, M.L. Rickkole, *Microchem. Acta* 11 (1989) 77.
- [4] J. Maslowska, S. Starzynski, *Chromatographia* 28 (1989) 519.
- [5] S. Dilli, P.R. Haddad, A.K. Htoon, *J. Chromatogr.* 500 (1990) 313.
- [6] D.A. Roston, *Anal. Chem.* 56 (1984) 241.
- [7] X. Ming, Y. Wu, G. Schewdt, Fresenius J., *Anal. Chem.* 342 (1992) 556.
- [8] Y. Zhao, C. Fu, *Anal. Chim. Acta* 230 (1990) 23.
- [9] Y. Yuen, Y. Wang, *Talanta* 36 (1989) 777.
- [10] H. Hoshino, K. Nakano, T. Yolsuyanagi, *Analyst* 115 (1990) 133.
- [11] R.B. Singh, B.S. Gorg, R.P. Sing, *Talanta* 25 (1978) 619.
- [12] A.G. Azuero, M. Gonzalez-Balairon, *Macrochem. J.* 25 (1980) 14.
- [13] E. Crislofol, F. Sanchez Rojas, J.M. Cano-Pavon, *Talanta* 38 (1991) 448.
- [14] J.L. Gonez Ariza, J.M. Cano-Pavon, F. Piano, *Talanta* 23 (1976) 460.
- [15] K. Harumi, B. Norikagu, K. Satoski, O. Takeo, *Bunseki Kagaku* 20 (1971) 1371.
- [16] A.K. Singh, K.C. Trikha, R.P. Singh, M. Katyal, *Talanta* 22 (1975) 551.
- [17] S. Kasavan, B.S. Greg, R.P. Singh, *Talanta* 24 (1977) 51.
- [18] P. Heizmann, K. Ballsmiter, *J. Chromatogr.* 137 (1977) 153.
- [19] S. Hoshi, N. Takahashi, S. Inone, M. Matsubara, *Bunseki Kagaku* 35 (1986) 819.
- [20] N. Uehara, K. Morimoto, Y. Shijo, *Analyst* 117 (1992) 977.
- [21] M.Y. Khuhawar, Z.P. Memon, S.N. Lanjwani, *Chromatographia* 41 (1995) 236.
- [22] Y. Qiam, J. Fritz, *J. Chromatogr.* 602 (1992) 103.
- [23] S. Hoshi, H. Fujisawa, K. Nakamura, S. Nakata, M. Uto, K. Akatsuka, *Talanta* 41 (1994) 503.
- [24] N. Uehara, M. Mirota, Y. Shijo, *Bunseki Kagaku*, 43 (1994) 195.

Mixed ligand complexes of benzimidazole and pyrimidine hydroxy azo dyes with some transition metals and glycine, DL-alanine or DL-leucine

Ahmed H. Amrallah *, Nadia A. Abdalla, Esam Y. El-Haty

Chemistry Department, Faculty of Science, South Valley University, Aswan, Egypt

Received 12 November 1996; received in revised form 18 April 1997; accepted 11 July 1997

Abstract

The overall formation constants of 1:1:1 ternary complexes of Cu(II), Zn(II), Cd(II) with glycine, DL-alanine or DL-leucine as primary ligands and *o*-hydroxyphenylazo derivatives of 2-cyanomethyl benzimidazole (ABI) and barbituric acid (ABA) as secondary ligands have been investigated potentiometrically in 40% (v/v) EtOH. Formation constants of binary systems were also determined under the same experimental conditions (37°C and $\mu = 0.15 \text{ mol dm}^{-3}$). The stability of ternary complexes have been quantitatively compared with those of the corresponding binary complexes in terms of the parameters $\Delta \log K$, $\log X$ and $\log X'$. The data were interpreted on the basis of statistical considerations and the nature of complexes. The concentration distribution of various species formed in solution was evaluated. The Cu(II) complexes have been synthesized and the coordination sites of the ligands were characterized by means of IR spectroscopy. © 1998 Elsevier Science B.V. All rights reserved.

Keywords: Amino acids; Azo dyes; Complexes; pH-metric

1. Introduction

It has been shown that the arylazo derivatives of benzimidazole and barbituric acid play an important role in biochemistry because their imidazole and barbiturate moieties were the principle sites on the proteins, enzymes and nucleic acids [1–5]. Much attention has been paid recently to the study of ternary complexes of transition metals with molecules of biological and pharmaceutical interest [6–9]. Mixed complexes of transi-

tion metals containing an imidazole or pyrimidine group as ligands are commonly found in biological media and may have important roles in processes as catalysis of drugs interaction with biomolecules [10,11]. Furthermore, it has been suggested that the presence of metal ions in biological fluids, could have a significant effect on the therapeutic action of drugs [12,13]. The work reported on the interaction of Cu(II), Zn(II) and Cd(II) with imidazole derivatives and amino acids demonstrated that imidazole moiety is the principal site responsible for metal binding [10,14,15]. This was attributed to its capacity to form both σ and π bonds with metal ions.

* Corresponding author.

To obtain a more understanding of the driving forces leading to complexation in biological systems, we are reporting in the present paper, the results of pH-metric studies on the mixed ligand complexes of Cu(II), Zn(II) and Cd(II) with glycine (GLY), DL-alanine (ALA) and DL-leucine (LEU) as primary ligands and expected biologically important 2-[-*o*-hydroxyphenylazo] 2'-cyanomethyl benzimidazole (ABI) and 5-[-*o*-hydroxyphenylazo]barbituric acid (ABA) as secondary ligands. The work is aimed to establish the various equilibria that exist in solution, and to determine the dissociation constants of the free ligands and stability constants of binary and ternary complexes in 40% (v/v) EtOH-H₂O at 37°C and $\mu = 0.15 \text{ mol dm}^{-3} \text{ NaClO}_4$. Although the aqua-organic solvent mixtures are of little interest, since these media are not present in the human body, these systems were studied for comparison.

2. Experimental

2.1. Materials and solutions

All the chemicals used were of A.R. grade (Merck) and were used without further purification. The azo compounds 2-[-*o*-hydroxyphenylazo]-2-cyanomethyl benzimidazole (ABI) and 5-[-*o*-hydroxyphenylazo] barbituric acid (ABA) were synthesized by the usual procedure as described by Vogel [16]. The Cu(II) complexes were prepared as described in our earlier paper [17]. Ligand stock solutions were prepared by dissolving the calculated amounts in 20% (v/v) EtOH-H₂O mixture and were standardized by pH-titration with standard HClO₄. Solutions of the metal ions Cu(II), Zn(II) and Cd(II) (Merck or BDH products) were prepared in doubly-distilled water and the metal content was determined by complexometric EDTA titration [18]. Carbonate-free solutions of NaOH (0.1 mol dm⁻³) was prepared and standardized against standard potassium hydrogen phthalate solution. 1.0 mol dm⁻³ NaClO₄ and 0.1 mol dm⁻³ HClO₄ stock solutions were prepared from analytical grade samples and freshly used. The solutions were diluted as necessary.

2.2. Apparatus and procedure

The Vis. and IR spectral measurements were the same as described before [19]. PH-metric titrations were carried out at 37°C (± 0.1) in a double-walled glass cell. Temperature control was achieved by means of a liquid circulation proceeding from a thermostat. pH measurements were carried out on a MV 87 digital pH-Messgerate accurate to ± 0.005 unit and equipped with a glass electrode and saturated calomel electrode.

In both the acidic and alkaline regions, the electrode system was calibrated in terms of hydrogen ion concentrations instead of activities. The following mixtures (total volume of 50 ml) were titrated against CO₂-free 0.0825 NaOH, HClO₄ (a); a + amine (b); b + metal ion (c); a + azo dye (d); d + metal ion (e), and a + amine + azo dye + metal ion (f). The ionic strength was adjusted to 0.15 mol dm⁻³ by addition of NaClO₄ as supporting electrolyte. Magnetic stirrer was used during all titrations. Oxygen free nitrogen gas was bubbled through the solution before and during titrations. Multiple titrations were carried out for each system. All titrations were made in 40% (v/v) EtOH-H₂O in order to overcome the weak solubility of the studied systems in pure aqueous medium. The pH meter reading (*B*) recorded in 40% (v/v) EtOH-H₂O solutions were converted to hydrogen ion concentration [H⁺] by means of relation of Van Uitert and Hass [20] namely

$$-\log [H^+] = B + \log U_H - \log(1/\gamma^2)$$

Where γ is the activity coefficient of the solvent composition and is U_H the correction factor at zero ionic strength for the solution under investigation.

3. Results and discussion

3.1. Proton-ligand systems

Representative pH-metric equilibrium titration curves for the free and metal complexed ligands are depicted in Fig. 1. The acid dissociation constants of ABI and ABA in 40% (v/v) EtOH-H₂O are determined from curves (a) and (b) using

computer program based on Irving-Rossotti equations [21]. The details regarding the potentiometric method were reported in the experimental section. The values of the dissociation constants of amines: GLY ALA and LEU are also redetermined under the same experimental conditions (37°C, $\mu = 0.15 \text{ mol dm}^{-3} \text{ NaClO}_4$). The SUPERQUAD computer program [22], were used to refine the overall protonation or formation constants by minimizing the sum of squared residual, U between the observed, E_{obs} and calculated E_{calc} emf values

$$U = \sum W_i (E_{\text{obs}} - E_{\text{calc}})^2$$

The weighting factor, W_i is defined as the reciprocal of the error in the potential and volume readings, σ_E and σ_v , respectively. The W_i values were calculated from the equation

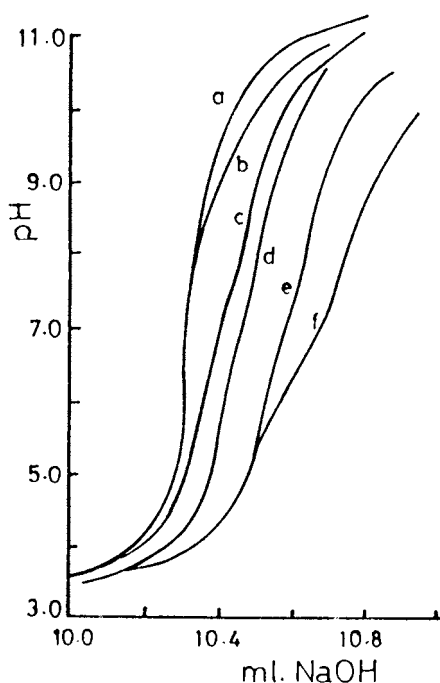


Fig. 1. Titration curves for the Cu(II)-GLY-ABA system at 37°C and equal to 0.15 and 40% EtOH; (a) 0.02 HClO₄; (b) solution (a) + 2×10^{-4} GLY; (c) solution (b) + 1×10^{-4} Cu(II); (d) solution (a) + 2×10^{-4} ABA; (e) solution (d) + 1×10^{-4} Cu(II); (f) solution (e) + 2×10^{-4} GLY, concentration of NaOH $0.0825 \text{ mol dm}^{-3}$.

Table 1
Ionisation constants of the free ligands and stability constants of binary systems

Constants	ABA	ABI	GLY	ALA	LEU
H⁺					
log β_1	7.27	8.02	—	—	—
log β_2	16.43	19.35	9.65	9.72	9.58
Cu(II)					
log β_1	5.65	5.52	7.97	7.74	7.66
log β_2	10.63	10.27	14.88	14.42	14.02
Zn(II)					
log β_1	5.22	5.03	5.48	5.36	5.24
log β_2	9.47	9.07	10.03	10.00	9.60
Cd(II)					
log β_1	5.04	4.85	5.13	5.09	4.21
log β_2	8.90	8.64	9.35	9.42	7.62

Temp = 37°C, $\mu = 0.15 \text{ M (NaClO}_4)$, error limit $\pm (0.02-0.06)$.

$$W_i = 1/\sigma^2 = 1/[\sigma_E^2 + (dE/\delta v)^2 \sigma_v^2]$$

The quality of the fit was judged by the values of the sample standard deviation, S , and the goodness of fit, X^2 , (Pearson's test). At $\sigma_E = 0.1 \text{ mV}$ (0.001 pH error) and $\sigma_v = 0.005 \text{ ml}$, the values of S in different sets of titrations were between 1.0 and 1.8, and X^2 was between 12.0 and 13.0, thus indicating good fit of the experimental data. The $\text{p}K_a$ values obtained through the refinement of several sets of potentiometric data are quoted in Table 1. The obtained $\text{p}K_a$ values of the studied amines show good agreement with the literature values after allowing for changes in experimental conditions as well as methods of calculation. It is worth mentioning that the $\text{p}K_{a1}$ values for amino acids studied are too low (≤ 2.35) [23], and exist only in strongly acidic solutions and thus these values are not used in calculations, since the pH-metric data are measured in the range $3 \leq \text{pH} \leq 10.5$.

3.2. Metal-ligand binary systems

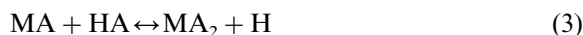
Analysis of the complexed ligands curves (e) and (d) (Fig. 1) indicates that the addition of metal ion to the free ligand solutions shifts the buffer region of the ligand to lower pH values. This shows that complexation reaction proceeds

by releasing of protons from such ligands. The curves reveals that the magnitude of the horizontal displacement of the complex curves (e) and (d) from the free ligand curves (b) and (c) is longer in case of Cu(II) than in case of Cd(II). This means that the Cu(II) strongly interacts than Cd(II) with the same ligand. Generally, it is observed that MA complexes (curve c) begin to form at lower pH range (~ 3.5) than MB complexes (curve e) ($\text{pH} \geq 4.3$). The complexes are quite stable up to high pH values. Precipitation occurred at $\text{pH} > 10.7$ and thus, no calculations have been performed beyond this point. Therefore, the hydroxo species likely to be formed after precipitation point could not be investigated.

The present study shows that 1:1 and 1:2 metal: ligand type of species are the important types in both metal ion-amino acid (A) and azo ligands (B) systems. This is based on the presence of two inflections in case of MA species and a single steep one in case of MB species, after addition of two moles of NaOH per 1 mol of ligand. This suggests the dissociation of two protons from amino acids in stepwise manner, while for MB systems the complexation is suggested to be simultaneous. These equilibria can be represented as follows, (charges are omitted for the sake of clarity)



$$\log K_{\text{MA}}^{\text{M}} = \log[\text{MA}] - (\log[\text{M}] + \log[\text{A}]) \quad (2)$$



$$\log K_{\text{MA}_2}^{\text{M}} = \log[\text{MA}_2] - (\log[\text{MA}] + \log[\text{A}]) \quad (4)$$

similarly, for azo ligands B

$$\log K_{\text{MB}}^{\text{M}} = \log[\text{MB}] - (\log[\text{M}] + \log[\text{B}]) \quad (5)$$

$$\log K_{\text{MB}_2}^{\text{M}} = \log[\text{MB}_2] - (\log[\text{MB}] + \log[\text{B}]) \quad (6)$$

Complex formation constants for binary systems expressed in terms of overall formation constants $\{\log \beta = \log K_{\text{MA}}^{\text{M}} + \log K_{\text{MA}_2}^{\text{M}}\}$ are computed using standard procedures based on the calculation of the average number of ligands bound per metal ion, n^- and the free ligand exponent, pL as described previously [21]. The best linear fit for the subject binary complexes are obtained by applying the relation $n^-/(1 - n^-)[L] = \beta_1 +$

$(2 - n^-)/(1 - n^-) \beta_2[L]$. The obtained values for $\log \beta_1$ and $\log \beta_2$ for different binary complexes are given in Table 1 and represented as shown in Fig. 2. The $\log \beta$ values reported in this Table were limited to those before the onset formation of hydroxo complexes. Other species were taken into consideration but were rejected during refinement for large sum of squared residual U and standard deviation σ .

The data listed in Table 1, clearly reveals that the stability of metal-amino acids are very close to those already published after allowing for changes in experimental conditions [10]. The results shows that the stability order of binary systems in terms of amino acids is $\text{GLY} > \text{ALA} > \text{LEU}$. This trend is not follows the basicities as expected, probably because the pK values of the amino acid studied are so similar. It is suggested that the absence of alkyl chain in GLY is responsible of the higher stability of its complex. Substitution of CH_3 group (ALA) or lengthening of GLY, skeleton (LEU) produces a small decrease in $\log \beta$ values. In terms of the nature of metal ion, the complex stability follow the trend $\text{Cu(II)} > \text{Zn(II)} > \text{Cd(II)}$, which is in agreements with the decrease in ionic potential (charge/ionic radius) of metal ions in the same direction. On the other hand, the results indicates that MA complexes are more stable than those of MB. This behaviour can be interpreted based on the bidentate nature of amino acids studied which coordinated through the α -amino nitrogen and the carboxylic oxygen atoms forming stable five-membered chelate ring, unlike the azo ligands ABI and ABA which act as monobasic tridentate ligands, coordinated through the o -hydroxy oxygen, the azo nitrogen atoms, and C=O of barbiturate or $N-3$ of benzimidazole moieties leading to the formation of five-six-membered rings. It is well known that 3-D metal ions prefer five-membered to six-membered rings during chelation [24].

3.3. Metal-ligand ternary systems

A set of typical titration curves for the different 1:1 Cu(II)-GLY, Cu(II)-ABA and 1:1:1 Cu(II)-GLY-ABA systems at (37°C and $\mu = 0.15 \text{ mol dm}^{-3} \text{ NaClO}_4$) are shown in Fig. 1 (curve f).

Table 2
Stability constants of M^{2+} amino acid-azo dye ternary systems

Metal ion	$\log \beta_{MAB}^M$	$\log K_{MAB}^{MA}$	$\log K_{MBA}^{MB}$	$-\Delta \log K$	$\log X$	$\log X'$	$\log \beta_{stat}$
M^{2+}-GLY-ABA							
Cu(II)	13.07	5.10	7.42	0.55	0.63	0.51	13.03
Zn(II)	10.00	4.52	4.78	0.70	0.50	0.23	9.78
Cd(II)	9.43	4.30	4.39	0.74	0.61	0.17	9.40
M^{2+}-GLY-ABI							
Cu(II)	12.93	4.96	7.41	0.56	0.71	0.50	12.86
Zn(II)	9.89	4.41	4.86	0.62	0.68	0.31	9.84
Cd(II)	9.38	4.25	4.53	0.60	0.77	0.21	9.26
M^{2+}-ALA-ABA							
Cu(II)	12.81	5.07	7.16	0.58	0.57	0.48	12.81
Zn(II)	10.06	4.70	4.84	0.52	0.65	0.17	10.01
Cd(II)	9.46	4.37	4.32	0.67	0.60	0.08	9.42
M^{2+}-ALA-ABI							
Cu(II)	12.63	4.89	7.11	0.63	0.57	0.33	12.60
Zn(II)	9.85	4.49	4.82	0.54	0.63	0.18	9.81
Cd(II)	9.36	4.27	4.51	0.58	0.66	0.18	9.31
M^{2+}-LEU-ABA							
Cu(II)	12.66	5.10	6.11	0.55	0.67	0.65	12.52
Zn(II)	9.88	4.64	4.66	0.58	0.69	0.30	9.78
Cd(II)	8.62	4.41	3.58	0.63	0.72	0.17	8.53
M^{2+}-LEU-ABI							
Cu(II)	12.54	4.88	7.02	0.64	0.79	0.66	12.45
Zn(II)	9.63	4.39	4.20	0.64	0.59	0.24	12.60
Cd(II)	8.47	4.26	3.62	0.59	0.68	0.21	8.42

Other mixed ligand systems show similar behaviour with Zn(II) and Cd(II) chelates. In our study, the amino acids (A) are considered as primary ligands and azo compound (B) as a secondary ligands, since MA species are formed at lower pH values than for MB species. The observed lowering of ternary MAB curve (f) in comparison to binary MA and MB curves (c) and (e) as well as its deviation from the theoretical composite curve (constructed by graphical addition of the horizontal distance of the 1:1 MA (or MB) curve to free ligand B (or A) titration curve), indicates the formation of ternary complexes in solution. The best-fit computer models in the investigated ternary systems showed the only 1:1:1 species, and the another species were very minor importance below pH 6.0. Further, it is worth mentioning that these systems show no precipita-

tion during titration. Thus, they not hydrolyzed under the experimental conditions, even in the high pH's. This behaviour may be explained on the basis that the electron density of the metal-ligand bonds in ternary chelates is redistributed in such a way that the ternary chelates are more polar than the binary chelates and hence, are not easily hydrolyzed in the high pH region.

Generally, the titration curves e and f (Fig. 1), reveals the overlapping of MA and MAB titration curves at low pH values, and then they diverges at higher pH's. This suggests that the azo ligands (B) does not participate in ternary system at lower pH values. Further, the formation of mixed ligand chelates MAB is proved by the observed and inflection point at $m = 1$, followed by buffer region in the higher pH range, ($m =$ the number of moles of alkali added per mol of metal ion). Up

to this point the MAB curve is almost coincident with MA curve, but beyond it, runs much below the MA curve.

To discuss the stabilization of ternary chelates, the following two methods has been considered. In the first method, the ternary complexes formation was considered to take place in simultaneous manner according to the following equilibria (charges omitted for brevity).

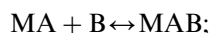


$$\log \beta_{MAB}^M = \log[MAB] - (\log[M] + \log[A] + \log[B]) \quad (7)$$

$$\text{since } \log[M] + \log[A] = \log[MA] - \log K_{MA}^M, \text{ Eq. (2)}$$

$$\therefore \log \beta_{MAB}^M = \log[MAB] - \log[MA] + \log K_{MA}^M + \log[B] \quad (8)$$

In the second method, the MAB chelate was consider to be formed in stepwise manner, assuming that the MA is practically formed in the lower buffer region followed by addition of the second ligand (B) in the upper buffer region. This equilibria can be represented as follows:



$$\log K_{MAB}^{MA} = \log[MAB] - (\log[MA] + \log[B]) \quad (9)$$

similarly:



$$\log K_{MBA}^{MB} = \log[MBA] - (\log[MB] + \log[A]) \quad (10)$$

The experimentally determined β_{MAB}^{MD} , is connected with K_{MAB}^{MA} and K_{MBA}^{MB} by the following equations

$$\log \beta_{MAB}^M - \log K_{MA}^M = \log K_{MAB}^{MA} \quad (11)$$

$$\log \beta_{MBA}^M - \log K_{MB}^M = \log K_{MBA}^{MA} \quad (12)$$

The average number of secondary ligand molecules associated with 1 mol of binary complex, n_{mix}^- was computed from the horizontal distance between curve (c) and (f). The values n_{mix}^- were used for compute the free secondary ligand exponent, pL_{mix} . The formation constants of ternary systems were evaluated from the n_{mix}^- - pL_{mix} curves (Fig. 3, Fig. 4). The results presented in Table 2 indicate that calculations based on Eq. (11) is more favoured than that based on Eq. (12), and thus, the ternary complex is formed simultaneously according to Eq. (7). This also confirms the assumption that the amino acids under study acts as primary ligands in our ternary systems. such observation is in line with those reported for ternary complexes of amines [25], and is contrary to earlier findings [26].

According to Sigel [6,27], the relative stability of ternary complex MAB as compared with that corresponding binary complex MB can be quantitatively expressed in different ways. The most suitable comparison is in terms of $\Delta \log K$. This parameter can be calculated from the reaction of secondary ligand (B) either with MA or with free metal ion, hence $\Delta \log K = \log K_{MAB}^{MA} - \log K_{MB}^M$. The above two reactions represent the following overall equilibrium, $MA + MB \leftrightarrow MAB + M$ and hence,

$$\Delta \log K_M = \log \beta_{MAB} - (\log K_{MA} + \log K_{MB}) \quad (13)$$

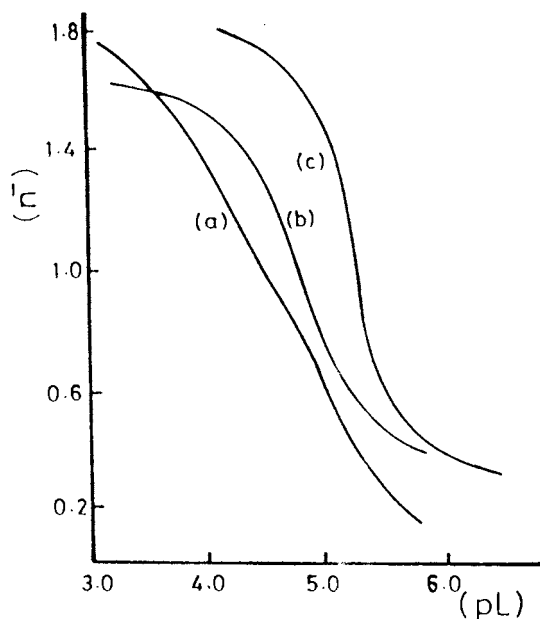


Fig. 2. Formation curves for metal ion-ABA binary systems. (a) Cd(II); (b) Zn(II); (c) Cu(II).

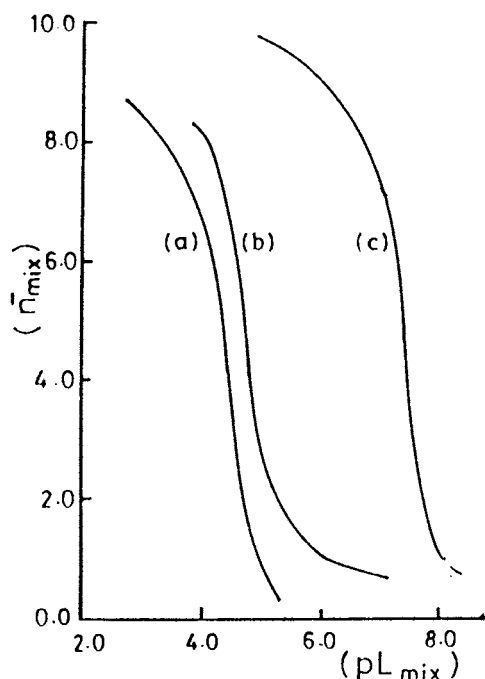


Fig. 3. Formation curves for metal ion-GLY—ABA (Fig. 3) or ABI (Fig. 4) systems (a) Cd(II); (b) Zn(II); (c) Cu(II).

A comparison of stability constants (Table 1) of binary complexes indicates that $K_1 > K_2$. Thus, in binary systems $\Delta \log K (= \log K_{MA_2}^{MA} - \log K_{MA}^M)$ values are generally negative which indicates the formation of 1:2 species. Similarly in case of ternary complexes formation, $\Delta \log K$ should also display the same trend. This behaviour can be explained on the base of the presence of fewer number of coordination sites on the MA mono-complexes than on the aquated metal ion. Thus, the secondary ligand (B) are expected to bind the MA complex with smaller stability constant than that with aquated metal ion. Therefore, $\Delta \log K$ should be negative values, generally between -0.5 and -2.0 [6,28], depending on the geometry of the complex. A positive or less negative $\Delta \log K$ value, suggests a significant stabilization of ternary system.

The quantitative stabilization of ternary complexes can also be expressed in terms of disproportionation constant X [29,30] as defined by the equation, $MA_2 + MB_2 \leftrightarrow 2MAB$, hence $X = [MAB]^2/[MA_2][MB_2]$

$$\log X = 2 \log \beta_{MAB}^M - (\log \beta_{MA_2}^M + \log \beta_{MB_2}^M) \quad (14)$$

The values for $\log X$ expected on statistical grounds is $+0.6$ [30] for all geometries. The more positive values than those expected statistically indicate the marked stabilities of ternary complexes. Further, the $\log X$ values can only indicate the coordination tendency of secondary ligand towards MA, but it fail to throw any light on the stabilizing order of metal-ligand bonds after the ternary complex formation. Hence to discuss the new stabilization constant $\log X'$, the following equilibria have been considered $MA_2 + MB \leftrightarrow MAB + MA$

$$\Delta \log X' = (\log \beta_{MAB}^M + \log K_{MA}^M) - (\log \beta_{MA_2}^M + \log K_{MB}^M) \quad (15)$$

The computed $\Delta \log K$, $\log X$ and $\log X'$ values for various ternary system are listed in Table 2. Some general observation about the behaviour of the various systems are as follows:

(a) The $\Delta \log K$ values obtained in the above ternary systems are generally do not deviate from the statistical expectations [27], where the statistical, steric and electrostatic factors result in the

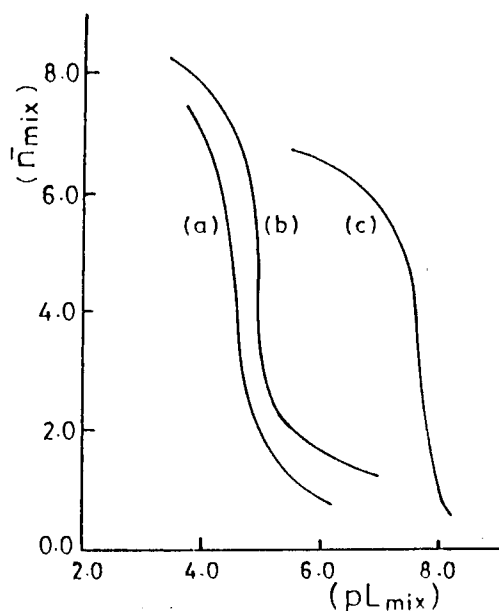


Fig. 4. Formation curves for metal ion-GLY—ABA (Fig. 3) or ABI (Fig. 4) systems (a) Cd(II); (b) Zn(II); (c) Cu(II).

lower stability constants for the ternary complexes as compared with the corresponding binary systems. The absence of stabilization is compatible with the explanations given by Sigel et al. [31–33] for the possible stabilization of ternary complexes. The data indicate that the $\Delta \log K$ values obtained for M-GLY-B species are more positive than the values obtained for M-ALA-B species indicating the marked stability of M-GLY-B. This is due to the limited tendency of alanine for interligand interaction [34] while glycine complexes sometimes exhibit exceptional stability [35]. Based on the fact that $\Delta \log K$ values depend on the coordination number of metal ion and the ligands [36,37], the change in $\Delta \log K$ values obtained may also be attributed to the change in the geometry of the complex. For square planar complexes with bidentate ligand, the $\Delta \log K$ values is -0.6 units. For a regular and distorted octahedral geometry, the values are -0.4 and -0.9 units, respectively [6].

(b) The $\log X$ values in the title systems are in general, found to be in the range of the statistically expected values (0.6). The statistically expected $\log X'$ value is 0.3. In Cu(II) ternary complexes, the $\log X'$ values are found to be greater than 0.3, suggesting that MA and MB bonds in ternary systems are stronger than those in corresponding binary systems. By varying the amino acid in ternary chelates, not much variation is observed in $\log X'$ values. This means that the stabilization of MA in ternary systems is influenced by the change in the size of amino acid. Hence $\log X$ values probably influenced by steric differences of ligands. The data reveals that $\log X'$ values of Cd(II) chelates (0.08–0.21) are smaller in magnitude than the statistical value, indicating the marked instability of Cd(II) ternary chelates compared with other species. Thus, it may be concluded that $\log X$ values probably influenced by the large size of Cd(II) ion.

(c) The stability of the studied ternary complexes is also calculated using statistical method [6,25] according to the equation:

$$\log \beta_{\text{state}} = \log 2 + 1/2 \log \beta_{\text{MA}_2}^{\text{M}} + 1/2 \log \beta_{\text{MB}_2}^{\text{M}} \quad (16)$$

The $\log \beta_{\text{stat}}$ values and the difference between stability constants measured and calculated ($\log \beta_{\text{MAB}} - \log \beta_{\text{stat}}$) are reported in Table 2. The results indicate that the above difference has a small positive values, reflecting that MAB system is more stable than both MA_2 and MB_2 . This stability enhancement is referred as a 'ligand effect' which is related to the electrostatic factors originated by charge neutralization, since in the formation of MAB^+ , one positive charge of MA^{2+} is neutralized by ligand B^- . This leads to increase in σ covalence. Moreover, the enhanced stability can also be explained in terms of metal to ligand $d_{\pi}-p_{\pi}$ back bonding which causes metal ion to be more positive or more electronegative [38], as compared with the hydrated metal ions. This permits stronger $\text{M} \leftrightarrow \text{B}$ interaction.

3.4. Distribution diagrams

Using the obtained stability constants of the complexes and equilibrium constants of the ligands under the same experimental conditions, the percentage concentration of each complex species involving metal ion and ligand as a function of pH has been calculated [39]. The pH species distribution profiles for the Cd-GLY binary and Cd-GLY ternary systems taken as a representative are shown in Fig. 4, Fig. 5 and Fig. 6, respectively. Similar trends were obtained for the other systems. The distribution profiles for binary systems show that at lower pH's (2.0–3.0) almost all Cd(II) ions will be present as free ions ($\infty = 88\%$). Over pH range 6.0–7.8 the predominant change is the conversion of Cd(II) into Cd-GLY with a maximum degree of formation 60% at pH 7.3. At pH circa 9.0 the Cd(II) ions are completely disappeared ($X = 3.09\%$) and Cd-GLY complex has low value ($\infty = 8.6\%$) while the concentration of $\text{Cd}(\text{GLY})_2$ predominates ($\infty = 78\%$).

In the case of ternary system, the plots (Fig. 6) show that between pH 7.5–9.3, the concentration of Cd-GLY complex decreases, while the concentration of Cd-GLY-B ternary systems increases. At pH = 8.9 the ternary system reaches maximums, $\infty = 57\%$ while the concentration of binary systems are of small values.

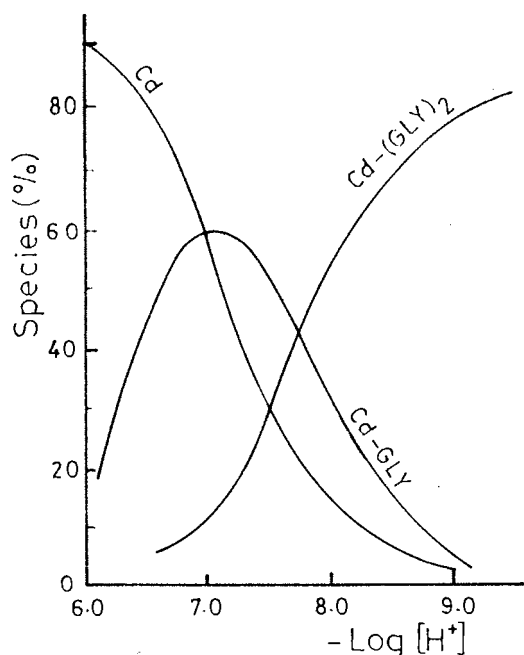


Fig. 5. Species-distribution diagrams for Cd(II)-GLY binary system.

3.5. Structure of the complexes

The synthesized complexes decompose above 300°C and soluble only in polar solvents. The

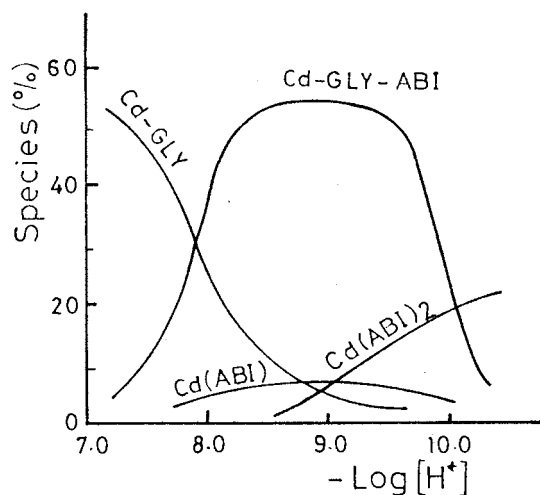


Fig. 6. Species-distribution diagrams for Cd(II)-GLY-ABI system.

electronic spectra of the solid complexes in DMF solutions show a weak band in the region 480–520 nm, can be assigned to $2E_{2g} - ^2T_{2g}d \rightarrow d$ transition in tetragonal distorted octahedral geometry about Cu(II) [40]. The two broad bands located at circa 410 and 430 nm are characterized by high molar absorptivity. Therefore, these bands may be due to *L*-M(CT) transition environment [41].

The bonding centres can be deduced on the basis of the following IR evidence:

(i) (I) The IR spectra of the azo ligands ABA and ABI exhibit a broad band at circa 3400 cm^{-1} due to the H-bond νOH mode, and a weak multiplet bands in the region 3180–3050 cm^{-1} assigned to νNH reflects strong intramolecular H-bonded to C=O group of the barbiturate ring. The absence of νOH in the IR spectra of the complexes suggests that the *o*-OH group is involved in bonding.

(ii) In ABA, the two strong bands at 1720 and 1660 cm^{-1} are due to free and H-bonded $\nu\text{C}=\text{O}$ stretching vibration, respectively. The absence of the first $\nu\text{C}=\text{O}$ on complexation indicating Cu-O interaction. The shifts of $\nu\text{C}=\text{O}$ stretching located at circa 1250 cm^{-1} in the free ligand, confirming the involvement of the phenolic-OH in chelation.

(iii) The IR spectra of ABI exhibit a band at 1610 cm^{-1} can be ascribed to $\nu\text{C}=\text{N}$ belonging to the imidazole ring. This band is shifted to lower frequencies on complexation, suggesting that N-3 imidazole ring involved in bonding.

(iv) The strong band appearing in the IR spectra of the free ligands ABA and ABI at 1445 and 1440 cm^{-1} , respectively, is attributed to $\nu\text{N}=\text{N}$ stretching mode [41]. On complexation, this band is located at lower frequencies (1430–1415 cm^{-1}) confirms the coordination of the nitrogen of the azo group to Cu(II).

Thus, the IR results reveal that the studied azo ligands in forming of the Cu(II) complexes are behaving as monobasic tridentate through the phenolic *o*-OH, N=N and C=O of barbiturate ring or the heterocyclic N-3 of benzimidazole moiety. This confirms our conclusion that only the phenolic *o*-OH group is deprotonated during complex formation in solution.

References

- [1] J.L. Berniter, J.P. Henichart, V. Warin, C. Trentesaux, J.C. Gardillier, *J. Med. Chem.* 13 (1985) 449.
- [2] J.K. Horten, M.F.G. Stevens, *J. Pharm. Pharmacol.* 33 (1981) 308.
- [3] H.K. Sinka, S.K. Dogra, *Chem. Phys.* 102 (1986) 337.
- [4] A.K. Mishra, S.K. Dogra, *J. Photochem.* 31 (1985) 333.
- [5] H.G. Gary, R.A. Sharma, *J. Pharm. Sci.* 59 (1970) 1691.
- [6] H. Sigel, *Metal Ions in Biological Systems*, Vol. 2., Marcel Dekker, New York, 1973.
- [7] H.C. Freeman, *Inorganic Biochemistry*, Elsevier, Amsterdam, New York, 1973.
- [8] P.M. May, D.R. Williams, P.W. Linder, *Metal Ions in Biological Systems*, Vol. 7, Marcel Dekker, New York, 1978.
- [9] P.G. Daniele, O. Zerbinati, V. Zelano, G. Ostacoli, *J. Chem. Soc., Dalton Trans.*, 2711 (1991).
- [10] A.K. Rao, P. Venkataiah, H.B. Bathina, M.S. Mohan, *J. Coord. Chem.* 20 (1989) 69.
- [11] H. Sigel, A.E. Martin, *Chem. Rev.* 82 (1982) 385.
- [12] S. Kirschner, Y.K. Wei, D. Francis, J.G. Bergam, *J. Med. Chem.* 9 (1966) 396.
- [13] J.R.J. Sornson, *Prog. Med. Chem.* 15 (1978) 211.
- [14] R. Tribolet, R.B. Martin, H. Sigel, *Inorg. Chem.* 26 (1987) 638.
- [15] K. Prasad, H. Bathina, M.S. Mohan, *J. Coord. Chem.* 17 (1988) 63.
- [16] A.I. Vogel, *A Text Book of Practical Organic Chemistry*, 3rd ed., Longmans, London, 1961.
- [17] M.T. El Haty, A.H. Amrallah, F.A. Adam, A.A. Gad, *J. Ind. Chem. Soc.* 67 (1990) 360.
- [18] T.S. West, *Complexometry with EDTA and Related Reagents*, Broglia Press, London, 1969.
- [19] F.A. Adam, M.T.EL-Haty, A.H. Amrallah, N.A. Abdalla, *Bull. Soc. Chim. Fr.*, 605 (1988).
- [20] L.G. Van Uitert, C.G. Hass, *J. Am. Chem. Soc.* 75 (1953) 451.
- [21] H.M. Irving, H.S. Rossotti, *J. Chem. Soc.*, 3397 (1953); 2904 (1954).
- [22] P. Gans, A. Sabatini, A. Vacca, *J. Chem. Soc. Dalton Trans.*, 1195 (1985).
- [23] R.C. Weast, *Hand Book of Chemistry and Physics*, 55th ed., CRC Press, 1975, 126 pp.
- [24] V.V. Ramanujam, V.M. Selvarajan, *Ind. J. Chem.* 20 (1981) 633.
- [25] A. Gergely, I. Sovago, I. Nagypal, R. Kiraly, *Inorg. Chim. Acta* 6 (1972) 435.
- [26] A.K. Rao, M.S. Mohan, H.B. Bathina, *Ind. J. Chem.* 29A (1990) 996.
- [27] H. Sigel, *Coordination Chemistry*, Vol. 20, Pergamon Press, Oxford, 1980.
- [28] B.E. Fischer, H. Sigel, *Inorg. Chem.* 18 (2) (1979) 425.
- [29] R.B. Martin, P. Prados, *J. Inorg. Nucl. Chem.* 36 (1974) 1665.
- [30] R. Dewitt, J.I. Watters, *Am. Chem. Soc.* 76 (1954) 3810.
- [31] H. Sigel, *Chimica* 21 (1967) 489.
- [32] H. Sigel, B.E. Fischer, B. Prijs, *J. Am. Chem. Soc.* 99 (1977) 4489.
- [33] H. Sigel, C.F. Naumann, *J. Am. Chem. Soc.* 98 (1976) 730.
- [34] H.A. Scherage, *Acc. Chem. Res.* 12 (1979) 7.
- [35] R.B. Martin, *Metal Ions in Biological Systems*, Vol. 9, Ch. 1, Marcel Dekker, New York, 1979.
- [36] B. Sen, *Anal. Chim. Acta*, 515 (1962).
- [37] V.S. Sharma, T.J. Schubert, *J. Chem. Educ.* 46 (1969) 506.
- [38] M.M. Srinivas, *Ind. J. Chem.* 20A (1981) 252.
- [39] M.T. Beck, *Chemistry of Complex Equilibria*, Van Nostrand Reinhold, London, 1970, pp. 73.195.
- [40] S.M. Parakewas, A.A. Danpoulos, *Inorg. Chim. Acta* 64L (1982) 151.
- [41] A.B.P. Lever, *Inorganic Electronic Spectroscopy*, 2nd ed., Elsevier, Amsterdam, 1984.

Spectrophotometric determination of isoproturon using *p*-aminoacetophenone and its application in environmental and biological samples

Omi Agrawal, Joyce V. Das, V.K. Gupta *

School of Studies in Chemistry, Pt. Ravishankar Shukla University, Raipur 492010 (M.P.), India

Received 4 March 1997; accepted 14 July 1997

Abstract

A simple and sensitive method for the determination of isoproturon, a widely used herbicide is described here which is based on alkaline hydrolysis of isoproturon to its corresponding primary amine followed by diazotization and coupling with *p*-aminoacetophenone in alkaline medium. The absorption maxima of the coloured compound formed is measured at 525 nm. Beer's law is obeyed over the concentration range of 0.5–5.0 μg in a final solution volume of 25 ml (0.02–0.2 ppm). The molar absorptivity and Sandell's sensitivity were found to be $8.6 \times 10^5 \text{ l mol}^{-1} \text{ cm}^{-1}$ and $0.0002 \mu\text{g cm}^{-2}$, respectively. The method has been satisfactorily applied to the determination of isoproturon in environmental and biological samples. © 1998 Elsevier Science B.V. All rights reserved.

Keywords: Spectrophotometry; Isoproturon; *p*-Aminoacetophenone; Biological samples

1. Introduction

The phenylurea herbicide *N,N*-dimethyl-*N'*-[4-(1-methylethyl)phenyl]urea popularly known as isoproturon used in wheat, grain, cereals and vegetables [1–3]. Isoproturon is similar to metoxuron in its action as an herbicide but with less toxic effects on crop cultivation [4]. Severe crop damage have been reported at 2 kg/ha, for isoproturon [5].

Few analytical methods such as titrimetric [6], GC [7], and UV-spectrophotometric [8], are available for the purpose of analysis. Spectropho-

metric methods using *p*-dimethylaminobenzaldehyde [9], and ethyl acetoacetate [1] as reagents are also available in the literature for the determination of isoproturon but these are less sensitive and use methanolic sodium hydroxide for the hydrolysis that can affect the colour development of the solution [1]. Hence, there is a need for a simple method for the routine analysis of isoproturon in environmental and biological samples.

Here is a simple, sensitive and selective method using a new reagent, *p*-aminoacetophenone, reported for the determination of isoproturon in various samples. The proposed method is based on the alkaline hydrolysis of isoproturon, followed by diazotization and coupling with *p*-

* Corresponding author.

aminoacetophenone in alkaline medium. The method has been satisfactorily applied for the determination of isoproturon in various environmental and biological samples.

2. Experimental

2.1. Apparatus

A Systronics UV-vis spectrophotometer model 108 with matched silica cells was used for all spectral measurements and a Systronics pH meter model no. 331 was used for pH measurements.

2.2. Reagents

Standard isoproturon solution (of certified grade)—1 mg/ml solution was prepared by dissolving 100 mg of isoproturon in 100 ml methanol [9]. Further working standard solution was prepared by appropriate dilution with deionised water. Sodium hydroxide—4 M aqueous solution. Hydrochloric acid—4 M aqueous solution. Sodium nitrite—1% aqueous solution. *p*-Aminoacetophenone (E. Merck, Germany)—a 2% solution in 25% ethanol. Sulphamic acid—1% aqueous solution.

2.3. Procedure

An aliquot of the test solution containing 0.5–5.0 µg of isoproturon was taken in calibrated tubes to which 1 ml of 4 M sodium hydroxide was added and allowed to stand for 15 min to ensure complete hydrolysis at room temperature. Then 2 ml of 4 M hydrochloric acid and 1 ml of 1% sodium nitrite was added at 0°C temperature, respectively, and allowed to stand in a ice bath for 10 min with thorough shaking. Then the tubes were removed from ice bath and 1 ml of 1% sulphamic acid was added to decompose the excess of nitrite and after 5 min 2 ml of 2% *p*-aminoacetophenone and 2 ml of 4 M sodium hydroxide solution were added

to each tube. Then the solution were kept for 15 min for complete colour development and made up to the mark with distilled water. The absorbance of the solutions were measured at 525 nm against distilled water.

2.4. Determination of isoproturon in polluted water

River water samples receiving run-off water from agricultural fields sprayed with isoproturon were collected. These samples were filtered through a Whatman no. 40 filter paper. Aliquots of water samples were taken in a 25 ml graduated tube [10] and analysed as described above (Table 1).

2.5. Determination of isoproturon in vegetables, foliages, and grains

Various samples, such as beans, onion bulb, oilseed, and wheat [11–14] were collected from the fields where isoproturon was used as a herbicide. The samples were weighed (50 g) and crushed with 20 ml of methanol and filtered. The filtrate was coloured due to presence of organic materials from the plants. The filtrate was passed through a silica gel column (10 × 1 cm) to remove chlorophyll and other interfering materials [15]. The column was washed with 10 ml methanol. The washings were collected in a 50 ml calibrated flask and made up to the mark with distilled water and aliquots were analysed as recommended above and in parallel by the reported method [9] (Table 1).

2.6. Determination of isoproturon in biological samples

Blood and urine samples were collected from the local pathology laboratory. Since these samples were found to be free of isoproturon, synthetic samples were prepared by adding a known amount of isoproturon to these samples and analysed as described above after adding 1 ml of trichloroacetic acid for deproteination and 2 ml EDTA for masking [16,17].

Table 1
Application of the method for the determination of isotroturon

Sample volume or mass*	Isotroturon originally found** (µg)		Isotroturon added (µg)	Total isotroturon found** (µg)		% Recovery (µg)	
	P	R		P	R	P	R
Natural water ^a	—	—	2.0	1.88	1.85	93.00	92.80
	—	—	2.0	1.90	1.80	95.00	90.47
Polluted water ^b	1.19	1.15	2.0	3.11	3.09	96.38	97.00
	1.21	1.16	2.0	3.18	3.12	98.50	98.00
Onion bulb ^c	0.98	0.92	2.0	2.86	2.76	94.00	92.00
Oilseed plant ^d	0.76	0.72	2.0	2.72	2.65	98.00	96.50
Wheat ^c	1.43	1.38	1.0	2.37	2.28	94.00	90.00
Beans ^f	0.82	0.80	2.0	2.74	2.67	96.00	93.50
Biological samples							
Blood ^g	—	—	3.0	2.76	2.72	92.00	90.66
Urine ^h	—	—	3.0	2.88	2.82	96.00	94.00

Size of sample: ^{a,b}100 ml; ^{c,d,e,f} = 50 g; ^{g,h} = 2 ml.

*Aliquot of the sample solution = 5 ml.

**Mean of three replicate analysis.

P, proposed method; R, reported method.

3. Results and discussion

The absorption maxima of the azo dye formed was found to be at 525 nm. The reaction conditions have been optimised to obtain maximum colour development varying one reagent at a time while keeping others constant. It was found that 1 ml of 4 M sodium hydroxide, waiting time of 15 min at room temperature and 2 ml of 4 M hydrochloric acid, 1 ml of 1% sodium nitrite, waiting time 10 min at 0°C temperature are required for complete hydrolysis and diazotization of isotroturon, respectively. One ml of 1% sulphamic acid was sufficient to destroy excess of nitrite. It has been reported that insufficient quantity of sulphamic acid leads to variation of the blank solution due to excess of nitrite [18]. Two ml of 2% *p*-aminoacetophenone followed by 2 ml of sodium hydroxide was sufficient for coupling. In acidic medium the colour obtained was negligible (Fig. 1).

Beer's law was obeyed over the concentration range of 0.5–5.0 µg of isotroturon of the final solution (0.02–0.2 ppm). The apparent molar absorptivity and Sandell's sensitivity were found to be $8.6 \times 10^5 \text{ l mol}^{-1} \text{ cm}^{-1}$ and $0.0002 \text{ µg cm}^{-2}$, respectively.

The validity of the method was assessed by investigating the effect of common foreign species and pesticides in the analysis of isotroturon. The tolerance limit values of different foreign species in a solution of isotroturon containing 3 µg per 25 ml of isotroturon are given below in ppm. Ethanol (3000), formaldehyde (2500), 2,4-D and 2,4,5-T (2300), Ca^{2+} , Cu^{2+} (2000), Ethion, Dimethoate (1800), Paraquat (950), SO_4^{2-} (500), Zineb (450).

The S.D. and R.S.D. of absorbance values were found to be ± 0.015 and 2.88%, respectively, for 3 µg/25 ml of isotroturon observed over a period of 7 days.

Application—the method has been satisfactorily applied for the determination of isotroturon in polluted water, environmental and biological samples. The results are in good agreement with the reported method [9]. The results are given in Table 1. To check the recoveries in environmental and biological samples a known amount of isotroturon were added to these samples and analysed by both the proposed and reported method [9]. The recoveries were found to be (92–98.5%). (Table 1).

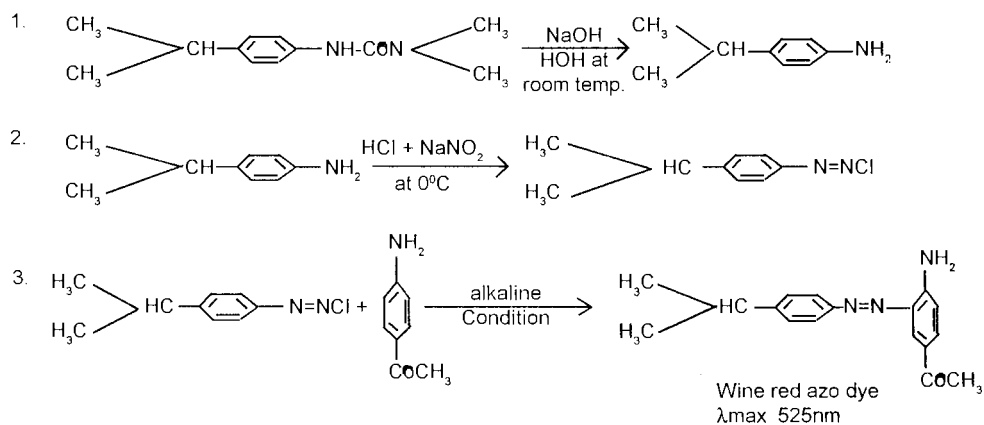


Fig. 1. Colour reaction. The colour reaction involves the following steps:

1. Hydrolysis of isotroturon to its corresponding primary amine;
2. Diazotisation of resulting primary amine;
3. Coupling of diazotised primary amine with *p*-aminoacetophenone under alkaline condition to form wine red coloured azo dye showing a λ_{max} at 525 nm.

Table 2
Comparison with other spectrophotometric methods

Parameter	<i>p</i> -Aminoacetophenone (proposed method)	Ethyl acetoacetate [1]	<i>p</i> -dimethylaminobenzaldehyde [9]
λ_{max} (nm)	525	398	438
Beer's law range ($\mu\text{g ml}^{-1}$)	0.5–5.0	1.5–15.0	1.125–11.25
Molar absorptivity ($\text{l mol}^{-1} \text{cm}^{-1}$)	8.60×10^5	1.37×10^4	3.09×10^4
Sandell's sensitivity ($\mu\text{g cm}^{-2}$)	0.0002	0.015	0.006

4. Conclusion

The proposed method has been compared with other spectrophotometric method and found to be more sensitive and selective (Table 2).

This method is a good alternative to some of the reported costly instrumental methods. The advantage of the proposed method is mainly its sensitivity, simplicity and selectivity and higher stability of the coloured solution. The proposed method has been successfully applied for the determination of isotroturon in polluted water, environmental and biological samples.

Acknowledgements

The authors are grateful to Pt. Ravishankar Shukla University Raipur for providing facilities. The authors are also thankful to SRF Fine Chemicals, Bangalore for providing the standard isotroturon sample.

References

- [1] K. Ramakrishnam Raju, S.R.K.M. Akella, J.V.S. Murthy, U.T. Balerao, Talanta 43 (1996) 577–581.

- [2] G. Krishnamurthy, Indian J. Pharm. Chem. 1 (1) (1983) 76.
- [3] V.P. Singh, J.P. Tiwari, S.P. Kurchania, Pesticides 23 (7) (1989) 39–47.
- [4] H.M. Lebaron, J. Gressel (Eds.), Herbicide Resistances In Plants, John Wiley and Sons, 1982, p. 1807.
- [5] A. Farahbakhsh, Tests Agrochem. Cultiv. 8 (1987) 116–117.
- [6] Z. Gunther, Analytical Methods for Pesticides and Plant Growth Regulators, Vol. 8, Academic Press, New York, 1976, 417.
- [7] H. Buser, K. Grolimund, J. Assoc. Anal. Chem. 57 (1) (1974) 1294.
- [8] Indian Standards Institution, Delhi, IS No. 12004, 1987.
- [9] K. Ramakrishnam Raju, T.N. Parthasarthy, S.R.K.M. Akella, Analyst 115 (1990) 455–457.
- [10] Z. Hammond, K.S. Moore, J.H. Walls, J. Chromatogr. 474 (1) (1988) 175.
- [11] K. Jozef, T. Jozef, K. Magola, Z. Lebenson, Unters Forsch. 184 (2) (1987) 96.
- [12] M. Raghav, J. Recent Adv. Appl. Sci. 2 (2) (1987) 335.
- [13] M. Raghav, A. Singh, S. Shrivastava, J. Recent Adv. Appl. Sci. 2 (1) (1987) 215.
- [14] W.G. Richardson, T.M. West, C.F. Flint, Tests Agrochem. Cultiv. 6 (1985) 148.
- [15] W.T. Haskins, Anal. Chem. 23 (11) (1951) 1672.
- [16] J.V. Das, V.k. Gupta, Chem. Anal. (Warsaw) 39 (1994) 693.
- [17] W.N. Aldrige, Analyst 69 (1944) 262.
- [18] M.I. Walsh, M. Rizk, A. El-Brashy, Talanta 35 (1988) 895.

Extraction of phenols using polyurethane membrane

Kathy Rzesutek, Art Chow *

Department of Chemistry, University of Manitoba, Winnipeg, MB R3T 2N2, Canada

Received 3 March 1997; received in revised form 14 July 1997; accepted 16 July 1997

Abstract

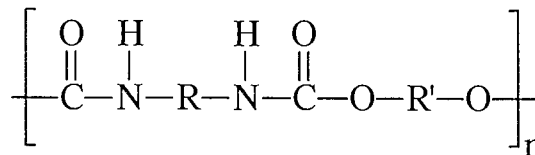
The extraction of various phenols from aqueous and organic solutions using polyurethane membrane has been investigated. The effects of solution concentration, extraction time, surface area, pH, salts, and temperature on extraction were studied. The phenols are extracted as neutral species and the extraction is governed by a combined effect of intra- and intermolecular hydrogen bonding and nonspecific hydrophobic interactions. The ether-type membrane showed higher extraction capability for the phenols than the ester-type polyurethane membrane. © 1998 Elsevier Science B.V. All rights reserved.

Keywords: Phenols; Polyurethane membrane; Extraction

1. Introduction

Polyurethanes have been conventionally used as elastic fibers, rubber foams, and coatings since the 1940s [1]. However, the use of these polymers as sorbents of various organic and inorganic species was proposed only in 1970 [2]. Since then, polyurethanes have been employed in many separation techniques [2]. Most recently, polymer membranes have been preferably used over other polyurethane materials in a variety of industrial, environmental and membrane science applications [3,4]. The extraction of inorganic species by thin polyurethane membrane has been already shown to be feasible [5,6]. The extraction of organic species, on the other hand, has not been as extensively studied. The most significant findings in-

volving extraction of organic compounds have been reported for thick polyurethane membranes by Aminabhavi and coworkers [7–10]. Most of these studies have been concerned either with the effects of organic solvents on the physical properties of the membrane, or with elucidation of the mechanism governing the extraction of the solvent. Nevertheless, a complete understanding of the sorption mechanism at the molecular level is still not well understood. Polyurethanes are linear block polymers containing the characteristic linkage group



where R is a substituted aromatic group and R' is usually a polyether or a polyester [1]. The bulk

* Corresponding author. Fax +1 204 2750905.

structure of polyurethanes is considered to consist of a microcrystalline domain (hard segments) separated by amorphous, random coil regions (soft segments). The isocyanates and the chain backbone comprise the hard regions. The soft segments are the polyether or polyester groups.

This study investigates an extraction mechanism of various phenols by thin polyurethane membrane. Phenols are widely used in industry and so far no single efficient method has yet been developed for their removal [3]. Information on the extraction of phenols can provide a basis for useful predictions of the sorption process of other organic compounds by polyurethane membrane.

2. Experimental

2.1. Apparatus

Spectra and absorbance readings were taken using a Hewlett-Packard Model 8452A diode-array spectrophotometer. Gas chromatographic data was obtained using a Hewlett-Packard 5710A gas chromatograph equipped with a Chromosorb W column coated with 5% bentone 34 and 5% diisodecyl phthalate. Solution pH was measured with an Orion Expandable Ion Analyser EA 940. A modified Burrell Wrist-Action shaker was used for sample agitation at room temperature. A Fisher Versa-Bath® shaking water bath was used for experiments at higher temperatures. Water was obtained from a Barnstead Nanopure II™ purification system fed with water purified by reverse osmosis. Polyurethane membranes, ether-type XPR625-FS and ester-type MP1495-SL were obtained from Stevens Elastomerics/Urethane Products, Northampton, MA. Three thicknesses of 0.025 mm, 0.051 mm, and 0.127 mm were used. All chemicals were of reagent grade. The apparatus used for membrane testing was a 40-ml Kimble Glass Inc. amber glass vial (60960A-912) with a plastic cap and a Teflon™-faced silicone liner. For experiments involving different surface areas of membrane exposed to the sample solution, glass containers having larger caps were used.

2.2. Procedure

Phenol stock solutions were prepared by accurately weighing an appropriate amount of phenol, dissolving it in the solvent and transferring this to a 500-ml volumetric flask which was then filled to volume. Sample solutions of about 2×10^{-4} M (unless otherwise specified) were prepared by transferring an aliquot of the phenol stock solution to a 100-ml volumetric flask. Parameters such as salt, acid, or base concentrations were adjusted prior to dilution to volume.

Sample solutions of *ortho*-, *meta*-, and *para*-xylenes were prepared by diluting a known amount of a particular xylene isomer to 25 ml using hexane. Ten-millilitre aliquots of the phenol and xylene sample solutions were then transferred, using volumetric pipettes, into the sample vials. The polyurethane membranes (ether-type 0.051 mm thick unless otherwise specified) were placed on the openings of the vials and covered with the Teflon™ silicone disks and screw caps and carefully tightened. The vials were then inverted to put the samples in contact with the membranes and shaken for 3 h, except when extraction with time was investigated. The surface of the membrane exposed to the sample solutions was 2.54 cm². For each experiment, triplicate samples were prepared and the experiment was repeated several times to establish reproducibility. The vials containing the samples were weighed prior to and after the extraction to determine if any loss due to leakage may have occurred. The UV visible spectra (190–820 nm) of the phenol sample solutions were taken and the absorbances (A_F) compared with the absorbances of the solutions prior to extraction (A_I). The absorbance readings for the *ortho* and *meta* isomers of bromo and chlorophenols were taken at 274 nm and the *para* isomers at 280 nm. The degree of extraction is reported as the % E which is the % decrease of absorption from the solution assuming a Beer's Law dependence.

$$\%E = 100(A_I - A_F)/A_I \quad (1)$$

Xylene sample solutions were analysed using gas chromatography. To determine whether a particular xylene was extracted by the membrane,

Table 1
Effect of concentration of phenols on extraction

Compound	% <i>E</i>				
	'natural' pH	2×10^{-6} M	2×10^{-5} M	1×10^{-4} M	3×10^{-4} M
<i>o</i> -Bromophenol	5.25	11	22	39	39
<i>m</i> -Bromophenol	5.42	33	39	43	41
<i>p</i> -Bromophenol	5.11	35	37	41	41
<i>o</i> -Chlorophenol	5.39	13	16	21	23
<i>m</i> -Chlorophenol	5.40	25	29	34	35
<i>p</i> -Chlorophenol	5.55	22	25	28	30

Conditions: $25.0 \pm 2.0^\circ\text{C}$, 10-ml aliquot of an aqueous phenol solution, 0.051 mm ether-type membrane, active surface area of 2.54 cm², % *E* \pm 3% at equilibrium at 3 h.

ratios of the xylene to the internal standard were obtained for the sample solutions and compared with those for the stock sample which was not exposed to the polyurethane membrane. A known amount of an internal standard was added to the sample solution after the extraction and to the same volume of the stock sample solution. *Ortho*-xylene was used as the internal standard for the analysis of *meta*-, and *para*-xylenes; *meta*-xylene was used as the internal standard for the analysis of *ortho*-xylene. The GC injection port and detector temperatures were 150°, the column temperature was 70°C, and the carrier gas (helium) flow rate was approximately 5 ml min⁻¹.

3. Results and discussion

3.1. Effect of phenol concentration on extraction

The choice of the concentration was limited by the solubility of various phenols in the solvents and by the detection limit of the UV-visible spectrophotometer. Solutions having concentrations of 2×10^{-6} M, 2×10^{-5} M, 1×10^{-4} M, and 3×10^{-4} M were extracted. Solutions having 2×10^{-6} M concentration of phenols were extracted more poorly with both ether- and ester-type membranes than the more concentrated solutions (Table 1). For later experiments, 2×10^{-4} M phenol solutions were used.

Table 1 shows that all of the phenols studied are extracted by the polyurethane membrane to a

greater extent when higher solution concentrations are used. During the extraction process three steps are occurring [11,12]: transfer of the phenol from the bulk solution to the solution–membrane interface, penetration of the phenol into the membrane surface, and migration of the phenol from the membrane surface into the bulk of the membrane.

phenol in solution

↓↑

phenol at solution–membrane interface

↑↓

phenol in membrane surface

↑↓

phenol in membrane bulk

(2)

The amount of phenol sorbed from the solution is controlled by the slowest of the above steps in the sorption process [11,13] which in this case may be the transfer of the phenol from the solution–membrane interface to the membrane surface or the migration of the phenol through the membrane bulk [11,13]. If the extraction efficiency was controlled by the distribution coefficient alone, an equal percent extraction of phenol would be expected regardless of the solution concentration. The fact that an increase in extraction was observed with the increase in concentration suggests that another factor must be influencing the sorption of the phenol. At lower phenol solution

concentrations, the concentration gradient created is smaller than at the higher phenol solution concentrations. For the less concentrated phenol solutions, although an equilibrium was attained between the phenol in solution and the phenol sorbed on the surface of the membrane, such an equilibrium may not have been reached within the bulk of the membrane. At lower phenol solution concentrations, the migration rate of the phenol from the surface through the bulk of the membrane will be slower due to the smaller concentration gradient. Since the number of the phenol molecules entering the membrane is lower, there are fewer of these phenol molecules to interact with the membrane. Therefore, there will be less disruption of the intramolecular forces between the membrane groups and migration deeper into the membrane will be slower than when a higher phenol solution concentration is used [13]. Consequently, a lower percentage of phenol is sorbed from the less concentrated solution at the observed equilibrium.

3.2. Effect of extraction time, surface area, and thickness of the membrane on extraction

An attempt was made to estimate the time needed for the extraction to reach equilibrium at room temperature. Extraction over a wide range of time (30 min to 48 h) was measured. All solutions were mechanically shaken for the desired amount of time, and samples were analysed after 30 min and subsequently at 1-h periods up to 10 h. Final readings were taken at 24 and 48 h. These experiments showed that equilibrium was attained within approximately 3 h for solutions containing 2×10^{-4} M concentration of phenols extracted with 0.051-mm thick ether- and ester-type polyurethane membranes. No significant increase in extraction was observed at 48 h as illustrated by the extraction of *m*-bromophenol (Fig. 1). The effects of an increased membrane surface and thickness of the membrane on sorption of phenols from solution were investigated. Results displayed in Table 2 show that the increase in surface area of the 0.051-mm thick membrane exposed to the phenol solution resulted in greater extraction nearly proportional to the area.

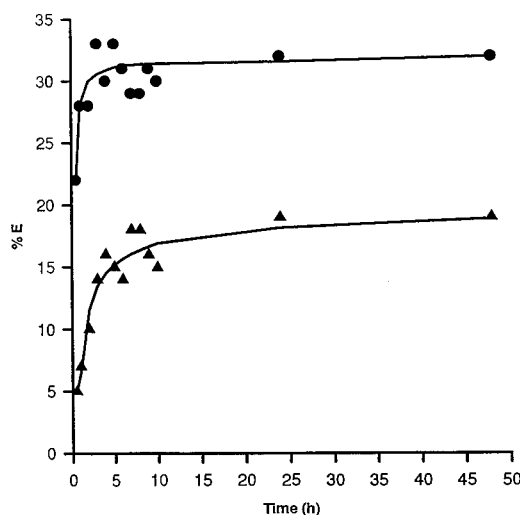


Fig. 1. Extraction of *m*-bromophenol with time using the ether- and ester-type polyurethane membranes. Conditions: $25.0 \pm 2.0^\circ\text{C}$, 10-ml aliquot of $\approx 2 \times 10^{-4}$ M aqueous phenol solution, 0.051 mm ether- and ester-type membranes, active surface area of 2.54 cm^2 , $\%E \pm 3\%$. Extraction with the ether-type membrane, ●; extraction with the ester-type membrane, ▲.

The thick membranes (0.051 mm and 0.127 mm) of identical surface area were found to have a higher sorptive capacity than the thin membranes (0.025 mm). This is shown by the results for the extraction of *m*-bromophenol (Table 3) over two time periods with both the ether- and ester-type polyurethane membranes.

When species extract into the solid phase from a solution, the steps shown in Eq. (2) are believed to take place [11,12]. The initial transfer of the phenol is from solution to the membrane surface followed by the migration of the molecule into the bulk of the polymer. Thus the overall sorption

Table 2
Effect of surface area on extraction of *m*-bromophenol

Active surface area (cm^2)	% <i>E</i>
2.00	36
2.54	44
7.07	85

Conditions: $25.0 \pm 2.0^\circ\text{C}$, 10-ml aliquot of $\approx 2 \times 10^{-4}$ M aqueous phenol solution, 0.051 mm ether-type membrane, $\%E \pm 3\%$ at equilibrium at 3 h.

Table 3

Extraction of *m*-bromophenol by ether- and ester-type polyurethane membranes having thicknesses of 0.025 mm, 0.051 mm, and 0.127 mm

Membrane type	Time (h)	% <i>E</i>		
		0.025 mm thick	0.051 mm thick	0.127 mm thick
Ether	3	26	42	59
	9	27	45	83
Ester	3	15	16	37
	9	16	23	46

Conditions: $25.0 \pm 2.0^\circ\text{C}$, 10-ml aliquot of $\approx 2 \times 10^{-4}$ M aqueous phenol solution, active surface area of 2.54 cm^2 , % *E* $\pm 3\%$.

process is basically an absorption and cannot be described solely as adsorption. However, the first step of this process could be considered analogous to the adsorption of gas on a solid surface as described by Langmuir [14]. According to Langmuir, the extent of adsorption is determined by the equilibrium that results from adsorption of gas molecules on the surface and their evaporation from the surface and is proportional to the area of the surface exposed to the gas [14]. Assuming that the phenol molecules in solution behave similarly to the gas molecules, we can represent the initial sorption of the phenol in solution onto the membrane surface, *y*, by a modified Langmuir equation

$$y = by_m C / (1 + bC) \quad (3)$$

where y_m is the amount of phenol sorbed from solution when the monolayer is complete, *C* is the concentration of phenol remaining in solution, and *b* is a sorption coefficient which is constant at a given temperature. Using the above analogy, the initial sorption of phenol from solution onto the membrane surface would be expected to proceed rapidly, which is in part controlled by the solubility of the phenol in the aqueous phase and attraction to the membrane surface, until an equilibrium is reached between the phenol in solution and the phenol sorbed on the surface of the membrane. If the sorption of the phenol by the membrane were only an adsorption process as the one described by Langmuir, no more phenol would be expected to be removed from the solution after an equilibrium at the solution–mem-

brane interface had been attained. We observed that the amount of phenol sorbed by the thin membranes (0.025 mm) does not significantly change with time, but membranes 0.051 mm and 0.127 mm thick sorbed more of the phenol when a longer extraction time was allowed. Because all of the membranes had an identical surface area exposed to the phenol solution, the results show that the phenol must be migrating into the bulk of the thicker membranes, and not back into the solution as described by the Langmuir model. As the phenol migrates into the polymer, the concentration at the solution–membrane interface will be depleted. A concentration gradient is therefore created and more phenol will be extracted by the membrane. No increase in sorption with extended times was observed for extractions with the 0.025-mm thick membranes probably because the material became saturated. Extraction of the phenol from solution using polyurethane membrane cannot therefore be described as an adsorption process because it involves migration of the phenol into the bulk of the membrane and not just its adsorption onto the surface of the polymer.

The smaller change in sorption over time observed for the 0.127-mm ester-type membrane indicates that migration of the phenol through this membrane is probably much slower than through the ether-type membrane. The difference in the rate of transfer of the phenol through the two membrane types suggests that the structure of the membrane may be an important factor in the extraction process. The ester-type polyurethane has a more compact structure than the ether-type

Table 4
Effect of base and acid addition

Acid or base added	% <i>E</i>				
	Zero addition	0.10 M final concentration	0.50 M final concentration	1.00 M final concentration	2.00 M final concentration
HCl	41	41	41	43	42
NaOH	41	9	0	0	0

Conditions: $25.0 \pm 2.0^\circ\text{C}$, 10-ml aliquot of $\approx 2 \times 10^{-4}$ M *m*-bromophenol solution, 0.051 mm ether-type membrane, active surface area of 2.54 cm^2 , % *E* $\pm 3\%$ at equilibrium at 3 h.

because the ester groups are more polar and have a better probability of forming intramolecular hydrogen bonds than the ether groups. Thus, the migration of the phenol through the ester-type membrane may be hindered due to more intramolecular interactions between the membrane ester groups. These interactions may be too strong to be disrupted effectively by the phenol and this can account for the consistently lower sorption obtained with the ester-type polyurethane membrane.

3.3. Effect of pH on extraction

Phenols can be involved in various equilibria with protons which result in neutral, positively, or negatively charged species. It was found that when substituent groups are ionizable, the pH plays an important role in extraction (Table 4). The addition of base resulted in a dramatic decrease in extraction due to the formation of a charged species. Addition of acid did not significantly alter the extraction. This suggests that the phenols must have already been protonated at the 'natural' pH (Table 1) prior to the addition of the acid. The oxygen present in the polyurethane ether and ester groups does not become protonated because the extraction capabilities of both membrane types did not change with the addition of acid. If protonation of the oxygen took place, a decrease in extraction would be observed due to formation of a charged surface which would interact with the neutral phenols less favourably.

3.4. Effect of salts on extraction

The extraction of phenols by polyurethane membrane from salt solutions is shown in Table 5. It is known that charged species which are not extracted by the membrane sometimes can be extracted as ion pairs [16]. Formation of ion pairs can be accomplished using the 'salting out' effect in which a highly concentrated salt solution is added to the solution so that an ion pair is formed which can then extract.

As shown in Table 5, no change in extraction was observed with the addition of salt, therefore no ion pair formation took place. This suggests that the phenols must be present in a non-ionized form in aqueous solution and extract as a neutral species. Furthermore, the ether groups in the membrane probably do not have an initial electrostatic charge when in contact with water because the addition of salt had no effect on sorption. If a charge was present on the membrane surface, the formation of an ion pair would have eliminated this charge resulting in a neutral surface. The neutral surface is more capable of extracting the uncharged phenol molecules, and therefore sorption would have increased. These results are consistent with the data obtained from the experiment involving the effect of pH on extraction.

3.5. Effect of solvent type on extraction

The initial experiments involved the extraction of phenols from water; however, the extraction from organic media could provide additional in-

Table 5
Effect of salt addition

Compound	% <i>E</i>		
	Zero addition	0.33 M NaCl final concentration	1.00 M NaCl final concentration
<i>o</i> -Bromophenol	39	39	41
<i>m</i> -Bromophenol	43	43	45
<i>p</i> -Bromophenol	41	44	42
<i>o</i> -Chlorophenol	21	21	23
<i>m</i> -Chlorophenol	34	34	32
<i>p</i> -Chlorophenol	29	29	28

Conditions: $25.0 \pm 2.0^\circ\text{C}$, 10-ml aliquot of $\approx 2 \times 10^{-4}$ M aqueous phenol solution, 0.051 mm ether-type membrane, active surface area of 2.54 cm^2 , % *E* $\pm 3\%$ at equilibrium at 3 h.

formation about the mechanism. The results of the extraction of phenols from various solvents are presented in Table 6. The *meta* and *para* isomers do not show a significant difference in extraction from water, hexane or cyclohexane. The *ortho* isomer, on the other hand, extracts well from water, but very poorly from hexane and cyclohexane. None of the compounds extracted from acetonitrile or ethyl acetate.

Water seems to be the best solvent from which to extract the halophenols. Water may interact with the polar groups of the polyurethane soft segments and swell the membrane. The movement of the larger phenol molecule into the membrane will therefore be easier because the soft segments of the membrane become more widely spaced. Therefore, the sites on the membrane, that may be important in extraction, become more accessible to the phenols. Water may also be acting as a carrier for the phenols which interact with water through hydrogen bonding. Water can bring the phenols into closer contact with the membrane groups and make the transfer of the phenols from the solution into the membrane more favourable. It has been shown that surface tension of the solvent has an effect on the extraction of organic compounds [17]. If the surface tension of the solvent is reduced by the solute, then the solute molecules will concentrate at the surface, whereas if the surface tension is raised, the solute will move away from the surface into the bulk of the solution. Most water-soluble organic compounds are known to reduce the surface tension of water

[17]. Therefore, phenols in water may tend to accumulate in regions of lower concentration, i.e. at the interface between the membrane and water, and then they may be carried by water into the membrane or interact directly with the membrane through nonspecific attraction forces. Hexane has a lower surface tension than water when in contact with the membrane, so the phenols would be expected to extract comparably well from hexane which is observed for the *meta* and *para* isomers but not for the *ortho* isomer. The *ortho* isomer possesses a higher localized charge than the other isomers since the hydroxyl and the halo substituents are closer together. Therefore, this isomer may not be solvated well by hexane or cyclohexane molecules. Since the membrane may itself hold some electrostatic charge in hexane, the *ortho*-phenol may be repelled from the membrane surface and less extraction will result. Extraction from polar organic solvents such as ethyl acetate and acetonitrile was not observed. The phenols are much more soluble in these solvents than in water or hexane. This suggests that the interactions of phenols with the membrane which are responsible for the extraction must be much weaker than the interactions with ethyl acetate and acetonitrile and thus no extraction can result.

3.6. Importance of hydrogen bonding and other nonspecific interactions

Intermolecular and intramolecular hydrogen bonding was found to be important in the extrac-

Table 6
Extraction of phenols from various solvents

Compound	% <i>E</i>				
	Water	Hexane	Cyclohexane	Acetonitrile	Ethyl acetate
<i>o</i> -Bromophenol	39	5	2	0	0
<i>m</i> -Bromophenol	42	41	30	0	0
<i>p</i> -Bromophenol	42	44	35	0	0
<i>o</i> -Chlorophenol	22	2	1	0	0
<i>m</i> -Chlorophenol	34	38	30	0	0
<i>p</i> -Chlorophenol	30	25	28	0	0

Conditions: $25.0 \pm 2.0^\circ\text{C}$, 10-ml aliquot of $\approx 2 \times 10^{-4}$ M phenol solution, 0.051 mm ether-type membrane, active surface area of 2.54 cm², % *E* \pm 3% at equilibrium at 3 h.

tion of phenols by the polyurethane membrane. An example of intermolecular hydrogen bonding would be the bonding between oxygen atoms on the membrane groups and the hydroxyl group or other substituents on the phenol. Intermolecular bonding can also occur between the ether and ester groups on the membrane segments or the membrane groups and solvent molecules. Intramolecular bonding can take place between the hydroxyl group and the other substituents present on the phenol ring. Such hydrogen bonding interactions can only be formed if the two interacting atoms are very close to each other. The bond is quite weak (8–41 kJ) and can be easily formed and broken [18]. The intra and intermolecular hydrogen bonds together appear to collectively influence the extraction of phenol by the polyurethane membrane. These effects can be shown by comparing the extraction of halophenols, in which an intramolecular hydrogen bond is unlikely, with alkyl phenols which can form such bonds. As shown in Table 7, the dialkyl phenols extract to a lesser extent than the halophenols in water (Table 6). The extraction of trialkyl phenols is comparable to the extraction of halophenols. The trialkyl phenols have one methyl group that is not involved in intramolecular hydrogen bonding which therefore is available for interactions with the membrane. The trialkyl phenols are also more non-polar and may preferentially partition into the membrane. The much lower extraction of alkyl phenols in hexane suggests that the phenols must be more soluble in hexane than in the mem-

brane, and thus tend to stay dissolved in the solvent. The isomers which can form the strongest intramolecular hydrogen bonds extract slightly poorer than those in which such bonding is less likely to take place. From this observation it follows that the ability to form intermolecular hydrogen bonds is equally important. Halophenols which are unlikely to form intramolecular hydrogen bonds, can be involved in intermolecular interactions with the membrane or the solvent through the hydroxyl group and the halo substituents. Therefore, they extract better than the dialkyl phenols in which the intramolecular interactions may be competing with the intermolecular interactions. Phenols with trialkyl substituents or compounds that can form more intramolecular hydrogen bonds with the membrane extract even better as shown in Table 7. Extractions obtained with the ether-type membrane are higher than those done with the ester-type membrane. This can be explained by the ability of the ester and ether groups to form hydrogen bonds. The $\text{p}K_{\text{a}}$ for the protonation of the ether oxygen is -3 and the $\text{p}K_{\text{a}}$ for the protonation of the carbonyl oxygen is -6 [19]. The ether oxygen is more basic and therefore better at forming hydrogen bonds with phenols or solvent molecules.

Other weak nonspecific hydrophobic interactions seem to be important in extraction as well. Molecules having a certain balance between the polar hydrogen bond-forming substituents and the non-polar substituents are extracted. Molecules which are either very polar (e.g. 2,4-di-

Table 7
Extraction of various organic compounds

Compound	Molecular structure	Water (% <i>E</i>)	Hexane (% <i>E</i>)
2,3-Dimethylphenol	(CH ₃) ₂ C ₆ H ₃ OH	20	4
2,6-Dimethylphenol	(CH ₃) ₂ C ₆ H ₃ OH	17	3
3,5-Dimethylphenol	(CH ₃) ₂ C ₆ H ₃ OH	17	6
2,3,5-Trimethylphenol	(CH ₃) ₃ C ₆ H ₂ OH	45	0
2,4,6-Trimethylphenol	(CH ₃) ₃ C ₆ H ₂ OH	34	0
2- <i>t</i> -Butyl-5-methylphenol	(<i>t</i> -bu)(CH ₃)C ₆ H ₃ OH	90	20
Phenol	C ₆ H ₅ OH	5	13
Diphenol	(C ₆ H ₄) ₂ (OH) ₂	45	46
Resorcinol	C ₆ H ₄ (OH) ₂	20	0
Benzoic acid	C ₆ H ₅ CO ₂ H	15	18
2,4-Dihydroxybenzoic acid	(OH) ₂ C ₆ H ₃ CO ₂ H	4	Not soluble
3,5-Dihydroxybenzoic acid	(OH) ₂ C ₆ H ₃ CO ₂ H	0	Not soluble
<i>o</i> -, <i>m</i> -, <i>p</i> -Xylenes	(CH ₃) ₂ C ₆ H ₄	*	0

Conditions: 25.0 ± 2.0°C, ≈ 2 × 10⁻⁴ M solutions, 0.051 mm ether-type membrane, active surface area of 2.54 cm², 10 ml solution, % *E* ± 3% at equilibrium at 3 h.

*Data were obtained using gas chromatography and therefore aqueous solutions were not extracted.

hydroxybenzoic acid, 3,5-dihydroxybenzoic acid) or non-polar (e.g. xylenes) do not extract, as illustrated in Table 7. Thus, sorption of phenols on the membrane is probably accounted for by a combined action of weak dispersion forces together with stronger hydrogen bond forces which depend on the proximity of the hydroxyl group to other substituents.

3.7. Effect of temperature on extraction

When phenols are being sorbed by the membrane, they can be thought of as distributing between the solution (a liquid phase) and the membrane (a solid phase). This can be represented by a distribution ratio, which is the equilibrium concentration in a liquid phase, K_s , divided by the concentration of the phenol in the solid phase, K_m . This ratio will change with temperature because the solubility of the phenol in the two phases changes with temperature. The extraction of organic molecules from liquids into solids is usually expressed as standard affinity, $\Delta\mu^\circ$, which, being a thermodynamic function, is exchangeable with Gibbs free energy [3], ΔG . Thus, if $\mu_m + RT \ln [K_m]$ is the free energy of the phenol in the membrane, and $\mu_s + RT \ln [K_s]$ is the free energy of phenol in aqueous solution,

these will be equal at equilibrium [3], i.e. $\mu_m + RT \ln [K_m] = \mu_s + RT \ln [K_s]$. Thus, at any temperature T , the affinity of the phenol will be

$$\begin{aligned}
 -(\mu_m + \mu_s) &= -\Delta\mu^\circ = RT \ln[K_m] - RT \ln[K_s] \\
 &= RT \ln[K_m]/[K_s] = RT \ln K \quad (4)
 \end{aligned}$$

where, K is the partition ratio. The heat (ΔH°) and entropy (ΔS°) of sorption can be calculated from the partition ratios at two different temperatures or over a temperature range [3]. The assumption is that ΔH° and ΔS° are independent of temperature which holds if a plot of $\log K$ vs $1/T$ is a straight line. Therefore,

$$\Delta H^\circ = -2.303RT_1T_2/(T_2 - T_1) \log K_1/K_2 \quad (5)$$

$$\Delta S^\circ = -2.303R \log K_1/K_2 \quad (6)$$

where T_1 and T_2 are the two temperatures, and K_1 and K_2 are the partition ratios at the two temperatures.

The percentage of extraction of bromophenols and chlorophenols was measured at equilibrium at various temperatures. The results of the extraction of various phenols by ester- and ether-type membranes are presented in Table 8. As an example, the plots of $\log K$ vs $1/T$ for the bromophenols are shown in Fig. 2 and Fig. 3. Extractions of all bromo and chlorophenols at low temperatures

Table 8
Effect of temperature

Compound	% <i>E</i>						
	4°C	12°C	25°C	37°C	50°C	70°C	90°C
<i>o</i> -Bromophenol							
Ether	30	31	39	21	19	17	13
Ester	12	13	16	14	14	13	11
<i>m</i> -Bromophenol							
Ether	44	43	43	33	25	20	13
Ester	32	28	24	20	18	13	11
<i>p</i> -Bromophenol							
Ether	42	44	41	27	20	16	6
Ester	29	24	21	18	13	13	6
<i>o</i> -Chlorophenol							
Ether	23	23	21	16	15	14	12
Ester	8	9	11	10	12	10	9
<i>m</i> -Chlorophenol							
Ether	34	32	34	21	17	10	9
Ester	16	13	16	14	13	9	8
<i>p</i> -Chlorophenol							
Ether	29	31	29	20	14	11	8
Ester	17	17	16	13	11	9	7

Conditions: 10-ml aliquot of $\approx 2 \times 10^{-4}$ M aqueous phenol solution, 0.051 mm ether- and ester-type membranes, active surface area of 2.54 cm², % *E* $\pm 3\%$ at equilibrium, temperature $\pm 1.0^\circ\text{C}$ (for extractions at 4 and 12°C using the ester-type membrane, the equilibrium was reached after 72 h rather than 3 h).

(4 and 12°C) using the ester-type polyurethane membrane (Fig. 3) required 72 h rather than 3 h to reach an equilibrium. The values for K , ΔH° , and ΔS° for bromo- and chlorophenols calculated for extractions with ester- and ether-type membranes are shown in Table 9.

Extractions of all bromophenol and chlorophenol isomers with the ether-type membrane and the *meta* and *para* isomers with the ester-type membrane (Table 8), show a gradual decrease in % *E* with an increase in temperature. Both ΔH° and ΔS° for these extractions are negative, and the entropy change for the sorption is quite small (Table 9). When these phenol isomers move from solution into the membrane, their motion becomes more restricted, and therefore we observe the negative entropy. Since the sorption process also involves a decrease in free energy, then from the thermodynamic relationship $\Delta G^\circ = \Delta H^\circ - T\Delta S^\circ$, it follows that ΔH° should be negative

which is confirmed by the data. Thus the sorption of these isomers on membrane is an exothermic process and from LeChatelier's principle, it would follow that the extent of sorption (under equilibrium conditions) should decrease with increasing temperature which is observed. Another explanation for the decrease in extraction with an increase in temperature is that the physical structure of the membrane may change at an increased temperature so that the matrix is less accessible to phenol molecules. The higher energy of the membrane segments and the phenol molecules provided by the increased temperature may prevent any stable interactions between the membrane groups and the phenol from forming, therefore producing a lower extraction. A smaller change in entropy observed for the extraction with the ester-type membrane suggests that the freedom of motion of the bromo and chlorophenol molecules in this membrane is higher. This indicates that dur-

ing extraction with the ester membrane, the phenols are more solvated and not as tightly bound as they are to the ether-type membrane.

The *ortho* bromo and chlorophenols showed a different sorption pattern when extracted with the ester-type polyurethane membrane over the 4–90°C temperature range. Extractions of the *ortho* isomers with the ester-type membrane show an extraction maximum at 25°C, and a slight decrease at higher and lower temperatures. Two sets of data were calculated corresponding to two straight line plots for which Eq. (5) and Eq. (6) are valid at equilibrium. The non-linearity of the $\log K$ vs $1/T$ plot for the extraction of the *ortho* isomers using the ester-type polyurethane membrane is due to the combined effect of structure of the *ortho* isomers and the more polar nature of the ester-type polyurethane membrane. Unlike the *meta* and *para* isomers, the *ortho* isomer undergoes a so-called *ortho* effect [15]. The proximity of the substituents allows for intermolecular noncovalent interactions such as hydrogen bonding and charge transfer which may result in the forma-

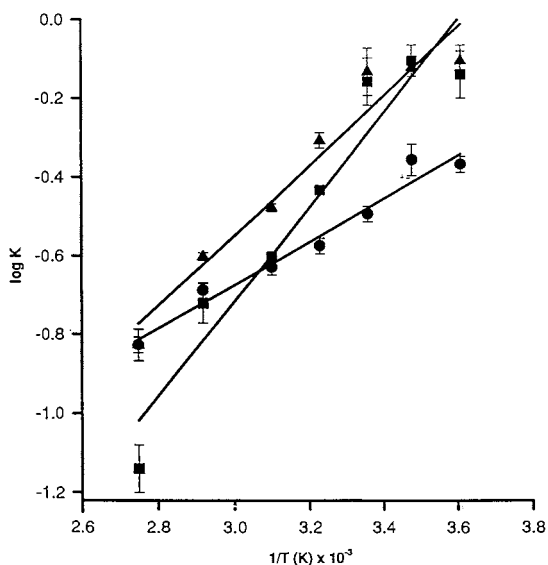


Fig. 2. Change in partition ratio with change in temperature for extraction of bromophenols using the ether-type polyurethane membrane. Extraction equilibrium was reached at 3 h. Bromophenols: ● *ortho*-, ▲ *meta*-, ■ *para*-.

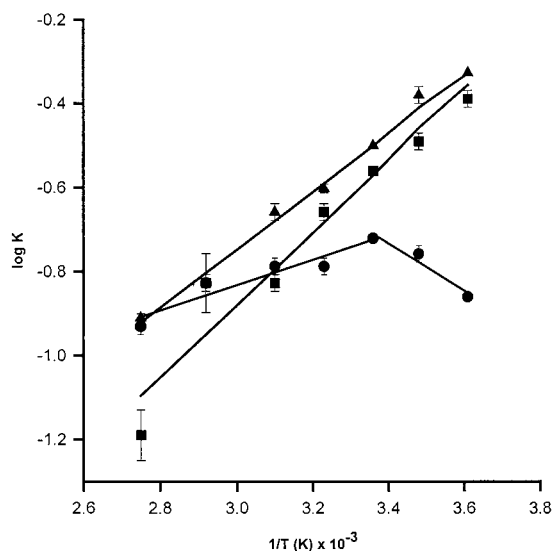


Fig. 3. Change in partition ratio with change in temperature for extraction of bromophenols using the ester-type polyurethane membrane. Extraction equilibrium was reached at 3 h except for solutions extracted at 4 and 12°C for which the equilibrium was attained after 72 h. Bromophenols: ● *ortho*-, ▲ *meta*-, ■ *para*-.

tion of a localized electronic field [15] in the molecule. The strength of this *ortho* effect is susceptible to temperature changes [15]. The overall sorption of the *ortho* phenols may be a result of a combined effect of the electrostatic interactions with hydrophobic interactions and hydrogen bonding. Because the ester-type membrane is more polar than the ether-type membrane, the electrostatic interactions between the phenol and the membrane are stronger and may induce the formation of more resonance structures of the *ortho* phenol which in turn contribute to the nonlinearity of the plot shown in Fig. 3. The extractions of the *ortho* phenols with both membrane types are generally lower compared to extractions of the *para* and *meta* isomers most likely due to the *ortho* effect. In the *para* and *meta* isomers, the hydroxyl group is separated from the substituent by the largest distance. Therefore, the hydroxyl group can interact more freely with the membrane substituents through hydrogen bonding interactions.

4. Conclusion

The study of the sorption of various phenols by the polyurethane membrane shows that these compounds are extracted in their neutral form.

Table 9
Partition ratio, enthalpy, and entropy change for extraction of phenols

Compound membrane type	K_1/K_2	ΔH° (kJ mol ⁻¹)	ΔS° (J mol ⁻¹ K ⁻¹)
<i>o</i> -Bromophenol			
Ether (4– 90°C)	2.879	–10.28	–8.79
Ester (4– 25°C)	0.716	10.85	–2.02
Ester (25– 90°C)	1.545	–6.52	–7.85
<i>m</i> -Bromophenol			
Ether (4– 90°C)	5.275	–16.17	–13.83
Ester (4– 90°C)	3.829	–12.97	–11.16
<i>p</i> -Bromophenol			
Ether (4– 90°C)	11.313	–23.19	–20.17
Ester (4– 90°C)	6.375	–17.89	–15.40
<i>o</i> -Chlorophenol			
Ether (4– 90°C)	2.199	–7.66	–6.55
Ester (4– 25°C)	0.710	11.11	2.85
Ester (25– 90°C)	1.265	–2.29	–1.96
<i>m</i> -Chlorophenol			
Ether (4– 90°C)	5.867	–16.13	–13.80
Ester (4– 90°C)	2.184	–7.54	–6.49
<i>p</i> -Chlorophenol			
Ether (4– 90°C)	4.690	–15.02	–12.85
Ester (4– 90°C)	2.720	–9.66	–8.32

Conditions: 10-ml aliquot of $\approx 2 \times 10^{-4}$ M aqueous phenol solutions, 0.051 mm ether- and ester-type membranes, active surface area of 2.54 cm². Extraction equilibrium was reached at 3 h except for solutions extracted at 4 and 12°C with the ester-type membrane for which the equilibrium was attained after 72 h.

Intra and intermolecular hydrogen bonding interactions of the phenols appear to be important factors governing the extraction process. An increased sorption of the phenol can be attained by providing either a larger surface area exposed to the phenol solution or a thicker membrane that has higher sorption capabilities. Strong intramolecular hydrogen bonding reduces the intermolecular interactions between the phenol and the membrane and results in a lower extraction. The relative solubility of the phenol in the liquid phase and the membrane was also found to influence the sorption. The ether-type polyurethane membrane showed a higher extraction capability for the phenols than the ester-type polyurethane membrane which is related to the differences in the structure of these two membrane types and their ability to interact with the phenols. Room temperature was shown to be optimal for the extractions of phenols. Future studies will involve investigation of these extractions for a wider range of organic compounds in order to obtain a clearer view of the extraction mechanism taking place.

Acknowledgements

The authors would like to thank Dr D.M. McKinnon, Dr W.G. Baldwin and Dr M. King for their assistance with the data analysis, and acknowledge the financial support of the Natural Sciences and Engineering Research Council of Canada.

References

- [1] H.R. Allcock, F.W. Lampe, Contemporary Polymer Chemistry, Prentice-Hall, Englewood Cliffs, NJ, 1990, p. 43.
- [2] H.J.M. Bowen, J. Chem. Soc. (A) (1970) 1082.
- [3] W.S. Winston Ho, K.K. Sirkar, Membrane Handbook, Van Nostrand Reinhold, New York, 1992.
- [4] U.S. Aithal, T.M. Aminabhavi, R.H. Balundgi, S.S. Shukla, JMS-Rev. Macromol. Chem. Phys. C30 (1) (1990) 43.
- [5] R.D. Oleschuk, A. Chow, Talanta 42 (1995) 957.
- [6] R.D. Oleschuk, A. Chow, Talanta 43 (1996) 1545.
- [7] U.S. Aithal, T.M. Aminabhavi, J. Chem. Eng. Data 35 (1990) 298.

- [8] U.S. Aithal, T.M. Aminabhavi, *J. Appl. Polym. Sci.* 42 (1991) 2837.
- [9] S.B. Harogopad, U.S. Aithal, T.M. Aminabhavi, *J. Appl. Polym. Sci.* 42 (1991) 3267.
- [10] R.S. Khinnavar, T.M. Aminabhavi, *J. Appl. Polym. Sci.* 46 (1992) 909.
- [11] G.D. Parfitt, C.H. Rochester, *Adsorption from Solution at the Solid/Liquid Interface*, Academic Press, New York, 1983, p. 367.
- [12] C.L. Bird, W.S. Boston, *The Theory of Coloration of Textiles*, The Dyers Company Publications Trust, 1975, p. 112.
- [13] I.D. Rattee, M.M. Breuer, *The Physical Chemistry of Dye Adsorption*, Academic Press, London, 1974, p. 227.
- [14] Gordon M. Barrow, *Physical Chemistry*, McGraw-Hill, New York, 1988, pp. 420–422.
- [15] K.A. Connors, *Chemical Kinetics: The Study of Reaction Rates in Solution*, VCH, New York, 1990, pp. 334–336.
- [16] L. Schumack, A. Chow, *Talanta* 34 (1987) 957.
- [17] C.L. Bird, W.S. Boston, *The Theory of Coloration of Textiles*, The Dyers Company Publications Trust, 1975, p. 47.
- [18] C.L. Bird, W.S. Boston, *The Theory of Coloration of Textiles*, The Dyers Company Publications Trust, 1975, p. 54.
- [19] G. Marc Loudon, *Organic Chemistry*, Addison-Wesley, Reading, MA, 1984, p. 1187.

Calix(6)arene carboxylate derivative for solvent extraction separation of iron(III)

R.M. Khandwe, S.M. Khopkar *

Department of Chemical Technology, University of Bombay, Matunga, Bombay 400019, India

Received 24 January 1997; received in revised form 25 July 1997; accepted 29 July 1997

Abstract

Hexaacetatocalix(6)arene was used for the solvent extraction of iron(III). About 7.5×10^{-2} M extractant was used at pH 7.0 for the quantitative extraction of iron(III). The metal from the organic phase was stripped with 1.0 M hydrochloric acid and determined spectrophotometrically as its thiocyanate complex at 480 nm. Iron(III) was separated from large excesses of alkali and alkaline earths in the ratio 1:20. The transition and main group elements were tolerated in the ratio 1:10. The method was extended for the analysis of iron from its mineral, alloy and pharmaceutical preparation. The method is reproducible with $SD \pm 1.10\%$. © 1998 Elsevier Science B.V. All rights reserved.

Keywords: Iron (III); Separation; Solvent extraction calix(6)arene; Spectrophotometry; Analysis of alloy; Mineral and pharmaceutical samples

1. Introduction

Calixarenes are a class of macrocyclic compounds which show promise as complexing ligands for metals due to their chemical architecture [1,2]. The existence of upper, as well as lower, rim permits effective substitution of the functional group. One such replaceable group is the carboxylene group, i.e. acetate. Hexaacetato calix(6)arene was used in the solvent extraction of cobalt [3] and palladium [4].

Solvent extraction of iron(III) was carried out using several chelating extractants, such as dibenzoylmethane, 8-hydroxyquinoline or dithizone [5]. These methods were not satisfactory however, as either many other metals were coextracted, or anions such as EDTA created strong interference. Extraction with oxygenated solvents, including ethers, were not satisfactory, as in few instances iron(III) was incompletely extracted.

An attempt to use macrocyclic polyethers for solvent extraction of iron was not very encouraging. Dicyclohexyl 18crown6 (DC18C6), dibenzo 18crown6 (DB18C6), or 18crown6 (18C6) extracted iron(III) from 0.1 M hydrochloric acid only in the presence of salting agents such as

* Corresponding author. Present address: Department of Chemistry, Indian Institute of Technology, Bombay 400076, India. Fax: +91 22 5783245; e-mail: cryptand@ether.chem.iit.ernet.in

lithium chloride [6]. In such extractions, iron(III) was extracted with dicyclohexyl 18crown6 in the presence of titanous chloride from 9 M hydrochloric acid, but in such extraction [7] bivalent iron was only partially extracted.

Supramolecular compounds were never used for the solvent extraction separation of iron(III). In view of our earlier work on extraction of cobalt and palladium [3,4] it was thought worthwhile to explore the possibility of extracting iron(III) with an acetyl derivative of calix(6)arene. An endeavour is made to present such systematic investigations in this paper.

2. Experimental

2.1. Apparatus and reagent

A Jasco V-530 UV-visible spectrophotometer with matched 10 mm glass cuvetts was used.

A stock solution of iron(III) was prepared by dissolving 1.08 g ferric chloride in 250 ml of distilled water containing 5 ml of hydrochloric acid. When the solution was standardised complexometrically [8], it contained 500 µg/ml of iron(III). A diluted solution containing 50 µg/ml of iron(III) was prepared by tenfold dilution of the stock solution.

Hexaacetato-calix(6)arene was synthesised by the procedure reported earlier [3]. Potassium thiocyanate was used in a 2% aqueous solution. Buffer solution of pH 7.0 was prepared in usual manner [8].

2.2. Procedure

An aliquot of a solution containing iron(III) was taken and its pH was adjusted to 7.0 with diluted solution of acetic acid or ammonia solution. The total volume of the solution was made up to 10 ml. Following this, 10 ml of buffer solution (pH 7) was added before extraction. This practice was generally followed during routine extraction in preference to adjusting the pH of the solution. The solution was then transferred to a separatory funnel. To this was added

Table 1
Extraction of iron(III) as a function of pH

pH	Extraction (%)	Distribution ratio
1.0–3.0	0	—
4.0	8.7	0.09
5.0	23.1	0.29
6.0	63.1	1.71
6.5	92.9	13.08
7.0	99.7	∞
7.5	94.5	17.18
8.0	89.1	8.17
9.0	75.2	3.03
10.0	26.7	0.36

10 ml of a 7.5×10^{-2} M solution of hexaacetato-calix(6)arene in toluene. The solution was then shaken for 7 min. The two phases were allowed to settle and separate. Iron(III) from organic phase was stripped with 1 M hydrochloric acid and was determined spectrophotometrically as its thiocyanate complex [9] at 480 nm against the reagent blank. The iron content was computed from the calibration curve.

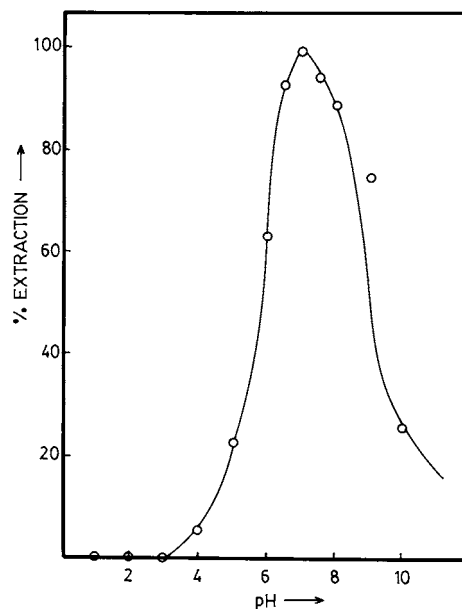


Fig. 1. Extraction of iron(III) as a function of pH.

Table 2
Extraction as the function of calix(6)arene concentration

Hexaacetatocalix(6)arene (1×10^{-2} M)	Volume of extractant (ml)	Extraction (%)	Distribution ratio (<i>D</i>)
0.01	10	0	—
0.1	10	54.0	1.17
1.0	10	74.3	2.89
2.5	10	89.1	8.17
5.0	10	93.1	13.49
7.5–20.0	10	99.9	∞
10.0	2.5	3.8	0.06
10.0	5.0	38.3	0.62
10.0	7.5	99.9	∞
10.0	10.0	99.9	∞
10.0	20.0	99.9	∞

Table 3
Extraction as a function of diluents

Diluents	Dielectric constant (ϵ)	Extraction (%)	Distribution ratio (<i>D</i>)
Benzene	2.28	38.3	0.62
Toluene	2.30	99.9	∞
Xylene	2.38	92.8	12.88
Nitrobenzene	34.80	81.7	4.46
Dichloromethane	9.08	58.1	1.38
Dichloroethane	10.50	41.3	0.70
Chloroform	4.80	33.1	0.49
Carbon tetrachloride	2.24	38.5	0.62
Cyclohexane	2.00	83.2	4.95

3. Results and discussion

3.1. Extraction as a function of pH

Iron(III) extracted in the pH range of 1.0–10.0 with 7.5×10^{-2} M hexaacetato calix(6)arene in toluene, when the extraction commenced at pH 4.0, was found to be 63% at pH 6.0 and was quantitative at pH 7.0 (Table 1; Fig. 1). Beyond pH 8.0 extraction began to decrease to 89.1%. Therefore, all extractions were carried out at pH 7.0 in the presence of the ammonium acetate–acetic acid buffer.

3.2. Extraction as a function of reagent concentration

Iron(III) was extracted with varying concentrations of hexaacetato calix(6)arene. The concentra-

tion of the reagent was varied from 1×10^{-2} to 10×10^{-2} M in toluene (Table 2). The extraction was 74% with 1×10^{-2} M extractant, but it was quantitative with 7.5×10^{-2} M of hexaacetato calix(6)arene. There was no special advantage in using higher concentrations of the reagent. The variation in the volume of reagent indicated that the large volume of 1×10^{-1} M of reagent led to no significant improvement in the extraction. Therefore, 10 ml of 10×10^{-2} M of extractant was used throughout these investigations for quantitative extraction of iron(III).

3.3. Extraction with various diluents

Iron(III) was extracted with 7.5×10^{-2} M hexaacetatocalix(6)arene with different solvents used as the diluents (Table 3). The extraction was quantitative only with toluene as the diluent. With

Table 4
Effect of various stripping agents

Stripping acid (M)	Extraction (%)				
	0.1	0.5	1.0	1.5	2.0
HCl	89.8	96.5	99.7	39.3	35.1
HNO ₃	89.1	94.9	99.6	89.8	86.1
H ₂ SO ₄	72.7	76.9	79.5	—	—
HClO ₄	49.6	71.0	80.9	54.1	44.4
CH ₃ COOH	3.80	42.4	60.9	63.4	70.2

Table 5
Effects of various ions

Ions	Ratio	Amount tolerated (µg)
K, Na, Ca, Sr, Ba, Cs, Mn(II)	1:20	1000
In, Al, Mg	1:10	500
Zn, Cd	1:5	250
Mo(VI), V(V)	1:1	50
Cl ⁻ , Br ⁻ , SO ₄ ²⁻ , SO ₃ ²⁻	1:60	3000
Ni, Pd, UO ₂ (II), Cu, Th(IV)	0	Interfere
Pt(IV), Rh(III), Co(II), Cr(IV)	0	Interfere

Fe(III), 50 µg.

all other solvents, it was incomplete. For instance, with xylene, nitrobenzene and cyclohexane it was less than 90%, while chloroform, carbon tetrachloride and benzene proved to be poor diluents. Therefore, for routine work, toluene was preferred as the diluent as it also allowed better phase separation.

3.4. Extraction with various stripping agents

After extraction of iron(III), the iron stripped using various mineral acids (Table 4). With 1 M

hydrochloric or 1 M nitric acid, the stripping was quantitative, while with all other acids stripping was incomplete. Stripping was 80% with perchloric acid and 70.0% with 2 M acetic acid. Therefore, 1 M hydrochloric acid was used as the stripping agent, as it facilitated colorimetric determination of iron(III) in chloride media.

3.5. Period of equilibration

The period of equilibration was varied from 1–10 min when iron(III) was extracted at pH 7.0 with 7.5×10^{-2} M hexaacetato-calix(6)arene. The extraction became quantitative within 5 min of shaking. Therefore, the equilibration period of 7 min was maintained during extraction.

3.6. Nature of extracted species

Iron(III) was extracted at pH 7 with varying concentration of an extractant. The plot of log *D* versus log [HR] where [HR] represents extractant concentration showed a slope of 1.45. Therefore, the probable composition of the extracted species is 1:2. Calixarene is a three dimensional network with varying annular space and basket like structure. The metal was trapped in the cone. In the absence of covalent bonding, the metal was held in winged the conformation, wherein aryl groups in the 1,4 position projected outwards like a pair of wings, perpendicular to the aryl groups viz. 2,3,5,6 forming a channel into which other molecules may sit. Thus, iron(III) was held firmly between two calixarene molecules by truly ionic attraction due to the substituted oxygen. However, these findings require further evidence in the form X-ray crystallographic investigations [10].

Table 6
Analysis of real samples

Sample	Iron(III) certified	Iron(III) found (g)	Recovery (%)	Error (±%)
Mineral	25.80	0.26	26.20	+0.40
Alloy	61.80	0.62	62.10	+0.30
Pharmaceutical preparation	36.00	0.025	36.05	+0.05

Average error, ±0.25%.

3.7. Effects of various ions

Iron(III) was extracted in the presence of varying proportions of different ions (Table 5). The tolerance limit was set as the amount of foreign ion causing an error of $\pm 2\%$ in the recovery of iron(III). Most of the anions were tolerated in the ratio 1:60, while alkali and alkaline earths were tolerated in the ratio of 1:20. Indium, aluminium and magnesium were tolerated in the ratio of 1:10 and zinc and cadmium were tolerated in the ratio of 1:5. Molybdenum(VI) and vanadium(V) were tolerated in the ratio of 1:1. However, nickel, copper, cobalt(II), chromium(VI), uranium(VI), palladium(II), platinum(VI) and thorium(IV) showed strong interference. Such interference was eliminated by using either sequestering agents or by resorting to the process of selective extraction.

3.8. Analysis of iron from real samples

The method was extended for the separation and determination of iron(III) from real samples. Such samples consisted of an alloy, mineral and pharmaceutical preparation.

The alloy or mineral samples (0.5 g) were dissolved in 10 ml of concentrated hydrochloric acid and diluted to 25 ml. An aliquot of solution (1 ml) was extracted at pH 7.0 with 10 ml of 7.5×10^{-2} M of hexaacetato calix(6)arene and iron(III) was stripped as usual. It was determined spectrophotometrically as its thiocyanate complex. The results of the analysis are shown in Table 6.

The sample of pharmaceutical (0.5 g) preparation containing iron(III) was dissolved in 10 ml of a mixture of nitric and hydrochloric acid (1:3) evaporated, dissolved in water and made up to a known volume. Iron(III) from the sample was extracted and was determined as per general procedure. The results are shown in Table 6.

4. Conclusion

The proposed method is simple, rapid and selective. It is suitable for separation of iron(III) from vanadium(V), molybdenum(VI), manganese(II) and aluminium(III), with which it is generally associated in minerals. The relative standard deviation was $\pm 1.1\%$ and the entire process of separation and determination requires just 30 min. As little as 10 μg of iron(III) can be easily separated and determined by the proposed method.

Acknowledgements

The Council for Scientific and Industrial Research as well as Department of Science and Technology are thanked for sponsoring this project. Thanks are also due to the Director, University Department of Chemical Technology, Bombay, for providing laboratory facilities.

References

- [1] M.N. Gandhi, S.M. Khopkar, Bull. Ind. Assoc. Nucl. Chem. Allied Sci. 10 (1994) 20.
- [2] D.M. Roundhill, Prog. Inorg. Chem. 43 (1995) 533.
- [3] A. Gupta, S.M. Khopkar, Talanta 42 (1995) 1493.
- [4] V.J. Mathew, S.M. Khopkar, Talanta 45 (1997) 1699.
- [5] A.K. De, S.M. Khopkar, R.A. Chalman, Solvent Extraction, Van Nostrand Reinhold, London, 1970.
- [6] H. Koshima, H. Onishi, Anal. Sci. 1 (1985) 389.
- [7] V.V. Yakshin, O.M. Vilkova, L.T. Makarova, N.A. Tarenko, B.N. Laskovin, Dokl. Acad. Nauk. 326 (1992) 117.
- [8] A.I. Vogel, Quantitative Inorganic Analysis, 3rd ed., Wiley, New York, 1962, p. 41.
- [9] F.D. Snell, Photometric and Fluorometric Methods of Analysis, Wiley, New York, 1978, p. 830.
- [10] U. Behrens, A.K. Brimah, T.M. Soliman, R.D. Fischer, D.C. Appcloy, N.A. Davies, R.K. Harris, Oragano Met. 11 (1992) 1718.

Determination of trace europium based on new fluorimetric system of europium(III) with thenoyltrifluoroacetone and *N,N'*-dinaphthyl-*N,N'*-diphenyl-3,6-dioxaoctanediamide

Wu Yang^a, Xiu-lan Teng^a, Miao Chen^a, Jin-zhang Gao^{a,*}, Li Yuan^a,
Jing-wan Kang^a, Qing-yu Ou^b, Shi-xia Liu^c

^a Department of Chemistry, Northwest Normal University, Lanzhou 730070, People's Republic of China

^b Lanzhou Institute of Chemical Physics, Chinese Academy of Sciences, Lanzhou 730000, People's Republic of China

^c Department of Chemistry, Lanzhou University, Lanzhou 730000, People's Republic of China

Received 17 April 1997; received in revised form 14 August 1997; accepted 19 August 1997

Abstract

In the present paper, *N,N'*-dinaphthyl-*N,N'*-diphenyl-3,6-dioxaoctanediamide acts as a specific reagent for enhancing the fluorescence intensity of Eu(III) complex with thenoyl trifluoroacetone (TTA), the spectrofluorimetric determination of trace amounts of Eu(III) based on the above system was carried out and its luminescence mechanism was studied. The excitation and emission wavelengths are 343.6 and 613.3 nm, respectively. The fluorescence intensities vary linearly with the concentration of europium(III) in the range 3.647×10^{-3} – $3.039 \mu\text{g ml}^{-1}$ for the original fluorescence with a detection limit down to $2.279 \times 10^{-4} \mu\text{g ml}^{-1}$ and the standard deviation is $0.063 \mu\text{g ml}^{-1}$ for 10 times measurements, and in the range 7.598×10^{-4} – $0.0243 \mu\text{g ml}^{-1}$ (SD = 0.035 for 15 times measurements), 0.06078 – $0.6100 \mu\text{g ml}^{-1}$ (SD = 0.52 for 10 times measurements) for the first derivative fluorescence signal with a detection limit down to $8.566 \times 10^{-5} \mu\text{g ml}^{-1}$. The interferences of other rare earths and some of inorganic ions are described. This method is a direct, rapid, selective and sensitive analytical method for the determination of trivalent europium in rare earth ore samples and high purity of rare earth oxides. © 1998 Elsevier Science B.V. All rights reserved.

Keywords: Europium determination; Fluorimetry; Thenoyltrifluoroacetone; *N,N'*-dinaphthyl-*N,N'*-diphenyl-3,6-dioxaoctanediamide

1. Introduction

The chemical properties of the rare earth elements are very similar, consequently, it is difficult to find specific reactions for individual ions, espe-

cially in their mixtures. Due to higher sensitivity and selectivity, fluorescence analyses of rare earth elements have attracted much attention and have also long since become a major subject of our studies [1–6].

Macrocyclic crown ethers, and their open-chain analogues show a high complexation selectivity,

* Corresponding author.

which makes them suitable reagents for investigation of separation and determination of lanthanide ions [7]. When delocalized groups, such as phenyl-, naphthyl-, are introduced onto these polyethers, they will serve as potential luminescent label reagents.

The purpose of this work is to develop a highly sensitive, well selective fluorescent system for the determination of trivalent europium based on the Eu^{3+} ternary complex with thenoyl trifluoroacetone (TTA) and *N,N'*-dinaphthyl-*N,N'*-diphenyl-3,6-dioxaoctanediamide (DDD) in *N*-cetylpyridium chloride (CPC) solution and study its luminescence mechanism.

2. Experimental

2.1. Reagents

Stock solution of Eu^{3+} was prepared by dissolving a desired amount of Eu_2O_3 (99.99% pure), purchased from Hunan rare earth metals institute, People's Republic of China, in concentrated hydrochloric acid, evaporating to near dryness and diluting to the scale with water. *N,N'*-dinaphthyl-*N,N'*-diphenyl-3,6-dioxaoctanediamide (DDD) was synthesized according to the literature [8] and recrystallized product was directly dissolved by acetone to prepare working solution. Other reagents used were of analytical reagent grade and were at least 99.5% pure. Ultrapure deionized water was employed for all dilutions. In experiments, acetone above 4% (V/V) strongly quenches the fluorescence of the complex, so the amount of acetone should be strictly controlled.

2.2. Apparatus

Fluorescence measurements were made on a Shimadzu RF-540 spectrofluorophotometer equipped with a Xenon light source, quartz cuvettes of 1 cm path length and a DR-3 data recorder. The excitation and emission slits were 10 nm. The pH of the solutions used was measured with a SPM-10 acidity meter made in Shanghai, People's Republic of China.

2.3. Procedure

Apparent fluorescence excitation and emission spectra were obtained at room temperature and optimum excitation and emission wavelengths were found from the recording spectra. An appropriate amount of Eu^{3+} , 0.30 ml of $1 \times 10^{-2} \text{ mol l}^{-1}$ TTA, 0.40 ml of $5 \times 10^{-3} \text{ mol l}^{-1}$ DDD, 0.50 ml of $5 \times 10^{-3} \text{ mol l}^{-1}$ CPC and 1 ml of NaAc-HAc (pH = 4.75) buffer were pipetted onto

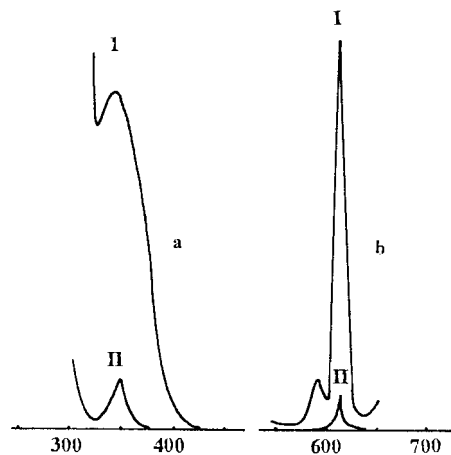


Fig. 1. Fluorescence excitation and emission spectra of the ternary system of $\text{Eu}(\text{III})$ with TTA and DDD(I) and the binary system of $\text{Eu}(\text{III})$ with TTA(II). (a) Excitation spectra; (b) emission spectra. $[\text{Eu}(\text{III})] = 1.0 \times 10^{-6} \text{ mol l}^{-1}$, $[\text{TTA}] = 2.0 \times 10^{-4} \text{ mol l}^{-1}$, $[\text{DDD}] = 1.0 \times 10^{-4} \text{ mol l}^{-1}$, $[\text{CPC}] = 2.5 \times 10^{-4} \text{ mol l}^{-1}$ and pH = 4.75.

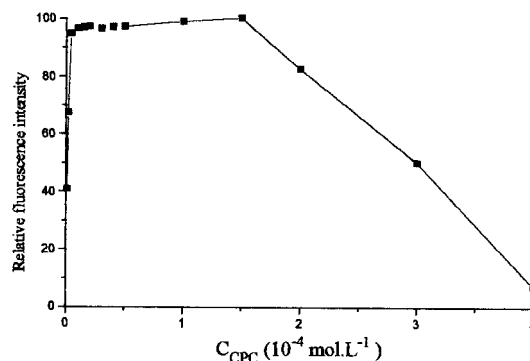


Fig. 2. The relationship between relative fluorescence intensity and the concentration of *N*-cetylpyridium chloride. $[\text{Eu}(\text{III})] = 0.06078 \mu\text{g ml}^{-1}$, $C_{\text{TTA}} = 1.2 \times 10^{-4} \text{ mol l}^{-1}$, $C_{\text{DDD}} = 8.0 \times 10^{-5} \text{ mol l}^{-1}$, pH = 4.75 and $\lambda_{\text{ex}} = 343.6 \text{ nm}$, $\lambda_{\text{em}} = 613.5 \text{ nm}$.

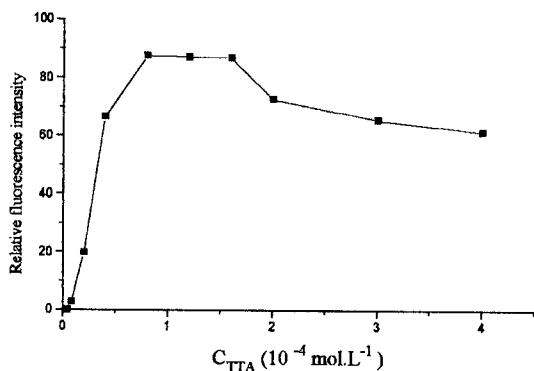


Fig. 3. The relationship between relative fluorescence intensity and the concentration of thenoyltrifluoroacetone. $[\text{Eu(III)}] = 0.06078 \mu\text{g ml}^{-1}$, $C_{\text{DDD}} = 8.0 \times 10^{-5} \text{ mol l}^{-1}$, $C_{\text{CPC}} = 1.0 \times 10^{-4} \text{ mol l}^{-1}$, $\text{pH} = 4.75$ and $\lambda_{\text{ex}} = 343.6 \text{ nm}$, $\lambda_{\text{em}} = 613.5 \text{ nm}$.

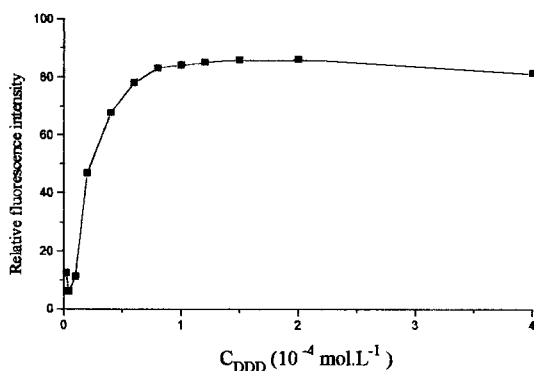


Fig. 4. The relationship between relative fluorescence intensity and the concentration of *N,N'*-dinaphthyl-*N,N'*-diphenyl-3,6-dioxaoctanediamide. $[\text{Eu(III)}] = 0.06078 \mu\text{g ml}^{-1}$, $C_{\text{TTA}} = 1.2 \times 10^{-4} \text{ mol l}^{-1}$, $C_{\text{CPC}} = 1.0 \times 10^{-4} \text{ mol l}^{-1}$, $\text{pH} = 4.75$ and $\lambda_{\text{ex}} = 343.6 \text{ nm}$, $\lambda_{\text{em}} = 613.5 \text{ nm}$.

a 25-ml calibrated tube, respectively. The mixture was diluted to 25 ml with deionized water. After 10 min, fluorescence determination was carried out at 613.5 nm keeping the excitation wavelength at 343.6 nm.

3. Results and discussion

3.1. Fluorescence spectra

The complex of europium(III) with TTA and DDD emits strong Eu^{3+} characteristic fluores-

cence sensitized by the ligands in surfactant CPC and NaAc-HAc ($\text{pH} = 4.75$) buffer solution, and Eu(III) is the only lanthanide ion which is appreciably fluorescent under these conditions. Other lanthanide ions do not show measurable fluorescence in this system except for trivalent samarium ion that shows a very weak luminescent signal.

Fig. 1 shows excitation and emission spectra of Eu(III)-TTA-DDD ternary system (I) in $2.5 \times 10^{-4} \text{ mol l}^{-1}$ CPC solution with $\text{pH} = 4.75$ and corresponding Eu(III)-TTA binary system(II).

Eu^{3+} -TTA binary system fluoresced weakly at $\lambda_{\text{em}} = 613.2 \text{ nm}$ when irradiated with ultraviolet light $\lambda_{\text{ex}} = 348.4 \text{ nm}$. But when DDD was introduced in the above system the fluorescence inten-

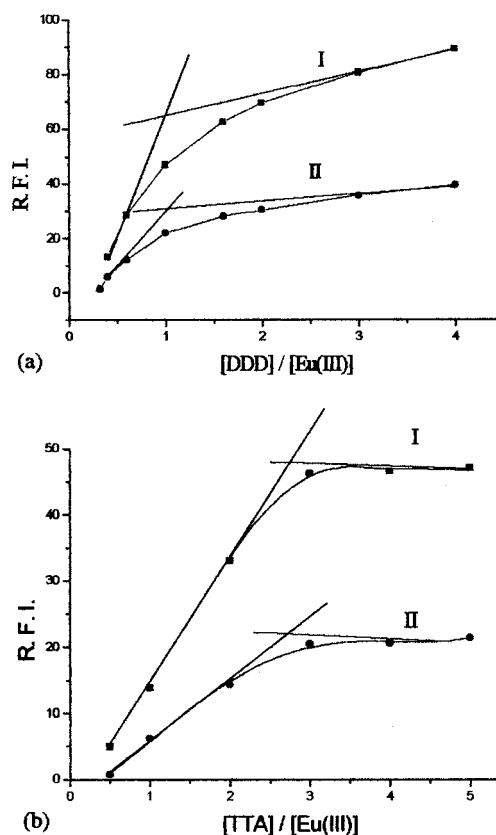


Fig. 5. Composition determination of the ternary complex. $C_{\text{CPC}} = 1.0 \times 10^{-4} \text{ mol l}^{-1}$, $\text{pH} = 4.75$ and $\lambda_{\text{ex}} = 343.6 \text{ nm}$, $\lambda_{\text{em}} = 613.5 \text{ nm}$. (I) $[\text{Eu(III)}] = 4.0 \times 10^{-7}$; (II) $[\text{Eu(III)}] = 2.0 \times 10^{-7} \text{ mol l}^{-1}$.

Table 1
Effect of foreign ions on the determination of $0.1520 \mu\text{g ml}^{-1}$ Eu(III)

Interference ions	Tolerance limit (M)/(Eu)	Interference ions	Tolerance limit (M)/(Eu)
La ³⁺	30	Mg ²⁺	500
Ce ³⁺	110	K ⁺	900
Pr ³⁺	250	Zn ²⁺	1500
Nd ³⁺	300	Pb ²⁺	1000
Sm ³⁺	100	Cu ²⁺	80
Gd ³⁺	80	Fe ²⁺	60
Tb ³⁺	50	Fe ³⁺	20
Dy ³⁺	460	NO ₃ ⁻	600
Ho ³⁺	60	SO ₄ ²⁻	800
Er ³⁺	60	Na ⁺	> 10000
Tm ³⁺	30	NH ₄ ⁺	> 10000
Yb ³⁺	10	Cl ⁻	> 10000
Lu ³⁺	20	Br ⁻	> 10000
Y ³⁺	50	Ac ⁻	> 10000
Ca ²⁺	800		

sity of the mixture solution was enhanced by 10–100-folds, λ_{ex} shifted to 343.6 nm and λ_{em} to 613.5 nm. For hydrate trivalent europium ion, very weak emission was observed at $\lambda_{\text{em}} = 609.2$ nm with 279.6 nm exciting. Under optimum conditions, no appreciable emissions at above emission wavelengths were observed for the free reagents without Eu(III) ion. It is evident that DDD sensitizes luminescence of europium(III) binary complex with TTA through intramolecular energy transfer [9].

Under the determinate conditions, other β -diketone, such as dibenzoyl methane, acetylacetone, benzoylacetone, or 1-phenyl-3-methyl-4-benzoyl-pyrazolene-5 as primary ligand and DDD as secondary ligand did not sensitize Eu(III) fluorescence.

3.2. Factors affecting relative fluorescence intensity

Because DDD does not dissolve in water, appropriate surfactant must be added to enhance its water-solubility. In this paper, two kinds of cationic surfactants, i.e. *N*-cetylpyridium chloride (CPC), cetyltrimethyl ammonium bromide (CTMAB); three kinds of anionic surfactants, i.e. sodium dodecylbenzene sulfonate (DBS), sodium naphthyl-1,5-disulfonate (NDS) and sodium lau-

ryl sulfate (LS); and two kinds of non-ionic surfactants, i.e. Triton X-100 and polyethylene glycol octaphenyl ether (emulsifier OP) were tested. It was shown that all of the surfactants mentioned above made DDD soluble in water media. However, in CPC solution the ternary complex of trivalent europium ion with TTA and DDD emits the strongest fluorescence, so CPC was applied in further experiments.

The effect of *N*-cetylpyridium chloride concentration on the fluorescence intensity was investigated. Fig. 2 shows that when CPC concentration is less than $4.0 \times 10^{-6} \text{ mol l}^{-1}$, the fluorescence intensity increases with CPC concentration increasing. When the concentration of CPC reaches $4.0 \times 10^{-6} \text{ mol l}^{-1}$ the fluorescence intensity reaches constant until $1.5 \times 10^{-4} \text{ mol l}^{-1}$ where the fluorescence intensity starts to decrease. In further experiments a $1.0 \times 10^{-4} \text{ mol l}^{-1}$ CPC solution was employed.

Fig. 3 shows the influence of the amount of TTA on luminescence intensity. When the concentration of TAA was controlled between 8.0×10^{-5} and $1.6 \times 10^{-4} \text{ mol l}^{-1}$, the system showed the strongest fluorescence intensity, and the excess of TTA made the complex fluorescence quench slightly owing to the reagent self-absorption. Therefore, $1.2 \times 10^{-4} \text{ mol l}^{-1}$ was selected as optimum TTA concentration. Fig. 4 shows the

Table 2
Determination of europium in high purity of Y₂O₃ matrix

Y ₂ O ₃ samples ^b	Added (μg ml ⁻¹)	Found (μg ml ⁻¹)	Average (μg ml ⁻¹)	Recovery (%)	RSD.% ^a
1	0	0.00415, 0.00415, 0.00417, 0.00418, 0.00418	0.00417		0.36
2	0.0152	0.0193, 0.0193, 0.0193, 0.0192, 0.0192	0.0193	99.5	0.28
3	0.0228	0.0260, 0.0260, 0.0261, 0.0261, 0.0258	0.0260	95.7	0.47
4	0.0304	0.0340, 0.0340, 0.0342, 0.0341, 0.0341	0.0341	98.5	0.25
5	0.0380	0.0419, 0.0422, 0.0419, 0.0427, 0.0423	0.0422	100	0.79

^a Relative standard deviation.

^b Containing 0.8891 μg ml⁻¹ Y(III).

effect of the DDD concentration on the determination signal fluoresced by the ternary complex solution containing 4.0×10^{-7} mol l⁻¹ of europium. The maximum fluorescence intensity lies between 6.0×10^{-5} mol l⁻¹ and 2.0×10^{-4} mol l⁻¹, and higher DDD concentration decreased the fluorescence intensity. Besides, in a solution containing higher concentration of DDD appeared some deposit. So a reagent concentration of 8.0×10^{-5} mol l⁻¹ was taken as optimum.

The pH effect was studied in the range of 2.00–11.00 by adjusting the pH with 0.5 mol l⁻¹ hydrochloric acid or the same concentration of sodium hydroxide solution. The results indicate that the emission intensity remained constant in the pH range of 4.50–6.50. After having studied a series of different buffer systems, it was found that the fluorescence was the strongest in sodium acetate—acetic acid buffer. Hence this buffer with pH = 4.75 was used. And the results showed that 1 ml was the optimum amount of NaAc-HAc buffer.

The effect of the time on the fluorescence intensity was investigated with 0.06078 μg ml⁻¹ Eu(III) in NaAc-HAc buffer solution (pH = 4.75). The results show that the solutions were allowed to stand under normal laboratory conditions. The maximum fluorescence intensity can keep at least 5 h. Continuous irradiation for 24 h caused reduction of 10.9% in the fluorescence intensity.

3.3. Composition of the ternary complex

The stoichiometry of the Eu(III)-TTA-DDD

ternary complex in CPC and NaAc-HAc buffer solution was measured by Job's continuous variation method. The results were shown in Fig. 5. As shown in Fig. 5(a), in the ternary complex the composition ratio of DDD and Eu(III) is 1:1, and similarly the composition ratio of TTA and Eu(III) is 3:1. So the ternary complex has a composition formula of Eu(TTA)₃DDD.

3.4. Calibration graph

The calibration graph for the determination of Eu(III) was constructed under the optimal conditions with original signal and the first derivative fluorescence signal ($\Delta\lambda = 5$ nm) respectively. Excellent linearity $F = 0.3174 + 117.52 C_{Eu}$ ($R = 0.99953$, and $SD = 0.063$ for 10 times measurements) was obtained over the range 3.647×10^{-3} – $3.039 \mu\text{g ml}^{-1}$ Eu³⁺ for the original fluorescence, and $F = 2.4317 + 1221.60 C_{Eu}$ ($R = 1$, $SD = 0.035$ for 15 times measurements) over the range 7.598×10^{-4} – $0.02431 \mu\text{g ml}^{-1}$ Eu³⁺ and $F = 3.4744 + 70.517 C_{Eu}$ ($R = 0.99932$, $SD = 0.52$ for 10 times measurements) over the range 0.06078 – $0.6100 \mu\text{g ml}^{-1}$ Eu³⁺ for the first derivative fluorescence signal. The detection limits were down to 2.279×10^{-4} and $8.566 \times 10^{-5} \mu\text{g ml}^{-1}$, respectively, that were calculated by multiplying the standard derivation of 15 blank measurements by three and dividing by the slope of the linear calibration curve. The results showed that the first derivative method is more sensitive than original fluorescence method in this system.

Table 3
Analysis of the rare earth ore sample

Baotou ore sample ^a	Known Eu ₂ O ₃ %	Found Eu ₂ O ₃ %	Average Eu ₂ O ₃ %	Recovery (%)	RSD (%)
	0.20%	0.205, 0.208, 0.213, 0.197, 0.215	0.208	103.8	3.43

^a Rare earth chloride ore sample was supplied as present by Baotou Rare Earth with a composition La₂O₃ (23.0%), CeO₂ (50.0%), Pr₆O₁₁ (4.60%), Nd₂O₃ (15.0%), Sm₂O₃ (1.10%–1.40%), Eu₂O₃ (0.20%), Gd₂O₃ (0.36%), all of other heavy rare earth oxides are less than 1.0%.

The effects of various ions on the determination of Eu(III) ion with a concentration of 0.1520 µg ml⁻¹ were investigated by the proposed method in order to determine its selectivity and its potential application to the assay of Eu(III) in ore samples and rare earth oxides. The results are given in Table 1. Tolerance limit in Table 1 is the highest tolerance amount of foreign ions when relative error is not more than 5% for europium determination.

4. Application of the method

The procedure was used to the determination of trace amounts of europium in high purity of Y₂O₃ matrix and Baotou rare earth ore samples. The results shown in Tables 2 and 3 revealed that the developed method is very suitable and can be successfully used. From the results presented it can be concluded that the proposed method is a simple, rapid, stable, sensitive and selective method for the determination of trace europium.

Acknowledgements

The authors are very grateful to Gansu Province Natural Science Foundation for Youth (ZQ-96-07) and Gansu Province Education commission of China for their financial support.

References

- [1] J.Z. Gao, J. He, X.W. Wang, Z.M. Wang, G.B. Bai, *Analyst* 112 (1987) 1080.
- [2] J.Z. Gao, J. He, X.W. Wang, G.B. Bai, *Inorg. Chim. Acta* 140 (1987) 273.
- [3] X.Z. Du, J.Z. Gao, Q. Xie, J.W. Kang, *Talanta* 41 (1994) 201.
- [4] J.Z. Gao, G.H. Zhao, J.W. Kang, C.Y. Li, *Analyst* 120 (1995) 2081.
- [5] J.Z. Gao, G.H. Zhao, J.W. Kang, *Talanta* 42 (1995) 1497.
- [6] G.H. Zhao, J.Z. Gao, J.W. Kang, *Bull. Soc. Chim. Belg.* 105 (1996) 445.
- [7] J.c.G. Bunzli, in: K.A. Gschneidner Jr., L. Eyring (Eds.), *Handbook on the Physics and Chemistry of Rare Earths*, Ch. 60, Elsevier, Amsterdam, 1987.
- [8] S.X. Liu, W.S. Liu, X.L. Wang, M.Y. Tan, *Polyhedron* 14 (1995) 3605.
- [9] G.Z. Chen, X.Z. Huang, Z.Z. Zheng, J.G. Xu, Z.B. Wang, *Fluorimetric Analytical Method (Chinese)*, 2nd Edn., Science Press, Beijing, 1990.

Determination of yttrium, scandium and other rare earth elements in uranium-rich geological materials by ICP–AES

G.V. Ramanaih *

Chemical Laboratory, Atomic Minerals Division, Department of Atomic Energy, Begumpet, Hyderabad-500 016, India

Received 6 March 1997; received in revised form 25 August 1997; accepted 28 August 1997

Abstract

A rapid method is described for the determination of yttrium, scandium, and other rare earth elements (REEs) in uranium-rich geological samples (containing more than 0.1% U) and in pitch blende type of samples by inductively coupled plasma atomic emission spectrometry (ICP–AES) after separation of uranium by selective precipitation of the analytes as hydroxides using $H_2O_2/NaOH$ in the presence of iron as carrier. Uranium goes into solution as soluble peruranate complex. The precipitated rare earth hydroxides (including Y and Sc) are filtered and dissolved in hydrochloric acid prior to their aspiration into plasma for their individual estimation after selecting interference free REE emission lines. The method has also been applied to some international reference standards like SY-2 and SY-3 (by doping a known amount of uranium) along with one in-house pitch blende sample and the REE values were found to be in agreement with the most usable values, offering an R.S.D. of 1–8.8% for all the REEs, Y and Sc. The method compared well, with the well-established cation exchange separation procedure. © 1998 Elsevier Science B.V. All rights reserved.

Keywords: Rare earth elements; Yttrium; Scandium; Geological materials; Inductively coupled plasma atomic emission spectrometry

1. Introduction

The determination of the rare earth elements in silicate rocks and their constituent minerals is of fundamental importance to modern petrological studies on the origin of igneous, metamorphic and sedimentary rocks. The processes by which rocks have formed have been greatly helped, by a knowledge of the rare earth elements (REE) con-

tents, and accurate determination of the concentrations of these elements in a wide variety of rocks has formed the basis for much research effort by geochemists in recent years. The comparative behaviour of the rare earths together with major elements, trace elements and selected isotopic concentrations are the most widely used data recorded in the recent geochemical literature.

The use of U, Th in nuclear reactors places stringent demands on the levels of impurities and about 35 trace elements are listed in the C787 [1] specifications issued by ASTM for UF_6 and high

* Tel.: +91 40 844101; +91 40 849940; e-mail: Dir@amdhyd.ernet.in

purity ThO₂. Therefore, some of the REEs' like Sm, Gd, Dy, Tb, Er, and Tm, if present in uranium are harmful to the efficient functioning of a nuclear reactor, even in sub microgram level due to their large neutron absorption cross-section. Furthermore, the determination of REEs' is important due to an increasing demand in the industrial and metallurgical fields. Accurate determination of the REEs' in uranium-rich geological materials, as well as in nuclear grade uranium, is therefore, essential prior to its use as a nuclear fuel at different stages.

In case of high uranium-bearing geological samples a preliminary separation of the REEs' is to be carried out to avoid spectral, as well as the matrix interferences of uranium on Sm, Gd, Tb, Er and Tm. Furthermore, uranium being a line rich emitter in inductively coupled plasma (ICP)-source, emits more than 1500 lines [2] thereby interfering on almost all emission lines of the studied elements. Therefore, uranium has to be separated from the trace REE as soluble peruranate complex by treating the sample solution with H₂O₂ in the presence of NaOH prior to their quantification by inductively coupled plasma atomic emission spectrometry (ICP-AES). Iron is used as carrier substrate for trace rare earth hydroxides during the separation of uranium.

A number of instrumental methods are now available for accurate determination of REEs' at various concentration levels viz. instrumental neutron activation analysis (INAA) [3], atomic absorption spectrometry (AAS) [4], spectrophotometry [5], X-ray fluorescence spectrometry (XRF) [6], DC arc emission spectrography [7], electron microprobe analysis (EMPA) [8], ICP-AES [9–13] and inductively coupled plasma mass spectrometry (ICP-MS) [14]. ICP-AES has now been established as a powerful analytical technique for the estimation of REEs' in the presence of high amounts of matrix elements preferably after separation of major elements by cation exchange column chromatography [15,16], solvent extraction [13] from uranium before quantification. Several workers have studied the applications of ICP-AES for the determination of REEs' in high uranium bearing samples [13,17–19] after chemical separation.

The present investigation reports separation of REE from U-dominant geological samples and subsequent estimation using ICP-AES. Uranium is separated as soluble peruranate complex formed using NaOH and H₂O₂ while REEs' are removed as insoluble hydroxides in the presence of 'Iron' as carrier. Furthermore, the proposed separation technique is very simple, rapid and without the need of costlier ion exchange resins. The method can be applied on a routine basis for such type of samples without adhering to any stringent operating conditions of acidity, elution rate, aqueous-to-organic volume ratio, etc. with more sample throughput, unlike in other cases of separation methods like ion exchange/solvent extraction technique.

2. Experimental

2.1. Instrumentation

All measurements were made using a ICP-AES model-8410 (GBC, Australia) plasmascan spectrometer, employing a computer controlled rapid scanning monochromator with the operating parameters presented in Table 1. The readings were obtained using a single point calibration method by calibrating the instrument with 1 µg/ml for, Sc, Eu, Yb, and Lu and 10 µg/ml for Y and the rest of the REE. The detection limits obtained under the above optimised conditions

Table 1
ICP-AES instrumental parameters and operating conditions

R.F. generator	27.12 MHz, crystal controlled
Forward power	1200 W
Reflected power	<5 W
Observation height	14 mm above load coil
PMT voltage	1000 V
Integration time	3 s (<i>n</i> = 3)
Entrance slit	20 µm and 3 mm height (fixed)
Exit slit	40 µm
Sample flush time	10 s
Argon gas flow rates:	
Coolant	14 l/min
Auxiliary	1.0 l/min
Sample	0.8 l/min
Solution uptake rate	3.0 ml/min

Table 2
Analytical results of REEs Y, Sc in in-house pitch blende type of sample as per procedure (data $\mu\text{g/g}$)

Element	Wavelength (nm)	Pitch blende		
		a (P.M.)	b (% R.S.D.)	c (I.E)
Sc	361.384	5.2	5.8	6.0
Y	371.030	447	1.1	440
La	333.749	740	1.2	750
Ce	418.660	2582	1.2	2572
Pr	422.293	422	1.1	425
Nd	430.358	1640	1.2	1677
Sm	442.434	398	1.0	398
Eu	381.967	39	3.8	39
Gd	364.619	301	1.7	304
Tb	350.917	14	5.7	15
Dy	353.170	100	1.5	102
Ho	345.600	9	4.5	11
Er	349.910	11	4.0	10
Tm	346.220	<5	—	<5
Yb	328.937	6	6.3	8
Lu	261.542	1.7	8.8	<5

(a) P.M, present method (average of five values).

(b) % R.S.D. by the present method.

(c) I.E, ion exchange method [15].

are in the range of 0.00014 $\mu\text{g/ml}$ in case of Lu (261.542 nm) to 0.0099 $\mu\text{g/ml}$ for Pr (422.293 nm), as reported [20] in an earlier publication from our laboratory.

2.2. Chemicals

All single element REE, Y, Sc (as oxides) 1.0 mg/ml standard stock solutions are made by dissolving Spec Pure rare earth oxides in hydrochloric acid, except CeO_2 (dissolved in a mixture of HNO_3 and H_2O_2 and later converted to HCl medium. Single element working standards were prepared (10 $\mu\text{g/ml}$) by dilution of the stock solution with 0.5 M HCl. Acids and all other chemicals used are of analytical reagent grade.

2.3. Procedure

2.3.1. Uranium rich samples (pitch blende) and other geological samples (U-content 0.1% and above)

Rock sample, 1.0 g, was weighed into 100 ml beaker and treated with 10 ml of 1:2 (HNO_3 :HCl)

mixture and evaporated to dryness on water bath (90°C). The process was repeated, and digested with 50 ml of 0.5 M HCl and filtered. The residue, after ignition in a platinum crucible, was treated with HF and then with HCl, finally fused with 1 g of Na_2CO_3 and dissolved in 0.5 M HCl solution. Both filtrate and residue solutions were combined. Ammonium chloride/ammonium hydroxide precipitation was carried out and if no precipitate was observed, 5 mg of iron solution was added as carrier. The resultant precipitate, after filtration, dissolved in a minimum quantity of HNO_3 and evaporated to dryness in a 100 ml beaker. The residue was digested with 5 ml of 1:4 HNO_3 and treated with 5 ml of H_2O_2 (100 vol) and 20 ml of NaOH (12.5 M) solution and digested in the cold with another 30 ml of distilled water and kept aside for 1 h to allow the precipitate to settle. The precipitate was filtered and washed with 1 M NaOH and 1% (v/v) H_2O_2 solution to make it free from uranium. The process repeated again to decontaminate uranium from the rare earth hydroxides. Finally, the precipitate was transferred from filter paper into a beaker with a few drops of

Table 3

Analytical data for Y, Sc, and REEs' in CCRMP standard reference sample SY-2, (Syenite) (data in $\mu\text{g/g}$)

Element	Wavelength (nm)	SY-2				
		a (P.M)	b (% R.S.D.)	c (I.E)	d (R.V)	e (R.V)
Sc	361.384	7.31	5.5	7.0	7.0	—
Y	371.030	120	1.25	116	128	126 \pm 1
La	333.749	80	1.25	75	75	73 \pm 1
Ce	418.660	166	1.20	164	175	164 \pm 2
Pr	422.293	19	6.3	19	18.8	21 \pm 0.5
Nd	430.358	75	1.3	74	73	80 \pm 2
Sm	442.434	18	6.1	18	16.1	16.5 \pm 0.5
Eu	381.967	3	7.3	2.7	2.42	2.6 \pm 0.1
Gd	364.619	15	6.6	14	17	17 \pm 1
Tb	350.917	4	6.2	3.8	2.5	3 \pm 0.5
Dy	353.170	19	6.3	21.8	18	21.3 \pm 0.3
Ho	345.600	3.3	6.1	4.3	3.8	5 \pm 0.2
Er	349.910	14	7.8	14.2	12.4	15.4 \pm 0.4
Tm	346.220	3.3	6.1	2.6	2.1	2.6 \pm 0.2
Yb	328.937	18	5.5	18.8	17	18.4 \pm 0.5
Lu	261.542	3.3	6.1	2.8	2.7	3.1 \pm 0.1

Sample solutions were doped with 200 mg of uranium and the decontamination for U was effected using the recommended procedure.

(a) P.M, present method ($\mu\text{g/g}$) (average of five values).

(b) % R.S.D., by the present method.

(c) I.E, ion exchange method ($\mu\text{g/g}$) [13].

(d) R.V, recommended value [23].

(e) R.V, recommended value [24].

concentrated HCl and distilled water and dissolved. The solution was made up to 100 ml in 0.5 M HCl.

The estimation of REEs', Y, Sc was carried out at the wavelengths listed in Table 2, Table 3, Table 4, and Table 5 using operating parameters presented in Table 1.

The above separation procedure was tested by adding a known amount of U (200 mg) to CCRMP standards like SY-2 and SY-3.

The method was applied to pitch blende sample and to geological samples. The geological sample solutions were doped with 200 mg of uranium and the decontamination of U was effected using the above recommended procedure. The results obtained along with their % R.S.D. are presented in Table 2, Table 3, Table 4 and Table 5 to validate the efficacy of the proposed procedure. The major matrix element composition of the inhouse pitch blende sample is presented in Table 6.

3. Results and discussion

Calcium, if present, in the sample solutions was found to adsorb uranium while separating uranium as peruranate with NaOH and H_2O_2 and incomplete separation of uranium was observed. For this reason calcium was separated at the stage of solution preparation by carrying out $\text{NH}_4\text{Cl}/\text{NH}_4\text{OH}$ precipitation. This also removes other matrix elements, e.g. Mg including Na from the Na_2CO_3 flux.

Fig. 1(a) shows the chondrite normalized (C_1) plot in respect of REEs' present in the pitch blende sample. $X_{(\text{CN})}$ represents the REE value in the sample divided by the respective REE value of chondrite [21]. The ratios of individual REEs' were plotted against the respective at. no. of the element. REE concentrations in rocks or minerals are usually normalized to a common reference standard, which most commonly comprises the values for chondritic meteorites. Chondritic mete-

Table 4

Analytical data for Y, Sc and REEs^a in CCRMP standard reference sample SY-3 (Syenite) (data in µg/g)

Element	Wavelength (nm)	SY-3				
		a (P.M)	b (% R.S.D.)	c (I.E)	d (R.V)	e (R.V)
Sc	361.384	7	5.5	—	6.8	—
Y	371.030	710	1.1	698	718	715 ± 4
La	333.749	1326	1.1	1360	1340	1350
Ce	418.660	2239	1.3	2237	2230	2250 ± 40
Pr	422.293	233	1.3	238	223	239
Nd	430.358	696	1.1	764	670	760 ± 4
Sm	442.434	146	1.4	145	109	134 ± 2
Eu	381.967	18	5.5	19.6	17	18.3 ± 0.4
Gd	364.619	100	1.5	112	105	121 ± 1
Tb	350.917	17	6.5	24	18	15 ± 0.2
Dy	353.170	130	1.1	131.6	118	138 ± 2
Ho	345.600	18	5.4	27.8	29.5	29 ± 0.5
Er	349.910	82	1.5	85	68	88 ± 1
Tm	346.220	12.7	8.7	12.5	11.6	12.5 ± 0.5
Yb	328.937	63.4	1.6	68.7	62	71 ± 1
Lu	261.542	9.7	5.2	8.3	7.9	8.6 ± 0.2

Sample solutions were doped with 200 mg of uranium and the decontamination of U was effected using the recommended procedure.

(a) P.M, present method (average of five values) (µg/g).

(b) % R.S.D., by the present method.

(c) I.E, ion exchange method (µg/g) [13].

(d) R.V, recommended value [23].

(e) R.V, recommended value [24].

orites were chosen because they are thought to be relatively unfractionated samples of the solar system dating from the original nucleosynthesis. However, the concentrations of REE in the solar system are very variable because of the different stabilities of the atomic nuclei. REE with even atomic numbers are more stable and, therefore, more abundant than the REE with odd atomic numbers, producing a zig-zag pattern on a composition abundance diagram.

Therefore, chondrite normalization (i.e. the REE value in the sample divided by the respective REE value of chondrite, $X_{(CN)}$) has two important functions:

1. it eliminates the abundance variation between odd and even atomic number elements; and
2. it allows any fractionation of the REE group relative to chondritic meteorites to be identified like in the case of the Eu- or Ce-anomaly.

The anomaly is positive if $(X_{(CN)} \div X_{(CN)}^*) > 1$ where $X_{(CN)}^*$ is the extrapolated value between the two successive points in the chondrite-normalised plot, and the anomaly, is negative, if the ratio < 1 , indicating oxidizing or reducing conditions or the environment, respectively, during the paragenesis of various crystallising phases. The value of $Y_{(CN)}$ was plotted between those for $Dy_{(CN)}$ and $Ho_{(CN)}$ because of the similarity in properties and ionic radii of the three elements. The crustal abundance [22] of yttrium, Fig. 1(b) shows an excellent agreement with the interpolated value. The REE pattern with a striking negative Eu-anomaly indicates that the studied pitch blende was formed either from Eu-depleted solutions or under a reducing environment during its paragenesis from the solidifying magma.

In geological samples containing high uranium (> 1000 ppm) due to its line rich emission spectra interferes on all the REE ion emission lines and although alternate (interference free) lines could

Table 5
Analytical results for REEs, Y, Sc and REEs' in geological samples (data $\mu\text{g/g}$)

Sample	Sc	Y	La	Ce	Pr	Nd	Sm	Eu	Gd	Tb	Dy	Ho	Er	Tm	Yb	Lu
4595																
a	4.8	206	277	461	52	206	42	1.8	32	6	36	6	24	3.2	22	2.7
b	4.2	1.4	1.4	1.1	1.3	1.40	2.4	8.0	1.9	8.3	3.0	8.3	5.8	7.0	3.6	6.5
c	4.9	210	264	471	54	207	45	2.6	33	6.5	38	7	26	3.5	24	3.5
4596																
a	1.3	366	70	115	9	62	24	1.2	28	10	64	14	58	10	60	8
b	7.1	1.1	1.4	1.0	3.3	2.2	4.2	8.6	2.9	5	1.9	4.2	1.4	5	1.2	6.0
c	1.4	379	69	117	10	65	26	1.6	29	9	69	16	61	9.5	63	8.6
4597																
a	20.3	68	111	209	16	84	19	1.7	14	8	12	<3	12	3.3	11	1.7
b	4.0	1.2	1.8	1.0	6.2	1.4	6.3	7.0	3.6	5	4.2		4.2	7.2	4.5	7.0
c	20.2	69	106	212	18	86	21	2.6	15	8.5	14	<3	10	<3	10	1.5
4598																
a	3.3	62.5	68	111	10	44	10	<1	6	<5	10	<3	6	<3	8.5	1
b	6.1	1.5	1.6	0.8	7.2	3.2	6.0		6.7		6		6.7		5.9	8
c	3.8	65	74	122	12	46	12	<1	<10	2	11	<3	7	<3	8	1
4605																
a	3.5	53.5	140	216	19	74	15	<1	9	<5	10	<3	4	<3	5	<1
b	5.7	1.6	1.4	1.0	5.8	1.6	5.3		5.6		6		6.8		6.0	
c	4.1	56	138	217	22	78	12	1	11	<5	11.5	<3	5	<3	5	<1
4606																
a	2.6	79	56	49	2.2	18	6	<1	<5	<5	11	<3	8	<3	9	1.3
b	6.9	1.4	2.7	2.4	9.1	6.1	8.3		—		5.4	5.0	5.0		4.7	7.8
c	3.5	80	50	51	<5	21	<10	<1	<5	<5	13	<3	9	<3	10	1.6

Wavelength (nm) of elements used for measurements: Sc (361.384), Y (371.030), La (333.749), Ce (418.660), Pr (422.293), Nd (430.358), Sm (442.434), Eu (381.967), Gd (364.619), Tb (350.917), Dy (353.170), Ho (345.600), Er (349.910), Tm (346.220), Yb (328.937), Lu (261.542).

Sample solutions were doped with 200 mg of uranium and the decontamination of U was effected using the recommended procedure.

(a) Present method (average of five values, $\mu\text{g/g}$)

(b) % R.S.D. by the present method.

(c) Ion exchange method [15].

be selected for some of the REE, extreme care has to be exercised in selecting the line for Sm, Tb, Er, and Tm. Since the correction factors due to inter REE interferences on some of the alternate emission lines do not follow the additive principle and

the spectral bias by uranium is also not always additive, a separation of the REE from uranium has been carried out by the above procedure. Separation of rare earths from high concentration of matrix elements and trace elements in the studied geological materials, including the pitch blende sample and uranium doped CCRMP certified reference standards SY-2 and SY-3 has also been carried out using the often-recommended cation exchange [15,16] separation method. The results obtained by both the methods are in very good agreement in case of all the studied samples including the certified reference standards, SY-2 and SY-3. The method is simple and rapid and easy to operate on a routine basis. The proposed

Table 6
Major matrix element composition of in-house pitch blende sample (data in wt%)

U_3O_8	74.10
PbO	1.02
SiO_2	15.10
Total Fe }	
As Fe_2O_3 }	1.18
P_2O_5	4.67

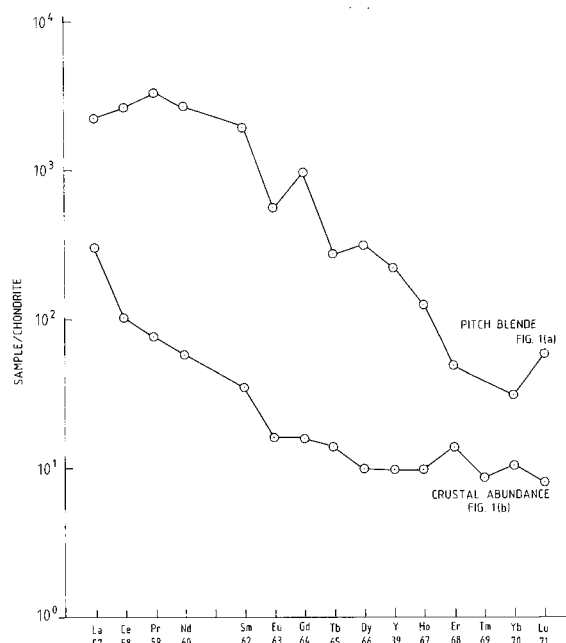


Fig. 1(a). Chondrite-normalized REE and Y pattern for pitch blende (21)

Fig. 1(b). Chondrite-normalized REE and Y pattern for crustal abundance (22)

Fig. 1. (a) Chondrite-normalized REE and Y pattern for pitch blende [21]. (b) Chondrite-normalized REE and Y pattern for crustal abundance [22].

method offers an R.S.D. of 1.0% at the 398 $\mu\text{g/g}$ level in the case of Sm and 8.8% at 1.7 $\mu\text{g/g}$ level in the case of Lu.

4. Conclusion

The determination of REE, Y, Sc and Th in several U-rich (> 0.1%) geological materials including the pitch blende type of samples has been successfully accomplished by ICP-AES, after separating the analytes from U-matrix by complexing uranium with NaOH/H₂O₂ system and the values are in very good agreement with the reported results. The method is simple, rapid, precise and accurate and has been applied to the certified reference standards, SY-2 and SY-3 (after doping with huge amount of U). In U-rich geological materials, it is important to separate the analytes from U-matrix before estimating by ICP-AES, due to its several spectral interferences on many

of the REE emission lines. In the present system, the U was efficiently complexed by H₂O₂ in presence of NaOH and all the analytes are precipitated quantitatively as hydroxides by using iron as the carrier before dissolving in hydrochloric acid for quantification by ICP-AES.

The proposed separative preconcentration method can be applied successfully to different type of U-rich samples like uraninite, pitch blende, brannerite, etc. on a routine basis.

Acknowledgements

The author wishes to thank colleagues of the laboratory and Dr K.K. Dwivedi, Director, AMD for his encouragement and permission to publish the paper.

References

- [1] J.P. Howe, in: H.A. Wilhem (Ed.), The metal Thorium, American Society of Metals, Cleveland, OH, Chap. (1958).
- [2] G.L. Moore, Introduction to inductively coupled plasma atomic emission spectrometry, Elsevier, Amsterdam, 1989, p. 8.
- [3] P.J. Potts, O.W. Thorpe, J.S. Watson, Chem. Geol. 34 (1981) 331.
- [4] J.G. Sen Gupta, Talanta 28 (1981) 31.
- [5] J. Havel, C. Moreno, A. Hrdlicka, M. Valiente, Talanta 41 (1994) 1251.
- [6] I. Roelandts, Anal. Chem. 53 (1981) 676.
- [7] J. Broekaert, Spectrochim. Acta 35B (1980) 225.
- [8] R. Amli, W.L. Griffin, Am. Mineral 60 (1975) 599.
- [9] J.N. Walsh, F. Buckley, J. Barker, Chem. Geol. 33 (1981) 141.
- [10] J.G. Sen Gupta, Talanta 34 (1987) 1043.
- [11] K.E. Jarvis, I. Jarvis, Geostand. Newsl. 12 (1988) 1.
- [12] R.K. Malhotra, K. Satyanarayana, D.S.R. Murthy, B.N. Tikoo, Proceedings of 6th ISAS National Symposium on Analytical Applications in Earth Sciences, held at Shillong, India, Associated Marketing Services Press, Bombay, 43, 1988.
- [13] K. Satyanarayana, Girija Srinivasan, R.K. Malhotra, B.N. Tikoo, Exploration and Research for Atomic Minerals. Vol. 2, 1989, pp. 235.
- [14] D.S. Braverman, J. Anal. At. Spectrom. 7 (1992) 43.
- [15] J.G. Crock, F.E. Lichte, G.O. Riddle, C.L. Beech, Talanta 33 (1986) 601.
- [16] I.W. Croudace, S. Marshall, Geostand. Newsl. 15 (1991) 139.

- [17] I. Roelandts, *Geostand. Newsl.* 14 (1990) 137.
- [18] P.S. Murthy, M. Barnes Ramon, Determination of trace rare earth elements by ICP–AES, *J. Anal. At. Spectrom.* 1 (1986) 145.
- [19] T. K Seshagiri, Y. Babu, M.L. Jayanth Kumar, A.G.I. Dalvi, M.D. Sastry, B.D. Joshi, Application of ICP–AES for the determination of Dy, Eu, Gd, Sm, and Th in uranium after chemical separation, *Talanta* 31 (1984) 773.
- [20] K. Satyanarayana, *At. Spectroscopy* 17 (2) (1996) 69.
- [21] H. Wakita, P. Rey, R.A. Schmitt, Proceedings of the second lunar science conference, Vol. 2, MIT Press, 1971, p. 1319–1329.
- [22] S.R. Taylor, *Geo. Chim. Cosmo-Chim. Acta* 28 (1964) 1280.
- [23] K. Govindaraju, *Geostand. Newsl.* 13 (1989) 1.
- [24] J.G. Crock, F.E. Lichte, *Anal. Chem.* 54 (1982) 1329.

Polymer-mediated extraction of 8-quinolinolato metal chelates for the determination of metal ions in water with graphite furnace atomic absorption spectrometry

Tohru Saitoh ^{a,*}, Toshihisa Ohyama ^a, Teruaki Sakurai ^a, Toshikazu Kaise ^a,
Kiyoko Takamura ^a, Yasuzo Suzuki ^b, Chiyo Matsubara ^a

^a School of Pharmacy and School of Life Science, Tokyo University of Pharmacy and Life Science, Horinouchi 1432-1, Hachioji, Tokyo 192-03, Japan

^b National Institute of Material and Chemical Research, Tsukuba 305, Japan

Received 2 June 1997; received in revised form 28 August 1997; accepted 29 August 1997

Abstract

Water-insoluble 8-quinolinolato metal chelates were formed and were stably solubilized in the aqueous solution of a water-soluble polymer, poly(*N*-isopropylacrylamide)(PNIPAAm), at room temperature. When the solution was heated at 50°C, PNIPAAm precipitated and then formed a gum-like aggregate (polymer phase) having a very small volume. Accompanying the polymer precipitation, hydrophobic 8-quinolinolato chelates with cobalt(II), iron(III), nickel(II), and copper(II) ions were efficiently incorporated into the polymer phase. At 0.5% (w/v) of PNIPAAm and 8.0 mM of 8-quinolinol, the recoveries in the incorporation of four metal chelates were quantitative. The fluorescence spectra of a probe suggests that the hydrated polymer in the aqueous solution provides hydrophobic portions which can incorporate hydrophobic metal chelates. The polymer phase was easily taken out from the solution and was dissolved with a small amount of acetonitrile. The resulting solution could be directly introduced into a graphite furnace of atomic absorption spectrometry. The signal intensities for the absorbance of cobalt after concentrating the chelate were 100-fold greater than those before the concentration. © 1998 Elsevier Science B.V. All rights reserved.

Keywords: Poly(*N*-isopropylacrylamide); 8-quinolinol; Concentration; Metal chelate; Atomic absorption spectrometry

1. Introduction

Aqueous solutions of a water-soluble polymer, poly(*N*-isopropylacrylamide) (PNIPAAm) (Fig. 1), when subjected to an increase in temperature, became turbid over a narrow temperature range,

which is referred to as their lower critical solution temperature (LCST) [1–3]. Above the LCST (32–34°C), the polymer becomes water-insoluble and then, forms gum-like precipitates (polymer phase) with a small amount of water separated from the bulk aqueous solution (aqueous phase) containing only a very small percentage (less than 0.001%) of the polymer. In contrast, the polymer phase becomes water-soluble when cooled below the

* Corresponding author. Tel.: +81 426 766793; fax: +81 426 765354; e-mail: saitoht@ls.toyaku.ac.jp

LCST. Therefore, we can conduct reversible precipitation and solubilization of the polymer by warming or cooling the solution.

Such reversible thermo-responsive properties of PNIPAAm have been extensively applied to the methodologies for the separation or the detection of biomolecules such as enzymes, antibodies, cell receptors and DNAs [4–6]. PNIPAAm–biomolecule conjugates and their complex with other biomolecules also exhibit precipitation phenomena at almost the same temperature as the LCST of PNIPAAm. Based on the bio-affinity between biomolecules and PNIPAAm-conjugated biomolecules, highly efficient recovery or highly specific detection of desired biomolecules in the presence of matrix components has been successfully achieved. In contrast, very few studies have been performed on the use of the thermo-responsive polymer as an extracting medium which can incorporate solutes [7].

Recently, we employed the precipitation phenomena of the thermo-responsive polymers, PNIPAAm and poly(vinylmethyl ether), to design a kind of efficient extraction system (polymer-mediated extraction) for hydrophobic compounds such as poly-aromatic hydrocarbons, steroid hormones, and lipids [8–11]. That is, in aqueous polymer solution, any hydrophobic materials present will be solubilized and incorporated into the thermo-responsive polymer assembly. As the polymer aggregates are condensed to an extremely small polymer phase, the hydrophobic compounds that are solubilized in the aqueous polymer solution are efficiently concentrated into this polymer phase. At room temperature, the polymer phase can be dissolved by adding small amounts of water or organic solvent. The resulting solutions containing highly concentrated analytes can be directly applied to several analytical methods such as absorption spectrophotometry, fluorescence spectrophotometry, or high-performance liquid chromatography [8–11].

The important advantage of using polymer-mediated extraction is in the ability to concentrate a variety of hydrophobic analytes (with high-concentration factors) by very simple and rapid procedures. The polymer precipitates could be condensed to a small piece of paste-like solid,

which can be easily taken up from the solution, by just heating and shaking the solution for a few seconds. Thus, instruments, such as a centrifuge, are not necessary for the phase separation. Next, the method is quite safe and cost-saving, because it requires only very small amounts of relatively nonflammable, nonvolatile and nontoxic polymers. This eliminates the need to use the larger volumes of organic solvent. Nontoxic properties of PNIPAAm have been clearly observed based on the extensive application of the polymer in the support of cell-growth [12,13]. Thus, using PNIPAAm is hazard free to the user and the environment. Additionally, the polymer phase can be easily disposed of, because the phase containing small amounts of water can be easily burned with other flammable materials. These facts indicate the great potential of the polymer-mediated extraction for concentrating hydrophobic analytes.

As yet, there appear to be no reports concerning the application of the polymer-mediated extraction to the concentration of hydrophobic metal chelates. Our idea was to use a relatively water-soluble chelating reagent to react with metal ions in water so that the resulting hydrophobic metal chelates would predominantly partition to the hydrated polymer media and thus, become concentrated to the polymer phase following the polymer precipitation. The method would provide a simple and rapid method for concentrating metal ions in water which is compatible with several spectrometric determinations of metals.

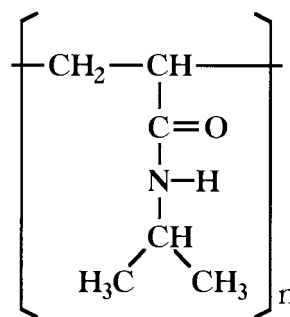


Fig. 1. Structure of PNIPAAm.

In this paper, we report the incorporation of metal chelates into the polymer phase to establish the basis for the use of the polymer-mediated extraction as a pre-concentration method of metal ions prior to their determination with graphite furnace atomic absorption spectrometry. 8-quinolinol (Hox) was employed as a chelating reagent, because it can form highly hydrophobic metal chelates with a variety of heavy metal ions. The conditions for achieving efficient concentration of the chelates were studied. Furthermore, the features in the solubilization and incorporation of hydrophobic metal chelates in hydrated polymer media were discussed on the basis of the spectral data of some spectrophotometric probes in the aqueous polymer solution.

2. Experimental

2.1. Apparatus

A Shimadzu atomic absorption spectrometer (AAS) with a graphite furnace atomizer GFA-4A was used for the determination of the metals in the polymer phase. A Jasco double-beam absorption spectrophotometer with 1-cm micro quartz cells (1-mm width) was employed for monitoring the formation or incorporation of metal chelates. The fluorescence spectra of a probe were measured using a Jasco spectrofluorometer FP-777 with a 1-cm quartz cell, in which the cell position was thermostated as $25 \pm 1^\circ\text{C}$.

2.2. Reagents

PNIPAAm was synthesized by free radical polymerization using 2,2'-azobis(isobutyronitrile) (AIBN) as an initiator [14]. *N*-isopropylacrylamide (NIPAAm), obtained from Aldrich (Milwaukee, WI), was purified by recrystallization from the mixture of diethyl ether and petroleum ether (1:10). A 10 g portion of NIPAAm and 0.10 g of AIBN were dissolved in 100 ml dry tetrahydrofuran. The solution was placed into a three-necked round bottom flask and heated at 40°C for 24 h under nitrogen atmosphere. After the solution volume was reduced to approximately 50 ml

by evaporation, it was poured into 1 l of dry diethyl ether. The white precipitates obtained were washed with dry ether and dried in vacuo (9.0 g, yields: 90%, average molecular weight; $M_w = 38\,000$ (by GPC)). A chelating reagent, 8-quinolinol (Hox), received from Wako (Tokyo, Japan) was used after triplicate recrystallization from 50% (v/v) aqueous ethanol. A fluorescence probe, 8-anilinonaphthalene sulfonate (spectrophotometric grade), was obtained from Tokyo Kasei (Tokyo, Japan). Other reagents used were of analytical grade.

2.3. Procedure for LCST determination

LCSTs of PNIPAAm were visually measured. The aqueous solution of PNIPAAm containing prescribed amounts of buffer components or salts were placed in a glass vial, and slowly warmed until it turned turbid. The slope of the temperature change was less than 1°C per 15 min. The temperature at which the solution became turbid was regarded as the LCST.

2.4. Procedure for the extraction of metal chelates

Prescribed amounts of the aqueous solution of 10.0% (w/v) PNIPAAm, 0.100 M Hox, and buffer components were added into the sample solution containing metal ions. The volume of the sample solution was typically 50 ml. After incubating at 50°C for 5 min, the solution was shaken to induce the condensation of the polymer phase. A piece of the polymer phase was taken from the solution and was then dissolved into 5 ml of acetonitrile. The recoveries of the metal chelates incorporated into the polymer phase were calculated from the absorbance at 480 nm for $[\text{Fe}(\text{ox})_3]$ or at 420 nm for other metal chelates.

2.5. Application to graphite furnace AAS

The sample solution (50.0 ml) containing cobalt(II) ion ($< 1 \times 10^{-8}$ M), 0.50% (w/v) PNIPAAm, 8.0 mM Hox, and 50 mM phosphate buffer (pH 7.0) was heated at 50°C . After shaking, the formed polymer phase was recovered

Table 1
Instrumental conditions for graphite furnace AAS

Temperature program	Step	Temperature (°C)	Hold (s)	Ramp (s)	Analytical wavelength (nm)
	1	150	30	0	—
	2	400	0	60	—
	3	500	20	0	—
	4	2300 (Co)	5	0	240.7
		2300 (Cu)	4	0	324.7
		2300 (Fe)	4	0	248.3
		2400 (Ni)	4	0	232.0

from the solution and dissolved using 250 μ l of acetonitrile. A 20 μ l portion of the resulting solution was introduced into the graphite furnace of AAS. The analytical conditions for the graphite furnace AAS are listed in Table 1.

3. Results and discussion

3.1. Phase separation of aqueous PNIPAAm under analytical conditions

Several investigators have studied the effect of salts on the LCSTs of PNIPAAm and other synthetic polymer and related it to the Hofmeister series [15,16]. Under analytical conditions, salts or buffer components are necessary for conducting the formation of metal chelates and thus, would influence the LCST of PNIPAAm.

Fig. 2 summarizes our observations regarding the sensitivity of the LCSTs of PNIPAAm to some salts and buffer components, which are often present in the aqueous solution for the complexation of metal chelates. The polymer precipitates in the region above the respective curves, while homogeneous aqueous solution is obtained below the curves. All of the salts and buffer components examined in this study lowered the LCST of PNIPAAm. Thus, they were useful for conducting the precipitation of PNIPAAm at a lower temperature of the LCST. Among them, sulfate and phosphate salt precipitate more effectively than acetate, chloride, nitrate, or perchlorate.

3.2. Formation and solubilization of metal chelates in aqueous PNIPAAm solution

Four metal ions tested in this study: cobalt(II), copper(II), iron(III), and nickel(II), formed metal chelates with Hox within 1 min in the aqueous solutions of PNIPAAm. Because the solution was homogeneous at room temperature, the complex formation could be conducted by just mild mixing of the solution. It is well-known that uncharged metal-ox chelates are barely dissolved in water [17]. However, the absorbance of the 0.20% (w/v) PNIPAAm aqueous solution containing 2.00×10^{-5} M of iron(III), 2.00 mM of Hox, and 50

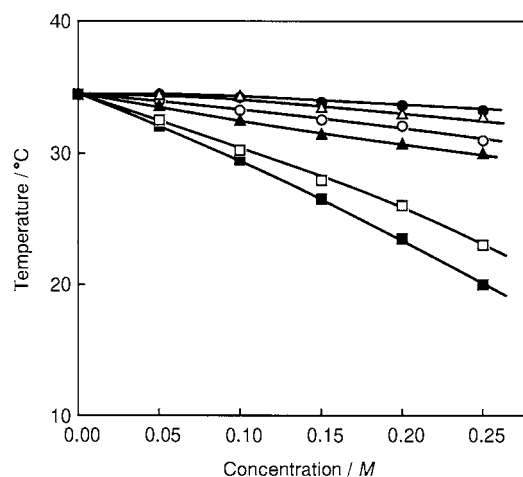


Fig. 2. LCST of 2.00% (w/v) of PNIPAAm as a function of the concentration of salt or buffer components. The solutions become turbid in the region above the respective curve, while clear solutions are obtained in the region below the curve. (○), NaCl; (●), NaNO₃; (△), NaClO₄; (▲), CH₃COONa; (□), Na₂SO₄; (■), NaH₂PO₄-Na₂HPO₄ (1:1).

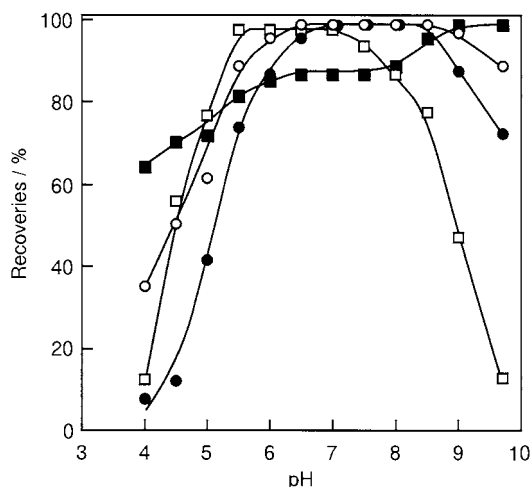


Fig. 3. Recoveries of 8-quinolinolato-metal chelates as a function of pH. Concentration of PNIPAAm is 0.50% (w/v), [metal ion] = 1.00×10^{-5} M, [Hox] = 8.00 mM, (○), Co(II); (●), Fe(III); (□), Ni(II); (■), Cu(II). The values of pH are those at room temperature.

mM of phosphate buffer (pH 7.0) at 480 nm was independent of time, at least for 48 h. This fact indicates quite stable solubilization of the $[\text{Fe}(\text{ox})_3]$ chelate in the aqueous solution of PNIPAAm. Other metal chelates were also stably solubilized in the aqueous polymer solution. PNIPAAm homogeneously solubilizing in the aqueous solution may provide portions which can incorporate hydrophobic chelates.

3.3. Extraction of metal chelates into the polymer phase.

When the solution was heated at 50°C, PNIPAAm precipitated and then formed a yellow-colored (dark gray colored in the case of iron(III) chelate) polymer phase due to the predominant incorporation of metal chelates. Fig. 3 illustrates the extent of metal-ox chelate incorporation into the polymer phase as a function of pH. The fraction of the respective metal chelates in the polymer phase increased with increasing solution pH, reflecting the pH-dependent formation of the metal chelate. At pH 7.0, the recoveries of iron(III), nickel(II), and cobalt(II) were almost quantitative, while they decreased over the higher

pH region probably due to their hydrolysis. In contrast, copper(II) chelate was predominantly incorporated into the polymer phase above pH 9.0. Obviously, the features in Fig. 3 indicate that this system can be regarded as a kind of solvent extraction where the polymer phase acts as an extracting solvent. In Fig. 3, there is a plateau region in the recoveries of the copper(II) chelate from pH 6.5 to 7.5, where the chelate was not quantitatively incorporated into the polymer phase. This plateau region reflects the distribution of 1:1 charged chelate, $[\text{Cu}(\text{ox})]^+$. The charged chelate is probably extracted accompanied by a counter ion such as phosphate. This is one of the unique features in the extraction to the polymer phase. To obtain high recoveries of four metal chelates, a pH 7.0 solution was selected in subsequent experiment.

The dependence of Hox concentration on the recoveries of the respective metal chelates was studied. Fig. 4(a) shows the recoveries of cobalt(II) into the polymer phase as a function of the concentration of Hox. Above 4.0 mM, the recoveries incorporated were quantitative. In the case of other metal chelates, 4.0 mM was adequate for obtaining sufficient recoveries. In this study, the concentration of Hox was adjusted to 8.0 mM.

The concentration of PNIPAAm also influences the recoveries of metal chelates. As illustrated in Fig. 4(b), the extent of cobalt(II) extraction increased with increasing concentration of PNIPAAm. The volume fraction of the polymer phase is expected to be almost proportional to the polymer concentration. The increase in recoveries was the result of increased volume of the phase which can incorporate the chelate. The concentration of PNIPAAm required for the almost quantitative recoveries of cobalt(II) was 0.3% (w/v). On the other hand, the addition of excess polymer lowered the concentration factor, as the formation of the polymer phase had a large volume fraction. The polymer concentration of 0.5% (w/v) was the foremost choice for easy recoveries of the polymer piece with quantitative recoveries and high-concentration factors of metal-ox chelates.

As previously described, the concentration of buffer components lowered the LCST of PNIPAAm.

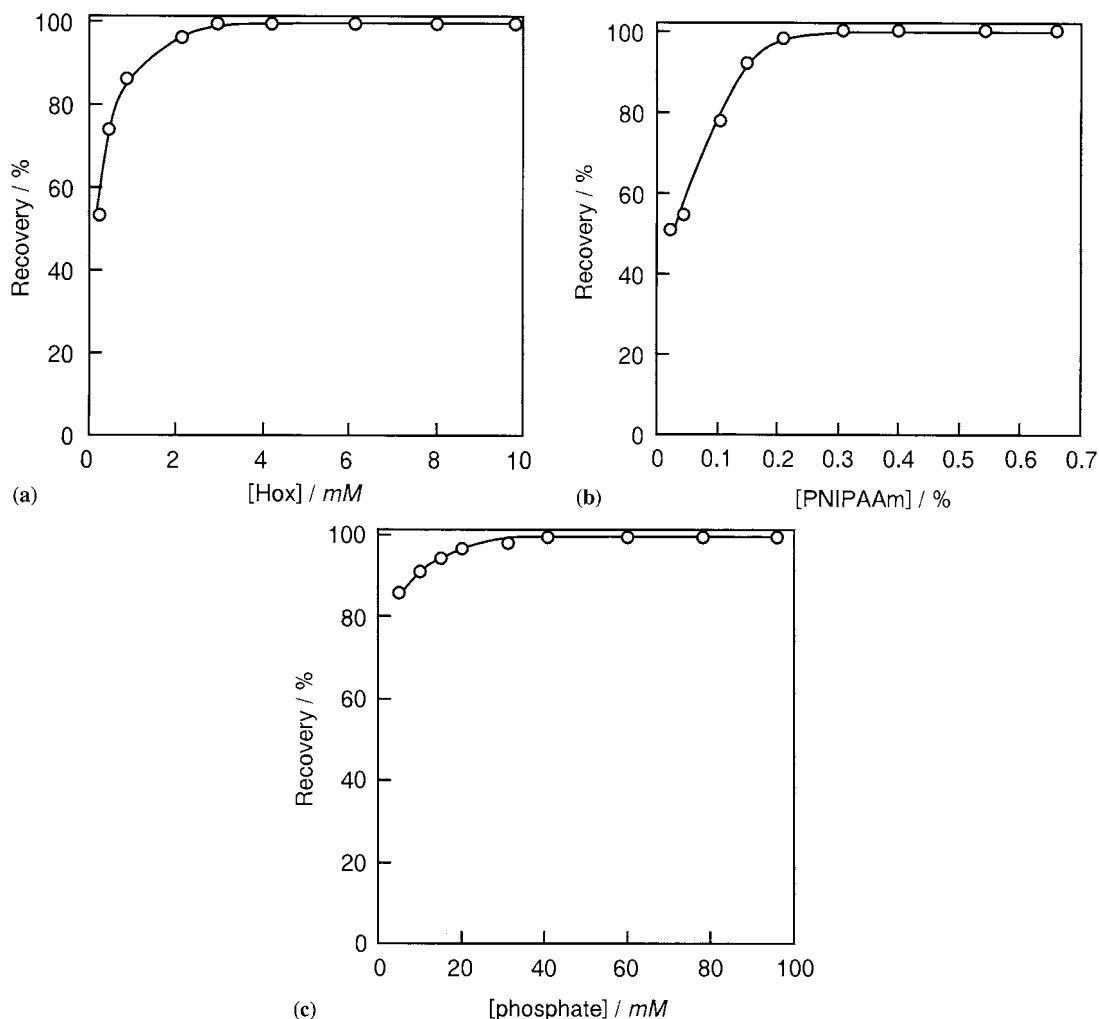


Fig. 4. Recoveries of cobalt(II) as a function of the concentration of Hox (a), PNIPAAm (b), or buffer components (c). (a), Concentration of PNIPAAm; 0.50% (w/v), $[\text{Co}^{2+}] = 1.0 \times 10^{-5}$ M, 0.05 M phosphate (pH 7.0); (b), $[\text{Co}^{2+}] = 1.0 \times 10^{-5}$ M, $[\text{Hox}] = 8.00$ mM, 0.05 M phosphate (pH 7.0); (c), Concentration of PNIPAAm; 0.50% (w/v), $[\text{Co}^{2+}] = 1.0 \times 10^{-5}$ M, phosphate (pH 7.0).

PAAm. In contrast, the temperature (50°C) for conducting polymer precipitation in this study is far higher than the LCST of PNIPAAm. Additionally, the 50 mM concentration of phosphate, described in Section 2 as an optimum condition for the recoveries of metal chelates, can only lower the LCST of PNIPAAm 2°C when it compared with the value in the aqueous solutions containing no buffer components. Thus, the concentration of buffer components does not seem to

be important for effective recoveries of metal chelates. As drawn in Fig. 4(c), however, the recoveries of cobalt(II) were not sufficient in the phosphate concentration region below 40 mM and increased with increasing concentration of phosphate buffer, while becoming almost quantitative above that concentration.

In the absence of salts or buffer components, the solution became turbid but the resulting precipitates still had a tendency to disperse. In con-

trast, the polymer precipitates efficiently condensed and formed a droplet of the polymer phase at the concentration of the phosphate above 40 mM. Buffer components were found to act not only as pH-adjusting reagents, but also as reagents for inducing the condensation of the polymer precipitates. When the phosphate was used as a buffer component, the concentration of 50 mM was recommended.

3.4. Mechanism of the extraction.

As previously mentioned, the stable solubilization of the water-insoluble metal chelates in the aqueous polymer solution strongly suggests that the hydrated PNIPAAm provides certain regions where hydrophobic metal chelates can be incorporated. In order to clarify the presence of these regions, we measured the fluorescence spectrum of 8-anilinonaphthalene sulfonate, ANS, which is a typical fluorometric probe responsible for the polarity of the media [18,19]. As shown in Fig. 5, the fluorescence intensity of ANS in the aqueous solution of PNIPAAm is significantly enhanced when

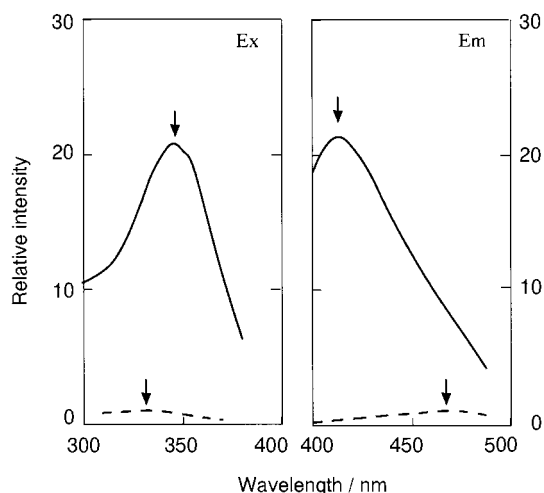


Fig. 5. Fluorescence spectra of ANS in the aqueous solution containing 1% (w/v) of PNIPAAm (solid lines), no PNIPAAm (dotted lines). $[ANS] = 1.0 \times 10^{-6}$ M, 25°C. Relative intensity is defined by the ratio of the fluorescence intensity against the maximum intensity in the aqueous solution containing no PNIPAAm. Arrows point to the wavelength at the maximum excitation or emission.

compared with that in the solution containing no polymers. Additionally, the wavelength at the maximum emission in the excitation spectrum shifts to the longer side, while that in the emission spectrum shifts to the shorter side. These facts indicate that the hydrated PNIPAAm in the aqueous solution provides hydrophobic regions rather than bulk aqueous solution and that some fractions of ANS were distributed in the regions. Rapid and efficient incorporation of hydrophobic metal-ox chelates into the precipitated polymer phase could be explained by their predominant distribution of the highly hydrophobic chelates into the hydrated polymer media. However, the specific sites for binding hydrophobic solutes in this polymeric material are obscure, because PNIPAAm, whose structure is illustrated in Fig. 1, seems to have no highly hydrophobic moieties. Probably, the hydrated polymer media would have only very low hydrophobicity.

It may be mentioned that the present method is comparable to the extraction of metal chelates on the basis of temperature-induced phase separation in aqueous micellar solutions of nonionic surfactants (termed 'cloud point extraction' in some articles) [20–22]. In contrast to the surfactant micelles, the polymer does not have a critical concentration for forming aggregates. Thus, higher concentration factors can be achieved, if the polymer concentration is set to be very low. The lack of requirement for instruments such as a centrifuge for inducing the phase separation is an additional advantage of the polymer-mediated extraction. The most important advantage of this method is that almost free ligands are present in the bulk aqueous phase. In cloud point extraction, relatively hydrophilic cationic (H_2ox^+), anionic (ox^-), and neutral (Hox) species of 8-quinolinol are also predominantly distributed into the micellar phase not only after but also before the phase separation [23]. The distribution lowers the activity of ox^- in the bulk aqueous phase, significantly decreasing the rate of complexation of ox^- with the metal ions [24]. The rapid formation of 8-quinolinolato-metal chelate in the aqueous PNIPAAm solution can be ascribed to the predominant distribution of free ligand to the bulk aqueous phase.

3.5. Application to graphite furnace AAS.

As already described, hydrophobic metal-ox chelates were efficiently concentrated into the small volume of the polymer phase. Thus, the concentration is expected to significantly enhance the signal intensity in analytical methods. In order to demonstrate the compatibility of the present method with a graphite furnace AAS, we examined the determination of cobalt(II) ion in mineral waters and their spiked samples by graphite furnace AAS after forming ox chelate and then extracting it into the polymer phase.

A piece of the polymer phase could be placed directly into the graphite furnace of AAS. However, the direct injection of the polymer piece had difficulties in the auto-sampling of a number of samples. Thus, we tested the solubilization of the polymer phase with some solvents including water, methanol, ethanol, methoxyethanol, *N,N*-dimethylformamide, dimethylsulfoxide, tetrahydrofurane, and acetonitrile. Among them, acetonitrile was the best choice for obtaining the least viscous sample solution by adding the smallest amounts of solvent.

The conditions for determining cobalt(II) in the sample solution, being composed from the aqueous-acetonitrile solution of concentrated polymer, are listed in Table 1. The conditions consisted of the same time course of temperature for drying and atomization as those recommended by the manufacture for determining cobalt(II) ion in water. Furthermore, the concentrated polymer matrix did not influence the signal intensity of cobalt or the background intensity. These facts indicate a good compatibility of the present method with the graphite furnace AAS.

Fig. 6 illustrates the signals of cobalt over the concentration range from 0 to 5.0×10^{-8} M before (a) and after (b) the concentration. When the concentration was carried out using procedures described in Section 2, approximately 100-fold concentration of cobalt was successfully achieved. The recoveries of cobalt(II) were almost quantitative and independent of its concentration. The relative deviation in the signal for 1.0×10^{-8} M cobalt(II) was 3% ($n=6$) which is almost the same as the measurement with the graphite fur-

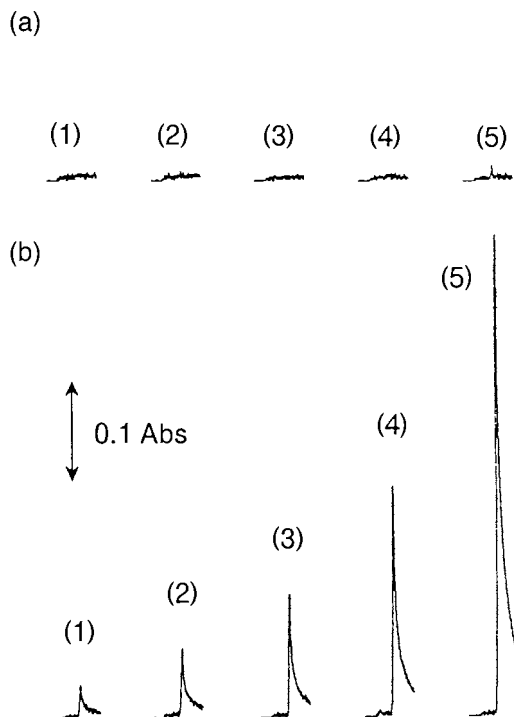


Fig. 6. Illustration of signals for cobalt in graphite furnace AAS. (a), before concentration; (b), after concentration. $[\text{Co}^{2+}]/10^{-8}$ M; (1), blank; (2), 0.5; (3), 1.0; (4), 2.0; (5) 5.0.

nance AAS, meaning quite high reproducibility of the concentration factor in the polymer-mediated extraction. Similarly, iron(III), copper(II), and nickel(II) were also effectively concentrated. The detection limit ($S/N=3$) and linear range of calibration curve were 1 nM, 2–100 nM ($r=0.995$) for cobalt(II), 5 nM, 10–250 nM ($r=0.998$) for iron(III), 1 nM, 2–100 nM ($r=0.998$) for copper(II), and 5 nM, 10–250 nM ($r=0.996$), respectively.

Table 2 lists the tolerance limits of various ions when 1.0×10^{-8} M cobalt(II) is determined by the present method. More than 0.1 M of lithium(I), sodium(I), potassium(I), chloride, bromide, nitrate, sulfate, phosphate, and acetate did not interfere with the signal intensity of cobalt(II). In contrast, the tolerance limit, 1×10^{-5} M, of calcium(II) and barium(II) was very low due to the precipitation of their phosphate salts. In order to heighten their tolerance limits up to 0.05 M, the

Table 2
Tolerance limits of foreign ions for the determination of cobalt (II)^a

Tolerance limit (M)	Foreign ion
>0.1	Na ⁺ , Li ⁺ , K ⁺ , Cl ⁻ , Br ⁻ , NO ₃ ⁻ , SO ₄ ²⁻ , ClO ₄ ⁻ , PO ₄ ³⁻ , acetate
0.05	Mg ²⁺
2 × 10 ⁻⁵	Citrate
1 × 10 ⁻⁵	(Al ³⁺ , Fe ³⁺ , Ni ²⁺ , Cu ²⁺ , Zn ²⁺) ^b (Ca ²⁺ , Ba ²⁺) ^c

^a Tolerance is the concentration which gives less than 5% error in the signal of 1.0 × 10⁻⁸ M of cobalt(II).

^b Not examined in the presence of more than 1 × 10⁻⁵ M foreign ion.

^c Tolerance limit was increased up to 0.05 M using HEPES as a buffer component.

use of 2-[4-(hydroxyethyl)-1-piperazinyl] ethane-sulfonic acid (HEPES) buffer components including 0.1 M sodium chloride was found to be a good alternative. In the case of metal ions which can complex with 8-quinolinol, no influences appeared in the signal of 1 × 10⁻⁸ M cobalt(II) even if 1 × 10⁻⁵ M of iron(III), aluminum(III), copper(II), and nickel(II) were present in the sample solution. The relatively low tolerance limit, 2 × 10⁻⁵ M, of citrate is ascribable to the strong

complexation with cobalt(II) ion.

Table 3 summarizes the recoveries and concentration factors of cobalt(II) when the polymer-mediated extraction is applied to the determination of cobalt(II) in real samples: mineral water and tap water taken from a water cooler. The concentrations of cobalt(II) in waters including spiked samples were successfully determined with very high reproducibility in the recovery and concentration factor. This result indicates that the polymer-mediated extraction of hydrophobic 8-quinolinolato-metal chelates provided an efficient method for concentrating metal ions in water prior to their determination with a graphite furnace AAS. The criteria for optimizing the concentration of metal chelates were almost the same as those for designing the liquid-liquid solvent extraction using the distribution of species between water and water-immiscible organic solvent. However, the procedures in the polymer-mediated extraction of metal chelates were simpler than those of conventional solvent extraction. The application of this method to other samples or the use of other chelating reagents, which form hydrophobic metal chelates, will greatly extend the potential of this method in the pre-concentration of metal ions for spectrometric analysis.

Table 3
Recoveries and concentration factors of cobalt (II)

	Added (10 ⁻⁹ M)	Detected (10 ⁻⁹ M)	Recovery (%)	Concentration factor ^a
Mineral water A	0.0	0.0	—	—
	5.0	4.8 ± 0.3 ^b	98.8 ± 0.5 ^b	96.3 ± 6.0 ^b
	10.0	10.1	99	101
	20.0	20.8	99	104
	50.0	49.4 ± 2.8 ^b	99.0 ± 0.3 ^b	98.8 ± 5.6 ^b
Mineral water B	0.0	0.0	—	—
	5.0	4.9	99	98.0
	50.0	49.3	99	98.6
Tap water ^c	0.0	2.5	—	—
	5.0	7.2	99	94.0
	50.0	54.8	99	104.0

^a Concentration factor = (AAS signal after concentration)/(AAS signal before concentration).

^b Results of five runs.

^c Taken from a water cooler.

Acknowledgements

Support of this work by the Grant-in-Aid for Encouragement of Young Scientist (No.09750891) and Grant-in-Aid for Scientific Research (B) (No.09558078) is gratefully acknowledged.

References

- [1] W.C. Wooten, R.B. Blanton, H.W. Coover Jr., *J. Polym. Sci.* 25 (1957) 403.
- [2] M. Heskins, J.E. Guillet, *J. Macromol. Sci. Chem. A2* (1968) 1441.
- [3] Y. Hirokawa, T. Tanaka, *J. Phys. Chem.* 81 (1984) 6379.
- [4] A.S. Hoffman, *Macromolecular Symposium* 98 (1995) 645, and references cited therein.
- [5] Y.G. Takei, T. Aoki, K. Sanui, N. Ogata, T. Okano, Y. Sakurai, *Bioconjugate Chem.* 4 (1993) 341.
- [6] M. Maeda, C. Nishimura, D. Umeno, M. Takagi, *Bioconjugate Chem.* 5 (1994) 527.
- [7] R.F.S. Freitas, E.L. Cussler, *Chem. Eng. Sci.* 42 (1987) 97.
- [8] C. Matsubara, N. Kikuchi, K. Takamura, *Bunseki Kagaku* 44 (1995) 311.
- [9] C. Matsubara, S. Izumi, K. Takamura, H. Yoshioka, Y. Mori, *Analyst (London)* 118 (1993) 553.
- [10] C. Matsubara, N. Kikuchi, K. Takamura, *Chem. Lett.* (1993) 849.
- [11] T. Ohyama, K. Arai, K. Takamura, C. Matsubara, *Bunseki Kagaku* 45 (1997) 59.
- [12] T. Okano, N. Yamada, H. Sakai, Y. Sakurai, *J. Biomed. Biomater. Res.* 27 (1993) 1243.
- [13] T. Takezawa, Y. Mori, T. Yonaha, K. Yoshizato, *Exp. Cell Res.* 208 (1993) 430.
- [14] G. Chen, A.S. Hoffman, *J. Biomater. Sci., Polym. Edn.* 5 (1994) 371.
- [15] M. Atman, *Colloid Polym. Sci.* 265 (1987) 19.
- [16] H.G. Schild, D.A. Tirrell, *J. Phys. Chem.* 94 (1990) 4325.
- [17] L. Lehman, *J. Am. Chem. Soc.* 56 (1934) 1836.
- [18] L. Stryer, *J. Mol. Biol.* 13 (1965) 482.
- [19] D.C. Turner, L. Brand, *Biochemistry* 7 (1968) 3381.
- [20] H. Ishii, J. Miura, H. Watanabe, *Bunseki Kagaku* 26 (1977) 252.
- [21] H. Watanabe, H. Tanaka, *Talanta* 25 (1978) 585.
- [22] W.L. Hinze, E. Pramauro, *Crit. Rev. Anal. Chem.* 24 (1993) 133, and references cited therein.
- [23] H. Hoshino, T. Saitoh, H. Taketomi, T. Yotsuyanagi, H. Watanabe, K. Tachikawa, *Anal. Chim. Acta* 147 (1983) 339.
- [24] S. Ito, K. Haraguchi, K. Yamada, *Nippon Kagaku Kaishi* 8 (1977) 1137.

Novel dye-attached macroporous films for cadmium, zinc and lead sorption: Alkali Blue 6B-attached macroporous poly(2-hydroxyethyl methacrylate)

A. Denizli ^{a,*}, K. Kesenci ^b, M.Y. Arıca ^c, B. Salih ^a, V. Hasırcı ^d, E. Pişkin ^b

^a Department of Chemistry, Hacettepe University, Ankara, Turkey

^b Department of Chemical Engineering, Hacettepe University, Ankara, Turkey

^c Department of Biology, Kırıkkale University, Kırıkkale, Turkey

^d Department of Biological Sciences, Biotechnology Research Unit, METU, Ankara, Turkey

Received 3 June 1997; received in revised form 8 August 1997; accepted 29 August 1997

Abstract

Alkali Blue 6B-attached poly(2-hydroxyethyl methacrylate) (poly(HEMA)) microporous films were investigated as chelate forming sorbents for heavy metal removal. Poly(HEMA) microporous films were prepared by UV-initiated photo-polymerization of HEMA in the presence of an initiator (azobisisobutyronitrile (AIBN)). Alkali Blue 6B was attached covalently. These films with a swelling ratio of 58%, and carrying 14.8 mmol Alkali Blue 6B m⁻² which were then used in the removal of Cd(II), Zn(II) and Pb(II) from aqueous media. Adsorption rates were very high, equilibrium was achieved in about 30 min. The maximum adsorption of heavy metal ions onto the Alkali Blue 6B-attached films were 41.4 mmol m⁻² for Cd(II), 52.4 mmol m⁻² for Zn(II), and 64.5 mmol m⁻² for Pb(II). When the heavy metal ions competed during the adsorption from a mixture the adsorption values for Cd(II), Zn(II) and Pb(II) were quite close. Heavy metal ions were desorbed by using 0.1 M HNO₃. A significant amount of the adsorbed heavy metal ions (up to 95%) could be desorbed in 30 min. Repeated adsorption/desorption cycles showed the feasibility of these novel dye-attached microporous films for heavy metal removal. © 1998 Elsevier Science B.V. All rights reserved.

Keywords: Alkali Blue 6B; Poly(HEMA) films; Heavy metal removal; Cadmium(II); Zinc(II); Lead(II)

1. Introduction

Heavy metal ions have become an ecotoxicological problem of prime interest and increasing sig-

nificance owing to their tendency to accumulate in living organisms. The necessity to reduce the amount of heavy metal ions in waste water streams of hydro-metallurgical and other industries, and subsequent possible re-use of these metal ions, has led to an increasing interest in selective sorbents [1–3]. Membrane separation, in which semipermeable membranes (mostly micro-

* Corresponding author. Mailing address: P.K. 51. Samanpazari, 06242 Ankara, Turkey. Tel. and fax: +90 312 2352330; e-mail: denizli@eti.cc.hun.edu.tr

porous) are used as selective barriers, is a promising technology from the energy-saving point of view for the selective separation of heavy metal ions [4]. There are basically three phases in the membrane extraction processes for heavy metal removal. Two immiscible phases are separated by a membrane phase which is immiscible with the other two phases. Extraction of metal ions is achieved by the mass transfer between two miscible phases through the membrane phase [5–8].

In the present study, we also utilized microporous membranes in our heavy metal removal system. However, in our case the microporous membrane (film) was not used as the rate and selectivity control phase, but rather as a carrier matrix. A swellable and macroporous carrier film was first prepared by photo-polymerization of 2-hydroxyethyl methacrylate (HEMA). Alkali Blue 6B was then attached covalently as a dye-ligand for heavy metal adsorption. This specific sorbent system in the film form was studied in adsorption/desorption of some selected heavy metal ions, i.e. Cd(II), Zn(II) and Pb(II) from aqueous media.

2. Experimental

2.1. Alkali Blue 6B-attached poly(HEMA) films

The poly(2-hydroxyethyl methacrylate) (poly(HEMA)) film was prepared as previously described [9]. The monomer, HEMA, was obtained from Fluka (Buchs, Switzerland), distilled under reduced pressure in the presence of hydroquinone and stored at 4°C until use. Two ml of HEMA containing 5 mg azobisisobutyronitrile (Fluka, Switzerland) as polymerization initiator was mixed with 3 ml 0.1 M SnCl₄. The mixture was then poured into a round glass mould (9 cm in diameter) and exposed to ultraviolet radiation (12 watt lamp, P.W. Allen, USA) for 10 min under a nitrogen atmosphere. The film obtained was washed several times with distilled water, and cut into square pieces (0.5 cm in length) with a perforator.

Preparation and characterization of the poly(HEMA) films are reported in our previous pa-

pers [10,11]. In order to prepare the films carrying 14.8 mmol Alkali Blue 6B m⁻², the following procedure was applied: 10 ml of solution containing 300 mg Alkali Blue 6B (BDH, UK) was poured into 90 ml of the solution of the poly(HEMA) film pieces in distilled water, and then 4.0 g of NaOH was added. These were then heated in a sealed reactor at 80°C for 4 h at a stirring rate of 400 rpm. The Alkali Blue 6B-attached poly(HEMA) films were filtered, and washed with distilled water and methanol several times until all the physically adsorbed dye molecules were removed. The amount of Alkali Blue 6B molecules covalently attached to the poly(HEMA) film was calculated from the elemental analysis data of the dried samples obtained using an elemental analysis device (Leco, CHNS-932, USA).

FTIR spectra of the Alkali Blue 6, plain poly(HEMA) and Alkali Blue 6B-attached poly(HEMA) films were obtained by using a FTIR spectrophotometer (FTIR 8000 Series, Shimadzu, Japan). The dry poly(HEMA) film (about 0.1 g) was thoroughly mixed with KBr (0.1 g, IR Grade, Merck, Germany), and pressed into a pellet, and the spectrum was then recorded.

2.2. Heavy metal adsorption/desorption

In the first group of experiments, adsorption of Cd(II), Zn(II) and Pb(II) from aqueous solutions containing single metal ions was investigated in batch adsorption–equilibrium experiments. Effects of the initial concentration of metal ion and pH of the medium on the adsorption rate and capacity were studied. 0.02 l Of aqueous metal ion solution with different concentrations (in the range 0.25–4.5 mmol l⁻¹) were treated with the plain and Alkali Blue 6B-attached poly(HEMA) films at different pH (in the range 2.5–7.5, adjusted with HCl and NaOH) at room temperature, in flasks agitated magnetically at 600 rpm. At the end of the adsorption process, the films were separated from the adsorption medium and the concentration of the metal ions in the aqueous phase was measured by using a graphite furnace atomic absorption spectrophotometer (GBC 932 AA, Australia). The amount of adsorbed ions per unit film surface was calculated from the following expression.

$$Q = [(C_0 - C) \cdot V] / A \quad (1)$$

Here, Q is the amount of metal ions adsorbed onto unit surface area of the poly(HEMA) film (mmol m^{-2}); C_0 and C are the concentrations of the metal ions in the solution initially and after adsorption, respectively (mmol l^{-1}); V is the volume of the aqueous phase (l); and A is the surface area of the poly(HEMA) film used (m^2).

In the second group of experiments, competitive adsorption of Cd(II), Zn(II) and Pb(II) from their mixture was investigated in a batch manner. A solution (20 ml) containing 1 mmol l^{-1} from each metal ion was incubated with a Alkali Blue 6B-attached poly(HEMA) film at a pH of 5.0 at room temperature, in flasks agitated magnetically at 600 rpm. After adsorption, concentration of the metal ions in the supernatant was determined with the atomic absorption spectrophotometer.

Desorption of heavy metal ions was studied in 0.1 M HNO_3 . The poly(HEMA) film loaded with metal ions were placed in this desorption medium and stirred at 600 rpm for 30 min at room temperature. The final metal ion concentration in the aqueous phase was determined by using an atomic absorption spectrophotometer. The desorption ratio was calculated from the initial amount of metal ions on the film and the final metal ion concentration in the desorption medium, by using the following equation.

Desorption ratio =

$$\frac{\text{Amount of metal ions desorbed to the elution medium}}{\text{Amount of metal ions adsorbed on the film}} \times 100 \quad (2)$$

In order to evaluate the reusability of the Alkali Blue 6B-attached poly(HEMA) films, the adsorption–desorption process was repeated 3 times with the same film.

3. Results and discussion

The poly(HEMA) films used in the present study were prepared and characterized in our previous papers [9–11]. These films are hydrophilic, cross-linked structures which swell but

do not dissolve in aqueous media depending on the degree of cross-linking density. The equilibrium swelling ratio is 58% (w/w).

Alkali Blue 6B was selected as the affinity dye-ligand, and covalently bonded to the poly(HEMA) films. In Fig. 1, the chemical structure of Alkali Blue 6B is shown. Note that the possible groups to react with divalent heavy metal ions are SO_3H –, NH and OH groups. FTIR spectra of plain poly(HEMA), Alkali Blue 6B and poly(HEMA)-Alkali Blue 6B are given in Fig. 2. FTIR spectra of both poly(HEMA) and poly(HEMA)-Alkali Blue 6B have the characteristic stretching vibration band of hydrogen bonded alcohol, O–H, around 3500 cm^{-1} . The FTIR spectra of Alkali Blue 6B-attached poly(HEMA) has some absorption bands different than those of poly(HEMA). These are at 3510 , 1500 and 670 cm^{-1} and characteristic of N–H stretching, N–H bending (scissoring) and S–O stretching, respectively observed also in Alkali Blue 6B (Fig. 1). Alkali Blue 6B-attached poly(HEMA) has a sharp shoulder absorption band at about 3500 cm^{-1} and is interpreted as the N–H absorption. The bands at 1075 and 1155 cm^{-1} represent symmetric stretching of S=O and asymmetric stretching of S=O, respectively, and are due to Alkali Blue 6B bonded to poly(HEMA). These bands, however, do not appear, because plain poly(HEMA) also has some absorption bands in the same region. Thus, absorption bands of plain poly(HEMA)

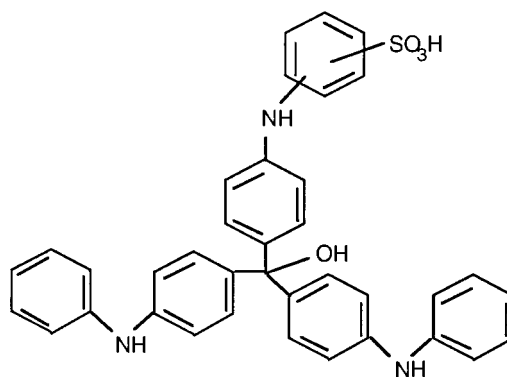


Fig. 1. Chemical structure of Alkali Blue 6B.

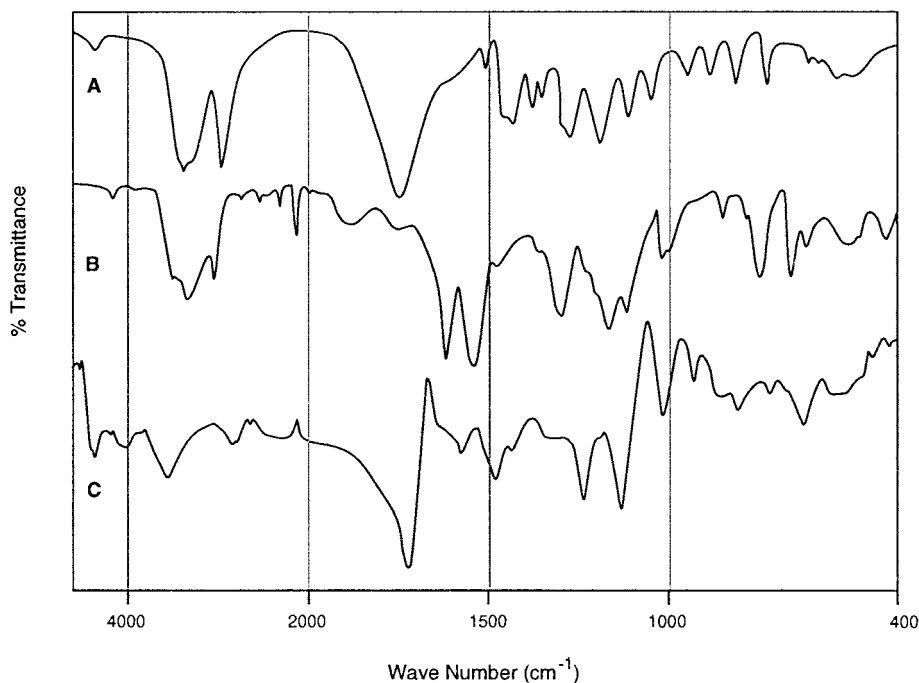


Fig. 2. FTIR Spectra of: (A) poly(HEMA); (B) Alkali Blue 6B; and (C) Alkali Blue 6B-attached poly(HEMA) film.

overlap with those of the Alkali Blue 6B at around these wavenumbers. The dye attached poly(HEMA) adsorption band intensities in this region are higher than those of poly(HEMA), but the intensity increase is quite small because of the low concentration of Alkali Blue 6B on the polymeric surface. On the other hand the hydrogen bonded alcohol O–H stretching band intensity of plain poly(HEMA) is higher than that of poly(HEMA)-Alkali Blue 6B film. The reason for the loss of the –OH groups is as a result of the condensation reaction between –OH groups of the poly(HEMA) and –NH groups of the Alkali Blue 6B.

Elemental analysis of the plain and Alkali Blue 6B-attached poly(HEMA) films were performed, and the incorporation of the Alkali Blue 6B was found to be 14.8 mmol m^{-2} from the nitrogen and sulphur stoichiometry.

Alkali Blue 6B leakage was also followed. There was no leakage in any of the adsorption and desorption media, which ensured that the washing procedure used for the removal of physi-

cally adsorbed Alkali Blue 6B molecules from the poly(HEMA) film was satisfactory.

3.1. Adsorption of heavy metal ions

3.1.1. Adsorption time

The equilibrium adsorption time of heavy metal ions (i.e. Cd(II), Zn(II) and Pb(II)) on the Alkali Blue 6B-attached poly(HEMA) film was investigated (Fig. 3). Note that these batch experiments were performed by using single (not mixed) solutions of the relevant ions. The initial concentrations of the ions within the aqueous phase were varied in the range $0.25\text{--}4.50 \text{ mmol l}^{-1}$. As seen from Fig. 3, adsorption amounts of metal ion were very high at the beginning of adsorption, and saturation levels were gradually reached within 30 min for all metal ions. Adsorption of metal ions was very fast especially, when the metal ion concentration was high. This may be due to the high driving force, which is the metal ion concentration difference between the liquid (i.e. adsorption medium) and the solid (i.e. the

film) phases, in the case of high metal ion concentration. Notice that Pb(II) was adsorbed

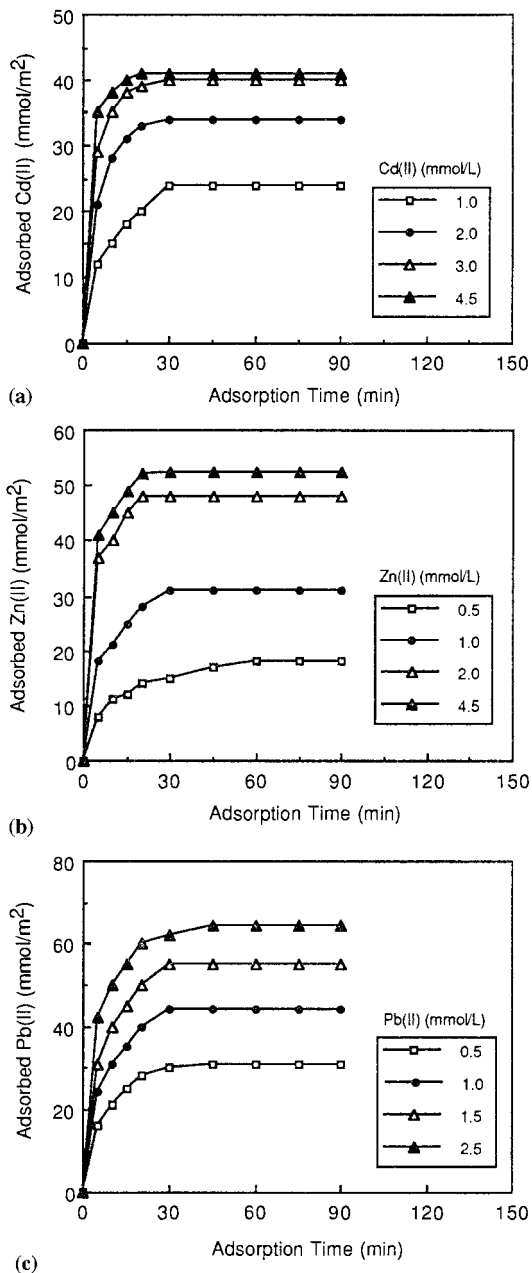


Fig. 3. Adsorption rates of heavy metal ions on the Alkali Blue 6B-attached poly(HEMA) film: (A) for Cd(II); (B) for Zn(II); and (C) for Pb(II). Temperature 20°C and pH 6.0; total film surface area in each batch 0.01 m² l⁻¹.

much faster than Cd(II) and Zn(II) due to the much higher affinity of the ligand (i.e. Alkali Blue 6B) molecules to these ions.

In the literature adsorption kinetics of heavy metal ions by various sorbent systems in film and microsphere form have shown a wide range of adsorption rates. For example, Marchese et al. [5] have investigated separation of cobalt, nickel and copper ions with alamine liquid films and they reported that equilibrium was achieved in about 4–5 h. Teramoto et al. [8] reported that a spiral type supported liquid film module reached the steady state in about 4 h. Reed and Matsumoto [12] have considered 6 h as a short equilibrium time in their cadmium adsorption kinetic studies, in which they have used activated carbon as sorbent. Shreedhara-Murthy and Ryan [13] have investigated mercury, copper, cadmium, lead and uranium adsorption on cellulose-dithiocarbamate resins and reported that the adsorption rates were very slow. Egawa [14] has studied uranium adsorption on polyacrylonitrile fibers containing amidoxime groups and reported 7 h equilibrium adsorption time. Denizli et al. [15] have used Alkali Blue 6B-attached poly(EGDMA-HEMA) sorbents for sorption of Cu(II), Cd(II), Zn(II) and Pb(II) ions and they reported that adsorption was completed in 30–90 min. Note that in such an adsorption process, there are several parameters which determine the adsorption rate, such as sorbent structural properties (e.g. size, porosity, topography and surface area), amount of sorbent, metal ion properties (e.g. hydrated ionic radius), initial concentration of metal ions, chelate-formation rate, and of course existence of other ions which may compete with the ions of interest for the active adsorption sites. All these studies published in the literature has been carried out under different experimental conditions. Hence, it is too difficult to compare the equilibrium adsorption times reported. However, the adsorption equilibrium times are less than 30 min in the case of our film-form sorbent system, which seems to be satisfactory.

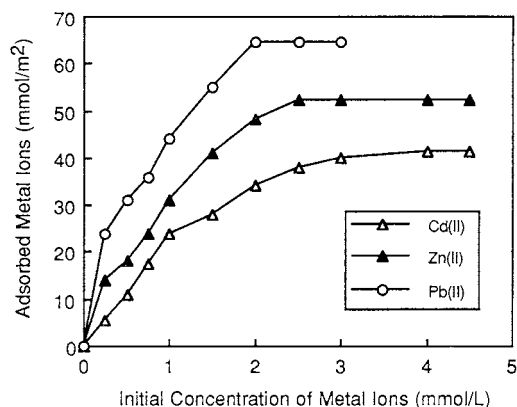


Fig. 4. Heavy metal ions adsorption capacity of the Alkali Blue 6B-attached poly(HEMA) films. Temperature 20°C and pH 6.0 and total film surface area in each batch $0.01 \text{ m}^2 \text{ l}^{-1}$.

3.2. Adsorption capacities

3.2.1. Effects of metal ion concentration

The heavy metal ion adsorption capacities of the Alkali Blue 6B-attached poly(HEMA) film are given as a function of the concentration of metal ions in the aqueous phase (Fig. 4). The amount of heavy metal ion adsorbed per unit surface area of the film (i.e. the adsorption capacity) first increased significantly with the initial concentration of metal ions, and then the change in adsorption was much less, after a heavy metal ion-concentration of 2–3 mmol l^{-1} depending on the metal ions. The maximum adsorption capacities achieved in the studied range are 41.4, 52.4 and 64.5 mmol m^{-2} of the sorbent film for Cd(II), Zn(II) and Pb(II), respectively. Note that the dye content of the adsorbent films used in this group of experiments was 14.8 mmol m^{-2} . It seems that a stoichiometry of around 3 metal ions per dye molecule depending on the metal ions. As mentioned before the possible groups to react with divalent heavy metal ions are SO_3H^- , NH and OH groups. N and O atoms with the unpaired electrons are available for these interactions, which means each dye molecule may adsorb more than 3 metal ions (see Fig. 4). But it was not the case here, maybe because of the low initial concentration of the metal ions. Note that it was not possible to get higher initial metal ion concentrations because of the precipitation problem.

It should also be noted that the non-specific adsorption values (adsorptions on the plain poly-(HEMA) film) of heavy metal ions were relatively low, 1.07, 0.94 and 1.21 mmol m^{-2} of the film for Cd(II), Zn(II) and Pb(II), respectively. This adsorption could actually be absorption (or entrapment) of heavy metal ions within the pores of the film. OH groups of HEMA (the unpaired electrons of O atoms) may contribute to these interactions.

Sorbents used in heavy metal removal are in particulate form in most of the cases. Reed and Matsumoto [12] reported 90–120 $\text{mmol Cd(II) m}^{-2}$ with activated carbon having different porosities. Egawa et al. [16] have found 62.1 $\text{mmol uranium m}^{-2}$ removal by amidoxime containing acrylonitrile–divinylbenzene copolymer beads. Maeda and Egawa [17] showed very low adsorption capacities which 1.5 $\text{mmol Pb(II) m}^{-2}$ and 1.6 $\text{mmol Cu(II) m}^{-2}$ with methylmethacrylate–divinylbenzene copolymer beads-amino methyl–phosphonic acid macroreticular chelating resin-containing poly(styrene-divinylbenzene) sorbents. Denizli and colleagues [10,11] used dye-affinity membranes for heavy metal adsorption. The maximum amounts of adsorption capacities achieved were 22.2–61.0 mmol m^{-2} Cd(II), 34.2–79.0 $\text{mmol Pb(II) m}^{-2}$ and 16.8 $\text{mmol Zn(II) m}^{-2}$. Comparing these data it seems that the adsorption capacities achieved with the dye-attached films are satisfactory.

3.2.2. Effect of pH

Heavy metal adsorption is pH dependent [15,18,19]. In the absence of complexing agents, the hydrolysis and precipitation of the metal ions are affected by the concentration and formation of soluble metal species. The solubility of metal ions is governed by hydroxide or carbonate concentration. As discussed in detail by Reed and Matsumoto [20], hydrolysis of metal ions becomes significant at basic pHs. In the present case, precipitation of Cd(II), Zn(II) and Pb(II) ions occur approximately pH 8.5, 7.0, and 7.5, respectively, which also depends on the concentration of metal ions in the medium. Therefore, here, in order to establish the effect of pH on the adsorption of metal ions onto the Alkali Blue 6B-attached

poly(HEMA) films, we repeated the batch equilibrium studies at different pH in the range 2.5–7.5 at low metal ion concentration. Fig. 5 shows the specific adsorption (i.e. adsorption by chelating with the Alkali Blue 6B molecules attached to the poly(HEMA) film) of metal ions. Adsorption of Cd(II), Zn(II) and Pb(II) ions first increased with increasing pH and almost reached a plateau value around pH 4.0–5.0 for all ions.

3.2.3. Competitive adsorption

Competitive adsorption of Cd(II), Zn(II) and Pb(II) ions were also studied. Solutions containing 1 mmol l^{-1} of each metal ion were incubated with the Alkali Blue 6B-attached poly(HEMA) films in batch fashion as described above. Fig. 6 shows that the amount of adsorption for each heavy metal ion is as follows: 31 mmol m^{-2} for Cd(II), 38 mmol m^{-2} for Zn(II), and 52 mmol m^{-2} for Pb(II). It is quite interesting to note that the competitive adsorption capacity of the Alkali Blue 6B-attached poly(HEMA) films for all metal ions were much higher than non-competitive conditions. The total heavy metal adsorption is much higher than one expects from considering the stoichiometry, i.e. the possible number of active sites on the dye molecules. It seems that heavy metal ions on the adsorbed form are interacting with each other, and therefore resulting a multi-

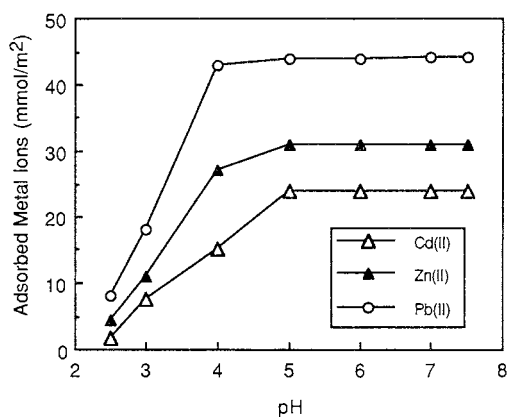


Fig. 5. Effect of pH on adsorption of heavy metal ions on the Alkali Blue 6B-attached poly(HEMA) film. Temperature 20°C and total film surface area in each batch $0.01 \text{ m}^2 \text{ l}^{-1}$. Initial concentration of metal ions 1.0 mmol l^{-1} .

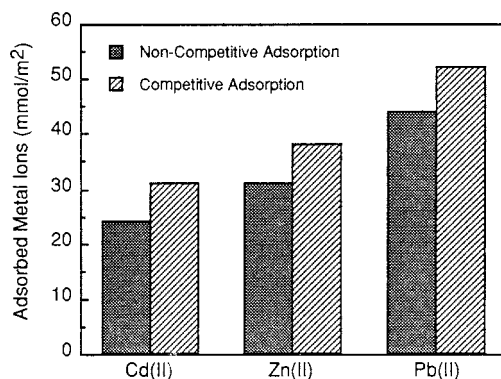


Fig. 6. Competitive adsorption of Cd(II), Zn(II) and Pb(II) ions on the Alkali Blue 6B-attached poly(HEMA) films. Initial concentration of metal ions 1 mmol l^{-1} ; temperature 20°C and pH 6.0; total film surface area in each batch $0.01 \text{ m}^2 \text{ l}^{-1}$.

layer type adsorption (non-Langmuir type). The order of affinity for competitive conditions is as follows: $\text{Pb(II)} > \text{Zn(II)} > \text{Cd(II)}$. This order is the same with non-competitive conditions.

3.3. Desorption and repeated use

Desorption of the adsorbed metal ions from the Alkali Blue 6B-attached poly(HEMA) films was also studied in a batch experimental set-up. The poly(HEMA) films loaded with the maximum amounts of the respective metal ions were placed in the desorption medium containing 0.1 M HNO_3 and the amount of metal ion desorbed in 30 min was measured. The desorption ratio was then calculated by using the expression given in Eq. (2). Table 1 clearly shows that the Alkali Blue 6B-attached poly(HEMA) films can be used repeatedly without significantly losing their adsorption capacities for all metal ions studied here.

4. Conclusions

Macroporous, hydrogel (swelling ratio: 58%) poly(HEMA) films were prepared by photo-polymerization of HEMA. Alkali Blue 6B was then covalently attached to these films with a film phase concentration of $14.8 \text{ mmol Alkali Blue 6B m}^{-2}$ as a dye-ligand. Adsorption/desorption of

Table 1

Heavy metal ions adsorption capacity of Alkali Blue 6B-attached poly(HEMA) films after consecutive adsorption and desorption

Cycle	Cd(II) (mmol m ⁻²)	Zn(II) (mmol m ⁻²)	Pb(II) (mmol m ⁻²)
1 Adsorption	24.1 ± 0.3	31.2 ± 0.4	44.1 ± 0.5
Desorption	23.8 ± 0.2	30.6 ± 0.2	43.8 ± 0.3
2 Adsorption	23.7 ± 0.3	30.4 ± 0.3	43.5 ± 0.4
Desorption	23.5 ± 0.2	30.1 ± 0.2	43.1 ± 0.3
3 Adsorption	23.4 ± 0.4	29.9 ± 0.1	42.7 ± 0.3
Desorption	23.2 ± 0.3	29.7 ± 0.2	42.4 ± 0.4

Total film surface area in each batch 0.01 m² l⁻¹. Initial concentrations of metal ions 1 mmol l⁻¹.

Cd(II), Zn(II) and Pb(II) from aqueous media on these films led to the following conclusions: adsorption equilibria were reached in about 30 min and therefore adsorption rates were very high. Adsorption capacities of these films were 41.4 mmol m⁻² for Cd(II), 52.4 mmol m⁻² for Zn(II) and 64.5 mmol m⁻² for Pb(II). When the heavy metal ions competed (in the case of the adsorption from their mixture) the amounts of adsorption for Cd(II), Zn(II) and Pb(II) were higher with respect to non-competitive conditions, which were 31 mmol m⁻² for Cd(II), 38 mmol m⁻² for Zn(II), and 52 mmol m⁻² for Pb(II). Adsorbed metal ions were desorbed up to 90% by using 0.1 M HNO₃ as the desorption agent. Repeated adsorption/desorption processes showed that these novel dye-attached films are very suitable for heavy metal removal.

References

- [1] C.S. Luo, S. Huang, Sep. Sci. Technol. 28 (1993) 1253.
- [2] D.A. Harkins, G.K. Schweitzer, Sep. Sci. Technol. 26 (1991) 345.
- [3] A. Sugii, N. Ogawa, H. Hashizume, Talanta 27 (1980) 627.
- [4] S. Hunt, in: H. Ecclos, S. Hunt (Eds.), Immobilisation of Ions by Bio-Sorption, Ellis Horwood, Chichester, UK, 1986.
- [5] J. Marchese, M. Campderros, A. Acosta, J. Chem. Technol. Biotechnol. 64 (1995) 293.
- [6] T. Saito, Sep. Sci. Technol. 26 (1991) 1519.
- [7] C.Y. Shiau, P.Z. Chen, Sep. Sci. Technol. 28 (1993) 2149.
- [8] M. Teramoto, N. Tahno, N. Ohnishi, H. Matsuyama, Sep. Sci. Technol. 24 (1989) 903.
- [9] M.Y. Arica, V. Hasirci, Biomaterials 8 (1987) 489.
- [10] A. Denizli, B. Salih, M.Y. Arica, K. Kesenci, V. Hasirci, E. Piskin, J. Chromatogr. 758 (1997) 217.
- [11] M.Y. Arica, A. Denizli, B. Salih, E. Piskin, V. Hasirci, J. Membr. Sci. 129 (1997) 65.
- [12] B.E. Reed, N.R. Matsumoto, Sep. Sci. Technol. 28 (1993) 2179.
- [13] R.S. Shreedhara-Murthy, D.E. Ryan, Anal. Chim. Acta 140 (1982) 163.
- [14] H. Egawa, M. Nakayama, T. Nonaka, E.E. Sugihara, J. Appl. Polym. Sci. 33 (1987) 1993.
- [15] A. Denizli, B. Salih, E. Piskin, React. Funct. Polym. 29 (1996) 11.
- [16] H. Egawa, T. Nonaka, S. Abe, M. Nakayama, J. Appl. Polym. Sci. 45 (1992) 837.
- [17] H. Maeda, H. Egawa, J. Appl. Polym. Sci. 33 (1987) 1275.
- [18] C. Kantipuly, S. Katragadda, A. Chow, H.D. Gesser, Talanta 37 (1990) 491.
- [19] Y. Konishi, S. Asai, Y. Midoh, M. Oku, Sep. Sci. Technol. 28 (1993) 1691.
- [20] B.E. Reed, M.R. Matsumoto, Carbon 29 (1991) 1191.

Spectrophotometric determination of methyl dopa and dopamine in pharmaceutical formulations using a crude extract of sweet potato root (*Ipomoea batatas* (L.) Lam.) as enzymatic source

Iolanda da Cruz Vieira, Orlando Fatibello-Filho *

Departamento de Química, Grupo de Química Analítica, Centro de Ciências Exatas e de Tecnologia,
Universidade Federal de São Carlos, Caixa Postal 676, CEP 13.560-970, São Carlos, SP, Brazil

Received 12 May 1997; received in revised form 2 September 1997; accepted 3 September 1997

Abstract

A rapid, precise and low cost spectrophotometric method is proposed for the determination of methyl dopa and dopamine in pharmaceutical formulations. The crude extract of sweet potato root (*Ipomoea batatas* (L.) Lam.) was used as an enzymatic source of polyphenol oxidase (PPO; EC.1.14.18.1). This enzyme catalyses the oxidation of catecholamines to the corresponding methyl dopaquinone and dopaminequinone. Those compounds are converted by a rapid spontaneous auto-oxidation to methyl dopachrome and dopaminechrome which have a strong absorption at 480 or 470 nm, respectively. The calibration graphs are linear from 2.0×10^{-4} to 6.0×10^{-3} M. The results obtained by the proposed enzymatic method are in close agreement with those obtained using a Pharmacopoeia procedure and also with the label values. The detection limit (three times the signal blank/slope) was 3.4×10^{-5} and 3.0×10^{-5} M for methyl dopa and dopamine, respectively, the recovery of methyl dopa and dopamine from three samples ranged from 97.5 to 102.9% of the added amount. © 1998 Elsevier Science B.V. All rights reserved.

Keywords: Methyl dopa; Dopamine; Polyphenol oxidase; Sweet potato (*Ipomoea batatas* (L.) Lam.); Pharmaceutical formulations

1. Introduction

Catecholamines are compounds that consist of amines attached to a benzene ring bearing two hydroxyl groups (catechol). The main sites of catecholamine production are the brain, chromaffin cells of the adrenal medulla and the sympathetic neurons [1]. Methyl dopa (α -methyl-3,4-

dihydroxyphenylalanine) is a centrally acting anti-hypertensive agent and dopamine (3,4-dihydroxyphenylethylamine) is a central neurotransmitter particularly important in the regulation of movement and possesses important intrinsic pharmacological properties. It is used for the correction of hemodynamic disorders associated with shock episodes [2].

Several methods have been employed to determine catecholamine drugs in biological specimens and/or pharmaceutical formulations. The determi-

* Corresponding author. Fax: +55 16 2748350; e-mail: doff@power.ufscar.br

nation of catecholamines in biological fluids normally requires the use of trace analysis techniques, mainly chromatography with fluorimetric or electrochemical detection [3]. Catecholamines are present in relatively large amounts in pharmaceutical formulations and much effort has been devoted to the development of simple, rapid, accurate and precise analytical procedures. Of those methods cited in the literature, some spectrophotometry has been used to determine methyl dopa [4–9] and dopamine [6,10].

A differential UV spectrophotometric procedure has been proposed for the determination of methyl dopa in pharmaceutical formulations in the presence of germanium dioxide at 292 nm. [4]. Methyl dopa has been determined in the visible region after reaction with vanillin [5], metaperiodate [6], potassium bromate [7], 2,3,5-triphenyltetrazolium chloride [8] and Fe(III)-*o*-phenantroline [9] at 420, 473, 485, 485 and 510 nm, respectively. Dopamine has been determined by vis spectrophotometry after a derivatization reaction with metaperiodate in a moderate acid medium [6] and an aqueous alcoholic medium [10], at 473 and 465 nm, respectively. However, there are no enzymatic spectrophotometric procedures for determining those catecholamines described in the literature and only dopamine biosensors using enzymes [12] and vegetal tissue [11,13–15] have been proposed.

In the present work, a spectrophotometric procedure is reported for determining methyl dopa and dopamine in pharmaceutical formulations. A crude extract of sweet potato root (*Ipomoea batatas* (L.) Lam.) was used as an enzymatic source of polyphenol oxidase (PPO; EC.1.14.18.1). This enzyme catalyses the *ortho*-hydroxylation of phenols and the oxidation of other catechol derivatives such as catecholamines to methyl dopaquinone and dopaminequinone. These quinones are converted to leucomethyl dopachrome and leucodopaminechrome and oxidized to methyl dopachrome and dopaminechrome which present a strong absorption at 480 and 470 nm, respectively. The use of an insoluble polyvinylpyrrolidone (Polyclar SB-100) to remove natural phenolic compounds (e.g. chlorogenic and isochlorogenic acids) from solution in the preparation of the crude extract of sweet potato root

led to a considerable increase in enzyme activity. The simple, sensitive and rapid enzymatic method proposed here for determining these catecholamines could be used as an economical alternative to those procedures that use chromogenic reagents [4–10] and/or biosensors [11–15].

2. Experimental

2.1. Apparatus

A DuPont Instruments (Newtown, CN) Model RC-5B centrifuge, provided with a Model SS-34 rotor, was used in the preparation of the crude extract of the sweet potato.

A Hewlett-Packard (Boise, ID) Model 8452A UV-visible spectrophotometer with a quartz cell (optical path 1 cm) was used in all spectrophotometric measurements.

2.2. Reagents and solutions

All reagents were of analytical reagent grade and all solutions were prepared with water from a Millipore (Bedford, MA) Milli-Q system (Model UV Plus Ultra-Low Organics Water). Standard catecholamines (methyl dopa or dopamine) were purchased from Aldrich (Milwaukee, WI); 1.0×10^{-2} M stock solutions were prepared daily in 0.1 M phosphate buffer of pH 7.0 and standardized using a conventional method [16]. Standard solutions from 2.0×10^{-4} to 6.0×10^{-3} M were prepared from stock solutions in 0.1 M phosphate buffer of pH 7.0.

Sucrose, glucose, fructose, lactose, starch, poly(ethylene glycol) 1500, sodium chloride and magnesium stearate were purchased from Sigma (St. Louis, MO). In the interference study, solutions containing 2.0×10^{-4} , 2.0×10^{-3} and 2.0×10^{-2} M of each one of the excipients was carried out using 2.0×10^{-3} M methyl dopa or dopamine solutions.

Polyclar SB-100 was used as a protective and/or stabilizer agent in the crude extract preparation and was kindly donated by GAF (Wayne, NJ). This polyvinylpyrrolidone was initially purified as described by McFarlane and Vader [17]. It was

boiled for 10 min in 10% v/v HCl and washed with distilled water until free of chloride ion, then washed with acetone and dried.

Healthy sweet potato roots (*Ipomoea batatas* (L.) Lam.) purchased from a local producer were selected, washed, hand-peeled, chopped and frozen in liquid nitrogen or in a freezer.

2.3. Preparation of the crude extract

Twenty-five grams of the frozen peeled sweet potato root were homogenized in a liquefier with 100 ml of 0.1 M phosphate buffer (pH 7.0), containing 2.5 g of Polyclar SB-100 for 2 min at 4–6°C. The homogenate was rapidly filtered through four layers of cheesecloth and centrifuged at $25\,000 \times g$ ($18\,000 \text{ rev min}^{-1}$) for 30 min at 4°C. The resulting supernatant was stored at this temperature in a refrigerator and utilized as the enzymatic source after the determination of polyphenol oxidase activity and total protein.

2.4. Measurement of polyphenol oxidase activity

The activity of soluble polyphenol oxidase (PPO) present in the crude extract was determined in triplicate by measuring the absorbance at 410 nm of melanin-like pigments formed in the polymerization of quinone produced by the reaction between 0.2 ml of supernatant solution and 2.8 ml of 0.05 M catechol solution in 0.1 M phosphate buffer (pH 7.0) at 25°C. The initial rate of the enzyme-catalyzed reaction was a linear function with time for 1.5–2.0 min. One unit of polyphenol oxidase activity is defined as the amount of enzyme that causes an increase of 0.001 absorbance min^{-1} under conditions described above [18,19].

2.5. Protein determination

The protein concentration was determined in triplicate using the Lowry et al. method [20] i.e. using bovine serum albumin as standard.

2.6. Spectrophotometric procedure

In a quartz cell, 0.2 ml of the crude extract containing $585 \text{ units ml}^{-1}$ PPO at pH 7.0 was

added to 2.8 ml of sample or standard solution in 0.1 M phosphate buffer (pH 7.0), shaken and the absorption of methyl dopachrome or dopaminechrome was measured at 480 and 470 nm, respectively; (after 10 min of homogenization). It is important to point out that 10 min sampling period is within the linear regime of the reaction.

2.7. Preparation of sample catecholamines in pharmaceutical formulations

The contents of twenty tablets, were mixed well; from the fine powder an accurately weighed portion was taken and dissolved in phosphate buffer (pH 7.0, 0.1 M at 25°C). Using a mechanical shaker or an ultrasonic bath, the powder was completely disintegrated and the solution was clarified by passing it through No. 1 filter-paper, after which appropriate dilutions were made.

For liquid samples an appropriate dilution with phosphate buffer solution was made (pH 7.0, 0.1 M at 25°C).

3. Results and discussion

3.1. Characteristics of the crude extract activity

The activity and total protein of the crude extract of the sweet potato root varied according to the extraction procedure and medium used. The buffer-to-tissue ratio was an important factor in the preparation of PPO from sweet potato root. In this study, the enzyme was extracted using ratios of 2–6:1 v/w and the highest specific activity was obtained at a ratio 4:1 v/w. It was also found that PPO could be extracted with a phosphate buffer solution of low concentration such as 0.05–0.4 M with the maximum yield achieved at a concentration of 0.1 M. The effect of buffer pH on the extraction of PPO was also investigated in the pH range of 6.0–8.0. The highest enzymatic activity was reached at pH 7.0. The natural phenolic compounds (chlorogenic and isochlorogenic acids) and the oxidation by atmospheric oxygen are responsible for the decrease of the PPO activity in the crude extract. In order to minimize this effect, a protective agent

and/or stabilizer such as polyvinylpyrrolidones (PVPs), ion-exchange resins, L-cysteine and/or other reducer compounds have been used. It was found that the Polyclar SB-100 in the concentration ratio of 2.5:25.0 w/w was the best protective agent, once it completely removes the natural phenolic compounds present in this root. The same concentration was found in our previous work [19]. The enzyme activity of crude extract obtained using this PVP did not vary for at least 5 months when it was stored in a refrigerator at 4°C.

3.2. Reaction between methyl dopa and/or dopamine with polyphenol oxidase

Fig. 1 shows the reaction steps of the enzymatic oxidation of catecholamines (methyl dopa and dopamine) [21,22] (A) by polyphenol oxidase of the crude extract to the methyl dopaquinone and dopaminequinone (B), respectively. Furthermore, these quinones are converted to leucomethyl dopachrome, leucodopaminechrome (C) by a fast spontaneous auto-oxidation which are in turn oxidized to the corresponding aminochromes (methyl dopachrome and dopaminechrome) (D), which have a strong absorption at 480 or 470 nm, respectively. The absorption of these chromophores increased rapidly for 9–10 min, than decreased very slowly when converted to 5,6-dihydroxyindole (E), indole-5,6-quinone (F) and finally melanin (G), as shown in this figure.

3.3. Effect of enzyme concentration, pH and temperature

The effect of PPO concentration from 7.8 to 62.6 units ml⁻¹ on the analytical signal (absorbance) for 5.0 × 10⁻³ M dopamine was investigated (Fig. 2). The absorbance signal increases with increasing concentration of enzyme solution used up to 37.0–39.0 units ml⁻¹ PPO and then leveled off between 39.0 and 62.6 units ml⁻¹. Consequently, a concentration of 39.0 units ml⁻¹ was used in this work.

The effect of pH in the range from 5.0 to 8.0 on the absorbance of 5.0 × 10⁻³ M methyl dopa and dopamine solution and 39.0 units ml⁻¹ PPO en-

zyme was also studied and is shown in Fig. 3. As observed, the optimum pH value for PPO activity was 7.0. The same optimum pH was found by Lourenço et al. [18] in pure and crude extracts of sweet potato and by us in previous work [19].

The effect of temperature was studied between 5 and 50°C. The enzyme exhibited highest activity in range 15–25°C after which a gradual decline in its activity by heat inactivation was observed (between 25 and 50°C), a temperature of 25°C was decided on and used in this work.

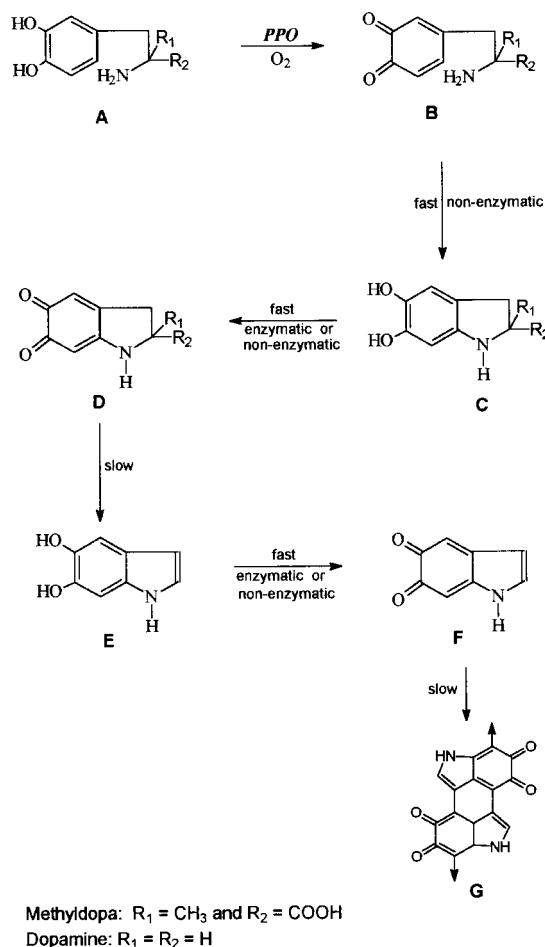


Fig. 1. Reaction steps of the catalytic oxidation of catecholamines by polyphenol oxidase.

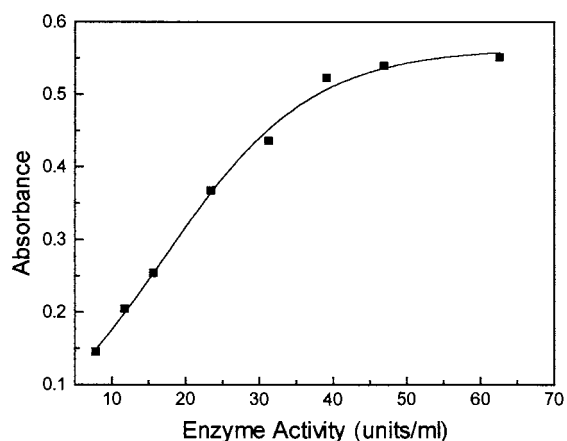


Fig. 2. Effect of polyphenol oxidase concentration from 7.8 to 62.6 units ml^{-1} on the absorbance signal for 5.0×10^{-3} M dopamine in 0.1 M phosphate buffer (pH 7), at 25°C.

3.4. Interference, recovery and repeatability studies

The effect of excipient substances frequently found with catecholamines in pharmaceutical formulations, such as sucrose, glucose, fructose, lactose, starch, poly(ethylene glycol), sodium chloride and magnesium stearate were evaluated using the developed method. The ratios of the concentrations of methyl dopa or dopamine to those of the excipient substances were fixed at 0.1, 1.0 and 10.0. None of these substances in-

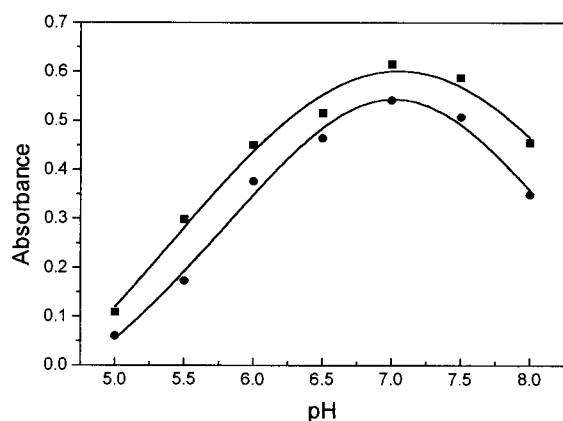


Fig. 3. Effect of the pH from 5 to 8 on the absorbance signal for 5.0×10^{-3} M catecholamines: (■ ■ ■), methyl dopa and (● ● ●), dopamine, at 25°C.

Table 1
Results of addition–recovery experiments using methyl dopa and dopamine with three different standard concentrations

Sample	Methyl dopa ^a or Dopamine ^b (mg) ^c		
	Added	Found	Recovery (%)
Aldomet tablet	2.38	2.45	102.9
	4.76	4.82	101.3
	7.15	7.09	99.2
Dopamine injection	1.90	1.87	98.4
	3.79	3.88	102.4
	5.69	5.55	97.5

^a Aldomet tablet.

^b Dopamine injection.

^c $n = 6$.

terfered with the proposed spectrophotometric method.

Recoveries varying from 97.5 to 102.9% of methyl dopa or dopamine from two pharmaceutical formulations samples ($n = 6$) were obtained using the spectrophotometric procedure (Table 1). In this study, 2.38, 4.76 and 7.15 mg of methyl dopa and 1.90, 3.79 and 5.69 mg of dopamine were added to each sample. This is good evidence of accuracy of the proposed method.

In the repeatability study, the relative standard deviations were 1.27 and 1.68% for solutions containing 5.0×10^{-3} M methyl dopa and dopamine ($n = 10$), respectively.

3.5. Analytical curves and applications

Under the optimum conditions established, i.e. enzyme concentration of 39.0 units ml^{-1} in 0.1 M phosphate buffer, pH 7.0, temperature of 25°C and reference solutions containing 2.0×10^{-4} – 6.0×10^{-3} M of methyl dopa or dopamine were employed to construct the calibration curve ($A = 0.014 + 125.11C_1$, $r = 0.9990$ and $A = 0.011 + 110.92C_2$, $r = 0.9988$ where C_1 and C_2 are the concentrations of methyl dopa and dopamine in M, respectively. Table 2 presents a comparison between the label values and the results obtained for these samples using the Pharmacopeia (HPLC: dopamine and spectrophotometric: methyl dopa)

Table 2

Determination of methyl dopa and dopamine in pharmaceutical formulations using the pharmacopeia and enzymatic spectrophotometric procedures

Sample	Catecholamine	Label value	Pharmacopeia	Enzymatic	Relative error(%)	
					(RE ₁)	(RE ₂)
Aldomet tablet	Methyl dopa ^a	250	254.3	248.7 ± 0.2	−0.5	−2.2
Dopamine injection	Dopamine ^b	50	48.4	47.3 ± 0.1	−5.4	−2.3

$n = 6$, confidence level 95%.

^a (mg tablet^{−1}) and ^b (mg ml^{−1}).

RE₁, enzymatic vs. label value; RE₂, enzymatic vs. pharmacopeia value.

[23] and proposed enzymatic spectrophotometric methods. The results are in close agreement with those reported and within an acceptable range of error. The detection limits (three times the signal blank/slope) were 3.4×10^{-5} M and 3.0×10^{-5} M methyl dopa and dopamine, respectively. The enzymatic method for determination of methyl dopa or dopamine in pharmaceutical formulations reported in this paper is rapid, precise and of low cost and it may be suitable for routine analysis.

Acknowledgements

Financial support of FAPESP (Process 91/2637-5) PADCT/CNPq (Process 62.0060/91-3), CNPq (Process 50.1638/91-1), and also the scholarship granted by CNPq to I.C.V. are gratefully acknowledged.

References

- [1] R.J. Whitley, A.W. Meikle, N.B. Watts, *Endocrinology*, in: C.A. Burtis, E.R. Ashwood (Eds.), *Tietz Textbook of Clinical Chemistry*, 2nd ed., W.B. Saunders, Philadelphia, 1994, 1739.
- [2] B.B. Hoffman, R.J. Lefkowitz, Catecholamines, sympathomimetic drugs, and adrenergic receptor antagonists, in: A.G. Gilman (Ed.), *The Pharmacological Basis of Therapeutics*, 9th ed., McGraw-Hill, New York, 1996, pp. 211–219.
- [3] A.J. Pesce, L.A. Kaplan, *Methods in Clinical Chemistry*, in: S. Bircher (Ed.), *The C.V. Mosby Company*, St. Louis, MO, 1987, pp. 944–963.
- [4] A.G. Davidson, *J. Pharm. Sci.* 73 (1984) 1582.
- [5] F.B. Salem, *Anal. Lett.* 18 (1985) 1063.
- [6] J.J.B. Nevado, J.M.L. Gallego, P.B. Laguna, *Fresenius J. Anal. Chem.* 353 (1995) 221.
- [7] W.I. Mohamed, F.B. Salem, *Anal. Lett.* 17 (1984) 191.
- [8] N.A. El-Rabbat, N.M. Omar, *J. Pharm. Sci.* 67 (1978) 779.
- [9] P.B. Issopoulos, *Fresenius J. Anal. Chem.* 336 (1990) 124.
- [10] M.E. El-Kommos, F.A. Mohamed, A.S. Khedr, *J. Assoc. Off. Anal. Chem.* 73 (1990) 516.
- [11] E.S. Forzani, G.A. Rivas, V.M. Solis, *J. Electroanal. Chem.* 382 (1995) 33.
- [12] Y. Hasebe, T. Hirano, S. Uchiyama, *Sensors and Actuators B* 24–25 (1995) 94.
- [13] J. Wang, M.S. Lin, *Anal. Chem.* 60 (1988) 1545.
- [14] L. Zhihong, Q. Wenjian, W. Meng, *Anal. Lett.* 25 (1992) 1171.
- [15] Y. Chen, T.C. Tan, *Talanta* 42 (1995) 1181.
- [16] C.A. Signori, O. Fatibello-Filho, *Quím. Nova* 17 (1994) 38.
- [17] W.D. McFarlane, M.J. Vader, *J. Inst. Brew.* 68 (1962) 254.
- [18] E.J. Lourenço, V.A. Neves, M.A. Da-Silva, *J. Agric. Food Chem.* 40 (1992) 2369.
- [19] O. Fatibello-Filho, I.C. da Vieira, *Analyst* 122 (1997) 345.
- [20] O.H. Lowry, N.J. Rosebrough, A.L. Farr, R.J. Randall, *J. Biol. Chem.* 193 (1951) 265.
- [21] M.D. Hawley, S.V. Tatawawadi, S. Piekarski, R.N. Adams, *J. Am. Chem. Soc.* 89 (1967) 447.
- [22] G.G. Guilbault, A.A. Suleiman, O. Fatibello-Filho, M.A. NabiRahni, *Immobilized bioelectrochemical sensors*, in: D.L. Wise (Ed.), *Bioinstrumentation and Biosensors*, Marcel Dekker, New York, 1990, p. 676.
- [23] United States Pharmacopeia National Formulary XXXIII, US Pharmacopeial Convention, Rockville, MD, 1995, pp. 549, 995.

Chemiluminescent detection of amines and amino acids using in situ generated $\text{Ru}(\text{bpy})_3^{3+}$ following separation by capillary electrophoresis

D.R. Bobbitt ^{a,*}, W.A. Jackson ^b, H.P. Hendrickson ^c

^a Department of Chemistry and Biochemistry, University of Arkansas, Fayetteville, AR 72701, USA

^b Arkansas Eastman Chemical Company, Batesville, AR 72501, USA

^c Department of Chemistry, Southern Illinois University at Edwardsville, Edwardsville, IL 62026, USA

Received 16 June 1997; received in revised form 27 August 1997; accepted 3 September 1997

Abstract

A new sensitive chemiluminescent detection method for capillary electrophoresis is described. Underivatized amines and amino acids were detected following capillary electrophoresis separation by their chemiluminescent reaction with $\text{Ru}(\text{bpy})_3^{3+}$ generated in situ at 35 μm carbon fibers. Detection limits for triethylamine and proline were 5 and 3 fmol, respectively at a SNR of three. The noise limiting the detectability of separated analytes was determined to exist at the level of the dark noise limit of the PMT used for these studies and additional noise reduction strategies are expected to improve the quantitative aspects of the method. Theoretical plate numbers for proline were approximately 20 000. End column addition of $\text{Ru}(\text{bpy})_3^{2+}$ coupled with in situ generation of $\text{Ru}(\text{bpy})_3^{3+}$, has been shown to be compatible with the nanoliter elution volumes characteristic of capillary electrophoresis. © 1998 Elsevier Science B.V. All rights reserved.

Keywords: Chemiluminescent detection; Amines and amino acids; $\text{Ru}(\text{bpy})_3^{3+}$; Capillary electrophoresis

1. Introduction

Since initial work involving electrophoretic separations in small diameter tubes by Mikkers et al. in 1979 [1], and Jorgenson and Lukacs, in 1981 [2], much interest has developed around separations based on the CE technique. This interest is primarily due to the unparalleled resolving power associated with CE and the relative simplicity of

the requisite instrumentation. Separation efficiencies approaching 400 000 theoretical plates for selected amino acid derivatives has been demonstrated [2].

The detection of analytes following CE separation is much more challenging than detection following HPLC. The characteristics which make CE an attractive separation technique also make detection difficult. This is due to the small dimensions of the capillary itself and the nanoliter injection volume necessary to maintain the separation efficiency of the CE process. Construction of off-

* Corresponding author. Tel.: +1 501 5754601; fax: +1 501 5754049; email dbobbitt@comp.uark.edu

column detection cells analogous to the detection cells used for UV-vis, fluorescence, and electrochemical detection in HPLC is problematic due to the small dead-volumes required to provide efficient detection without causing excessive zone broadening. Frequently absorbance, fluorescence, or other optical techniques employ on-column detection. In on-column detection, the polyamide coating on the capillary is removed at a position along the separation capillary, and this region is then used as the 'detection cell'. The pathlength of such a configuration is defined by the i.d. of the capillary and the sensitivity of absorbance detection is limited by this short pathlength [3].

An additional problem associated with detection following CE is the electric field used to drive the separation process. This electric field does not present a problem for optical techniques, but it presents a major problem for electrochemical (amperometric) forms of detection. Electrophoretic currents in the order of microamp are much larger than the nanoamp to picoamp Faradaic currents which would be expected for the micro-electrodes appropriate for amperometric detection in CE. Large electrophoretic currents make direct amperometric detection in CE difficult unless the electrophoretic potential field is first decoupled from the amperometric detection cell.

Effective decoupling of the electrophoretic field from the amperometric detection cell was first achieved by Wallingford and Ewing [4]. A porous glass capillary (decoupler) having an internal bore of the same diameter as the outside of the separation capillary was placed over a carefully formed fracture made in the separation capillary. The porous glass decoupler allowed ionic transport, but not bulk liquid flow. This results in a continuation of the electroosmotic flow past the fracture and into a section of capillary which extends beyond the capillary fracture. This region of the capillary is called the detection capillary and it is effectively decoupled from the electric field. Amperometric detection can then be performed by inserting a small electrode fiber into the end of the capillary. Other decouplers have been developed based on this general strategy [5–7]. End-column amperometric detection has also been demon-

strated in CE using small internal diameter capillaries ($< 25 \mu\text{m}$). Such capillaries produce small electrophoretic currents, in the order of nanoamps, a level which does not interfere with typical amperometric detection currents [8].

The development of an analytical methodology for the general detection of amino acids is challenging due to the absence of any easily identifiable property which is common to the 20 naturally occurring amino acids, and which can be exploited to facilitate detection. Thus, existing methodology has relied upon the formation of chemical derivatives to enhance detection. Pre-column derivatization is relatively straightforward and there have been a variety of recent reports describing new reagents and derivatization protocols [9–17]. Post-column derivatization has also been implemented [18–20], but it is more difficult because of the zone broadening which may be introduced by the post-column addition of the derivatization reagent. While derivatization schemes have greatly improved the quantitative aspects of amino acid detection, many of the derivatives are difficult to form, others are unstable, and some reagents form more than one adduct with the amino acid which complicates the analysis. In addition, since various experimental protocols rely upon either chromatographic retention or electrophoretic migration information for qualitative purposes, the added moiety may dominate the chromatographic or electrophoretic properties of the derivative thereby degrading the qualitative aspects of the analysis. Thus it would be advantageous to develop methodology which could provide for the sensitive detection of amino acids without requiring derivatization.

Native amino acids have been detected following CE separation using indirect methods. Kuhr and Yeung [21] have described the indirect laser induced fluorometric (LIF) detection of native amino acids, and Olefirowicz and Ewing have used indirect amperometry for the detection of underivatized amino acids [22]. The limit of detection for both of these techniques is in the micromolar range.

Direct amperometric detection of amino acids under strongly alkaline conditions has been reported at a copper wire electrode [23] following

CE separation. The copper electrode is the key to the success of this approach as other electrode materials do not provide a response for all amino acids. Alternately, pulsed amperometric detection (PAD) and integrated pulsed amperometric detection (IPAD) using a gold electrode have been successfully adapted to CE [24]. In these methods, detection limits at the 10 fmol level have been achieved with proper experimental design.

Chemiluminescence (CL) has been shown to be a very sensitive method for the detection of both derivatized [25] and underivatized [26,27] amino acids following HPLC separation. There has only been a few reports on the use of CL for detection of amines and amino acids following CE separation [17,28–33]. The first, [17], detection was accomplished by exploiting the energy transfer reaction between peroxalate and dansylated amino acid derivatives. The method required the use of two syringe pumps in addition to the electrophoretic apparatus. Detection limits were in the femtomole range. Other reports have shown that attomole detection limits are possible with proper experimental design using chemiluminescence detection in CE. The use of $\text{Ru}(\text{bpy})_3^{3+}$ -based chemiluminescence detection in CE has not been reported although previous work with this reaction scheme has suggested that this approach has much potential in terms of detection sensitivity and experimental simplicity.

This work will describe the instrumental development and subsequent application of in situ generated $\text{Ru}(\text{bpy})_3^{3+}$ -based chemiluminescence detection of underivatized amines and amino acids following CE separation. The experimental protocol uses a post-capillary reservoir of $\text{Ru}(\text{bpy})_3^{2+}$, which is then converted to $\text{Ru}(\text{bpy})_3^{3+}$ at a carbon microfiber for reaction with eluting amines and/or amino acids. This detection approach has been found to provide a reproducible electrophoretic separation and be compatible with the nanoliter detection volumes required to maintain CE separation efficiencies. The quantitative characteristics of the methodology will be evaluated and compared with existing analytical methods.

2. Experimental

2.1. Apparatus

2.1.1. Electrophoresis system

The high voltage (HV) for electrophoresis was applied using a Glassman (Whitehouse Station, NJ, model EH30R03.0) 30 kV power supply. Capillaries (75 and 100 μm i.d., 360 μm o.d.) were obtained from Polymicro Technologies (Phoenix, AZ). Capillaries were filled by pumping the desired solution into the capillary with a peristaltic pump. Electrical connection was made to both the anodic and cathodic ends of the capillary with Pt electrodes partially submerged in buffer. The HV (anode) end of the capillary was contained in a Plexiglas box which was equipped with an interlock to prevent accidental operator contact with the HV. A microammeter was placed in-line between the cathode and the common terminal of the HV power supply to allow monitoring of the electrophoretic current passing through the capillary. The entire apparatus was attached to and supported by a 2' \times 4' optical bread-board which was held at ground potential. Samples separated by CE were injected electrokinetically at 20 kV for 8 s. Oxygen ($\text{Ru}(\text{bpy})_3^{3+}$ luminescence quencher) was used as the marker for electroosmotic flow in order to determine the injection volume (45 nl). For the FIA study, injection was achieved hydrodynamically by placing the analyte solution 20 cm above the cathode for 5 s.

2.1.2. Preparation of the on-column Nafion joint

The electrochemical cell used to generate the $\text{Ru}(\text{bpy})_3^{3+}$ was decoupled from the electrophoretic field by the formation of an on-column fracture covered with a Nafion tube. The joint was located approximately 4 cm from the end of the capillary. This configuration is similar to that used by O'Shea et al. [5] for off-column amperometric detection following CE.

Microfiber electrodes were prepared from 35 μm carbon monofilament fibers (AVCO, Lowell, MA), 0.2 mm copper wire, and glass capillaries by following a procedure similar to that described earlier [5]. The final electrode length varied from 1 to 4 mm. Fig. 1 shows the cyclic voltammetric

(CV) response of $\text{Ru}(\text{bpy})_3^{2+}$ at one of these fibers.

2.1.3. Experimental arrangement for the observation of electrogenerated chemiluminescence

The electrochemical cell was assembled at the end of the detection capillary which extended beyond the Nafion joint and support beaker. The carbon fiber electrode assembly was mounted on a three-axis stage (Daedel, Harrison City, PA) using a small three-finger lab clamp (Fisher, Pittsburgh, PA). The three-axis stage was used to center the carbon fiber at the end of the detection capillary using $5\times$ magnification for precise placement. The carbon fiber served as the working electrode (WE) of a three-electrode assembly. A stainless steel (SS) spatula, held by a three-finger lab clamp served as the auxiliary electrode (AE). The spatula was held at one end by the lab clamp, and the other end acted as a support for a small pool of electrolyte which contacted the carbon fiber and the saturated calomel (SCE) reference electrode (RE). The end of the spatula which supported the electrolyte pool could be raised or lowered by varying the pressure of the adjustment screw of

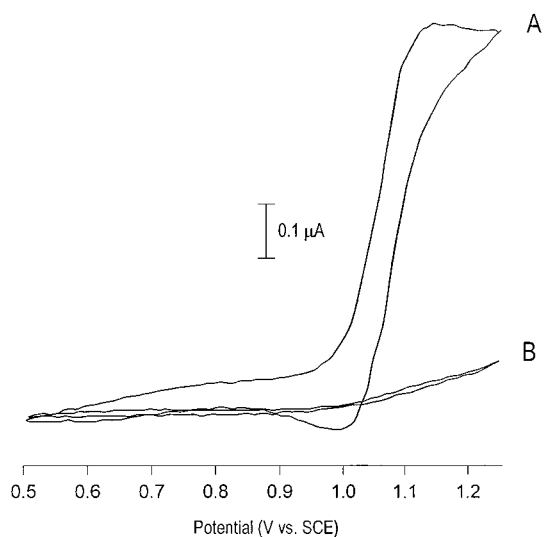


Fig. 1. Cyclic voltammetric response of $\text{Ru}(\text{bpy})_3^{2+}$ at a $35\ \mu\text{m}$ carbon microfiber electrode. Electrochemical electrolyte, 15 mM sodium borate; pH 9.8; sweep rate, $50\ \text{mV s}^{-1}$; electrode length, 3 mm. (A) 1.0 mM $\text{Ru}(\text{bpy})_3^{2+}$ present in the electrolyte; (B) No $\text{Ru}(\text{bpy})_3^{2+}$ present.

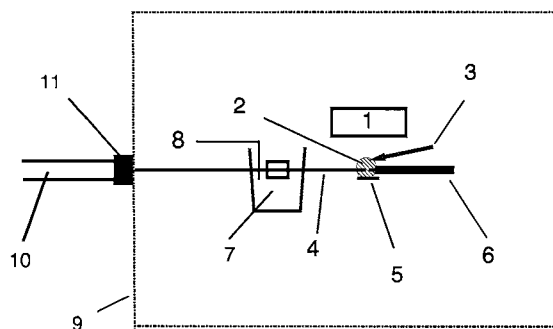


Fig. 2. Schematic diagram of the off-column electrochemical cell used for the in situ generation of $\text{Ru}(\text{bpy})_3^{2+}$ and the chemiluminescent detection of amines and amino acids. Components are as follows: (1) PMT; (2) $\text{Ru}(\text{bpy})_3^{2+}$ reservoir; (3) reference electrode (SCE); (4) detection capillary; (5) auxiliary electrode (stainless steel spatula); (6) carbon microfiber electrode assembly; (7) support beaker and Nafion joint; (8) Platinum cathode; (9) dark box; (10) PVC pipe; (11) rubber stopper.

the three-finger clamp holding the spatula. The SCE contacted the electrolyte pool at a point very close to the carbon fiber electrode, and it was supported by the spatula serving as the AE. The photomultiplier tube (PMT) (Hamamatsu, NJ, model R928) was mounted over the electrochemical cell so that the photocathode was positioned approximately 2 cm above the electrolyte solution. HV was supplied to the PMT by either a Bertan (Hicksville, NY, model 215) or Hewlett-Packard (Palo Alto, CA, model 6515A) HV power supply. Potential control of the electrochemical cell was accomplished using a Princeton Applied Research (Princeton, NJ) model 173 potentiostat and a model 363 universal programmer.

The beaker which supported the capillary joint, the electrochemical cell, and the PMT assembly were all contained in a light tight box. The segment of separation capillary located between the Plexiglas box and the light isolating box was contained inside a 0.75 inch diameter polyvinyl chloride tube which was sealed on both ends with a rubber stopper. The PVC tube prevented accidental operator contact with the capillary which was under high voltage, and helped to prevent light-piping by the capillary into the dark box. A schematic of the experimental arrangement is given in Fig. 2.

2.1.4. Data collection

The output of the PMT was sent to a Keithley (Cleveland, OH) model 485 picoammeter, the output of which was filtered by a 0.15 s time constant before undergoing analog to digital (A/D) conversion by a Stanford Research Systems (Stanford, CA) SR575 lock-in amplifier. Data were transferred to a personal computer (PC) for storage and analysis. Cyclic voltammetric data were also collected using this data system, with the exception that the electrode current during the CV experiments was filtered with a 5 ms time constant.

2.2. Reagents.

Amino acid standards were purchased from Sigma (St. Louis, MO) and were used without further purification. The water used for the preparation of the electrophoretic buffers was deionized by a mixed-bed ion-exchange cartridge (model # 09-034-3, Fisher). Triethylamine and $\text{Ru}(\text{bpy})_3\text{Cl}_2$ were purchased from Aldrich (Milwaukee, WI). $\text{Ru}(\text{bpy})_3\text{Cl}_2$ was converted to the perchlorate salt before use. Sodium hydroxide, used in the preparation of the electrophoretic buffers was reagent grade (Fisher).

Capillaries used for electrophoretic experiments were pretreated overnight with 0.1 M H_2SO_4 , unless otherwise noted.

3. Results and discussion

As described earlier, chemiluminescent detection in CE has several potential advantages which make it appropriate for such applications. Of most significance is the excellent quantitative characteristics demonstrated for CL detection in general, and the fact that the method does not have a path requirement for sensitive detection, as do absorption-based methods. In spite of these advantages, in many chemiluminescent protocols, the need to mix several reagents under the volume constraints of CE has proven problematic.

$\text{Ru}(\text{bpy})_3^{3+}$ based chemiluminescence has several advantages which suggest its application in CE. Excellent detection limits have been demon-

strated using $\text{Ru}(\text{bpy})_3^{3+}$ based chemiluminescence for both amines and amino acids separated by HPLC, or introduced into the detection system via flow injection analysis [26,27]. More importantly, the chemiluminescent reagent, $\text{Ru}(\text{bpy})_3^{3+}$ can be prepared in its active form at the site of interaction with the reagent. This simplifies the experimental arrangement eliminating the need for several reagent streams and subsequent mixing. Although much work has been reported involving the use of $\text{Ru}(\text{bpy})_3^{3+}$ as a chemiluminescent reagent [34–39], $\text{Ru}(\text{bpy})_3^{3+}$ based CL detection in capillary electrophoresis has not been demonstrated to date.

Fig. 3 shows the CE separation of triethylamine, proline, valine and serine at pH 9.5 with detection via $\text{Ru}(\text{bpy})_3^{3+}$ based chemiluminescence. The mixture was injected in triplicate. In this approach, the $\text{Ru}(\text{bpy})_3^{2+}$ is located in a 100 μl reservoir placed at the exit end (cathode) of the capillary. The 100 μl reservoir was adequate for over 4 h of operation, at which time the $\text{Ru}(\text{bpy})_3^{2+}$ solution was replenished. A 35 μm carbon fiber is used as the working electrode to convert the $\text{Ru}(\text{bpy})_3^{2+}$ to the active $\text{Ru}(\text{bpy})_3^{3+}$ form. The working electrode is placed as close as

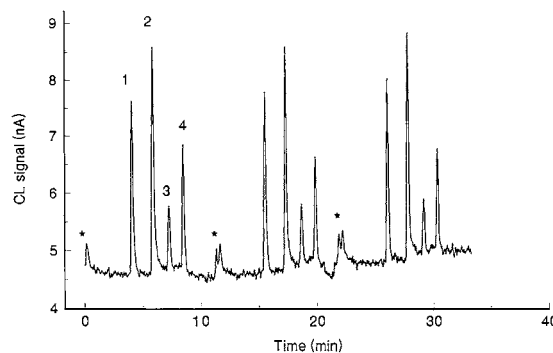


Fig. 3. Electropherogram of selected amino acids with end column addition of 1 mM $\text{Ru}(\text{bpy})_3^{2+}$. Separation conducted at 20 kV with injection of analytes for 8 s at 20 kV. Capillary, 75 μm i.d., 62 cm long with a 4 cm detection capillary. Buffer, 15 mM borate, pH 9.5. The electrode used for the in situ generation of $\text{Ru}(\text{bpy})_3^{3+}$ was a 35 μm diameter carbon fiber, 3 mm long held at 1.15 V vs. a SCE. The PMT was biased at 900 V. Peak identification: (1) 100 fmol TEA, (2) 70 fmol pro, (3) 1.6 pmol val, (4) 50 pmol ser. Injection points denoted by (*).

Table 1
Limit of detection for triethylamine and selected amino acids using $\text{Ru}(\text{bpy})_3^{3+}$ -based chemiluminescence following separation by CE

Compound	t_r (min.)	Concentration LOD	Mass LOD
Triethylamine (TEA)	4.4	120 nM	5.4 fmol
Proline (Pro)	6.2	68 nM	3.1 fmol
Valine (Val)	7.6	5.8 μM	0.3 pmol
Serine (Ser)	9.1	100 μM	4.5 pmol

possible to the exit without coming in physical contact with the capillary. Although the physical dimensions of the electrode are small, sufficient $\text{Ru}(\text{bpy})_3^{3+}$ is generated to react efficiently with the analyte eluting from the CE capillary. The carbon fiber did not require pretreatment.

From the data in Fig. 3, several points can be made. First, the detection sensitivity of the $\text{Ru}(\text{bpy})_3^{3+}$ -based chemiluminescent detection method is good, particularly when considering the analytes did not require derivatization prior to detection. Detection limits are summarized in Table 1 and they range from approximately 100 nM for TEA and proline, the most efficient luminescing species, to approximately 100 μM for serine. This difference in luminescence efficiency has been reported earlier and attributed to both the molecular characteristics of the reacting species [26], and the kinetics of the reaction [27]. The experimental precision is also very good considering the manual requirements of the injection procedure.

Second, the $\text{Ru}(\text{bpy})_3^{3+}$ based CL detection method using in situ generation of the active reagent is adequate to maintain the separation efficiency of the CE technique. The number of theoretical plates for the serine peak in Fig. 3 is estimated to be approximately 15 000 using the width at half-height. This plate number is smaller than previous reports involving derivatized amino acids and micelle enhanced running buffers [9]. However, the efficiency observed in the present study is comparable with that reported earlier in which underivatized amino acids were separated by CE and detected by an indirect method ([21]).

In order to thoroughly evaluate the quantitative characteristics of the CL detection approach described here, a capillary flow-injection technique was used to estimate the LOD and response linearity for leucine. Leucine was chosen for these more extensive studies since previous reports have shown that its response is approximately in the middle of the 20 naturally occurring amino acids [26]. Thus, from this data, one can judge the efficacy of this approach with respect to the other 20 amino acids. The FIA technique provided reproducible introduction of the analyte into the detection system. Further, by placing the $\text{Ru}(\text{bpy})_3^{2+}$ in the FIA buffer, data could be obtained over extended periods of time without depleting the $\text{Ru}(\text{bpy})_3^{2+}$ reservoir. For these flow injection experiments, a 75 μm i.d. \times 60 cm long capillary was used and samples were gravity injected by raising the injection end of the capillary 20 cm above the detection end of the capillary for 5 s. The buffer used for these studies was 15 mM borate at pH 9.8 with 1 mM $\text{Ru}(\text{bpy})_3^{2+}$ added for in situ detection. The LOD determined for leucine (SNR = 2) was 330 nM (15 fmol). A log-log plot of concentration versus signal for leucine showed a linear response from 1 μM to 100 μM injected leucine ($N = 6$, $y = 1.22(\pm 0.04)x - 0.18(\pm 0.05)$, $r^2 = 0.996$). This concentration LOD is not as low as an earlier report in which a larger flow cell and a glassy carbon disk working electrode (1 mm diameter) were utilized [27]. In that application, leucine was determined to have a LOD of 45 nM.

As described earlier, the likely reason for the slightly diminished detection limits with the capillary-based system is related to the very low light levels which must now be detected. The noise in the baseline which is limiting the detectability of the measurement is very periodic. It was determined in a separate experiment that the standard deviation in this background is essentially the same (approximately 0.2 nA) with, and without the electrochemical cell activated. From this data, it was concluded that the major contributor to the experimental noise with the capillary system is located within the electronics of the light detection system and not within the electrochemical system used to generate the $\text{Ru}(\text{bpy})_3^{3+}$. Although

the exact source of the noise is not known, random thermal emission from the photocathode of the PMT is a likely source. The PMT used for these studies is not designed for applications requiring the detection of ultralow light levels. According to specifications supplied by the manufacturer, the observed experimental noise is almost identical in magnitude to the random fluctuations in the dark current characteristic of this PMT at room temperature. Thus, cooling of the PMT or use of a PMT specifically designed for low light level detection should substantially improve the quantitative capabilities of the methodology. While these limits of detection in terms of amino acid concentrations are slightly higher than those demonstrated with the larger electrochemical cell [27], they are still very competitive with other methods used to detect native amino acids in CE [21,23]. By identifying the major contribution to the total noise, it is clear that these results can be substantially improved by improving the light detection system.

The $\text{Ru}(\text{bpy})_3^{3+}$ and eluting amine or amino acid are mixed by convection and diffusion. Although no design features were incorporated into the detection zone to enhance this mixing, this approach does appear to provide sufficient mixing such that the CL reaction can proceed with almost the same efficiency as when the $\text{Ru}(\text{bpy})_2^{2+}$ is present in the running buffer, as in the FIA study. The limit of detection for the two approaches is the same. The major advantage to this approach is that the electrophoresis will not be inhibited by the presence of $\text{Ru}(\text{bpy})_3^{3+}$ in the running buffer. Thus the method will be generally applicable to the separation and detection of all 20 amino acids and their important derivatives, such as the PTH amino acids which are products of protein sequence analysis.

4. Conclusion.

The chemiluminescent detection of amines and amino acids by reaction with in situ generated $\text{Ru}(\text{bpy})_3^{3+}$ at microcapillary dimensions has been demonstrated. The limit of detection for both triethylamine and proline were found to be below

the 10 fmol level. Leucine was analyzed by a capillary flow-injection technique and found to provide a linear response over two orders-of-magnitude in concentration with a LOD below 30 fmol. A noise analysis has shown that noise within the light-detection electronics is limiting the sensitivity of the technique. This is not expected to be a fundamental limitation and additional noise reduction measures will likely improve the quantitative aspects of the technique. Although neither the separation process nor the detection protocol are fully optimized, the results show the potential of the method for direct detection of amines or amino acids without requiring derivatization to enhance detection. Future work will focus on continued development of the end-column detection technique and its application to a wider range of amino acids including derivatives which may be produced as a consequence of protein sequence analysis.

Acknowledgements

The authors wish to thank Edward Earps for assistance in the construction of the electrophoresis instrument, Professors Craig and Susan Lunte of the University of Kansas for the gift of the carbon fibers, and Paul V. Anderson for assistance in the experimental work. Financial support from the Camille and Henry Dreyfus Foundation through a teacher–scholar fellowship (DRB), and from the National Science Foundation–Research Experience for Undergraduates program (PVA) is gratefully acknowledged.

References

- [1] F.E.P. Mikkers, F.M. Everaerts, Th.P.E.M. Verheggen, *J. Chromatogr.* 169 (1979) 11.
- [2] J.W. Jorgenson, K.D. Lukacs, *Anal. Chem.* 53 (1981) 1298.
- [3] A.G. Ewing, R.A. Wallingford, T.M. Olefirowicz, *Anal. Chem.* 61 (1989) 292A.
- [4] R.A. Wallingford, A.G. Ewing, *Anal. Chem.* 59 (1987) 1762.
- [5] T.J. O'Shea, R.D. Greenhagen, S.M. Lunte, C.E. Lunte, M.R. Smyth, D.M. Radzik, N. Watanabe, *J. Chromatogr.* 593 (1992) 305.

- [6] I.-C. Chen, C.-W. Whang, *J. Chromatogr.* 644 (1993) 208.
- [7] W.Th. Kok, Y. Sahin, *Anal. Chem.* 65 (1993) 2497.
- [8] X. Huang, R.N. Zare, S. Sloss, A.G. Ewing, *Anal. Chem.* 63 (1991) 189.
- [9] Y.-F. Cheng, N.J. Dovichi, *Science* 242 (1988) 562.
- [10] K.C. Waldron, N.J. Dovichi, *Anal. Chem.* 64 (1992) 1396.
- [11] T. Ueda, R. Mitchell, F. Kitamura, T. Metcalf, T. Kuwana, A. Nakamoto, *J. Chromatogr.* 593 (1992) 265.
- [12] T.J. O'Shea, P.L. Weber, B.P. Bammel, C.E. Lunte, S.M. Lunte, *J. Chromatogr.* 608 (1992) 189.
- [13] M. Jansson, J. Roeraade, *Anal. Chem.* 65 (1993) 2766.
- [14] J. Liu, Y.-Z. Hsieh, D. Wiesler, M. Novotny, *Anal. Chem.* 63 (1991) 408.
- [15] K.C. Chan, G.M. Janini, G.M. Muschik, H.J. Issaq, *J. Chromatogr.* 653 (1993) 93.
- [16] T. Fuchigami, T. Imasaka, *Anal. Chim. Acta* 282 (1993) 209.
- [17] N. Wu, C.W. Huie, *J. Chromatogr.* 634 (1993) 309.
- [18] D.J. Rose Jr., J.W. Jorgenson, *J. Chromatogr.* 447 (1988) 117.
- [19] S.L. Pentoney Jr., X. Huang, D.S. Burgi, R.N. Zare, *Anal. Chem.* 60 (1988) 2625.
- [20] M. Albin, R. Weinberger, E. Sapp, S. Moring, *Anal. Chem.* 63 (1991) 417.
- [21] W.G. Kuhr, E.S. Yeung, *Anal. Chem.* 60 (1988) 1832.
- [22] T.M. Olefirowicz, A.G. Ewing, *J. Chromatogr.* 499 (1990) 713.
- [23] J. Ye, R.P. Baldwin, *J. Chromatogr.* 687 (1994) 141.
- [24] W.R. LaCourse, G.S. Owens, *Electrophoresis* 17 (1996) 310.
- [25] K. Miyaguchi, K. Honda, K. Imai, *J. Chromatogr.* 316 (1984) 501–505.
- [26] S.N. Brune, D.R. Bobbitt, *Anal. Chem.* 64 (1992) 166.
- [27] W.A. Jackson, D.R. Bobbitt, *Anal. Chim. Acta* 285 (1994) 309.
- [28] R. Dadoo, L.A. Colon, R.N. Zare, *J. High Res. Chromatogr.* 15 (1992) 133.
- [29] S.D. Gilman, C.E. Silverman, A.G. Ewing, *J. Microcol. Sep.* 6 (1994) 97.
- [30] R. Dadoo, A.G. Seto, L.A. Colon, R.N. Zare, *Anal. Chem.* 66 (1994) 303.
- [31] J.-Y. Zhao, J. Labbe, N.J. Dovichi, *J. Microcol. Sep.* 5 (1993) 331.
- [32] W.R.G. Baeyens, B.L. Ling, K. Imai, A.C. Calokerinos, S.G. Schulman, *J. Microcol. Sep.* 6 (1994) 195.
- [33] M.A. Ruberto, M.L. Grayeski, *J. Microcol. Sep.* 6 (1994) 545.
- [34] J.B. Noffsinger, N.D. Danielson, *Anal. Chem.* 59 (1987) 865.
- [35] T.M. Downey, T.A. Nieman, *Anal. Chem.* 64 (1992) 261.
- [36] W.-Y. Lee, T.A. Nieman, *Anal. Chem.* 67 (1995) 1789.
- [37] D.R. Skotty, W.-Y. Lee, T.A. Nieman, *Anal. Chem.* 68 (1996) 1530.
- [38] J.B. Noffsinger, N.D. Danielson, *J. Chromatogr.* 387 (1987) 520.
- [39] M.A. Targove, N.D. Danielson, *J. Chromatogr. Sci.* 28 (1990) 505.

Response of a benzoxainone derivative linked to monoaza-15-crown-5 with divalent heavy metals

R.S. Addleman^{a,*}, J. Bennett^b, S.H. Tweedy^c, S. Elshani^a, C.M. Wai^a

^a Department of Chemistry, University of Idaho, Moscow, ID, 83843, USA

^b Department of Physics, Eastern Oregon State College, La Grande, OR, USA

^c Department of Chemistry, University of Washington, Seattle, WA, USA

Received 16 June 1997; received in revised form 28 August 1997; accepted 3 September 1997

Abstract

The response of a monoaza-15-crown-5 with an optically active aminobenzoxazinone moiety to divalent cations was investigated. The crown ether was found to undergo a strong emission shift to the blue when complexed with specific divalent metals that have ionic diameters between 1.9–2.4 Å. Consequently the photoactive macrocycle is responsive to Mg^{2+} , Ca^{2+} , Ba^{2+} , Sr^{2+} , Cd^{2+} , and particularly responsive to Hg^{2+} and Pb^{2+} . Macrocycle emission spectra are shown to be a function of cation concentration. Alkaline metal cations and smaller transition metals ions such as Ni^{2+} , Co^{2+} and Zn^{2+} do not cause significant changes in the macrocycle emission spectra. Emission, absorption, and complex stability constants are determined. Mechanisms of cation selectivity and spectral emission shifts are discussed. Challenges involving immobilization of the macrocycle while preserving its spectral response to cations are explored. © 1998 Elsevier Science B.V. All rights reserved.

Keywords: Benzoxainone derivative; Monoaza-15-crown-5; Divalent heavy metals

1. Introduction

Crown ethers are a class of organic compounds known to complex preferentially with metal ions. Cation selectivity in crown ethers has been shown to be a function of matching ionic radius and crown cavity size, crown structure, and charge transfer [1–7]. Attaching an optically active ligand to a crown ether can produce a photoactive ion selective compound, or a chromoionophore [8–21]. Without a photoactive group responsive

to the macrocycle cavity environment the spectral activity of crown ethers has been shown to have cation sensitivities in the millimolar range limiting their analytical utility [22,23]. For analysis of low concentrations of cations, micromolar and below, crown ethers with fluorescent groups are of interest since fluorescence is known to be more sensitive than absorption spectroscopy [24]. A fluorescent macrocyclic compound which is selective for regulated heavy metals such as Cd^{2+} , Pb^{2+} , and Hg^{2+} could be of particular interest for analysis of environmental samples. Ideally the macrocycle would provide the desired selectivity

* Corresponding author.

while the fluorescent ligand would provide the necessary sensitivity for trace level cation species analysis.

An optically active crown ether, reported in the literature [16] and shown in Fig. 1, is the photoactive benzoxazinone derivative of monoaza-15-crown-5 {3-(*p*-13-Aza-1,4,7,10-tetraoxa-cyclopentadecan-13-ylstyryl)-7-(dimethylamino)-1,4-benzoxazin-2-one}}, hence forth referred to as the BOZ-crown. The BOZ-crown ether was reported to have a high fluorescence quantum efficiency and selectivity for the divalent alkaline earths, particularly Ca^{2+} . The maximum wavelength of emission of the free ligand is shifted from 642 to 574 nm upon complexation with Ca^{2+} . Smaller spectral shifts occur for other alkaline earths. The absorption peak, centered at about 490 nm ($328\,200\text{ l mol}^{-1}\text{ cm}$) in acetonitrile, is only slightly perturbed by metal ion complexation. The quantum yield of the uncomplexed crown is 0.33 which increases to 0.64 when complexed with Ca^{2+} .

Despite the lack of reported information on complexation with any toxic heavy metal ions of interest, BOZ-crown was selected for further investigation for several reasons. (1) It has excellent emission characteristics (high quantum efficiency and a large peak shift upon complexation) and absorption in the blue which eliminates interferences from many ultraviolet absorbing species. (2) Azo-crown ethers with photoactive groups are known to be selective for the softer heavy metals [2,13,21]. Reported here are new studies on BOZ-crown, focusing on toxic heavy metals, with observations on; cation selectivity, emission mechanisms, effects of anions upon the complex, and issues concerning immobilization for analytical applications.

2. Experimental

The BOZ-crown was synthesized using previously reported procedures [16]—purified on silica columns and 50 μM stock solutions were utilized. All metal salts were of high purity (Aldrich) and 10 mM metal ion stock solutions

were prepared from these salts. All stock solutions were prepared by weighing out the compound into a 500 ml volumetric flask and diluting to the volume with acetonitrile. Aldrich HPLC reagent grade acetonitrile was chosen as the solvent since it has a very low fluorescence background and the BOZ-crown is insoluble in water. However, acetonitrile is a polar, aprotic solvent and is unable to solvate many materials. All perchlorate salts utilized were found to be soluble in acetonitrile. All hydrated nitrates with divalent cations were soluble in acetonitrile with the most readily soluble nitrate salts being the transition metals from manganese to zinc. Anhydrous nitrate salts including: the alkaline metals, alkaline earths, and most trivalent metals were found to be insoluble in acetonitrile at room temperature. Some iodide and chloride salts were soluble in acetonitrile at room temperature. Solutions were stirred until the salt completely dissolved. Those solutions in which the salt was not visually determined to go completely into solution were not utilized. All glassware was washed with nitric acid and then triple rinsed in acetonitrile.

All emission spectra were collected using a 0.25 m Chromex spectrometer with 150 grooves mm^{-1} grating, blazed at 500 nm, with a slit width of 200 μm . The detector was a 256×1024 element Princeton Instruments charge coupled device (CCD) cooled to -50°C with a thermoelectric cooler and controlled with a Princeton Instruments ST-130 Controller. The CCD was read out with a 16 bit A/D converter at 50 kHz and analyzed with a 486 PC computer. Unless otherwise noted a 30 s collection time was utilized with background subtraction. Since full slit illumination was achieved, the entire array was read out and the 256 vertical pixels were binned together to produce spectra with 1024 channels. Calibration of the spectrometer was achieved using Hg and Ar atomic line sources. Calibration was verified with a 632.8 nm dielectric notch filter. Absorption spectra were collected with a Guided Wave Model 200 Fiber Optic Spectrometer using a transmission probe with a 1.00 cm optical path.

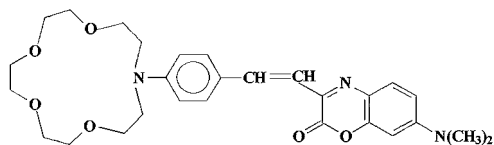


Fig. 1. The BOZ-crown ether. Ionic selectivity of the compound is determined by the monoaza-15-crown-5 cavity size (1.7–2.2 Å). Fluorescent properties of the compound are determined by the optically active aminobenzoxazinone moiety.

3. Results and discussion

3.1. Emission and selectivity

The BOZ-crown was previously reported to complex with alkaline earth and alkali metals [16]. We have found that the BOZ-crown complexes strongly with certain transition metal cations. As shown in Fig. 2, the 1 μM BOZ-crown in acetonitrile undergoes a strong blue shift of the emission peak and an increase in quantum efficiency when complexed with divalent cations with ionic diameters around 2Å. Consequently the BOZ-crown ether was found to be optically very responsive to Ca^{2+} , Ba^{2+} , Sr^{2+} , Cd^{2+} , Hg^{2+} , and Pb^{2+} .

Pb^{2+} and Hg^{2+} are particularly reactive with the BOZ-crown. At 15 μM , Pb^{2+} and Hg^{2+} ,

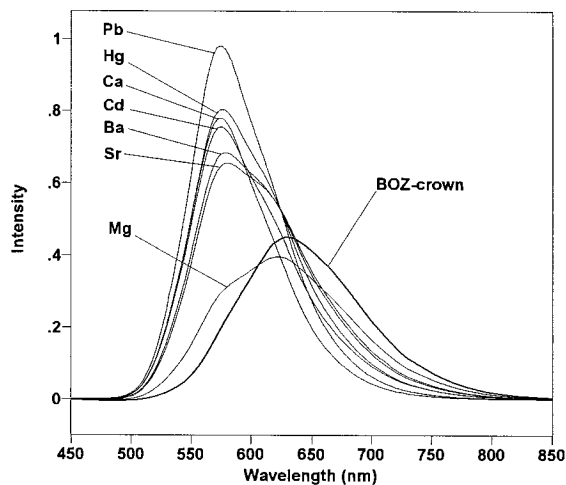


Fig. 2. Fluorescence spectra of cations with 1 μM BOZ-crown in acetonitrile. Pb^{2+} and Hg^{2+} are at 15 μM and other cations are at 1.5 mM. All cations are from perchlorate salts.

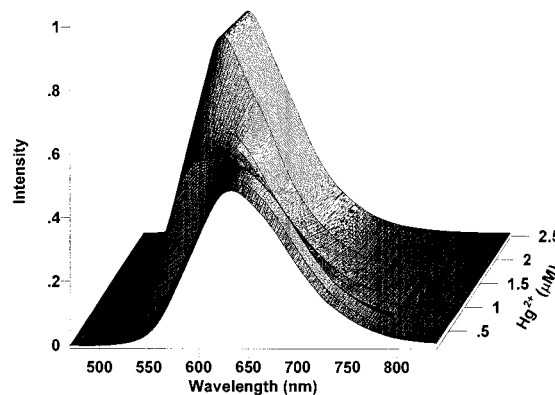


Fig. 3. BOZ-crown (1 μM) fluorescence spectrum with different concentrations Hg^{2+} in acetonitrile. Note the large 50 nm blue shift of the emission peak with increasing Hg^{2+} concentration. In addition to changing position, the peak intensity also increases with Hg^{2+} concentration until complete complexation has occurred at approximately 10 μM Hg^{2+} .

cause larger shifts in the BOZ-crown fluorescent peak wavelength and intensity than other cations at concentrations of 1.5 mM (Fig. 2). Other cations, such as Mg^{2+} , are observed to be only partially complexed at concentrations of 1.5 mM. The simultaneous shift in the spectral peak position and emission intensity with cation concentration can be observed in Fig. 3. The ion selectivity of the macrocycle and large dynamic range of the optical response shown in Figs. 3 and 4 demonstrate the potential of utilizing this fluorescing crown ether for trace level analysis of metals.

Unlike most macrocycle compounds with cavity sensitive fluorogenic groups, the emission of the BOZ-crown is not quenched upon complexation by spin orbit coupling, or the heavy atom effect [25,26]. The observed variations in the BOZ-crown emission spectrum with cation species is believed to be due to charge transfer between the BOZ-crown azo group and the aminobenzoxazinone moiety [16]. The macrocycle provides a rotational nonradiative deexcitation pathway for the ligand. Strong cation interactions with the macrocycles azo groups lone pair forces the nitrogen from an sp^3 configuration to a rigid sp^2 configuration deactivating the rotational nonradiative mechanism. Without the rotation deexcitation pathway the complex has larger quantum efficien-

cies and an increased Stokes shift in the emission spectrum with optical characteristics resembling the benzoxainone chromophore (BOZ-H). Those cations closely matching the crown cavity in size, complex stronger, binding to the nitrogen lone pair, creating the largest shift in the emission peak and intensity of the alkaline earths. This mechanism is supported by our observations of the BOZ-crown immobilized on a silica surface. The BOZ-crown was immobilized upon silica by slow evaporation from solvent (acetonitrile). This process has been shown to be a simple, effective method of immobilizing crown ethers without substantially altering their cation selectivity [27]. When surface immobilized upon silica the BOZ-crown becomes cation insensitive and has an emission maxima 568 nm very similar to that of the BOZ-H (463 nm) or a strong, solvated BOZ-crown-metal complex (474 nm). This cation insensitivity is interpreted as surface restricted rotation between the macrocycle and the aminobenzoxazine moiety similar to the restricted rotation resulting from complexation of the BOZ-crown with cations. Since surface restricted rotation renders

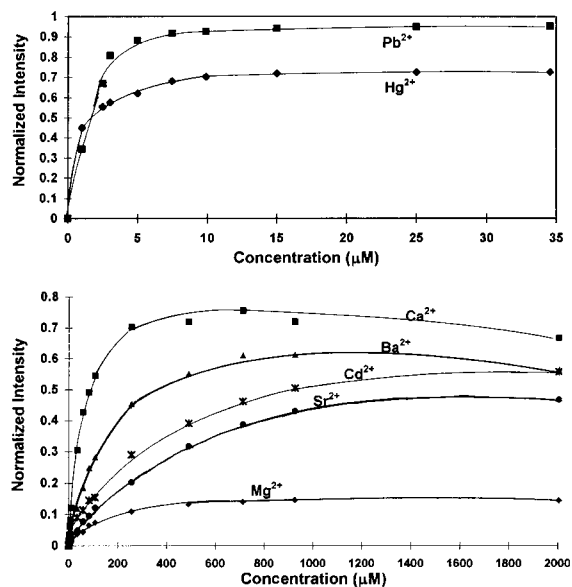


Fig. 4. Fluorescence intensity of 1 μM BOZ-crown in acetonitrile at 574 nm versus cation concentration. Note the difference in concentration range between Hg^{2+} , Pb^{2+} , and the other cations.

the BOZ-crown spectroscopically cation insensitive, any immobilization method must not sterically hinder the BOZ-crown. Liquid membranes and sol-gel are two techniques which might accomplish BOZ-crown immobilization without interfering with its spectroscopic response to cations.

Closely matching the crown cavity in size,— Ca^{2+} has been previously shown to complex strongly with the crown ether, binding with the lone pair of the macrocycle's azo group, creating the largest wavelength and intensity shift in the fluorescence emission peak of the alkaline earths [16]. The other alkaline earths cause significantly smaller shifts than Ca^{2+} while the univalent alkaline metals cations cause negligible shifts. The 15-crown-5 macrocycle complexes with univalent cations, but the univalent ions do not interact with the macrocycles nitrogen lone pair sufficiently to cause large changes in the fluorescence spectra.

The alkali metal cations (Li^+ , Na^+ , K^+), Ni^{2+} (1.38Å), Co^{2+} (1.10Å) and Zn^{2+} (1.48Å) do not cause significant changes in the BOZ-crown emission spectra. The univalent alkaline metals do not have sufficient charge to cause a shift in the emission spectra. While the divalent transition metals Ni^{2+} , Co^{2+} , Zn^{2+} have sufficient charge to affect the emission spectra, the small size precludes effective complexation in the 15-crown-5 cavity. The benzoxainone chromophore (BOZ-H) and consequently the BOZ-crown, complexes with Cu^{2+} to form an emission quenched purple complex which interferes with all other divalent complexes.

It can be seen in Fig. 2 that Ca^{2+} (2.00Å) and Cd^{2+} (1.90Å) have very similar spectroscopic responses while Mg^{2+} (1.44Å) and Zn^{2+} (1.48Å) which are more closely matched in ionic diameter, have very dissimilar emission characteristics. This difference in spectroscopic response for the two sets of divalent cations is particularly curious when the similarity in the electron configuration is examined. In each set the alkaline earth has a completely filled s shell and the transition metal has a completely filled d shell. Mg^{2+} will complex strong enough to cause the BOZ-crown spectrum to shift while Zn^{2+} will not. Since both Ca^{2+} and

Table 1
Fluorescence characteristics of BOZ-crown complexes

Cation	Ionic diameter ^a (Å)	λ_{em} (nm)	Φ^b	λ_{abs} (nm)	ϵ (l mol ⁻¹ ·cm ⁻¹)	log K_s^c	Conc. at peak intensity ^d (μ M)
BOZ-crown	1.7–2.2 ^e	629	.33	491	38 200	---	1
Li ⁺ -BOZ-crown ^f	1.52	612	.44	480	36 200	2.83	N.A.
Na ⁺ -BOZ-crown ^f	2.04	611	.38	476	34 400	2.23	N.A.
Mg ²⁺ -BOZ-crown	1.44	579	.42	488	34 900	2.75	2000
Ca ²⁺ -BOZ-crown	2.00	574	.64	474	33 000	4.28	713
Sr ²⁺ -BOZ-crown	2.52	577	.47	478	34 800	3.37	2000
Ba ²⁺ -BOZ-crown	2.84	577	.58	475	34 200	3.89	925
Cd ²⁺ -BOZ-crown	1.90	573	.50	475	34 000	3.98	2000
Hg ²⁺ -BOZ-crown	2.04	574	.55	474	32 000	6.15	35
Pb ²⁺ -BOZ-crown	2.40	573	.71	473	31 700	6.02	35
BOZ-H	---	567	.54	463	30 300	---	---

^a 75th ed. CRC Handbook of Chemistry and Physics, CRC Press, 1995.

^b Determined using reported values [16] of BOZ-crown and Ca²⁺-BOZ-crown as references and peak areas for 475–850 nm.

^c Measurement error approximately ± 0.1 .

^d Data points from titration of 1 μ M BOZ-crown in acetonitrile.

^e Diameter of crown cavity, not the ionic diameter [3].

^f Data from reference [16].

N.A., not available; Φ , quantum efficiency; $K_s = [ML^{2+}]/([M^{2+}][L])$.

Cd²⁺ shift the BOZ-crown spectra, the effect cannot be attributed to the difference between the alkaline earths and transition metals. The difference in behavior between Ca²⁺ and Cd²⁺ and Mg²⁺ and Zn²⁺ could be a function of solvation coordination. Ca²⁺, Cd²⁺ and Mg²⁺ have preferred coordination numbers (CN) of six while Zn²⁺ has a preferred coordination numbers of four. It appears solvation coordination significantly influences complexation into the BOZ-crown cavity with a coordination number six being preferred.

For a fixed concentration of BOZ-crown, the fluorescence intensity is proportional to cation concentration. Fig. 4 shows the response of 1 μ M BOZ-crown to cation concentration. The difference in concentration ranges clearly show the BOZ-crown-selectivity for Pb²⁺ and Hg²⁺. The decrease in emission intensity at higher cation concentrations is attributed to ionic quenching [16]. Ionic quenching can begin well before complete complexation occurs. BOZ-crown spectral intensities will increase with cation concentration up to a specific concentration unique to each metal ion. Subsequent increases in cation concentration will result in a blue shift of the fluores-

cence peak but with a net decrease in intensity.

Figs. 3 and 4 clearly show that the BOZ-crown spectra are a function of cation concentration. The monotonous dependence indicates a 1:1 stoichiometry within the concentration range investigated. Any particular BOZ-crown spectrum is a composite of fluorescence emissions from both the complexed and uncomplexed BOZ-crown ethers. The ratio of complexed to uncomplexed BOZ-crown is determined by the relative cation and ligand concentrations and the complex stability constant, K_s . Where the stability constant is given as: $K_s = [ML^{2+}]/([M^{2+}][L])$. K_s was determined with linear least squares analysis of $I_o/(I-I_o)$ vs. $1/[M]$. The intercept/slope of these plots provided K_s with correlation coefficients better than 0.96.

K_s and other constants for the BOZ-crown complexes are presented in Table 1. The maximum spectral shifts of the BOZ-crown peak, λ_{em} , occurs upon complete complexation with the cation. Due to ionic quenching, λ_{em} typically occurs at higher cation concentrations than the peak emission intensity.

The large stability constant and subsequent sensitivity of the BOZ-crown to Pb²⁺ and Hg²⁺ can be attributed to soft-soft interactions between

cations and the nitrogen in the macrocyle [28]. The softer nature of Pb^{2+} and Hg^{2+} can interact with the azo groups stronger than the harder alkaline earths. Similar selectivity effects for Pb^{2+} and Hg^{2+} by macrocycles containing azo groups have been noted in previous studies [1,2,13,21].

With the exception of Sr^{2+} , Fig. 5 shows the emission intensity of the BOZ-crown complexes improves with cavity fit, with the optimum cation ionic diameter ranging between 1.9 Å–2.4 Å. The emission intensities were divided by the complex's absorption coefficient, to adjust for differences in the molar absorptivities, and a trend line is shown. Fluorescent intensity of the BOZ-crown complex is affected by many factors including coordination number (CN), valence, and cation hardness but optical activity clearly increases as the macrocycle cavity and cation diameter are closer in size.

3.2. Complex stability

It can be seen in Fig. 6 that K_s increases with ionic diameter, regardless of cation hardness, until approximately 2.4 Å, after which the stability constant decreases significantly. This is very similar to the trend exhibited in Fig. 5. Unlike Fig. 5, Fig. 6 clearly shows that the stability of the complex is not a function of cavity fit alone. While complex stability improves as cation diameter approaches 1.9–2.4 Å it can be observed that

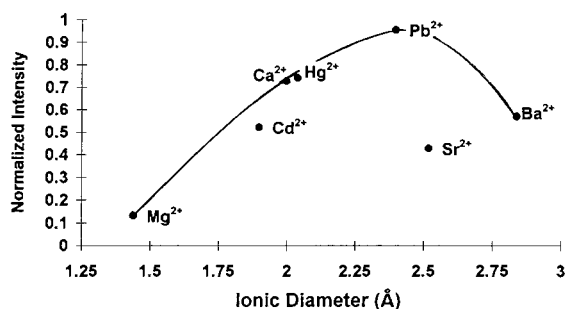


Fig. 5. BOZ-crown complex emission intensity (474 nm) versus ionic diameter. The macrocycle diameter is 1.7–2.2 Å. Emission intensities adjusted for different ϵ values and a line of best fit is shown. The complex peak emission intensities, which occur of different cation concentrations, and are listed in Table 1.

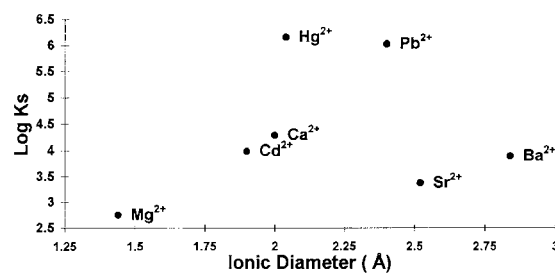


Fig. 6. BOZ-crown complex stability constant versus ionic diameter. Note the separation between the hard and soft cations. The macrocycle diameter is 1.7–2.2 Å. The uncertainty in K_s is ± 0.1 .

the softer cations form significantly stronger complexes than the hard cations of similar ionic diameters. For example, the BOZ-crown complexes with Hg^{2+} (2.04 Å) almost $100\times$ stronger than the similarly sized Ca^{2+} (2.00 Å).

As shown in Fig. 7, emission intensity is also related to the stability constant of the complex. The harder complexes, such as the alkaline earths, demonstrate an almost linear relationship. The large soft cation, Hg^{2+} and Pb^{2+} , with much higher K_s values are clearly separated from the hard cations. There is a nearly linear relationship between emission intensity and $\log K_s$ over almost four orders of magnitude. Clearly the stronger the complexation the more intense the emission from the complex.

The BOZ-crown is insoluble in polar solvents such as methanol and water. In low dielectric solvents which are partially miscible with water,

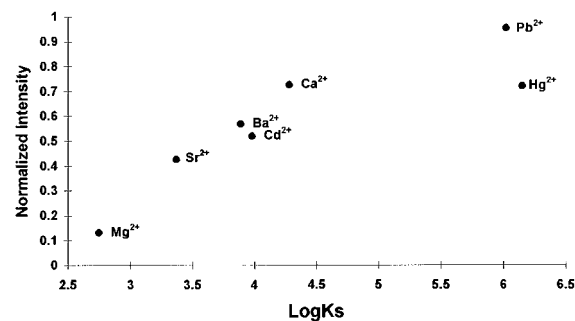


Fig. 7. BOZ-crown complex emission intensity (474 nm) versus complex stability constant. Note the near linear relationship over four orders of magnitude. The uncertainty in K_s is ± 0.1 .

such as methyl iso-butyl ketone and acetonitrile, the BOZ-crown emission intensity is reduced upon addition of water. The fluorescence of the BOZ-crown is quenched by the addition of high dielectric polar cosolvents such as ethanol and water. Therefore applications of the BOZ-crown to metal detection are limited to low dielectric constant lipophilic environments.

3.3. Quantum efficiency

The measured quantum efficiencies, Φ , of the BOZ-crown complexes is very dependent upon cation concentration and determination methods. Low concentrations result in incomplete complexation and high concentrations reduce the emission intensity through ionic quenching. The Φ values given in Table 1 were determined at peak intensity concentrations and referenced to the previously reported Φ values for the BOZ-crown (0.33) and Ca^{2+} -BOZ-crown complex (0.64). There is no simple functional relationship between Φ and K_s . However, in general quantum efficiencies can be observed to increase with K_s . Similarly, Φ generally improves with cavity fit between cation and macrocycle but other factors such as the cation hardness preclude any simple relationship.

3.4. Absorption

Absorption parameters are shown in Table 1. The changes in λ_{abs} and ϵ increase with the stability of the complex. Absorption spectra do not undergo the large shift seen in fluorescence spectra because cation complexation does not alter the excitation pathways as significantly as de-excitation pathways. However, changes in absorption spectra clearly do occur, with substantially larger changes for divalent cations than monovalent, indicating that electronic energy states in the BOZ ligand are being affected by the coulombic charge of the complexed cation. Like λ_{em} and Φ , measured values of λ_{abs} and ϵ change with cation concentration and determination of true complex values is difficult.

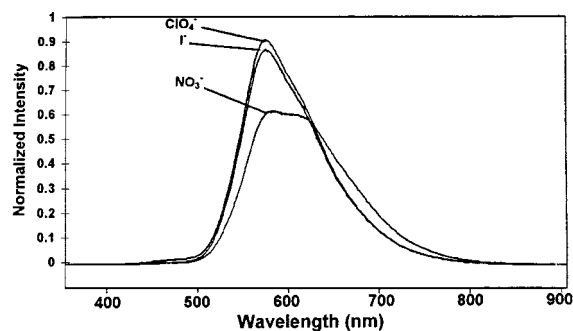


Fig. 8. Emission spectra of Cd^{2+} with different anions, competing with $1 \mu\text{M}$ BOZ-crown in acetonitrile.

3.5. Anion effects

Fig. 8 depicts the anion effects that are observed with BOZ-crown complexing with Cd^{2+} acetonitrile. CdCl_2 is insoluble in acetonitrile and is not shown. Soluble chloride, iodide, and perchlorate salts of the cations listed in Table 1 were found to have similar spectra with only slight differences in peak heights. Nitrate salts of the cations in Table 1 have a significantly different emission peak structure.

The mono-azo crown ether is known to be stable in nitrate solutions [2], however all nitrate salts soluble in acetonitrile were found to cause an intensity decay in the BOZ-crown emission spectrum. Nitrate, chloride, iodide, perchlorate salts were tested with a variety of cations and only nitrate salts were observed to cause the decay of emission spectra with time. The decay rate was found to be dependent upon the specific cation and the cation concentration. Simple addition of NaNO_3 will cause an intensity decay in the unshifted BOZ-fluorescence spectra. Addition of trace amounts of nitric acid will cause the peak to shift to 572 nm (protonation on the crown azo group) followed by a slow decay in fluorescence intensity. The decay in fluorescence intensity and change in emission spectra in nitrate solutions appear to be functions of the photoactive BOZ ligand and not caused by macrocycle interactions. Previous literature has shown the BOZ ligand (7-dimethylamino-3(*p*-formylstyryl)-1,4 benzoxazine-2-one) to be stable in a number of solvents

but there is no discussion of exposure or reactions of the BOZ ligand with nitrate [16,29–31]. A likely explanation for the observed behavior is a nitrate reaction with the highly conjugated chromophore group (BOZ ligand) resulting in loss of optical activity.

4. Conclusions

Reported here, is a fluorescing crown ether which increases emission intensity upon complexation with specific transition metal cations. The BOZ-crown undergoes a strong emission blue shift from 629 to approximately 574 nm when complexed with divalent cations that have ionic diameters between 1.9–2.4 Å. Consequently the BOZ-crown ether is responsive to Mg^{2+} , Ca^{2+} , Ba^{2+} , Sr^{2+} , Cd^{2+} , Hg^{2+} , and Pb^{2+} . Alkaline metal cations, Ni^{2+} , Co^{2+} and Zn^{2+} do not cause significant changes in the BOZ-crown emission spectra. Due to the soft-soft interactions of the macrocycles azo group, Pb^{2+} and Hg^{2+} have stability constants 100 times larger than any other metal cation and consequently induce changes in the BOZ-crown emission spectrum at substantially lower concentrations.

The measured constants such as K_s and Φ for Ba^{2+} , Ca^{2+} and Mg^{2+} are consistent with the values previously reported [16]. These constants have been determined and analyzed for many of the transition metals, particularly those of environmental interest. The large jump in K_s and emission intensity for Pb^{2+} and Hg^{2+} can be understood through soft-soft interaction with the macrocycles azo group. The lack of reaction for Zn^{2+} , Ni^{2+} , and Co^{2+} has been explained based on coordination number and ionic size. There is no apparent reason why Sr^{2+} has a lower K_s than Ba^{2+} with the BOZ-crown. Subsequent work is needed to explore and explain the observed differences in K_s and Φ , between Sr^{2+} and other divalent cations.

The BOZ-crown selectivity for the toxic heavy metals Pb^{2+} and Hg^{2+} coupled with the large optical response to the cations make the BOZ-crown a promising candidate for numer-

ous environmental analytical applications. Future work will examine immobilization issues, solvent extraction, and liquid membrane configurations for analytical applications.

References

- [1] R.M. Izatt, K. Pawlak, J.S. Bradshaw, Chem. Rev. 9 (1991) 1721.
- [2] J.S. Bradshaw, K.E. Krakwoiak, R.M. Izatt, Aza-Crown Macrocycles, Wiley, New York, 1993.
- [3] G. Gokel, Crown Ethers and Cryptands, Royal Society of Chemistry, Cambridge, 1991.
- [4] B. Dietrich, J. Chem. Educ. 62 (1985) 954.
- [5] C.M. Wai, Preconcentration Techniques for Trace Elements, CRC Press, Boca Raton, FL, 1991, Chap. 4.
- [6] C.M. Wai, H.S. Du, Y. Meguro, Z. Yoshida, Anal. Sci. 7 (1991) 41.
- [7] T. Wickstrom, J. Dale, W. Lund, S. Buen, Anal. Chim. Acta 211 (1988) 223.
- [8] H. Nishida, M. Tazaki, M. Takagi, K. Ueno, Mikrochim. Acta 1 (1981) 281.
- [9] H. Nakamura, H. Nishida, M. Takagi, K. Ueno, Anal. Chim. Acta 139 (1982) 219.
- [10] M. Shiga, H. Nishida, H. Makamura, M. Takagi, Anal. Chim. Acta 173 (1985) 193.
- [11] K. Sasaki, G. Pacey, Anal. Chim. Acta 174 (1985) 141.
- [12] H.G. Lohr, F. Vogtle, Acc. Chem. Res. 18 (1985) 65.
- [13] Y. Sakai, N. Kawano, H. Nakamura, M. Takagi, Talanta 33 (1986) 407.
- [14] Y. Katayama, R. Fukuda, M. Takagi, Anal. Chim. Acta. 185 (1986) 295.
- [15] Y. Katayama, R. Fukuda, T. Iwasaki, K. Nita, M. Takagi, Anal. Chim. Acta 204 (1988) 113.
- [16] S. Fery-Forgues, M.T. Le Bris, J.P. Guette, B.Valeur, J. Phys. Chem. 92 (1988) 6233.
- [17] H. Forrest, G.E. Pacey, Talanta 36 (1989) 335.
- [18] K. Wilcox, G.E. Pacey, Talanta 38 (1991) 1315.
- [19] T.L. Blair, J. Desai, L.G. Bachas, Anal. Lett. 25 (1992) 1823.
- [20] R.A. Bartsch, B.P. Chapoteau, J. Czech, A. Kumar, T.W. Robison, J. Org. Chem. 59 (1994) 616.
- [21] B. Vaidya, J. Zak, G.J. Bastiaans, M.D. Porter, J.L. Hallman, N.A. Nabuisi, M.D. Utterback, B. Strzelbicka, R.A. Bartch, Anal. Chem. 67 (1995) 4101.
- [22] J.F. Alder, D.C. Ashworth, R. Naryanaswamy, R.E. Moss, I.O. Sutherland, Analyst 112 (1987) 1191.
- [23] R. Escobar, C. Lamonedá, F. de Pablos, A. Guirum, Analyst 114 (1989) 533.
- [24] J.D. Ingle, S.R. Crouch, Spectrochemical Analysis, Prentice-Hall, Englewood Cliffs, NJ, 1988, Chap. 15.
- [25] R.S. Becker, J.B. Allison, J. Phys. Chem. 63 (1963) 2662.

- [26] S.P. McGlynn, T. Azumi, M. Kinoshita, *Molecular Spectroscopy of the Triplet State*, Prentice-Hall, Englewood Cliffs, NJ, 1966, pp 261–283.
- [27] M.K. Beklemishev, S. Elshani, C.M. Wai, *Anal. Chem.* 66 (1994) 3521.
- [28] R.G. Pearson, *J. Am. Chem. Soc.* 85 22 (1963) 3533.
- [29] M.T. Le Bris, J. Mugnier, J. Bourson, B. Valeur, *Chem. Phys. Lett.* 106 (1984) 124.
- [30] M.T. Le Bris, J. *Heterocyclic Chem.* 21 (1984) 551.
- [31] F. Dupuy, C. Rulliere, M.T. Le Bris, B. Valeur, *Opt. Commun.* 51 (1984) 36.

Photoinitiated gold sol generation in aqueous Triton X-100 and its analytical application for spectrophotometric determination of gold

Anjali Pal *

Civil Engineering Department, Indian Institute of Technology, Kharagpur 721 302, India

Received 20 June 1997; received in revised form 2 September 1997; accepted 3 September 1997

Abstract

Gold complex, HAuCl_4 has been transformed into pink-coloured stable gold sol having λ_{max} at 523 nm ($\epsilon = 3.06 \times 10^3 \text{ l} \cdot \text{mol}^{-1} \cdot \text{cm}^{-1}$) at room temperature in aqueous Triton X-100 (TX-100) upon photoirradiation. It is a very rapid and simple process and the absorbance at 523 nm is a direct measure of gold concentration. Beer's law is obeyed in the range of 0–150 ppm of gold. The relative standard deviation for 22.7 and 90.9 ppm of gold are 2.8 and 2.5% respectively. The 95% confidence limit (ten determinations) for 22.7 ppm of gold is 23.6 ± 0.5 ppm. Sandell sensitivity is $6.44 \times 10^{-2} \mu\text{g cm}^{-2}$. TX-100 acts both as a reducing agent and a stabilizer here. Statistical parameters, effects of TX-100 concentration, irradiation time and interferents are studied. The method is applicable for ore and synthetic mixture analysis. © 1998 Elsevier Science B.V. All rights reserved.

Keywords: Gold complex; Photoinitiated gold sol; Synthetic mixture analysis

1. Introduction

To discover a convenient method for gold sol preparation could be a challenging problem for many reasons. Colloidal gold could be used for staining proteins electrotransferred onto nitrocellulose membranes [1]. It could also serve as a medium for surface enhanced Raman scattering (SERS) [2]. There are many methods of gold colloid preparation, among which the method described by Moeremans et al. [3] is relatively trou-

blesome and requires refluxing. The method of Yamaguchi et al. [1] however, requires several hours stirring under appropriate pH conditions and for maturation of gold sol, an additional vigorous overnight stirring is necessary. In most cases, for obtaining SERS spectra, gold sol was prepared from gold(III) by various reducing agents but needed a control [4]. Generation of gold sol from gold(III)–gelatin complex using common reducing agents such as ascorbic acid, hydrazine etc. were also carried out [5], but required proper conditions. Light induced reactions could be an ideal alternative in this respect, because controlling the reaction may be less difficult

* Tel.: +91 3222 55221/55224, fax: +91 3222 55303, e-mail: tpal@hijli.iitkgp.ernet.in

here and the methodology could be very simple, quick and easy [6,7].

Several spectrophotometric methods for gold (III) determination involving binary complex formation between gold (III) and chromogenic reagents are known [8–12], but these methods lack sensitivity. Several extractants for the photometric determination of gold in complex materials have also been reported [13–17]. Conventional methods, in general, involve lengthy procedures due to the necessity of multiple extractions [14] and suffer from interference by other metal ions [12–18]. Sometimes, loss of photometric selectivity arising from the use of reagents such as amides [19] also results.

A very simple and quick photochemical method for gold determination through the formation of pink gold sol in poly (oxyethelene)isooctylphenyl ether known as Triton X-100, or TX-100, which acts both as a reducing agent and a stabilizer, is reported here.

2. Experimental

2.1. Apparatus

All absorbance measurements were carried out in a Shimadzu UV-160 digital spectrophotometer. Photochemical reactions were carried out in 1-cm well stoppered quartz cuvettes. Photoirradiations were carried out with an ordinary germicidal lamp (Sankyo Denki, Japan) of 15 W capacity. The cells were kept at a distance of 3 cm from the light source.

2.2. Reagents

All reagents were of AR grade. A stock solution of gold(III) chloride was prepared by dissolving 1 g of chloroauric acid (Johnson Matthey, Royston, Hertfordshire, UK) in 500 ml double distilled water and it was standardised by the quinol method [20]. TX-100 solutions were prepared by dissolving appropriate volumes of this in known volumes of distilled water.

2.3. Procedure

Aliquots of standard gold(III) solutions were taken in the quartz cuvettes and mixed with 10^{-2} M TX-100 so that the total volume is 2 ml for each and gold concentration varies from 2 to 150 ppm. Each was then irradiated for 20 min. Pink-coloured gold sol was produced. The absorbance value measured at 523 nm was proportional to the gold concentration. The colour was stable for more than a week at room temperature and for more than a month at $< 5^{\circ}\text{C}$.

3. Results and discussion

3.1. Photochemical reaction between HAuCl_4 and TX-100

Redox reactions occurring between gold(III) complex and air saturated aqueous solutions of poly (ethylene glycol) (PEG) and poly (vinyl alcohol) (PVA) have recently been reported [21] where gold(III) is converted to pink gold sol by PEG and PVA. This occurs at room temperature, but at a slow rate, requiring ~ 8 h for PEG and ~ 6 days for PVA. The fact that PEG polymers have been oxidised to acetoxy compounds has been confirmed from infrared (IR) spectral analysis. Recently, the photochemical reduction of aqueous HAuCl_4 in the presence of 2-propanol and acetone has been reported [22,23], using a steady-state xenon lamp or repetitive laser pulses to produce important and useful nanoscale gold particle. Sodium polyphosphate was used as a particle stabilizer in this system. The photooxidation of phenols [24] or alcohols [25] were used in synthetic organic chemistry but have not been used for analytical purposes. Here, we report our findings on the photochemical reaction of TX-100 in aqueous medium with gold(III) to form and stabilize small gold particles which may be very useful for material research [26]. The average size of the metal particles in the sol system produced was found using a Coulter N4 particle analyzer at an angle of 90° and was found to be 14 nm.

Curve A of Fig. 1 shows the surface plasmon absorption band of TX-100 stabilised zerovalent

gold ($\lambda_{\max} = 523 \text{ nm}$) obtained from the photoreduction of HAuCl_4 by TX-100. Curve B shows the spectrum of TX-100 after 20 min. irradiation. Without TX-100, gold(III) failed to give any colour, even after 1 h irradiation. If kept in the dark, aqueous TX-100 failed to generate gold sol, even after 8 h. However, if kept for more than 24 h, a slight pink colour was developed. Since the reagent blank did not absorb at 523 nm, it was not necessary to use a blank in the determinations. Deoxygenation of the sample followed by irradiation for 20 min. did not cause any change in the absorbance at 523 nm. The advantage of this method was that pH maintenance was not necessary. To the best of our knowledge, such a reaction has not been used for either gold sol preparation or gold determination.

Identification of the product formed in this process was attempted through infrared spectral analysis. A higher concentration of HAuCl_4 was attempted in this experiment in order to increase the product concentration. The resulting solution after irradiation was vacuum evaporated. The IR spectra obtained from the blank experiment without HAuCl_4 was compared with that of the sample. The appearance of a new band at 1613 cm^{-1} indicated the presence of the carboxylate group [21] generated due to the oxidation of the primary hydroxyl function of TX-100 by gold(III). Ultra-violet light of shorter wavelength ($\approx 254 \text{ nm}$) or visible light could not bring about such a reaction. This type of selectivity of wavelength is not un-

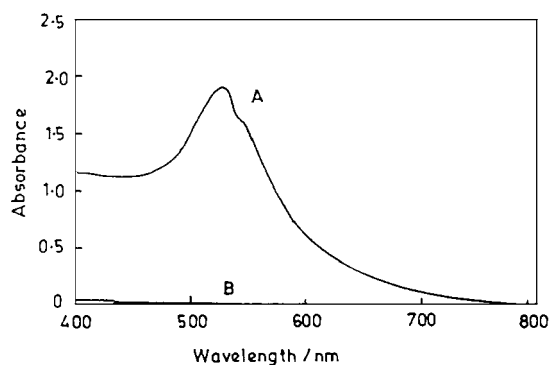


Fig. 1. Absorption spectra of: (a), gold sol (150 ppm) generated by the photoirradiation of HAuCl_4 in aqueous TX-100; (b), aqueous TX-100 after photoirradiation.

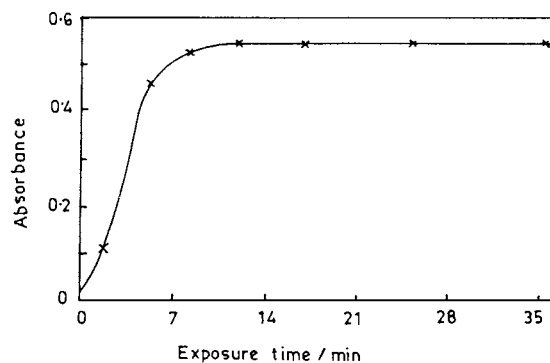


Fig. 2. Effect of irradiation time on the absorbance ($\lambda_{\max} = 523 \text{ nm}$) of gold sol (38 ppm).

usual and has been found in many reactions [6,7]. Photooxidation of aliphatic alcohols in aqueous medium are already known [25] and therefore, such a process is not unlikely. Yet, to gain a clear insight into the mechanism, further elaborative studies are needed.

3.2. Effect of irradiation time

As the reaction is based on the kinetic action brought about by the co-existence of TX-100 and gold(III) under UV light, it is enormously influenced by the exposure time. The kinetics were studied in order to obtain the optimum irradiation time for the system (the results are shown in Fig. 2). It was observed that an irradiation time of 12 min was sufficient to achieve the maximum absorbance at 523 nm, although further irradiation, at least up to 35 min, did not bring about any change. Hence, an irradiation time of 20 min was chosen for further studies.

3.3. Effect of TX-100 concentration

The use of TX-100 is vital, as the reduction of gold(III) to gold particle is carried out by TX-100 and light. TX-100 has another role: being a micelle forming agent it also acts as a stabilizer, otherwise, the particles may be precipitated. It also influences the particle size. In comparison to polymers and ligands, micelles have better size controlling capability with better reproducibility. Studies have been conducted with TX-100 in the

Table 1
Determination of gold in various samples

Sample (ppm)	Gold found ^a (ppm)	Relative standard error (%)
Synthetic samples		
Cu(II) (39)+Ag(I) (185)+Au(III) (50)	46.5	-7.0
Cd(II) (113)+Zn(II) (37)+Au(III) (50)	48.3	-3.4
Pt(IV) (39)+Pd(II) (45)+Au(III) (50)	47.0	-6.0
Gold ore (Au: 17 ppm)	15.0	-11.7

^a Average of three determinations.

concentration range of 10^{-1} – 10^{-4} M and 10^{-1} – 10^{-3} M was found to be the optimum. TX-100 of 10^{-4} M, which is below the critical micelle concentration, caused the λ_{\max} to be red shifted and absorbance to be decreased. When TX-100 \cong 1 M it was too viscous to be used. Other neutral surfactant and polymers such as Triton X-114, PEG and PVA were tried and found to produce very faint blue colour after 20 min irradiation.

3.4. Calibration graph and other statistical parameters

The sample solutions containing TX-100 (10^{-2} M) and gold(III) (0–150 ppm final concentrations) were exposed to UV light for 20 min. A linear calibration graph was obtained over this range of gold concentration. Linear regression performed over the linear response region provided a correlation coefficient of 0.999 with an intercept of 5.4×10^{-3} and a slope of 1.4×10^{-2} ppm. It was observed that gold can be determined down to a concentration level of 1 ppm. The molar absorptivity of pink gold sol was 3.06×10^3 l·mol⁻¹ cm⁻¹. The precision of the method (RSD, five determinations) was found to be ± 2.8 and $\pm 2.5\%$ for 22.7 and 90.9 ppm of gold, respectively. The Sandell sensitivity (with respect to gold) was 6.44×10^{-2} μ g cm⁻². The 95% confidence limit for 22.7 ppm of gold was 23.6 \pm 0.5 (for ten replicates).

3.5. Effects of diverse ions

Ag(I), Cu(II), Ni(II), Cd(II), Pt(IV), Pd(II), Zn(II) did not produce any colour during the procedure discussed. With 50 ppm of gold(III), the presence of the following anions SO₄²⁻, NO₃⁻, Cl⁻, NO₂⁻ (up to 250 ppm) did not cause any change in the absorbance value at 523 nm.

3.6. Applicability of the method

In order to confirm the applicability of the proposed method, it was applied to the determination of gold in three synthetic mixtures and to a concentrate of low grade Canadian RM gold ore. In aqua regia, on a low Bunsen flame, 1 g of ore was digested and finally evaporated to dryness in a water bath. During this process, all nitric acid was expelled. The dry residue was then extracted in distilled water and filtered, giving a final volume of 1 ml. The gold in the sample was then determined using the procedure described above. The results are summarised in Table 1.

4. Conclusion

A novel photochemical method of gold sol preparation is described, which has been used for spectrophotometric determination of gold. The method is simple, quick and reliable and has been used for the analysis of gold in synthetic mixtures and an ore sample.

Acknowledgements

The author is grateful to CSIR for financial support.

References

- [1] K. Yamaguchi, H. Asakawa, Anal. Biochem. 172 (1988) 104.
- [2] I.R. Nabiev, R.G. Efremov, G.D. Chumanov, Sov. Phys. Usp. 31 (1988) 241.
- [3] M. Moeremans, G. Daneels, J.D. Mey, Anal. Biochem. 145 (1985) 315.

- [4] O. Siiman, L.A. Bumm, R. Calaghan, C.G. Blatchford, M. Kerker, *J. Phys. Chem.* 87 (1983) 1014.
- [5] T. Pal, A. Ganguly, *Analyst* 112 (1987) 1327.
- [6] A. Pal, *Analyst* 119 (1994) 1899.
- [7] A. Pal, *Bull. Chem. Soc. (Japan)* 67 (1994) 2420.
- [8] F.E. Beamish, J.C. Van Loon, *Analysis of Noble Metals*, Ch. 3, Academic Press, New York, 1977.
- [9] H.R. Das, S.N. Bhattacharyya, *Talanta* 23 (1976) 535.
- [10] A. Diamantatos, *Anal. Chim. Acta* 66 (1973) 147.
- [11] M.A. Anuse, S.R. Kuchekar, N.A. Mote, M.B. Chavan, *Talanta* 32 (1985) 1008.
- [12] M.A. Anuse, N.A. Mote, M.B. Chavan, *Talanta* 33 (1983) 323.
- [13] M.Y. Mirza, *Talanta* 27 (1980) 101.
- [14] P.S. Patil, V.M. Shinde, *Microchim. Acta* 2 (1973) 331.
- [15] M. Mojski, *Talanta* 25 (1978) 163.
- [16] P.N. Nesterenko, V.M. Ivanov, G.V. Kudryavtsev, G.V. Lisichkim, *Zh. Anal. Khim* 39 (1984) 456.
- [17] K.S. Patel, K.U. Lieser, *Anal. Chem.* 58 (1986) 1547.
- [18] Z. Marczenko, K. Jankowski, *Talanta* 32 (1985) 291.
- [19] S. Jaya, T.P. Rao, T.V. Ramakrishna, *Analyst* 108 (1983) 1151.
- [20] A.I. Vogel, *A Text Book of Quantitative Inorganic Analysis*, Longman, London, 1973, p. 464.
- [21] L. Longenberger, G. Mills, *J. Phys. Chem.* 99 (1995) 475.
- [22] K.C. Yi, V.S. Mendieta, R.L. Castanares, F.C. Meldrum, C. Wu, J.H. Fendler, *J. Phys. Chem.* 99 (1995) 9869.
- [23] A. Henglin, P. Mulvaney, T. Linnert, *Faraday Discuss.* 92 (1991) 31.
- [24] T. Pal, A. Pal, *J. Ind. Chem. Soc.* 67 (1990) 387.
- [25] H.D. Becker, in: S. Patai (Ed.), *The Chemistry of the Hydroxyl Group (Part 2)*, Ch. 16, Wiley-Interscience, New York, 1971.
- [26] T. Pal, T.K. Sau and N.R. Jana, *Corr. Sci.* 39 (1977) 981.

Determination of milk-oxidised ketone bodies as an acetone derivative by electron capture gas chromatography

I. Sarudi *, É. Visi-Varga

Department of Chemistry, Faculty of Animal Science, Pannon University of Agriculture, PO Box 16, Guba S.u. 40, 7401 Kaposvár, Hungary

Received 12 December 1996; received in revised form 4 August 1997; accepted 5 September 1997

Abstract

Following the deproteination of the milk sample by means of zinc hexacyanoferrate, acetoacetic acid was decarboxylated by heating; the acetone originally present was then determined together with the acetone formed. The essence of the determination was that acetone reacted with bromine in the presence of sulphuric acid, following which, the bromoacetone formed was extracted into toluene, separated by gas chromatography and measured using an electron capture detector. The calibration curve was found to be linear up to a concentration of 2 mmol l^{-1} acetone. The detection limit calculated from the threefold noise level and the slope of the calibration curve was $9 \times 10^{-7} \text{ mol l}^{-1}$. The reliability of the method meets the practical requirements. Its application may be recommended above all for the establishment of subclinical ketosis. © 1998 Elsevier Science B.V. All rights reserved.

Keywords: Oxidised ketone bodies; Milk; Bromoacetone; Gas chromatography

1. Introduction

An increase in acetone, acetoacetic acid and 3-hydroxybutyric acid in biological fluids generally indicates some kind of energy metabolism disturbance in animals or humans. Thus, their estimation in blood, milk or urine is important with respect to diagnosis. In clinical chemistry the collective term ketone bodies is used for these compounds, while the sum of acetone and acetoacetic acid (given in mmol l^{-1}) is termed oxidised ketone bodies. Ketosis is a common disease

in dairy cows of high milk yield and it has been established that the level of oxidised ketone bodies in milk correlates closely with the concentration of blood ketone bodies [1,2].

In practice, the determination of oxidised ketone bodies is generally based on the assay of acetone, which is obtained after the decarboxylation of acetoacetic acid by heating. Some decades ago various non-automated photometric methods were most frequently used for the determination of milk acetone and in the 1980s photometric flow injection analysis [2] also began to appear in the specialist literature. Although traditional photometric methods provide accurate results, they are too time-consuming for serial tests. This is due to

* Corresponding author. +36 82 314155; fax: +36 82 313562.

the fact that photometric measurement in the presence of milk matrix is impossible, so acetone must be separated from the sample beforehand, by distillation [3,4], extraction [5,6] or diffusion [7–9]. Gas chromatography is now preferred to these laborious techniques. Out of all of the methods of gas chromatography previously developed [9–16], including the applications of the head-space technique [12–15], flame ionisation detection is used.

The present paper demonstrates another potential method for the determination by gas chromatography of oxidised ketone bodies in milk. The principal objective of this study was to achieve a high level of sensitivity by the application of electron capture detection.

2. Experimental procedure

2.1. Chemicals and solutions

Analytical reagent grade chemicals and triply distilled water were used throughout the study. The clarifying agents used were 4.8 g/100 ml ZnSO_4 and 3.7 g/100 ml $\text{K}_4[\text{Fe}(\text{CN})_6]$. Other solutions and chemicals used were: ca. $4.5 \times 10^{-2} \text{ mol l}^{-1}$ Br_2 solution prepared by the dilution of saturated bromine water in a ratio of 1:4; 4 mol l^{-1} H_2SO_4 ; aqueous 5 g/100 ml phenol solution; and in addition toluene purified by vacuum distillation at a pressure of ca. 15 mbar once every 2 weeks.

Aqueous standard solutions containing 0.10, 0.25, 0.50, 0.75, 1.00, 1.50, 2.00, 2.50 and 3.00 mmol l^{-1} acetone respectively, were diluted from a 0.10 mol l^{-1} stock solution, which was made up using acetone (99.5% p.a.) obtained from Merck AG, Germany. Acetone was redistilled before use. The stock solution could be kept in a refrigerator for about 3 weeks, but the calibrating standards were replaced with fresh ones once a week.

In the preparation of a 0.1 M acetoacetate solution lithium acetoacetate (supplied by Aldrich Chemical) was used. As acetoacetic acid and its salts dissolved in water are unstable, even at low temperatures, the lithium acetoacetate solution was made up directly prior to use.

2.2. Apparatus and conditions for chromatography

The gas chromatograph used was a Chrompack model 437 S, equipped with a ^{63}Ni electron capture detector and a fused silica capillary column ($50 \text{ m} \times 0.25 \text{ mm}$) coated with CP-Sil-8CB (supplied by Chrompack, The Netherlands). Nitrogen, at an inlet pressure of 90 kPa, was used as the carrier gas. The tests were performed under isothermal conditions. The temperatures of the column, the inlet and the detector were 110°C , 250 and 270°C , respectively. The split ratio and the degree of electrometer attenuation were 50:1 and 2^7 respectively.

2.3. Procedure

In a 30 ml centrifuge tube, 10 ml of the milk sample was mixed with 7 ml water and 1.5 ml of both clarifying agents. After a 10 min period of centrifuging at $750 \times g$, a portion of 5 ml of the clear supernatant was measured into a 10 ml

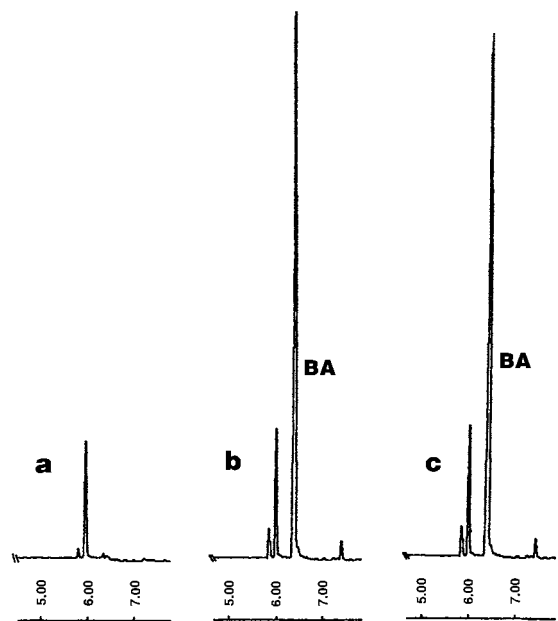


Fig. 1. Chromatograms of oxidised ketone bodies analysed as bromoacetone (BA): (a) reagent blank; (b) standard of 1.50 mM; and (c) a milk sample containing 1.42 mmol l^{-1} oxidised ketone bodies.

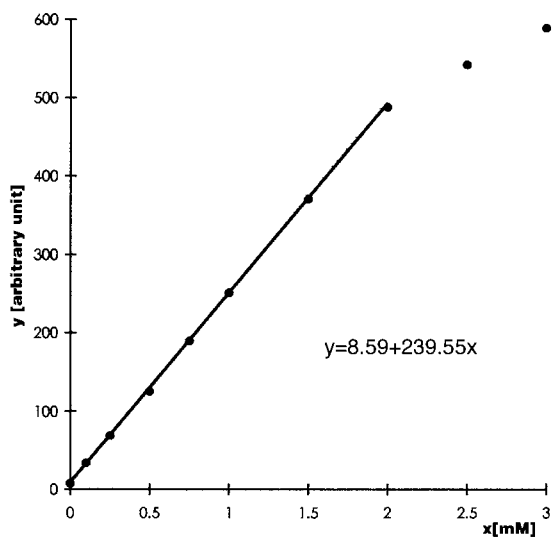


Fig. 2. Detector response (y) as a function of the concentration of acetone (x) in aqueous solution.

glass-stoppered test tube; the latter was then closed and kept in a boiling water bath for 35 min.

After cooling, 1.5 ml of the Br_2 solution, 1 ml of the H_2SO_4 solution and 2.5 ml toluene were added to the carboxylated sample solution, then the test tube was sealed and allowed to stand at room temperature for an hour and a half, with vigorous shaking every 15 min.

In order to bind the excess of bromine, 0.2 ml of the phenol solution was added to the mixture in the test tube (this reaction was also advanced by vigorous shaking until the brownish colour disappeared). Finally, 1 μl aliquots of the organic phase were injected manually into the gas chromatograph using a micropipette. For each sample, three injections were made. The peak area was used for quantitation and for the calculations. With the exception of heating in the water bath, the blank (triply distilled water) and the standard acetone solutions were subjected to the same procedure as that described above.

If the concentration of milk-oxidised ketone bodies was found to be more than 2 mmol l^{-1} , the analysis was repeated using 4 ml of the milk sample and 13 ml water instead of 10 and 7 ml,

respectively and the result obtained in such a manner was accepted.

3. Results and discussion

First, the milk sample was deproteinated by means of zinc hexacyanoferrate precipitate, then acetoacetic acid was decarboxylated by heating [2]. Following this, the acetone formed due to the decomposition of acetoacetic acid and the acetone which already existed in the sample were determined together. The procedure for this was as follows: acetone was allowed to react with bromine in the presence of sulphuric acid and the propanone derivative formed was extracted into toluene, then measured by gas chromatography using electron capture detection. Prior to gas chromatography, the excess bromine was bound by phenol.

The conditions detailed above yielded a single propanone derivative, namely monobromoacetone, the peak corresponding to which appeared on the chromatogram after the retention time of 6.4 min (Fig. 1). The identification of this substance was performed by gas chromatography with the aid of a monobromoacetone standard solution prepared according to the method of Maros et al. [17], where the bromoacetone preparation is described in connection with the bromine determination.

In the initial stage of the study *n*-hexane and also toluene were tried out as solvents for the extraction of the bromoacetone formed in the aqueous medium. As the partition coefficient of the propanone derivative mentioned above was found at room temperature to be 0.7 between *n*-hexane and water and 1.5 between toluene and water, it was decided to use toluene. In the latter case, the contact time of the two phases did not significantly affect the results for contact times up to 2 h. The amount of reaction product in the toluene extract when separated from the aqueous solution was stable.

The detector response to bromoacetone into toluene was directly proportional to the acetone concentration (or more precisely, the concentration of the oxidised ketone bodies) in the sample up to 2 mmol l^{-1} . Fig. 2 also shows a typical

Table 1
Results of recovery tests for acetoacetate added to different samples

Sample	Sum of acetone and acetoacetate determined in the original sample ^a (mmol l ⁻¹)	Acetoacetate	
		Added (mmol l ⁻¹)	Recovered (%)
1 mM acetone	0.985	0.54	105.7
Cow's milk (I)	0.375	0.27	91.9
Boiled cow's milk (I) ^b	0.008	0.27	94.8
Cow's milk (II)	0.610	0.81	103.5
Cow's milk (III)	1.728	1.08	95.8
Cow's milk (IV)	3.231	1.08	101.7
Mare's milk	0.182	0.27	113.0
Sheep's milk	0.264	0.27	96.7

^aThe number of replicates analyses was three in each case.

^bThe sample was boiled in an open vessel for 20 min prior to analysis.

standard curve. The standard deviations of the intercept and the slope are 1.48 and 1.46, respectively. It was shown by the *t*-test that the intercept differs significantly from zero ($p < 0.01$), probably due to impurities in the reagents used.

To establish the limit of detection, the blank (triply distilled water) was subjected twelve times to the procedure detailed above, with the excep-

tion of heating following the use of the clarifying agents. The mean and the standard deviation of the signals obtained were 5.080 and 0.072 respectively, in arbitrary units. The limit of detection (LOD) was calculated from the standard deviation of the blank signals (noise, N) and the slope of the calibration curve mentioned previously (S), as follows [18]: $LOD = 3N/S = 9 \times 10^{-7} \text{ mol l}^{-1}$ oxidised ketone body in the sample. The concentration value thus calculated corresponds to 52 pg of acetone in the sample if 10 ml of the milk sample is measured and a 1 μl aliquot of the organic phase is injected into the gas chromatograph.

In order to check the reproducibility, the complete procedure described above was repeated fifteen times with one milk sample taken from a non-ketotic cow and twelve times with another sample from a cow suffering from hyperketonaemia. The mean and the relative standard deviation (RSD) of the results obtained were 0.36 mmol l⁻¹ and 7.5% respectively, for the healthy cow and 4.57 mmol l⁻¹ and 3.8% respectively, for the hyperketonaemic cow.

To estimate the day-to-day reproducibility, the oxidised ketone bodies in a milk sample were determined once a day on five consecutive days. Each time the complete procedure (including the deproteination, as previously described, with clarifying agents) was carried out. The mean of the results obtained was 1.48 mmol l⁻¹, their RSD

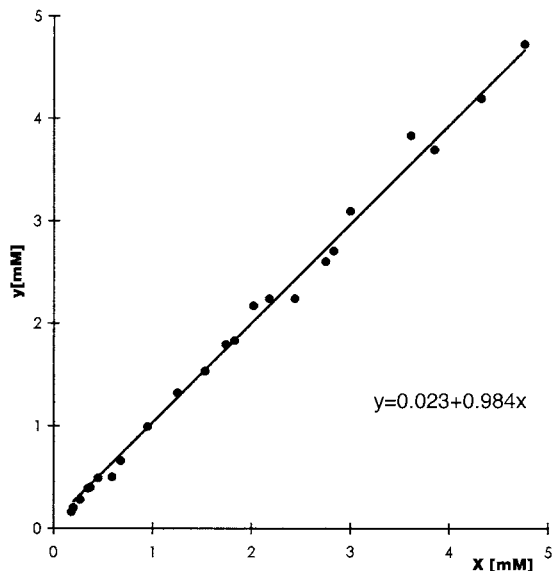


Fig. 3. Comparative results obtained by the gas chromatographic method (x) and a widely accepted spectrophotometric method (y) for oxidised ketone bodies in various milk samples.

being 6.6%. The sensitivity of the measuring system applied was not higher than 4.5%.

The accuracy of the method described in the present paper was also checked by means of a recovery test and a method comparison study. As Table 1 indicates, recovery of the acetoacetic acid added to the sample ranged from 92 to 113%, the mean being 100.4%. This gas chromatographic method and a widely accepted spectrophotometric method [9] were used to analyse 23 samples. It was proven by regression analysis that the results obtained by the two methods were in close agreement (Fig. 3). The regression coefficient scarcely diverged from the value of one and the regression constant was not significantly different from zero ($p > 0.1$).

4. Conclusion

On the basis of the results obtained in this study, it can be ascertained that the reliability of the gas chromatographic method developed meets practical requirements. The forte of this method is its high sensitivity, in consequence of which it is suitable for the establishment of even subclinical ketosis. The determination procedure is quite simple to perform, but necessitates a gas chromatograph equipped with an electron capture detector, together with distilled water of extremely high quality and very pure chemicals.

Acknowledgements

The financial support of the Hungarian National Fund for Scientific Research (OTKA) is gratefully acknowledged.

References

- [1] H. Steger, H. Girschewski, B. Piatowski, J. Voigt, *Arch. Tiernähr.* 22 (1972) 157.
- [2] P. Marstorp, *Anal. Chim. Acta* 149 (1983) 281.
- [3] H.G. Schuster, G. Baasch, *Z. Med. Labortechn.* 12 (1971) 312.
- [4] E. Mehnert, *Arch. Exp. Veterinärmed.* 24 (1970) 1269.
- [5] H. Göshke, *Clin. Chim. Acta* 28 (1970) 359.
- [6] A.D. Woolhouse, *N. Z. J. Med. Lab. Technol.* 25 (1971) 82.
- [7] C. Thin, A. Robertson, *Biochem. J.* 51 (1952) 218.
- [8] H. Steger, J. Voigt, *Arch. Tiernähr.* 20 (1970) 631.
- [9] B. Piatowski, J. Voigt, H. Girschewski, H. Steger, *Mh. Vet.-Med.* 29 (1974) 532.
- [10] J.D.H. Cooper, *Clin. Chim. Acta* 33 (1971) 483.
- [11] M.D. Trotter, M.J. Sulway, E. Trotter, *Clin. Chim. Acta* 35 (1971) 137.
- [12] C.J.P. Erikson, *Anal. Biochem.* 47 (1972) 235.
- [13] N.C. Jain, R.H. Cravey, *J. Chromatogr. Sci.* 10 (1972) 263.
- [14] I.A. McDonald, L.P. Hackett, L.J. Dusci, *Clin. Chim. Acta* 63 (1975) 235.
- [15] P. Hradecky, P. Jagos, *J. Chromatogr.* 146 (1978) 327.
- [16] F. Mangani, *J. Chromatogr.* 437 (1988) 294.
- [17] L. Maros, M. Káldy, S. Igaz, *Anal. Chem.* 61 (1989) 733.
- [18] E. Pungor, *Analitikusok Kézikönyve (Analysts' Handbook)*, vol. 17, Müszaki Könyvkiadó, Budapest, 1987, p. 380 (in Hungarian).

Further development of catalase, tyrosinase and glucose oxidase based organic phase enzyme electrode response as a function of organic solvent properties

L. Campanella *, G. Favero, M.P. Sammartino, M. Tomassetti

Department of Chemistry, University 'La Sapienza', p.le A. Moro, 5, 00185 Rome, Italy

Received 7 February 1997; received in revised form 1 August 1997; accepted 5 September 1997

Abstract

Using three enzyme sensors (tyrosinase, catalase and glucose oxidase), capable of functioning also in non-aqueous solvents, we found new correlations between classical indicators, e.g. the log *P* value of several organic solvents and new empirical indicators such as 'maximum current variation' (MCV) and above all the 'current variation rate' (CVR), the values of which may be monitored with the biosensor considered dipping directly into the organic solvent. The trend of the immobilised specific activity of the tyrosinase enzyme dipping into different organic solvents was evaluated and compared with that determined by the spectrophotometric method. Lastly, an investigation was performed to experimentally verify the relation between hydrophobicity of the solvent and its ability to draw back the water from the enzyme microenvironment using the Karl Fischer method and thermogravimetric analysis to estimate the residual water in the enzyme microenvironment after having treated the enzyme with the organic solvent, then allowing it to dry. © 1998 Elsevier Science B.V. All rights reserved.

Keywords: OPEEs; Catalyse; Tyrosinase; GOD

1. Introduction

As the catalytic performance of an enzyme is strictly dependent on the characteristics of the solvent in which the enzyme operates, many attempts have been made in recent years to obtain empirical and theoretical rules for the optimization of the whole reaction system [1–11].

Authors such as Laane [4], Zacks [5], Klivanov [7], Dordick [8], and coworkers have repeatedly pointed to the correlation between enzymatic activity and dielectric constant, or log *P* values of the solvent considered. More recently, Cernia et al. [12] employed microbial immobilized lipase to catalyse the esterification of aromatic chiral alcohols, using organic solvents as reaction media. They reached very interesting conclusions regarding the correlation between the above cited indicators and enzyme activity and selectivity.

Our increased knowledge concerning the possible use of a large number of enzymes also in

* Corresponding author. Tel.: +39 6 49913744; +39 6 490375; e-mail: campanella@axrma.uniroma1.it

non-aqueous solvents recently encouraged the development of enzymatic sensors capable of operating in organic solvents. Several different authors, including Turner and coworkers and Wang et al., have published papers in this field [13–25].

In recent years we have carried out detailed studies into the correlation between the nature of the organic solvent used and the sensitivity of the response of an original tyrosinase enzymatic sensor dipping into this solvent [26,27]. What was really being looked for was a possible correlation between biosensor sensitivity (and, therefore, enzymatic activity) and indicators, such as the dielectric constant value (DEC), or the log P value of the solvent used; the results seemed to be of great interest [27].

Two different papers published last year [22,28] demonstrate the ability of catalase (from bovine liver) to operate in an organic phase. We, therefore, recently studied a new catalase biosensor, sensitive to hydrogen peroxide, capable of operating both in several non-aqueous anhydrous solvents [29] and in water saturated chloroform [30], employing the new catalase biosensor to continue the experimental research that our laboratory has been actively pursuing [26,27] into the dependence of biosensor sensitivity and lifetime (and ultimately also the greater or lesser activity displayed by the enzyme operating in organic solvents) on the different hydrophobicity and polarity of the solvent used. Results, obtained using the biosensor dipped in four different organic solvents, were excellent also in this case [29] and mostly confirmed what we expected to find on the basis of the previous experiments carried out using the tyrosinase sensor [27].

The aspect investigated in recent months and described in this paper, using catalase or tyrosinase biosensors dipping into several organic solvents, is the correlation between classical indicators such as the log P value of the solvent and empirical new indicators such as 'maximum current variation' (MCV) or 'current variation rate' (CVR) of the enzyme biosensor dipping into the solvent considered. The results discussed herein seem of particular interest as re-

gards the correlation between log P and the CVR.

The interest inherent in experimental investigations aimed at determining possible correlation among certain easily measurable indicators, using a biosensor, and chemical indicators such as the log P values (which is known to describe the hydrophobicity of the considered solvent [4,7,10]), derives from the fact that an enzyme, even when working in an organic solvent, needs a minimal quantity of water in order to carry out its catalytic activity [3,5,8]. The actual amount varies from enzyme to enzyme and depends also on the solvent used. Usually, enzymatic activity is related directly to hydrophobicity. On the other hand, hydrophobicity is measured using the value of log P (P is the distribution coefficient of the solvent used in a standard two-phase octanol/water system [4,7,10]). For instance, solvents with log P lower than 2 are strongly hydrophilic. They, thus, remove water needed by the enzyme and consequently tend to substantially enhance the structural rigidity of the latter's molecule, which results in a loss of catalytic activity. This removal of the water molecule from the enzymatic microenvironment has been both postulated and indirectly verified by various authors [3,5,6,8,31]. However, more direct experimental evidence in this connection is still needed. To achieve this it will nevertheless be necessary to develop specific, somewhat complex methods. The present paper represents also an attempt to make an experimental contribution to the study of this problem. We think that, although qualitative in nature, the results of studies can be of some interest also from the methodological point of view. In practice, it has been attempted to correlate the log P trend of the solvents considered with the percentage of water (as determined experimentally using two different analytical methods) still present in the microenvironment of the enzyme glucose oxidase chosen as an enzyme model, after the enzyme was treated with different organic solvents and then allowed to dry; the first data are reported and discussed in this paper.

2. Experimental

2.1. Materials

Catalase (EC 1.11.1.6) (from bovine liver, 11 000 U/mg), tyrosinase (EC 1.14.18.1) (from mushroom, 4400 U/mg), glucose oxidase (EC 1.1.3.4), (from *Aspergillus niger*, 150–203 U/mg) and the dialysis membrane (D-9777) were supplied by Sigma, St. Louis, MO, USA. The phenol and the κ -Carrageenan were purchased from Fluka AG, Buchs, Switzerland; n-heptane, n-hexane, n-pentane, toluene, acetonitrile and ethyl acetate (RPE ACS), hydrogen peroxide, glucose, phosphate (used for the buffer preparation) and all the other chemical reagents, of analytical reagent grade, were supplied by Carlo Erba, Milan, Italy; 1,4-dioxane (extra pure) was from Merck, Darmstadt, Germany; chlorobenzene (spectrophotometric grade) from Aldrich, Milan, Italy; chloroform (Chromasolv) was supplied by Riedel de Haen, Seelze-Hannover, Germany.

The reagent and solvent used for water content determination using the Karl Fischer method were supplied by Merck, Darmstadt, Germany, art. 9243 and art. 9241, respectively. Using this method the water content of the anhydrous solvents used is generally lower than 0.01–0.02% by weight [26,27].

2.2. Apparatus

The oxygen electrode was a mod. 4000-1 obtained from Universal Sensors Inc., New Orleans, USA, the original membrane of which was replaced by a Teflon one. The O-ring, as well as the external body of the electrode, was also custom made of Teflon [27].

Tyrosinase biosensor measurements were performed using a Digital pH meter multimeter apparatus, model 200, supplied by Bell Engineering, USA. A Metrohm (Switzerland) 641 VA-Detector was used as potentiostatic power supply and to transform the 'current' signal into a 'tension' signal.

For the catalase biosensor measurements an Amel mod. 551 potentiostat equipped with an Amel adapter mod. 551/R from Amel, Milan

Italy, and a digital multimeter Mitek-MK 5001 (Taiwan) were used.

Glucose biosensor measurements were carried out using an Amperometric Biosensor Detector supplied by Universal Sensors Inc., New Orleans, USA.

In all cases, the responses were recorded on an Amel (Italy) model 868 recorder and the tests were carried out at 25°C in a thermostatted glass cell equipped with a forced water circulation jacket coupled to a model VC 20B Julabo (Germany) thermostat. The solvents used in the tests were kept under constant magnetic stirring using a microstirrer from Velp Scientifica (Italy).

Measurements of the water content were performed using both a Karl Fischer automatic titrator, model DL18, supplied by Mettler (Switzerland) and a Mettler TG50 thermobalance, coupled with a Mettler TC10 A-TA processor system and a Swiss Dot-Matrix printer, all from Mettler (Switzerland).

2.3. Methods

2.3.1. Enzyme immobilization.

The same enzymatic immobilization method to make the biosensors was used throughout. It consisted essentially in the κ -Carrageenan gel immobilization method, which had proved very effective on previous occasions [27,29].

Briefly, a 2% (w/w) solution of κ -Carrageenan was prepared by dissolving 0.2 g of the polysaccharide in 10 ml of distilled water, gradually heating the solution and maintaining it under constant stirring. The warm solution was placed on a Petri dish and, after cooling, some disks (1 cm diameter) were cut from it. After drying at room temperature, the κ -Carrageenan disks can be stored as long as needed. To obtain the enzyme membrane, 25 μ l of the enzymatic solution was added to each disk, which was then stored overnight at 5°C. The concentrations of the enzymatic solutions (all in 1/15 M phosphate buffer, at pH 7) used to make the three different enzyme biosensors employed in this study, were about 55 000, 2000, 7500–10 000 U/ml, for tyrosinase, catalase and glucose oxidase, respectively.

2.3.2. Biosensors assembly

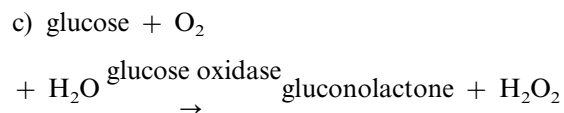
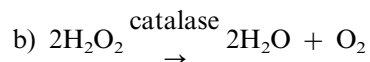
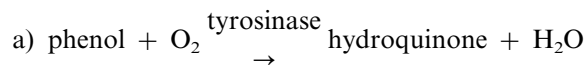
The κ -Carrageenan layer entrapping the enzyme, prepared as described above, was placed on the head of an amperometric gas diffusion electrode for oxygen, between the gas permeable membrane of the electrode and a dialysis membrane; the whole system was fixed to the Teflon cap by means of a Teflon O-ring (see the drawing of the biosensor assembly in a previous paper [27]).

Before use, the biosensor was immersed for about 15 min in phosphate buffer; after use it was first washed with the solvent used and then with phosphate buffer, before being stored at 5°C in a humid atmosphere.

If the dialysis membrane is deteriorated, the O-ring must be removed and the Teflon cap dipped into phosphate buffer for a short time, so that the dialysis membrane can easily be removed without disturbing the κ -Carrageenan layer containing the enzyme. A new dialysis membrane and the same enzyme-containing layer are then mounted on the cap using the Teflon O-ring.

2.3.3. Measurements

When the biosensor is dipped into 15 ml of the organic solvent, under stirring, and the substrate added, measurements are carried out by recording the signal variations related to the oxygen consumption, or production, in solution, due to one of the following enzymatic reactions:



For each biosensor and for each solvent, calibration curves were obtained by successive additions of small volumes (a few μl) of the non-aqueous standard solution of the substrate (i.e. phenol, hydrogen peroxide, or glucose) and

recording the signal variation between the two steady states before and after each addition of substrate. A procedure to obtain calibration curves using biosensors is reported in greater detail in previous papers [26,27,29,30]. Of course, the MCV was easily checked when the trend of the calibration curve reached the plateau (see example of graphical measurement of MCV in Fig. 1).

2.3.4. Measurement of the CVR and the immobilized specific activity using biosensors

To perform the measurements of CVR, the enzymatic sensor was immersed in 15 ml of non-aqueous solvent contained in a glass cell thermostatted at 25°C, under constant atmospheric pressure of 1013.1 (± 6.1) mbar and stirred magnetically, waiting until the signal became stable. With the onset of stabilization the measurement was performed by adding a fixed small volume (generally 25.0 μl) of the proper standard non-aqueous solution of the substrate [27,29], to bring the final concentration to 0.6 mM in hydrogen peroxide, or 1.0 mM in phenol, or 0.06 mM in glucose, respectively, and the signal variation (corresponding to the oxygen decrease, in the case of tyrosinase and glucose oxidase biosensors, or increase, for the catalase biosensor), was recorded until a new steady state was reached. The CVR value was obtained by plotting the recorded signal vs. the time, and calculating the value of the angular coefficient of the straight line portion of the recorded curve, see example in Fig. 3. To calculate the immobilized specific activity, the signal was converted into consumed or produced oxygen and, taking into account the stoichiometry of the enzymatic reaction, the number of μmol of substrate converted into the product per min was determined. Lastly, from the diameter (1.0 cm) of the κ -Carrageenan disk, it was possible to obtain the value of the immobilized specific activity (as described in greater detail in a previous paper [32]).

Because of the very low solubility of glucose in organic solvents, above all in non-polar solvents, the reaction rate measurements performed using the glucose oxidase sensor were performed only in saturated chloroform containing 0.09% (v/v) of

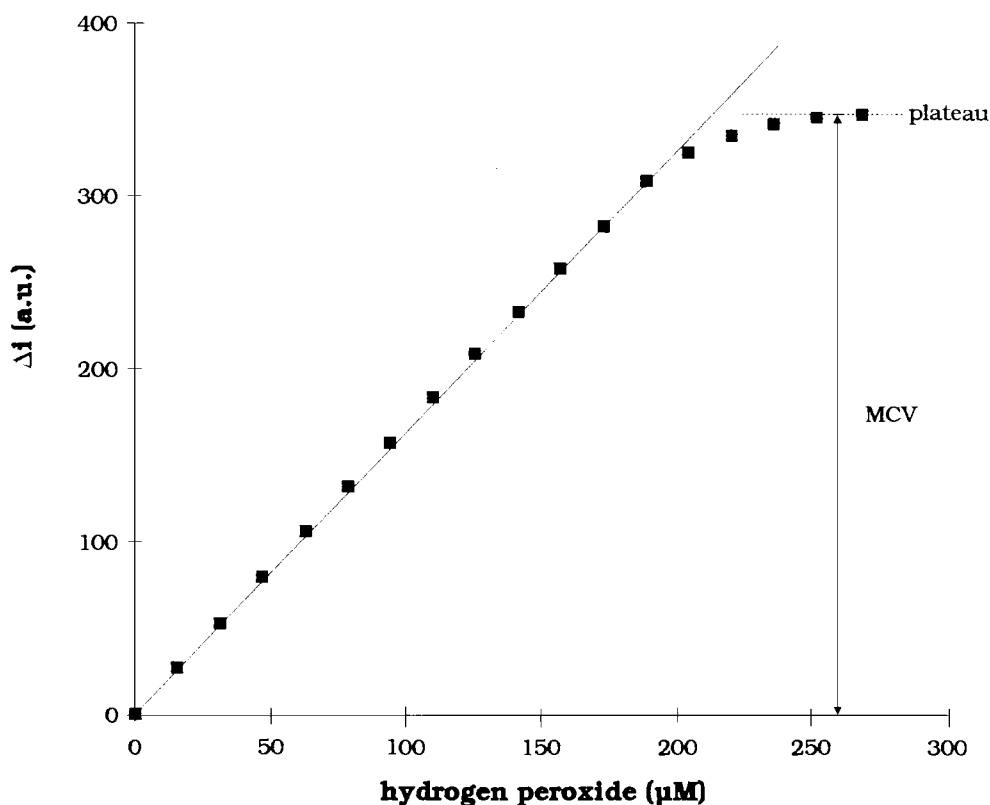


Fig. 1. Calibration graph obtained using the catalase biosensor with chloroform as organic solvent and graphical measurement of MCV indicator for catalase biosensor in chloroform.

water, as well as in ethyl acetate and in acetonitrile, 1.5 and 2.5% (v/v) in aqueous solution, respectively, (i.e. containing the minimum percentage of water below which no biosensor response could be observed). The small percentage of water contained in these solvents is, in fact, necessary to increase, albeit slightly, the solubility of the substrate in the solvent considered.

2.3.5. Measurement of the immobilized specific activity by the spectrophotometric method

In the case of the tyrosinase enzyme layer data on immobilized specific activity as a function of the organic solvent considered and determined using the tyrosinase biosensor were compared with analogous data obtained using a classical spectrophotometric method based on the use of Folin Ciocalteu reagent [33]. To this end a κ -

Carrageenan enzymatic layer was dipped in 25 ml of the non-aqueous solution 2.1 mM of phenol and thermostatted at 25°C. At different times a small volume of the solution was tested for phenol content by the following procedure: 0.5 ml of Folin Ciocalteu reagent, followed by 1.5 ml of 20% (w/v) sodium carbonate solution, were added to 1.0 ml of the above standard solution. The mixture was then diluted to 5 ml with water and heated in a water bath at 35°C for 20 min, to allow the colour to develop completely. The absorbance was measured at $\lambda = 760$ nm against a white reagent. Concentration values were obtained by the direct method using a calibration graph. It was, thus, possible to determine the decrease in concentration of the substrate (phenol) as a function of time, in practice, the reaction rate. Lastly, the immobilized specific activity was

obtained taking into account of the diameter of the κ -Carrageenan disk (generally 1.0 cm).

2.3.6. Treatment of the glucose oxidase enzyme with different organic solvents to check the solvent ability to draw the water from the enzyme microenvironment

About 200 mg of glucose oxidase were weighed out for each test. Four different procedures were preliminarily tested:

- a) The enzyme was placed in a glass Petri dish, about 20 ml of the organic solvent were added and then after stirring allowed to evaporate at constant humidity (25% RH), temperature (25°C) and atmospheric pressure (1013.1 mbar).
- b) The enzyme was placed in a dialysis tube filled with the solvent and closed at each end; the tube was then placed in about 20 ml of the same solvent; the latter was renewed three times and then the dialysis tube was opened and the solvent containing the enzyme allowed to dry at constant humidity (25% RH), temperature (25°C) and atmospheric pressure (1013.1 mbar).
- c) The enzyme was placed in a Gooch crucible incorporated in a filtering apparatus. The Gooch crucible was filled three times with volumes of about 20 ml of the organic solvent considered. The enzyme was then allowed to dry in a desiccator under a moderate vacuum.
- d) The enzyme was placed in a Gooch crucible in a filtering apparatus. The Gooch crucible was filled three times with volumes of about 20 ml of the organic solvent considered. The enzyme was then allowed to dry at constant humidity (25% RH), temperature (25°C) and atmospheric pressure (1013.1 mbar).

The determination of the water content after each of the above treatments, carried out using the methods described in the present paper, showed that treatment (a) is comparatively inefficient; in practice, the enzyme retains about the same water content as at the outset; treatments (b) and (d) are practically equivalent as far as the results are concerned, but treatment (b) is much slower, taking several days instead of several hours. Lastly, treatment (c), which differs from (d) only in the way the drying is performed, gives rise to a product (enzyme) that retains a smaller

quantity of water than in all other cases. Above all, however, this quantity remains practically constant whatever the method and solvent used. Using this method to dry the enzyme is practically the only drying treatment that affects the water retained by the enzyme, eliminating the differences due to treatment with the various solvents. In conclusion, taking these results into account, the treatment that was subsequently systematically adopted in all the experiments carried out using different solvents was the treatment (d). Probably, also in this way, the water content of the product is partially affected by the method used for drying (it is indeed possible that the enzyme is partially rehydrated). However, the differences in water content due to treatment with solvents at different degrees of hydrophilicity, may still be highlighted by means of careful determination of the water content, as the experimental results have shown.

2.3.7. Determination of the water content in the glucose oxidase enzyme whether treated or not by organic solvent

For measurements using the Karl Fischer method, 30–40 mg of the enzyme, treated or not treated with the organic solvent considered, were weighed and rapidly added to the Karl Fischer cell. Titration, performed by the automatic titrator, was started after 30 s of stirring at 25°C, in a nitrogen stream.

For the measurements of water content by thermogravimetry an amount of enzyme of the order of 10 mg was accurately weighed and analysed under the following experimental conditions: heating between 20 and 150°C at a rate of 5°C/min in an air stream at a flow rate of 50 cm³/min.

3. Results and discussion

As stated in the introduction of this paper, in recent work we investigated catalase biosensor response to hydrogen peroxide, which we studied in four different anhydrous organic solvents [29]. Fig. 1 shows the unpublished calibration graph in anhydrous chloroform. In the curve in Fig. 1, as well as in other similar curves, obtained using the

other solvents investigated (chlorobenzene, toluene, ethyl acetate), a fairly long straight line section is found, at the end of which the curve tends to flatten out rapidly. As observed in the case of the tyrosinase biosensor [27], also in this case it was possible to ascertain experimentally that a correlation existed between indicators, such as the slope of the straight line section of the calibration graph in the various solvents (in practice the biosensor's sensitivity) and the value of $\log P$ of the solvent considered. It is sufficient to compare the trends of the (a) and (b) series of histograms shown in Fig. 2 for this purpose. However, an improved correlation has now been found. In this case it should also be noted that, instead of biosensor sensitivity, in order to highlight another interesting correlation with $\log P$ value, it would also be possible to use the MCV of the enzyme sensors as a new empirical indicator, recorded for high concentrations of substrate, in practice when the calibration curve obtained using the catalase biosensor dipping in the organic solvent flattens out (see Fig. 1). With this purpose in mind a comparison should be made between the trends in the (a) and (c) series of histograms in Fig. 2.

Lastly, the histogram (b) of Fig. 4 also shows the trend of the value of the CVR of the catalase biosensor dipping into different organic solvents, as determined for high substrate concentrations (0.6 mM) and measured as shown in Fig. 3. Clearly, according to the common definition of enzymatic activity, the measured CVR, is related to the variation of the oxygen concentration in solution, due to the enzymatic reaction and therefore also to the reaction rate. CVR is thus essentially an empirical indicator that should correlate more closely with enzymatic activity than the previously [27,29] investigated indicators. Experimental tests actually also indicate a trend in perfect agreement with the value of $\log P$ (see Fig. 4(a)). On the other hand, in this connection, it is not surprising that the CVR trend is in perfect agreement with the value of $\log P$, if the latter is to be a truly realistic indicator of enzymatic activity in the solvent considered [11,13,27,29,31].

Furthermore, using the previous rate data, in order to calculate the reaction rate and thus the

immobilized specific activity of the enzyme in the various solvents, it is obvious that the plot obtained for the latter will be very similar to that of the CVR indicator and of course in good correlation with the trend of $\log P$ values (Fig. 4). It is equally obvious that, despite the objection that, since the classic operating conditions required for the activity measurement in aqueous solvent [20] were not fully achieved and so the 'absolute values' of the immobilized specific activity found

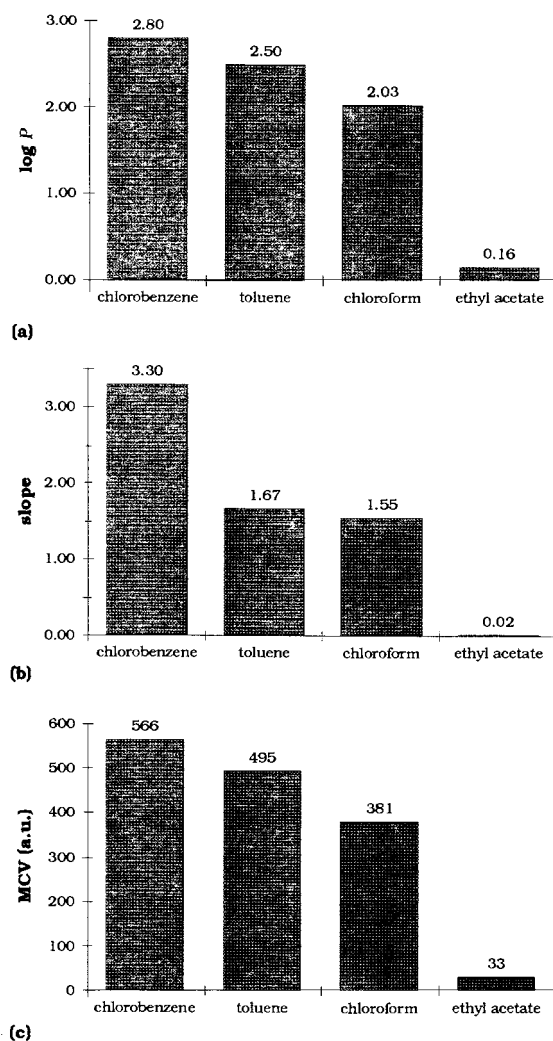


Fig. 2. Trend of: (a) $\log P$ values of several organic solvents; (b) the slope of the calibration graphs; (c) the MCV for the catalase biosensor as a function of the organic solvents considered.

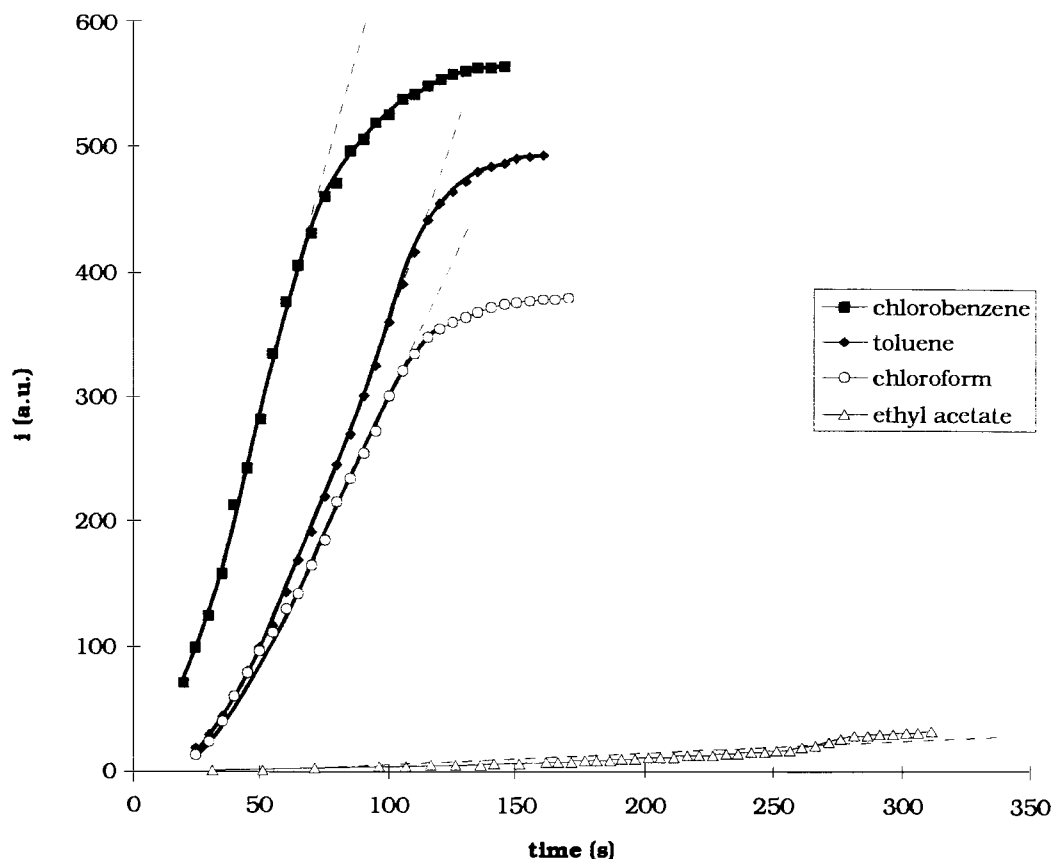


Fig. 3. Response of catalase biosensor dipping into different solvents, as a function of time, recorded for a high value of the hydrogen peroxide concentration: 0.6 mM. The value of the angular coefficient of the straight line section of the recorded response curve of the biosensor allows the value of the CVR indicator to be checked.

might not be completely accurate, the histogram trends of the relative activity values, measured using the biosensor dipping into the different solvents, may certainly be considered reliable, as the operating conditions remained the same in spite of the change of solvent.

In view of the interest and satisfaction at having found this further correlation, we also set out to determine whether the highly significant correlation between $\log P$ values of different solvents and the CVR indicator (and therefore also the specific immobilized activity), or MCV indicator, could again be experimentally verified using another enzymatic sensor, i.e. the tyrosinase biosensor, which is also capable of being used in non-aqueous solution and was recently studied by us [26,27].

The experimental results of this investigation are shown graphically in Fig. 5 and Fig. 6. By means of the histograms in Fig. 5 a comparison was made of $\log P$ trends for the same solvents as were considered in a previous paper [27] and those of sensitivity values of the tyrosinase enzyme sensor (e.g. the slope values of the straight line section of the calibration curve obtained using the tyrosinase biosensor in the organic solvent considered), or else with those of the new indicator MCV. On the other hand, Fig. 6 shows the trend of CVR values of the tyrosinase biosensor response dipping into the different organic solvents considered, determined for a high substrate concentration (1.0 mM). It is interesting to note that the $\log P$ trend and that of the sensitivity values

are in good agreement when the following solvents are used: acetonitrile, chloroform, toluene and n-heptane, whereas, when n-hexane or n-pentane are used as solvent, the trend continues to rise if the sensitivity values are taken, while it is inverted and decreases if $\log P$ values are considered. Conversely, the same inversion is found in the trends of MCV values (Fig. 5) and in those of the CVR values (Fig. 6). However, while in the first case the MCV trend, although quite com-

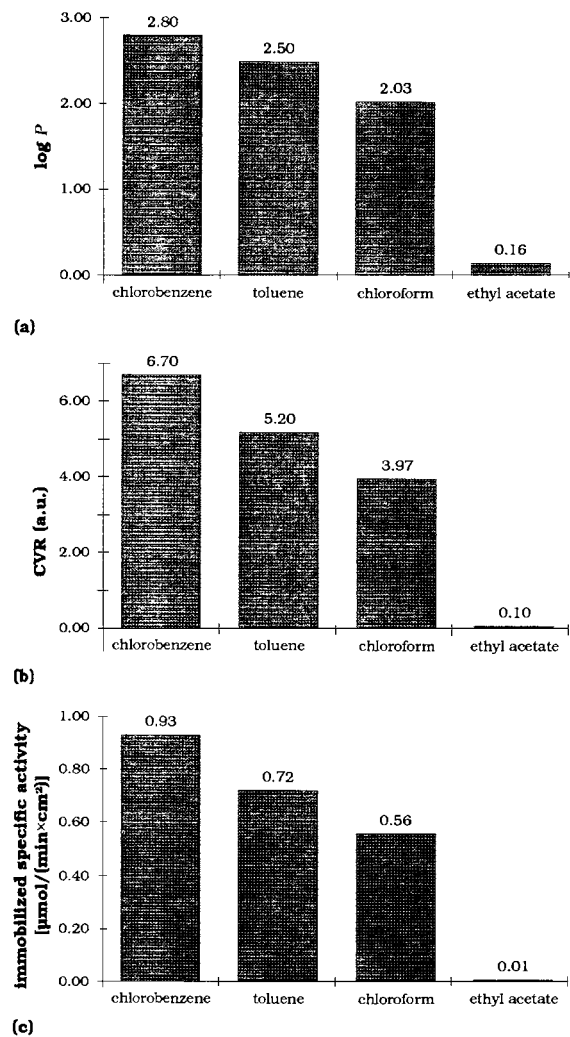


Fig. 4. Trend of: (a) $\log P$ values of several organic solvents; (b) the CVR; (c) the immobilized specific activity, for the catalase biosensor, as a function of the organic solvents considered.

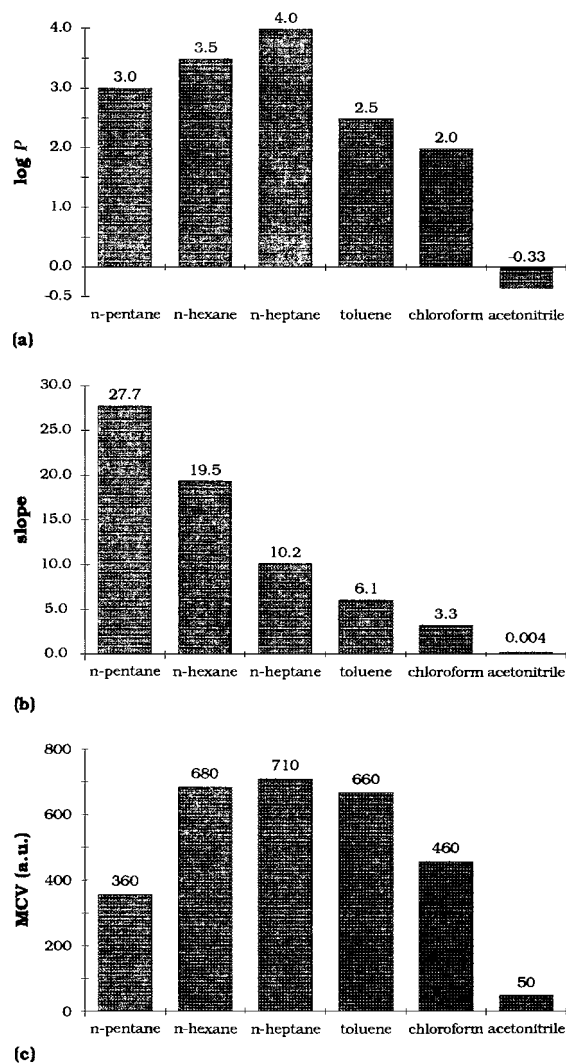


Fig. 5. Trend of: (a) $\log P$ values of several organic solvents; (b) the slope of the calibration graphs; (c) the MCV for the tyrosinase biosensor as a function of the organic solvents considered.

parable to those of $\log P$, are not exactly the same, in the second case the CVR trend and that of $\log P$ are in almost perfect agreement.

Also in this case, as in that of the catalase electrode, it is obviously possible to estimate the values of the immobilized specific activity of the enzyme. Although also for these data the same reservations apply as for the accuracy of the

absolute value of the activities obtained using the enzyme sensor, it is nevertheless comforting to observe how the actual values of the activity, determined independently, also by means of the absorption spectrophotometry, not only obviously display an analogous trend regardless of the method used to obtain them, but the values are not in absolute terms much different from those determined using the biosensor immersed directly in the organic solvent (compare both the trends and the values of the histograms (b) and (c) in Fig. 6).

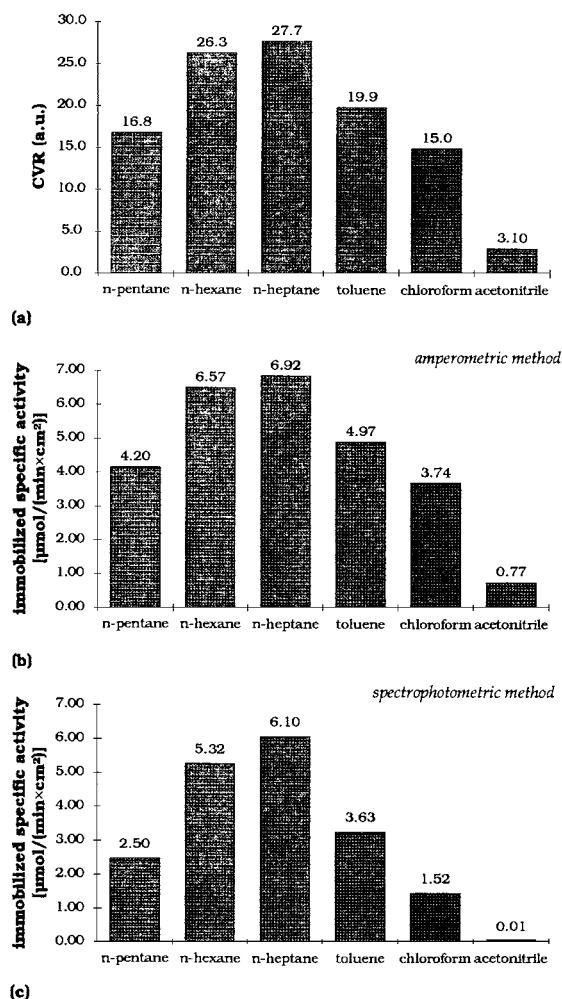


Fig. 6. Trend of: (a) the CVR; (b) the immobilized specific activity for the tyrosinase biosensor; (c) the immobilized specific activity measured using the spectrophotometric method, as a function of the organic solvents considered.

Lastly, as briefly stated in the introduction of this paper, the role played by the aqueous microenvironment constantly surrounding the enzyme is well known, and is thus a key factor in optimizing the enzymatic activity [3,5,8] and, thus, also the biosensor response [13,14,27,29]. Therefore, we carried out an experimental study to determine the water content of a typical common enzyme both in the lyophilized form and after treatment with an organic solvent and then allowing the organic solvent to evaporate. Taking into account that this study requires a large amount of enzyme, glucose oxidase was used as an enzyme model, even though it certainly does not represent one of the most interesting enzymatic systems from the point of view of possible uses in non-aqueous solvents. The main reason for this choice was the enzyme's relatively low cost and the fact that it was recently shown [34] to be capable of operating also in non-aqueous solvents, or mixtures of solvents. To this end several organic solvents with different hydrophobicity were employed; in practice a weighed amount of the lyophilized glucose oxidase enzyme was treated with each of the organic solvents considered in turn, according to the procedure described in Section 2 of this paper. Therefore, after allowing the organic solvent to evaporate, the water content that was still found to be held by the enzyme itself was determined. The techniques used for this study were thermogravimetric analysis and Karl Fischer titration. Although only in qualitative mode, the results seem to confirm the reverse correlation between the hydrophobicity of the solvents considered and their ability to withdraw water from the enzyme aqueous microenvironment. The data referring to the water content of the treated enzyme as determined independently using two different methods of analysis, confirm what we actually expected to find, namely that the enzyme treated with less hydrophilic solvent (i.e. with a higher $\log P$ value) retains a higher water content than the enzyme treated with a more hydrophilic solvent (i.e. with a low $\log P$ value) [11,13,27,29,31]. Clearly, for the reasons briefly set out in Section 2, in performing this kind of experiment, whatever the procedure adopted in treating

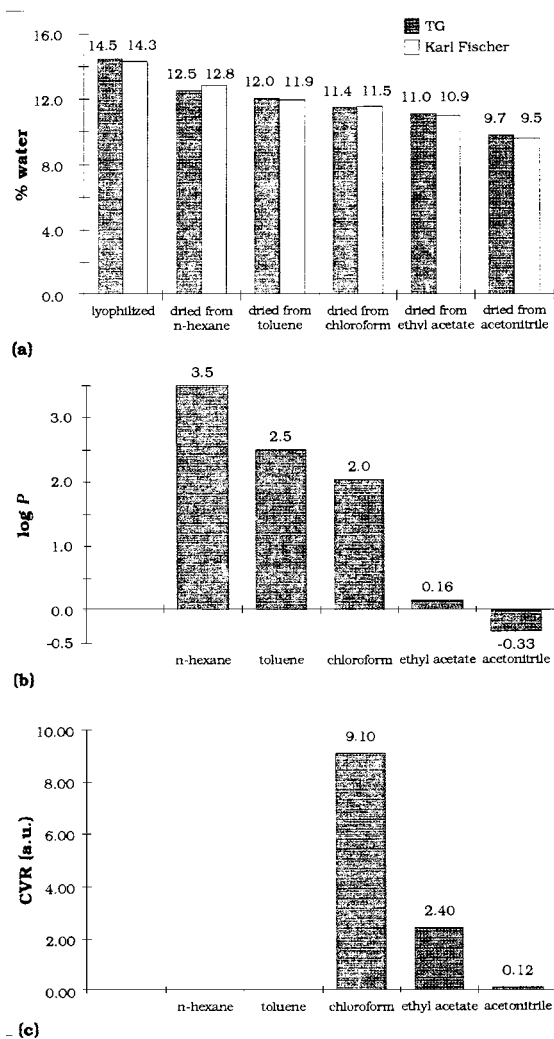


Fig. 7. (a) % Water content of glucose oxidase enzyme, either lyophilised or after treatment with the solvent considered, then allowed to dry, found using the thermogravimetric (TG) or Karl Fischer method; trend of: (b) $\log P$ values of the organic solvents considered; (c) the CVR measured using the glucose oxidase biosensor, as a function of the organic solvents considered.

the enzyme with the organic solvent and, to an even greater extent, that used to evaporate the organic solvent in the enzyme thus treated, inevitably had a systematic influence on the water content associated with the enzyme, thus determined using the above methods, nevertheless the trend that emerges from the histogram (a) in Fig.

7 shows that it still retains practically the original information; since by constantly operating in the same experimental conditions, the procedure adopted had only a systematic effect on the analytical data. Indeed an appreciable correlation was found between the $\log P$ trends of the solvents used and the water content retained by the glucose oxidase which was subjected to treatment using one of the organic solvents considered. Incidentally, it is interesting to observe the good agreement of the analytical results yielded by the two methods used to determine the water retained by the enzyme even though they are based on quite different principles.

Furthermore, some experiments using a glucose oxidase enzyme sensor dipping into an organic solvent yielded results in agreement with those found using two other catalase and tyrosinase biosensors. Indeed, the last set of histograms (c) in Fig. 7 clearly show how by considering the CVR indicator for the glucose oxidase enzyme sensor, working in different organic solvents, also in this case the value of this indicator increases with increasing $\log P$, i.e. with the degree of solvent hydrophobicity. Of course, in these experiments using the glucose oxidase biosensor, the investigation was limited to just three different organic solvents in view of the very low solubility of the substrate in organic solvents, above all in solvents that were more hydrophobic than those considered (e.g. toluene and n-hexane). In conclusion, even the limited experiments carried out using the glucose oxidase enzyme sensor confirm the more general results found in this research using the other two enzymatic biosensors.

In other words, we can conclude that a close correlation exists between the trend in the classic $\log P$ indicator and that of the CVR indicator proposed here. Subsequently, the latter indicator, also because it can be measured simply and rapidly by the enzyme sensor dipped directly into the organic solvent, may be used as an indicator of enzymatic activity in the organic solvent considered; in fact, its trend closely follows that of $\log P$, in many cases even more closely than the biosensor's sensitivity, which is the indicator that we have studied and proposed over the last 2 years in previous papers [27,29] and which itself

has often provided very good results in this connection.

Lastly, it must be pointed out that, in carrying out the research described, and in evaluating and discussing the results obtained, several reasonable assumptions were made: in the first place, that, as in all sensors of this kind (OPEEs), the enzyme molecules involved in the catalytic action are essentially those at the interface. Therefore, also in view of the considerable (albeit different) hydrophobicity of the organic solvents considered, it would appear legitimate, in discussing the results obtained, to neglect in the first instance, any diffusion phenomena in the κ -Carrageenan gel or any solvent effects on the gel itself (in any case, this assumption is supported by the long lifetime of the biosensors considered and the good reproducibility of their response [27,29,30]). Furthermore, the enzyme immobilized in the gel and certainly still completely surrounded by water molecules was considered as though it was practically free in an aqueous solution, so as to be able to discuss the effects of the solvent on the enzymatic microenvironment, using the same criteria and the same indicators as in the majority of literature articles on the subject, many of which are cited also in the references of the present paper [1–13,26–31]. The good agreement between the experimental results and what was reasonable to expect on the strength of the literature data [1–14,27,29,31], may in any case, be deemed to justify the assumptions made, albeit a posteriori.

Acknowledgements

We are indebted to Dr Umberto Martini for his contribution to the development and characterisation of the catalase probe in organic solvents. This work was supported by the National Research Council (CNR) of Italy. Target Projects ‘Solid State Electronic Materials’ (MADESS) and ‘Tecnologie Chimiche Innovative’.

References

- [1] C. Laane, S. Boeren, K. Vos, *Trends Biotechnol.* 3 (1985) 251.
- [2] R.Z. Kazandjian, J.S. Dordick, A.M. Klibanov, *Biotechnol. Bioeng.* 28 (1986) 417.
- [3] M. Reslow, P. Adlercreutz, B. Mattiasson, *Appl. Microb. Biotechnol.* 26 (1987) 1.
- [4] C. Laane, S. Boeren, K. Vos, C. Veeger, *Biotechnol. Bioeng.* 30 (1987) 81.
- [5] A. Zacks, A.J. Russell, *J. Biotechnol.* 8 (1988) 259.
- [6] Y.L. Khmelitsky, A.V. Levashov, N.L. Klyachko, K. Martinek, *Enzyme Microb. Technol.* 10 (1988) 710.
- [7] A. Zacks, A.M. Klibanov, *J. Biol. Chem.* 263 (1988) 3194.
- [8] J.S. Dordick, *Enzyme Microb. Technol.* 11 (1989) 194.
- [9] A. Guagliardi, M. Rossi, S. Bartolucci, *Chim. Oggi* May (1989) 31.
- [10] K. Ryu, J.S. Dordick, *J. Am. Chem. Soc.* 111 (1989) 8026.
- [11] V.S. Narayan, A.M. Klibanov, *Biotechnol. Bioeng.* 41 (1993) 390.
- [12] E. Catoni, E. Cernia, C. Palocci, *J. Molecular Catalysis* 105 (1996) 79.
- [13] S. Saini, G.F. Hall, M.E.A. Downs, A.P.F. Turner, *Anal. Chim. Acta* 249 (1991) 1.
- [14] J. Wang, in: G.G. Guilbault, M. Mascini (Eds.) *Uses of Immobilized Biological Compounds*, Kluwer, Dordrecht, The Netherlands 1993, pp. 255–262.
- [15] G.F. Hall, D.J. Best, A.P.F. Turner, *Anal. Chim. Acta* 213 (1988) 113.
- [16] J. Wang, A. Reviejo, S. Mannino, *Anal. Lett.* 25 (1992) 1399.
- [17] L. Campanella, M.P. Sammartino, M. Tomassetti, *Sensors and Actuators B* 7 (1992) 383.
- [18] Q. Deng, S. Dong, *Anal. Chem.* 67 (1995) 1357.
- [19] D.O. Hitzamm, T.R. Hopkins, *Eur. Pat. Appl.*, 0214336A1, 1987.
- [20] G.F. Hall, A.P.F. Turner, *Anal. Lett.* 24 (1991) 1375.
- [21] F. Schubert, S. Saini, A.P.F. Turner, *Anal. Chim. Acta* 245 (1991) 133.
- [22] J. Wang, Y. Lin, L. Chen, *Analyst* 118 (1993) 277.
- [23] J. Wang, G. Rivas, J. Liu, *Anal. Lett.* 28 (1995) 2287.
- [24] G.F. Hall, D.J. Best, A.P.F. Turner, *Enzyme Microb. Technol.* 10 (1988) 543.
- [25] J. Wang, Y. Lin, A.V. Eremenko, A.L. Ghindilis, I.N. Kurochkin, *Anal. Lett.* 26 (1993) 197.
- [26] L. Campanella, A. Fortuney, M.P. Sammartino, M. Tomassetti, *Talanta* 41 (1994) 1397.
- [27] L. Campanella, G. Favero, M.P. Sammartino, M. Tomassetti, *Talanta* 41 (1994) 1015.
- [28] E. Magner, A.M. Klibanov, *Biotechnol. Bioeng.* 46 (1995) 175.
- [29] L. Campanella, U. Martini, M.P. Sammartino, M. Tomassetti, *Electroanalysis* 8 (1996) 1150.
- [30] L. Campanella, U. Martini, M.P. Sammartino, M. Tomassetti, *Analisis* 24 (1996) 288.
- [31] L.A.S. Gorman, J.S. Dordick, *Biotechnol. Bioeng.* 39 (1992) 392.
- [32] M. Mascini, M. Tomassetti, M. Iannello, *Clin. Chim. Acta* 132 (1983) 7.
- [33] R.F. Milton, W.A. Waters (Eds.) *Methods of Quantitative Micro-Analysis*, Edward Arnold (Publ.) Ltd., 1955, p. 356.
- [34] E.I. Iwuoha, M.R. Smith, *Anal. Proc. Incl. Anal. Comm.* 31 (1994) 19.

Differential pulse anodic stripping voltammetry of lead (II) benzoylacetate in chloroform: Application to the analysis of free-lead gasoline and gas oil samples

M.H. Pournaghi-Azar *, A.H. Ansary-Fard

Electroanalytical Chemistry Laboratory, Faculty of Chemistry, University of Tabriz, Tabriz, Iran

Received 29 April 1997; received in revised form 22 August 1997; accepted 5 September 1997

Abstract

The voltammetric characteristics of lead(II) benzoylacetate in chloroform at the mercury electrode are investigated. The conditions for nearly reversible reduction of lead(II) were optimized. Anodic stripping voltammetry for the determination of trace-lead was developed using differential pulse technique to strip amalgamated lead from hanging mercury drop electrode. The experimental conditions, such as scanning rate of electrode potential and deposition time of lead were optimized. The calibration graph was linear over concentration range 5×10^{-8} – 10^{-6} M of lead(II). The detection limit was 2.5×10^{-9} and the relative standard deviation for the determination of 4×10^{-7} M Pb(II) was 2%. Preceded by decomposition of organolead compounds with concentrated nitric acid, then ashing at 300°C and a solvent extraction of Pb(II) benzoylacetate in chloroform, the suitability of the proposed method for the determination of lead in free-lead gasoline and gas oil was demonstrated as a typical example of application. © 1998 Elsevier Science B.V. All rights reserved.

Keywords: Pulse polarography; Anodic stripping voltammetry; Chloroform; Lead(II) benzoylacetate; Gasoline; Gas oil

1. Introduction

Direct application of electroanalytical methods to the determination of analytes in pure extracts following solvent extraction seem to be simple and sensitive [1–7]. The previous studies revealed that a preliminary separation and preconcentration of some metal ion chelates by solvent extraction into chloroform and application of

electroanalytical methods for the determination of the analyte in pure extracts provide good selectivity and sensitivity [1,2]. Anodic stripping voltammetry (ASV) has always been regarded as one of the most sensitive technique for trace-metal analysis in water. A little works, exploiting non aqueous solvent for stripping techniques were reported [8,9]. To our knowledge, there are no reports on the use of stripping techniques in organic solvents of low dielectric constant, convenient for solvent extraction.

* Corresponding author. Fax: +98 041 344013.

The present work deals with the study of polarographic characteristics of Pb(II) benzoylacetate in chloroform in the presence of a suitable supporting electrolyte. It was intended to investigate the suitability of the proposed method for the determination of lead in complex matrices, such as gasoline and gas oil, after its mineralization and extraction as lead(II) benzoylacetate in chloroform.

2. Experimental

2.1. Chemicals and reagents

Chloroform, perchloric acid, benzoylacetone (purified by recrystallization or sublimation), tetrabutylammonium chloride (TBACl) and piperidine were from E. Merck p.a grade. The supporting electrolytes used were 0.5 M tetrabutylammonium perchlorate (TBAP) or 0.75 M piperidinium perchlorate (PP) + 0.25 M piperidine (P). PP was prepared by gradual neutralization of a given volume of perchloric acid 1:1, with the required amount of piperidine while cooling the solution in iced water. PP formed in slightly acid solution was crystallized by successive concentration on the water bath and cooling at room temperature. The crystals formed were dried at 50°C.

2.2. Standard lead solutions

A 10^{-2} M aqueous solution of Pb(II) nitrate from E. Merck was prepared as a stock solution. The standard solutions were prepared by successive dilution of this stock solution.

2.3. Extraction solution

A 0.01 M chloroform solution of benzoylacetone was used. $\text{Pb}(\text{C}_2\text{H}_5)_4$, at least 99% purity, was from Octel (Manchester, UK) and gasoline sample with a certified amount of $\text{Pb}(\text{C}_2\text{H}_5)_4$ was obtained from Tabriz refinery. The free-lead gasoline sample (with no deliberate addition of $\text{Pb}(\text{C}_2\text{H}_5)_4$) was obtained from petroleum chemistry laboratory of our faculty.

2.4. Apparatus

All voltammograms were recorded with a three electrode system. A polarograph E 626 was used with a VA-Stand 663 and VA-controller E608 (from Metrohm) to plot the polarograms. A multipurpose instrument from EG and G including potentiostat/galvanostat model 273, electrochemical analysis software 300 model 270 coupled with an IBM personal computer and an Epson FX 850 printer was used to record the cyclic voltammograms with IR compensation.

2.5. Electrodes

The reference electrode Ag/AgCl (sat.), TBACl (sat.) and TBAP 0.5 M in chloroform in a separated compartment was directly immersed in the reaction cell. The working electrodes were DME and HMDE, the auxiliary electrode was a platinum wire.

2.6. Procedures

2.6.1. Extraction and polarography of Pb(II) benzoylacetate

A 1 ml portion of aqueous standard or sample solutions of Pb(II) was transferred into a 100 ml separating funnel, the pH of the solution was buffered with 10 ml of 0.1 M ammonia buffer at 9, at which the extraction of lead(II) benzoylacetate was complete, this solution was shaken with an equal volume of 0.01 M chloroform solution of benzoylacetone for 20 min on a mechanical shaker. The chloroform phase was separated and transferred into a polarographic cell and a required amount of supporting electrolyte (PP 0.75 + P 0.25 M) was added, the solution was deaerated for 20 min with the nitrogen gas (99.999) presaturated with chloroform. The polarograms were recorded by sweeping the potential from 0.4 to -0.6 V vs reference electrode (the potential range of electroactivity of Hg in chloroform is $+0.45$ – -0.70 V).

2.6.2. Anodic stripping voltammetry of Pb(II) benzoylacetate

A 10 ml portion of chloroform extract of 5×10^{-8} – 10^{-6} M Pb(II) benzoylacetate with 0.01 M benzoylacetone, obtained from the standard or sample solutions was transferred into an electrolysis cell and required amount of supporting electrolyte was added. The solution was deaerated by N_2 gas for 20 min. Metallic lead was deposited on a hanging mercury drop electrode at -0.5 V for 10 min, while stirring the solution. The amalgamated lead was stripped by differential pulse polarography by scanning of potential of the electrode between -0.5 and 0.0 V with scan rate of 5 mV s^{-1} and pulse amplitude of 50 mV .

2.6.3. Mineralization and anodic stripping voltammetry of free-lead gasoline and gas oil

An aliquot of the sample (2 ml) was transferred into a porcelain crucible and 1 ml of concentrated nitric acid (65%) was added. The mixture was heated on a hot plate at 90°C for about 15 min to form a viscous product, then the crucible was placed in a furnace at 300°C for 20 min. After cooling the crucible, the residue was taken with 5 ml water. Then lead(II) benzoylacetate was extracted into chloroform, as described, for pure lead(II). The standard addition procedure or calibration graph were used.

2.6.4. Spectrophotometric analysis of free-lead gasoline

An aliquot of the gasoline sample (2 ml) was shaken with 5 ml of 1 M aqueous solution of ICl [12] in a separating funnel for 2 min. The aqueous phase was separated and heated for 5 min to mineralize the organolead compounds, then a saturated solution of sodium sulfite was added until the aqueous phase become colourless. The mineralized Pb(II) was extracted by a 2.5% dithizone solution in chloroform. The absorbance was measured at 520 nm and the amount of Pb was determined via a calibration graph constructed by means of standard solutions of Pb(II) over a concentration range of 0 – 50 mg l^{-1} .

3. Results and discussion

3.1. Preliminary polarographic investigations.

Considering that the presence of β -diketones in chloroform do not restrict the potential range for mercury electrode and that Pb(II) may be extracted quantitatively into chloroform as benzoylacetates, we have first investigated the polarographic characteristics of lead(II) benzoylacetate in chloroform in the presence of two different supporting electrolytes.

In chloroform, in the presence of 0.5 M TBAP as supporting electrolyte, the lead(II) benzoylacetate did not reduce at mercury electrode, but with PP 0.75 + P 0.25 M merged as suitable electrolyte, the reduction of lead (II) benzoylacetate exhibited one cathodic wave with half-wave potential of -0.32 V. A plot of $\log[(i_d - i)/i]$ vs E for DC polarogram of lead(II) benzoylacetate gives a straight line with a slope of about 48 mV . A typical cyclic voltammogram monitored between 0.2 and -0.6 V is shown in Fig. 1. For all scan rates (20 – 2000 mV s^{-1}) one cathodic and corresponding anodic peaks were observed. The peak separation potential $\Delta E = E_p^a - E_p^c$ for scan rates less than 50 mV s^{-1} was 63 mV , the current

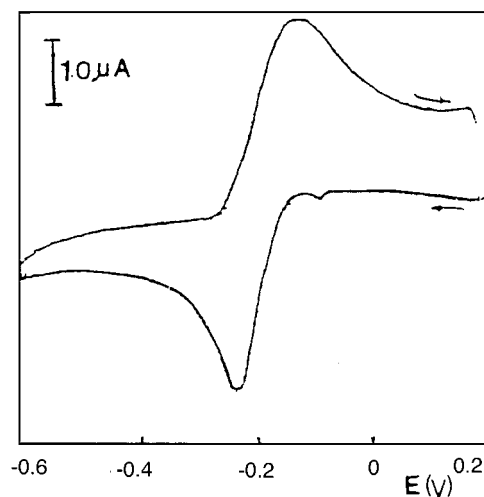


Fig. 1. Cyclic voltammograms of 1 mM Pb(II) benzoylacetate in the presence of 0.75 M PP/0.25 M P as supporting electrolyte, scan rate: 50 mV s^{-1} .

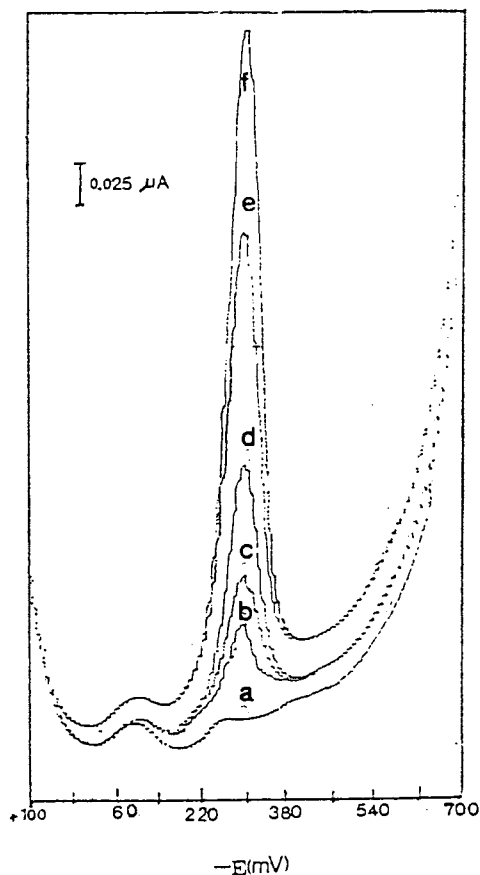


Fig. 2. Differential pulse polarograms of Pb(II) benzoylacetonate: (a) 0, (b) 5 μM , (c) 10 μM , (d) 20 μM , (e) 40 μM , (f) 60 μM in the presence of 0.75 M PP/0.25 M P as supporting electrolyte, scan rate: 5 mV s^{-1} . Pulse amplitude: 50 mV.

function ($i_p / V^{1/2}$) decreases with increasing scan rate. These confirmed that the reduction of Pb(II) benzoylacetonate was a two electron quasi-reversible process. On the other hand, the plot of i_p vs $V^{1/2}$ was linear, with a correlation coefficient better than 0.999, confirming the diffusion nature of the reduction current. The i_p^a/i_p^c ratio was about 1 for scan rate of 20–2000 mV s^{-1} . Differential pulse (DP) polarography presented well-defined peaks (Fig. 2) with E_p -0.31 V, very close to $E^{1/2}$. The calibration graph constructed with the aid of a 10^{-3} M Pb(II) benzoylacetonate solution in chloroform was linear over concentration range 5×10^{-6} – 10^{-4} M. The detection limit (LOD) of DP procedure ($\text{LOD} = y_B + 3S_{y/x}$) was suggested

5×10^{-7} M and the relative standard deviation for five replicate determinations of 2.5×10^{-5} M of Pb(II) was 1.2%.

3.2. Extraction efficiency of Pb(II) benzoylacetonate in chloroform

Quantitative extraction of Pb(II) benzoylacetonate from aqueous solution of pH 7–10, with a 0.1 M solution of benzoylacetonate in benzene was reported [10]. An extensive study showed that the Pb^{2+} ion may also be quantitatively extracted from a 0.1 M ammonia buffer solution of pH 8–9 by 0.01 M benzoylacetonate in chloroform. The optimum shaking time with a mechanical shaker was determined to be ~ 15 min. The average recovery of five replicate extractions of 10 ml 2×10^{-5} M aqueous solution of Pb^{2+} at the conditions mentioned above, was 98.5% ($\text{rsd} = 1.2\%$). The calibration graph, constructed by means of the chloroform extracts using various aqueous solutions of Pb^{2+} over concentration range 5×10^{-6} – 10^{-4} M, was linear. The slope (0.06 ± 0.008) was very close to that of calibration graph (0.062 ± 0.008) constructed by direct addition of Pb(II) benzoylacetonate in chloroform. This agreement confirmed the completeness of Pb(II) extraction into chloroform.

3.3. Anodic stripping voltammetry

On the basis of the results obtained from DP polarography of Pb(II) benzoylacetonate in chloroform, it can be concluded that the differential pulse anodic stripping voltammetry (DPASV) may be used for ultra-trace determinations of lead (10^{-7} – 10^{-10} M). The stripping voltammograms for lead deposited on the hanging mercury drop electrode (with the deposition potential and deposition duration of -0.5 V and 12 min, respectively), from the quiescent solutions of 4×10^{-7} – 10^{-6} M Pb(II) benzoylacetonate in the presence of 0.01 M benzoylacetonate and 0.75 M PP + 0.25 M P as supporting electrolyte, are shown in Fig. 3. In this experiment, the amalgamated lead is oxidized at -0.3 V followed by an unknown peak at -0.05 V. The peak at -0.05 V appeared to be a copper impurity, since it

increased in magnitude when Cu(II) was deliberately added to the solution. However, very sharp and reproducible lead stripping peaks were observed in all cases.

3.4. Effect of scan rate on the lead-stripping peak

On the basis of Randles-Sevcik equation, the anodic stripping peak current i_p increases with square root of scan rate $V^{1/2}$, while the charging current i_c increases with V . Therefore, an optimum scan rate providing a maximum 'analyt signal/residual current' ratio is desirable. For this purpose, the stripping voltammograms were recorded for the blank and 4×10^{-7} M Pb(II) benzoylacetate solutions with various electrode potential scan rates ranging from 2–50 mV s^{-1} . The deposition potential and deposition time were -0.5 V and 12 min, respectively.

On the basis of the results obtained, the maximum value of this ratio appeared at scan rate of 5 mV s^{-1} .

3.5. Effect of preconcentration time

Using three solutions of 0.1, 0.2 and 0.4 μM Pb(II) benzoylacetate, the effect of preconcentration time on lead stripping peak current has

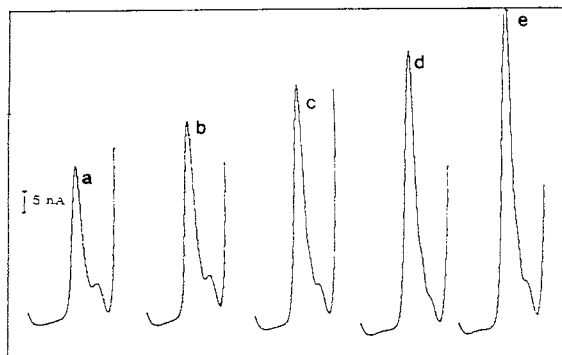


Fig. 3. Anodic stripping voltammograms at the hanging mercury drop electrode of Pb(II) benzoylacetate (a) 0.1 (b) 0.2 (c) 0.3 (d) 0.4 (e) 0.5 μM in the presence of 0.01 M benzoylacetone and 0.75 M PP/0.25 M P as supporting electrolyte, preconcentration potential was -0.5 V and preconcentration time was 10 min, scan rate: 5 mV s^{-1} , pulse amplitude: 50 mV.

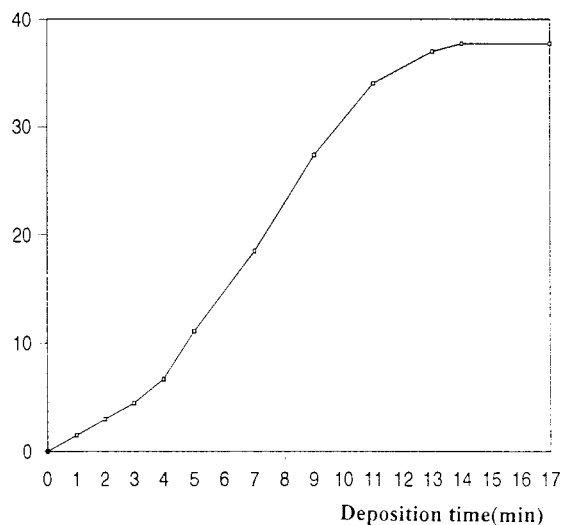


Fig. 4. Plot of average 'signal/noise' ratio of anodic stripping voltammograms of Pb vs deposition time, scan rate 5 mV s^{-1} . Deposition potential: -0.5 V, solutions concentration: 0.1, 0.2 and 0.4 μM of Pb(II) benzoylacetate.

also been studied. Preconcentration has been carried out at -0.5 V and the voltammograms have been simultaneously recorded for the blank and Pb(II) solutions, at a potential scan rate of 5 mV s^{-1} . The plot of average signal/noise ratio vs deposition time for the results obtained, is shown in Fig. 4. As seen in this figure, a preconcentration duration of 10 min may be suitable for this purpose.

3.6. Analytical performances

The calibration graph was constructed: (i) by direct addition of lead(II) benzoylacetate over concentration range 5×10^{-8} – 10^{-6} M in chloroform solution of 0.01 M benzoylacetone; and (ii) by means of chloroform extracts using the aqueous solutions of lead(II) nitrate over concentration range 5×10^{-8} – 10^{-6} M. The regression equations were $I(\mu\text{A}) = (0.013 \pm 0.004) + (0.015 \pm 0.0007) C$ (M) and $I(\mu\text{A}) = (0.0125 \pm 0.004) + (0.015 \pm 0.0007) C$ (M), respectively. These findings suggested that the two calibration graphs were nearly overlapped and therefore, the extraction efficiency of lead(II) benzoylacetate at low concentration range was $\sim 100\%$. The detection

limit of the method ($LOD = Y_B + 3S_{x/y}$) found to be 2.5×10^{-9} M of Pb(II). The standard deviation of three replicate determinations of 4×10^{-7} M lead(II) solution was $\sim 2\%$.

3.7. Interference study

Among the metal ions, Cd(II), Bi(III), Cu(II), Zn(II), Co(II), Ni(II), Mn(II), Ti(IV), Mo(VI), U(VI), La(III) and Be(II) are extractable with benzoylacetone in chloroform at pH 9 [10]. Cu(II), Bi(III), U(VI) and Mo(VI) seem to be electroreducible under the polarographic conditions for the determination of Pb(II) benzoylacetate in chloroform. We have demonstrated that the reduction potential of Cu(II) benzoylacetate is sufficiently different and did not interfere in the Pb(II) determination. We have also found that the presence of great amount of Mo(VI) and Bi(III) in aqueous solution of Pb(II) did not cause any serious interference. However U(VI) is undesirable [2], but natural occurrence of uranium in gasoline has not been reported. The presence of I⁻ ion in aqueous solution of Pb(II) masks it as PbI_4^{2-} and prevents the quantitative extraction of Pb(II) benzoylacetate into chloroform, therefore the mineralization of organolead compounds in petroleum product with ICl is undesirable.

3.8. Impurity and contamination effects

An extensive study in this area showed that a serious impurity problem appeared by benzoylacetone only (evaluated 5×10^{-8} M of Pb in voltammetric cell). This problem was solved by further purification of the commercial benzoylacetone and using its 0.01 M chloroform solution, instead of 0.1 M mentioned in Section 2.6.

3.9. Application to the analysis of gasoline and gas oil samples

The preliminary experiments showed that the alkyllead compounds are not reducible in chloroform in the polarographic conditions described above, therefore the mineralization of these compounds was required. The mineralization of organolead compounds in chloroform with a 1 M

iodine chloride (ICl) solution [11] in this solvent, seemed to be fast and suitable, but the experimental investigations showed that this procedure was unsuccessful.

Following a mineralization procedure in aqueous solution as described in [12], the alkyllead converted completely into an inorganic lead, the iodide ion formed in the solution however, was a interferent masking Pb(II) as PbI_4^{2-} and decreasing the extraction efficiency of lead(II) benzoylacetate into chloroform, therefore it was omitted in this work.

The mineralization of organolead compounds with nitric acid at convenient temperature and taking the residue in pure water [13] as described in Section 2, was found to be most suitable for the present extraction polarographic method in chloroform.

3.10. Optimization of mineralization temperature of gasoline

The ashing of gasoline–nitric acid mixture was performed at various temperature ranging from 200–600°C. Preceded by an ashing of gasoline–nitric acid mixture and solvent extraction of lead(II) benzoylacetate in chloroform, the pulse polarograms of Pb(II) were recorded and on the basis of the results, obtained the optimum temperature of 300°C.

Preceded by a mineralization process, as described above, the average recovery of lead (monitored by present extraction dp polarography) from five different tetraethyllead spiked free-lead gasoline samples ranging from 3×10^{-7} – 3×10^{-5} M was about 99%. The standard deviation in all cases was nearly 3% ($n = 3$).

3.11. Determination of lead in free-lead gasoline and gas oil

The free-lead gasoline and gas oil samples were mineralized according to procedure described in Section 2 and analyzed by anodic stripping voltammetry via a calibration graph. A typical stripping voltammogram is shown in Fig. 5 and the average amount of three replicate determinations are given in Table 1. The accuracy of the

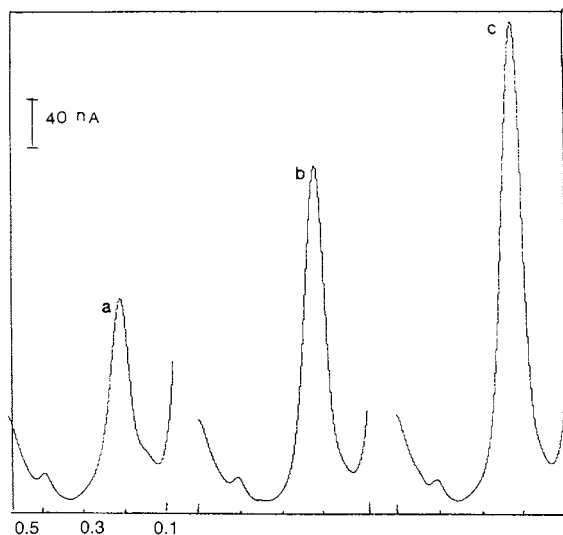


Fig. 5. Anodic stripping voltammograms of Pb for (a) 2 ml free-lead gasoline, mineralized at 300°C (b) *a* + 0.6 ml and (c) *a* + 1.2 ml of 5 μ M Pb(II) benzoylacetate. Experimental conditions as Fig. 4.

proposed method was investigated: (i) By parallel analysis of the sample with the standard spectrophotometric method of ASTM [12]; and (ii) by recovery study of spiked samples. The results obtained from these studies are also given in Table 1. As can be seen from the results in Table 1, the agreement between the lead amount obtained by two methods is good and the recovery of spiked tetraethyllead is acceptable. Since a standard method for the determination of lead in gas oil was not reported in the literature, the

accuracy of gas oil analysis was confirmed by recovery study of spiked samples (Table 1).

4. Conclusion

The results obtained from DC polarography and cyclic voltammetry revealed that the Pb(II) benzoylacetate reduced according to a two electron quasi-reversible process at about -0.3 V in the presence of 0.75 M PP + 0.25 M P as suitable supporting electrolyte in chloroform. The mass transfer is controlled by diffusion. The Pb(II) benzoylacetate is extractable in chloroform at buffered pH 9 and extraction efficiency was $> 98.5\%$. The determination of Pb(II) in extracted phases was carried out by differential pulse polarography, the limit of detection (LOD) found is 5×10^{-7} M.

Differential pulse anodic stripping voltammetry can be successfully used for the determination of trace-lead in chloroform as an organic solvent of very low permittivity, after quantitative extraction of lead in chloroform as Pb(II) benzoylacetate. The calibration graph is linear over concentration range 5×10^{-8} – 10^{-6} M of lead at optimized conditions. The limit of detection is relatively low and found to be 2.5×10^{-9} M. The proposed stripping method is selective, precise, sensitive and usable for ultra-trace lead determination in complex matrices such as petroleum products. The reliability of the method was established by parallel determination of lead against the spectrophotometric standard method.

Table 1
Determination of lead in free-lead gasoline and gas oil samples

Pb added (mg l^{-1})	Pb found (mg l^{-1}) \pm SD*	
Free lead sample	Stripping method	Spectrophotometric method
Gasoline	—	0.078 ± 0.002
Gasoline	0.100	0.098 ± 0.003
Gas oil	—	0.062 ± 0.001
Gas oil	0.062	0.060 ± 0.002

* Results based on three replicate determinations per sample

References

- [1] M.H. Pournaghi-Azar, R. Zargarian, *Anal. Chim. Acta* 328 (1996) 33.
- [2] M.H. Pournaghi-Azar, J. Ordoukhanian, *Talanta* 38 (1991) 1469.
- [3] Y. Nagaosa, K. Kobayashi, *Talanta* 31 (1984) 593.
- [4] S.M. Golabi, D. Nematollahi, *J. Pharm. Bioanal.* 10 (1992) 1053.
- [5] M.H. Pournaghi-Azar, S.M. Golabi, *Talanta* 35 (1988) 959.
- [6] T. Fujinaga, H.L. Lee, *Talanta* 24 (1977) 395.
- [7] D. Wilson, R.K. Webster, G.W.C. Milner, G.A. Barmett, A.A. Smales, *Anal. Chim. Acta* 23 (1960) 505.
- [8] G. Schulze, W. Frenzel, *Anal. Chim. Acta* 159 (1984) 95.
- [9] J.F. Coetzee, M.J. Ecoff, *Anal. Chim. Acta* 63 (1991) 975.
- [10] A.K. De, S.M. Khopkar, R.A. Chalmers, *Solvent Extraction of Metals*, Van Nostrand Reinhold, London.
- [11] *IP Standards for Petroleum and its Products Part I*, vol. 2, IP 270/77, Institute of Petroleum, London, 1985.
- [12] *ASTM Standard D-3116. 77, Part 5*, American society for testing and materials, Philadelphia, PA, 1981.
- [13] J.L. Guinon, R. Griman, *Analyst* 113 (1988) 613.

Direct determination of copper and zinc in cow milk, human milk and infant formula samples using electrothermal atomization atomic absorption spectrometry

N. Campillo, P. Viñas, I. López-García, M. Hernández-Córdoba *

Dpto. de Química Analítica, Facultad de Química, Universidad de Murcia, E-30071 Murcia, Spain

Received 28 May 1997; received in revised form 9 September 1997; accepted 9 September 1997

Abstract

Infant formula and powdered milk samples were suspended in a medium containing 20% ethanol, 0.65% nitric acid, 6% hydrogen peroxide and 0.1% ammonium dihydrogenphosphate and directly introduced in the electrothermal atomizer. Liquid milk samples were diluted with this suspension solution. The build-up of carbonaceous residues inside the atomizer was avoided by using a combination of hydrogen peroxide and nitric acid. Fast programs were used to simplify the heating cycles. Calibration was carried out using aqueous standards and the detection limits for copper and zinc were found to be 70 and 15 pg, respectively. The metal contents of several milk samples obtained by direct introduction of the samples agree with those obtained by means of a conventional procedure based on the total dissolution of the samples. The reliability of the methods was also confirmed by analyzing three certified reference materials. The free and protein binding fractions were measured by ultrafiltration membrane permeability of the milk samples. © 1998 Elsevier Science B.V. All rights reserved.

Keywords: Atomic absorption spectrometry; Copper; Milk; Zinc

1. Introduction

Milk is an important food in the human diet, and the main source of metals for infants and children. Milk is considered a rich source of some essential trace metals such as zinc, but it is poor in

copper. A large amount of zinc in a diet interferes with the copper absorption system, resulting in copper deficiency. Hence, zinc antagonizes copper absorption. Zinc and copper have been associated with cholesterol metabolism and the maintenance of cardiovascular integrity. Hypercholesterolemia due to copper deficiency has been observed in humans and in a variety of animal species [1]. The improved availability of zinc in human milk over cow milk for infants has been explained by a

* Corresponding author. Tel.: +34 68 307100/2177; fax: +34 68 364148; e-mail: hcordoba@fcu.um.es.

low-molecular-mass zinc-binding ligand [1] as well as by differences in protein composition. Cow milk has a low copper content and, therefore, infants provided solely with a milk diet may develop copper deficiency and anemia.

Electrothermal atomic absorption spectrometry (ETAAS) is a useful technique for the analysis of metals in milk and previous studies concerning determination of copper and zinc have been published [2–13]. However, such determinations are not without problems, since conventional acid-mineralization procedures are lengthy and there is a risk of contamination, which is particularly severe in the case of zinc. For this reason, some authors prefer to introduce the liquid samples directly into the electrothermal atomizer and, when dealing with powdered samples, to prepare a suspension [14,15], which is also analyzed without further treatment. Such procedures can also be problematic due to high background values and to the accumulation of carbonaceous residues inside the atomizer, both drawbacks being overcome by inclusion of an air or oxygen ashing step [16] in the heating program. Recently, it has been demonstrated [17–22] that the addition of hydrogen peroxide to the samples also alleviates these problems. The hydrogen peroxide decomposes during the heating cycle and the organic matter is partially destroyed with no apparent harmful effect on the pyrolytic graphite atomizers.

This paper describes procedures for the direct determination of copper and zinc in cow and human milk and infant formula samples using hydrogen peroxide as a chemical modifier. The removal of organic matter is very effective and allows fast-program methodology [23,24] to be used. The procedures, which were checked by analyzing three standard reference materials, are rapid and reliable, and were subsequently used to assess the fraction of the metal ions bound to milk proteins. For this purpose, various fractions of milk samples were separated using ultrafiltration membrane permeability, in which the solvents and solutes are forced through the membrane under centrifuge pressure while the movement of large molecules is restricted by the pore size [25].

2. Experimental

2.1. Instrumentation

A Perkin-Elmer Model 1100B atomic absorption spectrometer equipped with deuterium-arc background correction and a HGA-400 (Perkin-Elmer) graphite furnace atomizer were used. Pyrolytic graphite coated tubes (part number B013-5653) and pyrolytic graphite platforms (part number B012-1092) inserted into pyrolytic graphite coated tubes were obtained from Perkin-Elmer. Measurements were performed at 324.8 and 213.9 nm for copper and zinc, respectively, using hollow cathode lamps operated at 5 mA and bandwidths of 0.7 nm. Argon was used as the inert gas, the flow rate being 300 ml min⁻¹ during all stages, except during atomization, when the flow was stopped for copper or reduced to 150 ml min⁻¹ for zinc in order to adjust sensitivity. A Branson ultrasonic bath of 14 W constant power was used. Ultrafiltration of milk samples was carried out using a Centricon-SR3 filter system (3000 Da pore size) and an ultracentrifuge operated at 7500 × g.

2.2. Reagents

High-quality water, obtained using a Milli-Q system (Millipore), was used exclusively. Copper and zinc standard solutions (1000 µg ml⁻¹) were obtained from Panreac (Spain) and diluted as necessary to obtain working standards. High-quality ethanol (Riedel-deHaër), concentrated (65%) nitric acid (Merck), concentrated (30%) hydrogen peroxide (Fluka), concentrated acetic acid (Probus, Spain) and ammonium dihydrogenphosphate (Fluka) were also used.

2.3. Reference materials

Three reference materials were used. Non-fat milk powder SRM 1549 was obtained from NIST (USA); skim milk powder CRM 063 from BCR (Belgium) and whole milk powder 8435 from CLBRR (Canada).

Table 1
Heating furnace programs for copper and zinc

Step	Copper			Zinc		
	Temperature (°C)	Ramp (s)	Hold (s)	Temperature (°C)	Ramp (s)	Hold (s)
Dry	190	1	35	400	10	15
Atomize	2400	0	2 ^a	1600	0	3 ^b
Cleaning	2650	1	3	2600	1	3

^a Internal gas flow rate = 0 ml min⁻¹.

^b Internal gas flow rate = 150 ml min⁻¹.

2.4. Procedures

Infant formulas and powdered and liquid milk samples were purchased in specialized markets. Human milk samples were obtained from a volunteer. The samples of powdered milk were dried at 45°C. Homogeneous dispersions of dried milk were prepared by adding 25 ml of the suspension medium to an accurately weighed amount of sample (typical amounts ranged from 0.05 to 0.4 g for copper and from 12 to 50 mg for zinc). The suspensions were sonicated for a few minutes to ensure the absence of lumps and sampled while they were being continuously stirred with a magnetic stirrer. Liquid milk samples were diluted as necessary with the suspension medium and treated as mentioned for powdered milk. The suspension solution was prepared by mixing 0.1 g of ammonium dihydrogenphosphate, 20 ml of absolute ethanol, 20 ml of 30% hydrogen peroxide and 1 ml of 65% nitric acid in 100 ml deionised water, for both copper and zinc determinations. Aliquots of 20 µl were injected into the furnace. The heating programs given in Table 1 (where the quoted temperatures are values set on the HGA-400 power supply) were run and the background-corrected peak areas due to the analytes were obtained. Calibration was performed by injecting aqueous standards prepared in the suspension medium and using the same experimental conditions. Standard reference milk samples were analyzed in the same way.

The samples were previously analyzed for comparison purposes. Fractions of 0.5 ml or 0.1–0.5 g of liquid or powdered samples, respectively, were dried and then calcined at 450°C for 8 h. The

ashes were treated with 5 ml concentrated nitric acid and 2 ml concentrated hydrogen peroxide solution and heated to almost dryness; they were then diluted up to appropriate volumes with a solution containing 0.1% ammonium dihydrogenphosphate to analyze copper. A suitable dilution was used to analyze zinc by ETAAS.

2.5. Ultrafiltration of milk

A fraction of 2 ml milk was treated with 300 µl concentrated acetic acid, stirred and centrifuged at 3000 × *g* for 10 min. The two phases obtained were separated. The supernatant was filtered through a Centricon-SR3 filter system (3000 Da pore size) using an ultracentrifuge at 7500 × *g* for 1 h. The solid fraction remaining in the filter was resuspended with 2 ml suspension solution and sonicated for 5 min. Copper and zinc were measured in both the filtrated fraction (with proteins smaller than 3000 Da) and in the resuspended fraction (larger than 3000 Da). The metal contents in the fraction precipitated with acetic acid were determined by difference. The absence of membrane adsorption phenomena was studied using aqueous standards of Cu and Zn. No differences between the initial concentrations and the concentrations found in the ultrafiltrable were observed, thus discarding membrane adsorption. Contamination of the sample by the addition of acetic acid or by the micropartition process was evaluated by carrying out a blank using the suspension medium. This blank was repeated three times using different membranes and the results were reproducible.

3. Results and discussion

3.1. Optimization of the experimental conditions

Following the rules of analytical minimalism recently discussed by Halls [24], fast-program methodology, in which the conventional drying and ashing steps are replaced by a single modified drying step, was used throughout the work.

Preliminary experiments were carried out using 20 mg ml^{-1} suspensions prepared from a powdered milk sample in the presence of 0.65% nitric acid and 3% hydrogen peroxide. These experiments showed poor reproducibility, the relative standard deviation (R.S.D.) of copper being close to $\pm 20\%$. Consequently, to obtain a good dispersion and stabilization of the suspensions, the addition of different chemicals was tried. Addition of glycerol proved inadequate since abundant smoke was evolved during the atomization stage. Triton X-100 also proved problematic due to foam. Excellent results were obtained by adding ethanol to the suspensions. Fig. 1 shows that by increasing the ethanol percentage, the drying temperature could be increased without sputtering and, consequently, the hold time necessary for a totally dried sample to be obtained could be shortened and reproducibility improved due to a better homoge-

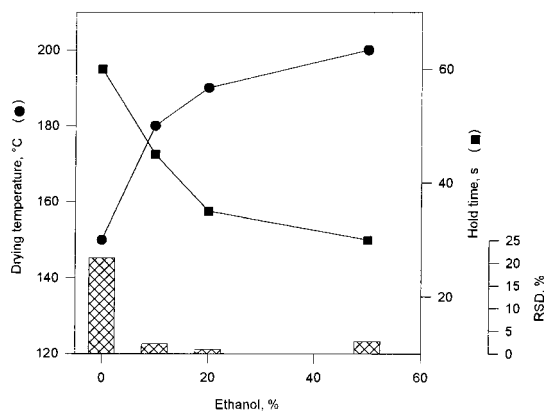


Fig. 1. Influence of ethanol percentage on the drying step (drying temperature and hold time) and the reproducibility of the analytical signal for copper. The bar graph represents the variation of the relative standard deviation for 10 identical injections.

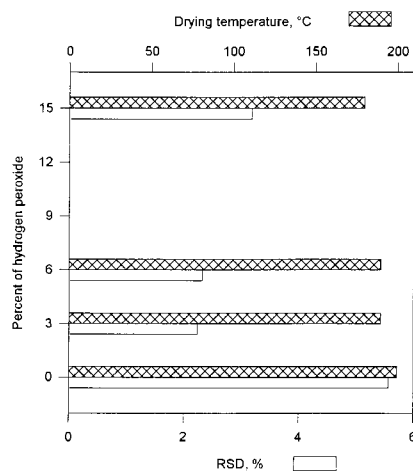


Fig. 2. Effect of the hydrogen peroxide percentage on the drying temperature and the relative standard deviation of 10 successive injections of a 2% liquid cow milk sample for copper atomization.

nization. The bar graph in Fig. 1 shows the R.S.D.s obtained for 10 successive injections of milk. Thus, 20% ethanol was added to the suspensions in all the other samples considered in this work. Similar results were obtained for zinc. To ensure zinc stabilization and to avoid a premature signal during atomization, 1 mg ml^{-1} ammonium dihydrogenphosphate was routinely incorporated to all the samples [26].

The hydrogen peroxide percentage was optimized for the atomization of copper using a 20 mg ml^{-1} suspension prepared from powdered cow milk in the presence of 0.65% nitric acid. Fig. 2 shows the influence of this variable on the reproducibility and the drying temperature. The R.S.D. for 10 successive injections considerably decreased in the presence of the oxidant. The drying temperature was also slightly affected by the presence of hydrogen peroxide and percentages higher than 15% produced bubbling, it proving necessary to decrease the temperature to avoid sputtering of the sample. A concentration of 6% hydrogen peroxide was finally selected, which avoided the deposition of carbonaceous residues inside the atomizer even after a high number of firings. The influence of the addition of nitric acid was assayed in the 0–0.65% range. There was no

modification in the analytical peaks whereas an important decrease in the background values was observed in the presence of the acid [21,22]. Thus, a 0.65% nitric acid was added. These problems were not so important for zinc because the suspensions were prepared with lower amounts of solid matter.

Preliminary experiments for copper determination were carried out by using both platform and wall atomization. No advantages were observed when platform atomization was used. In addition, this atomization mode required lengthy times for the complete profile to be obtained. Thus, wall atomization was finally selected for copper, well defined atomization profiles being obtained by programming 2 s for the holding time of this stage. Following the guidelines of fast-program methodology, the drying temperatures and holding times to be used in the modified drying stage were studied in an attempt to find the highest temperature possible which did not produced sputtering. The optimal drying temperature for copper determination was found to be 190°C. A holding time of 35 s allowed the sample to be dried completely and smoke to be removed before atomization. The atomization temperature was varied between 1500 and 2400°C as shown in Fig. 3 and the best profile was found at 2400°C.

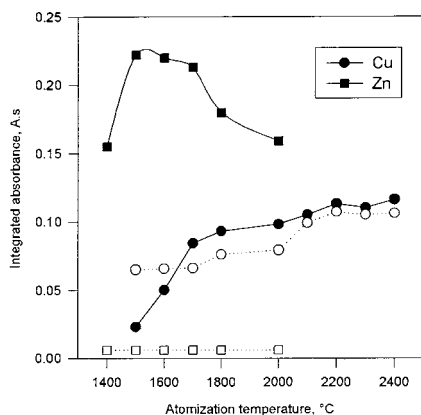


Fig. 3. Effect of atomization temperature on the integrated absorbance for the analytical signals for copper and zinc (—) and the backgrounds (---). Dilutions of 10 and 0.5% of liquid cow milk were used for copper and zinc atomization, respectively.

Although the analytical signal appeared very quickly, in non-isothermal conditions, both the reproducibility and results were excellent.

Platform atomization was used for zinc determination. The optimal drying temperature was found to be 400°C with a slow heating ramp (10 s) and a 15 s holding time. It is important to note that the temperatures and holding times here indicated are values programmed on the HGA-400 power supply although the actual temperature reached inside the atomizer and that programmed are not always identical [23]. So, these parameters must be taken as indicative rather than absolute and it is advisable to check and adapt them to the particular characteristics of the instrumentation used. The atomization temperature was varied in the 1400–2000°C range both for aqueous zinc and for milk samples, the maximum signal with a fully developed profile in 3 s being obtained at 1600°C. The optimized programs for copper and zinc are shown in Table 1.

It must be pointed out that the high sensitivity of zinc in ETAAS led to signals outside the linear response range being obtained, for which reason a small flow of argon was maintained during the atomization stage. This way of adjusting sensitivity can pose practical problems, since atomization takes place in a non-isothermal environment and, in addition, good reproducibility in the gas flow is necessary. Thus, the effect of the gas flow on both the slope of the calibration graph and the reproducibility of the analytical signal was studied. It was experimentally shown that a 150 ml min⁻¹ argon miniflow was suitable to obtain signals within the linear range when suspensions containing 0.5–2 mg ml⁻¹ powdered milk were used. In these conditions, the R.S.D. (10 measurements) was $\pm 3\%$.

3.2. Influence of the milk concentration, calibration and results

The variation of the atomic signal obtained for copper when varying the concentration of a powdered cow milk sample is shown in Fig. 4. Linearity was obtained up to 60 mg ml⁻¹. The precision of the method was demonstrated by repeated analyses calculating the R.S.D. for 10 replicate

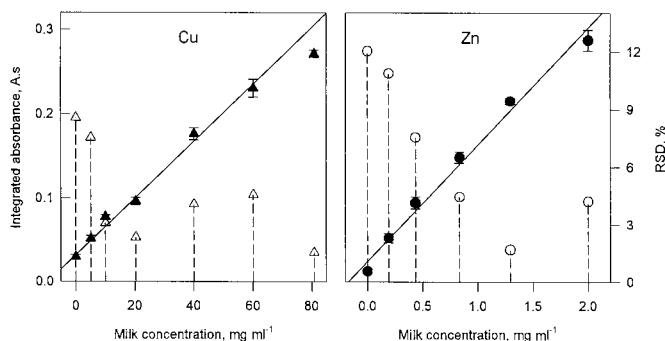


Fig. 4. Influence of the slurry concentration on the copper and zinc signals using a cow milk sample ($n = 10$). The points joined to the x -axis by broken lines indicate the relative standard deviations for 10 successive injections at each concentration level.

determinations at each concentration level. The bars indicate the standard deviations and the points joined to the x -axis by broken lines indicate the R.S.D. values. A similar study was carried out for zinc using suspensions prepared from powdered milk in the $0.5\text{--}2\text{ mg ml}^{-1}$ concentration range. Values of R.S.D. were between $\pm 10\%$ for very diluted suspensions and $\pm 3\text{--}4\%$ for more concentrated suspensions, linearity being obtained between 0.5 and 2.0 mg ml^{-1} . It is important to note that, because the sensitivity is in this case adjusted by using a miniflow condition, this concentration range must be taken as orientative and adapted to the characteristics of the instrumentation used.

The standard additions method was used to investigate the possible interference caused by the matrix. Each graph was constructed from five points and each point was measured three times. The slopes obtained with aqueous standards were similar (95% confidence level) to those obtained

for the standard additions graphs (Table 2). In addition, the analyte contents obtained by extrapolation of the graphs agreed with those obtained by a conventional procedure involving the complete dissolution of the samples. Thus, calibration with aqueous standards was valid. The detection limits (DL) calculated by 10 repeated injections of the blank and using the 3σ criterion were 70 and 15 μg for Cu and Zn, respectively. The limits of detection could also be estimated using the regression line obtained for aqueous standards or a regression line obtained from a plot of the analytical signal against the milk concentration for a representative sample. The regression line should provide a more accurate estimation of the blank than the single measured blank value [27]. Using this approach, the DL for Cu and Zn were, respectively, 94 and 55 μg when using the regression lines from aqueous standards. When using the maximum recommended suspension concentration, DL was 60 ng g^{-1} for copper in the 60 mg ml^{-1} powdered cow milk suspension and 400 ng g^{-1} for zinc in the 2 mg ml^{-1} powdered cow milk suspension. It must be noted that the high values obtained in the detection limits for zinc are a consequence of the adjustment of the sensitivity needed to obtain signals within the linear response range.

Table 3 shows the results obtained when analyzing different types of milk using the proposed suspension procedure and another based on the total calcination of the milk samples. As can be seen, the results are in good agreement (95%

Table 2
Slopes of the standard additions calibration graphs

Sample	Slope (mean \pm S.D., $n = 3$) ($\text{A s}^{-1}\text{ ng}^{-1}$)	
	Cu	Zn
Aqueous standards	0.53 ± 0.02	1.01 ± 0.02
Powdered cow milk	0.54 ± 0.03	1.016 ± 0.03
Infant formula	0.52 ± 0.03	1.02 ± 0.02
Maternal milk	0.52 ± 0.03	1.02 ± 0.02

Table 3
Results for the determination of copper and zinc in milk samples^a

Sample	Copper mean \pm S.D. ($n = 9$)		Zinc mean \pm S.D. ($n = 9$)	
	Suspension	Reference	Suspension	Reference
Infant powdered milk				
1	5.33 \pm 0.15	5.35 \pm 0.13	35.5 \pm 0.4	36.0 \pm 0.6
2	4.58 \pm 0.14	4.55 \pm 0.15	33.0 \pm 0.5	32.8 \pm 0.8
3	5.12 \pm 0.15	5.08 \pm 0.10	15 \pm 1	15.3 \pm 0.7
Powdered milk	0.37 \pm 0.01	0.371 \pm 0.015	23.5 \pm 0.3	23.7 \pm 0.6
Bottled cow milk	0.062 \pm 0.005	0.059 \pm 0.007	3.0 \pm 0.2	3.2 \pm 0.2
Maternal milk	0.283 \pm 0.004	0.278 \pm 0.009	1.12 \pm 0.05	1.01 \pm 0.08
Skim milk powder 063R	0.61 \pm 0.02	0.60 \pm 0.02 ^b	49.7 \pm 0.75	49.0 \pm 0.6 ^b
Whole milk powder 8435	0.462 \pm 0.025	0.46 \pm 0.08 ^b	28 \pm 2	28 \pm 3 ^b
Non-fat milk powder 1549	0.689 \pm 0.065	0.7 \pm 0.1 ^b	47 \pm 2	46 \pm 2 ^b

^a Results for liquid samples are given in $\mu\text{g ml}^{-1}$ and for powdered samples in $\mu\text{g g}^{-1}$.

^b Certified values.

confidence level). The highest amounts of copper and zinc appeared in the infant formula and powdered cow milk. The methods were validated using three certified reference milk samples. The results are also included in Table 3.

3.3. Distribution of both copper and zinc free and protein binding

The main cow milk proteins are casein, lactalbumin, lactoferrin and lactoglobulin, the most important being casein. When milk is acidified with acetic acid, casein flocculates while the whey proteins remain in solution [28]. A distribution of the content of both free metals and protein binding in the milk samples was carried out. The study of speciation of copper and zinc in milk hardly depends on the method used [7,8]. The samples selected were human milk (collected 1 month after the birth), powdered fortified infant formula (60% casein and 40% lactalbumin) and whole bottled cow milk. Experiments were carried out in triplicate. After precipitation of the casein by means of acetic acid, the supernatant was ultrafiltered through a 3000 Da membrane. The degree to which individual proteins are filtered through the membrane is normally a function both of their molecular size and of their concentration. The low-molecular-mass proteins are forced into the filtrate while the high-molecular-mass proteins only appear in the filtrate in trace amounts.

It was found (Fig. 5) that the fractions containing higher concentrations of both metals were those having a particle size lower than 3000 Da (probably free copper or zinc) for the maternal milk and infant formula samples. For the non-fat cow milk, the fraction showing higher concentrations was that with a particle size greater than 3000 Da (probably proteins which are non-precipitable with acetic acid). These different distributions are in accordance with the literature, which cites a low-molecular-mass zinc-binding ligand

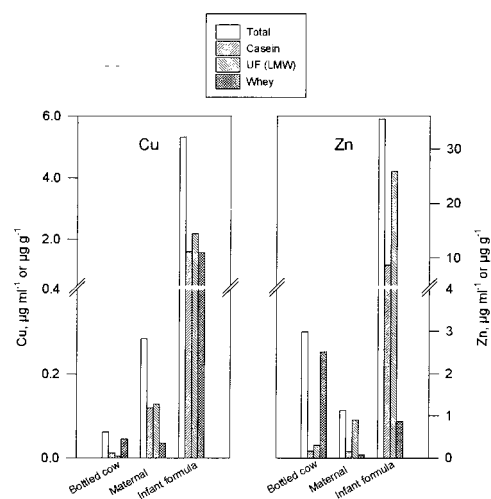


Fig. 5. Distribution of the free copper and zinc contents and protein binding in the milk samples ($n = 3$).

which facilitates zinc absorption as the explanation for the improved availability of zinc in human milk over cow milk, and the reported higher plasma zinc levels of breast-fed over bottle-fed infants [29]. It must be noted that the distribution of zinc and copper, as well as of other metals [30], is also influenced by the first step using acetic acid precipitation. Using acid could increase the ultrafiltrable part. Moreover, a prolonged storage at -20°C could also modify the distribution of copper and zinc.

4. Conclusion

The use of hydrogen peroxide is confirmed to be a useful way to decrease the background and to avoid the build-up of carbonaceous residues when concentrated milk suspensions are introduced into the electrothermal atomizer. The effect of such a modifier is so effective that fast-program methodology can be used. In this way, the sample manipulation is minimal and the risk of contamination is decreased.

Acknowledgements

The authors are grateful to the Spanish DGI-CYT (Project PB96-1100) and to Comunidad Autónoma de la Región de Murcia for financial support. N. Campillo holds a fellowship from Caja Murcia, Spain.

References

- [1] R.A. Jacob, in: N.W. Tietz (Ed.), *Textbook of Clinical Chemistry*, Saunders, Philadelphia, 1986.
- [2] Z.A. Khammas, J. Marshall, D. Littlejohn, J.M. Ottaway, S.C. Stephen, *Mikrochim. Acta* 1 (1985) 333.
- [3] J.L. Munro, J. Sneddon, *At. Spectrosc.* 8 (1987) 92.
- [4] D. Wagley, G. Schmiedel, E. Mainka, H.J. Ache, *At. Spectrosc.* 10 (1989) 106.
- [5] U.K. Kunwar, D. Littlejohn, D.J. Halls, *Talanta* 37 (1990) 555.
- [6] E. Coni, A. Stacchini, S. Caroli, P. Falconieri, *J. Anal. At. Spectrom.* 5 (1990) 581.
- [7] J. Arnaud, A. Favier, J. Alary, *J. Anal. At. Spectrom.* 6 (1991) 647.
- [8] J. Arnaud, A. Favier, *Analyst* 117 (1992) 1593.
- [9] J. Arnaud, M.C. Bouillet, J. Alary, A. Favier, *Food Chem.* 44 (1992) 213.
- [10] A.M. Aziz-Alrahman, *Anal. Lett.* 27 (1994) 411.
- [11] M.A. de la Fuente, G. Guerrero, M. Juarez, *At. Spectrosc.* 16 (1995) 219.
- [12] M.A. de la Fuente, G. Guerrero, M. Juarez, *J. Agric. Food Chem.* 43 (1995) 2406.
- [13] P. Bermejo-Barrera, R. Domínguez González, A. Bermejo-Barrera, *Fresenius' J. Anal. Chem.* 357 (1997) 457.
- [14] C. Bendicho, M.T.C. de Loos-Vollebregt, *J. Anal. At. Spectrom.* 6 (1991) 353.
- [15] N.J. Miller-Ihli, *Fresenius' J. Anal. Chem.* 345 (1993) 482.
- [16] S.C. Stephen, D. Littlejohn, J.M. Ottaway, *Analyst* 110 (1985) 1147.
- [17] P. Viñas, N. Campillo, I. López-García, M. Hernández-Córdoba, *Fresenius' J. Anal. Chem.* 349 (1994) 306.
- [18] P. Viñas, N. Campillo, I. López-García, M. Hernández-Córdoba, *Food Chem.* 50 (1994) 317.
- [19] P. Viñas, N. Campillo, I. López-García, M. Hernández-Córdoba, *Analyst* 119 (1994) 1119.
- [20] P. Viñas, N. Campillo, I. López-García, M. Hernández-Córdoba, *At. Spectrosc.* 16 (1995) 86.
- [21] P. Viñas, N. Campillo, I. López-García, M. Hernández-Córdoba, *Talanta* 42 (1995) 527.
- [22] I. López-García, P. Viñas, N. Campillo, M. Hernández-Córdoba, *J. Agric. Food Chem.* 44 (1996) 836.
- [23] D.J. Halls, *Analyst* 109 (1984) 1081.
- [24] D.J. Halls, *J. Anal. At. Spectrom.* 10 (1995) 169.
- [25] D.J. Holme, H. Peck, *Analytical Biochemistry*, 2nd ed., Longman, Essex, 1993.
- [26] D.L. Tsalev, V.I. Slaveykova, P.B. Mandjukov, *Spectrochim. Acta Rev.* 13 (1990) 225.
- [27] J.C. Miller, J.N. Miller, *Statistics for Analytical Chemistry*, 3rd ed., Ellis Horwood, Chichester, 1993.
- [28] H.D. Belitz, W. Grosch, *Química de los Alimentos*, Acribia, Zaragoza, 1985.
- [29] P.J. Aggett, J.T. Harries, *Arch. Dis. Child.* 54 (1979) 909.
- [30] P. Brätter, B. Gercken, U. Rösick, A. Tomiak, in: P. Brätter, P. Schramel (Eds.), *Trace Elements in Analytical Chemistry, Medicine and Biology*, de Gruyter, Berlin, 1988.

Simultaneous voltammetric determination of toxic metals in sediments

Clinio Locatelli *, Giancarlo Torsi

Department of Chemistry 'G. Ciamician', University of Bologna, Via F. Selmi 2, I-40126 Bologna, Italy

Received 11 June 1997; received in revised form 9 September 1997; accepted 9 September 1997

Abstract

Voltammetric methods are very suitable, versatile and rapid techniques for the simultaneous metal determination in complex matrices. The work, regarding the determination of As(III), Se(IV) and Mn(II), is a very interesting example of the possibility for simultaneously determining each single element in real samples in a wide range of concentration ratios. The differential pulse (DPV) measurements were carried out using a conventional three-electrode cell, while ammonia–ammonium chloride buffer (pH 9.6) was employed as the supporting electrolyte. The analytical procedure was verified by the analyses of standard reference materials: estuarine sediment BCR-CRM 277 and river sediment BCR-CRM 320. Precision and accuracy, expressed as relative S.D. and relative error, respectively, were in all cases of the order of 3–5%, while the detection limit for each element was around 10^{-8} M. The standard addition technique improved the resolution of the voltammetric method, even in the case of very high element concentration ratios. © 1998 Elsevier Science B.V. All rights reserved.

Keywords: Toxic metals; Sediments; Simultaneous determination; Voltammetry

1. Introduction

The simultaneous determination of several elements at trace and ultratrace level concentration in real matrices is one of the main aims of an analytical procedure, which however must always have both good selectivity and very high sensitivity.

The accumulation of toxic and persistent substances in the environment continuously increases owing to anthropogenic activities. Particular at-

tention is being paid to the presence of heavy metals, because of their irreversible effects on man [1]. In fact such elements tend to concentrate in all aquatic environmental matrices [2,3], biota and sediment, and for this reason they are present in the aquatic food chain, becoming dangerous for humans too, as a consequence of the consumption of marine products.

In metal determination, several techniques are employed such as neutron activation analysis, atomic absorption spectrometry, atomic emission spectrometry with inductively coupled plasma excitation, and X-ray fluorescence. Usually such techniques need enrichment steps and, further-

* Corresponding author. Tel.: + 39 51 259534; fax: + 39 51 259456.

more, as regards selectivity and sensitivity, often favour only one of these two aspects. For these reasons, the voltammetric techniques are shown to be very suitable, versatile and rapid for multi-component determinations, having good selectivity and sensitivity without requiring metal enrichments before the analytical measurements [4–6].

In previous studies [7,8] sensitive and selective voltammetric methods were employed for the simultaneous determination of various elements in real matrices. The present study, regarding the simultaneous determination of arsenic(III), selenium(IV) and manganese(II), is the continuation of that endeavour. In fact the problem of selenium(IV) and arsenic(III) determination at trace level [9] has received much attention as a consequence of the biological importance of the former, in fact selenium(IV) is an essential nutrient at trace level, but toxic in excess [10,11]. Frequently they are simultaneously present in several matrices together with manganese(II), but such a simultaneous presence produces effects on the electrochemical behaviour of both elements [12]. Furthermore manganese(II) is an essential micronutrient: in fact it is very important in various biochemical cycles regarding man, animals and plants, and it is present in a great deal of inorganic matrices, in which arsenic(III) and selenium(IV) are also almost always present.

Adsorption stripping voltammetry was proposed for the determination of manganese(II) in the presence of several interferences [13] and in real samples [14]. Differential pulse anodic stripping voltammetry was also employed successfully for determining manganese(II) in natural water [15–17] and sea water [18,19].

Lastly, manganese(II) was also determined in real matrices by a potentiometric stripping technique [20], taking into account either interference problems [21] or batch and flow procedures [22–24].

For this reason it seems to be interesting to set up a new selective and sensitive analytical procedure for simultaneously determining arsenic(III), selenium(IV) and manganese(II) in the presence of each other in a wide range of concentration ratios in real samples, employing differential pulse

voltammetry (DPV) as the voltammetric technique.

2. Experimental

2.1. Apparatus

Voltammetric measurements were carried out with an AMEL Mod. 433 employing, as the working electrode, a hanging mercury drop electrode (HMDE), consisting of a glass capillary having an internal diameter of 0.1 mm and a cone-shaped tip. An Ag/AgCl, KCl sat. electrode and a platinum wire were used as the reference and the auxiliary electrode, respectively. The voltammetric cell was thermostated at $20.0 \pm 0.5^\circ\text{C}$. The solutions were deaerated with pure nitrogen for 5 min prior to measurements, while a nitrogen blanket was maintained above the solution during the analysis. The solutions were deaerated for 1 min after each standard addition.

2.2. Reagents and reference solutions

All solutions were prepared with deionized water (Millipore, Milli-Q). Suprapure grade acids, ammonia and sodium hydroxide were used. Ammonia–ammonium chloride buffer solution (pH 9.6) was prepared by mixing an appropriate amount of hydrochloric acid and ammonia solu-

Table 1
Experimental conditions for the determination of As(III), Se(IV) and Mn(II) by differential pulse voltammetry (DPV)

Instrumental parameters	
E_i	–1.050
ΔE	50
dE/dt	10
τ	0.065
ν	0.250

Supporting electrolyte: ammonia–ammonium chloride buffer (pH 9.6). Experimental peak potentials E_p (V/Ag, AgCl, KCl sat.): -1.350 ± 0.005 [As(III)]; -1.445 ± 0.005 [Se(IV)]; -1.595 ± 0.005 [Mn(II)].

E_i , initial potential (V/SCE); ΔE , pulse amplitude superposed (mV); dE/dt , potential scan rate (mV s^{-1}); τ , pulse duration (s); ν , pulse repetition (s).

Table 2
Analytical calibration functions^a and relative mono and bivariate analysis

	As(III)	Se(IV)	Mn(II)
Calibration functions of each single element	$I_p = (0.01 \pm 0.02) + (2.13 \pm 0.07) \times 10^6 c,$ $r = 0.9991^b, s_r = 2.9\%^c,$ D.L. = 4.69×10^{-9} M ^d	$I_p = (0.02 \pm 0.02) + (7.75 \pm 0.10) \times 10^5 c,$ $r = 0.9993, s_r = 3.2\%,$ D.L. = 1.29×10^{-8} M	$I_p = (0.01 \pm 0.01) + (9.69 \pm 0.09) \times 10^5 c,$ $r = 0.9991, s_r = 3.4\%,$ D.L. = 1.03×10^{-8} M
Monovariate analysis ^c	$I_p = (0.01 \pm 0.01) + (2.06 \pm 0.09) \times 10^6 c,$ $r = 0.9996, s_r = 2.1\%,$ $e = -3.3, \text{D.L.} = 4.85 \times 10^{-9}$ M	$I_p = (0.01 \pm 0.02) + (7.58 \pm 0.10) \times 10^5 c,$ $r = 0.9990, s_r = 3.5\%, e = -2.2,$ D.L. = 1.32×10^{-8} M	$I_p = (0.01 \pm 0.02) + (9.90 \pm 0.09) \times 10^5 c,$ $r = 0.9988, s_r = 4.9\%, e = +2.2,$ D.L. = 1.01×10^{-8} M
Bivariate analysis ^c	$I_p = (0.01 \pm 0.01) + (2.05 \pm 0.11) \times 10^6 c_{\text{As}} + (6.9 \pm 0.2) \times 10 c_{\text{Se}},$ $r = 0.9992, s_r = 2.8\%,$ $e = -3.8\%,$ D.L. = 4.88×10^{-9} M	$I_p = (0.01 \pm 0.01) + (7.49 \pm 0.14) \times 10^5 c_{\text{Se}} + (2.3 \pm 0.3) \times 10 c_{\text{As}},$ $r = 0.9989, s_r = 4.8\%, e = -3.4\%,$ D.L. = 1.34×10^{-8} M $I_p = (0.01 \pm 0.01) + (7.41 \pm 0.09) \times 10^5 c_{\text{Se}} + (9.6 \pm 0.6) \times 10 c_{\text{Mn}},$ $r = 0.9990, s_r = 4.5\%,$ $e = -4.4\%,$ D.L. = 1.35×10^{-8} M	$I_p = (0.01 \pm 0.02) + (9.99 \pm 0.15) \times 10^5 c_{\text{Mn}} + (7.6 \pm 0.8) \times 10 c_{\text{Se}},$ $r = 0.9989, s_r = 3.9\%, e = +3.1\%,$ D.L. = 1.00×10^{-8} M

^a The errors correspond to a probability of 95%; I_p , peak current (μA); c , concentration of the electroactive species (M).

^b r , correlation coefficient.

^c s_r , mean residual S.D.

^d D.L., limit of detection, expressed according to IUPAC [28] and corresponds to a probability of 99%.

^e In monovariate analysis interferences from neighbouring elements are neglected; it is considered, however, in bivariate analysis [25–27].

tions. Aqueous stock solutions of arsenic(III), selenium(IV) and manganese(II) were prepared by dilution of the respective standard 1000 mg l⁻¹ (BDH, UK) solutions. The Teflon voltammetric cell was rinsed every day with suprapure concentrated nitric acid in order to prevent any contamination. Estuarine sediment BCR-CRM 277 and river sediment BCR-CRM 320 were chosen as standard reference materials for testing the accuracy and precision of the analytical procedure.

3. Results and discussion

3.1. Aqueous reference solutions

Prior to the analysis of the standard reference materials, a preliminary study was carried out employing aqueous reference solutions. The experimental conditions are reported in Table 1.

The standard addition method was used for the determination of the element analytical calibration functions (Table 2). The correlation coefficient was found to be satisfactory in all cases, while the precision of the technique, expressed in terms of the residual S.D. was good (s_r smaller than 5%). Table 2 also reports the detection limits for each element.

The simultaneous determination of arsenic(III), selenium(IV) and manganese(II) was studied in a large range of concentration ratios of the components. More precisely, employing the experimental conditions in Table 1, the element concentration ratios, within which each single element could be determined without mutual interference, were investigated. To a fixed, but very small concentration of the element of interest, standard additions of the interfering element were added in such a way as to change their concentration ratios. The peak current values of the former element were

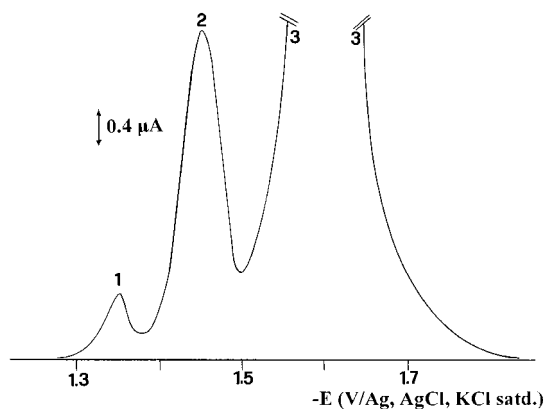


Fig. 1. Differential pulse voltammogram of a mixture of As(III), Se(IV) and Mn(II) in ammonia–ammonium chloride buffer solution (pH 9.6) as supporting electrolyte. Peak 1, As(III); peak 2, Se(IV); peak 3, Mn(II). Concentrations: 2.6×10^{-7} M [As(III)]; 4.2×10^{-6} M [Se(IV)]; 6.6×10^{-6} M [Mn(II)]. For experimental conditions see Table 1.

then compared to those determined by using the analytical calibration function of the individual element (Table 2) and the relative errors were calculated.

The determination of the single metals is possible, within a maximum error of 5%, in the concentration ranges $49:1 > c_{\text{Se}}:c_{\text{As}} > 1:58$ and $77:1 > c_{\text{Se}}:c_{\text{Mn}} > 1:69$. Such concentration ratios have been confirmed also by mono- and bivariate [25–27] analysis. In all cases, within the considered concentration ratios interval, the slopes of the statistical functions were practically equal to

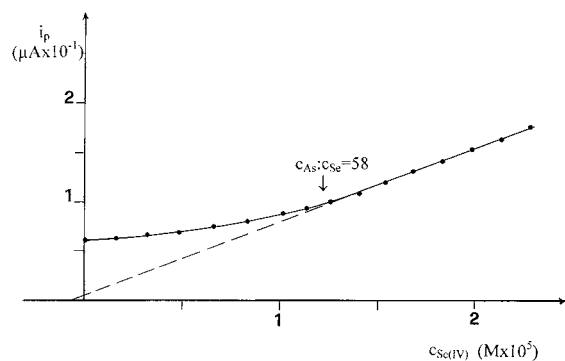


Fig. 2. Determination of 4.90×10^{-7} M Se(IV) in the presence of 6.96×10^{-4} M As(III) (concentration ratio $c_{\text{As}}:c_{\text{Se}} = 1420$). For experimental conditions see Table 1.

the analytical calibration function of the single element, and, moreover, the slope of the interfering element (bivariate analysis) was negligible (Table 2), thus indicating the non-interference between neighbouring species. Also, if the peak potential differences are of the order of 100 mV, the three metals, in the interval concentration ratios above, show well defined peaks. A typical voltammogram is shown in Fig. 1.

However the interesting aspect of this study is in regards to the determination of the metal with the lowest concentration and an unfavourable concentration ratio to the interferent species, that is outside the concentration ratios interval where the regression function obtained from bivariate analysis of the data was valid.

In this situation, bringing the concentration ratio within the interval valid for bivariate analysis by appropriate addition of the standard solution of the metal with the lowest concentration was enough to determine the metal itself. In fact, the I_p versus concentration plots showed a non linear behaviour. A linear section was obtained when the concentration ratios attain values within the validity of the bivariate analysis. An extrapolation of this linear section permitted the evaluation of the metal content in the mixture with acceptable accuracy. For example, Fig. 2 shows the fitting of the experimental data for the determination of selenium(IV) in the presence of a very high arsenic(III) concentration. The limit within which linearity prevails was well defined and statistically evaluated according to the method of Liteanu et al. [29] using the *t*-test criteria.

3.2. Standard reference materials

Once set up on the aqueous reference solutions, the method was transferred to the standard reference materials, in order to confirm and verify the applicability of the analytical procedure and to determine its accuracy and precision.

Estuarine Sediment BCR-CRM 277 and River Sediment BCR-CRM 320 were prepared as follows. Approximately 1.0 g, weighed accurately in a pyrex digestion tube, was dissolved in 15 ml 1:1 diluted 69% (m/m) nitric acid. The tube was inserted into the cold home-made block digester,

Table 3
Analytical sensitivities ($\mu\text{A M}^{-1}$) and merits of the analytical calibration functions in the standard reference materials^a

Element	Estuarine Sediment BCR-CRM 277	River Sediment BCR-CRM 320	Analytical calibration function ^b
As(III)	$(2.24 \pm 0.6) \times 10^6$, $r = 0.9990$, $s_r = 3.7\%$, $e = +5.2\%$, D.L. = 4.49×10^{-9} M	$(2.23 \pm 0.5) \times 10^6$, $r = 0.9989$, $s_r = 3.9\%$, $e = +4.7\%$, D.L. = 4.48×10^{-9} M	$(2.13 \pm 0.07) \times 10^6$, $r = 0.9991$, $s_r = 2.9\%$, D.L. = 4.69×10^{-9} M
Se(IV)	$(7.46 \pm 0.21) \times 10^5$, $r = 0.9991$, $s_r = 3.0\%$, $e = -3.7\%$, D.L. = 1.34×10^{-8} M	$(7.47 \pm 0.23) \times 10^5$, $r = 0.9989$, $s_r = 3.0\%$, $e = -3.6\%$, D.L. = 1.34×10^{-8} M	$(7.75 \pm 0.10) \times 10^5$, $r = 0.9993$, $s_r = 3.2\%$, D.L. = 1.29×10^{-8} M
Mn(II)	$(9.93 \pm 0.27) \times 10^5$, $r = 0.9993$, $s_r = 2.6\%$, $e = +2.5\%$, D.L. = 1.01×10^{-8} M	$(9.89 \pm 0.29) \times 10^5$, $r = 0.9990$, $s_r = 3.0\%$, $e = +2.1\%$, D.L. = 1.02×10^{-8} M	$(9.69 \pm 0.09) \times 10^5$, $r = 0.9991$, $s_r = 3.4\%$, D.L. = 1.03×10^{-8} M

^a For r , s_r , e and D.L. see footnote in Table 2.

^b See Table 2.

which gradually increased the temperature up to 125°C and kept it there for all the mineralization time. A further two aliquots of concentrated nitric acid were added: 10 ml after 15 min and 5 ml after 30 min. At the end (after 45 min), 10 ml of 37% (m/m) hydrochloric acid were added, keeping the temperature at 125°C for a further 15 min. After light cooling, the solution was filtered through a Whatman No. 541 filter paper, evaporated almost to dryness, and then, again after cooling, the soluble salts were dissolved in 25.0 ml ammonia–ammonium buffer solution (pH 9.6).

The solutions were analyzed under the experimental conditions listed in Table 1. Table 3 shows the slopes and merits of the analytical calibration functions calculated in the standard reference materials for each element together with those determined in the aqueous reference solutions (Table 2). Their comparison emphasizes that, in all cases, no matrix interference was present, not showing analytical sensitivities of significant differences at the 5% error level. Furthermore, problems of possible hydrolysis of iron ions, present at a very low concentration level in the digested solution, were not found experimentally during the voltammetric measurements.

For both standard reference materials, the arsenic(III) and manganese(II) determinations (being the elements with higher concentrations) were possible by employing the respective calibration curves (Table 2).

On the contrary, the selenium(IV) determination was very difficult in both standard reference materials since the concentration ratios were $c_{\text{Mn}}:c_{\text{Se}} > 69$ in both cases ($c_{\text{Mn}}:c_{\text{Se}} = 1.6 \times 10^3:2.04 = 784.3$ for Estuarine Sediment BCR-CRM 277 and $c_{\text{Mn}}:c_{\text{Se}} = 0.8 \times 10^3:0.214 = 3738.3$ for River Sediment BCR-CRM 320) and $c_{\text{As}}:c_{\text{Se}} > 58$ in the case of the River Sediment BCR-CRM 320 ($c_{\text{As}}:c_{\text{Se}} = 76.7:0.214 = 358.4$). For this reason, being outside the non-interference concentration ratio intervals, selenium(IV) has been determined employing the standard addition method, extrapolating the linear section of the I_p versus metal concentration curve. The experimental data fall, at the 95% confidence level, in the interval of the certified values for each element of the standard reference materials (Table 4).

The precision, expressed as relative S.D., and accuracy, expressed as relative error, were good in all cases, thus confirming the validity of the proposed method.

3.3. Practical application

The analytical procedure, set up on the standard reference materials, was transferred to real samples: sediments sampled in the Marecchia River (Rimini, Italy), in the river-bed (Verucchio zone) and in the estuary (Rimini zone).

The sampling (May and October, 1996) was performed by means of a plexiglass device. Single samples of superficial sediment (height 5 cm) were

Table 4
Analytical results obtained in the standard reference materials^a

		Estuarine Sediment BCR-CRM 277	River Sediment BCR-CRM 320
As(III)	Certified (mg kg ⁻¹)	48 ± 2	77 ± 3
	Determined (mg kg ⁻¹)	46 ± 2	80 ± 4
	<i>e</i> (%) ^b	-4.1	+3.9
	R.S.D. (%) ^b	2.3	3.7
Se(IV)	Certified (mg kg ⁻¹)	2.0 ± 0.2	0.21 ± 0.03
	Determined (mg kg ⁻¹)	2.0 ± 0.1	0.20 ± 0.02
	<i>e</i> (%)	0	-4.8
	R.S.D. (%)	3.2	5.2
Mn(II)	Certified (mg kg ⁻¹)	1.6 × 10 ³	0.80 × 10 ³
	Determined (mg kg ⁻¹)	1.7 × 10 ³	0.75 × 10 ³
	<i>e</i> (%)	+6.3	-6.3
	R.S.D. (%)	4.1	5.0

^a Number of samples 5

^b *e*, relative error; R.S.D., relative S.D.

drawn out and put in polyethylene bottles, previously washed with a diluted 1:1 suprapure HNO₃ solution for 48 h, in order to avoid any contamination. The sample was dried at 60°C for 48 h and then passed through a 40 mesh sieve to eliminate coarse material and successively through a second 150 mesh sieve, and finally powdered by means of a corundum ball mill. The sediments were then mineralized with the HNO₃-HCl acidic mixture, following the same digestion procedure employed in the case of the standard reference materials.

The element concentration ratios, in almost all cases, were higher than the interference values ($c_{As}:c_{Se} = 58$ and $c_{Mn}:c_{Se} = 69$), notwithstanding this the metal analytical determinations have all been carried out employing the same standard

addition procedure described above (Table 5).

Also, though the environmental aspects are beyond the aim of this study, a comment can be made. Table 5 shows that the concentrations of the three elements change according either to the sampling time or the sampling site: higher in autumn, after the winter and spring floods followed by the summer dry weather, and in the vicinity of the estuary. However the concentrations in Table 5, if compared with those found in the sediments sampled in different ecosystems and with the native concentration level of each element [30], show substantial agreement, so indicating that, in the investigated area, no manifest pollution load seems to be present.

In conclusion, the present study confirms once more that the voltammetric techniques, together

Table 5
Determination of As(III), Se(IV) and Mn(II) in the superficial sediments (0–5 cm) sampled in the Marecchia River (Rimini, Italy)^a

Sampling Time	May, 1996		October, 1996	
	Riverbed	Estuary	Riverbed	Estuary
As(III)	24 ± 1, <i>s_r</i> = 4.5%	37 ± 2, <i>s_r</i> = 4.8%	23 ± 1, <i>s_r</i> = 5.2	49 ± 2, <i>s_r</i> = 4.3%
Se(IV)	1.8 ± 0.1, <i>s_r</i> = 4.5%	2.6 ± 0.1, <i>s_r</i> = 4.2%	1.7 ± 0.1, <i>s_r</i> = 3.6%	2.9 ± 0.2, <i>s_r</i> = 5.2%
Mn(II)	(0.69 ± 0.03) × 10 ³ , <i>s_r</i> = 4.3%	(0.93 ± 0.04) × 10 ³ , <i>s_r</i> = 4.3%	(0.73 ± 0.04) × 10 ³ , <i>s_r</i> = 5.5%	(1.02 ± 0.03) × 10 ³ , <i>s_r</i> = 2.8%

^a Concentration: mg kg⁻¹. The residual S.D. *s_r* is determined on 5 independent measurements.

with the appropriate choice of supporting electrolyte and the standard addition method, have been shown to be a sensitive and selective analytical procedure, especially suitable for multicomponent element determination in complex real samples (sediments in the present case).

Acknowledgements

The authors wish to thank Dr Leonardo Ronchini for his cooperation. The work was supported by Funds for Selected Research Topics of the University of Bologna (Italy).

References

- [1] K. Honda, H. Sahrul, H. Hidaka, R. Tatsukawa, *Agric. Biol. Chem.* 47 (1983) 2521.
- [2] P. Chapman, G. Romberg, G. Vigers, *J. Water Pollut. Control Fed.* 54 (1982) 292.
- [3] G.P. Thomas, L.C. Goldstone, *Int. Lab.* 24 (1994) 13.
- [4] A.M. Bond, *Modern Polarographic Methods in Analytical Chemistry*, Marcel Dekker, New York, 1980.
- [5] Kh.Z. Brainina, E. Neyman, *Electroanalytical Stripping Methods*, Wiley, New York, 1993.
- [6] J. Wang, *Stripping Analysis—Principles, Instrumentation and Applications*, VCH, Deerfield Beach, FL, 1985.
- [7] F. Fagioli, C. Locatelli, S. Landi, R. Vecchiotti, *Electroanalysis* 1 (1989) 449.
- [8] C. Locatelli, F. Fagioli, T. Garai, *Anal. Chem.* 63 (1991) 1409.
- [9] S. Caroli, *Element Speciation in Bioinorganic Chemistry*, chap. 12 and 13, Wiley, New York, 1996.
- [10] R.W. Andrews, D.C. Johnson, *Anal. Chem.* 47 (1975) 294.
- [11] R.A. Zingaro, W.C. Cooper, *Selenium*, Van Nostrand Reinhold, New York, 1974, p. 594.
- [12] W. Holak, *Anal. Chem.* 52 (1980) 2189.
- [13] J. Wang, J.S. Mahmoud, *Anal. Chim. Acta* 182 (1986) 147.
- [14] L. Wang, C. Ma, X. Zhang, J. Wang, *Anal. Lett.* 26 (8) (1993) 1711.
- [15] M.P. Colombini, R. Fuoco, *Talanta* 30 (1983) 901.
- [16] D. Kalavská, *Int. J. Environ. Anal. Chem.* 45 (1991) 159.
- [17] V. Stara, M. Kapanica, *Electroanalysis* 5 (7) (1993) 595.
- [18] R.J. O'Halloran, H. Blutstein, *J. Electroanal. Chem.* 125 (1981) 261.
- [19] R.J. O'Halloran, *Anal. Chim. Acta* 140 (1982) 51.
- [20] J.K. Christensen, L. Kryger, *Anal. Chim. Acta* 118 (1980) 53.
- [21] Y. Zhang, K. Jiao, C. Liu, X. Liu, *Anal. Chim. Acta* 282 (1993) 125.
- [22] H. Eskilsson, D.R. Turner, *Anal. Chim. Acta* 161 (1984) 293.
- [23] M. Betti, L. Almestrand, D. Jagner, L. Renman, *Ann. Chim. (Rome)* 82 (1992) 339.
- [24] E. Beinrohr, P. Csemi, F.J. Rojas, H. Hofbauerova, *Analyst* 119 (1994) 1355.
- [25] A. Hald, *Statistical Theory with Engineering Applications*, Wiley, London, 1952.
- [26] H.L. Youmans, *Statistics for Chemistry*, Charles E. Merrill, Columbus, OH, 1973.
- [27] F. Fagioli, T. Garai, J. Devay, *Ann. Chim. (Rome)* 64 (1974) 633.
- [28] IUPAC, Analytical Chemistry Division, *Spectrochim. Acta B* 33 (1978) 219.
- [29] C. Liteanu, I.C. Popescu, E. Hopirtean, *Anal. Chem.* 48 (1976) 2010.
- [30] E. Merian, *Metals and Their Compounds in the Environment—Occurrence, Analysis and Biological Relevance*, VCH, Weinheim, Germany, 1991.

Simultaneous determination of arsenic, antimony, selenium and tin by gas phase molecular absorption spectrometry after two step hydride generation and preconcentration in a cold trap system

Susana Cabredo ^a, Javier Galbán ^{b,*}, Jesús Sanz ^a

^a *Chemistry Department, Analytical Chemistry Section, University of La Rioja, Logroño-26001, Spain*

^b *Analytical Chemistry Department, Faculty of Sciences, University of Zaragoza, Zaragoza-50009, Spain*

Received 8 July 1997; received in revised form 9 September 1997; accepted 9 September 1997

Abstract

A cold trap system for the simultaneous determination of arsenic, antimony, selenium and tin by continuous hydride generation and gas phase molecular absorption spectrometry is described. The hydride generation is carried out in two steps; first, tin hydride is generated at low acidity and second, arsenic, antimony and selenium hydrides are formed at higher acidity. All the hydrides are collected in a liquid nitrogen cryogenic trap and transported to the flow cell of a diode array spectrophotometer, where molecular absorption spectra are obtained in the 190–250 nm range. Five calibration solutions containing arsenic, antimony, selenium and tin are solved using multiple linear regression analysis. Tests are performed in order to extend the same manifold to other hydrides but no signals are obtained for bismuth, cadmium, lead, tellurium and germanium. Under the optimum conditions found and using the wavelengths of maximum sensitivity (190, 198, 220 and 194 nm), the analytical characteristics of each element are calculated. The detection limits are 0.050, 0.020, 0.12 and 1.1 $\mu\text{g ml}^{-1}$ and the RSD values are 3.7, 3.1, 3.5 and 3.0% for As, Sb, Se and Sn, respectively. The method is applied to As, Sb, Se and Sn determination in natural spiked water samples. © 1998 Elsevier Science B.V. All rights reserved.

Keywords: Simultaneous determination; Gas phase molecular absorption spectrometry; Cryogenic preconcentration; Hydrides

1. Introduction

The adaptation of a preconcentration step to the hydride generation (HG) process has been

extensively developed. When acid–metal reducers were used initially, this step was necessary because hydride generation was slow; preconcentration is still used nowadays to improve sensitivity. Preconcentration can be performed at room temperature [1,2] or at low temperature (mainly using liquid nitrogen) [3–5]. Cryogenic traps are

* Corresponding author. Tel.: +34 76 761292; fax: +34 76 671292; e-mail: jgalban@msf.unizar.es

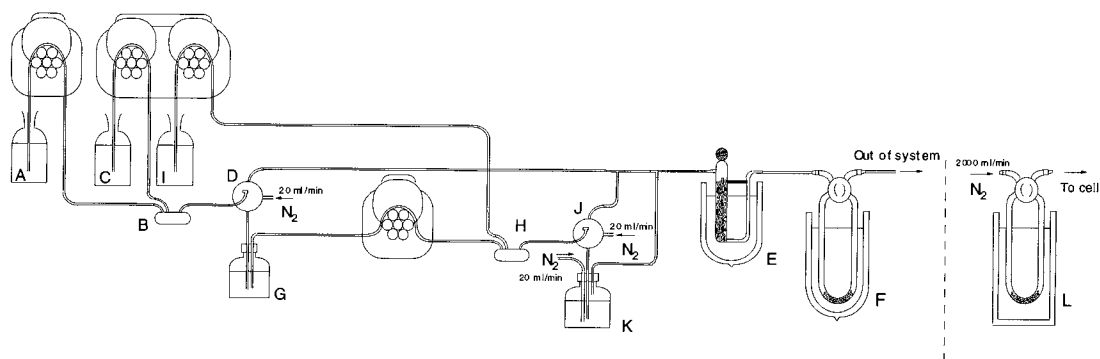


Fig. 1. Manifold used for simultaneous generation of As, Sb, Se and Sn hydrides. (A) sample solution at 35 ml min^{-1} containing As, Sb, Se and Sn in 0.05 M HCl ; (B) first generator; (C) $4\% \text{ NaBH}_4$ at 4 ml min^{-1} ; (D) first gas-liquid separator; (E) water trap (an ice and salt bath at $\approx -10^\circ\text{C}$); (F) hydrides trap (liquid nitrogen); (G) closed vessel; (H) second generator; (I) 2 M HCl solution at 4 ml/min ; (J) second gas-liquid separator; (K) third gas-liquid separator; (L) hot water bath at $\approx 80^\circ\text{C}$.

now the most common. Very useful information about hydride generation and preconcentration in a cold trap is provided by Dedina [6,7].

A survey of the literature indicates that there are not many papers describing analytical methods to determine four or more hydride-forming elements simultaneously. The difficulties result from the interelement interferences and the different oxidation states involved, which affect the generation kinetic. One of the more widely used techniques for simultaneous determination (without the preconcentration step) is HG-Induced Coupled Plasma-Atomic Emission Spectrometry (HG-ICP-OES), which has been used for arsenic and antimony [8–10], arsenic and lead [11], arsenic, antimony and selenium [12–15], arsenic, antimony and bismuth [16] or arsenic, antimony, bismuth, selenium and tin [17]. Speciation analysis is also possible, for example, As(III) and As(V) [18]. Sensitivity is good, but the cost of such equipment compared with other techniques has prevented it from becoming commonplace in analytical laboratories. A preconcentration system can also be combined with HG-ICP-OES [19]. Atomic absorption spectrometry is another technique which is widely used for speciation analysis of hydride-forming elements, such as arsenic [20] or tin [21].

In the last few years, we have studied in depth the analytical possibilities of Gas Phase Molecular

Absorption Spectrometry (GPMAS) for the determination of 1, 2 or 3 compounds (which have been recently reviewed [22]), mainly hydride forming elements and as a detector in gas chromatography [23]. In all those previous papers, the volatilization conditions for all the elements composing the mixtures have been the same. In this paper, we have tried to approach a new problem: the simultaneous determination of a mixture of elements in which different volatilization conditions have to be used. As a result, we have solved mixtures of arsenic, antimony, selenium and tin by GPMAS combined with a robust direct multivariate calibration method.

2. Experimental

2.1. Apparatus

All measurements were performed by using a Hewlett-Packard model HP 8451A diode-array spectrophotometer furnished with a quartz flow cell of 1 cm path length (Hellma 174 QS) and equipped with a keyboard HP98155A (Hewlett-Packard), a floppy disk drive for bulk data storage (Hewlett-Packard HP9121) and a graphics plotter (HP7475A).

For mathematical treatment, a Hewlett-Packard Vectra microprocessor with Eureka[®] software was used.

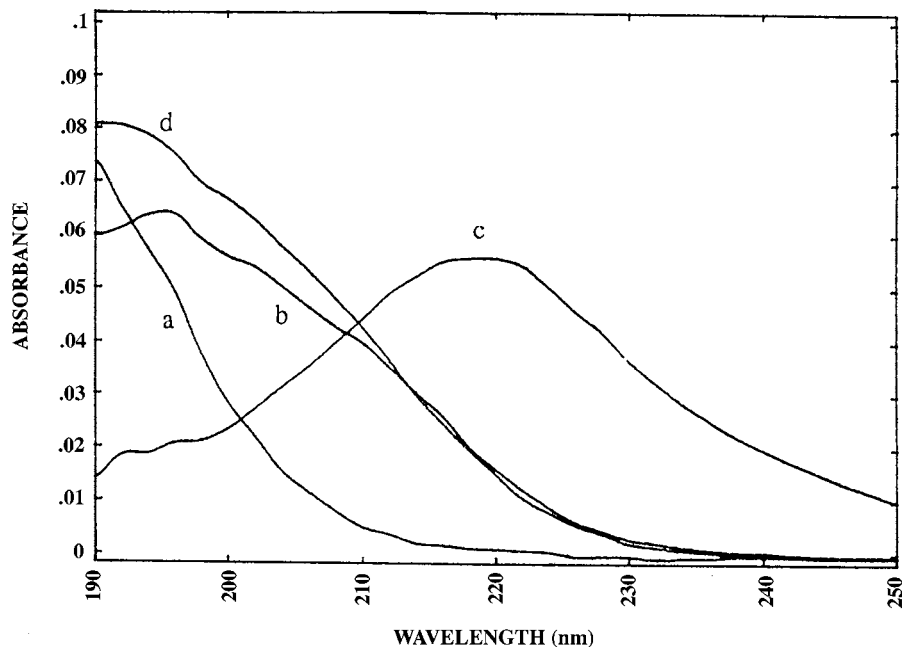


Fig. 2. Molecular absorption spectra in the gas phase of As (a), Sb (b), Se (c) and Sn (d) hydrides.

Reagents were pumped using two Masterflex peristaltic pumps, models 7518-10 and 7016-20 (Cole Parmer, Chicago, IL 60648) and one peristaltic pump model MS-4 Reglo (Ismatec S.A., Spain).

2.2. Reagents

All reagents used were of analytical grade quality. Doubly distilled water was used.

- Stock arsenic solution, 1000 mg l⁻¹, prepared by dissolving As₂O₃ (Merck) in 5 M NaOH, neutralizing with 5 M HCl and diluting with 0.5 M HCl.
- Stock antimony solution, 1000 mg l⁻¹, prepared by dissolving potassium antimony (III) oxide tartrate hydrate extra pure (Merck) in water and acidifying to 0.5 M with respect to HCl.
- Stock selenium solution, 1000 mg l⁻¹, prepared by dissolving extra-pure selenium metal (Merck) (1 g) in the minimum volume of 60% (w/w) HNO₃ and evaporating the solution nearly to dryness. Doubly distilled water (2 ml)

was added and the solution evaporated nearly to dryness (this was repeated twice). The residue was subsequently diluted to 1 l with 10% (v/v) HCl.

- Stock tin solution, 1000 mg l⁻¹, prepared by dissolving SnCl₂ (Merck) in diluted HCl.
- Concentrated HCl 1.19 g ml⁻¹ and 35% (w/w) (Carlo Erba).

Working standards were prepared by serial dilution of the stock solutions with distilled water, immediately before use.

- Aqueous solutions of NaBH₄ (Merck) were prepared immediately before use. The same solution can be used for three or four measurements. By dissolving the NaBH₄ in water, the acidity can be controlled better than if dissolved in a basic medium.

2.3. System description. Recommended procedure

The system (Fig. 1) can be conveniently considered to consist of five sections: first generator (B), first gas-liquid separator (D), second generator (H), second gas-liquid separators (J and K), water

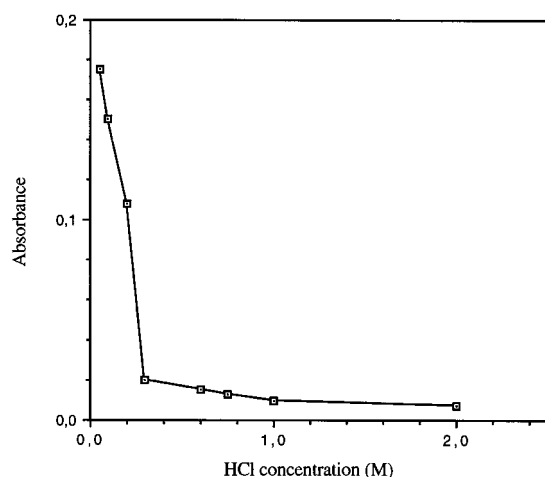


Fig. 3. Effect of HCl concentration on Sn hydride absorbance.

trap (an ice and salt bath at $\approx -10^{\circ}\text{C}$) (E) and the cryogenic trap (F). These components have been described previously [24].

The sample solution at 35 ml min^{-1} (A) containing arsenic, antimony, selenium and tin in 0.05 M HCl is mixed (B) with 4% NaBH_4 at 4 ml min^{-1} (C). All the tin hydride and a low amount (between 10 and 20%) of arsenic, antimony and selenium hydrides are generated. The resultant gas–liquid mixture enters the first gas–liquid separator (D); the hydrides are transported by a carrier gas stream of nitrogen (20 ml min^{-1}) to the water trap (E) and finally to the hydride trap (F).

The liquid remaining at D goes to a hermetically closed vessel (G). The liquid is pumped into a generator (H), where it comes together with a 2

Table 1
Optimization of HCl concentration for the hydride generation of As, Sb and Se in the second generator

HCl concentration (M)	Absorbance		
	As	Sb	Se
3	0.0091	0.0098	0.0088
2.5	0.0100	0.0128	0.0094
2	0.0103	0.0158	0.0105
1.5	0.0085	0.0105	0.0068
1	0.0064	0.0085	0.0043

M HCl solution at 4 ml min^{-1} (I); arsenic, antimony and selenium hydrides are generated. The gas–liquid mixture is then passed through two gas–liquid separators (J and K); in J, a carrier nitrogen flow of 20 ml min^{-1} is used and in K, nitrogen gas is bubbled at 20 ml min^{-1} . The volatiles generated are also transported to the water trap (E) and hydride trap (F) consecutively.

After 5 min of generation and retention, the hydride trap is removed from the liquid nitrogen and left at room temperature for 5 min. Finally, it is placed in hot water ($\approx 80^{\circ}\text{C}$) for 1 min (L). In this way, the hydrides are volatilized and are then transported to the flow cell, with a nitrogen flow of 2000 ml min^{-1} . Molecular absorption spectra of the hydrides in the $190\text{--}250\text{ nm}$ range are obtained, which are subjected to multiple linear regression analysis.

3. Results and discussion

3.1. Previous tests

As has been mentioned, we had previously carried out the simultaneous determination of arsenic, antimony and selenium using continuous hydride generation with cryogenic preconcentration [24]. According to other authors [7] and our previous experience [25], tin forms its hydride under similar generation conditions. Based on this, the system employed for arsenic, antimony and selenium determination was tested for the simultaneous determination of the four elements (including tin). Unexpectedly, the results obtained were not satisfactory and high concentrations of tin were necessary to obtain a good analytical signal. As a consequence, we reconsidered the generation and trapping conditions for tin hydride and later the manifold design for continuous generation.

3.2. Continuous tin hydride generation: Optimization

Tin hydride presents a molecular absorption spectrum with a maximum at 194 nm (Fig. 2). The main parameters affecting tin hydride genera-

Table 2
Analytical characteristics for the simultaneous determination of As, Sb, Se and Sn

Element	Sensitivity (ml μg^{-1})	Quantification limit ($\mu\text{g ml}^{-1}$)	LD ($\mu\text{g ml}^{-1}$)	RSD* (%)
As	0.0950	0.050	0.050	3.7
Sb	0.1510	0.050	0.020	3.1
Se	0.0195	0.20	0.12	3.5
Sn	0.0030	1.5	1.1	3.0

* Obtained for $n = 8$.

tion are the concentration of the reducing agent (NaBH_4) and the acidity of the medium. The NaBH_4 concentration is very important, not only for a quantitative tin hydride generation but also to get a good preconcentration in the cryogenic trap. Different NaBH_4 concentrations from 1 to 7% (w/v) were tested. By using low NaBH_4 concentrations, a low quantity of hydrogen is also generated and the total gas flow passing through cryogenic trap is low. Nitrogen gas therefore, becomes trapped also; when the trap is submitted to room temperature, the nitrogen suddenly escapes from the valve and allows the volatiles to escape. NaBH_4 concentrations equal to or above 4% w/v avoid this problem. From the GPMAS point of view, the optimum acidity for tin hydride generation in the batch method is about 0.6 M [25]; however, using this continuous method, the results were very different. Hydrochloric acid at various concentrations was used in order to look for the optimum acidity; as can be seen in Fig. 3, the higher the concentration, the lower the absorbance value obtained. In addition, it was necessary to employ a low concentration (0.05 M) to obtain a good generation yield. We also tried generating the tin hydride by mixing a basic solution (0.1 M NaOH) containing tin and NaBH_4 with different concentrations of HCl (0.5, 0.05 and 0.025 M), but we did not observe better absorbance values. Given these points, the optimum acidity for tin hydride generation in our system was set at HCl equal to 0.05 M.

3.3. Continuous As + Sb + Se + Sn hydride generation: Optimization

The main problem which appears when 0.05

M HCl is used, is that the arsenic, antimony and selenium hydrides are not generated quantitatively. Therefore, if simultaneous generation and determination of the four hydrides is required, it is necessary to modify the system in order to change the acidity of the medium during the generation process. A new system was therefore designed (Section 2.3). As can be seen, a two step generation process is proposed, first at low acidity (principally generating tin hydride) and second, at high acidity (arsenic, antimony and selenium hydrides are generated quantitatively). Several tests were also made using the contrary mode, with prior generation at high acidity and later alkalization, but the results were not satisfactory.

Considering 0.05 M HCl as optimum for the first step, optimization of the HCl concentration for the second step was then carried out. Since selenium is the element which shows the lowest sensitivity in GPMAS, the study was undertaken with this element, although it was later tested for As and Sb, also showing an agreement with the results for selenium. The results obtained are shown in Table 1; it can be seen that the optimum acidity is 2 M HCl.

In order to investigate if the acidity in the second generator (H) affects the tin hydride generation, some studies were made using tin solution in 0.05 M HCl (solution A) and modifying the HCl concentration in the second generator; different solutions were used as solution I: doubly distilled water, 0.05 M HCl, 0.5 M HCl and 2 M HCl. The results proved that the tin hydride signal is independent of the acidity of solution I, showing that tin hydride is generated quantitatively in the first generator.

Table 3
Results for simultaneous determination of As, Sb, Se and Sn

Mixture	Real concentration ($\mu\text{g ml}^{-1}$)				Found concentration ($\mu\text{g ml}^{-1}$)			
	As	Sb	Se	Sn	As	Sb	Se	Sn
1	0.10	0.10	1.0	10.0	0.09	0.08	1.1	11.0
2	0.10	1.0	1.0	10.0	0.08	0.86	0.93	11.3
3	1.0	0.10	1.0	10.0	1.2	0.12	1.0	9.2
4	0.10	0.10	1.0	40.0	0.12	0.10	0.90	42.0
5	0.10	0.10	5.0	10.0	0.11	0.12	4.8	8.6

3.4. Analytical characteristics

Fig. 2 shows the gas-phase molecular absorption spectra of As, Sb, Se and Sn hydrides. It can be seen that the maxima appear at 190, 198, 220 and 194 nm, respectively.

Under the optimum conditions found and using the wavelengths of maximum sensitivity, the analytical characteristics of each element were calculated. Table 2 shows the sensitivity (the slopes of the calibration graphs), detection limits (the concentration corresponding to a signal of twice the standard deviation of the blank¹ signal), reproducibility (expressed as Relative Standard Deviation) and quantification limits (obtained experimentally) for each element.

It is necessary to note that the analytical figures of merit obtained for As, Sb and Se were slightly worse; so when simultaneous determination of these three elements was carried out [24], detection limits of 0.022, 0.015 and 0.065 $\mu\text{g ml}^{-1}$ and quantification limits of 0.050, 0.030 and 0.200 $\mu\text{g ml}^{-1}$ were obtained for As, Sb and Se respectively. However, this is compensated for by the possibility of carrying out the simultaneous determination of four elements.

3.5. Simultaneous determination

Resolution of five calibration solutions containing As, Sb, Se and Sn was carried out by using multiple linear regression analysis (MLR), based on resolving a system of ' n ' equations with four

unknowns (n = number of wavelengths used). In all cases, all the absorbance values were experimentally obtained in the 190–250 nm range. The optimum wavelength range to be used for MLR resolution (190–220 nm) was obtained by testing empirically different ranges. Table 3 shows a matching of the real mixture concentrations and the results obtained. RSD was in all cases better than 4% ($n = 4$).

3.6. Application

The method was applied for As, Sb, Se and Sn determination in drinking water. Following the procedure described previously, the samples were analyzed and in all cases, the endogeneous amounts of the elements were below the detection limit, so these elements were added to the drinking water samples. After As, Sb, Se and Sn addition, the samples were analyzed in quadruplicate by the proposed method and the results obtained are shown in Table 4. In all cases, the RSD was better than 4%.

3.7. Incorporation of other hydride-forming elements

Once the new system had been prepared for the simultaneous determination of As, Sb, Se and Sn, the incorporation of other hydride-forming elements, such as Bi, Cd, Pb, Ge and Te was tested.

3.7.1. Bismuth

It was not possible to determine bismuth using this methodology because its hydride is very unstable and the preconcentration is not effective

¹ The blank signal is obtained following the procedure, but using 0.05 M HCl as solution (A).

Table 4
Results for simultaneous determination of As, Sb, Se and Sn in drinking water samples

Sample	Added concentration ($\mu\text{g ml}^{-1}$)				Found concentration ($\mu\text{g ml}^{-1}$)			
	As	Sb	Se	Sn	As	Sb	Se	Sn
1	0.30	0.52	1.0	10.4	0.26	0.48	1.2	11.0
2	0.15	0.26	2.0	20.8	0.11	0.23	2.1	19.3

[26]. This was checked by using both molecular absorption spectrometry and atomic absorption spectrometry techniques. The bismuth hydride signal was obtained just before the nitrogen liquid trap; the signal disappeared after trapping in the cryogenic trap.

3.7.2. Cadmium and lead

When simultaneous determination of As, Sb and Se was performed, cadmium and/or lead showed a positive interference (Cd and/or Pb increase the hydride absorbance) on the signal. However, it was not possible to obtain a signal from hydrides of these elements in the absence of As, Sb and Se.

3.7.3. Germanium and tellurium

Based on our own experience [27,28], hydrides of these elements using a batch method are better generated from a basic medium. Nevertheless, considering the results obtained for tin hydride generation (in the batch method the optimum acidity is ten times higher than in the continuous method), a complete study using different Ge and Te hydride generation conditions from acid media was made. Several tests were made modifying the concentrations of HCl (0.5–6 M) and NaBH_4 (2–6%), and no signal was found in any case for germanium or tellurium.

In conclusion, we think that it will be possible to obtain a GPMAS signal from these elements in a continuous flow system (by using a different manifold), but that this will not be possible at the same time as investigating As, Sb, Se and Sn.

Acknowledgements

This work was partly supported by Caja Rioja-University of La Rioja agreement. S. Cabredo would like to thank the 'Instituto de Estudios Riojanos' of La Rioja (Spain) for the FPI grant.

References

- [1] R. Merry, B. Zarcinas, *Analyst* 105 (1980) 558.
- [2] K. Yamaya, T. Aoki, I. Kim, *Bunseki Kagaku* 41 (1992) 263.
- [3] U. Örnemark, J. Pettersson, Å. Olin, *Talanta* 39 (1992) 1089.
- [4] P.N. Vijan, C.Y. Chan, *Anal. Chem.* 48 (1976) 1788.
- [5] M. Burguera, J.L. Burguera, M.R. Brunetto, M. de la Guardia, A. Salvador, *Anal. Chim. Acta* 261 (1992) 105.
- [6] J. Dedina, *Prog. Anal. Spectrosc.* 11 (1988) 251.
- [7] J. Dedina, D.L. Tsalev, *Tydride generation atomic absorption spectrometry*, vol. 130, in: *Chemical Analysis*, Wiley, Chichester, 1995.
- [8] B. Pahlavanpour, M. Thompson, L. Thorne, *Analyst* 105 (1980) 756.
- [9] B. Pahlavanpour, M. Thompson, L. Thorne, *Analyst* 106 (1981) 467.
- [10] B.L. Huang, *Can. J. App. Spect.* 39 (1994) 117.
- [11] H.W. Chen, J.Z. Wu, I.D. Brindle, *Talanta* 42 (1995) 353.
- [12] K.A. Wolnik, F.L. Fricke, M.H. Hahn, J.A. Caruso, *Anal. Chem.* 53 (1981) 1030.
- [13] D.D. Nygaard, J.H. Lowry, *Anal. Chem.* 53 (1981) 803.
- [14] M.H. Hahn, K.A. Wolnik, F.L. Fricke, J.A. Caruso, *Anal. Chem.* 54 (1992) 1048.
- [15] E. de Oliveira, J.W. McLaren, S.S. Berman, *Anal. Chem.* 55 (1983) 2047.
- [16] L. Zhang, X. Shan, Z. Ni, *Fresenius Z. Anal. Chem.* 332 (1988) 764.
- [17] P. Schramel, Xu Li-Qiang, *Fresenius Z. Anal. Chem.* 340 (1991) 41.
- [18] Y.L. Feng, J.P. Cao, *Anal. Chim. Acta* 293 (1994) 211.

- [19] X.O. Wang, Z.X. Zhuang, P.Y. Yang, B.L. Huang, *Microchem. J.* 51 (1995) 88.
- [20] R. Torralba, M. Bonilla, L.V. Perezarribas, A. Palacios, C. Cámara, *Spectrochim. Acta Part B* 49 (1994) 893.
- [21] Y. Cai, J.M. Bayona, *J. Chromatogr. Sci.* 33 (1995) 89.
- [22] J. Galbán, S. Cabredo, F. Gallarta, I. Sanz-Vicente, M. Pérez, J. Sanz, *Fresenius J. Anal. Chem.* 355 (1996) 406.
- [23] I. Sanz-Vicente, S. Cabredo, F. Sanz, J. Galbán, *Chromatographia* 42 (1996) 356.
- [24] S. Cabredo, J. Sanz, J. Galban, *Anal. Chim. Acta* 300 (1995) 321.
- [25] J.R. Castillo, J. Sanz, F. Gallarta, J. Galban, XXVI Colloquium Spectroscopicum Internationale, vol. VIII, selected papers, 1989, pp. 177.
- [26] D.S. Lee, *Anal. Chem.* 54 (1982) 1682.
- [27] J. Sanz, L.A. Ortega, J. Galban, J.R. Castillo, *Microchem. J.* 41 (1990) 29.
- [28] J. Sanz, J. Galban, F. Gallarta, J. Benito, *Anal. Lett.* 28 (1995) 121.

Differential electrolytic potentiometry, a detector in flow injection analysis for precipitation reactions

A.M.S. Abdennabi *, M.E. Koken

Chemistry Department, Box 5048, King Fahd University of Petroleum and Minerals, Dhahran 31261, Saudi Arabia

Received 14 May 1997; received in revised form 10 September 1997; accepted 11 September 1997

Abstract

The application of differential electrolytic potentiometry as a detection system in flow injection analysis for precipitation reactions is described. Different combinations of electrodes were investigated. The optimum conditions for the current density and the flow rate were elucidated. In the case of chloride, an Ag/AgCl–Pt pair was found to be successful. For iodide a combination of Ag–Pt electrodes was found to give good results. The relation between the concentration of analyte and the measured signal was found to be linear. © 1998 Elsevier Science B.V. All rights reserved.

Keywords: Differential electrolytic potentiometry; Flow injection analysis; Chloride and iodide detection

1. Introduction

Differential electrolytic potentiometry (dc DEP) consists of polarising two identical electrodes with a stabilised current and measuring the potential difference (ΔE) between them. This method has been applied to various types of titrimetric reactions in both aqueous [1–4] and non-aqueous [5–9] media using different types of electrodes. In this technique the polarized electrodes respond faster, the apparatus is simple and the salt bridge problems of the reference cell are eliminated.

The determination of chloride by flow injection analysis has been based mainly on spectrophotometrical procedures where the reaction between thiocyanate and mercury complex leads to the

displacement of thiocyanate and the formation of an intensely colored complex of iron(III) [10–12]. This method has been found to suffer from poor detection limits, however, Slanina et al. [13] have improved the method and were able to detect chloride in the range of 0.2–15 ppm using both photometric and potentiometric detectors. Chloride was also determined by Cireloogamina and Brindle [14] using a UV-photometric flow injection method. Taylor and Grate [15] determined chloride by means of a flow injection technique with a reflectance detector for the determination of chloride.

The technique of differential electrolytic potentiometry has not as yet been applied as a detection system in flow injection analysis. This paper describes the application of this technique for certain precipitation reactions. The behaviours of different combinations of polarized electrodes

* Corresponding author. Tel.: +966 3 8602111; fax: +966 3 8604227; e-mail: abdallam.@dpc.kfupm.edu.sa

were investigated. Suitable combinations of electrodes for chloride and iodide determination is reported.

2. Experimental

2.1. Reagents

Chloride ion solutions were prepared using Thorn Smith Standard sodium chloride. Supporting electrolyte solutions were prepared from AnalaR sodium nitrate and potassium nitrate. Hydrochloric acid (Fisher) and Baker Analyzed nitric acid were used for the required purposes. Fluka iron(III) chloride was used for the preparation of the solution that is required in the plating of silver electrodes with silver chloride.

Fluka silver nitrate was used for the preparation of silver nitrate solution. Degussa mercury was used for the preparation of the amalgamated electrode. A stock solution of 0.01 M sodium chloride was prepared by dissolving 0.585 g of NaCl in distilled deionized water in 1000 ml volumetric flask. Working solutions were prepared by dilution. The same procedure was applied to prepare stock solutions of silver nitrate, sodium nitrate and potassium nitrate.

A solution of 0.5 M iron(III) chloride was prepared by dissolving the required weight of iron(III) chloride in 8.06 ml of concentrated hydrochloric acid and 50 ml of distilled deionized water in a 100 ml flask then completing to the mark with distilled deionised water.

Nitric acid solution (6 M) was prepared in the usual way from concentrated nitric acid. Fluka sodium iodide was used to prepare iodide solution. A standard solution of 0.01 M iodide was prepared in water.

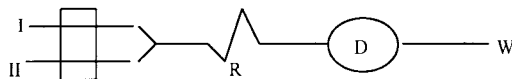


Fig. 1. Manifold used in the determination of chloride. I, silver nitrate carrier; II, supporting electrolyte solution; R, reactor; D, detector; W, waste.

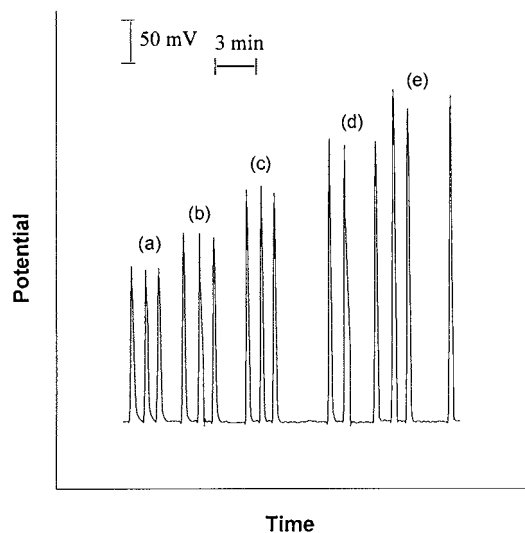


Fig. 2. Current density–peak height relationship. Electrode pair, Ag–Ag; flow rate, 0.93 ml min^{-1} , volume, $140 \mu\text{l}$ of 3.55 ppm Cl^- ; (a) $1.98 \mu\text{A cm}^{-2}$; (b) $3.96 \mu\text{A cm}^{-2}$; (c) $5.95 \mu\text{A cm}^{-2}$; (d) $7.93 \mu\text{A cm}^{-2}$; (e) $9.91 \mu\text{A cm}^{-2}$.

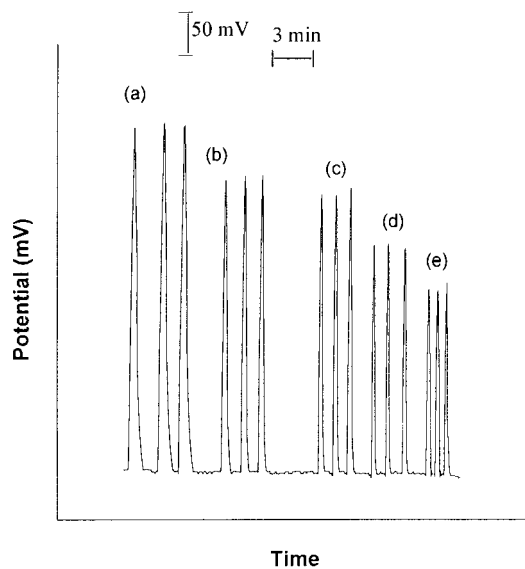


Fig. 3. Flow rate–peak height relationship. Electrode pair, Ag–Ag; current, $5.95 \mu\text{A cm}^{-2}$; vs, $140 \mu\text{l}$ 3.55 ppm Cl^- ; (a) 0.55 ml min^{-1} ; (b) 0.93 ml min^{-1} ; (c) 1.17 ml min^{-1} ; (d) 1.26 ml min^{-1} ; (e) 1.45 ml min^{-1} .

2.2. Apparatus

Keithley Instruments 225 Constant Current Source was used to polarize the electrodes.

The potentiometer used is Corning Scientific Instruments Model 12 research pH meter for oxidation reactions and changed to digital Fisher

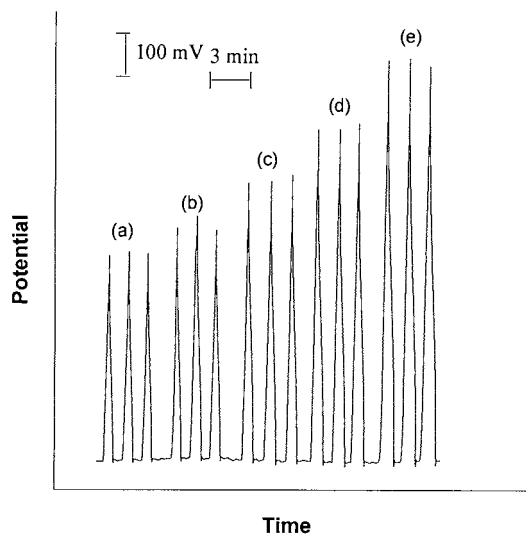


Fig. 4. Calibration curve. Electrode pair, Ag–Ag; current, $5.95 \mu\text{A cm}^{-2}$; flow rate, 0.93 ml min^{-1} , volume, $140 \mu\text{l}$; (a) 3.55 ppm; (b) 10.7 ppm; (c) 17.8 ppm; (d) 24.8 ppm; (e) 32.0 ppm.*

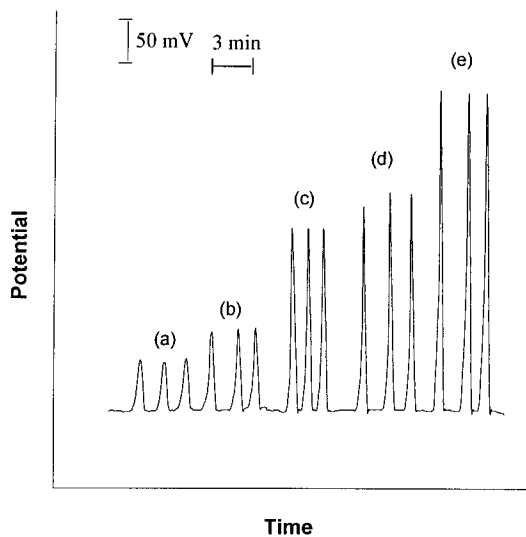


Fig. 5. Current density–peak height relationship. Electrode pair, Ag/AgCl–Pt; flow rate, 0.93 ml min^{-1} , volume, $100 \mu\text{l}$ of 6.4 ppm Cl; (a) $1.98 \mu\text{A cm}^{-2}$; (b) $9.91 \mu\text{A cm}^{-2}$; (c) $19.8 \mu\text{A cm}^{-2}$; (d) $29.7 \mu\text{A cm}^{-2}$; (e) $39.6 \mu\text{A cm}^{-2}$.

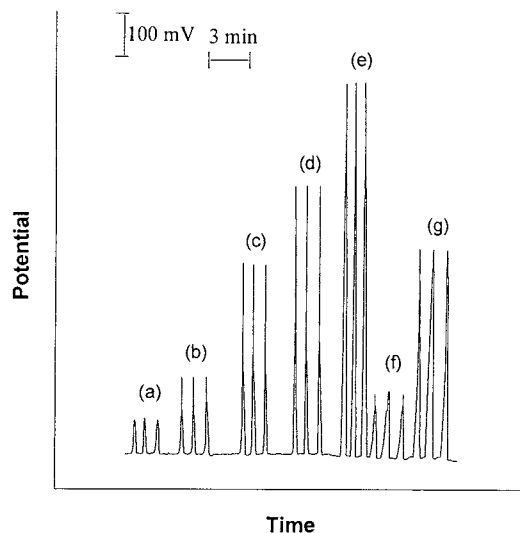


Fig. 6. Calibration curve. Electrode pair Ag/AgCl–Pt, current density, $19.82 \mu\text{A cm}^{-2}$; flow rate, 0.93 ml min^{-1} , volume, $100 \mu\text{l}$ of Cl^- ; (a) 3.0 ppm; (b) 4.8 ppm; (c) 29 ppm; (d) 48 ppm; (e) 68 ppm; (f) signal of sample 1; (g) signal of sample 2.

Accumet Selective Ion Analyzer Model 750 for the other experiments.

A Cole Parmer chart recorder was used and the data was recorded with a speed of 0.3 cm/min .

The test solutions were propelled by a peristaltic pump of Alitea USA/ FIA laboratory for all experiments.

Gateway 2000 computer with RS 332-098 4 phase unipolar stepper motor drive board introduced into the hard disk was used for the injection of samples into carrier streams to provide highly precise and reproducible volume. The injector used was a plastic syringe with the metallic needle replaced by a plastic one to prevent corrosion.

A two line manifold system was used as shown in Fig. 1. Silver nitrate solution was passed from one line and the supporting electrolyte from the other. The reactor was made of a coiled tube formed from a plastic tube of 25 cm length and 1.14 mm inner diameter. This tube was mounted on a glass cylinder of diameter 0.7 cm. The detector was made of Teflon in the form of a cylinder 3 cm in length where the two electrodes were placed and this detector was connected to the reactor.

Table 1
Results for the determination of chloride in real samples by precipitation and FIA-DEP methods

Sample No.	Cl ⁻ (found by pptn method) in ppm	Cl ⁻ (found by FIA-DEP) in ppm	% Recovery
1	3.50	3.58	102.3
2	32.0	32.1	100.3

rsd, 0.2%

2.3. Electrodes

Silver wire electrodes were used in the first part of the chloride and iodide analysis. They were cleaned with 6 M nitric acid as a pretreatment before each experiment. The electrodes were then rinsed with distilled deionized water and placed in the cell.

The platinum electrodes were SargentWelch type 30-415 and 30-415 respectively. They were cleaned with concentrated sulfuric and/or nitric acid before each experiment as a pretreatment, rinsed with distilled deionized water and placed in the cell.

Platinum electrode were cleaned by dipping in boiling aqua regia and then rinsed with distilled deionized water. It was then immediately immersed into pure mercury for 30 s to prepare a Pt/Hg electrode.

Silver/silver chloride electrodes were prepared by surface oxidation of silver electrodes in a solution of 0.5 M Fe(III) chloride solution which was found to be more effective than the traditional anodic oxidation process [16]. The electrode was immersed in the solution, left overnight then rinsed with distilled deionized water and placed in the cell.

3. Results and discussion

Fig. 1 shows the manifold used in this study where silver nitrate was delivered as reactant from line I. The supporting electrolyte solution was passed through line II. At the start of this work, the proper current density was determined by injecting a volume of 140 μ l of 3.55 ppm chloride solution into a stream of 0.01 M KNO₃ and 10⁻³ M AgNO₃ as shown in Fig. 1. Different current

densities were employed to polarise two identical silver electrodes. Fig. 2a shows that the heights of the resulting peaks increased with the current densities employed. It was noted that at lower current densities, for instance 1.98 μ A cm⁻², the electrodes were found to have a slow response. This is reflected in the small heights of the resulting peaks. However, at current densities greater than 7.93 μ A cm⁻², the electrodes response becomes abnormal. Consequently the resulting peaks will show poor reproducibility as seen from peaks at d and f of Fig. 2. This abnormal behaviour is probably due to the fact that higher currents will increase the concentration overpotentials of both the anode and the cathode. Consequently the measured signal which is the difference between the potentials of these two electrodes will be affected. Fig. 2 shows that the three peaks at point (c) are symmetrical, reproducible and of a considerable height. These peaks were obtained at a current density of 5.95 μ A cm⁻², hence, this value is considered to be an optimum under the employed conditions. The relation between peak height and current density employed to polarise the silver electrodes is shown in table. 2.

The effect of flow rate on the produced signal was also studied and the results are depicted in Fig. 3. It is obvious from this figure that the peak height decreases with an increase in flow rate. The peaks of point b are symmetrical, having a reasonable width and they are considerably high, therefore, the flow rate at this point which is 0.93 ml min⁻¹ was considered to be appropriate for the experimental measurements.

A calibration curve was constructed by injecting standard chloride solutions of concentrations that range from 3.55–35.5 ppm. This calibration curve is shown in Fig. 4 and it has a regression

coefficient of 0.991. During the course of this work it was observed that the response of the silver electrodes became sluggish. This can be attributed to the fact that the resulting silver

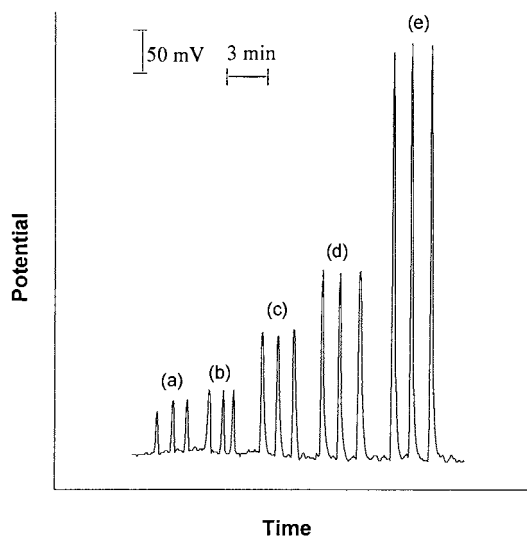


Fig. 7. Current density–peak height relationship. Electrode pair, Ag/AgCl–Pt/Hg; flow rate, 0.93 ml min^{-1} , volume $100 \mu\text{l}$ of 4.5 ppm Cl^- ; (a) $0.99 \mu\text{A cm}^{-2}$; (b) $2.97 \mu\text{A cm}^{-2}$; (c) $11.89 \mu\text{A cm}^{-2}$; (d) $14.9 \mu\text{A cm}^{-2}$; (e) $19.8 \mu\text{A cm}^{-2}$.

Table 2

The relation between the peak heights and the current densities employed for different combinations of electrodes used for chloride determination

Type of electrodes	Current density ($\mu\text{A cm}^{-2}$)	Height of peak (mV)
Ag–Ag	1.98	183
	3.96	225
	5.95	283
	7.93	333
	9.91	400
Ag/AgCl–Pt	1.98	58
	9.91	100
	19.8	225
	29.7	258
	39.6	400
Pt/Hg–Ag/AgCl	0.99	58
	2.97	75
	11.89	141
	14.9	225
	19.8	500

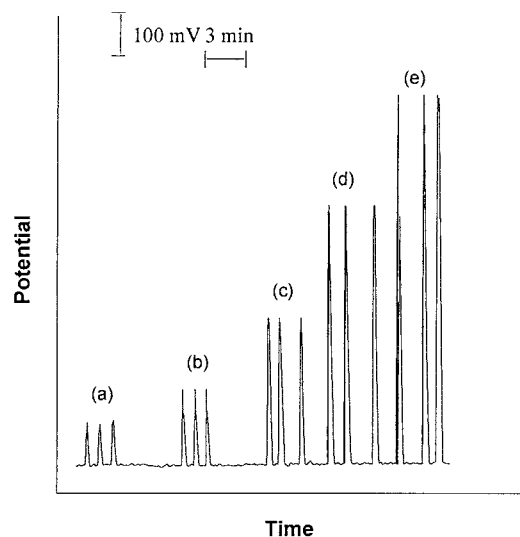


Fig. 8. Calibration curve. Electrode pair, Ag/AgCl–Pt/Hg; current density, $19.8 \mu\text{A cm}^{-2}$; flow rate, 0.93 ml min^{-1} , volume, $100 \mu\text{l}$ of Cl^- ; (a) 1.8 ppm ; (b) 3.0 ppm ; (c) 18.2 ppm ; (d) 29.8 ppm ; (e) 42.7 ppm .

chloride dissociates and the ions formed will affect the behaviour of the polarised electrodes. A pair of Ag/AgCl electrodes has been used for the determination of chloride [17]. However, the use of Ag/AgCl electrode as a cathode in DEP will lead to the dissolution of AgCl coating and the electrode will eventually become a silver electrode. Consequently, the resulting signal will differ from the previous ones and abnormal behaviour becomes inevitable.

Polarised platinum electrodes have also been used for chloride analysis using silver nitrate as a titrant [18]. The response of the platinum electrode was attributed to the adsorption of silver chloride precipitate on the surface of the electrode. It was decided to make a combination of a platinum electrode with a Ag/AgCl electrode where the platinum electrode would act as cathode. This combination was employed for the determination of chloride by injecting the latter into a stream containing silver nitrate. When the sample is injected, a potential difference develops between the anode and the cathode, consequently, a peak is formed. The relation between the height of the peak and the current density was studied and the results are shown in Fig. 5 and Table 2. It

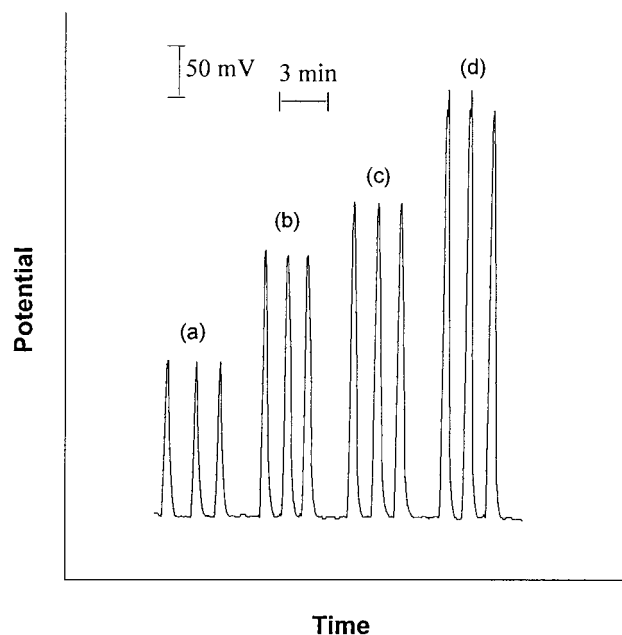


Fig. 9. Effect of change in the current density employed. Electrode pair, Ag–Ag; flow rate, 0.93 ml min^{-1} ; volume, $140 \mu\text{l}$ of 12.7 ppm I^{-} ; (a) $1.98 \mu\text{A cm}^{-2}$; (b) $3.96 \mu\text{A cm}^{-2}$; (c) $5.95 \mu\text{A cm}^{-2}$; (d) $9.91 \mu\text{A cm}^{-2}$.

is evident from this figure that the peak height increases with current density and the value of $19.82 \mu\text{A cm}^{-2}$ was chosen for experimental measurements because the resulting peaks are symmetrical and have similar heights.

A calibration curve was established by applying the above mentioned conditions. Standard chloride solutions of concentrations that range from $3.0\text{--}68 \text{ ppm}$ were injected. The resulting calibration curve is depicted in Fig. 6. This curve was found to be linear with $r = 0.997$ and can be applied to determine chloride in real water samples where the sulphate ion if exists is expected to pose no effect on the response of the indicating system. Fig. 6 shows the results of applying DEP in combination with Ag/AgCl–Pt as a detection system for the analysis of chloride in two samples of drinking water. Peaks (f) and (g) shown in Fig. 6 represent the signals for these two samples. Table 1 gives a comparison between the results obtained by this technique and that of standard precipitation titration. It is apparent from this table that DEP can be applied as a detector in FIA and better sensitivity is expected compared

with direct titration methods including the classical DEP technique. In this technique two identical electrodes are employed to obtain a symmetrical peak which gives the end point. The morphology of the peak depends on the completion of both anodic and cathodic reactions that take place on the two electrodes. However, the use of the DEP technique as a detector in flow injection analysis does not require the completion of the reaction. Therefore different combinations of electrodes can be employed to obtain a better signal. In this regard, a combination of Pt/Hg–Ag/AgCl electrodes was used for the determination of chloride. The proper conditions were found using the univariant method. Fig. 7 shows the effects of changing current density on the height of the signal and the optimum current density that gives the highest reproducible signal was found to be $19.82 \mu\text{A cm}^{-2}$. The relation between the peak height and the current density employed is shown in Table 2.

On applying these conditions, a calibration curve that covers a chloride concentration range between 1 and 45 ppm was constructed and is depicted in Fig. 8. It is apparent that this curve is

linear with $r = 0.996$. However when the combination of Pt/Hg–Ag/AgCl electrodes were used for the determination of chloride in real water samples, higher signals resulted. A similar observation

Table 3

The relation between the peak heights and the current densities employed for combinations of electrodes used for iodide determination

Type of electrodes	Current density ($\mu\text{A cm}^{-2}$)	Height of peak (mV)
Ag–Ag	1.98	158
	3.96	266
	5.95	316
	9.91	416
Ag–Pt	4.95	17
	9.91	41
	29.73	166
	39.4	383
Pt/Hg–Ag/AgCl	0.99	58
	2.97	75
	11.89	141
	14.9	225
	19.8	500

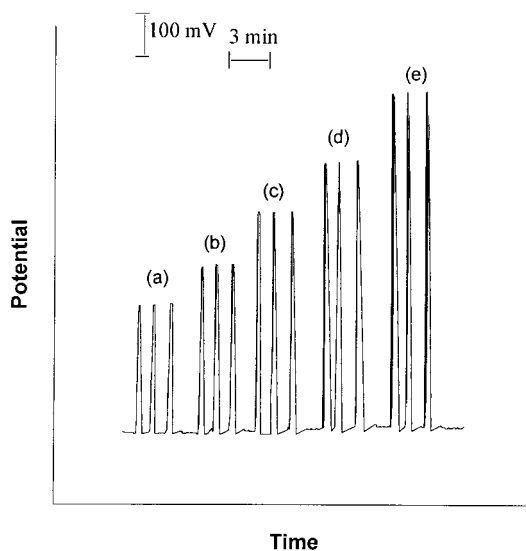


Fig. 10. Calibration curve. Electrode pair, Ag–Ag; current density, $5.95 \mu\text{A cm}^{-2}$; flow rate, 0.93 ml min^{-1} ; volume, $140 \mu\text{l}$; (a) 12.7 ppm; (b) 38.1 ppm; (c) 63.5 ppm; (d) 88.9 ppm; (e) 114 ppm.

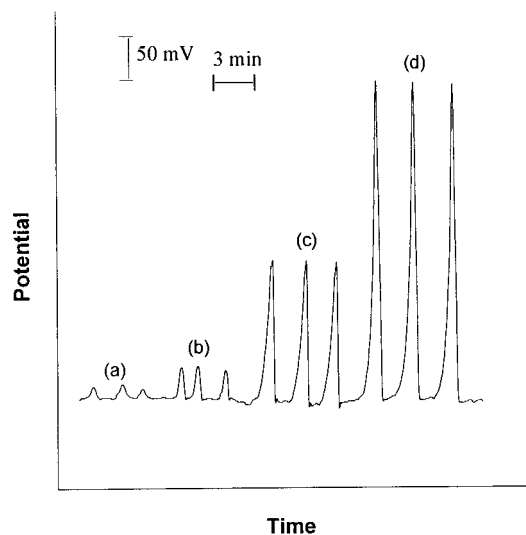


Fig. 11. Effect of the change in the current density employed. Electrode pair, Ag–Pt; flow rate, 0.93 ml min^{-1} ; volume $100 \mu\text{l}$ of 1.27 ppm I^- ; (a) $4.95 \mu\text{A cm}^{-2}$; (b) $9.91 \mu\text{A cm}^{-2}$; (c) $29.73 \mu\text{A cm}^{-2}$; (d) $39.64 \mu\text{A cm}^{-2}$.

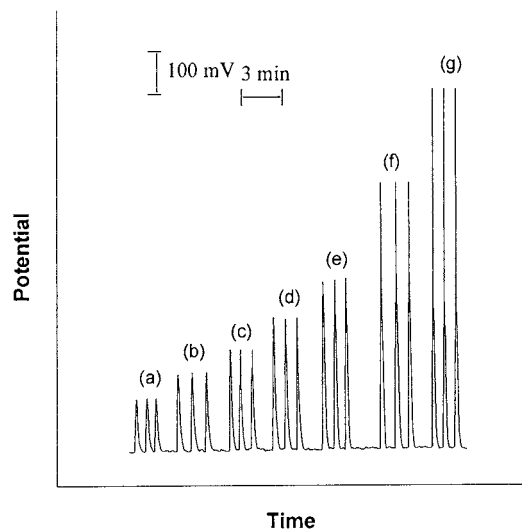


Fig. 12. Calibration curve. Electrode pair, Ag–Pt, current density, $35 \mu\text{A cm}^{-2}$, flow rate: 0.93 ml min^{-1} ; volume of I^- , 140 ml ; (a) 1.27 ppm; (b) 3.81 ppm; (c) 6.35 ppm; (d) 7.62 ppm; (e) 8.89 ppm; (f) 11.4 ppm; (g) 19.0 ppm; (h) 31.8 ppm.

was noted by others [19] where sulfate was found to interfere. Therefore the combination of Pt/Hg–Ag/AgCl is recommended for the determination of chloride in the absence of interfering ions such as sulphate.

The applicability of the DEP technique as a detector in FIA for precipitation reactions was extended to include iodide. Since the solubility of silver iodide is very low, a combination of two identical silver electrodes were expected to give satisfactory results. The appropriate current density gives symmetrical and reproducible peaks of considerable height which was found to be $5.95 \mu\text{A cm}^{-2}$ as shown in Fig. 9. The relation between peak height and current densities employed is shown in Table 3. A calibration curve was constructed for standard iodide solutions of concentrations from 12.7 to 127 ppm. Fig. 10 depicts this curve which has an excellent correlation coefficient of 0.998.

In order to examine the applicability of other combinations of electrodes, one silver electrode was replaced by a platinum electrode in iodide determination. The height of the signal was found to increase with an increase in current density employed as shown in Fig. 11. Its optimum value was chosen as $34.7 \mu\text{A cm}^{-2}$ and Table 3 shows the relation between the peak height and the current densities employed. A calibration curve was established for a concentration range of 1.27–31.8 ppm. This curve is shown in Fig. 12 and it has a correlation coefficient of 0.997 which indicates the applicability of the DEP technique as a detector in flow injection analysis.

4. Conclusion

The technique of DEP which depends on polarising two identical electrodes using a small current and measuring the potential difference between them can be used as a detector in FIA. A combi-

nation of Ag/AgCl–Pt electrodes can be applied for the determination of chloride. For iodide determination Ag–Pt combination was found to give acceptable results. The appropriate conditions of flow rate and current density were investigated.

Acknowledgements

M. Koken wishes to thank KFUPM for donating the scholarship to read for MS degree.

References

- [1] E. Bishop, G.D. Short, *Analyst* 87 (1962) 467.
- [2] G.D. Short, E. Bishop, *Analyst* 87 (1962) 724.
- [3] G.D. Short, E. Bishop, *Analyst* 89 (1964) 415.
- [4] E. Bishop, R.B. Dhaneshwer, *Analyst* 87 (1962) 207.
- [5] A.M.S. Abdennabi, E. Bishop, *Analyst* 107 (1982) 1032.
- [6] E. Bishop, A.M.S. Abdennabi, *Analyst* 108 (1983) 1349.
- [7] A.M.S. Abdennabi, E. Bishop, *Analyst* 108 (1983) 71.
- [8] A.M.S. Abdennabi, M. Rashid, *A.J.S.E* 12 (1986) 82.
- [9] A.M.S. Abdennabi, E. Bishop, *Analyst* 108 (1983) 1227.
- [10] J. Ruzicka, J.W.B. Stewart, E.A. Zagatto, *Anal. Chim. Acta.* 81 (1976) 387.
- [11] E.H. Hansen, J. Ruzicka, *Anal. Chim. Acta.* 87 (1976) 353.
- [12] J. Ruzicka, E.H. Hansen, H. Mosbaek, *Anal. Chim. Acta.* 49 (1977) 1958.
- [13] J. Slanina, F. Bakker, A. Bruyn-Hes, J.J. Mols, *Anal. Chim. Acta.* 33 (1980) 33.
- [14] J. Cirelloegamino, I.D. Brindle, *Analyst* 120 (1995) 183.
- [15] R.H. Taylor, J.N. Grate, *Talanta* 42 (1995) 257.
- [16] M. Trojanowickz, W. Matuszewski, *Anal. Chim. Acta.* 151 (1983) 77.
- [17] E. Bishop, R.G. Dhaneshwar, *Anal.Chem.* 36 (1964) 726.
- [18] R.W. Freedman, *Anal. Chem.* 31 (1959) 214.
- [19] E.P. Serjeant, *Potentiometry and Potentiometric Titrations*, Chemical Analysis vol.69, Wiley, Canada, 1984.

Salting-out extraction technique for pretreatment in the liquid chromatographic determination of copper(II), aluminum(III), iron(III) and manganese(II) in biological samples

Y. Nagaosa *, K. Sakata

Department of Applied Chemistry and Biotechnology, Faculty of Engineering, Fukui University, Bunkyo, Fukui 910, Japan

Received 5 February 1997; received in revised form 28 August 1997; accepted 12 September 1997

Abstract

A solvent extraction method for the simultaneous determination of Cu, Al, Fe and Mn by reversed phase liquid chromatography is presented. The metal chelates with 5-chloro-8-quinolinol are extracted into an acetonitrile phase with tetrabutylammonium perchlorate and ammonium sulfate as salting-out agents, followed by LC separation and determination using an ODS column. The experimental parameters such as the composition of mobile phase and concentration of the salting-out agent for phase separation have been investigated. The mobile phase is a mixture of 3:1 (v/v) acetonitrile-0.02 mol l⁻¹ sodium acetate solution containing 5 × 10⁻³ mol l⁻¹ 5-chloro-8-quinolinol. The proposed method has been applied to the trace analysis of Cu, Al, Fe and Al in bovine liver and citrus leaves. © 1998 Elsevier Science B.V. All rights reserved.

Keywords: Salting-out extraction; Liquid chromatography; 5-Chloro-8-quinolinol; Metal ions

1. Introduction

Trace metals like copper, zinc, manganese as well as iron are essential elements of plants and animals [1]. We need to develop simple and sensitive methods for analyzing these constituents in biological bodies—for human consumption of agricultural products and environmental conservation. Determination of metals in samples has usually been carried out using spectrometric and chromatographic methods [2,3].

Over the past decade, the simultaneous determination of metal ions in aqueous samples by liquid chromatography (LC) with spectrophotometric detection has received much more attention [4,5]. A number of papers have been published on the LC of metal complexes with various chelating agents such as dithiocarbamates [6,7], 8-quinolinol (8-HQ) [8] and 2-pyridylazo compounds [9,10] as derivatization agents.

In order to increase the selectivity and sensitivity of metal determinations, preconcentration methods using solvent extraction [11–13] and on-line enrichment system [14] has been developed. Direct injections of organic solvents into ODS

* Corresponding author. Fax: +81 776 278747; e-mail: nagaosa@acbio.acbio.fukui-u.ac.jp

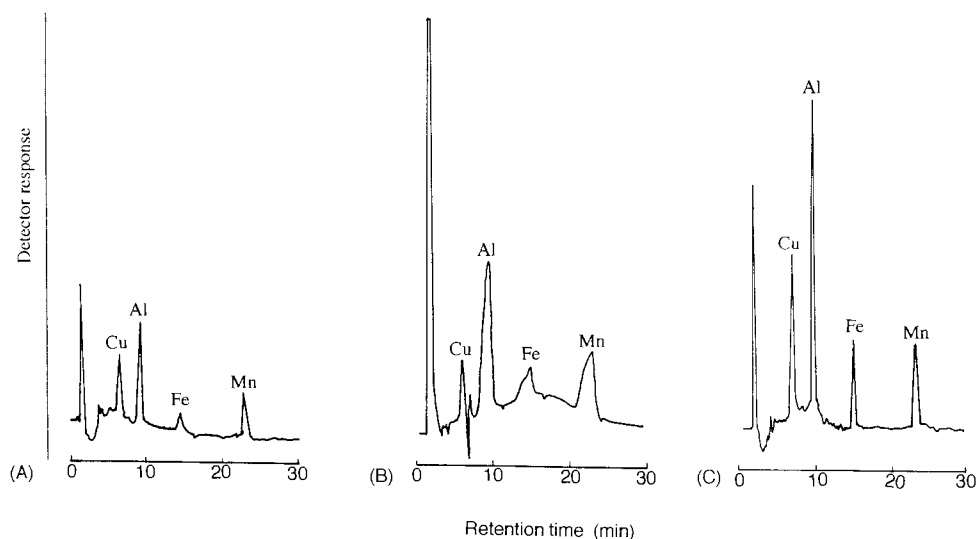


Fig. 1. Chromatograms obtained for metal complexes with 8-quinolinol (8-HQ) by reversed phase LC. The sample solution (A) was prepared by mixing 5.0 ml of a $0.1 \mu\text{g ml}^{-1}$ metal ion solution with 5.0 ml of a 0.02 mol l^{-1} 8-HQ solution in acetonitrile; the acetonitrile extract sample (B) was obtained by adding 2.0 g of ammonium sulfate to the sample (A); The sample (C) was obtained by dilution of the acetonitrile extract sample (B) (with water at a volume ratio of 1:1), the mobile phase was a mixture of 2:3 (v/v) acetonitrile- 0.02 mol l^{-1} acetate buffer (pH 5.9) containing $5.0 \times 10^{-3} \text{ mol l}^{-1}$ 8-HQ. Other conditions are described in Section 2 of the text.

columns often causes chromatographic distortions on the elution curves due to the solubility problem of the organic extract in the mobile phase [13,15]. Kaneko et al. [16] reported chloroform extraction followed by evaporation of the extract and addition of dimethylsulfoxide for sample preparation; the procedure was very tedious and time-consuming, and LC peaks obtained were quite sharp. Mueller et al. [11] used a salt-induced (salting-out) extraction technique using acetonitrile as a solvent to overcome this drawback. Sodium chloride as the salting-out agent, however, was inappropriate because an emulsion formed between the two phases.

Here we propose using tetrabutylammonium perchlorate (TBAP) for inorganic salt-induced extraction to achieve a simple and effective pretreatment method for LC analyses of complex samples like biological materials. This method is based on the extraction of metal complexes with 5-chloro-8-quinolinol (5-Cl-8-HQ) into an acetonitrile phase by using TBAP and ammonium sulfate as the composite salting-out agent, followed by direct injection of the extract into an ODS column. This

LC method has been applied to the determination of copper, aluminum, iron and manganese in bovine liver and citrus leaves.

2. Experimental

2.1. Reagents

Standard reference materials (citrus leaves 1572, bovine liver 1577a) were used to evaluate the proposed method. Tokyo Kasei supplied 8-HQ, 5-Cl-8-HQ and tetrabutylammonium perchlorate (TBAP). Metal ion standards (1000 ppm) for atomic absorption spectrometry and ammonium sulfate were from Wako Junyaku. All other chemicals and solvents were of analytical or HPLC grade. Water was purified with a Millipore Milli-Q water purification system after distillation.

2.2. Apparatus

The LC equipment comprised of the following components: Tosoh Model CCPD pump (Tokyo,

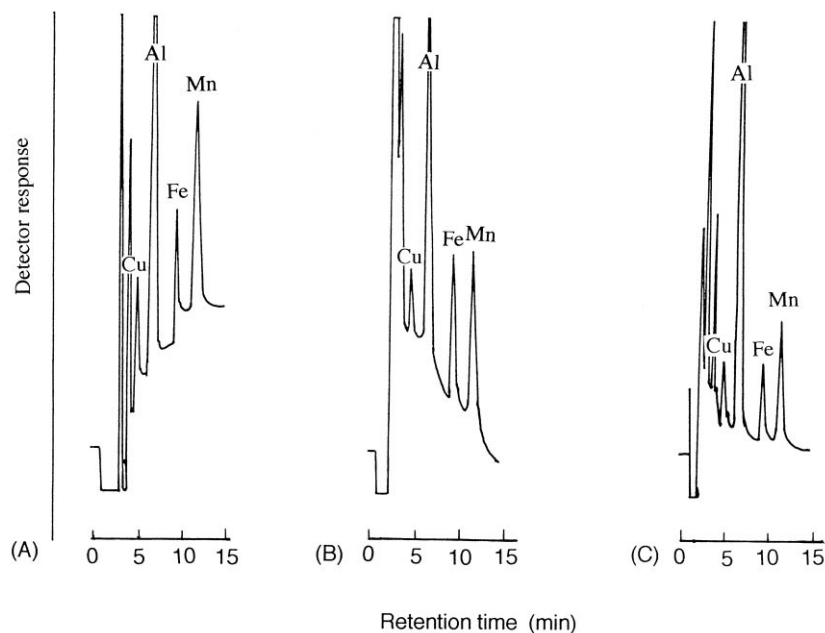


Fig. 2. Chromatograms obtained for metal complexes with 5-chloro-8-quinolinol (5-Cl-8-HQ) after sample treatment with various salting-out agents. The concentration of metal ions: $0.1 \mu\text{g ml}^{-1}$ of each of the extract samples (A), (B) and (C) were obtained by adding 1.0 g of ammonium sulfate, 1.0 mmol TBAP and a mixture of 1.0 g of ammonium sulfate and 0.5 mmol TBAP to a mixed solution of 2.0 ml of 0.02 mol l^{-1} 5-Cl-8-HQ in acetonitrile and 5.0 ml of metal ion solution; the mobile phase was a mixture of 3:1 (v/v) acetonitrile- 0.02 mol l^{-1} sodium acetate solution containing $5 \times 10^{-3} \text{ mol l}^{-1}$ 5-Cl-8-HQ.

Japan) and Reodyne Model 7125 injector valve with a $100 \mu\text{l}$ sample loop (Cotati, California); for UV detection at 390 nm, a Shimadzu Model SPD-6AV spectrophotometer (Kyoto, Japan). Data was processed using a Shimadzu Model CR-6A integrator/recorder. A Toa Denpa Model HM-30s pH meter was used to measure the pH of the solution. LC analyses were carried out on a Tosoh TSKGEL ODS column ($5 \mu\text{m}$, $4.6 \times 150 \text{ mm}$).

2.3. Procedures

5-Cl-8-HQ solution (2 ml of a 0.02 mol l^{-1}) in acetonitrile was added to 4.0 ml of a moderately acidic aqueous sample solution containing the metal ions. To the resultant solution, 1.0 ml

of a 2.0 mol l^{-1} sodium acetate solution was added. After complete complex formation, the metal complexes were extracted by adding a mixed salt of 2.5 g ammonium sulfate and 0.5 mmol (0.17 g) TBAP as the salting-out agent followed by vigorous shaking for about 1 min. The recovered volume of the acetonitrile phase was 2.0 ml under experimental conditions. A $100\text{-}\mu\text{l}$ portion of the acetonitrile extract was injected into the analytical column. The complexes were eluted with a 3:1 (v/v) acetonitrile- 0.02 mol l^{-1} sodium acetate solution containing $5 \times 10^{-3} \text{ mol l}^{-1}$ 5-Cl-8-HQ as the mobile phase. The flow rate was 1.0 ml min^{-1} , and the detector was operated at 390 nm.

About 1 g of the standard reference materials, citrus leaves (NBS, SRM 1572) and bovine liver

(NBS, SRM 1577a), was separately treated by the wet digestion method using a mixed acid of nitric acid–sulfuric acid–perchloric acid at about

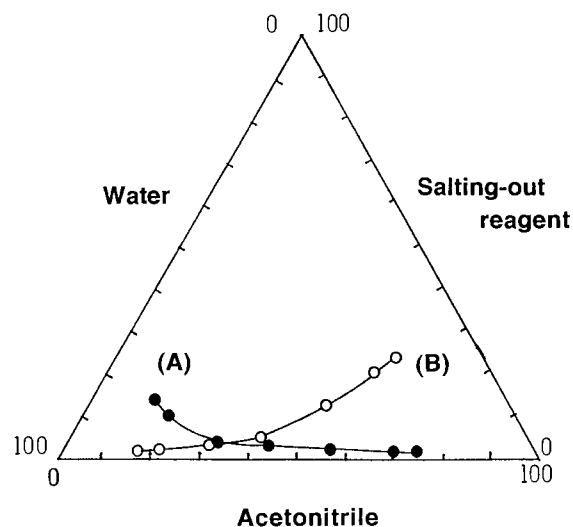


Fig. 3. Ternary phase-diagram for the water/salting-out agent/acetonitrile system (A), ammonium sulfate; (B), TBAP; the lines indicate the composition of the three compounds under which homogeneous solutions form.

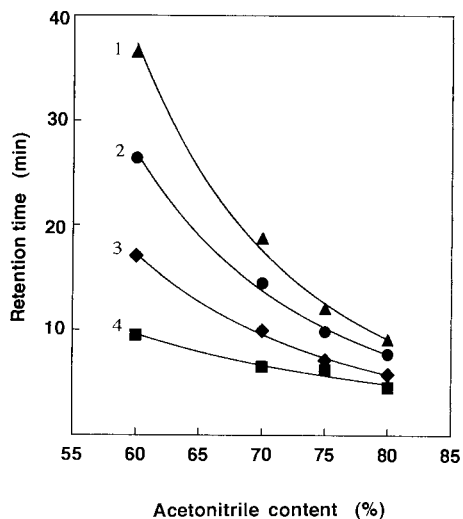


Fig. 4. Effect of acetonitrile content in the mobile phase on retention times. The concentration of metal ions, $0.1 \mu\text{g ml}^{-1}$; the experimental conditions are described in Section 2.3; (1), Mn(II); (2), Fe(III); (3), Al(III); (4), Cu(II).

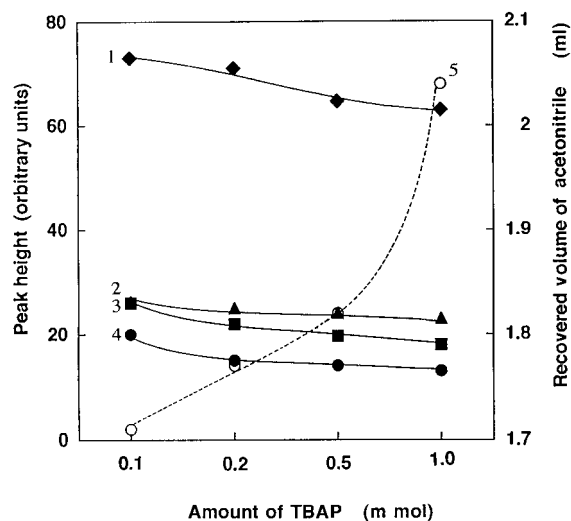


Fig. 5. Effect of TBAP amounts on peak heights. The solid lines are the same as those shown in Fig. 4; the dotted line (5) indicates the recovered volume of acetonitrile after phase separation. The chromatographic conditions are given in Section 2 of the text.

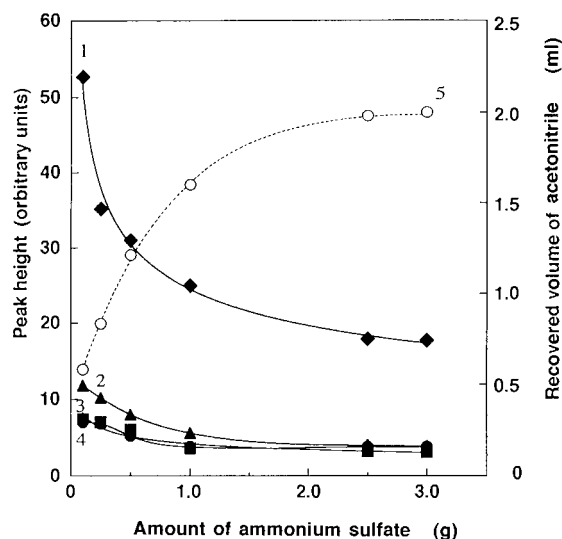


Fig. 6. Effect of ammonium sulfate amounts on peak heights. The chromatographic conditions are given in Section 2 of the text.

200°C. The sample solutions were adjusted to about pH 2 with 2 mol l^{-1} sodium hydroxide and then diluted to 100 ml with water.

Table 1
Statistical analyses and detection limits

Metal ion	Regression line	Correlation coefficient	Detection limit (ng ml ⁻¹)
Cu(II)	$Y = 4.91 + 140X$	0.9966	3.1
Al(III)	$Y = 24.2 + 244X$	0.9972	4.8
Fe(III)	$Y = 1.46 + 94.6X$	0.9997	2.7
Mn(II)	$Y = 0.40 + 173X$	0.9952	3.3

X and Y are metal concentrations in $\mu\text{g ml}^{-1}$ and peak height in arbitrary unit, respectively.

3. Results and discussion

3.1. LC separation of metal complexes

Acetonitrile has been used as a modifier of mobile phases for the separation of a variety of compounds by the reversed phase LC method. Usually aqueous samples are injected into an ODS column and are then eluted with a mixture of acetonitrile and aqueous solution. Fig. 1(A) shows a typical chromatogram obtained for the separation of Al(III), Cu(II), Fe(III) and Mn(II) complexes with 8-HQ where the sample solution was a mixture of 1:1 (v/v) acetonitrile-0.02 mol l⁻¹ acetate buffer (pH 5.9) containing 5×10^{-3} mol l⁻¹ 8-HQ. Elution peaks were very sharp and good separation was achieved. When the acetonitrile extract obtained with the salt-induced phase separation was directly injected into the column, the peaks were broader and a little distorted, as shown in Fig. 1(B). This is probably because the sample was much different from the mobile phase in composition [17]: the acetonitrile extract was about 4:1 (v/v) acetonitrile-aqueous solution containing 0.25 mol l⁻¹ TBAP. A well-defined chromatogram illustrated in Fig. 1(C) was obtained when the acetonitrile extract was injected after diluting it (at a volume ratio of 1:1) with water. The injected sample was finally a mixture of 2:3 (v/v) acetonitrile–water; the experimental procedure is somewhat tedious and therefore seems inappropriate for LC analysis.

We have tried developing LC analysis using direct injections of the acetonitrile extract which can be obtained by the salting-out extraction with TBAP and/or ammonium sulfate. For the purpose

of this study, 5-Cl-8-HQ was selected as a derivatization agent for LC determination of metals. Fig. 2 shows typical chromatograms for Al(III), Cu(II), Fe(III) and Mn(II) complexes with the chelating agent, with a mobile phase of 3:1 (v/v) acetonitrile-0.02 mol l⁻¹ sodium acetate. In Fig. 2, the salting-out agents used were TBAP (A), ammonium sulfate (B) and their mixture (C), respectively. The metal complexes were found to be more strongly retained on the ODS column than the 8-HQ complexes. The volume ratio of acetonitrile/aqueous solution in the mobile phase was almost the same as that of the acetonitrile extract sample injected. The salting-out agent, however, affected the elution behavior as shown in Fig. 2; the baseline increased (A) and decreased (B) when TBAP and ammonium sulfate were used, respectively. This is because the two substances have opposite effects on the retention of 5-Cl-8-HQ in the reversed phase LC system. The mixture of both salts was chosen because the best result was obtained (C).

3.2. Phase separation with salting-out agents

The salt-induced phase separation between acetonitrile and aqueous solution was observed by addition of a variety of inorganic and organic electrolytes. Water-miscible organic solvents have drawbacks over water-immiscible ones in that the phase volumes depend on added amounts of the salting-out agent. A constant and possibly large amount of the salt must be added to get constant recovered-volumes of the two phases. In the present study, a relatively small amount of TBAP

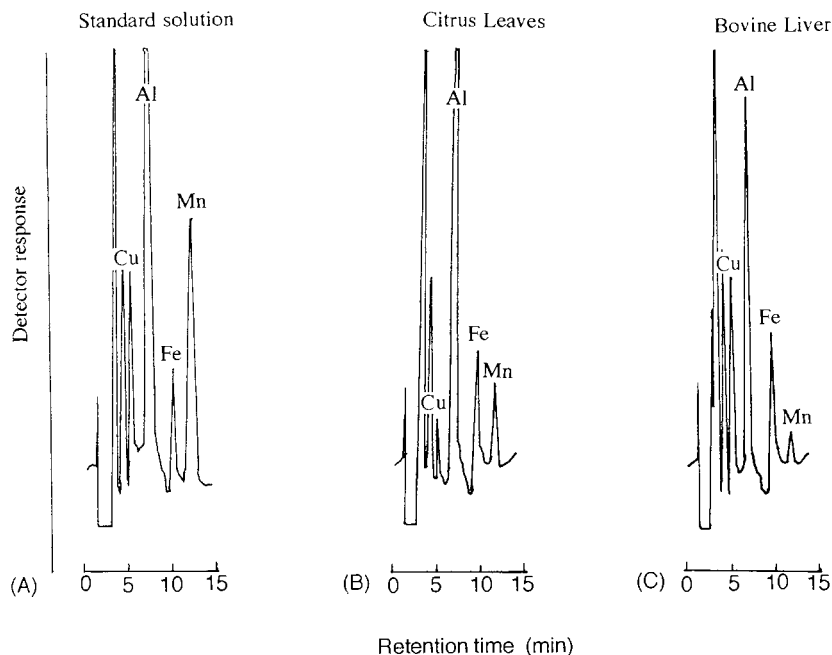


Fig. 7. Determination of aluminum, copper, iron and manganese in biological samples. (A), $0.1 \mu\text{g ml}^{-1}$ of each metal ion solution; (B), citrus leaves; (C), bovine liver.

was added together with ammonium sulfate to achieve a rapid and clear phase separation between acetonitrile and aqueous solution. Fig. 3 shows a ternary phase-diagram expressed in weight percent for the water/salting-out agent/acetonitrile system. The lines indicate minimum amounts of the salt at which the two phases begin to separate, and no phase separation takes place under the lines.

3.3. Experimental conditions for LC determination of metals

The mobile phase was tested by changing the ratio of acetonitrile and 0.02 mol l^{-1} sodium acetate solution. The results shown in Fig. 4 indicate that the retention times gradually decreased as the acetonitrile content of the mobile phase increased. At an acetonitrile content of 80%, the peak-to-peak separation was incomplete. The mobile phase contained 75% acetonitrile, corresponding 3:1 (v/v) acetonitrile- 0.02 mol l^{-1} sodium acetate solution, was selected.

The effects of experimental parameters such as the amounts of TBAP and ammonium sulfate on the peak heights of the metals was investigated. Fig. 5 shows the relationship between the amount of TBAP and peak heights for Al(III), Cu(II) and Fe(III) and Mn(II). The recovered volume of the acetonitrile phase was also plotted against the amount of TBAP as the salting-out agent. It can be seen that all peaks gradually decreased in height as the amount of TBAP increased from 0.1 to 1.0 mmol. The recovered volume of acetonitrile phase increased from 1.71 to 2.04 ml without addition of ammonium sulfate. Fig. 6 shows the relationship between the amount of ammonium sulfate and peak heights for all metal ions investigated. It can be seen that the addition of ammonium sulfate ranging from 2.5 to 3.0 g gave approximately constant values in peak height even though an emulsion formed between the two phases. When 0.2–1.0 mmol TBAP and 2.5–3.0 g ammonium sulfate were added together as the salting-out agents, the recovered volume of the acetonitrile phase (2.0 ml) and the peak heights

Table 2
Analytical results for standard reference materials

Sample	Metal	Concentration found ($\mu\text{g g}^{-1}$)	Certified value ($\mu\text{g g}^{-1}$)
Bovine liver	Cu	157 ± 2	158 ± 2
	Al	- ^a	2
	Fe	190 ± 3	194 ± 20
	Mn	9.6 ± 0.7	9.9 ± 0.8
Citrus leaves	Cu	15.6 ± 0.7	16.5 ± 1
	Al	88.2 ± 1.1	92 ± 15
	Fe	91.6 ± 1.8	90 ± 10
	Mn	22.1 ± 0.5	23 ± 1

^a No detection

were kept almost constant. In the present study, 0.5 mmol (0.17 g) of TBAP and 2.5 g of ammonium sulfate were added because a rapid and clear separation of the two phases could also be achieved.

3.4. Calibration graphs and detection limits

From the results obtained using the procedures described above, calibration graphs of peak height (Y) and metal concentration (X) were constructed for the four metals. Linear relationships were obtained over the concentration of each metal up to $10 \mu\text{g ml}^{-1}$ for $100 \mu\text{l}$ injections. The equations of the graphs and their regression results are listed in Table 1, together with the detection limits defined as the metal concentration giving a signal-to-noise ratio of 3.

3.5. Analytical applications

In order to validate the proposed method, determination of Al, Cu, Fe and Mn in two biological samples were investigated. Fig. 7 shows the chromatograms obtained using the procedure described in Section 2.3. The analytical results (replicate five determinations) listed in Table 2 were in good agreement with the certified values, except for aluminum in bovine liver; the concentration of aluminum in bovine liver was too low to be determined. It can be concluded that the method is acceptable and seems very useful for the analysis of trace metals in biological materials. We expect that interference from matrices or large

amounts of foreign ions can be removed using the present method.

4. Conclusion

A salting-out extraction method as a pretreatment step is described for the liquid chromatographic determination of aluminum, copper, iron and manganese in biological samples of bovine liver and citrus leaves. The results indicate that the present LC method including the acetonitrile extraction gives a simple and rapid technique to eliminate interference due to matrix effect and coexisting constituents in biological samples. Moreover, effective preconcentration with higher enrichment factors can be achieved by changing the volume ratio of the two phases and the amount of salting-out agents.

References

- [1] S.S. Brown (Ed.), *Clinical Chemistry and Clinical Toxicology of Metals*, Elsevier, Amsterdam, 1997.
- [2] E. Bergman, *Toxic Metals and Their Analysis*, Heyden and Son, London, 1980.
- [3] G.V. Lyengan, W.E. Kollmer, J.M. Bowman, *The Elemental Composition of Human Tissue and Body Fluids*, Verlag Chemie, Weinheim, Germany, 1978.
- [4] J.G. Dorsey, W.T. Cooper, J.F. Wheeler, H.G. Barth, J.P. Foley, *Anal. Chem.* 66 (1994) 500R.
- [5] K. Robards, P. Starr, E. Patsalides, *Analyst* 116 (1991) 1247.
- [6] S. Ichinoki, M. Yamazaki, *Anal. Chem.* 57 (1985) 2219.

- [7] A.M. Bond, R.W. Knight, J.B. Reust, D.J. Tucker, G.G. Wallace, *Anal. Chim. Acta* 182 (1986) 47.
- [8] Y. Nagaosa, T. Kobayashi, *Int. J. Environ. Anal. Chem.* 61 (1995) 231.
- [9] Y. Zao, C. Fu, *Analyst* 116 (1991) 621.
- [10] C.S. Lin, X.S. Zhang, *Analyst* 112 (1987) 1659.
- [11] B.J. Mueller, R.J. Lovett, *Anal. Chem.* 59 (1987) 1405.
- [12] Y. Shijo, K. Takada, N. Uehara, *Anal. Sci.* 9 (1993) 315.
- [13] Y. Nagaosa, T. Suenaga, A.M. Bond, *Anal. Chim. Acta* 235 (1990) 279.
- [14] S. Ichinoki, M. Yamazaki, S. Suzuki, *J. Chromatogr. Sci.* 30 (1992) 233.
- [15] S. Ichinoki, M. Yamazaki, *Anal. Sci.* 5 (1989) 465.
- [16] E. Kaneko, H. Hoshino, T. Yotsuyanagi, *Chem. Lett.* (1992) 955.
- [17] T. Fujinaga, Y. Nagaosa, *Bull. Chem. Soc. Jpn.* 53 (1980) 416.

Differential pulse polarographic determination of trace amounts of vanadium and molybdenum in various standard alloys and environmental samples after preconcentration of their morpholine-4-carbodithioates on microcrystalline naphthalene or morpholine-4-dithiocarbamate cetyltrimethyl-ammonium bromide-naphthalene adsorbent

S. Puri, R.K. Dubey, M.K. Gupta¹, B.K. Puri*

Chemistry Department, Indian Institute of Technology, Hauz Khas, New Delhi-110016, India

Received 10 June 1997; received in revised form 5 September 1997; accepted 12 September 1997

Abstract

A highly selective, sensitive, and fairly rapid and economical differential pulse polarographic (DPP) method has been reported for the determination of trace amounts of vanadium and molybdenum in standard alloys and various environmental samples. The morpholine-4-carbodithioates of these metals were retained (> 99% recovery) quantitatively on microcrystalline naphthalene in the pH range 4.5–6.9 for vanadium and 1.5–4.5 for molybdenum. These metals were determined by DPP after desorption with 10 ml of 1 M HCl. Vanadium and molybdenum may also be preconcentrated by passing their aqueous solutions under similar conditions on morpholine-4-dithiocarbamate CTMAB-naphthalene adsorbent packed in a column at a flow rate of 1–5 ml min⁻¹ and determined similarly. The detection limits are 0.20 ppm for vanadium and 0.04 ppm for molybdenum at minimum instrumental settings (signal to noise ratio = 2). The linearity is maintained in the following concentration ranges, vanadium 0.50–10.0 and molybdenum 0.10–9.0 ppm, with a correlation factor of 0.9996 (confidence interval of 95%, slopes 0.0196 and 0.01497 $\mu\text{A } \mu\text{g}^{-1}$, intercepts 3.65×10^{-3} and -1.92×10^{-3} respectively) and relative standard deviation of 1.1% in the microcrystalline method, while in the column method, the linearity is maintained in the concentration ranges, 0.50–6.5 for vanadium and 0.10–5.5 ppm for molybdenum with correlation factor of 0.9994 (with confidence interval of 95%, slopes 0.0194, 0.015 $\mu\text{A } \mu\text{g}^{-1}$, intercepts 3.60×10^{-3} and -1.90×10^{-3} respectively) and relative standard deviation of 1.4%. Various parameters such as the effect of pH, reagent, naphthalene and CTMAB concentrations, volume of aqueous phase and interference of a large number of metal ions on the estimation of vanadium and molybdenum have been studied in detail to optimize the conditions for their voltammetric determination at trace level in various standard alloys and environmental samples. © 1998 Elsevier Science B.V. All rights reserved.

Keywords: Molybdenum and vanadium determination; Preconcentration; Differential pulse polarography; Morpholine-4-carbodithioate; Standard alloys and environmental samples

* Corresponding author.

¹ On study leave from Zakir Husain College, University of Delhi, Delhi-110007, India.

1. Introduction

Vanadium and molybdenum are the most important elements which affect the physical properties of steel, alloys and high purity metals. Vanadium is widely distributed in the earth's crust, its compounds can be highly toxic to man and animals and cause environmental diseases when released in the atmosphere [1]. It has also been noted that the environmental background levels of vanadium have been slowly rising as a result of the combustion of fossil fuels which have high vanadium content [2]. Vanadium is therefore, important not only because of its toxicity at high levels but also because it is an environmental pollutant [3]. Occupational exposure to vanadium has been observed in several industrial processes, for example, in iron and steel production, in the manufacture of pigments, printing inks and paints, in the glass industry, in the cleaning and repairing of oil fired boilers, particularly in electricity power stations [4–6]. Molybdenum is an essential element to all living organisms. Its biological role is extremely important in the nitrogen metabolism of plants. However, an excess of this element becomes harmful to ruminants since the adsorption of copper by the liver is depressed [7]. Very low concentrations of molybdenum and vanadium are present in various matrices such as plants, soils, sea-water, etc. Therefore, it is very important from the analytical point of view to develop sensitive, selective, rapid and economical methods for their quantitative determination even when present in trace amounts. These metals may be determined spectrophotometrically after extraction of their metal complexes into suitable organic solvents, but these methods have a limited sensitivity and may have many types of interferences [8–12]. NAA, AAS, graphite furnace AAS, ICP-AES, ICP-MS may be used for the trace determination of metals in complex materials, but these instruments are highly expensive, their day to day maintenance cost is high and they are not free from various types of interferences [13–16].

Vanadium and molybdenum may also be determined polarographically after the extraction of their metal complexes into various organic solvents [17–23]. However, the method has poor

sensitivity since the organic phase has to be mixed with a solvent of high dielectric constant to obtain well defined polarograms, and is also time consuming as pure nitrogen gas has to be passed for 15–20 min, which may also result in partial evaporation of the organic solvent and thus effects the reproducibility of the method. Catalytic [24–26], adsorptive stripping voltammetric (AdSV) [27–29] and square wave adsorptive stripping voltammetry methods [30] are very sensitive for the determination of these metals, but in such cases the reproducibility depends upon a number of parameters like the rigid control of temperature, pH, reagent concentration, surface area of the electrode and the rate of formation of the film on the electrode. Adsorptive stripping voltammetry methods are also time consuming due to prolonged deposition and stripping steps and removal of oxygen with highly pure nitrogen gas and are not selective [27–30]. The preconcentration step proposed in the present method not only concentrates the sample from a large volume (300–350 ml) to a small volume (10–15 ml) to make the differential pulse polarography successful for the trace estimation of the metal ions, but also makes the method highly selective because different metal ions are adsorbed at different pH values. The various parameters developed are highly flexible and can be applied over a wide range while in the case of stripping voltammetric methods the various parameters related to them need rigid control to obtain reproducible results. The removal of oxygen hardly takes 2–5 min in the present method, while it takes 15–20 min in other electrochemical methods [17–30].

In the present work, we have developed a simple, rapid, economical, sensitive and selective method for the direct differential pulse polarographic determination of vanadium and molybdenum after adsorption of their morpholine-4-carbodithioates on microcrystalline naphthalene. Alternatively, these metal ions may be preconcentrated after passing their aqueous solutions over morpholine-4-dithiocarbamate CTMAB-naphthalene adsorbent placed in a column. The microcrystalline method is rapid but the column method gives a better preconcentration factor (2.5 times). This reagent is fairly sensitive,

selective, can be easily prepared in the laboratory and does not interfere in the polarographic determination of metals [31]. Various parameters have been evaluated and the procedure developed has been successfully employed for the determination of trace and ultratrace amounts of vanadium and molybdenum in various standard alloys and environmental samples.

2. Experimental

2.1. Apparatus

Polarograms were recorded with an Elico Model CL-90 three electrode polarograph. It was outfitted with a model LR-108 *X-Y* recorder. All atomic absorption measurements were made using a Varian Model 475 AAS. An Elico model LI-120 pH meter was used for pH measurements. A funnel tipped glass tube (60 × 6 mm i.d.) was used as a preconcentration column. It was plugged with poly(propylene) fibres and filled with the slurry (adsorbent) to a height of 1.0–1.2 cm after slightly pressing the adsorbent in the column with a flat glass rod.

2.2. Reagents

All reagents were of analytical grade and double distilled water was used whenever required. Molybdenum(VI) solution was prepared by dissolving 12.8800 g of $(\text{NH}_4)_6\text{Mo}_7\text{O}_{24}\cdot 4\text{H}_2\text{O}$ in water in the presence of a few millilitres of concentrated HCl, and made-up to 1000 ml in a calibrated flask with distilled water. Vanadium(V) solution was prepared by dissolving 2.3000 g of NH_4VO_3 in a few ml of 1 M NaOH, acidified with dilute HCl and then diluted to 1000 ml in a standard flask. Both solutions were standardized by known methods [32] and made 1000 ppm corresponding to pure metal by approximate dilution. Potassium morpholine-4-dithiocarbamate (MCDT) was prepared, by the method described in the literature [31]. Morpholine (17.5 g) in dry ether was placed in a 250 Erlenmeyer flask and to this solution, stoichiometric amounts of carbon disulphide (nearly 25 ml) was added dropwise

with constant stirring. The reaction mixture was cooled thoroughly in an ice-salt mixture and to this solution stoichiometric amount of potassium hydroxide ~12 g (dissolved in a minimum amount of water) was added dropwise with constant stirring. The addition was completed in about 3–4 h. The crude product was filtered over suction and washed several times with solvent ether. The residue was recrystallized twice from isopropyl alcohol. The pure product is white needle shaped crystals, highly soluble in water. The melting point 175°C was found to be the same as reported in the literature. A 0.2% aqueous solution of MCDT was prepared. For the preparation of MCDT CTMAB-naphthalene

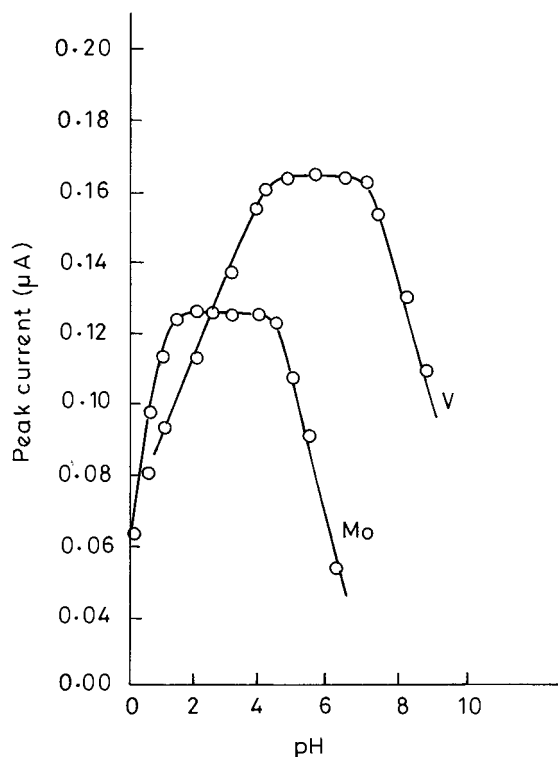


Fig. 1. Effect of pH on adsorption/retention of molybdenum and vanadium complex; molybdenum, 100.0 µg; vanadium, 100.0 µg; reagent, 2.0 ml; (0.2%), naphthalene, 2.0 ml (20%), reference reagent blank, supporting electrolyte Mo: HCl, 10 ml (1 M), pyridine 2 ml (1 M), water 3 ml, (total 15 ml); V: HCl, 10 ml (1 M), pyridine 2 ml (1 M), NaOH, 3 ml (1 M), (total 15 ml); instrumental settings: scan rate = 12 mV s⁻¹, modulation amplitude = 50 mV and drop time = 0.5 s.

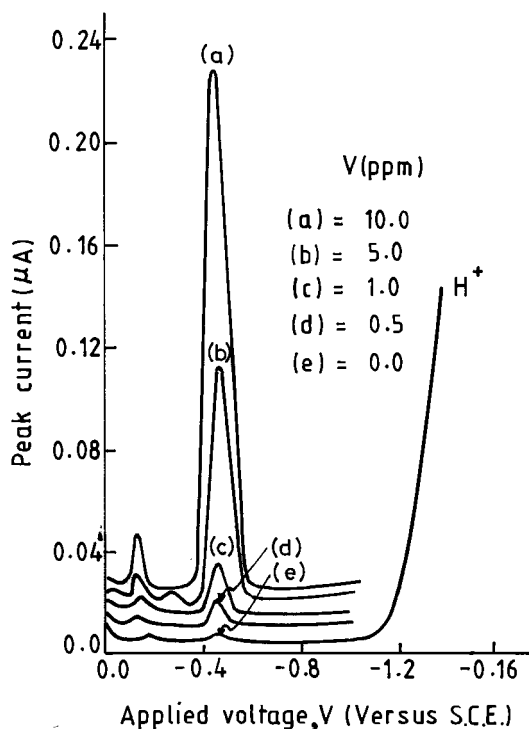


Fig. 2. Typical differential-pulse polarograms in a series of vanadium solutions (ppm). Conditions same as Fig. 1.

adsorbent, a solution of naphthalene was prepared by dissolving a 10 g sample in 100 ml of acetone followed by 1 l of distilled water containing 0.050 g cetyltrimethyl ammonium bromide. It was stirred at 25–30°C on a hot plate/stirrer, followed by 100 ml of 0.2% MCDT solution in distilled water. The mixture was stirred for 3 h and kept for 5 h at room temperature. The supernatant liquid was aspirated with a siphon and the residue was washed twice with double-distilled water. The final adsorbent was a slurry of MCDT CTMAB-naphthalene and stored in a bottle for subsequent use. Solutions of naphthalene in acetone (20%), pyridine 1 M, alkali metal salts (1%) and various metal salts (0.1%) in distilled water were used. Buffer solutions were prepared from 0.2 M acetic acid and 0.2 M ammonium acetate for pH 3–6.

2.3. Pretreatment of standard alloys and environmental samples

The solution of the standard alloys was prepared as described in the literature [31]. A 0.1–1.0 g sample of each of the standard alloy was dissolved in 30–60 ml of 6 M HCl by heating on a hot plate; then 3–5 ml of 30% hydrogen peroxide was added. The excess of peroxide was decomposed by heating. The solution was cooled, filtered if needed, and diluted to 100 ml with distilled water in a calibrated volumetric flask.

Solid environmental samples were oven dried at 200°C for 2 h. A 0.1–0.5 g sample of each was decomposed with 50–60 ml of 6 M HCl and 10 ml of concentrated HNO₃. The mixture was heated on a hot plate almost to dryness. The residue was then dissolved in 10 ml of 1 M HCl and diluted with 10 ml of distilled water and filtered if needed. Finally, the solution was made up to 100 ml with distilled water in a calibrated volumetric flask [31].

The liquid environmental sample (100–500 ml of each) was taken and 5 ml of concentrated nitric acid was added to it. The solution was heated

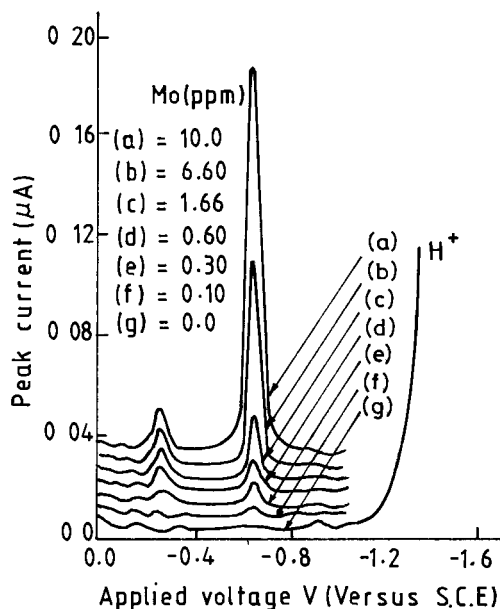


Fig. 3. Typical differential-pulse polarograms in a series of molybdenum solutions (ppm). Conditions same as Fig. 1.

almost to dryness on a hot plate, the residue was then dissolved in 5 ml of 1 M HCl and finally the solution was made up to 100 ml with distilled water in a calibrated volumetric flask [31]. The tap water samples may be analysed directly without the above treatment using the standard addition method. The recovery is more than 95% in each case.

2.4. General procedure

An aliquot of vanadium (V) or molybdenum (VI) (100 μg each) solution was taken individually in a 250 ml Erlenmeyer flask with a tightly fitting stopper. MCDT (2 ml of 0.2% reagent) was added and the solution was then diluted to 30–40 ml. The pH was adjusted with 2.0 ml of a buffer of pH 5.5 and 3.0, for vanadium and molybdenum, respectively. The solution was mixed well and allowed to stand for a few seconds. Then, 2.0 ml of a 20% solution of naphthalene in acetone was added to it while continuously shaking. The solid mass so formed was separated by filtration on a Whatman filter paper No. 1041. The residue was dried in the fold of a filter paper and transferred to an Erlenmeyer flask. It was shaken vigorously with 10 ml of 1 M HCl solution, and then transferred to the polarographic cell. In the column method, the adsorbent was conditioned to pH 5.5 for vanadium and 3.0 for molybdenum, with 5 ml of the buffer solutions, before passing the test solutions through the column at a flow rate of 1–5 ml min^{-1} . The column was finally washed with distilled water. Desorption of the metals was carried out by passing 10 ml of 1 M HCl at the same flow rate and the solution was transferred to the polarographic cell. Pyridine (2 ml of 1 M) was added to the polarographic cell. In case of vanadium, in addition to pyridine 3 ml of 1 M NaOH solution was also added. The total volume was made up to 15 ml with the addition of distilled water if needed. The differential pulse polarograms were recorded after oxygen was removed by passing nitrogen gas for 2–5 min.

3. Results and discussion

Preliminary observations indicated that vanadium(V) and molybdenum(VI) give well defined differential pulse polarograms with $E_p = -0.44$ V (pH ~ 1) and -0.68 V (pH ~ 1) vs. S.C.E. in pyridine–hydrochloric acid sodium chloride and pyridine–HCl solutions, respectively. The half peak width was 50 ± 3 for V(V) and 80 ± 1 mV for Mo(IV). Under these conditions, the cyclic voltammograms using mercury pool as the working electrode were recorded. In both cases only cathodic waves were obtained. It clearly indicates that these metal ions were reduced irreversibly under these conditions. The effect of the supporting electrolyte (1 M pyridine solution) concentration was studied on the polarograms of molybdenum and vanadium. The peak height and peak potential were almost constant in 1.0–6.0 ml of 1 M pyridine solution for molybdenum and 1.0–4.0 ml of 1 M pyridine solution for vanadium. Therefore, 2 ml of 1 M pyridine was used as the supporting electrolyte throughout this work.

3.1. Effect of pH on the differential pulse polarograms

The effect of pH was studied by adding a dilute solution of NaOH to the polarographic cell solution keeping other variables constant after the preconcentration step. In case of vanadium, two waves were obtained with peak potentials of (E_p) = -0.11 V and -0.44 V vs. S.C.E. The wave height of the first wave is very small as compared with the second wave. The shape and wave height of the second wave was found to be constant in the pH range of 1.0–4.0, however, E_p was shifted towards the more negative direction. The plot of E_p vs. pH was not linear indicating that protonation reaction is not taking part in the overall electrode process [33]. In case of molybdenum, the effect of pH could not be studied because the wave became ill-defined with the addition of NaOH.

Table 1
Effect of salts and metal ions

Salt or metal ion added	Tolerance Limit		Remarks
	Molybdenum (mg)	Vanadium (mg)	
Na ₂ SO ₄ , NaCl, NaBr, NaF, NaI, Na ₂ CO ₃ , CH ₃ COONa, potassium sodium tartrate, Na ₂ HPO ₄ , Na ₂ C ₂ O ₄ , Na ₂ S ₂ O ₃ , sodium citrate, KCNS, KNO ₃	100	100	—
Na ₂ EDTA	0.75	0.75	—
U(VI), Se(IV), Ti(III), Cr(III), Mn(II), Te(IV), Al(III), As(III), Sb(III), Ir(III), Os(VIII)	50.0	50.0	—
Mo(VI)	—	10.0	—
Zn(II)	50.0	25.0	—
Fe(III), Cu(III)	5.0	5.0	Iron masked with 5 ml of 20% triethanolamine and copper with 5 ml of 5% NaCN solution.
Ni(II)	10.0	50.0	—
V(V)	10.0	—	—
Bi(III), Co(II)	10.0	10.0	—
Sn(II)	50.0	10.0	—
Tl(I)	10.0	0.10	—
Pb(II)	5.0	0.5	After masking with 0.5 ml of 1% Na ₂ EDTA solution.
Cr(VI)	5.0	10.0	—
Rh(III)	50.0	5.0	—
Ru(III)	50.0	5.0	—
Pd(II)	50.0	5.0	—
Cd(II)	10.0	50.0	After masking with 5 ml of 5% NaCN solution.
In(III)	2.0	5.0	—

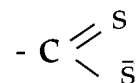
Mo: 100 µg, V: 100 µg, reagent (0.2%): 2 ml, naphthalene (20%): 2 ml, pH: Mo: 3.0, V: 5.5. E_p (V) vs. S.C.E.; Mo: -0.68 V, V: -0.44V.

3.2. Effect of pH on adsorption

The effect of pH on adsorption of the metal complex on naphthalene was studied at different pH values keeping other variables constant (Fig. 1). It was found that morpholine-4-carbodithioates of molybdenum and vanadium were quantitatively retained on naphthalene in the pH range 1.5–4.5 and 4.4–6.9 respectively. Analogous to the case in the column method. Addition of 1–5 ml of buffer did not have any effect on the adsorption, therefore, 2.0 ml of the buffer of respective pH was used in the subsequent studies.

3.3. Retention characteristics of MCDT.

The chelating agent has the functional groups



of the dithiocarbamate molecules which is coordinated with the metal. Hence, molybdenum and vanadium form chelates with four and two molecules of dithiocarbamate respectively [11]. The retention capacity of morpholine-4-dithiocarbamate supported on naphthalene was determined by the batch method. This experiment was carried out by taking a solution containing 5 mg each of

metal, 2.0 ml of required buffer solution, a suitable amount of the adsorbent in a 100 ml separatory funnel. The mixture was diluted to 30 ml. It was shaken for 30 min, and filtered through a filter paper. The amount of the metal ion in the filtrate was determined by AAS. The naphthalene-chelating agent material was dried on a filter paper, and the solid mass was weighed on a balance. The retention capacity of the metal ion for the adsorbent was found to depend on the amount of adsorbent. The maximum amount of retention per gram of the adsorbent was 1.3 mg of molybdenum and 1.6 mg for vanadium.

3.4. Reaction conditions

Reaction conditions were established using 100 μg of molybdenum or vanadium individually. The effect of HCl concentration on the desorption of metal complexes with 10 ml of 0.1–5.0 M HCl keeping other variables constant was studied. The peak height and shape of the differential pulse polarograms were found to be constant in the concentration range 0.5–2.0 M for molybdenum and 0.5–5.0 M for vanadium. Therefore, 10 ml of 1 M HCl was used throughout the present work. The reagent concentration was varied over a range of 0.1–7.0 ml (0.2%). It was found that adsorptions were quantitative and maximum for the concentration range, molybdenum 0.5–4.5 and vanadium 0.6–4.0 ml (0.2%). Therefore, 2.0 ml of 0.2% reagent solution was used in the subsequent studies. Various amounts of naphthalene (20% solution in acetone) was added to the sample solutions keeping other variables constant. It was found that 0.6–4.5 and 0.8–5.0 ml of 20% naphthalene solution was required for the quantitative retention of the molybdenum and vanadium complexes respectively. However, 2.0 ml of 20% naphthalene solution was used to be on the safe side. The effect of shaking time on the adsorption of the metal complexes on naphthalene indicates that the retention was constant and maximum over a range of 0.5–7.0 min and 1 min of shaking time was recommended. In case of the column method, the flow rate was varied from 0.5–8.0 ml min^{-1} . It was found that a flow rate of 0.5–5.0 ml min^{-1} in both cases did not effect the retention of the metal

complex on the adsorbent. Hence, a flow rate of 1–5 ml min^{-1} was recommended for the present work. The volume of the aqueous phase was varied—in the range of 10–700 ml under optimum conditions, keeping other variables constant. It was found that retention was almost constant up to 120 ml of the aqueous phase for molybdenum and vanadium (preconcentration factor 8) whereas in the case of the column method, the peak height was constant up to 350 ml for molybdenum (preconcentration factor ~ 23) and 300 ml for vanadium (preconcentration factor ~ 20). However, in both the cases, 40 ml of aqueous phase was maintained for convenience.

3.5. Calibration:

Calibration graphs for the determination of molybdenum and vanadium were prepared according to general procedure (Figs. 2 and 3). The detection limits were 0.04 ppm for molybdenum and 0.20 ppm for vanadium at the minimum instrumental settings (signal to noise ratio = 2). The linearities were maintained in the following concentration range, molybdenum 0.10–9.0 ppm and vanadium 0.50–10.0 ppm, with a correlation factor of 0.9996 (confidence interval of 95%, slopes 0.0196 and 0.1497 $\mu\text{A } \mu\text{g}^{-1}$, intercepts 3.65×10^{-3} and -1.92×10^{-3} respectively) and relative standard deviation of 1.1% in the microcrystalline method and molybdenum 0.10–5.5 ppm and vanadium 0.50–6.5 ppm with a correlation factor of 0.9994 (with confidence interval of 95%, slopes 0.194 and 0.015 $\mu\text{A } \mu\text{g}^{-1}$, intercepts 3.60×10^{-3} and -1.90×10^{-3} respectively) and relative standard deviation of 1.4% in the column methods.

3.6. Effect of diverse ions

The effect of various salts of anions and cations on the adsorption and subsequently on the differential pulse polarographic determination of 100 μg of molybdenum and vanadium taken individually was studied. Among the various ions examined (Table 1), many could be tolerated up to milligrams levels except EDTA. EDTA ($\sim 700 \mu\text{g}$) could be tolerated probably due to the high

Table 2
Determination of molybdenum and vanadium in standard alloys

Name	Certified (%)	Molybdenum (%)	Vanadium found
JSS 503-4 (Ni–Cr–Steel)	Mo, 0.013; V, 0.004; Ni, 1.24; Cr, 0.70; Mn, 0.63; Si, 0.27; C, 0.33; P, 0.029; S, 0.02; N, 0.0115; Cu, 0.084	0.0135 ± 0.0003	0.0044 ± 0.00012
JSS 607-6 High Speed Steel	Mo, 0.30; V, 0.86; Cu, 0.028; Ni, 0.058; Co, 4.72; Cr, 4.14; Mn, 0.030; W, 16.96; Si, 0.32; C, 0.75; P, 0.012; S, 0.006	0.294 ± 0.005	0.874 ± 0.013
NKK No. 916 (Al–alloy)	Ni, 0.06; Bi, 0.03; V, 0.02; Zn, 0.30; Si, 0.41; Pb, 0.04; Zr, 0.05; Co, 0.03; Sb, 0.01; Fe, 0.54; Cu, 0.27; Mg, 0.10; Cr, 0.05; Ti, 0.10; Sn, 0.05; Ca, 0.03; B, 0.006; Mn, 0.11	—	0.0197 ± 0.0005
NKK No. 920 (Al–alloy)	Ni, 0.29; V, 0.15; Cu, 0.71; Co, 0.10; Cr, 0.27; Si, 0.78; Ti, 0.15; Sn, 0.20; Pb, 0.10; Fe, 0.72; Bi, 0.06; Ga, 0.05; Zn, 0.80; Sb, 0.10; Ca, 0.03; Mg, 0.46; Mn, 0.20	—	0.146 ± 0.0003
NKK No. 1021 (Al–alloy)	V, 0.007; Ni, 0.14; Fe, 0.99; Zn, 1.76; Ti, 0.04; Sn, 0.10; Si, 0.10; Mn, 0.20; Mg, 0.29; Cr, 0.03; Pb, 0.18; Zr, 0.01; Bi, 0.01; Sb, 0.01; Ca, 0.004	—	0.0073 ± 0.0002
NBS SRM-163 Cr–Steel	Mo, 0.029; Cu, 0.087; Ni, 0.081; Cr, 0.982; Mn, 0.897; Si, 0.488; C, 0.933; P, 0.007; S, 0.027; N, 0.007	0.0297 ± 0.0008	—

Average of five determinations, ± S D.

In steel samples, Fe³⁺ was eliminated by pre-extraction as trifluoroethylxanthate.

In the case of Al–alloys, Cu²⁺ and Cd²⁺ were masked with 5 ml of 5% NaCN solutions, while Fe³⁺ with 5 ml of triethanolamine solution.

value of formation constants of these metals than their dithiocarbamates. In the case of metal ions, many did not interfere up to milligram levels. Fe(III), Cu(II) and Cd(II) interfered in both cases. Fe(III) was masked with 5 ml of 20% triethanolamine solution, while Cu(II) and Cd(II) with 5 ml of 5% solution of sodium cyanide during the preconcentration step. Tl(I) and Pb(II) interfered in the determination of vanadium only. Pb(II) could be masked with 0.5 mg of EDTA (0.5 ml of 1% EDTA solution) while 0.1 mg of Tl(I) could be tolerated by the controlling the pH. The concentration of Cu(II), Pb(II), Tl(I) and Cd(II) are higher than 5 mg in a sample, these could be easily removed by preextraction of their trifluoroethylxanthates into chloroform at pH 8.5–9.5 [11]. Thus the method is highly selective and has been applied safely in the estimation of these metals in various complex samples.

3.7. Application to the analysis of standard alloys and environmental samples

The accuracy and applicability of the proposed method was evaluated by its application on various standard alloys and environmental samples.

In the case of aluminium alloys and environmental sample, an aliquot of the sample (40–100 ml) was taken, 5 ml of 5% sodium cyanide and 5 ml of 20% solution of triethanolamine were added and then the general procedure was applied. For steel analysis, the excess of iron was removed by the preextraction of iron as trifluoroethylxanthate at pH 9 [11]. Relatively low results were obtained when Fe(III) was removed as hydroxide with NaOH solution [34] since iron oxide and iron hydroxides are well known adsorbents. After removal of Fe(III), molybdenum and vanadium were determined using the general procedure. In the case of environmental samples, the results were compared with atomic absorption spectrometry after the preconcentration step developed in the present method. The results are given in Tables 2 and 3.

4. Conclusion

Catalytic and stripping voltammetric methods are more time consuming and also depend on the rigid control of conditions. The proposed method has solved most of these problems and has been

Table 3
Determination of molybdenum and vanadium in environmental samples

Sample	Amount found by the present method ($\mu\text{g g}^{-1}$)/($\mu\text{g ml}^{-1}$)		Amount ^a found by AAS method ($\mu\text{g g}^{-1}$)/($\mu\text{g ml}^{-1}$)	
	Molybdenum	Vanadium	Molybdenum	Vanadium
Flyash near, Indraprastha (IP) power station, New Delhi, India.	28.4 ± 0.5^b	198 ± 3^b	28.2 ± 0.4^b	200 ± 4^b
Soil, near Wazirpur Industrial area, New Delhi, India.	23.93 ± 0.14^b	85 ± 2^b	23.9 ± 0.07^b	87 ± 3^b
Soil, near Indraprastha (IP) power station, New Delhi, India.	26.12 ± 0.15^b	172 ± 4^b	26.08 ± 0.4^b	175 ± 48^b
Water, Okhla canal near Okhla Industrial area, Okhla, New Delhi, India.	0.415 ± 0.006^b	0.193 ± 0.004^b	0.425 ± 0.007^b	0.195 ± 0.005^b
Waste water near Indraprastha (IP) power station, New Delhi, India.	0.0126 ± 0.005^c	0.115 ± 0.003^b	0.012 ± 0.0007^c	0.120 ± 0.004^b
Water, Yamuna river near Indraprastha (IP) power station, New Delhi, India.	0.0114 ± 0.0003^c	0.027 ± 0.0007^c	0.0122 ± 0.0004^c	0.029 ± 0.0005^c
Tap water from IIT Delhi, New Delhi, India.	0.0087 ± 0.0005^c	0.0024 ± 0.0001^c	0.009 ± 0.0007^c	0.0020 ± 0.0001^c

Average of five determinations, \pm S D.

^a After preconcentration by the present method.

^b Microcrystalline method

^c Column method

Standard addition method was also applied for water samples.

successfully applied to the determination of molybdenum and vanadium in various complex materials. Atomic adsorption spectrometric method may be used following the preconcentration step after removal of naphthalene by filtration, but it is expensive, day to day maintenance is high and it is not free from matrix effect. The column method improves the preconcentration factor by 2.5 times that of the microcrystalline method but is relatively more time consuming as compared with the microcrystalline method. The developed procedure can also be employed for the determination of these metals in biological samples like bovine liver, human hair, nails and various vegetable products. Simultaneous determination of these metal ions is possible if the preconcentration is carried out at pH 4.5.

References

- [1] D.H.K. Lee, *Metallic Contaminants and Human Health*, Academic Press, New York, 1972, p. 153.
- [2] W.L. Nelson, *Oil Gas J.* 71 (1973) 54.
- [3] V.W. Vouk, W.T. Piver, *Environ. Health. Perspec.* 47 (1983) 201.
- [4] M. Pyy, L. Kiviluoto, A. Pakarinen, *Int. Arch. Occup. Environ. Health* 48 (1981) 51.
- [5] B. Gylseth, H. Leira, E. Steinnes, Y. Thomassen, *Scand. J. Work Environ. Health* 5 (1979) 188.
- [6] E. Sabbioni, M. Maroni, *A Study on Vanadium in Workers from Oil Fired Power Plants*. Commission of the European Communities, Publication No. EUR. 9005, Luxembourg, 1983.
- [7] E.J. Underwood, *Trace Elements in Human and Animal Nutrition*, Academic Press, New York, 1977.
- [8] S.K. Jain, B.K. Puri, A.L. Singla, A.L.J. Rao, *Chim. Acta. Turc.* 16 (1988) 327.
- [9] J.L. Martinez-Vidal, C.D. Cervantes, R. Fernandez-Alba, F. Salinas, *An. Quim.* 87 (1991) 375.
- [10] S.P. Arya, J.L. Malla, *J. Indian Chem. Soc.* 68 (1991) 635.
- [11] M.F. Hussain, *Analytical Applications of Some Substitution Xanthates*, Ph.D. Thesis, Indian Institute of Technology, Delhi, India, 1985.
- [12] T. Kiriya, R. Kuroda, *Talanta* 31 (1984) 472.
- [13] K.W. Jackson, H. Qiao, *Anal. Chem.* 64 (1992) 50R.
- [14] K.W. Jackson, T.M. Mahmood, *Anal. Chem.* 66 (1994) 252R.
- [15] C.J. Kantipuly, A.D. Westland, *Talanta* 35 (1988) 1.
- [16] A. Ramesh, J. Krishnamacharayulu, L.K. Ravindranath, S.B. Rao, *Analyst* 117 (1992) 1037.
- [17] S.K. Bhowal, M. Bhattacharyya, *Talanta* 36 (1989) 989.

- [18] J. Alary, J. Esclassan, J. Vandaele, *Analyst* 111 (1986) 593.
- [19] B.J. Basu, D.K. Padma, S.R. Rajagopalan, *Talanta* 38 (1991) 1431.
- [20] Y. Nagaosa, K. Kobayashi, *Talanta* 31 (1984) 593.
- [21] G.K. Budnikov, N.K. Shakurova, N.A. Ulakhovich, R. Charkasov, V.V. Ovchinnikov, G.A. Kuttyrev, V.F. Toropova, *Zh. Anal. Khim.* 32 (1977) 1326.
- [22] A.T. Pilpenke, E.A. Shpak, A.I. Samchuk, *Zh. Anal. Khim.* 30 (1975) 1086.
- [23] M.F. Grigoieva, E.F. Teranlengaran, I.A. Tserkovnit-skaya, *Izv. Vyssh. Uchebn. Zavod. Khim. Khim. Tekhnol.* 26 (1983) 1426.
- [24] E. Barrado, V. Alvarez, R. Pardo, P.S. Batanero, *Electroanalysis* 3 (1991) 715.
- [25] N. Kato, K. Aoki, *J. Electroanal. Chem.* 261 (1989) 309.
- [26] T.E. Edmonds, *Anal. Chim. Acta* 116 (1980) 323.
- [27] A.G. Fogg, R.M. Alonso, *Analyst* 113 (1988) 361.
- [28] J. Wang, B. Tian, J. Lu, *Talanta* 39 (1992) 1273.
- [29] J. Wang, J. Lu, Z. Taha, *Analyst* 117 (1992) 35.
- [30] M.M.P.M. Neto, M.M.G.S. Rocha, C.M.A. Brett, *Talanta* 41 (1994) 1597.
- [31] R.K. Dubey, B.K. Puri, *Talanta* 42 (1995) 65.
- [32] A.I. Vogel, *A Text Book of Quantitative Inorganic Analysis*, 4th ed., Longmans, London, 1978.
- [33] A. Bobrowski, *Anal. Chem.* 61 (1989) 2178.
- [34] A.I. Jimenez, F. Jimenez, J. Arias, *Analyst* 114 (1989) 93.

Extractive spectrophotometric determination of some phenothiazine derivatives in pharmaceutical preparations

K. Basavaiah ^{a,*}, G. Krishnamurthy ^b

^a *Department of Studies in Chemistry, University of Mysore, Manasagangotri, Mysore-570 006, India*

^b *Department of Chemistry, PES College of Science, Mandya-571 401, India*

Received 28 April 1997; received in revised form 10 September 1997; accepted 15 September 1997

Abstract

A simple, accurate, rapid and sensitive spectrophotometric method has been developed for the assay of six phenothiazine derivatives in bulk drug and their pharmaceutical preparations. The method is based on ion-pair complex reaction of phenothiazines with bromocresol green in aqueous acidic buffer. The chromogen, being extractable with chloroform, could be measured quantitatively at 420 nm. All variables were studied in order to optimize the reaction conditions. The proposed method has been successfully applied to the analysis of the bulk drugs and their dosage forms, tablets and injections. No interference was observed from common pharmaceutical adjuvants. Statistical comparison of the results with those of an official method shows excellent agreement and indicates no significant difference in precision. © 1998 Elsevier Science B.V. All rights reserved.

Keywords: Phenothiazine derivatives; Pharmaceutical preparations; Spectrophotometric method

1. 1. Introduction

Phenothiazine derivatives make valuable pharmacological preparations. Owing to their relatively low toxicity, high physiological activity and versatile pharmacological action, they are widely used in therapeutics, particularly as psychotropic drugs. Over 30 phenothiazine drugs and 100 formulations are commercially available. The importance of these drugs prompted the development of many methods for their determination, reviewed by Blazek [1], Fairbrother [2] and Belikov and

Moiseeva [3]. Apart from official methods based on uv-spectrophotometry and non-aqueous titrimetry, two-phase, tetraphenylborate, ammonium reineckate, complexometric and oxidative titrations have also been used. A variety of spectrophotometric methods based on coloured complex formation or oxidative reactions have also been proposed, some lacking sensitivity and specificity [4–9] or requiring long heating times [10–13]. Some other spectrophotometric methods have very narrow limits of detection [14–16] and a few require the use of a very high concentration (50% v/v) of sulphuric acid [17,18].

Despite the large number of spectrophotometric methods available, the literature on extractive

* Corresponding author. Tel.: +91 821 515525; fax: +91 821 421263.

spectrophotometric methods for the assay of phenothiazine drugs is scanty, although these methods are well suited for the determination of phenothiazine drugs in pharmaceutical formulations and body fluids.

In this paper, a study of the determination of six phenothiazine drugs is described. The proposed method is based on the formation of an ion-association complex between phenothiazines and the acid-dye, bromocresol green in acidic buffer. The reaction conditions were thoroughly studied and the molar-ratio was also calculated. The procedure provides a highly sensitive method for the determination of phenothiazine drugs.

2. Experimental

2.1. Apparatus

A Systronics Model 106 spectrophotometer with 1-cm matched glass cells was used for all absorbance measurements. pH measurements were made with an Elico Model LI-120 digital pH-meter.

2.2. Reagents

All chemicals were of analytical reagent grade and solvents were of spectroscopic grade. Buffer solutions of required pH were prepared by mixing appropriate volumes of 0.2 M KCl and 0.2 M HCl. A 0.04% (m/v) bromocresol green (BDH) solution was prepared in buffer solutions.

2.3. Standard solutions of phenothiazines

Aqueous solutions of chlorpromazine hydrochloride (CPH; British Pharma., India), thioridazine hydrochloride (TH; Sandoz, India) trifluoperazine dihydrochloride (TFPH; SmithKline Beecham, India) triflupromazine hydrochloride (TPH; Sarabhai Chemicals, India), prochlorperazine dimaleate (PCPM; Rhône-Poulenc, India) and thioproperazine mesylate (TPPM; Rhône-Poulenc, India) were prepared by dissolving the requisite amount of the samples in distilled water. Insoluble PCPM was dissolved in a few

drops of dilute hydrochloric acid. Working solutions were prepared as required by dilution.

2.4. Standard procedure for the determination of phenothiazines

Accurately measured volumes of drug solutions equivalent to 2–8, 2–18, 2–12, 2–10, 2–10 and 2–12 $\mu\text{g ml}^{-1}$ final solution of CPH, TH, TFPH, TPH, PCPM and TPPM respectively, were transferred into a series of 125-ml separating funnels. Buffer (5 ml) of recommended pH (Table 1) and of bromocresol green solution (2 ml) were added to each separating funnel. The total volume was adjusted to 15 ml by adding distilled water. Chloroform (10 ml) was added to each separating funnel and the contents were shaken for exactly 1 min. The two phases were allowed to separate and the chloroform layer was passed through anhydrous sodium sulphate. The absorbance was measured at 420 nm against a reagent blank. A calibration graph was drawn or regression equation calculated.

2.5. Procedure for pharmaceutical formulations

Twenty tablets were weighed and powdered. An accurately weighed portion of the powder, equivalent to 20 mg of active ingredient, was transferred into a 100 ml calibrated flask and diluted to volume with water. Using a mechanical stirrer, the powder was completely disintegrated and the solution was filtered. An aliquot of this solution was further diluted with distilled water to obtain a concentration of calibration graph and assayed as

Table 1
Optimum reaction conditions

Phenothiazine	pH range	Stoichiometry (drug:dye)
CPH	1.0–1.8 (1.4)	1:1
TH	1.0–2.2 (1.6)	1:1
TFPH	1.0–2.0 (1.6)	1:2
TPH	1.2–2.2 (1.6)	1:1
PCPM	1.4–1.8 (1.4)	1:2
TPPM	1.2–2.0 (1.6)	1:2

Working pH values are shown in parentheses.

described under standard procedure (for dissolving PCPM a few drops of dilute HCl were used).

For the determination of the drug in injectable dosage form, the mass of the drug per ml was determined. A quantity of injectable dosage form equivalent to 20 mg of drug was transferred to a 100 ml volumetric flask and diluted to the mark with distilled water. This solution was further diluted with distilled water so that the final solution contained about $20 \mu\text{g ml}^{-1}$ of drug, before analysis using the described procedure. The results of the analysis are given in Table 3.

3. Results and Discussion

Ion-pair extractive spectrophotometry has received considerable attention for quantitative estimation of many pharmaceutical compounds [19–24]. Phenothiazines were previously determined by colorimetric methods [25] based on yellow or blue colour formed, using buffered orange II ($\lambda_{\text{max}} = 495 \text{ nm}$) or brilliant blue ($\lambda_{\text{max}} = 620 \text{ nm}$). In the present investigation, bromocresol green being an anionic dye, forms with phenothiazines, in acidic pH, a yellow coloured ion-pair complex which is soluble in chloroform and can be measured at 420 nm.

3.1. Optimization of conditions

The optimum conditions for quantitative estimation of the associated ion-pair formed were established via a number of preliminary experiments. The effect of pH was studied by extracting the coloured complex formed in the presence of various buffers of different acidic pH values. Of the various buffers tried, Clark and Lubs (pH 1.0–2.2) was found to be more suitable compared to Walpole or Sorenson buffer. Table 1 shows the pH range over which the absorbances were constant for the drugs studied. Complexation was found to be unaffected when 0.5–12.5 ml of buffer of selected pH was used. Hence, 5 ml of buffer was used in all the cases in a total volume of 15 ml. A 2.0-ml addition of

0.04% bromocresol green solution was found to be optimal for complexation, since the absorbance was practically constant in the range of 1–5 ml of 0.04% dye solution.

A number of immiscible organic solvents were tested in order to provide an applicable extraction procedure. Chloroform was preferred for its selective extraction of the drug–dye complex from the aqueous phase. A ratio of 3:2 of aqueous to chloroform phases was required for efficient extraction of the coloured species. Shaking times of 0.5–4 min produced a constant absorbance, hence a shaking time of 1 min was used throughout. Only one extraction was adequate to achieve a quantitative recovery of the complex. Absorbances of the separated extracts were stable for more than 1 h. The blanks did not absorb at λ_{max} .

The phenothiazines being basic in nature, form an ion-association complex with the acidic dye, bromocresol green, which is extractable into chloroform from the aqueous phase. The stoichiometric ratio of phenothiazine to bromocresol green was determined by the mole–ratio method [26] and the findings are presented in Table 1.

3.2. Linearity of calibration graphs.

The Beer's law limits, molar absorptivity and Sandell's sensitivity values, regression equations and correlation coefficients found for various phenothiazine drugs are given in Table 2. A linear relationship was found between absorbance at λ_{max} and the concentration of drugs in the range 2–18 $\mu\text{g. ml}^{-1}$ in the final measured solutions (10 ml.). Regression analysis of the Beer's law plots at λ_{max} reveal a good correlation ($r = 0.9289$ – 0.9986). The graphs show negligible or zero intercept except for CPH and TH and are described by the regression equation, $Y = a + bx$ (where Y is the absorbance of a 1-cm. Layer, b is the slope, a is the intercept and x the concentration of the measured solution in $\mu\text{g. ml}^{-1}$) obtained by the least-squares method [27]. The apparent molar absorptivities of the resulting coloured products range from 1.74×10^4 to $2.65 \times 10^4 \text{ l. mol.}^{-1} \text{ cm.}^{-1}$ and indicate the high sensitivity of the proposed procedure.

Table 2
Optical characteristics, precision and accuracy data

Parameter	CPH	TH	TFPH	TPH	PCPM	TPPM
Beer's Law limits ($\mu\text{g ml}^{-1}$)	2–8	2–18	2–16	2–10	2–10	2–12
Molar absorptivity ($1. \text{mol.}^{-1} \text{cm.}^{-1} \times 10^4$)	2.63	2.13	1.74	2.02	1.94	2.65
Sandell's sensitivity ($\mu\text{g cm}^{-2}$ per 0.001 <i>A</i> unit)	0.0054	0.0190	0.0270	0.0192	0.0312	0.024
Correlation coefficient, <i>r</i>	0.9964	0.9289	0.9977	0.9924	0.9986	0.9964
Regression equation (<i>Y</i>) ^a						
Slope, <i>b</i>	0.0255	0.0158	0.0194	0.0325	0.029	0.027
Intercept, <i>a</i>	0.1875	0.242	0.0979	0.087	0.016	0.07
Relative standard deviations (%) ^b	0.38	0.28	0.39	0.48	0.38	0.33
Range of error (95% confidence limit) ⁺	0.40	0.30	0.41	0.50	0.40	0.35

^a $Y = a + bx$ where *x* is the concentration in $\mu\text{g ml}^{-1}$.

^b For six replicate analyses within Beer's law limits.

3.3. Quantification, accuracy and precision

The validity of the proposed procedure for the determination of the studied drugs in their pure state and in their pharmaceutical formulations, was tested by analysing these products using the proposed procedure and the official method [28]. The results obtained for pure drugs (Table 2) were reproducible with low relative standard deviations (0.28–0.48%) and the mean recoveries were comparable to those obtained using the official method (Table 4) for each of the studied drugs. The results of analysis for dosage forms obtained by the proposed and the official methods are in good agreement (Table 3).

3.4. Statistical analysis of the results in comparison with the BP method

The performance of the proposed method was judged by calculating the student's *t*- and *F*-values. At 95% confidence level, the calculated *t*- and *F*-values do not exceed the theoretical values (Table 5). Therefore, there is no significant difference between the proposed method and the official method, indicating that the proposed method is as accurate and precise as the official method.

3.5. Application

The applicability of the method to the assay of sample dosage forms was examined by analysing

various formulations. Table 3 shows the quantities obtained by the proposed method and labelled amount. The percent recoveries (97.20–101.24%) indicate good accuracy and the independence of the matrix effect over the absorbance measurements.

4. Conclusion

The proposed method is advantageous when compared to many of the reported methods in having higher sensitivity [29,30] and stability [31,32] of the coloured species. The method is sufficiently sensitive to permit determination even up to $2 \mu\text{g ml}^{-1}$. A significant advantage of the extractive spectrophotometric method is that it can be applied to the determination of individual components in a multicomponent mixture. This aspect of spectrophotometric analysis is of major interest in analytical pharmacy, since it offers distinct possibilities in the assay of a particular component in a complex dosage formulation. In the present study, some phenothiazine drugs were estimated successfully as pure compounds, as well as components in representatives dosage formulations. The commonly used additives and excipients in the dosage forms of phenothiazines, such as starch, lactose, galactose, glucose, sugar, talc, gelatin, magnesium stearate, sodium lauryl sulphate, sodium sulphite, sodium chloride, calcium chloride, ethanol, formaldehyde and sodium salt

Table 3
Assay of Phenothiazine derivatives in dosage forms

Formulation	Labelled amount (mg/tablet or ml)	Amount found (mg)		% Recovery by proposed method ^a
		Proposed method	Reference method	
CPH				
Tablet 1	25	24.63	24.68	98.52
Tablet 2	50	50.01	49.12	100.02
Tablet 3	100	98.16	98.76	98.16
Tablet 4	200	196.24	197.58	98.12
Injection	25	24.60	24.82	98.40
TH				
Tablet 1	10	9.78	9.85	97.80
Tablet 2	25	25.31	24.38	101.24
Tablet 3	50	49.04	48.56	98.08
Tablet 4	100	98.15	99.64	98.15
TFPH				
Tablet 1	5	4.91	5.02	98.20
Tablet 2	10	9.77	9.98	97.70
TPH				
Tablet	10	10.02	9.92	100.20
Injection	10	9.72	9.96	97.20
PCPM				
Tablet	5	4.96	5.00	99.20
Injection	12.5	12.23	12.30	97.84
TPPM				
Tablet	5	4.88	—	97.60

^a Average of five determinations.

of EDTA were found not to interfere in the analysis. The method is simple and rapid, with

Table 4
Analysis of phenothiazines in bulk drugs by the proposed method and official method

Drug	Amount taken ($\mu\text{g ml}^{-1}$)	% Recovery (\pm SD)	
		Proposed method	Official method
CPH	5	100.03 \pm 1.15	101.12 \pm 1.08
TH	10	100.00 \pm 1.45	99.84 \pm 1.11
TFPH	10	99.99 \pm 2.20	98.96 \pm 1.65
TPH	10	100.00 \pm 1.85	99.94 \pm 1.20
PCPM	10	100.00 \pm 0.46	100.31 \pm 0.80
TPPM	10	99.68 \pm 0.21	—

reasonable accuracy and does not involve any critical reaction conditions or tedious sample preparation. It is unaffected by slight variations in experimental conditions such as pH, dye concentration, shaking time and temperature. The wide applicability of the new procedure for routine quality control is well established by the assay of phenothiazine in pharmaceutical formulations.

Acknowledgements

The authors are grateful to SmithKline Beecham, India, Ltd., Rhone-Poulenc India, Ltd., Sarabhai Chemicals Ltd., British Pharmaceuticals, India, Ltd, for the supply of pure drug samples.

Table 5

Statistical Analysis of results for bulk drugs by proposed method compared with official method

Drug	Proposed method			Official method		
	% Recovery (mean \pm SD)	N	CV	% Recovery (mean \pm SD)	N	CV
CPH	100.03 \pm 1.15 $t = 1.80$ (2.18); $F = 1.13$ (3.97)	6	1.15	101.12 \pm 1.08	8	1.07
TH	100.00 \pm 1.45 $t = 0.19$ (2.31); $F = 1.71$ (9.01)	6	1.45	99.84 \pm 1.11	4	1.11
TFPH	99.99 \pm 2.20 $t = 0.90$ (2.18); $F = 1.78$ (8.81)	10	2.20	98.96 \pm 1.65	4	1.67
TPH	100.00 \pm 1.85 $t = 0.06$ (2.26); $F = 2.38$ (8.94)	7	1.85	99.94 \pm 1.20	4	1.20
PCPM	100.00 \pm 0.46 $t = 0.82$ (2.20); $F = 3.02$ (4.07)	9	0.46	100.31 \pm 0.80	4	0.79

Figures in the parantheses are the tabulated values of t - and f -values at the 95% confidence level.

N , Number of determinations; CV, Coefficient of variation (%).

References

- [1] J. Blazek, Pharmazie 22 (1967) 129.
- [2] J.E. Fairbrother, Pharm. J. 222 (1979) 271.
- [3] V.G. Belikov, G.F. Moiseeva, Farmatsiya 36 (1986) 87.
- [4] F. Gurka, R.E. Kolinski, J.W. Myrick, C.E. Wells, J. Pharm. Sci. 69 (1980) 1069.
- [5] P.G. Ramappa, H.S. Gowda, A.N. Nayak, Analyst 105 (1980) 663.
- [6] W. Jim, L. Qian, Yaowu Fenxi Zazhi 11 (1991) 106.
- [7] M.M. El-Kerdwy, S.M. Hassan, S.M. El-Ashy, Mikrochim. Acta 108 (1992) 323.
- [8] V.P. Kalashnikov, A.I. Shkadova, T.G. Popova, Farm. Zh. 5–6 (1992) 68.
- [9] F. Arioiez, L. Ersoy, Pharmazie 49 (1994) 536.
- [10] A.F. Fell, B.J. Clark, J. Pharm Pharmacol. 35 (1983) 22.
- [11] S.R. El-Shabouri, A.R. Yousif, F.A. Mohamed, A.M.I. Rageh, J. Assoc. Off. Anal. Chem. 69 (1986) 821.
- [12] M.S. Mahrous, M.M. Abdel-Khalk, Talanta 31 (1984) 289.
- [13] K.M. Emara, Anal. Lett. 25 (1992) 99.
- [14] P.G. Ramappa, H.S. Gowda, A.N. Nayak, Microchem. J. 28 (1986) 586.
- [15] M. Rizk, N.A. Zakhari, F. Ibrahim, M.I. Waksh, Talanta 33 (1986) 111.
- [16] O.N. Shesherbina, Farm. Zh. 3 (1992) 76.
- [17] A.M. Taha, A.E. Namal, E. Michael, H.R. Ibrahim, Analyst 108 (1983) 1500.
- [18] I. Serdar Ates, E. Gok, Anal. Lett. 20 (1987) 117.
- [19] Y.M. Dessouky, B.A. Mousa, H.M. Nour El-Din, Pharmazie 29 (1974) 573.
- [20] S. Tosunglu, S. Atmaca, Ibid 44 (1989) 498.
- [21] M.H. Barary, A.M. Wahbi, Drug Dev. Ind. Pharm. 17 (1991) 457.
- [22] O.H. Abdelmageed, P.Y. Khasaba, Talanta 40 (1993) 1289.
- [23] J.C. Botello, G.P. Caballero, Talanta 42 (1994) 105.
- [24] C.S.P. Sastry, K. Rama Rao, D. Sivaprasad, Talanta 42 (1995) 311.
- [25] S.L. Bhongade, A.V. Kasture, Talanta 40 (1993) 1525.
- [26] T. Rose, Advanced Physicochemical Experiments, Pitman, London, 1964.
- [27] E.L. Baner, Statistical Manual for Chemists, Academic Press, London, 1971, p 61.
- [28] British Pharmacopoeia, HMSO, London, 1993.
- [29] S.M. Sultan, Talanta 40 (1993) 681.
- [30] J. Martinez Calatayud, S. Narasquillo Sarion, A. Sanchez Sampedro, C. Gomez Berito, Microchem. J. 45 (1992) 129.
- [31] M.A.-A. Enami Khoi, J. Pharm. Sci. 72 (1983) 704.
- [32] K.M. Emara, Anal. Lett. 25 (1992) 99.

Spectrophotometric determination of nitrate and nitrite in water and some fruit samples using column preconcentration

G.F. Wang, M. Satake, K. Horita *

Faculty of Engineering, Fukui University, Fukui 910, Japan

Received 4 April 1997; received in revised form 15 September 1997; accepted 16 September 1997

Abstract

A sensitive analytical method for the simultaneous assay of nitrate and nitrite in water and some fruit samples is presented. The method is based on nitrite determination using the diazotization-coupling reaction by column preconcentration and on the reduction of nitrate to nitrite using the Cd–Cu reductor column. Nitrite is diazotized with sulfanilamide (SAM) in the pH range 2.0–5.0, sulfamethizole (SM) in pH 1.8–5.6 and sulfadimidine (SD) in pH 1.8–4.0 in a hydrochloric acid medium to form water-soluble colourless diazonium cations. These cations were coupled with sodium 1-naphthol-4-sulfonate (NS) in the pH range 9.0–12.0 for the SAM–NS system, pH 8.6–12.0 for the SM–NS system and pH 9.4–12.0 for the SD–NS system to be retained on naphthalene-tetradecyldimethylbenzylammonium (TDBA)–iodide (I) adsorbent packed in a column. The solid mass is dissolved out from the column with 5 ml of dimethylformamide (DMF) and the absorbance is measured by a spectrophotometer at 543 nm for SAM–NS, 537 nm for SM–NS and 530 nm for SD–NS. The calibration graph was linear over 30–600 ng NO₂-N and 22–450 ng NO₃-N in 15 ml of final aqueous solution (i.e. 2–40 ng NO₂-N ml⁻¹ and 1.5–30 ng NO₃-N ml⁻¹ in aqueous sample) for three systems. The detection limits were 1.4 ng NO₂-N ml⁻¹ and 1.1 ng NO₃-N ml⁻¹ for SAM–NS, 1.2 ng NO₂-N ml⁻¹ and 0.89 ng NO₃-N ml⁻¹ for SM–NS, 1.0 ng NO₂-N ml⁻¹ and 0.75 ng NO₃-N ml⁻¹ for SD–NS, respectively. The concentration factor is eight for SAM–NS and SM–NS, and 12 for SD–NS. Interferences from various foreign ions have been examined and the method was successfully applied to the determination of low levels of nitrate and nitrite in water and some fruit samples. © 1998 Elsevier Science B.V. All rights reserved.

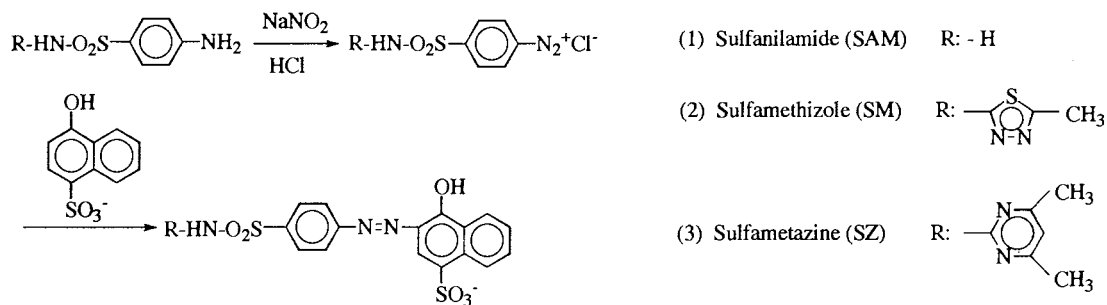
Keywords: Nitrate and nitrite determination; Spectrophotometry; Naphthalene column preconcentration; Sulfanilamide; Sulfamethizole; Sulfadimidine; Sodium 1-naphthol-4-sulfonate; Diazotization-coupling reaction; Water; Fruit samples

1. Introduction

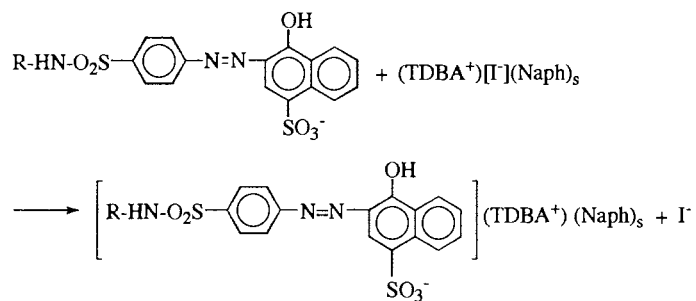
Nitrate and nitrite are commonly monitored for environmental protection purposes in agriculture and food control. Owing to the formation of carcinogenic *N*-nitrosamines [1] and being also

* Corresponding author. Fax: +81 776 278767; e-mail: d930725@icpc00.icpc.fukui-u.ac.jp(K.Horita)

Diazization-coupling reaction:



Adsorption reaction:



Scheme 1.

essential to indicate organic pollution in water [2], the determination of the exact concentration of nitrate and nitrite is desirable. In recent years, an increasing interest in the determination of nitrate levels in food products has been observed, essentially due to the potential reduction of nitrate to nitrite, which is known to have adverse effects on human and animal health. Nitrite and nitrate are intermediate states in the nitrogen cycle, and the high concentration of nitrite in water generally indicates poor quality [3]. From these points of view, the determination of nitrate and nitrite in water, fruit samples is of vital importance. Numerous methods for the determination of nitrate and nitrite in mixtures are based on the reduction of nitrate to nitrite by reducing agents, such as zinc [4], cadmium [5], amalgamated [6] or copperized cadmium [7], and on the reaction of nitrite with various aromatic amines in acidic medium to form a diazonium salt coupled with an aromatic amine to produce a highly coloured azo dye com-

pound which is subsequently determined colorimetrically [8].

Based on considerations of simplicity, rapidity, colour stability, adherence to Beer's law and sensitivity, we propose a simple and convenient pre-concentration method of the azo dye made from nitrite with the diazotizable and coupling reagents and TDBA-I ion-pair loaded on naphthalene. Preliminary observations revealed that the nitrite ion is quantitatively retained as the azo dye on naphthalene. The adsorbed mixture was dissolved out from the column with 5 ml DMF solution and the trace nitrite was estimated spectrophotometrically. The same reaction is used to determine nitrate using the Cd-Cu column which converts nitrate to nitrite. When the sample was not passed through the Cd-Cu column, the only response was due to nitrite present in the sample. Nitrate can therefore be determined by measuring the difference between responses with and without the converter. For nitrite analysis of natural waters,

Table 1
Optimum experimental conditions for NO_2^-

Experimental condition	SAM-NS	SM-NS	SD-NS
Wavelength (nm)	543	537	530
Diazotisable agent (0.1%, ml)	0.5–2.0 (1.0)	0.2–2.0 (1.0)	0.5–2.0 (1.0)
pH for diazotization (min)	2.0–5.0 (3.5)	1.8–5.6 (3.0)	1.8–4.0 (2.8)
Time of diazotization (min)	5–20 (10)	5–20 (10)	5–20 (10)
NS coupling agent (0.1%, ml)	2.5–7.0 (5.0)	3.0–7.0 (5.0)	2.0–7.0 (4.0)
pH for coupling reaction	8.9–11.8 (10.5)	8.6–12.0 (10.5)	9.4–12.0 (10.5)
Time of coupling reaction (min)	5–30 (10)	5–20 (10)	5–20 (10)
Flow rate (ml min^{-1})	0.5–12.5 (1.0)	0.5–12.5 (1.0)	0.5–12.5 (1.0)
Aqueous phase (ml)	10–40 (15)	10–40 (15)	10–60 (15)

NO_2^- (SAM-NS), 0.067 mg l^{-1} ; NO_2^- (SM-NS), 0.06 mg l^{-1} ; NO_2^- (SD-NS), 0.053 mg l^{-1} .

diazotization-coupling reaction with sulfanilamide and *N*-(1-naphthyl) ethylenediamine is recommended as the official standard method by the Japanese Industrial Standard (JIS) [9], but the sensitivity of the method is not sufficient to permit the direct colorimetric measurement of nitrite in unpolluted natural water samples. In such cases, the preconcentration techniques such as solvent extraction or adsorption are required for the analysis of water samples. The conditions have been optimized and the method has been used for analysis of low levels of nitrate and nitrite in water and some fruit samples without prior separation.

2. Experimental

2.1. Reagents and apparatus

Standard nitrate solution, 1 mg l^{-1} , was prepared by diluting 1000 mg l^{-1} standard nitrate solution (Wako, Osaka, Japan) with oxygen-free water. Standard nitrite solution, 1 mg l^{-1} , was prepared by diluting 1000 mg l^{-1} standard nitrite solution (Wako, Osaka, Japan) with oxygen-free water. The working solutions containing 1 ml of chloroform were stored in a brown bottle. Solutions (0.1% m/v) of SAM, SM and SD were prepared by dissolving 0.2 g of the reagent in 2 ml of 6 mol l^{-1} hydrochloric acid and diluting to 200 ml with water. A solution of NS (0.1% m/v) was prepared by dissolving 0.3 g of the reagent in 300 ml of water. Buffer solution was prepared by

mixing an appropriate ratio of 0.5 mol l^{-1} ammonium acetate and 0.5 mol l^{-1} acetic acid or 0.5 mol l^{-1} aqueous ammonia. All chemicals used were of analytical-reagent grade or the highest purity available. Doubly distilled water was used throughout.

A Hitachi Model 200-20 spectrometer and a Toa-Dempa HM-6A pH meter were used. A glass tube ($5 \text{ cm} \times 6 \text{ mm i.d.}$) with a tapered end was used as a simple separatory column. The column was plugged with polypropylene fibres and then slurry-packed with the naphthalene material to a height of 1.0–1.5 cm, pushing it with a flat-topped glass rod. The Cu–Cd reductor column was made from a glass funnel ($12 \text{ cm} \times 6 \text{ mm i.d.}$) filled with the copperized cadmium (particle size: 0.5–1.0 mm, Wako, Osaka, Japan).

2.2. Preparation of naphthalene-TDBA-I adsorbent

A solution of naphthalene (20 g) was prepared by dissolution in acetone (40 ml) on a stirring-hot plate at 35°C . This solution was added to water (1500 ml) containing TDBA (2 g) with constant stirring, and then KI (6 g) in 500 ml water was slowly added. The naphthalene, coprecipitated with TDBA^+ and I^- , and stirred for 2 h. The supernatant solution was drained off by decantation and the mixture was washed twice with water. The slurry of naphthalene–TDBA–I adsorbent in water was stored in a bottle.

The preparation of adsorbent is very simple and is completed by mixing the acetonetic solution

of naphthalene with water. The naphthalene adsorbent, stored in aqueous solution, is very stable and has no effect on the adsorption of the azo dye for over a year.

2.3. General procedure

An aliquot (10 ml) of sample solution containing 30–600 ng $\text{NO}_2\text{-N}$ for the three systems was transferred to a 20 ml beaker, 1.0 ml of 0.1% SAM, SM or SD solution was added as the diazotizable reagent. The solution was adjusted to pH 3.5 for SAM–NS system, pH 3.0 for SM–NS system and pH 2.8 for SD–NS system with 1 mol l^{-1} HCl and allowed to stand for 10 min for complete diazotization. To each solution 5.0 ml of 0.1% NS was added to the three systems as a coupling agent and the volume made up to 15 ml with water. Then the pH was adjusted to 10.5 with ammonia buffer solution, leaving it to stand for 10 min allowing the complete coupling reaction for the three systems. The mixture was passed through a column packed with the adsorbent at the natural flow rate of 1 ml min^{-1} . The packing was washed with small volumes of water and aspirated for a few seconds to eliminate excess water attached to naphthalene. The azo dye along with naphthalene was dissolved out from the column with 5 ml of DMF. The absorbance of the solution was measured at 543 nm for SAM–NS, 537 nm for SM–NS and 530 nm for SD–NS against a reagent blank. An aliquot of aqueous solution containing 11–230 ng $\text{NO}_3\text{-N}$ solution for the three systems was passed through the Cd–Cu column, then reduced nitrite was determined using the same method.

3. Results and discussion

3.1. Diazotization-coupling reaction and adsorption characteristics

The diazotization-coupling reaction and adsorption reaction of the azo dye are depicted as follows Scheme 1. Nitrite ion reacts with diazotizable aromatic amines such as SAM, SM and SD in a hydrochloric acid medium to form colourless

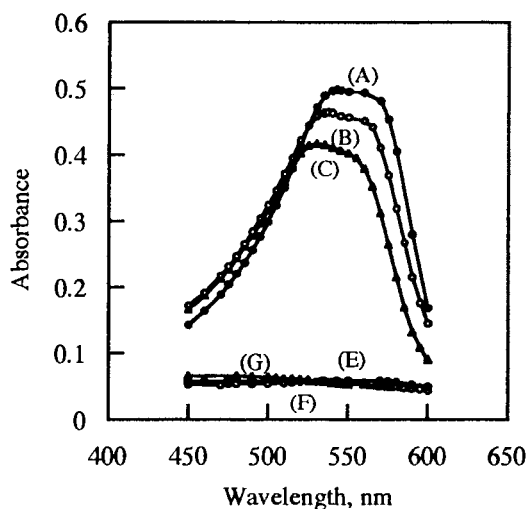


Fig. 1. Absorption spectra of the reagent blanks and the azo dyes in naphthalene–DMF solution. (A), NO_2^- (SAM–NS system), 1.0 μg ; 0.1% SAM, 1.0 ml; pH for diazotization, 3.5; 0.1% NS, 4.0 ml; pH for coupling reaction, 10.5. (B), NO_2^- (SM–NS system), 0.9 μg ; 0.1% SM, 1.0 ml; pH for diazotization, 3.0; 0.1% NS, 5.0 ml; pH for coupling reaction, 10.5. (C), NO_2^- (SD–NS system), 0.8 μg ; 0.1% SD, 1.0 ml; pH for diazotization, 2.8; 0.1% NS, 5.0 ml; pH for coupling reaction, 10.5. (D), Reagent blank (SAM–NS system). (E), Reagent blank (SM–NS system). (F), Reagent blank (SD–NS system). Reference, DMF.

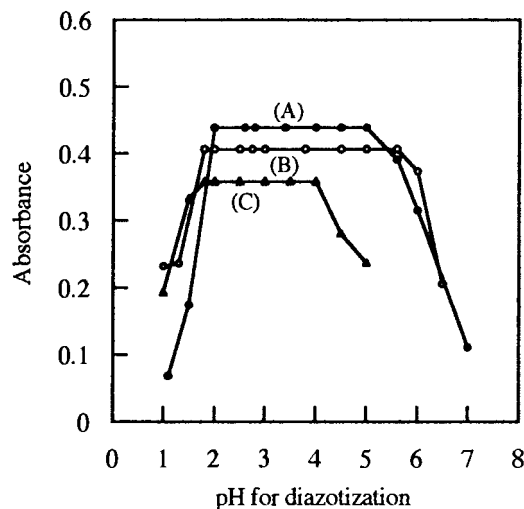


Fig. 2. Effect of pH on diazotization. (A), NO_2^- (SAM–NS system), 1.0 μg ; 0.1% SAM, 1.0 ml; 0.1% NS, 4.0 ml; pH for coupling reaction, 10.5; wavelength, 543 nm. (B), NO_2^- (SM–NS system), 0.9 μg ; 0.1% SM, 1.0 ml; 0.1% NS, 5.0 ml; pH for coupling reaction, 10.5; wavelength, 537 nm. (C), NO_2^- (SD–NS system), 0.8 μg ; 0.1% SD, 1.0 ml; 0.1% NS, 4.0 ml; pH for coupling reaction, 10.5; wavelength, 530 nm. Reference, reagent blank.

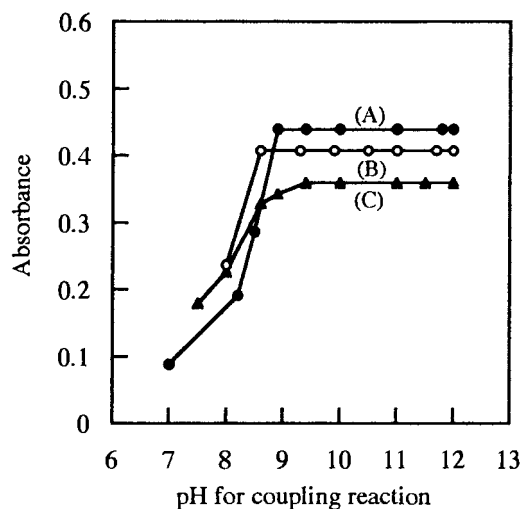


Fig. 3. Effect of pH on the coupling reaction. (A), NO_2^- (SAM–NS system), 1.0 μg ; 0.1% SAM, 1.0 ml; pH for diazotization, 3.5; 0.1% NS, 4.0 ml; wavelength, 543 nm. (B), NO_2^- (SM–NS system), 0.9 μg ; 0.1% SM, 1.0 ml; pH for diazotization, 3.0; 0.1% NS, 5.0 ml; pH for coupling reaction, 10.5; wavelength, 537 nm. (C), NO_2^- (SD–NS system), 0.8 μg ; 0.1% SD, 1.0 ml; pH for diazotization, 2.8; 0.1% NS, 5.0 ml; wavelength, 530 nm. Reference, reagent blank.

diazonium ions. These ions produce the coloured azo dyes with NS. Among the ion-pair adsorbents i.e. TDBA-I, CTMA (cetyltrimethylammonium bromide)-I, CTMA–SCN, CPA (cetylpyridiniumammonium chloride)–SCN and CTMA– ClO_4 , only naphthalene–TDBA–I adsorbed the azo dyes completely for the three systems because the exchange reaction of azo dye with the TDBA–I adsorbent occurs easily.

3.2. Optimum experimental conditions for NO_2^-

Table 1 presents the optimum experimental conditions for NO_2^- . Fig. 1 shows the absorption spectra of the reagent blanks and azo dyes in the naphthalene–DMF solution, measured against DMF. It was observed that the absorption spectra of azo dyes shifts slightly to the longer wavelength side in the order SD–NS (λ_{max} 530 nm) < SM–NS (λ_{max} 537 nm) < SAM–NS (λ_{max} 543 nm). All absorbance measurements were made at 530 nm for SD–NS, 537 nm for SM–NS and 543 nm for SAM–NS. Figs. 2 and 3 shows the effect of pH

on diazotization and coupling reactions, respectively. The pH range of diazotization decreases in the order SM–NS (pH 1.8–5.6) > SAM–NS (pH 2.0–5.0) > SD–NS (pH 1.8–4.0). The coupling reactions for the three systems were in a pH 8.6–12.0 medium.

3.3. Choice of solvent and colour stability

Various solvents were tried to dissolve out the azo dye along with naphthalene from the column. The solid material is soluble in solvents such as DMF, acetonitrile, dimethyl sulfoxide, propylene carbonate, ethanol and 1,4-dioxane. As these solvents are miscible with water, there is no need to remove excess water attached to the naphthalene, unlike non-polar solvents such as benzene or chloroform. Since the solid mass is also dissolved in a small volume of solvent, it is necessary to select a solvent in which the compound is highly soluble. In the three systems, DMF was the most suitable and sensitive solvent. The azo dyes in the DMF solution were very stable, even after standing for more than 90 min, the relative changes of the absorbance with time being < 0.2%.

3.4. Linearity, sensitivity and precision

Under optimal conditions, the absorbance of various concentrations of nitrite were measured at 543 nm for SAM–NS, 537 nm for SM–NS and 530 nm for SD–NS. Beer's law holds well in the concentration range 2–40 ng $\text{NO}_2\text{-N ml}^{-1}$ and 1.5–30 ng $\text{NO}_3\text{-N ml}^{-1}$ in the sample solution for the three systems. The replicate determinations of seven sample solutions containing 0.067 mg l^{-1} of nitrite for SAM–NS, 0.06 mg l^{-1} of nitrite for SM–NS and 0.053 mg l^{-1} of nitrite for SD–NS gave mean absorbances of 0.439, 0.407 and 0.359 with relative standard deviations of 0.48, 0.35 and 0.47%, respectively. The molar absorptivity was 10^5 order, estimated to be $1.01 \times 10^5 \text{ l}^{-1} \text{ mol}^{-1} \text{ cm}^{-1}$ for SAM–NS, $1.04 \times 10^5 \text{ l}^{-1} \text{ mol}^{-1} \text{ cm}^{-1}$ for SM–NS and $1.03 \times 10^5 \text{ l}^{-1} \text{ mol}^{-1} \text{ cm}^{-1}$ for SD–NS. The detection limits, calculated as three times the standard deviation ($n = 10$) of the reagent blanks, were 1.4 ng $\text{NO}_2\text{-N ml}^{-1}$ and 1.1 ng $\text{NO}_3\text{-N ml}^{-1}$ for SAM–NS, 1.2 ng $\text{NO}_2\text{-N}$

Table 2
Effect of diverse salts and ions

Salt or ion	Tolerance limit ^c		
	SAM–NS	SM–NS	SD–NS
Na ₂ SO ₄ , NaH ₂ PO ₄ , Na–citrate, KNO ₃ , NaCl	30 mg ^a	30 mg ^a	30 mg ^a
CH ₃ COONa.3H ₂ O	10 mg	30 mg	30 mg
Na ₂ CO ₃	5 mg	30 mg	30 mg
Na–tartrate	5 mg	5 mg	5 mg
Na ₂ SO ₃	5 mg ^b	5 mg ^b	5 mg ^b
Cu ²⁺ , Ni ²⁺ , Zn ²⁺ , Mg ²⁺ , Ca ²⁺ , Cd ²⁺	300 µg ^a	300 µg ^a	300 µg ^a
Al ³⁺	100 µg	300 µg	100 µg
Co ²⁺	100 µg	50 µg, 100 µg ^c	50 µg, 100 µg ^c
Mn ²⁺	20 µg, 300 µg ^d	20 µg, 300 µg ^d	20 µg, 300 µg ^d
Fe ²⁺ , Fe ³⁺	<1 µg, 20 µg ^d	<1 µg, 20 µg ^d	<1 µg, 20 µg ^d

^a Maximum value tested. NO₂⁻ (SAM–NS), 1.0 µg; NO₂⁻ (SM–NS), 0.9 µg; NO₂⁻ (SD–NS), 0.8 µg.

^b Masked with 1.0 ml of 1% barium chloride.

^c Masked with 0.5 ml of 1% sodium tartrate.

^d Masked with 1.0 ml of 2% EDTA.

^e Evaluated as ± 3% on absorbance.

ml⁻¹ and 0.89 ng NO₃-N ml⁻¹ for SM–NS, 1.0 ng NO₂-N ml⁻¹ and 0.75 ng NO₃-N ml⁻¹ for SD–NS, respectively.

3.5. Effect of diverse ions

Possible interferences of various ions were examined in the determination of nitrite. Various amounts of alkali metal salts and metal ions were added individually to a solution containing 1.0, 0.9 and 0.8 µg of nitrite for SAM–NS, SM–NS and SD–NS systems, respectively and the procedure applied. The tolerance limit was taken as the amount causing a change of ± 3% in the absorbance. The results obtained are given in Table 2. The same procedure was also carried out for the determination of NO₃⁻. Differences were not observed in the tolerance limit between NO₂⁻ and NO₃⁻. Hence, the proposed method is considerably selective and has been applied to the determination of trace nitrate and nitrite in unpolluted water and some fruit samples without any previous separation.

3.6. Determination of nitrite and nitrate in water and some fruit samples

Water samples from various sources were col-

lected and analysed within 1 h after sampling because nitrite is potentially unstable, and all food and water samples should be analyzed as soon as possible after collection [10]. The sample collected was filtered through a filter paper (No. 5C, Toyo Roshi, Japan). An aliquot (10 ml) of the filtrate was taken in a beaker and the general procedure applied. The fruit sample was chopped and 5.0 g of the slurry was transferred to a 150 ml beaker, with 100 ml of distilled water. After shaking for 60 min and filtering through a membrane filter (pore size 0.45 µm), the nitrite it was diluted in a 100 ml standard flask and nitrite was analyzed using the general procedure outlined above. From the calibration curve, the nitrite content in some fruit samples was determined and calculated. The results given in Table 3 agreed reasonably with alternative methods [11]. The recovery test was carried out for spiked water and pear samples. The recovery of the obtained nitrite was good.

For the analysis of nitrate, an aliquot (10 ml) of the filtrate was taken in a beaker, passed through the Cd–Cu column, and the nitrate content was determined in the same manner as nitrite (Table 3). These results indicate that this analytical method can be successfully applied to determine low levels (ng ml⁻¹) of nitrite and nitrate which are

Table 3
Determination of nitrite and nitrate in water and some fruit samples

Sample		Concentration of nitrogen (ng ml ⁻¹)			
		SAM-NS ^a	SM-NS ^a	SD-NS ^a	Alternative ^a
River water	NO ₂ -N	4.0 ± 0.1	4.4 ± 0.2	4.1 ± 0.2	4.0 ± 0.2
	NO ₃ -N	43.2 ± 0.2	43.0 ± 0.3	43.1 ± 0.4	43.4 ± 0.3
Snow	NO ₂ -N	8.2 ± 0.1	8.6 ± 0.2	8.5 ± 0.1	8.5 ± 0.1
	NO ₃ -N	545.8 ± 0.7	544.8 ± 0.4	543.7 ± 0.6	548.2 ± 0.6
Ground	NO ₂ -N	1.2 ± 0.1	1.2 ± 0.3	1.2 ± 0.2	1.2 ± 0.1
Water	NO ₃ -N	38.4 ± 0.2	38.3 ± 0.3	38.1 ± 0.2	38.5 ± 0.3
Fruit ^c					
Apple	NO ₂ -N	0.40 ± 0.02	0.42 ± 0.02	0.41 ± 0.02	0.41 ± 0.02
	NO ₃ -N	0.27 ± 0.01	0.26 ± 0.02	0.26 ± 0.01	0.27 ± 0.01
Pear	NO ₂ -N	0.18 ± 0.01	0.19 ± 0.02	0.17 ± 0.01	0.18 ± 0.01
	NO ₃ -N	0.09 ± 0.01	0.08 ± 0.01	0.10 ± 0.01	0.08 ± 0.02
Persimmon	NO ₂ -N	0.30 ± 0.02	0.31 ± 0.02	0.31 ± 0.01	30 ± 0.01
	NO ₃ -N	0.06 ± 0.01	0.05 ± 0.01	0.06 ± 0.01	0.06 ± 0.01

^a Average ± SD (*n* = 5).

^b Mean recovery of five determination (*n* = 5).

^c The concentration of nitrogen in fruit samples are given in µg g⁻¹.

normally present in water and some fruit samples.

4. Conclusions

The proposed method is the first attempt at separating and preconcentrating trace nitrite and nitrate using diazotization-coupling reaction and ion-pair loaded on naphthalene-TDBA-I adsorbent. Nitrate was reduced 100% through the Cd-Cu column. Since the method requires only simple glassware, such as glass tubes, small volume beakers, and a small volume of organic solvent, it is very economical. As the procedure is free from the interference of diverse alkali salts and metal ions, it has been applied to analyzed lower concentrations of nitrite and nitrate in water and some fruit samples. The primary purpose of the present study is to develop various adsorbents for the preconcentration of trace nitrite and nitrate using conventional instruments, which are available in all laboratories. The proposed method is

characterized by the fact that the solid adsorbent in the column can only be used once, instead of being re-usable as in ion-exchange resin and chelex-100 methods. The method may be improved further by using ion-exchange resin and the adsorbent supported with an ion-pair on silica combined with optical analytical techniques like flow injection and/or fluorimetry.

References

- [1] W. Lijinsky, S.S. Epstein, Nature (London) 21 (1970) 225.
- [2] J. Gabbay, Y. Almog, M. Davidson, A.E. Donagi, Analyst 371 (1977) 102.
- [3] K. Nagashima, M. Matsumoto, S. Suzuki, Anal. Chem. 57 (1985) 2065.
- [4] M. Aoyama, T. Hobo, S. Suzuki, Bunseki Kagaku (Japan) 31 (1982) E163.
- [5] M. Bernard, G. Macchi, Automation in Analytical Chemistry, Technicon Symposia 1965, Mediad, N.Y., 1966, p. 252.
- [6] A.W. Morris, J.P. Riley, Anal. Chim. Acta 29 (1963) 272.

- [7] J.F. Van Staden, *Anal. Chim. Acta* 138 (1982) 403.
- [8] L. Anderson, *Anal. Chim. Acta* 110 (1979) 123.
- [9] Japanese Industrial Standard, JIS K0101, 1979, 123.
- [10] J.F. van Staden, M.A. Makhafola, D. de Weal, *Appl. Spectrosc.* 50 (1996) 991.
- [11] M. Pandurangappa, N. Balasubramanian, *Mikrochim. Acta* 124 (1996) 137.

An optical fiber sensor for berberine based on immobilized 1,4-bis(naphth[2,1-d]oxazole-2-yl)benzene in a new copolymer

Wan-Hui Liu ^{a,b}, Ying Wang ^a, Jiang-Hong Tang ^a, Guo-Li Shen ^a, Ru-Qin Yu ^{a,*}

^a Department of Chemistry and Chemical Engineering, Hunan University, Changsha, 410082, People's Republic of China

^b Analytical Center, Yantai University, Yantai, 264005, People's Republic of China

Received 9 July 1997; received in revised form 13 September 1997; accepted 16 September 1997

Abstract

A new copolymer made of 8-quinolyl methacrylate, methyl methacrylate and *n*-butyl acrylate (PQMB) has been used as a solid substrate for the preparation of an optical fiber berberine sensor. The sensing is based on the fluorescence of 1,4-bis(naphth[2,1-d]oxazole-2-yl)benzene (BNOB) immobilized in the copolymer quenched by berberine with the formation of 1:1 complex between them. The membrane composition was optimized using the orthogonal experimental design. Using the sensor described above, berberine in a sample solution from $4.02 \times 10^{-7} \text{ mol l}^{-1}$ to $2.82 \times 10^{-4} \text{ mol l}^{-1}$ can be detected. The sensor has satisfactory reversibility and a short response time of less than 30 s. The relative standard deviations for repeated measurements ($n = 15$) of $8.05 \times 10^{-6} \text{ mol l}^{-1}$ and $4.02 \times 10^{-5} \text{ mol l}^{-1}$ berberine are 0.43% and 0.33%, respectively. The sensor shows good selectivity over alkali and alkali-earth metal salts and some common pharmaceutical species and can be used for the determination of berberine in pharmaceutical preparations. © 1998 Elsevier Science B.V. All rights reserved.

Keywords: 1,4-bis(naphth[2,1-d]oxazole-2-yl)benzene; Berberine; Optical fiber sensor

1. Introduction

A fluorescence optical fiber sensor can be prepared by immobilizing a fluorophore on a solid substrate and monitoring the change in optical properties of the sensing layer upon interaction with the analyte. Various methods of immobilizing fluorophores such as adsorption [1,2], entrapment [3–5], and covalent bonding [6,7] have been used for this purpose. The fluorophores without suitable bonding groups attached to polymers are

often trapped in plasticized poly(vinyl chloride) (PVC) membranes [8–10]. The PVC type polymeric membrane material has numerous disadvantages such as dye leaching and poor adhesion of the membrane on quartz glass located at the distal end of the optical fiber. Finding new membrane materials with reduced dye leaching and improved adhesion characteristics is of considerable interest.

Methacrylate–acrylate based polymers are a class of promising membrane materials for chemical sensor design [11,12] with fine adhesion abilities on ceramics, silicon and quartz glass. In this

* Corresponding author.

paper, we describe a new methacrylate–acrylate based copolymer prepared from 8-quinolyl methacrylate, methyl methacrylate and *n*-butyl acrylate (PQMB) for trapping 1,4-bis(naphth[2,1-d]oxazole-2-yl)benzene (BNOB) to prepare an optical fiber sensor for berberine.

Berberine, being a quaternary ammonium salt, has been used as a medicine for stomach and intestinal disorders. For analytical determination of berberine, a number of methods have been proposed including extraction spectrophotometry [13,14], high performance liquid chromatography [15], ion-selective electrodes [16,17], flow-injection [18], and fluorometry [19]. Most of these methods demand a cumbersome sample pretreatment and suffer from interference of many co-existing species. We report on a fluorescence sensor for detection of berberine, which was based on fluorescence quenching of 1,4-bis(1,3-benzoxazolyl-2-yl)benzene (BBOB) immobilized on a plasticized PVC membrane [20]. This method's response is quick and has good reversibility, though BBOB tends to leach from the PVC membrane. In this study, we report on a new optical fiber sensor for berberine based on immobilizing BNOB on a new membrane material. This membrane material has good adhesion properties on quartz glass and fair compatibility with BNOB because of the existence of quinolyl groups in PQMB copolymer which reduces the BNOB leaching from the membrane phase. Furthermore, the sensor made of PQMB exhibits a fast response time, high sensitivity, good reversibility and durability. The newly proposed sensor can be used in the determination of berberine in commercial pharmaceutical preparations.

2. Experimental

2.1. Apparatus

Fluorescence measurements were conducted on a Hitachi M-850 spectrofluorimeter with both excitation and emission bandpasses set at 5.0 nm. Berberine sensing measurements were carried out using a home-made poly(tetrafluoroethylene) (PTFE) flow-through cell (Fig. 1). A randomly

distributed bifurcated bundle (30 + 30 quartz fibers, length 1 m, 6 mm in diameter at the common end) from Glass Institute of Beijing, was sealed into a mounting screw nut (26 mm in length, 32 mm in outer diameter and 26 mm in inner diameter) to carry the light to and from the cell. A quartz glass plate (12 mm in diameter) covered with the sensing membrane was positioned on the top of the flow chamber (ca. 75 μ l) and fixed by the mounting screw nut. The solution inlet and outlet channels were drilled through the cell body (28 mm in length, 20 mm in diame-

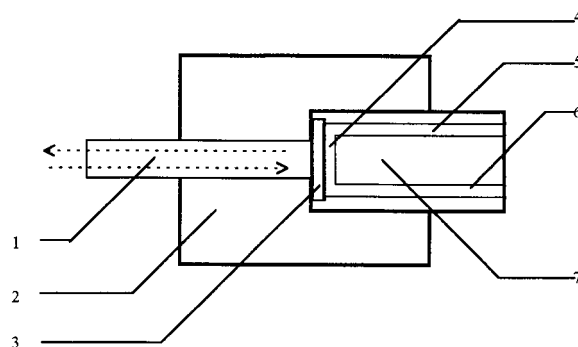


Fig. 1. Schematic diagram of the flow cell arrangement. (1), Bifurcated optical fiber; (2), quartz glass plate mounting screw nut; (3), quartz glass plate covered with sensing membrane; (4), flow chamber; (5), solution inlet channel; (6), solution outlet channel; (7), cell body.

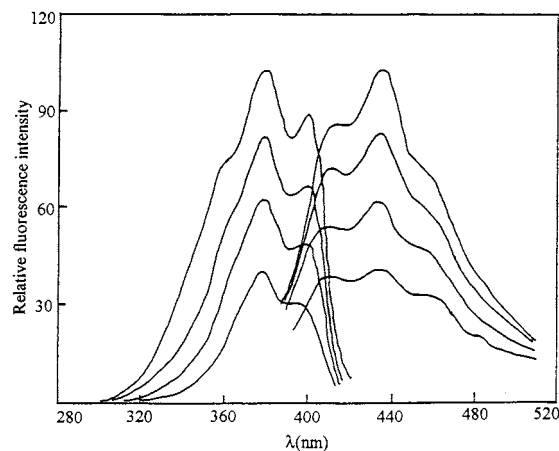


Fig. 2. Fluorescence excitation (left) and emission spectra (right) of the berberine sensor on exposure to (curves from top to bottom): reagent blank, 2.01×10^{-5} mol l⁻¹, 4.02×10^{-5} mol l⁻¹, 9.07×10^{-5} mol l⁻¹.

ter) to the flow chamber and connected to two 2 mm Teflon tubes. The sample solution was continuously circulated in and out of the cell at a flow rate of 1.2 ml min^{-1} with a peristaltic pump (Guokang Instruments, Zhejiang, People's Republic of China). In order to avoid ambient light penetrating the sensing membrane, the flow-through cell was covered with black cloth during measurements. Measurements of pH were performed using a Model PH-3C pH meter equipped with a combination electrode calibrated using two standards.

2.2. Chemicals

The copolymer PQMB was synthesized from 8-quinolyl methacrylate, methyl methacrylate and *n*-butyl acrylate by free-radical polymerization. A detailed description is presented in other studies [21]. BNOB was obtained by a condensation reaction of 1-amino-2-naphthol hydrochloride with *p*-phthalic acid [22], tetrahydrofuran (THF) and dinonyl sebacate (DNS) were from Changsha Chemical Reagents. Berberine was used as received from Shanghai Pharmaceutical.

A stock standard aqueous berberine solution of $2.012 \times 10^{-3} \text{ mol l}^{-1}$ was prepared. The working solutions were obtained by serial dilutions of this stock with chloroacetic acid buffer prepared by dissolving 24 g of chloroacetic acid in 500 ml of water and adjusting it to pH 2.16 with 6 mol l^{-1} NaOH solution. All reagents were of analytical grade, and freshly redistilled water was used in all experiments.

2.3. Preparation of optode membrane

A membrane cocktail was obtained by dissolving 40 mg of PQMB and 80 mg of DNS in 0.8 ml of THF saturated with BNOB and 0.2 ml of THF without BNOB. With the help of a spin-on device [3], a membrane of approximately $4 \mu\text{m}$ in thickness was cast on a quartz glass (12 mm in diameter).

2.4. Fluorescence measurement

The membrane was positioned on the top of a

flow chamber (Fig. 1). The detection of membrane fluorescence quenched by berberine was made under batch conditions at the maximum excitation wavelength of 380.0 nm and the maximum emission wavelength of 435.0 nm using an emission filter of 390 nm. Berberine solution was pumped through the flow cell at a rate of 1.2 ml min^{-1} . The sensor was allowed to equilibrate with the sample solution, so that a stable fluorescence signal could be recorded. The fluorescence reading of the optode membrane was recovered by flowing the blank buffer solution prior to the next measurement.

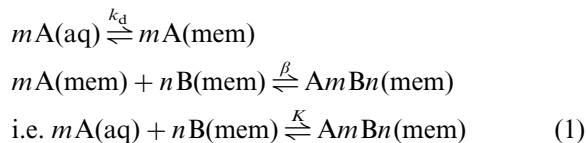
2.5. Sample preparation

The powder (50 mg) of ground berberine tablets was dissolved in boiling water, and the cooled solution together with the residue was diluted to a final volume of 100 ml. With the initial portion discarded, the filtrate was collected and used for analytical determination.

3. Results and discussion

3.1. Principle of operation

The lipophilic fluorophore BNOB newly synthesized in our laboratory has a large conjugated double bond system and exhibits strong fluorescence emission. Benzoxazole compounds were referred to as good charge-donors [23] capable of forming charge-transfer complexes with charge-acceptor molecules. Fig. 2 shows the fluorescence excitation and emission spectra of the optode membrane containing BNOB on exposure to the blank and berberine solutions of different concentrations. It is evident from Fig. 2 that berberine can strongly quench the fluorescence of the membrane, accompanied by the formation of a possible charge-transfer complex. The process can be expressed as follows:



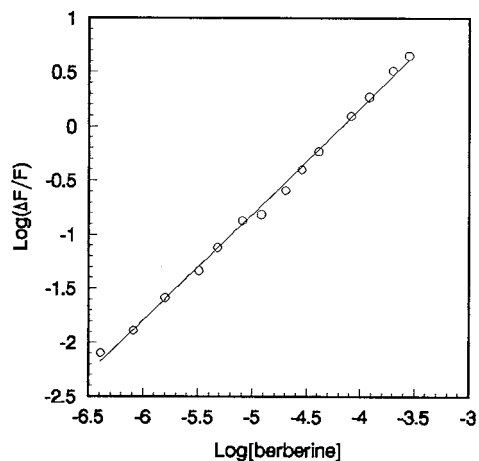


Fig. 3. A plot of $\log(\Delta F/F)$ as a function of the logarithm of berberine concentration.

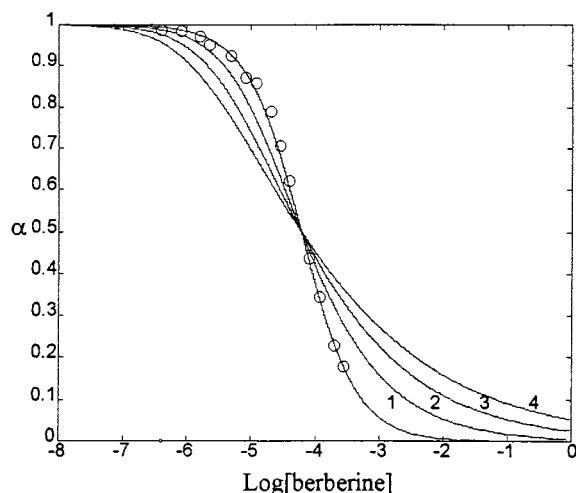


Fig. 4. Relative fluorescence intensity (α) as a function of $\log[\text{berberine}]$. The curves fitting the experimental data were calculated from Eq. (4). The circles are experimentally observed data points. (1), $m:n = 1:1$ $K = 1.67 \times 10^4$; (2), $m:n = 1:2$ $K = 2.72 \times 10^6$; (3), $m:n = 1:3$ $K = 4.87 \times 10^8$; (4), $m:n = 1:4$ $K = 9.49 \times 10^{10}$.

where A and B represent berberine and BNOB, respectively; m/n are the complexing ratio of berberine and BNOB; k_d is the distribution coefficient of berberine between aqueous and membrane phases; β is the formation constant of the complex of berberine with BNOB in PQMB membrane and K is the equilibrium constant of Eq. (1). The relationship between fluorescence signal

changes, berberine concentration and the amount of BNOB can be expressed as:

$$\frac{F_0 - F}{F} = K[B]_{(\text{mem})}^{n-1}[A]_{(\text{aq})}^m$$

$$\log\left(\frac{\Delta F}{F}\right)$$

$$= \log K + (n-1) \log[B]_{(\text{mem})} + m \log[A]_{(\text{aq})}$$

$$\Delta F = F_0 - F \quad (2)$$

where F_0 and F denote the fluorescence intensities of the optode membrane in the absence and presence of berberine, respectively; $[A]_{(\text{aq})}$ is the total concentration of berberine in aqueous phase and $[B]_{(\text{mem})}$ is the total concentration of BNOB in the membrane phase. It is obvious from Eq. (2) that m is the slope of the plot of $\log(\Delta F/F)$ versus $\log[A]_{(\text{aq})}$ (Fig. 3), which was calculated to be 1 from Fig. 3.

Relative fluorescence intensity α is defined as the ratio of free BNOB, $[B]_f$, and the total amount of BNOB, $[B]_{(\text{mem})}$ in the membrane which can be determined experimentally by measuring the fluorescence intensity of the optode membrane:

$$\alpha = \frac{[B]_f}{[B]_{(\text{mem})}} = \frac{F_2 - F_{(\text{limit})}}{F_1 - F_{(\text{limit})}} \quad (3)$$

where F_1 is the fluorescence intensity of the optode membrane in the blank solution, and $F_{(\text{limit})}$ is the fluorescence intensity when BNOB in the membrane is completely complexed with berberine, F_2 is the fluorescence intensity of the

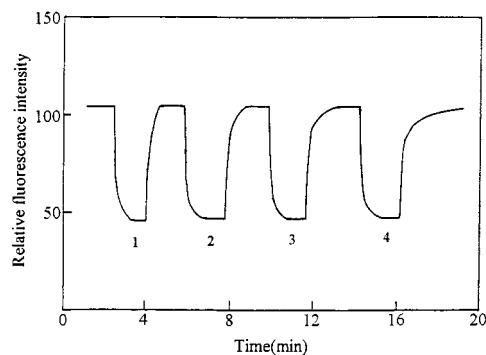


Fig. 5. Fluorescence intensity, response and recovery times of berberine sensor operated at different pH. (1), pH 2.65; (2), pH 5.01; (3), pH 6.92; (4), pH 8.29.

Table 1
Fluorescence response characteristics for the optode membranes of different composition

Membrane	Membrane cocktail composition			Fluorescence intensity	Linear range (mol l ⁻¹)	Response slope (l mol ⁻¹)
	PQMB (mg)	DNS (mg)	BNOB (ml) ^a			
M ₁	20	0	0.6	66.7	4.02 × 10 ⁻⁷ ~ 6.00 × 10 ⁻⁵	1.27 × 10 ⁴
M ₂	20	40	0.8	80.0	4.02 × 10 ⁻⁷ ~ 1.00 × 10 ⁻⁴	1.32 × 10 ⁴
M ₃	20	80	1.0	106.0	4.02 × 10 ⁻⁷ ~ 2.00 × 10 ⁻⁵	1.29 × 10 ⁴
M ₄	40	0	1.0	79.0	4.02 × 10 ⁻⁷ ~ 1.00 × 10 ⁻⁴	1.20 × 10 ⁴
M ₅	40	40	0.6	101.7	4.02 × 10 ⁻⁷ ~ 2.82 × 10 ⁻⁴	1.29 × 10 ⁴
M ₆	40	80	0.8	109.8	4.02 × 10 ⁻⁷ ~ 2.82 × 10 ⁻⁴	1.35 × 10 ⁴
M ₇	60	0	0.8	98.8	4.02 × 10 ⁻⁷ ~ 6.00 × 10 ⁻⁵	1.45 × 10 ⁴
M ₈	60	40	1.0	126.0	4.02 × 10 ⁻⁷ ~ 2.82 × 10 ⁻⁴	1.19 × 10 ⁴
M ₉	60	80	0.6	107.7	4.02 × 10 ⁻⁷ ~ 2.82 × 10 ⁻⁴	1.19 × 10 ⁴

^a Volume of THF solution saturated with BNOB.

optode membrane actually measured when in contact with berberine solutions of different concentrations. The relationship between the fluorescence signal and berberine concentration $[A]_{(aq)}$ can be expressed by as:

$$\frac{\alpha^n}{1 - \alpha} = \frac{1}{nK[B]_{(mem)}^{n-1}[A]_{(aq)}^m} \quad (4)$$

It is noticed that $m = 1$. The functional relationship between α and the concentration of berberine is governed by different n and K . Fig. 4 shows the theoretical curves calculated by Eq. (4). Obviously, only curve 1 of 1:1 complex ratio and a reasonable $K = 1.66 \times 10^4$ is the best fit for the experimental data.

Based on the formation of the 1:1 complex, the quenching efficiency as a function of the berberine concentration is given by the Stern–Volmer equation:

$$\frac{F_0}{F} = 1 + K[A]_{(aq)} \quad (5)$$

In subsequent experiments, Eq. (5) is employed to evaluate the analytical performance of the sensor and is used as the basis of quantitative analysis.

3.2. Effect of acidity

In order to determine the optimum experimental conditions, the suitable pH range was investigated by recording fluorescence intensity, response and recovery times of the sensor. The fluorescence quenching efficiency (F_0/F) and the response time of the sensor are almost independent of pH, while the recovery time is affected by the acidity of solutions. Fig. 5 shows the response curves of the berberine sensor operated at different pH. A pH of 2.16 chloroacetic acid buffer solution was selected as the working buffer in the following experiments.

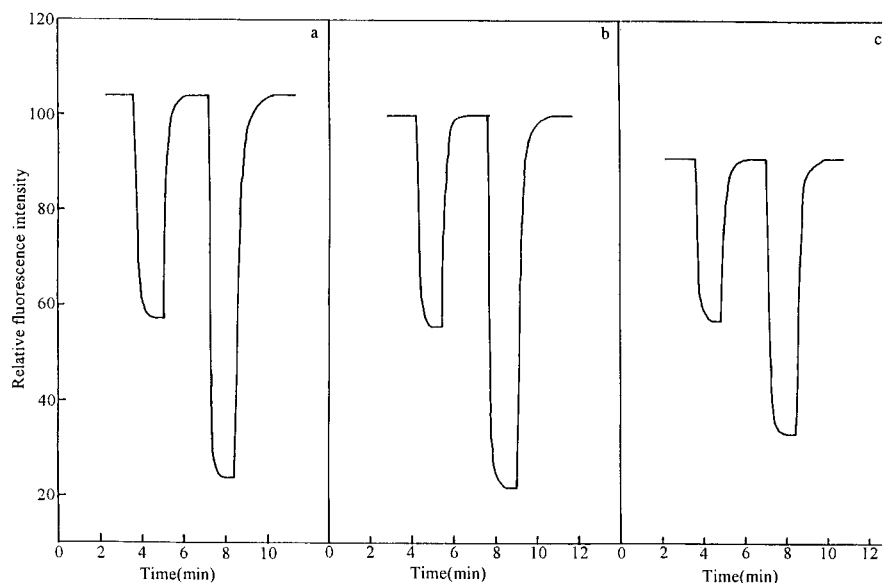


Fig. 6. Response of the sensor membranes exposed to $6.03 \times 10^{-5} \text{ mol l}^{-1}$ (left) and $2.01 \times 10^{-4} \text{ mol l}^{-1}$ (right) berberine: (a), DNS plasticized PQMB membrane; (b), PQMB membrane; (c), PQM membrane.

3.3. Optimization of membrane composition

For optimization of the optode membrane composition, a membrane cocktail containing PQMB, BNOB and DNS was prepared, approximately 0.1 ml of the solution was used for the preparation of the optode membrane. The optimization of the optode membrane composition including PQMB, BNOB and DNS was performed using the $L_9(3^4)$ orthogonal experimental table. The solubility of BNOB in THF solution is rather low owing to the presence of a large conjugated system in the molecule. THF solution saturated with BNOB was used instead of the weighting of BNOB in optimization experiments.

As described above, the response of the sensor is based on the fact that berberine can quench the membrane fluorescence. The sensing performance is determined by the quenching curve and the quenching constant in Stern–Volmer Eq. (5). The analytical range and the slope of the Stern–Volmer curve were employed in the evaluation of optode membrane optimization. The experimental results are showed in Table 1. Relatively narrow linear ranges were obtained from membranes without DNS or with small amounts of DNS. No

distinct effects of the amount of PQMB and DNS on the linear ranges and response slopes were observed, though fluorescence intensities increased with increasing amounts of PQMB and DNS in the membranes. A membrane cocktail containing 80 mg of DNS, 40 mg of PQMB and 0.8 ml of THF saturated with BNOB and 0.2 ml of THF without BNOB was selected for the optode membrane preparation.

3.4. Response time and possible response mechanism

The response time of a polymer membrane based optical sensor is closely related to the diffusion of the analyte within the membrane phase and its extraction from the sample solution [24]. Usually, an appropriate plasticizer should be added to the membrane phase to facilitate the diffusion and extraction processes. In our experiments, however, the response time of a DNS-free PQMB membrane was actually the same as that of a DNS-plasticized PQMB membrane (Fig. 6). A new copolymer of 8-quinolyl methacrylate and methyl methacrylate (PQM) was prepared to test whether the *n*-butyl group in PQMB has a func-

tion as ‘internal’ plasticizer. It turned out that the response time of the PQM based sensor was quite similar to that of the two PQMB based sensors (Fig. 6). It seems that the diffusion of berberine within the membrane and the extraction of berberine from the aqueous phase into the membrane phase are not substantially affected by the presence of plasticizer or some functional groups acting as ‘internal’ plasticizer. On exposure to water the PQM and PQMB based membranes would undergo swelling as a result of the slight hydrophilicity of the quinolyl group in the copolymer. This might facilitate the diffusion and extraction of hydrophilic berberine in the membrane phase and results in the fast response of the berberine sensor.

The aforementioned reasoning should not be applicable to lipophilic analytes. Nitrobenzene is a lipophilic molecule, it can quench the fluorescence of BNOB. A comparison was made for PQMB, DNS-plasticized PQMB and PQM mem-

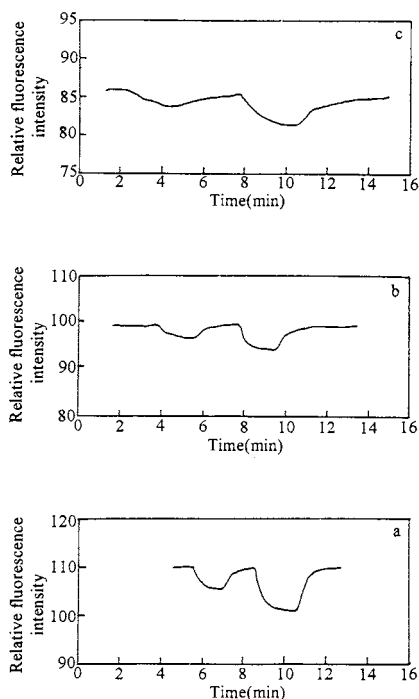


Fig. 7. Response of the sensor membranes exposed to $2.00 \times 10^{-4} \text{ mol l}^{-1}$ (left) and $2.01 \times 10^{-4} \text{ mol l}^{-1}$ (right) nitrobenzene: (a), DNS plasticized PQMB membrane; (b), PQMB membrane; (c), PQM membrane.

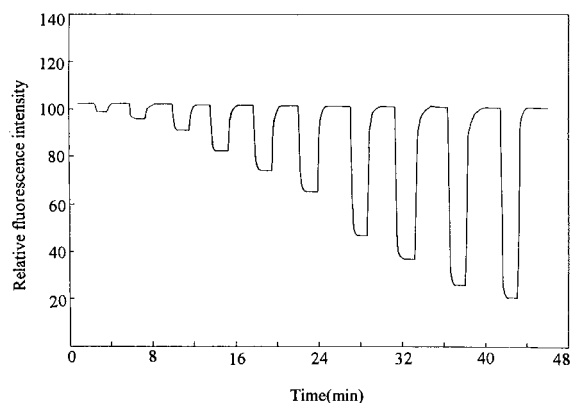


Fig. 8. Reversibility of the sensor upon step changes of the berberine concentrations (mol l^{-1}). From left to right: 3.219×10^{-6} , 4.829×10^{-6} , 8.048×10^{-6} , 2.012×10^{-5} , 2.817×10^{-5} , 4.024×10^{-5} , 8.048×10^{-5} , 1.207×10^{-4} , 2.012×10^{-4} , 2.817×10^{-4}

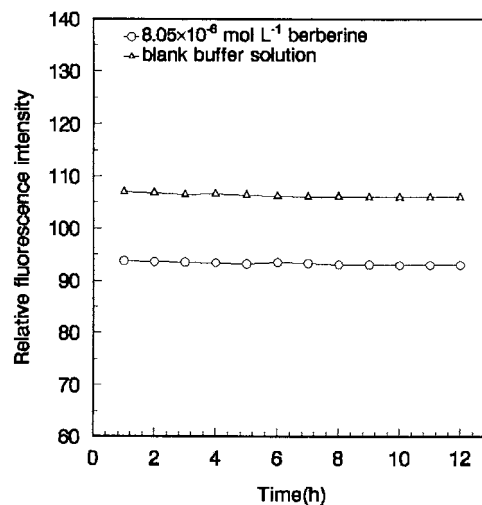


Fig. 9. The stability of the sensor exposed to buffer solution and 8.05 mol l^{-1} berberine. Fluorescence intensities were recorded over a period of 12 h with an interval of 1 h

branes for sensing nitrobenzene. Among these membranes, one would expect that membranes with the addition of a plasticizer (PQMB/DNS) or ‘internal’ plasticizer (PQMB) should have shorter response times in comparison with the PQM membrane. This was in agreement with experimental observations (Fig. 7). The response times of the PQMB membrane and the DNS plasticized PQMB membrane exposed to nitrobenzene solu-

Table 2

Effect of interferants on fluorescence intensity of the optode membrane. Each sample solution contains a fixed concentration of 4.02×10^{-5} mol l⁻¹ berberine in buffer solution

Interferant	Concentration (mol l ⁻¹)	Fluorescence change value ^a (ΔF) = ($F_2 - F_1$)	Relative error ($\Delta F/F_1$) × 100
KCl	1.06×10^{-2}	0.3	-0.64
NaNO ₃	1.02×10^{-2}	0.3	-1.89
NH ₄ Cl	1.03×10^{-2}	0.5	-1.51
MgSO ₄	1.05×10^{-2}	0.2	-1.32
CaCl ₂	1.00×10^{-2}	0.75	-1.60
Lidocaine	1.03×10^{-3}	0.0	0.00
Amobarbital	1.00×10^{-3}	-0.6	1.71
Theophylline	1.00×10^{-3}	0.0	0.00
Levamisole	1.20×10^{-3}	0.5	0.43
Vitamin B ₁	9.70×10^{-4}	0.6	0.00
Diphenhydramine	1.05×10^{-3}	0.6	0.00
Benzazole	1.51×10^{-3}	-0.6	0.43
Sulfaguanidine	1.00×10^{-3}	-1.0	1.71
Ethacrynic acid	4.74×10^{-4}	0.1	2.14
Pentoxifyverine	1.00×10^{-3}	0.0	0.00
Promethazine	2.03×10^{-4}	0.1	0.00
Sulfadiazine	1.00×10^{-3}	1.0	0.43
Naproxen	1.00×10^{-3}	0.4	1.07
Tropocanide	1.00×10^{-3}	-0.1	0.00
KC-404	1.00×10^{-3}	0.0	0.00
Clindamycin	1.00×10^{-3}	0.0	0.00

^a F_1 and F_2 are the fluorescence intensities of the optode membrane in contact with 4.02×10^{-5} mol l⁻¹ berberine solution without and with the interferant, respectively.

tions are nearly the same as those membranes in contact with the berberine samples. Here the role of DNS as a plasticizer or, *n*-butyl group as 'internal' plasticizer seems to facilitate the extraction of nitrobenzene from sample solution into these membranes and the quick diffusion of nitrobenzene within them. The unplasticized PQM membrane has a substantially longer response time for nitrobenzene than for berberine as a result of the difficult extraction of nitrobenzene from the water phase into the unplasticized membrane phase and a slower diffusion of nitrobenzene within it.

3.5. Reversibility, reproducibility, short-time stability and life time

The sensor was successively exposed to a series of berberine solutions of different concentrations, with the blank buffer in-between. By recording the fluorescence intensity changes vs. time, the

reversibility of the sensors was evaluated. The result is shown in Fig. 8. It can be seen that the sensor is completely reversible. The relative standard deviations in fluorescence intensities recorded from 15 consecutive measurements of 8.05×10^{-6} mol l⁻¹ and 4.02×10^{-5} mol l⁻¹ berberine with the blank in between were 0.43% and 0.33%, respectively. The sensor shows good reproducibility in the detection of berberine.

For the evaluation of short-term stability of the sensor, experiments were carried out by dipping two similar sensors into a blank buffer and 8.05×10^{-6} mol l⁻¹ berberine solution, respectively. Fluorescence intensities of these sensors were recorded over a period of 12 h at intervals of 1 h (Fig. 9). The relative standard deviations was calculated as 0.33% and 0.29%. In order to monitor BNOB leakage from the membrane into the sample, the fluorescence intensity changes of the optode membrane were recorded. The fluorescence intensity of the sensor dropped ca. 6.5%

Table 3
Response characteristics of the berberine sensors

Sensor characteristics	Sensor	
	BNOB trapped in PQMB membrane	BBOB trapped in PVC membrane ^a
Complexing ratio	1:1	1:1
Response time (s)	< 30	< 30
Linear range (mol l ⁻¹)	4.02 × 10 ⁻⁷ ~ 2.82 × 10 ⁻⁴	1.62 × 10 ⁻⁵ ~ 6.76 × 10 ⁻⁴
Response slope (mol ⁻¹ l)	1.35 × 10 ⁴	1.00 × 10 ³
Detection limit (mol l ⁻¹)	2 × 10 ⁻⁷	—
Relative standard deviation for repeated measurements	0.43 (n = 15, [HB] = 8.05 × 10 ⁻⁶ mol ⁻¹ l) 0.33 (n = 15, [HB] = 4.02 × 10 ⁻⁵ mol ⁻¹ l)	1.67 (n = 12, [HB] = 8.05 × 10 ⁻⁶ mol ⁻¹ l)
Dye leaching	Slight	Serious

^a Data from literature [20]

from the initial value, after 200 measuring cycles (sensing and regeneration). The existence of the quinolyl group in the PQMB copolymer (having good compatibility with BNOB), seems beneficial in reducing the leakage of BNOB from the membrane phase. The optode membrane can be stored in wet conditions without losing its sensitivity for at least one month.

3.6. Interference

The effect of interferants on the fluorescence intensity of the proposed sensor was tested. Alkali and alkali earth metal salts as well as many

common pharmaceutical species do not have a substantial effect on the fluorescence intensity (Table 2). The sensor has sufficient selectivity towards berberine, making it feasible for practical applications in pharmaceutical analysis.

3.7. Comparison of the berberine sensors

The sensor response characteristics including complexing ratio, response time, linear range, response slope, detection limit, etc. are summarized in Table 3 and compared with a berberine sensor reported earlier [20]. The proposed sensor in this paper has a wider linear range, higher sensitivity and better reproducibility. Moreover, one can expect the PQMB based sensor to have a longer life time owing to the reduced dye leaching from the membrane phase.

3.8. Preliminary application

The proposed sensor was used for the direct determination of berberine in pharmaceutical preparations. The sample solutions as prepared according to the Section 2 were diluted with buffer solution at pH 2.16 analyzed by the calibration curve method using the BNOB sensor. The results are in agreement with those obtained using the pharmacopoeia method [25] (Table 4).

Table 4
Results for berberine in commercial tablets using the proposed method and the pharmacopoeial method

Sample	Berberine content (%)	
	The proposed method	The pharmacopoeial method
	Mean ^a ± SD	Mean ^a ± SD
1	24.7 ± 0.31	24.6 ± 0.35
2	60.5 ± 0.57	60.7 ± 0.65
3	12.0 ± 0.20	12.0 ± 0.15

^a Mean of six determinations. SD, standard deviation.

Acknowledgements

This work was supported by the Foundation for Ph.D. Thesis Research of the National Education Commission, the Foundation for the Technological Development of Machinery Industry and Natural Science Foundation of Hunan Province, People's Republic of China.

References

- [1] W.A. Wyatt, F.V. Bright, G.M. Hieftje, *Anal. Chem.* 59 (1987) 2272.
- [2] J.Zh. Lu, Zh.J. Zhang, *Anal. Chim. Acta* 318 (1996) 175.
- [3] H.H. Zeng, K.M. Wang, Ch.L. Liu, P.Q. Yu, *Talanta* 40 (1993) 1569.
- [4] K. Seiler, K.M. Wang, M. Kuratli, W. Simon, *Anal. Chim. Acta* 244 (1991) 151.
- [5] M. Kuratli, E. Pretsch, *Anal. Chem.* 66 (1994) 85.
- [6] G. Orellana, A.M. Gomez-Cameros, G. Dios, A.A. Garcia-Martinez, M.C. Morenno-Bondi, *Anal. Chem.* 67 (1995) 2231.
- [7] T. Rosatzin, P. Holy, K. Seiler, B. Rusterholz, W. Simon, *Anal. Chem.* 64 (1992) 2029.
- [8] Y. Wang, W.H. Liu, J.H. Wang, K.M. Wang, G.L. Shen, R.Q. Yu, *Anal. Lett.* 30 (1997) 221.
- [9] M. Lerchi, F. Orsini, Z. Cimerman, E. Pretsch, D.A. Chowdhury, S. Kamata, *Anal. Chem.* 68 (1996) 3210.
- [10] H.H. Zeng, K.M. Wang, R.Q. Yu, *Anal. Chim. Acta* 298 (1994) 271.
- [11] L.Y. Heng, E.A.H. Hall, *Anal. Chim. Acta* 324 (1996) 47.
- [12] C.E. Hall, D. Datta, E.A.H. Hall, *Anal. Chim. Acta* 323 (1996) 87.
- [13] H.M.N.H. Riving, J.J. Markham, *Anal. Chim. Acta* 39 (1967) 7.
- [14] G.V. Scott, *Anal. Chem.* 40 (1968) 768.
- [15] Ch. Yu, Y.C. Hong, H. Zhang, X.R. Xu, *Seppu* 10 (1992) 167.
- [16] G.L. Shen, Sh.Zh. Yao, X.H. Jiang, *Fenxi Huaxue* 11 (1983) 1.
- [17] X.Y. Zhou, Y. Luo, M. Shuai, *Fenxi Huaxue* 20 (1992) 42.
- [18] S. Tadao, *Analyst* 116 (1991) 187.
- [19] S. Tadao, C.Y. Soon, O. Noriko, *Anal. Sci.* 8 (1992) 377.
- [20] Y. Wang, K.M. Wang, W.H. Liu, G.L. Shen, R.Q. Yu, *Analyst* 122 (1997) 69.
- [21] W.H. Liu, Y. Wang, J.H. Tang, G.L. Shen, R.Q. Yu, Quinolyl methacrylate copolymer as an immobilization matrix for fluorophore in optical fiber sensor, in preparation.
- [22] Y. Wang, Ph.D. Thesis, Hunan University, Changsha, People's Republic of China, 1997.
- [23] B.N. Ying, P. Huan, J.R. Tu, *Guangguang Kexue Yu Guanghuaxue* 12 (1994) 342.
- [24] K.M. Wang, *Theories and Methods of Optical Chemical Sensors*, Hunan Education Press, Changsha, China, p. 316 (in Chinese).
- [25] Sanitation Faculty (Ed.) *Pharmacopoeia of the People's Republic of China, Part III*, Sanitation Press, Beijing, 1990, p. 358 (in Chinese).

Spectrophotometric measurement of uranium(VI)-tributylphosphate complex in supercritical carbon dioxide

Takayuki Sasaki *, Yoshihiro Meguro, Zenko Yoshida

Advanced Science Research Center, Japan Atomic Energy Research Institute, Tokai, Naka, Ibaraki 319-11, Japan

Received 16 June 1997; received in revised form 22 September 1997; accepted 23 September 1997

Abstract

UV-visible absorption spectra of uranium(VI)-tributylphosphate (U(VI)-TBP) complex dissolved in supercritical CO₂ at 40–60°C and 100–250 kg cm⁻² were recorded. Wavelengths and molar extinction coefficients for the absorption peaks of U(VI)-TBP were determined and confirmed to be in good agreement with those of UO₂(NO₃)₂(TBP)₂ complex dissolved in organic solvents such as *n*-hexane. The absorbance at a given wavelength was proportional to the concentration of U(VI) species in supercritical CO₂, indicating a feasibility of in-situ determination of U(VI) concentration in CO₂ phase. A lower detection limit of U(VI)-TBP complex was estimated to be ca. 1×10^{-3} M. The molar extinction coefficient of U(VI)-TBP in supercritical CO₂ decreased slightly with an increase of the density of CO₂ medium, suggesting that the solute–solvent interaction of U(VI)-TBP complex with CO₂ was affected by the density. On the basis of the spectra obtained, phase behavior and solubility of UO₂(NO₃)₂(TBP)₂ + H(NO₃)(TBP) + TBP in supercritical CO₂ were elucidated. © 1998 Elsevier Science B.V. All rights reserved.

Keywords: Spectrophotometry; Uranium(VI); Tributylphosphate; Supercritical carbon dioxide; Density; Solubility; Phase behavior

1. Introduction

A supercritical CO₂ fluid is one promising substitute for metal-extraction media because of its potential for minimizing the amount of solvent waste and for simplifying the process. It is also attractive in that CO₂ is easily recyclable, non toxic, chemically and radiochemically stable and

less expensive[1,2]. We have been developing the supercritical fluid extraction (SFE) method for the separation of U(VI), Pu(IV) and fission product elements in nitric acid solution using supercritical CO₂ containing relatively low concentrations of tributylphosphate (TBP) and have demonstrated a high feasibility of SFE in a metal-separation processes, in particular to such nuclear technology fields as the reprocessing of nuclear spent-fuel [3–5]. Although continuous and in-situ measurement of the concentration of U(VI) and/or Pu(IV)

* Corresponding author. Tel.: +81 292 825532; fax: +81 292 825927; e-mail: sas@analchem.tokai.jaeri.go.jp

extracted in the SF-CO₂ phase is indispensable to attain normal operation of the SFE process, an analytical method applicable to this purpose is very limited.

Absorption spectrophotometry of a solute in dissolving supercritical fluids provides information on the concentration of the solute [6,7], which implies the feasibility of spectrophotometry for monitoring the metal concentration in SF-CO₂. UV absorption spectrometry was employed for direct measurement of the concentration of the uranium/ β -diketone complex extracted into SF-CO₂ [8]. In addition, spectrophotometric measurement has been used as a very powerful means for the observation of the solute–solvent or solute–solute interactions of organic dye dissolved in supercritical fluid [9–11]. The distribution and solvation behaviors of the extracted species in SFE can be elucidated by measuring the absorption characteristics of the extracts.

In the present study, we measured the UV-visible spectrum of uranium(VI)-tributylphosphate (U(VI)-TBP) complex, which was involved in the SFE of U(VI) from nitric acid solution [3–5], dissolved in SF-CO₂ under different conditions of pressure and temperature. The feasibility of spectrophotometry for analytical application will be evaluated. A phase behavior and solubility of U(VI)-TBP/SF-CO₂ system will be discussed.

2. Experimental

2.1. Apparatus

A stainless steel cell (JASCO), of 2.35 ml inner volume, consisting of a pair of sapphire windows of 10 mm diameter and 6 mm thickness, was installed in a UV-visible spectrophotometer (JASCO, Ubest-30). The light path was calibrated to be 0.992 cm by measuring the absorption spectra of a standard solution of potassium dichromate [12]. The cell was maintained at a given temperature using a water-jacket type thermostat with a water circulator, (THOMAS TRL-108H) and was connected to a syringe pump (ISCO, series D). A stainless steel capillary of 0.1 mm ϕ i.d. and 20 cm in length was used as a restrictor (ISCO).

2.2. Measurement of spectra

An aliquot of U(VI)-TBP solution, prepared as described below, was taken in the cell. Carbon dioxide fluid was introduced into the cell using the syringe pump and the pressure and the temperature inside the cell were maintained at P higher than the critical pressure, P_c , of CO₂ (75.2 kg cm⁻²) and at T higher than the critical temperature, T_c , of CO₂ (31.2°C). The mixture of the sample and CO₂ was stirred using a magnetic stirrer for 5 min. The mixture was allowed to stand for 5 min after stirring, following which the absorption spectrum was measured. The pressure was varied stepwise from the lower to the higher pressure, after which the procedure of stirring followed by spectrum-measurement at a given pressure was repeated. After the experiment, the sample–CO₂ mixture was allowed to flow through the restrictor into the collection vessel containing ca. 100 ml of 0.1 mol dm⁻³ (M) HNO₃ where U(VI) and TBP were recovered from the CO₂ medium being gasified under atmospheric pressure and temperature.

2.3. Chemicals

Uranium(VI) stock solution: uranium metal, JAERI U-4, 99.99% purity, was dissolved with 7 M HNO₃ in the presence of hydrogen peroxide. After the solution was heated to near dryness, the residue was dissolved in 1 M HNO₃ to prepare a 0.10 M U(VI) solution.

U(VI)-TBP solution: aqueous solution, 100 ml of 7 M HNO₃ + 0.10 M U(VI), was mixed with 10 ml of TBP of $\geq 97\%$ purity. Uranium(VI) and H⁺ were extracted into the TBP phase as UO₂(NO₃)₂(TBP)₂ and H(NO₃)(TBP), resulting in a mixture of U(VI)-TBP, H⁺-TBP and uncombined TBP. The composition of the mixture prepared was confirmed to be 0.991 M U(VI) + 1 M H⁺ + 0.7 M free TBP from analytical results of U(VI) by inductively coupled plasma atomic emission spectrometry and H⁺ by alkali titration, as well as by subtracting the combined TBP from total TBP concentration, i.e. 3.7 M. The solution obtained was dehydrated in contact with molecular sieves for 30 min and then stored in a desiccator with silica-gel.

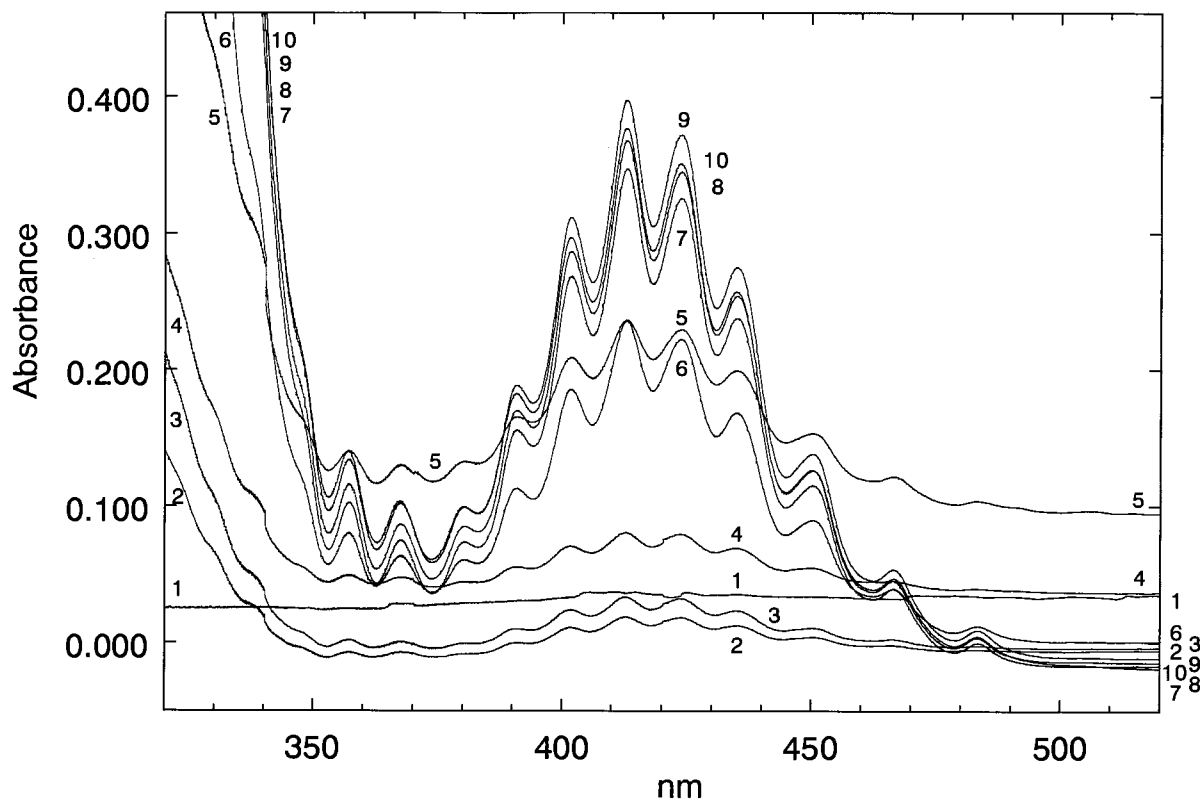


Fig. 1. Absorption spectra of U(VI)-TBP complex in supercritical CO_2 . Sample: 4.55×10^{-2} M $\text{UO}_2(\text{NO}_3)_2(\text{TBP})_2 + 5 \times 10^{-2}$ M $\text{H}(\text{NO}_3)(\text{TBP}) + 3.5 \times 10^{-2}$ M free TBP in CO_2 . Pressure (kg cm^{-2}): (1) 100; (2) 125; (3) 150; (4) 151; (5) 152; (6) 153; (7) 154; (8) 155; (9) 175; (10) 250.

All chemicals used were of reagent grade. Liquid CO_2 cylinder of 99.99% purity supplied by Shin Tokyo, Teisan, was used.

3. Results and discussion

An aliquot of U(VI)-TBP solution was taken in the cell to which CO_2 was added in order to obtain a mixture of 4.55×10^{-2} M U(VI)-TBP + 5×10^{-2} M H^+ -TBP + 3.5×10^{-2} M free TBP and supercritical CO_2 at 50°C and 100 kg cm^{-2} . Since the mixture prepared was slightly turbid initially, the measurement of the spectrum was performed after the mixture was stirred for 5 min and then allowed to stand for 5 min. The result thus obtained is shown by spectrum 1 in Fig. 1. A slight positive shift of

baseline absorbance over a wide range of wavelength is observed, which shows that the mixture is still turbid at $P = 100 \text{ kg cm}^{-2}$. No characteristic absorption peak due to U(VI) in the CO_2 phase is detected in spectrum 1. Spectra 2–10 were recorded identically to spectrum 1, but at different pressures, which were varied stepwise from 125 kg cm^{-2} to 250 kg cm^{-2} . In these spectra, 11 clear peaks are observed at wavelengths specific to absorption of U(VI), indicating distinct aspects as follows.

(i) Spectra 2 and 3 measured at $P = 125$ and 150 kg cm^{-2} respectively, show a slight increase of absorbance of U(VI), although the absorption intensity is not so strong and is hardly dependent on the pressure. It is noteworthy that a turbid characteristic of the mixture observed in spectrum 1 completely disappears in spectra 2 and 3.

(ii) Spectra 4–6 measured in very narrow pressure range, $P = 151–153 \text{ kg cm}^{-2}$, show the most remarkable variation. The absorption intensity of U(VI) starts to increase rapidly, indicating the sudden enhancement of the dissolution of U(VI)-TBP in the CO_2 phase with an increase in pressure greater than 151 kg cm^{-2} . Coincidentally, with the steep rise in the U(VI) absorption intensity, the positive shift of the baseline is again noted, as shown typically by spectra 4 and 5. The shift is assumed to be due to a formation of suspension under such transient conditions of the mixture of U(VI)-TBP, H^+ -TBP, free TBP and CO_2 from heterogeneous to homogeneous phases, although this is not yet fully understood.

(iii) Spectra 7–10 measured at $P = 154–250 \text{ kg cm}^{-2}$ indicate the complete dissolution of U(VI)-TBP complex over this pressure range resulting in a homogeneous supercritical CO_2 phase containing $4.55 \times 10^{-2} \text{ M U(VI)-TBP}$.

The wavelengths of 11 absorption peaks of U(VI)-TBP complex in supercritical CO_2 at 50°C and 200 kg cm^{-2} are listed in Table 1. All wavelengths determined agree well with those of U(VI)-TBP complex dissolved in neat TBP at 25°C and atmospheric pressure; the results are given in the last column of the table. From these results, it is confirmed that the chemical form of U(VI)-TBP complex dissolved in CO_2 is $\text{UO}_2(\text{NO}_3)_2(\text{TBP})_2$ as expected.

Table 1
Wavelengths λ and molar extinction coefficients ϵ of absorption bands of U(VI)-TBP complex in (1) supercritical CO_2 (50°C , 200 kg cm^{-2}) and (2) tributylphosphate (25°C , 1 kg cm^{-2}) media.

Band no.	CO ₂ media		TBP media
	λ (nm)	$\epsilon_{\text{UO}_2^{+}}$	λ (nm)
1	483.3	0.45 ± 0.01	485.9
2	466.4	1.44 ± 0.03	467.9
3	450.1	3.36 ± 0.07	452.4
4	434.9	6.47 ± 0.13	437.5
5	423.6	8.68 ± 0.15	425.6
6	412.7	9.30 ± 0.11	415.0
7	401.4	7.43 ± 0.09	403.9
8	390.7	4.64 ± 0.02	393.2
9	380.1	2.62 ± 0.04	382.7
10	367.3	2.67 ± 0.07	368.5
11	357.0	3.49 ± 0.08	358.5

A small discrepancy (1.2–2.6 nm) in wavelengths between the U(VI)-TBP complex in CO_2 and that in neat TBP is attributable to the difference in solvation behavior of the complex with the TBP and CO_2 molecules. In regard to this, a slight temperature-dependence of wavelength was observed, e.g. the highest peak was at 412.6 nm (40°C), 412.7 nm (50°C), or 412.9 nm (60°C). Similar temperature-dependence was reported by Bell et al.[13] in the absorption spectra of U(VI) in aqueous perchlorate media. This temperature-dependence of the wavelength, i.e. 0.02 nm longer shift per 1°C increase, does not coincide with the shorter shift as shown in Table 1. The effect of temperature on the peak position is so small that the measurement of the absorbance at a given wavelength is not disturbed by the variation of temperature over the range from 40 to 60°C , or even higher.

Fig. 2a shows the plot of absorption intensity at 412.7 nm, at which the highest U(VI) absorption peak appears, against the pressure. The absorption intensity after subtracting the baseline is shown in this figure. Plots 1, 2 and 3 correspond to results at 40, 50 and 60°C , respectively. From these results, one can recognize a sudden increase of the absorption with increasing pressure. The absorbance decreases slightly and gradually, with an increase of the pressure in the higher pressure range even where the complete dissolution of U(VI)-TBP is achieved. It is evident from the plots in Fig. 2(a) that the minimum pressure for achieving complete dissolution of U(VI)-TBP complex is lower at lower temperatures.

In Fig. 2(b), the results are reproduced as the plot of absorbance against the density of CO_2 [14–16]. It can be concluded that the complete dissolution of U(VI)-TBP complex is achieved more effectively, i.e. with CO_2 of the lower density, when the dissolving temperature is at its highest. There has been a suggestion that the solubility, S , of a solute in supercritical CO_2 can be expressed using the density, ρ , of CO_2 and S increases with an increase of ρ , as given by Eq. (1) [17]:

$$\ln S = a \ln \rho + b \quad (1)$$

where constant a is assumed to be an indication of the solvation of the solute in the supercritical

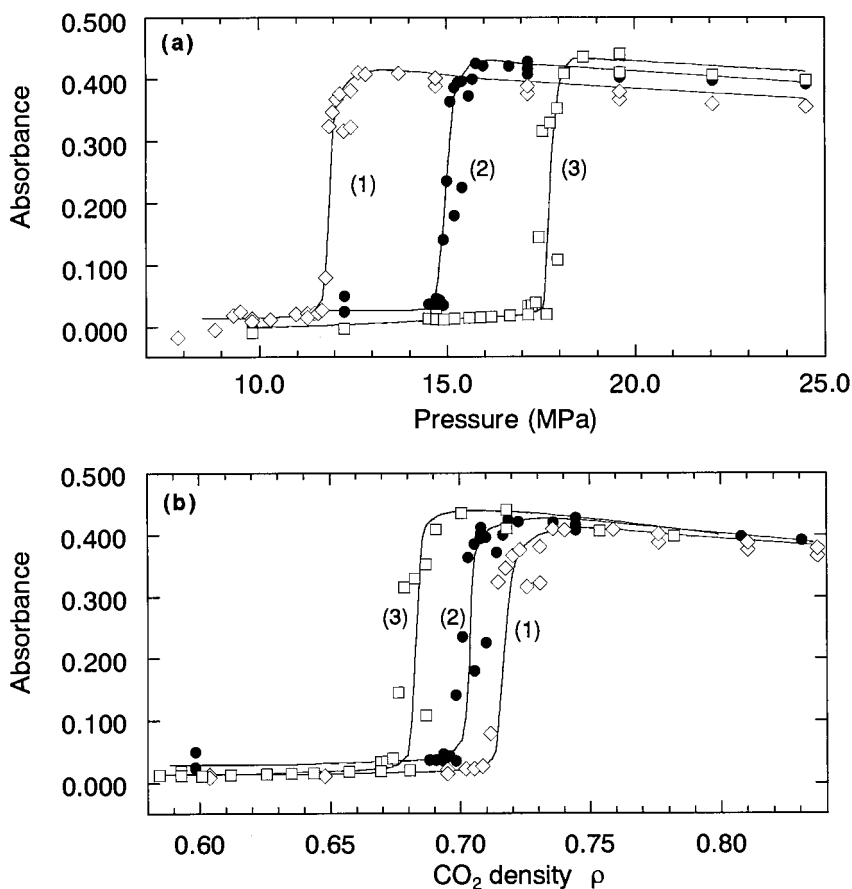


Fig. 2. Relation between U(VI)-absorbance at 412.7 nm and (a) pressure or (b) density of supercritical CO₂. Sample: identical as that in Fig. 1, temperature (°C): (1) 40; (2) 50; (3) 60.

CO₂ and b is a temperature-dependent constant correlated to the volatility of the solute. The temperature effect is attributable to the contribution of the constant b to the overall solubility, as shown in Fig. 2(b), the solubility of U(VI)-TBP complex in CO₂ of a given density is higher at higher temperatures.

The low absorbance of less than 0.02 which is observed at the lower pressure in Fig. 2(a) and in the lower CO₂-density region in Fig. 2(b), (see also spectra 2 and 3 in Fig. 1) hardly depends on the pressure, i.e. the density of the CO₂ medium. Simple solubility theory expressed by Eq. (1), cannot be applied to simulate the dissolution behavior of U(VI)-TBP complex in such a lower solubility region. One difficulty in the simulation

may arise from the variation of the composition of U(VI)-TBP + H⁺-TBP + free TBP mixture, depending strongly on the experimental conditions.

Molar extinction coefficients for absorption peaks of U(VI)-TBP spectra in supercritical CO₂ (50°C, 200 kg cm⁻²) are summarized in Table 1, calculated from results obtained with a supercritical CO₂ phase containing 2.28×10^{-2} , 4.55×10^{-2} and 6.83×10^{-2} M U(VI)-TBP. No appreciable change in the molar extinction coefficients was observed, even when the contents of H⁺-TBP complex or of free TBP in the sample were increased in the concentration range of 5×10^{-2} – 2×10^{-1} M or 3×10^{-2} – 8×10^{-2} M, respectively. The calibration curves representing the

linear relation between absorption intensity at 412.7 nm and the concentration of U(VI)-TBP complex in supercritical CO₂ are illustrated in Fig. 3. The slope of the linearity decreases slightly with increase of the pressure.

A lower detection limit, which is estimated as the concentration giving an absorption intensity of 0.01 with a cell of 1 cm light path, is ca. 1×10^{-3} M of U(VI)-TBP complex in CO₂, if the absorption at 412 nm is employed (Fig. 3). High reproducibility was obtained in the measurement of the absorption intensity, since peak position was almost independent of pressure, temperature and the concentration of coexisting free TBP and nitric acid species. A relative standard deviation (%) in the measurements (repeated six times) of a given sample of 4.55×10^{-2} M U(VI)-TBP + 5×10^{-2} M H⁺-TBP + 3.5×10^{-2} M free TBP in SF-CO₂ is less than $\pm 1\%$. Pu(IV) species extracted together with U(VI) gives a positive error in the measurement of absorption of U(VI) at 412.7 nm. The concentration of U(VI) in the presence of Pu(IV) can be determined by correcting the Pu(IV) contribution estimated from the absorbance of Pu(IV) at the other wavelength.

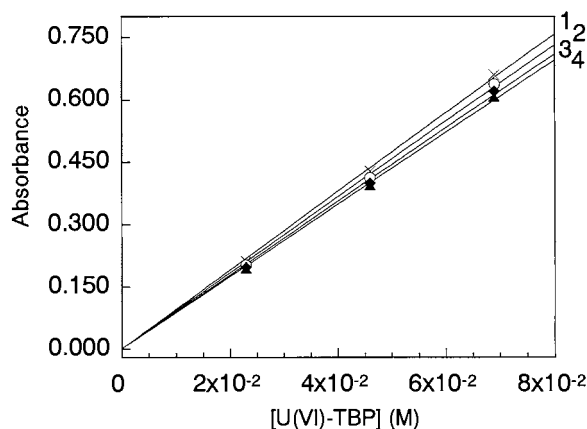


Fig. 3. Relation between U(VI)-absorbance at 412.7 nm and the concentration of U(VI)-TBP complex dissolved in supercritical CO₂. Pressure (kg cm⁻²): (1) 175; (2) 200; (3) 225; (4) 250.

4. Conclusion

The UV-visible spectrophotometry was demonstrated for studying the U(VI)-TBP complex dissolved in supercritical CO₂ under different conditions of pressure and temperature. The wavelength and intensity of absorption peaks are in good agreement with those for U(VI)-TBP complex dissolved in neat TBP at 25°C and atmospheric pressure, indicating that the chemical form of U(VI) species dissolved in CO₂ is UO₂(NO₃)₂(TBP)₂. The results also suggest the feasibility of using the spectrophotometric method for the determination of U(VI) concentration in the CO₂ phase, even in the presence of Pu(IV).

A solubility or phase behavior of an objective compound in the supercritical fluid medium should be properly examined in the experimental system containing the compound as a single component solute such as UO₂(NO₃)₂(TBP)₂ complex in the present case. This is because a presence of the other species such as H⁺-TBP and/or free TBP may affect the behavior of the solute of interest. However, from a practical viewpoint concerning the U(VI)-TBP extraction process using supercritical CO₂ medium, information from a more intricate system is required, e.g. the information on the solubility behavior of U(VI)-TBP complex in the mixture of UO₂(NO₃)₂(TBP)₂ + H(NO₃)(TBP) + free TBP and supercritical CO₂ as studied in the present work. In relation to this, it was not easy to synthesize UO₂(NO₃)₂(TBP)₂ complex as an isolated form.

Acknowledgements

The present research is partially supported by the REIMEI Research Resources of Japan Atomic Energy Research Institute.

References

- [1] Y. Lin, C.M. Wai, Anal. Chem. 66 (1994) 1971.
- [2] C.M. Wai, S. Wang, Y. Liu, V. Lopez-Avila, W.F. Beckert, Talanta 43 (1996) 2083.
- [3] S. Iso, Y. Meguro, Z. Yoshida, Chem. Lett. (1995) 365.

- [4] Y. Meguro, S. Iso, H. Takeishi, Z. Yoshida, *Radiochim. Acta* 75 (1996) 185.
- [5] Y. Meguro, T. Sasaki, S. Iso, Z. Yoshida, *Proceedings of the Fourth International Symposium on Supercritical Fluids*, 11–14 May, 1997, Sendai, Japan, vol. B, pp. 447.
- [6] G.L. Röbling, E.U. Franck, *Ber. Bunsenges. Phys. Chem.* 87 (1983) 882.
- [7] H. Ebeling, E.U. Franck, *Ber. Bunsenges. Phys. Chem.* 88 (1984) 862.
- [8] K.G. Furton, L. Chen, R. Jaffé, *Anal. Chim. Acta* 304 (1995) 203.
- [9] A. Morita, O. Kajimoto, *J. Phys. Chem.* 94 (1990) 6420.
- [10] S. Kim, K.P. Johnston, *Ind. Eng. Chem. Res.* 26 (1987) 1206.
- [11] S.P. Kelley, R.M. Lemert, *AIChE. J.* 42 (1996) 2047.
- [12] G.W. Haupt, *J. Res. Natl. Bur. Stand. Research Paper* 48 (1952) 414.
- [13] J.T. Bell, R.E. Biggers, *J. Mol. Spectrosc.* 18 (1965) 247.
- [14] P. Schofield, *Phys. Rev. Lett.* 22 (1969) 606.
- [15] P. Schofield, J.D. Litster, J.T. Ho, *Phys. Rev. Lett.* 23 (1969) 1098.
- [16] G.A. Chapela, J.S. Rowlinson, *J. Chem. Soc. Faraday Trans. I* 70 (1974) 584.
- [17] N.G. Smart, T. Carleson, T. Kast, A.A. Clifford, M.D. Burford, C.M. Wai, *Talanta* 44 (1997) 137.

Determination of nickel in human urine by ion chromatography with series bulk acoustic wave detection

Xiaorong Yang, Zhanchao Qiao, Wanzhi Wei, Shouzhuo Yao *

College of Chemistry and Chemical Engineering, Hunan University, Changsha, 410082, People's Republic of China

Received 7 July 1997; received in revised form 23 September 1997; accepted 24 September 1997

Abstract

By using ion chromatography with series bulk acoustic wave detection, a method for the determination of nickel at microgram per liter levels in urine has been developed. The highly sensitive response of series bulk acoustic wave (SBAW) detection has been combined with the selectivity of ion chromatography and hence sensitivity and precision have been improved. The detection and determination limits of the method for nickel are 0.4 and 2.0 ng ml⁻¹, respectively. For the IC analysis, the analytical column is a Shim-pack IC C1 column and the mobile phase is 4.5 mM tartaric acid solution. The method allows the determination of nickel in the presence of some ions commonly co-occurring with it. Urine samples from individuals with no occupational exposure to nickel were analysed successfully. © 1998 Elsevier Science B.V. All rights reserved.

Keywords: Ion chromatography; Series bulk acoustic wave; Nickel; Human urine

1. Introduction

Toxicological and physiological research on nickel have been a subject of growing interest over recent years. Nickel is immunotoxic and causes allergy and skin sensitization [1,2]. The concentration of nickel in biological materials in populations is known to be altered by acute myocardial infarction [3]. In particular, the carcinogenicity of this element has been extensively reviewed in the report by the International Committee on Nickel Carcinogenicity in Man [4,5] and the International Agency for Research on Cancer has concluded that nickel compounds are carcinogenic to

humans. Hence, the determination of nickel in biological materials in populations with and without occupational exposure is usually necessary.

As nickel occurs at very low levels in biological materials, a sensitive, selective and accurate method for its determination is desirable. Useful methods include electrothermal atomization spectrometry (ETAAS) [6,7], inductively coupled plasma mass spectrometry (ICP-MS) and voltametry [7,8]. These methods are powerful techniques for the determination of trace elements, but are not applicable to certain kinds of samples. For human urine and blood serum matrix effects are apparent for the ETAAS measurements. If the sample matrix contains large amounts of calcium, the determination of Ni by

* Corresponding author.

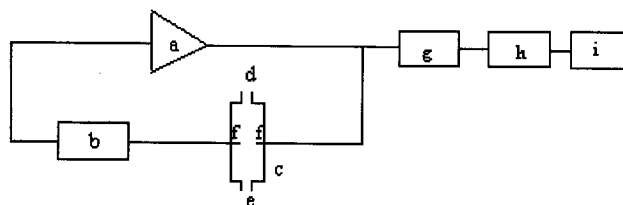


Fig. 1. Schematic diagram of the SBAW detector. (a) TTL-IC oscillator; (b) piezoelectric quartz crystal; (c) detection cell; (d) mobile phase inlet; (e) mobile phase outlet; (f) conductivity electrode; (g) frequency counter; (h) F/V converter; (i) computer.

ICP-MS is troublesome [9–13]. In addition, the sensitivity of these methods is not always sufficient for direct determination in every conceivable sample. This paper reports a method for the determination of nickel at ultra-trace levels by ion chromatography with a series bulk acoustic wave (SBAW) detection system.

Originally, ion chromatography (IC) was developed as a chromatographic method for inorganic ions, with an ion-exchange resin as the stationary phase and using conductometric detection. At present, the scope of IC has been extended to include the determination of organic ions and other species. In addition to conductometric detection, many detection techniques have been used. In this work, an SBAW was used in the detection technique.

Bulk acoustic wave (BAW) sensing devices have been developed rapidly and utilized widely as chemical and biomedical microsensors [14–16]. The frequency of the BAW sensor in liquid is affected by properties of liquids such as density, viscosity, specific conductivity and permittivity [17–19].

A new type detection system for IC known as a SBAW has been developed [20]. It responds only to solution conductivity and permittivity and has been successfully applied as a BAW detector for IC monitoring. This device was designed and constructed in our laboratory [21,22] and its theory and application have been summarized [23,24]. Compared with conventional conductometric detection for IC, SBAW detection is advantageous in its high sensitivity, high resolving power and good reproducibility, as it can eliminate the interfering effect of double layer capacitance. In this work, an SBAW detector was used

to develop a procedure for the determination of nickel in human urine, when incorporated into a non-suppressed anion exchange chromatographic system.

2. Experimental

2.1. Reagents

All chemicals were of analytical reagent grade or better and were used as received. De-ionized water was used throughout. A stock standard solution of Ni (II), Fe (III), Co (II), Cu (II), Zn (II) and Ca (II) was prepared from the nitrate or sulphate salts and standardized gravimetrically. Working standard solutions were prepared by appropriate dilution as necessary. Standard solution was prepared daily. A 4.5 mM tartaric acid solution was used as the mobile phase. The mobile phase, standard and sample solutions were filtered through a 0.45 μm membrane (Millipore, USA)

2.2. Instrumentation

2.2.1. SBAW detector

A new SBAW detection system for IC was designed and constructed in our laboratory [14,15], a schematic diagram of which is shown in Fig. 1. The SBAW detector was composed of a quartz crystal oscillator connected in series and a conductivity detection cell. The oscillator was assembled by coupling a 9 MHz AT-cut quartz crystal to a TTL-IC oscillating circuit. The detection cell was made as follows. Two 1 mm platinum wires (pretreated with 6 M HNO_3 and then

with water and acetone), as conductivity electrodes, were inserted oppositely at the middle of the detection cell, with a distance of 0.5 mm between them. The body of the detector was made of two Plexiglass plates with a thickness of 5 mm, within which a cylindrical trough (2 mm diameter and 8 mm length) was used as the detection cell. The detector volume was about 25 μl . The cell constant 3.2 cm^{-1} was used. Two 0.5mm stainless steel tubes were connected at opposite ends of the detection cell separated by 7 mm and used as the mobile phase inlet and outlet. One of the platinum electrodes was connected to the quartz crystal which together with another platinum wire served as the feedback network of the IC-TTL oscillator. The frequency signal from the detector was sent either to the digital counter to give a direct frequency recording or to the F/V conversion circuit connected to the chromatography workstation to obtain voltage information. The base noise and hence sensitivity of the SBAW is influenced by temperature. When the SBAW detector temperature is equal to that of the column, the lowest noise and drift levels are achieved. Hence, the temperature of the SBAW detector was kept the same as that of the column, 37°C.

2.2.2. F/V converter

A universal frequency counter (Model SC-7201, Iwatsu, Japan) was used to investigate the performance of the BAW sensor with respect to frequency shift. As the frequency data must be transformed into a format which can be used by the chromatographic workstation, a frequency-to-voltage converter (made in our laboratory) was used to transform the frequency signal of the BAW detector to a CR-4A Chromatopac data processor (Shimadzu, Japan), which is used to record chromatograms in real time and integrate peak areas.

2.2.3. Chromatographic apparatus

Chromatographic separation was accomplished by means of a Shimadzu LP-6A liquid delivery pump, an SLC-6B system controller, an SIL-6B auto injector and a CTO-6AS column oven. The analytical column was a Shim-pack IC-C1 column (5.0 mm ID*15 cm, stainless), packed with a

surface functional group cation exchange resin on a polystyrene–divinylbenzene support with a particle size of 10 μm , incorporating a sulphonic acid base as a functional group. A Shim-pack IC-GC1 guard column (4.0 mm ID*10 mm) preceded the analytical column.

2.3. Chromatographic conditions

The mobile phase was 4.5 mM tartaric acid used at a flow rate of 1.2 ml min^{-1} and the injection volume was 100 μl . To obtain the optimum response of the SBAW detector and lowest noise level, the temperatures of both column and detector were set at 37°C.

2.4. Sample preparation

The human urine was acidified to 1% (v/v) with concentrated HNO_3 and stored frozen until analysed for nickel. The protein in human urine is removed by means of nitric acid and centrifugation. The supernatant was passed through a Sep-pak C18 cartridge to remove organic interference and then filtered through a 0.45 μm filter membrane. Following this, 100 μl of filtrate was applied to the IC column.

3. Results and discussion

3.1. Analytical conditions

3.1.1. Choice of the concentration of the mobile phase

The SBAW response vs conductivity change relationship is

$$\Delta f = k \Delta G$$

where Δf is frequency shift, ΔG is the conductivity change between the sample solution and the mobile phase, k is the constant depending on the construction of the SBAW detector and the conductivity of the mobile phase (G_0) [19,20]. Provided that all design parameters of the detector remain unchanged, as was the case in our work, the detector sensitivity is mainly affected by the conductivity of the mobile phase (G_0). It is well

known that the concentration of the mobile phase affects not only its conductivity but also the retention time and resolution of analytes. Hence, the proper choice of concentration of the mobile phase is very important. In order to achieve a sensitive response and good resolution with acceptable analytical time, various dilutions of the tartaric acid solution were evaluated. Fig. 2 shows the chromatogram of the mixture standard solution containing Ni(II) and the other ionic species tested, where 4.5 mM tartaric acid solution can clearly separate the Ni(II) peak from the other metal ions within a reasonable retention time. The concentration (in ppm) of the metal ions in the mixture standard solution are as follows: Fe(III), 1; Cu, 0.4; Zn, 0.6; Ni, 0.5; Co, 0.3; and Ca, 2. As can be seen in Fig. 3, the detector sensitivity increases with increasing concentration of the mobile phase until a maximum is reached and then decreases as the concentration of the mobile phase increases further. The maximum sensitivity is reached at 4.5 mM tartaric acid solution.

3.1.2. Effects of the detector temperature

As the SBAW detector responds to the solution conductivity and permittivity, which are affected by the temperature, the resonant and the oscillation frequency of the piezoelectric quartz crystal are influenced by temperature variation. Hence, the base line and the noise level of the SBAW vary with temperature change. In order to evaluate the behavior of the SBAW detector as a

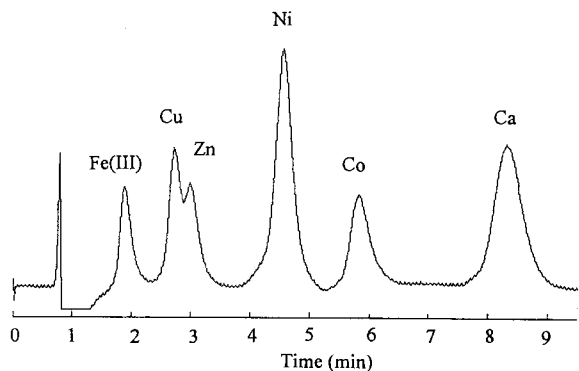


Fig. 2. Chromatogram (obtained using IC-SBAW) of a mixture standard solution containing Ni(II) and the interfering ions tested.

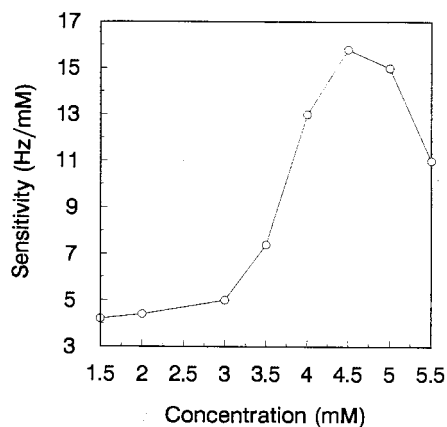


Fig. 3. Effect of eluent concentration on detector response sensitivity.

function of temperature, experiments were carried out. According to Table 1, when the SBAW detector temperature is equal to that of the column, the lowest noise and drift levels are obtained. Therefore, the SBAW detector was maintained at the same temperature as the column, 37°C.

3.2. Analysis of real samples

The proposed IC-SBAW method was used to determine nickel levels in urine from individuals with no occupational exposures to nickel. Fig. 4 is a typical chromatogram of a real sample, where the peak for Ni was identified by the method of standard additions. Table 2 shows the results of the determination of Ni in human urine. According to the tentative reference value ($< 3 \text{ ng ml}^{-1}$) proposed by Templeton et al. [25], the individuals examined have no nickel-poisoning except for individual No. 2. For a person with no occupational exposures to nickel, nickel-poisoning is probably caused by handling metal objects such as jewellery and coins, dietary intake of nickel, or implantation of medical prostheses containing nickel.

Table 1
Effect of temperature on noise and drift of SBAW detector

T (°C)	25	30	33	35	37	40	45	50
Noise (Hz)	5	4	2	2	2	2	3	6
Drift (Hz h ⁻¹)	7	7	4	3	3	5	5	8

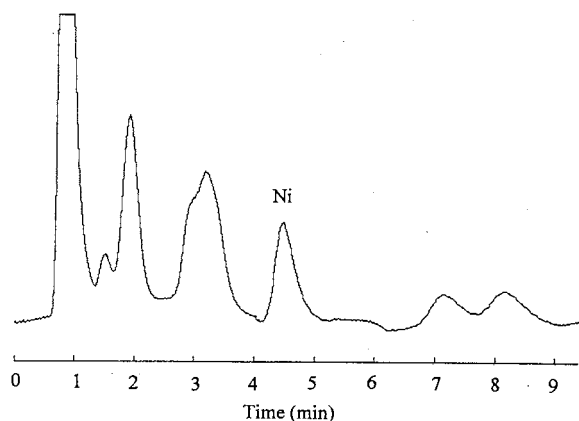


Fig. 4. Chromatogram (obtained using IC-SBAW) of urine from individuals having no occupational exposure to nickel.

3.3. Sensitivity, precision and accuracy

Under the optimized chromatographic and detector conditions, the detection and determination limits for nickel were 0.4 and 2.0 ng ml⁻¹, respectively. The precision of the IC-SBAW was tested using a standard solution of 5.0 ng ml⁻¹ analysed nine times on different days. The maximum relative standard deviation obtained was 3.6%.

In order to investigate the accuracy of the proposed method, the results obtained by IC-SBAW were compared to those from graphite-furnace atomic absorption spectrometry (GFAAS) [7], as shown in Table 2. The results obtained by the proposed method were in agreement with those obtained for the same sample types using GFAAS. Recovery experiments were also per-

Table 2
Determination of Ni in human urine using IC-SBAW and GFAAS

Sample No.	IC-SBAW (ng ml ⁻¹)	GFAAS(ng ml ⁻¹)
1	2.6 ± 0.1	2.3 ± 0.5
2	4.7 ± 0.1	5.1 ± 0.2
3	1.8 ± 0.3	1.7 ± 0.1
4	1.2 ± 0.4	1.1 ± 0.3
5	0.9 ± 0.3	1.3 ± 0.6
6	1.6 ± 0.2	1.2 ± 0.2

Values are expressed in mean ± SD (*n* = 5).

formed by spiking real urine samples with aliquots of Ni standard solutions. The nickel content was determined by the recommended procedure using standard additions and the results are shown in Table 3. Recoveries were found to be from 96 to 104%.

3.4. Comparison with BAW detector and conductometric IC detector

The proposed SBAW detector is based on its non-mass effect, i.e. conductivity change in the course of chromatographic separation. As there is no mass deposition on the detector surface, no intermittent removal of the deposited mass is required to restore the detector, as is the case with mass-effect-based conventional BAW detection techniques. Hence, the proposed detector can be used continuously.

Although the conductivity cell is among the most commonly used detectors in ion chromatography, the detection limit of this method is subject to background interference from the mobile phase, especially in single-column ion chromatography.

In a conductometric cell, double electric layer capacitance or Faradaic impedance can take place, causing the effective applied potential to change. This may affect sensitivity and accuracy in the determination of ions. To solve these problems, methods involving the use of alternating electrode potential and bipolar pulse conductance have been proposed, but the instrumentation is rather complicated. In the proposed SBAW detection technique, the interfering effect of the double layer capacitance on the detector response is eliminated and there was no use of the complicated alternating electrode potential technique or multiple electrodes method. Moreover, the SBAW detector has a long life-span and since the platinum electrode is chemically stable, the proposed detector can be used for at least two years.

The detection limit for Ni by ion chromatography with conductometric detection is more than 0.1 ppm [26], which is not adequate for determination of Ni in human urine. Using ion chromatography with SBAW detection, the detection and determination limits for Ni are 0.4 and 2.0 ng ml⁻¹, respectively.

Table 3
Recovery of Ni from spiked samples

Sample No.	Ni present (ng ml ⁻¹)	Ni spiked (ng ml ⁻¹)	Ni found (ng ml ⁻¹)	Recovery (%)
1	2.6	5.0	7.6	100
2	4.7	5.0	9.6	98
3	1.8	10.0	11.5	97
4	1.2	2.5	3.6	96
5	0.9	10.0	10.8	99
6	1.6	2.5	4.2	104

3.5. Comparison with graphite-furnace atomic absorption spectrometry

Current analytical methods for trace determination of nickel involve mainly the use of spectroscopic techniques, such as GFAAS. Although this technique is available in more laboratories, it has some serious drawbacks, including high equipment costs and matrix interference effects, as well as slow analysis, since only one element can be determined at a time. Cano Pavón and Vereda Alonso et al. [27] presented a method for the determination of nickel by GFAAS involving the prior extraction of the metal into methyl isobutyl ketone with 1,5-bis(di-2-pyridylmethylene) thio-carbonohydrazide. Although this method can determine Ni at ultra-trace (ng ml⁻¹) level, it is cumbersome, since it necessitates preconcentration.

In conclusion, the ion chromatographic method using the SBAW detector is advantageous in its rapidity, simplicity, sensitivity and accuracy. The high sensitivity, low equipment cost, simple construction and great potential for automation of the SBAW detector portend its development in the analysis of inorganic, organic and biological ions. The susceptibility of the proposed method to matrix effects is the subject of further study.

References

- [1] T. Menne, *Sci. Total. Environ.* 148 (1994) 275.
- [2] IARC Monographs on the evaluation of carcinogenic risks to humans, vol. 52: including cobalt and cobalt compounds, IARC, Lyons, France, 1991.
- [3] C.N. Leach Jr., J.V. Linden, S.M. Hopfer, M.C. Crisostomo, F.W. Sunderman Jr., *Clin. Chem.* 31 (1985) 556.
- [4] R. Doll, J. Scand, *Work. Environ. Health* 16 (1990) 1.
- [5] P. Grandjean, G.D. Nielsen and O. Andersen, Human nickel exposure and chemobiokinetics, in: T. Menne, H.I. Maibach (Eds.), *Nickel and the Skin: Immunology and Toxicology*, CRC Press, Boca Raton, FL, 1989, p. 9.
- [6] F.W. Sunderman Jr., S.M. Hopfer, M.C. Crisostomo, *Methods Enzymol.* 158 (1988) 382.
- [7] D.M. Templeton, Nickel, in: R.F.M. Herber, M. Stoepller (Eds.), *Trace Element Analysis in Biological Specimens*, Elsevier, Amsterdam, 1994, p. 469–487.
- [8] E. Vereda Alonso, J.M. Cano Pavon, A. Garciade Torres, M.T. Siles Cordero, *Anal. Chim. Acta* 283 (1993) 224.
- [9] M.A. Vaughan, D.M. Templeton, *Appl. Spectrosc.* 44 (1990) 1685.
- [10] M.R. Plantz, J.S. Fritz, F.G. Smith, R.S. Houk, *Anal. Chem.* 61 (1989) 149.
- [11] D. Beauchemin, S.S. Berman, *Anal. Chem.* 61 (1989) 1857.
- [12] J.W. McLaren, A.P. Mykytiuk, S.N. Willie, S.S. Berman, *Anal. Chem.* 57 (1985) 2907.
- [13] L.C. Alves, L.A. Allen, R.S. Houk, *Anal. Chem.* 65 (1993) 2468.
- [14] S. Yao, L. Nie, *Anal. Proc.* 24 (1987) 336.
- [15] S. Yao, L. Nie, *Sci. China (Series B)* 36 (1993) 796.
- [16] S. Si, Y. Xu, L. Nie, S. Yao, J. *Biochem. Biophys. Methods* 31 (1996) 135.
- [17] S. Yao, T. Zhou, *Anal. Chim. Acta* 212 (1988) 61.
- [18] T. Zhou, L. Nie, S. Yao, *J. Electroanal. Chem.* 293 (1990) 1.
- [19] M. Yang, M. Thompson, *Anal. Chim. Acta* 269 (1992) 167.
- [20] S. Yao, B. Yu, P. Chen, L. Nie, M. Yang, W. Zhu, *Instr. Sci. Tech.* 24 (1996) 247.
- [21] P. Chen, L. Nie, S. Yao, *J. Chromatogr. Sci.* 33 (1995) 268.
- [22] Z. Mo, S. Yao, *Anal. Chim. Acta* 229 (1990) 167.
- [23] D. Shen, W. Zhu, L. Nie, S. Yao, *Anal. Chim. Acta* 276 (1993) 87.
- [24] Z. Mo, L. Nie, S. Yao, *J. Electroanal. Chem.* 316 (1991) 79.
- [25] D.M. Templeton, F.W. Sunderman Jr., R.F.M. Herber, *Sci. Total Environ.* 148 (1994) 243.
- [26] J.S. Fritz, D.T. Gjerde and C. Pohlandt, *Ion Chromatography*, Shanghai Science and Technology Literature Press, Shanghai, China, 1990, p.145–168. (in Chinese).
- [27] J.M. CanoPavón, E. VeredaAlonso, C. BoschOjeda, A. GarciadeTorres, *Anal. Lett.* 24 (1991) 153.

Spectrophotometric determination of lithium ion using a water-soluble octabromoporphyrin in aqueous solution

M. Tabata *, J. Nishimoto, T. Kusano

Department of Chemistry, Faculty of Science and Engineering, Saga University, 1 Honjo-machi, Saga 840, Japan

Received 8 July 1997; received in revised form 24 September 1997; accepted 25 September 1997

Abstract

A water-soluble porphyrin, (2,3,7,8,12,13,17,18-octabromo-5,10,15,20-tetrakis(4-sulfonatophenyl)porphyrin; $H_2obtpps^{4-}$) was synthesized and developed for the determination of lithium ion in aqueous solution. The octabromo groups lower the basicity of the porphyrin by their electron-withdrawing effect, and enable the porphyrin to react with the lithium ion in alkaline solution to form the lithium complex along with a shift of absorption maximum: λ_{max}/nm ($\log \epsilon/mol^{-1} dm^3 cm^{-1}$) of the lithium porphyrin are 490.5 nm (5.31) and 734 nm (4.36). Sodium and potassium ions did not react with the porphyrin. The equilibrium constant for the reaction $Li^+ + Hobtpps^{5-} \rightleftharpoons [Li(obtpps)]^{5-} + H^+$ was found to be $10^{-8.80}$ and the conditional formation constant of the $[Li(obtpps)]^{5-}$ at pH 13 is $10^{4.21}$. The above results were applied to the determination of lithium ion in aqueous solution. The interference from transition and heavy metal ions was masked by using *N,N'*-1,2-ethanediybis[*N*(carboxyl-methyl)glycinato]magnesium(II) ($[Mg(edta)]^{2-}$) solution. Absorbance at 490 nm was measured against a blank solution. A calibration graph was linear over the range of $0.007-0.7 \mu g cm^{-3}$ ($1 \times 10^{-6}-1 \times 10^{-4} mol dm^{-3}$) of lithium(I) with a correlation factor of 0.967. Lithium ion less than ppm level was determined spectrophotometrically in aqueous solution. The proposed method was applied to the determination of lithium in human serum and sea water samples. © 1998 Elsevier Science B.V. All rights reserved.

Keywords: Lithium porphyrin; Spectrophotometry; Serum; Sea water

1. Introduction

Lithium ion has been used widely in science, medicine and technology in the treatment of manic depression and its use in the lithium battery [1]. In light of such applications, the methods for the determination and separation of the lithium

ion are receiving considerable attention. Many efforts have used synthetic multidentate ligands to form complexes with lithium ion. Since lithium ion is a hard acid, it prefers hard donor atoms [2]. Therefore, the stability constants of Li^+ complexes are expected to increase as ligand donor atoms change $S \ll N \ll O$. Crown ethers have been utilized for the determination and separation of lithium ion. Takagi et al. [3] first succeeded in synthesizing chromogenic crown ethers for alkali

* Corresponding author. Tel.: +81 952 288560; fax: +81 952 288548; e-mail: tabatam@cc.saga-u.ac.jp

metal ions in 1977 and extracted the colored complexes of the alkali metal ions into chloroform. Following from this, various monoaza-crown ethers [4,5] and cryptands [6] with chromophores bound to the ring nitrogen were synthesized, and spectral change upon the addition of alkali metal was observed. All these reagents, however, are insoluble in water and the measurement of lithium ion was limited to organic solvent system. Chromogenic ionophores soluble in homogeneous mixed aqueous solution containing DMSO or 2-(2-ethoxyethoxy)ethanol were synthesized [7–9] and applied to the determination of lithium ion in blood serum without solvent extraction [10].

The selectivity of alkali metal ion depends on the cavity size of crown ethers [11] and the chromogenic response upon metal complexation is enhanced when the chromogenic ligand has ionizable protons [4]. Porphyrins show high selectivity for metal ions due to rigid cavity size (400 pm in diameter) that accommodates medium-sized metal ions like nickel(II), copper(II) and zinc(II) [12,13]. Furthermore, porphyrins give high molar absorptivities (about $500\,000\text{ mol}^{-1}\text{ dm}^3\text{ cm}^{-1}$) at the

Soret band by metalation resulting in release of ionizable pyrrole protons [14]. We noticed that the ionic size of lithium ion (73 pm) is comparable with zinc(II) (74 pm) [15] that was selectively determined in a large excess of cadmium(II) and lead [16,17]. A weak point of porphyrins is that the ionization of protons occur at high pH > 14 [18]. In order to solve this problem, we synthesized a new water-soluble porphyrin with eight bromine atoms which decrease the basicity of the porphyrin and make it easy to release protons bound to the pyrrole nitrogen atom of porphyrin. We report here on a selective and sensitive colorimetric determination method for lithium ion in aqueous solution without using any organic solvents.

2. Experimental

2.1. Apparatus

Absorption spectra were recorded on a Shimadzu UV-2100 and a Jasco Ubest spectrophotometers. The pH values were determined with a radiometer Ion 85 analyzer with a combined electrode (GK2401C). A $1.000 \times 10^{-2}\text{ mol dm}^{-3}$ nitric acid solution containing 0.09 mol dm^{-3} sodium nitrate was employed as the standard hydrogen ion concentration ($-\log[\text{H}^+] = 2.000$). From the pH meter readings on various hydrogen ion concentrations, the pH meter and electrode system was calibrated in terms of $-\log[\text{H}^+]$ at an ionic strength of 0.1 mol dm^{-3} ($\text{HNO}_3 - \text{NaNO}_3$). All experiments were carried out at 25°C .

2.2. Synthesis of the porphyrin

2,3,7,8,12,13,17,18 - Octabromo - 5,10,15,20 - tetrakis(4-sulfonatophenyl)porphyrin ($\text{H}_2\text{obtpps}^{4-}$, Fig. 1) was synthesized by the bromination and sulfonation of 5,10,15,20-tetraphenylporphyrin (H_2tpp) as follows: H_2tpp (1g, 1.63 mmol) was treated with *N*-bromosuccinimide (NBS, 3 g, 16.8 mmol) instead of bromine as previously reported [19] in dibromomethane which was sufficiently dried by molecular sieve (4 \AA) before use. The

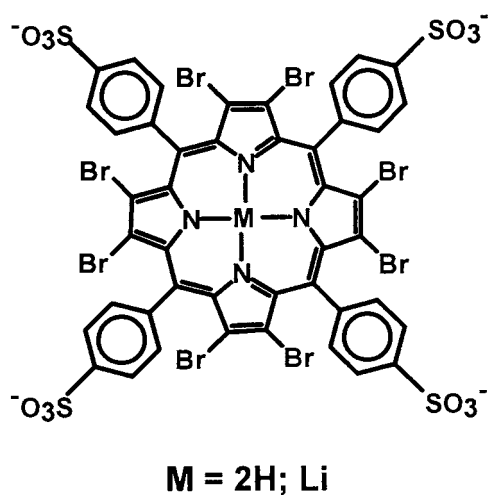


Fig. 1. 2,3,7,8,12,13,17,18-Octabromo-5,10,15,20-tetrakis(4-sulfonatophenyl)porphyrin ($\text{H}_2\text{obtpps}^{4-}$) and its Lithium porphyrin ($\text{Li}(\text{obtpps})^{5-}$).

crude product gave three bands on an activated alumina chromatography (300 mesh, Wako, Japan) using chloroform as eluent and the first band was collected. Yield was 53%. Absorption maximum-wave length and chemical shifts of ^1H NMR of the product, 2,3,7,8,12,13,17,18-octabromo-5,10,15,20-tetraphenylporphyrin (H_2obtpp , 1), were observed at 370, 469, 569, 626 and 743 nm in chloroform, and at 7.79 ppm (m, 12 H, for *m*- and *p*-H of phenyl) and 8.19 ppm (d, 8H, *o*-H of phenyl) in CDCl_3 vs. TMS, respectively. Compound 1 was sulfonated in concentrated sulfuric acid. The product was precipitated by the careful addition of small amounts of water and purified by a Sephadex column LH-20 which was soaked in a water-methanol (7:3) mixed solvent. Absorption maximum-wave length ($\log \epsilon/\text{mol}^{-1} \text{dm}^3 \text{cm}^{-1}$) and ^1H NMR data (δ/ppm) of the final product, H_6obtpps , were as follows: 376 (4.54), 478 (5.30), 657 (4.25) and 760 nm (4.07) in aqueous solution at pH 7.0; 8.62 (d, 8H, *o*-H of phenyl) and 8.09 (d, 8H, *m*-H of phenyl) in d_6 -dimethyl-sulfoxide.

2.3. Reagents

Sodium nitrate used for adjusting ionic strength was purified by solvent extraction using phenyldiazene-carbothionic acid 2-phenylhydrazide (dithizone) in carbon tetrachloride to remove transition and heavy metal ions like Cu(II), Zn(II), Fe(II) and Pb(II), and followed by recrystallization from hot water. Otherwise these metal ions form their metalloporphyrins in alkaline pH. Other metal nitrates were of analytical-reagent grade and were used without further purification. The buffer solutions were prepared by addition of nitric acid or sodium hydroxide to solutions of sodium acetate for pH 4–6, 2-morpholinoethanesulfonic acid (MES) for pH 6–7, 2-(4-(2-hydroxyethyl)-1-piperazinyl)-ethanesulfonic acid (HEPES) for pH 7–8.5 and sodium borate for pH 8.5–10 (Wako, Osaka, Japan). All solutions were prepared in water, treated with a Mill-Q SP TOC (Nippon Millipore, Japan).

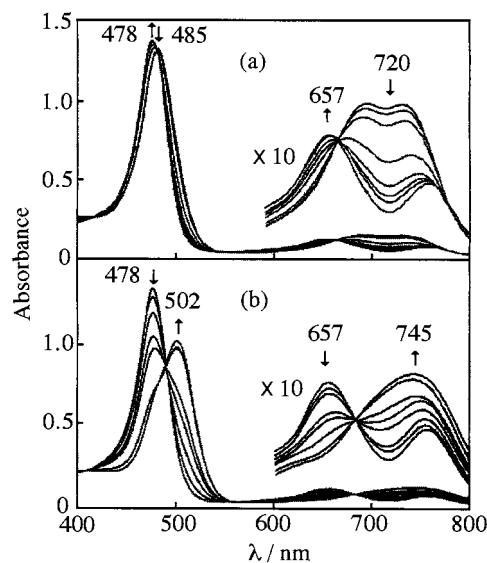
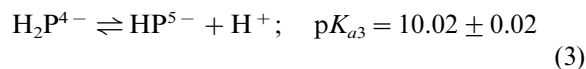
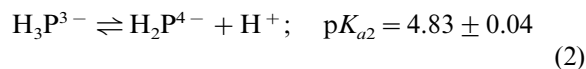
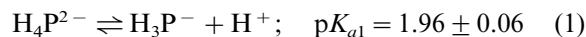


Fig. 2. Change in absorption spectra of $\text{H}_2\text{obtpps}^{4-}$ at pH 4–6 (a) and 10–12 (b).

3. Results and Discussion

3.1. Acid-dissociation constants of $\text{H}_4\text{obtpps}^{2-}$

Absorption spectra of the porphyrin were measured at various pH values at ionic strength of 0.1 mol dm^{-3} (NaNO_3) and at 25°C . The absorption maximum-wave lengths were observed in three pH regions: 490 and 740 nm at pH lower than 2478 and 657 nm at pH 6–8.2 and 502 and 745 nm at pH higher than 11 (Fig. 2). The change in absorbance suggests three steps for the acid-dissociation equilibrium and their equilibrium constants as given in Eqs. (1)–(3)



where H_2P^{4-} denotes free-base form of the porphyrin which is the main chemical species at neutral pH. The acid-dissociation constants of the porphyrin were determined by using a nonlinear least-squares minimization program in two pH

ranges: one region, 1–8 and other pH 8–13. The octabromo groups lower the basicity of the porphyrin by their electron-withdrawing effect, and the deprotonation process of the free-base form, $\text{H}_2\text{obtpps}^{4-}$, producing Hobtpps^{5-} , occurred at pH 10.

3.2. Formation of lithium(I) porphyrin.

Lithium hydroxide reacted with $\text{H}_2\text{obtpps}^{4-}$ to shift the absorption spectrum towards a shorter wavelength. Sodium hydroxide and potassium hydroxide did not alter the absorption spectra (Fig. 3). The absorption maximum-wave length ($\log \epsilon/\text{mol}^{-1} \text{dm}^3 \text{cm}^{-1}$) of the lithium(I) porphyrin complex are 490.5 nm (5.31) and 734 nm (4.36). Non-brominated porphyrin like 5,10,15,20-tetrakis(4-sulfonatophenyl)porphyrin did not give any spectral change even in $0.1 \text{ mol dm}^{-3} \text{LiOH}$. This behavior is unique to $\text{H}_2\text{obtpps}^{4-}$. The equilibrium constant of the lithium(I) porphyrin complex was determined as follows. Absorption spectra were measured at different concentrations of lithium ion (10^{-5} – $10^{-2} \text{ mol dm}^{-3}$) and sodium hydroxide (pH 11.7–12.3). If we assume that n molecules of lithium ions react with HP^{5-} to form lithium porphyrin with the release of m molecules of hydrogen ions, the equilibrium constant for the formation lithium porphyrin is given by Eqs. (4) and (5):

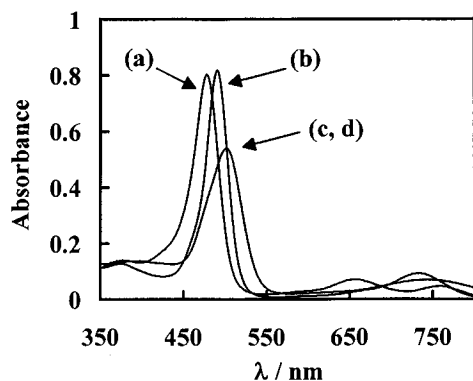


Fig. 3. Change in absorption spectra of $\text{H}_2\text{obtpps}^{4-}$ in pH 7.0 (a); $0.1 \text{ mol dm}^{-3} \text{LiOH}$ (b); $0.1 \text{ mol dm}^{-3} \text{NaOH}$ (c); and $0.1 \text{ mol dm}^{-3} \text{KOH}$ (d).

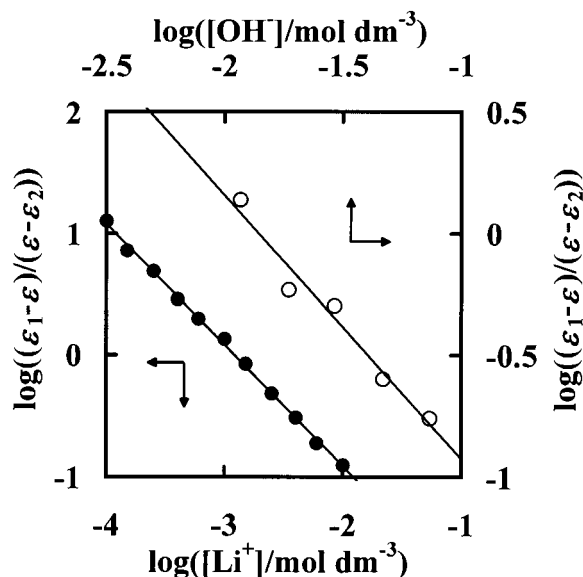
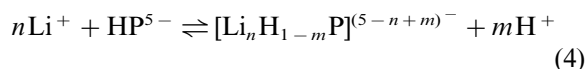


Fig. 4. Plot of $\log((\epsilon_1 - \epsilon)/(\epsilon - \epsilon_2))$ against $\log([Li^+]/\text{mol dm}^{-3})$ and $\log([OH^-]/\text{mol dm}^{-3})$ in order to determine the equilibrium constant of the lithium porphyrin complex and the number of lithium ions and protons in the lithium porphyrin.



$$K = \frac{[\text{Li}_n\text{H}_{1-m}\text{P}^{(5-n+m)-}][\text{H}^+]^m}{[\text{Li}^+]^n[\text{HP}^{5-}]} \quad (5)$$

The observed apparent molar absorptivity ($\epsilon = \text{absorbance}/C_{\text{H}_2\text{P}}$) at different concentrations of lithium and sodium hydroxide is correlated to the equilibrium constant as follows:

$$\begin{aligned} \log((\epsilon_1 - \epsilon)/(\epsilon - \epsilon_2)) \\ = -n\log[Li^+] - m\log[OH^-] + m\log K_w - \log K \end{aligned} \quad (6)$$

where ϵ_1 and ϵ_2 are the molar absorptivities of the lithium and nonmetalated porphyrins, respectively. The plots of the left-hand side of Eq. (6) against $\log[Li^+]$ and $\log([OH^-]/\text{mol dm}^{-3})$ give straight lines with a slope of one for both Li^+ and OH^- (Fig. 4). Thus, one lithium ion reacts with HP^{5-} to form $[\text{LiP}]^{5-}$ by releasing one hydrogen ion. The equilibrium constant of Eq. (5) was found to be $\log(K_{\text{LiP}}) = -8.80 \pm 0.02$ at 25°C and $I = 0.1 \text{ mol dm}^{-3}$ (NaNO_3).

Arnold et al. isolated lithium porphyrins and reported that two lithiums can interact with the porphyrin nitrogen in nonpolar solvents like THF and that one lithium can be bound to all four nitrogens in the porphyrin in polar solvents like alcohol [20,21]. Since water is a high polar solvent, the 1:1 $[\text{LiP}]^{5-}$ is formed for $\text{H}_2\text{obtpps}^{4-}$ in aqueous solution. In the lithium porphyrin, lithium is incorporated well in the porphyrin core like zinc(II) [22], due to the comparable ionic radius of lithium(I) (73 pm) to that of zinc(II) (74 pm) [15]. However, sodium and potassium ions do not form stable complexes with the porphyrin under the same experimental conditions because of the large ionic radii of sodium (113 pm) and potassium (151 pm) [15]. The octabromo groups decrease the basicity of the porphyrin so that the proton in the pyrrole group is released even at pH 10. This makes it easy for lithium ion to react with the porphyrin.

It is interesting to know how $[\text{LiP}]^{5-}$ is stable compared with lithium(I) crown-ether complexes. Although the equilibrium constant for the reaction $\text{Li}^+ + \text{P}^{6-} \rightleftharpoons [\text{LiP}]^{5-}$ could not be determined, the conditional formation constant defined by $K' = [\text{LiP}^{5-}][\text{Li}^+]^{-1}[\text{P}^{6-}]^{-1}$ was calculated as $10^{4.21}$ in 0.1 mol dm^{-3} NaOH from the formation constant (K) of $[\text{LiP}]^{5-}$ and acid-dissociation constant of $\text{H}_2\text{obtpps}^{4-}$ ($\text{p}K_{\text{a}3}$) values, where $[\text{P}^{6-}]$ denotes the total concentration of the porphyrin unbound to lithium(I). The equilibrium constant is much larger than the formation constant of Li with crown-ethers [11].

3.3. Determination of lithium

The above results were applied to the determination of lithium ion in aqueous solution. The general procedure is as follows. A 5-cm^3 water sample containing $0.014\text{--}1.4 \mu\text{g}$ of lithium(I) was placed in a 10-cm^3 calibrated flask. Then, 1 cm^3 of N,N' -1,2-ethanediybis[N (carboxylmethyl)—glycinato]magnesium ($[\text{Mg}(\text{edta})]^{2-}$) solution ($C_{\text{Mg}} = 1.1 \times 10^{-2} \text{ mol dm}^{-3}$; $C_{\text{H}4\text{edta}} = 1.0 \times 10^{-2} \text{ mol dm}^{-3}$), 1 cm^3 of $\text{H}_2\text{obtpps}^{4-}$ ($3.8 \times 10^{-5} \text{ mol dm}^{-3}$), and 0.5 cm^3 of 1 mol dm^{-3} NaOH were added to the flask. Distilled water was added to

the mark (10 cm^3) and absorbance was measured at 490 nm against a blank solution. A calibration graph was linear over the range of $1 \times 10^{-6}\text{--}1 \times 10^{-4} \text{ mol dm}^{-3}$ of lithium(I) with a correlation factor of 0.967. Lithium ion less than ppm level was determined spectrophotometrically in aqueous solution.

3.4. Effect of foreign ions on the determination of lithium

Since $\text{H}_2\text{obtpps}^{4-}$ forms stable complexes with transition and heavy metal ions like copper(II), zinc(II) and lead(II), these metal ions were masked by the addition of $[\text{Mg}(\text{edta})]^{2-}$ solution as a ligand buffer. Nakagawa and Tanaka have proposed the use of a ligand buffer solution for the polarographic determination of zinc(II) in the presence of cadmium(II) [23]. We determined the optimum conditions for the ligand buffer solution to mask transition and heavy metal ions in order to determine lithium in a sample solution. In order to mask metal M as completely as possible, most of M (zinc(II); copper(II) etc.) should be the form of $[\text{M}(\text{edta})]^{2-}$ and lithium should be a free ion. Magnesium(II) used as a component of the ligand buffer for masking metal M should satisfy the conditions: $K_{\text{M}(\text{edta})} > K_{\text{Mg}(\text{edta})} > K_{\text{Li}(\text{edta})}$. The formation constants (logarithmic values) of copper(II), zinc(II), magnesium(II) and lithium(I) are 18.70, 16.44, 8.83 and 2.79, respectively [24]. Thus, $[\text{Mg}(\text{edta})]^{2-}$ completely masks metal ions such as copper(II) and zinc(II). The results are listed in Table 1. Cations usually encountered in environmental samples are masked by $[\text{Mg}(\text{edta})]^{2-}$ and anions do not interfere with the determination of lithium(I). Even, chloride as high as $10^{-1} \text{ mol dm}^{-3}$ did not have any effect on the determination of lithium(I).

The high concentration of mercury(II) was not masked completely by $[\text{Mg}(\text{edta})]^{2-}$, therefore NaCN was used to mask mercury(II). Such high concentrations of mercury(II) are rare in environmental samples as such the addition of NaCN may not be required for the determination of lithium in environmental samples.

Table 1

The effect of foreign ions on the determination of Li⁺ using the present method

Ions	Concentration (mol dm ⁻³)	Recovery (%)	Ions	Concentration (mol dm ⁻³)	Recovery (%)
Al ³⁺	1.0 × 10 ⁻⁵	91	Na ⁺	1.0 × 10 ⁻¹	105
Fe ³⁺	1.0 × 10 ⁻⁵	102		1.0 × 10 ⁻²	101
Cd ²⁺	1.0 × 10 ⁻⁵	100		1.0 × 10 ⁻³	99
Zn ²⁺	1.0 × 10 ⁻⁵	92	F ⁻	1.0 × 10 ⁻⁵	97
Cu ²⁺	1.0 × 10 ⁻⁵	93	Cl ⁻	1.0 × 10 ⁻¹	96
Pb ²⁺	1.0 × 10 ⁻⁵	95		1.0 × 10 ⁻²	101
Mn ²⁺	1.0 × 10 ⁻⁵	94		1.0 × 10 ⁻³	97
Co ²⁺	1.0 × 10 ⁻⁵	98	Br ⁻	1.0 × 10 ⁻⁵	107
Ca ²⁺	1.0 × 10 ⁻⁵	95	SCN ⁻	1.0 × 10 ⁻⁵	99
Mg ²⁺	1.0 × 10 ⁻⁵	99	CO ₃ ²⁻	1.0 × 10 ⁻⁵	101
Hg ²⁺	1.0 × 10 ⁻⁵ a	105	SO ₄ ²⁻	1.0 × 10 ⁻⁵	107
	1.0 × 10 ⁻⁶	102	PO ₄ ³⁻	1.0 × 10 ⁻⁵	103
K ⁺	1.0 × 10 ⁻³	92			

^a NaCN (1.0 × 10⁻² mol dm⁻³) was added for masking mercury(II).

3.5. Application of the proposed method to real samples

The present method was applied to the determination of lithium ion(I) in human blood serum, sea water and hot spring water.

3.5.1. Human blood sample

Protein reacts with the porphyrin and reduces absorbance. Thus, protein in serum was removed using the following procedure. Human blood was centrifuged at 3000 rpm, and 1 cm³ of the upper serum was transferred slowly to a trichloroacetic acid solution (5 g and 50 cm³) under constant stirring. The sample was left for 10 min and was followed by centrifugation at 3000 rpm for 30 min—protein precipitated. Trichloroacetic acid in the supernatant was completely removed by extraction (repeated five times using diethyl ether). The aqueous phase was concentrated to ca. 1 cm³ of volume, and the sample was analyzed after dilution (100 times) using the method described above. Since serum contains millimolar quantities of Mg²⁺, H₄edta ([H₄edta] = 1.00 × 10⁻⁴ mol dm⁻³) in place of [Mg(edta)]²⁻ was added to mask other metal ions in serum. We checked the recovery of lithium ion by the addition of accurate amounts of standard lithium concentration in the order (1–10) × 10⁻⁵ mol dm⁻³. The results are shown in Fig. 5. The lithium concentration

was sufficiently recovered after removing protein. The recovery decreased if protein remained. Protein binds to the porphyrin and interferes with the formation of the lithium porphyrin.

3.5.2. Sea water and hot spring water

In the present method large amounts of sodium ions did not interfere with the determination of lithium ions, however, magnesium(II) ions more than 10⁻⁴ mol dm⁻³ interfered a little. Thus, an equivalent amount of H₄edta to the total quantity of magnesium ion in sea water was added to mask magnesium in the sea water sample. Lithium ions in the sea water sample was determined by the

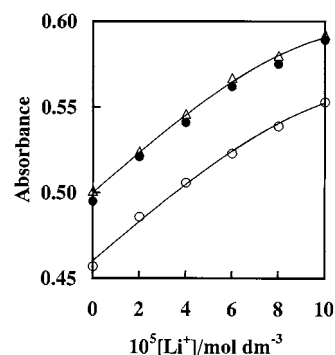


Fig. 5. Recovery of lithium by the addition of accurate amounts of lithium to serum before (○) and after (●) removing protein and to pure water (Δ).

standard addition method using a calibration graph measured at the same ionic strength as sea water. The concentration of lithium was found to be $(1.99 \pm 0.04) \times 10^{-5} \text{ mol dm}^{-3}$. The concentration of lithium ion was deduced by flame photometry and the concentration was $(1.57 \pm 0.09) \times 10^{-5} \text{ mol dm}^{-3}$. The small difference observed in concentration of lithium using the two methods may be caused by the interference of sodium ions in the flame method. The concentration of lithium in hot-spring water was so small, less than $10^{-6} \text{ mol dm}^{-3}$ that its concentration could not be determined using the present method, but a recovery test using the hot-spring water was sufficient: zinc and iron in the hot-spring water were completely masked by $[\text{Mg}(\text{edta})]^{2-}$.

4. Conclusion

This work proposes the first example for the direct spectrophotometric determination of lithium, when present at less than 1 ppm in water using a water-soluble porphyrin. The method is sensitive, simple and selective, using a ligand buffer of $[\text{Mg}(\text{edta})]^{2-}$. It was used to determine lithium in serum and sea water. The method will be developed to a flow injection analysis.

Acknowledgements

We are grateful for the Grant-in Aid for Scientific Research (No 08454238) from the Ministry of Education, Science and Culture of Japan.

References

- [1] R.O. Bach, *Lithium-Current Application in Science, Medicine and Technology*, Wiley, New York, 1985.

- [2] R.G. Pearson, *Hard and Soft Acids and Bases*, Dowden Hutchinson and Ross, Stroudsburg, PA, 1973.
- [3] M. Takagi, H. Nakamura, K. Ueno, *Anal. Lett.* 10 (1977) 1115.
- [4] H.G. Löhr, F. Vögtle, *Acc. Chem. Res.* 18 (1985) 65.
- [5] J.P. Dix, F. Vögtle, *Angew. Chem., Int. Ed. Engl.* 17 (1978) 857.
- [6] A.F. Sholl, I.O. Sutherland, *J. Chem. Soc., Chem. Commun.*, (1992) 1716.
- [7] C. Bazzicalupi, A. Bencini, M. Ciampolini, V. Fusi, M. Micheloni, N. Nardi, I. Razzolini, B. Valtancoli, *Supramol. Chem.* 7 (1996) 61.
- [8] E. Chapoteau, M.S. Chowdhary, B.P. Czech, A. Kumar, W. Zazulak, *J. Org. Chem.* 57 (1992) 2804.
- [9] W. Zazulak, E. Chapoteau, B.P. Czech, A. Kumar, *J. Org. Chem.* 57 (1992) 6720.
- [10] E. Chapoteau, B.P. Czech, W. Zazulak, A. Kumar, *Clin. Chem.* 38 (1992) 1654.
- [11] R.M. Izatt, K. Pawlak, J.S. Bradshaw, R.L. Bruening, *Chem. Rev.* 91 (1991) 1721.
- [12] W.R. Scheidt, *Porphyrin stereochemistry*, in: D. Dolphin (Ed.), *The Porphyrins*, vol.III, part A, Academic Press, New York, 1978, pp. 463–511.
- [13] J.L. Hoard, *Stereochemistry of porphyrins and metalloporphyrin*, in: K.M. Smith (Ed.), *Porphyrins and Metalloporphyrins*, Elsevier, New York, 1975, pp. 317–380.
- [14] M. Tabata, M. Tanaka, *Trends Anal. Chem.* 10 (1991) 128.
- [15] R.D. Shannon, *Acta Crystallogr.* A32 (1976) 751.
- [16] M. Tabata, K. Osita, M. Tanaka, *Mikrochim. Acta*, [Wien], I (1985) 397.
- [17] M. Tabata, N. Kajihara, *Anal. Sci.* 5 (1989) 719.
- [18] M. Tabata, M. Tanaka, *J. Chem. Soc., Chem. Commun.*, (1985) 42.
- [19] P. Bhyrappa, V. Krishnan, *Inorg. Chem.* 30 (1991) 239.
- [20] J. Arnold, D.Y. Dawson, C.G. Hoffman, *J. Am. Chem. Soc.* 115 (1993) 2707.
- [21] H. Brand, J.A. Capriotti, J. Arnold, *Inorg. Chem.* 33 (1994) 4334.
- [22] W.R. Scheidt, J.U. Mondal, C.W. Eigenbrot, A. Adler, L.J. Radonovich, J.L. Hoard, *Inorg. Chem.* 25 (1986) 795.
- [23] G. Nakagawa, M. Tanaka, *Talanta* 19 (1972) 559.
- [24] A.E. Martell, R.M. Smith, *Critical Stability Constants*, vol.1, Plenum, New York, 1974, pp. 203–211.

Short communication

Electrochemical quartz crystal microbalance characterization of I^- and its amperometric detection by microelectrode

W. Zhang ^{a,*}, H. Zha ^a, B. Yao ^a, C. Zhang ^a, X. Zhou ^a, S. Zhong ^b

^a Department of Chemistry, Wuhan University, Wuhan 430072, People's Republic of China

^b Research Center of Experimental Medicine, Tongji Medical University, Wuhan 430030, People's Republic of China

Received 1 January 1997; received in revised form 15 September 1997; accepted 16 September 1997

Abstract

The electrochemical redox mechanism of I^- ion under different concentrations on gold electrodes was studied in detail using the EQCM technique (a combination of the QCM technique and cyclic voltammetry). The redox behavior of the I^- ion on a gold microelectrode when no supporting electrolyte was added was compared with a conventional gold microelectrode. Due to the small current and the very low solution iR drop of the microelectrode, the actual oxidation potential of I^- on the microelectrode was much more negative than that of the conventional electrode and its anodic peak was better defined. Therefore the gold microelectrode was employed for the determination of I^- . A linear range of 1.0×10^{-5} – 0.1 mol l^{-1} with a detection limit of $1.0 \times 10^{-6} \text{ mol l}^{-1}$ was obtained on the microelectrode in pure KI aqueous solution. Two samples were measured using this method and the results were in good agreement with those indicated or calculated. © 1998 Elsevier Science B.V. All rights reserved.

Keywords: Electrochemical quartz crystal microbalance; I^- ; Amperometric detection; Microelectrode

1. Introduction

Compared with the conventional electrode with a diameter in the order of 1 mm, microelectrodes offer several significant advantages in voltammetric experiments [1–3]. These include: (1) a steady-state response at appropriately low sweep rates; (2) the ability to determine moderately fast heterogeneous chemical reactions through steady-

state measurements; (3) the ability to decrease distortion from iR drop, which allows less polar solvents, lower electrolyte concentration, and faster sweep rates to be used; (4) rapid measurement of Faradaic processes due to a very small RC time constant; and (5) a favorable ratio of Faradaic current to charging current.

QCM is a new sensitive mass sensor which can respond to mass change in the order of 1 ng. The combination of the QCM technique and CV (cyclic voltammetry) is very useful to study a variety of electrochemical processes, such as ad-

* Corresponding author. Tel.: +86 27 7882712; fax: +86 27 7882661.

sorption and deposition of metal ions, migration of ions in polymers modified on the electrode [4–9], etc.

The iodide ion, which is a clinically important, is generally determined using the ion selective electrode (ISE). The disadvantage of this method is that some coexisting anions such as Br^- , Cl^- and CN^- will interfere with the detection of I^- . The redox mechanism of iodide in iodide or iodide + iodine solutions has been studied extensively on the conventional electrode using a variety of electrochemical techniques such as voltammetry, chronoamperometry, RDE and RDDE techniques [10–13]. In this paper, we applied the QCM to investigate the redox mechanism of iodide in iodide solution on the gold electrode. The redox behavior of I^- on the gold micro-electrode was studied and compared with the conventional electrode. Because of the very small iR drop and the favorable signal to noise ratio, the gold microelectrode was selected for the measurement of I^- . A linear range of $0.1\text{--}1.0 \times 10^{-5} \text{ mol l}^{-1}$ with a detection limit of $1.0 \times 10^{-6} \text{ mol l}^{-1}$ was obtained. This electrode was also used for the measuring two samples, man-made sea water and table salt. Their results were in good agreement with those indicated or calculated.

2. Experimental

2.1. Apparatus and materials

The planar AT-cut quartz crystal, with diameter of 12 mm, fundamental frequency of 9 MHz, and two gold electrodes connected on both sides of the crystal with a diameter of 6 mm, was supplied by Beijing 707 Plant, People's Republic of China. An oscillator circuit was constructed from a transistor-transistor logic integrated circuit. The crystal frequency was monitored by a model GFC-8010G universal frequency counter (Good Mill Taiwan, People's Republic of China). The potential signal was generated by the model-366 biopotentiostat (EG&G, Princeton Applied Research, Princeton, USA). The curves of current \sim voltage, $I \sim E$, and frequency \sim voltage,

$f \sim E$, were recorded by a type-3086 xy recorder (Yokogawa Hukushin Electric, Japan). A model-485 autoranging picoammeter was used to amplify the current signal from the microelectrode. Gold microwires with a diameter of 30 μm were purchased from Goodfellow, UK. The gold disk microelectrode was home-made by sealing a gold wire in a pulled glass capillary or a small pipette. All solutions were prepared in deoxygenated double distilled water with analytical grade reagents. KI aqueous solution (0.1 mol l^{-1}) was prepared as stock solution. No supporting electrolyte was added to the KI solution.

2.2. Procedure

The working electrode used was either the gold electrode on the crystal ($d = 6 \text{ mm}$), or the conventional gold-disk electrode ($d = 4 \text{ mm}$), or else the gold-disk microelectrode ($d = 30 \mu\text{m}$). A potassium chloride saturated calomel electrode (SCE) was used as a reference electrode, and a platinum wire was used as a counter electrode ($d = 1 \text{ mm}$, $L = 0.5 \text{ cm}$). All the potential values were recorded against SCE. When the microelectrode was used as the working electrode, the electrochemical cell was set in a electrically shielded copper cage. In cyclic voltammetry, the potential was swept between -0.20 V and $+0.80 \text{ V}$. Before the experiment, all working electrodes were conditioned by potential cycling between -0.20 V and $+0.80 \text{ V}$ until steady voltammograms were obtained.

3. Results and discussion

3.1. Characterization of I^- by QCM

The QCM was composed of a piezoelectric crystal on which electrode pads were deposited; an oscillator circuit was appropriately employed to the system. For the stiff deposit on the crystal electrode, the changes of frequency as a function of mass changes can be expressed by the well known Sauerbrey equation [14].

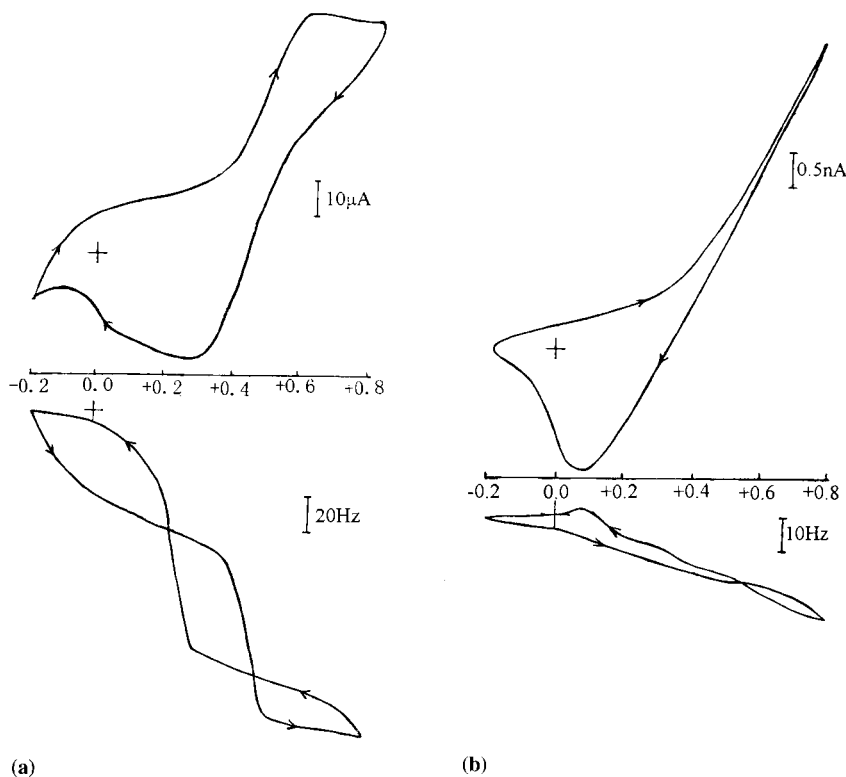


Fig. 1. EQCM characterization of I^- : (a), in 0.1 mol l^{-1} KI solution; (b), in $8.0 \times 10^{-5} \text{ mol l}^{-1}$ KI solution. The potential was swept between -0.2 V and $+0.80 \text{ V}$ at 100 mV s^{-1} .

$$\Delta f = -2\Delta m(f_0)^2/[nA(\mu\rho)^{1/2}] \quad (1)$$

When the properties of the solution remain the same, the frequency changes are also the function of mass changes and can also be described by the Sauerbrey equation. In cyclic voltammetry, the relationship of the frequency changes and the peak currents, i_p , is given by the following equation.

$$i_p = -nFvA(\mu\rho)^{1/2}[d(\Delta f)/dE]E_p/2f_0^2M_w \quad (2)$$

Here, Δf is the observed frequency changes; Δm , the mass changes at the electrode surface; f_0 , the fundamental frequency of the crystal; n , the order of the harmonic oscillator; A , the electrode area on the crystal; μ , the shear modulus of quartz; ρ , the density of quartz and v , the scan rate of electrode potential.

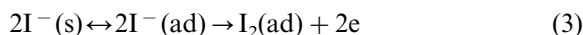
However, the above-mentioned equation, is valid only for adlayers of uniform thickness both

in vacuum and in solution while operating with the QCM. When crystals and electrode pads of a finite size are employed, the mass sensitivity across the surface of QCM is non-uniform. Fortunately, most of time, not all of the electrogenerated material would deposit on the electrode. Thus, from the frequency changes we can calculate the mass of the deposit by using Eq. (2). Combining the cyclic voltammogram, it is very easy to determine the electrode reaction mechanism of some redox systems.

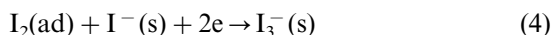
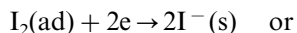
In the EQCM experiment, the $I \sim t$ and $f \sim t$ curves were recorded simultaneously and shown in Fig. 1a and Fig. 1b, for 0.1 mol l^{-1} KI and $8.0 \times 10^{-5} \text{ mol l}^{-1}$ KI solutions, respectively, by using gold electrode on the crystal ($d = 6 \text{ mm}$). Both the $I \sim E$ curve and the $f \sim E$ curve depends on the concentration of the KI solution. In 0.1 mol l^{-1} KI solution, shown in Fig. 1a, an anodic peak at $+0.60 \text{ V}$ and a cathodic peak at $+0.25$

V was observed when the potential was cycled between -0.20 V and $+0.80$ V. The oxidative process was controlled by the diffusion rate. The frequency decreased when the potential was scanned from -0.20 V to $+0.80$ V, and increased when the scan was reversed. This indicated that I^- was oxidized to I_2 and deposited on the electrode. On the anodic curve of $f \sim E$, three sections were observed. When it becomes more negative than $+0.40$ V, the decrease of the frequency may be caused by the slow oxidation of I^- to the deposited I_2 or the direct absorption of I^- on the electrode. From $+0.40$ V to $+0.50$ V, the sharp fall of frequency was caused by the fast oxidation of I^- and the following deposit of I_2 . When it becomes more positive than $+0.50$ V, a frequency plateau was observed due to the depletion of the diffusion layer. The cathodic curve can also be divided into three parts. From $+0.80$ V to $+0.30$ V, the slow rise of the frequency may be caused by the reductive stripping of the deposited I_2 at a slow rate. Between $+0.30$ V and $+0.10$ V, the sharp increase of frequency was caused by the fast reduction of I_2 to I^- . When more negative than $+0.10$ V, a plateau was observed due to the complete reduction of I_2 . From the above results the redox process of I^- may be proposed as:

Sweeping anodically



Sweeping cathodically



In 8.0×10^{-5} mol l^{-1} KI solution, shown in Fig. 1b, no anodic peak was observed. Since the concentration of 8.0×10^{-5} mol l^{-1} was very low compared with the concentration of 0.1 mol l^{-1} and no supporting electrolyte was added, the resistance of the solution was larger, thus the iR drop of the solution was greater, hence the oxidative potential of the I^- ion was higher and no anodic peak was observed within the potential window (the anodic peak may be seen at a potential more positive than $+0.8$ V). Consequently, the frequency variation in 8.0×10^{-5} mol l^{-1} KI solution was smaller than that in 0.10 mol l^{-1} KI

solution due to its lower concentration. When the potential was swept anodically, the frequency fell gradually with the potential resulting from the deposit of I_2 . When the scan reversed, the frequency decreased smoothly with the scan, and finally reached a plateau. This can be explained— I_2 was continually deposited on the electrode at first, then it was reduced to I^- . When the deposited I_2 was completely reduced, the frequency came back to the original no further change was observed. Because the KI concentration was very low, the variation of frequency was smaller.

3.2. Effect of the electrode size on the redox behavior of I^-

A cyclic voltammogram of KI on a conventional gold electrode with a radius of 2 mm was shown in Fig. 2a. No anodic peak but a well defined cathodic peak was observed within the potential window on the cyclic voltammogram. In

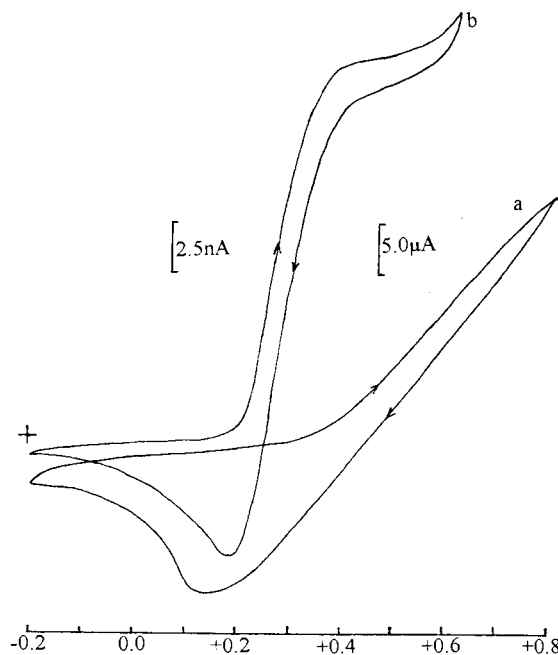


Fig. 2. Cyclic voltammograms of 1.0 mmol l^{-1} KI solution on the conventional electrode ($d = 4$ mm) (a) and the microelectrode ($d = 30$ μ m) (b) at $\nu = 100$ $mV s^{-1}$. No supporting electrolyte was added.

Fig. 2b, however, an anodic plateau was observed. The anodic peak is at +0.50V, which is more negative than that of the conventional gold electrode, and the cathodic peak potential is +0.38 V. The ΔE_p value, 120 mV, was larger than that of the reversible redox system, indicating a quasi-reversible redox process for I^- on this electrode. The ratio of i_{pa} to i_{pc} was smaller than unity, indicating the absorption of I_2 on the electrode.

Since the area of the conventional electrode is larger than that of the counter electrode and the concentration of the KI solution was lower and no supporting electrolyte was added, the iR drop of the conventional electrode system was considerably larger resulting in a more positive oxidation peak potential and a large ΔE_p value. On the other hand, the area of the microelectrode is one percent of that of the counter electrode, the iR drop was very small, which brings about a well defined anodic plateau, a microelectrode character at steady-state diffusion. The well-defined cathodic peaks in the two cases were caused by the reductive stripping of the adsorbed I_2 on the electrodes. Therefore I^- was easily oxidized on the microelectrode and the oxidation peak was not distorted under low analyte concentration solution. The addition of the supporting electrolyte was unnecessary. Moreover, the charging current of the microelectrode was very small, hence the ratio of signal to noise improved.

3.3. Detection of I^- on the microelectrode

A gold microelectrode was selected for the determination of I^- , since I^- was easier to oxidize on the microelectrode and the addition of supporting electrolyte (which may bring about other interference since its concentration was usually high) was unnecessary. Fig. 3 shows that the anodic peak current, i_p , was linearly related to the concentration of I^- between 1.0×10^{-5} and 0.10 mol l^{-1} with a detection limit of $1.0 \times 10^{-6} \text{ mol l}^{-1}$. Because the range of the concentration was very wide, $\log(i_p)$ was plotted against $\log C$. The calibration curve can be expressed as $i(nA) = 3.16 \times 10^4 C (\text{mol l}^{-1})$.

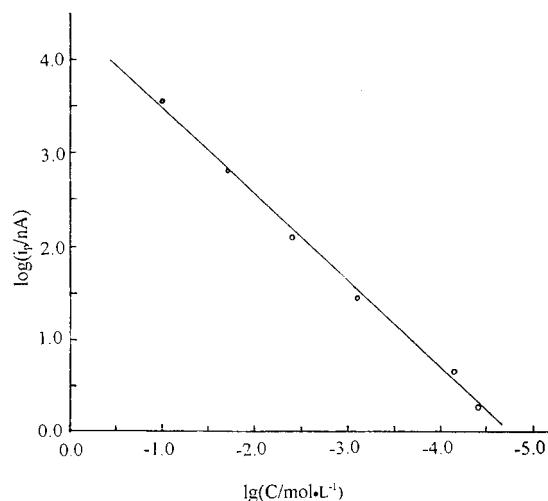


Fig. 3. $\log(i_p) \sim \log C$ plot for the gold microelectrode in a series of KI solution without supporting electrolyte added. $v = 100 \text{ mV s}^{-1}$.

3.4. Interference

Negative ions such as Br^- , Cl^- did not interfere with the detection of I^- , because these ions can only be oxidized at potentials more positive than +0.80 V, which was 300 mV higher than the oxidation potential of I^- . Other ions such as CN^- , F^- , NO_3^- , SO_4^{2-} , PO_4^{3-} and K^+ , Na^+ , Ca^{2+} , Mg^{2+} , Fe^{3+} , Cu^{2+} , Zn^{2+} , Cd^{2+} did not interfere with the detection of I^- .

3.5. Effect of pH

When the pH value of the solution ranged from 1 to 7, the oxidative potential and current of I^- were not affected. Hence no buffer solution was used. The standard KI solutions used to obtain the $\log(i_p) \sim \log C$ plot were prepared with distilled water as shown in Fig. 3.

3.6. Measurement of I^- in samples

The man-made sea water was prepared by dissolving 6.0 g NaCl, 1.5 g $MgCl_2$, 0.5 g $CaCl_2$, 1.0 g $NaSO_4$, 0.8535 g KI and 0.0799 g KBr in 500 ml distilled water. The table salt was commercially obtained; its solution was prepared by dissolving

Table 1
Determination of samples by the microelectrode

Sample	Indicated amount	Measured value	Average value	Mean RSD %
Sea water (mg ml ⁻¹)	1.306	1.305	1.305	10.1
		1.300		
		1.310		
		1.302		
		1.308		
Table salt (mg ml ⁻¹)	2.452	2.450	2.457	12.8
		2.460		
		2.473		
		2.448		
		2.455		

1.0 g of this salt in 100 ml distilled water. Since the linear range for KI on the microelectrode was very wide, the two sample solutions were directly measured without further dilution. Results listed in Table 1 show that the measured values were in good agreement with the indicated values. The average anodic peak currents for sea water and table salt solution were 324.74 nA and 6.11 nA, respectively.

4. Conclusion

The method of combining QCM and CV together is a very useful technique both to study the redox process or to detect the content of I⁻. By using this technique, more information about the redox process from the $f \sim E$ and $i \sim E$ curves of I⁻ can be obtained. Compared with the conventional electrode, a better voltammogram could be observed using the gold microelectrode, and the oxidation-potential was relatively lower when the analyte concentration was low and no supporting electrolyte was added. The linear range of $1.0 \times 10^{-5} \sim 0.10 \text{ mol l}^{-1}$, was very wide. A detection limit of $1.0 \times 10^{-6} \text{ mol l}^{-1}$ was obtained. It is safe to say that the method is very useful, practical, and deserves more research.

Acknowledgements

The authors would like to thank the National Natural Sciences Foundation of China for supporting this work.

References

- [1] R.M. Wightman, Anal. Chem. 53 (1981) 1125A.
- [2] M. Fleischmann, S. Pons, D.R. Robinson, P.P. Schmidt, Ultramicroelectrodes, Datatech Systems Publisher, Moranganton, NC, 1987.
- [3] R.M. Wightman, E. Stroye, R.N. Admas, Nature (London) 262 (1976) 145.
- [4] R.R. McCaffrey, S. Bruckenstein, P.N. Prasad, Langmuir 2 (1986) 228.
- [5] B.J. Feldman, O.R. Melroy, J. Electroanal. Chem. 234 (1987) 213.
- [6] D. Orata, D.A. Buttry, J. Am. Chem. Soc. 109 (1987) 3574.
- [7] R. Schumacher, J.G. Gordon, O. Melroy, J. Electroanal. Chem. 216 (1987) 127G.
- [8] S. Bruckenstein, M. Shay, J. Electroanal. Chem. 188 (1985) 131.
- [9] S. Bruckenstein, S. Swathhirajan, Electrochim. Acta. 30 (1985) 851.
- [10] T. Bejerano, E. Gileadi, J. Electroanal. Chem. 82 (1977) 209.
- [11] T. Bejerano, E. Gileadi, J. Electrochem. Soc. 124 (1977) 1720.
- [12] S. Swathirajan, S. Bruckenstein, J. Electroanal. Chem. 112 (1980) 25.
- [13] S. Swathirajan, S. Bruckenstein, J. Electroanal. Chem. 143 (1983) 167.
- [14] G. Sauerbrey, J. Phys. 155 (1959) 206.

Nanoscale analysis of pharmacologically active catechins in body fluids by HPLC using borate complex extraction pretreatment¹

Hironori Tsuchiya ^{a,*}, Masaru Sato ^b, Hirotsugu Kato ^a, Hidetoshi Kureshiro ^b, Nobuhiko Takagi ^a

^a Department of Dental Pharmacology, Asahi University School of Dentistry, 1851 Hozumi, Hozumi-cho, Motosu-gun, Gifu 501-02, Japan

^b Department of Oral Microbiology, Asahi University School of Dentistry, 1851 Hozumi, Hozumi-cho, Motosu-gun, Gifu 501-02, Japan

Received 19 February 1997; received in revised form 26 May 1997; accepted 26 May 1997

Abstract

A pretreatment method based on borate complex formation is described for the selective and simultaneous quantitation of pharmacologically active catechins in human plasma and saliva. This method is based on the interaction of catechins with diphenylborate (as a complexing agent) and tetra-*n*-butylammonium (as a counter ion) in alkaline media to give the catechin–diphenylborate complex and ion-pair that are extractable to the organic phase. The complex extracted in an organic solvent is dissociated by shaking with an aqueous trifluoroacetic acid solution to back-extract free catechins to the aqueous phase, followed by high-performance liquid chromatography (HPLC) analysis with fluorometric and diode array detection. Under optimal conditions, all catechins originating from green tea extracts were selectively purified from plasma and saliva samples, and they were stabilized during the extraction procedures by forming the complex. The nano-scale quantitative analysis of eight catechins was achieved with high recovery and analytical reproducibility. The proposed method would be a useful tool for pharmacokinetic studies of catechins in plasma and saliva. © 1998 Elsevier Science B.V. All rights reserved.

Keywords: Borate complex; Catechins; High-performance liquid chromatography; Plasma; Pretreatment; Saliva

1. Introduction

Catechins (3,3',4',5,7-pentahydroxyflavan and its derivatives) contained in tea leaves (*Camellia sinensis*) are known to possess various biological activities [1,2]. Among the known pharmacological effects, the practical applications of catechins are in the treatment of acute viral hepatitis [3] and in the prevention of dental caries [4]. The medi-

* Corresponding author: Tel./fax: + 81 58 3291432; e-mail: hiro@dent.asahi-u.ac.jp

¹ Presented at the First Asia-Pacific International Symposium on Capillary Electrophoresis, and other Nano- and Microscale Analytical Techniques, held in Singapore, December 17–20, 1996.

nal effectiveness of catechins depends on their concentrations in blood after oral administration and on their concentrations in saliva after application to the oral cavity. Therefore, a quantitative method for catechins that are present or retained in body fluids has been needed for their pharmacokinetic studies.

Catechins in widely used tea extracts are composed of catechin (*trans*-2-[3,4-dihydroxyphenyl]-3,4-dihydro-1[2H]-benzopyran-3,5,7-triol: C), epicatechin (*cis*-catechin: EC), gallocatechin (*trans*-2-[3,4,5-trihydroxyphenyl]-3,4-dihydro-1[2H]-benzopyran-3,5,7-triol: GC), epigallocatechin (*cis*-gallocatechin: EGC), catechin-3-gallate (CG), epicatechin-3-gallate (ECG), gallocatechin-3-gallate (GCG) and epigallocatechin-3-gallate (EGCG) [5]. The prepurification selective for these eight catechins is essential to successful analysis of body fluids. Although several pretreatment methods were previously reported to purify catechins in biological samples [6–10], they are unsatisfactory in selectivity, sample-size and procedural simplicity.

Since borate specifically forms a complex with 1,2-diols [11], such borate complex formation has been used for the purification of catechol compounds [12–14]. Eight tea catechins possess the same 1,2-dihydroxyl structure. Hence, they are speculated to be selectively extracted from body fluid samples by forming the borate complex and ion-pair as shown in Fig. 1. The back-extracted catechins would be separately analyzed by high-performance liquid chromatography (HPLC).

To achieve a nano-scale analysis of catechins based on this speculative system, analytical conditions were optimized for their pretreatment using the borate complex extraction method. After treating human plasma and saliva under optimal conditions, all the purified catechins were subjected to HPLC analysis with fluorometric and diode array detection.

2. Experimental

2.1. Reagents

Standard C, EC, EGC, ECG and EGCG were supplied by Dr Munekazu Iinuma, Gifu Pharma-

ceutical University (Gifu, Japan). GC, CG and GCG were purchased from Funakoshi (Tokyo, Japan). Their stock solutions (1.0 mg ml^{-1} of each) were prepared by dissolving the standards in 0.01 N HCl, and then they were stored at 4°C . They were diluted as required with 0.01 N HCl before use. Pyrocatechol (PC) from Nacalai Tesque (Kyoto, Japan) and 4-methylcatechol (4-MC) from Tokyo Kasei (Tokyo, Japan) were used as an internal standard for plasma and saliva analysis, respectively. Diphenylborate–ethanolamine complex was obtained from Aldrich (Milwaukee, WI, USA). Catechin-containing green tea extract was supplied from Taiyo Kagaku (Yokkaichi, Japan). Tetra-*n*-alkylammonium bromides with different alkyl chains were of ion-pair chromatographic grade (Nacalai Tesque). Acetonitrile of HPLC grade (Kishida, Osaka, Japan) was used for the mobile phase preparation. All other reagents were of the highest analytical grade available. Water was redistilled by an all-glass apparatus after purifying by a Milli-Q water purification system (Nihon Millipore, Tokyo, Japan).

2.2. Pretreatment procedures and optimization of conditions

Extraction procedures were performed using polypropylene tubes with screw caps ($101 \times 14 \text{ mm}$; Sarstedt, Nümbrecht, Germany). All of the glassware used for quantitative analyses was silanized to avoid the adsorption of analytes onto the glass surfaces [15]. After adding $50 \mu\text{l}$ of a 4-MC solution in 0.01 N HCl (1.0 mg ml^{-1}), 0.5 ml of the sample solution was vortex-mixed for 1 min with 0.5 ml of 0.15% (w/v) diphenylborate in 2.0 M potassium phosphate buffer (pH 8.5) containing 5% (v/v) ethanol and 4.0 ml of 5 mM tetra-*n*-butylammonium bromide in *n*-octanol/*n*-hexane (20:80, v/v). The mixture was centrifuged at $1200 \times g$ for 3 min. The organic phase was vortex-mixed for 1 min with 0.25 ml of 7.5% (v/v) trifluoroacetic acid. After centrifugation at $1200 \times g$ for 3 min, the aqueous phase was subjected to HPLC separation.

Standard catechin solutions ($5.0 \mu\text{g ml}^{-1}$ of each) were treated by varying the diphenylborate concentration (0–0.2%, w/v), the phosphate

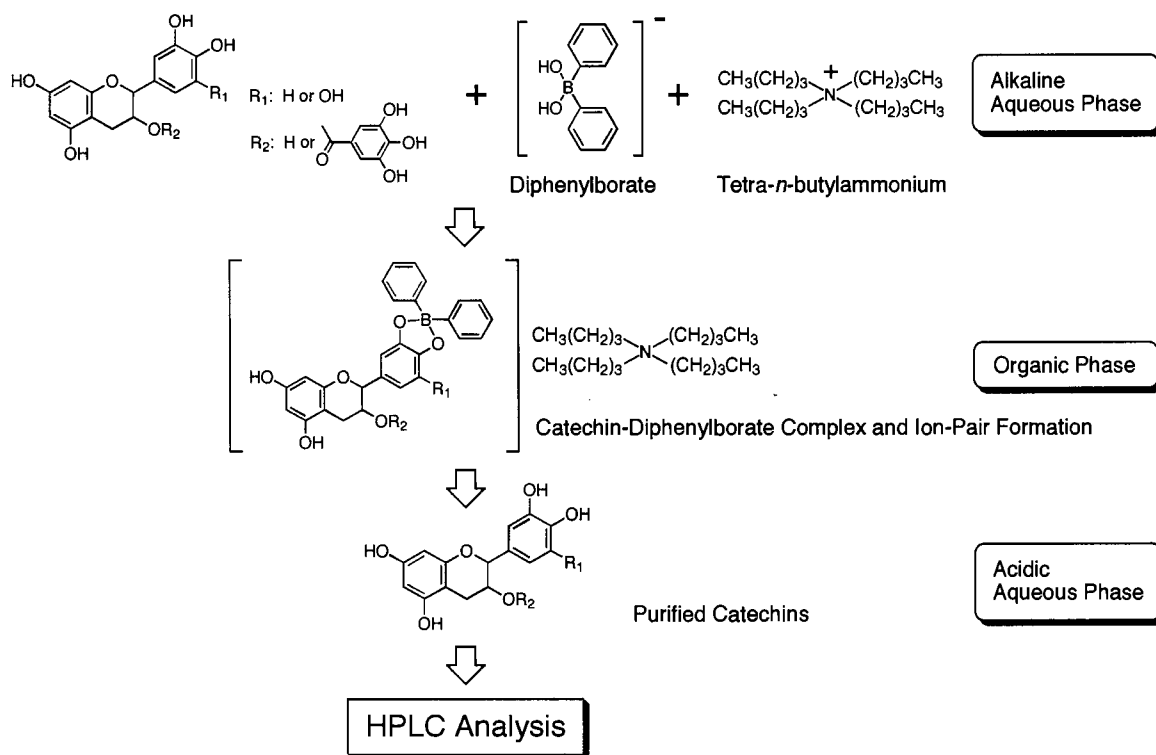


Fig. 1. Schematic analytical procedure using the extraction pretreatment based on diphenylborate complex and ion-pair formation.

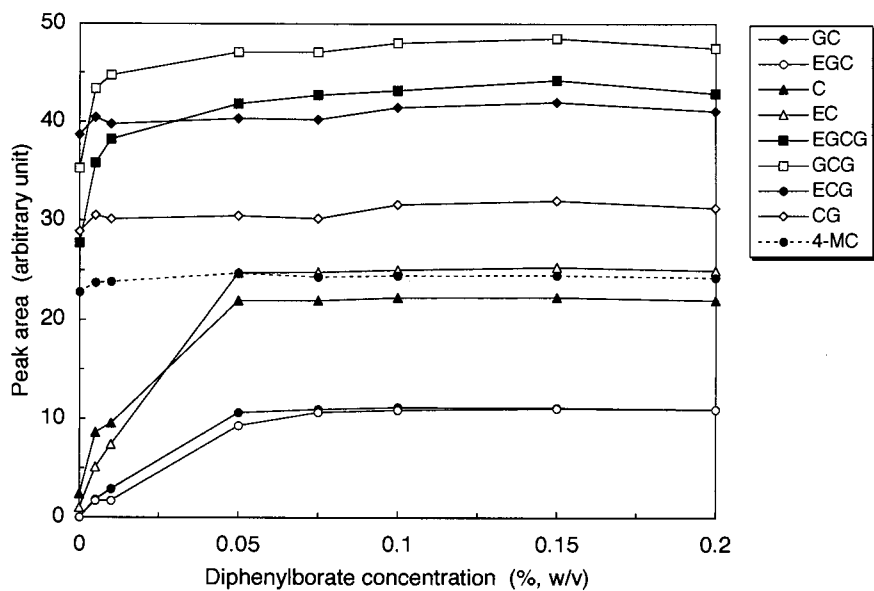


Fig. 2. Effect of diphenylborate concentration on catechin extraction.

buffer pH (3.0–10.0), the type (alkyl chains of $(C_3H_7)_4^-$ to $(C_{10}H_{21})_4^-$) and concentration (0–10 mM) of tetra-*n*-alkylammonium bromide, the type of extraction solvent (*n*-alcohol: $C_5H_{11}-OH$ to $C_{10}H_{21}-OH$ and *n*-hydrocarbon: C_5H_{12} to $C_{10}H_{22}$), the solvent composition (*n*-alcohol in *n*-hydrocarbon: 5–40%, v/v), and the trifluoroacetic acid concentration (0.1–12.5%, v/v). The analytical conditions were optimized by comparing the relative peak areas obtained throughout all procedures (extractions and HPLC with diode array detection). The results were expressed as the means of duplicated experiments.

2.3. Stability of catechins

To 0.5 ml of a standard catechin solution (10.0 $\mu\text{g ml}^{-1}$ of each) was added 0.5 ml of 2.0 M potassium phosphate buffer (pH 2.0, 7.0, 8.5 or 10.0) or 2.0 M potassium phosphate buffer (pH 8.5) containing 0.15% (w/v) diphenylborate. The mixtures were allowed to stand for 2.5–30 min at room temperature. A 0.5 ml aliquot of each resulting solution was analyzed as described in Section 2.2. The relative stability of catechins under different conditions was evaluated by comparing the mean peak areas of duplicated experiments to the original peak areas (0.01 N HCl solution).

2.4. Sample preparation

2.4.1. Plasma

Heparinized blood plasma was collected from male subjects, all aged 44 years. To 150 μl of plasma samples was added 100 μl of 50 mM citrate buffer (pH 4.5) containing 0.02% (w/v) EDTA–2Na. The mixture was vortex-mixed with 100 μl of 5% (v/v) perchloric acid containing PC (5.5 $\mu\text{g ml}^{-1}$), and centrifuged at $20000 \times g$ for 10 min. To 300 μl of the supernatant were added 0.5 ml of 0.1% (w/v) diphenylborate in 5% (v/v) ethanol/2.0 M potassium phosphate buffer (pH 8.5) and 4.0 ml of 15 mM tetra-*n*-butylammonium bromide in *n*-octanol/*n*-hexane (20:80, v/v), and then treated as de-

scribed in Section 2.2. The back-extraction was performed with 0.2% (v/v) trifluoroacetic acid instead of 7.5% (v/v) trifluoroacetic acid.

2.4.2. Saliva

Unstimulated whole saliva was collected from male subjects, all aged 44 years, and then diluted 2–10 times with 0.01 N HCl. After adding 50 μl of a 4-MC solution in 0.01 N HCl (1.0 mg ml^{-1}), 0.5 ml of saliva diluent was treated as described in Section 2.2.

2.5. Liquid chromatography

2.5.1. Plasma sample

An LC-10AD liquid chromatograph (Shimadzu, Kyoto, Japan) controlled by an SCL-10A system controller (Shimadzu), a DGU-4A degasser (Shimadzu), a 7125 sample injector (injection volume of 100 μl ; Rheodyne, Cotati, CA, USA), a Shim-pack CLC-C8 (M) column (250 \times 4.6 mm, particle size 5 μm ; Shimadzu) placed in a CTO-6A column oven (Shimadzu), and an RF-550 spectrofluorometric detector (Shimadzu) connected to a C-R 6A Chromatopac data processor (Shimadzu) were used. Separation was performed by delivering the mobile phase, acetonitrile/trifluoroacetic acid/water (16.5:0.2:83.3, v/v/v), at a flow rate of 1.0 ml min^{-1} and at a column temperature of 50°C. C, EC and PC were detected at 282 nm for excitation and 314 nm for emission. C and EC were quantified based on the peak area ratios to PC by reference to the calibration graphs.

2.5.2. Saliva sample

An LC-9A liquid chromatograph (Shimadzu) connected to a KMT-30A auto sampler with an injection volume of 40 μl (Kyowa Seimitsu, Tokyo, Japan), a Shim-pack CLC-C8 (M) column (250 \times 4.6 mm, particle size 5 μm ; Shimadzu) placed in a thermo-controller (Kyowa Seimitsu), and an SPD-M10AVP diode array detector (Shimadzu) controlled by an FMV-5133D5 personal computer (Fujitsu, Tokyo, Japan) were used. The mobile phase, A: acetonitrile/trifluoroacetic acid/water (10:0.3:89.7, v/v/v), and B: acetonitrile/

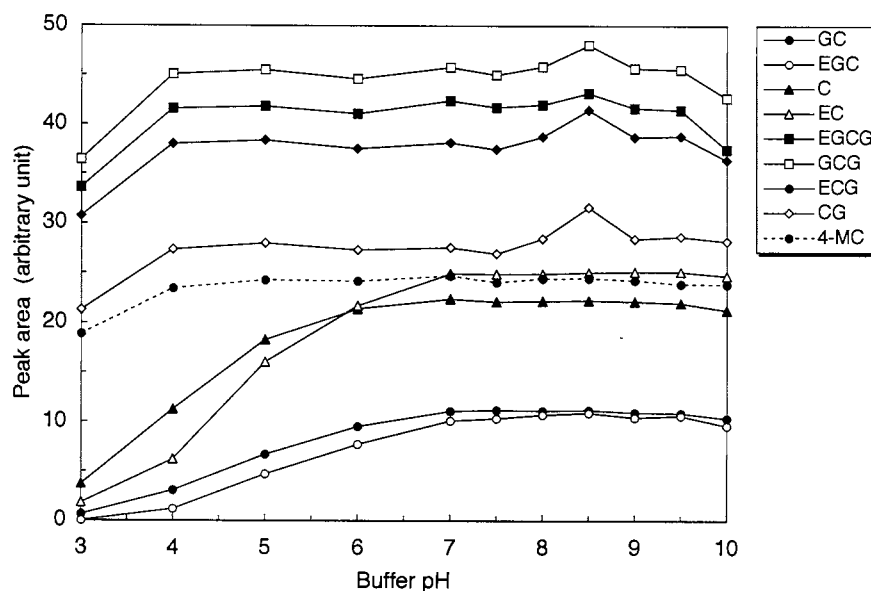


Fig. 3. Effect of buffer pH on catechin extraction.

Table 1
Relative stability of catechins under different circumstances

	Original	pH 2.0		pH 7.0				pH 8.5 without complex formation				pH 8.5 with complex formation				pH 10.0
		30	30	30	30	2.5	5	10	30	2.5	5	10	30	30 (min)		
GC	1.00	1.01	0.97	0.97	0.97	0.97	0.79	0.99	0.99	1.04	0.96	0.14				
EGC	1.00	0.99	0.92	0.81	0.67	0.52	0.18	0.99	1.00	1.06	0.96	0.00				
C	1.00	0.99	0.99	1.01	1.00	0.95	0.98	1.01	1.02	1.01	0.98	0.63				
EC	1.00	0.99	0.99	1.03	1.01	0.98	1.02	1.02	1.03	1.02	1.00	0.82				
EGCG	1.00	1.03	0.94	0.84	0.75	0.57	0.21	0.98	1.00	0.99	0.93	0.05				
GCG	1.00	1.03	0.99	0.93	0.89	0.76	0.53	0.96	0.98	0.95	0.90	0.09				
ECG	1.00	1.01	0.98	0.92	0.92	0.81	0.77	0.95	0.96	0.94	0.89	0.55				
CG	1.00	1.01	0.97	0.94	0.94	0.82	0.72	0.93	0.95	0.90	0.84	0.46				

Standard catechins ($5.0 \mu\text{g ml}^{-1}$ of each) were allowed to stand in phosphate buffer of different pH values (2.0, 7.0, 8.5 or 10.0) or phosphate buffer (pH 8.5) containing diphenylborate. They were analyzed after the indicated time. The values indicate the mean relative peak areas of duplicated experiments.

water (30:70, v/v), was delivered at a flow rate of 1.0 ml min^{-1} and at a column temperature of 50°C in a linear gradient elution mode. The gradient was prepared as follows: 100% A at 0 min to 25% A and 75% B at 17 min. The UV absorbances of the analytes were detected at 269, 274, 277 and 278 nm. All catechins were quantified based on the peak area ratios to 4-MC by reference to the calibration graphs.

3. Results and discussion

3.1. Optimal conditions

Various analytical conditions were optimized for the procedures schematically shown in Fig. 1. Among the borate compounds commercially available [13], diphenylborate was chosen as a complexing agent because it showed the highest

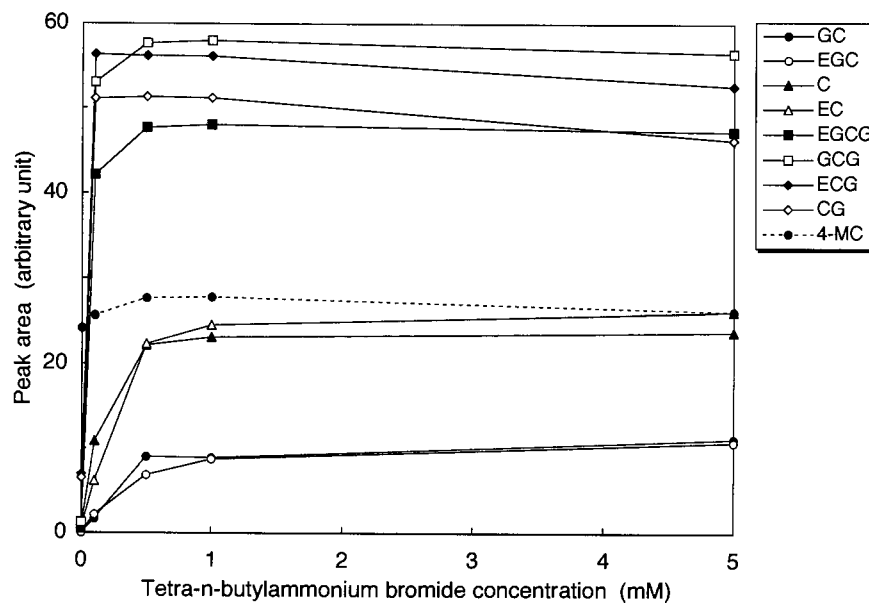


Fig. 4. Effect of tetra-*n*-butylammonium bromide concentration on catechin extraction.

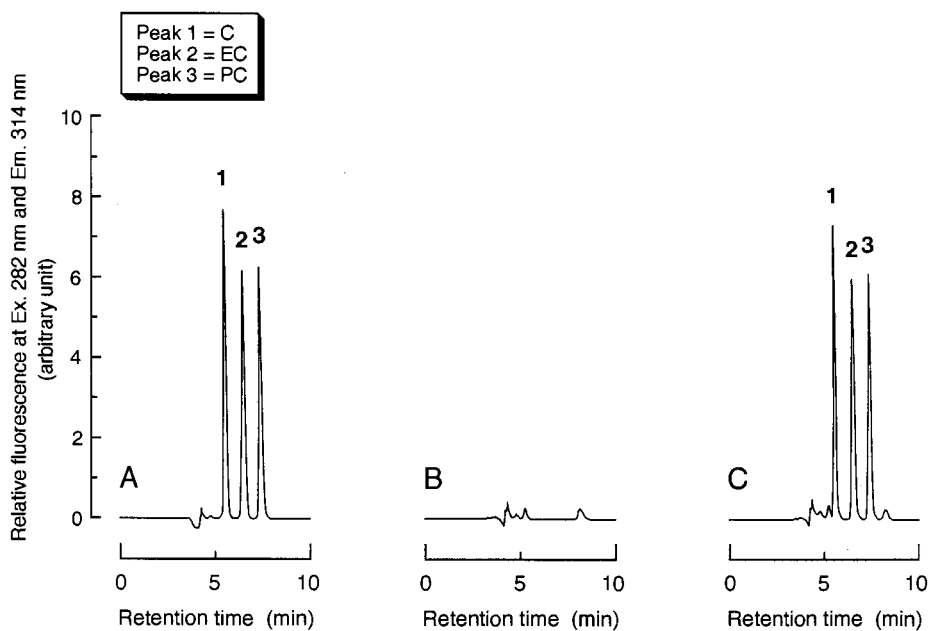


Fig. 5. Chromatograms obtained from standard and plasma samples. (A) Standard catechins (72.5 ng ml^{-1} of each); (B) blank plasma; (C) plasma added with standard catechins (72.5 ng ml^{-1} of each). Fluorometric detection: 282 nm for excitation and 314 nm for emission.

Table 2
Comparative analytical evaluation of HPLC methods with fluorometric and diode array detection

	Fluorometric detection for plasma analysis	
	C	EC
Mean recovery ^a (%)	90.0	99.2
CV (%)	2.2	2.9
Quantitative range (ng ml ⁻¹)	7.25–300	7.25–300
Detection limit (ng injection ⁻¹)	0.35	0.35

	Diode array detection for saliva analysis							
	GC	EGC	C	EC	EGCG	GCG	ECG	CG
Mean recovery ^b (%)	98.0	96.9	98.7	99.0	95.9	96.8	95.9	96.3
CV (%)	1.2	1.2	1.5	1.4	1.5	1.6	1.7	1.8
Quantitative range (µg ml ⁻¹)	0.1–20	0.1–20	0.05–20	0.05–20	0.025–20	0.025–20	0.025–20	0.025–20
Detection limit (ng injection ⁻¹)	4.0	4.0	2.0	2.0	1.0	1.0	1.0	1.0

^a Recovery and reproducibility were evaluated by analyzing replicate plasma samples spiked with standards (72.5 ng ml⁻¹ of each, $n = 5$).

^b Recovery and reproducibility were evaluated by analyzing replicate saliva samples spiked with standards (5.0 µg ml⁻¹ of each, $n = 5$).

extractability for catechins. The peak areas of catechins varied with the diphenylborate concentrations as shown in Fig. 2. The peak areas of all the tested catechins increased with the addition of diphenylborate, indicating that their extraction is improved by the complex formation. The use of diphenylborate was especially effective on the extraction of GC, EGC, C and EC. Their extractability was significantly elevated by increasing the concentrations. In contrast, this effect was lesser on EGCG, GCG, ECG and CG, suggesting that their extraction is primarily based on relatively high lipophilicity. The concentrations of 0.1–0.15% (w/v), at which the peak areas of all the catechins became plateau, were used.

The complex formation between borate and catechol compounds proceeds in weakly alkaline media [12–14]. As shown in Fig. 3, catechins also formed the complex with diphenylborate depending on an increase of phosphate buffer pH, and

showed the largest and/or constant peak areas at pH 8.5. The peak areas tended to decrease above pH 9.0, indicating the possible decomposition of catechins.

C was recently reported to be stable in acidic media, but oxidatively decomposed above pH 5.0 [10]. Although catechins most efficiently formed the diphenylborate complex at pH 8.5, they had been presumed to be unstable under such alkaline conditions. When catechins were allowed to stand in phosphate buffer of different pH, their peak areas changed as shown in Table 1. After 30 min, catechins showed no change at pH 2.0. They were also relatively stable at pH 7.0. At pH 10.0, however, all catechins showed a reduction to 0–82% of their original concentrations. Catechins did decompose at pH 8.5 (the optimal extraction condition) and their concentrations decreased with time. Significant decomposition occurred especially in EGC, EGCG and GCG, which reduced to

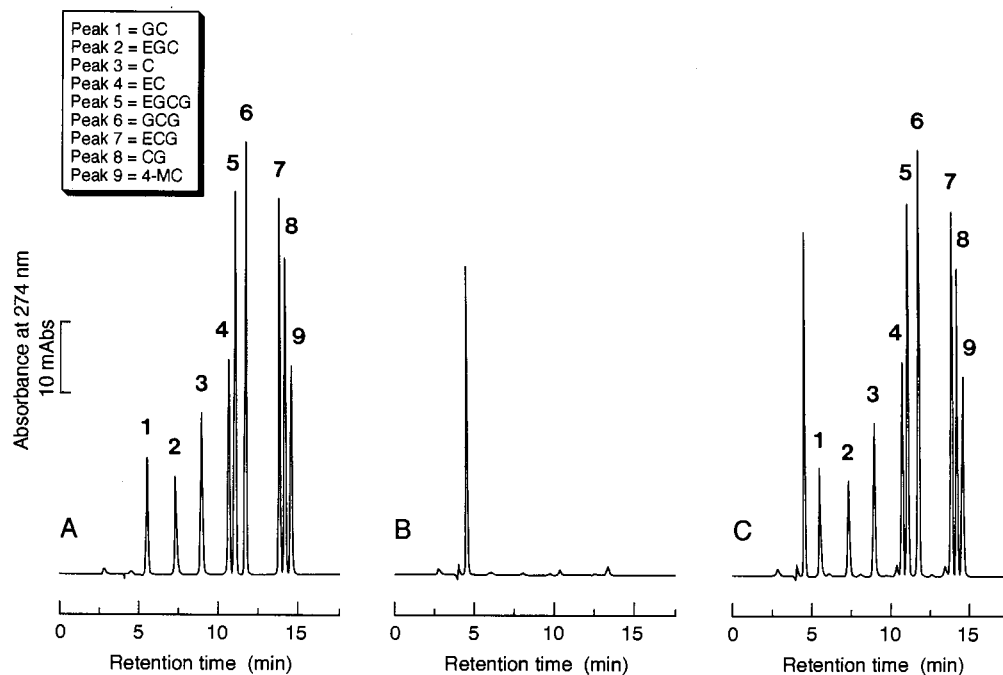


Fig. 6. Chromatograms obtained from standard and saliva samples. (A) Standard catechins ($5.0 \mu\text{g ml}^{-1}$ of each); (B) blank saliva; (C) saliva added with standard catechins ($5.0 \mu\text{g ml}^{-1}$ of each). UV detection: 274 nm.

52, 57 and 76%, respectively, after 10 min. In contrast, after mixing with diphenylborate, no or significantly less reduction was observed in all catechins even at pH 8.5. As the vortex-mixing time is only 1 min under such alkaline conditions, the decomposition of catechins is negligible at the step of complex formation and extraction. Although catecholamines, like catechins, are unstable at alkaline pH, they are stabilized by forming a complex with alumina [16]. Catechins in the diphenylborate complex form are similarly considered to be stable.

Since diphenylborate is negatively charged in alkaline media, it is speculated to form an anionic complex with catechins [12]. Therefore, ion-pair extraction using a cationic counter ion is favorable for increasing the extractability of the catechin-diphenylborate complex (Fig. 1). When using tetra-*n*-alkylammonium with different alkyl chains, $(\text{C}_3\text{H}_7)_4^-$ to $(\text{C}_{10}\text{H}_{21})_4^-$, tetra-*n*-butylammonium with $(\text{C}_4\text{H}_9)_4^-$ showed the highest extractability. The peak areas of catechins varied with tetra-*n*-butylammonium bromide concentrations, as shown in Fig. 4. The use of this counter-ion was so

effective that the extractability of all catechins was significantly enhanced by increasing the concentrations of tetra-*n*-butylammonium, although they were scarcely extracted without it. The peak areas of all catechins became constant over 5 mM. The reproducible extraction of C and EC from plasma samples required a concentration of 15 mM, suggesting the consumption of tetra-*n*-butylammonium by anionic compounds in plasma other than the catechin-diphenylborate complex.

The diphenylborate complex dissociates under acidic conditions to give free catechins back-extractable to the aqueous phase (Fig. 1). This dissociation easily occurs in a short time by shaking with an acidic aqueous solution [13]. GC, EGC, C and EC were back-extracted to the aqueous phase by vortex-mixing their diphenylborate complex with 0.2% (v/v) trifluoroacetic acid solution for 1 min. The efficient back-extraction for the other catechins needed a higher concentration of trifluoroacetic acid, 7.5% (v/v). These acidic back-extraction conditions are also advantageous for the stability of catechins.

3.2. HPLC analysis of plasma

Among catechins, C has been used for the treatment of acute viral hepatitis [3]. When the tea extract is orally administered, C and its isomer, EC, are expected to occur at ng ml^{-1} levels in blood [8,17]. The nanoscale separative analysis of C and EC was performed by HPLC with fluorometric detection. Fig. 5 shows the chromatographic results after the diphenylborate complex extraction pretreatment. Plasma C, EC and PC were simultaneously separated without interfering peaks, indicating that the present pretreatment is selective for catechins in plasma.

The quantitative evaluation is summarized in Table 2. Plasma samples spiked with standards were analyzed throughout all procedures. Plotting the peak area ratios of C and EC to PC against the known concentrations showed good linearity in the ng ml^{-1} concentration range for both C and EC. In replicate spiking experiments, the recovery and analytical reproducibility of C and EC were high enough for the quantitative analysis of plasma samples. The mean recovery ($n = 5$) of PC was 92.7%, which was determined by analyzing standard catechin and plasma samples added to 100 μl of the PC solution ($5.5 \mu\text{g ml}^{-1}$).

The present method is superior in selectivity for plasma C and EC to previous methods [8,9], in which plasma samples were purified by solid-phase or liquid-phase extraction, but the major unknown peaks appeared on chromatograms. Its plasma sample-size is only 150 μl volume, which is less than the 0.25–2 ml needed in other methods [6,8,10]. It is also effective for stabilization of C and EC during analysis, but in other methods [7–9,18] no attention was paid to their stability. The pretreatment procedure, consisting of simple two-step extractions, is applicable to multi-sample analysis.

The proposed method was applied to the analysis of plasma collected from human subjects after the oral administration of green tea extract (1.0 g) containing C and EC. Since the major fractions of flavanoids are conjugated in human blood [19], plasma was analyzed after enzymatic hydrolysis [9]. Neither C nor EC was detected in any plasma samples before administration. However, both C

and EC in plasma were found to increase in a time-dependent manner after their administration. The peak plasma levels of total (free plus conjugated) C and EC were reached 60–120 min after administration, which agrees with the report of Lee et al. [9].

3.3. HPLC analysis of saliva

The caries-preventive effects of catechins have been considered to be derived from their antibacterial activity against cariogenic bacteria [20] and inhibitory activity against plaque formation [21]. Since GC, EGC, EC, EGCG, GCG and ECG show such activities at $\mu\text{g ml}^{-1}$ levels [4,20,21], the nano- and microscale analysis of these catechins in saliva is needed to assess their retentivity in the oral cavity after mouth-rinsing with tea catechins. However, catechins other than C and EC did not possess fluorescent properties suitable for their simultaneous detection. Therefore, a diode array detector was employed to detect all of the eight catechins showing absorption maxima in the range 269–278 nm. Fig. 6 shows the chromatographic results after the diphenylborate complex extraction pretreatment. Eight catechins and 4-MC were simultaneously separated without major interfering peaks, indicating that the present pretreatment is selective for catechins in UV detection as well as in fluorometric detection.

The quantitative evaluation is summarized in Table 2. Calibration graphs prepared by plotting the peak area ratios of catechins to 4-MC were linear in the concentration range $\text{ng}–\mu\text{g ml}^{-1}$. The replicate spiking experiments showed high recovery and reproducibility applicable to the quantitative analysis for all salivary catechins of active concentrations. The mean recovery ($n = 5$) of 4-MC was 97.2%, which was determined by analyzing standard catechin and saliva samples added to 50 μl of the 4-MC solution (1.0 mg ml^{-1}).

Previous HPLC methods separately analyzed only some catechins, not all catechins [9,22,23]. The present method is the first to be successfully applied to the simultaneous analysis of all the eight catechins in saliva.

Saliva was analyzed after mouth-rinsing with an aqueous solution of green tea extract (5.0 mg ml⁻¹, 100 ml) for 2.5 min. The eight salivary catechins were found to show the µg ml⁻¹ concentrations 1–60 min after mouth-rinsing, although no catechins were detected in saliva before mouth-rinsing.

4. Conclusion

A pretreatment based on diphenylborate-complex formation and ion-pair extraction has been proven to be effective not only for the selective purification of catechins but also for their stabilization during analysis. The HPLC procedure combined with this pretreatment allows the nanoscale quantitative analysis of catechins in plasma and saliva. The proposed method is applicable to the pharmacokinetic study of pharmacologically active catechins in body fluids.

Acknowledgements

The authors thank Dr Munekazu Inuma and Taiyo Kagaku for kindly supplying standard catechins and tea extracts. This study was supported by Grant 07307018 from the Ministry of Education, Science and Culture of Japan and by Grant-97 from the Miyata Science Research Foundation.

References

- [1] D. Pathak, K. Pathak, A.K. Singla, *Fitoterapia* 62 (1991) 371.

- [2] K. Muramatsu, *Tea Science*, Asakura-Shoten, Tokyo, 1995, pp. 124–183 (in Japanese).
- [3] A.L. Blum, P. Berthet, W. Doelle, H. Goebell, K. Kortum, S. Pelloni, P. Peter, H. Poulsen, G. Strohmeyer, N. Tygstrup, *Lancet* 2 (1977) 1153.
- [4] S. Otake, M. Makimura, T. Kuroki, Y. Nishihara, M. Hirasawa, *Caries Res.* 25 (1991) 438.
- [5] H.N. Graham, *Prev. Med.* 21 (1992) 334.
- [6] A.R. Giles, A. Gumma, *Arzneim.-Forsch.* 23 (1973) 98.
- [7] A.M. Hackett, L.A. Griffiths, A. Broillet, M. Wermeille, *Xenobiotica* 13 (1983) 279.
- [8] H.Y. Pan, D.L. Liu, P.P. Xu, M.L. Lu, *Acta Pharm. Sinica* 26 (1991) 371 (in Chinese).
- [9] M.-J. Lee, Z.-Y. Wang, H. Li, L. Chen, Y. Sun, S. Gobbo, D.A. Balentine, C.S. Yang, *Cancer Epidemiol. Biomarkers Prev.* 4 (1995) 393.
- [10] Y. Ho, Y.-L. Lee, K.-Y. Hsu, *J. Chromatogr.* 665 (1995) 383.
- [11] A. Bergold, W.H. Scouten, Borate chromatography, in: W.H. Scouten (Ed.), *Solid Phase Biochemistry. Analytical and Synthetic Aspects*, Wiley-Interscience, New York, 1983, pp. 149–187.
- [12] F. Smedes, J.C. Kraak, H. Poppe, *J. Chromatogr.* 231 (1982) 25.
- [13] H. Tsuchiya, T. Hayashi, *J. Chromatogr.* 491 (1989) 291.
- [14] H. Tsuchiya, T. Hayashi, *J. Pharmacol. Methods* 23 (1990) 21.
- [15] H. Tsuchiya, S. Ohtani, N. Takagi, T. Hayashi, *Biomed. Chromatogr.* 3 (1989) 157.
- [16] H. Todoriki, T. Hayashi, H. Naruse, A.Y. Hirakawa, *J. Chromatogr.* 276 (1983) 45.
- [17] L. Balant, B. Burki, M. Wermeille, G. Golden, *Arzneim.-Forsch.* 29 (1979) 1758.
- [18] I.C. Shaw, A.M. Hackett, L.A. Griffiths, *Xenobiotica* 12 (1982) 405.
- [19] N.P. Das, *Biochem. Pharmacol.* 20 (1971) 3435.
- [20] S. Sakanaka, M. Kim, M. Taniguchi, T. Yamamoto, *Agric. Biol. Chem.* 53 (1989) 2307.
- [21] S. Sakanaka, T. Sato, M. Kim, T. Yamamoto, *Agric. Biol. Chem.* 54 (1990) 2925.
- [22] P.J. Hayes, M.R. Smyth, I. McMurrough, *Analyst* 112 (1987) 1205.
- [23] D. Madigan, I. McMurrough, M.R. Smyth, *Analyst* 119 (1994) 863.

A new method for the preparation of polyacrylamide gradient gel-filled capillaries with low UV detection background¹

Yi Chen *

Institute of Chemistry, Chinese Academy of Sciences, Beijing 100080, People's Republic of China

Received 19 February 1997; accepted 17 June 1997

Abstract

A simple but reproducible method has been explored for the preparation of polyacrylamide gradient gel-filled capillaries with low UV detection background. The principle is to fill a capillary by plugging it into a wide tube already filled with gradient gelling solutions including a section of buffer. Void-free capillaries can be prepared with a full success for gels below 13%T + 5%C (immobilised completely). For gels between 15%T and 25%T + 5%C, the preparation success rate is 80–95%, depending on the gel immobilisation methods. The resulting capillaries allow the use of any available wave-length for sensitive detection and in the separation of polylysines, a great improvement of their detection sensitivity has been achieved, up to 10^3 – 10^4 fold as compared to the common gel-filled capillaries. Unlabelled polysaccharides from the sacculi of *Escherichia coli* can hence directly be detected at 200 nm. These capillaries can continuously be used for more than 2 months in separating the biological polysaccharides at -200 V cm^{-1} and pH 7.8 while at pH 4.7, they can still be used for more than 400 injections (~ 1 month) of the polylysines at $+180$ V cm^{-1} . As expected by stacking effect, the gradient gels yield higher efficiency or running speed (1-fold) and even higher UV detection sensitivity (> 2 -fold) than the homogeneous gels. © 1998 Elsevier Science B.V. All rights reserved.

Keywords: Low background polyacrylamide gradient gel-filled capillaries; Capillary gradient gel electrophoresis; Polyamino acids; Direct detection of unlabelled polysaccharides

1. Introduction

Capillary gradient gel electrophoresis (CGGE) is in theory an attracting model for the separation of closely-sized molecules or complicated samples

according to slab gradient gel electrophoresis [1–3], but the preparation of gradient gel-filled capillaries seems to be very difficult. Different from a wide slab chamber or column, capillaries have only microlitres of volume, their flowing rate is hardly controlled which varies part by part and from capillary to capillary. Consequently, gel gradients cannot precisely be located in the capillaries, resulting in irreproducible preparations (and separations). This is also different from pro-

* Tel: +86 10 62618240; fax: +86 10 62569564.

¹ Presented at the First Asia-Pacific International Symposium on Capillary Electrophoresis, and other Nano- and Microscale Analytical Techniques, held in Singapore, December 17–20, 1996.

ducing the homogeneous gel-filled capillaries used for capillary gel electrophoresis (CGE) [4].

To control the location of the gradients, we have suggested a step filling method (SFM) [5,6] which can be used for the preparation of not only homogeneous but also stepped and smooth gradient gel-filled tubes [5–8]. However, it needs 20 steps (1.5 cm per step) and 20 ml (1 ml per step) of monomer solutions to prepare a 30 cm smooth gradient gel. The capillary should hence be transferred from solution to solution for 19 times. This is somehow tedious and the transferring, if too slow, may introduce air bubbles in between the steps. By adjacently arranged wells, the transferring distance or time was reduced [6] but the problem has not yet been removed.

We have then tried to use paraffin membrane-separated wells so that a capillary can reach any well by breaking through the membranes. This is theoretically a method to eliminate the transferring problem but not ideal. It is labour-intensive to build up the 20 wells while the built wells can only be used for one time. An alternative way is to use a sort of liquid connected or continuous ‘wells’, that is, layering the gelling solutions inside a wide tube. This is thus a two-stepped filling (TsF) method: The first step is to prepare the gradient gelling solutions inside the tube, and the second step is to transfer the pre-gradient solutions from the tube into a capillary. Similar to SFM, TsF can also be used for producing both of the gradient and homogeneous gel-filled capillaries with low UV background.

In this paper, we will discuss the preparation of polyacrylamide gel-filled capillaries with smooth gradients and low UV detection background. The obtained capillaries are tested by both of negatively charged polysaccharides from the sacculi of *Escherichia coli* [9] and positively charged polylysines. Such samples are difficult to separate and have serious detection problem in CGE with common gel-filled capillaries [10–12] which yield no peak at 210 nm or shorter [5,8]. Different from the common tubes, the new capillaries, which allow the use of any available wave-length for sensitive UV detection, generate

a high detection sensitivity and fast separation of the tested samples. Their UV detection sensitivity is 10^3 – 10^4 fold higher than the common capillaries and at least 2-fold higher than the homogeneous gel-filled capillaries with also low detection background. A direct detection of unlabelled polysaccharides can thus be achieved at 200 nm. Their running speed is about 1-fold higher than the homogeneous gel-filled columns while their efficiency is similar to or better than the latter columns. The experiments also show that resulted capillaries are quite stable: They can be used for more than 400 injections (~ 1 month) of polylysines at pH 4.7, 25°C and +180V cm^{-1} and for more than 2 months at pH 7.8 and -200V cm^{-1} .

2. Experimental

2.1. Chemicals

Tris [tris(hydroxymethyl)aminomethane], EDTA, TEMED [*N,N,N',N'*-tetramethyl-ethylenediamine] and γ -MPS [γ -methacryloxypropyltrimethoxysilane] came from Sigma (St. Louis, MO). Acrylamide and BIS [*N,N'*-methylenebis(acrylamide)] were research reagent grade from Beijing Purchasing Station, Chinese Pharmacy (Beijing, PR China). Boric acid, APS [ammonium persulfate], phosphates, acetic acid, sodium acetate and other chemicals were all analytical reagent grade from Beijing Chemical Works (Beijing, PR China). Water used was triply distilled.

2.2. Sample

Poly(Lys)₃₈ and poly(Lys)₁₂₆ [poly-L-lysine hydrobromides, with polymerisation degree of 38 and 126 each, obtained from the viscosity measurements, Sigma products were dissolved in water at 0.05–100 mg ml^{-1} . The very diluted samples ($< 5 \text{ mg ml}^{-1}$) were prepared every morning to eliminate the hydrolysis problem. Poly(GlcNAc-Mur) is a mixture of $\alpha(1 \rightarrow 4)$ linked regular interpolymers of *N*-acetylglucosamine-2

(GlcNAc) and muramic acid (Mur). It was prepared by enzymatic digestion of the murein peptidoglycan from the sacculi of *E. coli* KN126 (detailed preparation see [9]) and desalted by dialysing against water for 3×4 h at 4°C , with Spectra/Por membrane (MWCO 1000, from Carl Roth GmbH., Karlsruhe, Germany). The desalted sample is blown to dry with nitrogen gas and stored at -20°C . Before use, it was dissolved in water at a total concentration of 1 mg ml^{-1} .

2.3. Preparation of capillaries

The main point is to fill a capillary and a tunnel with sufficiently short steps (≤ 1.5 cm) of gelling solutions. The stepwise distributions will spontaneously change to smooth gradients [6]. The detection background is reduced just by replacing the gels at the detection part of the capillary with UV-transparent buffers [5,6]. To stabilise the capillaries, the gels are immobilised by forming chemical bonds along the entire tubing wall. This is realised by coating the capillaries just before filling. The suggested filling method is TsF.

2.3.1. Coating

A fast coating procedure modified from those of our previous works [5–8] is as follows: A new capillary (J&W) is filled with a solution of 0.5% γ -MPS and 0.5% acetic acid in dichloromethane. After 30 min of reaction at room temperature, it is washed with acetonitrile and water for 2 min each and then filled with a gelling solution of 1.5%T + 5%C², allowed to react at $50\text{--}70^\circ\text{C}$ for 30 min. This capillary is washed with water for 2 min and dried by inrush of air for 1 min.

2.3.2. Filling

Step 1: Into the mixing well (Fig. 1A-3), a volume (V_0) of buffer (pH 7.8–8.4) containing TEMED and APS is filled and a $V_{F(0)}$ volume of

it is allowed to flow into the tunnel till the mark 1T . The left buffer is then mixed with a volume [$V_{A(1)}$] of a concentrated gelling solution. Following the buffer, the mixed solution is filled into the tunnel till the buffer reaches the mark 2T . The left gelling solution is then diluted with the buffer and filled into the tunnel step by step until the buffer reaches the mark $^{\text{end}}T$ which is at the position including the mechanically untouchable volume (V_{un}) in between the valve and the well so that the final solution can flow into the tunnel. About 10 steps (1 cm per step) is required to fill a capillary with 20 steps of gelling solutions. The theoretical

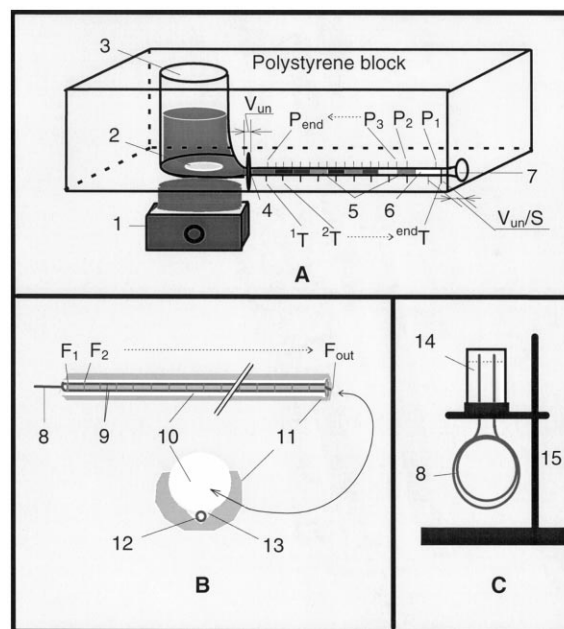


Fig. 1. A, Device for preparing gradient gelling solutions; B, a method for viewing amplification of capillaries; C, hanging polymerisation. (1) Magnetic stirrer; (2) stir bar; (3) mixing well; (4) valve for filling control; (5) pre-gradient gelling solutions ready for filling a capillary; (6) buffer; (7) $\phi 2\text{--}3 \text{ mm} \times 11\text{--}12 \text{ cm}$ tunnel; (8) capillary; (9) amplified view of the capillary; (10) glass rod; (11) recessed plastic casing; (12) capillary outlet; (13) guide slot; (14) sealed vial with ice-cooled water; (15) Shelf. V_{un} , untouchable volume; S , cross sectional area; $P_1, P_2, \dots, P_{\text{end}}$, capillary plugging positions marked at 0.3–0.5 cm from $^{\text{end}}T$ and 2–2.5 cm from P_1 and then at every 0.5 cm; $^1T, ^2T, \dots, ^{\text{end}}T$, position symbols for filling the tunnel marked at every 1 cm except for $^{\text{end}}T$ which includes $V_{\text{un}}/S \approx 1$ cm; $F_1, F_2, \dots, F_{\text{out}}$, capillary filling symbols marked at 12–13 cm from the tip and then at every 1.5 cm.

² By gelling solution is meant the monomer solution added with TEMED and APS. The concentration of a gelling solution is given by $x\%T + y\%C$ where x is the grams of acrylamide and BIS in 100 ml solution and y the grams of BIS per 100 g monomers.

concentrations in the middle part of step i (C_i) and at the boundary ($C_{(i+1)/i}$) are

$$C_{(i+1)/i} = (C_{i+1} + C_i)/2$$

$$C_{i+1} = \frac{C_i[V_i - V_{F(i)}] + V_{A(i+1)}C_{A(i+1)}}{V_i - V_{F(i)} + V_{A(i+1)}}$$

$$i = 0, 1, 2, 3, \dots$$

$$V_i = V_0 - V_{un} + \sum_1^i V_{A(i)} - \sum_0^{i-1} V_{F(i)} \quad (1)$$

where $V_{A(i)}$ is the newly added volume of the solution at step i and $C_{A(i)}$ its concentration ($= 0$ except for $i = 1$), $V_{F(i)}$ is the volume filled into the tunnel at step i . C_i has thus a value sequence of $C_0 (= 0) < C_1 > C_2 > C_3 > \dots > C_{end}$. By this equation we can see that non-linear gradients will be resulted if $V_{A(i)}$ is kept constant. To produce linear gradient [$(C_{i+1} - C_i) = \text{constant}$], $V_{A(i)}$ should be changed at different steps which can be calculated by re-writing the Eq. (1) as follows:

$$V_{A(i+1)} = \frac{C_{i+1} - C_i}{C_{A(i+1)} - C_{i+1}} (V_i - V_{F(i)}) \quad (2)$$

In the case of continuous dilution and filling, the concentration of the mixed gelling solution at time t [$C(t)$] is given by

$$C(t) = C_{A(1)} V_{A(1)} \left\{ V_0 - V_{un} + \int [v_A(t) - v_F(t)] dt \right\} \quad (3)$$

where $v_A(t)$ is the volume flow rate of the solution for dilution at time t and $v_F(t)$ that of the mixed gelling solution flowing into the tunnel. $C(t)$ can be transformed to the concentration distribution along the tunnel [$C(L)$] through $L = \int v_F(t) dt / S$, where S is the cross sectional area of the tunnel.

Step 2: The coated capillary is marked at the required filling positions and mounted in a glass rod amplifying device (Fig. 1B). It (F_1 end) is then horizontally inserted in the tunnel at the position P_1 (Fig. 1A). As soon as the buffer flows, by surface tension, to mark F_1 , the capillary is further plugged in and stopped at P_2 until the buffer reaches F_2 . Repeatedly, the capillary

will pass through all the marked positions till it meets the P_{end} . When the buffer inside the capillary moves to F_{out} , the capillary is quickly pulled out and both its ends are plugged into a sealed glass vial (Beckman, 358807), followed by injection of about 4 ml of ice-cooled water into the vial to form a slight pressure and to cool the pressurised ends [5]. The capillary is hung (Fig. 1C) for at least 5 h to accomplish the polymerisation.

After polymerisation, the capillary is pulled out and a detection window is created at 2 cm away from the gel-buffer boundary (at the F_{out} end) by manually removing the capillary overcoating with a scalpel. The capillary is then mounted in Beckman P/ACE system and equilibrated with a running buffer at -200 V cm^{-1} and 35°C for > 30 min. The equilibrated capillary is stored at room temperature for 2–3 days with both its ends dipped into the running buffer. This storage increases the stability and separation efficiency of the gels. The reasons are not clear but we suggest that this is due to the over-bending or over coiling of the capillaries inside the cartridges. The gels should thus be re-shaped which is not easy and may take a long time.

All the gel-filled capillaries are described by $X \mu\text{m ID} \times L_g(x_1 \rightarrow x_2\%T + 5\%C) + 2/L$ cm where X is their inner diameter, L_g is the gel length located at 2 cm before the detection window and L is the total tube length; $x_1 \rightarrow x_2\%T + 5\%C$ shows the gradient range and migration direction.

2.4. Electrophoresis

All separation was performed at 25°C using the Beckman P/ACE system (model 2050) controlled by a computer with the System Gold software. The electric field strength is $+180 \text{ V cm}^{-1}$ for the separation of poly(Lys) $_i$ ($i = 38/126$) and -200 V cm^{-1} for the separation of poly(GlcNAc-Mur). Poly(Lys) $_i$ is introduced into the gel end at $+5 \text{ kV}$ for seconds and poly(GlcNAc-Mur) at -5 kV cm^{-1} for 15 s. The separated bands were detected at 200 nm and 1 s rise-time while the peak data acquired at 1 Hz.

3. Results and Discussion

3.1. Control of polymerisation speed and direction

It is needed to prevent the gelling solutions from polymerisation before filling is finished. A glass tube is not suitable for preparing the pre-gradient gelling solutions because the polymerisation sometimes starts just in the half way of filling. By lowering the amount of TEMED and/or APS is a way to decrease the speed but not preferred: For gels below 10%T, the polymerisation may not happen at all or the resulted gels may be unstable if TEMED and APS are < 0.02%. Another way is to cool the gelling solutions in an ice-bath. This method may also results in unstable or irreproducible capillaries.

Interestingly, the polymerisation can effectively be inhibited by preparing the gelling solutions in teflon or polystyrene plastic tubes and can be recovered by transferring the solutions into the glass vials. Although the mechanism is not clear (it seems that some plastics prevent the radicals from passing to acrylamide), a polystyrene filling device is used to control the polymerisation speed. This transparent plastic allows an easy observation of the solution flow.

The formation of voids in polyacrylamide gels due to their volumetric losses during polymerisation is a common but serious problem, this problem will become even more serious in the preparation of concentrated gels and when the gels are immobilised along the entire capillary wall [7]. The voids can be eliminated by programmed initiation of the polymerisation so that the volumetric losses in the polymerised parts of can be compensated for by attracting the not-yet-polymerised solutions. A successful way reported to introduce APS and TEMED into a monomer solution-filled capillary by isotachopheresis [10]. It is also theoretically possible to control the polymerisation direction by sequentially warming or cooling the filled capillaries. We suggest here a fast way, that is, using gradient TEMED and/or APS. This is impossible with a normal sucking or pressing filling method but TsF allows a regulation of TEMED and APS concentrations at each mixing step.

Gradient gels themselves will form in a direction from high to low concentrations at a given amount of APS and TEMED. This can be enhanced by adding more TEMED or APS to the concentrated solutions and can be reversed if we change the gradient direction of APS or TEMED. This control, associated with cooling and pressurising the tube end, was shown to be effective and fast. The pressure assists the solution flowing to the polymerised part and the cooling prevent the tubing ends from polymerisation before other parts.

As a result, void-free capillaries can be prepared with a full success for gels below 13% + 5%C, independent of the gel immobilisation methods and buffers used for the preparation of the gelling solutions, both of which have shown to influence on the formation of voids [7]. The preparation success rate will be reduced but still higher than 80% for the gels above 15%T but < 25%T (higher gels were not tried). The rate can be improved up to 95% if the gels are not immobilised but stabilised by stoppers [5,6]

3.2. Reproducibility

A lot of factors which influence the reproducibility of a homogeneous gel-filled capillary will also affect the quality of the gradient gel-filled capillaries. However, the most special one for the gradients gels is their locations as mentioned at the beginning.

Using TsF, the gradient gels can quite easily be located at the required positions in any size of capillaries (< 25 μm ID), with a deviation < 3%. By passing a monomer solution-filled capillary (without over-coating) through a UV-detector (model 166 from Beckman) at 2 mm s⁻¹ [6], an absorption curve parallel to the gradients or concentrations can be measured at 285 nm. The gradient location deviation (GLD) at different parts of the capillary can thus be defined and calculated by

$$\text{GLD (\%)} = 100 [A(L)_{\text{grad}} - A_{\text{homo}}]/A_{\text{homo}} \quad (4)$$

where $A(L)_{\text{grad}}$ is the absorbency of the gradient gel-filled capillary at position L and A_{homo}

that of an identically sized capillary filled with only one monomer solution at the expected concentration. The measurements were performed with five capillaries at five positions per capillary. The overall GLD was 2.53%

The location deviation mainly depends on the tunnel size, the capillary plugging process and the following of the solution flow inside the capillaries. The tunnel should be wide enough for plugging a capillary without seriously disturbing the pre-gradient solutions but it should also be sufficiently narrow to keep the solutions stable. According to our experience, a $\phi 2\text{--}3$ mm tunnel is suitable for plugging a $375\ \mu\text{m}$ OD capillary. If a wider tunnel is used, the solutions can also be maintained by raising the tunnel outlet up. The capillary should gently be plugged into the tunnel along its one side. To correctly follow the solution flow, the observation field of the capillary is suggested to be amplified. This can easily be achieved with a glass rod (Fig. 1B).

3.3. Stability

The capillaries prepared by TsF have been shown to be stable. In the separation of polylysines, they can normally be used for about 400 injections (ca 45 min per run, including the reconditioning time to be discussed below) even at pH 4.7. The total running time is then 300 h (~ 1 month). By checking 10 capillaries, we found that there was a capillary which was used for only 1 week (ca. 100 injections) but there was also a capillary used for 1.5 months (ca. 800 injections). Most of the capillaries were injected for 400–500 times, with quite an acceptable reproducibility (Fig. 2). At pH 7.7–8.4, the capillaries can be used for more than 2 months as demonstrated in the separation of poly(GlcNAc-Mur). This is due to the great reduction of the gel hydrolysis.

Importantly, to run the capillaries for a longer time it is needed to recondition them every 5–10 separations, at an electric field countering that for separation. The reconditioning may take as long a time as the 5–10 runs but can be reduced to < 1 h if the applied electric field strength is increased to $\pm 400\ \text{V cm}^{-1}$ or higher.

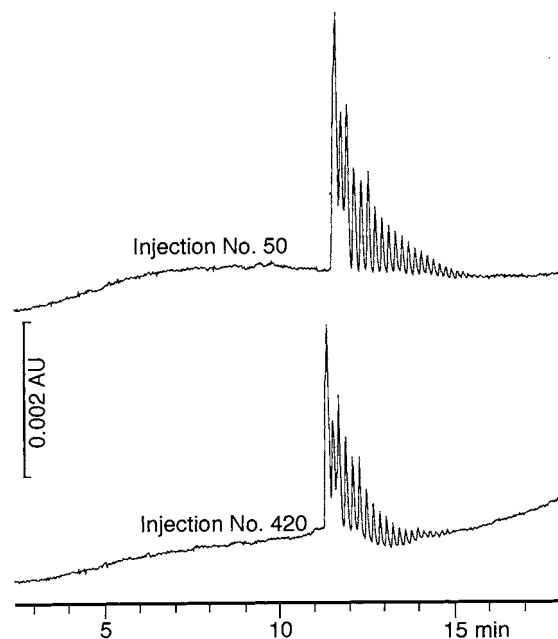


Fig. 2. Reproducible CGGE of poly(Lys)₃₈ at $0.05\ \text{mg ml}^{-1}$. Capillary: $75\ \mu\text{m ID} \times 30\ \text{cm}$ ($5 \rightarrow 10.1\%T + 5\%C$) + $2/38.8\ \text{cm}$; buffer: $20\ \text{mmol l}^{-1}\ \text{NaH}_2\text{PO}_4$ in $10\ \text{mmol l}^{-1}$ sodium acetate/acetic acid at pH 4.71; injection: $+5\ \text{kV}$ for 1 s.

3.4. Detection sensitivity and separation efficiency

Detection is another serious problem in using the CGE and CGGE as well. Nevertheless, it can at least partially be overcome with the low background capillaries: They allow the use of any available UV wave-length for sensitive detection. As a result, the poly(Lys)₃₈ can be detected at 200 nm at a concentration as low as $0.05\ \text{mg ml}^{-1}$, requiring only 1 s of injection (Fig. 2). In the case of common gel-filled capillaries, the most sensitive detection wave-length is 220 nm and the sample should be injected for > 10 s at a concentration of $50\text{--}100\ \text{mg ml}^{-1}$ [7,10]. The detection sensitivity is thus improved by the new capillaries for at least $50 \times 10 / 0.05 \times 1 = 10^4$ -fold. This may be an extreme case. For more complicated samples such as poly(Lys)₁₂₆, a suitable concentration is $0.5\ \text{mg ml}^{-1}$ (see Fig. 3). The sensitivity improved is thus 10^3 -fold. With such a sensitivity, direct detection of unlabelled poly(GlcNAc-Mur) can be achieved as shown in Fig. 4. This polysaccharides has no reducing end and we have not yet found out an acceptable labelling method.

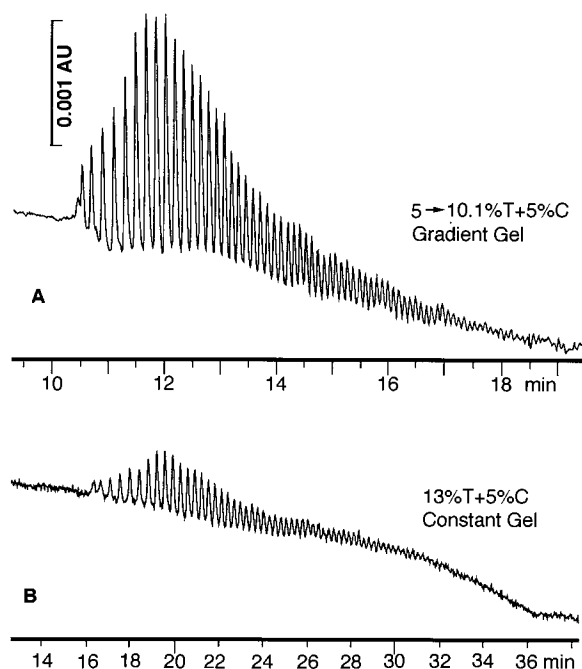


Fig. 3. Comparison of CGGE (A) with CGE (B) using 0.5 mg ml^{-1} poly(Lys)₁₂₆ as a testing sample. Capillary: $50 \text{ }\mu\text{m ID} \times 30 \text{ cm}$ (gels) + $2/38.8 \text{ cm}$; buffer: $20 \text{ mmol l}^{-1} \text{ NaH}_2\text{PO}_4$ in 10 mmol l^{-1} sodium acetate/acetic acid at pH 4.71; injection: + 5 kV for 2 s.

Fig. 3 shows that gradient gel-filled capillaries yield higher detection sensitivity (> 2 -fold) than homogeneous ones although their background is reduced using the same way. There might be different reasons responsible for this phenomenon but the stacking effect generated by the gradient gels is clearly the most important one. We can predict that this effect will increase not only the detection sensitivity but also the separation effi-

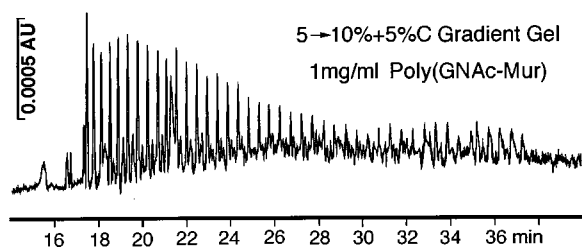


Fig. 4. CGGE of polysaccharides from the sacculi of *E. coli*. Capillary: $75 \text{ }\mu\text{m ID} \times 28 \text{ cm}$ (gradient gel) + $2/36.8 \text{ cm}$; buffer: 100 mol l^{-1} Tris and 250 mol l^{-1} boric acid.

ciency. In other words, if the efficiency is maintained, CGGE should be faster than CGE. This can also be seen from Fig. 3: About 1-fold improvement of the running speed can be achieved by CGGE without reducing the solution. More interestingly, the very complicated biological polysaccharides can be finely be separated at a fairly low concentration of gradient gels (Fig. 4) It should be noted that, to obtain a fine separation of these substances by CGGE, the running conditions should be optimised which will be discussed elsewhere.

4. Conclusion

TsF is an easy method for the preparation of gradient gel-filled capillaries, requiring fairly small volume of gelling solutions ($< 3 \text{ ml}$) and without the capillary transferring problem. It can in principle be used for filling any size of capillaries with different materials, including polyacrylamide gradient and non-gradient gels, non-polyacrylamide gels and non-gels (such as buffer, radicals, or additives). Automatic operation of TsF is also possible, which is being in exploration.

CGGE with low back ground gradient gel-filled capillaries is surely superior to CGE with both of the common and low background capillaries in some separations but further investigations are required to make a conclusion. Increasing the detection sensitivity of CGE and CGGE by lowering the background of the capillaries is a simple and reliable method but the detected base-lines may drift positively or negatively, depending on wave-length, buffers and samples which has already been discussed in our previous work [5].

Acknowledgements

We would like to thank for the financial supports of this project from the Natural Science Foundation of China, the Chinese National Council of Education, the Chinese National Division of Personnel, the Director Funds of the Institute of Chemistry, the President funds and the Academic funds of the Chinese Academy of

Sciences, and the Chinese National Council of Sciences. The kind donation of the Beckman P/ACE system from Alexander von Humboldt Foundation is specially acknowledged.

References

- [1] D.E. Hames, D. Rickwood (Eds.), *Gel Electrophoresis of Proteins*, IRL Press, Washington D.C., 1983.
- [2] A.R. Oller, W.G. Thilly, *J. Mol. Biol.* 228 (1992) 813–826.
- [3] S.G. Fischer, L.S. Lerman, *Proc. Nat. Acad. Sci. USA* 80 (1983) 1579–1583.
- [4] S. Hjerten, *J. Chromatogr.* 270 (1983) 1–6.
- [5] Y. Chien, J.-V. Holtje, U. Schwarz, *J. Chromatogr. A* 685 (1994) 121–129.
- [6] Y. Chen, F.-L. Wang, U. Schwarz, *J. Chromatogr. A*, submitted in Oct. 1996.
- [7] Y. Chen, J.-V. Holtje, U. Schwarz, *J. Chromatogr. A* 680 (1994) 63–71.
- [8] Y. Chen, J.-V. Holtje, U. Schwarz, *J. Chromatogr. A* 700 (1995) 35–42.
- [9] H. Harz, K. Burgdorf, J.-V. Holtje, *Anal. Biochem.* 190 (1990) 120–128.
- [10] V. Dolnik, M.V. Novotny, *Anal. Chem.* 65 (1993) 563–567.
- [11] J. Liu, O. Shirota, M. Novotny, *Anal. Chem.* 64 (1992) 973–975.
- [12] J. Liu, V. Dolnik, Y.-Z. Hsieh, M. Novotny, *Anal. Chem.* 64 (1992) 1328–1336.

Mannitol influence on the separation of DNA fragments by capillary electrophoresis in entangled polymer solutions¹

Futian Han, Jun Xue, Bingcheng Lin *

Dalian Institute of Chemical Physics, Chinese Academy of Sciences, 457 Zhongshan Road, Dalian 116023, People's Republic of China

Received 19 February 1997; received in revised form 16 July 1997; accepted 17 July 1997

Abstract

A new kind of sieving matrix is presented in this paper to allow satisfactory separation of DNA fragments in a relatively low viscous solution. When a certain amount of mannitol was added to cellulose solution not concentrated enough to separate PGEM-3Zf(+) /HaeIII standards well, a polymer solution with low viscosity but with very good separation effects was obtained. The separation result of this sieving buffer was comparable with those using highly concentrated cellulose solutions. The sieving ability of solutions with different cellulose concentrations and different amounts of mannitol has been investigated. It was proved that 0.5% was the minimum hydroxypropylmethylcellulose (HPMC) concentration that could be used to separate DNA fragments satisfactorily. HPMC solutions with a concentration of less than 0.5% could not separate the standard DNA fragments even in the presence of mannitol. It was found that 6% was the optimized mannitol concentration because either more or less mannitol will lead a decrease of resolution. The principle of the positive influence of mannitol has also been discussed. © 1998 Elsevier Science B.V. All rights reserved.

Keywords: Capillary electrophoresis; DNA separation; Mannitol

1. Introduction

Capillary electrophoresis (CE) has thrown a new light on the separation of biomolecules such as protein, peptides and nucleic acids since it

came into being more than a decade ago. High performance, high resolution, automation and versatility of CE seem to be the main advantages over traditional slab electrophoresis, which is labor intensive and time consuming. It has found widespread application in the analysis and separation of DNA fragments, which is very important in forensic sciences, clinical diagnosis, biological researches, etc. [1–6]. Polymerase chain reaction (PCR) is a very strong tool which can amplify specific genes or gene fragments conveniently and efficiently. PCR coupled with CE plays a more

* Corresponding author. Fax: +86 411 3622302; e-mail: Linbc@dlut.edu.cn

¹ Presented at the First Asia-Pacific International Symposium on Capillary Electrophoresis, and other Nano- and Microscale Analytical Techniques, held in Singapore, December 17–20, 1996.

and more important role in DNA HPA (heteroduplex polymorphism analysis) [7], DNA STR (short tandem repeats) [8], DNA VNTR (variable number of tandem repeats) [9], DNA RFLP (restriction fragment length polymorphism) [10] and DNA SSCP (single strand conformation polymorphism) [11–13] analysis.

The mobility of DNA fragments is independent of length because the charge to mass ratio of DNA fragments with different lengths is almost the same. Introducing a sieving mechanism into CE seems very useful because it is impossible to separate DNA fragments using capillary free zone electrophoresis. Two kinds of sieving media are employed in capillary electrophoresis: gels and entangled polymer solutions. They are called capillary gel electrophoresis (CGE) and entangled solution capillary electrophoresis (ESCE), respectively. It is difficult to prepare a gel-filled capillary because it is very sensitive to bubble forming. Gel capillaries have a very limited lifetime since the gel is easily destroyed by high current densities and Joule heating. Great care must be taken while preparing or using gel capillaries [14]. The reproducibility of CGE is not satisfactory and is not suitable for routine use. Researchers prefer to use entangled polymer solutions as sieving media because they can be replaced after each run and therefore are much easier to operate [15,16].

The viscosity of entangled polymer solutions are always very high in order to obtain satisfactory separation of DNA fragments in PCR-based CE studies. Those DNA fragments are always no more than several hundred base pairs (bp) in length; hence, they are not able to be separated in dilute polymer solutions. It is difficult to pump those high viscous solutions into or out of the capillary. Cheng and coworkers [17] have found that glycerol can enhance the separation of DNA fragments in cellulose derivative solutions. Another additive is presented in this paper that can enhance the separation of DNA fragments significantly. When mannitol was used as additive to the HPMC solution, a less viscous polymer solution was obtained. The sieving effect was very good.

2. Experimental

2.1. Apparatus

All the ESCE experiments were performed with the Bio-Focus 3000™ capillary electrophoresis system (Bio-Rad Company, Hercules, CA, USA). This capillary electrophoresis system was equipped with a UV high-speed scanning detector. The data were collected and analyzed with a CE3000 software at 260 nm. The capillaries (30 cm × 50 μm ID with the effective length of 25.5 cm) used in this study were internally coated with polyacrylamide using our coating process.

2.2. Chemicals

HPMC (viscosity of 2% aqueous solution is 4000 cp. at 25°C) and γ -methacryloxypropyltrimethoxysilane (MAPS) were purchased from Sigma (St. Louis, MO, USA). Acrylamide, ammonium persulfate and *N,N,N',N'*-tetramethylethylene diamine (TEMED) were obtained from Bio-Rad Labs (Hercules, CA, USA). Tris(hydroxymethyl) aminomethane, mannitol, boric acid and EDTANa₂ (sodium ethylene diamine tetracetate) were obtained domestically. DNA standard sample PGEM-3Zf(+)/HaeIII was purchased from the Sino-American Biotechnology Company (Shanghai, People's Republic of China). The sample was diluted with the storage buffer (10 mM Tris-HCl, 10 mM NaCl, 1 mM EDTA, pH = 7.5) and kept at -20°C until use. The concentration of the sample was about 20 μg ml⁻¹.

2.3. Coating of the capillary inner wall

The uncoated capillary was purchased from Yongnian Optical Factory (Yongnian, Heibei, China). The capillaries were first washed with 1 N NaOH for 2 h and then rinsed with water for a few minutes. Secondly, the capillaries were rinsed with 1 N HCl for another 2 h followed by water rinsing for 10 min. The capillaries thus treated were then washed with methanol for 10 min. After that, the capillaries were filled with MAPS and methanol mixture, then the two ends of the capil-

larities were sealed with gel and incubated at room temperature for several hours. The capillaries were washed with methanol and water for several minutes, respectively, and then were ready for coating. Pump the reaction reagent (5% acrylamide, 0.6% TEMED and 3% ammonium persulfate) into the capillaries and keep for 2 h at room temperature. Then the reaction reagent was washed out with water and the capillaries were dried with nitrogen gas. The capillaries thus treated can be used for at least 100 runs without any decrease in efficiency.

2.4. Preparation of the polymer solutions

The carrier electrolyte used in this study was TBE (100 mM Tris–borate, 2 mM EDTA, pH = 8.3) buffer that was frequently used by other researchers. HPMC solutions at concentrations of 0, 0.2, 0.3, 0.4, 0.5, 0.8, 1.0 and 1.2% (w/v) were prepared using the above buffer. Add the HPMC powder slowly into the container with TBE buffer while stirring and then keep the container at 4°C overnight until all the powder was solved. Mannitol at concentrations of 2, 4, 6 and 8% (w/v) was added to the above HPMC solutions (except the 1.2% HPMC solution). All the solutions were prepared using double-distilled water and then filtered with 0.45 µm nylon membrane. Buffers thus prepared were kept at 4°C for storage.

2.5. Entangled solution capillary electrophoresis

The capillary was rinsed with water for 2 min first and then with sieving buffer for another 2 min. Before injection, the inlet end of the capillary was dipped two times in a water container in order to clean the outside wall. This washing process can prevent the sample from contamination by the viscous buffer solution. The sample was injected at 10 kV for 15 s. The running voltage was 4 kV from negative to positive. While running, the capillary was kept at 30°C by liquid cooling and the sample vials were also kept at 30°C by a computerized device.

3. Results and discussion

HPMC at concentrations of 0, 0.2, 0.3, 0.4, 0.5, 0.8, 1.0 and 1.2% was used as sieving buffer to separate PGEM-3Zf(+)/HaeIII standards first. HPMC solutions with different amounts of mannitol were then used to separate the same sample in order to investigate the influence of mannitol on the separation. From the results, a significant enhancement of separation was observed when adding mannitol to HPMC solutions of any investigated concentration, but there was no good separation of all those fragments when the HPMC concentration was below 0.5% (data not shown). This indicates that 0.5% is the minimum HPMC concentration that can form a network in the solution, i.e., the threshold concentration. The electropherograms using 0.5% HPMC containing 0, 2, 4, 6 and 8% mannitol were presented here (Fig. 1). It can be seen from Fig. 1 that the smaller fragments were gradually separated while the concentration of mannitol was increased. The separation of larger fragments was also enhanced. Fig. 1(d) and (e) showed that all the fragments are resolved (11 and 18 bp fragments are undetectable because the concentration of these fragments was not high enough). As for solutions with concentration higher than 0.5%, the mannitol amount added to the buffer in order to obtain complete separation became smaller. For 0.8 and 1.0% HPMC solutions, only 2% mannitol was needed, and for HPMC solutions with concentration greater than 1.2%, it was not necessary to add mannitol to the buffer.

Although HPMC solutions at concentrations of 1.2% or more can resolve the separation satisfactorily without the presence of mannitol, this is difficult to achieve because of the high viscosity. High pressure or a long time must be needed to pump the sieving buffer into or out of the capillary. Adding mannitol to HPMC solution makes it possible to separate DNA fragments using a lower concentration of HPMC solution. The viscosity data of the solutions are not available in this paper but can be evaluated through the fluidity of those buffers. The viscosity of two kinds of buffers (0.5% HPMC + 6% mannitol and 1.2% HPMC without mannitol) was evaluated by an

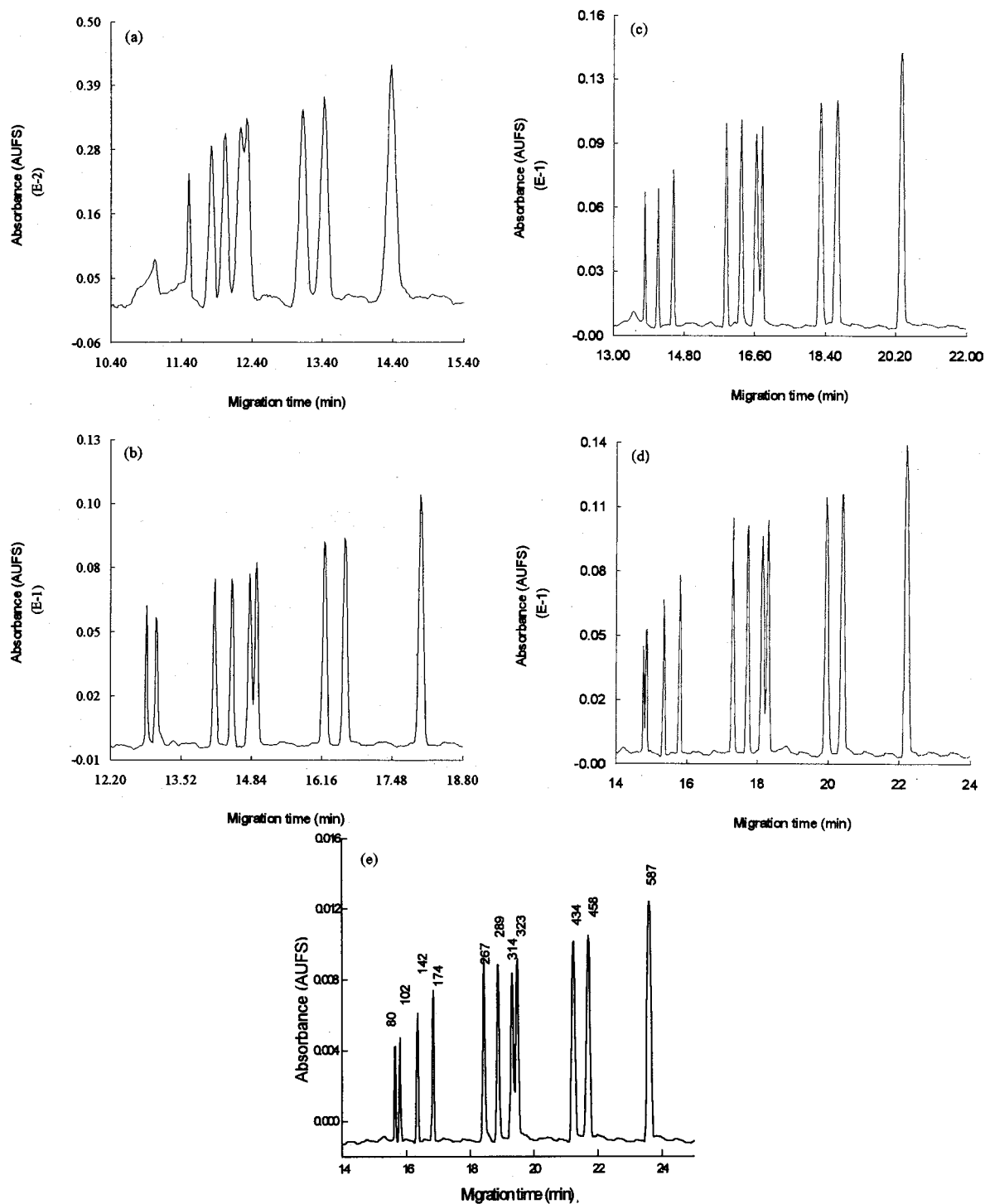


Fig. 1. Electropherograms of PGEM-3Zf(+)/HaeIII standard fragments in 0.5% HPMC sieving buffer at different mannitol concentrations: (a) 0% mannitol, (b) 2% mannitol, (c) 4% mannitol, (d) 6% mannitol, and (e) 8% mannitol. Injection: 10 kV \times 15 s; running at 4 kV from negative to positive. Other conditions are as listed in Section 2.

indirect method. It took only 4 s for the first buffer to fill a 30 cm × 50 μm ID capillary under a pressure of 3.1 MPa. For the latter buffer, the time is 10 s. It is obvious that the viscosity of the solutions decreases with decreasing HPMC concentration. Although adding mannitol to these buffers raises the viscosity slightly, they are still much easier to work with than those buffers with a high HPMC concentration.

The resolution of the 314/323 fragment pair was calculated using a traditional chromatographic equation (Eq. (1)). Where t_2 and t_1 are the migration time of the two fragments, and $W_{1,0.5}$ and $W_{2,0.5}$ are the halfwidth of the two peaks:

$$R = \frac{1.18(t_2 - t_1)}{W_{1,0.5} + W_{2,0.5}} \quad (1)$$

Fig. 2 demonstrates the change of resolution according to cellulose concentration and mannitol concentration. It may be noticed that the resolution increased when the concentration of HPMC changes from 0.2 to 1.0%, as may be expected. The pore size of the network decreases and then influences the resolution. The resolution also goes upward when the mannitol concentration changes from 0 to 6% and then decreases when the mannitol concentration is 8%.

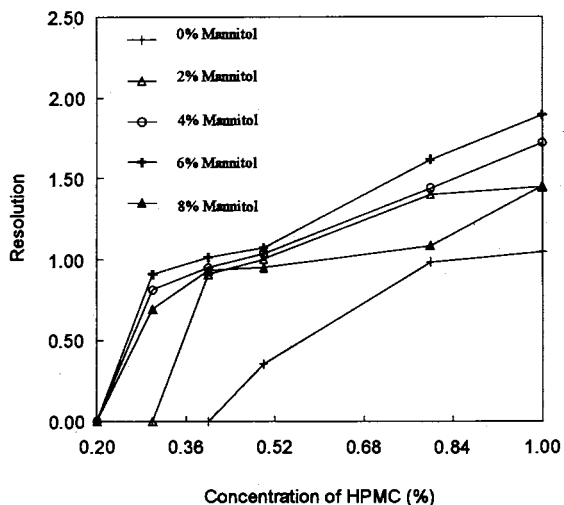


Fig. 2. Plot of resolution of 314/323 bp fragments vs. HPMC concentration (%) at different mannitol concentrations (%).

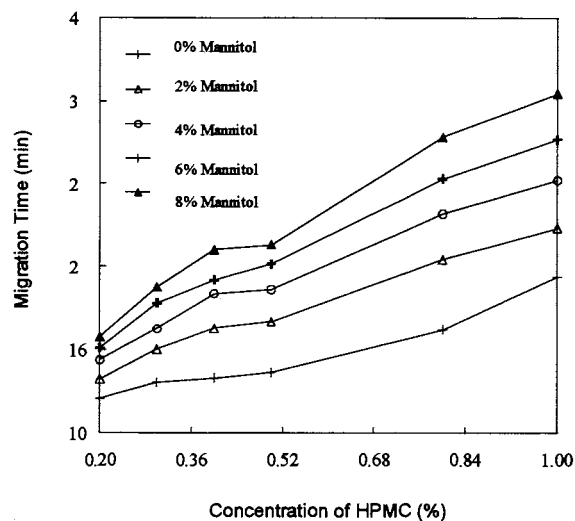


Fig. 3. Plot of migration time (min) of the 587 bp fragment vs. HPMC concentration (%) at different mannitol concentrations (%).

The mobility of the DNA fragments decreases when adding mannitol to the HPMC solution since the migration time becomes longer. The greater the concentration of mannitol, the longer the migration time. The plot of the migration time versus mannitol concentration is almost linear, which means that the mobility of the DNA fragment is inversely proportional to the mannitol concentration. This phenomenon indicates that mannitol interacts with HPMC and the pore size becomes smaller and, as a result, the obstruction becomes larger. From the plot of migration time versus HPMC concentration (Fig. 3), we can say that the migration time increases with increasing HPMC concentration. This is also due to the decrease of the pore size of the network with increasing HPMC concentration.

The migration time versus DNA fragment length in 0.5% HPMC + 2, 4, 6 and 8% mannitol gave perfect linear relationships. The linear coefficients were more than 0.9991. This phenomenon indicates that we can use a (CE-based) calibrating method to calculate the length of a DNA fragment such as PCR products more precisely than using the traditional slab gel electrophoresis method.

Fig. 4 is the Ferguson plot that illustrates the sieving effect of HPMC solutions with 6% mannitol additive. All the curves of the four selected fragments are similar in shape. This result implies that under certain sieving matrix conditions, the sieving mechanism is the same for these fragments. This is the reason why the mobility of the DNA fragments are proportional to the fragment length. It may also be noticed that the curves are non-linear. This result does not match with what Schwartz and coworkers observed [18]. In the same work, they also found that there would still be certain separation of DNA fragments in CZE without any sieving media, which also did not match with our result. It was found in our experiments that when the HPMC concentration reaches zero, there was no separation of the DNA fragments.

The influence of mannitol on the separation of the DNA fragments may be due to the specific structure of this substance. The structure of mannitol is special because the hydroxyl groups are on the opposite side of the chain (Fig. 5). It is well known that boric acid can complex with carbohydrates to form tetraborate structure as shown in Eq. (2). This may also happen between mannitol, HPMC and boric acid. The tetrabo-

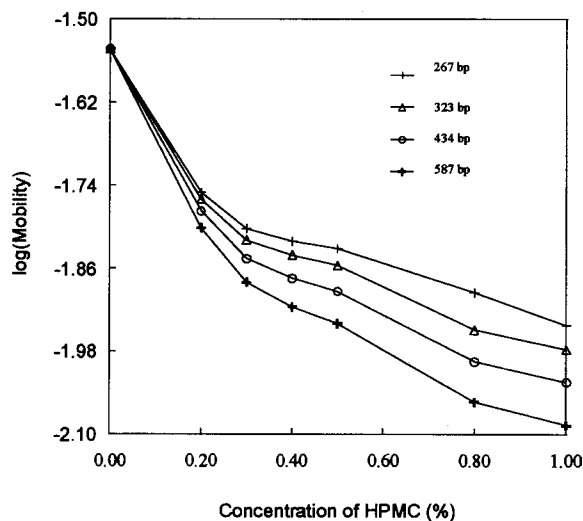


Fig. 4. Ferguson plot of 267, 323, 434 and 587 bp fragments in HPMC buffer with the existence of 6% mannitol.

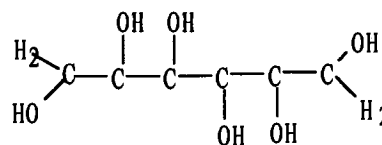
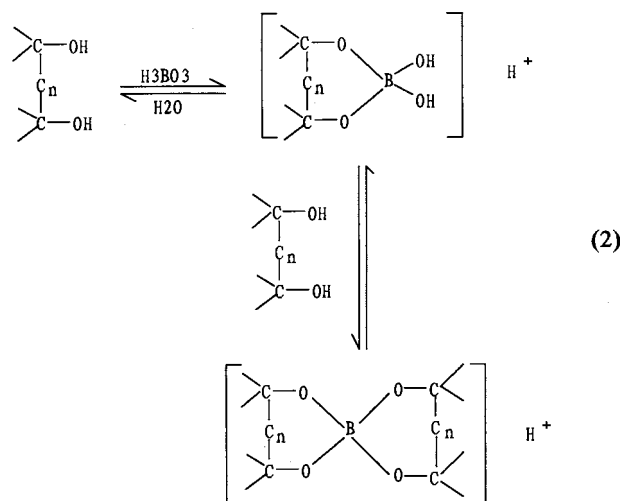


Fig. 5. Structure of mannitol.

rate structure can form a bridge between HPMC chains and then influence the dynamic sieving network in the entangled solution. Fig. 6 illustrates the linkage of HPMC chains through mannitol and tetraborate. Mannitol's influence on the separation is superior to that of glycerol because glycerol has fewer hydroxyl groups and cannot form the bridge chain.



The formation of tetraborate can be proved by the increasing of the running current when adding mannitol to the HPMC solution. The plot of running current versus mannitol concentration is shown in Fig. 7. This current increase results from the formation of the tetraborate structure. When the tetraborate structure is formed, a hydrogen ion is released, increasing the ionic strength of the buffer. When the mannitol concentration is above 6%, the current remains constant, which implies that the formation of tetraborate has reached equilibrium and that there are no more free polyhydroxy groups on the HPMC chains.

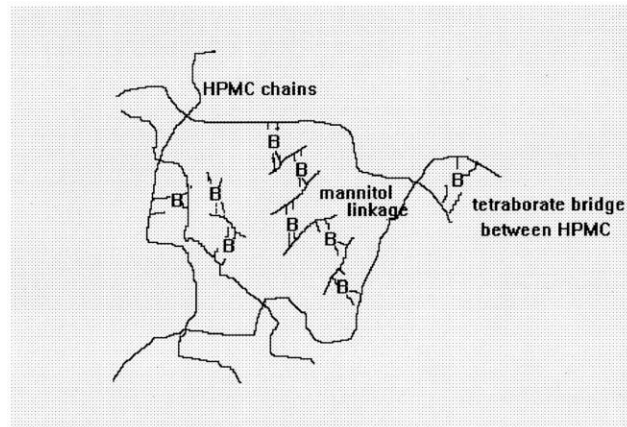


Fig. 6. Illustration of the entanglement of HPMC molecules and the tetraborate bridge through mannitol and HPMC chains.

This kind of linkage decreases or shapes the dynamic pore size of the polymer solution and results in the enhancement of the separation. When there is an overdose of mannitol, the resolution will be reduced because the saturation of mannitol prolongs the migration time, broadens the peak and then affects the resolution of 314/323. The electropherograms also show that the resolution of 80/102 is enhanced when the mannitol concentration is changed from 4 to 8%. No

resolution of these two smallest fragments is observed when the mannitol concentration is less than 4%.

4. Conclusion

Mannitol can interact with HPMC in the presence of boric acid to form a dynamic flexible network in the sieving matrix. A less concentrated HPMC solution is then able to be used as a sieving buffer to separate smaller DNA fragments. Because its viscosity is much lower than that of the more concentrated sieving matrix, it is much easier to operate. After examining a series of sieving buffers with different amounts of HPMC and mannitol, it can be concluded that 0.5% HPMC with 6% mannitol can give the optimum results. This kind of sieving matrix can be used to analyze PCR products conveniently and precisely. PCR CE may prove to be a potential method in clinical diagnosis, forensic analysis and molecular biology research.

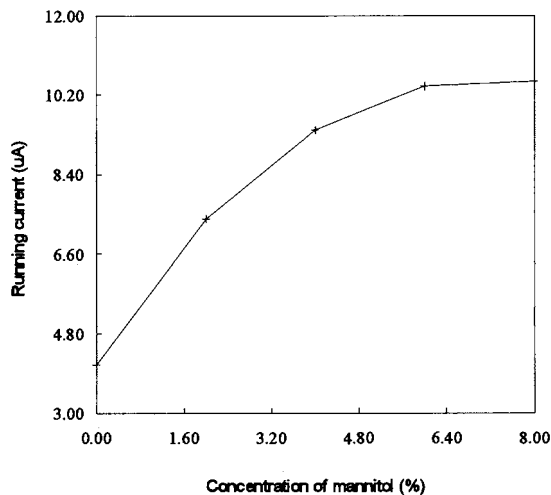


Fig. 7. Plot of running current at different mannitol concentrations (%).

Acknowledgements

The authors appreciate the research grant from the National Nature Science Foundation of China (NNSFC) and the support of Bio-Rad Labs (Hercules, CA, USA).

References

- [1] B.R. McCord, J.M. Jung, E.A. Holleran, J. Liquid Chromatogr. 16 (1993) 1963.
- [2] C. Gelfi, P.G. Righetti, V. Brancolini, L. Cremonesi, M. Ferrari, Clin. Chem. 40 (1994) 1603.
- [3] C. Heller, J. Chromatogr. A 698 (1995) 19.
- [4] J.P. Landers, Clin. Chem. 41 (1995) 495.
- [5] W. Thormann, S. Molteni, J. Caslavská, A. Schmutz, Electrophoresis 15 (1994) 3.
- [6] N. Zhang, E.S. Yeung, Anal. Chem. 68 (1996) 2927.
- [7] J. Cheng, T. Kasuga, K.R. Mitchelson, E.R.T. Lightly, N.D. Watson, W.J. Martin, D. Atkinson, J. Chromatogr. A 677 (1994) 169.
- [8] J.M. Butler, B.R. McCord, J.M. Jung, R.O. Allen, Bio-Techniques 17 (1994) 1062.
- [9] Y. Baba, R. Tomisaki, C. Sumita, I. Morimoto, S. Sugita, M. Tsuhako, T. Miki, T. Ogihara, Electrophoresis 16 (1995) 1437.
- [10] K.J. Ulfelder, H.E. Schwartz, J.M. Hall, F.J. Sunzeri, Anal. Biochem. 200 (1992) 260.
- [11] F. Barros, I. Munoz-Barus, M.V. Lareu, M.S. Rodriguez-Calvo, A. Carracedo, Electrophoresis 15 (1994) 566.
- [12] A.W.H.M. Kuypers, P.M.W. Willems, M.J. van der Schans, P.C.M. Linssen, H.M.C. Wessels, C.H.M.M. De Bruijn, F.M. Everaerts, E.J.B.M. Mensink, J. Chromatogr. Biomed. Applic. 621 (1993) 149.
- [13] M. Oto, T. Suehira, Y. Yuasa, Clin Chem. 41 (1995) 1787.
- [14] H. Yin, J.A. Lux, G. Schomburg, J. High Resolution Chromatogr. 13 (1990) 624.
- [15] Y. Baba, N. Ishimaru, K. Samata, M. Tsuhako, J. Chromatogr. A 653 (1993) 329.
- [16] Y.F. Pariat, J. Berka, D.N. Heiger, T. Schmitt, M. Vilenchik, A.S. Cohen, F. Foret, B.L. Karger, J. Chromatogr. A 652 (1993) 57.
- [17] J. Cheng, K.R. Mitchelson, Anal. Chem. 66 (1994) 4210.
- [18] H.E. Schwartz, K. Ulfelder, F.J. Sunzeri, M.P. Busch, R.G. Brownlee, J. Chromatogr. 559 (1991) 267.

Separation of enantiomers of drugs by capillary electrophoresis Part 8. β -Cyclodextrin as chiral solvating agent¹

B. Lin^a, X. Zhu^a, S. Wuerthner^b, U. Epperlein^b, B. Koppenhoefer^{b,*}

^a Institute of Chemical Physics, Dalian, People's Republic of China

^b Institute of Organic Chemistry, Eberhard-Karls-University Tübingen, Aur der Morgenstelle 18, 72076 Tübingen, Germany

Received 19 February 1997; received in revised form 6 August 1997; accepted 7 August 1997

Abstract

As part of a comprehensive screening program on the separation of chiral drugs by capillary zone electrophoresis, we have investigated the enantio-separation of 54 drug racemates with β -cyclodextrin as a chiral solvating agent (CSA), thus complementing previous studies on 34 drug racemates. Fourteen out of the 54 analytes investigated have been separated into the enantiomers, yielding an overall success rate of 24.4% for 86 drug racemates investigated in total. © 1998 Elsevier Science B.V. All rights reserved.

Keywords: Capillary electrophoresis; Chiral drugs; β -Cyclodextrin; Enantiomer separation

1. Introduction

Stimulated by the extensive development of enantio-specific analytical methods in the recent decades, the world market of single enantiomer drugs has grown to a multi-billion dollar business [1], paralleled by enantio-pure pesticides, flavors and fragrances [2]. For the approval of new chiral drugs, enantio-specific analyses are now demanded in all industrial countries [3].

Capillary electrophoresis (CE) bears the advantage of enantiomer determination directly from compound mixtures in aqueous solution [4,5]. According to our database Chirbase/CE (available from the authors on request), capillary zone electrophoresis (CZE) [6] and micellar electrokinetic chromatography (MEKC) [7,8] are most commonly used for enantiomer separation by CE, contributing to 72 and 20%, respectively, of articles published in this field. Other modes add to approximately 10% of all original research articles, including reports on several modes in the same document.

Apparently, Chirbase/CE provides a solid basis for further studies on structure–enantio-selectivity relationships. However, in view of the lack of

* Corresponding author. Tel.: +49 7071 2972037; fax: +49 7071 292037; e-mail: koppenhoefer@uni-tuebingen.de

¹ Presented at the First Asia-Pacific International Symposium on Capillary Electrophoresis, and other Nano- and Microscale Analytical Techniques, held in Singapore, December 17–20, 1996.

Table 1

Analytes separated into enantiomers upon addition of β -CD to the run buffer (phosphate, pH 2.5) in CE

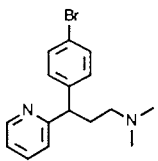
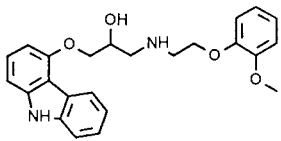
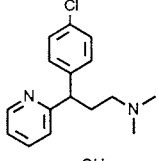
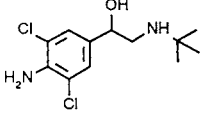
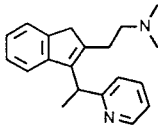
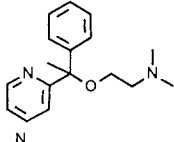
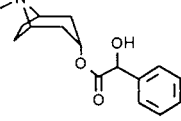
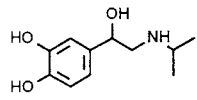
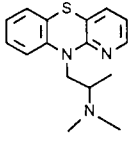
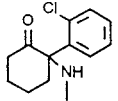
Analyte name	Analyte structure	tm1	tm2	tm2/tm1	Cond.
Bromphenamine		6.57	6.66	1.014	b
Carvedilol		13.43	13.81	1.028	c
Chlorphenamine		5.34	5.39	1.009	b
Clenbuterol		7.04	7.24	1.028	a
Dimetindene		5.29	5.47	1.030	d
Doxylamine		4.08	4.17	1.022	b
Homatropine		8.78	9.15	1.040	d
Isoprenaline		6.48	6.59	1.017	a
Isothipendyl		10.87	11.00	1.010	d
Ketamine		7.42	7.51	1.012	b

Table 1 (continued)

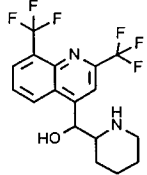
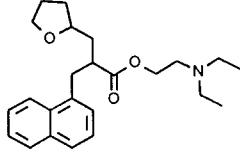
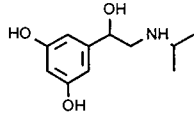
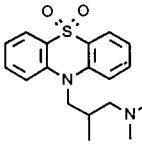
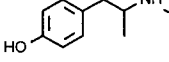
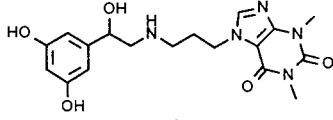
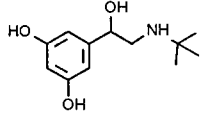
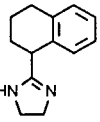
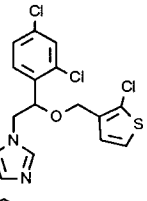
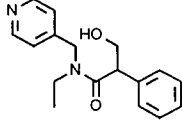
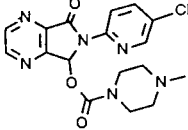
Analyte name	Analyte structure	tm1	tm2	tm2/tm1	Cond.
Mefloquine		7.44	7.58	1.020	d
Naftidrofuryl		12.71	12.84	1.010	d
Orciprenaline		7.94	8.25	1.039	a
Oxomemazine		10.77	10.97	1.020	d
Pholedrine		9.09	9.40	1.034	a
Reproterol		9.80	9.96	1.020	d
Terbutaline		8.72	9.20	1.055	a
Tetryzoline		6.99	7.27	1.040	d
Tioconazole		13.28	13.38	1.010	d
Tropicamide		9.65	10.09	1.046	b

Table 1 (continued)

Analyte name	Analyte structure	t_{m1}	t_{m2}	t_{m2}/t_{m1}	Cond.
Zopiclone		10.72	11.42	1.065	c

t_{m1} , Migration time of the first eluted enantiomer in 15 mmol l⁻¹ β -CD containing buffer; t_{m2} , migration time of the second eluted enantiomer in 15 mmol l⁻¹ β -CD containing buffer.

Cond.: Total column length (a) 29, (b) 30, (c) 36 and (d) 32 cm, respectively; effective length 4.5 cm shorter in each case. For other conditions, see Section 2.

consistent data for marketed drugs in the literature, a dedicated ‘German–Chinese Chiral Drug Screening Program’ [9] was started. Meanwhile, a huge amount of reliable data has been collected under constant experimental conditions for a large set of analytes and chiral solvating agents (CSAs) [10–13]. In this article, we report on hitherto unpublished results with β -cyclodextrin (β -CD) as the CSA, applied to CZE of 54 enantiomeric pairs of drugs.

2. Experimental

All experiments were carried out on a Bio-Focus 3000 automatic capillary electrophoresis system (Bio-Rad Laboratories, Hercules, CA, USA), equipped with a variable wavelength detector operated at 200 or 210 nm. Operating parameters were as follows: injection, 15 kV for 3 s; analysis, 15 kV + \rightarrow -; capillary temperature, 25°C. Fused silica capillaries (0.05 mm ID, 0.375 mm OD) were obtained from Yongnian Optical Conductive Fiber Plant (Yongnian, Province Hebei, People’s Republic of China). In the laboratory these were coated with polyacrylamide on the inner surface.

The plain run buffer contained 100 mmol l⁻¹ sodium dihydrogenphosphate and was adjusted to pH 2.5. β -Cyclodextrin was added to the plain buffer in concentrations of 15 mmol l⁻¹. The analytes were dissolved in the run buffer to give a sample concentration of 0.1 mg ml⁻¹.

β -Cyclodextrin was kindly donated by Wacker Chemie (Munich, Germany). The drug samples

were donated by a large number of German and international manufacturers. Internal purity standards of the manufacturers apply to all drug samples. All other chemicals were analytical grade.

3. Results and discussion

In order to facilitate later investigations on structure–enantio-selectivity relationships, attention was focussed on entries with one stereogenic center, mounting to a collection of 123 drug racemates. Two prerequisites, a solubility of 0.1 mg ml⁻¹ (0.2–0.6 mmol l⁻¹) in aqueous phosphate buffer at pH 2.5, and migration towards the cathode, were met by a subset of 86 drugs thereof. The results for 52 enantiomeric pairs presented in this article complement a previous report [12] on the screening of 34 drugs with β -CD as the CSA.

A report on the analytes separated is listed in Table 1, in alphabetic order. Based on the observation that the electro-osmotic flow (EOF) could be neglected, the ratio t_{m2}/t_{m1} of the migration times of the second and first eluted enantiomer, respectively, was taken for a measure of the degree of enantio-discrimination [12]. This definition bears the advantage over the peak resolution of being independent of most experimental parameters, such as solvent viscosity, capillary length, the electric field strength, etc.

Because of the limited solubility of β -CD in the run buffer, the concentration had to be kept at 15 mmol l⁻¹. A total of 12 (23%) drug racemates out of 52 analytes investigated could be resolved in

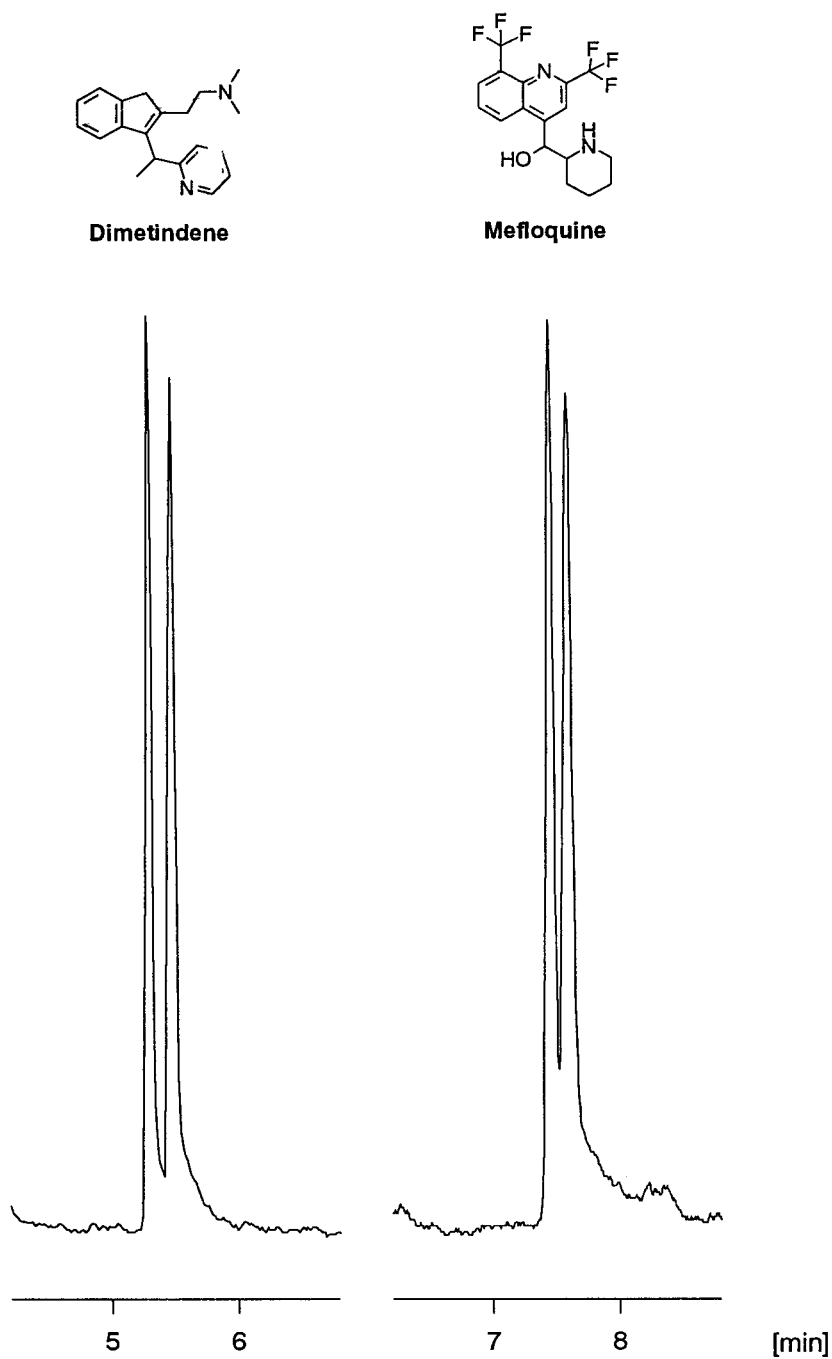


Fig. 1. Two representative electropherograms of drug enantiomers with 15 mmol l^{-1} β -CD; for other conditions see Section 2. Left panel, dimetindene with one stereogenic center; right panel, mefloquine with two stereogenic centers. The second peak pair may be caused by the minor diastereomer.

Table 2
Analytes not separated into enantiomers under the conditions of Table 1

Analyte name	t_{m1}	Cond.	Analyte name	t_{m1}	Cond.
Alimemazine	13.34	d	Meclozine	18.41	c
Alprenolol	10.21	a	Mepindolol	7.31	b
Amorolfine	13.20	b	Metaclazepam	9.73	d
Atropine	11.37	d	Metoprolol	12.27	a
Azelastine	13.81	c	Nicardipine	9.26	d
Baclofen	6.09	a	Norfenefrine	4.93	a
Bamethan	6.99	a	Ornidazole	9.88	a
Benproperine	12.86	d	Oxprenolol	7.07	a
Bisoprolol	14.05	a	Oxybutynin	12.89	b
Bupranolol	10.60	a	Phenoxybenzamine	8.86	b
Butamirate	14.16	a	Phenylpropanolamine	5.46	a
Carteolol	6.97	b	Procyclidine	16.68	a
Celiprolol	8.59	a	Promethazine	12.86	d
Chloroquine	3.37	b	Propranolol	9.03	b
Chlorphenoxamine	12.14	b	Sulpiride	6.81	b
Cicletanine	12.80	d	Synephrine	6.12	a
Clobutinol	12.74	a	Talinolol	13.60	b
Dipivefrine	15.47	a	Theodrenaline	8.73	d
Fendiline	13.27	d	Trihexyphenidyl	13.91	d
Gallopamil	10.20	b	Verapamil	12.43	b

t_{m1} , Migration time in 15 mmol l⁻¹ β -CD containing buffer.

Cond.: Total column length (a) 29, (b) 30, (c) 36 and (d) 32 cm, respectively; effective length 4.5 cm shorter in each case. For other conditions, see Section 2.

this straightforward approach. In addition, two drugs (isothipendyl and naftidrofuryl) could now be separated that had not been resolved previously [12], presumably because of insufficient peak resolution. The migration separation factor of isothipendyl and naftidrofuryl in our study is, however, still at the limit of the method, with migration separation factors of only 1.010 each.

Two representative examples for the many electropherograms obtained are shown in Fig. 1. A satisfactory migration separation factor, $\alpha_m > 1.015$, was attained for 10 analytes. For the less well separated enantiomeric pairs and even for some not yet resolved examples, there is still a chance of achieving sufficiently high separation factors by adjusting the operation variables, especially CSA concentration and pH [14,15].

Many of the drug racemates separated into enantiomers in this study have been separated by

CE quite often, some also with β -CD (bromphenamine, clenbuterol, doxylamine, homatropine, isoprenaline, oxomemazine, terbutaline, tioconazole), although under different conditions (concentrations, modifiers, pH), others with different CSAs (dimetindene, isothipendyl, mefloquine, pholedrine); whereas, to the best of our knowledge, the enantiomer separation of naftidrofuryl and reproterol by capillary electrophoresis was not yet published.

The new results, including the failure of separation in several cases (as documented in Table 2), constitute a valuable complement to the increasing amount of data accumulated in our extended screening study. These data are of interest in their own right; moreover, systematic insight into the underlying molecular recognition phenomena may also prove valuable in other fields. A dedicated publication on this topic is in due preparation.

Acknowledgements

We are indebted to Fonds der Chemischen Industrie, Deutsche Forschungsgemeinschaft and National Natural Science Foundation of China for grants, to Bio-Rad Labs (Hercules, CA, USA) for support, to various pharmaceutical companies for drug samples and to Wacker Chemie for cyclodextrin samples.

References

- [1] S.C. Stinson, *Chem. Eng. News*, October 9 (1995) 44.
- [2] B. Koppenhoefer, R. Behnisch, U. Epperlein, H. Holzschuh, A. Bernreuther, P. Piras, C. Roussel, *Perfum. Flavor.* 19, September (1994) 1.
- [3] J. Caldwell, *Chim. Oggi* 14, October (1996) 65.
- [4] S. Fanali, *J. Chromatogr. A* 735 (1996) 77.
- [5] H. Nishi, *J. Chromatogr. A* 735 (1996) 57.
- [6] E. Gassmann, J.E. Kuo, R.N. Zare, *Science* 230 (1985) 813.
- [7] S. Terabe, M. Shibata, Y. Miyashita, *J. Chromatogr.* 480 (1989) 403.
- [8] A. Dobashi, T. Ono, S. Hara, J. Yamaguchi, *Anal. Chem.* 61 (1989) 1984.
- [9] B. Lin, X. Zhu, B. Koppenhoefer, U. Epperlein, *HPCE '96*, Orlando, FL, USA, 21–25 January, 1996.
- [10] B. Koppenhoefer, U. Epperlein, B. Christian, Y. Ji, Y. Chen, B. Lin, *J. Chromatogr. A* 717 (1995) 181.
- [11] B. Lin, Y. Ji, Y. Chen, U. Epperlein, B. Koppenhoefer, *Chromatographia* 42 (1996) 106.
- [12] B. Koppenhoefer, U. Epperlein, B. Christian, B. Lin, Y. Ji, Y. Chen, *J. Chromatogr. A* 735 (1996) 333.
- [13] B. Koppenhoefer, U. Epperlein, X. Zhu, B. Lin, *Electrophoresis* 18 (1997), 924.
- [14] S.A.C. Wren, R.C. Rowe, *J. Chromatogr.* 603 (1992) 235.
- [15] Y.Y. Rawjee, G. Vigh, *Anal. Chem.* 66 (1994) 619.

Separation of polycyclic aromatic hydrocarbons by micellar electrokinetic chromatography with aqueous short-chain alcohol solvent¹

Xiaoyun Fu *, Jiande Lu, Yaozu Chen

Analytical and Testing Center, Zhejiang University, Hangzhou 310027, People's Republic of China

Received 19 February 1997; received in revised form 20 October 1997; accepted 20 October 1997

Abstract

Micellar electrokinetic capillary chromatography (MEKC) with aqueous organic solvent has been developed to separate polycyclic aromatic hydrocarbons (PAHs). Methanol, ethanol or propanol as an organic modifier was added to sodium dodecyl sulfate (SDS) micellar solution in order to increase the solubility of very hydrophobic solutes in mobile phase. Both methanol and ethanol can be used as co-solvents for the separation of PAHs. Use of ethanol resulted in a shorter analysis time than use of methanol. The separations of some PAHs were unsatisfactory using propanol although the analysis time was much shorter than with ethanol. The influence of ethanol content, SDS concentration and temperature on the separations was studied. Benzene and nine polycyclic aromatic hydrocarbons were successfully separated using 50 mM SDS–20 mM phosphate–5 mM borate, containing 40% (v/v) ethanol at 35°C. The relative standard deviation (R.S.D.) of t_R ranged from 0.5 to 1.5% for six repeat injections. © 1998 Elsevier Science B.V. All rights reserved.

Keywords: Micellar electrokinetic capillary chromatography; Polycyclic aromatic hydrocarbons; Separation of aromatic compounds

1. Introduction

Micellar electrokinetic chromatography (MEKC) combined capillary electrophoresis with chromatography has been proven to be a very

useful separation method for the determination of neutral compounds [1,2]. The separation mechanism is based on the difference in the partition between the electro-osmotically pumped aqueous phase (mobile phase) and the ionic micellar phase (pseudostationary phase). Naturally, this technique has been introduced for the separation of PAHs. However, it is difficult to separate highly hydrophobic PAHs by conventional MEKC because their partition coefficients are so high that they tend to co-elute with the micelles [3].

* Corresponding author.

¹ Presented at the First Asia-Pacific International Symposium on Capillary Electrophoresis, and other Nano- and Microscale Analytical Techniques, held in Singapore, December 17–20, 1996.

Walbroehl and Jorgenson [4] first reported the separation of limited PAHs by EKC and proposed a solvophobic interaction mechanism for the separation of aromatic compounds. Later, Terabe et al. [5] reported that PAHs could be separated by cyclodextrin-modified MEKC. Cole et al. [6] separated PAHs by MEKC with bile salt in the presence of organic modifier. In addition, a monomolecular pseudostationary-phase MEKC [7] was demonstrated to separate PAHs. Hydrophobic interaction electrokinetic chromatography [8] and an organic modifier MEKC [9,10] were also found to improve the resolution of hydrophobic solutes.

Sodium dodecyl sulfate (SDS)-MEKC with organic co-solvent is a convenient and effective method for the separation of hydrophobic compounds. The addition of organic solvent decreases the relative affinity between the hydrophobic solute and micellar phase, and increases the solubility of hydrophobic solute in mobile phase. However, it has been reported that this method is not appropriate for the separation of PAHs [5,6] because a high concentration of organic solvents is required and the micelles may not be stable in the presence of a high amount of organic solvents [11]. In this work, we studied the influence of the properties and content of short-chain alcohol, SDS concentration and temperature on the separation of PAHs by MEKC.

2. Experimental

Many of the experiments were performed with laboratory-constructed apparatus, consisting of a high-voltage d.c. power supply and a fixed wavelength UV detector of Shimadzu IP-2A Isotachophoresis instrument (Kyoto, Japan). Other experiments were performed with a Waters Quanta 4000 CE system (Milford, MA, USA). The UV detector was operated at 254 nm. Electrokinetic chromatograms were recorded with a Shimadzu Chromatopac C-RIB data processor (Kyoto, Japan). A fused-silica capillary of 0.05 mm ID was used without any special wall treatment. Sample solutions were injected into the end of the capillary by the siphoning method. The

siphoning height was 9.8 cm and the injection time was 15 or 20 s. The separation temperature was controlled by circulating air.

All reagents were of analytical-reagent grade. SDS, sodium tetraborate ($\text{Na}_2\text{B}_4\text{O}_7 \cdot 10\text{H}_2\text{O}$), potassium dihydrogen phosphate (KH_2PO_4), methanol, ethanol, 1-propanol, benzene, naphthalene, and 2-methyl naphthalene were purchased from Shanghai Chemicals (Shanghai, People's Republic of China). Other PAHs were obtained from Sigma Chemicals (St. Louis, MO, USA).

Samples were dissolved in ethanol or micellar solution with 40% (v/v) ethanol. The concentration of each component in the samples ranged from 50 to 500 mg l^{-1} . The micellar solutions were filtered through a membrane filter of 0.45 μm and degassed by ultrasonic cleaner before being used. The capillary was rinsed with the operating micellar solution for 3 min before and between runs, and with the 70% (v/v) ethanol-water for 15 min before and after the experiment.

3. Results and discussion

3.1. Influence of short-chain alcohol co-solvent on the separation of PAHs

PAHs are highly hydrophobic compounds and have a great affinity for the micellar phase. Consequently, using only micellar aqueous solution, it is impossible to separate PAHs by MEKC. We have chosen short-chain alcohols as organic co-solvent because of their low viscosity, relatively high dielectric constant and low influence on the stability of SDS micelles. To study the influence of different short-chain alcohol co-solvent on the separation of PAHs, the experiments were carried out with a micellar solution of 40 mM SDS–20 mM KH_2PO_4 –5 mM $\text{Na}_2\text{B}_4\text{O}_7$, containing the different contents of methanol, ethanol and propanol, respectively. As expected, the addition of alcohol caused two different effects on retention time of the solute (t_R). The presence of alcohols decreased electro-osmotic flow, resulting in longer t_R . The results showed that the elution time of the electro-osmotic flow marker (t_0) in-

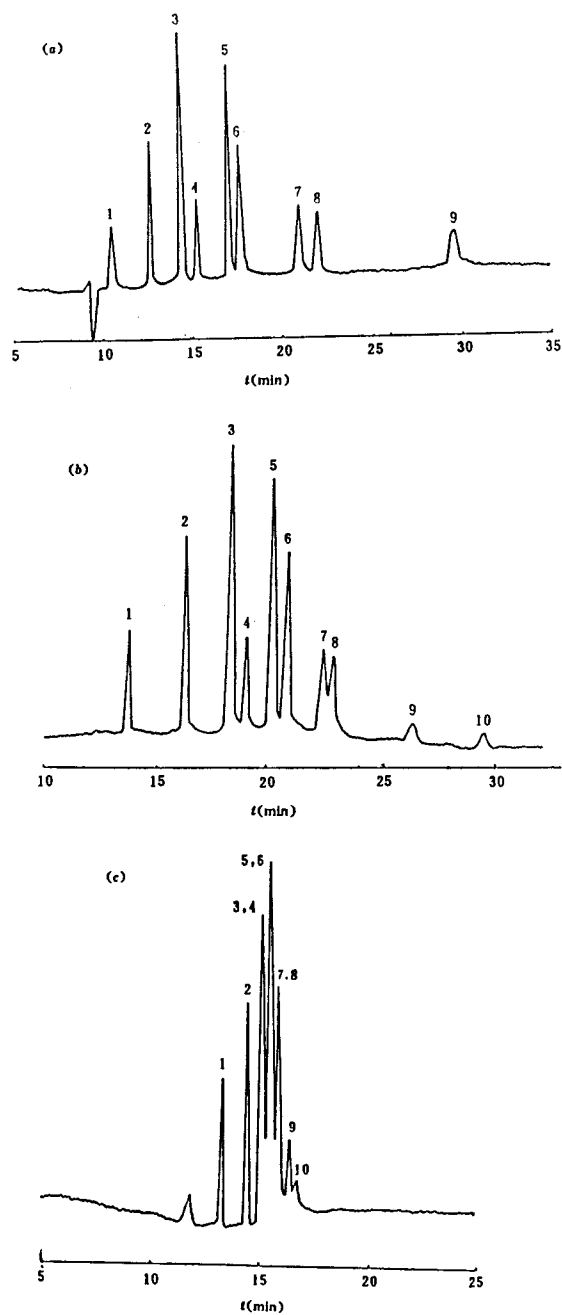


Fig. 1. Influence of short-chain alcohol co-solvent on the separation of PAHs. 1. benzene; 2. naphthalene; 3. 2-methyl naphthalene; 4. acenaphthene; 5. phenanthrene; 6. anthracene; 7. fluoranthene; 8. pyrene; 9. chrysene; 10. perylene. Micellar solution: 40 mM SDS–20 mM KH_2PO_4 –5 mM $\text{Na}_2\text{B}_4\text{O}_7$, containing (a) 50% (v/v) methanol, (b) 40% ethanol, (c) 30% propanol. Capillary: 0.05 mm i.d. \times 450 mm (400 mm to detector). Voltage: (a) 16 kV, (b) 16 kV, (c) 11 kV. Temperature: 35°C.

creased with the molecular weight of alcohol and/or alcohol content because the ratio of dielectric constant to viscosity decreased. The addition of alcohol, on the other hand, increased the solubility of PAHs in mobile phase and lowered t_R . Hence, the different alcohols had different optimum contents. Fig. 1 showed the separation of benzene and nine PAHs using methanol, ethanol and propanol as organic co-solvent under the given conditions. Good separations of PAHs were obtained in the presence of 50% methanol or 40% ethanol as organic co-solvent. The presence of methanol produced better separation of PAHs, but longer analysis time and higher content were needed compared to ethanol. Using propanol, which has stronger hydrophobicity than ethanol and methanol, as an organic co-solvent resulted in a shorter analysis time, but the resolution for some PAHs was unsatisfactory. Although different alcohols showed various improvements in resolution, no elution order change was observed. The higher the hydrophobicity of the solute, the higher the t_R value.

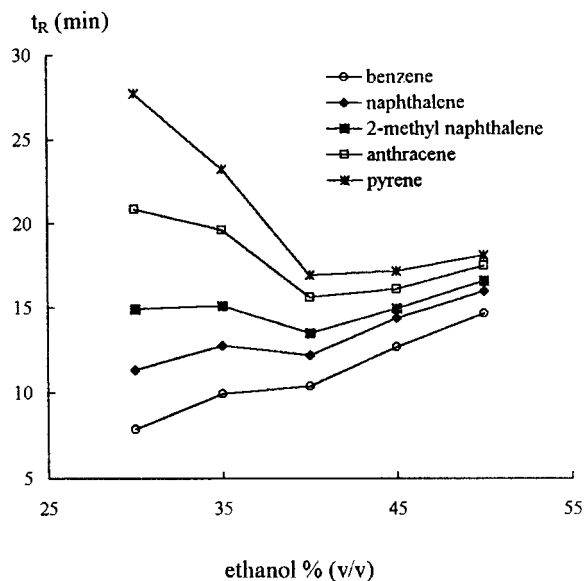


Fig. 2. Influence of ethanol content on t_R . Voltage, 18 kV, other conditions as in Fig. 1(b), except for ethanol content.

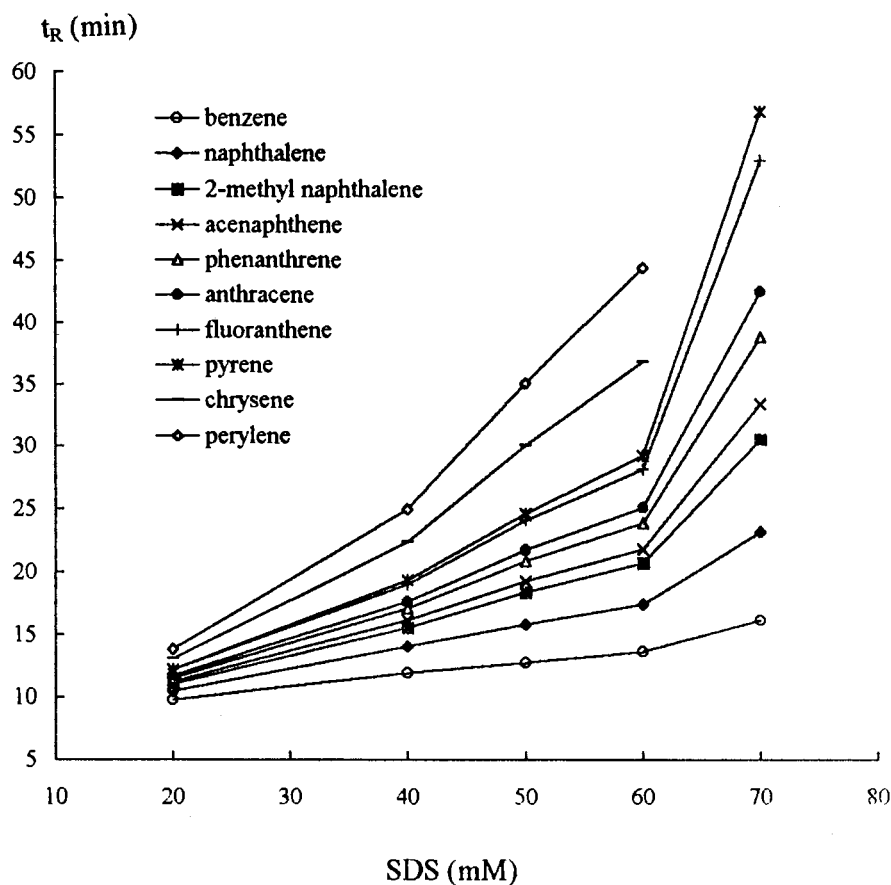


Fig. 3. Dependence of t_R on SDS concentration. Voltage, 18 kV, other conditions as in Fig. 1(b), except for SDS concentration.

3.2. Influence of alcohol content on separation

We studied the influence of ethanol content on the separation of PAHs. It was found that the addition of a small amount of ethanol co-solvent did not improve the separation sufficiently. Ethanol content in the range 30–50% (v/v) was investigated. Fig. 2 illustrates the influence of ethanol content on t_R . As the ethanol content increased, t_R of PAHs decreased and then increased because both the partition coefficient and the electro-osmotic flow were reduced. The change in the partition coefficient was predominant when ethanol content was less than 40%. It was also observed that the separation efficiency increased significantly with increasing ethanol content from 30 to 45%, but decreased when the ethanol content was 50%. Furthermore, when

ethanol content reached 60%, poor separation of PAHs was obtained. A similar result was observed with 40% propanol. The reason may be mainly that such a high alcohol content leads to micelle breaking.

3.3. Influence of SDS concentration on the separation

In order to optimize the separation, we studied the influence of SDS at concentrations from 20 to 70 mM. As in conventional MEKC, both t_R and resolution increased with increasing SDS concentration. Fig. 3 illustrates the dependence of the t_R on SDS concentration. When 70 mM SDS was used, the retention times of chrysene and perylene were longer than 60 min. It can be seen that the

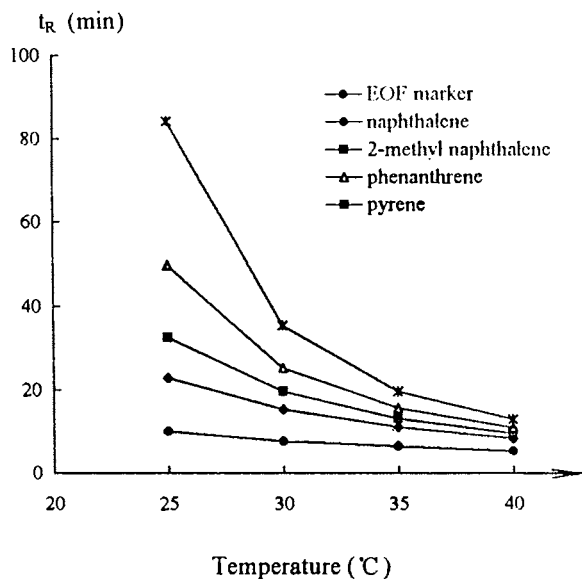


Fig. 4. Influence of temperature on t_R . Micellar solution: 40 mM SDS–10 mM $\text{Na}_2\text{B}_4\text{O}_7$, 40% ethanol. Voltage: 28 kV. Capillary: 0.05 mm i.d. \times 465 mm (390 mm to detector), other conditions as in Fig. 1.

baseline separation of benzene and nine PAHs was achieved when SDS concentration increased to 50 mM.

3.4. Influence of temperature on the separation

Temperature is another important factor which affects separation and retention time. Fig. 4 demonstrates the influence of temperature on t_R . The temperature was raised from 25 to 35°C, the t_R of pyrene decreased from 84.4 to 12.9 min. These results may be attributed to the increase of electro-osmotic flow and the decrease of the partition coefficient. The separation efficiency, in terms of the number of theoretical plates (N), raised slightly with increasing temperature, but decreased when the temperature was higher than 35°C. It may be explained in terms of micelle–monomer exchange. The rate of micelle–monomer exchange was increased by increasing the temperature. It may reduce the loss in efficiency due to micelle polydispersity [11], but a higher temperature may lead to an increase in molecular dispersion.

3.5. Separation of PAHs

Fig. 5 showed that benzene and nine PAHs were separated successfully using 50 mM SDS–10 mM $\text{Na}_2\text{B}_4\text{O}_7$, containing 40% ethanol. The separation efficiency was about 10^5

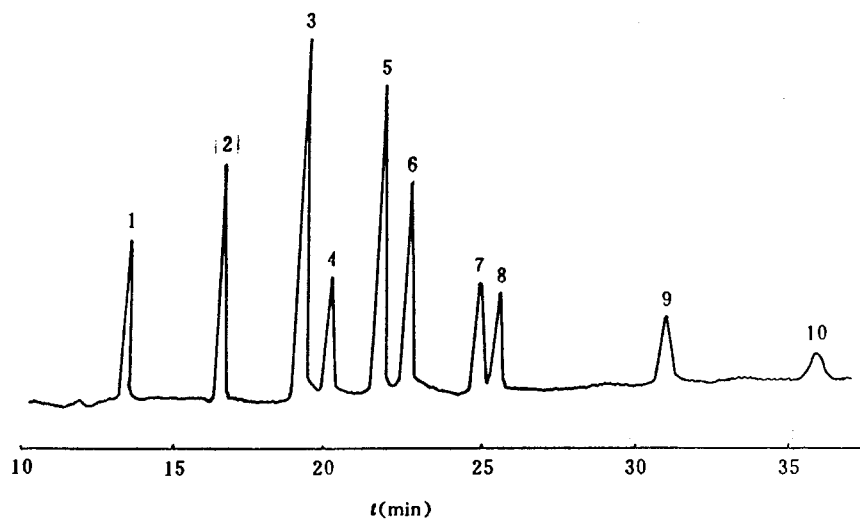


Fig. 5. Separation of benzene and nine PAHs. Micellar solution: 50 mM SDS–10 mM $\text{Na}_2\text{B}_4\text{O}_7$, 40% ethanol. Voltage: 18 kV, other conditions as in Fig. 1.

theoretical plates per meter. To demonstrate the stability of micellar in mobile phase, the reproducibility of t_R was investigated under the conditions given in Fig. 4 (35°C). The relative standard deviation (R.S.D.) of t_R ranged from 0.5 to 1.5% for six repeat injections. This indicated that the micelles were still present under the given conditions. The separation mechanism may be mainly based on solute–micelle interaction.

In conclusion, PAHs were successfully separated by MEKC with short-chain alcohol co-solvent. The MEKC condition can be optimized by changing the alcohol content, SDS concentration and separation temperature.

Acknowledgements

The authors are grateful for financial support from Nature Science Foundation of China (NSFC).

References

- [1] S. Terabe, K. Otsuka, K. Ichikawa, A. Tsuchiya, T. Ando, *Anal. Chem.* 56 (1984) 111.
- [2] A. Zhu, X. Fu, J. Lu, P. Zheng, *Se Pu* 7 (1989) 193.
- [3] M.A. Garcia, M.L. Marina, J.C. Diez-Masa, *J. Chromatogr. A* 732 (1996) 345.
- [4] Y. Walbroehl, J.W. Jorgenson, *Anal. Chem.* 58 (1986) 479.
- [5] S. Terabe, Y. Miyashita, O. Shibata, *J. Chromatogr.* 516 (1990) 23.
- [6] R.O. Cole, M.J. Sepaniak, W.L. Hinze, J. Gorse, K. Oldiges, *J. Chromatogr.* 557 (1991) 113.
- [7] C.P. Palmer, M.Y. Khaled, H.M. McNair, *J. High Resolution Chromatogr.* 15 (1992) 756.
- [8] E.S. Ahuja, J.P. Foley, *J. Chromatogr. A* 680 (1994) 73.
- [9] X. Fu, J. Lu, A. Zhu, *Fenxi Huaxue* 18 (1990) 791.
- [10] P.L. Desbene, C.M. Rony, *J. Chromatogr. A* 689 (1995) 107.
- [11] M.J. Sepaniak, A.C. Powell, D.F. Swaile, R.O. Cole, Fundamentals of micellar electrokinetic capillary chromatography, in: P.D. Grossman, J.C. Colburn (Eds.), *Capillary Electrophoresis: Theory and Practice*, Academic Press, New York, 1992, pp. 159–189.

Short communication

Determination of plasma heparin by micellar electrokinetic capillary chromatography¹

Xiao-Mian Zhou *, Jian-Wu Liu, Meng-En Zhang, Shun-jin Chen

Department of Medical Laboratory, NanFang Hospital, Guangzhou 510515, People's Republic of China

Received 19 February 1997; received in revised form 14 August 1997; accepted 18 August 1997

Abstract

The micellar electrokinetic capillary chromatography (MECC) method is reported for the separation of heparin, and for the possibility of direct determination of free heparin in plasma. The conditions for MECC were: pH 8.5, 25 mM sodium dodecyl sulfate (SDS), 25 mM borate buffer, with a 30 cm × 50 μm ID fused-silica capillary. The sample was detected with a UV-detector at 270 nm with heparin as external standard. The recovery rate was 95.6–98.7%. This method was linear in the range 80–7000 U l⁻¹. The within-run and between-run relative standard deviations were lower than 3.1 and 4.5%, respectively. It is suggested that this MECC method may be used to determine blood samples containing high levels of heparin. © 1998 Elsevier Science B.V. All rights reserved.

Keywords: Heparin; High-performance capillary electrophoresis; Plasma

1. Introduction

Blood coagulation tests are used mostly to monitor plasma heparin levels in clinical therapy: tests such as the thrombin time (TT), activated partial thrombokinase time (APTT), etc., which measure anticoagulation activity of heparin in blood. However, these methods cannot quantitate the concentration of plasma heparin. Several tech-

niques have been investigated for the analysis of heparin preparations. Gradient polyacrylamide gel electrophoresis (PAGE) [1] and strong anion exchange high-performance liquid chromatography (HPLC) [2] have been the methods of choice for the qualitative and quantitative analysis of heparin preparations. Recently, a number of workers who carried out investigations [3–5] reported that high-performance capillary electrophoresis (HPCE) was a sensitive, high-resolution method for the determination of the heparin fragment. However, the samples described above in the papers were non-biological samples. Mao et al. [6] reported that free heparin

* Corresponding author.

¹ Presented at the First Asia-Pacific International Symposium on Capillary Electrophoresis, and other Nano- and Microscale Analytical Techniques, held in Singapore, December 17–20, 1996.

in plasma was separated and its concentration was successfully determined by HPLC. HPLC is, however, a time-consuming, labor-intensive and high-cost method.

This paper describes and compares different methods for determining plasma heparin. The MECC method is simple, rapid, highly sensitive, especially suitable for determining a high dosage of heparin, and not affected by fibrin decomposing product (FDP) and other factors.

2. Material and methods

2.1. Instrument

The instrument used in this work is the automated BioFocus 3000 capillary electrophoresis system (Bio-Rad, USA) with a diode array UV detector, an automatic injector, and a fluid cooled cartridge. The capillary cassette used was filled with a 50 μm ID fused-silica column, 30 cm in length (to detector). Injection of the sample was by pressure for 8 s. All electrophoresis was carried out at 20°C, with an applied voltage of 20 kV and UV detection at 270 nm. The electrophoresis buffer was boric acid (25 mmol l^{-1}), sodium dodecyl sulfate (SDS) (25 mmol l^{-1}), adjusted to pH 8.5 with 1 N sodium hydroxide. Sodium heparin solution (250000 u l^{-1}) was purchased from Shangshia Biochemistry Pharmaceutical Factory. The anticoagulation activity of sodium heparin was calibrated with the standard solution of sodium heparin (355000 u l^{-1} , US Pharmacopeia). The sodium heparin accorded with the unit marked by the factory.

2.2. Methods

Object of study: 10 extraneous circulation patients (360–500 units sodium heparin per kg body weight), 15 dialysis patients (10 patients, 65 u kg^{-1} ; five patients, 10.5 u kg^{-1}).

Preparation of samples: after 30 min of intravenous injection, 2 ml blood was collected. Plasma was isolated by centrifugation at 3000 \times

g for 10 min. A total of 200 μl plasma was deproteinized by mixing with 300 μl acetonitrile for 2 min and then centrifuging for 5 min at 3000 \times g. Heparin plasma may be stored at -20°C for 1 week, but cannot be subjected repeatedly to a freeze/thaw cycle.

Stock standard solution: stock standard solution was prepared by diluting 250000 u l^{-1} sodium heparin 50-fold with redistilled water.

Working standard solutions: the stock standard solution was diluted to concentration levels that bracketed the concentration level of interest, prior to analysis.

Electrophoresis: the supernatants from the acetonitrile deproteinization were introduced into the capillary by pressure injection. After each sample, the capillary was washed with water (1 min); 1 N NaOH (1 min); and fresh buffer by pressure injection. The capillary was washed daily with NaOH, 1 N (2 min); water (1 min); and finally, electrophoresis buffer.

3. Results

Sodium heparin has maximum absorbance at 270 nm. Fig. 1 illustrates the peak of sodium heparin, which is single, intact, symmetrical, with good separation, its migration time being 2.58 ± 0.02 min.

The working standard solution was diluted to 0.08, 0.1, 0.5, 1.0, 2.0, 3.0, 4.0, 5.0, 6.0 and 7.0 u ml^{-1} . The peak area and the amount of heparin were linear in the range 80–7000 u l^{-1} with the detection limit of 25 u l^{-1} ($y = 131253.1x - 13895.6$, $r = 0.998$). A known amount of heparin was added to 1 ml plasma of a normal person in the manner described above, and the peak area and the standard peak area were measured. Recovery rates of 95.6–98.7% were obtained. With regard to the reproducibility of different concentrations of heparin, the within-run R.S.D. and between-run R.S.D. were 1.5–3.0 and 2.0–4.4%, respectively.

For comparison, the results of the improved TT [7] and HPCE were similar ($P > 0.05$) (see Table 1).

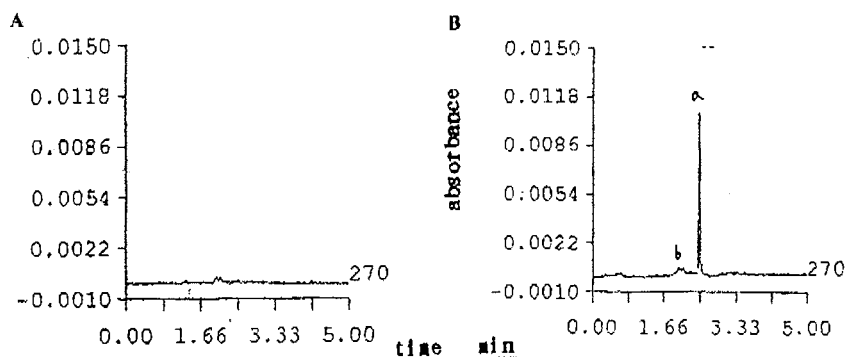


Fig. 1. (A) Electrophoretograms of blank plasma. (B) Electrophoretograms of heparin plasma: (a) sodium heparin; (b) protein peak. Conditions: pH 8.5; 25 mmol l^{-1} SDS; 25 mmol l^{-1} borate buffer.

4. Discussion

Our experimental results show good separation of heparin by HPCE. The peak is single, intact and symmetrical. The peak area and the concentration of plasma heparin are strongly linear. HPCE may quantitate free heparin in plasma. During deproteinization, deproteinization with acetonitrile was greater than with methanol, ethanol, trichloroacetic acid, or methanol combined with acetone. Acetonitrile deproteinization allows a larger sample volume to be introduced into the capillary and increases the plate number and peak height [8], thereby increasing the sensitivity of the material determined.

When heparin was injected into the blood circulation, its anticoagulation activity depended on the amount of heparin in blood. Our results

show that free heparin in plasma is basically in direct proportion to the dose of heparin. The concentration of free heparin measured by HPCE was similar to the activity of plasma heparin determined by the improved TT. Hence, the concentration of plasma heparin determined by HPCE may stand for the activity of heparin anticoagulation.

It is essential to monitor high doses of heparin in plasma in clinical therapy. The HPCE method may determine higher doses of heparin: the results of three patients were measured at 5958, 6270 and 5876 u l^{-1} , respectively. However, the clotting tests were difficult to use to measure them and their reproducibility was very poor. When the concentrations of FDP of two patients were 75 and 96 mg l^{-1} , the concentrations of free heparin by HPCE were 152 and 276 u l^{-1} , respectively. However, it is very difficult to measure the levels of heparin by the improved TT method. HPCE has the advantage that it is not affected by the level of fibrinogen, FDP and antithrombin-III, and the operation is simple to perform.

Table 1
Comparison of the results from the two methods

Group	n	Conc. of plasma heparin (u l^{-1} , $\bar{x} \pm s$)	
		TT	HPCE
Extraneous circulation	10	5100 ± 510	5230 ± 490
Blood dialysis			
Dose of 65 u kg^{-1}	10	290 ± 100	300 ± 110
Dose of 10.5 u kg^{-1}	5	100 ± 20	110 ± 30

5. Conclusion

The HPCE method may be used to quantitate plasma heparin and is especially suitable for measuring high doses of heparin in clinical therapy. Its operation is simple, rapid, and highly sensitive.

References

- [1] R.E. Edens, A. Al-Hakim, J.W. Weiler, et al., *J. Pharm. Sci.* 81 (1992) 823–827.
- [2] R.J. Linhardt, K.G. Rice, Y.S. Kim, et al., *Biochem. J.* 254 (1988) 781–787.
- [3] U.K. Desai, H.M. Wang, S.A. Ampofo, et al., *Anal. Biochem.* 213 (1993) 120–127.
- [4] J.B.L. Damm, G.J. Overkolift, *J. Chromatogr. A* 678 (1994) 151–165.
- [5] K. Malsch, J. Harenberg, D.L. Heene, *J. Chromatogr. A* 716 (1995) 259.
- [6] P. Mao, S. Huang, C. Li, et al., *Chin. J. Med. Lab. Technol.* 18 (6) (1995) 358–360.
- [7] Z.K. Shihabi, *J. Chromatogr. A* 652 (1993) 471–475.
- [8] P. Mao, F. Chen, C. Li, *Chin. J. Med. Lab. Technol.* 18 (5) (1995) 295.

Review

Application of ternary and multicomponent complexes to spectrophotometric and spectrofluorimetric analysis of inorganics

T. Prasada Rao *, M.L.P. Reddy, A. Ramalingom Pillai

Regional Research Laboratory (CSIR), Trivandrum 695 019, India

Received 11 March 1997; received in revised form 6 August 1997; accepted 7 August 1997

Abstract

The application of ternary and multicomponent complexes in spectrophotometric and spectrofluorimetric determination of trace elements is reviewed. Newer types of colour systems employing mixed ligand, surfactant sensitized, ion-association, flotation, derivative and FIA systems are described. Separate sections are devoted to advances in both spectrophotometric and spectrofluorimetric determination of individual elements. Future trends in spectrophotometric and spectrofluorimetric analysis are discussed. © 1998 Elsevier Science B.V. All rights reserved.

Keywords: Spectrophotometric; Spectrofluorimetric; Complexes

1. Introduction

Atomic absorption and inductively coupled plasma emission and mass spectrometry, rapidly developed during the past two decades, have

Abbreviations: A, aqueous; BPR, Bromopyrogallol red; CPB, cetylpyridinium bromide; CPCI, Cetylpyridinium chloride; CTAB Cetyltrimethyl ammonium bromide; CTACI, Cetyltrimethyl ammonium chloride; DMG, Dimethylglyoxime; EDTA, Ethylenediamine tetra acetic acid; Erio T, Eriochrome Black T; E, Extraction; NTA, Nitrilotriacetic acid; 1,10-Phen, 1,10-Phenanthroline; PAR, 4,2-pyridylazo Resorcinol; Q, Quenching; TTA, Thenoyltrifluoroacetone; TEA, Triethanolamine; TOPO, Trioctylphosphine oxide.

* Corresponding author. Fax: +91 471 490186.

diminished the role of spectrophotometry as the routine analytical technique in many laboratories. The low detection limits and enhanced selectivity of atomic spectrometric techniques together with the use of sequential multi-element determination capabilities makes these techniques better suited than spectrophotometry and spectrofluorimetry. However, the latter two techniques continue to be widely popular in view of their speed, simplicity, precision, accuracy and common availability of the instrumentation. This has resulted in extensive literature being published over the years [1–16].

Ternary complexes, wherein central ion reacts with two different ligands, have aroused considerable interest in the past two decades. West [17]

has classified ternary complexes into two major categories: coordination unsaturated type and ion-association type. The coordination unsaturated ternary complex results when a binary complex ('binary' here refers to a complex containing one type of central ion and another type of ligand, regardless of their stoichiometric ratio) has free coordination positions available on the central ion, allowing further reaction with a different ligand. Alternatively, if the binary complex is charged, the ion-association with an ion of opposite charge (usually dye stuff) may occur. In addition, multicomponent complexes (metal ion with more than two reagents) are used for spectrophotometric and spectrofluorimetric determination of inorganics. The modes of formation of all three types of complexes together with improvements in selectivity and sensitivity which accompany their formation, have been extensively discussed in a series of reviews [18–26]. Since the publications relating to the use of ternary and multicomponent complexes are rapidly increasing in frequency in the chemical literature of spectrophotometry and spectrofluorimetry and also possible simultaneous analysis based on multiwavelength and derivative measurements and being the most widely used detection technique in flow injection analysis (FIA), it is appropriate to present, in this review, a detailed evaluation of various procedures reported since 1980 on this subject.

2. Advances in colour systems

Most spectrophotometric and spectrofluorimetric determination of inorganic species are based on the formation of coloured compounds or complexes by their reaction with unidentate or chelating ligands. These methods are usually not sufficiently sensitive, excepting for those involving charge transfer transition, as the sensitivity, in general, is controlled by the extent of π -conjugation present in the ligand. Selectivity, most often, is achieved either by the proper choice of a reagent or by the use of masking agents. The sensitivity and selectivity can be improved through the synthesis of organic ligands possess-

ing extensively delocalized π -electron system along with appropriately placed ligating sites. However, apart from the synthesis being an arduous task, the reactivity of such ligands towards metal ions is restricted by the steric factors.

In recent years, this problem of designing model ligands for improving sensitivity and selectivity have been circumvented by reacting the metal ion with two different ligands, instead of one, to form a ternary complex [17]. The increase in sensitivity observed in these systems is due to the complex organic envelope around the central metal ion. The improvement in selectivity can be explained as due to the decreased probability of similar interaction with other metal ion. Even if other metal ions should react in a similar manner, they can effectively be masked, for now the system can tolerate more masking agents due to the increased stability of the complex.

3. Spectrophotometry

Ternary and multicomponent systems in spectrophotometry can be classified into:

1. Mixed ligand systems
2. Surfactant sensitized systems
3. Flotation-spectrophotometric methods
4. Ion-association systems

In addition, ternary and multicomponent systems are used in signal processing (derivative) and sample processing (FIA) analytical techniques in spectrophotometry and these are also included in the present review.

3.1. Mixed ligand systems

The mixed ligand systems makes use of coloured complexes, charged or neutral, consisting of metal ion and two different ligands. One of these ligands is anionic and the other can be anionic or neutral. Thus in $[\text{Fe}(\text{OH})(\text{EDTA})]^{2-}$ both the ligands are anionic while in $\text{Ni}(\text{HDz})_2(\text{Py})_2$ both an anionic and a neutral ligand are involved. Table 1 surveys ternary and multicomponent mixed ligand complexes with various metal ions for the determination of the latter.

3.2. Surfactant sensitized systems

The surfactant sensitized systems are based on the ability of certain surfactants to sensitize the binary complexes of the metal ion with chromogenic ligands. The ligands, most often, are metallochromic indicators and for sensitization, cationic surfactants are used. Sensitization can result either due to the replacement of acidic protons of the ligated dye molecule by surfactant cations as is the case in Pb-bromopyrogallol red-CTAB/CPB colour systems [318] or by adsorption of the metal-reagent complex on the micelles of the cationic surfactant as with Th-phenylfluorone-CPB [377] system. The applications of surfactant sensitized systems in spectrophotometric analysis are summarized in Tables 2–4.

3.3. Flotation-spectrophotometric methods

Basic non-chelating dyes enjoy high popularity in spectrophotometric analysis due to a high molecular extinction coefficient ($\approx 1 \times 10^5 \text{ l mol}^{-1} \text{ cm}^{-1}$). They are able to form extractable ion-pairs with monovalent or bivalent anionic complexes of metals leading to a variety of sensitive methods. Polyvalent anionic metal complexes also react with basic dyes but the reaction products cannot be extracted by slightly polar solvents. Instead, the compounds formed accumulate during shaking on the phase boundary or on the wall of the separating funnel. The precipitate can be separated off and dissolved in a polar solvent, producing an intensely coloured solution that forms the basis of a flotation-spectrophotometric method of determination. Flotation-spectrophotometric methods developed so far since 1980 are listed in Table 5.

3.4. Ion-association systems

Ion-association systems, in a more general way, could be said to result from the interaction of charged binary complexes with oppositely charged ions. When a neutral ligand, e.g. a nitrogenous base, is used, the primary complex produced is cation, possessing the same charge as that of metal. Such complexes were made to associate

with anionic dyes like eosin, rose bengal etc. to form ion-associates that are extractable into organic solvents. When charged ligands, e.g. halides, thiocyanate or carboxylic acids, are used, the primary complex produced is anionic which can be associated with onium compounds like tetraphenylarsonium and phosphonium chlorides or cationic dyes. Onium compounds are used when the primary complex is chromophoric in nature. Thus the thiocyanato complexes of Fe(III), Co(II) and W(VI) have been extracted with tetraphenyl salts and the extracts, when subjected to spectrophotometry, were shown to provide improved sensitivity over the methods that simply involve the extraction of the primary complex. When the primary complex formed is anionic and colourless, they can be made to ion-associate with oppositely charged dye molecules. The particular advantage of such colour systems containing dye molecules over the onium salts is the increased sensitivity arising from the high molar absorptivity of the dyes which usually lie in the range 6.0×10^4 to $1.25 \times 10^5 \text{ l mol}^{-1} \text{ cm}^{-1}$. The selectivity is also improved due to the inability of most other ions to react with two ligands to form an ion-association complex of the same nature as the desired ion. Tables 6 and 7 lists various ternary and multicomponent ion-association complexes utilized for the trace determination of inorganics.

3.5. Derivative systems

Derivative systems have enjoyed extensive activity during the last 10 years due to the incorporation of electronic differentiators in most of the commercial spectrophotometers. These, together with associated software, are able to compute derivatives up to n th order of the spectrum. Today, this technique has proved to be very useful, providing both qualitative and quantitative information derived from mathematical processing of UV and VIS spectra. Derivative spectrophotometry leads to an increase in selectivity and in some cases, sensitivity of determination due to elimination of errors resulting from overlapping bands. It permits measurements in turbid media (even in the UV range) thus eliminating the need for centrifugation and allowing in situ measurements us-

Table 1
Mixed ligand complexes

Element	Reagents [R]	Medium for determination	pH/acidity	λ_{max} , nm	$\epsilon \times 10^{-4}$	Beer's law range (ppm)	Applications
Ag	1,10-phen, phloxin [27]	H ₂ O	5	590	13	$\leq 15 \mu\text{g}$	—
	2(3,4-phenylazo phenyl)triazeno phenol-TEA [28]	H ₂ O	10.2	545	12.8	$\leq 0.28 \text{ ppm}$	—
Al	1,10-phen, bromopyrogallol red [29]	H ₂ O	6.5–7.5	640	—	—	—
	Bromopyrogallol red, diphenyl guanidine [30]	Butanol	4.2	535	3.1	0.1–1.1	—
	5-bromosalicylfluorone, 5,7-dibromo-8-hydroxyquinoline [31]	H ₂ O	6	530	6.2	0.05–0.8	—
Bi	Iodide, nitron [32]	—	—	490	—	0.5–25	—
	Xylenol orange, 4-chloro <i>N</i> - <i>M</i> -tolyl benzohydroxamic acid [33]	CHCl ₃	4.5	530	2	0.33–16.7	—
	Bromide, nitron [34]	1,2-Dichloroethane	—	388	0.96	—	Wood's metal
Cd	Alizarin violet, <i>N,N</i> -bis(aminopropyl) hexadecylammonium chloride [35]	—	—	600	4.8	0.8 $\mu\text{g}/25 \text{ ml}$	—
	Alizarin Red S, diphenyl guanidine [36]	—	4	500	—	—	—
	Dithiozone, 1,10-phenanthroline [37]	—	3	505	—	0–20 μg	—
	Diphenylcarzone, 1,10-phenanthroline [38]	—	—	536	9.4	—	—
	Crystal violet, bromopyrogallol red [39]	H ₂ O	—	654	17.9	0–0.4	High purity Zn
Ce	1,10-Phenanthroline, cation [40]	CHCl ₃	9–10	490	9.2	—	—
	Chromazurol S, quinoline-8-ol [41]	—	6–6.8	610	2	0.1–2.8	—
	SCN ⁻ , ephedrin [42]	IBMK	—	620	0.43	0.5–19.5	—
Co	2-(5-bromo-2-pyridylazo)5-diethylamino-phenol benzoate, sodium dodecyl sulphate [43]	—	—	595	7.93	0.02–0.52	Alloy steel
Cr	Methylthymol blue, diphenylguanidine [44]	—	—	—	—	—	—
Cu	1,10-phen, 2,4-dinitrophenylazo catechol [45]	—	—	—	—	—	—
	SCN ⁻ , 2,3 or 4-picolinel [46]	—	3–8	410, 405 or 400	—	2.5–30	—
Er	NTA, Tiron [47]	—	6.5–11	379	—	0.13–1.34	—
Fe	Eriocyanine R, Diphenylguanidine [48]	—	5.5–6.5	610	4.75	4.8–22.4 μg	—
	SCN ⁻ , monoethyl α -(4-chlorobenzylamino)salicylphosphonate [49]	CHCl ₃ or benzene	0.1–3.3	451	0.99	—	—
	Erio T, <i>meso</i> tetra(4-sulphophenyl)-porphyrin [50]	—	4	392	20.7	—	Pure Cu, tea leaves, tobacco
Zn	SCN ⁻ , <i>N</i> -hydroxy- <i>N</i> - <i>m</i> -atolyl- <i>N</i> -(3,4-xylyl)-benzamide [51]	—	—	460 or 520	1.2 or 0.4	0.2–40 or 0.8–13	Drugs
	1,10-phen, SCN ⁻ , Tween-80 [53]	—	2	525	—	—	Plants, soils, blood
Mn	Oxalate, purpurin [54]	—	—	600	0.57	0.05–0.2	Zn, W, sherry and urine
	Azide, <i>N</i> -hydroxy <i>N,N'</i> -diphenyl benzamide [55]	CHCl ₃	—	530	—	1–12	—

Table 1 (continued)

Element	Reagents [R]	Medium for determination	pH/acidity	λ_{max} , nm	$\epsilon \times 10^{-4}$	Beer's law range (ppm)	Applications
Ga	PAR, diphenylguanidine [56]	—	—	—	—	—	—
Hg	1,10-phen, 2,4-dinitrophenylazocatechol [57] Xylenol orange, diphenylguanidine [58]	Isoamyl alcohol- CHCl ₃	8	590	2.3	0.25–5.8	—
In	Erio T, diphenylguanidine [59]	—	—	—	—	—	—
K	Benzo-15-crown-5, dipicrylamine [60]	—	—	420	2.7	0.2–4	Rocks, soil, plants
La	Antipyrine-A, diphenylguanidine [61]	—	—	—	—	—	—
Lu	Pyrogallol Red, 1,10-phen [62]	—	7–8	620	2.39	0.15–1.2	—
Mn	Bromopyrogall Red, 1,10-phen [62]	—	3.7–7.0	620	1.87	0.1–0.5	—
	1,10-phen, TTA [63]	—	11.5	375	3.6	—	—
	1,10-phen, dithizone [64]	—	6	507	4.6	<5 µg	Carbonate rocks
Mo	SCN ⁻ , thioacetanilide [65]	Benzene	—	470	1.9	—	Steel, coal ash and ores
	Bromopyrogallol red, ethyl violet [66]	—	—	535	17	Up to 0.16	—
	SCN ⁻ , Amidopyridine [67]	Benzene	—	470	1.9	0.5–4.4	—
	SCN ⁻ , Pyrogallol [68]	IBMK	—	465	10	0.04–1.0	—
	SCN ⁻ , Nitron [69]	—	—	465	—	1.2–12	Steels
	SCN ⁻ , ethyl isobutazine HCl [70]	CHCl ₃	—	460	3.9	0.5–5.6	Steels
	SCN ⁻ , 2-acetyl pyridine thiosemi-carbazone [71]	CHCl ₃	—	470	1.7	0.1–6.5	Steels
	N-phenylbenzohydroxamic acid, 2-nitrophenyl-fluorone [72]	—	1.0–1.5	520	7	0.08–1.4	—
Nb	N,N'-di(2-hydroxy-5-sulphophenyl)-c-cyan formazan, diantipyryl methane [73]	Butanol, benzene	—	660	—	—	Geological materials
	SCN ⁻ , promethazine HCl [74]	—	—	400	2.72	—	Ores
	SCN ⁻ , 1-naphthylmethyltriphenyl-phosphonium chloride [75]	—	393	3.72	Up to 20 µg	—	—
	Dibenzo-18-crown-6, SCN [76]	Benzene	—	398	3.85	—	—
	Pyrogallol, 2,3,5-triphenyltetrazolium chloride [77]	CHCl ₃	—	390	—	—	—
	Catechol, 2-(4-iodophenyl)-3-(4-nitrophenyl)-5-phenyl-tetrazolium chloride [78]	CHCl ₃	—	400	—	—	—
	SCN ⁻ , 1,2,4,6-tetraphenyl pyridinium perchlorate [79]	—	—	395	2.82	0.1–2.5	—
	Motocatechuric acid, 1,2-diaminocyclohexane tetracetic acid [80]	—	—	395	2.82	0.1–2.5	—
Ni	1,10-Phen, dithizone [81]	—	11.5	514	4.95	—	—
	1,10-Phen, cadion [82]	CHCl ₃	—	505	1.0	—	—
	Rubeanic acid, quinoline [83]	—	7.5–9.0	390	—	0.63–4.4	—
	Ethylxanthate, pyridine [84]	—	—	—	—	—	—
Os	Pyrocatechol, N-hydroxy,N,N'-diphenyl benzamide [85]	CHCl ₃	8.5	—	39.5	≤0.035	Low grade ores
Pb	1,10-Phen, bismuthiol-II [86]	CHCl ₃	3–7	342 or 370	—	0.3–30	—

Table 1 (continued)

Element	Reagents [R]	Medium for determination	pH/acidity	λ_{max} , nm	$\epsilon \times 10^{-4}$	Beer's law range (ppm)	Applications
Pd	SCN ⁻ , 2,4,6-Collidine [87]	CHCl ₃	1.2–2.1	304	3.21	—	—
	2-Thiopyrogallol, β -mercaptoresorcylic acid [88]	60% ethanol	5	430	—	0.5–6	—
	Rubeanic acid, collidine [89]	Ethanol	—	410	1.02	1.87–4.3	—
	Phloxine, thiamine [90]	—	4.6	565	10.2	≤ 8 μg	—
	Thiosalicylic acid, hexylamine [91]	CHCl ₃	—	—	1.54	0.91–6.92	Pd charcoal
	1,10-Phen, cadion HSC [92]	—	—	518	9.4	≤ 0.4	Catalysts
	Phenothiazine, promazine [93]	Ethanol	—	450	0.92	0.2–23	—
	PAR, Diphenyl guanidine [94]	—	5.3	530	9.4	0.21–191	—
	KI, diantipyrylmethane [95]	CHCl ₃	—	365	2.2	—	—
	SCN ⁻ , α -benzildioxime [96]	Isoamylacetate	—	430	2.9	0.2–8.8	Reflector flue dust
Rh	SCN ⁻ , DMG [97]	—	—	430	—	Up to 4	Flue dust
	SCN ⁻ , potassium hexacyanoferrate [98]	Isopentyl alcohol	—	440	2.98	Up to 4	—
	Diphenylcarbazine, 2-picoline [99]	MIBK	—	560	4.01	0.1–3	—
	2-mercaptoacetamide, 4-picoline [100]	CHCl ₃	3.3–6.0	585	1.48	1.5–4.75	—
	1,10-Phen, SCN ⁻ [101]	—	—	490	0.8	0.2–10	—
	Eriocyanine R, phosphatidylcholine [102]	—	6.7	605	3.7	—	—
	5-Dimethylamino-2-(thiazolazo)-phenol, 1,3-diphenylguanidine [103]	—	4.5	605	—	2–18 μg	—
	Eriocyanine R, chloropromazine [104]	—	—	600	—	0.7–3.3	Monazite
	Tiron, diantipyryl methane [105]	—	4.5	400	—	—	Ni based alloys
	Tannin, thioglycolic acid [106]	—	4	400	0.8	0.2–5	—
Ru	Bromopyrogallol red, EDTA [107]	—	—	—	—	—	—
	Catechol, adainone-1-carboximide [108]	CHCl ₃	1.5–2.0	410	1	—	Steels, Ni based alloys
	Thiazolylzocatechol, diantipyryl methane [109]	CHCl ₃	3.2–3.9	530	4.8	0.05–0.4	—
	Mandelic acid, stilbazo [110]	—	—	535	11.0	≤ 8	Silica
	PAR, <i>N</i> -octylacetamide [111]	—	5.5–6.5	530	3.2	Up to 5	Dolomite rocks
	Pyrogallol, chloropromazine HCl [112]	CHCl ₃	7.5 \pm 0.2	380	—	0.8–18	Mineral samples
	SCN ⁻ , <i>N</i> -phenyleinanamohydroxamic acid [113]	CHCl ₃	—	590	—	0.8–6.4	—
	Catechol violet, chloropromazine [114]	—	—	675	—	—	—
	PAR, <i>N</i> -phenylbenzohydroxamic acid [115]	—	—	560	—	≤ 2	Steels, Ti alloys
	SCN ⁻ , <i>N</i> - <i>m</i> -TMBHA [116]	CHCl ₃	—	580	0.71	0–4.8	Blood, urine, plant materials
U	SCN ⁻ , salicylhydroxamic acid [117]	MIBK	3	540	—	0.4–12	Alloy steels
	SCN ⁻ , hydroxymidine [118]	CHCl ₃	1.7–3.0	605	0.62	≤ 7.2	Steels
	SCN ⁻ , <i>N</i> -cinnamoyl- <i>N</i> -phenylhydroxylamine [119]	—	—	580	0.7	0.4–12	Alloy steels and ores
	SCN ⁻ , benzohydroxamic acid [120]	—	4	535	—	—	Steels and rocks
	4-Hydroxybenzaldehyde, hydroxy amidine [122]	—	—	—	—	—	—
	SCN ⁻ , diphenylguanidine [123]	H ₂ O	—	340	17	0.07–7	—

Table 1 (continued)

Element	Reagents [R]	Medium for determination	pH/acidity	λ_{max} , nm	$\epsilon \times 10^{-4}$	Beer's law range (ppm)	Applications
W	BPR, diphenylguanidine [124]	—	—	510	6.8	—	—
	SCN ⁻ , propiciozine [125]	CHCl ₃	—	410	1.82	0.6–14.8	Steel
	SCN ⁻ , chlorpromazine [126]	—	—	406	1.14	0.5–16.6	Steel
Zn	Phenylfluorone, diphenyl guanidine [128]	—	—	554	8.4	0.04–0.4	Clays and silicates
Zr	BPR, malonic acid [129]	H ₂ O	5.5	690	8.4	0.2–4	Ores
	Erio T, 1,1-diantipyrinyl butane [130]	CHCl ₃	—	520	—	1–100 μ M	Water

Table 2
Surfactant sensitized systems

Element	Reagents [R]	Medium for determination	pH/acidity	λ_{max} , nm	$\epsilon \times 10^{-4}$	Beer's law range (ppm)	Applications
Ag	1,10-Phen, tetrabromofluorescein, CTAB [131]	H ₂ O	4	545	8.4	Up to 0.8	Waste water and minerals
	Cation 2B, sodium dodecyl sulphate [132]	H ₂ O	9.2	560	12.3	Up to 0.64	Water
	Dithizone, CTAB [133]	H ₂ O	12.5–13	565	—	1	—
	5(2,4-dihydroxy(benzylidene) rhodamine, CPB [134]	H ₂ O	—	547	7.1	≤45 µg	Silicate rocks
	Rhodamine derivative, CTAB [135]	H ₂ O	—	—	—	—	—
	Phenol, TEA, sodium dodecyl sulphate [136]	H ₂ O	5–6	565	6	≤0.6	Waste water
	4-(3,5-dibromo-2-pyridylazo) <i>N,N</i> -diethylamylene, sodium dodecyl sulphate, peregol O [137]	H ₂ O	5.5	600	—	0.1–1.0	—
	5-Cl-PADAB, sodium dodecyl sulphate, peregol O [138]	H ₂ O	8–11	515	4.7	0–1	Ores
	2-nitrophenylfluorone, CTAB [139]	H ₂ O	6.5	568	16	Up to 4.2 µg/25 ml	—
	Chromazurol S, benzyl(dodecyl dimethyl ammonium bromide [140]	H ₂ O	5	615	—	0.02–0.2	—
	9-(2-chlorophenyl)fluorone, CTAB [141]	H ₂ O	—	568	10.5	Up to 0.2	—
	Chromazurol S, OP [142]	H ₂ O	6.2–7.0	620	—	0–4 µg/25 ml	—
	<i>o</i> -Chlorophenylfluorone, CTAB [143]	H ₂ O	6	570	10.8	≤11 µg/25 ml	—
Chromazurol S, CTA Cl, OP-10 [144]	H ₂ O	0.2 M HCl-pH 2	640	—	0.1–1 µg/25 ml	—	
Al	Chromazurol S, CPB, OP [145]	H ₂ O	6.7–7.0	630	13.5	0.04–0.4	—
	Chromazurol S, Dodecylpyridinium bromide [146]	H ₂ O	5.3–5.8	610	—	0–0.24	—
	Sodium 2'-bromo-4',5'-dihydroxyazo-benzene-4'-sulphonate, CTAB [147]	H ₂ O	6.7–8.0	527	6.9	≤10 µg	—
	Catechol violet, CTAB [149]	H ₂ O	6–7.2	675	7.3	—	—
	Chromazurol S, CTAB [150]	H ₂ O	6.2–6.25	625	—	—	—
	Chromazurol S, CPB [151]	H ₂ O	—	627	—	0.1–0.4	—
	Bromopyrogallol red, CTAB [152]	H ₂ O	—	627	—	0.1–0.4	—
	Xylenol orange, CPB [153]	H ₂ O	6.5–7.5	520	1.6	—	Alloys
	Aluminon, CTAB [154]	H ₂ O	4.5	545	3.11	0–0.67	Water
	Chromefast blue B, CTAB [155]	H ₂ O	6	645	12.5	0.01–0.08	Steel, soil, plant ash
	Chromal blue G, CTAB [156]	H ₂ O	6.0–7.2	660	16.2	—	Mg based alloys
	Chromazurol S, hexadecyl(dimethyl ammonium acetate [157]	H ₂ O	5.5–6.0	620	13	0–0.2	Bronze
	Chromazurol S, OP [158]	H ₂ O	—	650	—	—	—
	Bromphenol blue, CPCl [159]	CHCl ₃	6–7	605	—	0.03–0.3	—
	Pyrogallol red, CTAB [160]	H ₂ O	6.8–7.2	610	4.8	0–0.5	—
	Salicylfluorone, CTAB [161]	H ₂ O	5.7–6.5	559	14	0–0.2	Alloys and water
	Chromazurol S, CTAB [162]	H ₂ O	—	—	—	—	—
Ferron, CTAB [163]	H ₂ O	—	—	—	—	—	

Table 2 (continued)

Element	Reagents [R]	Medium for determination	pH/acidity	λ_{\max} , nm	$\epsilon \times 10^{-4}$	Beer's law range (ppm)	Applications
Au	I ⁻ , CTAB [164]	CHCl ₃	—	290 or 360	—	Up to 15	—
	Michler's thioketone, Tween-80 [165]	H ₂ O	—	560	14.6	0–0.6	Ores
	Curcumin, CPB [166]	H ₂ O	—	560	1.8	≤3 µg/25 ml	—
	Eriocyanine R, CPCl [167]	H ₂ O	10	530	5.4	—	Water
Be	4,5-Dibromophenyl fluorone, CTAB, polysorbate 60 [168]	H ₂ O	8–9	568	170	Up to 6.8 ppb	Be–Cu alloys and minerals
	Chromazurol S, Zephiramine [169]	H ₂ O	5.5	615	—	—	—
Bi	Chromazurol S, benzyl dimethyl tetradecylammonium bromide [170]	H ₂ O	4.3	620	11	—	—
	Phenylfluorone, OP [171]	H ₂ O	8.2	545	7.56	Up to 0.08	—
	Chromazurol B, CPCl [172]	H ₂ O	5	615	9.9	Up to 3.5 µg/25 ml	—
	Chromazurol S, Benzyl dimethyl tetradecylammonium chloride [173]	H ₂ O	10.2	525	5.9	—	—
Ca	Eriochrome cyanine R, Septonex [174]	H ₂ O	5.9	590	—	—	—
	Chromazurol S, zephiramine [175]	H ₂ O	10	525	5.4	0.4–13 µM	—
	Eriochromeazurol B, CTAB [176]	H ₂ O	6.5–7.5	628	13.3	2–80 ppb	—
	Chromazurol S, benzyl dodecyl dimethyl ammonium bromide [177]	H ₂ O	—	610	10.5	0.002–0.2	—
	Chromazurol S, CTAB [178]	H ₂ O	8.5–11	520	3.3	0–20 µg/50 ml	Ores
	<i>m</i> -Fluorophenylfluorone, thiourea, CTAB [179]	H ₂ O	6.2	560	18.3	Up to 5	—
	I ⁻ , Benzyl dimethylanilinium chloride [180]	CH ₂ Cl ₂	—	490	—	4–40	—
	Pyrogallol Red, CTAB [181]	H ₂ O	—	615	—	1–5	—
	Pyrogallol Red, CTAB [182]	H ₂ O	2	615	2	0–300 µg/50 ml	—
	Baromopyrogallol red, CPB [183]	H ₂ O	—	630	—	0.6–2.5 µg/25 ml	—
Cd	Chromazurol S, 1,10-phen, CTAB [184]	H ₂ O	—	620	4.2	0–1	Ferrosilicon
	Xylenol orange, CTAB [185]	H ₂ O	—	605	4.5	≤0.48	—
Co	Cadion 2B, sodium dodecyl sulphate [186]	H ₂ O	—	520	11.90	0–0.5	Cu alloys and Zn
	PAR, CTAB [187]	H ₂ O	10	505	—	—	—
	2-(5-Bromo-2-pyridylazo)-5-diethyl-aminophenyl, OP [188]	H ₂ O	9	560	11.6	0–0.8	—
Co	Salicylfluorone, CTAB [189]	H ₂ O	—	573	24.7	≤6 µg/25 ml	Waste water
	PAR, CPCl [190]	H ₂ O	9	—	—	—	—
	8-Hydroxy-7-nitrosoquinoline-5-sulphonic acid, Zephiramine [191]	CHCl ₃	3.5–8.0	530	—	0–30	Sea water
	4,5-Dibromophenylfluorone, CPB [192]	H ₂ O	10.5	640	12.7	Up to 0.8	Ores
	SCN ⁻ , CTAB [193]	CHCl ₃	—	625	2.2	—	Vitamin B ₁₂
Co	Eriochrome Azural B, 4,4'-bipyridyl, CTAB [194]	H ₂ O	10.7	632	7.8	—	Ni and NiSO ₄
	PAN, CTAB [195]	H ₂ O	5	572	2.2	0.1–1	Vitamin B ₁₂
	Phenylfluorone, CPCL [196]	H ₂ O	—	—	—	—	—
	—	—	—	—	—	—	—

Table 2 (continued)

Element	Reagents [R]	Medium for determination	pH/acidity	λ_{\max} , nm	$\epsilon \times 10^{-4}$	Beer's law range (ppm)	Applications	
Cr	Chromazurol S, CTAB, OP [197]	H ₂ O	—	625	13	Up to 6.5 $\mu\text{g}/25$ ml	—	
	Triphenylmethane reagents, CTAB [198]	H ₂ O	6	520	6.8	1–20 $\mu\text{g}/25$ ml	—	
	Chromazurol S, CTAB [199]	—	4.0–4.04	618	8.4	0.04–0.4	—	
	Bromopyrogallol red, Septonex [200]	H ₂ O	4	640	—	0.1–0.4	—	
	1-(2-thiazolylazo)2-naphthol, CTAB [201]	H ₂ O	5.7	575	1.46	5–60 μg	—	
	Salicylfluorone, CPCI [202]	H ₂ O	5.6–6.6	580	26	0–0.25	Steel	
	Chromazurol S, OP [203]	H ₂ O	4.7	625	12	0–0.28 ppb	Steel	
	Eriochromeazuro B, CTAB [204]	H ₂ O	—	630	13.5	$\leq 8 \mu\text{g}/25$ ml	Steel	
	<i>o</i> -Hydroxyquinol phthalein, CTAB [205]	H ₂ O	5.8	560	16.4	—	Ferro silico steel	
	Eriochrome cyanine R, CTAB [206]	H ₂ O	—	590	7–8	0–14 $\mu\text{g}/25$ ml	—	
	Salicylfluorone, CTAB [207]	H ₂ O	—	565	12	0–11 $\mu\text{g}/50$ ml	—	
	Bromopyrogallolred, CTAB [208]	H ₂ O	5.3–5.8	635	3.6	0–0.28	—	
	Eriocyanine R, CTAB [209]	H ₂ O	7.6–8.7	590	9.6	0.05–0.6	—	
	Chromazurol B, quinoline, CTAB [210]	H ₂ O	5.6	587	—	Up to 0.6	—	
	Phenylfluorone, CPB [211]	H ₂ O	5.4	565	—	Up to 0.12	Human hair	
	Methyl orange, CTAB [212]	H ₂ O	—	580	295	0.1–0.6	Si–Cu intrauterine device	
	Chromazurol B, CDCAB [213]	H ₂ O	—	677	22	0.03–1	—	
	Cu	Phenylfluorone, Zephiramine [214]	H ₂ O	9	562	9.3	Up to 0.42	—
		PAR, Benzylidimethyl phenyl ammonium chloride [215]	Iso-butanol	7	625	1.29	0.4–5	Alloys
		Eriochrome cyanine R, bipyridyl, anionic surfactant [216]	H ₂ O	10.4	575	4.6	0–159 $\mu\text{g}/50$ ml	—
PAR, benzylidimethyl tetradecyl ammonium chloride [217]		CHCl ₃	9.7	510	8	0.1–0.5	—	
Xylenol orange, CPCI [218]		H ₂ O	9	605	—	—	—	
Chromal Blue G, CTACI [219]		H ₂ O	10.5	542	4.8	0.1–16 ppb	—	
5-Br-PADAP, CTAB [220]		H ₂ O	1.5–4.0	565	8.5	≤ 0.8	—	
Chromazurol S, CTAB [221]		H ₂ O	8	615	—	0.03–0.55	—	
10-(benzoxazol-2-ylazo)phenanthren-9-ol, surface active agent [222]		1,4-Dioxan	5.1 \pm 0.1	542	5.1	0–0.8	—	
Chromazurol S, CTAB [223]		—	—	—	—	—	—	
Chromazurol S, CPCI [224]		H ₂ O	10	530	4.2	2.5–40 $\mu\text{g}/25$ ml	—	
Eriochrome cyanine R, CPCI [225]		H ₂ O	7.0–7.75	593	—	0–0.6	—	
5-Dimethylamino-2-nitrosophenol, Zephiramine [226]	CHCl ₃	—	468	3.6	—	Iron, steel, Al alloy		
PAR, Triton X-305, CPCI [227]	H ₂ O	10	540	7.2	Up to 2 ppm	—		

Table 2 (continued)

Element	Reagents [R]	Medium for determination	pH/acidity	λ_{\max} , nm	$\epsilon \times 10^{-4}$	Beer's law range (ppm)	Applications
Fe	4,5-Dibromophenylfluorone, CTAB, Triton X-100 [228]	H ₂ O	—	470	117	Up to 50 ppb	Zn alloys, glass, human hair
	SCN ⁻ , CTAB [229]	Benzene	1	475	—	—	—
	Pyrocatechol violet, CTAB [230]	CHCl ₃	5.15	595	6.55	≤ 4 µg	—
	Chromal Blue G, CTACl [231]	H ₂ O	—	693	14.3	0.04–0.4	Mg alloys
	Chromazurol S, cationic surfactant [233]	H ₂ O	4	645	—	—	—
	Chromazurol S, dodecyl bis-(polyoxyethylene)ammonioformic [234]	H ₂ O	—	630	—	—	—
	Methylthymolblue, CTAB [235]	H ₂ O	4–6.5	540	2.75	0–60 µg/50 ml	—
	Bromopyrogallol Red, Quaternary ammonium salt [236]	H ₂ O	5.5	635	5.6	0.08–0.5	—
	Eriocyanine R, Zephiramine [237]	H ₂ O	4.3	630	—	0–10 µg	—
	Alizarin yellow R, CTAB [238]	H ₂ O	—	520	9.3	0–8.5 µg/25 ml	—
	Bromopyrogallolred, CTAB [239]	H ₂ O	—	630	5.2	0.005–0.5	—

Table 3
Continuation of Table 2

Element	Reagents [R]	Medium for determination	pH/acidity	λ_{max} , nm	$\epsilon \times 10^{-4}$	Beer's law range (ppm)	Applications
Ga	<i>o</i> -Chlorophenylfluorone, CTAB [240]	H ₂ O	8.6–9.8	505	15.7	0.04–0.64	Ores
	Dibromophenylfluorone, CPB [241]	H ₂ O	3.5–6.5	570	13.5	Up to 0.4	Ores
	Eriocyanine R, Zephiramine [242]	H ₂ O	4–4.5	580	12.3	—	—
	<i>o</i> -Chlorophenylfluorone, CPB [243]	H ₂ O	5.7–6.5	578	17	Up to 0.4	Ores
	Eriocyanine R, CPB [244]	H ₂ O	4.5	585	—	0.7–3.1 $\mu\text{g}/25$ ml	—
	Chromazurol S, benzyl dimethyl lauryl ammonium bromide [245]	H ₂ O	3.5–4.0	620	11	—	Al, AlCl ₃
	Morin, sodium dodecyl sulphate, Triton X-100 [246]	H ₂ O	—	510	—	2–120 ppb	—
	ChromalBlue G, CTACl [247]	H ₂ O	6.5	662	14.4	1.15 $\mu\text{g}/25$ ml	—
	Baromopyrogallol red, CTAB [248]	H ₂ O	4.8–5.2	625	13.00	0.1–0.4	—
	Phenylfluorone, pyridine, CPB [249]	H ₂ O	4–5.5	570	14.8	Up to 4.3 μM	—
	<i>o</i> -Chlorophenylfluorone, hexadecyl dimethyl ammonium acetate, Triton X-100 [250]	H ₂ O	7.5	565	17.4	Up to 0.24	—
	5'-Nitrosalicylfluorone, CTAB [251]	H ₂ O	7.3–8.0	555	19.10	0–7 $\mu\text{g}/25$ ml	Pb ores
	Alizarin S, CPB [252]	H ₂ O	3.3	505	—	0–0.28	—
	4,5-Dibromophenylfluorone, CTAB [253]	H ₂ O	6–8	580	17.1	0–9 $\mu\text{g}/25$ ml	Ores
	4,5-Dibromophenyl fluorone, CTAB [254]	H ₂ O	7.8–8.5	588	25.9	0–0.35	Rocks and minerals
Ge	Chromazurol B, amphoteric surfactant [255]	H ₂ O	6.1	638	—	0.1–14	—
	4-Aminophenylfluorone, CTAB [256]	H ₂ O	6.2–8.4	550	15.8	0–10 $\mu\text{g}/50$ ml	Ores, Pb and Zn
	Eriochrome cyanine R, CTAB [257]	H ₂ O	5	535	—	0–1	Al, AlCl ₃
	Chromazurol S, CPB [258]	H ₂ O	4.9–5.3	640	10.2	0.35–3.5	Semiconductors, alloys
	Vanilylfluorone, CTAB [259]	H ₂ O	—	510	12.4	—	Alloys
	<i>o</i> -Chlorophenylfluorone, CTAB [260]	H ₂ O	—	512	16	0–0.2	—
	<i>p</i> -Chlorophenylfluorone, Tween-60 [261]	H ₂ O	6–7	518	18	—	—
	Phenylfluorone, CTAB [262]	H ₂ O	—	505	15	Up to 0.28	—
	9-(2-chlorophenyl)-2,6,7-trihydroxyanthene-3-one, CTAB [263]	H ₂ O	—	516	18.2	Up to 0.2	—
	2,4-Dichlorophenylfluorone, CTAB [264]	H ₂ O	—	513	17	0–9 $\mu\text{g}/50$ ml	—
Phenylfluorone, zephiramine [265]	H ₂ O	—	505	13.8	0–0.4	—	
Salicylfluorone, CTAB [266]	H ₂ O	—	515	15.1	0–0.5	—	
Phenylfluorone, Dodecyltrimethyl- ammonium bromide [268]	H ₂ O	—	530	17.2	0–0.4	—	
BPR, CTAB [269]	H ₂ O	—	670	6.3	≤ 1.6	—	
Dithiazone, CPCl [270]	H ₂ O	12.9	555	8.4	1–10 μM	—	
Oxne-5-sulphonic acid, CPCl [271]	—	4.4	390	—	0–41 μg	—	

Table 3 (continued)

Element	Reagents [R]	Medium for determination	pH/acidity	λ_{\max} , nm	$\epsilon \times 10^{-4}$	Beer's law range (ppm)	Applications
In	BPR, CTAB [272]	H ₂ O	—	620	—	3–23 $\mu\text{g}/25$ ml	—
	Chromazurol S, benzyl(dodecyl)-dimethylammonium bromide [273]	H ₂ O	—	625	17.4	0.04–0.448	—
Ln	Alizarin violet, CPCl [274]	H ₂ O	5	620	3.5	—	Sn foil, Pb mining samples
	9-(2-chlorophenyl)2,6,7-trihydroxy-xanthene-3-one, CTAB [275]	H ₂ O	5–6.6	583	19.2	Up to 0.5	—
	Eriochrome cyanine R, CTAB [276]	H ₂ O	—	585	11	0–0.8	—
	Salicylfluorone, cetrinide [277]	H ₂ O	6.2	570	15	—	—
	Phthalexon S, CPB [278]	H ₂ O	8	605	2.6	0.05–5	—
	<i>p</i> -Sulphamoylchlorophosphonazo, CTAB [279]	H ₂ O	—	680	18.9	—	—
	BPR, Septonex [280]	H ₂ O	—	670	—	—	—
	Chromazurol S, 5-nitro, 1,10-phen, CTAB [281]	H ₂ O	9.5	—	—	0–0.8	—
	Chromazurol S, 2,2'-bipyridyl, CPCl [282]	H ₂ O	9.5–11.5	640	10.8	0.1–1.0	—
	Eriochromeazuro B, 5-nitro-1,10-phen, CTAB [283]	H ₂ O	10–10.5	—	—	0–0.8	—
Lu	Glycine thymol blue, CPCl, benzylthiourea [284]	H ₂ O	8–8.5	660	—	0.035–3	—
	Methylthymol blue, CPCl [285]	H ₂ O	5.0	635	—	Up to 55 $\mu\text{g}/25$ ml	—
	Xylidyl blue, CTAB, OP [286]	H ₂ O	9.8–11.5	520	2.5	Up to 0.32	—
Mg	4,5-Dibromophenylfluorone, CTAB [287]	H ₂ O	11	610	13.8	Up to 0.4	Minerals
	Eriochromeazuro B, 2,2'-bipyridyl, CTAB [288]	H ₂ O	9.5–10.5	625	8.3	Up to 0.6	—
Mn	<i>o</i> -Nitrophenylfluorone, CTAB, OP [289]	H ₂ O	8.4–11.0	615	15.3	—	—
	2-Nitrophenylfluorone, CPB [290]	H ₂ O	9.4–9.9	—	13	40–240 ppb	Mn, Al, Se alloys
Mo	Chromazurol S, 1,10-phen, CTAB [291]	H ₂ O	10.5	618	9.6	0.04–1	Rocks and minerals
	Phenylfluorone, CPB [292]	H ₂ O	8.5–9.8	590	12.3	≤ 10	—
	2,6,7-Trihydroxy-9-(2-hydroxy-phenyl)fluorone, CTAB [293]	H ₂ O	—	525	—	≤ 20 $\mu\text{g}/50$ ml	Ta and Nb
	Quinalizarin, CPCl [294]	H ₂ O	3.8	580	12.7	≤ 0.6	—
	<i>p</i> -Diethylaminophenylfluorone, CPB [295]	H ₂ O	2.8	532	11	0–14 $\mu\text{g}/25$ ml	Steels
	7,8-Dihydroxy 4-methylcoumarin, CTAB [296]	H ₂ O	5.8	400	13.2	Up to 0.6	—
	<i>o</i> -Nitrophenylfluorone, CTAB [297]	H ₂ O	—	530	15.5	Up to 0.4	—
	BPR, CPB, OP [298]	H ₂ O	—	620	5.9	0.1–1.2	—
	Salicylfluorone, CTAB [299]	H ₂ O	—	532	—	≤ 1 $\mu\text{g}/25$ ml	—
	9-(4-Formylphenyl)2,6,7-trihydroxyxanthene, CTAB [300]	H ₂ O	—	530	8.3	0–0.4	Steel
	4,5-Dibromophenylfluorone, cetrinide [301]	H ₂ O	—	538	12	0–0.55	—
	Oxine-5-sulphonic acid, methyltriocetyl ammonium chloride [302]	CHCl ₃	—	570	—	38–228 μg	—
BPR, CTAB [303]	H ₂ O	—	630	8.4	—	Sea water	
BPR, CTAB [304]	H ₂ O	—	640	6.1	—	—	
Hematoxylin, CTAB [305]	H ₂ O	5.6–6.8	610	—	—	Steel	
Pyrogallol red, CTAB [306]	H ₂ O	3.6	610	—	—	—	
Payrogallol red, CPCl [307]	H ₂ O	4.7	610	—	—	—	

Table 3 (continued)

Element	Reagents [R]	Medium for determination	pH/acidity	λ_{\max} , nm	$\epsilon \times 10^{-4}$	Beer's law range (ppm)	Applications
Nb	BPR, CPCI [308]	H ₂ O	6.5–7.0	635	14.1	0–22 $\mu\text{g}/50$ ml	—
	4,5-Dibromophenylfluorone, CTAB [309]	H ₂ O	—	540	21	≤ 0.3	—
Ni	Chromazurol S, CTAB [310]	H ₂ O	10.5	640	14.8	Up to 0.4	—
	2-(Benzothiazol-2-ylazo)5-dimethyl-aminophenol, DMF, dodecylpyridinium chloride [311]	—	7–8.5	545	10.7	0–160 ppb	Waters
Pb	Xylenol orange, CTAB [312]	H ₂ O	9.5	614	—	0–360 ppb	Steels and soils
	1,10-Phen, phloxine, polyoxyethylene glycol [313]	H ₂ O	8	566	4.7	1–15 $\mu\text{g}/25$ ml	Steel
	Dithiazone, methyltriocetylammmonium chloride [314]	H ₂ O	5.2	503	2.4	0–0.6	—
	Catechol violet, CPCI [315]	H ₂ O	7.6	645	5.07	0.5–4	—
	Salicylfluorone, CPCI [316]	H ₂ O	5.5	565	9	—	—
	Pyrogallol Red, CTAB [317]	H ₂ O	6.5	610	2.1	Up to 60 μg	—
	BPR, CTAB or CPB [318]	H ₂ O	5	630	2.6	10–40 $\mu\text{g}/25$ ml	Brass
	2-(5-bromo-2-pyridylazo)5-diethyl aminophenol, CTAB [319]	H ₂ O	7	575	5.1	0.5–4.9	—
	Sodium 2-bromo-4'-5'-dihydroxy azobenzene-4-sulphonate, CTACl [320]	H ₂ O	8.7	530	4.5	0–80	—
	3',4'-Dimethoxyphenylfluorone, CTAB [321]	H ₂ O	7.2–8.4	587	11.1	0–0.6	Catalysts
Pd	<i>p</i> -Bromophenylfluorone, CTAB [322]	H ₂ O	7.8	598	9.3	0–0.5	Catalysts
	Chromazurol B, hexadecyldimethyl ammonium acetate, Triton X-100 [323]	H ₂ O	6.8	645	13	0–4 $\mu\text{g}/25$ ml	—
	I ⁻ , CTAB [324]	CHCl ₃	2–10	340	2.04	Up to 5	—
	4'-Hydroxy-3'-methoxy phenylfluorone, CTAB [325]	H ₂ O	7.2	582	—	Up to 0.16	—
	Phenylfluorone, CPCI [326]	H ₂ O	—	—	8.5	Up to 75 μM	Ti–Pd alloys
	1,4-Dihydrazinophthalazine, CPCI [327]	H ₂ O	—	400	2.6	Up to 2	Catalysts
	2,6,7-Trihydroxy 9-(3,5-dibromo-4-hydroxy phenyl)3-fluorone, CTAB [328]	H ₂ O	6.4	—	9.5	Up to 0.7	—
	5-(3,4-Methoxyhydroxybenzylidene) rhodamine, CTAB [329]	H ₂ O	9.7	530	—	0.32–1.56	—
	Chromazurol S, CTAB or CPB [330]	—	—	583	11.7	0–16 $\mu\text{g}/25$ ml	Catalysts
	Salicylfluorone, CTAB [331]	H ₂ O	6.2	530	—	—	—
Pr	Dithiazone, methyltriocetylammmonium chloride [332]	H ₂ O	5–8	540	2.9	0–3.6	Catalysts
	PAR, CTAB [333]	H ₂ O	3.8–5	630	8.80	0.2–0.8	—
	Chromazurol S, CTAB [334]	H ₂ O	>9.4	613	10.2	0–15 $\mu\text{g}/25$ ml	—
	Eriochrome cyanine R, 1,10-phen, CTAB [335]	H ₂ O	—	290	5.4	Up to 3	—
Pt	I ⁻ , CTAB [336]	Ethylacetate	4.2	540	83	Up to 0.35	—
	4,5-Dibromophenylfluorone, CTAB [337]	H ₂ O	4.5	650	—	25–290 $\mu\text{g}/50$ ml	—
	Chromazurol S, CPB [338]	H ₂ O	—	—	—	—	—

Table 4
Continuation of Tables 2 and 3

Element	Reagents [R]	Medium for determination	pH/acidity	λ_{max} , nm	$\epsilon \times 10^{-4}$	Beer's law range (ppm)	Application
Rh	PAR, CPCl [339]	CHCl ₃	5.2	520	—	0.08–1	—
	2,6,7-Trihydroxy-9-(3,5-dibromo-4-hydroxy)phenylfluorone, CTAB [340]	—	—	610	2.9	≤0.5	Alloys
Sb	Salicylfurone, CTAB [341]	H ₂ O	—	595	11	Up to 0.4	Catalysts
	4,5-Dibromophenylfluorone, CTAB [342]	H ₂ O	—	578	39.6	0–35 $\mu\text{g}/25 \text{ ml}$	Cu alloys
	Dibromophenylfluorone, CPB [343]	H ₂ O	—	550	5.6	0–35 $\mu\text{g}/25 \text{ ml}$	Cu alloys
Sc	Salicylfurone, I ⁻ , emulsifying agent [344]	H ₂ O	—	510	7.1	0–15	—
	Chlorophosphonazo, tetradecyl-pyridinium chloride [345]	H ₂ O	—	677	5.2	Up to 0.8	Alloys
	<i>o</i> -Chlorophenylfluorone, CTAB [346]	H ₂ O	—	560	12.1	Up to 0.48	Ores
	<i>o</i> -Chlorophenylfluorone, CTAB [347]	H ₂ O	—	560	12.1	0–6 $\mu\text{g}/25 \text{ ml}$	—
	Chromazurol S, benzyldimethyl dodecyl ammonium bromide [348]	—	—	610	13.7	0.02–0.3	Cu and Mg
Sn	Chromazurol S, CTAB or CPB [349]	H ₂ O	5.7	645	14.9	0.04–0.4	—
	Chromazurol S, zephiramine [350]	H ₂ O	5.2	614	16.4	—	—
	Eriocyanine R, CPB [351]	H ₂ O	—	600	9.2	—	—
	Chlorophosphonazo, tetradecyl pyridinium chloride [352]	—	2.0	677	4.5	—	Alloys
	Chlorophosphonazo, octylpyridinium bromide [353]	—	—	727	10.6	0.2–0.6	—
	<i>o</i> -Hydroxyquinolphthalein, CPCl [354]	—	5.4	555	10	0–4.5 μg	—
	Chromazurol S, trimethyloctyl ammonium bromide [355]	—	—	597	19	1–6 $\mu\text{g}/25 \text{ ml}$	—
	Eriochromeazuro B, zephiramine [356]	H ₂ O	5–6	603	—	0.5–8 $\mu\text{g}/25 \text{ ml}$	—
	Salicylfurone, NTA, CTAB [357]	H ₂ O	3.8	532	27.4	53.6–874.4 ppb	—
	4,5-Dibromophenylfluorone, NTA, CTAB [358]	H ₂ O	2.8–3.9	560	14.2	—	Alloys
	Vamyl fluorone, CPB [359]	H ₂ O	—	515	18.4	Up to 6 μg	—
	4-(4-Iodophenylazo)pyrogallol, CTAB [360]	—	—	500	—	Up to 1.6	—
	BPR, CPB [360]	H ₂ O	2.6–2.9	530	37.2	0.2–5 $\mu\text{g}/25 \text{ ml}$	Pb(NO ₃) ₂
	Phenylfluorone, polyoxyethylene glycol [362]	H ₂ O	—	520	12.3	≤15 $\mu\text{g}/50 \text{ ml}$	—
	Trihydroxyfluorone, CPB [363]	—	—	—	—	—	—
4-Nitrophenylfluorene, CTAB [364]	H ₂ O	—	515	9.1	—	Cu and brass	
2,6,7-Trihydroxy xanthene-3-one, CTAB [365]	H ₂ O	—	512	—	0–0.2	—	
Phenylfluorone, CTAB [366]	H ₂ O	—	505	—	—	Alloys	
Salicylfurone, CTAB [367]	H ₂ O	—	510	17.9	0–8 $\mu\text{g}/25 \text{ ml}$	Steels	
Catechol violet, CPB [368]	H ₂ O	—	665	9.8	0–1.8	—	
Catechol violet, CTAB [369]	—	—	—	—	—	—	
Bromopyrogallol red, CPB [370]	H ₂ O	0.9–1.3	550	3	0.05–1	Steels and iron Plastics, granite and foods	
Ta	Phenylfluorone, dodecyl trimethyl ammonium bromide [371]	H ₂ O	—	508	14.3	1–50 μg	—
	2,7-Dihydroxyfluorescein, tartaric acid, CPB [372]	H ₂ O	—	510	20.3	—	Minerals and rocks
	2,4-Dichlorophenylfluorone, CTAB [373]	H ₂ O	—	520	—	0–40 $\mu\text{g}/50 \text{ ml}$	—
4-Carboxy-6,7-dihydroxy-2-phenylbenzopyrylium chloride, CTAB [374]	H ₂ O	3–5.5	—	—	—	—	
4,5-Dibromophenylfluorone, tartaric acid, CTAB [375]	H ₂ O	—	540	10	—	—	

Table 4 (continued)

Element	Reagents [R]	Medium for determination	pH/acidity	λ_{max} , nm	$\epsilon \times 10^{-4}$	Beer's law range (ppm)	Application
Th	Eriochrome cyanine R, CPCl [376]	H ₂ O	5.5–5.9	595	—	0.2–1.1	—
	Phenylfluorone, CPB [377]	H ₂ O	10.2	568	16	0.1–1.66	—
	<i>m</i> -Carboxychlorophosphonazo, CPCl [378]	H ₂ O	—	685	15	Up to 0.4	RE–Si–Mg alloys
	Chlorophosphonazo, CTAB [379]	H ₂ O	—	685	35	≤0.2	—
	5-Dimethylamino(2-thiazolylazo) phenol, CPCl [380]	H ₂ O	4.3–4.8	570	8.5	0–2.4	—
	Chlorophosphonazo, CPB [381]	H ₂ O	—	707	24.1	0–0.4	Water
	Chromazurol S, Dodecyl dimethyl- ammonium acetate [382]	H ₂ O	—	625	16	0–1	—
	4,5-Diphenylfluorone, tartrate, CTAB [383]	H ₂ O	4.3	625	30.2	≤0.12	Steels and rocks
	2,3,7-Trihydroxy-4-chlorophenyl- fluorone, NTA, CTAB [384]	H ₂ O	5.8–6.6	573	—	Up to 140 ppb	Rocks and Al alloys
	<i>o</i> -Hydroxyquinol, phthalein, Tween-20 [385]	H ₂ O	4.7	595	19.1	0.03–0.24	—
	Phenylfluorone, <i>N</i> -phenyldodecano- hydroxamic acid [386]	H ₂ O	—	560	12.3	≤0.4	—
	4,5-Dibromophenylfluorone, Tween-80 [387]	H ₂ O	—	530	—	0–4 µg/25 ml	—
	Erichrome cyanine R, CTAB [388]	H ₂ O	—	560	4.1	0–0.4	—
	Catechol violet, hydroxylamine, CTAB [389]	H ₂ O	3	730	9.4	0.08–0.4	—
	Bromopyrogallol red, CPB [390]	H ₂ O	—	630	—	—	—
	Phenylfluorone, CPB [391]	H ₂ O	—	535	14.6	≤10 µg	—
	Barompyrogallol red, CPB [392]	H ₂ O	3	630	2.6	0.2–2	—
Catechol violet, tridodecylethyl-ammonium bromide [393]	CCl ₄	—	586	5.2	0.06–1.0	—	
Salicylfluorone, CTAB [394]	H ₂ O	—	540	16.4	0–0.2	—	
Chromazurol S, CTAB [395]	H ₂ O	—	565	7.3	—	—	
4,5-Dibromophenylfluorone, NTA, CTAB [396]	H ₂ O	—	576	21.3	≤0.4	—	
Disulphophenylfluorone, Triton X-305 [397]	H ₂ O	3.1–3.4	592	14	2–150 ppb	—	
Bromopyrogallol red, CPB [398]	H ₂ O	2.5	625	—	—	—	
Alizarin Yellow, CTAB [401]	H ₂ O	—	450	—	0–0.6	—	
Chromazurol S, BPR, CTAB [402]	H ₂ O	1–1.5	590	7.5	0–0.4	Alloys	
Gallein, CPCl [403]	H ₂ O	—	610	140	Up to 0.1	Alloys	
Bromopyrogallol red, CTAB [404]	H ₂ O	—	410	—	0.08–1	—	
Eriochromeazurol B, Septonex [405]	H ₂ O	5.6	635	—	1.5–9 µM	—	
Chromazurol S, CTAB [406]	H ₂ O	5.4	628	—	0.6–2.6	—	
Chromazurol S, benzyldimethylauryl ammonium bromide [407]	H ₂ O	5	610	9.2	0.04–2.8	—	
Ti	Eriocyanine R, Septonex [408]	H ₂ O	5.6	596	8	Up to 26 µg	—
	Alizarin green, CTAB [409]	H ₂ O	4.7	645	—	0.5–15	—
	Salicylfluorone, Zephiranine [410]	H ₂ O	—	555	12.7	≤1	—
	Chromazurol S, CTAB [411]	H ₂ O	4.5	620	8.1	—	—
	4(2-Thiazolylazo)resorcinol, Zephiranine [412]	H ₂ O	7	540	0.35	0–6	—
V	Eriocyanine R, benzyl dodecyl methylammonium bromide [413]	—	5.00	580	8.4	1–16 µg/25 ml	—
	<i>o</i> -Hydroxyquinol phthalein, CTAB [414]	H ₂ O	5.4	—	—	Up to 0.8	Water
	Alizarin red S, CPB [415]	H ₂ O	3.3	520	—	0.4–2.4	—
	PAR, H ₂ O ₂ , CTAB [416]	H ₂ O	5	584	4	0–0.25	—
	Alizarin complexan, CPCl [417]	H ₂ O	2.1–2.7	520	—	—	—
	Catechol violet, CTAB [418]	—	—	—	—	—	—

Table 4 (continued)

Element	Reagents [R]	Medium for determination	pH/acidity	λ_{max} , nm	$\epsilon \times 10^{-4}$	Beer's law range (ppm)	Application
W	Eriochrome cyanine R, CTAB [419]	H ₂ O	5.7	585	6.6	≤ 18 µg	—
	Chromazurol S, CTAB [420]	H ₂ O	3.8	580	—	0.2–1.63	—
	Gallein, Sodium dodecyl sulphate [421]	H ₂ O	4.5	535	1.6	0–3.4	—
	Alizarin green, Septonex [422]	H ₂ O	2–6.5	—	—	—	—
	3,4,5,6-Tetrachloro gallein, CPCl [423]	H ₂ O	—	385	70	0–0.8 µg	—
	<i>o</i> -Chlorophenylfluorone, NTA, CTAB [424]	H ₂ O	—	520	12.4	Up to 1	—
	Dibromoalazarin violet, CTAB [425]	H ₂ O	—	620	8.2	0–0.01	—
	Saicylfluorone, polysorbate, CTAB [427]	H ₂ O	—	519	14.3	0–1	—
	Sodium 2-bromo 4'-hydroxyazobenzene-4-sulphonate, CTACl [428]	H ₂ O	3	490	4.3	≤ 74 µg	—
	Pyrogallol red, CTAB, OP emulsifier [429]	H ₂ O	5.6	580	—	0–74 µg	—
	4,5-Dibromophenylfluorone, CTAB [430]	H ₂ O	—	528	13.2	≤ 0.6	—
	Saicylfluorone, CTAB [431]	—	—	518	—	—	—
	Catechol violet, CTAB [432]	—	—	650	—	—	—
	2-(2-Thiazolyazo) <i>p</i> -cresol, zephiramine [433]	H ₂ O	7.5–8	610	—	0–1.2	—
	Chromazurol S, 1,10-phen, dimethyldodecyl ammonio acetic acid [434]	—	7–11	638	14	0–16 µg/25 ml	—
Zn	PAN, diphenylguanidine, CTAB [435]	CHCl ₃	10	555	6	0.1–1.2	—
	Chromazurol B, quinoline, CTAB [436]	H ₂ O	8.7	590	11.3	Up to 18 µg	—
	Dithiazone S, CPB [437]	H ₂ O	12	582	—	—	—
	Methylthymol blue, oxine, CPCl [438]	H ₂ O	—	620	—	3	—
	Sulpharsazen, CPCl [439]	Butanol-CHCl ₃	9	460	—	0.2–1.6	—
	Phenylfluorone, Pyridine, CPB [440]	—	7.7–8.2	585	8	≤ 15.3 µm	—
	PAR, CTAB [441]	CHCl ₃	9.7	505	9.8	≤ 0.3	—
	2-(3,5-Dibromo-2-pyridylazo)-5-diethylammonophenol, sodium dodecyl sulphate [442]	H ₂ O	8.2	570	13.5	≤ 7	—
	Vamylfluorone, polysorbate 20 [443]	H ₂ O	—	530	13.9	Up to 0.48	—
	2,3,7-Trihydroxyphenylfluorone, dodecyl dimethylbenzylammonium bromide [444]	—	—	—	13.8	0.02–0.144	—
Zr	BPR, CTACl [445]	—	—	—	—	Up to 37 µg/25 ml	—
	Chlorophosphonazo DBC, CTAB [446]	H ₂ O	—	650	6.3	0–0.5	Alloys
	<i>p</i> -Acetylchlorophosphonazo, sodium dodecyl benzene sulphate [448]	H ₂ O	—	419	60.3	0–0.12	—
	<i>m</i> -Nitrophenylfluorone, CTAB [449]	H ₂ O	—	538	17	0–7 µg	—
	4,5-Dibromophenylfluorone, polysorbate 60, CTAB [450]	H ₂ O	—	540	19	0–0.38	Steels and alloys
	Chromazurol B, hexadecyldimethyl ammonium acetate, OP [451]	H ₂ O	1.6–1.7	660	21.7	1–16	—
	5-Br PADAP, Polysorbate 80 [452]	H ₂ O	2.6–3.6	585	12	0–0.4	Alloys
	5-Br PADAP, sodium dodecyl sulphate [453]	H ₂ O	3–5	634	31.5	—	—
	Morin, polysorbate 80, CPB [454]	H ₂ O	—	420	8.7	0–0.6	—

Table 5
Flotation—spectrophotometric methods

Element	Anion(Dye)[R]	Flotation solvent	λ_{max} nm	$\epsilon \times 10^{-4}$	Beer's law range (ppm)	Applications
Ag	SCN ⁻ (Rhodamine 6G) [455]	Diisopropyl ether	530	15.2	0.3–4	River water
Au	I ⁻ , SnCl ₂ (CI basicgreen 4) [456]	—	620	270	1.2–64 ppb	Tap water, Li ₂ CO ₃
	Cl ⁻ (crystal violet) [457]	—	603	63.5	0.05–0.4	—
Hg	I ⁻ , (Methylene blue) [458]	Diisopropyl ether	655	34	—	Blister copper
	Br ⁻ (Rhodamine 6G) [459]	Diisopropyl ether	545	116	—	Blister copper
	SCN ⁻ (Rhodamine 6G) [460]	Diisopropyl ether	530	21	50–1000 ppb	CaCl ₂ , sediment
	I ⁻ Methylene blue [461]	Cyclohexane	655	34	0.1–3	Cd and CdO
Ir	I ⁻ (Brilliant green) [462]	Cyclohexane	625	59.60	0.004–0.5	Paper industry effluent
	SnCl ₂ (Rhodamine B) [463]	Pentane	553	47.7	Up to 0.72	—
	SnCl ₂ (Rhodamine 6G) [464]	Diisopropyl ether	530	36	0.08–0.4	—
Mo	SCN ⁻ (Catechol violet) [465]	Toluene	590	18.7	0.025–0.42	—
Nb	3,5-Dinitrocatechol(Rhodamine B) [466]	Cyclohexane	555	21	0.01–0.3	Soil and rocks
Os	Cl ⁻ (Rhodamine 6G) [467]	Toluene	530	4	—	Pt metals
	SCN ⁻ (Capri blue) [468]	—	630	—	0–16 μg	—
	SCN ⁻ (methylene blue) [469]	Toluene	655	—	0–0.8	Pt
	SnCl ₂ (Rhodamine B) [470]	Cyclohexane	560	—	Up to 0.4	Pt group metals
	SnCl ₂ (Rhodamine B) [471]	Toluene	560	62	0.04–0.3	—
	SnCl ₂ (Crystal violet) [472]	Cyclohexane	600	20	—	Pt
	Molybdate (Malachite green) [473]	Butyl acetate	620	27	Up to 0.1	Fe, Co, Ni and Zn
	SnCl ₂ (Rhodamine 6G) [474]	Diisopropyl ether	530	28	0.05–0.35	Ag metal
	SCN ⁻ (methylene blue) [475]	Toluene	660	—	—	Ag
	Br ⁻ (Safranin T) [476]	Benzene	520	22	—	—
Pr	5,7-dichlorooxime (Rhodamine 6G) [477]	Hexane	530	18.3	40–240 ppb	Al and steel
Pt	SnCl ₂ (Rhodamine B) [478]	—	555	33.6	—	—
Rh	SnCl ₂ (Malachite green) [479]	Diisopropyl ether	627	34	$\leq 8 \mu\text{g}$	—
	SnCl ₂ (Rhodamine 6G) [480]	Diisopropyl ether	530	40	0.04–0.5	Pd metal
Ru	SnCl ₂ (Crystal violet) [481]	Toluene	600	—	0.04–0.56	—
	Cl ⁻ (Rhodamine 6G) [482]	Toluene	530	51	0.07–0.25	Crucible Pt
Si	Cl ⁻ (Rhodamine 6G) [483]	Toluene	530	10.9	0–0.6	—
	SnCl ₂ (Malachite green) [484]	—	621	100	0.05–0.8 $\mu\text{g}/25 \text{ ml}$	—
	SnCl ₂ (Rhodamine B) [485]	Hexane	530	50	0.04–0.2	Crucible Pt
	Molybdate (Malachite green) [486]	Cyclohexane – IBMK (8:1)	620	42	10 nM	—
Sn	Molybdate (Chromopyrazol II) [487]	Toluene–acetone (1:1)	590	21.5	2–20 ppb	—
	SnCl ₄ (Rhodamine 6G) [488]	Diisopropyl ether	530	8.7	0.1–2	Sn(IV) chloride
Te	Papaverine (Butyl Rhodamine B) [489]	—	565	—	1–20	Cu
V	I ⁻ (Nile blue A) [490]	Benzene	640	—	Up to 2	—
	3,5-Dinitrocatechol (Rhodamine B) [491]	Hexane	555	21	0.003–0.3	Plants, vegetable
	3,5-Dinitrosalicylic acid (Rhodamine B) [492]	Cyclohexane	555	59	0.002–0.06	Marine sediments

Table 6
Ion-association systems

Element	Reagents [R]	Medium for determination	pH/Acidity	λ_{\max} nm	$\epsilon \times 10^{-4}$	Beer's law range (ppm)	Applications
Ag	1,10-Phen-eosine, PVA, Triton X-100 [493]	H ₂ O	5	550	9.72	0.004–0.8	—
	SCN ⁻ , Rhodamine B [494]	H ₂ O	—	588	27.3	0.02–0.25	Captis root and human hair
	Adenine, eosine [495]	H ₂ O	—	560	11	0.2–15 μ g	Solder and protein
	Bathophenanthroline, eosine, PVA, Triton X-100 [496]	H ₂ O	5.5	559	1	—	Waste liquor and anodic mud
	1,10-Phen, eosine [497]	—	5.3–5.4	548	—	—	—
	Bathophen, methyl orange [498]	CHCl ₃	6–7	384	3.13	0–2.5	—
	1,10-Phen, cadion [499]	CHCl ₃	—	525	—	—	—
	1,10-Phen, Phloxine [500]	—	6.3–7.4	—	4.8	0–0.5	—
	Cyanide, methylene blue [501]	—	—	657	—	—	—
	1,10-Phen, eosine [502]	—	5.8–6.4	540	—	0.16–1.03	—
As	I ⁻ , Rhodamine B [503]	H ₂ O	—	600	16.5	1–12 μ g/25 ml	—
	Catechol, Brilliant green [504]	Toluene	—	—	—	—	—
	Molybdate, ethyl Rhodamine B [505]	H ₂ O	—	586	22	Up to 0.1	Steel, chemical reagents
	Molybdate, ethyl Rhodamine B, PVA [506]	H ₂ O	—	589	30	Up to 0.2	—
	Molybdate, Rhodamine B, PVA [507]	H ₂ O	—	595	19	1–7 μ g/25 ml	Flue dust and plants
	Molybdate, Rhodamine 6G [508]	Toluene	—	530	—	—	—
	Molybdate, crystal violet [509]	—	—	550	12.40	0–0.5	—
	Bromide, chromopyrazol I [510]	Toluene	0.6–3.9	580	7.5	0.05–2.5	Cu, Sb and Pb
	SCN ⁻ , Rhodamine B [511]	—	—	595	12.3	Up to 0.32	—
	Chloride, methylene blue [512]	CHCl ₃	—	—	—	0.1–18	—
Au	Chloride, Tryphan blue [513]	—	4	595	—	1.3–2.5	—
	I ⁻ , Butyl Rhodamine B, OP [514]	H ₂ O	2–3	610	59	1–8	Plating waste liquors
	Br ⁻ , Victoria pure blue BO [515]	—	—	636	—	0.2–1	—
	SCN ⁻ , Rhodamine B [516]	—	—	600	6.7	—	Inorganic compounds, dental alloys
	SCN ⁻ , methylene blue [517]	benzene	0.2–2.6	674	8.4	0.05–2	Zn concentrate
	Chloride, toluidine [518]	—	—	635	—	—	—
	Chloride, acridine yellow [519]	Dichloro-ethane, ethylacetate	1.00	455	6	—	—
	2,4-Dinitronaphthalene 1,8-diol, Brilliant green [520]	Toluene	—	637	—	<0.5 μ g	Steel
	Resorcinol, fluorescein [521]	H ₂ O	5–6	510	1.8	0.02–1.0	—
	Mandelic acid, Malachite green [522]	Benzene	3.2	630	—	Up to 1.5 μ g	Steel
B	Hydroxyphenylacetic acid, Malachite green [523]	Benzene	3.2	637	5.3	0.5–15 μ M	MgO
	Hydroxyphenylacetic acid, Malachite green [524]	—	5.00	595	10	1.6–8 μ M	—
	3,5-Di- <i>t</i> -butylcatechol, ethyl violet [525]	Toluene	6.3–8.7	610	10.5	0–0.45 μ g	Sea water
	Resorcinol, Thionine [526]	H ₂ O	—	510	1.1	40–400 ppb	—
	I ⁻ , Ethyl violet [527]	—	18–28 μ M HCl	540	20.5	Up to 0.96	ores
	I ⁻ , Butyl Rhodamine B [528]	—	—	586	150	Up to 0.1	—

Table 6 (continued)

Element	Reagents [R]	Medium for determination	pH/Acidity	λ_{max} nm	$\epsilon \times 10^{-4}$	Beer's law range (ppm)	Applications
Cd	Alizarin red S, Brilliant green [529]	Ethanol	5	630	—	0.02	—
	I ⁻ , Rhodamine B [530]	—	—	586	150	Up to 0.1	—
	2,6-Dihydroxybenzoic acid, crystal violet [531]	—	1.8–2.8	600	9.8	80–1600 ppb	—
	I ⁻ , Malachite green [532]	Toluene	—	615	16.1	0–1.4	—
	I ⁻ , Janus green [533]	—	—	—	—	—	—
	I ⁻ , crystal violet, triton X-100, PVA [534]	H ₂ O	—	550	17.7	Up to 0.32	Waste water, rice
	4-Mecyclam-14, erythrocin A [535]	CHCl ₃	—	545	—	—	—
	I ⁻ , pyronine G [536]	H ₂ O	4	575	9	0–15 µg/25 ml	Pure Zn materials
	I ⁻ , Malachite green [537]	—	—	654	7.2	Up to 5	—
	I ⁻ , Butylrhodamine B [538]	—	—	600	114	0–0.06	Al alloy and electrolytic Zn
	I ⁻ , ethyl violet, PVA [539]	H ₂ O	—	550	73	Up to 0.08	—
	1,10-Phen, Thymol blue [540]	CHCl ₃	8.5	410	106	0.05–1	Solder, In and Zn compounds
	I ⁻ , Rhodamine B [541]	—	—	610	50.3	Up to 0.2	—
	I ⁻ , Methyl violet [542]	H ₂ O	4	590	15	Up to 0.2	—
I ⁻ , Rhodamine 6G [543]	H ₂ O	3.5	575	8.90	0–0.6	Zn metal and Zn salts	
Cryptate 2,2,1-triiodofluorescein [544]	Nitrobenzene-Toluene (1:4)	—	545	11	—	—	
Ce	I ⁻ , ethyl violet [545]	H ₂ O	5	540	28	0.02–0.2	Ores
	I ⁻ , ethyl Rhodamine B [546]	H ₂ O	—	605	130	0.1–1.5 µg/25 ml	Tapwater and ZnSO ₄
	I ⁻ , Brilliant green [547]	—	—	670	12	0.04–0.6	—
	I ⁻ , Rhodamine B [548]	—	—	600	42	4–200 ppb	Zn salts
	1,10-Phen, Bromophenol Blue [549]	—	—	570	39.6	0.5–24 ppb	—
	Molybdate, butyl Rhodamine B [550]	—	—	—	—	1–20 µg	—
	Nitroso-R-salt, crystal violet [551]	—	—	510	41	Up to 3 µg Co	—
	1,10-Phen, eosine BNX [552]	—	4.6	560	5	0.06–1.68	—
	SCN ⁻ , Brilliant green [553]	—	6.5	635	—	—	—
	1,10-Phen, chromeazurol S [554]	—	6–10	—	—	—	—
	1,10-Phen, eosine [555]	CHCl ₃	7–8	545	9.1	0.01–1.7	—
	SCN ⁻ , Brilliant green [556]	H ₂ O	2	660	14.7	0–0.6	Rocks
	SCN ⁻ , 2,4-Dichlorobenzyltriphenyl phosphonium ion [557]	1,2-dichloroethane	—	328	1.10	0–4	—
	SCN ⁻ , methyl violet [558]	—	—	—	—	0–0.5	Water
I ⁻ , Crystal violet [559]	Toluene	—	607	17	Up to 2.5 µM	—	
Cu	Cl ⁻ , ethyl violet [560]	Toluene	5	612	9.65	—	—
	2,2'-Biquinoyl, picrate [561]	Dichloro-ethane	—	550	—	0.04–0.3	Metal salts and plants
	Neocuproine, eosine Y [562]	CHCl ₃	—	544	6.83	1	Drugs
	Bathocuproine, ethyl eosine [563]	CHCl ₃ -cyclohexanol (30:1)	4.6	545	—	—	—
	SCN ⁻ , Rhodamine B [564]	—	—	610	5	Up to 0.4	Steel and alloys
	2,2'-Biquinoyl, rosebengal [565]	—	6–7	572	—	—	—
	2-(2-Quinoline)benzoquinoline, bromophenol blue [566]	CHCl ₃ -isopentanol	5	421	2.5	—	Al–Mg alloys
	1,10-Phen, Bromophenol blue [567]	—	—	—	—	—	—
	Solochrome Red B, Brilliant green [568]	—	6.00	522	1.30	—	—

Table 6 (continued)

Element	Reagents [R]	Medium for determination	pH/Acidity	λ_{\max} nm	$\epsilon \times 10^{-4}$	Beer's law range (ppm)	Applications
Eu	Hexaaza-18-crown-6, erythroisine [569]	CHCl ₃	11	550	—	0.76 μg	—
Fe	1,10-Phen, tetraiodofluorescein [570]	Nitrobenzene	8	555	21	3–30 n mol	—
	1,10-Phen, picrate [571]	1,2-dichloro-ethane	—	510	13	0.1–3.6	—
	SCN ⁻ , Rhodamine 6G [572]	—	—	510	61.4	Up to 0.12	—
	SCN ⁻ , crystal violet [573]	H ₂ O	—	536	25	0–2.8 $\mu\text{g}/25$ ml	—
	SCN ⁻ , crystal violet [574]	—	0.04–0.12 M H ₂ SO ₄	550	110	Up to 0.1	Alloys and pure salts
Ga	Cl ⁻ , Rhodamine B [575]	Benzene	—	565	—	—	—
Gd	Catechol, Brilliant green [576]	—	2.5	655	20	0.05–0.8	—
	3,5-Diiodosalicylic acid, Rhodamine B [577]	—	5.5	550	—	—	—
Ge	Molybdate, Butyl Rhodamine B [578]	—	—	595	27.2	Up to 0.2	Cu–Cd slag
Hf	Mandelic acid, Malachite green [579]	Chloro- benzene	3	628	13.3	0.17–8.63 μM	—
	Molybdolanthanate, Nile blue [580]	—	—	590	150	Up to 10 ppb	Minerals
Hg	1,10-Phen, Bromophenol blue [581]	CHCl ₃	6.90	610	10	0.2–2	—
	Thiazacrown ether, Bromocresol green [582]	CHCl ₃	3.5	420	—	0.5–12	—
	Br ⁻ or I ⁻ , tetrazoviolet [583]	—	—	250	10.2	1–14 μg	Soils
	I ⁻ , Methylene blue [584]	—	—	560	4.3	0.2	Waste water
	I ⁻ , Ethyl Rhodamine B [585]	H ₂ O	—	605	114	Up to 0.1	—
In	Br ⁻ , Rhodamine B [586]	Ethylacetate-Toluene (1:3)	—	504	15	—	—
	I ⁻ , Pyronine G [587]	Benzene	6.5	515	8.2	0–1.8	—
	Br ⁻ , Rhodamine 6G [588]	H ₂ O	0.5–4.5	528	8.2	0–20	Sea water
	Br ⁻ , ethyl violet [589]	Benzene	—	594	8.2	0–2	—
	Br ⁻ , Crystal violet [590]	Isopentyl-acetate	0.9–1.2	595	9.6	0.1–5	—
	I ⁻ , Rhodamine B [591]	H ₂ O	—	600	52.2	0–0.6	—
	1,10-Phen, Phloxine [592]	1,2-Dichloro-ethane	8.0	564	8.2	≤ 20 μg	—
	SCN ⁻ , crystal violet [593]	—	—	535	—	—	—
	SnCl ₂ , Malachite green [594]	H ₂ O	0.48–0.96 M HCl	600	14.5	Up to 0.8	—
	K	Dibenzo-18-crown-6, Bromothymol blue [595]	CHCl ₃	5.1	410	1.8	—
Cryptand, Methyl orange [596]		CHCl ₃	—	415	2.2	0.3–3.5	—
18-Crown-6, Metanil yellow [597]		—	—	—	—	—	—

Table 7
Continuation of Table 6

Element	Reagents [R]	Medium for determination	pH/Acidity	λ_{\max} nm	$\epsilon \times 10^{-4}$	Beer's law range (ppm)	Applications
Mg	5,7-Diiodoquinolin-8-ol, Rhodamine S [598]	Toluene	9.3	540	6.5	—	—
Mo	SCN ⁻ , Nile blue [599]	H ₂ O	—	630	18	Up to 1.2	Steel and ores
	SCN ⁻ , Rhodamine B [600]	H ₂ O	—	570	38	1.2–220 ppb	Fe–Ni–Mo thin films
	SCN ⁻ , β -cyclodextrin, malachite green [601]	—	—	652	38	Up to 0.2	—
	SCN ⁻ , Malachite green [602]	—	—	640	10	≤ 400 ppb	Ores
	SCN ⁻ , Rhodamine 6G [603]	H ₂ O	—	570	10	0.04–0.24	—
	Tetrabromocatechol, Brilliant green [604]	CCl ₄	—	630	6.6	—	—
	SCN ⁻ , Rhodamine B [605]	H ₂ O	—	580	15	—	Steel
	Catechol, neotetrazolium chloride [606]	CH ₂ Cl ₂	—	650	0.98	0–4.2	—
	Dibromodibenzo-18-crown-6, bromocresol green [607]	CHCl ₃	3–6	418	—	—	—
	Benzo-15-crown-5, Bromocresol green [608]	CHCl ₃	3–4.7	410	0.5	0–3	Water, iron ore
Nd	Benz-15-crown-5, bromophenol blue [609]	CHCl ₃	—	415	0.3	0.5–7	—
	5,7-Dichlorooxine, Rhodamine 6G [610]	Toluene	8.5	535	10.5	Up to 0.5	Al metal
Ni	CN ⁻ , 2,6-Dihydroxy-3-(4'-5'-dimethyl-2-thiazolylo)benzoic acid [611]	—	—	538	3.5	0.05–0.47	Steels
	1,10-Phen, eriochrome red B [612]	CHCl ₃	5.5	490	—	—	—
	1,10-Phen, tetraiodofluorescein [613]	—	7.8	556	19	0.02–0.18	—
	1,10-Phen, eosine [614]	—	8	530	7.1	0–0.4	Water
	4-Chloro-2-nitrosol-1-naphthol, crystal violet [615]	Toluene	7	611	—	0–10 μ M	—
	1,10-Phen, rosebengal [616]	—	7.00	570	—	0.05–1.05	—
	Molybdate, Rhodamine B [617]	—	—	576	260	Up to 1.2 μ g/25 ml	Catalysts, ores
	SnCl ₂ , Brilliant green [618]	H ₂ O	—	434	560	4–28 ppb	Pure Ni
	SnCl ₂ , Malachite green [620]	H ₂ O	—	690	160	Up to 0.16	Precious metal
	Molybdate, malachite green [621]	H ₂ O	—	605	12	—	—
Os	Molybdate, ethylrhodamine B [622]	H ₂ O	—	584	130	Up to 0.01	—
	Molybdate, Rhodamine B [623]	H ₂ O	1.5 MHCl	572	14	—	—
	Molybdate, Malachite green [624]	H ₂ O	—	550	13	0–3.5 μ g/25 ml	NaOH
	Molybdozircono Blue, crystal violet [625]	H ₂ O	—	514	—	0–6.8 μ g/25 ml	—
	Dicyclohexyl-18-crown-6, Dithizone [626]	CHCl ₃	—	514	—	—	—
	Cryptand 2.2.2, eosine [627]	Chlorobenzene	—	545	11.50	—	High purity metals and alloys
	18-Crown-6, Tropaeoline III [628]	CHCl ₃	—	490	—	0.5–10 μ g	—
	I ⁻ , chromopyrazole I [629]	—	—	630	1.12	0.02–4	—
	Cryptand 2.2.2, eosine [630]	—	—	545	—	0–10 μ M	—
	Pd	Molybdate, Rhodamine B [631]	H ₂ O	11	585	41	Up to 4 μ g/25 ml
SCN ⁻ , Malachite green [632]		—	—	—	—	—	—
SCN ⁻ , Rhodamine B [633]		Butylacetate	—	555	—	0.1–8.8 μ g	Catalysts
I ⁻ , Rhodamine B [634]		H ₂ O	—	590	65	≤ 80 ppb	—
SCN ⁻ , Rhodamine B [635]		—	—	590	—	1.12 μ g/25 ml	Catalysts
SCN ⁻ , crystal violet [636]		—	—	582	—	0.02–1.8	Pt
Br ⁻ , Rhodamine 6G [636]		—	0.6	530	—	0–0.3	Pt
I ⁻ , Pyronine G [638]		DMF	2.5	575	—	1–7 μ g/25 ml	Steels, alloys
I ⁻ , Rhodamine 6G [639]		H ₂ O	3.5	575	8.8	0–10 μ g/25 ml	Catalysts
SCN ⁻ , Rhodamine 6G [640]		H ₂ O	4	575	8.8	0–10 μ g/25 ml	Catalysts

Table 7 (continued)

Element	Reagents [R]	Medium for determination	pH/Acidity	λ_{\max} nm	$\epsilon \times 10^{-4}$	Beer's law range (ppm)	Applications
Pt	I ⁻ , pyronine G [641]	H ₂ O	—	575	10.7	0–20 μ g/25 ml	Pd foil
	I ⁻ , Rhodamine 6G [642]	H ₂ O	3	575	12.6	0–14 μ g/25 ml	Catalysts
	SCN ⁻ , Rhodamine 6G [643]	H ₂ O	3	575	14.1	0–10 μ g/25 ml	Catalysts
	SCN ⁻ , crystal violet [644]	—	1.7–2.5	600	4.8	0.05–2.5	—
	SnCl ₂ , Rhodamine B [645]	H ₂ O	—	600	10	Up to 18 μ g/25 ml	Catalysts
	Molybdate, Butyl Rhodamine B [646]	H ₂ O	—	570	93	—	—
	Molybdate, Butyl Rhodamine B [647]	H ₂ O	—	570	93	Up to 3 μ g/25 ml	Catalysts and ores
	Molybdate, Rhodamine B [648]	H ₂ O	—	570	58	0.14 ppb	Catalysts and minerals
	SnCl ₂ , Malachite green [649]	—	—	621	45	0–0.6	—
	I ⁻ , Butyl Rhodamine B [650]	H ₂ O	—	590	30	16–180 ppb	—
Rh	I ⁻ , Rhodamine B [651]	H ₂ O	3–3.8	605	12	\leq 1.2	—
	SnBr ₂ , Malachite green [652]	H ₂ O	—	650	16.7	0–10 μ g/25 ml	Catalysts
	Crystal violet [653]	Benzene	—	590	—	0.1–6	—
	Astrazone Blue G [654]	—	—	650	—	0.45–3.72	—
	SnCl ₂ , Rhodamine 6G [655]	H ₂ O	—	558	15.2	0–12 μ g/25 ml	Alloys
	SnCl ₂ , Rhodamine 6G [656]	H ₂ O	4	565	13	$<$ 0.2	Thermocouple wires
	SnCl ₂ , Crystal violet [657]	H ₂ O	—	540	100	0–0.2	—
	Molybdate, Rhodamine B [658]	—	—	570	90.5	—	Ores
	SnCl ₂ , crystal violet [659]	H ₂ O	—	550	110	0.008–0.1112 μ g	—
	SCN ⁻ , Rhodamine 6G [660]	H ₂ O	4	575	10	—	—
Sb	Cl ⁻ , Brilliant green [661]	—	—	640	9.9	Up to 20 μ g	—
	SnCl ₂ , crystal violet [662]	Toluene-methyl	—	590	—	10–250	—
	Cl ⁻ , Methylene blue [663]	Toluene-methylpentanone	675	—	—	150 nM	—
	Mandelic acid, Malachite green [664]	Chloro- benzene	3	628	—	0.19–11.5 μ g	—
	Cl ⁻ , Janus blue [665]	—	—	—	—	—	—
	I ⁻ , Rhodamine B [666]	—	—	595	—	—	—
	2-Hydroxyisocaproic acid, Malachite green [667]	—	—	628	4.7	0.19–11.5 μ g	—
	Molybdate, Nile blue [668]	H ₂ O	—	585	36	Up to 2 μ g/25 ml	—
	SCN ⁻ , crystal violet [669]	—	—	—	—	—	—
	Se	ICl ₂ , Rhodamine 6G [670]	—	—	525	—	0.1–0.9 μ g
SCN ⁻ , Rhodamine B [671]		H ₂ O	3.8	606	7.9	\leq 3 μ g/25 ml	—
1,10-Phen, eosine [672]		—	3.5–10	530	—	2–35 μ M	—
Si	Molybdate, ethyl Rhodamine B [673]	—	—	584	34	\leq 1.3 μ g/25 ml	—
	Molybdate, Rhodamine B [674]	—	—	578	22	Up to 200 ppb	—
	Molybdate, ethyl Rhodamine B [675]	—	—	595	110	Up to 29 ppb	—
	Molybdate, Rhodamine B [676]	—	—	585	45	Up to 3.5 μ g/50 ml	Pig iron alloys
Sn	3-Nitroalizarin, Brilliant green [677]	—	—	630	20	0.1–2	—
	I ⁻ , 5,7-Dichlorooxine [678]	CHCl ₃	1.3–1.6	401	1–20	—	—
	SCN ⁻ , crystal violet [679]	—	—	550	25	Up to 0.2	Alloys, steel

Table 7 (continued)

Element	Reagents [R]	Medium for determination	pH/Acidity	λ_{\max} nm	$\epsilon \times 10^{-4}$	Beer's law range (ppm)	Applications
Sr	Cryptand 222, erythrosine B [680]	Toluene–Nitro benzene (4:1)	9	547	—	Up to 12 μM	—
Ta	Molybdate, Nile blue [681]	—	—	625	22.6	Up to 2.6 $\mu\text{g}/25$ ml	—
	SCN^- , ethyl violet [682]	—	5.50	560	1900	Up to 0.02	—
	Molybdate, Butyl Rhodamine B [683]	—	3.7	588	36.2	Up to 0.2	Rocks
	N-(4-Chlorophenyl)3,4,5-trimethoxy- cinnamohydroxamic acid, Brilliant green [684]	CHCl_3	—	635	2.3	—	—
Te	F^- , victoria blue B [685]	Benzene	—	630	—	30–220	Ores
	F^- , brilliant green [686]	Benzene	—	640	—	—	Steel
	I^- , Rhodamine B [687]	—	—	560	280	20–70 ppb	Ores, smoke dust
	SCN^- , ethyl violet [688]	—	—	560	155	0–0.2	Semiconducting films
Ti	Cl^- , Cationic red violet [689]	Toluene	—	570	3.8	0.6–17.8	Steel, pig iron
	I^- , Rhodamine B [690]	—	—	600	165	Up to 40 ppb	—
	Tetrachlorocatechol, Brilliant green [691]	CCl_4	—	640	10	0.01–0.1	—
	I^- , Rhodamine 6G [692]	H_2O	—	560	11.4	0.04	—
Tl	Cl^- , pyronine G [693]	—	—	530	12	1–14 $\mu\text{g}/25$ ml	Cd sponge, rocks
	Br^- , cresyl violet [694]	Toluene–ethyl methyl ketone (3:2)	—	610	6.7	2.5–3.5 μg	Alloys
U	Br^- , victoria blue B [695]	—	—	625	—	0.4–20	—
	Br^- , Phenosafranine [696]	—	—	529	6.7	0–2	Fly ash and ores
	Oxine, Butyl Rhodamine [697]	Benzene	5.7–5.8	564	—	0.3–4	Monazite sand
	SCN^- , ethyl violet [698]	—	—	—	57.1	Up to 800 ppb	Ores
V	Anthranilic acid, Rhodamine 6G [699]	H_2O	4.5	575	6.3	0.04–4	Monazite sand
	Benzilic acid, Rhodamine B [700]	—	—	546	—	0–100 μg	—
	Salicylic acid, Rhodamine B [701]	—	3.3–4.0	570	92.5	—	—
	3,5-dinitrocatechol, Brilliant green [702]	CCl_4	5–7	630	17	≤ 0.3	—
W	SCN^- , Crystal violet [703]	—	—	540	41	Up to 0.44 ppb	—
	SCN^- , Ethyl Rhodamine B [704]	—	—	585	190	Up to 0.06	Lake and well water
Zn	1,10-Phen, tetraiodofluorescein [705]	CHCl_3	9.3	549	—	0.2–2 $\mu\text{g}/25$ ml	Bronze, alloys
	1,10-Phen, rosebengal [706]	CHCl_3	6.5–7.5	575	10	0–0.5	Soils
	SCN^- , Rhodamine 6G [707]	H_2O	4	575	8	0–5 $\mu\text{g}/25$ ml	—
	SCN^- , Malachite green [708]	—	—	600	11.3	—	Al
Zr	SCN^- , victoria blue 4R [709]	—	—	570	—	—	—
	SCN^- , crystal violet [710]	—	—	—	—	—	—
	F^- , Alizarin [711]	MIBK	8.9	556	15.2	0–20 μg	Alloys

Table 8
Derivative systems

Element	Reagents [R]	Derivative mode	Medium for determination	pH/H ⁺	Range (ppm)	Detection limit (ppb)	Applications
Co	1,0-Phen, Rosebengal [712]	⁴ D	CHCl ₃	8 ± 1.0	1–8 µg/25 ml	6	Rare earth oxides
Fe	1,10-Phen, ClO ₄ ⁻ [713]	² D	Mesityloxiide	2–9	0–50 µg/100 ml	0.5	Rare earth oxides
Hg	I ⁻ , pyronine G [714]	³ D	H ₂ O	4	1–20 µg/25 ml	2.5	Industrial effluents
Mo and Ti	Salicylfluorone, CTAB [715]	³ D	—	—	Up to 0.4	—	—
Nd and Er	Oxine-5-sulphonic acid, Triton X-100 [716]	³ D	H ₂ O	6.5	25 Nd, 30 Er	—	—
Nd	Bromopyrogallol red, Triton X-100 [717]	⁴ D	—	9.0	Up to 3.6	150	RE mixtures
Nd	Methylthymol blue, CPCI [718]	⁴ D	—	9.3	0–3.5	200	RE mixtures
P	Molybdate, Rhodamine 6G [719]	³ D	H ₂ O	—	0–0.24	1.5	Steels, milk, powder, sediments
Pr, Nd, Ho and Er	Sulphosalicylic acid, EDTA [720]	⁴ D	H ₂ O	11.5	—	—	—
Pr, Ho	Oxine-5-sulphonic acid, CPCI [721]	³ D	H ₂ O	Hexamine buffer	—	—	—
Ru	2,4,6-Tri(2-pyridyl)-1,3,5-triazine Picrate [722]	¹ D	1,2-dichloroethane	5	0.007–0.4	—	—
Sm	Methylthymolblue, CTAB [723]	³ D	H ₂ O	6.0–8.0	0–30 µg/25 ml	30	—

Table 9
FIA systems

Element	Reagents [R]	pH/H ⁺	λ_{max} , nm	$\epsilon \times 10^{-4}$	Range (ppm)	Applications
Al	Chromazurol S, CPCl [724]	5.7	625	13.4	Up to 400 ppb	—
Ca and Mg	Xylenol orange, CTAB [725]	10.5	605	—	Up to 8	Waters
Cd	I ⁻ , Malachite green [726]	4	685	—	0.1–3	—
Fe	Chromazurol S, HDMAA [727]	7.5	—	—	—	—
Hg	Br ⁻ , crystal violet [728]	5	664	7.15	0.2–4	—
Ln	Chromazurol S, CTAB/CPB [729]	9.4	620	—	—	—
Ln	Xylenol orange, CPB [730]	5.5	600	—	2.5–25 μM	—
Mo, V	Caraminic acid, CTAB [731]	4	—	—	0.76–28.8	—
Pd	Orange G, CPB [732]	—	—	—	1–10	—
Re	Dicyclohexano-18-crown-6, Brilliant green [733]	—	640	—	Up to 1.5	—
Si	Molybdate, Rhodamine B [734]	—	590	—	0.2–2	Waters
Sm, Eu	Molybdate, Malachite green [735]	—	627	—	Up to 9 ppb	—
	TTA, TOPO, nonaoxyethylene glycol dodecylether [736]	3.5	596	—	—	—

Table 10
Summary of fluorimetric methods using ternary complexes

Element	Reagents [R]	Type of method	pH/H ⁺	$\lambda_{\text{ex}}/\lambda_{\text{em}}$ (nm)	Calibration range (ppm)	Applications
Ag	1,10-Phen, eosine B [737]	A	4.5	550/600	0.8–6	—
	I ⁻ , Brilliant green [738]	A	3	256/521	0.25–5 $\mu\text{g}/50 \text{ ml}$	—
	Benzothiacrownether, eosine [739]	E	—	536/558.8	2–15 ppb	—
Al	Oxine-S-sulphonic acid, CTAB [740]	A	5	390/493	—	—
Au	Cl ⁻ , Acridine yellow [741]	E	≤ 2.7	490/—	0.01–0.5	—
	Cl ⁻ , Acridine yellow [742]	E	—	—/495	6–400 ppb	Ores
	SCN ⁻ , Rhodamine [743]	E	—	—/530	—	—
	Br ⁻ , Rivanol [744]	E	—	370/490	0.1–4.7	Ores
B	2,2,4-Trimethylpentane 1,3-diol, caramimic acid [745]	E	—	547/567	9–120 ppb	Plants
Bi	2,6,7-Trihydroxy(4,5-dibromophenyl) fluorone, CTAB [746]	Q	—	535/563	0.02–0.4	Rocks and minerals
	SCN ⁻ , Rhodamine B [747]	Q	—	—/610	—	Cast iron
Ca	Cryptand 221, eosine [748]	E	8.5	535/552	1.5–100 ppb	Sugar
Cd	Ferron, CTAB [749]	A	5.5–6.5	365/524	0.1–4	Wheat flour
	Ferron, CTAB [750]	A	—	400/510	—	—
	Cryptand 221 or 222, eosin [751]	E	—	536/552	0.5–150 ppb	—
	I ⁻ , Rhodamine [752]	Q	—	365/551	4–20 ppb	—
	Cryptand 221, eosine [753]	E	—	536/555	0.5–150 ppb	High purity Zn
	Oxine-S-sulphonic acid, methyltriethyl ammonium ion [754]	—	8.1–8.5	400/524	1–10 μg	—
CN ⁻	Iodine, Fluorescein [756]	—	6.4	494/514	—	—
Cr	I ⁻ , crystal violet [757]	E	2	256/521	Up to 60 ppb	Water
Cu	1,10-Phen, 4,5-dibromofluorescein [758]	E	8.5	530/565	1–10 μM	—
Dy	Salicylic acid, EDTA [759]	A	13.2	—/577	50 ppb	—
	Thron, CTAB [760]	A	—	—/577	10 nM–4 μM	—
Eu	1,10-Phen, TTA [761]	A	5.5	345/614	7 ppb	—
	N ⁻ (2-Hydroxyethyl) EDTA, TTA [762]	A	8.3	365/613	1–8 $\mu\text{g}/25 \text{ ml}$	—
	TTA, diphenylguanidine [763]	A	6.1	374/611	0–0.16 μg	—
	1,10-Phen, TTA, Triton X-100, Tb [764]	A	—	371/612	10 nM–10 pM	RE oxides
	1,10-Phen, TTA [765]	A	5	374/613	0.07–30 ppb	Ores
	4,7-Diphenyl, 1,10-phen, TTA [766]	A	5.3	346/613	0.08–40 μg	Gd ₂ O ₃ , Nd ₂ O ₃
	TTA, TOPO, Gd(III) [767]	A	5.5–6.5	343/615	0.13–38 ng	—
	Benzoyltrifluoroacetone, CTAB [768]	A	8.6	363/612	Up to 100 ppb	—
	TTA, Trialkylammonium chloride [769]	A	9.6	363/612	0.5–60 nM	—
	Dibenzoylmethane, Diphenylguanidine, Tb [770]	A	6.5–7.5	390/612	0.5–60 nM	—
	Dibenzoylmethane, Diphenylguanidine, Y [771]	A	7	390/612	0.1–50 nM	—
	Sodium benzoate, TOPO, Triton X-100 [772]	A	5.5	280/592	1 μm –1 mm	—
	Benzoylacetonone, 1,10-Phen [773]	A	—	370/612	1–200 nM	RE oxides
	Dibenzoylmethane, TOPO, Triton X-100 [774]	A	7.8	363/617	20 pM–110 nM	Gd ₂ O ₃
	TTA, CTAB, Triton X-100 [775]	A	—	370/612	1–100 nM	—
	Dibenzoylmethane, diethylamine, Gd [776]	A	9.6	390/612	10 pM–4 nM	—
	1,10-Phen, TTA [777]	A	5.5–8.2	365/612	0.05–4 nM	—
	Benzoyltrifluoroacetone, TOPO [778]	E	6	335/620	Up to 100 ppb	—
	TTA, Dibenzo-18-crown-6, Triton X-100, Tb [779]	A	7.0–9.0	371/614	10 ⁻¹¹ to 10 ⁻⁶ M	La ₂ O ₃ , Pr ₆ O ₁₁ and Dy ₂ O ₃

Table 10 (continued)

Element	Reagents [R]	Type of method	pH/H ⁺	$\lambda_{\text{ex}}/\lambda_{\text{em}}$ (nm)	Calibration range (ppm)	Applications
Ga	Salicylfluorone, CTAB [780]	Q	8.8	400/510	50–250 $\mu\text{g}/25 \text{ ml}$	—
	Cl ⁻ , Butyl Rhodamine B [781]	E	—	-/584	Up to 0.25 ppm	—
Hg	Cryptand 221, eosine [782]	E	8.5	539/550	Up to 125 ppb	Coal and flyash
	I ⁻ , Rhodamine 6G [783]	A	—	365/554	4–40 ppb	—
Li	I ⁻ , Brilliant green [784]	A	3	256/521	5–100 ppb	—
	I ⁻ , Cryptand 222, eosine [785]	Q	—	528/540	0.3–2 $\mu\text{g}/25 \text{ ml}$	—
Mo	Dichlorofluorescein, CPCl [786]	Q	—	528/540	0.3–2 $\mu\text{g}/25 \text{ ml}$	—
	Crown ethers, Rhodamine 200 B [787]	E	2–12	-/548	—	—
Nb	7-Iodo-oxine-5-sulphonic acid, CTAB [788]	A	7.5	381/501	Up to 1 ppm	—
	SCN ⁻ , Rhodamine B, sodium dodecyl-benzyl sulphionate [789]	A	—	354/600	0.1 ppm	—
Nd	o-Chlorophenylfluorone, CTAB [790]	A	5	400/510	2–80 ppb	—
	Morin, CPCl [791]	A	—	436/510	0.8–20 ppb	—
P	4,5-Dibromophenylfluorone, CTAB [792]	A	—	420/470	Up to 0.24	—
	Xylenol orange, Ethonium [793]	A	7.5	546/850	—	Y ₂ O ₃ , La ₂ O ₃
Pb	Molybdate, Rhodamine 6G [794]	E	—	530/548	Up to 100 μg	—
	Molybdate, Rhodamine 6G [795]	Q	—	350/550	3–5 ppb	—
Pd	18-Crown-6, eosine [796]	E	8.3	537/549	—	—
	Cryptand 222, eosine [797]	E	1.5	536/549	—	—
Pt	Br ⁻ , acridine orange [798]	E	—	-/530	≤ 2	—
	Cl ⁻ , Rhodamine 6G [799]	E	9	-/570	15 ppb	—
Ru	Cl ⁻ , Rosebengal [800]	E	6.5	550/568	—	—
	Oxine, CTAB [801]	A	—	388/520	4–2400 ppb	—
Sb	1,10-Phen, sodium dodecylsulphate [802]	A	—	437/617	Up to 2	—
	SnCl ₂ , Rhodamine B [803]	A	—	450/510	0.10–0.25	—
Sc	4,5-Dibromophenylfluorone, CTAB [804]	A	—	-/555	Up to 0.2	—
	5,7-Dinitroxine, Rhodamine B [805]	E	3.5	420/520	0–2 ppb	—
Sm	5,7-Dinitroxine, Rhodamine B [806]	E	—	420/582	0.02–4	—
	Oxine-5-sulphonic acid, CTAB [807]	A	4.8	393/505	0.4–3 μM	—
Sn	1,10-Phen, TTA, Gd [808]	A	—	349/648	Up to 4 nM	—
	1,10-Phen, TTA, La, Triton X-100 [809]	A	—	—	10 nM–8 μM	—
Tb	Hexafluoroacetylacetone, TOPO [810]	A	—	—	—	—
	Hexafluoroacetylacetone, TOPO, Triton X-100 [811]	A	—	330/565	1–100 μM	—
Ti	1,10-Phen, TTA, Y, Triton X-100 [812]	A	5–10	370/565	—	—
	BMPHD ₂ , CTAB, Gd [813]	A	5.5	300/650	—	—
U	Dibenzoylmethane, NH ₃ , acetone [814]	A	8.5	406/565	10–500 nM	—
	TTA, TOPO, Triton, X-100, Tb [815]	A	6.4–8.7	—	6 nM–1 μM	—
V	1,10-Phen, TTA, Triton X-100 [816]	A	4.5–8.5	368/565	1–60 nM	—
	2-Chlorophenylfluorone, CTAB [817]	A	4.2	530/550	20–120 ppb	Ores
Zn	NTA, Tiron [818]	A	12	320/545	0.53–52.8 ppb	—
	5-Bromosalicylfluorone, CTAB [819]	A	—	515/533	Up to 4 ng/25 ml	Steel, Ti–Al alloys
Mn	Cl ⁻ , Methylene blue [820]	E	—	468/730	—	—
	Cl ⁻ , Pyronine B [821]	E	—	560/590	—	MnO ₂ ore
Co	Cl ⁻ , Rivanol [822]	E	—	369/491	—	—
	EDTA, oxalic acid [823]	A	—	360/455	100 μg –1 mg/ml	—
Ni	TTA, Rhodamine B [824]	E	6	545/570	0.05–1	—

Table 10 (continued)

Element	Reagents [R]	Type of method	pH/H ⁺	$\lambda_{\text{ex}}/\lambda_{\text{em}}$ (nm)	Calibration range (ppm)	Applications
V	PAR, Safranin T [825]	E	5.5–6	515/581	—	—
W	Salicylfluorone, CTAB [826]	Q	—	500/520	Up to 0.1	—
Zn	Ferron, <i>m</i> -tetra- <i>p</i> -sulphophenylporphyrin [827]	—	—	400/650	—	Al alloys
	Oxine-5-sulphonic acid, methyl trioctyl-ammonium chloride [828] Ferron, CTAB [829]	A A	8 6	400/522 400/510	5–150 nM —	— Alloys
Zr	Ferron, Zephiramine or CTAB [830]	A	4.3	396/526	Up to 0.32	—
	Ferron, β -cyclodextrin [831]	A	3	365/490	Up to 2	—
	<i>o</i> -Hydroxy hydroquinone phthalatein, tetradecyltrimethylammonium chloride [832] Salicylic acid, Rhodamine B [833]	A E	4.5 1.4–1.6	345/543 546/575	Up to 36 ppb —	— Hf metal

A, Aqueous; E, Extraction; Q, Quenching.

ing fibre optics. It has proved particularly useful in eliminating matrix interferences. The derivative spectrophotometric methods utilizing ternary and multicomponent complexes in inorganic analysis are summarized in Table 8.

3.6. FIA systems

During the past decade FIA has rapidly grown in popularity. This is because of its simplicity, versatility, precision, high sampling rate, low sample consumption, low cost and ease of automation. This technique involves the injection of the sample into a stream of chromogenic reagent and ligand which transports it to the detector. The analysis requires a small amount of sample (10–300 μl) which, together with a light path of 10 mm usually used, is responsible for relatively high sensitivity. Virtually each colour reaction in a homogenous medium, provided it is sufficiently fast, can be adapted to flow injection processing resulting in a flow injection spectrophotometric method. Table 9 shows several FIA procedures, reported so far, for inorganics which make use of ternary and multicomponent complexes.

4. Spectrofluorimetry

A summary of fluorometric methods based on ternary complex formation until 1975 is given in a review article by Haddad [20]. A summary of spectrofluorimetric luminescence methods described so far since 1976 for inorganics is given in Table 10.

4.1. Ternary complexes with anionic binary complexes

Ternary complexes formed by ion-association of an anionic complex with a basic dye cation comprise the vast majority of ternary complexes used in spectrofluorimetry as in the case of spectrophotometry. The fluorescent dyes of the xanthene series (i.e. rhodamine dyes) serve as the cationic counter-ion in the ternary complex. Ion-association ternary complexes formed from these dyes may be classified into two groups—those contain-

ing an anionic binary complex formed between a metal and electronegative ligand and those formed from an anionic chelate binary complex.

4.2. Ternary complexes with cationic binary complexes

The availability of fluorescent anionic dyes of the fluorescein series has led to the possibility of fluorescent ion-association ternary complexes wherein the binary complex is cationic. Fluorescein dyes (often referred to as phthalein dyes) are very closely related in structure to the xanthene (Rhodamine) dye series.

4.3. Coordination unsaturated ternary complexes

Coordination unsaturated complexes do not suffer from the lack of selectivity often experienced with the ion-association type. This is generally attributed to a reduction in the likelihood of unwanted side reactions, because of the increased complexity in conditions required for two ligands to react. Fluorescent ternary complexes of rare earth ions are typified by the reaction of europium and samarium with TTA and 1,10-phenanthroline [764] and TTA-dibenzo-18-crown-6 [779] wherein terbium acts as an activator.

4.4. Advances in spectrophotometric and spectrofluorimetric methods for individual elements

4.4.1. Group I (H, Li, Na, K, Rb, Cs, Fr, Cu, Ag, Au)

Until the last decade, lithium, sodium, potassium, rubidium and cesium had not generally been determined spectrophotometrically or spectrofluorimetrically. A rapid development in synthetic chemistry, however, brought a dramatic increase in the number of spectrophotometric methods developed for these elements.

Selective ion-association procedures were developed for sodium using crown ether and triphenyl methane dyes [607–609]. A mixed ligand procedure was developed for the determination of potassium [60] in rocks, soil and plants by using benz-15-crown-5 and dipicrylamine. Selective extraction spectrophotometric methods were devel-

oped based on ion-association complex formation using crown ethers [595,597] and cryptand [596] in the presence of triphenylmethane dyes.

Of the various mixed ligand procedures developed for copper, the method based on the SCN^- and 2,3 or 4 picoline [46] is selective and applicable over a wide pH range 3–8. A number of reasonably sensitive spectrophotometric procedures were developed using surfactant sensitized systems [209–226]. Of these, the procedure based on chromal blue G and CTA Cl [219] is highly sensitive as it is useful to determine as low as 0.1–16 ppb of copper. The ion-association procedures developed for copper utilize both cationic and anionic dyes [559–568]. Amongst these, the procedure based on thiocyanate and Rhodamine B [564] is useful in determining traces of copper in steel and alloys. Ion-association procedure using 1,10-phenanthroline and 4,5-dibromofluorescein [758] forms the basis for sensitive spectrofluorimetric determination of copper.

Mixed ligand complex based on 2[3,4-phenylazophenyl]triazeno]phenol and TEA [28] is highly sensitive ($\epsilon = 1.28 \times 10^5 \text{ l mol}^{-1} \text{ cm}^{-1}$) for the determination of traces of silver by spectrophotometry. Of the various surfactant sensitized systems developed for silver [131–138] cadion 2B and sodium dodecyl sulphate [132] is highly sensitive ($\epsilon = 1.23 \times 10^5 \text{ l mol}^{-1} \text{ cm}^{-1}$). Flotation spectrophotometric method based on I^- , SnCl_2 and CI basic green [456] is more sensitive than SCN^- and Rhodamine 6G [455] for the determination of silver. The determination of silver based on thiocyanate and Rhodamine B [494] is more sensitive than other similar ion-association procedures [493–504]. As low as 2–15 ppb of silver can be determined spectrofluorimetrically by the use of benzothiacrown ether and eosine [739]. This procedure is more sensitive than the two other similar spectrofluorimetric procedures [737,738].

The surfactant sensitized procedures developed for gold [164–166] are not at all selective and sensitive. The halide and thiocyanate complexes form ion-associates with basic dyes, which were proposed for sensitive determination of gold either after extraction [510–519] or flotation [457–459]. As low as 6 ppb of gold can be determined by spectrofluorimetry using chloride and acridine yellow [742]. Other spectrofluorimetric procedures

[741,743,747] developed for gold are only reasonably sensitive.

4.4.2. Group II (Be, Mg, Ca, Sr, Ba, Ra, Zn, Cd, Hg)

Of the seven surfactant sensitized systems evaluated for spectrophotometric determination of beryllium [167–173], the use of 4,5-dibromophenylfluorone, CTAB and polysorbate 60 is the best as it gives highest sensitivity ($\epsilon = 1.7 \times 10^6 \text{ l mol}^{-1} \text{ cm}^{-1}$) and is applied to the determination in Be–Cu alloys and minerals.

Of the two surfactant sensitized systems developed for magnesium [286,287] sensitization of Mg-4,5-dibromophenylfluorone complex with CTAB [287] is more sensitive ($\epsilon = 13.8 \times 10^4 \text{ l mol}^{-1} \text{ cm}^{-1}$) and has been successfully used for its determination in minerals. An extractive spectrometric method was developed for the determination of traces of magnesium based on the formation of ternary ion-association complex with 5,7-diiodoquinolin-8-ol and Rhodamine S [598]. The sensitization of chromeazurol S-1,10-phenanthroline [184] and Ca-xylene orange [185] complexes by CTAB formed the basis for reasonably sensitive spectrophotometric procedures for the determination of calcium. The latter system was also used in flow injection mode [724]. Up to 12 μM of strontium could be determined by extractive spectrophotometric determination using cryptand 222 and erythrosine B [680].

A mixed ligand system, based on phenylfluorone and diphenyl guanidine [128], was developed for the determination of traces of zinc in clays and silicates. Of the various surfactant sensitized systems developed for zinc [435–440], chromeazurol B-quinoline-CTAB system [436] is more sensitive ($\epsilon = 1.13 \times 10^5 \text{ l mol}^{-1} \text{ cm}^{-1}$). However, none of the procedures are applicable for the determination of zinc in real samples. Formation of binary complexes with 1,10-phenanthroline or thiocyanate and subsequent association with anionic or cationic dyes respectively formed the basis for trace determination of zinc [705–710]. Of these, the procedure based on thiocyanate and Rhodamine 6G [707] is an aqueous procedure and has been used for its determination in soils. Among the four systems described for spectrofluorimetric determination of zinc [827–830], the procedure

based on the use of ferron-CTAB is applicable for its determination in alloys.

A highly sensitive mixed ligand system based on the use of crystal violet and bromopyrogall red [39] was developed for the determination of traces of cadmium in high purity zinc. Three other procedures [37–40] in this category involve extraction and have not been applied to real samples. Sixteen ion-association procedures [534–549] were described for the trace determination of cadmium and most of these utilise iodide for the formation of binary anionic complex and associate with different oppositely charged cationic dyes. A few of them [536,538,543] are successfully applied for the determination of traces of cadmium in high purity zinc materials. Amongst the spectrofluorimetric procedures developed for cadmium [749–755], the method based on the quenching of fluorescence of I^- -Rhodamine S [752] is more sensitive and is useful in the determination of as low as 4–20 ppb.

Though two mixed ligand systems are mentioned in the literature for mercury [57,58] the details of the former are not available and the sensitivity of the latter is very low ($\epsilon = 2.3 \times 10^4 \text{ l mol}^{-1} \text{ cm}^{-1}$) and involves extraction. Of the three flotation spectrophotometric procedures developed for mercury [460–462], the method based on the use of ternary system iodide and Brilliant green [462] is more sensitive ($\epsilon = 5.96 \times 10^5 \text{ l mol}^{-1} \text{ cm}^{-1}$) and is applicable to its determination in paper industry effluents. Of the 12 ion-association systems developed for mercury [581–592], the formation of anionic mercury-halide complex and association with oppositely charged cationic dyes are more popular. A third order derivative spectrophotometric procedure was developed for mercury [714] based on the formation of ternary ion-associate $Hg-I^-$ -pyronine G. This procedure has been applied to the determination of traces of mercury in industrial effluents. Three spectrofluorimetric procedures were developed during this period for the determination of mercury [782–784]. Amongst these, the procedure based on extraction of ternary ion associate formed with cryptand 221 and eosine [782] is most sensitive and is applied to coal and fly ash samples.

4.4.3. Group III (B, Al, Ga, In, Tl, Sc, Y, lanthanides, actinides)

A rapid development in the methods based on the formation of ion-associates with anionic boron complexes were observed [520–526]. The extraction of boron with 3,5-di-*t*-butylcatechol and ethyl violet [522] is most sensitive ($\epsilon = 1.05 \times 10^5 \text{ l mol}^{-1} \text{ cm}^{-1}$) and has been applied to sea water samples. Similarly, an extractive spectrofluorimetric method was developed for the determination of as low as 8–120 ppb of boron in plants [745].

Mixed ligand system based on 5-bromosalicylfluorone and 5,7-dibromo-8-hydroxyquinoline [31] is more sensitive ($\epsilon = 6.2 \times 10^4 \text{ l mol}^{-1} \text{ cm}^{-1}$) than that with bromopyrogallol red and diphenyl guanidine [30] ($\epsilon = 3.1 \times 10^4 \text{ l mol}^{-1} \text{ cm}^{-1}$). The latter procedure involves extraction with butanol. Of the 15 aqueous spectrophotometric methods developed for aluminium [139–163] based on surfactant sensitized systems, the reaction based on the sensitization of Al chromeazulur S complex by CPB and OP [145] is more sensitive ($\epsilon = 1.35 \times 10^5 \text{ l mol}^{-1} \text{ cm}^{-1}$) and is applicable for the determination of 0.04–0.4 ppm of aluminium. The Al-chromeazurol S-CPCl system has been carried out in FIA mode also [724]. The only mixed ligand system described for gallium [56] is based on the formation with PAR and diphenylguanidine. Among the surfactant sensitized systems developed for gallium [240–258] the reaction based on *o*-chlorophenyl fluorone and CPB is more sensitive ($\epsilon = 1.7 \times 10^5 \text{ l mol}^{-1} \text{ cm}^{-1}$) and has been applied for its determination in ores [243]. A number of metal triphenylmethane dye complexes sensitized by cationic surfactants formed the basis for sensitive determination of indium [272–277]. Of these, the procedure based on 9-(2-chlorophenyl)2,6,7-trihydroxyxanthene-3-one-CTAB [275] is most sensitive ($\epsilon = 1.92 \times 10^5 \text{ l mol}^{-1} \text{ cm}^{-1}$) and has been applied to Sn foil and lead mining samples. Two surfactant sensitized systems [403,404] were developed for the sensitive determination of thallium based on the sensitization of Tl-gallein and Tl-bromopyrogallol red complexes by cationic surfactants. The anionic binary complex formed with halide and association with oppositely charged cationic dyes [692–

696] formed the basis for sensitive spectrophotometric determination of thallium. Of these, the ion-associate formed with chloride and pyronine G is most sensitive ($\epsilon = 1.2 \times 10^5 \text{ l mol}^{-1} \text{ cm}^{-1}$) and found application to thallium in Cd sponge and rocks.

Barring one each of mixed ligand [102] and ion-association system [669], the most frequently developed spectrophotometric procedures for scandium are based on the formation of surfactant sensitized systems [345–356]. Of these, the sensitization of Sc-chromeazurol S complex with zephiramine [350] is most sensitive ($\epsilon = 1.64 \times 10^5 \text{ l mol}^{-1} \text{ cm}^{-1}$). A multicomponent surfactant sensitized system based on Y-chromeazurol S, 1,10-phenanthroline and dimethyldodecylamino acetic acid [434] formed the basis for sensitive determination of yttrium ($\epsilon = 1.4 \times 10^5 \text{ l mol}^{-1} \text{ cm}^{-1}$).

Two mixed ligand systems are described for the trace determination of lanthanum with antipyrine A and diphenylguanidine [61] and lutetium with pyrogallol red or bromopyrogallol red and 1,10-phenanthroline [62]. The ternary complexes with methylthymol blue-CPCl [285] and Hexaazo-18-crown-6-erythrosine A [569] formed the basis for the sensitive determination of lutetium and europium, respectively. However, the above ternary systems developed for a particular lanthanide are not selective as other lanthanides react in a similar way. The development of derivative techniques has increased the potential of many of the old methods by allowing the poor selectivity of sensitive reagents to be circumvented. The resolution of complex absorption spectra of ternary complexes of rare earth ion by using derivative mode allowed the determination of single or a few target elements in a mixture. Thus, a few derivative procedures were developed for the determination of neodymium [717,718], samarium [723] and mixtures of neodymium and erbium [717], praseodymium, neodymium, holmium and erbium [720] and praseodymium and holmium [721] in other rare earth oxides. Sensitive and selective spectrofluorimetric procedures were developed over the last five years for the determination of europium [761–779] and samarium [809–816]. Of these, few procedures find application for the determination of europium in other rare earth oxides [764,766,773,774,779].

4.4.4. Group 4 (C, Si, Ge, Sn, Pb, Ti, Zr, Hf)

The methods developed for silicate invariably use molybdate to form binary complex and subsequently associated with malachite green [486] or chromopyrazol II [487] methods. Similar ion-association complexes were used both in flotation spectrophotometric determination [673–675] or in FIA mode [734,735]. Ten surfactant sensitized procedures were developed for the trace determination of germanium [259–268]. Of these, the sensitization of Ge-*p*-chlorophenylfluorone by Tween-60 is more sensitive ($\epsilon = 1.8 \times 10^5 \text{ l mol}^{-1} \text{ cm}^{-1}$) [261]. Germanium is also determined by formation of two ternary ion-association complexes based on molybdate-butyl Rhodamine B [578] and mandelic acid-malachite green [579]. The former one is an aqueous procedure and has been applied to trace determination of germanium in Cu–Cd slag.

Surfactant sensitized systems are mostly investigated for the determination of trace amounts of tin, with as many as 15 procedures [357–371] are described during the last two decades. The sensitization of Sn-bromopyrogallol red complex with CPB is more sensitive ($\epsilon = 3.72 \times 10^5 \text{ l mol}^{-1} \text{ cm}^{-1}$) and has been used for its determination in $\text{Pb}(\text{NO}_3)_2$. The association of binary complex of tin formed with 3-nitroalizarin, iodide and thiocyanate and with oppositely charged Brilliant green [677], 5,7-dichlorooxine [678] and crystal violet [679], formed the basis for sensitive determination of tin. The sensitization of Sn-2-chlorophenylfluorone complex with CTAB [817] formed the basis for spectrofluorimetric determination of 20–120 ppb of tin. The extraction of lead with bismuthiol II in presence of 1,10-phenanthroline allows the determination of 0.3–30 ppm of lead [86]. The sensitization of lead-salicylfluorone complex with CPCl [316] is more sensitive ($\epsilon = 9 \times 10^4 \text{ l mol}^{-1} \text{ cm}^{-1}$) compared to other surfactant sensitized procedures developed for lead [315–320]. Lead-crown ether or cryptand binary complexes and their association with oppositely charged anionic dyes [626–630] resulted in development of sensitive spectrophotometric procedures. Only Pb-cryptand 2,2,2-eosine [762] procedure has been successfully applied for the determination of traces of lead in highly purity metals and alloys. Similarly, ion association com-

plexes formed with eosine in the presence of 18-crown-6 or cryptand 2,2,2 are used for sensitive determination of lead by spectrofluorimetry. Of the few mixed ligand system investigated for titanium [105–110], none of them are sensitive enough to find application in trace analysis. On the other hand, of the various surfactant sensitized systems [383–402] almost all of them, excepting one, are aqueous determinations and are reasonably sensitive. The first two of these procedures finds application to steels and rocks [383] and rocks and alloys [384]. As in the case of titanium, surfactant sensitized systems are most often investigated [443–454] for the sensitive determination of zirconium. Of these, the sensitization of Zr-*p*-acetylchlorophosphonazo complex with sodium dodecyl benzene sulphonate [448] is most sensitive ($\epsilon = 6.03 \times 10^5 \text{ l mol}^{-1} \text{ cm}^{-1}$) and allows the determination of as low as 0–0.12 ppm of zirconium. An ion association complex formed with fluoride and alizarin and subsequent extraction into MIBK formed the basis for the determination of 0–20 μg of zirconium in alloys [711].

4.4.5. Group V (*N, P, As, Sb, Bi, V, Nb, Ta*)

The flotation of ternary complex of phosphate with molybdate and malachite green [473] using butyl acetate formed the sensitive determination of phosphate and has been applied to Fe, Co, Ni and Zn samples. Similarly, formation of ion association complexes of phosphate in the presence of molybdate with various cationic dyes [621–625] formed the basis for development of sensitive spectrophotometric procedures. A third order derivative spectrophotometric procedure was developed for phosphate which is also based on the formation of ternary ion-association complex with molybdate and Rhodamine 6G [719]. Similar ion-association complexes formed by arsenic in the presence of molybdate and different cationic dyes [505–509] are the basis for its sensitive determination. Similar procedures using ethyl rhodamin B [505] and Rhodamine B, PVA [507] as counter cations have been applied to the determination of arsenic in steel and chemical reagents and flue dust and plants, respectively.

Three surfactant sensitized procedures [342–344] were developed for the determination of

traces of antimony. Of these, sensitization of Sb-4,5-dibromophenyl fluorone complex by CTAB [342] is most sensitive ($\epsilon = 3.96 \times 10^5 \text{ l mol}^{-1} \text{ cm}^{-1}$) and has been applied to copper alloys. Ion-association systems are the most often studied for the determination of antimony [661–668]. None of these procedures have been applied to real samples. The mixed ligand systems described for bismuth [32–36] are not sensitive, in spite of using extraction in two cases [33,34]. Among the surfactant sensitized systems described for bismuth [179–183] the sensitization of Bi-*m*-fluorophenylfluorone complex with CTAB is more sensitive ($\epsilon = 1.83 \times 10^5 \text{ l mol}^{-1} \text{ cm}^{-1}$) [179] and none of these are applied to real samples. The formation of binary anionic complex with iodide and subsequent association with cationic dyes resulted in the development of a few sensitive spectrophotometric procedures for the determination of bismuth [527–533]. Two fluorescence quenching procedures have been described for the determination of 0.02–0.4 ppm of bismuth in rocks and minerals [746] and cast iron [747].

Of the various mixed ligand systems described for vanadium [113–123], the one based on thiocyanate and diphenylguanidine [123] is most sensitive ($\epsilon = 1.7 \times 10^5 \text{ l mol}^{-1} \text{ cm}^{-1}$) while the other procedures are very low sensitive. Among the 11 surfactant sensitized systems described for vanadium [413–423], the V-3,4,5,6-tetrachlorogallein-CPCl [423] is most sensitive ($\epsilon = 7.0 \times 10^5 \text{ l mol}^{-1} \text{ cm}^{-1}$). Highly sensitive flotation-spectrophotometric procedures were developed for vanadium [491,492]. These are based on the formation of floatable ion-associates with 3,5-dinitrocatechol-Rhodamine B and 3,5-dinitrosalicylic acid-Rhodamine B using hexane and cyclohexane, respectively. Both these procedures have been applied to real samples. The extraction of vanadium as its ion-association complex with 3,5-dinitrocatechol and Brilliant green [702] into CCl_4 formed the basis for its sensitive determination ($\epsilon = 1.7 \times 10^5 \text{ l mol}^{-1} \text{ cm}^{-1}$). FIA-spectrophotometric procedure was described for vanadium based on sensitization of caraminic acid by CTAB [731]. An extractive spectrofluorimetric procedure was developed for vanadium based on the ternary complex PAR and safranin T [825]. Nine mixed

ligand systems are described for niobium [73–81] and none of them are sensitive enough to be mentioned here. Of the two surfactant sensitized systems described for niobium [308,309], the one based on Nb-4,5-dibromophenylfluorone-CTAB [309] was more sensitive ($\epsilon = 2.1 \times 10^5 \text{ l mol}^{-1} \text{ cm}^{-1}$). Aqueous spectrofluorimetric procedures [791,792] were developed based on sensitization of Nb-morin [791] and Nb-4,5-dibromophenylfluorone complexes [792] by cationic surfactants. Among the surfactant sensitized systems developed for tantalum [372–375], the one based on sensitization of Ta-2,7-dihydroxyfluoresein complex by CPB [372] has been applied to minerals and rocks. Ion-association systems are the most popular for the determination of tantalum and as many as six procedures [681–686] were described. Of these two procedures based on molybdate-butyl Rhodamine B [683] and fluoride-Brilliant green [686] have been applied to the determination of tantalum in rocks and ores respectively.

4.4.6. Group VI (O, S, Se, Te, Po, Cr, Mo, W)

Of the three ion-association procedures reported for selenium [670–672], indirect determination by formation of ICl_2^- which associate with Rhodamine 6G [670] procedure is good and finds application in bark and copper ore. Two flotation spectrophotometric procedures were developed based on papaverine-butyl Rhodamine B [489] and iodide-Nile blue A [490] and the former is applicable to copper. Ion-association systems based on halide or thiocyanate complexes of tellurium in association with suitable cationic dyes [687–690] formed the basis for its sensitive determination and all these procedures were applied to real samples.

Surfactant sensitized systems [197–208] are the most often studied for the trace determination of chromium. The sensitization of Cr-*o*-hydroxyquinol phthalein complex by CTAB [205] is most sensitive ($\epsilon = 1.64 \times 10^5 \text{ l mol}^{-1} \text{ cm}^{-1}$) and finds application in ferrosilicon and steel samples. The formation of iodocomplex with chromium and subsequent ion-association with crystal violet [757] formed the basis for the determination of ppb amounts by an extractive spectrofluorimetry. Of the few mixed ligand systems described for

molybdenum [65–72], the one based on the use of bromopyrogallol red and ethyl violet [66] is more sensitive ($\epsilon = 1.7 \times 10^5 \text{ l mol}^{-1} \text{ cm}^{-1}$). Among the various surfactant sensitized systems [293–307], the sensitization of Mo-*o*-nitrophenylphenylfluorone complex with CTAB and OP [297] is more sensitive ($\epsilon = 1.53 \times 10^5 \text{ l mol}^{-1} \text{ cm}^{-1}$) and has not been applied to real samples. The flotation of molybdenum thiocyanate-catechol violet complex with toluene formed the basis for flotation spectrophotometric determination of molybdenum [465]. Of the eight ion-association procedures described for molybdenum [599–606], the procedure based on thiocyanate and Rhodamine B [600] allows the determination of as low as 12–220 ppb of molybdenum and has been applied to Fe–Ni–Mo thin films. A third order derivative spectrophotometric procedure was developed for the simultaneous determination of Mo and Ti [715]. Mo and V have been determined in FIA mode by sensitization of their caraminic acid complexes by CTAB [731]. A multicomponent system based on Mo–SCN–Rhodamine B and sodium dodecyl benzene sulphonate [789] formed the basis for the determination of as low as 0.1 ppm of Mo by spectrofluorimetry. As low as 2–80 ppb of molybdenum could be determined spectrofluorimetrically based on the sensitization of Mo-*o*-chlorophenylfluorone complex by CTAB [790]. Of the four mixed ligand systems described for tungsten [124–127] none of them are sensitive enough to mention here. Surfactant sensitized systems [424–432] are the most often investigated for tungsten. The multicomponent system, W-salicylfluorone-polysorbate-CTAB [427] offers high sensitivity though not applicable to real samples. Ion-association with crystal violet [703] and ethyl Rhodamine B [704] with anionic thiocyanate complexes of tungsten results in its sensitive determination. A fluorescence quenching procedure was developed for tungsten [826] based on the sensitization of salicylfluorone with CTAB.

4.4.7. Group VII (F, Cl, Br, I, At, Mn, Tc, Re)

Ternary complexes of manganese based on 1,10-phenanthroline-TTA [63] and 1,10-phenanthroline-dithizone [64] were described for its determination but these are not sensitive with ϵ values of 3.6×10^4 and $4.6 \times 10^4 \text{ l mol}^{-1} \text{ cm}^{-1}$.

Of the five surfactant sensitized systems described for manganese [288–292], the sensitization of Mn-*o*-nitrophenylfluorone complex with CTAB and OP is most sensitive ($\epsilon = 1.53 \times 10^5 \text{ l mol}^{-1} \text{ cm}^{-1}$). Mixed ligand systems described for rhenium utilize thiocyanate as one of the ligand [96–98] and none of them are sensitive enough to mention here. An FIA procedure is developed for the determination of rhenium based on the formation of ternary ion-association complex viz. Re-dicyclohexano-18-crown-6-Brilliant green [733].

4.4.8. Group VIII (Fe, Co, Ni, Ru, Rh, Pd, Os, Ir, Pt)

A large number of methods are developed for iron based on the mixed ligand formation [48–55]. None of these procedures, excepting the one based on the use of erio T, mesotetra(4-sulphophenyl)porphyrin [50] are sensitive. Of the 12 surfactant sensitized procedures described for iron [228–239], the sensitization of Fe-alizarin yellow complex by CTAB provides highest molar absorptivity ($\epsilon = 9.3 \times 10^4 \text{ l mol}^{-1} \text{ cm}^{-1}$). The formation of cationic or anionic binary complexes with 1,10-phenanthroline [570,571] or thiocyanate [572–574] and subsequent association with oppositely charged reagents formed the basis for sensitive determination of iron. Of these the formation of ternary ion-association complex with thiocyanate and crystal violet [574] is most sensitive ($\epsilon = 1.1 \times 10^6 \text{ l mol}^{-1} \text{ cm}^{-1}$) and has been applied to the determination of traces of iron in alloys and pure salts. A second order derivative spectrophotometric procedure was developed for iron [713] based on the extraction of ternary ion-associate formed with iron in presence of 1,10-phenanthroline and perchlorate. One FIA procedure is described for iron by using chromeazourol S and HD MAA, but the details are not available. Of the six surfactant sensitized systems described for cobalt, the reaction based on sensitization of Co-4,5-dibromophenylfluorone complex with CPB [192] is more sensitive ($\epsilon = 1.27 \times 10^5 \text{ l mol}^{-1} \text{ cm}^{-1}$) and has been applied to ore samples. As in the case of iron, the formation of charged binary complexes with 1,10-phenanthroline [552,554,555] and thiocyanate [553,556–558] and association with oppositely

charged triphenyl methane or xanthene dyes formed the basis for the sensitive determination of cobalt. The procedure based on formation of ternary complex with thiocyanate and Brilliant green [556] is most sensitive ($\epsilon = 1.47 \times 10^5 \text{ l mol}^{-1} \text{ cm}^{-1}$) and has been applied to rock samples. The mixed ligand systems described for nickel [82–84] are not that sensitive to mention here. The sensitization of nickel-chromeazourol S complex [310] by CTAB is the most sensitive ($\epsilon = 1.48 \times 10^5 \text{ l mol}^{-1} \text{ cm}^{-1}$) of the various other similar systems described during this period [311–314].

Flotation spectrophotometric procedures are most often investigated for noble metals during this period [463,464,467–472,474–476,478–485]. These reactions are highly sensitive and have been applied to various real samples. The highest sensitive reactions are SnCl₂-Rhodamine B (for Ir) [463], SnCl₂-Rhodamine B (for Os) [471], SnCl₂-Rhodamine 6G (for Rh) [480] and Cl⁻-Rhodamine 6G (for Ru) [482]. In addition, four ion-association systems are described for the determination of osmium [617–620]. Of these, the sensitivity obtainable by ternary complex Os-SnCl₂-Brilliant green is more sensitive ($5.6 \times 10^6 \text{ l mol}^{-1} \text{ cm}^{-1}$) than flotation spectrophotometric procedures. This procedure has been applied to the determination of traces of osmium in pure nickel. Of the three ion-association systems described for ruthenium [658–660] during this period, the formation of ternary complex with SnCl₂-crystal violet allows the determination of as low as 8 ppb [659] and is most sensitive ($\epsilon = 1.1 \times 10^6 \text{ l mol}^{-1} \text{ cm}^{-1}$). A first order derivative spectrophotometric procedure was developed for the determination of as low as 7 ppb of ruthenium [722] using ternary mixed ligand system 2,4,6-tri(2-pyridyl)1,3,5-triazine and picrate. Two aqueous spectrofluorimetric procedures were developed for ruthenium [801,802] based on the ternary complexes formed with oxine-CTAB and 1,10-phenanthroline-sodium dodecylsulphate. Surfactant sensitized systems are the most often investigated for palladium [321–334]. Of these, the sensitization of Pd-salicylfluorone complex with CTAB is most sensitive ($\epsilon = 1.17 \times 10^5 \text{ l mol}^{-1} \text{ cm}^{-1}$) and has been applied to catalyst

samples. The formation of anionic binary complex with halide or thiocyanate with palladium and subsequent association with cationic dyes formed the basis for its determination [635–640]. The reaction based on iodide and pyronine G is most sensitive ($\epsilon = 9.5 \times 10^4 \text{ l mol}^{-1} \text{ cm}^{-1}$) and has been applied to steels and alloy samples. A FIA procedure is described for palladium [731] based on the sensitization of Pd-orange G complex by CPB. An extraction-fluorimetric procedure was developed for the determination of ≤ 2 ppm of palladium after formation of ternary ion-association complex with bromide and acridine orange [798]. Of the three surfactant sensitized systems described for platinum [336–338], the reaction based on Pt-4,5-dibromophenylfluorone-CTAB [337] is most sensitive ($\epsilon = 8.3 \times 10^4 \text{ l mol}^{-1} \text{ cm}^{-1}$). As many as 12 ion-association complexes are utilized for the determination of traces of platinum [641–652]. Among these, the procedure based on formation of ion-association complex with SnBr_2 -malchite green [652] is most sensitive ($\epsilon = 1.67 \times 10^5 \text{ l mol}^{-1} \text{ cm}^{-1}$) and has been applied to catalyst samples. Extractive spectrofluorimetric procedures were developed for the determination of traces of platinum based on the formation of ternary ion-association complexes with chloride-Rhodamine 6G [799] and chloride-rose bengal [800]. The former procedure allows the determination of as low as 15 ppb of platinum. Three sensitive and aqueous spectrophotometric procedures were described during this period for the determination of traces of rhodium [655–657]. Of these, the ion-association complex formed with SnCl_2 -crystal violet [657] is more sensitive ($\epsilon = 1.0 \times 10^6 \text{ l mol}^{-1} \text{ cm}^{-1}$) and allows the determination of 0–0.2 ppm of rhodium. A similar ion-association system Ir– SnCl_2 -malachite green was described for the sensitive determination of iridium ($\epsilon = 1.45 \times 10^5 \text{ l mol}^{-1} \text{ cm}^{-1}$) [594].

5. Future trends

Despite being regarded by many analysts as obsolete, spectrophotometry still enjoys great popularity, which seems to be increasing in some fields. Advances in the synthesis of new organic

reagents will occur, but whether they will be able to bring about a breakthrough in analytical spectrophotometry or spectrofluorimetry is rather doubtful. Examination of various mixed ligand ternary and multicomponent systems, developed over the last two decades, indicates there is little scope in the future as they are unlikely to surpass in sensitivity over ion-association and surfactant sensitized systems. The use of multicomponent systems in surfactant sensitized procedures are finding increasing attention over the last five years. This trend is likely to continue in improving the sensitivity and selectivity of surfactant sensitized procedures. Flotation spectrophotometric procedures developed over the last decade are mainly for noble metals. In the coming years, one could see the development of flotation spectrophotometric procedures for the transition elements and *p*-block elements in view of their superior sensitivity. There is a shift in ion-association procedures over the last 15 years in the development of rapid, reliable, selective and sensitive aqueous procedures in place of extractive spectrophotometric procedures. This trend will continue with an emphasis on the application of developed procedures to real samples and in analysis of reference materials. Derivative and FIA spectrophotometric procedures are the novel and emerging areas where we will see many developments in the future. However, growing interest in automatic sample processing can place spectrophotometry as a detection technique due to the relatively low cost of the equipment and above all, its far easier and cheaper maintenance. The drawback of poor selectivity is frequently overcome by powerful signal processing techniques. These all make spectrophotometry a competitive technique, if not in ultra trace, at least in trace analysis.

Prior to 1980s, spectrofluorimetric procedures developed for inorganics utilize extraction and in most cases with xanthene dyes as one of the ligands in ternary and multicomponent complexes. In the last two decades also, this trend continued. During the last five years there is a trend towards the development of aqueous spectrofluorimetric procedures based on the quenching of the fluorescence of the dye. This trend is likely to increase in the future. A mention has to

be made here in the development of novel spectrofluorimetric procedures for europium and samarium wherein another rare earth ion acts as an activator. The development of such novel spectrofluorimetric systems may find increasing attention from various researchers throughout the world in view of its ramifications in the development of procedures for the determination of individual lanthanides in high purity rare earth oxides [834].

References

- [1] R. Lobinski, Z. Marczenko, *Crit. Rev. Anal. Chem.* 23 (1992) 55.
- [2] Z. Marczenko, *Crit. Rev. Anal. Chem.* 11 (1981) 195.
- [3] H. Onishi, *Photometric determination of traces of metals: Part IIA—Individual Metals Aluminium to Lithium*, Wiley, New York, 1986.
- [4] H. Onishi, *Photometric determination of traces of metals: Part IIB—Individual Metals Magnesium to Zirconium*, Wiley, New York, 1989.
- [5] Z. Marczenko, *Separation and Spectrophotometric Determination of Elements*, Horwood, Chichester, 1986.
- [6] A. Knowles, C. Burgess (Eds.), *Techniques in visible and ultraviolet spectrometry*, vol. 3, Practical Absorption Spectrometry, Ultraviolet Spectrometry Group, Chapman and Hall, London, 1984.
- [7] E. Upor, M. Mohali, G. Novak, *Comprehensive Analytical Chemistry*, vol. 20, Photometric Methods in Inorganic Analysis, Elsevier, New York, 1985.
- [8] T. Nowicka-Jankowska, *Comprehensive Analytical Chemistry*, vol. 19, Analytical Visible and Ultraviolet Spectrometry, Elsevier, Amsterdam, 1986.
- [9] M.I. Bulatov, I.P. Kalinkin, *Practical Manual on Photometric Analysis Methods*, Khimiya, Leningrad 1986.
- [10] C.L. Bashford, D.A. Harris, *Spectrophotometry and Spectrofluorimetry, A Practical Approach*, IRL Press, Oxford, 1987.
- [11] C. Burgess, K.D. Mielenz (Eds.), *Analytical Spectroscopy Library*, vol. 2, Advances in Standards and Methodology in Spectrophotometry, Elsevier, Amsterdam, 1987.
- [12] L. Sommer, *Analytical Absorption Spectrophotometry in The Visible and Ultraviolet, The Principles*, Elsevier, Amsterdam, 1989.
- [13] L. Sommer, M. Langova, *Crit. Rev. Anal. Chem.* 19 (1988) 225.
- [14] J.A. Howell, L.G. Hargis, *Anal. Chem.* 64 (1992) 66R.
- [15] L.G. Hargis, J.A. Howell, *Anal. Chem.* 66 (1994) 72R.
- [16] I.M. Warner, L.B. McGown, *Anal. Chem.* 64 (1992) 343R.
- [17] T.S. West, *Chemical Spectrometry in Trace Characterisation—Chemical and Physical*, NBS Monograph, 100, in: Meinke, B.F. Ecribner (Eds.), 1987, p. 215.
- [18] A.G. Fogg, C. Burgess, D.T. Burns, *Talanta* 18 (1971) 1175.
- [19] A.T. Pilipenko, M.M. Tananaiko, *Talanta* 21 (1974) 501.
- [20] P.R. Haddad, *Talanta* 24 (1977) 1.
- [21] D.P. Shcherbov, R.N. Plotnikova, *Zavodsk Lab.* 41 (1975) 129.
- [22] A.T. Pilipenko, M.M. Tananaiko, *Zh. Analit. Khim.* 28 (1973) 745.
- [23] S. Koch, G. Ackermann, *Z. Chem.* 12 (1972) 410.
- [24] X. Xia, G. Shao, *Fenxi Shiyanshi* 7 (1988) 41.
- [25] A.K. Babko, *Talanta* 15 (1968) 721.
- [26] S.B. Savvin, R.F. Gureva, *Zh. Anal. Khim.* 35 (1980) 1818.
- [27] X. Wu, *Fenxi Shiyanshi* 6 (1987) 29.
- [28] W. Chen, X. Jiang, J. Pan, Z. Xu, Lihua, Jianyan, *Huaxue Fence* 27 (1991) 267.
- [29] Z. Qiu, *Fenxi Huaxue* 10 (1982) 635.
- [30] I. Rudzitis, L. Cermakova, K. Nodomova, M. Malat, *Chem. Anal.* 26 (1981) 1045.
- [31] V.A. Nazarenko, I.G. Kostenko, E.A. Biryuk, *Zh. Anal. Khim.* 34 (1979) 1937.
- [32] A. Dimitrova, A. Shishkov, *Dokl. Bolg. Akad. Nauk* 32 (1979) 1679.
- [33] Y.K. Agarwal, V.J. Bhat, *Analyst* 109 (1984) 1287.
- [34] M.J.S. Delgado, L.M. Polo Diez, L.E. Gabeiran, *An. Quim.* 81 (1985) 88.
- [35] D. Shu, W. Yang, *Fenxi Shiyanshi* 8 (1989) 55.
- [36] G.V. Flyantikova, A.T. Isakhanova, O.A. Tataev, I.P. Kovalevska, *Zh. Neorg. Khim.* 25 (1980) 2769.
- [37] H. Akaiwa, H. Kawamotoand, F. Yoshimatsu, *Bull. Chem. Soc. Jpn.* 52 (1979) 3718.
- [38] E. Yamada, T. Kuwamoto, T. Fujinaga, E. Nakayama, *Anal. Chim. Acta* 138 (1982) 409.
- [39] Z. Zhao, R. Gao, L. Zhao, *Talanta* 39 (1992) 643.
- [40] N. Kuishen, F. Wei, Q. Qi, *Anal. Lett.* 14 (1981) 1565.
- [41] P.B. Granovskaya, M.M. Akhmedli, *Zh. Anal. Khim.* 37 (1982) 405.
- [42] R.A.L. Ferreira, M.L. Ensenat, Y. Barea, F.B. Martinez, *Anal. Lett.* 22 (1989) 1819.
- [43] G.V. Rathaiah, M.C. Eswar, *Analyst* 111 (1986) 61.
- [44] A.I. Postoronko, S.A. Aleshkevich, *Vopr. Khim. Khim. Technol.* 82 (1986) 67.
- [45] I.K. Guseinov, N. Kh. Rustamov, *Azerb. Khim. Zh.* 2 (1986) 115.
- [46] P. Chattopadhyay, S.K. Mazumdar, *Indian J. Chem.* 21 (1982) 857.
- [47] S. Lis, Z. Hnatejko, B. Makowska, M. Elbanowski, *Chem. Anal.* 39 (1994) 47.
- [48] L. Chermakova, O. Stirkska, E. Jansons, G. Rudzitis, H. Saldone, *Latv. PSR Zinat. Akad. Vestis, Kim. Ser. I* (1989) 352.
- [49] J. Siepak, *Z. Chem.* 29 (1989) 183.
- [50] Q.D. Ni, Y.H. Zhang, *Fenxi Huaxue* 22 (1994) 980.
- [51] P.K. Sharma, R.K. Mishra, *Acta Cienc. Indica* 8 (1982) 159.
- [52] A. Jha, R.K. Mishra, *J. Indian Chem. Soc.* 59 (1982) 694.

- [53] K. Ning, J. Fan, Fensi Huaxue 13 (1985) 952.
- [54] F.C. Garcia, A.A. Ramirez, C.J. Linares, Analyst 110 (1985) 819.
- [55] G. Moges, B.S. Chandravanshi, Ann. Chim. 74 (1984) 627.
- [56] I.V. Guseinov, N. Kh. Rustanov, Azerb. Khim. Zh. 5 (1985) 116.
- [57] I.V. Pyatnitsku, S.G. Mamuliya, L.L. Kotomietes, Ukr. Khim. Zh. 48 (1982) 181.
- [58] R.I. Hornillos, J.L.P. Fernandez, A.C. Mastin, R.G. Andreu, Microchem. J. 30 (1984) 114.
- [59] A.A. Kafarova, Izv. Akad. Nauk Graz. SSR, Ser. Khim. 8 (1982) 192.
- [60] F. Zhang, J. Liao, Fenxi Huaxue 12 (1984) 513.
- [61] D.N. Askerov, I.K. Guseinov, E.A. Bashirov, A.A. Melikov, Azerb. Khim. Zh. 3 (1985) 102.
- [62] L.I. Ganago, L.A. Alinovskaya, Zh. Anal. Khim. 35 (1980) 279.
- [63] M. Deguchi, S. Hayakawa, Bunseki Kagaku 31 (1982) 612.
- [64] H. Akaiwa, H. Kawamoto, S. Kogure, Bunseki Kagaku 28 (1979) 498.
- [65] N. Mishra, A. Ghosh, R.K. Mishra, K.S. Patel, Anal. Sci. 6 (1990) 407.
- [66] H. Shen, Y. Liu, Gaodeng Zuexiao Huaxue Xuebao 9 (1988) 897.
- [67] K.S. Patel, R.K. Mishra, Talanta 29 (1982) 791.
- [68] P.B. Barrera, J.F. Vazquez, F.B. Martinez, Microchem. J. 35 (1987) 1.
- [69] J.K. Thomas, A.G. Parker, Anal. Chim. Acta 113 (1980) 389.
- [70] A.J. Gowda, N.M.M. Gowda, Analyst 110 (1985) 743.
- [71] K.N. Thimmaiah, H.S. Gowda, K.K. Murthy, Microchem. J. 32 (1985) 8.
- [72] A.T. Pilipenko, A.I. Samchuk, O.S. Zulfigarov, Zh. Anal. Khim. 40 (1985) 1262.
- [73] W. Fan, X. Wang, Fenxi Huaxue 12 (1984) 620.
- [74] B. Keshavan, K.P. Krishna Prasad, Indian J. Chem. 30A (1991) 299.
- [75] D.T. Burns, D. Chimpalee, Anal. Chim. Acta 256 (1992) 307.
- [76] D.B. Gomis, S.A. Jimeno, A.S. Medel, Talanta 29 (1982) 761.
- [77] S. Kostova, A. Aleksandrov, M. Vrchlabsky, Ser. Fac. Sci. Nat. Univ. Purkynianae Brun 14 (1984) 103.
- [78] A. Aleksandrov, S. Kostova, O. Navratil, Collect. Czech. Chem. Commun. 50 (1985) 2369.
- [79] J. Aznarez, M.P. Cipres, L. Marco, A. Ferrer, Analyst 110 (1985) 1329.
- [80] C.V. Rao, M.S. Rao, K. Srinivasulu, Indian J. Chem. 19 (1980) 931.
- [81] H. Akaiwa, H. Kawamoto, M. Konishi, Bunseki Kagaku 28 (1979) 690.
- [82] N.K. Shen, F.S. Wei, Q.P. Qi, W.T. Chu, Mikrochim. Acta II (1983) 405.
- [83] M.B. Saha, A.K. Chakraborty, J. Indian Chem. Soc. 60 (1983) 281.
- [84] N.A. Ulakovich, I.V. Postnova, G.K. Budnikov, Zh. Anal. Khim. 40 (1985) 484.
- [85] M.K. Deb, R.K. Mishra, Int. J. Environ. Anal. Chem. 48 (1992) 151.
- [86] K. Watanabe, Y. Imaed, K. Kawagaki, Bull. Chem. Soc. Jap. 55 (1982) 3147.
- [87] P. Chattopadhyay, S.K. Mazumdar, Indian J. Chem. 22 (1983) 91.
- [88] S.P. Bag, B. Bhattacharya, J. Indian Chem. Soc. 60 (1983) 204.
- [89] M.B. Saha, A.K. Chakraborty, J. Indian Chem. Soc. 59 (1982) 1109.
- [90] Y. Fugita, I. Mori, M. Toyoda, Y. Nakahashi, K. Kato, M. Nakamura, Bull. Chem. Soc. Jap. 62 (1989) 3260.
- [91] A.K. Chakkar, L.R. Kakkar, Fr. J. Anal. Chem. 347 (1993) 483.
- [92] P.P. Sun, B. Wu, H.O. Liu, Lihua Jianyan Huaxue Fence 29 (1993) 327.
- [93] H.S.Y. Jayarama, M.V. D'Souza, S. Rangaswamy, Indian J. Chem. 25A, 1986, 703
- [94] O. Coufalova, G. Rudzite, G. Mezaraups, L. Cermakova, Microchem. J. 32 (1985) 24.
- [95] K. Sharma, A.K. Chhakar, L.R. Kakkar, Ann. Chim. 85 (1995) 577.
- [96] A. Wahi, L.R. Kakkar, Fr. J. Anal. Chem. 352 (1995) 387.
- [97] A. Wahi, L.R. Kakkar, Anal. Sci. 9 (1993) 409.
- [98] A. Wahi, L.R. Kakkar, Anal. Sci. 10 (1994) 509.
- [99] K. Sarma, H.K. Das, J. Indian Chem. Soc. 62 (1985) 631.
- [100] A.K. Das, J. Das, Indian J. Chem. 23 (1984) 359.
- [101] T.V. Babilseva, V.I. Fadeeva, Zh. Anal. Khim. 36 (1981) 518.
- [102] Y. Xu, X. Chen, Z. Hu, Anal. Lett. 20 (1987) 1001.
- [103] Ch. Tsurumi, K. Furuya, H. Kamada, Analyst 106 (1981) 944.
- [104] J. Valero, An. Quim. 83 (1987) 106.
- [105] S.J. Tsai, H. Hwang, J. Chin. Chem. Soc. 36 (1989) 187.
- [106] S. Banerjee, Talanta 33 (1986) 360.
- [107] S. Koch, G. Achermann, H. Mosler, Talanta 31 (1984) 667.
- [108] B.I. Nabivanets, E.N. Knyazeva, K.P. Klimenko, N.L. Dovgan, Zh. Anal. Khim. 37 (1982) 247.
- [109] H. Nguyen, V.M. Ivanov, Zh. Anal. Khim. 36 (1981) 1953.
- [110] Q. Liu, Fenxi Shiyanshi 5 (1986) 9.
- [111] A. Ghosh, K.S. Patel, R.K. Mishra, J. Radioanal. Nucl. Chem. 152 (1991) 243.
- [112] B. Keshavan, K.P. Krishnaprasad, J. Indian Chem. Soc. 69 (1992) 895.
- [113] A. Mulugeta, B.S. Chandravanshi, Mikrochim. Acta 1 (1983) 255.
- [114] J. Valero, Afinidad 40 (1983) 288.
- [115] Y. Anjaneyulu, M.R.P. Reddy, P.V.S. Kumar, C.S. Kavipurapu, B.V. Rao, Mikrochim. Acta I (1990) 87.
- [116] A.K. Baveja, V.K. Gupta, Int. J. Environ. Anal. Chem. 17 (1984) 299.

- [117] A.B. Chatterjee, S.P. Bag, A. Chakraborti, P.R. Chakraborty, *Mikrochim. Acta* III (1983) 307.
- [118] A.R. Jha, R.K. Mishra, *J. Indian Chem. Soc.* 59 (1984) 1177.
- [119] S.P. Bag, A.B. Chatterjee, A.K. Chakraborti, P.R. Chakraborty, *J. Indian Chem. Soc.* 59 (1982) 630.
- [120] S.P. Bag, A.B. Chatterjee, A.K. Chakraborti, P.R. Chakraborty, *Talanta* 29 (1982) 526.
- [121] N.A. Verdizade, Z.B. Ragimova, *Azerb. Khim. Zh.* 3 (1985) 109.
- [122] R.S. Kharsan, K.S. Patel, R.K. Mishra, Fresenius, *J. Anal. Chem.* 297 (1979) 159.
- [123] N.A. Kerdizade, Z.B. Ragimova, *Azerb. Khim. Zh.* 3 (1978) 116.
- [124] V.A. Nazarenko, E.N. Poluektova, G.G. Shitareva, R. Yalykko, *Ukr. Khim. Zh.* 45 (1979) 878.
- [125] A.T. Gowda, K. Rangappa, *Anal. Chem.* 58 (1986) 827.
- [126] P.G. Ramappa, H. Sanke Gowda, S. Manjappa, *Curr. Sci.* 48 (1979) 1016.
- [127] N.A. Verdizade, S.M. Shiraliev, *Azerb. Khim. Zh.* 6 (1983) 136.
- [128] A.P. Rubel, L.I. Vinasova, V.P. Antonovich, E.S. Ivanova, *Zh. Anal. Khim.* 41 (1986) 1206.
- [129] Y. Cai, X. Chen, *Fenxi Huaxue* 14 (1986) 201.
- [130] M.I. Shtokalo, E.F. Kostenko, *Zh. Anal. Khim.* 45 (1990) 296.
- [131] Z. Yang, *Fenxi Huaxue* 17 (1989) 450.
- [132] Y. Zhu, L. Yang, Y. He, *Hangzhou Daxue Xuebao, Ziran Kexueban* 18 (1991) 60.
- [133] R. Shah, S. Devi, *Indian J. Chem.* 34A (1995) 925.
- [134] F.M. El-Zawawy, M.F. El-sahaat, A.A. Mohammed, M.T.M. Zaki, *Analyst* 120 (1995) 549.
- [135] A.A.Y. El-Saeed, *Bull. Chem. Soc. Jap.* 67 (1994) 3216.
- [136] G. Xue, *Fenxi Huaxue* 14 (1986) 50.
- [137] K. Oshita, H. Wada, G. Nakagawa, *Anal. Chim. Acta* 182 (1986) 157.
- [138] Y. Zhu, H. Chen, W. Qi, *Fenxi Huaxue* 12 (1984) 369.
- [139] Z. Luo, G. Li, *Fenxi Huaxue* 16 (1988) 437.
- [140] F. Buhl, G. Kwapulinska, *Chem. Anal.* 32 (1987) 1013.
- [141] J. Yang, *Lihua Jiannan, Huaxue Fence* 24 (1988) 351.
- [142] Y. Chen, L. Lin, *Huaxue Fence* 23 (1987) 9.
- [143] Z. Luo, Z. Lin, *Yankuangcishi* 7 (1988) 104.
- [144] L.I. Savranskii, O. Yu Nadzafova, *Zh. Anal. Khim.* 47 (1992) 1613.
- [145] T. Zhang, X. Li, *Lihua Jiannan, Huaxue Fence* 27 (1991) 150.
- [146] W. Cheng, F. Yao, Y. Ci, *Fenxi Huaxue* 12 (1984) 394.
- [147] S. Tong, F. Zhao, L. Zhang, Z. Zhong, Q. Yang, *Huaxue Shiji* 7 (1985) 311.
- [148] S. Tagashira, *Anal. Chim. Acta* 157 (1984) 343.
- [149] V.N. Tikhonov, O.K. Pavlova, *Zh. Anal. Khim.* 37 (1982) 1809.
- [150] E. Peskova, K. Pliska, L. Sommer, *Ser. Fac. Sci. Nat. Univ. Purkynianae Brun.* 11 (1981) 395.
- [151] S. Liu, *Analyst* 107 (1982) 428.
- [152] C. Wyganowski, M. Kolczynska, *Microchem. J.* 27 (1982) 37.
- [153] Y. Ren, Y. Zhao, Y. Tong, *Fenxi Huaxue* 13 (1985) 881.
- [154] Y. Yuan, *Huaxue Shiji* 8 (1986) 85.
- [155] C. Martire, L. Hainberger, *Mikrochim. Acta* II (1985) 223.
- [156] M. Miyawaki, K. Uesugi, *Mikrochim. Acta* III (1985) 319.
- [157] M. Zang, Z. Hu, *Fenxi Huaxue* 15 (1987) 80.
- [158] Y. Zhu, G. Peng, *Fenxi Shiyanshi* 5 (1986) 62.
- [159] M.M. Tananaiko, L.I. Gorcnshtcin, *Ukr. Khim. Zh.* 52 (1986) 288.
- [160] C. Lyganowski, *Microchem. J.* 26 (1981) 45.
- [161] Z. Tan, S. Wu, *Huaxue Shiji* 7 (1985) 319.
- [162] V.N. Tikhonov, S.G. Danilvova, *Zh. Anal. Khim.* 35 (1980) 1264.
- [163] X. Ding, *Fenxi Huaxue* 13 (1985) 340.
- [164] P.K. Paria, T.K. Thokdar, S.K. Mazumdar, *Curr. Sci.* 58 (1989) 694.
- [165] G. Xu, *Fenxi Huaxue* 14 (1986) 679.
- [166] X. Feng, *Fenxi Huaxue* 7 (1988) 60.
- [167] N. Yamaguchi, T. Nishida, H. Nishida, *Bunseki Kagaku* 38 (1989) 48.
- [168] J. Zhang, D. Wang, H. Shu, Q. Pan, *Fenxi Huaxue* 15 (1987) 874.
- [169] H. Nishida, *Bunseki Kagaku* 39 (1990) 805.
- [170] M. Jarosz, I. Biernat, *Chem. Anal.* 33 (1988) 693.
- [171] Y. Yang, Y. Chen, *Fenxi Huaxue* 17 (1989) 365.
- [172] Y. Wu, D. Yang, *Lihua Jiannan, Huaxue Fence* 23 (1987) 343.
- [173] H. Nishida, *Bunseki Kagaku* 35 (1986) 368.
- [174] I. Buresova, V. Kuban, L. Sommer, *Collect. Czech. Chem. Commun.* 47 (1982) 1321.
- [175] H. Nishida, *Bunseki Kagaku* 31 (1982) 156.
- [176] Y. Zheng, L. Li, S. Sun, *Fenxi Huaxue* 12 (1984) 828.
- [177] G. Kwapulinska, F. Buhl, *Mikrochim. Acta* 1 (1984) 333.
- [178] J. Zhu, *Fen Hsi Hua Hsueh* 9 (1981) 53.
- [179] S. Li, H. Zhang, Z. Gu, *Fenxi Shiyanshi* 10 (1991) 29.
- [180] K.C. Bayan, H.K. Das, *Curr. Sci.* 53 (1984) 312.
- [181] C. Wyganowski, *Chem. Anal.* 26 (1981) 307.
- [182] Q. Xu, X. Xu, *Huaxue Xuebao* 40 (1982) 419.
- [183] I. Nemkova, H. Pesinova, V. Suk, *Microchem. J.* 30 (1984) 27.
- [184] Z. Liano, C. Li, *Fenxi Huaxue* 14 (1986) 370.
- [185] J. Kuang, G. Liu, C. Huang, *Fenxi Huaxue* 12 (1984) 736.
- [186] X. Liu, *Fenxi Shiyanshi* 5 (1986) 41.
- [187] D. Nonova, S. Pavlova, *Anal. Chim. Acta* 123 (1981) 289.
- [188] Y. Sun, X. Han, B. Zhao, *Fenxi Huaxue* 14 (1986) 917.
- [189] S. Li, Y. Xie, *Fenxi Huaxue* 14 (1986) 938.
- [190] M.M. Tananaiko, T.I. Vysotskaya, *Ukr. Khim. Zh.* 48 (1982) 629.
- [191] T. Ozaki, *Anal. Lett.* 15 (1982) 595.
- [192] D. Xia, Y. Wu, *Huaxue Shiji* 10 (1988) 45.
- [193] M.A. Pujar, P. Nagraj, *Ind. J. Technol.* 27 (1989) 503.
- [194] D. Cheng, Y. Ma, Z. Li, *Huaxue Shiji* 10 (1988) 42.
- [195] J. Kobylecka, *Chem. Anal.* 37 (1992) 369.

- [196] O.A. Tataev, I. Kh. Abakasova, D. Gasanova, *Fiz. Khim. Metody Anal. Kontroyla Proizvod I* (1981) 126.
- [197] Y.M. Li, H.M. Shen, *Lihua Jianyan, Huaxue Fence* 32 (1996) 175.
- [198] M. Jarosz, I. Biernat, *Chem. Anal.* 33 (1988) 685.
- [199] W. Qi, B. Pu, *Huaxue Xuebao* 42 (1984) 27.
- [200] I. Nemcova, J. Hrachovska, V. Suk, *Microchem. J.* 31 (1985) 233.
- [201] G.V. Rathiah, M.C. Eshwar, *Bull. Chem. Soc. Jap.* 58 (1985) 2447.
- [202] T. Chen, Y. Xiao, *Fenxi Huaxue* 15 (1987) 234.
- [203] L. Zheng, J. Luan, *Fenxi Shiyanshi* 5 (1986) 29.
- [204] D. Chen, Z. Li, *Fenxi Shiyanshi* 5 (1986) 35.
- [205] I. Mori, Y. Fujita, T. Enoki, *Bunseki Kagaku* 28 (1979) 707.
- [206] D. Xia, *Fen Hsi Hua Hsueh* 9 (1981) 196.
- [207] G. Xi, D. Liang, *Fenxi Huaxue* 12 (1984) 209.
- [208] H. Wong, G. Gong, *Fenxi Huaxue* 11 (1983) 291.
- [209] B.E. Evtimova, T.A. Chemleva, V.I. Fadeeva, *Zh. Anal. Khim.* 43 (1988) 1610.
- [210] X.H. Guo, *Yankuang Ceshi* 11 (1992) 359.
- [211] H. Hu, *Yankuang Ceshi* 10 (1991) 114.
- [212] L.H. Chen, W.X. Gu, *Fenxi Shiyanshi* 14 (1995) 61.
- [213] W. Lan, X. Wu, *Lihua Jianyan, Huaxue Fence* 26 (1990) 145.
- [214] M.T.M. Zaki, S.M. Attiya, *Anal. Sci.* 6 (1990) 579.
- [215] K.C. Bayan, H.K. Das, *J. Indian Chem. Soc.* 64 (1987) 198.
- [216] S. Zou, W. Liang, B. Xu, S. Wu, *Fenxi Huaxue* 12 (1984) 525.
- [217] D. Nonova, K. Stoyanov, *Anal. Chim. Acta* 138 (1982) 321.
- [218] S. Feng, X. Wang, *Fenxi Huaxue* 10 (1982) 289.
- [219] K. Uesugi, M. Miyawaki, T. Nagahiro, *Microchem. J.* 32 (1985) 332.
- [220] G. Xue, *Fenxi Shiyanshi* 5 (1986) 27.
- [221] B.E. Evtimova, *Dokl. Bolg. Akad. Nauk* 39 (1986) 61.
- [222] S. Okawa, *Bunseki Kagaku* 35 (1986) 101.
- [223] V.N. Tikhonov, E.S. Tikhonov, *Org. Reakt. Anal.* 3 (1979) 48.
- [224] Y. Zhu, Z. Luo, H. Xu, *Fen Hsi Hua Hsueh* 9 (1981) 438.
- [225] X. He, D.P. Poe, *Anal. Chim. Acta* 131 (1981) 195.
- [226] S.C. Rui, S. Motomizu, K. Toei, *Bunseki Kagaku* 34 (1985) 643.
- [227] I. Mori, J. Fujita, M. Toyoda, S. Kimura, *Anal. Lett.* 25 (1992) 1345.
- [228] D. Wang, W. Liao, X. Huang, Q. Pan, *Fenxi Huaxue* 15 (1987) 689.
- [229] P.K. Paria, T.K. Thokdar, S.K. Mazumdar, *J. Indian Chem. Soc.* 66 (1989) 465.
- [230] M.T.M. Zaki, W.H. Mahmoud, A.Y. Elsayed, *Talanta* 35 (1988) 253.
- [231] M. Miyawaki, K. Uesugi, *Mikrochim. Acta* 1 (1985) 135.
- [232] S. Liu, *Huaxue Shiji* 7 (1985) 128.
- [233] Z. Marczenko, H. Kalowska, *Anal. Chim. Acta* 123 (1981) 279.
- [234] X. He, H. He, H. Shi, *Fenxi Huaxue* 14 (1986) 565.
- [235] Q. Liu, *Fenxi Shiyanshi* 5 (1986) 27.
- [236] C. Wyganowski, *Microchem. J.* 29 (1984) 143.
- [237] Z. Marczenko, M. Krasiejko, *Chem. Anal.* 26 (1981) 297.
- [238] Y. Chen, M. Sha, Z. Chen, *Huaxue Shiji* 8 (1986) 365.
- [239] X. He, D.P. Poe, *Talanta* 28 (1981) 419.
- [240] Y. He, Y. Liu, J. Zhao, Z. Zhao, F. Wang, *Fenxi Huaxue* 16 (1988) 341.
- [241] G. Zhao, *Fenxi Shiyanshi* 6 (1987) 21.
- [242] M. Jarosz, *Chem. Anal.* 33 (1988) 675.
- [243] S. Zuo, J. Li, *Fenxi Shiyanshi* 8 (1989) 35.
- [244] W. Qi, D. Liu, *Yankuangceshi* 8 (1989) 91.
- [245] G. Kwapulinska, *Chem. Anal.* 40 (1995) 783.
- [246] J. Li, Y.L. He, J.D. Zhao, Z.Y. Zhao, F.P. Wang, *Fenxi Huaxue* 21 (1993) 1296.
- [247] K. Uesegi, M. Miyawaki, *Microchem. J.* 26 (1981) 288.
- [248] W. Czeslaw, *Microchem. J.* 27 (1982) 13.
- [249] S. Sakuraba, *Talanta* 37 (1990) 637.
- [250] L. Hou, B. Jin, *Yankuangceshi* 9 (1990) 187.
- [251] S. Cao, Z. Lu, Y. Cai, *Kuangye Gongcheng* 10 (1990) 55.
- [252] A.T. Pilipenko, E.G. Malesimiyuk, *Ukr. Khim. Zh.* 53 (1987) 58.
- [253] D. Xia, H. Liu, *Fenxi Huaxue* 15 (1987) 59.
- [254] D. Wong, P. Wu, Z. Xiao, Q. Pon, *Huaxue Shiji* 8 (1986) 138.
- [255] J. Li, H. Shi, J. Pan, Y. Yao, *Huaxue Shiji* 7 (1985) 249.
- [256] J. Wang, G. Xi, D. Liang, *Fenxi Huaxue* 13 (1985) 593.
- [257] Z. Marczenko, H. Kalowska, *Mikrochim. Acta* 2 (1979) 507.
- [258] L.I. Ganago, N.N. Ishchenko, *Zh. Anal. Khim.* 35 (1980) 1718.
- [259] Y. Tang, *Fenxi Huaxue* 18 (1990) 1.
- [260] Y. Zhang, H. Wang, J. Xu, *Huaxue Shiji* 12 (1990) 146.
- [261] J. Zhuang, D. Wang, Z. Xic, X. Zeng, *Lihua Jianyan, Huaxue Fence* 26 (1990) 221.
- [262] G. Xu, Z. Wang, C. Yao, *Yankuangceshi* 8 (1989) 254.
- [263] H. Shen, Z. Wang, G. Xu, *Analyst* 112 (1987) 887.
- [264] G. Xi, P. Liang, *Fenxi Huaxue* 14 (1986) 284.
- [265] Z. Marczenko, M. Krasiejko, A. Klebeck, *Microchem. J.* 34 (1986) 121.
- [266] M. Cai, G. Huang, Y. Huang, *Yankuangceshi* 6 (1987) 30.
- [267] H. Shen, L. Wang, *Huaxue Xuebao* 41 (1983) 700.
- [268] H. Kurihara, H. Kuwabara, *Bunseki Kagaku* 31 (1982) 50.
- [269] Q. Xu, *Huaxue Shiji* 6 (1984) 191.
- [270] L.A. Albota, L.S. Serdyuk, M.M. Zaverach, *Zh. Anal. Khim.* 36 (1981) 270.
- [271] N. Wang, P. Qi, *Fenxi Huaxue* 17 (1989) 960.
- [272] S.G. Jadav, C. Venkateswarlu, *Ind. J. Chem.* 28A (1989) 820.
- [273] G. Kwapulinska, F. Buhl, *Chem. Anal.* 33 (1988) 801.
- [274] R. Zhang, H. Wang, *Huaxue Shiji* 9 (1987) 269.
- [275] C. Jiang, S. Liu, *Fenxi Shiyanshi* 7 (1988) 30.
- [276] Z. Marczenko, H. Kalowska, *Chem. Anal.* 25 (1980) 555.

- [277] X. Chen, C. Han, Z. Yuan, Fenxi Huaxue 12 (1984) 135.
- [278] A.I. Krilov, G.M. Kotromitnova, G.N. Koroleva, L.N. Korsun, N.A. Kostromina, Zh. Anal. Khim. 36 (1981) 1323.
- [279] Q. Wong, C. Ouyang, Fenxi Huaxue 14 (1986) 67.
- [280] N. Irena, P. Pavla, H.C. Tran, Collect. Czech. Chem. Commun. 47 (1982) 503.
- [281] S. Sun, C. Ho, Kohsueh Tung Pao 26 (1981) 797.
- [282] Y. Ci, M. Yang, Huaxue Shiji 5 (1983) 7.
- [283] S. Sun, Y. Shen, Koxue Tongbao 28 (1983) 220.
- [284] A.I. Kirillov, L.P. Shaulina, O.D. Alckscceva, Zh. Anal. Khim. 39 (1984) 161.
- [285] E.G. Maksimiyuk, A.T. Pilipenko, Ukr. Khim. Zh. 56 (1990) 37.
- [286] M. Xiao, Lihua Jianyan, Huaxue Fence 25 (1989) 8.
- [287] D. Xia, J. Zhang, W. Xie, Huaxue Shiji 11 (1989) 186.
- [288] D. Cheng, Z. Li, Fenxi Huaxue 15 (1987) 308.
- [289] M. Ding, D. Xia, F. Wang, Y. He, Huaxue Shiji 9 (1987) 260.
- [290] N.N. Ishchenko, L.I. Ganago, L.G. Starobinets, Vestsi Akad. Navuk BSSR, SerKhim. Navuk 2 (1990) 3.
- [291] D. Xia, C. Zhao, Fenxi Huaxue 13 (1985) 923.
- [292] Z. Li, C. Li, Fenxi Shiyanshi 23 (1986) 61.
- [293] X.Y. Wu, S.A. Zhang, Fenxi Huaxue 22 (1994) 536.
- [294] M. Tarck, M. Zaki, F.M. El-Zawawy, A.K. Abdel Kader, M.M. Abdalla, Anal. Sci. 6 (1990) 61.
- [295] S. Zeng, H. Zhang, S. Xie, Wuhan Daxue Xuebao, Ziran Kexuban (1990) 92.
- [296] M. Tarek, M. Zaki, A.K. Adbelkader, M.M. Abdalla, Talanta 37 (1990) 1091.
- [297] Z. Hsu, X. Liao, Talanta 35 (1988) 1007.
- [298] M.M. Tananaiko, L.I. Gorenstein, Zh. Anal. Khim. 43 (1988) 303.
- [299] R. Qu, W. Lin, H. Yang, H. Chang, Fenxi Huaxue 13 (1985) 732.
- [300] R. Zhou, P. Zhen, X. Wu, Fenxi Shiyanshi 5 (1986) 10.
- [301] D. Wang, J. Bai, J. Chen, Fenxi Huaxue 12 (1984) 140.
- [302] M. Sugawara, M. Uto, T. Kambara, Bull. Chem. Soc. Jpn. 56 (1983) 3179.
- [303] I. Yu Andreeva, L.I. Lebedeva, G.L. Kavelina, Zh. Anal. Khim. 37 (1982) 2202.
- [304] J. Lin, Fen Hsi Hua Hsuch 8 (1980) 345.
- [305] J. Valero, Afinidad 38 (1981) 50.
- [306] C. Wyganowski, M. Czeslaw, Microchem. J. 25 (1980) 147.
- [307] I. Mori, Y. Fujita, Y. Kamata, M. Maeyama, T. Enoki, Bunsekikagaku 29 (1980) 638.
- [308] H. Zhang, Z. Mu, R. Zhang, Fenxi Huaxue 12 (1984) 824.
- [309] D. Wang, J. Chen, J. Bai, Q. Pon, Gaodeng Xuexiao Huaxue 4 (1983) 809.
- [310] H. Li, Z. He, X. Song, Yankuangceshi 8 (1989) 185.
- [311] D. Qi, F. Miao, R. Xie, X. Sun, Huaxue Shiji 8 (1986) 10.
- [312] G. Liu, Y. Liu, C. Xiuong, W. Zhong, X. Ma, Fenxi Shiyanshi 6 (1987) 20.
- [313] S. Feng, Z. Gao, Huaxue Tongbao 3 (1986) 34.
- [314] A. Hideo, K. Hiroshi, H. Etsuo, Bunseki Kagaku 31 (1982) 117.
- [315] M. Jarosz, A. Swietlow, Microchem. J. 37 (1988) 322.
- [316] L.A. Alinowskaya, L.V. Kovaleva, L.N. Bhukteeva, R.S. Famenko, Vcstsi Akad. Navuk BSSR, SerKhim. Navuk 6 (1990) 6.
- [317] K.K. Namboothiri, T.V. Ramakrishna, Indian J. Technol. 27 (1989) 201.
- [318] T. Prasada Rao, T.V. Ramakrishna, Talanta 27 (1980) 439.
- [319] A.Z. Abu Zuhri, Spec. Lett. 19 (1986) 333.
- [320] Y. Wakamatsu, Bunseki Kagaku 31 (1982) 538.
- [321] S. Hu, Z. Zeng, Fenxi Huaxue 18 (1990) 250.
- [322] S. Hu, Z. Zeng, Lihua Jianyan, Huaxue Fence 26 (1990) 103.
- [323] D. Yang, Fenxi Shiyanshi 9 (1990) 66.
- [324] T.K. Thokdar, P.K. Paria, S.K. Mazumdar, Ind. J. Chem. 28A (1989) 443.
- [325] S. Hu, Z. Zeng, Fenxi Shiyanshi 8 (1989) 13.
- [326] S. Sakuraba, K. Oguma, Fresenius J. Anal. Chem. 369 (1994) 523.
- [327] D.L. Xu, M.Y. Gong, G.S. Li, L.X. Xiang, S.Y. Gao, Fenxi Shiyanshi 15 (1996) 47.
- [328] Z.X. Guo, M.Y. Yuan, S.Y. Zhang, Fenxi Shiyanshi 14 (1995) 18.
- [329] A.A.Y. El-Saeed, Mikrochim. Acta 117 (1995) 161.
- [330] R.R. Srivastava, Omprakash, Croat. Chem. Acta 54 (1982) 465.
- [331] S. Li, L. Wong, G. Fang, W. Mo, Fenxi Huaxue 13 (1985) 926.
- [332] H. Akaiwa, H. Kawamoto, E. Yoshimatsu, Nippon Kagaku Kaishi 1 (1981) 79.
- [333] S. Hu, X. Kou, Fenxi Shiyanshi 5 (1986) 23.
- [334] V.N. Tikhonov, N.P. Aleksandrova, Zh. Anal. Khim. 36 (1981) 242.
- [335] Y. Ci, K. Hu, C. Zheng, Y. Tan, Ko Hsuch Tung Pao 24 (1979) 879.
- [336] P.K. Paria, T.K. Thokdar, S.K. Mazumdar, Curr. Sci. 58 (1989) 69.
- [337] D. Wang, J. Zhuang, Y. Zhuang, S. Tian, Q. Pan, Fenxi Huaxue 18 (1990) 766.
- [338] J. Sabartova, M. Herrmannova, M. Malat, L. Cermakova, Chem. Zvesti 34 (1980) 111.
- [339] A. Alte, L. Cermakova, Chem. Pap. 42 (1988) 483.
- [340] Z.X. Guo, M.Y. Yuan, S.Y. Zhang, Fenxi Shiyanshi 14 (1995) 36.
- [341] S. Hu, C. Shu, Q. Li, S. Cheng, A. Yin, Fenxi Huaxue 15 (1987) 814.
- [342] D.J. Wang, H.M. Wang, Y.C. Tan, Fenxi Huaxue 22 (1994) 643.
- [343] R. Lai, Z. Zhang, Fenxi Huaxue 12 (1984) 392.
- [344] R. Wu, Fenxi Huaxue 12 (1984) 921.
- [345] Z. Zhou, W. Xu, Lihua Jianyan, Huaxue Fence 23 (1987) 72.
- [346] Z. Luo, W. He, Talanta 37 (1990) 641.
- [347] D. Yiang, Yankuangceshi 10 (1991) 209.
- [348] G. Kwapulinska, F. Buhl, J. Poledniok, Chem. Anal. 38 (1993) 201.
- [349] J. Jurkevicinte, M. Malat, Collect. Czeck. Chem. Commun. 44 (1979) 3236.
- [350] Y. Ci, Y. Zhao, H. Hu, L. Wen, Fen. Hsi Hua Hsuch 9 (1981) 64.

- [351] M. Jarosz, Z. Marczenko, *Anal. Chim. Acta* 159 (1984) 309.
- [352] Z. Zhou, J. Gu, *Fenxi Shiyanshi* 5 (1986) 46.
- [353] Z. Zhou, J. Gu, *Fenxi Huaxue* 14 (1986) 46.
- [354] I. Mori, Y. Fujita, K. Fujita, A. Usami, H. Kawabe, Y. Koshiyama, T. Tanaka, *Bull. Chem. Soc. Jpn.* 59 (1986) 1623.
- [355] Y. Zheng, S. Zhou, *Fenxi Huaxue* 11 (1983) 210.
- [356] Y. Zheng, S. Zhou, *Huaxue Shiji* 5 (1983) 198.
- [357] G. Huang, W. Li, *Yankuangceshi* 10 (1991) 38.
- [358] D. Wang, Z. Xie, Q. Wu, Y. Song, S. Jin, *Analyst* 116 (1991) 1189.
- [359] W. Lin, X. Wu, *Lihua Jiannan, Huaxue Fence* 25 (1989) 281.
- [360] C. Gao, J. Pan, H. Zhu, *Huaxue Fence* 25 (1989) 339.
- [361] Y. Xu, Y. Zhao, Y. Ci, *Fenxi Huaxue* 15 (1987) 1028.
- [362] Y. Zhou, C. Ma, *Fenxi Huaxue* 11 (1983) 435.
- [363] V.P. Antonovich, E.N. Suvorova, E.I. Shelikina, *Zh. Anal. Khim.* 37 (1982) 429.
- [364] X. Wu, H. Ding, *Fenxi Shiyanshi* 5 (1986) 26.
- [365] H. Shen, L. Wong, *Huaxue Shiji* 5 (1983) 262.
- [366] J. Li, *Fenxi Shiyanshi* 6 (1987) 63.
- [367] G. Xu, H. Shen, *Fenxi Huaxue* 10 (1982) 334.
- [368] J. Zhao, *Fen Hsi Hua Hsueh* 9 (1981) 430.
- [369] J. Wu, Z. Yang, *Kang Tieh* 15 (1980) 40.
- [370] H.C. Tran, I. Nemcova, I. Nemecek, V. Suk, *Anal. Chim. Acta* 115 (1980) 279.
- [371] H. Kurihara, H. Kuwabara, *Bunseki Kagaku* 33 (1984) 199.
- [372] Z. Chen, Q. Pan, Q. Rong, J. Luo, *Huaxue Shiji* 8 (1986) 141.
- [373] G. Xi, D. Liang, Z. Pai, *Fenxi Huaxue* 14 (1986) 281.
- [374] F. Zang, Z. Wang, *Xiyou Jinshu* 5 (1986) 287.
- [375] G. Qin, Y. Tong, *Huaxue Shiji* 5 (1983) 347.
- [376] J. Valero, *An. Quim.* 84 (1988) 130.
- [377] M.T.M. Zaki, A.Y. Elsaed, *Anal. Lett.* 28 (1995) 1525.
- [378] X. Liao, Z. Xu, J. Pan, *Lihua Jiannan, Huaxue Fence* 27 (1991) 324.
- [379] B. Wu, N. Zhang, Y. Qu, H. Liu, *Huaxue Shiji* 7 (1985) 66.
- [380] Ch. Tsurumi, K. Furuya, H. Kamada, *Bunseki Kagaku* 28 (1979) 754.
- [381] N. Guo, *Fenxi Huaxue* 15 (1987) 105.
- [382] H. Shi, J. Li, G. Zhang, *Fenxi Huaxue* 11 (1983) 826.
- [383] D.J. Wang, Q.L. Wu, J.L. Huang, S.M. Zhang, *Yejin Fenxi* 13 (1993) 19.
- [384] D. Wang, Z. Xie, Q. Fan, W. Cai, B. Huang, Z. Zhang, *Yankuangceshi* 9 (1990) 115.
- [385] I. Mori, Y. Fujita, K. Sakaguchi, *Bull. Chem. Soc. Jpn.* 55 (1982) 3649.
- [386] H.D. Gunawardhana, *Analyst* 108 (1983) 952.
- [387] D. He, K. Ma, Y. Feng, *Fenxi Shiyanshi* 5 (1986) 62.
- [388] J. Wu, H. Wang, *Fenxi Huaxue* 14 (1986) 860.
- [389] D. Zhang, X. Zeng, *Fenxi Huaxue* 14 (1986) 498.
- [390] L.V. Kovaleva, L.I. Gonago, *Vestsi. Akad. Navuk. BSSR Serkhim. Navuk* 2 (1983) 3.
- [391] T. Wu, X. Chen, X. Chen, *Fenxi Huaxue* 11 (1983) 529.
- [392] L.I. Gonago, L.V. Kovaleva, *Zh. Anal. Khim.* 37 (1982) 1209.
- [393] Y. Shijo, T. Shimizu, K. Sakai, *Bull. Chem. Soc. Jpn.* 55 (1982) 3187.
- [394] H. Shen, Z. Wang, *Fenxi Huaxue* 9 (1981) 665.
- [395] Z. Marczenko, H. Kalowska, *Microchem. J.* 27 (1982) 174.
- [396] D. Wong, N. Zheng, F. Luo, Q. Pon, *Fenxi Huaxue* 12 (1984) 819.
- [397] A. Yu, Nazarenko, *Zh. Anal. Khim.* 40 (1985) 828.
- [398] Z. Hausenblasova, J. Nemcova, U. Sule, *Microchem. J.* 26 (1981) 262.
- [399] L. Zhang, R. Tai, Z. Zhang, *Fenxi Huaxue* 12 (1984) 398.
- [400] M.E.D. Garuia, E.B. Gonzalez, A.S. Medel, *Microchem. J.* 30 (1984) 211.
- [401] Y. Chen, L. Zheng, Y. Lin, *Fenxi Shiyanshi* 6 (1987) 25.
- [402] H. Cao, *Fenxi Shiyanshi* 6 (1987) 10.
- [403] R. Zhang, H. Wang, J. Wen, *Fenxi Huaxue* 16 (1988) 111.
- [404] H. Ladzinska-Kulinska, *Chem. Anal.* 31 (1986) 843.
- [405] L. Jancar, B. Slezackova, L. Sommer, *Talanta* 36 (1989) 549.
- [406] M. Jarosz, *Chem. Anal.* 31 (1986) 553.
- [407] G. Kwapulinska, B. Janoszka, *Fresenius J. Anal. Chem.* 338 (1990) 641.
- [408] J. Havel, A. Vankova-Kotranova, *Script J. Fac. Sci. Masaryk Univ. Brno.* 20 (1990) 323.
- [409] J. Simek, E. Ruzicka, *Acta Univ. Palocki. Olomoc, Fac. Rerum. Nat.* 76 (1983) 97.
- [410] X. Yuan, *Fenxi Huaxue* 12 (1984) 183.
- [411] S. Kumar, R. Kant, O. Prakash, *Rev. Roum. Chem.* 29 (1984) 383.
- [412] T. Ozaki, *Anal. Lett.* 15 (1982) 581.
- [413] K. Kania, F. Buhl, *Chem. Anal.* 35 (1990) 775.
- [414] Y. Nakahashi, A. Yoshii, *Anal. Lett.* 20 (1987) 747.
- [415] N.L. Babenko, M.Sh. Blokh, G.N. Tashuta, *Zh. Anal. Khim.* 42 (1987) 1829.
- [416] N. Jie, X. Lin, *Huaxue Shiji* 12 (1990) 190.
- [417] N.L. Babenko, M.Sh. Blokh, Z.V. Medvedov, G.N. Tashuta, *Zh. Anal. Khim.* 45 (1990) 1755.
- [418] M.N. Gordeeva, D.N. Meshcheryakova, *Probl. Sovrem. Anal. Khim.* 1 (1983) 16.
- [419] D. Xia, *Fenxi Huaxue* 11 (1983) 845.
- [420] C.K. Verma, S. Kulsreshtha, O. Prakash, *Chem. Anal.* 28 (1983) 669.
- [421] I. Mori, Y. Fujita, K. Sakaguchi, *Bunseki Kagaku* 31 (1982) 193.
- [422] N.T. Son, E. Ruzicka, *Chem. Zvesti* 33 (1979) 758.
- [423] I. Mori, Y. Fujita, K. Fujita, Y. Koshiyama, T. Tanaka, *Bull. Chem. Soc. Jpn.* 59 (1986) 3997.
- [424] Z. Luo, Y. Wu, *Huaxue Tongbao* 6 (1989) 42.
- [425] H. Shen, *Huaxue Shiji* 2 (1982) 79.
- [426] J. Lin, *Fen Hsi Hua Hsueh* 9 (1981) 443.
- [427] M. Ding, D. Xia, F. Wang, Y. He, *Fenxi Shiyanshi* 6 (1987) 22.
- [428] Y. Wakamatsu, *Bunseki Kagaku* 31 (1982) 575.
- [429] S. Zheng, *Fenxi Huaxue* 11 (1983) 684.

- [430] D. Wong, J. Chen, J. Bai, Q. Pan, *Huaxue Shiji* 6 (1984) 139.
- [431] V.A. Nazarenko, V.P. Antonovich, N.A. Veshchikova, *Talanta* 34 (1987) 215.
- [432] T. Chang, Yung-Kang, Fen Hsi Hua Hsueh, 7 (1979) 160.
- [433] Ch. Tsurumi, K. Furuya, H. Kamada, *Anal. Lett.* 13 (1980) 319.
- [434] H. Shi, X. He, G. Chang, Fen Hsi Hua Hsueh 9 (1981) 127.
- [435] J. Galban, M.L. Urate, M.D. Mariscal, C. Diaz, J. Aznarez, *Microchem. J.* 40 (1989) 94.
- [436] D. Xia, H. Li, Fenxi Huaxue 18 (1990) 760.
- [437] A.T. Pilipenko, E.N. Arendaryuk, *Ukr. Khim. Zh.* 56 (1990) 260.
- [438] I. Mori, Y. Fujita, K. Sakaguchi, H. Tsuji, T. Gnuki, *Bunseki Kagaku* 29 (1980) 723.
- [439] M.M. Tananaikio, N.V. Popovich, N.L. Ozerova, *Ukr. Khim. Zh.* 48 (1982) 505.
- [440] S. Sakuraba, *Talanta* 31 (1984) 840.
- [441] D. Nonova, K. Stoyanov, *God. Sofil. Univ., Khim. Fak*
- [442] T. Zhe, S.S. Wu, *Talanta* 31 (1984) 624.
- [443] Y. Tang, Fenxi Shiyanshi 10 (1991) 31.
- [444] K. Kania, F. Buhl, *Chem. Anal.* 37 (1992) 691.
- [445] B. Xu, J. Yao, Yegin Fenxi 13 (1993) 37.
- [446] Y. Ren, L. Gu, Fenxiceshi Tongbao 9 (1990) 76.
- [447] Z. Guan, X. Yuan, Fenxi Huaxue 16 (1988) 172.
- [448] Q.Z. Zai, *Analyst* 119 (1994) 1895.
- [449] H. Shen, L. Wong, Fenxi Huaxue 11 (1983) 576.
- [450] D. Wong, S. Shi, Y. Fu, Q. Pon, *Huaxue Shiji* 5 (1983) 337.
- [451] J. Li, H. Shi, Fenxi Huaxue 13 (1985) 418.
- [452] Z. Li, J. Chen, L. Shi, *Huaxue Shiji* 7 (1985) 330.
- [453] H. Shen, H. Li, *Huaxue Shiji* 8 (1986) 63.
- [454] Z. Li, H. Lin, S. Tan, F. Fan, *Huaxue Shiji* 8 (1986) 20.
- [455] K. Kalinowski, Z. Marczenko, *Chem. Anal.* 32 (1987) 941.
- [456] S.H. Zhang, X.T. Chen, Z.K. Wang, *Huaxue Shiji* 14 (1992) 239.
- [457] Z. Liu, J. Liu, W. Li, J. Shang, *Lihua Jianyan, Huaxue Fence* 27 (1991) 34.
- [458] Z. Marczenko, K. Jankowski, *Talanta* 32 (1985) 291.
- [459] Z. Marczenko, K. Jankowski, *Anal. Chim. Acta* 176 (1985) 185.
- [460] M. Zaros, P. Lubowski, *Quim. Anal.* 13 (1994) 19.
- [461] Z. Marczenko, R. Lobinski, *Chem. Anal.* 34 (1989) 87.
- [462] L. Mathew, M.L.P. Reddy, T.R. Ramamohan, C.S.P. Iyer, A.D. Damodaran, *Microchim. Acta* (in press).
- [463] G. Yang, M. Zhao, Z. Li, Fenxi Huaxue 18 (1990) 836.
- [464] Z. Marczenko, K. Kalinowski, *Anal. Chim. Acta* 144 (1982) 173.
- [465] L.I. Ganago, I.F. Ivanova, V.N. Yashchuk, *Zh. Anal. Khim.* 45 (1990) 1729.
- [466] R. Lobinski, Z. Marczenko, *Anal. Chim. Acta* 226 (1989) 281.
- [467] Z. Marczenko, M. Balcerzak, H. Pasek, *Microchim. Acta II* (1982) 371.
- [468] Z. Marczenko, J. Uscinska, *Microchem. J.* 26 (1981) 453.
- [469] Z. Marczenko, J. Uscinska, *Anal. Chim. Acta* 123 (1981) 271.
- [470] M. Balcerzak, *Analyst* 113 (1988) 129.
- [471] M. Balcerzak, A. Kowalczyk, *Chem. Anal.* 33 (1988) 519.
- [472] M. Balcerzak, *Anal. Chim. Acta* 242 (1991) 185.
- [473] M. Chen, *Fresenius J. Anal. Chem.* 343 (1992) 613.
- [474] K. Kalinowski, Z. Marczenko, *Anal. Chim. Acta* 186 (1986) 331.
- [475] Z. Marczenko, M. Jarosz, *Analyst* 106 (1981) 751.
- [476] Q. Xu, X. Xu, Z. Li, *Huaxue Shiji* 10 (1988) 81.
- [477] V. Bhagavathy, T. Prasada Rao, A.D. Damodaran, *Anal. Chim. Acta* 280 (1993) 169.
- [478] G. Jin, Fenxi Huaxue 16 (1988) 424.
- [479] Z. Marczenko, E. Kowalczyk, *Anal. Chim. Acta* 108 (1979) 261.
- [480] K. Kalinowski, Z. Marczenko, *Mikrochim. Acta I* (1985) 167.
- [481] M. Balcerzak, *Analysis* 18 (1990) 365.
- [482] M. Balcerzak, *Mikrochim. Acta II* (1985) 389.
- [483] M. Balcerzak, *Chem. Anal.* 31 (1986) 859.
- [484] Z. Li, M. Zhao, Fenxi Huaxue 17 (1989) 966.
- [485] M. Balcerzak, W. Wozniak, *Microchem. J.* 37 (1988) 326.
- [486] S. Motomizu, M. Oshima, T. Ikegami, *Analyst* 114 (1989) 1679.
- [487] E.N. Dorokova, N.A. Gracheva, L.V. Dracheva, *Zh. Anal. Khim.* 43 (1988) 265.
- [488] K. Kalinowski, Z. Marczenko, *Microchem. J.* 39 (1989) 198.
- [489] V.G. Skripchuk, *Zh. Anal. Khim.* 36 (1981) 1362.
- [490] T. Kowlaski, *Chem. Anal.* 32 (1987) 379.
- [491] R. Lobinski, Z. Marczenko, *Anal. Sci.* 4 (1988) 629.
- [492] L. Mathew, M.L.P. Reddy, T. Prasada Rao, C.S.P. Iyer, A.D. Damodaran, *Fresenius J. Anal. Chem.* 350 (1994) 180.
- [493] W. Qi, H. Luo, Fenxi Shiyanshi 7 (1988) 17.
- [494] S.H. Li, S.Q. Li, *Huaxue Shiji* 14 (1992) 68.
- [495] Y. Fujita, I. Mori, M. Toyoda, T. Matsuo, *Anal. Sci.* 9 (1993) 829.
- [496] J.Y. Jin, L.Q. Wang, Z.H. Wang, *Lihua Jianyan, Huaxue Fence* 30 (1994) 347.
- [497] Ch. Fan, W. Lin, *Hua Hsueh Tung Pao* 4 (1980) 212.
- [498] Y. Xiao, Fenxi Huaxue 11 (1983) 279.
- [499] Q. Qi, F. Wei, N. Shen, *Huaxue Shiji* 5 (1983) 269.
- [500] Z. Hu, F. Su, C. Li, *Lanzhou Daxue Xuebao, Ziran Kexueban* 19 (1983) 65.
- [501] T. Koh, M. Katon, *Anal. Chim. Acta* 109 (1979) 167.
- [502] K.S. Idriss, M.M. Seleim, M.S. Abubaker, *Proc. Indian Acad. Sci.* 89 (1980) 519.
- [503] S. Liu, Z. Liu, Y. Liu, Fenxi Huaxue 11 (1983) 641.
- [504] E.A. Biryuk, L.I. Vinarova, R.V. Ravitskaya, *Ukr. Khim. Zh.* 47 (1981) 760.
- [505] S.J. Xu, Y.Z. Zhang, Fenxi Huaxue 21 (1993) 685.
- [506] X. Zhao, S. Xu, Fenxi Huaxue 15 (1987) 625.
- [507] K. Palanivelu, T.V. Ramakrishna, *Indian J. Technol.* 28 (1990) 67.

- [508] E. Wieteska, F. Wieckowska, *Biul. Wojsk. Acad. Tech.* 30 (1981) 103.
- [509] D. Chen, F. Liu, *Fenxi Huaxue* 11 (1983) 245.
- [510] P.N. Nesterenko, V.M. Ivanov, *Zh. Anal. Khim.* 37 (1982) 1977.
- [511] S. Xu, F. Bai, *Fenxi Shiyanshi* 10 (1991) 18.
- [512] K. Rakhmatullaev, A.Sh. Giyasov, *Uzb. Khim. Zh.* 1 (1989) 5.
- [513] C. Patroescu, F. Pioara, I. Patroescu, *Rev. Chim.* 40 (1989) 605.
- [514] Z. Yi, *Fenxi Shiyanshi* 6 (1987) 63.
- [515] C. Cecilia, C.G. Constantinescu, *Rev. Chim.* 30 (1979) 248.
- [516] C. Sanchez-Peelreno, M.H. Cordoba, I.L. Garcia, *Quim. Anal.* 4 (1985) 387.
- [517] R.N. Nesterenko, V.M. Ivanov, G.V. Kudryovtsev, G.V. Lisichkin, *Zh. Anal. Khim.* 39 (1984) 456.
- [518] M.H. Cordoba, C.S. Pedreno, I.L. Garcia, *Afinidad* 39 (1982) 169.
- [519] V.M. Tarayan, G.I. Mikaelyan, *Arm. Khim. Zh.* 34 (1981) 545.
- [520] K. Toei, S. Motomizu, M. Oshima, H. Watari, *Analyst* 106 (1981) 776.
- [521] V.A. Nazarenko, G.V. Flyantileava, T.N. Chekirda, *Zh. Anal. Khim.* 39 (1984) 35.
- [522] A. He, Lihua Jianyan, *Huaxue Fence* 24 (1988) 17.
- [523] T. Wu, Y. Wang, Y. Xia, *Huaxue Fence* 28 (1992) 164.
- [524] S. Sato, S. Uchikawa, *Bunseki Kagaku* 29 (1980) 729.
- [525] M. Oshima, S. Motomizu, K. Toei, *Anal. Chem.* 56 (1984) 948.
- [526] G.V. Flyantikova, T.N. Chekirda, V.A. Nazarenko, *Zh. Anal. Khim.* 37 (1982) 1982.
- [527] Z. Wang, J. Zhao, Z. Zhao, F. Wang, Y. He, *Yankuangcishi* 7 (1988) 187.
- [528] X. Li, X. Ma, *Fenxi Huaxue* 16 (1988) 797.
- [529] G.V. Flyantikova, A.T. Isakhanova, *Zh. Anal. Khim.* 37 (1982) 1452.
- [530] S. Liu, Z. Liu, *Fenxi Huaxue* 10 (1982) 321.
- [531] M.H. Cordoba, I.L. Garcia, C.S. Pedreno, *An Quim. Ser. B.* 83 (1987) 71.
- [532] Q. Xu, S. Liu, J. Liu, *K'o Hsueh Tung Pao* 25 (1980) 302.
- [533] A.B. Abdullaeva, I.K. Guseinov, Ya.A. Agnimov, *Az-erb. Khim. Zh.* 1 (1979) 126.
- [534] J. Hu, W.B. Qi, B.Y. Pu, *Mikrochim. Acta* 109 (1992) 295.
- [535] W. Szczepaniak, W. Ciszewska, B. Juskowiak, *Chem. Anal.* 30 (1985) 369.
- [536] T. Prasada Rao, T.V. Ramakrishna, *Analyst* 107 (1982) 704.
- [537] P.P. Kish, I.S. Balog, *Zh. Anal. Khim.* 34 (1979) 2326.
- [538] L. Zhang, C. Zhang, *Yejin Fenxi* 11 (1991) 7.
- [539] N. Jie, J. Guo, S. Jiang, *Fenxi Huaxue* 16 (1988) 431.
- [540] L. Mathew, C.S.P. Iyer, T. Prasada Rao, A.D. Damodaran, *Mikrochim. Acta* 111 (1993) 231.
- [541] X.N. Ge, A.P. Xu, S.Q. Ying, Y.M. Liu, X.Y. Xu, Lihua Jianyan, *Huaxue Fence* 29 (1993) 362.
- [542] D.S. Nair, T. Prasada Rao, C.S.P. Iyer, A.D. Damodaran, *Ind. J. Chem.* 33A (1994) 445.
- [543] S. Kartikeyan, T. Prasada Rao, C.S.P. Iyer, A.D. Damodaran, *Talanta* 40 (1993) 771.
- [544] W. Szczepaniak, B. Juskowiak, *Chem. Anal.* 32 (1987) 121.
- [545] Z. Wang, J. Zhao, Z. Zhao, F. Wang, Y. He, *Fenxi Shiyanshi* 7 (1988) 35.
- [546] S. Xu, L. Wan, *Fenxi Shiyanshi* 8 (1989) 1.
- [547] X. Liu, Z. Kou, T. Chen, Lihua Jianyan, *Huaxue Fence* 25 (1989) 149.
- [548] S. Liu, Y. Liu, Z. Liu, *Mikrochim. Acta* III (1983) 355.
- [549] F. Buhl, B. Mikula, *Chem. Anal.* 28 (1983) 779.
- [550] J.L. Wang, Z.B. Li, Q.H. Xu, *Fenxi Huaxue* 24 (1996) 344.
- [551] H. Shen, R. Ling, *Fenxi Huaxue* 18 (1990) 700.
- [552] G. Popa, N. Dumitrescu, *Bul. Inst. Politech. Gheorghie Gheorghiv-Dej Bucurest Ser. Chim.-Metal* 40 (1978) 17.
- [553] D.T. Burns, N. Tungkananuruk, *Anal. Chim. Acta* 189 (1986) 383.
- [554] N.L. Shestidesyatnaya, L.V. Gaevskaya, *Ukr. Khim. Zh.* 50 (1984) 275.
- [555] M.A. Matveets, S.D. Akhmetova, D.P. Shcherbov, *Zh. Anal. Khim.* 35 (1980) 1640.
- [556] Y. He, D. Huang, *Fenxi Huaxue* 12 (1984) 389.
- [557] D.T. Burns, P. Hanprasopwathana, B.P. Murphy, *Anal. Chim. Acta* 134 (1982) 397.
- [558] C. Zhan, S. Liu, *Huaxue Shiji* 5 (1983) 177.
- [559] K. Yamamoto, S. Motomizu, *Bunseki Kagaku* 38 (1989) 103.
- [560] K. Yamamoto, S. Motomizu, *Analyst* 112 (1987) 1011.
- [561] A. Morales, I. Valladares, *Fresenius J. Anal. Chem.* 334 (1989) 53.
- [562] J. Yan, Z. Bei, M. Zhu, *Fenxiceshi Tongbao* 9 (1990) 63.
- [563] F. Buhl, K. Kania, *Chem. Anal.* 32 (1987) 1005.
- [564] J. Yang, *Fenxi Shiyanshi* 9 (1990) 69.
- [565] F. Buhl, K. Kania, *Chem. Anal.* 27 (1982) 191.
- [566] L.P. Adamovich, S.A. Shapovalov, *Zh. Anal. Khim.* 37 (1982) 1782.
- [567] M.M. Tananaiko, L.I. Gorenstein, *Org. Reagents Anal. Khim.* 5 (1985) 126.
- [568] H. Khalifa, A.A. El-Sirafy, *Egypt J. Chem.* 19 (1976) 389.
- [569] W. Szczepaniak, W. Ciszewska, B. Juskowiak, *Chem. Anal.* 37 (1992) 465.
- [570] S. Hoshi, H. Hosokawa, S. Inoue, M. Matsubara, *Bunseki Kagaku* 35 (1986) 139.
- [571] A. Morales, M.I. Toral, *Analyst* 110 (1985) 1445.
- [572] Z. Liu, S. Liu, H. Cao, *Fenxi Huaxue* 19 (1991) 309.
- [573] S. Jiang, W. Shen, M. Sun, Y. Wang, Lihua Jianyan, *Huaxue Fence* 27 (1991) 104.
- [574] Z. Li, Q. Xu, *Fenxi Huaxue* 17 (1989) 453.
- [575] Y. Hasegawa, T. Inagake, Y. Karosawa, *Talanta* 30 (1983) 721.
- [576] V.A. Nazarenko, E.A. Biryuk, L.I. Vinanova, R.V. Ravitskaya, *Zh. Anal. Khim.* 36 (1981) 1315.
- [577] E.I. Tselik, N.S. Poluektov, V.T. Mischenko, *Ukr. Khim. Zh.* 48 (1982) 303.

- [578] G. Deng, L. Guan, Q. Li, Y. Wang, *Lihua Jianyan*, *Huaxue Fence* 28 (1992) 148.
- [579] S. Sato, H. Tanaka, *Talanta* 36 (1989) 391.
- [580] Z.B. Li, Q.H. Xu, *Fenxi Huaxue* 21 (1993) 1254.
- [581] M.M. Tananaiko, L.F. Gorenshstein, *Zh. Anal. Khim.* 37 (1982) 589.
- [582] B. Saad, S.M. Sultan, *Talanta* 42 (1995) 1349.
- [583] M. Kamburova, *Chem. Anal.* 40 (1995) 791.
- [584] G.C. Zhao, J.Y. Jin, Y.J. Chen, *Fenxi Shiyanshi* 11 (1992) 30.
- [585] G. Cheng, S. Xu, *Fenxi Huaxue* 17 (1989) 112.
- [586] A.F. Danet, M. Popescu, *Rev. Chim.* 41 (1990) 59.
- [587] Y. Anjaneyulu, N. Suguna, M.R.P. Reddy, K. Chandrasekhar, *Analysis* 14 (1986) 200.
- [588] J.R. Mudakavi, Y.S. Ramaswamy, *J. Indian Inst. Sci.* 66 (1986) 155.
- [589] Ch. Liu, J. Long, S. Ma, *Fenxi Huaxue* 10 (1982) 34.
- [590] V.M. Taryan, E.N. Ovsepyan, S.P. Lebedeva, *Arm. Khim. Zh.* 33 (1980) 617.
- [591] Y. Liu, S. Liu, *Huaxue Shiji* 6 (1984) 125.
- [592] A. Guo, Y. Zhang, S. Huang, L. Dou, *Fenxi Huaxue* 12 (1984) 728.
- [593] S. Liu, Z. Liu, *Huaxue Shiji* 12 (1990) 210.
- [594] Z. Li, M. Zhao, *Fenxi Huaxue* 16 (1988) 647.
- [595] R. Escobar, C. Lamonedá, F.D. Pablos, A. Guiraum, *Analyst* 114 (1989) 533.
- [596] P.A. Abrodo, D.B. Gomis, A.S. Medel, *Microchem. J.* 32 (1985) 296.
- [597] I.V. Pyatnitski, N.P. Aleksyuk, A. Yu Nazarenko, *Zh. Anal. Khim.* 38 (1983) 2176.
- [598] G. Roebisch, A. Rericha, *Anal. Chim. Acta* 153 (1983) 281.
- [599] Z. Li, Q. Xu, *Fenxi Shiyanshi* 7 (1988) 13.
- [600] L.I. Ganago, L.F. Ivanova, *Zh. Anal. Khim.* 42 (1987) 1641.
- [601] C. Huang, W. Qi, *Fenxi Shiyanshi* 8 (1989) 20.
- [602] X. Zhong, *Xiyou Jinshu* 6 (1987) 71.
- [603] T. Prasada Rao, T.V. Ramakrishna, *Bull. Chem. Soc. Jpn.* 53 (1980) 2380.
- [604] L.I. Vinanova, E.V. Malinka, I.V. Stoyanova, *Zh. Anal. Khim.* 38 (1983) 2013.
- [605] G. Gong, H. Wang, *Fenxi Huaxue* 13 (1985) 410.
- [606] A.K. Singh, D. Kumar, *Analyst* 110 (1985) 751.
- [607] A. Yu Nazarenko, *Ukr. Khim. Zh.* 49 (1983) 279.
- [608] G. Xi, X. Yong, *Fenxi Huaxue* 13 (1985) 452.
- [609] R. Escobar, C. Lamonedá, F.J. Barragan, A. Guiraum, *Analysis* 16 (1988) 189.
- [610] V. Bhagavathy, M.L.P. Reddy, T. Prasada Rao, A.D. Damodaran, *Ind. J. Chem.* 32A (1993) 463.
- [611] M.J. Sanchez, M.A. Rodriguez, M.F. Garcia, *Anal. Lett.* 22 (1989) 2075.
- [612] M.C.P. Conde, A.M.G. Carreras, M.C.R. DeMiguel, L.M. Polodicz, *Quim. Anal.* 5 (1986) 67.
- [613] S. Hoshi, Y. Takamatsu, S. Inoue, M. Matsubara, *Bunseki Kagaku* 35 (1986) 864.
- [614] Kumari Asha, T. Prasada Rao (to be communicated).
- [615] K. Toei, S. Motomizu, H. Yokosu, *Anal. Chim. Acta* 110 (1979) 110.
- [616] V.P. Rao, Y. Anjaneyulu, P. Sasisekhar, P. Chandramouli, *Talanta* 26 (1979) 1059.
- [617] Z.B. Li, J.L. Wang, Q.H. Xu, Y.J. Liu, *Fenxi Shiyanshi* 14 (1995) 18.
- [618] Y.Z. Lu, Z.X. Chen, H.W. Zhou, W.G. Sun, B. Ning, *Fenxi Shiyanshi* 12 (1993) 48.
- [619] S. Jaya, T.V. Ramakrishna, *Bull. Chem. Soc. Jpn.* 55 (1982) 2633.
- [620] Z. Li, M. Zhao, *Fenxi Huaxue* 17 (1989) 118.
- [621] M. Ishikuro, M. Hosoya, K. Takada, *Bunseki Kagaku* 40 (1991) 71.
- [622] X.W. He, S. Liu, X.Y. Liu, S.J. Xu, *Fenxi Shiyanshi* 15 (1996) 63.
- [623] L. Sommer, J. Dolezal, *Scr. Fac. Sci. Nat. Univ. Purkyniana Brun.* 19 (1989) 159.
- [624] C. Pan, J. Pan, *Huaxue Shiji* 8 (1986) 367.
- [625] X. Wong, *Fenxi Huaxue* 12 (1984) 857.
- [626] E.A. Novikov, L.K. Shpigun, Yu A. Zoltov, *Zh. Anal. Khim.* 44 (1989) 422.
- [627] W. Szczepaniak, B. Juskowiak, *Mikrochim. Acta*, I (1987) 237.
- [628] V.V. Sukhan, A. Yu Nazarenko, *Izv. Vyssh. Uchben. Zaved. Khim. Khim. Technol.* 31 (1988) 39.
- [629] P.P. Kish, Ya R. Bazel, K.I. Zikan, *Zh. Anal. Khim.* 41 (1986) 1061.
- [630] W. Szczepaniak, B. Juskowiak, *Anal. Chim. Acta* 140 (1982) 261.
- [631] J.L. Wang, Z.B. Li, Q.H. Xu, *Anal. Lett.* 28 (1995) 147.
- [632] R.W. Manko, *Chem. Anal.* 36 (1991) 7.
- [633] I.L. Garcia, J.M. Aviles, M.H. Cordoba, *Talanta* 33 (1986) 411.
- [634] Y. Ci, J. Zhang, *Fenxi Huaxue* 14 (1986) 321.
- [635] I.L. Garcia, C.S. Pedrino, J.M. Aviles, *An. Quim. Ser. B.* 82 (1986) 86.
- [636] Z.M. Khvatkova, V.V. Golovinai, *Zh. Anal. Khim.* 34 (1979) 2035.
- [637] Z. Marczenko, M. Jarosz, *Talanta* 28 (1981) 561.
- [638] S. Jaya, T. Prasada Rao, T.V. Ramakrishna, *J. Less Comm. Met.* 91 (1983) 261.
- [639] A. Ramalingom Pillai, P.P. Ouseph, K.K. Ramachandran, T. Prasada Rao, *Ind. J. Chem.* (in Press).
- [640] A. Ramalingom Pillai, P.P. Ouseph, K.K. Ramachandran, T. Prasada Rao, *Chem. Anal.* 42 (1997) 75.
- [641] S. Jaya, T. Prasada Rao, T.V. Ramakrishna, *Analyst* 109 (1984) 1405.
- [642] A. Ramalingom Pillai, P.P. Ouseph, K.K. Ramachandran, T. Prasada Rao, communicated to *Indian J. Chem.*
- [643] A. Ramalingom Pillai, P.P. Ouseph, K.K. Ramachandran, T. Prasada Rao, *Chem. Anal.* 41 (1996) 787.
- [644] A.T. Pilipenko, Z.M. Khvatkova, V.V. Golovina, *Zh. Anal. Khim.* 43 (1988) 1664.
- [645] L. Li, G. Jin, S. Zhu, *Huaxue Shiji* 10 (1988) 78.
- [646] Z.B. Li, J.L. Wang, Q.H. Xu, *Mikrochim. Acta* 118 (1995) 43.
- [647] Z.B. Li, J.L. Wang, Q.H. Xu, *Fenxi Huaxue* 23 (1995) 52.
- [648] Z.B. Li, J.L. Wang, Q.H. Xu, *Fenxi Shiyanshi* 14 (1995) 15.
- [649] Z. Li, *Fenxi Shiyanshi* 11 (1992) 29.

- [650] Y. Ci, A. Wang, *Fenxi Shiyanshi* 5 (1986) 1.
- [651] J.R. Mudakavi, T.V. Ramakrishna, *J. Indian Inst. Sci.* 64B (1983) 57.
- [652] Z. Li, M. Zhao, *Fenxi Huaxue* 13 (1985) 698.
- [653] A.G. Gaibakyan, A.G. Kachatryan, S.A. Karapetyan, *Zh. Anal. Khim.* 42 (1987) 2093.
- [654] C. Cecilia, C. Gheorghe, *Rev. Roum. Chim.* 25 (1980) 1421.
- [655] L. Li, Y. An, *Huaxue Shiji* 12 (1990) 274.
- [656] S. Jaya, T. Prasada Rao, T.V. Ramakrishna, *Analyst* 108 (1983) 1151.
- [657] M. Zhao, *Kexue Tongbao* 31 (1986) 1547.
- [658] Z.B. Li, J.L. Wang, Q.H. Xu, Y.J. Liu, *Fenxi Huaxue Xuebao* 11 (1995) 28.
- [659] M. Zhao, S. Hu, *Fenxi Huaxue* 16 (1988) 865.
- [660] S. Jaya, T.V. Ramakrishna, *Analyst* 107 (1982) 828.
- [661] D.T. Burns, D. Chimpalee, H.J. Bullick, *Anal. Chim. Acta* 284 (1993) 195.
- [662] L.A. Shevchuk, V.N. Baskin, S.N. Zaitsev, *Zavod. Lab.* 57 (1991) 18.
- [663] E.V. Bastrakova, T.V. Popova, *Zavod Lab.* 56 (1990) 1.
- [664] S. Sato, S. Uchikawa, E. Iwamoto, Y. Yamamoto, *Anal. Lett.* 16 (1983) 827.
- [665] F.S. Mamedova, I.K. Guseinov, A. Ya Azimov, *Azerb. Khim. Zh.* 5 (1980) 83.
- [666] S. Liu, Z. Liu, *Fenxi Huaxue* 10 (1982) 464.
- [667] S. Sato, S. Uchikawa, *Anal. Sci.* 2 (1986) 47.
- [668] Z.B. Li, J.L. Wang, Q.H. Xu, *Anal. Sci.* 12 (1996) 259.
- [669] L.I. Ganago, L.A. Alinobskaya, L.V. Kobaleva, *Vestsi Akad. Navuk BSSR, SerKhim. Navuk* 5 (1986) 10.
- [670] A. Ramesh, T.V. Ramakrishna, M.S. Subramanian, *Bull. Chem. Soc. Jpn.* 67 (1994) 2121.
- [671] L.J. Hu, *Fenxi Shiyanshi* 13 (1994) 36.
- [672] K.A. Adriss, M.M. Seleim, M.S. Abu-Bakr, *Mikrochim. Acta II* (1980) 179.
- [673] X. He, S. Xu, B. Wang, *Fenxi Huaxue* 16 (1988) 1086.
- [674] J. Fu, *Fenxi Shiyanshi* 6 (1987) 61.
- [675] S. Li, S. Li, C. Liu, *Gaodeng Xuexiao Huaxue, Xuebao* 9 (1988) 998.
- [676] M.H. Zhang, Q.R. Zhang, T.G. Xu, X.R. Liang, L. Luo, M.S. Yang, *Fenxi Huaxue* 23 (1995) 699.
- [677] G.V. Flyantikova, T.N. Chekirda, O.N. Lasovskaya, L.V. Chebolar, *Zh. Anal. Khim.* 37 (1982) 1043.
- [678] A.M. Gutierrez, M.V. Laorden, A.S. Medel, J.L. Nieto, *Anal. Chim. Acta* 184 (1986) 317.
- [679] X. Yu, *Yejin Fenxi* 13 (1993) 27.
- [680] B. Juskowiak, *Chem. Anal.* 37 (1992) 471.
- [681] Q. Xu, Z. Li, *Fenxi Shiyanshi* 11 (1992) 1.
- [682] Z. Li, Q. Xu, *Fenxi Shiyanshi* 10 (1991) 11.
- [683] Z. Luo, J. Liang, *Yankuang Ceshi* 10 (1991) 89.
- [684] Y.K. Agarwal, K.T. John, *Analyst* 110 (1985) 1041.
- [685] Y. Inokuma, J. Endo, *Bunsekikagaku* 37 (1988) 242.
- [686] E.M. Donaldson, *Talanta* 30 (1983) 497.
- [687] H. Luo, *Mikrochim. Acta* 106 (1992) 21.
- [688] Z. Li, Q. Lu, *Fenxi Huaxue* 18 (1990) 638.
- [689] P.P. Kish, V.A. Andruk, I.S. Balog, *Zh. Anal. Khim* 46 (1991) 2328.
- [690] S. Liu, Z. Liu, *Gaodengxuexiao Huaxue Xuebao* 9 (1988) 774.
- [691] V.A. Nazarenko, E.A. Biryuk, L.I. Vinarova, K.A. Mukelo, *Zh. Anal. Khim.* 37 (1982) 252.
- [692] H.Q. Luo, S.P. Liu, Z.F. Liu, *Fenxi Huaxue* 21 (1993) 1179.
- [693] K.K.G. Nambodiri, N. Balasubramanian, T.V. Ramakrishna, *Talanta* 38 (1991) 945.
- [694] J. Skadauskas, I. Naruskevicius, O. Skadauskiene, *Zavod Lab.* 55 (1989) 7.
- [695] C. Cecilia, C. Gheorghe, *Rev. Roum. Chim.* 25 (1980) 1411.
- [696] C. Liu, H. Zhou, H. Guen, L. Qion, *Fenxi Huaxue* 14 (1986) 142.
- [697] I.P. Alimarin, A.P. Golovina, V.K. Runov, *Zh. Anal. Khim.* 37 (1982) 855.
- [698] Z. Liu, S. Liu, *Analyst* 116 (1991) 95.
- [699] T.V. Ramakrishna, R.S. Sheedhara Murthy, *Talanta* 27 (1980) 442.
- [700] E.I. Tselik, S.V. Beityukova, L.I. Kononenko, *Ukr. Khim. Zh.* 46 (1980) 1222.
- [701] S. Jiang, X. Wang, *Huaxue, Xuebao* 43 (1985) 1005.
- [702] Z. Marzenko, R. Lobinski, *Talanta* 35 (1988) 1001.
- [703] S. Feng, X. Zhang, *Fenxi Huaxue* 17 (1989) 820.
- [704] H. Zhang, S. Xu, *Fenxi Huaxue* 18 (1990) 987.
- [705] S. Hoshi, S. Inoue, M. Matsubara, *Bunseki Kagaku* 34 (1985) 549.
- [706] Y. Anjaneyulu, P. Chandramouli, L.N. Murthy, *Proc. Indian Natl. Sci. Acad.* 51 (1985) 458.
- [707] T. Prasada Rao, T.V. Ramakrishna, *Analyst* 105 (1980) 674.
- [708] S. Liu, Z. Liu, *Huaxue Shiji* 1 (1982) 20.
- [709] S. Liu, Z. Liu, *Huaxue Tongbao* 4 (1982) 208.
- [710] K.A. Abshidze, *Izv. Akad. Nauk. Gruz. SSR, Ser. Khim.* 6 (1980) 302.
- [711] R.I. Nunez, M. Callejon, A.G. Purez, *Anal. Chim. Acta* 192 (1987) 119.
- [712] T. Jyothi, M.L.P. Reddy, T. Prasada Rao, A.D. Damodaran, *Anal. Lett.* 20 (1987) 1729.
- [713] R. Sukumar, T. Prasada Rao, A.D. Damodaran, *Talanta* 36 (1989) 694.
- [714] S. Mathew, R. Sukumar, T. Prasada Rao, A.D. Damodaran, *Anal. Lett.* 25 (1992) 1941.
- [715] H. Shi, L. Kong, J. Li, L. Wang, *Huaxue Shiji* 12 (1990) 321.
- [716] S. Zhou, N. Wang, *Talanta* 37 (1990) 337.
- [717] N.X. Wang, L. Lin, *Fresenius J. Anal. Chem.* 350 (1994) 365.
- [718] N.X. Wang, P. Qi, K.H. Jiang, *Mikrochim. Acta* 116 (1994) 191.
- [719] S. Kartikeyan, T. Prasada Rao, C.S.P. Iyer, A.D. Damodaran, *Mikrochim. Acta* 113 (1994) 71.
- [720] W. Yang, J.Z. Gao, J.W. Kang, Z.M. Wang, G.B. Bai, C.X. Li, *Analyst* 119 (1994) 2463.
- [721] P. Qi, N. Wang, *Fenxi Huaxue* 17 (1989) 1128.
- [722] A. Morales, M.I. Toral, P. Richter, M. Silva, *Anal. Lett.* 25 (1992) 1765.
- [723] V. Bhagavathy, T. Prasada Rao, A.D. Damodaran, *Anal. Lett.* 21 (1988) 901.

- [724] B. Bowzid, A.M.G. McDonald, *Anal. Chim. Acta* 207 (1988) 337.
- [725] Y. Yuan, Y. Wang, K. Qu, *Fenxi Huaxue* 16 (1988) 546.
- [726] I.L. Garcia, P.N. Navarro, M.H. Cordoba, *Talanta* 35 (1988) 885.
- [727] L. Zhou, G.D. Shao, X.P. Guo, *Fenxi Shiyanshi* 15 (1996) 35.
- [728] M.H. Cordoba, P.N. Navarro, I.L. Garcia, *Int. J. Environ. Anal. Chem.* 32 (1988) 97.
- [729] D.B. Gladilovic, V. Kuban, *Chem. Pap.* 42 (1988) 607.
- [730] J. Havel, C. Moreno, A. Hardlicka, M. Valiente, *Talanta* 41 (1994) 1251.
- [731] T. Perez-Ruiz, C. Martinez-Lozano, V. Tomas, C. Paredes, *Mikrochim. Acta* 118 (1995) 203.
- [732] L. Ma, X. Chen, Z. Hu, *Fenxi Huaxue* 20 (1992) 339.
- [733] H. Koshima, H. Onishi, *Anal. Chim. Acta* 232 (1990) 287.
- [734] F. Mas, J.M. Estela, V. Cerda, *Anal. Chim. Acta* 239 (1990) 151.
- [735] J.P. Susanto, M. Oshima, S. Motomizu, *Analyst* 120 (1995) 2605.
- [736] M. Alihara, T. Nakashimada, *J. Flow Inj. Anal.* 6 (1989) 128.
- [737] H. Wang, Z. Liu, *Fenxi Huaxue* 14 (1986) 773.
- [738] V. Kabasakalis, *Anal. Lett.* 27 (1994) 2789.
- [739] M. Oue, K. Kimura, T. Shono, *Analyst* 113 (1988) 551.
- [740] W. Cui, J. Wang, H. Shi, *Fenxi Huaxue* 11 (1983) 900.
- [741] L.A. Grigoryan, D.A. Mikaelyan, V.M. Tarayan, *Arm. Khim. Zh.* 33 (1980) 545.
- [742] L.A. Grigoryan, D.A. Mikaelyan, V.M. Tarayan, *Zh. Anal. Khim.* 35 (1980) 45.
- [743] S.V. Kachin, L.P. Poddubnykh, V.K. Runov, *Zavod Lab.* 9 (1991) 1.
- [744] D.A. Mikaelyan, A.G. Khachatryan, *Ukr. Khim. Zh.* 54 (1988) 522.
- [745] J. Aznarez, A. Ferrer, J.M. Rabadan, L. Marco, *Talanta* 32 (1985) 1156.
- [746] D.X. Chen, Y.Z. Li, *Fenxi Huaxue* 22 (1994) 502.
- [747] H. Zhao, I. Zhang, *Fenxi Shiyanshi* 11 (1992) 40.
- [748] D.B. Gomis, E.A. Garcia, E.F. Alonso, P.A. Abrodo, *Mikrochim. Acta* 3 (1990) 259.
- [749] Q. Liu, S. Si, J. Xu, *Huaxue Shiji* 10 (1988) 106.
- [750] N. Jie, C. Wang, S. Jiang, *Fenxi Huaxue* 15 (1987) 243.
- [751] D.B. Gomis, E.A. Garcia, *Analyst* 115 (1990) 89.
- [752] G. Wang, Y.L. He, Z.Y. Zhao, F.P. Wang, *Fenxi Huaxue* 21 (1993) 695.
- [753] D.B. Gomis, E.F. Alonso, E.A. Garcia, P.A. Abrodo, *Talanta* 36 (1989) 1237.
- [754] Y. Kondon, M. Kataoka, T. Kambara, *Bull. Chem. Soc. Jpn.* 55 (1982) 434.
- [755] C.F. Ishak, R.T. Pflaum, *Analyst* 113 (1988) 941.
- [756] G.Q. Gong, H. Zhao, L.F. Wang, *Anal. Lett.* 27 (1994) 2797.
- [757] V. Kabasakalis, *Anal. Lett.* 26 (1993) 2269.
- [758] K.P. Stolyarov, V.V. Firyulin, *Zh. Anal. Khim.* 38 (1983) 625.
- [759] J.W. Gao, H.G. Huang, *Fenxi Huaxue* 20 (1992) 761.
- [760] G. Zhu, J. Yang, Y. Niu 23 (1988) 80.
- [761] H. Huang, X. Zeng, *Bunseki Kagaku* 35 (1986) 579.
- [762] Y. Ci, K. Hu, J. Liu, H. Ma, *Fenxi Huaxue* 10 (1982) 232.
- [763] H. Shi, W. Cui, *Fenxi Huaxue* 10 (1982) 561.
- [764] J. Yang, G. Zhu, B. Wu, *Anal. Chim. Acta* 198 (1987) 287.
- [765] T. Zhou, X. Ping, H. Zhang, *Yankuangceshi* 7 (1988) 294.
- [766] Y. Ci, Z. Lan, *Anal. Lett.* 21 (1988) 1499.
- [767] Y. Ci, Z. Lin, *Analyst* 113 (1988) 1453.
- [768] G.Y. Zhu, Z.K. Si, B. Zhang, W. Jiang, J.T. Hu, *Guangpuxue Yue Guangpu Fenxi* 15 (1995) 109.
- [769] L. He, Y. Ren, *Fenxi Huaxue* 20 (1992) 541.
- [770] Z. Si, G. Zhu, B. Zhang, W. Jiang, *Anal. Lett.* 25 (1992) 321.
- [771] G. Zhu, W. Jiang, Z. Si, B. Zhang, *Fenxi Huaxue* 20 (1992) 223.
- [772] S. Peter, B.S. Panigrahi, K.S. Viswanathan, C.K. Mathews, *Anal. Chim. Acta* 260 (1992) 135.
- [773] J. Yang, H. Zhou, X. Ren, C. Li, *Anal. Chim. Acta* 238 (1990) 307.
- [774] S. Zheng, J. Wang, J. Hu, G. Chen, Y. Zheng, *Huaxue Shiji* 13 (1991) 132.
- [775] Z. Si, G. Zhu, J. Li, *Analyst* 116 (1991) 309.
- [776] G. Zhu, Z. Si, P. Liu, *Anal. Chim. Acta* 245 (1991) 109.
- [777] J. Yang, G. Zhu, H. Wang, *Analyst* 114 (1989) 1417.
- [778] E. Shirakawa, T. Honjo, K. Terada, *Fresenius J. Anal. Chem.* 334 (1989) 37.
- [779] N.M. Sita, T. Prasada Rao, C.S.P. Iyer, A.D. Damodaran, *Talanta* 44 (1997) 423.
- [780] J. Zhao, Y. He, Z. Wu, F. Mang, Z. Zhao, *Yankuangceshi* 7 (1988) 88.
- [781] G. Gong, S. Yang, N. Wang, *Xiyou Jinshu* 7 (1988) 283.
- [782] E. Andres, E. Fuente, D. Blanco, *Anal. Lett.* 26 (1993) 1037.
- [783] G. Wang, W. He, Z.Y. Zhao, J.D. Zhao, F.P. Wang, *Yan-Kuangcheshi* 12 (1993) 159.
- [784] V. Kabasakalis, R. Tsitouridu, C.A. Alexiades, *Int. J. Environ. Anal. Chem.* 43 (1991) 267.
- [785] E. Andres, E. Fuente, D. Blanco, *Anal. Lett.* 27 (1994) 775.
- [786] G.Q. Gong, L. Jia, C. Su, *Fenxi Huaxue* 22 (1994) 465.
- [787] N.O. Mechdlov, E.A. Cordova, S.I. Egorova, E.A. Cordova, *Zh. Anal. Khim.* 49 (1994) 1177.
- [788] L.M. He, Y. Ren, *Fenxi Huaxue* 21 (1993) 465.
- [789] G.I. Song, Y.T. Liu, J.X. Zhang, *Lihua Jianyan, Huaxue Fence* 29 (1993) 142.
- [790] M. Guo, J. Li, J. Zhao, Z. Zhao, F. Wang, Y. He, *Huaxue Shiji* 12 (1990) 305.
- [791] J. Gao, Y. Shi, *Lihua Jianyan Huaxue Fence* 26 (1990) 51.
- [792] R.D. Zhang, J.H. Chao, H.G. Wang, *Fenxi Huaxue* 20 (1992) 819.
- [793] N.V. Rusakova, S.B. Meshkova, *Zh. Anal. Khim.* 45 (1990) 1914.
- [794] M. Taga, M. Kan, T. Nasu, *Fresenius Z. Anal. Chem.* 334 (1989) 45.

- [795] X. Wang, Q. Shao, Z. Bai, F. Yang, *Guang Puxue Yu Guangpu Fenxi* 8 (1988) 51.
- [796] A.S. Medel, D.B. Gomis, E. Fuente, S.A. Jimeno, *Talanta* 31 (1984) 515.
- [797] D.B. Gomis, E.F. Alonso, A.S. Medel, *Talanta* 32 (1985) 915.
- [798] D.A. Mikaelyan, L.A. Grigoryan, V.M. Tarayan, *Arm. Khim. Zh.* 36 (1983) 697.
- [799] D.A. Mikaelyan, L.A. Grigoryan, E.N. Ovsepyan, *Zabod Lab.* 53 (1987) 14.
- [800] M.E.M. Izquiere, J.S.D. Alegria, A.C. Martin, R.G. Andrew, *Analyst* 109 (1984) 377.
- [801] S. Li, D. Zheng, M. Ma, P. Li, *Yankuangceshi* 7 (1988) 130.
- [802] S. Li, D. Zheng, P. Li, M. Ma, *Yankuangceshi* 7 (1988) 221.
- [803] J. Xu, S. Wang, W. Yang, H. Wang, *Fenxi Huaxue* 16 (1988) 622.
- [804] W. Cai, Y. Ouyang, L. He, J. Xu, *Fenxi Huaxue* 15 (1987) 828.
- [805] N. Yu Kuzyakova, A.P. Golovina, T.A. Chemleva, N.V. Ilyakova, *Vestn. Mosk. Univ., Zh. Khim.* 25 (1984) 58.
- [806] N. Yu Kuzyakova, A.P. Golovina, *Zh. Anal. Khim.* 38 (1983) 1023.
- [807] W. Cui, H. Shi, *Fenxi Huaxue* 11 (1983) 778.
- [808] Y. Ci, Z. Lan, *Anal. Chem.* 61 (1989) 1063.
- [809] G. Zhu, J. Yang, G. Liu, *Guangpuxue Yu Guangpu Fenxi* 10 (1990) 60.
- [810] J. Li, Y. Zeng, G. Chen, *Talanta* 37 (1990) 809.
- [811] G. Zhu, Z. Si, J. Yang, J. Ding, *Anal. Chim. Acta* 231 (1990) 157.
- [812] G. Zhu, J. Yang, Y. Sun, *Fenxi Huaxue* 17 (1989) 127.
- [813] J.H. Yang, H.M. Ge, N.Q. Jie, X.Z. Ren, N.X. Wang, H.B. Zhou, *Fresenius J. Anal. Chem.* 349 (1994) 728.
- [814] G. Zhu, J. Yang, W. Jiang, D. Liu, *Lihua Jianyan, Huaxue Fence* 25 (1989) 322.
- [815] G. Zhu, J. Yang, W. Jiang, C. Yin, *Yejin Fenxi* 10 (1990) 20.
- [816] G. Zhu, J. Yang, L. Wang, *Shandong Daxue, Xuebao Ziran Kexueban* 23 (1988) 56.
- [817] J. Zhao, X. Cao, M. Guo, Y. He, *Yankuangceshi* 8 (1989) 182.
- [818] S. Lis, Z. Hnatejko, M. Elbanowski, *Chem. Anal.* 38 (1993) 505.
- [819] S. Li, H. Zhang, D. Gao, X. Ma, *Lihua Jianyan, Huaxue Fence* 25 (1989) 130.
- [820] L. Li, H. Lin, *Yankuangceshi* 9 (1990) 24.
- [821] D.A. Mikaelyan, V.Zh. Artsruni, A.G. Kachatryan, *Zh. Anal. Khim.* 50 (1995) 162.
- [822] C.S. Pedreno, M.H. Cordoba, C.L. Erroz, *Afindad* 42 (1985) 399.
- [823] H.W. Peng, R. Zhang, *Guang Puxue Yu Guangpu Fenxi* 14 (1994) 113.
- [824] T. Naganuma, S. Tuzuki, J. Jin, *Bunseki Kagaku* 39 (1990) 197.
- [825] T.L. Shevchenko, A.T. Pilipenko, A.I. Volkova, *Ukr. Khim. Zh.* 45 (1979) 456.
- [826] G. Gong, Y. Zhang, H. Wang, *Fenxi Huaxue* 18 (1990) 383.
- [827] G. Huang, X. Xun, *Fenxi Shiyanshi* 11 (1992) 42.
- [828] K. Yukuhiro, K. Masamitsu, K. Tomihito, *Bunseki Kagaku* 30 (1981) 109.
- [829] S. Jiang, N. Jie, Y. Shi, *Fenxi Huaxue* 14 (1986) 934.
- [830] L. Li, Q. Zhao, *Fenxi Huaxue* 16 (1988) 636.
- [831] F.G. Sanchez, J.C.M. Gomcz, M.H. Lopez, *Anal. Lett.* 23 (1990) 923.
- [832] T. Mori, T. Matsuo, M. Toyoda, Y. Fujita, C. Matoba, K. Akagiri, *Anal. Lett.* 28 (1995) 649.
- [833] T.V. Ramakrishna, M.S. Subramanian, *Bull. Chem. Soc. Jpn.* 56 (1983) 321.
- [834] V. Bhagavathy, T. Prasada Rao, A.D. Damodaran, in: K.A. Gschneidner, L. Eyring (Eds.), *Handbook on Physics and Chemistry of Rare Earths*, Ch. 146, vol. 21, 367, 1995.

Review

Fluorimetric analysis of pesticides: Methods, recent developments and applications

Atanasse Coly¹, Jean-Jacques Aaron*

Institut de Topologie et de Dynamique des Systèmes de l'Université Denis Diderot Paris 7, Associé au CNRS, URA 34, 1, rue Guy de la Brosse, 75005, Paris, France

Received 27 December 1996; received in revised form 27 October 1997; accepted 4 November 1997

Abstract

The fluorimetric analysis of pesticides is reviewed with emphasis on the description of direct and indirect fluorimetric methods, including chemical derivatization, fluorogenic labelling, and photochemically-induced fluorescence. The use of fluorescence detection in TLC, HPLC and FIA as well as applications to environmental samples are discussed in detail. © 1998 Elsevier Science B.V. All rights reserved.

Keywords: Pesticides; Fluorimetry; Analysis

1. Introduction

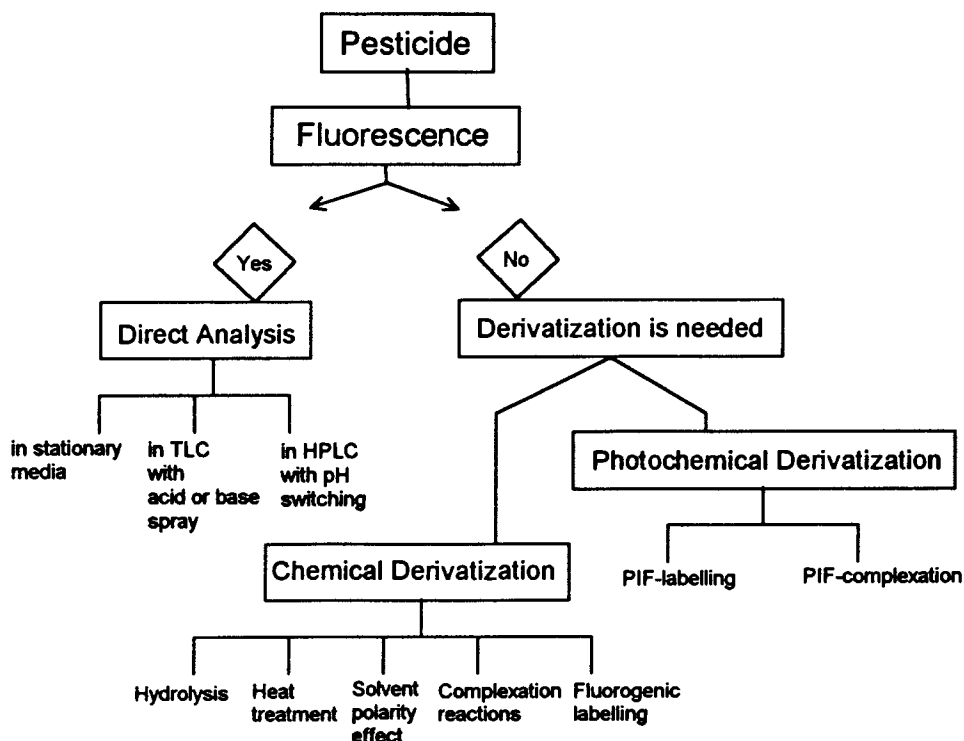
Confined to inorganic or organic compounds until the second world war, the list of pesticides—antiparasitic products for agricultural purposes—has rapidly grown in the last thirty years, because of the development of synthetic organic chemistry and the urgent need for intensive agriculture. At present, the number of different pesticides used widely for plant protection has exceeded several hundred [1–4]. Therefore, the input of agrochemical pollutants in the environment has increased

proportionally and has required the use of more sensitive and selective analytical methods in order to monitor the pesticide residue levels and to control the bioaccumulation process.

Important progress has occurred in the development and applications of various analytical tools including separation methods such as gas chromatography (GC) and high performance liquid chromatography (HPLC) and detection techniques such as electrochemistry, spectrophotometry and spectrofluorimetry. These techniques have allowed the identification and determination (at low concentration levels) of pesticide residues in a number of food and environmental samples [1,2,4–7]. Although several classes of pesticides (e.g. carbamates, phenylureas and some organo-

* Corresponding author. Fax.: +33 1 44 276814.

¹ On leave from the Université Cheikh Anta DIOP, Faculté des Sciences et Techniques, Département de Chimie, Dakar, Sénégal.



Scheme 1.

phosphorus insecticides) are rapidly degraded, by various biological, chemical or photochemical processes in soil, ground water and/or surface water [4,6,8], others (e.g. organochlorinated insecticides), are not biodegradable, and have been forbidden in many countries after evidence has been found of their toxicity and bioaccumulation in the environment and biosphere.

Currently, GC remains the main analytical method used for pesticide residue analysis because of its excellent separation and detection potential, especially when combined with MS [1,2]. However, it has some drawbacks such as the need for pre-treatment procedures in the case of weakly volatile and/or thermally labile pesticides (e.g. carbamates, phenylureas and sulfonylureas). The second most utilized method is HPLC, with UV-visible absorption detectors; it remains the technique of choice for screening work.

The use of fluorescence techniques for organic pesticide residue analysis has been limited by the fact that, relatively few of these compounds are

strongly fluorescent. However, many compounds possess the necessary degree of aromaticity and may be converted to fluorescent species using a variety of methods. Hence, two distinct cases (Scheme 1) have to be considered. (i) If the pesticide under study is fluorescent, then it can be determined directly by fluorimetry; (ii) if the pesticide is non or weakly fluorescent, it can be converted into a fluorescent compound using various physicochemical means, including chemical and/or photochemical reactions.

Generally speaking, literature results [9–19] show that fluorimetric detection is much more selective and sensitive than most other detection systems. Some laboratories involved in HPLC analysis of pesticide residues have chosen fluorimetry with post-column chemical and/or photochemical reactor rather than the classical UV-visible absorption for detection purposes [13,17,19].

Derivatization is an important aspect of pesticide analysis in fluorimetry as well as in GC and

other methods, since many pesticides have one or more functional groups and can be converted into more stable derivatives to successfully ensure environmental analysis. This increase in the use of derivatization is demonstrated by the number of papers, especially reviews [9–13] and books [15–18] published on the subject. In the present review, only the most important publications describing significant advances in the fluorescence methodology, instrumentation and applications to environmental analysis of pesticides are reported. The main advantages as well as the drawbacks of each method are outlined or discussed. Other aspects of the fluorimetric technique concerning bioanalysis (i.e. fluoroimmunoassays) will not be considered.

The scope of this review covers the available literature of the last twenty years up to the middle of 1996. It is intended to assist workers involved in the areas of trace spectrofluorimetric analysis of pesticides in environmental matrices and to provide readers with a critical summary of primary papers concerning the application of fluorescence to pesticide analysis. Recent instrumentation including sophisticated electronics and precise optical systems makes fluorescence a powerful method for pesticides residues determination because of its high sensitivity and selectivity.

The summary of the review is outlined in Scheme 1.

2. Fluorimetric methods

The original work on the fluorescence of pesticides has been carried out in stationary solutions, (i.e. batch procedure) by Hornstein [20] and has been limited to naturally-fluorescent pesticides such as guthion, pomsan, warfarin and piperonyl butoxide. The aim of this early fluorimetric assay was to investigate the possibility of quantifying low levels of pesticide residues. The promising results of this first attempt has led to the development of a number of direct fluorimetric methods and derivatization techniques allowing the transformation of non fluorescent pesticides into fluorescent derivatives.

2.1. Direct fluorimetric methods

The direct methods are based on the fluorescence detection of analyte and are mainly applied to those pesticides exhibiting an intrinsic fluorescence strong enough to be analytically useful. Therefore, the fluorescence properties of anticoagulant rodenticides including indanediones [21–23] and coumarins [21–31], carbamates insecticides such as aminocarb [32], bendiocarb [23,33], benomyl [29,34], carbaryl [33,35–38] and carbofuran [37,38], and some organophosphorus insecticides, including coumaphos [33] and pirimiphos-methyl [21], and other classes of pesticides [33] have been investigated. For example, Krause [33] has selected seventy-five pesticides, metabolites and a number of industrial chemicals for HPLC studies based on their known fluorescence or on chemical structures indicating possible fluorescence. The main analytical results obtained using these methods are shown in Table 1.

Direct fluorimetry has also been applied to herbicides [39–41], and fungicides [42–45]. In most cases, the fluorimetric detection of pesticides has been performed on solid support by thin layer chromatography (TLC) [34,46], in combination with dynamic systems including HPLC [22,24–33,35–39,42–44,47–50], flow injection analysis (FIA) [23,45], and by using specific techniques such as synchronous and/or derivative spectra in batch procedures [40,41].

2.1.1. Fluorimetric detection on solid support, (TLC)

At present, this type of pesticide analysis is not frequently used. Among the various existing solid substrates, silica gel plates [34,46] are the most utilized. TLC is inexpensive and rapid, but lacks sensitivity and selectivity.

Recent ameliorations in support quality, involving layers prepared from particles with narrow size distributions and mean diameters between 5 and 15 μm [51]—associated to modern quantitative, instrumental high performance TLC (HPTLC) [52] has improved the analytical performance of the method. For example, the limits of detection, (LOD) of four different aromatic pesticides in several environmental water matrices

Table 1
Fluorimetric methods for the determination of pesticides in the environment without derivatization

Recovery					
Method	Pesticide	Matrices	(%)	LOD (ng ml ⁻¹) ^a	Reference
SM	Chlorophacinon	Formulation	94–116	8	[21]
SM	Coumatetralyl	Formulation	86–102	0.07	[21]
SM	Pirimiphos-methyl	Formulation	88–99	0.3	[21]
HPLC	Coumatetralyl	Animal tissues	—	2	[22,27]
HPLC	Difenacoum	Animal tissues	—	2	[22,27]
HPLC	Brodifacoum	Animal tissues	—	2	[22,27]
HPLC	Bromadiolone	Animal tissues	86–95	8	[22]
HPLC	Warfarin	Animal tissues	95–97	10	[22]
FIA	Bendiocarb	Tap water	97–101	22 ^b	[23]
FIA	Chlorophacinon	Tap water	93–102	2 ^b	[23]
HPLC	Warfarin	Plasma, urine	—	0.18 ^b	[24]
HPLC	7-OH-warfarin	Plasma, urine	—	0.06 ^b	[24]
HPLC	Brodifacoum	Serum	86–100	20	[25]
HPLC	Difenacoum	Liver tissue	87–100	20	[25]
HPLC	Coumatetralyl	Liver tissue	87–93	20	[25]
HPLC	Warfarin	Serum	90–98	50	[25]
HPLC	Coumatetralyl	Liver tissue	93–94	2	[26]
HPLC	Difenacoum	Liver tissue	95–99	2	[26]
HPLC	Brodifacoum	Liver tissue	89–91	2	[26]
HPLC	Bromadiolone	Liver tissue	82–93	10	[26]
HPLC	Warfarin	Liver tissue	90–95	20	[26]
HPLC	Bromadiolone	Blood serum	91–98	20	[29]
HPLC	Warfarin	Blood serum	68–80	20	[29]
HPLC	Brodifacoum	Blood serum	86.7	10	[29]
HPLC	Coumatetralyl	Blood serum	81–82	10	[29]
HPLC	Difenacoum	Blood serum	89–90	10	[29]
HPLC	Aminocarb	Lake, rain water	76–84	0.05	[32]
HPLC	Carbaryl	—	—	0.5 ^b	[33]
HPLC	Carbofuran	—	—	10 ^b	[33]
HPLC	Coumaphos	—	—	0.5 ^b	[33]
HPLC	<i>o</i> -Phenylphenol	—	—	0.5 ^b	[33]
TLC	Benomyl	Sea water	100–107	0.04	[34]
TLC	Morestan	Sea water	103–105	0.15	[34]
TLC	<i>o</i> -Phenylphenol	Tap water	99–103	0.08	[34]
HPLC	Carbaryl	Plant tissue	93	—	[35]
HPLC	Carbaryl	Plant tissue	72–81	—	[36]
HPLC	Carbaryl	Plant tissue	102–108	—	[38]
HPLC	Carbofuran	Plant tissue	102–108	—	[38]
HPLC	MCPA ^c	River water	81	0.035	[39]
HPLC	Mecoprop	River water	97	0.040	[39]
HPLC	MCPB ^c	River water	85	0.030	[39]
NSF	Naphthylacetic acid	Apple	95–105	4	[40]
1DSF	Naphthylacetic acid	Apple	95–101	1.1	[40]
2DSF	Naphthylacetic acid	Apple	97–103	1.6	[40]
NSF	Flurecol	Ground soil	92–103	54	[41]
1DSF	Flurecol	Ground soil	91–105	128	[41]
2DSF	Flurecol	Ground soil	88–102	41	[41]
HPLC	<i>o</i> -Phenylphenol	Fruits, vegetables	90–104	—	[42]
HPLC	Carbendazim	Blubberies	76–94	15	[43]
HPLC	Diphenyl	Oranges	99–100	100	[44]
HPLC	<i>o</i> -Phenylphenol	Oranges	98–100	50	[44]

Table 1 (continued)

Recovery					
Method	Pesticide	Matrices	(%)	LOD (ng ml ⁻¹) ^a	Reference
HPLC	Thiabendazole	Oranges	98–99	50	[44]
FIA	Fuberidazole	Water	102–107	0.1	[45]
FIA	Thiabendazole	Water	104–105	0.7	[45]
VASS/CD	Aminocarb	Water	99.5	89	[69]
VASS/CD	Carbendazim	Water	104	55	[69]
VASS/CD	Coumatetralyl	Water	106	17	[69]
SM/CD	Warfarin	Water	95–105	59	[75]

^a Unless otherwise mentioned.

^b In nanograms.

^c MCPA, 2-methyl-4-chlorophenoxyacetic acid; MCPB, 4-(2-methyl-4-chlorophenoxy) butyric acid.

SM, stationary media; HPLC, high performance liquid chromatography; FIA, flow injection analysis; TLC, thin layer chromatography; NSF, normal synchronous fluorimetry; 1DSF, first derivative synchronous fluorimetry; 2DSF, second derivative synchronous fluorimetry; VASS, variable angle synchronous spectrometry; CD, cyclodextrins.

were in the range 0.04–0.15 ng ml⁻¹ according to the molecular structure of the pesticides [34].

2.1.2. Fluorimetric detection in combination with HPLC

Fluorimetric detection has been closely bound to the important development of HPLC instrumentation since it is generally more sensitive than the classical UV absorption detection. In addition, fluorescence detectors are very selective, eliminating matrix interference. However, it must be mentioned that several research groups have recently used HPLC with diode array UV and MS detection for extensive and successful analytical studies of many classes of pesticides and their mixtures in real samples [53–64]. HPLC is particularly useful because of the effectiveness of the various separative columns. Several types of HPLC systems have been reported for the fluorimetric determination of pesticides. As an example, the following LOD values are compared for the same series of rodenticides: (i) 2–20 ng ml⁻¹ for normal phase HPLC [22,26], (ii) 2–20 ng ml⁻¹ for reversed-phase HPLC [22,25,26,29,33], (iii) 2–10 ng ml⁻¹ for ionic column HPLC [22]. Finally, in other HPLC applications, fluorimetric detectors are connected in series with UV or electrochemical detectors [39,42,50].

2.1.3. Fluorimetric detection in stationary media

Although relatively time-consuming, this fluorimetric method has gained widespread acceptance because of enhanced selectivity brought about by the use of first and/or second derivative spectra in conjunction with a specific technique such as synchronous spectrofluorimetry [40,41]. The sensitivity and selectivity of this approach has been demonstrated by Garcia-Sanchez and co-workers [65–68]. The simplification of the spectral profile and the band-narrowing effect coupled with the derivative technique (very useful for the reduction of band overlapping) makes both identification of weak bands and magnification of the overall fluorescence signal feasible. For instance, a LOD value of 1 ng ml⁻¹ was achieved using the first derivative approach in the determination of the plant growth regulator naphthylacetic acid [40], recoveries from spiked apple samples ranged from 97 to 99%.

The potential of variable angle synchronous spectrometry (VASS) for the resolution of fluorescent mixtures was assessed in the case of the cyclodextrin-enhanced fluorescence determination of ternary mixtures of aminocarb, carbendazim and coumatetralyl [69]. The method was compared with the rank annihilation method (RAM). Fluorescence spectral distribution exhibits a great overlap that precludes the direct determination of this type of mixture. VASS shows better analytical

performance (recovery: 99–104%) than RAM (recovery: 84–130%) due to better resolution of mixtures of overlapping fluorescent compounds.

The use of organized media viz. cyclodextrins [70], micelles [71] and liposomic vesicles [72] for resolution of mixtures of analytes [69], enhancement of fluorescence detection [73] and reduction of interferences from impurities [74] has continued to grow rapidly. However, the application of such media in analytical spectrofluorimetry generally involves other organic aromatic compounds rather than pesticides [69,73,75].

In conclusion, the fluorimetric detection in stationary media or in combination with TLC or HPLC techniques proves to be highly sensitive and selective. LODs are in the low ng or ng ml⁻¹ range but these values must be used cautiously because they depend on enrichment during sample pretreatment (Table 1). Unfortunately, the number of pesticides presenting an intrinsic fluorescence is rather limited. For this reason, several derivatization reactions have been proposed.

2.2. Fluorimetric pretreatment methods

Chemical derivatization is generally used for non or weakly fluorescent compounds in order to convert them into fluorescent species following pretreatment. The type of chemical derivatization reaction applied to the analyte depends essentially on the pesticide class [9,11,13,76–79]. The principle of the method—which is designed to improve the quantum fluorescence yield—generates a fluorophore by means of a reagent, a thermal treatment or solvent polarity effect. The choice of reagent or treatment utilized dictates the type and mechanism of the derivatization reaction scheme. Hydrolysis, heat treatment, solvent polarity effect, complexation reactions and fluorogenic labelling are the most widely applied derivatization methods in pesticide fluorimetric analysis.

2.2.1. Hydrolysis

Hydrolysis is the most simple pretreatment method for pesticide residue analysis. It is accomplished in a strongly alkaline aqueous medium (NaOH) and at a high temperature (50–100°C). It

leads to the formation of fluorescent anions. The method has been successfully applied to the determination of carbamates such as carbaryl [34,80,81], benomyl [34] and organophosphorus insecticides such as guthion [82] and quinalphos [83] with LODs in the low nanogram range.

For instance, a LOD of 6 ng per spot has been found for carbaryl hydrolyzed in α -naphthol on a TLC plate by spraying with 1 M NaOH, and using scanning fluorimetry [80].

Moreover, for many pesticides, the sensitivity of the method was improved after heat treatment of the hydrolysis products.

2.2.2. Heat treatment

In this procedure, the pesticide sample is put on a chromatoplate, thermally decomposed during a specific time at a given temperature (75–225°C) and fluorimetrically monitored in situ. Although the mechanism of fluorescence thermal production is not completely established, it probably occurs through decomposition or rearrangement of the original molecule into a more stable and/or more conjugated species; a number of fluorescent products have been obtained. In fact, the only necessary criterion for the thermal production of fluorescence is a certain degree of aromaticity within the structure of the compound under investigation.

The TLC technique has been employed for determining non fluorescent organophosphorus insecticides [84] and other pesticides exhibiting native fluorescence [84,85]. Significant changes in excitation and emission spectra occur for the naturally-fluorescent compounds as well as an increase or decrease in their fluorescence signal upon heating (Table 2). The effect of a variety of external reagents such as acids, bases [85] and inorganic salts [86] on a number of pesticides heated on silica gel thin layers was also investigated. The spray of alkali reagents was found to be more efficient as fluorescence intensifiers than that of acid reagents. Background fluorescence, which affects many fluorogenic spraying techniques is absent here, ensuring more reproducible results. The LODs are in the low nanogram range (Table 2).

Table 2
Effect of heat treatment on the TLC fluorescence analytical properties of several aromatic pesticides

Pesticide	Optimum heating conditions	Maximum wavelength (nm)	LOD (ng)	Reference
	Temp./time (°C min ⁻¹)	Before/after heating λ_{ex} , $\lambda_{em}/\lambda_{ex}$, λ_{em}	Before/after heating	
Bayrusil	100/30	—/353, 441	—/20	[84]
Bayrusil	200/30 (1 M NaOH) ^a	—/356, 440	—/4	[84]
Bayrusil	100/30 (1 M KOH) ^a	—/356, 440	—/6	[84]
Bayrusil	100/30 (0.5 M H ₂ SO ₄) ^a	—/373, 510	—/8	[84]
Benomyl	200/45	298, 422/362, 464	60/20	[84]
Captan	100/45 (0.1 M AlCl ₃) ^b	—/360, 465	—/20	[86]
Chlorpyrifos	200/30 (1 M KOH) ^a	—/370, 510	—/40	[84]
Coumaphos	200/20	—/344, 440	—/1	[84]
Coumaphos	200/20	—/366, 400	—/10	[52]
Coumatetralyl	200/45 (0.1 M NH ₄ OH) ^a	—/358, 450	—/10	[85]
Cythioate	200/45 (1 M NaOH) ^a	—/350, 458	—/10	[84]
Cythioate	200/45 (1 M KOH) ^a	—/345, 450	—/60	[84]
Dervinol	RT ^c /30 (1 M AlCl ₃) ^a	355, 428/—	8/—	[86]
Difolatan	100/45 (0.1 M AlCl ₃) ^b	—/360, 465	—/20	[86]
Diphacinon	200/45 (2.5 M KOH) ^a	—/330, 514	—/2000	[85]
Diquat	RT ^c /30 (0.1 M AlCl ₃) ^a	375, 472/—	20/—	[86]
Fospirate	200/45	—/351, 440	—/200	[84]
Fospirate	150/45 (1 M NaOH) ^a	—/353, 439	—/1000	[84]
Fospirate	150/45 (1 M KOH) ^a	—/357, 436	—/1000	[84]
Fuberidazole	200/45 (0.1 M HCl) ^a	—/333, 410	—/6	[85]
Maretin	200/20	364, 482/352, 435	8/—	[84]
Maretin	200/20 (1 M NaOH) ^a	—/370, 500	—/2	[84]
Maretin	200/20 (1 M KOH) ^a	—/365, 492	—/6	[84]
Maretin	75/20 (0.5 M H ₂ SO ₄) ^a	—/355, 440	—/1	[84]
Maretin	RT ^c /20 (0.1 M AlCl ₃) ^b	358, 412/—	2/—	[86]
Menazon	225/30	—/370, 475	—/9	[88]
Menazon	200/30 (1 M KOH) ^a	—/350, 495	—/80	[88]
Menazon	RT ^c /5 (0.1 M H ₂ SeO ₃) ^b	366, 466/—	10/—	[86]
Methabenzthiazuron	200/45	—/353, 439	—/2	[85]
Naptalam	200/45	—/361, 455	—/80	[85]
Naptalam	220/30 (2.5 M KOH) ^a	—/298, 455	—/40	[85]
Naptalam	200/45 (1 M AlCl ₃) ^a	—/312, 482	—/10	[86]
Noltran	200/45	—/351, 440	—/80	[84]
Noltran	200/45 (1 M KOH) ^a	—/377, 505	—/100	[84]
Paraquat	100/45 (0.1 M Na ₂ B ₄ O ₇) ^b	—/420, 510	—/40	[86]
Phosalone	200/120	—/370, 489	—/20	[84]
Propyl isome	200/45 (0.1 M HCl) ^a	—/352, 472	—/8	[85]
Quinomethionate	200/45 (0.05 M H ₂ SO ₄) ^a	—/337, 458	—/40	[85]
Quinomethionate	200/45 (0.1 M NH ₄ OH) ^a	—/335, 455	—/10	[85]
Quinomethionate	200/45 (0.1 M HCl) ^a	—/362, 417	—/60	[85]
Rotenone	200/45	362, 453/370, 440	800/600	[85]
Rotenone	100/45 (0.1 M AlCl ₃) ^b	—/362, 450	—/60	[86]
Thioquinox	200/45	—/329, 441	—/40	[85]
Thioquinox	200/45 (0.1 M NH ₄ OH) ^a	—/329, 435	—/80	[85]
Warfarin	200/45	—/363, 456	—/60	[85]
Zinophos	225/30	—/365, 450	—/80	[84]

^a Chromatoplates were sprayed with a strong acid or base or an inorganic salt prior to heat treatment.

^b The inorganic salt reagent was incorporated into the sorben layer prior to heat treatment.

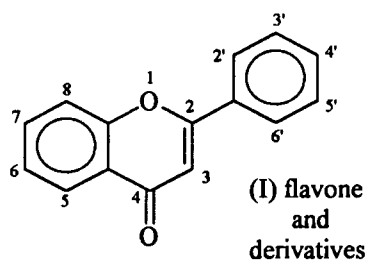
^c RT, room temperature.

2.2.3. Solvent polarity effect

A series of flavone derivatives (II–VI, Scheme 2) were proposed as fluorogenic reagents to spray upon polar pesticides deposited on cellulose [87] and silica gel [88] thin layers. A number of flavonol (II) derivatives (unsubstituted in the five position) almost non fluorescent in non polar media, exhibited a dramatic fluorescence enhancement in a polar environment [87].

Mallet and Frei [87,88] exploited such polarity effects to detect a large variety of pesticides separated by TLC. The developed chromatoplates were sprayed with flavone compounds, resulting in a fluorescent spot appearing at the location of the pesticide on a weakly-fluorescent or non fluorescent background. It was theorized that the pesticide increased the medium polarity locally, producing a fluorescence enhancement of the flavone in the spot area. Although not selective, the technique was applied to carbamates, organophosphorus insecticides *s*-triazine herbicides, organochlorine pesticides, chlorophenoxy-acid herbicides, and phenylurea insecticides, with LODs between 10 and 100 ng [87,88].

Among the flavones derivatives under study, robinetin produced the best result and was preferred over fisetin and flavonol because of its low background fluorescence [88].



(II) flavonol: (3- hydroxyflavone)

(III) fisetin: (3, 3', 4' 7- tetrahydroxyflavone)

(IV) robinetin: (3, 3', 4', 5', 7- pentahydroxyflavone)

(V) morin: (2', 3, 4', 5, 7- pentahydroxyflavone)

(VI) quercetin: (3, 3', 4', 5, 7- pentahydroxyflavone)

Scheme 2.

2.2.4. Complexation reactions

Complexation reactions have been widely used for pesticide residue determination in the environment. Two approaches have been developed for this purpose, including (i) a direct complexation method which leads to the formation of a strongly fluorescent pesticide–ligand complex [79,89–93]; and (ii) an indirect approach, based on a ligand-exchange reaction [94].

Organotin compounds have been frequently employed in agriculture as fungicides and insecticides. Flavonol(II), morin(V) and quercetin(VI) can form fluorescent complexes with both inorganic and organic tin compounds [79,89,90]. The morin–organotin complexes are the most convenient, because they form rapidly at room temperature and lead to a very sensitive assay. They are also stable for long periods in organic solvents [89], (*n*-hexane, ethylacetate) but are poorly soluble in aqueous media [90]. Morin is especially sensitive to dialkyltin compounds. In a stationary medium, LODs are 10^{-9} M for dialkyltins, 10^{-7} M for monoalkyltins, 5×10^{-7} M for trialkyltins, and 10^{-7} M for triphenyltins [79]. The recoveries of the same organotins compounds in spiked human urine and various rat organs at 1–100 nmol levels range from 91.0 to 99.7%, depending on the organotin species. A simultaneous determination of dialkyltin compounds and their possible metabolites was conducted using HPLC on a cyanopropyl-bonded column after post-column morin derivatization. LODs between 0.1 and 1 ng and recoveries of 91–99% were found for dialkyltin compounds added to animal tissues at the 5 nmol level. Langseth [90,91] has described a method requiring only a single HPLC pump by incorporating the ligand in the mobile phase. This approach is based on an eluent containing morin or another complexing agent; it appears to have considerable potential for determining different organotins compounds at low picogram levels. Furthermore, the use of an epifluorescence microscope as an imaging detector [92] and micellar solutions [93] permits the improvement of detection limits for ultratrace measurements and to increase the solubility of organotin–morin complexes in aqueous media.

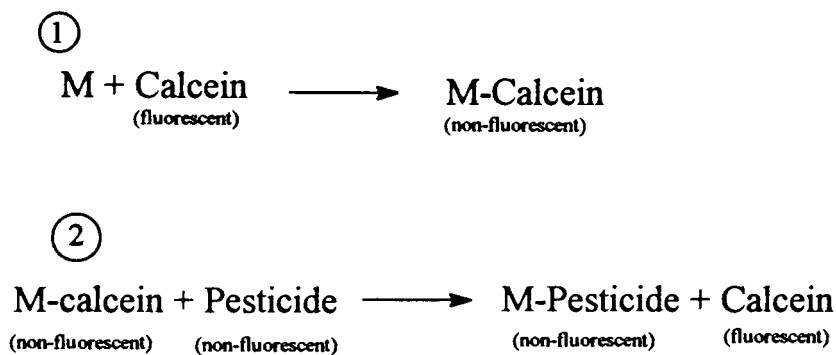


Fig. 1. Ligand exchange reaction scheme between non fluorescent metal/calcein and pesticide/metal complexes

Metal chelates have also been utilized for the fluorimetric analysis of pesticides. A complexation technique named ligand-exchange reaction has been applied by Bidleman et al. [94] to the TLC analysis of 16 organophosphorus pesticides. In this method, based on the fluorescence of a metal chelate, calcein [94]—two steps take place successively: (i) formation of a complex between a fluorescent ligand and a metal (M); and (ii) introduction of the pesticide which induces the release of the fluorescent ligand and then recomplexes with the free metal, (Fig. 1). The amount of added pesticide is proportional to the free calcein concentration, measured by its fluorescence signal.

Calibration curves are linear over a 10–15 fold range, according to the insecticide and calcein-metal spray used. LODs are 10–50 ng for phosphorodithioate and 50–100 ng for phosphorothioate pesticides. Relative standard deviations are less than 15%. The mean recovery of cygon from spiked samples of local lake water is $102 \pm 8\%$. The reaction between palladium and pesticides does not readily occur in solution but only in the adsorbed state.

Although the spray techniques are rapid and simple, they are not selective, and are therefore rather susceptible to interference. An alternative method is fluorogenic labelling, which involves fixing a fluorophore to the analyte, it can be determined fluorimetrically, using TLC or HPLC rather than batch procedures.

2.2.5. Fluorogenic labelling

This pretreatment method is the most widely used for pesticide analysis, probably because of its high sensitivity, which depends on the type of fluorogenic labelling reagent [9,13]. Fluorogenic labelling involves fixing a fluorophore molecule to a non fluorescent analyte; in this process, only a hydrogen atom or a single atom of the analyte is substituted by the fluorophore moiety. Lawrence and Frei [95,96] determined pesticides using fluorogenic labelling with dansyl chloride (dans-Cl). At present, four types of labelling reagents, including dans-Cl, NBD chloride (NBD-Cl), fluorescamine and orthophthalaldehyde with 2-mercaptoethanol (OPA/2-ME) or with 3-mercaptopropionic acid (OPA/3-MP) are used in pesticide residue analysis [9–11,97]. They react easily with alkylamines, arylamines, thiols and phenols, which are widely found among the pesticide reaction products. For instance, carbamates are hydrolyzed into amines and phenols [96,98], urea herbicides lead to aniline derivatives [99,100], many organophosphorus insecticides yield thiols and phenols upon hydrolysis [101], and the *s*-triazine herbicides are hydrolyzed into alkylamines [102]. For numerous pesticides, the labelling reaction mechanism is usually a two-step process which is simple, rapid, and selective, the first step is pesticide alkaline hydrolysis, the second step, fluorogenic labelling of the hydrolysis products. Dans-Cl and NBD-Cl are generally used as pre-column derivatization reagents, while fluorescamine and OPA/2-ME are more suitable for

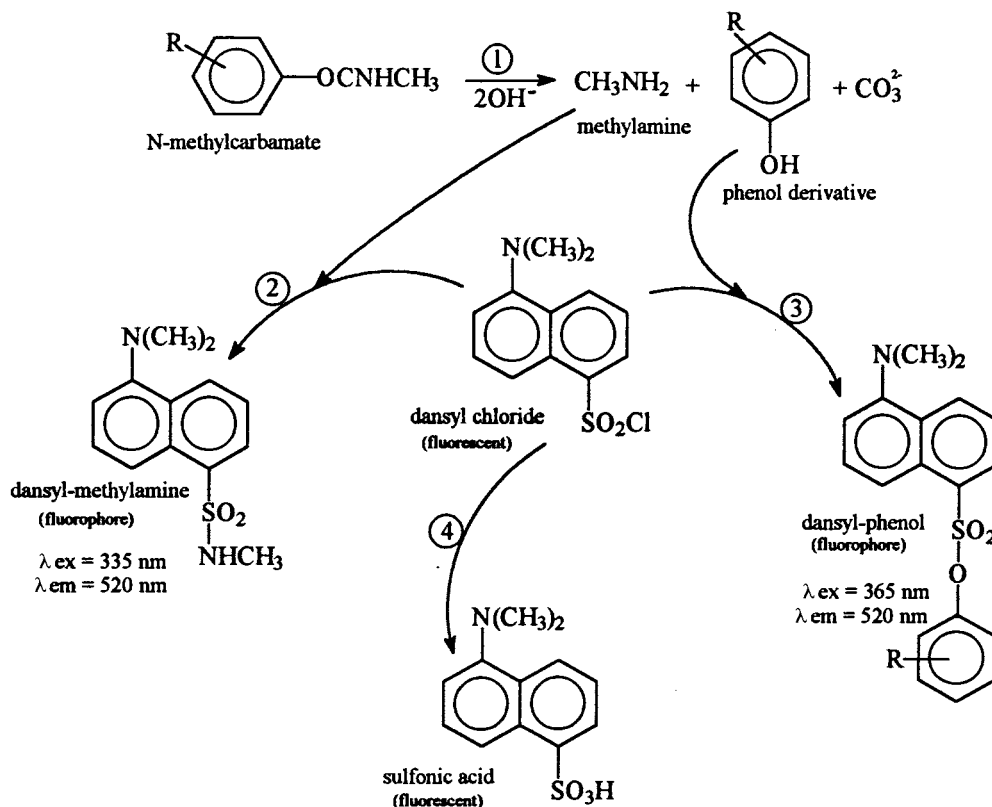


Fig. 2. Reaction scheme for dans–Cl labelling of *N*-methylcarbamate insecticides, ([95,96]). (1) Hydrolysis of the carbamate into phenol and methylamine: performed in 1 M sodium carbonate solution for 10–30 min at 45°C. (2) and (3) labelling of the hydrolysis products: the coupling reaction proceeds faster than the carbamate or the reagent hydrolysis, and it was generally carried out in a water-miscible solvent (acetone, dioxane, acetonitrile) for 20 min at 45°C. (4) Complete hydrolysis of dans–Cl by carbonate into sulfonic acid. Then, the dans–Cl derivative is extracted from the alkaline aqueous solution with non-polar solvents (hexane, benzene, cyclohexane), while sulfonic acid remains in the aqueous phase. The organic phase is then dried and used for analysis. Such a reagent would obviously not be suitable for post-column derivatization, since the reagent is highly fluorescent itself and the reaction kinetic is too slow.

post-column derivatization. Several examples of labelling reaction mechanisms are given, for several classes of pesticides, in the following paragraphs

2.2.5.1. Labelling with dansyl chloride. Dans–Cl readily reacts with primary and secondary amines, at slightly higher pH, with phenols, some thiols and to a lesser extent, with aliphatic alcohols. The derivative products are more fluorescent than dans–Cl [95,96,103–105].

The procedure employed by Lawrence and Frei [95,96], i.e. the hydrolysis of carbamate into phenol and methylamine, is followed by the reaction

of dans–Cl with both hydrolysis products. (Fig. 2) Generally, the phenol derivative is chosen for quantitation since it is characteristic for each carbamate [96]. The technique has been applied to the detection of carbamates in water and soil samples [103] without additional clean-up procedures. LODs are in the low nanogram range (Table 3).

Solvents also have a significant effect on both the dansylation reaction and the extraction process [105]. The fluorescence characteristics of dansyl–phenol derivatives vary significantly with the dielectric constant of the solvent. Apolar solvents such as hexane, cyclohexane and benzene generally increase the fluorescence intensity and shift

Table 3
Determination of pesticides by fluorogenic labelling

Method	Pesticide	Matrice	Labelling reagent	Derivatization duration (Time, temp.) (1 st step), (2 nd step)	Recovery (%)	LOD (ng ml ⁻¹ or ng*)	Reference
HPLC	Fenchlorphos	Water	Dans-Cl	(45 min, 80°C), (90 min, 80°C)	—	10*	[101]
HPLC	Cruformate	Water	Dans-Cl	(45 min, 80°C), (90 min, 80°C)	—	5*	[101]
HPLC	Fenthion	Water	Dans-Cl	(45 min, 80°C), (90 min, 80°C)	—	5*	[101]
HPLC	Carbofuran	Food	Dans-Cl	(30 min, 45°C), (30 min, 45°C)	50–69	10	[104]
HPLC	3-Keto carbofuran	Food	Dans-Cl	(30 min, 45°C), (30 min, 45°C)	55–75	10	[104]
HPLC	3-Hydroxy carbofuran	Food	Dans-Cl	(30 min, 45°C), (30 min, 45°C)	61–80	10	[104]
SM	Promecarb	Air	Dans-Cl	(20 min, 55°C), (10 min, 55°C)	—	100	[105]
NSF	Propam	Water	Fluoresc. ^a	(40 min, 100°C), (— ^b)	103–150	13.5	[110]
1DSF	Propam	Water	Fluoresc.	(40 min, 100°C), (— ^b)	93–108	7.2	[110]
2DSF	Propam	Water	Fluoresc.	(40 min, 100°C), (— ^b)	81–107	12.8	[110]
NSF	Asulam	Peaches	Fluoresc.	(—), (— ^c)	96–120	43	[111]
1DSF	Asulam	Peaches	Fluoresc.	(—), (— ^c)	86–106	43	[111]
HPLC	Carbaryl	Vegetables	OPA/2-ME	(16 s, 100°C), (1.3 s, RT)	85–90	10	[114]
HPLC	Carbofuran	Vegetables	OPA/2-ME	(16 s, 100°C), (1.3 s, RT)	82–93	10	[114]
HPLC	Methiocarb	Vegetables	OPA/2-ME	(16 s, 100°C), (1.3 s, RT)	78–85	10	[114]
HPLC	Aldicarb sulphone	Sub soil	OPA/2-ME	(17 s, 100°C), (4 s, 5°C)	92	2	[115]
HPLC	Oxamyl	Top soil	OPA/2-ME	(17 s, 100°C), (4 s, 5°C)	96	2*	[115]
HPLC	Methomyl	Top soil	OPA/2-ME	(17 s, 100°C), (4 s, 5°C)	95	2	[115]
HPLC	Aldicarb sulphoxide	Water	OPA/2-ME	(17 s, 100°C), (4 s, 5°C)	77–83	2	[115]
HPLC	Carbaryl	Water	OPA/2-ME	(2 min, 100°C), (na)	104–106	2*	[116]
HPLC	Aldicarb sulphoxide	Water	OPA/2-ME	(30 s, 85°C), (13 s, RT)	99–101	1	[117]
HPLC	Oxamyl	Water	OPA/2-ME	(30 s, 85°C), (13 s, RT)	100–101	1	[117]
HPLC	Methomyl	Water	OPA/2-ME	(30 s, 85°C), (13 s, RT)	99–103	1	[117]
HPLC	3-Hydroxy carbofuran	Water	OPA/2-ME	(30 s, 85°C), (13 s, RT)	100–101	1	[117]
HPLC	Carbofuran	Crop	OPA/2-ME	(12 s, 95°C), (na)	83–97	—	[118]
HPLC	Oxamyl	Crop	OPA/2-ME	(12 s, 95°C), (na)	77–99	—	[118]
HPLC	Methomyl	Crop	OPA/2-ME	(12 s, 95°C), (na)	80–96	—	[118]
HPLC	Mesurool	Crop	OPA/2-ME	(12 s, 95°C), (na)	81–98	—	[118]
HPLC	Aldicarb	Grape	OPA/2-ME	(16 s, 100°C), (1.3 s, RT)	79–90	10	[119]
HPLC	Carbofuran	Grape	OPA/2-ME	(16 s, 100°C), (1.3 s, RT)	98	10	[119]
HPLC	Methiocarb	Grape	OPA/2-ME	(16 s, 100°C), (1.3 s, RT)	97–99	10	[119]
HPLC	Oxamyl	Grape	OPA/2-ME	(16 s, 100°C), (1.3 s, RT)	88–92	10	[119]
HPLC	Aldicarb	Potato	OPA/2-ME	(16 s, 100°C), (1.3 s, RT)	91–93	10	[119]
HPLC	Bufencarb	Potato	OPA/2-ME	(16 s, 100°C), (1.3 s, RT)	96–98	10	[119]

Table 3 (continued)

Method	Pesticide	Matrice	Labelling reagent	Derivatization duration (Time, temp.) (1 st step), (2 nd step)	Recovery (%)	LOD (ng ml ⁻¹ or ng*)	Reference
HPLC	Carbofuran	Potato	OPA/2-ME	(16 s, 100°C), (1.3 s, RT)	97–103	10	[119]
HPLC	Methomyl	Potato	OPA/2-ME	(16 s, 100°C), (1.3 s, RT)	92–96	10	[119]
HPLC	Aldicarb sulphoxide	Watermelon	OPA/2-ME	(12 s, 95°C), (na)	74–76	—	[122]
HPLC	Aldicarb sulphoxide	Water	OPA/2-ME	(30 s, 85°C), (26 s, RT)	75–77	0.04	[123]
HPLC	Aldicarb sulphphone	Water	OPA/2-ME	(30 s, 85°C), (26 s, RT)	71–73	0.06	[123]
HPLC	Aldicarb	Water	OPA/2-ME	(30 s, 85°C), (26 s, RT)	77–80	0.06	[123]
HPLC	Aldicarb	Fruits	OPA/2-ME	(40 s, 100°C), (0.2 s, RT)	86–98	0.05*	[124]
HPLC	Bendiocarb	Vegetables	OPA/2-ME	(40 s, 100°C), (0.2 s, RT)	81–93	0.100*	[124]
HPLC	Isoprocab	Fruits	OPA/2-ME	(40 s, 100°C), (0.2 s, RT)	83–96	0.100*	[124]
HPLC	Landrin	Vegetables	OPA/2-ME	(40 s, 100°C), (0.2 s, RT)	86–98	0.050*	[124]
HPLC	Propoxur	Diet	OPA/2-ME	(4 s, 100°C), (0.2 s, RT)	71–73	1.6*	[125]
HPLC	Carbofuran	Diet	OPA/2-ME	(4 s, 100°C), (0.2 s, RT)	82–83	1.6*	[125]
HPLC	Propoxur	Diet	OPA/2-ME	(4 s, 100°C), (0.2 s, RT)	85–89	1.6*	[125]
HPLC	Bufencarb	Food	OPA/2-ME	(59 s, 140°C), (na)	—	0.1*	[129]
HPLC	Dioxacarb	Food	OPA/2-ME	(50 s, 110°C), (na)	—	0.05*	[130]
HPLC	Butocarbexim	Food	OPA/2-ME	(45 s, 150°C), (na)	—	0.05*	[130]
HPLC	Thiofanox	Food	OPA/2-ME	(47 s, 150°C), (na)	—	0.05*	[130]
HPLC	Trimethacarb	Corn	OPA/2-ME	(na), (na)	80–100	40	[132]
HPLC	Tranid	Surface water	OPA/2-ME	(50 s, 140°C), (0.2 s, RT)	99–112	0.02	[134]
HPLC	Carbomolate	Surface water	OPA/2-ME	(50 s, 140°C), (0.2 s, RT)	82–100	0.02	[134]
HPLC	Ethiofencarb	Surface water	OPA/2-ME	(50 s, 140°C), (0.2 s, RT)	92–108	0.02	[134]
HPLC	Aminocarb	Soil	OPA/2-ME	(40 s, 95°C), (17 s, 40°C)	96–97	0.1*	[135]
HPLC	Mexacarbate	Water	OPA/2-ME	(40 s, 95°C), (17 s, 40°C)	94–98	0.1*	[135]
HPLC	Carbofuran	Vegetables	OPA/2-ME	(30 s, 80°C), (80 s, 20°C)	—	20	[140]
HPLC	Aldicarb	River water	OPA/2-ME	(45 s, 100°C), (1.6 s, RT)	—	0.1*	[142]
HPLC	Methomyl	River water	OPA/2-ME	(45 s, 100°C), (1.6 s, RT)	—	0.3*	[142]
HPLC	Methiocarb	River water	OPA/2-ME	(45 s, 100°C), (1.6 s, RT)	—	0.85*	[142]
HPLC	Methomyl	Surface water	OPA/2-ME	(53 s, 90°C), (2.7 s, RT)	—	0.4*	[145]
HPLC	Aldicarb	Surface water	OPA/2-ME	(53 s, 90°C), (2.7 s, RT)	—	0.5*	[145]
HPLC	Oxamyl	Potatoes	OPA/2-ME	(na), (na)	90–94	20	[145]
HPLC	Glyphosate	Cereals	OPA/2-ME	(210 s, 20°C), (30 s, RT) ^d	80	200	[147]
NSF	IAA ^e	—	OPA/2-ME	(15 min, RT), (— ^f)	—	0.80	[148]

Table 3 (continued)

Method	Pesticide	Matrice	Labelling reagent	Derivatization duration (Time, temp.)	Recovery (%)	LOD (ng ml ⁻¹ or ng ^a)	Reference
1DSF	IBA ^e	—	OPA/2-ME	(15 min, RT), (— ^f)	—	0.19	[148]
2DSF	IPA ^e	—	OPA/2-ME	(15 min, RT), (— ^f)	—	0.27	[148]

TLC, thin layer chromatography; HPLC, high performance liquid chromatography; SM, stationary media; NSF, normal synchronous fluorimetry; 1DSF, first derivative synchronous fluorimetry; 2DSF, second derivative synchronous fluorimetry.

^a Fluoresc., fluorescamine.

^b The second step is instantaneous.

^c No hydrolysis step, but direct coupling reaction for the carbamates.

^d The first step is an oxidation reaction.

^e IAA, indole-3-acetic acid; IBA, indole-3-butyric acid; IPA, indole-3-propanoic acid.

^f Single stage derivatization; na, not available; RT, room temperature.

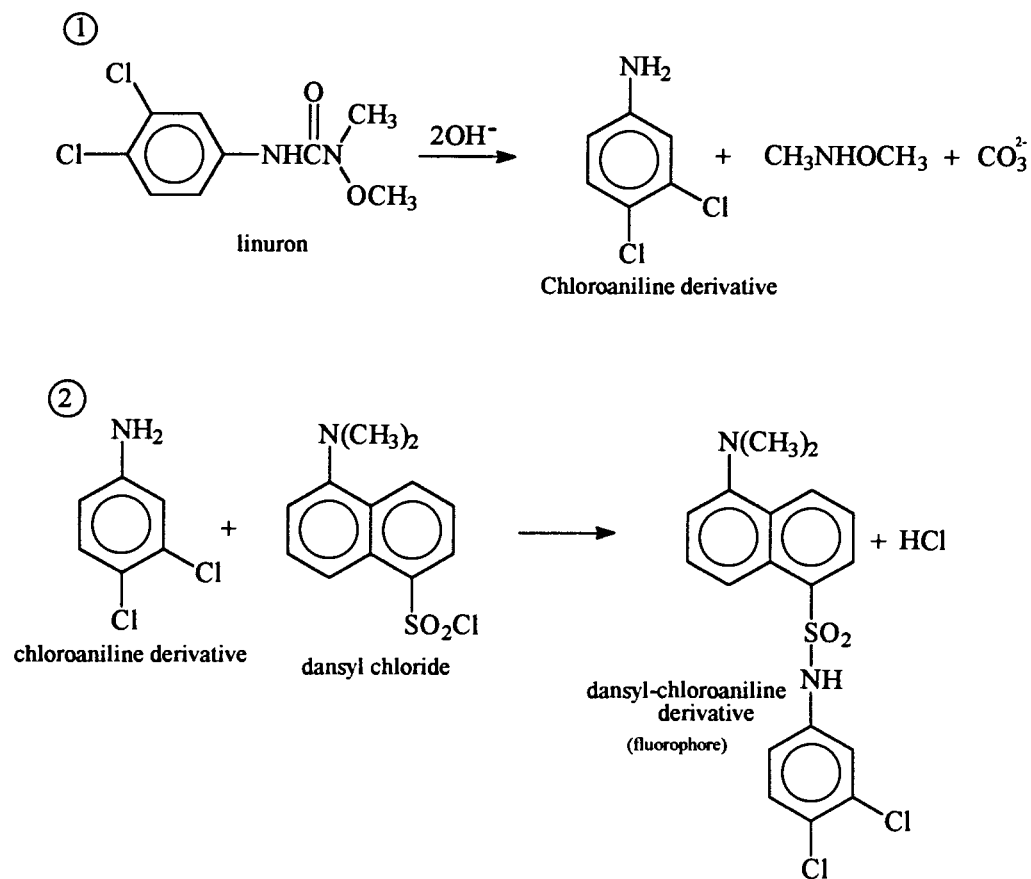


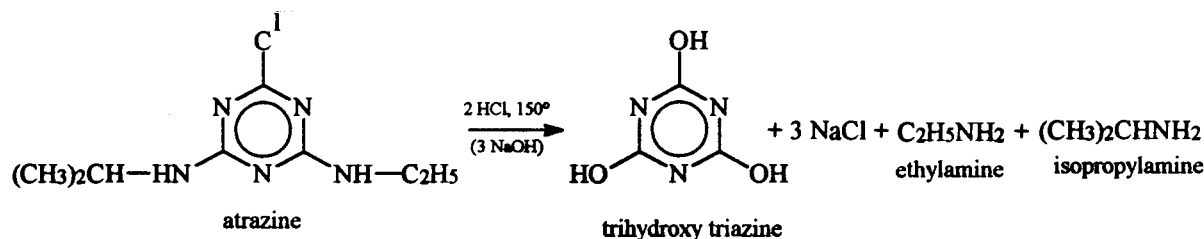
Fig. 3. Reaction scheme for the dans–Cl labelling of linuron, ([99]). (1) Hydrolysis of the urea herbicide into chloroaniline. (2) Labelling of the released chloroaniline with dans–Cl.

the emission wavelength towards the blue, whereas polar hydrosoluble solvents reduce the fluorescence intensity and produce a red-shift of the emission maxima. The dansylation reaction of most carbamates does not occur in non hydrosoluble solvents such as chloroform and methyl isobutyl ketone (MIBK). In contrast, a two-phase solvent system is preferred for organophosphorus pesticides while the phenylureas hydrolysis products have to be extracted before the coupling reaction. A concentration excess of dans–Cl (10 times) over carbamate is required, and complete hydrolysis of the remaining dans–Cl into sulfonic acid is necessary to avoid high blank signals.

Fig. 3 shows an example of the labelling mechanism with linuron, a phenylurea herbicide [99].

After alkaline hydrolysis of the herbicide the released aniline derivative is extracted with hexane from the hydrolysis mixture, spotted on a TLC plate, and reacts in situ with a 10-fold excess of dans–Cl. A 300 ng linear dynamic range, a 1-ng detection limit and reproducibility (3–5%) are obtained (Table 3).

Dans–Cl labelled organophosphorus insecticides such as fenthion, ruelene, fenchlorphos and parathion, yield phenols upon hydrolysis and are detected in the low nanogram range [101]. After alkaline hydrolysis the coupling reaction is carried out in a two-phase system, at the interface—water:MIBK, the resulting dansyl–phenol is extracted with benzene and analyzed by quantitative in situ TLC and HPLC. (Table 3)



Scheme 3.

Dans-Cl labelling has also been applied to *s*-triazine herbicides (atrazine, simazine, propazine) [102]. Hydrolysis (Scheme 3) is carried out in an acidic medium, the resulting mixture is then made alkaline: the released alkylamines are coupled with dans-Cl (Fig. 2).

2.2.5.2. Labelling with NBD chloride. NBD-Cl only reacts with primary and secondary aliphatic amines under weakly basic conditions to form highly fluorescent derivatives. It is more selective than dans-Cl since it does not form fluorescent derivatives with phenols, thiols, alcohols or anilines. Unlike dans-Cl, the NBD-Cl hydrolysis product is non fluorescent and does not interfere in quantitative analysis. In addition, the NBD-Cl fluorescence excitation ($\lambda_{\text{ex}} \approx 470\text{--}480$ nm) and emission ($\lambda_{\text{em}} \approx 530\text{--}550$ nm) maximum wavelengths are located in the visible region of the spectrum, where there is no interference from naturally fluorescent compounds that may be present as co-extractives. Therefore, a quantitative labelling method based on NBD-Cl has been developed for the determination of *N*-methyl and *N,N*-dimethylcarbamate pesticides in aqueous solutions [106] (Fig. 4). The reaction rates, as well as fluorescence and TLC properties were investigated to optimize the technique, subnanogram quantities of pesticides were detected.

The advantage of NBD-Cl labelling method is its selectivity, since only one fluorescent derivative is produced with most carbamates, which eliminates possible interference. Its disadvantages include its inability to distinguish between carbamates of different classes.

2.2.5.3. Labelling with fluorescamine. Fluorescamine, a powerful fluorogenic reagent, was synthesized by Weigle et al. [107]. It reacts directly with primary aliphatic amines in aqueous medium (pH 8–10) at room temperature in less than a second, yielding a highly fluorescent derivative. Fluorescamine itself is non fluorescent and excess reagent is hydrolyzed in a few seconds, producing non fluorescent products [108]. The large rate of the reaction and its good selectivity makes it suitable for post-column HPLC detection of primary amines, (Scheme 4). In addition to its affinity for aliphatic amines, fluorescamine can react with primary aromatic amines in aqueous media [109].

Fluorescamine has been widely used as a labelling compound for the determination of amine-generating pesticides [9,110–112]. The reaction mechanism is similar to dans-Cl labelling of amines and has been carried out on amines obtained either by hydrolysis of carbamates [110,111], or by reduction of some nitrosubstituted pesticides such as fenitrothion, and parathion methyl [112], LODs are in the ng ml^{-1} range (Table 4).

2.2.5.4. Labelling with orthophthalaldehyde/2-mercaptoethanol (OPA/2-ME). Initially OPA was applied to the HPLC analysis of seven *N*-methylcarbamate insecticides [97]. OPA selectively reacts with primary aliphatic amines. The reaction mechanism involves two steps: the alkaline hydrolysis of carbamate into methylamine and alcohol, and the derivatization of the released methylamine with OPA in the presence of 2-mercaptoethanol (2-ME) [97,113–135] or 3-mercapto-propionic acid (3-MP) [129,136] to form a highly

Table 4
Determination of pesticides using photochemically-induced fluorimetry (PIF) or photosensitized fluorimetry (PSF) detection

Method ^a	Pesticide	Matrices	Solvent ^b	Photolysis time (s)	Recovery (%)	LOD (ng ml ⁻¹) ^c	Reference
FIA	Fenitrothion	Formulations	DMSO/H ₂ O ^d	52	96–107	3 ^e	[23]
FIA	Fenvalerate	Formulations	MeOH	52	97–106	4 ^e	[23]
FIA	Fenvalerate	Tap water	MeCN	95	93–102	10 ^e	[23]
FIA	Deltamethrin	Formulations	EtOH	95	—	18 ^e	[23]
FIA	Deltamethrin	Tap water	EtOH	95	94–104	—	[23]
FIA	Diflufenzuron	Formulations	2-PrOH	89	88–106	19 ^e	[23]
SM	Fenitrothion	Formulations	DMSO	96	96–105	0.7	[149]
SM	Fenvalerate	Formulations	MeCN	600	99–108	8.7	[149]
SM	Deltamethrin	Formulations	MeOH	1380	88–98	33	[149]
SM	Diflufenzuron	Formulations	2-PrOH	1380	96–107	4.9	[149]
SM	MCPBP ^f	River water	MeOH/pH 5 ^g	900	92–116	36	[150]
SM	2,4-D ^f	—	MeOH/pH 5 ^g	900	—	103	[150]
SM	2,4,5-T ^f	—	MeOH/pH 5 ^g	900	—	119	[150]
SM	Fenvalerate	—	MeCN	600	—	16	[151]
SM	Fenvalerate	Unt. formul. ^h	SDS	720	89–99	7	[151]
SM	Deltamethrin	—	MeOH	1380	—	27	[151]
SM	Deltamethrin	Unt. formul. ^h	SDS	2100	96–113	11	[151]
HPLC	Alachlor	Ground water	MeOH	168	100–105	5	[152]
HPLC	Butachlor	Ground water	MeOH	168	97–110	12	[152]
HPLC	Carbetamide	Ground water	MeCN/H ₂ O+0.02% aceton tone	168	95–115	38	[152]
HPLC	Carboxin	Ground water	MeOH/H ₂ O	168	95–110	5	[152]
HPLC	Diphenamid	Ground water	MeOH/H ₂ O	168	—	50	[152]
HPLC	Fenoxycarb	Ground water	MeOH/H ₂ O	168	—	5	[152]
FIA	MCPA ^f	River water	MeOH/pH5	90 ⁱ	96.5	26	[153]
FIA	MCPBP ^f	River water	MeOH/pH5	90 ⁱ	97.2	23	[153]
FIA	MCPBP ^f	River water	MeOH/pH5	90 ⁱ	103.7	30	[153]
FIA	2,4-D ^f	River water	MeOH/pH5	720 ^j	108.4	98	[153]
FIA	2,4-DP ^f	River water	MeOH/pH5	600 ^j	103.9	82	[153]
HPLC	2-Chlorophenol	River water	MeOH/H ₂ O ^j	40	96–104	4 ^e	[154]
HPLC	3-Chlorophenol	Urine	MeOH/H ₂ O ^j	25	95–100	1 ^e	[154]
HPLC	4-Chlorophenol	River water	MeOH/H ₂ O ^j	25	96–104	1 ^e	[154]
HPLC	2,4-Dichlorophenol	River water	MeOH/H ₂ O ^j	60	96–104	50 ^e	[154]
HPLC+OPA/2-ME	Diuron	Carrots	MeCN/H ₂ O	44	—	12 ^e	[155]
HPLC+OPA/2-ME	Linuron	Carrots	MeCN/H ₂ O	44	—	24 ^e	[155]
HPLC+OPA/2-ME	Monuron	Carrots	MeCNH ₂ O	44	—	4 ^e	[155]
HPLC+OPA/2-ME	Thiobencarb	Vegetables	MeCN/H ₂ O	336	58–140	—	[156]
HPLC+OPA/2-ME	Methiocarb	Ground water	MeCN/H ₂ O	336	—	3.4 ^e	[156]
HPLC+OPA/2-ME	Neburon	Ground water	MeCN/H ₂ O	336	—	0.8 ^e	[157]
HPLC+OPA/2-ME	Aldicarb	Ground water	H ₂ O	336	83–95	1 ^e	[157]
HPLC+OPA/2-ME	Aldicarb	Ground water	H ₂ O	336	83–110	0.9 ^e	[157]

Table 4 (continued)

Method ^a	Pesticide	Matrices	Solvent ^b	Photolysis time (s)	Recovery (%)	LOD (ng ml ⁻¹) ^c	Reference
HPLC+OPA/2-ME	Propoxur	Ground water	H ₂ O	336	72–104	1.3 ^c	[157]
HPLC+OPA/2-ME	Thiram	Ground water	H ₂ O	336	36–96	1.5 ^c	[157]
HPLC+OPA/2-ME	Neburon	Ground water	MeCN/H ₂ O	336	87–113	0.8 ^c	[157]
HPLC	Monuron	—	MeCN/H ₂ O	336	—	24 ^c	[157]
HPLC+OPA/2-ME	Monuron	—	MeCN/H ₂ O	336	—	1.3 ^c	[157]
HPLC	Fluometuron	—	MeOH/H ₂ O	336	—	1.4 ^c	[157]
HPLC+OPA/2-ME	Fluometuron	—	H ₂ O	336	—	5.1 ^c	[157]
HPLC	Chlorbromuron	—	MeCN/H ₂ O	336	—	1.2 ^c	[157]
HPLC+OPA/2-ME	Chlorbromuron	—	MeOH/H ₂ O	336	—	42 ^c	[157]
HPLC+OPA/2-ME	Diphenamid	Water	H ₂ O	168	90–100	0.5	[158]
HPLC+OPA/2-ME	Diphenamid	—	MeOH/H ₂ O	168	—	0.2 ^c	[158]
HPLC+OPA/2-ME	EPTC	Water	H ₂ O	168	100–106	1.3	[158]
HPLC+OPA/2-ME	EPTC	—	MeCN/H ₂ O	168	—	0.4 ^c	[158]
HPLC+OPA/2-ME	Molinate	Water	H ₂ O	168	100–104	7.4	[158]
HPLC+OPA/2-ME	Molinate	—	MeOH/H ₂ O	168	—	1 ^c	[158]
HPLC+OPA/2-ME	Thiobencarb	Water	H ₂ O	168	96–110	1.3	[158]
HPLC+OPA/2-ME	Thiobencarb	—	MeCN/H ₂ O	168	—	0.3 ^c	[158]
HPLC+OPA/2-ME	Daminozide	—	MeCN/H ₂ O	168	—	1 ^c	[158]
HPLC+OPA/2-ME	Trifluralin	—	MeOH/H ₂ O	168	—	2 ^c	[158]
HPLC+OPA/2-ME	Paraquat	—	MeOH/H ₂ O	168	—	0.7 ^c	[158]
HPLC+OPA/2-ME	Dinoseb	—	MeOH/H ₂ O+0.5% acetone	168	—	5 ^c	[158]
HPLC	Fenarimol	Ground water	MeCN/H ₂ O	78	—	1.5 ^c	[159]
HPLC+OPA/2-ME	Fenarimol	Ground water	MeCN/H ₂ O	78	—	9.5 ^c	[159]
HPLC	Napropamide	Ground water	MeCN/H ₂ O	78	—	0.6 ^c	[159]
HPLC+OPA/2-ME	Napropamide	Ground water	MeCN/H ₂ O	78	—	3.4 ^c	[159]
HPLC	Propanil	Ground water	MeCN/H ₂ O	78	—	0.5 ^c	[159]
HPLC+OPA/2-ME	Propanil	Ground water	MeCN/H ₂ O	78	—	5.4 ^c	[159]
HPLC+morin	TCT ^k	Surface water	<i>n</i> -H/THF/AA ^l	9	67–114	30	[160]
HPLC+morin	TCT	Sediments	<i>n</i> -H/THF/AA ^l	9	125–130	3000	[160]
HPLC+morin	TCT	Soils	<i>n</i> -H/THF/AA ^l	9	95–100	0.3	[160]
HPLC+morin	FBTO ^k	Surface water	<i>n</i> -H/THF/AA ^l	9	61–97	20	[160]
HPLC+morin	FBTO	Sediments	<i>n</i> -H/THF/AA ^l	9	100–135	20	[160]
HPLC+morin	FBTO	Soils	<i>n</i> -H/THF/AA ^l	9	91–93	20	[160]
HPLC+morin	TPT ^k	Surface water	<i>n</i> -H/THF/AA ^l	9	72–101	20	[160]
HPLC+morin	TPT	Sediments	<i>n</i> -H/THF/AA ^l	9	65–105	300	[160]
HPLC+morin	TPT	Soils	<i>n</i> -H/THF/AA ^l	9	44–59	1000	[160]
SM	Benfluralin	—	MeCN/H ₂ O ^m	240	—	300	[184]
SM	Isopropalin	—	MeCN/H ₂ O ^m	120	—	3300	[184]

Table 4 (continued)

Method ^a	Pesticide	Matrices	Solvent ^b	Photolysis time (s)	Recovery (%)	LOD (ng ml ⁻¹) ^c	Reference
SM	Oryzalin	—	MeCN/H ₂ O ^m	120	—	4200	[184]
SM	Trifluralin	—	MeCN/H ₂ O ^m	240	—	300	[184]

^a FIA, flow injection analysis; SM, stationary medium; HPLC, high performance liquid chromatography.

^b All solvents used are either pure or 50:50 (v/v).

^c Unless otherwise mentioned.

^d Water is used only as mobile phase.

^e In nanograms.

^f Chlorophenoxyacid herbicides: 2,4-D, 2,4-dichlorophenoxyacetic acid; 2,4,5-T, 2,4,5-trichlorophenoxyacetic acid; 2,4,-DP, 2-(2,4-dichlorophenoxy) propionic acid; MCPA, 2-methyl-4-chlorophenoxyacetic acid; MCPB, 4-(2-methyl-4-chlorophenoxy) butyric acid; MCPP or mecoprop, 2-(2-methyl-4-chlorophenoxy) propionic acid.

^g Buffer pH 5.

^h Untreated formulations.

ⁱ Stopped flow time in FIA.

^j MeOH/H₂O (60:40, v/v).

^k Organotin pesticides: TCT, tricyclohexyltin hydroxide; FBTO, fenbutatin oxide; TPT, triphenyltin chloride.

^l Ternary mixture of *n*-hexane/THF/acetic acid (96:2:2, v/v).

^m MeCN/H₂O, (20:80, v/v).

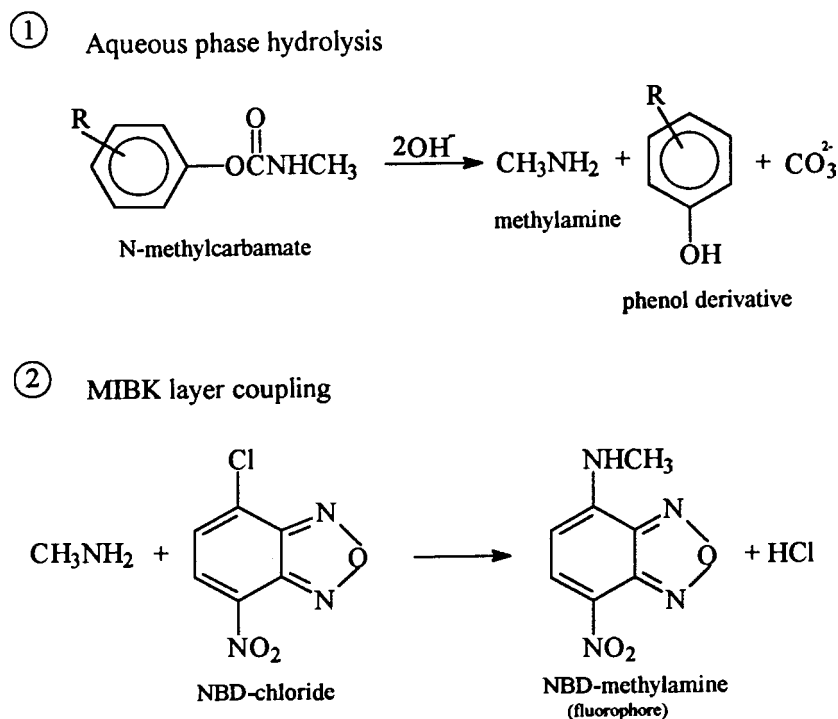


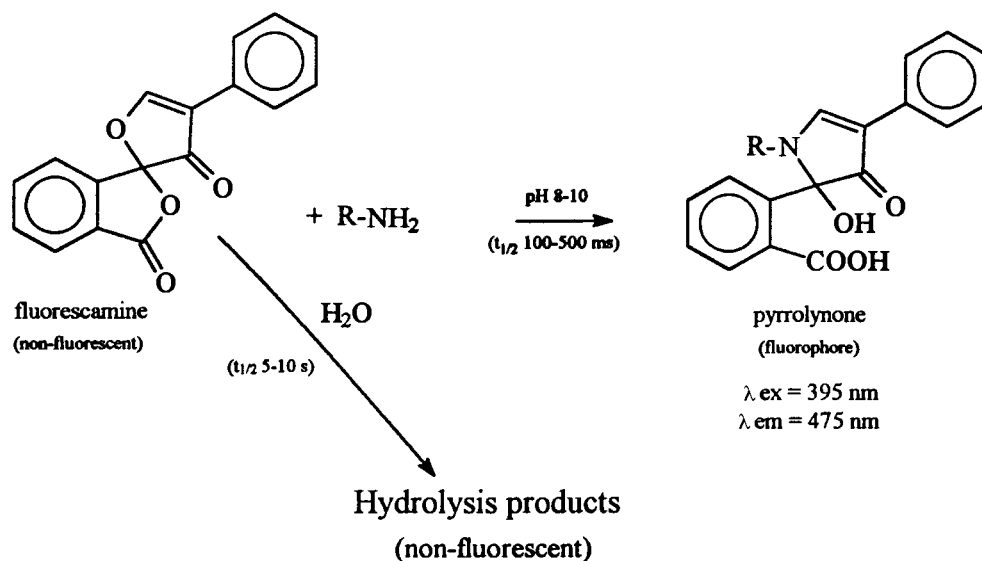
Fig. 4. Reaction scheme of the labelling of *N*-methylcarbamate insecticides with NBD-Cl, ([106]). (1) Hydrolysis of the insecticide in aqueous buffer phase. (2) Labelling of methylamine in an organic methyl isobutyl ketone (MIBK) phase. Due to the low solubility of NBD-Cl in water, the labelling reaction with methylamine was carried out at a water:MIBK interface. The coupling reaction is faster in polar solvents such as alcohols and ketones. Performed at 80°C, using a 1% NBD-Cl in MIBK solution, the reaction completed in about 30 min. NBD-Cl is not suitable for post-column derivatization because the reaction kinetics is too low.

fluorescent isoindole derivative identified by NMR and mass spectrometry [137] (Fig. 5). Most studies employing OPA and 2-ME or 3-MP are based on post-column HPLC derivatization, since the reagents can be easily introduced in the reaction system by successive pumps (Fig. 6).

HPLC post-column reaction derivatization parameters have been optimized by Krause [138,139] and Engelhardt et al. [140]. The OPA/2-ME HPLC method which has been recognized by the US Environmental Protection Agency (EPA) [141] is widely used as a multiresidue method for *N*-methylcarbamate and carbamoyloxime insecticides determination in food [119,120,139] as well as in a variety of media including water [115–117,123,127,131,134,135,142], soils [115,132,135], and plant tissues [114,118,121,122,124,126,132,133,140]. De Kok et al. [124] extended the method

to other *N*-methylcarbamates, and developed a simple clean-up method which is applicable to various types of crop samples.

Nondek et al. [142,143] significantly improved the OPA/2-ME method, by hydrolyzing carbamates at 100–120°C, in a catalytic solid-phase reactor packed with a strong anion exchanger resin, (e.g. Aminex A-28, a tetralkylammonium anion exchanger). This approach eliminates one of the post-column reagent delivery pumps avoiding possible mixing problems and flow pulsations. Moreover, it suppresses band broadening due to dilution of the analyte in the mobile phase, thus improving the sensitivity and selectivity of the method. In these conditions, as little as 0.1 ng aldicarb and 0.3 ng methomyl can be detected [143]. Jansen et al. [144] miniaturized the catalytic solid-phase reactor using 1-mm i.d. narrow-bore HPLC columns, and obtained LODs in low



Scheme 4.

nanogram range. Furthermore, De Kok et al. [130] applied solid-phase catalysis to the determination of 22 *N*-methylcarbamates and their major metabolites in crop samples. Magnesium oxide was substituted as anion exchanger resin, which minimized band broadening.

Another useful simplification—the hydrolysis and derivatization steps were combined by means of a single reagent, (OPA/2-ME in 0.01 M KOH) delivered by a single post-column pump [129]. This feature eliminates the need for both an alkali post-column pump and solid-phase or photolytic reactors. LODs were about 0.1 ng for 11 *N*-methylcarbamates. This single-step technique has also been applied to the analysis of oxamyl in potatoes [145] and oxamyl and methomyl in crops and water samples (LOD: 1 ng) [146]. This single-step post-column derivatization method is more convenient than the two-step conventional technique since sensitivity is increased, the hardware and cost are reduced and the daily procedure is simplified.

Among all the derivatization methods, OPA/2-ME labelling remains the most sensitive and practical for the analysis of pesticides yielding primary amines under hydrolysis or photodegradation. *N*-methylcarbamate and carbamoyloxime insecti-

cides, and to a lesser extent, herbicides [147], plant growth regulators [148], and phenylureas [113,139,144] have been determined using this technique. Generally the LODs range from the low ng ml⁻¹ to upper pg ml⁻¹ according to the compound (Table 3).

2.2.5.5. Labelling with other reagents. Other pesticide labelling reagents [76,78] exist, but have not as yet gained widespread acceptance. For example, Suzuki et al. [76] used 9-anthryldiazomethane, as a labelling reagent to detect about 500 pg of chlorophenoxyacid herbicides in ground water. A rapid determination of glufosinate was also performed in environmental water samples using 9-fluorenylmethoxycarbonyl, with pre-column derivatization at 0.25 ng ml⁻¹ in less than 15 min [78].

2.2.5.6. Advantages and drawbacks of fluorogenic labelling. Generally speaking, fluorogenic labelling constitutes a sensitive analytical procedure which as yet presents poor selectivity. As compared with other derivatization methods (hydrolysis, heat treatment etc.), fluorogenic labelling offers a number of advantages, simplified optimization procedures, dual or multiresidue methods, wide range

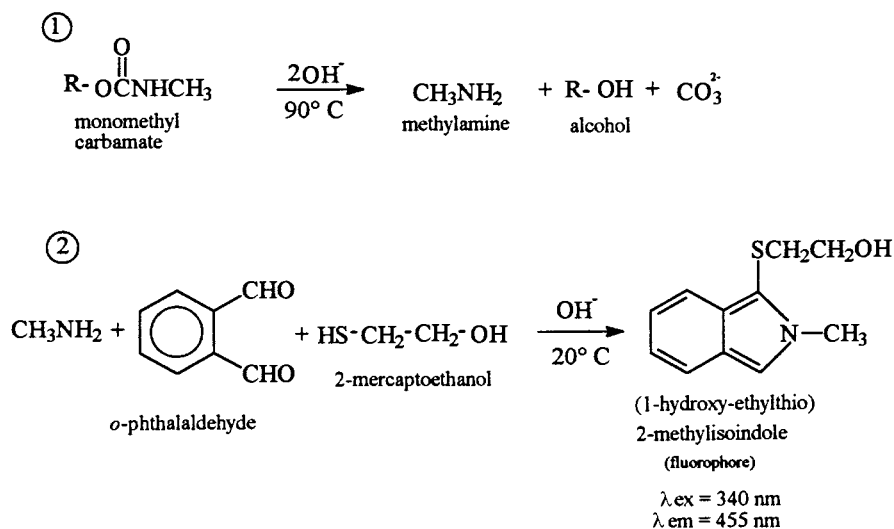


Fig. 5. Reaction scheme of OPA/2-ME labelling of a monomethyl carbamate insecticide. ([132]). (1) Hydrolysis. (2) Labelling of the liberated methylamine to (1-hydroxy-ethylthio)-2-methylisindole,

of labels and accessible experimental variables with ideal sensitivity. However, limitations exist due to problems associated with the simultaneous detection of individual components in mixtures, the development of HPLC has significantly improved the selectivity of the labelling method relative to the originally-used TLC [95,96], and other time-consuming procedures in stationary solutions [105].

The labelling reagents should be sufficiently stable and the derivatization reaction must be fairly rapid to provide a short residence time in the post-column reactor.

3. Photochemically-induced fluorimetric (PIF) methods

The concept of photochemically-induced fluorimetry (PIF) is based on the conversion of non fluorescent analytes into strongly fluorescent photoproduct. PIF is more recent than chemical derivatization and has been much less applied to pesticide quantitative analysis. Several chapters in various books have been devoted to PIF methods [16–18]. In addition to its simplicity, these methods present several advantages, but also have

some drawbacks, relative to derivatization methods.

The main advantages are as follows: (i) the use of photons for analyte conversion instead of a chemical reagent means it does not require a mixing system, and therefore, the analyte must not be diluted; (ii) since most photochemical reactions take place via free radicals, the reactions rates are generally fast, resulting in short conversion times; (iii) the use of room temperatures constitutes an advantage of a photoinitiated in situ analyte conversion, relative to thermally-initiated derivatization; (iv) the technique is very easy to implement, requires inexpensive equipment and is suitable for various experimental conditions such as stationary liquid solutions [149–151], dynamic systems, including flow injection analysis (FIA) [23,152,153], HPLC [154–160] and TLC[161].

Obviously, PIF provides a selective fluorogenic transformation of non fluorescent compounds since it does not require the usual separation of fluorescent photoproduct from other photoproducts in the reaction medium. This simplicity is brought about by the fact that the photochemical conversion of pesticides in solution occurs either by the direct photolysis mechanism in which the

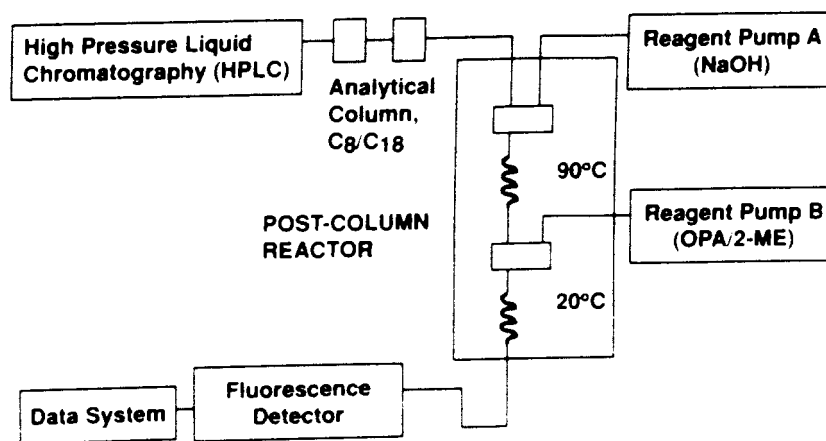


Fig. 6. Schematic diagram of carbamates post-column HPLC derivatization, using OPA/2-ME, ([132], with permission).

compound directly absorbs the incident radiation, or by an indirect photolysis process in which an additional compound acts as a photosensitizer and transfers absorbed energy or generates an active oxidizing species.

From an analytical point of view, another advantage is that it is not really necessary to identify the structure of the fluorescent compound(s) formed after UV irradiation, provided that reproducible PIF signals are obtained. However, photoproducts identification could be helpful and is recommended not only for academic relevance, but to ensure the applicability of PIF to the quality control of different types of samples, especially in environmental studies. In some cases, PIF simultaneous determination of a mixture can be performed without a prior separation step, using different optimum UV irradiation time (t_{opt}) values—characteristic of each compound—[149,162] or by applying specific techniques, such as derivative PIF spectra, and/or partial least square (PLS) multivariate method [163].

PIF has some drawbacks, such as the formation of non fluorescent photoproducts; secondary thermal reactions and/or photoreactions leading to non stable and difficult to identify photoproducts, particularly those responsible for fluorescence emission [18].

Generally, PIF conversion methods have proven to be efficient fluorophore-generating systems for stationary media [149–151] as well as

flowing devices such as HPLC post-column photoreaction [152,154–158] or FIA [23,152,153] method. Several parameters affecting the analyte conversion reactions have been investigated. It was found that two parameters affect the sensitivity of the method, namely the UV irradiation time [149,162] and the type of solvent used [149,152,156,162]. In fact, t_{opt} and PIF intensity values vary considerably with solvent polarity and its protic or aprotic character. For example, pesticides such as fenvalerate, deltamethrin and diflubenzuron have a good affinity for protic solvents (i.e. high PIF intensity with short t_{opt}), while for fenitrothion and chlorpyrifos, polar aprotic solvents are a better choice [149,162]. Therefore, for analytical purposes, the solvent selected should be one giving the shortest t_{opt} and the largest PIF signal. When these ideal conditions are not matched by any solvent, the solvent having the shortest t_{opt} is generally chosen even if PIF intensity is not the strongest [162].

3.1. Photochemical reactivity and photodegradation pathways

The photochemistry and photodegradation pathways of several classes of pesticides have been investigated by a number of workers [164–181].

The photochemical degradation of herbicides is well documented. Plimmer [164] has summarized the photochemical loss of chlorine mechanism

from halogenated aromatic herbicides. Crosby [165] has reviewed in detail the effect of UV irradiation time on nitrophenol and chlorophenol derivative herbicides. The photolytic dehalogenation is a well known and an important degradation pathway for chlorophenoxyacid herbicides, and the main photoproducts are identified as lower chlorinated phenols, dihydroxylated products, phenols and polymers [166–168]. Hence, the occurrence of a photolytic dechlorination mechanism explains the relatively high fluorescence efficiency generally observed for chlorophenoxyacid and chlorophenol pesticide photoproducts [150,153,154].

The study of the photodegradation pathway of phenylurea herbicides indicates that one of the photoproducts is dimethylamine [169,170]. This observation led Luchtefeld [155] to believe that the photolysis of phenylureas herbicides may also produce methylamine which could then react with OPA/2-ME.

The photodegradation mechanism of pyrethroid insecticides has been widely investigated. Ruzo et al. [171–174] have elucidated the photodecomposition steps of several pyrethroid insecticides including deltamethrin [172], while Mikami et al. [175] found that fenvalerate photodegradation rates and pathways depended on environmental conditions (soils, water, ...).

The photolytic degradation of organophosphorus insecticides [176–180], carbamates [21,180] and chlorotriazines [180] have also been studied. Sometimes, in the presence of a sensitizer, several compounds, otherwise inert may undergo photodegradation reactions. For instance, Ross and Crosby [181] have shown that the addition of acetone as a sensitizer increased the disappearance of ethylenethiourea under natural and artificial light. Furthermore, it has been demonstrated that photolysis reactions can improve the indirect fluorescence detection of several aromatic or non aromatic compounds [16–18].

3.2. PIF related mechanisms

Since the application of PIF to pesticide determination is relatively new, very few and fragmentary studies have been devoted to describing the

photoinduced mechanisms of formation of fluorescent photoproduct(s) [149,152,154]. No systematic identification of the exact nature of fluorescent (or non fluorescent) photoproduct(s) formed during the photolysis reactions has been reported. Some authors [149,152] have suggested that the photodegradation pathways of aromatic pesticides probably involve some changes in the aromatic moiety of the molecules under study. However, the identification of a number of photoproducts during the photolysis of fenitrothion [177], fenvalerate [175] and deltamethrin [171,172] in various experimental conditions demonstrates the great complexity of photolysis mechanisms.

In the case of the photolysis of four aromatic pesticides, including deltamethrin, diflubenzuron, fenitrothion and fenvalerate, Coly and Aaron [149] have proposed the existence of two distinct types of mechanisms based on different curves of PIF intensity vs. irradiation time. Further investigations have allowed the same authors [162] to identify the nature of the fluorescent photoproducts obtained during the photolysis reaction of three of these pesticides, (fenitrothion, fenvalerate and deltamethrin) (Fig. 7).

3.3. PIF application to pesticides analysis

Comparing the analytical performances of the PIF method with other fluorogenic derivatization techniques, several workers have highlighted the main advantages of this technique, including simplicity, shorter analysis time, enhanced sensitivity and selectivity. The following results have been reported for pesticide PIF analysis.

Werkhoven-Goewie et al. [154] were probably the first to apply PIF to the liquid chromatographic analysis of chlorophenol pesticides in effluent water samples and biological fluids. The fluorescence signals of photolysed chlorophenols were linearly related to the amounts of analyte over 2–3 orders of magnitude. The LODs were in the low nanogram range and recoveries from spiked river water samples were $100 \pm 4\%$.

Since the chemical hydrolysis of urea compounds was generally inefficient [139], Luchtefeld [155] modified this step to produce a larger amount of methylamine which can react with

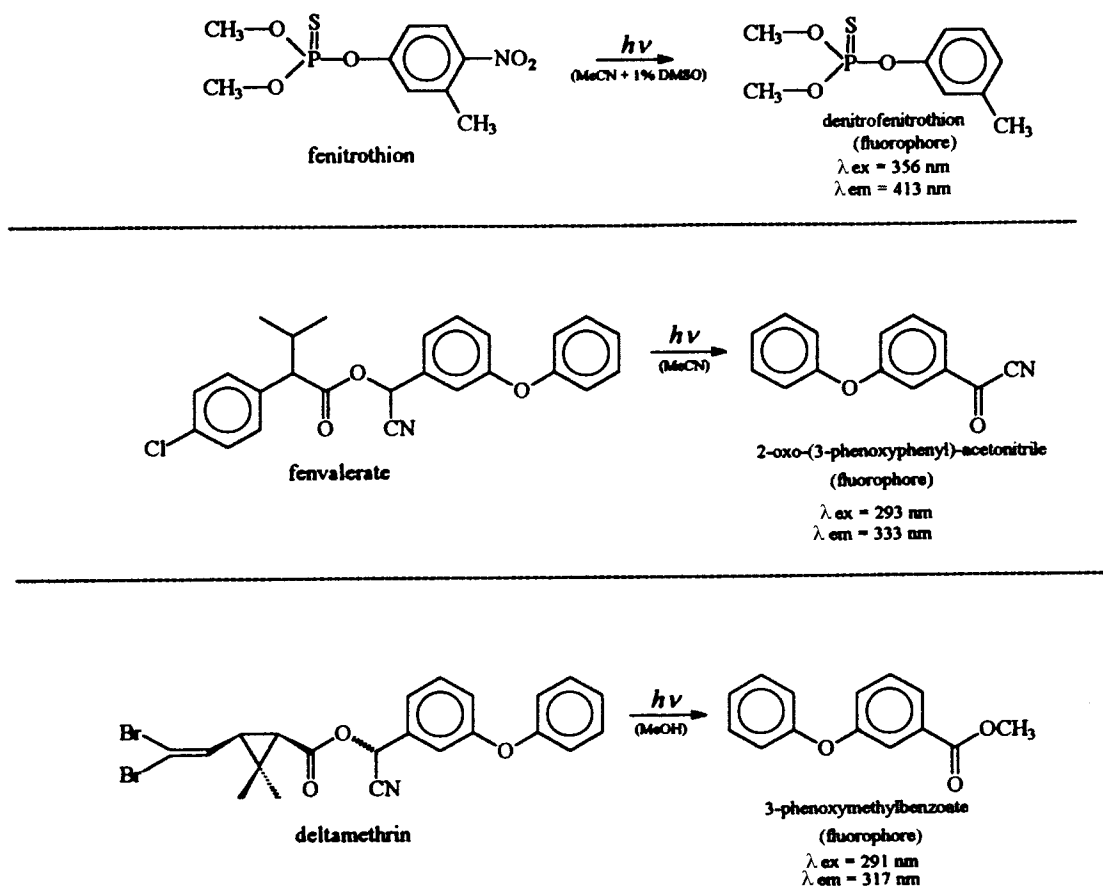


Fig. 7. Reaction scheme for the photolysis of fenitrothion (acetonitrile + 1% DMSO), fenvalerate (acetonitrile), and deltamethrin (methanol) into fluorescent derivatives, (Coly and Aaron, (unpublished)).

OPA/2-ME after photolytic degradation of 14 phenylurea herbicides. Linear dynamic ranges between 2 and 48 ng, with correlation coefficients larger than 0.99 were found. Herbicides with *N,N*-dimethyl group give a greater response than those with an *N*-methyl, *N*-methoxy moiety. The selectivity of the PIF method was compared with that of UV absorption detection in the case of herbicides extracted from carrots. This PIF labelling technique has the advantage of eliminating the need for the alkali reagent post-column pump shown in Fig. 6.

The applicability of the amine-generating photolysis reaction of pesticides OPA/2-ME derivatization was extended by Moye et al. [152,156–158] to a broad range of different

classes of nitrogenous pesticides including carbamates, carbamoyloximes, carbamothioic acids, dithiocarbamates, organophosphorus, sulfonyleureas, thiadiazolureas, thioureas, bipyridiniums, triazines, dinitrophenols, amides, acetamides and amines. Among the various compounds, carbamoyloximes produced the highest yield of methylamine [157]. PIF detection was used with [152,155–159] and without OPA/2-ME [152,156,157].

A post-column photolysis fluorescence detector, combining HPLC and PIF allowed these researchers to determine several classes of pesticides such as phenylcarbamates, phenylamides and phenylurea herbicides [157]. Linear calibration curves were obtained over two orders of magni-

tude, while LODs were in the low nanogram range. The same authors applied HPLC post-column photolysis and fluorogenic labelling with OPA/2-ME to the analysis of five pesticides including aldicarb sulfoxide, aldicarb, propoxur, thiram and neburon, in three fortified ground water samples, at 10–50 ng ml⁻¹ level, (Table 4). Using the same HPLC or FIA apparatus, Patel et al. [152,158] measured the PIF signal of several nitrogenous pesticides. Several solvent systems were evaluated as typical reversed-phase mobile phase, and the use of surfactants as photosensitizing agent was found to increase the PIF response of most pesticides. The LODs [152] ranged between 5 and 50 ng ml⁻¹, (Table 4). This laboratory-made post-column PIF detector gave satisfactory results with and without OPA/2-ME. Another interesting feature is that many pesticides that gave a good PIF response did not give any signal when the alkaline hydrolysis OPA/2-ME detection system was used [113]. However, aromatic carbamates were found to be rather slowly photolysed [21,180], thus leading to a low yield of methylamine photoproducts. Therefore, in the case of the latter compounds as well as non aromatic pesticides (i.e. aldicarb, aldicarb sulfone, methomyl...), the use of a sensitizing agent such as acetone [152,158] is recommended to enhance the photoconversion ratio.

PIF application with a normal-phase HPLC, on a cyanopropyl-bonded silica stainless steel column coupled on-line with post-column photoconversion and morin (V) complexation has been described by Stab et al. [160] for the determination of low nanogram amounts of triorganotin pesticides in surface water, sediments and soils. An advantage of this PIF complexation technique was the very short reaction times (Table 4). Another useful PIF approach based on complexation with morin and combined with TLC was also applied by Brown et al. [161] to screen phenyltin fungicides in potato extracts down to 0.01 ppm.

PIF detection coupled with FIA has been also reported by Aaron et al. [23,153] for the determination of several types of aromatic pesticides. The interest in this system for improving the sampling rate has been clearly demonstrated. Indeed, as many as 60 samples can be analysed per hour,

with satisfactory recoveries (88–109%) and LOD values ranging from lower nanogram to upper picogram levels (Table 4).

PIF has been used in stationary media, allowing fluorescent photoproducts to be obtained from four naturally non fluorescent aromatic insecticides viz., fenitrothion, fenvalerate, deltamethrin and diflubenzuron [149]. The PIF properties of these insecticides were investigated in various solvents. The LODs range from 0.7 to 33 ng ml⁻¹ according to the compound, with relative standard deviations of about 2.5%. The use of aqueous anionic micellar media improves the sensitivity of PIF in some cases [151]; i.e. the LODs of pyrethroid insecticides are 2.2–2.5 times lower in sodium dodecyl sulfate (SDS) micelles than in the common organic solvents. Eremin et al. [150] used the same procedure to determine several widely-used chlorophenoxyacid herbicides in spiked river water samples. The photolysis time is about 15 min. LODs vary from 36 to 179 ng ml⁻¹.

We can conclude that the usefulness of PIF for quantifying several classes of pesticides with good sensitivity and selectivity has been demonstrated. The combination of the PIF technique with dynamic systems (TLC, HPLC, FIA) is currently making progress and future developments of this method are expected.

4. Photosensitized fluorimetric (PSF) methods

When the analyte is weakly or non fluorescent and its irradiation also leads to weakly or non fluorescent photoproducts, it becomes necessary to photosensitize the photoreaction. In this case, anaerobic photoreduction reactions of sensitizers such as aromatic ketones by hydrogen atom-donating (HAD) compounds like aliphatic alcohols, aldehydes, saccharides, glycosides, amines and steroides are generally used [182–185]. The aromatic ketones employed as sensitizing reagent are quinone [182,183] and anthraquinone derivatives [19,184,185]. The mechanism of photosensitizing process is known to occur via the sensitizer triplet state [19]. An asset of the photosensitized fluorimetric (PSF) method is that it can be applied either to

the detection of HAD compounds [19,184] or to that of quinones themselves [182,183].

However, the use of this method in pesticide residue analysis has been very limited until now. Traore and Aaron [184] have sensitized the fluorescence of four naturally non fluorescent dinitroaniline herbicides, using anthraquinone. The PSF signal was found to be proportional to the herbicide concentration. The LODs ranged from 0.3 to 4 $\mu\text{g ml}^{-1}$, and the optimal irradiation times were short (<5 min), resulting in a decrease in analysis time. PSF can be considered a rapid and precise method for the analysis of dinitroaniline herbicides.

5. Conclusions and future trends

Obviously, pesticide residues from crops and environmental samples can be handled and analysed using a number of techniques. Pesticide analysis requires selective as well as sensitive detectors. At present, an important trend is to directly monitor the analytes by GC and/or HPLC with UV (including diode array) plus MS detection, since these tools generally yield the type of information required by the environmental and health legislations.

Due to its great sensitivity, fluorescence detection is very useful in pesticide analysis, but because of its selectivity, it cannot be the recommended method for pesticides screening or early-warning procedures. Nevertheless fluorescence detection is an important aid in environmental analysis, especially when monitoring specific analytes and, occasionally, a class of compounds such as carbamates and chlorophenoxy acids. Moreover, derivatized fluorescence and photochemically-induced fluorescence (PIF) are adaptable to various experimental conditions such as TLC, stationary liquid solutions, and flow systems, including HPLC and FIA. As a result of its procedural simplicity PIF seems to be more convenient and rapid than fluorogenic derivatization, for pesticides analysis. In addition, the inability of direct or indirect fluorimetric methods for determination of pesticides containing neither chromophores nor fluorophores should be overcome

in some specific cases by using photosensitized fluorimetry.

Other developments, including the use of organized media, (cyclodextrins, micelles, liposomic vesicles), special spectral techniques (synchronous, derivative spectra, variable angle scanning spectra,...), and statistical treatments of the spectral data such as partial least squares regression (PLS), should help fluorescence and photochemically-induced fluorescence to become valuable complementary approaches for environmental analysis of pesticides.

No doubt, because of these recent technological advances and their inherent sensitivity, selectivity, and versatility, fluorescence methods will continue in the future to find numerous applications in environmental complex matrices and to be widely employed for trace analysis in pesticide research.

References

- [1] J. Sherma, *Anal. Chem.* 67 (1995) 1R.
- [2] J. Sherma, *Anal. Chem.* 65 (1993) 40R.
- [3] *The Agrochemical Handbook* 3rd ed., The Royal Society of Chemistry, London, 1991.
- [4] D. Barcelo, *Analyst* 116 (1991) 681.
- [5] A.R. Newman, *Anal. Chem.* 61 (1989) 861A.
- [6] D.A. Hinckley, T.F. Bidleman, *Environ. Sci. Technol.* 23 (1989) 995.
- [7] W. Liao, T. Joe, W.G. Cusick, *J. Assoc. Off. Anal. Chem.* 74 (1991) 554.
- [8] A. Noble, *J. Chromatogr.* 642 (1993) 3.
- [9] J.F. Lawrence, R.W. Frei, *J. Chromatogr.* 98 (1974) 253.
- [10] R.W. Frei, W. Santi, *Z. Anal. Chem.* 277 (1975) 303.
- [11] J.F. Lawrence, *J. Chromatogr. Sci.* 17 (1979) 147.
- [12] J.-J. Aaron, *Anal. Proc.* 30 (1993) 72.
- [13] B.D. McGarvey, *J. Chromatogr.* 642 (1993) 89.
- [14] *Vogel's Textbook of Quantitative Chemical Analysis*, 5th ed., Longman Scientific and Technical, Burnt Mill, Harlow, UK, 1989, pp. 224–227.
- [15] J.F. Lawrence, R.W. Frei, in: *Chemical Derivatization in Liquid Chromatography*, Elsevier, Amsterdam, 1976.
- [16] I.S. Krull, W.R. Lacourse, *Reaction detection in liquid chromatography*, in: I.S. Krull (Ed.), Marcel Dekker, New York, 1986.
- [17] J.R. Poulsen, J.W. Birks, *Chemiluminescence and photochemical reaction detection in chromatography*, in: J.W. Birks (Ed.), VCH Publishers, New York, 1989, chap. 6.
- [18] J.J. Aaron, *Molecular Luminescence Spectroscopy: methods and applications*, in: S.G. Schulman (Ed.), Wiley, New York, 1993, pp. 85.

- [19] M.S. Gandelman, J.W. Birks, U.A.Th. Brinkman, R.W. Frei, *J. Chromatogr.* 282 (1983) 193.
- [20] I. Hornstein, *J. Agric. Food Chem.* 6 (1958) 32.
- [21] A. Coly, J.-J. Aaron, *Talanta* 41 (1994) 1475.
- [22] K. Hunter, *J. Chromatogr.* 321 (1985) 255.
- [23] A. Coly, J.-J. Aaron, *Analisis* 24 (1996) 107.
- [24] S.H. Lee, L.R. Field, *Anal. Chem.* 53 (1981) 467.
- [25] D.E. Mundy, A.F. Machin, *J. Chromatogr.* 234 (1982) 427.
- [26] K. Hunter, *J. Chromatogr.* 270 (1983) 267.
- [27] K. Hunter, *J. Chromatogr.* 270 (1983) 277.
- [28] W. Langseth, U. Nymoene, *Fresenius' Z. Anal. Chem.* 339 (1991) 249.
- [29] L.J. Felice, T. Chalermchaikit, M.J. Murphy, *J. Anal. Toxicol.* 15 (1991) 126.
- [30] T. Chalermchaikit, L.J. Felice, M.J. Murphy, *J. Anal. Toxicol.* 17 (1993) 56.
- [31] M.J. Kelly, J. Chambers, A.D. Mac Nicoll, *J. Chromatogr., Biomed. Appl.* 620 (1993) 105.
- [32] G.L. Brun, R.M. Mac Donald, *Bull. Environ. Contam. Toxicol.* 24 (1980) 886.
- [33] R.T. Krause, *J. Chromatogr.* 255 (1983) 497.
- [34] J. Rohand, J.L. Vilchez, L.F. Capitan-Vallvey, R. Avidad, A. Navalon, *Euroanalysis VIII*, Edinburgh, Scotland, UK, September 5–11, 1993, Book of Abstracts, PG7.
- [35] T. Cairns, E.G. Siegmund, G.M. Doose, W.S. Langham, K.S. Chiu, *Bull. Environ. Contam. Toxicol.* 32 (1984) 310.
- [36] T.D. Spittler, R.A. Marafioti, G.W. Helfman, R.A. Morse, *J. Chromatogr.* 352 (1986) 439.
- [37] R.J. Argauer, *Pesticide Analytical Methodology*, in: J. Harvey Jr., G. Zweig (Eds.), ACS symposium series 136, American Chemistry Society, Washington, DC, 1980, pp. 103–126.
- [38] R.T. Krause, E.M. August, *J. Assoc. Off. Anal. Chem.* 66 (1983) 234.
- [39] W. Schussler, *Chromatographia* 29 (1990) 24.
- [40] F. Garcia-Sanchez, C. Cruces-Blanco, *Mikrochim. Acta* 21 (1989) 49.
- [41] F. Garcia-Sanchez, C. Cruces-Blanco, *J. Agric. Food Chem.* 37 (1989) 937.
- [42] W.H. Newsome, P. Collins, *J. Chromatogr.* 472 (1989) 416.
- [43] R.J. Bushway, H.L. Hurst, J. Kugabalasooriar, L.B. Perkins, *J. Chromatogr.* 587 (1991) 321.
- [44] N. Motohashi, H. Nagashima, R. Meyer, *J. Liq. Chromatogr.* 14 (1991) 3591.
- [45] L.F. Garcia, J.-J. Aaron, *Mikrochim. Acta* 126 (1997) 289.
- [46] J.L. Vilchez, R. Avidad, J. Rohand, A. Navalon, L.F. Capitan-Vallvey, *Anal. Chim. Acta* 282 (1993) 445.
- [47] J.A. Jamieson, H.J. Duncan, *Potato Res.* 32 (1989) 123.
- [48] B. Wyhowsky de Bukanski, J.M. Degroodt, H. Beer-naert, *Z. Lebensm.-Unters. Forsch.* 193 (1991) 130.
- [49] C. De Ruiter, W.A. Minnaard, H. Lingeman, E.M. Kirk, U.A.T. Brinkman, R.R. Otten, *Int. J. Environ. Anal. Chem.* 43 (1991) 79.
- [50] D.M. Gilvydis, S.M. Walters, *J. Assoc. Off. Anal. Chem.* 73 (1990) 753.
- [51] C.F. Poole, S.K. Poole, *Anal. Chem.* 66 (1994) 27A.
- [52] M.B. Taccheo, M. De Paoli, C. Spessotto, *Pestic. Sci.* 25 (1989) 11.
- [53] E.R. Brouwer, S. Kofman, U.A.T. Brinkman, *J. Chromatogr., A* 103 (1995) 167.
- [54] E.R. Brouwer, E.A. Struys, J.J. Vreuls, U.A.T. Brinkman, *Fresenius' Z. Anal. Chem.* 350 (1994) 487.
- [55] H. Bagheri, E.R. Brouwer, R.T. Ghijssen, U.A.T. Brinkman, *J. Chromatogr.* 647 (1993) 121.
- [56] J. Slobodnik, S.J.F. Hoekstra-Oussoren, M.E. Lager, M. Honing, B.L.M. Van Baar, U.A.T. Brinkman, *Analyst* 121 (1996) 1327.
- [57] I. Feerer, D. Barcelo, *J. Chromatogr., A* 737 (1996) 93.
- [58] C. Molina, P. Grasso, E. Benfenati, D. Barcelo, *J. Chromatogr. A* 737 (1996) 47.
- [59] D. Barcelo, M. Honing, S. Chiron, *Applications of LC-MS in environmental chemistry*, *J. Chromatogr. Lib.* 59 (1996) 219–261.
- [60] S. Lacorte, D. Barcelo, *Anal. Chem.* 68 (1996) 2464.
- [61] S. Lacorte, D. Barcelo, *J. Chromatogr. A* 725 (1996) 85.
- [62] M. Honing, J. Riu, D. Barcelo, B.L.M. Van Baar, U.A.T. Brinkman, *J. Chromatogr. A* 733 (1996) 283.
- [63] S. Chiron, S. Papilloud, W. Haerdi, D. Barcelo, *Anal. Chem.* 67 (1995) 1637.
- [64] D. Barcelo, M.C. Hennion, *Anal. Chim. Acta* 318 (1995) 1.
- [65] C. Cruces-Blanco, F. Garcia-Sanchez, *Anal. Chem.* 56 (1984) 2035.
- [66] F. Garcia-Sanchez, A. Navas, M. Santiago, *Anal. Chim. Acta* 167 (1985) 217.
- [67] F. Garcia-Sanchez, C. Cruces-Blanco, A. Heredia-Bayona, *Talanta* 34 (1987) 345.
- [68] F. Garcia-Sanchez, M. Hernandez-Lopez, J.C. Marquez-Gomez, *Spectrochim. Acta* 43 (1987) 101.
- [69] F. Garcia-Sanchez, M. Cedazo, J. Lovillo, A. Navas-Diaz, *Talanta* 43 (1996) 1327.
- [70] S. Li, W.C. Purdy, *Chem. Rev.* 92 (1992) 1457.
- [71] R. Zana, *Surfactant Sci. Ser.* 22 (1987) 241.
- [72] M.J. Gonzalez-Alvarez, M.E. Diaz-Garcia, A. Sanz-Medel, *Anal. Chim. Acta* 234 (1990) 181.
- [73] M. De la Guardia, M.L. Hernandez, S. Sancenon, J.L. Carrion, *Colloids Surf.* 48 (1990) 57.
- [74] A. Berthod, J.M. Asensio, J.J. Laserna, *J. Liq. Chromatogr.* 12 (1989) 2621.
- [75] J.C. Marquez, M. Hernandez, F. Garcia-Sanchez, *Analyst* 115 (1990) 1003.
- [76] T. Suzuki, S. Watanabe, *J. Chromatogr.* 541 (1991) 359.
- [77] S.V. Prabhu, R.J. Varsolona, T.A. Wehner, R.S. Egan, P.C. Tway, *J. Agric. Food Chem.* 40 (1992) 622.
- [78] J.V. Sancho, F.J. Lopez, F. Hernandez, E.A. Hogendoorn, P. Van Zoonen, *J. Chromatogr.* 678 (1994) 59.
- [79] Y. Arakawa, O. Wada, M. Manabe, *Anal. Chem.* 55 (1983) 1901.
- [80] R.W. Frei, J.F. Lawrence, P.E. Belliveau, *Z. Anal. Chem.* 254 (1971) 271.

- [81] J.-J. Aaron, M. Some, *Analisis* 10 (1982) 481.
- [82] F. Garcia-Sanchez, A. Aguilar-Gallardo, *Analyst* 117 (1992) 195.
- [83] F. Garcia-Sanchez, M. Hernandez-Lopez, A. Garcia-Pareja, *Anal. Chim. Acta* 255 (1991) 311.
- [84] G.L. Brun, V. Mallet, *J. Chromatogr.* 80 (1973) 117.
- [85] V. Mallet, D.P. Surette, *J. Chromatogr.* 95 (1974) 243.
- [86] D.P. Surette, V. Mallet, *J. Chromatogr.* 107 (1975) 141.
- [87] V. Mallet, R.W. Frei, *J. Chromatogr.* 56 (1971) 69.
- [88] R.W. Frei, V. Mallet, C. Pothier, *J. Chromatogr.* 59 (1971) 135.
- [89] T. Yu, Y. Arakawa, *J. Chromatogr.* 258 (1983) 189.
- [90] W. Langseth, *Talanta* 31 (1984) 975.
- [91] W. Langseth, *J. Chromatogr.* 315 (1984) 351.
- [92] W.R. Blair, E.J. Parks, G.J. Olson, F.E. Brinckman, M.C. Valeiras-Price, J.M. Bellama, *J. Chromatogr.* 410 (1987) 383.
- [93] L. Ebdon, J.I. Garcia-Alonso, *Analyst* 112 (1987) 1551.
- [94] T.F. Bidleman, B. Nowland, R.W. Frei, *Anal. Chim. Acta* 60 (1972) 13.
- [95] R.W. Frei, J.F. Lawrence, *J. Chromatogr.* 61 (1971) 174.
- [96] J.F. Lawrence, R.W. Frei, *Int. J. Environ. Anal. Chem.* 1 (1972) 317.
- [97] H.A. Moye, S.J. Scherer, P.A. St. John, *Anal. Lett.* 10 (1977) 1049.
- [98] R.W. Frei, J.F. Lawrence, *Methods in residue analysis*, in: A.S. Tahori (Ed.), *Pesticides Chemistry*, vol. 4, Gordon and Breach, New York, 1971, 193.
- [99] R.W. Frei, J.F. Lawrence, D.S. Le Gay, *Analyst* (London) 98 (1973) 9.
- [100] J.F. Lawrence, G.W. Laver, *J. Assoc. Off. Anal. Chem.* 57 (1974) 1022.
- [101] J.F. Lawrence, C. Renault, R.W. Frei, *J. Chromatogr.* 121 (1976) 343.
- [102] J.F. Lawrence, G.W. Laver, *J. Chromatogr.* 100 (1974) 175.
- [103] R.W. Frei, J.F. Lawrence, J. Hope, R.M. Cassidy, *J. Chromatogr. Sci.* 12 (1974) 40.
- [104] J.F. Lawrence, R. Leduc, *J. Chromatogr.* 152 (1978) 507.
- [105] F. Garcia-Sanchez, C. Cruces-Blanco, *Analyst* 116 (1991) 851.
- [106] J.F. Lawrence, R.W. Frei, *Anal. Chem.* 44 (1972) 2046.
- [107] M. Weigele, S.L. De Bernardo, J.P. Teng, W. Leimgruber, *J. Am. Chem. Soc.* 94 (1972) 5927.
- [108] S. Udenfriend, S. Stein, P. Bohlen, W. Dairman, W. Leimgruber, M. Weigele, *Science* 178 (1972) 871.
- [109] J.A.F. De Silva, N. Strojny, *Anal. Chem.* 47 (1975) 714.
- [110] F. Garcia-Sanchez, C. Cruces-Blanco, *Anal. Chem.* 58 (1986) 73.
- [111] F. Garcia-Sanchez, A. Aguilar-Gallardo, C. Cruces-Blanco, *Talanta* 39 (1992) 1195.
- [112] J.G. Zakrevsky, V.N. Mallet, *J. Chromatogr.* 132 (1977) 315.
- [113] R.T. Krause, *J. Chromatogr.* 185 (1979) 615.
- [114] G.L. Muth, F. Erro, *Bull. Environ. Contam. Toxicol.* 24 (1980) 759.
- [115] A. Dekker, N.W.H. Houx, *J. Environ. Sci. Health* 18 (1983) 379.
- [116] L.K. She, U.A.T. Brinkman, R.W. Frei, *Anal. Lett.* 17 (1984) 915.
- [117] K.M. Hill, R.H. Hollowell, L.A. Dal Cortivo, *Anal. Chem.* 56 (1984) 2465.
- [118] K.C. Ting, P.K. Kho, A.S. Musselman, G.A. Root, G.R. Tichelar, *Bull. Environ. Contam. Toxicol.* 33 (1984) 538.
- [119] R.T. Krause, *J. Assoc. Off. Anal. Chem.* 68 (1985) 726.
- [120] R.T. Krause, *J. Assoc. Off. Anal. Chem.* 68 (1985) 734.
- [121] N. Aharonson, L. Muszkat, M. Klein, *Phytoparasitica* 13 (1985) 129.
- [122] K.C. Ting, P.K. Kho, *Bull. Environ. Contam. Toxicol.* 37 (1986) 192.
- [123] D. Chaput, *J. Assoc. Off. Anal. Chem.* 69 (1986) 985.
- [124] A. De Kok, M. Hiemstra, C.P. Vreeker, *Chromatographia* 24 (1987) 469.
- [125] C.E. Goewie, E.A. Hogendoorn, *J. Chromatogr.* 404 (1987) 352.
- [126] D. Chaput, *J. Assoc. Off. Anal. Chem.* 71 (1988) 542.
- [127] S. Lesage, *LC-GC* 7 (1989) 268.
- [128] M.S. Ali, *J. Assoc. Off. Anal. Chem.* 72 (1989) 586.
- [129] B.D. Mc Garvey, *J. Chromatogr.* 481 (1989) 445.
- [130] A. De Kok, M. Hiemstra, C.P. Vreeker, *J. Chromatogr.* 507 (1990) 459.
- [131] K.W. Edgell, L.A. Biederman, J.E. Longbottom, *J. Assoc. Off. Anal. Chem.* 74 (1991) 309.
- [132] W. Blass, *Fresenius' Z. Anal. Chem.* 339 (1991) 340.
- [133] M.W. Reeve, L.P. O'Connell, S. Bissell, J. Ross, *Bull. Environ. Contam. Toxicol.* 49 (1992) 105.
- [134] A. De Kok, M. Hiemstra, U.A.T. Brinkman, *J. Chromatogr.* 623 (1992) 265.
- [135] K.M.S. Sundaram, J. Curry, *J. Chromatogr.* 672 (1994) 117.
- [136] P. Kucera, H. Umagat, *J. Chromatogr.* 255 (1983) 563.
- [137] S.S. Simons Jr., D.F. Johnson, *J. Am. Chem. Soc.* 98 (1976) 7098.
- [138] R.T. Krause, *J. Chromatogr. Sci.* 16 (1978) 281.
- [139] R.T. Krause, *J. Assoc. Off. Anal. Chem.* 63 (1980) 1114.
- [140] H. Engelhardt, B. Lillig, *Chromatographia* 21 (1986) 136.
- [141] U.S. Environmental Protection Agency; EPA/600/4-85/054; U.S. GPO: Washington, DC, 1985; method 531.
- [142] L. Nondek, R.W. Frei, U.A.T. Brinkman, *J. Chromatogr.* 282 (1983) 141.
- [143] L. Nondek, U.A.T. Brinkman, R.W. Frei, *Anal. Chem.* 55 (1983) 1466.
- [144] H. Jansen, U.A.T. Brinkman, R.W. Frei, *Chromatographia* 20 (1985) 453.
- [145] B.D. McGarvey, Th.H.A. Olthof, J.L. Townshend, *J. Agric. Food Chem.* 38 (1990) 1608.
- [146] S.C. Stafford, W. Lin, *J. Agric. Food Chem.* 40 (1992) 1026.
- [147] L.G.M.Th. Tuinstra, P.G.M. Kienhuis, *Chromatographia* 24 (1987) 696.

- [148] F. Garcia-Sanchez, C. Cruces-Blanco, A.L. Ramos-Rubio, M. Hernandez-Lopez, J.C. Marquez-Gomez, C. Carnero, *Anal. Chim. Acta* 205 (1988) 149.
- [149] A. Coly, J.-J. Aaron, *Analyst* 119 (1994) 1205.
- [150] S. Eremin, B. Laassis, J.-J. Aaron, *Talanta* 43 (1996) 295.
- [151] J.-J. Aaron, A. Coly, *Analyst* 121 (1996) 1545.
- [152] B.M. Patel, H.A. Moye, R. Weinberger, *Talanta* 38 (1991) 913.
- [153] L.F. Garcia, S. Eremin, J.-J. Aaron, *Anal. Lett.* 29 (1996) 1447.
- [154] C.E. Werkhoven-Goewie, W.M. Boon, A.J.J. Praat, R.W. Frei, U.A.T. Brinkman, C.J. Little, *Chromatographia* 16 (1982) 53.
- [155] R.G. Luchtefeld, *J. Chromatogr. Sci.* 23 (1985) 516.
- [156] C.J. Miles, H.A. Moye, *Chromatographia* 24 (1987) 628.
- [157] C.J. Miles, H.A. Moye, *Anal. Chem.* 60 (1988) 220.
- [158] B.M. Patel, H.A. Moye, R. Weinberger, *J. Agric. Food Chem.* 38 (1990) 126.
- [159] C.J. Miles, *J. Chromatogr.* 592 (1992) 283.
- [160] J.A. Stab, M.J.M. Rozing, B. Van Hattum, W.P. Cofino, U.A.T. Brinkman, *J. Chromatogr.* 609 (1992) 195.
- [161] K.K. Brown, P. Tomboulian, S.M. Walters, *J. Res. Natl. Bur. Stand. (USA)* 93 (1988) 301.
- [162] A. Coly, Ph.D. Thesis, Université C. A. Diop, Dakar, Sénégal, 1994.
- [163] M. Sanchez Peña, A. Munoz de la Peña, F. Salinas, M.C. Mahedero, J.-J. Aaron, *Analyst* 119 (1994) 1177.
- [164] J.R. Plimmer, *Residue Rev.* 33 (1971) 47.
- [165] D.G. Crosby, *Herbicides: chemistry, degradation and mode of action*, in: P.C. Kearney and D.D. Kaufman, (Eds.), Marcel Dekker, New York, 1976, vol. 2, 835.
- [166] L.L. Lamparski, R.H. Stehl, R.L. Johnson, *J. Environ. Sci. Technol.* 14 (1980) 196.
- [167] K. Omura, T. Matsuura, *Tetrahedron* 27 (1971) 3101.
- [168] H. Parlar, P.G.W. Steven, R. Bauman, F. Korte, *Z. Naturforsch.* 34 (1979) 113.
- [169] D. Kotzias, F. Korte, *Ecotoxicol. Environ. Saf.* 5 (1981) 503.
- [170] P.H. Mazzocchi, M.P. Rao, *J. Agric. Food Chem.* 20 (1972) 957.
- [171] L.O. Ruzo, R.L. Holmstead, J.E. Casida, *Tetrahedron Lett.* 35 (1976) 3045.
- [172] L.O. Ruzo, R.L. Holmstead, J.E. Casida, *J. Agric. Food Chem.* 25 (1977) 1385.
- [173] L.O. Ruzo, J.E. Casida, *J. Chem. Soc. Perkin Trans. I*, (1980) 728.
- [174] L.O. Ruzo, J.E. Casida, *J. Agric. Food Chem.* 29 (1981) 702.
- [175] N. Mikami, N. Takahashi, K. Hayashi, J. Miyamoto, *J. Pest. Sci.* 5 (1980) 225.
- [176] H. Ohkawa, N. Mikami, J. Miyamoto, *Agric. Biol. Chem.* 38 (1974) 2247.
- [177] R. Greenhalgh, W.D. Marshall, *J. Agric. Food Chem.* 24 (1976) 708.
- [178] N. Mikami, K. Imanishi, H. Yamada, J. Miyamoto, *J. Pest. Sci.* 10 (1985) 263.
- [179] G. Durand, D. Barcelo, J. Albaiges, M. Mansour, *Chromatographia* 29 (1990) 120.
- [180] G. Durand, N. De Bertrand, D. Barcelo, *J. Chromatogr.* 554 (1991) 233.
- [181] R.D. Ross, D.G. Crosby, *J. Agric. Food Chem.* 21 (1973) 335.
- [182] J.R. Poulsen, J.W. Birks, *Anal. Chem.* 61 (1989) 2267.
- [183] M.F. Lefevre, R.W. Frei, A.H.M.T. Scholten, U.A.T. Brinkman, *Chromatographia* 15 (1982) 459.
- [184] S. Traore, J.-J. Aaron, *Anal. Lett.* 20 (1987) 1995.
- [185] M.S. Gandelman, J.W. Birks, *J. Chromatogr.* 242 (1982) 21.

Simultaneous determination of iron and zinc by pH gradient construction in a flow-injection system¹

Shulin Zhao ^{a,*}, Xinquan Xia ^a, Gang Yu ^b, Bo Yang ^a

^a Department of Polymer Chemical Engineering, Shenyang Institute of Chemical Technology, Shenyang, China

^b Department of Chemical Engineering, Shenyang Polytechnic University, Shenyang, China

Received 2 January 1997; received in revised form 24 July 1997; accepted 29 July 1997

Abstract

A flow-injection method for the simultaneous determination of iron and zinc in the human hair with 2-(5-bromo-2-pyridylazo)-5-diethylaminophenol (5-Br-PADAP) using a pH gradient technique has been developed. The linear range for the determination of iron is 0.1 ~ 1.8 $\mu\text{g ml}^{-1}$ and for zinc is 0.2 ~ 5.0 $\mu\text{g ml}^{-1}$. About 20 ~ 30 samples can be determined in 1 h. The proposed method is simple, rapid and accurate. It has been applied to the simultaneous determination of trace amounts of iron and zinc in the human hair with satisfactory results. © 1998 Elsevier Science B.V. All rights reserved.

Keywords: Iron; Zinc; Simultaneous determination; Flow injection

1. Introduction

Flow injection analysis (FIA) is a simple, rapid, precise, highly reproducible technique which has advantages of exhausting little reagent and can be easily automated. It has recently, developed very quickly. Owing to the need for simultaneous fast monitor and control of multicomponents in clinical, environmental, industrial in-line analyses and other fields, much attention has been paid to simultaneous determination of multicomponents by FIA [1–8]. A pH gradient technique, constructed from a flow-injection system, is that ac-

ording to the different pH value of the reaction of chromogenic reagent with different metallic ions, simultaneous determination of multicomponents is realized by making different metallic ions encolor at the same time in pH gradient between sample plug and carrier. By this method, D. Betteridge et al. reported simultaneous determination of lead and vanadium [9]; nickel and copper [10]. S. Baban, reported simultaneous determination of bismuth, thorium and copper [11] and R. Liu et al. of copper and zinc [7]. But simultaneous determination of iron and zinc has not been reported.

This paper proposes a pH gradient technique in the FIA system for simultaneous determination of iron and zinc by using 2-(5-bromo-2-pyridylazo)-5-diethylaminophenol (5-Br-PADAP) as a chromogenic reagent with satisfactory results.

* Corresponding author. Fax: +86 24 5850082.

¹ Project supported by the Natural Sciences Foundation of Liaoning Province, China.

5-Br-PADAP is an analytical reagent with a high degree of sensitivity [12], it reacts with iron at pH 3 ~ 8 and with zinc at pH 5 ~ 8, the absorption maximum wavelength of the two complexes are the same and the determination conditions were identical. When iron and zinc were determined by using the pH gradient technique, a large volume of pH 3.0 sample solution was injected into the pH 7.5 carrier stream. A constant pH gradient might be formed between the sample plug and the carrier in a flowing process of the sample solution with the carrier. Because the pH value at the center of the sample band was 3.0, only the iron complex could be formed, while the pH value at the two ends of the sample band was 7.5 because the dispersion of the carrier and the two complexes of iron and zinc could be produced simultaneously. Thus, from the absorbance signals at the center and at the two ends of the sample band, iron and zinc were quantified, respectively and simultaneous determination of them was realized.

2. Experimental

2.1. Reagents

Analytical-reagent grade chemicals and deionized water were used throughout.

2.1.1. An iron (III) stock solution

An iron (III) stock solution (1.000 mg ml^{-1}) was prepared by dissolving 1.0000 g of pure iron (99.99%) in 15 ml of 8 M nitric acid and diluted to volume in a 1000-ml calibrated flask with water. Working solutions were prepared by suitable dilution of the stock solution with masking agent solution.

2.1.2. A zinc stock solution

A zinc stock solution (1.000 mg ml^{-1}) was prepared by dissolving 1.0000 g of pure zinc (99.99%) in 15 ml of 6 M hydrochloric acid and diluted to volume in a 1000-ml calibrated flask with water. Working solutions were prepared by suitable dilution of the stock solution with masking agent solution.

2.1.3. Mixed chromogenic reagent solution

80 ml of $5 \times 10^{-4} \text{ M}$ 5-Br-PADAP ethanol solution and 120 ml of 1% emulsifier OP solution were mixed and the pH value of the solution was adjusted to 3.0.

2.1.4. Carrier

A total of 6.8 g of potassium dihydrogen phosphate and 1.6 g of sodium hydroxide were dissolved in 900 ml of water. The pH of the solution was adjusted to 7.5 and the solution diluted to 1000 ml.

2.1.5. Masking agent

Ten g of thiourea and 2.0 g of ascorbic acid were dissolved in 1000 ml of water and the pH value of the solution was adjusted to 3.0.

2.2. Apparatus

The flow-injection manifold used is shown in Fig. 1. The peristaltic pump and injection valve were supplied by Shenyang Zhaofa Analytical Instruments Research Institute. A Model 722 spectrophotometer (Shanghai Third Analytical Instruments Factory) with a flow cell was used as the detector. Absorbance signals were recorded with a Model WXT-204 Table-type equilibrium automatic recorder (Shanghai Dahua Instruments Factory). A Model pHS-3 pH meter (Shanghai Second Analytical Instruments Factory) was used to measure the pH values of the solutions.

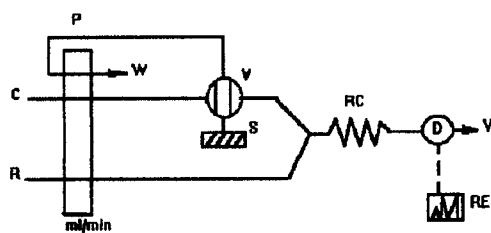


Fig. 1. Schematic diagram of FI system. P, peristaltic pump; V, injection valve; D, spectrophotometer; RE, recorder; C, carrier; S, sample; R, chromogenic reagent; RC, reaction coil; W, waste.

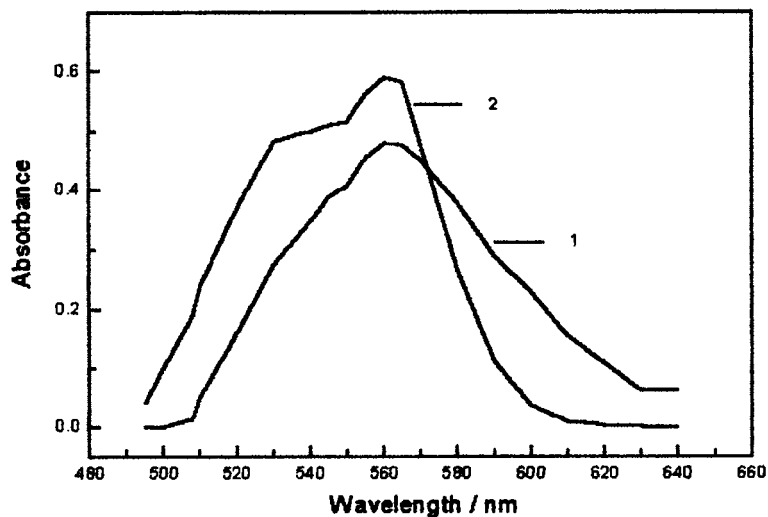


Fig. 2. Absorption spectra of iron and zinc complexes. 1. iron-5-Br-PADAP; 2. zinc-5-Br-PADAP.

2.3. Procedure

The flow injection system is shown in Fig. 1. Teflon pipes with an interior diameter of 0.7 mm were used as reaction tubes and linking tubes. The pH of the sample solutions was adjusted to 3.0 with the masking agent and the main parameters of the adjusted apparatus were: pump rate, 4.2 ml min⁻¹; the volume of the sample cycle of taking sample valve, 1000 μ l; the interval of taking sample, every 80 s; injecting time, every 60 s. Then the sample solutions were injected into the carrier stream and the absorbance was measured in the flow cell at 560 nm. The transient signal was recorded as a peak, the height of which was proportional to the iron and zinc concentration in the sample. The first and third peaks correspond to the sum of iron and zinc present, and the second to iron only.

3. Results and discussion

3.1. Measurement wavelength

In the presence of nonionic surfactant OP, 5-Br-PADAP reacts with iron and zinc to form red

soluble complexes. The absorption spectra of complexes are shown in Fig. 2. The absorption maximum of two complexes was located at 560 nm. Therefore, a wavelength of 560 nm was chosen for the determination.

3.2. Effect of reaction acidity

The effect of acidity on the absorbance of the complexes was studied. The results obtained are shown in Fig. 3. 5-Br-PADAP reacts with iron at pH 3 ~ 8 and with zinc at pH 5 ~ 8. Based on this characteristic, when a large volume of pH 3.0 sample solution was injected into pH 7.5 carrier, the transient signal shown in Fig. 4 could be obtained according to the principle of pH gradient. Only iron complex could be formed because the pH value was 3.0 at the center of sample plug, so the absorbance signal of the zinc complex went back to the basic line and only the absorbance signal of the iron complex appeared at the center of the mixed signals. But at the two ends of the mixed signals the absorbance was the sum of iron and zinc complexes because the pH value was 7.5 as a result of the dispersion and buffering of the carrier.

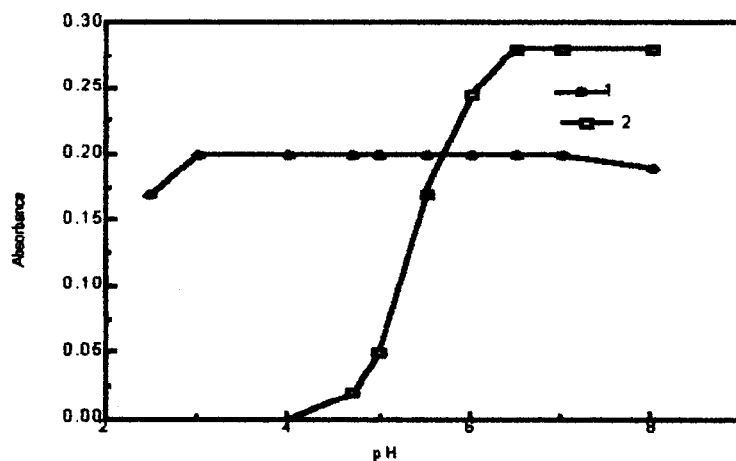


Fig. 3. Effect of pH on the absorbance. 1. iron complex; 2. zinc complex.

3.3. Effect of concentration of reagents

The experiment results showed that both complexes had a higher and more suitable absorbance in the reagent solution containing $1.75 \times 10^{-4} \sim 2.75 \times 10^{-4} \text{ mol l}^{-1}$ of 5-Br-PADAP and 0.4 ~ 0.8% of emulsifier OP. So the optimum concentrations of 5-Br-PADAP and OP were selected as $2.0 \times 10^{-4} \text{ mol l}^{-1}$ and 0.6% in the experiment, respectively.

In this system, thiourea was added to prevent the interference of copper. Ascorbic acid was added to reduce Fe^{3+} to Fe^{2+} and to increase the sensitivity of the iron determination. Neither of them affected the measurement in the masking reagent solution which contained < 1% thiourea and < 0.25% ascorbic acid. So the concentrations of the ascorbic acid and thiourea in the masking reagent solution were chosen as 0.2 and 1%, respectively.

3.4. Effect of flow rate of carrier and reagent solution

Under the conditions where both carrier rate and reagent solutions rate were the same, there was no effect on the absorbance for zinc over the range $2.0 \sim 5.4 \text{ ml min}^{-1}$, while the sensitivity to iron decreased with the increasing of the flow rate, but the change was minimal between 4.0 and 5.4

ml min^{-1} . Therefore, the flow rate of carrier and chromogenic reagent solution was selected as 4.2 ml min^{-1} for this experiment.

3.5. Selection of the reaction coil length

The effect of the reaction coil length was investigated in the range 100–250 cm. The experiment results showed that when the reaction coil length was changed from 180 to 250 cm, using a 0.7 mm interior diameter for the reaction coils, there was a maximum and agreeable sensitivity for both iron and zinc. Hence a coil length of 200 cm was chosen as optimal.

3.6. Sample injection volume

The sample injection volume is a key to realizing simultaneous determination of both iron and zinc. In order to ensure that the second peak corresponds only to iron, a pH gradient must be formed in the sample plug and the carrier. The influence of the sample injection volume on the determination was studied by injecting zinc solution into the carrier. The results indicated that two separate peaks corresponding to zinc could be observed when the sample injection volume was larger than 0.8 ml. Therefore, 1.0 ml of sample injection volume was employed in the experiment.

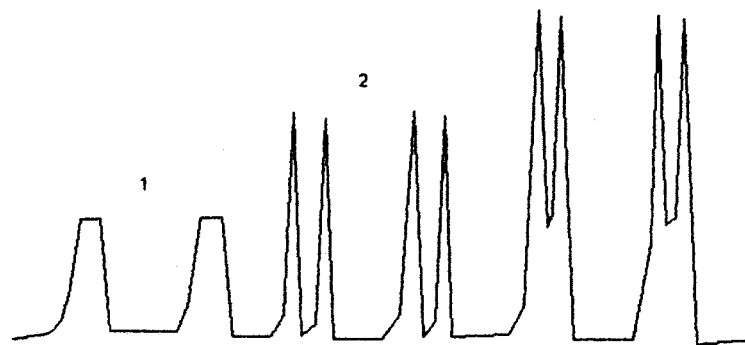


Fig. 4. Typical recording of absorbance. 1. iron only; 2. zinc only; 3. the mixture.

3.7. Calibration graph

Under the condition described, a mixed standard solution of iron and zinc was measured. The calibration graph was linear in the range $0.1 \sim 1.8 \mu\text{g ml}^{-1}$ for iron with the regression equation $A = 0.5277C - 0.0082$ ($r = 0.9994$), and $0.24 \sim 4.4 \mu\text{g ml}^{-1}$ for zinc with the regression equation $A = 0.2272C - 0.0048$ ($r = 0.9998$). Where A is the absorbance, C is the content of iron or zinc in $\mu\text{g ml}^{-1}$ and r is the correlation coefficient.

3.8. Effect of diverse ions

The effect of interference from diverse ions was investigated in a 25 ml solution containing $15 \mu\text{g}$ of iron and $50 \mu\text{g}$ of zinc. There was no interference from $1500 \mu\text{g}$ of Mg^{2+} , $1000 \mu\text{g}$ of Ca^{2+} , $300 \mu\text{g}$ of Mo(VI) , $150 \mu\text{g}$ of W(VI) , $100 \mu\text{g}$ of Mn^{2+} , Cr(VI) , Cu^{2+} , $50 \mu\text{g}$ of Sr^{2+} , $30 \mu\text{g}$ of Pb^{2+} , Ba^{2+} , Bi^{3+} , $20 \mu\text{g}$ of Cd^{2+} , $15 \mu\text{g}$ of Al^{3+} , $10 \mu\text{g}$ of Ni^{2+} , Co^{2+} , $5 \mu\text{g}$ of Ti(IV) . The above results showed that there was no effect on the determination of iron and zinc in the presence of diverse ions below the physiological content in human hair.

4. Determination of mixed standard solutions

Mixed standard solutions of different mass ratios of zinc and iron between 1:2 and 9:1 were measured. Recovery of both zinc and iron for

these solutions is given in Table 1. A recovery of between 95–101% for zinc and iron can be obtained.

5. Determination of iron and zinc in human hair

A 2.0 g sample of rinsed, dried hair was placed in a 100-ml flask, 15 ml of nitric acid and nitrate were added at low temperature. After the solution turned clear, 5 ml of perchloric acid was added. The temperature of the solution was raised until white fumes of perchloric acid were produced and the solution color changed from yellow to colorless. The solution was then evaporated to nearly dry. After it was cooled, 40 ml of water was added and the solution was then heated to dissolve the salt. The pH value was adjusted to 3.0. The solution was then transferred into a 50-ml calibrated flask and diluted to the mark with water. A portion of the sample solution was

Table 1
The determination of mixed standard solution ($\mu\text{g ml}^{-1}$)

Sample	Added		Found		Recovery (%)	
	Zn	Fe	Zn	Fe	Zn	Fe
1	0.80	1.60	0.79	1.58	98.8	98.8
2	1.60	1.20	1.60	1.21	100.0	100.8
3	2.60	0.80	2.60	0.79	100.0	98.8
4	3.60	0.60	3.63	0.58	100.8	96.7
5	3.60	0.40	3.63	0.38	100.8	95.0

Table 2
Results for the determination of zinc and iron in hair ($\mu\text{g g}^{-1}$)

Sample	AAS method		Proposed method	
	Fe	Zn	Fe	Zn
1	49.0	136.5	50.0 (0.8)*	134.4 (1.2)*
2	51.5	168.5	51.3 (1.1)	170.5 (0.9)
3	43.5	128.1	41.6 (1.5)	125.6 (0.8)
4	58.7	210.0	56.3 (1.7)	210.9 (1.6)
5	43.8	145.0	44.5 (1.7)	142.9 (2.2)

^a Values in parentheses are the relative S.D. of five determinations.

pipetted into a 25-ml calibrated flask and diluted to the mark with masking agent solution. The operation was carried out by the proposed method and the results are shown in Table 2.

6. Conclusions

This paper proposes a new method for simultaneous determination of iron and zinc with a single detector by a pH gradient technique in a flow injection system. The results obtained by the pro-

posed method, when applied to the hair, were in agreement with those obtained by atomic absorption spectrophotometry. The proposed method is a rapid, simple, precise, highly sensitive and highly selective technique.

References

- [1] M.D. Lague de Castro, M. Valcarcel, *Analyst* 109 (1984) 413.
- [2] M. Valcarcel, M.D. Luque de Castro, F. Lazaro, A. Rios, *Anal. Chim. Acta* 216 (1988) 275.
- [3] S. Kozuka, K. Saito, K. Oguma, R. Kuroda, *Analyst* 115 (1990) 431.
- [4] T. Yamana, E. Goto, *Talanta* 38 (1991) 139.
- [5] M.G.M. Andrade, S.L.C. Ferreiar, B.F. Santos, A.C.S. Costa, *Talanta* 39 (1992) 1229.
- [6] R. Liu, D. Liu, A. Sun, G. Liu, *Analyst* 120 (1995) 565.
- [7] R. Liu, D. Liu, A. Sun, G. Liu, *Analyst* 120 (1995) 569.
- [8] N. Teshima, K. Ayukawa, T. Kawashima, *Talanta* 43 (1996) 1755.
- [9] D. Bettridge, B. Fields, *Anal. Chem.* 50 (1978) 654.
- [10] D. Betteridge, B. Fields, *Anal. Chim. Acta* 132 (1981) 139.
- [11] S. Baban, *Anal. Proc* 17 (1980) 535.
- [12] W. Fusheng, Z. Yudan, S. Naikui, *Huaxue Shiji* 2 (1980) 52.

Development of flow-injection liposome immunoanalysis (FILIA) for imazethapyr

Myoyong Lee ^{a,*}, Richard A. Durst ^a, Rosie B. Wong ^b

^a Department of Food Science and Technology, Cornell University, Geneva, NY 14456-0462, USA

^b American Cyanamid Agricultural Research Center, Princeton, NJ 08543-0400, USA

Received 12 June 1997; received in revised form 19 August 1997; accepted 20 August 1997

Abstract

Imazethapyr is the herbicide developed for use in leguminous crops. In this study, flow-injection liposome immunoanalysis (FILIA) has been shown to be capable of measuring imazethapyr in a buffered solution with a detection limit of 0.1 ppb through the optimization process. Protein A coated glass beads covalently conjugated with antibody were contained in a glass column, and this column was used as an immunoreactor. Liposomes which encapsulated a fluorescent dye, sulforhodamine B (SRB) or carboxyfluorescein (CF), generated the analytical signal. By loading larger volumes of sample onto the column, it was shown that the detection limit could be lowered. Liposomes containing carboxyfluorescein gave more sensitive response and a lower detection limit than those with sulforhodamine B. Also, improved response was obtained by using a smaller flow cell in the fluorescence detector due to the reduced dilution effect. © 1998 Elsevier Science B.V. All rights reserved.

Keywords: Flow-injection liposome immunoanalysis (FILIA); Imazethapyr; Liposomes; Immunoassay; Herbicide

1. Introduction

Imazethapyr [5-ethyl-2-(4-isopropyl-4-methyl-5-oxo-2-imidazolin-2-yl)nicotinic acid] belongs to the imidazolinone class of herbicides and is the active ingredient of PURSUIT^{®1} herbicide. The structure of imazethapyr is shown in Fig. 1. Imazethapyr is currently approved for soybean

[*Glycine max* (L.) Merr] and all edible legumes [1]. The herbicidal activity is from inhibiting acetoxy acid synthase, the feedback enzyme in the biosynthesis of branched chain amino acids [2,3]. Mammals, birds, and fish do not have this enzyme and are known to be unaffected by imazethapyr. In general, tolerant species can convert imazethapyr to a more polar and less phytotoxic metabolite by hydroxylation of the ethyl substituent on the pyridine ring [4,5]. This hydroxylated metabolite has herbicidal activity, although it is less active than the imazethapyr. However, in soybean, imazethapyr is metabolized to nontoxic form by the conjugation of the hydroxylated metabolite to glucose.

* Corresponding author. Present address: Department of Chemistry, Tufts University, Medford, MA 02155, USA; tel.: +1 617 6273675; fax: +1 617 6275773; e-mail: mlee5@emerald.tufts.edu

¹ Registered trademark of American Cyanamid

The conventional analytical techniques for monitoring agrochemicals are time-consuming and expensive. The demand for a rapid and inexpensive analytical method has increased. As an alternative or complement to classical analytical methods, immunoassays have gained the attention of many researchers. Recently, many papers are published which are about the application of immunochemical methods for environmental analysis. Hammock and Gee reported that more research has been done in the last few years than in the preceding two decades [6]. Immunoassays exploit the specificity and selectivity of antibody–antigen reactions. These factors, as well as the reduced need for sample preparation and short analysis times, make immunoassays a good choice to replace the traditional analytical methods.

A liposome is a uni- or multilamellar vesicle containing an aqueous cavity which can be used for the encapsulation of drugs, genetic material or markers depending on its intended application. Liposomes can be used in immunoassays by preparing them to have appropriate antibodies or antigens on their surface [7]. To achieve this, antigen- or antibody-conjugated phospholipids are used as a component of lipid mixture for the preparation of liposomes. Alternatively, this conjugation step can be done after the liposomes are prepared. The advantage of liposomes in immunoassay is that the amplification of response can be obtained immediately upon lysis, because they have many marker molecules in their aqueous interiors. The incubation step for color production is not necessary, unlike the enzyme linked immunosorbent assay (ELISA).

Flow-injection analysis (FIA) has been developed during the last twenty years into a well established laboratory technique [8,9]. The scope of applications of FIA covers clinical, food, pharmaceutical and environmental fields [10,11]. Flow-injection systems can be easily automated and adapted to a wide variety of analysis formats.

Liposomes have been used in solid-phase assays [12] and an ELISA-type immunoassay [13]. The flow-injection immunoanalysis system has also been demonstrated to function well with liposomes as the detectable label [14–17]. In these papers, immunoreactor columns were prepared by

conjugating antibody to some functional groups on the matrix or injecting the same amount of antibody into the column for each analysis. The disadvantages of those methods are the loss of antibody activity as a result of randomly oriented conjugation and the reduced reproducibility by introducing one more variable step. To overcome these problems, glass beads coated with protein A were covalently bound to the non-antigen binding Fc region of antibody and used for the immunoreactor packing material in this study. In this research, we describe flow-injection liposome immunoanalysis (FILIA) for the measurement of imazethapyr and the optimization process for improving the detection limit and sensitivity in the FILIA.

2. Methods

2.1. Materials

Imazethapyr, monoclonal antibody to imazethapyr and dipalmitoyl phosphatidyl ethanolamine-analyte (DPPE-analyte) were supplied by American Cyanamid (Princeton, NJ). Sulforhodamine B (SRB) was purchased from Eastman (Rochester, NY), and 5-(and-6)-carboxyfluorescein (CF) was obtained from Molecular Probes (Eugene, OR). Dipalmitoyl phosphatidyl choline (DPPC) and dipalmitoyl phosphatidyl glycerol (DPPG) were purchased from Avanti Polar Lipids (Alabaster, AL). Polycarbonate syringe filters of 3, 0.4 and 0.2 μm pore sizes were purchased from Poretics (Livermore, CA). Dimethylpimelimidate (DMP) was obtained from Pierce (Rockford, IL). Protein A immobilized on porous silica glass was from Bioprocess-

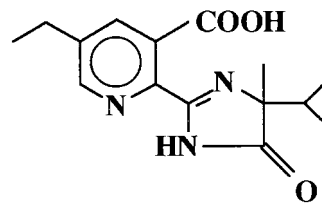


Fig. 1. Structure of imazethapyr.

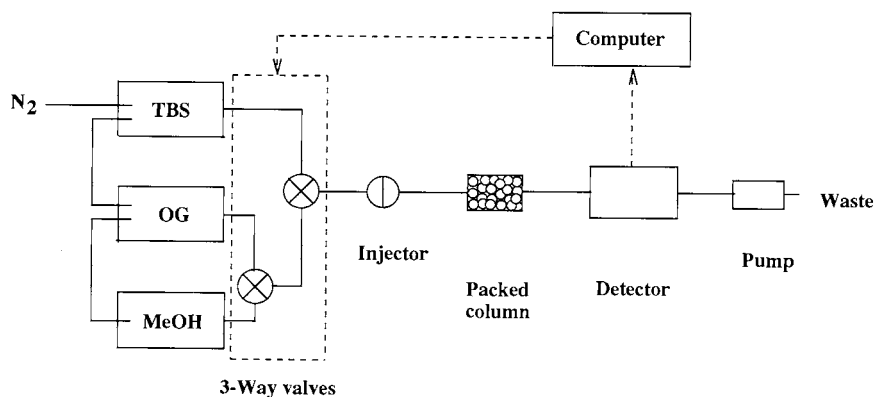


Fig. 2. Flow injection liposome immunoanalysis system. TBS, Tris-buffered saline with 0.01% sodium azide, pH 7.0; OG, 30 mM *n*-octyl- β -D-glucopyranoside in TBS; MeOH, 40% methanol solution.

ing (Princeton, NJ), and all other chemicals from Sigma (St. Louis, MO).

2.2. Apparatus

Fig. 2 shows a diagram of the FILIA system. A 20- μ l, 500- μ l or 1-ml sample loop (Rainin, Emeryville, CA) was used in the injector (Rheodyne Model 7725, Rainin, Emeryville, CA). Two three-way 12-V solenoid pinch valves (Biochem Valve, East Hanover, NJ) directed the flow of reagent into the FILIA system and were computer-controlled through a valve controller (Solenoid Interface, Rainin). All connecting PEEK tubing (0.02 in. i.d.) and standard fingertight fittings were purchased from Upchurch (Oak Harbor, WA). A peristaltic pump (Rainin) at the outlet of the system was used to maintain a flow rate of 1.3 ml min⁻¹ of TBS (Tris buffered saline) in conjunction with 41 kPa (6 psi) head pressure on each of the mobile-phase bottles. A HPLC pump used for achieving a constant flow rate was from Varian (Walnut Creek, CA). A MacIntegrator I data analysis package, used for valve operation, data collection and integration, was purchased from Rainin. The fluorescence detectors used were a Model FD-300 with a 24- μ l flow cell obtained from GTI/Spectrovision (Concord, MA) and a Model FL-1 with a 3.5- μ l flow cell from Rainin.

2.3. Preparation of immunoreactor column

Anti-imazethapyr monoclonal antibody was covalently linked to protein A glass beads according to the method described by Wong et al. [6]. Two batches were prepared by using different amounts of anti-imazethapyr antibody. One batch had a binding capacity of 6.6 μ g ml⁻¹ for imazethapyr and the other had 0.15 μ g ml⁻¹. The beads were packed in a glass column (6 \times 50 mm, Omnifit, New York, NY) and held in place with two polyethylene frits. An adjustable column endpiece was used to make a bed length of 1 mm. For the determination of non-specific binding, protein A coated beads which were covalently bound to rabbit anti-mouse IgG were prepared by the same method used for the production of beads conjugated with antibody to imazethapyr, a modification of Brew [18] and Schneider [19] methods. The beads were mixed with the desired amount of antibody in 1 M glycine/0.15 M NaCl (pH 8.6) buffer and incubated overnight. After washing with glycine buffer and 0.2 M triethanolamine (TEA, pH 8.2), cross-linking was done by resuspending the beads in 20 volumes of 25 mM DMP in 0.2 M TEA for 45 min. The beads were washed with 0.1 M ethanolamine (pH 8.0) and incubated overnight. After rinsing with TEA, the beads were stored in TBS buffer (pH 7.0) at 4°C.

2.4. Production of liposomes

Liposomes were prepared by the reverse-phase evaporation method [20–22] from a mixture of DPPC, cholesterol, DPPG, and DPPE-analyte in a molar ratio of 5:5:0.5:0.02. This mixture was dissolved in a solvent system containing chloroform, isopropyl ether and methanol (6:6:1, v/v). The dye solution of 150 mM sulforhodamine B, or 150 and 200 mM carboxyfluorescein, was added with swirling. This mixture was sonicated for 5 min under a low flow of nitrogen. The organic phase was removed under vacuum on a rotary evaporator at 45°C. An additional aliquot of the dye solution was added, and the liposomes were then extruded through three polycarbonate filters of decreasing pore sizes of 3, 0.4 and 0.2 μm . To remove any unencapsulated dye the liposomes were gel filtered on a 1.5×25 cm Sephadex G-50-150 column and finally dialyzed overnight against TBS at 4°C.

2.5. Flow-injection liposome immunoanalysis (FILIA)

The imazethapyr sample in TBS was introduced onto the immunoreactor column by manual injection. This was followed by injection of the liposomes. These two steps were done in the flow of the TBS carrier solution. After all unbound liposomes were eluted, a detergent solution (30 mM *n*-octyl- β -D-glucopyranoside in TBS) was passed through the column. The detergent caused rupture of the bound liposomes, and the fluorescence of the released dye was generated and measured. Finally, 40% methanol solution was passed through the column to regenerate the antibody binding sites by dissociating bound analyte, and the column is then reconditioned for the next analysis by returning the mobile phase to TBS. All solutions were degassed under vacuum before use each day, because introduction of the methanol solution created a large temperature differential and caused bubbles to form.

3. Results and discussion

3.1. FILIA assay

A typical trace for an analytical run is shown in Fig. 3. Peak B shows the inverse response to the amount of imazethapyr in the sample. The sample containing imazethapyr is first introduced onto the immunoreactor column. A 30 μl aliquot containing ca. 10^{10} tagged liposomes are next injected and bind to the unoccupied antibody binding sites in the column. Peak A represents the signal from unbound liposomes and traces of free dye passing through the fluorescence detector. Peak B is the analytical signal produced by the lysis of bound liposomes and consequent release of the fluorescent marker. Response is measured as the area of peak B. For samples containing a high concentration of imazethapyr, most of the antibody sites are occupied by imazethapyr, resulting in few remaining antibody sites available to liposomes. As a result, few liposomes can bind in the column and thus give a small peak upon lysis. Conversely, when a low concentration of imazethapyr is injected, a large number of liposomes bind to the unoccupied antibody binding sites thereby producing a large peak.

3.2. Displacement of the dose–response curve by loading larger sample volumes

The antibody in the column binds to imazethapyr contained in the flow of TBS buffer solution. In principle, until all antibody binding

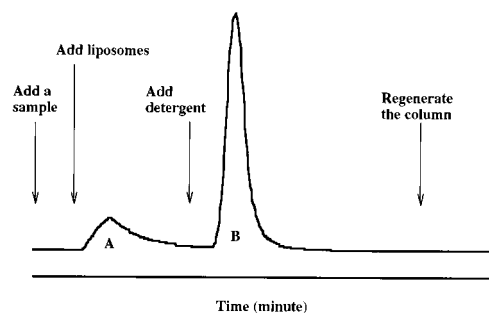


Fig. 3. Typical FILIA run. One analysis can be performed in 15 min.

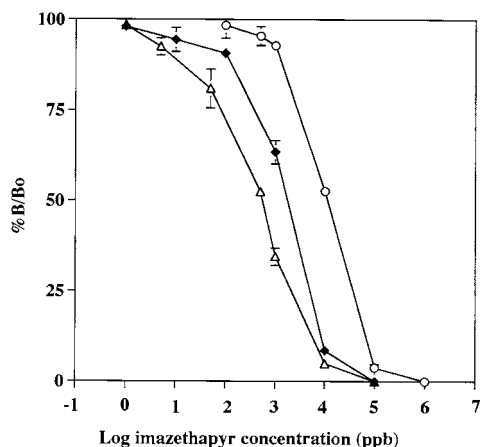


Fig. 4. Dose–response curves for imazethapyr with 20- μ l (○), 500- μ l (◆) and 1-ml (△) sample loops in the injector. Liposome encapsulating 150 mM SRB and the fluorescence detector with a 24- μ l flow cell were used. The column capacity for imazethapyr was 6.6 μ g ml⁻¹. Each point represents the mean of three measurements with error bars representing ± 1 SD.

sites are saturated with imazethapyr, they can continue to bind imazethapyr from the sample passing through the immunoreactor column. Therefore, even though a low concentration of imazethapyr sample is injected, the total amount of imazethapyr bound to the antibody can be increased by loading a larger amount of sample. To demonstrate this concept, 20-, 500- and 1000- μ l sample loops were used in the injector for increasing the sample volume. In this system, liposomes encapsulating 150 mM SRB were used with the Model FD-300 fluorescence detector from GTI/Spectrovision. The antibody used in this experiment had a very high affinity to imazethapyr and did not show any significant dissociation during the sample loading. Fig. 4 shows the comparison of three response curves obtained using the three different loop sizes. The fluorescence data were recorded as arbitrary units using MacIntegrator software and transformed as in Eq. (1), where F is the fluorescence at a given concentration of imazethapyr, F_0 is the fluorescence at zero imazethapyr, and F_∞ is the fluorescence in the presence of excess imazethapyr.

$$\%B/B_0 = (F - F_\infty / F_0 - F_\infty) \times 100 \quad (1)$$

$\%B/B_0$ represents the percentage of liposomes bound to the immunoreactor column. As the size of the loop, that is, the volume of sample increases, the dose–response curve is shifted toward lower concentration. That means the system with a larger sample loop has a lower detection limit than the one with a smaller loop. In Fig. 4, the dose–response curve from the 1-ml sample shows the most sensitive response for lower concentrations of imazethapyr than two others. However, introducing a larger volume of sample into the system takes a longer period of time. As a result, a compromise must be made between the detection limit and the analysis time.

3.3. Comparison of responses by two fluorescent dyes, SRB and CF

Liposomes containing 150 mM CF were prepared and compared to those containing 150 mM SRB. Fig. 5 shows two dose–response curves produced by the same amount of the two different types of liposomes using the same sample loop of 500- μ l. CF liposomes gave ca. 3.5 times larger response than the SRB liposomes. The free fluorescent dyes showed the same results, CF giving ca. 3.5-fold more sensitive response. This

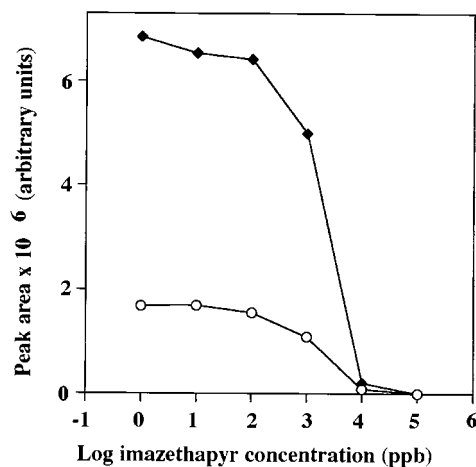


Fig. 5. Dose response curves with 500- μ l sample loop when SRB (○) and CF (◆) liposomes were used. The concentration of two fluorescent dyes for preparation of liposomes was 150 mM. The fluorescence detector with a 24- μ l flow cell was used and the column capacity for imazethapyr was 6.6 μ g ml⁻¹.

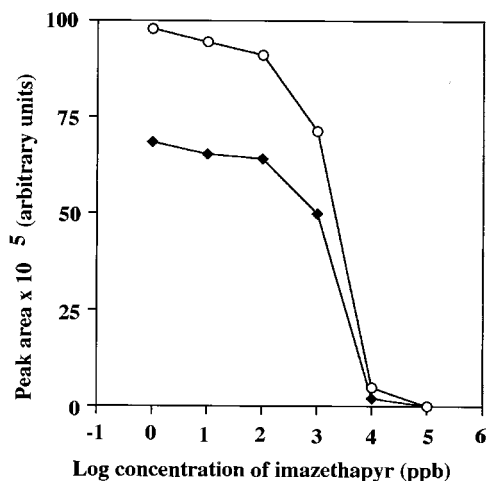


Fig. 6. Comparison of responses by liposomes containing 150 mM (◆) and 200 mM CF (○). A 500- μ l sample loop was used and the column capacity for imazethapyr was 6.6 μ g ml⁻¹.

difference results from the spectral response of the photomultiplier tube (PMT) in the fluorescence detector. A PMT is a device that generates a current when photons of light strike it and has different wavelength sensitivities. The PMT used in the GTI/Spectrovision fluorescence detector has ca. 3.5 times higher sensitivity at the emission wavelength (520 nm) of CF than at that (583.5 nm) of SRB according to the specifications of the PMT manufacturer (Hamamatsu, Shizuoka-ken, Japan). Therefore, the sensitivity variance of the PMT corresponds to the response difference shown by the liposomes containing SRB and CF. As a result, in this system, imazethapyr can be detected with higher sensitivity using the liposomes encapsulating CF.

The comparison of responses by liposomes containing two different concentrations of CF is given in Fig. 6. The liposomes containing 200 mM CF produce ca. 1.4 times higher response than those with 150 mM CF. In principle, liposomes encapsulating 200 mM CF are expected to have ca. 1.3-fold more dye molecules in the aqueous cavity than the ones with 150 mM CF. This response increase shows a good correlation with the concentration differences between the liposomes.

3.4. Effect of the column capacity on the response

The glass beads, which had a binding capacity of 0.15 μ g ml⁻¹ for imazethapyr, were packed in the glass column and used to investigate the effect of the column capacity on the sensitivity (Fig. 7). For the above study, the glass beads having a binding capacity of 6.6 μ g ml⁻¹ were used. In comparison with the higher capacity beads, the response from the lower capacity column is very small. The high capacity column has many antibody binding sites, and a large amount of imazethapyr is needed for saturation of the antibody binding sites. Therefore, the dynamic dose-response range is shown only over quite high concentrations of imazethapyr. To overcome this limitation and improve the detection limit, the column binding capacity was reduced. However, this results in a decrease in the number of liposomes that can bind to the antibody of the column and, as a result, the detector response was too small to quantify the amount of imazethapyr in the sample. From this result, it was decided that a significant improvement of the detection limit was not attainable by a simple optimization process but could be achieved only by an instrumental change to increase the sensitivity.

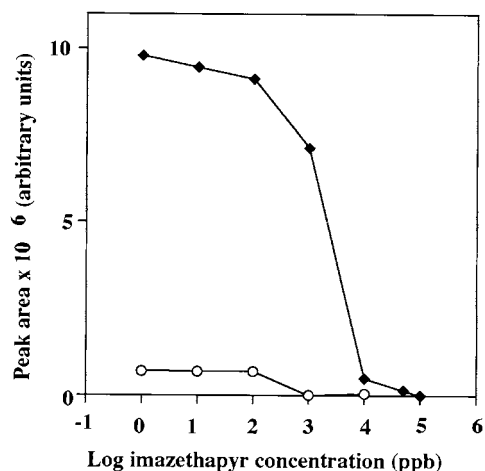


Fig. 7. Comparison of two columns having the binding capacities of 0.15 (○) and 6.6 (◆) μ g ml⁻¹ for imazethapyr. A 500- μ l sample loop, liposomes encapsulating 200 mM CF and the fluorescence detector with a 24- μ l flow cell were used.

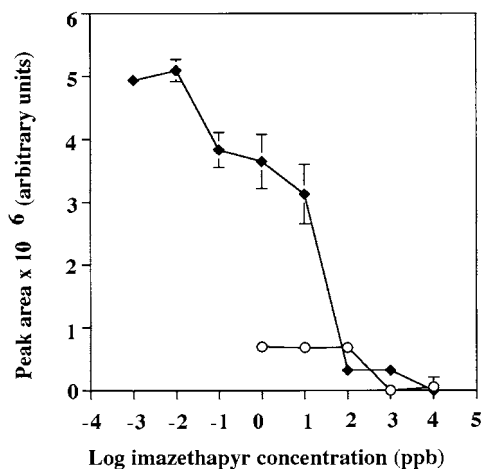


Fig. 8. Comparison of two sizes of flow cells. (○) was obtained from the fluorescence detector with a 24- μl flow cell and (◆) was from the one with a 3.5- μl flow cell. A 1-ml sample loop and the column with 0.15 $\mu\text{g ml}^{-1}$ binding capacity for imazethapyr were used. Each point represents the mean of three measurements with error bars representing ± 1 SD.

3.5. Influence of the flow cell size on the response

A model FL-1 fluorescence detector from Rainin was used instead of the GTI/Spectrovision fluorescence detector. A pulsed xenon lamp was used as an excitation source in both fluorescence detectors. The main difference between the two fluorescence detectors was the size (volume) of the flow cell. The flow cell is a quartz tube which allows for the transmission of the excitation and emission radiation. The fluorescence detector from Rainin has a 3.5 μl flow cell volume and that from GTI/Spectrovision has a 24 μl . Fig. 8 shows two dose–response curves obtained with the two different sizes of flow cells when the beads of 0.15 $\mu\text{g ml}^{-1}$ binding capacity were used. The total response increases over five times with the 3.5- μl flow cell. However, for the fluorescence detector having the 3.5- μl flow cell, the liposome solution was diluted ten-fold because, if the same amount of liposomes was injected, the detector response was off scale. For the determination of the actual response increase, free CF dye was injected into both detectors, and the concentration of the free dye required to produce the same peak area was obtained and compared. From this study, it was

determined that the response with the fluorescence detector having the 3.5- μl flow cell is ca. 50 times more sensitive than that with the 24- μl flow cell. While a part of this increased sensitivity results from the reduction of the flow cell volume giving rise to the decreased dilution of the dye, this difference in the sensitivity may also be caused by other instrumental differences.

3.6. Non-specific binding study

In Fig. 8, the dose–response curve from the 3.5- μl flow cell appears to show that 0.1 ppb of imazethapyr can be easily detected. However, the shape of the curve is not the typical sigmoidal form obtained in an immunoassay, instead showing two leveling-off regions in the low concentration range of imazethapyr. In this case, it was found that non-specific binding (F_{∞}) accounted for about 60% of the total response, and this high non-specific binding may cause the unusual shape of the curve. The graph showed only specific binding portion ($F_0 - F_{\infty}$). In the above study with the beads of 6.6 $\mu\text{g ml}^{-1}$ binding capacity, less than 30% of the total response was from non-specific binding. The uncoated glass sites are thought to bind to liposomes and give the non-specific binding response. Also, while not directly observed, liposomes captured in the pores of the glass beads could give the non-specific binding response. Fig. 9 shows the results obtained when the beads conjugated with different amounts of rabbit anti-mouse IgG were used in the column. For rabbit polyclonal antibody, a typical capacity of 37 mg ml^{-1} of glass beads was given in the manufacturer's instructions (Bioprocessing). This amount of antibody was used for conjugation with protein A beads, and these beads were designated as 100% saturation. By the reference to this amount, the other bead loadings were prepared. The binding of liposomes obtained from the beads without antibody was considered as 100% non-specific binding. At the level of 100% saturation with IgG, 25% of the total non-specific binding remains, and this results from the binding to the frits and tubing. This indicates that, when the high capacity beads were used, about 30% of non-specific binding is mainly from the binding to

the frits and tubing. From the beads 50% saturated with rabbit anti-mouse IgG, the non-specific binding decreased considerably, and this may result from the inhibition by antibody of the liposome access to the pores and uncoated sites of the glass beads.

Total amount of antibody molecules (specific and non-specific) attached to the beads was larger for the smaller capacity beads. For the high capacity beads, 5 mg anti-imazethapyr antibody was used per ml of the glass beads. In the case of the low capacity beads, after binding 1 mg anti-imazethapyr antibody per ml of the glass beads, the beads were incubated with 5 mg of mouse IgG to block the unoccupied protein A sites giving rise to total 6 mg of antibody binding. Therefore, the total amount of antibody on the column has only an indirect relationship with the degree of non-specific binding, suggesting that imazethapyr bound to the antibody binding sites makes the nearby uncoated glass sites and pores inaccessible to liposomes by steric hindrance and/or ionic interactions. In case of the low capacity beads, 5 mg of mouse IgG used for blocking was not enough to saturate the protein A binding sites, and many glass sites and pores were still accessible to liposomes. In the beads having a larger amount of anti-imazethapyr antibody, even

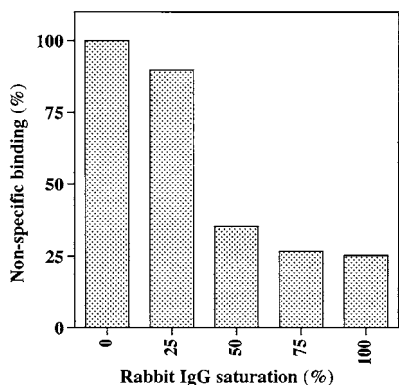


Fig. 9. Non-specific binding related to the antibody amount on the column. 37 mg ml^{-1} of rabbit anti-mouse IgG was used for preparation of 100% saturated beads, and by the reference to this amount, the other beads were prepared. The binding of liposomes obtained from the beads without antibody was regarded as 100% non-specific binding.

though total antibody amount was smaller, the quantity of imazethapyr bound to the antibody binding sites is high when a high concentration imazethapyr is injected. As a result, liposomes cannot easily access the uncoated glass sites and pores giving the low degree of non-specific binding.

3.7. Achieving a constant flow rate

In this FILIA system, a constant flow rate could not be maintained within and between days because it was difficult to regulate gas pressure precisely. It was observed that the flow rate changed slowly as the amount of solution in the bottles decreased. To achieve a constant flow rate, the peristaltic pump at the outlet of the system was replaced with a HPLC pump. Because the HPLC pump has quite a large holdup volume, it was not appropriate to connect it into the front part of this system which needed the switching of three solutions within a short time period. The HPLC pump was not sufficient by itself for drawing solutions due to the amount of resistance between the pump and the mobile-phase bottles which still needed the application of head pressure. However, the flow rate was no longer influenced by the pressure applied to the solution bottles. Another concern was that without enough back pressure, the pump would not work properly. This problem was solved by connecting an old HPLC column at the outlet of the pump.

4. Conclusions

FILIA was successfully used for the detection of imazethapyr herbicide. The detection limit could be lowered by loading larger volume of sample. Also, the sensitivity increased by using liposomes encapsulating CF instead of SRB. The dose–response study with a smaller flow cell and a low capacity column suggests that FILIA can be used for imazethapyr quantitation over a broader linear range, if the non-specific binding is reduced. For future study, a capillary column will be derivatized with protein A conjugated to the inside of the capillary wall. Due to the reduction of

the surface area-to-volume ratio and the elimination of the frits, the non-specific binding should be significantly lowered. Also, a constant flow rate achieved by using a HPLC pump will improve the reproducibility of response.

Acknowledgements

We would like to thank Dr. Stuart Reeves and Sui Ti Siebert for their help and suggestions, and Geoffrey Rule for assistance during this research.

References

- [1] M.M. Loux, K.D. Reese, *Weed Technol.* 7 (1993) 452.
- [2] P.C. Anderson, K.A. Hibberd, *Weed Sci.* 33 (1985) 479.
- [3] D.L. Shaner, P.C. Anderson, *Plant Physiol.* 76 (1984) 545.
- [4] D.L. Shaner, S.L. O'Connor (Eds.), *The Imidazolinone Herbicides*, CRC Press, Boca Raton, FL, 1991.
- [5] N.M. Mallipudi, A. Lee, R. Fiala, A.R. daCunha, M. Safarpour, *J. Agric. Food Chem.* 42 (1994) 1213.
- [6] J.O. Nelson, A.E. Karu, R.B. Wong (Eds.), *Immunoanalysis of Agrochemicals: Emerging Technologies*, American Chemical Society, Washington, DC, 1995.
- [7] H. Rongen, *Immunoassays: Development and Application of Chemiluminescent and Liposome Labels*, Universiteit Utrecht, Utrecht, 1995.
- [8] R.D. Schmid (Ed.), *Flow Injection Analysis (FIA) Based on Enzymes or Antibodies*, VCH, New York, 1991.
- [9] J. Ruzicka, E.H. Hansen, *Flow Injection Analysis*, Wiley, New York, 1988.
- [10] B. Karlberg, G.E. Pacey, *Flow Injection Analysis: A Practical Guide*, Elsevier, New York, 1989.
- [11] M. Valcárcel, M.D. Luque de Castro, *Flow-Injection Analysis: Principles and Application*, Halsted Press, New York, 1987.
- [12] D. Monroe, *J. Liposome Res.* 13 (1990) 339.
- [13] A.L. Plant, M.V. Brizgys, L. Locascio-Brown, R.A. Durst, *Anal. Biochem.* 176 (1989) 420.
- [14] L. Locascio-Brown, A.L. Plant, V. Horváth, R.A. Durst, *Anal. Chem.* 62 (1990) 2587.
- [15] L. Locascio-Brown, A.L. Plant, R. Chesler, M. Kroll, M. Ruddel, R.A. Durst, *Clin. Chem.* 39 (1993) 386.
- [16] G. Gregoriadis (Ed.), *Liposome Technology*, CRC Press, Boca Raton, FL, 1993.
- [17] G.S. Rule, D.A. Palmer, S.G. Reeves, R.A. Durst, *Anal. Proc. Anal. Commun.* 31 (1994) 339.
- [18] K. Brew, J.H. Shaper, K.W. Olsen, I.P. Trayer, R.L. Hill, *J. Biol. Chem.* 250 (1975) 1434.
- [19] C. Schneider, R.A. Newman, D.R. Sutherland, U. Asser, M.F. Greaves, *J. Biol. Chem.* 257 (1982) 10766.
- [20] F. Szoka, F. Olson, T. Heath, W. Vail, E. Mayhew, D. Papahadjopoulos, *Biochim. Biophys. Acta* 601 (1980) 559.
- [21] J.P. O'Connell, R.L. Campbell, B.M. Fleming, T.J. Mercolino, M.D. Johnson, D.A. McLaurin, *Clin. Chem.* 31 (1985) 1424.
- [22] S.T.A. Siebert, S.G. Reeves, M.A. Roberts, R.A. Durst, *Anal. Chim. Acta* 311 (1995) 309.

Rate study of reduction of 2-heptanone with samarium iodide by gas chromatography

M.-R.S. Fuh *, T.-Y. Lin, S.-C. Chang

Department of Chemistry, PO Box 86–72, Soochow University, Taipei, Taiwan, ROC

Received 21 July 1997; accepted 15 September 1997

Abstract

This article describes a newly developed method of gas chromatography (GC) for the rate study of the reduction of organic compounds by samarium iodide. Solvent extraction was used to reduce the interference of GC analysis by inorganic species. Adequate recoveries ranged from 88.3 to 94.5 % and good linearity ranging from 0.1 to 2.1 mM was determined. An internal standard, decane, was used to enhance the precision of this test. The coefficient variations of intra-day and inter-day ranged from 0.22 to 3.00%. The stability of the reacted sample was also assessed. In addition, the reaction rates of the reduction of 2-heptanone by samarium iodide in the presence of hexamethylphosphoramide were examined. The results presented herein demonstrate the utility of this method in kinetic studies. © 1998 Elsevier Science B.V. All rights reserved.

Keywords: 2-heptanone; Samarium iodide; Gas chromatography

1. Introduction

The samarium iodide (SmI_2) reduction of organic compounds has been one of the most interesting research topics in recent decades, since Girard et al. And others reported its reactivity towards various functional groups [1–4]. Although some mechanisms were proposed for these reductions, reaction rates were seldom studied [3,4]. Hasegawa and Curran measured the first bimolecular rate constants for the SmI_2 reduction of a primary alkyl radical by using a competitive hexenyl radical clock [5]. Sturino and Fallis ob-

tained the rate constants of competitive ‘radical clock’ type cyclization of hydrazones and alkenes by SmI_2 [6]. However, the above rates only reflected the reactivity of the radicals formed. The measurement of the rate for the first electron transfer step by SmI_2 to organic substrate remains an unsolved problem. We therefore present a method for further understanding the speed of this step. Owing to the characteristic absorption of SmI_2 solution, we attempted to trace SmI_2 concentration by UV/Vis spectroscopy [7–10]. Unfortunately, the results were extremely complicated and the experiments were difficult to control. This may be attributed to air sensitivity of SmI_2 and different absorption coefficients of various forms of the complexes.

* Corresponding author. Tel.: + 886 02 8819471; fax: + 886 02 8811053; e-mail: msfuh@mbm1.scu.edu.tw

Another approach for investigation of the reaction is to monitor the reduced reactants. Since these reactants are small organic molecules, gas chromatography (GC) can be used to monitor the amount of reactant in the mixture during the reaction. In this paper, we describe a newly developed GC method to determine the reduction of 2-heptanone by SmI_2 . In this analysis, inorganic species were removed from the reaction mixture by HCl solution to minimize their effect on GC analysis. 2-Heptanone was extracted to hexane and then determined by GC. An internal standard, decane, was used to minimize experimental variation. External standards were used to quantitatively measure 2-heptanone. The linearity, detection limit and precision associated with this are also discussed. Furthermore, this method is applied to investigate the reduction of 2-heptanone by SmI_2 in the presence of hexamethylphosphoramide, which is an efficient catalyst.

2. Experimental

2.1. Chemicals

Samarium iodide, decane, 2-heptanone and hexamethyl phosphoramidate (HMPA) were purchased from Aldrich (Milwaukee, WI, USA). Hydrochloric acid and iodine were purchased from Nacalai Tesque (Kyoto, Japan) and Wako Pure Chemical Industries (Osaka, Japan). Hexane was purchased from Tedia (Fairfield, OH, USA). The chemicals were used as received, without further purification. Tetrahydrofuran (THF) was obtained from Labscan (Dublin, Ireland). THF was freshly distilled before use and immediately transferred to a glove box. GC system A Shimadzu 14B GC with a flame ionization detector (FID) and a 14AO autosampler (Shimadzu Scientific Instruments, Tokyo, Japan) were used for analysis. A split/splitless injector was used for analysis. A Scientific Information Service Corporation (SISC; Taipei, Taiwan) chromatography data system and a personal computer were used for data acquisition and processing. Separation was carried out in a DB-1 column (15 m., 0.53 mm i.d., 1 mm film thickness; Supelco, Bellefonte, PA, USA).

The instrument settings for GC–FID were as follows: injector temperature, 250°C; FID temperature, 250°C; oven temperature, 50°C initially, increased to 95°C at 10°C min⁻¹, then to 240°C at 40°C min⁻¹ and finally held for 3 min at 240°C. The injector split ratio was set at 30/1. The injection volume for GC analysis was 6 µl.

2.2. Standard solutions

A solution of hexane with added decane (1.46 mM) was prepared and used to develop 2-heptanone standards (2.06, 1.03, 0.52, 0.25 and 0.10 mM). These standards were used to establish the calibration curve for quantitative analysis.

2.3. Reaction sample preparation

The concentration of SmI_2 was determined by I_2 titration prior to reaction. 0 µl of 2-heptanone (0.25 M) in hexane was injected into a 5.0 ml of SmI_2 solution and thoroughly mixed. Subsequently, at each time interval, 0.50 ml of reaction mixture was transferred into 0.50 ml of hexane containing decane and I_2 . This procedure ensured that unreactive Sm(II) is quenched by I_2 . This I_2 quenching solution was freshly prepared with equal concentrations of SmI_2 . After the mixture was removed from the glove box, 0.50 ml of 0.12 M HCl solution was added to each quenched solution and mixed for 3 min using a Virtex mixer. This procedure extracts most inorganic species into the aqueous phase and minimizes their effect on GC analysis. The solution was left at room temperature (1–2 min.) until organic and aqueous layers were well separated. Finally, the clear organic layer was injected into the GC apparatus for analysis.

3. Results and discussion

Fig. 1 depicts typical GC chromatograms of standard and reaction extract. Adequate separation was achieved in approximately 10 min. The retention time of 2-heptanone was 3.5 min. To minimize experimental variation and volume change due to the mixing of tetrahydrofuran and

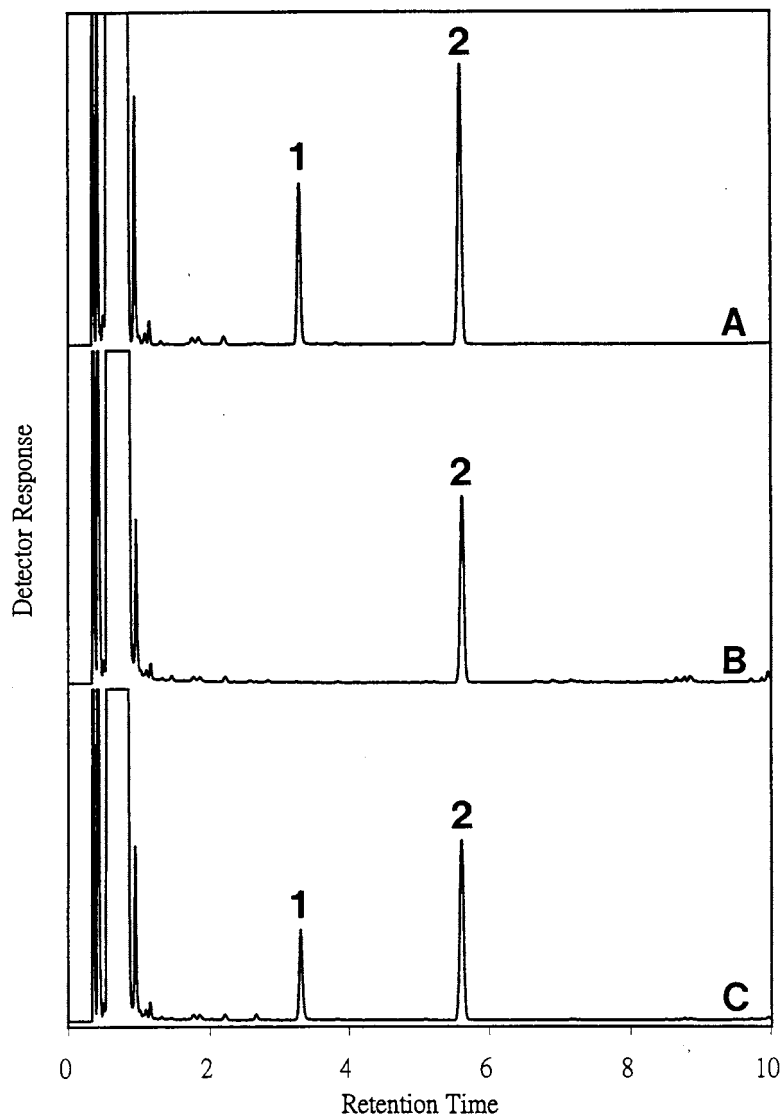


Fig. 1. Typical chromatograms of: (A) standard solution; (B) samarium(II)/THF solution after quenching with I_2 ; and (C) reacted sample. Peak 1, 2-heptanone, peak 2, decane.

hexane, decane was added as an internal standard and eluted at 5.7 min. As reported elsewhere, 2-heptanol was the reaction product in the presence of a proton source [1]. Therefore, we also examined the separation of 2-heptanol (eluted at 4.1 min) to ensure that there is no proton source in the reaction mixture which may create other reaction routes. Additional unidentified peaks appeared in the reac-

tion extract; however, these did not interfere with 2-heptanone or decane.

The calibration curve was constructed by plotting the ratio of the peak area of 2-heptanone to that of decane versus the concentration of 2-heptanone. The linearity was good, being from 2.1 to 0.1 mM ($r_2 = 0.9998$). The detection limit was about 0.001 mM based on a signal-to-noise ratio of 3.

Table 1
Intra-day and inter-day precision study

Added amount (mM)	Intra-day ^a			Inter-day ^b		
	Mean (mM)	SD	CV	Mean (mM)	SD	CV
2.06	2.06	0.005	0.25	2.06	0.005	0.24
1.50	1.51	0.005	0.33	1.50	0.006	0.40
1.03	1.02	0.002	0.22	1.03	0.005	0.48
0.74	0.75	0.004	0.53	0.75	0.004	0.53
0.52	0.53	0.001	0.22	0.53	0.003	0.57
0.25	0.23	0.001	0.49	0.24	0.001	0.42
0.10	0.09	0.001	1.11	0.10	0.003	3.00

^a The mean and SD represent three measurements of each amount.

^b The inter-day reproducibility was determined from five different runs over a 2 week period.

The precision of this test method was evaluated by replicate analysis of 2-heptanone spiked n-hexane solution. The intra-day precision revealed a coefficient of variation (CV) of 0.22–1.11 %. The inter-day variation was similarly evaluated for five days. The inter-day CV ranged from 0.24 to 3.00%. Details of the precision study are summarized in Table 1.

The extraction efficiency of 2-heptanone by hexane was investigated and the results are summarized in Table 2. In this study, SmI₂/THF solution was first oxidized by air. A different amount of 2-heptanone was added to Sm(III)/THF solution, while hexane and HCl solution was added subsequently, as described in Section 2. The extracted 2-heptanone was evaluated by GC.

In order to match the sample matrix of the reaction mixture, SmI₂/THF solution was quenched with I₂/decane/hexane and 0.12 M HCl solution, as described in Section 2.3. Some 2-heptanone was added to the mixture and mixed by a Virtex mixer. The clear organic layer was injected into the GC apparatus for analysis. Recoveries ranged from 90.7 to 101.4%, as determined through the concentration range examined herein.

Fig. 2 summarizes the stability of the sample. The extracted samples were stored at room temperature (about 26°C). Samples were withdrawn from solutions daily and analyzed by GC to examine their stability under storage. The first day sample served as a control. The difference between the results of each of subsequent measure-

Table 2
Recovery of 2-heptanone extraction

Sample number	Amount added (mM)	Amount found ^a (mM ± SD)	Recovery ^a (% ± SD)
1	1.88	1.778 ± 0.004	94.6 ± 0.2
2	1.88	1.766 ± 0.003	93.9 ± 0.1
3	1.88	1.764 ± 0.005	93.8 ± 0.2
4	1.00	0.887 ± 0.003	88.7 ± 0.3
5	1.00	0.890 ± 0.002	89.0 ± 0.2
6	1.00	0.916 ± 0.001	91.6 ± 0.1
7	0.50	0.451 ± 0.001	90.2 ± 0.2
8	0.50	0.455 ± 0.001	91.0 ± 0.2
9	0.50	0.446 ± 0.001	89.2 ± 0.1
10	0.25	0.224 ± 0.001	89.6 ± 0.5
11	0.25	0.222 ± 0.001	88.8 ± 0.5
12	0.25	0.227 ± 0.001	90.8 ± 0.5

SD, standard deviation.

^a Average of three measurements.

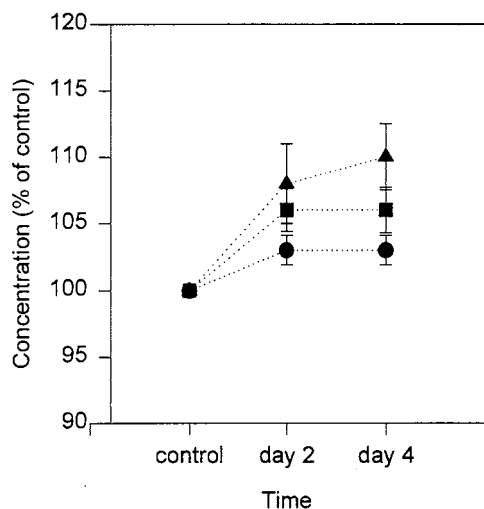


Fig. 2. Stability of 2-heptanone (●, 0.8 mM; ■, 0.5 mM; ▲, 0.2 mM) in reacted mixture versus time, which stored at room temperature. Values are represented as percentile changes of control (mean \pm SEM; $n = 3$).

ments and the control was examined by a one-tail student t -test. Statistical significance was taken as $P < 0.05$. The response significantly decreased after storage at room temperature over the period of study. Therefore, all collected samples were measured immediately after preparation.

This newly developed method was used to examine the reduction rate of 2-heptanone with

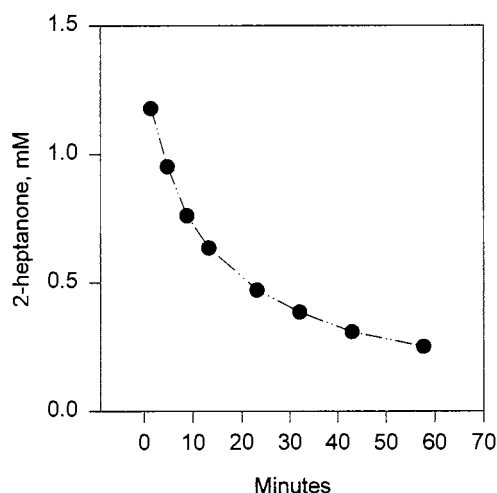


Fig. 3. Unreacted 2-heptanone in the mixture.

SmI₂. According to these results, 2-heptanone was reduced by this powerful reagent surprisingly slowly. In a reaction mixture of 0.12 M SmI₂ and 1.5 mM 2-heptanone, only 28% of the ketone reacted 16 days. However, in the presence of 0.11M HMPA, the reaction under the same conditions was nearly complete in 1 h, as shown in Fig. 3. The initial rate constant can be estimated as 0.062 M⁻¹ min⁻¹ if both reactants were assumed to be first order.

4. Summary

This paper presents a simple, accurate and sensitive GC method for the rate studying the rate of reduction of 2-heptanone with SmI₂. A simple sample preparation procedure was utilized to remove inorganic species in the organic phase and increase the sensitivity of the GC analysis. Good linearity ($r_2 = 0.999$) in the range of 0.1 to 2.1 mM was determined. In addition, the precision of this method is also very good. This method was used to assess the reduction rate of 2-heptanone by Sm(II). The reaction rate was significantly affected by HMPA.

This method can be easily applied to examine the reduction rate of other organic compounds with Sm(II). Currently, we have applied this newly developed method to investigate the reduction of other carbonyl group compounds with Sm(II).

Acknowledgements

This work was supported by National Science Council of Taiwan.

References

- [1] P. Girard, J.L. Namy, H.B. Kagan, J. Am. Chem. Soc. 102 (1980) 2693.
- [2] D.P. Curran, T.L. Fevig, C.P. Jasperse, M.J. Totleben, Synth. Lett. (1992) 943.
- [3] G.A. Molander, Chem. Rev. 92 (1992) 29.
- [4] N.E. Brandukova, Y.S. Vygodskii, S.V. Binogradova, Russ. Chem. Rev. 63 (1994) 345.

- [5] E. Hasegawa, D.P. Curran, *Tetrahedron Lett.* 34 (1993) 1717.
- [6] C.F. Sturino, A.G. Fallis, *J. Org. Chem.* 59 (1994) 6514.
- [7] J.L. Namy, P. Girard, H.B. Kagan, P.E. Caro, *Nouv. J. Chim.* 5 (1981) 479.
- [8] A.N. Kamenskya, N.B. Mikheev, N.P. Kholomogorova, *Zh. Neorg. Khim.* 28 (1983) 2499; *Russ. J. Inorg. Chem.*, 28 (1983) 1420.
- [9] A.N. Kamenskya, *Zh. Neorg. Khim.* 29 (1984) 439; *Russ. J. Inorg. Chem.*, 29 (1984) 251.
- [10] Y. Okaue, T. Isobe, *Inorg. Chim. Acta* 144 (1988) 143.

Arsenic speciation in iron hydroxide precipitates

Birgit Daus *, Holger Weiß, Rainer Wennrich

UFZ Umweltforschungszentrum Leipzig-Halle GmbH, Permoser Str. 15, D-04318 Leipzig, Germany

Received 14 May 1997; received in revised form 12 September 1997; accepted 15 September 1997

Abstract

In this study a special sequential extraction method is proposed to discriminate between arsenic adsorbed and co-precipitated in precipitates arising mainly from iron hydroxides or bound in low solubility mineral phases. Synthetic iron hydroxide precipitates were prepared to investigate the influence of the amount of arsenate, of the manganese additionally added and of the valence state of arsenic on the remobilisation of arsenic. After preparing the precipitates with arsenate no arsenic could be detected in the supernatant solution. About 82% (w/w) of the arsenate is adsorbed to the precipitate and the remaining part can be dissolved by shaking with an oxalate buffer. A significant difference between the amount of arsenic added and the amount analysed in the two steps was not found. Consequently, compounds with a low solubility, such as scorodite, were not formed in the synthesized precipitates. The valence of the arsenic and addition of manganese influence significantly the uptake of arsenic by iron hydroxides. Natural precipitate samples from a percolate water of tin mill tailings were investigated using this method. © 1998 Elsevier Science B.V. All rights reserved.

Keywords: Arsenic; Speciation; Sequential extraction

1. Introduction

Mining activities have both local and regional impacts on terrestrial and aquatic ecosystems. Mines produce large quantities of waste-rock and mill tailings which require disposal [1]. Tin ore has been mined in the Erzgebirge in the east of Germany for a long time. Near the city of Altenberg a settling pond for the tailings was constructed by isolating a segment of the Biela River valley by two dams. The pond covers an area of about 0.53 million m². Presently, about 30 l s⁻¹

of seepage water percolates through the main dam. This effluent water contains arsenic in concentrations up to 1 mg l⁻¹ [2]. Precipitates are formed under oxidizing conditions in the effluent water and consist mainly of iron hydroxides. These contain arsenic in concentrations up to 8% w/w.

The well known sequential extraction methods after Tessier et al. [3] or Förstner [4] were designed to deal with M²⁺ metal ions. However, the behavior of arsenic is very different. The use of the method after Förstner for the precipitate samples from Biela River valley leads to the expected result, that the arsenic is bound to the amorphous iron hydroxide. However, to understand the im-

* Corresponding author. Tel.: +49 341 2352058; fax: +49 341 2352126; e-mail: daus@pro.ufz.de

mobilisation or possible remobilisation processes of arsenic it is important to know, how the arsenic is incorporated into the precipitate. To discriminate between arsenic adsorbed or co-precipitated to iron hydroxides and bound in minerals like scorodite, a two step sequential extraction method was applied in this study.

Pierce and Moore [5] investigated the adsorption of arsenite and arsenate on amorphous iron hydroxide. They found that at pH values higher than 10, no adsorption takes place. Therefore, 1 mol l⁻¹ NaOH is used for the desorption of the arsenate. Such a solution would be able to solve also organic substances (e.g. humic acids) [6,7]. However, the concentrations of organic material in the precipitates described are very low. In this case a determination of the arsenic adsorbed to the iron hydroxide surface should be possible.

Amorphous and poorly crystallized iron hydroxides, as well as manganese hydroxides are the main components in the precipitate and can be dissolved in an oxalate buffer (pH = 3) [7,8] or with a hydroxylamine solution [9,10]. The arsenates which are bound to these compounds can be determined after the dilution of the hydroxides. The low solubility compounds, such as iron arsenate (solubility product = 5.7×10^{-21} [11]) or other heavy metal arsenates, remain in the residue.

Synthesized precipitates from iron, manganese and arsenate were prepared with different amounts of arsenic to test this sequential extraction scheme. Precipitate samples from the seepage water of the tailings pond in the Biela River valley were investigated for comparison.

2. Experimental

2.1. Reagents

Deionized water (Millipore) was used throughout. All reagents were of analytical reagent grade or higher purity. Fe(II) stock solution containing 0.5 g Fe/10 ml was prepared by dissolving (NH₄)₂Fe(SO₄)₂·6 H₂O (Merck). As(V) and Mn(II) as nitrates were taken from standard solutions (Merck, 1000 mg l⁻¹).

The As(III) stock solution containing 1 mg As l⁻¹ was prepared by dissolving NaAsO₂ (Merck). The oxalate buffer was prepared by dissolving ammonium oxalate and oxalic acid (0.2 mol l⁻¹ ammonium oxalate, 0.2 mol l⁻¹ oxalic acid).

2.2. Analysis

Iron, manganese, and arsenic concentrations in the solutions were determined using ICP-AES (Spectroflame, SPECTRO A.I.) with pneumatic nebulization (cross flow).

The total content of these elements in the solid samples from the Biela River valley was determined with wavelength-dispersive X-ray fluorescence spectrometry (WDXRF, SRS 3000, Siemens) using pellets prepared in stearine wax (4 + 1 g).

2.3. Synthetic precipitates

In a first experiment different amounts of As(V) (0.5–5.0 mg) were mixed with 10 ml of the Fe(II) stock solution (0.5 g). The mixture was diluted with water up to a total volume of 30 ml. The pH of this mixture was adjusted with a NaOH solution to a value of 6.8 to form the iron hydroxide precipitates. This pH-value was measured in the effluent water in the sampling area. To accelerate the oxidation process oxygen was bubbled into the suspension for about 5 min until the precipitate had changed its colour into reddish-brown. After 18 h the precipitate was separated from the solution by centrifugation and the supernatant liquid was decanted. The concentrations of iron and arsenic were determined in this solution by ICP-AES to calculate the amounts of the elements precipitated. Additionally, some precipitates were prepared using As(III) instead of As(V) and a few precipitates containing manganese in different amounts. These precipitates were prepared in the same way. Three replicates of each precipitate were done.

2.4. Natural samples

The precipitate samples were collected from different site locations in the Biela River valley as

surface samples. Three samples were taken near the dam and one about 50 m downstream. The slurry was filled in 1000 ml polyethylene bottles and stored at 4°C. For the extraction wet material was used and the dry weight was calculated by weighing a different part of the sample after drying at 40°C. Each sample was analysed in three replicates.

2.5. Sequential extraction

An amount of 20 ml 1 mol l⁻¹ NaOH was added to the synthesized precipitates or to the natural samples to solubilize the adsorbed arsenate. After shaking for 1 h the suspension and the liquid phase were separated by centrifugation (step I).

Two different solutions were tested to extract arsenic bound to the iron hydroxide precipitate. An extraction with a 0.04 mol l⁻¹ NH₂OH·HCl solution in 25%(v/v) CH₃COOH (heating at 96°C, [12]) was chosen first. This method was inappropriate for our purpose, because only a small amount of the synthetic iron hydroxide precipitate was dissolved. Next a method based on an oxalate buffer (pH = 3) [9] was investigated. The synthesized precipitate was totally dissolved in this way. The volume of 20 ml of the oxalate buffer was added to the residue of step I and the mixture was shaken over night and the liquid phase was separated by centrifugation (step II).

The amount of arsenic bound in sparingly soluble compounds (e.g. heavy metal arsenates) can be calculated from the difference of the total amount determined by WDXRF and the sum of step I and step II.

3. Results and discussion

3.1. Synthetic precipitates

In a first experiment synthetic precipitates were prepared with varying amounts of As(V) (0.5–5.0 mg) to study the influence of the concentration of the arsenic on its binding to the iron hydroxide precipitate. The different amounts of arsenic were added to 10 ml Fe(II) stock solution and the

mixture was filled with deionized water up to a volume of 30 ml. The precipitate was formed in the described way and leached sequentially with the NaOH solution and the oxalate buffer.

The discussion of all results is done with the mass of the elements to avoid confusion originating from the dilutions in the different steps of extraction.

After preparing the precipitates no arsenic was detectable in the supernatant liquid, which means that the precipitation of the arsenic was complete. As shown in Fig. 1 the average recovery for arsenic added was 95% in the two steps of leaching. Most of the arsenic was found in the NaOH leaching solution. About 82% (w/w) of the arsenic was leached in this step of the procedure. The same pattern was observed in the oxalate buffer solution with approximately 13% (w/w). There was no significant difference between the arsenic added and found, which suggest that no significant quantity of arsenic is bound up in sparingly soluble forms.

In Fig. 2 the behaviour of iron in this experiment is shown. Surprisingly, about 94% (w/w) of the iron remains in solution.

The iron concentrations in the water (soluble) was for all arsenic concentrations the same with a standard deviation smaller than 2%. Obviously the amount of iron precipitated was not affected by the arsenate concentrations. As expected, no iron was determined after the extraction with 1 mol l⁻¹ NaOH. This means that the arsenic

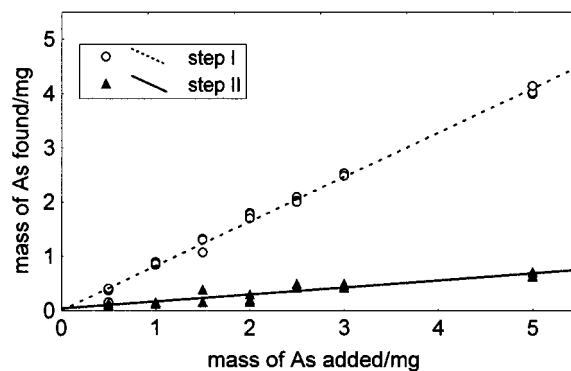


Fig. 1. Correlation plot of the arsenic amount added and found in the different extraction steps (step I, NaOH solution; step II, oxalate buffer).

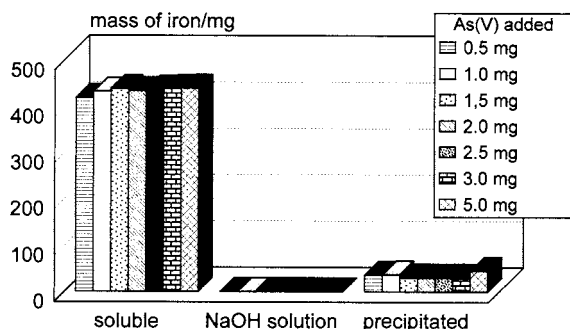


Fig. 2. Iron amounts analysed in the different fractions.

which is determined after this extraction step is extracted from the precipitate without dissolving.

The extraction scheme seems to be suitable to discriminate between the arsenic species described above.

In a further step the influence of an additional redox species was investigated using synthetic precipitates. Different amounts of manganese (Mn^{2+}) were added to the mixture of Fe^{2+} (0.5 g) and AsO_4^{3-} (2 mg As) in a total volume of 30 ml. During the procedure of preparing the precipitates, described above, Mn^{2+} is also oxidised forming MnO_2 . The various amounts of manganese (2, 4, and 6 mg) showed no influence on the amount of iron precipitated (Fig. 3). This is in agreement with the results found, when varying the As(V) concentrations.

However, the addition of manganese leads to significant changes in the binding of arsenic (Fig. 4). As shown, even small additional amounts of

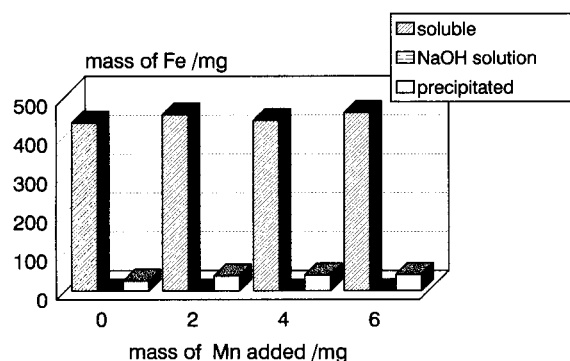


Fig. 3. Behaviour of iron depending on the amount of manganese added.

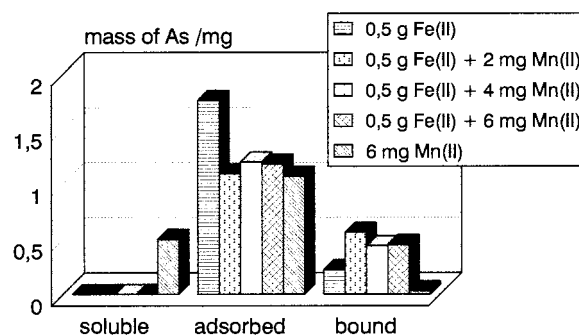


Fig. 4. Arsenate binding as a function of the amount of manganese added.

manganese (2 mg) have the effect of more arsenate being bound to the precipitate. The amount of manganese is obviously not important in this range of concentrations. Less than 3% of the manganese amount added was detected in the precipitate (step II). Most of the manganese remain in the solution. The small amounts of manganese detected in the precipitate seems to change the structure of the precipitate with the result of binding more arsenic. The precipitation of arsenic was incomplete if only manganese (6 mg Mn(II)) without any iron was used.

The influence of the valence of arsenic on its binding was studied in an additional experiment with synthetic iron hydroxide precipitates. Again 2 mg As (III) were added to 0.5 g iron corresponding to a total volume of 30 ml. Additionally manganese (2 mg) was added to a few samples before preparing the precipitate. Using As(III) instead of As(V), an identical behavior of iron and manganese was found, but the valence of arsenic has a significant influence on its binding as illustrated in Fig. 5.

As shown above, the addition of manganese leads to changes in the binding form of arsenic if As(V) was used. When As(III) instead of As(V) was added, again more arsenic is bound to the iron hydroxides (more than 1 mg As). However, the difference between the results with and without manganese was not significant ($t = 2.89$, $t(0.95;3) = 3.18$) in this experiment with As(III). A small amount of arsenic (about 0.1 mg) was still in solution after the precipitation, according to a concentration of about 3 mg l^{-1} . The con-

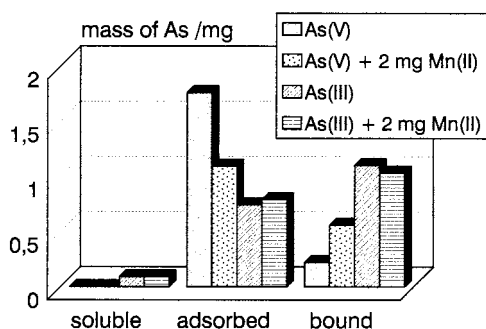


Fig. 5. Influence of the valence of arsenic on its binding.

centrations of arsenic measured in the effluent water were about 1.5 mg l^{-1} [2]. The slow oxidation process of As(III) to As(V) may be the reason for such high concentration in these water samples.

Additional oxidizable substances in the system are able to change the structure of the precipitate. In both cases, if Mn(II) or As(III) was used, the amount of arsenic bound to the precipitate increased.

3.2. Natural samples

Three different precipitate samples (sample 1–3) taken near the dam of the tailings and one additional taken about 50 m downstream (sample 4) were extracted sequentially with 1 mol l^{-1} NaOH and the oxalate buffer. The total contents of the analytes were determined by XRF for comparison. The results of the elements arsenic and iron are summarized in Tables 1 and 2.

More than 80% (w/w) of the total arsenic of the original samples can be removed by an extraction with NaOH. This means that a remobilisation of this part is easily possible without dissolving the

iron precipitate. The arsenic amounts analysed in the solution of step II (oxalate buffer) were always lower than 4% (w/w) of the total content. This fraction is much smaller in the natural samples than in the synthesized precipitates (> 13%). The highest total arsenic concentration was measured in the sample taken 50 m downstream. In this sample the amount analysed in step I is similar to the total contents.

This results prove the absence of any redistribution or re-adsorption processes discussed often for sequential extraction methods ([13–15]). This phenomenon can be excluded in the case of this simple two step method for iron hydroxide precipitates.

A calculation of the difference between the total contents and the sum of step I and II is not possible in all cases. The standard deviation in the different steps is too high considering the error propagation [16] to find a significant value for this difference. A significant difference was determined only for the samples 1 and 2. There was no difference between the results of the sequential extraction and the total content of the sample taken 50 m downstream. Consequently arsenic compounds existing in these samples taken near the dam, which have a low solubility in the used extraction solutions. A transport of particles from the tailings should be discussed to explain the presence of these compounds only in these samples.

From the samples near the dam (sample 1–3) only about 50% (w/w) or less of the total iron can be dissolved by the oxalate buffer, whereas almost all iron was detected in this extraction solution of the sample taken 50 m downstream. In this sample the iron is obviously bound in amorphous or poorly crystallized iron hydroxides. The absence

Table 1

Arsenic results of the original samples (mean value \pm S.D., mg g^{-1} dry substance)

	Sample 1	Sample 2	Sample 3	Sample 4
Total content (RFA)	50 ± 1	63 ± 1	29 ± 1	78 ± 1
NaOH leaching (step I)	45 ± 3	51 ± 3	26 ± 4	78 ± 5
Oxalic buffer leaching (step II)	0.33 ± 0.12	2.32 ± 0.16	0.77 ± 0.04	1.26 ± 0.20
Difference (RFA–step I–step II)	5 ± 3	12 ± 3	3 ± 4	

Table 2

Iron results of the original samples (mean value \pm S.D., mg g⁻¹ dry substance)

	Sample 1	Sample 2	Sample 3	Sample 4
Total contents	279 \pm 3	245 \pm 3	176 \pm 2	269 \pm 3
Oxalic buffer leaching (step II)	72 \pm 8	139 \pm 4	93 \pm 12	245 \pm 2

of crystallized iron compounds, which should be formed as a consequence of aging of the amorphous iron hydroxide precipitates, confirm with the findings of Paige et al. [17]. They have found that iron hydroxide precipitates containing more than 3 mol% (As/(As + Fe)) do not crystallize even at a temperature of 60°C and a pH of 12. The concentration of arsenic in the sample taken 50 m downstream is about 18 mol%.

In the area near the dam, where the other samples have been taken, the precipitate contains other iron compounds in different quantities. This confirms the hypotheses of a particle transport of hardly soluble minerals containing iron as well as arsenic. These particles settle a few meters after the seepage water source.

4. Conclusions

The synthesized precipitates prepared under controlled conditions and the sample taken 50 m downstream which obviously contains mainly amorphous or poorly crystallized iron hydroxides lead to similar results of the arsenic binding. The only difference was found in the extraction step II, where arsenic bound to the iron hydroxides is dissolved with the oxalate buffer. Only 1.6% of the total arsenic content in the natural sample 4 was detected in the extraction solution of step II. Values up to 40% of the total arsenic of the synthetic precipitates were detected in step II, if additional manganese or As(III) instead of As(V) was added. Values in this range were expected, because the concentrations of As(III) are remarkable high. Obviously the simple combination of two or three components is not able to describe

this complex process of precipitation satisfactorily. Nevertheless, it was a useful tool for checking the extraction method and for understanding the influence of the different components on the system. The developed procedure will be used for further investigations, which are aimed to immobilize the arsenic by modification of the precipitate.

Acknowledgements

The authors wish to thank Dr I.L. Marr from the University of Aberdeen (UK) for his critical review of the manuscript and the two anonymous referees for their helpful comments.

References

- [1] R.J. Allen, in: W. Salomons, U. Förstner, P. Mader (Eds.), *Heavy Metals*, Springer, Berlin, 1995, pp. 119–140.
- [2] R. Wennrich, J. Mattusch, H.J. Stärk, D. Schlegel, P. Morgenstern, U. Fankhänel, *Vom Wasser* 88 (1997) 1–12.
- [3] A. Tessier, P.G.C. Cambell, M. Bisson, *Anal. Chem.* 51 (1979) 844–851.
- [4] U. Förstner, *Intern. J. Environ. Anal. Chem.* 51 (1993) 5–23.
- [5] M.L. Pierce, C.B. Moore, *Water Res.* 16 (1982) 1247–1253.
- [6] G. Abbt-Braun, F.H. Frimmel, P. Lipp, *Z. Wasser-Abwasser-Forschung* 24 (1991) 285–292.
- [7] S. Kuwatsuka, A. Watanabe, I. Kazuhito, A. Shigemitsu, *Soil Sci. Plant Nutr.* 38 (1992) 23–30.
- [8] U. Förstner, *Z. Fresenius, Anal. Chem.* 316 (1983) 604–611.
- [9] U. Förstner, W. Calmano, *Vom Wasser* 59 (1982) 83–92.
- [10] E.E. van der Hoek, R.N.J. Comans, *Environ. Sci. Technol.* 30 (1996) 517–523.

- [11] R. Wagemann, *Water Res.* 12 (1978) 139–145.
- [12] N. Belzile, A. Tessier, *Geochim. Cosmochim. Acta* 54 (1990) 103–109.
- [13] C. Kheboian, C.B. Bauer, *Anal. Chem.* 59 (1987) 1417–1423.
- [14] P.M.V. Nirel, F.M.M. Morel, *Water Res.* 24 (8) (1990) 1055–1056.
- [15] M. Raksataya, A.G. Langdon, N.D. Kim, *Anal. Chim. Acta* 332 (1996) 1–14.
- [16] K. Doerffel, *Statistik in der analytischen Chemie*, VEB Deutscher Verlag für Grundstoffindustrie, Leipzig, 1987, p. 51.
- [17] C.R. Paige, W.J. Snodgrass, R.V. Nicholson, J.M. Scharer, *Water Environ. Res.* 68 (1996) 981–987.

A potentiometric study of protonation and complex formation of xylenol orange with alkaline earth and aluminum ions

M.B. Gholivand *, F. Bamdad, J. Ghasemi

Department of Chemistry, Razi University, Kermanshah, Iran

Received 1 July 1997; received in revised form 26 August 1997; accepted 23 September 1997

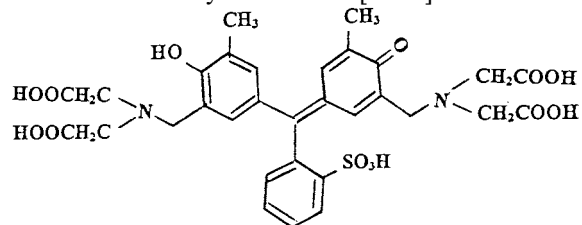
Abstract

Xylenol orange (XO) is one of the complexometric indicators, that can bind to metal cations at both their amino and acidic groups. In this study the protonation constants and distribution diagrams of XO were studied pH-metrically, and the corresponding six protonation constants were calculated. The complex formation between XO (L) and alkaline earth ions (M) was investigated and the formation constants of the resulting complexes ML, MHL, M₂L and M₂HL were determined. The stabilities of both ML and M₂L complexes were found to vary in the order Mg²⁺ > Ca²⁺ > Sr²⁺ > Ba²⁺. Studying the complex formation between Al³⁺ ion (M) and XO (L), it was observed that four complexed species with stoichiometries ML, ML₂, MHL and MH₂L could be formed in solution. It was also found that the Al L₂ complex can act as a chelating agent for further complexation with two cations other than Al³⁺ ion (i.e. Ba, L, Al, L, Ba, Mg, L, Al, L, Mg, and Mg, L, Al, L, Ba). The formation constants of the resulting mixed complexes were determined and their distribution diagrams were investigated. © 1998 Elsevier Science B.V. All rights reserved.

Keywords: Xylenol orange; Complexation of alkaline earth aluminum ions; Mixed complexes

1. Introduction

Xylenol orange (I) is an excellent complexometric indicator and potentiometric reagent for determination of many metal ions [1–15].



* Corresponding author.

Xylenol orange [3,3'-bis-*N,N*, di(carboxy methyl)-aminomethyl-*o*-cresol sulphonphthalein]. Due to the existence of more than one chelating system and the various acidic and basic properties of the XO molecule which can form various complexes, the investigation of such a system can be difficult. Therefore the differences in the composition of the XO-metal ion complexes and their stabilities [1–15] are due to this and the methods employed. To solve this problem the program developed by Martell and his coworkers [16] for potentiometric titration has been used. By using this method not only can the composition and stability of XO-metal ion complexes be solved but

Table 1
Protonation constants of XO ($t = 25^\circ\text{C}$, $\mu = 0.1$ (KNO₃))

Functional group	Calculated values ($\sigma_{\text{fit}} = .023$)	Reported values [20] [21]	
		(20)	(21)
$\log K_1$ $\equiv\text{NH}^+$	12.61	12.00	12.6
$\log K_2$ $\equiv\text{NH}^+$	9.68	10.30	10.5
$\log K_3$ $-\text{OH}$	7.34	7.50	6.40
$\log K_4$ $-\text{COOH}$	3.56	4.49	3.23
$\log K_5$ $-\text{COOH}$	2.16	2.74	2.58
$\log K_6$ $-\text{COOH}$	2.06	2.00	1.15
$\log K_7$ $-\text{COOH}$	—	—	0.76
$\log K_8$ $-\text{OH}^+$	—	—	-1.09
$\log K_9$ $-\text{SO}_3\text{H}$	—	—	-1.74

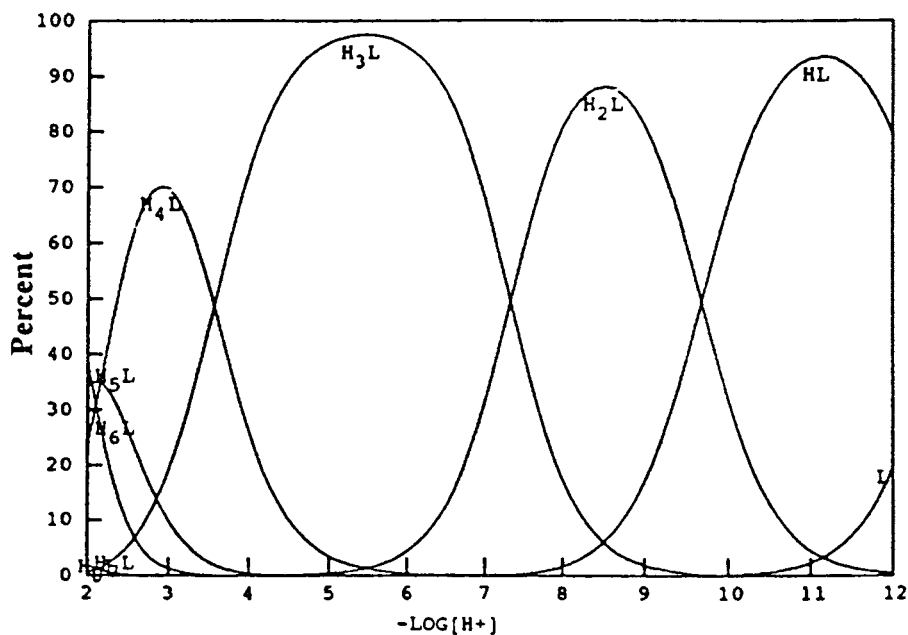


Fig. 1. Distribution of major species as a function of $-\log[\text{H}^+]$ for XO.

the study of mixed complexes using iterative methods and the FORTRAN program Best [16] is possible.

In this paper the composition and the protonation constants of XO and the stability constants of its complexes with alkaline earth, aluminum ions and mixed metals have been investigated.

2. Experimental section

2.1. Potentiometry

The apparatus consisted of a custom-designed, thermostated 80-ml capacity all-glass vessel. It was fitted with a cover having a 50-mm 'O' ring seal, through which was inserted a combined

Table 2
Formation constants of alkaline earth cation complexes with XO ($t = 25^\circ\text{C}$, $\mu = 0.1$ (KNO₃)) log K

Reaction	Mg ²⁺ (σ_{fit})	Ca ²⁺ (σ_{fit})	Sr ²⁺ (σ_{fit})	Ba ²⁺ (σ_{fit})	
$\text{M}^{2+} + \text{L}^{6-} \rightleftharpoons \text{ML}^{4-}$	8.96 (.036)	8.64 (.027)	7.46 (.023)	5.51 (.023)	[18]
	9.02	8.65	7.71	6.67	
$\text{H}^+ + \text{ML}^{4-} \rightleftharpoons \text{MHL}^{3-}$	10.08 (.036)	10.10 (.027)	10.11 (.023)	10.86 (.023)	
	10.3	10.41	10.4	10.5	[18]
$\text{M}^{2+} + \text{ML}^{4-} \rightleftharpoons \text{M}_2\text{L}^{2-}$	5.28 (.020)	4.69 (.027)	4.42 (.019)	3.45 (.022)	
	6.74	6.02	4.89	4.57	[18]
$\text{H}^+ + \text{M}_2\text{L}^{2-} \rightleftharpoons \text{M}_2\text{HL}^-$	8.15 (.020)	8.47 (.027)	8.40 (.019)	9.30 (.022)	
	6.8	6.9	7.6	8.0	[18]

glass electrode, a delivery tube for a Metrohm piston buret, and inlets and outlets for prepurified nitrogen. Each experiment was preceded by standardization of the pH meter, which was calibrated to display $-\log[\text{H}^+]$ using dilute standard HCl and KOH solutions. The system was maintained

at an ionic strength of $\mu = 0.10$ M with KNO₃ as a supporting electrolyte.

In general, an experimental run involves collecting equilibrium data points throughout the entire pH range, between 2.0 and 11.0 as a function of millimoles standard KOH, added using the piston buret through a fine capillary tip immersed in the solution. In titration, after each addition, the required time was allowed to reach chemical equilibrium. The concentration of the reactants in the experimental solution were in the order 10^{-3} M for each component. The hydrogen concentration was measured using a Metrohm model 686 titro-processor connected to a confident 286 PC for data transfer and computation.

The potentiometric equilibrium measurements of the ligand solution in the absence and presence of metal ions was calculated using the program Best [16]. The protonation and formation constants of all species were obtained through the least-squares refinement of its $\text{p}[\text{H}^+]$ profiles. Throughout this investigation the function minimized was the weighted average of the sums of squares of deviations between calculated and observed $\text{p}[\text{H}^+]$ value (σ_{fit}).

2.2. Electronic spectra

The electronic spectra were produced on a Beckman 34 spectrophotometer and the absorbance measurements were carried out on a Metrohm 662 probe-type photometer.

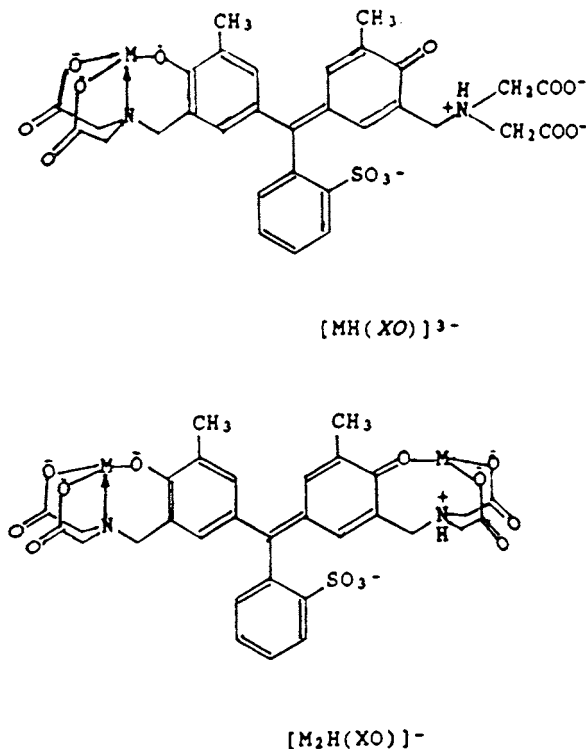


Fig. 2. The structure of alkaline earth-XO complexes

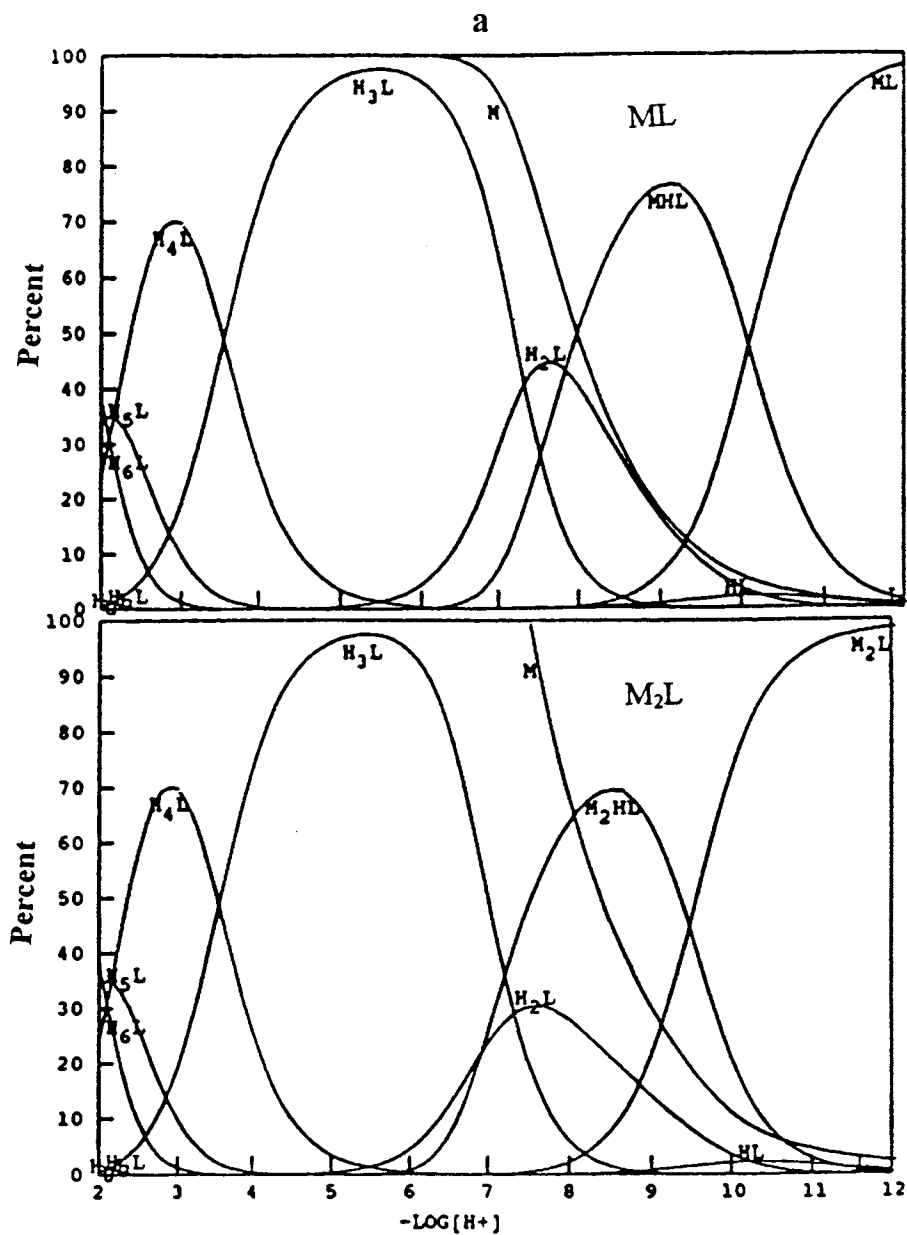


Fig. 3. Distribution of major species as a function of $-\log[H^+]$ for 1:1 and 2:1 molar ratio of XO to Mg^{2+} and Ba^{2+} ions, (a) (Mg^{2+}); (b) (Ba^{2+}).

2.3. Reagents

Xylenol orange and metal salts (nitrate) were of reagent grade (Merck) and were used without any

further purification. KOH solution (titrisol) was prepared and eluted from an anion exchange column to remove carbonate, and standardized with potassium hydrogen phthalate (KHP).

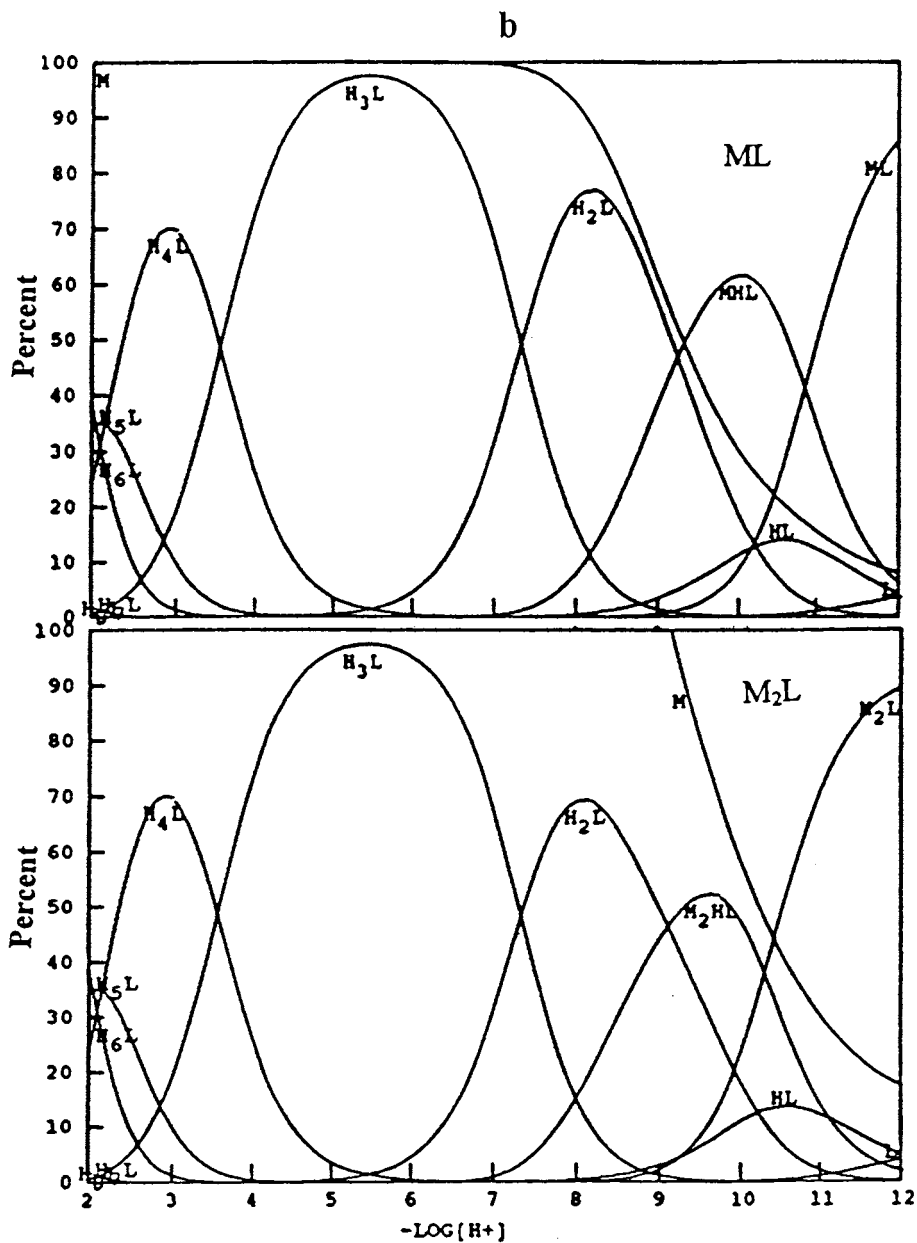


Fig. 3. (Continued)

3. Results and discussion

3.1. Protonation constants

The protonation constants of xylenol orange

(XO) were calculated from the potentiometric titration of free ligand using the program Best. XO can be represented by the symbolic formula H_6L showing the presence of six ionizable hydrogens. In the absence of metal ions, depending on

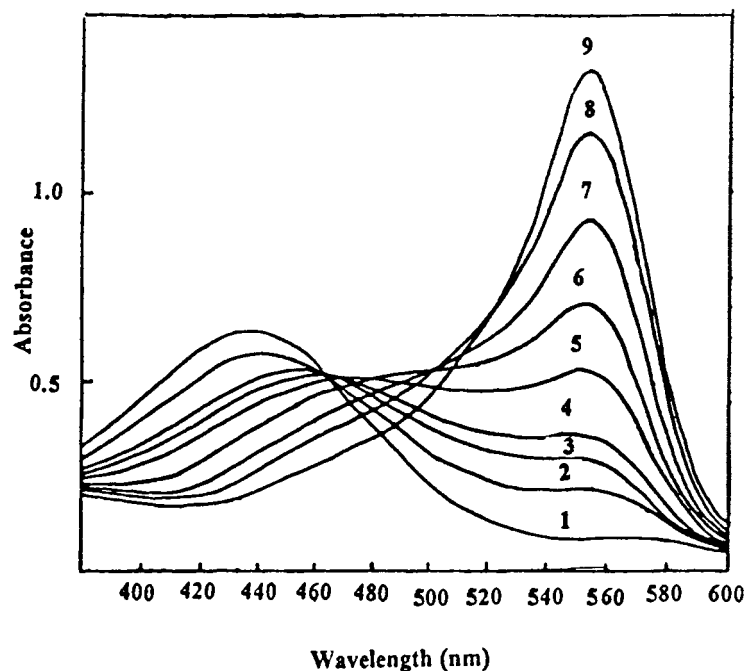


Fig. 4. Visible absorption spectra for titration of XO (5.0×10^{-5} M) with Al^{3+} ion; $\text{CaAl}^{3+} = 1(0.0)$, $2(1.0 \times 10^{-5})$, $3(2.0 \times 10^{-5})$, $4(2.5 \times 10^{-5})$, $5(3.0 \times 10^{-5})$, $6(4.0 \times 10^{-5})$, $7(5.0 \times 10^{-5})$, $8(6.0 \times 10^{-5})$, $9(7 \times 10^{-5}$ M).

the pH there are several possible forms that XO can adopt. In addition XO can acquire up to three positive charges. The resulting protonation constant values are listed in Table 1. The small differences between our values and previously reported values are in part due to the more accurate nature of the present computational technique compared with graphical or approximate methods used by earlier workers.

It can be seen from the distribution curves of XO (Fig. 1) and Table 1, the two last constants are too low and, after dissolution, XO immediately loses these protons. Therefore at pH 2, H_8L and H_9L make no contribution to the distribution curve, the concentration of H_7L is so low that it can be ignored. The other six species are distributed (in considerable concentrations) from pH 2.0 to pH 12.0.

According to previous reports [17], the first two protonation constants are due to protonated nitrogen atoms, the remaining constants are due to one-OH group and three carboxylic acid groups of the iminodiacetate arms of XO. These three

latter protonation steps have no effect on the color change of XO, the color of the solution is yellow and has an absorption maximum at 435

Table 3
Formation constants of aluminum and mixed metal complexes with XO ($t = 25^\circ\text{C}$, $\mu = 0.1$ (KNO_3))

Reaction	$\log K$ (σ_{fit})
$\text{Al}^{3+} + \text{L6}^- = = \text{AIL}^{3-}$	18.18 (.015)
$\text{H}^+ + \text{AIL}^{3-} = = \text{AIHL}^{2-}$	7.45 (.015)
$\text{H}^+ + \text{AIHL}^{2-} = = \text{AIH}_2\text{L}^-$	5.14 (.015)
$\text{L}^{6-} + \text{AIL}^{3-} = = \text{AIL}_2^{9-}$	5.22 (.038)
$2\text{Mg}^{2+} + \text{AIL}_2^{9-} = = (\text{Mg})_2\text{AIL}_2^{5-}$	4.03 (.042)
$2\text{Ba}^{2+} + \text{AIL}_2^{9-} = = (\text{Ba})_2\text{AIL}_2^{5-}$	1.12 (.019)
$\text{Ba}^{2+} + \text{Mg}^{2+} + \text{AIL}_2^{9-} = = \text{BaMgAIL}_2^{5-}$	2.79 (.021)

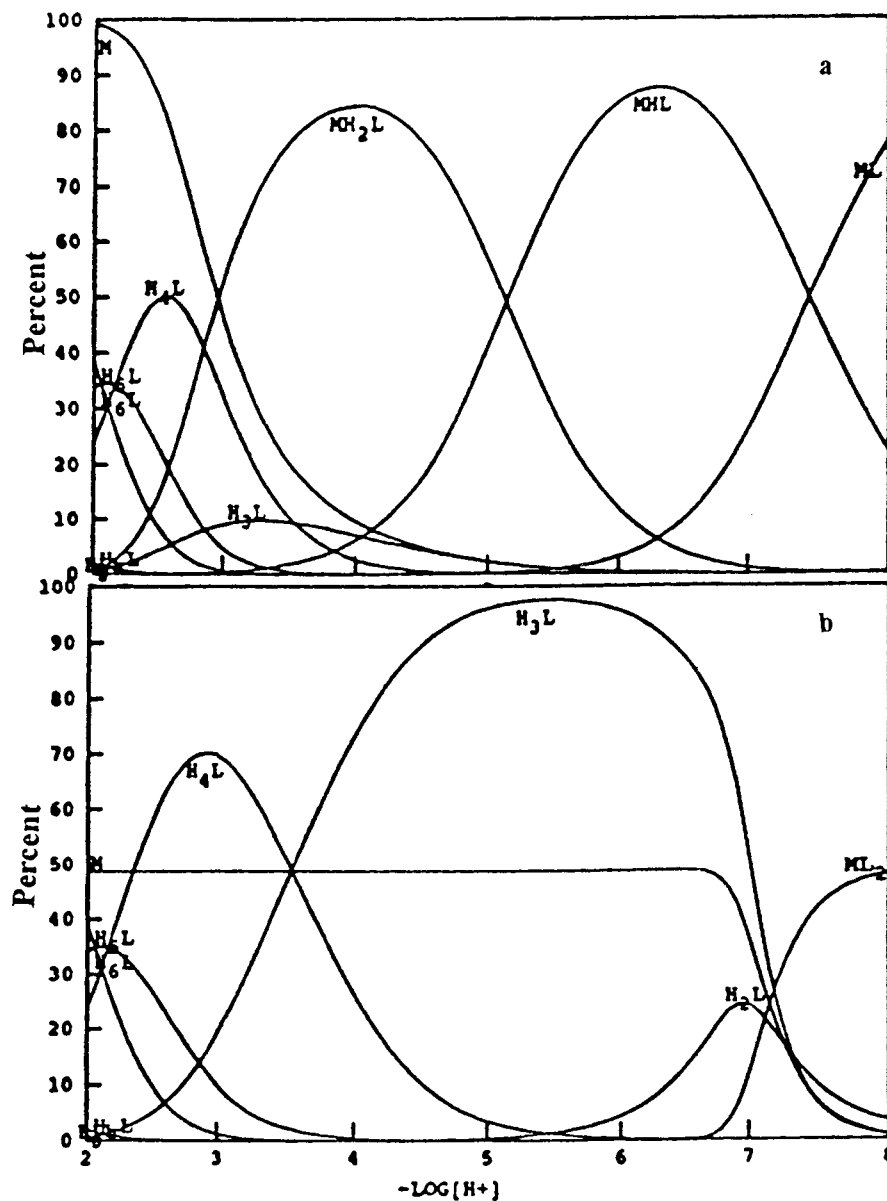


Fig. 5. Distribution of major species as a function of $-\log[H^+]$ for a 1:1 (a) and 1:2 (b) molar ratio of XO to Al^{3+} ion.

nm. At a pH of 6.5 another maximum appears at 580 nm, becoming prominent at pH 7.0 and being the only one at pH > 8, the color then changes to red.

3.2. Alkaline earth complexes

Alkaline earth cations react with XO at a pH above 6 in aqueous solutions. The program Best

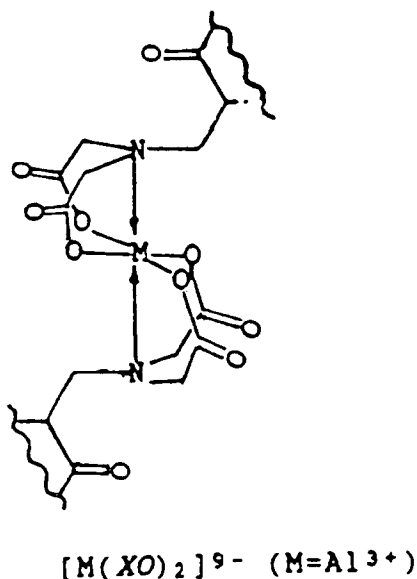


Fig. 6. The structure of Aluminum–XO with mole ratio 1:2.

allowed us to calculate the formation constants reported in Table 2. All cations used form four species, namely ML^{4-} , MHL^{3-} , M_2L^{2-} , and M_2HL^- . Fig. 2 shows the possible structures of alkaline earth–XO complexes [18]. The metal ion may bind with one of the phenol groups and with two carboxyl groups of the iminodiacetate arm at the same side as sulphonphthalein. As a result of this combination, a proton of MHL from the nitrogen atom of the iminodiacetate arm of the XO dissociates to form the ML complex.

The M_2HL complex is a result of the second metal ion binding with the vacant coordination sites located at the other side of the XO molecule—with an arrangement similar to the first coordinated metal. A proton of M_2HL can dissociate to form the M_2L complex.

The distribution curves for various dissociated forms of the ligand and its alkaline earth complexes are shown in Fig. 3. These curves show the complication of the complexation reactions. For all alkaline earth–XO systems used, the ML and M_2L complexes can be formed in an alkaline pH range. It is obvious from distribution curves that the contributions of MHL and M_2HL complexes are smaller than ML and M_2L types. With the exception of the XO– Ba^{2+} system, all distribu-

tion curves have relatively similar features. Barium ion having the smallest stability constant in the series, shows complex formation with XO at higher pH values than any other metal ion used, and thus a fair amount of the free ligand species HL and L exist in the barium distribution curve which are negligible in other cation systems.

Table 2 shows a decrease in the stability of the XO–alkaline earth complexes for M_2L and ML, in the order $Mg^{2+} > Ca^{2+} > Sr^{2+} > Ba^{2+}$. The same stability order has been previously reported [18]. This sequence shows that the interaction between XO and alkaline earth cations increases with increasing charge density of the metal ion. However, it should be noted that the stability constants result from a balance between the binding energy and the solvation energies of all charged species involved in complexation reactions.

3.3. Aluminum and mixed metal complexes

The three charges on the small aluminum cation causes the cation to react strongly with XO forming two major complexes, with metal to ligand stoichiometries of 1:1 and 1:2 (i.e. ML and ML_2) [19]. From the absorption curve (Fig. 4) it is apparent that two complexes can be formed. The existence of 1:1 and 1:2 (metal to ligand) complex has been proven using the molar-ratio and continuous variation methods, measuring the absorbance at 550 nm (Fig. 4) at a pH 5. The aluminum ion is capable of forming protonated complexes, as well as normal 1:1 (ML) complexes. Two protonated forms of the ML complex were found in this study and their formation constant, were calculated using the program Best (Table 3). A comparison of the normal stability constants (K_{mL}) and their protonation constants reveal a concerted two-proton reaction, going from Al_2L to AlH_2L . Such behavior seems to involve a change in the coordination geometry and/or coordination number of the complexes involved. According to the corresponding distribution diagram (Fig. 5) these protonated species ($AlHL^{2-}$ and AlH_2L^-) are formed at low pH ranges.

In the ML_2 system, however, the protonated complexes (MHL_2 , MH_2L_2 etc.) were not found

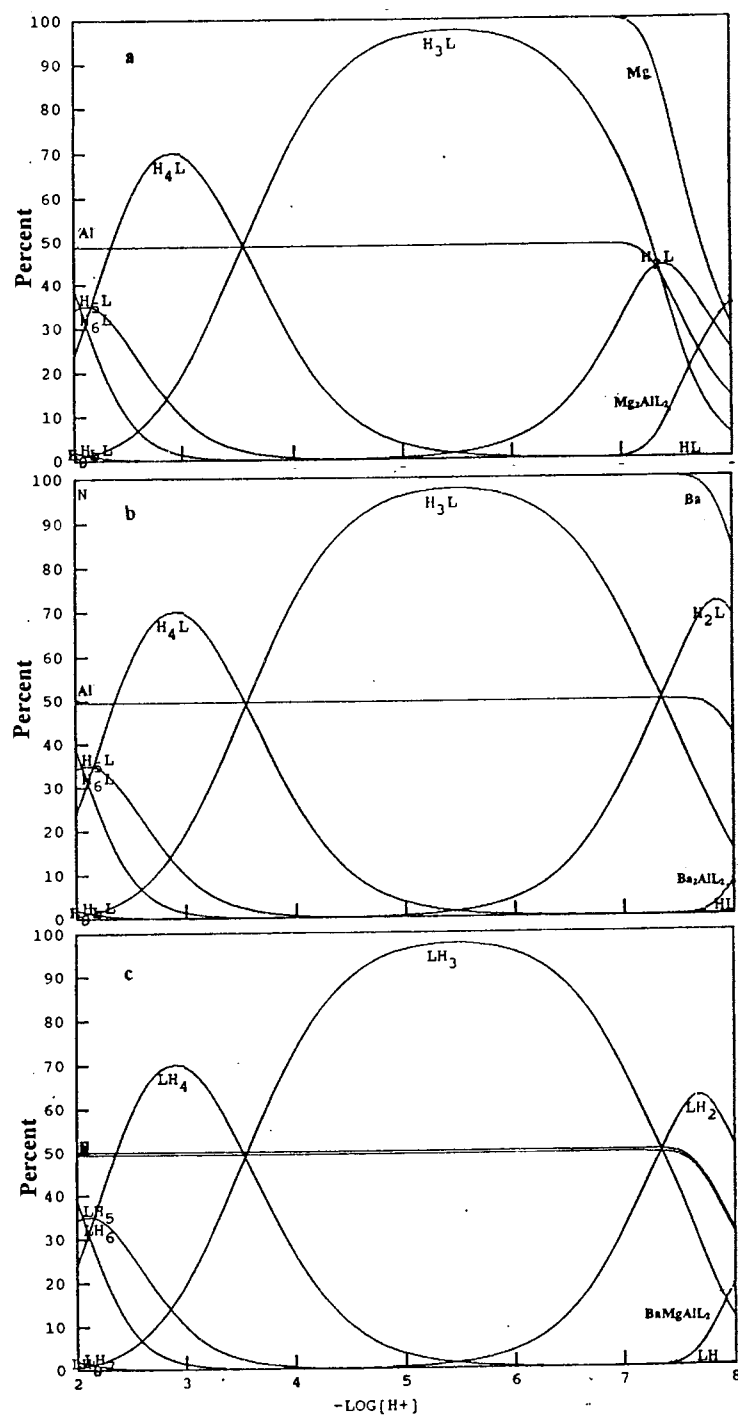


Fig. 7. Distribution of major species as a function $-\log[H^+]$ for 2:1:2 mole ratio of alkaline earth-Aluminum-XO, (a) $(Mg_2Al(L_2)_2)$, (b) $(Ba_2Al(L_2)_2)$, (c) $(BaMgAl(L_2)_2)$, (L = XO).

by the program, the deprotonated complex has the unique form of the $Al^{3+}-XO$ complex, in the corresponding distribution curve (Fig. 5). According to the literature [20], XO forms complexes at each of the iminodiacetate arms independently, hence in the ML_2 complex a metal cation can be coordinated by the other arms of two XO molecules (Fig. 6).

Further complexation of the ML_2 complex with other cations such as Ba^{2+} and Mg^{2+} indicates that the free sites of the resulting ML_2 complex can act as a chelating agent for mixed metal complexation. Using this property the Ba, L, Al, L, Ba, Mg, L, Al, L, Mg and Mg, L, Al, L, Ba mixed metal complexes were studied. The existence of these complexes was proven using the program Best. They are the major species that can be found in the $2M^{2+}:Al:2XO$ mixture in aqueous solution. The search for other species as well as protonated complexes ($2M^{2+}:Al:H_n:2XO$) gave results that did not correlate well with experimental data. From Table 3 it can be clearly observed that the formation constant of the $MgBa(XO)_2Al$ complex falls between the calculated values for the two complexes $Mg_2(XO)_2Al$ and $Ba_2(XO)_2Al$. The distribution curve for mixed metal complexes (Fig. 7) shows, that the $Mg:XO:Al:XO:Ba$ complex is formed between the pH range of formation of $Mg_2(XO)_2Al$ and $Ba_2(XO)_2Al$.

References

- [1] J. Körbl, R. Pribil, A. Emr, Collect. Czech. Chem. Commun. 22 (1957) 961.
- [2] J. Körbl, R. Pribil, Chemist-Analyst 46 (1956) 102.
- [3] K.L. Cheng, Talanta 2 (1959) 61.
- [4] K.L. Cheng, Talanta 2 (1959) 266.
- [5] K.L. Cheng, Anal. Chim. Acta 28 (1963) 41.
- [6] K.L. Cheng, Talanta 3 (1959) 81.
- [7] M. Otomo, Bull. Chem. Soc. Jpn. 36 (1963) 140.
- [8] B. Budesinsky, Collect. Czech. Chem. Commun. 27 (1962) 226.
- [9] K.L. Cheng, Talanta 3 (1959) 147.
- [10] H. Onishi, N. Ishiwatari, Bull. Chem. Soc. Jpn. 33 (1960) 1581.
- [11] H. Onishi, N. Ishiwatari, Talanta 8 (1961) 753.
- [12] K.L. Cheng, Talanta 5 (1960) 254.
- [13] K. Studlar, J. Janousek, Talanta 8 (1961) 203.
- [14] K. Tonosaki, M. Otomo, Bull. Chem. Soc. Jpn. 35 (1962) 1983.
- [15] M. Otomo, Bull. Chem. Soc. Jpn. 36 (1963) 140.
- [16] R.J. Molekalis, A.E. Martell, Can. J. Chem. 60 (1982) 2403.
- [17] A. Hulanicki, S. Glab, G. Ackermann, Pure Appl. Chem. 55 (1988) 1173.
- [18] T. Yoshino, H. Okasoki, S. Murakam, M. Kagawa, Talanta 21 (1974) 676.
- [19] V.A. Nazarenko, E.M. Nevskaya, Zh. Anal. Khim. 29 (1969) 536.
- [20] M. Yamada, Bunseki Kagaku, 25 (1976) 850.
- [21] B. Budesinsky, Xylenol Orange and Methylthymol Blue as chromogenic reagents, in: H.A. Flaschka, A.J. Barnard, Jr., (Eds.), Chelates in Analytical Chemistry, vol. 1, Marcel Dekker, New York, 1967, p. 15.

New cesium ion-selective electrodes based on anilino-(1,3-dioxo-2-indanylidene) acetonitrile derivatives

Mohamed B. Saleh *

Chemistry Department, Faculty of Science, Minia University, Minia, Egypt

Received 27 May 1997; received in revised form 1 September 1997; accepted 23 September 1997

Abstract

Cesium ion-selective PVC membrane electrodes based on anilino-(1,3-dioxo-2-indanylidene) acetonitrile derivatives as a novel class of neutral ionophores were examined. The ionophores were *p*-methoxyanilino-(1,3-dioxo-2-indanylidene) acetonitrile, *p*-methylanilino-(1,3-dioxo-2-indanylidene) acetonitrile and *p*-*N,N*-dimethylanilino-(1,3-dioxo-2-indanylidene) acetonitrile. The anilino-(1,3-dioxo-2-indanylidene) acetonitrile proved to work well with cesium, the corresponding electrodes display a response to this ion. The most favourable ionophore was *p*-methoxyanilino-(1,3-dioxo-2-indanylidene) acetonitrile, especially when the secondary ion exchanger potassium tetrakis (4-chlorophenyl) borate was incorporated in 2-nitrophenyl octyl ether for ion-selective electrode membrane construction. The response function was linear within the concentration range 10^{-1} – 2.5×10^{-5} mol l⁻¹ and the slope was 52 mV decade⁻¹. The detection limit remained at 6.3×10^{-6} mol l⁻¹. The selectivity and response time of the electrode was studied and it was found that the electrode exhibited good selectivity for cesium over alkali, alkaline earth and some transition metal ions. The electrode response was stable over a wide pH range. The lifetime of the electrode was about 1 month. © 1998 Elsevier Science B.V. All rights reserved.

Keywords: Anilino-(1,3-dioxo-2-indanylidene) acetonitrile; Cesium ion-selective electrodes; Potentiometry

Crown ethers have been used as neutral ionophores in Cs⁺ ion-selective electrodes (ISE_S). Those based on 15-crown-5 functionality have produced excellent Nernstian response slopes, detection limits (DL_S), and short response times of less than 1 min. However, the selectivities for interferents was relatively high [1]. The bis(benzo-18-crown-6) derivatives seem to produce the best Cs⁺ electrodes [2], since the *cis*-form is capable of forming sandwich-type Cs⁺

complexes. The electrode developed by Attiyat et al. [3] which incorporates a dibenzo dioxatetraazacylotetradecin-carbonitrile exhibited a twenty-five-fold selectivity over Rb⁺ and K⁺ respectively. A dibenzo-24-crown-8 has been proposed as a promising Cs⁺ PVC-based ISE [4]. The plasticizing agent was dibutyl phthalate (DBP) as opposed to the more frequently employed 2-nitrophenyl octyl ether (2-NPOE). Moreover, the influence of membrane components such as secondary ion exchangers [5], plasticizers [6] and polymer base [7] on electrode

* Tel.: +20 86 323011; fax: +20 86 342601.

performance has been examined in the literature. Recently, Michael et al. [8] constructed cesium-selective electrodes based on crowned benzoquinones with 2-NPOE, and incorporating the secondary ion exchanger potassium tetrakis(4-chlorophenyl) borate (KTCIPB). The selectivity coefficients of the cesium electrode based on the best ionophore 2,3-benzoquinol[15]crown-5 to Rb^+ , K^+ and Na^+ ($\log K_{\text{Cs,M}}^{\text{Pot}}$) were -0.47 , -0.99 and -2.38 , respectively. There was interference from Ag^+ ($\log K_{\text{Cs,Hg}}^{\text{Pot}} = 0.94$) and Hg^{2+} ($\log K_{\text{Cs,Hg}}^{\text{Pot}} = 2.12$). In this work, anilino-(1,3-dioxo-2-indanylidene) acetonitrile derivatives are examined as a novel class of neutral ionophores in cesium-selective PVC membrane electrodes.

1. Experimental

1.1. Materials

The neutral ionophores [anilino-(1,3-dioxo-2-indanylidene) acetonitrile derivatives] used in this work (Fig. 1) were synthesized as previously described [9,10].

The plasticizer dioctyl adipate (DOA), diethyl phthalate (DEP), dibutyl adipate (DBA), tris(2-ethylhexyl) phosphate (TEHP) and dibutyl phthalate (DBP) were obtained from Aldrich (Milwaukee, WI) and 2-nitrophenyl octyl ether (2-NPOE) from Fluka (Buchs, Switzerland).

The lipophilic salts (as membrane additives) used were obtained as follows: sodium tetraphenylborate (NaTPB) from BDH (Poole, UK), sodium tetrakis (4-fluorophenyl) borate (NaTFPB) from Aldrich and KTCIPB from Fluka. High molecular mass poly(vinyl chloride) (PVC) was obtained from Fluka and tetrahydrofuran (THF) from Aldrich. All solutions were prepared from salts of reagent grade using doubly-distilled water.

1.2. Electrode preparation

The membrane components outlined in Table 1 were mixed and dissolved in THF overnight. The resulting homogeneous mixture was poured into a glass ring [11] with an inner diameter of 30 mm

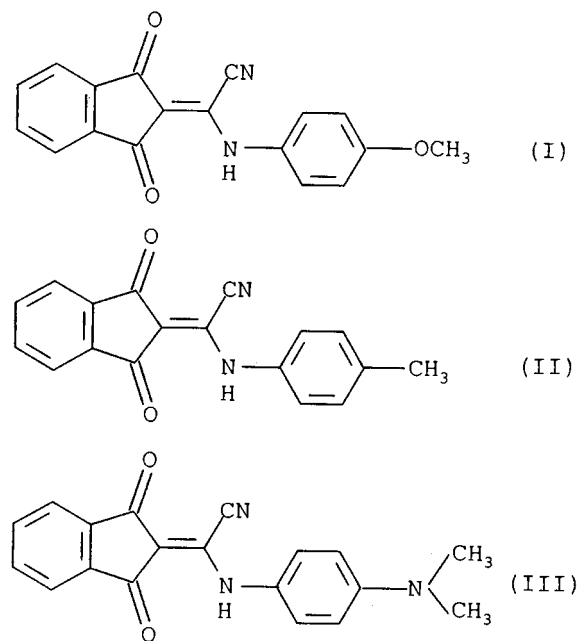


Fig. 1. Ionophores employed in this work: I, *p*-methoxyanilino-(1,3-dioxo-2-indanylidene) acetonitrile; II, *p*-methylanilino(1,3-dioxo-2-indanylidene) acetonitrile; III, *p*-*N,N*-dimethylanilino-(1,3-dioxo-2-indanylidene) acetonitrile.

resting on a smooth glass plate and the THF was evaporated at room temperature. Transparent PVC membranes were obtained with an average thickness of 0.2 mm. A 1 mm (approximately) diameter piece was cut out from the PVC membrane and attached to a PVC tube by means of PVC-THF solution (250 mg of PVC powder in 5 ml of THF). The PVC tube with the membrane was then connected to an Ag-AgCl wire electrode. After filling with a solution of $10^{-3} \text{ mol l}^{-1}$ CsCl as internal solution, the electrode was conditioned for 24 h by soaking in $10^{-3} \text{ mol l}^{-1}$ CsCl solution.

Table 1
Membrane components used in ISE membrane construction

Component	Amount (% m m ⁻¹)	Mass (mg)
Ionophore	0.99	1.8
Lipophilic salt	0.27	0.5
Plasticizer	65.83	120
PVC	32.91	60
THF	—	2 ml

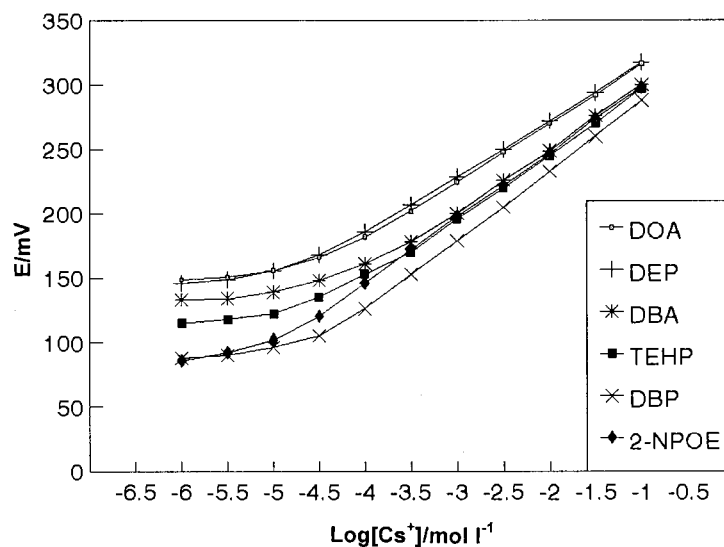


Fig. 2. Effect of plasticizers on the responses of cesium ion-selective electrodes based on ionophore I.

1.3. Measurements of electrode potentials

All potential measurements were made with a Fisher Scientific Computer-Aided pH-meter (Model 450). The sample solutions were stirred and thermostated at $25 \pm 1^\circ\text{C}$. The electrochemical system was as follows: Ag–AgCl/internal solution ($10^{-3} \text{ mol l}^{-1} \text{ CsCl}$)/PVC membrane/sample solution/saturated KCl/AgCl–Ag. The external reference electrode was a double-junction Ag–AgCl (Cole-Parmer 7425 N). Standard CsCl solutions for calibration was obtained by the gradual dilution of $0.1 \text{ mol l}^{-1} \text{ CsCl}$ solution. Response times were determined as follows: after the potential of one cesium solution becomes constant, similar measurements were carried out in another

solution, of 100-fold concentration. Potentiometric selectivity coefficients were determined by the separate solutions method [12] using aqueous 0.1 mol l^{-1} solutions of metal chlorides in accordance with the equation

$$\log K_{\text{Cs},\text{M}}^{\text{Pot}} = \frac{E_{\text{M}} - E_{\text{Cs}^+}}{S} + \left(1 - \frac{Z_{\text{Cs}}}{Z_{\text{M}}}\right) \log[\text{M}] \quad (1)$$

where $K_{\text{Cs},\text{M}}^{\text{Pot}}$ is the selectivity coefficient, E_{Cs^+} is the potential measured in $0.1 \text{ mol l}^{-1} \text{ CsCl}$ solution, E_{M} is the potential measured in 0.1 mol l^{-1} solution of the chloride of the interfering cation, Z_{Cs}^+ and Z_{M} are the charges of cesium and the interfering ions, respectively, and S is the slope of the response function. For monovalent interferent ions, Eq. (1) simplifies to

Table 2

Effect of plasticizers on the selectivities of cesium ion-selective electrodes based on ionophore I

Plasticizer	$\log K_{\text{Cs},\text{M}}^{\text{Pot}}$						
	Li^+	Na^+	K^+	Rb^+	NH_4^+	Mg^{2+}	Ca^{2+}
DOA	−1.13	−0.86	−0.35	−0.30	−0.68	−2.96	−3.20
DEP	−1.71	−1.33	−0.64	−0.49	−0.98	−3.08	−3.10
DBA	−0.76	−0.46	−0.02	−0.03	−0.35	−2.55	−2.74
TEHP	−0.93	−0.71	−0.27	−0.17	−0.39	−2.88	−3.28
DBP	−1.72	−1.15	−0.35	−0.17	−0.78	−3.07	−3.33
2-NPOE	−3.33	−2.72	−1.22	−0.70	−1.59	−3.70	−4.13

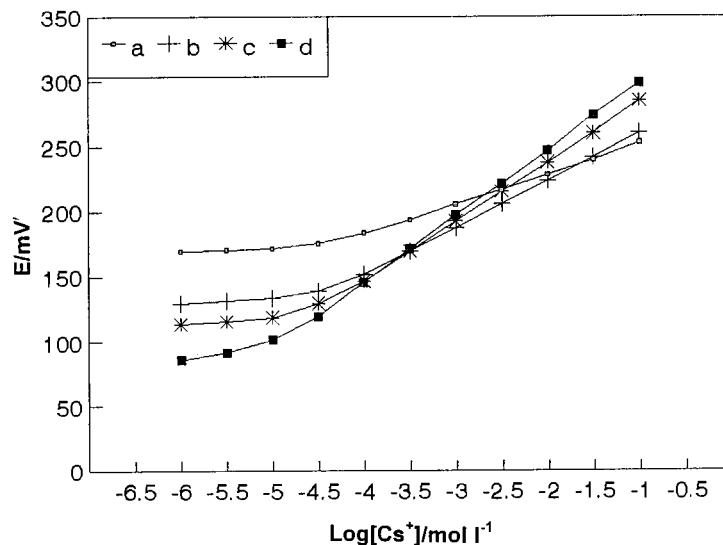


Fig. 3. Effect of anionic membrane components on responses of cesium ion-selective electrodes based on ionophore I: (a) ionophore I + PVC + 2-NPOE; (b) a + TPB; (c) a + TFPB and (d) a + TCIPB.

$$\log K_{Cs,M}^{Pot} = \frac{E_M - E_{Cs^+}}{S} \quad (2)$$

The influence of pH on the electrode response was examined by adjusting the pH of the measured solution with 1 mol l⁻¹ sodium hydroxide and hydrochloric acid. Electrode lifetimes were also examined by monitoring the slope of Cs⁺ calibrations periodically.

2. Results and discussion

The effect of plasticizers DOA, DEP, DBA, TEHP, DBP and 2-NPOE on cesium-selective PVC membrane electrodes based on ionophore I were studied. The electrode properties are shown

in Fig. 2 and summarized in Table 2. They demonstrate that the electrode based on ionophore I with 2-NPOE as plasticizer gives a good response to the cesium ion with a slope of 52 mV decade⁻¹ and a detection limit of 6.3 × 10⁻⁶ mol l⁻¹. With other plasticizers, the performance of the electrode was inferior to that containing 2-NPOE. Table 2 reveals that the selectivity coefficients of the 2-NPOE systems are generally much smaller than those of other systems. The variation in observed electrode response and selectivity using different plasticizers may be attributed to different carrier mechanisms [13]. Moreover, polar plasticizer 2-NPOE leads to the lowering of the membrane resistance as compared with apolar plasticizers DOA, DEP, DBA,

Table 3

Effect of anionic membrane components on selectivities of cesium ion-selective electrode based on ionophore I

Anionic membrane component	log $K_{Cs,M}^{Pot}$				
	Li ⁺	Na ⁺	K ⁺	Rb ⁺	Mg ²⁺
(a) Ionophore I + 2-NPOE + PVC	-1.91	-1.57	-0.77	-0.44	-2.47
(b) a + TPB	-1.99	-1.81	-0.96	-0.52	-2.88
(c) a + TFPB	-2.70	-2.48	-1.07	-0.55	-3.57
(d) a + TCIPB	-3.33	-2.72	-1.22	-0.70	-3.70

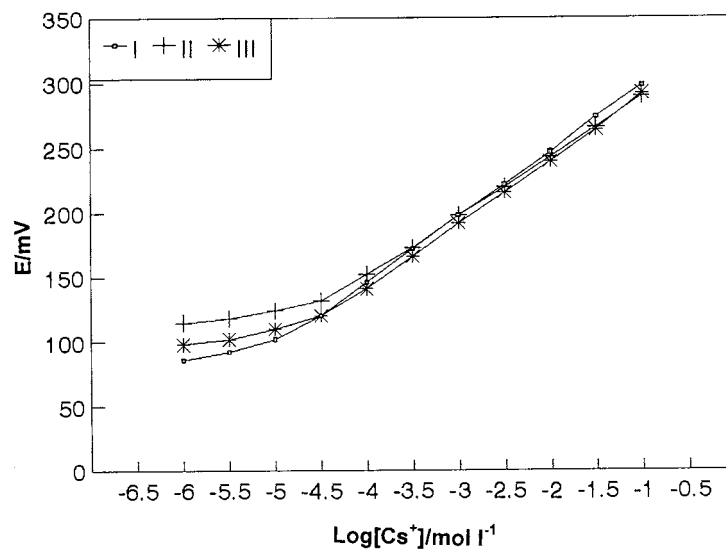


Fig. 4. Potential responses of cesium ion-selective electrodes based on ionophores I–III.

TEHP and DBP. 2-NPOE was presented as the best plasticizer for the proposed PVC membrane electrode systems.

The dependence of the electrode response and selectivity coefficient of the cesium-selective PVC membrane electrode on the anionic membrane components is shown in Fig. 3 and presented in Table 3. The results indicate that the membrane containing ionophore I with 2-NPOE, in the ab-

sence of anionic sites in the membrane phase (membrane component a, Fig. 3) gives a response to cesium ion with a sub-Nernstian slope of $24 \text{ mV decade}^{-1}$ and a detection limit of $4.0 \times 10^{-5} \text{ mol l}^{-1}$. The response of this electrode, however, is linear in the range 10^{-1} – $10^{-4} \text{ mol l}^{-1}$ and the electrode selectivity for Cs^+ over Li^+ , Na^+ , K^+ , Rb^+ and Mg^{2+} is fairly high (Table 3). Several neutral ionophores are known that do not induce

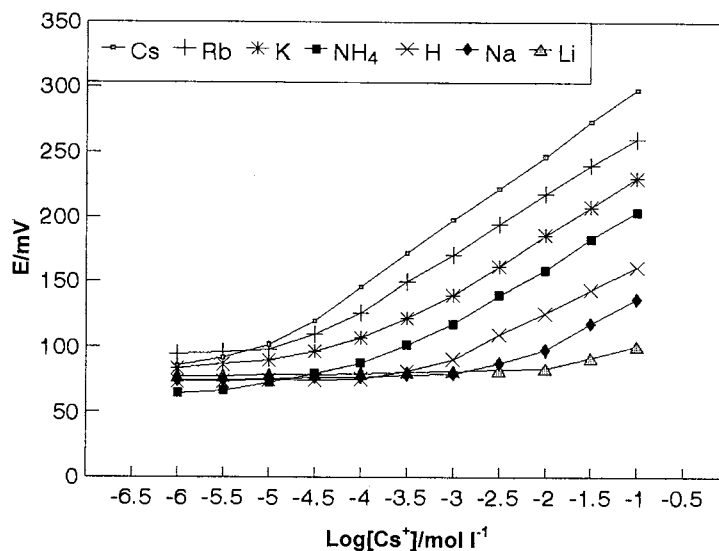


Fig. 5. Calibration of the ionophore I electrode for alkali metal and ammonium ions.

Table 4
Effect of anionic additives (TCIPB) on selectivities of cesium ion-selective electrodes

Anionic additives	$\log K_{Cs,M}^{Pot}$					
	H ⁺	Li ⁺	Na ⁺	K ⁺	Rb ⁺	NH ₄ ⁺
(a) 0.5 mg TCIPB+2-NPOE+PVC	-2.19	-2.87	-2.40	-0.98	-0.53	-1.42
(b) 1.5 mg TCIPB+2-NPOE+PVC	-2.18	-2.90	-2.39	-1.00	0.54	-1.45
(c) 3.0 mg TCIPB+2-NPOE+PVC	-2.20	-2.92	-2.42	-1.01	-0.56	-1.46

any selectivity in membranes, in the absence of additional anionic sites [5,14]. The selectivity data of the membrane without anionic site additives is possibly due to interfacial kinetic limitations in the transfer of ions from the sample solution to the membrane phase and vice versa. Lipophilic anionic components can efficiently catalyze this cation transfer [15].

Incorporation of TPB or TFPB as a lipophilic anion with ionophore I (membrane components (b) and (c), Fig. 3) in the membrane phase improves the detection limits (2.2×10^{-5} and 1.8×10^{-5} mol l⁻¹, respectively), increases the slope of the electrode response (36 and 46 mV decade⁻¹,

respectively) and increases the membrane selectivity (Table 3). It is obvious from Fig. 3 that the incorporation of a highly lipophilic anion, TCIPB, with ionophore I (membrane component (d)) in the membrane phase leads to a decrease in the detection limit (6.3×10^{-6} mol l⁻¹), increase in the calibration slope (52 mV decade⁻¹) and an increase in membrane selectivity compared with TPB or TFPB. This occurs because its water solubility is lower than that of TPB and TFPB [16], and as such decreases membrane resistance and increases the permselectivity of the membrane for cations.

The potential response of the PVC cesium-selective electrode based on ionophore I (Fig. 1) using of 2-NPOE as plasticizer, and incorporating the secondary ion exchanger KTCIPB is shown in Fig. 4. The electrode seems to exhibit a linear response to cesium ions within the concentration range 10^{-1} – 2.5×10^{-5} mol l⁻¹ CsCl with a slope of 52 mV decade⁻¹ and a detection limit of 6.3×10^{-6} mol l⁻¹. For ionophores II and III, as shown in Fig. 4, linear responses in the concentration range 10^{-1} – 6.3×10^{-5} and 10^{-1} – 4.0×10^{-5} mol l⁻¹, respectively were also observed, they showed slopes of 48 and 51 mV decade⁻¹ and detection limits of 2.0×10^{-5} and 1.3×10^{-5} mol l⁻¹, respectively. The alkali metal ion calibration plot of the electrode based on ionophore I, i.e., *p*-methoxyanilium-(1,3-dioxo-2-indanylidene) acetonitrile, is given in Fig. 5. The corresponding plots for this electrode for other metal ions indicate high Cs⁺ selectivity over divalent ions. All cations produced responses with slopes and detection limits values lower than the Cs⁺ response. The cation response order for metal ions is Cs⁺ > Rb⁺ > K⁺ > NH₄⁺ > H⁺ > Na⁺ > Li⁺. This series is similar to the 2-NPOE plasticized PVC

Table 5
Interferent selectivity values ($\log K_{Cs,M}^{Pot}$) using the separate solution method

Interferent	I	II	III
H ⁺	-2.31	-2.20	+0.17
Li ⁺	-3.33	-2.74	-2.92
Na ⁺	-2.72	-2.48	-2.62
K ⁺	-1.22	-0.98	-1.14
Rb ⁺	-0.70	-0.40	-0.57
NH ₄ ⁺	-1.59	-1.40	-1.50
Ag ⁺	-1.77 ^a	-1.34 ^a	-1.61 ^a
Mg ²⁺	-3.70	-3.65	-3.69
Ca ²⁺	-4.13	-3.86	-3.92
Sr ²⁺	-4.16	-3.88	-3.95
Ba ²⁺	-3.97	-3.41	-3.70
Mn ²⁺	-4.65	-4.27	-4.41
Co ²⁺	-4.58	-4.12	-4.31
Ni ²⁺	-4.60	-4.21	-4.40
Cu ²⁺	-4.45	-4.16	-2.82
Zn ²⁺	-3.58	-3.30	-1.39
Pb ²⁺	-3.87	-3.66	-3.71
Cd ²⁺	-4.72	-4.47	-4.51
Hg ²⁺	-1.55	-1.18	-1.28

^a Determined at 10^{-2} mol l⁻¹.

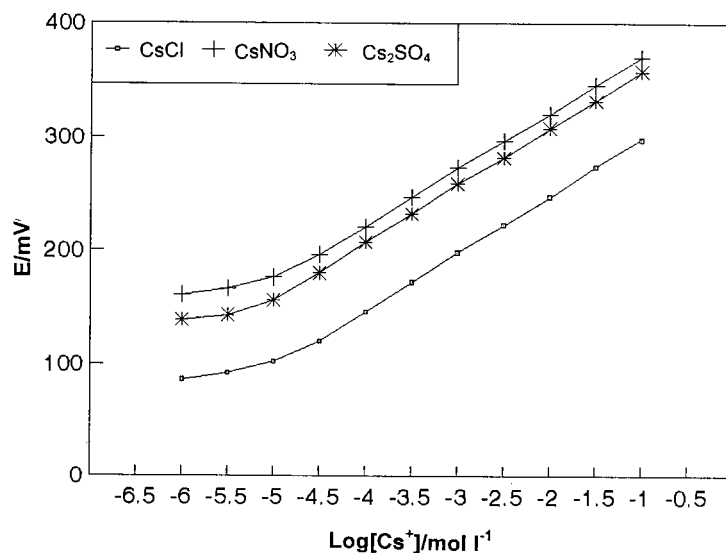


Fig. 6. Effect of sample anion on responses of cesium ion-selective electrodes based on ionophore I.

electrodes incorporating the KTC1PB secondary ion exchanger (see Table 4), where the logarithm of selectivity coefficient is inversely proportional to the free energy of hydration.

The cation response order for alkaline earth ions was $\text{Mg}^{2+} > \text{Ba}^{2+} > \text{Ca}^{2+} > \text{Sr}^{2+}$. The response for Mg^{2+} was $12 \text{ mV decade}^{-1}$, whereas responses for other divalent cations was consider-

ably less. The transition metal ion responses were very poor with the response order being $\text{Zn}^{2+} > \text{Pb}^{2+} > \text{Cu}^{2+} > \text{Co}^{2+} \sim \text{Ni}^{2+} > \text{Mn}^{2+}$. Both Mn^{2+} , Co^{2+} and Ni^{2+} produced no response (zero slope) across the calibration concentration range. The slope was obtained for Ag^+ ($44 \text{ mV decade}^{-1}$) in the concentration range 10^{-3} – $10^{-2} \text{ mol l}^{-1}$ followed by a sharp drop in potential at

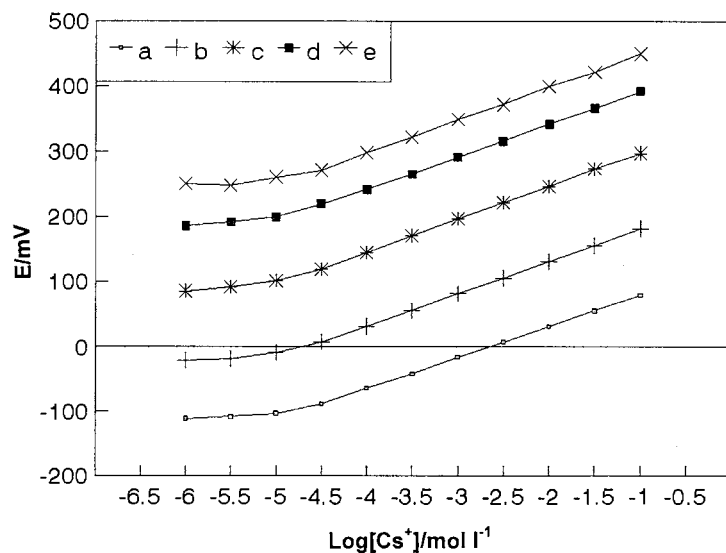


Fig. 7. Effect of internal solution concentration on the responses of cesium ion-selective electrodes based on ionophore I: (a) 10^{-1} ; (b) 10^{-2} ; (c) 10^{-3} ; (d) 10^{-4} and (e) $10^{-5} \text{ mol l}^{-1}$.

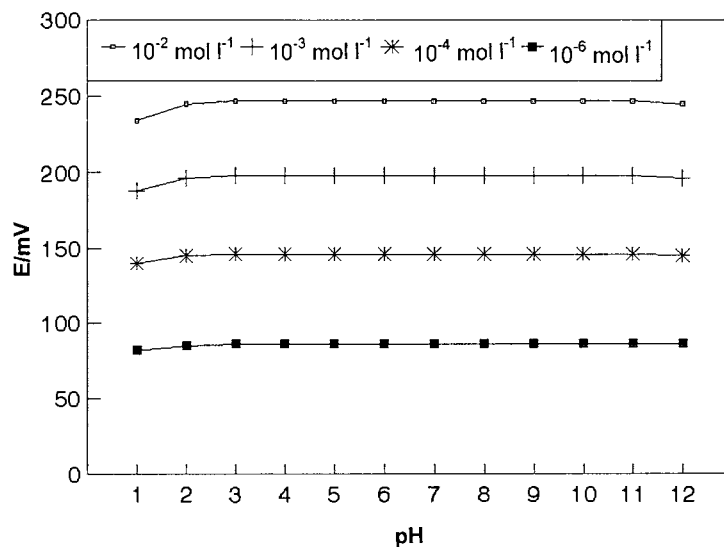


Fig. 8. Dependence of electrode response on pH.

$10^{-1} \text{ mol l}^{-1}$. The Ag^+ calibration plot has a higher detection limit ($4.0 \times 10^{-4} \text{ mol l}^{-1}$) than the Cs^+ calibration ($6.3 \times 10^{-6} \text{ mol l}^{-1}$).

The selectivity coefficients ($\log K_{\text{Cs},\text{M}}^{\text{Pot}}$) for a wide range of metal ions determined by the separate solutions method at 0.1 mol l^{-1} are presented in Table 5. The results in Table 5 reveal that the electrode based on ionophore I (*p*-methoxyanilino-(1,3-dioxo-2-indanylidene) acetonitrile shows a high selectivity for cesium ions over other metal ions compared with ionophores II, III. The incorporation of the *p*-methyl group instead of *p*-methoxy for electrode II leads to a

decrease in selectivity of cesium over metal cations studied. Electrode III incorporating the *p*-*N*-*N*-dimethyl group on anilino-(1,3-dioxo-2-indanylidene) acetonitrile is significantly different from the other electrodes (I and II) with an increase in the selectivity coefficients, H^+ ($\log K_{\text{C},\text{H}}^{\text{Pot}} = +0.17$), Cu^{2+} ($\log K_{\text{Cs},\text{Cu}}^{\text{Pot}} = -2.82$) and Zn^{2+} ($\log K_{\text{Cs},\text{Zn}}^{\text{Pot}} = -1.39$). This is accompanied by an increase in the response to H^+ , Cu^{2+} and Zn^{2+} ions and is attributed to the presence of the nitrogen atom of tert-amine capable of accepting protons and coordination to Cu^{2+} and Zn^{2+} ions on the anilino group.

The results in Fig. 4 and Table 5 indicate that the changes in the structures of ionophores I–III affect the detection limit, the slope of the electrode response and selectivity. These in turn are expected to affect the formation constants and distribution coefficients of cesium complexes. Introduction of an electron donor substituent to the ionophore molecule [$-\text{OCH}_3$ (ionophore I) instead of $-\text{CH}_3$ (ionophore II)] increases the electron density in the anilino group, which in turn is reflected in the high stability of the complex formed. On the other hand, the presence of the nitrogen atom of tert-amine in the ionophore III which is capable of accepting protons, decreases the electron density on the anilino group com-

Table 6
Lifetime studies of cesium ion-selective electrodes based on ionophore I

Day	Detection limit (mol l^{-1})	Slope (mV decade^{-1})
1	6.3×10^{-6}	52
2	6.3×10^{-6}	52
7	6.3×10^{-6}	52
10	6.3×10^{-6}	52
14	6.3×10^{-6}	52
18	6.3×10^{-6}	51
24	7.9×10^{-6}	49
30	7.9×10^{-6}	48
39	8.9×10^{-6}	43
45	1.8×10^{-5}	40

Table 7
Comparison studies of cesium ion-selective electrodes based on ionophore I (in the present electrode) and previously described ionophores

Ionophore	Response time (s)	Linearity (mol l ⁻¹)	Detection limit (mol l ⁻¹)	Slope (mV decade ⁻¹)	log $K_{Cs,M}^{Pot}$				
					Li ⁺	Na ⁺	K ⁺	Rb ⁺	NH ₄ ⁺
15-Crown-5 phosphotungstic acid precipitate (I1)	<60	0.1–10 ⁻⁴	1.0 × 10 ⁻⁵	60	-0.89	-0.46	-0.31	-0.46	—
2,3-Benzo-quinone [15]	<3	0.1–10 ⁻⁴	5.0 × 10 ⁻⁵	51.9	-3.00	-2.38	-0.99	-0.47	-1.40
<i>p</i> -Methoxy-anilino(1,3-dioxo-2-indanylidene) acetonitrile (tonophore)	= 60	0.1–2.5 × 10 ⁻⁵	6.3 × 10 ⁻⁶	52	-3.33	-2.72	-1.22	-0.70	-1.59

pared with $-\text{OCH}_3$ group in ionophore I. In brief, the membrane response and selectivity can be arranged in terms of ionophore molecular structure in the order $\text{I} > \text{III} > \text{II}$. Thus, the electrode of ionophore I [*p*-methoxyanilino-(1,3-dioxo-2-indanylidene) acetonitrile] has the best response and cesium selectivity, which might be due to the favourable structure of ionophore I which forms a stable complex with the cesium ion.

The effect of the sample anion on the responses of cesium ion-selective electrodes based on ionophore I has been studied and no significant change was observed using various anions such as Cl^- , NO_3^- and SO_4^{2-} (Fig. 6). The potential response of the electrode was found to be linear over the concentration range 10^{-1} – 2.5×10^{-5} mol l^{-1} for CsCl , 10^{-1} – 8×10^{-5} mol l^{-1} for CsNO_3 and 10^{-1} – 1.0×10^{-5} mol l^{-1} for Cs_2SO_4 with a slope of 52–53 mV decade $^{-1}$. According to IUPAC recommendations [17], the practical detection limits, taken as the concentration corresponding to the point of intersection of the two extrapolated lines, are 6.3×10^{-6} , 6.0×10^{-6} and 5.6×10^{-6} mol l^{-1} for chloride, nitrate and sulfate, respectively.

The concentration of the internal solution affects both the transmembrane electric potential and the stability of the cell potential [18]. The effect of the internal solution concentration on the responses of cesium ion-selective electrodes based on ionophore I has also been studied (Fig. 7) and it can be seen that 10^{-3} mol l^{-1} CsCl appears to be the optimum concentration of the internal solution to obtain the best response function. The response time and reproducibility were measured to elucidate the practical properties of cesium-selective electrode. By the 'dip to read' measurements, a response time of within 1 min was obtained with this electrode system. To evaluate the reproducibility of the potential response of the electrode, alternating measurements were performed in 10^{-4} and 10^{-3} mol l^{-1} CsCl . The potential difference in these two solutions was found to be reproducible to 52 ± 0.3 mV ($s, n = 3$) for an upward change in concentration and 52 ± 0.4 mV ($s, n = 3$) for the reverse change. A 1 min period was needed to achieve stable and reproducible potential readings. The potential response curves retrace themselves

without any appreciable hysteresis on increasing and decreasing the concentration of cesium ion.

Measurements of pH dependence of the electrode response was made using the electrode of ionophore I (Fig. 8). In the pH range 2–11, the slope of the potential response seems to indicate no significant change, but at $\text{pH} < 2.0$ and $\text{pH} > 11.0$ the slope decreased. This is perhaps due to a change in the activity coefficients superimposed.

The experimental results in Table 6 show that the lifetime of the present electrode was about 30 days. During this time, the detection limit of the electrode slightly increased from 6.3×10^{-6} to 7.9×10^{-6} mol l^{-1} and the slope of the electrode response decreased from 52 to 48 mV decade $^{-1}$. After this time, the electrochemical behaviour of the electrode gradually deteriorated. This is attributed to the decrease in quantity of plasticizer and ionophore resulting in their migration from a PVC membrane into a PVC tube [19].

The electrode with ionophore I compares well with previously described electrodes (Table 7). The proposed cesium electrode based on ionophore I exhibits much better linearity (10^{-1} – 2.5×10^{-5} mol l^{-1}), detection limit (6.3×10^{-6} mol l^{-1}) and potentiometric selectivity for cesium over metal ions (e.g. Li^+ , Na^+ , K^+ , Rb^+ and NH_4^+) when compared with previously described electrodes. On the basis of these results, the superiority of ionophore I over other reported reagents for cesium is attributed to the high stability of its complex with cesium ion.

3. Conclusion

Anilino-(1,3-dioxo-2-indanylidene) acetonitrile as a new class of neutral ionophores induces useful selectivities for Cs^+ . A cesium-selective PVC membrane electrode based on ionophore I [*p*-methoxyanilino-(1,3-dioxo-2-indanylidene) acetonitrile] exhibits good selectivity compared with ionophores II and III (ionophores under investigation) and previously described electrodes. The present electrode can be used over a wide pH range (2–11). It also has good detection limit (6.3×10^{-6} mol l^{-1}), reproducibility and a short response time (≈ 1 min).

References

- [1] D. Wang, S.J. Shih, *Analyst* 110 (1985) 635.
- [2] K.W. Fung, K.H. Wong, *J. Electroanal. Chem.* 111 (1980) 359.
- [3] A.S. Attiyat, Y.A. Ibrahim, G.D. Christian, *Microchem. J.* 37 (1988) 122.
- [4] S.K. Srivastava, V.K. Gupta, M.K. Dwivedi, S. Jain, *Anal. Proc.* 32 (1995) 21.
- [5] R. Eugster, P.M. Gehrig, W.E. Morf, U.E. Spichiger, W. Simon, *Anal. Chem.* 63 (1991) 2285.
- [6] R. Eugster, T. Rosatzin, B. Rusterholz, B. Aebersold, U. Pedrazza, D. Rüegg, A. Schmid, U.E. Spichiger, W. Simon, *Anal. Chim. Acta* 289 (1994) 1.
- [7] Y. Tsujimura, M. Yokoyama, K. Kimura, *Anal. Chem.* 67 (1995) 2401.
- [8] G.F. Michael, M. David, S.M. William, D.G. Jeremy, *Analyst* 121 (1996) 127.
- [9] H. Juenk, H. Aigner, H. Fischer-Colbrrie, *Monatsh. Chem.* 103 (1972) 639.
- [10] Z. Rappoport, D. Ladkani, *J. Chem. Soc. Perkin II* (1973) 1045.
- [11] G.J. Moody, J.D.R. Thomas, in: T.E. Edmonds (Ed.), *Chemical Sensors*, Blackie, London, 1988.
- [12] G.G. Guilbault, R.A. Drust, M.S. Frant, H. Freiser, E.H. Hansen, T.S. Light, E. Pungner, G. Rechnitz, N.M. Rice, T.J. Rohm, W. Simon, J.D.R. Thomas, *Pure Appl. Chem.* 48 (1976) 127.
- [13] E. Pungner, K. Toth, *Anal. Proc.* 22 (1985) 352.
- [14] W.E. Morf, G. Khar, W. Simon, *Anal. Lett* 7 (1974) 9.
- [15] P. Gehrig, W.E. Morf, M. Welti, E. Pretsch, W. Simon, *Helv. Chim. Acta* 73 (1990) 203.
- [16] D. Ammann, W.E. Morf, P. Anker, P.C. Meier, E. Pretsch, W. Simon, *Ion-Selective Electrode Rev.* 5 (1983) 3.
- [17] G.G. Guilbault, *Ion-Selective Electrode Rev.* 139 (1979) 1.
- [18] M.V. Rouilly, M. Badertscher, E. Pretsch, G. Suter, W. Simon, *Anal. Chem.* 60 (1988) 2013.
- [19] U. Oesch, W. Simon, *Anal. Chem.* 52 (1980) 692.

Chemometrical optimization FIA of perphenazine assay

Salah M. Sultan *, Anthony D. Walmsley

School of Chemistry, Cottingham Road, The University of Hull, Hull HU6 7RX, UK

Received 1 August 1997; received in revised form 22 September 1997; accepted 23 September 1997

Abstract

A flow injection method for the assay of perphenazine using cerium(IV) as oxidant in a sulphuric acid media was adopted. Different chemometric techniques, considered the main objective of this work, were utilised to optimise sensitivity and sample throughput as a function of five experimental variables. The optimum conditions obtained by the super modified simplex method were, 0.170 M sulphuric acid, 2.13 mM cerium(IV), 2.56 ml min⁻¹ flow rate, 52 cm coil length, and 136 µl sample loop size. A central composite design was successfully employed, characterising the relation between these variables and the response surface, and hence validating the optimum conditions obtained by the simplex method. Regression analysis of the data from the experimental design, demonstrated that a second order polynomial model is an adequate description of the surface over the factor limits studied. Further analysis of the response surface revealed the presence of a broad maximum around the simplex method optimum. A linear calibration curve in the range 50–500 ppm together with a sampling frequency of at least 120 s h⁻¹ and a relative standard deviation of less than 0.8% were obtained for the determination of perphenazine in its pure analytical grade. Results of the perphenazine assay in pharmaceutical preparations indicates that the method does not suffer interference from excipients rendering the method suitable for the assay of perphenazine in drug formulations. © 1998 Elsevier Science B.V. All rights reserved.

Keywords: Perphenazine; Cerium(IV); Flow injection; Central composite design; Experimental design; Response surface; Simplex optimization

1. Introduction

Chemometrics has been shown to be successful for the optimization of chemical reactions in flow injection procedures [1–7] and also proven to be

an efficient technique when four or more interacting variables are involved. Experimental design can be a powerful tool when used as part of the optimisation. Ruggedness testing and modelling of chemical analysis procedures usually employed to understand the relationship between experimental factors and their corresponding responses, as well as a need to determine the optimum operating conditions at which small changes of these factors can be tolerated. Screening designs, such as a two level factorial or fractional design

* Corresponding author. Present address: Chemistry Department, King Fahd University of Petroleum and Minerals, KFUPM Box No. 2026, Dhahran 31261, Saudi Arabia. Tel.: +966 3 8602111; fax: +966 3 8604227; e-mail: smsultan@kfupm.edu.sa

Table 2
Coded levels of the central composite design and their respective experimental set-up

Factor	Central composite design levels				
	2.4378	1	0	−1	−2.4378
[H ₂ SO ₄] A, (M)	0.285	0.220	0.170	0.120	0.05
[Ce(IV)] B, (mM)	4.21	3.03	2.13	1.23	0.05
Flow rate C, (ml min ^{−1})	4.56	3.47	2.56	1.65	0.47
Coil length D, (cm)	105	88	75	62	45
Loop size E, (μl)	164	148	136	124	110

nation of perphenazine. In addition to the optimisation study, an attempt to model the response surface and so correlate the effect of the experimental factors and the kinetics of the reaction to the response function will be described. Cerium(IV) was used as an oxidant in a sulphuric acid media. The coloured product of the oxidised form of perphenazine is followed spectrophotometrically at 525 nm using the FIA technique.

2. Experimental

2.1. Reagents

Cerium(IV) stock solution (0.01 M) was prepared by dissolving 16.0 g of cerium(IV) sulphate dihydrate (Merk, UK) in 250 ml of 0.05 M sulphuric acid. This solution has been used after 24 h.

Stock sulphuric acid solutions were prepared by diluting Analar grade concentrated acid.

The pure perphenazine solution (1000 ppm) was prepared by dissolving 0.1 g of the pure analytical reagent grade compound (May and Baker products, supplied by Rhone-Poulenc, batch No.D11) in 100 ml of 0.01 M sulphuric acid.

2.2. Apparatus

An Alitea, USA/FIA Lab (Medina, WA) apparatus described in a previous communication [15] was used for FI measurements. The apparatus consists of a peristaltic pump, injector, reactor module and a spectronic Mini 20 Spectrophotometer

connected to a single-channel strip-chart recorder (Cole-Parmer, Chicago, IL).

Fig. 1 shows the double-line FI manifold used. The carrier was pumped through a poly(vinyl chloride) (PVC) pump tubing 1.3 mm i.d. The sample injector was a Rheodyne (Cotati, CA) Model 5041 four-way PTFE rotary valve with a 136 μl injection loop. The reactor coil was 52 cm PTFE tubing 0.5 mm i.d. A Unovic (Plainsville, NY) ultramicro flow cell of 20 μl and path-length 1.0 mm was used.

2.3. Procedure

The drug sample (136 μl) was injected into 0.170 M H₂SO₄, which acts as a carrier solution. The carrier solution together with the injected drug zone, was then mixed with 2.13×10^{-3} M cerium(IV) solution and propelled through a reaction coil of 52 cm length to the spectrophotometer detector. The absorbance of the resulting solution was monitored at 525 nm with the chart recorder operated at a speed of 0.5 cm min^{−1}.

2.4. Experimental design

The super modified simplex procedure [6,7] was initially utilised for the optimization of five parameters; sulphuric acid concentration, cerium(IV) concentration, flow rate, coil length, and sample loop size. The criteria on which the performance of the analytical system can be evaluated, so that an optimum set of operating conditions can be obtained, was selected to include sample throughput and sensitivity, in one expression:

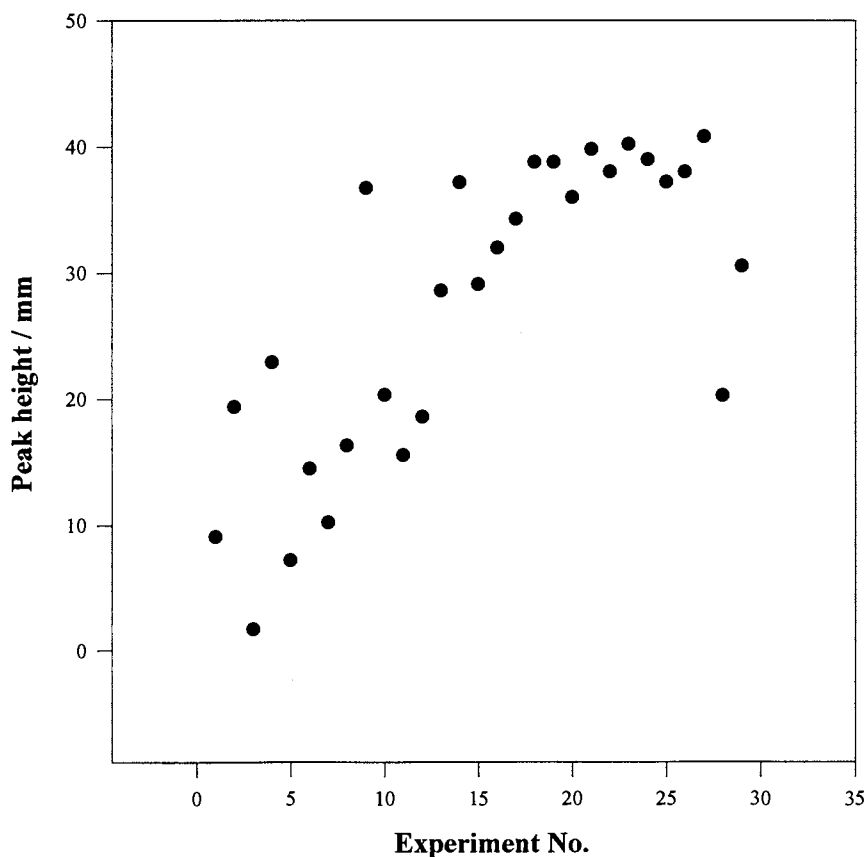


Fig. 2. Response function progress of the simplex.

$$R = \frac{A_{\text{exp}}}{A_{\text{base}} \cdot t_b} \times 100 \quad (1)$$

where R is the response function, A_{exp} is the peak absorbance at the peak maximum for a given set of conditions, A_{base} is the peak absorbance for the reference set of conditions, and t_b is the peak width at baseline. The response function is related to sensitivity by the term $A_{\text{exp}}/A_{\text{base}}$ and sample throughput by t_b . The range of experimental variables investigated are given in Table 1.

The response surface was then mapped and explored using a rotatable five factor central composite design [10,11], the centre of which was located on the simplex optimum. The central composite design, introduced by Box and Wilson [16], consists of a 2^k factorial or fractional facto-

rial design augmented by 2^k axial points and a number of centre points (N_0). The five factor central composite design is composed of 42 experiments plus six centre experiments, so that a total of 48 experiments were performed. The coded levels of the variables together with their real experimental values are given in Table 2. The centre point represents the set of optimum conditions obtained by the simplex, save the coil length which was changed from 52 cm to 75 cm in order to simultaneously cover a broad region of factor space, within the factor limit, and to maintain the desired properties of the experimental design [10,11]. The sigma plot software package was used to generate the full design in two blocks and to randomise the time order of the experiments within each block. All experiments were performed on the same day.

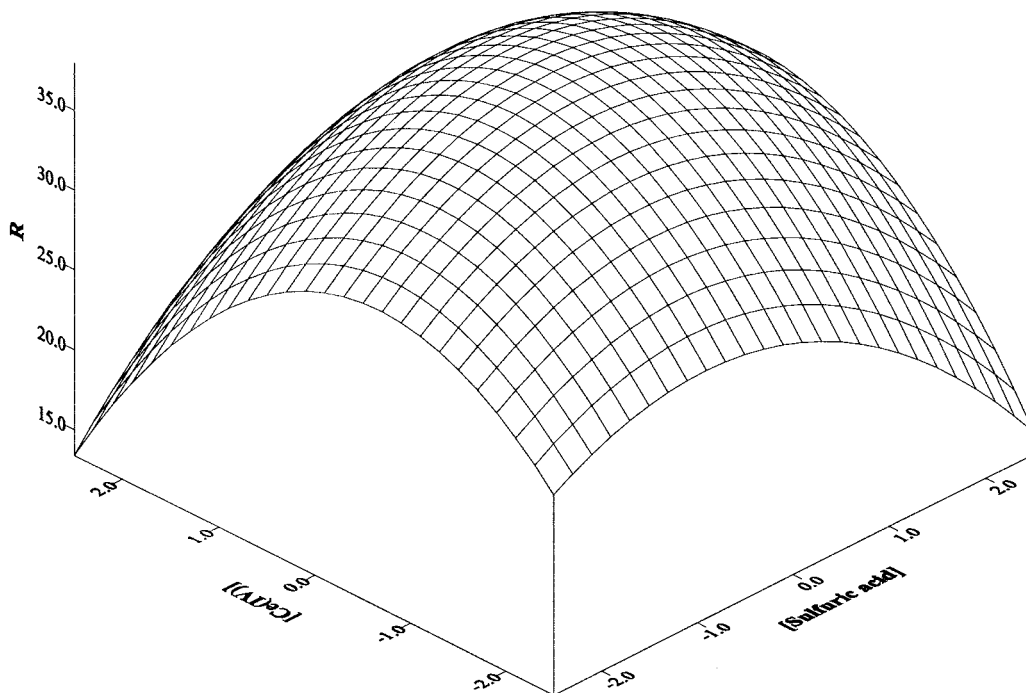


Fig. 3. Surface plot of the response vs. sulphuric acid and cerium(IV), all other factors are kept constant at their zero levels.

3. Results and discussion

Before undertaking any optimization study, it is important to delineate clearly the boundaries of the selected system and to define the performance criterion or response function. In this study, five factors namely, sulphuric acid concentration, cerium(IV) concentration, flow rate, coil length and sample loop size were investigated. The lower and upper levels of these five factors are shown in Table 1 which are limited by the physical distances of the apparatus or those beyond where no response was observed.

One way of treating multiple competing objectives is to select a criterion as primary and the remaining criteria as secondary. The primary criterion is then used as an optimization performance measure, while the secondary criteria are assigned acceptable minimum or maximum values and treated as system constraints [4,5,17]. The performance criterion or the response function was formulated (Eq. (1)) in a single expression as

a compromise between sensitivity and the time of analysis. The super modified simplex program was employed to obtain optimum operating conditions. The progress of simplex is given in Fig. 2 showing a gradual improvement in the response function and clear levelling towards maximisation. The simplex results given in Fig. 2 were obtained by injecting 200 ppm drug standard solution. A total of 29 experiments were needed to decide on optimum conditions. The optimum conditions were obtained by calculating the average of the four sets of conditions that give rise to the top four responses. The maximum response functions obtained are more or less similar and range between 39.8 and 40.8. The set of conditions that generated these maximum responses vary within a very narrow range. Therefore, the optimum operating condition obtained by the simplex technique for the determination of perphenazine are 0.170 M sulphuric acid, 2.13×10^{-3} , cerium(IV) concentration flow rate of 2.56 ml min^{-1} , coil length of 52 cm and sample loop size of 136 μl .

Table 3
Multiple regression analysis

Regressor variable		^a Parameter	Parameter estimate	^b Significant level (%)
Intercept		β_0	37.9350	100
Sulphuric acid	A	β_1	-0.2630	85
	AA	β_{11}	-1.2006	99.5
[Cerium(IV)]	B	β_2	-0.5423	99.6
	BB	β_{22}	-1.8316	100
Flow rate	C	β_3	4.4814	100
	CC	β_{33}	-2.3700	99.9
Coil length	D	β_4	-0.9065	99.5
	DD	β_{44}	-0.5780	99.9
Loop size	E	β_5	0.5126	99.3
	EE	β_{55}	-0.7631	99.9
AB		β_{12}	0.7844	99.9
AC		β_{13}	-0.2844	82.7
AD		β_{14}	0.2594	78.7
AE		β_{15}	-0.01563	6.0
BC		β_{23}	-0.8094	99.5
BD		β_{24}	-0.2781	81.8
BE		β_{25}	0.3469	90.1
CD		β_{34}	0.003125	1.2
CE		β_{35}	0.06563	24.7
DE		β_{45}	0.4719	71.7

^a See Eq. (2).

^b Level at which the null hypothesis ($H_0, \beta = 0$) can be rejected.

3.1. Response surface modelling

Response surface methodology (RSM) was used to assemble the model in order to describe the way in which the variables are related and the way in which they influence the response function. The form of the relationship between response function and experimental variables is initially assumed to be unknown. Therefore, the data obtained from the set of conditions employed by the central composite design were fit to the following parametric equation (full second order polynomial)

$$R = \beta_0 + \sum_{i=1}^5 \beta_i X_i + \sum_{i=1}^5 \beta_{ii} X_i^2 + \sum_{i < j} \beta_{ij} X_i X_j \quad (2)$$

where R is the response (given by Eq. (1)), β_0 is the intercept, X_i s are the five main variables, β_i is the linear parameter, β_{ii} is the quadratic parameter, β_{ij} represents the interaction parameters. Table 3 gives the estimates of 21 parameters, contained in Eq. (2), obtained by the matrix least squares [11,18].

The adjusted correlation coefficient of regression (R^2) was found to be 0.956. The significance of regression was tested by the F -ratio of the mean square due to the factors divided by the mean of squares due to the total error, and was found to be highly significant. Analysis of the residuals from the regression model and the lack of a fit test [11,18], revealed that the second order polynomial model, tentatively assumed, would be an adequate description of the surface over the region studied.

3.2. Response surface plots

Response surfaces for all two factor interactions were produced using the second order polynomial model. All plots were generated to describe two factors at a time by holding the other factors constant at the zero level. Only a few plots are illustrated here, i.e. factors with considerable interaction.

Fig. 3 shows the response surface as a function of sulphuric acid and cerium(IV) concentration,

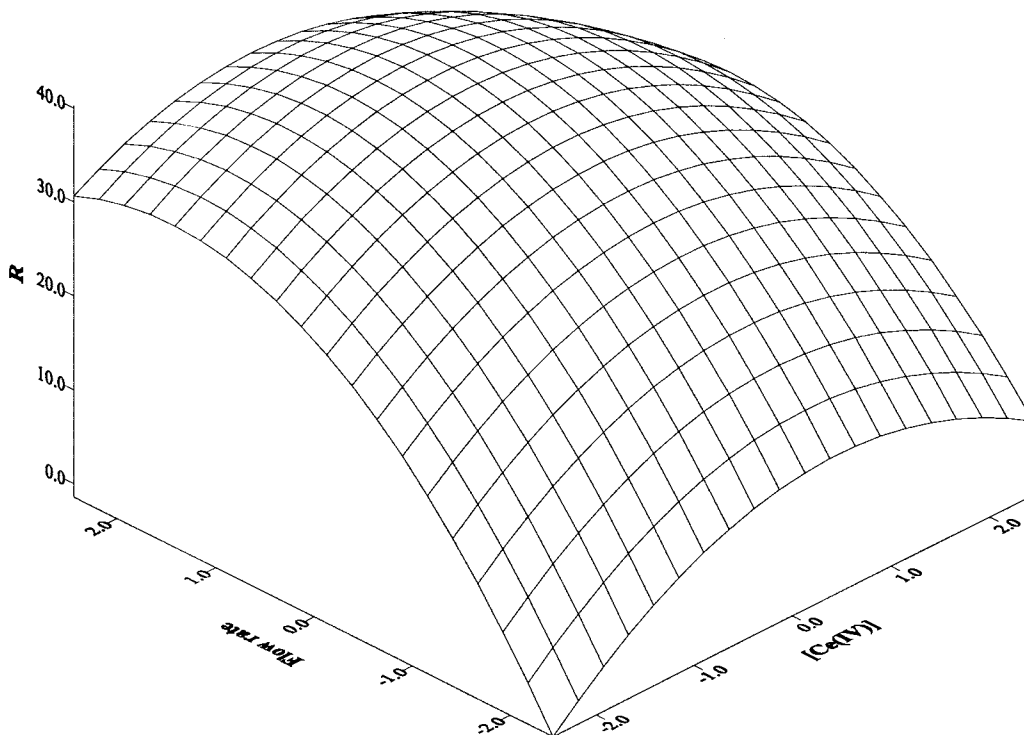


Fig. 4. Surface plot of the response vs. cerium(IV) and flow rate, all other factors are kept constant at their zero levels.

other factors are at their zero levels. Both factors exhibit significant main effects as well as highly significant interaction effects (Table 3). It is evident from Fig. 3 that a broad optimum is obtained at the middle levels of both factors. Moving away from the optimum to high acid concentration and low cerium(IV) concentration, a sharp decrease in the response is observed. Response surface plots demonstrating the effect of varying cerium(IV) concentration versus flow rate, loop size versus cerium(IV) concentration, and coil length versus loop size are shown in Figs. 4, 5 and 6, respectively.

4. Analytical application

The optimum operating conditions obtained by the simplex procedure and those obtained from the stationary point of the experimental design are shown in Table 1. Series of standard perphenazine

solutions were run using the set of conditions obtained by the super modified simplex optimization procedure, and the stationary point conditions one at a time. Peak absorbance versus concentration was found to be linear between 50 and 500 ppm for both methods, an almost two-fold improvement in the linear range as compared with the previous study [14]. The calibration equations obtained for the simplex optimized method and the experimental design stationary point are as follows:

$$A = -0.02812 + 1.916 \times 10^{-3}C, \quad R^2 = 0.998$$

$$A = -0.034 + 2.233 \times 10^{-3}C, \quad R^2 = 0.997$$

Where A is the peak absorbance and C is the concentration of perphenazine in ppm. The relative standard deviation was found to be 0.74 and 0.77%, when the simplex and experimental design method set of conditions were performed, using five repeated determinations of 200 ppm drug,

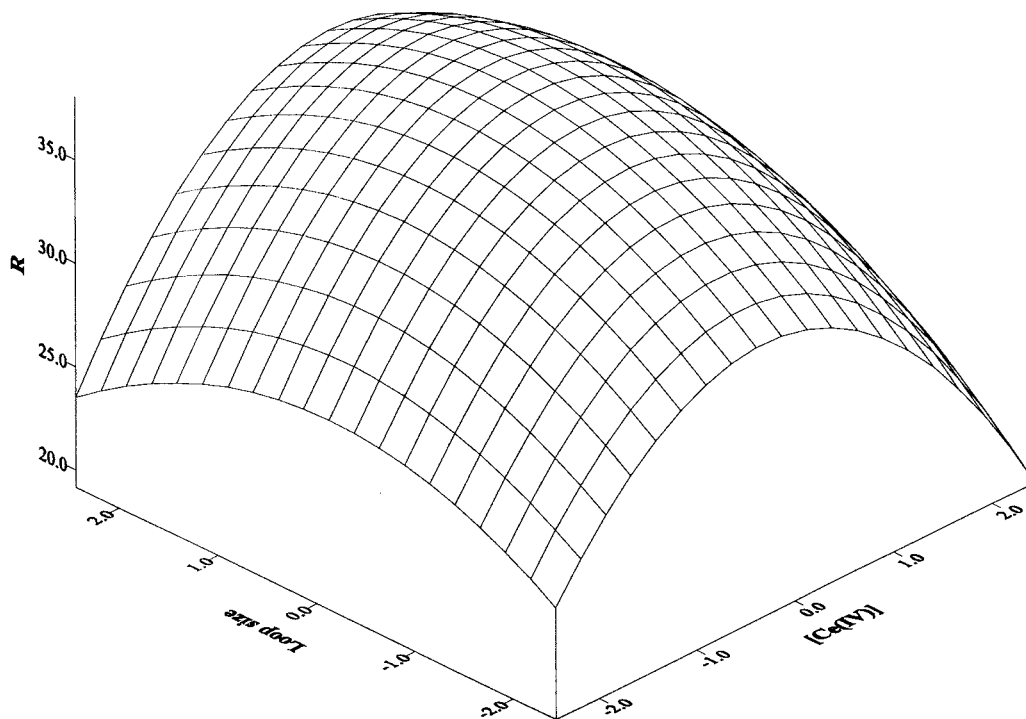


Fig. 5. Surface plot of the response vs. loop size and cerium(IV), all other factors are kept constant at their zero levels.

respectively. A standard deviation of less than 0.10 was obtained from the slopes and less than 1.1 at y -intercepts. Three calibration standards were present per calibration relation. The stationary point of the experimental design was found to be characterised by a higher sampling frequency, 190 S h^{-1} as compared with the simplex depicted method of only 120 S h^{-1} .

The tolerance of the two sets of optimum operating conditions to excipients which could be present in a typical pharmaceutical preparation containing perphenazine, was investigated. Synthetic solutions of 200 ppm perphenazine in the presence of 2000 ppm interfering compounds, such as starch, glucose, lactose and maltose, have been analysed using the two optimum conditions. The percent recovery, standard deviation (SD) and the student t -test values are given in Table 4. The student t -test values reveal that a similar degree of accuracy is obtained by the two set of conditions. Foreign compounds expected to be present in drug formulations show minimum or no interference in both cases.

5. Conclusion

This work outlines the important application of a systematic optimization of many variables for such a complicated system in order to obtain a rapid, sensitive and reproducible quantitative FIA procedure. The super modified simple method successfully attained optimum conditions which were further confirmed by experimental design techniques. Response surface modelling helped in understanding the effect of each factor on the response and enabled a good correlation to the kinetics of the chemical reaction to be achieved.

The chemometrics applied in this work is not new, but its application in analytical chemistry is seldom represented. The growing interest of the industrial sectors to acquire data and information rapidly with minimal measurement during the manufacturing process, would suggest that simplex optimization is best suited for the final refinement stage of a method, especially if the method provides a simple and well characterized response

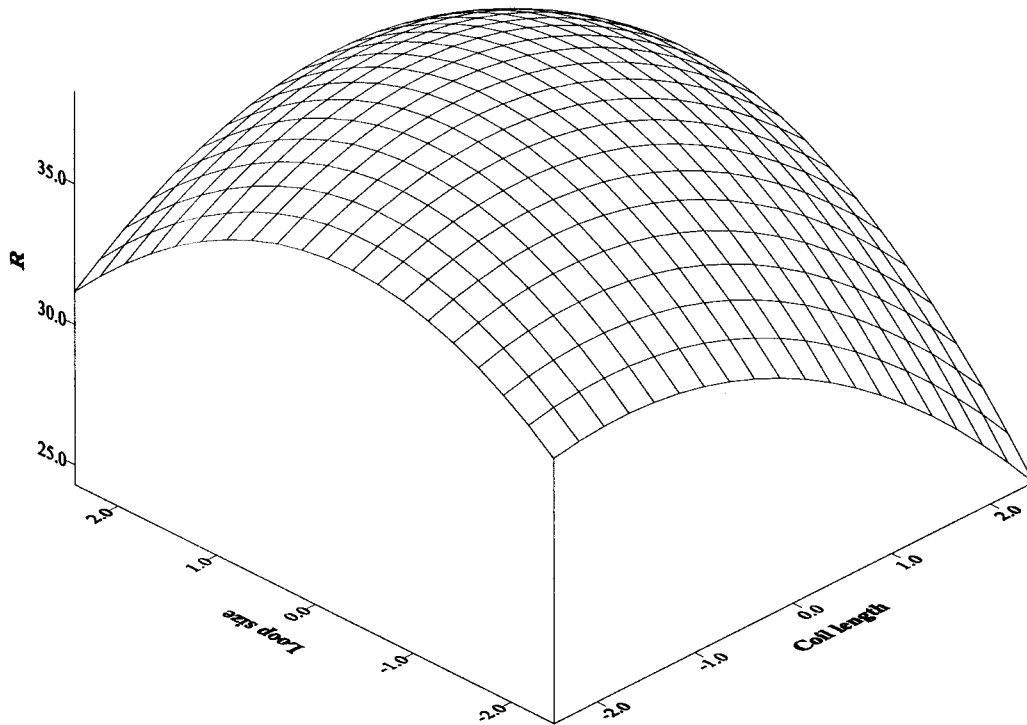


Fig. 6. Surface plot of the response vs. coil length and loop size, all other factors are kept constant at their zero levels.

like FIA. The results generated and presented in tables and figures demonstration this reduction of data thus indicating the novelty of the outcome.

Table 4

Results of statistical analysis of synthetic samples containing perphenazine using optimum conditions obtained by the simplex method compared with those obtained by experimental design stationary point

Species added ^a	%Recovery \pm SD ^b		<i>t</i> [*]
	Simplex method	Experimental design method	
Starch	99.98 \pm 0.57	99.11 \pm 0.46	0.21
Glucose	97.74 \pm 0.50	95.46 \pm 0.59	0.56
Lactose	101.84 \pm 0.48	100.18 \pm 0.58	0.40
Maltose	101.54 \pm 0.75	99.98 \pm 0.77	0.53

^a Concentration of interferant is 10 times that of the drug.

^b Standard deviation calculated from 5 determinations.

^{*} Student *t*-test calculated, theoretical value = 2.228 (*P* = 0.05).

It is postulated that simplex optimization will be used more frequently when it becomes easier to use. Once a given algorithm proves successful then the next step leading to common acceptance is a user friendly computer programme. Maybe future applications need to focus less on insignificant comparisons of similar algorithms in favour of providing a uniform algorithm or software package. The results presented in this manuscript indicate that ruggedness testing is the more logical application of simplex optimization because this application makes use of the response surface around optimum parameter values.

Acknowledgements

Prof. Salah M. Sultan wishes to thank KFUPM for the year sabbatical leave spent at the University of Hull, UK. Thanks is also extended to Prof. A. Townshend, The Dean of Science, and the University of Hull for allowing the visit and use of all the university's facilities.

References

- [1] S.M. Sultan, F.O. Suliman, *Analyst* 117 (1992) 1523.
- [2] S.M. Sultan, F.O. Suliman, *Anal. Sci.* 8 (1992) 841.
- [3] S.M. Sultan, F.O. Suliman, *Talanta* 40 (1993) 623.
- [4] S.M. Sultan, F.O. Suliman, *Analyst* 118 (1993) 573.
- [5] F.O. Suliman, S.M. Sultan, *Talanta*, in press.
- [6] D. Betteridge, T.J. Sly, A.P. Wade, J.E.W. Tillman, *Anal. Chim.* 55 (1983) 1292.
- [7] D. Betteridge, A.P. Wade, A.G. Howard, *Talanta* 37 (1985) 723.
- [8] Y. Vander Heyden, M.S. Khots, D.L. Massart, *Anal. Chim. Acta* 276 (1993) 189.
- [9] M. Mullholand, J. Waterhouse, *Chromatographia* 25 (1988) 769.
- [10] R.H. Myers, *Response Surface Methodology*, Allyn and Bacon, Boston, MA, 1971.
- [11] D.C. Montgomery, *Design and Analysis of Experiments*, 2nd ed., Wiley, New York, 1984.
- [12] R.T. Matthews, S.R. Goode, S.L. Morgan, *Anal. Chim. Acta* 133 (1981) 169.
- [13] A.P. Wade, P.M. Shiundue, P.D. Wentzell, *Anal. Chim. Acta* 237 (1990) 361.
- [14] S.M. Sultan, A.M. Abdennabi, *Microchem. J.* 48 (1993) 343.
- [15] S.M. Sultan, *Analyst* 116 (1991) 177.
- [16] G.E.P. Box, K.B.J. Wilson, *J. R. Stat. Soc.* 13 (1951) 1.
- [17] G.V. Reklaitis, A. Ravindran, K.M. Ragsdell, *Engineering Optimization; Methods and Application*, Wiley, New York, 1983.
- [18] N.R. Draper, H. Smith, *Applied Regression Analysis*, Wiley, New York, 1966.

Development of a bimodal polarimetric response model for improved quantitation of enantiomeric mixtures under conditions of poor chromatographic resolution

R.G. Lodevico^a, D.R. Bobbitt^{a,*}, T.J. Edkins^b

^a *Department of Chemistry and Biochemistry, University of Arkansas, Fayetteville, AR 72701, USA*

^b *Analytical Development, The R.W. Johnson Pharmaceutical Research Institute, Spring House, PA, 19477-0776, USA*

Received 03 July 1997; accepted 29 September 1997

Abstract

The combination of a chiral-selective separation mode with polarimetric detection was investigated in terms of its ability to quantitate enantiomeric mixtures of the dansylated derivatives of phenylalanine, threonine, and valine under conditions of poor chromatographic resolution. Using the difference between two Gaussian functions to model the bimodal response obtained using polarimetric detection and incomplete chiral resolution, correlation coefficients as high as 0.999 were obtained when actual enantiomeric fractions were plotted against observed enantiomeric fractions calculated from the fitting procedure. The methodology was evaluated at different levels of chromatographic resolution, and as a function of the sign and magnitude of the specific rotation of the model compounds. Limits of quantitation calculated at different levels of enantiomeric excess demonstrate the potential of the method to quantitate enantiomeric mixtures even under conditions of poor chromatographic resolution. Minimum measurable quantities (MMQ) at, or below the 1.0% enantiomeric excess (ee) level were obtained for the three amino acid derivatives tested under various conditions of chromatographic resolution when the polarimetric data were fit to the bimodal response model. Even under the lowest resolution conditions tested, the MMQ was determined to be at the 5% ee level. © 1998 Elsevier Science B.V. All rights reserved.

Keywords: Chromatographic resolution; Enantiomeric mixtures; Polarimetric detection

1. Introduction

The quantitation of mixtures in chromatographic analysis frequently utilizes either peak height or peak area as the basic analytical descriptor. For baseline-resolved peaks, the measurement

of these parameters is easy, straightforward, and accurate. However, the distortion caused by excessive overlap of peaks has presented problems with respect to precision due to uncertainties in the determination of baselines and peak boundaries [1,2].

In response to problems which arise in situations involving overlapping peaks in chiral separations, the use of peak height and area in the

* Corresponding author. Tel.: +1 501 5754601; fax: +1 501 5754049; e-mail: dbobbitt@comp.uark.edu

determination of enantiomeric excess in a mixture was investigated in a recent study [3]. Using conventional enantiomeric separation methods, a laser-based polarimetric detection system was interfaced with a chiral-selective separation mode (CSS/PD) for the precise quantitation of enantiomeric mixtures even under conditions of poor chromatographic resolution. Quantitation was achieved using this combined technique as a consequence of the unique bimodal response function of the polarimetric detector when presented with a mixture of enantiomers in the detection cell. The bimodal response results from the fact that enantiomers rotate the plane of polarized light in opposite directions. With peak height and peak area as the analytical descriptors, the experimentally obtained bimodal response function provided a well-defined crossing point that served as a reference in the determination of these parameters [3].

The goal of this study was to extend the analytical capabilities of the CSS/PD method for the quantitation of enantiomeric mixtures. The development of an appropriate response function was proposed as a way to offset the problems of baseline stability and integration limits on the determination of peak areas. The bimodal response obtained from the polarimetric detection scheme is well-characterized by the difference between two Gaussian functions. By fitting the data to this model, the entire data set can be used which allows the relative concentration of the two enantiomers in a mixture to be determined with excellent measurement precision. The analytical capabilities of this analysis procedure will be compared to both peak height and area for three model compounds at various levels of enantiomeric resolution.

2. Theoretical analysis

Various approaches have been developed in order to characterize chromatographic peak profiles and provide a clearer understanding of the physical and chemical processes occurring in the chromatographic column. Under conditions where random processes shape the analyte distri-

bution in a column, peak shapes can be adequately described by a Gaussian function [4–6], which is represented by:

$$h(t) = [A/\sqrt{(2\pi\sigma^2)}] \exp[-(t-m)^2/2\sigma^2] \quad (1)$$

In Eq. (1), $h(t)$ is the height or amplitude at time, t ; s is the standard deviation of the distribution; m is the peak position along the time axis; and A is the peak area of the function.

Theoretically, the ideal shape of this function is approached when an analyte undergoes a sufficiently large number of random sorption and desorption processes in a column [7]. Representing the frequency distribution of the analyte migrating through the system, a chromatographic peak can functionally be taken as a time distribution of the chromatographic height, $h(t)$ at any retention time, t . At the center of the distribution lies the 'average' position that is used to characterize a particular analyte. It has been shown that a Gaussian function can accurately describe the concentration profile of an eluting substance [8,9].

A pair of enantiomers have the unique property that they rotate plane polarized light to the same extent, but in opposite directions. A distribution consisting of two incompletely resolved enantiomers will produce a bimodal response with polarimetric detection and this response can be characterized as the difference between two Gaussian functions, as given in Eq. (2) below

$$h(t) = [A_1/\sqrt{(2\pi\sigma_1^2)}] \exp[-(t_1-m_1)^2/2\sigma_1^2] - [A_2/(\sqrt{2\pi\sigma_2^2})] \exp[-(t_2-m_2)^2/2\sigma_2^2] \quad (2)$$

where $h(t)$ is the height or amplitude at time, t ; s is the standard deviation of the peak; m is the peak position along the time axis; and A is the peak area.

By fitting the polarimetric response obtained for an incompletely resolved enantiomeric pair to this difference function, the entire response is used for quantitation of each enantiomer thereby enhancing the precision of the methodology.

In this study, the application of Eq. (2) to polarimetric data obtained at different levels of chromatographic resolution and specific rotation will be evaluated in order to more fully characterize and apply the CSS/PD technique.

3. Experimental

3.1. Reagents

The dansylated amino acids (Dns-D- and L-phenylalanine, Dns-L-threonine and Dns-L-valine), as well as the underivatized forms (D-threonine and D-valine) were obtained from Sigma (St. Louis, MO). Dns-D- and L-phenylalanine were available in the free acid form while Dns-L-threonine and Dns-L-valine were purchased as cyclohexylammonium salts. The derivatizing agent, 5-[dimethyl-amino]naphthalene-1-sulfonyl chloride (DnsCl) and the HPLC solvents acetonitrile and methanol were also obtained from Sigma.

3.2. Derivatization of amino acids

The derivatization of the amino acid samples was carried out as described previously [3,10]. DnsCl was dissolved in acetonitrile (1.5 mg ml^{-1}) while the amino acid (0.75 mg ml^{-1}) was dissolved in 40 mM lithium carbonate buffer adjusted to pH 9.5 with HCl. A 1-ml volume of the DnsCl solution was rapidly added to 2 ml of the amino acid solution, the mixture was shaken for 2 min and then allowed to stand overnight at room temperature (22–23°C). Termination of the reaction was accomplished by adding 100 μl of a 2% ethylamine hydrochloride solution. Containers were wrapped with aluminum foil to exclude light.

For polarimetric detection, the quantity of the derivatizing agent as well as the amino acid, was increased to 0.0500 and 0.0250 g, respectively. DnsCl was dissolved in 20.0 ml of acetonitrile while the amino acid was dissolved in 10.0 ml of 40 mM lithium carbonate buffer adjusted to pH 9.5. The mixture was heated to about 55°C for 1 h and the reaction was terminated, as before, using the 2% ethylamine hydrochloride solution. Solvents were evaporated at the same temperature under a vacuum.

3.3. Determination of specific rotation

Samples of commercially available, dansylated amino acids (DNS-L- and D-phenylalanine, DNS-

L-threonine and DNS-L-valine) were dissolved in a 70/30 (v/v) acetonitrile/ NH_4NO_3 solvent mixture at a level of 0.100 g/10.00 ml. Specific rotations were obtained using a conventional polarimetric system at a measurement wavelength of 488.0 nm. The specific rotation of each compound was calculated from α , the actual rotation measured, c , the concentration of the solute in g ml^{-1} of solution, and l , the pathlength, in decimeters.

3.4. UV and polarimetric detection

The UV detector (Shimadzu, Kyoto, Japan, model LC-6), was equipped with a solvent delivery module, a UV-VIS spectrophotometric detector and a CR 601 integrator. The laser-based polarimetric detection system has been described in detail previously [11,12]. Briefly, the source was an argon ion laser (Lexel, Palo Alto, CA, model 85) mounted on a 4×6 ft optical breadboard. The source light passed through a pair of Glan-Thompson polarizing prisms, (Karl Lambrecht, Chicago, IL, model MGT-E8). The source light was modulated using an in-house constructed Faraday cell driven by a signal generator (Wavetek, model 190). The modulation and detection cells had volumes of 1.1 ml and 29 μl , and pathlengths of 0.85 and 0.38 dm, respectively. The polarized laser light passing through the analyzer was detected with a photomultiplier tube (PMT), (Hamamatsu, Middlesex, NJ, model 928) powered by a high-voltage supply, (Bertran Associates, Hicksville, NY, model 215). The signal from the PMT was demodulated, amplified and digitized using a lock-in amplifier, (Stanford Research Systems, Palo Alto, CA, model SR 510). The digitized data were transferred to a PC Computer over an IEEE interface, (National Instruments, Austin, TX, model PC-2A) for storage and analysis. The Faraday coil used as an internal standard was made from a 10 cm \times 0.125 o.d. piece of stainless-steel tubing wrapped with 8000 turns of a 30 A WG magnet wire (Bendon, Geneva, IL). A DC current of 0.266 A produced a rotation of 3.85×10^{-40} at 488 nm, as calculated from the results of Ingersoll and Liebenberg [13].

3.5. Chromatographic analysis

The 25 cm × 4.6 mm i.d. Cyclobond column was purchased from Astec, (Whippany, NJ). The stationary phase for this column is a chiral β -cyclodextrin chemically bound to a spherical gel support through a non-nitrogen-containing spacer arm.

Enantiomeric mixtures of D and L dansylated amino acids were prepared using different D to L ratios: 1/0, 0/1/, 1/1/, 1/2/, 2/1, 1/3, 3/1, 1/4, 4/1. In these mixtures, the total amount (L + D) of amino acid dissolved in the methanol solvent was prepared such that the amount of material injected with the polarimetric detection system was 15 μ g for phenylalanine, 40 μ g for threonine and 60 μ g for valine using a 20 μ l injection loop. With UV detection, the concentration of all three samples was set at 1.50 mg/250.0 ml. All separations were achieved at a flow rate of 1.00 ml min⁻¹ using a degassed solvent system consisting of combinations of acetonitrile and NH₄NO₃. Since near baseline separation for DNS-D- and L-phenylalanine was obtained with a solvent system of 80/20 acetonitrile/NH₄NO₃, other solvent systems were prepared, for example, 70/30, 50/50 and 40/60, to decrease resolution. For the 40/60 solvent, the [NH₄NO₃] was 0.10 M. Chromatographic analyses were performed using the different D:L ratios and a combination of four eluent systems. Concentrations for the derivatized samples (Dns-D-threonine and Dns-D-valine) were determined using known concentrations of the corresponding Dns-L-amino acid and UV absorption spectroscopy. Resolution values for the dansylated enantiomers of phenylalanine, valine and threonine as a function of eluent composition are given in Table 1.

A minimum of three determinations for each enantiomeric mixture were obtained for all three amino acids using four solvent systems and different L/D mixtures.

3.6. Analysis of bimodal response function

The bimodal response function was simulated using the difference of two Gaussian functions, as given in Eq. (2). This simulated bimodal response

model was then fit to the polarimetric response data for various enantiomeric mixtures using standard techniques. Correlation coefficients were obtained using actual and calculated enantiomer concentrations after taking the ratio of areas for the L and D enantiomers and translating these area ratios into concentration ratios.

4. Results and discussion

In order to adequately evaluate the use of a bimodal response model for polarimetric detection under conditions of low enantioselective resolution, both the magnitude of the specific rotation and the extent of separation must be varied. Dansylation of the three amino acid test compounds produced a range of specific rotations (phe, -131; val, 65.3; and thr, -18.7; units °(g ml⁻¹)⁻¹ dm⁻¹). This range of chirality provides a good test of the methodology and the model compounds also encompass a sign change in their respective specific rotations. In order to create a range of chromatographic resolutions, various eluent compositions were evaluated and the corresponding resolutions are given in Table 1. As is evident for these eluent compositions, experimentally determined resolutions varied from approximately 1.0–0.3. Even under the highest

Table 1
Enantiomeric resolution for three dansylated amino acids

DNS-AA	Euent ^a	Resolution
PHE	80/20	1.00
	70/30	0.66
	50/50	0.34
	40/60	0.32
THR	80/20	1.06
	70/30	0.86
	50/50	0.43
	40/60	0.37
VAL	80/20	1.03
	60/40	0.90
	50/50	0.44
	40/60	0.34

^a ACN/NH₄NO₃ (0.025 M, pH 4.0) except the 40/60 eluent (0.10 M, pH 4.0).

resolutions tested, conventional approaches to enantioselective analysis would not be able to provide accurate and precise compositional information on an enantiomeric mixture. Thus this range of chromatographic resolutions provides a rigorous test of the proposed methodology.

In Fig. 1, a simulated response for a single enantiomer is compared to the experimentally determined profile obtained using polarimetric detection. The simulated response was calculated using the first segment of Eq. (2). It is clear that the CSS/PD system provides a well characterized response which can be modeled precisely by a Gaussian function. In Fig. 2, both parts of Eq. (2) were used to simulate the bimodal response expected for two enantiomers which are incompletely resolved. As is evident, the simulated and experimental profiles agree well. In order to prepare the simulated response, only the distance between the maximum and minimum of the bimodal response and the width of the profile were used. Therefore, with Eq. (2) as the model, polarimetric data obtained for incompletely resolved enantiomeric mixtures can be used to obtain quantitative information on each enantiomer separately. It should be emphasized that this approach does not require baseline separation, although the obtainable resolution would be expected to effect the quality of the measurement.

Table 2 summarizes the correlation coefficients obtained when experimentally determined enantiomeric fractions were plotted against actual enantiomeric fractions for DNS-phenylalanine, DNS-threonine and DNS-valine. The experimentally determined values were obtained by fitting the bimodal response function given in Eq. (2) to the polarimetric data. Several points are evident in these results. First, for most eluents tested, excellent correlation is noted between the experimentally determined and actual values. Even under conditions of incomplete chromatographic resolution, the quantitative capability of the CSS/PD methodology is very good. For this range of chromatographic resolutions, a non-selective detector would not produce a response which could be used to differentiate the various enantiomeric fractions. It also is clear that the quality of the determination is affected, to some extent by the

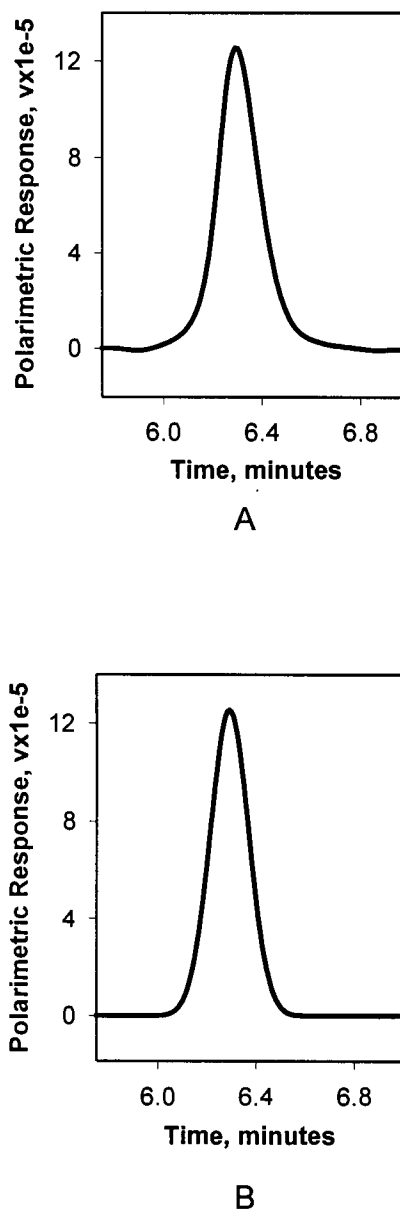
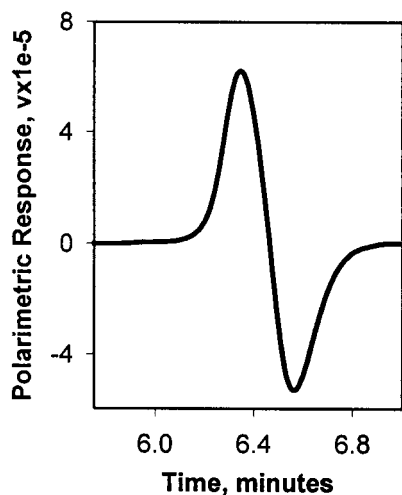


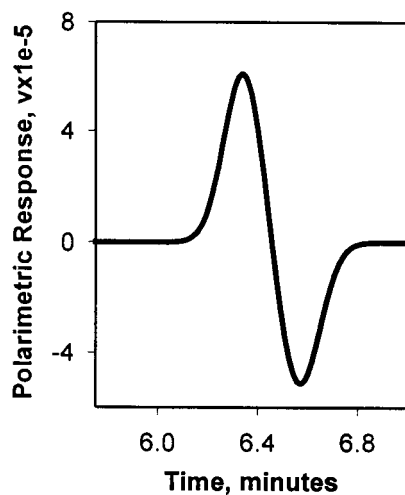
Fig. 1. Polarimetric response curves for Dns-L-Phenylalanine. (A) and (B) represent the experimental and simulated response curves obtained using a β -cyclodextrin column, 15.0 μg of injected material and a mobile phase system consisting of 70/30 ACN/ NH_4NO_3 . Flow rate was 1.0 ml min^{-1} .

chromatographic resolution. However, valuable quantitative information can still be obtained with the CSS/PD system under conditions which would be problematic or impossible for a non-chiral-se-

lective detector. This approach could have merit, for example in synthetic development studies where changes in the enantiomeric fraction of the product mix is monitored as a function of experimental conditions in order to optimize the yield of



A



B

Fig. 2. Polarimetric response curves for a 1/1 mixture of L and D Dns-Phenylalanine. (A) and (B) represent the experimental and simulated response curves obtained by injecting a total quantity of 15.0 μg of the enantiomers. Chromatographic conditions are given in Fig. 1.

Table 2

Correlation coefficient (r) for actual and observed fractions of dansylated amino acid enantiomers as a function of enantioselective resolution

DNS-AA	Euent ^a	L peak	D peak
PHE	80/20	0.997	0.998
	70/30	0.999	0.999
	50/50	0.999	0.999
	40/60	0.985	0.985
THR	80/20	0.997	0.996
	70/30	0.999	0.999
	50/50	0.989	0.995
	40/60	0.994	0.994
VAL	80/20	0.995	0.996
	60/40	0.997	0.997
	50/50	0.996	0.996
	40/60	0.991	0.988

^a ACN/NH₄NO₃ (0.025 M, pH 4.0) except the 40/60 eluent (0.10 M, pH 4.0).

a desired product. In such situations, chiral columns are easily degraded by the conditions since the composition of the injected sample can vary greatly and, due to the uncontrolled nature of the sample, irreversible absorption of material to the column could degrade the chiral resolution. Even under such conditions, the CSS/PD approach could provide useful information. Finally, it should be noted that the quality of the data does not appear to be affected by the magnitude or sign of the specific rotation of the enantiomeric pair over the range of linearity for the polarimetric detection system.

The data in Table 2 serves to establish that a relationship exists between the CSS/PD response and the amount of each enantiomer in a mixture. Of more importance is the ability of the methodology to provide accurate and precise quantitative information on each enantiomer under conditions of poor enantioselective resolution. For such an evaluation, the limit of quantitation, in terms of enantiomeric excess can provide information about the quantitative capability of the methodology as a function of the relative amounts of the two enantiomers. The enantiomeric excess (ee) is defined as the difference between the amount of the two enantiomers in a mixture divided by their total. For example, 0% ee is equivalent to a

racemic mixture that contains equal amounts of the two enantiomers, 60% ee contains 80% L and 20% D while –40% ee, in the interest of this study, contains 30% L and 70% D. In this study, the limit of quantitation (LOQ) constitutes the confidence interval (2σ) for the quantitation of one enantiomer in an enantiomeric mixture at a particular level of enantiomeric excess, as determined by the calibration function and the standard error of the slope of this function. The LOQ may vary over the range of enantiomeric excess and as a function of chromatographic resolution and elution order.

Tables 3–5 show the LOQs obtained for dansylated phenylalanine, threonine, and valine at three different values of enantiomeric excess. At 0% ee, the range varied from 49.3–50.8, 49.0–51.0, to 48.8–51.3, for phenylalanine, threonine, and valine, respectively, using the 80/20 solvent system. Values obtained using the 70/30 and 50/50 or 60/40 solvent systems are comparable with these numbers, although, the LOQ range obtained for the 40/60 solvent system was larger. These numbers suggest that low levels of each enantiomer can be detected in the presence of the other. For example, the LOQs for Dns-L-phenylalanine using the 80/20 and 40/60 eluent systems were 29.6–30.5 and 28.4–31.8 at the –40% ee level, suggesting that the minimum measurable change in

Table 3
Limits of quantitation for DNS-phenylalanine enantiomers as a function of enantiomeric excess and enantioselective resolution

Eluent ^a	Parameter	±40% ee ^b	0% ee ^c	±60% ee ^d
80/20	L peak	29.6–30.4	49.3–50.8	78.8–81.2
	D peak	29.6–30.4	49.3–50.7	79.0–81.1
70/30	L peak	29.7–30.3	49.5–50.5	79.2–80.8
	D peak	29.7–30.3	49.5–50.5	79.2–80.8
50/50	L peak	29.7–30.3	49.6–50.5	79.3–80.7
	D peak	29.7–30.3	49.5–50.5	79.3–80.7
40/60	L peak	28.4–31.8	47.4–52.9	75.8–84.7
	D peak	28.4–31.8	47.4–52.9	75.8–84.7

^a ACN/NH₄NO₃ (0.025 M, pH 4.0) except the 40/60 eluent (0.10 M, pH 4.0).

^b +40% ee defined as 30% L, 70% D; –40% ee, 30% D, 70% L.

^c 50% L, 50% D.

^d +60% ee defined as 80% L, 20% D; –60% ee, 20% L, 80% D.

Table 4
Limits of quantitation for DNS-threonine enantiomers as a function of enantiomeric excess.

Eluent ^a	Parameter	±40% ee ^b	0% ee ^c	±60% ee ^d
80/20	L peak	29.4–30.6	49.0–51.0	78.4–81.6
	D peak	29.4–30.6	49.0–51.0	78.4–81.7
70/30	L peak	29.7–30.3	49.5–50.6	79.2–80.9
	D peak	29.7–30.3	49.5–50.6	79.2–80.9
50/50	L peak	28.8–31.3	48.0–52.2	76.8–83.5
	D peak	29.2–30.8	48.7–51.4	77.9–82.2
40/60	L peak	29.2–30.8	48.7–51.4	78.0–82.2
	D peak	29.2–30.8	48.7–51.4	77.9–82.2

^a ACN/NH₄NO₃ (0.025 M, pH 4.0) except the 40/60 eluent (0.10 M, pH 4.0).

^b +40% ee defined as 30% L, 70% D; –40% ee, 30% D, 70% L.

^c 50% L, 50% D.

^d +60% ee defined as 80% L, 20% D; –60% ee, 20% L, 80% D.

enantiomeric excess that can be detected with this approach is less than 1% ee for Dns-L-phenylalanine at a resolution of 1.0, and approximately 3% ee at a resolution of 0.3. It is important to note that at these resolution values, traditional approaches would not be able to provide useful quantitative information. The bimodal response model also is superior to simple peak height or area analysis. In a previous study [3] in which peak area was used for quantitation of

Table 5
Limits of quantitation for DNS-valine enantiomers as a function of enantiomeric excess and enantioselective resolution

Eluent ^a	Parameter	±40% ee ^b	0% ee ^c	±60% ee ^d
80/20	L peak	29.3–30.8	48.8–51.3	78.1–82.0
	D peak	29.4–30.7	48.9–51.1	78.3–81.8
70/30	L peak	29.5–30.5	49.2–50.8	78.7–81.3
	D peak	29.5–30.5	49.2–50.8	78.7–81.3
50/50	L peak	29.4–30.7	48.9–51.1	78.3–81.8
	D peak	29.4–30.7	48.9–51.1	78.3–81.8
40/60	L peak	29.0–31.1	48.3–51.4	77.4–82.8
	D peak	28.9–31.2	48.2–51.9	77.3–83.1

^a ACN/NH₄NO₃ (0.025 M, pH 4.0) except the 40/60 eluent (0.10 M, pH 4.0).

^b +40% ee defined as 30% L, 70% D; –40% ee, 30% D, 70% L.

^c 50% L, 50% D.

^d +60% ee defined as 80% L, 20% D; –60% ee, 20% L, 80% D.

partially separated enantiomers, corresponding minimum measurable changes at these resolution values were 2 and 6%, respectively. Over the range of enantiomeric excess and resolutions evaluated, the minimum measurable change varied from 1 to 2% ee at low enantiomeric excess, to 2–3% ee at 0% enantiomeric excess, to 3–6% ee at high enantiomeric excess. Similar results were obtained for the three test compounds with differing sign and magnitudes of specific rotation.

As described earlier, one important application of the CSS/PD technique may be as an aid in the development and optimization of an enantio-selective synthetic strategy for a new target compound, for example, a therapeutic pharmaceutical. In such applications, a large number of synthetic variables may be evaluated in an attempt to control the enantiomeric composition of the final product. In these situations, rapid feedback is necessary with respect to the composition of the reaction mixture and the CSS/PD methodology may be able to provide this information without the need for extensive chromatographic development work.

The success of this methodology is limited by the sensitivity of the polarimetric detection system, the quality of the separation and the innate optical activity of the enantiomeric pair. Recently, a commercially available, laser source polarimeter has been introduced based upon the same operational principles as the experimental instrument used for this work, and which has demonstrated similar performance specifications [15]. Thus the method is not limited by available polarimetric instrumentation. Although polarimeters do not provide a response for racemic mixtures, a situation which will occur under conditions of extremely low enantio-selective resolution, as long as a modest degree of resolution has been achieved ($R_s \sim 0.3$), the method may be used to provide a reasonable estimate of the enantiomeric composition of the sample.

5. Summary and conclusions

This study combined a chiral selective separation mode with polarimetric detection for the

analysis of enantiomeric mixtures at low enantioselective resolution. A bimodal response function was developed using the difference between two symmetrical Gaussian functions, and found to fit the polarimetric response well. Excellent quantitative results were obtained for assessing enantiomeric excess and the bimodal response model was found to provide equivalent results over a range of specific rotations and enantioselective resolutions. At the lowest resolutions tested, conventional approaches would not be able to provide any useful quantitative information on an enantiomeric mixture.

In many circumstances, symmetrical peak profiles may not be obtained for one, or both of the eluting enantiomers. In such situations, the symmetrical Gaussian peak model may not be appropriate. Recent work has demonstrated that an exponentially modified Gaussian function (EMG) can be used as a valid model of a tailed analyte distribution [14]. Thus, in such situations, modification of the methodology described herein by the use of the EMG in place of a symmetrical Gaussian function may allow similar results to be obtained even on tailed analyte distributions.

References

- [1] A. Papas, *CRC Crit. Rev. Anal. Chem.* 20 (1989) 359.
- [2] A. Janik, *J. Chromatogr. Sci.* 13 (1975) 93.
- [3] R.G. Lodevico, D.R. Bobbitt, T.J. Edkins, *Talanta* 44 (1997) 1353.
- [4] J.C. Giddings, *Dynamics of Chromatography, Part I: Principles and Theory*, M. Dekker, New York, 1965, p. 20.
- [5] S.M. Roberts, *Anal. Chem.* 44 (1972) 502.
- [6] R.D.B. Fraser, E. Suzuki, *Anal. Chem.* 41 (1969) 37.
- [7] J.M. Miller, *Chromatography: Concepts and Contrasts*, Wiley, New York, 1988, p. 12.
- [8] R. Shinnar, G.H. Weiss, *Sep. Sci.* 11 (1976) 377.
- [9] K. De Clerk, T.S. Buys, *Sep. Sci.* 7 (1972) 371.
- [10] Y. Tapuhi, N. Miller, B.L. Karger, *J. Chromatogr.* 205 (1981) 325.
- [11] E.S. Yeung, L.E. Steenhoek, S.D. Woodruff, J.C. Kuo, *Anal. Chem.* 52 (1980) 1399.
- [12] P.D. Rice, *Analytical applications of laser-based polarimetry*, Ph. D. Thesis, University of Arkansas, 1992.
- [13] L.R. Ingersoll, D.H. Liebenberg, *J. Opt. Soc. Am.* 46 (1956) 538.
- [14] J.P. Foley, J.G. Dorsey, *J. Chromatogr. Sci.* 22 (1984) 40.
- [15] PDR Chiral Detector, PDR, Palm Beach Gardens, FL, 1997.

Methods for determination of hexachlorobenzene and pentachlorophenol in soil samples

Luciana Polese *, Maria Lúcia Ribeiro

Departamento de Química Orgânica, Instituto de Química, UNESP 14800-900, CP 355, Araraquara, SP, Brazil

Received 08 July 1997; received in revised form 29 September 1997

Abstract

The efficiency of methods for the determination of hexachlorobenzene (HCB) and pentachlorophenol (PCP) in soil samples was evaluated. An on-line method was applied for HCB determination. Soil samples were transferred to chromatographic columns prepacked with alumina. The HCB elution was processed with n-hexane. The PCP was extracted from soil samples with n-hexane–acetone in an ultrasonic bath. After re-extraction with K_2CO_3 solution PCP was acetylated with acetic anhydride. The pentachlorophenyl acetate derivative was then extracted with n-hexane. The HCB and PCP derivative were analyzed by gas chromatography with electron capture detection (GC-ECD). Mean recoveries obtained from soil samples fortified at levels of 0.5; 4 and 20 $ng\ g^{-1}$, ranged from 91 to 100% for HCB, and for PCP, at levels of 10; 40 and 200 $ng\ g^{-1}$, ranged from 88 to 101%. These results demonstrated the efficiency of the proposed methods. © 1998 Elsevier Science B.V. All rights reserved.

Keywords: Hexachlorobenzene; Pentachlorophenol; Soil; GC-ECD

1. Introduction

As a result of agricultural practices and industrial waste disposal, the environment is being continually polluted by pesticides and industrial chemicals. The behaviour of these polluting compounds in the environment is determined by the physicochemical properties of the compounds and their relationship to processes such as adsorption, leaching, vaporization, and degradation.

Hexachlorobenzene (HCB), a fungicide and by-product resulting from the manufacture of many chlorinated hydrocarbons [1], and pen-

tachlorophenol (PCP), an insecticide, fungicide and herbicide [2], were dumped by a chemical company near a populated area in the town of São Vicente, in the State of São Paulo, Brazil. Whereas governmental norms have been established for controlling water pollution by pesticides, none exist concerning soil pollution [3], it is therefore important to develop suitable, accurate, and sensitive methods to determine the extent of soil contamination.

Many methods for the determination of contaminants which include HCB and PCP in soils and sediments have been described in the literature [4–12]. Seidel et al. [4] made a comparison of simultaneous steam distillation-solvent extraction

* Corresponding author. Fax.: + 55 162 227932.

(SDE) with two preconcentration techniques (Soxhlet extraction-SE and supercritical fluid extraction-SFE) for the determination of organochlorine pesticides (OCPs) and HCB in soil and oleagineous matrices. A new SDE apparatus was developed and the extraction efficiency for OCPs proved to be better for SDE than for SE or SFE.

Several studies have described the optimization of SFE for the extraction of OCPs, HCB, and polychlorinated biphenyls from soils [5–7]. Although SFE has been shown to be a viable alternative to conventional extraction techniques, it presents certain limitations such as the high cost of equipment, the influence of soil-water content in the recovery of pesticides, and the low recovery of polar substances [3].

The application of the SFE technique for determination of polar compounds such as PCP and other chlorophenols in soil samples was demonstrated by Lee et al. [8]. Phenols were extracted from soil and acetylated *in situ* with supercritical carbon dioxide in the presence of triethylamine and acetic anhydride. This procedure increases the extractability of polar compounds since acetyl derivatives are in general less polar.

Phenol derivatization prior to gas chromatography (GC) analysis is not a new technique. However, the advantages of different procedures for derivatizing such as sensitivity, and improved gas chromatographic performance are still being discussed and continue to be recommended [8,9,11,13,14].

Despite differences in the chemical properties between HCB and PCP, analytical methods for simultaneous determination of these compounds in soil and sediments have been developed [9,12]. Kolb et al. [9] proposed a method for the analysis of a wide variety of compounds. After extraction at different pH values, first high molecular matrix compounds were separated by gel permeation chromatography and fractionation of the samples into five groups of substances was performed by column chromatography; phenols were derivatized by pentafluorobenzoylchloride. Recoveries of most of the compounds were higher than 80%. Lopez-Avila et al. [12] used a commercially available system (Soxtec) for extracting organic com-

pounds from soils and sediments. Average recoveries of 62.7% were obtained for PCP and ranged from 52.5 to 85.6% for HCB.

The aim of this study is to evaluate the applicability of two methodologies for determination of HCB and PCP in soil samples.

The determination of HCB was made by means of an on-line method combining extraction and cleanup in a single step. Soil samples were transferred to chromatographic columns and HCB was quantitatively eluted with n-hexane. The PCP was extracted from soil samples with a solvent mixture followed by a K_2CO_3 solution. The addition of acetic anhydride led to the formation of pentachlorophenyl acetate which was then extracted with n-hexane. The HCB and PCP derivative were analyzed by gas chromatography with electron capture detection (GC-ECD).

2. Experimental

2.1. Apparatus

A Varian 3300 gas liquid chromatograph equipped with 200 cm \times 2 mm i.d. glass column packed with 1.5% OV 17/1.95% QF 1 on 100–120 mesh Chromosorb WHP, a constant current ^{63}Ni electron capture detector (ECD) and a Varian 4290 integrator were used. The operating conditions were as follows: injector temperature, 230°C; column temperature, 180°C; detector temperature, 300°C; nitrogen flow rate, 30 ml min⁻¹; ECD range, 10; ECD attenuation, 4; and chart speed, 0.5 cm min⁻¹.

2.2. Reagents

n-Hexane (Mallinckrodt) and acetone (Merck) were of pesticide grade. Acetic anhydride (Merck), anhydrous potassium carbonate (Grupo Química) and sulphuric acid (Merck) were of analytical grade. Anhydrous sodium sulphate (pesticide grade, Merck) was heated at 130°C for 24 h. Alumina 90 neutral (70–230 mesh, Merck) was deactivated according to the procedure described by Ribeiro et al. [15]. Reference standards of HCB and PCP were obtained from the Envi-

ronmental Protection Agency (Triangle Park, NC). Standard solutions were made up in n-hexane and stored at -18°C .

2.3. Sample preparation and fortification

Soil samples were air-dried, homogenized, ground, sieved (48–150 mesh) and stored in stoppered glass flasks at -18°C . Fortified soil samples were prepared by adding 1.0 ml of each standard solution to 5.0g of soil. The standard solution was added to the sample drop by drop while verifying that the solution covered the soil particles completely. After fortification the samples were homogenized with the use of a glass rod and kept at room temperature for 1 h to allow evaporation of the solvent.

2.4. Analytical procedures

2.4.1. Hexachlorobenzene

A glass chromatographic column (350 \times 10 mm i.d.) was prepared by adding, in this order: a small plug of glass wool, n-hexane up to 30 mm, and 2.0 g of 4.6% deactivated alumina as a slurry. The column was tapped gently and 5.0 g of the soil sample was transferred to the column. The elution was processed with 60 ml of n-hexane at 2 ml min^{-1} . The eluate was collected in a 100 ml round-bottom flask and concentrated to 3 ml using a rotary evaporator. The final extract was reconstituted to an adequate volume with n-hexane.

2.4.2. Pentachlorophenol

An analytical sample of 5.0 g was adjusted to a $\text{pH} < 1$ with approximately 1 ml of H_2SO_4 (1:1) and extracted twice with 20 ml of n-hexane–acetone (1:1) in an ultrasonic bath (Branson) for 20 min. Following each extraction, the soil was allowed to settle and the supernatant was transferred to a separatory funnel. The organic layer was extracted three times with 20 ml of potassium carbonate solution (5%), and after the last extraction the organic layer was discarded. To combined aqueous extracts 1.0 ml of acetic anhydride and 20 ml of n-hexane were added. The separatory funnel was stirred slowly until the evolution

of CO_2 subsided, and then stirred vigorously for 2 min. The acetylation extraction process was repeated twice. The combined organic layers were dried through anhydrous sodium sulphate, concentrated, and diluted as described above

2.5. Gas chromatographic analysis

Suitable aliquots of soil extracts and standard solutions were injected into a gas chromatograph. The percentages of recoveries were calculated by comparing the average chromatographic peak areas of the standard, fortified samples and unfortified samples. Standard solutions of PCP were extracted with potassium carbonate solution and acetylated as described previously.

3. Results and discussion

The efficiency of the proposed methods was evaluated by means of recovery studies with soil samples fortified at three different levels. The physicochemical properties of the soil samples are presented in Table 1. The fortification levels and recovery values of HCB and PCP are shown in Table 2.

3.1. HCB procedure

The development of the HCB procedure was based on an on-line method previously developed in our laboratory [16] for determination of

Table 1
Physicochemical characteristics of soil samples.

Parameters	Samples	
Phosphorus (ppm)	5	2
Potassium (mEq/100 g)	0.03	0.01
Calcium (mEq/100 g)	0.3	0.7
Magnesium (mEq/100 g)	—	—
pH	5.2	3.7
Cation exchange capacity (mEq/100 g)	1.0	1.6
Organic carbon (%)	0.1	0.3
Sand (%)	94.6	97.1
Silt (%)	1.5	2.5
Clay (%)	3.9	0.4

Table 2
Recoveries of HCB and PCP in fortified soil samples

Compound	Fortification level (ng g ⁻¹)	Recovery ^a (%)		
		Range	Mean	Standard deviation
HCB	0.5	89–110	100	9.3
	4	85–99	92	4.7
	20	86–93	91	3.2
PCP	10	91–110	101	6.9
	40	80–101	88	7.6
	200	89–106	99	6.2

^a Eight analyses.

organochlorine pesticides in soil. Preliminary analyses were performed by using n-hexane–dichloromethane (7:3) for HCB elution from the column. Low recovery data (44 and 65%) were obtained when the elute was concentrated to dryness. Then, n-hexane was tested for elution of HCB in place of n-hexane–dichloromethane (7:3); this substitution is of interest due to the carcinogenic properties of dichloromethane and the need to remove dichloromethane before GC-ECD analysis [17]. The concentration step was performed as described in the experimental section and the recovery values ranged from 85 to 110% for soil samples fortified at 0.5; 4 and 20 ng g⁻¹. Different solvent systems such as toluene and n-hexane–dichloromethane were tested for the elution of PCP from the column. Recovery results were very low in all cases and demonstrated that this method was not adequate for PCP determination.

3.2. PCP procedure

The establishment of the experimental conditions followed a described methodology [18] developed for the analysis of chlorophenols in sediments. In this method, after acidification, sediment samples were Soxhlet extracted with a mixture of acetone-hexane for 20 h. Phenols in the organic extract were extracted with KHCO₃ solution, and then acetylated with acetic anhydride. After extraction with petroleum ether, the acetates were cleaned on a silica gel chromatographic column.

In the present study, after acidification, PCP was extracted from soil in an ultrasonic bath. In the first step, n-hexane and n-hexane–acetone were tested for their efficiency to extract PCP. Low percentages of recovery (64 and 65%) were obtained with n-hexane, however by using the mixture of n-hexane–acetone (1:1) better recoveries were obtained (80 and 83%). The extraction and acetylation of PCP were achieved by using a K₂CO₃ solution and acetic anhydride. n-hexane was used for extraction of the PCP derivative. Recovery data from samples fortified at 10; 40 and 200 ng g⁻¹, ranged from 80 to 110%. These values are in good agreement with the results reported by Lee et al. [18] but the procedure presented in this study has certain advantages such as time saving and reduction of solvents required for extraction; also, no further cleanup steps were necessary.

Capillary columns instead of packed columns have been widely used in residue determination. However the isothermal GC analysis on a packed column provided satisfactory separation of PCP from other compounds that could interfere in the analysis. In addition, gas chromatograms obtained for HCB determination were free of interfering compounds. The detection limits for HCB and PCP, determined by the described procedure [19], were 0.2 and 5 ng g⁻¹, respectively. The reproducibility of these methods was demonstrated by standard deviation values that ranged from 3.2 to 9.3%. Although the proposed methods do not allow for the simultaneous determination of HCB and PCP, they are efficient, selective, and

Table 3
Concentrations^a of HCB and PCP in soil samples

Sample number	Depth (cm)	Distance from the dumping site (m)	HCB (ng g ⁻¹)	PCP (ng g ⁻¹)
1	0–3	10	29298	21
2	5–10	10	81300	135
3	23–28	10	1.7	— ^b
4	42–47	10	0.6	—
5	60–62	10	31	—
6	65–68	10	0.4	—
7	78–81	10	2.3	—
8	8	20	87	—
9	14–16	20	8.5	—
10	25–26	20	0.2	—
11	33–35	20	0.2	—
12	43–45	20	6.4	—
13	60–63	20	0.6	—
14	3–6	47	3.6	—
15	27	47	13	—
16	33	47	8.7	—
17	40–43	47	0.3	—
18	54–57	47	0.5	—
19	65–68	47	0.2	—

^a Mean of two determinations.

^b Dashes indicate not detected.

can be employed in monitoring studies to estimate the contamination of soil by HCB and PCP.

In order to evaluate the dispersion and retention of HCB and PCP in soil, the methods were applied using soil samples from the Samaritá, a district in the city of São Vicente, São Paulo. The samples were taken at different depths and sampling points, pre-selected by pedological criteria. The concentrations of HCB and PCP are given in Table 3. The fungicides HCB and PCP were detected in 100 and 11% of the analyzed samples, respectively. When the concentrations of HCB and PCP were compared, HCB had the highest levels of contamination of all the soil samples. The concentrations of HCB ranged from 0.2 to 81300 ng g⁻¹. These data show the applicability of the proposed method to a wide range of concentrations.

The HCB concentrations found in the deeper soil layers indicated a vertical dispersion of HCB.

In this study, the distance from the dumping site appears to be one of the main factors in

determining the levels of HCB and PCP in soil samples. The highest levels of HCB (29298 and 81300 ng g⁻¹) and PCP (21 and 135 ng g⁻¹) were obtained from soil samples collected at about 10 m from the dumping site. It was observed that concentrations of these compounds decreased depending on the distance from the dumping site.

A comparison was not made of the proposed methods with other extraction techniques as the methods did not require specific optimizations for naturally contaminated samples and in addition the statistical analyses of recovery values confirmed the precision and accuracy of these methods.

Acknowledgements

The authors would like to thank Professor Nádia Regina do Nascimento from IGCE-UNESP for her assistance in collecting samples and Elaine F.G. Jardim and Professor Elizabeth V. Minelli for technical support.

References

- [1] L.G. Costa, C.L. Galli, S.D. Murphy, *Toxicology of Pesticides: Experimental, Clinical and Regulatory Perspectives*, Springer, Berlin, 1987, p. 133.
- [2] C. Tomlin, *The Pesticide Manual—Incorporating the Agrochemical Handbook*, 10th ed., British Crop Protection Council, The Royal Society of Chemistry, Bath Press, UK, 1994, pp. 780–782.
- [3] E. Barriuso, *Anal. Magazine* 22 (1994) 13.
- [4] V. Seidel, W. Lindner, *Anal. Chem.* 65 (1993) 3677.
- [5] E.G. van der Velde, W. de Haan, A.K.D. Liem, *J. Chromatogr.* 626 (1992) 135.
- [6] E.G. van der Velde, M. Dietvorst, C.P. Swart, M.R. Ramlal, P.R. Kootstra, *J. Chromatogr. A* 683 (1994) 167.
- [7] B.W. Wenclawiak, G. Maio, Ch.v. Holst, R. Darskus, *Anal. Chem.* 66 (1994) 3581.
- [8] H.B. Lee, T.E. Peart, R.L. Hong-You, *J. Chromatogr.* 605 (1992) 109.
- [9] M. Kolb, H.B. Böhm, M. Bahadir, *Fresenius J. Anal. Chem.* 351 (1995) 286.
- [10] A. Besner, R. Gilbert, P. Tétreault, L. Lépine, J.F. Archambault, *Anal. Chem.* 67 (1995) 442.
- [11] K. Abrahamsson, A. Ekdahl, *J. Chromatogr.* 643 (1993) 239.
- [12] V.L. Lopez-Avila, K. Bauer, J. Milanes, W.F. Beckert, *J. Assoc. Off. Anal. Chem. Int.* 76 (1993) 864.
- [13] P. Mußmann, K. Levsen, W. Radeck, *Fresenius J. Anal. Chem.* 348 (1994) 654.
- [14] A. Kramer, J. Angerer, *Fresenius J. Anal. Chem.* 351 (1995) 327.
- [15] M.L. Ribeiro, L. Polese, M.S. Draetta, E. V. Minelli, A. Del Acqua, *J. Braz. Chem. Soc.* 2 (1991) 102.
- [16] L. Polese, E.V. Minelli, E.F.G. Jardim, M.L. Ribeiro, *Fresenius J. Anal. Chem.* 354 (1996) 474.
- [17] T. Cairns, J. Sherma, *Emerging Strategies for Pesticide Analysis—Modern Methods for Pesticide Analysis*, CRC Press, Boca Raton, FL, 1992, 81 pp.
- [18] H.B. Lee, Y.D. Stokker, A.S.Y. Chau, *J. Assoc. Off. Anal. Chem.* 70 (1987) 1003.
- [19] H.P. Their, H. Zeumer, *Manual of Pesticide Residue Analysis*, Deutsche Forschungsgemeinschaft, Pesticides Comm. Verlag Chemie, Weinheim New York, 1987, pp. 37–44.

Radiometric determination of trace amounts of zinc using liquid scintillation counting

D. Sandhya, M.S. Subramanian *

Department of Chemistry, Indian Institute of Technology, Madras, Chennai-600 036; Madras, India

Received 7 July 1997; received in revised form 30 September 1997

Abstract

A sensitive and selective radiometric method of substoichiometric isotope dilution analysis for the determination of trace amounts of zinc is described. The activity of ^{65}Zn used as a tracer in this method was measured by liquid scintillation counting and its counting efficiency was found to be $76 \pm 2.7\%$. The method is based on the extraction of the ion-association complex of zinc from thiocyanate medium at pH 7.9 using substoichiometric amount of Aliquat-336 in toluene. The method is sensitive to 20 ng of Zn(II) in an aqueous phase volume of up to 15 ml and its reliability was tested by applying it to a certified reference material—magnesium alloy and pharmaceutical samples. © 1998 Elsevier Science B.V. All rights reserved.

Keywords: Zinc determination; Liquid scintillation counting; Substoichiometric isotope dilution analysis; Aliquat-336

1. Introduction

Traditionally, liquid scintillation counters have been used primarily to measure the radioactivity of soft β^- emitters. It is now being used to measure the activity of a wide range of radioactive emissions like α , γ and also electron-capture decay. Advances in LSC has led to its use in environmental monitoring of a number of radionuclides [1].

The use of LSC as an analytical tool was described by Gibson and Lally [2]. Recent methods have been reported detailing the routine trace analysis of elements like indium [3], thallium [4]

and selenium [5] using liquid scintillation counting (LSC). These methods provide very low detection limits which were attained by the high counting efficiency and low background activity of LSC. Our aim here is to develop a sensitive analytical method for zinc using LSC which has not been considered in any of the standard methods.

The main drawback with zinc is the lack of selectivity with organic reagents used for its detection and determination [6]. However, substoichiometric extractions can improve the selectivity for zinc in the sense that at least those metal ions which possess lower extractions constants than that of zinc will not interfere in its estimation [7]. Nevertheless, a few reagents [8–10] have been used as substoichiometric reagents in the isotope dilution analysis of zinc—either poor sensitivity

* Corresponding author. Tel.: +91 44 2351365; fax: +91 44 2350509; e-mail: mss@chandra.iitm.ernet.in

or selectivity or the poor stability of the substoichiometric reagent used imposes a limitation on these methods.

Numerous methods have been reported detailing the extraction of zinc as its $\text{Zn}(\text{NCS})_4^{2-}$ anion with brilliant green [11], 2-hexylpyridine, [12], rhodamine-6G [13], tributyl phosphate [14], etc. as counter cations for either the spectrophotometric determination of zinc or for separation by solvent extraction. In any case these counter cations were added in excess. We found that Aliquat-336 (tri-caprylmethylammonium chloride) was a very effective extractant in the extraction of this anionic complex. This reagent is very stable and works very well under substoichiometric conditions. In the present study a ^{65}Zn radioisotope was used as the tracer and its activity was measured using LSC. The counting efficiency of ^{65}Zn that decays by electron-capture was found to be $76 \pm 2.7\%$. The developed method is very sensitive and selective, down to 20 ng of zinc from a final volume of 15 ml could be determined.

2. Experimental

2.1. Apparatus

A Packard Tri-Carb 1500 Liquid Scintillation Analyser was used to measure the activity of ^{65}Zn .

2.2. Optimum window settings

In a liquid scintillation counter, the entire energy dissipated by a radioactive particle is converted from analog pulse to a digital value by a high speed analog to digital converter (ADC) which is the address of a memory slot of a spectralyzer spectrum analyzer. This spectralyzer spectrum analyzer consists of many storage slots or channels covering an energy range from 0 keV to 2000 keV and the optimum window settings are made from 0 keV to E_{max} of the radionuclide to obtain maximum counting efficiency and at the same time to exclude all unwanted radiation falling outside the region of interest [15]. The activity measurements of ^{65}Zn were made using a window-width of 0–1115 keV so that both the

electron capture decay of ^{65}Zn as well as the γ transitions of its daughter, ^{65}Cu will be counted.

2.3. Reagents

Analytical-reagent grade chemicals were used throughout. A ^{65}Zn tracer of specific activity 14×10^{11} dpm g^{-1} was procured from the Board of Radiation and Isotope Technology (BRIT), Mumbai, India.

A bulk solution of 1000 $\mu\text{g ml}^{-1}$ of standard Zn(II) solution was first prepared by dissolving 0.4398 g of pure $\text{ZnSO}_4 \cdot 7\text{H}_2\text{O}$ in doubly distilled water and diluting to 100 ml. Suitable aliquots of this solution were diluted to obtain the working standards.

Radioactive Zn(II) solution, 10 $\mu\text{g ml}^{-1}$ (1.5×10^{-4} M) was prepared by mixing a 10 ml volume of 100 $\mu\text{g ml}^{-1}$ of Zn(II) solution with approximately 51×10^6 dpm of ^{65}Zn tracer and diluting to 100 ml with doubly distilled water.

A stock solution of 8.5×10^{-3} M Aliquat-336 solution was prepared by dissolving 0.1886 g of it (Merck; 442 g mol^{-1}) in 50 ml toluene. From this a working solution of 3.06×10^{-5} M was prepared by appropriate dilution with toluene. A 5 ml volume of this solution was used for each extraction.

A Packard Scint-A XF scintillator solution was used for activity measurements.

2.4. Calibration

To a 1 ml volume of 10 $\mu\text{g ml}^{-1}$ (1.5×10^{-4}) solution of radioactive Zn(II), in a separatory funnel, 2 ml of borax buffer, pH 7.9 and 1 ml of a 25% solution of NH_4SCN was added. After dilution to 10 ml the resulting anionic tetrakis(isothiocyanato) zincate (II) complex was extracted with 5 ml of 3.06×10^{-5} M Aliquat-336 in toluene. A blank experiment was performed under identical conditions without the use of Aliquat-336 to eliminate the activity caused by the extraction of zinc in any other form. The activity in each case was determined by mixing 2 ml of organic extract with 10 ml of cocktail and measuring the activity using a window-width of 0–1115 keV. The blank-corrected activity (a_s) was

then calculated. Another set of experiments was performed as above by adding varying amounts of inactive Zn(II), taken in a series of separatory funnels to 10 μg of radioactive Zn(II). The solution thus gets isotopically diluted. The blank-corrected activities (a) were similarly determined. A plot of a_s/a versus the concentration of inactive Zn(II) served in calibration (see Fig. 1). It was found to be linear in the range 0–3 μg of zinc. The regression equation obtained was $Y = 0.076 X + 0.9998$.

To determine zinc in various samples, suitable aliquots of the diluted sample digest were analyzed using the procedure described above and was repeated to obtain the 'a' value. Using the a_s/a value, the amount of zinc present in these samples was obtained from the calibration plot.

3. Results and discussion

3.1. Quenching studies:

The method of internal standardisation was employed to determine the presence of any kind

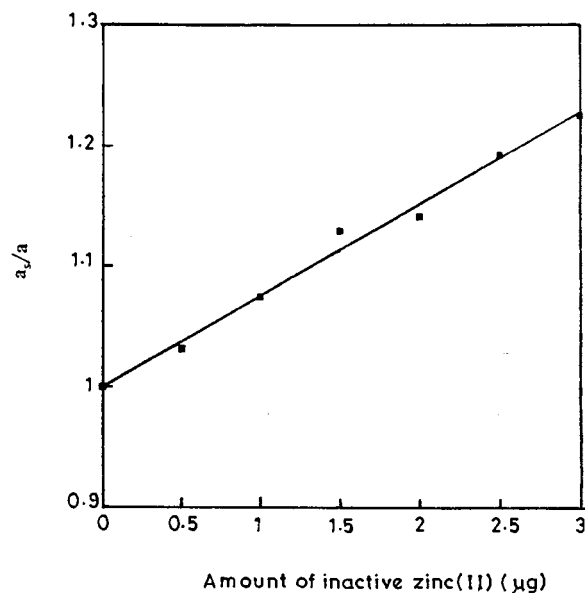


Fig. 1. Calibration plot ratio of activities versus amounts of inactive zinc(II).

of quenching, when using LSC to measure the activity of ^{65}Zn .

To about 10 ml of the scintillation cocktail, ^{65}Zn radioisotope of known activity was added and its count rate was measured. The counting efficiency 'E' was calculated using the formula, $E = \text{counts per minute (cpm)} / \text{disintegrations per minute (dpm)} \times 100$. It was found to be $76 \pm 2.7\%$. Inactive Zn(II) (10 μg) was extracted at pH 7.9 from thiocyanate medium using 5 ml of 3.06 ± 10^{-5} M solution of Aliquat-336 in toluene. Toluene extract (2 ml) was added to the above cocktail and ^{65}Zn mixture, the count rate was again measured to determine the counting efficiency. It was found that there was no decrease in the counting efficiency, indicating the absence of quenching due to inactive zinc solution, thiocyanate and chemicals used in the extraction.

3.2. Effect of variable

The optimum pH for maximum extraction of the complex was determined by extracting 10 μg ml^{-1} of radioactive Zn(II) from excess thiocyanate medium at different pH conditions. Maximum extraction was achieved in the pH range 7.7–8.1. Hence a borate buffer of pH 7.9 was used in all subsequent experiments. An equilibration time of 3 min was sufficient for maximum extraction and an aqueous phase volume of up to 15 ml was tolerated using this method.

The effect of various solvents on extraction showed toluene to be the most suited one with maximum blank-corrected activity even though blank activities were negligible with all other solvents. The results are summarized in Table 1. The use of halogenated or oxygenated hydrocarbons was avoided as they would cause chemical quenching effects on the LSC measurements.

Extractions carried out under optimum conditions with varying concentrations of NH_4SCN maintaining an aqueous volume of 10 ml, showed that for maximum activity, the addition of at least 1 ml of 15% solution was required, beyond which the activity remained constant. However, a 1 ml volume of 25% solution of NH_4SCN was added in all extractions.

Table 1
Choice of solvent for the extraction of zinc(II) with aliquat-336 from thiocyanate medium

Solvent	Sample activity (cpm)	Blank activity (cpm)	Blank-corrected activity (cpm)
Toluene	108 419	98	108 321
Xylene	98 035	24	98 011
Benzene	63 047	19	63 028
<i>n</i> -Pentane	6028	10	6018
Cyclohexane	33 633	12	33 621

3.3. Verification of reproducibility of substoichiometric extraction

This is an important parameter and is verified using this method. It ensures that under substoichiometric conditions, extractions are reproducible.

In this experiment varying concentrations of radioactive Zn(II) ranging from 1 to 16 μg (1.51×10^{-5} – 2.4×10^{-4} mM) were extracted from a solution containing 1 ml of 25% NH_4SCN at pH 7.9 using 5 ml of 3.06×10^{-5} M Aliquat-336 in toluene. The activity of the extract (2 ml) was measured after mixing with 10 ml of cocktail. A blank extraction was performed in the absence of Aliquat-336 and the activity of 2 ml of the extract after mixing with 10 ml cocktail was again measured. The blank-corrected activity in each case was determined. A plot of blank-corrected activity versus the concentration of radioactive ^{65}Zn is shown in Fig. 2. As can be seen, the activity reaches a saturation point corresponding to 7.1×10^{-5} mM concentration of Zn(II) indicating a 1:2 stoichiometric ratio of zinc to Aliquat-336. Beyond this concentration of zinc the amount of Aliquat-336 used in the extraction studies becomes substoichiometric and it can be seen that in the substoichiometric region (beyond 7.1×10^{-5} mM concentration of zinc) extractions are reproducible with the activity remaining fairly constant with further increase in zinc concentration.

3.4. Precision and detection limit

The relative standard deviation at the 2 μg level of zinc (ten determinations) was found to be 2.16%. The detection limit was calculated on the basis of its definition $C_B + 3\sigma_B$ (where $C_B =$

blank activity and $\sigma_B =$ standard deviation of the blank activity) [16] was found to be 16 ng from an aqueous phase volume of 15 ml, i.e. (2.1×10^{-8} M).

3.5. Effect of interfering ions

An investigation was carried out to determine the effect of a number of cations and anions on 2 μg of Zn(II). Ions that are capable of forming complexes with thiocyanate were examined as well as a number of other ions. A 1 mg amount of each ion was added prior to the addition of other reagents and determinations were carried out as previously outlined. The ions examined and their interference effects are summarized in Table 2.

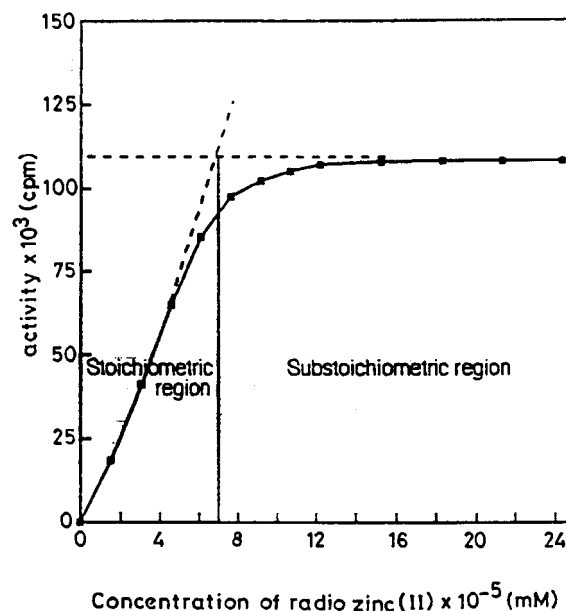


Fig. 2. Verification of reproducibility of substoichiometric extraction.

Table 2
Interference studies

Ion added, (1 mg level)	Remarks
Ba ²⁺ , Sr ²⁺ , Mg ²⁺ , Ni ²⁺ , Cd ²⁺ , Bi ³⁺ , Cu ²⁺ , Tl ⁺ , Sb ³⁺ , WO ₄ ²⁻ , tartrate, S ₂ O ₃ ²⁻ , citrate, PO ₄ ³⁻ , C ₂ O ₄ ²⁻ , SO ₃ ²⁻ , Br ⁻ , Cl ⁻ , I ⁻ , Cr ₂ O ₇ ²⁻ , AsO ₄ ³⁻ , VO ₃ ⁻ , Pb ²⁺ (500 µg) ^a	No interference
Co ²⁺ , Hg ²⁺ , Sn ²⁺ , Fe ³⁺ , Al ³⁺ , Mn ²⁺ , F ⁻	Interfered by decreasing the counts

^a Corresponds to tolerance limit.

The interfering effects of Hg²⁺ (1 mg) and up to 500 µg of Co²⁺ could be overcome by masking with 1 ml of 4% sodium thiosulphate solution. Fe³⁺, Al³⁺ (1 ml) and up to 500 µg of Mn²⁺ were removed using 2 ml of 4% solution of sulphosalicylic acid. The interference of Sn²⁺ (1 mg) could be removed by complexing it with 1 ml of 4% tartrate solution.

3.6. Application studies

The city waste incineration ash sample was decomposed using H₂SO₄-KMnO₄-H₂O₂ mixture [17]. The Fourts-B tablets (Fourts India, Chennai, India) was carefully boiled with dilute HNO₃ and the magnesium alloy sample with 1:1 HCl. The Boro-plus ointment sample (Himani, Calcutta, In-

dia) was decomposed using HNO₃-H₂SO₄-HClO₄ [18]. The digest in each instance was filtered, if necessary, and diluted to known volumes. Suitable aliquots were taken and analyzed for zinc as described earlier in Section 2.4. Known amounts of zinc were then added to the samples before decomposition and the above procedure was repeated to check the recovery of zinc.

Simultaneously the method of internal standardisation was repeated with aliquots of all the sample solutions taken for analysis (as mentioned in Section 3.1) to verify the presence or absence of quenching arising from matrix constituents of these samples. However it was found that the counting efficiencies remained the same which was confirmed by the absence of any kind of quenching.

Table 3
Application studies

Sample	Zinc present (µg)	Zinc added (µg)	Zinc found by the proposed method ^a (µg)	Recovery
City waste incineration ash (CRM ^c 176) 0.02 g 500 ml ⁻¹	516	---	511 ± 3.2	-
		250	764 ± 3.8	101.2
Fourts-B tablet 0.02 g 250 ml ⁻¹	494 ^b	---	496 ± 1	---
		125	620 ± 0.9	99.2
		250	747 ± 1.9	100.4
Magnesium alloy 0.05 g 250 ml ⁻¹	500	---	492 ± 2.5	---
		125	615 ± 3.9	98.4
		250	741 ± 2.1	99.6
Boro-plus ointment 0.03 g 250 ml ⁻¹	435 ^b	---	438 ± 4.6	---
		250	685 ± 2.7	98.8

^a Average of three determinations.

^b Determined by inductively coupled plasma-atomic emission spectrometry (ICP-AES).

^c CRM = certified reference material.

The results obtained in the case of Fourts-B tablet and Boro-plus ointment samples were compared with those obtained by inductively coupled plasma-atomic emission spectrometry (ICP-AES) to assess the reliability of the method since the certified values were not available. A 213.856 nm zinc emission line was used for the analysis of zinc which is relatively free from spectral interference. The results of the application studies are shown in Table 3 which indicates a close agreement between the proposed method and that of ICP-AES or the certified values.

4. Conclusion

The proposed method has demonstrated the feasibility of using LSC for the routine analysis of zinc by measuring the electron-capture decay activity of ^{65}Zn with fairly good efficiency. The advantage of carrying out solvent extraction prior to LSC measurements is the minimization of quenching due to the elimination of extraneous matrix constituents, as demonstrated in this method. Also elaborate sample preparation is not required. The method is simple and reliable and can be used to determine as low as 16 ng of Zn(II) from an aqueous phase volume of up to 15 ml. The method has been successfully applied to the determination of zinc in pharmaceutical preparations, magnesium alloy and a certified reference material. The sensitivity of the method can be further improved by the use of a radioisotope of higher specific activity.

References

- [1] G.T. Cook, *Anal. Proc. (London)* 29 (1992) 4.
- [2] J.A.B. Gibson, A.E. Lally, *Analyst* 96 (1971) 681.
- [3] N. Rajesh, M.S. Subramanian, *Analyst* 117 (1992) 1953.
- [4] N. Rajesh, J. Jacob, M.S. Subramanian, *Radiochim. Acta* 62 (1993) 101.
- [5] A. Ramesh, K. Raghuraman, M.S. Subramanian, T.V. Ramakrishna, *Analyst* 119 (1994) 2067.
- [6] Z. Holzbecher, L. Divis, M. Kral, L. Sucha, F. Vlácil, *Handbook of Organic Reagents in Inorganic Analysis*, 1st ed., Wiley, New York, 1976, p. 423.
- [7] J. Ruzicka, J. Stary, in: M. Williams (Ed.), *Stoichiometry in Radiochemical Analysis*, Pergamon, London, 1968, p.25.
- [8] C. Ballaux, R. Dams, J. Hoste, *Anal. Chim. Acta* 35 (1966) 141.
- [9] K. Ashoka Rao, P. Chandrasekhar Reddy, B. Ranganannar, *Radiochem. Radioanal. Lett.* 56 (1983) 149.
- [10] H. Akaiwa, H. Kawamoto, K. Ogura, *Talanta* 24 (1977) 394.
- [11] Z. Zhau, C. Wei, F. Huasue, *Anal. Abstr* 13 (1985) 215; 47 (1985) 12B73
- [12] M.S.Bhatti, Shamasud-Zuha, *J. Radioanal. Chem.* 62 (1981) 23.
- [13] T. Prasada Rao, T.V. Ramakrishna, *Analyst* 105 (1980) 674.
- [14] D. Singh, O.V. Singh, S.N. Tandon, *Anal. Chim. Acta* 115 (1980) 369.
- [15] Packard Operation Manual, Tri-Carb1500 Liquid Scintillation Analyzer, Model 1500, Packard Instrument, 1988.
- [16] D.A. Skoog, J.L. Leary, *Principles of Instrumental Analysis*, 4th ed., Saunders, New York, 1992, p.7.
- [17] Foster Dee Snell, *Photometric and Fluorometric Methods of Analysis, Metals, Part 1*, Wiley-Interscience, New York, 1978, p.112.
- [18] C. Feldman, *Anal. Chem.* 46 (1974) 1606.

Separation study of cadmium through an emulsion liquid membrane using triisooctylamine as mobile carrier

Quan-Min Li *, Qi Liu, Qing-Fen Zhang, Xian-Jun Wei, Jin-Zhi Guo

Department of Chemistry, Henan Normal University, Xinxiang 453002, People's Republic of China

Received 14 March 1997; received in revised form 15 September 1997; accepted 1 October 1997

Abstract

A study of the transport of Cd^{2+} ions through a triisooctylamine (TIOA)—sorbitan monooleate (Span 80)—dimethylbenzene liquid membrane has been performed with varying concentrations of HCl, KI, TIOA, Span 80 and NaOH in the feed, membrane and stripping solutions. Maximum transport was observed with 0.025 M HCl, 0.01 M KI, 0.02 M TIOA, 3% (w/v) Span 80 and 0.05 M NaOH. With this system cadmium could be completely separated with Cu^{2+} , Zn^{2+} , Fe^{2+} , Co^{2+} , Ni^{2+} , Mn^{2+} , Cr^{3+} and Al^{3+} . The transport mechanism of this metal ions through the membrane has been discussed. © 1998 Elsevier Science B.V. All rights reserved.

Keywords: Ions; Transport; Mechanism

1. Introduction

As a new method, the emulsion liquid membrane (ELM) has been studied for the preconcentration and separation of metal ions [1–3], because of its advantage of high efficiency and low expense. Tri-*n*-octylamine (TOA) has been studied as an ELM mobile carrier to separate metal ions [4,5], but triisooctylamine (TIOA) has not been applied for the separation of cadmium from coexistence ions. As an important extractant, TIOA can be combined with CdI_4^{2-} ions after its protonation [3].

In this paper, an ELM with TIOA as mobile carrier is studied for the transport of cadmium. Various parameters influencing the transport of cadmium across the membrane have been optimized to separate cadmium from Cu^{2+} , Zn^{2+} , Fe^{2+} , Co^{2+} , Ni^{2+} , Mn^{2+} , Cr^{3+} and Al^{3+} , and the transport mechanism of this metal ions through the membrane has been discussed.

2. Experimental

2.1. Reagents

A standard (1 mg ml^{-1}) solution of cadmium was prepared from metal cadmium (99.99%) dis-

* Corresponding author.

solved in nitric acid and distilled, deionized water. TIOA (analytical grade) was obtained from Aldrich. Sorbitan monooleate (Span 80; chemical grade) was obtained from Shanghai Dazhong Medical Company (Shanghai, People's Republic of China). A 0.10 M solution of TIOA and a 3% (w/v) solution of Span 80 in dimethylbenzene were used in this work.

2.2. Apparatus

The following instruments were used: a motor-driven emulsifier (range 0–6000 rpm); motor-driven stirrers (range 0–600 rpm); and a model 722 spectrophotometer (Shanghai Analytical Instrument Factory, People's Republic of China).

2.3. Procedure

2.3.1. Preparation of ELM

A 20 ml portion of solution TIOA and Span 80 in dimethylbenzene are emulsified at a stripping speed of 2000 rpm. Stripping solution was added at a rate of 20 ml min⁻¹ until the volume ratio of organic membrane solution to stripping solution was 1:1. The solution was then stirred continuously for 15 min to obtain a stable white ELM.

2.3.2. Transport of metal ions

To small beakers containing 10 ml metal ion feed solutions was added 2 ml of ELM and the contents stirred at 200 rpm for a given transfer time; the phases were allowed to separate, clear feed solution was pipetted into a 25 ml volumetric flask and analyzed for the amount of cation remaining.

2.3.3. Determination of cadmium [6]

Three millilitres of 5 × 10⁻⁴ M 4-(2-pyridylazo) resorcinol (PAR) alcohol solution was added to 5 ml of 0.1 M Na₂B₄O₇·10H₂O buffer solution (pH = 9.2) in a 25 ml volumetric flask containing cadmium ions, after diluting to the mark the absorbance was read at 495 nm against the reagent blank.

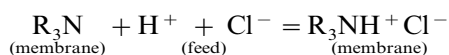
In separation experiment, the concentration of cadmium as well as other cations was determined by inductively-coupled plasma atomic emission spectrometry (ICP-AES).

3. Results and discussion

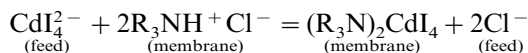
3.1. The effect of hydrochloric acid concentration in the feed

The relationship between the concentration of hydrochloric acid in the feed solution and extraction of cadmium is shown in Fig. 1. An acid concentration of 0.025 M was found to be best for transport of Cd²⁺ through ELM. In Fig. 1, it also is found that the transport of cadmium is completed in 5 min, this is because extraction and back-extraction occur simultaneously, and the degree of dispersion of the ELM in the feed solution is high [7]. In the presence of HCl and KI in the feed solution, the transport process of cadmium through an ELM is illustrated by the following equations:

1. TIOA (shown as R₃N) in the membrane phase reacts with hydrochloric acid in the feed phase.



2. In the feed, CdI₄²⁻ exchanges with Cl⁻ of R₃NH⁺Cl⁻ in the membrane phase.



3. NaOH in the stripping solution reacts with (R₃NH)₂CdI₄²⁻ to strip cadmium into the stripping solution.

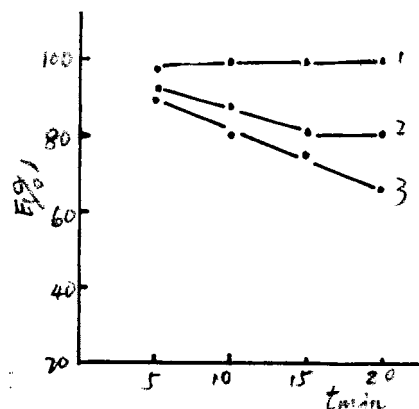


Fig. 1. Effect of HCl conc. in the feed on the percent extraction of Cd²⁺ membrane phase: 0.02 M TIOA + 3% (w/v) Span 80 + dimethylbenzene; stripping phase: 0.05 M NaOH; feed phase: 50 μg ml⁻¹ Cd²⁺ + 0.01 M KI + HCl (M): 1–0.01–0.10, 2–0.005, 3–1.0.

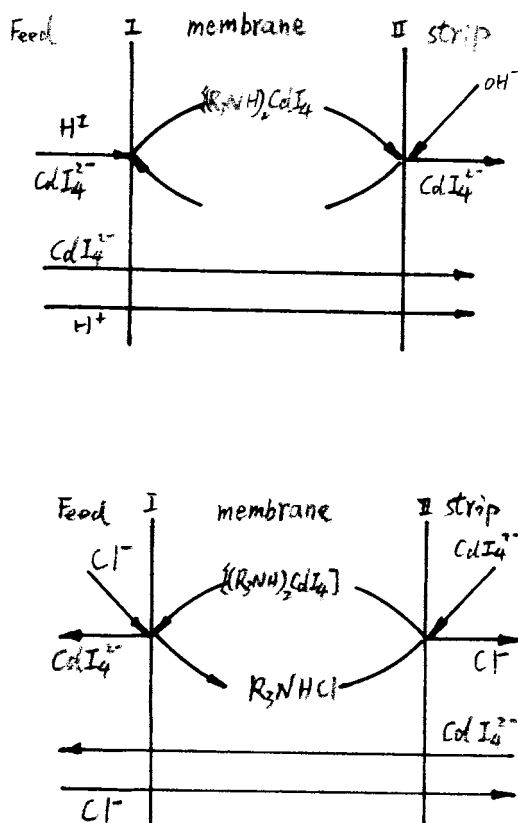
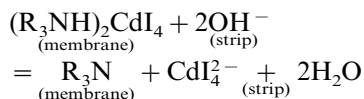


Fig. 2. (a) Co-transport of CdI_4^{2-} with H^+ . (b) Counter-transport of CdI_4^{2-} with Cl^- co-transport or counter-transport of CdI_4^{2-} with protonated triisooctylamine as carrier.



The expected mechanism of cadmium transport in the present case is shown in Fig. 2a. Cd^{2+} and H^+ were transported from the feed solution to the stripping solution where H^+ was neutralized by NaOH . The transport of H^+ along a concentration gradient supplied the energy for the transport of cadmium against a concentration gradient. It was discovered that the decrease of H^+ concentration in the feed solution was more considerable than that of cadmium. This was due to the formation of $\text{R}_3\text{NH}^+\text{Cl}^-$ -type species and their transport into the stripping phase. When the concentration of HCl was < 0.005 M, transport of cadmium

abruptly decreases with time. This is because less H^+ is available to protonate R_3N , and precipitation of Cd^{2+} as $\text{Cd}(\text{OH})_2$ blocks the membrane. These can be proved by finding white $\text{Cd}(\text{OH})_2$ precipitation in the stripping solution after demulsification. When the concentration of $\text{H}^+ > 0.1$ M, the extraction of cadmium decreased too, this is because a great amount of H^+ transport into the stripping where OH^- is neutralized immediately, then the original transport direction of cadmium is changed (the cadmium transport from the stripping to the feed) [8]. This process is shown in Fig. 2b.

3.2. The effect of the concentration of surfactant

Span 80 is better than other surfactant when used in ELM [2]. Both the stability of the emission and the viscosity of the liquid membrane were altered by the proportion of surfactant in the organic phase. An increase in the concentration of Span 80 increased the stability of the emulsion, however as follows from Table 1, the extraction of cadmium decrease. When the concentration of Span 80 was $< 2\%$ by weight in the organic phase, the ELM was easy to break with transfer time. A concentration of 3% (w/v) in the organic phase resulted in good extraction and stability.

3.3. The effect of the concentration of TIOA

The effect of the concentration of TIOA (mobile carrier) in the organic phase on the extraction of cadmium is shown in Fig. 3. The optimum concentration range of carrier was 0.02–0.03 M. When the concentration of TIOA was 0.01 M, less H^+ entered the stripping, Cd^{2+} precipitated as $\text{Cd}(\text{OH})_2$ and clogged the membrane, the extraction of Cd^{2+} decreased. When the concentration of TIOA was > 0.05 M, H^+ transported into the stripping and neutralized OH^- immediately, then the cadmium transported inversely from the stripping to the feed [8] (see Fig. 2b). In the experiment 0.02 M concentration of TIOA was selected for a rapid and complete transport of cadmium.

Table 1
The effect of concentration of surfactant

Conc. of Span 80 [(w/v)]	1	2	3	4	5
Percent extraction	93.3	94.7	99.0	96.5	96.8

Membrane phase: 0.02 M TIOA+Span 80; feed phase: 0.025 M HCl+50 $\mu\text{g ml}^{-1}$ Cd(II)+0.01 M KI. Stripping phase: 0.05 M NaOH; transfer time: 10 min.

3.4. The effect of the concentration of NaOH in the stripping solution

The NaOH in the stripping phase functioned as a back-extracting solution. When the composition of emulsion was fixed, the maximum extraction was obtained in different stripping solution at 0.01–0.05 M NaOH. It has been observed that above a concentration of 0.2 M NaOH, the transport decreased markedly (see Fig. 4). This may be because more H^+ transported the stripping, formed more water, made the membrane swell and break. When the concentration of NaOH increased to 1.0 M, CdI_4^{2-} precipitated $\text{Cd}(\text{OH})_2$ and the membrane was clogged as soon as the transport began. In the experiment, 0.05 M NaOH was selected.

When the concentrations of NaOH were 0.025 and 0.5 M, by changing the transfer time (from 0.5 to 2.5 min) measured the natural logarithm of the ratio of initial concentration (C_0) to give time

concentration (C) of cadmium the kinetic curve can be obtained (see Fig. 5). In $C_0/C - t$ curve line is a good straight line, they are (1) $\ln C_0/C = 1.479 \times 10^{-2}t + 0.6386$, $r = 0.9908$; (2) $\ln C_0/C = 1.285 \times 10^{-2}t + 0.2556$, $r = 0.9985$, respectively. This shows that transport of cadmium is near kinetic pseudo-first-order reaction. The transfer rate constant of Cd^{2+} was 0.0148 and 0.0128 s^{-1} , which are similar. This shows that the transfer rate of Cd^{2+} was controlled only by $(\text{R}_3\text{NH})_2\text{CdI}_4$ concentration on the feed-side interface. Its kinetic equation is illustrated by the following equation

$$-d[\text{Cd}(\text{II})] = k[(\text{R}_3\text{NH})_2\text{CdI}_4] dt$$

3.5. The effect of other reagents in the feed solution

With a suitable acid concentration of the feed solution, the concentration of KI in the feed was

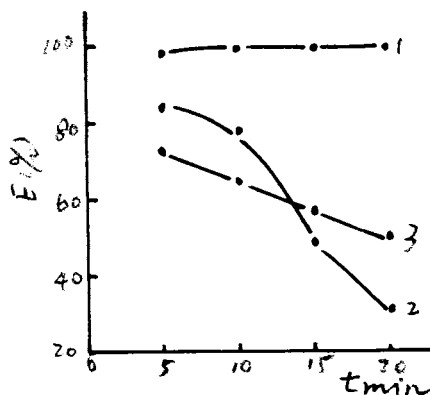


Fig. 3. Effect of TIOA conc. in the membrane phase on the percent extraction of Cd^{2+} feed phase: 50 $\mu\text{g ml}^{-1}$ Cd^{2+} + 0.01 M KI + 0.025 M HCl; stripping phase: 0.05 M NaOH; membrane phase: 3% (w/v) Span 80 + TIOA (M): 1–0.02 ~ 0.03, 2–0.01, 3–0.05.

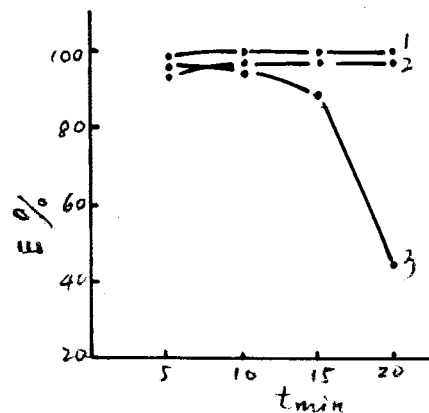


Fig. 4. Effect of concentration of NaOH on the percent extraction of Cd^{2+} membrane phase: 0.02 M TIOA + 3% (w/v) Span 80 + dimethylbenzene; feed phase: 50 $\mu\text{g ml}^{-1}$ Cd^{2+} + 0.025 M HCl + 0.01 M KI; stripping phase: NaOH (M): 1–0.01–0.05, 2–0.10, 3–0.20.

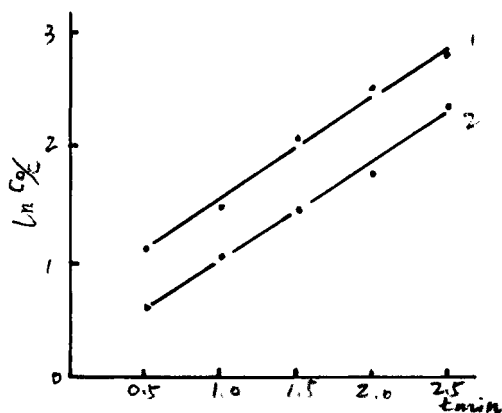


Fig. 5. Kinetic curve line of transport of Cd²⁺ membrane phase: 0.02 M TIOA + 3% (w/v) Span 80 + dimethylbenzene; feed phase: 50 µg ml⁻¹ Cd²⁺ + 0.025 M HCl + 0.01 M KI; stripping phase: NaOH (M): 1–0.025, 2–0.05.

> 0.01 M, the extraction efficiency of cadmium was always > 98%. If KI was replaced by KBr or KSCN in turn, the extraction of cadmium decreased greatly, it is because the logarithm of their cumulative stability constants ($\log \beta_4$) of CdI₄²⁻, CdBr₄²⁻ and Cd(SCN)₄²⁻ are respectively 5.35, 2.93 and 2.91 [9], the $\log \beta_4$ of CdI₄²⁻ is the highest. If KCl, KNO₃, K₂SO₄ or KClO₄ were added to above systems in turn, the results were shown in Fig. 6, ClO₄⁻ is the biggest anion and so its association with TIOA resulted in the most significant decrease in the transport of cadmium (see curve 4 in Fig. 6). The smallest anion Cl⁻ did not interfere the transport of cadmium (see curve 1 in Fig. 6).

3.6. Separation of cadmium from other metal ions

Under suitable conditions, transport of Cu²⁺, Zn²⁺, Fe²⁺, Co²⁺, Ni²⁺, Mn²⁺, Cr³⁺ and Al³⁺ were studied. Results for the competitive transport of cadmium and other common cations in mixed solution are shown in Table 2. (Note that the data of Table 2 comes from ICP-AES measurements. All other data are from colorimetric measurements.) Selectivity of separation of cadmium was excellent and the transport of Cu²⁺, Zn²⁺, Fe²⁺, Co²⁺, Ni²⁺, Mn²⁺, Cr³⁺ and Al³⁺ was found to be negligible.

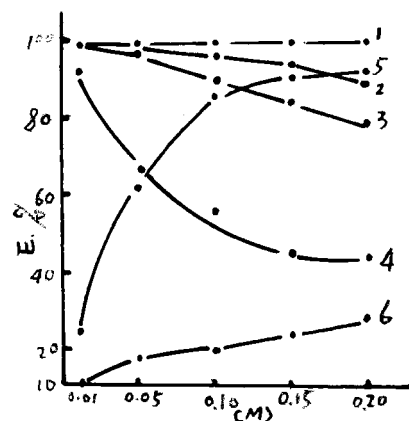


Fig. 6. Effect of different salts in the feed solution on the percent extraction of Cd²⁺ membrane phase: 0.02 M TIOA + 3% (w/v) Span 80 + dimethylbenzene; stripping phase: 0.05 M NaOH; feed phase: 50 µg ml⁻¹ Cd²⁺ + 0.05 M HCl + salt: 1–0.01 M KI + KCl, 2–0.01 M KI + K₂SO₄, 3–0.01 M KI + KNO₃, 4–0.01 M KI + HClO₄, 5–0.01 M Br, 6–0.01 M KSCN; transfer time: 10 min.

The TIOA-Span 80-dimethylbenzene liquid membrane is feasible to separate cadmium from other common cations, specifically from Zn²⁺, because the character of Zn²⁺ is significant.

4. Conclusion

In this paper, transport of cadmium through a TIOA-Span 80-dimethylbenzene ELM was studied. The mechanism of transport of cadmium was discussed and is presented in Fig. 2a, b. The optimum conditions of transport have been found to be 0.01 M KI and 0.025 M HCl in the feed

Table 2

The percent extraction of Cd²⁺ in a mixed solution

Initial amount of each co-ions (Fe ²⁺ , Zn ²⁺ , Co ²⁺ , Ni ²⁺ , Al ³⁺ , Mn ²⁺ , Cr ³⁺)	The percent extraction of Cd ²⁺
10 µg ml ⁻¹	99.3
50 µg ml ⁻¹	97.6
100 µg ml ⁻¹	95.8

Initial amount of Cd²⁺: 50 µg ml⁻¹; membrane phase: 0.02 M TIOA + 3% (w/v) Span 80 + dimethylbenzene; feed phase: 0.05 M HCl + 0.025 M KI; stripping phase: 0.05 M NaOH; transfer time: 10 min.

solution, 0.02 M TIOA and 3% (w/v) Span 80 in the liquid membrane, and 0.05 M NaOH in the stripping solution. It is concluded that this method can be applied for the selective separation of cadmium from a mixed solution of Cu^{2+} , Zn^{2+} , Fe^{2+} , Co^{2+} , Ni^{2+} , Mn^{2+} , Cr^{3+} and Al^{3+} or as a preconcentrating step of measuring cadmium. Small amount of carriers are involved and the extraction efficiency is high.

References

- [1] R.M. Izatt, G.C. Lindh, R.L. Bruening, *Anal. Chem.* 60 (1988) 1694.
- [2] Y. Li, A. Wang, J.C. Van Loon, R.R. Barefoot, *Talanta* 39 (1992) 1337.
- [3] C. Malik, A. Li, *Sep. Sci. Technol.* 25 (3) (1990) 263.
- [4] Q. Li, K. Li, C. Zhou, S. Tong, *Chem. J. Chin. Univ.* 14 (2) (1993) 171.
- [5] Q. Cai, Z. Yan, H. Chao, *Sci. Technol. Membr.* 9 (4) (1989) 33.
- [6] F. Liu, K. Li, J. Lu, Y. Shun, S. Tong, *Ion-Exch. Adsorpt.* 8 (5) (1992) 400.
- [7] T.L. Largman, S. Sifniades, *Hydrometallurgy* 3 (1978) 153.
- [8] W.C. Babcock, *J. Membr. Sci.* 7 (1980) 71.
- [9] Analytical Chemistry Studio of Zhongnan Mineral College, *Handbook of Chemical Analysis*, Science Press, Beijing, People's Republic of China, 1984, pp. 624–630.

Resolution of ternary mixtures of Tartrazine, Sunset yellow and Ponceau 4R by derivative spectrophotometric ratio spectrum-zero crossing method in commercial foods

J.J. Berzas Nevado *, J. Rodríguez Flores, C. Guiberteau Cabanillas,
M.J. Villaseñor Llerena, A. Contenido Salcedo

Department of Analytical Chemistry and Food Technology. University of Castilla-La Mancha, 13071 Ciudad Real, Spain

Received 14 May 1997; received in revised form 10 September 1997; accepted 2 October 1997

Abstract

A very simple spectrophotometric method is described for resolving ternary mixtures of the food colorants Tartrazine, Sunset Yellow and Ponceau 4R by using the first derivative of the ratio spectra with measurements at zero-crossing wavelengths. Calibration graphs are linear up to 20 mg l^{-1} of Tartrazine (E-102), 40 mg l^{-1} of Sunset Yellow (E-110) and 32 mg l^{-1} of Ponceau 4R (E-124). Standard deviations of 0.9, 0.8 and 2.4% were obtained for nine standards of 8 mg l^{-1} of Tartrazine, 8 mg l^{-1} of Sunset Yellow and 8 mg l^{-1} of Ponceau 4R, respectively. This method was satisfactorily used for determining synthetic mixtures of these colorants in different ratios (from 1:1:1 to 1:5:5 or even higher) with recoveries in 94–105% range and it was successfully applied over three commercial products containing the three dyes and it did not require any separation step. The results were compared with those obtained by HPLC and very similar values were found by both methods. © 1998 Elsevier Science B.V. All rights reserved.

Keywords: Derivative spectrophotometry; Tartrazine; Sunset Yellow; Ponceau 4R

1. Introduction

Food colorants may often be considered simply cosmetic in nature, but their role in the food industry is actually very significant. Colour is the first sensory quality by which foods are judged and food quality and flavour are closely associated with colour. Consumers are conditioned to expect foods of certain colours and to reject any

deviation from their expectations. The psychological basis for the need of food colours is well established [1].

Colorants also play a significant role in enhancing the aesthetical appeal of food. They are very important ingredients in many convenience food such as confectionery products, gelatin desserts, snacks and beverages, since many of these would be colorless and would thus appear undesirable without the inclusion of dyes.

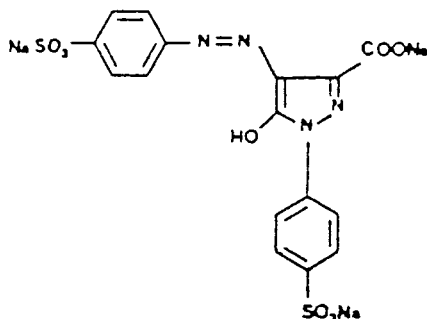
The term colour additive can be applied to any dye, pigment or other substance made (artificial

* Corresponding author. Tel.: +34 26295339; fax: +34 26295318; e-mail: jjberzas-cr@qata-cr.uclm.es

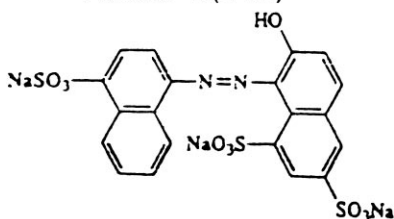
colorant) or obtained from a vegetable, animal, mineral or another natural source, that are capable of colouring food, drugs or cosmetics [2].

Tartrazine (T), Sunset Yellow (S) and Ponceau 4R (P), subjects of this work, are three synthetic dyes available as yellow, orange and red powders, respectively, that can be present in common food (drinks, yoghurts, ice cream, sweets, etc...). The content of these dyes must be controlled because its presence and/or contact with some kinds of drugs (aspirin, benzoic acid and other analgesics) in the human body can induce allergic and asthmatic illness in sensitive people. Development of regulations for using food colorants was reviewed by Haveland-Smith [3].

Tartrazine (E-102)



Ponceau 4R(E-124)



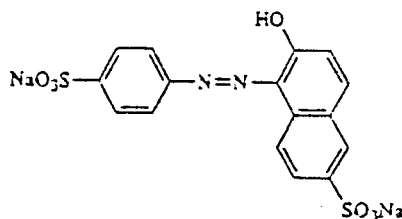
Taking into account the chromogenic characteristics of the three compounds, spectrophotometric methods can be used for their quantitative analysis. However, the absorption spectra of T, S and P are very much overlapping and direct measurement of the absorbance is not suitable for resolving ternary mixtures of these dyes without a separation step. Derivative spectrophotometry, particularly with digital processing [4] is an analytical technique of great utility to resolve binary mixtures with overlapping spectra.

Recently, spectrophotometric methods have been developed by us in order to resolve binary mixtures of dyes [5–8]. These methods were successfully applied to several commercial foods.

On the other hand, chromatographic methods have been used for colorant analysis in food and they are recommended when mixtures contain many different colorants [9–11], but ternary mixtures can be easily resolved by means of a spectrophotometric method [12,13], which is based on the simultaneous use of ‘zero-crossing’ and ‘ratio spectra derivative’ methods.

Adsorptive stripping voltammetry has been also applied by the authors in order to quantify sepa-

Sunset Yellow (E-110)



rately two dyes (Tartrazine and Sunset Yellow) of this ternary mixture in different commercial products [14,15].

The aim of this work is to propose a simple method for resolving ternary mixtures of Tartrazine, Sunset Yellow and Ponceau 4R dyes in commercial products without prior separation. In the same way, this method yields accurate and reproducible results in three different commercial products.

2. Experimental

2.1. Apparatus

A Beckman Instruments DU-70 spectrophotometer connected to an IBM PS/2 fitted with Beckman Data Leader Software [16] was used for all measurements and treatment of data.

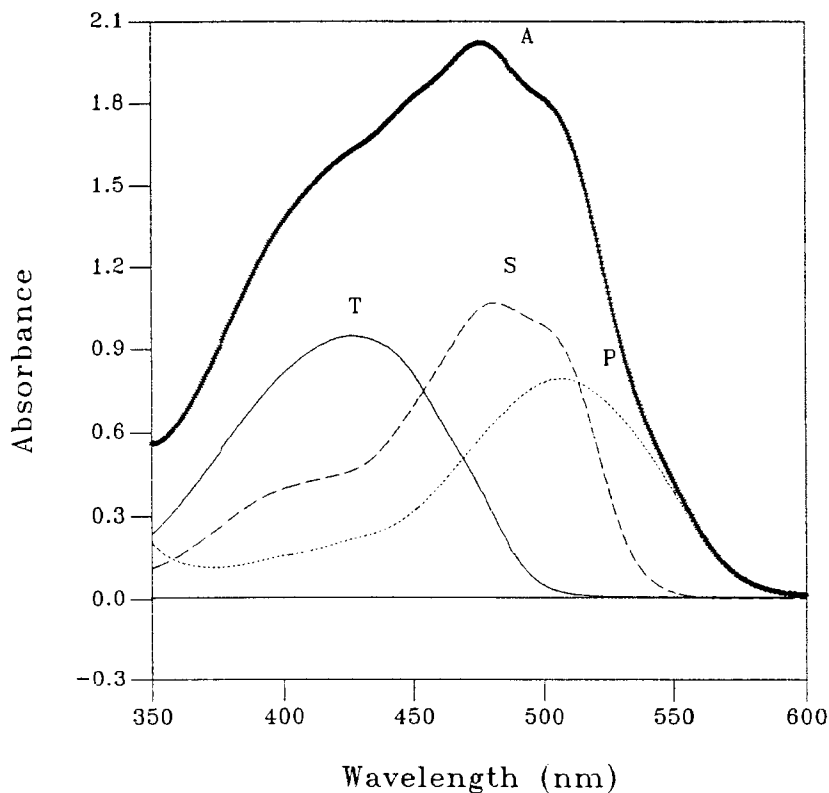


Fig. 1. Absorption spectra of 20.0 mg l^{-1} of Tartrazine (T), 24.0 mg l^{-1} of Sunset Yellow (S), 28.0 mg l^{-1} of Ponceau 4R (P) and their mixture (T + S + P).

The HPLC equipment used was: a SHIMADZU model LC-10A with a diode-array detector model SPD-M10A, equipped with a double pump system, that permitted us to work in the gradient mode and, as stationary phase, a chromatographic column Apex C_{18} (25 cm of length \times 3.9 mm i.d. and 5 μm as particle diameter).

2.2. Solutions

All solvents and reagents were of analytical reagent-grade unless otherwise indicated. Tartrazine (T) was supplied by Sigma Products (Sigma number T0388); Sunset Yellow (S) was obtained from Sancolor S.A. enterprise and Ponceau 4R (P) was provided by ALDRICH (number 19973-7). T, S and P stock aqueous solutions with a concentration of 200 mg l^{-1} were prepared. Acetic acid/sodium acetate (0.1 M and pH = 4.8) was used as buffer solution.

In order to achieve all chromatographic assays, the following solutions were also used: an $\text{NaH}_2\text{PO}_4/\text{Na}_2\text{HPO}_4$ buffer (0.1 M and pH = 7.1) and methanol (HPLC quality).

2.3. Procedure

2.3.1. Spectrophotometric procedure

The general procedure for 'derivative ratio spectrum-zero crossing' method was the following: samples were prepared in 25 ml calibrated flasks containing $2\text{--}20 \text{ mg l}^{-1}$ of T, $4\text{--}40 \text{ mg l}^{-1}$ of S and $4\text{--}32 \text{ mg l}^{-1}$ of P or their ternary mixtures, 5 ml of buffer solution and diluted with water to the mark. The absorption spectra of the samples thus prepared were recorded and stored in the computer.

The determination of two of the dyes in a ternary mixture can be done by the use of a

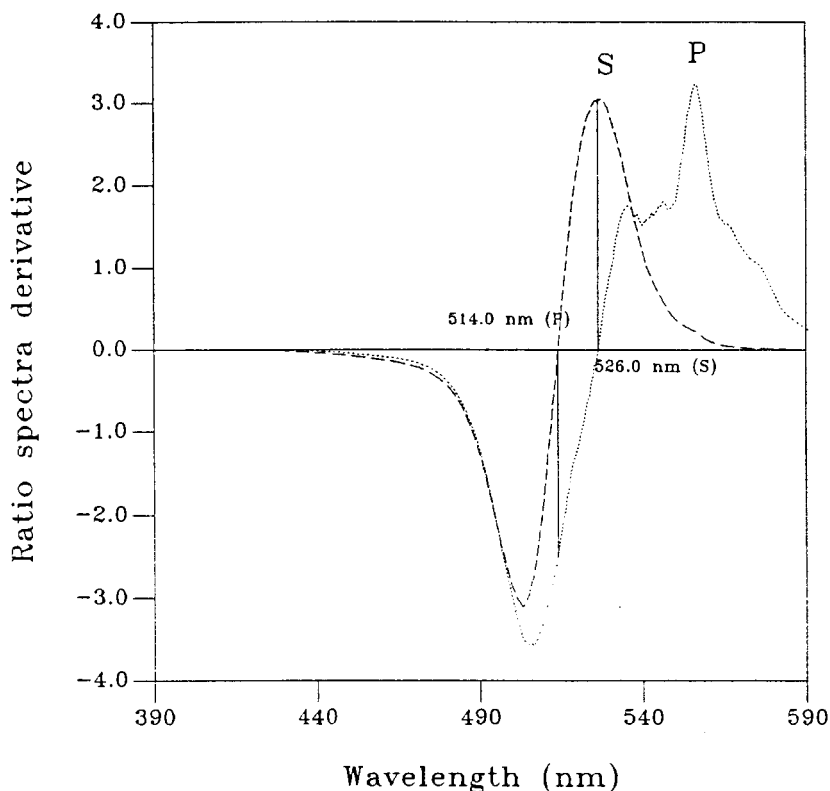


Fig. 2. Ratio spectra derivative of 24.0 mg l^{-1} of S and 28.0 mg l^{-1} of P when the divisor is a spectrum of 8.8 mg l^{-1} of T.

standard spectrum of the third colorant of this mixture as divisor. The ratio spectra is obtained by dividing the amplitudes of the absorption spectrum of the ternary mixture by a standard spectrum of one of the components; the first derivative of this ratio spectra is achieved and the measurements have to be done in the previously selected zero-crossing wavelengths of the other two dyes.

The determinations carried out by this method are the following:

(a) When a spectrum of T (whose concentration is 8.8 mg l^{-1}) is used as divisor, S is determined at 526.0 nm (${}^1\text{DD}_{526.0}$) (zero-crossing point for ratio spectra derivative of P) and P can be determined by measuring at 514.0 nm (${}^1\text{DD}_{514.0}$) (zero-crossing point for ratio spectra derivative of S), using a $\Delta\lambda = 8 \text{ nm}$ and a smoothing function of 23 experimental points in order to reach their first derivative spectra.

(b) When a standard spectrum of 16 mg l^{-1} of S is used as divisor, T is determined by measuring at 445.0 nm (${}^1\text{DD}_{445.0}$) (zero-crossing for ratio spectra derivative of P) and also a calibration graph was used to measure P at 514.0 nm (${}^1\text{DD}_{514}$) (zero-crossing point for ratio spectra derivative of T); $\Delta\lambda = 6 \text{ nm}$ and a smoothing of 16 experimental points were applied to obtain first derivative spectra.

(c) When a spectrum of P of 8 mg l^{-1} is used as divisor, a calibration graph for T determination is established at 444.0 and 430.0 nm (${}^1\text{DD}_{444.0}$ and ${}^1\text{DD}_{430.0}$) (zero-crossing points for ratio spectra derivative of S). On the other hand, similar graphs were used in order to measure S at 526.0 nm (${}^1\text{DD}_{526.0}$) (zero-crossing point for ratio spectra derivative of T). In order to reach these first derivative spectra, a $\Delta\lambda = 14 \text{ nm}$ and a smoothing of 15 experimental points were applied.

Table 1
Statistical data

Equation	Regression coefficient	Linearity range (mg l ⁻¹)	Detection limit (mg l ⁻¹) ^a
Divisor T			
¹ DD _{526.0} = 0.06860 + 0.1213 C _S	1.0000	4.0–40.0	0.032
¹ DD _{514.0} = -0.00065 + 0.0899 C _P	0.9999	4.0–32.0	0.107
Divisor S			
¹ DD _{445.0} = 0.00100 + 0.0033 C _T	0.9999	2.0–20.0	0.130
¹ DD _{514.0} = -0.00002 + 0.0020 C _P	0.9999	4.0–32.0	0.108
Divisor P			
¹ DD _{444.0} = 0.00400 + 0.0141 C _T	1.0000	2.0–20.0	0.110
¹ DD _{526.0} = 0.00250 + 0.0046 C _S	0.9998	4.0–40.0	0.032

C_T = mg l⁻¹ of T; C_S = mg l⁻¹ of S; C_P = mg l⁻¹ of P.

^a C_L = 3S_B/m, where C_L = detection limit; S_B = standard deviation of blank; and m = slope of calibration.

The proposed method was applied to determine T, S and P in three commercial products:

Gelatin, flavour pineapple: with sugar, gelatin, acidulant (E-334, E-331), flavorings, authorized artificial dyes (E-102, E-110 and E-124) and ascorbic acid. From the enterprise Royal Brands, S.A. (Spain).

Gelatin, flavour tropical: with sugar, gelatin, acidulant (E-334, E-331), flavorings, authorized artificial dyes (E-102, E-110 and E-124) and ascorbic acid. From the enterprise Royal Brands, S.A. (Spain).

Creamy dessert, flavour vanilla: with sugar, modified starch, preservatives (E-450, E-401 and E-339), acidulant (E-263), salt, flavorings and authorized artificial dyes (E-102, E-110 and E-124). From the enterprise Royal Brands, S.A. (Spain).

The ingredients are in all products in decreasing order of concentration.

The preparation of the samples was very similar in the three cases:

- For the determination of the three dyes in the first product, 50 g (exactly known) were dissolved in 250 ml of hot water. From this stock solution aliquots of different volumes were

taken in order to apply standard additions method for each dye.

- In the second product, the procedure was almost the same, dissolving a mass of 12 g of commercial product in 250 ml of hot water.
- With regard to the third product, the stock solution was obtained by dissolving 30 g in 250 ml of hot water in strong stirring conditions; a centrifugation step was also necessary to remove the starch from the sample; after that, different aliquots were taken in order to achieve standard additions of each dye over the clarified solution.

2.3.2. Chromatographic procedure

The determination of contents of T, S and P in the three commercial products was also verified by HPLC using a diode-array detector with measurements at 430, 483 and 507 nm (wavelengths where the absorbance was maximal for each dye) and using the stationary phase already mentioned in Section 2.1; as mobile phase, we have employed a mixture of methanol and 0.1 M NaH₂PO₄/Na₂HPO₄ buffer solution (pH = 7.1), with the following gradient of concentrations:

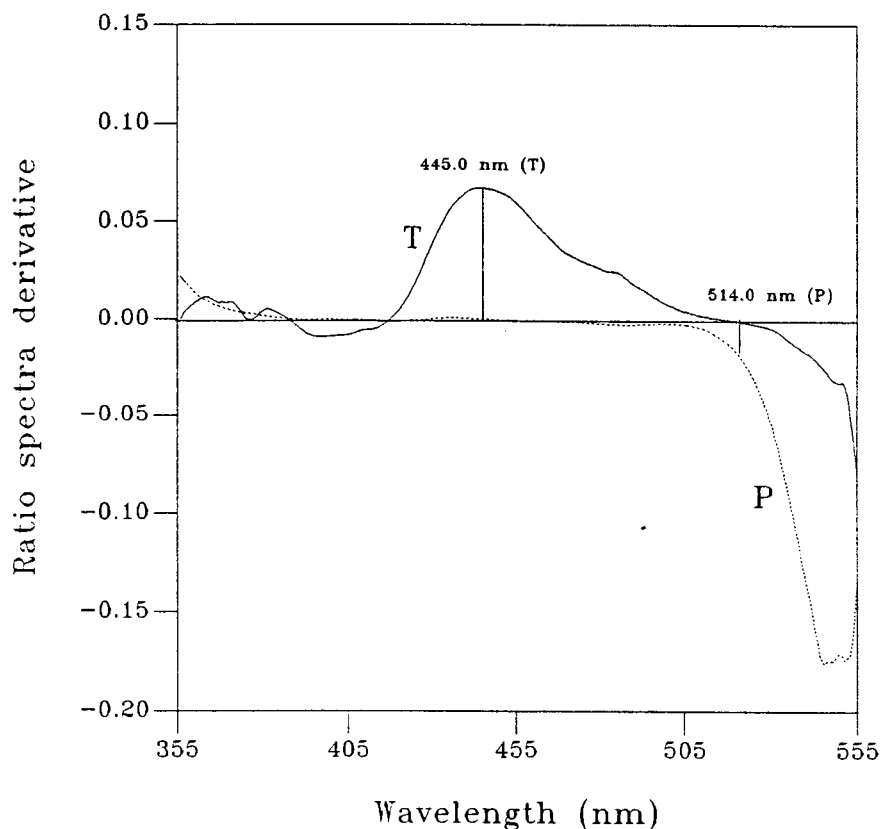


Fig. 3. Ratio spectra derivative of 20.0 mg l^{-1} of T and 4.0 mg l^{-1} of P when the divisor is a spectrum of 16.0 mg l^{-1} of S.

Time (minutes)	Concentrations
0.0–2.0	20–35% Methanol in linear gradient
2.0–12.0	35% Methanol constant
12.0–17.0	35–20% Methanol in linear gradient

The flow rate was 1.0 ml min^{-1} ; under these conditions the retention times were 4.1 min for T, 8.6 min for P and 9.6 min for S.

3. Results and discussion

3.1. Method development

The influence of pH on the absorption spectra of T, S and P was studied. In order to establish suitable pH values for this study, a range of values were examined between pH 1.5 and 12. The following results were obtained. The spectra of T showed a maximum at 430.0 nm between 1.0 and 9.0 pH values, whereas for higher pH values this maximum decreases; S shows a maximum at 483.0 nm, which is stable between 1.0 and 10 pH values, decreasing for higher values; with regard to P, its

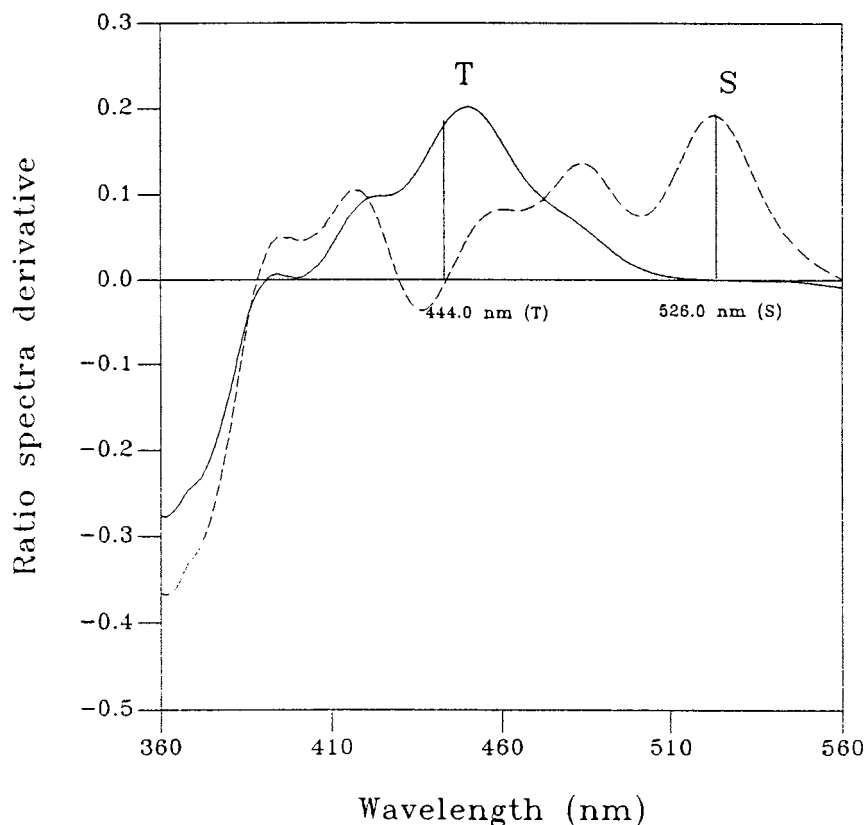


Fig. 4. Ratio spectra derivative of 12.8 mg l^{-1} of T and 40.0 mg l^{-1} of S when the divisor is a spectrum of 8 mg l^{-1} of P.

absorbance spectrum shows a maximum at 507.0 nm, whose absorbance remains constant between 1 and 9 pH units, decreasing from this last value. We have chosen a pH value of 4.8 as optimum. Under these conditions diluted aqueous solutions of T, S and P were stable for 7 days at least.

In Fig. 1 the zero order spectra of T, S and P in the 350–600 nm wavelength range are shown. It can be seen that the absorption spectra of the three dyes are strongly overlapped and as a result, only P could be determined from direct measurements of absorbance in a very small zone around 570 nm. In order to resolve this ternary mixture we have applied the proposed method, based on the simultaneous use of the first derivative of ratio spectra and zero-crossing measurements.

3.2. Derivative ratio spectrum zero-crossing method

According to the proposed method, we can determine two dyes by means of the third colorant which is used as divisor. The ratio spectrum is obtained by dividing the amplitudes of the absorption spectrum of the mixture by a standard spectrum of one of the three components and obtaining the first derivative of this ratio spectrum, where the other two dyes can be determined by measuring at their respective zero-crossing points, that has been previously established by means of a similar study for each dye of the ternary mixture.

Table 2
Results obtained for ternary mixtures of T, S and P by derivative ratio spectrum-zero crossing method

T (mg l ⁻¹)	S (mg l ⁻¹)	P (mg l ⁻¹)	T (8.8 mg l ⁻¹) ^a		S (16.1 mg l ⁻¹) ^a		P (8.0 mg l ⁻¹) ^a	
			S (%)	P (%)	T (%)	P (%)	T(%)	S(%)
			¹ DD _{526.0}	¹ DD _{514.0}	¹ DD _{445.0}	¹ DD _{514.0}	¹ DD _{444.0}	¹ DD _{526.0}
32.0	20.0	2.0	98.4	94.9	96.8	46.2	95.8	98.9
20.0	20.0	20.0	94.6	100.5	97.0	96.7	95.9	99.0
20.0	4.0	20.0	87.3	98.4	96.9	97.7	96.5	97.2
4.0	20.0	20.0	94.2	102.5	96.5	99.0	92.3	98.3
20.0	20.0	4.0	98.0	102.1	97.0	81.3	95.9	98.9

^a Spectrum used as divisor.

In order to obtain the best recoveries for the three dyes, it is necessary to study and to optimize the following parameters: concentration of the standard spectrum used as divisor, $\Delta\lambda$ to obtain the first derivative, smoothing function and zero-crossing wavelengths.

3.2.1. Selection of optimal instrumental conditions

3.2.1.1. Determination of S and P in the presence of T. The above mentioned variables were studied and the following values were chosen as optima: a standard spectrum of T of 8.8 mg l⁻¹, an $\Delta\lambda$ of 8 nm for the first derivative ratio spectra and a smoothing function of 23 experimental points. In these conditions, the first derivative ratio spectra of S/T and P/T are shown in Fig. 2. We can see that the S content can be measured at 526 nm (zero-crossing point for ratio spectra derivative of P), whereas P is determined at 514 nm (zero-crossing point for ratio spectra derivative of S) and in a very small zone around 570 nm. Calibration graphs were obtained at the previously selected wavelengths up to 40 mg l⁻¹ of S and 32 mg l⁻¹ of P (Table 1).

3.2.1.2. Determination of T and P in the presence of S. Once studied the usual variables we have established as optimal values: a standard spectrum of S of 16 mg l⁻¹, an $\Delta\lambda$ of 6 nm for the ratio spectra derivative and a smoothing function of 16 experimental points. In these conditions, the first derivative ratio spectra for T/S and P/S ob-

tained are shown in Fig. 3. It can be seen that T content can be determined at 445 nm (zero-crossing point for ratio spectra derivative of P) and, in the same way, P content is measured at 514 nm (zero-crossing point for ratio spectra derivative of T). Two calibration graphs were obtained at the previously selected wavelengths giving straight lines up to 20 mg l⁻¹ of T and 32 mg l⁻¹ of P (Table 1).

3.2.1.3. Determination of T and S in the presence of P. The determination of these two dyes was realized using the same method. The optimal values established were: a standard spectrum of 8 mg/l of P as divisor, an $\Delta\lambda$ of 14 nm for the first derivative ratio spectra and a smoothing function of 15 experimental points. Fig. 4 shows the first derivative ratio spectra of T/P and S/P in these conditions. As can be observed in this figure, the determination of T can be made at 444 nm (zero-crossing point for ratio spectra derivative of S), whereas the S content can be measured at 526 nm (zero-crossing point for ratio spectra derivative of T). Calibration graphs were obtained at the previously selected wavelengths up to 20 mg l⁻¹ for T and 40 mg l⁻¹ for S.

4. Statistical data

In Table 1, the most characteristic data obtained from the different calibrations, from the repeatability of the reagent-blank and from nine

Table 3
Contents of T, S and P in commercial products^a

Product	Derivative spectrophotometry			HPLC		
	T	S	P	T	S	P
Gelatin flavour pineapple	1.9×10^{-3} (-6.2%)	1.1×10^{-3} (2.6%)	2.5×10^{-4} (2.3%)	2.0×10^{-3}	1.1×10^{-3}	1.2×10^{-4}
Gelatin flavour tropical	4.4×10^{-2} (-2.5%)	7.5×10^{-3} (11.1%)	2.6×10^{-3} (8.7%)	4.2×10^{-2}	8.0×10^{-3}	2.5×10^{-3}
Creamy dessert of vanilla	2.3×10^{-2} (0.0%)	1.5×10^{-3} (7.4%)	1.5×10^{-3} (-11.6%)	2.2×10^{-2}	1.3×10^{-3}	1.2×10^{-3}

() Percentages of deviation between the slopes of calibration graphs and that obtained for each dye in the three products by standard additions procedure.

^a Contents expressed as percentage mass/mass.

standards of 8 mg l^{-1} of T, nine standards of 8 mg l^{-1} of S and nine standards of 8 mg l^{-1} of P, respectively have been summarized. Standard deviations of 0.9, 0.8 and 2.4% were recorded for each dye.

On the other hand, we can see in this table that very good regression coefficients are reached in all cases for the tested concentration ranges; with regard to detection limits, similar values are obtained for each dye when different dyes are used as divisor as it is shown in Table 1, obtaining the best detection limit for S determination.

5. Applications

The method under study was tested to determine of T, S and P in artificial mixtures (Table 2). The recoveries obtained in most cases were in the range 94–105% except for those ones in which the dye to be determined was present in very small concentrations with regard to the other two dyes (ratio 1:5:5 or even lower). Nevertheless, taking into account the results shown in Table 2, we advise the use of a standard spectrum of P as divisor for S determination, the use of a standard spectrum of T as divisor for P determination, and the use of S as divisor for determining T in all ratios shown in this table.

Lastly, the proposed method was applied to determine T, S and P in the commercial products described in Section 2.3.

The percentages of the dyes in the three commercial products were calculated by direct measurement and standard addition method (in order to check the presence of matrix effects) using selected wavelengths. We do not advise the use of direct measurements because of the low levels of dyes in the three commercial applications, the reason being, it would be necessary to work with high volumes of stock commercial solutions that would involve matrix effects and consistently it could produce erroneous results.

When the standard addition procedure was applied for each dye in the three commercial products, slopes very similar to those of the calibration graphs were obtained, as it can be deduced from the percentages of deviation between the slopes of the calibration and standard addition method for each dye in the three applications (Table 3). In this table the contents obtained by standard additions are also shown for each dye in the three products, given as percentage mass/mass.

Under the conditions already described in Section 2.3 for the HPLC study, the calibration graphs established for each dye at wavelength corresponding to its maximum are given in Table 4.

Chromatographic results are also summarized in Table 3. They are in agreement with values provided by the derivative ratio spectrum-zero crossing method, except for the determination of Ponceau 4R dye in the product 'Gelatin dessert of pineapple'. In this case spectrophotometric and

Table 4
Data for the chromatographic determination of studied dyes

Dye	λ max (nm)	Linearity range (mg l ⁻¹)	t_r (min)	Equation ^a	Regression coefficient
T	430	0.2–12.0	4.1	Area (μ V s) = 74.32 + 6382.9 C_T	0.9999
S	483	0.8–16.0	8.6	Area (μ V s) = 285.1 + 5897.0 C_S	0.9999
P	507	0.8–16.0	9.6	Area (μ V s) = 289.2 + 5452.0 C_P	1.0000

^a C_T , C_S and C_P are concentrations of Tartrazine, Sunset Yellow and Ponceau 4R given as mg l⁻¹.

chromatographic values differ because of interference from matrix gelatin in the spectrophotometric determination of very low levels of Ponceau 4R in this product. For this reason, the chromatographic method seems to be appropriate in this case since it provides separation of dyes from matrix interferences.

6. Conclusions

Satisfactory results are reached when the derivative ratio spectrum-zero crossing method was applied over this ternary mixture. In order to resolve synthetic mixtures and taking into account the recoveries shown in Table 2, we advise the use of a standard spectrum of P as divisor for S determination, and a standard spectrum of T as divisor for P determination, as well as the suitable use of S and P as divisors for determining T for all ratios showed in Table 2, except for those in which the dye to quantify was in the ratio 1:5:5 or lower.

We also recommend the proposed spectrophotometric method due to the simplicity of determination, inexpensive instrumentation and the satisfactory results obtained in the analysis of complex matrix such as gelatins and creamy dessert.

Acknowledgements

The authors are grateful to the DGICYT of the

Ministerio de Educación y Ciencia (Spain) for supporting this study (Project PB 94-0743).

References

- [1] M. Amerind, R. Pangborn, E. Roessler, Principles of Sensory Evaluation of Food, Academic Press, New York, 1965.
- [2] A. Branen, P. Davidson, S. Salminen, Food Additives, Marcel Dekker, New York, 1989.
- [3] R. Combes, R. Haveland-Smith, Mutat. Res. 98 (1982) 101.
- [4] A. Savitzky, M. Golay, Anal. Chem. 36 (1964) 1627.
- [5] J. Berzas Nevado, J. Rodríguez Flores, M. Villaseñor Llerena, Analisis 21 (1993) 395.
- [6] J. Berzas Nevado, J. Rodríguez Flores, M. Villaseñor Llerena, Anal. Lett. 27 (1994) 1009.
- [7] J. Berzas Nevado, J. Rodríguez Flores, M. Villaseñor Llerena, Talanta 40 (1993) 1391.
- [8] J. Berzas Nevado, M. Guiberteau Cabanillas, A. Contento Salcedo, Fresenius J. Anal. Chem. 350 (1994) 606.
- [9] M. Puttemans, L. Dryon, D. Massart, J. Assoc. Off. Anal. Chem. 65 (1982) 737.
- [10] M. Puttemans, L. Dryon, D. Massart, J. Assoc. Off. Anal. Chem. 66 (1983) 1039.
- [11] M. Puttemans, L. Dryon, D. Massart, J. Assoc. Off. Anal. Chem. 67 (1984) 880.
- [12] J. Berzas Nevado, M. Guiberteau Cabanillas, F. Salinas, Talanta 39 (1992) 547.
- [13] J. Berzas Nevado, J. Rodríguez Flores, J. Villaseñor Llerena, Bull. Soc. Chim. Belg. 102 (1993) 527.
- [14] J. Berzas Nevado, J. Rodríguez Flores, M. Villaseñor Llerena, Talanta 44 (1997) 467.
- [15] J. Berzas Nevado, J. Rodríguez Flores, M. Villaseñor Llerena, Fresenius J. Anal. Chem. 357 (1997) 989.
- [16] Beckman Instruments, Spectroscopy 2 (1987) 16.

Pentacoordinate organotin complexes as neutral carriers for salicylate-selective PVC membrane electrodes

Li Zhi-Qiang, Yuan Ruo, Ying Min, Song You-Qun, Shen Guo-Li *, Yu Ru-Qin

Department of Chemistry and Chemical Engineering, Center for Chemometrics and Sensing Technology, Hunan University, Changsha 410082, China

Received 14 April 1997; received in revised form 17 September 1997; accepted 2 October 1997

Abstract

Selectivity properties are established for three new electrodes prepared by incorporating three pentacoordinate organotin(IV) complexes, mono(2,4-pentanedionato-*o,o'*) tri(phenylmethyl)tin (DMTBS), mono(benzoylacetonato-*o,o'*) tri(phenylmethyl)tin (MPTBS) and mono(dibenzoylmethanato-*o,o'*) tri(phenylmethyl)tin (DPTBS) into plasticized PVC membranes. These electrodes exhibit linear response to salicylate and an anti-Hofmeister selectivity pattern with high specificity for salicylate over many common anions. The results show that the potentiometric response characteristics are related to the structure of organic ligands. The detection limit and the slope of the electrodes based on these pentacoordinate organotin complexes exhibit a tendency to decrease as the substituent in organic ligands changes from a methyl group to a phenyl group. Electrodes prepared with DMTBS have the best detection limit and the highest degree of selectivity and sensitivity for salicylate. The response mechanism is also investigated by use of a.c. impedance and i.r. spectroscopic techniques. © 1998 Elsevier Science B.V. All rights reserved.

Keywords: Pentacoordinate organotin complex; Neutral carrier; Salicylate-selective PVC membrane electrode

1. Introduction

Recently, electrodes using a plasticized PVC membrane incorporating derivatives of vitamin B₁₂, Co(III), Sn(IV), Mo(IV) and Mn(III) porphyrin complexes and electropolymerized Co(II) porphyrin derivative films demonstrated potentiometric anion selectivity sequences which deviated from the Hofmeister pattern [1–5]. These deviations resulted from the direct interactions between the central metal and the analyte ions. Thus, this

unusual anion selectivity behaviour was based on the properties of the central metal and the chemical environment around the central metal. Since the 1960s, hundreds of thousands of organometallic compounds have been synthesized and some of them have been applied in many fields. Some new anion-selective electrodes based on organometallic species, such as metallocenes, alkyl-substituted derivatives of Hg(II), Sb(III) and Sn(IV), have been reported [6–13]. Although these electrodes exhibited an unusual response to respective anions (e.g. chloride, nitrate, dibasic phosphate and salicylate), the research on new carriers for improve-

* Corresponding author. Fax: +86 731 8824525

Table 1
Elemental analysis and important i.r. spectra data of the complexes

No.	Formula	Elemental analysis (%) ^a			I.r. spectra (cm ⁻¹)		
		C	H	N	ν C=O	ν C=C	ν Sn–O
1	C ₂₆ H ₂₈ O ₂ Sn	64.10 (63.58)	5.63 (5.75)	24.02 (24.16)	1743.7	1579	550
2	C ₃₁ H ₃₀ O ₂ Sn	67.54 (67.30)	5.50 (5.42)	21.30 (24.16)	1711.6	1555	543.2
3	C ₃₆ H ₃₂ O ₂ Sn	69.86 (70.27)	5.33 (5.20)	19.01 (19.29)	1702.6	1536	529.7

29.7

^a Calculated values are given in parentheses.

ment the potentiometric response characteristics of these electrodes was of considerable interest in order to be applied for the analysis in actual samples. Because of the stereospecific configurations of organometallic compounds, they are expected to be used as components in anion-selective electrodes and accelerate the development of novel anion ionophores.

Salicylate and its analogues, including acetyl-salicylate (aspirin), are available to the public in a wide variety of formulations. The most widely used analytical method for the detection of salicylate is based on the Trinder reaction in which sample salicylate reacts with ferric ions to form a colored complex in acid solution [14]. Since similar complexes can be formed under the same experimental conditions, this method always lacks adequate selectivity over many common anions. Polymeric membrane electrodes based on quaternary ammonium salts of salicylate suffered from the same problem [15,16]. Electrodes prepared by incorporating Mn(III) and Sn(IV) porphyrin complexes into PVC membranes exhibited high selectivity towards salicylate, but it is necessary to improve some potentiometric response characteristics such as linear range, detection limit and detection sensitivity, etc. [17]. In the present work, we report on the anion-selective properties of pentacoordinate organotin complexes (DMTBS, MPTBS and DPTBS). The results indicate that electrodes based on DMTBS offer a wide linear response range, high selectivity and high sensitivity to salicylate. The novel electrodes have been used for the detection of salicylate in human urine with satisfactory results.

2. Experimental

2.1. Reagents and materials

All chemicals used were of analytical-reagent grade. Twice-distilled water was used throughout all experiments. Tribenzyltin chloride was prepared by the method described previously [18]. The melting point was found to be 141–142°C, the same as the reported value in the reference. Pentacoordinate organotin complexes were synthesized by the reaction of tribenzyltin chloride with 2,4-pentanedione, benzoylacetone and dibenzoylmethane according to published procedures [19,20]. They were characterized by elemental analysis and i.r. spectra (see Table 1) and will be reported elsewhere.

2.2. Apparatus

The PVC membrane electrodes were fabricated from various carriers and assembled according to Thomas and co-workers [21,22]. The membrane compositions were 2.5 wt.% ionophores (DMTBS, MPTBS or DPTBS), 66.5 wt.% membrane solvent (*o*-nitrophenyl octyl ether) and 31 wt.% PVC. Before use, the electrodes were conditioned in 0.1 mol · l⁻¹ sodium salicylate aqueous solution for 24 h. Potentiometric and pH measurements were made with a model PHS-3E digital ion analyzer (Jiangshu instruments). The cells for millivolt measurements were of the following type:

Hg – Hg₂Cl₂/KCl(satd.)/sample solution/
membrane/0.01 mol · l⁻¹ KCl/AgCl – Ag

The a.c. impedance of the electrode membrane was recorded with a PAR M386-2 System (EG&G Princeton Applied Research) in $\text{KH}_2\text{PO}_4\text{--Na}_2\text{HPO}_4$ buffer at pH 5.0. The frequency region used was from 10^5 to 10^{-2} Hz (25°C). For the infrared measurements and the spectra manipulations, a Fourier infrared spectrophotometer, model AQS-20 (Analect instruments, USA) was used.

3. Results and discussion

3.1. Response characteristics of the electrodes

The structures of pentacoordinate organotin complexes are shown in Fig. 1, and potentiometric response characteristics of the electrodes containing different carriers are shown in Fig. 2. The electrodes incorporating DMTBS show a specific response to salicylate ranging from 1.0×10^{-1} to 1.0×10^{-4} mol \cdot l $^{-1}$ in a $\text{KH}_2\text{PO}_4\text{--Na}_2\text{HPO}_4$ buffered solution adjusted to pH 5.0 with a detection limit of 3.4×10^{-5} mol \cdot l $^{-1}$ and a slope of 96.0 mV per decade. The d.c. resistance of the DMTBS membrane is 645.5 ± 0.3 k Ω ($n = 6$). The response time ($t_{90\%}$) is less than 1 min in the linear response range which implies the reversible anion exchange is rapid, these novel prepared electrodes do not display any hysteresis effects. The standard deviation of the DMTBS-based electrode potential readings over a period of 12 h in 0.001 mol l $^{-1}$ sodium salicylate buffered with $\text{KH}_2\text{PO}_4\text{--Na}_2\text{HPO}_4$ to pH 5.0 is 0.8 mV ($n = 72$). The potential readings for the same electrode dipped

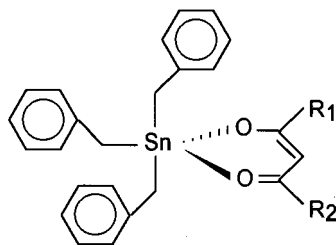


Fig. 1. Structure of the carriers studied. DMTBS, $R_1 = R_2 = \text{CH}_3$; MPTBS, $R_1 = \text{CH}_3$, $R_2 = \text{C}_6\text{H}_5$; DPTBS, $R_1 = R_2 = \text{C}_6\text{H}_5$.

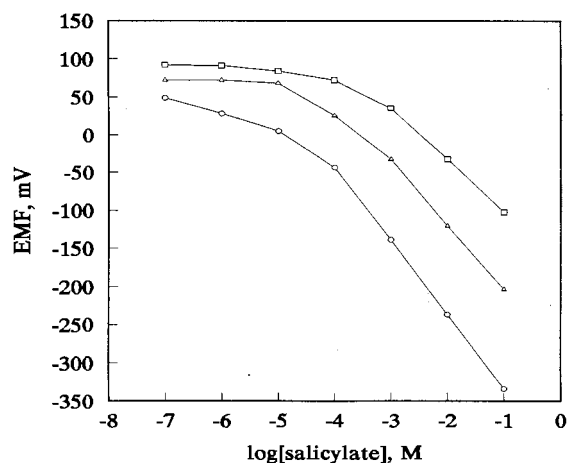


Fig. 2. Potentiometric response to salicylate for the electrodes based on various carriers: (○) DMTBS; (△) MPTBS; (□) DPTBS.

alternatively into stirred solutions of 1.0×10^{-3} and 1.0×10^{-4} mol \cdot l $^{-1}$ sodium salicylate show a standard deviation of 1.3 mV over 4 h ($n = 12$). Detectable loss of performance characteristics has not been found after these electrodes have been used for 5 months, which implies that this type of organotin complex is stable in the presence of water. The electrodes based on MPTBS and DPTBS exhibit similar potentiometric response characteristics, but their slopes decrease to 80.6 and 69.0 mV per decade, respectively, while the

Table 2
Selectivity coefficients, $\log K_{ij}^{\text{pot}}$ for the solvent polymeric membrane containing different carriers

Anion	Aliquat 336 Sal ^a	DMTBS	MPTBS	DPTBS
Salicylate	0.0	0.0	0.0	0.0
Perchlorate	2.2	-1.8	-1.5	+0.2
Benzoate	-1.0	-1.8	-1.1	-1.6
Thiocyanate	1.0	-2.3	-1.3	-1.5
Iodide	0.6	-2.6	-2.0	-1.7
Nitrite	-1.8	-3.2	-2.3	-2.5
Nitrate	-1.0	-3.4	-2.7	-2.2
Acetate	-2.2	-3.7	-3.0	-3.0
Bromide	-1.2	-3.8	-2.5	-3.0
Chloride	-2.0	-4.0	-2.8	-3.3
Citrate	-1.6	-4.2	-2.5	-3.0

^a From Ref. [28].

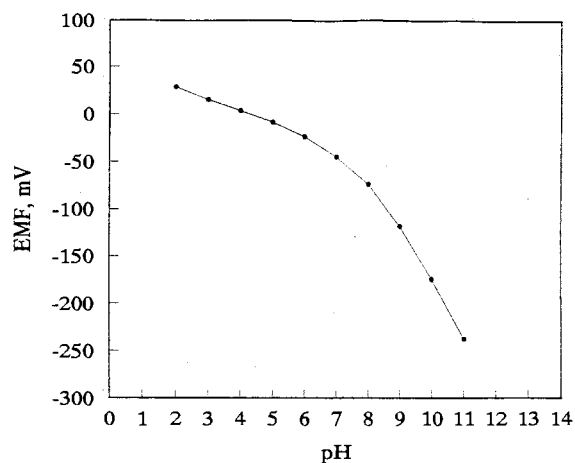


Fig. 3. pH response of membrane electrode based on DMTBS.

detection limits change to 2.0×10^{-4} and $3.2 \times 10^{-4} \text{ mol} \cdot \text{l}^{-1}$ respectively. It is obvious that the potentiometric response characteristics have a close relationship with the chemical environment around the central metal.

3.2. Selectivity

Possible interferences from a number of mono-valent anions were studied. Anion selectivity coefficients, $\log K_{ij}^{\text{pot}}$ were determined by the separate solution method according to IUPAC recommendations and were obtained with the respective $0.1 \text{ mol} \cdot \text{l}^{-1}$ anion solutions of sodium salts [23]. The single-ion activities were calculated by the extended Debye–Hückel equation. The results shown in Table 2 indicate that the new electrodes based on mono(2,4-pentanedionato-*o,o'*) tri(phenylmethyl)tin (DMTBS) demonstrate excellent selectivity towards salicylate anion and exhibit a selectivity sequence of anions in the following order: salicylate > benzoate \cong perchlorate > thiocyanate > iodide > nitrite > nitrate > acetate > bromide > chloride > citrate. The most striking feature of these data is the apparent relationship between the selectivity and the substituent in the ligands. As the substituent changes from the methyl group to the phenyl group, the selectivity for salicylate deteriorates.

3.3. Effect of pH on response characteristics of the electrodes

The effect of pH on the response of the potential readings of the DMTBS-based electrode was examined by recording the emf of a cell which contained sodium salicylate solutions ranging from 1.0×10^{-6} to $1.0 \times 10^{-1} \text{ mol} \cdot \text{l}^{-1}$ in a buffered solution ($\text{KH}_2\text{PO}_4\text{--Na}_2\text{HPO}_4$) adjusted to the respective pH values. The results show that the linear range, the detection limit and the detection sensitivity deteriorate to some extent as the pH increases. The results in Fig. 3 indicate that the change in pH has less effect on the electrode potential within the pH range of 2–7 (average slope of $14.5 \text{ mV} (\text{pH unit})^{-1}$), but the slope of the descending part of the curve within the pH range of 7–11 is nearly Nernstian (average slope of $48.1 \text{ mV} (\text{pH unit})^{-1}$) pointing out a hydroxyl ion exchange at the membrane surface. In accordance with previous research, the deterioration of potentiometric response characteristics at higher pH values was due to an increasing level of interference from hydroxyl [24].

3.4. Mechanism of salicylate response

Some lipophilic organometallic compounds were reported as unusual anion ionophores, and exhibited specific anion-selective behaviour which was different from the so-called Hofmeister sequence. Their anion selectivities were mainly governed by the specific interactions between organometals and anions, rather than the lipophilicity of anions or simple opposite charge interactions with anions. That the electrodes based on pentacoordinate organotin complexes exhibited high potentiometric selectivity for salicylate, must be related to the strong interactions between the central Sn(IV) atom in organotin complexes and salicylate anions. In order to investigate the interactions between the carriers and salicylate in membrane phase, infrared spectra of a DMTBS membrane, which had been conditioned in $\text{KH}_2\text{PO}_4\text{--Na}_2\text{HPO}_4$ buffer for 24 h was carried out with a PVC membrane as the background (see curve 2 in Fig. 4). Certain relative features of the bands at 1743.6, 1574 and 504

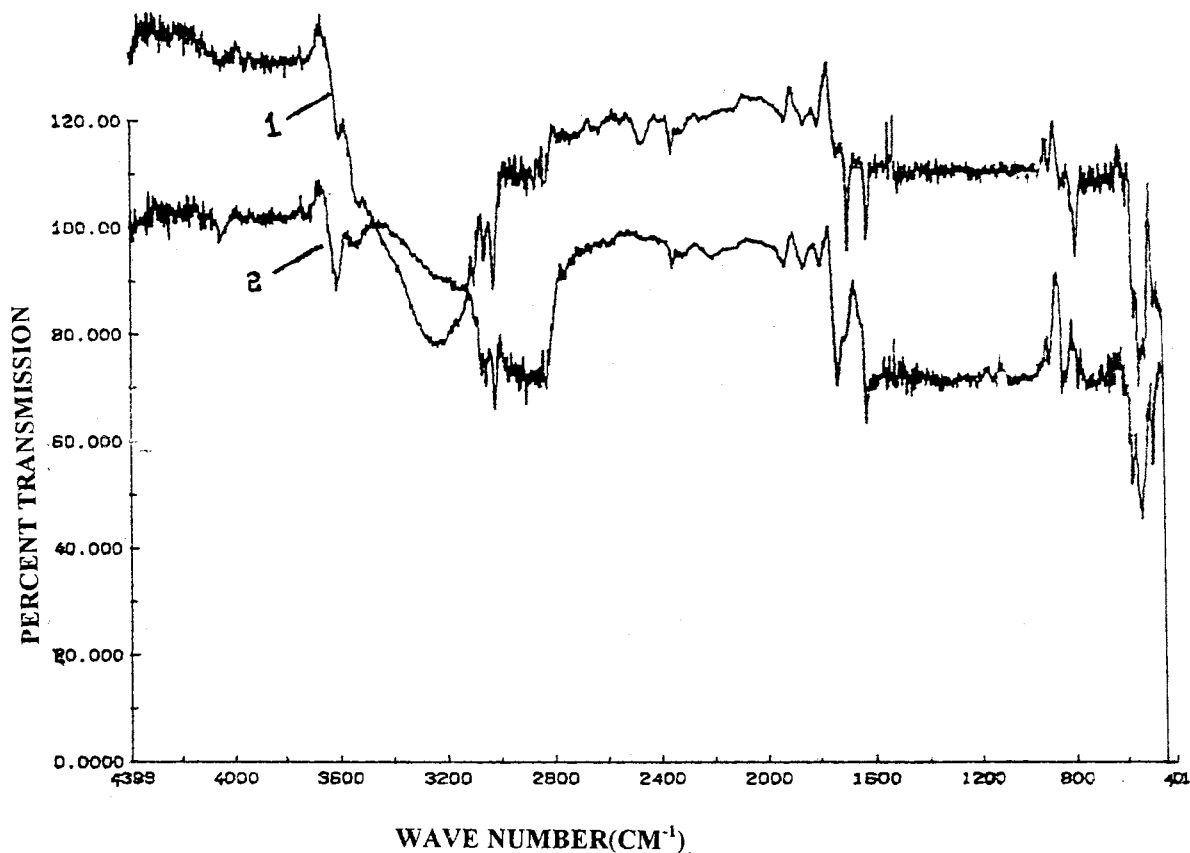


Fig. 4. Comparison of infrared spectra (2) of a DMTBS membrane with that (1) of the same membrane which has been dipped into $0.1 \text{ mol} \cdot \text{l}^{-1}$ salicylate for 24 h using a blank PVC membrane as background.

cm^{-1} are due to the vibrations of C=O, C=C and Sn–O bonds, respectively. The $\nu\text{C}=\text{O}$ stretch (1743.6 cm^{-1}) in DMTBS membrane corresponding to the free ligand (acetylaceton) indicates that the strength of chelation is relatively weak in solution and the coordinate carbonyl group in this kind of complex may be replaced by solvent molecule reversely. This agrees with the results in pentacoordinate triphenyltin complexes obtained by Gopinathan et al. [19]. Obvious changes are observed in infrared spectra after the same membrane has been dipped into $0.1 \text{ mol} \cdot \text{l}^{-1}$ salicylate for 24 h (see curve 1 in Fig. 4). A strong broad band appearing at $3117\text{--}3508 \text{ cm}^{-1}$ shows that the phenolic hydroxyl of salicylate can form an adduct with the carbonyl of the ligands by hydrogen bonding. The band at 1743.6 cm^{-1} shows a considerable red shift at about 1702

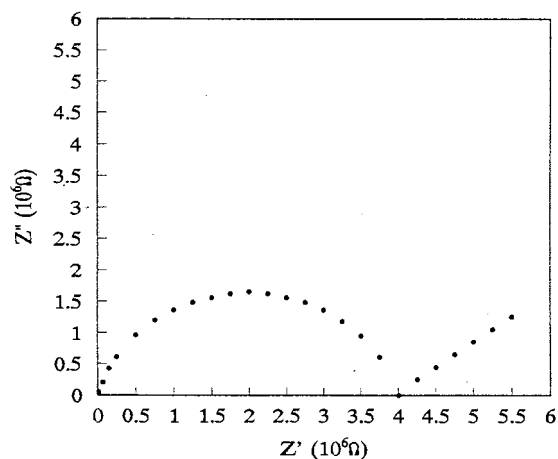


Fig. 5. Impedance plot of a DMTBS membrane with *o*-nitrophenyl octyl ether as plastizer immersed in $1.0 \times 10^{-4} \text{ mol} \cdot \text{l}^{-1}$ salicylate buffered with $\text{KH}_2\text{PO}_4\text{--Na}_2\text{HPO}_4$ to pH 5.0.

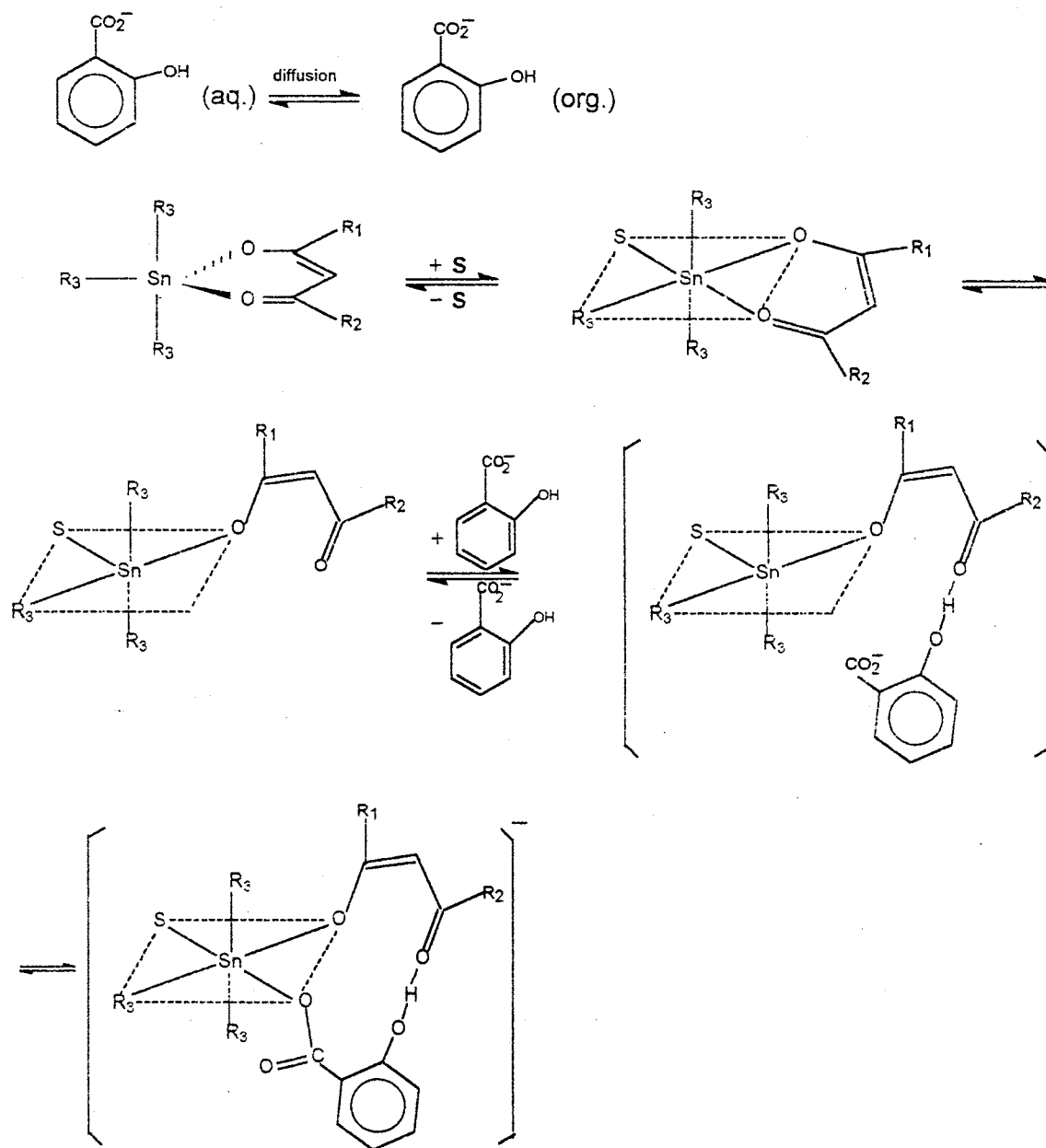


Fig. 6. The suggested mechanism of the unusual potentiometric response characteristics and high selectivity of the electrodes based on pentacoordinate organotin compounds for salicylate.

cm^{-1} , this red shift may be caused by the formation of a hydrogen bond between the phenolic hydroxyl of salicylate and the carbonyl of the carrier. Bands at 1574 and 550.3 cm^{-1} rise to higher frequencies, 1635.7 and 560.6 cm^{-1} , re-

spectively, which indicates coordinate exchange takes place between the central Sn(IV) atom and the carboxyl of salicylate in the membrane phase.

Fig. 5 shows the a.c. impedance of a DMTBS membrane with *o*-nitrophenyl octyl ether as plas-

Table 3

Comparison of results of electrode and spectrophotometric methods for the detection of salicylate concentration ($\text{mmol} \cdot \text{l}^{-1}$) in urine samples

Method	1	2	3	4	5	6	7	8
Electrode	0.82	0.86	0.68	0.97	1.03	1.11	1.20	1.32
Spectrophotometry	0.78	0.82	0.72	0.94	1.07	1.05	1.15	1.40

ticizer immersed in $\text{KH}_2\text{PO}_4\text{--Na}_2\text{HPO}_4$ buffer at pH 5.0 for 4 h. A well-resolved semicircle at high frequencies and Warburg impedance at low frequency intervals are observed. As the concentration of salicylate increases, the bulk resistance decreases as follows: $2.00 \times 10^6 \Omega$ in $10^{-4} \text{ mol} \cdot \text{l}^{-1}$ salicylate, $1.65 \times 10^6 \Omega$ in $10^{-3} \text{ mol} \cdot \text{l}^{-1}$ and $1.50 \times 10^6 \Omega$ in $10^{-2} \text{ mol} \cdot \text{l}^{-1}$ salicylate. The results obtained indicate that the transfer process of salicylate across the PVC membrane is controlled by the diffusion process [25].

The suggested mechanism of salicylate response and selectivity is shown in Fig. 6. Coordination-unsaturated tin complexes can form adducts with the solvent molecule [26]. A similar process takes place in pentacoordinate organotin complexes used in this paper. The Sn(IV) atom in this kind of compound is a typical Lewis acid and seems to exhibit an unusual coordinate behaviour with anions [27]. The high potentiometric selectivity for salicylate (see Table 2) must be related to the unique interactions with salicylate [28]. The most striking feature of these data is the apparent relationship between the potentiometric response characteristics of these new electrodes and the substituent in the ligands. As the substituent changes from the methyl group to the phenyl group, the selectivity for salicylate deteriorates, accompanied by a lowering of the slope and a narrowing of linear range. The results have led us to hypothesize that a suitable electron density of the central Sn(IV) atom was important for the unique interaction between the carriers and salicylate. As the amount of phenyl groups increases, the electron-withdrawing power of the ligands increases, with the enhancement of hyperconjugation which decreases the electron density of the

central Sn(IV) atom. The low electron density could weaken the coordinate exchange interactions between salicylate and the central metal which resulted in the deterioration of the potentiometric response characteristics and selectivity for salicylate. Under the conditions of our experiments (pH 5), part of the salicylate in the sample solutions forms salicylic acid with hydrogen ions. Both salicylate and salicylic acid could transfer across the PVC membrane by diffusion simultaneously, and form adducts with the carrier molecule. Only the reversible transfer of salicylate anions is a potential-developing process, while the reversible transfer of salicylic acid does not contribute to the membrane potential. We presume that salicylate and salicylic acid transfer across the membrane phase at the same rate, the average charge of total salicylate (including salicylate and salicylic acid) which takes part in the transfer process from the sample solutions to the membrane phase corresponds to half of the negative charge. The super-Nernstian response to salicylate may be due to the transfer of salicylate with half of the negative charge.

3.5. Analytical application

The DMTBS-based electrode was shown to be useful in the potentiometric determination of salicylate in human urine samples, which can be easily prepared by 10-fold dilution of urine with $\text{KH}_2\text{PO}_4\text{--Na}_2\text{HPO}_4$ buffer adjusted to pH 5.0. The results (shown in Table 3) showed a standard deviation of 0.053(%), indicating that the DMTBS-based electrode can be applied for the determination of salicylate in actual samples with satisfactory results as compared with the conventional method.

Acknowledgements

This work was supported by the Chinese National Education Committee Foundation for Ph.D. thesis Research, Natural Science Foundation of Hunan Province and the Foundation for the Technological Development of Machinery Industry.

References

- [1] P. Schulthess, D. Amoman, B. Krautler, C. Caderas, R. Steplanek, W. Simon, *Anal. Chem.* 57 (1985) 1397.
- [2] N.A. Chaniotakis, A.M. Chasser, M.E. Meyerhoff, J.T. Groves, *Anal. Chem.* 60 (1988) 185.
- [3] A. Hodinar, A. Tyo, *Anal. Chem.* 61 (1989) 1169.
- [4] Q. Chang, M.E. Meyerhoff, *Anal. Chim. Acta* 186 (1986) 81.
- [5] S. Daunert, S. Wallace, A. Florido, G. Bachas, *Anal. Chem.* 63 (1991) 1676.
- [6] M.S. Frant, J.W. Ross, US Patent 3,406,102, 1968.
- [7] V.A. Zarinskii, L.K. Shpigun, V.M. Shkinev, *Russ. J. Anal. Chem.* 35 (1980) 381.
- [8] V.M. Shkinev, B.Y. Spivakov, G.A. Vorobeva, Y.A. Zolotov, *Anal. Chim. Acta* 167 (1985) 145.
- [9] U. Wuthier, H.V. Pham, W. Simon, *Anal. Chem.* 56 (1984) 535.
- [10] Liu Dong, Chen Wen-Can, Shen Guo-Li, Yu Ru-Qin, *Chem. J. Chinese Univ.* 17 (1996) 1528.
- [11] S.A. Glazier, M.A. Arnold, *Anal. Chem.* 60 (1988) 2542.
- [12] S.A. Glazier, M.A. Arnold, *Anal. Lett.* 22 (1989) 1075.
- [13] S.A. Glazier, M.A. Arnold, *Anal. Chem.* 63 (1991) 754.
- [14] P. Trinder, *Biochem. J.* 57 (1954) 301.
- [15] K.K. Choi, K.W. Fung, *Anal. Chim. Acta* 138 (1982) 385.
- [16] P.A. Mitsana, E.P. Diamantis, *Anal. Chim. Acta* 159 (1984) 193.
- [17] N.A. Chaniotakis, S.B. Park, M.E. Meyerhoff, *Anal. Chem.* 61 (1989) 566.
- [18] K.J. Sisido, *J. Am. Chem. Soc.* 83 (1961) 538.
- [19] S. Gopinathan, C. Gopinathan, J. Gupta, *Indian J. Chem.* 12 (1974) 626.
- [20] Liang Yong-Min, Song Qing-Bao, Huang Guo-Sheng, Ma Yong-Xiang, *Synth. React. Inorg. Met.-Org. Chem.* 25 (1995) 105.
- [21] G.J. Moody, R.B. Oke, J.D.R. Thomas, *Analyst* 95 (1970) 910.
- [22] A. Craggs, G.J. Moody, J.D.R. Thomas, *J. Chem. Educ.* 51 (1974) 541.
- [23] IUPAC, IUPAC Recommendation for Nomenclature of ion-selective electrodes, *Pure Appl. Chem.* 48 (1976) 129.
- [24] Yuan Ruo, Chai Ya-Qin, Gao De, Yu Ru-Qin, *Anal. Chem.* 65 (1993) 2572.
- [25] Li Jun-Zhong, Peng Xin-Yu, Yu Ru-Qin, *Anal. Chim. Acta* 297 (1994) 437.
- [26] M. Arshadi, D. Johnels, U. Edlund, *J. Chem. Soc., Chem. Commun.* 11 (1996) 1279.
- [27] Li Qing-Shan, Wang Hong-Fei, Guo Mao-Lin, *Chem. J. Chinese Univ* 17 (1996) 1165.
- [28] Liu Dong, Chen Wen-Can, Shen Guo-Li, Yu Ru-Qin, *Analyst* 121 (1996) 1495.

Acid–base equilibria of diazepam and prazepam in montmorillonite suspensions

A.E.M. Ismail Mohamed *

Department of Pharmaceutical Analytical Chemistry, University of Assiut, Assiut, Egypt

Received 24 February 1997; received in revised form 22 September 1997; accepted 2 October 1997

Abstract

The distribution of ionic species of diazepam and prazepam in aqueous and aqueous montmorillonite clay suspensions at several pH conditions (pH 1–12) was monitored spectrophotometrically. Measurements were performed at 284 and 365 nm for diazepam and 285 and 361 nm for prazepam. The interaction between the negative clay surface and protonated species of the drugs studied relative to the unchanged species is responsible for the apparent displacement of pK_a values from 3.3 and 2.7 to 4.4 and 3.9 for diazepam and prazepam respectively. Changes in the partial molar free energy of the ionic species of both drugs (ΔG_i) as a result of interactions with montmorillonite suspensions was -1.47 and -1.72 for diazepam and prazepam respectively. The effect of an additional ionic solute i.e. sodium chloride was also studied. The recovered amounts of both drugs from five different concentrations of veegum at pH 2, 5 and 10 indicates the effect of drug–clay interactions in drug analysis. © 1998 Elsevier Science B.V. All rights reserved.

Keywords: Diazepam; Prazepam; Acid–base equilibria in montmorillonite suspensions; Drug–clay interactions

1. Introduction

Diazepam (Valium) and prazepam (prazene) are important drugs, widely used in the treatment of several anxiety states, sometimes as anticonvulsants, for premedication in anesthesiology and in spastic disorders [1,2]. Silicate clays were widely used in the manufacture of dosage forms of many drugs [3]. They have also been suggested as vehicles for controlled release formulations [4,5].

The effect of the clay surface on acid–base equilibria of weak bases in aqueous clay suspensions was investigated for some drugs [6–8]. Previous investigations have shown that, protonation was enhanced as a result of base–clay interactions and consequently the rate of hydrolysis.

Knowledge of the degree of equilibrium displacement and the fractions of studied drugs bound in the presence of clay suspensions may be of great value in the analysis of such drugs.

The effect of montmorillonite on the acid–base equilibria of diazepam and prazepam and the determination of quantities recovered from five different veegum concentrations at three pH levels was investigated in this study.

* E-mail: aimrageh@aun.eun.eg

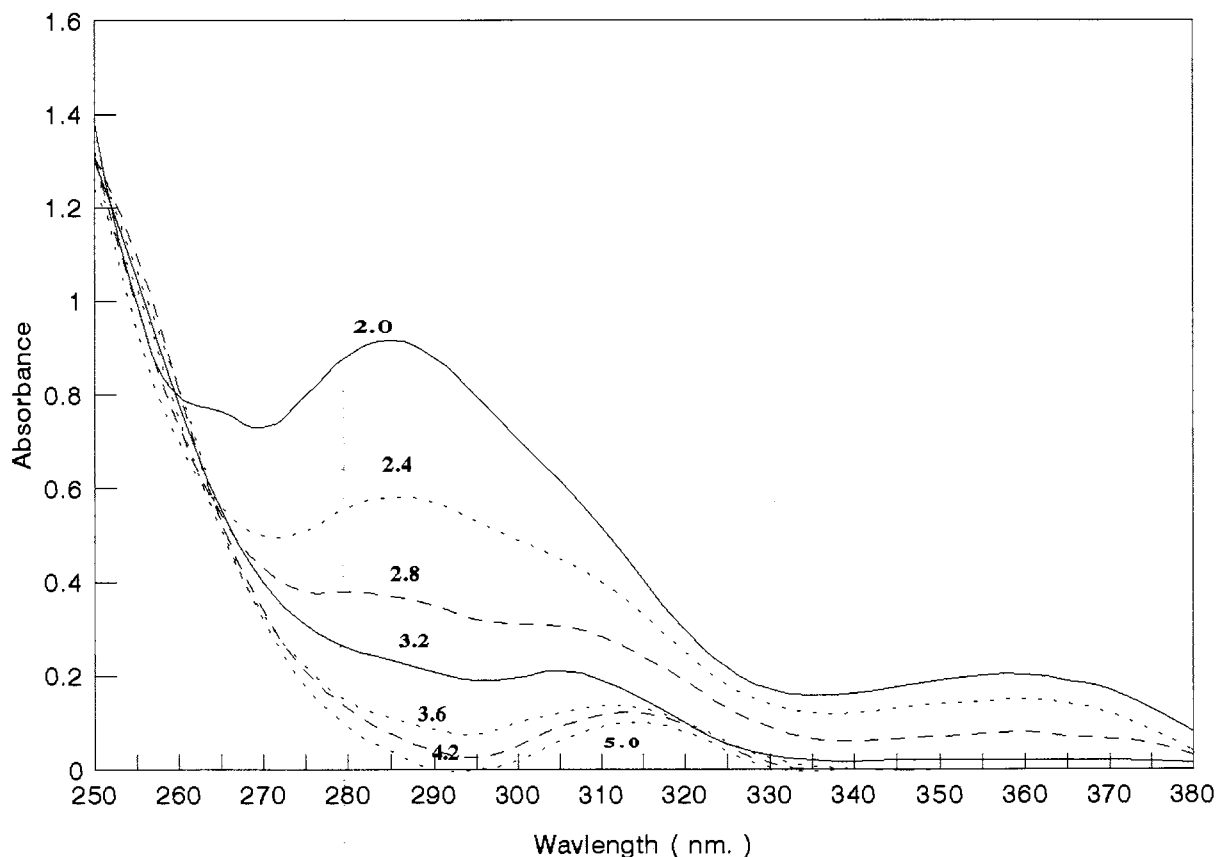


Fig. 1. UV-absorption spectra for prazepam ($10 \mu\text{g ml}^{-1}$) in aqueous solutions at different pH values.

2. Experimental

2.1. Apparatus

Measurements were performed with,

1. Uvidec-320 spectrophotometer (Jasco, Tokyo, Japan).
2. Unicam-SP 1750 spectrophotometer (Pye-Unicam, Cambridge, UK).
3. pH-Meter, Model 3305 (Jenway, UK).

2.2. Materials and reagents

Diazepam (Hoffmann-La-Roche AG, 7889 Grenzach-Wyhlen, Germany), and prazepam (Gödecke AG, Freiburg, Germany) were used as working standards without further treatment. All chemicals and solvents used throughout this work were of analytical grade.

1. Montmorillonite suspension: (Veegum HV as a source of montmorillonite used: R.T. Vanderilt, New York, USA): Veegum HV was finely pulverized and passed through $63 \mu\text{m}$ sieve to remove any extraneous matter and then weighed and diluted with distilled water to obtain 1% w/v veegum suspension.
2. Standard drug solution: Into a 100 ml volumetric flask, 100 mg of the studied drug (accurately weighed) was dissolved in about 80 ml ethanol and then completed to the mark with the same solvent. The standard drug solution was kept refrigerated in a light protected flask.
3. Buffer solutions (pH 1–12); were prepared in freshly boiled and cooled water [9].
4. Sodium chloride solution: 1 N solution in distilled water.

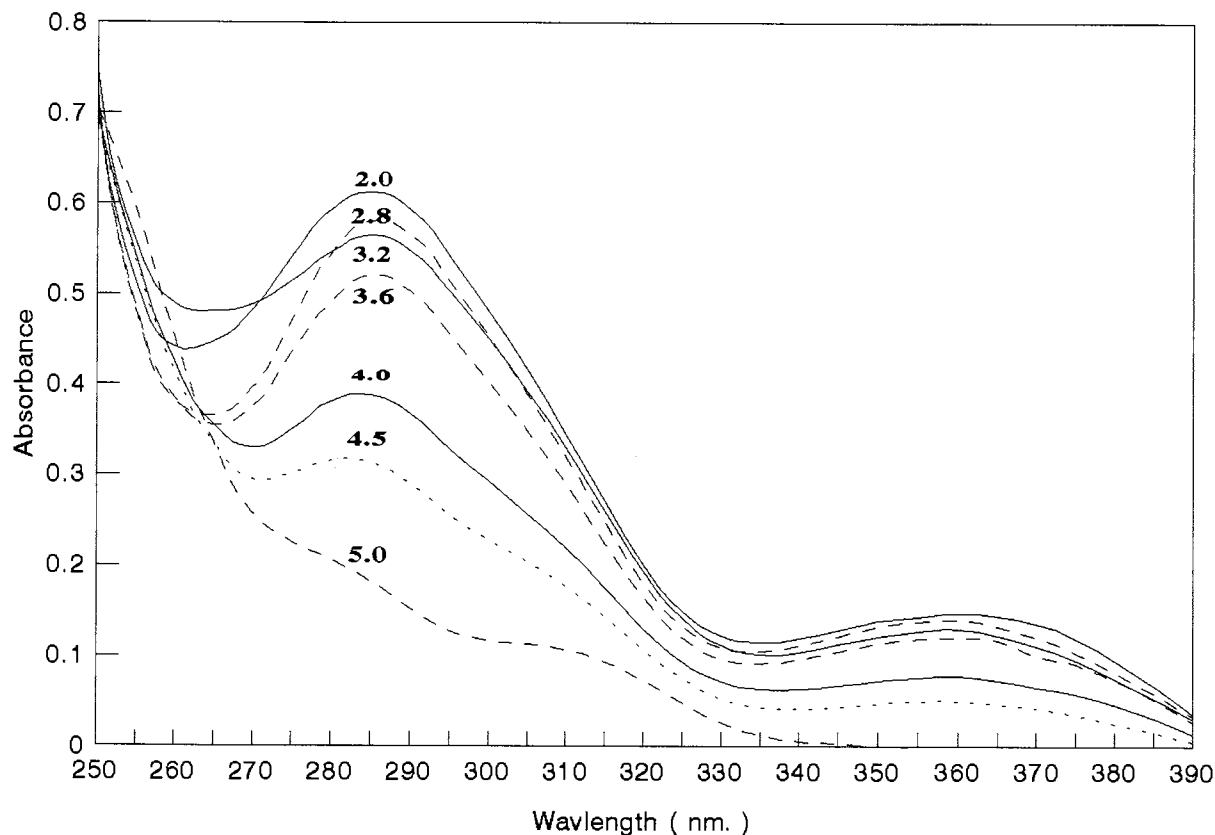


Fig. 2. UV-absorption spectra for prazepam ($20 \mu\text{g ml}^{-1}$) in aqueous veegum suspensions at different pH^b values.

2.3. General procedure

The standard drug solution (2 ml) was transferred to a 100 ml volumetric flask containing about 25 ml buffer solution at the desired pH, the volume was completed to about 95 ml with water. The veegum suspension (2 ml) was added to the flask prior to dilution to 100 ml with water to minimize the change in pH while mixing the drug with clay. The exact pH^b (the bulk pH of the suspension) of the stirred suspension was measured after the pH^b had stabilized. About 50 ml of the solution was then separated from the solid by centrifugation. Absorbance of the clear supernatant was measured at 284 and 365 nm for diazepam and at 285 and 361 nm for prazepam against a blank treated similarly using 2 ml of ethanol instead of the drug solution.

2.4. Effect of presence of sodium chloride

The standard drug solution (2 ml) was transferred to a 100 ml volumetric flask containing about 25 ml buffer solution at the desired pH, followed by 10 ml of sodium chloride solution, then completed as in Section 2.3 starting from “then the volume was completed...”.

3. Results and discussion

The absorption spectra of prazepam (as a representative example), in aqueous solutions and montmorillonite suspensions at different pH levels are illustrated in Figs. 1 and 2. These figures show that veegum suspensions significantly affect the absorption profiles and intensities of the drugs at certain pH values.

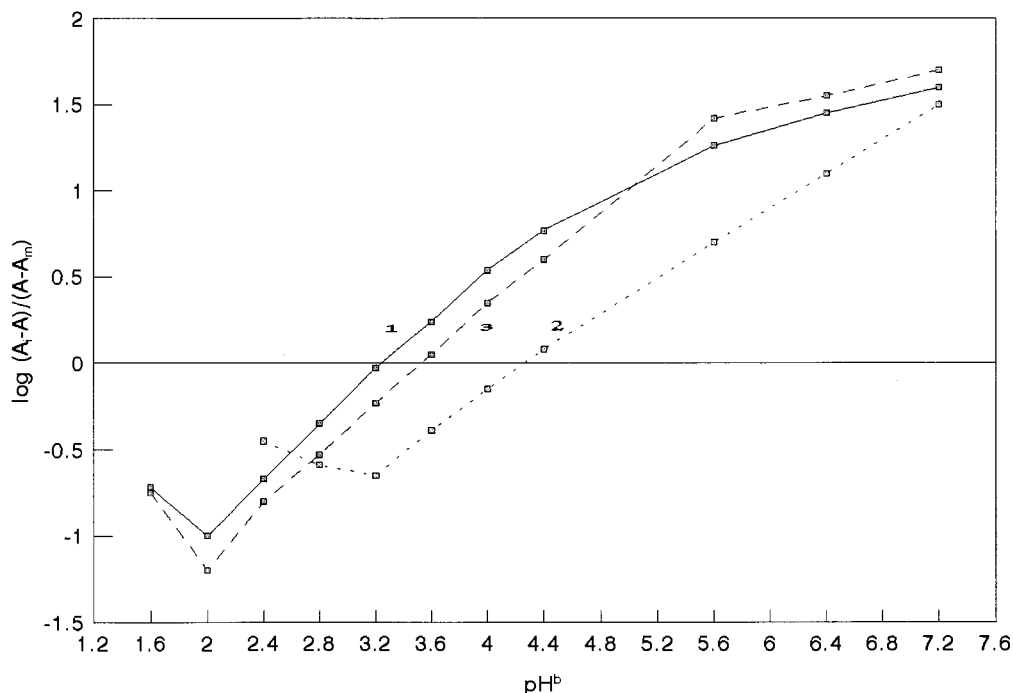


Fig. 3. pK_a values of diazepam in aqueous solutions (1), aqueous veegum suspensions (2), and aqueous veegum suspensions containing 0.1 N NaCl (3).

The acid–base equilibria of both drugs were markedly influenced by the presence of montmorillonite suspensions. In aqueous solutions, pK_a values of diazepam and prazepam were 3.3 and 2.7 respectively which agree well with the reported values [10,11]. However, in the presence of veegum, pK_{eff} were 4.4 and 3.9 (Figs. 3 and 4 and Table 1). The interaction of protonated species of diazepam and prazepam with the negative clay surface was responsible for these shifts.

ΔG_i ($i = \text{BH}^+, \text{B}$) is the change in partial molar Gibbs free energy for the constituent i , accompanying the addition of clay to the system at constant temperature, pressure and composition. ΔG_{B} and ΔG_{BH^+} could be related to the equilibrium constants by Eq. (1),

$$\Delta G_{\text{BH}^+} - \Delta G_{\text{B}} = RT \ln K_{\text{eff}}/K \quad (1)$$

For any individual species (i) in a reaction mixture, the free energy is described by Eq. (2),

$$G_i = G_i^* + RT \ln a_i \quad (2)$$

where G_i represents the free energy of formation of the substance, at activity a_i , from its elements in their standard state; G_i^* is the standard free energy of formation [7,12,13]. Because the system is heterogenous, external electric fields are present (due to the charged clay). As a consequence, ΔG_i may be identified using electrochemical potential, and the activity a_i is regarded as the total activity as described by Low [13]. This activity is not to be confused with the that commonly applied to homogenous systems (i.e. solutions for which the activity is defined in terms of the chemical potential and relates to field-free systems). Consequently, the values K_{eff}/K or $pK_{\text{eff}}-pK$ serve as reliable parameters indicating the degree of equilibrium displacement due to the BH^+ –clay and B–clay interactions.

If the system is sufficiently diluted with respect to clay and all other solutes, ΔG_{BH^+} and ΔG_{B} values can be calculated individually from Eqs. (7) and (8) [6,7]. As $C_i \rightarrow 0$ K_{eff} and ΔG_i values approach a definite value that reflects an intrinsic

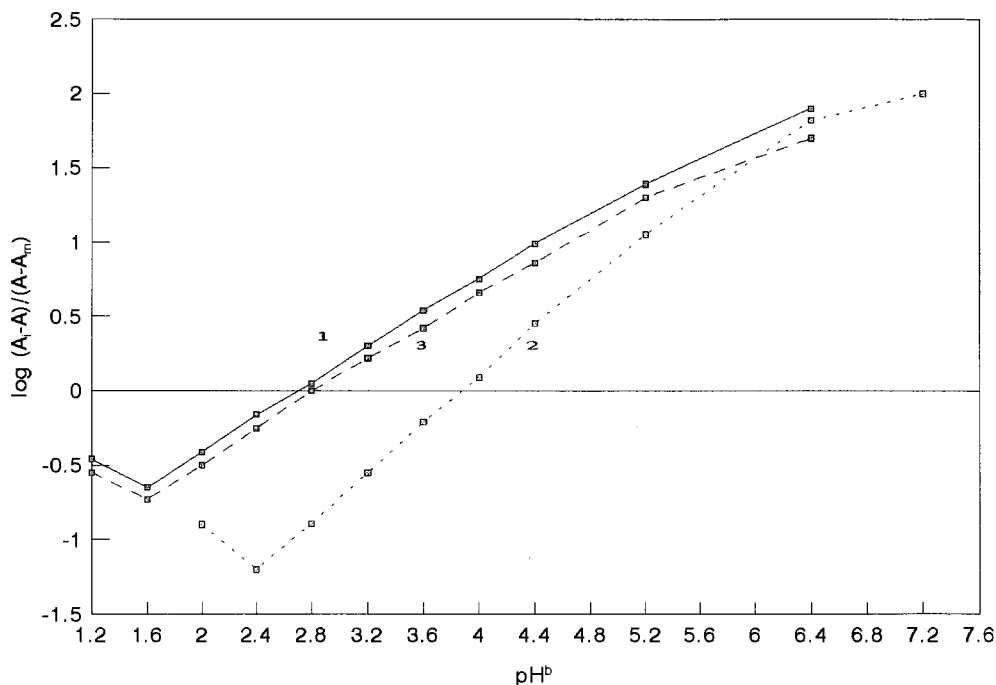


Fig. 4. pK_a values of prazepam in aqueous solutions (1), aqueous veegum suspensions (2), and aqueous veegum suspensions containing 0.1 N NaCl (3).

interaction of species i with the clay surface, independent of C_p .

As seen in Table 1, ΔG_{BH^+} values were -1.47 and -1.72 Kcal mol $^{-1}$ for diazepam and prazepam respectively, indicating a greater stabilization of the protonated species than the free bases ($\Delta G_B = -0.04$ and -0.06 for diazepam and prazepam respectively).

The interaction of protonated drugs with veegum was affected by other ionic species in the system. As seen in Figs. 3 and 4 and Table 1, the

shift in the pK_{eff} values were reduced in the presence of 0.1 N sodium chloride solutions. It is hypothesized that sodium ions compete with BH^+ for the negative sites on the clay surface, or equivalently, that sodium ions screen the negatively charged clay surface, thereby reducing the apparent negative charge of the clay surface. Sodium chloride may also affect the interaction by altering the dispersion state of the clay, so that negative sites are less accessible to BH^+ species. Thus, the values for pK_{eff} calculated approached

Table 1
Effect of veegum on the acid–base equilibria of diazepam and prazepam

Sample (Kcal mol $^{-1}$)	Diazepam			Prazepam		
	pK_{eff}	ΔG_B (Kcal mol $^{-1}$)	ΔG_{BH^+} (Kcal mol $^{-1}$)	pK_{eff}	ΔG_B (Kcal mol $^{-1}$)	ΔG_{BH^+} (Kcal mol $^{-1}$)
Aqueous solution	3.3	—	—	2.7	—	—
Aqueous veegum suspensions	4.4	-0.04	-1.47	3.9	-0.06	-1.72
Aqueous veegum suspensions containing 0.1 N NaCl	3.5	-0.05	-0.16	2.8	-0.07	-0.27

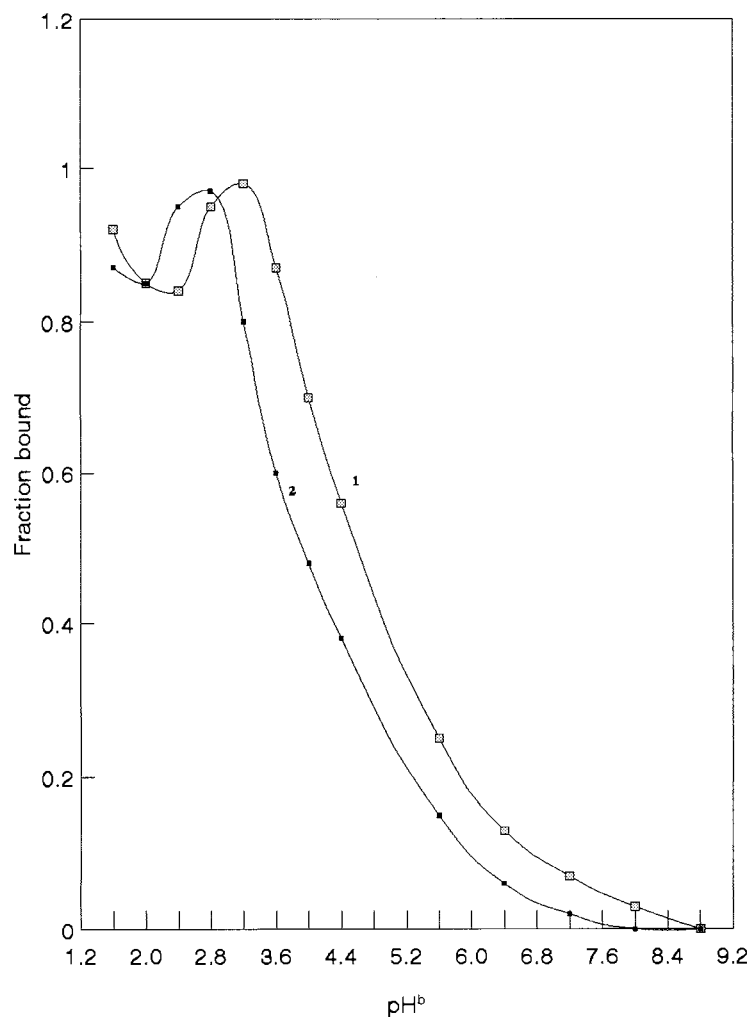


Fig. 5. Effect of pH^b on the fractions of diazepam (1) and prazepam (2) bound to the clay surface.

normal pK_a values (3.5 and 2.8 for diazepam and prazepam respectively) and ΔG_{BH^+} values approached zero (-0.052 and -0.066 for diazepam and prazepam respectively).

The fraction bound curves in Fig. 5 indicate that, the fraction of the drug bound to the clay surface increased with pH^b until a maximum was observed at pH^b 3.3 for diazepam and 2.6 for prazepam. At lower pH^b values, protons apparently compete with BH^+ for the negative clay sites. The fraction of drug bound to montmorillonite decreased rapidly in all conditions because pH^b conditions allowed the unionized form of the

drug to appear in the system. The ΔG_{B} values which range from -0.035 to -0.062 for both drugs indicates little interaction with the clay surface.

The recovered quantities of diazepam and prazepam from five different veegum concentrations at three pH levels (pH 2, 5 and 10) were listed in Table 2. It is clear from the table that, the drug concentration in solution is greatly affected in acid medium, while in alkaline medium, there is no significant effect due to the presence of the drug in its unionized form. The magnitude of the fraction bound as well as the shift in the pK_a

Table 2

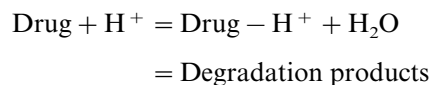
Recovered amounts^a (% ± RSD) of diazepam (1) and prazepam (2) from different veegum suspensions compared with aqueous solutions

	Milileters added of 0.2% veegum suspension				
	1.0	2.0	3.0	4.0	5.0
(1) pH 2	89 ± 2	77 ± 1	62 ± 2	46 ± 2	29 ± 2
(1) pH 5	98 ± 1	96 ± 2	95 ± 2	94 ± 2	93 ± 2
(1) pH 10	100 ± 1	99 ± 2	98 ± 2	98 ± 2	98 ± 2
(2) pH 2	85 ± 2	73 ± 2	60 ± 2	44 ± 2	27 ± 2
(2) pH 5	99 ± 2	98 ± 2	96 ± 2	95 ± 2	93 ± 2
(2) pH 10	101 ± 1	100 ± 1	99 ± 2	99 ± 2	99 ± 2

^a Average of five measurements.

value of drug at a given pH range due to the interaction with the clay surface may explain the failure of some analytical procedures to determine the exact quantities of drugs due to the presence of certain additives such as silicates.

The distribution of ionized and nonionized species of prazepam as representative example, in aqueous solutions and aqueous montmorillonite suspensions, based on the respective values of pK_a and pK_{eff} found in this study as shown in Fig. 6. The changes in the acid–base equilibria of both drugs due to the stabilizing effect of the montmorillonite clay surface favored the protonated forms to be present over a wider pH range than expected with acid–base equilibria in solutions and consequently may lead to an accelerated hydrolysis rate.



In contrast, stability might be increased due to the drug–clay interaction as a result of increasing the activation energy for the hydrolysis reaction. The net effect on the hydrolysis rate will vary for each system, depending on the relative magnitude of each factor.

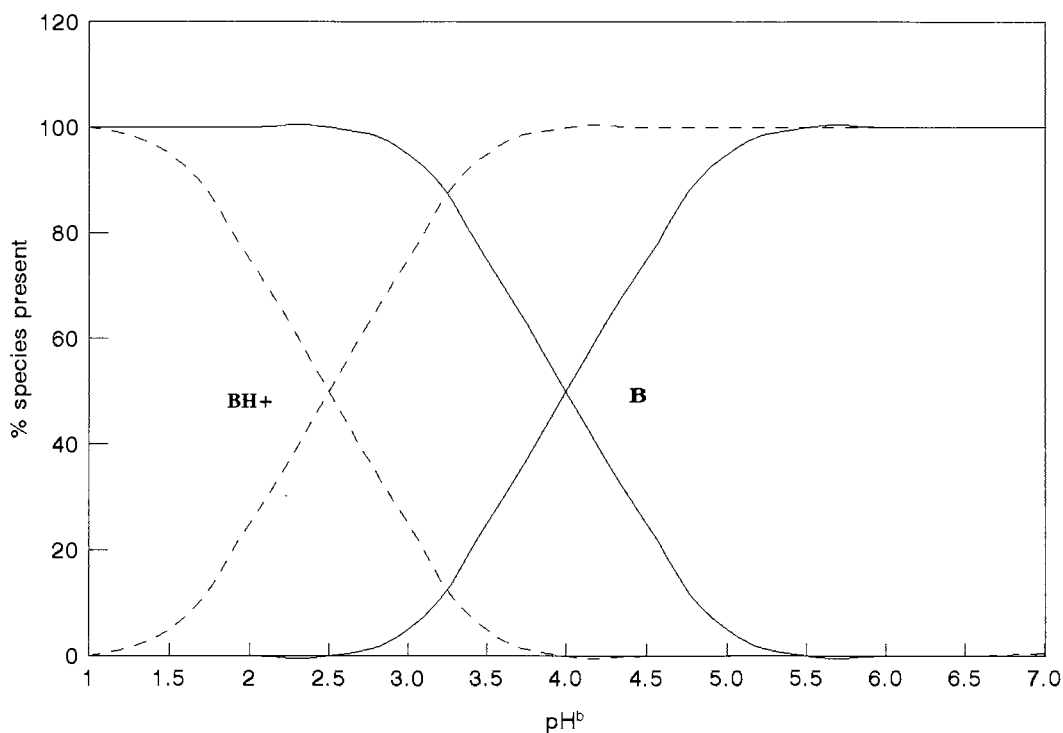


Fig. 6. Distribution of the ionized and unionized species of prazepam. (---), aqueous solutions; (—), veegum suspensions.

4. Conclusion

The acid–base equilibria of diazepam and prazepam could be significantly affected by interaction with the clay surface. Clays may be found as vehicles in many dosage forms. Therefore, understanding their effect on the acid–base equilibria of the drug under investigation should provide the information needed to select the proper analysis method and pH at which the determination must be carried out. K_{eff} and ΔG_i are useful values for following the drug–clay interactions.

Appendix A. Determination of the effective equilibrium constant (pK_{eff})

UV-spectrophotometric determinations were performed at the previously given maxima to determine $C_{\text{B}}/C_{\text{BH}^+}$ as required for determination of K and K_{eff} by Eqs. (3) and (4).

$$K = \alpha\text{H}^+ \frac{\alpha\text{B}}{\alpha\text{BH}^+} \quad (3)$$

Where a_i is the activity of the species i ($i = \text{B}, \text{BH}^+, \text{H}^+$). In very dilute solutions (clay free) $C_{\text{B}}/C_{\text{BH}^+} = \alpha\text{B}/\alpha\text{BH}^+$ (in our case 7×10^{-5} and 6×10^{-5} M solutions of diazepam and prazepam were used respectively).

$$K_{\text{eff}} = \alpha\text{H}^+ \frac{C_{\text{B}}}{C_{\text{BH}^+}} \quad (4)$$

Where, C_i ($i = \text{B}, \text{BH}^+$) is the average suspension concentration of the species i .

Molar absorptivity (ϵ) of the drugs studied, is related to $C_{\text{B}}/C_{\text{BH}^+}$ by Eq. (5),

$$\frac{C_{\text{B}}}{C_{\text{BH}^+}} = \frac{\epsilon - \epsilon_{\text{BH}^+}}{\epsilon_{\text{B}} - \epsilon} \quad (5)$$

The symbols ϵ_{B} and ϵ_{BH^+} represent the molar absorptivities when all of the studied drug is present as B and BH^+ respectively, while ϵ represents the observed molar absorptivity at a given pH^{b} value.

For graphical representation, the theoretical lines for the drugs studied was calculated from Eq. (6)

$$\text{p}K_{\text{eff}} = \text{pH}^{\text{b}} + \log\left(\frac{\epsilon_{\text{B}} - \epsilon}{\epsilon - \epsilon_{\text{BH}^+}}\right) \quad (6)$$

to fit experimental points.

Appendix B. Determination of ΔG_i

If the system is sufficiently dilute with respect to clay and other solutes, ΔG_{BH^+} and ΔG_{B} values are given by Eqs. (7) and (8),

$$\Delta \overline{G}_{\text{BH}^+} = RT \ln(1-f) \left(\frac{K_{\text{eff}} + \alpha\text{H}^+}{K + \alpha\text{H}^+} \right) \quad (7)$$

$$\Delta \overline{G}_{\text{B}} = RT \ln(1-f) \left(\frac{K}{K_{\text{eff}}} \right) \left(\frac{K_{\text{eff}} + \alpha\text{H}^+}{K + \alpha\text{H}^+} \right) \quad (8)$$

where f is the fraction of base initially added to the system that is bound to clay. The fraction bound (f) was calculated from, $f = (A_i - A_s)/A_i$; where A_i represents the absorbance of a solution only containing the protonated species (BH^+), having a concentration equal to the initial concentration (C_o), while A_s represents the absorbance of the sample supernatant of initial concentration (C_o) measured against a blank treated similarly.

References

- [1] J.N. Delgado, W.A. Remers, Textbook of Organic Medicinal and Pharmaceutical Chemistry, 9th ed., Lippincott Company, Philadelphia, 1991, pp. 364–368.
- [2] Martindal, The Extra Pharmacopoeia, 29th ed., Pharmaceutical Press, London, 1989.
- [3] K. Wai, H.G. Dekay, G.S. Banker, J. Pharm. Sci. 55 (1966) 1244.
- [4] J.W. McGinity, J.I. Lach, J. Pharm. Sci. 66 (1977) 63.
- [5] J.L. White, S.L. Hem, Ind. Eng. Chem. Prod. Res. Dev. 22 (1983) 665.
- [6] J.R. Feldkamp, J.L. White, J. Colloid Interface Sci. 69 (1979) 97.
- [7] J.E. Browne, J.R. Feldkamp, J.L. White, S.L. Hem, J. Pharm. Sci. 69 (1980) 811.
- [8] A.M. El-Sayed, A.El-M. Ismail, A.El-A. Assi, Acta Pharm. Hung. 63 (1993) 257–266.
- [9] M. Pesez, J. Bartos, Colorimetric and Fluorimetric Analysis of Organic Compounds and Drugs, Marcel Dekker, New York, 1974, 628.

- [10] A.C. Moffat, J.V. Jakson, M.S. Moss, B. Widdop, Clark's Isolation and Identification of Drugs, 2nd ed., Pharmaceutical Press, London, 1986, pp. 526–527.
- [11] L. Meites, An Introduction to Chemical Equilibrium and Kinetics, Pergamon Press, Oxford, 1981, pp. 17–27.
- [12] R.A. Alberty, Physical Chemistry, 7th ed., Wiley, New York, 1987, pp. 110–287.
- [13] P.F. Low, Soil Sci. 71 (1951) 409.

Cerium (IV)-based chemiluminescence analysis of hydrochlorothiazide

J. Ouyang^a, W.R.G. Baeyens^{a,*}, J. Delanghe^{a,b}, G. Van der weken^a,
A.C. Calokerinos^{a,c}

^a University of Ghent, Faculty of Pharmaceutical Sciences, Department of Pharmaceutical Analysis,
Laboratory of Drug Quality Control, Harelbekestraat 72, B-9000 Ghent, Belgium

^b University of Ghent, Faculty of Medicine, Central Laboratory, De Pintelaan 185, B-9000 Ghent, Belgium

^c University of Athens, Chemistry Department, Laboratory of Analytical Chemistry, Panepistimiopolis 157 71, Athens, Greece

Received 10 July 1997; received in revised form 23 September 1997; accepted 2 October 1997

Abstract

A flow-injection analytical method for the determination of hydrochlorothiazide is presented. The method is based on the chemiluminescence reaction of hydrochlorothiazide with cerium(IV) in sulphuric acid, sensitized by the fluorescent dye rhodamine 6G. The proposed procedure allows quantitation of hydrochlorothiazide in the concentration range of 0.33–130 $\mu\text{mol l}^{-1}$ with a detection limit of 0.15 $\mu\text{mol l}^{-1}$, an RSD of 2.4% at 10 $\mu\text{mol l}^{-1}$ and a sample measurement frequency of 200 h^{-1} . The method was successfully applied to the determination of hydrochlorothiazide in pharmaceutical preparations containing, amongst others, lactose, maize starch, calcium phosphate, magnesium stearate, potassium chloride and E 110 (disodium-6-hydroxy-5-(4-sulphonatophenylazo) naphthalene-2-sulphonate) as the concomitant species. Apart from the single formulation, hydrochlorothiazide was also determined in tablets combined with the antihypertensive lisinopril. © 1998 Elsevier Science B.V. All rights reserved.

Keywords: Chemiluminescence; Hydrochlorothiazide; Cerium (IV); Rhodamine 6G; Flow-injection analysis; Pharmaceutical analysis

1. Introduction

Hydrochlorothiazide (6-chloro-3,4-dihydro-2H-1,2,4-benzothiadiazine-7-sulphonamide-1,1-dioxide) is a powerful thiazide diuretic. It has been used as such and in combination with other drugs,

e.g. amiloride [1], captopril [2], lisinopril [3] and fosinopril [4] for the treatment of hypertension and related disorders.

Hydrochlorothiazide is classically determined using electrochemical [5,6] or spectrophotometric [4,7] methods, the latter being recommended by the British Pharmacopoeia [8]. As hydrochlorothiazide is sometimes combined with other drugs in tablet formulations, liquid chromatographic procedures with UV detection have been suggested

* Corresponding author. Tel.: + 32 92 648097; fax: + 32 92 648196; e-mail: willy.baeyens@rug.ac.be

for its determination [9–11]. Multicomponent analyses based on derivative or multiwavelength spectrophotometry have been considered as simple and selective methods, the analysis of hydrochlorothiazide in a mixture with amiloride in tablet formulation being an excellent example [1]. The accuracy of this technique, however, mostly depends on the knowledge of all components present that contribute to the mixture absorbance [1,4]; a complicated mathematical calculation might also be needed. Therefore the method for the analysis of hydrochlorothiazide still requires improvement.

Analytical procedures applying chemiluminescence (CL) measurements in flow-injection (FI) set-ups combine the advantages of instrument simplicity (no monochromator required) and rapidity in signal detection (normally 0.1–10 s) and have been extensively used for the analysis of pharmaceutical compounds [12,13]. An early electrochemiluminescent study of hydralazine briefly mentioned the reaction of hydrochlorothiazide with $\text{Ru}(\text{bpy})_3^{3+}$ [14]. This system was further investigated by Holeman and Danielson in 1993 [15]. The main disadvantages of this proposed system for the determination of hydrochlorothiazide is the complicated instrumental set-up used for the electro-generation of CL, and the serious interference by organic amines which react with $\text{Ru}(\text{bpy})_3^{3+}$. Also, compounds combined with hydrochlorothiazide in tablet formulations such as amiloride and lisinopril may cause significant interferences in the hydrochlorothiazide determination.

The CL reaction of cerium(IV)-ions with drugs containing a thiol-group, sensitized by fluorescent dyes has been proposed by the present group for the analysis of captopril, penicillamine and tiopronin [16–18]. One of the advantages of the system is a certain degree of selectivity for S-containing compounds. When coupled with FI analysis (FIA), the method proves to be cheap, rapid, simple, and reproducible, which is essential in drug quality control studies.

The primary aim of the present work was to develop a simple and selective CL-based FIA method, applying the CL reaction of cerium(IV), sensitized by fluorescent dyes, for the routine de-

termination of hydrochlorothiazide in pharmaceutical preparations, in single form or combined with other drugs such as amiloride and lisinopril.

2. Experimental

2.1. Chemicals and Reagents

All chemicals were of analytical grade unless specified otherwise. Hydrochlorothiazide was obtained from Sigma (St. Louis, MO, USA), lisinopril and amiloride were purchased from Merck (Brussels, Belgium), cerium(IV) sulphate, rhodamine B and rhodamine 6G from UCB (Leuven, Belgium). All solutions were prepared with de-ionized water. An aqueous stock standard solution of hydrochlorothiazide ($130 \mu\text{mol l}^{-1}$) was freshly prepared in 20% (v/v) methanol. The cerium(IV) solution (10 mmol l^{-1}) was prepared by dissolving the ceric salt ($\text{Ce}(\text{SO}_4)_2 \cdot 4\text{H}_2\text{O}$) in $0.1 \text{ mol l}^{-1} \text{ H}_2\text{SO}_4$; the 0.1 mmol l^{-1} rhodamine 6G solution was similarly prepared by dissolving rhodamine 6G in $0.1 \text{ mol l}^{-1} \text{ H}_2\text{SO}_4$ medium.

2.2. Apparatus

The FI system consists of a Gilson peristaltic pump (Minipuls 2 from Gilson, Villier-le-Bel, France; two channels, variable speed), provided with PTFE tubing. An HPLC isocratic pump (SP8770, Spectraphysics, CA) and an injector (VALCO, home-made loop $100 \mu\text{l}$) was installed as shown in Fig. 1. CL emission was measured using a CL detector (Chemlab, The Netherlands). CL data were handled by an IBM-compatible computer employing the luminometer software (Bio-orbit, Turku, Finland) for graphical viewing of the measured values and for calculation.

2.3. Procedure

2.3.1. Procedure for calibration

Working standard solutions containing hydrochlorothiazide in the range of $0.33\text{--}130 \mu\text{mol l}^{-1}$ were prepared by diluting a concentrated fresh standard solution of hydrochlorothiazide

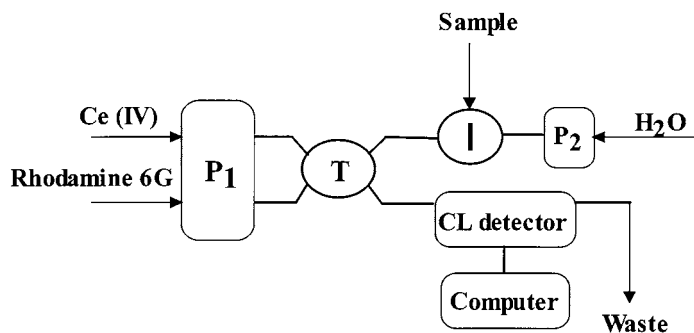


Fig. 1. FI manifold for hydrochlorothiazide determination: Ce(IV), 10 mmol l^{-1} in $0.1 \text{ mol l}^{-1} \text{ H}_2\text{SO}_4$; Rhodamine 6G, 0.1 mmol l^{-1} in $0.1 \text{ mol l}^{-1} \text{ H}_2\text{SO}_4$; P1, peristaltic pump; P2, HPLC pump; T, mixing cross; I, injector ($50 \mu\text{l}$).

($130 \mu\text{mol ml}^{-1}$) with 20% (v/v) methanol solution. The CL signal was measured by injecting $100 \mu\text{l}$ of the working standard solution into the carrier stream, which then joined the reagent streams (10 mmol l^{-1} Ce(IV) and 0.1 mmol l^{-1} rhodamine 6G in $0.1 \text{ mol l}^{-1} \text{ H}_2\text{SO}_4$ solutions). Peak heights of the CL light emission versus hydrochlorothiazide concentration were used for the calibration.

2.3.2. Procedure for tablets

Two types of tablets containing 12.5 and 50.0 mg of hydrochlorothiazide, single and in combination with lisinopril, respectively, were analyzed using the proposed method. Ten tablets were weighed so as to obtain the mean tablet weight.

An accurately weighed portion of the homogenized powder corresponding with 10 mg of hydrochlorothiazide was treated with HPLC-grade methanol up to 50 ml in the ultrasonic generator for 1 h. Then 2.5 ml of the solution was diluted with 20% (v/v) of methanol to 50.0 ml for the CL-FIA, providing a theoretical hydrochlorothiazide concentration of $10 \mu\text{g ml}^{-1}$.

3. Results and Discussion

3.1. Optimization

The effects of Ce(IV), sulphuric acid, methanol, rhodamine concentrations and the reagent flow-

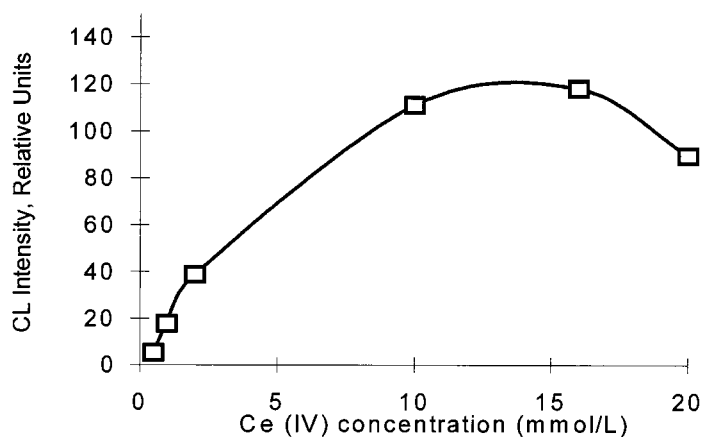


Fig. 2. Effect of Ce(IV)-concentration on the hydrochlorothiazide CL emission. Ce(IV) solutions prepared by dissolving $\text{Ce}(\text{SO}_4)_2 \cdot 4\text{H}_2\text{O}$ in $0.1 \text{ mol l}^{-1} \text{ H}_2\text{SO}_4$; rhodamine 6G-concentration, 0.10 mmol l^{-1} in $0.1 \text{ mol l}^{-1} \text{ H}_2\text{SO}_4$; hydrochlorothiazide-concentration, $10 \mu\text{mol l}^{-1}$ in 20% (v/v) aqueous methanol.

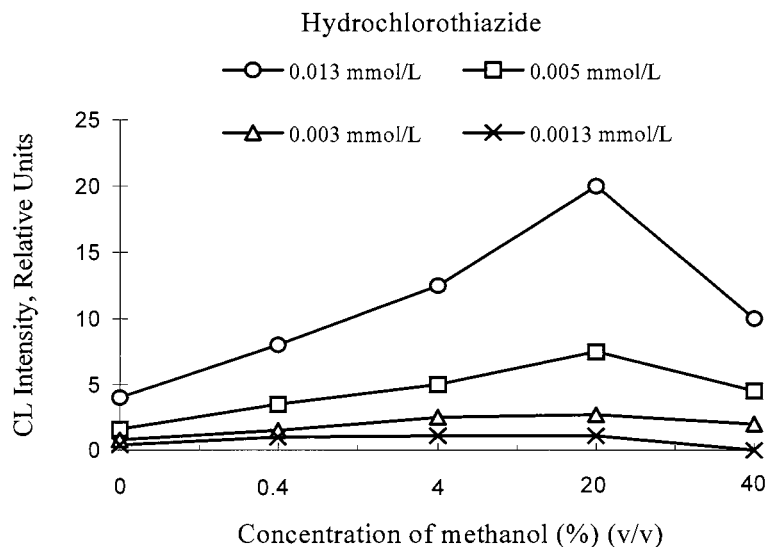


Fig. 3. Effect of methanol concentration on the CL emission of hydrochlorothiazide. Ce(IV)-concentration, 10.0 mmol l^{-1} ; rhodamine 6G concentration, 0.10 mmol l^{-1} , both in $0.1 \text{ mol l}^{-1} \text{ H}_2\text{SO}_4$.

rates on the CL emission were investigated, together with the effects of sample injection volume and some micellar reagents.

3.1.1. Effect of Ce(IV) concentration

The concentration effect of Ce(IV) upon the CL behaviour of hydrochlorothiazide was examined over the range $0.5\text{--}20 \text{ mmol l}^{-1}$ in $0.1 \text{ mol l}^{-1} \text{ H}_2\text{SO}_4$. The results are shown in Fig. 2. Maximum emission intensity was observed at Ce(IV)-concentrations of $10\text{--}15 \text{ mmol l}^{-1}$. Lower concentrations of oxidant cause decreased CL emission. Higher concentrations produce self-absorption of the emitted radiation by the deep yellow colour from the Ce(IV) solution. Therefore, a concentration of 10 mmol l^{-1} of the ceric salt was used for further work.

3.1.2. Effect of H_2SO_4 concentration

Since acidic Ce (IV) reacts with hydrochlorothiazide yielding measurable CL emission, the effect of acid added to the Ce(IV) and rhodamine 6G solutions was examined. The highest CL signal was observed in the concentration range $0.1\text{--}0.2 \text{ mol l}^{-1}$ of H_2SO_4 . Higher and lower concentrations of the acid produced a decrease of CL. Hence, $0.1 \text{ mol l}^{-1} \text{ H}_2\text{SO}_4$ solution was chosen to

prepare and dilute the Ce(IV) and rhodamine 6G solutions.

3.1.3. Effect of methanol concentration

As hydrochlorothiazide is practically water-insoluble, methanol was used to dissolve the compound from the samples. It is known that organic solvents in general influence CL behaviour, hence the effect of methanol was examined. As shown in Fig. 3, an increase in CL intensity was observed when the methanol concentration was increased up to 20% (v/v). Methanol concentrations higher than 20% (v/v) caused a decrease in CL intensities, as illustrated with hydrochlorothiazide concentrations ranging from $0.0013 \text{ mmol l}^{-1}$ to $0.013 \text{ mmol l}^{-1}$. Therefore 20% (v/v) methanol was selected as the optimum concentration for the present work. It should be stated that the 20% (v/v) methanol concentration used will also be of benefit in the separation of this diuretic drug using HPLC. In this respect the effect of acetonitrile was also tested, but caused a strong suppression of the hydrochlorothiazide CL emission.

3.1.4. Effect of rhodamine concentration

A few fluorescing compounds were tested as energy transfer-reagents in the CL reaction of

Ce(IV) with thiol-containing drugs [16,17]. The rhodamine series and quinine produced a remarkable increase of CL efficiency. These fluorophores were therefore examined in this study. As shown in Table 1, both rhodamine dyes as sensitizers increase the CL efficiency 25 to 40-fold. The effects of the concentration of rhodamine 6G and rhodamine B were further examined. The results in Fig. 4 show that 0.1 and 0.5 mmol l⁻¹ of rhodamine 6G and rhodamine B, respectively, provide maximum CL intensities. Higher concentrations cause self-absorption of the emission by the sensitizers and therefore lower CL intensity. As rhodamine 6G produces higher emission yields than rhodamine B, this dye was used in further experiments.

Table 1
Effect of different fluorophores on the CL emission from Ce(IV)-hydrochlorothiazide

Fluorescer	Optimized Concentration (mmol l ⁻¹)	Relative CL
None	—	1.0
Eosine	0.2	1.3
Lucigenin	0.1	3.3
Quinine	1.0	10.0
Riboflavine	0.1	13.0
Rhodamine B	0.5	25.4
Rhodamine 6G	0.1	40.5

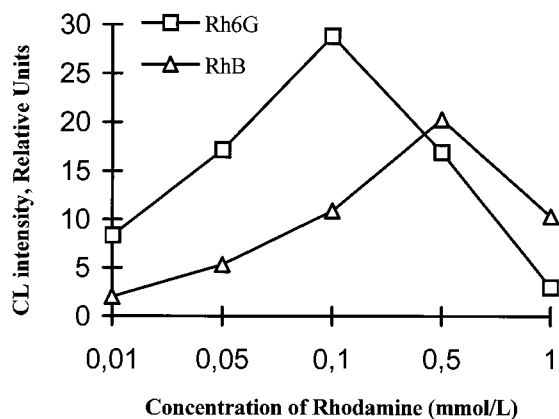


Fig. 4. Effect of rhodamine 6G and rhodamine B on the CL emission of hydrochlorothiazide. Ce(IV)-concentration, 10.0 mmol l⁻¹; hydrochlorothiazide-concentration, 10 μmol l⁻¹ in 20% (v/v) methanol (Rh 6G, rhodamine 6G; Rh B, rhodamine B).

Table 2
Effect of some organized solutions on CL emission

Surfactant, cyclodextrin	Relative CL intensity ^a
Triton X-100	25
β-Cyclodextrin	86
Cetyltrimethylammoniumbromide	90
Tetrabutylammoniumbromide	99
None	100
Sodium dodecyl sulphate	105
Heptanal sodium bisulfite	110
Brij 35	135

^aConcentration: 10 mmol l⁻¹.

3.1.5. Effect of reagents flow-rate

The flow-rate of the reagent solutions was optimized in order to obtain satisfactory CL emission. The highest intensity was achieved at 1.0 ml min⁻¹ for both Ce(IV) and rhodamine 6G reagents. Decreasing the flow-rate from 1.0 to 0.7 ml min⁻¹, significantly spared the consumption of reagents with only a slight loss of CL intensity. Further study was therefore carried out using a flow-rate of 0.7 ml min⁻¹ for each reagent. In spite of the effect of the sample carrier stream on CL emission, the carrier stream flow-rate of 1 ml min⁻¹ was installed so as to easily couple the system with an HPLC set-up. Increasing sample carrier stream flow-rates may be applied to increase the CL emission intensity and thus improve detection limits.

3.1.6. Effect of sample injection volume

It is well-known that the sample injection volume in a FI set-up affects the signal intensity. An increase in sample volume normally leads to an increase in the emitted CL signal. The present study shows that a change in loop size from 50–200 μl can improve the CL intensity by a factor of 2, further increase in sample volume from 200–500 μl increases the CL intensity much slower. Therefore, 200 μl was considered the optimum sample injection volume in the FI system. The final purpose of this work is to couple the CL detector to an HPLC separation set-up, hence a sample volume of 50 μl was used throughout. Obviously, the injection volume, when applied to

Table 3
Recovery of 10 $\mu\text{mol l}^{-1}$ of hydrochlorothiazide applying various additives used as excipients

Additive	Concentration ratio additive/hydrochlorothiazide (w/w)	Recovery (%) ($n = 4$)
CaHPO ₄	100	100.0
KCL	100	98.5
Lactose	100	105.7
Magnesium stearate	100	100.0
Mannitol	100	101.0
Maize starch	100	100.0
Maize starch, pregelatinized	100	103.0
E110	10	102.0

HPLC set-ups should be appropriately reduced so as to prevent overload and subsequent peak deformation.

3.1.7. Effect of some micellar solutions

The effect of some organized systems, including two neutral surfactants (Brij 35, Triton X-100), two cationic surfactants (tetrabutylammonium-bromide and cetyltrimethylammoniumbromide), and two anionic surfactants (heptanal sodium bisulfite (1-hydroxy-1-heptanesulphonic acid monosodium salt) and sodium dodecyl sulphate) and β -cyclodextrin upon the cited CL reaction was similarly investigated. As can be seen from Table 2, apart from Brij 35 most of these systems could not enhance CL emission; on the contrary, substantial signal decreases were noticed. About

35% of increase in CL intensity was observed by the Brij 35 surfactant. As the increase is not significant for determination, the micellar solutions were not used for further FI work.

3.2. Determination of hydrochlorothiazide

Under optimum conditions described above, the hydrochlorothiazide calibration graph was linear in the range 0.33–130 $\mu\text{mol l}^{-1}$ and the regression line was $I = 1.8155C + 6.4564$, $r = 0.9993$ ($n = 10$), where I is the relative peak intensity and C the concentration of hydrochlorothiazide. The relative standard deviation (RSD) for 10 $\mu\text{mol l}^{-1}$ hydrochlorothiazide was 2.4% ($n = 10$). The detection limit, defined as three times the standard deviation for the reagent blank signal is 0.15 $\mu\text{mol l}^{-1}$ hydrochlorothiazide.

Table 4
Determination of hydrochlorothiazide with amiloride and lisinopril in synthetic mixtures using the proposed method

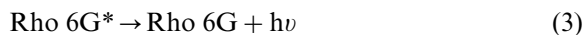
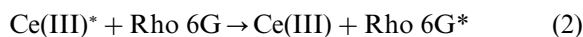
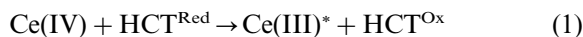
Amount added ($\mu\text{g ml}^{-1}$)		Amount found ($\mu\text{g ml}^{-1}$)		Recovery (%)
Hydrochlorothiazide	Amiloride	Hydrochlorothiazide	Hydrochlorothiazide	
0	8.0	0	—	—
4	8.0	4.39	109.2	109.2
4	4.0	4.26	106.1	106.1
4	1.6	4.14	103.0	103.0
4	0.8	3.96	99.2	99.2
4	0.4	3.98	100.5	100.5
4	0.2	4.04	101.3	101.3
Hydrochlorothiazide	Lisinopril	Hydrochlorothiazide	Hydrochlorothiazide	
0	120	0	—	—
4	120	3.96	99.5	99.5
4	90	4.08	102.8	102.8
4	60	4.11	103.1	103.1
4	30	3.99	100.7	100.7

Table 5
Determination of hydrochlorothiazide in pharmaceutical formulations

Sample	Amount (mg)		Official method found \pm SD ($n = 5$)	Added (mg)	Recovered (mg)	Recovery (%)
	Label	Proposed method found \pm SD ($n = 10$) ^a				
Dichlotride [®]	50.0	49 \pm 1	49 \pm 2	50	97.9	97.9
				100	155.8	106.8
				150	201.2	101.5
Zestoretic [®]	12.5	12.5 \pm 0.8	12 \pm 2	12.5	25.3	102.4
				25	36.6	96.6
				50	62.1	99.3

^a Data obtained by the determination of 10 independent samples (including sample preparation and measurements).

The mechanism of the CL reaction using Ce(IV) and the energy transfer to rhodamine dyes has been discussed [16]. The possible reactions are as following:



where, HCT, hydrochlorothiazide; Rho 6G, rhodamine 6G; $h\nu$, chemiluminescence emission; Red, reduced form; Ox, oxidized form.

3.3. Interference studies

The influence of commonly used excipients and additives in pharmaceutical dosage forms of hydrochlorothiazide was investigated in the determination of 10 $\mu\text{mol l}^{-1}$ hydrochlorothiazide. No interference was observed using the proposed method in the presence of lactose, mannitol, CaHPO_4 , magnesium stearate, KCl, maize starch and pregelatinized maize starch even when present in 100-fold excess. E110 (disodium-6-hydroxy-5-(4-sulphonatophenylazo) naphthalene-2-sulphonate) decreases the CL emission at a 100-fold higher concentration (1 mmol l^{-1}) than hydrochlorothiazide due to the deep orange colour of this dye, which results in the absorption of CL emission produced by the reaction of Ce(IV) with the analyte in the acidic medium. However, once the concentration of E110 is decreased to 0.1 mmol l^{-1} (1:10 ratio), no significant influence on

CL intensity is noticed. The results are shown in Table 3.

3.4. Application

In order to determine hydrochlorothiazide content in a mixture with lisinopril in tablet formulation, the interference of lisinopril with the hydrochlorothiazide CL reaction was examined. A 30-fold higher concentration of lisinopril did not cause significant interference in the determination of hydrochlorothiazide. Compared with only a 2-fold higher concentration of lisinopril in the pharmaceutical tablet, the proposed method was reliable for the analysis of hydrochlorothiazide in the mixture preparation. Similar experiments were carried out so as to investigate the feasibility of analysing preparations containing hydrochlorothiazide mixed with amiloride. The results listed in Table 4 show that, apart from two cases, no significant interference from amiloride was observed in the ratios listed, which offers the possibility of determining hydrochlorothiazide in the mixture preparation with amiloride. The cited interference of amiloride concentration in two cases was not relevant because the concentration of amiloride in tablet formulations is generally about 10-fold lower than hydrochlorothiazide. However, it should be noted that the antihypertensive thiol captopril has a significant effect on the determination of hydrochlorothiazide due to the CL reaction between captopril with Ce(IV) in the given CL system. A HPLC separation of captopril with

hydrochlorothiazide will be considered in future work.

The proposed method was successfully applied to the determination of hydrochlorothiazide alone and in a mixture formula containing 12.5 mg of hydrochlorothiazide and 20 mg of lisinopril (tablet formulation). The results of some synthetic mixtures are shown in Table 5. As can be seen, an acceptable correlation was found between the label values and the results obtained using the proposed method. In order to evaluate the validity of this method for hydrochlorothiazide determination in pharmaceuticals, recovery studies were carried out on samples where known amounts of hydrochlorothiazide were added. The recoveries for the different concentration levels varied from about 96–107%, as shown in Table 5. The reliability of the proposed method was also evaluated using an official method [8]. No significant differences were observed between the results obtained by the official method and the proposed method (Table 5). The method shows promise for routine control analysis of pharmaceutical preparations containing hydrochlorothiazide, or mixed with lisinopril. In view of the unpredictable effects on CL emission by decomposition products of the active principle, column liquid chromatographic analysis based on the proposed technique will be further evaluated.

Acknowledgements

The company Chemlab Instruments (The Netherlands) is greatly acknowledged for the use of their CL-based detector.

References

- [1] E. Martín, O. Hernández, F. Jiménez, J.J. Arias, *Anal. Lett.* 28 (1995) 1449.
- [2] J.M. Chillon, C. Capdeville-Atkinson, I. Lartaud, J. Guillou, P.M. Mertes, J. Atkinson, *Br. J. Pharmacol.* 107 (1992) 710.
- [3] G.M. Reaven, C. Clinkingbeard, J. Jeppesen, P. Maheux, D. Pei, J. Foote, C.B. Hollenbeck, Y.D. Chen, *Am. J. Hypertens.* 8 (1995) 461.
- [4] A.L. Magri, F. Balestrieri, A.D. Magri, D. Marini, *Talanta* 42 (1995) 1719.
- [5] A.L. Woodson, D.E. Smith, *Anal. Chem.* 42 (1970) 242.
- [6] J.T. Stewart, S.S. Clark, *J. Pharm. Sci.* 75 (1986) 413.
- [7] F.P. Bigley, R.L. Grob, G.S. Brenner, *Anal. Chim. Acta* 181 (1986) 241.
- [8] *British Pharmacopoeia*, HM Stationery Office, London, 1980.
- [9] P. Timmins, *Drug Dev. Ind. Pharm.* 12 (1986) 2301.
- [10] S. Erram, H.P. Tipnis, *Indian Drugs* 29 (1992) 553.
- [11] V. Ulvi, H. Keski-Hynnili, *J. Pharm. Biomed. Anal.* 12 (1994) 917.
- [12] W.R.G. Baeyens, D. De Keukeleire, K. Korkidis (Eds.), *Luminescence Techniques in Chemical and Biochemical Analysis*, Practical Spectroscopy Series, Marcel Dekker, New York, vol.12, 1991.
- [13] F. McCapra, I. Beheshti, in: K. Van Dyke (Ed.), *Bioluminescence and Chemiluminescence: Instruments and Applications*, CRC Press, Boca Raton, FL, vol.1, 1985, pp. 9–42.
- [14] W.K. Nonidez, D.E. Leyden, *Anal. Chim. Acta* 96 (1978) 401.
- [15] J.A. Holeman, N.D. Danielson, *Anal. Chim. Acta* 277 (1993) 55.
- [16] X.R. Zhang, W.R.G. Baeyens, G. Van Der Weken, A.C. Calokerinos, K. Nakashima, *Anal. Chim. Acta* 303 (1995) 121.
- [17] Z.D. Zhang, W.R.G. Baeyens, X.R. Zhang, G. Van Der Weken, *Analyst* 121 (1996) 1569.
- [18] Y. Zhao, W.R.G. Baeyens, X. Zhang, A.C. Calokerinos, K. Nakashima, G. Van Der Weken, *Analyst* 122 (1997) 103.

Full automated robotic method for the determination of chloride, nitrite and nitrate in cured meat products

A. Velasco-Arjona^a, J.A. García-Garrido^b, R. Quiles-Zafra^b,
M.D. Luque de Castro^{a,*}

^a Department of Analytical Chemistry, Faculty of Sciences, University of Córdoba, E-14004 Córdoba, Spain

^b Research Department, Navidul S.A., E-45500 Torrijos, Toledo, Spain

Received 6 June 1997; received in revised form 24 September 1997; accepted 2 October 1997

Abstract

A completely automated method to determine the most common parameters in cured meat products is proposed. The approach to full automation is based on the coupling of a robotic station for development of preliminary operations (namely weighing of the sample, grinding, leaching, filtration and transport to the aspiration zone) and a continuous unsegmented manifold for derivatisation and spectrophotometric monitoring of the reaction coloured products. This assembly works in an unattended fashion thus eliminating the bottleneck produced by the determination of these parameters in routine laboratories. The good agreement between results obtained by the proposed method and those from conventional methods for target analytes confirms its excellent performance and usefulness. © 1998 Elsevier Science B.V. All rights reserved.

Keywords: Robotic; Chloride–nitrite–nitrate; Meat; Continuous flow

1. Introduction

Curing is one of the most widely used technologies in meat manufacturing. The different curing modes (namely dry curing, wet curing, injection curing [1]) are based on the same principle, addition of a mixture of sodium chloride, either nitrite or nitrite plus nitrate salts to the fresh product. Even though the use of these curing agents involve some minor disadvantages, the advantages are so overwhelming [2] that no alternatives are

available at present. In the case of nitrite and nitrate, some of the most remarkable beneficial aspects of the curing process [3] are as follows; appearance of a red colour due to a reaction between muscular hemoglobin and the nitric oxide generated in nitrite reduction; reaction of nitrite and different compounds such as sugars, alcohols, amines, etc. to yield products which contribute to the typical aroma of meat cured products; antioxidant effect on lipid rancidity; antimicrobial activity, which hinders the growth of pathogenic microorganisms, such as *C. Botulinum*. The negative effects of curing anions only appear in products with excess amounts of

* Corresponding author. Tel.: +34 57 218615; fax: +34 57 218606; e-mail: qallucam@uco.es

these agents [4]. Some of the well-known undesirable effects are; the oxidant action of nitrite on the hemoglobin–Fe(II) complex, which can produce poisonous symptoms; formation of *N*-nitrosocompounds in the presence of both nitrosamine formers and acid pH; and the toxic action of nitrate, not per se but due to reduction to nitrite. For these reasons, the routine analysis of nitrite and nitrate is common practice in the meat industries in order to keep their levels within a range which ensures the development of the beneficial effects without the toxic aspects. The presence of sodium chloride in the curing process is advantageous, its protective effect hinders or makes it difficult for germ development by decreasing water activity; its conserving action by potentiating the effects of other preservative agents and inhibiting fungi and yeast proliferation, it also increases flavour. High salt concentration in cured products results in consumer rejection.

We have developed a fully automated method based on the coupling of a robotic station for sample weighing and pretreatment and a continuous flow system for derivatisation and detection in order to help big meat industries in the development of routine determinations of these three more commonly determined parameters.

2. Experimental section

2.1. Instruments and apparatus

The flow injection (FI) manifold was built using a Gilson Minipuls-HP3 peristaltic pump, a Rheodyne 5041 injection valve (adapted for use as switching valve), reduction columns of copperised cadmium of different lengths (1.8 mm i.d.) and a Pye Unicam SP6-500 spectrophotometer furnished with a Hellma 178. 12QS flow-cell and connected to the AD (Analog-Digital) converter of the PEC via its analog output for data acquisition, processing and delivery of the results via a computer program designed in our laboratory, which permits the use of so-called electronic dilution FIA technique [5–7]. All tubing used to construct the hydrodynamic system was of PTFE of 0.5 mm i.d.

The robotic station consisted of a Zymate II Plus robot (Zymark, Hopkinton), a System V controller, and the following peripherals.

2.1.1. Master laboratory station (MLS)

The proposed method uses two MLSs (MLS1 and MLS2), which consist of three syringes each, intended to dispense liquids in conjunction with the dilute and dissolve unit. Only two of the syringes of MLS1 were used, one of them was connected to a water bath and the other to a filter. Both were also connected to a dispenser; one of the syringe-dispenser assembly was used to dispense water; the other one to dispense filtered solution.

2.1.2. Small-size object all-purpose (SSOAP), big-size object all-purpose (BSOAP) and solid dispenser (SD) hands

The SSOAP hand allows the robot to seize centrifuge tubes and objects of similar size. The BSOAP hand allows the robot to seize 250 ml fleakers and objects of similar size. The SD hand (designed by the authors) allows the robot to manipulate solid samples. This hand is installed on the SSOAP hand forming 180° with its fingers and consists of a pair of tweezers which have a basket at their ends (see details in Fig. 1A).

2.1.3. Power and event controller (PEC)

The PEC module acts as an interface between the controller, peripherals and robot.

2.1.4. System V controller

This module sends orders to the rest of the units, including the robot and controls additional units such as a peristaltic pump, a photometer, switching valves, etc. The RS232 outputs of these units allow them to be operated by the System V via the PEC.

2.1.5. Balance

The balance plate for tube weighing was modified as shown in Fig. 1A (closer to the top of the balance), thus allowing the fleaker to be manoeuvred to and from the balance by the robot.

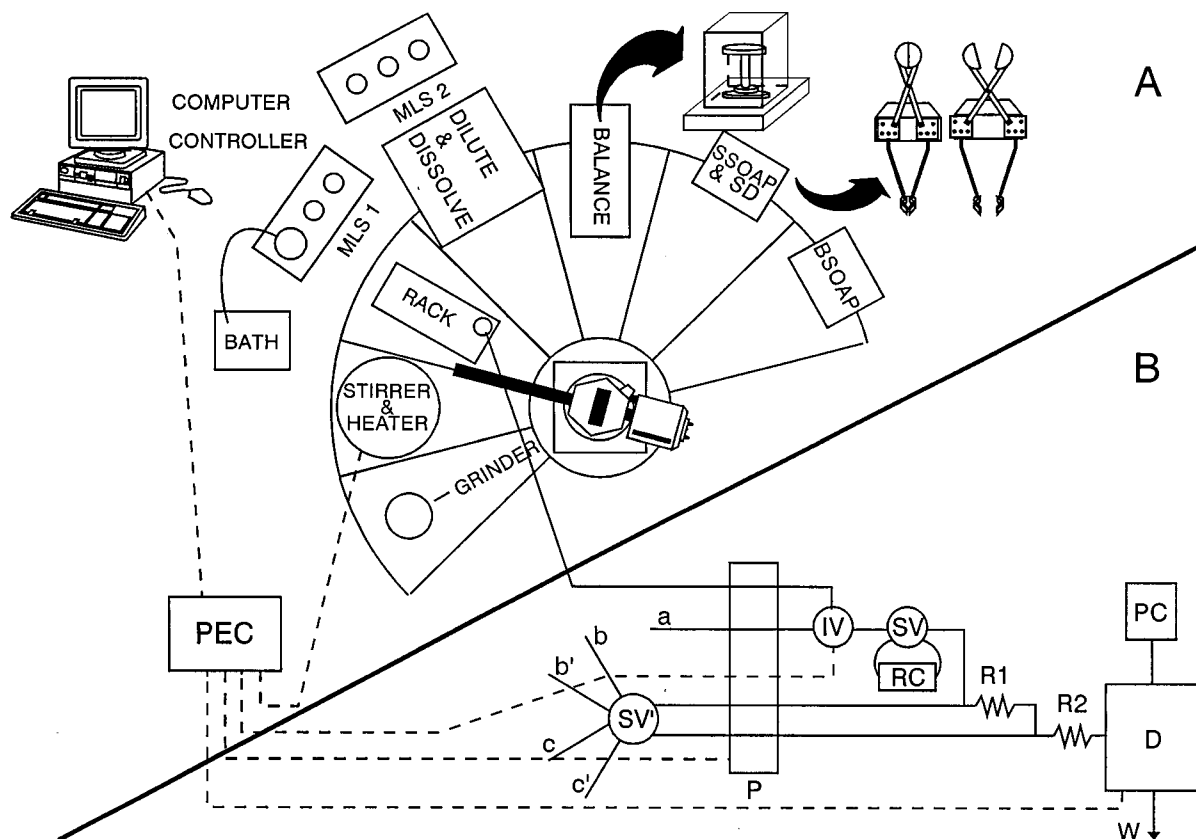


Fig. 1. Robotic station (A) coupled to a FI manifold (B) for the determination of nitrate, nitrite and chloride in cured meat products. MLS, master laboratory station; SSOAP, small-size object all-purpose hand; BSOAP, big-size object all-purpose hand; SD, solid dispenser hand; PEC, power and event controller; IV, injection valve; SV, selecting valve; RC, redox column; R, reactor; PC, personal computer; D, detector; W, waste; A, carrier solution; b, and c, reagents.

The following units in the flow manifold are also controlled by the robotic station: The peristaltic pump, the HPLC injector (only its valve is employed for automatic injection of the sample into the FI system), the injection valves used as switching valves and the photometer. The controller also makes absorbance readings at short intervals and stores that which is followed by a lower value; that is the maximum absorbance.

In addition, an Agimatic-N stirrer, a coffee grinder and a Technicon stainless steel filter were used. The System V controller was interfaced to a Netset 286/400 personal computer.

2.2. Reagents and solutions

2.2.1. Sample pretreatment

A 5% di-sodium tetraborate decahydrate aqueous solution and Carrez reagents (a 15% potassium ferrocyanide aqueous solution and a 30% zinc acetate aqueous solution) are used.

2.2.2. Derivatisation

Manual method [8]. Determination of chloride, a 0.1 N AgNO_3 and a 10% K_2CrO_4 aqueous solution. Determination of nitrate and nitrite, 37 g l^{-1} CdSO_4 aqueous solution, 5% NH_4OH aqueous solution and Zambelli reagent

(52 ml of 1.18 g ml^{-1} HCl aqueous solution in a 100 ml volumetric flask is made to volume with distilled water). This solution is transferred to a 200 ml volumetric flask. Sulphanilic acid (1 g) and 1.5 g of phenol are added in this order while heating to 100°C . The solution is cooled down and made to volume with a saturated NH_4Cl aqueous solution. FI method. Determination of nitrate and nitrite, a $0.001 \text{ M HAcO} + 1 \text{ g l}^{-1} \text{ Na}_2\text{EDTA}$ solution is used as carrier. Sulphonylamide solution, a volume of 10 ml of HCl containing 0.95 g of sulphonylamide diluted to 250 ml with distilled water. *N*-1-naphthylethylenediamine solution, 0.36 g of *N*-1-naphthylethylene-diamine and 2.9 g of sodium chloride is made to volume with distilled water in a 250 ml volumetric flask. Copperisant solution, a $0.1 \text{ M Na}_2\text{EDTA} + 0.1\% \text{ CuSO}_4$ solution. Determination of chloride, 0.86 ml of concentrated HNO_3 added to an aqueous solution containing 0.086 g of potassium thiocyanate and 0.169 g of $\text{HgCl}_2 \cdot 2\text{H}_2\text{O}$ and then 12.650 g of $\text{Fe}(\text{NO}_3)_3 \cdot 9\text{H}_2\text{O}$ are added. The mixture is made to volume with distilled water in a 250 ml volumetric flask.

2.2.3. Preparation of the copperised minicolumns

FI method. A representative amount (ca. 10 g) of cadium granules are rinsed with a 1 N HCl solution and then with distilled water. The metal is placed in a precipitate vessel where 50 ml of a 0.1% CuSO_4 solution is added and then stirred until the blue colour of the solution disappears and then rinsed for 10 min with distilled water in order to remove all the semi-colloidal copper formed. The granules of the treated metal are packed in a cylindrical glass column which is coupled to the FI manifold.

Manual method. The column is packed with a bed of glass wool and then 20–25 cm of cadmium powder. The packed column is successively rinsed with a 0.1 N HCl solution, distilled water and a 5% NH_4OH solution.

All reagents were supplied by Merck.

2.3. Manual sample pretreatment and determination

2.3.1. Sample pretreatment

The meat sample is ground and homogenised. A representative amount (ca. 10 g) of the sample is

weighed (within 1 mg precision) and introduced into a 250 ml Erlenmeyer flask where 5 ml of 5% di-sodium tetraborate decahydrate solution and about 150 ml of distilled water at 60°C is added. The resultant suspension is maintained warm and stirred for 30 min, after which, it is transferred to a 200 ml volumetric flask and 2 ml of each Carrez reagent is added. The suspension is stirred, let cool down and made to volume. Then, it is filtered and the filtrate transferred to a 250 ml Erlenmeyer flask.

2.3.2. Determination of nitrite

Between 5 and 10 ml of filtrate is taken and introduced into a 25 ml volumetric flask. Distilled water ca. 20 ml and 1 ml of Zambelli reagent are added and the solution stirred, then stood at room temperature for 10 min. After this, 1 ml of an ammonia concentrated solution is added and made to volume with distilled water. It is let cool down for a further 10 min and the absorbance of the solution is then measured at 436 nm.

2.3.3. Determination of nitrate

The filtrate (20 ml) is transferred to a 25 ml Erlenmeyer flask. NH_4OH (5 ml) of a 5% solution is added and the mixture is heated until it starts to softly boil it is then passed through the cadmium column. The eluate is collected in a 100 ml volumetric flask. The column is rinsed for 3 min with hot water and the liquid is added to a volumetric flask which is then made up to volume. The nitrite obtained after this treatment is determined in solution by the method previously described.

2.3.4. Determination of chloride

The filtrate (10 ml), ca. 100 ml of distilled water and some drops of a 10% K_2CrO_4 solution are added to a 250 ml Erlenmeyer flask. This solution is titrated with 0.1 N AgNO_3 solution until a red colour appears.

2.4. Proposed procedure

2.4.1. Sample pretreatment

The robot gets the BSOAP hand, catches a 250 ml fleaker and tares it. The sample is ground using a coffee grinder connected to an AC output (AC2) of the PEC. After this, the robot takes the SSOAP

hand, adds the sample into the fleaker until the sample weight is between 10 and 12 g. The controller collects the weight-datum, and the robot takes the fleaker out from the balance, sets it under the dilute and dissolve dispenser, adds 5 ml of 5% sodium tetraborate solution inside the fleaker and then places it on the stirrer. It takes the distilled water dispenser, sets it over the fleaker and adds 150 ml of distilled water which is aspirated from a reservoir in a thermostated bath at 60°C. The controller drives the AC output (AC1) of the PEC, the stirrer is turned on and the sample stirred for 30 min maintaining the temperature at 60°C. The robot carries the fleaker from the stirrer and 2 ml of each Carrez reagent is added and then returns it to the stirrer for 20 s. Now, the robot catches the fleaker, places it in the rack and, once the solution is cooled down adds distilled water until the weight is 200 g, homogenises the solution by stirring, takes the filter, introduces it into the solution and acts on the MLS2 syringe, connected to the filter. The syringe is filled with filtered solution and emptied into a clean fleaker. This operation is repeated twice in order to rinse the filter from stuck particles. The filtered solution is aspirated to the continuous manifold.

The hydrodynamic system (FI configuration) for the determination of nitrite and nitrate is shown in Fig. 1B. Valve SV lets the sample merge directly with the reagents for nitrite determination (filling position). In the inject position the sample passes through the reduction column before mixing with the reagents. The original nitrite, and nitrite resulting from the reduction of nitrate are thus determined. The concentration of nitrate is calculated by the difference.

The continuous manifold for the determination of nitrate is also used for chloride determination. Sulphonylamide and *N*-1-naphthylethylenediamine solutions are exchanged by distilled water and chloride reagent solution, respectively. The carrier is distilled water in all instances.

2.4.2. Calibration

This is accomplished by running a calibration curve with seven standards every week. Three standards are inserted every day in order to correct the slope, if necessary.

2.4.3. Overall procedure

Once the filtrate has been acquired by the robot, it is aspirated by means of the aspiration probe connected to the injection valve of the flow injection manifold with the aid of the peristaltic pump. First, the nitrite is determined, then the nitrate, in both cases by interpolation of the peak absorbance of the sample in the corresponding calibration line stored in the computer, and finally the chloride is determined using electronic dilution for collection and data treatment.

2.4.4. Computer program for electronic dilution

Two main reasons make the use of a computer program necessary for chloride determination. (1) The wide determination range of this analyte (between 3 and 18% w/w) which makes mandatory signal measurement at times longer than the residence time without significant errors. (2) Management of the huge numbers of data obtained in routine analysis of a large series of samples (up to 400 sample day⁻¹).

Fig. 2 shows the flow-chart of the designed program. Signal–time data is collected by the computer at preset intervals from the maximum of the peak. This data is stored either for individual samples or batch samples. In the former case the computer works like a recorder. In the latter case the time at which the absorbance is measured is selected when the data from all the samples have been acquired. Depending on the concentration of the target sample, the time selected can correspond to the maximum or a longer time in the tail of the diagram where the absorbance is lower due to a higher dispersion. Once the time is selected, the computer provides the absorbance signal, which is imported to a LOTUS chart from which the calibration line corresponding to the selected time is run and the absorbance of the sample interpolated.

3. Results and discussion

3.1. Chemical systems

The determination of nitrite is based on the Griess reaction, adopting Shin's modification [9]

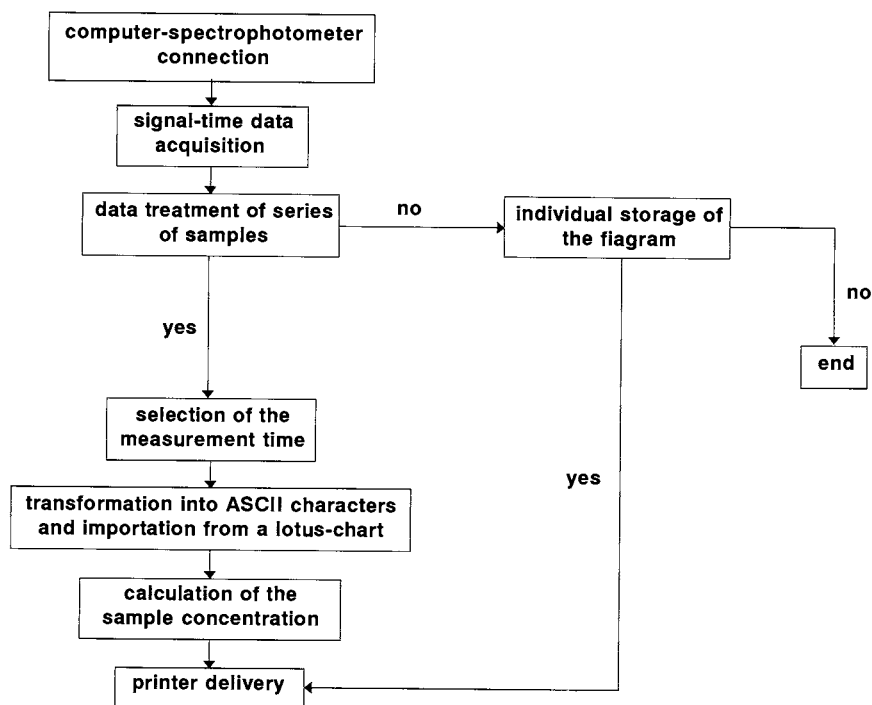


Fig. 2. Flow-chart of the computer program for electronic dilution.

in order to avoid the manipulation of carcinogenic reagents. The determination of nitrate is based on the same derivatisation reaction after reduction to nitrite. The determination of chloride is based on displacement of thiocyanate in the mercury–thiocyanate complex. Then, the displaced thiocyanate forms a red complex with ferric ion, which is monitored at 480 nm. As the overall process consists of two parts (discontinuous or robotic and continuous or FI), the optimisation of each was accomplished separately.

3.2. Discontinuous or robotic stage: sample pretreatment

A computer program was developed to control the different unitary operations (UOs) carried out by the robotic station. The performance of both the program and the different UOs was then checked.

In order to obtain a ground sample suitable for handling by the robot (not sticky mass but di-

vided in small particles) the grinding time must be short (about 10 s is sufficient).

The solutions were made to weight (as described in Section 2.4) rather than to volume as the robot was a sensorless device.

3.3. Determination step

Detailed methods for the determination of nitrite, nitrate and chloride by flow techniques are abundant in the literature. The ruggedness of the method for chloride is guaranteed because of its routine use since 1960 in segmented-flow analysers, and since 1975 in FI. As the aim of this research was focused on overall automation rather than the development of new determination methods, some variables such as reagent concentration, diameter of the tubing system, length of reactors and geometry of the reduction column were not optimised and the values developed by our research team in previous studies [10–12] were used (see Table 1).

Table 1
Optimum values of variables for the determination of NO_2^- , NO_3^- and Cl^-

Parameter	Optimum value
Injection volume ($\text{NO}_2^-/\text{NO}_3^-$) (μl)	100
Injection volume (Cl^-) (μl)	10
Flow-rate (ml min^{-1})	1.1
R1 length (cm)	15
R2 length (cm)	200
Column length (cm)	8.5
Column diameter (mm)	3

3.4. Features of the methods

3.4.1. Nitrite and nitrate determination

This method requires running three calibration lines. One for nitrate and two for nitrite (with and without passage of the sample through the reduction minicolumn). A series of solutions were prepared from solutions of both anions within a wide range of concentrations and subjected to sample pretreatment to minimise matrix effects. The data treatment gives the values shown in Table 2(A). Linear ranges between $0.1\text{--}15\text{ mg l}^{-1}$ for nitrite and between $0.5\text{ and }30\text{ mg l}^{-1}$ for nitrate were obtained. These ranges are appropriate for the determination of these anions in meat. The RSD obtained for 11 samples of 5 mg l^{-1} injected in

triplicate was lower than 1.5% in all instances. The sampling frequency was 30 h^{-1} .

3.4.2. Chloride determination

The characteristics of this system makes it necessary to run only one calibration line. The so called electronic dilution was used in order to adapt the method to the usual wide range of concentrations of this anion in meat (between 3 and 18% (w/w)). The data was acquired and processed using a computer program designed in our laboratory (see flow-chart in Fig. 2). Standards were prepared in a wide range of concentrations. The features of the calibration lines obtained at different times from the maximum of the transient signal are listed in Table 2(B).

3.5. Applications of the method to meat samples

The proposed method was validated by applying it to 10 samples of fresh and cured meat from Navidul. The content of the samples was also determined using the manual method. In both cases the concentrations are referred to the filtrated solution. The excellent agreement between both approaches is shown in Table 3, where the precision of the proposed method for each sample, expressed as SD, and that of the manual method, expressed as a reproducibility study during a

Table 2
Features of the methods

Anion	Linear range (mg l^{-1})	Calibration line		r	RSD(%)
		Slope	Intercept		
(A) Determination of NO_3^- and NO_2^-					
NO_2^- ^b	0.1–15	0.178	0.012	0.999	1.20 ^a
NO_2^- ^c	0.1–30	0.065	0.033	0.999	1.42 ^a
NO_3^-	0.5–30	0.022	0.005	0.999	1.31 ^a
(B) Determination of Cl^-					
t (s) ^d					
0	5–1000	1.473	63.5	0.99	0.18
20	6–1000	1.490	49.3	0.99	2.77
30	100–2000	0.300	34.8	0.99	3.77
400	500–4000	0.079	84.8	0.99	3.92

^a Values calculated from triplicate injection of 11 samples containing 5 mg l^{-1} of the target analyte.

^b Without passage through the minicolumn.

^c With passage through the minicolumn.

^d Time from the maximum

Table 3
Determination of NO_2^- , NO_3^- and Cl^- in meat

Samples	Concentration found					
	Proposed method			Manual method ^a		
	NO_2^- mg l ⁻¹	NO_3^- mg l ⁻¹	Cl^- g l ⁻¹	NO_2^- mg l ⁻¹	NO_3^- mg l ⁻¹	Cl^- g l ⁻¹
1	3.2 ± 0.2	46.2 ± 1.3	3.55 ± 0.05	3.1	45.4	3.65
2	2.2 ± 0.1	37.0 ± 1.2	3.35 ± 0.10	2.3	33.2	3.25
3	3.4 ± 0.2	49.2 ± 0.6	3.15 ± 0.05	3.4	42.0	3.05
4	3.8 ± 0.2	48.5 ± 0.9	3.20 ± 0.05	2.7	47.7	3.25
5	3.6 ± 0.3	41.4 ± 1.2	3.85 ± 0.15	2.6	35.1	3.60
6	2.7 ± 0.2	25.4 ± 1.0	3.35 ± 0.10	2.7	23.4	3.35
7	2.5 ± 0.1	48.8 ± 1.3	3.50 ± 0.10	3.8	58.9	3.50
8	1.9 ± 0.1	44.9 ± 0.8	2.85 ± 0.15	2.7	41.1	2.85
9	5.3 ± 0.3	35.1 ± 1.0	3.50 ± 0.05	3.5	28.9	3.50
10	3.7 ± 0.2	47.1 ± 1.1	3.35 ± 0.05	3.3	46.7	3.35

^a The 1-month reproducibility ($n = 7$) was as follows: RSD (NO_2^-) = 5.5%; RSD (NO_3^-) = 3.5%; RSD (Cl^-) = 0.5% for 1.4 mg l⁻¹, 3.1 mg l⁻¹ and 3.55 g l⁻¹, respectively.

month, demonstrated that the automatic method is more precise than its manual counterpart.

4. Conclusions

A completely automated method for the determination of nitrite, nitrate and chloride in cured meat based on the coupling of discontinuous (robotic)/continuous (flow injection) automated alternatives is proposed.

The assembly works in an unattended fashion thus eliminating human intervention with results in a subsequent decrease in the overload created in routine laboratories.

The method also allows a reduction in analysis time, as the conventional method involves a number of steps which are deleted in the automated counterpart. This shortening in the time required for the overall process is mainly due to the faster development of the derivatisation/monitoring step, which takes place in non-equilibrium conditions characteristic of FI methods. A decrease in the time required for this step from 20 to 3 min was achieved.

The time required for the development of the robotic preliminary operations is similar to that required by the conventional method, the most significant advantage of its implementation being

the elimination of human intervention which makes a 24 h working-day feasible.

Acknowledgements

The authors are grateful to the Spanish Dirección General de Investigación Científica y Técnica (DGICYT) for financial support in the form of Grant PB96/0505.

References

- [1] K. Möhler, *El curado*, Editorial Acirbia, Zaragoza, Spain, 1982.
- [2] L. Tóth, *Fleischwirtsch* 63 (1993) 208.
- [3] S.H. Lee, R.G. Cassens, O.R. Fenneman, *J. Food Sci.* 41 (1976) 969.
- [4] W. Vösgen, *Fleischwirtsch* 72 (1992) 1675.
- [5] J. Ruzicka, *Philos. Trans. R. Soc. London* 5 (1982) 645.
- [6] J. Ruzicka, E.H. Hansen, *Anal. Chim. Acta* 145 (1983) 1.
- [7] S. Olsen, J. Ruzicka, E.H. Hansen, *Anal. Chim. Acta* 136 (1982) 101.
- [8] N.W. Hanson (Ed.), *Official, Standardised and Recommended Methods of Analysis*, The Society for Analytical Chemistry, 2nd ed. London, 1973, pp. 155 and 158–160.
- [9] M.B. Shinn, *Ind. Eng. Chem. Anal. Educ.* 13 (1941) 33.
- [10] F. Cañete, A. Ríos, M.D. Luque de Castro, M. Valcárcel, *Analyst* 113 (1988) 739.
- [11] B. Bermúdez, A. Ríos, M.D. Luque de Castro, M. Valcárcel, *Talanta* 35 (1988) 810.
- [12] J.S. Cosano, J.L. Calle, J.L. Pinillos, P. Linares, M.D. Luque de Castro, *Téc. Lab.* 147 (1989) 32.

Kinetic and equilibrium studies on mercury(II)-coproporphyrin-I. Metal ion exchange reaction with cobalt(II) and application to determination of trace mercury(II)

Rita Giovannetti ^{a,*}, Vito Bartocci ^b

^a *Centro Interdip. Grandi Apparecchiature, P.le G. da Varano, Università degli Studi di Camerino, 62032, Camerino, Italy*

^b *Dipartimento di Scienze Chimiche, Via S. Agostino 1, Università degli Studi di Camerino, 62032, Camerino, Italy*

Received 8 July 1997; received in revised form 1 October 1997; accepted 2 October 1997

Abstract

The reaction of 3,8,13,18-tetramethyl-21H,23H-porphine-2,7,12,17-tetrapropionic acid or coproporphyrin-I (CPI) with mercury(II) was studied spectrophotometrically, and kinetic and equilibrium constants were determined; the influence of temperature on the reaction rate was also studied. It was verified that mercury(II) accelerates the incorporation reaction of cobalt(II) into CPI; the kinetics and mechanism of this reaction at high alkaline pH were studied. Sensitive kinetic methods for the determination of mercury(II) at ppb levels have been established; the apparent molar absorptivity and Sandell's sensitivity for the recommended procedure, at 368 nm, and 400 s after the start of the reaction, were: 4.23×10^5 ($1 \text{ mol}^{-1} \text{ cm}^{-1}$) and 0.474 (ng cm^{-2}) (for $A = 0.001$). © 1998 Elsevier Science B.V. All rights reserved.

Keywords: Mercury(II); Cobalt(II); Spectrophotometry; Coproporphyrin-I

1. Introduction

In recent years many articles and reviews have been published on the mechanisms and kinetics of metal-ion incorporation reactions into the porphyrin nucleus [1–5]. The rate of metallo-porphyrin formation is generally much slower than that of complex formation with other open-chain ligands [6] and, in order to study these reactions, different organic catalysts such as pyridine and

imidazole have been proposed [7–9]; these reactions can also be accelerated using several metal-ions with high atomic radii, such as mercury(II), cadmium(II) and lead(II) [10–14]. In fact the coordination reactions of these metal-ions are very fast and cause the deformation of porphyrin ring helping the attack from the back side of other metal-ions with smaller ionic radii. This property has been suitably used for the catalytic determination of low concentrations of different metals [12,14,15].

In this paper we detail a study on the reaction mechanism of 3,8,13,18-tetramethyl-21H,23H-

* Corresponding author. Tel.: +39 737 40369; fax: +39 737 40370.

porphine-2,7,12,17-tetrapropionic acid or coproporphyrin-I (CPI) with mercury(II), the aim being to determine the equilibrium and kinetic constants of the reaction. The catalytic effect of mercury(II) on the formation of $\text{Co}^{\text{II}}(\text{CPI})$ complex, highlighting the presence of the reactive intermediate $\text{Hg}^{\text{II}}(\text{CPI})$, was also studied and a reaction mechanism was suggested. On the basis of these results a kinetic method for the spectrophotometric determination of sub-microgram amounts of mercury(II), founded on the catalytic effect of mercury(II) on the $\text{Co}^{\text{II}}(\text{CPI})$ complex formation, was developed. The optimum conditions for the determination of mercury(II) was discussed.

2. Experimental

2.1. Reagents

All reagents were of analytical-reagent grade and used without further purification. All the solutions were prepared using ultrapure water treated by a Milli-Q-Plus 185.

2.1.1. CPI solution

Stock solution containing $4.40 \times 10^{-5} \text{ mol l}^{-1}$ was prepared by dissolving 16.0 mg of CPI–dihydrochloride in 500 ml of 4.8 mmol l^{-1} sodium hydroxide solution.

2.1.2. Standard mercury(II) and cobalt(II) solutions

Stock aqueous solutions containing ca. 5 or 0.05 mmol of HgCl_2 and ca. 4 mmol $\text{CoCl}_2 \cdot 6\text{H}_2\text{O}$ per litre, and sufficient nitric acid to prevent precipitation, were prepared; these solutions were standardized by ICP.

2.2. Apparatus

Absorption spectra were recorded on a Hewlett–Packard 8452A diode array spectrophotometer with a 1 cm quartz cell connected to Lauda K2R thermostat. The pH values were determined using a Metrohm 655 pH meter with a combined electrode (Inlab 413). The stock metal solutions were standardized by an Inductively Coupled Plasma (ICP) Jobin Yvon JY 24R.

2.3. Recommended procedure for catalytic determination of mercury(II)

The reactions were started by mixing (with magnetic stirring) 2 ml of an alkaline CPI solution ($\text{NaOH } 0.5 \text{ mol l}^{-1}$) with 20 μl of a solution containing cobalt(II) and up to 75 μl of mercury(II) solutions. The rates of the $\text{Co}^{\text{II}}(\text{CPI})$ complex formation was monitored spectrophotometrically by recording the disappearance of free CPI at 368 nm (λ_{max} of CPI) or the increase of $\text{Co}^{\text{II}}(\text{CPI})$ at 412 nm (λ_{max} of $\text{Co}^{\text{II}}(\text{CPI})$), as a function of mercury(II) concentrations, at fixed times. The absorbances were measured in a 10-mm thermostated cell at 20°C and at ionic strength of 0.5 mol l^{-1} , against blank.

3. Results and discussion

3.1. Determination of the stability constant of $\text{Hg}^{\text{II}}(\text{CPI})$ complex

Aqueous solutions of CPI at high alkaline pH, ionic strength of 0.5 mol l^{-1} and temperature of 20°C, was pale pink and presented absorption maxima at 368 nm (Soret band; $\epsilon = (1.015 \pm 0.006) \times 10^5$), 500, 538, 558 nm, and a shoulder of about 606 nm. Adding excess mercury(II), the colour of the solution changed to yellow and the resulting spectrum showed absorption maxima at 348, 414 nm (Soret band; $\epsilon_{348} = (3.392 \pm 0.032) \times 10^4$, $\epsilon_{414} = (5.707 \pm 0.033) \times 10^4$), 538 and 558 nm. The spectra of CPI and $\text{Hg}^{\text{II}}(\text{CPI})$ complex are shown in Fig. 1.

The stoichiometry of the of $\text{Hg}^{\text{II}}(\text{CPI})$ formation reaction, has been determined, applying two different experiments, the Job method in which the sum of metal ion and ligand concentrations ($C_{\text{Hg}} + C_{\text{CPI}}$) were 8.796×10^{-6} or $4.398 \times 10^{-6} \text{ mol l}^{-1}$; the results suggest the formation of a 1:1 complex (Fig. 2).

It was previously reported that mercury(II) does not fit well into the porphyrin core and is displaced over its plane forming 1:1, 2:1 and 3:2 species (mercury(II)/porphyrins), that changed at alkaline pH into a 1:1 complex [4]. For this reason the equilibrium between mercury(II) and CPI, in

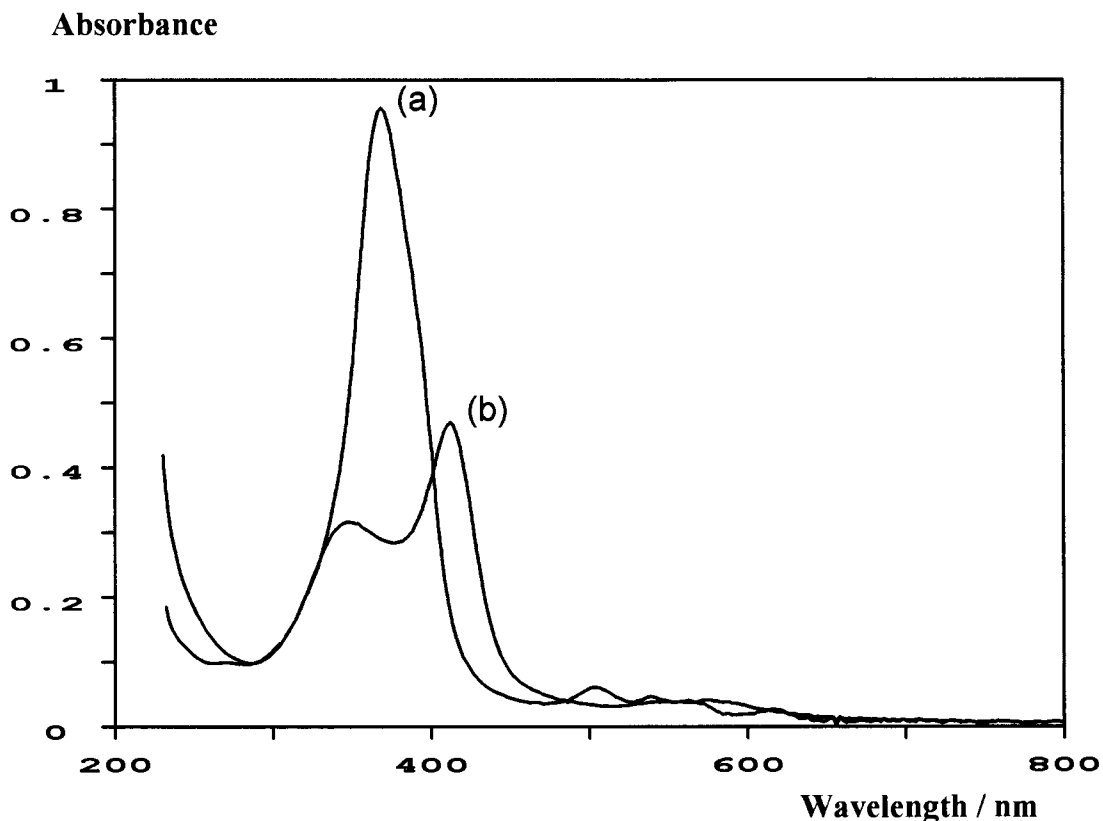
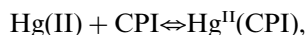


Fig. 1. Absorbance spectra of 8.796×10^{-6} M CPI (a) and 8.796×10^{-6} M $\text{Hg}^{\text{II}}(\text{CPI})$ (b), at 0.5 mol l^{-1} ionic strength ($T = 20^\circ\text{C}$).

0.5 mol l^{-1} NaOH can be represented by the equation



and the equilibrium constant,

$$K = [\text{Hg}^{\text{II}}(\text{CPI})][\text{Hg}(\text{II})]^{-1}[\text{CPI}]^{-1}$$

where $[\text{Hg}(\text{II})]$ and $[\text{CPI}]$ denote the equilibrium concentrations of Hg(II) and CPI respectively. Mercury(II) is known to form numerous hydroxo complexes as a function of pH and concentration [16], in the studied equilibrium, at alkaline pH, it was mainly in the form of $\text{Hg}(\text{OH})_2(\text{aq.})$, $\text{Hg}^{\text{II}}(\text{CPI})$ must be considered as mercury(II) hydroxo–CPI complex; consequently, the corresponding equilibrium constant known as the ‘conditional’ constant. The presence of chloro-complexes in this alkaline medium can be excluded [17]. In order to calculate the stability constant, this reaction was studied at mercury(II)

concentrations of 2.199×10^{-6} – 1.992×10^{-3} mol l^{-1} and CPI concentrations of 2.199×10^{-6} – 1.759×10^{-5} mol l^{-1} . When $C_{\text{Hg}} = C_{\text{CPI}}$ and $[\text{Hg}(\text{II})] = [\text{CPI}]$, the stability constant K can be calculated from the intercept of the straight line obtained by plotting $\log[\text{Hg}^{\text{II}}(\text{CPI})]$ versus $2 \cdot \log[\text{CPI}]$, where $[\text{Hg}^{\text{II}}(\text{CPI})] = (A_1 - A_2)/(\epsilon_{\text{CPI}} - \epsilon_{\text{HgCPI}})$ and $[\text{CPI}] = C_{\text{CPI}} - [\text{Hg}^{\text{II}}(\text{CPI})]$, where A_1 and A_2 denote the absorbance in the absence and presence of mercury(II), ϵ_{CPI} and ϵ_{HgCPI} the absorbivities of CPI and complex, respectively, at $\lambda = 368 \text{ nm}$ (corresponding to CPI absorbance maximum). The value of K was $(2.64 \pm 0.01) \times 10^3 \text{ l mol}^{-1}$.

When $C_{\text{Hg}} \gg C_{\text{CPI}}$,

$$[\text{Hg}^{\text{II}}(\text{CPI})] = \frac{A_1 - \epsilon_{\text{CPI}}C_{\text{CPI}}}{(\epsilon_{\text{HgCPI}} - \epsilon_{\text{CPI}})}$$

and

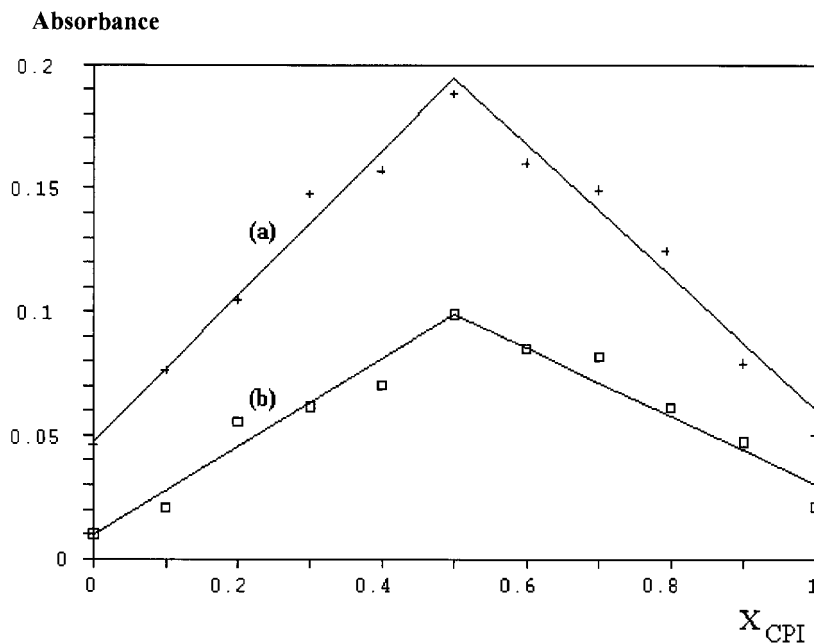


Fig. 2. Job's diagram for the reaction between CPI and Hg(II) at 0.5 mol l^{-1} ionic strength ($T = 20^\circ\text{C}$). $C_{\text{Hg}} + C_{\text{CPI}} = 8.796 \times 10^{-6} \text{ mol l}^{-1}$, $\lambda = 414 \text{ nm}$ (a) and 368 nm (b).

$$[\text{CPI}] = \frac{(\varepsilon_{\text{HgCPI}}C_{\text{CPI}} - A_l)}{(\varepsilon_{\text{HgCPI}} - \varepsilon_{\text{CPI}})},$$

where A_l is the absorbance measured at 414 nm (corresponding to $\text{Hg}^{\text{II}}(\text{CPI})$ absorption maximum); the value of K obtained by plotting $\log[\text{Hg}^{\text{II}}(\text{CPI})]$ versus $\log[\text{CPI}]$, was $(2.56 \pm 0.01) \times 10^3 \text{ l mol}^{-1}$, is in good agreement with previous results.

3.2. Reaction rate for the formation of $\text{Hg}^{\text{II}}(\text{CPI})$ complex

The reaction of CPI with mercury(II) studied at six different 1:1 ratios at concentrations of $2.199 - 8.796 \times 10^{-6} \text{ mol l}^{-1}$, at alkaline solutions and temperature of 20°C , was completed within 100 s . The results obtained are shown in Fig. 3 where the values of $[\text{Hg}^{\text{II}}(\text{CPI})]$ against time are reported, the reaction rate increases with the concentration of the reaction product as a typical autocatalytic reaction [18]. In this case, the kinetic equation for the reaction is given by:

$$-d[\text{CPI}]/dt = k_3 [\text{CPI}][\text{Hg}^{\text{II}}][\text{Hg}^{\text{II}}(\text{CPI})]$$

where k_3 represents the 'conditional' rate constant. Since we have carried out measurements at $C_{\text{Hg}} = C_{\text{CPI}}$, the kinetic equation has been changed

$$-d[\text{CPI}]/dt = k_3 [\text{CPI}]^2[\text{Hg}^{\text{II}}(\text{CPI})],$$

integration between t_1 and t gives,

$$-K_3 t = \frac{1}{C_{\text{CPI}}^2} \ln \frac{C_{\text{CPI}} - [\text{CPI}]_{t_1}}{C_{\text{CPI}} - [\text{CPI}]_t} \cdot \frac{[\text{CPI}]_t}{[\text{CPI}]_{t_1}} + \frac{1}{C_{\text{CPI}}^2} \left(\frac{C_{\text{CPI}}}{[\text{CPI}]_{t_1}} - \frac{C_{\text{CPI}}}{[\text{CPI}]_t} \right).$$

Plotting the right term of the equation versus time, for different 1:1 concentration ratios of metal and ligand, we obtained good straight lines, the slopes of which represent the values of the rate constant k_3 , confirming presence of an autocatalytic reaction. The average value of k_3 , from the mean of six experiments, at 20°C , was $(2.463 \pm 0.051) \times 10^9 \text{ l}^2 \text{ mol}^{-2} \text{ s}^{-1}$ and the constant for the reverse reaction, got from $k_{-3} = k_3/K$, was $9.329 \times 10^{-5} \text{ l mol}^{-1} \text{ s}^{-1}$.

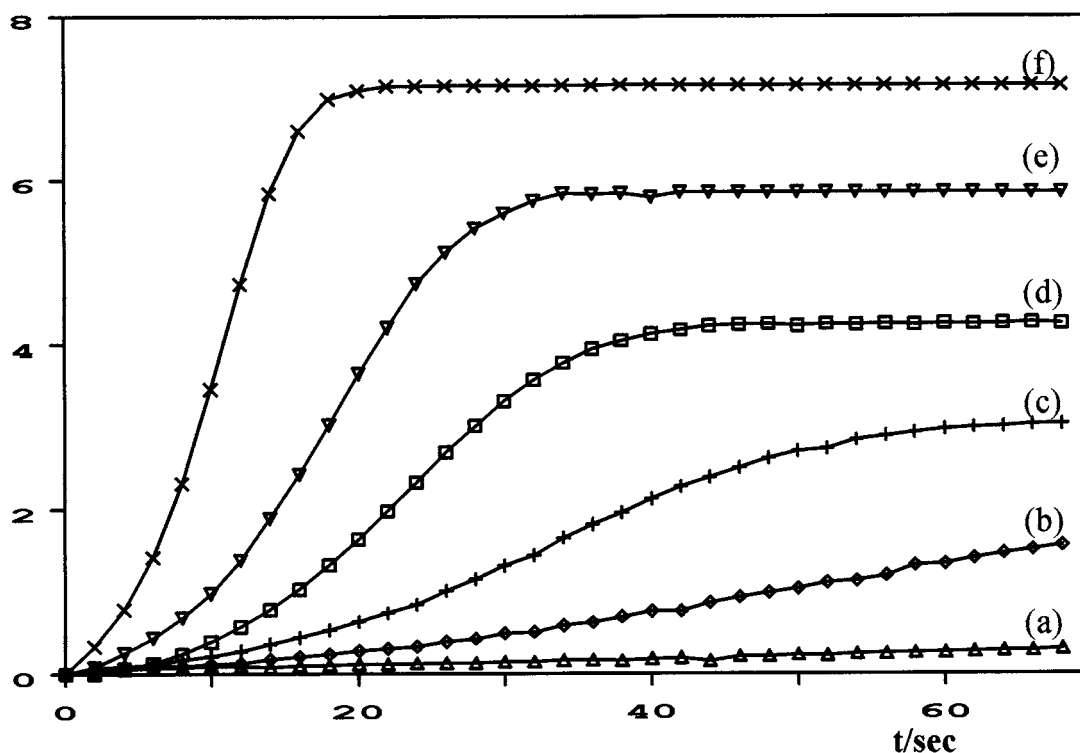
$10^6 [\text{Hg}^{\text{II}}(\text{CPI})] / \text{mol l}^{-1}$


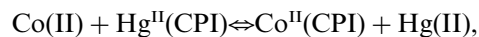
Fig. 3. Change of $[\text{Hg}^{\text{II}}(\text{CPI})]$ against time for different $\text{CPI} = \text{Hg}(\text{II})$ concentrations: (a) 2.20×10^{-6} ; (b) 3.08×10^{-6} ; (c) 4.40×10^{-6} ; (d) 6.60×10^{-6} ; (e) 7.50×10^{-6} ; (f) $8.80 \times 10^{-6} \text{ mol l}^{-1}$. Ionic strength, 0.5 mol l^{-1} ($T = 20^\circ\text{C}$).

Measurements performed at temperatures of 5–35°C have shown an increase in the reaction rate (about 0.2 times per degree). Plots of $\ln k_3$ against $1/T$ at different wavelengths, enables the activation energy E_a to be determined according to the well-known relationship, $\ln k_3 = \ln A - (E_a/RT)$. The mean value for a series of five measurements was $E_a = (4.234 \pm 0.026) \times 10^4 \text{ J mol}^{-1}$.

3.3. Catalytic effect of mercury(II) on the formation of $\text{Co}^{\text{II}}(\text{CPI})$ complex

The rate of $\text{Co}^{\text{II}}\text{CPI}$ complex formation was very low [9] but could be accelerated in the presence of mercury(II). The reaction of CPI ($2.099 \times 10^{-6} \text{ mol l}^{-1}$) with cobalt(II) ($3.914 \times 10^{-5} \text{ mol l}^{-1}$) was studied in the presence of mercury(II) concentrations from 4.750×10^{-7} to 1.782×10^{-6}

mol l^{-1} in $\text{NaOH } 0.5 \text{ mol l}^{-1}$. The rate of CPI complex formation with cobalt(II) was monitored spectrophotometrically every 3 s at 20°C, by measuring the change in absorbance at 412 and 368 nm for the $\text{Co}^{\text{II}}(\text{CPI})$ complex and CPI respectively. Fig. 4 shows this change in absorbance against time, in which biphasic kinetic behaviour can be observed. The first-step reaction was completed in a few seconds, and was related to the formation of the $\text{Hg}^{\text{II}}(\text{CPI})$ complex with third order kinetics, as described above; the second-step corresponded to $\text{Hg}^{\text{II}}(\text{CPI})$ disappearance, and to the simultaneous formation of $\text{Co}^{\text{II}}(\text{CPI})$ by the exchange reaction,



with a second order kinetic according to the equation:

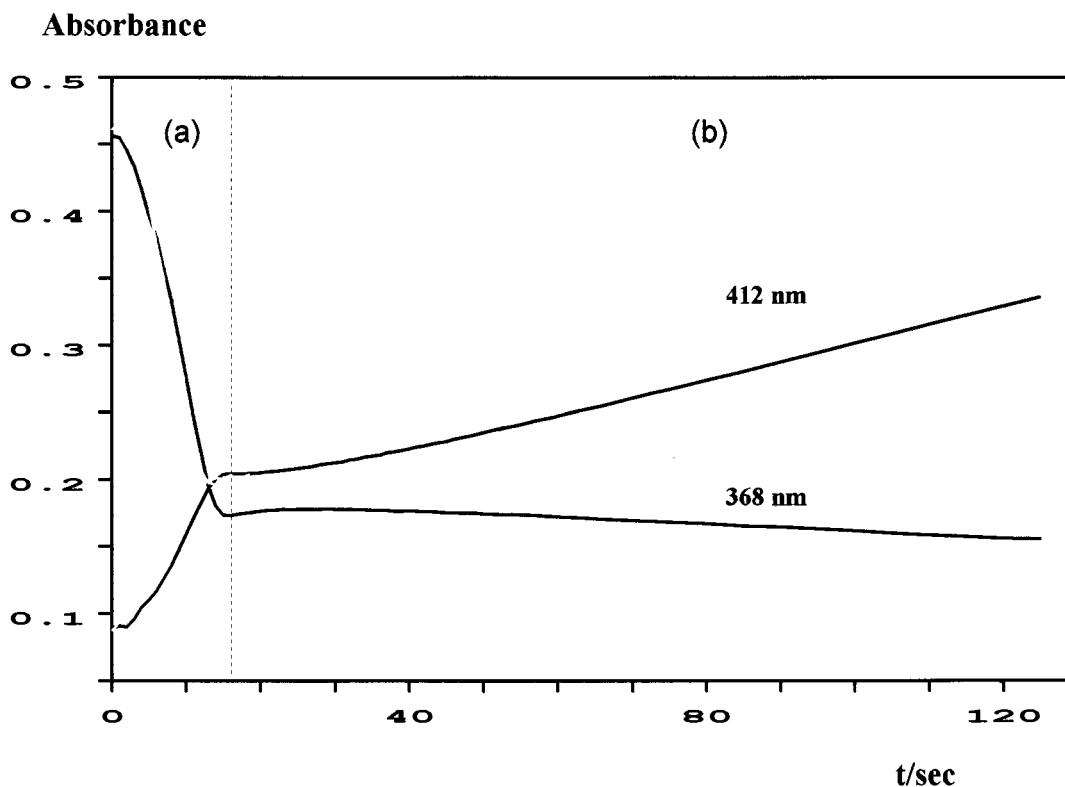


Fig. 4. Typical kinetic runs showing the two-step reaction of CPI with Co(II) in the presence of Hg(II). [CPI] = 4.31×10^{-6} mol l^{-1} , [Co(II)] = 4.02×10^{-5} mol l^{-1} , [Hg(II)] = 4.89×10^{-5} mol l^{-1} , ionic strength, 0.5 mol l^{-1} ($T = 20^\circ C$). (a) First step: $CPI + Hg(II) \rightarrow Hg^{II}(CPI)$; (b) second step: $Hg^{II}(CPI) + Co(II) \rightarrow Co^{II}(CPI) + Hg(II)$.

$$\begin{aligned} -\frac{d[Co^{II}(CPI)]}{dt} &= -\frac{d[Hg^{II}(CPI)]}{dt} \\ &= k_2[Co(II)][Hg^{II}(CPI)] \end{aligned}$$

The rate constant k_2 was determined from the slope of the straight line obtained from the plot

$$\frac{1}{(C_{Co} - C_{HgCPI})} \ln \frac{[Co(II)]}{[Hg^{II}(CPI)]} \text{ vs. } t,$$

where,

$$[Co(II)] = C_{Co} - \frac{A_t - A_\infty}{\epsilon_{CPI} - \epsilon_{CoCPI}}$$

and

$$[Hg^{II}(CPI)] = \frac{A_t - A_\infty}{\epsilon_{CPI} - \epsilon_{CoCPI}}$$

C_{Co} and [Co(II)] denote the total and the equilibrium concentrations of Co(II) and ϵ_{CoCPI} the

molar absorptivity of the $Co^{II}(CPI)$ complex. The value of k_2 at $20^\circ C$, obtained from a mean of four measurements, was $(2.25 \pm 0.04) \times 10^7$ $l \text{ mol}^{-1} \text{ s}^{-1}$.

3.4. Catalytic determination of mercury(II)

3.4.1. Calibration graphs

In an alkaline medium the rate constant of $Co^{II}(CPI)$ formation depends only on the mercury(II) concentration, therefore this metal-ion can be determined by means of its catalytic effect. The reaction of CPI (4.198×10^{-6} mol l^{-1}) with cobalt(II) (3.914×10^{-5} mol l^{-1}) was studied in the presence of mercury(II) concentrations from 0 to 1.785×10^{-6} mol l^{-1} . The increase of absorbance at 412 nm (ΔA_{412}) or its decrease at 368 nm (ΔA_{368}) measured at two fixed times (300 and 400 s) depends on the concentration of mer-

cury(II), the plots of these (ΔA) values against [Hg(II)] gave good straight lines. Apparent molar absorptivities ($l \text{ mol}^{-1} \text{ cm}^{-1}$) and Sandell's sensitivities (ng cm^{-2}) of the calibration graphs at 412 nm were 2.54×10^5 , 0.789 (after 300 s), 3.67×10^5 and 0.546 (after 400 s), while at 368 nm, 3.24×10^5 and 0.619 (after 300 s), 4.23×10^5 and 0.474 (after 400 s). The equations for the straight lines, obtained according to the procedure described were,

- after 300 s Hg(II) (ng ml^{-1}) = 619 (ΔA_{368}) = 789 (ΔA_{412})
- after 400 s Hg(II) (ng ml^{-1}) = 474 (ΔA_{368}) = 546 (ΔA_{412})

The suggested kinetic method allowed the determination of small amounts of mercury(II) with a detection limit of $3.5 \times 10^{-9} \text{ mol l}^{-1}$. The present method obtained detection limit similar to that described by Tabata and Tanaka [12] where similar results were obtained but with a ten fold pre-concentration of the sample by distillation.

3.4.2. Effect of foreign ions

Synthetic solutions containing mercury(II) (7.140×10^{-7} and $1.070 \times 10^{-6} \text{ mol l}^{-1}$), cobalt(II) ($3.914 \times 10^{-5} \text{ mol l}^{-1}$), and various amounts of foreign ions were prepared. The effects of foreign ions according to the procedure described, were examined. The tolerance limits of foreign ions are summarized in Table 1. Pd(II) and Fe(II) interfere with the determination, but the interference of Pd(II) can be re-

Table 1
Tolerance limits of foreign ions for the determination of mercury(II) ($7.140 \times 10^{-7} \text{ mol l}^{-1}$) at 20°C

Tolerance limit ($\text{mol}^{-1} \text{ l}$)	Ion
4.0×10^{-3}	Ca(II), Mg(II), Sr(II), Ba(II)
1.0×10^{-4}	Fe(III)
1.0×10^{-6}	Mn(II), Cu(II), Ni(II)
5.0×10^{-7}	Cd(II), Pb(II), Zn(II)
1.0×10^{-2}	F ⁻ , NO ₃ ⁻ , I ⁻ , Br ⁻ .
5.0×10^{-2}	Cl ⁻
4.0×10^{-4}	SO ₄ ²⁻

moved by adding 0.01 mol l^{-1} potassium iodide, while Fe(II) can be initially oxidated to Fe(III). The results obtained using the proposed kinetics has given values with a standard deviation lower than 2%.

4. Conclusions

The kinetic study of equilibrium between mercury(II) and CPI at alkaline pH, has emphasized the formation of 1:1 complex (Hg^{II}(CPI)) with a constant of $K = (2.64 \pm 0.01) \times 10^3 \text{ l mol}^{-1}$. The study of the mechanism has shown that this reaction is autocatalytic with kinetics of a third order with respect to Hg^{II}(CPI), CPI and mercury(II) concentrations.

Mercury(II) significantly accelerates the rate of the reaction of cobalt(II) with CPI to give Co^{II}(CPI); to highlight this increase with respect to the uncatalyzed reaction, we have contrasted this result with that obtained by other authors [9], although in different conditions, the rate can become about 10^7 times faster. In the study of this reaction biphasic kinetics was observed: in the first-step Hg^{II}(CPI) was formed, while in the second-step Hg^{II}(CPI) reacted with cobalt(II), (a metal substitution reaction) to give Co^{II}(CPI) and mercury(II). In the first-step the formation of Hg^{II}(CPI) was favoured, for the higher reaction rate with respect to Co^{II}(CPI); mercury(II) does not fit well in CPI and was displaced over the porphyrin plane, deforming CPI in the second-step, promoted the incorporation of cobalt(II). As was observed, deformation of the porphyrin plane is the most important factor governing the reaction mechanism [4].

The absorbance of the Co^{II}(CPI) complex at 412 nm (λ_{max}) depends only on the mercury(II) concentration allowing the determination of mercury(II) by means of its catalytic effect. Trace amounts of mercury(II) at concentration as low as $10^{-9} \text{ mol l}^{-1}$ on the basis of a clearly defined chemical reaction can be determined with high sensitivity. Recovery tests for mercury(II) in synthetic solutions in the presence of

various cations and anions was 98–102%. The present method permitted quick determination of mercury(II) at ppb levels without manipulation of the samples: only 400 s for each measurement on the calibration graph are necessary.

The best experimental conditions can be easily set, knowing the rate and equilibrium constants.

References

- [1] M. Tabata, *J. Mol. Liq.* 65/66 (1995) 221.
- [2] P. Hambright, in: K.M. Smith (Ed.), *Porphyryns and Metalloporphyryns*, Elsevier, Amsterdam, 1975.
- [3] P. Hambright, P.B. Chock, *J. Am. Chem. Soc.* 96 (1974) 3123.
- [4] M. Tabata, W. Miyata, N. Nahar, *Inorg. Chem.* 34 (1995) 6492.
- [5] D.K. Lavallee, *Coord. Chem. Rev* 61 (1985) 55.
- [6] D.W. Margerum, G.R. Cayley, in: A.E. Martell (Ed.), *Coordination Chemistry*, American Chemical Society, Washington, 1978.
- [7] K. Kawamura, S. Igarashi, T. Yotsuyanagi, *Anal. Sci.* 4 (1988) 175.
- [8] M. Tabata, M. Tanaka, *Inorg. Chem.* 27 (1988) 203.
- [9] R. Giovannetti, V. Bartocci, S. Ferraro, M. Gusteri, P. Passamonti, *Talanta* 42 (1995) 1913.
- [10] M. Tabata, M. Tanaka, *Trends Anal.Chem.* 10 (1991) 128.
- [11] M. Tabata, M. Tanaka, *J. Chem. Soc. Dalton Trans.* (1983) 1955.
- [12] M. Tabata, M. Tanaka, *Anal. Lett.* 13A (1980) 427.
- [13] M. Tabata, M. Tanaka, *Mikrochim. Acta II* (1982) 149.
- [14] M. Tabata, *Analyst* 112 (1987) 141.
- [15] H.A. Mottola, H.B. Mark, *Anal. Chem* 264R (1986) 58.
- [16] L.R. Robinson, P. Hambright, *Inorg. Chem.* 31 (1992) 652.
- [17] C. Baes, R.E. Mesmer, *The Hydrolysis of Cations*, Wiley, New York, 1976, p. 310.
- [18] P.W. Atkins, *Physical Chemistry*, Oxford University Press, 1990.

Cyclic voltammetry determination of epinephrine with a carbon fiber ultramicroelectrode

P. Hernández, I. Sánchez, F. Patón, L. Hernández *

Departamento de Química Analítica, Universidad Autónoma de Madrid, 28049 Madrid, Spain

Received 22 July 1997; received in revised form 1 October 1997; accepted 2 October 1997

Abstract

A carbon fiber ultramicroelectrode was used for the electroanalytical determination of epinephrine in biological fluids (urine) by cyclic voltammetry. The ultramicroelectrode was subjected to an electrochemical pretreatment in order to improve the epinephrine adsorption on the electrode surface. With this preconcentration step, detection limits of 7.8 ng ml^{-1} and determination limits of 27.6 ng ml^{-1} can be reached. The method was contrasted with native fluorescence determination—similar results were obtained. © 1998 Elsevier Science B.V. All rights reserved.

Keywords: Epinephrine; Adrenaline; Carbon fiber ultramicroelectrode

1. Introduction

Epinephrine or adrenaline is a hormone in the catecholamine family which is secreted by the suprarenal gland along with norepinephrine. It was first isolated in 1901 by Takamine and Aldrich, and was synthesized in 1904 by Stolz and Dalkin [1].

Catecholamines stimulate the nervous system. One of its more important functions is the increase in strength and frequency of cardiac contraction in the heart.

Epinephrine is synthesized naturally in the body from L-tyrosine by the action of different enzymes. Almost 50% of the secreted hormone appears in urine as free and conjugated, 3% as

vanilmandelic acid, (VAM), the most abundant metabolite in urine [2]. Only small amounts of free epinephrine is excreted.

All methods for determining catecholamines in urine require careful purification of the sample due to the many related amines and catecholes in urine. The oldest methods for epinephrine analysis are based on the native fluorescence of original amines. The trihidroxiindol method requires prior separation in a weak cationic resin for subsequent determination by fluorescence. Another method involves condensation with ethylenediamine after absorption in alumina.

Current methods focus on the use of high performance liquid chromatography (HPLC) with fluorimetric or electrochemical detection [3] and capillary electrophoresis [4].

As with other catecholamines, epinephrine has electroactive groups, the oxidation process to

* Corresponding author. Tel.: +34 1 3974149; fax: +34 1 3974931; e-mail: lucas.hernandez@uam.es

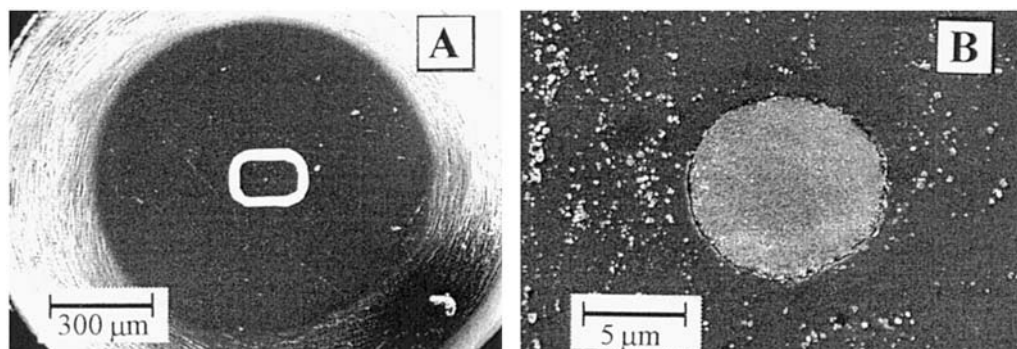


Fig. 1. Photograph of the working ultramicroelectrode after being polished with the alumina suspension (a). The surface of the carbon fibre which constitutes the working ultramicroelectrode can be appreciated in photograph (b).

quinone has been widely studied from an electrochemical point of view [5]. Wightman et al. used ultramicroelectrodes to detect a second oxidation wave for adrenaline, a secondary amine, at high scan rates [6]. In this work we used an adsorption process for adrenaline on a carbon fiber ultramicroelectrode previously activated to reduce the detection limit of epinephrine.

2. Experimental

2.1. Equipment and reagents

The carbon fiber ultramicroelectrode was constructed using a 10 μm diameter carbon fiber (Textron) as the working electrode.

Electrochemical measurements were taken with an EG&G Princeton Applied Research Corporation (PARC) model 263 potentiostat with an Ag/AgCl 3 M reference electrode and a platinum counter-electrode. The potentiostat is equipped with an EG&G PARC model 181 current pre-amplifier and a faraday box. The data obtained was stored in a personal computer.

Solutions of epinephrine, norepinephrine and ephedrine (Aldrich) were prepared from the solid product dissolved in perchloric acid 0.1 M. Separation of biological fluids was accomplished using an ion exchange column with 'Amberlite C-G 50' resin and alumina.

The pH of the epinephrine solutions was changed using buffer solutions ranging from pH

2–12 on the basis of phosphoric, acetic and boric acid, using KOH to adjust the pH. All reagents used were Reagent Analysis Quality and the water was deionised using MilliRO-MilliQ (Water System) equipment.

2.2. Working ultramicroelectrode construction.

The working ultramicroelectrode was constructed from 10 μm diameter carbon fiber, which was fed into a 0.5 mm i.d. polypropylene tube. This tube was carefully sealed using a mild heat source in order to slowly melt the end of the tube where the fibre had entered so as to completely wrap it with polypropylene. The electrode was perfectly sealed [7]. At the other end of the tube, we fed a copper wire and mercury droplets to make electrical contact between the carbon fiber and the copper wire. This end was then closed using a fast-dry glue.

Finally the carbon fiber had to protrude from the polypropylene. To achieve this, we included an electrode polishing stage: P-1200 (PRESI) sandpaper was first used to reach the carbon fibre, then smoother paper (P-4000) and finally an alumina suspension (1 μm particle size) on a felt pad was used to produce a flat, easily reproducible disk surface (Fig. 1).

2.3. Activation and regeneration of the working electrode

The working ultramicroelectrode performance was checked against a 50 mM solution of potas-

The working ultramicroelectrode performance was checked against a 50 mM solution of potassium hexacyanoferrate(III) in a H_2SO_4 0.1 M medium. A cyclic voltammogram was recorded at 50 mV s^{-1} scan rate, obtaining a sigmoidal wave as corresponds to an ultramicroelectrode (Fig. 2). The current intensity of the steady-state may be used to calculate the radius of the electrode's active surface, as with an ultramicroelectrode we find that,

$$i_{\text{lim}} = 4nFDC^*r$$

[8]where i_{lim} is the limiting current (A), n is the number of electrons involved in the reaction, F is the Faraday constant, D is the diffusion coefficient of the electroactive substance ($7.2 \cdot 10^{-6} \text{ cm}^2 \text{ s}^{-1}$) [10], C^* is the concentration of the electroactive substance within the solution (mol cm^{-3}) and r is the electrode radius (cm). The limiting current we measured was 50 nA, and the active electrode surface was $3.6 \text{ } \mu\text{m}$.

In order to obtain a reproducible response in solutions of epinephrine, the electrode should be subjected to an activation process prior to use. This activation step was performed once after assembly, using cyclical scans from 0.0 to 1.500 V at 200 mV s^{-1} in a $\text{H}_3\text{PO}_4/\text{H}_2\text{PO}_4^-$ 0.04 M buffer at pH 3. This procedure produced a constant residual current indicative of the electrode activation. This activation process was only necessary once after polishing the electrode.

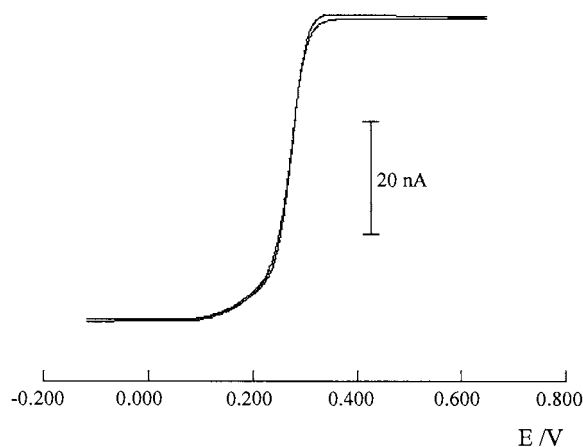


Fig. 2. Cyclic voltammogram of potassium hexacyanoferrate(III) 50 mM in a 0.1 M H_2SO_4 medium. $v = 50 \text{ mV s}^{-1}$.

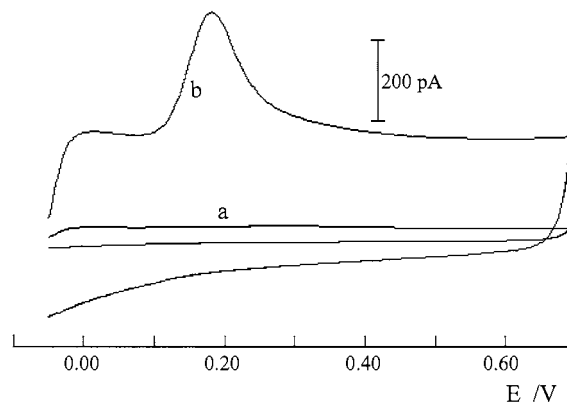


Fig. 3. Cyclic voltammograms recorded for a $2.0 \text{ } \mu\text{g ml}^{-1}$ epinephrine solution in a $0.04 \text{ M H}_2\text{PO}_4^-/\text{HPO}_4^{2-}$ buffer at pH 8; $v = 100 \text{ mV s}^{-1}$; $T_{\text{ac}} = 100 \text{ s}$: (a) before the activation step; (b) after the activation step.

We found in epinephrine, an adsorption process (of the molecule) that occurs on the electrode surface, facilitated by our activation step of the ultramicroelectrode (Fig. 3). We also found that the electrode cleaning treatment is not necessary after each measurement, since the product of epinephrine oxidation is not retained on the electrode surface, thus maintaining the active surface constant.

3. Results and discussion

Initially, the effect of the medium's pH on the electrochemical signal was analysed. The pH of the epinephrine solutions was changed using buffer solutions ranging from pH 2–12. The buffer solution concentrations were 0.04 M, and the measurements were made with a variable accumulation potential in accordance with the solution pH, at 60 s accumulation time, 100 mV s^{-1} scan rate and $2.0 \text{ } \mu\text{g ml}^{-1}$ concentration of epinephrine.

Fig. 4 shows the voltammograms recorded for pH below 9. The epinephrine had no oxidation wave in experimental conditions above pH 9. This is not the observed behaviour for other catecholamines [5]. This behaviour is due to the deprotonation of epinephrine ($\text{p}K_{\text{a}}$ around 8) this prevents its adsorption to the electrode surface, and removes the oxidation wave [10,11].



Fig. 4. Cyclic voltammograms recorded for a $2.0 \mu\text{g ml}^{-1}$ concentration solution of epinephrine with an accumulation time of 60 s and scan rate 100 mV s^{-1} at different pH levels.

There was also a shift in the peak potential when the pH was changed. The potential shifted to lower values as the pH increased according to the equation:

$$E_p(\text{V}) = 0.60 - 0.06 \text{ pH} \quad r = 0.999$$

the intervention of H^+ in the electrochemical reaction correlates with the mechanism proposed by other authors for the oxidation of catecholamines (Fig. 5).

The best relationship between peak current and its resolution is found at a buffer concentration of 0.04 M and pH 8, we took this as the optimum pH and used it in the subsequent experiments.

After selecting the working pH, the accumulation potential was analysed. A solution of epinephrine ($2 \mu\text{g ml}^{-1}$) was used in a phosphate medium at pH 8, varying the accumulation potential (-0.1 – 0.0 V), with a 60 s accumulation time, and 100 mV s^{-1} scan rate. Because we did not find any significant variation in the peak intensity, we chose an accumulation potential of -0.050 V , since the wave is well defined and the electrode is

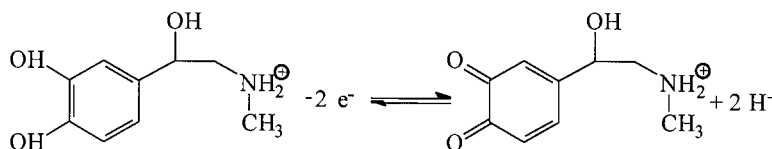


Fig. 5. Oxidation mechanism for epinephrine.

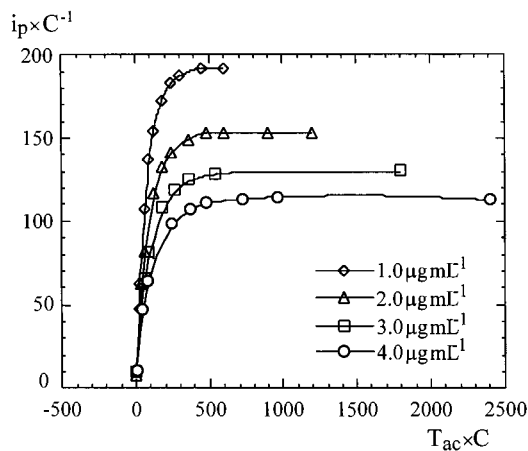


Fig. 6. Isotherm of adsorption for different concentrations of epinephrine. Peak current (i_p) is in pA, T_{ac} is in seconds and C is in $\mu\text{g ml}^{-1}$.

not subjected to drastic conditions that might alter its performance, especially for values below -0.1 V .

The study of the variation of accumulation time enabled us to ascertain the level of epinephrine adsorption on the electrode surface. To accomplish this, we varied the accumulation time between 0 and 600 s for different concentrations of epinephrine in the measurement cell, in all cases without shaking, i.e. the hormone only reached the electrode by electrostatic attraction or chemical attraction. Measurements were carried out in a phosphate buffer at pH 8, applying an accumulation potential of -0.05 V and a scan rate of 100 mV s^{-1} . Fig. 6 shows the isotherms of epinephrine adsorption. For long accumulation times, an equilibration between substance concentration on the surface of the electrode and epinephrine concentration of the solution was reached. This occurs at shorter times when the epinephrine concentration is increased. In light of

these results, we chose 100 s as the accumulation time for subsequent analyses. Because epinephrine concentrations found in biological fluids are lower than those analysed, an accumulation time must be chosen that varies according to the sample—without considering any time as optimum the isotherms follow a similar pattern.

We then analysed the effect of scan rate on the electroanalytical signal. For this purpose we used optimum conditions from previous studies and varied the scan rate between 10 and 250 mV s^{-1} . The accumulation time was 100 s.

The voltammograms recorded (Fig. 7) revealed that the peak intensity increases, the peak potential shifted towards more anodic values with increasing scan rate. While the intensity increases with scan rate, there is also an increase in the width at half height and the peak definition worsened. The peak intensity reaches a maximum at 250 mV s^{-1} , a compromise must be reached between peak intensity and width at half height, 100 mV s^{-1} was chosen as the optimum scan rate.

When i_p is plotted against $v^{1/2}$, and E_p against $\log v$, we obtain a linear relationships that fits the following equations:

$$i_p \text{ (pA)} = -43.9 + 33.5v^{1/2} \quad r = 0.998$$

$$E_p \text{ (V)} = 0.037 + 0.064 \log v \quad r = 0.991$$

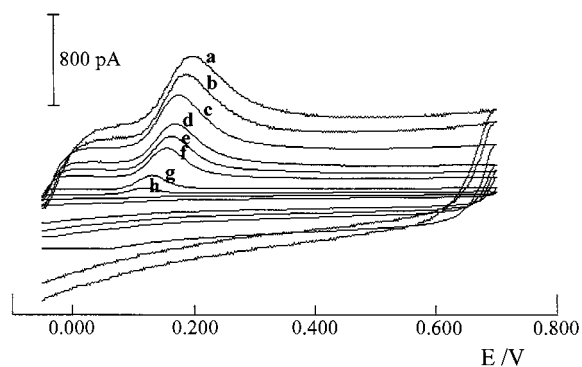


Fig. 7. Cyclic voltammograms recorded at different scan rates from -0.05 to $+0.70$ V. A $2 \mu\text{g ml}^{-1}$ epinephrine solution was used at pH 8, 0.04 M phosphate buffer: (a) 250 mV s^{-1} ; (b) 200 mV s^{-1} ; (c) 150 mV s^{-1} ; (d) 125 mV s^{-1} ; (e) 100 mV s^{-1} ; (f) 75 mV s^{-1} ; (g) 25 mV s^{-1} ; (h) 10 mV s^{-1} . $T_{ac} = 100$ s and $E_{ac} = -0.05$ V.

indicating that the electrochemical process is irreversible, a similar behaviour observed in the conventional sized electrode [9].

We also analysed the effect of buffer concentration on electrochemical measurement. To determine this we employed previously established conditions and changed the concentration of the phosphate buffer at pH 8 from 1 to 0.02 M. We found that the peak intensity falls exponentially as the concentration of the buffer increases. The maximum intensity is thus obtained for a 0.02 M concentration of the buffer electrolyte.

With a view to the future applicability of this method, and taking into consideration the range of epinephrine concentrations in urine, we opted to use two regression lines for calibration, one for high and the other for low concentrations, using 100 and 600 s accumulation time respectively.

At an accumulation time of 100 s, there were two linear sections in the regression line, which fit the following equations:

For concentrations below $4.0 \mu\text{g ml}^{-1}$,

$$i_p \text{ (pA)} = 54.1 + 102.3 C \text{ (}\mu\text{g ml}^{-1}\text{)} \quad r = 0.997$$

For concentrations above a $4 \mu\text{g ml}^{-1}$,

$$i_p \text{ (pA)} = 267.6 + 40.9 C \text{ (}\mu\text{g ml}^{-1}\text{)} \quad r = 0.998$$

Using 600 s as the accumulation time, concentrations in the order of 10 ng ml^{-1} can be measured. Plotting the values of peak intensity against concentration (Fig. 8), we find, as in the previous case, two linear sections in the regression line which fit the following equations:

For concentrations below 100 ng ml^{-1} ,

$$i_p \text{ (pA)} = 0.72 + 1.06 C \text{ (ng ml}^{-1}\text{)} \quad r = 0.998$$

For concentrations above 100 ng ml^{-1} ,

$$i_p \text{ (pA)} = 42.02 + 0.65 C \text{ (ng ml}^{-1}\text{)} \quad r = 0.994$$

The analytical characteristics of this method were established, taking into consideration the measurements made under optimum conditions. The statistical treatment of the data obtained indicates that the procedure has a standard error that ranges between 6.7 and 14.3%, and a standard deviation ranging between 2.6 and 27.6% ($n = 10$) for epinephrine concentrations $10\text{--}150 \text{ ng ml}^{-1}$, with an accumulation time of 600 s.

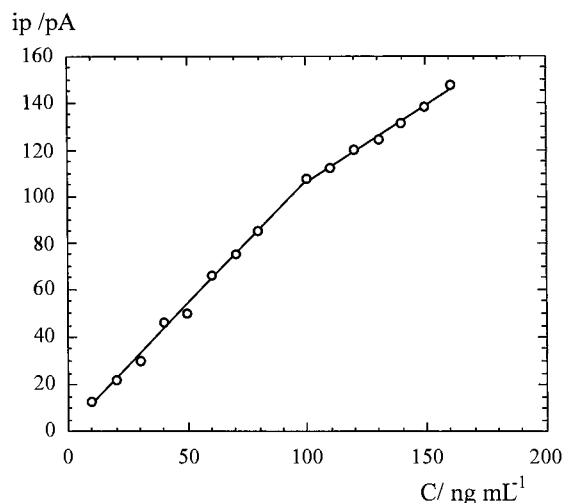


Fig. 8. Regression line according to the epinephrine concentration in the medium for an accumulation time of 600 s at an accumulation potential of -0.05 V and a scan rate of 100 mV s^{-1} . Scan limits are -0.05 and $+0.75$ V in pH 8, 0.02 M phosphate buffer.

At the same time, a value was found for the typical standard deviation of the background current (3 pA). Hence, the detection limit, considered to be three times the typical deviation of the background current, is 7.8 ng ml^{-1} , and the determination limit, considered to be ten times the value of the typical deviation of the background current, is 27.6 ng ml^{-1} with an accumulation time of 600 s [12].

In the analysis of potential interferences that might change the signal of our compound, we chose two principal compounds with similar characteristics, norepinephrine and ephedrine. The interference of these substances was analysed under the same measurement conditions as those used to study the effects of epinephrine concentration.

The presence of norepinephrine in the medium produces an increase in ip , a similar percentage to epinephrine concentration, although the presence of norephedrine can be detected under these measurement conditions, the norephedrine wave reduction is detected as it is a quasi-reversible system, presenting the reduction wave at 100 mV. The presence of ephedrine does not cause significant interference, until additions exceed 300% of the

adrenaline concentration. Because of the interference produced by these compounds, it is necessary to perform a separation pretreatment for epinephrine before analytical measurement.

4. Application

4.1. Determination in urine

Pre-treatment is a specific, standardized method for determining epinephrine in biological fluids [3]. Urine (5 ml) is mixed with a pH 7 phosphate buffer. The solution is passed through an Amberlite CG-50 ion exchange column. The catecholamines retained in the resin are eluted with an ammonium sulphate solution (2 M) and mixed with alumina powder for 10 min. The mixture is centrifuged and the solution is discarded. Catecholamines are extracted from the alumina with phosphoric acid (0.3 M).

The extract is raised to pH 8 with 2 M NaOH, a final volume of 3 ml is obtained using the appropriate buffer solution i.e. 0.02 M $\text{H}_2\text{PO}_4^-/\text{HPO}_4^{2-}$.

This solution is fed into the measurement cell, the voltammogram (Fig. 9) is recorded under conditions used for calibration, using 600 s accumulation time. In order to quantify the epinephrine

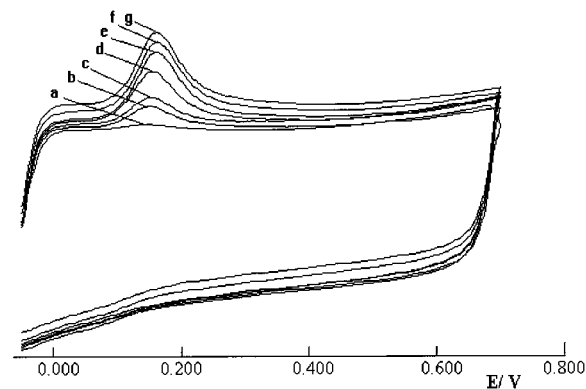


Fig. 9. Cyclic voltammograms corresponding to standard additions applied to the urine extract. Accumulation potential was -0.05 V; $T_{ac} = 600$ s, $v = 100$ mV s^{-1} in pH 8, 0.02 M phosphate buffer: (a) sample; (b) 132 ng ml^{-1} ; (c) 198 ng ml^{-1} ; (d) 333 ng ml^{-1} ; (e) 533 ng ml^{-1} ; (f) 600 ng ml^{-1} ; (g) 666 ng ml^{-1} .

concentration we used the standard addition method.

A regression line is obtained which fits the equation:

$$ip \text{ (pA)} = 8.08 + 219.44 C \text{ (ng ml}^{-1}\text{)}$$

$$r = 0.997$$

by extrapolation we detected a concentration of 18.8 ng ml⁻¹ for the sample in the measured extract. Taking into consideration the fact that the recovery index for the whole process is 40%, we find that the epinephrine concentration in the initial sample is 47.11 ng ml⁻¹, a range considered normal for the excretion of human fluids in a state of repose [2].

4.2. Determination by native fluorescence

After analysing the extract electrochemically, the above method was contrasted using the native fluorescence determination of epinephrine [3]. This determination was carried out at an excitation wave length of 200 nm and emission in the range of 300–600 nm. The urine extract and successive additions of epinephrine of known concentration were recorded in the range of 10–50 ng ml⁻¹, obtaining a regression line which fits the equation,

$$I_{em} = 16.7 + 0.84 C \text{ (ng ml}^{-1}\text{)} \quad r = 0.999$$

and a concentration of 19.1 ng ml⁻¹ at 420 nm, similar to the result obtained using the ultramicroelectrode.

Acknowledgements

The authors gratefully acknowledge financial support from the DGICYT (Spain) Project PB94-178.

References

- [1] R. Greene, in: S.A. Guadarrama (Ed.), *Las hormonas del organismo humano. Introducción a la Endocrinología*, chap. 5, 1950.
- [2] F. Ganong William, *Manual de fisiología médica. El manual moderno S.A., Mexico D.F., 7th ed., chaps. 13, 15, 20*, 1980.
- [3] K. Pesce, *Química Clínica. Métodos, Médica Panamericana*, chap. 125, 1990.
- [4] M. Chicharro, A. Zapardiel, E. Bermejo, J.A. Pérez-López, L. Hernández, *J. Liq. Chromatogr.* 18 (1995) 117–123.
- [5] A. Brun, R. Rosset, *Electroanal. Chem. Interfacial Electrochem.* 49 (1974) 287.
- [6] K. Pihel, T.J. Schroeder, R.M. Wightman, *Anal. Chem.* 66 (1994) 4532–4537.
- [7] P. Hernández, F. Patón, L. Hernández, *Anal. Chim. Acta.* 327 (1996) 117–123.
- [8] K. Aoki, K. Akito, K. Tokuda, H. Matsuda, J. Osteryoung, *J. Electroanal. Chem.* 171 (1984) 219.
- [9] J. Koryta, J. Dvorak, *Principles of Electrochemistry*, Wiley, 1987, 128.
- [10] *Stability Constants of Metal Ion-Complexes*, (Suppl. n.1.), Special Publication no. 17. The Chemical Society, Burlington House, London W1V 0BN, 1971, 584.
- [11] A. C. Andrews, T.D. Lyons, T.D. O'Brien, *J. Chem. Soc.* (1962) 1776.
- [12] H.H. Kaiser, *Anal. Chem.* 42 (1970) 26A.

Electrocatalysis of cytochrome *c* at a C₆₀- γ -cyclodextrin and Nafion chemically modified electrode

Mei-Xian Li, Nan-Qiang Li *, Zhen-Nan Gu, Xi-Huang Zhou, Yi-Liang Sun, Yong-Qing Wu

Department of Chemistry, Peking University, Beijing 100871, People's Republic of China

Received 9 July 1997; received in revised form 3 October 1997; accepted 4 October 1997

Abstract

The C₆₀- γ -cyclodextrin and Nafion chemically modified electrode exhibits two redox waves by cyclic voltammetry. Such an electrode will effect reduction and oxidation of cytochrome *c* and be capable of mediating the electron transfer to cytochrome *c*. © 1998 Elsevier Science B.V. All rights reserved.

Keywords: Electrocatalysis; Cytochrome *c*; C₆₀- γ -cyclodextrin; Nafion; Chemically modified electrode

1. Introduction

The electrochemical behavior of C₆₀ films has been widely investigated in non-aqueous solution since the large-scale method for successful laboratory synthesis of the fullerenes became available [1–8]. It indicates that reduction can form insoluble films with incorporated cations or lead to dissolution. The electrochemical behavior of C₆₀ films in an aqueous solution is also reported [9,10], showing that both the reduction and the oxidation are completely irreversible. In order to study the interaction between C₆₀ and biomacromolecules, water-soluble derivatives of C₆₀-C₆₀- γ -cyclodextrin inclusion complexes were synthesized according to the paper described [11–13]. Their electrochemical behavior has been studied in an

aqueous solution and the electrochemical behavior and electrocatalysis of hemoglobin by a thin coating of C₆₀- γ -cyclodextrin (C₆₀- γ -CD) and Nafion, deposited by evaporation on a glassy carbon electrode in an aqueous solution, have been investigated [14].

This paper is concerned with the electrocatalysis of cytochrome *c* at a C₆₀- γ -CD and Nafion chemically modified electrode. It was found that C₆₀- γ -CD is capable of mediating the electron transfer to cytochrome *c*.

2. Experimental

2.1. Reagents

C₆₀ was prepared in our laboratory. Its purity was 99.9%, as determined by mass spectrometry. The γ -cyclodextrin was bought from Tokyo Kasei

* Corresponding author. Fax: +86 10 62751708; e-mail: lmwx@chemms.chem.pku.edu.cn

and the 5% Nafion (Dupont) was from Aldrich and was diluted to 1% with ethanol before use. Horse heart cytochrome *c* (Type III) was obtained from BDH Chemicals, Poole. The water-soluble C_{60} - γ -CD inclusion complexes were prepared according to the literature [11–13]. Other reagents used were of analytical grade. Water was triply distilled from an all-quartz still and experiments were carried out at room temperature ($25 \pm 2^\circ\text{C}$).

2.2. Electrochemical measurements

The electrochemical cell consisted of a single-compartment glass cell with an Au counter electrode and a saturated calomel reference electrode located near the working electrode. The solutions were routinely deaerated by purging with high purity nitrogen. Cyclic voltammetric experiments were performed with a Princeton applied research (PAR) Model 273 potentiostat/galvanostat. The UV-Vis spectra were recorded using a Shimadzu Model UV-3100 spectrophotometer.

2.3. Electrodes and preparation

The working electrode was glassy carbon (GC) ($d = 4$ mm). Before use in electrochemical experiments and also before the start of modification procedures, the surface of the GC electrode was polished on fine emery paper and chamois leather containing Al_2O_3 slurry and then rinsed thoroughly with water in an ultrasound bath. Chemically modified electrodes (CME) were prepared by evaporation of a few microliters of C_{60} - γ -CD (1:2) in an aqueous solution on the electrode surface with an infrared lamp and then by casting a Nafion protection film. The experiments showed that there was an optimal CME response for the C_{60} - γ -CD reaction with $10 \mu\text{l}$ $2.0 \times 10^{-5} \text{ mol l}^{-1}$ C_{60} - γ -CD (1:2) dripped on the surface of the GC electrode. As C_{60} - γ -CD is soluble in water, to avoid a desorptial C_{60} - γ -CD layer, a thin film of Nafion was used to coat the C_{60} - γ -CD layer on the GC electrode surface. Experimental results demonstrate that the optimum electrode performance for the C_{60} - γ -CD reaction is obtained when C_{60} - γ -CD layer is coated with $4 \mu\text{l}$ 1% Nafion.

3. Results and discussion

3.1. Electrochemistry of CME

In Fig. 1, the curve a shows the cyclic voltammogram of C_{60} - γ -CD (1:2)/Nafion CME in a 0.10 mol l^{-1} KCl (pH = 6.4) medium. The curve exhibits two redox peaks P_1 and P_1' , with $E_{P_1} = -0.60 \text{ V}$ and $E_{P_1'} = -0.56 \text{ V}$. Furthermore, the corresponding peak currents were a linear function of the scan rates. Based on the experimental results and the papers reported [14–16], the electroreduction of the C_{60} - γ -CD (1:2)/Nafion CME is a reversible, surface-confined one-electron-transfer process. Possibly due to the effect of the heterogeneous kinetic factor and other factors (such as IR drop, ionic strength, solvent effect etc.), the peak potential difference between the redox peaks is not 0 V.

In order to examine the stability of the CME, it was exposed to air for 24 h, after which the currents remained unchanged. Furthermore, scanning more than 100 complete CV cycles at a scan rate of 500 mV s^{-1} between -0.20 and -0.80 V produced no significant decrease in cathodic and

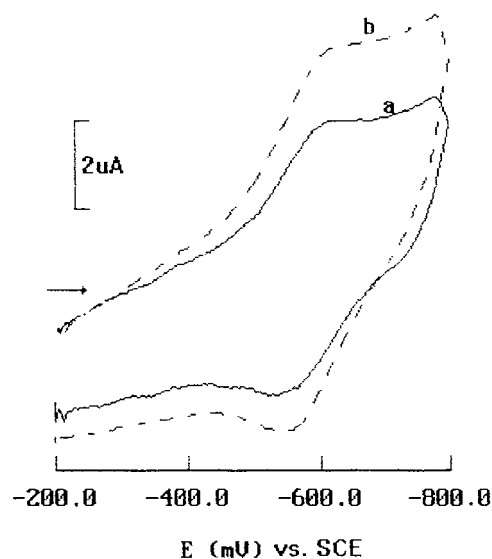


Fig. 1. C_{60} - γ -CD (1:2) electrocatalysis cyclic voltammograms for: (a) 0.10 mol l^{-1} KCl; (b) 0.10 mol l^{-1} KCl + $3.3 \times 10^{-5} \text{ mol l}^{-1}$ cytochrome *c*; initial potential, $E_i = -200.0 \text{ mV}$; scan rate, 200 mV s^{-1} .

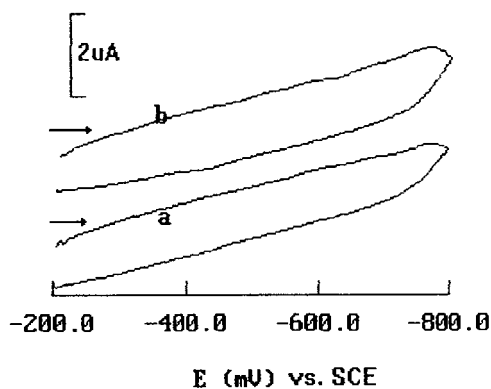


Fig. 2. Cyclic voltammograms for $3.3 \times 10^{-5} \text{ mol l}^{-1}$ cytochrome *c*, 0.10 mol l^{-1} KCl; initial potential, $E_i = -200.0 \text{ mV}$; scan rate, 100 mV s^{-1} . (a) bare GC electrode; (b) γ -CD/Nafion CME.

anodic peak currents, indicating that CME in the neutral form has good stability.

3.2. Electrocatalysis of cytochrome *c* at the CME

The experiments show that cytochrome *c* demonstrates no evident electrochemical response at a bare GC electrode and a γ -CD/Nafion CME between -0.20 and -0.80 V in a 0.10 mol l^{-1} KCl medium (Fig. 2). This implies that the electron-transfer rate of cytochrome *c* at two kinds of electrodes is very slow in the absence of C_{60} - γ -CD.

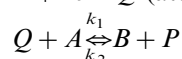
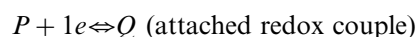
Cyclic voltammograms obtained with C_{60} - γ -CD (1:2)/Nafion CME and run in 0.10 mol l^{-1} KCl both with and without added cytochrome *c* are shown in Fig. 1. The voltammograms obtained upon addition of cytochrome *c* showed an increase in both the C_{60} - γ -CD (1:2) reduction current and oxidation current, but with little change in the peak potentials. This behavior persisted even at a scan rate as fast as 3 V s^{-1} . C_{60} - γ -CD (1:1)/Nafion CME was tested in the same way and it was found that there is an increase in both the C_{60} - γ -CD (1:1) reduction and oxidation currents in 0.10 mol l^{-1} KCl containing cytochrome *c*, but that this effect is weaker than that of C_{60} - γ -CD (1:2)/Nafion CME. This indicates that C_{60} - γ -CD is capable of mediating the electron-transfer rate of cytochrome *c*. However, the formal potential of

the C_{60} - γ -CD system may not be close to that of cytochrome *c* according to papers described [17,18].

Hinnen and Niki [17] have studied the roles of surface modifies (4-pyridyl derivatives) in the electron-transfer reaction of cytochrome *c* at a gold electrode surface. They concluded that the formal potential of the adsorbed cytochrome *c* is about 440 mV more negative than the potential of native cytochrome *c*. Wrighton and his co-workers [18] reported the preparation of nearly reversible electrode for cytochrome *c*. They pointed out that in principle, it should be possible to effect a redox reaction when the E^0 's of the surface mediator and biological system are unfavorable.

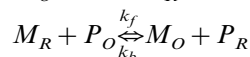
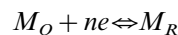
In order to examine whether cytochrome *c* has penetrated into the Nafion film, Nafion coating was prepared by transferring $40 \mu\text{l}$ of 1% solution onto a quartz microscopic slide and allowing the solution to evaporate. Following this, the quartz microscopic slide was soaked in 0.10 mol l^{-1} KCl containing $5.0 \times 10^{-5} \text{ mol l}^{-1}$ cytochrome *c* for 1 h and the surface was rinsed thoroughly with water after removal from the solution. The spectrum of cytochrome *c* in Nafion is shown in Fig. 3. Penetration of cytochrome *c* into the Nafion film is indicated by the appearance of the Soret band of porphyrin in the spectrum.

Andrieux and Saveant have discussed some cases of the following system by redox polymer film CME [19]:



where *A* and *B* are oxidized and reduced forms of the substrate, respectively and $K = k_1/k_2$ is the equilibrium constant.

Based on above theory, Dong et al. proposed a reversible catalytic reaction mechanism in the research of dye CMEs promoting redox of protein [20]:



where *M* is the mediator, *P* the redox protein, *O* and *R* correspond to oxidation and reduction, respectively and *k* is the rate constant of the catalytic reaction.

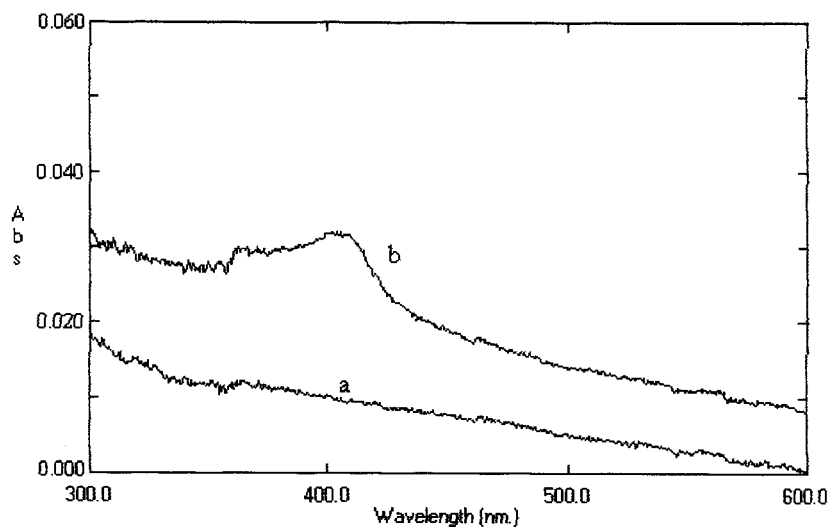
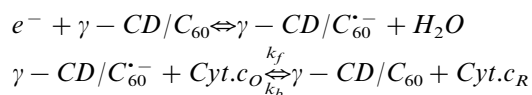


Fig. 3. UV-Vis spectra: (a) no cytochrome *c*; (b) incorporating cytochrome *c*.

Fig. 4 shows that the ratio of the catalytic cathodic peak current I_{k_1} to the reversible cathodic peak current I_{p_1} of C_{60} - γ -CD (1:2)/Nafion CME at different scan rates in 0.10 mol l^{-1} KCl containing $1.2 \times 10^{-5} \text{ mol l}^{-1}$ cytochrome *c*. It indicates that I_{k_1}/I_{p_1} first increases and then decreases slowly, finally approaching a constant as the scan rate increases.

According to the experimental results and the literature [14–20], electrocatalytic reaction mecha-

nism of cytochrome *c* at C_{60} - γ -CD/Nafion CMEs can be expressed as follows:



In conclusion, this work presents the first reported observation for reversible electrocatalytic activity of cytochrome *c* at C_{60} - γ -CD/Nafion CMEs in aqueous solution.

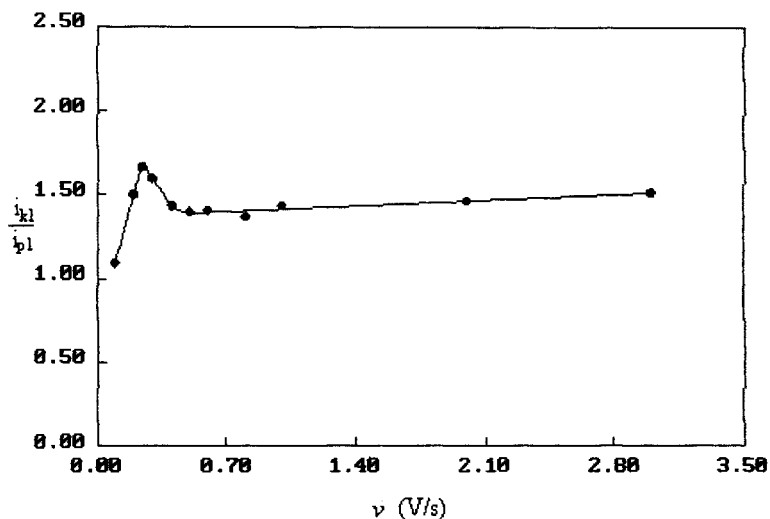


Fig. 4. The effect of scan rate on i_{k_1}/i_{p_1} . 0.10 mol l^{-1} KCl; $1.2 \times 10^{-5} \text{ mol l}^{-1}$ cytochrome *c*; initial potential, $E_i = -200.0 \text{ mV}$.

Acknowledgements

This project was jointly supported by No.9400120 of the Foundation of Doctoral Program of the State Commission of Education and No.29575192 of the National Natural Science Foundation of China.

References

- [1] W. Kratschmer, L.D. Lamb, K. Fostiropoulos, D.R. Huffman, *Nature* 347 (1990) 354.
- [2] C. Jehoulet, A.J. Bard, F. Wudl, *J. Am. Chem. Soc.* 113 (1991) 5456.
- [3] C. Jehoulet, Y.S. Obeng, Y.T. Kim, F. Zhou, A.J. Bard, *J. Am. Chem. Soc.* 114 (1992) 4237.
- [4] R.G. Compton, R.A. Spackman, D.J. Riley, R.G. Wellington, J.C. Eklund, A.C. Fisher, M.L.H. Green, R.E. Doothwaite, A.H.H. Stephens, J. Turner, *J. Electroanal. Chem.* 344 (1993) 235.
- [5] M. Nishizawa, T. Matsue, I. Uchida, *J. Electroanal. Chem.* 353 (1993) 329.
- [6] W. Koh, D. Dubois, W. Kutner, M.T. Jones, K.M. Kadish, *J. Phys. Chem.* 96 (1992) 4163.
- [7] L.T. Jin, M.S. Zhou, Z.L. Shi, T. Liu, *Anal. Chem. (Chinese)* 23 (1995) 163.
- [8] W.B. Caldwell, K. Chen, C.A. Mirkin, S.J. Babinec, *Langmuir* 9 (1993) 1945.
- [9] A. Szucs, A. Loix, J.B. Nagy, L. Lamberts, *J. Electroanal. Chem.* 397 (1995) 191.
- [10] A. Szucs, A. Loix, J.B. Nagy, L. Lamberts, *J. Electroanal. Chem.* 402 (1996) 137.
- [11] D.D. Zhang, Q. Liang, J.W. Chen, M.K. Li, S.H. Wu, *Chin. Sci. Bull.* 39 (1995) 383.
- [12] M.X. Li, N.Q. Li, Z.N. Gu, X.H. Zhou, Y.L. Sun, Y.Q. Wu, *Electrochim. Acta* 41 (1996) 2897.
- [13] M.X. Li, N.Q. Li, Z.N. Gu, X.H. Zhou, Y.L. Sun, Y.Q. Wu, *Electroanalysis* 9 (1997) 490.
- [14] M.X. Li, N.Q. Li, Z.N. Gu, X.H. Zhou, Y.L. Sun, Y.Q. Wu, *Electroanalysis* (in press).
- [15] P. Boulas, W. Kutner, M.T. Jones, K.M. Kadish, *J. Phys. Chem.* 98 (1994) 1282.
- [16] N.M. Dimitrijevic, P.V. Kamat, *J. Phys. Chem.* 97 (1993) 7623.
- [17] T. Sagara, K. Niwa, A. Sone, C. Hinnen, K. Niki, *Langmuir* 6 (1990) 254.
- [18] S.C. Chao, J.L. Robbins, M.S. Wrighton, *J. Am. Chem. Soc.* 105 (1983) 181.
- [19] C.P. Andrieux, J.M. Saveant, *J. Electroanal. Chem.* 142 (1982) 1.
- [20] T. Chen, S.J. Dong, Y.W. Xie, *Chin. Electrochem.* 1 (1995) 125.

Complexation of trivalent cations (Al(III), Cr(III), Fe(III)) with two phosphonic acids in the pH range of fresh waters

Stella Lacour, Véronique Deluchat, Jean-Claude Bollinger *, Bernard Serpaud

Laboratoire de Chimie Analytique, Sciences de l'Eau et de l'Environnement, Faculté des Sciences, 123 avenue Albert-Thomas, 87060 Limoges, France

Received 3 June 1997; received in revised form 3 October 1997; accepted 6 October 1997

Abstract

The complex formation constants of two phosphonic acids, HEDP and ATMP, with three trivalent metallic cations, Al(III), Cr(III) and Fe(III), have been determined by acid–base titration at 25°C and constant ionic strength (0.1 mol l⁻¹, KNO₃), using Martell and Motekaitis' computer programs. Species distribution curves showed that all three cations are in complex form in the pH range of fresh waters (5–9). The study of different cation/ligand ratios proved that both ligands mainly form anionic soluble complexes for systems having an excess of ligand—as protonated and unprotonated forms and especially ternary complexes with HEDP. For higher metal concentrations (excess of cation), weakly soluble species of HEDP and ATMP were formed with Al(III) and Cr(III). Two insoluble complexes with ATMP have been identified by SEM/EDAX as AlH₃X_(s) and Cr₂X_(s). Regarding Fe(III) species, Fe(OH)_{3(s)} precipitate seems to predominate in solution. © 1998 Elsevier Science B.V. All rights reserved.

Keywords: Complexation; Phosphonic acids; Speciation; Trivalent cations

1. Introduction

Due to a growing increase in public environmental concern, the use of sodium tripolyphosphate has been banned in domestic detergents. In recent years phosphonate derivatives have been used in washing powder formulations. However, some concerns still exist about their behaviour when released in lakes or rivers, as they can complex with toxic elements previously immobilized in sediments. We have studied two com-

monly used phosphonic acids, 1-hydroxyethane-1,1'-diphosphonic acid (HEDP) and aminotris(methylenephosphonic acid) (ATMP) (Scheme 1), whose acid/base and complexation behaviours with divalent cations have recently been characterized [1].

After domestic use, these phosphonic acids are released along with the rest of the domestic waste waters. In municipal waste treatment plants, a phosphorus elimination step can reduce phosphonate levels by 80% [2]. This step is however costly and is not always included in the treatment process. Phosphonates can enter aquatic ecosystems, and later flow through water potabilization plants

* Corresponding author. Fax.: +33 555 457459; e-mail: jcbollinger@unilim.fr

where a common process—coagulation/flocculation with ferric or aluminium hydroxides occurs. These complexing agents (including HEDP and ATMP) have recently been shown to retard hydration of cement slurries [3], possibly by preventing the formation of gelatinous Fe(III) hydroxide during the hydration of a calcium/aluminium/iron(III) cement as a result of iron chelation. It is therefore important to study the possible interactions of HEDP and ATMP with Fe(III) and Al(III).

The toxicity of Al(III) in drinking water is now well documented [4], and its contribution to Alzheimer's disease has been detailed [5]. Although Cr(III) is an essential oligoelement for animal life, its oxidation to toxic Cr(VI) can lead to ecological problems [6]. Both Al(III) and Cr(III) salts are commonly used in the tannery industry [7].

Trivalent cation complexation with multidentate ligands bearing phosphonate groups has previously been reported, but very few papers deal with HEDP and ATMP and frequently these studies only give qualitative results [8–13].

In this study we present the metal complex formation constants of HEDP and ATMP with three trivalent cations (Al(III), Cr(III) and Fe(III)), determined using protometric titration. Some insoluble compounds have been characterized using a SEM/EDAX technique and their solubility has been estimated by flameless AA. The potential impact of these complexes on natural systems is discussed using speciation diagrams.

2. Materials and methods

2.1. Chemicals

All chemicals were analytical grade reagents (Fluka or Prolabo) dissolved in ultra-pure water produced by the Millipore Milli-Q Plus system (resistivity of 18.2 M Ω cm and T.O.C. lower than 10 ppb). Solutions of metal cations were prepared from nitrate salts and standardized by acid–base titration in the presence of ligand. Phosphonic acid concentration was also determined by pH-metric titration.

2.2. Acid–base titrations

All experiments were carried out in a constant temperature cell at $25 \pm 0.5^\circ\text{C}$, at constant ionic strength $I = 0.1 \text{ mol l}^{-1}$ (KNO₃) under a purified nitrogen stream. In these conditions, the water ion concentration product is $\text{p}K_w = 13.78$ [14].

The pH-metric titrations were performed with a Metrohm 716 DMS automatic titrator using the dynamic equivalent point titration (DET) mode. The correct response of the combined glass electrode (Ag/AgCl, KCl 3 mol l⁻¹, Metrohm 6.0233.100) was verified with standard buffer solutions at pH 4, 7 and 10 and especially with a calibration in H₃O⁺ concentrations using strong acid–strong base titration as suggested by Irving et al. [15]. Experimental and calculated pH values are therefore equal to $-\log[\text{H}_3\text{O}^+]$.

The sodium hydroxide solution was prepared from pure grade (Prolabo) anhydrous solid dissolved in boiled and degassed ultra-pure water in order to prevent carbonate interference. This solution was standardized by hydrochloric acid titration. The extent of NaOH carbonation was measured using the Gran method [16,17]. It never exceeded 0.5% but was taken into account for the determination of protonation constants.

Solutions having metal ion/ligand molar ratios of 1/1, 1/2 and 1/5 were analysed. The ligand concentration was always 0.002 mol l⁻¹. For each ratio, three different titrations were repeated in triplicate, thus giving at least nine experimental data sets per ratio to be computed.

2.3. SEM/EDAX

Insoluble complex stoichiometry was characterized from atomic percentages produced by the scanning electron microscope.

The apparatus was either a Philips microscope (XL30 model), associated with a spectrometric X-ray detector (EDAX 9100/60) or a JEOL microscope (JSM 820 model) with a KEVEX system. The detection limit was 1% of analysed volume.

Precipitates were isolated according to the following procedure: Insoluble complexes were prepared from solutions at three cation/ligand molar

ratios: 1/1, 1/2 and 2/1. These were filtered on a cellulose nitrate Whatman membrane (pore diameter 0.2 μm) and recovered solids were dried for 48 h in a 96°C oven.

2.4. Flameless atomic absorption spectrometry

We determined the solubility of the studied precipitates using a SpectrAA-800, Graphite Furnace Spectrometer GTA 100 (Varian). A known precipitate amount was placed in a solution containing KNO_3 0.1 mol l^{-1} and stirred at a constant temperature ($25 \pm 2^\circ\text{C}$) sheltered from light. The solution was sampled regularly and the pH measured each time, until equilibrium was reached. Samples were acidified, filtered (on the cellulose nitrate membrane) and analysed.

2.5. Computer programs

Protonation and metal complex formation constants were calculated from pH-metric titration data using PKAS and BEST computer programs [18].

These computer programs use experimental data (concentration, volume, pH_{exp}). The known or estimated values of the overall stability constants are used to calculate pH_{calc} and minimize the sum of weighted squares of pH residuals ($\text{pH}_{\text{exp}} - \text{pH}_{\text{calc}}$). Constants are calculated according to an iterative method until minimisation is no longer possible. The overall and stepwise stability constants are defined as:

$$\beta_{ijk} = [\text{M}_i\text{H}_j\text{L}_k]/[\text{M}]^i[\text{H}]^j[\text{L}]^k \text{ and}$$

$$K_{ijk} = [\text{M}_i\text{H}_j\text{L}_k]/[\text{M}_i\text{H}_{j-1}\text{L}_k][\text{H}]$$

or

$$\beta_{ijk} = [\text{M}_i(\text{OH})_j\text{L}_k][\text{H}]^j/[\text{M}]^i[\text{L}]^k \text{ and}$$

$$K_{ijk} = [\text{M}_i(\text{OH})_j\text{L}_k][\text{H}]/[\text{M}_i(\text{OH})_{j-1}\text{L}_k]$$

where L is the HEDP or ATMP ligand (Y^{4-} or X^{6-} respectively), charges are omitted for simplification.

Calculated overall stability constants were averaged from a large number of experiments, good agreement exists between theoretical and experimental pH-metric curves, confirming their reliabil-

ity. The standard deviation ($\sigma_{(n-1)}$) was determined from all stability constants calculated for each titration. Stepwise stability constants were calculated from the overall constants determined for each individual experiment, not from averaged overall constants. This explains the gap sometimes observed between the errors in $\log K$ and in $\log \beta$.

A calculation method recently described [1] was used and validated (by two different workers) by the IUPAC procedure [19] with the glycine/nickel(II) system.

The SPE computer program developed by Martell and Motekaitis [18] was also used to draw speciation diagrams from calculated stability constants.

All protometric titration data were computed in the pH range 2–10 for the determination of metal complex formation constants. Protonation constants were determined in a pH range of 2–12 [1]. For more clarity, only complex metal forms were represented on species distribution curves in the pH range of fresh waters, i.e. 5–9.

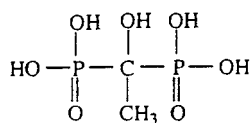
3. Results and discussion

3.1. Protonation constants of ligands

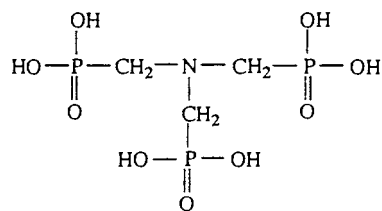
The values for stepwise protonation constants determined here are identical to those previously reported [1] using the same experimental procedure i.e. calculated at 25°C with an ionic strength of 0.1 mol l^{-1} (KNO_3), using the PKAS computer program (Table 1). The protonation constant relative to the acidity of the HEDP hydroxide group was not considered [1,13].

3.2. Complexing properties of HEDP (H_4Y)

The pH-metric titration curves for free ligand and ligand in the presence of metallic cations at 1/2 cation/ligand molar ratio are shown in Fig. 1. It can be assumed that the phosphonate anion Y^{4-} forms relatively stable complexes with the three cations in the entire pH range studied and its complexing behaviour towards Al(III) and Fe(III) is similar. Up to pH 7, HEDP complexes



1-Hydroxyethane-1,1'-Diphosphonic Acid

HEDP H₄Y

Nitrilotris(Methylenephosphonic Acid)

ATMP H₆XScheme 1. Representation of HEDP (H₄Y) and ATMP (H₆X)

with Al(III) and Fe(III) are more stable than those of Cr(III). At pH > 7, there is an inversion of complex stability. The use of fresh metallic solutions in the presence of excess ligand allowed a good reproductibility of experiments at 25°C, with a stable electrode response.

These acid–base titration data were computed with BEST for the determination of metal complex formation constants. Several authors have shown the importance of taking into account both soluble and insoluble hydroxide complexes of trivalent metal ions because they can influence complexation reactions by their easy formation in solution [20–23]. In the presence of organic ligands with stronger affinity, such species could be inhibited. MY(OH)_x^{1-x} ternary complexes must also be considered. They can result from the hydrolysis of species like MY⁻ or be formed from M(OH)_x^{3-x} in the basic pH range as shown for divalent cations in the same system [1] and for Al(III) with other phosphonate ligands [24,25].

The calculation procedure previously described for the determination of metal-complex equi-

Table 1
Stepwise protonation constant values of HEDP and ATMP [1]

	HEDP (H ₄ Y)	ATMP (H ₆ X)
Log K _{a1}	11.0 ± 0.2	12.5 ± 0.2
Log K _{a2}	6.9 ± 0.1	7.22 ± 0.03
Log K _{a3}	2.7 ± 0.1	5.90 ± 0.02
Log K _{a4}	1.6 ± 0.2	4.59 ± 0.03
Log K _{a5}		1.6 ± 0.3
Log K _{a6}		0.5 ± 0.3

I = 0.1 mol l⁻¹ (KNO₃), t = 25°C. K_{ai} = [H_iL]/[H] [H_{i-1}L].

librium constants [1] was used with iterations only with Y⁴⁻ complexes formed, while the protonation constants and metal hydrolysis constants were fixed. These last values (Table 2) were taken from reported data [26–28] and recalculated for our experimental conditions using the Davies equation. Hydrolysis constants recalculated using the semiempirical equation of Daniele et al. [29] for Fe(III), and relations given by Baes and Mesmer [28] for Al(III) and Cr(III) agree with ours, with differences not exceeding 0.1 in log β.

Values of metal complex formation constants for each system at the 1/2 cation/ligand ratio (Table 3) clearly show that there are no significant differences between stability constants of Al(III), Cr(III) and Fe(III) complexes. The highest stabil-

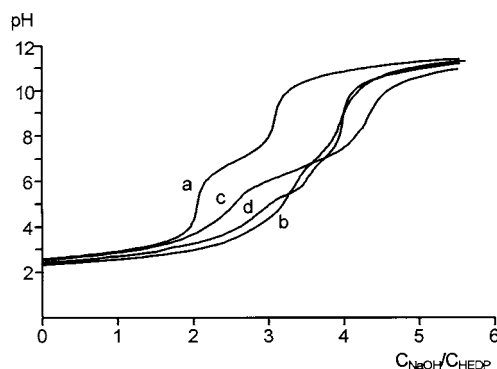


Fig. 1. Titration curves of free HEDP and metal ion/HEDP complex at a 1/2 M/L molar ratio by NaOH (0.1 mol l⁻¹). [HEDP] = 0.002 mol l⁻¹, I = 0.1 mol l⁻¹ (KNO₃), t = 25°C (a) free HEDP; (b) Fe(III)/HEDP; (c) Cr(III)/HEDP; (d) Al(III)/HEDP.

Table 2
Overall metal hydrolysis constant values and solubility quotient for $I = 0.1 \text{ mol l}^{-1}$ (KNO_3), $t = 25^\circ\text{C}$

	Log β_{xy}		
	Fe(III) ^a	Cr(III) ^b	Al(III) ^c
MOH^{2+}	-2.6	-4.6	-5.4
M(OH)_2^+	-6.3	-11.0	-10.0
M(OH)_3^0	-12.6 ^b	-19.3	-15.8
M(OH)_4^-	-22.0	-28.2	-23.5
$\text{M}_2(\text{OH})_2^{4+}$	-2.9	-5.1	-7.7
$\text{M}_3(\text{OH})_3^{5+}$	-6.1	-8.2	-13.7
$\text{M}_4(\text{OH})_6^{6+}$		-15.9	
$\text{M}_{12}(\text{OH})_{34}^{2+}$	-56.0 ^d		
$\text{M}_{13}\text{O}_4(\text{OH})_{24}^{7+}$			-102.7
Solubility quotient		log Q_s	
$\text{M(OH)}_{3(s)}$	2.3	13.3	9.2

$$\beta_{xy} = [\text{M}_x(\text{OH})_y] [\text{H}]^y / [\text{M}]^x, Q_s = [\text{M}^{3+}] / [\text{H}]^3$$

^{a, b, c, d} Recalculated from values at $I = 0 \text{ mol l}^{-1}$ [26–29] respectively.

ity of MY^- complexes corresponds to the lowest stability of the corresponding protonated MHY^0 species. This stability inversion was also observed by Gaizer et al. [24] and could be due to a strong electron transfer from ligand to metal, which would decrease the basicity of uncoordinated donor oxygen atoms. The same tendency is also observed for the MH_2Y^+ species of Cr and Al systems (the calculation of formation constants for FeH_2Y^+ and $\text{AlH}_3\text{Y}^{2+}$ species was not possible because of their low concentration in solution). Moreover, the gap between MY^- and MHY^0 successive constants, and also for MY_2^{5-} and MHY_2^{4-} in the case of Cr, is quite vast. This is probably due to the interference caused by the HEDP hydroxyl group in the cation complexation, as has been previously suggested with other di- and tri-valent cations [9,30].

In all three systems, the formation of mono and/or binuclear hydroxophosphonate complexes indicates the easy hydrolysis of these metal ions.

Standard deviations on stability constants are quite high. Such gaps are however in no way reflective of data treatment, regarding the high stability of complexes.

Comparison of our constant values with those in the literature was difficult as the latter were very scarce and experimental procedures for constant determination were often either not identical to ours or not specified. Nevertheless, for the Cr/HEDP system, our values for MHY^0 and MH_2Y^+ conditional constants ($\log K_1^* = 13.9$; $\log K_2^* = 11.0$) are close to those of Yamashita et al. [12] ($\log K_1^* = 14.6$; $\log K_2^* = 10.4$ where $K_j^* = [\text{M}(\text{H}_j\text{Y})]/[\text{M}][\text{H}_j\text{Y}]$). For Al and Fe/HEDP systems, the overall constant values of Kabachnik et al. [9] and Vasil'ev et al. [13] differ somewhat for several complexed species.

Speciation diagrams were drawn from the metal complex formation and protonation constant values for a 1/2 cation/ligand molar ratio for the pH range 5–9 of fresh waters (Fig. 2). This confirms that even at the acidic end of this pH range, each metal ion is present as a complex. Unlike ternary complexes, free metal cations and hydroxide species are negligible in solution, over the pH range (2–10) that was studied. Species such as M(OH)_4^- are present only at $\text{pH} \geq 12$. No polynuclear hydroxide species was observed in the pH range studied. Below pH 7, interfering protonated and unprotonated complexes have the highest constant values for Al(III) and Fe(III); for $\text{pH} \geq 7$ the predominant species are Al(OH)Y^{2-} and Fe(OH)Y^{2-} with stability constant values lower than those of CrY_2^{5-} .

Acid–base titration data for Al and Cr/HEDP systems with a 1/1 ratio could not be computed by BEST. Interference might occur from insoluble species slowly formed and dissolved during titration. Unfortunately, BEST cannot calculate formation constants when insoluble complexes predominate in solution because it does not take into account solubility products.

When the metal concentration increased (solution containing an excess of cation), insoluble hydroxide complexes such as $\text{Fe(OH)}_{3(s)}$ were formed at $\text{pH} \geq 8$ for the Fe/HEDP 1/1 system, but this was not observed for the other two systems. Tchoubar and Bottero [23] studied the hydrolysis and condensation behaviour of Al and Fe oxy-hydroxides $\text{M}_x\text{O}_y(\text{OH})_z^{(3x-2y-z)}$. They observed the formation of polynuclear hydroxide

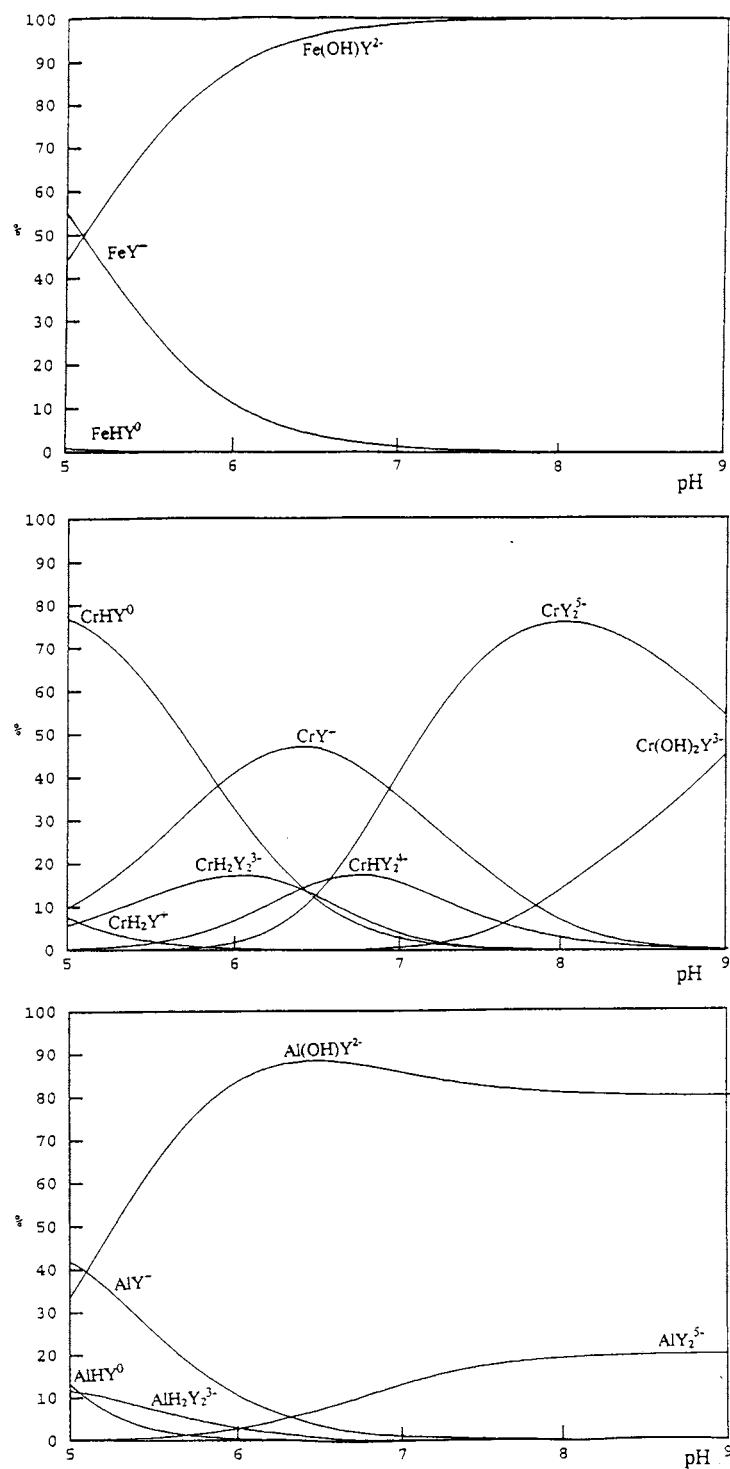


Fig. 2. Distribution curves of Fe(III), Cr(III) and Al(III)/HEDP (Y^{4-}) complexed species, as percentage of total metal vs. pH.

Table 3

Metal complex formation constants of HEDP (Y^{4-}) with Fe(III), Cr(III) and Al(III), calculated for $I = 0.1 \text{ mol l}^{-1}$ (KNO_3) and $t = 25^\circ\text{C}$

	Fe(III)/HEDP		Cr(III)/HEDP		Al(III)/HEDP	
	Log β_{ijk}	Log K_{ijk}	Log β_{ijk}	Log K_{ijk}	Log β_{ijk}	Log K_{ijk}
MY ⁻	24.2 ± 0.2	24.2 ± 0.2	19.0 ± 0.2	19.0 ± 0.2	22.7 ± 0.1	22.7 ± 0.1
MHY ⁰	27.4 ± 0.2	3.2 ± 0.2	24.9 ± 0.1	6.0 ± 0.1	27.2 ± 0.2	4.4 ± 0.2
MH ₂ Y ⁺			28.9 ± 0.1	4.0 ± 0.1	29.1 ± 0.3	1.8 ± 0.3
MH ₃ Y ²⁺			31.1 ± 0.4	2.2 ± 0.4		
M ₂ HY ³⁺					38.7 ± 0.5	
MY ₂ ⁵⁻			26.7 ± 0.1	26.7 ± 0.1	31.1 ± 0.4	
MHY ₂ ⁴⁻			33.3 ± 0.2	6.6 ± 0.2		
MH ₂ Y ₂ ³⁻			39.7 ± 0.1	6.3 ± 0.1	43.1 ± 0.5	
M(OH)Y ²⁻	19.1 ± 0.2				17.6 ± 0.1	
M(OH) ₂ Y ³⁻			3.3 ± 0.2			

$$\beta_{ijk} = \frac{[M_i H_j L_k]}{[M]^i [H]^j [L]^k} \quad K_{ijk} = \frac{[M_i H_j L_k]}{[M_i H_{j-1} L_k] [H]}$$

$$\beta_{ijk} = \frac{[M_i (OH)_j L_k]}{[M]^i [L]^k} \quad K_{ijk} = \frac{[M_i (OH)_j L_k] [H]}{[M_i (OH)_{j-1} L_k]}$$

metallic species at $\text{pH} \geq 4$. In the presence of organic ligands, they reported the formation of heterogeneous aggregates where metals were coordinated by two or three ligands rather than hydroxide ions. Moreover, Spiccia et al. [31,32] and Avena et al. [22] noted the predominance of insoluble mono- and poly-nuclear Cr(III) species in fresh and aged solutions, respectively.

This suggests that such species interfere in solutions containing high concentrations of metal, and that the titration time and age of solutions can lead to the evolution of species. No attempt was made to identify them.

3.3. Complexing properties of ATMP (H_6X)

No titration data could be obtained for the Al/ATMP system due to immediate precipitation of an insoluble complex. This precipitate was therefore characterized by the SEM/EDAX technique at the three different cation/ligand molar ratios: 1/1, 1/2 and 2/1. From the phosphorus/aluminium P/Al = 3.1 ± 0.2 atomic ratio, we can create the simplified formula AlH_3X (without any indication of water molecules). NaOH titration showed the solubilization of this species at $\text{pH} \geq 7$. The titration of the 1/5 ratio solution also led to the formation of an insoluble complex.

Nikitina et al. [10] studied this complexation between ATMP and Al(III) using IR spectroscopy. Employing high metal concentrations (0.1 mol l^{-1}), they observed the formation of both sparingly ($Al_3H_3X_2$ and Al_2X) and readily soluble ($AlHX^{2-}$ and AlX^{3-}) compounds, but gave no stability constants. We can assume that other complexes interfere when metal concentrations are lower, particularly the AlH_3X insoluble species. The kinetic study of precipitate solubilization showed that equilibrium was reached after 33 days and at a pH of 3.67 ± 0.03 . The solubility of the AlH_3X complex, determined by AA, is $s = (4.8 \pm 0.5) \times 10^{-6} \text{ mol l}^{-1}$. The apparent solubility product is directly dependent on the pH value; with $K_s = [Al^{3+}][X^{6-}][H^+]^3 = s^2[H^+]^3$, we calculated $\text{p}K_s = 21.6 \pm 0.1$.

pH -titration curves for the Cr/ATMP and Fe/ATMP systems at 1/2 ratio are presented in Fig. 3. For $\text{pH} < 7.5$, ATMP complexing behaviour towards Cr(III) and Fe(III) is similar and for $\text{pH} \geq 7.5$, Cr(III) is the most complexed. As has been observed in the Al/ATMP system, the formation of insoluble complexes perturbed the Cr/ATMP study for the 1/2 and 1/1 ratios. During titration, the solution became cloudy in the pH range 4–9 and this induced irregularities on the curve. Morozova et al. [11] studied the complexation properties of ATMP with transition metals

and Cr(III). They also observed the formation of a precipitate during titration with a 1/1 ratio. The precipitate in solutions with cation/ligand ratios of 1/1, 1/2 and 2/1 was the same. It was isolated and identified by SEM/EDAX from the P/Cr = 1.6 ± 0.1 atomic ratio as Cr_2X (without indicating the number of water molecules). Unlike the Al/ATMP system, the solubility of Cr_2X species could not be determined because the results in five replicates were not reproducible.

Acid–base titration data for the 1/5 ratio could be analysed using BEST.

Calculated overall and stepwise metal complex formation constants for the Cr/ATMP 1/5 and Fe/ATMP 1/2 systems (Table 4) are very similar. The large decrease in stability of MHX^{2-} species might be caused by the broken bond between the metal and the ATMP amino group. The first protonation of these complexes should, therefore, occur on the nitrogen atom and the following ones on oxygen phosphonate groups as in the case of the free ligand. This phenomenon was described by Bollinger and Roundhill [33] for Fe(III) complexes with aminodiphosphonic acids, and by Nikitina et al. [10] and Sawada et al. [34,35] for various trivalent cation complexes with ATMP. A crystallographic study by Rajendram and Hoggard [36] showed that the coordination of monoprotonated aminophosphonates with Cr(III) occurred on the oxygen atom of phosphonate groups as it probably did for our MHX^{2-} species.

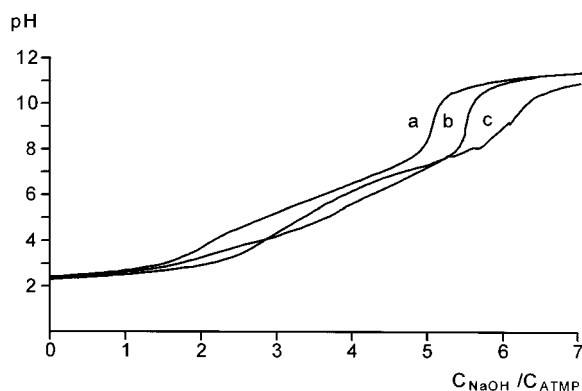


Fig. 3. Titration curves of free ATMP and metal ion/ATMP complex at a 1/2 M/L molar ratio by NaOH (0.1 mol l^{-1}). $[\text{ATMP}] = 0.002 \text{ mol l}^{-1}$, $I = 0.1 \text{ mol l}^{-1}$ (KNO_3), $t = 25^\circ\text{C}$ (a) free ATMP; (b) Fe(III)/ATMP; (c) Cr(III)/ATMP.

Table 4

Metal complex formation constants of ATMP (X^{6-}) with Fe(III) and Cr(III), calculated for $I = 0.1 \text{ mol l}^{-1}$ (KNO_3) and $t = 25^\circ\text{C}$

	Fe(III)/ATMP		Cr(III)/ATMP	
	Log β_{ijk}	Log K_{ijk}	Log β_{ijk}	Log K_{ijk}
MX^{3-}	21.1 ± 0.2	21.1 ± 0.2	20.67 ± 0.04	20.67 ± 0.04
MHX^{2-}	28.1 ± 0.2	7.0 ± 0.3	27.1 ± 0.1	6.5 ± 0.2
MH_2X^-	33.1 ± 0.4	4.8 ± 0.4	32.3 ± 0.2	5.22 ± 0.06
MH_3X^0			36.4 ± 0.2	4.05 ± 0.03
MH_4X^+			39.8 ± 0.2	3.4 ± 0.1
MX_2^{9-}			27.6 ± 0.1	

$$\beta_{ijk} = [\text{M}_i\text{H}_j\text{L}_k]/[\text{M}]^i[\text{H}]^j[\text{L}]^k \quad K_{ijk} = [\text{M}_i\text{H}_j\text{L}_k]/[\text{M}_i\text{H}_{j-1}\text{L}_k][\text{H}]$$

Literature concerning Cr/ATMP complexes gives only qualitative data. No complex formation constant values could be found. Nevertheless, constant values determined here seem to be reliable as a small standard deviation value was obtained between calculated and experimental pH-metric curves (0.03 pH unit).

The study of the Fe/ATMP system was somewhat difficult because of the formation of $\text{Fe}(\text{OH})_{3(s)}$ during titration. Indeed, the speciation diagram shows that $\text{Fe}(\text{OH})_{3(s)}$ becomes the major species at $\text{pH} \geq 5.2$. Titration data were only exploited at $\text{pH} \leq 6.5$ because above this, Fe(III) is totally complexed with hydroxide ligand as $\text{Fe}(\text{OH})_{3(s)}$. Vuceta and Morgan [37] showed that the degree of $\text{Fe}(\text{OH})_{3(s)}$ precipitation was only slightly influenced by complexing agents. Although our calculated and experimental data are very similar (without taking into account the solubility quotient Q_s value (see Table 2) for the $\text{Fe}(\text{OH})_3$ precipitate), stability constants for this system have to be used with caution. Other reported constant values [8] differ from ours. Moreover, at lower metal and ligand concentrations, the present author obtained a colloidal precipitate, which slowly dissolved above pH 5. It would therefore be necessary to precisely characterize the interfering species in this solution in order to verify our results.

Our calculated constants are in agreement with the complexing behaviour of ATMP towards

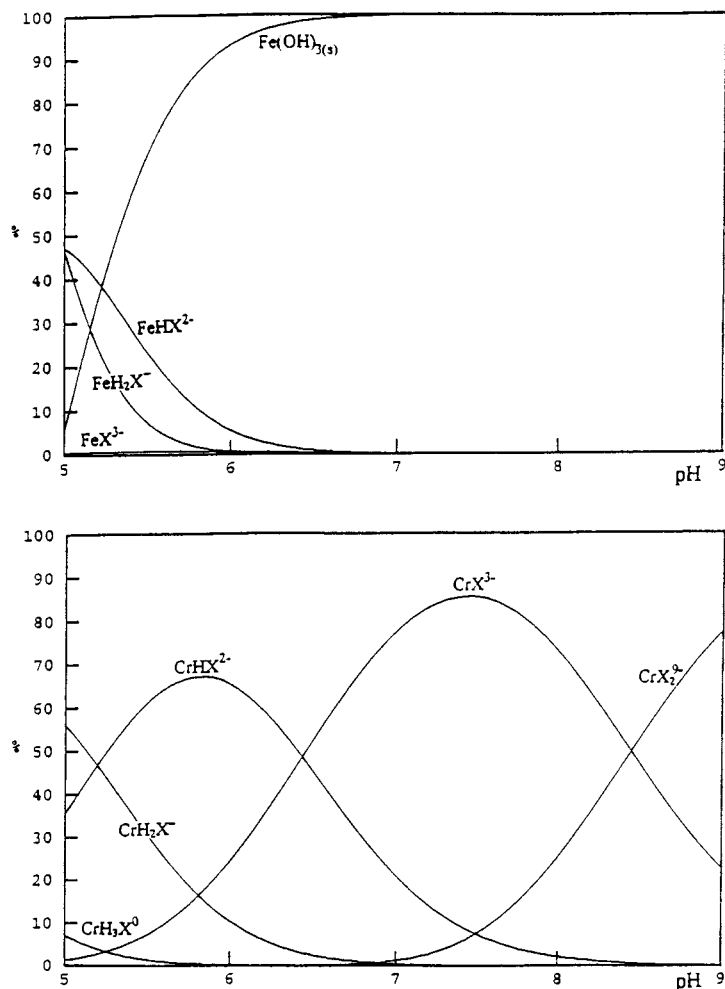


Fig. 4. Distribution curves of Fe(III) and Cr(III)/ATMP (X^{6-}) complexed species, as percentage of total metal vs. pH.

these two metallic cations as it appears on the species distribution curves (Fig. 4). Below pH 7, the interfering complexed species are FeH_2X^- , $FeHX^{2-}$ and FeX^{3-} and CrH_3X^0 , CrH_2X^- , $CrHX^{2-}$ and CrX^{3-} with similar overall constant values. Above pH 7, the major species is the $Fe(OH)_{3(s)}$ precipitate for the Fe/ATMP system, and the ATMP ligand is in its free form. The gap observed between the pH-metric curves for the free ligand and the ligand in the presence of Fe(III) (Fig. 3) corresponds to the decrease in the hydroxide ion concentration in solution due to the formation of $Fe(OH)_{3(s)}$ species. Concerning the

Cr/ATMP system, the CrX^{3-} and CrX_2^{9-} species predominate at basic pH values.

Quantities of hydroxide species, ternary complexes and free metals were negligible for the Cr/ATMP 1/5 solution, as was the Cr_2X^0 soluble species (which precipitates at higher metal concentrations). Ternary complexes and free metals did not appear in the Fe/ATMP 1/2 solution.

4. Conclusion

HEDP and ATMP form strong complexes with the three trivalent cations Al(III), Cr(III) and

Fe(III) studied. These phosphonates could therefore have a major impact on metal speciation in fresh waters or in waste water treatment plants.

With an excess of ligand, there is a predominance of anionic complexed species in the pH range of non acidic natural waters, and therefore little chance that such species can be adsorbed electrostatically onto natural solids. With metal and phosphonate concentrations close to those encountered in natural waters, these metallic complexes would potentially persist in the liquid phase and could increase water contamination.

With an excess of metallic cation, weakly soluble complexes of HEDP seem to form (even though they were not in evidence here), insoluble complexed metals appear in the presence of ATMP as $\text{AlH}_3\text{X}_{(s)}$ and $\text{Cr}_2\text{X}_{(s)}$. Concerning Fe(III), $\text{Fe}(\text{OH})_{3(s)}$ precipitate predominates and its formation is independent of phosphonate concentration. A recent study on the behaviour of phosphonates during wastewater treatment [2] has shown that their elimination rate can reach 80%. This would be due to their adsorption onto or co-precipitation with sludge containing high levels of precipitated iron or aluminium oxides. These phosphonates would not therefore perturb the coagulation/flocculation step when metals are at quite high concentrations.

The presence of insoluble species makes computation of data difficult because only formation constants relative to soluble complexes can be calculated. At present, no computer program amongst those commonly used for analysing the data from acid–base titration can take into account solubility products. This is due to the lack of chemical equilibrium during precipitation.

Our experimental methods did not provide precise information on the coordination and structure of metallic complexes. A study of these complexes using ^{31}P NMR is in progress. Other species that exist in fresh waters, such as carbonates, calcium and magnesium ions, which could interfere in the complexation phenomena between phosphonates and metal ions will also be studied.

Acknowledgements

The authors wish to extend their gratitude to A.K. Bourg for her editing of the English text, R. Al-Shukry, P. Lortholary and J.C. Noulhaguët for their contributions to precipitate analysis, and Prof. K. Sawada for useful discussions. The Regional Council, the 'Contrat de Plan Etat-Région' and the program 'Environnement-Détergents' are gratefully acknowledged for partial financial support.

References

- [1] V. Deluchat, J.C. Bollinger, B. Serpaud, C. Caullet, *Talanta* 44 (1997) 897.
- [2] B. Nowack, submitted to *Wat. Res.* (1996).
- [3] P.V. Coveney, W. Humphries, *J. Chem. Soc. Faraday Trans.* 92 (1996) 831.
- [4] R.B. Martin, *Acc. Chem. Res.* 27 (1994) 204.
- [5] H. Jacqmin, D. Commenges, L. Letenneur, P. Barberger-Gateau, J.F. Dartigues, *Am. J. Epidemiol.* 139 (1994) 48.
- [6] P.M. Outridge, A.M. Scheuhammer, *Rev. Environ. Contam. Toxicol.* 130 (1993) 31.
- [7] R.J. Langlais, *J. Am. Leather Chem. Assoc.* 86 (1991) 413.
- [8] H.S. Hendrickson, *Anal. Chem.* 39 (1967) 998.
- [9] M.I. Kabachnik, R.P. Lastovskii, T.Ya Medved', V.V. Medyntsev, I.D. Kolkpova, N.M. Dyatlova, *Dokl. Chem. (Engl. Transl.)* 177 (1967) 1060.
- [10] L.V. Nikitina, A.I. Grigor'ev, N.M. Dyatlova, *Dokl. Chem. (Engl. Transl.)* 217 (1974) 819.
- [11] S.S. Morozova, L.V. Nikitina, N.M. Dyatlova, G.V. Serebryakova, *Russ. J. Inorg. Chem. (Engl. Transl.)* 20 (1975) 228.
- [12] H. Yamashita, K. Omori, T. Nosaki, *Nippon Kagaku Kaishi* (1991) 168.
- [13] V.P. Vasil'ev, E.V. Kozlovskii, V.V. Serdyukov, *Russ. J. Inorg. Chem. (Engl. Transl.)* 35 (1990) 210.
- [14] M. Maeda, O. Hisada, Y. Kinjo, K. Ito, *Bull. Chem. Soc. Jpn.* 60 (1987) 3233.
- [15] H.M. Irving, M.G. Miles, L.D. Pettit, *Anal. Chim. Acta* 38 (1967) 475.
- [16] G. Gran, *Analyst* 77 (1952) 661.
- [17] F.J.C. Rossotti, H. Rossotti, *J. Chem. Educ.* 42 (1965) 375.
- [18] A.E. Martell, R.J. Motekaitis, *Determination and Use of Stability Constants*, 2nd ed., VCH, New York, 1992.
- [19] A. Braibanti, G. Ostacoli, P. Paoletti, L.D. Pettit, S. Sammartano, *Pure Appl. Chem.* 59 (1987) 1721.
- [20] J.R. Duffield, J.R. Johns, F. Marsicano, D.R. Williams, *Polyhedron* 10 (1991) 1121.
- [21] F.C. Richard, A.C.M. Bourg, *Wat. Res.* 25 (1991) 807.

- [22] M.J. Avena, C.E. Giacomelli, C.P. De Pauli, J. Colloid Interface Sci. 180 (1996) 428.
- [23] D. Tchoubar, J.Y. Bottero, C.R. Acad. Sci. Paris 322 (II a) (1996) 523.
- [24] F. Gaizer, G. Hägele, S. Goudetsidis, H. Papadopoulos, Z. Naturforsch. 45b (1990) 323.
- [25] K. Atkari, T. Kiss, R. Bertani, R.B. Martin, Inorg. Chem. 35 (1996) 7089.
- [26] R.M. Smith, A.E. Martell, Critical Stability Constants, vol. 6, (Suppl. 2), Plenum Press, New York, 1989.
- [27] J. Kragten, Atlas of Metal-Ligand Equilibria in Aqueous Solution, Ellis Horwood, Chichester, UK, 1978.
- [28] C.F. Baes, R.E. Mesmer, The Hydrolysis of Cations, Wiley, New York, 1967.
- [29] P.G. Daniele, C. Rigano, S. Sammartano, V. Zelano, *Talanta* 41 (1994) 1577.
- [30] E.N. Rizkalla, M.T.M. Zaki, M.I. Ismail, *Talanta* 27 (1980) 715.
- [31] L. Spiccia, Inorg. Chem. 27 (1988) 432.
- [32] A. Drljaca, L. Spiccia, Polyhedron 15 (1996) 2875.
- [33] J.E. Bollinger, D.M. Roundhill, Inorg. Chem. 32 (1993) 2821.
- [34] K. Sawada, M. Kuribayashi, T. Suzuki, H. Miyamoto, J. Solution Chem. 20 (1991) 829.
- [35] K. Sawada, T. Ichikawa, K. Uehara, J. Chem. Soc. Dalton Trans. (1996) 3077.
- [36] C.R.A. Rajendram, P.E. Hoggard, J. Coord. Chem. 33 (1994) 15.
- [37] J. Vuceta, J.J. Morgan, Environ. Sci. Technol. 12 (1978) 1302.

Complexation of trivalent cations (Al(III), Cr(III), Fe(III)) with two phosphonic acids in the pH range of fresh waters

Stella Lacour, Véronique Deluchat, Jean-Claude Bollinger *, Bernard Serpaud

Laboratoire de Chimie Analytique, Sciences de l'Eau et de l'Environnement, Faculté des Sciences, 123 avenue Albert-Thomas, 87060 Limoges, France

Received 3 June 1997; received in revised form 3 October 1997; accepted 6 October 1997

Abstract

The complex formation constants of two phosphonic acids, HEDP and ATMP, with three trivalent metallic cations, Al(III), Cr(III) and Fe(III), have been determined by acid–base titration at 25°C and constant ionic strength (0.1 mol l⁻¹, KNO₃), using Martell and Motekaitis' computer programs. Species distribution curves showed that all three cations are in complex form in the pH range of fresh waters (5–9). The study of different cation/ligand ratios proved that both ligands mainly form anionic soluble complexes for systems having an excess of ligand—as protonated and unprotonated forms and especially ternary complexes with HEDP. For higher metal concentrations (excess of cation), weakly soluble species of HEDP and ATMP were formed with Al(III) and Cr(III). Two insoluble complexes with ATMP have been identified by SEM/EDAX as AlH₃X_(s) and Cr₂X_(s). Regarding Fe(III) species, Fe(OH)_{3(s)} precipitate seems to predominate in solution. © 1998 Elsevier Science B.V. All rights reserved.

Keywords: Complexation; Phosphonic acids; Speciation; Trivalent cations

1. Introduction

Due to a growing increase in public environmental concern, the use of sodium tripolyphosphate has been banned in domestic detergents. In recent years phosphonate derivatives have been used in washing powder formulations. However, some concerns still exist about their behaviour when released in lakes or rivers, as they can complex with toxic elements previously immobilized in sediments. We have studied two com-

monly used phosphonic acids, 1-hydroxyethane-1,1'-diphosphonic acid (HEDP) and aminotris(methylenephosphonic acid) (ATMP) (Scheme 1), whose acid/base and complexation behaviours with divalent cations have recently been characterized [1].

After domestic use, these phosphonic acids are released along with the rest of the domestic waste waters. In municipal waste treatment plants, a phosphorus elimination step can reduce phosphonate levels by 80% [2]. This step is however costly and is not always included in the treatment process. Phosphonates can enter aquatic ecosystems, and later flow through water potabilization plants

* Corresponding author. Fax.: +33 555 457459; e-mail: jcbollinger@unilim.fr

Flow injection spectrophotometric determination of trace amounts of selenium

M.F. Mousavi *, A.R. Ghiasvand, A.R. Jahanshahi

Department of Chemistry, Tarbiat Modarres University, P.O. Box 14155-4838, Tehran, Iran

Received 11 December 1996; received in revised form 8 October 1997; accepted 10 October 1997

Abstract

A simple, rapid and sensitive flow injection spectrophotometric method for determination of selenium ($0.005\text{--}1.5\ \mu\text{g ml}^{-1}$) is described. The method is based on the catalytic effect of Se(IV) on the reduction reaction of thionine (TN) with sulphide ion, monitored spectrophotometrically at 598 nm. The detection limit is $5\ \text{ng ml}^{-1}$ the relative standard deviation for eight replicate measurements is 1.1% for $1\ \mu\text{g ml}^{-1}$ of selenium. The sampling rate is 25–30 samples h^{-1} . The procedure was applied successfully to the determination of selenium in real samples. © 1998 Elsevier Science B.V. All rights reserved.

Keywords: Flow injection; Spectrophotometry; Catalytic; Selenium; Thionine; Sulphide; Trace metal

1. Introduction

There is a rather narrow range of concentration levels for several essential elements such as Se in most organisms. Low concentrations result in different abnormalities because of pertinent specific biochemical changes. High concentrations result in toxicity [1].

Selenium is used in photocells, metal rectifiers, in colouring glass a red or reddish tint and in the production of flame-proof insulated electric wires [2]. Selenium compounds are also used in lubricating oils as oxidation inhibitors, in the improvement of the detergent properties of lubricating oils, and in shampoo (small amounts) as a dan-

druff inhibitor. Adding selenium to certain stainless steels is believed to improve their machining properties [3].

There is an increasing demand for sensitive determination methods for selenium in different samples. Many extraction-spectrophotometric [4,5], catalytic-spectrophotometric [6,7], fluorimetric [8], neutron activation [9,10], ICP-AE [11], voltammetric [12], chromatographic [13], hydride generation [14], ICP-MS [15], X-ray fluorescence spectrometric [16], electrothermal [17], and flow injection analysis [18,19] methods that have been developed for determination of selenium. Some of these methods give good selectivity and sensitivity, but require very expensive reagents and are time consuming and complicated procedures.

This paper describes a simple, sensitive and rapid method for the determination of Se(IV)

* Corresponding author. Fax: +98 21 8006544; e-mail: mousavim@net1cs.modares.ac.ir

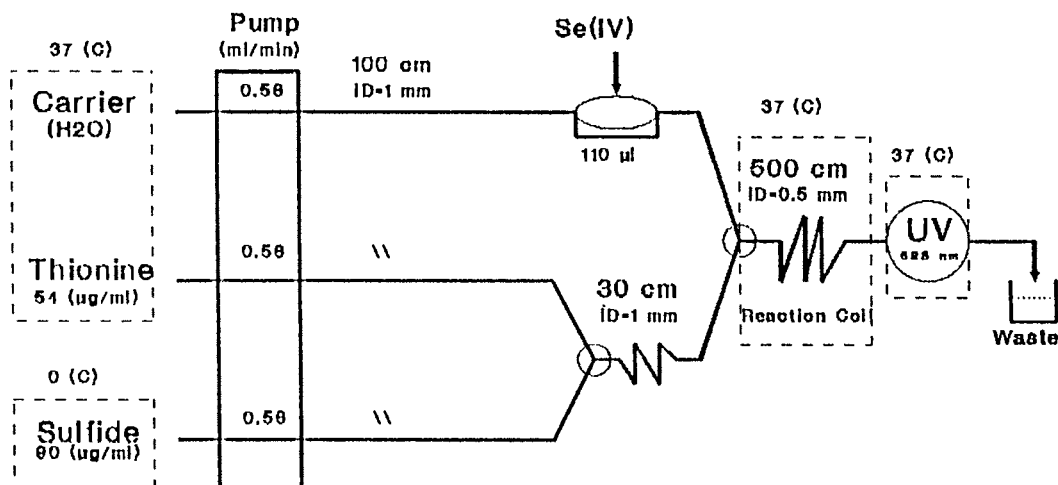


Fig. 1. Schematic diagram of the FIA system for the determination of Se(IV).

based on its catalytic effect on the reduction reaction of thionine (TN) with sulphide ion.

2. Experimental

2.1. Reagents

All chemicals used were of the highest purity available and used without any further purification. Doubly distilled water was used throughout.

Sulphide stock standard solution ($1000 \mu\text{g ml}^{-1}$) was prepared by dissolving 0.7500 g of $\text{Na}_2\text{S}\cdot x\text{H}_2\text{O}$ ($7 < x < 9$, Merck) in water and diluting to 100 ml in a calibrated volumetric flask. This solution was prepared daily and standardized iodometrically [20]. Working solutions were prepared by appropriate dilution of the stock solution with water.

Selenium stock solution ($1000 \mu\text{g ml}^{-1}$) was prepared by dissolving 0.1405 g of SeO_2 (Merck) in water and diluting to 100 ml in a volumetric flask. The solution was standardized iodometrically [20].

A $200 \mu\text{g ml}^{-1}$ stock solution of TN was prepared by dissolving an appropriate amount of dyestuff (Merck) in water this was kept refrigerated.

2.2. Apparatus

The flow injection configuration that was employed is outlined in Fig. 1. Silicon tubing of 0.5 and

1 mm i.d. was used for the manifold and mixing coil, tees were made of glass. A twelve-channel peristaltic pump (PLG, Desaga) was used for propelling the solutions. Samples were injected using a rotating Rheodyne valve (VALCO-C8W) with a sample loop of 110 μl . A double beam UV-Vis spectrophotometer (Shimadzu, 2100) with a thermostated flow cell was used to record the absorbance of TN at 598 nm. Except for the sulphide solution, all other reagents were placed in a 37°C thermostated water bath.

The sulphide solution was kept at 0°C, to ensure solution stability during the course of the reaction.

The reaction coil was placed in a 37°C water bath. The flow cell was also maintained at 37°C by circulation of the thermostated water. A thermostated bath (Shimadzu, TB-85) and a water bath (GFL-D 3600) were used. Measurement of pH was made using a Metrohm (691) pH-meter.

2.3. Recommended procedure

A $54 \mu\text{g ml}^{-1}$ TN solution (containing 20% citrate-phosphate buffer [21], pH 7.2) and a $90 \mu\text{g ml}^{-1}$ sulphide solution were each pumped at a flow rate of 0.56 ml min^{-1} . An 110 μl sample volume containing selenium ($0.005\text{--}1.5 \mu\text{g ml}^{-1}$) was injected into the carrier which was also pumped at a flow rate of 0.56 ml min^{-1} . The absorbance of the mixture was measured and recorded at 598 nm.

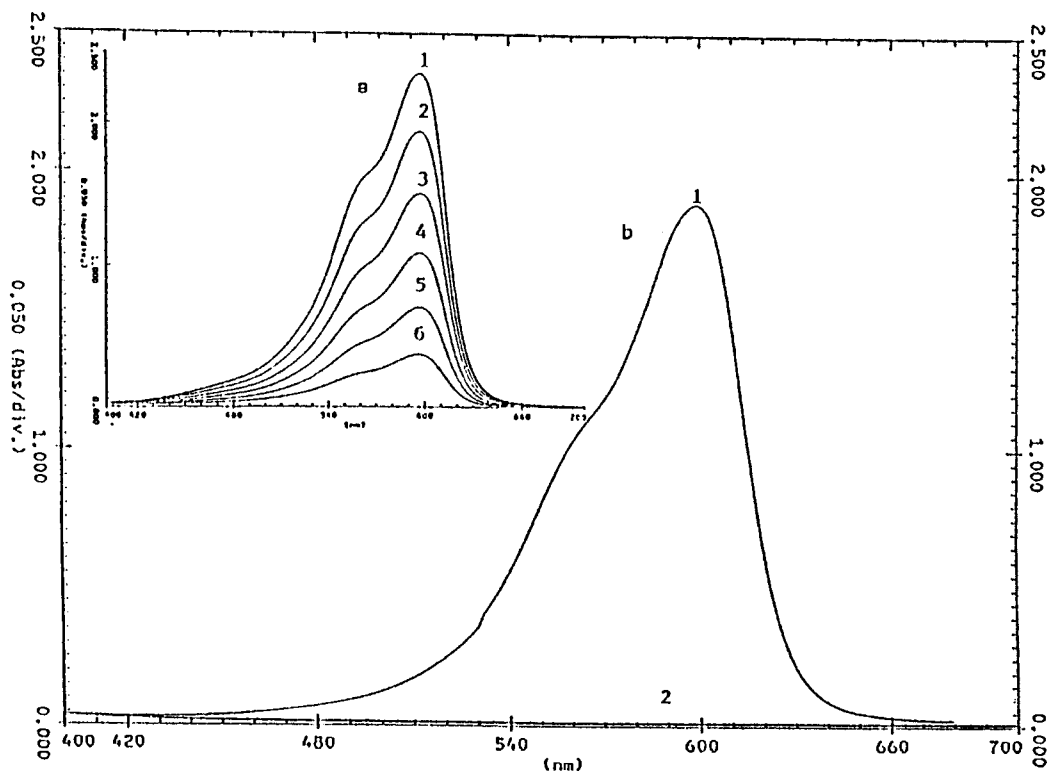


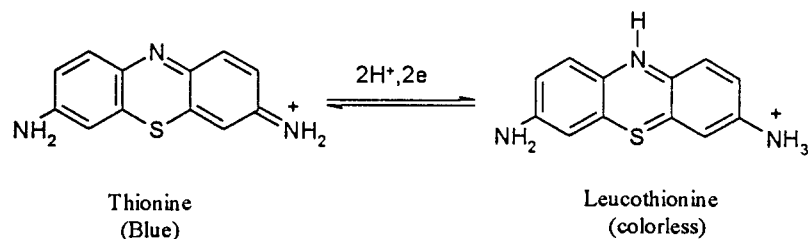
Fig. 2. Absorbance spectra of thionine ($18 \mu\text{g ml}^{-1}$) in the presence of sodium sulphide ($30 \mu\text{g ml}^{-1}$) at pH 7.2, time intervals 70 s, $T = 37^\circ\text{C}$, (a) in the absence of Se(IV), (b) in the presence of $0.33 \mu\text{g ml}^{-1}$ of Se(IV).

Under optimum conditions the peak height was proportional to selenium concentration.

3. Results and discussion

3.1. Batchwise studies

The reaction for the reduction of TN is as follows [22]:



This reaction proceeds slowly without a catalyst (see Fig. 2). However, trace amounts of Se(IV) catalyzes the reaction so that it proceeds much faster (Fig. 2 curve b). The accelerating effect of Se(IV) has been explained [23] by the formation of $[\text{S}\dots\text{Se}]^{2-}$, after the initial reduction of Se(IV) to its elemental state [24]. This compound can reduce the dye molecule faster than the sulphide ion and then reform Se(IV). The reaction can be

monitored spectrophotometrically, because the reduced TN (leucothionine) is colorless.

3.2. Effect of chemical reaction variables

3.2.1. Effect of pH

The effect of pH on peak height was studied in the range of 2.2–10.3 using a mixture of citrate and phosphate buffers, and NaOH. The reaction exhibits its largest peak height at about pH 7.2. This was used as the optimum pH for further studies.

3.2.2. Effects of dye and sulphide concentrations

The influence of thionine and sulphide concentrations on peak height was investigated (Fig. 3). The concentrations of thionine and sulphide were adjusted in the range 15–72 and 30–126 $\mu\text{g ml}^{-1}$ respectively. An increase in peak height was observed when the concentration of dye was varied from 15–54 $\mu\text{g ml}^{-1}$, at higher dye concentration a slight change in response was observed. Sulphide concentrations higher than 90 $\mu\text{g ml}^{-1}$ causes a decrease in the response peak. A concentration of 54 and 90 $\mu\text{g ml}^{-1}$ was selected for dye and sulfide respectively.

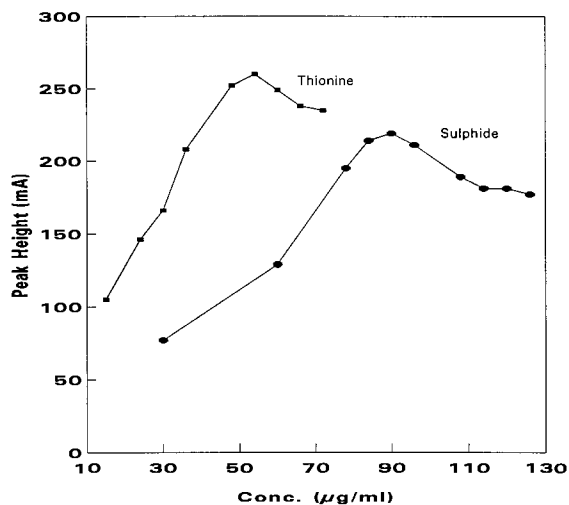


Fig. 3. Effects of thionine and sulphide on peak height. Conditions, Se(IV), 1 $\mu\text{g ml}^{-1}$; pH, 7.2; T, 25°C; sample loop volume, 110 μl ; reaction coil length, 1.5 m; flow rate, 0.56 ml min^{-1} ; thionine, 30 $\mu\text{g ml}^{-1}$ for sulphide curve; sulphide, 90 $\mu\text{g ml}^{-1}$, for thionine curve.

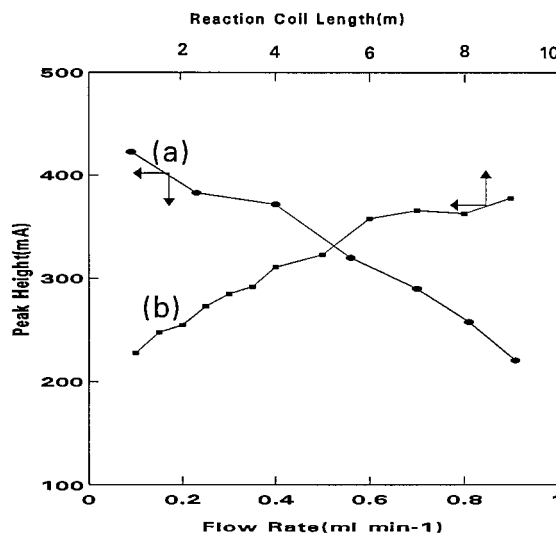


Fig. 4. Effects of the reaction coil length and flow rate on the peak height. Conditions: Se(IV), 1 $\mu\text{g ml}^{-1}$; pH, 7.2; T, 25°C; sample loop volume, 110 μl ; thionine, 54 $\mu\text{g ml}^{-1}$; sulphide, 90 $\mu\text{g ml}^{-1}$; flow rate 0.56 ml min^{-1} , for curve (a); reaction coil length, 5 m for curve (b).

3.2.3. Effect of temperature and ionic strength

The effect of temperature on peak height was studied. A continuous increase in the response peak was observed when the temperature was varied from 20–39°C. A temperature of 37°C was selected for further studies.

The effect of ionic strength on the response was studied using NaNO_3 . Up to a value of about 0.6 M of NaNO_3 , change in ionic strength had no considerable effect on peak height. A further increase in ionic strength caused a slight increase in peak height.

3.3. Effect of flow injection variables

In the application of any flow injection method, the change in absorbance depends on the residence time of the sample zone in the system i.e. on the flow rate and the reaction coil length. The effect of the flow rate on the peak height was studied over a range 0.1–0.9 ml min^{-1} in each stream (Fig. 4, curve a). Lower flow rates produced higher peaks, but flow rates lower than 0.56 ml min^{-1} resulted in peak broadening leading to lower sample output. High flow rates (higher than

0.8 ml min⁻¹) had two drastic effects, decreasing sensitivity by decreasing peak height and second, the driving force of each peristaltic pump roller was seen as noise (small peak) on the baseline. The latter effect decreases reproducibility and makes the detection limit of the system worse, hence a flow rate of 0.56 ml min⁻¹ was selected.

Reaction coil lengths of 1–9 m were tested (Fig. 4, curve b). The peaks became higher as the length of coil increased from 1 to 7 m, but a further increase did not result in any significant change in sensitivity lengths of exceeding 5 m caused peak broadening, a reaction coil length of 5 m was chosen.

To obtain the best overall response the effect of sample volume was also investigated in the range 20–200 µl (Fig. 5). The peak height increased up to a sample volume of 110 µl and then remained more or less constant. A sample volume of 110 µl was chosen.

3.4. Calibration curve, reproducibility and detection limit

Under optimum conditions described above, a selenium concentration range of 0.005–1.5 µg ml⁻¹ produced a quite linear calibration curve ($r = 0.9992$, $n = 14$).

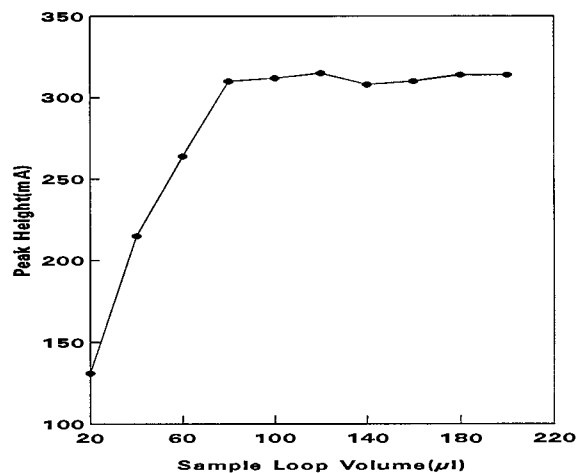


Fig. 5. Effect of sample volume on peak height. Conditions, Se(IV), 1 µg ml⁻¹; pH, 7.2; T, 25°C; thionine, 54 µg ml⁻¹; sulphide, 90 µg ml⁻¹; reaction coil length, 5 m; flow rate 0.56 ml min⁻¹.

Table 1

Tolerance limits of diverse ions on the determination of 1 µg ml⁻¹ selenium at optimum conditions

Ion	Tolerated ratio of foreign ion to Se(IV)
K ⁺ , Na ⁺ , NO ₃ ⁻ , Cl ⁻	0.1M
HPO ₄ ²⁻ , CH ₃ COO ⁻ , I ⁻	2000 ^a
Ca(II), CO ₃ ⁻	500
Ag(I), Pb(II), Cu(II), Hg(II), Fe(III)	200 ^b
Zn(II), HCO ₃ ⁻ , tartarate	200
SO ₃ ²⁻	150 ^c
Cr(III), Br ⁻ , H ₂ PO ₄ ⁻ , OCN ⁻ , N ₃ ⁻ , B ₄ O ₇ ²⁻	100
Mg(II), NH ₄ ⁺ , SO ₃ ²⁻ , BrO ₃ ⁻	40
Ni(II), IO ₃ ⁻	10
Mn(II), Cd(II), Co(II), S ₄ O ₆ ²⁻	5

^a Above of which was not tested.

^b After removal with cation exchange resin.

^c After masking with formaldehyde (2×10^{-5} M).

Using a signal to noise ratio of three, as a limiting requirement, the experimental detection limit was found to be 0.005 µg ml⁻¹.

For eight replicate measurements of standard selenium solution (1 µg ml⁻¹), the relative standard deviation was 1.1%. The sampling rate was 25–30 samples h⁻¹.

3.5. Effect of foreign ions

The effects of various cations and anions on the determination of 1 µg ml⁻¹ of Se(IV) was studied. The results are summarized in Table 1. The tolerance limit was taken as the concentration of added ion causing less than 3% relative error.

Almost all anions (with respect of SO₃²⁻) and many cations used have no effect on the determination of selenium. However, as expected the presence of cations which can form insoluble precipitates with the sulphide ion cause interference.

3.5.1. Removal of interfering ions

Cations such as Ag(I), Pb(II), Cu(II), Hg(II), Fe(III), interfere with the determination of the Se(IV) ion. These cations can be removed using a cation exchanger resin (Aldrich, strongly acidic form) [25]. A series of 10 ml solutions containing 7.5 µg of Se(IV) plus 1500 µg of the desired cation

Table 2
Determination of selenium in Kjeldahl tablets

Sample taken (ml)	Se ($\mu\text{g ml}^{-1}$)		Recovery (%)
	Contained	Found	
0.5	0.100	0.976	97.6
1.0	0.200	0.207	103.5
1.5	0.300	0.295	98.3
2.0	0.400	0.418	104.5
2.0	0.400	0.410	102.5

were prepared. Each solution (10 ml) was passed through a 20 cm column containing the cation exchanger resin. The column was washed with distilled deionized water (four times, with 10 ml of water) and the eluent was transferred to a 50 ml volumetric flask. The solution was diluted to the mark with distilled deionized water and the amount of Se(IV) was determined using the recommended procedure.

Among the anions studied, the presence of sulphite ion causes serious interference. The interfering effect of this anion was removed using formaldehyde [25].

3.6. Application

To evaluate the analytical applicability of this method, it was applied to the determination of selenium in Kjeldahl tablets and a health-care product (a shampoo for the treatment of dandruff) respectively. One tablet (1.1151 g) containing 0.05 g of selenium was dissolved in an appropriate volume of 4 M HCl solution and was then boiled for 15 min. This stage converts Se(VI)

completely to Se(IV) [26]. The solution was neutralized by the addition of 2 M NaOH solution and diluted with water to 100 ml in a volumetric flask. This solution (2 ml) was diluted to 100 ml with water. During the final stage different volumes of the resulting solution were transferred to a 50 ml volumetric flask and was determined using the recommended procedure after diluting to volume with water. The results are given in Table 2.

A shampoo sample dissolution was carried out using the procedure described by Afkhami et al. [27]. Approximately 1 g of the sample was weighted into a 100 ml Kjeldahl flask. Concentrated sulphuric acid (1 ml) was added and the mixture was heated to fuming for 15 min. The solution was allowed to cool and 5 ml of 30% w/v hydrogen peroxide was added. The mixture was boiled vigorously to eliminate excess hydrogen peroxide, the flask was then allowed to cool. The mixture was diluted to 1.0 l with doubly distilled water. A 1 ml volume of this solution was taken for the determination of selenium(IV) as in the recommended procedure. The results are given in Table 3.

4. Conclusion

The method adopted was significant with respect to the development of a simple, precise and rapid flow injection method for the analysis of selenium in real samples. The high sensitivity, selectivity, broad dynamic range of selenium determination and mild pH conditions required are just some of the advantages of this method. The

Table 3
Determination of selenium in shampoo

Sample taken (ml)	Se (ng)		Se in sample (ng)	Recovery (%)
	Added	Found		
1.0	0	28.96	28.96	—
1.0	10	39.2	29.2	102.4
1.0	20	49.63	29.63	103.3
1.0	30	58.18	28.18	97.4
1.0	40	67.05	27.05	95.2

Table 4
Comparison of merit of the present work with previously reported results

References	Dynamic range ($\mu\text{g ml}^{-1}$)	Detection limit ($\mu\text{g ml}^{-1}$)	Precision (RSD %)
[6]	2.5–25	1	1.1
[28]	—	0.0003	2.6
[29]	0.005–0.150	0.0015	<5
[30]	0.005–0.1	—	4.7
The present work	0.005–1.5	0.005	1.1

merits of this present work over previously reported FIA methods [28–30] are summarized in Table 4.

Acknowledgements

The support of this work by the Tarbiat Modarres University Research Council is gratefully acknowledged.

References

- [1] S.M. Alaejos, D.C. Romero, *Chem. Rev.* 95 (1995) 227.
- [2] R.E. Kirk, D.F. Othmer, *Encyclopedia of Chemical Technology*, vol. 12, John Wiley & Sons, New York, 1980, p. 145.
- [3] J.W. Bagnall, *The Chemistry of Selenium, Tellurium and Polonium*, Elsevier, Amsterdam, 1966.
- [4] H. Manish, K.N. Ramachandran, V.K. Gupta, *Talanta* 41 (1994) 1623.
- [5] I.L. Lambert, P. Arthur, T.E. Moor, *Anal. Chem.* 23 (1951) 1101.
- [6] C.M. Lozano, T.P. Ruiz, V. Tomas, C. Abellen, *Analyst* 114 (1986) 715.
- [7] W. Hewkes, *Anal. Chim. Acta* 183 (1986) 197.
- [8] H.F. Bayfield, L.F. Romalis, *Anal. Biochem.* 144 (1985) 569.
- [9] J. Yang, M.H. Yang, S. Lin, *Anal. Chem.* 62 (1990) 146.
- [10] G.D. McOrist, J. Fardy, R. Sleet, *J. Radioanal. Nucl. Chem.* 158 (1992) 293.
- [11] R. Bye, *Talanta* 37 (1990) 1029.
- [12] B. Huang, H. Zhang, J. Pu, F. Yin, S. Zheng, H. Yang, *Anal. Lett.* 18 (1985) 279.
- [13] G.S. Bldew, J.J.M. Goeiji, N.P.E. Vermeulen, *J. Chromatogr.* 496 (1989) 11.
- [14] I. Hansson, J. Pttersson, A. Olin, *Talanta* 34 (1987) 829.
- [15] M. Janghorbani, B.T.G. Ting, *Anal. Chem.* 61 (1989) 701.
- [16] V. Bethel, V. Hamm, A. Knochel, *Fresenius Z. Anal. Chem.* 335 (1989) 855.
- [17] G.R. Carnrick, D.C. Manning, W. Slavin, *Analyst* 108 (1983) 1297.
- [18] B. Welz, M. Schubert-Lacobs, *At. Spectrosc.* 12 (1991) 91.
- [19] C.M. Lozano, T.P. Ruiz, V. Tomas, C. Abellan, *Analyst* 114 (1989) 715.
- [20] A.I. Vogel, *A Text Book of Quantitative Inorganic Analysis*, 3rd ed., Longman, London, 1961.
- [21] J.A. Dean, *Lange's Hand Book of Chemistry*, 12th ed., McGraw-Hill, New York, 1979, pp. 5–82.
- [22] M. Jiang, F. Jiang, J. Duan, X. Tang, Z. Zhao, *Anal. Chim. Acta* 234 (1990) 403.
- [23] F. Feigel, P.W. West, *Anal. Chem.* 19 (1947) 351.
- [24] A. Safavi, A. Afkhami, A. Massoumi, *Anal. Chim. Acta* 232 (1990) 351.
- [25] M.F. Mousavi, M. Shamsipur, *Bull. Chem. Soc. Jpn.* 65 (1992) 2770.
- [26] H. Parham, M. Shamsipur, *Bull. Chem. Soc. Jpn.* 64 (1991) 3067.
- [27] A. Afkhami, A. Safavi, A. Massomi, *Talanta* 39 (1992) 993.
- [28] C.Y. Chan Chris, S. Sadana Ram, *Anal. Chim. Acta* 270 (1992) 231.
- [29] M.G. Fernandez Cobo, M.A. Palacios, C. Carmen, *Anal. Chim. Acta* 283 (1993) 386.
- [30] D.W. Bryce, A. Izquierdo, M.D. Luque de Castro, *Anal. Chim. Acta* 308 (1995) 96.

Orthogonal array design (OAD) for the optimization of mercury extraction from soils by dilute acid with microwave heating

Wei Gu, Chao Yan Zhou, Ming Keong Wong *, Leong Ming Gan

Department of Chemistry, National University of Singapore, Lower Kent Ridge Road, Singapore 119260, Singapore

Received 8 July 1997; received in revised form 9 October 1997; accepted 10 October 1997

Abstract

The use of dilute acid for mercury extraction from geological samples with microwave assisted heating was investigated. An orthogonal array design $OA_{16}(4^1 \times 2^{12})$ was applied to select the optimum conditions. The effects of the concentration of HNO_3 , the additions of HCl and H_2SO_4 , the extraction time and their interactions were evaluated by the mixed-level orthogonal array design (OAD). The results indicated that the addition of small amount of HCl would improve significantly the extraction of mercury from soil matrices. From the study, it is seen that the mercury in the soil matrices could be extracted completely by 14% (v/v) HNO_3 with small quantity of HCl . The effects of the pressure within the digestion vessel and the sample mass were studied under the optimum conditions derived from the OAD. The extraction methods with optimum conditions were evaluated by determining mercury in NIST SRM 1645 River Sediment, NIES CRM No. 2 Pond Sediment and NRCC BCSS-1 Marine Sediment. Recoveries of 78–109% were achieved. Good mean recoveries of 95–98% were also obtained from real soil samples spiked with different species of mercury. © 1998 Elsevier Science B.V. All rights reserved.

Keywords: Dilute acid; Mercury; Microwave digestion; Soil; Orthogonal array design

1. Introduction

Mercury is a toxic element sparsely distributed in the lithosphere. Its concentration has been estimated to be 0.08–0.4 mg kg^{-1} in igneous and sediment or soil samples [1]. Industrial and other human activities have resulted in increased localized concentration of Hg. Since soils and sediments are the principal sinks of most of these

localized discharges [2], they are good indicators of the extent of environmental contamination [3].

The most widely used procedure for the determination of Hg in geological samples is digestion by mineral acids and then the Hg in solution is measured by cold vapor atomic absorption spectrometry (CVAAS). The technique of CVAAS is highly sensitive for mercury with a method detection limit of 0.2 $\mu g l^{-1}$ and has gained generalized acceptance for routine mercury analysis. However, there are a variety of methods for the chem-

* Corresponding author.

ical pretreatment of the sample. The wet ashing method is recommended for the mercury determination by CVAAS methods. For most wet digestion with open vessel, different mixtures of acids and chemicals are used to increase the oxidizing power and the boiling temperature of the digestion medium [3–6]. Generally, several hours are needed for completely extracting the mercury from sample matrices for most of these methods.

In the past few years, closed vessel microwave dissolution procedures have been developed to reduce sample preparation/pretreatment times from hours to minutes and to prevent the loss of the volatile analytes [7–10]. Pressure dissolution procedures have been recommended for the determination of mercury in different types of samples using different acid mixtures [11,12]. Most of these methods also use the concentrated acid mixtures with strong oxidizing nature, such as nitric-sulfuric acid mixtures [11] and concentrated nitric hydrochloric acid mixtures [10,12]. In the closed vessel digestion, the oxidizing power of the acids is increased with increasing digestion temperature and the loss of the volatile component is limited.

The optimum conditions of extraction were evaluated by a chemometric method—orthogonal array design (OAD). In OAD [20], orthogonal arrays are used to assign factors to a series of experiment combination, the results of which can then be analyzed by analysis of variance (ANOVA) and other common mathematical methods. The main effects of the variables and interaction effects between variables can be extracted separately. This statistical method can be used to optimize experimental conditions and reduce the number of experiments [8,18,21]. This method was introduced into the area of analytical chemistry in 1989 by Oles and Yankovich [22], who used OAD to optimize operation conditions of gas chromatographic analysis. Since then, OAD was applied in gas chromatography [23], liquid chromatography [24] and microwave digestion of biological samples [25].

It was reported that the poor recoveries of Hg were obtained when nitric acid alone was used to extract mercury in soil samples [13]. However,

dilute nitric acid has been successfully used to extract mercury from traditional Chinese medicines with heating [17]. In this work, the OAD was used to investigate the mercury extraction from soil samples by dilute acid in a closed vessel digestion system. The effectiveness of the various extraction methods was compared using the National Institute for Environmental Studies (NIES) Certified Reference Materials (CEM) No. 2 Pond Sediment. Other standard reference materials were also used to verify the selected extraction conditions.

2. Experimental

2.1. Instrumental

A flow injection analysis system (Perkin-Elmer FIAS-200) interfaced to an atomic absorption spectrometer (Perkin-Elmer Model 4100ZL) was used. This system consists of two peristaltic pumps, Tygon pump tubing, 1.0 mm-i.d. Teflon manifold tubing, a gas-liquid separator and a quartz T-cell with resistive furnace heating. Pump action, injection time, quartz cell temperature and all data processing were controlled through Perkin-Elmer FIAS200 software on a personal computer. Specific instrumental parameters for mercury analysis in this system are given in Table 1.

Soil samples were digested in the MDS-2000 Microwave Sample Preparation System with 630

Table 1
FIA instrumental parameters for the determination of mercury

Wavelength	253.6 nm
Light source	EDL
Lamp current	6 mA
Measurement time	Peak area in 30 s
FIAS fill time	10 s
FIAS inject time	15 s
Carrier 3% (v/v)	HCl
Reductant	0.25% (w/v) NaBH ₄ in 0.05% (w/v) NaOH
Cell temperature	150°C
Sample Loop	500 µl

W power (CEM, Matthews, NC). An internal pressure and temperature control system allowed for programming to control pressure from 0 to 1380 kPa (200 psi) and temperature up to 200°C in five separate stages. The system can digest 12 samples using low pressure screw-top polytetrafluoroethylene (PTFE) digestion vessels.

2.2. Reagents

Deionized distilled water was used in all final washings and in the dilution of all chemicals. Analytical grade concentrated nitric acid (65% w/v), sulfuric acid (98% w/v) and hydrochloric acid (37% w/v) (Merck, Germany) were used throughout the study. Mercury standards were prepared by appropriately diluting a 1000 mg/l mercury nitrate aqueous standard solution (BDH, UK). Sodium tetrahydroborate (NaBH_4) (Fluke, Buchs, Switzerland) reducing agent (0.25% w/v) in 0.05% (w/v) sodium hydroxide (ARISTA grade, BDH, UK) was prepared fresh daily by dissolving the appropriate mass of NaBH_4 and NaOH in deionized distilled water. The solution was then filtered with 0.45 μm Millipore filter. Oxidative stabilizing agent was prepared fresh by dissolving 5 g of analytical-grade potassium permanganate (AJAX, Australia) in 100 ml deionized distilled water.

2.3. Procedure

2.3.1. Drying of sample

Separate real world soil samples obtained from the campus (Singapore) and standard references were dried in the oven at 110°C for 4 h to obtain mass loss data. Undried samples were analyzed to avoid the effects of mercury loss. The results for the undried samples were multiplied by the mean undried to dried sample mass ratio obtained from the separate drying experiment. All reported values are based on the dried sample.

2.3.2. Preparation of sample spiking

HgO/HgS/HgAc of 0.05 g were weighed and mixed well with 100 g soil. The mixtures were finely ground in an agate mortar. Then 0.10 g mixtures were further mixed with another 100 g

soil. The finely ground final mixtures were kept in a desiccator.

2.3.3. Microwave digestion procedure

In the optimization procedure, the digestion parameters of 14 ml 2–20% (v/v) HNO_3 , 1 ml conc. HCl, 1 ml conc. H_2SO_4 and extraction time were changed according to the arrangement of orthogonal array design (Table 2). The digestion was carried out under pressure setting 1035 kPa (150 psi). The optimized parameters were then used for the analysis of 'application' samples.

Approximately 0.25 g samples and blanks were digested using the different parameter settings. After the digestion, the vessels were cooled in the air until the pressure in the vessels was reduced to below 345 kPa (50 psi). The vessels were opened and the digest was filtered and then diluted with deionized distilled water to 50.0 ml in a volumetric flask.

2.4. Analysis

Ten millilitres of digested solution (and blanks) were transferred to test tubes (used for auto sampler AS-90) and 0.2 ml of 5% (w/v) potassium permanganate solution was added as an oxidative stabilizing agent before analysis. The mixtures were introduced to the FIA system by AS-90 auto sampler. A continuously flowing HCl acid carrier stream transported the sample from the valve to the mixing manifold, where it was merged with NaBH_4 reductant. The reaction mixture was then purged with argon gas stream and transported to the gas–liquid separator, where the cold vapor mercury was swept to the absorption cell, and the peak area signal was measured. Mercury concentration in the sample solution was determined by direct comparison to a calibration curve prepared using solutions from 0.5 to 20 $\mu\text{g l}^{-1}$ that were matched in acid and stabilizer concentration with that of the sample.

2.5. Assignment of experiments

In the closed vessel microwave assisted extraction system, the extraction is carried out under high pressure and high temperature. The extrac-

Table 2
Assignment of variables and level settings after a randomization process for the microwave digestion by an $OA_{16}(4^1 \times 2^{12})$ matrix

	Column No.															
	1	2	3	4	5	6	7	8	9	10	11	12	13			
Level	<i>A</i>	<i>B</i>	$(A \times B)_1$	$C \times D$	$(A \times B)_2$	$(A \times B)_3$	<i>C</i>	$(A \times C)_1$	$B \times D$	$(A \times C)_2$	$(A \times C)_3$	$B \times C$	$(A \times D)_1$	<i>D</i>	$(A \times D)_2$	$(A \times D)_3$
1	2	15				1								0		
2	14	30				0								1		
3	20															
4	8															

A, concentration of HNO_3 (%); *B*, extraction time (min); *C*, addition of conc. H_2SO_4 (ml); *D*, addition of conc. HCl (ml).

Table 3
The $OA_{16}(4^1 \times 2^{12})$ matrix and the experimental results

No.	Column No.													R
	1	2	3	4	5	6	7	8	9	10	11	12	13	
1	1	1	1	1	1	1	1	1	1	1	1	1	1	66.6
2	1	1	1	1	1	2	2	2	2	2	2	2	2	66.7
3	1	2	2	2	2	1	1	1	1	2	2	2	2	84.4
4	1	2	2	2	2	2	2	2	2	1	1	1	1	63.8
5	2	1	1	2	2	1	1	2	2	1	1	2	2	68.5
6	2	1	1	2	2	2	2	1	1	2	2	1	1	83.1
7	2	2	2	1	1	1	1	2	2	2	2	1	1	95.0
8	2	2	2	1	1	2	2	1	1	1	1	2	2	71.9
9	3	1	2	1	2	1	2	1	2	2	1	2	2	90.7
10	3	1	2	1	2	2	1	2	1	2	1	2	1	71.5
11	3	2	1	2	1	1	2	1	2	2	1	2	1	72.5
12	3	2	1	2	1	2	1	2	1	1	2	1	2	90.9
13	4	1	2	2	1	1	2	2	1	1	2	2	1	86.5
14	4	1	2	2	1	2	1	1	2	2	1	1	2	59.9
15	4	2	1	1	2	1	2	2	1	2	1	1	2	76.6
16	4	2	1	1	2	2	1	1	2	1	2	2	1	80.7
K1	281.5	593.5	605.6	619.7	610.0	640.8	617.5	609.8	631.5	619.6	551.3	626.6	619.7	
K2	318.5	635.8	623.7	609.6	619.3	588.5	611.8	619.5	597.8	609.7	678.0	602.7	609.6	
K3	325.6													
K4	303.7													

tion efficiency is increased dramatically with rising temperature and pressure. The relation between pressure and temperature in the extraction vessel is affected by the sample matrix, the composition and the concentration of acid mixture used. When using volatile acid such as HNO_3 for extraction, the pressure control is critical. When the extraction is carried out with less volatile acids such as H_2SO_4 or $HClO_4$ [15], the temperature control is important. From the literature and our experience, the following six variables were chosen for evaluation in this study. They are: the concentration of HNO_3 (variable i); the addition of H_2SO_4 (variable ii); the addition of HCl (variable iii); the extraction time (variable iv); the mass of sample (variable v); and the pressure setting (variable vi). The first four variables were optimized by a mixed-level OAD. The mass of sample and the pressure setting were studied separately. In the mixed-level OAD, the concentration of HNO_3 (variable I) was evaluated in four-level, the additions of H_2SO_4 (variable ii) and HCl (variable iii) and the extraction time were evaluated in two-level. Since there were one four-

level and three two-level variables to be evaluated, the $OA_{16}(4^1 \times 2^{12})$ matrix was used to assign the variables considered. After a randomization process, the variable assignment and level setting in the mixed-level orthogonal array design were listed in Table 2. The randomization process for the level setting was to reduce the error from personal inclination on level assignment. In this paper, the interactions among the variables $A \times B$, $A \times C$, $A \times D$, $B \times C$, and $C \times D$ were considered. The interaction A and B ($A \times B$) was obtained by the sum of $(A \times B)_1$, $(A \times B)_2$ and $(A \times B)_3$. The other interactions $A \times C$ and $A \times D$ were similarly obtained.

The variable assignment, the level setting and experimental arrangement in the mixed-level orthogonal array design are shown in Table 3. A total of 16 experiments are listed in the column of trial. The numbers 1, 2, 3 and 4 under the various column number in the table represent the level setting in the experiment. The K_m ($m = 1-4$) values in the last four rows are the sum of response (R) with variable m . K_m is used to estimate the effect of the variable.

Table 4
ANOVA results for output responses in the $OA_{16}(4^1 \times 2^{12})$ matrix

Source	SS	Df	MS	F	Percent contribution	Best level
<i>A</i>	284.732	3	94.910	7.08 ^b	16.5	<i>A</i> 3
<i>B</i>	111.830	1	111.830	8.34 ^c	6.5	<i>B</i> 2
<i>C</i>	170.955	1	170.955	12.75 ^c	9.9	<i>C</i> 1
<i>D</i>	1003.305	1	1003.305	74.82 ^a	58.0	<i>D</i> 2
<i>A</i> × <i>B</i>	32.255	3			1.9	
(<i>A</i> × <i>B</i>) ₁ <i>C</i> × <i>D</i>	20.475	(1)				
(<i>A</i> × <i>B</i>) ₂	6.375	(1)				
(<i>A</i> × <i>B</i>) ₃	5.405	(1)				
<i>A</i> × <i>C</i>	78.890	3		1.96 ^d	4.6	
(<i>A</i> × <i>C</i>) ₁ <i>B</i> × <i>D</i>	2.030	(1)				
(<i>A</i> × <i>C</i>) ₂	5.880	(1)				
(<i>A</i> × <i>C</i>) ₃	70.980	(1)				
<i>A</i> × <i>D</i>	48.200	3			2.8	
<i>B</i> × <i>C</i> (<i>A</i> × <i>D</i>) ₁	6.125	(1)				
(<i>A</i> × <i>D</i>) ₂	6.375	(1)				
(<i>A</i> × <i>D</i>) ₃	35.700	(1)				
Error	80.455	6	13.409			
Total	1730.167	15			100.2	

^a $P = 0.01$ (99% confidence level) $F_{(1,6)} = 13.75$.

^b $P = 0.05$ (95% confidence level) $F_{(3,6)} = 4.76$.

^c $P = 0.05$ (95% confidence level) $F_{(1,6)} = 5.99$.

^d $P = 0.25$ (75% confidence level) $F_{(3,6)} = 1.78$.

For evaluating the effects of the variables at different levels from 16 experimental trials, the concentration of mercury in the NIES CRM No. 2 Pond Sediment was used as response function. The mercury was analyzed by CVAAS. The output response (*R*) in our work is defined as:

$R = \text{accuracy of mercury analysis (\%)} = \frac{\text{mercury content from experiment}}{\text{certified value given by CRM No. 2}} \times 100\%$

The optimization was performed under the pressure setting at 1035 kPa (150 psi) and the sample mass at about 0.25 g. The effects of the pressure setting and the mass of sample were then studied separately.

3. Results and discussion

After implementing the 16 experimental trials

which were designed according to the $OA_{16}(4^1 \times 2^{12})$ matrix, the corresponding results of output response for each experimental trial were calculated and listed in Table 3. The analysis of variance (ANOVA) technique was used and the results of ANOVA and *F*-test are shown in Table 4. From Table 4, it is seen that factor *D* (addition of HCl) is statistically the most significant at $P < 0.01$, whereas no statistical differences are observed for any other variable or interaction considered at $P < 0.01$. The percent contribution was over 50%. The factor *A* (concentration of HNO_3), factor *B* (extraction time) and factor *C* (addition of H_2SO_4) are statistically significant at $P < 0.05$. The percent contributions of the interactions of *A* × *B* and *A* × *D* are quite low and contribute < 5%, thus they can be pooled as error. The effect of interaction of *A* × *C* was also discussed. The effects of pressure setting and sample mass were studied later after the other variables had been optimized.

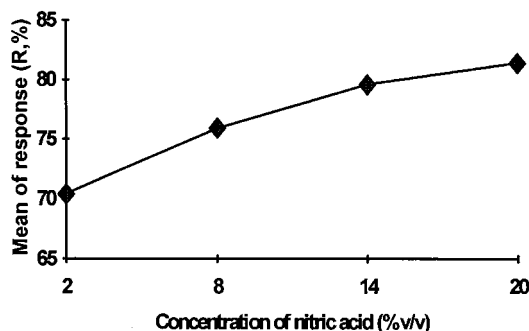


Fig. 1. Effect of the concentration of nitric acid on mean of response (R) for extraction.

3.1. Effect of the concentration of HNO_3

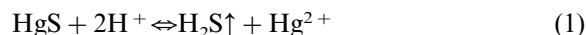
The effect of the concentration of HNO_3 as factor A was evaluated at four different levels in the $\text{OA}_{16}(4^1 \times 2^{12})$ matrix. The ANOVA results indicated that the concentration of HNO_3 significantly influenced the mercury extraction since the F -test result is significant at $P < 0.05$, but its effect was less than that of other factors evaluated. Fig. 1 shows the relationship between the concentration of HNO_3 and the mean responses (R) which are the mean values of K_m ($m = 1-4$). From Fig. 1, the best level is 20% (v/v) HNO_3 , but the increase in mercury recovery was very small from 79.6 to 81.4% when the concentration of HNO_3 was increased from 14 to 20%. From the four-by-two table of the interaction between the HNO_3 concentration (factor A) and the addition of HCl (factor D) (Table 5), it is seen that the mercury recoveries increased substantially from 75.6 to 89.1% as the HNO_3 concentration was increased from 2 to 14% with the addition of HCl . Table 5 was obtained from the mean values of R containing different level settings of variables A

and D in 16 trials. When the concentration of HNO_3 in the extract solutions with HCl was further increased from 14 to 20%, no significant difference (89.1–90.8%) was observed from the mercury recoveries. Thus the 14% (v/v) HNO_3 was used in the subsequent study.

3.2. Effect of addition of HCl

The addition of other acids such as HCl and H_2SO_4 along with HNO_3 was to improve the oxidizing ability and enhance the partition coefficient of mercury between vapor and solution [13,15]. Most of these added acids in the digestion mixtures were no longer decisive factors when closed-vessel microwave digestion was used, since the selected parameter settings could produce similar effects. However, the addition of HCl in the extraction or digestion mixtures is still critical, since it would result in better recovery of mercury from soil samples.

Most of the mercury in soil or sediment samples exists in the form of HgO , HgS and organic mercury. Both organic mercury and HgO are soluble in acid [14,15,17]. However, HgS is only very slightly soluble in acid which is the main reason for the reduced recovery of mercury in the commonly used wet digestion and microwave digestion methods. HgS is often present in geological materials such as rock, soils and sediments [14,16]. When HgS is placed in dilute HNO_3 , the following equilibrium exists:



Since HgS is only slightly soluble in dilute HNO_3 , the concentration of Hg^{2+} is very low. When HCl is added to the solution, the stable $[\text{HgCl}_4]^{2-}$ complex formed will shift the equi-

Table 5

Mean response (R) for four-by-two table of the interaction between the concentration of HNO_3 (variable A) and the addition of HCl (variable D)

	Concentration of HNO_3			
	2% (level 1)	8% (level 4)	14% (level 2)	20% (level 3)
Addition of HCl				
0 ml (level 1)	65.2	68.3	70.2	72.0
1 ml (level 2)	75.6	83.6	89.1	90.8

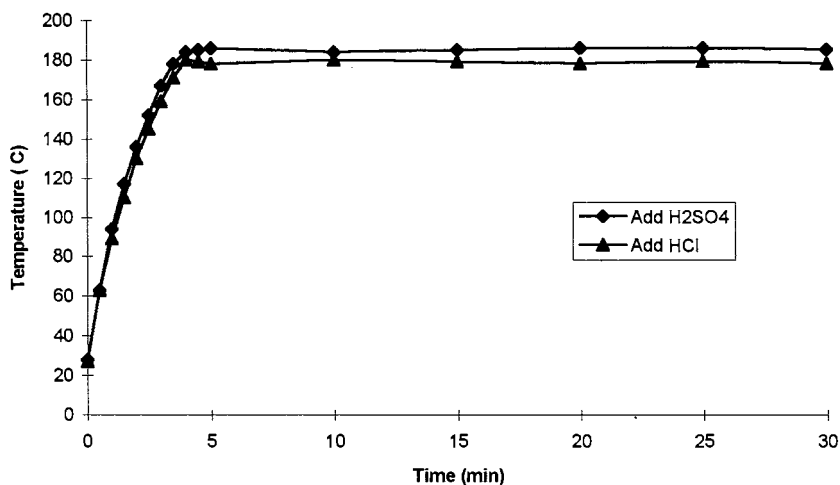


Fig. 2. Temperature change with the addition of 1 ml different acids in 14% (v/v) HNO_3 .

librium to the right and hence more HgS will be dissolved. Thus the addition of HCl would improve the extraction of Hg from soil samples. From the results of ANOVA, the addition of HCl was statistically significant at $P < 0.01$ and the percent contribution is 58%. As shown in Table 5, good recoveries ($\sim 90\%$) were obtained when 1 ml of HCl was added to 14 ml of extract solutions of either 14 or 20% (v/v) HNO_3 . The addition of 1 ml of HCl in the extraction solution thus was used in the subsequent study.

3.3. Effect of addition of H_2SO_4

In the closed vessel microwave digestion of soil samples with acid mixtures containing H_2SO_4 , the temperature setting was considered first, because the temperature increased quickly during initial digestion time and reached easily to vessel tolerance [15]. In the soil sample digestion with acid mixtures with high ratio of H_2SO_4 , the temperature control is preferred and the single pressure control can not be used to control the digestion. The acid mixtures with low ratio content of H_2SO_4 could be used in microwave digestion with pressure control. In this study, only 1 ml of H_2SO_4 was added in the acid mixture, and acid mixtures with and without H_2SO_4 were evaluated. The addition of H_2SO_4 was found to be significant at $P < 0.05$ but the percent contribution in SS

(Table 4) is only 9.9. It means that the addition of 1 ml of H_2SO_4 had improved the extraction of mercury from the soil sample but was not the main factor to be considered. To study the effect of the addition of H_2SO_4 in our present study, the temperature was recorded during the closed-vessel microwave digestion process and is shown in Fig. 2. It is seen that the addition of the H_2SO_4 had increased the digestion temperature $\sim 7^\circ$ during most of the digestion period. High temperature would increase the oxidizing power of the acid which would improve the mercury extraction efficiency. Comparing the results of digestion medium with and without H_2SO_4 in the four-by-two Table 6 which is similarly obtained as that of Table 5, the addition of 1 ml H_2SO_4 in HNO_3 (2–14%) had improved the mercury extraction efficiency from 75.5 to 81.8%. However, when 20% HNO_3 were used to extract mercury from the soil samples, no advantage could be obtained by adding 1 ml H_2SO_4 .

3.4. Effect of extraction time

With the assistance of microwave oven, the extraction time can be reduced from several hours even a day to within an hour. In this work, the extraction time was evaluated at two levels of 15 and 30 min, respectively. From the results of ANOVA, the effect of the extraction time was

Table 6

Mean response (R) for four-by-two table of the interaction between the concentration of HNO_3 (variable A) and the addition of H_2SO_4 (variable C)

Addition of H_2SO_4	Concentration of HNO_3			
	2% (level 1)	8% (level 4)	14% (level 2)	20% (level 3)
0 ml (level 2)	65.3	70.3	77.5	81.2
1 ml (level 1)	75.5	81.6	81.8	81.6

statistically significant at $P < 0.05$. From our earlier work [8,18], it is known that extraction time is an important factor to be considered. Fig. 3 shows the effect of extraction time on the mercury recoveries. The results indicate that increasing the extraction time from 15 to 30 min had improved the extraction efficiency from 85 to $100 \pm 2\%$. Considering the different matrix of soils, extraction time of 30 min was subsequently used in the study.

3.5. The interaction effect

The interactions among the variables A , B , C and D were considered. The interaction $A \times B$ was obtained by the sum of $(A \times B)_1$, $(A \times B)_2$, $(A \times B)_3$, and similarly for $A \times C$ and $A \times D$. The interaction $C \times D$ is in the same column of $(A \times B)_1$, $B \times D$ in the same column of $(A \times C)_1$ and $B \times C$ in the same column of $(A \times D)_1$. It is difficult to separate the effects from different interactions in the same column. Since the SS of $B \times D$ and $(A \times C)_1$ and $B \times C$ and $(A \times D)_1$ are 2.030 and 6.125 (Table 4), the effects of $B \times D$ and $B \times C$ can be ignored in the study. The effects of $B \times D$ and $B \times C$ were merged in $A \times C$ and $A \times D$, respectively. The SS of $(A \times B)_1$ and $C \times D$ is 20.475 (Table 4). Even if all the SS came from $C \times D$, the percent contribution from $C \times D$ would still be $< 1.2\%$. Thus the effect of $C \times D$ was not considered in later study. The sum of the SS from $(A \times C)_1$, $(A \times C)_2$ and $(A \times C)_3$ is 78.890. Hence, the interaction $A \times C$ is considered separately. The effects of $A \times B$ and $A \times D$ are not significant, they were pooled as error. The interaction $A \times C$ was evaluated in Table 6 and its effect was discussed in the section in the effect of addition of H_2SO_4 .

3.6. Effect of pressure

The extraction of mercury from soil samples by microwave oven depends on the quantities of acids used, the extraction time, the sample mass and the parameter settings of the microwave oven. The concentration of HNO_3 , the addition of HCl and H_2SO_4 and the extraction time were evaluated using the $\text{OA}_{16}(4^1 \times 2^{12})$ orthogonal array design. During the study, the pressure setting was fixed at 1035 kPa (150 psi) for the 16 runs. After optimizing the other conditions (acid mixture, 14% HNO_3 (v/v) + 1 ml HCl ; the sample mass, 0.3 g; the digestion time, 30 min), the effect of pressure setting was studied. The results are listed in Table 7. Good recoveries were obtained at pressures higher than 828 kPa (120 psi). Considering the complex nature of soils and sediments, the pressure setting of 1035 kPa (150 psi) was selected.

3.7. Effect of sample mass

Sample mass is also an important factor for the extraction of mercury from soil sample, especially for the dilute acid extraction. For the closed-vessel digestion or extraction of trace metals from soil samples, the sample mass is dependent on the vessel volume, the quantity of the acid mixture and the concentrations of the acids [15]. Most of the sample sizes used in the microwave digestion were < 0.50 g [15,19]. Under the selected conditions, samples ranging from 0.15 to 0.55 g of the NIES CRM No. 2 Pond Sediment were tested. Results are listed in Table 8. When the sample mass was over 0.35 g, the recoveries of the mercury were reduced significantly. It indicates that the selected acid mixture cannot extract mercury completely from soil sample matrices under the

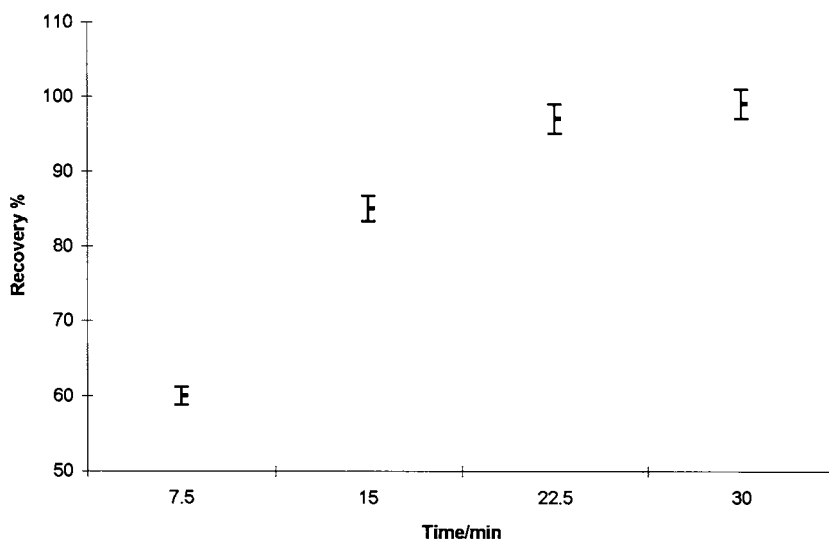


Fig. 3. Effect of the extraction time on mercury recovery using 14 ml 14% (v/v) HNO_3 + 1 ml HCl.

recommended conditions. Although good recovery of mercury was obtained at the sample mass of 0.3 g, considering the complex and varied nature of soil samples, a sample size of 0.25 g was recommended for dilute acid extraction.

3.8. Application to samples

From our previous discussion, the use of 14% (v/v) HNO_3 combined with the addition of 1 ml concentrated HCl was recommended for the extraction of mercury from 0.25 g soil samples using closed vessel microwave digestion. The digestion was carried out under the pressure setting at 1035 kPa (150 psi) and 30 min for the extraction time. To further verify this extraction method, three standards of NIST SRM 1645 River Sediment,

NIES No. 2 Pond Sediment and NRCC BCSS-1 Marine Sediment and one real world soil sample spiked with different mercury compounds were tested. The analytical results are listed in Table 9. Good recoveries were obtained for standard samples and the real world soil sample spiked with different mercury species. Thus the proposed method is suitable for different sample matrices. There was no loss of either organic and inorganic mercury during extraction.

4. Conclusion

In conclusion, with the use of microwave-assisted closed vessel extraction system, mercury

Table 7
Analytical results of mercury in NIES CRM No. 2 Pond Sediment^a with different pressure settings

Pressure settings/kPa	Test result ($\mu\text{g g}^{-1}$)
552 (80 psi)	0.99 ± 0.02
828 (120 psi)	1.33 ± 0.08
1035 (150 psi)	1.30 ± 0.03

^a Certified value of NIES CRM No. 2 Pond Sediment is $1.3 \mu\text{g g}^{-1}$.

Table 8
The analytical results of mercury in NIES CRM No. 2 Pond Sediment with different sample mass

Mass of sample/g	Found value ($\mu\text{g g}^{-1}$)
0.15	1.31 ± 0.06
0.25	1.17 ± 0.03
0.30	1.24 ± 0.03
0.35	1.10 ± 0.02
0.45	0.78 ± 0.10
0.55	0.71 ± 0.12

Table 9

Analytical results of mercury ($\mu\text{g g}^{-1}$) in different standard materials and a real soil sample spiked with different mercury compounds extracted by the acid mixture with 14 ml of dilute nitric acid (14% v/v) and 1 ml of concentrated HCl ($n = 3$)

Sample	Certified value ($\mu\text{g g}^{-1}$)	Spiked	Added ($\mu\text{g g}^{-1}$)	Amount found ($\mu\text{g g}^{-1}$)	Recoveries (%)
NIST SRM 1645 River Sediment	1.1 ± 0.5	—	...	1.07 ± 0.05	93–102
NIES CRM No.2 Pond Sediment	1.3	—	...	1.29 ± 0.03	98–102
NRCC BCSS-1 Marine Sediment	0.129 ± 0.012	—	...	0.12 ± 0.02	78–109
Soil sample	0.41 ± 0.05	HgO	2.40	2.34 ± 0.30^a	98
Soil sample	0.41 ± 0.05	HgS	2.40	2.28 ± 0.22^a	95
Soil sample	0.41 ± 0.05	HgAc	2.40	2.36 ± 0.19^a	98

^a After subtracting the amount of Hg originally present in soil.

could be extracted from 0.25 g soil samples using 14% (v/v) HNO_3 within 30 min. The addition of a small amount of HCl in the dilute nitric acid improved the extraction efficiency significantly by forming the stable $[\text{HgCl}_4]^{2-}$. This recommended method had been successfully applied to the analysis of different soil samples.

References

- [1] A.A. Levinson, Introduction Geochemistry, Applied Publishing, Calgary, 1974.
- [2] D. Purves, Trace-element contamination of the environment, Elsevier, Amsterdam, 1985, p. 66.
- [3] S. Landi, F. Fagioli, Anal. Chim. Acta 298 (1994) 363–374.
- [4] J.W.B. Stewart, J.R. Bettany, in: A.L. Page, R.H. Miller, D.R. Keeney (Eds.), Methods of Soil Analysis, Part 2, American Society of Agronomy (ASA), Soil Science Society of America (SSSA), Madison, WI, 1982, p. 367.
- [5] U.S. Environmental Protection Agency, Test Methods for Evaluating Solid Wastes, SW 864, vol. 1, Washington, DC, 3rd ed., 1986, Sec. A, (A) Method 7471, (B) Method 7470.
- [6] Association of Official Analytical Chemists (AOAC), Official Methods of Analysis, in: K. Helrich (Ed.), Arlington, VA, 15th ed., vol. 1, 1990, (A) Sec. 971.21, (B) 977.15.
- [7] A. Morales-Rubio, M.L. Mena, C.W. McLoed, Anal. Chim. Acta 308 (1995) 364.
- [8] C.Y. Zhou, M.K. Wong, L.L. Koh, Y.C. Wee, Anal. Chim. Acta 314 (1995) 121.
- [9] H.M. Kingston, L.B. Jassie, (Eds.), Introduction to Microwave Sample Preparation: Theory and Practices, American Chemical Soc., Washington, DC, 1988.
- [10] R. Saraswati, C.M. Beck, M.S. Epstein, Talanta 40 (1993) 1477.
- [11] C. Koopmann, A. Prange, Spectrochim. Acta 46B (1991) 1395.
- [12] P. Quevauviller, J.L. Imbert, M. Olle, Mikrochim. Acta 112 (1993) 147.
- [13] S.B. Adeloju, H.S. Dhindsa, R.K. Tandon, Anal. Chim. Acta 285 (1994) 359.
- [14] H. Sakamoto, T. Tomiyasu, N. Yonehara, Anal. Sci. 8 (1992) 35–39.
- [15] C.Y. Zhou, M.K. Wong, L.L. Koh, Y.C. Wee, Anal. Sci. 12 (1996) 471.
- [16] A. Kuldvere, Analyst 115 (1990) 559.
- [17] P.Y.T. Chou, T.H. Chua, K.F. Tang, B.Y. Ow, Analyst 120 (1995) 1221.
- [18] W.G. Lan, M.K. Wong, N. Chen, Y.M. Sin, Analyst 119 (1994) 1659.
- [19] H. Matusiewicz, R.E. Sturgeon, Prog. Anal. Spectrosc. 12 (1989) 21.
- [20] R.N. Kacker, E.S. Lagergren, J.J. Filliben, J. Res. Natl. Inst. Stand. Technol. 96 (1991) 577.
- [21] W.G. Lan, M.K. Wong, N. Chen, Y.M. Sin, Analyst 119 (1994) 1669.
- [22] P.J. Oles, A. Yankovich, LC–GC 7 (1989) 579.
- [23] P.J. Oles, J. Assoc. Off Anal. Chem. 73 (1990) 724.
- [24] H.B. Wan, W.G. Lan, M.K. Wong, C.Y. Mok, Anal. Chim. Acta 289 (1994) 371.
- [25] C.Y. Zhou, M.K. Wong, L.L. Koh, J. Anal. At. Spectrom. 11 (1996) 585.

Stability studies and purification procedure for nitrite solutions in view of the preparation of isotopic reference materials¹

Jean-Claude Wolff *, Ulf Örnemark ², Philip D.P. Taylor, Paul De Bièvre

Institute for Reference Materials and Measurements (IRMM), European Commission-JRC, B-2440 Geel, Belgium

Received 15 July 1997; received in revised form 9 October 1997; accepted 10 October 1997

Abstract

The lack of reference materials, accurately certified for nitrite, is a problem in view of the importance of this species for environmental and medical reasons. This work outlines a plan for the preparation of nitrite isotopic reference materials (IRMs) in the form of high purity solutions, certified for their nitrite–nitrogen isotopic composition and nitrite concentration. To achieve the desired accuracy (expanded uncertainty U with a coverage factor $k = 2$ of $\leq 2\%$), primary methods of measurement such as isotope dilution mass spectrometry (IDMS), gravimetry, and titrimetry must be used. The main difficulty is the stability of nitrite. Other problems expected in the preparation and certification of nitrite IRMs are described. Results from long term stability studies (up to 1.5 years) and a procedure for the purification of the candidate nitrite IRMs are presented. The purpose is to use these IRMs for high accuracy method calibrations and as anchor points for SI-traceable nitrite concentrations. Reference values linked to the SI system are useful to demonstrate the degree of international comparability of nitrite measurements in intercomparison programmes such as the IRMM—International Measurement Evaluation Programme (IMEP). © 1998 Elsevier Science B.V. All rights reserved.

Keywords: Nitrite; (Isotopic) Reference Materials; Stability; Purification

1. Introduction

Among nitrogen species occurring in waters, nitrite represents a relatively unstable and toxic

intermediate in the nitrification and denitrification processes of the nitrogen cycle. Nitrite may indicate incomplete oxidation and bring to light recent water pollution. The sources of nitrite for humans are mainly consumption of contaminated drinking water, cured meat and fish. However, 75% of nitrite entering the stomach originates from nitrate reduced in saliva. The toxicity of nitrite is far more severe from contaminated water than from food, as ascorbic acid (vitamin C) may react competitively with nitrite and thus protect the organism. Nitrite may cause methemoglobinemia, i.e. the reduction of the oxygen-carrying

* Corresponding author. Present address: SmithKline Beecham Pharmaceuticals, Analytical Sciences, New Frontiers Science Park, Harlow, Essex CM19 5AW, UK. Tel.: +44 1279 627446; fax: +44 1279 627655; e-mail: Jean-Claude_Wolff-1@sbphrd.com

¹ Presented at BERM-7 (Seventh International Symposium on Biological and Environmental Reference Materials), Antwerp, Belgium, 21–25 April 1997.

² Present address: SP Swedish National Testing and Research Institute, Box 857, SE-501 15 Borås, Sweden.

Table 1
Overview of preservation methods for nitrite

Method of preservation	Water type	Duration of preservation and/or study	Reference
Filtration through 0.45 μm membrane filter, stored at 4°C after addition of 40 mg l ⁻¹ of Hg ²⁺	Estuarine water (low organic content)	30 days	[7]
Storage at 4°C	Reagent grade water	> 30 days	[6]
Storage at 4°C	Surface water	8 days	[6]
Storage at 4°C, addition of NaOH (pH = 12)	Ground water, surface water, and leachate water	37 days	[6]
Storage at 4°C, addition of 1 ml l ⁻¹ of a saturated HgCl ₂ Solution	Lake water	6 days	[8]
Addition of a saturated HgCl ₂ solution	Strongly polluted water (high biological activity)	17 days	[9]
Addition of 22, 42 and 66 mg l ⁻¹ of HgCl ₂	Surface water without and with 20% settled sewage	20 days	[10]
Filtration through 0.45 μm membrane filters	River and lake water	21 days	[11]
Autoclaving	Seawater	27 months	[12]

capacities of blood, especially in infants and concern exists about the role nitrite may play in carcinogenesis [1].

Due to its toxicity, the nitrite concentration of drinking water has been regulated by the European Community Directive 80/778/EEC, which states the maximum admissible concentration i.e. 0.1 mg l⁻¹ [2]. Thus intercomparison of results is needed in order to provide legal and political authorities with values they can base decisions on. With the search for comparability and traceability of results, an IMEP-round (International Measurement Evaluation Programme) has been requested by the Austrian government services (K. Schwaiger, personal communication). In such an IMEP-round the anchor points are SI-traceable reference values, which rely on primary methods of measurement (as defined by the Comité Consultatif pour la Quantité de Matière [3], mostly isotope dilution mass spectrometry (IDMS) [4]. In order to carry out IDMS measurements, isotopic reference materials (IRMs), certified for isotopic composition and concentration (spikes) with an expanded uncertainty U of $\leq 2\%$, are needed. The concept of uncertainty is used to describe the reliability of the measurements and the terminology introduced by ISO is employed [5].

A prerequisite for establishing a spike IRM, which should have a shelf-life of at least 2–5 years, is stability and purity. Nitrite is known to be quite unstable, especially in natural water, due to chemical and biological processes. After a few weeks in oxic water it transforms readily into nitrate [6]. To avoid deterioration of nitrite, water samples and calibration solutions are often treated with biocidal or bioinhibitory agents, such as mercury salts or chloroform [7–10]. Filtration [7,11], cold storage [6–8] and autoclaving [12] are also used (Table 1). Besides the importance and diversity of biological life, factors such as the chemical composition of water, the influence of light, the storage temperature as well as the material and history of storage containers may have a considerable impact on the preservation method adopted. The candidate nitrite IRMs are prepared from ‘pure’ chemicals and sub-boiling distilled water so that instability caused by biological activity becomes a minor problem. Aminot and K erouel [13] found that unpreserved nitrite calibration solutions were stable for several months, but recommend a storage period of 1–2 months. In this work the influence of bottle material, pH and biocidal agents (chloroform and phenyl mercury chloride) on the stability of nitrite solutions was investigated in order to find conditions that guarantee the stability of the candidate IRMs.

A preliminary analysis of two commercially available ^{15}N -enriched sodium nitrite materials (Medgenix Diagnostics GmbH, Ratingen, Germany and Euriso-top, Groupe CEA Saclay, Gif-sur-Yvette, France), revealed that these contained approximately 8.8 and 1.3% mass fractions of nitrate respectively [14]. For the NLM-1535-Q ^{15}N -enriched potassium nitrite salt (CIL, Woburn, MA), the manufacturer stated a nitrate content of 5–10% mass fraction. The thermal ionisation mass spectrometric measurement procedure for nitrite is identical to that for nitrate, as nitrite is measured via nitron–nitrate and negative ionisation of nitrogen dioxide after oxidation to nitrate [14–17]. Hence a chemical clean-up procedure for the removal of interfering nitrate was investigated.

2. Experimental

2.1. Chemicals, reagents and solutions

Analytical grade chemicals from Merck (Darmstadt, Germany) and water, purified in a MilliQ system (MilliQ-water), were used unless otherwise stated. Nitrite solutions with $c(\text{NO}_2^-) = 1 \mu\text{g ml}^{-1}$ were prepared from NaNO_2 . Solutions were acidified using $1 \text{ mol l}^{-1} \text{H}_2\text{SO}_4$, or rendered alkaline using $1 \text{ mol l}^{-1} \text{NaOH}$. Chloroform (0.02 ml l^{-1}) or phenyl mercury chloride (0.01 ml l^{-1} of a 1% solution) were added to some of the nitrite solutions.

The nitrite solutions were stored in daylight and room temperature ($20\text{--}25^\circ\text{C}$) either in FEP (fluorinated ethylene propylene from Nalgene®, Nalge, Rochester, NY) or in PE (polyethylene from Kartell, Italy) bottles. Table 2 gives an overview of the nitrite solutions investigated during the stability studies.

For column experiments, 0.050, 0.50 and $1.00 \text{ mol l}^{-1} \text{HCl}$ were prepared by dilution of stock acid and standardised against sodium hydroxide.

2.2. Spectrophotometry

Nitrite was measured spectrophotometrically ($\lambda_{\text{max}} = 543.9 \text{ nm}$) using Aquaquant® nitrite test (Merck), which is based on the classical Griess

reaction [18]. To 2 ml of nitrite solution, approximately 20 mg Aquaquant® reaction powder was added. The solution was shaken for 30 s and allowed to stand for 10 min. The measurements were made in 1 cm plastic cells using a Cecil CE 1010 spectrophotometer (Cecil Instruments, Cambridge, UK).

2.3. Ion chromatography

Ion chromatography was used to monitor possible formation of nitrate in the stored solutions and to check the separation of nitrite and nitrate on anion exchange resins. The ion chromatography system consisted of an isocratic HPLC pump, fitted with a titanium analytical pump head (Knauer, Berlin, Germany), an Ion-Pac AG12A guard column, an Ion-Pac AS12A separator column, an anion self-regenerating suppressor ASRS-1 and a CD20 conductivity detector with DS3-1 detection stabiliser cell (Dionex, Sunnyvale, CA). Chromatograms were recorded on a Shimadzu Chromatopac C-R6A integrator (Kyoto, Japan). The injection valve (Knauer) as well as all tubings and connections were made of inert polyether ether ketone (PEEK). The injection volume was $20 \mu\text{l}$ and the flow rate of the eluent ($\text{Na}_2\text{CO}_3 \text{ } 2.7 \text{ mmol l}^{-1}/\text{NaHCO}_3 \text{ } 0.3 \text{ mmol l}^{-1}$) was 1.5 ml min^{-1} . The background conductivity was typically $14.1 \mu\text{S}$, and the backpressure 14.5 MPa . Samples were injected using disposable 2 ml plastic syringes (B. Braun Melsungen AG, Germany). The injection loop was flushed with at least 1 ml of solution, thus avoiding cross-contamination.

Table 2
Summary of the experimental conditions for the nitrite solutions investigated

Solution	Chemicals added	pH	Bottle material
1A	None	6	FEP
2A	H_2SO_4	3	FEP
6A	NaOH	9	FEP
B	None	6	PE
C	CHCl_3	6	PE
D	NaOH , CHCl_3	10.5	PE
E	$\text{C}_6\text{H}_5\text{HgCl}$	6	PE
F	NaOH	12	PE

2.4. Low pressure anion exchange chromatography for the separation of nitrite and nitrate

The AG 1X8 anion exchange resin, 100–200 mesh, chloride form (Bio-Rad, Nazareth, Belgium), was used. The capacity is approximately 2.6 eqv kg^{-1} (dry weight) or 1.2 eqv l^{-1} . Fines were removed by decantation and the resin was washed with 1 mol l^{-1} NaOH, MilliQ-water, 1 mol l^{-1} HCl and finally, MilliQ-water in which the resin was stored until further use. Columns, 1.5–2 ml (0.75–1 g dry weight) bed volume, were prepared by packing the resin under a small piece of quartz wool in 10 ml Poly-Prep plastic tubes (Bio-Rad). Conditioning was achieved by passing 10 ml of 1 mol l^{-1} HCl followed by MilliQ-water through the column.

Initial column experiments were aimed at optimising analytical separation and verifying chromatographic predictions. Nitrite and nitrate (100–500 μg) from neutral solutions were put on the column. Elution (flow rate $1\text{--}1.2 \text{ ml min}^{-1}$) was performed with HCl of various concentrations and fractions of 5 or 10 ml were collected. The fractions were pre-treated using Ag-OnGuard cartridges (Dionex) to remove chloride prior to injection on the ion chromatograph. The contributions of metal impurities from the Ag-OnGuard column were checked by flushing with water and analysing the effluent using a VG Plasma Quad2+ (VG Elemental, Winsford, UK) inductively coupled plasma mass spectrometer (ICP-MS). The influence of dissolved oxygen on nitrite solutions was investigated. Solutions, $5 \mu\text{g ml}^{-1}$ in nitrite, prepared from deaerated or normal HCl, were monitored for the $\text{NO}_3^-/\text{NO}_2^-$ ratio at regular intervals during a 6 h period. Finally, the influence of pH on the fraction containing nitrite was studied. Eluted nitrite was collected in NaOH to render the solution alkaline. By using an acid–base indicator (chlorophenol red), the pH can easily be adjusted to conditions required for the Ag-OnGuard column and ion chromatographic analysis.

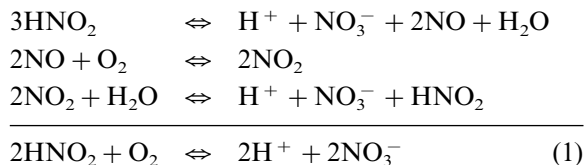
3. Results and discussion

3.1. Stability

As it was intended to measure relative changes in the nitrite concentration of solutions, it was estimated that the precision provided by the rapid, cost-effective Aquaquant® nitrite test would be sufficient to indicate which storage conditions should pertain. The (combined) uncertainty depicted in the figures was chosen arbitrarily and is deliberately large, i.e. 5%, in order to take into account all possible non-controlled sources of uncertainty, and does not represent the relative standard uncertainty of the measurements, which were typically about 1%.

3.1.1. Influence of pH

Fig. 1 shows that the NaOH-preserved solution (6A) was stable for almost 1.5 years at a concentration level of 1 mg l^{-1} . The ion chromatographic analysis of this solution did not show any appearance of nitrate whereas in the neutral solution (1A), nitrate was detected after 200 days. Alkaline preservation avoids the use of toxic mercury and prevents the liberation of nitrous acid as well as the disproportionation reaction which nitrite undergoes in acidic medium (HNO_2 ; $\text{p}K_a = 3.14$) according to Eq. (1).



Solution F stored in PE bottles (pH = 12.5) remained stable for almost 1 year, the decrease in NO_2^- concentration after 1.5 years can still be considered to be within the uncertainty of measurement. The same is held for solution D which had a pH of about 10.5. Acid preservation (2A) must be precluded.

3.1.2. Influence of the bottle material

Bottle material apparently plays an important role in the stability of NO_2^- (Fig. 2). The neutral solution stored in the PE bottle showed a clear

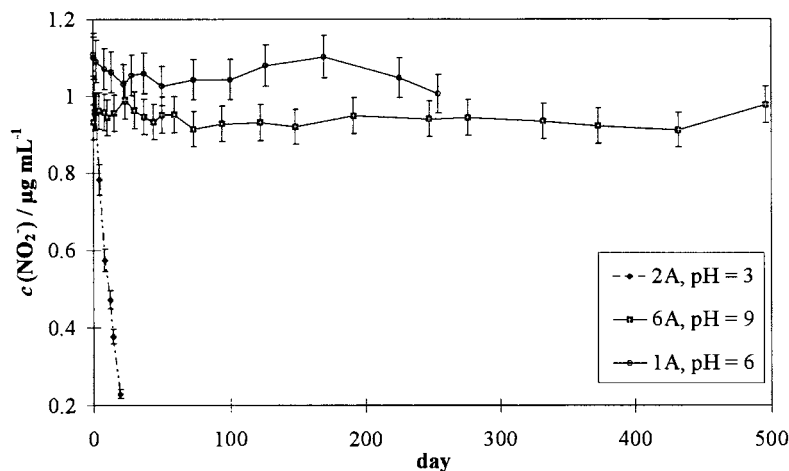


Fig. 1. Influence of pH on the stability of NO_2^- solutions stored in FEP bottles.

decrease in NO_2^- concentration, whereas the latter remained constant in the FEP bottle. The decrease observed at pH 6 could be linked to the manufacturing process (use of catalysts) of the two plastics investigated. Leaching of Zn from PE could lead to the reduction of NO_2^- to NH_4^+ . At higher pH (D and F, Fig. 3) the decrease in nitrite concentration was slower. Storage in PE bottles even at higher pH did not appear as satisfactory as using FEP bottles (Fig. 1). Adsorption of NO_2^- on the walls of the PE bottle, or the higher porosity of PE to NO_x and/or CO_2 compared with that of FEP, could explain the difference in stability observed. The nitrate concentration, increased to a large extent than if only due to the transformation of nitrite into nitrate. This fact supports the hypothesis that nitrate increase is due to the adsorption of NO_x which diffuses from the air through the PE into solutions. The NO_x adsorption by the solution was favoured in neutral or acidic medium.

3.1.3. Influence of biocidal agents

The unpreserved solution B as well as the mercury-preserved solution E showed a slight decrease in NO_2^- concentration after approximately 50 days of storage (Fig. 3). Chloroform is a poor method of preservation as shown by the results for solution C where nitrite concentration decreased drastically after 100 days of storage.

Chloroform is commonly used together with NaOH to stabilise nitrite calibration solutions prior to spectrophotometric measurements [19,20]. From the present work, it seems that stability depends mainly on NaOH (solution D, Fig. 3).

Addition of HgCl_2 and/or storage at 4°C are the methods chiefly used for short term preservation of water samples (< 1 month, c.f. Table 1). The former method proved unsuitable for the preservation of our nitrite solution (E), as we observed formation of nitrate in the order of 5%. The present work confirms results reported by Kremling and Wenck [21] and Aminot and Kérrouel [13], who showed that mercury had a rather adverse effect on the preservation of nitrite. After 20–30 days of preservation, mercury induced the disappearance of nitrite. It is thought [13] that Hg(II) oxidises NO_2^- to NO_3^- . Due to the presence of dissolved oxygen, the Hg(I) formed is re-oxidised to Hg(II) , thus enabling nitrite oxidation to proceed.

3.2. Purification of the candidate nitrite IRM

Several possibilities were envisaged for the removal of interfering nitrate. These were based either on the reduction of nitrate to nitrite or on the separation of both species using anion exchange chromatography.

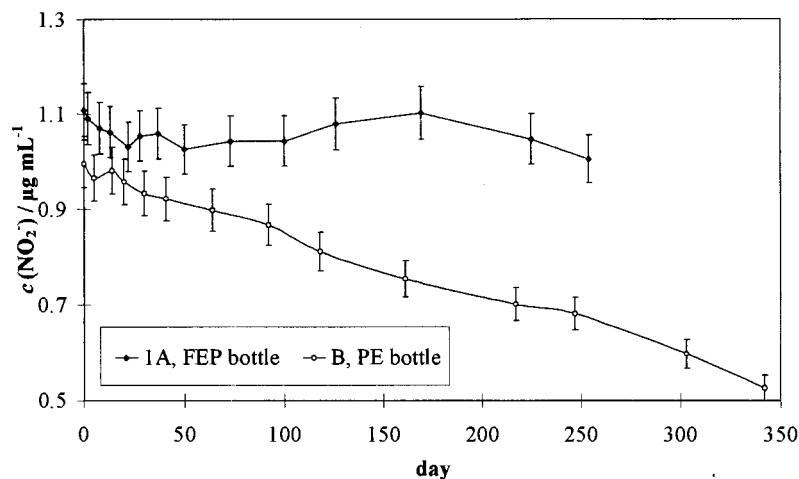


Fig. 2. The influence of bottle material (PE and FEP) on the stability of NO_2^- solutions at pH 6.

3.2.1. Reduction of nitrate to nitrite

Nitrate could be reduced to nitrite since both the nitrite concentration and the nitrogen isotope amount ratio in nitrite species, are measured after purification and storage in adequate vials. The reduction could employ a Cd-column [22] or Zn [23] as used for spectrophotometric measurements of nitrate via nitrite (Griess reaction) in a great number of flow injection systems. However, the reaction is often not quantitative, sometimes proceeds to lower oxidation states (i.e. NH_4^+) and introduces Cd^{2+} or Zn^{2+} to the solution. Photolytic reduction [24,25], is a very clean way of removing nitrate, as no additional chemicals are brought into contact with the candidate IRM. This approach was abandoned since equilibrium between both species was always established in the system investigated in our laboratory [26].

3.2.2. Separation of nitrite and nitrate

With the development of ion chromatography, nitrate–nitrite trace determinations are now done on a routine basis using a variety of instrumentation and column materials [6,27–30]. The number of practical procedures, used in analytical or preparatory applications with classical ion exchange chromatography is limited [31]. The procedure should allow microgram to milligram amounts of nitrite to be quantitatively separated from nitrate in a reasonable time and from the

simplest possible matrix. For both reasons, the procedure described by Gürtler and Holzapfel [32] is less suitable. The authors used the hydroxide form of the strongly basic anion exchanger Wofatit and separated nitrite from nitrate using litre volumes of $1 \text{ mol l}^{-1} \text{ NaCl}$ – $0.1 \text{ mol l}^{-1} \text{ NaOH}$ or $0.5 \text{ mol l}^{-1} \text{ Na}_2\text{SO}_4$ – $0.1 \text{ mol l}^{-1} \text{ NaOH}$. Gilbert and Dobbs [33] demonstrated a fast and efficient separation on Dowex 2 but used $1.25 \text{ mol l}^{-1} \text{ NaCl}$.

Recovery of nitrite seems to be quantitative or near quantitative in most ion exchange applications [34–36]. A high recovery is desirable in this work, especially for the enriched materials due to their price and availability. Both nitrate and nitrite are adsorbed from neutral or weakly acid solutions on anion exchange resins in various forms and efficient separation is achieved from all cations [31]. The difference in resin selectivity is approximately a factor of three for these ions [37] but poor column efficiency can hinder fast separations. Previous attempts in our laboratory, using sodium sulphate proved unsatisfactory for this reason. We decided to exploit the possibility of using acid conditions to separate nitrite as nitrous acid. In an analytical application aimed at direct accurate quantification, this approach would (due to the stability of nitrite) be less attractive. However, in preparatory work there are some advantages. Minor losses on the column are not

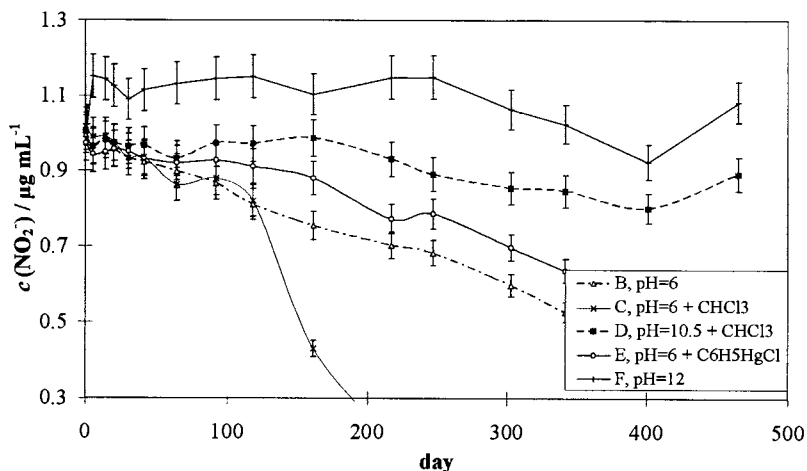


Fig. 3. Influence of biocidal agents (CHCl_3 and $\text{C}_6\text{H}_5\text{HgCl}$) and NaOH on the stability of NO_2^- solutions stored in PE bottles.

important as long as the integrity of the purified (eluted) solution, on which the assay is later done, can be maintained. Short contact times also lowers the levels of impurities released from the resin. Chemical manipulations after separation should be limited to additional purification and those which assure stabilisation. Davenport and Johnson [38] demonstrated the potential of acid separation conditions using 0.010 mol l^{-1} perchloric acid on Amberlite IRA-900 at 0.2 ml min^{-1} .

Eqs. (2) and (3) were derived to predict the behaviour and the retention volume V_R of nitrite and/or nitrate on the preparatory ion exchange column [39].

$$V_R(\text{NO}_x^-) = V_m + w \cdot \frac{E_{\text{Cl}^-}^{\text{NO}_x^-} \cdot [\text{Cl}^-]_R}{[\text{Cl}^-]_{\text{aq}}} \quad (2)$$

$$V_R(\text{NO}_2^-) = V_m + w \cdot \frac{E_{\text{Cl}^-}^{\text{NO}_2^-} \cdot [\text{Cl}^-]_R}{[\text{Cl}^-]_{\text{aq}} + \beta \cdot [\text{H}^+]_{\text{aq}} \cdot [\text{Cl}^-]_{\text{aq}}} \quad (3)$$

$[\text{Cl}^-]_{\text{aq}}$ is the counter ion concentration in the eluent (mol l^{-1}), E is the selectivity coefficient, w is the dry mass of resin (kg) and V_m is the column dead volume (l). $[\text{Cl}^-]_R$ is approximately equal to the resin capacity for analytical applications. Eq. (2) is used in the absence of side reactions. However, while nitrate corresponds to a strong acid, nitrite also exists in the nitrous acid form ($\text{p}K_a(\text{HNO}_2) = 3.14$). This is considered in Eq. (3)

where β is the protonation constant for nitrite ($\log \beta = \text{p}K_a$) and $[\text{H}^+]_{\text{aq}}$ reflects the acidity (mol l^{-1}) in the aqueous phase. E -values for nitrite (1.2) and nitrate (3.8) relative to chloride on this resin type, were taken from [37]. By insertion of this data into Eqs. (2) and (3) and varying the concentration of chloride (derived from NaCl or HCl), Fig. 4 was obtained. Examining this figure reveals that both anions ought to be readily pre-concentrated on the column from solutions having $[\text{Cl}^-] < 10^{-4} \text{ mol l}^{-1}$ and that ‘separation’ could be significantly improved using 0.010 mol l^{-1} HCl compared with 0.010 mol l^{-1} NaCl .

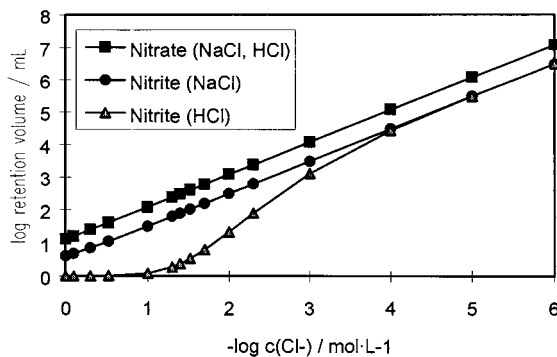


Fig. 4. Predicted retention volumes (ml) for nitrite and nitrate on Bio-Rad AG1X8 as function of chloride concentration. The curves are derived from Eqs. (2) and (3) and the following column data: $\log \beta = 3.14$; $V_m = 0.001 \text{ l}$; $w = 0.001 \text{ kg}$; $E_{\text{Cl}^-}^{\text{NO}_2^-} = 1.2$; $E_{\text{Cl}^-}^{\text{NO}_3^-} = 3.8$; resin capacity = 2.6 eqv kg^{-1} .

Experimental results agreed well with the predicted results. A flow rate of 1 ml min^{-1} could be maintained during the separation. Using $0.010\text{--}0.050 \text{ mol l}^{-1}$ HCl, nitrite can be quantitatively collected in a fraction of $\leq 25 \text{ ml}$ with no trace of nitrate. Conversion of nitrite during the preparation of the solution or on the ion exchange column is not critical. However, as soon as the solution leaves the resin, conditions must be such that sample integrity is preserved. The time elapsed between collecting the fractions and ion chromatographic analysis, i.e. a few hours, was enough to result in a solution with the same, or higher levels of nitrate than initially present in the spike material. A possible explanation is that the resin contributes compound(s) which catalyse the oxidation of nitrite. Removal of dissolved oxygen had no influence on the conversion rate, as could have been anticipated from Eq. (1).

Collecting the effluent in NaOH so as to obtain a neutral solution provides the basis for the subsequent removal of chloride using the Ag-OnGuard column. Once excess chloride has been removed, the solution is further stabilised by increasing the pH to about 10. No nitrate could be detected in solutions treated this way whereas non-stabilised solutions showed approximately 19% conversion after 4 h. The acid–base indicator provides a simple means of adjusting the pH of the solution. However, in subsequent removal of chloride some of the indicator passes the silver column—this is why a potentiometric measurement of pH should be considered in the final procedure. The capacity of the silver cartridge is $1.8\text{--}2.0 \text{ meqv}$. The cartridges work well for solutions $0.01\text{--}0.05 \text{ mol l}^{-1}$ in chloride where usually $1\text{--}2 \text{ }\mu\text{g ml}^{-1}$ remains in the effluent. This is sufficient to evaluate the neighbouring nitrite peak using the ion chromatographic procedure. Low $\mu\text{g kg}^{-1}$ levels of B, Ca, Zn, Ni, Pb, Al, Ca, Fe, Cr, Mo, Zr, Sn and Hg were noted in effluents from cartridges when rinsed with MilliQ-water. The levels of Ag were $10\text{--}30 \text{ }\mu\text{g l}^{-1}$. No attempts have been made so far to prepare ‘our own’ Ag-column. Possible difficulties are associated with flow restrictions and efficient trapping of the precipitate. This would probably require a pressurised system. The drawback of the commercial cartridge is its lim-

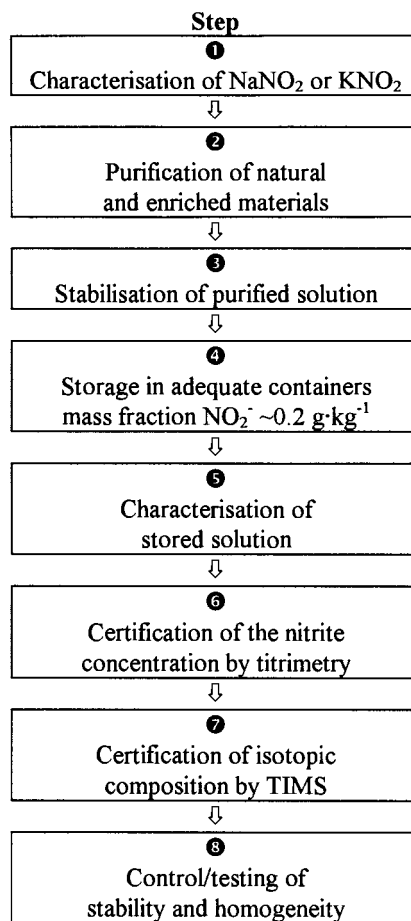


Fig. 5. Flowchart outlining the procedure for the preparation of nitrite IRMs.

ited capacity, it also becomes impractical if filtration is carried out manually.

3.3. Outline of the certification procedure

Fig. 5 indicates the procedure requirements for preparing a nitrite IRM. Characterisation, purification and stabilisation have been discussed in previous paragraphs. The alkaline medium creates an additional problem i.e. the storage container to be used. Storage in quartz ampoules seems unlikely, as silicon, released by the alkaline etching of the surface will decrease the pH of the solution with time. The use of plastic containers on the other hand raises the question of water loss due to

evaporation and also the question of diffusion and permeation of gases like CO_2 and NO_x , which could potentially affect the integrity of the candidate nitrite IRM. Data from the National Institute of Standards and Technology (NIST) shows that annual losses of 0.1% are about the best that can be obtained from 60 ml plastic containers inside a foil lined bag (J.R. Moody, personal communication). Evaporative losses of this magnitude could be tolerated since the combined uncertainty of the certified nitrite amount content will be in the order of 1%. Storage in small FEP bottles inside a foil lined bag are preferred.

The nitrite mass fraction (200 mg kg^{-1}) has been chosen to allow spiking of natural waters, resulting in blends having ‘easy-to-measure’ isotope amount ratios, and containing an amount of nitrite permitting chemical treatment of the sample, especially the ‘indirect’ isolation of nitrite via precipitation (Fig. 6). The stored candidate IRM

can be characterised for impurities using ion chromatography and ICP-MS. The purification procedure effectively removes interfering nitrate, reduces the chloride content but adds traces of silver. The NaOH used for stabilisation, introduces chloride, nitrite and traces of alkali and alkaline earth elements.

The certification of nitrite–nitrogen isotopic composition is carried out using negative thermal ionisation mass spectrometry (NTI-MS) based on the procedure described by Wolff et al. [16] to establish a nitrate isotopic reference material. Fig. 6 outlines the major steps for nitrite NTI-MS measurement. Adopting this procedure, a certified isotope amount ratio $n(^{14}\text{NO}_2^-)/n(^{15}\text{NO}_2^-)$ can be established with a combined uncertainty u_c of about 2% for both ^{15}N -enriched and natural nitrite solutions.

The nitrite concentration of candidate IRM has to be measured using a primary method of measurement. This assay can be done by titrimetry to a combined uncertainty of 1% using tetravalent manganese or permanganate [40,41]. Reverse IDMS cannot be used, as no primary nitrite RM exists.

3.4. Future work and use of nitrite reference materials

The present materials will be certified employing primary methods of measurement. An uncertainty budget, accounting for all known sources of uncertainty during the preparation will be created [15,16]. Both these conditions are prerequisites for obtaining SI-traceable values which can then be used as anchor points for comparability in a measurement evaluation programme such as IMEP [4] and for calibration of other instrumental methods. This is important as commercial nitrite calibration solutions have proven (from our experience) to be somewhat unreliable. These solutions are often made up in deionised water having a pH of about 6, which inherently leads to solution instability and serious potential errors. Providing the IRMs in small volumes, in containers for single use, is preferred rather than the larger bottles commercially available.

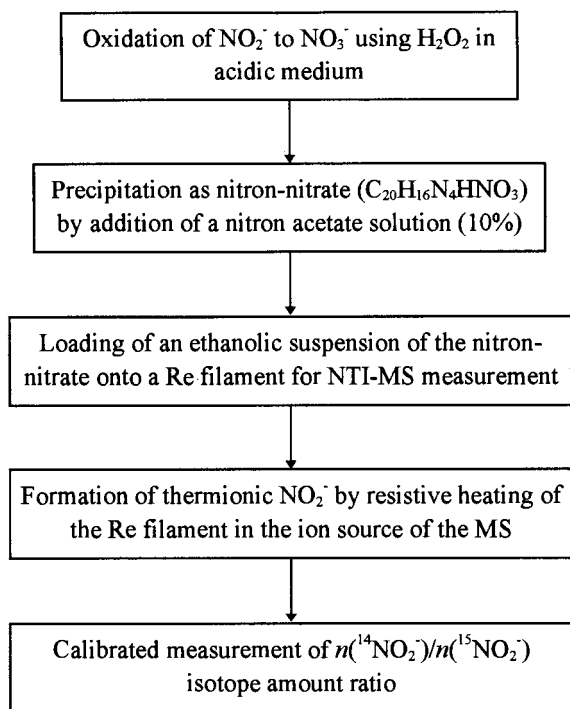


Fig. 6. NTI-MS procedure for the measurement of the isotopic composition of nitrite.

Acknowledgements

The authors wish to thank the Luxembourg 'Ministère de l'Éducation Nationale et de la Formation Professionnelle, Recherche Scientifique et Recherche Appliquée' for financial support given to JCW, and the European Commission for the research grant awarded to UÖ, which enabled this work to be carried out under the 4th Framework Programme of the European Union. They are also grateful to Hedin Joensen (Technical University of Lyngby, Denmark) for his contribution to some stages of the work.

References

- [1] P.F. Swann, *J. Sci. Food Agric.* 26 (1975) 1761.
- [2] Council directive of the 15th July 1980 relating to the quality of water intended for human consumption 80/778/EEC. *Off. Pub. Eur. Commun.* 229 (1980) 11.
- [3] Comité Consultatif pour la Quantité de Matière, Report of 1st meeting, BIPM Sèvres, April 1995.
- [4] A. Lamberty, L. Van Nevel, J.R. Moody, P. De Bièvre, *Accred. Qual. Assur.* 1 (1996) 71.
- [5] Guide to the expression of uncertainty in measurement, ISBN 92-67-10188-9, ©International Organisation for Standardisation, 1993.
- [6] M. Roman, R. Dovi, R. Yoder, F. Dias, B. Warden, *J. Chromatogr.* 546 (1991) 341.
- [7] D. Jenkins, *J. Water Pollut. Control Fed.* 39 (1967) 159.
- [8] P.L. Brezonik, F.G. Lee, *Int. J. Air Water Pollut.* 10 (1966) 549.
- [9] D.H.R. Hellwig, *Int. J. Air Water Pollut.* 8 (1964) 215.
- [10] L.H. Howe, C.W. Holley, *Environ. Sci. Technol.* 3 (1969) 478.
- [11] W.T. Sullivan, *J. Am. Water Works Assoc.* 67 (1975) 146.
- [12] A. Aminot, R. Kérrouel, *Mar. Chem.* 49 (1995) 221.
- [13] A. Aminot, R. Kérrouel, *Mar. Chem.* 52 (1996) 173.
- [14] J.-C. Wolff, C. Lathen, P.D.P. Taylor, P. De Bièvre, D. Lakkis, Internal report, IRMM, GE/R/SIM/9/95, 1995.
- [15] J.-C. Wolff, Ph.D. Thesis, University of Antwerp, 1997.
- [16] J.-C. Wolff, B. Dyckmans, P.D.P. Taylor, P. De Bièvre, *Int. J. Mass Spectrom. Ion Process.* 156 (1996) 67.
- [17] M. Unger, K.G. Heumann, *Fresenius Z. Anal. Chem.* 320 (1985) 525.
- [18] P. Griess, *Chem. Ber.* 12 (1879) 426.
- [19] B.F. Rider, M.G. Mellon, *Ind. Eng. Chem. Anal. Ed.* 18 (1946) 96.
- [20] M.F. Giné, H. Bergamin, E.A.G. Zagatto, B.F. Reis, *Anal. Chim. Acta* 114 (1980) 191.
- [21] M. Kremling, A. Wenck, *Meeresforsch.* 31 (1986) 69.
- [22] F. Nydahl, *Talanta* 23 (1976) 349.
- [23] T.S. Chow, M.S. Johnstone, *Anal. Chim. Acta* 27 (1969) 441.
- [24] Y. Zhang, L. Wu, *Analyst* 111 (1986) 767.
- [25] S. Motomizu, M. Sanada, *Anal. Chim. Acta* 308 (1995) 406.
- [26] H. Joensen, J.-C. Wolff, Internal Report, IRMM, GE/R/SIM/22/96, 1996.
- [27] C. McNeff, Q. Zhao, P.W. Carr, *J. Chromatogr. A.* 684 (1994) 201.
- [28] S.A. Everett, M.F. Dennis, G.M. Tozer, V.E. Prise, P. Wardman, M.R.L. Stratford, *J. Chromatogr. A.* 706 (1995) 437.
- [29] J. Chen, *J. Chromatogr. A* 739 (1996) 273.
- [30] J. Korkisch, *Handbook of Ion Exchange Resins: Their Applications to Organic Analytical Chemistry*, vol. 1, CRC Press, Boca Raton, FL, 1989, pp.53–110.
- [31] J. Korkisch, *Handbook of Ion Exchange Resins, Their Application to Inorganic Analytical Chemistry*, vol. VI, CRC Press, Boca Raton, FL, 1989, pp. 149–165.
- [32] O. Gürtler, H. Holzapfel, *Angew. Macromol. Chem.* 7 (89) (1969) 194.
- [33] T.W. Gilbert, R.A. Dobbs, *Anal. Chem.* 45 (1973) 1390.
- [34] B.C. Lippsmeyer, M.L. Tracy, G. Möller, *J. Assoc. Off. Anal. Chem.* 73 (1990) 457.
- [35] J.E. Varner, W.A. Bulen, S. Vanecko, R.C. Burrell, *Anal. Chem.* 25 (1953) 1528.
- [36] P.L. Buldini, D. Ferri, E. Pauluzzi, M. Zambianchi, *Microchim. Acta* 1 (1984) 43.
- [37] R.M. Wheaton, W.C. Bauman, *Ind. Eng. Chem.* 43 (5) (1951) 1088.
- [38] R.J. Davenport, D.C. Johnson, *Anal. Chem.* 46 (1974) 1971.
- [39] U. Örnemark, Å. Olin, *Talanta* 41 (1994) 67.
- [40] U. Muralikrishna, K. Subrahmanyam, M. Krishnamurthy, *Microchem. J.* 33 (1986) 376.
- [41] Vogel's textbook of Quantitative Chemical Analysis, 5th ed., Longman Scientific & Technical, Essex, UK, 1989, pp. 373–374.

Sequential liquid–liquid extraction graphite furnace atomic absorption spectrometric (GFAAS) and spectrophotometric determination of zirconium(IV) with calixarene hydroxamic acid

Yadvendra K. Agrawal *, Malika Sanyal, Pranav Shrivastav, Sobhana K. Menon

Department of Chemistry, School of Sciences, Gujarat University, Ahmedabad, 380009, India

Received 19 August 1997; received in revised form 9 October 1997; accepted 10 October 1997

Abstract

A new calixarene hydroxamic acid, 25,26,27,28-tetrahydroxy-5,11,17,23-tetrakis (*N-p*-chlorophenyl) calix[4]arene hydroxamic acid (CPCHA) is synthesized and used for the extraction and graphite furnace atomic absorption determination of zirconium(IV). The extract is also determined spectrophotometrically as CPCHA–SCN complex having maximum absorbance at 447 nm with molar absorptivity $9.4 \times 10^3 \text{ l mol}^{-1} \text{ cm}^{-1}$. The Beer's law obeys in the range of 1.0–9.5 ppm of zirconium. The graphite atomic absorption (GFAAS) increases the sensitivity by about 50 folds. The method is applied to the trace determination of zirconium(IV) in standard samples. © 1998 Elsevier Science B.V. All rights reserved.

Keywords: Liquid–liquid extraction; Graphite furnace atomic absorption spectrometric (GFAAS); Spectrophotometric determination; Zirconium(IV); Calixarene hydroxamic acid

1. Introduction

The literature continues to be enriched by many different methods for the determination of zirconium at various levels. Several organic reagents, in particular, the metallochromic indicators like arsenazo-III [1–5], xylenol orange [6–8], pyrocatechol violet [9], alizarin red S [10–12], phenyl fluorone [13,14], bromopyrogallol red [15], morin [16–18] etc. have been used for spectrophotometric determination of zirconium, however, hafnium

interferes seriously. Zirconium has a good chemical stability, high melting and hence, its method of determination by atomic absorption spectrometry is not very sensitive and zirconium cannot be determined at less than 8 ppm [19]. However, this can be overcome by preconcentration by liquid–liquid extraction technique. The combination of liquid–liquid extraction and GFAAS is rather effective and versatile hybrid technique for trace analysis [20]. The primary reason for the wide use of extraction in combination with GFAAS is the improvement in sensitivity arising partly from increased element concentration and also because nebulization of organic solvents can produce a more finely dispersed aerosol [21].

* Corresponding author. Tel.: +91 79 6440969; fax: +91 79 6441654.

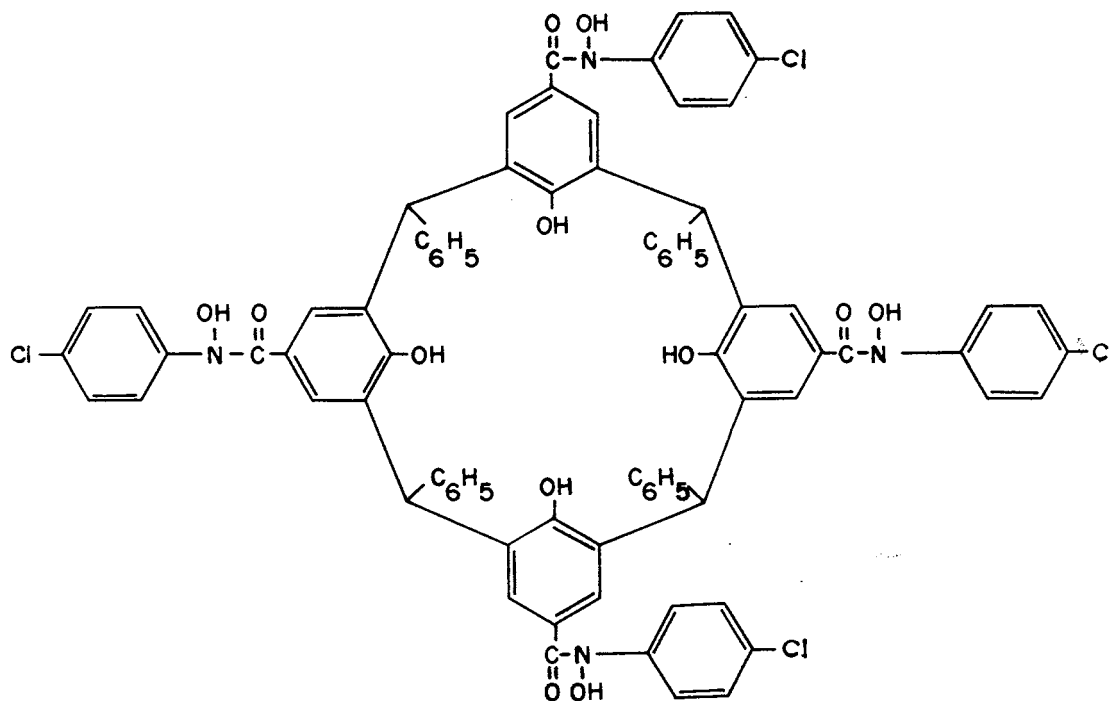


Fig. 1. 25,26,27,28-tetrahydroxy-5,11,17,23-tetrakis(*N-p*-chlorophenyl calix[4]arene hydroxamic acid (CPCHA).

Calixarenes are baskets that can serve as vehicles of transport for chemical baggage such as metal ions and molecules [22–25]. They are amenable to chemical modifications [26] and their derivatives with donor groups containing soft bases (N or S) have proved to be effective receptors that can selectively bind a range of transition metals [27–31]. The hydroxamic acids, are bidentate ligands and have remarkable versatility for the organic and inorganic analysis [32–37]. They have achieved tremendous importance as analytical reagents for the separation and determination of large number of metal ions [38–42].

In the present investigation, the reagent 25,26,27,28-tetrahydroxy-5,11,17,23-tetrakis(*N-p*-chlorophenyl calix[4]arene hydroxamic acid (CPCHA), Fig. 1, have been synthesized [43] and used for the liquid–liquid extraction, pyrolytic graphite furnace AAS which increases the sensitivity 50 times, and simultaneous spectrophotometric determination of zirconium(IV). The zirconium(IV) is extracted as Zr(IV)-calixarene hydroxa-

mate–thiocyanate complex into ethyl acetate and determined spectrophotometrically.

2. Experimental section

2.1. Apparatus

A Hitachi (Tokyo, Japan) 3210 UV-Visible spectrophotometer with matched quartz-cells was used for spectral measurements. AAS measurements were made on Perkin Elmer Model 420 with pyrolytically coated HGA-76 graphite furnace. A zirconium wavelength 360.1 nm with a spectral width of 0.2 nm, lamp current 15 mA.

2.2. Reagents

All the chemicals were of analytical reagent grades of E. Merck (Bombay, India). Glass distilled and deionized water was used throughout. A 0.2% solution of the ligand CPCHA was prepared

Table 1
Extraction of zirconium(IV) with various calixarene hydroxamic acids

Compound No.	Calixarene hydroxamic acid	λ_{\max}	Molar absorptivity ($1 \text{ mol}^{-1} \text{ cm}^{-1}$)
I	<i>N</i> -phenyl-	447	7.2×10^3
II	<i>N-p</i> -chlorophenyl-	447	9.4×10^3
III	<i>N-p</i> -bromophenyl-	447	7.8×10^3
IV	<i>N-p</i> -iodophenyl-	447	7.8×10^3
V	<i>N-p</i> -methylphenyl-	447	6.8×10^3

Zirconium: 6.30 ppm.
KSCN: 10 ml (20%).
HCl: 4 M.
Solvent: Ethyl acetate.

in ethyl acetate. Zirconium(IV) stock solution was prepared by dissolving 0.089 g zirconyl chloride hydrate in minimum volume of dilute hydrochloric acid and diluting up to 500 cm^3 with double distilled water. Its final concentration $9.9 \times 10^{-4} \text{ M}$ was determined spectrophotometrically [44]. It was further diluted as and when required. A 20% solution of KSCN was prepared in double distilled water.

2.3. Calix[4]arene hydroxamic acids

Calix[4]arene was synthesized by the acid catalyzed reaction of *p*-hydroxy benzoic acid with benzaldehyde. Further the calix(4)arene acid chlo-

Table 2
Effect of varying solvents on the extraction of zirconium(IV)-CPCHA-SCN complex

Solvent	Extraction (%)	Molar absorptivity ($1 \text{ mol}^{-1} \text{ cm}^{-1}$)
Chloroform	NE	—
Carbon tetra-chloride	NE	—
Ethyl acetate	100	9.4×10^3
Benzene	39.4	3.7×10^3
Toluene	37.2	3.5×10^3
Nitrobenzene	78.6	7.3×10^3
Isoamyl acetate	86.4	8.1×10^3

Zirconium: 6.30 ppm.
CPCHA: 10 cm^3 (0.2% in ethyl acetate).
KSCN: 10 cm^3 (20%).
HCl: 4 M.
 λ_{\max} : 447 nm.
NE: no extraction occurs

ride was prepared by reacting calix[4]arene with thionyl chloride and finally coupling it with hydroxylamine to get the desired hydroxamic acids [43].

2.4. Standard geological samples

In a 200 cm^3 Teflon beaker, 1 g of the sample was digested on a steam bath with 10 cm^3 of $1 \times 10^{-3} \text{ mol dm}^{-3}$ hydrofluoric acid and evaporated to dryness. Then, 25 cm^3 of (1 mol dm^{-3}) hydrochloric acid was added and transferred into

Table 3
Effect of varying acidity on the extraction of zirconium(IV)-CPCHA-SCN complex

HCl (M)	Extraction (%)	Molar absorptivity ($1 \text{ mol}^{-1} \text{ cm}^{-1}$)
0.25	73.40	6.9×10^3
0.5	80.79	7.6×10^3
1.0	94.90	8.9×10^3
2.0	98.60	9.2×10^3
2.5	100.0	9.4×10^3
3.0	100.0	9.4×10^3
3.5	100.0	9.4×10^3
4.0	100.0	9.4×10^3
4.5	100.0	9.4×10^3
5.0	95.80	8.9×10^3
6.0	79.20	8.3×10^3

Zirconium: 6.30 ppm.
CPCHA: 10 cm^3 (0.2% in ethyl acetate).
KSCN: 10 cm^3 (20%).
Solvent: Ethyl acetate.
 λ_{\max} : 447 nm.
The zirconium concentration in aqueous phase was determined by GFAAS.

Table 4
Effect of varying concentration of CPCHA for the extraction of zirconium(IV) -CPCHA-SCN complex

CPCHA (M $\times 10^{-4}$)	-log(CPCHA)	Zirconium conc. (M)		log D_M
		[Zr] _{org} $\times 10^{-4}$	[Zr] _{laq} $\times 10^{-4}$	
3.69	3.43	2.45	4.54	-0.27
5.62	3.25	3.50	3.49	0.00
7.39	3.13	4.14	2.85	0.16
8.86	3.05	4.16	2.33	0.30
10.78	2.97	5.05	1.94	0.41
14.77	2.83	6.99	<0.01	>2.89
22.10	2.66	6.99	<0.01	>2.89

Zirconium in the aqueous phase was determined by GFAAS.

Zirconium: 6.30 ppm.

KSCN: 10 cm³ (20%).

HCl: 4 M.

Solvent: Ethyl acetate.

λ_{\max} : 447 nm.

a 200 cm³ Pyrex beaker and digested on a sand bath for 1 h to dryness. The residue was redissolved in 10–15 cm³ of concentrated hydrochloric acid along with 0.5 g ammonium persulphate and centrifuged at 3000 rpm. The solution is finally diluted to 100 cm³ with distilled water.

2.5. Soil samples

1–2 g sample of dried solid was digested with 50 cm³ of concentrated hydrochloric acid and 10 cm³ of concentrated nitric acid for 1 h on sand-bath, then the solution was evaporated to dryness. The residue was boiled with 10 cm³ 5 M hydrochloric acid, filtered and diluted to 100 cm³ with distilled water.

2.6. Extraction procedure

An aliquot of zirconium(IV) solution (25–237.5 ppm) was transferred into a 60-cm³ separatory funnel. The molarity of the aqueous phase was adjusted to 4 M with concentrated hydrochloric acid. 10 cm³ of 0.2% CPCHA solution in ethyl acetate was added. The mixture was shaken for 5 min and the organic phase was separated. To ensure the complete recovery of zirconium, the extraction was repeated with 5 cm³ of CPCHA

solution and the combined organic phase was dried over 1 g of anhydrous sodium sulphate and transferred into 25 cm³ calibrated flask. The sodium sulphate was washed with 2 \times 2 cm³ ethyl acetate. The extracts and washings were diluted up to the mark with ethyl acetate and the extract was injected into furnace for GFAAS measurements. For spectrophotometric determination the ethyl acetate extract was shaken with 10 cm³ of KSCN the organic layer was separated and determined spectrometrically at 447 nm against blank.

3. Results and discussion

3.1. Absorption spectra, adherence to Beer's law and sensitivity

The determination of zirconium by the GFAAS has a sensitivity 15 ng/0.005 absorbance, detection limit 0.1 μ g cm³ zirconium using 100 μ l volume, precision 1–2% CV. Reproducibility of sensitivity is very good. About 100 determinations could typically be performed without significant drops in sensitivity. Since the automatization signal is generated slowly, a larger time constant can be used with recorder tracing to improve noise levels without loss of sensitivity. The extraction of zirco-

Table 5
Effect of varying concentration of thiocyanate for the extraction of zirconium(IV)

Thiocyanate (M)	-log(SCN)	Zirconium conc. (M)		log D_M
		$[Zr]_{org} \times 10^{-4}$	$[Zr]_{aq} \times 10^{-4}$	
0.05	1.30	3.99	3.00	0.12
0.10	1.00	4.80	2.19	0.34
0.15	0.82	5.15	1.84	0.45
0.25	0.60	5.59	1.40	0.60
1.02	-0.01	6.45	0.54	1.08
2.05	-0.31	6.99	<0.01	>2.89
2.50	-0.40	6.99	<0.01	>2.89

Zirconium in the aqueous phase was determined by GFAAS.

Zirconium: 6.30 ppm.

KSCN: 10 cm³ (20%).

HCl: 4 M.

Solvent: Ethyl acetate.

λ_{max} : 447 nm.

nium(IV) was carried with the various calixarene hydroxamic acids (Table 1). It is observed that the *N-p*-chlorophenyl-calixarene hydroxamic acid (CPCCHA) has the highest sensitivity compared to others and hence the extraction of zirconium was studied in detail. The absorption spectrum of zirconium(IV) -CPCCHA-SCN complex recorded against a reagent blank has maximum absorbance between 440–450 nm. At 447 nm, the absorbance was reproducible and hence all measurements were made at this wavelength. The molar absorptivity of the complex at 447 nm is 9.4×10^3 l mol⁻¹ cm⁻¹. The system obeys Beer's law in the range 1.0–9.5 ppm. The regression analysis represents Conc. = $4.76 \times$ Absorbance - 0.05 ($r = 0.999$).

3.2. Choice of extracting solvents

Chloroform, carbon tetrachloride, benzene, toluene, ethyl acetate, isoamyl acetate and nitrobenzene were tested as extracting solvents of zirconium(IV) -CPCCHA-SCN system. Of these, ethyl acetate was found to be most suitable (Table 2). No extraction occurs in chloroform and carbon tetrachloride, however, the extraction is incomplete in isoamyl acetate and nitrobenzene.

3.3. Effect of acidity and time of equilibration

The percentage extraction and formation of

chelate is influenced by the molarity of solution. The extraction % is obtained as $\%E = 100D/D + [V_{aq} \setminus V_{org}]$ where V_{aq} and V_{org} are the volume of the aqueous and organic phases and distribution coefficient, $D =$ Concentration of zirconium in organic phase/(total zirconium taken-zirconium in organic phase). The extraction of zirconium complex from 2.5 to 4.5 M HCl is rapid and selective. The data given in (Table 3) shows that the extraction at lower and higher molarity is incomplete. It was observed that 5 min. for equilibration is sufficient for quantitative extraction of zirconium.

3.4. Effect of CPCCHA concentration

The effect of CPCCHA was studied by extracting zirconium with different amounts of CPCCHA, keeping the concentration of thiocyanate fixed. It has been observed (Table 4) that 10 cm³ of 0.2% solution of CPCCHA is adequate for the complete extraction of zirconium. Lower concentration of CPCCHA reduces the percentage extraction, while an excess of reagent can be used without any difficulty.

3.5. Effect of thiocyanate concentration

The influence of thiocyanate was studied by extracting zirconium with different amounts of thiocyanate, keeping the concentration of ligand

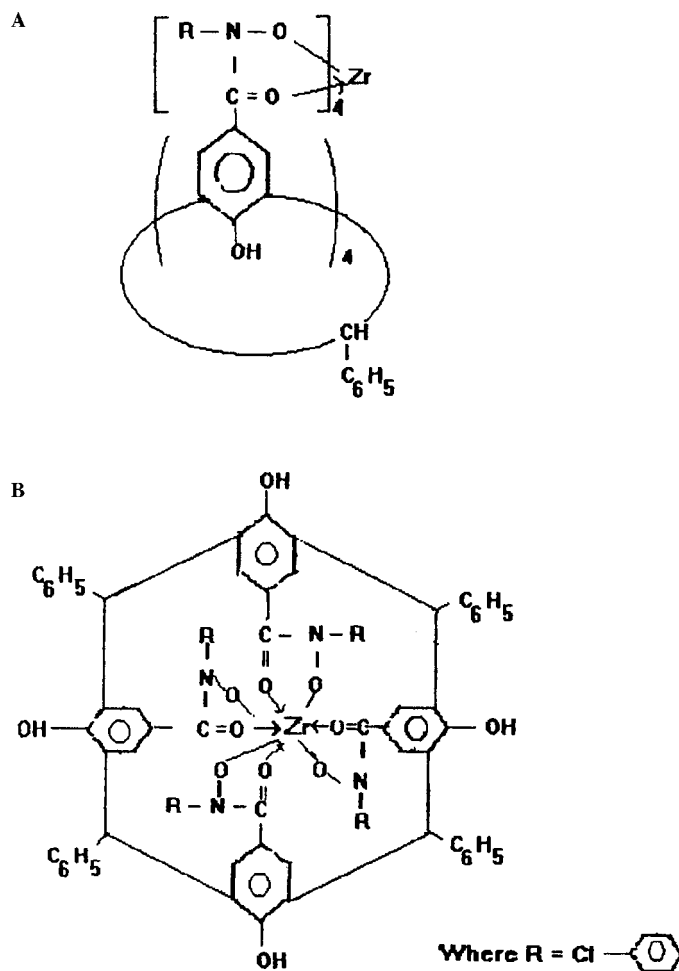


Fig. 2. (A) General structure of the complexes of zirconium with calix[4]arene hydroxamic acid (CPCHA). (B) Complexes of zirconium with calix[4]arene hydroxamine acid (CPCHA) (top view).

CPCHA fixed. It was observed that 10 cm³ of 20% KSCN solution is adequate for obtaining maximum absorbance of extracted complex (Table 5).

3.6. Stoichiometry of the complex

The composition of zirconium(IV) -CPCHA-SCN complex extracted into ethyl acetate has been studied by slope ratio method [44,45]. i.e. by plotting a graph of logarithm of distribution coefficient of the metal ($\log D_M$) against the negative logarithm of ligand concentration ($-\log$ ligand). Two sets of extractions were carried out.

One, by taking fixed amount of zirconium and thiocyanate solution and varying amounts of CPCHA. The second, by varying concentration of thiocyanate keeping zirconium and CPCHA concentrations fixed. The graph of $\log D_M$ against $-\log(\text{CPCHA})$ and $\log D_M$ against $\log \text{SCN}^-$ gives a straight line of slope 0.90 and 0.98, respectively. Hence the expected stoichiometry of extracted species is Zr(IV):CPCHA:SCN⁻: (1:1:1). The possible reactions are as

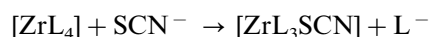
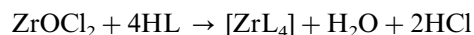


Table 6
Effect of diverse ions on the extraction of zirconium(IV)-CPCHA–SCN complex

Ion	Added as	Amount added (mg)	Recovery of zirconium (ppm)	
			Spectrophotometry	GFAAS
Ag ⁺	AgNO ₃	35	6.32	6.34
Ag ³⁺	As ₂ O ₃	40	6.32	6.33
Be ²⁺	BeSO ₄	30	6.29	6.32
Mg ²⁺	MgSO ₄	35	6.31	6.33
Ca ²⁺	Ca(NO ₃) ₂	35	6.29	6.31
Sn ²⁺	Sn(NO ₃) ₂	40	6.31	6.33
Cd ²⁺	CdSO ₄	40	6.30	6.31
Co ²⁺	CoCl ₂	35	6.32	6.32
Cu ²⁺	CuSO ₄	35	6.30	6.30
Cr ³⁺	CrCl ₃	35	6.30	6.31
Hg ²⁺	HgCl ₂	40	6.31	6.31
Ni ²⁺	NiCl ₂	40	6.31	6.32
Fe ²⁺	FeSO ₄	40	6.32	6.33
Fe ³⁺	FeCl ₃	30	6.32	6.32
Mn ²⁺	MnCl ₂	35	6.31	6.32
Zn ²⁺	ZnSO ₄	35	6.32	6.33
Al ³⁺	AlCl ₃	40	6.32	6.32
^a UO ₂ ²⁺	UO ₂ (NO ₃) ₂	25	6.33	6.34
^b Ti ⁴⁺	TiCl ₄	30	6.34	6.34
^a V ⁵⁺	NH ₄ VO ₃	30	6.34	6.34
^b MO ₆ ⁺	(NH ₄) ₆ MO ₇ O ₂₄ –4H ₂ O	30	6.34	6.35
Nb ⁵⁺	Nb ₂ O ₅	25	6.31	6.31
Ta ⁵⁺	Ta ₂ O ₅	25	6.29	6.31
^c Hf ⁴⁺	HfCl ₄	30	6.33	6.34
Cl [–]	NaCl	50	6.30	6.31
Br [–]	NaBr	50	6.30	6.31
I [–]	NaI	50	6.30	6.30
CH ₃ COO [–]	CH ₃ COONa	50	6.30	6.30
PO ₄ ^{3–}	Na ₃ PO ₄	30	6.29	6.31
SO ₄ ^{2–}	Na ₂ SO ₄	50	6.30	6.31

Zirconium: 6.30 ppm.

KSCN: 10 cm³ (20%).

HCl: 4 M.

Solvent: Ethyl acetate.

λ_{\max} : 447 nm.

^a Stripped with 0.25 M sodium oxalate.

^b Stripped with 0.3 M tartarate.

^c Stripped with 20% hydrogen peroxide.

The CPCHA consists of four groups of hydroxamic acid (4L) hence, forms a (1:1) complexes with Zr(IV) (Fig. 2) which are extracted with ethyl acetate. On addition of SCN[–] it gives (1:1:1) complexes of [Zr(IV):CPCHA:SCN].

3.7. Effect of foreign ions

In order to examine the utility of this method in

the presence of other commonly associated ions, a systematic study of their interferences was carried out. Moderate amounts (20–40 mg) of many commonly occurring metal ions with zirconium were tolerated and did not interfere in the determination of zirconium (Table 6). Interference was determined by measuring the absorbance of the extracted organic phase and also by making the measurements by GFAAS from both extract as

Table 7
Estimation of zirconium in Geological (USGS) and IAFA Soil-5 Samples

Sample	Standard value (ppm)	Zirconium found ^a (ppm)	
		Spectrophotometry	GFAAS
W-1	100	100.2 ± 0.3	99.97 ± 0.8
AGV-1(74/19)	200	199.7 ± 0.5	200.03 ± 0.10
G2(108/15)	290	289.4 ± 0.3	288.92 ± 0.09
PCC-1 (2/1)	10	10.0 ± 0.1	9.99 ± 0.04
Soil-5	220	220.4 ± 0.2	220.12 ± 0.5

^a Average of ten determinations.

well as aqueous phase. The tolerance limit was set as the amount of foreign ions causing a change of ± 0.02 absorbance or 2% error in the recovery of zirconium. Moderate amounts of various metal ions, commonly associated with zirconium were tolerated and also most anions. The interference of molybdenum and titanium, vanadium and uranium were eliminated either by masking or stripping them with 0.3 M tartarate and 0.25 M sodium oxalate, respectively. Zirconium, is separated and determined in presence of large amount of hafnium by it with 20% solution of hydrogen peroxide, as described by Cheng [46,47].

The determination of zirconium in standard samples is given in (Table 7).

Acknowledgements

The authors are grateful to DST New Delhi for financial support.

References

- [1] A. Ashton, A.G. Frogg, D.T. Burns, *Analyst* 99 (1974) 108.
- [2] P. Pakalns, *Anal. Chim. Acta* 57 (1971) 51.
- [3] V.G. Goryushina, E.V. Romanova, T.A. Archakova, *Zavodsk Lab.* 27 (1961) 795.
- [4] H. Onishi, K. Sekine, *Anal. Chim. Acta* 62 (1972) 204.
- [5] D.A. Vita, W.A. Levier, E. Litteral, *Anal. Chim. Acta* 42 (1968) 87.
- [6] K.L. Cheng, *Talanta*, 1959, 2, 61, 186, 266.
- [7] P.M. Champion, P. Crowther, D.M. Kemp, *Anal. Chim. Acta* 36 (1966) 413.
- [8] A.K. Babko, Sutokalo M.I. *Ukr. Khim. Zh.* 27 (1961) 566.
- [9] H. Flaschka, M.Y.Z. Farah, *Anal. Chem.* 152 (1956) 401.
- [10] D.E. Green, *Anal. Chem.* 20 (1948) 370.
- [11] G.B. Wengert, *Anal. Chem.* 24 (1952) 1449.
- [12] O. Gilbeti, A. Jacob, *Hel. Chim. Acta* 38 (1955) 1026.
- [13] K. Kimura, Sano H. *Bull. Chem. Soc. Jpn.* 30 (1957) 80.
- [14] F.G. Zharovskii, A.T. Pilipenko, *Zavodsk. Lab.* 23 (1957) 1407.
- [15] T. Sakai, Y. Funaki, *Bull. Chem. Soc. Jpn.* 42 (1969) 2272.
- [16] H. Tuma, N. Tietz, *Collect. Czech. Chem. Commun.* 23 (1958) 142.
- [17] H. Tuma, V. Kabicky, *Talanta* 8 (1961) 749.
- [18] A.B. Blank, I.I. Mirenskaya, L.P. Eksperiandova, *Zh. Analit. Khim.* 28 (1973) 1331.
- [19] L.H.J. Lajuen, *Spectrochemical Analysis of Atomic Absorption and Emission*, Royal Society of Chemistry, London, 1992.
- [20] A.B. Volynsky, B.Y. Spivakov, Y.A. Zolotov, *Talanta* 31 (6) (1984) 449.
- [21] M.S. Cresser, *Solvent Extraction in Flame Spectroscopic Analysis*, Butterworths, London, 1978.
- [22] R. Ludwig, K. Inoue, T. Yamamoto, *Solvent Extr. Ion Exch.* 11 (2) (1993) 311.
- [23] S.K. Chang, M.J. Jang, S.Y. Han, J.H. Lee, M.H. Knag, K.T. No, *Chem. Lett.* 10 (1992) 1937.
- [24] F. Hamada, T. Fukugaki, K. Murai, G.W. Orr, J.L. Atwood, *J. Inclus. Phenom. Mol. Recognit. Chem.* 10 (1) (1991) 57.
- [25] K. Ohto, T. Yamamoto, M. Goto, F. Nakashio, T. Nagasaki, S. Shinkai, *Proc. Symp. Solvent Extr.* 61 (1991).
- [26] M.A. McKervey, V. Bohmer, *Chem. Br.* 28 (8) (1992) 724.
- [27] C.D. Gutsche, *Calixarenes*, The Royal Society of Chemistry, Cambridge, 1989.
- [28] R. Ungaro, A. Pochini, *Calixarenes, a versatile class of Macrocyclic Compounds*, in: J. Vicens, V. Bohmer (Eds.), Kluwer, Dordrecht, 1991, p. 127.

- [29] S. Shinkai, Calixarenes, a versatile class of Macrocyclic Compounds, in: J. Vicens, V. Bohmer (Eds.), Kluwer, Dordrecht, 1991, p. 173.
- [30] J.C.G. Bunzli, J.M. Harrowfield, Calixarenes, a versatile class of Macrocyclic Compounds, in: J. Vicens, V. Bohmer (Eds.), Kluwer, Dordrecht, 1991, p. 211.
- [31] M.J. Schwing-Weill, M.A. McKervey, Calixarenes, a versatile class of Macrocyclic Compounds, in: J. Vicens, V. Bohmer (Eds.), Kluwer, Dordrecht, 1991, p. 149.
- [32] A.D. Shendrikar, *Talanta* 16 (1969) 51.
- [33] V.K. Gupta, S.G. Tandon, *Anal. Chim. Acta* 66 (1973) 39.
- [34] C.E. Meloan, M. MAuck, C. Huffman, *Anal. Chem.* 33 (1961) 104.
- [35] E.M. Donaldson, *Talanta* 17 (1970) 583.
- [36] Y.K. Agrawal, *Talanta* 20 (1973) 1213.
- [37] Y.K. Agrawal, *Anal. Lett.* 5 (1972) 863.
- [38] Y.K. Agrawal, *Rev. Anal. Chem.* 3 (2) (1980) 51.
- [39] Y.K. Agrawal, S.A. Patel, *Rev. Anal. Chem.* 4 (4) (1980) 237.
- [40] Y.K. Agrawal, R.D. Roshania, *Bull. Soc. Chim. Belg.* 89 (1980) 159.
- [41] Y.K. Agrawal, R.K. Jain, *Rev. Anal. Chem.* 6 (1982) 49.
- [42] Y.K. Agrawal, *Anal. Chem.* 47 (1975) 940.
- [43] Y.K. Agrawal, M. Sanyal, *Supramol. Chem.*, communicated.
- [44] S.B. Savvin, *Talanta*, 1961, 8, 673, 1964, 11, 1, 7.
- [45] D.A. Skoog, D.M. West, *Fundamentals of Analytical Chemistry*, 3rd edn., Holt, Rinehart and Winston, New York, 1976.
- [46] K.L. Cheng, *Talanta* 3 (1959) 86.
- [47] K.L. Cheng, *Anal. Chim. Acta* 28 (1963) 45.

Effects of capacity on the preconcentration of trace metals and matrix elimination by an iminodiacetate chelating adsorbent

Barbro Noresson *, Payman Hashemi, Åke Olin

Department of Analytical Chemistry, Uppsala University, P.O. Box 531, S-751 21 Uppsala, Sweden

Received 7 July 1997; received in revised form 13 October 1997; accepted 14 October 1997

Abstract

Low capacity adsorbents, based on iminodiacetic acid and a crosslinked agarose, Novarose™, have been synthesised for the enrichment of metal ions. Test ions Cu^{2+} with high, and Cd^{2+} with a moderate affinity for the sorbent were selected. The study includes the effect of specific capacity and matrix composition on the rate of uptake and recovery of these ions. Using a column packed with 0.25 ml of a sorbent and a sample volume of 100 ml, Cu^{2+} is quantitatively accumulated from all of the matrices studied even at a capacity of $6 \mu\text{mol ml}^{-1}$ of adsorbent and a flow rate as high as 100 ml min^{-1} . The enrichment of Cd^{2+} is affected by the matrix and for quantitative recovery the flow rate and capacity must be properly adjusted. In the presence of 0.01 M Ca^{2+} , a specific capacity of $45 \mu\text{mol ml}^{-1}$ is needed for quantitative retention and a flow rate of 100 ml min^{-1} , whereas a capacity of $10 \mu\text{mol ml}^{-1}$ suffices at 10 ml min^{-1} . The advantage of low specific capacity on the removal of matrix elements has been demonstrated. A method based on the determination of conditional stability constants of the metal sorbent complex is suggested for predicting the sorbent capacity needed to acquire quantitative recovery and optimal matrix elimination. © 1998 Elsevier Science B.V. All rights reserved.

Keywords: Iminodiacetate adsorbent; Low capacity; Preconcentration; Matrix elimination

1. Introduction

Sorbents are used in trace metal determinations for different purposes such as preconcentration of analyte [1–3], elimination of major cations or anions from the matrix [4,5], and speciation [6,7].

The capacity of sorbents range from $\mu\text{mol ml}^{-1}$ of bed volume in low capacity sorbents to mmol ml^{-1} in high capacity sorbents [8]. The efficiency

of a sorbent in the removal of analytes from the matrix ions is determined by its selectivity towards the ions of interest and its total capacity. Since most sorbents are non-selective, major cations will often saturate the sorbent. Complexing sorbents are often charged at the pH of accumulation and non-complexing ions may therefore be taken up by ion exchange. On elution of the preconcentration column, these ions will accompany the analytes to the detector and may cause interference. In such cases, loosely held disturbing ions can be pre-eluted by a more ‘innocent’ ion

* Corresponding author. E-mail: Barbro.Noresson@kemi.uu.se

such as the ammonium ion, but it requires an additional step in the procedure and some analytes may be lost during the washing.

The concentration of the co-eluted ions may become quite high at column capacities normally used. For a column of total capacity 250 μmol eluted into 0.5 ml, the concentration of a major ion could reach 0.5 M and interfere with the measurements of some elements by, for instance, ICP-AES. Such interferences could be even more problematic in ICP-MS or GFAAS since with these techniques matrix modification is often more important than preconcentration [4,5,9]. A sorbent column of low capacity, which collects less matrix ions, would be preferable. The equilibrium constant of the sorption reaction and its kinetics will determine the extent of analyte uptake from the percolating test solution. Therefore, quantitative accumulation of analyte will be facilitated by the high specific capacity of the sorbent. Hence, arguments can be raised both in favour of large and low capacity sorbents in trace element preconcentration.

No systematic study, to our knowledge, has been made on the effect of the specific capacity of a sorbent and its performance in trace element preconcentration. The reason might be practical difficulties in controlling the capacity by synthesis or unfavourable kinetics, which requires high capacities for quantitative uptake. In a recent paper [10], the kinetics and equilibrium properties of a fast iminodiacetate chelating ion exchanger was reported. This sorbent can conveniently be prepared with different specific capacities which makes it suitable for investigation of capacity effects. As test ions Cu^{2+} with a high, and Cd^{2+} with a moderate affinity for the sorbent were selected. In particular, the influence of specific capacity, flow rate and buffer concentration on the accumulation process were elucidated.

2. Experimental

2.1. Chemicals

A highly crosslinked agarose called Novarose™ Act^{High}-100/40 (Inovata AB, Stockholm, Sweden)

was used as the support material for the adsorbent. Test solutions were made by dilution of AAS standards (Referensmaterial AB, Sweden). Other solutions were prepared from analytical grade chemicals and Milli-Q filtered deionized water.

2.2. Apparatus and analysis

The determination of the metal ion binding capacity of the adsorbent was carried out with the TraceCon computer controlled flow analysis equipment (Knapp Logistics, Graz, Austria), and for the preconcentration measurements the same flow system was used as previously reported [10].

Glass columns of 6.5 mm i.d. and of variable length (Omnifit) held the adsorbent. Endpieces were made of PTFE and porous polyethylene frits kept the adsorbent in place.

Determination of metal ion concentrations were performed by FAAS (PerkinElmer 2380) for the capacity measurements or by ICP-AES (Spectroflame, Spectro, Kleve, Germany). The manufacturers recommendations for instrumental settings were followed in both cases.

2.3. Synthesis and capacity determination

The low capacity adsorbents were synthesised according to the method described by Inovata AB [11], with minor modifications. To 5 ml of suction dry Novarose™ (about 5 g) in a 20 ml PE (polyethylene)-bottle the appropriate amount (fig. 1) of a 10% iminodiacetate solution in 0.1 M NaOH, pH 13, and 5 ml of 0.5 M Na_2CO_3 were added. The bottle was agitated on a shaker for 17 h. The adsorbent was then transferred onto a Millipore glass filter holding a membrane filter (HA, 0.45 μm) and washed with 50 ml portions of 1 M NaOH, 0.1 M HCl and Milli-Q water. The adsorbent was next returned to the PE-bottle and deactivated by adding 15 ml of 1 M NaOH. After shaking for 24 h, the adsorbent was washed with Milli-Q water and then stored in 20% ethanol.

The capacity was determined using a previously described procedure [12], packing a known volume of the adsorbent in a column and saturating

it with Cu^{2+} . After washing with 0.1 M acetate buffer, pH 5.5, the copper was eluted with 1 M HCl and determined by FAAS. The specific capacity was calculated as the quotient between the number of μmol of copper found and the bed volume. The adsorbents are named by their functional group imino diacetic acid, IDA, followed by their capacity in $\mu\text{mol ml}^{-1}$. For example, IDA45 refers to the IDA-Novarose adsorbent with a capacity of $45 \mu\text{mol ml}^{-1}$.

2.4. Adsorption rate and equilibrium concentrations

The measurements of the adsorption rate and equilibrium concentrations were performed in batch mode as described earlier [10] with some minor changes. A test solution of 100 ml of $3 \mu\text{M}$ Cd^{2+} , and/or Cu^{2+} , buffered to pH 5.5 by acetate–acetic acid, was added to a beaker. The solution was continuously sampled through a filter into the ICP-AES instrument by a peristaltic pump at 2 ml min^{-1} . When the signal stabilised, 0.5 ml of IDA-Novarose was quickly added to the stirred solution. The adsorption of the metals was followed by recording the emission signal every other second for at least 10 min. Equilibrium concentrations were also determined in the off-line mode by sampling after 2 and 24 h. The concentrations were found by ICP-AES calibrated against matched standards.

2.5. Enrichment

The FIA-ICP-AES system and the procedures used in the enrichment studies were essentially the same as reported earlier [10]. The preconditioning of the column was performed by either 0.005 or 0.1 M acetic acid–acetate buffer, depending on the buffer concentration of the sample. The enrichment flow rates were between 10 and 100 ml min^{-1} . The column was usually washed with 4 ml of 0.1 M acetate buffer before elution and eluted with 1 ml of 2 M hydrochloric acid. In the recovery measurements the eluates were collected in an off-line mode and determined by ICP-AES against matched standards.

3. Results and discussion

3.1. The sorbent

The preparation of the sorbents followed the recommendations of the manufacturer of Novarose™ (the crosslinked, bromohydrine activated agarose), as described in Section 2. Thus for a fixed reaction time, the concentration of iminodiacetate in the reaction mixture can be used as the sole parameter to control the specific capacity. Fig. 1 shows the capacities obtained as a function of the amount of IDA added per ml of Novarose™, for the capacity range $0\text{--}45 \mu\text{mol ml}^{-1}$. Sorbents with capacities up to about $150 \mu\text{mol ml}^{-1}$ can be prepared in a reproducible way. The sorbent was kept and handled in the zwitterion form, $\text{R-NH}^+(\text{CH}_2\text{COO}^-)(\text{CH}_2\text{COOH})$. The intrinsic acidity constants were determined in a previous study, $\text{p}K_{\text{li}} \cong 3.0$ and $\text{p}K_{\text{zi}} = 8.7$ [10]. At pH 5.5, the sorbent is present almost solely in the monoprotonated form.

A low capacity adsorbent must be more thoroughly packed than a high capacity adsorbent, since in a loosely packed column, channels may form resulting in analyte losses. For a high capacity adsorbent ($> 20 \mu\text{mol ml}^{-1}$) the number of active groups in such channels is sufficient for quantitative uptake and few packing problems were encountered.

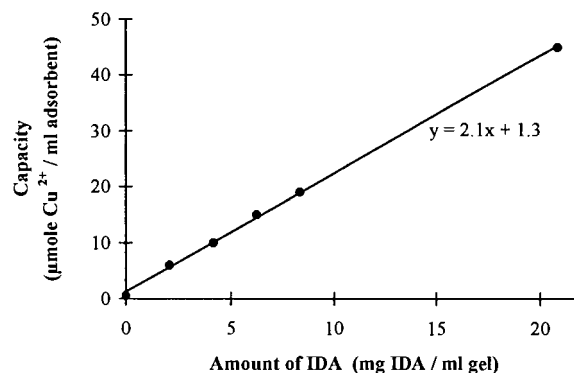


Fig. 1. The capacity obtained in the synthesis of IDA-Novarose as a function of the amount of imino diacetic acid (IDA) added per ml of Novarose™. The regression line levels at higher capacities and a practical upper limit is set at about $150 \mu\text{mol ml}^{-1}$.

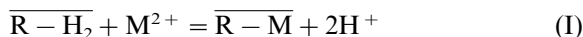
3.2. Influence of the specific capacity on retention

One way of discussing the influence of specific capacity on the uptake of small amounts of a metal ion at low concentration is to apply the basic chromatographic relationship

$$V_R = V_M(1 + k') \cong V_M k' \quad (1)$$

to the enrichment process in the sorbent column. As usual V_R is the retention volume, V_M the volume of the mobile phase and k' the capacity factor. Initially sorbed metal ions are thus regarded as being eluted by subsequent portions of the sample under equilibrium conditions and V_R becomes an estimate of the sample volume which can be processed before a break-through occurs. The rapid uptake shown by IDA-Novarose and its high dynamic capacity in relation to the static capacity, even at high flow rates [10], indicates that the assumption of equilibrium conditions is a reasonable approximation. However, with increasing flow rates and decreasing capacity, kinetic and other effects can be expected to increase the dispersion of the analyte in the column substantially. The ability of the model to predict the permissible enrichment volume will decrease correspondingly.

The exchange reaction between the metal ion, M^{2+} , and the sorbent in zwitterion form, $R-H_2$, is



with

$$\beta = \frac{[H^+]^2 [\overline{R-M}]}{[M^{2+}] [\overline{R-H_2}]} \quad (2)$$

Bars indicate the species in the resin phase, CAP signifies specific capacity, expressed in $\mu\text{mol ml}^{-1}$. For divalent ions, CAP would be equal to the concentration of IDA-groups. Under normal conditions an enrichment is made from a solution with constant electrolyte background and at constant pH. Consequently, the free metal ion concentration in the mobile phase, $[M^{2+}]$, will be a constant fraction, α_1 , of the corresponding total metal ion concentration, $[M^{2+}]_t$, in equilibrium with the sorbent. Furthermore, the resulting $[\overline{R-M}]$

is generally much smaller than CAP (not more than 1%) so that the total concentration of IDA-groups will be

$$\begin{aligned} [\overline{R-H_2}]_t &= [\overline{R-H_2}] + [\overline{R-H^-}] + [\overline{R-M}] \\ &\cong [\overline{R-H_2}] + [\overline{R-H^-}] \end{aligned} \quad (3)$$

thus $[\overline{R-H_2}]$ constitutes a constant fraction, α_2 , of $[\overline{R-H_2}]_t$. This fraction is determined by the acidity constant of $R-H_2$ and pH. Eq. (2) can now be rewritten

$$\beta = \frac{[H^+]^2 [\overline{R-M}]}{\alpha_1 \alpha_2 [M^{2+}]_t [\overline{R-H_2}]_t} = \frac{[H^+]^2}{\alpha_1 \alpha_2} \beta' \quad (4)$$

and the conditional constant, β' , is

$$\beta' = \frac{[\overline{R-M}]}{[M^{2+}]_t [\overline{R-H_2}]_t} \cong \frac{[\overline{R-M}]}{[M^{2+}]_t \text{CAP}} \quad (5)$$

The expression k' can then be written as,

$$k' = \frac{V_s [\overline{R-M}]}{V_M [M^{2+}]_t} = \frac{V_s}{V_M} \beta' \cdot \text{CAP} \quad (6)$$

The volume of the stationary phase, V_s , equals the bed volume since concentrations in this phase are expressed with reference to unit bed volume. Eqs. (1) and (6) gives

$$V_R = \beta' V_s \cdot \text{CAP} \quad (7)$$

If the volume which can be enriched is assumed to be roughly equal to V_R , this volume would be proportional to the total capacity, $V_s \cdot \text{CAP}$, of the column under equilibrium conditions according to Eq. (7).

Column capacity can be diminished if the sample volume for enrichment, V_0 , is less than V_R . The ratio between the analyte and interferent concentrations will increase and use of a low capacity sorbent is advantageous. When V_R approaches V_0 , no improvement in the above ratio can be achieved by lowering the specific capacity. A low CAP value must be compensated for by a longer column in order to reach the total capacity needed.

Table 1 presents recoveries from enrichments of Cu^{2+} and Cd^{2+} on 0.25 ml columns of IDA-Novarose of different capacities. Two flow rates, 10 and 100 ml min^{-1} , were used corresponding to

Table 1

Recovery of Cu^{2+} and Cd^{2+} from enrichment of 100 ml of 10 ppb Cu^{2+} and Cd^{2+} in 0.1 M ammonium acetate–acetic acid buffer, pH 5.5, at different specific capacities and flow rates

Sorbent	Recovery (%)			
	Cu		Cd	
	Flow rate (ml min^{-1})			
	10	100	10	100
IDA45	100	100	99	98
IDA20	96	99	100	94
IDA15	98	99	99	83
IDA10	99	98	93	67
IDA6	98	98	67	42

Column, 6.5 (i.d.) \times 9 mm; $n = 3$, RSD = 2–3%.

the residence times of about 0.8 and 0.08 s, respectively. The loading of a column did not exceed 1% of the total capacity. The recovery in all experiments with Cu^{2+} was close to quantitative. With this metal, which has a high affinity for the iminodiacetate group [10], it could be possible to diminish the amount of unwanted ions by decreasing the capacity of the column even further. Use of a sorbent with a low CAP is required for this ion. The Cd^{2+} ion has a much smaller β -value than Cu^{2+} and the sorbent incompletely accumulates the ion from 0.1 M acetate buffer below a CAP of about $20 \mu\text{mol ml}^{-1}$. Hence the lower limit for quantitative collection has been reached and further reduction in the amount of accumulated matrix ions by lowering the capacity is not possible at the prevalent level of β' . When an increase in the total capacity is needed for quantitative enrichment it can be achieved by increasing the column length or the specific capacity. Experiments with column lengths of 5 and 9 mm, and flow rates between 10 and 100 ml min^{-1} indicates no marked difference between the options except for the increased back pressure when the column length was extended.

3.3. Enrichment in batch

The previous discussion was based on an equilibrium model. The results presented in Table 1

and other column enrichments at different flow rates indicate that the kinetic aspects of the enrichment process must also be considered. For instance, the recovery of Cd^{2+} in 0.1 M acetate buffer, pH 5.5, decreased steadily from 97 to 64% on a 6.5 mm i.d. \times 5 mm IDA15 column when the flow rate was gradually increased from 10 to 100 ml min^{-1} . Measurements of the rate of metal accumulation by the sorbent was carried out in batch mode and the removal of test ions from 100 ml of solution by 0.5 ml of sorbent was followed at pH 5.5. Three series of experiments were run with different electrolyte backgrounds, viz. 0.1 M ammonium acetate–acetic acid buffer, 0.005 M acetate buffer + 0.095 M ammonium nitrate and 0.005 M acetate buffer only. The use of a 0.1 M NH_4^+ medium was based on the assumption that the addition of ammonium ions to a water sample would effectively diminish the uptake of Ca^{2+} , which was found to interfere with the determination of some metal ions [10].

Fig. 2 shows the results obtained in 0.1 M acetate buffer. The kinetic curves for Cu^{2+} were similar and no systematic trend with CAP was observed. The small differences most likely reflect the difficulties in establishing a reproducible addition of sorbent and stirring of the test solution. These problems affect the curve shapes particularly at the start of an experiment before the sorbent has been homogeneously distributed. The Cu^{2+} concentration drops below the detection limit ($\approx 2 \text{ ppb}$) in about 3–4 min and the decline follows a first order reaction with a half-time of about 10 s.

The results for Cd^{2+} show that sorption reaches a steady state after about 5 min. The steady state concentrations follow the expected order and only with IDA45 does the concentration reach the detection limit ($\approx 2 \text{ ppb}$). Assuming that the steady state concentrations are equilibrium concentrations, the conditional constant β' (Eq. (5)) can be calculated. The values obtained ranged between 1.1 and $0.4 \times 10^5 \text{ M}^{-1}$ with a steady decrease in the numerical value with CAP. A similar trend was observed in previous determinations of β and reasons for this trend were suggested [10]. The equilibrium constant of

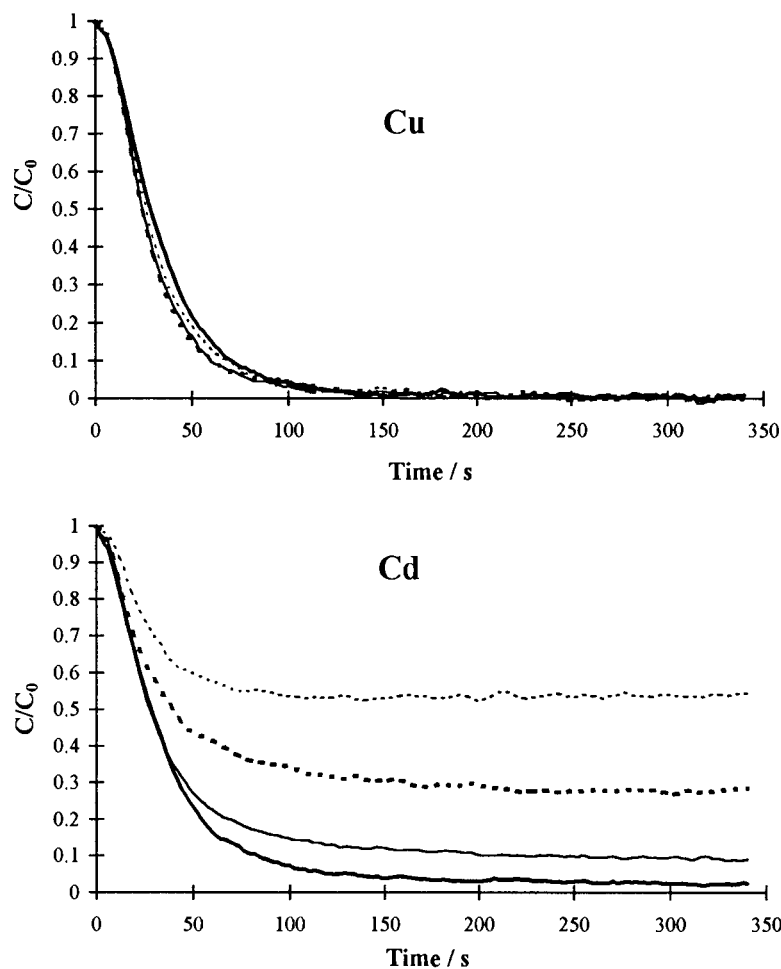


Fig. 2. Adsorption profiles of Cu^{2+} and Cd^{2+} on IDA-Novarose adsorbents of different specific capacity. Start solution, 100 ml of $3 \mu\text{M}$ Cd^{2+} and Cu^{2+} . Sorbent, 0.5 ml. Background electrolyte, 0.1 M ammonium acetate–acetic acid buffer, pH 5.5. (---, IDA6; — — —, IDA10; —, IDA20 and —, IDA45).

the sorption reaction is known from determination with high capacity IDA-Novarose. $\log \beta = -2.85$ was obtained at $I = 0.1 \text{ M}$ and the first apparent acidity constant of R-H_2 at this ionic strength should be close to $\text{p}K_{a1} = 3.0$ [10]. Using the presented equilibrium constants and Eq. (4), the predicted value of β' is $1.6 \times 10^5 \text{ M}^{-1}$, in agreement with the present results.

Since the acetate ion is known to complex with Cd^{2+} and thereby render the sorption more difficult, a second series was run at an acetate buffer concentration of 0.005 M. The NH_4^+ concentration was still kept at 0.1 M by the addition

of ammonium nitrate. The diminished acetate concentration led to lower equilibrium concentrations of Cd^{2+} . The calculated β' values ranged between 2.3 and $0.8 \times 10^5 \text{ M}^{-1}$ and the same trend with CAP was present as before. The quotient between the two sets of stability constants was 2.5 ± 0.4 from which the formation constant of the cadmium acetate complex is estimated at 15 M^{-1} . The value reported in 0.1 M NaClO_4 is 40 M^{-1} [13].

Using the β' values from the batch experiments, the retention volumes in the column experiments (Table 1) can be estimated from Eq. (7). The V_R

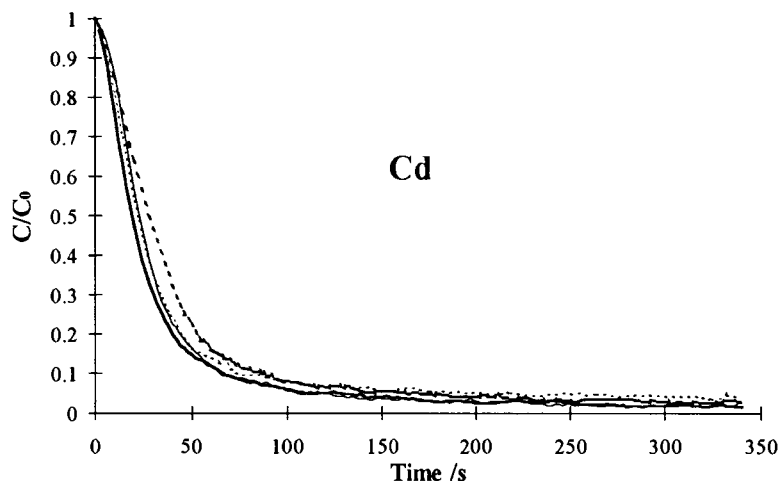


Fig. 3. Adsorption profiles of Cd^{2+} on IDA-Novarose adsorbents of different specific capacity. Start solution, 100 ml of $3 \mu\text{M}$ Cd^{2+} . Sorbent, 0.5 ml. Background electrolyte, 0.005 M ammonium acetate–acetic acid buffer. (---, IDA6; - - -, IDA10; — — —, IDA20 and —, IDA45)

values obtained for IDA20, IDA10 and IDA6 are 550, 135, and 50 ml, respectively. With IDA20 quantitative uptake is indicated and also found at a low flow rate. At a high flow rate, some loss occurs and the residence time, about 0.1 s, is apparently too short for equilibrium to be established. With IDA10 the retention volume is only slightly larger than the sample volume so that some loss can be expected also at a low flow rate. Low recoveries are anticipated and also found for IDA6 since the retention volume is smaller than the sample volume.

The result for the sorption from 0.005 M acetate buffer is shown in Fig. 3. A striking decrease is observed in equilibrium concentrations when the ionic strength of the buffer is lowered (cf Fig. 2). The half-times are independent of CAP and close to 10 s. Hence, no significant difference in the sorption rates between Cu^{2+} and Cd^{2+} was found.

Equilibrium data from the three matrices studied are summarised in Table 2.

3.4. Influence of the matrix on recovery

Table 3 shows the influence of buffer concentration on the recovery of Cd^{2+} by IDA6 and IDA10 at flow rates between 10 and 80 ml min^{-1} .

As predicted, the larger retention volume in a 0.005 M buffer, results in improved recoveries and almost quantitative recovery (96%) was achieved even for the lowest capacity tested (IDA6) at 80 ml min^{-1} .

An attempt to clarify the reason for the much improved performance at low ionic strength might begin at Eqs. (1) and (2). It is well known that an increase in the ionic strength increases the apparent acidity constant of R-H_2 [14]. Membrane (Donnan) equilibria are responsible for this effect. A decrease in the ionic strength at constant pH leads to an increase in the activity of R-H_2 . This

Table 2
Equilibrium concentration of Cd^{2+} in batch enrichments at pH 5.5 for different specific capacities and background electrolytes.

Background	Equilibrium concentration (μM)			
	IDA6	IDA10	IDA20	IDA45
I	1.55	0.83	0.24	0.05
II	0.89	0.40	0.13	0.03
III	0.11	0.05	0.02	0.03

Start solution, 100 ml of $3 \mu\text{M}$ Cd^{2+} ; Sorbent, 0.5 ml. Background electrolyte, (I) 0.1 M ammonium acetate–acetic acid buffer, (II) 0.005 M acetate buffer in 0.095 M ammonium nitrate, (III) 0.005 M acetate buffer

Table 3

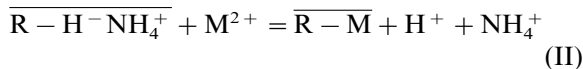
Recovery of Cd²⁺ from enrichment of 100 ml of 10 ppb Cd²⁺ in ammonium acetate–acetic acid buffers, pH 5.5, at different specific capacities and flow rates

Flow rate (ml min ⁻¹)	Recovery (%)			
	IDA6		IDA10	
	0.1 M	0.005 M	0.1 M	0.005 M
10	67	96	94	99
30	61	93	95	98
60	47	97	89	99
80	42	96	73	98

Column, 6.5 (i.d) × 9 mm; *n* = 3, RSD = 2–3%.

in turn leads to an increase in the ratio $\overline{[R - M]}/[M^{2+}]$ resulting in improved accumulation of M²⁺. In order to quantify the effect, the somewhat simplified approach by Pesavento et al. [14] was applied to calculate the activity of R–H₂. The result is shown in Fig. 4 which depicts the relative activity change as a function of ammonium ion concentration. The range of a pronounced Donnan effect increases with CAP since electrolyte invasion, which eventually suppresses the differences in potential between the two phases, starts at increasingly higher electrolyte concentrations. Even though calculations point out the benefits of keeping the electrolyte content of the sample low, the observed effect of a decrease in ionic strength is considerably larger than predicted.

An alternative approach would be to consider the effect of a diminished NH₄⁺ concentration in terms of an ion exchange equilibrium



The equilibrium constant of the exchange would be a ‘true’ constant since an equal number of charges is passed in both directions across the phase boundary. At pH 5.5 the sorbent is almost completely in the RH⁻NH₄⁺ form and the ratio $\overline{[R - M]}/[M^{2+}]$ is predicted to be inversely proportional to [NH₄⁺]. This model seems to overestimate the effect but again emphasises the advantages of keeping electrolyte additions to a minimum.

Since the electrolyte concentration is of such importance, the uptake of the analytes will be influenced by major matrix ions occurring in the sample. For instance, concentrations of alkali and alkaline earth metal ions have to be considered for samples of natural waters. To estimate the influence of such a matrix the adsorption of Cd²⁺ and Cu²⁺ at different concentrations of Ca²⁺ was measured. Table 4 presents equilibrium concentrations of Cd²⁺ in 0.005 M acetate buffer containing 0, 0.001 M and 0.01 M CaCl₂. The equilibrium concentrations in the 0.01 M Ca²⁺ solution are similar to those in 0.1 M acetate buffer. The recoveries of Cd²⁺ at 0.01 M Ca²⁺ and different flow rates by an IDA10 column were 98, 92, 86 and 78% at 10, 30, 60 and 80 ml min⁻¹, respectively. These figures are similar to those obtained in 0.1 M acetate buffer and presented in Table 3. Thus, at flow rates greater than 10 ml min⁻¹, a natural water matrix could affect the recovery of Cd²⁺ when an IDA-Novarose of lower capacity than 45 μmol ml⁻¹ is used. However, in comparison with other adsorbents, which are used at flow rates generally less than 10 ml min⁻¹, a low capacity IDA-Novarose could have the advantage of yielding smaller concentrations of the matrix ions in the enriched sample.

For Cu²⁺ no influence on recovery by the matrices studied was observed, probably due to the high affinity of this ion for the IDA-Novarose sorbent. Quantitative recovery was always obtained.

3.5. Recovery and retention volume

The recoveries from enrichment experiments at 10 and 100 ml min⁻¹ are presented in Fig. 5. In all cases 100 ml of 10 ppb Cd²⁺ at pH 5.5 were enriched on columns of varying volume and capacity. The NH₄⁺ and Ca²⁺ concentrations of the test solutions were also varied. The corresponding values of β' were found by batch experiments and used to calculate V_R. The recovery appears to be a smooth function of V_R. The sample volume has been marked out in the graphs, which indicates that a V_R-value of twice the sample volume is sufficient for quantitative recovery at a flow rate

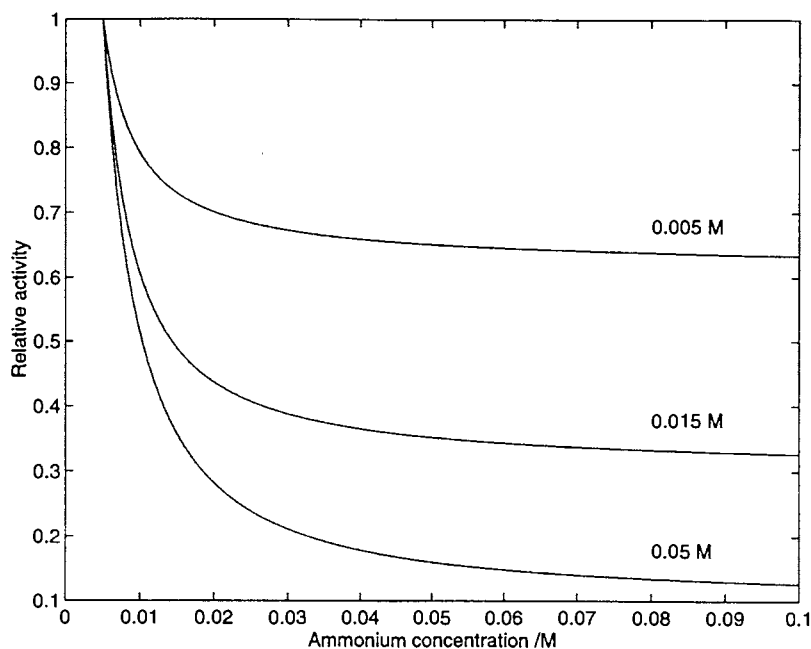


Fig. 4. The relative change of the activity of the R-H₂ groups as a function of the ammonium ion concentration at three specific adsorbent capacities (in M = 10⁻³ μmol ml⁻¹). The activity at [NH₄⁺] = 0.005 M is used as reference.

of 10 ml min⁻¹, while the V_R -value needs to be about 10 times the sample volume at 100 ml min⁻¹.

The empirical relationship between recovery and V_R is a useful means of selecting the conditions for enrichment of metal ions which can be accumulated at near equilibrium conditions. The β' -values of the ions can be determined simultaneously for all ions in the appropriate matrix using a batch experiment. Calculated V_R -values

Table 4
Equilibrium concentration of Cd²⁺ in batch enrichments in 0.005 M acetate buffer at pH 5.5 containing Ca²⁺, for different specific capacities

Background	Equilibrium concentration (μM)			
	IDA6	IDA10	IDA20	IDA45
I ^a	0.16	0.04	<0.01	<0.01
II	0.49	0.14	0.03	0.04
III	1.51	0.73	0.25	0.01

^a Same conditions as in Table 2 (III).

Start solution, 100 ml of 3 μM Cd²⁺, Sorbent, 0.5 ml.

Calcium concentration, (I) 0 M, (II) 0.001 M, (III), 0.010 M.

can then be used to find preliminary conditions for quantitative enrichment of the analytes at a low total capacity so that the concentrations of the concomitants can be kept low in the eluate.

Fig. 6 shows the enrichment of 1 μg of Cu²⁺ and Cd²⁺ from volumes between 50 and 400 ml on an IDA10 column. The solutions also contain 0.01 M Ca²⁺ and the pH was adjusted to 5.5 by 0.005 M acetate buffer. The V_R value for Cd²⁺ is about 230 ml, > 2000 ml for Cu²⁺ in this matrix. Quantitative retention of the latter ion is observed for all sample volumes as expected. For Cd²⁺ significant losses start at a sample volume of about 175 ml which shows that V_R is a reasonable predictor at low flow rates. The adverse effect of calcium concentration is demonstrated for a sample volume of 300 ml by an increase in recovery from about 75 to 100% when the Ca²⁺ concentration decreases from 0.01 to 0.004 M.

3.6. Matrix elimination

The presence of major matrix ions not only diminishes the sample volumes that can be en-

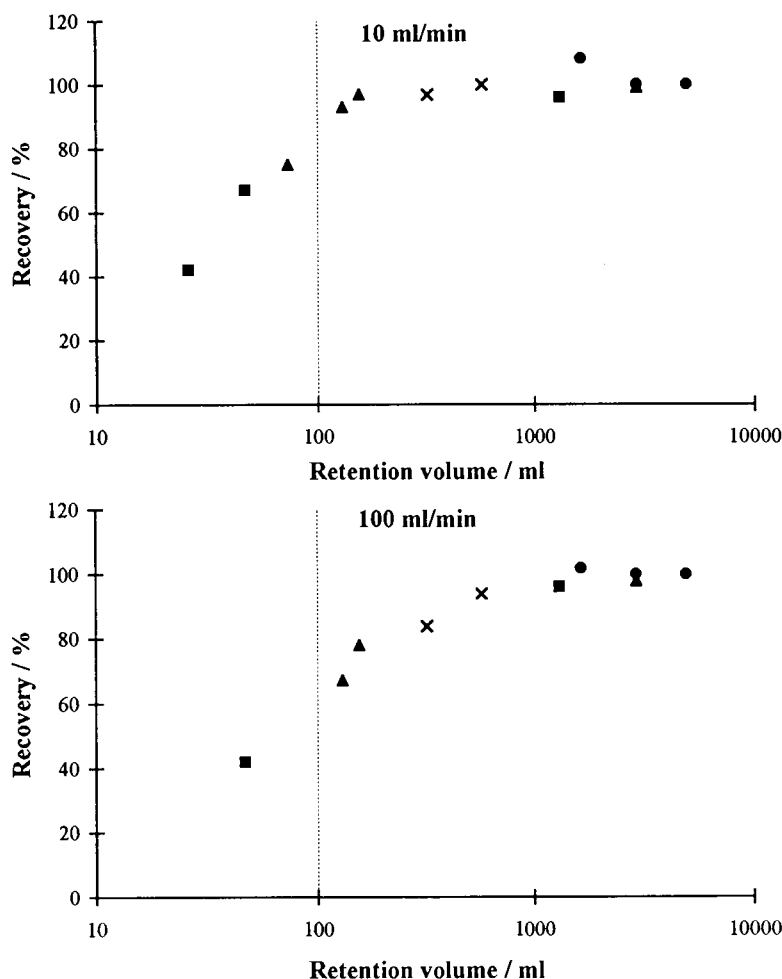


Fig. 5. The recovery of cadmium by columns of different capacity as a function of the calculated retention volume (logarithmic scale). A 100 ml portion of 10 ppb Cd^{2+} at pH 5.5 in different matrices was enriched at 10 and 100 ml min^{-1} . The matrices were, 0.005 and 0.1 M acetate buffer, 0.01 M Ca^{2+} + 0.005 mM acetate buffer. Columns: 6.5 mm i.d. \times 5 or 9 mm. (■, IDA6; ▲, IDA10; ×, IDA20 and ●, IDA45).

riched by a column, but can also cause disturbances in the spectrochemical finish by ICP-AES. This can be exemplified by the determination of Cd^{2+} in natural waters with preconcentration and determination performed in a flow system. Fig. 7 shows elution profiles from IDA10 and 45 initially in equilibrium with a 0.005 M Ca^{2+} solution at pH 5.5. Before elution the columns were washed with 0, 2 or 4 ml of 0.1 M ammonium acetate–acetic acid buffer. The washing was carried out in an attempt to replace Ca^{2+} with NH_4^+ .

The shape of the initial parts of the elution curves for Ca^{2+} is partly caused by the manifold used in the experiment and can be as such ignored. The important features are the peaks, most clearly seen for IDA45, which follow upon elution of the adsorbent by acid. Incomplete removal of Ca^{2+} by NH_4^+ gives rise to peaks on the elution curve for Cd^{2+} which would lead to errors in the determination of cadmium. With IDA10, 2 ml of the washing solution suffices to remove Ca^{2+} to a level that does not disturb the cadmium signal. The results point to the advan-

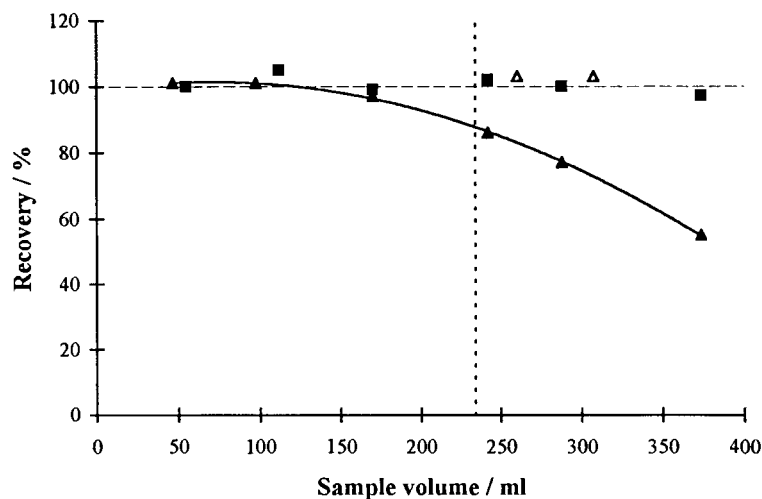


Fig. 6. The recovery of Cu^{2+} (■) and Cd^{2+} (▲) enriched on IDA10 at 10 ml min^{-1} , from a matrix of 0.01 M Ca^{2+} and 0.005 M acetate buffer, pH 5.5, as a function of sample volume. Each sample contained $1 \mu\text{g}$ of both metals. The estimated retention volume (V_R) for Cd^{2+} is 230 ml. Two results from solutions containing 0.004 M Ca^{2+} are also included for Cd^{2+} (△).

tage of a low specific capacity, namely easier removal of concomitants, but it must be kept in mind that it only holds as long as the total capacity is large enough for quantitative recovery.

3.7. Dispersion

Since the analytes will be spread out into a larger volume when the adsorbent capacity is lowered, the elution profile might change with the specific capacity. Therefore, such profiles were studied for IDA45, 20 and 10 after enrichment of 60 ml of 20 ppb Cd^{2+} and Cu^{2+} in 0.005 M acetate buffer, pH 5.5. The flow rate was 25 ml min^{-1} , which is known to yield quantitative recovery. The elution of the test ions by 1 ml of 2 M HCl at 4 ml min^{-1} was followed by ICP-AES. The elution profiles did not differ between Cd^{2+} , having a moderate, and Cu^{2+} , having a high affinity to the adsorbent. They were also independent of capacity, resulting in the same peak sensitivity for the three adsorbents. Washing the column before elution with 4 ml of 0.1 M acetate buffer did not effect the shape of the elution peak.

One might argue that the similarities between elution profiles for different capacities is a result of large contributions from the ICP nebulizer and

other parts of the system to total dispersion. This could mask small effects by the sample distribution in the column. The extent of the non-column dispersion was studied by collection of 0.1 ml fractions of the eluate at the column outlet in an off-line experiment. The elution profiles obtained in this way had essentially the same width as the on-line signals (about 1 ml). This indicates that minor extra dispersion is caused by the ICP instrument and the manifold. A narrower column with 3 mm i.d. increased the sensitivity by about 40%, but the increased back pressure made work with this column difficult and it was not further used.

A study of the effect of the nature and concentration of the eluent on dispersion showed that there was no advantage of nitric acid or perchloric acid over hydrochloric acid at a concentration of 1 mol l^{-1} . Increase in the concentration of hydrochloric acid to 2 M resulted in a signal enhancement of about 10%. Hence, 2 M hydrochloric acid was generally used as eluent. The effect of the elution flow rate was studied and signal enhancements of about 5 and 10% were achieved by diminishing the elution flow rate from 4 to 3 and 2 ml min^{-1} , respectively. However, the peak widths, in millilitres, were essentially the

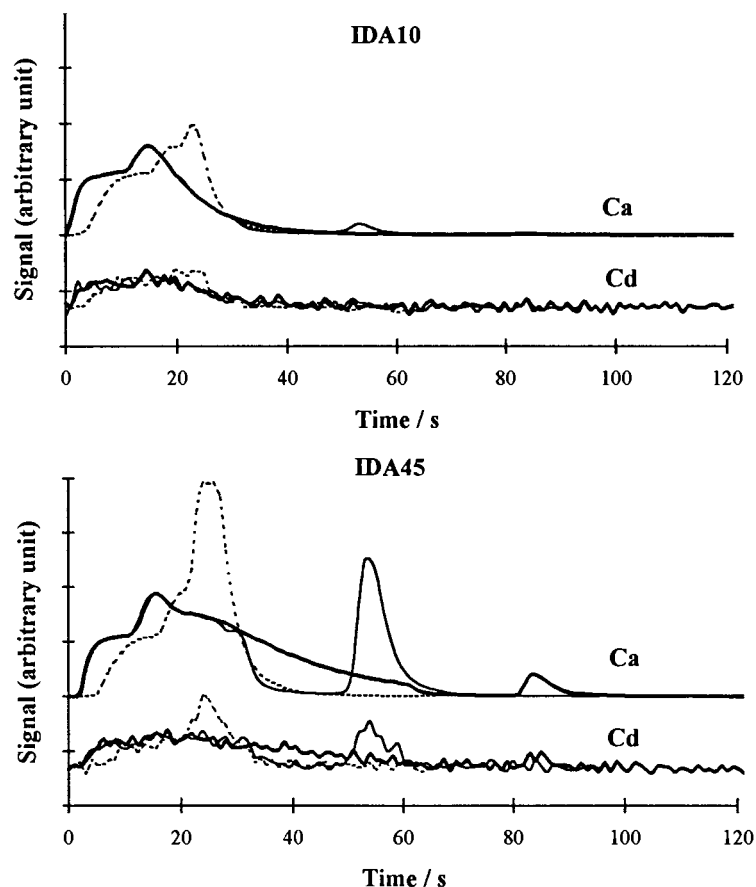


Fig. 7. Calcium and cadmium signals from the solution leaving a calcium saturated enrichment column during washing and elution. Washing was performed with 0, (---); 2, (—) and 4, (— · —) ml of 0.1 M acetate buffer. Calcium was measured by ICP-AES at 317.933 and cadmium at 228.802 nm.

same for the different flow rates indicating that sensitivity enhancement was due to limitations in the ICP input capacity at higher flow rates rather than by a change in the peak dispersion.

4. Conclusions

The general properties and simple preparation of an IDA-Novarose adsorbent with a desired specific capacity make this adsorbent suitable for studies and applications in which specific capacity can be an important parameter.

Conditional metal ion—sorbent stability constants pertaining to the sample matrix can be

readily determined in batch experiments. Due to the rapid kinetics of the adsorbent, an equilibrium approach based on the conditional constant can be used to predict proper conditions for an attempted preconcentration.

The negative effect of the ionic strength on the value of the conditional constant implies that any buffering required should be made using as low a buffer concentration as possible.

The peak height and peak area of the ICP-AES signal from on-line eluates are independent of specific capacity. Use of a low capacity adsorbent results in less interference in the analytical finish from matrix ions—these can be easily replaced by a non-interfering ion by simply washing the en-

richment column before elution. Hence the total capacity of the enrichment column should be kept as low as possible. Adjustment of the total capacity can be carried out by varying the specific capacity of the sorbent at a fixed column length or by changing the column length at a fixed specific capacity.

With Cu^{2+} , having great affinity for the IDA-Novarose sorbent permits 100% recovery even at a flow rate of 100 ml min^{-1} and a specific capacity of $6 \mu\text{mol ml}^{-1}$. For Cd^{2+} , with a moderate affinity, the recovery is dependent on the matrix composition, adsorbent capacity and flow rate. In this case proper condition must be chosen for quantitative recovery.

Acknowledgements

Dr Göran Lindgren, Inovata AB, is greatly acknowledged for his kind gift of the support material. We would also like to thank Dr Jean Pettersson, Department of Analytical Chemistry, Uppsala University, for valuable discussions and suggestions during this work.

References

- [1] R.A. Nickson, S.J. Hill, P.J. Worsfold, *Anal. Proc. Incl. Anal. Commun.* 32 (1995) 387.
- [2] S. Caroli, A. Alimonti, F. Petrucci, Zs. Horvath, *Anal. Chim. Acta* 248 (1991) 241.
- [3] Y. Liu, J.D. Ingle Jr., *Anal. Chem.* 61 (1989) 520.
- [4] S.M. Nelms, G.M. Greenway, R.C. Hutton, *J. Anal. At. Spectrom.* 10 (1995) 929.
- [5] S.F. Durrant, A. Krushevska, D. Amarasiriwardena, M.D. Argentine, S. Romon-Guesnier, R.M. Barnes, *J. Anal. At. Spectrom.* 9 (1994) 199.
- [6] J.Y. Lu, C.L. Chakrabarti, M.H. Back, A.L.R. Sekaly, D.C. Gregoire, W.H. Schroeder, *J. Anal. At. Spectrom.* 11 (1996) 1189.
- [7] M. Groschner, P. Appriou, *Anal. Chim. Acta* 297 (1994) 369.
- [8] M. Torre, M.L. Marina, *Crit. Rev. Anal. Chem.* 24 (1994) 327.
- [9] H.M. Kingston, I.L. Barnes, T.J. Brady, T.C. Rains, M.A. Champ, *Anal. Chem.* 50 (1978) 2064.
- [10] P. Hashemi, Å. Olin, *Talanta* 44 (1997) 1037.
- [11] Application Note No. 305, Inovata AB, Annedalsvägen 39, S-168 65 Bromma, Sweden.
- [12] L. Steinmann, J. Porath, P. Hashemi, Å. Olin, *Talanta* 41 (1994) 1707.
- [13] *Stability Constants of Metal-Ion Complexes*, (Suppl. 1), The Chemical Society, London, UK, Alden and Mowbray, Oxford, 1971.
- [14] M. Pesavento, R. Bicusuz, M. Gallorini, A. Profumo, *Anal. Chem.* 65 (1993) 2522.

pH-dependent spectral behavior of substituted quinolones: potential fluorophore for metallofluorescent indicators

Geraldine M. Huitink *

Department of Chemistry, Indiana University South Bend, South Bend, IN 46634, USA

Received 4 August 1997; received in revised form 13 October 1997; accepted 14 October 1997

Abstract

The 7-methoxy and 7-hydroxy derivatives of 2,3-dimethyl-4-quinolone have been characterized with respect to absorbance, steady-state fluorescence excitation and emission, and acid-base behavior in perchloric acid ($H_0 = 5.68$ —pH 2.0) and aqueous buffers (pH 2.2–14.2); susceptibility to alkaline hydrolysis has been examined absorptometrically. 7-Hydroxy-2,3-dimethyl-4-quinolone is resistant to attack by hydroxide ion. Aqueous solutions of it exhibit moderate to high fluorescence emission, which is dependent on solution acidity. It is recommended for incorporation into metallofluorescent indicators of the Calcein Blue type. © 1998 Elsevier Science B.V. All rights reserved.

Keywords: pH-dependent spectral behavior; Substituted quinolones; Potential fluorophore; Metallofluorescent; Indicators

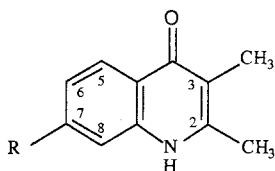
1. Introduction

Metallofluorescent indicators of the Calcein Blue type consist of a fluorophore and one or more methyleneiminodiacetic acid groups. When an indicator of this type is used in spectrofluorometric determinations of metal ions that form weak complexes with methyleneiminodiacetic acid an alkaline medium must be employed. The alkaline medium eliminates competition between protons and metal ions for methyleneiminodiacetic acid; however, if the fluorophore is susceptible to alkaline hydrolysis, indicator function is compromised.

A study of 7-hydroxychromones [1] has identified

2,3-dimethyl substitution as providing the 7-hydroxybenzo-4-pyrone nucleus with high fluorescence intensity and high resistance to attack by hydroxide ion. Might this substitution pattern provide the nitrogen analog of 7-hydroxychromone with desired indicator properties also? As a γ -amide the nitrogen analog should exhibit greater resistance to alkaline hydrolysis than the corresponding γ -ester, but is the material sufficiently fluorescent? The parent 4-quinolone, referred to as 4-hydroxyquinoline in the early literature, has been the subject of several investigations [2–8]. In the present study we characterize the 7-hydroxy and 7-methoxy derivatives of 2,3-dimethyl-4-quinolone—structures and numbering shown below—with respect to absorbance, fluorescence excitation and emission, and acid–base behavior.

* Tel.: +1 219 2374259; fax: +1 219 2376589; e-mail: ghuitink@iusb.edu



2,3-dimethyl-4-quinolone

I. R = OCH₃ (7-methoxy-2,3-dimethyl-4-quinolone)

II. R = OH (7-hydroxy-2,3-dimethyl-4-quinolone)

2. Experimental

2.1. Synthesis

7-Methoxy-2,3-dimethyl-4-quinolone (I) was synthesized according to Mallams and Israelstam [9]: m.p. 303–305° (acetic acid); reported 293–295° (ethanol). Found C 70.99%, H 6.18%, N 6.77%; calculated for C₁₂H₁₃NO₂ (*M*_w 203.2) C 70.92%, H 6.45%, N 6.89%.

7-Hydroxy-2,3-dimethyl-4-quinolone (II) was prepared by boiling I (1 g) and hydriodic acid (10 ml; d, 1.7) under reflux for 1 h. After adding 50 ml of water, the pH was adjusted to 7.0 with a concentrated solution of potassium hydroxide which also contained sodium hydroxide. The precipitate was recrystallized four times from aqueous ethanol: m.p. 335–339°d. Found C 69.83%, H 5.90%, N 7.29%; calculated for C₁₁H₁₁NO₂ (*M*_w 189.2) C 69.82%, H 5.87%, N 7.40%.

2.2. Reagents and procedures

All chemicals were of analytical reagent-grade quality.

Water was demineralized and was further purified by passage through a Milli-Q⁵⁰ system until it exhibited resistance of 18 MΩ.

For the acidity range *H*₀ – 5.68 to +0.04 perchloric acid, 70% (GFS) was diluted with water. Weighed samples were assayed by titration with sodium hydroxide that had been standardized against primary standard potassium acid phthalate, and *H*₀ values were obtained through

interpolation of the corrected Hammett acidity scale of Yates and Wai [10]. Perchloric acid, rather than sulfuric acid, was used to avoid the possibility of sulfonating the 4-quinolones.

Solutions in the pH region 0–2.0 were prepared by dilution of 1 M perchloric acid.

For the range pH 2.20–11.60 buffer solutions of ionic strength 0.01 were prepared following the method of Perrin [11].

For the range pH 10.5–14.2, ionic strength 1.60, appropriate masses of 45.7% w/w potassium hydroxide solution (Baker analyzed) and potassium chloride were diluted with water which had been boiled to remove carbon dioxide.

Stock solutions 3.11 × 10^{–3} M in the 4-quinolones were made up in 95% ethanol. Absorption spectra were run on solutions 2.61 × 10^{–5} M in I and 2.24 × 10^{–5} M in II; fluorescence excitation and emission spectra were obtained on solutions 1.9 × 10^{–6} M in the fluorophore. All solutions were prepared by adding appropriate volumes of stock solution to 25 ml volumetric flasks by means of a Micro Metric Model SB2 buret and Model S5Y syringes and diluting to the mark with buffer solution.

Absorbance measurements were obtained using a Perkin–Elmer λ-6 spectrophotometer interfaced with an Epson Equity III+ computer and an Okidata Microliner 320 printer.

Fluorescence measurements were made using a Perkin–Elmer LS-5 spectrofluorometer interfaced with a Model 3600 data station. Excitation and emission spectra were scanned at rates of 120 nm min^{–1}; the resulting peak intensity and wavelength were processor controlled by the Perkin–Elmer PECLS application program and are uncorrected. An Epson Model FX-85 printer was used to record fluorescence spectra.

The spectrophotometer and spectrofluorometer were equipped with water-circulating cell holders and maintained at 25 ± 0.01°C with Lauda RM6 circulating baths (Brinkman); all absorbance and fluorescence spectra were obtained immediately after solution preparation in 10 × 10 μm quartz cuvettes.

An Accumet[®] 925 pH/ion meter equipped with a semi-micro calomel, glass body, combination

electrode was employed for pH measurement; standardization was accomplished using the two-point calibration procedure. Determination of pH was made in the thermostatted cuvette immediately after each spectrum was run.

Acid dissociation constants were determined using the relationship

$$pK_a = \text{pH} + \log \frac{D_I - D}{D - D_M} \quad (1)$$

where D_I is the absorbance or fluorescence of the ionic form, D_M is the absorbance or fluorescence of the molecular form, and D is the absorbance or fluorescence of mixtures of both quinolone forms measured at a wavelength at which the difference in the absorbance or fluorescence emission of the two forms is greatest and $\text{pH} = \text{p}K_a \pm 0.0, \pm 0.2, \pm 0.4, \pm 0.6$. Plots of absorbance or fluorescence emission as a function of H_0 or pH yield sigmoid curves extending over approximately two and one half H_0 or pH units. For fluorescence work excitation was, in all cases, at the long wavelength isosbestic point in the absorption spectrum.

To avoid making measurements in potassium hydroxide solutions more concentrated than 1.60 M, absorbance and fluorescence of the fully deprotonated quinolones were determined indirectly. Recasting Eq. (1) as

$$D = D_I - \frac{[H^+](D - D_M)}{K_a} \quad (2)$$

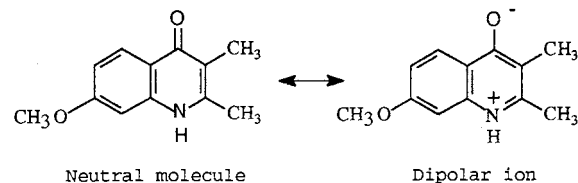
and plotting D versus $[H^+](D - D_M)$, the absorbance or fluorescence of the fully deprotonated material was obtained as the y intercept [12]. Best straight line fits were obtained by linear regression analysis of the experimental data.

Susceptibility of the compounds to alkaline hydrolysis in pH 13 solution at 25°C was determined by monitoring changes in the absorption spectrum of each compound over a period of 8.5 h.

3. Results and discussion

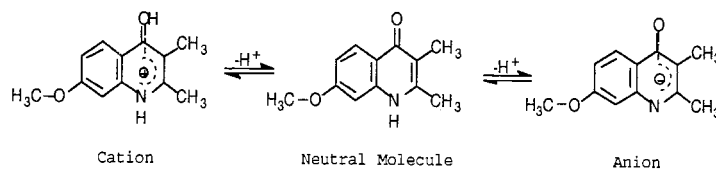
3.1. 7-Methoxy-2,3-dimethyl-4-quinolone (I)

As solution acidity increases in the interval pH 5.0–1.0 carbonyl oxygen is protonated, and the long wavelength absorption maximum shifts from 310 to 326 nm (isosbestic points: 262.4, 286.9 and 326.5 nm) (Fig. 1; Table 1). Basicity of the carbonyl group is attributed to strong resonance between the neutral molecule and its dipolar ion [4]. Fluorescence emission, which follows the ground state prototropic reaction, shifts from 362 to 385 nm and increases as acidity increases over the same pH interval (Fig. 2). The $\text{p}K_a$ value obtained fluorimetrically (2.68 ± 0.05) is identical, within experimental error, to that obtained absorptometrically (2.64 ± 0.03).



Deprotonation of the ring nitrogen occurs at pH greater than 10.5 and is accompanied by a decrease in molar absorptivity. The long wavelength absorption maximum (310 nm at pH 10.5) shifts to 305.5 nm, and an unresolved peak (321 nm) shifts to 325.5 nm at pH 14.0 (isosbestic point: 328.8 nm); $\text{p}K_a$, 12.46 ± 0.02 ($I = 1.60$). Changes in the emission spectrum parallel changes in the absorption spectrum, an intense band centered at 409 nm emerging above pH 10.5; $\text{p}K_a$, 12.44 ± 0.02 ($I = 1.60$).

Three forms of I were detected: the anion exists at pH 14 and higher, the neutral molecule is the dominant species in the range pH 4.5–10.5, and the cation exists at pH 1 and lower in both the



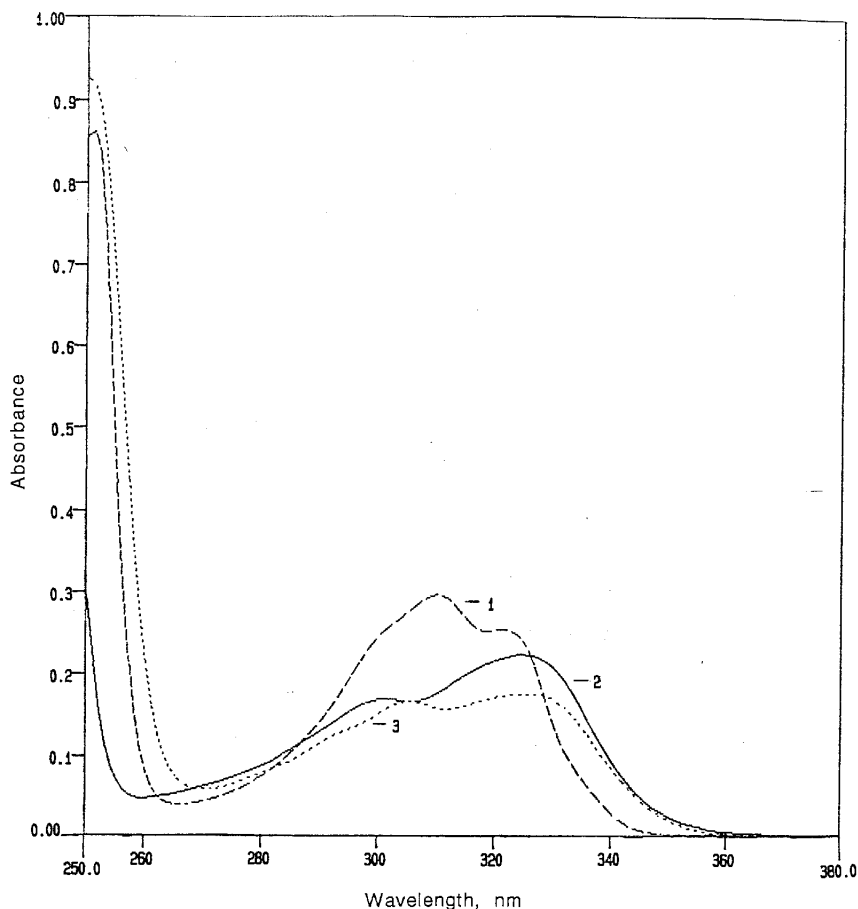


Fig. 1. Absorption spectrum of 7-methoxy-2,3-dimethyl-4-quinolone (Compound I) at (1) pH 5.0; (2) $H_0 + 0.04$; (3) pH 14.0.

ground and S_1 states. The correspondence of pK_a values obtained absorptometrically and fluorometrically and of maxima shifts suggests that fluorescence proceeds from excited ground-state forms, and prototropic equilibria are not established during the lifetime of the first excited singlet state.

3.2. 7-Hydroxy-2,3-dimethyl-4-quinolone (II)

Below pH 5 ground state acid–base behavior of II parallels that of I. As carbonyl oxygen is protonated the absorption spectrum, which at pH 5 consists of a 314.3 nm maximum, a 306 nm shoulder and a lesser maximum at 326 nm, is red-shifted and transformed into a broader band

having one maximum at 327 nm and a lesser maximum at 301 nm (isosbestic points: 262.6, 286.4 and 330.2 nm) (Fig. 3); pK_a , 2.72 ± 0.06 .

The neutral molecule is the dominant ground state species between pH 4 and 7. With neutralization of the phenolic proton over the range pH 7.0–9.5 the absorption spectrum is red-shifted: the 306 nm shoulder and 314.3 nm peak coalesce into a peak centered at 313.9 nm, and a broad band arises at 339 nm. A short wavelength maximum centered at 245.9 nm shifts to 261.9 nm over the same pH range (isosbestic points: 276.9, 307.8, 322.4, and 330.4 nm); pK_a , 8.20 ± 0.04 .

Deprotonation of the ring nitrogen is accompanied by a decrease in molar absorptivity, the maximum shifting from 313.9 nm at pH 12.0 to

309 nm at pH 14.2 (isosbestic point: 296.3 nm); pK_a , 13.86 ± 0.05 ($I = 1.60$). The N proton of II is a weaker acid than that of I owing to greater difficulty in removing a proton from an anion than an uncharged molecule. The small spectral shift observed upon ionization of the N proton is in agreement with studies on 4-hydroxyquinoline [2]. Both I and II are stable in pH 13 solution; absorption spectra change by less than 1.5 per cent over a period of 8.5 h.

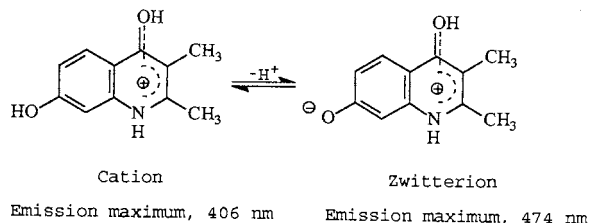
In $H_0 = -3.65$ solution the cation is the dominant species and is responsible for both absorption and fluorescence emission. The shift in the wavelength of maximum emission from 406 to 474 nm in pH 1.0 solution (Fig. 4) is attributed to ionization of the phenolic proton; no corresponding change occurs in the emission spectrum

Table 1

Absorption maxima and molar absorptivities of 7-methoxy-2,3-dimethyl-4-quinolone and 7-hydroxy-2,3-dimethyl-4-quinolone; wavelength range, 250–450 nm

Compound (designation)	Wavelength, nm	Molar absorptivity, $\text{cm}^{-1} \text{mol}^{-1} \text{l}$
<i>7-Methoxy-2,3-dimethyl-4-quinolone (I)</i>		
Cation	301	6.5×10^3
	326	8.5×10^3
Neutral molecule	301.5 sh	9.7×10^3
	310	1.1×10^4
	321	9.7×10^3
Anion	305.5	6.4×10^3
	325.5	6.7×10^3
<i>7-Hydroxy-2,3-dimethyl-4-quinolone (II)</i>		
Cation	301	6.1×10^3
	327	8.3×10^3
Neutral molecule	251 sh	2.6×10^4
	306 sh	9.9×10^3
	314.3	1.1×10^4
	326	9.2×10^3
Anion	261.9	4.2×10^4
	313.9	1.3×10^4
	339	8.0×10^3
Dianion	261	3.9×10^4
	309	8.1×10^3
	337	6.9×10^3

of I, which does not contain a phenolic group. The species responsible for fluorescence emission at 474 nm is presumed to be a zwitterion. Absence of change in the absorption spectrum of II over this acidity range indicates that the phenol is a stronger acid than the protonated carbonyl in the S_1 state; the reverse order prevails in the ground state.



Plots of the decreasing 406 nm emission and the rising 474 nm emission as a function of Hammett acidity yield complementary sigmoid curves with inflection points at $H_0 = -1.37 \pm 0.04$ and -1.34 ± 0.05 , respectively (Fig. 5). Identical inflection points indicate that prototropic equilibrium is established within the lifetime of the first excited singlet state [13], the H_0 value at the inflection points being equal to the excited state pK_a .

As acidity continues to decrease between pH 1.0 and 4.0 the 474 nm emission maximum decreases in intensity and shifts to shorter wavelength (470 nm) while a second maximum emerges at 355 nm; isoemissive point, 425.9 nm. Continued decrease in solution acidity between pH 3.8 and 6.0 is accompanied by further shift of the long wavelength emission maximum to 466 nm (isoemissive point: 437.6 nm). There is little change in the emission intensity of either the 355 nm or the 466 nm bands above pH 4.6. The changes in the emission spectrum appear to be linked to changes in the status of the ground-state carbonyl group, the pK_a value determined fluorometrically (2.76 ± 0.05) agreeing with the value determined absorptiometrically.

The 355 and 466 nm emission bands have identical excitation spectra, which indicates that they originate from the same ground state species. Both bands have about equal emission in-

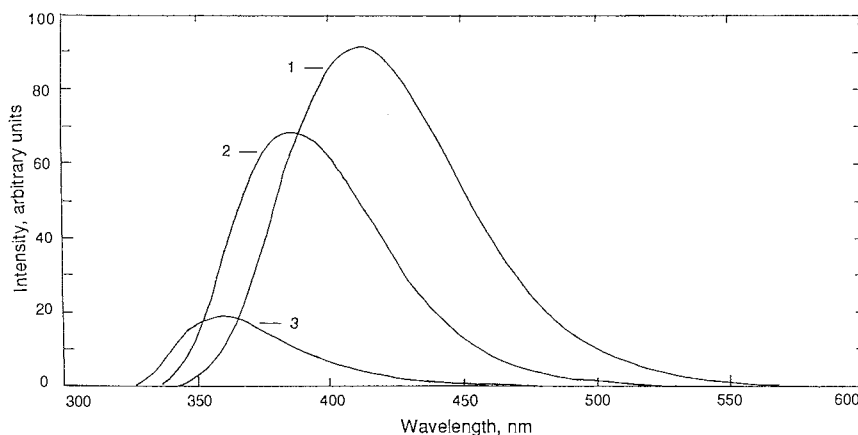
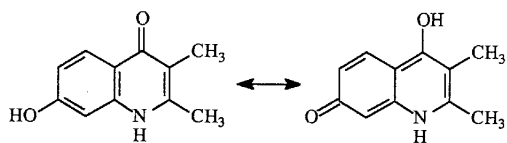


Fig. 2. Fluorescence emission spectrum of 7-methoxy-2,3-dimethyl-4-quinolone (Compound I) at (1) pH 14.2, excitation monochromator set at 323 nm; (2) $H_0 + 0.04$, excitation monochromator set at 322 nm; (3) pH 5.0, excitation monochromator set at 306 nm.

tensity, the 466 nm band being a little more intense than the 355 nm band. Comparison with the 362 nm emission maximum of I suggests that the 355 nm band originates from the excited neutral molecule. The 466 nm band is thought to originate from the excited neutral ketotautomer.



Neutral molecule

Neutral ketotautomer

Emission maximum, 355 nm

Emission maximum, 466 nm

It should be noted that a variety of excited-state species have been proposed to account for long-wavelength emission in similar compounds, and a variety of mechanisms have been posited to explain how a proton may be transferred from a phenolic group to a carbonyl group several atoms away [14–20].

In the pH interval 7.0–9.5 fluorimetric titration of II follows ground-state neutralization of the phenolic proton: emission at 355 nm decreases while the 466 nm band shifts to 431 nm and triples in intensity; pK_a , 8.20 ± 0.04 . Emission at 431 nm is attributed to the excited anion.

Above pH 11 fluorescence emission of II decreases, and the wavelength of maximum emission

intensity appears to shift to shorter wavelength being centered at 428 nm in pH 14.2 solution. The data are insufficient to provide an excited-state pK_a , but it is presumed to be greater than 14.

7-Hydroxy-2,3-dimethyl-4-quinolone exhibits complex excited-state behavior. Strongest fluorescence is observed in perchloric solutions of $H_0 - 3.65$ and higher, emission being from the excited cation. Fluorescence from what is presumably a zwitterion is strongest near pH 1, but, with conversion of the ground-state cation into the neutral molecule, the dominant excited-state species is converted to the neutral molecule and neutral ketotautomer, and moderate fluorescence is observed. Molecular formulas of the zwitterion, uncharged molecule and ketotautomer are identical. Each has the same number of protons. In the zwitterion and ketotautomer the protons are attached to the same atoms, but the two forms have different electronic arrangements. The emission maxima of the species tentatively identified as zwitterion and ketotautomer differ by only 8 nm, and each may possess a certain amount of the others character. The anionic form of II is approximately 15 percent as fluorescent as the anionic form of 7-hydroxy-4-methylcoumarin, the fluorescent moiety of Calcein Blue, still II is strongly fluorescent. This strong fluorescence and resistance to attack by hydroxide ion indicate that II is an excellent candidate for incorporation into metallofluorochromic indicators.

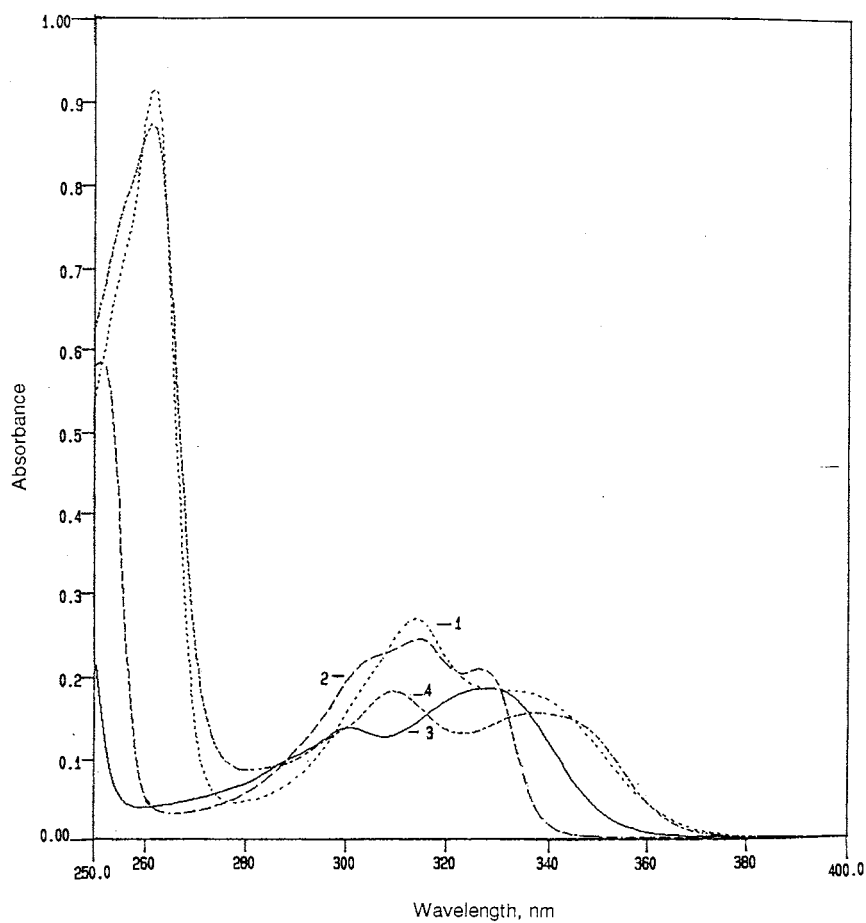


Fig. 3. Absorption spectrum of 7-hydroxy-2,3-dimethyl-4-quinolone (Compound II) at (1) pH 10.5; (2) pH 5.0; (3) $H_0 + 0.04$; (4) pH 14.2.

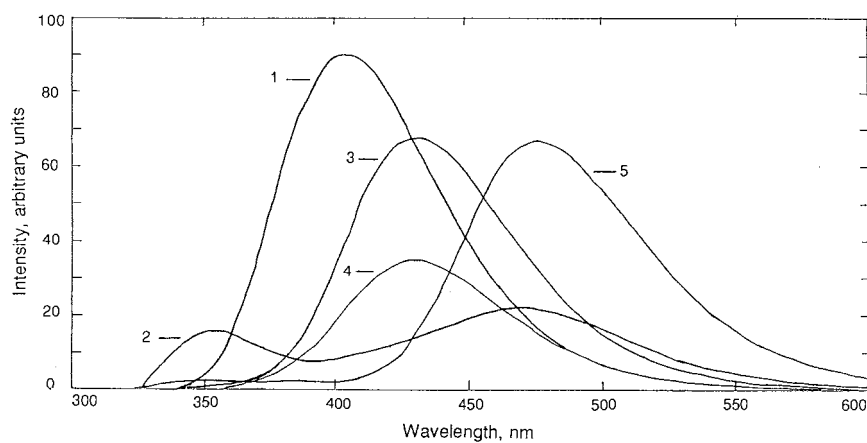


Fig. 4. Fluorescence emission spectrum of 7-hydroxy-2,3-dimethyl-4-quinolone (Compound II) at (1) $H_0 - 3.65$, excitation monochromator set at 323 nm; (2) pH 5.0, excitation monochromator set at 309 nm; (3) pH 10.1, excitation monochromator set at 310 nm; (4) pH 14.2, excitation monochromator set at 335 nm; (5) pH 1.0, excitation monochromator set at 324 nm.

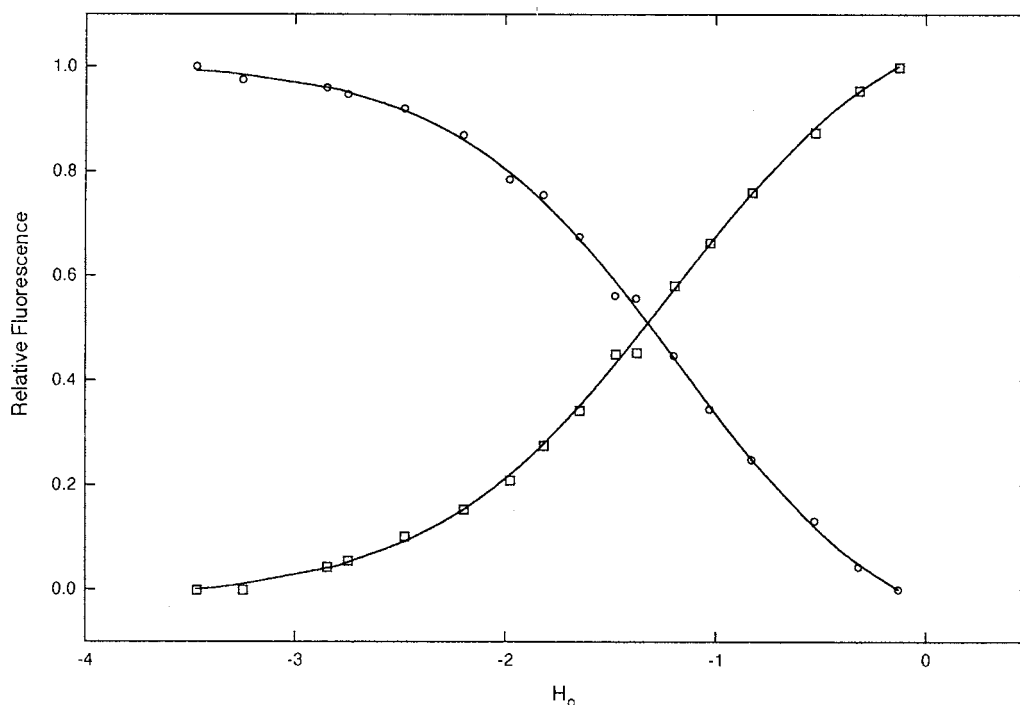


Fig. 5. Variation of fluorescence of 7-hydroxy-3,4-dimethyl-4-quinolone (Compound II) with Hammett acidity, excitation monochromator set at 321 nm. (1) Emission monochromator set at 406 nm. (2) Emission monochromator set at 474 nm.

Acknowledgements

The author recognizes the following undergraduates for their contributions to this project: Charles Doyle, Mark Mankowski, William Nowatski, Debrada Smith, and Sahana Mollah. She acknowledges financial support from Indiana University South Bend in the form of Grant-in-Aid of Research funds and an Undergraduate Research Award to S.M. She is grateful to the late Professor Harvey Diehl for advise and encouragement.

References

- [1] G.M. Huitink, *Talanta* 27 (1980) 977.
- [2] G.W. Ewing, E.A. Steck, *J. Am. Chem. Soc.* 68 (1946) 2181.
- [3] S.F. Mason, *J. Chem. Soc.* (1958) 674.
- [4] A. Albert, J.N. Phillips, *J. Chm. Soc.* (1956) 1294.
- [5] G.F. Tucker, J.L. Irvin, *J. Am. Chem. Soc.* 76 (1951) 1923.
- [6] K. Kimura, L.S. Foster, *J. Phys. Chem.* 71 (1967) 2744.
- [7] S.G. Schulman, A.C. Capomacchia, B. Tussey, *Photochem. Photobiol.* 14 (1971) 733.
- [8] S.G. Schulman, B.S. Vogt, *J. Phys. Chem.* 85 (1981) 2074.
- [9] A.K. Mallams, S.S. Israelstam, *J. Org. Chem.* 29 (1964) 354.
- [10] K. Yates, H. Wai, *J. Am. Chem. Soc.* 86 (1964) 5408.
- [11] D.D. Perrin, *Aust. J. Chem.* 16 (1963) 572.
- [12] A. Albert, E.P. Serjeant, *The Determination of Ionization Constants*, 3rd ed., Chapman and Hall, New York, 1984, p. 84.
- [13] N. Lasser, J. Feitelson, *J. Phys. Chem.* 77 (1973) 1011.
- [14] P.E. Zinsli, *J. Photochem.* 3 (1974) 55.
- [15] G.S. Beddard, S. Carlin, R.S. Davidson, *J. Chem. Soc. Perkin 2* (1977) 262.
- [16] S.G. Schulman, L.S. Rosenberg, *J. Phys. Chem.* 83 (1979) 447.
- [17] R.K. Bauer, K. Kowalczyk, *Z. Naturforsch* 35a (1980) 946.
- [18] T. Moriya, *Bull. Electrochem. Lab.* 45 (1981) 129.
- [19] R. Schipfer, O.S. Wolfbeis, A. Knierzinger, *J. Chem. Soc. Perkin Trans. 2* (1981) 1443.
- [20] E. Bardez, P. Boutin, B. Valeur, *Chem. Phys. Lett.* 191 (1992) 142.

Neotetrazolium chloride: a new reagent for spectrophotometric determination of manganese

M. Kamburova

Department of Chemistry, Higher Institute of Agriculture, BG-4000 Plovdiv, Bulgaria

Received 24 March 1997; received in revised form 4 August 1997; accepted 20 October 1997

Abstract

The interaction of Mn(VII) and the Neotetrazolium chloride has been examined. The ion-associate formed is extracted into 1,2-dichloroethane. The optimum conditions have been established. The molar absorptivity of the complex is $(9.1 \pm 0.08) \times 10^5 \text{ l mol}^{-1} \text{ cm}^{-1}$. The sensitivity of the method is $6.04 \times 10^{-5} \mu\text{g cm}^{-2}$. It is possible to extract and determine manganese in the presence of large number of cations and anions. The characteristic values for the extraction and the aqueous phase equilibria were determined: extraction constant $K_{\text{ex}} = 3.21 \times 10^9$, distribution constant $K_D = 33$ and association constant $\beta = 9.72 \times 10^7$. The method is applicable to analysis of soils and steels. © 1998 Elsevier Science B.V. All rights reserved.

Keywords: Extraction-spectrophotometry; Manganese determination; Soils; Steels

1. Introduction

The determination of microquantities of manganese in soils and other naturally occurring materials is of particular importance in connection with the growing interest in environmental problems. New accurate and reliable methods for analysis of various objects containing traces of manganese should be searched for this element.

Manganese is a microelement actively absorbed by plants and has an effect on the fertility of soils [1]. The reagents suggested for determination of manganese include: ethylenebis(triphenylphosphonium) [2]; isophthalaldihydroxamic acid [3]; 1,10-phenantroline [4]; 8-hydroxyquinoline [5]; 4-(2-pyridylazo)resorcinol

[6]; 1-(2-pyridylazo)-2-naphthol [7,8]; *N*-diphenyl benzamidine [9]. Some of the above mentioned extraction methods are characterized by a long procedure, are not very selective [4–8], low stability of the complexes obtained [2,3], low sensitivity [3].

In the literature there is data on the use of Neotetrazolium chloride for determination of chromium(VI) [16], zinc(II) [17,18], cobalt(II) [19] and molybdenum(VI) [20]. No data about determination of manganese with Neotetrazolium chloride can be found in the literature. The tetrazolium salt Neotetrazolium chloride we suggest is a new reagent for determination of microquantities of manganese. Mn(VII) forms stable an ion-pair with NTC. This can be used in developing an extraction-photometric

method for determination of manganese. The nature of the interaction between the manganese(VII) with the cation of the tetrazolium salt should be studied. The present paper represents the conditions needed for determination of manganese with Neotetrazolium chloride (NTC). This is an extremely simple and direct extraction for determination of microquantities of manganese.

The goal is to develop an extraction–photometric method using NTC for determination of manganese in soils and steels, superior, in some respects, to the existing methods.

2. Experimental

2.1. Reagents

All the chemicals used were of analytical grade. A 1×10^{-3} M stock solution of Neotetrazolium chloride (NTC) Fluka was prepared by dissolving 0.0702 g of NTC in distilled water and diluting to 100 ml. Other NTC concentrations were prepared by appropriate dilution. The solutions were stable for several months.

Stock manganese(VII) solution. A 1×10^{-2} M aqueous solution was prepared by dissolving 0.395 g of KMnO_4 in 250 ml of distilled water. After 8 days the exact concentration of manganese(VII) was checked by oxalate titration. Working solution containing 1×10^{-4} M Mn(VII) was prepared by dilution.

Solutions of ions for interference studies were prepared by dissolving the amount of each compound needed to give 10 mg ml^{-1} of the ion concerned.

Phosphoric, nitric, hydrochloric, sulfuric and perchloric acids at concentrations of 2, 1.55, 1.2, 2 and 9 M, respectively, were used; 1,2-Dichloroethane.

2.2. Apparatus

Absorbance measurements were made with spectrophotometer VSU 2-P (Carl Zeiss, Jena, Germany), 1 cm light path cuvette, 240 nm.

2.3. Procedures

2.3.1. Calibration

In a 100 ml separatory funnel place 0.5 ml of 2 M phosphoric acid, 2 ml of 1×10^{-4} M Neotetrazolium chloride, and a known volume of manganese(VII) solution containing up to $\sim 17 \mu\text{g}$ of manganese. Dilute to 10 ml with distilled water and shake with 3 ml of dichloroethane for 5 s. Transfer the organic layer through a dry filter paper into a 1-cm cuvette and measure the absorbance at 240 nm against a reagent blank similarly prepared.

2.3.2. Determination of manganese in steel

Samples of 0.1 g of steel types were dissolved in 50 ml HNO_3 (1:3) and evaporated to remove vapours of nitric oxides. 0.1 g of ammonium persulphate was added, and boiled for 10 min for oxidation of the carbon compounds and the destruction of the excess of the persulphate. It was diluted up to 70 ml with water and portions of 3 ml conc. H_2SO_4 , 2 ml conc. H_3PO_4 and 0.2 g potassium periodate were added for the oxidation of Mn(II) to Mn(VII) [10,11]. It was heated to boiling point and the temperature was maintained for 10 min. Then the solution was cooled. It was transferred into a volumetric flask of 100 ml and diluted to the mark with distilled water. Aliquot parts of this solution were taken for analysis with addition of 0.5 ml of 2 M phosphoric acid, 2 ml of 1×10^{-4} M NTC and 2 ml of saturated ascorbic acid solution (to mask interfering ions). It was diluted to a volume of the aqueous phase of 10 ml with distilled water, extracted with 3 ml of dichloroethane for 5 s, and the organic layer was then transferred through paper filter into 1 cm cuvette and absorbance was measured at 240 nm.

The determination of manganese was carried out using the analytical graph.

2.3.3. Determination of manganese in soils

4 g of the air-dried soil sample is weighed and introduced into a platinum crucible, then heated for 3 h in a muffle furnace at 500–550°C to digest the organic matter. After cooling, the sample is transferred into a platinum bowl and 5 ml conc. H_2SO_4 , 5 ml of conc. HNO_3 and 2 ml H_2O_2 are

added. The sample was heated until the white fumes of SO_3 appeared. Next, 1 ml of H_2SO_4 and 3 ml of HNO_3 was added and evaporated to dryness. 5 ml of conc. HCl and 2 ml of conc. HClO_4 were added to the dry residue, then heated to dryness evaporating chromium as chromylchloride with destruction of the organic compounds [12]. The dry residue is then dissolved in bidistilled water and acidified with hydrochloric acid. The solution obtained is then neutralized with concentrated ammonia solution to precipitate the iron(III) and aluminium(III) as the hydroxide. The precipitate is filtered through filter paper and the filtrate is evaporated until the volume is 30 ml. 3 ml of conc. H_2SO_4 , 2 ml of conc. H_3PO_4 and 0.2 g of potassium periodate are added, the solution is heated to the boiling point and the temperature maintained for 10 min [13]. Then the solution was cooled and transferred into a 50 ml volumetric flask, and diluted to the mark with distilled water. To mask the interfering ions 0.5 ml of 2 M phosphoric acid, 2 ml of 1×10^{-4} M NTC and 3 ml of ascorbic acid saturated solution were added to 3 ml of soil solution. The solution was diluted to 10 ml with distilled water, then shaken for 5 s with 3 ml 1,2-dichloroethane. The organic phase was filtered through a dry paper into a 1-cm cuvette and the absorbance was measured at 240 nm. A blank was run in parallel in the absence of the soil sample. A calibration graph was constructed with standards similarly treated.

3. Results and discussion

3.1. Extraction of the complex into organic solvents and determination of the wavelength of maximum absorption

Manganese(VII) forms an ion-pair with Neotetrazolium chloride. The solubility of the ion-associate in various organic solvents was investigated. Benzene, chloroform, 1,2-dichloroethane, dimethyl ketone, isobutanol, toluene, alcohols, ethers, xylene were tested. Our studies showed that the ion associate of MnO_4^- with NTC was quantitatively extracted into 1,2-dichloroethane. The absorption spectra of solutions of tetrazolium

salt and ion-association complex in phosphoric acid show that the absorption maxima are around 260 nm (Fig. 1).

3.2. Stability and composition of the ion-association complex

The organic phase containing 1.78×10^{-5} M manganese was extracted as described in Section 2.3. The absorption was measured at 260 nm against time in 1-cm cells with dichloroethane in the reference cell. It was established that the ion-pair had high stability. The absorption did not change for 20 days. Variations in temperature of the test solution from 18 to 24°C had a negligible effect on the light absorption.

The stoichiometric coefficients of the ion-associate were established by various methods [14]: the method of molar ratios, the method of isomolar series. The results show that in the ion-associate, the reagent ratio is $\text{NTC}:\text{MnO}_4^- = 1:2$. The extraction equilibrium was reached in 5 s.

3.3. Photometric characteristics

The molar absorptivity of the complex, calculated by the method of Komar-Tolmatchov [14] is $(9.1 \pm 0.08) \times 10^5 \text{ l mol}^{-1} \text{ cm}^{-1}$. This demonstrates the high sensitivity of the given reaction. A

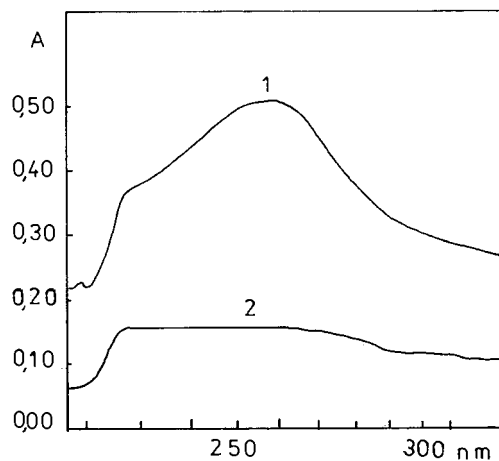


Fig. 1. Absorption spectra of ion-association complex (1) and NTC (2) in dichloroethane: $C_{\text{Mn(VII)}} = 1.33 \times 10^{-5}$ M, $C_{\text{NTC}} = 1 \times 10^{-5}$ M, $C_{\text{H}_3\text{PO}_4} = 0.1$ M.

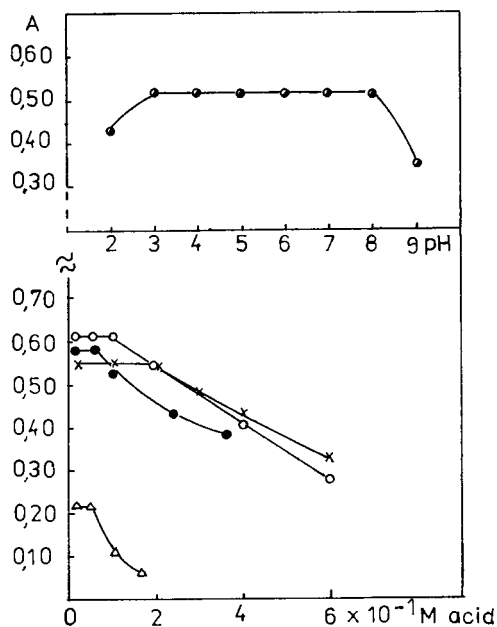


Fig. 2. Investigation of the influence of acidity on the extraction of Mn(VII) with NTC: $C_{\text{Mn(VII)}} = 1.78 \times 10^{-5}$ M, $C_{\text{NTC}} = 1 \times 10^{-5}$ M; (○)— H_3PO_4 , (●)— HCl , (×)— H_2SO_4 , (△)— HNO_3 .

plot of the concentration of aqueous phase manganese(VII) vs. absorbance of the organic layer showed good linearity in the range 0.1–1.7 μg of manganese(VII) per 1 ml of aqueous phase. The sensitivity of the method according to Sandell [13] is 6.04×10^{-5} $\mu\text{g cm}^{-2}$. The relative standard deviation (12 determinations with 1 μg of Mn(VII), 95% confidence level) is $\pm 0.85\%$.

3.4. Effect of reagents and conditions on absorbance measurements

The effect of the acidity of the solution on the extraction of the ion associate of manganese is given in Fig. 2. The optimum acidity of the extraction was over a rather wide range: pH 3–8 and 0.2×10^{-1} – 1×10^{-1} M H_3PO_4 . The effect of various acids (H_3PO_4 , H_2SO_4 , HCl , HNO_3 and HClO_4) on the extraction equilibrium was studied. In the presence of perchloric acid, the manganese associate could not be extracted by the organic phase. The change of the absorbance of the ion-associate in the pH range 2–9 was also studied with buffers.

The influence of Neotetrazolium chloride concentration on the ion-associate absorbance was studied. At an aqueous phase acidity 1×10^{-1} M of H_3PO_4 , the maximum extraction of the ion-associate was reached at a concentration of NTC in the range 1.5×10^{-5} – 3.5×10^{-5} M (Fig. 3).

3.5. Interferences

Analyses were performed as described in Section 2.3 with 1 μg of manganese and the amounts of the various elements shown in Table 1. The results obtained show the possibility of extractive-photometric determination of manganese(VII) in the presence of numerous ions without separation beyond the extraction procedure described above. Ascorbic acid was used to eliminate the interference of W(VI) and Mo(VI). $\text{S}_2\text{O}_3^{2-}$ is serious interference. The ratios of the accompanying ions at which the deviations in the results reached $S_r = 0.04\%$ ($n = 3$) are given in Table 1.

3.6. Quantitative characteristics of the extraction equilibrium

The quantitative investigation of the interaction in the aqueous phase and extraction of the ion-associate complex with dichloroethane has been performed.

(1) Distribution of the ion associate between the aqueous and the organic phase and the corresponding distribution constant

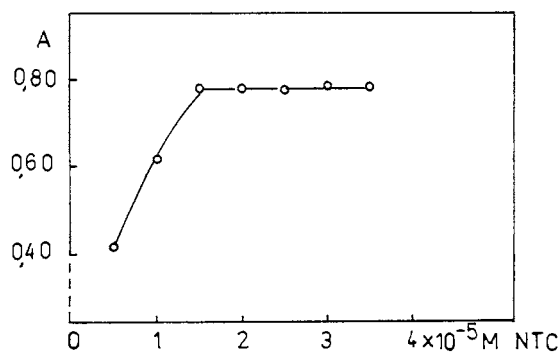


Fig. 3. Dependence of the absorbance on the concentration of NTC: $C_{\text{Mn(VII)}} = 1.78 \times 10^{-5}$ M, $C_{\text{H}_3\text{PO}_4} = 0.1$ M.

Table 1
Effect of diverse ions on determination of 1 µg of manganese

Foreign ion	Limiting amount (mg)
K(I)	200
Zn(II), Na(I), SO ₄ ²⁻ , Cl ⁻ , CO ₃ ²⁻ , C ₂ O ₄ ²⁻	60
HCO ₃ ⁻	50
Cd(II)	40
Ni(II)	20
Sr(II)	10
Ag(I)	6
Cu(II)	5
Al(III), Pb(II)	2
Fe(III), Co(II), Cr(VI), NO ₃ ⁻	1
V(V)	0.6
Mg(II)	0.5
CrO ₄ ²⁻	0.3
Ca(II)	0.2
Mo(VI)	0.3 and 1.2*
W(VI)	0.02 and 0.4*
S ₂ O ₃ ²⁻	Interfere

* In the presence of ascorbic acid as masking agent.

$$K_D = \frac{\{NTC[MnO_4]_2\}_0}{NTC[MnO_4]_2} \quad (1)$$

(2) The entire process of the extraction is described by the corresponding equilibrium constant which is regarded as the extraction constant

$$K_{ex} = \frac{\{NTC[MnO_4]_2\}_0}{[NTC^{2+}] \cdot [MnO_4^-]} = K_D \cdot \beta \quad (2)$$

(3) The formation of the ion associate in aqueous phase is characterised by the corresponding equilibrium constant

$$\beta = \frac{NTC[MnO_4]_2}{[NTC^{2+}] \cdot [MnO_4^-]} \quad (3)$$

The following solutions are introduced into 100 ml separating funnels: 4 ml of 1×10^{-4} M NTC, 0.5 ml of 2 M phosphoric acid and the corresponding amounts of manganese(VII). The volume of the aqueous phase is brought to 10 ml with distilled water, then is extracted with 3 ml of dichloroethane for 5 s. After the separation of the two phases, the organic phase is transferred through filter paper into a 25 ml flask and is diluted to the mark with dichloroethane. The light

absorption of the organic phase is measured at 240 nm with a 1-cm light path cuvette.

To determine the distribution coefficient of NTC, the absorptions obtained are compared to the one obtained after three extractions of the aqueous layer:

$$D_{NTC} = A / (A_{max} - A)$$

(A = light absorption for a single extraction, A_{max} = light absorption for three extractions.)

Using the logarithmic values of D_{NTC} and the concentration of manganese, the plot $\log D_{NTC}$ vs. $\log C_{Mn}$ (Fig. 4), allows determination of the distribution constant graphically by extrapolation of the straight line parallel to the X -axis up to the point of intersection with the Y -axis [21]. The value obtained was:

$$K_{D \text{ NTC}[MnO_4]_2} = 33.00 \pm 0.09$$

The extraction constant was determined by the method of Likussar and Boltz [15] by means of an isomolar series and their equation for a 1:2 complex. The extraction constant found was

$$K_{ex \text{ NTC}[MnO_4]_2} = (3.21 \pm 0.05) \times 10^9$$

The stability constant of the ion-association complexes in the aqueous phase was calculated from $K_{ex} = K_D \cdot \beta$. The value found was

$$\beta_{NTC[MnO_4]_2} = (9.72 \pm 0.15) \times 10^7$$

The results show that the ditetrazolium salt Neotetrazolium chloride is superior in terms of completeness of extraction.

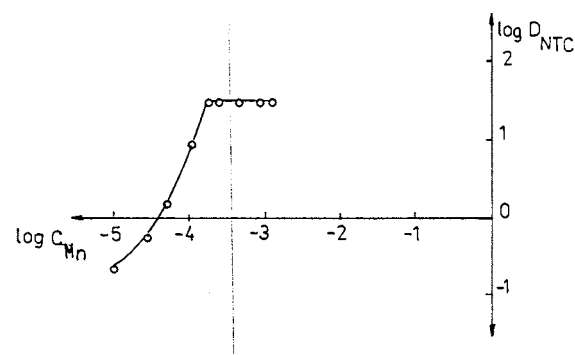


Fig. 4. Logarithmic dependence of D_{NTC} on the manganese concentration: $C_{NTC} = 4 \times 10^{-5}$ M, $C_{H_3PO_4} = 0.1$ M.

Table 2
Determination of manganese in steels and soils

Steel	NTC method (%)	Certified manganese (%)	RSD* (%)
CO-C 14a	0.320	0.305	1.5
CO-C 37	1.25	1.35	1.8
Soil	NTC method (%)	Atomic absorption	RSD* (%)
Pseudopodzolic	6.15×10^{-3}	6.30×10^{-3}	1.2
Black	7.0×10^{-3}	7.18×10^{-3}	1.5
Deluvial	4.50×10^{-3}	4.35×10^{-3}	1.9

* Relative standard deviation (based on three determinations).

3.7. Applications

The developed method with NTC has been used for determination of manganese in standard samples of steels. Steel type CO-C 14a contains (%): Mn—0.305, V—0.208, Cu—0.128, Cr—1.84, Ni—0.162, W—0.293, Al—0.56, S—0.0058, P—0.0074, C—0.364, Si—0.50; steel type CO-C37: Mn—1.35, Cr—17.6, Si—0.5, C—0.05, Ni—12, Cu—0.2, Nb—1.2. The results obtained for standard steel samples are given in Table 2. The relative standard deviation of the method was $S_r = 2.0\%$ in the analysis of the standard sample CO-C 14a and $S_r = 1.4\%$ in the case of CO-C 37.

The method was used for the determination of microquantities of manganese in soils. A few types of soils were studied: pseudopodzolic, black, deluvial (Table 2).

The data obtained were checked up by the atomic absorption method. The good agreement of the results obtained by both methods shows that NTC can be used as a reagent for determination of microquantities of manganese. Preisolation of manganese or most other ions is not necessary. The method we developed has a high selectivity and sensitivity.

References

- [1] V. Savich, O. Sidorenko, *Agrokhimiya* 2 (1990) 74.
- [2] D. Burns, D. Chimpalee, *Anal. Chim. Acta* 199 (1987) 241.
- [3] F. Salinas, J. Jiménez, M. Mahedero, *Anal. Lett. A* 16 (1983) 1449.
- [4] D. Masakasu, H. Shuichi, *Bunseki Kagaku* 31 (1982) 612.
- [5] M. Kaselau-Macan, D. Popovic, S. Gerian-Stefanovic, *Prehramb. Technol. Biotechnol. Rev.* 24 (1986) 115.
- [6] Y. Anjaneyklu, M. Reddy, K. Chandrasekhar, F. Chandramouli, *Proc. Indian Nat. Sci. Acad. A* 53 (1987) 295.
- [7] M. Bulatov, I. Evtuhovich, N. Muhovikova, *Izv. Vuzov. Himiya i Him. Technol.* 31 (9) (1988) 49.
- [8] K. Vytras, J. Jenik, A. Kaden-Ková, *Sb. Ved. Pr. VSCHT Pardubice* 45 (1982) 173.
- [9] D. Ayele, V. Chandravaushi, *Anal. Lett.* 23 (9) (1990) 1729.
- [10] G. Waterbury, A. Hayes, D. Martin, *J. Am. Chem. Soc.* 74 (1952) 15.
- [11] J. Strickland, G. Spicer, *Anal. Chim. Acta.* 3 (1949) 517.
- [12] I. Vazhenin, *Method for Determination of Microelements in Soils, Plants and Waters*, Moscow, 1974.
- [13] E. Sandell, *Colorimetric Determination of Traces of Metals*, 3rd ed., Interscience, New York, 1959.
- [14] M. Bulatov, I. Kalinkin, *A Practical Manual of Photocolometric and Spectrophotometric Methods of Analysis*, 3rd ed., Khimiya, Leningrad, 1972.
- [15] J.W. Iikussar, D.F. Boltz, *Anal. Chem.* 43 (1971) 1265.
- [16] M. Kamburova, *Anal. Lett.* 30 (2) (1997) 305.
- [17] A. Alexandrov, M. Kamburova, *Mikroch. Acta.* 2 (1976) 61.
- [18] A. Alexandrov, M. Kamburova, *Mikroch. Acta.* 3 (1985) 159.
- [19] A. Singh, D. Kumar, M. Katyal, *Bull. Chem. Soc. Jpn.* 58 (12) (1985) 3673.
- [20] A. Singh, D. Kumar, *Analyst* 110 (6) (1985) 752.
- [21] A. Alexandrov, O. Budevsky, A. Dimitrov, *J. Radioanal. Chem.* 29 (1976) 43.

Binding of polyanions by biogenic amines. II. Formation and stability of protonated putrescine and cadaverine complexes with carboxylic ligands

Concetta De Stefano ^{a,*}, Antonio Gianguzza ^b, Roberta Maniaci ^b, Daniela Piazzese ^b,
Silvio Sammartano ^a

^a *Dipartimento di Chimica Inorganica, Chimica Analitica e Chimica Fisica dell'Università, Salita Sperone 31, I-98166, Messina, Vill. S. Agata, Italy*

^b *Dipartimento di Chimica Inorganica dell'Università, Via Archirafi 26, I-90123, Palermo, Italy*

Received 14 May 1997; received in revised form 14 October 1997; accepted 20 October 1997

Abstract

The formation and stability of protonated diamines–carboxylic ligand complexes was studied potentiometrically (H^+ -glass electrode). Species formed are ALH_r (A = cadaverine, putrescine, L = acetate, malate, tartrate, malonate, citrate, 1,2,3-propanetricarboxylate, 1,2,3,4-butanetetracarboxylate and glutamate; $r = 1 \dots m + 1$, where m is the maximum degree of protonation of the carboxylic ligand), and their stability is a function of charges involved in the formation reaction. For the equilibrium $H_i A^{i+} + H_j L^{(j-z)} = ALH_{i+j}^{(i+j-z)}$ the following linear relationships can be written: $\log K_{1j} = -0.25 + 0.75 |j - z|$, $\log K_{2j} = 0.50 + 0.90 |j - z|$ (by also considering some ethylenediamine and 1,2-diaminopropane complexes). Medium effects were considered. Comparison was made with analogous inorganic polyanion complexes. The simplest relationships $-\Delta G^0 = 6.5 \pm 0.3$ and $-\Delta G^0 = 7.9 \pm 0.6 \text{ kJ mol}^{-1} n^{-1}$ (n = number of possible salt bridges) were found for carboxylic and inorganic anions, respectively. © 1998 Elsevier Science B.V. All rights reserved.

Keywords: Biogenic amines; Carboxylic ligands; Anion coordination chemistry; Speciation of biological fluids

1. Introduction

Carboxylic acid anions (including those of aminocarboxylic acids) form complexes with protonated polyamines whose stability is proportional to the charges of the reagents. In our own laboratories and in those of colleagues, 32 + 13 at

other universities, this type of complex, in particular with $C_{(2n-2)}N_nH_{(5n-2)}$ type amines, has been studied [1,2].

In the first of this series of studies [1] we included stability data relative to the formation of biogenic diamine–inorganic anions complexes. Here we examine the same diamines with organic polyanions [acetic (*ac*), 32 + 13 malonic (*mal*), malic (*mala*), tartaric (*tar*) and glutamic acids (*glu*)] potentially involved in biological cycles. In

* Corresponding author. Tel.: +39 90 393659; fax: +39 90 392827; e-mail: destefano@chem.unime.it

addition, in order to give a fuller picture of amine–anion interactions we also considered other diamines, and 1,2,3-propantricarboxylate (tricarallylate, *tca*) and 1,2,3,4-butanetetracarboxylate (*btc*) polyanions.

2. Experimental

2.1. Materials

Amines [1,4 diaminobutane (putrescine, *ptr*), 1,5 diaminopentane (cadaverine, *cdv*), ethylenediamine (*en*), Sigma] were purified by transformation into the corresponding hydrochlorides, and were used in this form. Carboxylic acids (Fluka and/or C. Erba pure or puriss.) were used without further purification. Their purity, checked by potentiometric titrations, was always >99.5%. Other experimental details, apparatus, procedure and calculations are as reported previously [1].

3. Results and discussion

3.1. Protonation constants

Protonation constants of amines, carboxylic ligand and glutamic acid have already been reported [1,3–7]. In all the calculations we have taken the formation of protonated amine-Cl⁻ and carboxylic ligand-Na⁺ complexes into account. Note that, owing to the fairly high formation constants of high charged polyanion-Na⁺ complexes, interferences with the sodium cation must be avoided, and this is why we worked in the absence of background salt.

3.2. Protonated amine–carboxylic ligand complexes

Table 1 shows overall formation constants of mixed species studied in this work together with the equilibrium constants relative to the reaction



In this Table some other systems of protonated diamines [ethylenediamine (*en*) and histamine

(*hm*)] and carboxylic anions [succinate (*succ*), oxalate (*ox*), 1,2,4,5-benzenetetracarboxylate (pyromellitate, *pymel*) and benzenhexacarboxylate (mellitate, *mlt*)] are shown too [8–12]. In all the systems investigated we found the formation of ALH_r species ($r = 1 \dots m + 1$, $m =$ maximum degree of protonation of carboxylic ligand), with a maximum formation constant value corresponding to reactions which involve the maximum value of $[i + (j - z)]$. This is in accordance with previous results for similar systems (see Table 1 and refs. [2,4–7]). Glutamic acid behaves as a dicarboxylic ligand (such as malate, tartrate and malonate). Figs. 1 and 2 show the distribution of the species vs. pH for the system H⁺-*ptr-cit*³⁻ and H⁺-*cdv-btc*⁴⁻.

3.3. Charge–stability relationships

As can be seen in Table 1, log K_{ij} equilibrium constants mainly depend on the charges involved in the formation reaction. This behaviour has already been observed for several other protonated amine–polyanion systems [1,2]. In Table 2, we give log K_{ij} mean values for each type of reaction considered, and in Fig. 3 these values are reported vs. polyanion charge. For these data we can use the linear relationship

$$\log K_{ij} = a + b|j - z| \quad (2)$$

$a = -0.25, 0.50$ and $b = 0.75, 0.90$, for $i = 1$ and 2 , respectively. Alternatively we can write the equation

$$\log K_{ij} = -1.83 + 1.18i + 0.88|j - z| \quad (3)$$

The above results are in accordance with the basic hypothesis of the non-covalent nature of protonated amine–polyanion interaction. Recent calorimetric measurements for similar systems [8] showed that ΔH^0 values associated to reaction in Eq. (1) are also consistent with this hypothesis, being positive and dependent on charges.

3.4. Comparison with inorganic complexes

In order to compare the stability of inorganic [1] and organic complexes, we may use the very simple relationship

Table 1
Formation constants^a of diamines^b with anions^b at $I = 0 \text{ mol dm}^{-3}$ and $T = 25^\circ\text{C}$

Species	log K		Species	log K	
$H_jL^{(z-j)-}$	HA^+	H_2A^{2+}	$H_jL^{(z-j)-}$	HA^+	H_2A^{2+}
A = en^c			A = en^c		
<i>ac</i> ⁻	-0.1	0.7	<i>btc</i> ⁴⁻	2.2	4.2
<i>mal</i> ²⁻	0.9	2.5	$H(btc)^{3-}$	—	3.1
$H(mal)^-$	—	1.7	$H_2(btc)^{2-}$	—	2.0
<i>mala</i> ²⁻	0.7 (10.65 ± 0.06)	2.1 (18.84 ± 0.02)	$H_3(btc)^-$	—	1.1
$H(mala)^-$	—	0.9 (22.79 ± 0.05)	<i>pymel</i> ⁴⁻	1.7	4.0
<i>tar</i> ²⁻	0.9(10.80 ± 0.14)	2.2 (10.01 ± 0.03)	$H(pymel)^{3-}$	—	3.0
$H(tar)^-$	—	0.9 (22.13 ± 0.05)	$H_2(pymel)^{2-}$	—	1.5
<i>cit</i> ³⁻	1.5	3.6	<i>mlt</i> ⁶⁻	3.5	6.8
$H(cit)^{2-}$	—	2.5	$H(mlt)^{5-}$	—	5.4
$H_2(cit)^-$	—	1.6	$H_2(mlt)^{4-}$	—	4.4
<i>tca</i> ³⁻	1.8	3.3	$H_3(mlt)^{3-}$	—	3.2
$H(tca)^{2-}$	—	2.4	$H_4(mlt)^{2-}$	—	2.3
$H_2(tca)^-$	—	1.6			
A = dap^d			A = hm^e		
<i>mal</i> ²⁻	1.0	2.6	<i>succ</i> ²⁻	1.4	1.9
$H(mal)^-$	—	1.8	<i>cit</i> ³⁻	2.1	3.2
<i>succ</i> ²⁻	0.7	2.5	$H(cit)^{2-}$	—	1.9
$H(succ)^-$	—	1.5	$H_2(cit)^-$	—	0.8
<i>ox</i> ²⁻	1.2	2.6	<i>tca</i> ³⁻	1.8	3.0
$H(ox)^-$	—	1.4	$H(tca)^{2-}$	—	1.7
			<i>btc</i> ⁴⁻	2.4	4.0
			$H(btc)^{3-}$	—	2.8
			$H_2(btc)^{2-}$	—	1.6
A = ptr			A = ptr		
<i>ac</i> ⁻	1.4 (11.87 ± 0.08)	1.8 (21.35 ± 0.05)	<i>tca</i> ³⁻	2.0 (12.5 ± 0.2)	3.2 (22.82 ± 0.06)
<i>mala</i> ²⁻	1.7 (12.20 ± 0.06)	2.5 (22.10 ± 0.04)	$H(tca)^{2-}$	—	2.3 (28.37 ± 0.06)
$H(mala)^-$	—	1.6 (26.27 ± 0.07)	$H_2(tca)^-$	—	1.6 (32.6 ± 0.1)
<i>tar</i> ²⁻	2.0 (12.49 ± 0.08)	2.9 (22.50 ± 0.06)	<i>btc</i> ⁴⁻	3.2 (13.7 ± 0.3)	4.1 (23.70 ± 0.08)
$H(tar)^-$	—	2.4 (26.37 ± 0.12)	$H(btc)^{3-}$	—	3.1 (29.82 ± 0.08)
<i>cit</i> ³⁻	2.5 (12.98 ± 0.06)	3.7 (23.24 ± 0.05)	$H_2(btc)^{2-}$	—	2.2 (34.76 ± 0.09)
$H(cit)^{2-}$	—	2.6 (28.57 ± 0.06)	$H_3(btc)^-$	—	1.4 (38.5 ± 0.2)
$H_2(cit)^-$	—	1.8 (32.55 ± 0.11)	<i>glu</i> ²⁻	1.8	2.9
			$H(glu)^-$	—	2.0
A = cdv			A = cdv		
<i>ac</i> ⁻	—	—	<i>tca</i> ³⁻	3.0 (13.8 ± 0.4)	3.3 (23.65 ± 0.15)
<i>mal</i>	1.5 (12.3 ± 0.3)	2.3 (22.70 ± 0.08)	$H(tca)^{2-}$	—	2.2 (29.10 ± 0.12)
$H(mal)$	—	0.9 (27.0 ± 0.3)	$H_2(tca)^-$	—	1.5 (33.3 ± 0.2)
<i>mala</i> ²⁻	1.1 (11.85 ± 0.15)	2.1 (22.44 ± 0.05)	<i>btc</i> ⁴⁻	3.6 (14.4 ± 0.3)	4.2 (24.55 ± 0.13)
$H(mala)^-$	—	0.9 (26.4 ± 0.2)	$H(btc)^{3-}$	—	3.0 (30.6 ± 0.2)
<i>tar</i> ²⁻	1.3 (12.04 ± 0.08)	2.2 (22.59 ± 0.04)	$H_2(btc)^{2-}$	—	1.8 (35.2 ± 0.2)
$H(tar)^-$	—	1.0 (25.8 ± 0.2)	$H_3(btc)^-$	—	1.0 (38.9 ± 0.4)
<i>cit</i> ³⁻	1.9 (12.68 ± 0.12)	3.2 (23.62 ± 0.05)	<i>glu</i> ²⁻	1.9 (12.64 ± 0.07)	2.7 (23.08 ± 0.04)
$H(cit)^{2-}$	—	2.2 (29.04 ± 0.09)	$H(glu)^-$	—	2.1 (32.44 ± 0.05)
$H_2(cit)^-$	—	1.5 (33.0 ± 0.2)			

^a Overall formation constants, together with errors (3 S.D.) are reported in parentheses for the complexes studied in this work.

^b *en* = ethylenediamine, *dap* = 1,2-diaminopropane, *hm* = histamine, *ptr* = 1,4-diaminobutane, (putrescine), *cdv* = 1,5-diaminopentane, (cadaverine), *ac* = acetate, *mal* = malonate, *mala* = malate, *tar* = tartrate, *succ* = succinate, *ox* = oxalate, *cit* = citrate, *tca* = 1,2,3-propantricarboxylate (tricarballilate), *btc* = 1,2,3,4-butanetracarboxylate, *pymel* = 1,2,4,5-benzenetetracarboxylate (pyromellitate), *mlt* = benzenehexacarboxylate (mellitate) and (*glu*) = glutamate.

^c Ref. [9,10].

^d Ref. [11].

^e Ref. [12].

$$\log K_{ij} = a\xi \quad (4)$$

where $\xi = |z_{\text{anion}}z_{\text{cation}}|$

If we make the rough assumption $\xi = 2n$ (n = number of possible salt bridges), the following equation is valid for the ΔG^0 value of a single bond (as mean) $-\Delta G^0 = 11.42a$. We found $a = 0.69 \pm 0.05$ and 0.57 ± 0.03 ; $\Delta G^0 = -7.9 \pm 0.6$ and $-6.5 \pm 0.3 \text{ kJ mol}^{-1} n^{-1}$, for inorganic and organic anions, respectively. In a recent review [8] this analysis was performed for several amine–inorganic and organic polyanion complexes, and it was found that $\Delta G^0 = -7.5 \pm 0.3$ (inorganic) and -6.4 ± 0.4 (organic), in excellent agreement with our own findings. In the first work of this series [1] it was found that the stability of protonated diamines–inorganic polyanion complexes is a function of $n[\text{NH}_2 - (\text{CH}_2)_n - \text{NH}_2]$, whilst this is not true (as a first approximation) for organic

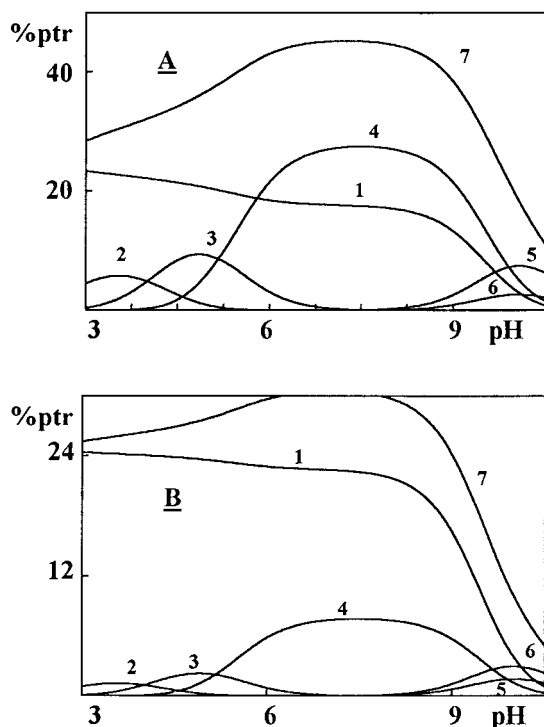


Fig. 1. Distribution diagram of the species vs. pH for the system $\text{H}^+ - \text{ptr} - \text{cit}^{3-}$, $I = 0.15 \text{ mol dm}^{-3}$ (NaCl), $T = 25^\circ\text{C}$. A. $C_{\text{ptr}} = 2 \text{ mmol dm}^{-3}$, $C_{\text{cit}} = 5 \text{ mmol dm}^{-3}$. B. $C_{\text{ptr}} = 0.1 \text{ mmol dm}^{-3}$, $C_{\text{cit}} = 1 \text{ mmol dm}^{-3}$. 1. $\text{ptr}(\text{Cl})\text{H}_2^+$, 2. $\text{ptr}(\text{cit})\text{H}_4^+$, 3. $\text{ptr}(\text{cit})\text{H}_3^0$, 4. $\text{ptr}(\text{cit})\text{H}_2^-$, 5. $\text{ptr}(\text{cit})\text{H}^{2-}$, 6. $\text{ptr}(\text{Cl})\text{H}^0$, 7. $\Sigma[(\text{ptr})(\text{cit})\text{H}_r + (\text{ptr})\text{ClH}_2]$.

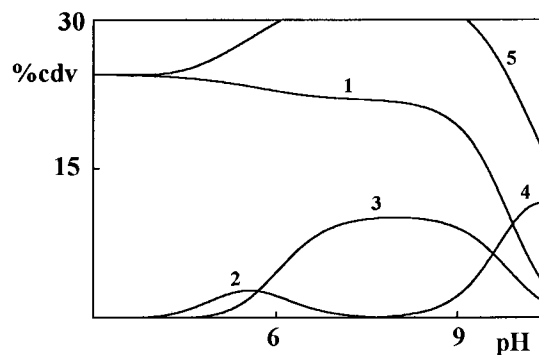


Fig. 2. Distribution diagram of the species vs. pH for the system $\text{H}^+ - \text{cdv} - \text{btc}^{4-}$, $I = 0.15 \text{ mol dm}^{-3}$ (NaCl), $T = 25^\circ\text{C}$. $C_{\text{cdv}} = 1 \text{ mmol dm}^{-3}$, $C_{\text{btc}} = 2 \text{ mmol dm}^{-3}$ (species with $\% < 2$ were neglected). 1. $\text{cdv}(\text{Cl})\text{H}_2^+$, 2. $\text{cdv}(\text{btc})\text{H}_3^-$, 3. $\text{cdv}(\text{btc})\text{H}_2^{2-}$, 4. $\text{cdv}(\text{btc})\text{H}^{3-}$, 5. $\Sigma[(\text{cdv})(\text{btc})\text{H}_r + (\text{cdv})\text{ClH}_2]$.

polyanions. The higher dispersion of the negative charge in organic polyanions may explain this difference, and, moreover, would justify the difference in mean value of ΔG^0 .

3.5. Errors associated with equilibrium constants

It is important to bear in mind that the speciation model, together with formation constants obtained for each system, is valid strictly within

Table 2
Mean values of $\log K_{ij}$ for protonated diamine–polyanion complexes^a, at $I = 0 \text{ mol dm}^{-3}$ and $T = 25^\circ\text{C}$

Reaction	$\log K_{ij} \pm e^b$	N^c
$\text{HA}^+ + \text{L}^{2-} = \text{ALH}^-$	1.2 ± 0.3	11
$\text{HA}^+ + \text{L}^{3-} = \text{ALH}^{2-}$	2.1 ± 0.4	6
$\text{HA}^+ + \text{L}^{4-} = \text{ALH}^{3-}$	2.7 ± 0.7	4
$\text{H}_2\text{A}^{2+} + \text{L}^- = \text{ALH}_2^+$	1.4 ± 0.4	11
$\text{H}_2\text{A}^{2+} + \text{HL}^- = \text{ALH}_3^+$	1.4 ± 0.5	11
$\text{H}_2\text{A}^{2+} + \text{H}_2\text{L}^- = \text{ALH}_4^+$	1.6 ± 0.2	6
$\text{H}_2\text{A}^{2+} + \text{H}_3\text{L}^- = \text{ALH}_5^+$	1.2 ± 0.3	3
$\text{H}_2\text{A}^{2+} + \text{L}^{2-} = \text{ALH}_2^0$	2.4 ± 0.2	11
$\text{H}_2\text{A}^{2+} + \text{HL}^- = \text{ALH}_3^+$	2.4 ± 0.1	6
$\text{H}_2\text{A}^{2+} + \text{H}_2\text{L}^- = \text{ALH}_4^+$	2.0 ± 0.2	3
$\text{H}_2\text{A}^{2+} + \text{L}^{3-} = \text{ALH}_2^-$	3.4 ± 0.2	6
$\text{H}_2\text{A}^{2+} + \text{HL}^{3-} = \text{ALH}_3^-$	3.1 ± 0.1	4
$\text{H}_2\text{A}^{2+} + \text{L}^{4-} = \text{ALH}_2^{2-}$	4.1 ± 0.1	4

^a Diamines: *en*, 1,2-*dap*, *ptr*, *cdv*; polyanions of Table 1 (but *mlt*); for symbols see footnote to Table 1.

^b e –99% confidence interval.

^c N = number $\log K_{ij}$ considered.

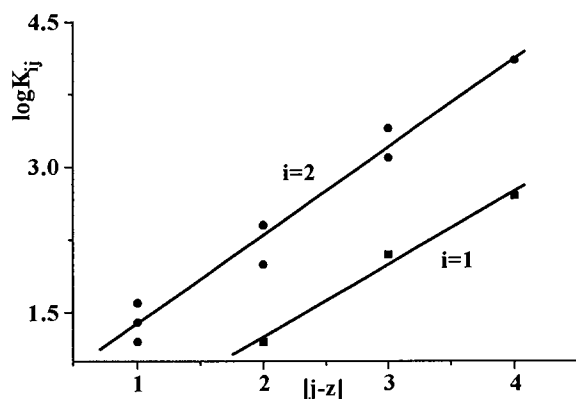


Fig. 3. The effect of polyanion charge on the stability of protonated diamine complexes; see Eq. (2).

experimental conditions; in fact, it is not possible to exclude the formation of other species when concentrations of reactant are higher than those used in the present work. Moreover, it is possible that some quaternary species such as $AL(Cl)H_r$, $AL(Na)H_r$ are formed if NaCl is added in significant amounts. Nevertheless, the speciation model proposed in this work can be considered satisfactory, since other possible minor species may account for at least 5% with respect to total concentration of amines and anions. The formation of major species in protonated amine–polyanion systems has also been confirmed recently by UV–CD measurements [8]. Errors associated with overall formation constants are reported in Table 1 as three times the standard deviation. In general these uncertainties can be considered satisfactory, but we must consider that by including small systematic errors, formation constants may be affected by substantially higher uncertainties. Values of $\log K_{ij}$ (Table 2) are reported with only one decimal figure since they are affected by an error $3s > 0.1$ ($s = S.D.$).

3.6. Ionic strength and medium effects

The dependence on ionic strength of effective formation constants can be taken into account by a Debye Hückel type equation (see ref. [1] and references therein), when considering the formation of Na^+ –polyanion with Cl^- -protonated

amine complexes. Often in literature only apparent formation constants, which do not consider the formation of these species, are reported. Apparent formation constants are lower than effective ones and can be calculated as previously reported [8]. As an example, the interfering effect of Cl^- can be seen in Figs. 1 and 2 (high percentage of chloride complexes). For the main species (i.e. those of diprotonated amines with unprotonated polyanions, $\log K_{20}$) we have, at $I = 0.1 \text{ mol dm}^{-3}$ (NaCl) [8]:

$$\log K_{\text{effective}}(I = 0.1) = \log K(I = 0) - 0.34|z|$$

$$\begin{aligned} \log K_{\text{apparent}}(I = 0.1) \\ = \log K(I = 0) + 0.12 - 0.40|z| \end{aligned}$$

3.7. Relevance of protonated diamine–organic polyanion complexes

The relevance of these complexes can be deduced from Figs. 1 and 2. As one can see, high formation percentages are obtained even in very low concentration conditions. In the system H^+ - ptr - cit^{3-} , for $C_{ptr} = 0.1$ and $C_{cit} = 1 \text{ mmol dm}^{-3}$, at $pH = 7-8$, the species $(ptr)(cit)H_2^-$ accounts for $\sim 10\%$ of total ptr , and if we also consider chloride complexes, $\%[(ptr)(cit)H_2^- + (ptr)ClH_2^+] > 30$. Similar considerations can be made for the system H^+ - cdv - btc^{4-} (note that for this system Na^+ causes strong interferences, since Na^+ - btc^{4-} complexes are fairly stable, refs. [3–7]).

3.8. Comparison with analogous Na^+ and Ca^{2+} complexes

Inorganic anion–protonated diamine complexes show similar stability with respect to analogous Na^+ and Ca^{2+} species. As regards organic anions, we have a similar trend for double charged cations, Ca^{2+} and H_2A^{2+} (refs. [3,5,6] and this work), whilst there is a remarkable difference for Na^+ and HA^+ , as reported in Fig. 4. At present, too few data are available to make any inference from this fact. Nevertheless, since $\log K(\text{ammonium cation}) \geq \log K(Na^+, Ca^{2+})$, it is possible to affirm that the competitive interaction of the ammonium cation must be taken into account in biological fluids.

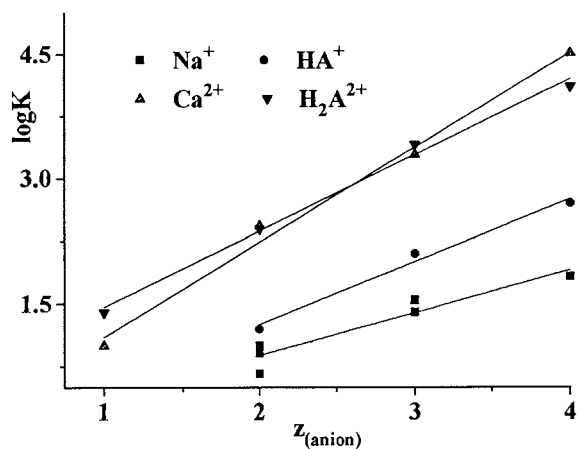


Fig. 4. Formation constants vs. anion charge for the reactions, $\text{M}^{2+} + \text{L}^{z-} = \text{ML}^{(2-z)}$, $\text{M}^+ + \text{L}^{z-} = \text{ML}^{(1-z)}$, ($\text{M}^+ = \text{Na}^+$, HA^+ ; $\text{M}^{2+} = \text{Ca}^{2+}$, H_2A^{2+} ; L = carboxylic anion).

3.9. Conclusions

The conclusions of this study can be summarized in the following points.

1. Organic polyanions form (as do inorganic ones) fairly stable complexes with protonated diamines (Table 1).
2. The stability of these species is strictly dependent on the charges involved in the formation reactions [Eqs. (2) and (3), Fig. 3, and Table 2].
3. For analogous species of inorganic and organic systems we have higher stability for inorganic species.
4. A simple relationship for ΔG^0 of single bond is proposed [Eq. (4)].

Acknowledgements

We thank MURST and CNR for financial support.

References

- [1] A. De Robertis, C. De Stefano, A. Gianguzza, S. Sammartano, *Talanta* 46 (1998) 1089.
- [2] A. De Robertis, C. De Stefano, O. Giuffrè, S. Sammartano, *J. Chem. Soc. Faraday Trans.* 92 (1996) 4219.
- [3] P. G. Daniele, A. De Robertis, C. De Stefano, S. Sammartano, C. Rigano, *J. Chem. Soc. Dalton Trans.* (1985) 2353.
- [4] P. G. Daniele, A. De Robertis, C. De Stefano, A. Gianguzza, S. Sammartano, *J. Chem. Res.* (1990) (S) 300, (M) 2316.
- [5] C. De Stefano, C. Foti, A. Gianguzza, *Talanta* 41 (1994) 1715.
- [6] A. De Robertis, C. Foti, A. Gianguzza, *Ann. Chim. Rome* 83 (1993) 485.
- [7] C. De Stefano, C. Foti, A. Gianguzza, C. Rigano, S. Sammartano, *Chem. Speciat. Bioavailability* 7 (1994) 1.
- [8] P.G. Daniele, A. De Robertis, C. De Stefano, C. Foti, O. Giuffrè, E. Prenesti, S. Sammartano, *Ann. Chim. Rome* 87 (1997) 415.
- [9] A. De Robertis, C. De Stefano, C. Foti, O. Giuffrè, S. Sammartano, *J. Chem. Res.* (1996) (S) 60.
- [10] A. De Robertis, A. Gianguzza, G. Patanè, S. Sammartano, *J. Chem. Res.*, (1994) (S) 182.
- [11] P.G. Daniele, A. De Robertis, C. De Stefano, D. Gastaldi, S. Sammartano, *Ann. Chim. Rome* 83 (1993) 575.
- [12] A. De Robertis, C. De Stefano, C. Foti, A. Gianguzza, S. Sammartano, *J. Chem. Soc. Faraday Trans.* 91 (1995) 1619.

Binding of polyanions by biogenic amines. I. Formation and stability of protonated putrescine and cadaverine complexes with inorganic anions

Alessandro De Robertis ^a, Concetta De Stefano ^{a,*}, Antonio Gianguzza ^b,
Silvio Sammartano ^a

^a *Dipartimento di Chimica Inorganica, Chimica Analitica e Chimica Fisica dell'Università, Salita Sperone 31, I-98166, Messina, Vill. S. Agata, Italy*

^b *Dipartimento di Chimica Inorganica dell'Università, Via Archirafi 26, I-90123, Palermo, Italy*

Received 14 May 1997; received in revised form 14 October 1997; accepted 20 October 1997

Abstract

The formation and stability of proton diamine-inorganic anion [Cl^- , SO_4^{2-} , HPO_4^{2-} , $\text{P}_2\text{O}_7^{4-}$ and $\text{Fe}(\text{CN})_6^{4-}$] complexes was studied potentiometrically [(H^+) -glass electrode] at 25°C. Several general formula ALH_r complexes are formed in these various systems. The stability of complexes formed between H_2A^{2+} and different anions ranges from one to six (log formation constants). The formation constants are slightly dependent on the length of the alkylic chain whilst they strongly depend on the anion charge. A general relationship [$\log K = -0.85 + 1.81z - 0.055n$] was found for the reaction $\text{H}_2\text{A}^{2+} + \text{L}^{z-} = \text{ALH}_r^{(2-z)}$ [L = inorganic anions, $\text{A} = \text{NH}_2 - (\text{CH}_2)_n - \text{NH}_2$ diamines with $n = 2 \dots 8$]. © 1998 Elsevier Science B.V. All rights reserved.

Keywords: Biogenic amines; Inorganic ligands; Anion coordination chemistry; Speciation of biological fluids

1. Introduction

Biogenic amines are low molecular weight, highly charged polyamines and are present in all the cells of animal organisms and in those of many micro-organisms. The positively charged sites make the polyamines highly reactive towards a series of cellular molecules including DNA and RNA in all its forms. It has been demonstrated

that the addition of polyamines causes the accelerated entry of cells into the DNA duplication phase. Indeed, in vivo synthesis of biogenic amines manifests itself as soon as cells begin to replicate their own DNA and is due to the activity of the ornithine decarboxylase enzyme. Polyamines are, therefore, critical to the functioning of the cellular cycle, their main biological function being to stabilize the structure and activity of DNA and RNA. The most straightforward explanation of the stabilizing effect of polyamines on DNA is the neutralization of phosphate

* Corresponding author. Tel.: +39 90 393659; Fax: +39 +90 392827; e-mail: destefano@chem.unime.it

groups through the formation of very stable complex species. This hypothesis is confirmed, moreover, by the precipitation of DNA in the presence of high concentrations of polyamines because of the formation of intermolecular complexes. On the other hand, in highly concentrated (high ionic strength) cellular liquids, the presence of large amounts of Mg^{2+} hinders the protective action of these molecules presumably as a result of competition with it against phosphate groups.

Interactions between polyamines and phosphate groups have been demonstrated by Labadi et al. [1] who studied interactions between the pyrophosphate ion and various polyamines in aqueous solution using potentiometric and calorimetric methods. Their findings show that the presence of wholly protonated amines significantly increases the apparent acidity of the $\text{HP}_2\text{O}_7^{3-}$ and $\text{H}_2\text{P}_2\text{O}_7^{2-}$ ions. The most straightforward explanation for these apparent changes in protonation seems to be the formation of an adduct among the negatively charged phosphate ions and protonated ions. These results have been confirmed by a recent study in our laboratories [2]. The higher the charge of the interacting ions is, the more stable one can expect the adduct to be.

The stabilizing effect of mono and polycharged cations, and therefore of polyamines too, has also been demonstrated for the various forms of RNA including tRNA. The tRNA molecule in particular is converted from an inactive to an active form by the addition of monovalent cations (Na^+ , K^+) or Mg^{2+} and polyamines, the latter two in lower concentrations [3]. The tRNA molecule presents up to five strong bond sites for magnesium with formation constants in the order of $10^5 \text{ mol}^{-1} \text{ dm}^3$ [3], which proves the importance of this cation to the maintenance of the original structure and biological functions of tRNA. In vitro trials have shown that certain polyamines can replace magnesium, at least partially, in the stimulation of the biological activity of tRNA [4]. In general, all polyamines increase the stabilization of the structure and activity of nucleic acids, but the concentration necessary to achieve maximum stabilizing capacity varies according to the amines. Spermine has been shown to have the greatest stabilizing capacity with a maximum con-

centration of $1.67 \times 10^{-5} \text{ mol dm}^{-3}$, while higher concentrations of spermidine and diamines (cadaverine and putrescine) are necessary. A similar stabilizing effect is demonstrated by bivalent cations: Mg^{2+} and Mn^{2+} are always present in the stabilizing processes of phosphate groups as an effect of the formation of complex species. It is interesting to note that the protective effect of spermine is reduced in the presence of citrate. The formation of a particularly stable spermine–citrate complex would explain this behaviour. The free cellular concentration of polyamines can be estimated to be in the range $10\text{--}100 \text{ mmol dm}^{-3}$; however, considering that those present are in the main bonded with nucleic acids, it can be estimated that their overall concentration in cells is in the order of mmol dm^{-3} .

Despite the well recognized biological importance of polyamines (having been amply proven), few studies have been performed on their chemical behaviour, and in particular into their acid–base behaviour in biological fluids. Recently we reported several data on the formation of protonated amine-organic and inorganic polyanions [2,5–13].

This study describes an investigation of the formation and stability of the diamines putrescine (1,4-diaminobutane, *ptr*) and cadaverine (1,5-diaminopentane, *cdv*) with inorganic anions (Cl^- , SO_4^{2-} , HPO_4^{2-} , $\text{P}_2\text{O}_4^{4-}$ and $\text{Fe}(\text{CN})_6^{4-}$). Some other diamines were also considered [ethylenediamine (*en*), 1,2-diaminopropane (1,2-*dap*), 1,3-diaminopropane (1,3-*dap*), 1,6-hexanediamine (1,6-*d*) and 1,8-octanediamine (1,8-*d*)] for comparison. The study was performed using the (H^+ -glass electrode) potentiometric technique, at 25°C .

2. Experimental

2.1. Materials

Amines (ethylenediamine, 1,3-diaminopropane, 1,4-diaminobutane, 1,5-diaminopentane, Sigma products) were purified by transformation into the corresponding hydrochlorides, and were used in this form. Tetrasodium diphosphate (Analar BDH), hexacyanoferrate(II) [used in the form of

tetrasodium salt (Fluka, puriss.), sulphuric and phosphoric acids (Fluka purum.) were used without further purification. The purity of all the ligands, checked by potentiometric titrations, was always > 99.5%. Solutions of NaOH and HCl were prepared by diluting concentrated Fluka ampoules and were standardized against potassium biphthalate and sodium carbonate, respectively. Grade A glassware and twice distilled water were used for all solutions.

2.2. Apparatus

Potentiometric measurements were carried out with two different equipments: a) an Amel 337 potentiometer coupled with a Metrohm glass saturated calomel electrode; b) a Metrohm 654 potentiometer coupled with a combination Ross type electrode 8102; the titrant was delivered by a Metrohm Dosimat 665 dispenser. The estimated accuracy of both systems was ± 0.15 mV and ± 0.003 cm³ for e.m.f. and titrant volume readings, respectively. A computer program was used for the acquisition of the potentiometric data. The titration program allows the evaluation of equilibrium potential values and determines the amount of titrant based on the actual buffering properties on the titrated solution, so that there is a difference in pH values of 0.05–0.08 between two successive readings; the e.m.f. was considered to be stable when the variation was less than 0.1 mV within 5 min.

2.3. Procedure

25 ml of the solution containing the inorganic ligand, and the amine hydrochloride under study were titrated with standard NaOH up to 80–90% neutralization. Titrations were performed without adding background salt (except for the protonation of amines) in order to minimize the interference of Na⁺ (which forms complexes with polyanions) and Cl⁻ (which forms complexes with amines, see Section 3, Results). Concentrations used in the experiments were: $C_{\text{amine}} = 5\text{--}20$ mmol dm⁻³, $C_{\text{anion}} = 2.5\text{--}40$ mmol dm⁻³ (lower concentrations for higher charged polyanions; for Cl⁻ 0.1–1 mol dm⁻³). Separate titrations of HCl

at about the same ionic strength (adjusted with NaCl) as the sample under study, were carried out to determine the standard electrode potential E^0 . A stream of purified and presaturated N₂ was bubbled through all solutions in order to exclude the presence of CO₂ and O₂. Small quantities of Na⁺ (titrant NaOH) and Cl⁻ (amine hydrochlorides) are brought into the solution and the relative interactions with polyanions and diamines were taken into account in the calculations.

2.4. Calculations

The computer program ESAB2M [14] was used to calculate the purity of the reagents and to refine all the parameters related to the calibration of the electrode system. The computer programs BSTAC [15] and STACO [11] were used to calculate the formation constants. The dependence of formation constants on ionic strength was taken into account by using the Debye–Hückel type equation [11,16]

$$\log \beta = \log {}^T\beta - z^* \frac{\sqrt{I}}{(2 + 3\sqrt{I})} + CI + DI^{3/2} \quad (1)$$

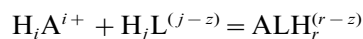
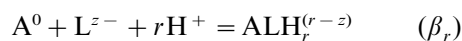
$$C = c_0 p^* + c_1 z^*$$

$$D = d_1 z^*$$

$$p^* = \sum p_{\text{reactants}} - \sum p_{\text{products}}$$

$$z^* = \sum z_{\text{reactants}}^2 - \sum z_{\text{products}}^2$$

(β = formation constants; ${}^T\beta$ = formation constant at zero ionic strength; p and z are the stoichiometric coefficients and the charges, respectively). For the calculations performed in this work we used the values of $c_0 = 0.10$, $c_1 = 0.23$ and $d_1 = -0.1$ [16]. The computer programs STACO and BSTAC are able to perform calculations in non constant ionic strength. The different equilibria considered in this work were expressed as follows:



$$(K_{ij}, \quad r = i + j) \quad (2)$$

Table 1

Protonation and chloride complex formation constants of diamines^a at $I = 0 \text{ mol dm}^{-3}$ and $T = 25^\circ\text{C}$

Reaction ^b	log $K \pm 3 \text{ S.D.}$						
	<i>en</i> ^c	1,2- <i>dap</i> ^d	1,3- <i>dap</i> ^e	<i>ptr</i> ^c	<i>cdv</i> ^e	1,6 <i>d</i> ^f	1,8 <i>d</i> ^f
$\text{H}^+ + \text{A}^0 = \text{HA}^+$	9.91	9.77	10.45 ± 0.01	10.49 ± 0.02	10.79 ± 0.01	10.93	10.88
$2\text{H}^+ + \text{A}^0 = \text{H}_2\text{A}^{2+}$	16.77	16.23	18.88 ± 0.01	19.59 ± 0.02	20.38 ± 0.02	20.79	20.94
$\text{HA}^+ + \text{H}^+ = \text{H}_2\text{A}^{2+}$	6.86	6.46	8.43	9.10	9.59	9.86	10.06
$\text{HA}^+ + \text{Cl}^- = \text{AHCl}^0$	9.80	9.53	10.27 ± 0.12	10.20 ± 0.15	10.51 ± 0.15	10.7	10.6
$2\text{H}^+ + \text{A}^0 + \text{Cl}^- = \text{AH}_2\text{Cl}^+$	17.43	17.26	19.69 ± 0.09	20.30 ± 0.09	21.09 ± 0.11	21.50	21.47
$\text{HA}^+ + \text{Cl}^- = \text{AHCl}^0$	-0.1	-0.2	-0.2	-0.3	-0.3	-0.2	-0.3
$\text{H}_2\text{A}^{2+} + \text{Cl}^- = \text{AH}_2\text{Cl}^+$	0.66	1.0	0.81	0.71	0.71	0.71	0.53

^a Symbols: *en* = ethylenediamine; 1,2-*dap* = 1,2-diaminopropane; 1,3-*dap* = 1,3-diaminopropane; *ptr* = 1,4-diaminobutane; *cdv* = 1,5-diaminopentane; 1,6*d* = 1,6-hexanediamine and 1,8*d* = 1,8-octanediamine.

^b A = amine;

^c Ref. [22];

^d Ref. [5];

^e This work;

^f Ref. [7].

3. Results and discussion

3.1. Protonation constants

Protonation constants of polyanions have already been studied [17–20]. As is known, these polyanions form weak complexes with the sodium ion [21], whose stability increases with the negative charge. These complexes were taken into account in the calculation relative to the formation of mixed proton–polyanion–amine species (experiments were performed without adding background salt, but Na^+ (coming from titrant NaOH). Protonation constants of 1,3-*dap*, *ptr* and *cdv* were determined in this work and are reported in Table 1, together with those of *en*, 1,2-*dap*, 1,6*d*, and 1,8*d* previously reported [5,7,22]. The dependence on ionic strength of amines was taken into account in two ways, i.e. a) by considering the formation of chloride complexes (see below) and b) by considering only apparent protonation constants. Apparent protonation constants vs. I can be expressed by Eq. (1) with $D = 0$ and $C(\log K_1^{\text{H}}) = 0.31 \pm 0.01$, 0.33 ± 0.02 and 0.26 ± 0.02 ; $C(\log \beta_2^{\text{H}}) = 0.61_5 \pm 0.015$, 0.57 ± 0.03 and 0.59 ± 0.03 for 1,3-*dap*, *ptr* and *cdv*, respectively.

3.2. Chloride complexes

Protonated diamines form weak complexes with chloride (AClH^0 and AClH_2^+), whose stability constants are reported in Table 1. These constants follow the general trend found for several other amine–chloride complexes [21]. A mean value $\log K_{20} = 0.73$ is observed which is equal to that of analogous species of some other amines [22–24] (diethylenetriamine, triethylenetetramine, tetraethylenepentamine and pentaethylenhexamine), i.e. $\log K = 0.73$. Though quite weak, AClH ,

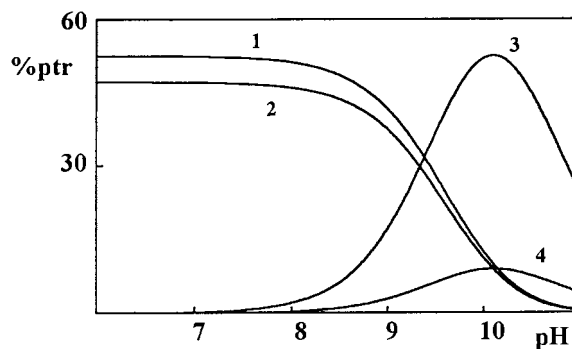


Fig. 1. Distribution of species in the system H^+ -putrescine- Cl^- vs. pH. $C_{\text{Na}} = C_{\text{Cl}} = 0.5 \text{ mol dm}^{-3}$; $C_{\text{ptr}} = 1 \text{ mmol dm}^{-3}$. 1. $(\text{ptr})\text{ClH}_2^+$; 2. $(\text{ptr})\text{H}_2^+$; 3. $(\text{ptr})\text{H}^+$; 4. $(\text{ptr})\text{ClH}^0$.

Table 2

Sulphate complex formation constants of diamines^a at $I = 0 \text{ mol dm}^{-3}$ and $T = 25^\circ\text{C}$

Reaction ^b	log $K \pm 3 \text{ S.D.}$				
	<i>en</i> ^c	1,2- <i>dap</i> ^d	1,3- <i>dap</i> ^c	<i>ptr</i> ^c	<i>cdv</i> ^c
$\text{H}^+ + \text{A}^0 + \text{SO}_4^{2-} = \text{A}(\text{SO}_4)\text{H}^-$	10.78 ± 0.12	10.78	11.35 ± 0.25	11.83 ± 0.15	11.49 ± 0.15
$2\text{H}^+ + \text{A}^0 + \text{SO}_4^{2-} = \text{A}(\text{SO}_4)\text{H}_2^0$	19.19 ± 0.05	18.73	21.17 ± 0.06	22.15 ± 0.06	22.43 ± 0.04
$\text{HA}^+ + \text{SO}_4^{2-} = \text{A}(\text{SO}_4)\text{H}^-$	0.9	1.0	0.9	1.3	0.7
$\text{H}_2\text{A}^{2+} + \text{SO}_4^{2-} = \text{A}(\text{SO}_4)\text{H}_2^0$	2.42	2.5	2.29	2.56	2.05

^a For symbols, see footnote to Table 1.^b A = amine;^c This work;^d Ref. [7].

complexes may be relevant in the speciation of natural fluids where Cl^- ions are generally present in high concentrations. As an example, in Fig. 1 we report the distribution of the species in the system $\text{H}^+ - \text{ptr} - \text{Cl}^-$ ($C_{\text{Cl}} = 0.5 \text{ mol dm}^{-3}$), vs. pH. As can be seen the species $(\text{ptr})\text{ClH}_2^+$ is present in a large pH range (< 8) in a very high percentage, $> 50\%$, with respect to putrescine.

3.3. Sulphate and hydrogen phosphate complexes

Protonated amines form two species with SO_4^{2-} , i.e. $\text{A}(\text{SO}_4)\text{H}^-$ and $\text{A}(\text{SO}_4)\text{H}_2^0$, and three species with HPO_4^{2-} , i.e. $\text{A}(\text{PO}_4)\text{H}_2^-$, $\text{A}(\text{PO}_4)\text{H}_3^0$ and $\text{A}(\text{PO}_4)\text{H}_4^+$, whose formation constants are reported in Tables 2 and 3. The mean value $\log K_{20} = 2.5$ is in accordance with the values found for several diprotonated amines with L^{2-}

type anions, both organic and inorganic [13]. For the complex $(\text{tetren})(\text{HPO}_4)\text{H}_2^0$ (tetraethylenepentamine, *tetren*) we found previously $\log K_{20} = 2.3$. As regards the complex $\text{A}(\text{HPO}_4)\text{H}^-$ and $\text{A}(\text{SO}_4)\text{H}^-$, it is interesting to note that the value of $\log K_{10}$ for both anions is fairly close to the values of NaSO_4^- and $\text{NaH}(\text{PO}_4)^-$ stability constants ($\log K = 0.73$ and 1.1 respectively) [17,18].

3.4. Pyrophosphate complexes

Diamines form four species with $\text{P}_2\text{O}_7^{4-}$, namely $\text{A}(\text{P}_2\text{O}_7)\text{H}_r^{(r-4)}$, $r = 1 \dots 4$. The stability of these complexes (Table 4) is quite high, as can be seen in the speciation diagram (Fig. 2). In a previous work [2] we reported the stability of several protonated amine–pyrophosphate complexes, where we found that for the equilibrium $\text{H}_2\text{A}^{2+} + \text{P}_2\text{O}_7^{4-} = \text{A}(\text{P}_2\text{O}_7)\text{H}_2^{2-}$ $\log K = 5.4, 5.5,$

Table 3

Phosphate complex formation constants of diamines^a at $I = 0 \text{ mol dm}^{-3}$ and $T = 25^\circ\text{C}$

Reaction ^a	log $K \pm 3 \text{ S.D.}$			
	<i>en</i>	1,3- <i>dap</i>	<i>ptr</i>	<i>cdv</i>
$2\text{H}^+ + \text{A}^0 + \text{PO}_4^{3-} = \text{A}(\text{PO}_4)\text{H}_2^-$	23.7 ± 0.2	24.0 ± 0.3	24.3 ± 0.2	24.5 ± 0.3
$3\text{H}^+ + \text{A}^0 + \text{PO}_4^{3-} = \text{A}(\text{PO}_4)\text{H}_3^0$	32.10 ± 0.05	33.69 ± 0.05	34.53 ± 0.05	35.03 ± 0.06
$4\text{H}^+ + \text{A}^0 + \text{PO}_4^{3-} = \text{A}(\text{PO}_4)\text{H}_4^+$	37.9 ± 0.2	39.5 ± 0.2	40.83 ± 0.10	41.33 ± 0.15
$\text{HA}^+ + \text{HPO}_4^{2-} = \text{A}(\text{PO}_4)\text{H}_2^-$	1.5	1.2	1.5	1.4
$\text{H}_2\text{A}^{2+} + \text{HPO}_4^{2-} = \text{A}(\text{PO}_4)\text{H}_3^0$	3.0	2.5	2.6	2.3
$\text{H}_2\text{A}^{2+} + \text{H}_2\text{PO}_4^- = \text{A}(\text{PO}_4)\text{H}_4^+$	1.6	1.1	1.7	1.4

^a For symbols, see footnote to Table 1.^b A = amine;

Table 4
Pyrophosphate complex formation constants of diamines^a at $I = 0 \text{ mol dm}^{-3}$ and $T = 25^\circ\text{C}$

Reaction ^b	log $K \pm 3 \text{ S.D.}$				
	<i>en</i> ^c	<i>ptr</i> ^d	<i>cdv</i> ^d	1,6 <i>d</i> ^c	1,8 <i>d</i> ^c
$\text{H}^+ + \text{A}^0 + \text{P}_2\text{O}_7^{4-} = \text{A}(\text{P}_2\text{O}_7)\text{H}^{3-}$	12.64 13.0	15.3 ± 0.2	16.09 ± 0.12	13.7	13.4
$2\text{H}^+ + \text{A}^0 + \text{P}_2\text{O}_7^{4-} = \text{A}(\text{P}_2\text{O}_7)\text{H}_2^{2-}$	22.53 22.86	25.35 ± 0.09	26.02 ± 0.06	25.66	25.20
$3\text{H}^+ + \text{A}^0 + \text{P}_2\text{O}_7^{4-} = \text{A}(\text{P}_2\text{O}_7)\text{H}_3^-$	30.17 30.32	33.1 ± 0.2	33.86 ± 0.06	33.99	33.45
$4\text{H}^+ + \text{A}^0 + \text{P}_2\text{O}_7^{4-} = \text{A}(\text{P}_2\text{O}_7)\text{H}_4^0$	35.4 35.5	38.8 ± 0.3	39.45 ± 0.15	39.7	39.0
$\text{HA}^+ + \text{P}_2\text{O}_7^{4-} = \text{A}(\text{P}_2\text{O}_7)\text{H}^{3-}$	2.7 3.1	4.8	5.3	2.7	2.5
$\text{H}_2\text{A}^{2+} + \text{P}_2\text{O}_7^{4-} = \text{A}(\text{P}_2\text{O}_7)\text{H}_2^{2-}$	5.8 6.1	5.8	5.6	5.0	4.4
$\text{H}_2\text{A}^{2+} + \text{HP}_2\text{O}_7^{3-} = \text{A}(\text{P}_2\text{O}_7)\text{H}_3^-$	3.9 4.0	3.9	3.9	3.6	3.1
$\text{H}_2\text{A}^{2+} + \text{H}_2\text{P}_2\text{O}_7^{2-} = \text{A}(\text{P}_2\text{O}_7)\text{H}_4^0$	2.4 2.5	2.9	2.8	2.6	1.9

^a For symbols, see footnote to Table 1.

^b A = amine;

^c Ref. [7] (first row), ref. [2] (second row);

^d This work

4.7 and 5.0 for diethylenetriamine, triethylenetetramine, tetraethylenepentamine and pentaethylenhexamine, respectively, in excellent agreement with values reported here for diamines. It is to be noted that stability decreases appreciably with n (n = number of $-\text{CH}_2-$ in the alkylic chain) and this will be discussed later. Labadi et al. [1] studied 1,3-*dap*, *ptr* and *cdv*- $\text{P}_2\text{O}_7^{4-}$ complexes potentiometrically and calorimetrically, in $(\text{CH}_3)_4\text{NCl}$ 0.5 or 1 mol dm^{-3} . In their experimental conditions only the species $\text{A}(\text{P}_2\text{O}_7)\text{H}_2^{2-}$ was found. At $I = 0.5 \text{ mol dm}^{-3}$ log K_{20} was 2.5, 2.1 and 1.9 for the three amines, respectively. Also for pyrophosphate complexes we observe that the formation constants of amine species have values similar to those of Na^+ species [19] (in particular for *en*, 1,6*d* and 1,8*d*, log $K_{10} \cong 2.6$; log $K_1 = 2.4$ for Na^+ species).

3.5. Hexacyanoferrate(II) complexes

Diamine complexes formed with $\text{Fe}(\text{CN})_6^{4-}$ are the same as for pyrophosphate. Their stability

(Table 5) is quite high and is comparable to that of mono and diprotonated amines- $\text{Fe}(\text{CN})_6^{4-}$ species already studied [8]. For the reaction $\text{H}_2\text{A}^{2+} + \text{Fe}(\text{CN})_6^{4-} = \text{A}[\text{Fe}(\text{CN})_6]\text{H}_2^{2-}$ we have a mean value log $K_{20} = 4.5$. In a previous work [8], we found log $K_{20} = 4.9$ and 4.4 for diethylenetriamine and triethylenetetramine, respectively. The same remarks, as in Sections 3.3 and 3.4, can be made on the similarity in the stability of Na^+ and HA^+ complexes.

3.6. Triphosphate complexes

These complexes have been studied previously [11] (for *en*, 1,6*d* and 1,8*d*), and their relative formation constants, log K_{ij} , range between 3.3 and 6.9. On the basis of the general trend of data in this work, we also estimated log K_{ij} values for 1,3-*dap*, *ptr* and *cdv*, namely 6.6, 6.3 and 6.0 (log K_{20}); 4.6, 4.5, 4.4 (log K_{21}) and 3.4, 3.4 3.3 (log K_{22}). According to the high charge of $\text{P}_3\text{O}_{10}^{5-}$, the species formed with diammonium cations are very stable. The stability of these complexes fol-

lows the same trend as HPO_4^{2-} and $\text{P}_2\text{O}_7^{4-}$; it increases linearly with the anion charge.

3.7. Structure and charge-stability relationships

The amines studied here have a general formula $\text{NH}_2 - (\text{CH}_2)_n - \text{NH}_2$ (except 1,2-diaminopropane, which can be assimilated to ethylenediamine, $n = 2$). In a previous work [7], on the basis of much fewer data, it was hypothesized that the stability of $\text{ALH}_r^{(r-z)}$ complexes is an inverse function of n , (i.e. the distance between the two aminogroups negatively influences the formation of anion complexes). In Fig. 3, where $\log K_{2j}$ ($j = 1$ for all the systems, but pyrophosphate

where, $j = 1$ and 2) is reported vs. n , we can see that this hypothesis is confirmed. The $d \log K_{ij}/d n$ slope is about -0.1 , which is quite significant. Moreover, one can observe that this slope is rather more negative for complexes of polyanions with higher charges. Data from ref. 1 are also in accordance with this trend, $\log K_{20} = 3.4 - 0.3n$ (diamine–pyrophosphate complexes, $I = 0.5 \text{ mol dm}^{-3}$). However, the most important factor influencing the stability of protonated amine–polyanion complexes is the charge of the polyammonium cation. The relationship between $\log K_{ij}$ and z is linear, and an example is shown in Fig. 4 (cadaverine complexes). In this Figure, and in the subsequent calculations, hexacyanoferrate(II) complexes are neglected (see below). Data in Fig. 4 can be expressed by the equation

$$\log K_{2j} = -1.0 + 1.63 (\pm 0.10)z$$

with a correlation coefficient > 0.99 and a mean deviation (in $\log K_{2j}$) < 0.1 . Now dependence on both z and n can be taken into account together, by the equation

$$\log K_{ij} = -0.85 + 1.81 (\pm 0.03)z - 0.05 (\pm 0.005)n \quad (3)$$

with a mean deviation (in $\log K_{2j}$) < 0.15 .

The stability of hexacyanoferrate(II) complexes is considerably lower than expected on the basis of Eq. (3). This is not surprising since in $\text{Fe}(\text{CN})_6^{4-}$ anion charge dispersion must be higher than in the other polyanions.

3.8. Relevance of inorganic polyanion-protonated diamine complexes

Data reported in this work, together with previous findings, confirm that in solutions containing protonated diamines and polyanions a significant part of these components form mixed species, $\text{ALH}_r^{(r-z)}$. In particular, biogenic amines having high $\log K^{\text{H}}$ values, form stable mixed diprotonated species in the physiological pH range. In the speciation diagram of the pyrophosphate–putrescine system, we see that even for very low concentrations (Fig. 2B, $C_{\text{ptr}} = C_{\text{pyrophosphate}} = 10 \mu\text{mol dm}^{-3}$), very high percentages of mixed species are found: at $\text{pH} = 7.4$ % $[(\text{ptr})(\text{P}_2\text{O}_7)\text{H}_3^-] +$ %

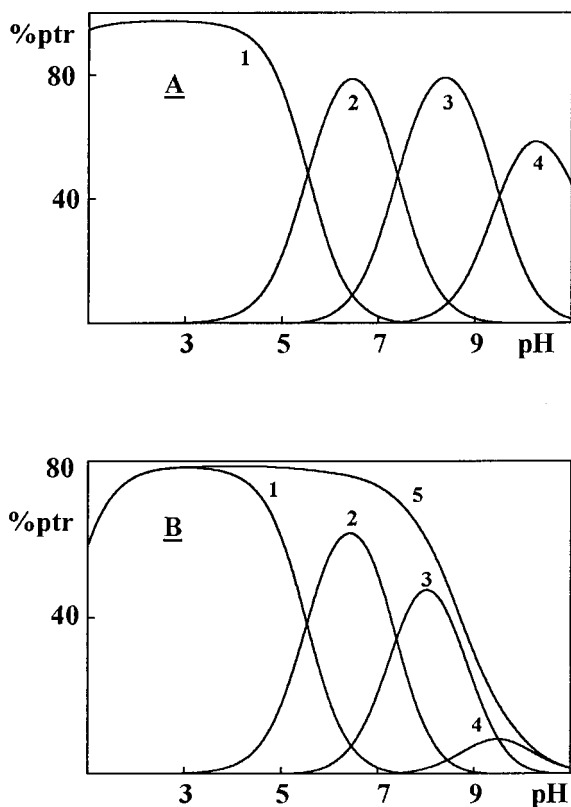


Fig. 2. Distribution of species in the system H^+ –putrescine– $\text{P}_2\text{O}_7^{4-}$ vs. pH. (A) $C_{\text{NaCl}} = 0.15 \text{ mol dm}^{-3}$; $C_{\text{ptr}} = C_{\text{P}_2\text{O}_7} = 1 \text{ mmol dm}^{-3}$; (B) $C_{\text{ptr}} = C_{\text{P}_2\text{O}_7} = 10 \mu\text{mol dm}^{-3}$. 1. $(\text{ptr})(\text{P}_2\text{O}_7)\text{H}_4^0$; 2. $(\text{ptr})(\text{P}_2\text{O}_7)\text{H}_3^-$; 3. $(\text{ptr})(\text{P}_2\text{O}_7)\text{H}_2^{2-}$; 4. $(\text{ptr})(\text{P}_2\text{O}_7)\text{H}_3^{3-}$; 5. $\Sigma (\text{ptr})(\text{P}_2\text{O}_7)\text{H}_r$; (other species are neglected in this diagram).

Table 5

Hexacyanoferrate (II) complex formation constants of diamines^a at $I = 0 \text{ mol dm}^{-3}$ and $T = 25^\circ\text{C}$

Reaction ^b	$\log K \pm 3 \text{ S.D.}$		
	<i>en</i> ^c	<i>ptr</i> ^d	<i>cdv</i> ^d
$\text{H}^+ + \text{A}^0 + \text{Fe}(\text{CN})_6^{4-} = \text{A}[\text{Fe}(\text{CN})_6]\text{H}^3^-$	12.7	13.1 ± 0.3	13.6 ± 0.3
$2\text{H}^+ + \text{A}^0 + \text{Fe}(\text{CN})_6^{4-} = \text{A}[\text{Fe}(\text{CN})_6]\text{H}_2^{2-}$	21.55	23.91 ± 0.13	24.74 ± 0.12
$3\text{H}^+ + \text{A}^0 + \text{Fe}(\text{CN})_6^{4-} = \text{A}[\text{Fe}(\text{CN})_6]\text{H}_3^-$	24.71	27.4 ± 0.2	28.1 ± 0.2
$4\text{H}^+ + \text{A}^0 + \text{Fe}(\text{CN})_6^{4-} = \text{A}[\text{Fe}(\text{CN})_6]\text{H}_4^0$	26.44	29.1 ± 0.3	29.9 ± 0.3
$\text{HA}^+ + \text{Fe}(\text{CN})_6^{4-} = \text{A}[\text{Fe}(\text{CN})_6]\text{H}^3^-$	2.8	2.6	2.8
$\text{H}_2\text{A}^{2+} + \text{Fe}(\text{CN})_6^{4-} = \text{A}[\text{Fe}(\text{CN})_6]\text{H}_2^{2-}$	4.8	4.3	4.4
$\text{H}_2\text{A}^{2+} + \text{H}[\text{Fe}(\text{CN})_6]^{3-} = \text{A}[\text{Fe}(\text{CN})_6]\text{H}_3^-$	3.6	3.4	3.3
$\text{H}_2\text{A}^{2+} + \text{H}_2[\text{Fe}(\text{CN})_6]^{2-} = \text{A}[\text{Fe}(\text{CN})_6]\text{H}_4^0$	2.9	2.7	2.7

^a For symbols, see footnote to Table 1.^b A = amine;^c Ref. [8];^d This work.

$[(ptr)(\text{P}_2\text{O}_7)\text{H}_2^{2-}] > 70\%$ of total components. This means that the hypothesis that in vivo these reactions can be of some interest, is now quantitatively confirmed. Moreover, if we consider other important natural fluids, such as seawater ($\text{pH} = 8.2$), it is possible to infer that low molecular ligands containing aminogroups interact significantly with polyanions. Data reported in this work refer to a temperature of 25°C , whilst natural and biological fluids generally have very different temperatures (e.g. 37°C). A few calorimetric

measurements [1,25] showed that for the reaction in Eq. (2) we have fairly low ΔH^0 values, and therefore quantitative data at $T \neq 25$ should be not very different from ours. The relevance of inorganic anion–diamines cation complexes can also be considered in comparison with the relative alkali and alkaline earth cation complexes. As discussed in preceding sections, Na^+ complexes have similar stability in comparison with diammonium complexes studied here. As regards Ca^{2+} and Mg^{2+} complexes for SO_4^{2-} $\log K = 2.29$ and

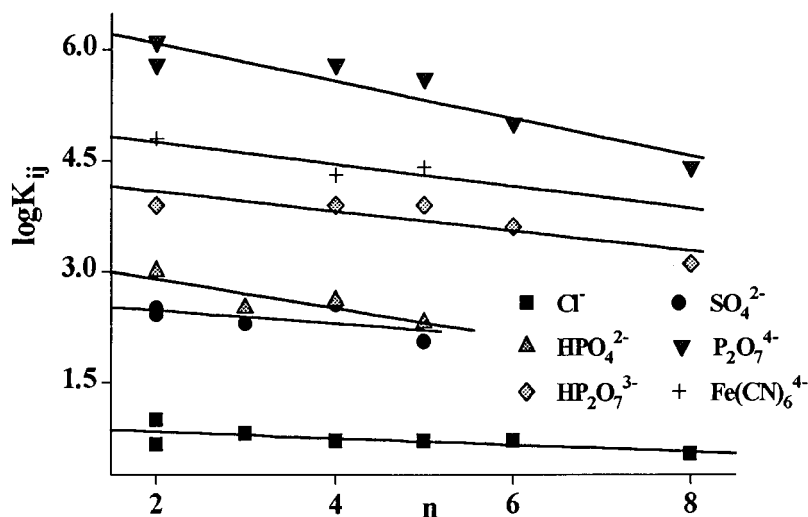


Fig. 3. Values of $\log K_{ij}$ vs. n , amines: $\text{NH}_2-(\text{CH}_2)_n-\text{NH}_2$ (1,2-diaminopropane $n = 2$) [$i = 2$; $j = 1$ for all anions, but for pyrophosphate, $j = 1$ and 2].

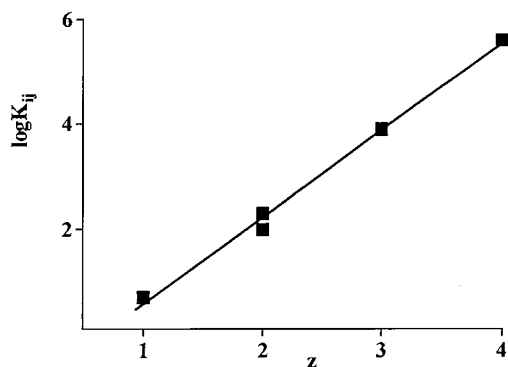


Fig. 4. Values of $\log K_{ij}$ vs. z (charge of polyanions), for cadaverine-anion species, at $I=0 \text{ mol dm}^{-3}$ and $T=25^\circ\text{C}$ [$i=2$; $j=1$ for all anions, except for pyrophosphate, $j=1$ and 2].

2.31 [26], and for $(en)(\text{SO}_4)\text{H}_2$ $\log K = 2.42$, i.e. in this case too stability is similar. Therefore the hypothesized competition between inorganic and ammonium cations in biochemical reactions is explained here quantitatively.

3.9. Conclusions

The main conclusions of this investigation are as follows:

1. Different diamines $\text{NH}_2-(\text{CH}_2)_n-\text{NH}_2$ ($n = 2\dots 8$) form complexes $\text{ALH}_r^{(r-z)}$ with polyanions L^{z-} having similar stability.
2. The stability of $\text{ALH}_r^{(r-z)}$ species depends on n (fairly) and z (strongly), [see Eq. (3)].
3. Mixed proton-amine-polyanion species are formed in significant amounts even at very low concentrations (see Fig. 2B).
4. The stability of Na^+ and Ca^{2+} complexes with inorganic anions is comparable to that of corresponding protonated amine complexes.

Acknowledgements

We thank CNR and MURST for financial support.

References

- [1] I. Labadi, E. Jenei, R. Lahti, H. Lönnberg, *Acta Chem. Scand.* 45 (1991) 1055.
- [2] C. De Stefano, C. Foti, O. Giuffrè, S. Sammartano, *Talanta* 43 (1996) 707.
- [3] P.H. Bolton, D.R. Kearns, *Biochemistry* 16 (1977) 5729.
- [4] S.S. Cohen, *Nature* 274 (1978) 209.
- [5] P.G. Daniele, A. De Robertis, C. De Stefano, D. Gastaldi, S. Sammartano, *Ann. Chim. (Rome)* 83 (1993) 575.
- [6] A. De Robertis, A. Gianguzza, G. Patanè, S. Sammartano, *J. Chem. Res. (S)* (1994) 182.
- [7] P.G. Daniele, C. De Stefano, E. Preresti, S. Sammartano, *J. Solution Chem.* 24 (1995) 325.
- [8] C. De Stefano, C. Foti, O. Giuffrè, *J. Solution Chem.* 25 (1996) 155.
- [9] A. De Robertis, C. De Stefano, O. Giuffrè, S. Sammartano, *J. Chem. Soc. Faraday Trans.* 92 (1996) 4219.
- [10] A. De Robertis, C. De Stefano, C. Foti, O. Giuffrè, S. Sammartano, *J. Chem. Res. (S)* (1996) 60.
- [11] C. De Stefano, C. Foti, O. Giuffrè, P. Mineo, C. Rigano, S. Sammartano, *Ann. Chim. (Rome)* 86 (1996) 257.
- [12] C. De Stefano, C. Foti, A. Gianguzza, O. Giuffrè, S. Sammartano, *J. Chem. Soc. Faraday Trans.* 92 (1996) 1511.
- [13] P.G. Daniele, A. De Robertis, C. De Stefano, C. Foti, O. Giuffrè, E. Preresti, S. Sammartano, *Ann. Chim. (Rome)* 87 (1997) 415.
- [14] C. De Stefano, P. Princi, C. Rigano, S. Sammartano, *Ann. Chim. (Rome)* 77 (1987) 643.
- [15] C. De Stefano, P. Mineo, C. Rigano, S. Sammartano, *Ann. Chim. (Rome)* 83 (1993) 243.
- [16] A. Casale, P.G. Daniele, A. De Robertis, S. Sammartano, *Ann. Chim. (Rome)* 78 (1988) 249.
- [17] C. De Stefano, C. Rigano, S. Sammartano, R. Scarcella, *J. Chem. Res. (S)* (1988) 372.
- [18] P.G. Daniele, A. De Robertis, C. De Stefano, A. Gianguzza, S. Sammartano, *J. Solution Chem.* 20 (1991) 495.
- [19] C. De Stefano, C. Foti, A. Gianguzza, *J. Chem. Res., (S)* 464, (M) 2639 (1994).
- [20] S. Capone, A. De Robertis, S. Sammartano, C. Rigano, *Thermochim. Acta* 102 (1986) 1.
- [21] P.G. Daniele, C. De Stefano, E. Preresti, S. Sammartano, *Curr. Topics Sol. Chem.* 1 (1994) 95.
- [22] A. Casale, A. De Robertis, F. Licastro, C. Rigano, *J. Chem. Res., (S)* 204, (M) 1601 (1990).
- [23] A. De Robertis, C. De Stefano, G. Patanè, S. Sammartano, *J. Solution Chem.* 22 (1993) 927.
- [24] A. De Robertis, C. De Stefano, G. Patanè, *Thermochim. Acta* 7 (1992) 209.
- [25] C. De Stefano, O. Giuffrè, S. Sammartano, *J. Chem. Soc. Faraday Trans.*, in press.
- [26] A. De Robertis, C. De Stefano, A. Gianguzza, S. Sammartano, *Chem. Spec. Bioavail.* 6 (1994) 65.

On-line preconcentration of mercury by sorption on an anion-exchange resin loaded with 1,5-bis[(2-pyridyl)-3-sulphophenyl methylene] thiocarbonohydrazide and determination by cold-vapour inductively coupled plasma atomic emission

P. Cañada Rudner, A. Garcia de Torres, J.M. Cano Pavón *, F. Sanchez Rojas

Department of Analytical Chemistry, Faculty of Sciences, University of Malaga, E29071, Malaga, Spain

Received 14 May 1997; received in revised form 14 October 1997; accepted 20 October 1997

Abstract

1,5-Bis[(2-pyridyl)-3-sulphophenyl methylene] thiocarbonohydrazide (PSTH) immobilized on an anion-exchange resin (Dowex) has been used for the on-line preconcentration of mercury from biological samples and waters prior to its determination by inductively coupled plasma atomic emission spectroscopy. The metal was eluted from the column using a solution of 2 M HNO₃ and mixed on-line with SnCl₂. The optimum experimental conditions were evaluated for the continuous preconcentration of Hg, the direct generation of mercury vapour and the final determination of this element by ICP–AES. The enrichment, together with low blank levels of the optimized procedure, allow the simple determination of this toxic element at concentrations down to a few nanograms per milliliter. The proposed method has a linear calibration range 5–1000 ng ml⁻¹ of mercury, with a detection limit of 4 ng ml⁻¹ (*S/N* = 3) and a sampling rate of 40 h⁻¹, investigated with a 9 ml sample volume. The precision of the method (evaluated as the relative standard deviation obtained after analyzing ten series of ten replicates) was ± 3.6% at the 10 ng ml⁻¹ level of Hg(II) and ± 1.3% at the 100 ng ml⁻¹ level. The accuracy of the method was examined by the analysis of certified reference materials. © 1998 Elsevier Science B.V. All rights reserved.

Keywords: Mercury; Preconcentration; Ion-exchange; Inductively coupled plasma atomic emission spectrometry

1. Introduction

The toxic effects of mercury are well known. For this reason, sensitive, fast, reproducible and

accurate analytical methods are required for the determination of this element. In routine laboratory measurements, Hg is determined in its atomic form in the vapour phase using atomic spectroscopic methods. However, the direct determination of (ultra)trace amounts of mercury in complicated matrices is usually difficult owing to

* Corresponding author. Tel.: +34 5 2131887; fax: +34 5 2132000; e-mail: jm_cano@uma.es

matrix interferences and/or insufficient detection power. Consequently, a preliminary preconcentration and/or separation is required. Thus, recently, Burrini et al. [1] have developed a sensitive and accurate method for the determination of mercury in urine by ET–AAS using complexation with dithizone and extraction with cyclohexane. However, this extraction procedure cannot be combined with ICP–AES due to the difficulties of introducing organic solvents into the plasma of an ICP spectrometer. In addition, the use of a common batch-type solvent extraction procedure was found to be time consuming and incompatible with the intrinsic speed of ICP–AES analysis.

Column solid-phase extraction has some advantages over liquid–liquid extraction: the possibility of combination with AAS as well as with ICP–AES, allows preconcentration from a larger sample volume, establishing higher concentration factors, simple storage and transportation of the pre-treated samples [2–5]. Column preconcentration using chelating resins such as Chelex-100 [6,7], quinolin-8-ol immobilized on porous glass [8], or silica [9] and poly(dithiocarbamate) [10] have been used for the enrichment of natural waters and biological materials. However, some resins, such as those based on poly(dithiocarbamate), are reluctant to release the bound analyte, and the resin is usually dissolved prior to analysis [11,12]. Thus, Alexandrova et al. [13] report a method for the preconcentration of trace metals prior to their measurements by AAS or ICP–AES; for ICP–AES measurements a quantitative elution was obtained with 4 M HNO₃ permitting the determination of Cd, Mn, Cu, Fe, Ni and Pb, however, the procedure was found to be inappropriate for Hg or Co determination, owing to the formation of stable dithiocarbamate complexes, which cannot be destroyed at an HNO₃ concentration of 4 M. Arpadjant et al. [14] presented an alternative method for preconcentration of Hg from water samples, for ICP–AES measurements the physically immobilized organic chelating ligand together with the analyte–dithiocarbamate complex were completely dissolved in methanol; the methanol solution was diluted with water and then nebulized into the ICP–AES system. For each sample a new sorption column was applied.

From data presented it can be concluded that a detection limit of 0.12 ng ml⁻¹ can be achieved by processing 150 ml samples. However, this type of elution, or more correctly, of dissolution of the preconcentrated element is undesirable as it is labour intensive, time consuming and a potential source of contamination.

Chelation exchange resins containing iminodiacetate functional groups have been used extensively to isolate the first-row transition metals and analytes such as cadmium and lead from complex matrices such as sea-water and biological samples. Such uses have been reviewed [15]. However, many of these techniques were performed off-line.

The incorporation of column solid-phase extraction in the FI systems coupled on-line to atomic spectrometers offer some interesting improvements. The major improvements are, in general, the possibility of working in a closed system with a significant reduction of airborne contamination and a fairly high sampling frequency, which justifies current trends towards an increasing use of this preconcentration technique. To date, various kinds of separation techniques have been adapted to FI on-line separation and preconcentration ICP–AES systems, these procedures were compiled in a recent monograph [16]. The majority of work conducted in this area has been associated with preconcentration on packed columns either by exchange or by adsorption. Of particular importance, is the use of chelating resins as packing materials due to their ability to preconcentrate metal ions from very dilute solutions, thus allowing detection limits to be greatly improved [17]. For this reason, synthesis of chelating resins having good selectivity is a subject of continuing interest and importance. Thus, in the last years, a number of chelating resins containing various functional groups have been reported [18–21].

In this article, a FI-ICP–AES method for the determination of trace amounts of mercury is described. A new chelating ion-exchange resin was prepared for the separation and preconcentration of mercury from different matrices. The efficiency of the resin for Hg(II) preconcentration was studied in detail, with respect to pH, flow rate, precision, interferences of the other ions, etc. The

manifold used involve a column included within the sample loop of an injection valve, in this FI system the metal was eluted from the column and mixed on-line with SnCl_2 , mercury vapour was generated directly and separated via a gas–liquid separator. The accuracy of this automatic method was examined by the analysis of certified reference materials.

2. Experimental

2.1. Apparatus

The ICP–AES system used was a Perkin–Elmer 40 sequential emission spectrometer equipped with the Perkin–Elmer AS-90 autosampler and controlled by an IBM XT-486 personal computer. The spectrometer output was connected to a PE Nelson Model 1020 personal integrator. The plasma operating conditions used in this work are summarized in Table 1.

Table 1
Optimum operating conditions for FI-ICP determination of Hg

ICP system	
Wavelength	253.652 nm
R.f. generator	
Frequency	40 MHz
Incident power	1.1 kW
Photomultiplier voltage	600 V
Plasma gas flow rate	12 l min ⁻¹
Auxiliary gas flow rate	0.6 l min ⁻¹
Plasma viewing height	15 mm (above the induction coil)
FI system	
Internal diameter of coils	0.8 mm
Mixing coil length	100 cm
Sample flow rate	9 ml min ⁻¹
Elution flow rate	5 ml min ⁻¹
Argon carrier flow rate	80 ml min ⁻¹

A schematic diagram of the automatic on-line preconcentration system modified from the Perkin–Elmer FIAS 400 is presented in Fig. 1. Pump P_2 was connected to the sampler capillary and the microcolumn through the four-way rotary valve, this valve had the column connected within the sample loop. The micro-column was a glass tube (3 cm × 3 mm i.d.), and packed with the chelating resin to a height of 1 cm, in both ends of microcolumn polyethylene frits (Omnifit) were fixed to prevent material losses. Transport lines and mixing coils were made using 0.8 mm i.d. PTFE tubing. A classical gas–liquid separator [22] was used. The mini-column was initially flushed with 2 M nitric acid; subsequent use of 2 M HNO_3 as eluent in each operating cycle was sufficient to make it ready for re-use.

For sample digestion, a microwave oven, Pro-labo TX-32, was used.

All glassware used were washed with 10% nitric acid for one day and rinsed with deionized water just before use.

2.2. Reagents

Analytical-reagent grade chemicals were used throughout. Doubly de-deionized water prepared from a Milli-Q purification system (Millipore) was used throughout this work.

A stock solution of Hg(II) was prepared from the nitrate (Merck) and standardized complexometrically; standards of working strength were made by appropriate dilution as required, immediately prior to use.

1,5-bis[(2-pyridyl)-3-sulphophenyl methylene] thiocarbonohidrazide (PSTH) was prepared and purified as described under Synthesis of the chelating agent. The anion-exchange resin used was Dowex 1 × 8–200, 100–200 mesh (Aldrich). The 0.03 M tin(II) chloride solution was prepared from $\text{SnCl}_2 \cdot 2\text{H}_2\text{O}$ (Carlo Erba). A pH 4.7 buffer was prepared by mixing 25 ml of 0.5 M sodium acetate and 25 ml of 0.5 M acetic acid and diluting to 100 ml with deionized water.

2.3. Synthesis of the chelating agent

A 2 g mass of 2-benzoylpyridine (Aldrich) was

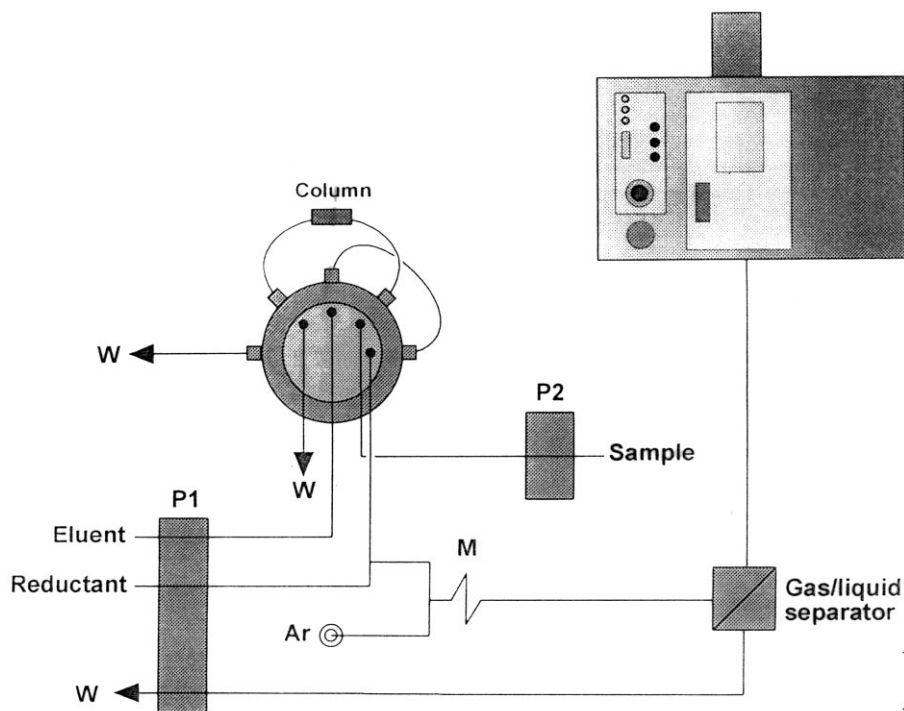


Fig. 1. Schematic diagram of FI manifold for the determination of mercury: P₁, P₂, peristaltic pumps; M, mixing coil (length 100 cm, i.d. 0.8 mm); Ar, stream of argon (80 ml min⁻¹); W, waste. See text for other details.

dissolved in 20 ml of concentrated sulphuric acid (Merck) at 0°; the solution was allowed to stand for about 2 h. and mixed with 180 ml of ether. The mixture was then cooled in a refrigerator and the product that formed, 2-benzoyl(3-sulphonyl) pyridine, was filtered, washed with ether, recrystallized from ethanol:water (1:1) and dried. A solution of 1.54 g of this product in 75 ml of deionized water was mixed with a solution of 0.12 g of thiocarbonohydrazide (Aldrich) in 10 ml of deionized water, then ten drops of glacial acetic acid were added. The mixture was refluxed and stirred for 2 h. After cooling to room temperature, the reaction mixture was placed in a refrigerator and, after a short time, orange crystals were formed. The solid (PSTH) was filtered, washed with deionized water, dried and stored in a vacuum desiccator. Yield is about 78%. Elemental analysis confirmed the purity of the reagent and its structure was verified by IR and NMR spectroscopy.

2.4. Preparation of the chelating resin

After removal of the fines, the Dowex ion-exchange resin was treated with 1 M HCl, collected by filtration and washed with deionized water until pH 7. Then was coupled to PSTH by adding to it 10 ml of a 0.01 M solution of PSTH in 5 M NaOH for each gram of resin. The mixture was stirred and allowed to stand for about 24 h.

2.5. General procedure

2.5.1. On-line preconcentration and elution

With the manifold described in Fig. 1 and under the optimum instrumental conditions show in Table 1. During the 1 min sample loading period, valve in the 'fill' position, a 9 ml min⁻¹ flow of sample (standard or blank) at pH 4.7 buffered with sodium acetate-acetic acid is pumped (via pump P₂) through the microcolumn (located in the loop of the valve) The metal is adsorbed on the sorbent mini-column and the

sample matrix sent to waste. During preconcentration, a 5 ml min^{-1} flow of eluent (2 M HNO_3) and reductant (0.03 M SnCl_2) are being aspirated from the containers by the pump P_1 to establish the baseline of the readout and to stabilize the plasma. At the beginning of the 30 s elution stage, the valve position is changed and the sample pump P_2 is stopped. When the valve is in the 'inject' position, the eluant passes through the column. Thus, the accumulated mercury ion is eluted at an elution rate of 5 ml min^{-1} and merges with a 5 ml min^{-1} flow of reductant in the mixing coil M (length 100 cm, i.d. 0.8 mm), where direct generation of mercury vapour takes place. The gas generated and the solvent are then passed into the gas-liquid separator which provides a separation of gases from liquid. The liquid is drained and the generated mercury vapour is swept into the ICP torch by a stream of argon (80 ml min^{-1}). Calibration plots for Hg were measured from six standard solutions within the concentration range $5\text{--}1000 \text{ ng ml}^{-1}$. Peak heights were used as analytical measurements.

2.5.2. Sample preparation

The certified reference materials (CRMs) analyzed to determine the accuracy of the proposed procedure were: Community Bureau of Reference (BCR), CRMs 397 Human Hair; Institute of Standards and Technology (NIST), Standard Reference Materials (SRMs) 2670 freeze-dried urine. The samples were first dried in accordance with the instructions of the respective analysis certificates and were prepared by microwave digestion. The working conditions of the microwave oven are listed in Table 2. After digestion, the pH of the solutions were adjusted to 4.7 with concentrated NaOH and buffer solutions and finally, the samples were diluted to 50 ml with deionized water in a calibrated flask. Analysis of each sample, in triplicate, was carried out as described in Section 2.5, General procedure, using a calibration graph.

Sea water was collected in polypropylene bottles previously cleaned by soaking in 0.1 M hydrochloric acid. Samples were filtered by using a membrane of $0.45 \mu\text{m}$ pore size, acidified to 0.1% (v/v) with concentrated HNO_3 and stored frozen until analysis.

3. Results and discussion

3.1. Characteristics of the PSTH

The solubilities in several solvents of the organic ligand was determined. The reagent is easily soluble in polar organic solvents, e.g. dimethylformamide, ethanol, methyl isobutyl ketone and is also soluble in alkaline solution and slightly soluble in water.

Thermogravimetric curves were recorded, the reagent was stable up to 100° ; a decrease occurs between 100 and 200° , this fact can be attributed to the loss of six molecules of water. Thus, elemental analysis gave the following results: C 44.01%, H 4.37%, N 11.99%; $\text{C}_{25}\text{H}_{18}\text{N}_6\text{S}_3\text{O}_6 \cdot 6\text{H}_2\text{O}$ requires: C 44.77%, H 4.47%, N 12.53%.

The infrared spectrum of the reagent (KBr pellet) is complicated because the aromatic portion of the molecule produces numerous bands, the overlap of which makes detailed assignments difficult. The band at 1204 cm^{-1} was attributed to C=S stretching and the bands at 3107 cm^{-1} and at 1503 cm^{-1} were assigned to N-H and C=N stretching, respectively.

The ultraviolet spectra of the reagent in various solvents showed intense $n \rightarrow \pi^*$ bands between 200 and 390 nm, as expected for this system. On the other hand, the ultraviolet spectra of aqueous PSTH solutions are pH dependent. Because sulphonic groups are acid-strong, PSTH acts habitually in solution as a charged compound. The other pK values (pK_2 and pK_3) were calculated from the variation of absorbance with pH applying the customary Stenstrom and Goldsmith [23] and Sommer [24] methods. The values obtained are: $pK_2 = 3.3$ and $pK_3 = 10.2$. The pK values are the arithmetic means of the values obtained from measurements at three different wavelengths. The second ionization constant can be attributed to the deprotonation of the nitrogen atom in the pyridine rings (on comparison with those of similar compounds); owing to the large distance between the two pyridine nitrogen atoms, the values of their ionization constants would be expected to be similar and hence they are not distinguishable by spectrometry. pK_3 is due to the deprotonation

Table 2
Working conditions for microwave oven

Step	Reagent	Volume (ml)		Power (%)		Time (min)	
		Toxic metals in freeze-dried urine SRM2670	Human hair CRM397	Toxic metals in freeze-dried urine SRM2670	Human hair CRM397	Toxic metals in freeze-dried urine SRM2670	Human hair CRM397
1	HNO ₃		10	6	5	5	2
2	—		—	—	15	10	3
3	—		—	—	30	10	6
4	H ₂ O ₂		—	3	30	10	5
5	H ₂ O ₂		5	3	30	5	5
6	H ₂ O ₂		5	—	25	5	—

of the –SH group (which is in tautomeric equilibrium with the C=S group), this process is typical of all thiocarbonhydrazones and thiosemicarbazones. Since the ligand is an anion above pH 10, it is strongly retained by anion exchange resins.

The reaction of different cations with PSTH were tested at different pH values. The characteristics of the most important complexes are summarized in Table 3. The data were obtained from the appropriate spectra, which were measured in the presence of an excess of the reagent at those pH values which facilitate the formation of the different complexes. Since the reagent reacts with many metal ions forming stable complexes, if a solution of these ions at the appropriate pH are passed through such a column, the metals should be complexed and removed from solution.

3.2. Separation and determination of mercury

To optimize the system, main efforts were focused on the conditions for sample loading and mercury eluting from the column, as well as the analytical flow system which was coupled on-line with the preconcentration and separation unit in order to obtain highly sensitive, accurate and reproducible results.

3.2.1. Optimization of experimental parameters

Chemical parameters including sample acidity, reductant concentration, FI variables (mixing coil, sample flow rate, eluent flow rate, etc) and ICP–

AES parameters were optimized according to the procedure described in Section 2.5.1, On-line preconcentration and elution.

It is known that strong acids are effective in dissociating complexes and releasing free metal ions. In this study a 2 M HNO₃ solution was chosen as eluant. In the initial study the stability of the PSTH–Dowex resin was studied experimentally in acidic, neutral and basic media by observing any physical changes occurring in the material, the results obtained showed that the resin was stable over a wide pH range of pH < 0–13.

Since the solution pH affects the extent of complexation which in turn determines the percentage of metal retained by the resin, the preconcentration of mercury from solutions buffered at different pH was studied. The pH from 2.0 to 5.0 was adjusted using sodium acetate–acetic acid buffer and from pH 5.0 to 11.0 using borax–boric acid buffer. The results (mean ± S.D. for three replicate measurements) are shown in Fig. 2. These results indicated that the optimum pH range was around 4.5–6.5. All subsequent studies were carried out at pH 4.7.

Preliminary tests showed that the sample volume was not an important factor when the mass of analyte arriving at the column was kept constant. The influence of the sample flow rate was studied using a constant flow rate of eluant and reductant. For this purpose, 50 ml of samples containing 800 ng of mercury were brought to pH 4.7 and passed through the column at different sample flow rate (the flow rate was varied by changing the speed of the sample pump). The results were essentially the same for flow rate of 6, 8 and 9 ml min⁻¹. It is probable that even faster flow rates would have been successful with a faster pump.

The effect of sample loading time on the emission signal of 100 ng ml⁻¹ Hg was tested at a sample flow rate of 9 ml min⁻¹. The signal increased almost linearly up to 12 min preconcentration time, after which the slope decreased gradually, presumably as a result of an insufficient capacity of the resin. Sensitivity enhancements gained by increasing the sample loading time, however, the loading time selected in the experi-

Table 3
Photometric properties of complexes

Metal ion	λ_{\max} (nm)	pH	ϵ (l mol ⁻¹ cm ⁻¹) × 10 ⁴
Zn(II)	414	5.0	3.23
Co(II)	410	2.6	3.47
Ni(II)	418	8.0	2.62
Bi(III)	424	2.6	5.13
Cd(II)	402	8.0	5.07
Zr(IV)	418	5.0	2.41
Fe(III)	408	4.0	3.53
Ga(III)	422	5.0	3.43
Cu(II)	428	2.6	2.48
Hg(II)	376	7.0	2.14

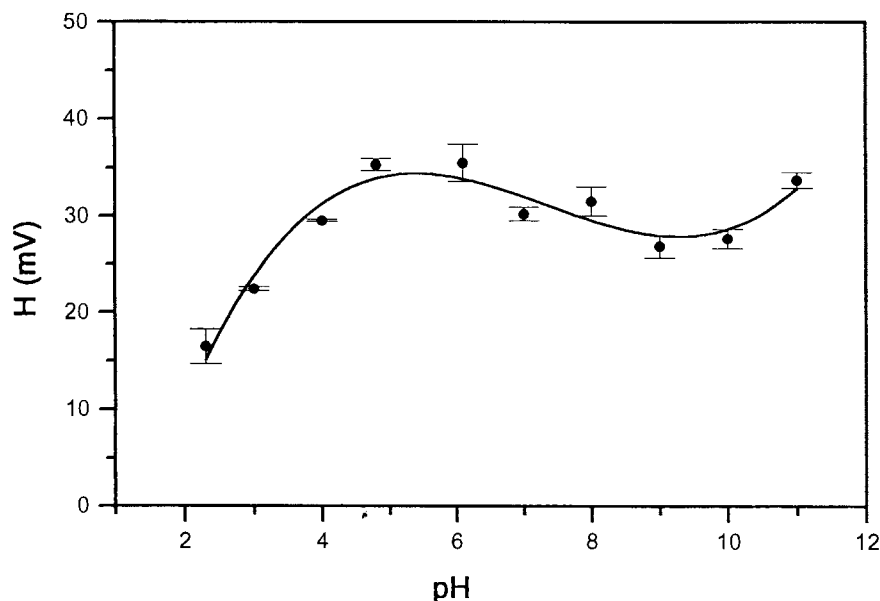


Fig. 2. Influence of pH on the preconcentration of mercury.

ment was 60 s, in order to achieve high sampling frequency with a reasonable degree of sensitivity. Loading time may be higher for samples with low concentrations of mercury.

The influence of the flow rate of elution on sensitivity and precision for triplicate determinations of 100 ng ml^{-1} Hg was investigated in the range $1\text{--}6 \text{ ml min}^{-1}$. The results (mean \pm S.D., $n = 3$) are shown in Fig. 3. As can be seen, the peak height increases with increasing elution flow rate. The precision, however, worsened at flow rates $> 5 \text{ ml min}^{-1}$, possibly due to the high pressures produced. As a compromise between analytical sensitivity and precision, a elution flow rate of 5 ml min^{-1} was chosen. The recommended dissolution period is 30 s.

The influence of mixing coil length was also examined to ensure a homogeneous mixture between the sample and SnCl_2 solutions. Tubing coils (0.8 mm i.d.) of different lengths (0–200 cm) were tested. The ICP emission signals were constant for coil lengths ≥ 50 cm, so a 100 cm coil was chosen. To determine the reductant concentration necessary to quantitative generation of mercury vapour, 50 ml volumes of sample containing 800 ng of mercury at pH 4.7 were passed

through the resin and the SnCl_2 concentration was varied from 0.0005 to 0.03 M. At each corresponding reductant level, 5 ml min^{-1} flow of reductant was used. The results obtained showed that the peak heights remains constant for reductant concentrations equal or greater than 0.02 M. A concentration of 0.03 M was used in practice.

The effect of the argon carrier flow rate on emission signals was also examined. The results obtained showed that the peak height increased with increasing argon flow rate up to 80 ml min^{-1} ; at values $> 80 \text{ ml min}^{-1}$ the peak decrease. Therefore, an argon flow rate of 80 ml min^{-1} was chosen.

Using the minimum background equivalent concentration, BEC, as the optimization criterion, the following wavelengths were investigated: 194.227, 253.653, 296.728, 435.835, 265.204, 302.150 and 365.483 nm. From these wavelengths, measurement made at 253.653 nm produced the most intense emission, thus, this Hg line was selected for this work. Other operating ICP–AES variables such as photomultiplier voltage and plasma observation height were established to achieve the best signal-to-noise (S/N) ratios. The results are given in Table 1.

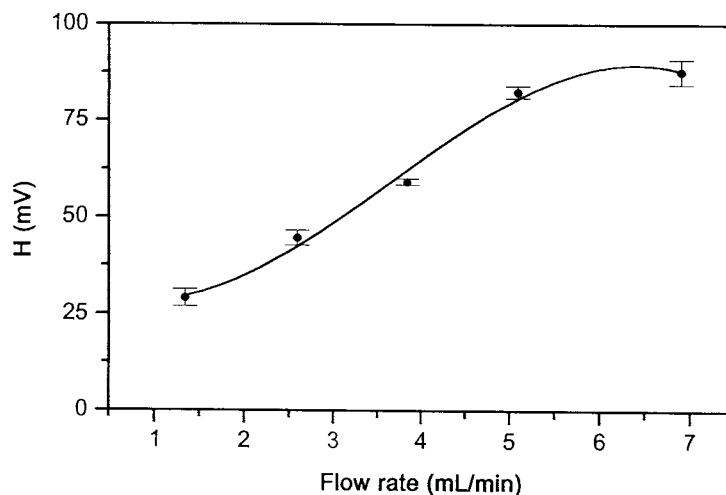


Fig. 3. Influence of eluent flow rate (ml min^{-1}).

3.2.2. Performance of the method

Under the optimum conditions, with the use of a 60 s preconcentration time, a sample flow rate of 9 ml min^{-1} and an elution flow rate of 5 ml min^{-1} , a linear calibration graph was obtained at least from 5 to 1000 ng ml^{-1} of Hg(II) with a regression coefficient of 0.999. The signal appeared 10 s after sample injection. Within 30 s after injection, the FI system was ready for the next injection, thus giving a sampling rate of about 40 per h.

The enrichment factor (EF), defined as the ratio of the slopes of the linear section of the calibration curves before and after the preconcentration, was 10.1. The concentration efficiency (CE) defined as the product of the enrichment factor EF and the sampling frequency in number of samples analyzed per hour was 7.8 and the consumptive index defined as the volume of sample, in milliliters, consumed to achieve a unit EF, was 0.8 ml. The phase transfer factor (P), defined as the ratio between the analyte mass in the original sample and in the concentrate was 0.6.

The detection limit defined as the concentration of analyte giving a signal equivalent to three times the standard deviation of blank signal plus the net blank intensity was measured to be 4 ng ml^{-1} , the absolute blank value was obtained by using the preconcentration and determination procedures with deionized water buffered at pH 4.7.

The results of including significant levels of possible interferences are presented in Table 4. The elements which can be chelated by the column will compete with mercury for the active sites. If the interferent is more strongly chelated on the column, or in a sufficiently high concentration, the preconcentration of mercury will be reduced.

The precision of the method (evaluate as the relative standard deviation obtained after analyzing ten series of ten replicates) was $\pm 3.6\%$ at the 10 ng ml^{-1} level of Hg(II) and $\pm 1.3\%$ at the 100 ng ml^{-1} level.

Table 4
Interference of foreign ions in the determination of mercury with PSTH

Ion	Tolerance ratio (w/w)	Recovery (%)
Br^-	5×10^3	97
ClO_4^-	2×10^4	99
SO_4^{2+}	10^4	87
EDTA	2×10^2	82
Triton X-100	500	100
Humic Acid	10	99
Ca(II)	2×10^3	95
Mg(II)	4×10^3	98
Zn(II)	500	100
Cr(III)	250	100
Ni(II)	250	100
Co(II)	250	100
Cu(II)	80	100

Table 5
Results for the determination of mercury in real and spiked samples

Sample	Certified value (ng ml ⁻¹)	Added (ng ml ⁻¹)	Found value* (ng ml ⁻¹)	Recovery (%)
CRM 397	12.3 ± 0.5 ^a		11.9 ± 0.1 ^a	97.5
SRM 2670	105 ± 8		104 ± 1	99.1
Synthetic sea water		25	24.2 ± 1.0	96.8
Sea water		25	25.1 ± 0.1	100.4
Tap water		25	24.5 ± 0.5	98.0

* Mean ± S.D. for three replicate measurements of three individual sample preparations.

^a Values in µg g⁻¹.

In order to test the accuracy and applicability of the proposed method to the analysis of the real samples, two biological reference materials were analyzed. The results, as the average of three separate determinations are shown in Table 5. These results showed that this automatic system provides analytical data within the ranges of the certified values.

In view of the application of the method to the determination of mercury in water, standard solutions containing Hg(II) were added to tap-water, sea water and synthetic sea water. The results, shown in Table 5, indicate excellent recovery.

4. Conclusion

Two of the most frequently stated advantages of the ICP as a source for emission spectrometry are its multi-element capability and low detection limits. However, in certain instances the detection limits possible with the ICP are still inadequate, especially when the sample has a complex matrix. There are also many sample matrices that present difficulties in their own right. Problems may arise due to the high dissolved solids content of the sample solution, other matrix-induced problems include spectral interferences, which result in measurement errors. In these circumstances, a preliminary preconcentration and/or separation is required. Conventional off-line procedures for separation and preconcentration, although, effective, are usually time consuming and tedious, and are vulnerable to contamination and analyte loss.

This study has shown that the FI-ICP method described allows the rapid determination of Hg.

The analytical scheme of the proposed system is more simple than other off-line procedures due to the fact that it combines trace enrichment, derivation and detection in one analytical set-up. The high speed, ease of use and automation, selectivity and relative freedom from random contamination by sample handling make this method suitable for Hg determination in waters and biological samples. The detection limit, obtained with a 60 s loading time at a sample flow rate of 9 ml min⁻¹, was 4 ng ml⁻¹, which compares favourably with other obtained using column solid-phase extraction in FI systems coupled on-line to conventional atomic spectrometers. For example, detection limits obtained by Greenway et al. [17] using different chelating agents (quinolin-8-ol-5-sulfonic acid, dithiocarbamate, dithizone and cysteine) ranged from 10 to 50 ng ml⁻¹ Hg.

Acknowledgements

The authors thank the Dirección General de Investigación Científica y Técnica (DGICYT) for supporting this study (Projects PB 93-1007 and PB 96-0702) and also the Junta de Andalucía.

References

- [1] C. Burrini, A. Cagnini, *Talanta* 44 (1997) 1219.
- [2] P. Burba, J.C. Rocha, A. Schulte, *Fresenius J. Anal. Chem.* 346 (1993) 414.
- [3] A. Tong, Y. Akama, *Anal. Chim. Acta* 230 (1990) 175.
- [4] J. Jambor, T. Javorek, *Collect. Czech. Chem. Commun.* 58 (1993) 1821.

- [5] C. Kantipuly, S. Katragadd, A. Chow, H. Gesser, *Talanta* 37 (1990) 491.
- [6] E.A. Novikov, L.K. Shpigum, A.Y. Zolotov, *Anal. Chim. Acta* 230 (1990) 157.
- [7] Y. Liu, J.D. Ingle, *Anal. Chem.* 61 (1989) 525.
- [8] V. Porta, O. Abollino, E. Mentalti, C. Sarzanini, *J. Anal. At. Spectrom.* 6 (1991) 119.
- [9] D. Beauchemin, S.S. Berman, *Anal. Chem.* 61 (1989) 1857.
- [10] X.R. Wang, R.M. Barnes, *J. Anal. At. Spectrom.* 4 (1989) 509.
- [11] R.S.S. Murthy, Z. Horvath, R.M. Barnes, *J. Anal. At. Spectrom.* 1 (1986) 269.
- [12] M. Sperling, X. Yin, B. Welz, *Analyst* 117 (1992) 629.
- [13] A. Alexandrova, S. Arpadjan, *Analyst* 118 (1993) 1309.
- [14] S. Arpadjan, L. Vuchkova, E. Kostadinova, *Analyst* 122 (1997) 243.
- [15] L. Ebdon, A.S. Fisher, S.J. Hill, P.J. Worsford, *J. Autom. Chem.* 13 (1991) 281.
- [16] Z. Fang, *Flow Injection Atomic Absorption Spectrometry*, Wiley, Chichester, 1995.
- [17] G.M. Greenway, A. Townshend, *Anal. Proc.* 30 (1993) 438.
- [18] R. Pathak, G.N. Rao, *Talanta* 44 (1997) 1447.
- [19] M.E. Mahmoud, E.M. Soliman, *Talanta* 44 (1997) 1063.
- [20] S. Blain, P. Appriou, H. Handel, *Anal. Chim. Acta* 272 (1993) 91.
- [21] A. Seubert, G. Petzold, J.W. McLaren, *J. Anal. At. Spectrom.* 10 (1995) 371.
- [22] R.R. Liversage, J.C. Van Loom, J.M. Andrade, *Anal. Chim. Acta* 161 (1984) 275.
- [23] W. Strenström, N. Goldsmith, *J. Phys. Chem.* 30 (1926) 1683.
- [24] L. Sommer, *Folia Fac. Sci. Nat. Univ. Purkynianae Brn.* 5 (1964) 1.

Preconcentration of trace cobalt with the ion pair of 2-(5-bromo-2-pyridylazo)-5-diethylaminophenol and tetraphenylborate onto microcrystalline naphthalene or column method and its determination by derivative spectrophotometry

J. Patrick Pancras^a, Bal Krishan Puri^{a,*}, Mohammad Ali Taher^b,
Ali Mostafavi Dehzoee^b, Ali Sheibani^b

^a Department of Chemistry, Indian Institute of Technology, Delhi, Hauz Khas, New Delhi, 110 016, India

^b Department of Chemistry, Shahid Bahonar University of Kerman, Kerman, Iran

Received 12 May 1997; received in revised form 15 October 1997; accepted 20 October 1997

Abstract

Cobalt-2-(5-bromo-2-pyridylazo)-5-diethylaminophenol (5-Br-PADAP)-tetraphenylborate ion associated complex is quantitatively adsorbed on microcrystalline naphthalene in the pH range 3.5–9.5 from a fairly large volume of the aqueous samples (preconcentration factor ~30). After filtration, the solid mass consisting of the cobalt complex and naphthalene was dissolved with 5 ml of dimethylformamide (DMF) and the metal determined by first-derivative spectrophotometry. The cobalt-5-Br-PADAP complex can alternatively be quantitatively retained on ammonium tetraphenylborate-naphthalene adsorbent filled in a column (preconcentration factor 120) in the same pH range and determined similarly. The detection limit is 30 ppb (signal-to-noise ratio = 2) and the calibration curve is linear over 0.3–8.0 µg of cobalt in 5 ml of the final DMF solution. Eight replicate determinations of 1.0 µg of cobalt gave a mean peak height of 0.208 (at 611.5 nm) with a relative standard deviation of 1.2%. The sensitivity of the method is 1.04 (dA/dmm) ml µg⁻¹ found from the slope of the calibration curve. The interference of a large number of anions and cations on the determination of cobalt has been studied and the optimized conditions developed were utilized for its trace determination in various standard alloys and biological samples. © 1998 Elsevier Science B.V. All rights reserved.

Keywords: Cobalt determination; Derivative spectrophotometry; 5-Br-PADAP; TPB; Naphthalene; Standard alloys; Biological samples

1. Introduction

Sodium tetraphenylborate has been used as a counter ion in the extraction and adsorption of some metal complexes into molten naphthalene

* Corresponding author. e-mail: bkpuri@chemistry.iitd.ernet.in

[1–3] and microcrystalline naphthalene respectively [4–6]. A survey of the literature reveals that metal ions may be preconcentrated using various adsorbents [7]. Although some of these adsorbents are fairly effective for the preconcentration of metal ions, but their methods of preparation are lengthy and involve rigid control of conditions. The desorption of the metal is carried out by the slow process of elution, hence the procedure is time consuming. Solvent extraction is another technique which may be used for the preconcentration of metal ions, but it can not be applied directly to metal ions which form stable complexes with the chelating agents at elevated temperature. This difficulty can be overcome by using molten naphthalene as the extractant for thermally stable metal chelates [8]. Solid–liquid separation after adsorption of metal chelates on microcrystalline naphthalene is more rapid and convenient and can be applied to many types of metal complexes [4–6]. The preconcentration of metal ions is also possible by passing their aqueous solutions over naphthalene-NH₄-TPB adsorbent taken in a column. The microcrystalline naphthalene method is rapid but the column method gives a better preconcentration factor (four times in the present case).

In the present communication, we have developed a simple, rapid, sensitive and highly selective first-derivative spectrophotometric method for the trace determination of cobalt in various complex materials using 2-(5-bromo-2-pyridylazo)-5-diethylaminophenol (5-Br-PADAP) as the complexing agent, tetraphenylborate as the counter ion and naphthalene as the absorbent. In general, spectrophotometry lacks sensitivity and selectivity. This preconcentration technique is very simple, economical and practical. It not only concentrates the metal ions from large volume (~150 ml in case of microcrystalline method and 600 ml in the column method) to 5 ml of the final solution for the analysis but also improves the selectivity of the method because different metal ions are adsorbed at different pH. The combination of this preconcentration technique and derivative spectrophotometry further improve the selectivity and sensitivity of the method. Various reagents may be used for the spectrophotometric

determination of cobalt [9–11] but 5-Br-PADAP and its derivatives are highly sensitive and selective [12]. The other metal ions also react with the reagent under these conditions and may interfere in the determination of cobalt. However, the cobalt complex of this reagent once formed is highly stable in the acidic solution while the other metal complexes are completely decomposed under these conditions and will not interfere in its determination. Moreover, in the acidic conditions, the nitrogen atom of diethylamino group of 5-Br-PADAP is protonated readily. The resultant quaternary ammonium ion forms instantaneous water insoluble ion-pair with TPB and makes the column method free from the control of flow rate. Various parameters have been evaluated and the optimized conditions utilized for the trace determination of cobalt in certified alloys, ores and biological samples.

2. Experimental

2.1. Apparatus

An Unicam 8700 series UV-Vis spectrophotometer with 1.0 cm quartz cell were used. A Beckman pH meter was employed for pH measurements. The glass column used for the preconcentration was 50 mm long and had an i.d. of 6 mm. All atomic absorption measurements were made with an atomic absorption spectrometer (Shimadzu AA670). All glasswares were washed with a mixture of concentrated sulphuric and nitric acids (1 + 1) before use.

2.2. Reagents

All the reagents were of analytical reagent grade. Cobalt (II) chloride was dissolved in distilled water and standardized complexometrically [13]. A 2 ppm solution of cobalt was prepared by appropriate dilution of the standard solution. A 0.05% solution of 5-Br-PADAP in methanol was prepared. Buffer solutions of pH ~4.5 was prepared by mixing appropriate volume of a 0.5 M acetic acid–0.5 M sodium acetate. A 1% solution of sodium tetraphenylborate (TPB)

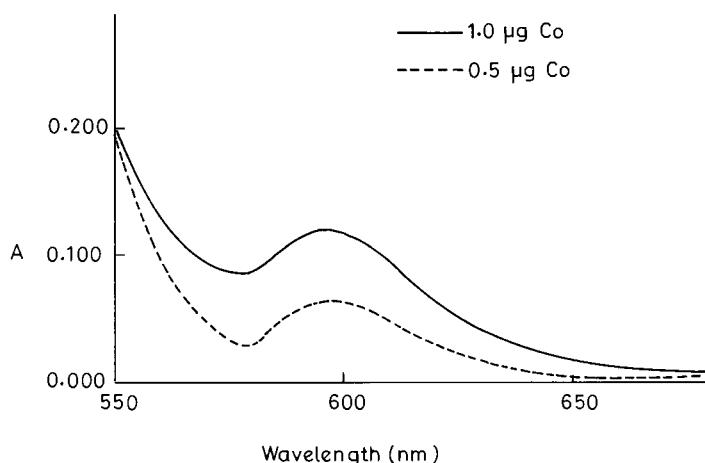


Fig. 1. Zero order spectrum of the naphthalene-Co-(5-Br-PADAP)-TPB complex. Co: 1 μg ; buffer: 2.0 ml; (pH: 4.5); 5-Br-PADAP: 2.0 ml(0.05%); Flow rate: 1 ml min^{-1} ; solvent: 5 ml DMF; reference: reagent blank.

and 20% solution of naphthalene were prepared in water and acetone, respectively. The naphthalene-ammoniumtetrphenylborate adsorbent was prepared as described in our previous paper [7].

2.3. Pre-treatment of standard alloys and biological samples

The solution of standard alloy was prepared by dissolving 0.5 g of the alloy in 20 ml of hydrochloric acid (1 + 1) by heating on a water bath and then 2 ml of 30% hydrogen peroxide was added to it. The excess of peroxide was decomposed by heating the solution on a water bath. The solution was cooled, filtered if needed and the filtrate was diluted to 100 ml with double distilled water in a calibrated flask.

A 0.2 g of biological sample was taken in a beaker and dissolved in concentrated nitric acid (~5 ml) by heating. The solution was cooled, diluted and filtered. The filtrate was made to 100 ml with water in a calibrated flask.

2.4. General procedure

An aliquot of solution containing 0.3–8.0 μg of cobalt was taken in a 150 ml conical flask and the total volume was adjusted to ~25 ml. A 2 ml of buffer solution (pH ~4.5) and 2.0 ml of 0.05% 5-Br-PADAP were added and it was allowed to

stand for 3–5 min. Then its acidity was re-adjusted to ~2.0 N with the addition of 6.5 ml of Concentrated hydrochloric acid and 2 ml of 1% solution of TPB was added to it with shaking. Then a 2 ml of 20% naphthalene in acetone was added to it and the solution shaken continuously for 2–3 min. The solid mass was separated by filtration on a Whatman filter paper (No. 1041), dried in folds of a filter paper, and dissolved in 5 ml of DMF. While in the case of column method, the Co-5-Br-PADAP complex in acid medium was passed through the column containing ammonium tetrphenylborate-naphthalene adsorbent at a flow rate of 2–3 ml min^{-1} . Finally, the column was aspirated strongly for 2–3 min and the solid mass was dissolved out with 5 ml of DMF. In both the cases, the first-derivative spectrum with $\Delta\lambda = 1$ for the final DMF solution was recorded against the reagent blank prepared in the similar way. The peak height at 611.5 nm was measured from the base line at various concentrations to construct a calibration curve.

3. Results and discussion

3.1. Spectrophotometric measurements

The zero order and first order derivative spectra of the complex are shown in Figs. 1 and 2,

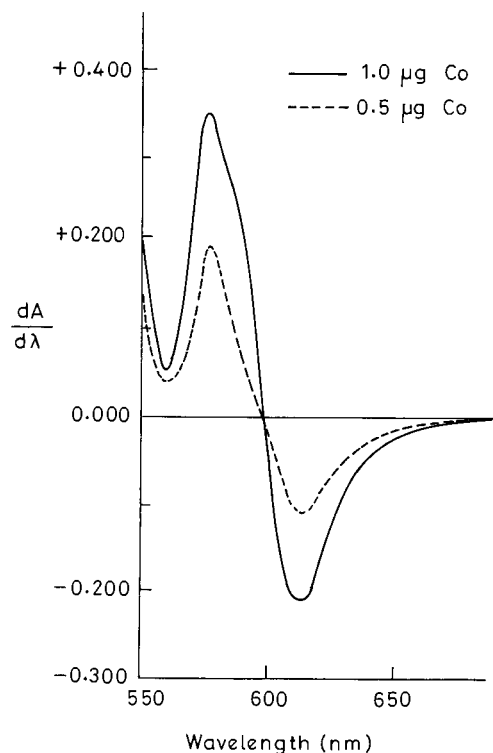


Fig. 2. First-derivative spectrum of the naphthalene-Co-(5-Br-PADAP)-TPB complex. For conditions, see Fig. 1.

respectively. As can be seen, the higher wavelength peaks of the derivative spectra are more significant. Derivative leads to sharper zero-order bands and gives higher signals in the resulting spectra. The characteristics of derivative spectra, such as peak height and noise level depend on the choice of various parameters [14]. The optimum

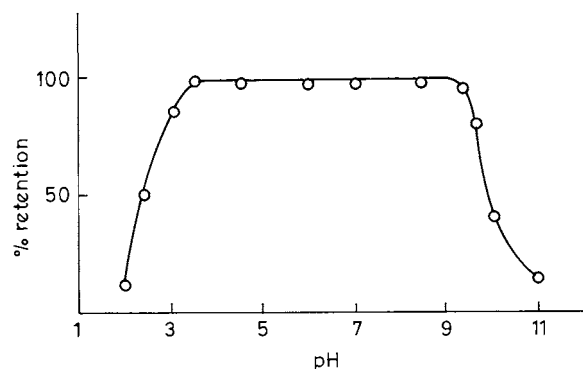


Fig. 3. Effect of pH. For conditions, see Fig. 1.

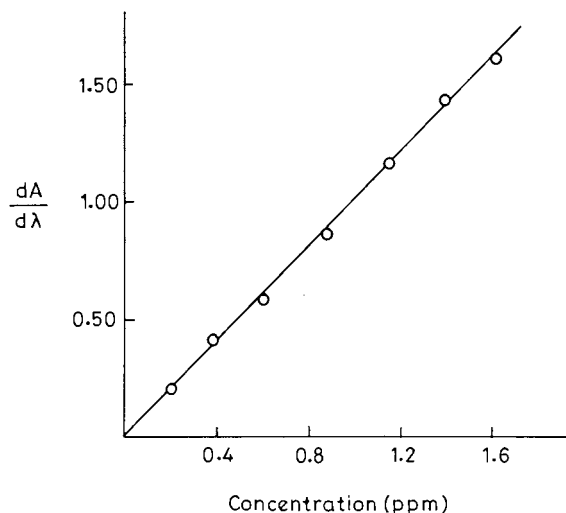


Fig. 4. Calibration curve for Co by first-derivative spectrophotometry. For conditions, see Fig. 1.

parameters were chosen from the preliminary experiments. The best results were obtained from first-derivative with wavelength interval ($\Delta\lambda$) 1 nm and with the scan speed of 120 nm min^{-1} . In the present work, the peak height at 611.5 nm was measured from the base line in all instances against the reagent blank because the reagent does not absorb at this wavelength at all. Although at 575 nm the intensity is high but the peaks are not well defined and at the same time blank is high too.

3.2. Reaction conditions

These were established with the use of $1 \mu\text{g}$ of cobalt. The adsorption of cobalt was found to be maximum in the pH range 3.5–9.5 (Fig. 3). In the subsequent studies, the pH was maintained at approximately 4.5 to avoid interferences of other metals. Addition of 0.5–8.0 ml of the buffer (pH 4.5) did not affect the retention of cobalt and the use of 2.0 ml was recommended. Various amounts of 0.05% alcoholic solution of 5-Br-PADAP were tried. Cobalt was quantitatively adsorbed on the absorbent over the range 0.1–5.0 ml of the reagent. Therefore, 2 ml of the reagent is recommended in the present study (Co:reagent mole ratio is 1:170). The acidity was varied from 0.1 to

Table 1
Analysis of cobalt in standard alloys

Sample	Certified composition (%)	Cobalt found* (%)
JSS 651-7 stainless steel	Co, 0.22; C, 0.047; Si, 0.072; P, 0.028; Cr, 18.60; S, 0.0063; Mo, 0.84; Al, 0.002; N, 0.0312; Mn, 1.72; Cu, 0.082; Ni, 9.20	0.217 ± 0.005 ^a
JSS 653-7 stainless steel	Co, 0.35; C, 0.068; Si, 0.63; Cr, 22.53; Ni, 13.91; N, 0.0276; Mn, 1.72; Cu, 0.030	0.34 ± 0.01 ^b
NKK No. 916 aluminium alloy	Co, 0.03; Si, 0.41; Fe, 0.54; Mg, 0.10; Cr, 0.05; Zn, 0.30; Ti, 0.10; Sb, 0.01; B, 0.04; Zr, 0.05; Bi, 0.03; Ni, 0.06; Mn, 0.11; Cu, 0.27; V, 0.02; Sn, 0.05; Pb, 0.04	0.029 ± 0.001 ^a
NKK No. 920 aluminium alloy	Co, 0.1; Cr, 0.27; Si, 0.78; Ti, 0.15; Sn, 0.20; Pb, 0.10; Fe, 0.72; Bi, 0.06; Ga, 0.05; Zn, 0.80; Sb, 0.10; Ca, 0.03; Mg, 0.46; Ni, 0.29; Mn, 0.20; Cu, 0.71; V, 0.15	0.102 ± 0.003 ^b

* Average of five determinations, ± S.D. ($n = 4$), 0.5 g of thiourea was added as masking reagent.

^a Column method was applied.

^b Microcrystalline naphthalene method was applied.

5.0 M with concentrated HCl. The peak height was constant and maximum in the range 0.1–3.0 M. Therefore, the acidity was maintained ~2 M with the addition of 6.5 ml of concentrated HCl.

In the case of microcrystalline naphthalene method, the concentration of TPB solution was varied. The retention of cobalt was maximum between 0.2–4.0 ml of 1% TPB, 1 ml was recommended. Various amounts of naphthalene (20% solution of naphthalene in acetone) were added to the sample solution keeping other variables constant. It was observed that the signal height remained constant with the addition of 1.0–5.0 ml of 20% naphthalene solution and 2.0 ml of 20% naphthalene solution was recommended in the present work. The effect of shaking time on the adsorption indicated that the signal height remained constant over a range of 0.5–7.0 min. Therefore, 1.0 min of shaking time was maintained in the present work. While in the case of column method, the flow rate was varied. It was found that a flow rate of 0.5–10.0 ml min⁻¹ did not affect the retention of the complex. A flow rate of 2–3 ml min⁻¹ was recommended in the present study. Various solvents were tried to dissolve the solid mass containing the metal complex. DMF was found to be best and it was used in the present work due to the high absorbance and stability of the metal complex (5 days). The

volume of the aqueous phase was varied in the range of 10–700 ml under the optimum conditions, keeping other variables constant. It was observed that the signal height was almost constant up to 150 ml (preconcentration factor of 30) in microcrystalline method and 600 ml (preconcentration 120) in the case of column method. The column material can be dissolved out with 2–3 ml of DMF. Hence a preconcentration factor of ~200 may be achieved.

3.3. Retention capacity of the adsorbent

The retention capacity of the adsorbent was determined by a batch method. The experiment was performed by taking 500 µg of cobalt, 2 ml of buffer solution (pH = 4.5), the suitable amount of reagent 5-Br-PADAP solution and 40 ml of water in a beaker. This solution was transferred into a separating funnel and then a suitable amount of the naphthalene-NH₄-TPB adsorbent was added. The separatory funnel was shaken vigorously on a mechanical shaker for 5 min. The solid mass was separated by filtration and cobalt was determined from the filtrate by AAS. The solid mass on the filter-paper was dried in an oven, kept in a desiccator and then weighed to determine the mass of the adsorbent. The maximum amount of cobalt retained was 1.5 mg g⁻¹ of adsorbent.

Table 2
Analysis of cobalt in biological samples

Sample	Certified composition ($\mu\text{g g}^{-1}$)	Found**a ($\mu\text{g g}^{-1}$)
NIES, No. 1 pepperbush	Co, 23.3 ± 3 ; K, $1.5 + 0.06$; Mn, $0.203 + 0.10$; Mg, 0.408 ± 0.020 ; Ca, $1.38 \pm 0.07\%$; Cd, 6.7 ± 0.5 ; Ni, 8.7 ± 0.6 , Fe, 205 ± 17 ; Pb, 5.5 ± 0.8 ; Ba, 165 ± 10 ; Na, 106 ± 13 ; Rb, 75 ± 4 ; Sr, 36 ± 4 ; As, 2.3 ± 0.3 ; P(1100); Cr(1.3); Cs, (1.2); Tl, (0.13); Hg, (0.056); Cu, 12 ± 1 ; Zn, 340 ± 20	22 ± 1^b
NIES No. 3, chlorella	Co, 0.87 ± 0.05 ; K, 124 ± 0.06 ; Ca, 0.49 ± 0.03 ; Fe, 0.185 ± 0.010 ; Mg, 0.33 ± 0.02 ; P, (1.7%); Mn, 69 ± 5 ; Zn, 20.5 ± 1.0 ; Sr, 40 ± 3 ; Cu, 3.5 ± 0.3 ; Cd(0.026); Pb, (0.60); Sc, (0.013)	0.84 ± 0.04^c
NIES, N. 5 human hair	Co, 0.10; Pb, 6.0; Cd, 0.20; Sb, 0.07; Zn, 169; Al, 240; Fe, 225; Mg, 208; Hg, 4.4; K, 34; Rb, 0.19; Sc, 0.05; Se, 1.4; Na, 26; Sr, 2.3; Ti, 22; Ca, 728; Cr, 1.4; Ba, 2.2; Ni, 1.8; Mn, 5.2; Cu, 16.3	0.104 ± 0.05^c
NIEs, No. 7 tea leaves	Co, 0.12; Pb, 0.80; Cd, 0.030; Sb, 0.014; Zn, 33; Cr, 0.15; Al, 775; Mg, 1530; Ba, 5.7; K, 18600; Sc, 0.011; Na, 15.5; Sr, 3.7; Ca, 3200; Cs, 0.22; Ni, 6.5; Mn, 7.00; Cu, 7.0	0.117 ± 0.006^c

* Average of five determinations, \pm S.D. ($n = 4$), 0.5 g thiourea was added as masking reagent.

^a Column method was applied.

^b Microcrystalline naphthalene method was applied. NIES: National Institute of Environmental studies reference materials. NIES: 1 and 3 (values in parentheses were approximate and not certified).

^c Standard addition method was applied.

3.4. Calibration, sensitivity and precision

On the basis of the optimum conditions developed above a calibration graph was constructed according to the general procedure. It was linear over the concentration range 0.3–8.0 μg of cobalt in 5 ml of the final DMF solution (Fig. 4). Eight replicate determinations of 1.0 μg of cobalt in 5 ml of the DMF solution gave a mean intensity in the first-derivative spectrum, measured from the peak height at 611.5 nm, of 0.208 with a relative standard deviation of 1.2%. The sensitivity was 1.04 (dA/dmm) $\text{ml } \mu\text{g}^{-1}$ from the slope of the calibration curve and the detection limit was 30 ppb (signal-to-noise ratio = 2).

3.5. Effect of diverse ions

Various salts of anions and cations were added individually to a solution containing 1.0 μg of cobalt and the general procedure applied. The tolerance limit was set as the ion concentration required to cause a $\pm 3\%$ error in the determination. The following amounts shown in the parentheses did not interfere: Sodium acetate, sodium chloride, potassium nitrate (1 g); ammonium chloride, ammonium bromide, ammonium sulphate (500 mg); thiourea (600 mg); potassium iodide

(400 mg); potassium carbonate (100 mg); potassium sodium tartrate (10 mg); potassium thiocyanate, trisodium citrate (5 mg); disodium EDTA (5 μg); Ca(II), Mg(II), Al(III) (5 mg); Pb(II), Zn(II), Fe(III), Ni(II) (300 μg); Rh(III), Cr(III), Cd(II), Mn(II) (2.0 mg); Zr(IV), Bi(III), Ga(III), (250 μg); Ir(III), W(VI), Ag(II), Pt(IV) (600 μg); Cu(II) (400 μg after masking with 500 mg of thiourea). Palladium interfered seriously. However, it can be eliminated by pre-extraction using dimethylglyoxime [13].

3.6. Analysis of cobalt in standard alloys and biological samples

The accuracy and applicability of the proposed method was evaluated by the analysis of cobalt in Nippon Keikinokogyo (NKK) CRM 916 and NKK No.920 aluminium alloy and Japanese standards of iron and steel (JSS) CRM 651-7, 653-7 stainless steel, National Institute of Environmental Studies Reference Materials (NIES) No. 1 pepperbush; No. 5 human hair, No. 3 chlorella and No. 7 tea leaves. An aliquot (10–50 ml) of the pre-treated sample solution was taken and analyzed by the general procedure. The results are given in Tables 1 and 2 which are in good agreement with the certified values.

4. Conclusion

A solid ion-pair compound produced from 5-Br-PADAP and TPB⁻ on naphthalene provides a simple and economical method for the preconcentration of cobalt from a large volume of alloys and biological samples using 5-Br-PADAP as the complexing agent. This reagent is fairly sensitive and selective for cobalt. With the preconcentration step and the use of derivative spectrophotometry its sensitivity and selectivity have been further improved and thus the developed method can be used safely for the estimation of cobalt in a number of complex materials such as environmental samples. Since the adsorbent provides TPB⁻ as the counter anion, therefore it may be used for the preconcentration of various types of cationic metal complexes. As a whole the proposed method is highly sensitive, selective, simple and highly economical (it requires simple glassware, and a small volume of the organic solvent to dissolve the solid mass) for the estimation of cobalt.

References

- [1] M. Satake, T. Nagahiro, B.K. Puri, *Analyst* 109 (1984) 31.
- [2] T. Nagahiro, K. Uesugi, M. Satake, B.K. Puri, *Bull. Chem. Soc. Jpn.* 85 (1985) 1115.
- [3] L.F. Cheng, M. Satake, T. Kuwamoto, B.K. Puri, *Microchem. J.* 33 (1986) 46.
- [4] T. Nagahiro, M. Satake, J.L. Lin, B.K. Puri, *Analyst* 109 (1984) 163.
- [5] J.L. Lin, M. Satake, B.K. Puri, *Analyst* 110 (1985) 1351.
- [6] M.C. Mehra, T. Nagahiro, M. Satake, *Microchem. J.* 33 (1985) 198.
- [7] M.A. Taher, B.K. Puri, *Talanta* 43 (1996) 247.
- [8] M. Satake, G. Kano, S. Usami, B.K. Puri, *Indian J. Chem.* 27A (1988) 265.
- [9] R. Lundquist, G.E. Markle, D.F. Boltz, *Anal. Chem.* 27 (1955) 1731.
- [10] K.J. McNaught, *Analyst* 67 (1942) 97.
- [11] S. Shibata, M. Furukawa, Y. Ishiguro, S. Sasaka, *Anal. Chim. Acta* 55 (1971) 231.
- [12] J. Zbiral, L. Sommer, *Fresenius Z. Anal. Chem.* 306 (1981) 129.
- [13] A.I. Vogel, *A Text Book of Quantitative Inorganic Analysis*, 5th edn., Longmans, London.
- [14] J. Medinilla, F. Alers, F.G. Sanchez, *Talanta* 33 (1986) 329.

Sequential extraction of U, Th, Ce, La and some heavy metals in sediments from Ortigas river, Spain

R. Martin ^{a,*}, D.M. Sanchez ^a, A.M. Gutierrez ^b

^a *Unidad de Química Analítica, Programa de Química, C.I.E.M.A.T., Av. Complutense 22, E-28040 Madrid, Spain*

^b *Dpto. Química Analítica, Facultad C.C. Químicas, Universidad Complutense de Madrid, Av. Complutense s/n, E-28040 Madrid, Spain*

Received 25 June 1997; received in revised form 14 October 1997; accepted 20 October 1997

Abstract

The extractable contents of U, Th, Ce, La, Cu, Cr, Ni and Zn in two sediment samples collected from the Ortigas river have been analysed using the three step sequential extraction procedure (SEP) described by BCR, Community Bureau of Reference (now Standards Measurements and Testing Programme) of the European Union. In order to perform a mass balance, a fourth step has been included, i.e. digestion of the residue from the third extraction step. ICP-AES was used for the determination of Cu, Cr, Ni, Zn, Th, Ce and La. Because of the inadequate sensitivity of ICP-AES for the analysis of uranium, ICP-MS was used for the determination of this element. Standard addition method was required, because of the matrix effects. Finally, SEP was applied to the Ortigas river sediments, showing that most of the elements were found mainly associated with the residual sediment fraction, except for uranium, which was found as an exchangeable species in approximately 60% of its total content. Recoveries of 86–108% have been obtained. © 1998 Elsevier Science B.V. All rights reserved.

Keywords: Speciation; Sequential extraction; Sediment; ICP

1. Introduction

The study of metal distribution in different sediment phases, by applying sequential extraction schemes, may help to predict metal behaviour, giving information about the mobility of metals and the possible transfer from sediment to the aquatic media [1,2]. Thus, not only the total concentration but the concentration of the differ-

ent forms of metals must be determined in these materials in order to evaluate their bioavailability and related eco-toxicity [3].

Sequential extraction procedures (SEP) are operationally defined methods proposed for speciation in solid samples.

The European Communities Bureau of Reference (BCR) recently proposed a SEP for use throughout the E.U. [4]. It harmonizes different extraction schemes for sediment analysis [5–7] and allows the comparison between results obtained in different laboratories [8], because the

* Corresponding author. Tel.: +34 1 3466561; fax: +34 1 3466005.

operation conditions (i.e. extractant agents, time and form of shake, operation sequence, etc.) are concentered. This protocol is usually applied to the study of heavy metal distribution in sediments.

This paper describes the development of methods for the determination of Cu, Cr, Ni, Zn, U, Th, Ce and La in nitric acid, acetic acid, hydroxylammonium chloride and ammonium acetate extracts by ICP-AES and ICP-MS. Due to the presence of reagents and co-extracted species from the sediment, the matrix standard addition method was required to correct for interference effects observed.

The methods developed were applied to the determination and speciation study of analytes in two sediment samples taken from the Ortigas river, Spain. This river is located in a granitic zone near to two uranium mines (the El Lobo and Pedregal mines).

The uranium content of these sediments comes from two sources: (1) from uranium mines and (2) from some accessory minerals in the granitic host rocks of these U deposits (e.g. xenotime and/or uraninite). Thorium is held in inherited monazite. La and Ce are closely associated with Th in some accessory granitic minerals, mainly in monazite. Cu is associated with U in secondary uranyl minerals (e.g. torbernite). Zinc is present in granitic rocks as sulphides (e.g. sphalerite).

To validate the applied methodology, and assess the quality of the results, a sediment LS-1, supplied by the University of Barcelona has been analysed and the results obtained of total and extractable contents of some of the heavy metals have been compared with those obtained by Fiedler [9].

2. Experimental

2.1. Instrumentation

Sequential spectrometer induction coupled plasma Jobin Ivon JY38PLUS (France) with radiofrequency generator JY2300 with 2.3 KW of power and frequency of 40.68 MHz.

Mass spectrometer with plasma source Finnigan MAT SOLA (UK).

2.2. Reagents

All reagents used were of analytical grade, Merck (Germany), and their dilutions were made with double deionized water, of conductivity < 18 Ω cm, obtained by purification of deionized water in a MILLI-Q system (Millipore, Molsheim, France).

2.3. Standard solutions

Monoelemental solutions 1000 mg l⁻¹ of Ce, La, Th and U in HNO₃ 5% (ALFA, Johnson Matthey, Karlsruhe, Germany).

Zn, Cu, Cu and Cr standard solutions were obtained by digestion of 1.0000 g of each metal (Johnson Matthey, Germany) with nitric acid and made up to 100 ml.

Low concentration solutions were obtained by successive dilutions with MILLI-Q water.

2.4. Sampling points description

The studied area is located in the central-west of Spain Fig. 1. This area is composed of granitic materials with two uranium mines and three streams flowing parallel to these mines. The Ortigas river collects water from these three streams [10].

Two sediments, S-1 and S-2, were taken of the Ortigas river upstream and downstream respectively, at the confluence of the three streams. About 500 g of each sample were taken

Sediments were dried at 110°C during 24 h period, ground and homogenized in agate mortar, and sieved with an AISI-304 mesh to obtain a particle size < 63 μ m (Norm UNE 7050) which retains trace metals [11]. They were stored in PTFE containers until the analyses were performed.

2.5. Procedure

2.5.1. Sample digestion for total contents analysis [12]

Dried sediment (0.5 g) was transferred into teflon PFA microwave reactors. HF/HCl/HNO₃ (12 ml of (5/5/2)) acid mixture was added. The

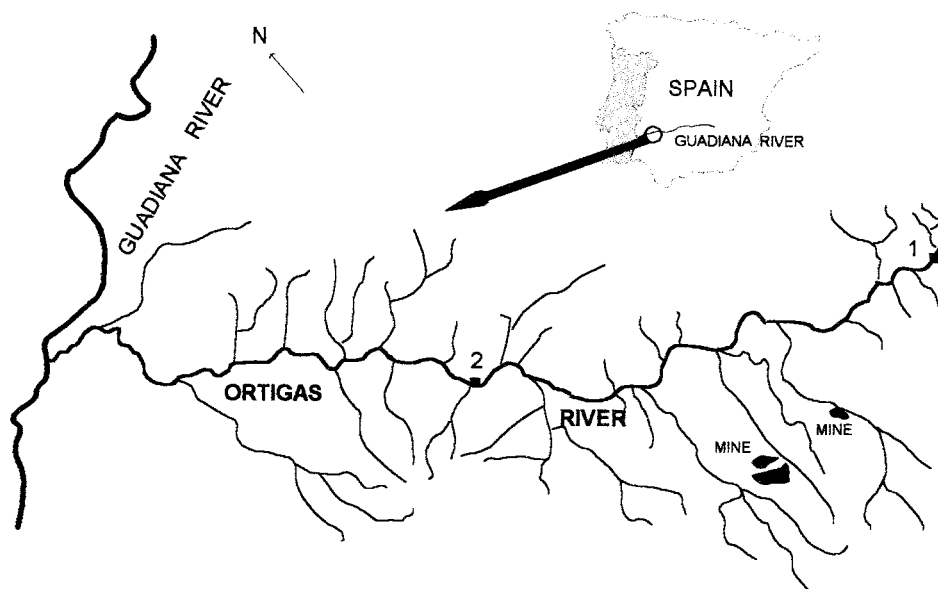


Fig. 1. Sampling point sites.

reactors were sealed and heated in the microwave oven. The program followed was:

1st step: 630 W Power, 80 psi Press during 20 min

2nd step: 630 W Power, 100 psi Press during 60 min

The digests, when cooled, were transferred to teflon capsules. Then 2 ml of HClO_4 was added, and heated to dryness to remove HF completely. Followed by the addition of 2 ml of HNO_3 , to dissolve dry residues, and heated until complete dissolution. They were finally made up to 25 ml with MILLI-Q water. The digests were analysed using the standard addition method.

Table 1
Reagents used in the sequential extraction procedure (SEP)

Reagent	Extracted specie
$0.11 \text{ mol l}^{-1} \text{ CH}_3\text{COOOH}$	Exchangeable and soluble in water and acids
$0.1 \text{ mol l}^{-1} \text{ NH}_2\text{OH} \cdot \text{HCl}$ (pH 2)	Reducible
$8.8 \text{ mol l}^{-1} \text{ H}_2\text{O}_2$ followed by $1 \text{ mol l}^{-1} \text{ CH}_3\text{COONH}_4$ (pH 2)	Oxidizable

2.5.2. Sequential extraction procedure (SEP)

The reagents used in the BCR sequential extraction procedure together with the nominal sediment phases dissolved at each step are given in Table 1. The experimental procedure is summarized below:

Step one: treatment of 0.5 g of sediment in a centrifuge tube with 20 ml 0.11 mol l^{-1} acetic acid solution, shaken for 16 h at room temperature, using an end-over-end shaker. The residue is separated by centrifugation and the supernatant retained for analysis.

Step two: treatment of residue obtained in step one with 20 ml of 0.1 mol l^{-1} hydroxylamine chloride solution (adjusted to pH 2 with nitric acid) and operated as described above.

Third step: treatment of the residue from step two with 5 ml of $8.8 \text{ mol l}^{-1} \text{ H}_2\text{O}_2$ (adjusted to pH 2 with nitric acid) keeping 1 h at room temperature and another hour at 85°C . It was evaporated to near dryness, the treatment was repeated with H_2O_2 heating until dryness. Ammonium acetate (25 ml of 1 mol l^{-1}) was added (adjusted to pH 2 with nitric acid) and the operations were repeated as described in previous steps.

Table 2
Direct and standard addition calibration slopes

Calibration slopes in each medium								
0.11 mol l ⁻¹ CH ₃ COOH		0.1 mol l ⁻¹ NH ₂ OH HCl		1 mol l ⁻¹ CH ₃ COONH ₄		0.5 mol l ⁻¹ HNO ₃		
Direct	Std.add.	Direct	Std.add.	Direct	Std.add.	Direct	Std.add.	
Zn	256.6 ± 2.5	299.3 ± 2.1	205.8 ± 4.5	279.3 ± 3.1	442.7 ± 3.1	517.5 ± 5.0	136.8 ± 1.8	212.1 ± 2.3
Ni	150.3 ± 1.8	172.1 ± 2.4	130.7 ± 2.0	170.0 ± 2.5	168.3 ± 1.2	207.1 ± 4.8	106.2 ± 0.3	151.2 ± 1.5
Cu	1076 ± 6	1342 ± 7	937.6 ± 8.1	1310 ± 5	758.5 ± 5.4	958.8 ± 7.9	1095 ± 8	1329 ± 9
Cr	983.5 ± 4.5	1106 ± 8	902.4 ± 9.4	1048 ± 4	535.8 ± 4.3	624.5 ± 5.3	1065 ± 8	980.9 ± 5.4
Th	776.6 ± 4.9	891 ± 5.1	706.0 ± 5.2	914.4 ± 5.1	500.2 ± 4.6	682.7 ± 6.2	932.6 ± 2.3	813.0 ± 1.7
La	807.2 ± 5.2	1164 ± 6	845.2 ± 7.8	1155 ± 5	600.8 ± 6.3	1020 ± 7	1132 ± 10	1750 ± 11
U	301.5 ± 3.7	385.9 ± 5.4	285.2 ± 3.0	358.4 ± 3.1	236.5 ± 4.2	347.6 ± 6.2	323.1 ± 2.5	242.0 ± 5.1
Ce	89.2 ± 1.2	121.0 ± 2.5	89.2 ± 2.1	121.1 ± 3.8	71.6 ± 2.0	95.2 ± 3.1	111.1 ± 0.5	124.7 ± 1.4

Uranium calibration graphs by ICP-MS is ($I = f(\text{conc.}(\mu\text{g l}^{-1}))$). Calibration graphs of the rest of the elements by ICP-AES are ($I = f(\text{conc.}(\text{mg l}^{-1}))$). The errors quoted are ± 1 s.

To obtain an indication of the concentration of these elements associated with the residual components of the sediment matrix a fourth step was introduced, which involves the total digestion of the residue from the third step, with 12 ml of (5/5/2) HF/HCl/HNO₃ acid mixture in a microwave oven, following the program described in the sample digestion for analysis of total contents.

All the extracts were made up to 25 ml with MILLI-Q water.

3. Results and discussion

3.1. Development of the analytical methodology

Analytical wavelengths for determination of Cu

Table 3
ICP-AES (or ICP-MS for uranium) detection limits in sequential extraction reagents ($\mu\text{g g}^{-1}$ sediment dry mass)

	0.11 mol l ⁻¹ CH ₃ COOH	0.1 mol l ⁻¹ NH ₂ OH HCl	1 mol l ⁻¹ CH ₃ COONH ₄	0.5 mol l ⁻¹ HNO ₃
Zn	0.42	0.81	1.1	0.40
Ni	0.41	0.62	1.1	0.28
Cu	0.46	0.52	0.50	0.34
Cr	0.40	0.44	0.90	0.36
Th	0.18	0.44	0.50	0.06
La	0.20	0.42	0.42	0.20
U	0.0074	0.0068	0.013	0.0042
Ce	0.36	0.90	1.2	0.84

Detection limits were calculated on the basis of 3 s (blank solution).

(327.396 nm), Cr (357.870 nm), Ni (232.003 nm), Zn (206.200 nm), Th (401.913 nm), Ce (456.236 nm) and La (408.672 nm) by ICP-AES, were chosen taking into account their sensitivity and the absence of interferences.

Because of the inadequate sensitivity of ICP-AES for uranium analysis, ICP-MS was chosen for determination of this element.

To determine the matrix effects of reagents used in the extraction, slopes of calibration graphs for each element obtained from standards in 0.5 mol l⁻¹ HNO₃, were compared with those obtained in different reagents (0.11 mol l⁻¹ acetic acid, 0.1 mol l⁻¹ hidroxilamonium chloride and 1 mol l⁻¹ ammonium acetate). In all cases, the correlation coefficients were $r \geq 0.9999$. Results are shown in Table 2. The analytical signals were affected by

Table 4
Results ($\mu\text{g g}^{-1}$) obtained in validation of the method using the sediment LS-1

Extraction phase		Zn	Ni	Cu	Cr
0.11 mol l ⁻¹ CH ₃ COOH	Obtained	235 ± 15	8 ± 1	7.5 ± 0.6	0.5 ± 0.1
	Fiedler	238 ± 4	7.5 ± 0.6	7.15 ± 0.1	0.49 ± 0.08
0.1 mol l ⁻¹ NH ₂ OH.HCl	Obtained	139 ± 8	4.7 ± 0.7	3.1 ± 0.5	0.6 ± 0.1
	Fiedler	145 ± 9	4.3 ± 0.3	2.3 ± 0.5	0.5 ± 0.1
1 mol l ⁻¹ CH ₃ COONH ₄	Obtained	236 ± 10	11.0 ± 0.8	129 ± 6	21.4 ± 0.7
	Fiedler	245 ± 22	11.0 ± 0.6	137 ± 6	23.4 ± 0.9
Residual	Obtained	261 ± 16	49 ± 3	121 ± 2	104 ± 6
Total contents	Obtained	831 ± 14	79 ± 9	241 ± 12	115 ± 7
	Fiedler	821 ± 6	72 ± 4	248 ± 10	110 ± 2

The procedure was carried out by quadruplicate and the results are expressed as $x \pm s$.

the presence of reagents. In the case of Zn and Ni an increase in the signal was observed, whereas for other elements a decrease in the signal occurred. The higher effects were caused by ammonium acetate.

To evaluate the matrix effects of the components associated with each particular sediment fraction, S-2 sediment was chosen. After application of SEP, standard addition calibrations were

made for all the extracts. The slopes obtained were compared with those from direct calibrates (Table 2). In all cases the differences were higher than 8%. Some authors [13] consider that there will be matrix effects when the differences between direct and standard addition slopes are higher than 6%. In this work, with a 't' statistic assay, for a 95% level confidence, significant differences were found between standard addition

Table 5
Results ($\mu\text{g g}^{-1}$) of analysis of total contents and the extracts obtained in SEP applied to sediments S-1 and S-2

	Total	F-1	F-2	F-3	F-4	Σ total	%Recovery
S-1							
Zn	59.7 ± 2.5	6.12 ± 1.70	3.72 ± 0.42	8.33 ± 2.70	46.2 ± 5.3	64.4 ± 6.2	107
Ni	17.0 ± 0.6	2.38 ± 0.44	<0.62	2.92 ± 0.36	12.4 ± 0.6	17.7 ± 2.5	104
Cu	14.5 ± 0.7	1.12 ± 0.18	0.74 ± 0.03	3.34 ± 0.15	8.80 ± 0.30	14.0 ± 0.4	97
Cr	40.3 ± 6.8	0.90 ± 0.11	0.92 ± 0.04	3.31 ± 0.23	35.9 ± 2.4	37.7 ± 2.4	93
Th	14.0 ± 0.6	0.49 ± 0.01	0.35 ± 0.04	0.79 ± 0.05	11.7 ± 0.8	13.3 ± 0.8	95
La	33.0 ± 0.4	0.76 ± 0.06	1.58 ± 0.24	2.70 ± 0.21	23.9 ± 2.2	28.9 ± 2.2	88
U	7.35 ± 0.35	1.36 ± 0.85	0.65 ± 0.46	2.63 ± 0.14	2.73 ± 0.70	7.37 ± 1.2	100
Ce	67.0 ± 2.8	1.51 ± 0.30	3.24 ± 0.40	7.43 ± 0.33	51.1 ± 3.9	63.3 ± 3.9	94
S-2							
Zn	114 ± 2	3.44 ± 0.43	7.97 ± 1.20	19.4 ± 2.0	80.5 ± 4.2	111 ± 4	98
Ni	43.0 ± 5.3	2.34 ± 0.42	2.68 ± 0.27	7.07 ± 1.50	33.4 ± 4.7	45.5 ± 5.0	106
Cu	27.5 ± 2.1	1.09 ± 0.17	5.93 ± 0.30	5.54 ± 0.25	12.3 ± 1.0	24.9 ± 1.1	90
Cr	108 ± 4	0.69 ± 0.12	3.12 ± 0.20	15.2 ± 0.7	81.0 ± 6.6	100 ± 7	93
Th	23.0 ± 1.4	0.19 ± 0.01	0.39 ± 0.13	6.41 ± 0.32	12.8 ± 0.3	19.8 ± 0.4	86
La	36.0 ± 0.6	0.38 ± 0.02	1.08 ± 0.62	7.31 ± 0.68	25.3 ± 0.7	34.1 ± 1.1	95
U	8.80 ± 0.78	1.04 ± 0.14	2.67 ± 0.35	1.90 ± 0.48	3.37 ± 0.47	8.98 ± 0.77	102
Ce	118 ± 6	1.09 ± 0.22	31.3 ± 1.2	15.5 ± 1.3	57.2 ± 2.6	104 ± 3	89

The procedure was carried out by quadruplicate and the results are expressed as $x \pm s$.

Total, total contents; F-1, 0.11 mol l⁻¹ CH₃COOH; F-2, 0.1 mol l⁻¹ NH₂OH HCl; F-3, 1 mol l⁻¹ NH₄COOCH₃; F-4, Residual, S, F-1+F-2+F-3+F-4. Also expressed is the recovery percentage with respect to total contents.

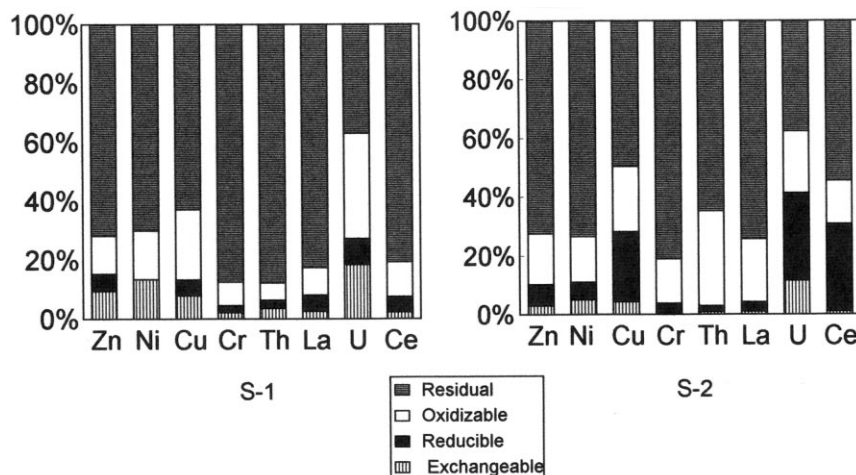


Fig. 2. Distribution of contents in S-1 and S-2 fractions sediments

slopes and direct calibration slopes. This confirms the matrix effects which will have some influence on the determination of the analytes. The standard addition method was necessary to carry out the analysis.

Detection limits for each analyte in each of the reagents, calculated as three times the standard deviation of results obtained in the analysis of 10 blank solutions, are shown in Table 3. Higher detection limits were obtained using ammonium acetate for all the analytes owing to the poorer precision of the ICP signals.

A study following the same previous process, was carried out for the determination of U in the extracts and in total digestion sediments solutions by ICP-MS. Detection limits were established and calibrated slopes were calculated for each medium (Tables 2 and 3).

By comparison of direct calibrated slopes and standard addition slopes, interfering effects were observed (Table 2) as such the standard addition method was necessary to determine this element.

Validation of the method was carried out using the sediment LS-1 from Flumendosa lake, Cerdèña, Italy, and prepared by J.R.C. Ispra, Italy. Sequential extraction procedure was carried out with this sediment. Cu, Cr, Ni and Zn, were analysed in the extracts. The results were compared with those obtained by Fiedler [9] (Table 4).

There were no significant differences found between values with 95% of confidence level found.

3.2. Distribution of contents in S-1 and S-2

The extractable contents of Zn, Ni, Cu, Cr, Th, Ce, La and U from SEP applied to S-1 and S-2 Ortigas river sediments are shown in Table 5.

All the elements suffer with some differences, along a distribution of the four phases, they are basically retained in the residual sediment fraction. The distribution obtained for each element along different extraction phases are shown in Fig. 2.

The distribution of Zn, Ni and Cr is similar in the two sediments. They are retained in the residual fraction approx. 70–80% of their total content.

With respect to Cu and Ce, 60% of Cu and 80% of Ce are associated with residual fraction in S-1. Otherwise, there is an increase in more labile forms of these elements, particularly reducible species in S-2, 50% in the residual fraction.

Th and La in S-2 are shown to be more extractable than in S-1 increasing the proportion of these elements associated with the oxidizable sediment fraction.

In the case of uranium, the obtained results clearly show that the proportion retained in residual fraction is significantly lower than in the case

of other elements. Approx. 60% of the total content of this element is exchangeable. In addition, the distribution of uranium between sediment fractions is slightly different in each sediment. In S-1, the percentage in extractable and oxidizable sediment fractions increase, while the proportion of U associated with the reducible sediment fraction in S-2 is higher than S-1.

Comparison of the sum of metal concentrations in the individual fractions after application of SEP (Table 5) with total metal concentration shows good agreement for all trace metals. The total recovery percentages obtained were 86–108%.

Acknowledgements

The authors are grateful to Dr R. Rubio of the University of Barcelona for supplying the sediment LS-1, Dr M.T. Crespo and Dr J.L. Gascon for supplying the sediment samples S-1 and S-2 and Dr L. Perez del Villar for information on geological materials.

References

- [1] U. Förstner, *Int. J. Environ. Chem.* 51 (1993) 5–23.
- [2] R. Morabito, *Fresenius'Z. Anal. Chem.* 351 (1995) 378–385.
- [3] Ph. Quevauviller, G. Rauret, H. Muntau, A.M. Ure, R. Rubio, J.F. Lopez-Sanchez, H.D. Fiedler, *Fresenius'Z. J. Anal. Chem.* 349 (1994) 808–814.
- [4] A.M. Ure, Ph. Quevauviller, H. Muntau, B. Griepink, EUR Report No. 14763, CEC, Brussels, 1992.
- [5] A. Tessier, P.G.C. Campbell, M. Bisson, *Anal. Chem.* 51 (1979) 844.
- [6] A.K. Das, R. Chakraborty, M.L. Cervera, M. de la Guardia, *Talanta* 42 (1995) 1007–1030.
- [7] G.E. Batley (Ed.), *Trace Element Speciation. Analytical Methods and Problems*, CRC Press, Boca Raton, FL, 1989, pp. 285–286.
- [8] R. Rubio, J.F. Lopez-Sanchez, G. Rauret, *Verh.- Int. Ver. Limnol.* 25 (1993) 1147–1149.
- [9] H.D.L. Fiedler, Ph.D. Thesis, University of Barcelona, Spain, March 1995.
- [10] M. Jurado Vargas, Ph.D. Thesis, University of Extremadura, Spain, May 1994.
- [11] R. Rubio, J.F. Lopez-Sanchez, G. Rauret, *An. Quim.* 87 (1991) 599–605.
- [12] R. Martin. Master Degree, University Complutense of Madrid, Spain, June 1996.
- [13] A. Sahuquillo, J.F. Lopez-Sanchez, R. Rubio, G. Rauret, V. Hatje, *Fresenius'Z. Anal. Chem.* 351 (1995) 197–203.

Supercritical fluid extraction of phenol compounds from olive leaves

F. Le Floch, M.T. Tena, A. Ríos, M. Valcárcel *

Department of Analytical Chemistry, Faculty of Sciences. University of Córdoba, E-14004 Córdoba, Spain

Received 14 July 1997; received in revised form 21 October 1997

Abstract

A clean, highly selective supercritical fluid extraction (SFE) method for the isolation of phenols from olive leaf samples was examined. Total phenol extracts were determined using the Folin-Ciocalteu reagent. Dried, ground, sieved olive leaf samples (30 mg) are subjected to SFE, using carbon dioxide modified with 10% methanol at 334 bar, 100°C (CO₂ density 0.70 g ml⁻¹) at a liquid flow-rate of 2 ml min⁻¹ for 140 min. Diatomaceous earth is used to reduce the void volume of the extraction vessel. The influence of extraction variables such as modifier content, pressure, temperature, flow-rate, extraction time, and collection/elution variables, were studied. Supercritical fluid extracts were screened for acid compounds such as carboxylic acids and phenols using Electrospray-MS (in the negative ionization mode). SFE was found to produce higher phenol recoveries than sonication in liquid solvents such as *n*-hexane, diethyl ether and ethyl acetate. However, the extraction yield obtained was only 45%, using liquid methanol. © 1998 Elsevier Science B.V. All rights reserved.

Keywords: Supercritical fluid extraction; Phenol; Olive leaves

1. Introduction

The determination of polyphenols in plants is of great interest because of the natural antioxidant activity of these compounds. Phenol compounds are synthesized by plants as a defence mechanism against microorganisms and strong UV radiation [1]. Antioxidants are added to fat-containing foods to prevent the formation of off-flavour and toxic compounds resulting from lipid oxidation. Plant extracts are natural alternatives

to synthetic antioxidants as they possess similar or even higher antioxidant activity.

Several studies on the chemical composition of the olive leaf and oil have been carried out [2–7]. Very little information is available on the chemical composition of olive leaves, the primary site of plant metabolism for primary and secondary plant products. Luteolin, luteolin-7-glucoside, rutin, quercitrin and chlorogenic acid have been identified in methanol extracts from the olive leaf [2]. Extraction of highly-hydroxylated flavonoids using supercritical methanol-modified carbon dioxide is difficult [8]. In fact, compounds in SFE extracts that react with the Folin-Ciocalteu

* Corresponding author. Tel.: +34 57 218614; fax: +34 57 218606; e-mail: qalricaa@uco.es

reagent are more likely to be phenolic acids such as salicylic, hydroxybenzoic, coumaric, caffeic, protocatechuic or ferulic acid. These compounds have been found in aqueous hydrochloric acid and ethyl acetate extracts from olive leaves [3]. Montedoro et al. [4], using HPLC-UV, identified hydroxytyrosol, tyrosol, vanillic acid, caffeic acid, syringic acid, *p*-coumaric acid and ferulic acid in methanol extracts from virgin olive oil; the major peaks in the chromatogram, correlated with total phenol, autoxidation stability, could not be assigned. In a subsequent study [5], these compounds were characterized as oleuropein aglycon and three hydrolysable phenols containing hydroxytyrosol or tyrosol. Angerosa et al. [6], using GC-MS, also detected the presence of linked phenols containing tyrosol and hydroxytyrosol in virgin olive oil.

Polyphenols in leaves are different from those in flowers, stems, roots and fruits. Indeed, the types of phenols present on the surface (e.g. in leaf waxes), are usually different from those occurring within the plant. Surface flavonoids are usually highly methylated and lack sugar substitution [9], so they should be more readily extracted using SC-CO₂.

SFE [10–14] offers special advantages over conventional liquid-solvent extraction such as increased selectivity, expeditiousness, automaticity and environmental safety, in addition to dramatically decreased use of organic solvents. Several SFE-based methods for determining phenol pollutants in environmental samples including waters, dust and waste solids have been proposed [15–17]. Also, SFE with carbon dioxide is the most favored method for the isolation of phenol compounds with antioxidant properties from spices and agricultural by-products [18–21].

The Folin reagent is widely used in this context and is recommended for the determination of total phenols; it reacts with compounds other than the target phenols, as such interfering reductants must be removed prior to the assay [22,23]. Solution-ionizable polar compounds not suitable for gas chromatography analysis can be detected by mass spectrometry following electrospray ionization [24,25]. Electrospray-MS in the ion mode

has been used to detect phenolic diterpenes in rosemary SFE extracts [18].

The aim of this work was to develop an SFE-based method for the determination of total phenols in plant samples. Olive leaves were chosen as the plant model because they are by-products of olive farming, one of the most important agricultural activities in the Mediterranean region, and because phenols with a high pharmacological activity are particularly commonplace in plants of warm, dry regions.

2. Experimental

2.1. Apparatus

All SFE experiments were performed on a 7680T Hewlett Packard supercritical fluid extractor equipped with a Hewlett Packard 1050 isocratic modifier pump and furnished with a 7 ml extraction vessel, an automated variable restrictor and a solid-phase trap packed with octadecylsilica (ODS) or PorapakQ material. A Hewlett Packard 8453 diode array spectrophotometer was used to determine the total phenol content in olive leaf extracts. A Fisons VG Platform electrospray and a Fisons VG Autospec mass spectrometer were used to screen acid compounds in the SFE extract.

2.2. Chemicals

Caffeic acid and diatomaceous earth (acid-washed, approximately 95% SiO₂) were purchased from Sigma and used as received. All solvents and reagents were HPLC-grade and analytical reagent grade, respectively. SFC-grade carbon dioxide from Air Liquide (Paris, France) was used as extraction fluid.

Calibration solutions containing 1, 2, 4, 6, 8 and 10 µg ml⁻¹ caffeic acid were prepared from a 1 g l⁻¹ stock solution in ethanol by appropriate dilution in *n*-hexane. Appropriate volumes of ethanol were also added in order to equalize its content in all calibration solutions. Since no significant differences were found between the signals produced by hexane, diethyl ether or ethyl

acetate solution containing the same amount of caffeic acid, calibration solutions prepared in *n*-hexane were used to determine total phenol in water-immiscible solvents. For methanol extracts, calibration solutions containing 10, 25, 50, 75 and 100 $\mu\text{g ml}^{-1}$ caffeic acid were prepared from 1 g l^{-1} methanol stock solution by appropriate dilution in methanol.

An aqueous solution of 2% (v/v) Folin-Ciocalteu phenol reagent (Merck) and a 0.2 M aqueous solution of sodium bicarbonate (Merck) adjusted to pH 12.4 with sodium hydroxide (Merck) was also used.

Olive (*Olea europaea* L.) leaves were collected from trees in the surrounding countryside, dried at 100°C for 2 h, ground and sieved $\leq 500 \mu\text{m}$.

2.3. Supercritical fluid extraction

CO_2 was aspirated from a cylinder furnished with a dip tube, pressurized to 155–334 bar (corresponds to 0.35–0.70 g ml^{-1} density at 100°C) and mixed on-line with 0–20% (v/v) methanol. Ethanol was also assayed as CO_2 modifier. The flow-rate of liquid carbon dioxide was varied from 1 to 4 ml min^{-1} . The sample amount used was 30–200 mg. Extractions were conducted in 7 ml thimbles that were filled with diatomaceous earth in most cases in order to reduce the void volume. Each extraction was carried out in duplicate and the extraction recoveries reported are the averages of the two. Samples were subjected to dynamic extraction for 5–140 min, depending on the particular experiment. A static extraction period of 1 min was used. Extraction curves at different temperatures were obtained by performing consecutive extractions of the same sample and plotting the cumulative concentration obtained. Extracted analytes were collected on an ODS or PorapackQ trap. After extraction, the analytes were eluted from the trap at 20°C with 1.5 ml of HPLC-grade methanol or *n*-hexane. When the rinse solvent was methanol, an additional rinse with *n*-hexane was necessary in order to remove methanol non-soluble coextractives from the trap. The trap temperature was raised to 70°C in order to avoid undesirable modifier condensation on the trap during extraction/collection.

2.4. Sonication with a liquid-solvent

Ground, sieved olive leaf sample (100 mg) was extracted four times with *n*-hexane (4 ml + 3 \times 2 ml). The extraction was performed using ultrasonication at room temperature and the duration of the first and subsequent steps was 30 and 15 min, respectively. The same procedure was followed for ethyl acetate, diethyl ether and methanol extractions; the amount of sample and volume of solvent used in the first step was 30 mg and 6 ml, respectively. After each step, the mixture was centrifuged and the supernatant separated. The amount of total phenol was determined using the water-immiscible solvent calibration procedure for *n*-hexane, diethyl ether and ethyl acetate, and the water-miscible solvent calibration procedure for methanol.

2.5. Photometric determination

Total phenol in the SFE and liquid-solvent extracts was quantified using the Folin-Ciocalteu reagent and either of two procedures depending on the particular rinse/extraction solvents used. Amounts of phenols are given in micrograms of caffeic acid.

Water-immiscible solvents (*n*-hexane, diethyl ether and ethyl acetate): Two aliquots of Folin-Ciocalteu and buffer solutions (2.5 ml) were mixed in a test-tube and 1 ml of *n*-hexane solution containing the phenols was added. The mixture was stirred for 1 min and allowed to stand for 30 min. The absorbance of the aqueous phase was measured at 750 nm after centrifugation.

Water miscible solvent (methanol): Two aliquots of Folin-Ciocalteu and buffer solutions (2.5 ml) were mixed in a test-tube and a volume of 0.5 ml of methanol solution containing the phenols was added. The mixture was stirred for 1 min and allowed to stand for 30 min before its absorbance at 655 nm was measured.

2.6. Mass spectrometric screening of the SFE extract

The SFE extract was screened by electrospray MS (in the negative ionization mode) in order to

detect acid compounds such as carboxylic acids and phenols from their M-1 peaks. A volume of 10 μl of SFE extract was injected into a 50:50 methanol/water carrier solution at 20 $\mu\text{l min}^{-1}$. The source temperature and cone voltage were 60°C and 30 V, respectively. The voltage of the capillary and high-voltage lenses were 3 kV and 0.5 kV, respectively. The M-1 peaks obtained by Electrospray MS of an SFE extract are listed in Table 1. Those compounds previously found in olive leaf or virgin olive oil [2–6] that could have provided an M-1 signal at each m/z ratio are also tabulated. Obviously, tentative assignments are

Table 1
MS screening (M-1 peaks) of SFE extract from olive leaves

m/z (relative abundance (%))	Tentative compound(s)
101 (10), 107 (12), 117 (29), 119 (13), 123 (9), 127 (100), 129 (9), 137 (9)	Tyrosol, hydroxybenzoic acid ^a
143 (16), 147 (10), 151 (24), 153 (9)	Cinnamic acid ^a
157 (14), 159 (17), 161 (9), 163 (9), 173 (8), 177 (10), 179 (33), 181 (43), 185 (9), 191 (13), 195 (9), 197 (15), 213 (33), 223 (9), 241 (12), 265 (24), 287 (19), 297 (32)	Hydroxytyrosol, protocatechuic acid ^a
	Caffeic acid ^a
	Homovanillic acid ^a
	Syringic acid ^a
	Elenolic acid ^a
	4'-Methoxytectochoylin ^c
309 (17), 311 (91), 312 (14), 313 (17), 325 (70), 326 (9), 339 (34), 353 (13), 403 (42), 523 (9), 539 (25)	Caftaric acid ^b
	Cirsimaritin ^c
	Fertaric acid ^b
	Chlorogenic acid ^a
	Ligstroside ^a
	Oleuropeine ^a

^a Present in olive.

^b Present in wine.

^c Flavones present in rosemary.

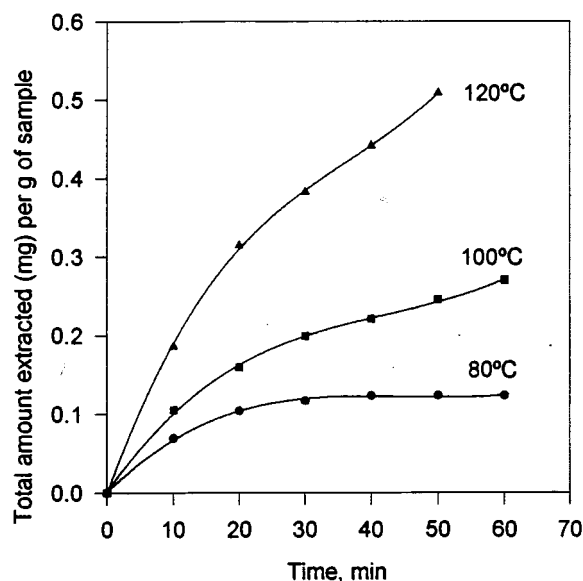


Fig. 1. Effect of the extraction temperature on the SFE efficiency of phenols. Amount of sample, 100 mg. SFE conditions: CO₂ modified with 10% methanol; CO₂ pressure, 334 bar; flow-rate, 2 ml min⁻¹; ODS trap; nozzle and trap temperature during collection 45 and 70°C, respectively; rinse solvent, *n*-hexane; rinse volume, 1.5 ml; nozzle and trap temperature during rinse, 20°C. Amounts of phenols per gram of sample expressed as milligrams of caffeic acid.

only an approximation and should be further investigated by HPLC fractionation followed by electron impact mass spectrometry analysis.

3. Results and discussion

Preliminary experiments demonstrated that the addition of a modifier to CO₂ was mandatory in order to extract phenols, the extraction yield was strongly influenced by pressure and, especially, the extraction temperature. The restrictor was plugged and overloaded by samples larger than 100 mg (especially at high temperatures) which caused overpressure problems.

3.1. Influence of the extraction temperature on the SFE efficiency

The effect of the extraction temperature on the amount of phenols extracted was studied at con-

stant pressure (334 bar). Fig. 1 shows the extraction curves obtained at three different temperatures (80, 100 and 120°C), corresponding to CO₂ densities of 0.78, 0.70 and 0.63 g ml⁻¹, respectively. Although the solvating power of methanol-modified carbon dioxide decreased with decreasing density, raising the temperature increased both the extraction rate and extraction efficiency through increased diffusion and desorption. The amount of phenols extracted at 80°C increased with increasing extraction time up to 40 min beyond which it remained constant. However, greater amounts were extracted at 100 or 120°C and no plateau was observed over the period studied (1 h). The datum for 60 min at 120°C could not be obtained owing to the short lifetime of the thimble cap. Indeed, the manufacturer recommends that thimble caps be used only once, if the extraction is performed at 120°C. In fact, caps were dramatically deformed and became useless after five extractions. An extraction temperature of 100°C was selected for further experiments as a compromise between extraction efficiency and thimble cap lifetime.

3.2. Void volume

Since the extraction vessel volume (7 ml) was much larger than the sample size (< 0.5 ml), an inert solid (diatomaceous earth) was added to the vessel in order to fill any extra void volume. The void volume was thus reduced and no additional extraction time was required to sweep the SC-extract out of the vessel. Diatomaceous earth was placed at the thimble edge of the CO₂ inlet. Diatomaceous earth (1 g) was extracted under the same conditions in order to check for the absence of interferents extracted from this material. The amount of phenols extracted was markedly increased by the addition of 1 g of diatomaceous earth to the thimble (see Table 2).

3.3. Influence of collection variables

ODS and PorapackQ were tested as packing materials for the analyte trap. Methanol and *n*-hexane were used as rinse solvents with both packings. The amounts of phenols found in the

SFE extracts obtained under the same conditions with the four collection/elution systems are shown in Table 2. As can be seen, the amounts eluted from ODS and PorapackQ trap were much larger (34–21 fold) with methanol than with *n*-hexane. Methanol proved to be a better rinse solvent than *n*-hexane with both traps. However, methanol was not efficient enough to completely remove other extracted substances (yellow/green pigments), so a subsequent rinse using *n*-hexane was mandatory in order to make the trap ready for a new extraction. Indeed, the use of an ODS/methanol or PorapackQ/methanol collection system to extract phenols allowed on-line clean-up of the supercritical extracts. It seems that methanol dissolves the more polar phenols, which may be insoluble in *n*-hexane. A volume of 1.5 ml of rinse solvent (*n*-hexane or methanol) at 2 ml min⁻¹ and 20°C was sufficient to remove all soluble phenols from the trap. No analytes were detected after a subsequent rinse. The nature of the trap packing affected the amount of phenols to a lesser extent than the nature of the rinse solvent. Slightly greater amounts of phenols (about 10%) were obtained with ODS than with PorapackQ. However, PorapackQ provided cleaner extracts, so it was selected for subsequent experiments.

Table 2

Influence of the collection system (trap/rinse solvent) and void volume used on the SFE efficiency of phenols from olive leaves

SFE conditions	Concentration in olive leaves ^a (mg g ⁻¹)
PorapackQ/MeOH, no DE	2.6
PorapackQ/MeOH, DE	3.8
PorapackQ/ <i>n</i> -Hexane, DE	0.11
ODS/MeOH, DE	4.2
ODS/ <i>n</i> -Hexane, DE	0.20

Amount of sample, 30 mg. SFE conditions: CO₂ modified with 10% methanol; pressure, 334 bar; extraction temperature, 100°C; flow-rate, 2 ml min⁻¹; extraction time, 20 min; nozzle and trap temperature during collection, 45 and 70°C, respectively; rinse volume, 1.5 ml; nozzle and trap temperature during rinse, 20°C. DE, addition of 1 g of diatomaceous earth.

^a Expressed as caffeic acid.

Table 3
Influence of the extraction pressure on the SFE efficiency of phenols from olive leaves

Pressure (bar)	(CO ₂ density (g ml ⁻¹))	Mean concentration ^a (mg g ⁻¹)	rsd (%)
155	(0.35)	0.59	13
207	(0.50)	1.9	12
256	(0.60)	2.6	9
334	(0.70)	3.4	5

Amount of sample, 30 mg. SFE conditions: CO₂ modified with 10% methanol; extraction temperature, 100°C; flow-rate, 2 ml min⁻¹; extraction time, 20 min; PorapackQ trap; nozzle and trap temperature during collection, 45 and 70°C, respectively; rinse solvent, methanol; rinse volume, 1.5 ml; nozzle and trap temperature during rinse, 20°C. Addition of 1 g of diatomaceous earth.

^a Expressed as caffeic acid.

3.4. Influence of pressure

The effect of extraction pressure on the amount of phenols dynamically extracted from olive leaves using CO₂ modified with 10% methanol for 20 min was studied at a constant temperature of 100°C. The amounts extracted increased linearly with increasing CO₂ density (Table 3, intercept -2.2 mg g⁻¹, slope 8.1 mg ml g⁻², *r*² 0.9996). An extraction pressure of 334 bar and a temperature of 100°C (viz. a CO₂ density of 0.70 g ml⁻¹) were chosen for subsequent extractions.

3.5. Influence of the modifier

The amount of total phenols extracted from olive leaves with pure CO₂ and various methanol-CO₂ mixtures is shown in Fig. 2. The effect of the modifier content on the extraction yield was examined at 100°C and 334 bar. As can be seen, the addition of methanol to CO₂ was mandatory in order to fully extract these compounds. A 10% methanol-CO₂ mixture provided the highest recovery of phenols while a modifier content of 20% produced undesirable methanol condensation on the analyte trap.

Because the proposed SFE of phenols could be implemented by the food, cosmetic and pharmaceutical industry provided the modifier used is non-toxic, the feasibility of replacing methanol with ethanol as modifier was investigated. Ethanol was found to be useful as a modifier, but less effective than methanol: the extraction yield of phenols obtained with 10% ethanol as modifier was 2.0 mg g⁻¹ (rsd 2.5%), the yield obtained

with 10% methanol under the same conditions was 3.6 mg g⁻¹ (rsd 5.6%).

3.6. Influence of the flow-rate and extraction time

There was no significant difference between the results obtained at a flow-rate of 1 and 2 ml min⁻¹ at 80°C; however, the extraction yield in-

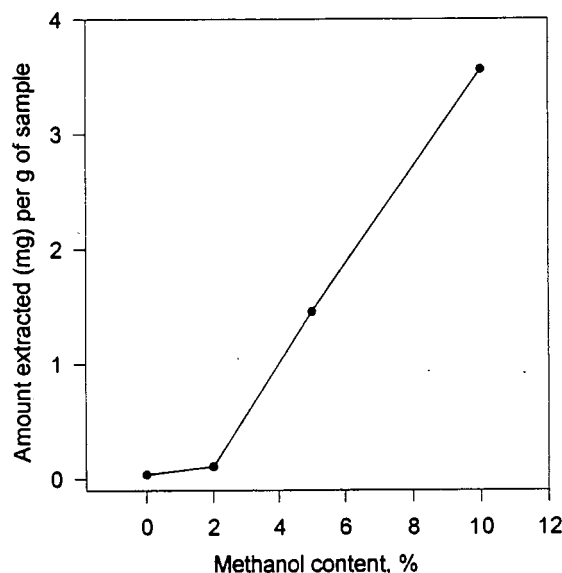


Fig. 2. Influence of methanol content on the SFE efficiency of phenols from olive leaves. Amount of sample, 30 mg. SFE conditions: pressure, 334 bar; extraction temperature, 100°C; flow-rate, 2 ml min⁻¹; extraction time, 20 min; PorapackQ trap; nozzle and trap temperature during collection 45 and 70°C, respectively; rinse solvent, methanol; rinse volume, 1.5 ml; nozzle and trap temperature during rinse, 20°C. Addition of 1 g of diatomaceous earth. Amounts of phenols per gram of sample expressed as milligrams of caffeic acid.

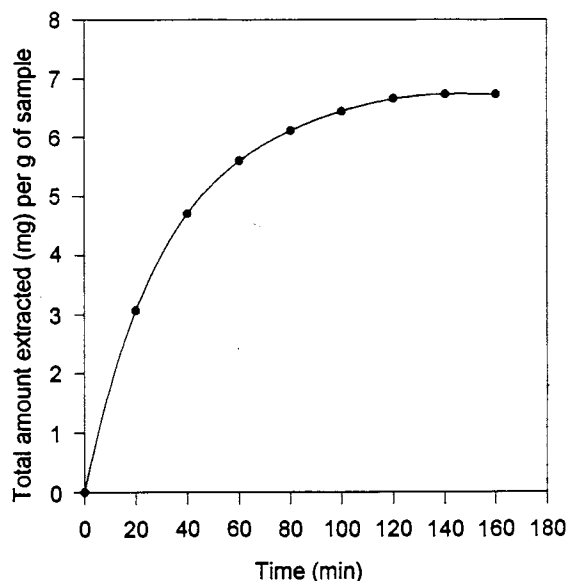


Fig. 3. Influence of the extraction time on the SFE efficiency of phenols from olive leaves. Amount of sample, 30 mg. SFE conditions: CO₂ modified with 10% methanol; pressure, 334 bar; extraction temperature, 100°C; flow-rate, 2 ml min⁻¹; PorapakQ trap; nozzle and trap temperature during collection, 45 and 70°C, respectively; rinse solvent, methanol; rinse volume, 1.5 ml; nozzle and trap temperature during rinse, 20°C. Addition of 1 g of diatomaceous earth. Amounts of phenols per gram of sample expressed as milligrams of caffeic acid.

creased with increasing flow rate at 100°C (from 6.4 mg g⁻¹ at 1 ml min⁻¹ to 8.0 mg g⁻¹ at 2 ml min⁻¹). Extraction from plant materials at low temperature seems to be limited primarily by desorption/diffusion since the flow rate has no effect on the extraction rate. However, the process is solubility-controlled at increased extraction temperatures. The behaviour of spiked phenols [8] was different at 50°C; increasing the flow-rate resulted in increased recoveries because solubilization was the limiting step. Undesirable methanol condensation on the analyte trap that could result in analyte loss (by ejection of methanol drops) was observed above 2 ml min⁻¹.

In order to ensure complete methanol evaporation, the trap temperature was raised from 70 to 100°C, which reduced collection efficiency. The extraction yields fell from 7.6 to 6.7 mg g⁻¹ as a result.

Fig. 3 shows the extraction curve obtained under the optimal SFE conditions. Exhaustive extraction was achieved after 140 min of dynamic extraction. A comparison of the cumulative amount of phenols per gram of sample obtained after seven 20-min extractions (6.7 mg g⁻¹) with that obtained in a single 140-min extraction (8.0 mg g⁻¹) revealed the absence of analyte losses after a long extraction time. In absence of losses, the amount obtained by seven 20-min extractions or by a single 140-min extraction must be the same. Determination of low phenol concentrations was difficult, particularly in extracts obtained from the last 20-min steps. It may explain the decreased result of 6.7 mg g⁻¹.

The precision of the whole method (SFE + colorimetry), expressed as percent relative standard deviation (extraction time = 20 min, $n = 5$) was 5.6%.

3.7. Comparison of SFE and sonication in a liquid solvent

SFE and liquid solvent extraction were compared in terms of phenol yields (Table 4). The data for liquid solvents was obtained in four successive extractions of triplicate samples. Only

Table 4
Concentration of total phenols found in olive leaves using the Folin-Ciocalteu reagent after SFE or sonication in a liquid solvent

Solvent	Concentration in olive leaf ± SD ^a ($n = 3$) (mg g ⁻¹)
<i>n</i> -Hexane	0.18 ± 0.03
Diethyl ether	1.1 ± 0.3
Ethyl acetate	1.6 ± 0.4
Methanol	16.8 ± 0.8
CO ₂ + 10% Methanol	7.6 ± 0.5

Sonication time: 75 min, SFE conditions: pressure, 334 bar; extraction temperature, 100°C; flow-rate, 2 ml min⁻¹; extraction time, 140 min; PorapakQ trap; nozzle and trap temperature during collection, 45 and 70°C, respectively; rinse solvent, methanol; rinse volume, 1.5 ml; nozzle and trap temperature during rinse, 20°C. Addition of 1 g of diatomaceous earth. Amount of sample, 30 mg.

^a Expressed as caffeic acid.

with methanol was the olive leaf sample exhaustively extracted. The results reveal that the higher the solvent polarity, the higher the phenol extraction yield. Thus, SFE provided much greater amounts of phenols than extraction with *n*-hexane, diethyl ether or ethyl acetate; however, carbon dioxide modified with 10% methanol recovered 45% of the amounts extracted by liquid methanol.

4. Conclusions

A clean, highly selective, automated method for the isolation of phenols from olive leaves was investigated. Because solvent polarity increases extraction rate and efficiency, the addition of a polar modifier (e.g. methanol or ethanol) to non-polar supercritical CO₂ is essential. Modifier contents and flow-rates higher than 10% and 2 ml min⁻¹, respectively, give rise to methanol condensation on the trap. Ethanol was found to be a less efficient modifier than methanol. PorapackQ packing and methanol was the best combination for collecting and eluting extracted analytes. This collection system affords on-line clean-up of plant extracts. Supercritical CO₂ modified with 10% methanol was found to be a more efficient solvent than *n*-hexane, diethyl ether and ethyl acetate, but was surpassed by liquid methanol in terms of yield.

Acknowledgements

The Spanish Comisión Interministerial de Ciencia y Tecnología (CICYT) is gratefully acknowledged for financial support in the form of Grant PB95-0977. M.T.T. would also like to thank the University of Córdoba for the award of a postdoctoral fellowship. The authors are also indebted to the Servicio Central de Espectrometría de Masas of the University of Córdoba for MS analyses.

References

- [1] K. Robards, M. Antolovich, *Analyst* 122 (1997) 11R.
- [2] D. Heimler, A. Pieroni, M. Tattini, A. Cimato, *Chromatographia* 33 (1992) 369.
- [3] D. Heimler, A. Pieroni, *Chromatographia* 38 (1994) 475.
- [4] G. Montedoro, M. Servili, M. Baldioli, E. Miniati, *J. Agric. Food Chem.* 40 (1992) 1571.
- [5] G. Montedoro, M. Servili, M. Baldioli, E. Miniati, *J. Agric. Food Chem.* 40 (1992) 1577.
- [6] F. Angerosa, N. d'Alessandro, P. Konstantinou, L. Di Giacinto, *J. Agric. Food Chem.* 43 (1995) 1802.
- [7] F. Angerosa, N. d'Alessandro, F. Corana, G. Mellerio, *J. Chromatogr. A.* 736 (1996) 195.
- [8] M.T. Tena, A. Rios, M. Valcárcel, *Fresenius' J. Anal. Chem.* (in press, 1998).
- [9] E. Wollenweber, in E. Rodriguez, P.L. Healey and I. Mehta (Eds.), *Biology and Chemistry of Plant Trichomes*, Plenum, New York, 1984, pp. 53–70.
- [10] M.D. Luque de Castro, M. Valcárcel, M.T. Tena, *Analytical Supercritical Fluid Extraction*, Springer-Verlag, Berlin, 1994, pp. 299–304.
- [11] M. Valcárcel, M.T. Tena, *Fresenius' Z. Anal. Chem.* 358 (1997) 561.
- [12] R.M. Smith, *LC-GC Int.*, January (1996) 8.
- [13] C.D. Bevan, P.S. Marshall, *Nat. Prod. Rep.* 11 (1994) 451.
- [14] P. Castioni, P. Christen, J.L. Veuthey, *Analisis* 23 (1995) 95.
- [15] E.D. Ramsey, B. Minty, M.A. McCullagh, D.E. Games, A.T. Rees, *Anal. Commun.* 34 (1997) 3.
- [16] T.S. Reighard, S.V. Olesik, *Anal. Chem.* 68 (1996) 3612.
- [17] H.B. Lee, T.E. Peart, R.L. Hong-You, *J. Chromatogr.* 636 (1993) 263.
- [18] M.T. Tena, M. Valcárcel, P.J. Hidalgo, J.L. Ubersa, *Anal. Chem.* 69 (1997) 521.
- [19] Z. Djarmati, R.M. Jankov, E. Schwirtlich, B. Djulinac, A. Djordjvic, *JAOCS* 68 (1991) 731.
- [20] S.V. Shobha, B. Ravindranath, *J. Agric. Food Chem.* 39 (1991) 2214.
- [21] T. Tsuda, K. Mizuno, K. Ohshima, S. Kawakishi, T. Osawa, *J. Agric. Food Chem.* 43 (1995) 2803.
- [22] T. Swain, J.L. Goldstein, in J.B. Pridham (Ed.), *Methods in Polyphenol Chemistry*, Pergamon, Oxford, 1964, pp. 131–146.
- [23] A. Vázquez-Roncero, C. Janer del Valle, M.L. Janer del Valle, *Grasas Aceites* 24 (1973) 350.
- [24] J.M.E. Quirke, C.L. Adams, G.J. Van-Berkel, *Anal. Chem.* 66 (1994) 1302.
- [25] B. Mason-Hughes, D.E. McKenzie, K.L. Duffin, *J. Am. Soc. Mass Spectrom.* 4 (1993) 604.

Electrochemical oxidation of bentazon at a glassy carbon electrode

Application to the determination of a commercial herbicide

E. Manuela Garrido^{1,a}, José L. Costa Lima^a, C. M. Delerue-Matos^{1 a},
Ana Maria Oliveira Brett^{b,*}

^a *CEQUP/Departamento de Química-Física, Faculdade de Farmácia, Universidade do Porto, 4050 Porto, Portugal*

^b *Departamento de Química, Faculdade de Ciências e Tecnologia, Universidade de Coimbra, 3000 Coimbra, Portugal*

Received 5 August 1997; received in revised form 10 October 1997; accepted 22 October 1997

Abstract

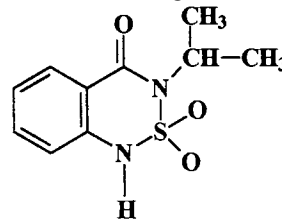
The electrochemical methods cyclic, differential pulse and square wave voltammetry were applied to develop an electroanalytical procedure for the determination of the herbicide bentazon in a commercial product, containing bentazon as the active ingredient, used to treat rice and corn crops. The oxidation mechanism is complex, consisting of an electrochemical step followed by chemical dimerization reaction of the products, which causes severe adsorption problems and consequent poisoning of the electrode surface. The effect of adding Triton surfactant is to enable determinations with good reproducibility to be carried out; the analytical conditions were studied and optimized. The limit of detection obtained was 10^{-5} M. © 1998 Elsevier Science B.V. All rights reserved.

Keywords: Bentazon; Herbicides; Square wave voltammetry

1. Introduction

Bentazon is the common name for the herbicide 3-isopropyl-1H-2,1,3-benzothiadiazin-4-(3H)-one-2,2-dioxide and is used as a post-emergence herbicide to control broadleaf and sedges in beans, rice, corn, peanuts and mint [1]. It is a contact herbicide, which means that it only functions in

the part of the plant where it is applied and its activity is short-lived [2]. Commercially, it is available in the form of soluble concentrate which contains the sodium salt of bentazon as the active ingredient and is referred to as sodium bentazon. Bentazon has the following structure



* Corresponding author. Tel./fax: + 351 39 35295; e-mail: brett@cygnus.ci.uc.pt

¹ Present address: Instituto Superior de Engenharia do Porto, 4200 Porto, Portugal.

Analytical techniques used for the determination of bentazon in water, soils and fruits are gas chromatography [3–6] and high performance liquid chromatography (HPLC) [7–14]. The latter has the advantage of not requiring derivatization to obtain good resolution. However, the UV detector employed has low sensitivity and selectivity, making preconcentration and clean-up steps necessary.

The electrochemical oxidation properties of bentazon were studied and an electrochemical method was developed for determination of bentazon in a commercial product used to protect rice and corn crops.

2. Experimental

2.1. Reagents and solutions

Bentazon was from Riedel de Haen. All reagents were of analytical grade and aqueous solutions were prepared using purified water from a Millipore Milli-Q system (conductivity $< 0.1 \mu\text{S cm}^{-1}$). The stock solution of bentazon was prepared in ethanol at a concentration of 9.6×10^{-3} M. The buffer solutions used were in the pH range 1.2–12.8. Quantitative determinations were carried out in a 0.2 M acetate buffer of pH = 3.4.

2.2. Commercial sample preparation

In the commercial product (Basagran, BASF), bentazon is in the basic form; therefore, the sample stock solution was prepared by accurately weighing 0.46 g of the commercial sample and adding a few drops of glacial acetic acid until complete precipitation of the acid form of bentazon occurred. Ethanol was added to the mixture until complete dissolution occurred and the total volume was adjusted to 100.0 cm³. The sample stock solution was diluted with buffer electrolyte in order to obtain a concentration within the calibration curve range.

2.3. Apparatus

All experiments were performed using a 663 VA Metrohm system containing a glassy carbon working electrode (Metrohm 6.1204.000) ($d = 3.0$ mm), a glassy carbon rod counter electrode (Metrohm 6.1247.000) and an Ag/AgCl reference electrode (Metrohm 6.0728.000) attached to a Autolab PSTAT 10 potentiostat/galvanostat running with model GPES version 3 software (Eco-Chemie, The Netherlands). The potential range studied was from +0.2 to +1.2 V.

The glassy carbon working electrode was polished every day using a polishing kit (Metrohm 6.2802.010), first with $\alpha\text{-Al}_2\text{O}_3$ (0.3 mm) and water for 60 s and then with water only, for 60 s. After polishing, the electrode surface was thoroughly washed with purified water.

The pH measurements were obtained with a pH-meter E 520 from Metrohm with a combined glass electrode (Metrohm 6.0202.000).

HPLC experiments for the AOAC Method were carried out using a HPLC Sykan system, model A1210 with a variable wavelength detector.

3. Results and discussion

The oxidation of bentazon was first studied by cyclic voltammetry in order to probe the oxidation mechanism. The electrochemical oxidation of bentazon occurs at +0.96 V vs Ag/AgCl in 0.2 M acetate buffer of pH = 3.4 (Fig. 1) and is an irreversible process. The oxidation products adsorb very strongly on the electrode surface, causing irreproducibility. A plot of I vs $\nu^{1/2}$ is a straight line passing through the origin, indicating that the oxidation is a diffusion-controlled process.

Due to the high adsorption of the products formed during the oxidation of bentazon and in order to attain good reproducibility and increase the sensitivity, an electrochemical cleaning procedure was developed. This electrochemical treatment of the electrode surface was carried out after mechanical polishing and consisted of applying a constant potential of -1.0 V for 60 s and $+1.0$ V for 60 s, followed by a square wave scan at 50

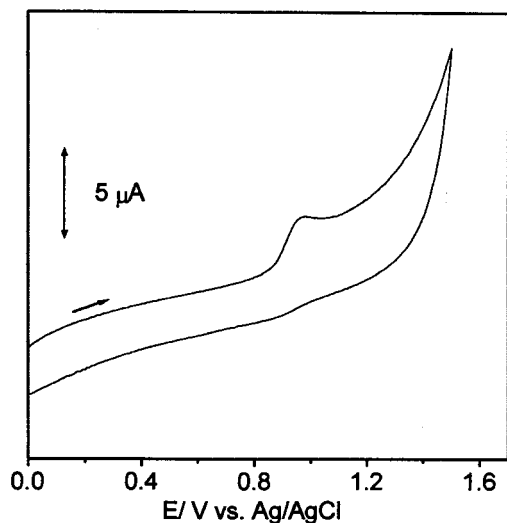


Fig. 1. Cyclic voltammogram of bentazon, 1.0×10^{-4} M, in 0.2 M acetate buffer of pH = 3.4. Scan rate 100 mV s^{-1} , pulse amplitude 50 mV.

Hz between +0.6 and +1.2 V, the potential range of interest for bentazon, in a 0.2 M acetate buffer solution of pH = 3.4. The use of potentials more negative than -1.0 V or more positive than +1.0 V leads to worse reproducibility and longer conditioning times did not improve the results further.

The best results were obtained when, in addition to this mechanical/electrochemical cleaning, a surfactant (Triton) was added to the solution in order to prevent adsorption of the oxidation products. Table 1 shows the results obtained for the peak current for different % V/V Triton added to the solution. It was possible to use high concentrations of Triton without problems of foam formation. For low percentages of Triton, adsorption effects occur and the reproducibility was not

Table 1
Dependence of the peak current on the % (v/v) of Triton for a bentazon solution of 1.90×10^{-5} M

Triton added % (v/v)	$I_p \mu\text{A}^{-1}$
0.1	0.447
1.0	0.338
5.0	0.106

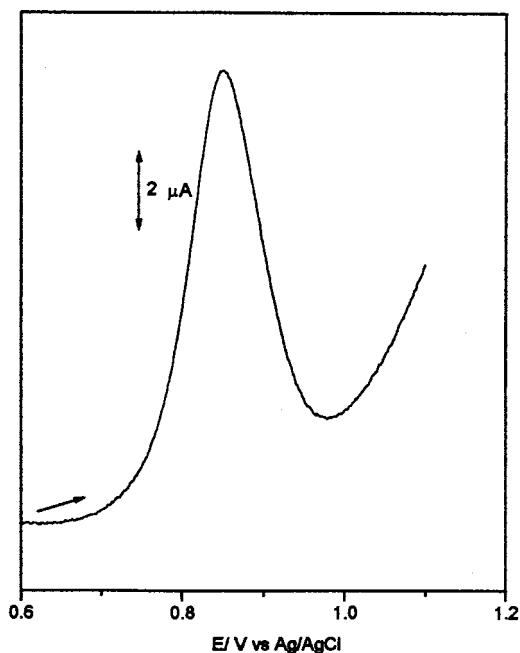


Fig. 2. Differential pulse voltammograms of bentazon, 2.0×10^{-5} M, in 0.2 M acetate buffer of pH = 3.4. Pulse amplitude 50 mV, scan rate 5 mV s^{-1} .

good; at high percentages greater adsorption of the surfactant itself on the electrode surface caused diminution of the peak current, but good reproducibility was obtained. Addition of 1% Triton to the solution was found to be most suitable and in these optimized conditions of 0.2 M acetate buffer of pH = 3.4 with 1% Triton the detection limit was 10^{-5} M.

3.1. The effect of pH

The electrochemical behaviour of bentazon was studied over a large pH range between 1.2 and 12.8, using differential pulse voltammetry (Fig. 2) and scanning from +0.6 to +1.2 V. Plots of E_p vs pH for 2×10^{-5} M solutions of bentazon (Fig. 3) show that the peak potential is dependent on pH in acid media, becoming independent above pH ~ 3.5 ; no peak was observed for pH values greater than 8.4. Bentazon is a weak acid with $pK_a = 3.2$ [14], corresponding to the intersection of the two lines. The dependence of the peak potentials on pH in acid media corresponds to 40

mV per unit of pH, meaning that it is likely that the reaction mechanism corresponds to an electron transfer followed by a chemical reaction, probably a dimerization, leading to irreversible product adsorption on the electrode surface. A plot of I_p vs pH (Fig. 4) shows that higher currents are observed for $\text{pH} \sim \text{p}K_a$.

3.2. Application of the method to a commercial product

The electroanalytical method developed for the determination of bentazon was used to analyse a commercial compound, Basagran, that contains bentazon as the active ingredient. The sample and calibration standards, between 1.51×10^{-5} and 2.26×10^{-5} M were prepared according to the description in Section 2. The square wave voltammograms obtained for both sample and standards are shown in Fig. 5. The calibration plot gave a straight line ($r = 0.998$, $n = 5$) for bentazon.

These results were compared with those obtained using the AOAC method [15]. This method is an isocratic reversed-phase liquid chromatogra-

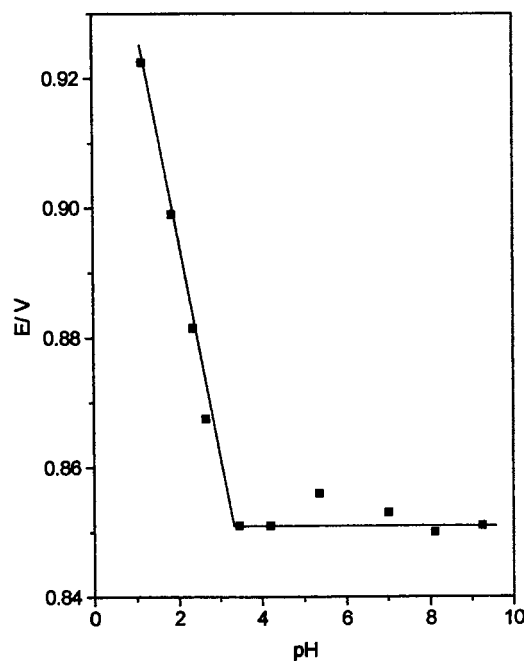


Fig. 3. Plot of E_p vs pH for 2.0×10^{-5} M solutions of bentazon in 0.2 M buffer electrolyte.

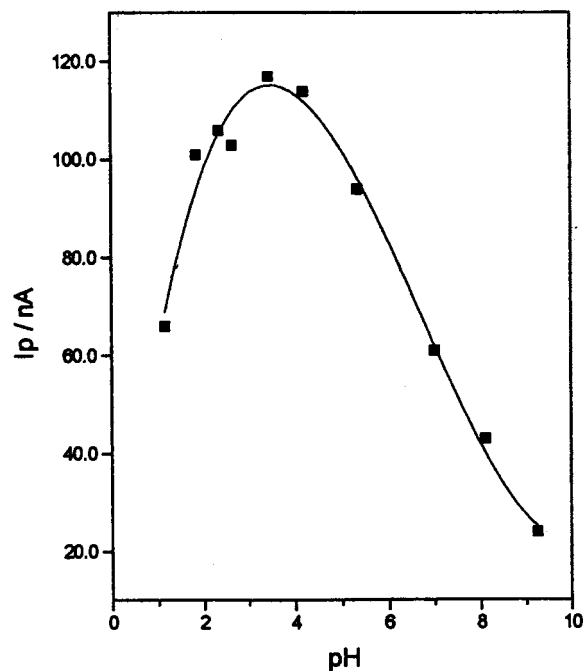


Fig. 4. Plot of I_p vs pH for 2.0×10^{-5} M solutions of bentazon in 0.2 M buffer electrolyte.

phy (LC) procedure for measuring bentazon in commercial herbicide products and aqueous formulations. The samples are dissolved in LC eluent (0.075 M sodium acetate + methanol (60 + 40)) and analysed by LC on a 30 cm \times 3.9 mm octadecylsilyl column with detection by UV absorption at 340 nm. The quantity of active ingredient is determined by comparing the mean response factor (RF) of the sample to the mean RF of the standards injected immediately before and after each pair of sample injections.

The results obtained with the electrochemical and AOAC methods were in good agreement and the reproducibility was good. The mean and standard deviation obtained for eight determinations by the electrochemical method were 41.61% w/w and 1.42%, respectively and by the AOAC procedure 42.36% w/w and 0.72%. The recovery data for these eight determinations using the electrochemical method was $99 \pm 4\%$. The accuracy of these results was assessed by comparing the electrochemical results with those obtained by the AOAC method, the relative error being 2.4%.

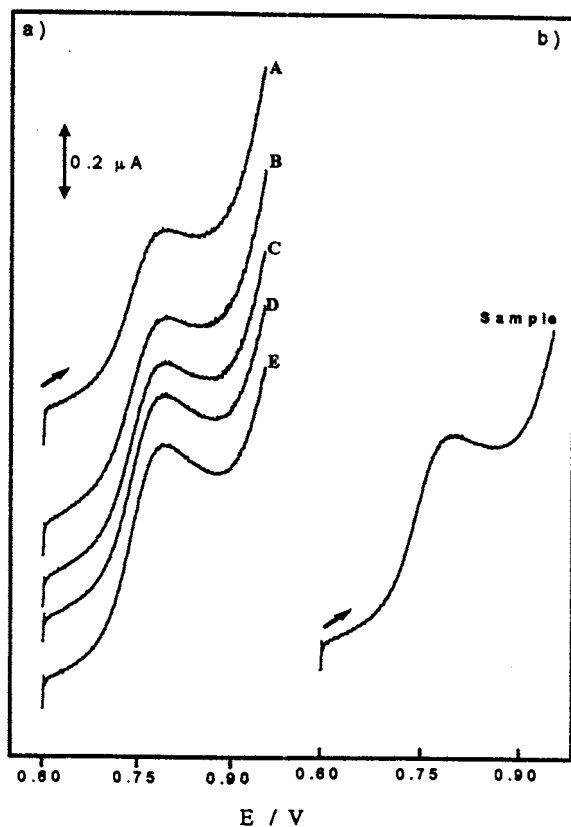


Fig. 5. Square wave voltammograms of bentazon in 0.2 M acetate buffer of pH = 3.4, scan rate 50 mV s^{-1} and pulse amplitude 50 mV: (a) successive additions of standard solutions for constructing the calibration plot (A, 1.51×10^{-5} ; B, 1.70×10^{-5} ; C, 1.89×10^{-5} ; D, 2.07×10^{-5} ; E, 2.26×10^{-5} M); (b) commercial sample solution.

4. Conclusions

Electrochemical methods can be successfully used to quantify the herbicide bentazon in a commercial product. The electrochemically-developed method is simple, enables faster determinations and also permits the study of the oxidation mech-

anism of bentazon which is complex and involves the formation of strongly adsorbed products on the electrode surface. A comparative evaluation of the data showed that the results obtained electroanalytically were in good agreement with those obtained by the AOAC chromatographic method.

Acknowledgements

The authors wish to thank the Junta Nacional de Investigação Científica e Tecnológica (JNICT) for financial support through project PEAM/SEL/516/95 and PRODEP for a research grant (E. Manuela Garrido).

References

- [1] A. Cessna, *J. Agric. Food Chem.* 33 (1985) 108–110.
- [2] J.D. Gaynor, D.C. Mactavish, *J. Agric. Food Chem.* 29 (1981) 626–629.
- [3] K. Kadokami, M. Morimoto, K. Haraguchi, M. Kojima, Shinohara, *Anal. Sci.* 7 (1991) 247–252.
- [4] G. Durand, V. Bouvot, D. Barceló, *J. Chromatogr.* 607 (1992) 319–327.
- [5] M. Akerblom, G. Alex, *J. Assoc. Anal. Chem.* 67 (1984) 653–655.
- [6] C.J. Miles, H.A. Moye, *Anal. Chem.* 60 (1988) 220–226.
- [7] S. Chiron, E. Martinez, D. Barceló, *J. Chromatogr. A* 665 (1994) 283–293.
- [8] R.B. Geerdink, A.M.B.C. Graumans, J. Viveen, *J. Chromatogr.* 547 (1991) 478–483.
- [9] R.T. Krause, *J. Chromatogr.* 255 (1983) 497–510.
- [10] E.A. Hogendoorn, U.A.Th. Brinkman, P. Van Zoonen, *J. Chromatogr.* 644 (1993) 307–314.
- [11] E.A. Hogendoorn, C.E. Goewie, *J. Chromatogr.* 475 (1989) 432–441.
- [12] E.A. Hogendoorn, P. Van Zoonen, *Fresenius J. Anal. Chem.* 343 (1992) 73–74.
- [13] R. Schuster, A. Gratzfeld-Hüsgen, *Analisis* 19 (1991) 45–48.
- [14] M. Chen, Y. Wang, *Fenxi-Huaxue* 13 (1985) 445–447.
- [15] T.M. Schmitt, *J. AOAC Int.* 77 (1994) 328–330.

Selective determination of Ni(II) and Co(II) by flow injection analysis and adsorptive cathodic stripping voltammetry on a wall jet mercury film electrode

A. Economou *, P.R. Fielden

Department of Instrumentation and Analytical Science, UMIST, PO Box 88, Manchester, M60 1QD, UK

Received 18 July 1997; received in revised form 23 October 1997; accepted 24 October 1997

Abstract

Ni(II) and Co(II) have been determined simultaneously by means of adsorptive cathodic stripping voltammetry (AdCSV) in a computerised flow injection system. The working electrode was a glassy carbon disk that was fitted in a wall-jet flow cell. The electrode was initially electrochemically coated with a mercury film at -1.0 V by injecting a Hg(II) solution in the flow stream. Then, the sample, containing Ni(II) and Co(II), was mixed on-line with a solution containing dimethylglyoxime (DMG) at pH 9 in order to selectively complex the metal ions and was injected in the flow system. After a number of successive injections during which accumulation took place under controlled potentiostatic conditions, the surface-bound complexes were reduced in ammonia buffer at pH 9 by a cathodic scan of the potential of the working electrode in the square wave mode and the current-potential response was recorded. Finally, the electrode surface was regenerated by a potentiostatic polarisation at -1.4 V in the same buffer. The apparatus could be easily converted for continuous flow accumulation in order to increase the sensitivity; in this mode of operation, instead of performing discrete injections, the sample was continuously pumped through the cell. Various parameters associated with the preconcentration, stripping and regeneration steps were optimised for the determination of Ni(II) and Co(II). The selectivity of the method was demonstrated for the analysis of high purity iron; the accuracy for the determination of Ni(II) and Co(II) was 11 and 3%, respectively while the coefficient of variation was 10 and 8%, respectively. © 1998 Elsevier Science B.V. All rights reserved.

Keywords: Nickel; Cobalt; Adsorptive cathodic stripping voltammetry; Flow injection analysis

1. Introduction

Since the discovery of the analytical utility of the adsorptive properties of the Ni(II) and Co(II) complexes with dimethylglyoxime, methodologies have been developed to determine Ni(II) and Co(II) by AdCSV in various matrices (for example [1,2]) that make use of the HMDE and con-

* Corresponding author. Present address: University of Athens, Laboratory of Analytical Chemistry, Department of Chemistry, Panepistimiopolis, Athens 157 71, Greece; tel.: +30 1 7231608; fax: +30 1 7231608.

ventional batch measuring configurations. Mercury film electrodes (MFEs) can replace the HMDE for adsorptive stripping measurements in the reductive regime [3]. While MFEs are mechanically stable and simple to make and to maintain, their main drawback lies with the difficulty in regenerating the active mercury surface after the irreversible adsorption of surface active compounds after prolonged use [4]. Despite these complications, MFEs plated on a rotating disk electrode have been applied previously with success to the AdCSV analysis of various samples for their Ni(II) and Co(II) content [5–7]. However, the recent trend is towards the use of flow analysers on account of the ease of use, cost, throughput and reliability that such systems typically offer. The HMDE has been occasionally used in flow-through systems [8,9] but is not particularly well suited to operate in flowing systems due to the practical problems of its limited mechanical stability and the difficulty associated with the disposal of liquid mercury. On the other hand, several applications exist that make use of MFEs for the selective accumulation of the Ni(II) and Co(II) complexes with different oximes in flow systems [10–12] or in the batch injection analysis (BIA) mode [13].

In this work, Ni(II) and Co(II) have been determined simultaneously by square wave AdCSV (SWAdCSV) and flow injection analysis (FIA) with high selectivity and sensitivity. The square wave modulation, combined with AdCSV, offers speed, high analytical sensitivity, low background current and insensitivity to dissolved oxygen compared to other scanning waveforms [14]. On the other hand, operation in the FIA mode allows convenient medium exchange in the stripping step and removes the need for the time consuming deoxygenation stage. The cleaning-regeneration of the mercury film working electrode was exhaustively assessed and optimised. Other parameters affecting the combined stripping signal (such as the accumulation time, the concentration ratios of the two metals, the preconcentration potential and the sample volume injected) were also investigated. The selectivity of the method was demonstrated for the analysis of an iron sample for its nickel and cobalt content.

2. Experimental

2.1. Reagents-apparatus

1000 ppm Ni(II) and Co(II) atomic absorption standard solutions were purchased from BDH (Poole, England) and used for the preparation of standards by serial dilution. DMG was also purchased from BDH and a 0.1 M stock solution was prepared in 95% ethanol. A 0.1 M Hg(II) stock solution was prepared by dissolving the appropriate amount of $\text{HgCl}_2 \cdot 6\text{H}_2\text{O}$ (BDH) in 1 mM HNO_3 and the 1 mM mercury plating solution was prepared by dilution with 0.1 M $\text{KNO}_3/0.01$ M HNO_3 . The 0.1 M ammonia buffer (pH 9) was prepared by dissolving the appropriate amounts of concentrated HCl and NH_3 (BDH, Aristar grade). Distilled and deionised water (resistance > 18 M Ω) was used for the preparation of the solutions.

The flow system was a modified version of an earlier FIA apparatus [15]. The configuration of the system for the present work is schematically illustrated in Fig. 1(a). Sampling was carried out for 8 s under stopped-flow conditions and the sample loop was flushed with carrier for 22 s in order to transport the sample to the cell. This timing resulted in a sampling rate of 2 samples min^{-1} . The potentiostat and the wall jet flow cell have also been reported earlier [15]. The loop volume was 200 μl .

2.2. Preparation of the sample

The iron sample (0.250 g) was weighed, dissolved in 10 ml of 4 M HNO_3 and diluted to 100 ml in a volumetric flask. For the analysis, 0.5 g of potassium tartrate was added to a 5.0 ml portion of this solution (in order to complex Fe(III) and avoid precipitation as $\text{Fe}(\text{OH})_3$ in the later stages in alkaline pH). Then 40.0 ml of the ammonia buffer (pH 9) was added and the pH adjusted to 9 with concentrated ammonia. Finally, the solution was diluted to 100.0 ml and was ready for the analysis. A blank solution not containing iron was prepared in the same way.

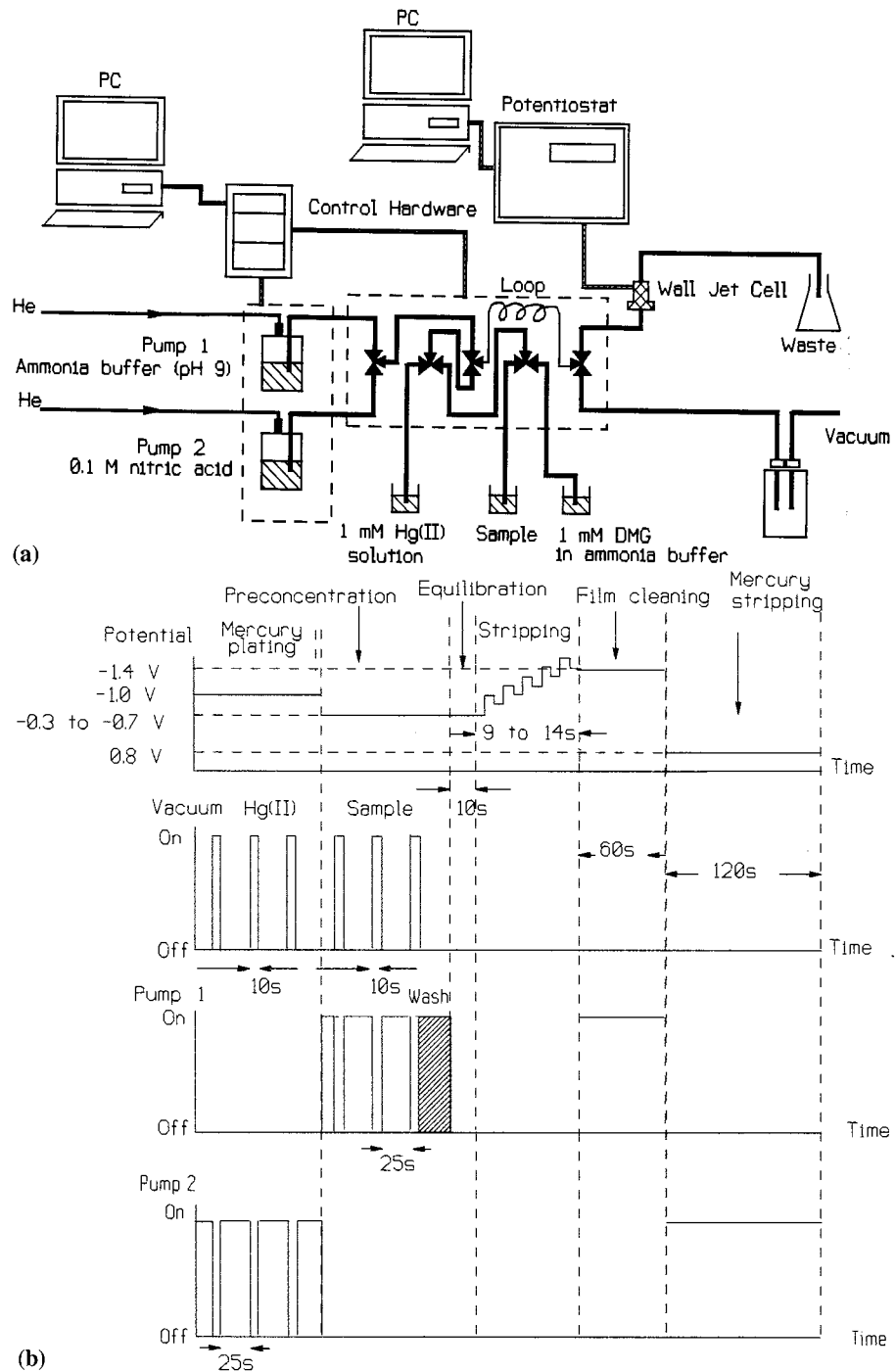


Fig. 1. (a) Experimental configuration for the determination of Ni(II) and Co(II). (b) Schematic diagram of the sequence of operations and the experimental parameters for the determination (times not drawn to scale for the sake of clarity).

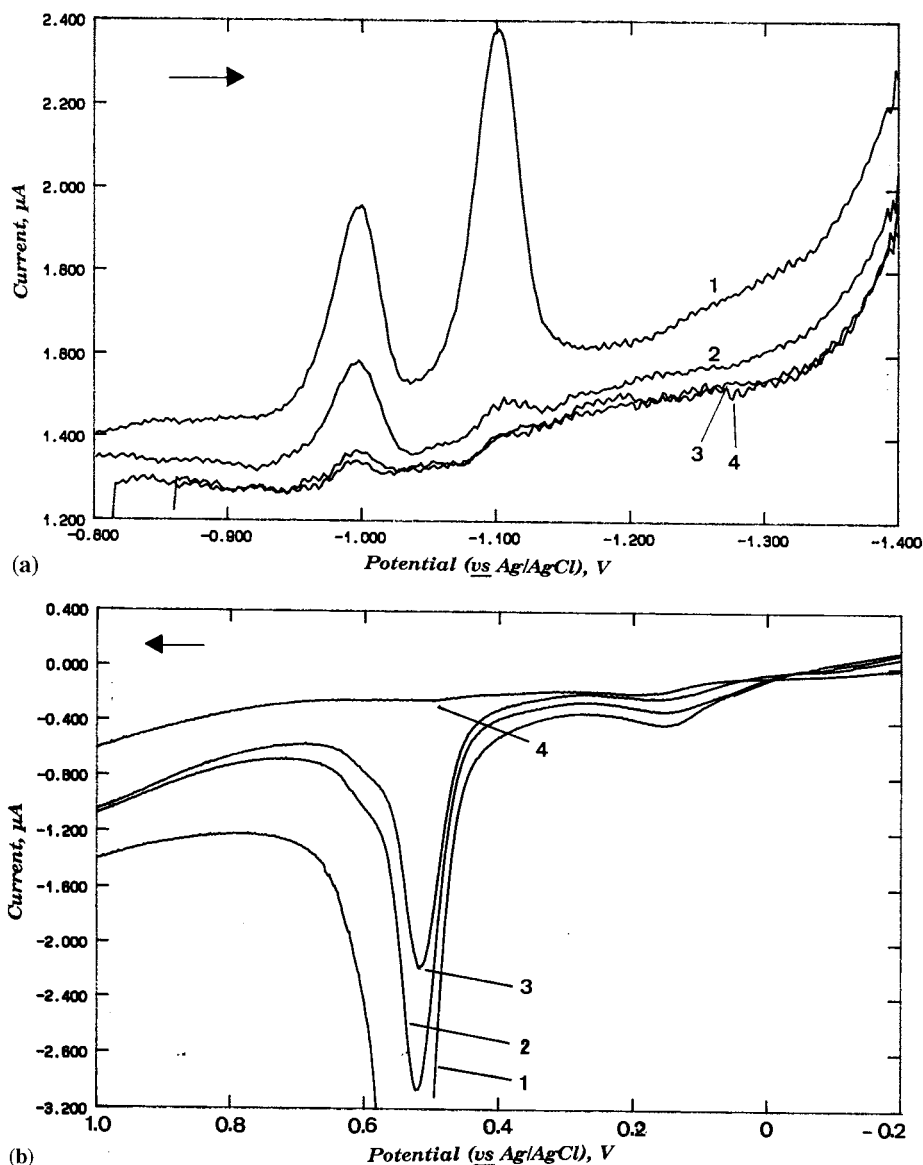


Fig. 2. (a) Voltammograms demonstrating the efficiency of the in situ cleaning of the complexes at different cleaning times. (1), (2), (3) and (4) correspond to 0, 10, 20, and 40 s cleaning at -1.4 V. $[\text{Ni}(\text{II})]$ and $[\text{Co}(\text{II})]$ 100 nM; DMG 1 mM; deposition at -0.7 V; 3 sample injections; SW frequency 40 Hz, pulse height 10 mV, scan increment 2 mV. (b) Voltammograms demonstrating the efficiency of the mercury stripping from the surface of the glass carbon electrode after electrochemical cleaning in 0.1 M HNO₃ and 0.8 V at different cleaning times. (1), (2), (3) and (4) correspond to 0, 30, 60, and 120 s cleaning at 0.8 V. Scan rate 0.1 V s⁻¹.

2.3. Experimental procedure

The different steps of the experimental procedure together with the physical parameters used for the determination are schematically illustrated in Fig. 1(b).

2.3.1. Coating of the mercury film

The electrode was polished as described previously [6] and then was coated with mercury by injecting three aliquots of the 1 mM Hg(II) plating solution at a potential of -1.0 V using 0.1 M nitric acid as the carrier with a flow rate of 2 ml l⁻¹.

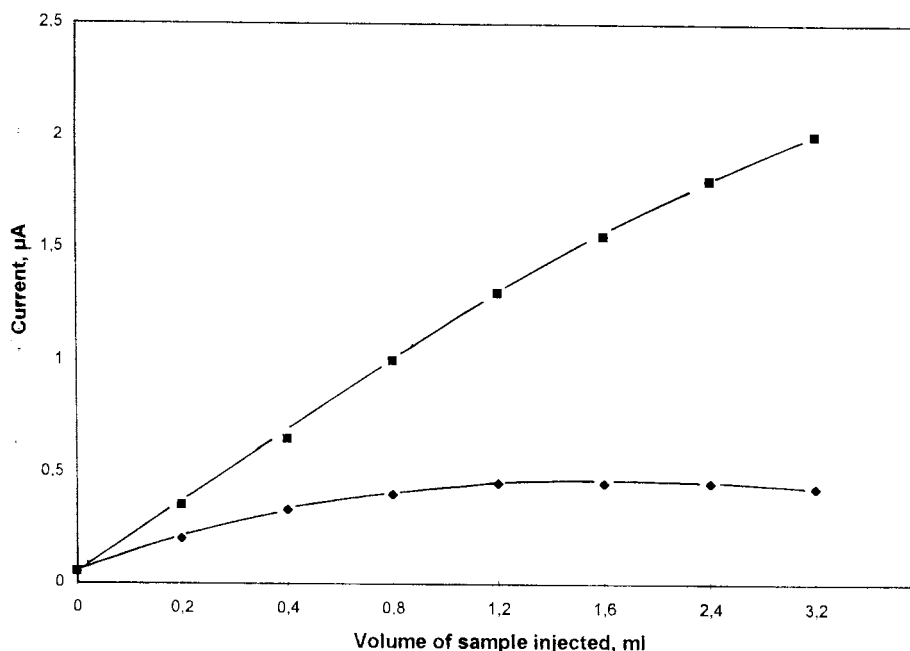


Fig. 3. Plot of the magnitude of the stripping peak current of Ni(II) (◆) and Co(II) (■) as a function of the total injected sample volume. [Ni(II)] and [Co(II)] 50 nM. Other conditions as in Fig. 2(a).

2.3.2. Preconcentration and measurement

The blank solution was mixed with the 1 mM DMG solution and injected into the carrier stream of ammonia buffer while the potential of the electrode was maintained at the preconcentration potential (ranging from -0.3 to -0.7 V). After three successive injections, the flow was stopped and, after a 10 s rest period, the square

wave scan was initiated from the preconcentration potential to -1.4 V with a frequency of 40 Hz, pulse height 10 mV and scan increment 2 mV while the current-potential response was recorded and stored. After measuring the background, the same procedure was repeated by replacing the blank with the sample and the spiked sample solutions.

Table 1

Calibration parameters for the determination of Ni(II) and Co(II) by SWAdCSV using FIA and continuous flow accumulation

Metal	Deposition mode			
	FIA		Continuous flow	
	Ni(II)	Co(II)	Ni(II)	Co(II)
Sensitivity ($\mu\text{A mol l}^{-1}$)	5.2×10^6	1.0×10^7	2.2×10^7	4.8×10^7
Intercept (μA)	0.12	0.14	0.14	0.22
LOD (nM) at 3σ	4.3	2.9	0.76	0.68
Linear range (mol l^{-1})	From LOD to 1×10^{-6}	From LOD to 1×10^{-6}	From LOD to 1×10^{-7}	from LOD to 1×10^{-7}
Correlation coefficient	0.998	0.997	0.995	0.999

Continuous flow involved 30 s adsorption of the sample flowing through the cell at 2 ml min^{-1} .

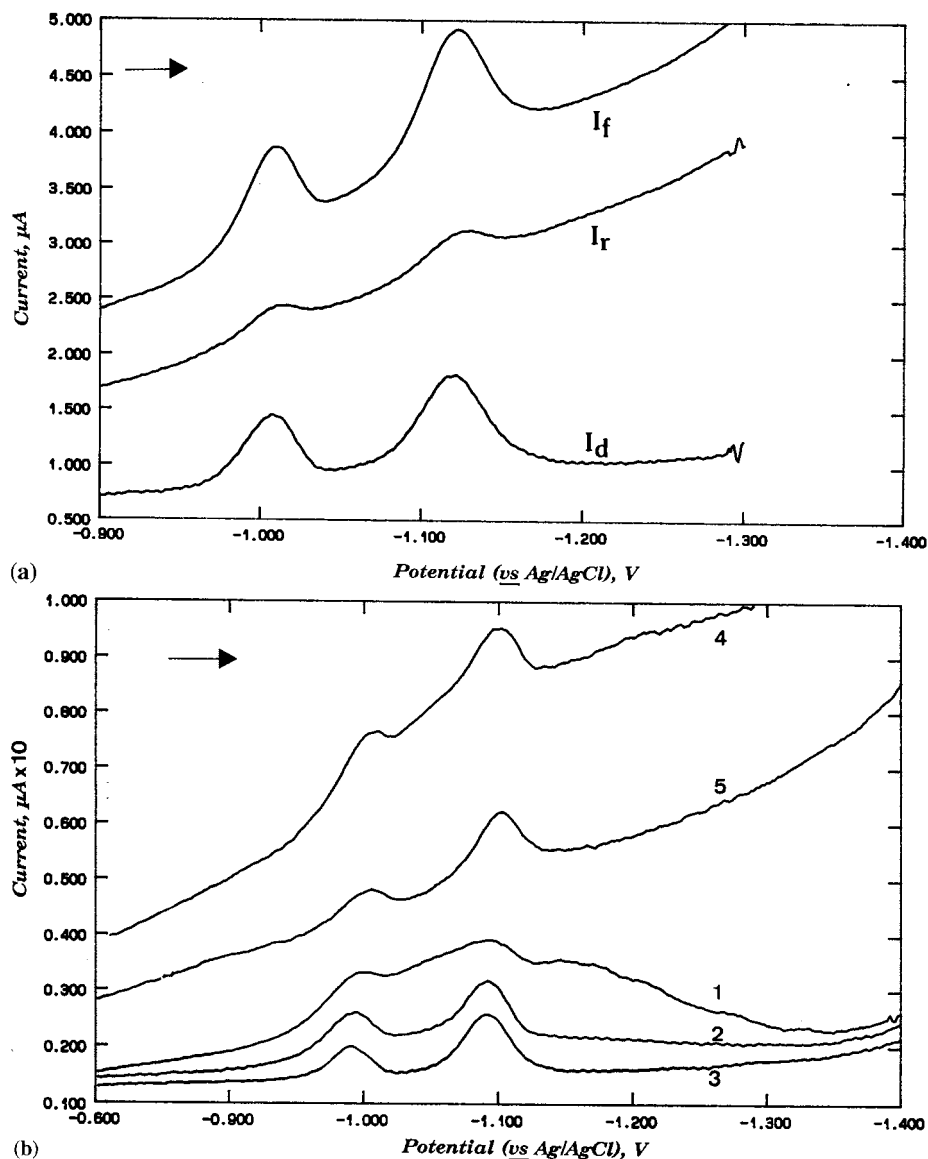


Fig. 4. (a) Current components of a SW voltammogram of Ni(II) and Co(II) after preconcentration of a deoxygenated sample. [Ni(II)] 100 nM and [Co(II)] 50 nM. Other conditions as in Fig. 2(a) (b) Effect of oxygen on the SW and SC voltammograms of Ni(II) and Co(II). SW after deoxygenation for: (1) 0 s; (2) 60 s; (3) 240 s. SC after deoxygenation for (4) 60 s; (5) 240 s. Other conditions as in Fig. 2(a).

2.3.3. Cleaning of the mercury film

After each measurement, the mercury film was reactivated by potentiostatic polarisation at -1.4 V

in a stream of ammonia buffer flowing at 2 ml min^{-1} . The mercury film was stripped by polarisation at $+0.8$ V in 0.1 M nitric acid flowing at 2 ml min^{-1} .

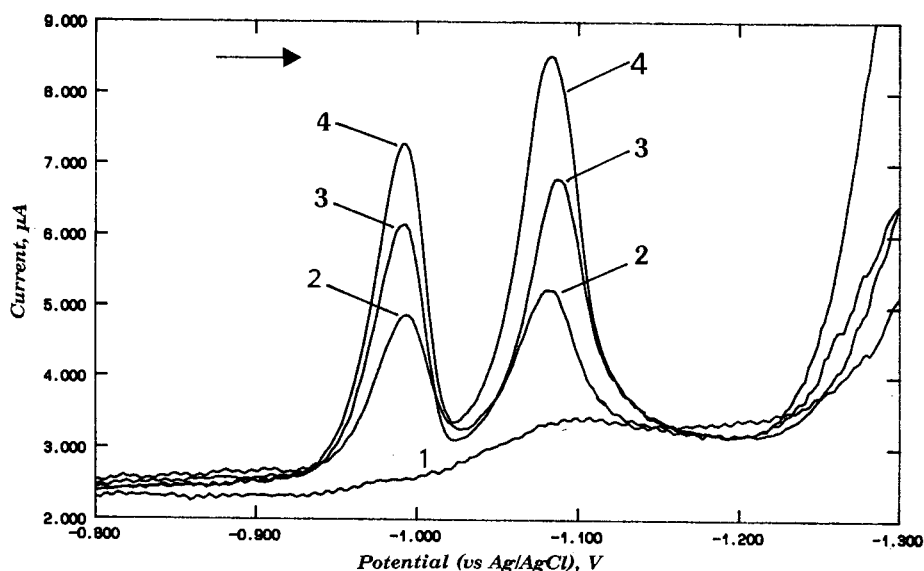


Fig. 5. (a) Analysis of the 149/3 BCR iron sample for its Ni and Co content. (1) blank; (2) sample; (3), (4) successive additions of $6 \mu\text{g l}^{-1}$ Ni(II) and $12 \mu\text{g l}^{-1}$ Co(II). Deposition at -0.5 V. Other conditions as in Fig. 2(a).

3. Results and discussion

3.1. Mercury film cleaning/regeneration

In order to develop the analytical procedure, a stable and renewable electrode surface was required. Despite the recognition of the fact by most authors that the cleaning/regeneration method of the mercury deposit is one of the most important factors determining the precision of the results in AdCSV, no comprehensive study exists related to this subject. In this work, both the reactivation of the electrode after each measurement and the stripping of the mercury film were assessed.

Initial experiments demonstrated that plating of a new mercury film before each measurement resulted in poor reproducibility in the Ni(II) and Co(II) stripping peaks (coefficient of variation for repetitive measurements was 20–25%). This lack of precision associated with MFEs is attributed to variations in the active surface of these electrodes (i.e. the ‘between-film’ precision is poor). For this reason, it was decided to investigate in situ regeneration of the mercury film as suggested in earlier work and it was found that efficient reactivation could be achieved by polarisation of the electrode

at -1.4 V in flowing ammonia buffer. Under these conditions, the complexes of Ni(II) and Co(II) with DMG were reduced and desorbed from the electrode surface. No memory effects from the reduction and amalgamation of the liberated Ni(II) and Co(II) at -1.4 V were observed. It was assumed that the ions were swept downstream by the flowing solution after desorption and reduction of the complex before they could be reoxidised to the zero oxidation state, in view of the low solubility of nickel and cobalt in mercury. It must be noted that the nickel complex took longer to desorb than the cobalt complex but complete removal of both species could be eventually achieved. The time of the cathodic polarisation depended on the amount of complexes adsorbed but, in general, a cleaning time ranging from 40 to 60 s was sufficient. Fig. 2(a) illustrates the effect of the in situ cleaning time on the magnitude of the stripping response. This procedure decreased the coefficient of variation of successive determinations on the same mercury film (referred to as ‘within-film’ reproducibility) to around 3%. To summarise, in contrast to the method based on the formation of a new film before each analysis resulting in significant ‘between-film’ uncertainty, in situ regeneration of the

same film enabled to achieve a much lower 'within-film' uncertainty and the overall precision of results increased. Each electrode could be used for twenty or more complete preconcentration/stripping/regeneration cycles, depending on the matrix. In situ deposition of the mercury film achieved by adding Hg(II) in the sample solution was found to be unsuccessful, probably due to the alkaline pH of the sample that causes the hydrolysis of Hg(II).

The stripping of the mercury from the electrode surface was also investigated. The objective of this study was the efficient, rapid and reproducible removal of the old coating from the electrode surface. The efficiency of the cleaning was monitored by scanning the potential of the electrode from 0.0 to +1.0 V and recording the magnitude of the stripping peak for the oxidation of mercury. Three cleaning methods were studied: i) the first method was based on the strong complexing activity of tetraethylpentamine (tetren) towards mercury [16]. For this purpose a 0.1 M tetren solution was allowed to flow through the cell while the potential of the working electrode was maintained at +0.4 V. Despite efficient and fast removal of mercury (cleaning time was 60 s for a typical film) this method was found to be unsatisfactory because tetren itself is a strong surface active compound. As a result, tetren fouled the active sites of the electrode surface and subsequent mercury plating to form a new film was erratic as demonstrated by small plating currents and small and irreproducible stripping peaks for Ni(II) and Co(II); ii) the second method involved oxidation and complexation of mercury in the form of the very stable $[\text{HgI}_4]^{2-}$ complex in a medium containing iodide and I^- ions [17]. To carry out the cleaning, a solution containing 0.005M I_2 /0.5 M KI was allowed to flow through the cell. It was found that short cleaning times (cleaning time 40 s for a typical film) were sufficient to remove the mercury coating. However, thorough rinsing (~3 min) of the cell was necessary before plating a new mercury film in order to expel any remaining I^- ions and, thus, avoid the formation of insoluble Hg_2I_2 on the electrode surface and tubings [16]. A common practical disadvantage of both the methods mentioned

above was that they require a more complex flow system (i.e. additional pumps and valves) capable of providing the cleaning medium; iii) the third method involved electrochemical oxidation of mercury at +0.8 V in a 0.1 M HNO_3 solution [15]. Although this method was more time consuming (a cleaning time of 120 s was required for a typical film), any risk of contamination or poisoning of the electrode surface and the flow manifold was eliminated and the experimental procedure was simplified as the nitric acid medium was also used as the carrier for the mercury plating. The traces in Fig. 2(b) demonstrate the cleaning efficiency after polarisation at +0.8 V in 0.1 M HNO_3 for different cleaning times. Electrochemical cleaning was selected for all the subsequent experiments.

3.2. Effect of the total injected sample volume and the flow rate

In batch analysis, the effective preconcentration time is calculated as the total time during which accumulation of the adsorbable species is carried out. In this case, the bulk concentration of the species is assumed to be constant with time. In FIA, preconcentration occurs only when each injected sample plug passes over the electrode and, even then, preconcentration is more efficient at the centre of the plug rather than at the edges where diffusion is predominant. So, In FIA it is more meaningful to relate the stripping current on the volume of the injected sample (or, equivalently, to the number of injections) rather than on the total preconcentration time. The relevant plot for the simultaneous determination of Ni(II) and Co(II) is illustrated in Fig. 3. The response, typically for an adsorptive process, increased with the

Table 2
Analysis of the 149/3 BCR iron sample for its nickel and cobalt content by SWAdCSV ($n = 5$)

Certified content (%)		Content found (%)	
Ni	Co	Ni	Co
0.0036	0.0073	0.0040	0.0075
± 0.0008	± 0.0005	± 0.0008	± 0.0006

total injected volume and levelled off at higher preconcentration times for both Ni(II) and Co(II). The pattern is that the equilibrium surface concentration for Ni(II) was lower and was achieved earlier for Ni(II) than for Co(II) and it was similar to the pattern obtained for the rotating disk electrode and the HMDE [6,18]. This is probably due to the fact that the adsorption coefficient of Ni(II) is larger than the adsorption coefficient of Co(II) at the preconcentration potential of -0.7 V, as already noted in earlier studies [6,18].

Varying the carrier flow rate between 1 and 3 ml min⁻¹ did not affect the peak currents significantly, probably because the increase in the preconcentration efficiency afforded at higher flow rates was counterbalanced by the decreased residence time of the sample in the flow cell. However, higher flow rates enabled higher sampling frequencies and faster rinsing of the cell. A flow rate of 2 ml min⁻¹ was adopted for most of the experiments in this work.

3.3. Calibration parameters—FIA vs continuous flow preconcentration

The calibration curve for the determination of Ni(II) and Co(II) with FIA was linear up to 1 μ M. For higher concentrations the electrode surface saturated and the calibration curve levelled off. The calibration parameters are shown in Table 1. While the linear range was extended to higher concentrations, the limit of detection was higher than in batch analysis using the HMDE or the rotating disk electrode [6,18]. This sensitivity was not sufficient to determine Ni(II) or Co(II) in ultratrace levels (e.g. seawater) without some sort of preconcentration but was enough for the determination of traces of the two metals in pure iron samples. The sensitivity can be increased by employing continuous flow, instead of FIA, preconcentration. This preconcentration mode involves continuous flow of the sample through the cell during the accumulation period rather than discrete injections of sample. Conversion of the FIA manifold to continuous flow

manifold can be achieved in a matter of minutes by repositioning the electrochemical flow cell in the flow manifold, as reported earlier [19]. The calibration parameters with continuous flow preconcentration are also, shown in Table 1.

3.4. Optimisation of the background response

In most reductive voltammetric procedures, dissolved oxygen interferes by producing a wide reduction irreversible peak and capacitive currents arise as a result of the potential scan. In this work two methods were combined to alleviate the deterioration in the background due to these effects: i) the SW potential scanning waveform, and; ii) the medium exchange approach. A third method, involving the use of concentrated CaCl₂ (which has a low oxygen content) [20] was considered impractical due to the possibility of calomel formation on the electrode surface.

The SW provides a means of discrimination of reduction processes according to their reversibility because it enhances the redox current of reversible processes and suppresses less reversible processes. In this case, since the reduction of Ni(II) and Co(II) is irreversible [6], the SW modulation affords no improvement on the classical digitally generated staircase waveform (SC) as far as the sensitivity (peak heights) is concerned. This is due to the same polarity of the forward, I_p , and reverse currents, I_r , which result in a decreased differential current, I_d , (Fig. 4(a)). This is further demonstrated by inspection of the traces in an unpurged solution which clearly demonstrate that no discrimination against oxygen is provided by the SW scan (Trace 1 in Fig. 4(b)). Thus, not only is sensitivity compromised by the use of SW but also the oxygen interference remains. In view of these results, the utility of the SW mode can be questioned. However, a significant improvement in the capacitive component can be obtained as a result of the differential nature of this technique (Fig. 4(a) and Traces 3 and 5 in Fig. 4(b)). On the other hand, the effect of oxygen can be eliminated by exchanging the sample solution with purged ammonia buffer (Trace 3 in Fig. 4(b)).

3.5. Analytical application

The method developed was applied to the analysis of high purity iron for its nickel and cobalt content. The sample was dissolved in nitric acid to oxidise the metals and convert them to their cations, Ni(II) and Co(II). Tartrate was added to the sample solution to prevent Fe(III) from precipitating as Fe(OH)₃ when making the pH alkaline. As explained in the previous section, the sample was not deliberately deoxygenated since the stripping was carried out in the purged buffer. The method of standard additions was used for the quantitative evaluation of the nickel and cobalt content in order to avoid any matrix effects. In agreement with the findings of previous work and, since cobalt is in excess of nickel in the sample, the preconcentration was carried out at -0.5 V in order to increase the ratio of Ni(II)-to-Co(II) peak heights [6]. The peaks for Ni(II) and Co(II) were well defined and no interfering peaks due to other constituents of the sample were present. A series of traces after standard additions in the sample is illustrated in Fig. 5(a). The results for the standard additions analysis are shown in Table 2. It was noted that, after repetitive measurements without in situ electrode cleaning an increase in the background current close to the Co(II) peak was observed. This effect was not investigated further as cleaning of the electrode at -1.4 V restored the background to its initial value.

References

- [1] J. Perez Pena, J.J. Hernandez Brito, J. Herrera Melian, C. Callado Sanchez, C.M.G. van den Berg, *Electroanalysis* 6 (1994) 1069.
- [2] M.M. Palrecha, *Fresenius. J. Anal. Chem.* 351 (1995) 800.
- [3] A. Economou, P.R. Fielden, *TrAC* 16 (1997) 286.
- [4] A. Economou, P.R. Fielden, *Analyst* 118 (1993) 1399.
- [5] H.J. Diederich, S. Meyer, F. Scholz, *Fr. Z. Anal. Chem.* 349 (1994) 670.
- [6] A. Economou, P.R. Fielden, *Analyst* 118 (1993) 47.
- [7] J.M. Zen, M.L. Lee, *Anal. Chem.* 65 (1993) 3238.
- [8] R.I. Mrzljak, A.M. Bond, T.J. Cardwell, R.W. Cattrall, R.W. Knight, O.M.G. Newton, B.R. Champion, *Analyst* 119 (1994) 1057.
- [9] M.P. Newton, C.M.G. van den Berg, *Anal. Chim. Acta* 199 (1987) 59.
- [10] C.M.A. Brett, A.M.C.F. Oliveira Brett, J.L. Pereira, *Electroanalysis* 3 (1991) 683.
- [11] M.M.G.S. Rocha, M.M.P.M. Neto, M.O. Torres, A. de Varennes, *Electroanalysis* 9 (1997) 145.
- [12] C.M.A. Brett, M.B.Q. Garcia, J.L.F.C. Lima, *Electroanalysis* 8 (1996) 1169.
- [13] C.M.A. Brett, A.M.C.F. Oliveira Brett, L. Tugulea, *Electroanalysis* 8 (1996) 639.
- [14] A. Economou, P.R. Fielden, *Anal. Chim. Acta* 273 (1993) 27.
- [15] A. Economou, P.R. Fielden, A.J. Packham, *Analyst* 119 (1994) 279.
- [16] M. Wasberg, A. Ivaska, *Anal. Chim. Acta* 179 (1986) 433.
- [17] H. Eskilsson, C. Haraldsson, D. Jagner, *Anal. Chim. Acta* 175 (1985) 79.
- [18] S.B. Adeloju, A.M. Bond, M.H. Briggs, *Anal. Chim. Acta* 164 (1984) 181.
- [19] A. Economou, P.R. Fielden, *Analyst* 121 (1996) 1903.
- [20] D. Jagner, L. Renman, Y.D. Wang, *Electroanalysis* 4 (1992) 267.

Non-protected fluid room temperature phosphorescence of several naphthalene derivatives

Longdi Li *, Yu Zhao, Yingguang Wu, Aijun Tong

Department of Chemistry, Tsinghua University, Beijing 100084, China

Received 8 May 1997; received in revised form 27 October 1997; accepted 28 October 1997

Abstract

In our previous work, we reported that with TINO_3 as a heavy atom perturber and Na_2SO_3 as a deoxygenator, room temperature phosphorescence (RTP) emission of dansyl chloride and its amino acid derivatives can be induced directly from their aqueous solution without a protective medium. Is this kind of fluid luminescence phenomenon unique for the dansyl chloride compounds? The present work has shown that many naphthalene derivatives can also exhibit RTP emission in their aqueous solutions under similar conditions in the absence of a protective medium. Such an RTP emission phenomenon could be denoted as nonprotected fluid room temperature phosphorescence (NP-RTP). In order to further understand this new luminescence phenomenon, the substituent group effects and the favorable chemical structure of compounds for NP-RTP emissions are discussed in detail. © 1998 Elsevier Science B.V. All rights reserved.

Keywords: Naphthalene derivatives; NP-RTP; Substituent group

1. Introduction

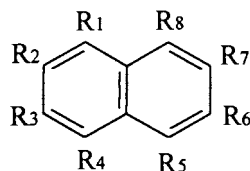
As $S_0 \rightarrow T_1$ is a spin-forbidden transition, the triplet state has a long lifetime. During this moment, the nonradiative decay processes of luminophores, the collisions with solvent and conversion of energy, as well as the possibility of photochemical reaction, can easily take place. As a result, the intensity of the phosphorescence will be attenuated and the detection of phosphorescence in solution or gas phases becomes very difficult.

Donkerbroek et al. [1,2] investigated the room temperature phosphorescence (RTP) of various phosphorescent compounds in solution, concluding that RTP intensities of solutes in liquid solution are generally too low to be useful in direct analytical work. This is mainly due to the long lifetime of the triplet state, which favors collision quenching by oxygen and other quenchers in solution at room temperature.

Turro et al. [3] first reported that RTP in fluid solution could be observed in the presence of micelles, heavy atoms and deoxygenation by nitrogen. On the basis of that report, Cline Love [4] established the micelle-stabilized room temperature phosphorescence (MS-RTP) as an analytical

* Corresponding author.

Table 1
Chemical structure, name and code of the 26 derivatives studied



Code	Structure and name	Code	Structure and name
1	Naphthalene; $R_1 = R_2 = R_3 = R_5 = R_6 = R_8 = H$	14	Dansyl amine
2	1-Naphthol; $R_1 = -OH$	15	1-Amino-5-naphthalenesulfonic acid sodium salt; $R_1 = NH_2$, $R_5 = -SO_3Na$
3	2-Naphthol; $R_2 = -OH$	16	1-Nitroso-2-naphthol; $R_1 = -NO$, $R_2 = -OH$
4	α -Naphthalene chloride; $R_1 = -Cl$	17	2-Nitroso-1-naphthol; $R_1 = -OH$, $R_2 = -NO$
5	α -Naphthalene bromide; $R_1 = -Br$	18	Diaminoethylene naphthyl hydrochloride; $R_1 = -CH=C(NH_2 \cdot HCl)_2$
6	1-Naphthamine; $R_1 = -NH_2$	19	8-Phenylamine-1-naphthalenesulfonic acid; $R_1 = -SO_3H$, $R_8 = -NHPh$
7	1-Naphthamine hydrochloride; $R_1 = -NH_2 \cdot HCl$	20	Nitroso red salt; $R_1 = -NO$, $R_2 = -OH$, $R_3 = R_6 = -SO_3Na$
8	β -Naphthol ethyl ether; $R_2 = -OCH_2CH_3$	21	TAN; $R_1 = -N=N-SNC_3H_7$, $R_2 = -OH$
9	α -Naphthylacetic acid; $R_1 = -CH_2COOH$	22	1,5-Dinaphthalenesulfonic acid; $R_1 = -SO_3H$, $R_5 = -SO_3H$
10	α -Naphthoxyacetic acid; $R_1 = -OCH_2COOH$	23	1-Hydroxy-2-naphthoic acid; $R_1 = -OH$, $R_2 = -COOH$
11	β -Naphthoxyacetic acid; $R_2 = -OCH_2COOH$	24	Anthracene
12	β -Naphthalenesulfonic acid sodium; $R_2 = -SO_3Na$	25	Phenanthrene
13	Dansyl chloride; $R_1 = -N(CH_3)_2$, $R_5 = -SO_2Cl$	26	Pyrene

method. The phase behavior of micelles changes the microscopic environment and raises the stability of the triplet state, so that phosphorescence intensity increases to a remarkable degree. Following the successful application of protected medium in fluid RTP, cyclodextrin-induced RTP (CD-RTP) [5], vesicle-stabilized RTP (VS-RTP) [6], microemulsion-stabilized RTP (ME-RTP) [7] etc., have been developed subsequently.

Therefore, it seems necessary to provide a protective ordered medium to minimize self-quenching and bimolecular quenching (for example, in CD-RTP, cyclodextrins are the microscopically ordered medium and phosphors are protected in their cavities) and to organize reactants on a molecular level to increase the proximity of heavy atoms and analyses which can increase the quan-

tity of the triplet state and lead to a intense phosphorescence emission. Using these methods, RTP can be observed after deoxygenation.

However, based on the recent discovery, our group has reported that the RTP emission of dansyl chloride (DNS-Cl) and its derivatives can be directly induced in aqueous systems only by the addition of thallos nitrate as a heavy atom perturber and sodium sulfite as the deoxygenator [8,9]. In order to discover whether this phenomenon occurs only for some unique compounds or if the others also display this characteristic, the properties of RTP emission in a series of solutions of naphthalene derivatives without protective medium (the chemical names of these derivatives studied and their respective codes in this paper are shown in Table 1) were

studied in the present work. The experimental results demonstrated that DNS-Cl is not the only compound to produce RTP without protective ordered medium. The RTP of many derivatives can also be induced under the same conditions. Following our research into the mechanism of this phenomenon, the name non-protected fluid room temperature phosphorescence (NP-RTP) is suggested for this new type of RTP emission.

2. Experimental

2.1. Chemicals

Aqueous solutions (2.0 mmol l^{-1}) were prepared for the code 7, 12, 15, 18, 19, 20 and 22 compounds, 2.0 mmol l^{-1} acetone–water (1:9 v:v) solutions were prepared for code 2, 3, 6, 9, 16 and 23 compounds and 2.0 mmol l^{-1} acetone solutions were prepared for the remaining compounds. Thallous nitrate (TlNO_3 , CP), sodium sulfite (Na_2SO_3 , AR) were purchased from Beijing Chemical Plant (China) and a 0.25 mol l^{-1} solution of TlNO_3 and a 0.1 mol l^{-1} solution of Na_2SO_3 were used in experiments. The water used was sub-boiled and distilled twice.

2.2. Instruments

All spectra and luminescence intensities were obtained with a Perkin–Elmer LS-50B luminescence spectrometer. Data acquisition and manipulation were facilitated by a King computer interfaced directly to the spectrometer.

2.3. Methods

All glassware used was washed with analytical grade acetone or doubly distilled water before use.

2.3.1. Determination of fluorescence

A 0.1 ml aliquot of 2.0 mmol l^{-1} naphthalene derivative solution was added to a 5 ml quantitative tube and the solution was filled to the mark with water. After shaking, the fluorescence spectra were measured with a 1 cm quartz cell (Ex slit = Em slit = 3 nm).

2.3.2. Determination of phosphorescence

A 0.1 ml aliquot of 2.0 mmol l^{-1} naphthalene derivative solution was added to a 5 ml quantitative test tube. A 1.0 ml aliquot of 0.25 mol l^{-1} TlNO_3 and 0.5 ml aliquot of 0.1 mol l^{-1} Na_2SO_3 were added and the solution was filled to the mark with water. Following shaking, the phosphorescence and mixed spectra (fluorescence spectra in the presence of a heavy atom perturber) were measured with a 1 cm quartz cell (for phosphorescence spectra: Ex slit = 15.0 nm ; Em slit = 20.0 nm ; delay time = 0.1 ms ; gate time = 2.0 ms ; for mixed spectra: Ex slit = Em slit = 3.0 nm).

3. Results and discussion

3.1. NP-RTP spectra of naphthalene derivatives

Under the above conditions, the NP-RTP spectra and characterization of several naphthalene derivatives are shown in Fig. 1 and Table 2. In particular, we choose 1-amino-5-naphthalenesulfonic acid sodium salt as a typical example (see Fig. 2). It can be seen that the phosphorescence emission wavelength is much longer than that of the fluorescence, but the excitation wavelengths are very similar. Moreover, it is well known that fluorescence lifetime is 10^{-8} s order of magnitude; however, the RTP life time of naphthalene derivatives that were measured was 10^{-4} s . These results clearly illustrate that what we observed is indeed RTP.

Therefore, the conclusion is drawn that with TlNO_3 as a heavy atom perturber and Na_2SO_3 as a chemical deoxygenator, many derivatives can emit RTP without a protective medium. Furthermore, the RTP intensities are high enough to be useful in analytical work.

3.2. Effect of TlNO_3 on the NP-RTP of dansyl chloride

With fixed concentrations of dansyl chloride and Na_2SO_3 , the intensities of fluorescence and RTP of DNS-Cl change with the change in TlNO_3 concentration (Fig. 3). While increasing TlNO_3 content, its fluorescence intensity decreases and

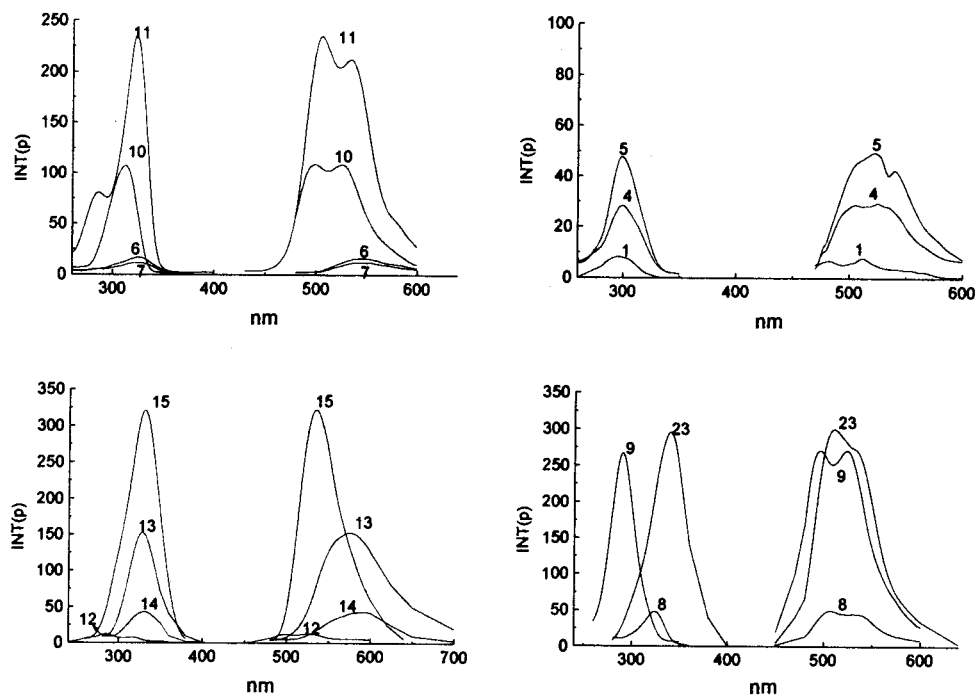


Fig. 1. RTP spectra of partial naphthalene derivatives (code as in Table 1; $C = 4.0 \times 10^{-5} \text{ mol l}^{-1}$).

the RTP intensity increases. Therefore, TINO_3 is a spin-forbidden transition enhancer, increasing intersystem-crossing efficiency.

3.3. Time-stability of RTP emission

For the purpose of using NP-RTP properties of naphthalene derivatives as an analytical tool, the time stability of RTP emission was studied. As shown in the time-scanning spectrum (Fig. 4), there are three cases for the compounds studied: (1) for dansyl chloride in acetone solution, it is necessary to irradiate for 30 s with the apparatus light source in order to obtain a stable RTP signal; (2) for 1-amino-5-naphthalene-sulfonic acid sodium salt in aqueous solution, the RTP intensity is stable; and (3) for some derivatives, including β -naphthoxyacetic acid and α -naphthylacetic acid, the intensity falls with increasing irradiative time. The mechanisms leading to these differences remain to be further investigated.

3.4. Analytical curve and detection limit

Since the RTP intensities of 1-hydroxy-2-naphthoic acid, α -naphthalic acid and 1-amino-5-naphthalenesulfonic acid sodium salt are quite strong under the experimental conditions, the relationship between NP-RTP intensity and the concentration of these derivatives has been investigated and a good linearity has resulted (Table 3).

3.5. Discussion

All the experimental results show that in the presence of a heavy atom perturber to increase the efficiency of the triplet state and a deoxygenator to decrease the quenching of oxygen, the NP-RTP of many naphthalene derivatives without microscopically ordered medium can be observed.

As shown in the literature [10,11], a few compounds such as bridged biphenyls, octahelicene

Table 2
RTP and fluorescence properties of 26 naphthalene derivatives

Code	Phosphorescence			Fluorescence		Mixed spectra	
	$\lambda_{\text{ex}}/\lambda_{\text{em}}$	I_{P}	τ_{p} (ms)	$\lambda_{\text{ex}}/\lambda_{\text{em}}$	I_{F}	$\lambda_{\text{ex}}/\lambda_{\text{em}}$	I_{m}
1	296/482, 512	8.0	—	207, 224, 287, 307/334	125.0	296, 352/404	51.1 ^b
2	—	—	—	297/467	67.8	—	—
3	—	—	—	231, 273, 326/361, 409	998.0	—	—
4	300/525	29.4	0.3977	230, 298/343	26.0	300/340	39.4 ^c
5	299/523, 540	49.4	0.4461	237, 299, 350/397	23.0 ^c	297, 338/385	55 ^b
6	326/546	16.0	0.3517	315/447	388.8	327/450	48.5
7	325/545	11.9	0.2791	314/448	776.7	326/445	55.4
8	324/507	49.4	0.4083	213, 325/352	507.1	327/353	48.7
9	290/495, 523	270.7	0.4182	210, 228, 284/340	750.2	291/341	6.3
10	312/499, 525	108.8	0.3240	220, 309/366	119.5	316/368	18.3
11	286, 323/505, 534	234.0	0.3320	208, 233, 272, 325/350	353.0 ^d	327, 381/442	—
12	284/500, 528	12.7	0.2230	231, 271/329, 341, 354	319.9 ^d	285, 321/341	13.6
13	328/574	152.6	0.5405	320/504	120.6	328/491	19.0
14	331/591	43.1	0.7780	326/531	22.9	336/520	16.5
15 ^a	331/534	322.5 ^b	0.4643	327/424	566.1 ^d	331/422	217.8
16	—	—	—	375/431	—	—	—
17	—	—	—	361/421	—	—	—
18	—	—	—	326/428	389.5 ^d	—	—
19	—	—	—	—	—	—	—
20	—	—	—	338/495	3.8	—	—
21	—	—	—	—	—	—	—
22	—	—	—	227, 286/338	983.9	296/338	150
23	340/510	300.2	0.2397	341/415	338.0	341/417	180
24	—	—	—	336, 353, 372, 394/405, 422, 446	423.1	—	—
25	292/477	6.5	—	303, 334, 350, 364/392, 412, 436	219.3	—	—
26	334/600	1.2	—	320, 334/376, 395, 456	314.2	—	—

^a Ex slit = Em slit.

^b 10 nm.

^c 5 nm.

^d 2.5 nm.

etc., can produce RTP emission without protective medium. This was attributed to the specific rigidity of the luminophor or the existence of a spin-forbidden transition enhancer. It was regarded as a particular phenomenon belonging to this kind of compound. However, our studies show NP-RTP is not an exceptional phenomenon of certain derivatives but a regular characteristic of naphthalene derivatives. Clearly, the existence of a specific intersystem-crossing enhancement reagent is an important external condition. After studying the structure of naphthalene derivatives, we concluded that RTP emission depends mainly on the chemical structure of the derivatives and the nature of the lowest excited triplet state.

3.5.1. Favorable chemical structure and the nature of the lowest excited triplet state

The basic structure of naphthalene derivatives is the naphthalene nucleus, which has a specific rigidity. The molecular configuration is planar, leading to a high fluorescence efficiency. If the conjugated system grows with the substituent group, the electron is easily excited and fluorescence and phosphorescence are engendered. Turro [12] has pointed out that if phosphorescence can be obtained at 77 K, it can also generally be observed in fluid solution at room temperature, if two conditions are fulfilled: (1) impurities capable of quenching triplet states are rigorously excluded; (2) the triplet state does not undergo an

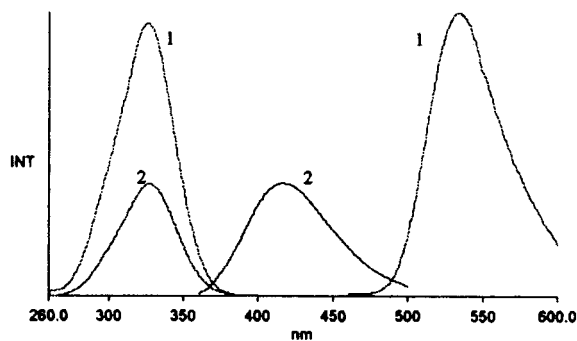


Fig. 2. NP-RTP and fluorescence spectra of 1-amino-5-naphthalenesulfonic acid sodium salt ($C = 1.6 \times 10^{-6} \text{ mol l}^{-1}$). 1, NP-RTP (Ex slit = 15 nm, Em slit = 20 nm); 2, fluorescence (Ex slit = Em slit = 3.0 nm).

activated unimolecular deactivation having a rate constant (3k_m) greater than or equal to 10^4 times the rate constant for phosphorescence (k_p). In other words, phosphorescence can be observed at room temperature in fluid solution provided that ${}^3k_m < 10^4 k_p$ and that the phosphorescence quantum yield (Φ_p) can be expressed approximately by Eq. (1) based on the dynamic graph (Fig. 5)

$$\Phi_p = \frac{k_p}{{}^3k_m + k_q[q]} \quad (1)$$

where k_q is the rate constant for bimolecular deactivation of the triplet state and $[q]$ is the concentration of quencher. A typical value of k_p for a molecule in an (n, π^*) triplet state (T_1) is 10^2 s , while in a (π, π^*) triplet state is 10^{-1} s [13]. With these k_p values and other assumptions, it is

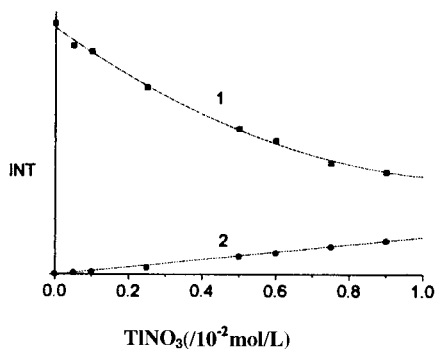


Fig. 3. Effect of TINO_3 on Fluorescence and RTP of DNS-Cl. 1, fluorescence; 2, RTP.

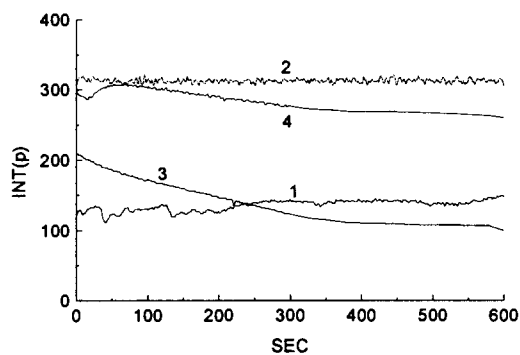


Fig. 4. Time-scanning spectra of RTP. 1, dansyl chloride; 2, 1-amino-5-naphthalenesulfonic acid sodium salt; 3, β -naphthoxyacetic acid; 4, α -naphthylacetic acid.

possible to calculate the limiting concentration of quencher for the observation of phosphorescence if the quenching is diffusional controlled, such as oxygen. To observe phosphorescence, the Φ_p should be at least 10^{-4} , while for non-viscous organic solvent, the rate constant of diffusion (k_{dif}) is about $10^{10} \text{ l mol}^{-1} \text{ s}^{-1}$. In general, it is assumed that $k_{\text{dif}} = k_q$, then the condition for observing phosphorescence is: for $T_1(n, \pi^*)$, $k_{\text{dif}}[q] < 10^6 \text{ s}$, therefore $[q] < 10^{-4} \text{ mol l}^{-1}$; and for $T_1(\pi, \pi^*)$, $k_{\text{dif}}[q] < 10^3 \text{ s}$, therefore $[q] < 10^{-7} \text{ mol l}^{-1}$.

A concentration of $10^{-4} \text{ mol l}^{-1}$ for q can be readily obtained experimentally, but to obtain a concentration of $10^{-7} \text{ mol l}^{-1}$ is more difficult. Thus, it is easy to observe fluid RTP of compounds with $T_1(n, \pi^*)$ states, whereas it is quite difficult with $T_1(\pi, \pi^*)$ states. This conclusion is in accordance with our experimental results. For example, the NP-RTP emission of naphthalene, anthracene, phenanthrene and pyrene are very weak or cannot be observed because their triplet states are $T_1(\pi, \pi^*)$ states, even in very pure solvents (impurity level including oxygen below $10^{-9} \text{ mol l}^{-1}$), the quantum yields of phosphorescence (Φ_p) are in the order of 10^{-6} .

3.5.2. The substituent group effects

1. Electron-donating substituent groups, particularly those with an n electron, tend to increase the phosphorescence intensity, since they can increase the mobility of the electrons of the naph-

Table 3
Characterization of analytical curve

Compound	Linear range (mol l ⁻¹)	Slope	Intercept	Correlation co- efficient	Detection limit (mol l ⁻¹)
1-Hydroxy-2-naphthoic acid	4.0×10^{-7} $\sim 2.0 \times 10^{-5}$	1.16×10^7	2.10	0.997	1.5×10^{-7}
α -Naphthylacetic acid	8.0×10^{-6} $\sim 8.0 \times 10^{-5}$	4.02×10^6	3.44	0.990	5.9×10^{-7}
1-Amino-5-naphthalenesulfonic acid sodium salt	1.6×10^{-7} $\sim 4.0 \times 10^{-6}$	3.84×10^7	5.30	0.999	3.0×10^{-8}

thalene ring and can form a $T_1(n, \pi^*)$ state such as 1-naphthylamine, β -naphthyl ethyl ether etc...

2. Substituent groups with a negative charge can enhance the phosphorescence intensity. In aqueous solution, the proximity between luminophor and inorganic heavy atom perturber Tl^+ can be increased owing to attraction based on static electricity and can increase the efficiency of intersystem crossing to the triplet state, such as for the code 15 compound, 1-amino-5-naphthalenesulfonic acid sodium salt, which contained not only the electron-donating (with n electron) group $-NH_2$ but also contained the SO_3^- group at position 5. Therefore, its NP-RTP intensity is the highest in the compounds studied.

3. For heavy atom substituted compounds, phosphorescence intensity is relatively strong. In molecules containing heavy atoms, this condition favors a higher probability of intersystem-crossing $S_1 \rightarrow T_1$. Frequently, one sees a decrease in the fluorescence quantum yield Φ_f and an increase in

the phosphorescence quantum yield Φ_p when the heavy-atom effect occurs, such as the Φ_f and Φ_p are 0.55, 0.0016 and 0.051, 0.27 at 77 K for naphthalene and α -naphthalenebromide, respectively [14]. The introduction of additional halogen atoms into naphthalene nuclei also results in a red-shift in the phosphorescence.

4. If the carbonyl group is present, the lowest excited singlet state of derivative is the $S_1(n, \pi^*)$ state. The $S_1 \rightarrow T_1$ intersystem crossing efficiency is high [15] and the NP-RTP of the compound is usually observed, such as code 9, 10, 11 and 23 compounds.

5. Compounds with $-NO$ or $-OH$ groups substituted, such as code 16, 20, 2 and 3 compounds, do not favor phosphorescence emission in solution. When the substituted group is $-NO$, it is easy to produce $T_1 \rightarrow S_0$ non-irradiative intersystem-crossing or photochemical reaction, owing to the reactivity of $-NO$. In aqueous solution, there are hydrogen bonds between the $-OH$ substituent group and H_2O and this may lead to quenching of the phosphorescence. If a suitable amount of β -CD is added into the corresponding α - or β -naphthol (code 2, 3) system, the phosphorescence may be observed as a result of the protective effect of CDs, which isolates luminophor and water.

6. For 1,8-ANS, the group at position 8 is phenylamine, which is connected with naphthalene nucleus through single bond. Since rotation configuration causes energy dissipation, not only can NP-RTP not be detected, but the fluorescence intensity is also very weak.

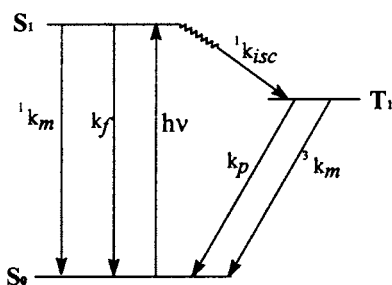


Fig. 5. The dynamic graph of fluorescence and phosphorescence.

Although it is problematic to illustrate the mechanism of NP-RTP clearly at present, we can predict, based on the above, whether a compound with an n electron and negative charge substituent group, 1-dimethylamino-5-naphthalenesulfonate, it will give intensive NP-RTP emission.

Compared with CD-RTP, MS-RTP etc., NP-RTP has some unique advantages:

1. First and most important, without the microscopically ordered protective medium, NP-RTP not only makes the method itself simple, but also can avoid interference with the analysis due to the addition of the medium. It is particularly suitable for biological samples.

2. RTP can be a useful and powerful technique for detection in liquid chromatography and flow injection analysis (FIA). The investigated system is a transparent, stable solution, which makes it possible to associate it with these analytical techniques and perform automatic on-line analysis.

NP-RTP is a new method for fluid RTP technique. The scope of this luminescence technique is very broad. For example, DNS-Cl, DNS-NH₂ etc., are important and widely used fluorescence derivative reagents, whose derivatives can also be used for NP-RTP. In addition, for sensitized/quenched-RTP (S/Q-RTP) [16], the NP-RTP quantum yield of naphthalene derivatives is high and they can be used as acceptors. Thus, the limits of acceptors for S/Q-RTP will be extended.

Acknowledgements

This work was supported by the National Science Foundation and the Beijing Natural Science Foundation.

References

- [1] J.J. Donkerbroek, C. Gooijer, N.H. Velthorst, R.W. Frei, *Anal. Chem.* 54 (1982) 891.
- [2] J.J. Donkerbroek, J.J. Elzas, C. Gooijer, R.W. Frei, N.H. Velthorst, *Talanta* 28 (1981) 717.
- [3] N.J. Turro, Kou-chang Liu, M.F. Chow, P. Lee, *Photochem. Photobiol.* 27 (1978) 523.
- [4] L.J. Cline Love, M. Skrolec, *Am. Lab.* 13 (1981) 103.
- [5] S. Scypinski, L.J. Cline Love, *Anal. Chem.* 56 (1984) 322.
- [6] M.R. Fernandez de la Campa, Y.M. Liu, M.E. Diaz Garcia, A. Sanz-Medel, *Anal. Chim. Acta* 238 (1990) 297.
- [7] G.R. Romos, I.M. Khasawneh, M.L. Garcia-Alvarez-Coqua, J.D. Winefordner, *Talanta* 35 (1988) 41.
- [8] L.D. Li, Y.L. Chen, A.J. Tong, *Huaxue Tongbao (Lett.)* 6 (1996) 3.
- [9] L.D. Li, Y.L. Chen, Y. Zhao, A.J. Tong, *Anal. Chim. Acta* 341 (1997) 241.
- [10] R.B. Bonner, M.K. DeArmond, G.H. Wall Jr., *J. Am. Chem. Soc.* 94 (1972) 988.
- [11] E. Vander Donckt, M. Matagne, M. Sapir, *Chem. Phys. Lett.* 20 (1973) 81.
- [12] N.J. Turro, *Modern Molecular Photochemistry*, Benjamin-Cummings, Redwood City, CA, 1978, p. 129.
- [13] R.J. Hurtubise, *Phosphorimetry: Theory, Instrumentation and Applications*, VCH, Weinheim, 1990, p. 100.
- [14] X.Q. Song et al., *Guang Hua Xue Yuan Li (Principles of Photochemistry)*, Tsinghua, Beijing, 1983, p. 38.
- [15] G.Z. Chen et al., *Fluorimetry*, 2nd ed., Science in China Press, Beijing, 1990, p. 44.
- [16] J.J. Donkerbroek, N.J.R. Van Eikema Hommes, C. Gooijer, N.H. Velthorst, R.W. Frei, *J. Chromatogr.* 255 (1983) 281.

Determination of tin in marine materials by using hydride generation–high resolution inductively coupled plasma mass spectrometry

Yong-Lai Feng, Hisatake Narasaki *

Department of Chemistry, Faculty of Science, Saitama University, Shimo-Okubo, Urawa 338, Japan

Received 7 July 1997; received in revised form 28 October 1997; accepted 29 October 1997

Abstract

A hydride generation system combined with high-resolution inductively coupled plasma mass spectrometry was used to determine tin in marine materials. The optimization conditions for determination of tin in this system are 0.015 M of sulfuric acid solution as medium, 0.2% (w/v) of sodium tetrahydroborate(III) in 0.015 M of sodium hydroxide solution as a reductant and argon as the carrier gas at a flow rate of 1.1 l min⁻¹. In order to remove the interferences from transition element ions, a strongly basic anion exchanger was used in this method. Tin was converted to its chlorostannate with 2 M hydrochloric acid followed by passing to an anion exchanger. The tin absorbed on the column was then eluted with 1 M nitric acid. Under the optimized conditions, the detection limit of the method was 12 ng l⁻¹ without using the anion column as preconcentration method. The results obtained using this method were in good agreement with the certified values of marine standard reference materials. The recoveries for the method when applied to determine trace tin in river water were 95–115%. © 1998 Elsevier Science B.V. All rights reserved.

Keywords: Inductively coupled plasma mass spectrometry; Tin; Strongly basic anion exchanger

1. Introduction

Hydride generation, as a separation and pre-concentration technique for the determination of hydride-forming elements, has been used recently for the rapid determination of the presence of tin by combination with atomic absorption spectrometry (AAS), inductively coupled plasma

atomic emission spectrometry (ICP-AES) or inductively coupled plasma mass spectrometry (ICP-MS). Of these methods, ICP-MS is the most highly-sensitive. However, with marine materials, because of interference from large amounts of matrix, especially from transition element ions, it is difficult to determine tin by the hydride generation method without interference removal or matrix separation. In the literature on hydride generation technique combined with atomic spectrometry, masking agents [1–8] and ion exchange

* Corresponding author. Tel.: +81 488 522111; fax: +81 488 583378.

resins [9,10] are usually used to reduce or remove the interference from transition element ions. Strongly basic anion exchanger resin such as Amberlite CG400 [9] and Dowex 1-X8 [10] are usually used in the separation column to remove these interferences. Silica gel was also described as a cleanup method for removal of the interferences from transition element ions and preconcentration of trace amounts of tin [11]. Many other masking agents were reported to mask the interference ions in order to reduce their interference in the hydride generation system [1–8]. In a previous paper [12], L-cysteine hydrochloride monohydrate was used as a masking agent to reduce interference from transition metal ions in the hydride generation ICP-AES. In this paper, tin in marine materials and river waters was determined by high-resolution inductively coupled plasma mass spectrometry combined with hydride generation technique. Since tin can be converted into chlorostannate anion in concentrated hydrochloric acid and reconverted into cation with dilute nitric acid, prior to analysis, DIAION PA316, a strongly basic anion exchanger, was used to remove the interferences from transition ions as well as some other hydride-forming elements and CrO_4^- etc. DIAION PA316 is composed of polystyrene crosslinked with 8% divinylbenzene and has functional groups of trimethylammonium.

2. Experimental

2.1. Apparatus

The schematic diagram of the hydride generation system is described elsewhere [13]. A high resolution inductively coupled plasma-mass spectrometer (JMS PLASMAX2, Japan Electron Optics Laboratory, Akishima, Japan) equipped with a computer with a 'HUeLine' operating system to control the instrument operations, data conversion and storage, was used in this study. Two single-channel peristaltic pumps (SJ-1211H, Atto Corporation, Tokyo, Japan) were used to pump the sample and sodium tetrahydroborate(III) solutions, respectively. The waste solution was

drained by an electromagnetic solenoid valve (Pinch Valve PK-305-NO, 13W, Takasago Electric Industries, Nagoya, Japan). The operating conditions of the spectrometer are listed in Table 1. The setup of the electric circuit for this hydride generation system was described elsewhere [13].

2.2. Reagents

The stock standard solution ($1000 \mu\text{g ml}^{-1}$) of Sn(IV) was obtained from Wako Pure Chemical Industries (Tokyo, Japan). The working standard solution (20 ng ml^{-1}) of Sn(IV) and four point calibration solutions composed of blank, 0.2, 0.4 and 0.6 ng ml^{-1} of Sn(IV) in 0.015 M sulfuric acid solution were prepared daily from the stock solution. All acids used were Tamapure-AA-100 (Tama Chemical Industries, Tokyo, Japan). Milli-Q ultrapure water (Japan Millipore, Tokyo, Japan) was used throughout in this study. The stock solution of sodium tetrahydroborate(III) (2% w/v) was prepared by dissolving sodium te-

Table 1
Operating conditions of ICP-MS

Plasma incident power	1.2 kW
Radiofrequency	40.68 MHz
Coolant gas flow rate (argon)	14.5 l min^{-1}
Auxiliary gas flow rate (argon)	0.9 l min^{-1}
Carrier gas flow rate (argon)	1.1 l min^{-1}
Carrier gas pressure	16 kPa
Sampling cone and skimmer cone	Copper
Acceleration voltage	6.0 kV
Acceleration time	0 min
Magnetic field radius	310 mm
Magnetic field angle	40°
Electric field radius	223 mm
Electric field angle	85°
Mass resolution	10 000
Frequency of filter	1000 Hz
Sweep width	2000 ppm
Sweep rate	2000 ms
Repetition number	3
Accumulation	10
Main slit	70 m
Alpha slit	0.76 mm
Collector slit	13 m
Pullout	0
Q lens	0
Torch	Normal MS torch
Sn (m/z)	117.9016

trahydroborate(III) powder (Morton International, Tokyo, Japan) in 0.15 M sodium hydroxide solution and storing in a polyethylene bottle in a refrigerator at 4°C. The usage period for the stock solution of sodium tetrahydroborate(III) is within 1 week. The working solution of sodium tetrahydroborate(III) (0.2% w/v) with 0.015 M sodium hydroxide was prepared by diluting the stock solution daily. Stock solutions of interference ion ($1000 \mu\text{g ml}^{-1}$ and $10 \mu\text{g ml}^{-1}$) were prepared from their corresponding salts. The column (8 mm i.d. \times 100 mm high) was loaded with a strongly basic anion exchange resin DIAION PA 316 (Mitsubishi Chemical, Tokyo, Japan). The resin was used in the chloride form without any conditioning and was discarded after use. All other reagents used were of analytical reagent grade or better.

2.3. Sample pretreatment

For Marine Sediment Reference Material, PACS-1 (National Research Council, Ottawa, Canada), 0.1 g of the material was weighed in a 100-ml platinum dish. Nitric acid (10 ml; 68% w/w Tamapure-AA-10), 2 ml of perchloric acid (70% w/w Tamapure-AA-100) and 0.5 ml of sulfuric acid (98% w/w) were added to the dish. The mixture was left overnight at room temperature. Then 5 ml of hydrofluoric acid (38% w/w) was added and the platinum dish was heated at 80°C on a temperature controllable electric heater plate for 2 h followed by heating continuously at about 150°C until white fumes of perchloric acid were produced, indicating the end of the digestion procedure. The residue was diluted to 100 ml with water and 1 ml of this solution was diluted to 25 ml with 2 M hydrochloric acid followed by passing through the anion exchanger column and washing the column with 15 ml of 2 M hydrochloric acid three times. The tin adsorbed on the column was then eluted with 18 ml of 1 M nitric acid. After the pH of the eluate was adjusted to about 6 with 6 M sodium hydroxide, 0.5 ml of 1.5 M sulfuric acid was added and finally diluted to 50 ml with water.

For Marine Biological Reference Material, TORT-1 (National Research Council, Ottawa, Canada), 0.015 g of the material was treated following a similar procedure to that for the Marine Sediment, but without using hydrofluoric acid.

For river water, 20 ml of concentrated hydrochloric acid was added to 100 ml of river water, giving it an acidity of 2 M. The acidified river water was left overnight, before undergoing a procedure similar to that described above. Finally, the solution was diluted to 50 ml.

3. Results and discussion

3.1. Effect of sulfuric acid concentration on the tin peak area

Prior to optimization of the other conditions, the effect of sulfuric acid concentration on the tin peak area was investigated. Fig. 1 shows the effect of sulfuric acid concentration on the area at 400 ppt of tin. The area increased and reached a maximum with increasing concentration of sulfuric acid. Thereafter in the experiment, 0.015 M sulfuric acid was used. High acidity of sample solution can cause the corrosion of sampling and skimmer cones. The pH values of hydride reaction solution caused by mixing the sample solution with the sodium tetrahydroborate(III) solution decreased with increasing acidity, as shown in Fig. 1. This indicates that the pH of the mixing solution may be a key factor for the hydride generation of tin, the kind of acid being immaterial.

3.2. Effects of concentrations of sodium tetrahydroborate(III) and sodium hydroxide on the tin peak area

The effects of sodium tetrahydroborate(III) concentrations and sodium hydroxide on the tin peak area were investigated. As a result of several experiments, it was found that both concentrations of sodium tetrahydroborate(III) and sodium hydroxide affect the determination of tin. However, when compared with sodium hydroxide, the concentration of sodium tetrahydroborate(III) has

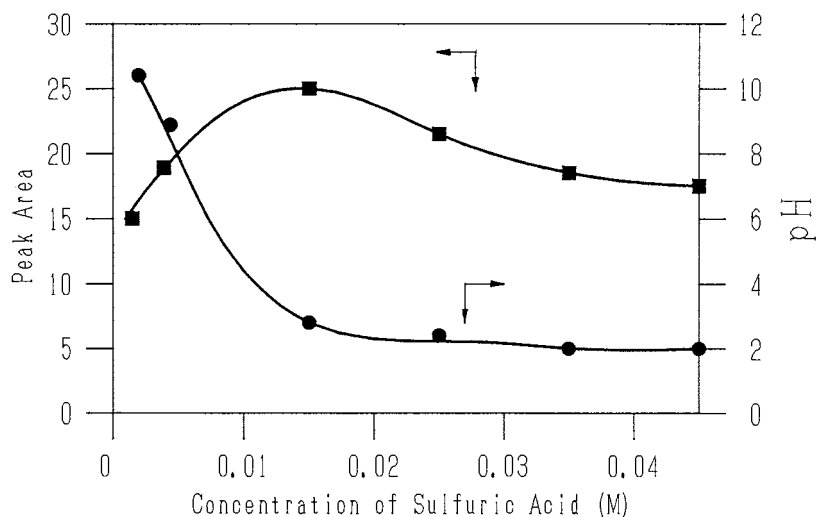


Fig. 1. Effect of concentration of sulfuric acid on the tin peak area. $[\text{Sn(IV)}] = 400$ ppt, concentration of sodium tetrahydroborate(III) is 0.2% in 0.015 M NaOH solution. The flow-rate of the carrier gas (argon) is 1.04 l min^{-1} . ■, concentration of H_2SO_4 versus peak area; ●, concentration of H_2SO_4 versus pH.

a key effect on the area of tin in this system. Finally, 0.2% (w/v) of sodium tetrahydroborate(III) and 0.015 M sodium hydroxide were found to be most suited to the system. To investigate the factor controlling the hydride generation reaction in this system, the pH value of the hydride reaction solution from mixing sample and sodium tetrahydroborate(III) solutions was sur-

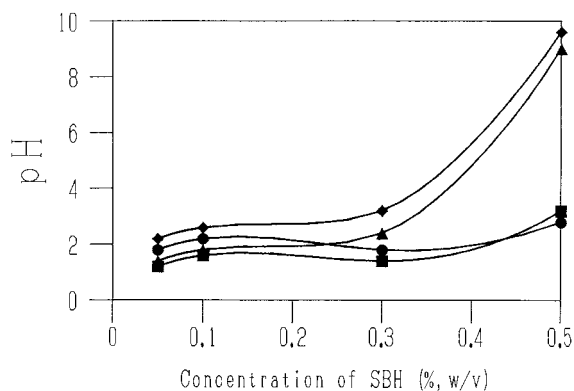


Fig. 2. Effect of concentration of NaBH_4 and NaOH on the pH of the mixed solution. $[\text{Sn(IV)}] = 400$ ppt, concentration of sulfuric acid 0.015 M, flow-rate of carrier gas 1.04 l min^{-1} , concentration of sodium hydroxide: ■, 0.008 M; ●, 0.015 M; ▲, 0.025 M; ◆, 0.035 M.

veyed during the hydride generation procedure. From Fig. 2, it can be seen that the pH value of the mixed solution increased with increasing concentration of sodium hydroxide and sodium tetrahydroborate(III). However, when compared with sodium tetrahydroborate(III), the concentration of sodium hydroxide has little influence on pH in this system, meaning that the variation in pH of the mixed solution may be mainly caused by sodium tetrahydroborate(III), rather than by sodium hydroxide, under the above conditions.

3.3. Effect of carrier gas flow-rate on the tin peak area

The effect of the carrier gas flow-rate on the tin peak area is shown in Fig. 3. It can be seen that the area of tin varied considerably with variation of the carrier gas flow-rate and reached a maximum at about 1.1 l min^{-1} . Separation of the hydride gas from the liquid in the gas-liquid separator may be greatly affected by the flow-rate of the carrier gas. Therefore, in this work, a 1.1 l min^{-1} flow-rate was chosen for the following experiment.

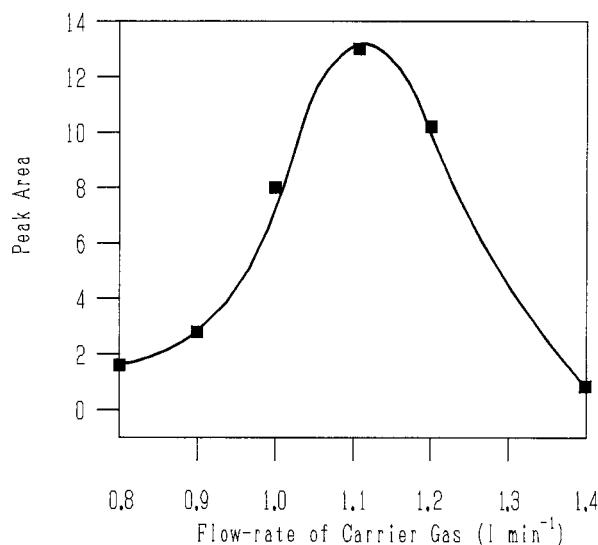


Fig. 3. Effect of carrier gas (argon) flow-rate on the tin peak area. [Sn(IV)] = 400 ppt. The concentrations of sulfuric acid, sodium tetrahydroborate(III) and sodium hydroxide are 0.015 M, 0.2% (w/v) and 0.015 M, respectively.

3.4. Optimization of flow-rate of the sample and sodium tetrahydroborate(III) solutions

Under above optimization conditions, the effect of flow-rates of the sample and sodium tetrahydro-

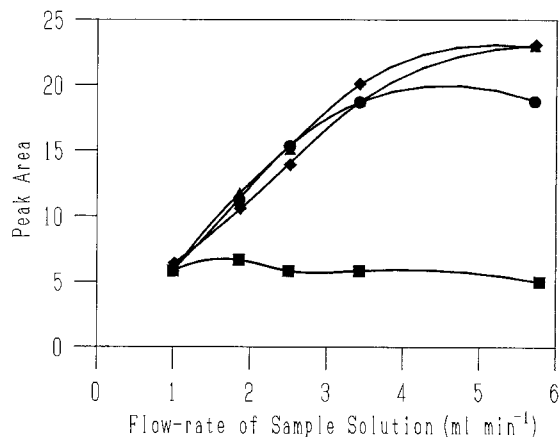


Fig. 4. Effect of flow rate of sodium tetrahydroborate(III) solution and sample solution on the tin peak area. [Sn(IV)] = 400 ppt, the concentrations of H₂SO₄, NaBH₄ and NaOH are 0.015 M, 0.2% (m/v) and 0.015 M, respectively. The carrier gas (argon) flow rate is 1.1 l min⁻¹. The flow rate of sodium tetrahydroborate(III): ■, 0.86 ml min⁻¹; ●, 2.15 ml min⁻¹; ▲, 3.8 ml min⁻¹; ◆, 6.0 ml min⁻¹.

droborate(III) solutions was investigated (Fig. 4). It can be seen that the optimization flow-rates of the sample and sodium tetrahydroborate(III) solutions are 3.6 and 2.15 ml min⁻¹, respectively.

3.5. Effect of kinds of plastic tube on conveyance of stannane

Several plastic tubes (silicone, PVC and Tygon) were checked for their ability to convey stannane from the separating trap to the ICP torch. A silicone tube was found to be most suitable for that purpose, while a PVC tube absorbed stannane and decreased the area.

3.6. Interference study

Table 2 shows the interference from transition metal ions. It can be seen that they greatly affect the determination of tin in this system without using any masking method or separation technique, especially from copper, cobalt and iron. During the investigation of interference from the transition metal ions, the pH values of the mixed solution were also investigated. However, the results showed that the pH values changed little in the presence of interference ions, meaning that the interference from transition metal ions may not be mainly due to reaction of the transition metal ions with sodium tetrahydroborate(III) causing the change in pH value of the mixed solution, but may be due to some other mechanism. In PACS-1, a marine sediment reference material, concentrations of copper, cobalt and iron are about 452 mg kg⁻¹, 17.5 mg kg⁻¹ and 6.96% (as Fe₂O₃), respectively and in TORT-1, a marine biological reference material, concentrations of copper and cobalt are about 439 mg g⁻¹ and 0.42 mg g⁻¹, respectively. Therefore, it is indispensable to eliminate these metals from the materials prior to determination of tin using the hydride generation method. For this reason, a strongly basic anion exchanger resin was investigated to separate and preconcentrate tin, thereby removing interference from transition metal ions. Tin can be converted to the form of anionic chlorostannate complexes in 2 M hydrochloric acid medium, which can be

Table 2
Interference study^a

Ions	Amounts of ions mg l ⁻¹	Recovery without using column %	Recovery using column %
Cd(II)	0.4	100	None ^b
	2	79	None
	5	68	117
	10	45	104
Ni(II)	0.4	91	None
	2	100	131
	5	90	142
Cu(II)	0.04	90	None
	0.4	79	None
	2	1	107
	5	0.4	41
Zn(II)	0.4	91	None
	2	90	116
	5	89	121
Co(II)	0.4	103	None
	2	86	127
	5	15	114
Mn(II)	0.4	95	None
	2	94	None
	5	98	97
	10	96	96
Cr(III)	0.4	99	None
	2	98	122
	5	87	103
Cr(VI)	0.04	87	None
	0.4	83	None
	2	90	101
	5	97	95
Mo(VI)	0.04	97	None
	0.4	86	None
	2	66	88
	5	68	114
Fe(II/III)	0.4	83	None
	2	44	121
	5	11	119

^a Concentrations of tin, NaBH₄ in 0.015 M NaOH solution and sulfuric acid are 0.5 ng l⁻¹, 0.2% w/v and 0.015 M, respectively.

^b Not determined.

adsorbed to the strongly basic anion exchanger resin. This adsorbed tin can then be eluted out when 1 M nitric acid is passed through the anion exchanger resin column [14]. In this study, 2 M hydrochloric acid and 1 M nitric acid were chosen separately and the strongly basic anion exchanger was DIAION PA 316. Fig. 5 shows the elution

curve of DIAION PA 316 column using 1 M nitric acid as the eluant. It can be seen that the adsorbed tin can be completely eluted with 16 ml of the eluant. Therefore, from this point onwards 18 ml of 1 M nitric acid was used to elute the tin chlorostannate. Also evident from Fig. 5, is the long tail of the elution curve, which is similar to

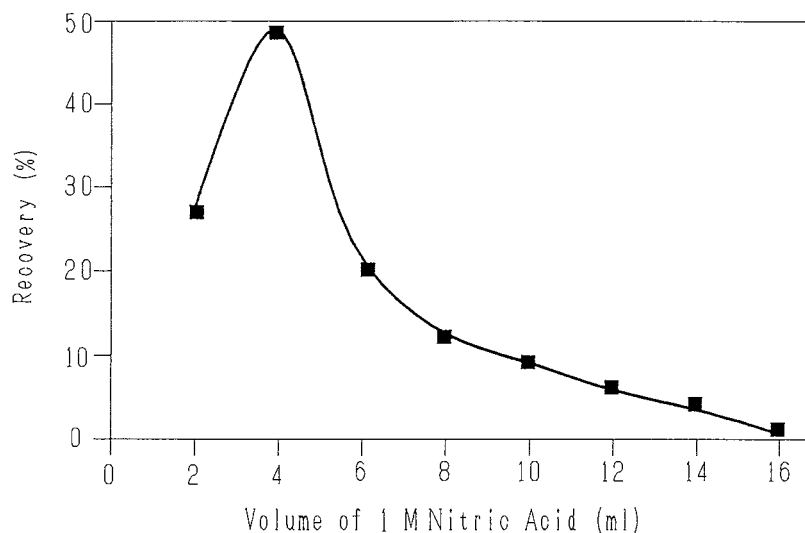


Fig. 5. Elution curve for tin by using 1 M nitric acid. The quantity of Sn(IV) is 4 ng.

Dowex 1X8 described by Fang et al. [10]. Table 2 shows that this anion exchanger resin column can remove interference from transition metal ions, as well as anions which cannot be converted to the form of cations when eluted with 1 M nitric acid.

3.7. Sample analysis

Since there are three kinds of organotins in PACS-1, before the method was applied to determine tin in PACS-1, two kinds of organotins, tributyltin and triphenyltin, were investigated to determine whether they can be converted to inorganic tin by using the same pretreatment conditions. The results (Table 3)

Table 3
Recoveries of organotins

Organotin	Added as tin (ppm)	Recovery (%)
Tributyltin	2.0	96
	0.5	105
	0.1	103
Triphenyltin	2.5	97
	0.5	108
	0.1	94

showed that both kinds of organotins can be completely converted to inorganic tin from 0.1 to 2.5 ppm under the pretreatment conditions. Based on the above investigation, the method was applied to determine tin levels in marine materials and river water. As shown in Table 4, the results obtained by this method are within the certified values of marine standard reference materials.

The river water samples were taken from several sites along the River Arakawa which flows through the Saitama District and into Tokyo Bay. The contents and recoveries of tin in the river water by standard addition are shown in Table 5. The results showed that the recoveries were within the range of the standard deviation.

Table 4
Determination of tin in reference materials

Sample	Measured value ^a (mg kg ⁻¹)	Certified value	
		(mg kg ⁻¹)	Organotin (as Sn)
PACS-1	41.1 ± 3.1	45.4 ± 5.9	2.71 ± 0.57
TORT-1	144 ± 17	139 ± 11	—

^a Mean of four determinations with standard deviation.

Table 5
Analysis of river water

Site	Added (ppb)	Determined (ppb)	Recovery (%)
Mitsumineguchi	0	0.89 ± 0.21^a	—
	0.5	1.53	102
	1	1.85	98
	2	2.97	104
Kami-nagatoro	0	0.53 ± 0.10^a	—
	0.5	1.09	115
	1	1.57	104
	2	2.43	95

^a Mean of three determinations with standard deviation.

References

- [1] H. Narasaki, M. Ikeda, *Fresenius J. Anal. Chem.* 336 (1990) 5.
- [2] X.-C. Le, R. Cullen, K.J. Reimer, I.D. Brindle, *Anal. Chim. Acta* 258 (1992) 307.
- [3] J. Zhang, X. Zeng, Z. Zhang, J. Yang, S. Guan, Q. Guan, *Fenxi Huaxue* 18 (1990) 806.
- [4] M. Legret, L. Divet, *Anal. Chim. Acta* 189 (1986) 313.
- [5] Y. Liu, X.-L. Zhang, C. Luo, *Fenxi Huaxue* 12 (1984) 218.
- [6] I.D. Brindle, X.-C. Le, *Analyst* 113 (1988) 1377.
- [7] P. Schramel, L.-Q. Xu, *Fresenius J. Anal. Chem.* 340 (1991) 41.
- [8] A.M. Abdallah, M.M. El Defrawy, N Nawar, M.M. El Shamy, *J. Anal. At. Spectrom.* 8 (1993) 759.
- [9] T. Kiriya, R. Kuroda, *Mikrochim. Acta (Wien)* 1 (1991) 261.
- [10] Z.-L. Fang, L.-J. Sun, E.H. Hansen, J.E. Olesen, L.M. Henriksen, *Talanta* 39 (1992) 383.
- [11] T. Tsuda, M. Wada, S. Aoki, Y. Matsui, *J. Assoc. Off. Anal. Chem.* 71 (1988) 373.
- [12] Y.-L. Feng, H. Narasaki, H.-Y. Chen, L.-C. Tian, *Fresenius J. Anal. Chem.* 357 (1997) 822.
- [13] H. Narasaki, J.-Y. Cao, *Anal. Sci.* 12 (1996) 623.
- [14] J.D. McCrackan, M.C. Vecchione, S.L. Longo, *At. Absorpt. Newsl.* 8 (1969) 102.

Fluorometric determination of 3,4-dihydroxyphenylalaine in pharmaceutical formulation by reaction with paracetamol

Nianqin Jie ^{a,*}, Duanling Yang ^a, Qiang Zhang ^a, Jinghe Yang ^a, Zhongqing Song ^b

^a Department of Chemistry, Shandong University, Jinan, 250100, China

^b Chemistry Teaching-Research Section, Dalian Maritime University, Jinan, China

Received 4 March 1997; received in revised form 15 October 1997; accepted 30 October 1997

Abstract

A new method has been developed for the fluorometric determination of 3,4-dihydroxyphenylalaine (L-dopa) in pharmaceutical formulations. The reaction product, belonging to fluorescent species, has the excitation and emission maxima at 410 and 510 nm, respectively. Under the optimum conditions, responses were linear between 0.06–4.0 and 4.0–12.0 $\mu\text{g ml}^{-1}$. The detection limit, corresponding to a signal-to-noise ratio of 3, was 1 ng ml^{-1} . The relative standard deviation ($n = 10$) was 0.6%. The proposed method was applied to determination of L-dopa in pharmaceutical formulations. © 1998 Elsevier Science B.V. All rights reserved.

Keywords: Potassium periodate; Paracetamol; L-dopa; Fluorometry

1. Introduction

L-3,4-dihydroxyphenylalaine is also named L-dopa, which is a forerunner of L-dopamine, and it is a catecholamine which is important in neurotransmitter. L-dopa was employed in the treatment of Parkinson disease which is in relation to lack of dopamine in brain tissue, but dopamine can not permeate into brain tissue. In order to increase the concentration of dopamine, we can administer L-dopa which can permeate into brain

tissue and then be converted into dopamine in the presence of decarboxylase.

So it is important to determine L-dopa and its metabolites in biological and pharmaceutical formulations. At present, many methods have been developed for its determination. Spectrophotometry [1] has been used for the determination of L-dopa in pharmaceutical formulations, at 280 nm. Double-wavelength spectrophotometry [2] and derivative spectrophotometry [3] can deplete the interference of carbidopa or benserazida.

Chromatography techniques and thinlayer chromatography has also been used for the separation and determination of L-dopa [4]. Gas chromatography has been used to study the effect of

* Corresponding author. Present address: College of Basic Science and Technology, Agricultural University, Beijing, P.R. China.

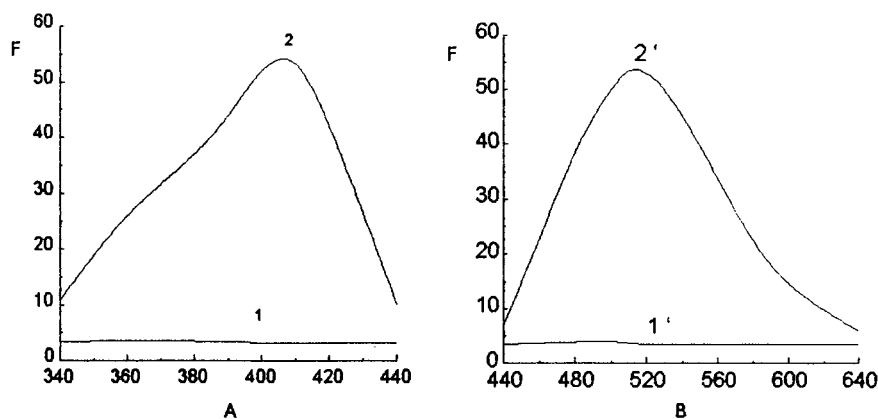


Fig. 1. fluorescence spectra. 1,1'-blank 2,2'-fluorescent species. Conditions: PRT 1.0×10^{-3} mol l^{-1} , H_2SO_4 0.6 mol l^{-1} , KIO_4 4.2×10^{-3} mol l^{-1} , NTA 1.75×10^{-2} mol l^{-1} , NaOH 0.7 mol l^{-1} , L-dopa 8 μg ml^{-1} .

L-dopa in rat brain [5]. High performance liquid chromatography has been widely used for the determination of L-dopa in brain, plasma, urine, liver, serum, tissues and biological fluids using electrochemical detection [6–11], or fluorescence detection [12].

Fluorometry has also been used to determine L-dopa and its metabolites. L-dopa reacts with ethylenediamine to product the fluorescent species [13]. L-dopa can also be oxidized to fluorescent species by I_2 [14], $NaIO_4$ [15] or $K_3[Fe(CN)_6]$ [16].

The purpose of the present investigation is to develop a new simple and sensitive method for the determination of L-dopa in pharmaceutical formulations by fluorometry. Compared with other methods, the proposed method is more sensitivity, precise, simple. The recovery and determination results are satisfactory.

2. Experimental

2.1. Apparatus

All fluorescence measurements were made with a 850-spectrofluorometer (Hitachi, Japan).

2.2. Reagents

All reagents were of analytical grade and demineralized distilled water was used throughout.

L-dopa solution ($100 \mu g$ ml^{-1}) was prepared by dissolving 0.0100 g L-dopa (Beijing) in 100 ml of distilled water.

Paracetamol solution (1×10^{-2} mol l^{-1}) was prepared by dissolving 0.1510 g Paracetamol (Beijing) in 100 ml of distilled water.

Potassium periodate stock solution (1.67×10^{-2} mol l^{-1}) was prepared by dissolving 0.9584 g Potassium periodate (Tianjin University) in 250 ml distilled water.

Nitriilotriacetic acid (NTA) (5×10^{-2} mol l^{-1}) was prepared by dissolving 0.9557 g NTA (Beijing) in 100 ml of 2 mol l^{-1} NaOH solution

L-dopa sample (Guangxi Donglan). A L-dopa tablet includes 0.25 g L-dopa

H_2SO_4 solution (6.0 mol l^{-1}) and propanone solution

2.3. Procedure

In a 10 ml volumetric flask, adding 1 ml of 1×10^{-2} mol l^{-1} PRT, 1 ml of 6.0 mol l^{-1} H_2SO_4 , 2.5 ml of 1.67×10^{-2} mol l^{-1} KIO_4 . The mixture was heated in a boiling water-bath for 10 min, then was cooled with tap water. Appropriate volumes of L-dopa standard solution ($100 \mu g$ ml^{-1}) to give a final concentration between 0.06 and $12 \mu g$ ml^{-1} , 3.6 ml of 2 mol l^{-1} NaOH (including 5×10^{-2} mol l^{-1} NTA) were added into the solution. The mixture was in a boiling water-bath for 30 min, then cooled with tap water to room tempera-

ture. Adding 2 ml propanone to the solution, then the solution was diluted to 10 ml. The fluorescence intensity was measured in a 1 cm quartz against reagent blank at excitation and emission wavelengths of 410 nm and 510 nm, respectively.

The experimental procedure of determination of L-dopa was as following: Random sampling five tablets L-dopa, lapped to powder, weight out 0.0130 g, dissolved in water and diluted to 100 ml. Determine the concentration by standard addition method.

3. Results and discussion

3.1. Fluorescence spectra

The excitation and emission spectra of the system were shown in Fig. 1. The fluorescent species has excitation and emission maxima at 410 and 510 nm, respectively. The reagent blank is no fluorescence at above wavelength.

3.2. Factors affecting the fluorescence intensity of the system

3.2.1. Effect of the PRT concentration on the reaction

The influence of the concentration of PRT on the fluorescence intensity of the system was

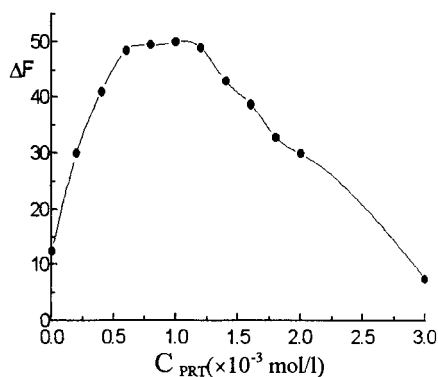


Fig. 2. Effect of PRT concentration. Condition: H_2SO_4 0.6 mol l^{-1} , KIO_4 4.2×10^{-3} mol l^{-1} , NTA 1.75×10^{-2} mol l^{-1} , NaOH 0.7 mol l^{-1} , L-dopa 10 $\mu\text{g ml}^{-1}$.

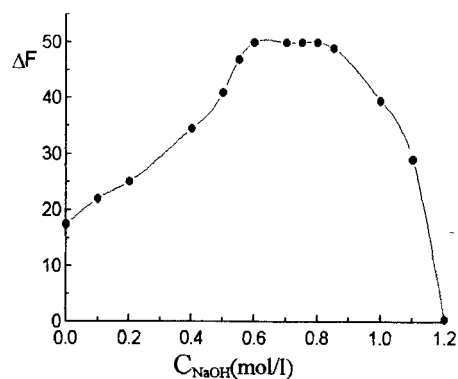


Fig. 3. Effect of sodium hydroxide concentration. Condition: PRT 1.0×10^{-3} mol l^{-1} , H_2SO_4 0.6 mol l^{-1} , KIO_4 4.2×10^{-3} mol l^{-1} , NTA 1.75×10^{-2} mol l^{-1} , L-dopa 10 $\mu\text{g ml}^{-1}$.

shown in Fig. 2. It can be seen that the fluorescence intensity of the system remained constant and reached a maximum value in the range of 6.0×10^{-4} – 1.2×10^{-3} mol l^{-1} PRT. When the concentration of PRT was less than 6.0×10^{-4} or more than 1.2×10^{-3} mol l^{-1} , the fluorescence of the system was decreased. So 1.0×10^{-3} mol l^{-1} PRT solution was selected. The hydrolysate of PRT is of stronger fluorescence, and the reagent blank is increase in presence of an excess of PRT, therefore the excess of PRT have the negative effect on the fluorescence of the system.

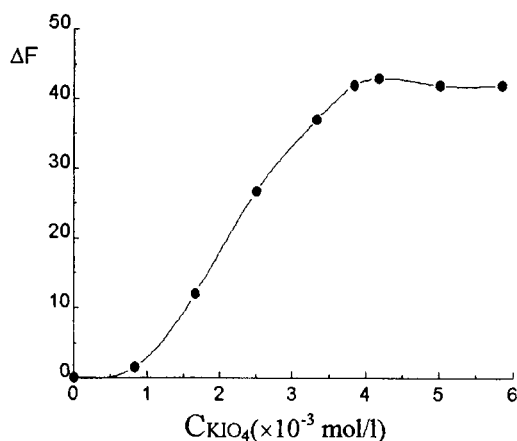


Fig. 4. Effect of periodate concentration. Condition: PRT 1.0×10^{-3} mol l^{-1} , H_2SO_4 0.6 mol l^{-1} , NTA 2.0×10^{-2} mol l^{-1} , NaOH 0.85 mol l^{-1} , L-dopa 10 $\mu\text{g ml}^{-1}$.

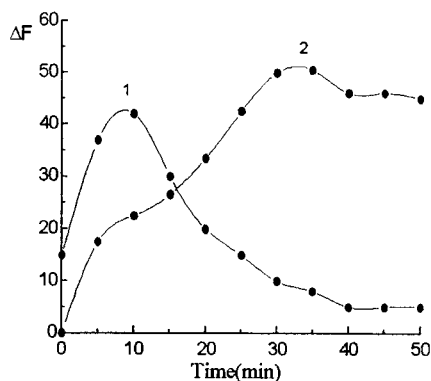


Fig. 5. Effect of heating time. Curve 1 for the hydrolysis time of PRT. Curve 2 for the reaction time. Condition: PRT $1.0 \times 10^{-3} \text{ mol l}^{-1}$, H_2SO_4 0.6 mol l^{-1} , KIO_4 $4.2 \times 10^{-3} \text{ mol l}^{-1}$, NTA $1.75 \times 10^{-2} \text{ mol l}^{-1}$, NaOH 0.85 mol l^{-1} , L-dopa $10 \mu\text{g ml}^{-1}$.

3.2.2. Effect of sodium hydroxide solution

The effect of sodium hydroxide solution was shown in Fig. 3. The result indicated that the fluorescence intensity of the system increased with increasing NaOH concentration up to about 0.6 mol l^{-1} , the fluorescence intensity of the system remained constant and reached a maximum value in the range of $0.6\text{--}0.8 \text{ mol l}^{-1}$. Concentration of NaOH above 0.8 mol l^{-1} caused a decrease in the fluorescence intensity of the system. So 0.7 mol l^{-1} NaOH was selected.

3.2.3. Effect of periodate concentration

Fig. 4. showed that the fluorescence intensity

of the system increased from zero with increasing KIO_4 concentration. The fluorescence intensity of the system remained constant and maxima when the concentration of periodate is above $3.84 \times 10^{-3} \text{ mol l}^{-1}$. So $4.2 \times 10^{-3} \text{ mol l}^{-1}$ KIO_4 was selected.

3.2.4. Effect of heating time

The effect of heating time on the fluorescence intensity was shown in Fig. 5. (Curve 1 for the first heating time, Curve 2 for the second heating time). It was found that heating for 10 min (first time) and 30 min (second time) in a boiling water-bath gave maximum fluorescence intensity.

3.2.5. Effect of solvents

In this study, the following solvents were examined: methanol, ethanol, isopropanol, propanone, ammonia water. The result indicated that in presence of methanol, ethanol, isopropanol and propanone, the fluorescence intensity of the system was increased. The propanone is the best one. The sensitivity of the system with the propanone as solvent can increase by 1.5-fold as compared with that with water as solvent. The result also showed that the ammonia water can decrease the fluorescence intensity of the system to zero. The quenching effect of NH_3 probably owing to the formation of hydrogen bond of benzoquinoneimine and NH_3 , which prevent forming fluorescent product of benzoqi-

Table 1

Effect of ions, amino acids and excipients (L-dopa $10 \mu\text{g ml}^{-1}$)

Ions, amino acids	Ratio to L-dopa ($\mu\text{g}/\mu\text{g}$)	Amino acids and excipients	Ratio to L-dopa ($\mu\text{g}/\mu\text{g}$)
SO_4^{2-}	2400	Val	50
K^+	1000	Glu	40
PO_4^{3-}	480	Arg	30
Ala	270	Citric acid	15
Gly	230	Creatine	14
His	80	Starch	8
Phe	80	Lys	5.4
Ca^{2+}	70	Cys	2.8
Mg^{2+}	60	Leu	2
Asp	50	Try	2
Ser	40	Tyr	1.2
Cl^-	13	Pro	1.2

Table 2
Recovery test and sample analysis

Sample (μg)	Added (μg)	Found ^a (μg)	Recovery (%)	Concentration	
				Proposed method (w/w)	Reference value ^b (w/w)
6.5	0.00	5.46 ± 0.24	—	84.00%	84.71%
	5.0	10.66 ± 0.60	104.1		
	10.0	15.76 ± 0.75	103.0		
	20.0	25.42 ± 0.84	99.8		

^a Average values found \pm S.D. corresponding to five independent analyses.

^b Obtained using spectrophotometric method [2].

noneimine with L-dopa. In this study, we also examined the effect of surfactants, such as β -CD, CTMAB, OP, SDS, CTAB, Triton x-100. The results showed that the surfactants have no effect on the fluorescence intensity of the system.

3.2.6. Stability of the fluorescent species

The fluorescent species can remain stable for more than 2 h.

3.2.7. Standard curve and detection limit

The fluorescence intensity of the system exhibits linear responses towards 0.06–4 and 4–12 $\mu\text{g ml}^{-1}$ L-dopa. The detection limit is 1 ng ml^{-1} with a signal-to-noise ratio (S/N) of 3.

A calibration graph of a series of standard solutions of L-dopa (0.06–4 and 4–12 $\mu\text{g ml}^{-1}$) provided two typical calibration line with the following analytical regression features.

$$0.06 - 4 \mu\text{g ml}^{-1}: \Delta F = -0.049 + 8.64C_{\text{L-dopa}}$$

$$4 - 12 \mu\text{g ml}^{-1}: \Delta F = 18.23 + 4.08C_{\text{L-dopa}}$$

with regression coefficient r of 0.9999 and 0.9999 respectively.

The relative standard deviation for ten replication measurements was 0.6%.

3.2.8. Interference of some ions, amino acids and excipients

The effect of some other ions, amino acids and excipients on the determination of L-dopa was shown in Table 1. An error of 5% in the intensity values was considered tolerable. Table 1 indicates

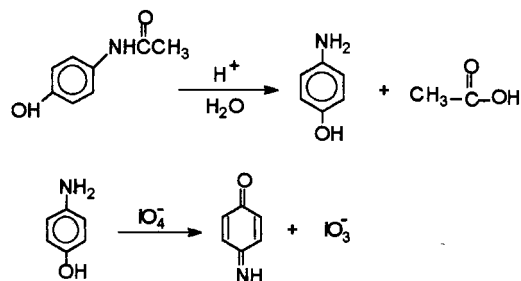
that ions almost have no interference, but Cys, leu, Try, Tyr, Pro caused severe interference.

3.2.9. Sample analysis

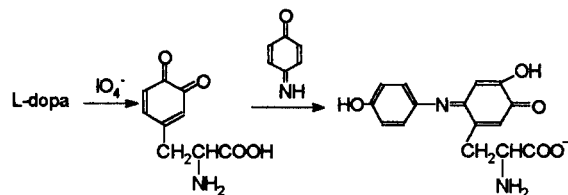
The standard addition method was applied in the recovery test and for the determination of the sample. The results of recovery test and sample analysis were shown in Table 2. From Table 2, it can be seen that the precision and accuracy of the proposed method are satisfactory.

3.2.10. Mechanism of the reaction

PRT hydrolyzes in acidic medium, then is oxidized by periodate:



The product is benzoquinoneimine which reacts readily with the free *para*-position of phenolic compounds by an electrophilic attack [17]. The product is fluorescent species:



References

- [1] Chinese Medicine Dictionary, vol. 2., 1985 p. 72.
- [2] Dongmei Fei, *Zhong Guo Yao Xue Za Zhi* 24 (1989) 669.
- [3] Zhandi Hu, *Zhong Guo Yi Yao Gong Ye Za Zhi* 24 (1993) 313.
- [4] K. Guenther, J. Martens, M. Schickedanz, *Fresenius J. Anal. Chem.* 322 (1985) 513.
- [5] J.D. Edward, S.P. Doshi, *J. Chromatogr.* 210 (1981) 305.
- [6] S. Sarre, Y. Michotte, P. Herregodts, D. Deleu, N. Deklippel, G. Ebinger, *J. Chromatogr. Biomed. Appl.* 113 (1992) 207.
- [7] J. Cummings, M.L. Matheson, F.J. Smyth, *J. Chromatogr.* 93 (1990) 43.
- [8] M.J. Cedarbaum, R. Williamson, H. Kutt, *J. Chromatogr.* 59 (1987) 393.
- [9] R.C. Benedict, *J. Chromatogr.* 385 (1987) 369.
- [10] E. Nissinen, J. Jaskinen, *J. Chromatogr. Biomed. Appl.* 20 (1982) 459.
- [11] Y. Michotte, M. Moors, D. Deleu, P. Herregodts, G. Ebinger, *J. Pharm. Biomed. Anal.* 5 (1987) 659.
- [12] K. Jeonk, H. Nohta, *Anal. Biochem.* 200 (1992) 332.
- [13] F. Eichhorn, A. Rutenberg, E. Kott, *Clin. Chem.* 17 (1971) 296.
- [14] J.C. Johnson, G.J. Gold, D.H. Clouet, *Anal. Biochem.* 54 (1973) 129.
- [15] A.H. Anton, D.F. Sayre, *J. Pharmacol.* 145 (1964) 326.
- [16] H. Takahashi, T.B. Fitzpatrick, *J. Invest. Dermatol.* 42 (1964) 161.
- [17] B.A. Hasan, K.D. Khalaf, M. De La Guardia, *Talanta* 42 (1995) 627.

Trace analysis of BTEX compounds in water with a membrane interfaced ion mobility spectrometer

C. Wan^a, P. de B. Harrington^{a,*}, D.M. Davis^b

^a Department of Chemistry, Center for Intelligent Chemical Instrumentation, Ohio University, Athens, OH 45701-2979, USA

^b Edgewood Research Development and Engineering Center, Chemical and Biological Detection Research Team, Aberdeen Proving Ground, MD, 21010-5423, USA

Received 21 July 1997; accepted 30 October 1997

Abstract

A tubular silicone membrane interface has been developed for trace detection of benzene, toluene, ethyl benzene, and xylene (BTEX) compounds in water with a portable ion mobility spectrometer. Effects of flow rate, membrane length and stirring conditions on the IMS signals have been systematically investigated. Besides conventional dynamic mode operation, static mode sampling has been demonstrated for the first time and high sensitivities were achieved by sampling of BTEX contaminated water with static mode operation. A toluene concentration of 0.101 mg l^{-1} in purified water, corresponding to a headspace concentration of $2.75 \text{ } (\mu\text{g m}^{-3})$, was determined by static mode sampling. Headspace sampling without the membrane interface could not detect toluene at this concentration. This method has high sensitivity for trace concentrations of gasoline components in river water with a response time of several seconds. The apparatus developed is portable and can be used for sensitive detection of organic contaminants in water, with improved performance compared to conventional modes of IMS sampling. © 1998 Elsevier Science B.V. All rights reserved.

Keywords: IMS; Tubular silicone membrane; BTEX; Interface

1. Introduction

Gasoline contamination of ground and surface water by leaking gas tanks, pipelines and vehicles is a recognized environmental and health problem [1]. For fuel as well as some other petroleum products, benzene, toluene, ethyl benzene and xylene (*o*-, *m*-, *p*-) (BTEX) compounds are useful

for detecting contamination. Various analytical methods have been employed for water analysis. The common methods include gas chromatography/flame ionization detection (GC/FID) analysis with direct aqueous injection [2], GC/FID with solid-phase micro-extraction [3], GC/FID with headspace solid-phase micro-extraction [4], gas chromatography/mass spectrometric detection (GC/MSD) analysis with solid-phase micro-extraction [5], capillary GC with membrane extraction [6] and gas chromatography/infrared

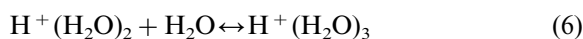
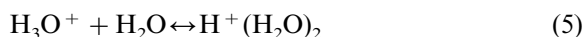
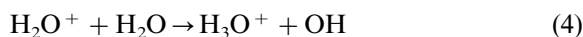
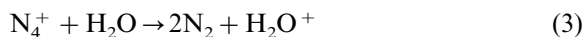
* Corresponding author. Tel.: +1 614 5932099; fax: +1 614 5930148; e-mail: harrington@helios.phy.ohiou.edu

detection (GC/IRD) [7,8]. These GC related methods offer high resolution and low detection limits, however they are generally time-consuming and sample preparation may be required. Laser induced fluorescence has been investigated for on-line oil contamination analysis in an industrial sewage system [9], but this method suffers from its complex data and expensive instrumentation.

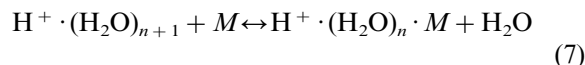
With the implementation of Phase II of the Clean Air Act [10], the development and deployment of portable instruments with satisfactory detection limits is growing in importance for routine on-line water contamination analysis. Ion mobility spectrometry (IMS) offers instruments that may satisfy this demand. IMS instrumentation are sensitive to volatile organic compounds (VOC) and offer the advantages of portability, low cost, rapid response and high sensitivity.

A typical IMS instrument [11] consists of a reaction region and a drift region, with both regions maintained at ambient pressure. An ionization source such as a ^{63}Ni foil or a corona discharge element is used to produce reactant ions in the reaction region. These ions will exchange charge with the analyte through competitive charge transfer reactions. The ions are directed from the reactant region and through the drift region by external electric fields.

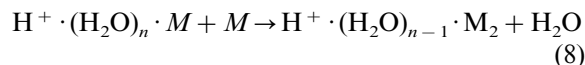
The IMS instrument used in this work can detect ions in either positive or negative modes. The positive ion mode was used for BTEX compounds, because their chemistries favored the formation of positive ions. For positive mode, the reactant ions formed from air tend to be protonated water clusters $\text{H}^+ \cdot (\text{H}_2\text{O})_n$. These ions are formed by the atmospheric pressure reaction sequence outlined by Good et al. [12] and Shahin [13], which are given in Eq. (1) and Eq. (6).



The IMS spectrum is a measure of ion current at the detector with respect to ion drift time. The instrument readout is typically converted to voltage. When a blank air sample is measured by IMS, only the reactant ion peak (RIP) appears in the spectrum. When analyte vapors (M) enter the reaction region through the IMS inlet, they may be ionized to form monomer product ions by proton transfer:



As a result of conservation of charge and competitive charge transfer among ions, the RIP intensity decreases while the monomer product ion peak intensity increases with concentration. For high concentrations of analytes, cluster ions may appear. The dimer product ion may form by the procedure below:



The analytes may be identified by their characteristic drift times. Ions with different charge to size ratios will have different drift times. The product ion peak intensity or area provides a means for measuring the analyte concentration [14–16].

Typical IMS instruments are convenient for vapor sampling, but they are not amenable to liquid phase samples. For IMS measurements of liquids, headspace sampling may be used. However, in some cases the analyte concentration in the headspace may not be high enough to be detected by the IMS. For example, toluene in water of concentration 0.101 mg l^{-1} is not detectable by headspace sampling with a chemical agent monitor (CAM), a hand-held IMS developed for use by the US army. By employing a membrane interface, aqueous samples can be sampled and pre-concentration may be achieved. Additional advantages of the membrane interface are that the ion mobility spectrometer is less susceptible to contamination and pre-concentration by the membrane may allow detection of analytes of lower concentrations than headspace sampling. For example, previous studies have used a tubular membrane-based inlet coupled with an ion mobility spectrometer to monitor aniline in hexane or

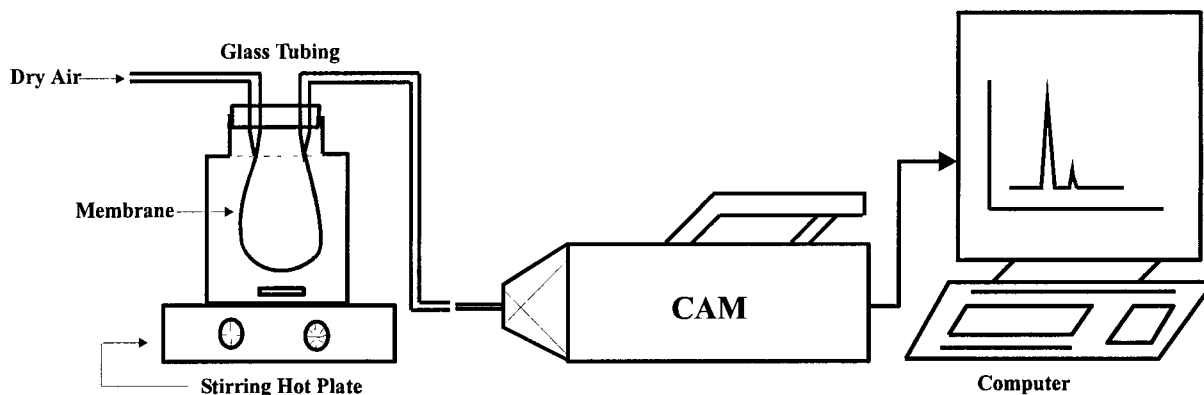


Fig. 1. Schematic of the experimental setup.

water [17]. Also, a sheet silicon membrane interface coupled with an ion mobility spectrometer has been used for on-line monitoring aqueous ammonia [18]. Also, IMS coupled with a solid phase enrichment and thermal desorption apparatus has been used for field screening of phthalate esters in water [19]. Despite this work, BTEX compounds in environmental samples have not been studied with a membrane interfaced ion mobility spectrometer. This paper extends the previous studies by developing a tubular silicon membrane interfaced sampling apparatus to screen BTEX compounds in water with a handheld ion mobility spectrometer. The effects of experimental parameters on the performance of the system and its feasibility for real-time ground water monitoring of gasoline contamination are presented.

2. Experimental

2.1. Description of the system

The schematic diagram of the system is given in Fig. 1. Silicone tubular membranes (i.d. 0.034 cm, o.d. 0.040 cm; VWR cat. no. 62999-199) of various length (5.0–200.0 cm) were used. The membrane interface was constructed by connecting a silicone membrane to a dry airline (i.d. 0.60 cm), in which house air was dried using a Whatman Model 76-02 air drying tower. The air pressure

was maintained at 20 psig with a regulator. The drying line connected two drying towers (i.d. 4.0 cm, length 17.0 cm) in series that are used to scrub the air of residual organic compounds. The drying towers were packed with 2–3 cm layers of grade 44 indicating silica gel (3–8 mesh size), a 1:1 mix of 13X and 5A molecular sieves, and Pyrex Fiberglas glass wool.

The ion mobility spectrometer used in this work was a CAM (NSN, Serial No. 1420, Type 482-301N, GIL 1995, Graseby Ionics, Watford, Herts, UK) unless otherwise specified. This instrument was used with a single modification. Typically, a CAM uses acetone chemistry for the production of ions, whereas for this work, water chemistry was used. This modification was accomplished by removing the reagent gas source from the re-circulating gas system of the instrument and replacing the internal molecular sieves in the CAM.

A wide mouth glass bottle (500 ml) was used as a sample compartment. A rubber stopper (4.70 cm) with two holes (0.53 cm) was used to seal the bottle. Two Pyrex glass tubes (0.56 cm), bent at right angles, were used for carrier gas input and output. The ends of the glass tubes were tapered by drawing the tubes in a flame. The diameter of the tapered glass tip is slightly smaller than the membrane inner diameter. The glass tubes were inserted into the holes in the rubber stopper. The membrane connects the two tapered ends of the glass tube inside the glass bottle. The membrane and the tubes form a gas-tight connection.

The air flow rate through the membrane was regulated with a Cole-Parmer flow meter (part number FM064-62). Flow rates from 5 ml s^{-1} to 50 ml s^{-1} were verified using a soap bubble flow meter (P/N 29-000086-00, Varian). Stirring of the solution is controlled by a Thermix stirring hot plate (Model 310T, Fisher Scientific).

2.2. Sample preparation

Standard solutions of toluene (AR, Mallinckrodt Chemical Works, St. Louis, USA) were prepared using a $500.00 \pm 0.15 \text{ ml}$ volumetric flask and an analytical electronic balance ($\pm 0.1 \text{ mg}$; Model BP210s, Sartorius). Water purified by reverse osmosis was used to prepare standard solutions unless indicated otherwise and toluene standards of 0.101, 0.202 mg, 1.01, 2.02, 5.05, 10.1 and 20.2 mg l^{-1} were prepared. The standard solutions for other BTEX compounds were prepared in a similar manner. Benzene was obtained from Andover, MA. *m*-Xylene (lot no. 782730) and *p*-xylene (lot no. 952739) were from Fisher Scientific. *o*-Xylene (lot no. IFI 151) was from Spectrum Chemical, CA and Ethyl benzene (CAS no. 100-41-4) was purchased from Mallinckrodt.

Fresh river water from the Hocking River was collected near the campus of Ohio University, Athens for analysis. BTEX spiked river water was prepared using the method mentioned above. Gasoline samples obtained from a local gas station were used to prepare spiked river water standards for analysis.

Upon initial testing, the membrane, as obtained from the manufacturer, gave three product ion peaks at IMS drift times of 11.00, 12.03 and 13.56 ms, indicating the existence of residual volatile organic compounds in the membrane. Heating the membrane in a vacuum oven (Model 5830, National Appliance) at 373 K for 1 h removed these peaks. The clean membrane was stored in a desiccated vessel for later use. The bottle, glass tubes and rubber stopper were cleaned with hot water and concentrated cleaning solution (Micro, cat. no. 6731), following which the apparatus was flushed with tap water, purified water and dried before use.

2.3. Data collection procedures

Data was collected using the WASP software package (Graseby Ionics). All spectra were collected in positive ion mode and each spectrum was the average of 50 instrument scans. Baseline correction of each spectrum was applied by calculating the average intensity from 1.50 to 3.00 ms and then subtracting the average intensity from all spectral intensities. Each spectrum had 900 points that were collected with an 80 kHz data acquisition rate. The gating pulse frequency was 40 Hz with 180 μs pulse width and 1.00 ms delay. IMS was used to evaluate the cleanliness of the cell and membrane before use. A volume of 500 ml of purified water was imported to the bottle and ten background spectra were collected. Subsequently, the water was poured out and the bottle dried by compressed air. For dynamic mode operation, the standard solution was transferred to the bottle and data was immediately collected for 15 min with the carrier gas turned on; approximately 300 spectra were collected. The toluene product ion peak area or peak intensity of the 110th spectrum, which is obtained 5 min after the start of spectra collection, was used for the construction of the calibration curve. For the static mode operation, the membrane is immersed in the solution for some time (optimum 10 min) with the carrier gas turned off, then the carrier gas is turned on and data is collected for 15 min.

3. Results and discussions

3.1. Selectivity of the membrane

To demonstrate that toluene contaminated water can be distinguished from uncontaminated water, the spectrum of a blank sample (Fig. 2(a)) is compared with that of purified water (Fig. 2(b)). It was observed that under the conditions used, sampling water through the membrane interface did not affect the RIP intensity or drift time. In contrast, a product ion peak (Fig. 2(c)) can be rapidly detected when sampling purified water spiked with toluene, indicating that toluene vapor can selectively pervaporate through the membrane.

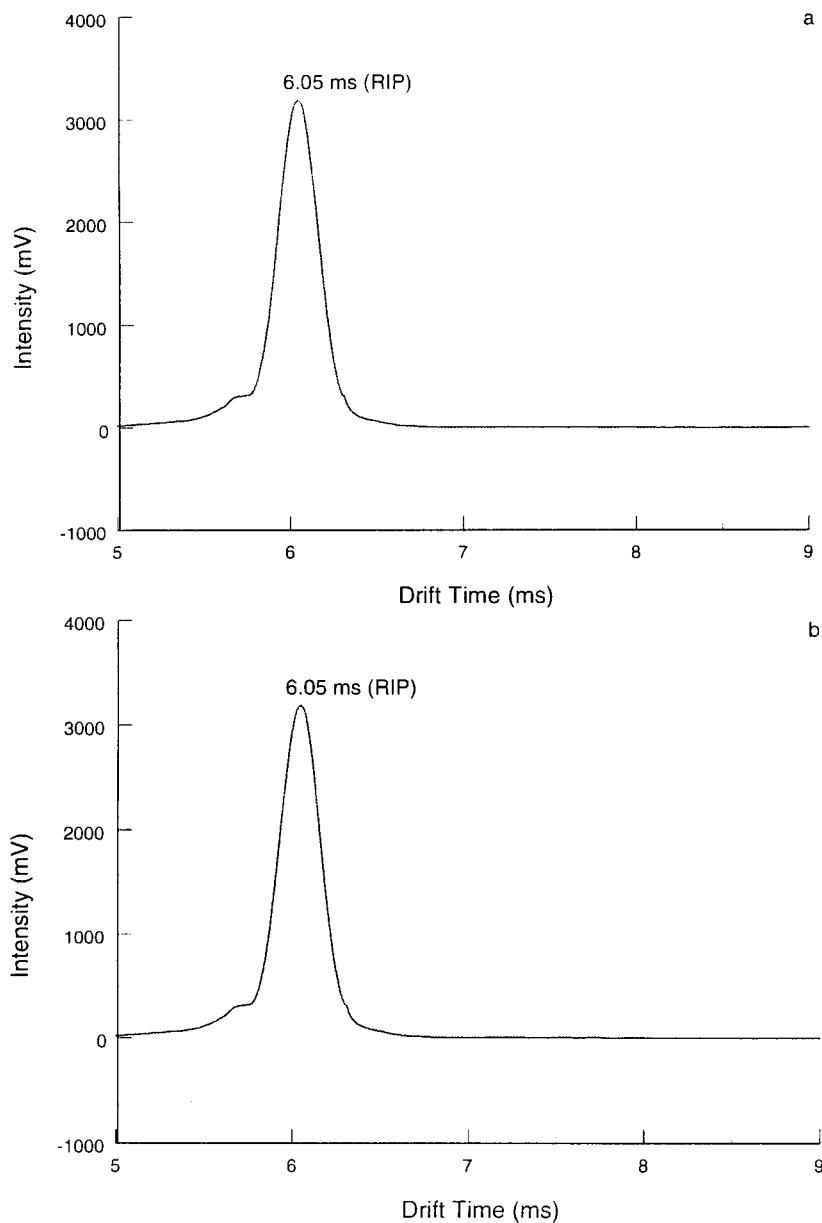


Fig. 2. IMS spectrum of: (a) blank; (b) purified water; and (c) toluene in water (10.1 mg l^{-1}).

To verify that the product ion peak in Fig. 2(c) is due to toluene, the toluene vapor from a small vial containing toluene was flushed into the tip of the ion mobility spectrometer by dry air. A product ion peak at 6.85 ms was observed and the RIP drift time of 6.00 ms did not

change. Another product ion peak at 8.66 ms was also observed when the toluene vapor concentration was high. The product ion peak at 6.84 ms is due to the toluene monomer ion, while that at 8.66 ms may be due to the toluene dimer ion.

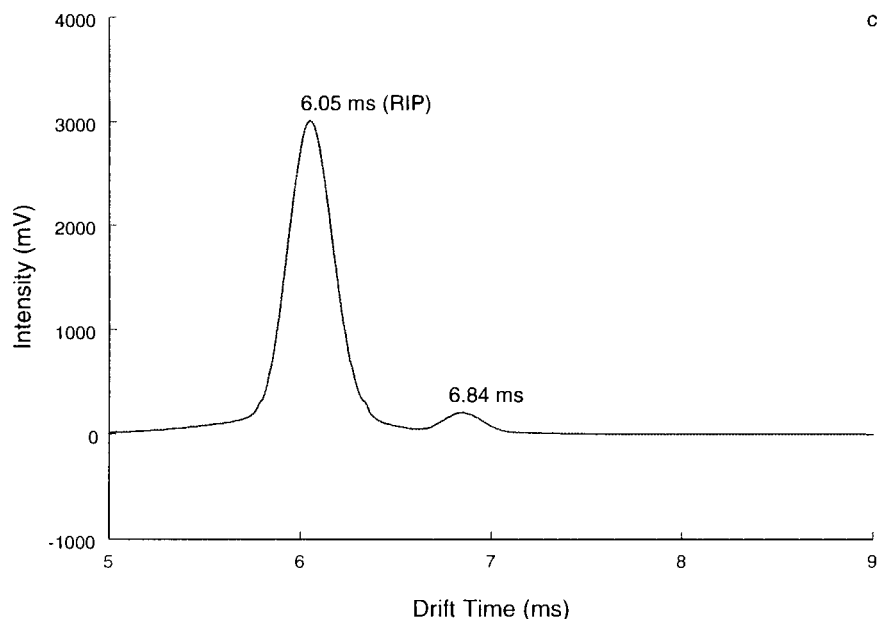


Fig. 2. (Continued)

3.2. Effects of experimental parameters

It was observed that many experimental parameters influence toluene peak intensity. Among the most important of these parameters are the carrier gas flow rate, the membrane length and stirring conditions. Each of these parameters was studied to determine the optimal configuration for the proper analysis of BTEX compounds in water.

Carrier gas flow rate is potentially the most important parameter affecting detection using the membrane interface. The effects of flow rate on the peak area are given in Fig. 3(a) for 8.4 mg l^{-1} of toluene in purified water. The peak area reached a maximum when the carrier gas flow rate was 50 ml s^{-1} . The toluene peak area was smallest for 5 ml s^{-1} , largest for 50 ml s^{-1} and decreased for flow rates greater than 50 ml s^{-1} . At carrier gas flow rates of 5 ml s^{-1} , dilution from the surrounding ambient air decreased the peak area. Furthermore, interference from the ambient air gave spurious peaks when the carrier gas flow rate was at 5 ml s^{-1} . The interface between the instrument and the sampling apparatus was open to the surrounding air.

The IMS instrument samples air through its inlet at a rate of 8 ml s^{-1} . Carrier gas (i.e. dry air) flow rates below the instrument sampling rate results in a dilution of the carrier gas by the surrounding air. At carrier gas flow rates above the IMS sampling rate, only a portion of the carrier gas and the entrained toluene vapor is directed into the instrument. However, the mass of toluene delivered to the instrument is increased at flow rates of up to 50 ml s^{-1} . This increase is due to the relatively fast diffusion of toluene through the membrane. At flow rates greater than 50 ml s^{-1} , the analytical signal was attenuated. This decrease is probably due to dilution of toluene in the carrier gas, because the flow rate exceeds the diffusion rate of the membrane. Thus, the optimal carrier gas flow rate was approximately 50 ml s^{-1} for the membrane.

Membrane length is another important measurement parameter. The effect of membrane length was studied using a toluene solution of 1.01 mg l^{-1} (the results of this study are given in Fig. 3(b)). Immersion of the membrane into the solution interferes with the mixing of the solution. When the membrane is not long enough to signifi-

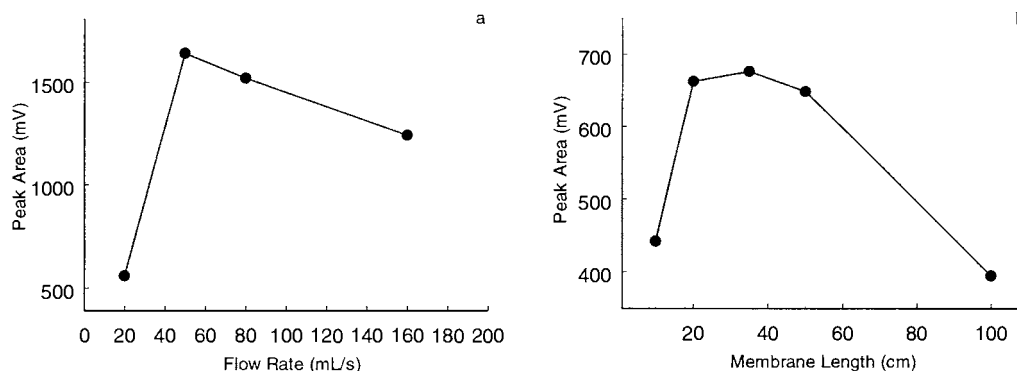


Fig. 3. (a) Effects of flow rate on the analyte signals (toluene concentration: 10.1 mg l^{-1} ; membrane length: 20.0 cm); (b) effects of membrane length on the analyte signals (toluene concentration: 1.01 mg l^{-1} ; flow rate: 50 ml s^{-1}).

cantly interfere with the mixing, the sensitivity increases with the membrane length for membrane lengths between 10.0 and 20.0 cm (Fig. 3(b)). However, it can be seen that the analytical signal is almost constant for membrane lengths between 20.0 and 50.0 cm . Longer membranes interfere with the mixing of the solution and offset the benefit of the increased membrane surface area. The adverse effects of membrane length on solution stirring are further exhibited by using membranes longer than 50.0 cm . In these experiments, the analytical signal was decreased. When the membrane is approximately 2 m long, there is almost no mixing of the solution and almost no toluene peak is observed. For this system, a membrane length of 20.0 cm was considered optimal. It should be noticed that stirring of the solution and membrane length influence toluene peak with different mechanisms. Stirring of the solution increases the diffusion rate of the toluene molecules in the membrane, while a longer membrane has a greater sampling surface area. These results depend on the geometry of the sample cell. Long membrane lengths may be useful for cylindrical flow through cell designs.

Using the optimized system, toluene peak intensities and area with respect to the toluene concentration in water are given in Fig. 4. The intensities and area are obtained in the dynamic mode of operation. In the dynamic mode of operation, the carrier gas flow is maintained when the sample solution is added to the sample cell. Two linear

ranges for the curve of peak area with respect to toluene concentration may be observed in Fig. 4. The sensitivity is greater at low concentrations. At lower concentrations, only toluene monomer ion is present and the curve is linear. As the concentration increases, toluene dimer ions begin to appear. The peak areas now exhibit a more complex relationship with concentration, because the contribution of monomer and dimer must be included. At even higher concentrations, the contribution to the spectrum is dominated by the dimer ion and a new linear range is realized. Similarly, the curve of peak intensity with respect to toluene concentration shows the same effect. At higher concentrations of toluene, silicone membranes have been known to swell, which decreases the pore size and the pervaporation rates of toluene through the tubular membrane. This behavior would result in a loss of sensitivity for this sampling method.

3.3. Static mode operation

In addition to the dynamic mode operation described above, a static mode operation was also studied. In static mode operation, the tubular membrane is immersed into a stirred toluene solution for a preset period of time to achieve pre-concentration. The effect of immersion time on the analytical signal is given in Fig. 5a. It can be seen that higher IMS signal intensities can be obtained with static mode operation than dy-

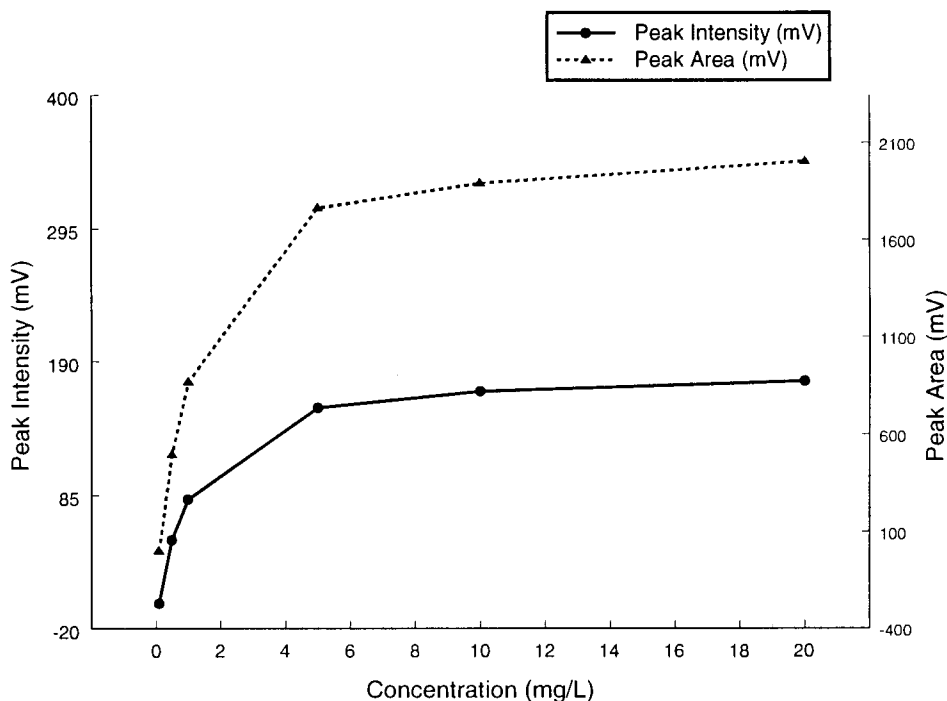


Fig. 4. Calibration curves of toluene in water obtained by dynamic mode operation (flow rate: 50 ml s^{-1} ; membrane length: 20.0 cm).

dynamic mode operation, with the strongest signal obtained with an immersion time of 10 min. The reproducibility of the static mode operation was evaluated with two separate toluene solutions of 20.0 mg l^{-1} . The two solutions were analyzed several days apart using two different membranes of the same length. The reproducibility in this paper is defined as the difference of peak area or peak intensities between two measurements and a reproducibility of 121 mV was obtained for standard toluene solutions of 20.0 mg l^{-1} . This reproducibility is considered satisfactory, because the difference of the peak area has relative standard deviation of 6.2% for the two replicate measurements. Based on the results of reproducibility research, only a single measurement was made for a standard toluene solution of 1.01 mg l^{-1} and no abnormality was noticed during the experiments. Pre-concentration of the sample may be achieved with static mode operation, as the membrane is saturated by toluene vapor in 10 min. For dy-

dynamic mode operation, no equilibrium is ever achieved due to the continuous flow of carrier gas. Thus, signals are smaller than those of static mode operation. It is therefore concluded that higher sensitivity can be achieved with static mode operation.

Fig. 5(b) shows the difference in toluene peak area between static mode operation and dynamic mode operation. It can be seen that the difference decreases with increasing toluene concentration. Little difference is observed for the samples with toluene concentrations higher than 20.0 mg l^{-1} . Note that a toluene peak is observed for 0.101 mg l^{-1} of toluene in static mode, corresponding to a headspace concentration of $2.75 \mu\text{g m}^{-3}$. Toluene was undetected with either dynamic mode operation or headspace sampling of the solution. Therefore, static mode is an effective pre-concentration method for trace analysis of the BTEX in aqueous solution.

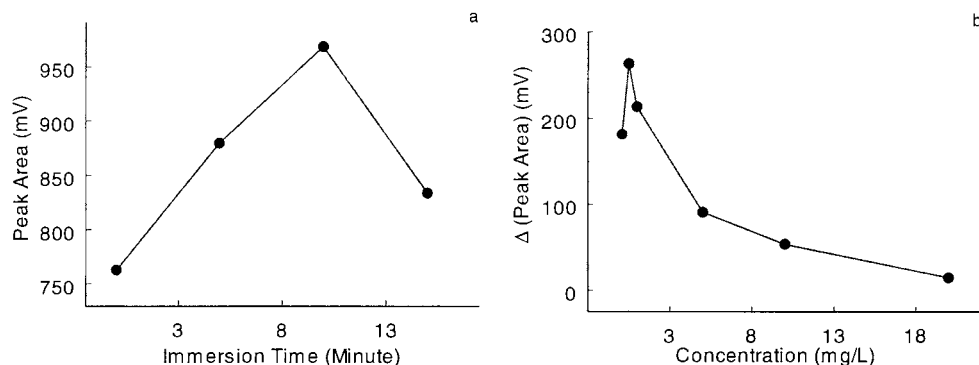


Fig. 5. (a) Effects of immersion time on the toluene peak area in static mode (toluene concentration: 1.01 mg l^{-1} ; membrane length: 20.0 cm ; flow rate: 50 ml s^{-1}); (b) difference of peak area between static mode operation and dynamic mode operation (membrane length: 20.0 cm ; flow rate: 50 ml s^{-1}).

3.4. Detection of toluene in Hocking River water

The peak intensity of product ions in an IMS spectrum changes not only with the concentration of the product itself, but also with the concentration of the other matrix compounds present, due to competitive charge transfer reactions. For purified water, matrix effects are not problematic, because only a single analyte is competing for charge with the reactant ions. However, river water contains organic compounds that may deleteriously affect the product ion peak intensity or generate interfering peaks in the spectrum.

This study used dynamic mode sampling with the spectra acquired 10 min after the solution is added to the sample cell. With the membrane interface, the background IMS spectrum indicates that no detectable contamination is present (Fig. 6(a)). An untreated river water sample was spiked with toluene to generate a 1.04 mg l^{-1} concentration. This solution has a peak intensity of 67 mV (Fig. 6(b)), which is about 20 mV lower than the spiked purified water obtained from the same concentration (Fig. 4). The reproducibility, defined as above, is typically 5 mV for the pure water measurement. The attenuation of the toluene in the river water sample may be due to organic speciation (e.g. adsorption to humic substances). This technique may be a useful measurement tool for studying organic species directly in environmental samples.

3.5. Analysis of other BTEX compounds and gasoline in Hocking River water

To explore the feasibility of detecting other BTEX compounds and gasoline in river water, standards BTEX and gasoline solutions were prepared with Hocking river water. The static mode operation was used for all spectra collection. IMS spectra of ethyl benzene, *m*-xylene and benzene that obtained with a CAM (NSN, Serial No. 216-M-00002, Type 482-310N, GIL 1994, Graseby Ionics¹, Watford, Herts, UK) are given in Fig. 7(a–c), respectively. The ethyl benzene at 0.668 mg l^{-1} produces a single peak at 7.38 ms with an RIP at 6.21 ms (Fig. 7(a)) and the drift time of *m*-xylene (0.112 mg l^{-1}) is 7.30 ms (Fig. 7(b)). The intensities of the product ion peaks indicate that ethyl benzene and *m*-xylene can be detected at even lower concentrations.

Low concentrations of benzene in river water were readily detected with static mode operation, as demonstrated by the monomer and dimer peaks in the spectra (Fig. 7(c)). Dimer ions are indicative of higher concentrations. The membrane was immersed in benzene river water solutions spiked to 0.416 mg l^{-1} for 10 min with carrier gas disconnected to achieve pre-concentration. A peak at 7.05 ms (not shown) with this CAM was obtained when a toluene/river water

¹ A different ion mobility spectrometer than described previously.

solution of 0.104 mg l^{-1} was sampled. Again, headspace sampling and dynamic mode sampling of the same concentration of toluene produced no

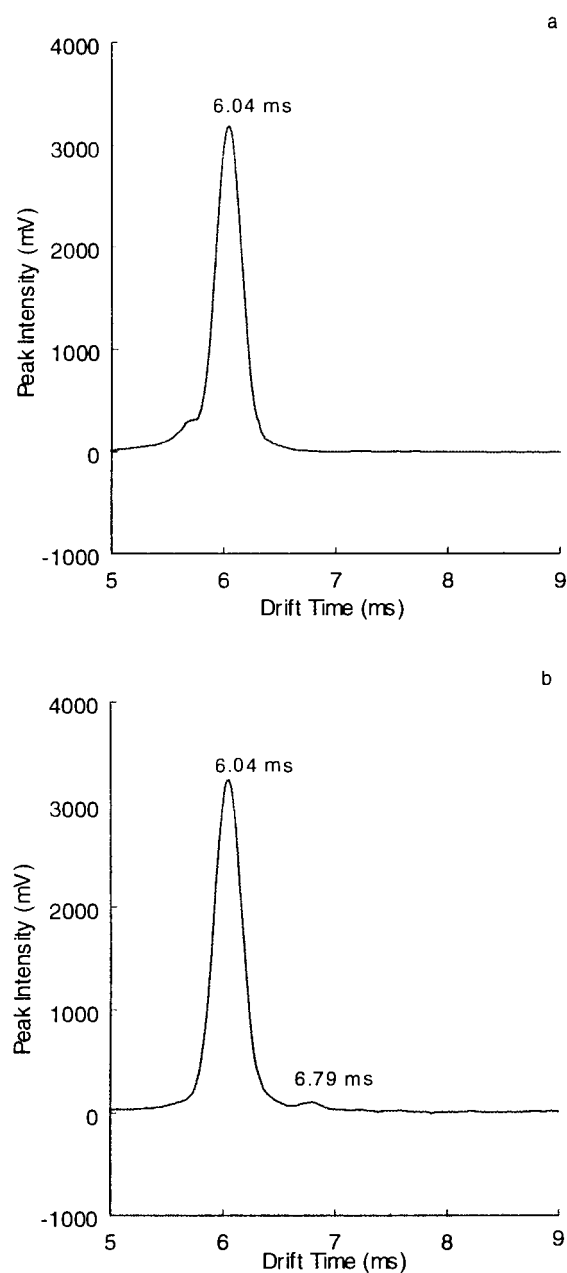


Fig. 6. IMS spectrum of: (a) background; and (b) toluene in the river water (toluene concentration: 1.04 mg l^{-1} ; flow rate: 50 ml s^{-1} ; membrane length: 20.0 cm).

detectable peaks, indicating the higher sensitivity of the static mode operation.

For the IMS scan of river water spiked with gasoline to 0.748 mg l^{-1} (Fig. 7(d)), the spectrum has two broad product ion peaks. Wide peaks are obtained from complex mixtures such as gasoline. The integrated product ion peak area may be a useful indicator of gasoline contamination levels. IMS can also yield a general analysis method by measuring the decrease in RIP. Furthermore, the advantages of portability and low cost of the detection units offer the potential for sensitive detection of contaminants at remote sites that may be hostile or inaccessible by other methods.

4. Conclusions

A simple tubular membrane interfaced ion mobility spectrometer apparatus has been developed for trace analysis of BTEX compounds in water. Effects of experimental parameters such as carrier gas flow rate, membrane length and stirring conditions on analyte signals have been systematically investigated. The optimal carrier gas flow rate is 50 ml s^{-1} for the presented design. The optimal membrane length is related to stirring conditions and sample cell geometry. An optimal membrane length of 20.0 cm was found for this design. Higher sensitivity was achieved by operating the apparatus in static, rather than dynamic mode. BTEX compounds in purified and river water at sub-ppb level were detected with this method when operated in static mode. Benzene gave the greatest sensitivity compared to toluene, ethyl benzene and *m*-xylene. Detection of a gasoline spike in river water at 710 ppb was demonstrated. Similar results were obtained using two different IMS instruments. The developed apparatus is portable and inexpensive and the detection limits for BTEX compounds are better than those obtainable with conventional IMS or other competitive methods. This methodology may be adapted to real-time monitoring of water streams. Although semi-quantitative models may be possible, this method may be useful for the direct screening of environmental water samples for organic pollutants, such as BTEX.

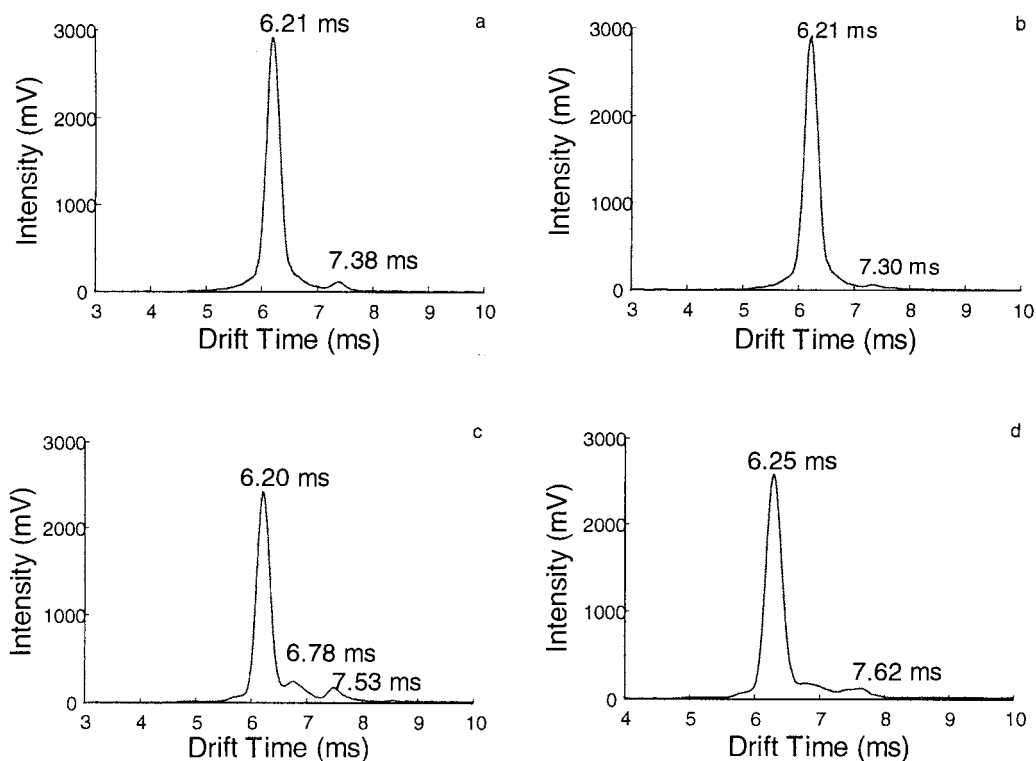


Fig. 7. IMS spectra of: (a) ethyl benzene; (b) *m*-xylene; (c) benzene; and (d) gasoline in water obtained with a membrane interfaced ion mobility spectrometer operated in dynamic mode.

Acknowledgements

This work was funded by US army DAAM01-95-C-0042 and was presented at PITCON'97 on Analytical Chemistry and Applied Spectroscopy, Atlanta, GA, March 19, 1997. Jared Butcher is thanked for his help of instrumentation. The reviewers are thanked for their valuable suggestions.

References

- [1] J.D. Beavers, J.S. Himmerelstein, S.K. Hammond, T.J. Smith, E.M. Kenyon, C.P. Sweet, J. Occup. Environ. Med. 38 (1996) 35.
- [2] T.L. Potter, Ground Water Monit. Remediat. 16 (1996) 157.
- [3] S.P. Thomas, R.S. Ranjan, G.R.B. Webster, L.P. Sarna, Environ. Sci. Technol. 30 (1996) 1521.
- [4] Z.Y. Zhang, J. Pawliszyn, Anal. Chem. 65 (1993) 1843.
- [5] J.J. Langenfeld, S.B. Hawthorne, D.J. Miller, Anal. Chem. 68 (1996) 144.
- [6] M.J. Yang, S. Harms, Y.Z. Luo, J. Pawliszyn, Anal. Chem. 66 (1994) 1339.
- [7] J. Diehl, J. Finkbiner, F. DiSanzo, Anal. Chem. 64 (1992) 3202.
- [8] J. Diehl, J. Finkbiner, F. DiSanzo, Anal. Chem. 67 (1995) 2015.
- [9] W. Schade, J. Bublitz, Environ. Sci. Technol. 30 (1996) 1451.
- [10] T. William, J. Winberry, Environ. Lab. 5 (1993) 46.
- [11] G.A. Eiceman, Z. Karpas, Ion Mobility Spectrometry, CRC Press, Boca Raton, FL, 1994.
- [12] A. Good, D.A. Dueden, P. Kebarle, J. Chem. Phys. 52 (1970) 212.
- [13] M.M. Shahin, J. Chem. Phys. 45 (1965) 2600.
- [14] G.A. Eiceman, A.P. Snyder, Int. J. Envir. Anal. Chem. 38 (1990) 415.
- [15] G.A. Eiceman, Crit. Rev. Anal. Chem. 22 (1991) 471.
- [16] H.H. Hill, W.F. Siems, R.H. St. Louis, D.G. McMinn, Anal. Chem. 38 (1990) 1201A.
- [17] G.A. Eiceman, L.G. Gonzalez, Y.F. Wang, B. Pittman, G.E. Burroughs, Talanta 39 (1992) 459.
- [18] A.R.M. Przybylko, C.L.P. Thomas, P.J. Anstice, P.R. Fielden, J.B. Brokenshire, F. Irons, Anal. Chim. Acta 311 (1995) 77.
- [19] E.J. Poziomek, G.A. Eiceman, Environ. Sci. Technol. 26 (1992) 1313.

Solvent extraction separation of tin (IV) with 2-ethylhexyl phosphonic acid mono-2-ethylhexyl ester (PC-88A)

Sunita V. Bandekar, P.M. Dhadke *

Department of Chemical Technology, Inorganic Chemistry Laboratory, University Of Mumbai, Matunga, Mumbai 400 019, India

Received 28 July 1997; received in revised form 24 October 1997; accepted 30 October 1997

Abstract

Solvent extraction of tin(IV) from hydrochloric acid media was carried out with 2-ethylhexyl phosphonic acid mono-2-ethylhexyl ester (PC-88A) in toluene. Tin(IV) was quantitatively extracted with 2.5×10^{-2} M PC-88A in toluene from 0.1–0.3 M HCl when equilibrated for 5 min. Tin(IV) from the organic phase was stripped with 4 M HCl and determined spectrophotometrically by both the morin and pyrocatechol violet method. The nature of the extracted species was determined from the log–log plots. Various other diluents such as xylene, hexane and cyclohexane also gave quantitative extraction of tin. The metal loading capacity of the reagent was found to be 0–15 ppm of tin(IV). The extraction of tin(IV) was carried out in the presence of various ions to ascertain the tolerance limit of individual ions. Tin(IV) was successfully separated from commonly associated metal ions such as antimony(III), bismuth(III), lead(II), thallium(I), copper(II), nickel(II), etc. The method was extended for determination of tin in real samples. © 1998 Elsevier Science B.V. All rights reserved.

Keywords: Solvent extraction; Separation; Stripping agent; Tin(IV); Phosphonic acid

1. Introduction

Since the last decade, organophosphorus compounds have been widely used as extractants for solvent extraction of various metal ions. An acidic organophosphorus extractant, 2-ethylhexyl phosphonic acid mono-2-ethylhexyl ester (PC-88A) has been used for various transition and rare earth metals [1].

Bis(2-ethylhexyl) hydrogen phosphate was used for extraction of tin(IV) but masking agent [2],

longer period of equilibration and salting out agent [3] were required. Tin(IV) was extracted with various reagents such as 2-(salicylideneamino) benzenethiol [4], methyltrioctylammonium chloride [5], trioctylphosphine oxide [6], trialkyl ammonium nitrate and bis(2-ethylhexyl) hydrogen phosphorodithioate [7], as well as 8-hydroxy-7-iodoquiniline-5-sulfonic acid and tribenzylamine [8]. However, with these methods interference and co-extraction of commonly associated ions was observed. Extraction of tin was also carried out with reagents such as quinoline-8-ol [9], salicylaldehyde [10], 1,1,1-trifluorotridecan-1,3-dione [11] and tetrabromophenolphthalein

* Corresponding author: Tel.: +91 22 4145616; fax: +91 22 4145614.

ethyl ester [12], but these suffered from the limitations of critical pH conditions.

In the present investigation, tin(IV) has been quantitatively extracted from hydrochloric acid media with PC-88A in toluene. The method is applied for the separation of tin from commonly associated metals and analysis of tin in real samples.

2. Experimental

A UV-visible spectrophotometer (model GBC 911A) with 10 mm matched quartz cells was used for absorbance measurement and a digital pH meter (model LI-120) was used to adjust the required pH of the solution.

The stock solution of tin(IV) was prepared by dissolving stannic chloride in 2 M HCl and was standardised by known method [13]. The required solution concentration of tin(IV) was prepared by diluting the stock solution with 2 M HCl. The extractant 2-ethylhexyl phosphonic acid mono-2-ethylhexyl ester was kindly supplied by Dai-hachi Chemical Industries, Japan and it was used without further purification. All chemicals used were of analytical grade.

An aliquot of the solution containing 60 μg of tin(IV) was taken in a separating funnel, hydrochloric acid concentration was adjusted to 0.2 M on dilution to 10 ml and equilibrated with 10 ml of 2.5×10^{-2} M PC-88A in toluene for 5 min. The two phases were allowed to settle and separate. Tin(IV) from the organic phase was back extracted with 4M HCl and determined spectrophotometrically using the morin [14] or pyrocatechol violet method [15].

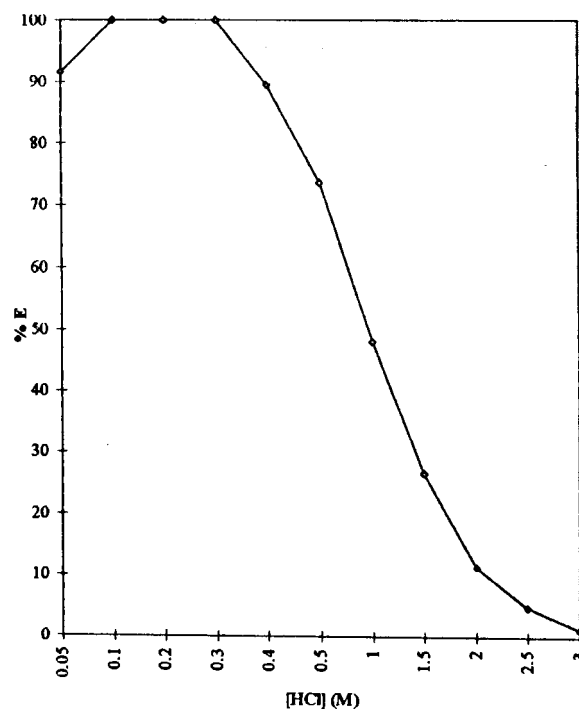


Fig. 1. Effect of hydrochloric acid concentration on percentage extraction of tin(IV) with 2.5×10^{-2} M PC-88A in toluene.

3. Result and discussion

3.1. Effect of acid concentration

The hydrochloric acid concentration of the aqueous phase was varied from 0.05–3.0 M and the extraction was found to be quantitative with 0.1–0.3 M HCl (Fig. 1). Hence, the acidity of the aqueous phase was maintained at 0.2 M HCl for other experimental studies.

Table 1
Effect of PC-88A concentration

[PC-88A] 1×10^{-2} M	0.10	0.25	0.50	0.75	1.00	2.00	2.50	5.00	10.00
%E	6.06	24.20	54.54	62.96	81.81	93.94	99.22	99.22	99.22
D	0.06	0.32	1.20	1.70	4.50	15.50	127.21	127.21	127.21

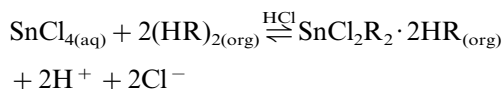
3.2. Effect of reagent concentration

Tin(IV) was extracted with varying concentrations of PC-88A ranging from 1×10^{-3} – 1×10^{-1} M dissolved in toluene. The minimum concentration of PC-88A required for quantitative extraction was 2.5×10^{-2} M (Table 1).

3.2.1. Nature of the extracted species

The nature of the extracted species was investigated by the slope analysis method. A graph of $\log D$ vs $\log [\text{PC-88A}]$ was plotted and the slope was found to be 1.88. Therefore, metal to reagent stoichiometry of the tin(IV):PC-88A complex was 1:2. A graph of $\log D$ vs $\log [\text{Cl}^-]$ was also plotted and the slope was equal to 2.05. These results suggested that tin(IV) was extracted by PC-88A from HCl media as $\text{Sn}^{+4}\text{R}_2\text{Cl}_2 \cdot 2\text{HR}$. It has already been found that tin(IV) was extracted by bis(2-ethylhexyl) phosphoric acid (HR) as a complex of the type $\text{Sn}^{+4}\text{R}_2\text{X}_2 \cdot 2\text{HR}$ from aqueous HCl or HBr solution where $\text{X} = \text{Cl}$ or Br [16].

The probable reaction mechanism may be given as,



where HR represents PC-88A which is dimeric in toluene [1].

3.3. Effect of diluents

Various diluents were used for the extraction of tin(IV) with PC-88A. The extraction was quantitative with toluene, hexane and cyclohexane, whereas with xylene (83.64%), benzene (65.45%), chloroform (84.85%), carbon tetrachloride (80.6%) and dichloromethane (89.7%) it was incomplete. Toluene was preferred as it gave better phase separation.

3.4. Effect of stripping agents

Tin(IV) from the loaded organic phase was stripped with different concentrations of mineral acids such as HCl, HClO_4 , HNO_3 and H_2SO_4 .

Table 2

Effect of stripping agent on the percentage extraction of tin

Concentration (M)	% Stripping of Sn(IV) with various mineral acids			
	HCl	HClO_4	H_2SO_4	HNO_3
1.0	4.85	18.88	22.93	6.45
2.0	49.25	34.4	40.0	17.36
3.0	76.82	—	—	30.42
4.0	100	—	—	45.16
5.0	91.96	—	—	—
6.0	86.2	—	—	—

The quantitative stripping was only observed with 4 M HCl (Table 2).

3.5. Effect of equilibrium time

The aqueous phase containing tin(IV) was shaken with 2.5×10^{-2} M PC-88A in toluene for different periods of equilibration from 1–20 min. and the minimum equilibrium time required was 5 min. It was observed that there was no decrease in the percentage extraction of tin when shaken for a longer time period.

3.6. Effect of metal loading

The concentration of tin(IV) was varied to determine the loading capacity of PC-88A. The loading capacity was found to be 0–15 ppm of tin(IV) with 2.5×10^{-2} M PC-88A in toluene.

3.7. Effect of various diverse ions

The effect of various diverse ions was tested when tin(IV) was extracted with PC-88A in toluene. The tolerance limit of the individual diverse ion was determined with an error of $\pm 1\%$. Alkali metal ions (Li^+ , Na^+ , K^+ , Rb^+ , Cs^+) were tolerated in the ratio 1:30 while alkaline earth metal ions (Be^+ , Mg^{2+} , Ca^{2+} , Ba^{2+} , Sr^{2+}), transition metal ions (Hg^{2+} , Cu^{2+} , Zn^{2+} , Co^{2+} , Fe^{3+} , Mn^{2+} , V^{5+} , Ni^{2+}) and some main group metal ions such as Al^{3+} , Ga^{3+} , In^{3+} were tolerated in the ratio 1:10. Cr^{3+} , Cd^{2+} , Au^{3+} , Bi^{3+} and Pb^{2+} were tolerated in the ratio 1:5.

Table 3
Effect of diverse ions

Ratio of ions (Sn:ions)	Cations	Anions
1:50	—	SO ₄ ²⁻ , SO ₃ ²⁻ , Cl ⁻
1:30	Li ⁺ , Na ⁺ , K ⁺ , Rb ⁺ , Cs ⁺	—
1:20	Hg ²⁺ , Al ³⁺ , Be ²⁺ , Cu ²⁺ , Zn ²⁺ , Co ²⁺ , Mg ²⁺ , Ca ²⁺ , Ba ²⁺ , Sr ²⁺ , Fe ³⁺ , Mn ²⁺ , Ga ³⁺ , In ³⁺ , V ⁵⁺ , Ni ²⁺	NO ₂ ⁻ , NO ₃ ⁻ , Br ⁻ , I ⁻ , citrate
1:10	Ru ³⁺ , Rh ³⁺ , Pd ²⁺ , Pt ⁴⁺ , Tl ⁺	HPO ₄ ²⁻ , SCN ⁻ , EDTA, oxalate, tartrate, thiourea
1:5	Cr ³⁺ , Cd ²⁺ , Au ³⁺ , Bi ³⁺ , Pb ²⁺	—
1:1	Sb ³⁺	—
1:0	As ³⁺	—

The amount of tin(IV) is 60 µg.

Sb³⁺ was tolerated in the region of 1:1 while As³⁺ was found to interfere. Anions such as SO₄²⁻, SO₃²⁻ and Cl⁻ were tolerated in the ratio 1:50 whereas NO₂⁻, NO₃⁻, Br⁻, I⁻ and citrate were tolerated in the ratio 1:20. Anions such as HPO₄²⁻, SCN⁻, EDTA, oxalate, tartarate and thiourea were tolerated in the ratio of 1:10 (Table 3).

3.8. Separation of tin(IV) from associated metals

Tin(IV) was separated from commonly associated metal ions by taking advantage of the difference in the extraction conditions between metals. Tin(IV) and antimony(III) were quantitatively ex-

tracted with 1.5×10^{-1} M PC-88A in toluene from 0.1 M HCl. These two metal ions were quantitatively separated by differential stripping. Tin(IV) was first stripped with 4 M HCl followed by antimony(III) with 8.5 M H₂SO₄. Tin(IV) was separated from bismuth(III), lead(II), thallium(I) and nickel(II) by taking advantage of the fact that these metal ions were unextracted when tin(IV) was extracted with 2.5×10^{-2} M PC-88A in toluene from 0.2 M HCl. Tin(IV) was separated from Copper(II) in the presence of thiourea with 2.5×10^{-2} M PC-88A in toluene when the acidity was maintained at 0.1 M HCl. Tin(IV) was also separated from ternary mixtures. An aliquot con-

Table 4
Separation of tin(IV) from multicomponent mixture

Metal ions	Concentration (µg)	pH/acidity	Reagent Concentration (M)	Stripping agent	% Recovery
Sn(IV)	50	0.1 M HCl	1.5×10^{-1}	4 M HCl	99.2
Sb(III)	50			8.5 M H ₂ SO ₄	99.14
Sn(IV)	50	0.1 M HCl+th ^a	2.5×10^{-2}	4 M HCl	99.2
Cu(II)	200			—	98.6
Sn(IV)	50	0.1 M HCl	1.5×10^{-1}	4 M HCl	99.2
Sb(III)	50			8.5 M H ₂ SO ₄	99.14
Bi(III)	200		Unextracted	—	100.0
Sn(IV)	50	0.1 M HCl	1.5×10^{-1}	4 M HCl	99.2
Sb(III)	50			8.5 M H ₂ SO ₄	99.14
Pb(II)	100		Unextracted	—	98.75
Sn(IV)	50	0.1 M HCl	2.5×10^{-2}	4 M HCl	99.2
Bi(III)	150	0.1M AN	6×10^{-3}	2 M HNO ₃	99.4
Tl(I)	100	At pH = 1.5	Unextracted	—	99.1

The diluent is toluene. AN, ammonium nitrate; th, thiourea.

^a Masking agent.

Table 5
Analysis of tin in real samples

Samples	Amount of tin			% Recovery (D)	R.S.D. (%; F)
	Present (A)	Found (B)	Mean (C) ^a		
Alloys (%)					
Leaded gun metal (BCS-183/4)	7.27	7.22 7.22 7.16 7.27 7.22	7.22	99.31	0.69
Leaded gun metal (ITA-LAB-4382)	4.86	4.97 4.75 4.97 4.70 4.86	4.85	99.79	0.20
Foodstuffs ($\mu\text{g g}^{-1}$)					
Pineapple slices	123.6 ^b	123.1 121.5 124.1 122.5 123.1	122.86	99.40	0.60
Orange pulp	98.3 ^b	97.2 97.8 97.2 97.8 98.3	97.66	99.35	0.65

% Recovery (D) = $C/A \times 100$; R.S.D. (F) = $A - C/A \times 100$.

^a Average of number of assays per sample.

^b Determined by the AAS method.

taining tin(IV), antimony(III) and bismuth(III) was equilibrated with 1.5×10^{-1} M PC-88A in toluene in the presence of 0.1 M HCl. Tin(IV) and antimony(III) were extracted in the organic phase, while bismuth(III) was unextracted. Tin(IV) from the organic phase was first stripped with 4 M HCl followed by antimony(III) with 8.5 M H_2SO_4 . Similarly, tin(IV) was separated from the mixtures of tin(IV), antimony(III) and lead(II), as well as tin(IV), antimony(III) and thallium(I), where lead(II) and thallium(I) were unextracted (Table 4).

3.9. Applications

3.9.1. Determination of tin in alloys

The proposed method was tested by analysing tin in leaded gunmetal. Alloy (50 mg) was dissolved in aqua regia, followed by the addition of

5 ml of perchloric acid. The solution was evaporated to dryness, leached with water and diluted to 100 ml with 2 M HCl. An aliquot of each solution was taken for extraction and determination of tin by the recommended procedure.

3.9.2. Determination of tin in canned foods

The sealed tins of various canned food samples such as pineapple slices and orange pulp were collected from local shops. The canned food samples were treated by the HNO_3 -HCl digestion procedure described previously [17].

A 5 g sample was dried in an oven at 120°C for 24 h in a 250 ml beaker. 30 ml of concentrated nitric acid was added, the mixture was gently heated on a hot plate to initiate digestion and then boiled down to about 3 ml. Following this, 25 ml of concentrated hydrochloric acid was added and gently boiled down to 10–15 ml. It

was cooled, transferred into a 100 ml standard flask and diluted with distilled water. Aliquots of each sample were taken and the tin content was determined using the proposed method. The results obtained with this method were compared with the AAS method. Recovery of tin in these real samples was found to be in good agreement with the theoretical values (Table 5).

4. Conclusion

The present method permits quantitative extraction of tin with a very low concentration of PC-88A within a short period of equilibration. Tin is quantitatively separated from commonly associated metals. The proposed method is used to separate and determine tin in real samples.

Acknowledgements

The authors thank Professor S.M. Khopkar, Professor Emeritus, IIT Bombay, for his guidance in the research work and Dai-hachi Chemical Industries, Japan, for supplying PC-88A.

References

- [1] E. Otu, A. Westland, *Solvent Extr. Ion Exch.* 8 (1990) 759.
- [2] V.A. Tarasova, I.S. Levin, I.A. Bykhovskaya, T.F. Rodina, R.D. Trershitskaya, *Zh. Anal. Khim.* 32 (5) (1977) 981.
- [3] I.G. Yudelevich, E.N. Gilbert, I.S. Levin, J.A. Kondratenko, *Izh. Sib. Otd. Akad. Nauk.* 1 (1979) 446.
- [4] H. Imura, N. Suzuki, *Anal. Chim. Acta.* 118 (1) (1980) 129.
- [5] I. Tsukahara, T. Yamamoto, *Anal. Chim. Acta.* 135 (2) (1982) 235.
- [6] I. Janousek, *Hutn. Listy* 48 (12) (1982) 30.
- [7] V.V. Denisov, U.P. Skvortsova, V.T. Yatsenko, G.V. Verevkin, *Zh. Anal. Khim.* 42 (1) (1987) 95.
- [8] S.P. Arya, S.C. Bhatia, A. Bansal, *Fresenius Z. Anal. Chem.* 345 (11) (1993) 679.
- [9] D.T. Burns, M. Harriott, F. Glocking, *Fresenius Z. Anal. chem.* 327 (7) (1987) 701.
- [10] J.T. Azngraz, J.C. Vidal, J.M. Rabandand, *Analyst* 11 (6) (1986) 619.
- [11] S.R.D. Biswas, A.K. Das, *Anal. Lett.* 22 (3) (1989) 741.
- [12] N. Kaneko, N. Shinohara, H. Nazu, *Bunseki Kagaku* 42 (5) (1993) 229.
- [13] W.W. Scott, *Standard Methods of Chemical Analysis*, 6th ed., vol. 1, 1963.
- [14] K. Kodama, *Methods of Quantitative Inorganic Analysis*, Wiley-Interscience, New York, 1963, p. 203
- [15] W.J. Ross, J.C. White, *Anal. Chem.* 33 (1961) 421.
- [16] I.S. Levin, V.A. Tarasova, V.A. Varnek, T.F. Rodina, *Zh. Neorg. Khim.* 22 (1977) 761.
- [17] R.W. Dabeka, A.D. McKenzie, R.H. Albert, *J. Assoc. Off. Anal. Chem.* 68 (1985) 209.

Extraction behaviour of copper(II) and silver(I) with a thiacycrown ether carboxylic acid, 2-(3,6,10,13-tetrathiacyclotetradec-1-oxy)hexanoic acid

Keiitsu Saito *, Ichiro Taninaka, Satomi Murakami, Akihiko Muromatsu

Division of Natural Environment and Chemistry, Faculty of Human Development, Kobe University, Tsurakabuto, Nada, Kobe 657, Japan

Received 24 April 1997; received in revised form 30 October 1997; accepted 31 October 1997

Abstract

The extraction behaviour of copper(II) and silver(I) with 2-(3,6,10,13-tetrathiacyclotetradec-1-oxy)hexanoic acid (TTCTOHA) was investigated at $25 \pm 0.1^\circ\text{C}$ and ionic strength of 0.1. The value of the logarithmic distribution coefficient, $\log K_{\text{DR}}$ of TTCTOHA between octan-1-ol and aqueous phases was determined to be 4.13. Copper(II) was extracted with TTCTOHA into octan-1-ol as CuL_2 , where L represents the anionic species of TTCTOHA. The logarithmic extraction constant, $\log K_{\text{ex}(10)}$, was determined at -7.42 . Silver(I) was extracted with TTCTOHA into octan-1-ol as AgL and Ag_2L_2 . The logarithmic distribution constant, $\log K_{\text{DC}}$, of AgL was estimated to be 0.49. On the other hand, silver(I) was extracted into 1,2-dichloroethane as AgL and the logarithmic extraction constant, $\log K_{\text{ex}(10)}$, was determined to be -2.24 . © 1998 Elsevier Science B.V. All rights reserved.

Keywords: Extraction; Copper(II); Silver(I); Thiacycrown ether carboxylic acid

1. Introduction

The complexing properties of macrocyclic polythioethers (thiacycrown ethers) have been studied and metal complexes with macrocyclic polythioethers have been isolated and characterized [1–12]. Thiacycrown ethers have also been studied as analytical reagents which are selective for soft metal ions [13–16]. The extraction behaviour of some metal ions with thiacycrown ethers has been

examined stoichiometrically [17–21]. Chromogenic thiacycrown ethers which contain a dissociative group such as hydroxyl or picrylamino group functioning as a counter anion have been synthesized and the extraction of metal ions with chromogenic thiacycrown ethers has been detailed [22–24]. As acid dissociation constants of the chromogenic thiacycrown ethers are small, high extraction efficiency of metal ions was obtained under alkaline media. In general, extraction of metal ions from alkaline media is unfavourable because of metal ion hydrolysis. Thiacycrown ethers with a dissociative group in acidic media, such as

* Corresponding author. Fax: +81 78 8031261; e-mail: saito@natura.h.kobe-u.ac.jp

a carboxyl group, are expected to extract metal ions from acidic media. Although crown ether carboxylic acids have been synthesized and the separation of alkali-metal and alkaline-earth cations from aqueous solutions has been reported by Bartsch et al. [25–33], there are few studies carried out on thiacycrown ether carboxylic acids. Recently, we synthesized two new thiacycrown ether carboxylic acids and examined their characteristics as extracting reagents for various metal ions [34]. It was found that copper(II) and silver(I) are selectively extracted with 2-(3,6,10,13-tetrathia-cyclotetradec-1-oxy)hexanoic acid (TTCTOHA, Fig. 1). The extraction efficiency of copper(II) and silver(I) with TTCTOHA differed from that previously studied with thiacycrown ethers. Although copper(II) is classified as a borderline Lewis acid [35], the extractability was higher than that of soft metal ions such as silver(I) and copper(I). Therefore, it is of interest to study the extraction equilibria of copper(II) and silver(I) with TTCTOHA. Moreover, the results of equilibrium studies should provide significant information in devising a procedure for copper and silver separation from various metal ions and designing new polythioether carboxylic acids for metal ion extraction. Thus, the extraction behaviour of copper(II) and silver(I) with TTCTOHA was stoichiometrically examined in this study. The distribution of TTCTOHA between octan-1-ol and aqueous phases and the back-extraction of copper(II) and silver(I) from octan-1-ol into aqueous acid solutions were also examined.

2. Experimental

2.1. Reagents

The thiacycrown ether carboxylic acid was synthesized and purified using a method previously described [34]. Copper and silver sulphate (analytical-reagent grade) were used to prepare 1×10^{-2} M copper(II) and 2×10^{-2} M silver(I) stock solutions. Their concentrations were determined by EDTA titration and potentiometric titration with sodium chloride, respectively. Octan-1-ol and 1,2-dichloroethane were purified as previously de-

scribed [34]. Other reagents were of analytical-reagent grade.

2.2. Apparatus

Extraction was performed in a Taiyo M-100 incubator at $25 \pm 0.1^\circ\text{C}$. A Seiko SAS-725 atomic absorption spectrometer was used for the determination of copper(II) and silver(I). The UV-vis absorption spectra were measured with a Hitachi U-3200 spectrophotometer. The pH of the aqueous phase was measured with a Toa HM-5ES pH meter.

2.3. Distribution of TTCTOHA between octan-1-ol and aqueous phases

An aqueous solution (10 ml) containing acetic acid and sodium acetate buffer solution (1×10^{-2} M) and sodium sulphate to maintain the ionic strength at 0.1 and an octan-1-ol solution (10 ml) containing 5×10^{-3} M TTCTOHA were placed in a 50 ml glass cylindrical tube and shaken for 30 min at 200 inversions min^{-1} at $25 \pm 0.1^\circ\text{C}$. After shaking the solution it was then centrifuged for 5 min at 2000 rounds min^{-1} , the aqueous phase was separated. A definite volume of the aqueous phase, buffer solution (sodium tetraborate and sodium hydroxide, pH 9.4) and bis[2-(5-chloro-2-pyridylazo) - 5 - diethylaminophenolato]cobalt(III) chloride (Co-5-Cl-PADAP) were placed in another glass cylindrical tube and diluted to 10 ml with water. The final concentrations of the buffer solution and Co-5-Cl-PADAP were 1×10^{-2} and 1×10^{-4} M, respectively. The residual aqueous solution was used for measuring pH. The hydro-

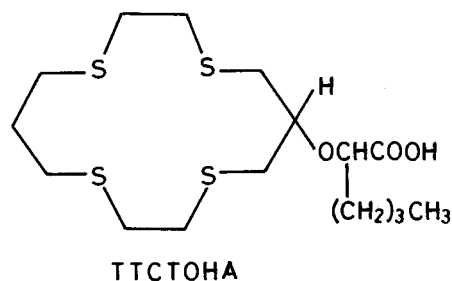


Fig. 1. The investigation of thiacycrown ether carboxylic acid.

gen ion concentration, $-\log[\text{H}^+]$, was calculated from the pH value [36]. After the addition of chlorobenzene (10 ml) the mixture was shaken for 5 min at 200 inversions min^{-1} and then centrifuged at 2000 rounds min^{-1} . The absorbance of the chlorobenzene phase was measured at 566 nm against a reagent blank. The concentration of TTCTOHA in the aqueous phase was determined from the calibration graph which was a straight line passing through the origin.

2.4. Distribution of copper(II) and silver(I)

An aqueous solution (10 ml) containing the metal ion and a buffer solution was placed in a 50 ml glass cylindrical tube. The buffer solution was prepared with disodium hydrogenphosphate and potassium dihydrogenphosphate (5×10^{-3} M) or acetic acid and sodium acetate (1×10^{-2} M). The ionic strength was maintained at 0.1 with sodium sulphate. After the addition of an organic solution (10 ml) of TTCTOHA the mixture was shaken for 30 min at 200 inversions min^{-1} at $25 \pm 0.1^\circ\text{C}$ and then centrifuged for 5 min at 2000 rounds min^{-1} . After the two phases had separated the pH of the aqueous phase was measured. The concentration of the metal ion in the aqueous phase was determined by atomic absorption spectrometry. The metal ion concentration in the octan-1-ol phase was determined as follows: Copper(II) or silver(I) in the organic phase was back-extracted into nitric acid (0.1 M) or hydrochloric acid (3 M), respectively, and the concentration in the stripped solution was determined by atomic absorption spectrometry. The concentration of silver(I) in the 1,2-dichloroethane phase was determined as previously outlined [20].

3. Results and discussion

3.1. Distribution coefficient of TTCTOHA between octan-1-ol and aqueous phases

The distribution ratio, D_R , of TTCTOHA between octan-1-ol and the aqueous phases was examined at various hydrogen ion concentrations. After the octan-1-ol solution containing TTC-

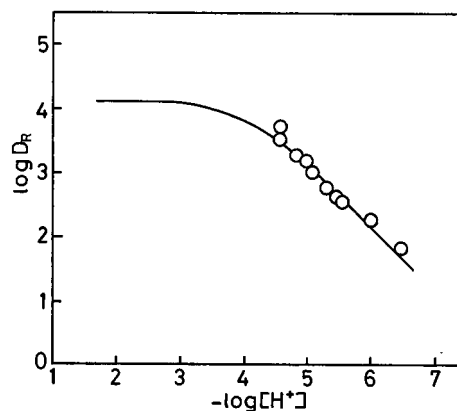


Fig. 2. Distribution ratio of TTCTOHA as a function of $-\log[\text{H}^+]$. Initial TTCTOHA concentration, 5×10^{-3} M. Ionic strength, 0.1 (Na_2SO_4). The solid line is the calculated curve based on $K_a = 10^{-4.05}$ and $K_{DR} = 10^{4.13}$.

TOHA (5×10^{-3} M) was equilibrated with an aqueous phase at a certain hydrogen ion concentration, the total concentration of TTCTOHA in the aqueous phase, $[\text{HL}]_t$, was determined spectrophotometrically by extraction as the ion associate with Co-5-Cl-PADAP. The value of D_R was calculated from the following equation.

$$D_R = (C_{\text{HL}} - [\text{HL}]_t)/[\text{HL}]_t$$

where C_{HL} denotes the initial concentration of the ligand.

Fig. 2 shows the logarithmic distribution ratio as a function of $-\log[\text{H}^+]$. Since carboxylic acid does not form a dimer in octan-1-ol [37], the distribution ratio of TTCTOHA between octan-1-ol and aqueous phases can be expressed as Eq. (1) and is rewritten as Eq. (2) using the proton dissociation constant, K_a , and the distribution coefficient, K_{DR} ,

$$D_R = [\text{HL}]_o/([\text{HL}] + [\text{L}^-]) \quad (1)$$

$$D_R = K_{DR}/(1 + K_a/[\text{H}^+]) \quad (2)$$

where subscript o denotes the concentration in the organic phase. Eq. (3) gives the logarithmic expression,

$$\log D_R = \log K_{DR} - \log(1 + K_a/[\text{H}^+]) \quad (3)$$

The value of K_a has been determined [34], $\log K_{DR}$ can be calculated from $\log D_R$ and the

hydrogen ion concentration. The value of $\log K_{DR}$ was determined as 4.13 from Eq. (3) and data from Fig. 2.

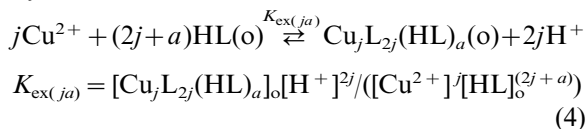
3.2. Back-extraction of copper(II) and silver(I)

Since TTCTOHA is a weak acid, the metal ions in the organic phase should be back-extracted into an aqueous acid solution by adjustment of the acid concentration. Copper(II) was quantitatively back-extracted into nitric acid (0.1 M) from octan-1-ol phase. However, silver(I) was rarely back-extracted into nitric acid (1 M). This may be due to the formation of the ion associate. Therefore, sulphuric acid and hydrochloric acid solutions were tested as stripping solutions for silver(I). Silver(I) was back-extracted to some degree (40%) into sulphuric acid (1 M) from the octan-1-ol phase. Silver(I) was quantitatively back-extracted into hydrochloric acid (1.2 M or above). This is due to the formation of a complex—silver(I) with chloride ions i.e. $[\text{AgCl}_2]^-$.

3.3. Equilibria of the extraction of complexes with TTCTOHA

3.3.1. Extraction of copper(II) with TTCTOHA.

If the extracted species in the organic phase are represented by $\text{Cu}_j\text{L}_{2j}(\text{HL})_a$ the extraction equilibrium and the extraction constant are given by,



where (o) and subscript o denotes the species in the organic phase. When only $\text{Cu}_j\text{L}_{2j}(\text{HL})_a$ is responsible for the extraction of the total concentration of copper(II) in the organic phase it can then be expressed as:

$$\log C_{\text{Cu,o}} = j(\log[\text{Cu}^{2+}] - 2 \log[\text{H}^+]) + (2j+a) \log[\text{HL}]_{\text{o}} + \log j + \log K_{\text{ex}(ja)} \quad (5)$$

If copper(II) species other than the Cu^{2+} ion

in the aqueous phase can be neglected compared with Cu^{2+} ion concentration Eq. (5) becomes,

$$\log C_{\text{Cu,o}} = j(\log C_{\text{Cu,w}} - 2 \log[\text{H}^+]) + (2j+a) \log[\text{HL}]_{\text{o}} + \log j + \log K_{\text{ex}(ja)} \quad (6)$$

The degree of polymerization of the extracted species can be determined from the slope of the plot $\log C_{\text{Cu,o}}$ against $(\log C_{\text{Cu,w}} - 2 \log[\text{H}^+])$ at constant concentration of TTCTOHA. The result is shown in Fig. 3. The plot in Fig. 3 falls on a straight line with a slope of 1.0. Then only the monomeric species were expected to be responsible for the extraction of copper(II) with TTCTOHA. When the monomeric copper(II) species is extracted the following relation can be derived:

$$\log C_{\text{Cu,o}} - \log C_{\text{Cu,w}} + 2 \log[\text{H}^+] = \log K_{\text{ex}(1a)} + (2+a) \log[\text{HL}]_{\text{o}} \quad (7)$$

From the plot of the left-hand side value in Eq. (7) against $\log[\text{HL}]_{\text{o}}$, the number of ligand molecules involved in the monomeric copper(II) species can be estimated. Fig. 4 shows the value of the left-hand side in Eq. (7) as a function of TTCTOHA concentration in the organic phase. A straight line with a slope of 2.0 was obtained, which indicates $a=0$. This result shows that the

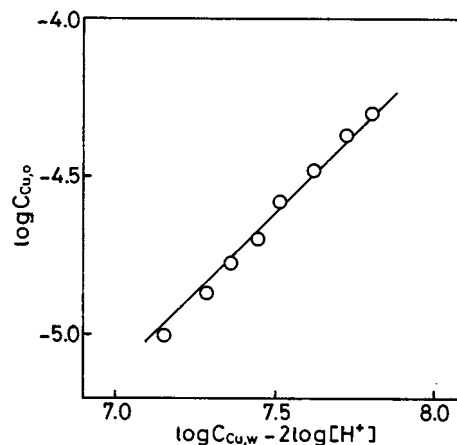


Fig. 3. Determination of the degree of polymerization of copper(II) TTCTOHA complex. Initial TTCTOHA concentration, 5×10^{-3} M. The solid line is straight with a slope of 1.0.

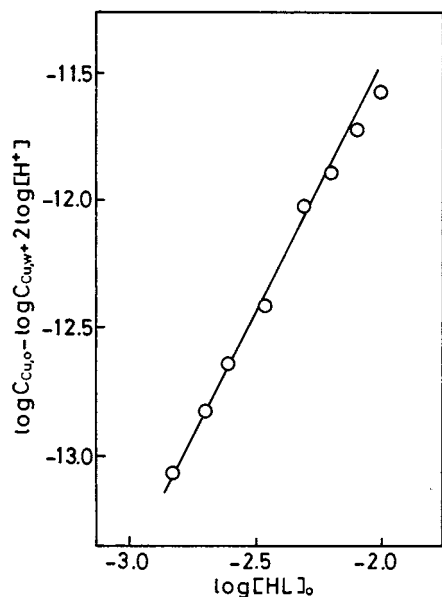
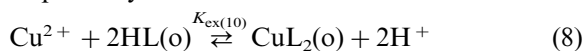


Fig. 4. Determination of the number of TTCTOHA involved in the monomeric complex. Initial copper(II) concentration, 5×10^{-5} M. The solid line is straight with a slope of 2.0.

monomeric species is CuL_2 , the extraction equilibrium and constant is given by Eqs. (8) and (9), respectively.



$$K_{\text{ex}(10)} = [\text{CuL}_2]_{\text{o}}[\text{H}^+]^2 / ([\text{Cu}^{2+}]_{\text{a}}[\text{HL}]_{\text{o}}^2) \quad (9)$$

From Eq. (7) and the results in Fig. 3 and 4, the logarithmic value of $K_{\text{ex}(10)}$ was found to be -7.42 .

3.3.2. Extraction of silver(I) with TTCTOHA.

When the concentration of the complex, silver(I) with TTCTOHA in the aqueous phase is negligible compared with the Ag^+ ion concentration, the extraction equilibria of silver(I) with TTCTOHA can be dealt with using the same method as the extraction of copper(II). However, the dependence of silver(I) extraction on the concentration of TTCTOHA indicates that the same treatment used for the extraction of copper(II) can not be applied. Fig. 5 shows the logarithmic distribution ratio of silver(I)— $\log D_{\text{Ag}}$ as a function of the logarithm of TTCTOHA concentration in the organic phase. When the concentration

of the complex of silver(I) with TTCTOHA in the aqueous phase is negligible compared with the concentration of Ag^+ ion the value of $\log D_{\text{Ag}}$ should depend on ligand concentration. Even though the value of $\log D_{\text{Ag}}$ gradually increases with increasing ligand concentration at $\log[\text{HL}]_{\text{o}} > -3.0$, it is substantially independent of ligand concentration at $-3.5 < \log[\text{HL}]_{\text{o}} < -3.0$. This result indicates that the species of silver(I) in the aqueous phase is similar to that in the organic phase at $-3.5 < \log[\text{HL}]_{\text{o}} < -3.0$. The composition of the extracted species at $\log[\text{HL}]_{\text{o}} < -3.0$ was examined using the molar ratio and the continuous variation method. As can be seen from Fig. 6, the results obtained using both methods indicates that the extracted species is the 1:1 complex, AgL , at $\log[\text{HL}]_{\text{o}} < -3.0$. As stated previously, the value of $\log D_{\text{Ag}}$ was almost constant at $-3.5 < \log[\text{HL}]_{\text{o}} < -3.0$ so that the species of silver(I) in the aqueous phase seems to be the AgL complex in this ligand concentration range. In order to confirm this, after the extraction of silver(I) (5×10^{-5} M) with 5×10^{-4} M TTCTOHA at $-\log[\text{H}^+] = 5.1$, the aqueous phase (8 ml) was shaken with octan-1-ol (8 ml) containing no TTCTOHA. When silver(I) predominantly exists as the hydrated ion, silver(I) should not be extracted. However, 51% of silver(I) in the aqueous phase was extracted into octan-1-ol. The extraction percentage was approximately analogous to that of the extraction of silver(I) with octan-1-ol, containing TTCTOHA in the same concentration as silver(I). This result sup-

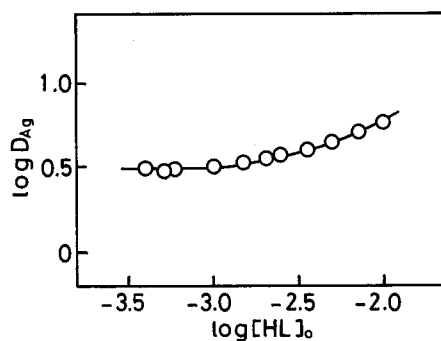


Fig. 5. Distribution ratio of silver(I) as a function of $\log[\text{HL}]_{\text{o}}$ at $-\log[\text{H}^+] = 5.1$ in octan-1-ol system. Initial silver(I) concentration: 5×10^{-5} M.

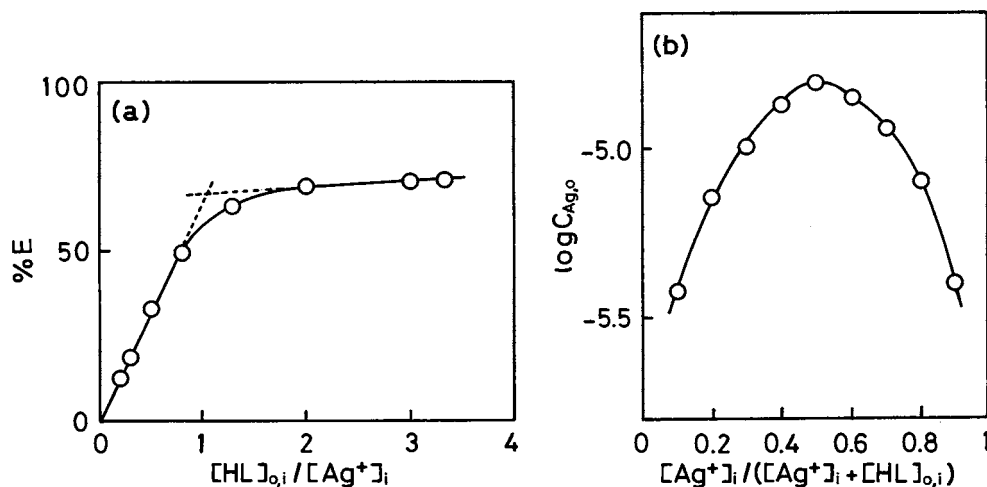
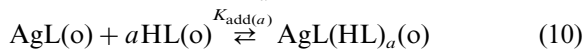


Fig. 6. Determination of the composition of the extracted silver(I) species at $\log[HL]_o < 3.0$ in octan-1-ol system. (a) Molar ratio method at $-\log[H^+] = 5.1$. Initial silver(I) concentration, 5×10^{-5} M. (b) Continuous variation method at $-\log[H^+] = 5.1$. $[Ag(I)]_i + [HL]_{o,i} = 5 \times 10^{-5}$ M.

ports the above consideration. The logarithmic distribution coefficient, $\log K_{DC}$, of AgL was estimated to be 0.49 from the values of $\log D_{Ag}$ at $-3.5 < \log[HL]_o < -3.0$. As shown in Fig. 5, the value of $\log D_{Ag}$ gradually increases with increasing TTCTOHA concentration at $\log[HL]_o > -3.0$. This suggests that the extracted species separate from AgL can be presented together with AgL. The formation of the monomeric adduct complex, $AgL(HL)_a$, in the organic phase could be a cause of ligand concentration dependence. In such a situation, the equilibrium and formation constant of $AgL(HL)_a$ are given by:



$$K_{add(a)} = [AgL(HL)_a]_o / ([AgL]_o [HL]_o^a) \quad (11)$$

From Fig. 2, the ligand concentration in the aqueous phase at $-\log[H^+] = 5.1$ is extremely low so that the formation of AgL_2 in the aqueous phase is negligible and the total concentration of silver(I) in the aqueous phase can be expressed as $C_{Ag,w} = [AgL]$ under the present condition. The logarithmic distribution ratio of silver(I) is given by:

$$D_{Ag} = C_{Ag,o} / C_{Ag,w} \\ = ([AgL]_o + [AgL(HL)_a]_o) / [AgL] \quad (12)$$

at constant $-\log[H^+]$. With appropriate substitutions using the expressions for K_{DC} and $K_{add(a)}$, Eq. (12) becomes Eq. (13).

$$\log C_{Ag,o} = \log K_{DC} + \log(1 + K_{add(a)}[HL]_o^a) \\ + \log C_{Ag,w} \quad (13)$$

The term $\log(1 + K_{add(a)}[HL]_o^a)$ is constant at constant ligand concentration so that the plot of $\log C_{Ag,o}$ against $\log C_{Ag,w}$ should be a straight line with a slope of unity. Fig. 7 shows the relationship between $\log C_{Ag,o}$ and $\log C_{Ag,w}$ at ligand concentration 1×10^{-3} and 5×10^{-3} M at constant $-\log[H^+]$. A straight line with a slope of 1.0 was obtained at 1×10^{-3} M of TTC-TOHA. On the other hand, the slope of the plot at 5×10^{-3} M of the ligand became progressively greater than unity with an increase in $\log C_{Ag,w}$, a straight line with a slope of 1.0 was obtained at lower $\log C_{Ag,w}$. These results indicate that the increase of $\log D_{Ag}$ at $\log[HL]_o > -3.0$ is not due to the formation of the $AgL(HL)_a$ complex. Another reason for this increase of $\log D_{Ag}$ at $\log[HL]_o > -3.0$ could be the formation of polymeric species. In this case, the value of $\log D_{Ag}$ should depend on ligand concentration, the slope of the plot of $\log C_{Ag,o}$ against $\log C_{Ag,w}$ should become greater than unity. Since the dependence

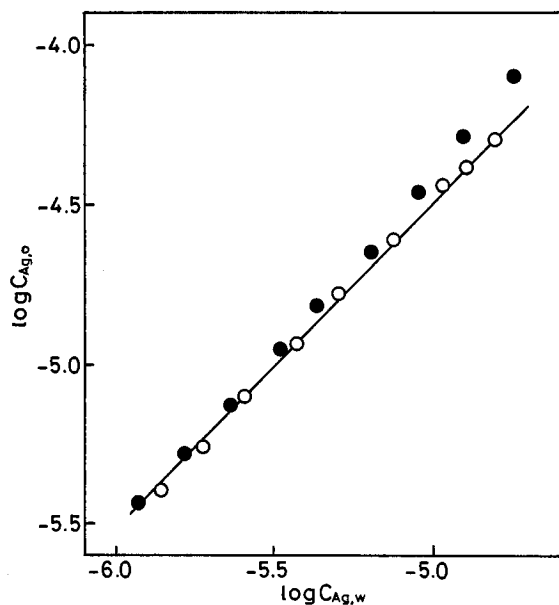


Fig. 7. Plots of $\log C_{Ag,o}$ vs. $\log C_{Ag,w}$ at $-\log[H^+] = 5.1$ in octan-1-ol system. Initial TTCTOHA concentration, (○) 1×10^{-3} M and (●) 5×10^{-3} M. The solid line is straight with a slope of 1.0.

of $\log D_{Ag}$ on ligand concentration is small and the slope of the plot of $\log C_{Ag,o}$ vs. $\log C_{Ag,w}$ is greater than unity but smaller than two, the dimeric species, Ag_2L_2 , is presumed to be ex-

tracted with the monomeric one. Even though silver(I) forms the stable AgL complex with TTC-TOHA and is extracted into octan-1-ol to some degree, the distribution constant between octan-1-ol and the aqueous phases is not as high as that of silver(I) and exists as the AgL complex in the aqueous phase. Furthermore, the dimeric species, Ag_2L_2 , seems to form with increasing concentrations of the AgL complex in the organic phase.

The extraction behaviour of silver(I) in 1,2-dichloroethane was also examined. The results are shown in Fig. 8. Considering the sharp O–H stretching absorption in the IR spectrum of TTC-TOHA [34], the rather high dielectric constant of 1,2-dichloroethane and the low ligand concentration—it is thought that TTC-TOHA exists predominantly as a monomer in the organic phase. Therefore, the value of $\log D_{Ag}$ was plotted against $\log[HL]_o$ in Fig. 8(a). A straight line with a slope of 1.0 was obtained, which is different from the extraction into octan-1-ol. After the extraction of silver(I) (5×10^{-5} M) with ligand (5×10^{-3} M) at $-\log[H^+] = 5.1$ the aqueous phase was shaken with the same volume of 1,2-dichloroethane (containing no TTC-TOHA). Silver(I) was not extracted, which also differs from the extraction in octan-1-ol. These results indicate that silver(I) exists predominantly as the hydrated

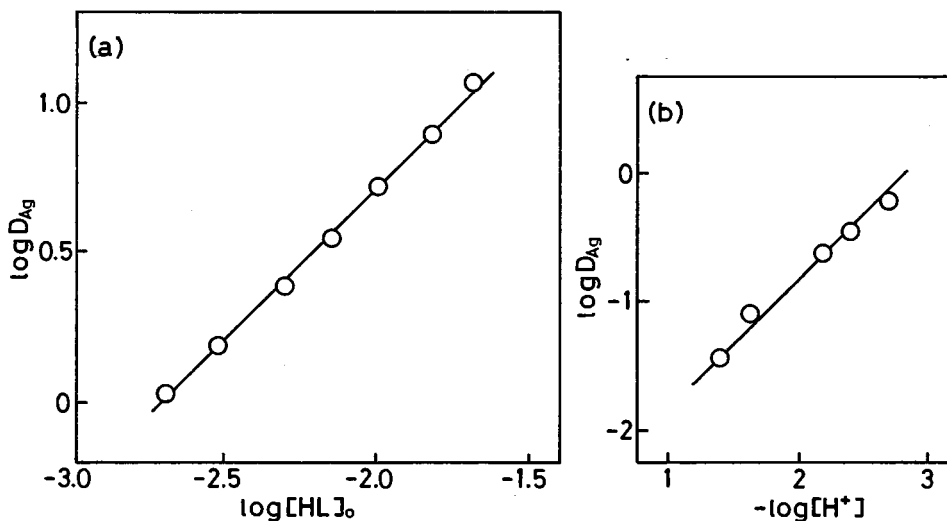
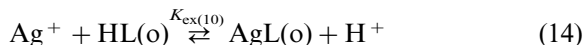


Fig. 8. Plots of (a) $\log D_{Ag}$ vs. $\log[HL]_o$ at $-\log[H^+] = 5.0$ and (b) $\log D_{Ag}$ vs. $-\log[H^+]$ in 1,2-dichloroethane system. Initial concentrations: Silver(I), 5×10^{-5} M for (a) and (b); TTC-TOHA, 5×10^{-3} M for (b). Solid lines are straight with a slope of 1.0.

ion in the aqueous phase when 1,2-dichloroethane was used as the organic solvent. From the results see Fig. 8(a) and 8(b), the extraction equilibrium and constant can be represented as follows:



$$K_{\text{ex}(10)} = [\text{AgL}]_{\text{o}}[\text{H}^+] / ([\text{Ag}^+][\text{HL}]_{\text{o}}) \quad (15)$$

The logarithmic distribution ratio of silver(I) is given by

$$\log D_{\text{Ag}} = \log K_{\text{ex}(10)} + \log[\text{HL}]_{\text{o}} - \log[\text{H}^+] \quad (16)$$

From Eq. (16) and the results in Fig. 8, the value of $\log K_{\text{ex}(10)}$ was calculated as -2.24 , when 1,2-dichloroethane was used as the organic solvent.

References

- [1] S.G. Murray, F.R. Hartley, *Chem. Rev.* 81 (1981) 365.
- [2] V.B. Pett, L.L. Diaddario Jr, E.R. Dockal, P.W.R. Corfield, C. Ceccarelli, M.D. Glick, L.A. Ochrymowycz, D.B. Rorabacher, *Inorg. Chem.* 22 (1983) 3661.
- [3] L.L. Diaddario Jr, E.R. Dockal, M.D. Glick, L.A. Ochrymowycz, D.B. Rorabacher, *Inorg. Chem.* 24 (1985) 356.
- [4] J.A. Clarkson, R. Yagbasan, P.J. Blower, S.C. Rawle, S.R. Cooper, *J. Chem. Soc., Chem. Commun.* (1987) 950.
- [5] H.J. Kuppers, K. Wiegardt, Y.H. Tsay, C. Krüger, B. Nuber, J. Weiss, *Angew. Chem.* 99 (1987) 583.
- [6] D. Sevdic, M. Curic, Lj. Tušek-Božić, *Polyhedron* 8 (1989) 505.
- [7] A.J. Blake, R.O. Gould, A.J. Holder, T.I. Hyde, M. Schröder, *Polyhedron* 8 (1989) 513.
- [8] A.J. Blake, M. Schröder, *Adv. Inorg. Chem.* 35 (1990) 1.
- [9] A.J. Blake, E.C. Pasteur, G. Reid, M. Schröder, *Polyhedron* 10 (1991) 1545.
- [10] A.J. Blake, G. Reid, M. Schröder, *Polyhedron* 11 (1992) 2501.
- [11] D. Collison, G. Reid, M. Schröder, *Polyhedron* 11 (1992) 3165.
- [12] H.J. Pietzsch, H. Spies, P. Leibnitz, G. Reck, *Polyhedron* 12 (1993) 2995.
- [13] K. Saito, Y. Masuda, E. Sekido, *Anal. Chim. Acta* 151 (1983) 447.
- [14] A. Ohki, M. Takagi, K. Ueno, *Anal. Chim. Acta* 159 (1984) 245.
- [15] K. Saito, Y. Masuda, E. Sekido, *Bull. Chem. Soc. Jpn.* 57 (1984) 189.
- [16] E. Sekido, H. Kawahara, K. Tsuji, *Bull. Chem. Soc. Jpn.* 61 (1988) 1587.
- [17] E. Sekido, K. Saito, Y. Naganuma, H. Kumazaki, *Anal. Sci.* 1 (1985) 363.
- [18] K. Saito, S. Murakami, A. Muromatsu, E. Sekido, *Anal. Chim. Acta* 237 (1990) 245.
- [19] K. Chayama, E. Sekido, *Anal. Chim. Acta* 248 (1991) 511.
- [20] K. Saito, S. Murakami, A. Muromatsu, E. Sekido, *Polyhedron* 12 (1993) 1587.
- [21] K. Saito, S. Murakami, A. Muromatsu, E. Sekido, *Anal. Chim. Acta* 294 (1994) 329.
- [22] E. Sekido, K. Chayama, M. Muroi, *Talanta* 32 (1985) 797.
- [23] M. Muroi, T. Tamiki, E. Sekido, *Bull. Chem. Soc. Jpn.* 62 (1989) 1797.
- [24] M. Muroi, E. Sekido, *Anal. Sci.* 9 (1993) 691.
- [25] R.A. Bartsch, G.S. Heo, S.I. Kang, Y. Liu, J. Strzelbicki, *J. Org. Chem.* 47 (1982) 457.
- [26] R.A. Bartsch, Y. Liu, S.I. Kang, B. Son, G.S. Heo, P.G. Hipes, L.J. Bills, *J. Org. Chem.* 48 (1983) 4864.
- [27] J. Strzelbicki, R.A. Bartsch, *Anal. Chem.* 53 (1981) 1894.
- [28] J. Strzelbicki, R.A. Bartsch, *Anal. Chem.* 53 (1981) 2247.
- [29] J. Strzelbicki, R.A. Bartsch, *Anal. Chem.* 53 (1981) 2251.
- [30] W.A. Charewicz, G.S. Heo, R.A. Bartsch, *Anal. Chem.* 54 (1982) 2094.
- [31] W.A. Charewicz, R.A. Bartsch, *Anal. Chem.* 54 (1982) 2300.
- [32] R.A. Bartsch, B.P. Czech, S.I. Kang, L.E. Stewart, W. Walkowiak, W.A. Charewicz, G.S. Heo, B. Son, *J. Am. Chem. Soc.* 107 (1985) 4997.
- [33] T. Hayashita, M.-J. Goo, J.C. Lee, J.S. Kim, J. Krzykawski, R.A. Bartsch, *Anal. Chem.* 62 (1990) 2283.
- [34] K. Saito, I. Taninaka, S. Murakami, A. Muromatsu, *Anal. Chim. Acta* 299 (1994) 137.
- [35] R.G. Pearson, *J. Am. Chem. Soc.* 85 (1963) 3533.
- [36] Y. Hara, K. Okamoto, J. Hidaka, H. Einaga, *Bull. Chem. Soc. Jpn.* 57 (1984) 1211.
- [37] H. Yamada, S. Suzuki, M. Tanaka, *J. Inorg. Nucl. Chem.* 43 (1981) 1873.

Multivariate analysis of Cd(II), In(III), Tl(I) and Pb(II) in mixtures using square wave anodic stripping voltammetry

H.N.A. Hassan ^{a,*}, M.E.M. Hassouna ^b, I.H.I. Habib ^a

^a *Microanalytical Research Laboratory, National Research Centre, El-Tahrir Str., Dokki, Cairo, Egypt*

^b *Chemistry Department, Faculty of Science (Beni-Suef), Cairo University, Beni-Suef, Egypt*

Received 6 June 1997; received in revised form 27 October 1997; accepted 4 November 1997

Abstract

Accurate qualitative and quantitative results were obtained by the application of parameter estimation methods, viz. Classical Least Squares 'CLS', Inverse Least Squares 'ILS' and Kalman Filter 'KF' algorithms. These methods were used to separate strongly overlapping electrochemical peaks produced by binary, ternary and quaternary mixtures of traces of cited poisonous heavy metals stripped from the hanging mercury drop electrode in an acetate–bromide electrolyte using the square wave anodic stripping voltammetry. The analysis was achieved using a single standard addition, the concentrations studied were down to 50 nM and molar ratios up to 1:6 for binary mixtures. A statistical analysis of the results was reported. The method was applied for the ultratrace analysis of the cited cations in a sample of sodium hydrogen carbonate AR. © 1998 Elsevier Science B.V. All rights reserved.

Keywords: Multivariate anodic stripping voltammetry; Cd(II), In(III), Tl(I), Pb(II)

1. Introduction

The polarographic and voltammetric methods are one of the well-known analytical tools used to give qualitative and quantitative information of electroactive species in a sample. Recent reported methods for the determination of both Pb and Cd in a variety of samples and matrices are numerous as their electrochemical peaks are separate enough to be estimated simultaneously. This is exem-

plified by the stripping voltammetry of both elements in unpurged sea water [1], in neutral zinc-plant electrolyte [2], in ammonium fluoride [3], in thioglycolic acid [4], in whole blood [5], in human gallstone [6] and in the urine of steel production workers [7]. Square-wave stripping voltammetry was also utilised in the determination of both elements [8,9]. Differential potentiometric stripping analysis was applied to determine Pb and Cd in serum [10].

When In or Tl are incorporated with either Pb, Cd or both, overlapping peaks are observed. To overcome this problem, various chemical and

* Corresponding author. Tel.: +20 233 71499; fax: +20 233 70931; e-mail: elsayed@frcu.eun.eg

statistical methods were employed to resolve the analytical data.

In and Cd were simultaneously determined by differential pulse polarography in the presence of poly- β -cyclodextrin [11] which increases the difference in their reduction potentials. The determination selectivity of traces of Cd, Pb, Tl and In is improved by direct coupling of liquid/liquid extraction and anodic stripping voltammetry [12,13]. Mutual interference of Pb and Tl was diminished by pre-electrolysis in the presence and absence of EDTA [14].

On the basis of chemometrics, Turnes et al. [15] used differential pulse polarography to resolve binary, ternary and quaternary mixtures of Cd, In, Tl and Pb in micromole levels using the generalized standard addition method with multiple linear regression. However, unsatisfactory results were obtained, especially with the binary mixture of Cd and In. Inadequate results were also achieved by the same authors [15] when a more sensitive technique, namely the linear anodic stripping voltammetry was applied with concentrations down to 50 nmol. Kalman filtering was used as a parameter estimator for the analysis of Cd/In and Cd/In/Pb systems by linear sweep [16], or analysis of Tl/Pb system by square wave voltammetry [17], both techniques were performed at the micromole scale, i.e. with concentrations down to 16 μ M for Cd and In, 14 μ M for Pb and 7 μ M for Tl. The relative error values obtained by Turnes [15], were significantly high and so the aim of the present work is to investigate the source of these errors, whether being in the electrochemical procedures or the statistical treatments.

2. Experimental

2.1. Reagents

All reagents used were of analytical-reagent grade. Stock solutions of 10 mM Cd(II) nitrate, In(III) chloride, Tl(I) nitrate and Pb(II) nitrate were prepared by dissolving the appropriate amounts of the cited salts in double distilled water acidified with 1 ml l⁻¹ concentrated nitric acid.

Diluted solutions were prepared daily and also acidified.

An acetate–bromide electrolyte [18,19] of pH 4.65 was prepared by dissolving 23.8 g KBr and 2.177 g sodium acetate in 100 ml distilled water. The pH of the solution was adjusted to 4.65 by the dropwise addition of 1 M HCl solution. The final concentrations of bromide, acetate and chloride ions should be 2, 0.16 and 0.08 M, respectively.

A matrix modifier used for Zeeman AAS was prepared by dissolving 0.05 mg ammonium dihydrogen phosphate (AR) and 0.003 mg magnesium nitrate (AR) in 1 l of deionized water.

2.2. Glassware

The glassware was initially allowed to stand (for 24 h) in an alkaline bath containing industrial detergent plus KOH, it was then transferred to an acidic bath of 5% HCl. It was washed with distilled water and then dried in a drying oven. Keeping it away from dust.

2.3. Apparatus

Direct current (DC) and Square wave (SW) anodic stripping voltammetric measurements were obtained from a Metrohm 693 VA processor equipped with a 694 VA stand involving three potentiometric electrodes. The working electrode was a hanging mercury drop electrode (HMDE) with a drop area of about 0.3 mm², while the auxiliary electrode was platinum wire. The reference electrode was Ag/AgCl in 3 M KCl. The instrumental settings used in all techniques are summarised in Table 1.

All voltammetric measurements were made in triplicate and all experiments were performed at room temperature (25°C).

After completing the sweep, the binary file was transferred on-line to an IBM-compatible PC computer and ASCII file was generated through the Metrodata 693 VA Backup program, version 1.1. For resolution of the multicomponent mixtures, the numerical data or ASCII file was entered in-line into the CASAP program [20] which was written in Turbo Pascal Language and com-

piled into an executable file run under MS DOS version 6. The program designed includes classical least squares CLS, inverse least squares ILS and Kalman filtering KF.

A Zeeman atomic absorption spectrometer, model 4100 of Perkin Elmer, was used for reference determinations.

2.4. Procedure

An appropriate volume of sample and 1 ml of the acetate–bromide electrolyte were placed in a 10 ml measuring flask, completed to the mark with distilled water and then transferred to the voltammetric vessel. The solution was stirred and de-aerated for 2 min by bubbling nitrogen gas at 1 atmospheric pressure. Cathodic reduction was then carried out at -900 mV for 1 min with continuous stirring. The stirrer was stopped and the solution was allowed to rest for 10 s, then the voltage was scanned using the selected mode in the anodic direction. The experiment was repeated three times with a fresh new mercury drop on the electrode in order to check the reproducibility up to 3%. A single standard addition, i.e. an individual standard for each sample, of 300 nM component was added to the sample and the procedure was repeated for each component. The vessel was washed thoroughly with 10% hydrochloric acid and then with double distilled water for each analyte.

Table 1
Experimental conditions used for DC and SW at hanging mercury drop electrode

Parameter	DC	SW
Stirring speed (rpm)	2000	2000
Purge and stirring time (s)	120	120
Deposition potential (mV)	-900	-900
Deposition time (s)	60	60
Delay before sweep (s)	10	10
Pulse Amplitude (mV)	—	10
Frequency (Hz)	—	25
Scan rate (mV s^{-1})	40	40
Initial potential (mV)	-900	-900
Final potential (mV)	-200	-300

The proposed method was applied to the ultra trace analysis of cations in sodium hydrogen carbonate 'ANALAR', reported to contain 99.5% NaHCO_3 and heavy metals in terms of Pb of $\approx 0.001\%$ (Batch No. 2093200, 500 g net). An aliquot of 5 ml solution of 10 g sample in 100 ml bidistilled water, was diluted to 10 ml and the same parameters of square wave technique illustrated in Table 1, were applied except for the time of preconcentration which was increased to 5 min.

3. Results and discussion

Using a thin mercury film on a glassy carbon electrode (MFGCE) in conjunction with SWASV reduces the detection and determination levels of poisonous metals to ppb and sub-ppb range, the hanging mercury drop electrode (HMDE) is still the most versatile and reliable method. Resurfacing of the glassy carbon support and replating the mercury film were not very successful, and often failed to restore the initial perfect response [21]. Furthermore, the HMDE is less sensitive to solution chemistry than the MFGCE and in fact suffers less from interference caused by the formation of intermetallic compounds [18].

Using direct current anodic stripping voltammetry (DCASV) leads to stripping peaks with a drawn-out shape, as shown in Fig. 1, owing to the slow diffusion of metal from the interior to the surface of the mercury drop. For this reason, it is necessary to use high-frequency waveforms for ASV at the HMDE [22,23]. The high effective scan rates of square wave technique responds only to dissolved metal at the surface of the mercury drop, and so the stripping peaks have a sharp, symmetrical and relatively high shape compared with that obtained by DCASV (Fig. 1). It is clear that peak widths obtained by SWASV are narrower than those produced by DCASV and so the degree of peak overlapping is less using the first method. Also, the peak currents obtained by SWASV are higher, nearly four fold higher than DCASV.

The optimum compositions required for the supporting electrolyte used in the determination of Cd, In, Tl and Pb at the HMDE were reported

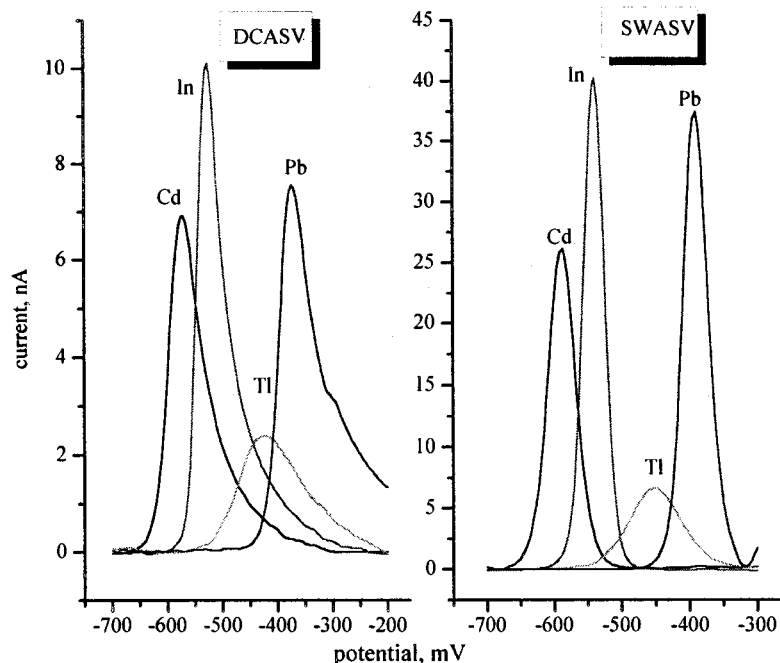


Fig. 1. Standard curves of 100 nM analyte in acetate–bromide medium after subtraction of the blank.

in the literature. The determination of In(III) by stripping voltammetry in aqueous solution at the HMDE requires a weakly acidic medium as well as the presence of halide or pseudohalide ions [18,19]. The most sensitive peaks were obtained in an acetate–bromide electrolyte [18,19] of pH 4.65, which is chosen for the present work. In non-complexing media such as nitrate and perchlorate electrolytes, In(III) did not produce a polarographic reduction wave [19]. Similar requirements must apply to the deposition and stripping of Cd(II) which produces much larger waves at the HMDE in halide ions than in perchlorate media [18]. These requirements may explain why the results achieved for the analysis of binary mixtures of Cd and In were unsatisfactory [15,16].

Errors due to the shift in peak position, may be caused by ligand concentration effects or by unknown synergistic effects in the mixture, these errors can be alleviated using a standard addition rather than calibration methods.

In the anodic stripping voltammetric techniques, the peak current i_j measured at a HMDE

and at a given potential ' $j = 1, 2, \dots, p$ ', is proportional to the electroactive analyte concentration ' c_i ' over a given concentration range and can be expressed as

$$i_j = k_j c + e_j \quad (1)$$

where k_j is the response constant of the analyte and e_j is the chemical and instrumental errors. For n components in a mixture, the total peak current, i_p , at a given potential will be

$$i_j = \sum_{i=1}^n k_{ij} c_i + e_j \quad (2)$$

where $i = 1, 2, \dots, n$ is the number of components. For a series of single standard additions ' $l = 1, 2, \dots, m$ ', i.e. an individual standard for each mixture component, each measured potential will provide an equation system in the form

$$i_{jl} = \sum_{i=1}^n k_{ij} c_{il} + e_{jl} \quad (3)$$

or in matrix notation, the empirical model is

$$I = \mathbf{K} \mathbf{C} + \mathbf{E} \quad (4)$$

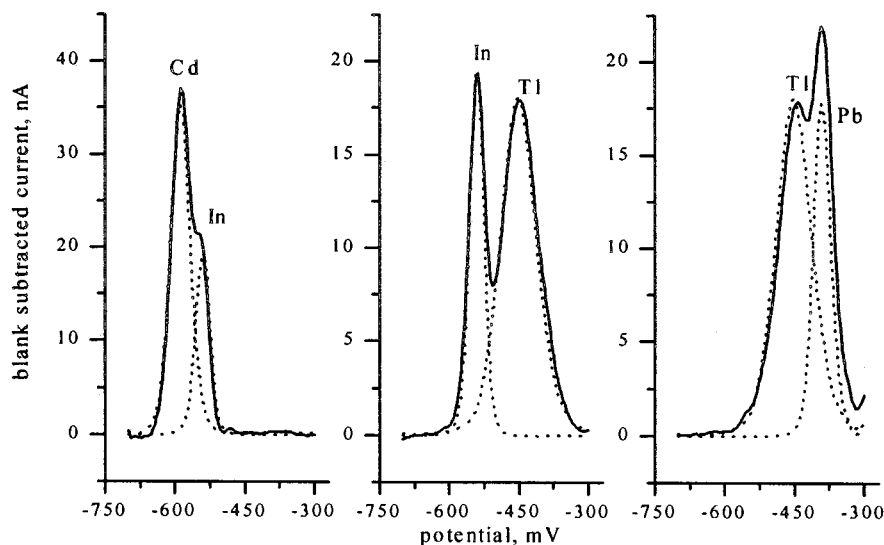


Fig. 2. Binary mixture square wave stripping peaks after subtraction of the blank (solid lines) and the corresponding fit components (dotted lines).

which involves \mathbf{K} ($p \times n$) matrix whose elements are response coefficients relating current I to analyte concentration C at given potential. The matrix \mathbf{E} is ($p \times m$) residual or error matrix in estimating the concentration of analytes. Most approaches to peak resolution rely on curve fitting of the standard empirical models to the overlapped electrochemical responses. In this work, three different multivariate calibration and prediction methods have been selected, which include classical least squares (CLS), inverse least squares (ILS) and Kalman filtering (KF).

The CLS and KF are capable of full-voltammogram calibration accounts for errors in the current measurements, while the ILS, sometimes called the P -matrix method, is a sensor-limited method, i.e. the number of sensors are selected and limited in order to avoid collinearity problems, and is inverse of CLS or KF models which account for errors in the concentration measurements and can be represented as a model by

$$C = \mathbf{P}I + \mathbf{E} \quad (5)$$

where \mathbf{P} is ($n \times p$) matrix with response coefficients relating analyte concentration C to current I at a given potential.

In most cases, the full-voltammogram methods are significantly better than the sensor-limited ILS method, since they have ability to achieve signal averaging effect over many or all the potentials included the analysis, while ILS is not capable of signal averaging [23]. However, all components of overlapping peaks should be known for optimal performance of CLS and KF, whereas at only one component needs to be known for ILS calibration.

An important consideration in the application of the least squares algorithms is the accurate estimation of the measurement model or empirical matrix \mathbf{K} or \mathbf{P} . This matrix was constructed by selecting the responses of every pure single component closest to the zero baseline. These were after background subtraction to remove the capacitive current component, by re-scanning anodically after the stripping step [16,17], or by scanning the blank.

To start the Kalman recursion KF, initial estimates of $x(0)$, $P(0)$ and $R(0)$ in the present case were assigned, according to Poulisse proposal [24], as 0, 1 and 1×10^{-6} , respectively. Figs. 2 and 3 and Fig. 4 shows the experimental voltammograms obtained for binary, ternary and quaternary mixtures, respectively, and the

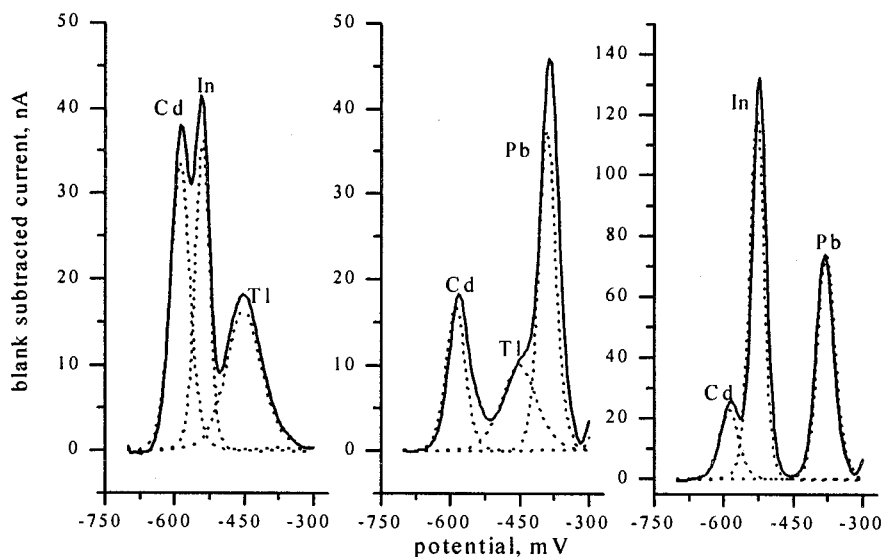


Fig. 3. Ternary mixture square wave stripping peaks after subtraction of blank (solid lines) and the corresponding fit components (dotted lines).

computer-fitted curves (dotted lines) of each component after resolving the multicomponent system by the KF method. As can be seen, the fitting is quite satisfactory and the problems encountered in the resolution of different components mentioned by Turnes [15] are improved by the KF. The same results might be obtained by employing full-voltammogram CLS as demonstrated in Table 2. Attempts to improve the error of propagation by minimisation of $\text{Cond}(K)$ [25] has been

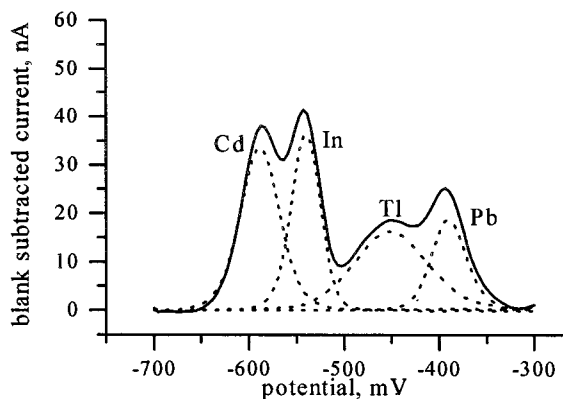


Fig. 4. Quaternary mixture square wave stripping peaks after subtraction of blank (solid lines) with the corresponding fit components (dotted lines).

made over the potential range lower than -700 to -300 mV, but results have not improved.

The optimal number of potentials used for ILS depends on the presence or absence of a random linear voltammetric base line, the degree of peak overlap of different electroactive components and the magnitude of the voltammetric noise [23]. Accordingly, the smallest error amplification, i.e. the smallest condition number of calibration, $\text{Cond}(K)$ [25], was a criterion to choose the optimal set of stripping potentials used for ILS analysis of Cd(II), In(III), Tl(I) and Pb(II). The potentials selected were -680 , -571 , -555 , -454 , -450 , -446 and -406 mV vs Ag/AgCl. Based on these selected potentials, the results are given in Table 2.

The metals can be identified as being Cd, In, Tl and Pb on the basis of their high estimates of concentrations obtained by parameter estimator (Table 3). If one component is not present in the sample, but its pure coefficients exist in the K matrix, the filter will produce a very small value for that component with respect to other components of the concentration.

In order to evaluate whether there are significant differences between the concentration found for each analyte and each method, the variance

Table 2
Comparative results obtained by different algorithms on the analysis of square wave stripping voltammograms

Taken (nM)		Found ^a (nM)												
		CLS			ILS			KF						
Cd	In	Pb	Cd	In	Tl	Pb	Cd	In	Tl	Pb	Cd	In	Tl	Pb
50	50	51.24 (2.54)	48.28 (1.02)	2.16 (1.22)	0.69 (0.42)	51.93 (3.45)	49.84 (2.09)	1.31 (1.12)	0.13 (0.08)	51.93 (1.91)	48.56 (2.26)	3.45 (3.25)	0.79 (1.00)	
	50	0.13 (0.35)	43.72 (2.02)	283.29 (13.81)	1.63 (2.13)	0.74 (1.25)	49.48 (1.54)	284.62 (14.34)	1.64 (2.03)	0.36 (0.56)	49.23 (1.63)	285.20 (12.89)	1.80 (2.16)	
	300	0.10 (0.25)	0.36 (0.24)	284.30 (9.32)	47.25 (5.89)	0.13 (0.31)	0.18 (0.21)	295.88 (6.91)	45.40 (2.34)	0.10 (0.24)	0.08 (0.20)	290.02 (6.49)	47.41 (5.93)	
150	100	144.25(2.06)	102.53 (0.97)	276.46 (2.34)	2.63 (0.06)	147.73 (1.78)	98.75 (1.23)	288.54 (1.12)	1.45 (0.24)	146.24 (1.91)	100.24 (1.24)	284.33 (2.53)	2.12 (0.94)	
	300	89.84 (4.37)	297.54 (3.58)	1.65 (2.26)	187.69 (0.19)	95.34 (3.76)	302.12 (2.48)	2.13 (1.00)	199.45 (2.04)	92.00 (3.97)	304.01 (2.88)	1.23 (0.00)	197.24 (1.45)	
	50	52.14 (2.91)	2.35 (0.23)	144.23 (2.67)	97.14 (1.27)	55.97 (1.98)	1.45 (0.33)	146.51 (1.86)	97.87 (1.12)	53.46 (3.07)	1.76 (0.17)	143.07 (2.37)	96.45 (1.34)	
	150	0.00 (0.00)	144.76 (3.50)	176.55 (10.37)	47.57 (2.23)	0.00 (0.00)	146.9 (2.48)	186.78 (8.76)	49.83 (2.03)	0.04 (0.00)	146.7 (3.16)	184.9 (11.78)	51.54 (3.45)	
	300	138.12 (11.46)	89.25 (5.80)	268.35 (3.45)	50.13 (4.51)	144.06 (6.46)	91.79 (4.78)	270.22 (2.68)	50.11 (3.30)	141.16 (7.84)	90.70 (6.78)	279.47 (3.89)	51.59 (3.76)	

^a Average of three determinations.

Values in parentheses represent standard deviation.

Table 3
Relative standard error of prediction (SEP) in validation data

	df	F_{critical} at $\alpha = 0.05$	CLS	ILS	KF
Cd	41	1.68	11.37	7.97	11.48
In	41	1.68	34.48	6.94	7.01
Tl	41	1.68	20.96	8.91	11.43
Pb	41	1.68	36.05	31.23	36.39

ratio test, F -test, was used to compare the relative standard error of prediction (SEP) [26] at the 95% confidence level. The values of SEP are shown in Table 3. It is clear that ILS gave the lowest SEP values for all components studied, this method offered the best results. This can be explained by the computational advantage that ILS has over CLS and KF in multicomponent data where wider potential ranges do not add any relevant analytical information, but noise. The results show no significant differences in any of the calibration methods for Pb determination. For In and Tl estimation, no significant differences have been found using ILS and KF. For Cd, there were significant differences between ILS and other calibration methods.

Applying the present method to a real sample of NaHCO_3 (ANALAR), it was possible to detect and determine the ultra traces of Pb, Cd and Tl present in the sample after 5 min preconcentration at -900 mV. As for In, it was clear that the bicarbonate medium is not suitable for its complexation similar to the effect of the previously mentioned anions [19]. This was confirmed by the standard addition of the cation itself where the In peak failed to develop in the predominantly bicarbonate medium, either in the presence or absence of the acetate–bromide electrolyte. Thus, subsequent measurements of Pb, Cd and Tl were performed in the absence of this supporting electrolyte to exclude the possibility of its contamination.

The peak potentials of Cd and Pb were shifted to a more negative value, -618 and -525 mV, respectively, while the Tl peak, at -445 mV, remained unaffected by the bicarbonate medium.

The baseline correction of the bicarbonate sample was performed through rapid square wave sweep after the stripping step.

Fig. 5 shows the voltammogram of the sample and the resolved peaks of Cd, Pb and Tl after applying the CLS method. The optimal set of stripping potentials used for ILS analysis of Cd(II), Pb(II) and Tl(I) was -618 , -525 and -445 mV. Comparative results obtained by CLS, ILS and KF for five replicate samples are outlined in Table 4.

The signal-to-noise ratio of the stripping peak, especially thallium, is generally very low, the relatively higher values of standard deviation (SD) obtained using the three techniques were expected, cf. Table 4. However, they still exist within the permissible limits for the determination of such ultra trace quantities. SD improvement may be attained if the enrichment time step was longer than 5 min.

For reference determinations, a Zeeman AAS, model 4100 of Perkin Elmer, was used. The measurements of cadmium, thallium and lead in sodium bicarbonate solution was carried out by adding a solution of ammonium dihydrogen phosphate and magnesium nitrate to the sample as matrix modifier [27]. The mean (and SD) values obtained are 26.202 (5.004), 0.716 (0.288), 1.180 (0.245) for lead, thallium and cadmium, respectively. The results are in accordance with those

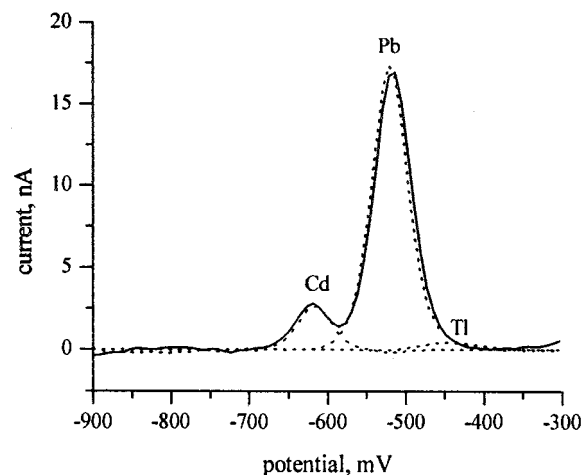


Fig. 5. Determination of Cd(II), Pb(II) and Tl(I) ions in sodium hydrogen carbonate (AR). Real mixture square wave stripping peaks after subtraction of blank (solid line) and the corresponding fit components obtained by CLS (dotted lines).

Table 4
Determination of Cd, Pb and Tl in sodium hydrogen carbonate sample using square wave anodic stripping voltammetry

Sample	Found ($\mu\text{g } 100 \text{ g}^{-1}$)								
	CLS			ILS			KF		
	Cd	Tl	Pb	Cd	Tl	Pb	Cd	Tl	Pb
1	0.969	0.829	18.942	0.998	0.117	18.018	0.942	0.712	18.867
2	1.377	3.022	31.754	1.186	2.483	33.494	0.834	0.412	30.168
3	1.410	0.000	27.894	1.267	0.000	32.631	0.976	0.000	26.464
4	1.115	0.000	22.557	1.120	0.000	22.778	1.068	0.000	22.446
5	1.151	2.228	29.146	1.188	1.787	30.519	1.120	2.169	28.905
Mean	1.204	1.216	26.059	1.152	0.877	27.488	0.988	0.659	25.370
SD	0.212	1.428	5.667	0.114	1.223	7.574	0.097	0.347	4.897

obtained in the present voltammetric method. It is noteworthy that in the voltammetric procedure as well as being simpler and cheaper, a matrix modifier is not required.

Acknowledgements

Our thanks are extended to the Volkswagen-Foundation, D-30505 Hannover, P.O. Box 810509, Germany for continuous assistance and support, and to Prof. Dr K. Brodersen, Institute of Inorganic and Analytical Chemistry, University of Erlangen-Nürnberg, D-91058 Erlangen, for his valuable advice.

References

- [1] C. Collado-Sanchez, J. Perez-Pena, M.D. Gelado-Caballero, J.A. Herrera-Melian, J.J. Hernandez-Brito, *Anal. Chim. Acta* 320 (1996) 19.
- [2] N. Elkenova, L. Ilcheva, Zh. Denchev, *Anal. Lab.*, 4 (1995) 98; *Anal. Abstr.* 58 (1996) 2E13.
- [3] T. Nedeltcheva, *Fresenius' Z. Anal. Chem.* 354 (1996) 370.
- [4] L. M. Maksimkina, L. N. Martynovskaya, N. V. Khitova, *Zavod. Lab.*, 62 (1996) 17; *Anal. Abstr.* 58 (1996) 10E32.
- [5] Kh. Brainina, H. Schafer, A. Ivanova, R. Khanina, *Anal. Chim. Acta* 330 (1996) 175.
- [6] N. Bouropoulos, D. Kararias, P.G. Koutsoukos, *Analisis* 24 (1996) 89.
- [7] C.J. Horng, *Analyst* 121 (1996) 1511.
- [8] J. Wang, S. Armalis, *Electroanalysis* 7 (1995) 958.
- [9] M.X. Shao, J.Z. Yu, X.L. Lu, H.J. Liu, G.H. Tan, C.Li, Lihua Jiayan. *Huaxue Fence*, 31 (1995) 337; *Anal. Abstr.*, 58 (1996) 4E99.
- [10] B. Fang, L. Wang, T. Wu, J. L. Wu, Lihua Jiayan *Huaxue Fence*, 31 (1995) 271; *Anal. Abstr.*, 58 (1996) 2F37.
- [11] T. Kurotu, *Fresenius' Z. Anal. Chem.* 355 (1996) 87.
- [12] C. Rounaghi, Z. Eshagi, E. Chiamati, *Talanta* 43 (1996) 1243.
- [13] J. Labuda, M. Vanickova, *Anal. Chim. Acta* 208 (1988) 219.
- [14] M.M. Palrecha, A.V. Kulkarni, R.G. Dhaneshwar, *Analyst* 111 (1986) 375.
- [15] G. Turnes, A. Cladera, E. Gómez, J.M. Estela, V. Cerdà, *J. Electroanal. Chem.* 338 (1992) 49.
- [16] T.F. Brown, S.D. Brown, *Anal. Chem.* 53 (1981) 1410.
- [17] C.A. Scolari, S.D. Brown, *Anal. Chim. Acta* 166 (1984) 253.
- [18] G.E. Batley, T.M. Florence, *J. Electroanal. Chem.* 55 (1974) 23.
- [19] T.M. Florence, G.E. Batley, Y.J. Farrar, *J. Electroanal. Chem.* 56 (1974) 301.
- [20] I.H.I. Habib, Ph.D. Thesis, Faculty of Science, Cairo University, 1997.
- [21] W. Frenzel, *Anal. Chim. Acta* 273 (1993) 123.
- [22] J.G. Osteryoung, R.A. Osteryoung, *Anal. Chem.* 57 (1985) 101A.
- [23] E.V. Thomas, D.M. Haaland, *Anal. Chem.* 62 (1990) 1091.
- [24] H.N.J. Poulisse, *Anal. Chim. Acta* 112 (1979) 361.
- [25] C. Jochum, P. Jochum, B.R. Kowalski, *Anal. Chem.* 53 (1981) 85.
- [26] P.J. Gemperline, J.R. Long, V.G. Greogoriosis, *Anal. Chem.* 63 (1991) 2313.
- [27] W. Slavin, G.R. Carnich, D.C. Manning, E. Pruszkowska, *At. Spectrosc.* 4 (1983) 69.

Adsorption of heavy metal ions onto dithizone-anchored poly (EGDMA-HEMA) microbeads

B. Salih^a, A. Denizli^{a,*}, C. Kavaklı^a, R. Say^b, E. Pişkin^c

^a Department of Chemistry, Hacettepe University, Ankara, Turkey

^b Department of Science, Hacettepe University, Ankara, Turkey

^c Chemical Engineering Department, Hacettepe University, Ankara, Turkey

Received 18 August 1997; received in revised form 4 November 1997

Abstract

The dithizone-anchored poly (EGDMA-HEMA) microbeads were prepared for the removal of heavy metal ions (i.e. cadmium, mercury, chromium and lead) from aqueous media containing different amounts of these ions (25–500 ppm) and at different pH values (2.0–8.0). The maximum adsorptions of heavy metal ions onto the dithizone-anchored microbeads from their solutions was 18.3, Cd(II); 43.1, Hg(II); 62.2, Cr(III) and 155.2 mg g⁻¹ for Pb(II). Competition between heavy metal ions (in the case of adsorption from mixture) yielded adsorption capacities of 9.7, Cd(II); 28.7, Hg(II); 17.6, Cr(III) and 38.3 mg g⁻¹ for Pb(II). The same affinity order was observed under non-competitive and competitive adsorption, i.e. Cr(III) > Pb(II) > Hg(II) > Cd(II). The adsorption of heavy metal ions increased with increasing pH and reached a plateau value at around pH 5.0. Heavy metal ion adsorption from artificial wastewater was also studied. The adsorption capacities are 4.3, Cd(II); 13.2, Hg(II); 7.2, Cr(III) and 16.4 mg g⁻¹ for Pb(II). Desorption of heavy metal ions was achieved using 0.1 M HNO₃. The dithizone-anchored microbeads are suitable for repeated use (for more than five cycles) without noticeable loss of capacity. © 1998 Elsevier Science B.V. All rights reserved.

Keywords: Dithizone; Poly(EGDMA-HEMA) microbeads; Heavy metal removal, cadmium, mercury, chromium and lead

1. Introduction

Dithizone (diphenylthiocarbazon) is considered a selective and sensitive ligand to prepare specific sorbents for heavy metal removal and preconcentration. Polymeric supports loaded with

dithizone were used for preconcentration of mercury from seawater but with little success [1–3]. Garcia et al. made a comparative study of silica, amberlite XAD2 and amberlite XAD7 loaded with diethyldithiocarbamate, pyrrolidine-1-ylthioformate and dithizone for on-line preconcentration of mercury [4]. Chow and Buksak have reported the use of dithizone-treated polyurethane foams for the preconcentration of ionic mercury from aqueous samples [5]. Griesbach and Lieser

* Corresponding author. Present address: P.K. 51, Samanpazari 06242, Ankara, Turkey. Tel.: +90 312 2352330; fax: +90 312 2352330. E-mail: denizli@eti.cc.hun.edu.tr

reported 15 sorbents, including one loaded with dithizone [6]. Uchiumi et al. utilized porous polymeric resin loaded with dithizone, thionalide and bismuthol II for the removal of As(III), Sb(III) and Cu(II) ions from industrial waste water [7]. Chwastowska and Kosiarska reported the anchoring of dithizone to a diazotised styrene-divinyl benzene support [8]. This chelating resin was utilized for the sorption of Ag(I), Cd(II), Cu(II), Pb(II), Ni(II), Co(II) and Zn(II) at different static and dynamic conditions. More recently, Shah and Devi attempted to apply dithizone anchored poly(vinyl pyridine) support for selective separation of mercury from binary and ternary mixtures of mercury, palladium, zinc and cadmium [9].

Recently, we produced microbeads (swell with water) made of ethylene glycol dimethacrylate (EGDMA) and hydroxyethyl methacrylate (HEMA) copolymer as a carrier matrix to prepare specific sorbents [10]. Several dye-ligands were attached covalently to these sorbents and used for selective removal of heavy metal ions from aqueous media [11–17]. In this study, we anchored dithizone on poly(EGDMA-HEMA) microbeads and attempted to use it in the adsorption of some selected heavy metal ions, i.e. Cd(II), Hg(II), Pb(II) and Cr(III). This study reports on the preparation and characterization of these dithizone-anchored poly(EGDMA-HEMA) microbeads and discusses the applicability of these sorbents in the adsorption/desorption/reuse of these heavy metal ions.

2. Experimental

2.1. Dithizone-anchored poly(EGDMA-HEMA) microbeads

Details of the preparation and characterization of the plain poly(EGDMA-HEMA) microbeads was previously detailed [10]. Ethyleneglycoldimethacrylate (EGDMA) (Röhm and Haas, Germany) and 2-hydroxyethylmethacrylate (HEMA) (Sigma, St. Louis, MO) were polymerized in suspension using benzoyl peroxide (BPO) and poly(vinylalcohol) (PVAL; M_w : 100000, 98%

hydrolyzed, (Aldrich)) as the initiator and stabilizer, respectively. Toluene (Merck, Germany) was included in the recipe as a pore former. Table 1 gives the polymerization conditions needed to obtain copolymer microbeads with a swelling ratio of 55%, in the size range of 150–200 μm .

In order to prepare microbeads containing 105.5 μmol dithizone g^{-1} polymer, the following procedure was applied: 10 ml of aqueous solution containing 500 mg dithizone (BDH, Poole, UK) was poured into 90 ml of the poly(EGDMA-HEMA) microbeads suspension in distilled water (containing 3.0 g of microbeads), 4.0 g of NaOH was then added. The medium was heated in a sealed reactor for 24 h at a stirring rate of 400 rpm, and at 80°C. The dithizone-anchored poly(EGDMA-HEMA) microbeads were filtered, and washed with distilled water and with 0.1 M NaOH several times until all of the physically adsorbed and/or absorbed dithizone molecules were removed. The extent of dithizone attachment was determined by elemental analysis data of the dried samples obtained using an elemental analysis device (Leco, CHNS-932, USA).

FTIR spectra of dithizone, untreated and dithizone-anchored microbeads were obtained using a FTIR spectrophotometer (FTIR 8000 Series, Shimadzu, Japan). The dry microbeads (about 0.1 g) were thoroughly mixed with KBr (0.1 g, IR Grade, Merck, Germany), and pressed into pellet form, the spectrum was then recorded.

Table 1
Polymerization conditions of the poly(EGDMA-HEMA) microbeads

Dispersion phase	Monomer phase
50 ml of distilled water	8 ml EGDMA
0.2 g PVAL	4 ml HEMA
	12 ml toluene
	0.06 g BPO
Polymerization conditions	
Reactor volume, 100 ml	
Stirring rate, 600 rpm	
Heating program, 65°C for 4 h, followed by 90°C for 2 h	

2.2. Heavy metal adsorption/desorption

Heavy metal ion adsorption from the single metal (nitrates were used) aqueous solutions was investigated in batch adsorption-equilibrium experiments. The effects of the initial concentration of metal ions and the pH of the medium on the adsorption rate and capacity was studied. Aqueous metal ion solutions of 20 ml with different concentrations (in the range of 25–500 ppm) was treated with the untreated and/or dithizone-anchored microbeads (100 mg microbeads per batch) at different pH values (in the range of 2.0–8.0, adjusted with universal buffer solution) at room temperature, in flasks magnetically agitated at 600 rpm. The adsorption time was selected as 60 min in preliminary experiments, which was assumed the equilibrium adsorption time, because there was no significant change in the amount of adsorption after 60 min. The microbeads were separated from the adsorption medium at the end of each adsorption experiment, and the concentration of the metal ions in the aqueous phase was measured by graphite furnace atomic absorption spectrophotometer (AAS, GBC 932 AA, Australia). Hg(II) concentration was determined by AAS connected with a Hydrid Generator (GBC HG 3000). All instrumental conditions were optimized for maximum sensitivity as described by the manufacturer. For each sample, the mean of 10 AAS measurements was recorded. The amount of adsorbed heavy metal ions was calculated as:

$$Q = [(C_o - C_A) \cdot V]/m \quad (1)$$

Where Q is the amount of metal ions adsorbed onto unit amount of the microbeads (mg g^{-1}); C_o and C_A are the concentrations of metal ions in the initial solution and in the aqueous phase after adsorption, respectively (mg ml^{-1}); V is the volume of the aqueous phase (ml); and m is the weight of the microbeads (g).

Competitive adsorption of heavy metal ions from their mixture was also investigated in batch wise form. A solution (20 ml) containing 50 ppm from each metal ions was treated with the dithizone-anchored microbeads at a pH of 7.0 at room temperature, in flasks stirred magnetically at 600

rpm. After adsorption, the concentration of the metal ions in the supernatant was acquired using an atomic absorption spectrophotometer.

Adsorption of heavy metal ions from artificial wastewater was also performed in batch wise form. A solution (20 ml) containing 50 ppm of each metal ion [i.e. Cr(III), Cd(II), Hg(II) and Pb(II)] was treated with the dithizone-anchored microbeads at a pH of 6.8 at room temperature, in flasks stirred magnetically at 600 rpm. Artificial wastewater also contains Ni(II), Cu(II), Zn(II), Fe(II), Co(II), Sn(II) and Ag(I). The concentration of each metal ion in artificial wastewater is 5 ppm. In order to adjust the salinity, 700 ppm NaCl was added to artificial wastewater. After adsorption, the concentration of metal ions in the supernatant was obtained using an atomic absorption spectrophotometer.

In order to determine the reusability of the dithizone-anchored microbeads, consecutive adsorption-desorption cycles were repeated five times using the same microbeads. Desorption of heavy metal ions was achieved using 0.1 M HNO_3 . The dithizone-anchored microbeads carrying 7.60 mg Cd(II) g^{-1} ; 14.05 mg Cr(III) g^{-1} ; 32.01 mg Pb(II) g^{-1} ; 12.30 mg Hg(II) g^{-1} were placed in this desorption medium and stirred at 600 rpm for 30 min at room temperature. The final metal ion concentration in the aqueous phase was determined using an atomic absorption spectrophotometer. The desorption ratio was calculated from the amount of metal ions initially loaded on the microbeads and the final metal ion concentrations in the desorption medium.

3. Results and discussion

3.1. Structure of chelating resin

The poly(EGDMA-HEMA) based microbeads which were prepared in this study have a rather hydrophilic structure. The equilibrium swelling ratio was about 55% [10]. As mentioned before, dithizone was selected as the chelating agent, and attached to the poly(EGDMA-HEMA) microbeads. Fig. 1 gives a schematical view of dithizone attachment to the carrier microbeads—the

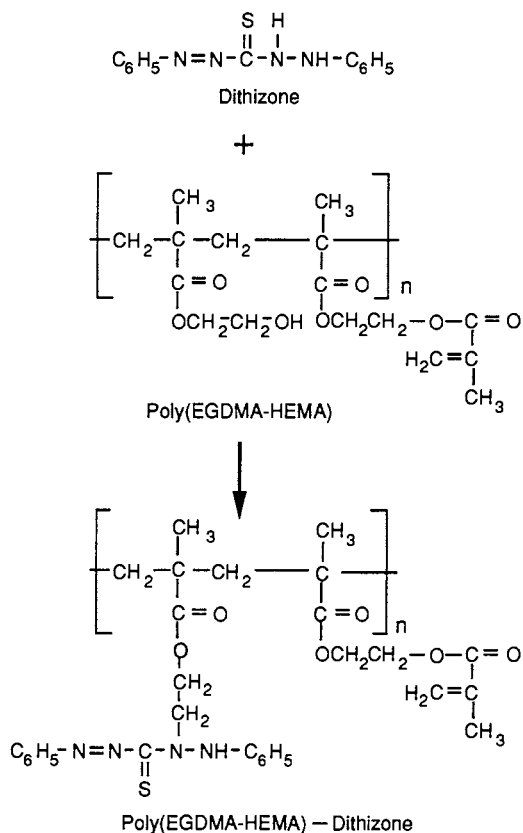


Fig. 1. Synthesis of the sorbent.

reaction of hydroxyl groups (coming from HEMA) on the carrier and the nitrogen atom of dithizone.

Fig. 2 gives the FTIR spectra of the untreated and dithizone-anchored microbeads. The bands observed at 3220 cm^{-1} are due to stretching of N–H, adjacent to the C=S functional group. The absorption band observed at 3370 cm^{-1} is assigned to the stretching of N–H that is adjacent to the aromatic ring. The N–H scissor absorption band is seen at 1500 cm^{-1} . The absorption band at 1625 cm^{-1} represents conjugation of the aromatic ring. The weak absorption band at 1575 cm^{-1} shows a N=N stretching band in the structure of dithizone. The absorption bands at 1100 cm^{-1} and 1450 cm^{-1} represent stretching of S=C and S=C–NH vibration, are due to the dithizone bonded to the poly(EGDMA-HEMA) microbeads. It is probable that not all of the OH

functional groups on the carrier reacted with dithizone. Therefore, the absorption band at 3370 cm^{-1} representing these unassociated OH groups is fairly broad in FTIR spectra of the dithizone-anchored poly(EGDMA-HEMA) microbeads. All of these absorption bands show the attachment of dithizone onto/into the microbeads.

Elemental analysis of untreated and dithizone-anchored microbeads was also carried out, the attachment of dithizone was found as $105.5\text{ }\mu\text{mol g}^{-1}$ from sulphur and nitrogen stoichiometry. This was the maximum attachment value achieved.

Dithizone leakage from the anchored microbeads was also studied. There was no dithizone leakage in any of the adsorption and desorption media used, a guarantee that the washing procedure was adequate for removal of physically adsorbed dithizone molecules from the microbeads.

3.2. Heavy metal adsorption

3.2.1. Effects of initial concentration of metal ions

The heavy metal ion adsorption capacities of the dithizone-anchored microbeads are given as a function of the initial concentration of metal ions within the aqueous phase in Fig. 3. These adsorption curves were obtained from experiments where adsorptions from the single metal aqueous solutions were studied. It was observed that the amount of adsorption was significantly increased with the initial heavy metal concentration especially in the case Pb(II) and also for Cr(III), in the studied concentration range. In order to eliminate the contribution made by the precipitation of heavy metal in the form of hydroxides, we did exceed metal ions concentrations of 500 ppm. The maximum adsorption capacities of the dithizone-anchored microbeads in the studied range are 18.3, 43.1, 62.2 and 155.2 mg g^{-1} for Cd(II), Hg(II), Cr(III) and Pb(II), respectively, at pH 7.0, which corresponds to an initial concentration of 500 ppm. The affinity order (weight basis) is Pb(II) > Cr(III) > Hg(II) > Cd(II). It should be noted that the maximum adsorption capacities (molar basis) of the dithizone-anchored microbeads are 160, 214, 749 and $1192\text{ }\mu\text{mol g}^{-1}$ of

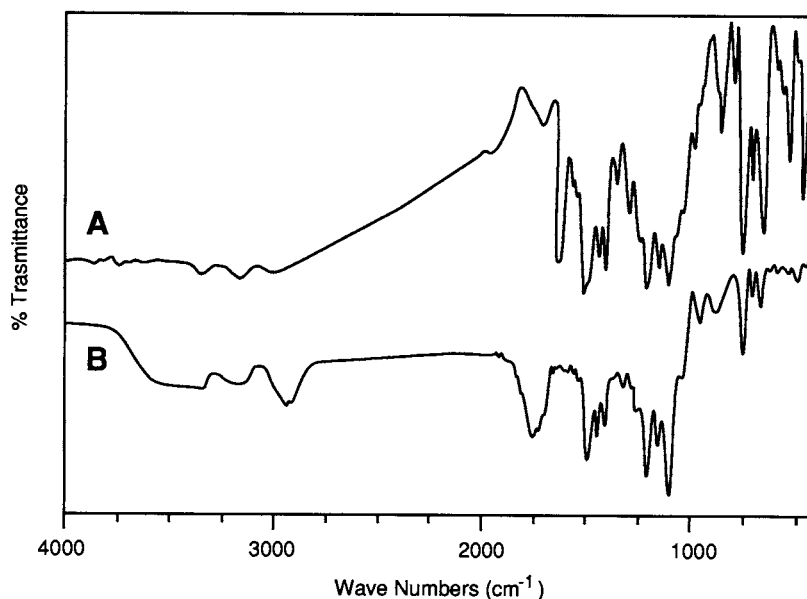


Fig. 2. FTIR Spectra of: (A) Dithizone; (B) Dithizone-anchored poly(EGDMA-HEMA) microbeads.

polymer for Cd(II), Hg(II), Pb(II) and Cr(III), respectively. The order of affinity based on micro-mole uptake by the sorbent differs according to weight base and is as follows: Cr(III) > Pb(II) > Hg(II) > Cd(II).

As mentioned previously, 1 g of sorbent carries 105.5 μmol dithizone which was determined by elemental analysis. From the stoichiometry, it

seems that one immobilized dithiozone molecule interacts with one to ten metal ions depending on the type of metal. The S and N atoms of dithiozone are available for interaction with heavy metal ions. The number of available active sites does not match the number of heavy metal ions adsorbed. Heavy metal ion adsorption on plain microbeads (carrying no dithiozone) is relatively low, about 8.3×10^{-3} , Cd(II), 10.5×10^{-3} , Hg(II), 59.3×10^{-3} , Cr(III) and $59.3 \times 10^{-3} \mu\text{mol g}^{-1}$ for Pb(II). Note that these microbeads are prone to swelling and are also porous, and therefore may absorb (or entrap) heavy metal ions within the matrix of the swollen microbead. In addition, the hydroxyl groups may interact with heavy metal ions (similar to solvation with water), causing these non-specific-adsorption capacities. These values do not explain the high adsorption (up to ten heavy metal ions per one dithiozone molecule, i.e. Cr(III) ions). It seems that the adsorbed heavy metal ions interact with heavy metal ions that arrive at the same adsorption site during the adsorption process, as such adsorption is not monolayer, but rather multilayer (non-Langmuir type).

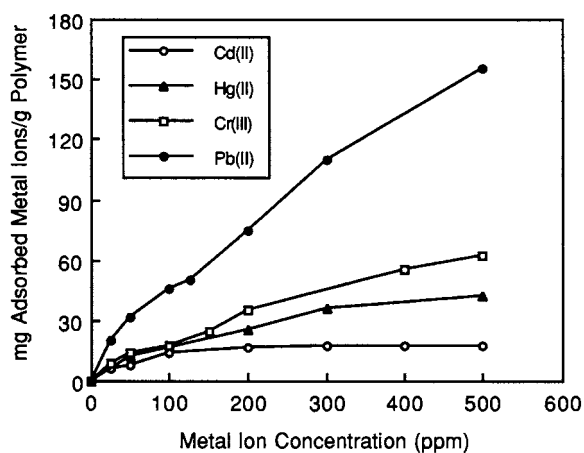


Fig. 3. Heavy metal ions adsorption capacity of the dithizone-anchored microbeads. Temperature 20°C; pH 7.0.

Different sorbents having a wide range of adsorption capacities for heavy metal ions have been used. Chwastowska and Kosiarska achieved 5.6 mg Cd(II) g⁻¹ and 10.4 mg Pb(II) g⁻¹ with dithizone loaded poly(styrene-divinylbenzene) copolymer [8]. Shah and Devi used dithizone-anchored poly(vinyl pyridine) support and they reported a specific mercury adsorption capacity of up to 144 mg Hg(II) g⁻¹ polymer [9]. Shreedhara-Murthy and Ryan found 3.9–14.4 mg Cd(II) g⁻¹ removal by cellulose-dithiocarbamate resins [18]. Roozmond et al. reported 40 mg Cd(II) g⁻¹ with pyrazole-containing poly(styrene-divinylbenzene) sorbents [19]. Konishi et al reported 4.8–96.3 mg Cd(II) g⁻¹ with alginic acid gels [20]. Liu et al. achieved 22.4 mg Cd(II) g⁻¹, 72.2 mg Hg(II) g⁻¹ and 93 mg Pb(II) g⁻¹ adsorption capacity with *N*-hydroxymethyl thioamide resin [21]. Sağ and Kutsal used *Zoogloea ramigera* microorganisms for heavy metal adsorption [22]. The maximum adsorption capacities achieved were 85 mg Pb(II) g⁻¹ dry weight of microorganisms. Denizli et al. used alkali blue 6B-attached P(EGDMA-HEMA) sorbents, in which the maximum adsorption capacities were 5.5 mg Cd(II) g⁻¹ and 125 mg Pb(II) g⁻¹ [13]. Dev and Rao reported 51.7 mg Cd(II) g⁻¹ and 80.8 mg Pb(II) g⁻¹ adsorption capacity for polystyrene-divinylbenzene macroreticular resin functionalized with bis-(*N,N'*-salicylidene)1,3-propanediamine [23]. Denizli et al. reported 136.2–174.2 mg Pb(II) g⁻¹ for diamine glow discharge treated polyhydroxyethylmethacrylate microbeads [15]. Aksu and Kutsal used *Chlorella vulgaris* microorganisms [24]. They reported 42.1 mg Cr(VI) g⁻¹ and 90 mg Pb(II) g⁻¹ maximum adsorption capacity. Jose and Pillai used ethylenediamine–triethyleneglycoldimethacrylate crosslinked polyacrylamide resin and reached 68 mg Cd(II) g⁻¹, 69 mg Cr(III) g⁻¹ and 164 mg Pb(II) g⁻¹ [25]. The adsorption capacities achieved in this study compare well with values reported in previous publications.

3.2.2. Effects of pH

Metal ion adsorption onto non-specific and specific sorbents is pH dependent [12–15]. In the absence of complexing agents, the hydrolysis and

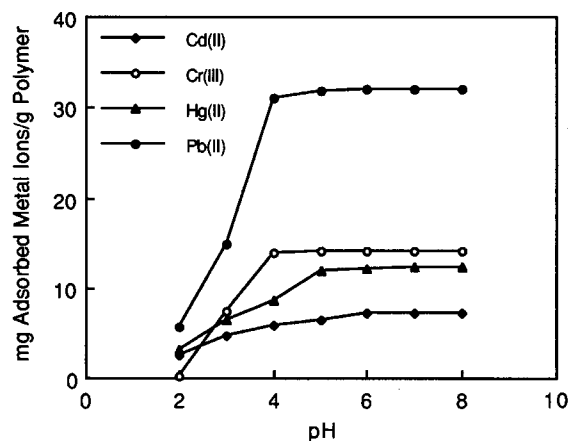


Fig. 4. Effect of pH on adsorption of heavy metal ions on the dithizone-anchored microbeads. Temperature 20°C. Initial concentrations of metal ions, 50 ppm.

precipitation of metal ions are affected by the concentration and form of soluble metal species. The solubility of metal ions is governed by hydroxide or carbonate concentration. As discussed in detail by Reed and Matsumoto [26], the hydrolysis of metal ions becomes significant at a pH of approximately 7.5–8.5. Therefore, in this study the pH range was adjusted to between 2.0 and 8.0. The effect of pH on heavy metal adsorption is illustrated in Fig. 4. It was noticed that the adsorption capacities increased with increasing pH, reaching plateau values at around pH 4–6 depending on the metal ions [8]. Our plateau values are 7.6, Cd(II), 12.3, Hg(II), 14.1, Cr(III) and 32 mg g⁻¹ for Pb(II), which correspond to initial metal ion concentrations of 50 ppm. The difference in adsorption values can be explained by the different affinities the heavy metal ions have for the donor atoms in the ligand dithizone.

3.3. Competitive adsorption

Adsorption capacities of dithizone-anchored microbeads for metal ions under competitive conditions (adsorption from solutions containing all heavy metal ions) for Cd(II), Hg(II), Cr(III) and Pb(II) are given in Table 2. Adsorption values are given both on a weight and molar basis. It should be noted that the competitive adsorption capac-

ities of the dithizone-anchored poly(EGDMA-HEMA) microbeads for all metal ions was much higher than non-competitive conditions. The non-competitive adsorption capacities are 7.60, Cd(II); 12.30, Hg(II); 14.05, Cr(III) and 32.01 mg g⁻¹ for Pb(II) at 50 ppm initial concentration. The competitive adsorption capacities are higher than the non-competitive adsorption capacities. They are 9.7, Cd(II); 28.7, Hg(II); 17.6, Cr(III) and 38.3 mg g⁻¹ for Pb(II). The dithizone-anchored microbeads exhibit the following metal ion affinity sequence (molar basis) under competitive adsorption conditions: Cr(III) > Pb(II) > Hg(II) > Cd(II). Contrary to previous publications, we did not observe any dithizone groups specificity for mercury ions, this maybe due to the adsorption conditions we studied [9].

3.4. Adsorption from artificial wastewater

Adsorption capacities of the dithizone-anchored microbeads from artificial waste-water for Cd(II), Hg(II), Cr(III) and Pb(II) are shown in Table 3. Adsorption values are given both in weight and molar basis. It is worth noting that the adsorption capacities of the dithizone-anchored microbeads from artificial wastewater for all metal ions was much lower than competitive conditions. The adsorption capacities are 4.3, Cd(II); 13.2, Hg(II); 7.2, Cr(III) and 16.4 mg g⁻¹ for Pb(II). The dithizone-anchored microbeads exhibit the following metal ion affinity sequence (molar basis): Cr(III) > Pb(II) > Hg(II) > Cd(II). Dithi-

Table 2

Competitive adsorption of heavy metal ions on the dithizone-anchored microbeads:

Ions	mg Adsorbed ion g ⁻¹ polymer ^a	μmol Adsorbed ion g ⁻¹ polymer ^a
Cd(II)	9.7 (7.60)	86.3 (67.6)
Hg(II)	28.7 (12.3)	143.1 (61.3)
Pb(II)	38.3 (32.01)	184.5 (154.5)
Cr(III)	17.6 (14.05)	338.5 (270.2)

^a Adsorptions from single metal ion solutions are given in parantheses.

Concentration of each metal ions, 50 ppm; pH 7.0, temperature 20°C.

Table 3

Adsorption of heavy metal ions from artificial wastewater on the dithizone-anchored microbeads

Ions	mg Adsorbed ion g ⁻¹ polymer	μmol Adsorbed ion g ⁻¹ polymer
Cd(II)	4.3	38.3
Hg(II)	13.2	65.6
Pb(II)	16.4	79.2
Cr(III)	7.2	138.4

Concentration of each metal ions, 50 ppm; pH 6.8, temperature 20°C.

zone-anchored microbeads adsorbed other metal ions. Therefore adsorption of other metal ions reduces the adsorption capacities of the microbeads for Cd(II), Hg(II), Cr(III) and Pb(II).

3.5. Regeneration of microbeads

To be of use in metal ion recycling processes, metal ions chelated should be easily desorbed under suitable conditions. Desorption experiments were performed with 0.1 M HNO₃ as the desorption agent. The dithizone-anchored microbeads loaded the maximum amounts of the respective metal ions when placed within the desorption medium, the amount of metal ions desorbed in 30 min was measured. Table 4 shows the adsorption-desorption values of heavy metal ions by dithizone-anchored microbeads after several cycles of consecutive adsorption and desorption. This table clearly shows that the dithizone-anchored microbeads can be used repeatedly without losing their adsorption capacities for all metal ions studied here.

4. Conclusion

Poly(EGDMA-HEMA) microbeads containing 105.5 μmol dithizone g⁻¹ polymer were used for adsorption/desorption of Cd(II), Hg(II), Cr(III) and Pb(II) ions from aqueous solution under non-competitive and competitive conditions. The maximum desorption capacities of these affinity microbeads from their single metal ions solutions were 18.3 mg g⁻¹ (160 μmol), Cd(II); 43.1 mg

Table 4
Adsorption-desorption cycles for heavy metal ions

Cycle no.	Cd(II)		Cr(III)		Pb(II)		Hg(II)	
	Adsorption (mg g ⁻¹)	Desorption (%)	Adsorption (mg g ⁻¹)	Desorption (%)	Adsorption (mg g ⁻¹)	Desorption (%)	Adsorption (mg g ⁻¹)	Desorption (%)
1	7.60	91.6	14.05	94.4	32.01	89.2	12.30	91.4
2	7.43	94.2	13.88	96.8	31.86	95.6	12.16	89.6
3	7.29	95.4	13.65	95.2	31.72	97.3	11.89	92.5
4	7.11	93.3	13.44	93.5	31.40	98.4	11.71	88.7
5	6.96	92.8	13.02	93.2	31.05	91.5	11.62	88.9

g^{-1} (214 μmol), Hg(II); 62.2 mg g^{-1} (1192 μmol), Cr(III) and 155.2 mg g^{-1} (749 μmol) for Pb(II). When the heavy metal ions competed (in the case of adsorption from their mixture) the amounts of adsorption was 9.7 mg g^{-1} (86.3 μmol), Cd(II); 28.7 mg g^{-1} (143.1 μmol), Hg(II); 17.6 mg g^{-1} (338.5 μmol), Cr(III) and 38.3 mg g^{-1} (184.5 μmol) for Pb(II). Dithizone-anchored microbeads exhibit the following metal ion affinity sequence under non-competitive and competitive conditions, Cr(III) > Pb(II) > Hg(II) > Cd(II). The adsorption capacities of the dithizone-anchored microbeads from artificial wastewater for all metal ions was much lower than competitive conditions. The adsorption capacities are 4.3, Cd(II); 13.2, Hg(II); 7.2, Cr(III) and 16.4 mg g^{-1} for Pb(II). Consecutive adsorption and desorption cycles showed the feasibility of these dithizone-anchored microbeads for heavy metal adsorption.

References

- [1] A. Chow, D. Buksak, Can. J. Chem. 5 (1975) 132.
- [2] Y.K. Lee, K.J. Whang, K. Ueno, Talanta 22 (1975) 535.
- [3] A.G. Howard, M.H. Arbab-Zavar, Talanta 26 (1979) 895.
- [4] M.F. Garcia, R.P. Garcia, N.B. Garcia, A.S. Medel, Talanta 41 (1994) 1833.
- [5] A. Chow, D. Buksak, Can. J. Chem. 53 (1975) 1373.
- [6] M. Griesbach, K.H. Lieser, Eur. Pat. Appl. 14222 (Cl. o8 F8/30), 1979.
- [7] A. Uchiumi, S. Tokunaga, T. Eyama, H. Shibayama, Int. Conf. Process. Mater. Prop. 1 (1993) 101.
- [8] J. Chwastowska, E. Kosiarska, Talanta 35 (1988) 439.
- [9] R. Shah, S. Devi, React. Funct. Polym. 31 (1996) 1.
- [10] K. Kesenci, A. Tuncel, E. Pişkin, React. Funct. Polym. 31 (1996) 137.
- [11] B. Salih, A. Denizli, B. Engin, E. Pişkin, React. Funct. Polym. 27 (1995) 199.
- [12] B. Salih, A. Denizli, E. Pişkin, Sep. Sci. Technol. 31 (1996) 715.
- [13] A. Denizli, B. Salih, E. Pişkin, React. Funct. Polym. 29 (1996) 11.
- [14] B. Salih, A. Denizli, B. Engin, A. Tuncel, E. Pişkin, J. Appl. Polym. Sci. 60 (1996) 871.
- [15] A. Denizli, B. Salih, E. Pişkin, J. Chromatogr. A 773 (1997) 169.
- [16] A. Denizli, K. Kesenci, M.Y. Arıca, B. Salih, V. Hasırcı, E. Pişkin, Talanta, 1997 (in press).
- [17] A. Denizli, B. Salih, M.Y. Arıca, K. Kesenci, V. Hasırcı, E. Pişkin, J. Chromatogr. 758 (1997) 217.
- [18] R.S. Shreedhara-Murthy, D.E. Ryan, Anal. Chim. Acta 140 (1982) 163.
- [19] D.A. Roozmond, Eur. Polym. J. 24 (1988) 367.
- [20] Y. Konishi, S.S. Asai, Y. Midoh, M. Oku, Sep. Sci. Technol. 27 (1992) 1985.
- [21] C.Y. Liu, H.T. Chang, C.C. Hu, Inorg. Chim. Acta 172 (1990) 151.
- [22] Y. Sağ, T. Kutsal, Chem. Eng. J. 60 (1995) 181.
- [23] K. Dev, G.N. Rao, Talanta 43 (1996) 451.
- [24] Z. Aksu, T. Kutsal, Environ. Technol. 11 (1990) 979.
- [25] L. Jose, V.N.R. Pillai, J. Appl. Polym. Sci. 60 (1996) 1855.
- [26] B.E. Reed, M.R. Matsumoto, Sep. Sci. Technol. 28 (1993) 2179.

Book reviews

Semiconductor Nanoclusters—Physical, Chemical and Catalytic Aspects by P.V. Kamat and D. Meisel (Eds.), Elsevier, Amsterdam, 1996, x + 474 pp. US\$272.00. ISBN 0-444-82064-7.

This book takes a wide-angle view of the rapidly expanding applications and greater sophistication in our understanding of the fundamentals of nanoparticles and nanostructured materials. Size quantization is defined and discussed in relation to single-size clusters, quantum dots, quantum wells and layered structures. Changes in electronic, optical, magnetic, catalytic, and mechanical properties in the nanometer regime are explored. Preparation, spectroscopic and electrochemical characterization of porous silicon, semiconductor metal oxide, II–VI, III–V nanoparticles, metal clusters and size-quantized structures, as well as devices based on them, are covered (e.g. H. Weller and A. Eychmüller). Some of the topics are only dealt with somewhat superficially, but through the references this book will be a good springboard to exploration of topics surrounding nano-materials.

The articles go beyond studies of isolated nanoparticles, describing a variety of nanoparticulate films and assemblies which employ the unique properties of nano-materials to develop electrodes (J.J. Fendler, P.V. Kamat, S. Gorer and G. Hodes), to imbed II–VI nanocrystals and carbon clusters in conducting polymers producing novel photoconductive imaging materials (Y. Wang) and to combine porous silicon with conducting polymers for displays (M.J. Sailor et al.). Electron transfer, carrier diffusion and relaxation are discussed (e.g. D. Meisel). Techniques for calculating

size quantization of optical properties in metal and semiconductor particles are presented (P. Mulvaney), and a good development of the use of a pseudopotential method for calculating optical and electronic properties of silicon quantum dots is included (L.-W. Wang and A. Zunger). An overview of applications of semiconductor nanostructures for solar energy conversion, electrochromic windows, luminescent diodes and intercalation batteries is given by M. Grätzel, while E. Pelizzetti and C. Minero describe applications in sensor technology, filtration, total organic carbon analysis and ferrofluids for medical imaging. Simple fabrication techniques are emphasized, with chemical solution deposition and electrodeposition utilized in most studies of films, although a nice treatment of molecular beam epitaxy in the fabrication of quantum wells is included (A.J. Nozik). Utilization of metal and semiconductor nanoparticles as catalysts for organic synthesis are discussed (Y. Li and L. Wang), as well as uses in environmental remediation of pollutants. A detailed study of the electronic states and carrier dynamics in TiO₂ and good introduction to application of TiO₂ to environmental photocatalysis in water (N. Serpone and R.F. Khairutdinov) and in air (X. Fu et al.) are presented. This book is recommended reading for both practitioners and newcomers who wish to keep up with the rapid developments in nano-materials, especially those treading the line between fundamental and applications.

N.J. Cherepy and J.Z. Zhang

PII S0039-9140(97)00413-X

Restoration and Rehabilitation of the Desert Environment. N. Al-Awadhi, M.T. Balba and C. Kamizam (editors), Elsevier, Amsterdam, 1996. xiii + 29 pp. US\$265.75. ISBN 0-444-824725.

This volume is the proceedings of the joint Kuwait–Japanese Symposium 3–4 March 1996. Nineteen papers are presented, and these are divided into three main categories: (1) Soil Bioremediation, (2) Greenery Development and (3) Water Utilisation for Greenery. It primarily focuses on rehabilitation of the desert environment in Kuwait post-Gulf War, and reflects current understanding of the technologies used to bioremediate oil-contaminated environments and of the ‘greening’ of desert environments. The connection between Japan and Kuwait in terms of rehabilitation of desert environments is not immediately obvious, but it appears that Japan does have water shortage problems and there are several good contributions by Japanese delegates on technologies for cleaning oil-contaminated soil and reuse of urban water. An author index and list of delegates are included.

The first section outlines the environmental problems facing Kuwait. During the Gulf War, large amounts of crude oil were released to the surface environment, forming huge oil lakes in the desert. While some of this oil has been extracted for processing, the remainder forms an oily sludge which must be degraded. An additional problem is that hundreds of oil wells were set on fire, necessitating the use of millions of gallons of sea water to put the fires out. This has resulted in oil sludges where microbial degradation is difficult because of the high salinity and desert environment. Various bioremediation treatments are detailed. These include composting to breakdown the heavier components of crude oil, allowing microbial degradation of the remaining light fraction. The overall conclusion is that bioremediation is aided by inoculation with a variety of bacterial strains to break down the different components of oil. Addition of nutrients increases bacterial activity, as does oxygenation (aerobic heterotrophs are far more efficient at oil degradation than anaerobic microorganisms). This first

section also includes an interesting paper on the use of photocatalysts such as TiO_2 to decompose crude oil spills. This method offers a promising approach to the remediation of heavier crudes.

The second section details strategies that can be employed to encourage plant growth in arid environments. This is of importance, not only in the rehabilitation of native plants in areas affected by oil contamination but also for dune stabilisation, agriculture and the urban environment. An interesting paper describes the propagation, via tissue culture, of individual plants that have tolerated conditions of fire and oil pollution. The authors hope that this will lead to tolerant ecotypes that can be planted in affected areas. Other topics covered include the role of microorganisms, notably VA (vesicular-arbuscular) mycorrhizal fungi and *Rhizobium* bacteria, in establishing plant growth. A plan for the ‘greening’ of Kuwait and Kuwait City is detailed. This plan is to create greenbelts and to improve the visual character of metropolitan areas. Planting will also aid energy conservation by providing shade for buildings.

The third sections deals with the implications of the ‘greening’ to water resources. There are two basic approaches: one is to plant indigenous species that are drought tolerant, and the other is to irrigate. Irrigation can be achieved through the reuse of reclaimed water from sewage treatment plants. Waste water is recycled using a combination of ultrafiltration and biological treatment. The efficiency of irrigation can also be improved with new technology.

This book is an interesting account of how the problems of oil contamination are currently being addressed by Kuwait. The results of these studies will underpin the treatment of any further man-made oil disasters. However, the sequence of papers could have been better thought about with introductory chapters at the beginning of each section. It is also very expensive for such a short book.

J. Cotter-Howells

PII S0039-9140(97)00414-1

Water Disinfection and Natural Organic Matter—Characterization and Control. R.A. Minear and G.L. Amy (editors), ACS, Washington, DC, 1996. Xi + 394 pp. US\$109.55. ISBN 0-8412-3464-7.

This book is one of the ACS Symposium Series and was developed from the proceedings of a symposium presented at the 210th National Meeting of the American Chemical Society held in Illinois on 23–24 August 1995.

Twenty papers are presented and these can be divided into four categories: (1) History, Overview and Regulatory Impact Analysis; (2) Chlorination–Chloramination Products and Reaction; (3) Natural Organic Matter Relationships and Characterization; (4) Other Processes—namely Bromate. A number of the authors contribute to more than one paper. Author, affiliation and subject indices are included.

This book may be of interest to scientists and engineers in the water industry as the concern and debate over disinfection by-products (DBPs) continues, and to water treatment companies themselves as they attempt to develop strategies to minimize and control the formation of DBPs. In Chapter 1, as a means of introduction, there is a review by the editors of the historical developments of water disinfection and an overview of the issues surrounding DBPs and natural organic matter. The second chapter discusses the use of regulatory impact analysis for disinfectants/disinfection by-products using total organic carbon (TOC) as a surrogate for DBP precursors. It was predicted that reductions in DBPs would parallel TOC reduction. A number of control strategies are reviewed using either precursor removal technologies such as coagulation, granular activated carbon or membranes, or alternative disinfectants such as chloramines, ozone or chlorine dioxide.

In Chapters 3–9, papers are presented on chlorination–chloramination reactions and products. Chloramines versus chlorine for the control of

dissolved organic halogens (DOX, i.e. all organic halogen-substituted DBPs) is examined and the influence of operational variables on their formation. Although chloramines are less reactive than free chlorine and produce fewer THMs, they are inherently unstable due to a complex set of reactions. Reaction pathways of chloramines and analytical techniques are considered in Chapters 7 and 8. Analytical techniques for the determination of cyanogen chloride, one particular chloramine DBP, are compared in Chapter 9.

Chapters 10–16 present papers dealing with natural organic matter relationships and characterization, including a case study of precursor removal using granular activated carbon compared to treatment by ozone–biological carbon. Significant improvements in the reduction of trihalomethanes, haloacetic acids and TOC were observed with the latter treatment.

Chapters 17–20 are a group of papers which relate to a number of issues which do not readily fall into the category of the other sections. Bromate formation from ozonation is the focus of Chapter 18, in particular the kinetic rate of formation which may be crucial in reactor design, ozone dose and other operational considerations. Chapter 19 outlines the development of an ion chromatography technique for the determination of oxalic, formic and acetic acids following the treatment of water in an ozonation and biofiltration pilot plant.

This book should provide a good reference and appeal for those with an interest in water treatment and to those analysts whose task is to identify and quantify the by-products and side-reactions associated with the disinfection of potable water.

R.W. Henderson

PII S0039-9140(97)00415-3

Review

Piezoelectric quartz crystal biosensors

Renee L. Bunde ^{a,*}, Eric J. Jarvi ^a, Jeffrey J. Rosentreter ^b

^a *Department of Pharmaceutical Sciences, Idaho State University, Pocatello, ID 83209 USA*

^b *Department of Chemistry, Idaho State University, Pocatello, ID 83209, USA*

Received 25 September 1997; accepted 4 November 1997

Abstract

Biosensing methods utilize the intrinsic selectivity of a biorecognition process to create relatively simple, low cost, analytical alternatives for a variety of research investigations. Here, biosensor applications of the piezoelectric quartz crystal (PQC) are reviewed. The discussion is divided into sections focusing on the development of PQC based analytical techniques, applications in solution phase sensing pertaining to PQC biosensors, and the current state of knowledge in PQC biosensing applications. Immobilization procedures, dip and dry assay techniques, and solution phase sensing methods are considered in detail. © 1998 Elsevier Science B.V. All rights reserved.

Keywords: Review; Piezoelectric quartz crystal; Biosensor

1. Introduction

Research trends suggest newly developing chemical and biological sensors, which are simple and inexpensive to design, will likely gain popularity over more complicated traditional techniques. Biological sensors, or biosensors, are measuring devices which incorporate a biologically active sensing element with an electronic transducer. Thus, biosensors harness the biological recognition processes created through evolution, providing enhanced selectivity capabilities. The biological component interacts with or senses

substance being investigated. The transducer recognizes the signal and converts the biological event into a response that can be further processed and displayed, such as a digital output. A variety of biological components (including enzymes, antibodies, antigens, nucleic acids, isolated receptors, whole cells, microorganisms, and plant and animal tissues) have been applied to sensing systems. Examples of signal transducing elements include electrochemical, optical, calorimetric, and acoustic sensors. The biological layer and the transducer in conjunction with the conditions of the assay environment dictate the overall applicability and sensitivity of biosensing systems. The design of an acoustic sensor, such as a piezoelectric quartz crystal (PQC) is relatively simple. Gen-

* Corresponding author. Tel.: +1 208 2363715; fax: +1 208 2364421; e-mail: bunderl@otc.isu.edu

erally, analyte detection is based on adsorbate recognition where selective binding causes a mass change which is identified by a corresponding change in the acoustic parameters of the PQC.

2. Development of PQC mass sensing

The piezoelectric effect occurs in crystals without a center of symmetry [1]. When pressure is applied to the crystal, the crystal lattice is deformed in such a manner that a dipole moment arises in the molecules of the crystal. Many types of crystals exhibit the piezoelectric effect, but the electrical, mechanical, and chemical properties of quartz make it the most common crystal type used in analytical applications [2]. PQC are quartz wafers sliced from a single crystal. Typically, alpha quartz is used for crystal fabrication [3]. The PQC is sandwiched between two electrodes which are generally composed of gold or silver and are prepared by thermal evaporation onto the quartz surface [2]. An alternating electric field is developed in the PQC by applying a potential difference between the electrodes. With this applied voltage, the physical orientation of the crystal lattice is distorted, resulting in a mechanical oscillation of a standing shear wave across the bulk of the quartz disk at a characteristic vibrational frequency (i.e. the crystal's natural resonant frequency). The direction of the oscillation depends on the orientation of crystal lattice in the electric field; in turn, the orientation of the crystal lattice depends on the exact geometry of the quartz disk with respect to the crystalline axes of the quartz from which the crystal is cut. Oscillation in the thickness shear mode (TSM) creates a displacement parallel to the surface of the quartz wafer. Only the region between the electrodes is piezoelectrically active; thus oscillation is maximum where the electrode pads overlap and diminishes rapidly from that point [4–6].

The frequency of the PQC vibration depends on parameters associated with the phases adjacent to the crystal and on the physical properties of the crystal itself (e.g. size, cut, density, and shear modulus). Of particular importance for analytical sensing devices is the proportional relation be-

tween the resonant frequency and the overall mass of the crystal. Most piezoelectric analytical applications utilize this mass relationship. The TSM of vibration is the mode most sensitive to mass change [3]. Two crystal orientations vibrate exclusively in the TSM, AT- and BT-cut crystals [7]. For the majority of piezoelectric work in analytical chemistry, AT-cut crystals have been used [1,3]. The AT-cut refers to quartz wafers cut at $+35^{\circ}15'$ angle from the z -axis. AT-cut crystals have a temperature coefficient of nearly zero, indicating the resonant frequencies are stable over a wide range of temperatures [1,3].

There are two methods to generate a signal using PQC [8,9]. In the first and most common method the crystal itself is part of an oscillator circuit. Here, the crystal vibrates at a frequency controlled by properties of the crystal. In the second method, the crystal is connected to an external instrument which applies an alternating voltage at various frequencies across the crystal. Here, the vibrational frequency is not determined by the crystal; the phase and amplitude of the crystal in response to electrical excitation is measured, e.g. monitoring the equivalent circuit parameters of a PQC. Subsequent discussions will focus primarily on the first analysis method since it represents the majority of experimental designs used.

There are two general classes of piezoelectric devices: BAW (bulk acoustic wave) and SAW (surface acoustic wave). PQC, as described in this paper, are BAW devices. Other terms used to reference (i.e. name) or describe these same PQC or BAW crystals are: QCM (quartz crystal microbalance) and TSM (thickness shear mode). The QCM term is often used because it describes the mass sensitivity of the crystal. TSM is used because it describes the motion of the crystal's vibration. SAW devices are an entirely different class of acoustic sensor. In a SAW device, electrodes are on the same side of the crystal. Interdigital transducers act as a transmitter and receiver to excite a wave that travels across the crystal face. The physical deformation of the wave is confined to the surface of the crystal. SAW devices have been applied to a number of sensing systems, including uses as biosensors [10–13].

SAW devices are more mass sensitive than PQC, but some SAW devices exhibit a variety of problems when applied to a biological sensing system because biological solutions can severely attenuate surface acoustic waves [14]. PQC sensing systems are used most in biological applications and thus will be the focus of subsequent discussion.

In 1959 Sauerbrey developed an empirical equation (equation 1) to describe the mass sensitivity of gas phase mass deposition on an PQC [15].

$$\Delta F = \frac{-2f_0^2 \Delta m}{A \sqrt{\mu_q \rho_q}} = -C \Delta m \quad (1)$$

where ΔF = measured frequency shift, in Hz; f_0^2 = the fundamental resonant frequency (squared), in Hz; Δm = mass change, in g; A = piezoelectrically active area (area of electrode surface), in cm²; μ_q = shear modulus of quartz = 2.947×10^{11} g cm⁻²; ρ_q = density of quartz = 2.648 g cm⁻³; C = mass sensitivity constant (based on type of crystal used), in (sg)⁻¹.

Sauerbrey's work demonstrated a thin film applied to a PQC could be treated as an equivalent mass change of the crystal. This approach is based on the deposition of rigid layers that are infinitesimally thin and, thus, dampen the propagation of the bulk shear wave in a fashion identical to quartz itself. A change in the mass of the crystal per unit area results in a change in resonant frequency. This equation forms the basis for the analytical use of PQC. As an analyte is physically or chemically adsorbed onto the PQC surface, it adds mass to the crystal. The change in mass is identified by a corresponding change in the frequency of vibration of the crystal. The Sauerbrey relation is based on the overall mass sensitivity of the PQC. Only the region under the electrode is piezoelectrically active; at the bare quartz, the mass sensitivity is negligible [4–6]. To interpret data based on Sauerbrey's relation the mass should be uniformly deposited over the entire active area of the PQC (i.e. the electrode surface). Also, there is a limit to the amount of mass that can be added to the PQC. When this limit is exceeded, the crystal ceases its oscillation.

Gas phase mass sensitivity is determined by the PQC's fundamental frequency as described in equation 1. Mass sensitivity increases as the fun-

damental frequency of the PQC increases; the fundamental frequency increases as the PQC thickness decreases. Thus, one approach to increase sensitivity is to fabricate thinner crystals, which in turn increases the operating frequency and sensitivity. Clearly, miniaturization can only be performed within physical limits. The size cannot be reduced below a certain value without affecting the durability of the device [14]. However, recent fabrication designs have been tested that provide fundamental frequencies of 30 MHz [16]. The most commonly used crystals are 5–15 MHz quartz disks with a 10–16 mm diameter. For a fundamental frequency of 10 MHz and an electrode surface area of 0.22 cm², the gas phase mass sensitivity is approximately 1 Hz per nanogram. Piezoelectric gas phase mass sensing is a well established technique and is currently applied to investigations in science and engineering in a wide array of assay conditions [1–3,17–22].

King, in 1964, is recognized as the first to utilize a PQC in an analytical chemical application [23]. PQCs were implemented into a gas chromatography system for detection of hydrocarbons. The detector selectivity was based on coatings on the PQC surface. The next two decades saw intensive research using PQC to monitor a number of gas phase species. For information on PQC techniques other than biosensing applications refer to the reviews by Alder and McCallum [1], Guibault and Jordan [3], McCallum [20], and Janta et al. [17].

Recent advances in gas phase detection schemes focus on modification of the crystal surface with organic compounds or biological components that will bind a particular gaseous substrate which can provide enhanced detection sensitivity. Guibault, in 1983, was the first to use a biological coating for direct assay in the gas phase [24]. Here, gas phase formaldehyde was monitored with an enzyme coated PQC. Ngeh-Ngwainbi et al. introduced gas phase immuno-sensing through a PQC coated with antibodies against parathion [25]. Wu and Wang immobilized an olfactory receptor protein on the PQC surface for quality assessment of sorghum liquor from measurement of head-space gas [26]. It is questionable whether gas phase biosensing can truly occur, however [27,28].

The structure of the immobilized biological component may retain waters of hydration when outside of their aqueous environment, but it is questionable if this is enough to ensure the integrity of the binding sites. Rajakovic et al. demonstrated gas phase adsorption of organics and pesticides to antibody coated PQC was completely reversible [28]. No signal corresponding to selective immunochemical binding was found. The true focus for PQC biosensing applications is in solution sensing, as discussed below.

3. PQC solution phase sensing

Early attempts to apply the PQC sensing system to liquid phase measurement failed because the crystal ceased to oscillate when submerged in solution. To sense solution phase analytes either the sample was converted into a gas or a tedious dipping procedure was used [1,3,20]. These problems have been addressed by developing oscillator circuits that allow for crystal immersion in solution [29] or through the use of specially designed crystal flow through and/or batch reaction cells where solution contacts only one crystal surface [30–38]. The first attempt to use an acoustic device as a liquid phase sensor was by Konash and Bastiaans in 1980 [39]. PQCs were used as a liquid chromatography detector where one crystal face was exposed to a flowing organic solution. The system had poor sensitivity and reproducibility, but they demonstrated the PQC could produce stable oscillations in liquid.

Sauerbrey's mass relation cannot be applied to a solution sensing system since the equation is applicable to only gas phase mass deposition of rigid layers. Pioneering studies to define what parameters govern the change in frequency seen for a PQC in liquid sensing systems have been conducted by a number of investigators. A summary of their findings follows.

Nomura and Okuhara were the first to attempt to characterize solution phase piezoelectric sensing [40]. The resonant frequency of a PQC in air was compared with the frequency response when the whole crystal was immersed in 17 non-conducting organic liquids. They developed an empir-

ical equation which related the frequency change to the square root of viscosity and density of a solution.

In 1985, Kanazawa and Gordon reported a theoretical model which described the frequency response in fluid phases in terms of the physical parameters of the PQC and analyte solution by considering the coupling of PQC shear wave to a dampened shear wave propagating into the fluid [41,42]. The depth of the shear wave penetration varied with the square root of the bulk liquid viscosity. The decay length corresponded to the effective thickness of the liquid in motion with the PQC. This liquid layer was treated as a sheet of mass attached to the PQC. The model treated the fluid layer as continuous; no slip boundary between the PQC surface and the fluid was allowed. The equation was verified by contacting a single PQC surface with solutions of glucose and ethanol. The oscillation frequency in pure water was taken as a reference. The decrease in frequency varied as the solution viscosity and density product increased.

In the same year, Bruckenstein and Shay described a model similar to that of Kanazawa and Gordon [43]. They assumed the liquid in contact with the PQC provided a viscous boundary layer at the PQC surface. The mass of this layer was considered as an additional mass load on the PQC. This mass is determined from the viscosity and density of solution. Therefore, the frequency change was again described in terms of the viscosity and density product. Here, the model was applied to solutions in contact with one or both surfaces of a PQC and they demonstrated good agreement between experimental results and the theoretical model. In the articles by both research groups, the additional mass load from the liquid layer was treated in the same manner as in the Sauerbrey relation. Although the physical properties of the liquid affect the operating frequency, the mass sensitivity was essentially unaffected.

Subsequent investigators experimentally demonstrated the validity of the equations for selected solutions but found deviations for highly viscous or conducting solutions [29,36,44–46]. Although they clearly showed the frequency response is affected by the viscosity and density of

the solution, the response is not controlled exclusively by these factors. Later work identified many parameters associated with the physical and chemical nature of the interfacial environment that influence the frequency. The frequency response is mediated by interfacial interactions such as the structure of the solid/solution interface with respect to surface roughness and surface stress [47–49]; conductivity, solution polarity, and temperature [36,45,50]; interfacial viscosity and surface free energy described in terms of hydrophilicity and hydrophobicity [9,38,46,51,52]; crystal coating uniformity [6]; and the extent of crystal contact with the solution phase [4].

Kurosawa et al. [45], Barnes [29], and Cavic-Vlasak and Rajakovic [46] found the change in PQC frequency was a linear function of the viscosity and density product except for high viscosity solutions, salt solutions, and solutions with high polymer concentrations. Since viscosity and density are temperature sensitive, this indicates the frequency may be temperature dependent. In 1987 Muramatsu et al. monitored the PQC frequency response in air, ethanol, sodium chloride solution, and purified water [36]. The response was evaluated in terms of the equations by Bruckenstein and Shay and Kanazawa and Gordon. They found the oscillating frequency was affected by the density, viscosity, temperature, and conductivity of the liquid, but they indicated each of the equations cannot predict all of the experimental factors involved. The deviations from the predictions were attributed to the solution conductivity and the dielectric polarization of water. Although, the difficulty in reading the frequency for high conductivity solutions may be associated with their method of solution contact. Both PQC electrodes were immersed in a conductive solution which may lead to short circuiting. In a later publication, Muramatsu et al. found the change in frequency responded linearly to the square root of the viscosity · density product for alcohol–water solutions but non-linearly when in contact with highly viscous solutions [44].

Yao and Zhou also found conductivity influenced the PQC frequency response [50]. The analyses were performed with the crystal submerged in liquids. They measured the frequency

when in contact with 47 pure organic liquids, water–organic mixtures, and electrolyte solutions and developed an empirical model similar to that of Nomura and Okuhara. Their equation identified a similar dependence on the square root of the density and viscosity but they improved their correlation by including terms for dielectric constant and conductivity. If the density and viscosity do not vary significantly with the electrolyte concentration, they suggested the influence of density, viscosity, and dielectric constant could be considered negligible. Thus, they proposed a method to describe the change in frequency in terms of specific conductance.

Other investigators found the frequency depends also on properties of the liquid/solid interface such as hydrophilicity and hydrophobicity of the metal electrodes and interfacial viscosity of the metal-to-water interface. Thompson et al. actually measured an increase in frequency with binding [38]. This result is contrary to what is expected based on all previous equations developed to describe mass addition to the PQC surface [15,40–43]. This frequency increase was attributed to differences between the hydrophilic and hydrophobic coating surfaces on the PQC. Thompson indicated hydrophilicity affects the interfacial viscosity which in turn affects the frequency. For PQC hydrophilic coatings, the resonant frequency required a greater time to stabilize due to equilibration of the boundary structure. Other investigators question whether Thompson's coatings were too thick to resonate in an aqueous environment [32]. However, Thompson's results did indicate the assumption of Bruckenstein and Shay and Kanazawa and Gordon of a no-slip boundary between the solid and liquid is invalid [38]. Hayward experimentally demonstrated the assumptions of continuity and no surface slip are groundless [53]. Rajakovic et al. found physical conditions of the interface mediate the transfer of acoustic energy into the liquid [51]. Hydrophobic surfaces have lower interfacial viscosity because of interfacial slip than hydrophilic surfaces. The PQC sensor responds to the extent to which the acoustic wave is propagated into the surrounding medium and to an alteration in interfacial viscosity. This indicates

the response to the addition of a rigid layer will differ from the response to the addition of a deformable layer like a protein. Duncan-Hewitt and Thompson proposed a theory to describe the PQC sensor response in polar liquids [52]. The paper characterizes the solid/liquid interface with respect to four liquid layers that wet the PQC surface to different extents. This model allows for a partial slip boundary condition at the interface. Yang and Thompson interpreted the PQC response in terms of kinetic energy transfer, acoustic energy dissipation, and formation of interfacial structures [9]. The structure of the solid/liquid interface can change if liquid properties (ionic strength, pH, buffer composition) change. The interfacial structure defines the interfacial viscosity; interfacial viscosity can influence the slip boundary condition at solid–liquid interface which in turn affects the resonant frequency.

To date, no unifying equation has been developed to describe the PQC response in a liquid medium since the response depends greatly on the exact interfacial structure formed between the coatings on the PQC surface and the solution environment. If the solutions are not highly viscous and only one electrode is in contact with the solution, good experimental agreement with the predictions of Bruckenstein and Shay and Kanazawa and Gordon can generally be expected. However, calibration of the PQC is vital for accurate use of the device. Ward and Delawski determined the radial mass sensitivity of a PQC in contact with a liquid [6]. The greatest sensitivity is in the center of the crystal, decreasing with increasing radius. Their results suggested coating uniformity is extremely important for accurate measurements. In 1992, Hillier and Ward determined mass changes occurring on the non-electrode portion of a PQC cannot be calibrated because the sensitivity constant would not be accurate due to field fringing [4]. These fringe effects can be minimized by contacting only the electrode portion of the PQC with solution. This suggests the best means of solution contact is through the use of crystal flow cells. In any case, the PQC response must be calibrated.

In summary, Sauerbrey demonstrated the PQC resonant frequency depends on the material

parameters of the PQC and on its overall mass [15]. This is strictly applicable to rigid layer behavior of gas phase mass deposition. Recent advances in solution sensing indicate the viscoelastic properties of the hydrodynamic layer in addition to mass deposition influence the frequency response. When vibrating in a liquid matrix, a layer of liquid moves with the PQC oscillation due to viscous drag. Binding of an analyte to the PQC surface will likely change the viscoelastic properties of the interface, but the overall change in frequency is likely to be different than that predicted by Sauerbrey. This indicates the need for characterizing the PQC system with the respective sensing environment. Application of solution phase sensing is paramount to the applicability of using PQC in biosensing systems.

4. PQC biosensors

The general approach to exploiting the piezoelectric effect for use in a biosensor is to coat a PQC with a material that interacts selectively with a target substance. Two general experimental designs are used in most PQC biosensing applications. In each, a biological entity is first immobilized on the crystal surface. One method is to measure the dry frequency of the crystal after the biological component is immobilized. Then the PQC is immersed in the reaction solution for a time period sufficient to allow for the target substance in solution to bind to the immobilized biological constituent. As the analyte interacts with the material coated on the PQC, it physically or chemically absorbs onto the PQC thereby adding to its overall mass. The PQC is then removed from the solution, rinsed, and dried. The additional mass is identified by measuring the corresponding change in the vibrational frequency of the PQC after the drying step. The limitations of this approach center on the tediousness of the dip and dry method. Additionally, the method provides no real-time data. The second approach addresses these limitations. Here, a PQC flow cell or some type of batch reaction cell is used to provide real-time data on the time course of binding events on the PQC surface. The analysis is

conducted wholly in the solution phase. Adsorption of the analyte on the PQC surface causes a change in the viscoelastic properties of the interfacial structure which are recognized by a decrease in the resonant frequency.

4.1. Immobilization methods for PQC biosensor applications

Optimization of immobilization techniques will need to be addressed before biosensors are used on a large scale [54]. There are four basic immobilization procedures used in which the species is bound to the PQC electrode or to an inert support on the electrode surface [54,55]. The first method utilizes crosslinking through glutaraldehyde. The second involves covalent attachment through a silane or via an avidin/biotin complex. The third uses entrapment in a matrix such as a gel or polymer. The fourth implements direct physical adsorption to the crystal's electrode surface. In many cases, a combination of these methods is used. Regardless of the procedure, it is advisable to clean the electrode surface prior to immobilization to remove any substances that may hinder the immobilization process. The cleaning procedure of Davis and Leary [32], or some modification of this general method, has been used in numerous cases.

Shons et al. immobilized albumin and gamma globulin through glutaraldehyde crosslinking to create the first PQC biosensor [56]. Many piezoelectric biosensors use crosslinking [18,38,55,57–66]. Chemical attachment through avidin and biotin has been conducted but is not routinely used [55,66,67]. Covalent binding through a thin silane layer is commonly employed [13,35,36,46,68–75]. Attachment via entrapment in a gel [33,34,38,76] or through a polymer [18,55,57–66,75,77] is also customary. Other procedures involve attachment to an immobilized Protein A layer [55,58–66,75,78]. The shortcomings of these immobilization procedures of crosslinking, covalent attachment, entrapment, or linking through Protein A rest in the large size and mass added to the PQC prior to analyte detection. This can increase the interfacial viscosity which will decrease the sensitivity and/or the

mass load may approach the PQC's limit for stable oscillation.

Many investigators have developed PQC sensors used for multiple dip and dry assays. Guilbault and Schmid indicated for multiple liquid assays immobilization through a stable layer is desired so the biological elements can withstand abrasive regeneration steps, such as contact with a solution of 8 M urea [18]. Prusak-Sochaczewski and Luong conducted multiple albumin assays and evaluated immobilization through protein A or a polyethylenimine layer with subsequent glutaraldehyde crosslinking [65]. In terms of reusability, pre-coating the crystal with protein A was superior to the polymer coating. In publications by Konig and Gratzel [58–63], Suri et al. [75], and Plomer et al. [64] three immobilization procedures were evaluated: through a silane layer (APTES) with subsequent glutaraldehyde crosslinking in addition to the above two methods. Based predominantly on their requirement for biosensor regeneration, Konig and Gratzel found the polymer coating to be superior in the case of detecting human T-lymphocytes [58], erythrocytes [60,62], and granulocytes [61]. For analysis of viruses and bacteria Konig and Gratzel found immobilization through protein A was the best [59,63]. Similarly, Plomer et al. and Suri et al. determined protein A was the best immobilization method for determination of insulin and enterobacteria, respectively [64,75]. Guilbault et al. [55] and Prusak-Sochaczewski et al. [66] tested the above three methods in addition to attachment via a biotin-avidin interaction. For *Salmonella typhimurium* detection, polyethylenimine was superior and the biotin-avidin procedure was far inferior to the other three immobilization methods. Again, the predominant qualifying factor was the ability to withstand harsh regeneration steps.

Immobilization via direct attachment to the PQC surface has also been conducted. Davis and Leary monitored the attachment of protein A to the surface of a gold electrode [32]. They indicated gold-protein A complexes are highly stable with an association constant of 10^8 M^{-1} ; the attractive forces are Van der Waals in nature. In general, protein adsorption to solid surfaces decreases as protein hydrophobicity decreases [79]. Subsequent

to Davis and Leary, a wide range of biological elements have been immobilized directly on a PQC electrode, including anti-human serum albumin [37], IgG [35], goat anti-ricin antibody [31], anti-vibro cholera [80], Herpes simplex virus type one [81], and recombinant protein fragments of HIV specific antibodies [82,83]. Bare PQC have also been used to monitor attachment of cells to its surface [84–86]. To date, no uniform immobilization standard has been identified. This indicates that for any particular method, the ‘best’ procedure should be identified and verified experimentally. Extensive details on immobilization techniques are provided in the literature mentioned above.

4.2. Dip and dry PQC biosensor applications

The fundamental procedure used for essentially all ‘dip and dry’ methods includes attachment of a selective binding agent to the PQC surface and quantifying the frequency of the PQC with the immobilized binding agent before and after interaction with the target analyte. Thus, the reaction occurs in the solution phase, but analysis and quantification occur under gas phase conditions. Before the frequency is measured, the PQC is subjected to one or more washing steps to remove non-specifically bound substances and dried by some means. In some cases measurement steps before immobilization of the biosensing element are also taken. The time allowed for interaction between the immobilized entity and the analyte is determined by the assay conditions and the type of analyte examined. The wash and dry conditions vary.

Shons et al. was the first to attempt to construct a PQC biosensor in 1972 [56]. Five MHz PQCs were coated with albumin or gamma globulin and immersed in anti-sera of varying concentration and specificity to determine antibody activity. They found the sensitivity was equal to or better than the conventional detection method of the day, passive agglutination. PQC biosensors did not receive any further research attention until the 1980s. An indirect, competitive binding assay for the determination of antigens was patented by Oliveira and Silver in 1980 [87]. Also in 1980, Rice

disclosed a method for identifying antibody subclasses [88]. Other microgravimetric PQC immunoassays have been developed for the detection of albumin [65], atrazine [57,89,90], human transferrin [78], insulin [75], cocaine [91], and IgM [71,76]. An enzymatic assay was designed by Grande et al. for detection of galactosyltransferase [92]. This work discussed some of the complications associated with conducting dip and dry PQC assays, such as solvent retention.

PQC biosensors have also been applied to the detection and quantification of cells. Muramatsu et al. were the first to perform a piezoelectric microbial assay [93]. *Candida albicans* concentrations were detected in the concentration range of 10^6 to 5×10^8 cells ml^{-1} . Assay specificity was confirmed; there was no reaction with other yeast species or other type of antigen. Subsequently, a number of bacterial, viral, and cellular entities have been analyzed: *Salmonella typhimurium* [66], *Listeria monocytogenes* [94], enterobacteria [64], granulocytes [61], human T-lymphocytes [58], human erythrocytes [60,62], viruses and bacteria that play a role in diarrhea [59], herpes viruses [63], and vibrio cholera [80]. In the work conducted by König and Gratzel a number of sample replicates were analyzed and thorough statistical analysis was performed [58–63]. Unfortunately, for many PQC studies this is the exception rather than the norm.

Reusable detectors for microbial assays have been reported [58–66]. Carter et al. also suggested their PQC sensor could be regenerated but indicated this was inadvisable due to contamination hazards associated with detection of cholera [80]. In most cases, the PQCs were regenerated by immersion in 8 M urea. König and Gratzel improved the reusability of a PQC immunosensor by developing a novel, competitive–regeneration step [62]. A PQC with an immobilized antibody and attached antigen was placed in a solution containing a synthetic peptide corresponding to the antigenic region of the antibody. After the peptide bound to the antigen, the antigen/peptide complex was removed from the antibody immobilized on the PQC with several washing steps. In a subsequent study for the determination of viral and bacterial agents, they were able to regenerate a single PQC for up to 18 analyses [63].

DNA hybridization studies have been conducted using the dip and dry method [72,74,77,95]. Fawcett et al. conducted the first study in 1988 where short, synthetic, single stranded nucleic acids were covalently attached to the PQC surface through a styrene–acrylic acid copolymer [77]. The PQC mass to frequency relationship was determined by adding 20 μl of polyvinyl alcohol to the surface of one PQC. Calibration was not performed on each PQC used in the analysis. Although their method of quantitation may be questionable, they did demonstrate the PQC biosensor could identify DNA hybridization. Later, Campbell et al. conducted a similar assay for monitoring Poly(U) hybridization to Poly(A) immobilized on a PQC [74]. The reusability of their sensor was demonstrated through sequential hybridization and denaturing steps. Wu et al. developed another hybridization assay [95]. Here, single stranded DNA isolated from salmon sperm were immobilized on the PQC through electro-blotting. In this procedure, the crystal electrode acts as positive electrode; the negatively charged DNA phosphate backbone is attracted to this positive electrode. Then, the PQC was irradiated with UV to covalently link the DNA probe to the PQC surface. Yamaguchi et al. monitored the direct adsorption of DNA onto gold and graphite PQCs modified with a silane (GPTMS) [72]. This portion of their assay was conducted in real-time but subsequent methods for monitoring hybridization used dip and dry procedures. Impedance measurements which can differentiate between mass addition to the crystal surface and solution viscosity changes were utilized to detect hybridization. All the above methods offer the opportunity to monitor DNA hybridization without the use of radio-isotopes.

Dip and dry piezoelectric sensing applications are advantageous in that the frequency signal can in some cases be interpreted through the use of the Sauerbrey relation; although, the method is sensitive to errors due to hydration, humidity, and solvent retention. The time consuming and tedious nature of the analysis scheme suggest the dip and dry method is not likely to ever become a routinely used analytical procedure. Furthermore, the application of solution phase piezoelectric

sensing is far superior in that real-time data analysis can be conducted and the system can be configured for on-line analysis.

4.3. Solution phase sensing PQC biosensor applications

Solution phase PQC sensing systems are designed using a myriad of conditions. The most common method employs the use of a contact cell where one crystal surface is adjacent to the solution. The contact cell is configured in a flow or batch mode and the solution is typically introduced using a peristaltic or syringe pump. In flow cells, the volume of solution flowing over the crystal surface is commonly less than 100 μl [31,35,38] but some flow cells have been designed for solution contact volumes of up to 7 ml [37]. No generalities can be made concerning the volume of solution in a batch contact cell; volumes range from a few microliters to nominally one liter. Alternatively, the whole crystal can be in contact with the solution phase. Here, either the PQC surface is masked to avoid solution contact [45,96,97] or the oscillator circuit is designed to allow the crystal to oscillate while immersed in solution [36,44,68,69]. Many conventional PQC's designs do not allow for dual electrode contact with a solution to avoid short-circuiting due to exposure to a common conductive solution. Further, with full solution contact more than just the piezoelectrically active surface interacts with the solution. This may cause calibration inconsistencies [4]. On the other hand, immersion in solution allows for detection of changes in solution conductivity. This could be advantageous, or a serious draw back, depending on the type of analysis performed.

For most biosensor techniques, a biological component is immobilized on the PQC surface. The signal is generated in response to adsorbate recognition. The sensitivity of direct analyte detection through an immobilized ligand is limited by the number of binding sites available to interact. This is beneficial for characterization of conditions associated with a reaction but may be a limitation in terms of detection sensitivity. One technique used to increase the sensitivity of PQC

biosensors is to relate the first-derivative of the change in frequency versus time to the analyte concentration [26,97–100]. Additionally, a number of analysis schemes have been proposed that do not rely on direct mass attachment to the crystal surface [32,50,67,85,86,96–106]. A summary of solution phase piezoelectric bio-sensing systems follows.

Roederer and Bastiaans were the first to conduct a piezoelectric immunoassay completely in solution phase [13]. A SAW device was coated with goat anti-human IgG for detection of IgG in solution in the range 0.0225–2.25 mg ml⁻¹. Thompson et al. were the first to study interfacial immunochemistry with a PQC in contact with a liquid phase [38]. Contrary to what was expected based on a microgravimetric signal, the binding of antibody to antigen (IgG) produced a frequency increase. The frequency increase was explained in terms of the change in surface free energy associated with binding. To our knowledge, no other frequency increase upon binding to the PQC surface has been documented in the literature. Muramatsu et al. determined antibody subclasses of IgG using a protein A modified crystal [36]. Their detection range of 10⁻⁶–10⁻² mg ml⁻¹ was markedly improved over Roederer and Bastiaans. Their measurements were conducted in the liquid phase, but their study was not in real-time. The crystal was washed with purified water before the frequency was measured; frequencies were not recorded over the time-course of the reaction. Minunni et al. conducted real-time detection of human-IgG adsorption directly to the PQC crystal surface [35]. A decrease in frequency was noted for successive increases in human-IgG concentrations; however, physical attachment to the crystal surface was never demonstrated. An indirect, competitive binding assay was also conducted. Antigen was covalently immobilized on the crystal and the assay solution contained both antigen (the target analyte) and antibody. The immobilized and free antigens competed for the antibody binding site. Thus, the frequency signal was inversely proportional to the analyte concentration. Muratsugu et al. determined microgram concentrations of human serum albumin [37]. The detection range for albumin was from 0.1 to 100 µg

ml⁻¹. They proposed using this detector for albumin in urine (normal range from 8.84 to 9.15 µg ml⁻¹) but all their analyses were conducted in purified solution. Selectivity for human albumin against bovine serum albumin was substantiated. Carter et al. detected ricin concentrations as low as 0.5 µg l⁻¹ [31]. Davis and Leary continuously monitored the reaction of immunoglobulins with protein A and the subsequent attachment of antibody to the immunoglobulin [32]. All investigations discussed above utilized adsorbate recognition through direct antibody–antigen interactions.

Binding interactions between lipopolysaccharide (LPS), an endotoxin, and LPS-binding peptides were monitored by Chang et al. [107]. The method allowed for crystal regeneration with an acidic buffer. Their work indicated the procedure may be useful for some drug screening studies. A cholestyramine coated PQC was used to determine bile acid concentrations in deionized water and phosphate buffer saline [108]. The detection limits were as low as 0.2–9 nmol in purified solution; however, no actual biological samples were assayed. The method showed excellent promise and the results even suggested the need for a drug modification that may increase the effectiveness of bile-salt sequestering drugs.

PQC sensing systems have been configured to determine protein analyte concentrations without immobilizing a biological constituent on the PQC surface. Imai et al. quantified total urine protein concentrations by a PQC technique based on sedimentation of proteins [103]. A protein precipitating agent was added to a protein solution; the protein consequently precipitated on the PQC surface causing a frequency decrease corresponding to the protein concentration. However, it is questionable whether simple precipitation, not physical or chemical bond formation, can be reliably correlated to the change in frequency [84,85].

The relationship between the PQC response and solution density and viscosity was applied to sensing gelation and agglutination. Muramatsu et al. determined endotoxin concentrations by monitoring the gelation of *Limulus ameobocyte* lysate [99]. Muramatsu et al. analyzed fibrinogen through a coagulation reaction with thrombin [98]. An assay

for C-reactive protein was developed by Kurosawa et al. based on the detection of changes in viscosity and density that occur when an antigen binds to an antibody coated on the surface of latex in solution [96]. The antigen induces an agglutination reaction of the antibody-bearing latex. Muratsugu et al. applied the latex assay to the detection of antistreptolysin O antibody [97]. Here, the first derivative of the change in frequency versus time was related to the analyte concentration. This concentration correlation greatly enhanced the method's sensitivity. Ghouchian and Kamo examined the effects of interfacial properties on the latex assay and found PQC surface modifications greatly affected the response to viscosity changes [105]. The latex assay was improved by developing a crystal cell allowing for a single PQC electrode to contact the solution [106]. Chu et al. developed an assay similar to the latex based assay where complement III was determined through another agglutination assay [109]. Again, detection was based on a change in the viscosity of the assay solution.

Escherichia coliform concentrations have been detected in solution [100,110]. Muramatsu et al. reported detection in the concentration range of 10^6 – 10^8 cells ml^{-1} [110]. To amplify the signal, polystyrene particles modified with anti-*E. coli* were added to the reaction mixture. After *E. coli* attached to the antibody immobilized on the PQC, anti-*E. coli* attached to polystyrene particles complexed to *E. coli*. Fengjiao et al. decreased the detection range to 10^1 – 10^6 cells ml^{-1} by implementing a frequency detection time method based on the detection of a change in conductivity of the solution [100]. The frequency detection time (FDT) was defined as the time required to see a shift in frequency above a threshold level where no response could be seen. A range of concentrations were analyzed and the FDT was determined for each concentration. The resulting calibration curve related the initial concentration to the FDT. Conductivity changes have also been used to determine aspirin and salicylic acid concentrations [104] and urease activity [111].

Herpes simplex virus type 1 was evaluated with a PQC biosensor [81]. HIV antibodies have been detected in rabbit immunosera at different anti-

serum dilutions [30] and in human sera [82,83]. Barnes et al. assayed for sugars and erythrocytes with a piezoelectric crystal coated with lectin [69]. Erythrocytes detection was based on recognition of the terminal sugar of the carbohydrate chains attached to the erythrocyte membranes as glycoproteins or glycolipids. Lasky and Buttry [33,34] developed a system for glucose sensing through immobilized hexokinase. This represents one of the few PQC biosensors based on an enzymatic interaction.

In situ piezoelectric techniques for monitoring cellular process have been described [84–86,101]. A cell growth sensor was developed by Ebersole et al. to detect metabolites without immobilization of a biological entity [101]. This was the first sensor capable of detecting metabolic responses and division rates of viable cells. The authors indicated production of metabolic acids is a useful marker of cell metabolism and growth and utilized this relation in their sensor design. Detection of metabolic processes was based on adhesion of a polymer to the PQC. The polymer precipitated from solution in response to titration of its carboxylate groups by the metabolic acids which converted the polymer to its isoelectric form. Ebersole et al. also reported solution phase detection of DNA hybridization [67]. The hybridization assay was based on an earlier method by the same primary author, amplified mass immunosorbent assay [102]. The signal is amplified enzymatically through production of a precipitate that settles on the crystal surface after the binding reaction occurs. Again, there is some question whether precipitate formation on the PQC surface can be reliably correlated to the change in frequency [84,85]. Matsuda et al. monitored real-time platelet adhesion in plasma [84]. The frequency decrease was associated with direct adhesion onto the crystal surface. When cell suspensions settled on the crystal surface, without forming a direct attachment, no measurable frequency decrease was observed. Gryte et al. monitored anchorage dependent cell adhesion and detachment to the surface of a PQC [85]. Here, the investigators demonstrated the decrease in frequency was a function of physical cell attachment not simple sedimentation. The frequency

change for cell attachment was compared to the frequency change for sedimentation of latex beads onto the crystal surface. The beads did not change the frequency appreciably. The formation of a biofilm of *Pseudomonas cepacia* was monitored by Nivens et al. [86]. The study was designed to simulate contamination in a sterile water system. The change in frequency was related to the number of attached cells; the number of attached cells was determined with a scanning electron microscope. This relationship was used to determine the number of cells attached over time by correlating the results with the change in frequency over time. Also, the rate of biofilm formation was determined from the first derivative of the change in frequency versus time.

Davis and Leary proposed using PQC biosensors to characterize reaction kinetics; however, no kinetic parameters were calculated [32]. Skladal et al. [73] and Steegborn and Skladal [112] utilized PQC methods to determine association and dissociation rate constants to characterize the affinity binding of an antibody to two herbicides, 2,4-dichlorophenoxyacetic acid and atrazine, respectively. Su et al. monitored DNA hybridization in solution in real-time by recording the PQC equivalent circuit parameters [113]. The actual mass added to the crystal through hybridization was quantified using radio-labels. The change in frequency correlating to this mass addition was approximately 18 times larger than that predicted by the Sauerbrey relation. This further substantiates the complexities associated with solution phase sensing. The authors indicated their analysis scheme could be used to study the kinetics of hybridization. Subsequently, two of the researchers from this group characterized the hybridization kinetics of a cDNA probe to single stranded DNA immobilized on a PQC [114].

5. Summary

PQC biosensing systems have been applied to a number of analytical problems because of the many advantages associated with using the detector. These advantages include the potential for on-line, automated, real-time analysis out-put;

high sensitivity and specificity; reduced influence of interferences; rapid response time; ease of use; small, readily transportable instrumentation; and cost effectiveness. The primary limitations of piezoelectric sensors are in the challenges associated with immobilization procedures; the lack of an exact correlation between mass addition and frequency change for solution phase sensing; and sensitivity to environmental conditions. These disadvantages can be addressed by investigating and determining the most appropriate immobilization procedure to use; through characterization and calibration of the sample matrix; and minimizing background effects through analysis of blanks and controls and with the use of reference crystals. Although a large body of work already exists, the potential applications yet to be investigated are exhaustive. Future studies will likely be applied to solving research problems in biochemical investigations, clinical diagnostics, and in environmental and industrial process monitoring.

References

- [1] J.F. Alder, J.J. McCallum, *Analyst* 108 (1983) 1169.
- [2] M.R. Deakin, D.A. Buttry, *Anal. Chem.* 61 (1989) 1147A.
- [3] G.G. Guibault, J.M. Jordan, *CRC Crit. Rev. Anal. Chem.* 19 (1988) 1.
- [4] A.C. Hillier, M.D. Ward, *Anal. Chem.* 64 (1992) 2539.
- [5] D.M. Ullevig, J.F. Evans, M.G. Albrecht, *Anal. Chem.* 54 (1982) 2341.
- [6] M.D. Ward, E.J. Delawski, *Anal. Chem.* 63 (1991) 886.
- [7] C. Lu, A.W. Czanderna, *Methods and Phenomena 7: Application of Piezoelectric Quartz Crystal Microbalance*, Elsevier, New York, 1984, p. 393.
- [8] M.D. Ward, D.A. Buttry, *Science* 249 (1990) 1000.
- [9] M. Yang, M. Thompson, *Anal. Chem.* 65 (1993) 1158.
- [10] J.C. Andle, J.F. Vetelino, M.W. Lade, D.J. McAllister, *Sens. Actuators B8* (1992) 191.
- [11] Y. Inoue, Y. Kato, K. Sato, *J. Chem. Soc. Faraday Trans.* 88 (1992) 449.
- [12] J. Kondoh, Y. Matsui, S. Shiokawa, *Jpn. J. Appl. Phys. Part 1* 32 (1993) 2376.
- [13] J.E. Roederer, G.J. Bastiaans, *Anal. Chem.* 55 (1983) 2333.
- [14] D.S. Ballantine Jr., H. Wohltjen, *Anal. Chem.* 61 (1989) 704A.
- [15] G. Sauerbrey, *Z. Phys.* 155 (1959) 206.

- [16] Z. Lin, C.M. Yip, I.S. Joseph, M.D. Ward, *Anal. Chem.* 65 (1993) 1546.
- [17] J. Janata, M. Josowic, D.M. DeVaney, *Anal. Chem.* 66 (1994) 207R.
- [18] G.G. Guilbault, R.D. Schmid, *Electrochemical, Piezoelectric, and fibre-optic biosensors*, in: A.P.F. Turner (Ed.), *Advances in Biosensors*, Jai, Greenwich, CN, 1991, pp. 257–289.
- [19] G.G. Guilbault, A. Suleiman, *Am. Biotech. Lab.* 8 (1990) 28.
- [20] J.J. McCallum, *Analyst* 114 (1989) 1173.
- [21] M. Minunni, M. Mascini, G.G. Guilbault, B. Hock, *Anal. Lett.* 28 (1995) 749.
- [22] A.A. Suleiman, G.G. Guilbault, *Analyst* 119 (1994) 2279.
- [23] W.H. King, *Anal. Chem.* 36 (1964) 1735.
- [24] G.G. Guilbault, *Anal. Chem.* 55 (1983) 1682.
- [25] J. Ngeh-Ngwainbi, P.H. Foley, S.S. Kuan, G.G. Guilbault, *J. Am. Chem. Soc.* 108 (1986) 5444.
- [26] T.-Z. Wu, H.-H. Wang, *Anal. Sci.* 7 (Suppl.) (1991) 867.
- [27] S. Borman, *Anal. Chem.* 59 (1987) 1161A.
- [28] L. Rajakovic, V. Ghaemmaghami, M. Thompson, *Anal. Chim. Acta* 217 (1989) 111.
- [29] C. Barnes, *Sens. Actuators A29* (1991) 59.
- [30] F. Aberl, H. Wolf, P. Woias, S. Koch, C. Koesslinger, S. Drost, *Biosens. Fundam. Technol. Appl.* 17 (1992) 123.
- [31] R.M. Carter, M.B. Jacobs, G.J. Lubrano, G.G. Guilbault, *Anal. Lett.* 28 (1995) 1379.
- [32] K.A. Davis, T.R. Leary, *Anal. Chem.* 61 (1989) 1227.
- [33] S.J. Lasky, D.A. Buttry, *Am. Biotechnol. Lab.* 8 (1990) 8.
- [34] S.J. Lasky, D.A. Buttry, *Sensors based on biomolecules immobilized on the piezoelectric quartz crystal microbalance: detection of glucose using hexokinase*, in: *Chemical Sensors and Microinstrumentation*, American Chemical Society, Washington, DC, 1989, pp. 237–246.
- [35] M. Minunni, P. Skladal, M. Mascini, *Anal. Lett.* 27 (1994) 1475.
- [36] H. Muramatsu, J.M. Dicks, E. Tamiya, I. Karube, *Anal. Chem.* 59 (1987) 2760.
- [37] M. Muratsugu, F. Ohta, Y. Miya, T. Hosokawa, S. Kurosawa, N. Kamo, H. Ikeda, *Anal. Chem.* 65 (1993) 2933.
- [38] M. Thompson, C.L. Arthur, G.K. Dhaliwal, *Anal. Chem.* 58 (1986) 1206.
- [39] P.L. Konash, G.J. Bastiaans, *Anal. Chem.* 52 (1980) 1929.
- [40] T. Nomura, M. Okuhara, *Anal. Chim. Acta* 142 (1982) 281.
- [41] K.K. Kanazawa, J.G. Gordon II, *Anal. Chim. Acta* 175 (1985) 99.
- [42] K.K. Kanazawa, J.G. Gordon II, *Anal. Chem.* 57 (1985) 1770.
- [43] S. Bruckenstein, M. Shay, *Electrochim. Acta* 30 (1985) 1295.
- [44] H. Muramatsu, E. Tamiya, I. Karube, *Anal. Chem.* 60 (1988) 2142.
- [45] S. Kurosawa, E. Tawara, N. Kamo, Y. Kobatake, *Anal. Chim. Acta* 230 (1990) 41.
- [46] B.A. Cavic-Vlasak, L.V. Rajakovic, *Fresenius J. Anal. Chem.* 343 (1992) 339.
- [47] R. Schumacher, G. Borges, K.K. Kanazawa, *Surface Sci.* 163 (1985) L621.
- [48] R. Schumacher, *Angew. Chem. Int. Ed. English* 29 (1990) 329.
- [49] K.E. Heusler, A. Grzegorzewski, L. Jaeckel, J. Pietrucha, *Ber. Bunsenges. Phys. Chem.* 92 (1988) 1218.
- [50] S.-Z. Yao, T.-A. Zhou, *Anal. Chim. Acta* 212 (1988) 61.
- [51] L. Rajakovic, B.A. Cavic-Vlasak, V. Ghaemmaghami, K.M.R. Kallury, A.L. Kipling, M. Thompson, *Anal. Chim. Acta* 217 (1989) 111.
- [52] W.C. Duncan-Hewitt, M. Thompson, *Anal. Chem.* 64 (1992) 94.
- [53] G. Hayward, *Anal. Chim. Acta* 264 (1992) 23.
- [54] M. Alvarez-Icaza, U. Bilitewski, *Anal. Chem.* 65 (1993) 525A.
- [55] G.G. Guilbault, J.H.T. Luong, E. Prusak-Sochaczewski, *Biotechnology* 7 (1989) 349.
- [56] A. Shons, F. Dorman, J. Najarian, *J. Biomed. Mater. Res.* 6 (1972) 565.
- [57] G.G. Guilbault, B. Hock, R. Schmid, *Biosens. Bioelectron.* 7 (1992) 411.
- [58] B. Konig, M. Gratzel, *Anal. Chim. Acta* 281 (1993) 13.
- [59] B. Konig, M. Gratzel, *Anal. Lett.* 26 (1993) 1567.
- [60] B. Konig, M. Gratzel, *Anal. Chim. Acta* 276 (1993) 329.
- [61] B. Konig, M. Gratzel, *Anal. Lett.* 26 (1993) 2313.
- [62] B. Konig, M. Gratzel, *Anal. Chim. Acta* 280 (1993) 37.
- [63] B. Konig, M. Gratzel, *Anal. Chem.* 66 (1994) 341.
- [64] M. Plomer, G.G. Guilbault, B. Hock, *Enzyme Microb. Technol.* 14 (1992) 230.
- [65] E. Prusak-Sochaczewski, J.H.T. Luong, *Anal. Lett.* 23 (1990) 401.
- [66] E. Prusak-Sochaczewski, J.H.T. Luong, G.G. Guilbault, *Enzyme Microb. Technol.* 12 (1990) 173.
- [67] R.C. Ebersole, J.A. Miller, J.R. Moran, M.D. Ward, *J. Am. Chem. Soc.* 112 (1990) 3239.
- [68] C. Barnes, C. D'Silva, J.P. Jones, T.J. Lewis, *Sens. Actuators B3* (1991) 295.
- [69] C. Barnes, C. D'Silva, J.P. Jones, T.J. Lewis, *Sens. Actuators B7* (1992) 347.
- [70] K.M.R. Kallury, V. Ghaemmaghami, U.J. Krull, M. Thompson, *Anal. Chim. Acta* 225 (1989) 369.
- [71] C.R. Suri, M. Raje, G.C. Mishra, *Biosens. Bioelectron.* 9 (1994) 325.
- [72] S. Yamaguchi, T. Shimomura, T. Tatsuma, N. Oyama, *Anal. Chem.* 65 (1993) 1925.
- [73] P. Skladal, M. Minunni, M. Mascini, V. Kolar, M. Franek, *J. Immunol. Methods* 176 (1994) 117.
- [74] N.F. Campbell, J.A. Evans, N.C. Fawcett, *Biochem. Biophys. Res. Comm.* 196 (1993) 858.
- [75] C.R. Suri, P.K. Jain, G.C. Mishra, *J. Biotechnol.* 39 (1995) 27.
- [76] X. Chu, Z.H. Lin, G.L. Shen, R.Q. Yu, *Analyst* 120 (1995) 2829.

- [77] N.C. Fawcett, J.A. Evans, L.-C. Chien, N. Flowers, *Anal. Lett.* 21 (1988) 1099.
- [78] E. Prusak-Sochaczewski, J.H.T. Luong, *Anal. Lett.* 23 (1990) 183.
- [79] D.R. Absolom, W. Zingg, A.W. Neumann, *J. Biomed. Mater. Res.* 21 (1987) 161.
- [80] R.M. Carter, J.J. Mekalanos, M.B. Jacobs, G.J. Lubrano, G.G. Guilbault, *J. Immunol. Methods* 187 (1995) 121.
- [81] S. Zupan, B. Filipic, M. Babic, *Acta Pharm.* 42 (1992) 361.
- [82] C. Koeslinger, S. Drost, F. Aberl, H. Wolf, *Fresenius J. Anal. Chem.* 349 (1994) 349.
- [83] C. Koeslinger, S. Drost, F. Aberl, H. Wolf, S. Koch, P. Woias, *Biosens. Bioelectron.* 7 (1992) 397.
- [84] T. Matsuda, A. Kishida, H. Ebato, Y. Okahata, *ASAIO J.* 38 (1992) M171.
- [85] D.M. Gryte, M.D. Ward, W.-S. Hu, *Biotechnol. Prog.* 9 (1993) 105.
- [86] D.E. Nivens, J.Q. Chambers, T.F. Anderson, D.C. White, *Anal. Chem.* 65 (1993) 65.
- [87] J.R. Oliveira, S.F. Silver, US Patent 4242096, 1980.
- [88] T.K. Rice, US Patent 4236893, 1980.
- [89] M. Minunni, P. Skladal, M. Mascini, *Life Chem. Rep.* 11 (1994) 391.
- [90] K. Yokoyama, K. Ikebukuro, E. Tamiya, I. Karube, N. Ichiki, Y. Arikawa, *Anal. Chim. Acta* 304 (1995) 139.
- [91] B.S. Attili, A.A. Suleiman, *Microchem. J.* 54 (1996) 174.
- [92] L.H. Grande, C.R. Geren, D.W. Paul, *Sens. Actuators* 14 (1988) 387.
- [93] H. Muramatsu, K. Kajiwara, E. Tamiya, I. Karube, *Anal. Chim. Acta* 188 (1986) 257.
- [94] M.B. Jacobs, R.M. Carter, G.J. Lubrano, G.G. Guilbault, *Am. Lab.* 27 (1995) 26.
- [95] T.-Z. Wu, H.-H. Wang, L.-C. Au, *Chinese J. Microbiol. Immunol.* 23 (1990) 147.
- [96] S. Kurosawa, E. Tawara, N. Kamo, F. Ohta, T. Hosokawa, *Chem. Pharm. Bull.* 38 (1990) 1117.
- [97] M. Muratsugu, S. Kurosawa, N. Kamo, *Anal. Chem.* 64 (1992) 2483.
- [98] H. Muramatsu, E. Tamiya, M. Suzuki, I. Karube, *Anal. Chim. Acta* 217 (1989) 321.
- [99] H. Muramatsu, E. Tamiya, M. Suzuki, I. Karube, *Anal. Chim. Acta* 215 (1988) 91.
- [100] H. Fengjiao, Z. Wenhong, G. Qing, N. Lihua, Y. Shouzhao, *Anal. Lett.* 27 (1994) 655.
- [101] R.C. Ebersole, R.P. Foss, M.D. Ward, *Biotechnology* 9 (1991) 450.
- [102] R.C. Ebersole, M.D. Ward, *J. Am. Chem. Soc.* 110 (1988) 8623.
- [103] S. Imai, H. Mizuno, M. Suzuki, T. Takeuchi, E. Tamiya, F. Mashige, A. Ohkubo, I. Karube, *Anal. Chim. Acta* 292 (1994) 65.
- [104] W. Wei, L. Nie, S. Yao, *Anal. Chim. Acta* 263 (1992) 77.
- [105] H.O. Ghouchian, N. Kamo, *Anal. Chim. Acta* 300 (1995) 99.
- [106] H.O. Ghouchian, N. Kamo, T. Hosokawa, T. Akitaya, *Talanta* 41 (1994) 401.
- [107] H.-C. Chang, C.-C. Yang, T.-M. Yeh, *Anal. Chim. Acta* 340 (1997) 49.
- [108] J.J. Chance, W.C. Purdy, *Anal. Chem.* 68 (1996) 3104.
- [109] X. Chu, G.-L. Shen, R.-Q. Yu, *Analyst* 121 (1996) 1689.
- [110] H. Muramatsu, Y. Watanabe, M. Hikuma, T. Ataka, I. Kubo, E. Tamiya, I. Karube, *Anal. Lett.* 22 (1989) 2155.
- [111] D. Shen, Q. Kang, Z. Liu, L. Wang, *Anal. Chim. Acta* 340 (1997) 55.
- [112] C. Steegborn, P. Skladal, *Biosens. Bioelectron.* 12 (1997) 19.
- [113] H. Su, K.M.R. Kallury, M. Thompson, A. Roach, *Anal. Chem.* 66 (1994) 769.
- [114] H. Su, M. Thompson, *Biosens. Bioelectron.* 10 (1995) 329.

Gravimetric determination of tin with sodium cyclotetramethylenedithiocarbamate and its applications in metal analysis

Zhou Nan *

Shanghai Research Institute of Materials, 99 Handan Lu, Shanghai 200437, People's Republic of China

Received 27 June 1997; received in revised form 10 September 1997; accepted 11 September 1997

Abstract

A gravimetric determination of tin is proposed with sodium cyclotetramethylenedithiocarbamate as precipitant at pH 5.0–5.5. By optimizing the reaction conditions the theoretical conversion factor 0.1687 can be used for determining $\geq 5\%$ of Sn. Its standard deviation ($n = 10$) at the level of 20 mg of Sn was found to be 0.08 mg. Effects of diverse cationic species can be eliminated by a clear-cut group precipitation at pH 9 with DDTC in the presence of tartrate and subsequent masking with EDTA. Provision is also made for removal of individual species in occasional cases. Hence, the proposed method is flexible and versatile and was successfully applied to the macro-determination of Sn in diverse alloys. © 1998 Elsevier Science B.V. All rights reserved.

Keywords: Gravimetric determination; Tin; Metal analysis

1. Introduction

Oxidimetry of Sn(II) with KIO_3 [1] is generally used for the macro-determination of tin, an important component of industrial alloys. This method is empirical, needs thorough exclusion of air, the titre of the titrant should be standardized each time [2] and its values may be inconsistent if different CRM's are used for standardization. The chelatometric titration of Sn is poorly selective [3]. More so are its gravimetric methods hitherto published which are time-consuming, hence, rarely

used. It reacts with *N*-benzoyl-*N*-hydroxylamine only in an ice bath for 4 h [4]. The precipitates formed with benzoate [5], phenylarsonic acid or *N*-nitroso-*N*-phenylhydroxylamine or as metatannic acid should be ignited to SnO_2 . Owing to the disproportionation of Sn(II) its electrodeposition is not quantitative. Indeed its macro-determination remains a problem and deserves further study.

Sodium cyclotetramethylenedithiocarbamate (TDTC) is proposed in this paper for precipitating Sn(IV). High selectivity can be achieved by incorporating a preliminary clear-cut group precipitation at pH 9 in the presence of tartrate with DDTC and a subsequent masking with EDTA.

* Fax: +86 21 5420554.

2. Experimental

2.1. Reagents

Deionized water was used for the preparation of all reagents and for dilutions. Analytical-reagent grade chemicals, supplied by Shanghai Reagent Chemicals, were used, unless otherwise specified. TDTC solution, 10% was prepared freshly from a product of Heyl, Germany. It was filtered through a 0.45 μm membrane before use. DDTC (sodium diethyldithiocarbamate) solution, 4% was prepared freshly and filtered before use. Tartaric acid solution, 0.5 M. HCl (3 M) and concentrated H_2SO_4 (9 M). Ammonia solution, 25% NaOH solution, 5 M TiCl_3 solution, ca. 15% in 3 M HCl. Al(III) solution, 0.1 M in 0.15 M NaOH by alkaline dissolution of $\geq 99.9\%$ pure Al metal. EDTA solution, 0.03 M. Buffer solution, pH of 5.2; containing 10 M of sodium acetate and 2 M of HCl. *m*-Nitrophenol solution, 0.3%. Screened indicator of pH 5.1, containing 0.08% of methyl red and 0.06% of bromocresol green in ethanol.

2.2. Wash solution A

To 100 ml of water add 2 ml of HCl conc., one drop of *m*-Nitrophenol solution and dropwise ammonia solution till the indicator colors yellow.

2.3. Wash solution B

To 100 ml of water add 2 ml of buffer solution and 1 ml of TDTC solution.

2.4. General procedure

Take 200 mg of the sample containing $\geq 5\%$ of Sn, weighing to the nearest 0.1 mg. Transfer it to a 250 ml conical flask and decompose with HCl alone or together with a few drops of HNO_3 (note 1). Cap the flask loosely and warm gently at 50–60°C till decomposition is complete (note 2). Dilute to 30 ml with water, add TiCl_3 solution in excess, cap the flask as before and boil gently for 10 min (note 3). Add an appropriate amount of tartaric acid (note 4), one or two drops of *m*-

Nitrophenol solution (note 5), neutralize with NaOH solution to pH 6–7, then with ammonia solution till yellow color appears (ca. pH 9) and dilute to 80–100 ml. Add DDTC solution dropwise with vigorous stirring till the precipitate forms slowly. Add 5 ml of Al solution (note 6), adjust the pH with HCl if necessary and continue the addition of DDTC till no further precipitate appears, then one or two drops more. Digest the precipitate in a water bath thermostated at 60°C for 5 min. Cool and filter off the precipitate through a 0.45 μm membrane and wash the precipitate and the original flask three or four times with wash solution A (note 7).

To a 250 ml beaker containing 1 ml of 9 M H_2SO_4 and 5 ml of HCl conc., pour in quantitatively by portionwise the combined filtrate and washings while stirring vigorously to make a clear solution. Boil to decompose the residual DDTC and concentrate the volume of the analyte solution to 60–70 ml. Add, while hot, 5–10 ml of EDTA solution (note 8), adjust pH to 4 with ammonia solution, then add one or two drops of the screened indicator solution and sufficient buffer solution till the indicator just turns green. Finally, add 10–30 ml (note 9) of TDTC solution dropwise with constant stirring.

Digest the precipitate in a water bath thermostated at 70°C for 15 min. Cool to room temperature, filter the precipitate quantitatively to an IG 4 filter crucible dried and weighed to constant mass at 95°C and wash the glass crucible and the original beaker three or four times with wash solution B. Dry the crucible at 95°C to constant mass and calculate the content of Sn in the sample as follows (note 10):

$$\text{Sn}\% = \frac{(m_2 - m_1) \times 0.1687}{G} \times 100 \quad (1)$$

where m_1 is the mass of the crucible itself, mg; m_2 is the mass of the crucible and precipitate, mg; G is the mass of the sample or its aliquot taken for the determination, mg; 0.1687 is the conversion factor of the precipitate to Sn (vide infra).

2.4.1. Note 1

For Ti alloys add 10 ml of HCl conc. alone; for Al-Sn alloys add 8 ml of HCl(1 + 3) first, then 8

ml each of water and HCl conc. only after vigorous reaction subsides. For Cu, Pb, Sn and fusible alloys add 10 ml of HCl conc. and a few drops of HNO₃ (just sufficient but no more) [6].

2.4.2. Note 2

If there is any insoluble matter left, filter it off through a medium-texture filter paper and wash the paper thoroughly with HCl.

2.4.3. Note 3

If As is present, transfer the analyte solution to a distillation flask in a smaller size, and distil till the temperature of the vapor in the flask reaches 108°C under standard pressure.

2.4.4. Note 4

Its optimum amount is 9 ml for Pb, Sn and fusible alloys; 13 ml for Cu alloys; 17 ml for Ti alloys; 30 ml for Al–Sn alloys. Sometimes heating is necessary, e.g. to complex Cr(III). If the sample contains ≥ 35% of Sn; or Mo or V or both, dilute its solution to a definite volume. For the determination take therefrom an appropriate aliquot (to which 3 ml of tartaric acid solution should be added) estimated after analyzing the other major elements.

2.4.5. Note 5

Omit its addition whenever colored species is present.

2.4.6. Note 6

Omit or reduce its addition if the analyte solution contains Al. This addition may raise the pH of the analyte solution.

2.4.7. Note 7

If V is present, add 10 ml of ethanol to the filtrate.

2.4.8. Note 8

Its amount depends on that of the species to be masked.

2.4.9. Note 9

Its amount depends on: (a) mg of Sn(IV) to be determined; (b) mg of Mo or V or both in the

analyte solution; 10 ml of it suffices to precipitate ≤ 30 mg of Sn alone.

2.4.10. Note 10

If Mo or V or both are present, the mass of the precipitate in the sintered glass crucible on drying is the sum of these two or three chelates. Hence, a correction for this co-precipitation should be made and Eq. (1) is modified as follows:

$$\text{Sn}\% = \frac{(m_2 - m_1 - 4.382m_a - 7.390m_b) \times 0.1687}{G} \times 100 \quad (2)$$

where m_a is the mass of Mo co-precipitated, mg; 4.382 is its conversion factor to MoO₂L₂ (L stands for the TDTC anion here), i.e. 420.453/95.94; m_b is the mass of V co-precipitated, mg; 7.390 is its conversion factor to VO(OH)L₂, i.e. 376.463/50.942.

Once m_1 and m_2 are known, m_a and m_b can be determined as follows. Dissolve the precipitate in aqua regia, dilute to a definite volume and take aliquots for determining Mo by photometry with thiocyanate and V by oxidimetry or 2,2'-iminodibenzoic acid method [8], respectively.

3. Results and discussion

3.1. Choice of the precipitant for Sn(IV)

Sn(IV) is the stable species in the aqueous medium, ligands of O,O-or S,S-donor type can react with it. Unfortunately, these reactions are poorly selective. Ligands of the latter type would be preferred, however, because reaction selectivity can be achieved by making use of the fact that they, like sulfide ion, do not precipitate Sn(IV) in an alkaline medium; but do most of the other precipitable species. Among them dithiocarbamates would be the candidates. It should be noted that those of the mono-substituted group tend to decompose readily in acidic and alkaline media [9], whereas the disubstituted group do so in the acidic medium only. Hence, the latter group would seem recommendable. The Sn(IV)-DDTC chelate was reported to be a mixture as the result

of its decomposition or simultaneous redox reaction between its components [10,11]. On the other hand, TDTC has the following special features: (1) very soluble in water, much more so than the corresponding ammonium salt [12]; (2) slight solubility of its chelates [13]; (3) stable to a considerable extent toward gently heating in the weakly acidic medium; (4) much less oxidizable than other dithiocarbamates, hence, precipitation in the absence of any accompanying redox reaction. Accordingly it was chosen as the precipitant.

3.2. Optimum conditions for quantitative precipitation of Sn(IV)

Our preliminary experiments showed that TDTC precipitates at $\text{pH} \leq 6$. Generally the decomposition rate of dithiocarbamates increases with increasing acidity of the medium, a pH range over 5.0–5.5 was chosen for the precipitation. This is easily controlled by the use of an acetate buffer of pH 5.2 with the aid of a screened indicator. Under such conditions the protonation effects of TDTC and the masking agent used would be minimized too. It is an added advantage.

An auxiliary complexing agent should be first chosen to meet the following requirements: It can prevent the hydrolysis of Sn(IV) and keep all the concomitant species in solution, yet exerts little effect on the main reaction. It was found that tartaric acid serves the purpose and in the presence of 0.5–1.0 g of it the precipitation of Sn(IV) runs normally. As it complexes cationic species in moles, its amount of addition vary widely for different kinds of alloys, as specified in note 4 of Section 2.4.

As revealed by our preliminary experiments, the mass of the precipitate $\approx 6 \times$ the mass of Sn added. Therefore, it can be inferred that the precipitate would be $\text{Sn}(\text{C}_5\text{H}_8\text{NS}_2)_4$, because its relative molecular mass, calculated on the basis of values of relative atomic mass of elements recently recommended by IUPAC [13] would be 703.74, which divided by 118.71, the relative atomic mass of Sn, gives the quotient 5.928.

This inference seems theoretically sound, because DDTC reacts with Sn(IV) in the same mole ratio [11]. Hence, the conversion factor from SnL_4 (L stands for the TDTC anion here) to Sn should be $1/5.928 = 0.1687$. With a view to applying this theoretical factor the reaction conditions were optimized as follows.

Different temperatures for drying the precipitate to constant mass were tested and their results are shown in Table 1. Evidently 95°C would be the optimum one, whereas low recovery of Sn was found if dried at higher temperatures, presumably owing to thermal decomposition of the precipitate. Drying at $< 95^\circ\text{C}$ takes much more time.

The optimum volume of the analyte solution for precipitating was found to be 80–100 ml. The precipitate formed at room temperature is difficult to filter. On the other hand, high precipitation temperature favors its filtrability, but accelerates the decomposition of the precipitant. As a compromise, 70°C was specified and found to be optimum. The precipitate should be aged for 15 min at this temperature and filtered only after cooling to room temperature. Otherwise the results may be poorly reproducible.

Different amounts of the precipitant were added for precipitating different amounts of Sn(IV) and the results are shown in Table 2.

Obviously addition of a large excess of TDTC does no harm. Its optimal amounts were specified to be 1–3 g. One g of it suffices to precipitate quantitatively ≤ 30 mg of Sn when present alone.

Table 1
Effect of drying temperature on determination of 15 mg of Sn

Drying temperature (°C)	Mass of precipitate (mg)	Sn found (mg)
105	87.7	14.8
	88.3	14.9
100	88.1	14.9
	88.5	14.9
95	89.2	15.0
	88.9	15.0

Table 2
Effect of amount of TDTC on the determination of Sn

Sn added (mg)	TDTC added (g)	Mass of precipitate found (mg)	Mass of Sn found (mg)
15.0	0.5	88.9	15.0
		89.1	15.0
30.0	0.8	178.4	30.1
		177.5	30.0
75.0	1.7	443.9	74.9
	3.0	444.3	75.0
		444.9	75.0

3.3. Effects of diverse ions and preliminary separation

As the preparation reaction with TDTC is not selective, most of other cationic species, if present, should be removed in advance. DDTC was reported to precipitate Sn(IV) over the whole pH range of 2–14 [14]. It is surely invalid. As an analog of TDTC, it has the same donor system, hence should behave similarly. Our experiments confirmed this since at $\text{pH} \geq 7$ no precipitate was found. Accordingly a preliminary group separation can be made by precipitation with DDTC at pH 9 in the presence of tartrate to remove at a single stroke: Ag(I), Au(III), Bi(III), Cd(II), Co(II), Fe(III), Hg(II), Mn(II), Ni(II), Pb(II), Sb(III), Te(IV), Tl(I) and Zn [14]. Although the removal of Se(IV) and Te(VI) is not quantitative, yet only a part of their residual portions would react with TDTC under the specified conditions [14]. Fortunately, they are usually present in very small amounts, hence, their interference might be ignored. The ionic species of platinum metals, if present, would be removed also. Once the filtrate is acidified to pH 2–6, the excess of DDTC left would precipitate Sn(IV) immediately. Therefore, it is advisable to overstep this pH region by pouring the alkaline filtrate portionwise to strong acids.

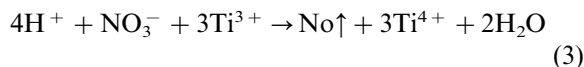
The possibly remaining species after this group separation would be: (a) cationic species of alkali and alkaline earth metals; (b) soluble tartrate complexes of B(III), Be(II), Al(III) and Ti(IV). All of them are tolerable even in macro amounts. Interferents are Cr(III), Ga(III), In(III) [14]. They can be masked, however, by EDTA, the excess of

which then reacts with Al(III) to constitute a ligand buffer, as their formation constants $\lg K_f$ were reported to be 23.4, 20.3, 25.0 and 16.3, respectively. Zr(IV), Hf(IV), Th(IV), U(VI) and most of the cationic species of rare earth metals would behave similarly, since they also form stronger chelates [15] with EDTA than Al(III). It was found that the precipitation of Sn(IV) runs normally in the presence of this ligand buffer, and that in the presence of Ce(III) or La(III), which itself is a non-interferent, a slight turbidity appears sometimes, and addition of EDTA helps to clear the solution.

Nb as an interferent may be present in some Ti alloys. If HCl alone is used for sample decomposition, it would remain undissolved and thus removed from the analyte solution [7]. So do W, Si and the platinum metals [7]. If necessary, the trace amount of Sn which might be occluded in the insoluble matter, can be recovered and determined separately as reported elsewhere [16].

Up to 1% of As may be present in some alloys of interest. As it is not separated by the preliminary group precipitation and reacts with TDTC, it would cause a positive error. Even 0.1 mg of it would increase the mass of the Sn-precipitate by 0.7 mg. Hence, it seems advisable to keep it in the trivalent state and distil off as AsCl_3 . Ge(IV) is an interferent [14] of rare occurrence. If present, it can be removed together with As.

Generally speaking, oxidants can oxidize TDTC, and hence interfere. The only oxidant introduced to the analyte solution is nitric acid. Accordingly its addition should be kept as small as possible. Its remnant can be completely removed by adding Ti(III):



Ti(III) was chosen for this purpose, since it serves to reduce also the higher valence states of As and Sb quantitatively to their trivalent ones, the presence of its excess is indicated by its own color and both Ti(III) and Ti(IV) are non-interferents. If sodium sulfite were used instead, the separation of Sb(III) would be incomplete owing to reoxidation [17]. Moreover, sulfite would react with hydrogen sulfide, one of the acid decomposition products of DDTC [18] to form colloidal elemental sulfur, and hence is the only interferent possibly used among the reductants.

The reaction between Mo(VI) and DDTC was reported to take place over the pH range of 2–9 [14]. This statement is questionable, as our experiments showed that it, like Sn(IV), reacts with either DDTC or TDTC at $\text{pH} \leq 6$ only. Hence, Mo(VI) would accompany Sn(IV) in the filtrate after the preliminary separation at pH 9. This interference from Mo can not be eliminated by masking with EDTA or hydroxylamine (which was used to mask the precipitation of MoS_3 in acid solution) [19] alone, nor as Mo(VI)– NH_2OH –EDTA [20].

V, like Mo, would accompany Sn(IV) in the filtrate too. As shown in its predominance-zone diagram, it is at pH 5.0–5.5 in the state of vanadyl vanadate, i.e. partly as V(IV) and partly as V(V) [21]. Hence, effects of both V(V) and V(IV) should be studied. It was found that in the presence of EDTA, TDTC does not precipitate either of them at the stated pH to form the same yellow product. The only difference lies in that this precipitation takes place at once in the case of V(V), but slows down somewhat in the case of V(IV).

It should be noted that at pH 9 V(V) is the predominate species in the filtrate; whereas at $\text{pH} \leq 0$ V(IV) is [21]. Therefore, subsequent acidification of the alkaline filtrate makes the unstable V(V) an oxidant. Under such conditions V(V) would oxidize DDTC or its decomposition products and thus render the analyte solution colloidal. In order to avoid this additional interference ethanol is purposely added prior to acidifi-

cation and preferentially oxidized. It was chosen since it is very pure, harmless and can be readily boiled off.

Attempts were made to eliminate interferences from Mo and V, but failed. Thus, we can not help taking another approach: to precipitate them altogether, determine their co-precipitated amounts and make corrections for them (Eq. (2)). Fortunately, their presence or absence can be readily detected by the naked eye: in their absence the precipitate is pure white; while in their presence it is colored (yellow if V is present and scarlet if Mo present). Their determinations are also an easy matter. Indeed, a clear-cut separation of Mo and V from Sn seems very much difficult, if not impossible, to incorporate conveniently in the proposed method.

For anions, some alloys may contain $\leq 1\%$ of P which is tolerable. Effects of some ionic species on the determination of Sn are shown in Table 3.

3.4. Applications

It should be noted that only Sn(IV) forms a precipitate with TDTC in the highest mole ratio of 1:4. Hence, its conversion factor is very small

Table 3
Effects of cations on the determination of 30.0 mg of Sn

Cation added (mg)	Mass of precipitate found (mg)	Mass of Sn found (mg)
As(III) 2	177.7	30.0 ^b
Bi(III) 100	177.5	29.9 ^c
Cu(II) 200	176.8	29.8 ^c
Fe(III) 30	177.9	30.0 ^c
Ni(II) 50	177.2	29.9 ^c
Pb(II) 200	177.0	29.9 ^c
Sb(III) 50	178.0	30.0 ^c
Zn(II) 80	177.4	29.9 ^c
Al(III) 200	178.5	30.1
Ti(IV) 200	178.3	30.1
Cr(III) 10	178.1	30.0 ^d
In(III) 23	178.2	30.1 ^d
Mo(VI) 5	200.6	30.1 ^a
V(V) 5	216.9	30.2 ^a

^a Corrected data by Eq. (2).

^b After volatilization.

^c After DDTC separation.

^d Masked by EDTA.

Table 4
Analytical data of some simulated samples

Sample composition (%)	Sn found (%)
Cu 5, Sb 12, Sn 73, Sb 10	72.8
As 0.5, Cd 2, Cu 3, Pb 73, Sb 15, Sn 6.5	6.55
Cu 83, Pb 4, Zn 6, Sn 7	6.95
Bi 45, In 10, Pb 25, Sn 20	20.10

(0.1687), even smaller than that of the well known nickel diacetyldioximate (0.2031). The proposed method is very suitable for the determination of 10–70 mg of Sn. Its standard deviation ($n = 10$) at the level of 20 mg of Sn was found to be 0.08 mg.

Its special features may be summarized as follows:

1. **Simplicity:** $\geq 5\%$ of Sn can be determined by taking 0.2 g of sample or even an aliquot there from. This makes the separation simpler and easier.
2. **Selectivity:** a single clear-cut precipitation in combination with masking suffices to eliminate most of the interferences and render the determination specific for Sn in most cases.
3. **Versatility:** provision is made for eliminating interferences in special cases, such as correction for Mo and V. This makes it also applicable to the analysis of Ti alloys.
4. **Flexibility:** it is flexible in the technique of sample decomposition and simplifications are possible in the absence of certain interferents.

Owing to these features the proposed method will find many industrial applications. The results for analysis of some simulated and industrial samples are shown in Tables 4 and 5 respectively.

4. Conclusion

A new gravimetric method is proposed for the macro-determination of Sn. It is simple, selective, versatile and flexible, hence would be very promising.

Acknowledgements

Grateful thanks are due to all members of the

Table 5
Determination of Sn in some certified reference materials (CRM)

CRM sample of alloys	Sn found (%)	Its certified value (%)
Al-Sn ^b	15.60	15.66
Cu-base	18.55	18.47 ^c
	9.83	9.80 ^a
Mg-base ^c	7.39	7.34
Pb-base ^c	8.81	8.88
Sn-base ^c	87.7	87.6
Ti-5Al-5Sn-5Zr ^b	5.20	5.13

Obtained from: ^a Bureau of Analysed Samples, UK; ^b Jinan Metallurgical Institute, China; ^c SRIM, a well known supplier of CRMs in China since 1952.

Directorate of SRIM for permission to publish this paper.

References

- [1] ASTM Standards E (1995) 478–89a.
- [2] ASTM Standards E (1995) 50–90.
- [3] R. Pribil, *Applied Complexometry*, Pergamon Press, Oxford, 1982, p. 140.
- [4] P. Belin, *Chim. Anal.* 44 (1962) 166.
- [5] D.E. Ryan, G.D. Lutwick, *Can. J. Chem.* 31 (1953) 9.
- [6] N. Zhou, R. Yu, X. Yao, Z. Lu, *Talanta* 32 (1985) 1129.
- [7] ASTM Standards E (1995) 120–189.
- [8] N. Zhou, C.X. He, *Analyst* 119 (1994) 2105.
- [9] S.J. Joris, K.I. Aspila, C.L. Chakrabarti, *Anal. Chem.* 42 (1970) 647.
- [10] G.K. Bratspies, J.F. Smith, J.O. Hill, *J. Anal. Appl. Pyrolysis* 2 (1980) 35.
- [11] H.P. Chang, K.L. Cheng, *Spectrosc. Lett.* 14 (1981) 795.
- [12] H. Malissa, *Anal. Chim. Acta* 27 (1962) 407.
- [13] IUPAC, *Pure Appl. Chem.* 66 (1994) 2423.
- [14] O.G. Koch, G.A. Koch-Dedic, *Handbuch der Spurenanalyse*, 2nd ed., Springer Verlag, Berlin, 1974, pp. 298–310.
- [15] S. Kotrlý, L. Sucha, *Handbook of Chemical Equilibria in Analytical Chemistry*, Ellis Horwood, Chichester, 1985, pp. 175–176.
- [16] N. Zhou, *Mikrochim. Acta* 108 (1992) 303.
- [17] H. Zintl, H. Wattenberg, *Berichte* 56 (1923) 472.
- [18] K.I. Aspila, V.S. Sastri, C.L. Chakrabarti, *Talanta* 16 (1969) 1099.
- [19] E. Lassner, *J. Less-Common Met.* 15 (1968) 143.
- [20] E. Lassner, P. Püschel, H. Schedle, *J. Less-Common Met.* 15 (1968) 151.
- [21] M. Pourbaix, *Atlas d'Equilibres Electrochimiques à 25°C*, Gautier-Villars, Paris, 1963.

Flow-injection spectrophotometric determination of calcium using murexide as a color agent

Kate Grudpan^{a,*}, Jaron Jakmune^a, Yuthsak Vaneesorn^a, Surasak Watanesk^a,
U Aye Maung^{1,a}, Ponlayuth Sooksamiti^b

^a Department of Chemistry, Faculty of Science, Chiang Mai University, Chiang Mai 50200, Thailand

^b Mineral Resource Region 3 (Chiang Mai), Chiang Mai 50200, Thailand

Received 27 August 1997; received in revised form 9 October 1997; accepted 10 October 1997

Abstract

FI spectrophotometric determination of calcium using murexide has been developed. The problem of the color of the dye fading and/or its complex in an alkaline medium in the batch method can be overcome by taking advantage of FIA. A calcium solution is injected into an ethylenediamine–ethylenediamine hydrochloride buffer (1 M, pH 11) which also serves as a masking agent, and is then merged with the aqueous murexide (0.005%, w/v) and continuously monitored. Simple FIA manifolds, including an LED colorimeter detector hooked up to a PC-based data acquisition and evaluation system are described. Optimization of FIA systems has been made. The proposed procedures have been validated by using reference materials and comparing the results with the standard methods, and then applied to ores and drug samples. © 1998 Elsevier Science B.V. All rights reserved.

Keywords: Calcium; Murexide; Flow injection; Spectrophotometry; Ores analysis; Drug analysis

1. Introduction

Calcium compounds are of concern to various industries, such as cement, pulp and paper, pharmaceutical, metallurgy and mining [1]. Determination of calcium is required for the quality control of raw material, process and/or product. Various techniques have been applied, for example titrimetry [2], spectrophotometry [3], atomic absorption

spectroscopy [4], ion-selective electrode [5] and ion chromatography [6]. In dealing with a large number of samples, a method which is rapid, accurate, precise and with low operation cost is required.

Flow injection (FI) techniques have increasingly served the above purposes. FI procedures for determination of calcium have been reported. Although some other techniques have also incorporated FI, such as flame AAS [7], flame photometry [8], ICP-AES [9], ISE [10], fluorimetry [11] and enthalpimetry [12], FI spectrophotometry has gained most attention owing to its simplicity.

A number of color reagents have been employed for FI determination of calcium. They

* Corresponding author. Tel.: +66 53 943345; fax: +66 53 892277; e-mail: kate@chiangmai.ac.th

¹ Permanent address: Department of Chemistry, Mawlamyine University, Myanmar.

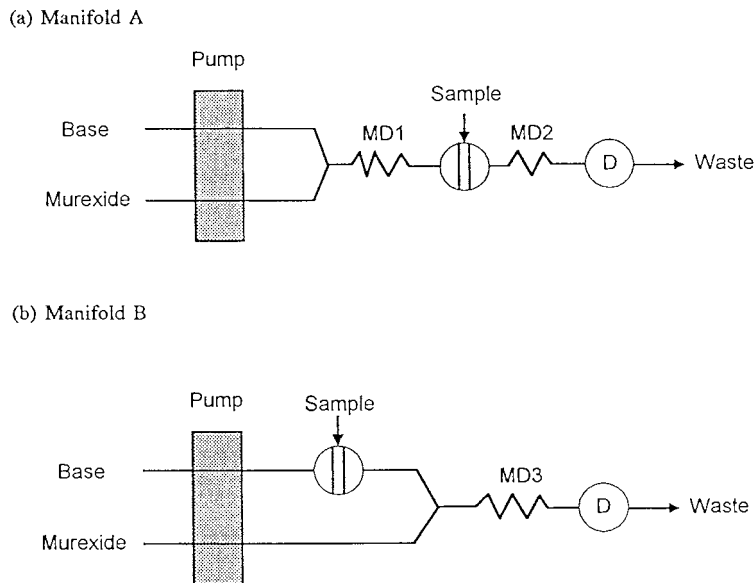


Fig. 1. The flow systems for the determination of calcium using murexide; MD1, MD2 and MD3, mixing devices (see text).

include complexon [13], chlorophosphonazo III [14], *o*-cresolphthalein [15], 3,3-bis[*N,N*-bis(carboxyl methyl)-*o*-cresolphthalein [16], 1-(2-hydroxy-4-diethylamine-1-phenylazo)-2-hydroxynaphthalene-3,6-disulfonic acid [17] and Arsenazo III [18].

Some reported FI procedures are based on chelatometric titration for calcium using EDTA and a color indicator, such as calmagite [19] or murexide [20].

Murexide is a metal ion indicator, commonly used in conventional EDTA titration determination of calcium. It was also proposed to be used as a chromogenic reagent for conventional spectrophotometric determination of calcium. The Ca(II)–murexide complex is formed in an alkaline solution, but its color fades rapidly [21].

In this work, attempts have been made to make use of the advantages of FI to overcome the problem on fading in the conventional method. Spectral characteristics of murexide and its metal complexes were re-investigated. FI direct spectrophotometric determination of calcium using murexide, which is a commonly available indicator, as a complexing color agent is proposed. A simple FI system with an LED detection device,

interfaced with a PC using 'CMUFIA II' software for data acquisition and evaluation, has been developed. The proposed system provides a simple, economical and precise determination of calcium using a cost-effective instrumentation. The procedures were validated by the analysis of reference materials, and applied for ores and pharmaceutical samples, and the results compared with standard methods.

2. Experimental

2.1. Reagents

All chemicals were analytical-reagent grade, except where otherwise stated; de-ionized water was used.

A stock standard calcium solution of 1000 mg l^{-1} was prepared by dissolving calcium carbonate (puriss, Fluka, 2.5800 g) in 50 ml of 0.1 M hydrochloric acid (proanalysis, Merck). The solution was boiled for a few minutes to remove carbon dioxide and diluted to 1 l with 0.1 M hydrochloric acid. Further dilutions with water were made for appropriate concentrations.

The stock color reagent was murexide solution (0.05%, w/v), obtained from murexide (ammonium purpurate, purum, Fluka, 0.05 g) dissolved in 100 ml of water. The stock was diluted with water for various concentrations.

Ethylenediamine–ethylenediamine hydrochloride (en/enHCl) buffer solution (1 M, pH 11) was prepared by dissolving ethylenediamine (purum, Fluka, 68.0 ml) in water (500 ml), mixing with concentrated hydrochloric acid (8.3 ml) and making up to a 1-l volume with water.

Certified reference materials for limestone, CRM1-J1s and CRM2-440/38, were obtained from The Geological Survey of Japan (GSJ) and The Department of Mineral Resources, Thailand, respectively. A mixed standard solution certified

for: Ca $1000 \pm 50 \text{ mg l}^{-1}$ (containing As, B, Be, Fe, Se and Zn, $100 \pm 5 \text{ mg l}^{-1}$; Ag, Al, Ba, Bi, Cd, Co, Cr, Cu, Ga, K, Li, Mg, Mn, Mo, Na, Ni, Pb, Rb, Sr, Te, Tl, U and V, $10.0 \pm 0.5 \text{ mg l}^{-1}$) was obtained from Merck.

2.2. Sample preparation

2.2.1. Calcite and limestone samples

Powdered sample (0.1000 g; ≥ 250 mesh USS) was put in a 50-ml beaker. One ml of water was added and concentrated hydrochloric acid was carefully added dropwise, until about 2 ml of the acid was used. The solution was evaporated until nearly dry. Then 20 ml of 0.1 M hydrochloric acid was added and the solution was filtered. The filtrate was made up to 100 ml with 0.1 M HCl. The solution for injecting into the FI system was prepared by suitable dilution of this solution with deionized water [22].

2.2.2. Drug samples

The samples were taken from drug stores then ground and accurately weighed, followed by dissolving with 5 ml of 1 M HCl. The solution was boiled on a hot plate until a clear solution was obtained. The solution was filtered and diluted to 100 ml with deionized water [23].

2.3. Apparatus

All spectrum measurements of the solutions of murexide and its metal ion complexes were made using a Shimadzu UV-265 spectrophotometer.

2.4. Flow manifold

The manifolds used are depicted in Fig. 1. The systems were assembled by using a peristaltic pump (FIALab, Alitea USA, or EVA pump, Eppendorf), an injection valve (Alitea) or a home-made two-loop injection valve with a suction system using an aquarium pump as described previously [8], a mixing device consisting of single-string glass beads (3.0 mm diameter) in a column of silicone tubing (3.2 mm I.D.) [24]. The detector was a Spectronic 21 (Bausch & Lomb, USA) with a flow-through cell (Hellma, 1 cm,

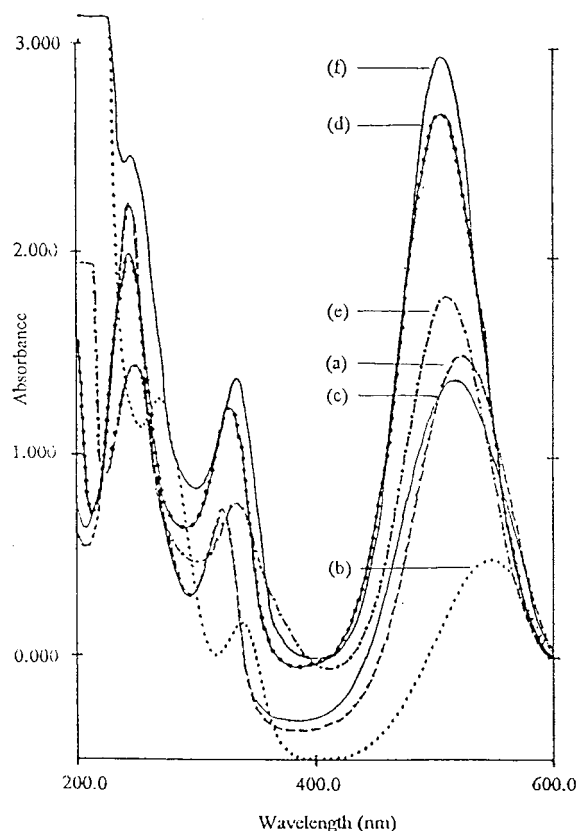


Fig. 2. Spectra of murexide and its Ca complex in various alkaline media (0.005% (w/v) murexide and 10 mg Ca l^{-1}). Murexide in (a) NaOH (pH 9), (b) en/enHCl buffer (pH 11). Ca–murexide in (c) NaOH (pH 9), (d) NaOH (pH 11), (e) NaOH (pH 13), and (f) en/enHCl buffer (1 M, pH 11).

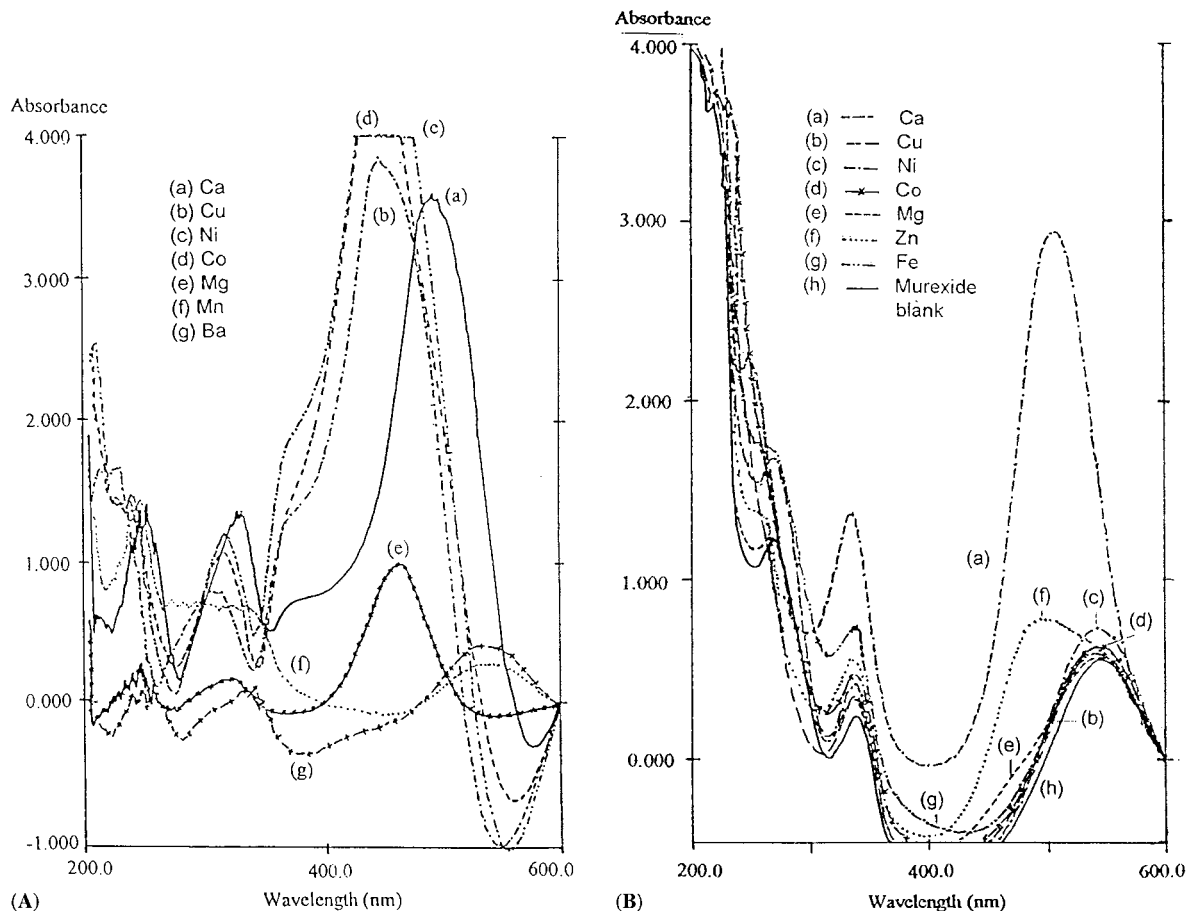


Fig. 3. The absorption spectra of metal complexes in (A) 0.002 M NaOH (vs. murexide blank as a reference) and (B) en/enHCl buffer (1 M, pH 11) (vs. H₂O as reference) (0.005% (w/v) murexide and 10 mg l⁻¹ metal ions).

Suprasil I window) or an LED colorimeter. Output signals were recorded by either a chart recorder (Omniscrite, Houston Instrument) or via a home-made 8-bits interface card linking with a PC using the 'CMUFIA II' software program [25] developed for data acquisition and evaluation.

3. Results and discussion

3.1. Spectral characteristics of murexide and its Ca complex

Three absorption maxima were observed in sodium hydroxide solutions for each dye spectrum

(Fig. 2) at 530 ± 15 , 335 ± 10 and 240 ± 5 nm, similar to the ones in a solution of en/enHCl buffer (1 M, pH 11).

Spectra of the Ca–murexide complex were also observed for three absorption maxima at 505 ± 5 , 335 ± 5 and 246 ± 5 nm in all the above alkaline solutions, except in the sodium hydroxide medium of pH 9, in which only the spectrum of the reagent was observed, but not that of the Ca–murexide complex. This agrees with the previous report [26].

Absorption spectra of the complexes of the dye with metal ions (Cu²⁺, Ni²⁺, Zn²⁺, Co²⁺, Fe²⁺, Mg²⁺, Ba²⁺ and Ca²⁺) were also recorded in sodium hydroxide (0.002 M) and in the en/enHCl

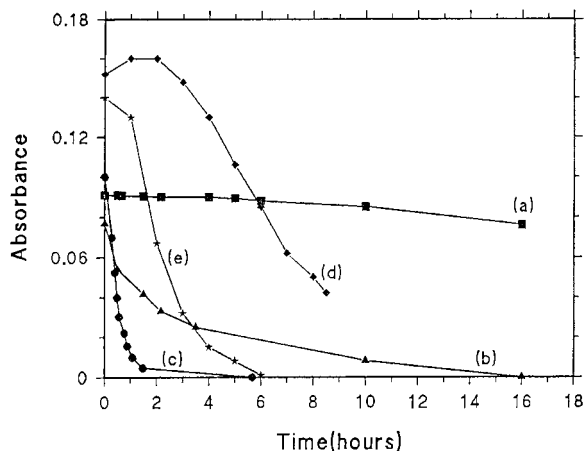


Fig. 4. Stability study (absorbance–time dependence at 520 nm (vs. H₂O)) of murexide solutions in (a) H₂O (pH 6), (b) 0.005 M NaOH (pH 11.7), and (c) en/enHCl buffer (1 M, pH 11), and of Ca–murexide complex in (d) 0.005 M NaOH and (e) en/enHCl buffer (1 M, pH 11); (a), (b) and (c) at 520 nm, and (d) and (e) at 505 nm Ca, 10 mg l⁻¹; murexide, 0.005% (w/v).

buffer (1 M, pH 11) as represented in Fig. 3. The dye complexes of some metal ions, such as Cu²⁺, Co²⁺ and Ni²⁺, also absorbed strongly at the absorption maximum wavelength of the Ca complex (505 or 498 nm against water or reagent blank, respectively). But absorbances of the com-

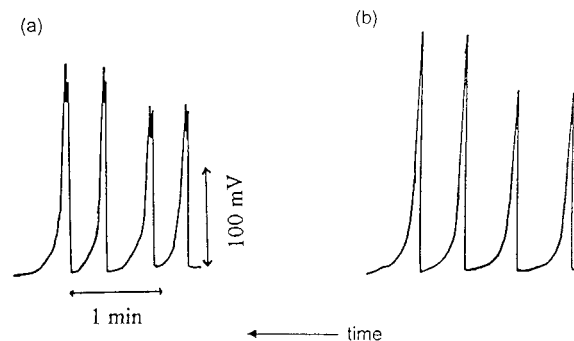


Fig. 6. FIA peaks observed when using (a) mixing coils and (b) glass bead columns as mixing devices.

plexes in the en/enHCl buffer were much less; only just about that of the reagent blank. This could be due to the fact that the metal ions form more stable complexes with en than the ones with murexide. The formation constants for the murexide complexes, log β , are 4.36, 3.11, 3.0, 2.66, 2.2, 2.0 and 2.68 for Cu²⁺, Ni²⁺, Zn²⁺, Co²⁺, Mg²⁺, Ba²⁺ and Ca²⁺, respectively [27], while those of the en complexes, log β , are 24.53, 21.29, 16.84, 16.76 and 0.37 for Cu²⁺, Ni²⁺, Zn²⁺, Co²⁺ and Mg²⁺, respectively [28]. This indicates that en could be used as a masking agent for the determination of calcium.

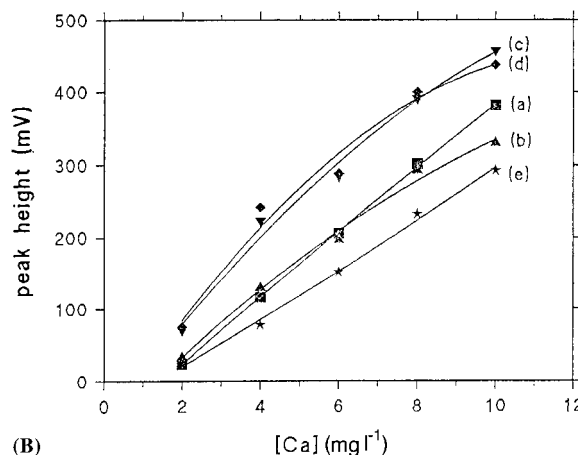
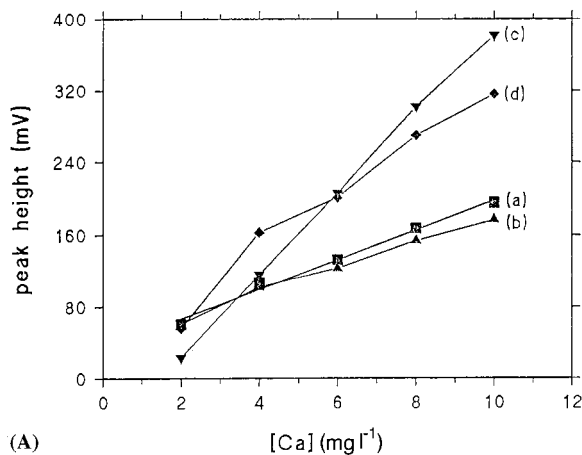


Fig. 5. Effect of reagent concentration on calibration curves: (A) murexide solution ((a) 0.0005, (b) 0.001, (c) 0.005 and (d) 0.010% (w/v)); [NaOH] = 0.01 M and (B) sodium hydroxide solution ((a) 0.01, (b) 0.02, (c) 0.03, (d) 0.04 and (e) 0.10 M); [murexide] = 0.005% (w/v).

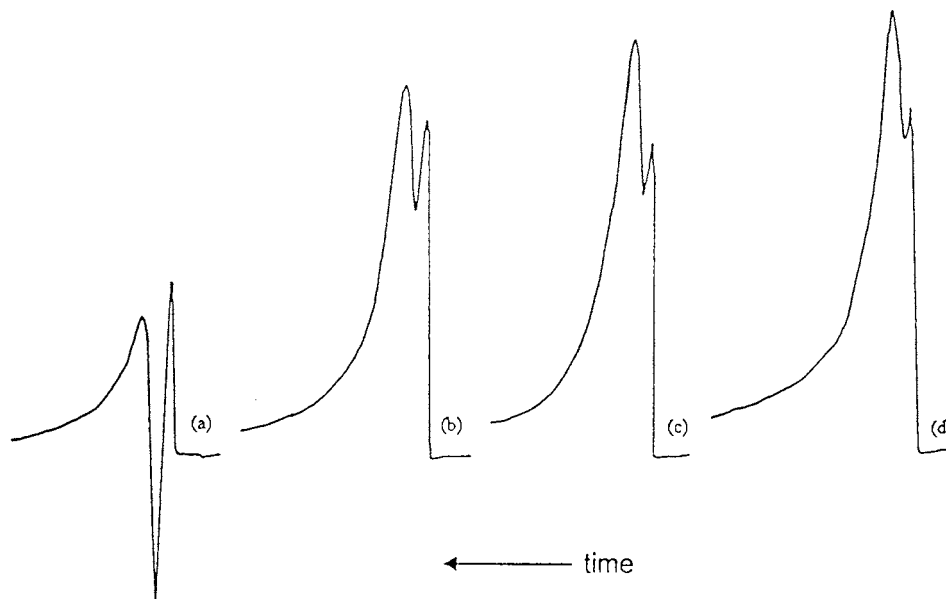


Fig. 7. Effect of sodium hydroxide concentration: (a) 0.001 M, pH 10.9; (b) 0.005 M, pH 11.7; (c) 0.010 M, pH 12.1; and (d) 0.050 M, pH 13.0.

Using the continuous ratio and the mole ratio methods, a 1:1 complex of Ca–murexide was confirmed as previously reported [26].

Fig. 4 represents a study on the stability of the Ca–murexide complex. A murexide solution (0.005%, w/v) in water was found to be stable for at least 6 h, while its solutions in sodium hydroxide (0.005 M) or in the en/enHCl buffer (1 M, pH 11) decomposed rapidly. Its Ca complex was observed to be more stable than the murexide alone.

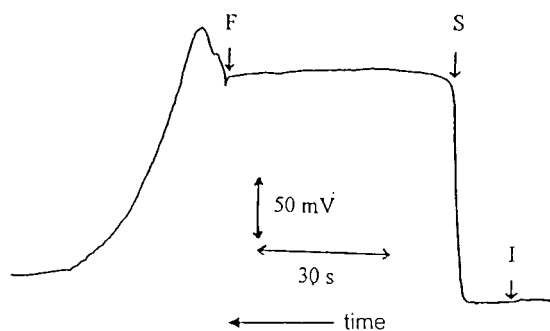


Fig. 8. Stopped-flow signal profile of FI stopped-flow experiment; (I) injection point; (S) stop the flow; and (F) start flow again.

3.2. Optimisation of the FI systems

3.2.1. The Manifold A

3.2.1.1. Effects of murexide and sodium hydroxide concentrations. Using manifold A (Fig. 1a) with mixing coils, MD-1 (145 cm long; 0.8 mm I.D.) and MD-2 (90 cm long; 0.8 mm I.D.); a flow-rate of 2.2 ml min^{-1} for each stream, effects of murexide concentration (0.0005–0.01%, w/v) and alkalinity of the medium (0.001–0.04 M NaOH) were studied. A series of standards ($2\text{--}10 \text{ mg Ca l}^{-1}$) was injected. From the results obtained (Fig. 5), 0.005% (w/v) murexide and 0.01 M NaOH were chosen for further study as the condition providing a good compromise between sensitivity and linearity of the signal.

3.2.1.2. Effect of mixing devices. The manifolds using mixing coils as the mixing devices yielded a doublet peak not found in usual FIA measurements. The peak height of each of them depended on the calcium concentration, but the first peak was consistently lower than the second one, as depicted in Fig. 6a. The second peak was better

Table 1
Effect of reagent flow-rate

Mixing device	Flow-rate of each line (ml min ⁻¹)	Residence time (s)	Peak height corrected for blank (mV) ^a	Peak width (s)
MD-1 (GBC 15 cm) without MD-2	0.8	13.5	273.2	99
	2.0	5.3	290.6	75
	6.0	2.3	284.9	36
	8.25	1.5	220.9	20
MD-1 (GBC 15 cm) and MD-2 (GBC 5 cm)	0.8	26.4	218.6	133
	2.0	12	246.5	92
	6.0	6.6	209.3	36
	8.25	5	274.4	18

^a Mean of triplicate injections of 8 mg l⁻¹ standard calcium solution (R.S.D. <4%).

correlated to calcium quantities than the first one. The doublet peak may be due to too high injected volume of sample; thus, when passing the second mixing coil of 90 cm length, the reagent cannot disperse well into the middle of the sample plug and the reaction will not occur there. The peaks may have been the result of the complex that formed at the beginning and the end zones of the sample plug. The glass bead column (GBC) mixing device provides better mixing of sample and reagent than mixing coils alone [24]. By using a 15-cm long GBC for MD-1 and a 10-cm long GBC for MD-2, the doublet peak profiles disappeared (Fig. 6b).

Doublet peaks may also be caused by pH gradi-

ent, i.e. a dispersion of NaOH solution into a sample plug. Fig. 7 shows that the higher concentration of sodium hydroxide decreased the depth of the valley of peaks. This would be due to the fact that the high concentration of NaOH solution would cause the NaOH to disperse into the middle of sample plug. The stopped-flow experiment indicated that no kinetic effects of reaction are responsible for the observed shapes (Fig. 8).

GBC was then chosen for use as a mixing device.

3.2.1.3. *Effect of GBC length.* The length of the MD-1 using a 15-cm GBC was fixed, while the

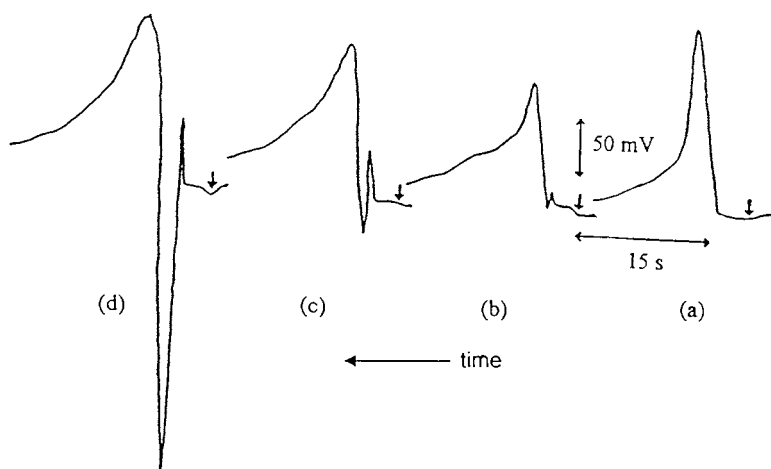


Fig. 9. Effect of sample volume on peak profiles: (a) 108 µl, (b) 144 µl, (c) 188 µl and (d) 280 µl.

Table 2
Effect of acidic sample

Conc. of HCl in buffer (M)	Observed pH	Sample volume (μl)	Blank corrected peak height (mV) ^a of 2 mg Ca l ⁻¹ in HCl (M)					
			0.00	0.10	0.25	0.50	0.75	1.00
0.001	11.4	65	88.3	102.3	111.6	83.7	116.2	93.0
		250	279.0	265.0	181.4	55.8	97.6	55.8
0.01	11.2	65	111.6	139.5	83.7	83.7	—	83.7
		250	269.7	265.0	190.6	106.9	69.8	74.4
0.1	10.4	65	88.4	116.3	97.6	106.9	—	88.4
		250	283.6	227.8	186.0	69.8	46.5	4.6

^a Mean of duplicate injections (R.S.D. <5%).

MD-2 GBC length was varied (3–30 cm long). A mixing chamber (0.8 ml) was also tried.

The results indicate that the longer GBC provided a wider linear determination range, but caused a longer residence time, thus reducing sample through-puts. As expected, the mixing chamber provided a wider linear range but broader peaks and lower sensitivity. Either 5- or 10-cm GBC could be suitable for the MD-2.

3.2.1.4. Reagent flow-rate. The flow-rate of each line was varied from 0.8 to 8.25 ml min⁻¹. It was found that 2.0 ml min⁻¹ was suitable for both manifolds, with and without MD-2, as reasonable peak height and acceptable residence time were obtained (Table 1).

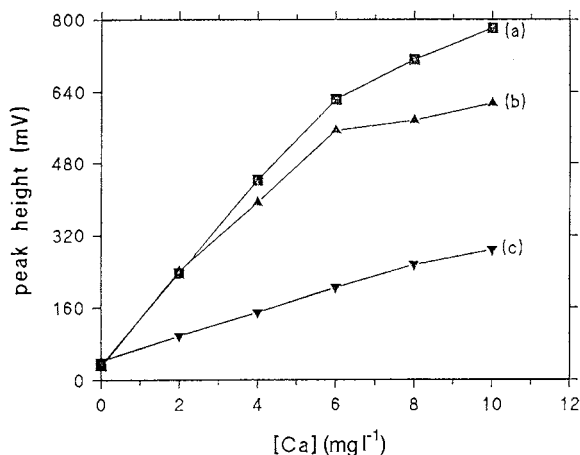


Fig. 10. Calibration curves of calcium standard in 0.1 M HCl using the en (1 M) buffers containing; (a) 0.001, (b) 0.01 and (c) 0.1 M HCl.

3.2.1.5. Sample volume. Injection volumes of three different loop lengths were measured by means of a spectrophotometric method using bromothymol blue as dye [29]. The effects of the injection volumes (108, 144 and 188 μl) of a series of Ca standard solutions were studied. Less volume injected provided good correlation in the calibration range of 0–10 mg Ca l⁻¹, although lower peak heights were obtained. Higher volumes cause doublet peaks (Fig. 9), possibly due to the fact that the reagent did not sufficiently disperse into the middle of the sample zone, as previously discussed.

3.2.2. Manifold B

To achieve a more efficient mixing, a sample was injected into a stream of buffer (Fig. 1b), followed by merging with a murexide solution stream before passing through a 10-cm long GBC. Only single positive peaks were obtained. By comparison with the same conditions for manifold A, a calibration curve of $y = 34.0x + 19.0$, $r = 0.96076$, resulted; manifold B yielded a calibration curve of better linearity, but with about 40% lower sensitivity ($y = 20.8x + 13.0$, $r = 0.99956$).

3.2.2.1. Effects of sample volume and mixing device length for manifold B. Three different volumes (45, 125 and 250 μl) were investigated for a series of Ca standards (0–10 mg l⁻¹) injected into a stream of the en/enHCl buffer (1 M, pH 11). The following calibration curves were obtained: for 45 μl , $y = 34.9x + 57.8$, $r = 0.99427$; for 125 μl , $y =$

Analyte : Calcium File : cal
 Comment : manifold A: 0.015%Ca, 1M en-enHCl, LED color, Flow 2.0 ml/min each
 A.U.

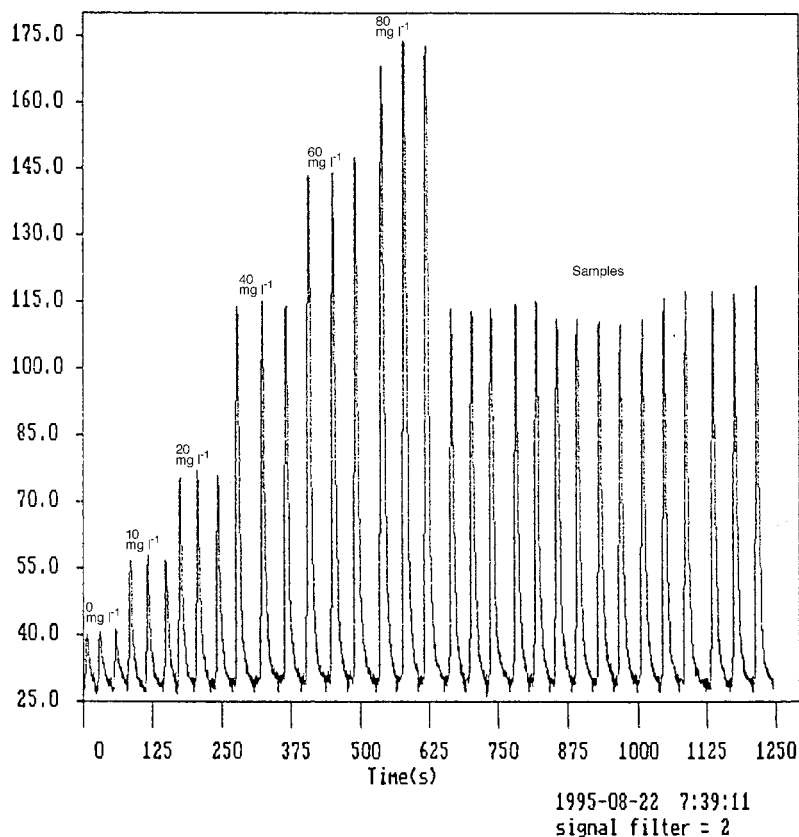


Fig. 11. FIAgram for the determination of calcium.

$40.2x + 40.0$, $r = 0.99810$; and for $250 \mu\text{l}$, $y = 55.2x + 79.7$, $r = 0.98173$. A volume of $125 \mu\text{l}$ provided a compromise of sensitivity and linearity in the determination.

The length of mixing device MD-3 was varied; GBC of 10–25 cm in length. The 15-cm GBC was found to give the most sensitivity and linearity, according to the calibration curves obtained: for the 10-, 15- and 25-cm GBCs, $y = 29.9x + 80.3$ ($r = 0.97826$), $y = 36.4x + 33.0$ ($r = 0.99396$) and $y = 25.5x + 25.9$ ($r = 0.99360$), respectively.

3.2.2.2. Effect of flow-rate. Using manifold B with the LED colorimeter detector, three flow-rates (3.7 , 5.0 and 8.0 ml min^{-1}) were tried for calibration curves (0 – 100 mg Ca l^{-1}). The flow-rate of

8.0 ml min^{-1} yielded high sensitivity with less residence time.

3.2.3. Effects of sample pH and of hydrochloric acid concentration for the en/enHCl buffer

As found earlier, a high pH medium favored the formation of a Ca–murexide complex and affected the observed absorbance. A sample solution is normally acidic since acids (especially HCl in this work) are used for dissolving samples. This affects the pH of the final mixture, after the sample solution is mixed with the reagent solution. The peak height observed decreased with decreasing pH values. The buffer solution, instead of NaOH solution, was required for maintaining the high pH conditions in the mixture. Ethylene-

Table 3
The conditions and analytical characteristics of the FIA systems developed

Parameters/features	Conditions				
	1	2	3	4	5
	Manifold A			Manifold B	
Detector	SPEC	LED	LED	SPEC	LED
Conc. of murexide (% w/v)	0.005	0.01	0.015	0.005	0.01
Buffer containing:					
en (M)	1	1	1	1	1
HCl (M)	0.001	0.001	0.001	0.001	0.001
Length of MD1 or MD3, GBC (cm)	15	15	15	15	15
Length of MD2, GBC (cm)	10	10	10	—	—
Recording system	Recorder	PC	PC	Recorder	PC
Amplifier gain	—	20	20	—	20
Baseline level (mV)	500	—	—	500	—
Full scale deviation of recorder (mV)	500	—	—	500	—
Injection volume (μl)	108	108	108	125	125
Reagent flow-rate:					
Murexide (ml min^{-1})	2	2	2	4	4
Base (ml min^{-1})	2	2	2	4	4
Linear range (mg Ca l^{-1})	0–8	0–20	0–80	0–20	0–100
Calibration equation	$y = 32.5x - 288.4$	$y = 79.8x + 816.3$	$y = 31.1x + 262.8$	$y = 23.8x + 33.7$	$y = 33.0x - 116.0$
Correlation coefficient	0.99610	0.99832	0.99780	0.99583	0.99338
Detection limit (mg Ca l^{-1})	0.7	1.3	6.8	2.0	11.8
Relative standard deviation (%)	2.9 ($n = 10$)	—	—	3.6 ($n = 11$)	0.8 ($n = 11$)

SPEC, spectrophotometer; LED, LED colorimeter.

diamine–ethylenediamine hydrochloride (pH 11) was introduced for this purpose, as well as being a masking agent. A HCl solution was added to the en solution (kept constant at 0.1 M en) to produce the required ethylenediamine salt. The buffer capacity and the pH of the buffer depend on the quantity of the HCl added, i.e. the ratio of

the en and the chloride salt.

Three different concentrations (0.001, 0.01 and 0.1 M) of HCl in the en (1 M) buffer resulted in pH values of 11.4, 11.2 and 10.4, respectively (Table 2). Solutions containing 2 mg Ca l^{-1} in various HCl concentrations were injected with two injection volumes (65 and 250 μl). It was found that the larger the volume injected, the more pronounced was the effect of the acidic sample. However, for the sample volume of 65 μl , a peak height due to 2 mg Ca l^{-1} in different concentrations of HCl did not yield significantly different results.

A calibration curve was constructed for each buffer by injecting a series of Ca standards in 0.1 M HCl (Fig. 10). Sensitivity was less when a high concentration of HCl was present in the buffer. This is due to the pH of the buffer being more acidic, a condition not suitable for calcium–murexide complex formation.

Table 4
Tolerance limit of some interfering ions for 4 mg Ca l^{-1} in the presence of 1 M en/enHCl buffer (pH 11) (see text)

Ions	Tolerance limit (mg l^{-1})
Al(III), ascorbic acid	≥ 1000
SO_4^{2-}	500
Cu(II) , PO_4^{3-} , Zn(II) , Fe(III) , CO_3^{2-}	25
Co(II)	20
Ni(II) , Ba(II) , Mn(II) , Fe(II) , Cr(VI)	10
Mg(II)	1

Table 5
The calcium contents of certified reference materials and limestones

Sample	Calcium content ^a (% w/w) found by method					
	FAAS ^f		FIA-SPEC ^b		FIA-LED ^b	
	Ca(II)	Mg(II)	Ca(II)	% diff. ^c	Ca(II)	% diff.
1. CRM 1-Jls-1 (39.48 ± 0.76% (w/w) Ca) ^d	—	—	40.8 ± 4.2	3.3	41.6 ± 0.9	5.4
2. CRM 2-440/38 (35.78 ± 0.52% (w/w) Ca) ^d	—	—	35.9 ± 3.1	0.3	37.6 ± 0.8	4.9
3. Certified standard solution (1000 ± 50 mg l ⁻¹ Ca ^e)	—	—	1024 ± 28	0.2	—	—
4. Limestone # 245	37.52	1.05	—	—	37.5 ± 0.7	0.1
5. Limestone # 2533	39.76	0.11	—	—	41.1 ± 0.5	3.4
6. Calcite # 2046	35.78	0.38	—	—	37.0 ± 0.9	3.4
7. Calcite no. 1	32.62	0.30	34.3 ± 1.5	-5.3	31.7 ± 0.6	-2.8
8. Calcite no. 2	30.31	0.25	32.2 ± 0.0	6.4	30.7 ± 0.5	1.3
9. Calcite no. 3	26.09	0.13	27.6 ± 0.2	6.0	25.6 ± 0.3	-1.7
10. Limestone no. 1	38.77	0.62	40.2 ± 0.0	3.6	39.0 ± 1.3	0.6
11. Limestone no. 2	38.18	0.32	40.4 ± 0.3	5.8	39.0 ± 1.1	2.1
12. Limestone no. 3	38.69	0.16	40.6 ± 0.0	5.0	40.3 ± 0.8	4.2
13. Limestone no. 4	38.45	0.24	39.7 ± 0.6	3.2	39.4 ± 0.8	2.6
14. Limestone no. 5	38.26	0.25	39.6 ± 0.0	3.5	39.4 ± 0.3	3.1
15. Limestone no. 6	38.19	0.28	39.0 ± 1.2	2.1	38.6 ± 0.8	1.0
16. Limestone no. 7	38.32	0.42	38.8 ± 0.5	1.2	39.4 ± 0.3	2.9
17. Limestone no. 8	38.46	0.25	39.9 ± 0.3	3.7	39.0 ± 0.7	1.4
18. Limestone no. 9	38.77	0.40	40.6 ± 0.8	4.6	40.3 ± 0.9	4.0

^a Mean of triplicate results.

^b SPEC, spectrophotometer; LED, LED colorimeter.

^c % diff. = ((%Ca, FIA - %Ca, FAAS) × 100) / (%Ca, FAAS) or = ((%Ca, FIA - %Ca, certified value) × 100) / (%Ca, certified value).

^d Certified values.

^e Certified value: Ca 1000 ± 50 mg l⁻¹ (As, B, Be, Fe, Se and Zn, 100 ± 5 mg l⁻¹; Ag, Al, Ba, Bi, Cd, Co, Cr, Cu, Ga, K, Li, Mg, Mn, Mo, Na, Ni, Pb, Rb, Sr, Te, Tl, U and V, 10.0 ± 0.5 mg l⁻¹). Nos. 3–6 determined by optimum condition of manifold A (200-fold sample dilution); nos. 1–2, 7–18 determined by optimum condition of manifold B (250-fold sample dilution).

^f Ref. [30].

Table 6
The calcium contents of calcium–drug formulations

Samples	Ca labeled (% w/w)	Calcium content (% w/w) ^a found by method				
		Ti ^b	FIA-SPEC ^b		FIA-LED ^b	
				% diff. ^c		% diff. ^c
1. Calcium Unison	13.6	9.9 ± 0.9	11.2 ± 0.2	13.6	10.0 ± 0.1	1.5
2. Chalkcap-285	34.0	38.7 ± 0.1	41.6 ± 0.6	7.4	38.9 ± 0.4	0.4
3. Sandoz vitamin C	3.9	3.5 ± 0.2	4.1 ± 0.4	15.0	3.7 ± 0.2	3.7
4. Dolomite	26.3	33.1 ± 5.4	31.2 ± 1.3	-5.9	33.2 ± 0.4	0.2

^a Mean of triplicate results.

^b Ti, The British Pharmacopoeia titrimetric method [23]; SPEC, spectrophotometer; LED, LED colorimeter.

^c % diff. = ((%Ca, FIA - %Ca, Ti) × 100) / (%Ca, Ti).

The buffer containing en (1 M) and HCl (0.001 M) should be best.

3.3. The FIA system for calcium using an LED colorimeter

A less-sensitive FIA system using an LED colorimeter can be used instead of a spectrophotometer for a sample containing high calcium contents, such as limestone, a raw material in the ceramic and cement industries. The system could be either hooked up to a recorder or to a computer-based data acquisition system controlled by the 'CMUFIA II' software [25]. Fig. 11 depicts an example of the FIAGram recorded.

3.4. Recommended conditions

The conditions and analytical characteristics of the FIA systems developed for calcium are summarized in Table 3.

3.5. Interference study

The interference of some expected ions was studied using condition 4 described in Table 3. Solutions of a 4-mg Ca l⁻¹ standard containing varying concentrations of diverse ions were injected. The tolerance limit for the given ions is defined as the amount of an interfering ion to cause a 5% deviation of calcium concentration alone. The tolerance limits of ions are summarized in Table 4.

All the ions studied interfered when 0.001 M NaOH was used as the alkaline medium. When 1 M ethylenediamine buffer was used, the tolerance limits of most ions increased. Therefore, ethylenediamine is effective as a masking agent. The properties of magnesium ion are similar to those of calcium, so the tolerance limit for magnesium ion was found to be very low. Despite the fact that 8-quinolinol has been reported as a masking agent for magnesium ion [13], it was not applied because, in the case of calcium minerals/ores samples that contain large amounts of calcium, magnesium contents are usually relatively low (Table 5). So this additional masking agent was avoided.

3.6. Accuracy and application of the methods

The accuracy of the FIA methods was checked by analysis of a certified standard solution and certified reference materials, and by comparison to the results obtained with the standard methods; flame atomic absorption spectroscopy (FAAS) [30] for ores samples (Table 5) and the British Pharmacopoeia titrimetric method for drug analysis (Table 6) [23].

The calcium contents obtained by the FIA methods agreed with the certified values and/or the standard methods.

Comparison of the results for calcite and limestone samples (Table 5) can be expressed by the following relationship: FI-SPEC = 0.98 × FAAS + 2.35, $r = 0.99362$; FI-LED = 1.12 × FAAS - 3.78, $r = 0.99158$ and FI-LED = 1.14 × FI-SPEC - 6.13, $r = 0.98962$.

The results for the drug analysis can be represented as follows: FI-SPEC = 1.00 × titrimetry + 0.66, $r = 0.99338$; FI-LED = 1.00 × titrimetry + 0.16, $r = 0.99999$ and FI-LED = 0.98 × FI-SPEC - 0.23, $r = 0.99360$.

4. Conclusion

The flow injection spectrophotometric method which has been developed for calcium, using a murexide color agent, is inexpensive and readily available, allows fast determination at low operating costs, and is simple. Use of an unstable reagent, alkaline murexide, for determination of calcium with the aid of FIA has been successfully applied. This emphasizes an additional advantage of FIA, even by using a very simple instrument. The application of the method to ores and pharmaceutical samples has been demonstrated.

Acknowledgements

Thailand National Science and Technology Development Agency (NSTDA) is acknowledged for part support of this research, especially the scholarship for J.J. UA.M. thanks the International

Atomic Energy Agency (IAEA) for his fellowship at Chiang Mai University. We thank Professor G.D. Christian for useful discussions.

References

- [1] M. Grayson, Encyclopedia of Chemical Technology, vol. 4, 3rd ed., John Wiley, New York, 1978, pp. 421–448.
- [2] K.C. Ghosh, B.C. Mukherjee, N.N. Garguly, M. Yasuf, V.N. Choudhury, Talanta 39 (1992) 675.
- [3] G.M. Huttink, Talanta 34 (1986) 423.
- [4] E.A.G. Zagatto, F.J. Krug, H. Bergarnin, S.S. Jorgensen, B.F. Reis, Anal. Chim. Acta 104 (1979) 279.
- [5] V.V. Cosofret, W.W. Olsen, S.A.M. Marzouk, M. Erdosy, T.A. Johnson, R.P. Buck, Anal. Lett. 29 (5) (1996) 725.
- [6] T. Williams, N.W. Barnett, Anal. Chim. Acta 259 (1992) 19.
- [7] M. Guardia, A. Morales-Rubio, V. Carbonell, A. Salvador, J.L. Burguera, M. Burguera, Fresenius Z. Anal. Chem. 345 (1993) 579.
- [8] K. Grudpan, C. Taylor, H. Sitter, C. Keller, Fresenius Z. Anal. Chem. 346 (1993) 882.
- [9] P.L. Kempster, J.F. Van Staden, H.R. Vliet, Fresenius Z. Anal. Chem. 332 (1988) 153.
- [10] J. Nyman, A. Ivaska, Talanta 40 (1992) 95.
- [11] W.A. Oliveiva, A.S. Mendes, Talanta 34 (1987) 543.
- [12] O.T. Thuy, D.D. Weever, W.T. Kok, P. Luan, T.V. Nghi, Anal. Chim. Acta 295 (1994) 151.
- [13] E.H. Hansen, J. Ruzicka, A.K. Ghose, Anal. Chim. Acta 100 (1978) 151.
- [14] M. Zenki, K. Ohmuro, K. Toei, Fresenius Z. Anal. Chem. 338 (1990) 707.
- [15] J.F. Van Staden, R.E. Taljaard, Anal. Chim. Acta 246 (1991) 329.
- [16] T. Yamato, E. Goto, Talanta 38 (1991) 139.
- [17] H. Wada, T. Ozawa, G. Nakagawa, Y. Asano, S. Ito, Anal. Chim. Acta 224 (1989) 23.
- [18] M. Blanco, J. Coello, J. Gene, H. Iturriaga, S. Maspocho, Anal. Chim. Acta 224 (1989) 23.
- [19] N. Ishibashi, T. Imato, Fresenius Z. Anal. Chem. 323 (1986) 244.
- [20] F. Canete, A. Rios, M.D. Luque de Castro, M. Valcarcel, Analyst 112 (1987) 267.
- [21] F.H. Pollard, J.F.W. Mcomie, J.V. Martin, Analyst 81 (1956) 353.
- [22] N.H. Furman (Ed.), Standard Methods of Chemical Analysis, vol. 1, Robert E. Krieger Publishing Company, NY, 1975, pp. 258–278.
- [23] British Pharmacopoeia, H.M. Stationary Office, London, 1993, pp. 101–105.
- [24] S. Hariratseree, M.S. Thesis in Chemistry, Chiang Mai University, 1994.
- [25] J. Jakmune, K. Grudpan, Data Acquisition and Evaluation for Flow Injection Analyzer, 20th Conference on Science and Technology of Thailand, Bangkok, October 1994, A-80, pp. 254–255.
- [26] M.B. Williams, J.H. Moser, Anal. Chem. 25 (1953) 1414.
- [27] G. Geier, Helv. Chim. Acta 50 (1967) 1879.
- [28] R.M. Smith, A.E. Martell, Critical Stability Constants, vol. 2, Plenum Press, New York, 1975, pp. 36–37.
- [29] B. Karlberg, G.E. Pacey, Flow Injection Analysis: A Practical Guide, Elsevier, Amsterdam, 1989, pp. 41–42.
- [30] L. Shapiro, Rapid Analysis for Silicate, Carbonate, and Phosphate Rocks, Revised Edition, US Geological Survey Bulletin, 1975, p. 1401.

Discrimination between arabica and robusta green coffee varieties according to their chemical composition

María J. Martín, Fernando Pablos, A. Gustavo González *

Department of Analytical Chemistry, Faculty of Chemistry, University of Seville, 41012, Seville, Spain

Received 14 July 1997; accepted 3 November 1997

Abstract

Arabica and robusta green coffee varieties have been differentiated by using pattern recognition procedures. Chlorogenic acid, caffeine, trigonelline, aqueous extract, amino acids and polyphenols have been analysed in 41 samples of green coffee and used as chemical descriptors. Principal component and cluster analysis in addition with the *K*-nearest neighbours method have been applied. © 1998 Elsevier Science B.V. All rights reserved.

Keywords: Coffee; Pattern recognition

1. Introduction

The two most important varieties of commercial coffee are *Coffea arabica* and *Coffea canephora*, usually known as arabica and robusta, respectively. Commercial coffee beverage is made from arabica or robusta beans or blends of them, the arabica being considered of better quality [1] and is therefore more expensive. Accordingly, it is interesting to have methods for differentiating between those two coffee varieties. Chemometric procedures applied to the data of chemical composition of the samples provide an interesting approach to the food quality control [2]. Within this realm several works on the discrimination of coffee varieties based on differences of their chem-

ical composition have been published. Some of them use as descriptors sterols [3,4], diterpenic alcohols [4], volatile components [5] and metals [6].

In the present paper the content of chlorogenic acid, caffeine, trigonelline, amino acids, polyphenols and aqueous extract have been determined in 41 samples of green coffee. By using these chemical data, principal component analysis (PCA), cluster analysis (CA) and the *K*-nearest neighbours (KNN) method have been applied to discriminate between arabica and robusta varieties.

2. Experimental

2.1. Reagents and solutions

Tannic acid (Fluka), Folin–Ciocalteu reagent (Fluka), glycine (Merck), ninhydrine (Sigma), 2-

* Corresponding author. Tel.: +34 5 455173; fax: +34 5 4557168; e-mail: agonzale@cica.es

metoxietanol (methylcellosolve) (Fluka), caffeine (Merck), chlorogenic acid (Fluka), trigonelline (Sigma) and concentrated hydrochloric acid (Merck) were of analytical grade. Methanol (Romil) of HPLC quality was also used. Milli-Q water (Millipore) was used throughout.

Glycine (0.3 g l^{-1}), tannic acid (0.1 g l^{-1}) and ninhydrine (10 g l^{-1}) in methylcellosolve with 0.03% of ascorbic acid were used. HPLC analysis was performed by using a mixture of 20:80 (v/v) methanol:water, buffered at pH 4.5 with a formate–formic acid buffer, as mobile phase. Ionic chromatography analysis was performed by using a 2 mmol l^{-1} aqueous hydrochloric acid (pH 3) as mobile phase.

2.2. Apparatus

A UV-V Phillips PU 9720 spectrophotometer equipped with 1.0 cm silica cells was used for absorption measurements. The HPLC equipment consisted of a 510 Waters HPLC pump, a Waters AGC-680 pump controller, a Rheodyne injection valve 7120 with a $20 \mu\text{l}$ sample loop, a Waters 440 UV detector operated at 254 nm and a CE Instruments DP700 integrator. A $150 \times 4 \text{ mm}$, $5 \mu\text{m}$ Lichrosorb RP-18 column was used and the flow rate of the mobile phase was 1.5 ml min^{-1} . The ion chromatographic system consisted of a 510 Waters HPLC pump, a Waters 440 absorbance detector (254 nm), a Rheodyne injector with a $100 \mu\text{l}$ loop and a Hewlett Packard HP3395 integrator. A $150 \times 3.9 \text{ mm}$, $5 \mu\text{m}$ Waters IC Pack C M/D column (silica base coated with polybutadiene-maleic acid) was used and the flow rate of the mobile phase was 1 ml min^{-1} .

2.3. Analytical procedures

Aqueous extract, total polyphenols, total free amino acids, caffeine, chlorogenic acid and trigonelline contents were carried out from assay solutions obtained by refluxing 3 g assay portions of dried sample with hot water (80°C) for 1 h. Before analysis, sample moisture was determined by drying at 103°C [7] until constant weight.

The aqueous extract was analysed by a gravimetric method according to the AOAC protocol [8].

The total polyphenols and the total free amino acids were determined by spectrophotometry using the Folin–Ciocalteu method [9] and a method based on ninhydrine [10], respectively.

Trigonelline was analysed by a single column ionic chromatography [11] with UV detection at 254 nm.

Caffeine and chlorogenic acid contents were evaluated by means of reversed-phase HPLC with UV detection at 254 nm. The procedure is a modification of previously reported works [12,13], performed at isocratic mode and using a mobile phase 20% v/v methanol/water (pH 4.5). Caffeine and chlorogenic peaks are well resolved and enable us to easy quantitation from calibration graphs based on peak heights.

The results were referred to dry base and expressed as the average weight percentage from triplicated measurements.

2.4. Coffee samples and data analysis

41 samples of green coffee, kindly provided by Kraft Jacobs Suchard, were studied. Arabica and robusta varieties from different geographic origin were included. Accordingly, they were labelled with a code. Table 1 shows the analysed samples with their origin and the assigned codes. All samples were ground, powdered and stored in polyethylene flasks.

Each green coffee sample (case) was considered as an assembly of six variables, i.e. the contents of aqueous extract (EXT), total polyphenols (POL), total free amino acids (AA), trigonelline (TRIG), chlorogenic acid (CHLOR) and caffeine (CAF) as chemical descriptors. A data matrix whose rows are the cases or samples and whose columns are the analysed variables was built as shown in Table 2.

Pattern Recognition (PR) techniques used in this paper were PCA [14], CA [15,16] and non parametric KNN [17,18]. The software packages and programs used for calculations were: CSS STATISTICA from Statsoft for performing PCA and CA. Software developed by us was used for KNN.

Table 1
Analysed green coffee samples

Variety	Origin	Code	Variety	Origin	Code
Arabica	Brazil	1A	Arabica	Salvador	22A
Arabica	Brazil	2A	Arabica	Nicaragua	23A
Robusta	Thailand	3R	Arabica	Brazil	24A
Arabica	Brazil	4A	Arabica	Brazil	25A
Robusta	Indonesia	5R	Arabica	Colombia	26A
Arabica	Salvador	6A	Robusta	Uganda	27R
Robusta	Ivory Coast	7R	Arabica	Brazil	28A
Arabica	Brazil	8A	Arabica	Brazil	29A
Arabica	Costa Rica	9A	Arabica	Nicaragua	30A
Robusta	Uganda	10R	Arabica	Brazil	31A
Arabica	Colombia	11A	Arabica	Brazil	32A
Robusta	Ivory Coast	12R	Arabica	Brazil	33A
Arabica	Honduras	13A	Arabica	Salvador	34A
Arabica	Nicaragua	14A	Arabica	Honduras	35A
Robusta	Camerun	15R	Robusta	Uganda	36R
Arabica	Guatemala	16A	Robusta	Indonesia	37R
Arabica	Colombia	17A	Arabica	Colombia	38A
Robusta	Ivory Coast	18R	Arabica	Nicaragua	39A
Robusta	Uganda	19R	Robusta	Camerun	40R
Arabica	Brazil	20A	Robusta	Vietnam	41R
Arabica	Honduras	21A			

3. Results and discussion

Before the PR analysis, the selected variables were tested for normality. In all cases, they did not follow the normal distribution according to the χ^2 criterion and the Kolmogorov test [19]. Therefore, this address us to call on non-parametric PR procedures as the best choice.

A preliminary study based on PCA and CA has been applied for a better understanding of the discriminating efficacy of the selected descriptors and, while, visualising samples trends.

3.1. PCA-based display methods

Biplots [20] are often used to observe the structure present in the data matrix. In these plots, both scores for samples (Q-mode) and scores for variables (R-mode), are represented in the space of the two principal components (PCs) obtained from PCA. Thus, relationships between samples, descriptors and between samples and descriptors can be seen on the same plot. Fig. 1 shows the biplot corresponding to our data, explaining the

57.1% of the total information. The first PC, PC1, explains 36.5% and the second, PC2, explains 10.6% of the total variance. At a glance, one can see that variables POL, CHLOR and CAF appear with similar loadings and they are the descriptors of highest contribution to PC1. So, these features happen to be the most discriminating ones and apparently, they are going to give the same kind of information. Descriptor AA has intermediate loading. Remaining variables such as EXT and TRIG have less importance since their loading is close to the zero value of PC1. On the other hand, robusta samples are situated at positive scores of PC1, except sample 40R, that appears at negative scores near to zero. Most of the arabica samples are at negative values of PC1 but there are four samples, 30A, 23A, 29A and 20A, which are at positive scores close to the robusta ones. As it can be seen, the biplot did not lead to a complete separation of the studied samples, although it enables us to assume that the descriptors with more discriminant power are POL, CHLOR and CAF. Moreover, these features appear at the right side of the plot with the robusta samples, that

Table 2
Data matrix (contents in % w/w, dry base)

Sample	EXT	POL ^a	AA ^b	TRIG	CHLOR	CAF	Sample	EXT	POL ^a	AA ^b	TRIG	CHLOR	CAF
1A	27.35	5.0	0.19	1.78	3.2	0.9	22A	24.50	7.0	0.23	1.14	3.4	1.3
2A	27.53	5.2	0.26	1.79	3.4	1.1	23A	25.97	7.5	0.26	1.10	4.0	1.2
3R	23.13	7.5	0.26	1.35	4.9	2.2	24A	24.89	5.0	0.18	1.31	2.8	1.3
4A	27.29	5.0	0.27	1.68	3.9	1.3	25A	22.08	5.0	0.15	1.41	2.7	1.3
5R	25.33	9.5	0.29	0.94	4.2	2.3	26A	23.66	4.9	0.23	1.20	3.3	1.3
6A	23.29	5.6	0.19	1.10	3.7	1.2	27R	24.50	6.8	0.25	1.14	4.2	2.2
7R	26.43	7.8	0.16	0.91	5.6	2.7	28A	25.11	4.6	0.25	1.45	4.3	1.3
8A	27.17	5.9	0.19	1.10	3.9	1.3	29A	25.11	6.4	0.23	1.45	4.8	1.4
9A	26.37	5.9	0.22	1.27	3.5	1.3	30A	23.18	6.8	0.26	1.00	5.0	1.4
10R	27.41	8.2	0.22	0.96	4.6	2.4	31A	27.21	7.5	0.24	1.39	3.4	1.2
11A	25.61	5.2	0.17	1.04	4.1	1.2	32A	24.13	5.5	0.23	1.51	3.3	1.1
12R	27.41	8.4	0.24	1.72	4.7	2.8	33A	29.54	5.5	0.24	1.42	3.1	1.1
13A	24.18	6.1	0.19	1.12	3.7	1.1	34A	26.61	4.4	0.19	1.26	3.2	1.3
14A	22.08	6.4	0.26	1.19	3.4	1.0	35A	23.08	5.1	0.20	1.18	3.6	1.4
15R	23.18	7.4	0.21	1.61	3.8	2.4	36R	25.50	6.0	0.18	1.11	3.8	2.3
16A	24.18	7.2	0.15	1.66	3.7	1.1	37R	23.86	8.2	0.26	1.24	3.8	2.2
17A	28.83	8.2	0.18	1.92	3.7	1.1	38A	22.03	6.2	0.20	1.28	3.3	1.1
18R	24.78	7.8	0.22	1.94	4.6	2.7	39A	20.93	6.6	0.24	1.24	3.4	1.0
19R	24.78	7.0	0.25	1.83	4.7	3.2	40R	22.42	8.1	0.16	1.10	3.3	1.7
20A	28.26	5.8	0.26	1.21	3.9	1.8	41R	27.47	8.1	0.17	1.30	3.6	1.6
21A	28.90	5.7	0.25	1.14	3.1	1.2							

^a Expressed as tannic acid.

^b Expressed as glycine.

present higher contents of the mentioned descriptors.

In order to obtain a good separation of the coffee samples, a hierarchical agglomerative CA of samples was done.

3.2. Cluster analysis

In spite of the a priori knowledge of the class membership of the coffee samples, CA has been carried out to find the natural grouping of the data trend. According to PCA, the most discriminating features are POL, CHLOR and CAF. They appeared with similar loadings, so it can be thought that these variables will provide similar information. Besides, from a non-parametric correlation study, the most correlated variable pairs according to the Spearman criterion are: CHLOR/CAF, POL/CHLOR and POL/CAF. Consequently, we have applied CA selecting only one of these three descriptors, CAF, together with AA, that appeared with intermediate loading.

Taking the Euclidean distance as a basis and the Ward's method as amalgamation rule [21], two clusters were obtained. Fig. 2 shows the corresponding dendrogram, where all arabica samples are grouped in one cluster and the rest of the cases, robusta samples, are forming a different cluster. Only cases 40R and 41R appear in the opposite group, but in the borderline between both clusters.

3.3. K-nearest neighbours

Aside from the results obtained by the display methods and CA, we have applied a supervised-learning PR technique, the KNN classification. KNN is a non-parametric classification procedure recommended when the descriptors do not follow the normal distribution. The validation procedure for evaluating the classification performance was the leave-one-out method [22]. The selected variables were AA and CAF. The results obtained as percentage of hits, against different *K* values, are

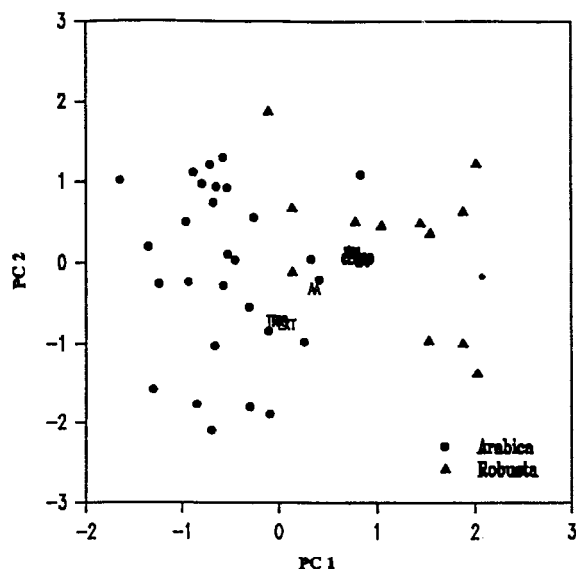


Fig. 1. PCA biplot for the first PCs.

presented in Table 3. As one can see, KNN leads to fairly good performances of classification. However, some samples are badly classified occasionally (40R, 41R for $K \geq 3$) or always (20A).

To assess that the performance cannot be improved by adding other descriptors, the KNN procedure was repeated using the following sets of

Table 3
Percentage of hits in the classification performance^a of coffees versus the number of K neighbours selected

K	% hits	Conflicts
1	97.6	Sample 20A is badly classified
2	97.6	
3	92.7	Samples 20A, 40R and 41R are badly classified
4	92.7	
5	92.7	

^a According to the leave-one-out method and using AA and CAF as descriptors.

non-correlated variables: {AA, CAF, EXT}, {AA, CAF, TRIG} and {AA, CAF, EXT, TRIG}. In all cases, similar results were obtained. This seems to emphasise that, in fact, the most discriminant descriptors are AA and CAF indeed. On the other hand, samples 20A, 40R and 41R exhibit some outlying features. Case 20A belongs to the arabica variety but presents a high content of caffeine, 1.8%, and samples 40R and 41R are robusta coffees with a very low content of caffeine, 1.7 and 1.6%, respectively.

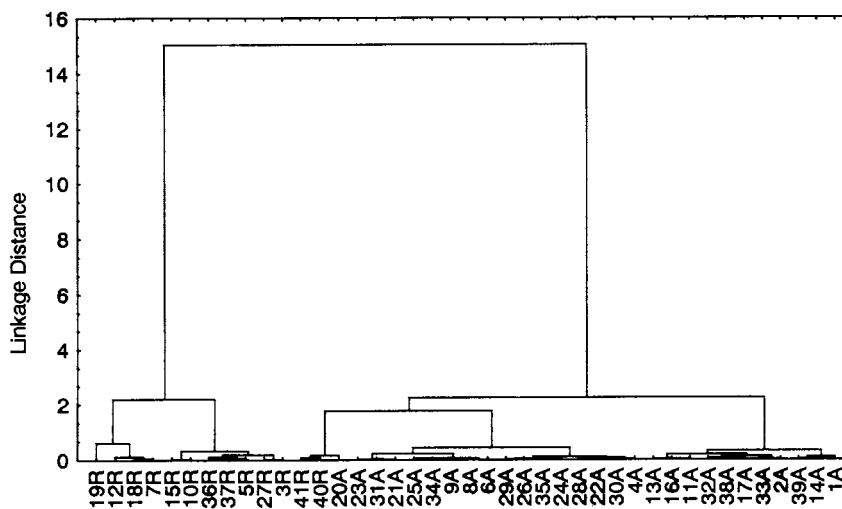


Fig. 2. Dendrogram of coffee samples by using CAF and AA variables.

4. Conclusion

After applying PR methods, with the exception of three outliers, green coffee varieties (arabica and robusta) can be easily differentiated according to their contents in caffeine and total free amino acids.

References

- [1] R.J. Clarke, R. Macrae (Eds.), *Coffee*, vol. 1, Elsevier, London, 1985.
- [2] J.R. Piggot (Ed.), *Statistical Procedures in Food Research*, Elsevier, London, 1986.
- [3] G. Lercker, N. Frega, F. Bocci, M.T. Rodriguez-Estrada, *Chromatographia* 41 (1995) 29.
- [4] N. Frega, F. Bocci, G. Lercker, *J. High Resolut. Chromatogr.* 17 (1994) 303.
- [5] A. Murota, *Biosci. Biotechnol. Biochem.* 57 (1993) 1043.
- [6] V. Krivan, P. Barth, A. Feria-Morales, *Mikrochim. Acta* 110 (1993) 217.
- [7] International Organization of Standardization ISO 11294, 1994.
- [8] Official Methods of Analysis of AOAC, 15th edn., Vol. 2, AOAC, Arlington, 1990.
- [9] V.L. Singleton, P. Esau, *Phenolic Substances in Grapes and Wines and their Significances*, Adv. Food Res., Suppl. 1, Academic Press, New York, 1969.
- [10] S. Moore, W.H. Stein, *J. Biol. Chem.* 176 (1955) 357.
- [11] M.J. Martín, F. Pablos, M.A. Bello, A.G. González, *Fresenius J. Anal. Chem.* 357 (1997) 357.
- [12] L.C. Trugo, R. Macrae, *Analyst* 109 (1984) 263.
- [13] L.C. Trugo, R. Macrae, *Food Chemistry* 15 (1984) 219.
- [14] C. Chatfield, A.J. Collins, *Introduction to Multivariate Analysis*, Chapman and Hall, London, 1980.
- [15] D.L. Massart, L. Kaufman, *Interpretation of Analytical Data by use of Cluster Analysis*, Wiley, New York, 1983.
- [16] B. Everitt, *Cluster Analysis*, Halsted (Wiley), New York, 1983.
- [17] D.L. Massart, A. Dijkstra, L. Kaufman, *Evaluation and Optimization of Laboratory Methods and Analytical Procedures*, Elsevier, Amsterdam, 1978.
- [18] A.M. Harper, D.L. Duewer, B.R. Kowalski, J.L. Fasching, ARTHUR and experimental data analysis. The heuristic use of a polyalgorithm, in: R.F. Gould (Ed.) *Chemometrics: Theory and Application*, Washington, 1981, p. 14.
- [19] W.J. Conover, *Practical Non-parametric Statistics*, Wiley, New York, 1971.
- [20] M. Meloun, J. Militky, M. Forina, *Chemometrics for Analytical Chemistry*, Ellis Horwood, New York, 1992.
- [21] J.H. Ward, *J. Am. Stat. Ass.* 58 (1963) 236.
- [22] A.J. Stuper, P.C. Jurs, *J. Pharm. Sci.* 67 (1978) 745.

Screening of antimony in PVC by solid sampling-graphite furnace atomic absorption spectrometry

Miguel A. Belarra *, Iñigo Belategui, Isela Lavilla, Jesús M. Anzano, Juan R. Castillo

Department of Analytical Chemistry, University of Zaragoza, E-50009, Zaragoza, Spain

Received 18 June 1997; received in revised form 24 October 1997; accepted 7 November 1997

Abstract

The development of two-stage control systems is of great interest when a large number of samples are analysed in order to check that they fulfil certain requirements. If the first stage is carried out using an inexpensive method with a high throughput which makes it possible to filter out the majority of the samples that fulfil the requirements, the procedure is not only less time-consuming but also more economical. Direct determination of metals in solid samples by graphite furnace atomic absorption spectrometry (GFAAS) appears, in principle, to be a suitable analytical technique for screening purposes since it provides sufficiently reliable results in a reasonably short time. In this paper it is applied with satisfactory results to antimony content control in a PVC sample. © 1998 Elsevier Science B.V. All rights reserved.

Keywords: Direct analysis; Solid samples; Antimony screening; Graphite-furnace atomic absorption spectrometry

1. Introduction

In the development of inspection or control procedures a number of factors which are not merely analytical (sensitivity, precision etc.) are increasingly important, such as expeditiousness, cost-effectiveness or personnel safety and comfort [1] and so the choice of an analytical method for a given purpose is not currently always dictated by accuracy but in many cases by throughput,

economic considerations and various other factors.

In many practical situations a large number of samples have to be analysed and what is important is not so much the exact content of the analyte but to determine whether it is higher or lower than a certain value. In these cases, a two-stage control system is recommendable from an economic viewpoint, with investigation of the samples in the first stage by an inexpensive method with a high throughput to filter out the majority of samples which fulfil the requirements [2].

The first analytical procedure is usually a screening method characterised by a high sample

* Corresponding author. Tel.: + 34 76 761175; fax: + 34 76 761292.

throughput, which enables a large number of samples to be sifted [3]. Screening methods based on immunochemical techniques are numerous [4] and are also used for the control of organic compounds, usually by chromatographic methods [5]. Their use in inorganic analysis, however, is far more limited [6].

Graphite furnace atomic absorption spectrometry (GFAAS) for direct determination of metals in solid samples [7] is, in principle, a suitable analytical technique for screening purposes as it provides sufficiently reliable results in a relatively short time, thus fulfilling the typical requirements of chemical analysis for industrial product control [8]. With this technique a result can be obtained in about 15 min and although the RSD values may well be higher than 10% [9], they can be kept within a range of 5–10% by correct control of the operating conditions. Although some papers pointed out that these characteristics meet the demands of those of a screening method [10,11] we have not found in the literature any practical application of the direct determination of metals from solid samples by GFAAS for screening purposes.

In order to obtain quick results the calibration should be carried out using aqueous solutions and too much time should not be spent on the preparation of the sample (homogenisation), although this could have a negative effect on precision [12].

In this paper we report the control of the concentration of antimony, used as a flame retardant to delay the initiation and burning in the production of polyvinyl chloride (PVC). The confirmatory technique may be flame-AAS after dissolution of the sample [13]. The minimum concentration of the product in this case should be 2.5%. Although this antimony content in the PVC is fairly high, which usually complicates the direct determination of metals in solid samples by GFAAS, [14,15] this sample was chosen because it is well known and so as to be able to compare the results with those obtained with a similar magnesium content in another PVC sample which had been previously homogenised [16].

2. Experimental

2.1. Reagents and sample

2.1.1. Antimony standard

1000 $\mu\text{g ml}^{-1}$, 2.74 g of potassium antimonyl tartrate hemihydrate were dissolved in water and diluted to 1 l with redistilled water.

2.1.2. Poly(vinyl chloride) resin and real sample

A commercially available PVC sample with an antimony content provided by the manufacturer of ca. 2.6% was used.

All solutions were prepared with analytical reagents and redistilled water and were stored in polyethylene vessels. Further dilutions of these elements were prepared from the standard solutions immediately prior to use.

2.2. Instrumentation

A Perkin–Elmer Model 3030 atomic absorption spectrometer was used together with a Perkin–Elmer HGA-400 graphite furnace furnished with a temperature programmer and an autosampler (Perkin–Elmer AS40) for liquid samples. The hollow-cathode lamp employed was purchased from Instrumentation Laboratory. Pyrolytic-coated graphite tubes with a platform were used; their dosing hole was mechanically enlarged to a diameter of about 4 mm.

Solutions and real samples were atomised electrothermally and the atomic absorption (integrated absorbance) of antimony was measured under the operating conditions summarised in Table 1.

Flame-AAS measurements were made on a Perkin–Elmer Model 2380 atomic absorption spectrometer.

2.3. Procedure for flame AAS

The procedures used to treat PVC samples and to determine antimony by flame-AAS are described in detail elsewhere [13].

Table 1
Instrumental parameters

Wavelength (nm)	211.4			
Lamp current (mA)	20			
Background correction	No			
Slit width (nm)	0.7			
Gas flow rate (ml min ⁻¹)	300			
Working range (µg)	0–120			
Injection volume (µl)	20			
Sample mass (mg)	1.5–4.0			
Step	Drying ^a	Pyrolysis	Atomization ^b	Cleaning
Temperature (°C)	120	800	2000	2700
Ramp (s)	20	6	0	1
Hold time (s)	30	30	1	3

^a Only for antimony solutions.

^b Without stop-flow.

Table 2
Study of wavelength suitability

Wavelength (nm)	Mass range (µg)	Slope of the calibration curve (s µg ⁻¹)	Adequate for antimony content ^a (%)	RSD _{x_o} ^b (%)
206.8	0–0.5	4.5	0.01	
211.4 ^c	0–120	0.0008	3	6.3 ± 0.5
212.7 ^c	0–40	0.008	1	
217.6	0–0.2	2.8	0.005	
231.2	0–0.5	2.7	0.01	

^a By placing ca. 3 mg of sample into the atomizer

^b Calculated as in ref. [20] (*n* = 4).

^c Without stop-flow in atomization step.

2.4. Procedure for the solid sampling technique

Small pieces of roughly the required mass of the PVC sample were cut off using stainless steel scissors while the plastic was handled with stainless steel pincers. The PVC pieces were weighed to within 1×10^{-5} g. Samples of 1.5–4 mg were used in different experiments.

Calibration graphs were run using aqueous solutions of antimony with the amounts given in Table 1. Each measurement was carried out three times.

An amount of ca. 2.5–3.5 mg solid PVC sample was introduced directly into a pyrolytic graphite tube through an inverted paper cone with its apex pierced and this was inserted into the enlarged

hole of the tube [16]. The antimony content of the sample was calculated as the median of five results obtained by interpolation on the pertinent calibration graph.

3. Results and discussion

3.1. Simplification of the procedure

The advantage of obtaining quick results due to the non-dissolution of the sample is lost to a considerable extent if the sample needs to be homogenised. Although in a recent work [17] we have proved that the non-homogeneity of the subsamples used is the principal cause of the poor

precision of the technique and so, atomisation in non-optimum conditions or possible changes in the deposition of the samples in the atomiser are hardly significant, the homogenisation process of the PVC was eliminated in order to give priority to obtaining quick results. Furthermore, the use of the median minimised the influence of possible anomalous results [18]. If the results obtained in the determinations of antimony (see median in Table 3) and magnesium [16] (for which the sample was homogenised) are compared, no significant differences can be seen with regard to precision.

Although the effect of the drying step on the time needed to carry out the measurements is considerably less than the influence of sample homogenisation, this step was omitted in the atomisation of the solid samples.

3.2. Solid sampling-GFAAS optimisation

The rapid determination of metals using GFAAS by direct atomisation of the solid samples poses three problems of a general nature: (1) adapting the sensitivity of the technique to the analyte content of the sample; (2) establishing the conditions for carrying out the calibration using aqueous solutions; and (3) establishing the range of sample mass which provides correct results.

Given the high antimony content in the sample, the lines proposed for the determination of the antimony by GFAAS [19] are too sensitive (see

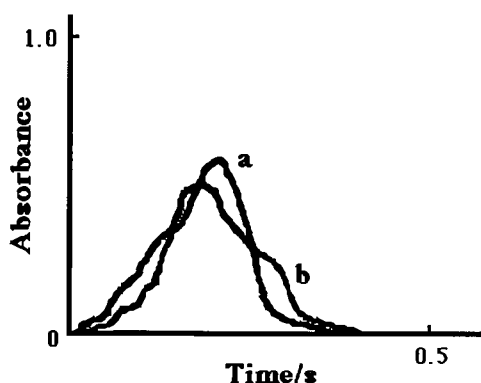


Fig. 1. Typical peaks for antimony: (a) 80 μg of Sb in water; and (b) 3.3 mg of PVC sample (82 μg of Sb).

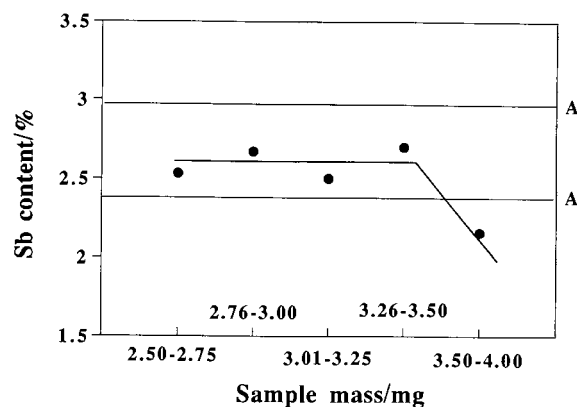


Fig. 2. Relationship between the antimony content found and the amount of sample used. (A) Average value $\pm 10\%$; (●) median of ten results.

Table 2). The line of 211.4 nm was therefore used and even with this wavelength it was necessary to maintain the gas flow during the atomisation step. Judging by the results obtained for tin [20], these non STPF working conditions should not cause a notable increase in imprecision, providing atomisation takes place from a platform. This is confirmed by the RSD_{x_0} value (6.3 ± 0.5 ; $n = 4$) which is similar to that of the least sensitive lines of tin [20].

In order to carry out the calibration using aqueous solutions, most of the matrix must be eliminated during the pyrolysis step. From previous work with PVC it was known that this elimination takes place at temperatures higher than 700–800°C [16,18], so a temperature of 800°C was used directly. The great similarity between the signals obtained with a solid sample and those obtained with an aqueous solution can be seen in Fig. 1. It can also be observed that no non-specific absorption is produced. The integration time was reduced to 0.5 s as marked instrumental noise appeared after 1 s because of d.c. emission from the tube.

With regard to the dependence of the results obtained on the amount of sample used, it was necessary to make a specific study as this dependence cannot be deduced from previous data [21]. By means of 60 measurements using masses of 1.5–4 mg, it was concluded that results which are

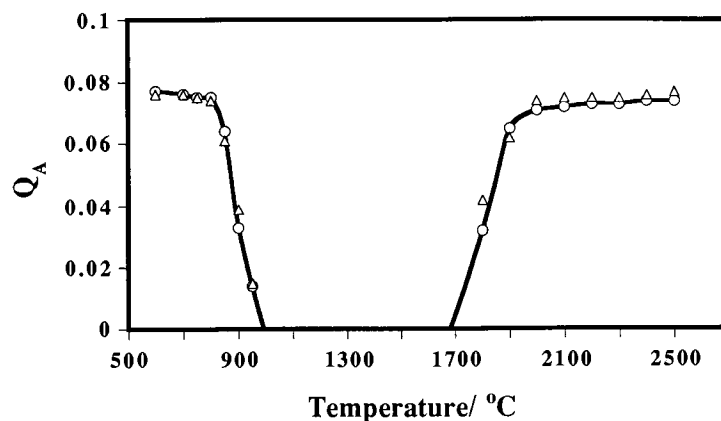


Fig. 3. Optimization of pyrolysis and atomisation temperature: (○) Sb in water; (△) Sb with PVC resin.

Table 3
Results for the determination of antimony in the PVC sample

Parameter	Solid sample		Solution
	Average value	Median	
No. of determinations	14	14	6
Average value (g per 100 g)	2.63	2.64	2.64
Range (g per 100 g)	2.04–3.34	2.37–3.03	2.53–2.82
Standard deviation (g per 100 g)	0.33	0.17	0.13
RSD (%)	12.6	6.4	4.8

$F = 1.79$.

$t = 0.015$.

in agreement with those provided by Flame-AAS can only be obtained in a range of 2.5–3.5 mg as can be seen in Fig. 2. Sample amounts greater than 3.5 mg lead to overestimated results while by using less than 2.5 mg the results obtained are very scattered.

3.3. Temperature programme-GFAAS optimisation

Apart from the problems of a general nature previously mentioned, each determination may pose specific problems. Although Frech et al. [22] report that antimony is stable up to 900°C, in the case under study there may well be antimony losses as $SbCl_3$ due to the high chloride content in the sample [23]. However, as can be seen in Fig. 3, the pyrolysis and atomisation curves of antimony

in the absence and in the presence of the PVC matrix are practically identical and no loss of antimony is observed below 800°C. Dahl et al. had previously reported that in the presence of chlorides antimony was more stable in some complex samples than in aqueous solution [24].

3.4. Screening of antimony

Over a 2-week period 14 determinations of antimony were carried out on seven different days. The result of each determination was taken as the median of five consecutive measurements carried out with a sample mass of 2.5–3.5 mg. The average of the 70 measurements carried out confirmed that the method has no systematic error (2.63% of antimony as an average value) and imprecision is high (RSD = 23.2%), although, ow-

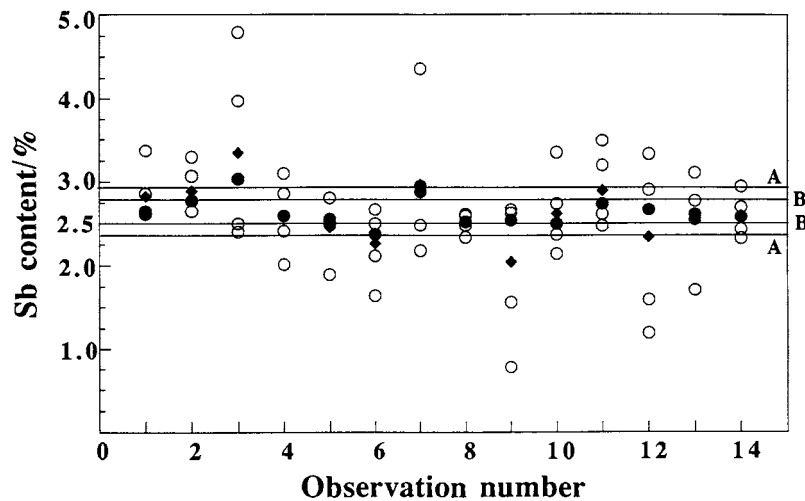


Fig. 4. Control chart for antimony screening (c.a. 2.6%): (A) Average value $\pm 10\%$; (B) Average value $\pm 5\%$; (○) Individual results; (●) Median; (◆) Average value.

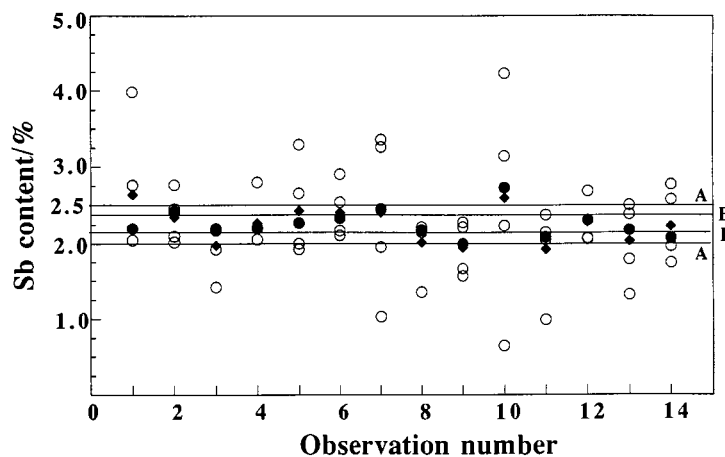


Fig. 5. Control chart for antimony screening (c.a. 2.25%): (A) Average value $\pm 10\%$; (B) Average value $\pm 5\%$; (○) Individual results; (●) Median; (◆) Average value.

ing to the large number of measurements, the confidence interval at a confidence level of 95% is small (2.49–2.78% of antimony). The proposed method has good reproducibility, as the ANOVA showed that there are no statistically significant differences at a confidence level of 95% between the results obtained on the seven days ($F = 1.62$; $p = 0.16$).

The results of the 14 determinations, taken as the mean and the median of the five replicates carried out in each case, are gathered in Table 3. The results are compared with those obtained

after aqueous dissolution of the sample. When either the mean or the median is used, the mean value is practically the same as that obtained after sample dissolution. However, as happened in the determination of cadmium [18], the median reduces the influence of anomalous results, so that the RSD is half the RSD obtained when the mean is used and is comparable to that obtained after sample dissolution.

Unfortunately, this RSD value cannot be extrapolated to all the series. If we observe the results gathered in Fig. 4 as a whole, it can be

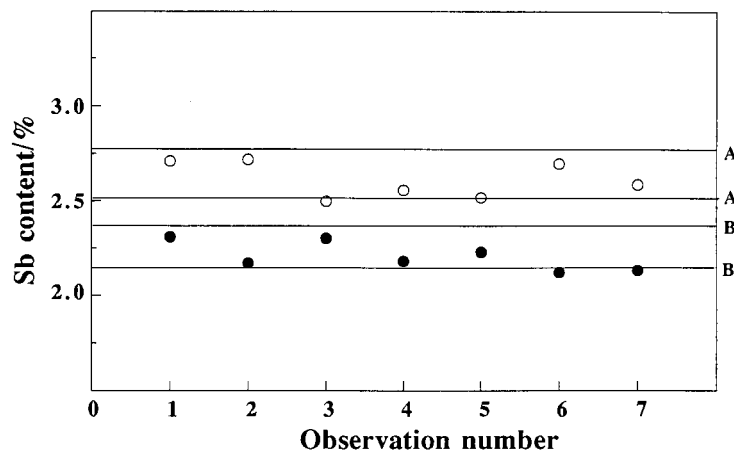


Fig. 6. Control chart for antimony screening (ten measurements): (A) Average value $\pm 5\%$ for the sample with a Sb content of c.a. 2.6%; (B) Average value $\pm 5\%$ for the sample with a Sb content of c.a. 2.25%; (○) Median for the sample with a Sb content of c.a. 2.6%; (●) Median for the sample with a Sb content of c.a. 2.25%.

seen that they are highly dispersed and each series displays a different behaviour from the others, with RSD values ranging from 5% in series 8 to 40% in series 9 and an average value of 20%. Despite this dispersion, the method carries out the screening task satisfactorily as only one (series 6) of the 14 controls has a value of antimony lower than 2.50%. Once again, the results obtained with the mean are worse: four series are lower than the reference value. The same conclusions can be reached more rapidly without carrying out a calibration curve. It is sufficient to compare the specific absorption ($3 * Q_A/\text{sample mass}$) of each measurement with that of a solution containing 75 μg of antimony (equivalent to 2.5% in 3 mg of the sample) measured three times.

The usefulness of a screening method depends on the characteristics of the method and the margin of tolerance accepted, which is understood as the difference between the real value and the maximum or minimum tolerated value (in this case c.a. 5%). The best way of generalising the benefits of this method is to evaluate the results on the basis of the frequency of their deviation above the mean value, which will also indicate whether there are false negatives [3]. With this method, if only the median is used,

ten of the 14 results are within the range of $\pm 5\%$, another two within the $\pm 10\%$ range, and only two are outside this interval. One of them is a false positive result and the other a false negative result. If a margin of error of $\pm 10\%$ is considered reasonable for these screening methods, the efficiency of the proposed method can be considered satisfactory. Although to obtain a result is necessary to carry out five measurements, the process is accomplished in less than 10 min and therefore is adequate for a screening purpose.

To check the former conclusions another sample of PVC with a content of ca. 2.25% in antimony (10% lower than the critical value) was subjected to the same control process. Results are shown in Fig. 5 and corroborate the performance of the method. Again only one (series 10) of the 14 controls has a value of antimony higher than 2.50%.

Naturally, the performance of the method improves if the number of replicates is increased, although this is logically more time-consuming. If, for example, the median of the ten replicates measured daily is taken as a result, all the results are within the interval of $\pm 10\%$ and only three lies outside the $\pm 5\%$ interval (see Fig. 6).

4. Conclusions

Atomic absorption spectrometry with direct atomisation of solid samples is efficient as the first stage in two-stage analysis design. It enables us to rapidly filter out a significant number of samples, which would otherwise need more careful determination, provided the tolerance limit is approximately 10%. Its application to the content control of antimony in a PVC sample is satisfactory.

As the method requires a previous study of the atomisation conditions in order to be able to calibrate using aqueous solutions and to determine the amount of sample to be used, the process is not suitable if only a small number of samples are to be analysed. However, it is highly profitable for routine control over a long period of time.

Acknowledgements

This work was financially supported by the Dirección General de Investigación Científica y Técnica (DGICYT) of the Spanish Ministry of Education and Science, in the framework of Project PB96/0720

References

- [1] M. Valcárcel, A. Ríos, *Anal. Chem.* 65 (1993) 781A.
- [2] W.G. de Ruig, F.A. Huf, A.A.M. Jansen, *Analyst* 117

- (1992) 425.
- [3] Draft Commission Decision, *Off. J. Eur. Comm.* L118 (1993) 64.
- [4] B. Hock, A. Dankwardt, K. Kramer, A. Marx, *Anal. Chim. Acta* 311 (1995) 393.
- [5] S. Butz, H.-J. Stan, *Anal. Chem.* 67 (1995) 620.
- [6] Z.H. Chohan, A.I. Shah, *Analyst* 117 (1992) 1379.
- [7] C. Bendicho, M.T.C. de Loos-Vollebregt, *J. Anal. At. Spectrom.* 6 (1991) 353.
- [8] P. Esser, *Fresenius Z. Anal. Chem.* 328 (1987) 410.
- [9] F.J. Langmyhr, G. Wibetoe, *Prog. Anal. At. Spectrosc.* 8 (1985) 193.
- [10] U. Völlkopf, Z. Grobowski, R. Tamm, B. Welz, *Analyst* 110 (1985) 573.
- [11] R.E. Sturgeon, *Spectrochim. Acta B* 44 (1989) 1209.
- [12] N.J. Miller-Ihli, *Anal. Chem.* 64 (1992) 964A.
- [13] M.A. Belarra, F. Gallarta, J.M. Anzano, J.R. Castillo, *J. Anal. At. Spectrom.* 1 (1986) 141.
- [14] G.R. Carnrick, B.K. Lumas, W.B. Barnett, *J. Anal. At. Spectrom.* 1 (1986) 443.
- [15] D.C. Baxter, W. Frech, *Fresenius J. Anal. Chem.* 337 (1990) 253.
- [16] M.A. Belarra, I. Lavilla, J.R. Castillo, *Anal. Sci.* 11 (1995) 651.
- [17] M.A. Belarra, M. Resano, J.R. Castillo, *J. Anal. At. Spectrom.*, 1998, in press.
- [18] M.A. Belarra, I. Lavilla, J.R. Castillo, *Analyst* 120 (1995) 2813.
- [19] M.L. Parsons, B.W. Smith, G.E. Bentley, *Handbook of Flame Spectroscopy*, Plenum Press, New York, 1975.
- [20] M.A. Belarra, M. Resano, J.R. Castillo, *Spectrochim. Acta B* 52 (1997) 1223.
- [21] M.A. Belarra, C. Crespo, M.P. Martínez-Garbayo, J.R. Castillo, *Spectrochim. Acta B*, 52 (1997) 1855.
- [22] W. Frech, E. Lundberg, A. Cedergren, *Prog. Anal. At. Spectrosc.* 8 (1985) 257.
- [23] B. Welz, S. Akman, G. Schlemmer, *Analyst* 110 (1985) 459.
- [24] K. Dahl, Y. Thomassen, I. Martinsen, B. Rudziuk, B. Salbu, *J. Anal. At. Spectrom.* 9 (1994) 1.

Preparation and chemical characterization of high purity fluorapatite

R. Fábrián^a, I. Kotsis^{a,*}, P. Zimány^a, P. Halmos^b

^a Department of Silicate and Materials Engineering, University of Veszprém, POB 158, Egyetem u.10., Veszprém, H-8201, Hungary

^b Department of Analytical Chemistry, Research Group for Anal. Chem. of Hungarian Academy of Sciences, University of Veszprém, POB 158, Egyetem u.10., Veszprém, H-8201, Hungary

Received 25 June 1997; received in revised form 5 November 1997; accepted 7 November 1997

Abstract

High purity fluorapatite (FAP) was prepared by solid state reaction, in flowing argon gas, at 1370°C for 60 min. For chemical characterization of $\text{Ca}_{10}(\text{PO}_4)_6\text{F}_2$, the accuracy and reproducibility of different analytical methods were assessed. Methods with a good accuracy for the determination of Ca, P and F content were: titrations with EDTA for Ca determination (accuracy: -0.8%), spectrophotometric method for P determination (accuracy: $+0.6\%$) and measurements with fluoride-selective electrode (accuracy $+5.4\%$) for F determination. © 1998 Elsevier Science B.V. All rights reserved.

Keywords: Fluorapatite; Preparation; Chemical characterization

1. Introduction

Synthetic fluorapatites are important materials for different applications like: preparation of phosphor for fluorescent lamps, laser host for neodymium, biocompatible materials. They are also used as humidity sensors, ion exchangers and dispersive additives for suspension polymer polymerization. For all these applications high purity fluorapatite is needed. This requirement can be assured by a well controlled preparation method and a sound and secure quality controlling of the final product. It is known that stoichiometric

apatite powders with high crystallinity could be prepared by solid state reaction by heating a mixture of $\text{Ca}_3(\text{PO}_4)_2$ and CaF_2 of 1:3 molar ratio at temperatures between 1100 and 1370°C and the reaction times could be about 1 for 4 h [1,2]. There is no data in the literature for optimal heat treating procedure (heat treating temperature and heat treating time). On the other hand, for the quality controlling of these materials is important to identify the most adequate analytical methods for their chemical characterization. Different authors refer to different methods, but the various methods used for determination of Ca, P and F content differ in their accuracy and precision, which depends strongly on the nature of analyzed samples. The aim of present study is to demon-

* Corresponding author. Tel.: +36 88 423091; fax: +36 88 423091; e-mail: kts040@almos.vein.hu

strate a solid state preparation method of good reproducibility and to compare, based on statistical calculations, the different analytical methods for each element, in terms of their accuracy and precision.

2. Experimental

2.1. Preparation

$\text{Ca}_{10}(\text{PO}_4)_6\text{F}_2$ (fluorapatite) was prepared by solid state reaction, by heating a stoichiometric (3:1 molar ratio) mixture of $\text{Ca}_3(\text{PO}_4)_2$ (Merck, 96.2% purity) and CaF_2 (Merck, 99.2% purity), in the presence of some CaF_2 upstream, to minimize volatilization of fluorine (as CaF_2) from the reaction mixture. Homogenization of raw materials was made using ethanol (abs. alcohol). The mixture of raw materials was heated at five different temperatures (1000, 1100, 1200, 1300, 1370°C) for two different heat treating times (30, 60 min). The furnace was first rinsed with H_2O - and CO_2 -free Ar gas (99.998%) and than a flush rate of 20 l h^{-1} of Ar was maintained during the heat treatment. Water-free character of the heating atmosphere was checked by scrubbing the gas leaving the furnace in P_2O_5 and by detecting the mass increase (if any) after the heating period. Prevention of CO_2 contamination was done by flowing the Ar gas through a KOH trap. Mineralogical composition of the samples was determined with a Philips PW 1825 type X-ray diffractometer. For identification of samples the following designations were made: FAP, T (°C), t (min), where FAP is fluorapatite.

2.2. Chemical analyses

2.2.1. Determination of Ca content

The calcium content of samples was determined by two different methods: by ICP [3] and by EDTA-titration in the presence of Fluorexon indicator [4]. Stock solutions were prepared as follows: the samples (approx. 0.1 g) were dissolved in 10 ml 1:1 HNO_3 solution and than were diluted to 100 ml (for ICP) and to 500 ml (for EDTA titrations). The measurements were carried out at

Table 1

Ca% (wt) content of the samples determined by ICP method at 317.993 nm

Sample	Ca% (wt)
FAP,1100,60	39.0 ± 0.6
FAP,1200,60	39.1 ± 0.7
FAP,1370,60	38.3 ± 0.7
FAP,1370,30	38.7 ± 0.7

317.993 nm, with an ARL 3410 MINITORCH type ICP.

2.2.2. Determination of P content

Two different methods were used for the determinations: ICP [3] and spectrophotometric method [5]. ICP measurements were carried out at 213.618 nm, with an ARL 3410 MINITORCH type ICP. The reagents used for spectrophotometric determinations were as follows:

1. 0.25% NH_4VO_3 pur. spec. solution
2. 5% $(\text{NH}_4)_6\text{Mo}_7\text{O}_{21} \cdot 4\text{H}_2\text{O}$ pur. spec. solution
3. 1:1 HNO_3 a.r. solution
4. 1 mg ml^{-1} KH_2PO_4 pur. spec. stock solution

The stock solutions were prepared as follows: the samples (approx. 0.07 g) were dissolved in 10 ml 1:1 HNO_3 solution and than the volume of solutions were adjusted to 200 ml. Measurements were done at 400 nm with a LAMBDA 20 UV/VIS, Perkin Elmer type spectrophotometer.

Table 2

Ca% (wt) content of the samples determined by EDTA titration in the presence of Fluorexon indicator

Sample	Ca% (wt)
FAP,1000,60	39.5 ± 0.4
FAP,1100,60	39.2 ± 0.7
FAP,1200,60	39.1 ± 0.4
FAP,1300,60	39.1 ± 0.4
FAP,1370,60	38.1 ± 0.4
FAP,1370,30	38.9 ± 0.7

Table 3

F-test for comparison between standard deviations of determinations of Ca, P content by two different methods

Samples	<i>F</i> -test for comparison between standard deviations of determinations of Ca content by ICP and EDTA titrations		<i>F</i> -test for comparison between standard deviations of determinations of P content by ICP and spectrophotometric method	
	<i>F</i> (95)	<i>F</i> _{calculated}	<i>F</i> (95)	<i>F</i> _{calculated}
FAP,1100,60	19.00	1.36	19.00	1.27
FAP,1200,60	19.00	3.06	19.00	1.30
FAP,1370,60	19.25	1.30	19.25	5.23
FAP,1370,30	19.00	1.00	19.00	1.27

2.2.3. Determination of *F* content

The methods used for fluoride determination were as follows:

1. Pyrohydrolytic method (distillation at 1000°C in the presence of Al₂O₃) [6]
2. Distillation with conc. H₂SO₄ (water vapor distillation at 165 ± 2°C) [7]. In both cases the fluoride content of the condensate was measured by thorium nitrate titration [8].
3. By ionchromatographic method [9]. The samples were dissolved in 4 ml 10% H₂SO₄ solution at 50°C. Ionchromatographic determinations were done with a DIONEX (DX 1000) ionchromatograph, using Na₂CO₃/NaHCO₃ eluent and AS9 column.
4. With fluoride selective electrode [10]. The samples (approx. 0.1 g) were dissolved in 10 ml 1:1 HNO₃ solution. The solutions were adjusted to pH = 5–6 using 1:1 NaOH solution, than 100 ml of TISAB was added and diluted to 500 ml.

According to some authors [11] the use of TISAB as buffer in fluoride determinations leads to an apparently lower result than by other methods. The use of citrate–hydrochloric acid buffer appears to avoid the fluoride loss that occurs with TISAB. The measurements were carried out using citrate–hydrochloric acid buffer too, but no differences were observed in the results. The pF values were obtained with the help of an OP-F-07 fluoride-selective electrode connected to a pH/ion Analyser OP-271 Radelkis. The reference electrode was a double-junction silver/silver chloride OP-0820P electrode (Radelkis).

3. Results and discussion

The following results were calculated based on 3–5 parallel measurements. The confidence intervals were determined considering a 95% confidence level and the convenient values of standard deviations and Student's *t*-test. The different analytical methods were compared based on *t*-test. The normal distribution of the results was supposed. Comparison of the standard deviations was done using *F*-test.

3.1. Ca determination

The theoretical value of calcium content was found to be 38.4% (wt), which value was calculated considering the purity of raw materials. Determination of Ca and P content of apatites by ICP is a routine method. The accuracy of this method is already mentioned in the literature to be ± 1–3% both for the Ca and the P determination [3]. However, for evaluation of the method's reproducibility and comparison with other methods, parallel measurements were necessary (Table 1).

Using EDTA titration method for Ca determination was mentioned in the literature [12], but no data for accuracy were available. To estimate the accuracy of the method, determination of the Ca content of a standard sample was needed. Selection of the most relevant standard was troublesome. It was necessary to find a standard sample containing all the elements which were present in the analyzed samples and having the same dissolution properties in 1:1 HNO₃ solution. Because

Table 4
t-test for comparison between determinations of Ca, P content by two different methods

Samples	<i>t</i> -test for comparison between determinations of Ca content by ICP and EDTA titrations		<i>t</i> -test for comparison between determinations of P content by ICP and spectrophotometric method	
	<i>t</i> (95)	<i>t</i> _{calculated}	<i>t</i> (95)	<i>t</i> _{calculated}
FAP,1100,60	2.776	0.931	2.776	2.501
FAP,1200,60	2.776	0.000	2.776	2.430
FAP,1370,60	2.447	0.884	2.447	0.000
FAP,1370,30	2.776	0.873	2.776	0.364

of the different dissolution properties, the stoichiometric mixture of the raw materials was ruled out. The same problem was faced also with $\text{Ca}_3(\text{PO}_4)_2$. In both cases the measured values of Ca and P contents were lower than the theoretical values. Based on the X-ray diffractograms of the samples prepared at different heating temperatures, unit cell parameters were calculated [13]. Unit cell parameters of sample FAP, 1000, 60 were found to be $a = 9.35 \pm 0.00296 \text{ \AA}$, $c = 6.86 \pm 0.00267 \text{ \AA}$, whereas those of the sample FAP, 1370, 60 were $a = 9.36 \pm 0.00243 \text{ \AA}$, $c = 6.87 \pm 0.0022 \text{ \AA}$, respectively. In Kanazawa's monography [1] $a = 9.36\text{--}9.37 \text{ \AA}$, $c = 6.87\text{--}6.89 \text{ \AA}$ parameters were given. Relying upon these findings, the sample prepared by heating at 1370°C for 60 min had a composition which best approaches the stoichiometric composition of fluorapatite. This sample was used as a standard for different analytical methods. Dissolution properties of the standard sample were identical to those of the other samples.

Using the sample mentioned above as a standard, the accuracy of the Ca content determination by EDTA titration method were found to be

Table 5
 P% (wt) content of the samples determined by spectrophotometric method at 400 nm

Sample	P% (wt)
FAP,1000,60	17.7 ± 0.8
FAP,1100,60	17.7 ± 0.9
FAP,1200,60	17.9 ± 0.8
FAP,1300,60	17.7 ± 0.9
FAP,1370,60	17.8 ± 0.8
FAP,1370,30	17.7 ± 0.9

–0.8% (Table 2), better than that of the ICP method. For a comparative evaluation of these two methods statistical calculations were done. Based on *F*-test was established that no differences among the standard deviations of the two methods, $F_{\text{calculated}} < F(95)$ (see Table 3). The results of *t*-test showed with an uncertainty at 95% confidence level that no differences among the average values of the two determinations, $t_{\text{calculated}} < t(95)$ (see Table 4). This results show that both of the methods (ICP and EDTA titration) are suitable for determination of Ca content if their accuracy is taken into consideration.

3.2. P determination

The theoretical P content was found to be: 17.7% (wt). The accuracy of the spectrophotometric method was found to be +0.6% (Table 5), better than experienced with ICP, $\pm 1\text{--}3\%$ (Table 6). Results of *F*-test and *t*-test showed no differences among the standard deviations and average values of P content determination by two different methods. Difference between the two methods was found only in their accuracy as compared to the standard sample.

Table 6
 P% (wt) content of the samples determined by ICP at 213,618 nm

Sample	P% (wt)
FAP,1100,60	18.4 ± 0.8
FAP,1200,60	18.5 ± 0.7
FAP,1370,60	17.8 ± 0.7
FAP,1370,30	17.8 ± 0.8

Table 7
F% (wt) content of the samples determined with fluoride-selective electrode

Sample	F% (wt)
FAP,1000,60	3.6 ± 0.2
FAP,1100,60	3.4 ± 0.2
FAP,1200,60	3.5 ± 0.2
FAP,1300,60	3.4 ± 0.3
FAP,1370,60	3.5 ± 0.2
FAP,1370,30	3.4 ± 0.2

3.3. F determination

The analysis of fluoride is one of the most difficult in analytical chemistry. The experiments demonstrated a strong dependence between the applicability of the methods and the nature of the samples as well as the quality of sample preparation. The difference between the first two methods (i.e. pyrohydrolytic method and distillation with conc. H₂SO₄) were merely in the sample preparation. Fluoride content of the solutions was determined by thorium nitrate titration. The results showed that neither of the methods is adequate for fluoride analysis, because the total fluoride content can not be extracted. The measured values were 45% (wt) less than the theoretical value 3.72% (wt).

3.3.1. F determination by ionchromatography

The precision of this method was satisfactory, but the accuracy was poor: –23%. This poor accuracy could be explained by the non-adequate sample preparation. The samples were dissolved in H₂SO₄ at 50°C, when a part of the fluoride content could be evaporated in the form of HF. Sample preparation by dissolution using an other acid (e.g. HNO₃) was not applicable because of the disturbing effect of NO₃[–] ions for the fluoride determination in this method.

3.3.2. F determination with a fluoride-selective electrode

Accuracy of the method was found to be: –5.4%. This method was of good precision but a moderate accuracy (Table 7). Nevertheless this latter method seems to be an acceptable compromise between precision and accuracy, especially in comparison with the formerly listed methods.

4. Conclusions

Fluorapatite with a composition (Ca:P:F = 10:6:1.9) which best approximates the theoretical stoichiometry (Ca:P:F = 10:6:2) was prepared by solid state reaction, heating a mixture of Ca₃(PO₄)₂ and CaF₂ of 3:1 molar ratio. Heating run was performed in flowing argon gas (20 l h^{–1}) with some CaF₂ upstream, at 1370°C for 60 min. Considering that this sample had the same unit cell parameters as the theoretic values, this one was selected for reference for Ca, P and F determination. Accuracy and precision of different analytical methods were determined. Methods with a good accuracy for the determination of Ca, P and F content were: titrations with EDTA for Ca (accuracy: –0.8%), spectrophotometric method for P (accuracy: +0.6%) and measurements with fluoride-selective electrode (accuracy: +5.4%) for F determination. Statistical results (*t*-test) demonstrated that all of the presented analytical methods (ICP, EDTA titrations, spectrophotometric method) were suitable for determination of Ca and P content in fluorapatites provided their accuracy, as compared to a standard sample, is considered during evaluation of results.

References

- [1] T. Kanazawa, Mater. Sci. Monogr. 52 (1989) 64.
- [2] J.R. Lehr, E.H. Brown, A.W. Frazier, J.P. Smith, R.D. Thrasher, Crystallographic properties of fertilizer compounds, National Fertilizer Development Center, Alabama, 1967, p. 11.
- [3] W.P. Rothwell, J.S. Waugh, J.P. Yesinowski, J. Am. Chem. Soc. 102 (1980) 2637.
- [4] I. Sajó, Complexometry, Műszaki Kiadó, Budapest, 1973, p. 194.
- [5] Z. Marczenko, Spectrophotometric determination of elements, Halsted Press, Toronto, 1976, p. 424.
- [6] P. Fodor, T. Tamás, Analytical Methods in Silicate Chemistry, Építésügyi Tájékoztatási Központ, Budapest, 1986, p. 37.
- [7] Hungarian Patent, MSZ-13-158-1990.
- [8] H. Monma, T. Kanazawa, Bull. Chem. Soc. Jpn. 49 (1976) 1421.
- [9] Dionex Product Selection Guide, 1994–1995.
- [10] D.J. Pietrzyk, C.W. Frank, Analytical Chemistry, Ed. Technica, Bucuresti, 1989, p. 533.
- [11] E.J. Duff, J.L. Stuart, Anal. Chim. Acta 52 (1970) 155.
- [12] D.R. Simpson, Am. Mineralogist 53 (1968) 432.
- [13] A. Boulton, D. Louer, J. Appl. Cryst. 24 (1991) 987.

ICP–AES determination of small amounts of zinc in copper-base alloys after separation by adsorption of the zinc–TAN complex on Sep Pak C18 cartridges

Leonardo S.G. Teixeira, José Oscar N. Reis, Antônio C.S. Costa, Sérgio L.C. Ferreira, Maria das Graças A. Korn, Jailson B. de Andrade *

Instituto de Química, Universidade Federal da Bahia, 40170-290, Salvador, Bahia, Brazil

Received 21 July 1997; received in revised form 10 November 1997; accepted 10 November 1997

Abstract

The use of ICP/AES for the determination of zinc, in low concentration levels, in matrices containing high levels of copper is difficult because copper interferes in the zinc main emission wavelength (213.856 nm). In the present work, a separation of zinc from copper matrices was possible, using the reaction of zinc(II) cation with 1-(2-tiazolylazo)-2-naphthol (TAN), in the pH range of 6.5–8.0, resulting in a stable red complex. Copper also reacts with TAN but its interference was avoided by the addition of ascorbic acid and thiosulphate in the reaction medium. In this way, the aqueous solution was passed through a SEP PAK C18 cartridge, in which the zinc(II)–TAN complex was quantitatively retained, but it did not occur with copper which passes through the cartridge, as $[\text{Cu}_2(\text{S}_2\text{O}_3)_2]^{2-}$, with the aqueous solution. The cartridge was washed with water and the complex eluted with ethanol. Then, the alcohol was evaporated and the complex decomposed by nitric acid. It results in both zinc pre-concentration and separation from copper. The zinc quantification was carried out by ICP/AES at 213.856 nm. The relative standard deviations, for ten different aliquots, were 5.7% and the average recovery found for zinc was 96%, even when the concentration ratio Cu/Zn was up to 500/1 ($\text{mg l}^{-1}:\text{mg l}^{-1}$). Other metals, like nickel, for example, can react with TAN in the same way as zinc but they do not interfere in the emission wavelength 213.856 nm. © 1998 Elsevier Science B.V. All rights reserved.

Keywords: ICP/AES; Zinc; Copper-base alloys

1. Introduction

The determination of zinc in low concentration levels has been widely done by spectroscopic methods such as ICP–AES and/or AAS. How-

ever, the determination of zinc traces in copper matrices using these analytical methods is difficult because of the spectral interference, due to the overlapping of the copper line at 213.853 nm with the zinc main emission wavelength (213.856 nm) [1–3]. A lack in *sensitivity* does not allow the quantification of zinc in its second emission wavelength at 334.502 nm. Thus, the determination of

* Corresponding author. e-mail: jailsong@ufba.br

zinc traces in copper matrices, by spectroscopic methods, requires a prior separation [4,5], which can be done by several ways. For example, Wunderlich and Haedeler [4] had determined zinc in pure copper, by atomic absorption spectrometry, after copper separation either as its sulfide with hydrogen sulfide, or by electrolysis. On the other hand, McCrackan et al. [5] determined zinc, cadmium and tin, at low concentration levels, in copper after copper separation by ion exchange.

In the present work, a new method for zinc separation from copper was investigated. It is based on the quantitative reaction between Zn(II) and TAN [6] and retention of the zinc(II)–TAN complex on a SEP PAK C18 cartridge. Copper also reacts with TAN, however, this reaction was masked with ascorbic acid and thiosulphate. After elution from the cartridge, zinc was quantified by ICP/AES, in the emission wavelength 213.856 nm, without any interference due to copper or other metals.

2. Experimental

2.1. Reagents

All reagents were analytical grade unless otherwise stated. Double distilled water was used in the preparation of the solutions. Nitric acid and hydrochloric acid were of Suprapur quality (Merck). The laboratory glassware was kept overnight in a 5% nitric acid solution. Before use, the glassware was washed with deionized water and dried in a dust-free environment.

The reagent solutions were prepared as follows: zinc stock solution [$1000 \mu\text{g ml}^{-1}$], by dissolving 1.000 g of granulated zinc metal (Baker) in concentrated nitric acid and taken up to 1000 ml, with water; Triton-X100 [10%], by dissolving 20.0 g in 200 ml of water; TAN [0.05%], by dissolving 0.10 g of 1-(2-tiazolylazo)-2-naphthol (Merck) in 5 ml of ethanol and taken up to 100 ml with the Triton-X100 solution; Hexamine buffer solution [pH 6.8], by dissolving 70 g of hexamethylenetetramine in 800 ml of deionized water and pH adjust with nitric acid and/or sodium hydroxide; Thiosulfate solution [10%], by dissolving 10.0 g of

sodium thiosulfate pentahydrate in 100 ml of deionized water; Ascorbic acid solution [10%], by dissolving 10.0 g in 100 ml of deionized water; Ethanol p.a. (Merck), SEP PAK C18 cartridges (Millipore Waters).

2.2. Apparatus

An Applied Research Laboratories model 3410 minitorch sequential inductively coupled plasma spectrometer, equipped with an IBM PC–AT computer was used. The emission intensity measurements were made under the conditions shown in Table 1. The calibration curves (five points) for zinc (without copper and using this method) concentration in the range of $0\text{--}2.0 \mu\text{g ml}^{-1}$ are shown in Table 2. The limit of detection and background equivalent concentration (BEC) were 16 and $98 \mu\text{g l}^{-1}$, respectively.

A 300 analyser pH meter was used to measure the pH values.

Table 1
Operating parameters for the inductively coupled plasma spectrometer

Incident output power	650 W
Reflected power	<5 W
Nebulizer	Glass, Meinhard
Plasma gas flow rate	7.5 l min^{-1}
Auxiliary gas flow rate	0.8 l min^{-1}
Aerosol carrier gas flow rate	0.8 l min^{-1}
Solution uptake rate	2.5 ml min^{-1}
Wavelength	213.856 nm
Signal integration time	5 s
Integration for determination	3

Table 2
Calibration curves for ICP/AES determination of zinc [$A = aC + b$], at 213.8 nm

Analytical Curves	<i>a</i>	<i>b</i>	<i>r</i> ²
Without copper	18.218	0.0428	0.9999
After copper separation	17.397	0.199	0.9999

$A = K$ counts; a = slope; C = concentration (mg l^{-1}); b = intercept; r = correlation coefficient.

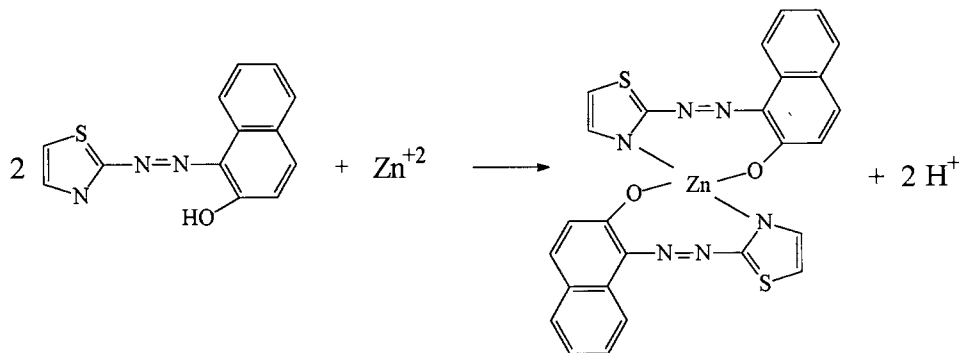


Fig. 1. Reaction between Zn(II) and TAN.

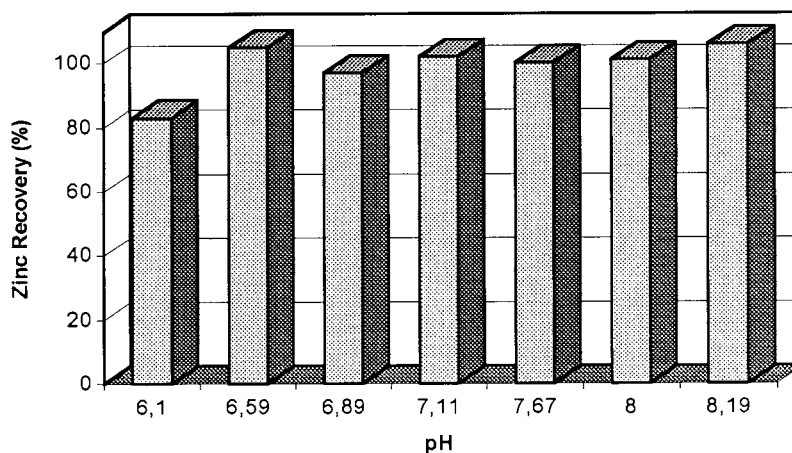


Fig. 2. Effect of acidity in Zn retention/recovery on SEP PAK C18 Cartridges.

2.3. Method

0.100 g of the sample was placed in conical flasks and 10 ml of concentrated nitric acid and 2 ml of concentrated hydrochloric acid per gram of sample were added. The system was heated up to promote the sample dissolution. The dissolved sample was placed in a volumetric flask and taken up to 1000 ml. Aliquots of 10.00 ml were placed in a 250 ml beaker. Then, 2.0 ml of ascorbic acid solution, 10.0 ml of hexamine buffer solution pH 6.8, 2.0 ml of 10% thiosulfate solution and 1.0 ml of TAN solution were added. Aliquots of 10.00 ml of the aqueous solution was passed through a SEP PAK C18 cartridge (using a 10 ml syringe) at an approximate

flow rate of 3 ml min⁻¹. In this way, the zinc(II)–TAN complex was quantitatively retained, but it did not occur with the copper which passes through the cartridge with the aqueous solution. Thus, the cartridge was washed with water and the complex was eluted with ethanol. Then, the alcohol was evaporated and the complex decomposed by nitric acid and sulfuric acid under heating. This solution was transferred to a 10.00 ml volumetric flask and taken up with water. The zinc quantification was carried out by ICP/AES at 213.856 nm. The samples can be pre-concentrated, if necessary, by passing a whole aqueous solution through a SEP PAK C18 cartridge, instead of aliquots of 10.00 ml.

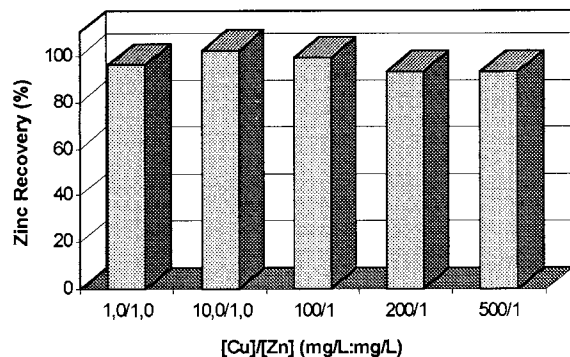


Fig. 3. Zinc determination in the presence of copper (the relative standard deviations for ten different aliquots were 5.7%).

3. Results and discussion

3.1. Characteristics of the zinc(II)-TAN complex

The zinc(II) cation reacts instantaneously with TAN, in the pH range of 6.5–8.0, in the presence of Triton-X100 to form a red complex (Fig. 1) [6], which is stable for at least 2 h. Both, TAN and its zinc(II) complex have low solubility in water but

the reaction in the presence of Triton-X100, increases the solubility. Due to the non polar character of the Zn–TAN complex it can be quantitatively retained on reversed phase SEP PAK C18 cartridges. The pH conditions did not affect the retention capacity if it were kept in pH range of 6.5–8.0, as can be seen in Fig. 2. In this conditions no breakthrough was observed in the Zn–TAN complex retention on the cartridges, even when the amount of zinc retained was up to 0.1 mg. A study showed that 5.0 ml of ethanol was sufficient to elute quantitatively the complex from the cartridge. Because the conditions (pH 6.5–8.0) are not aggressive to the reversed phase C18, the cartridge can be reused several times.

3.2. Masking of copper

Thiosulphate forms a strong complex with cuprous ion and has been used as masking agent for copper in zinc determinations by spectrophotometric methods and complexometric titrations with EDTA [7,8]. This is based on the reduction of copper(II) to copper(I) and complexation of copper(I) with thiosulfate $[\text{Cu}_2(\text{S}_2\text{O}_3)_2]^-$ [7,8].

Table 3

Emission intensity (K counts) measured when different zinc solutions are quantified by ICP/AES with and without copper, at 213.856 and 334.502 nm

Zn concentration (mg ml ⁻¹)	Without copper at 213.856 nm	Cu = 250 µg ml ⁻¹ at 213.856 nm	Cu = 250 µg ml ⁻¹ at 334.502 nm	Cu = 250 µg ml ⁻¹ at 213.856 nm, this method
0	0.172	0.469	0.009	0.177
0.40	7.579	11.36	0.138	7.180
0.80	14.27	18.31	0.242	13.87
2.00	36.25	39.83	0.904	35.48
3.20	58.54	63.13	1.401	55.62

Table 4

Concentrations (%) of zinc determined in copper-base alloys, from NBS and CEPED, by the procedure described in this work

Sample	Certified value	This work without copper separation	This work with copper separation
NIST 184	2.69	2.84 ± 0.03 (3)	2.65 ± 0.03 (3)
NIST 52C	2.12	2.34 ± 0.05 (3)	2.07 ± 0.05 (3)
CEPED 2150	0.41	0.68 ± 0.05 (3)	0.39 ± 0.05 (3)

NBS = National Bureau of Standards, USA.

CEPED = Research and Development Center, Bahia State, Brasil. It is the State reference bureau.

Numbers in parenthesis mean number of different aliquots analysed.

Table 5
Copper-base alloys composition

SAMPLE	Sn%	Cu%	Ni%	Pb%	Zn%	Fe%	As%	P%	Al%	Mn%
NIST 184	6.38	88.96	0.50	1.44	2.69	0.005	—	0.009	—	—
NIST 52C	7.85	89.25	0.76	0.011	2.12	0.004	—	—	—	—
CEPED 2150	8.16	90.48	0.06	0.81	0.41	0.024	<0.01	—	<0.05	0.005

However, this masking is efficient only up to pH 6.0, which is too low for optimum use with TAN. In this way, the use of a masking solution containing ascorbic acid and thiosulfate avoided the copper interference in pH range of 6.2–7.2 [6]. As $[\text{Cu}_2(\text{S}_2\text{O}_3)_2]^{2-}$, copper did not react with TAN and passed throughout the SEP PAK C18 cartridges without any retention. Fig. 3 shows the efficiencies in the recovery of zinc from solutions containing variable amounts of copper. The recovery efficiency was high (>90%) even in the presence of considerable amounts of copper (500 to 1 in relation to zinc concentration).

3.3. Zinc determination in copper-base alloys

In Table 3 it is shown the emission intensity measured when different zinc solutions are quantified, by ICP/AES, with and without copper. As can be seen in Table 3 the presence of $250 \mu\text{g ml}^{-1}$ can increase the signal up to 2.7 times depending on the zinc concentration. An alternative way *is to* quantify zinc at 334.502 nm, but it revealed a lack in sensitivity with the signal dropping up to 40 times depending on the zinc concentration (Table 3). Meanwhile, when copper is separated using the procedure proposed in this study, zinc can be quantified accurately and precisely in its main emission wavelength (213.856 nm), with a detection limit of $16 \mu\text{g l}^{-1}$. The relative standard deviations for ten different aliquots were 5.7%.

The method validation was made with three different copper-base alloys. The results are shown in Table 4, the application of the $t_{95\%}$ test in the result obtained at NIST and CEPED and in this work (Table 4) did not show significant differences. In the analyzed sample the concentra-

tions (%) of copper were in the range of 88.96–90.48% (Table 5) and its interference was avoided. Other metals like nickel, tin, iron, lead, aluminum, manganese and arsenic were present (Table 5) but they do not interfere in the emission wavelength 213.856 nm.

4. Conclusions

Copper is a serious interference in the determination of zinc by ICP/AES in the zinc main emission wavelength. The method proposed in the present work allows the determination of low levels of zinc in copper alloys by ICP/AES, at 213.856 nm.

Acknowledgements

The authors acknowledge the financial support of the CNPq, FINEP and CAPES.

References

- [1] M.G.A. Korn, E. Oliveira, Quím. Nova 19 (1996) 448.
- [2] V.A. Fassel, R.W. Winge, V.J. Peterson, Appl. Spectrosc. 33 (1979) 206.
- [3] B. Welz, Atomic Absorption Spectrometry, Weinheim, Deerfield Beach, Germany, 1985.
- [4] E. Wunderlich, W. Hädel, Z. Anal. Chem. 281 (1976) 300.
- [5] M.L. McCrackan, H.J. Webb, H.E. Hammar, C.B. Loadholt, Ass. Off. Agric. Chem. 50 (1967) 5.
- [6] S.L.C. Ferreira, N.M.L. Araújo, A.B. Santos, A.F. Dantas, A.C.S. Costa, Mikrochim. Acta 118 (1995) 123.
- [7] D.G. Davis, Anal. Chem. 30 (1958) 1729.
- [8] G. Schwarzenbach, H. Flaschka, Complexometric Titrations, Methuen, London, 1969.

Acid–base dissociation constants of 2,2'-bipyridyl in mixed protic solvents

Jing Fan *, Jianji Wang, Cunling Ye

Department of Chemistry, Henan Normal University, Xinxiang, Henan, 453002, China

Received 23 June 1997; received in revised form 10 November 1997; accepted 12 November 1997

Abstract

The acid dissociation constants (K_a), base dissociation constants (K_b) and the autoprotolysis constants (K_s) for 2,2'-bipyridyl in water and in water + alcohol (methanol, ethanol, iso-propanol) mixed solvents have been determined at 25°C and an ionic strength of 0.1 mol l⁻¹, from a direct potentiometric method based on the treatment of the data of a single pH titration. It has been shown that K_a increases, whereas K_b and K_s decrease, with increasing proportion of the alcohol in the mixed solvents. Linear relations between p K_a , p K_b , p K_s and the mole fraction of the alcohol were observed in the composition range investigated. These results are discussed in terms of the properties of solvent and the interactions of the different species existing in dissociation equilibrium with solvents. It is concluded that the higher stabilization of both 2,2'-bipyridyl and its protonated form by dispersion forces and of the proton by its interaction with solvent molecules in the mixed solvents compared with that in water are largely responsible for the observed changes of p K_a with composition. On the other hand, the low stabilization of OH⁻ in the mixed solvents relative to that in water and the electrostatic effect are the main factors in determining the solvent effect on p K_b . © 1998 Elsevier Science B.V. All rights reserved.

Keywords: Acid dissociation constant; Base dissociation constant; Autoprotolysis constant; Water + alcohol mixed solvent; 2,2'-bipyridyl

1. Introduction

In recent years, non-aqueous and mixed solvents have been widely used in analytical chemistry with the rapid development of non-aqueous analytical techniques and methods. Choosing acid-base titration as an example, there are essentially three reasons for this: (i) weak acid or weak base whose acid dissociation constant is less than

10⁻⁷ can not be titrated accurately in aqueous solution; (ii) the small solubility for a large number of organic compounds makes the titration impossible in water; (iii) the strong acids or bases in a mixture can not be titrated respectively, because of the leveling effect in aqueous solutions. Usually, these problems can be partially or entirely resolved by using proper non-aqueous solvents as the reaction medium.

Acid dissociation constant and base dissociation constant of organic compounds as well as the

* Corresponding author. Fax: +86 373 3383145.

autoprotolysis constant of solvent are the important basic data for non-aqueous titration. They may be used to choose the optimum analytical conditions and the best medium in which the titration is carried out [1,2]. Although a number of such constants in non-aqueous or mixed solvents have been determined and accumulated in literature [3–5], much more work in this respect is indispensable in order to meet the needs of practical applications and to clarify the nature of medium effect on the acid–base dissociation constants. As a part of the continuing studies on the use of ion selective electrode (ISE) in mixed solvents [6–9], we report here the acid dissociation constants, base dissociation constants and the autoprotolysis constants for 2,2'-bipyridyl in water and in water + alcohol (methanol, ethanol, iso-propanol) mixed solvents at 25°C and an ionic strength $I = 0.1 \text{ mol l}^{-1}$. These constants were determined from a direct potentiometric method [10] by which the acid, the base as well as the autoprotolysis constant can be obtained simultaneously from the data of a single pH titration. The effect of the solvents on the dissociation constants of 2,2'-bipyridyl have been discussed in terms of properties of the solvents and the interactions of the different species existing in dissociation equilibrium with the solvents.

2. Experimental

2.1. Reagents and stock solutions

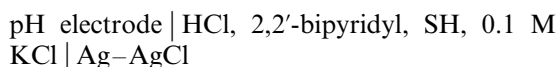
2,2'-bipyridyl (A.R., Beijing) was used after drying for 3 h under vacuum at 50°C. Methanol (MeOH), ethanol (EtOH) and iso-propanol (*i*-PrOH) (A.R., all from Shanghai) were dried over 4 Å type molecular sieves before use. Hydrochloric acid, potassium Chloride and sodium hydroxide (G.R., all from Shanghai) were used without further purification.

Stock solution of hydrochloric acid (0.2 mol l^{-1}) was obtained by direct dilution of the commercial hydrochloric acid with redistilled water, and that of sodium hydroxide (0.12 mol l^{-1}) was prepared by dissolving an accurate amount of sodium hydroxide in CO_2 free redistilled water.

The accurate concentration of these two stock solutions is determined by potentiometric titration. In order to prepare the stock solution of 2,2'-bipyridyl (0.05 mol l^{-1}) + hydrochloric acid (0.1 mol l^{-1}), the required amount of 2,2'-bipyridyl and pure water were added into a portion of the stock solution of hydrochloric acid. Generally, dilute solutions were prepared by appropriate dilution of the respective stocks. Water + alcohol mixed solvents were prepared by weight. The ionic strength in all solutions was supported with 0.1 mol l^{-1} potassium chloride.

2.2. Apparatus

The cell used in this work was



where SH denotes water + alcohol mixed solvent. The pH electrode was a pH glass electrode of type 231 (Shanghai). Ag–AgCl reference electrode without liquid junction was home-made by the thermal electrolytic method [11], the potentiometric titrations were carried out at $25 \pm 0.05^\circ\text{C}$ in a water jacketed glass cell as described in a previous paper [6]. The cell potentials were recorded by means of a precise pH meter (pHS-2D, Chengdu) readable to 0.2 mV. Before measurements, the glass electrode was prepared according to the manufacturer's instruction and calibrated with the standard aqueous potassium acid phthalate and sodium tetraborate buffers.

2.3. Procedure

Into two 50 ml volumetric flasks, transfer 5.00 ml of the stock solutions of 2,2'-bipyridyl + hydrochloric acid and sodium hydroxide, respectively. Add the required amount of alcohol and solid potassium chloride, dilute to the marks with redistilled water. Thus obtained solution containing 2,2'-bipyridyl + hydrochloric acid was used as the titrand, and that containing sodium hydroxide as the titrant. Here, the titrand and the titrant have the same proportion of the alcohol and the same ionic strength. Before measurements, Ag–AgCl and pH electrodes were soaked over night in a portion of the titrand.

Table 1

$E-V$ data of the potentiometric titrations, the specific constants of the cell both in the acidic and alkaline ranges and the calculated acid–base dissociation constants of 2,2'-bipyridyl in aqueous solution of 34.3 wt% methanol at 25°C and $I = 0.1$

V_{NaOH} (ml)	E (mV ^a)	E_a^0 (mV)	E_b^0 (mV)	pK_a	pK_s	pK_b
0.00	−241.5	−379.3				
0.50	−239.1	−379.3				
1.00	−236.8	−379.4				
1.50	−233.9	−379.4				
2.00	−231.2	−379.7				
2.50	−228.2	−379.6				
3.00	−224.8	−379.8				
3.50	−221.4	−379.9				
4.00	−217.8	−379.9				
10.00	−156.7			4.04		
10.50	−150.3			4.03		
11.00	−144.2			4.01		
11.50	−137.7			4.01		
12.00	−130.5			4.01		
12.50	−122.0			4.02		
13.00	−113.2			4.03		
19.50	273.0		440.4			
20.00	275.6		440.7			
20.50	277.8		441.1			
21.00	279.9		440.8			
21.50	281.4		441.1			
22.00	283.2		441.2			
22.50	284.5		441.3			
23.00	286.0		441.0			
23.50	287.2		441.0			
24.00	288.5		441.1			
Mean		-379.6 ± 0.2	441.0 ± 0.3	4.02 ± 0.01	13.87 ± 0.01	9.85 ± 0.01

^a The uncertainty in e.m.f. measurements is about ± 0.3 mV.

A 20.00 ml of the titrand was added to the cell. After thermal equilibrium was reached, the cell solution was titrated with small additions of the titrant. During titrations, the excess hydrochloric acid in the cell solution was titrated firstly before the first stoichiometric point. Then, 2,2'-bipyridyl hydrochloride was titrated up to the second stoichiometric point. E.m.f. readings were taken after every titrations when cell potential was constant within 0.5 mV for at least 3 min. $E-V$ (volume of the titrant added) data obtained (as shown in Table 1, column 1 and 2) are used firstly for the determination of the volume of the titrant, V_2 , added into the cell solution when the second stoichiometric point is reached. This is performed very accurately by

means of the second derivative method [12]. Since the mole ratio of 2,2'-bipyridylhydrochloride and hydrochloric acid in the titrand is exactly 1:1, the volume of the titrant added corresponding to the first stoichiometric point, V_1 , can be easily calculated from the V_2 value obtained.

3. Results

The whole titration process can be divided into three stages. Titration before the first stoichiometric point belong to the first stage. At this stage, the cell potential at 25°C is given by the following equation [13]

$$E = E_a^0 - 59.16 \log[\text{SH}_2^+] \quad (1)$$

Where E_a^0 is the specific constant of the cell in the acidic range, and includes the standard electrode potential of the glass electrode, the potential of the Ag–AgCl electrode and the activity factors. $[\text{SH}_2^+]$ is the concentration of solvated proton and can be expressed by

$$[\text{SH}_2^+] = c_{\text{HCl}} - c_{\text{NaOH}} \quad (2)$$

here c_{HCl} is the total analytical concentration of hydrochloric acid in the cell solution, constant throughout the experiment, c_{NaOH} is the total analytical concentration of the added sodium hydroxide.

Introducing Eq. (2) into Eq. (1), it follows that

$$E = E_a^0 - 59.16 \log(c_{\text{HCl}} - c_{\text{NaOH}}) \quad (3)$$

Using the measured E and c_{NaOH} values in every titration point before the first stoichiometric point, E_a^0 can be easily calculated from Eq. (3).

Titrations between the first and the second stoichiometric points belong to the second stage. The measured cell potential in every titration point in this range can be used to calculate the hydrogen ion concentration $[\text{H}^+]$ and the acid dissociation constant K_a by the following relations [14]

$$-\log[\text{H}^+] = \frac{(E - E_a^0)}{59.16} \quad (4)$$

and

$$\begin{aligned} \text{p}K_a &= -\log[\text{H}^+] \\ &+ \log \left\{ \frac{([\text{BH}^+] - [\text{SH}_2^+] + [\text{S}^-])}{([\text{B}] + [\text{SH}_2^+] - [\text{S}^-])} \right\} \\ &= -\log[\text{H}^+] + \log \left[\frac{(V_2 - V)}{(V - V_1)} \right] \end{aligned} \quad (5)$$

where $[\text{B}]$, $[\text{BH}^+]$ and $[\text{S}^-]$ are the equilibrium concentrations of 2,2'-bipyridyl, the protonated form of 2,2'-bipyridyl and the lyate ion in solution, respectively. V is the volume of the titrant (NaOH) added in every titration point.

Titrations after the second stoichiometric point are in the range of the third stage. The titrand at this region becomes 2,2'-bipyridyl and sodium hydroxide in the mixed solvent studied. The cell potential in every titration point is given by

$$E = E_b^0 + 59.16 \log[\text{S}^-] \quad (6)$$

where E_b^0 is the specific constant of the cell in the alkaline region, and includes also the standard electrode potential of the glass electrode, the potential of Ag–AgCl electrode and the activity factors. Under the conditions investigated here, the concentration of the lyate ion can be calculated by

$$[\text{S}^-] = c_{\text{NaOH}} - 2c_{\text{HCl}} \quad (7)$$

From Eqs. (6) and (7), it is evident that

$$E_b^0 = E - 59.16 \log(c_{\text{NaOH}} - 2c_{\text{HCl}}) \quad (8)$$

Similarly, using the measured E and c_{NaOH} values for every titration point after the first stoichiometric point, values of E_b^0 can be computed. Once E_a^0 , E_b^0 and $\text{p}K_a$ are known, the autoprotolysis constant K_s for the solvent and the base dissociation constant K_b can be obtained by means of the known relations [10]

$$\text{p}K_s = \frac{(E_b^0 - E_a^0)}{59.16} \quad (9)$$

and

$$\text{p}K_b = \text{p}K_s - \text{p}K_a \quad (10)$$

As an example, Table 1 lists the titration data for the three stages in aqueous solution of 34.3 wt% methanol as well as the calculated E_a^0 , E_b^0 , $\text{p}K_a$, $\text{p}K_s$ and $\text{p}K_b$ values. Values of $\text{p}K_a$, $\text{p}K_b$ and $\text{p}K_s$ ($I = 0.1$) for 2,2'-bipyridyl in water and in different water + alcohol mixed solvents are presented in Table 2.

4. Discussion

It is evident from Table 1 that E_a^0 and E_b^0 are constant throughout the experiment within the experimental error. This suggests that strong acid in the acidic range can be leveled to the strength of the solvated proton SH_2^+ and that strong base in the alkaline range can be leveled to the strength of the lyate S^- , in the investigated water + alcohol mixed solvents.

It can be seen from Table 2 that $\text{p}K_a$ value for 2,2'-bipyridyl obtained in water was 4.47, which is in excellent agreement with the values 4.48 or 4.44 reported in the literature [15,16]. The autoprotoly-

Table 2

Values of the acid–base dissociation constants for 2,2'-bipyridyl and the autoprotolysis constants in water + alcohol mixed solvents at 25°C and $I = 0.1$

Alcohol Wt%	H ₂ O+MeOH			H ₂ O+EtOH			H ₂ O+ <i>i</i> -PrOH		
	p <i>K</i> _a	p <i>K</i> _b	p <i>K</i> _s	p <i>K</i> _a	p <i>K</i> _b	p <i>K</i> _s	p <i>K</i> _a	p <i>K</i> _b	p <i>K</i> _s
0.0	4.47 ± 0.01	9.23	13.70	4.47 ± 0.01	9.23	13.70	4.47 ± 0.01	9.23	13.70
10.2	—	± 0.01	± 0.01	4.34 ± 0.01	± 0.01	± 0.01	4.27 ± 0.01	± 0.01	± 0.01
15.2	4.33 ± 0.02	9.41	13.74	4.30 ± 0.01	9.49	13.83	—	9.70	13.97
20.5	4.23 ± 0.02	± 0.03	± 0.02	4.17 ± 0.01	± 0.02	± 0.02	—	± 0.01	± 0.01
25.1	—	9.55	13.78	4.08 ± 0.01	± 0.01	± 0.01	3.94 ± 0.01	10.29	14.23
30.4	4.05 ± 0.01	± 0.03	± 0.02	4.08 ± 0.01	± 0.01	± 0.01	—	± 0.02	± 0.02
34.3	4.02 ± 0.01	9.85	13.87	—	9.98	14.06	—	—	—
35.8	—	± 0.01	± 0.01	—	± 0.01	± 0.01	3.66 ± 0.02	10.75	14.41
40.1	3.93 ± 0.02	9.94	13.87	3.85 ± 0.01	9.90	13.98	—	± 0.03	± 0.02
46.3	3.81 ± 0.01	± 0.03	± 0.02	—	± 0.01	± 0.01	—	± 0.03	± 0.02
48.9	—	10.05	13.86	—	—	—	3.52 ± 0.03	10.96	14.48
51.0	3.74 ± 0.01	± 0.03	± 0.03	3.74 ± 0.01	± 0.01	± 0.01	—	± 0.03	± 0.01
59.3	3.66 ± 0.01	10.13	13.87	—	10.45	14.30	3.43 ± 0.02	11.14	14.57
66.5	3.58 ± 0.01	± 0.01	± 0.01	3.43 ± 0.02	± 0.01	± 0.02	—	± 0.03	± 0.02
		10.27	13.93	—	—	—	—	—	—
		± 0.03	± 0.03	—	± 0.04	± 0.03	—	—	—
		10.39	13.97	—	—	—	—	—	—
		± 0.02	± 0.02	—	—	—	—	—	—

sis constant p*K*_s obtained for water was 13.70, which also agrees satisfactorily with the value 13.73 determined by Tencheva and co-workers [10]. As far as the dissociation constants in aqueous alcohol solutions are concerned, El-Gyar et al. [17] determined pH-metrically the acid dissociation constants of the protonated 2,2'-bipyridyl in aqueous media containing 30, 40, 50 and 60 wt% alcohol (methanol, ethanol) at 25°C

and $I = 0.1 \text{ mol l}^{-1}$. The standard deviations of our p*K*_a values and those determined by these authors in water + methanol and water + ethanol mixed solvents are 0.08 and 0.14, respectively. Data in Table 2 show that for 2,2'-bipyridyl, the acid dissociation constant (*K*_a) increases, whereas the base dissociation constant (*K*_b) and the autoprotolysis constant (*K*_s) decrease, with increasing proportion of the alcohol in the mixed solvents. A

careful analysis of these results reveals that in the composition range investigated, pK_a , pK_b and pK_s change linearly with the mole fraction (x_2) of the alcohol in aqueous solutions. These linear equations with correlation coefficients were listed in Table 3. As an example, the variation of pK_a , pK_b and pK_s as a function of x_2 in water + methanol mixed solvents was illustrated in Fig. 1.

It is generally recognized that the acid–base dissociation constants of acids and bases may be affected by electrostatic effect associated with the change in dielectric constant, acidic or basic strength of the solvents and the interactions of different species existing in dissociation equilibrium with solvents. The acid dissociation equilibrium of the protonated form of 2,2'-bipyridyl in mixed solvent can be represented by



If we disregard all participation of the solvent and the effect of ion activity coefficients, the difference of pK_a in mixed solvent and in water can be related to the Gibbs energy of transfer, $\Delta G_t^0(i)$, from water to the mixed solvent by

$$2.303RT[pK_a(SH) - pK_a(H_2O)] = \Delta G_t^0(H^+) + \Delta G_t^0(B) - \Delta G_t^0(BH^+) \quad (12)$$

Table 3

Linear equations between pK_a , pK_b , pK_s and the mole fraction of the alcohol, x_2 , in water + alcohol mixed solvents

Solvent	Linear equation	R^a	N^b
H ₂ O + MeOH	$pK_a = 4.44 - 1.767x_2$	-0.988	10
	$pK_b = 9.27 + 2.256x_2$	0.990	10
	$pK_s = 13.71 + 0.490x_2$	0.966	10
H ₂ O + EtOH	$pK_a = 4.45 - 2.786x_2$	-0.996	9
	$pK_b = 9.25 + 5.526x_2$	0.994	9
	$pK_s = 13.70 + 2.740x_2$	0.989	9
H ₂ O + <i>i</i> -PrOH	$pK_a = 4.46 - 6.459x_2$	-0.997	6 ^c
	$pK_b = 9.32 + 11.532x_2$	0.994	6 ^c
	$pK_s = 13.77 + 5.073x_2$	0.985	6 ^c

^a Correlation coefficient.

^b Number of the experimental points used in the regression analysis.

^c The last experimental point listed in Table 2 was not included in the regressions.

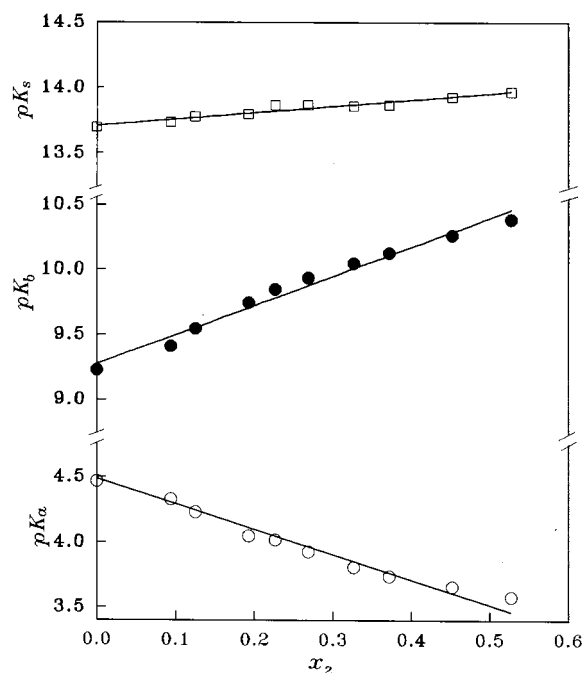


Fig. 1. Variation of pK_a , pK_b and pK_s as a function of mole fraction of methanol in the mixed solvents. \circ pK_a , \bullet pK_b , \square pK_s .

It is known that electrostatic effect operates only on the charged species. Its contribution to $\Delta G_t^0(i)$ is inversely proportional to the radius of the ionic species considered [3]. Consequently, the electrostatic term of $\Delta G_t^0(H^+)$ is larger than that of $\Delta G_t^0(BH^+)$, and K_a is expected to decrease with increasing proportion of the alcohol in aqueous medium. This is at variance with the observed changes in pK_a . Accordingly, electrostatic effect is of considerably less importance in explaining solvent effects on the isoelectric dissociation reaction, as indicated previously [3,17–19].

Wells [20–23], Popovych [24] and Lahiri et al. [25–27] determined the Gibbs energies of transfer of H^+ , B and BH^+ from water to water + alcohol (MeOH, EtOH, *i*-PrOH) mixtures. The results shown that values of $\Delta G_t^0(H^+)$, $\Delta G_t^0(B)$ and $\Delta G_t^0(BH^+)$ are increasingly negative with increasing proportion of the alcohol in aqueous solution, and that values of $\Delta G_t^0(B)$ are close to those of $\Delta G_t^0(BH^+)$ at the same composition in water-rich region. Thus, the magnitude of $pK_a(SH)$ relative

to $pK_a(\text{H}_2\text{O})$ is mainly determined by the sign of $\Delta G_i^0(\text{H}^+)$. Accordingly, K_a should increase with increasing proportion of alcohol in aqueous solution, which is in accordance with the results given in Table 2.

It has been stressed [25] that the basicity of the solvent mixtures and the H^+ -solvent interactions can best be determined from the Gibbs energy of transfer of H^+ from water to aquo-organic mixtures. The negative values of $\Delta G_i^0(\text{H}^+)$ indicate that the water + alcohol mixed solvents are more basic than water and that proton is more stable in the mixed solvents than in water. Similarly, the negative values of $\Delta G_i^0(\text{B})$ and $\Delta G_i^0(\text{BH}^+)$ means that B and BH^+ have lower energies or higher stabilization in the mixed solvents than in water. This is mainly due to their dispersion interaction with the alcohol in the mixed solvents because the effective density of dispersion centers of methanol, ethanol and propanol is higher than that of water [28,29]. Therefore, it is concluded that the higher stabilization of both 2,2'-bipyridyl and its protonated form by dispersion forces and of the proton by its interaction with solvent molecules in the mixed solvents compared with that in water are largely responsible for the observed changes of pK_a with composition of the mixed solvents.

The base dissociation equilibrium of 2,2'-bipyridyl in mixed solvent can be expressed by



As an approximation, $\Delta G_i^0(\text{S}^-)$ can be replaced by $\Delta G_i^0(\text{OH}^-)$ in the water-rich region. Under this condition, if we disregard the effect of ion activity coefficients, difference of pK_b in mixed solvent and in water is related to $\Delta G_i^0(i)$ by

$$2.303RT[pK_b(\text{SH}) - pK_b(\text{H}_2\text{O})] \\ = \Delta G_i^0(\text{BH}^+) + \Delta G_i^0(\text{OH}^-) - \Delta G_i^0(\text{B}) \quad (14)$$

Considering the fact that the Gibbs energies of transfer for OH^- from water to the water + alcohol solvents are increasingly positive with increasing proportion of the alcohol in aqueous media [20–23], it can be deduced from the similar analysis as above that electrostatic effects and low stabilization of OH^- in the mixed solvents

relative to that in water played major role in determining the solvent effect on the base dissociation process of 2,2'-bipyridyl.

Furthermore, it is interesting to note that at the same mole fraction of alcohols, K_a varies in the sequence $i\text{-PrOH} + \text{H}_2\text{O} > \text{EtOH} + \text{H}_2\text{O} > \text{MeOH} + \text{H}_2\text{O} > \text{H}_2\text{O}$, while K_b varies in the order $i\text{-PrOH} + \text{H}_2\text{O} < \text{EtOH} + \text{H}_2\text{O} < \text{MeOH} + \text{H}_2\text{O} < \text{H}_2\text{O}$. This behavior is expected as a result of increase in the basicity of the solvents or in the H^+ -solvent interaction, on going from H_2O , $\text{MeOH} + \text{H}_2\text{O}$, $\text{EtOH} + \text{H}_2\text{O}$ to $i\text{-PrOH} + \text{H}_2\text{O}$ mixed solvents. It has been observed [20–23] that at the same composition of different water + alcohol system, $\Delta G_i^0(\text{H}^+)$ is increasingly negative, while $\Delta G_i^0(\text{OH}^-)$ is increasingly positive, from $\text{MeOH} + \text{H}_2\text{O}$, $\text{EtOH} + \text{H}_2\text{O}$, $i\text{-PrOH} + \text{H}_2\text{O}$ mixtures. This strongly supports the above suggestion.

Acknowledgements

The authors are grateful to the Natural Science Foundation of Henan Province for financial support, and to the referees for their valuable suggestions.

References

- [1] J.J. Lagowski, Anal. Chem. 42 (1990) 305R.
- [2] J.J. Lagowski, Anal. Chem. 44 (1972) 524R.
- [3] R.G. Bates, J. Electroanal. Chem. 29 (1971) 1.
- [4] L. Chmurzynski, Anal. Chim. Acta 329 (1996) 267.
- [5] T. Mussini, A.K. Covington, P. Longhi, S. Rondinini, Pure Appl. Chem. 57 (1985) 865.
- [6] J. Fan, Talanta 42 (1995) 317.
- [7] J. Fan, J. Yan, W. Dong, Y. Wei, T. Liang, Chem. Sens. China 15 (1995) 280.
- [8] J. Fan, Chem. Sens. China 13 (1993) 39.
- [9] J. Fan, X. Shen, J. Wang, Anal. Lab. China 16 (1997) 66.
- [10] J. Tencheva, G. Velinov, O. Budevsky, J. Electroanal. Chem. 68 (1976) 65.
- [11] G.J. Ives, G.J. Janz, Reference Electrodes, Theory and practice, Academic press, New York, 1961.
- [12] J.A. Plambeck, Electroanalytical Chemistry: Basic Principles and Applications, John Wiley and Sons, 1982.

- [13] M. Georgieva, P. Ziklov, O. Budevsky, *Anal. Chim. Acta* 115 (1980) 411.
- [14] A. Albert, E.P. Serjeant, *Ionization Constants of Acids and Bases*, Wiley, New York, 1962.
- [15] K. Yamasaki, M. Yasuda, *J. Am. Chem. Soc.* 78 (1956) 1324.
- [16] H. Irving, D.H. Mellor, *J. Chem. Soc.* (1962) 5222.
- [17] S.A. El-Gyar, M.H.A. Hamed, E.M. Abdalla, M.R. Mahmoud, *Mona. Chem.* 124 (1993) 127.
- [18] A.S. Quist, W.L. Marshall, *J. Phys. Chem.* 72 (1968) 684.
- [19] A.S. Quist, W.L. Marshall, *J. Phys. Chem.* 72 (1968) 1536.
- [20] C.F. Wells, *J. Chem. Soc. Faraday Trans. 1* 69 (1973) 984.
- [21] C. F Wells, *J. Chem. Soc. Faraday Trans. 1* 70 (1974) 694.
- [22] C.F. Wells, *Aust. J. Chem.* 36 (1983) 1739.
- [23] C.F. Wells, *J. Chem. Soc. Faraday Trans. 1* 80 (1984) 2445.
- [24] O. Popovych, A.J. Dill, *Anal. Chem.* 41 (1969) 456.
- [25] D. Sengupta, S.C. Lahiri, *J. Chem. Soc. Dalton Trans.* 12 (1983) 2685.
- [26] A.K. Bhattacharyya, D. Sengupta, S.C. Lahiri, *Z. Phys. Chem. Leipzig* 265 (1984) 372.
- [27] S.K. Chakravorty, D. Sengupta, S.C. Lahiri, *Z. Phys. Chem. Leipzig* 267 (1986) 969.
- [28] M. Alfenaar, G.L. Deligny, *Rev. Trav. Chim.* 86 (1967) 292.
- [29] E. Grunwald, E. Price, *J. Am. Chem. Soc.* 86 (1964) 4517.

Flow injection analysis of potassium using an all-solid-state potassium-selective electrode as a detector

Shinichi Komaba ^a, Junko Arakawa ^b, Michiko Seyama ^a, Tetsuya Osaka ^{a,*},
Ikuro Satoh ^c, Sadako Nakamura ^b

^a Department of Applied Chemistry, School of Science and Engineering,

Kagami Memorial Laboratory for Materials Science and Technology, Waseda University, Shinjuku-ku, Tokyo, 169-8555, Japan

^b Department of Chemical and Biological Science, Faculty of Science, Japan Women's University, Mejirodai, Bunkyo-ku, Tokyo, 112-8681, Japan

^c Department of Applied Chemistry, Faculty of Engineering, Kanagawa Institute of Technology, 1030 Shimo-Ogino, Atsugi-shi, Kanagawa, 243-0292, Japan

Received 14 July 1997; received in revised form 21 October 1997; accepted 12 November 1997

Abstract

The concentration of potassium was determined by a combination of flow injection analysis (FIA) with an all-solid-state potassium sensor detection. The all-solid-state potassium-selective electrode possessing long-term potential stability was fabricated by coating an electroactive polypyrrole/poly(4-styrenesulfonate) film electrode with a plasticized poly(vinyl chloride) membrane containing valinomycin. The simple FIA system developed in this laboratory demonstrated sensitivity identical to that in the batch system and achieved considerably rapid assay (150 samples h⁻¹). Analyses of soy sauce and control serum samples by this FIA system yielded results in good agreement with those obtained by conventional measurements. © 1998 Elsevier Science B.V. All rights reserved.

Keywords: Flow injection analysis; Ion selective electrode; Potassium

1. Introduction

Determination of potassium contents of serum, urine, and foods is very important in clinical and medical fields [1], since the potassium contents are related to renal diseases. These diseases restrict patients to a diet containing a large amount of potassium. From the potassium determination,

medical information concerning physical conditions of the patient can be obtained. In the case of hypokalemia, alkalosis, cirrhosis of liver, diuretic drugs, etc. are suspected. On the other hand, when potassium concentration in human serum becomes higher than 9 mmol dm⁻³, heart often stops. Hence, accurate, easy and rapid sensing of potassium ions is very important.

Miniaturization of an ion-selective electrode (ISE) will bring improvements in determining ion contents in clinical and medical fields. Recently,

* Corresponding author. Tel.: +81 3 52863202; fax: +81 3 32052074; e-mail: osakatet@mn.waseda.ac.jp

we reported on the highly stable response of the all-solid-state K^+ ISE with an electropolymerized film [2,3], which, in general, is known to provide various functionalities [4–8]. This solid state electrode can be easily miniaturized. On the other hand, the method of flow injection analysis (FIA) allows fast and simple sample treatment, e.g. ion-selective electrodes have been employed previously as an FIA detector for analyses of real samples [9]. Because of the use of small diameter tubings, small volume injectors, flow-through detectors and fast flow rates, the FIA system offers rapid assay with high precision [10–14]. In this work, we combined the all-solid-state K^+ ISE with the simple flow injection system developed in this laboratory.

2. Experimental details

2.1. Reagents

Reagent grade pyrrole, valinomycin (Wako), poly(sodium 4-styrenesulfonate) (Aldrich, M_w ca. 70000 $g\ mol^{-1}$), poly(vinyl chloride) (PVC) (Kanto, $n = 1000 \pm 40$), *o*-nitrophenyl octyl ether (*o*-NPOE), and potassium tetrakis(*p*-chlorophenyl) borate (KTpCIPB) (Tokyo Kasei Kogyo) were used without further purification. A 2-amino-2-hydroxymethyl-1,3-propanediol (Tris) ($50\ mmol\ dm^{-3}$)-HCl ($0.1\ mol\ dm^{-3}$) buffer solution was used as pH buffer. All other chemicals used were of analytical-reagent grade. Deionized and distilled water was used in all experiments.

2.2. Preparation of solid state K^+ ISE

Details of the fabrication of the all-solid-state potassium ion selective electrode have been described in our previous papers [2]. A polypyrrole/poly(4-styrenesulfonate) (PPy/PSS) composite film was deposited potentiostatically on a Pt disk (1 mm in diameter) from an aqueous solution containing pyrrole and poly(sodium 4-styrenesulfonate) at 0.8 V vs. Ag/AgCl by passing a charge of $10^\circ C\ cm^{-2}$. After electropolymerization, the PPy/PSS composite film electrode was condi-

tioned in $1\ mol\ dm^{-3}\ KCl$ for 2 h and dried in laboratory atmosphere. The potassium-selective PVC membrane was formed on the PPy/PSS film electrode by casting from a tetrahydrofuran solution containing 7.0 wt.% valinomycin, 62.7 wt.% *o*-NPOE, 1.1 wt.% KTpCIPB and 29.2 wt.% PVC.

2.3. Flow injection analysis with K^+ ISE

A schematic diagram of the potentiometric flow system equipped with the K^+ ISE is illustrated in Fig. 1. Tris buffer (pH = 7.5 at room temperature) was continuously pumped through the system with a peristaltic pump (ATTO, AC-2120) at a flow rate of $2.8\ ml\ min^{-1}$. Sample solution was introduced via a rotary injection valve (Rheodyne, 7010). Fig. 1b shows a schematic drawing of the sensing part. A carrier stream was directed against the side of the reference electrode glass vessel. Employing this sensing configuration enabled

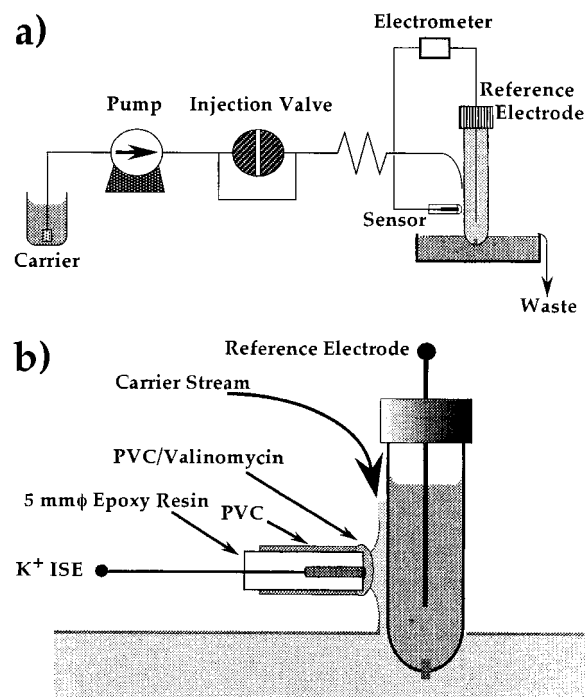


Fig. 1. a) Schematic diagram of the assay system using a flow-through potentiometric K^+ ion sensor and b) schematic configuration of the all-solid-state K^+ ISE in the FIA system.

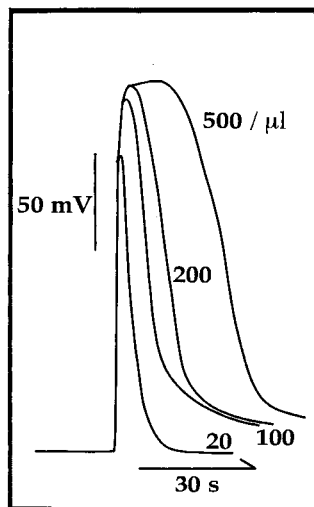


Fig. 2. Dependence of injection volume on potential response to 10 mmol dm^{-3} KCl with the use of the K^+ ISE based-simple FIA system. Carrier stream, 50 mmol dm^{-3} Tris (pH 7.5 adjusted with 0.1 mol dm^{-3} HCl); flow rate, 2.8 ml min^{-1} .

rapid assay owing to the absence of dead volume at the probe.

3. Results and discussion

3.1. Response properties and calibration

The all-solid-state K^+ ISE responded to the K^+ ion selectively even in a test solution containing Na^+ ion [2] and showed high stability as a potassium ion sensor in the batch system [3]. This K^+ ISE electrode displayed low potential drift in the response to potassium ion. First, by operating the K^+ ISE in the simple FIA system, injection volume was optimized as $200 \mu\text{l}$ for more sensitive and rapid determination as shown in Fig. 2. And more, flow rate and valve switching timing were optimized. The K^+ ISE based-simple FIA system demonstrated rapid potential responses with good sensitivity as shown in Figs. 3 and 4. In Fig. 3, a linear relationship was obtained in the range of K^+ activity from 10^{-5} – 10^{-1} with a slope of $57.6 \text{ mV decade}^{-1}$. The apparatus allowed 150 samples to be assayed per hour with a precision of 2.0% as illustrated in Fig. 4. As summarized in

Table 1, although the analytical precision varied with the concentration of potassium chloride, it was possible to determine potassium contents with satisfactory precision in the range of 10^{-5} – $10^{-1} \text{ mol dm}^{-3}$ potassium chloride. As previously analyzed by ac impedance for the batch system [3], the long-term stability of the K^+ ISE in the simple FIA was also confirmed, i.e. low potential drift and low impedance. We also evaluated time dependence of the sensitivity. Table 2 shows that the slope of the calibration curve remained almost independent of time during the period of 8 days after fabrication.

The results described above demonstrate that the simple FIA system equipped with the K^+ ISE allows rapid determination of potassium in KCl standard solutions with high precision.

3.2. Assay of food and serum samples

Figs. 5 and 6 show response curves obtained with two samples of Japanese soy sauce and one sample of control serum. In these determinations, soy sauce and control serum were diluted by factors of 200 and 20, respectively, in order to avoid interference by the presence of protein con-

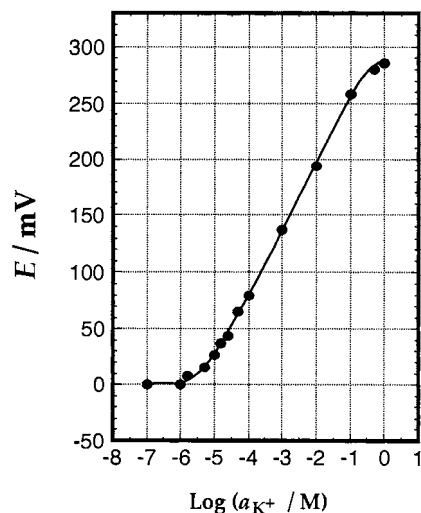


Fig. 3. Calibration graph for potassium ion using the FIA. Carrier stream, 50 mmol dm^{-3} Tris (pH 7.5 adjusted with 0.1 mol dm^{-3} HCl); flow rate, 2.8 ml min^{-1} ; injection volume, $200 \mu\text{l}$.

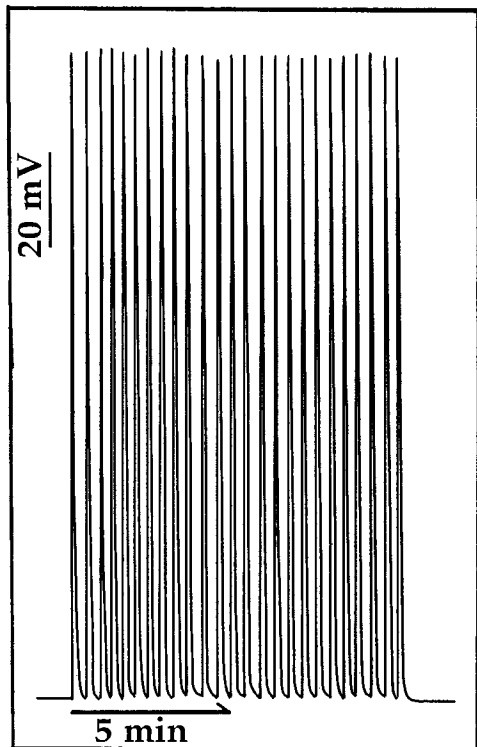


Fig. 4. Typical FIA peaks for 1 mmol dm⁻³ KCl standard solution. Operational, $n = 25$; carrier stream, 50 mmol dm⁻³ Tris (pH 7.5 adjusted with 0.1 mol dm⁻³ HCl); flow rate, 2.8 ml min⁻¹; injection volume, 200 μ l.

tained in the samples. Potassium concentrations estimated from the FIA analyses were; 0.143 mmol dm⁻³ (sample A) and 0.124 mmol dm⁻³ (sample B). These results agreed with flame photometric data. Furthermore, the potassium content of the control serum was determined to be 4.06 mmol dm⁻³, which also agreed with that listed for the specific serum lot used. In addition,

Table 1
Reproducibility of assay for standard potassium ion solution with various concentrations

KCl (mol dm ⁻³)	Precision (%)
1.0×10^{-1}	0.16
1.0×10^{-3}	2.00
1.0×10^{-5}	4.73

Table 2
Variations in the slope of calibration plots for potassium ion

Time (day)	Slope ^a (mV decade ⁻¹)
1	55.5
2	55.5
4	56.0
6	55.0
8	56.5

^a Slope was measured between $a_{K^+} = 1.0 \times 10^{-3}$ and 1.0×10^{-1} with more than 50 assays day⁻¹.

the recovery of potassium ions contained in diluted control serum samples is demonstrated in Table 3. At various dilution factors, recoveries were almost constant for determining potassium contents, and the mean recovery was 101.6%.

Soy Sauces

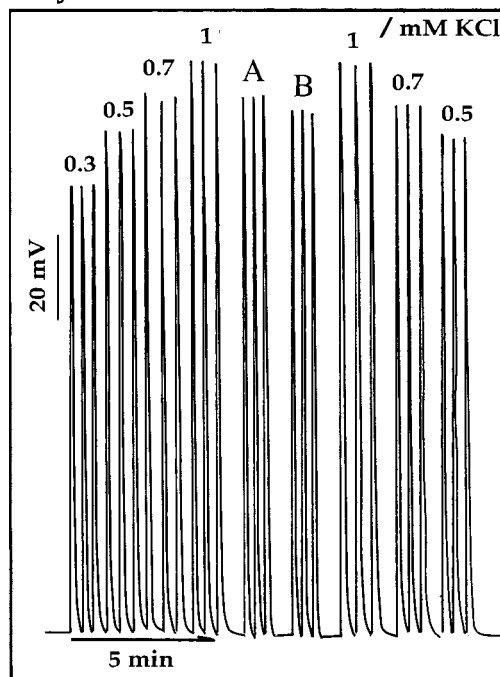


Fig. 5. FIA signals for determining potassium contents in two soy sauce samples. Carrier stream, 50 mmol dm⁻³ Tris (pH 7.5 adjusted with 0.1 mol dm⁻³ HCl); flow rate, 2.8 ml min⁻¹; injection volume, 200 μ l.

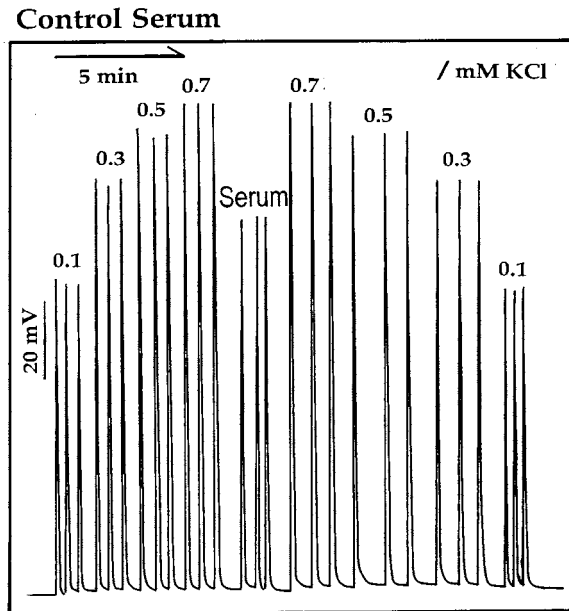


Fig. 6. FIA signals for determining potassium contents in control serum. Carrier stream, 50 mmol dm^{-3} Tris (pH 7.5 adjusted with 0.1 mol dm^{-3} HCl); flow rate, 2.8 ml min^{-1} ; injection volume, $200 \mu\text{l}$.

4. Conclusions

The potentiometric determination of potassium ions in the range between 10^{-5} and $10^{-1} \text{ mol dm}^{-3}$ was possible with the use of the simple flow injection cell equipped with the all-solid-state K^+ ISE developed in this laboratory. We achieved rapid ($150 \text{ samples h}^{-1}$) and continuous assay of potassium ions with good precision. It was demonstrated that samples of soy sauce and control serum can be assayed by this FIA system.

Table 3

Recovery of potassium added to control serum diluted (operational, $n = 25$)

Dilution rate	Recovery (%)
10	104
20	99.4
30	101
50	102

References

- [1] T.R. Harrison, R.D. Adams, I.L. Bennett, W.H. Resnik, G.W. Thorn, M.M. Wintrobe (Eds.), Principles of Internal Medicine, 5th edn., McGraw-Hill, New York, 1966.
- [2] T. Momma, S. Komaba, M. Yamamoto, T. Osaka, S. Yamauchi, Sensors Actuators B 24–25 (1995) 724–728.
- [3] T. Momma, M. Yamamoto, S. Komaba, T. Osaka, J. Electroanal. Chem. 407 (1996) 91.
- [4] T. Osaka, S. Komaba, M. Seyama, K. Tanabe, Sensors Actuators B 36 (1996) 463.
- [5] T. Osaka, S. Komaba, K. Fujihana, N. Okamoto, T. Momma, N. Kaneko, J. Electrochem. Soc. 144 (1997) 742.
- [6] W. Schuhmann, Mikrochim. Acta 121 (1995) 1.
- [7] F. Palmisano, D. Centonze, M. Quinto, P.G. Zambonin, Biosensors Bioelectron. 11 (1996) 419.
- [8] G.E. De Benedetto, F. Palmisano, P.G. Zambonin, Biosensors Bioelectron. 11 (1996) 1001.
- [9] P. Solich, P.E. Macheras, M.A. Koupparis, J. Pharm. Sci. 84 (1995) 889.
- [10] E.H. Hansen, F.J. Krug, A.K. Ghose, J. Ruzicka, Analyst 102 (1977) 714.
- [11] M.E. Meyerhoff, P.M. Kovach, J. Chem. Educ. 60 (1983) 765.
- [12] G.J. Moody, B.B. Saad, J.D.R. Thomas, Analyst 114 (1989) 15.
- [13] I. Satoh, Y. Aoki, Denki Kagaku 58 (1990) 1114.
- [14] I. Satoh, M. Akahane, K. Matsumoto, Sensors Actuators B 5 (1991) 241.

A modified catalytic–photometric method for the determination of vanadium in chloride rich hydro-geochemical samples

B.K. Balaji *, G. Saravanakumar, P. Murugesan, G. Mishra

Chemical Laboratory, Atomic Minerals Division, Department of Atomic Energy, Shradha buildings, R.V. Desai Road, Vadodara, Gujarat, 390 001, India

Received 21 July 1997; received in revised form 3 November 1997; accepted 12 November 1997

Abstract

The vanadium content in chloride rich hydrogeochemical samples has been determined through a modification in the existing standard gallic acid oxidation method which has severe interference problem from halides. The modification incorporates a preliminary fume-drying of the sample aliquot with a mixture of perchloric and sulphuric acids. This ensures total removal of halides and hence their interference. The estimation is completed as per the standard method after taking the sample in 10 ml of 1% nitric acid. Also mercuric nitrate addition which forms a part of the standard procedure to prevent halide interference, is also dispensed with keeping in view the toxic nature of mercury. The method has been tried on a number of samples having varying chloride content. The results obtained compare well with the standard PAR method. The method can be used to determine vanadium down to 1 ppb. The relative standard deviation obtained for vanadium contents in the range 400–10 ppb is in the range 4–8.2%. © 1998 Elsevier Science B.V. All rights reserved.

Keywords: Catalytic–photometric method; Determination; Vanadium; Chloride

1. Introduction

The determination of vanadium content at ppb level in potable water and hydrogeochemical samples has an important role to play because, (i) its presence in the range 20–150 ppb in drinking water has been reported to have beneficial role in the prevention of heart disease, and (ii) for locating the calcrite type of uranium deposit contain-

ing carnotite (a secondary mineral of uranium in association with vanadium and potassium having the composition $K_2O \cdot 2U_2O_3 \cdot V_2O_5 \cdot 2H_2O$). The procedure followed for the determination of vanadium is the catalytic–photometric method [1,2] that is based on the catalytic action of vanadium on the oxidation–coloration reaction of gallic acid by ammonium persulphate in acid medium. This method being highly sensitive is considered superior to other methods, [3–9] wherein different oxidizing agents and reagents that generate coloured product on oxidation, have

* Corresponding author. Fax: +91 265 432669.

been used. Although the persulphate–gallic acid procedure is accepted as the standard method, inherent defects of the method like reproducibility, accuracy and susceptibility to interference, calls for a cautious acceptance of the results. Weiguo [10] after a critical study suggested certain modifications which helped to achieve better reproducibility and improved sensitivity. However, the method continued to have serious interference problems from some cations and anions. Of the halides, chloride bromide and iodide, the latter two interfere seriously even when present at low levels. The tolerance limit for chloride, bromide and iodide are 100 ppm, 0.1 and 0.001 ppm respectively. Addition of mercuric nitrate (350 ppm) raises the tolerance limit for bromide and iodide to 0.25 ppm. However, when the levels of halides exceed the above limits, dilution of the sample solution is recommended so as to have the optimum suggested level of the halides, to pursue the determination. Mercuric ion itself acts as an interference when used beyond the suggested quantity of 350 ppm. Thus the knowledge of the halide content is essential to proceed with the vanadium determination.

During the analysis of hydrogeochemical samples from the semi-arid zones of Rajasthan, India, while surveying for carnotite mineralization, samples with high chloride contents ranging upto one lakh ppm and beyond, were encountered. Determination of vanadium in these chloride rich samples could not be carried out by the dilution technique as the dilution of the sample, many folds, resulted in bringing down the level of vanadium to an extent that was below the determination limit of the method. Also there is no easy way to ascertain the bromide and iodide content of the sample. In order to overcome the above problem, the present work has been developed after suitable modification of the existing method. It describes a simple and reliable procedure for determining vanadium in chloride rich hydrogeochemical samples. The procedure also excludes the use of mercury which is known for its toxicity.

2. Experimental

2.1. Apparatus

A cryostatic constant temperature waterbath model CB-701 from M/S Remi Instruments, Mumbai, India, with temperature control of $\pm 0.2^\circ\text{C}$ was used.

An ultrasonic cleaner IS-120 W/F from M/S IMECO ultrasonics, Mumbai, was used for cleaning glass ware.

A Elico (India) UV-Visible spectrophotometer ultraspecmodel CL-540 was used for making absorbance measurements.

2.2. Reagents

All chemicals used were of analytical reagent grade and the solutions were prepared using doubly distilled water.

2.3. Standard vanadium solution

100 $\mu\text{g ml}^{-1}$. It is prepared by dissolving 0.23 g of ammonium metavanadate in 1 l of water containing 7.5 ml of concentrated nitric acid. Working solutions of 1 and 0.1 $\mu\text{g ml}^{-1}$ were prepared fresh daily, for the work.

2.4. Ammonium persulphate–phosphoric acid solution (reagent A)

Prepared by dissolving 2.5 g of ammonium persulphate in 50 ml of 1:1 orthophosphoric acid solution. The solution is to be used after 29 h but is to be discarded after 48 h.

2.5. Gallic acid, 1% solution (reagent B)

1 g of gallic acid was dissolved in 100 ml of water and filtered before use. The solution is prepared fresh daily.

2.6. Mercuric nitrate solution

Prepared by dissolving 350 mg of mercuric nitrate in 1 l of water (350 $\mu\text{g ml}^{-1}$).

2.7. Procedure

The glass ware to be used are all initially cleaned in the ultrasonic cleaner using dilute nitric acid (3% v/v).

A known quantity of the sample aliquot containing not more than 0.4 μg of vanadium is taken in 50 ml beaker. It is treated with 0.5 ml of 1:1 sulphuric acid and 0.5 ml of perchloric acid (70% v/v) and heated on a hot plate till the evolution of dense white fumes ceased. The residue is taken up in 10 ml of 1% nitric acid which is added in small lots. The solution is transferred after warming, to vials having 10 ml marking. The final volume is adjusted to 10 ml with 1% nitric acid. A blank and a series of standards ranging from 0.05 to 0.4 μg vanadium were also processed similarly to obtain a calibration graph. The vials were stoppered and kept in the cryostatic bath set to 25°C along with the stoppered bottles containing ammonium persulphate–phosphoric acid solution (reagent A) and gallic acid [reagent B] for equilibration at the set temperature. After 45 min, 1 ml of reagent A is added to each of the vials, they are kept back in the water bath after swirling, for thorough mixing. After 15 min, 1 ml of reagent B is added to first vial which after mixing is placed again in the cryostatic bath. Addition of reagent B to other vials were continued at intervals of 2 min and were returned to the bath for equilibration. Exactly 60 min after the addition of reagent B, the absorbance of each solution was measured at 415 nm against distilled water as the blank. The vanadium content of the sample is computed from the calibration plot drawn for the standards. Beers law obeyed in the range 0.05–0.40 μg in 12 ml of the solution.

3. Results and discussion

Since it is known that the only effective way of driving out halides is by fuming with sulphuric acid, an attempt has been made in the present work to overcome the problem of interference of chloride in the vanadium determination. Fume drying of the sample with perchloric–sulphuric acid combination has been introduced as a pre-

liminary step in the existing procedure. This step ensures destruction of the dissolved organic matter with simultaneous conversion of all forms of vanadium to the pentavalent state and total removal of halides, thus paving way for vanadium determination. The following studies were also carried out to know the implications of the modification suggested.

3.1. Effect of sulphate ions

Varying quantities of sulphate ions were added to a series of solutions containing 0.1 μg vanadium and the absorbance of the solutions were measured after processing them as suggested in the procedure. It is noticed that presence of even upto 100000 ppm of sulphate, has no effect on the absorbance. Quantities beyond this were not tried. In order to fix the quantity of 1:1 sulphuric acid to be used and also to know their effectiveness for displacing chloride ions, experiments were carried out by adding 0.25, 0.50, 0.75 and 1.00 ml of 1:1 sulphuric acid along with 0.5 ml of perchloric acid, on solutions of 0.1 μg vanadium containing 5000–1 lakh ppm of chloride. After fume drying and processing as suggested above, the absorbance of the solutions were measured at 415 nm. In all the cases it is noticed that the fuming is effective in displacing the chloride ions as evidenced from the net absorbance values obtained which were comparable with the absorbance value of pure 0.1 μg vanadium solution, processed in a similar fashion. It was also noticed that, where quantities of sulphuric acid above 0.50 ml was used, there was a slight increase in absorbance values of both blank as well as that of the 0.1 μg vanadium solution.

Thus keeping in view the fuming time and the blank value, use of quantities beyond 0.5 ml of 1:1 sulphuric acid was discarded. Use of 0.25 ml of 1:1 sulphuric acid was also not continued as it may not be able to effectively displace chlorides in chloride rich samples. Hence a quantity of 0.50 ml was selected as the optimum quantity for further work. Further experiments also revealed that, use of 0.5 ml 1:1 sulphuric acid can comfortably fume of even around 1 lakh ppm of chloride. Fig. 1 shows the absorbance values obtained for solu-

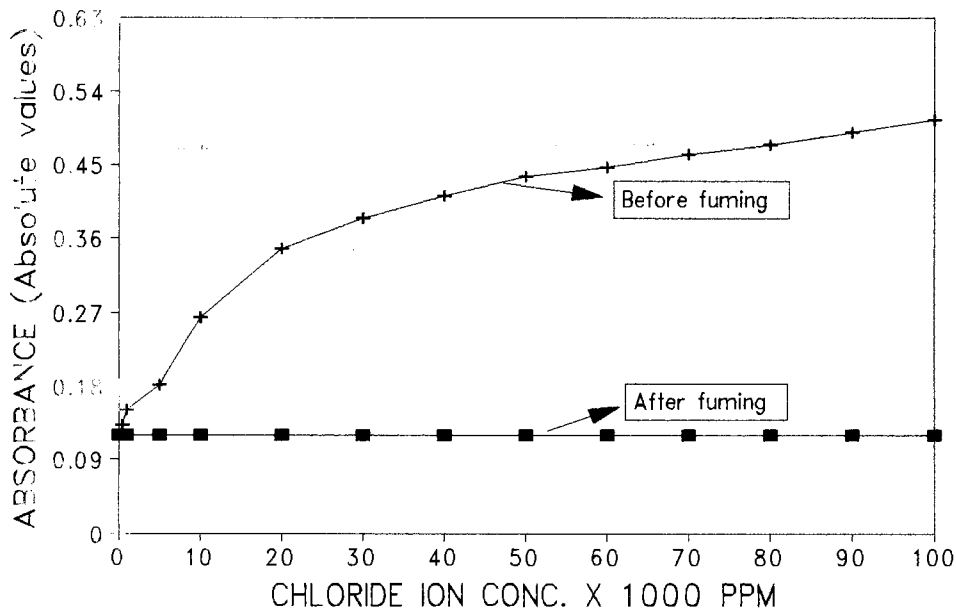


Fig. 1. Effect of chloride ion on absorbance of 0.1 µg vanadium.

tions containing 0.1 µg of vanadium, in presence of chloride and absorbance values obtained after fuming with perchloric and sulphuric acid.

3.2. Effect of metal ions

A fresh study was made with regard to the tolerance to various metal ions that are likely to interfere in view of the fact that certain modifications have been made. Table 1 gives the tolerance

Table 1
Tolerance limit for various cations and anions

Ions	Concentration (ppm)
U(VI)	10.0
Cr(VI)	1.5
Fe(III)	6.0
Mo(VI)	0.2
Co(III)	1.0
Cu(II)	0.05
Ni(II)	3.0
Ag(II)	1.0
F ⁻	15.0
Cl ⁻	100.0
Br ⁻	0.10
I ⁻	0.001

limits for various ions. It is seen that there is improved tolerance for iron. Further, the samples taken up for estimation of vanadium, were found to have the concentration of the interfering metal ions well below the tolerance limit given in the Table 1. From the results of the experiments carried out. It is evident that chlorides can effectively be removed from samples by simple fuming with a combination of perchloric and sulphuric acids. This obviously should ensure the removal of traces of bromides and iodides that may be present along with the chlorides. This aspect was confirmed by recording the absorbance value, after fuming with perchloric acid–sulphuric acid mixture, of a solution containing 0.10 µg vanadium along with 5000 ppm chloride, 10 ppm bromide and 10 ppm iodide. The absorbance value matched with that of the vanadium solution, not containing halides. Thus the suggested modification gets rid of the interference from the halides totally. The advantage of the modification suggested is that, there is no need to know the halide content of each sample, which however was a prerequisite for determining vanadium in the existing method for carrying out optimum dilutions in order to prevent halide interference. Yet

Table 2
Comparison of the values obtained by present method with standard PAR method

Sample No.	Chloride content (ppm)	Aliquot taken (ml)	Vanadium found (ppb)			
			Present method	RSD* (%)	PAR method	Standard addition technique
1	1435	10	10	8.2	9	11
2	2118	10	21	7.7	24	27
3	950	10	25	7.4	22	27
4	7875	5	33	7.3	40	35
5	2100	10	43	7.2	43	40
6	26425	2	43	6.8	48	48
7	23625	5	63	6.4	59	64
8	2188	2	98	5.9	92	95
9	140	2	113	5.3	126	122
10	1453	1	253	5.0	230	246
11	245	1	323	4.0	343	326
12	187 120	0.5	63	6.5	69	67

* Based on average of four determinations.

an other consequence of the modification suggested is that since there is total removal of halides, addition of mercuric nitrate, it was felt was unnecessary and superfluous. This in fact was confirmed experimentally, by processing a set of samples in duplicate and comparing the absorbance values of the set to which mercuric nitrate is added, with that of the set to which mercuric nitrate is not added. It was noticed that there was no difference in the absorbance values. Thus in the present work, use of mercuric nitrate has been dispensed with, completely. The exclusion of the use of mercuric nitrate is an added advantage in view of its poisonous nature and its possible pollution of the environment.

In order to validate the suggested method, the values obtained have been compared with the values obtained by standard PAR [11,12] method after preconcentration. Further validation was made by standard addition technique. The results obtained on a batch of 12 samples has been incorporated in Table 2 along with the relative standard deviation. The results obtained by PAR method and the standard addition technique are also given along with. Typical plots obtained for five random samples by standard addition technique are given in Fig. 2. It is seen that results compare well.

4. Conclusions

A simple, precise and accurate method has been suggested as a modification to the existing standard method, for determining vanadium in the chloride rich hydrogeochemical samples. It involves a preliminary fume drying of the sample with a mixture of perchloric and sulphuric acids. The procedure helps in overcoming the interference effects caused due to presence of halides. Depending on the nature (high or low total dissolved salt content) and quantity of the sample aliquot taken, the method can be extended to determine vanadium down to 1 ppb. The relative standard deviation ranges from 8.2 to 4.0% for the concentration range 10 to 400 ppb. Also the use of mercuric ion has been dispensed with.

Acknowledgements

The authors wish to thank the Regional Director, western region and the Head Chemistry Group, for their kind encouragement to carry out the above work. Sincere thanks are also due to Shari PK Shrivastava, Dr Ravikumar and Shri Hanumanthappa for providing water samples.

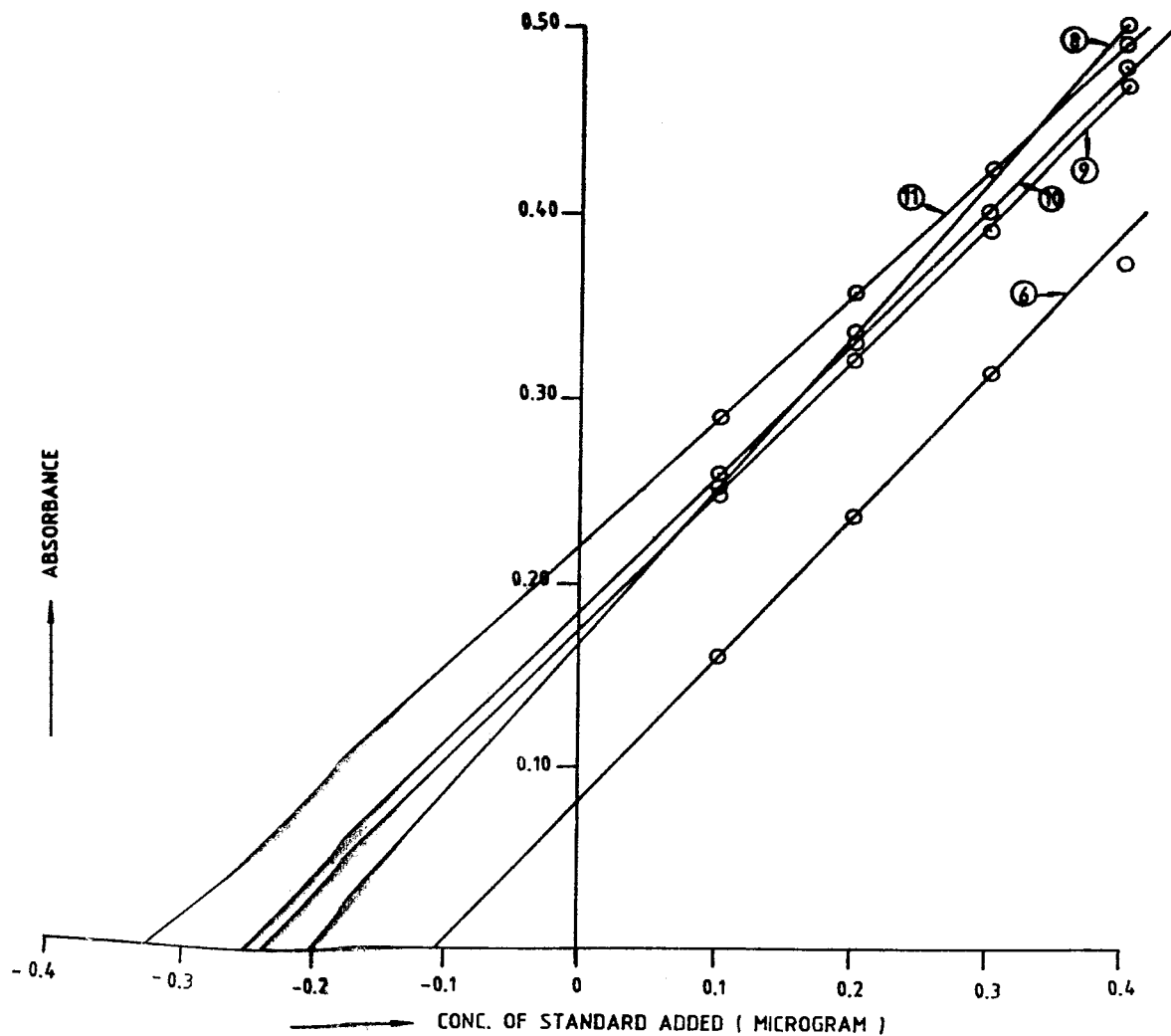


Fig. 2. Standard addition plot for selected samples.

References

- [1] M.J. Fishman, M.W. Skougstad, *Anal. Chem.* 36 (1964) 1643.
- [2] L. Clesceri, A. Greenberg, R.R. Trussell., *Standard Methods for the Examination of Water and Waste-water*, 17th edn., APHA, Washington, 1989, pp. 3–155.
- [3] D. Costache, *Chem. Abstr.* 79 (1973) 73233u.
- [4] C.W. Fuller, J.M. Ottaway, *Analyst* 95 (1970) 41.
- [5] S.U. Kreingol'd, A.A. Pantelemonova, R.V. Poponova, *Zh. Anal. Chim.* 28 (1973) 2179.
- [6] I.A. Il'icheva, I.F. Degetereva, I.F. Dolmanova, L.A. Petrukchina, *Chem. Abstr.* 89 (1978) 190385n.
- [7] G.S. Lisetskaya, G.F. Bakal, *Ukr. Khim. Zh.* 36 (1970) 709.
- [8] T. Motoharu, A. Norio, *Anal. Chim. Acta* 39 (1967) 485.
- [9] M.H. Cordoba, P. Vinas, C. Sanchez-Pedreno, *Analyst* 110 (1985) 1343.
- [10] Q. Weiguo, *Anal. Chem.* 55 (1983) 2043.
- [11] G. Chakrapani, D.S.R. Murty, B.K. Balaji, R. Rangaswamy, *Talanta* 40 (1993) 84–541.
- [12] H. Onishi, *Photometric Determination of Traces of Metals*, vol. 3., IIB., 4th edn., Wiley-Interscience, New York, 1989, p. 677.

Applying magnesium hydroxide coprecipitation method for trace analysis to dialysis concentrate

Latif Elçi *, Sibel Saraçoğlu

Chemistry Department, Art and Sciences Faculty, Erciyes University, 38039 Kayseri, Turkey

Received 28 July 1997; received in revised form 17 November 1997; accepted 20 November 1997

Abstract

A magnesium hydroxide coprecipitation technique for determination of Cd, Co, Cu, Mn, Ni in dialysis concentrate is described. The analytes are concentrated from 10 ml of dialysis concentrate into 1 ml of 1 M HNO₃ and subsequently determined by graphite furnace atomic absorption spectrometry. Coprecipitation parameters and matrix effects are discussed. The precision, based on replicate analysis, is around 5% for the analytes, and recovery is quantitative, based on analysis of spiked samples and solutions including matrix components. © 1998 Elsevier Science B.V. All rights reserved.

Keywords: Coprecipitation; Magnesium hydroxide; Dialysis concentrate

1. Introduction

Coprecipitation by hydroxides of metals is frequently used in the preconcentration of trace amounts of analytes, generally using a milligram quantity of carrier element [1,2]. Among metal hydroxides, magnesium hydroxide is the most attractive gathering precipitate due to the quantitative trace recovery of some elements and sufficient separation factors for alkaline elements [3–5]. It is especially useful for high salinity samples, such as sea water, dialysis concentrate, etc., including

magnesium ions at high enough concentration levels.

To the best of our knowledge, a magnesium hydroxide coprecipitation system has not been applied to the analysis of dialysis concentrate. Whereas, such a coprecipitation system would be ideal for analysis of dialysis concentrate because of an appropriate magnesium content. Furthermore, the contamination for the analysis would be significantly decreased, as it would only be from the sodium hydroxide solution used for pH adjustment.

In this study, the method of determination of the concentrations of cadmium, cobalt, copper, manganese and nickel in a dialysis concentrate has been critically discussed and extended.

* Corresponding author. Tel./fax: +90 352 4374933; e-mail: elci@zirve.erciyes.edu.tr

2. Experimental

2.1. Apparatus

A Hitachi Model Z-8000 atomic absorption spectrometer with a Zeeman background corrector was employed for the determination of analytes ions in the aqueous solution. An air–acetylene flame was used for the determinations related to model workings. The sample solutions were introduced into the nebulizer using an injection technique [6]. A Hitachi Model graphite furnace atomizer (Part no. 180-7400) was used for the determination of Cd, Co, Cu, Mn and Ni in the dialysis concentrate. The conditions for AAS measurements were as recommended by the instrument manufacturer.

A pH meter, Delta 320 Mettler, was employed for measuring pH values in the aqueous phase.

2.2. Reagents and solutions

Stock standard solutions of analytes, 1000 mg l⁻¹, were diluted daily for obtaining reference and test solutions. Water, redistilled in a quartz apparatus, was used in all the experiments. Sodium hydroxide (suprapure grade, Merck) was used for preparation of 6 M NaOH solutions and pH adjustment. Two mg ml⁻¹ Mg²⁺ as nitrate salt was prepared freshly from solid magnesium nitrate hexahydrate (suprapure grade, Merck). Nitric acid (65%) used for preparation of dilute acid solution was suprapure grade from Merck.

3. Procedures

3.1. Test working

The coprecipitation method was tested with model solutions prior to its application to dialysis concentrate. Five hundred microliters of 2 mg ml⁻¹ magnesium solutions were added to 10.0 ml of a solution containing 1–0.5 µg of Cd, Co, Cr, Cu, Mn, Ni and Pb. Then, a certain amount of 6 M NaOH solution was added to adjust the pH or NaOH concentration. After 10 min, the solution was centrifuged at 3500 rpm for 30 min. The

supernatant was removed. The precipitate remaining adhered to the tube was dissolved with 1 ml of 1 M HNO₃. To determine the analytes, 100 µl of this final solution was injected into the flame AAS nebulizer. There were three replicates for the test workings.

3.2. Analysis of dialysis concentrate

Exactly 10.0 ml of dialysis concentrate is placed into a 15-ml glass centrifugation tube. To form a magnesium hydroxide precipitate and to run coprecipitation, the pH of the concentrate is adjusted to 12.7 with 6 M NaOH solution. A certain amount of the NaOH solution is previously determined with a pH meter using a reference dialysis solution. The tube is slowly and carefully shaken for several seconds and allowed to stand for 10 min. The precipitate is centrifuged at 3500 rpm for 30 min, and the supernatant is discarded. A small precipitate adheres to the bottom of the tube. Then, 1 ml of 1 M HNO₃ is added to dissolve the precipitate. The analytes in this solution are determined with graphite furnace AAS using matrix matching standards.

4. Results and discussion

4.1. Coprecipitation of some metal ions with magnesium hydroxide

Initially, an attempt was made to examine the effect of magnesium concentration, due to the magnesium matrix, on the determination of the desired elements, using flame atomic absorption spectrometry. The absorbances for the elements remained almost constant up to about 40 mg ml⁻¹ Mg²⁺, however, above this concentration a decrease in the absorbances (increase for Pb) was observed. This indicates that the concentration of magnesium in the final solution for the combination of coprecipitation with flame AAS must be a maximum of 40 mg ml⁻¹.

The amount of magnesium ion needed for coprecipitation was selected experimentally. As can be seen from Table 1, the recoveries of desired metal ions from solution prepared with increasing

Table 1
Effect of magnesium amount on coprecipitation ($n = 3$)

Amount of Mg (μg)	Recovery (%)						
	Cd	Co	Cr	Cu	Mn	Ni	Pb
0	63	67	52	73	69	72	30
250	80	80	86	99	90	82	89
500	82	96	88	97	96	87	94
750	83	95	93	97	96	95	96
1000	85	98	97	100	98	95	95
1250	86	97	97	99	98	96	95
1500	88	96	95	99	96	97	96
3000	85	96	98	98	97	98	96
4500	89	97	95	97	95	100	95

amounts of magnesium ion in 0.05 M NaOH (pH 12.7) were quantitative after 0.25 mg Mg^{2+} for Cu, 0.50 mg Mg^{2+} for Mn and Co, 0.75 mg Mg^{2+} for Ni and Pb, and 1.0 mg Mg^{2+} for Cr. With these amount of Mg^{2+} , as the recoveries decrease, the precision of the results was also poor. The recoveries for Cd were lower than 88%. Magnesium hydroxide was precipitated at different pH values from test solution containing 1 mg magnesium and fixed trace amount of desired elements, such as 1 μg for Cu, Co, Cr, Mn, Ni, Pb and Fe, and 0.5 μg for Cd. pH values were adjusted with 6 M NaOH solution. A bulky precipitate of magnesium hydroxide formed with 0.005 M NaOH (pH 11.7), collecting significant amounts of Cu, Mn and Co as shown in Table 2. However, all metal ions of interest were virtually completely coprecipitated in the range of 0.01–1 M NaOH. In this work, the optimum concentration of NaOH was taken as 0.05 M (pH 12.7).

4.2. Effect of matrix ions

To detect potential interference on the coprecipitation of examined elements, various amounts of NaCl, KCl, CaCl_2 , CH_3COONa and dextrose, as the major components of dialysis concentrate, were added to a solution containing the examined elements at the fixed amounts, and then the procedure was followed. The maximum concentrations of the components were selected, based on the data given in Table 3 [7,8]. The results are listed in

Table 4. Of all the components (except NaCl) in the concentration ranges investigated, Pb and Cr were the ones which were generally affected. The others were not affected. From the comparison of dialysis concentrate compositions given in Table 3 with the tolerable concentrations found in Table 4, it can be concluded that Co, Cu, Mn and Ni will be recovered quantitatively from the dialysis concentrate. The tolerable concentrations for the matrices are defined as the concentration causing a relative error smaller than $\pm 5\%$ in relation to the determination of examined analytes. However, Cd can be determined with 85% recovery. The results are desirable in view of application to the dialysis concentrate sample. On the other hand, the precipitation of calcium ion, as a hydroxide in the dialysis concentrate, can be expected at the optimum pH 12.7. However, it may be concluded that this is not important because of the quantitative recoveries of the analytes. The coprecipitation of calcium hydroxide with analytes was not investigated in this work.

4.3. Accuracy, precision and detection limits

To ensure that this procedure was valid for real sample analysis by GFAAS, the recoveries of analytes spiked into dialysis concentrate as a real sample were also studied; satisfactory results were obtained, as shown in Table 5. The analytical errors for Cd, Cu, Mn, Ni are in the range of -4.1 to $+5.6\%$. The relative error in the deter-

Table 2
Effect of NaOH concentration on coprecipitation ($n = 3$)

NaOH Conc. (M)	Recovery (%)						
	Cd	Co	Cr	Cu	Mn	Ni	Pb
0.005	10	35	5	69	40	20	5
0.01	86	97	98	98	97	98	98
0.05	85	97	97	99	98	97	96
0.1	85	98	96	100	100	98	96
1	79	100	95	100	99	100	40

mination of Cd was higher than 10%. Also, the errors found from the test solutions with or without the matrix ion were at the same level as Cd (Tables 1, 2, 4 and 5). However, the results for the determination of cadmium are considerably replicable (R.S.D., 6.2%). Also, the accuracy of results was confirmed by use of a Co-DDTC coprecipitation method [9]. As seen from Table 6, there is no significant difference between the concentrations of analytes, except for Ni, obtained by the two methods.

The relative standard deviations for graphite furnace atomic absorption spectrometric measurements are between 4.7 and 7.7% in the case of $0.87\text{--}3.29 \mu\text{g l}^{-1}$ of analytes.

The detection limits, defined as the concentration equivalent to three times the standard deviation ($n = 10$) of the reagent blank, for graphite furnace atomic absorption spectrometric measurements, were $0.08 \mu\text{g l}^{-1}$ for Cd, $0.24 \mu\text{g l}^{-1}$ Co,

$0.33 \mu\text{g l}^{-1}$ Cu, $0.15 \mu\text{g l}^{-1}$ Mn and $0.74 \mu\text{g l}^{-1}$ Ni.

4.4. Analysis of dialysis concentrate

Based on the above findings, the procedure was applied to a dialysis concentrate analysis. The results are summarized in Table 6. The analytes in the final solution obtained with the coprecipitation were determined using a graphite furnace atomic absorption spectrometer using matrix matching standards. Previously, the magnesium content of dialysis concentrate was determined with flame AAS. The content of Mg^{2+} was found to be $390 \mu\text{g ml}^{-1}$. Accordingly, the standard solutions used for the calibration curves include $4 \text{ mg ml}^{-1} \text{ Mg}^{2+}$, calculated according to 10 ml of dialysis concentrate.

The concentrations given in Table 6 have been calculated on the assumption of 100% recovery of the analytes. The results from magnesium hydroxide coprecipitation are compared with results obtained by the Co-DDTC coprecipitation method [9], using a *t*-test at 95% C.L. The dialysis concentrates, having the same production date, analysed in this work and given in Ref. [9], are from the same company. With the exception of Ni, no significant difference is indicated between the results obtained by two techniques. For nickel, there is also a significant difference between the concentrations at 99% C.L. If the results in Ref. [9] are acceptable as a true value, the analytical errors for Cd, Cu and Mn (except Co and Ni) are less than 8%.

Table 3
Composition of typical dialysis concentrate

Ion	Concentration ranges ($\mu\text{g ml}^{-1}$)
Cl^-	$1 \times 10^5\text{--}1.5 \times 10^5$
CH_3COO^-	$5 \times 10^3\text{--}8.0 \times 10^4$
Na^+	$8 \times 10^4\text{--}1.2 \times 10^5$
K^+	$2 \times 10^3\text{--}3.0 \times 10^3$
Ca^{2+}	$1.5 \times 10^3\text{--}2.5 \times 10^3$
Mg^{2+}	$4 \times 10^2\text{--}7.0 \times 10^3$
Dextrose	$\sim 6.4 \times 10^4$

Table 4
Effect of matrix components on coprecipitation ($n = 3$)

Matrix	Amount (mg ml ⁻¹)	Recovery (%)						
		Cd	Co	Cr	Cu	Mn	Ni	Pb
NaCl	5	88	100	95	96	99	97	100
	10	92	100	95	96	98	98	99
	50	89	98	93	98	96	100	99
	100	90	99	90	99	98	100	98
	200	85	96	89	95	94	101	93
KCl	5	87	97	96	96	98	96	78
	10	89	95	95	98	99	97	80
	20	90	98	93	97	99	96	81
CaCl ₂	5	92	97	95	98	100	99	75
	10	94	97	90	98	100	100	66
CH ₃ COONa	20	90	98	90	100	98	96	33
	10	85	96	88	96	98	100	88
Dextrose	50	82	95	85	96	99	95	80
	100	80	90	82	92	98	85	78
	10	90	100	94	97	97	100	75
	50	91	98	78	98	99	96	70
Dextrose	75	87	98	80	96	98	94	66
	100	88	96	75	85	94	86	54

5. Conclusion

It can be concluded that the magnesium hydroxide coprecipitation method can be applied to

Table 5
Recovery of analyte spikes from dialysis concentrate ($n = 3$)

Analyte	Added (µg)	Found (µg)	Error (%)
Cd	0	0.0087	—
	0.005	0.0121	-11.7
	0.010	0.0160	-14.4
Co	0	0.0092	—
	0.010	0.0184	-4.2
	0.020	0.0305	+4.4
Cu	0	0.0329	—
	0.010	0.0436	+2.8
	0.020	0.0538	+1.7
Mn	0	0.0288	—
	0.010	0.0372	-4.1
	0.020	0.0499	+2.2
Ni	0	0.0115	—
	0.010	0.0227	+5.6
	0.020	0.0323	+2.5

Table 6
Results of dialysis concentrate analysis

Analyte	Conc. (µg l ⁻¹ ; $(x \pm ts/\sqrt{n})^a$)	
	Present method ($n = 7$)	Reference method [9] ($n = 9$)
Cd	0.87 ± 0.05	0.83 ± 0.04
Co	0.92 ± 0.04	—
Cu	3.29 ± 0.19	3.52 ± 0.14
Mn	2.80 ± 0.15	3.04 ± 0.09
Ni	1.25 ± 0.09	1.51 ± 0.08

^a Uncertainty at 95% confidence limit.

the determination of Cd, Co, Cu, Mn and Ni in dialysis concentrates with acceptable accuracy and precision.

References

- [1] J. Minczewski, J. Chwastowska, R. Dybczynski, in: Separation and Preconcentration Methods in Inorganic Trace Analysis, Ellis Harwood, Chichester, 1982.

- [2] A. Mizuike, in: *Enrichment Techniques for Inorganic Trace Analysis*, Springer-Verlag, Berlin, 1983.
- [3] A. Tsuyama, S. Nakashima, *Bunseki Kagaku* 29 (1980) 81.
- [4] Y. Shigetomi, *Bunseki Kagaku* 24 (1975) 699.
- [5] A.S. Buchanan, P. Hannaker, *Anal. Chem.* 56 (1984) 1379.
- [6] H. Bernd, E. Jackwerth, *Spectrochim. Acta* 30B (1975) 169.
- [7] M.R. Pereiro Garcia, A. Lopez Garcia, M.E. Diaz Garcia, A. Sanz-Medel, *J. Anal. Atom. Spectrom.* 5 (1990) 15.
- [8] M. Soylak, L. Elçi, M. Doğan, *Anal. Lett.* 26 (1993) 1997.
- [9] L. Elçi, U. Şahin, S. Öztaş, *Talanta* 44 (1997) 1017.

Determination of arsenic content in natural water by graphite furnace atomic absorption spectrometry after collection as molybdoarsenate on activated carbon

Toshio Kubota *, Tetuya Yamaguchi, Tadao Okutani

College of Science and Technology, Nihon University, 7-24-1, Narashinodai, Funabashi-shi, Chiba 274, Japan

Received 16 September 1997; received in revised form 20 November 1997; accepted 21 November 1997

Abstract

A sample solution containing less than 0.5 μg of As was adjusted to pH 2. As in the solution was collected on activated carbon (AC) as molybdoarsenate. The AC was directly introduced as an AC suspension into a graphite furnace atomizer, and the concentration of As was determined by atomic absorption spectrometry (AAS). This method is relatively free from interference caused by coexisting ions. The calibration curve was linear up to 0.1 mg l^{-1} , and limit of detection of As was 0.004 mg l^{-1} . When 1000 ml of sample solution is preconcentrated to 5 ml (enrichment factor is 200-fold) 0.02 $\mu\text{g l}^{-1}$ of As could be determined, and relative standard deviation was below 4.0% (by the deuterium background correction system). The method was applied to sea water and well water, and the sum of As(III) and As(V) was determined with satisfactory results. © 1998 Elsevier Science B.V. All rights reserved.

Keywords: Arsenic; Natural water; Graphite furnace atomic absorption spectrometry; Molybdoarsenate; Activated carbon

1. Introduction

Arsenic causes severe poisoning in man, and a chronic effect can appear from it in the body even at a low intake level. Carcinogenicity of the skin and the lungs has been attributed to As [1]. Therefore, accurate determination of As has become of increasing importance.

Determination of As content was previously carried out by spectrophotometry of 12-molybdoarsenic acid [2] and silver diethyldithiocarba-

mate [3]. For the determination of low concentrations of As, the extraction of 12-molybdoarsenic acid into 1-butanol [4], adsorption with thionalide loaded on silica gel [5], and preconcentration of molybdoarsenate–malachite green aggregate [6] were combined with the spectrophotometry.

Atomic absorption spectrometry (AAS) is an easy, rapid method and has been widely used for the determination of trace elements in natural water. However, it has not been used for direct determination of As because of poor sensitivity. The sensitivity is greatly enhanced by coupling a

* Corresponding author. Fax: +81 474 695324

hydride generation method with flame [7–10] and flameless [11,12] atomic absorption spectrometry. Walcerz et al. [13] and Sturgeon and Gregoire [14] reported unique preconcentration methods. That is, generated hydrides were transferred to the inner wall of the graphite furnace, then the furnace was heated at a high temperature, vaporized As was determined by AAS [13] and ICP-MS [14]. However, the hydride generation method has a tendency to interference by coexisting ions [15]. To remove this drawback, a flotation was reported [16] by which As is coprecipitated with Fe(III) hydroxide and determined by hydride generation AAS.

Other preconcentration methods for As without using the hydride generation method have been published. Hata et al. [17] reported that the As in natural water was preconcentrated on a membrane filter as an ion associate of molybdoarsenate and tetrapentylammonium, and the As was determined by inductively coupled plasma atomic emission spectrometry. Peräniemi et al. [18] reported that the As in aqueous solution was adsorbed onto zirconium-loaded AC and was determined by X-ray fluorescence spectrometry.

In this report, a trace level of As in natural water was collected as molybdoarsenate onto AC. The AC suspension was directly introduced into a graphite furnace (GF), and As was determined by AAS. This method is free from interference caused by coexisting ions, and furthermore, the sum of As(III) and As(V) in clean water was simultaneously determined without digestion. This method was applied to sea water and well water.

2. Experimental

2.1. Apparatus

A Seiko Model SAS 727 atomic absorption spectrometer equipped with a Model SAS 705V graphite furnace (GF) atomizer, an As hollow-cathode lamp and a deuterium background corrector were used. The optimum operating conditions are listed in Table 1. A Hitachi Model Z8270 polarized Zeeman atomic absorption spec-

trometer was also used for comparison with of another background corrector. An ultrasonic cleaner Model B2200 (Bransonic) was used for the preparation of the AC suspension.

2.2. Reagents

The standard As(III) solution (1000 mg l^{-1}) was prepared by dissolving 0.1320 g of As_2O_3 (Wako) in 5 ml of 6 M NaOH solution, neutralizing with 6 M HCl and diluting it to 100 ml with deionized water. The standard As(V) solution (1000 mg l^{-1}) was prepared by dissolving 0.4165 g of $\text{Na}_2\text{HAsO}_4 \cdot 7\text{H}_2\text{O}$ (Nakarai Tesque) in deionized water and diluting to 100 ml. Five percent (w/v) Mo solution ($0.52 \text{ mol Mo l}^{-1}$) was added to 9.20 g of $(\text{NH}_4)_6\text{Mo}_7\text{O}_{24} \cdot 4\text{H}_2\text{O}$ (Wako, super special grade) dissolved in deionized water and diluted to 100 ml. One percent (w/v) Zr solution was prepared by dissolution of 2.93 g of $\text{ZrO}(\text{NO}_3)_2 \cdot 2\text{H}_2\text{O}$ in deionized water and was diluted to 100 ml. Activated carbon (AC, Merck No. 2186, smaller than 300 Tyler mesh) was soaked in 3 M HCl for 1 day, washed with deionized water until it was neutral, and was then dried at 120°C for 2 h and kept in a desiccator. All other reagents were of analytical grade.

2.3. Preconcentration and determination procedure

Up to a 1000-ml portion of the sample solution containing less than $0.5 \mu\text{g}$ of As was placed in a

Table 1
Operating conditions of GF-AAS

Atomic absorption spectrometer ^a	
Light source	As-HCl, 10 mA
Wavelength	197.2 nm
Spectral band width	1.0 nm
Graphite furnace	
Drying conditions	150°C , 20 s (ramp mode)
Ashing conditions	1200°C , 60 s (ramp mode)
Atomization	2600°C , 3 s (temperature control mode)
Purge gas	Ar, 2.5 l min^{-1} (continuous)

^a Deuterium background correction system.

beaker. Acetic acid (3 M) was added to the sample solution to make 0.1 M acetic acid, which was adjusted to pH 2.0 with 1 M HCl. Then 0.1 ml of 5% (w/v) Mo solution per 100 ml of sample volume and 0.1 g of AC were added. The solution was stirred for 10 min with a magnetic stirrer. The AC with adsorbed As was separated from the aqueous phase through a membrane filter (MF, 3- μ m pore size), and the AC on the MF was dispersed in 5 ml of 0.1 M acetic acid (containing 0.1 ml of 1% (w/v) Zr solution) using an ultrasonic cleaner for 30 s (AC suspension). Ten μ l of magnetically stirred AC suspension was pipetted into the GF. The peak height of AAS was measured under the conditions shown in Table 1.

3. Results and discussion

3.1. Analytical conditions

As is an easily volatilized element in GF-AAS. However, in this method, As is not easily lost by volatilization without matrix addition, because there is up to 840 μ g Mo in 5 ml of the AC suspension and it should act as a matrix modifier. However, the peak height of As decreased according to the heating time of exposure in the GF. Therefore, 0.1 ml of 1% (w/v) Zr solution (1 mg of Zr) was added to 5 ml of the AC suspension as a matrix modifier in a manner similar to that described in the previous paper [19]. Under these conditions, using a pyrocoated graphite tube as the GF, the effects of the ashing and atomization temperatures were investigated at from 400 to 1400°C and from 2300 to 2800°C, respectively. The conditions under which stable and maximum peak heights were obtained were an ashing temperature of 1200°C and an atomization temperature of 2600°C. Atomic absorption measurement of As has been recommended using resonance lines at 193.7 and 197.2 nm. The line at 193.7 nm was more sensitive than at 197.2 nm according to this method. However, the absorbance of blanks at 193.7 and 197.2 nm, respectively, were 0.032 and 0.0064. This phenomenon did not occur without molybdenum. Therefore, there should be a spectral interference with molybdenum. From this

reason, the line at 197.2 nm was used for measurement of the atomic absorption of As.

3.2. Effect of pH on the adsorption of As onto the AC

The effects of pH on the adsorption of As(III) and As(V) onto the AC in 100 ml of sample solution were investigated from pH 1.0 to 6.0 with the procedure described in Section 2.3. The results are shown in Fig. 1. As was not contained in 5 ml of the filtrate obtained by the adsorption procedure of As(III) and As(V) in 5 ml of sample solution at pH 1.0 to 3.0. Furthermore, As contents in the AC suspension from 5 and 100 ml of the sample solution were in agreement. Therefore, As(III) and As(V) were quantitatively adsorbed onto AC in the pH range from 1.0 to 3.0. The method does not tend to suffer from interference from coexisting ions in a strong acidic range. Consequently, the optimum pH of 2.0 was employed for the adsorption of As(III) and As(V) onto the AC.

3.3. Effect of amount of Mo and AC

The suitable amount of Mo for the adsorption of As(III) and As(V) onto AC was determined. A 0.02–1.0-ml portion of 5% (w/v) Mo solution (1–50 mg Mo) was added to 100 ml of sample solution (containing 0.25 μ g of As) at pH 2.0, and the solution was stirred for 10 min. The amount of As(III) and As(V) adsorbed onto the AC was examined. The results are shown in Fig. 2. As(III) and As(V) were not adsorbed on AC without addition of Mo but were quantitatively adsorbed with the addition of 0.04–0.2 ml of 5% (w/v) Mo solution (2–10 mg of Mo). The recovery of As(III) and As(V) gradually decreased as the amount of Mo increased by more than 10 mg. Similarly, the amount of Mo necessary for the adsorption of As(III) and As(V) in 500 ml of sample solution was determined. The results are shown in Fig. 3. As(III) and As(V) were quantitatively adsorbed by the addition of 5–40 mg of Mo per 500 ml. The recovery of As decreased in the presence of more than 50 mg of Mo. Based on these results, 0.1 ml of 5% (w/v) Mo solution (5

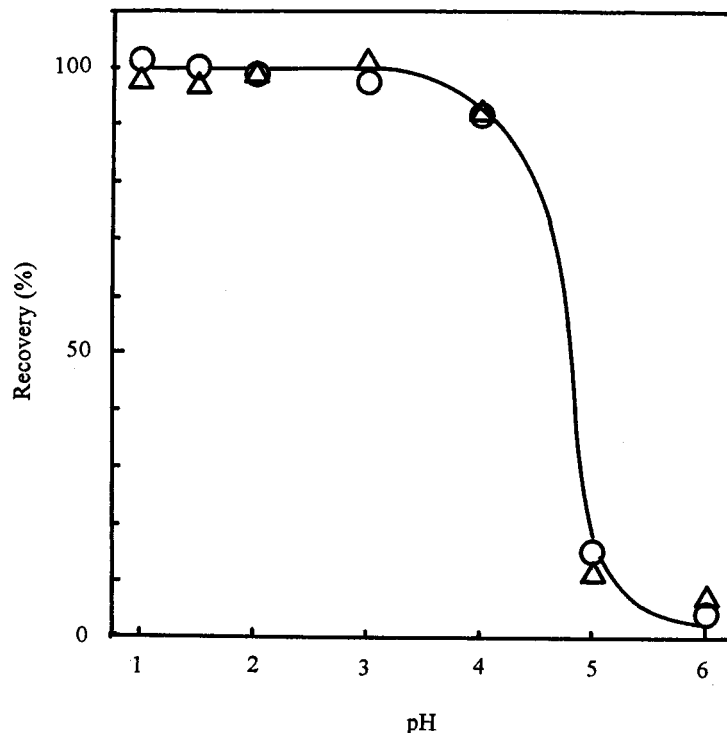


Fig. 1. Effect of pH on the adsorption of As onto the AC. (○) As(III); (△) As(V); As, 0.25 μg ; 5% (w/v) Mo solution: 0.1 ml. AC: 100 mg; stirring time, 10 min; 100 ml of sample solution was concentrated to 5 ml of sample suspension.

mg of Mo) per 100 ml of sample solution was employed for the proposed procedure.

The effects of the amounts of AC for adsorption of As(III) and As(V) at pH 2.0 were investigated. As(III) and As(V) were quantitatively adsorbed by the addition of 50–150 mg of AC. Therefore, 100 mg of the AC was employed for the proposed procedure.

3.4. Effect of the sample volume

The effect of the sample volume on the recovery of As(III) and As(V) onto AC was investigated by the proposed procedure. When 5 mg of Mo per 100 ml of sample solution was added and stirred for 10 min or more, As(III) and As(V) in 50–1000 ml of sample solution were quantitatively adsorbed onto AC.

3.5. Calibration curves

The values of the absorbance of As with matrix-matched standard solution without AC and the AC suspension differed according to the heating time of exposed GF. Therefore, a calibration curve was prepared from the AC suspension which was preconcentrated from 50 ml of the standard solution. The value of absorbance of the AC suspension did not change after 10 days. The calibration curves obtained by the AC suspension of As(III) and As(V) were in agreement and were linear up to 0.1 mg l^{-1} of As. The linear regression equation (absorbance and As concentration mg l^{-1}) was $y = 3.08x + 0.004$, and the correlation coefficient was 0.9997. Using this equation, the limit of detection of As was calculated to be 0.004 mg l^{-1} ($\bar{X}_{bl} + 3\sigma_{bl}$). When 1000 ml of sam-

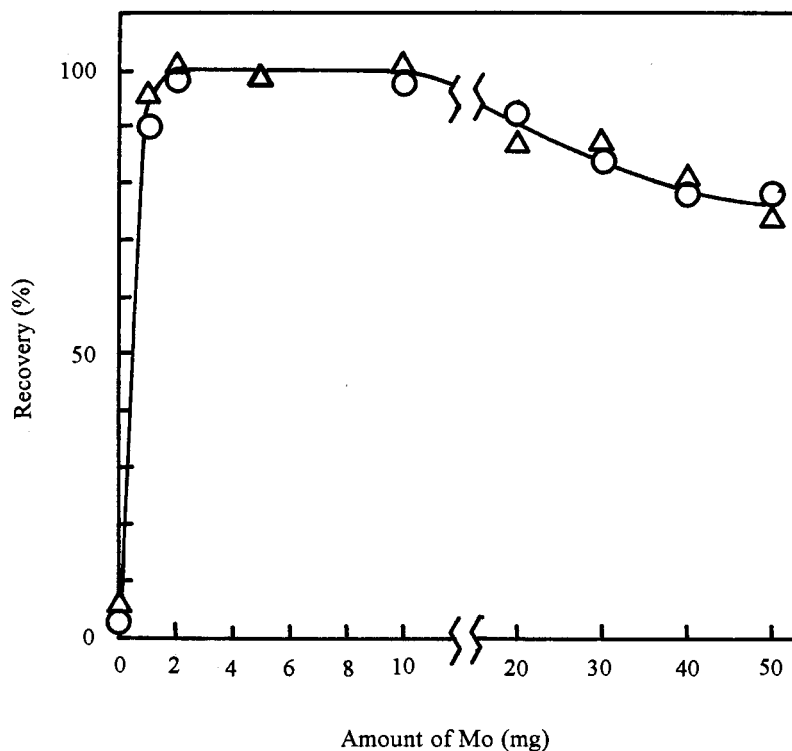


Fig. 2. Effect of amount of Mo addition on the adsorption from 100 ml of sample solution. (○) As(III); (△) As(V); As, 0.25 μg . AC, 100 mg; stirring time, 10 min; 100 ml of sample solution was concentrated to 5 ml of sample suspension.

ple solution was preconcentrated to 5 ml, 0.02 $\mu\text{g l}^{-1}$ of As could be determined.

3.6. Effect of foreign ions

The effect of foreign ions coexisting in sea water on the determination of As(III) and As(V) was investigated. A 100-ml portion of sample solution containing 0.25 μg of As and the foreign ions was concentrated to 5 ml of AC suspension, and the As content was determined by the proposed method. Because the recovery of As was $100 \pm 10\%$, the presence of foreign ions was regarded as having no effect. The experimental results are shown in Table 2. The sum of As(III) and As(V) in natural water which contains a sea water level concentration of foreign ions should be determined by the proposed method.

3.7. Determination of As in natural water

The proposed method was applied to the determination of As in natural water. The water samples were first filtered under pressure (0.8–1.0 atm) through a MF (0.45- μm pore size) to remove the suspended matter. The filtrate without digestion was then preconcentrated by the proposed method, and the sum of As(III) and As(V) was determined by AAS with the deuterium background correction system, and with the polarized Zeeman background correction system. The analytical results of the original sample solution and of this sample solution, to which a known amount of As(III) and As(V) was spiked, are shown in Table 3. The sum of As(III) and As(V) values with both systems was in good agreement. The recoveries of the spiked As(III) and As(V) were in the range of 95–110% for well water and in the

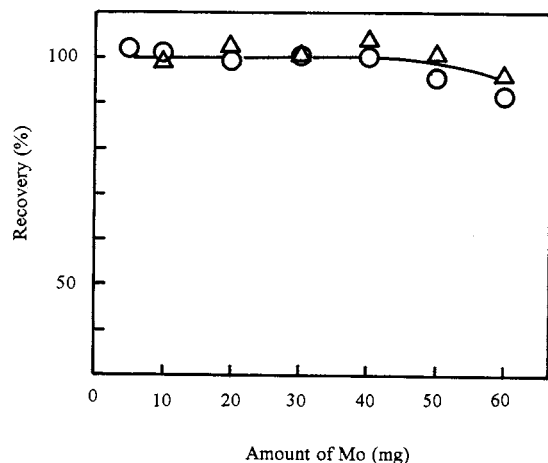


Fig. 3. Effect of amount of Mo addition on the adsorption from 500 ml of sample solution. (○) As(III); (△) As(V); As, 0.25 μg . AC, 100 mg; stirring time, 10 min; 500 ml of sample solution was concentrated to 5 ml of sample suspension.

range of 92–97% for the sea water. Sturgeon et al. [20] quantified As species in river water reference material. According to their data, the sum of As(III) and As(V) was about 65% of the total arsenic value. It is assumed that organic arsenic

Table 2
Effect of coexisting ions

Ion	Added (μg)	Recovery (%)	
		As(III)	As(V)
Na(I)	1.4×10^6	98	99
Mg(II)	2.5×10^5	103	97
Al(III)	20	100	105
Si(IV)	100	101	102
K(I)	2.1×10^6	98	101
Ca(II)	8.4×10^4	101	100
Sr(II)	50	104	100
Se(IV)	20	99	101
SO_4^{2-}	1.9×10^5	100	97
Cl^-	2.1×10^6	98	99
Br^-	3.4×10^4	107	100
F^-	1.0×10^3	99	97
I^-	10	99	100
PO_4^{3-}	10	100	100

As, 0.25 μg ; 5% (w/v) Mo solution, 0.1 ml. AC, 100 mg; 100 ml sample solution was concentrated to 5 ml of the sample suspension. When the recovery of As is within $100 \pm 10\%$, the foreign ion is regarded as having no effect.

species, such as disodium methyl arsonate, are also contained in sea water. Therefore, a digestion method for sea water was investigated. The tested digestion procedure [21] was as follows: 100 ml of filtrate, which had been filtered through a MF to remove the suspended matter, was placed in a beaker. Seven ml of 9 M H_2SO_4 and 5 ml of conc. HNO_3 were added and evaporated on an aluminum dry bath (bath temperature was about 155°C) until dense white fumes of SO_3 just appeared. The wall of the beaker was rinsed with a small amount of deionized water, and evaporation to the point fumes of SO_3 appeared was repeated. The sample was not dried during digestion. After cooling, the sample was diluted to about 100 ml of 0.1 M acetic acid and heated to almost boiling to dissolve the slowly soluble salt, and the solution was adjusted to pH 2.0 with 3 M HCl. The sample and blanks were analyzed with the procedure described in Section 2.3. The results are shown in Table 3. The obtained total As value was about 95% relative to the value of the sample without digestion. Kohno et al. [22] pointed out that As tends to be lost by volatilization during H_2SO_4 and HNO_3 digestion. From these results, further investigation of digestion should be done.

3.8. Discussion of the adsorption mechanism

It is well-known that 12-molybdoarsenate is formed by the reaction of As(V) and molybdate ions [17], but the reaction of As(III) and molybdate ions is little known. However, the proposed method in which As(III) and As(V) were adsorbed onto AC involved the presence of molybdate ions. Therefore, the mole ratio of As and Mo adsorbed onto AC was investigated. A 0.05-ml Mo solution (5% (w/v), 2.5 mg Mo) and 0.1 g of AC were added to 50 ml of pH 2.0 sample solution containing 0–0.5 μg of As, and the solution was stirred for 10 min. The AC with adsorbed As and Mo was separated from the solution through a MF. Mo and As on the AC were dissolved with successive conc. HCl and aqua regia treatment by heating at 145°C in the same manner shown in the previous paper [19]. According to this dissolution method, the Mo content was about 840 μg in 0.1 g of AC, and was independent of the As content.

Table 3
Analytical results of arsenic in natural water

	Added (μg)		Found ($\mu\text{g l}^{-1}$)	Recovery (%)	RSD ^g (%)
	As(III)	As(V)			
Well water ^{b,d}	—	—	0.57 ± 0.02^a	—	3.5
	0.1	—	0.79	110	—
	—	0.1	0.78	106	—
Well water ^{c,d}	—	—	0.56 ± 0.02^a	—	3.6
	0.1	—	0.78	110	—
	—	0.1	0.75	95	—
Sea water ^{b,e}	—	—	1.53 ± 0.05^a	—	3.3
	0.1	—	2.51	97	—
	—	0.1	2.49	96	—
Sea water ^{c,e}	—	—	1.51 ± 0.05^a	—	3.3
	0.1	—	2.45	95	—
	—	0.1	2.40	92	—
Digested ^f Seawater ^{b,c}	—	—	1.45 ± 0.05^a	—	3.4
	0.1	—	2.39	94	—
	—	0.1	2.36	91	—
Digested ^f Seawater ^{c,e}	—	—	1.43 ± 0.15^a	—	10.5
	0.1	—	2.39	96	—
	—	0.1	2.28	85	—

^a Average and standard deviation ($n = 6$).

^b By GF-AAS with deuterium background correction system.

^c By GF-AAS with polarized Zeeman background correction system. GF-AAS conditions were: drying, 80–150°C, 20 s; ashing, 150–500°C, 40 s (air flow-rate, 100 ml min⁻¹); 500–800°C, 40 s (Ar flow-rate, 200 ml min⁻¹); atomization, 2600°C, 4 s (Ar flow-rate, 20 ml min⁻¹).

^d Well water sample was taken on 2 August 1995, at Funabashi-shi Chiba (500 ml).

^e Sea water sample was taken on 7 May 1996, 1 km off the coast of Katuura in Chiba (100 ml).

^f Sea water was digested with H₂SO₄ and HNO₃.

^g RSD, relative standard deviation.

Therefore, the adsorption ratio of As and Mo onto AC could not be determined.

Next, in order to clarify the adsorption mechanism in the proposed method, the addition order of As, Mo and AC was varied. Method A: the solution containing As and Mo was adjusted to pH 2.0, and AC was immediately added. Method B: the solution containing As and Mo was adjusted to pH 2.0, stirred for 5 min, and then AC was added. Method C: AC was added to the Mo solution at pH 2.0 and stirred for 20 min. The AC with adsorbed Mo was separated from the solution through a MF. The wet AC on the MF was added to the As solution of pH 2.0. In methods A, B and C, each solution was stirred for the prescribed time and treated with the procedure described in Section 2.3. The results are shown in Fig. 4. As(V) is quantitatively adsorbed on the

AC within 2 min or above in every method. On the other hand, As(III) is adsorbed within 2 min or above in methods A and B, but in method C it is adsorbed at less than 15% of recovery up to 10 min. The molybdate ions are easily adsorbed on AC, and the AC adsorbs As(V), but it does not adsorb As(III) up to 10 min in method C. Based on these results, it is assumed that As(III) is oxidized to As(V) and is adsorbed as an molybdoarsenate complex onto AC. This assumption was investigated. The effects of dissolved oxygen in aqueous solution and adsorbed oxygen on AC for the oxidation of As(III) were examined. The procedure was as follows: dissolved oxygen in 1 mg l⁻¹ As(III) in pH 2.0 solution and in 5% (w/v) Mo solution were replaced separately with H₂ gas by blowing for 1 h. A 50-ml portion of pH 2.0 suspension containing 100 mg of AC was placed

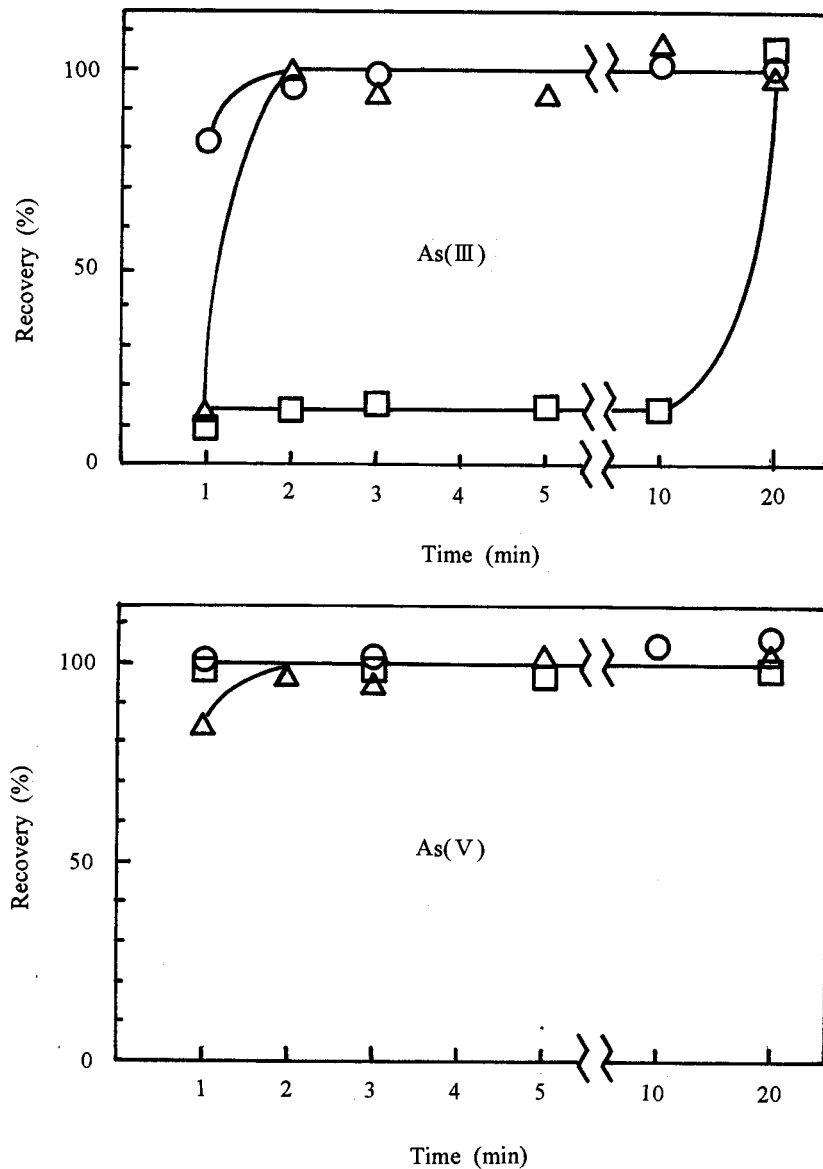


Fig. 4. Effect of addition order of As, Mo and AC. (○) Method A: the solution containing As and Mo was adjusted at pH 2.0, and AC immediately mixed. (△) Method B: the solution containing As and Mo was adjusted to pH 2.0, stirred for 5 min, and then AC is mixed. (□) Method C: AC was added to Mo solution at pH 2.0 and stirred for 20 min. The AC-adsorbed Mo was separated through a MF. The wet AC on the MF was added to the As solution at pH 2.0. *In methods A, B and C each solution was stirred for the prescribed time and treated with the procedure described in Section 2.3. *As, 0.25 μg ; 5% (w/v) Mo solution, 0.05 ml; AC, 100 mg; 50 ml sample solution were concentrated to 5 ml of sample suspension.

in a 100 ml cylindrical flask. The flask was covered with a rubber stopper, which was equipped with a H_2 gas inlet, an outlet glass tube with a stopcock, and a sample injection glass tube with a

rubber stopper. The suspension in the flask was replaced with H_2 gas by blowing for 1 h and by evacuating five times with an aspirator and then filled with H_2 gas. Then, 250 μl of 1 mg l^{-1}

As(III) solution and 50 μl of 5% (w/v) Mo solution were injected into the suspension in the cylindrical flask, stirred for 5 min, and finally treated by the procedure described in Section 2.3. Dissolved oxygen in the solution and physically adsorbed oxygen on the AC should be substantially removed by blowing H_2 gas and five evacuations. However, the investigation showed that As(III) was quantitatively adsorbed onto the AC. Kamegawa et al. [23] reported the catalytic oxidation of 50 ml of 1 mg l^{-1} As(III) in aqueous solution by 50 mg of AC (stirred for 24 h). They concluded the overall reaction mechanism to be: the dissolved oxygen oxidizes As(III) to As(V), and the active surface oxide of AC acts as a catalyst. The authors proposed a method in which As(III) and As(V) are adsorbed onto AC in the presence of molybdate ion, the concentration of As(III) solution is very dilute (0.005 mg l^{-1}), and the stirring time is very short (10 min). With regard to oxidation, the method also differs from the report of Kamegawa et al. [23]. Based on these results, As(V) and molybdate ions in solution and molybdate ion adsorbed on AC form a molybdoarsenate complex and adsorb onto the AC. On the other hand, As(III) is oxidized to As(V) by the surface oxide on the AC, and this As(V) reacts with molybdate ion in solution, forms a molybdoarsenate complex, and is adsorbed onto the AC. If the molybdate ion has already been adsorbed on the surface of the AC, this interferes with the oxidation of As(III).

References

- [1] Anon., International Agency for Research on Cancer, IARC Monographs, Vol. 23, Arsenic and Arsenic compounds, 1980, pp. 103–114.
- [2] D.F. Boltz, M.G. Mellon, *Anal. Chem.* 19 (1947) 873.
- [3] G. Stratton, H.C. Whitehead, *J. Am. Water Works Assoc.* 54 (1962) 861.
- [4] C. Wadelin, M.G. Mellon, *Analyst* 77 (1952) 708.
- [5] K. Terada, K. Matumoto, T. Inaba, *Anal. Chim. Acta* 158 (1984) 207.
- [6] C. Matubara, Y. Yamamoto, K. Takamura, *Analyst* 112 (1987) 1257.
- [7] W. Holak, *Anal. Chem.* 41 (12) (1969) 1712.
- [8] Kwok-Tai Kan, *Anal. Lett.* 6 (7) (1973) 603.
- [9] F.J. Schmidt, J.L. Royer, *Anal. Lett.* 6 (1) (1973) 17.
- [10] Y. Yamamoto, T. Kumamaru, *Z. Anal. Chem.* 281 (1976) 353.
- [11] E.J. Knudson, G.D. Christian, *Anal. Lett.* 6 (12) (1973) 1039.
- [12] A.U. Shakh, D.E. Tallman, *Anal. Chim. Acta* 98 (1978) 25.
- [13] M. Walcerz, S. Garbos, E. Bulska, A. Hulanicki, *Fresenius J. Anal. Chem.* 350 (1994) 662.
- [14] R.E. Sturgeon, D.C. Gregoire, *Spectrochim. Acta* 49B (1994) 1335.
- [15] H. Narasaki, *J. Anal. At. Spectrom.* 3 (1988) 517.
- [16] S. Nakashima, *Analyst* 103 (1978) 1031.
- [17] N. Hata, I. Kasahara, S. Taguchi, K. Goto, *Analyst* 114 (1989) 1255.
- [18] S. Peräniemi, S. Hannonen, H. Mustalahti, M. Ahlgrén, *Fresenius J. Anal. Chem.* 349 (1994) 510.
- [19] T. Kubota, T. Okutani, *Bunseki Kagaku* 39 (1990) 507.
- [20] R. Sturgeon, K.W. Michael, S.N. Willie, S. Berman, *Analyst* 114 (1989) 1393.
- [21] L.S. Clesceri, A.E. Greenberg, P.R. Trussell, *Standard methods for the examination of water and waste water*, American Public Health Association, Washington, DC, 1989, pp. 3–9.
- [22] H. Kohno, N. Nakagawa, K. Kuramoto, Y. Ohuchi, Y. Hattori, K. Shimizu, E. Chiba, S. Nakamura, K. Yamamoto, K. Donaga, S. Shigashikuni, in: *Proceedings of the 57th Symposium on Analytical Chemistry*, Matuyama, Japan, 1996, p. 5.
- [23] K. Kamegawa, H. Yoshida, S. Arita, *Nippon Kagaku Kaishi* 10 (1979) 1359.

Determination of total thallium in fresh water by electrothermal atomic absorption spectrometry after colloid precipitate flotation

Trajče Stafilov *, Katarina Čundeva

Institute of Chemistry, Faculty of Science, St. Cyril and Methodius University, P.O. Box 162, 91001 Skopje, Macedonia

Received 25 April 1997; received in revised form 26 November 1997; accepted 2 December 1997

Abstract

Tl(I) and Tl(III) are preconcentrated simultaneously from aqueous solutions by colloid precipitate flotation using two collectors: hydrated iron(III) oxide ($\text{Fe}_2\text{O}_3 \cdot x\text{H}_2\text{O}$) and iron(III) tetramethylenedithiocarbamate ($\text{Fe}(\text{TMDTC})_3$). After the coprecipitation step and the addition of foaming agents, Tl(I) and Tl(III) were separated from the water by a stream of air bubbles. Various factors affecting Tl(I) and Tl(III) recoveries during the separation from water, including the collector mass, the nature of the supporting electrolyte, pH, ζ potential of the collector particle surfaces, type of tenside, etc., were investigated. Within the optimal pH range (6–6.5), establishing by a recommended procedure, Tl(I) and Tl(III) were separated quantitatively (94.9–100.0%) with 30 mg Fe(III). Both Tl ions were simultaneously separated without any previous conversion of one type of Tl ion to the other. Total Tl determination was performed by electrothermal atomic absorption spectrometry by previous matrix modification of the concentrated samples. The determination limit of Tl by this method is $0.108 \mu\text{g l}^{-1}$. © 1998 Elsevier Science B.V. All rights reserved.

Keywords: Determination; Electrothermal atomic absorption spectrometry; Precipitate flotation; Thallium; Water

1. Introduction

Thallium can be found in nature as Tl(I) and Tl(III) ions. The total Tl quantity in fresh water is $0.01\text{--}14 \mu\text{g l}^{-1}$ [1]. Because the level of this element in uncontaminated fresh water is very low, it needs to be preconcentrated before its instrumental analysis. Among the preconcentra-

tion procedures, such as liquid–liquid extraction, ion-exchange, coprecipitation, etc., flotation techniques prove to be very simple. They allow handling of large volumes of sample and considerable saving in reagents and time [2–4]. Flotation studies have been performed on most elements [4], but there is only one report for flotation of Tl ions [5]. Hualing and Side's work [5] describes ion flotation of Tl(I) and Tl(III) from hydrochloric–nitric acid solution prior to determination by spectrophotometry, overlooking the interference of chlorides on Tl(I) recoveries.

* Corresponding author. Tel.: + 389 91 117055; fax: + 389 91 226865; e-mail: trajcest@iunona.pmf.ukim.edu.mk

The present paper is the first attempt of a precipitate flotation preconcentration of total Tl, previously establishing the experimental conditions for successful separation of both Tl ions. Similar to a previously suggested method for total chromium preconcentration [6], electrothermal atomic absorption spectrometry (ETAAS) has been applied. The determination of total Tl has been performed without previous reduction or oxidation of one type of Tl ion to the other. The procedure involves the use of two collectors: hydrated iron(III) oxide ($\text{Fe}_2\text{O}_3 \cdot x\text{H}_2\text{O}$) and iron(III) tetramethylenedithiocarbamate ($\text{Fe}(\text{TMDTC})_3$). The same combination of collectors has been applied for the separation of several metals from sea water using neutron activation [7] or atomic absorption spectrometry [6,8], but not for Tl(I) and Tl(III). The coprecipitation efficiency of Tl(I) and Tl(III) with $\text{Fe}_2\text{O}_3 \cdot x\text{H}_2\text{O}$ was investigated. The effect of $\text{Fe}(\text{TMDTC})_3$, as a compound with a bigger hydrophobicity than $\text{Fe}_2\text{O}_3 \cdot x\text{H}_2\text{O}$, on flotation recoveries of Tl(I) and Tl(III) was investigated. The interferences of chlorides on Tl(I) and Tl(III) flotation recoveries were studied. The method developed is simple, rapid and applicable to total Tl separation at $\mu\text{g l}^{-1}$ levels from a large volume of water.

2. Experimental

2.1. Apparatus

The apparatus employed in this work has been described previously [6]. A Tl Perkin-Elmer hollow cathode lamp was used as a source. The optimal instrumental parameters for ETAAS determination of Tl are given in Table 1. Inductively coupled plasma atomic emission spectrometry (ICP–AES) was performed using a Varian spectrometer Model Liberty 110 (Table 2). The flotation cell used to carry out the preconcentration and the equipment applied for electrophoretic determination of electrokinetic (ζ) potentials of the collector particle surfaces are the same as those used previously [6].

2.2. Reagents and standards

All chemicals used for preparation of solutions were of analytical-reagent grade except for ten-sides, sodium dodecyl sulfate (NaDDS) and sodium oleate (NaOL). The aqueous solutions were prepared in redistilled water. Stock solution of Tl(I) was made by dissolving a commercial standard solution (Titrisol, Merck) containing 1 g of Tl(I) in the form of TlNO_3 in 1 l water. The same commercial standard solution of TlNO_3 containing 1 g of Tl(I) was oxidized to Tl(III) with several drops of bromine. The solution was evaporated nearly to dryness (to expel the excess bromine) and the residue was diluted to 1 l. Before each investigation, series of Tl(I) and Tl(III) standards were freshly made by diluting these stock solutions of Tl(I) and Tl(III). Stock solution of $\text{Fe}(\text{NO}_3)_3$ was prepared by dissolving high purity Fe metal (21 g) in 60 ml conc. HNO_3 solution by heating. Thus all Fe was converted into the three-valent state. After cooling, redistilled water (500 ml) was added and the solution was filtered through the thickest filter paper. The

Table 1
Instrumental parameters for thallium determination by ETAAS

Wavelength	276.8 nm
Spectral width slit	0.7 nm
Calibration mode	Peak height
Lamp current	20 mA
Background correction	D ₂
Dry	
Temperature	110°C
Time	25 s
Ramp time	2 s
Charring	
Temperature	400°C
Time	25 s
Ramp time	1 s
Atomizing	
Temperature	2000°C
Time	5 s
Ramp time	0 s
Cleaning	
Temperature	2650°C
Time	3 s
Ramp time	1 s
Gas	Argon

Table 2
Instrumentation and operating conditions for ICP-AES system

ICP system	Varian, Liberty 110
RF generator	
Operating frequency	40.68 MHz
Coupling	Direct serial coupling, DISC ($\approx 70\%$ efficiency)
RF power	Auto tune, computer controlled, 1.5 kW for 190.790 nm
Spectrometer	
Optical arrangement	Czerny Turner, 0.75 m focal length
Grating	Holographic
Groove density	1800 lines mm^{-1}
Size	100 mm \times 90 mm
Optical spectral resolution	4 pm
Background corrector	Dynamic
Sample introduction area	
Plasma Argon flow rate	15 l min^{-1} (for 190.79 nm)
Auxiliary Argon flow rate	0.75 l min^{-1} (for 190.79 nm)
Nebulizer Argon flow rate	2 l min^{-1} (for 190.79 nm)
Sample nebulizer	Ultrasonic nebulizer, CETAC 5000 U+
Spray chamber	Inert Sturman-Masters
Sample flow rate	2 ml min^{-1}
Peristaltic pump	12 rollers, 1 turn min^{-1} increment
Integration time	2 s, smart integration 5 s, direct reading instrument

mass concentration was $\gamma(\text{Fe}) = 30 \text{ g l}^{-1}$. The stock solution of FeCl_3 ($\gamma(\text{Fe}) = 30 \text{ g l}^{-1}$) was prepared in the same way as described previously [6]. Series of standards with the mass concentration of Fe ranging from 2.5 to 100 mg ml^{-1} were obtained by diluting these Fe stock solutions. The solution of ammonium tetramethylenedithiocarbamate (NH_4TMDTC) was prepared as 0.1 mol l^{-1} dissolving an appropriate quantity of NH_4TMDTC in water. Before each investigation

it was filtered. The 0.5% solutions of tensides were prepared by dissolving appropriate amounts of NaDDS and NaOL in 95% ethanol. Solutions of HNO_3 (0.1 mol l^{-1}) and KOH (2.5% and 10%) were used to adjust the medium pH. Solutions of KCl (3.57 mol l^{-1}) and KNO_3 (2.78 mol l^{-1}) were used to regulate the ionic strength of the medium, i.e. the coagulation of the collector precipitates.

2.3. Recommended procedure

The procedure is for uncontaminated fresh water. The samples investigated were tap water from the city of Skopje and water from Lake Ohrid. Immediately after sampling, the lake water was filtered through a Sartorius membrane filter (0.5 μm pores) to remove plankton. The tap water was not filtered. To prevent the possible hydrolytic precipitation of some mineral salts present in natural water with standing, a few millilitres of concentrated HNO_3 had to be added to 1 l of natural water. The pH had to be 2.5–3.

An acidified water sample (1 l) was placed in a 1000 ml beaker. After adding 6 ml of KNO_3 and 1 ml of 30 g l^{-1} $\text{Fe}(\text{NO}_3)_3$ solution, pH was adjusted to 6.3 with a solution of KOH (2.5% or 10%). To the solution with yellow–brown precipitate of $\text{Fe}_2\text{O}_3 \cdot x\text{H}_2\text{O}$, 2 ml of NH_4TMDTC solution were added. The precipitate changed colour to black $\text{Fe}(\text{TMDTC})_3$. After stirring for 15 min (induction time), 0.6 ml of NaDDS and NaOL alcoholic solutions were added and the contents of the beaker were transferred quantitatively into the flotation cell with a small portion of 0.1 mol l^{-1} NH_4NO_3 . Air (50 ml min^{-1}) was passed through from the perforated bottom of the cell for 1–2 min. Then, a glass pipette was introduced into the cell through the foam layer and the water phase was sucked off. Hot concentrated HNO_3 solution (10 ml) was added to the cell to destroy the scum. The solution was sucked off and collected in a volumetric flask (25 ml) through the bottom of the cell. The cell was washed with 4 mol l^{-1} HNO_3 solution. The flask was filled up to the mark with the same solution of HNO_3 and the sample was ready for AAS measurement. Before ETAAS determination of total TI, a matrix mod-

Table 3

Dependence of Tl(I) flotation recovery R (%) on the iron mass concentration $\gamma(\text{Fe})$ coprecipitating with $\text{Fe}(\text{TMDTC})_3$ in the absence of chlorides ($n = 3$)

$\gamma(\text{Fe})$ (mg/l)	pH	$c(\text{KNO}_3)$ (mol l ⁻¹)	R (%)				
			$\gamma(\text{Tl}^+)$ 0.125 $\mu\text{g l}^{-1}$	$\gamma(\text{Tl}^+)$ 0.25 $\mu\text{g l}^{-1}$	$\gamma(\text{Tl}^+)$ 1.25 $\mu\text{g l}^{-1}$	$\gamma(\text{Tl}^+)$ 2.5 $\mu\text{g l}^{-1}$	$\gamma(\text{Tl}^+)$ 25 $\mu\text{g l}^{-1}$
2.5	5.5	0.02	34.2	40.6	44.3	34.1	59.1
5.0	5.5	0.02	41.1	44.1	57.4	55.3	81.5
10	5.5	0.02	58.5	64.9	72.3	58.2	89.6
20	5.5	0.02	79.9	87.5	88.6	82.3	94.7
30	5.5	0.02	94.9	95.2	96.1	95.1	98.5
40	5.5	0.02	96.3	96.6	96.2	95.8	97.1
60	5.5	0.02	97.8	96.9	95.5	100.0	96.4
80	5.5	0.02	97.8	98.1	96.7	100.0	95.5
100	5.5	0.02	98.1	99.0	100.0	97.9	95.2

ification with H_2SO_4 of each sample concentrated by flotation should be made by adding 0.5 ml concentrated H_2SO_4 to 10 ml of each Tl solution concentrated by flotation.

3. Results and discussion

3.1. Coprecipitation with hydrated iron(III) oxide

The coprecipitation of Tl(I) and Tl(III) in the sublate particles of $\text{Fe}_2\text{O}_3 \cdot x\text{H}_2\text{O}$, as the first collector, was investigated through the mass of Fe, as a constitutive element of this collector. The series of flotations were carried out by addition of different Fe quantities (2.5–100 mg l⁻¹) to the working solutions at a constant pH (5.5) and ionic strength (0.02 mol l⁻¹) regulated with KNO_3 . Fe was added as $\text{Fe}(\text{NO}_3)_3$. At pH 5.5, there is not any coprecipitation of Tl(I) and the coprecipitation of Tl(III) is insignificant (62%). These data show that the role of $\text{Fe}_2\text{O}_3 \cdot x\text{H}_2\text{O}$ as collector in the recommended procedure with two collectors at pH 5.5 was not decisive for Tl(I) and Tl(III) separation from water matrix. The first induction time used in the previous paper [6] can be reduced or omitted. The omission of the first induction time had shortened the performing of the method.

3.2. Influence of the $\text{Fe}(\text{TMDTC})_3$ mass and the presence of chlorides on flotation recoveries of Tl(I) and Tl(III)

Similarly as the previous investigations about the dependence of colligends recoveries on $\text{Fe}_2\text{O}_3 \cdot x\text{H}_2\text{O}$, the dependence of Tl(I) and Tl(III) recoveries on $\text{Fe}(\text{TMDTC})_3$ was determined through the mass of Fe. The influences of Cl^- were investigated, floating each colligend separately in the presence and in the absence of Cl^- . In the presence of Cl^- , Fe was added as a solution of FeCl_3 and a solution of KCl served as a ionic strength adjuster. To perform the investigations without Cl^- , Fe was added as a solution of $\text{Fe}(\text{NO}_3)_3$ and a solution of KNO_3 was used to regulate the ionic strength.

When FeCl_3 and KCl were used, Tl(I) was not quantitatively separated (maximum up to 84.6%). This means that Cl^- interfere with the Tl(I) recoveries. However, if $\text{Fe}(\text{NO}_3)_3$ and KNO_3 were used (Table 3), Tl(I) recoveries became quantitative (94.9–100.0%). In this case, the minimum mass of Fe used for flotation of Tl(I) was 30 mg.

The investigation of the influence of Fe mass on Tl(III) recoveries in the presence of chlorides and nitrates show that Tl(III) could not float successfully at pH 5.5 independently of that if the combination FeCl_3 – KCl or the combination $\text{Fe}(\text{NO}_3)_3$ – KNO_3 was used. Probably the proper

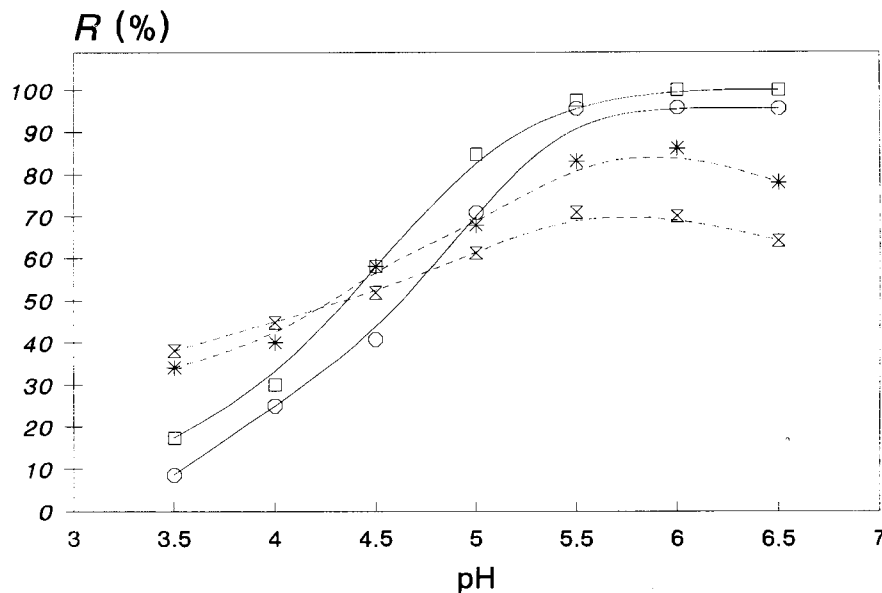


Fig. 1. Dependence of Tl(I) flotation recovery R (%) on medium pH values in the presence and in the absence of chlorides. In the presence of chlorides: \times , $\gamma(\text{Tl}^+) = 1 \mu\text{g ml}^{-1}$; $*$, $\gamma(\text{Tl}^+) = 2 \mu\text{g ml}^{-1}$. In the absence of chlorides: \square , $\gamma(\text{Tl}^+) = 1 \mu\text{g ml}^{-1}$; \circ , $\gamma(\text{Tl}^+) = 2 \mu\text{g ml}^{-1}$.

preconcentration of Tl(III) in the presence of nitrates might be carried out within another pH range.

All obtained results are the mean of three replicates. Relative standard deviations of these measurements vary from 1.2% to 2.9% and the confidence intervals (95%) of the recovery values vary from 0.4% to 1.9%.

3.3. Influence of pH

The influence of medium pH on the Tl(I), i.e. Tl(III) recoveries, was studied floating series of solutions containing 25 and 50 μg Tl, within the pH range 3.5–6.5, with 30 mg Fe at constant ionic strength (0.02 mol l^{-1}). Investigation of pH values higher than 6.5 was not performed because at pH higher than 6.5 the compound $\text{Fe}(\text{TMDTC})_3$ did not exist because of its hydrolysis. Fe was added as solutions of FeCl_3 or $\text{Fe}(\text{NO}_3)_3$. The ionic strength was regulated with KCl and KNO_3 , respectively.

When the combination $\text{Fe}(\text{NO}_3)_3$ – KNO_3 was used, the Tl(I) recoveries within the range 5.5–6.5

are 95.5–100.0% (Fig. 1). As expected, when FeCl_3 –KCl was applied, the Tl(I) recoveries, within the same pH range, are insufficient (a maximal value is 86.0%). The proper preconcentration of Tl(III) was carried out with 30 mg Fe(III) within the pH range 6–6.5, when Tl(III) recoveries are 98.9–100.0% (Fig. 2). The use of the combination FeCl_3 –KCl or $\text{Fe}(\text{NO}_3)_3$ – KNO_3 had no appreciable effect on the flotation efficiency of Tl(III). The presence of Cl^- did not interfere with Tl(III) preconcentration.

The Tl(I) as well as Tl(III) recoveries within the pH range 3.5–5 were lower because of the hydrolysis of NaDDS and NaOL as anion. Within this pH interval the medium acidity influenced the function of these tensides. At lower pH values they were not in the form of anions, but in the form of molecules which were not able to perform their function as surfactants. Thus, lower pH values decrease their efficiency as surfactants, the foaming is not good and both the Tl(I) and the Tl(III) recoveries obtained within the pH range 3.5–5 are poor.

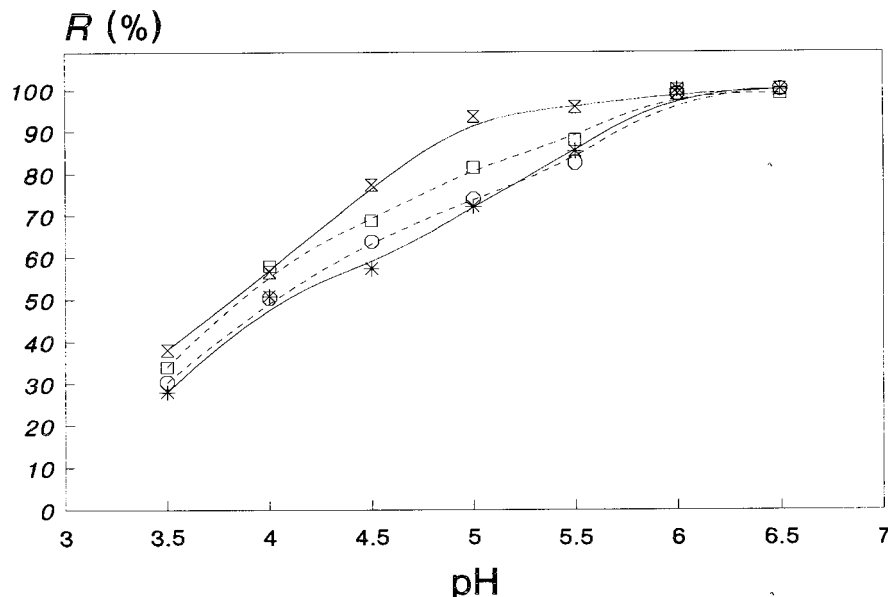


Fig. 2. Dependence of Tl(III) flotation recovery R (%) on medium pH values in the presence and in the absence of chlorides. In the presence of chlorides: ○, $\gamma(\text{Tl}^{3+}) = 1 \mu\text{g ml}^{-1}$; □, $\gamma(\text{Tl}^{3+}) = 2 \mu\text{g ml}^{-1}$. In the absence of chlorides: *, $\gamma(\text{Tl}^{3+}) = 1 \mu\text{g ml}^{-1}$; ×, $\gamma(\text{Tl}^{3+}) = 2 \mu\text{g ml}^{-1}$.

3.4. ζ potential of the collector flocs and choice of tenside

According to the signs of the $\text{Fe}_2\text{O}_3 \cdot x\text{H}_2\text{O}$ flocs (26.05 mV) as well as the ζ potentials of the $\text{Fe}(\text{TMDTC})_3$ flocs (46.5 mV), the two collectors needed anions for flotation. The anions NaDDS and NaOL were shown to be successful. The detergent NaDDS provides good foaming in hard water because of its soluble calcium and magnesium salts. The long flexible tail (the hydrocarbon chain) of NaOL increases the aerophilicity of collector particles. When NaOL was added to the system the air bubbles attached and fixed more easily to the collector particles surrounded by anions of tensides and the foaming was much better.

The more positive ζ potential of $\text{Fe}(\text{TMDTC})_3$ flocs than ζ potential of $\text{Fe}_2\text{O}_3 \cdot x\text{H}_2\text{O}$ flocs has indicated that the froth layer obtained by the second collector $\text{Fe}(\text{TMDTC})_3$ should be more stable [9]. Namely, the anions of NaDDS and NaOL, orientated with their negatively charged sides (the head groups) to the positive surface of

the floc particles, should create stronger association with $\text{Fe}(\text{TMDTC})_3$ than with $\text{Fe}_2\text{O}_3 \cdot x\text{H}_2\text{O}$. The experiment has demonstrated that if $\text{Fe}(\text{TMDTC})_3$ was used as collector the time of air bubbling during the step of flotation would be shorter (only 1 or 2 min). The froth layer obtained on the top of the liquid phase in the cell was better fixed at the gas–liquid interface and less exposed on reflux with standing. The separation of the froth layer of $\text{Fe}(\text{TMDTC})_3$ from the processed water phase was easier than the separation of $\text{Fe}_2\text{O}_3 \cdot x\text{H}_2\text{O}$.

3.5. Matrix modification of solutions concentrated by flotation

To destroy and dissolve the froth layer containing Tl(I) and Tl(III), a suitable acid should be used. The use of concentrated H_2SO_4 was unsuccessful. This acid helped to decompose the black $\text{Fe}(\text{TMDTC})_3$ compound but did not destroy the tensides. They hydrolysed, stood out as yellowish precipitate, made the system turbid and inappropriate for AAS determination. On the other hand,

when concentrated HNO_3 was used, due to its oxidizing properties the scum was destroyed and dissolved properly. A homogeneous clear yellow solution, suitable for AAS, was obtained, so the procedure was carried out using concentrated HNO_3 . However, it was shown that the nitrate form of Tl is inappropriate for ETAAS [10–13]. Namely, Tl nitrates start to atomize during the thermal pretreatment steps (drying and charring). So, before each Tl determination by ETAAS it was necessary to convert its compounds into more thermostable forms, i.e. to make the matrix modification. Because Tl sulfates are more thermostable than Tl nitrates [10–13], they should be transformed to sulfates. It was found experimentally that a matrix modification of the final solutions of Tl could be performed by adding 0.5 ml concentrated H_2SO_4 to 10 ml of each Tl solution concentrated by flotation.

3.6. Influence of Fe mass on Tl absorbance

The concentration of Tl made it possible to move its detection limit towards lower concentrations. However, it was important to examine the interferences resulting from the high Fe concentrated in the final testing solutions on the Tl absorbance during ETAAS determinations. For this purpose, a series of solutions with the same concentration of Tl ($0.05 \mu\text{g ml}^{-1}$) and different concentrations of Fe (from 0–1.6 mg ml^{-1}) were prepared and absorbance was measured. These investigations (Table 4) showed that the Tl absorbances changed insignificantly up to 1.6 mg ml^{-1} Fe, confirming the results of Dulski and

Table 4
Influence of iron mass on thallium absorbance

Sample no.	$\gamma(\text{Tl}) (\mu\text{g l}^{-1})$	$\gamma(\text{Fe})$ (mg l^{-1})	$(A/A_0) \cdot 100$
1	0.50	0	—
2	0.50	10.0	100.0
3	0.50	20.0	99.3
4	0.50	30.0	99.8
5	0.50	35.0	99.8
6	0.50	40.0	97.9

Bixler [14] and our previous results [12,13] about Fe interferences on Tl determination by ETAAS. This means that 30 mg of Fe added to 1 l of investigated water does not interfere in the final enriched solution.

3.7. Determination limit

To evaluate the detection limit of the method ten successive blank measurements were made. The detection limit ($0.08 \mu\text{g l}^{-1}$) was estimated as three values of the standard deviation ($0.027 \mu\text{g l}^{-1}$). The relative standard deviation for the blank was 5.02%. We found that the determination limit for Tl is $0.108 \mu\text{g l}^{-1}$ (as four values of standard deviation).

3.8. Analysis of natural water

The applicability of the proposed procedure has been verified by the ETAAS analysis of natural water samples with the method of standard additions. For this purpose, known amounts of Tl were added to 1 l aliquots of lake and tap water samples and then were floated and tested by ETAAS. The recoveries of 95.0–101.4% show that the preconcentration and separation of Tl are satisfactory (Table 5). The results obtained by ETAAS were compared with the results obtained by ICP–AES determinations. The samples for ICP–AES were prepared by concentration by evaporation (from a volume of 1 l to 25 ml) of tap and lake water (containing from 1–20 $\mu\text{g l}^{-1}$ Fe). A calculation of Student's *t*-test for the ETAAS and ICP–AES results gives the values in the range 2.04 for water sample from Labino to 2.65 for sample from Ljubaništa, whereas the theoretical value (95%) of *t* was 2.78. As can be seen, *t* values are smaller than theoretical values, there is no significant difference between the two methods.

4. Conclusion

The experimental conditions for ETAAS determinations of total Tl following colloid flotation have been established. To avoid the Cl^- interfer-

Table 5

Results of the determination of Tl in natural water with the method of standard additions (n = 5)

Sample of water	ETAAS				ICP-AES ^a
	Added ($\mu\text{g l}^{-1}$ Tl)	Estimated ($\mu\text{g l}^{-1}$ Tl)	Found ($\mu\text{g l}^{-1}$ Tl)	R (%)	Found ($\mu\text{g l}^{-1}$ Tl)
Ljubaniřta (Oh.) ^b , 6.75 DH [°] , pH 7.30	0.00	–	0.35	–	0.33 ± 0.02 ^c
	0.50	0.85	0.82	96.5	
	1.00	1.35	1.29	95.5	
Gradiřta (Oh.), 6.61 DH ^{°c} , pH 7.43	0.00	–	0.11	–	<0.1
	0.50	0.61	0.59	96.7	
	1.00	1.11	1.06	95.5	
Labino (Oh.), 3.91 DH [°] , pH 7.89	0.00	–	0.49	–	0.50 ± 0.02
	0.50	0.99	1.00	100.1	
	1.00	1.49	1.45	97.3	
Daljan (Oh.), 5.97 DH [°] , pH 7.68	0.00	–	0.20	–	–
	0.50	0.70	0.67	95.7	
	1.00	1.20	1.14	95.0	
Raře (Sk.) ^d , 20.26 DH [°] , pH 7.08	0.00	–	0.19	–	0.18 ± 0.01
	0.50	0.69	0.70	101.4	
	1.00	1.19	1.15	96.6	

^a ICP-AES results compared with ETAAS.^b Oh., water from localities at Lake Ohrid.^c DH[°] (*Deutsche Harte*), German degree of water hardness.^d Tap water from the city of Skopje (from Raře spring).^e Confidence interval (95% confidence level).

ences on the Tl(I) recoveries, reagents containing Cl^- should not be used. The use of $\text{Fe}(\text{TMDTC})_3$, as a second additional collector, improves separation of Tl(I) and Tl(III) from processed water phase. The dithiocarbamate added increases the hydrophobicity of the sublate which is the most important criterion for successful flotation. The value of ζ potential of the $\text{Fe}(\text{TMDTC})_3$ flocs is more positive than the ζ potential of $\text{Fe}_2\text{O}_3 \cdot x\text{H}_2\text{O}$ flocs, resulting in better separation efficiency. Matrix modifications of Tl salts of nitrates in sulfates improve the ETAAS determination.

Acknowledgements

We thank Stanimir Atanasov (University of Mining and Geology, Sofia, Bulgaria), for ICP-AES analysis.

References

- [1] V.A. Filova (Ed.), *Vrednye Khimicheskie Vshshestva*, Himiya, Leningrad, 1988, p. 238.
- [2] A. Mizuike, Flotation, in: *Enrichment Techniques for Inorganic Trace Analysis*, Springer-Verlag, Heidelberg, 1983, chapter 10, pp. 94–99.
- [3] A. Mizuike, M. Hiraide, *Pure Appl. Chem.* 54 (1982) 1556.
- [4] M. Caballero, R.J. Cela, A. Perez-Bustamante, *Talanta* 37 (1990) 275.
- [5] D. Hualing, H. Zhide, *Talanta* 36 (1989) 633.
- [6] K. Āundeava, T. Stařilov, *Fresenius J. Anal. Chem.* 352 (1995) 354.
- [7] X. Feng, D.E. Ryan, *Anal. Chim. Acta* 162 (1984) 47.
- [8] K. Āundeava, T. Stařilov, *Talanta* 44 (1997) 451.
- [9] S.D. Huang, T.P. Wu, C.H. Ling, G.L. Sheu, C.C. Wu, M.H. Cheing, *J. Colloid Interface Sci.* 124 (1988) 666.
- [10] G.P. Sighinolfi, *Atom. Absorp. Newsl.* 12 (1973) 136.
- [11] C.W. Fuller, *Anal. Chim. Acta* 81 (1976) 199.
- [12] T. Stařilov, T. Todorovski, B. Grozdanova, Lj. Spandeva, *Nucl. Instrum. Methods Phys. Res. A* 271 (1988) 321.
- [13] T. Stařilov, A. Lazaru, E. Pernicka, *Acta Chim. Slov.* 40 (1993) 37.
- [14] R.R. Dulski, R.R. Bixler, *Anal. Chim. Acta* 91 (1977) 199.

Cross-sections of spectrochromatograms for the resolution of overlapping peaks in diode-array high-performance liquid-chromatography

A. Garrido Frenich ^a, M. Martínez Galera ^a, M.D. Gil García ^a, J.L. Martínez Vidal ^a,
A. Muñoz de la Peña ^{b,*}, F. Salinas ^b

^a *Department of Analytical Chemistry, University of Almería, 04071 Almería, Spain*

^b *Department of Analytical Chemistry, University of Extremadura, 06071 Badajoz, Spain*

Received 14 July 1997; received in revised form 28 November 1997; accepted 2 December 1997

Abstract

Multi-wavelength detectors offer improved detection capabilities for liquid chromatographic methods, but require multivariate approaches to utilise all the available information. The photodiode-array detector in high-performance liquid chromatography (HPLC) generates a three-dimensional data matrix, which is conventionally presented as an isometric projection or a contour plot. In this work, a new graphical technique is described for improving the quantitative results obtained from HPLC, using the available spectrochromatographic information in both the time and wavelength domains. The technique consists of performing cross-sections through the data matrix to obtain the maximum analytical information for each of the analytes. Hence, the resolution of overlapping peaks and the sensitivity in the determination are optimised. In order to demonstrate the validity and simplicity of the approach, the method has been applied to the resolution of synthetic mixtures of iprodione, procymidone and chlorothalonil. Also, the method has been satisfactorily applied to the simultaneous determination of the pesticides in environmental groundwater samples. © 1998 Elsevier Science B.V. All rights reserved.

Keywords: Cross-sections; HPLC-DAD; Pesticides; Spectrochromatograms

1. Introduction

Multi-wavelength detectors for liquid chromatography have become increasingly available in analytical laboratories. UV-visible and, to a lesser extent, fluorescence based array detectors have

been used to gain more relevant analytical information from the mixtures of interest [1–3]. For example, the possibility of examination of the whole absorption spectrum at the peak allows the assignment of peak purity, and the investigation of homogeneity of a chromatographic peak.

In this context, it is very common to describe, as the most significant applications or advantages of high-performance liquid chromatography

* Corresponding author. Tel.: + 34 24 289378; fax: + 34 24 289375; e-mail: arsenio@unex.es

(HPLC) with diode-array detection, the following: (1) the simultaneous detection of two kind of compounds absorbing at different wavelengths, avoiding the need of performing two injections of the sample; (2) the development of methods of amplification and/or dilution of the sample, based on the reading of the absorbance of the standards at diverse wavelengths; (3) the verification of the spectral purity of the peaks, by scanning several absorption spectra at different zones of the chromatographic peaks. However, this multi-wavelength information is often not used for quantification, but instead a single wavelength is selected to obtain the calibration models. Much of the quantitative information available from these three-dimensional multi-wavelength (A, λ, t) data matrices is therefore wasted.

The spectrochromatographic data are usually represented as a three-dimensional projection, where slices in the time domain generate the elution profile at a fixed wavelength, while slices in the wavelength domain generate the absorption spectra at specified elution times. Alternatively, the data can be presented in two dimensions by using the cartographer's technique of contour plotting. Thus, the isoabsorptive contours are mapped in the (λ, t) plane. In this way, computer-aided manipulation of spectral and chromatographic data allows a number of digital methods to be exploited for enhanced detection sensitivity and selectivity [1,4], and opens up new approaches for the resolution of mixed solutes. Many of the algorithms developed for analytical spectroscopy can be used for data analysis in HPLC–UV-visible, and novel algorithms can be developed to exploit the combination of wavelength and time-domain data in the spectrochromatogram to extend the capabilities of liquid chromatography [5]. Various computer-aided graphical presentations such as spectral normalisation to aid visual assessment of the spectrochromatographic data matrix (A, λ, t) [6,7] and differentiation of the spectrochromatographic data have been applied [8–11]. A number of chemometric methods have also been proposed [7,12,13].

The objective of the present work is to examine the properties, limitations and potential applications of a new methodological approach, to extract the maximum analytical information from the data generated by a diode-array detector in HPLC. The method consists of the generation of cross-sections through the three-dimensional (A, λ, t) matrix, in a way similar to the several linear and non-linear synchronous techniques applied in luminescence spectroscopy, where a trajectory is performed through the three-dimensional (intensity, $\lambda_{\text{excitation}}, \lambda_{\text{emission}}$) luminescence matrix [14–17]. The proposed method allows the use of the spectral information for the deconvolution of overlapping peaks of analytes showing different absorption spectra, extending the potential applications of diode-array detectors in HPLC.

This method has been applied to the determination of iprodione, procymidone and chlorothalonil fungicides, in the presence of each other, in environmental groundwater samples. Generally, these compounds are determined by chromatographic methods, gas chromatography (GC) or HPLC. Methods of GC determination of iprodione, procymidone and chlorothalonil have been reported with thermoionic N-P [18], flame ionisation [19], electron-capture [20,21] and mass detection [22,23]. HPLC methods have been used with UV [24] and mass detection [22]. However, problems of selectivity can occur in multicomponent analysis because of the overlapping of peaks. Frequently, these pesticides are determined by using an a priori separation step [21,25,26], which is time consuming for routine analysis, and in some instances requires special and expensive instrumentation.

2. Experimental

2.1. Reagents

Analytical standards of known purity (99%, w/w) of iprodione, procymidone and chlorothalonil, were obtained from Riedel-de Haën (Seelze, Germany), and used without further purification. Acetonitrile (ACN) of analyti-

cal grade purity obtained from Panreac (Barcelona, Spain) was also used. Milli-Q water, obtained from Millipore Milli-Q filtration/purification system (Millipore, Bedford, MA) was used throughout.

2.2. Apparatus

A Waters (Milford, MA) 990 liquid chromatographic system was used, consisting of a Waters 600 E pump, a Rheodyne injection valve provided with a 20 μl loop, and a LC Waters 991 diode-array photometric detector. The spectral resolution used was 1.4 nm per diode in the range 200–250 nm.

2.3. Software

A compatible personal computer, provided with a 386 microprocessor and mathematical co-processor, was used for acquisition and treatment of the data. The LC system allows the acquisition of a series of chromatograms at different wavelengths (λ). The 991 Waters software controlling the instrument generates a three-dimensional file (A, λ, t) in binary format. Then, the three-dimensional file is converted in a series of n individual spectra, each of them corresponding to an absorption spectrum, acquired at a different time, with the ASCII converter included in the 991 Waters program. The resolution used in the time domain is 1.4 s.

A converter program in BASIC, developed by us, was used to transform the bidimensional files in ASCII format, to the software package SURFER [27]. The three-dimensional spectrochromatograms are obtained and presented as isometric plots (A, λ, t). Alternatively, the data are presented as a contour plot in the two dimensions of time and wavelength, by linking points of equal intensity to form the contour map. The SURFER program allows to generate cross-sections, and shows the trajectory followed in the contour or isometric plot. Cross-section data are plotted to produce a profile from the bidimensional data projection [$A-f(\lambda, t)$]. When the data are plotted, the absorbance value is plotted as the Y co-ordinate.

2.4. HPLC procedure

The column used was a Lichrospher[®] RP-C₁₈ 250 mm \times 4 mm (5 μm particle size) from Merck (Darmstadt, Germany). The mobile phase, under isocratic conditions, was ACN–water (70:30, v/v). This mobile phase composition was used to reduce the time of analysis and avoid too much dispersion of peaks. The solvents were daily filtered through a 0.45 μm cellulose acetate (water) or polytetrafluoroethylene (ACN) membrane filter before use, and de-gassed with helium during and before use.

Mixtures of iprodione, procymidone and chlorothalonil pesticides were prepared, in the concentration range 0.5–8.0 $\mu\text{g ml}^{-1}$. Sample volumes of 20 μl were injected into the HPLC system at a solvent rate of 1 ml min^{-1} and the spectrochromatographic data were recorded between 200 and 250 nm over an integration period of 1.4 s per spectrum. A cross-section was defined through the data matrix by the initial and final co-ordinate (λ, t) pairs (200, 300)–(210, 400) and (210, 400)–(250, 300). Cross-section data were plotted on the wavelength domain to produce a bidimensional projection that was used to determine the concentrations of iprodione, procymidone and chlorothalonil through the adequate calibration lines.

2.5. Procedure for the analysis of iprodione, procymidone and chlorothalonil in environmental groundwater samples

Three extractions with methylene chloride were carried out. Groundwater samples (500 ml) were filtered and shaken with 50 ml of the organic solvent for 2 min each. The combined organic extracts were dried, by passing them through anhydrous Na_2SO_4 and evaporated using a rotary vacuum evaporator. The samples thus concentrated were eluted with 1 ml of ACN. Amounts of 20 μl were injected in the chromatograph and the pesticides were determined as described above.

3. Results and discussion

The objective of the work is the investigation of the possibilities and limitations of a novel technique, taking advantages of the multivariate information produced by a diode-array detector in HPLC. For that, a mixture of three pesticides, iprodione, chlorothalonil and procymidone, has been selected for the discussion of the proposed approach.

The UV absorption spectra of each of the selected pesticides were recorded and are represented in the Fig. 1. The corresponding absorption maxima are located at 207.5 nm for iprodione, at 206.0 nm for procymidone, and at 233.5 nm for chlorothalonil. From the observation of the corresponding absorption spectra, it is evident that iprodione and procymidone present their absorption maxima at very close wavelengths, while chlorothalonil presents its maximum absorption at a longer wavelength, but its wide absorption spectrum overlaps in part with those of procymidone and iprodione.

Taking into account the absorption data of the mixture of interest, 220 nm was first selected as the monitoring wavelength, as a compromise value for the detection of the three compounds

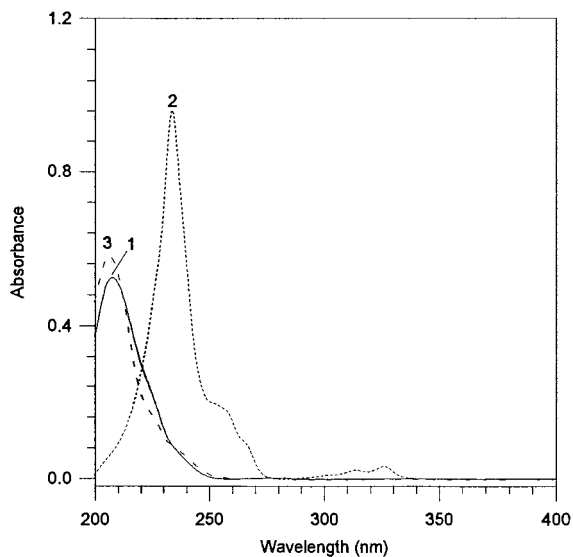


Fig. 1. Absorption spectra of: (1) $4 \mu\text{g ml}^{-1}$ iprodione; (2) $3 \mu\text{g ml}^{-1}$ chlorothalonil and (3) $4 \mu\text{g ml}^{-1}$ procymidone.

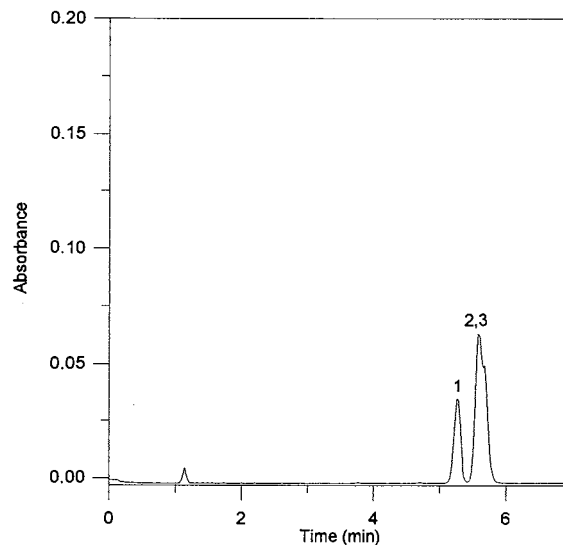


Fig. 2. Chromatogram at 220 nm of a sample containing: (1) $3 \mu\text{g ml}^{-1}$ iprodione; (2) $4 \mu\text{g ml}^{-1}$ chlorothalonil and (3) $5 \mu\text{g ml}^{-1}$ procymidone.

after the HPLC separation. The chromatogram corresponding to a mixture of iprodione, procymidone and chlorothalonil, using ACN–water (70:30, v/v) as the mobile phase, and monitoring the absorbance at 220 nm, is presented in Fig. 2. With these conditions, the complete chromatogram is obtained in 7 min.

The obtained retention times are 5.3 min for iprodione, 5.6 min for chlorothalonil and 5.7 min for procymidone. It is evident that, in the chromatographic profile taken at the fixed wavelength selected (220 nm), the peaks corresponding to chlorothalonil and procymidone are strongly overlapping, and that the complete resolution of the mixture is not accomplished. It can be observed in Fig. 2 that iprodione is well resolved from the other two components of the mixture, and that its determination would be possible from the chromatogram at 220 nm. Alternatively, to maximise the iprodione signal, 207.5 nm (wavelength of its maximum of absorption) can be selected for the analysis. In these conditions, the calibration graph found was $y = 0.02122I + 0.00195$ ($n = 10$) for iprodione concentrations ranging between 0.5 and $8.0 \mu\text{g ml}^{-1}$, where y is the peak height and I is the iprodione concentra-

tion. The standard deviations of the slope and the intercept were 0.00019 and 0.00080, respectively. Several synthetic mixtures were analysed for iprodione in these conditions, and the recoveries obtained ranged between 95.0 and 100.3%.

However, procymidone and chlorothalonil show overlapping peaks in the chromatographic profile, and the resolution of these two compounds is not possible by measuring at a fixed wavelength of 220 nm. A possible solution of the problem, in the case of using a diode-array detector, or a conventional photometric detector allowing the simultaneous measurement at two different wavelengths, would be the measurement of chlorothalonil at its absorption maximum at 233.5 nm. By measuring at 233.5 nm, the interference of procymidone on the analytical signal corresponding to chlorothalonil should be smaller, as its absorption maximum is at 206.0 nm. To explore this possibility, chromatograms of samples containing $0.5 \mu\text{g ml}^{-1}$ procymidone or $0.5 \mu\text{g ml}^{-1}$ chlorothalonil were recorded under the same chemical conditions, monitoring the absorbance at 233.5 nm.

The corresponding chromatograms are presented in Fig. 3. From an inspection of the chromatograms, it is evident that the presence of 0.5

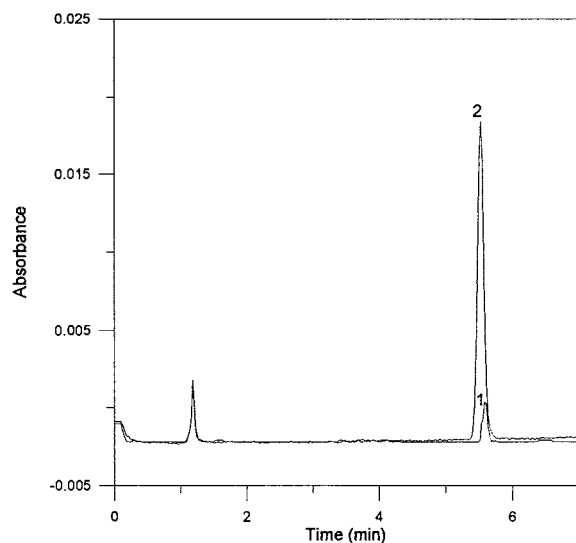


Fig. 3. Chromatogram at 233.5 nm of a sample containing: (1) $0.5 \mu\text{g ml}^{-1}$ procymidone and (2) $0.5 \mu\text{g ml}^{-1}$ chlorothalonil.

$\mu\text{g ml}^{-1}$ procymidone produces a small signal, practically at the same retention time, that would interfere in the determination of chlorothalonil at 233.5 nm. The reason is that, although the absorption maximum corresponding to procymidone is located at 206.0 nm, its wide spectrum still shows a small absorption signal at 233.5 nm.

We have found that the determination of chlorothalonil in mixtures with procymidone in concentration ranges between 0.5 and $2.0 \mu\text{g ml}^{-1}$ is only possible by measuring the absorbance at wavelengths higher than 250 nm, where procymidone absorption is negligible. However, the method suffers a dramatic decrease in sensitivity with respect to chlorothalonil determination, as its absorption at those wavelengths is much smaller than at 233.5 nm.

On the other hand, procymidone determination is not possible at any wavelength in the presence of chlorothalonil as, even at 200 nm, the wide absorption spectrum of chlorothalonil is overlapping, as can be observed from the corresponding absorption spectra profiles (Fig. 1).

This situation, with overlapping of peaks of several analytes of interest, or between analytes and interference substances, is frequent in multi-residue methods. The change of both stationary or mobile phases may resolve the problem, but with a multi-residue method applied to a high number of samples it is preferable to complete the determination without changing the analytical conditions. In consequence, the possibility of an approach to optimise the resolution of the peaks, avoiding as much as possible loss in sensitivity, seems interesting.

3.1. Three-dimensional spectrochromatograms

With the object of resolving the overlapping problem, using the total analytical information provided by the diode-array detector, the three-dimensional (A, λ, t) spectrochromatograms of each of the pesticides, and that of their mixture, were obtained.

In the Fig. 4, the spectrochromatographic profile of the mixture has been represented as an isometric projection. The spectrochromatogram of the selected mixture has been also represented,

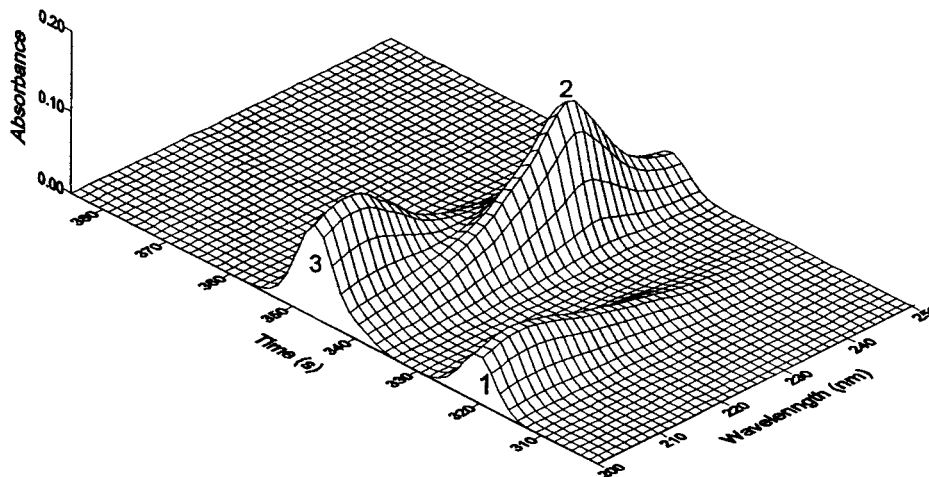


Fig. 4. Isometric (A , λ , t) representation of the spectrochromatogram of a mixture of (1) iprodione ($3 \mu\text{g ml}^{-1}$), (2) chlorothalonil ($4 \mu\text{g ml}^{-1}$) and (3) procymidone ($5 \mu\text{g ml}^{-1}$), captured at 1.4-s intervals during elution, and photometric detection effected in the range 200–250 nm.

in two dimensions, as a contour plot, where concentric isoabsorptive lines are plotted in the (λ , t) plane, so that all the data can be observed simultaneously. In the contour plots, the two normal axes represent time and wavelength, while absorbances are expressed as a series of contours connecting points of equal absorbance by contour lines. In the Fig. 5 the contour plot of a mixture of the three pesticides is presented.

From the three-dimensional representations, it is clearly evident that the signals corresponding to iprodione and procymidone show the absorption maxima at very close wavelengths, but at different retention times. However, the signals corresponding to procymidone and chlorothalonil appear at different wavelengths, but the chromatographic peaks are very overlapped in the time domain, and because of the wide spectral profiles some overlapping also exists in the wavelength domain.

3.2. Cross-sections optimisation through the three-dimensional data matrix

The contour presentation of the three-dimensional data matrix is more convenient than the isometric presentation, especially where quantitative data are needed. The contour plots are specially useful to make cross-sections through the

data matrix, in a way allowing to pass as close as possible to the wavelength maxima and elution times of the different peaks, with the object of optimising the resolution of the overlapping peaks in both, selectivity and sensitivity. Two trajectories have been selected through the contour plots to define the corresponding cross-sections. These trajectories have been defined by the initial and final co-ordinate (λ , t) pairs, that describe the different linear paths, of the corresponding cross-section.

The contour plot of a mixture containing $3 \mu\text{g ml}^{-1}$ iprodione, $4 \mu\text{g ml}^{-1}$ chlorothalonil and $5 \mu\text{g ml}^{-1}$ procymidone, in which the trajectories of the selected cross-sections are indicated, is presented in Fig. 6. In the present case, the two cross-sections selected are defined by two linear paths. In the cross-section I, the wavelength is first varying linearly from 200 to 210 nm, while the retention time is varying linearly between 300 and 400 s in the first path. In the second path, the wavelength is varying linearly between 210 and 250 nm, while the retention time is varying between 400 and 300 s. In this way, the initial and final co-ordinates (λ , t) are (200, 300)–(210, 400) for the first path, and (210, 400)–(250, 300) for the second path. Similarly, the co-ordinates for the cross-section II are (200, 300)–(215, 400) and (215, 400)–(250, 300).

The bidimensional projections on the wavelength domain, generated by the selected cross-sections through the data matrix, are represented in Fig. 7a, cross-section I, and Fig. 7b, cross-section II. The analytical signals obtained after this process are very different from the ones of the original chromatograms obtained at 220 nm. The separation of three peaks, corresponding to each one of the mixture components, is evident in both cross-section projections selected. In this way, the resolution of the mixture is accomplished, allowing the quantification of each of the analytes through the adequate calibration lines.

The two cross-sections tested have been selected in order to get bidimensional projections with the

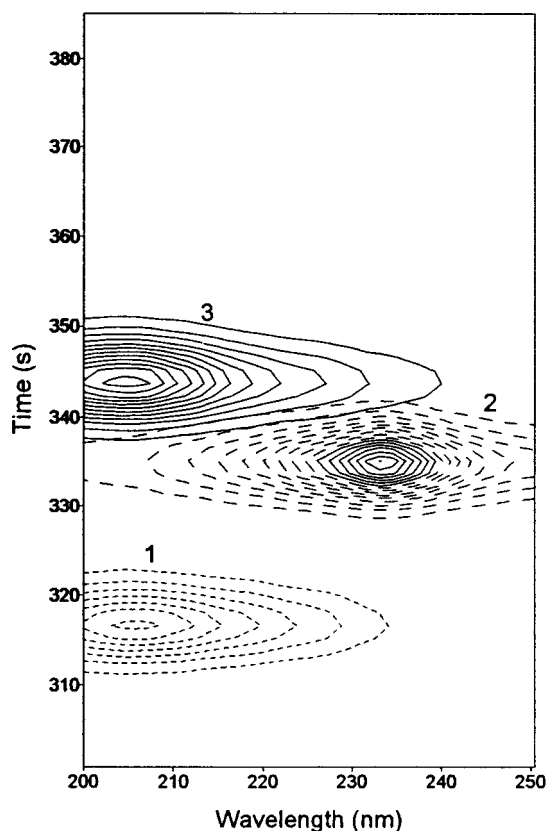


Fig. 5. Contour plot representation of the spectrochromatogram of standards of (1) iprodione ($3 \mu\text{g ml}^{-1}$), (2) chlorothalonil ($4 \mu\text{g ml}^{-1}$) and (3) procymidone ($5 \mu\text{g ml}^{-1}$), captured at 1.4-s intervals during elution, and photometric detection effected in the range 200–250 nm.

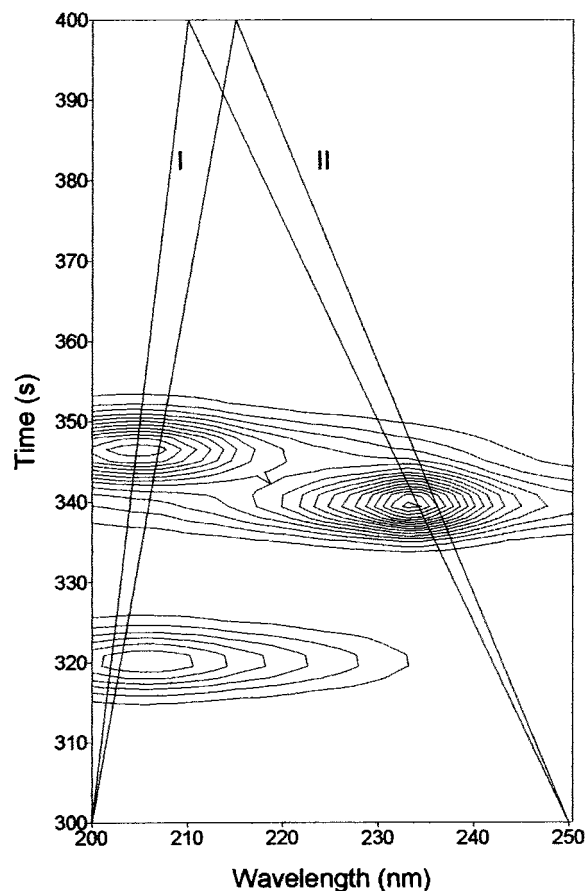


Fig. 6. The trajectories (I and II) and the two cross-sections selected for the analysis, plotted across the contour plot, of the spectrochromatogram of a mixture containing $3 \mu\text{g ml}^{-1}$ iprodione, $4 \mu\text{g ml}^{-1}$ chlorothalonil and $5 \mu\text{g ml}^{-1}$ procymidone.

best analytical characteristics (resolution and sensitivity). It is evident that the two trajectories selected in this work are not the unique possibilities. More complicated trajectories, with more than two linear paths, or even non-linear paths, may be selected for the analysis. Apart from maximising resolution, in order to obtain the highest sensitivity possible, in each particular case, the selected trajectories should pass as close as possible to each absorption maximum. In our case, comparing the results found for the two trajectories tested, the best bidimensional projection is the cross-section I. In Fig. 8, the isometric projection of the complete spectrochromatogram

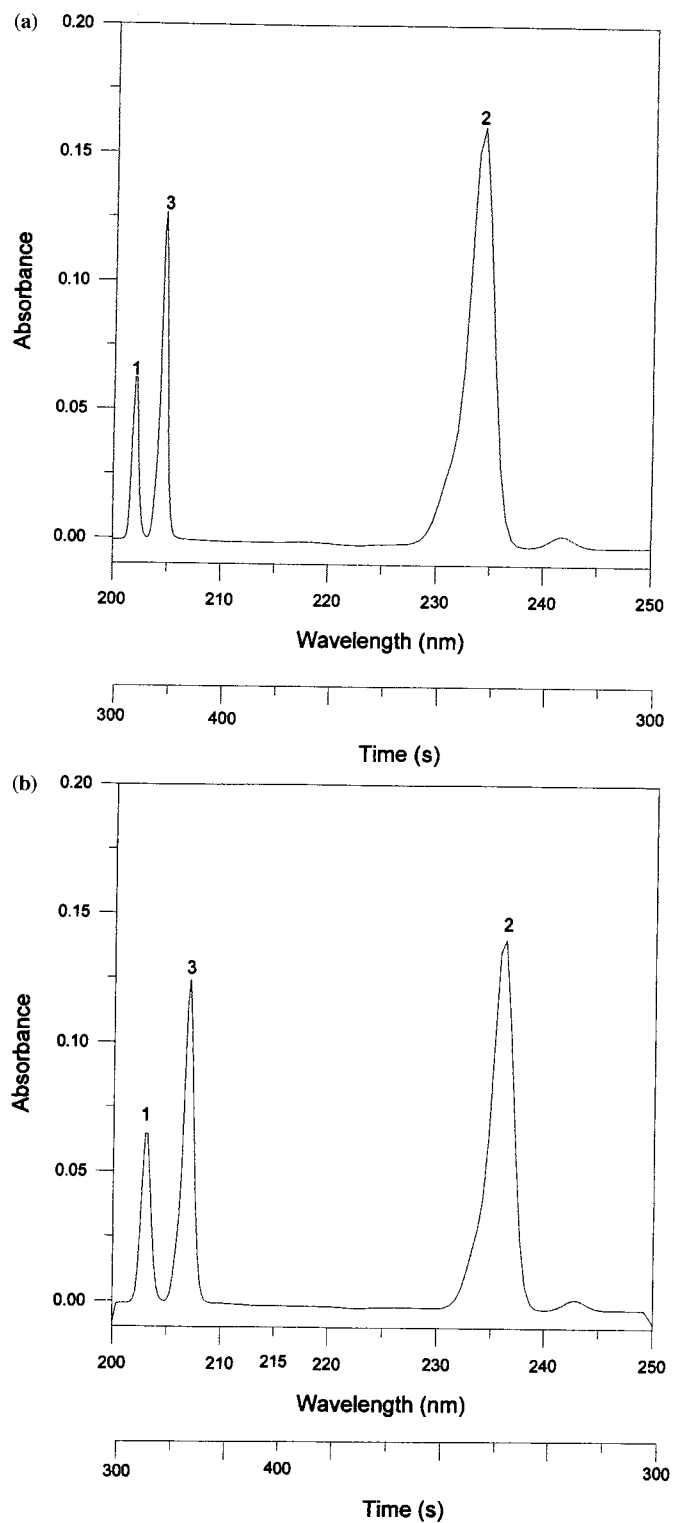


Fig. 7. Bidimensional projections of the cross-sections produced from the three-dimensional data, by plotting absorbance versus a function of wavelength and time: (a) trajectory I, (b) trajectory II.

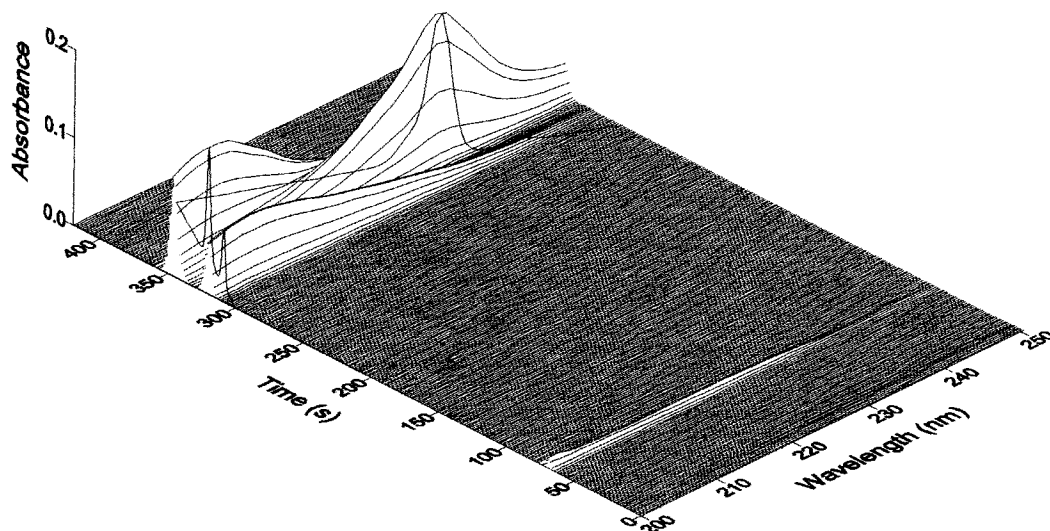


Fig. 8. Isometric projection of the spectrochromatogram of the mixture analysed, in which the trajectory of the selected cross-section, I, is marked.

of the mixture analysed, in which the trajectory of the selected cross-section I is marked, is presented.

With the aim of demonstrating that the trajectory taken is free from interferences, the selected cross-section I was applied to individual standards of iprodione, procymidone and chlorothalonil. The suitable bidimensional projections in the wavelength domain are superposed and represented in Fig. 9. It is clear that there is not interference in the determination of any analyte with the proposed cross-section. Hence, the combined use of chromatographical and spectral information allows to carry out the quantitation of each analyte, as the signal from one analyte is free from interferences from the other analytes. The above proves the advantage of this approach over the classic techniques of cutting through the three-dimensional matrix at constant wavelength, obtaining chromatograms, or at constant time, obtaining absorption spectra.

3.3. Calibration graphs

Calibration graphs, for the respective analytical signals constructed by measurement of the peak heights, were taken from the corresponding cross-section throughout the selected trajectory, for

samples of mixtures of the three compounds, containing different concentrations of iprodione, procymidone and chlorothalonil. Good linearity was obtained for all pesticides, in the range $0.5\text{--}8.0\ \mu\text{g ml}^{-1}$. Table 1 lists the straight-line equations obtained for the concentration intervals tested, and the corresponding statistical parameter values. The detection and quantitation limits [28], calculated statistically, are summarised in Table 2. In order to study the repeatability of the method, a series of six samples were prepared, containing $2.0\ \mu\text{g ml}^{-1}$ iprodione, $2.0\ \mu\text{g ml}^{-1}$ procymidone and $2.0\ \mu\text{g ml}^{-1}$ chlorothalonil, with results of 1.20, 0.85 and 0.78%, respectively, for the relative standard deviations. The values obtained show the high repeatability of the method.

3.4. Resolution of synthetic ternary mixtures

Mixtures of iprodione, procymidone and chlorothalonil, in the concentration range $1\text{--}8\ \mu\text{g ml}^{-1}$, were prepared, and the spectrochromatograms were recorded according to the described procedure. Table 3 presents the results of the analysis of different mixtures. Satisfactory results were obtained, with recovery values ranging from 95.0 to 99.8% for iprodione, from 96.7

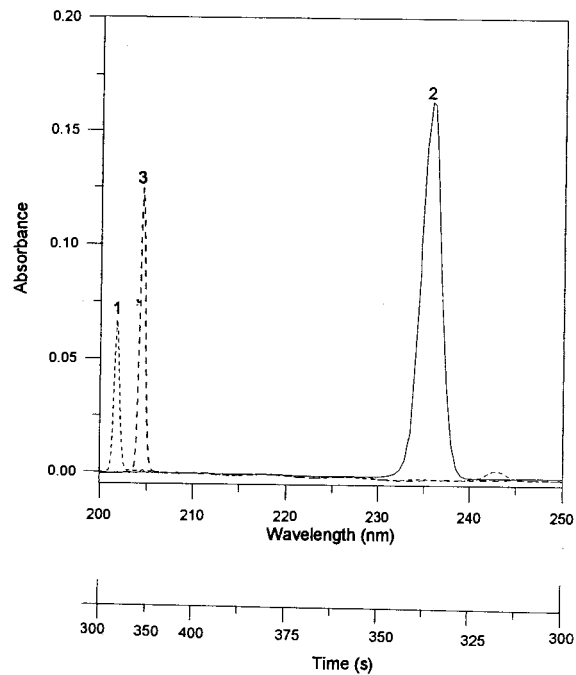


Fig. 9. Superimposed bidimensional projections of the cross-sections produced from the three-dimensional data, by plotting absorbance versus a function of wavelength and time, following the trajectory I.

to 103.7% for procymidone, and from 98.0 to 108.8% for chlorothalonil. The results indicate that the complete resolution of the mixture has been accomplished by the proposed approach, showing the high resolving power of the technique.

Table 1

Calibration graphs for the determination of iprodione (I), procymidone (P) and chlorothalonil (C) in mixtures, by measuring the peak heights at the selected projection of cross-section I

Pesticide	Equation ^a	R ²	Standard deviation	
			Slope	Intercept
Iprodione	$y = 0.02256I + 0.00260$	0.9997	0.00020	0.00090
Procymidone	$y = 0.02423P + 0.00199$	0.9999	0.00012	0.00056
Chlorothalonil	$y = 0.03850C + 0.00102$	0.9998	0.00025	0.00110

The results were obtained from ten calibration standards.

^a I, P, C are concentrations in $\mu\text{g ml}^{-1}$.

Table 2

Detection and quantitation limits

Pesticide	Detection limit ($\mu\text{g ml}^{-1}$)	Quantitation limit ($\mu\text{g ml}^{-1}$)
Iprodione	0.04	0.09
Procymidone	0.13	0.17
Chlorothalonil	0.10	0.16

3.5. Analysis of pesticides in environmental groundwater samples

To check the procedure in a real situation, the method was applied to determine the three pesticides in environmental samples of groundwater. The preconcentration step was carried out as described in Section 2. The study was performed with uncontaminated spiked groundwater samples.

Table 4 summarises the composition and the results of the analysis of different samples. Satisfactory recoveries were obtained, with values ranging from 90.0 to 108.0% for iprodione, from 93.7 to 107.7% for procymidone and from 87.0 to 107.0% for chlorothalonil. The results obtained indicate the suitability of the proposed approach to determine the pesticides in environmental water samples.

4. Conclusions

The determination of iprodione, procymidone and chlorothalonil mixtures has been performed by means of a novel technique with good re-

Table 3

Results obtained in the determination of iprodione, procymidone and chlorothalonil in synthetic ternary mixtures using the proposed approach

Iprodione		Procymidone		Chlorothalonil	
Added ($\mu\text{g ml}^{-1}$)	R (%)	Added ($\mu\text{g ml}^{-1}$)	R (%)	Added ($\mu\text{g ml}^{-1}$)	R (%)
2.0	97.0 (4.4)	2.0	97.5 (4.1)	1.5	99.3 (3.7)
5.0	99.8 (4.2)	5.0	100.2 (4.0)	3.0	101.3 (3.6)
2.0	96.0 (4.6)	8.0	98.1 (4.0)	1.0	98.0 (4.1)
1.0	95.0 (4.6)	3.0	103.7 (3.6)	5.0	105.0 (3.4)
2.0	95.5 (4.6)	4.0	103.0 (3.8)	6.0	104.2 (3.4)
2.0	95.0 (4.6)	2.0	100.5 (3.8)	4.0	101.7 (3.6)
2.4	97.1 (4.3)	2.4	96.7 (3.6)	3.5	108.8 (3.8)

The results are average of three determinations with R.S.D. in parentheses.

R, recovery.

peatability and sensitivity. The proposed technique is particularly useful for determining mixture of analytes in complex samples, as it is the case in multi-residue pesticide analysis. The usefulness of the proposed methodology is the resolution of overlapping chromatographic peaks maintaining, at the same time, as much sensitivity in the determination as possible. The technique presented here is applicable for such purpose if there exists at least one cross-section of the spectrochromatogram along which the peaks are resolved. In addition, the approach would allow a reduction in the time of analysis in certain cases. This can be the case in the separation of several analytes with similar polarities, from one of very different polarity. In con-

clusion, the combination of advanced computational capability, with the diode-array detector technology applied in HPLC, offers a powerful approach for the resolution of highly overlapping peaks, maximising at the same time the sensitivity of the method, as it is demonstrated in the particular case studied.

Acknowledgements

The authors gratefully acknowledge the DGI-CYT (Project PB95-1141 and Project PB95-1226) and the Consejería de Educación y Juventud de la Comunidad de Extremadura (Project EIA 95-36) for financial support.

Table 4

Recovery (R) results obtained in the determination of iprodione, procymidone and chlorothalonil in groundwater samples

Iprodione			Procymidone			Chlorothalonil		
Added ($\mu\text{g l}^{-1}$)	R (%)	R.S.D. ^a (%)	Added ($\mu\text{g l}^{-1}$)	R (%)	R.S.D. ^a (%)	Added ($\mu\text{g l}^{-1}$)	R (%)	R.S.D. ^a (%)
8.0	98.0	3.5	12.0	107.7	4.0	4.0	104.0	3.7
4.0	90.0	3.9	8.0	95.0	4.8	14.0	105.1	3.5
20.0	106.0	3.2	4.0	104.0	3.9	8.0	87.0	4.7
8.0	95.0	3.7	22.0	98.5	4.3	12.0	97.3	4.2
20.0	92.4	4.0	10.0	103.8	4.2	8.0	107.0	3.5
10.0	105.2	3.5	14.0	93.7	4.5	20.0	103.0	3.7
16.0	101.0	3.7	12.0	95.0	4.1	16.0	102.5	3.8
20.0	108.0	3.6	12.0	107.7	4.0	8.0	105.0	4.0

^a n = 3.

References

- [1] A.F. Fell, B.J. Clark, H.P. Scott, *J. Chromatogr.* 316 (1984) 423.
- [2] J.C. Gluckman, D.C. Shelly, M.V. Novotny, *Anal. Chem.* 57 (1985) 1546.
- [3] J. Wegrzyn, G. Patonay, M. Ford, I.M. Warner, *Anal. Chem.* 62 (1990) 1754.
- [4] E. Sánchez, L.S. Ramos, B.R. Kowalski, *J. Chromatogr.* 385 (1987) 151.
- [5] J.G. Dorsey, W.T. Cooper, J.F. Wheeler, H.G. Barth, J.P. Foley, *Anal. Chem.* 66 (1994) 500R.
- [6] B.J. Clark, A.F. Fell, H.P. Scott, D.J. Westerlund, *J. Chromatogr.* 286 (1984) 261.
- [7] B.J. Clark, A.F. Fell, *Chem. Brit.* November (1987) 1069.
- [8] A.A. Fasanmade, A.F. Fell, H.P. Scott, *Anal. Chim. Acta* 187 (1986) 233.
- [9] A.A. Fasanmade, A.F. Fell, *Anal. Chem.* 61 (1989) 720.
- [10] A. Muñoz de la Peña, F. Salinas, T. Galeano, A. Guiberteau, *Anal. Chim. Acta* 234 (1990) 263.
- [11] P. Parrilla, M. Martínez Galera, J.L. Martínez Vidal, A. Garrido Frenich, *Analyst* 119 (1994) 2231.
- [12] J.G.D. Marr, B.J. Clark, A.F. Fell, *Anal. Proc.* 25 (1988) 150.
- [13] T.L. Cecil, R.B. Poe, S.C. Rutan, *Anal. Chim. Acta* 250 (1991) 37.
- [14] J.N. Miller, *Analyst* 109 (1984) 191.
- [15] M.C. Gutiérrez, S. Rubio, A. Gómez-Hens, M. Valcárcel, *Talanta* 34 (1987) 325.
- [16] A. Muñoz de la Peña, F. Salinas, M.I. Durán, *Anal. Chim. Acta* 255 (1991) 317.
- [17] J.A. Murillo Pulgarín, A. Alañon Molina, *Comput. Chem.* 17 (1993) 341.
- [18] M.W. Brooks, D. Tessier, D. Soderstrom, J. Jenkins, J.M. Clark, *J. Chromatogr. Sci.* 28 (1990) 487.
- [19] M. Ogawa, T. Ohtsubo, S. Tsuda, K. Tsuji, *J. Assoc. Off. Anal. Chem.* 76 (1993) 83.
- [20] W.H. Newsome, P. Collins, *Int. J. Environ. Anal. Chem.* 38 (1990) 489.
- [21] A. Valverde García, E. González Pradas, J.L. Martínez Vidal, A. Agüera López, *J. Agric. Food Chem.* 39 (1991) 2188.
- [22] J. Simal Gandara, P. Paseiro Losada, V. González Rodríguez, A. Romero Rodríguez, *J. Agric. Food Chem.* 41 (1993) 674.
- [23] G.C. Mattern, G.M. Singer, J. Louis, M. Robson, J.D. Rosen, *J. Agric. Food Chem.* 38 (1990) 402.
- [24] M.A. Miron-Comas, M. Xirau-Vayreda, *Rev. Agroquim. Tecnol. Aliment.* 31 (1991) 352.
- [25] R.Ch. Hsu, I. Biggs, K.N. Saini, *J. Agric. Food Chem.* 39 (1991) 1658.
- [26] W. Harvey, P. Collins, *J. Chromatogr.* 472 (1989) 416.
- [27] GRAPHER and SURFER for Windows, Software Package Version 5.0, Golden Software, CO, 1993.
- [28] G.L. Long, J.D. Winefordner, *Anal. Chem.* 55 (1983) 713.

Lead ion selective PVC membrane electrode based on 5,5'-dithiobis-(2-nitrobenzoic acid)

Ahmad Rouhollahi ^a, Mohammad Reza Ganjali ^a, Mojtaba Shamsipur ^{b,*}

^a Department of Chemistry, Tehran University, Tehran, Iran

^b Department of Chemistry, Razi University, Kermanshah, Iran

Received 23 July 1997; received in revised form 1 December 1997; accepted 2 December 1997

Abstract

A PVC membrane electrode for lead ions based on 5,5'-dithiobis-(2-nitrobenzoic acid) as membrane carrier was prepared. The electrode exhibits a Nernstian response for Pb^{2+} over a wide concentration range (1.0×10^{-2} – 4.0×10^{-6} M). It has a relatively fast response time and can be used for at least 3 months without any divergence in potentials. The proposed electrode revealed good selectivities for Pb^{2+} over a wide variety of other metal ions and could be used in a pH range of 2.0–7.0. It was used as an indicator electrode in potentiometric titration of lead ions and in direct determination of lead in water samples. © 1998 Elsevier Science B.V. All rights reserved.

Keywords: 5,5'-Dithiobis-(2-nitrobenzoic acid); Lead ion selective electrode; PVC membrane; Potentiometry

1. Introduction

Ion-selective electrodes based on solvent polymeric membranes with incorporated ion carriers are well known as very useful tools for clinical, chemical and environmental analyses [1,2]. During the last two decades, a large number of neutral ionophores with high selectivities for specific metal ions have been developed and have found widespread applications in potentiometric and optical sensors for the determination of the respective metal ions in a variety of real samples [3,4].

Because of the increased industrial use of lead, on one hand, and its serious hazardous effect to

human health, on the other [5], the electrochemical properties and preparation of the lead ion selective membrane electrodes have been extensively studied by using different active materials. Besides the solid-state membranes [6–11] and liquid ion-exchange membranes [12,13], there has been recently increasing interest to the use of ionophore ligands as sensing materials for neutral carrier type lead ion selective electrodes, mainly due to the unique selectivities of these compounds [14–18].

We have recently prepared a lead-selective membrane electrode based on dibenzopyridino-18-crown-6 [18]. Since the sulphur donor atoms are well known to coordinate strongly with heavy metal ions [19,20], in this paper we employed 5,5'-dithiobis-(2-nitrobenzoic acid) (DTBNBA) as

* Corresponding author. Tel.: +98 831 94066; fax: +98 831 831618.

a suitable ion carrier to construct a PVC-based membrane electrode which exhibits significantly high selectivity to lead ion over alkali, alkaline earth and several transition metal ions.

2. Experimental

2.1. Reagents

Reagent grade dibutyl phthalate (DBP), oleic acid, 5,5'-dithiobis-(2-nitrobenzoic acid) (DTBNBA) and tetrahydrofuran (THF) were purchased from Merck and used as received. The nitrate salts of the cations used (all from Merck) were of the highest purity available and used without any further purification except for vacuum drying over P_2O_5 . Triply distilled deionized water was used throughout.

2.2. Electrode preparation

The general procedure to prepare the PVC membrane was to thoroughly mix 40 mg powdered PVC and 50 mg plasticizer DBP in 10 ml THF. To this mixture was added 20 mg oleic acid and 10 mg ionophore DTBNBA and the solution was mixed well. The resulting mixture was transferred into a glass dish of 2 cm diameter. The THF was evaporated slowly until an oily concentrated mixture was obtained. A Pyrex tube (3–5 mm o.d.) was dipped into the mixture for about 10 s so that a non-transparent membrane of about 0.3 mm thickness was formed. The tube was then pulled out of the solution and kept at room temperature for 1 h. The tube was filled with internal filling solution (1.0×10^{-3} M $Pb(NO_3)_2$ + 1.0×10^{-3} M NH_4Cl). The electrode was finally conditioned for 24 h by soaking in a 1.0×10^{-2} M solution of lead nitrate. A silver/silver chloride coated wire was used as an internal reference electrode.

2.3. e.m.f. measurements

All e.m.f. measurements were carried out with the following assembly: $Ag-AgCl/1.0 \times 10^{-3}$ M $Pb(NO_3)_2$, 1.0×10^{-3} M NH_4Cl/PVC membrane/test solution/ $Hg-Hg_2Cl_2$, KCl (satd.).

A Corning ion analyser 250 pH/mV meter was used for the potential measurements at $25.0 \pm 0.1^\circ C$. The e.m.f. observations were made relative to a double-junction saturated calomel electrode (SCE, Philips) with the chamber filled with an ammonium nitrate solution. Activities were calculated according to the Debye–Hückel procedure[21].

3. Results and discussion

Due to its negligible solubility in water and the existence of two donating sulphur atoms in its structure, DTBNBA seemed to be a potential ion carrier for soft heavy metal ions in the PVC membrane electrodes. Thus, in preliminary experiments, it was used to prepare PVC membrane ion-selective electrodes for a wide variety of metal ions, including alkali, alkaline earth, transition and heavy metal ions. The potential responses of these electrodes are illustrated in Fig. 1. As seen, among these cations, those of hard acid character

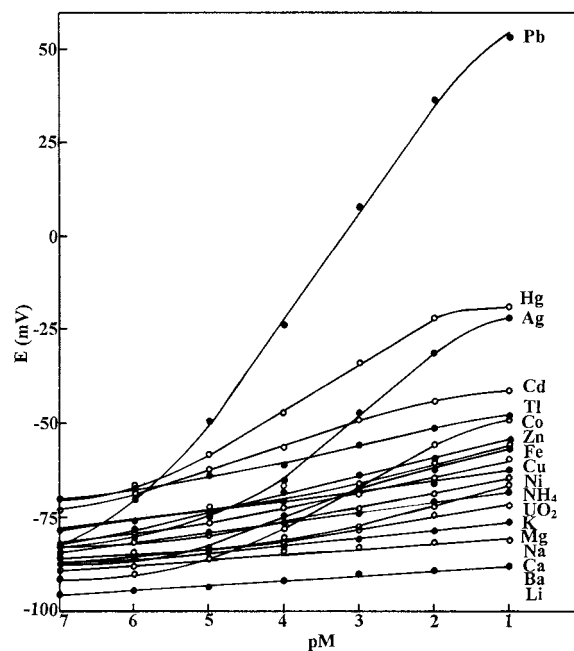


Fig. 1. Potential response of various ion-selective electrodes based on DTBNBA. Membrane composition: %33 PVC; %42 DBP; %9 DTBNBA; %16 oleic acid.

Table 1
Optimization of membrane ingredients

Membrane number	Composition (%)				Slope (mV per decade)	Linear range (M)
	PVC	DBP	DTBNBA	Oleic acid		
1	70	30	–	–	0	–
2	68	29	3	–	6	5.0×10^{-3} – 1.0×10^{-2}
3	67	28	5	–	9	5.0×10^{-3} – 1.0×10^{-2}
4	65	28	7	–	10	5.0×10^{-3} – 1.0×10^{-2}
5	64	27	9	–	11	5.0×10^{-3} – 1.0×10^{-2}
6	61	26	13	–	11	5.0×10^{-3} – 1.0×10^{-2}
7	58	25	9	8	24	7.0×10^{-5} – 1.0×10^{-2}
8	50	25	9	16	28	5.0×10^{-5} – 1.0×10^{-2}
9	42	33	9	16	29	6.0×10^{-6} – 1.0×10^{-2}
10	33	42	9	16	29	4.0×10^{-6} – 1.0×10^{-2}
11	25	50	9	16	29	8.0×10^{-6} – 1.0×10^{-2}
12	58	25	–	17	0	–

(i.e. alkali, alkaline earth and UO_2^{2+} ions [22]) show negligible responses, due to their weak interactions with the sulphur atoms of the carrier as soft bases. On the other hand, the metal ions of soft acid character (i.e. Tl^+ , Ag^+ , Cd^{2+} , Hg^{2+} and, especially, Pb^{2+} [22]) show the most sensitive potential response in the series, among which Pb^{2+} provides the most suitable ion-selective electrode. It is thus obvious that the Pb^{2+} ions are more easily attracted to the PVC–DTBNBA membrane which results in a Nernstian potential–concentration response over a wide range.

Since the sensitivities and selectivities obtained for a given ionophore depend significantly on the membrane ingredients and the nature of solvent mediators and additives used [18,23–25], we investigated the influence of membrane composition on the potential response of the Pb^{2+} sensor. The results are summarized in Table 1. It is seen that the increased amount of ionophore, up to a value of 9%, results in the best sensitivity and linear range, although the slope of e.m.f. versus log concentration plot in this case is about one-third of the expected Nernstian value. However, addition of 16% oleic acid will increase the sensitivity of the electrode response considerably, so that the membrane electrode demonstrates a Nernstian behavior. It is well known that the presence of lipophilic anions in cation-selective membrane electrodes not only diminishes the ohmic resis-

tance [26] and enhances the response behaviour and selectivity [27], but also, in cases where the extraction capability is poor, increases the sensitivity of the membrane electrodes [3].

In general, the thickness and hardness of the membrane depend upon the amount of PVC used. At higher PVC content, the membrane becomes too dense, which makes the transport of cations into the membrane more difficult and results in the increased resistance. A decrease in PVC causes an increased linear range of the electrode. However, at lower PVC content, the membrane becomes mechanically weak and swells up easily in aqueous solution. Therefore, the optimum composition of membrane 10 was used for further studies.

The concentration of the internal solution $\text{Pb}(\text{NO}_3)_2$ in the electrode was changed from 1.0×10^{-3} M to 1.0×10^{-5} M and the potential response of the Pb^{2+} selective electrode was obtained. It was found that the variation of the concentration of the internal solution does not cause any significant difference in the potential response, except for an expected change in the intercept of the resulting Nernstian plots. A 1.0×10^{-3} M concentration of the reference $\text{Pb}(\text{NO}_3)_2$ solution is quite appropriate for smooth functioning of the electrode system.

The PVC-based membrane of DTBNBA generates stable potentials when placed in contact with

Pb^{2+} solutions. The critical response characteristics of the Pb^{2+} selective electrode were assessed according to IUPAC recommendations [28]. The e.m.f. response of the membrane at varying activity of Pb^{2+} (Fig. 1) indicates a rectilinear range from 1.0×10^{-2} to 4.0×10^{-6} M. The slopes of the calibration curves were 29.0 ± 0.3 mV per decade of lead concentration. The limit of detection, as determined from the intersection of the two extrapolated segments of the calibration graph, was 1.5×10^{-6} M.

The average time required for the Pb^{2+} selective electrode to reach a potential within ± 1 mV of the final equilibrium value after successive immersion of a series of lead ion solutions, each having a 10-fold difference in concentration, was measured. The static response time thus obtained was 70 s for concentration $\leq 1.0 \times 10^{-3}$ M, and potentials stayed constant for more than 5 min, after which only a very slow divergence was recorded. The standard deviation of ten replicate measurements was ± 0.3 mV. The sensing behaviour of the membrane remained unchanged when the potentials recorded either from low to high concentrations or vice versa. The ion-selective membranes prepared could be used for at least 3 months without any measurable divergence.

The pH dependence of the membrane electrode was tested over the pH range 2–11 at Pb^{2+} concentration of 1.0×10^{-3} M and the results are shown in Fig. 2. As seen, the potential was constant from pH 2.0 to 7.0, beyond which a gradual

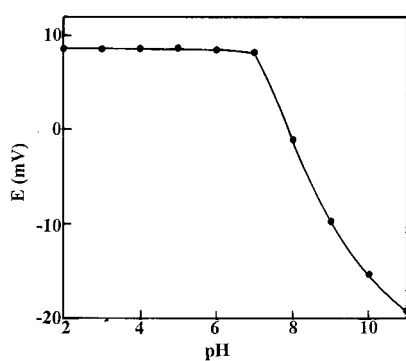


Fig. 2. Effect of pH of test solution on the potential response of the Pb^{2+} selective electrode.

Table 2
Selectivity coefficients of diverse ions

Diverse ion	$K_{\text{Pb}}^{\text{Pot}}$	Diverse ion	$K_{\text{Pb}}^{\text{Pot}}$
Li^+	1.5×10^{-4}	Co^{2+}	4.4×10^{-3}
Na^+	1.4×10^{-4}	Ni^{2+}	3.0×10^{-3}
K^+	1.3×10^{-4}	Cu^{2+}	9.1×10^{-3}
NH_4^+	1.4×10^{-4}	Zn^{2+}	7.8×10^{-3}
Ag^+	1.0×10^{-2}	Cd^{2+}	1.2×10^{-2}
Tl^+	2.9×10^{-3}	Hg^{2+}	4.3×10^{-2}
Mg^{2+}	2.7×10^{-4}	UO_2^{2+}	9.9×10^{-4}
Ca^{2+}	3.7×10^{-4}	Fe^{3+}	1.2×10^{-3}
Ba^{2+}	3.9×10^{-4}		

drift was observed. The observed drift at higher pH values would be due to the ionization of the ionophore and/or the formation of some hydroxy complexes of Pb^{2+} in solution.

In order to investigate the selectivity of the proposed Pb^{2+} selective electrode, perhaps as the most important characteristic of a membrane sensor, its response was examined in the presence of various foreign ions. The potentiometric selectivity coefficients ($K_{\text{Pb}}^{\text{Pot}}$) were evaluated graphically by the mixed solution method [29,30] from potential measurements on solutions containing a fixed amount of Pb^{2+} (1.0×10^{-3} M) and varying amounts of the interfering ions (M^{n+}) according to the equation:

$$K_{\text{Pb}}^{\text{Pot}} a_{\text{M}}^{1/n} = a_{\text{Pb}} \{ \exp[(E_2 - E_1)F/RT] \} - a_{\text{Pb}} \quad (1)$$

where E_1 and E_2 are the electrode potentials for the solution of Pb^{2+} alone and for the solution containing interfering ions (M^{n+}) and Pb^{2+} ions. According to Eq. (1), the $K_{\text{Pb}}^{\text{Pot}}$ values for diverse ions can be evaluated from the slope of the graph of $a_{\text{Pb}} \{ \exp[(E_2 - E_1)F/RT] \} - a_{\text{Pb}}$ versus $a_{\text{M}}^{1/n}$.

The resulting values are summarized in Table 2. As can be seen, with the exception of Ag^+ , Cu^{2+} , Cd^{2+} , and Hg^{2+} , for all diverse ions used, the selectivity coefficients are in the order of 10^{-3} or smaller, indicating they would not significantly disturb the functioning of the Pb^{2+} selective membrane. However, Ag^+ , Cu^{2+} , Cd^{2+} and Hg^{2+} with the selectivity coefficients in the order of 10^{-2} reveal some reversible interfering effect in the Pb^{2+} selective electrode functioning. It should be noted that an even more severe interference

effect from these cations on the functioning of other Pb^{2+} selective electrodes has been reported in the literature [16,17,31].

The proposed Pb^{2+} membrane electrode was found to work well under laboratory conditions. It was successfully applied to the titration of a Pb^{2+} solution with sodium chromate, and the resulting titration curve is shown in Fig. 3. As seen, the amount of Pb^{2+} in solution can be accurately determined with the electrode.

The electrode was also applied to the direct measurement of Pb^{2+} in local spring waters from the Calsimine lead and zinc mines (Dandi, Zanjan, Iran). The water samples were adjusted to pH of about 5.5 using 0.01 M ammonium nitrate buffer and their potentials were measured by direct potentiometry. The results obtained were compared with those from atomic absorption spectrometric (AAS) analysis (Table 3). The Zn^{2+} and Cd^{2+} contents of the water samples were also determined by AAS. As seen, the agreement is good and we conclude that the membrane electrode may have applications in the environmental monitoring of Pb^{2+} .

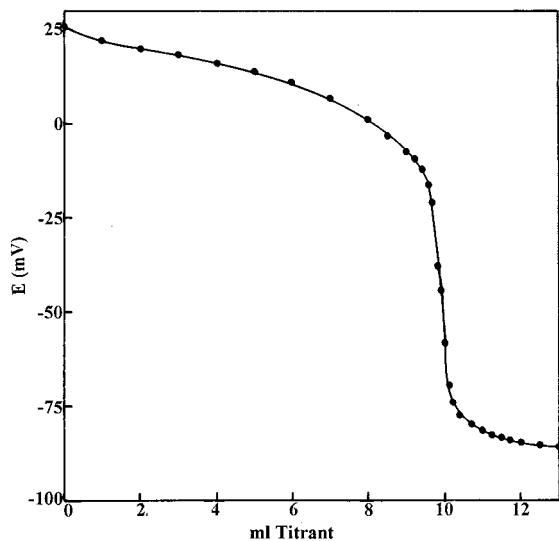


Fig. 3. Potentiometric titration curve of 25 ml of 4.0×10^{-3} M Pb^{2+} solution with 1.0×10^{-2} M Na_2CrO_4 , using the proposed sensor as an indicator electrode.

Table 3
Analytical data for the water samples

Method	Ion	\bar{x} (ppm)	S.D. ($n = 4$)	R.S.D. (%)
AAS	Zn^{2+}	21.7	0.4	1.8
	Cd^{2+}	1.8	0.1	5.5
ISE (direct)	Pb^{2+}	14.1	0.3	2.1
	Pb^{2+}	14.9	0.7	4.7
ISE (titration)	Pb^{2+}	14.1	0.6	4.2

4. Conclusions

This work demonstrates that 5,5'-dithiobis-(2-nitrobenzoic acid) as a new ionophore can be used in the development of a PVC-based lead ion-selective electrode. The electrode responds to Pb^{2+} in a Nernstian fashion and presents good selectivity and detection limit. The electrode is characterized by a relatively fast response, reasonable long-term stability and responsive potential stability. The proposed Pb^{2+} -membrane electrode was applied to the titration of Pb^{2+} solution with sodium chromate as well as the direct determination of lead in water samples.

References

- [1] G.J. Moody, B.B. Saad, J.D.R. Thomas, *Sel. Electrode Rev.* 10 (1988) 71.
- [2] M.E. Mayerhoff, M.N. Opdyche, *Adv. Clin. Chem.* 25 (1986) 1.
- [3] D. Ammann, W.E. Morf, P. Anker, P.C. Meier, E. Pretsch, W. Simon, *Ion-Sel. Electrode Rev.* 5 (1983) 3.
- [4] J. Janata, M. Jasowicz, D.M. DeVaney, *Anal. Chem.* 66 (1994) 207.
- [5] D.R. Lynarn, L.G. Plantanida, J.F. Cole, *Environmental Lead*, Academic Press, New York, 1975.
- [6] E.H. Hansen, J. Ruzika, *Anal. Chim. Acta* 72 (1974) 365.
- [7] P. Kivalo, R. Virtanen, K. Wickstrom, M. Wilson, E. Pungor, G. Horval, K. Toth, *Anal. Chim. Acta* 87 (1976) 41.
- [8] P.S. Thind, H. Singh, T.K. Bindal, *Indian J. Chem.* 21A (1982) 295.
- [9] E. Pungor, K. Toth, G. Nagy, L. Polos, M.F. Ebel, I. Wernisch, *Anal. Chim. Acta* 147 (1983) 23.
- [10] Ya. G. Vlasov, E.A. Bychkov and A.V. Legin, *Sov. Electrochem.* 22 (1987) 1379 (English translation).
- [11] J.F. Van Staden, *Fresenius Z. Anal. Chem.* 33 (1989) 226.

- [12] J. Ruzicka, J.C. Tjell, *Anal. Chim. Acta* 49 (1970) 346.
- [13] A.M.Y. Jaber, G.J. Moody, J.D.R. Thomas, *Analyst* 113 (1988) 1409.
- [14] E. Lindner, K. Toth, E. Pungor, *Anal. Chem.* 56 (1984) 1127.
- [15] S.R. Sheen, J.S. Shih, *Analyst* 117 (1992) 1691.
- [16] S. Kamata, K. Onoyama, *Anal. Chem.* 63 (1991) 1295.
- [17] S.K. Srivastava, V.K. Gupta, S. Jain, *Analyst* 120 (1995) 495.
- [18] N. Tavakkoli, M. Shamsipur, *Anal. Lett.* 29 (1996) 2269.
- [19] J.D. Lamb, R.M. Izatt, C.S. Swain, J.J. Christensen, *J. Am. Chem. Soc.* 102 (1980) 475.
- [20] R. Alberto, W. Nef, A. Smith, T.A. Kaden, M. Neuburger, M. Zehnder, A. Frey, U. Abram, P. August Schubiger, *Inorg. Chem.* 35 (1996) 3420.
- [21] S. Kamata, A. Bhale, Y. Fukunaga, A. Murata, *Anal. Chem.* 60 (1988) 2464.
- [22] R.D. Hancock, A.E. Martell, *J. Chem. Educ.* 73 (1996) 654.
- [23] J. Koryta, *Anal. Chim. Acta* 233 (1990) 1.
- [24] O.S. Wolfbeis, *Anal. Chim. Acta* 250 (1991) 181.
- [25] T. Rosatzin, E. Bakker, K. Suzuki, W. Simon, *Anal. Chim. Acta* 280 (1993) 197.
- [26] D. Ammann, E. Pretsch, W. Simon, E. Lindler, A. Bezegh, E. Pungor, *Anal. Chim. Acta* 171 (1991) 1380.
- [27] M. Huser, P.M. Gehring, W.E. Morf, W. Simon, E. Lindler, J. Jeney, K. Toth, E. Pungor, *Anal. Chem.* 63 (1991) 1380.
- [28] IUPAC Analytical Chemistry Division, Commission on Analytical Nomenclature, *Pure Appl. Chem.* 48 (1976) 127.
- [29] K. Srinivasan, G.A. Rechnitz, *Anal. Chem.* 41 (1969) 1203.
- [30] Y. Umezawa, K. Umezawa, H. Sato, *Pure Appl. Chem.* 67 (1995) 507.
- [31] D. Midgley, *Anal. Chim. Acta* 159 (1984) 63.

Simultaneous determination of selenium and lead in whole blood samples by differential pulse polarography¹

Recai İnam, Güler Somer *

Gazi Üniversitesi, Fen-Edebiyat Fakültesi, Kimya Bölümü, 06500 Ankara, Turkey

Received 1 August 1997; received in revised form 13 November 1997; accepted 2 December 1997

Abstract

The polarographic reduction of lead in the presence of selenite gives rise to an additional peak corresponding to the reduction of lead (Pb) on adsorbed selenium (Se) on mercury at -0.33 V. The selenium and lead content can be determined using this peak by the addition of a known amount of one of these ions first and then the second ion. The linear domain range of lead is 5.0×10^{-7} – 2.0×10^{-5} M and for selenium 5.0×10^{-7} – 1.0×10^{-5} M. Using this method 4.90×10^{-7} M Se(IV) and 1.47×10^{-6} M Pb(II) in a synthetic sample could be determined with a relative error of $+2.0\%$ and 1.8% , respectively ($n = 4$). A recovery test after acid digestion for a synthetic sample was 97% for selenium and 96.5% for lead. The method was applied to 1 ml of digested blood, and $328 \pm 23 \mu\text{g l}^{-1}$ Se(IV) and $850 \pm 62 \mu\text{g l}^{-1}$ Pb(II) could be determined with a 90% ($n = 5$) confidence interval. © 1998 Elsevier Science B.V. All rights reserved.

Keywords: Blood; Differential pulse polarography; Selenium and lead determination

1. Introduction

Determination of trace quantities of selenium has become increasingly important due to the important concern about its physiological significance and toxicity. It is an essential trace element in human body. A lack or an excess of selenium will lead to several diseases. A sensitive method of determining selenium is therefore necessary to study selenium deficiency disease or selenium poi-

soning. Blood contains iron (400 – 1000 mg l^{-1}), copper (600 – $1200 \mu\text{g l}^{-1}$), selenium (80 – $400 \mu\text{g l}^{-1}$), lead (100 – $800 \mu\text{g l}^{-1}$) and Sb, As, Bi, Cd, Cr, and Hg in very low quantities [1]. Voltammetric methods such as anodic stripping voltammetry (ASV) [2–5], cathodic stripping voltammetry (CSV) [2,6,7], adsorptive cathodic stripping voltammetry (AdsCSV) [2,8], differential pulse cathodic stripping voltammetry (DPCSV) [9,11] and differential pulse polarography (DPP) [10] have been used with priority because of their high sensitivities and inexpensive instrumentation. Determination of selenium in biological samples is usually difficult, because of long and tedious digestion procedures and risks of interference prob-

* Corresponding author. Tel.: $+90 312 2122900$; fax: $+90 312 2122279$; e-mail: kimya_a_quark.fef.gazi.edu.tr

¹ Presented at the XIth National Chemistry Congress, 16–20 June 1997, Van, Turkey.

lems. The interfering ions have to be separated by preconcentration techniques such as solvent extraction, ion exchange or hydride generation. These are all time-consuming procedures and losses of selenium are also possible. It is therefore very important to accomplish methods with minimum interference problems. In some voltammetric studies such as ASV [3] and CSV [12,13] it was mentioned that addition of selenite to a sample containing ions such as lead, copper or cadmium had a diminishing effect on their peak heights which would lead to erroneous results. Thorough investigation revealed formation at the mercury electrode surface of an intermetallic compound between selenium and the elements present [12,14]. The same kind of interference was also observed in DPP studies, a phenomenon not yet mentioned before in polarographic work, and was attributed to the formation of an intermetallic compound [15]. In fact, it was shown that, when selenium and lead were present together, a new peak belonging to an intermetallic compound appeared. This peak may be used for the quantitative determination of selenite. The present work takes advantage of this new peak and describes a new method for the determination of selenium in the presence of interfering ions without any separation procedure. It has been applied to blood samples analysis after acid digestion.

2. Experimental

2.1. Apparatus

A PAR Model 174 A polarographic analyser system, equipped with a PAR mercury drop timer, was used. The natural drop time of the mercury electrode was in the range 2–3 s (2.75 mg s⁻¹). A saturated calomel electrode (SCE) was used as the reference, and a platinum wire as the counter electrode. The polarograms were recorded with a Linseis LY 1600 X-Y recorder (Linseis, Selb, Germany). DP polarograms were recorded with drop time 1–2 s, scan rate 1–5 mV s⁻¹ and pulse amplitude 50 mV.

2.2. Reagents

All the reagents used were of analytical-reagent grade. Triply distilled water was used throughout. The mercury (proanalysis) used in the dropping mercury electrode was obtained from Merck (Darmstadt, Germany). Contaminated mercury was cleaned by passing it successively through dilute HNO₃ and water columns in the form of fine droplets. The collected mercury was dried between filter papers. Before use, a polarogram of this mercury was recorded in order to confirm the absence of impurities. A 0.1 M stock standard selenite solution was prepared by dissolving SeO₂ in hot water; 0.1 M lead and cadmium solutions were prepared by dissolving Pb(NO₃)₂ and Cd(NO₃)₂ in water, respectively. Dilute solutions were prepared daily from standard stock solutions to avoid aging.

2.3. Procedure

2.3.1. Sample digestion

To 5.0 ml of blood in a long-necked 100 ml flask, 6.0 ml of acid mixture (3 ml HNO₃ + 3 ml HClO₄) was added and after 10–15 min it was warmed up and evaporated until the half of the mixture was left. Before further warming up (to avoid explosion) 2.0 ml of HNO₃ was added and partly evaporated, then another 2.0 ml of HNO₃ was added. After evaporation to nearly dryness 2.0 ml HClO₄ was added and warmed up until white fumes were nearly finished; then a further 2 ml of HClO₄ were added, the sample became clear and was re-evaporated until nearly dryness. After cooling, 2.0 ml of HCl was added and evaporated until nearly dryness. The acidity was neutralized with 2 M NaOH and then it was diluted to 5.0 ml. After addition of 50 µl of concentrated HCl, the solution was kept as the digested blood sample solution.

2.3.2. Polarographic determination

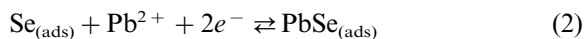
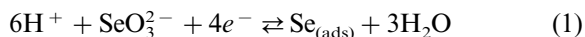
The 9.0 ml of 0.1 M HCl solution in the polarographic cell was deaerated by passing pure nitrogen gas (99.999%) for about 10 min. Polarogram was taken by scanning the potential from -0.1 V to about -0.8 V. Then 1 ml of digested

blood was added and the polarogram was recorded once more. A small peak at about -0.33 V and larger ones at -0.52 and -0.68 V were observed. The peak at about -0.33 V belongs to the intermetallic compound between lead and selenium. Firstly, a known amount of excess selenite ($50\text{--}200\ \mu\text{l}$ of 1×10^{-3} M Se(IV) solution) were added and the polarogram was recorded. After standard addition of $50\ \mu\text{l}$ of 1×10^{-4} M Pb(II) the peak at -0.33 V increased. Selenium and lead concentration in this peak was calculated from the increments. The conditions were: drop time, $1\text{--}2$ s; current range, 0.1 mA; pulse amplitude, 50 mV; scan rate, $1\text{--}5$ mV s^{-1} .

3. Results and discussion

In our earlier polarographic work [15] we observed that when selenium and lead were present together and when selenium concentration was higher than lead, two peaks were observed in acidic media. One corresponded to free selenium at -0.54 V and the second to an intermetallic compound between lead and selenium at -0.33 V. Fig. 1 shows the formation of the peak at -0.33 V by successive additions of Se(IV) to lead reduction in 0.1 M HCl. When standard additions of selenite were made in this solution, the peak for selenium at -0.54 V also increased. It was not possible, however, to determine selenium from this increment since one part of selenium was reduced to the intermetallic compound (at -0.33 V). In this case, both of these peaks have to be analysed for selenium.

Various solutions in different Pb/Se ratios were prepared in 0.1 M HCl solution. When the ratio was 1, only one peak at -0.33 V which belonged to the intermetallic compound (PbSe) was observed (see Eq. (2)) and since the reaction between selenium and lead is in equilibrium a very small peak at -0.54 V for selenium still existed.



When the lead concentration was larger than that of selenium (Fig. 1c–e), almost all of the selenium was reduced at -0.33 V with the formation of the intermetallic compound, while free lead ion appeared as a peak at -0.41 V. These two peaks are not well separated and therefore

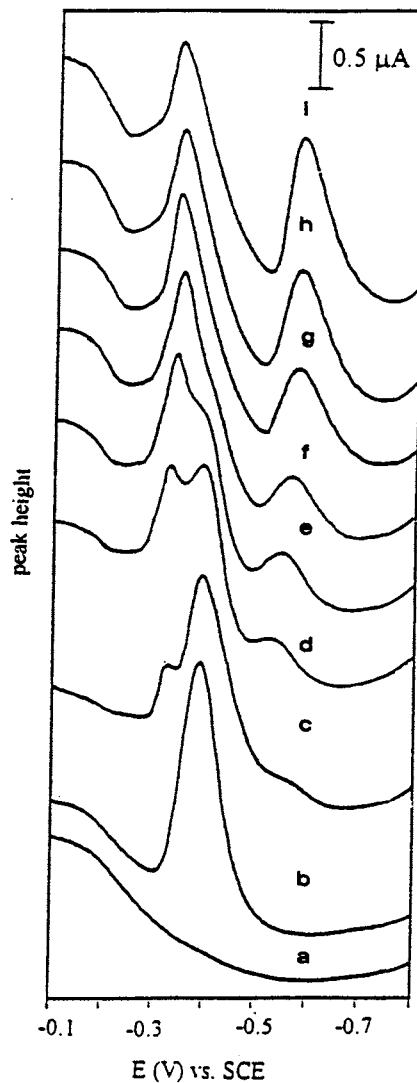


Fig. 1. Effect of selenite ion additions on the lead peak. (a) 10 ml 0.1 M HCl; (b) a + $200\ \mu\text{l}$ 1.0×10^{-3} M Pb(II); (c) b + $50\ \mu\text{l}$ 1.0×10^{-3} M Se(IV); (d) c + $50\ \mu\text{l}$ 1.0×10^{-3} M Se(IV); (e) d + $50\ \mu\text{l}$ 1.0×10^{-3} M Se(IV); (f) e + $50\ \mu\text{l}$ 1.0×10^{-3} M Se(IV); (g) f + $50\ \mu\text{l}$ 1.0×10^{-3} M Se(IV); (h) g + $50\ \mu\text{l}$ 1.0×10^{-3} M Se(IV); (i) h + $50\ \mu\text{l}$ 1.0×10^{-3} M Se(IV). Drop life, 1 s; scan rate, 5 mV s^{-1} ; pulse amplitude, 50 mV.

standard additions for selenium determination could not be applied under these conditions.

When the selenium concentration was larger than the lead concentration (Fig. 1g–i), two distinct peaks were observed, one for selenium at -0.54 V and the second for PbSe at -0.33 V. Since selenium reduction occurred in both of these peaks, they have to be analysed for selenium individually. The amount of selenium in the -0.54 V peak can be found by applying the standard addition method since it responds quantitatively to selenite additions in the concentration range 5.0×10^{-7} – 2.0×10^{-5} M. For the selenium content in the intermetallic compound, an indirect method is suggested. According to the above experiments, two conditions have to be considered. Either selenium or lead may be in excess in the solution under investigation. For these two situations two different methods have been suggested.

3.1. Samples containing excess selenite

A DP polarogram of 10.0 ml of 0.1 M HCl containing 1.47×10^{-6} M Se(IV) and 4.90×10^{-7} M Pb(II) was taken. As can be seen in Fig. 2b, two peaks were observed: the first at -0.33 V for PbSe and the second at -0.54 V for selenium. The selenium content in the sample can be determined by two different methods.

In the first method the selenium content in the -0.54 V peak can be calculated by standard additions of Se(IV). For the selenium content in the PbSe peak, a known amount of lead solution was added. As can be seen in Fig. 2d, while the selenite peak decreased, the peak for PbSe at -0.33 V increased. From this increase the lead and selenium content in this PbSe peak can be calculated. The total selenite content is the sum of the selenium present in both of these peaks. The above method was applied to two solutions of different composition. For a solution containing 1.47×10^{-6} M Se(IV) and 4.90×10^{-7} M Pb(II) after four successive measurements, values of $(1.63 \pm 0.01) \times 10^{-6}$ M for Se(IV) and $(5.40 \pm 0.49) \times 10^{-7}$ M for Pb(II) were obtained with relative standard deviations of 0.61% and 9.1%, respectively. The results are summarized in Table 1 as Ia and IIa.

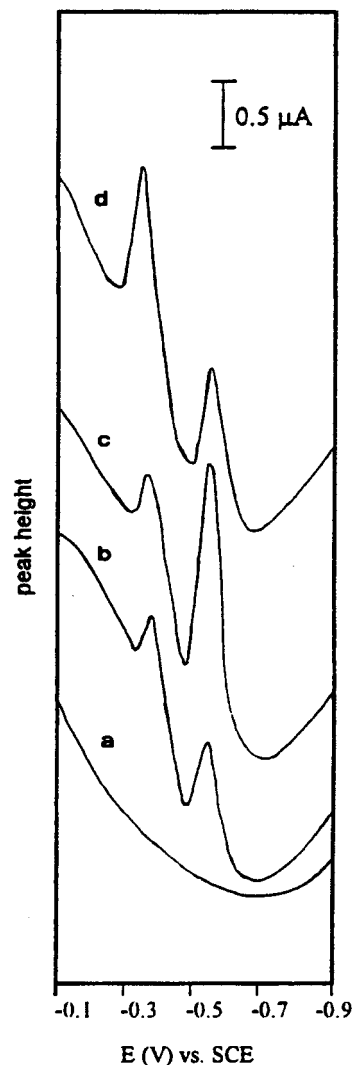


Fig. 2. DP polarogram of Se(IV) and Pb(II) with selenium in excess (first method). (a) 10 ml 0.1 M HCl; (b) a + 150 μ l 1.0×10^{-4} M Se(IV) and 50 μ l 1.0×10^{-4} M Pb(II); (c) b + 200 μ l 1.0×10^{-4} M Se(IV); (d) c + 100 μ l 1.0×10^{-4} M Pb(II). Conditions as in Fig. 1.

In the second method, the DP polarogram of a solution containing 1.94×10^{-5} M Se(IV) and 0.97×10^{-5} M Pb(II) was taken (Fig. 3b). A known amount of lead ion was added. The selenite peak at -0.54 V decreased and the PbSe peak at -0.33 V increased (Fig. 3c,d). From the decrease, the selenium content in the -0.54 V peak was calculated, since lead and selenium reacted in

Table 1
Determination of selenium and lead in synthetic samples in various concentration ratios

Sample no.	No. determinations	Pb and Se in synthetic sample (M)		Pb and Se found (M; $\bar{x} \pm ts/\sqrt{N}$)		Relative error (%)	
		Pb	Se	Pb	Se	Pb	Se
Ia	4	4.90×10^{-7}	1.47×10^{-6}	$(5.40 \pm 0.49) \times 10^{-7}$	$(1.63 \pm 0.01) \times 10^{-6}$	+10.2	+10.8
IIa	5	0.97×10^{-5}	1.94×10^{-5}	$(0.98 \pm 0.10) \times 10^{-5}$	$(1.91 \pm 0.13) \times 10^{-5}$	-1.0	-2.1
IIIb	5	0.97×10^{-5}	1.94×10^{-5}	$(0.89 \pm 0.04) \times 10^{-5}$	$(2.12 \pm 0.05) \times 10^{-5}$	-8.2	+9.2
IVc	4	1.47×10^{-6}	4.90×10^{-7}	$(1.50 \pm 0.07) \times 10^{-6}$	$(4.99 \pm 0.49) \times 10^{-7}$	+2.0	+1.8
Vc	4	2.83×10^{-5}	2.83×10^{-5}	$(2.63 \pm 0.03) \times 10^{-5}$	$(2.94 \pm 0.06) \times 10^{-5}$	-7.1	+3.9

t, 90% confidence interval.

a 1:1 ratio. From the increase of the PbSe peak the lead and selenium content in the PbSe peak were determined. Calculations showed that $(2.12 \pm 0.05) \times 10^{-5}$ M Se(IV) and $(0.89 \pm 0.04) \times 10^{-5}$ M Pb(II) were determined from the prepared synthetic sample. The relative standard deviations of selenium and lead were 2.4% and 4.5%, respectively. The result with its relative error is given in Table 1 as IIIb.

3.2. Samples containing excess lead:

A DP polarogram of 10.0 ml of 0.1 M HCl solution containing 4.90×10^{-6} M Se(IV) and 1.47×10^{-5} M Pb(II) was taken. Since the lead concentration was larger than that of selenium, a peak at -0.41 V for lead and a shoulder for PbSe at -0.33 V and the small peak at -0.54 V were observed (Fig. 4b). Because of the overlap of first two peaks, a known excess of selenite was added in order to bring all lead into PbSe phase. Thus, two peaks appeared: one for PbSe and a second one for selenite. With the addition of excess selenite, the first method could be applied. The selenium in the sample solution is equal to the difference between total selenite calculated and the added selenite. Lead and selenium contents of synthetic samples can be determined using this method. The above method was applied to more dilute solutions as encountered in biological samples such as blood where lead and selenite are present in similar molar quantities [1]. For four solutions with a composition of 4.90×10^{-7} M

Se(IV) and 1.47×10^{-6} M Pb(II), selenite and lead concentrations were found to be $(4.99 \pm 0.47) \times 10^{-7}$ M and $(1.50 \pm 0.06) \times 10^{-6}$ M with relative standard deviations of 9.4% and 4.0%, respectively. The results with their relative errors are given in Table 1 as IVc and Vc. As observed, when the lead concentration exceeded the selenium concentration, the peak of lead and the peak of PbSe overlapped. Since in most biological samples [16] lead concentration exceeds selenium concentration, it was decided to work with various solutions in which lead was in excess. The average results for three measurements are summarized in Table 2.

According to the above results, selenium and lead can be determined using DPP in fairly low concentrations with good precision and accuracy. As it was observed before [15], some kind of intermetallic compound formation happened in the presence of cadmium and copper. Although strong interference problems were observed in ASV and CSV studies with copper, in our DPP studies almost no effect was observed even when the copper concentration was more than ten times that of selenium (copper reduction peak is at -0.16 V).

3.3. Samples containing cadmium

A DP polarogram of a solution containing 4.90×10^{-6} M Se(IV) and 1.47×10^{-5} M Cd(II) in 0.1 M HCl showed two peaks. According to our previous [15] studies, the first peak at

−0.42 V belongs to the reduction of Cd(II) with formation of CdSe, and the second peak at −0.62 V belongs to Cd(II) reduction to CdHg (Fig. 5). For the determination of selenium and cadmium, a known amount of selenite was added. As can be seen from Fig. 5, the cadmium peak decreased and the CdSe peak increased. Since

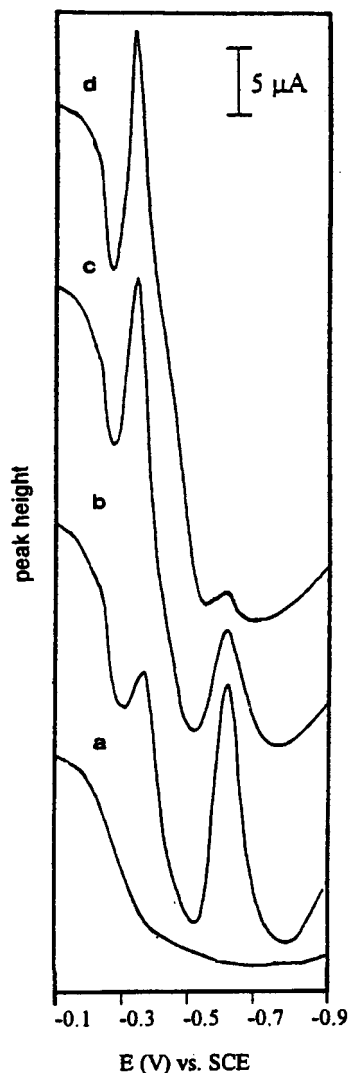


Fig. 3. DP polarogram of Se(IV) and Pb(II) with selenium in excess (second method). (a) 10 ml 0.1 M HCl; (b) a + 200 μl 1.0×10^{-3} M Se(IV) and 100 μl 1.0×10^{-3} M Pb(II); (c) b + 50 μl 1.0×10^{-3} M Pb(II); (d) c + 50 μl 1.0×10^{-3} M Pb(II). Conditions as in Fig. 1.

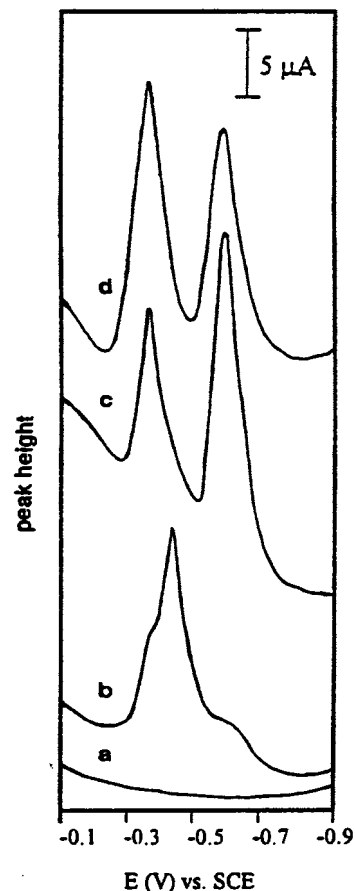


Fig. 4. DP polarogram of Se(IV) and Pb(II) with lead in excess. (a) 10 ml 0.1 M HCl; (b) a + 50 μl 1.0×10^{-3} M Se(IV) and 150 μl 1.0×10^{-3} M Pb(II); (c) b + 250 μl 1.0×10^{-3} M Se(IV); (d) c + 50 μl 1.0×10^{-3} M Pb(II). Conditions as in Fig. 1.

selenium and cadmium reacted in 1:1 ratio, the cadmium concentration can be calculated from the decrease of the cadmium peak, and the amount of cadmium and selenium in this peak can be calculated from the increase of the CdSe peak. By studying four solutions containing 4.90×10^{-6} M Se(IV) and 1.47×10^{-5} M Cd(II) the concentrations $(5.41 \pm 0.42) \times 10^{-6}$ M Se(IV) and $(1.38 \pm 0.12) \times 10^{-5}$ M Cd(II) were obtained at a 90% confidence interval with relative standard deviations of 7.8% and 8.7%, respectively.

Table 2

Determination of lead and selenium in synthetic samples when lead was in excess or equal to selenite

Pb and Se in synthetic samples (M)		Pb and Se found (M)		Relative error (%)	
Pb	Se	Pb	Se	Pb	Se
1.47×10^{-6}	4.90×10^{-7}	1.51×10^{-6}	4.70×10^{-7}	+2.7	-4.1
1.47×10^{-5}	4.90×10^{-6}	1.49×10^{-5}	4.75×10^{-6}	+1.4	-3.1
2.88×10^{-5}	0.96×10^{-5}	3.13×10^{-5}	0.87×10^{-5}	+8.6	-9.3
1.94×10^{-5}	0.97×10^{-5}	2.02×10^{-5}	1.01×10^{-5}	+4.1	+4.1
2.83×10^{-5}	2.83×10^{-5}	2.70×10^{-5}	2.97×10^{-5}	-4.5	+4.9

3.4. Determination of selenium and lead in whole blood

According to the above investigations, 4.90×10^{-7} M selenium can be determined using DPP in the presence of lead although they interfere with each other. It is known that blood contains lead and selenium, and their concentrations after digestion and dissolution are in the range 10^{-6} – 10^{-7} M. Thus the above method can be used for the determination of both of these ions in blood. Since, prior to the application of this method, blood samples have to be digested, the recovery of the elements during the digestion procedure has to be investigated. For this purpose synthetic samples were prepared and the digestion procedure given in Section 2.3.1 for blood was applied. For a solution containing $800 \mu\text{g l}^{-1}$ selenium and $2070 \mu\text{g l}^{-1}$ lead, recovery efficiencies of 97% for selenium and 96.5% for lead were obtained.

For the determination of lead and selenium in blood, one bag of group O Rh (–) blood (450 ml) was kindly provided from the university hospital. A sample of 5.0 ml was digested according to the digestion procedure. The acidity was neutralized and it was diluted to 5.0 ml; the pH was then adjusted to 1.0 by the addition of 50 μl of HCl. From this solution 1.0 ml was taken and it was added to 9.0 ml of oxygen-free 0.1 HCl solution. A DP polarogram was taken in cathodic potential direction; a small peak at about -0.33 V and two large peaks at about -0.52 and -0.68 V were observed. The peak at -0.33 V may belong to lead or PbSe. The lead ion peak should occur at -0.41 V and the selenite peak at -0.54 V

in this medium. To check whether these peaks (at -0.52 V and -0.33 V) belong to lead or selenium, lead ion addition was made and the polarogram taken once more. Neither the peak at -0.33 V nor the peak at -0.52 V changed by the addition of lead ion; only the peak for lead ion at -0.41 V increased. If the selenite peak were hidden in the -0.52 V peak, the peak at -0.33 V would increase by the addition of lead due to the formation of PbSe. This is an indication that the peak at -0.33 V does not belong to lead and the peak at -0.52 V does not include selenium, otherwise the latter peak would have been decreased because of the possible intermetallic compound formation. The peak at -0.33 V must belong to PbSe since it was shown to occur at this potential. To determine both ions, first 50 μl of 1.0×10^{-3} M Se(IV) was added and the polarogram was taken. (It should be remembered here that one of the ions—lead or selenium—in the solution has to be at a higher concentration than the other to complete the reaction between them). There was no change in the -0.33 V peak, which is an indication that all lead was in the PbSe form and that the lead and selenium molar quantities were similar. To find the quantity of these ions, 50 μl of 1×10^{-4} M Pb(II) additions were made. From the increment at the -0.33 V peak, the lead and selenium concentrations in blood were obtained. The changes in the -0.33 V peak during selenite and lead additions are shown in Fig. 6.

The results obtained for five separately digested blood samples taken from the same person were $328 \pm 23 \mu\text{g l}^{-1}$ Se(IV) and $850 \pm 62 \mu\text{g l}^{-1}$ Pb(II) in a 90% ($n = 5$) confidence interval with relative

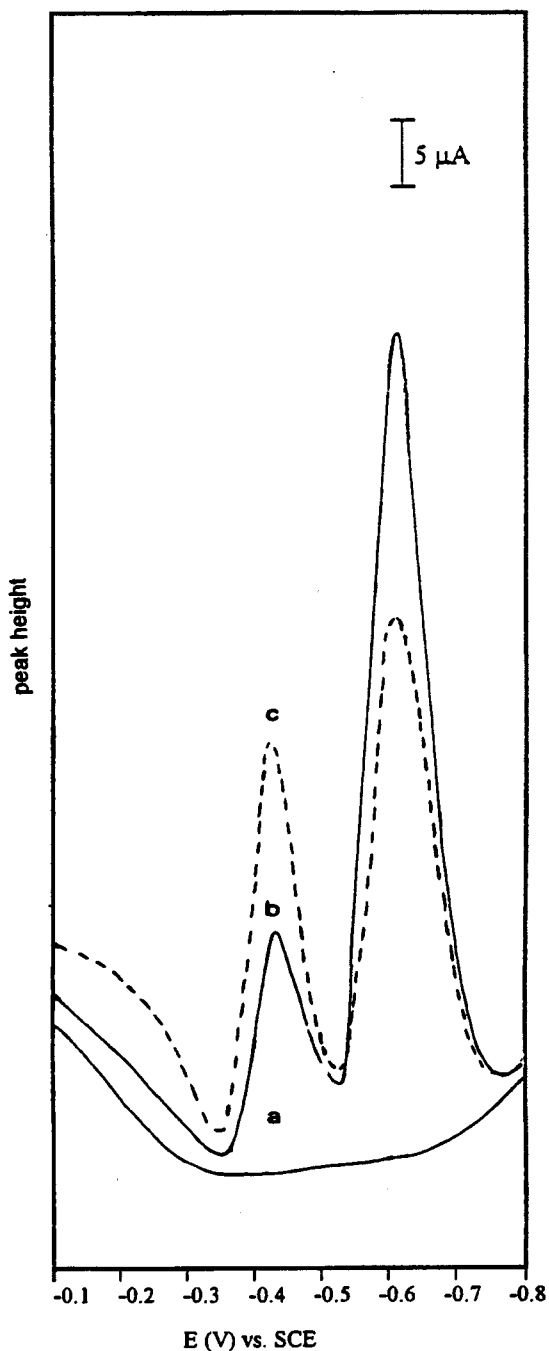


Fig. 5. DP polarogram of Se(IV) and Cd(II) in a synthetic sample. (a) 10 ml 0.1 M HCl; (b) a + 150 μl 1.0×10^{-3} M Cd(II) and 50 μl 1.0×10^{-3} M Se(IV); (c) b + 50 μl 1.0×10^{-3} M Se(IV). Conditions as in Fig. 1.

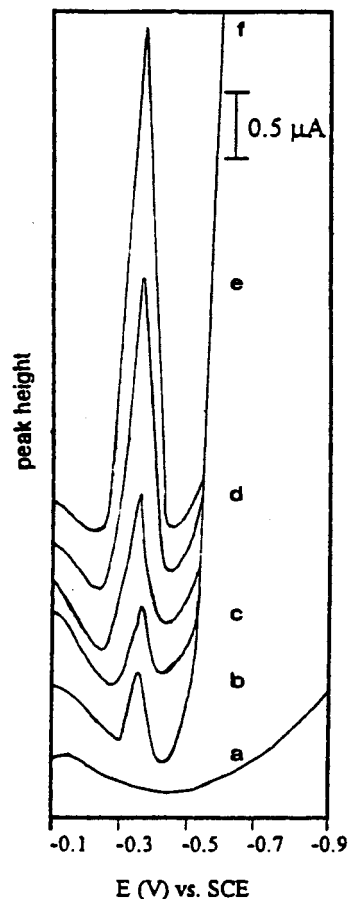


Fig. 6. DP polarogram of Se and Pb in blood sample. (a) 9.0 ml 0.1 M HCl; (b) a + 1.0 ml blood sample; (c) b + 50 μl 1.0×10^{-3} M Se(IV); (d) c + 50 μl 1.0×10^{-4} M Pb(II); (e) d + 50 μl 1.0×10^{-4} M Pb(II); (f) e + 50 μl 1.0×10^{-4} M Pb(II). Drop life, 2 s; scan rate 1.0 mV s^{-1} ; pulse amplitude, 50 mV.

standard deviations of 7.0% and 7.3%, respectively.

To check the validity of the method, the same blood sample was analysed for lead using ASV [5] and for selenium using AdsCSV [8] (Table 3). It can be seen that the results obtained with the proposed method are consistent with those given by other methods. The proposed method can be applied safely for many biological samples.

Table 3
Selenium and lead in blood determined by three different methods

Method	No. determinations	Se ($\mu\text{g l}^{-1}$; $\bar{x} \pm ts/\sqrt{N}$)	Pb ($\mu\text{g l}^{-1}$; $\bar{x} \pm ts/\sqrt{N}$)
This method	5	328 ± 23	850 ± 62
ASV	4	ND	827 ± 30
AdsCSV	4	345 ± 35	ND

ND, not determined; t , 90% confidence interval.

References

- [1] D.L. Tsalev, Atomic Absorption Spectrometry in Occupational and Environmental Health Practice, vol. II, 2nd ed., CRC Press, Boca Raton, FL, 1985, p. 167.
- [2] S.B. Adeloju, A.M. Bond, M.H. Briggs, Anal. Chem. 57 (1985) 1386.
- [3] H. Aydin, G. Somer, Anal. Sci. 5 (1989) 89.
- [4] M.S. Karacan, G. Somer, Microchim. Acta 127 (1998) 67.
- [5] G. Somer, H. Aydin, Analyst 110 (1985) 631.
- [6] R.B. Ahmad, J.O. Hill, R.J. Magee, Analyst 108 (1983) 835.
- [7] S.B. Adeloju, A.M. Bond, M.H. Briggs, Anal. Chem. 56 (1984) 2397.
- [8] R. İnam, G. Somer, Anal. Sci. 13 (1997) 653.
- [9] S.B. Adeloju, A.M. Bond, M.H. Briggs, H.C. Hughes, Anal. Chem. 55 (1983) 2076.
- [10] G.H. Batley, Anal. Chim. Acta 187 (1986) 109.
- [11] H. Bi-Xia, Z. Han-Chang, P.G. Gang, Y. Fang, Z.S. Chun, Y. Hong, Anal. Lett. 18 (B3) (1985) 276.
- [12] S.B. Adeloju, A.M. Bond, H.C. Hughes, Anal. Chim. Acta 148 (1983) 59.
- [13] W. Holak, J.J. Specchio, Analyst 119 (1994) 2179.
- [14] G. Somer, M.S. Karacan, Electroanalysis 6 (1994) 527.
- [15] R. İnam and G. Somer, Anal. Sci. (in press).
- [16] B. Searle, W. Chan, B. Davidow, Clin. Chem. 19 (1) (1973) 76.

Determination of pentoxifylline in pharmaceutical formulations using iodine as oxidizing agent

Chilukuri S.P. Sastry *, Petla Y. Naidu

Foods and Drugs Laboratories, School of Chemistry, College of Science and Technology, Andhra University, Visakhapatnam 530 003, India

Received 4 September 1997; received in revised form 24 November 1997; accepted 3 December 1997

Abstract

Simple, selective and sensitive spectrophotometric methods are described for the determination of pentoxifylline, based on the haloform reaction with a known and excess of standard iodine solution under alkaline conditions. The excess of iodine is determined at pH 3.0 with metol-isoniazid ($\lambda_{\max} = 620$ nm; method A) or wool fast blue BL ($\lambda_{\max} = 540$ nm, method B). All the variables have been optimised and the reaction mechanisms presented. Regression analysis of Beer's law plots showed good correlation in the concentration ranges 4.0–24.0 and 0.4–2.4 mg ml⁻¹ for methods A and B respectively. No interferences were observed from excipients and the validity of the methods was tested by analysing pharmaceutical formulations. Recoveries were 99.0–100.0%. The concentration measurements were reproducible within a relative standard deviation of 1.0%. © 1998 Elsevier Science B.V. All rights reserved.

Keywords: Iodine in alkaline medium; Isoniazid; Metol; Pentoxifylline; Pharmaceutical formulations; Spectrophotometry; Wool fast blue BL

1. Introduction

Pentoxifylline (PTF, 3,7-dimethyl-1-(5-oxo-hexyl)xanthine) is a vasodilator useful in the treatment of peripheral vascular disorders. Pentoxifylline is officially listed in the British Pharmacopoeia addendum as oxypentifylline [1]. Literature cites high-performance liquid-chromatographic methods [2–9], gas-chromatographic methods [10–12], fluorescence polarized im-

unoassay methods [13,14], visible [15] and UV [16] spectrophotometric methods for its determination. The reported visible spectrophotometric methods for pentoxifylline are based on treatment with reagents like picric acid [15] and 3,5-dinitrobenzoic acid [15]. These two methods suffer from disadvantages such as low λ_{\max} or limited sensitivity. It is therefore of interest to develop simple and sensitive procedures with higher λ_{\max} values for the determination of pentoxifylline in pure and pharmaceutical formulations. This paper describes two visible spectrophotometric methods for the determination of PTF, exploiting its structural features (i.e. methyl ketone).

* Corresponding author. Tel.: +91 891 554871; fax: +91 891 555547; e-mail: aulibra@md2.vsnl.net.in

It is well known that methyl ketones react with iodine under alkaline conditions leading to the formation of iodoform [17]. This reaction has been utilised for the quantification of PTF in pure and pharmaceutical formulations. These methods are based on the reaction of PTF with iodine under alkali, followed by the estimation of reacted iodine (amount originally taken minus unreacted) which corresponds to the drug amount, with either colour development with metol (*p*-*N*-methylaminophenol, PMAP)–isoniazid (INH) (method A) [18] or decrease in colour of an oxidizable dye such as wool fast blue BL (WFB, 5,9-dianilo-7-phenyl-4,10-disulphbenzo[α]phenazinium hydroxide inner salt) (C.I. No. 50316) (method B) [19]. We have applied these two sensitive procedures to the determination of PTF (methods A and B) in pure samples and pharmaceutical formulations.

2. Experimental

2.1. Apparatus

A Milton-Roy Spectronic 1201 Spectrophotometer with 1 cm matched quartz cells and an Elico LI-120 model digital pH meter were used for absorbance and pH measurements, respectively.

2.2. Reagents and solutions

All chemicals were of analytical or pharmacopoeial grade and doubly distilled water was used throughout.

Aqueous solutions of iodine 0.089% [0.0035 M I₂ (Merck) in 0.05 M potassium iodide (Merck)], metol (BDH, 0.3%), isoniazid (Wilson, 0.15%), sodium hydroxide (Merck, 1 M), hydrochloric acid (Merck, 1 M), and potassium hydrogen phthalate–HCl buffer (pH 3.0) [20] were prepared in the usual way for method A. Aqueous solutions of iodine 0.02% (0.786×10^{-3} M iodine (Merck) in 1.12×10^{-2} M potassium iodide), sodium hydroxide (Merck 1 M) and WFB (Chroma, 200 $\mu\text{g ml}^{-1}$) were prepared in the usual way for method B. Standard PTF solution (1 mg ml⁻¹) was prepared in distilled water. The working standard

solutions (200 $\mu\text{g ml}^{-1}$ for method A, 10 $\mu\text{g ml}^{-1}$ for method B) were obtained by further dilution of stock solutions with distilled water.

The pharmaceutical sample (tablet powder or injection) equivalent to 100 mg of the drug was accurately weighed or measured, transferred to a 100 ml volumetric flask and solutions were prepared as described for the standard solution and filtered, if insoluble material was present, prior to analysis as described for pure samples.

2.3. Procedures

2.3.1. Method A

Aliquots of a test solution of PTF (0.5–3.0 ml, 200 $\mu\text{g ml}^{-1}$) were transferred into a series of 25 ml graduated test tubes. Then 1.5 ml of the iodine and 1.0 ml of the sodium hydroxide solutions were added and the volume was adjusted to 6.0 ml with distilled water. The mixture was set aside for 5 min at 45–50°C for completion of reaction. Later 1.0 ml of hydrochloric acid, 15 ml of pH 3.0 buffer and 2.0 ml of metol solution were added. After 2 min, 1 ml of isoniazid solution was added. The absorbance was measured at 620 nm after 5 min and before 20 min against distilled water. In the same way a corresponding reference solution was prepared simultaneously, containing the sample, but with 2.0 ml of distilled water instead of 1.0 ml each of sodium hydroxide and hydrochloric acid. The difference in absorbance between the reference and test solutions corresponds to the iodine consumed by the drug. The amount of drug present in each pharmaceutical preparation was computed from the corresponding calibration graph or regression equation.

2.3.2. Method B

To each 25 ml graduated test tubes containing aliquots of a test PTF solution (1.0–6.0 ml, 10 $\mu\text{g ml}^{-1}$), 2.0 ml of 1.0 M NaOH solution was added and the volume was made up to 10 ml with distilled water. The contents were allowed to stand for 5 min at 45–50°C and cooled to room temperature, then 3.0 ml of iodine solution (200 $\mu\text{g ml}^{-1}$) and diluted to 19 ml with distilled water. After 5 min 6.0 ml of dye (WFB) solution was added and measured the absorbance, 5 min

later at 540 nm against distilled water. In the same way a corresponding blank (omitting drug) and dye (omitting drug and iodine) solutions were prepared and their absorbances were measured against distilled water. The decrease in absorbance corresponding to consumed iodine, which in turn corresponds to the drug content, was obtained by subtracting the decrease in absorbance of the test solution (dye-test), from that of the blank solution (dye-blank). The amount of drug present in each pharmaceutical preparation was computed from the corresponding calibration graph or regression equation.

3. Results and discussion

3.1. Method A

This involves two stages, namely oxidation with excess iodine in alkaline medium and the estimation of excess iodine using PMAP–INH reagent. Oxidation of PTF with 1.0–2.0 ml of iodine and 0.6–1.2 ml of 1 M NaOH solutions gave maximum and reproducible absorbance values. The absorption spectra of the reaction products in method A show characteristic λ_{\max} value (Fig. 1). The effect of time and temperature of oxidation on the absorbance of the coloured species was studied by conducting the oxidation at different temperatures for different time intervals. Oxidation times ranging from 5 to 10 min at (45–50°C) gave constant and reproducible absorbance values. Use of 0.6–1.2 ml of 1 M HCl was needed for the neutralization of excess alkali. Maintaining pH of the solution at 2.9 ± 0.3 was found to be best for attaining the highest sensitivity. Hence 15 ml of pH 3.0 potassium hydrogen phthalate–HCl buffer was used. Use of 1.5–2.5 ml of PMAP solution and 0.5–1.5 ml of INH solution afforded the highest absorbance values. A waiting period ranging from 1 to 4 min is necessary between the addition of PMAP solution and INH solution for the generation of *p*-*N*-methyl benzoquinone monoimine (PMBQMI) (by the action of iodine on PMAP). Prolonging the waiting period beyond 4 min results in low absorbance values, probably due to partial hydrolysis of the PMBQMI formed

in situ, to the quinone state. Maximum colour intensity was attained 5 min after the final dilution and remained stable for the next 20 min.

Fixed amount of iodine (1.5 ml, 0.089%), NaOH (1.0 ml, 1.0 M), HCl (1.0 ml, 1.0 M), buffer (15 ml, pH 3.0), metol (2.0 ml, 0.3%) and INH (1.0 ml, 0.15%) were used in a total volume of 25 ml in further investigation.

3.2. Method B

This method involves two stages: oxidation of PTF by iodine in alkaline medium and estimation of unconsumed iodine with wool fast blue BL.

In preliminary experiments, several phenazine and oxazine dyes such as neutral violet (NV; CA 3562-46-7), wool fast blue BL (WFB; CA 6378-88-7), azocarmin G (AG; CA 25641-18-3), lisamine blue BF (LBBF; CA 6448-97-1), gallocyanine (GC; CA 1562-85-2), solochrome prune AS (SPAS; CA 6416-51-9) and cresyl fast violet acetate (CFVA; CA 10510-54-0) were tested for reaction with iodine in alkaline medium. These investigations revealed that NV, WFB,

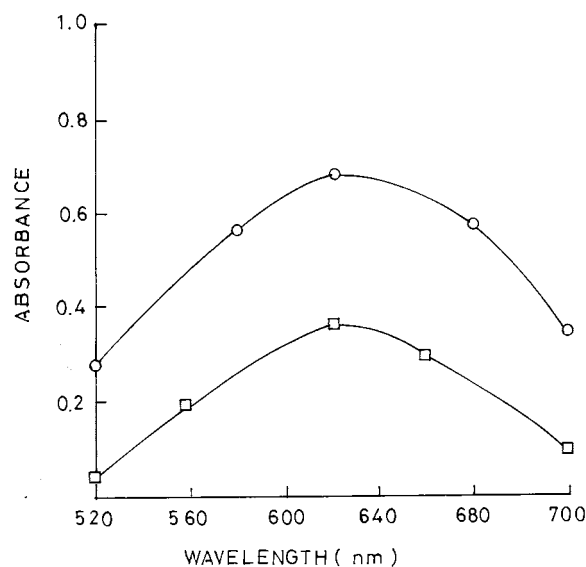


Fig. 1. Absorption spectra of PTF–I₂/PMAP–INH system (□) versus distilled water and reference solution (○) versus distilled water. Concentrations: PTF, 5.75×10^{-5} M; NaOH, 8.0×10^{-2} M; I₂, 1.75×10^{-4} M; PMAP, 6.97×10^{-4} M; INH, 4.36×10^{-4} M. pH 3.0.

Table 1
Optical and regression characteristics, precision and accuracy of the proposed methods

Parameters	Methods	
	A	B
Beer's law limits (mg ml ⁻¹)	4.0–24.0	0.4–2.4
Detection limits (mg ml ⁻¹)	0.68	0.016
Molar absorptivity (l mol ⁻¹ cm ⁻¹)	6.15 × 10 ³	5.16 × 10 ⁴
Sandell's sensitivity (mg cm ⁻² per 0.001 absorbance unit)	0.046	0.005
Regression equation ^a (A)		
Slope (<i>b</i>)	2.17 × 10 ⁻²	1.83 × 10 ⁻¹
Standard deviation on slope (<i>S_b</i>)	1.79 × 10 ⁻⁴	6.92 × 10 ⁻⁴
Intercept (<i>a</i>)	1.53 × 10 ⁻³	2.0 × 10 ⁻⁴
Standard deviation on intercept (<i>S_a</i>)	3.00 × 10 ⁻³	1.16 × 10 ⁻³
Standard error of estimation (<i>S_e</i>)	2.79 × 10 ⁻³	1.08 × 10 ⁻³
Correlation coefficient	0.9998	0.9999
% relative standard deviation ^b	0.86	0.32
% range of error ^b (95% confidence limits)	0.91	0.34

^a With respect to $A = a \pm bC$ where C is concentration (mg ml⁻¹) and A is absorbance unit.

^b Six replicate samples (concentrations 20 and 2.0 μg ml⁻¹ of pure drug for methods A and B, respectively).

SPAS and CFVA exhibit quantitative reactions, with iodine in alkaline medium by a definitive decrease in absorbance for a specific concentration of iodine in alkaline medium. As the difference in absorbance was found to be higher in the case of WFB, it was preferred over others in further investigation. The effect of reagent concentration (alkalinity, iodine and WFB), reaction temperature and period in each step were studied by means of controlled experiments varying one parameter at a time.

The above optimum conditions were incorporated in the recommended procedure (B).

3.3. Analytical data

The Beer's law limits, molar absorptivity, Sandell's sensitivity, detection limits [21], regression equation and correlation coefficients, ob-

tained by least squares treatment of these results are given in Table 1. Precision of each method was tested by analysing six replicate samples containing 500 and 50 μg of pure drug for methods A and B, respectively. The percent standard deviation and the percent range of error at 95% confidence level of each method are given in Table 1.

The values obtained by the proposed and reference [15] methods for pharmaceutical formulations are compared in Table 2, and are in good agreement. These results were compared statistically by the *t*- and *F*-tests and were found not to differ significantly. The results of the recovery experiments by the proposed methods are also listed in Table 2. Recoveries were determined by adding standard drug to the pre-analysed pharmaceutical formulations. The ingredients usually present in pharmaceutical formulations did not interfere in the proposed methods.

3.4. Chemistry of coloured species

Methods A or B involves the oxidation of PTF by iodine solution in excess under alkaline conditions which produce iodoform through the hydrolytic cleavage of methyl ketone group. The iodine unreacted at the end of the reaction was determined using metol–INH reagent after bringing the pH to 3.0 (method A) or decrease in the intensity of WFB colour (method B). The coloured complex in method A may be regarded as a charge-transfer [18] complex ($\lambda_{\text{max}} = 620$ nm) type, presumed to be taking place involving electron-transfer from the highest occupied π molecular orbital of INH to the lowest empty π^* molecular orbital of two adjacent *p*-*N*-methylbenzoquinone monoimine (formed in situ from metol and iodine) molecules. The colour intensity decreases at λ_{max} 540 nm in method B, is due to oxidation of WFB with iodine giving mixture of products from the dye with cleavage of conjugate system (i.e. chromophores and auxochromes). Even though the iodine oxidation of PTF or WFB under experimental conditions is not stoichiometric reproducible values are attained.

Table 2
Analysis of pharmaceutical formulations by proposed and reference procedures

Pharmaceutical preparation ^a	Labelled amount (mg)	Amount found ^b by proposed methods		Found by reference method[15]	Recovery by ^c proposed methods	
		A	B		A	B
Tablets I	200	199.2 ± 0.99 <i>t</i> = 1.22, <i>F</i> = 1.65	199.7 ± 0.54 <i>t</i> = 1.31, <i>F</i> = 2.09	199.1 ± 0.77	99.3 ± 0.5	99.5 ± 0.8
Tablets II	200	200.4 ± 0.52 <i>t</i> = 0.87, <i>F</i> = 2.20	200.6 ± 0.60 <i>t</i> = 1.38, <i>F</i> = 2.93	199.7 ± 0.35	99.8 ± 0.1	99.9 ± 0.4
Injection I	20 mg ml ⁻¹	19.94 ± 0.08 <i>t</i> = 0.94, <i>F</i> = 1.86	19.92 ± 0.17 <i>t</i> = 0.32, <i>F</i> = 2.34	19.86 ± 0.11	99.5 ± 0.9	99.6 ± 0.2
Injection II	20 mg ml ⁻¹	19.90 ± 0.21 <i>t</i> = 1.25, <i>F</i> = 1.72	20.09 ± 0.12 <i>t</i> = 1.08, <i>F</i> = 1.72	19.90 ± 0.16	99.6 ± 0.6	99.4 ± 0.5

^a Formulations that are manufactured by two different pharmaceutical companies.

^b Average ± standard deviation of six determinations, the *t*- and *F*-values refer to comparison of the proposed method with the reference method. Theoretical values at 95% confidence limits: *F* = 5.05, *t* = 2.57.

^c Recovery of 10 mg added to the pharmaceutical formulations.

4. Conclusion

The order of λ_{\max} values among the proposed methods and reference method (R) in the determination of pentoxifyllin is A > B > R. The higher λ_{\max} of the visible spectrophotometric methods over reported UV and visible spectrophotometric methods is a decisive advantage since the interference from the excipients should far less at higher wavelengths than at lower wavelengths. The sensitivity order of the methods is B > A > R.

Thus the proposed methods are simple sensitive (when compared to reported visible spectrophotometric methods) and can be used for the routine determination of pentoxifyllin in pure and pharmaceutical formulations. It is selective to compounds containing a methyl ketone portion in their molecule.

Acknowledgements

P.Y.N. is grateful to the CSIR, New Delhi, for the award of a Senior Research Fellowship.

References

- [1] British Pharmacopoeia, HMSO, London, 1993 (Addendum, 1994), p. 1357.
- [2] A. Mancinelli, S. Pace, A. Marzo, E.A. Martelli, G. Passetti, *J. Chromatogr.* 575 (13) (1992) 101.
- [3] M.R. Lockemeyer, C.V. Smith, *J. Chromatogr. Biomed. Appl.* 532 (26) (1990) 162.
- [4] D.M. Grasela, M.L. Rocci, *J. Chromatogr. Biomed. Appl.* 419 (7) (1987) 368.
- [5] D.R. Luke, M.L. Rocci, *J. Chromatogr. Biomed. Appl.* 374 (10) (1986) 191.
- [6] A.G. Moiroux, J.M. Poirier, G. Cheymol, P. Jaillon, *J. Chromatogr. Biomed. Appl.* 416 (24) (1987) 183.
- [7] W. Rieck, D. Platt, *J. Chromatogr. Biomed. Appl.* 305 (10) (1984) 419.
- [8] D.A. Chivers, D.J. Birkett, J.O. Miners, *J. Chromatogr. Biomed. Appl.* 225 (11) (1981) 261.
- [9] G.S. Sadana, A.B. Ghogre, *Indian Drugs* 27 (1990) 395.
- [10] G.S. Sadana, A.B. Ghogre, *Indian J. Pharm. Sci.* 53 (4) (1991) 159.
- [11] M.T. Bauza, R.V. Smith, D.E. Knuston, F.R. Witter, *J. Chromatogr. Biomed. Appl.* 310 (14) (1984) 61.
- [12] J.L. Burrows, *J. Chromatogr. Biomed. Appl.* 423 (25) (1987) 139.
- [13] M.R. Morton, R.C. Parigh, W.J. Spruill, *Ther. Drug Monit.* 11 (3) (1989) 347.

- [14] A. Cohen, C.E. Jonson, L. Wesolowicz, K.C. Swastek, *Clin. Pharmacol.* 7 (1988) 457.
- [15] S.N. Meyyanthan, B. Prasad, B. Suresh, *Indian Drugs* 33 (10) (1996) 514.
- [16] J.H. Heinz, *Arzneim-Forsch. Drug Res.* 21 (12) (1971) 2045.
- [17] C.L. Chakrabarti, in: Pt.C. Trahanovsky (Ed.), *Oxidation in Organic Chemistry*, Academic Press, New York, 1978, pp. 343–370.
- [18] C.S.P. Sastry, T.T. Rao, A. Sailaja, J.V. Rao, *Talanta* 38 (1991) 1107.
- [19] C.S.P. Sastry, S.G. Rao, P.Y. Naidu, K.R.S. Rao, *Talanta* (in press).
- [20] J. Lurie, *Handbook of Analytical Chemistry*, Mir, Moscow, 1975, p. 253.
- [21] IUPAC, *Spectrochim. Acta* 33 (1978) 241.

A selective voltammetric method for uric acid detection at Nafion[®]-coated carbon paste electrodes

Jyh-Myng Zen *, Chi-Teng Hsu

Department of Chemistry, National Chung-Hsing University, Taichung 402, Taiwan

Received 26 September 1997; received in revised form 25 November 1997; accepted 3 December 1997

Abstract

A square-wave voltammetric method together with Nafion[®]-coated carbon paste electrodes were used for the selective determination of uric acid in the presence of a high concentration of ascorbic acid. Since the oxidation potential of uric acid is about 200 mV more positive than that of ascorbic acid at the Nafion[®]-coated carbon paste electrode, the selectivity can be greatly improved simply by applying an electrolysis potential of +0.4 V vs. Ag/AgCl where only ascorbic acid is oxidised. The acceptable tolerance of ascorbic acid concentration for the determination of uric acid is as high as 1.5 mM. With 30 s of electrolysis time, a linear calibration curve is obtained over the 0–50 μ M range in 0.05 M citrate buffer solution, pH 4.0, with slope (μ A/ μ M) and correlation coefficient of 0.34 and 0.9984, respectively. The detection limit (3σ) is 0.25 μ M. The practical analytical utility is illustrated by selective measurements of uric acid in human urine without any preliminary treatment. © 1998 Elsevier Science B.V. All rights reserved.

Keywords: Carbon paste electrode; Nafion[®]; Uric acid

1. Introduction

Uric acid (UA), the primary end-product of purine metabolism, and ascorbic acid (AA) are both present in biological fluids such as blood and urine. It has been shown that extreme abnormalities of UA levels are symptomatic of several diseases [1]. Earlier electrochemical procedures based on the oxidation of UA at carbon-based electrodes in acidic solutions suffered from interference from AA which can be oxidised at a

potential close to that of UA [2,3]. Various methods, such as an adsorption/medium exchange approach [4,5], enzyme-based techniques [6–10], polymer-modified electrode with and without catalyst [10–13], and electrochemically pretreated carbon paste electrode or clay modified electrode [14,15], were developed to solve the UA detection problem. Indeed, the benefit of an enzyme-based method is that good selectivity is imparted by inclusion of the enzyme. Unfortunately, long-term stability is hardly achieved by any enzyme-based method. Until now, sensitive and selective methods still needed to be developed for the detection of UA due to its clinical significance.

* Corresponding author.

We report here an interesting approach for the selective determination of UA in urine samples using a Nafion[®]-coated carbon paste electrode (Nafion[®]-CPE) and square-wave voltammetry (SWV). The only means of achieving selectivity is by use of the Nafion[®] and applied potential. Since the oxidation potential of UA at the Nafion[®]-CPE is about 200 mV more positive than that of AA, the selectivity can be greatly improved simply by applying an electrolysis potential (P_p) where only AA is oxidised. The Nafion[®] membrane coating on the modified electrode can also prevent the organic interference from reaching the interface. In this paper, the optimal experimental conditions for the determination of UA as well as possible interferents, especially AA, were thoroughly investigated. The transport characteristics of UA in the Nafion[®]-CPE are also discussed.

2. Experimental

2.1. Chemicals and reagents

Nafion[®] perfluorinated ion-exchange powder, 5 wt% solution in a mixture of lower aliphatic alcohols and 10% water, was obtained from Aldrich. All buffers and supporting electrolyte solutions were prepared from Merck Suprapur reagents. Graphite powder (Aldrich), mineral oil (Sigma), UA (Sigma), AA (Wako), and all the other compounds (ACS-certified reagent grade) were used without further purification. Aqueous solutions were prepared with doubly distilled deionised water.

2.2. Apparatus

Electrochemistry was performed on a Bioanalytical Systems (West Lafayette, IN) BAS-100B electrochemical analyser. A BAS Model VC-2 electrochemical cell was employed in these experiments. The three-electrode system consisted of either a CPE or a Nafion[®]-CPE working electrode, a Ag/AgCl reference electrode (Model RE-5, BAS), and a platinum wire auxiliary electrode. Since dissolved oxygen did not interfere with the anodic voltammetry, no deaeration was performed.

2.3. Procedure

The Nafion[®]-CPE was made as follows. Carbon paste was prepared in a conventional fashion by thoroughly hand-mixing 70 wt% graphite powder and 30 wt% mineral oil in a mortar with a pestle. The carbon paste was packed into the hole of the electrode body and smoothed off on a sheet of weighing paper. A Nafion[®] solution (5 wt%) was then spin-coated on the CPE surface at 3000 rpm. The Nafion[®]-CPE was equilibrated in the test buffer solutions, by cyclic voltammetric scanning between 0.0 and +0.9 V until a steady background was attained, before measurements were made. Dependence of the anodic peak current of UA on pH at the Nafion[®]-CPE was evaluated using citrate-hydrochloric acid buffers. SW voltammograms were obtained by scanning the potential from +0.2 to +0.9 V at a SW frequency of 1.0 kHz, SW amplitude of 30 mV, and a step height of 4 mV for most cases. The UA quantification was achieved by measuring the current of the oxidation peak. For most of the experiments, a 0.05 M citrate buffer solution, pH 4.0, was used as supporting electrolyte.

Urine samples were obtained from laboratory personnel. After filtration through membrane filters (0.45 μ m), all samples were stored in the dark at 4°C. In order to fall into the linear range, all samples used for detection were diluted 200 times. The standard addition method was used to evaluate the content of UA in samples. The Nafion[®]-CPE can easily be renewed either by cleaning at +1.0 V in test solutions for 10 s or at +0.9 V for 15 s in 0.02 M NaOH.

3. Results and discussion

3.1. Voltammetric behaviour of UA at the Nafion[®]-CPE

The function of the Nafion[®]-CPE is illustrated in Fig. 1 for 50 μ M UA and 1.5 mM AA recorded at a bare CPE and the Nafion[®]-CPE by SWV. On scanning from 0.0 V towards a positive potential at the bare CPE, the interference from AA, which can be oxidised at a potential close to that

of UA, can be clearly seen, as shown in Fig. 1A(a). For comparison, Fig. 1A(b) shows that an anodic peak at around +0.5 V was observed for 50 μ M UA alone. This result indicates that there is a serious interference from AA in the detection of UA at a bare CPE. The appearance of a small peak at around +0.8 V correlating with the presence of AA will be discussed later. In contrast, separate peaks (at about 200 mV) of UA and AA were observed when the Nafion[®]-CPE was used, as shown in Fig. 1B(a). Similarly, for comparison, an anodic peak at the same peak potential was observed for UA alone at the Nafion[®]-CPE, as shown in Fig. 1B(b).

The basis for the practical utility of the Nafion[®]-CPE in the determination of UA is its discrimination against AA. Since the oxidation potential of UA at the Nafion[®]-CPE is about 200 mV more positive than that of AA, the interference from AA was found to be completely eliminated at the Nafion[®]-CPE by selecting a P_p of +0.4 V as shown in Fig. 2B. Note that such phenomenon, however, was not observed at the bare CPE. As can be seen in Fig. 2A, the shoulder

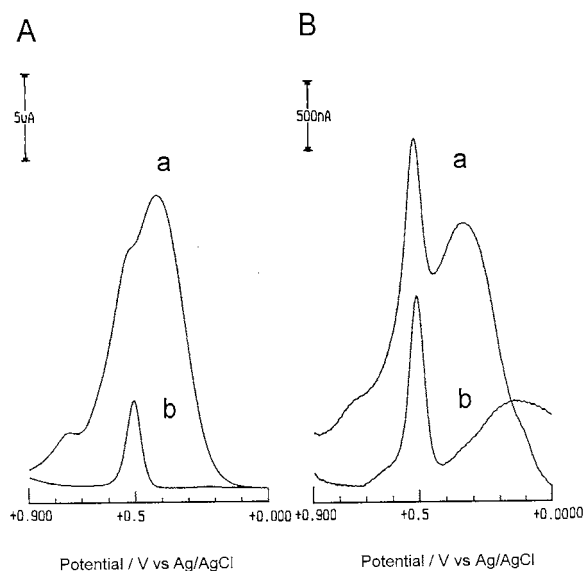


Fig. 1. SW voltammograms at (A) a bare CPE and (B) the Nafion[®]-CPE for (a) 50 μ M UA + 1.5 mM AA and (b) 50 μ M UA alone in 0.05 M citrate buffer solution, pH 4.0. $P_p = 0.0$ V; $t_p = 10$ s; SW amplitude, 20 mV; SW frequency, 50 Hz; step height, 4 mV.

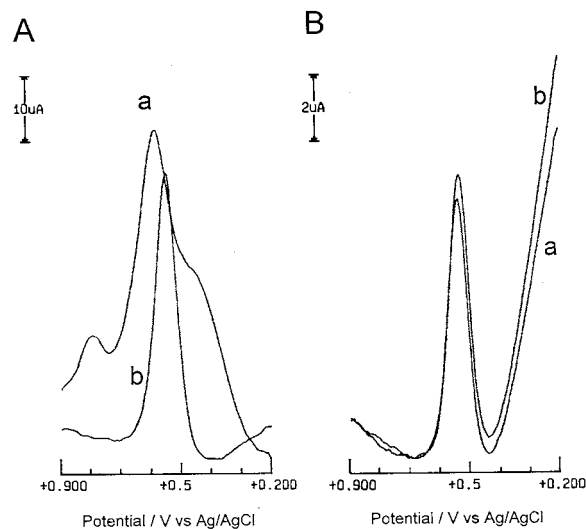


Fig. 2. SW voltammograms at (A) a bare CPE and (B) the Nafion[®]-CPE for (a) 50 μ M UA + 1.5 mM AA and (b) 50 μ M UA. $P_p = +0.4$ V; $t_p = 30$ s; SW amplitude, 30 mV; SW frequency, 1 kHz; step height, 4 mV.

that appears next to the UA peak can still cause interference in UA detection. The reason for this is that, at a bare CPE, even though the AA near the electrode surface is oxidised after the electrolysis step, the AA in the bulk solution can still diffuse rapidly to the electrode surface during the detection step. With the Nafion[®]-CPE, the diffusion process was apparently somewhat restricted by the existence of the Nafion[®] film during the detection step and hence the interference of AA can be completely removed. Note that the small peak at around +0.8 V was also removed at the Nafion[®]-CPE by selecting a P_p of +0.4 V as shown in Fig. 2B. This result further confirms that the appearance of the small peak around +0.8 V is indeed due to the existence of AA.

Further investigation was made into the transport characteristics of UA at the Nafion[®]-CPE. The current response of linear scan voltammetry for 50 μ M UA obtained at the Nafion[®]-CPE was found to be linearly proportional to the square root of the scan rate, indicating that the process was diffusion-controlled. More evidence for the non-adsorptive behaviour of UA was demonstrated by the following experiment. When the Nafion[®]-CPE was switched to a medium contain-

ing only pH 4.0 buffer solution after being used to measure a UA solution, no voltammetric peak signal was observed at all.

3.2. Optimisation of UA detection at the Nafion[®]-CPE

In order to arrive at the optimum conditions for UA determination, the major factors that should be considered are the solution pH, the P_p , the electrolysis time (t_p), and the SWV parameters. The effect of pH on the voltammetric oxidation of UA is shown in Fig. 3. As can be seen, the current response reaches a maximum around pH 4.0. The reason for the large drop in the current response when the pH is higher than 6 is because UA exists in the anionic form (pK_a 5.75) when the pH is higher than 6 and is consequently repulsed by the Nafion[®] film. A pH of 4.0 was therefore chosen for the subsequent analytical experiments. The trend of the peak potential (E_p) shifts linearly towards negative potentials with an increase in pH and indicates that protons are directly involved in the rate determination step of the UA oxidation reaction. The equation relating E_p (in

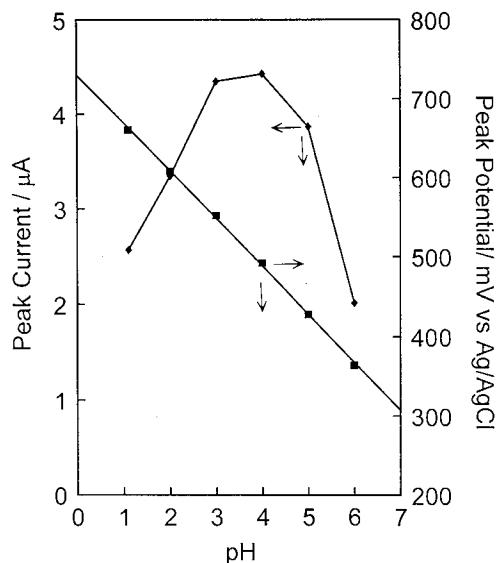


Fig. 3. Dependence of the anodic peak current and peak potential on pH in SWV for 50 μM UA at the Nafion[®]-CPE. Other conditions as in Fig. 1.

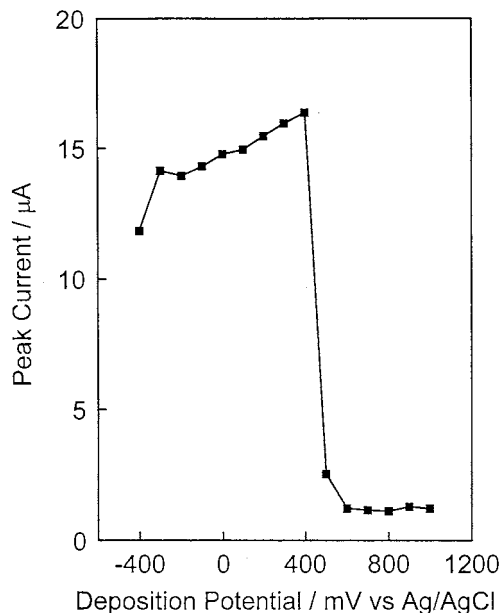


Fig. 4. Effect of P_p in SWV for 50 μM UA at the Nafion[®]-CPE. t_p = 30 s.

volts) and pH, over the pH range 1–6, was found to be: $E_p = 0.73 - 0.06\text{pH}$.

As mentioned earlier, by selecting a P_p of +0.4 V, the interference by AA can be removed at the Nafion[®]-CPE. The effect of the P_p on the SW response for UA detection was thoroughly studied and the results obtained are shown in Fig. 4. As expected, the peak current reaches a maximum at a P_p of +0.4 V for 50 μM UA with a t_p of 10 s. The large drop in peak current when the P_p was more positive than +0.5 V was due to the oxidation of UA since the E_p is around +0.5 V for UA at the Nafion[®]-CPE. The effect of the t_p on the SW response for UA has also been studied and the results are shown in Fig. 5. As can be seen, the peak current increases as the t_p increases and starts to level off around 60 s for 50 μM UA (Fig. 5A). A similar trend except with lower peak currents was also observed for a lower concentration of 10 μM UA as shown in Fig. 5B. For convenience, a t_p of 30 s was chosen for the subsequent analytical experiments. In order to increase the sensitivity of detection, a longer t_p is needed for a lower concentration of UA.

The peak current obtained in SWV is dependent on various instrumental parameters such as SW amplitude, SW frequency, and step height. These parameters are interrelated and have a combined effect on the response. When the SW amplitude was varied between 10 and 70 mV, the peak currents were increased with increasing amplitude up to 30 mV; the peak width was also increasing at the same time. Hence, 30 mV was chosen as the SW amplitude. The step height together with the frequency defines the effective scan rate. An increase of either the frequency or the step height results in an increase in the effective scan rate. The response for UA increases with SW frequency up to 1.0 kHz, above which the peak current was unstable and obscured by a large residual current. By maintaining the frequency at 1.0 kHz, the effect of step height was studied. At step heights greater than 5 mV, too few points were sampled, thus affecting the reproducibility of the detection, whereas the response is more accurately recorded at a step height of 4 mV. Overall, the optimised parameters can be summarised as follows: SW frequency, 1.0 kHz; SW amplitude, 30 mV; step height, 4 mV.

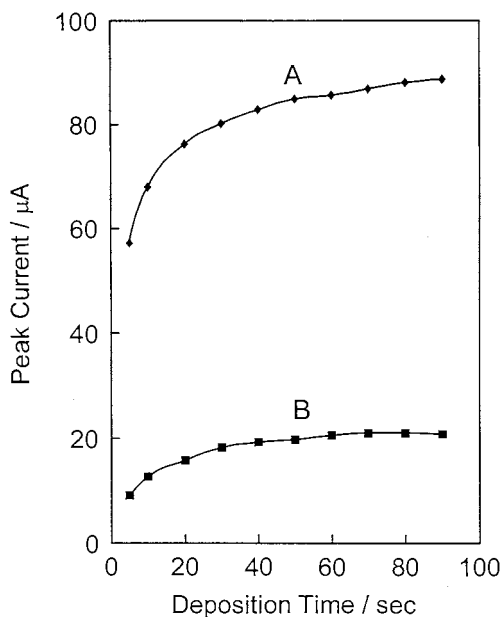


Fig. 5. Effect of t_p in SWV for (A) 50 μM and (B) 10 μM UA at the Nafion[®]-CPE. $P_p = +0.4$ V.

3.3. Analytical characterisations of UA detection at the Nafion[®]-CPE

Under optimal conditions, the SWV current response is linearly dependent on the concentration of UA between 0 and 50 μM in 0.05 M citrate buffer solution, pH 4.0, with slope ($\mu\text{A}/\mu\text{M}$) and correlation coefficient of 0.34 and 0.9984, respectively. The SW voltammograms and the calibration plot observed are shown in Fig. 6. The detection limit (3σ) is 0.25 μM .

To characterise the reproducibility of the modified electrode, repetitive electrolysis–measurement–regeneration cycles were followed. The Nafion[®]-CPE can be easily renewed by cleaning at +1.0 V for 10 s in test solutions or at +0.9 V for 15 s in 0.02 M NaOH. Before the next measurement, the renewed electrode was checked in the supporting electrolyte to ascertain that no peak appeared. The result of 25 successive measurements showed a very small relative standard deviation of 1.7% for 50 μM UA. The results indicate that the electrode renewal procedure gives an excellent reproducible surface. The long-term stability was also examined by measuring the response to various concentrations of UA for a period of 60 days. The result of measurements during this period showed almost no decrease in signal at the end of the lifetime test. Since the activity remains virtually constant during this period of time, the result indicates excellent long-term stability of the electrode.

Various possible interfering substances, such as purine, glucose, cysteine, cytosine, oxalate, hydrazine, and AA, were examined for their effect on the determination of 50 μM UA. The results obtained are summarised in Table 1. It is well known that AA co-exists with UA in many samples; therefore, its interference was investigated in more detail. Since the acceptable tolerance of AA concentration for the determination of UA is as high as 1.5 mM, the method is applicable to urine samples.

Three human urine samples from laboratory personnel were investigated using the method presented above. To fit into the linear range, all the samples used for detection were diluted 200 times. The dilution process can actually help in reducing

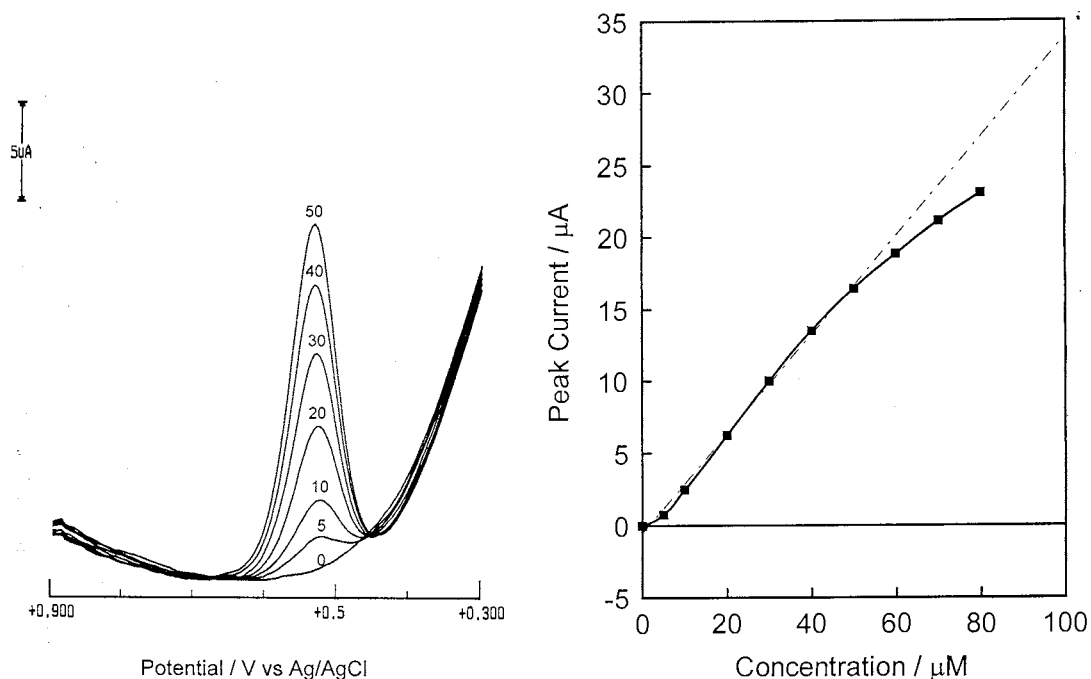


Fig. 6. Dependence of the SWV peak current with increasing UA concentrations of 0–80 μM . Other conditions as in Fig. 2.

the matrix effect of real samples. The results obtained are listed in Table 2. To determine the accuracy of the results, the samples were spiked with certain amounts of UA in about the same

concentration as found in the samples themselves. The recovery rates of the spiked samples were determined and found to range between 95.9% and 98.7% for the three human urine samples.

Table 1
Influence of potential interferences on the response of UA

Interferent	Concentration (mM)	Signal change ($i_{\text{UA}} = 100\%$)
AA	0.5	-3.8
	1.5	-6.1
	2.5	-11.4
Cytosine	0.05	-3.3
	0.5	-15.0
Purine	0.05	-7.0
	0.5	-9.2
Oxalate	2.5	0.0
Cysteine	0.05	-1.2
	0.5	-13.7
Glucose	0.5	0.0
	2.5	-2.2
Hydrazine	0.5	2.5
	1.5	-5.7

[UA] = 50 μM .

4. Conclusion

The present study demonstrates a very simple and improved SW voltammetric method to detect UA in the presence of a high concentration of AA at the Nafion[®]-CPE. The acceptable tolerance of AA concentration for the determination of UA is at least as high as 1.5 mM. The Nafion[®]-CPE can be applied to the detection of UA in urine samples with excellent sensitivity and selectivity. The recovery of the spiked UA was observed to be good in urine samples. The Nafion[®]-CPE possesses good selectivity and can be regenerated easily by cleaning at +1.0 V in test solutions for 10 s or at +0.9 V for 15 s in 0.02 M NaOH. The detection can be achieved without deoxygenation. Simplicity and long-term stability are further advantages of this method.

Table 2
Determination of UA in urine samples with the Nafion[®]-CPE

	Urine 1	Urine 2	Urine 3
Detected value, original (μM)	20.25 ± 0.70	15.94 ± 0.53	18.32 ± 0.95
Spike (μM)	10	10	10
Detected value, after spike (μM)	29.84 ± 1.23	25.80 ± 1.24	28.08 ± 1.34
Recovery (%)	95.9	98.7	97.7
Real value ($\mu\text{g l}^{-1}$)	680.8 ± 28.1	535.9 ± 25.8	615.9 ± 29.4

Total value is obtained by multiplying the detected value by the dilution factor of 200.

Number of samples assayed was 3.

Acknowledgements

The authors gratefully acknowledge financial support from the National Science Council of the Republic of China under grant NSC 87-2113-M-005-021.

References

- [1] V.S. Eswara Dutt, H.A. Mottola, *Anal. Chem.* 46 (1974) 1777.
- [2] G. Park, R.N. Adams, W.R. White, *Anal. Lett.* 5 (1972) 887.
- [3] T. Yao, Y. Taniguchi, T. Wasa, S. Musha, *Bull. Chem. Soc. Jpn.* 51 (1978) 2937.
- [4] J. Wang, B.A. Freiha, *Bioelectrochem. Bioenerg.* 12 (1984) 225.
- [5] T. Tatsuma, T. Watanabe, *Anal. Chim. Acta* 242 (1991) 85.
- [6] F.E. Keedy, P. Vadgama, *Biosens. Bioelectron.* 6 (1991) 491.
- [7] E. Gonzalez, F. Pariente, E. Lorenzo, L. Hernandez, *Anal. Chim. Acta* 242 (1991) 267.
- [8] M.A.T. Gilmartin, J.P. Hart, B. Birch, *Analyst* 117 (1992) 1299.
- [9] M.J. Rocheleau, W.C. Purdy, *Electroanalysis* 3 (1991) 935.
- [10] E. Miland, A.J.M. Ordieres, P.T. Blanco, M.R. Smyth, C.O. Fagain, *Talanta* 43 (1996) 785.
- [11] J.-M. Zen, J.-S. Tang, *Anal. Chem.* 67 (1995) 1892.
- [12] M.A. Gandour, E.-A. Kasim, A.H. Amrallah, O.A. Farghaly, *Talanta* 41 (1994) 439.
- [13] J.-M. Zen, Y.-J. Chen, C.-T. Hsu, Y.-S. Ting, *Electroanalysis* 9 (1997) 1009.
- [14] X. Cai, K. Kalcher, C. Neuhold, B. Ogorevc, *Talanta* 41 (1994) 407.
- [15] J.-M. Zen, P.-J. Chen, *Anal. Chem.* 69 (1997) 5087.

Pre-concentration of rare earths using silica gel loaded with 1-(2-pyridylazo)-2-naphthol (PAN) and determination by energy dispersive X-ray fluorescence

Lorena Cornejo-Ponce *, Patricio Peralta-Zamora, Maria Izabel Marette S. Bueno

Universidade Estadual de Campinas, Instituto de Química, C.P. 6154, 13083-970 Campinas-SP, Brazil

Received 29 July 1997; received in revised form 2 December 1997; accepted 4 December 1997

Abstract

The determination of a single rare earth element in a mixture with other species of this family is a very challenging problem in analytical chemistry due to the close similarity of their chemical properties. In this work, a liquid–solid extraction procedure for praseodymium, neodymium, samarium and yttrium mixtures and subsequent determination by energy dispersive X-ray fluorescence spectrometry is described. The pre-concentration procedure, which involves the use of silica modified with 1-(2-pyridylazo)-2-naphthol, permits complete recovery of the rare earths and significant sensitivity enhancement in comparison with direct determination in the aqueous phase. Determinations in quaternary mixtures show typical precisions and accuracies of 3% and 5%, respectively. © 1998 Elsevier Science B.V. All rights reserved.

Keywords: Pre-concentration; Rare earths; X-ray fluorescence

1. Introduction

Technological progress in recent years has increased the requirements for rare earth elements. Diverse and interesting applications of these elements are promoting their need in many activities, including glass and ceramic processing, metallurgy, nuclear chemistry, electronics, and, more recently, preparation of superconductor materials [1,2]. This massive demand has favored the progress of the analytical chemistry of these strategic

metallic species which is notably complex due to the great similarity of their chemical properties [1,2].

Classical spectrophotometric techniques are only useful for determination of the total amount of rare earth elements [3–6]. Simultaneous determination of several individual species is very troublesome due to the unavailability of selective chromogenic reactants. Other well-known analytical techniques such as atomic absorption and emission flame spectroscopy are of very restricted use, because rare earth elements, besides presenting complex absorption and emission spectra, manifest the important tendency to form refrac-

* Corresponding author. Fax: +55 197 883023; e-mail: lorenacp@iqm.unicamp.br

tory oxides as well as ionization [7,8]. Successful analytical methodologies are found only among modern instrumental techniques. Of these, plasma atomic emission spectroscopy [9,10], radiochemical analysis [11,12], chromatography [13], and fluorescence spectroscopy in the visible and X-ray regions [14,15], are the most efficient.

Energy dispersive X-ray fluorescence (EDXRF) is an instrumental technique with sufficient spectral resolution for the determination of rare earth mixtures without serious spectral interferences [16–21]. Nevertheless, the sensitivity of this technique is not enough for trace analysis. So, the application of pre-concentration procedures is an essential step in rare earth determination by this technique.

In this work, a procedure for pre-concentration and subsequent determination of praseodymium, neodymium, samarium and yttrium by EDXRF is proposed. The pre-concentration methodology involves the use of 1-(2-pyridylazo)-2-naphthol (PAN) immobilized on silica gel. The use of a liquid–solid pre-concentration step is a very favorable procedure, because, beyond permitting the elimination of potential matrix interferences, the solid phase is a convenient substrate for EDXRF measurements.

2. Experimental

2.1. Instruments

X-ray fluorescence measurements were performed using a Spectrace 5000 energy dispersive X-ray fluorescence spectrometer, equipped with a rhodium tube and a Si(Li) semiconductor detector. The samples were introduced on cylindrical plastic devices of about 2 cm in height with 3 cm i.d., using a Mylar film as sample support. Standard solution volumes were taken with a Metrohm microburette, using 0.5000 ml taps.

Analytical lines were: praseodymium, 5034 keV ($L\alpha_1$); neodymium, 5230 keV ($L\alpha_1$); samarium, 5,636 keV ($L\alpha_1$); yttrium, 14957 keV ($K\alpha_1$).

Instrumental conditions were: irradiation time, 100 s; tube voltage, 20 kV; tube current, 0.07 mA; atmosphere, air; filter, 0.127 mm aluminium film.

2.2. Reactants and standard solutions

The praseodymium standard solution was prepared from Pr_2O_3 (99.5%; Koch-Light), the neodymium standard solution from $Nd_2(CO_3)_3$ (reactant supplied by the Brazilian Federal Fiscal Service, without purity specifications), the samarium standard solution from Sm_2O_3 (99.9%; Aldrich) and the yttrium standard solution from Y_2O_3 (99%; Carlo Erba). All these solutions were prepared by direct dissolution of the reactants in $0.2 \text{ mol l}^{-1} \text{ HClO}_4$ (with heating in a water bath), and complexometrically standardized by the use of EDTA and xylenol orange [22].

Silica gel (Baker, 60–200 mesh) and 1-(2-pyridylazo)-2-naphthol (PAN; Baker) were used without further purification.

2.3. Working sample

The sample utilized is commercially distributed by NUCLEMON (Nuclebrás de Monazita e Associados Ltda., Brazil) as ‘rare-earth chloride’, corresponding to a concentrate obtained by chemical treatment of ‘Brazilian monazite’. The monazite is submitted to various physical and chemical processes for the separation of thorium, uranium, lead and other radioactive species. The resulting rare-earth chloride is then concentrated and packed as a final product, containing approximately 250 g of rare-earth oxides per litre of solution. The distribution of rare-earth elements in this product is presented in Table 1. The solution for analysis was obtained by precipitation of the hydroxides with an aqueous solution of NH_3 from a volume of 100 ml of the sample, with later dissolution in 100 ml of $2.0 \text{ mol l}^{-1} \text{ HClO}_4$.

2.4. Preparation of modified silica

A 10 g portion of silica (previously activated at 100°C for 3 h) was added to 50 ml of PAN solution (0.2% m/m in acetone). The mixture was vigorously stirred at room temperature to complete the solvent evaporation (approximately 3 h). The solid mass was homogenized in a mortar and stored in amber glass flasks.

Table 1
Distribution of the rare earths in the working sample

Element	% (as oxide)	g l ⁻¹ (original sample)	µg ml ⁻¹ (2500-fold dilution)
Pr	5.5	11.75	4.7
Nd	18.5	39.65	15.9
Sm	2.5	5.39	2.16
Y	1.3	2.56	1.02
Ce	47.5	101.38	40.55
La	22.0	46.90	18.76
Others	2.7	–	–

2.5. Extraction with modified silica

Aqueous solutions (50 ml) containing the rare earth mixtures were placed in 150 ml beakers and adjusted to suitable pH values with aqueous solutions of HCl or NH₃. To each solution, 0.2 g of the modified silica gel (minimal amount of sample necessary to cover the bottom of the cylindrical plastic device) was added. The mixture was magnetically stirred for 15 min and the solid was recovered by filtration with a Whatman 41 filter paper, washed with deionized water, dried at 60°C for 30 min and directly analysed by EDXRF.

2.6. Analytical curves and reproducibility

Using the optimized experimental conditions and the standard extraction procedure described above, calibration curves were obtained. The concentrations of each element in the rare earth mixtures ranged from 0.2 and 15 mg l⁻¹.

The reproducibility evaluation was performed using five determinations of two synthetic rare earth mixtures containing 4.0 or 10.0 mg l⁻¹ of each element.

3. Results and discussion

3.1. Optimization studies

The effect of pH on the rare earth extraction efficiency is seen in the extraction curves shown in Fig. 1. These curves presented a classical sigmoidal form with a very similar range of maximal extraction between pH 7.5 and 9.5. There is a

possibility of hydrolysis at these pH values since it is a particular tendency of the trivalent lanthanide elements. However, the physical phenomena that characterize the hydrolysis were not observed in our experimental conditions. On the contrary, the distinguishing purple colour that attests the formation of the lanthanide–PAN complexes was always observed. This is not a surprising; other studies have reported quantitative extractions of rare earth elements with PAN at pH values higher than 8 [14,21].

This result implies that there is no additional selectivity by application of the adsorption process. Fortunately, the high spectral resolution of the instrumental system permits the determination of the elements with little interference. A typical spectrum of rare earth elements adsorbed onto modified silica, isolated rare earth oxides and rare earths present in the work sample are shown in

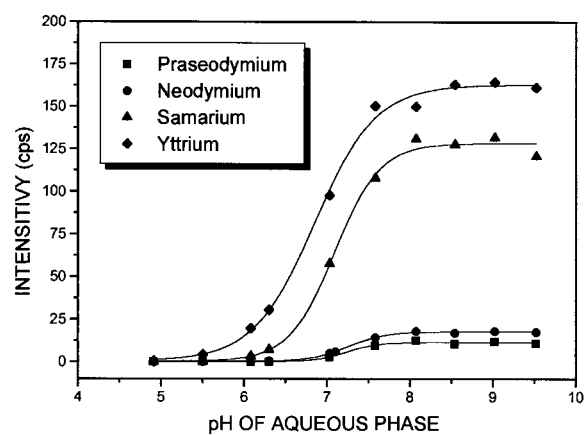


Fig. 1. Effect of aqueous phase pH on extraction of rare earths on silica–PAN. Rare earth concentration 10.0 mg l⁻¹.

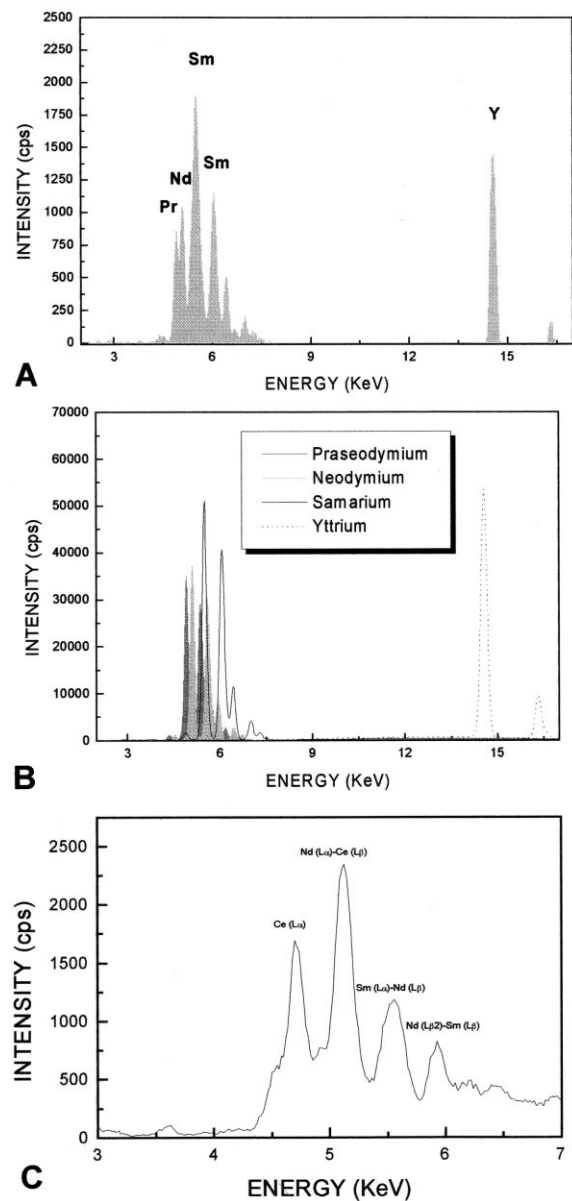


Fig. 2. X-ray fluorescence spectra of the rare earths. (A) Rare earth mixture adsorbed on modified silica. (B) Isolated rare earth oxides. (C) Working sample (expanded view).

Fig. 2A, Fig. 2B and Fig. 2C, respectively. In all these figures, it is possible to observe the existence of some spectral interferences, principally between

praseodymium, neodymium and samarium. Fig. 2C shows this effect of peak superposition most clearly.

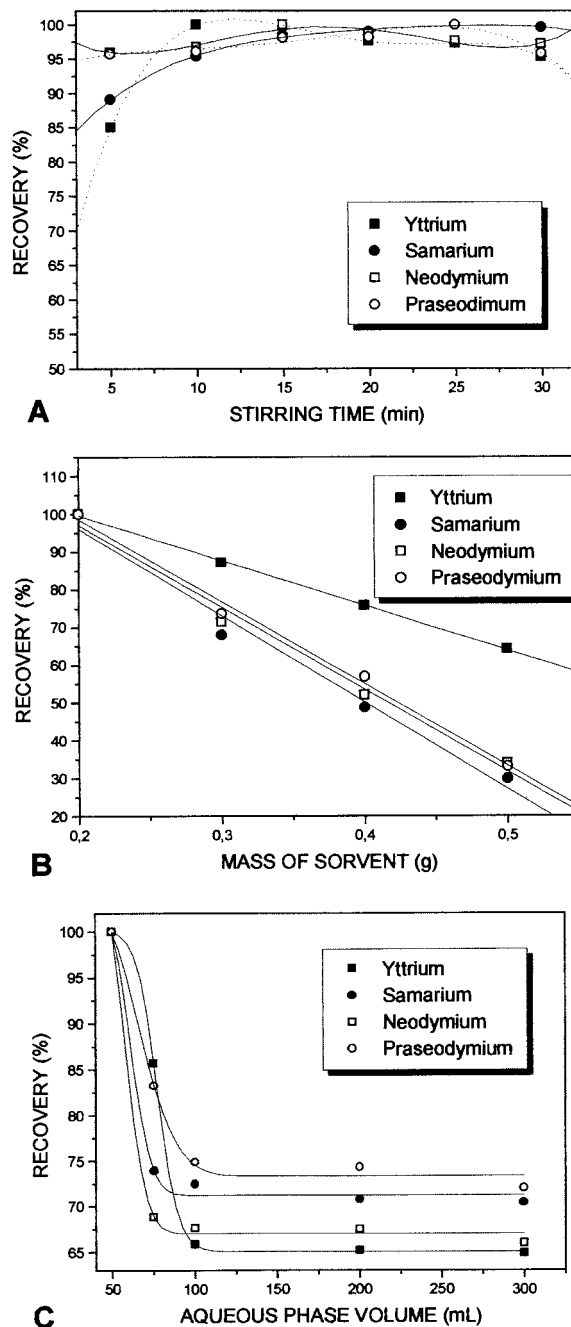


Fig. 3. Effect of stirring time (A), mass of solvent (B) and aqueous phase volume (C) on recovery of the rare earths.

Optimization studies show that the maximum extraction capacity of the sorbent is obtained with a stirring time of between 10 and 30 min (Fig. 3A). For subsequent experiments a stirring time of 15 min was selected. The effect of the variation on the mass of the sorbent (Fig. 3B) is negligible. So, whereas the sorbent mass is increased, the emission intensity of the element decreased in the same proportion, due to its dilution in the increasing mass of sorbent. For higher pre-concentration efficiency, a minimum mass of sorbent is necessary; thus, 0.2 g was selected for further experiments. Lower mass values have not been tested, because 0.2 g is the minimum amount necessary to cover the bottom of the sample device.

The effect of variation of the aqueous volume was tested between 50 and 300 ml. The results (Fig. 3C) show that the extraction is complete with volumes up to 50 ml. The use of volumes higher than 50 ml implies a significant reduction of the extraction efficiency, probably due to the drastic reduction of the contact among the phases. Between 100 and 300 ml the recovery is almost constant, with an efficiency of about 70%.

3.2. Analytical curves

The analytical curves presented in Fig. 4 were obtained using the optimized experimental conditions. These analytical curves are linear between 0.2 and 15 mg l⁻¹ with correlation coefficients higher than 0.999. Considering the sensitivity as a function of the slope of the analytical curves, the proposed method allows an enhancement equal to 176 for Pr, 172 for Nd, 167 for Sm and 84 for Y, compared to direct measurement of aqueous phases of these rare earths. These values are greater than those obtained by other extraction procedures [23].

3.3. Precision and figures of merit

To verify the precision of the proposed methodology, synthetic mixtures at two concentration levels (4.0 and 10.0 mg l⁻¹) were analysed using six replicates for each element. The results (Table 2) indicate that relative standard deviations (R.S.D.) lower than 5% can be obtained for these

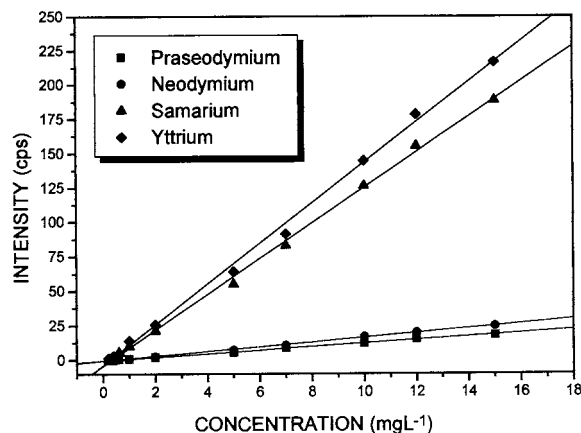


Fig. 4. Analytical curves for rare earths.

Praseodymium	$r = 0.9991$; cps = $(1.248 \times \text{mg l}^{-1}) - 0.394$
Neodymium	$r = 0.9990$; cps = $(1.686 \times \text{mg l}^{-1}) - 0.550$
Samarium	$r = 0.9992$; cps = $(12.911 \times \text{mg l}^{-1}) - 4.060$
Yttrium	$r = 0.9988$; cps = $(14.710 \times \text{mg l}^{-1}) - 3.708$

concentration levels, a value somewhat lower than that obtained by other methods (errors between 3 and 10% have been reported in determinations of binary, ternary and multielementor mixtures [18,20,24]).

Table 2
Reproducibility for six replicate study using two synthetic mixtures

	Amount (μg)			
	Nd	Pr	Sm	Y
Mixture 1				
Added amount	197	194	193	184
Found amount ^a	184	189	187	177
R.S.D. (%)	2.9	2.7	4.7	2.9
Error (%)	-6.6	-2.6	-3.1	-3.9
Mixture 2				
Added amount	490	487	487	490
Found amount ^a	494	483	491	492
R.S.D.	2.6	1.4	2.0	1.3
Error	+0.8	-0.8	+0.8	+0.4

^a Average of six replicates.

Table 3

Figures of merit of the developed pre-concentration methodology for the four elements (calculated under IUPAC recommendations)

Parameter	Praseodymium	Neodymium	Samarium	Yttrium
LDL (mg l^{-1})	0.26	0.06	0.06	0.61
R.S.D. (%) for 4.0 mg l^{-1}	2.7	2.9	4.7	2.9
S (cps mg l^{-1})	1.248	1.686	12.911	14.710

LDL (lower detection limit): $(3 \times \text{R.S.D. of blank})/S$.

R.S.D. (relative standard deviation): $S \times 100/\text{average of four replicates}$.

S (sensitivity): slope of analytical curve.

The principal figures of merit are shown in Table 3. The values obtained for the lower detection limit (LDL) and sensitivity (S) are comparable with the results reported in the literature [17,20].

3.4. Analysis of synthetic samples

By applying the proposed method to synthetic samples of variable elemental concentration (Table 4), it is observed that the interelemental spectral interferences are of little significance for those species in relatively high concentration and also when there is no appreciable difference in concentrations among the elements. In these cases the errors are of the same order of magnitude as those reported in the literature for similar procedures [10,18]. Nevertheless, it was verified here that, when one of the element is in relatively low concentration, the interelemental spectral interferences cause higher errors. This last case is critical in the determination of samarium, which suffers strong spectral interference from neodymium (see results of synthetic sample 3). It is important to observe that the error is produced not by the superposition of analytical lines but by the secondary $L\beta$ line of neodymium on the analytical $L\alpha$ line of samarium.

3.5. Analysis of working sample

The results for the quadruplicate analysis of the working sample are presented in Table 5. For samarium and yttrium, the results are very similar to the certified values. For neodymium, a large error was obtained, probably due to the interference of cerium which is present in large concen-

tration. Praseodymium was not detected due to its low concentration and poor sensitivity.

The large error obtained can be attributed to the great dilution factor used, 2500-fold. Nevertheless, the existence of concentrated samples is always provable. If a dilution is not made, the silica phase will be saturated and the extraction will be incomplete.

Another reason for these large errors can be spectral. In this case they can be improved by multivariate calibration, such as neural networks [25] and partial least squares [26] methods. In this sense, studies need to be done to solve the deficiencies in accuracy. So far, the great merit of the methodology described here consists of the high pre-concentration factors.

4. Conclusions

The proposed pre-concentration methodology consists of a simple, fast and low cost procedure which permits the complete recovery of rare earth elements from a large volume of aqueous phase. It permits high pre-concentration ratios for the determination of low concentrations of the rare earth elements by energy dispersive X-ray fluorescence spectrometry (EDXRF). In relation to the direct determination in aqueous phase, the pre-concentration procedure permits an enhancement of sensitivity of about 200 times for praseodymium, neodymium and samarium, and nearly 100 times for yttrium. This significant improvement in sensitivity expands the potential of the EDXRF technique which, by reason of its high spectral resolution, represents a valid alternative for applications in complex analysis.

Table 4
Analysis of synthetic samples

Run	Added amount (mg l ⁻¹)				Found amount (mg l ⁻¹)			
	Pr	Nd	Sm	Y	Pr	Nd	Sm	Y
1	0.39	5.77	1.95	9.60	0.20	7.24	2.63	11.7
2	5.80	0.39	9.57	1.96	9.37	0.26	6.20	1.89
3	1.95	9.67	0.39	5.88	0.20	10.54	2.66	6.17
4	9.60	1.96	5.71	0.39	12.25	0.26	4.87	0.75
5	9.60	9.67	5.71	1.96	9.77	9.60	6.96	2.31
6	9.60	9.67	9.57	9.60	9.66	9.88	9.82	9.84

Table 5
Analysis of working sample

Run	Certified amount (mg l ⁻¹)				Found amount (mg l ⁻¹)			
	Pr	Nd	Sm	Y	Pr	Nd	Sm	Y
1	4.70	15.90	2.16	1.02	ND	36.98	2.46	1.23
2	4.70	15.90	2.16	1.02	ND	35.81	2.47	1.29
3	4.70	15.90	2.16	1.02	ND	34.39	2.20	0.96
4	4.70	15.90	2.16	1.02	ND	36.39	2.46	1.20
Average	–	–	–	–	–	35.89	2.40	1.17
R.S.D. (%)	–	–	–	–	–	3.1	5.4	11.9
Error (%)	–	–	–	–	–	+125	+11	+15

ND, not detected.

The precision of the proposed method (R.S.D. of about 5%) is lower than those obtained by similar procedures [18]. Nevertheless, the accuracy is a function of the relative concentration of the species. For elements in high relative concentrations, the accuracy is satisfactory for analytical purposes. For the low concentration of one element in the presence of higher concentrations of another, the accuracy is prejudiced, probably due to spectral interferences by emission lines of the element present in the larger amount.

Acknowledgements

This work was supported by FAPESP (Brazil). We are grateful to Carol Collins for critically reading the manuscript.

References

- [1] T. Moeller, *The Chemistry of the Lanthanides*, Pergamon, New York, 1963.
- [2] Z. L Barbieri, *An. VI Simp. Anu. ACIESP* 1 (1982) 110.
- [3] S. Bhattacharya, S.J. Lyle, R.R. Maghjian, *Talanta* 27 (1980) 59.
- [4] S.J. Lyle, N.A. Zatar, *Anal. Chim. Acta* 135 (1982) 327.
- [5] N.S. Poluektov, M.A.J. Sandu, *J. Anal. Chem. U. S. S. R.* 25 (1970) 1302.
- [6] P.K. Spitsyn, V.S.J. Shvarev, *J. Anal. Chim. U. S. S. R.* 25 (1970) 1297.
- [7] A.P. Da Silva, R.N. Kniseley, V.A. Fassel, R.H. Curry, R.B. Myers, *Anal. Chem.* 36 (1964) 532.
- [8] V. A Fassel, R.H. Curry, R.N. Kniseley, *Spectrochim. Acta* 18 (1962) 1127.
- [9] L.H.J. Lajunen, G.R. Choppin, *Anal. Chem.* 9 (1989) 3.
- [10] O.N. Grebneva, N.M. Kuz'min, G.I. Tsysin, Y.A. Zolotov, *Spectrochim. Acta B* 51 (1996) 1417.
- [11] W.M. Jackson, G.I. Gleason, P.J. Hammons, *Anal. Chem.* 42 (1970) 1243.

- [12] W.M. Jackson, G.I. Gleason, *Anal. Chem.* 45 (1973) 2125.
- [13] K. Robards, S. Clarke, E. Patsalides, *Analyst* 113 (1988) 1757.
- [14] J. Gao, G. Hu, J. Kang, G. Bai, *Talanta* 40 (1993) 195.
- [15] R.H. Heidel, V.A. Fassel, *Anal. Chem.* 30 (1958) 176.
- [16] V. Bhagavathy, P.S.T. Sai, T. Prasada, A.D. Damodaran, *Anal. Lett.* 22 (1989) 197.
- [17] L.M. Marcó Parra, E.D. Greaves, J.L. Paz, L. Sajo-Bohus, *X-Ray Spectrom.* 22 (1993) 362.
- [18] F. Rastegar, D.E. Hady-Boussaad, R. Heimburger, C. Ruch, M.J.F. Leroy, *Analisis* 18 (1990) 497.
- [19] E. Bauer-Wolf, W. Wegscheider, S. Posch, G. Knapp, *Talanta* 40 (1993) 9.
- [20] A.N. Masi, R.A. Olsina, *Talanta* 40 (1993) 931.
- [21] V. Bhagavathy, L.P. Reddy, R.T. Prasada, A.D. Damodaran, *J. Radioanal. Nucl. Chem.* 149 (1991) 35.
- [22] S.J. Lyle, M. Rahman, *Talanta* 10 (1963) 1177.
- [23] P. Peralta-Zamora, L. Cornejo-Ponce, M.I.M.S. Bueno, *Talanta* 44 (1997) 811.
- [24] H. Onaga and M.I.M.S. Bueno, *J. Braz. Chem. Soc.* (submitted for publication).
- [25] I. Facchin, M.I.M.S. Bueno, C. Mello and R.J. Poppi, *X-Ray Spectrom.* (submitted for publication).
- [26] P. Peralta-Zamora, L. Cornejo-Ponce, N. Nagata, R.J. Poppi, *Talanta* 44 (1997) 1815.

Spectrophotometric determination of nitrite based on its catalytic effect on the oxidation of carminic acid by bromate

Jamshid L. Manzoori *, Mohammad H. Sorouraddin, Ali M. Haji-Shabani

Department of Analytical Chemistry, Faculty of Chemistry, University of Tabriz, Tabriz, Iran

Received 7 July 1997; received in revised form 8 December 1997; accepted 8 December 1997

Abstract

A highly sensitive and selective method is described for the determination of trace amounts of nitrite based on its effect on the oxidation of carminic acid with bromate. The reaction was monitored spectrophotometrically by measuring the decrease in absorbance of carminic acid at 490 nm after 3 min of mixing the reagents. The optimum reaction conditions were $1.8 \times 10^{-1} \text{ mol l}^{-1} \text{ H}_2\text{SO}_4$, $3.8 \times 10^{-3} \text{ mol l}^{-1} \text{ KBrO}_3$, and $1.2 \times 10^{-4} \text{ mol l}^{-1}$ carminic acid at 30°C. By using the recommended procedure, the calibration graph was linear from 0.2 to 14 ng ml^{-1} of nitrite; the detection limit was 0.04 ng ml^{-1} ; the R.S.D. for six replicate determinations of 6 ng ml^{-1} was 1.7%. The method is mostly free from interference, especially from large amounts of nitrate and ammonium ions. The proposed method was applied to the determination of nitrite in rain and river water. © 1998 Elsevier Science B.V. All rights reserved.

Keywords: Nitrite determination; Catalytic spectrophotometric method; Carminic acid–bromate redox reaction; Natural water

1. Introduction

Nitrite is an active intermediate in the nitrogen cycle, resulting from incomplete oxidation of ammonia or from reduction of nitrates. This ion is an important precursor of nitrosamines, which are potential carcinogens. Nitrite is one of the pollutants found in the atmosphere and natural water [1,2]. Nitrite salts is sometimes used as a preserva-

tive in the food industry and a corrosion inhibitor in industrial process water. Thus, its determination at ng ml^{-1} levels is important in environmental studies.

Many papers have been published on the determination of nitrite in different samples, but not all are suitable for routine trace determination. Among these methods spectrophotometry based on diazotization of an aromatic amine and subsequent coupling to form an azo dye are most widely used. These methods are characterized by high sensitivity but often have drawbacks of inter-

* Corresponding author. Tel.: +98 41 355998; fax: +98 41 340191.

ference by oxidizing and reducing agents, as well as relatively long reaction times and large sample volumes [3–7]. Other methods such as fluorometry [8,9], chemiluminescence [10,11], chromatography [12,13], pulse polarography [14,15] and flow injection [16–18] are also used but suffer from more or less time consuming procedures or complicated instrumentation.

A number of kinetic methods have been reported for nitrite determination [19–28]. Most of these procedures are based on its catalytic effect on bromate oxidation of organic compounds such as thionine [19], pyrogallol red [20], prochlorperazine [21], brilliant cresyl blue [22], methyl orange [23], pyridine-2-aldehyde 2-pyridylhydrazone [24], chlorophosphonazo-pN [25], and Nile blue A [26]. However, many of these methods are time consuming or have high limit of detection or need rigid control of acidity, temperature or reagents. The hydrogen peroxide oxidation of carminic acid has been used for the kinetic determination of cobalt [29] and iron [30], but its oxidation by bromate has not been used for nitrite determination so far.

The aim of this work was to study the catalytic oxidation of carminic acid with bromate in the presence of nitrite and to use the results obtained to develop a catalytic method for nitrite determination. The reaction was monitored spectrophotometrically and the method was successfully applied to the determination of nitrite in rain and river water.

2. Experimental

2.1. Reagents

Analytical-reagent grade chemicals and triply distilled water were used throughout.

A stock standard nitrite solution, $1000 \mu\text{g ml}^{-1}$, was prepared by dissolving 0.150 g sodium nitrite, pre-dried at 110°C for 4 h, in water. A small amount of sodium hydroxide was added to this solution to prevent its decomposition and a few drops of chloroform were also added to prevent bacterial growth. The resulting solution was made up to the mark in a 100 ml calibrated flask and was kept in a refrigerator and used within 2 weeks of preparation.

Potassium bromate solution ($3.8 \times 10^{-2} \text{ mol l}^{-1}$) was prepared by dissolving 1.5866 g KBrO_3 in water in a 250 ml volumetric flask. Carminic acid (Merck) (structure shown in Fig. 1) was used without further purification. A stock solution ($1.2 \times 10^{-3} \text{ mol l}^{-1}$) was prepared by dissolving 0.0591 g of carminic acid in water in a 100 ml standard flask and kept in a refrigerator. Sulphuric acid (1.8 mol l^{-1}) was prepared from concentrated H_2SO_4 (98%, Merck). Stock solutions ($1000 \mu\text{g ml}^{-1}$) of interfering ions were prepared by dissolving suitable salts in water, hydrochloric acid or sodium hydroxide solution.

2.2. Apparatus

A UV-265 FW spectrophotometer (Shimadzu) was used for measurements of absorption spectra. A model UV-120-02 spectrophotometer (Shimadzu) with 1.0 cm glass cuvettes was used to measure the absorbance at 490 nm. A thermostat (Tokyo Rikakika, LTD UA-1) was used to keep the reaction temperature at 30°C . A stop-watch was used for recording the reaction time.

2.3. Recommended procedure

1 ml 1.8 mol l^{-1} Sulphuric acid and 1 ml $1.2 \times 10^{-3} \text{ mol l}^{-1}$ carminic acid were added to each sample or standard solution containing 2–140 ng of nitrite in a 10 ml volumetric flask. Each solution was diluted to ca. 8 ml with water and was kept in a thermostated water-bath at 30°C for 10 min. 1 ml $3.8 \times 10^{-2} \text{ mol l}^{-1}$ Bromate previously brought to 30°C , was added and the solution was diluted to the mark with water. Time was measured from just after the addition of the

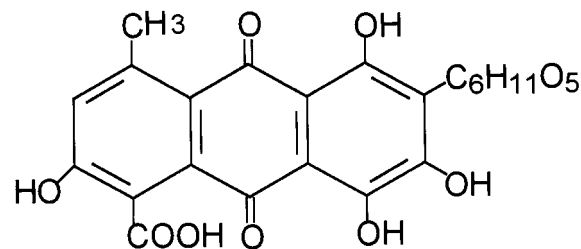


Fig. 1. The structure of carminic acid.

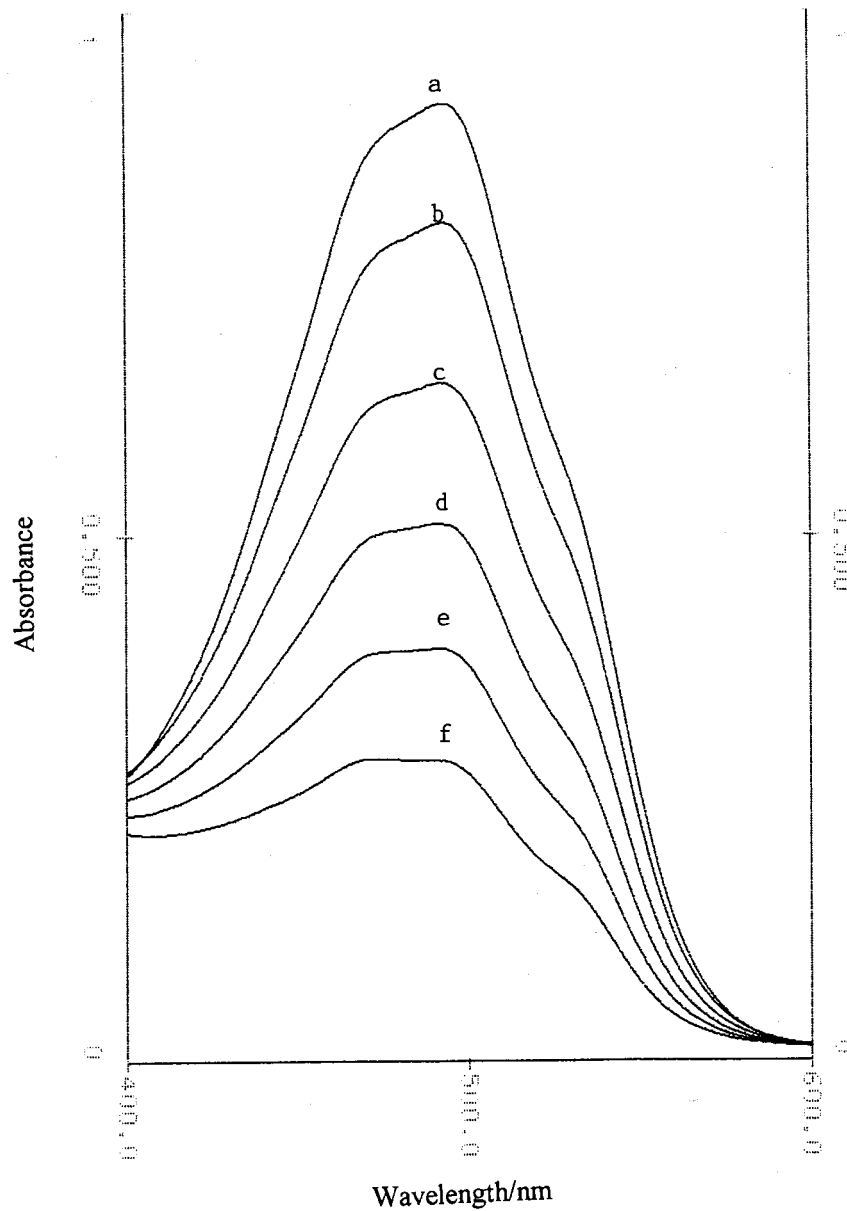


Fig. 2. Absorption spectra of the carminic acid– bromate system in the presence of nitrite, conditions: carminic acid, 1.2×10^{-4} mol l^{-1} ; sulphuric acid, 1.8×10^{-1} mol l^{-1} ; bromate, 3.8×10^{-3} mol l^{-1} ; nitrite, 5.0 ng ml^{-1} ; temperature, $30^{\circ}C$; after: a, 0.5; b, 1.5; c, 2.5; d, 3.5; e, 4.5; and f, 5.5 min from initiation of the reaction.

bromate solution. The blank solution was prepared by the same procedure. After 3.0 min, 0.1 g solid urea was added to the solutions to stop the catalysed reaction. The solutions were transferred into 1.0 cm glass cuvettes and after 3.5 min the absorbances of the solutions were measured

against water at 490 nm. The absorbances of the sample and blank were labeled A and A_0 respectively. Then the amount of nitrite was determined from a calibration graph which was constructed by plotting the $\log(A_0/A)$ versus the nitrite concentration.

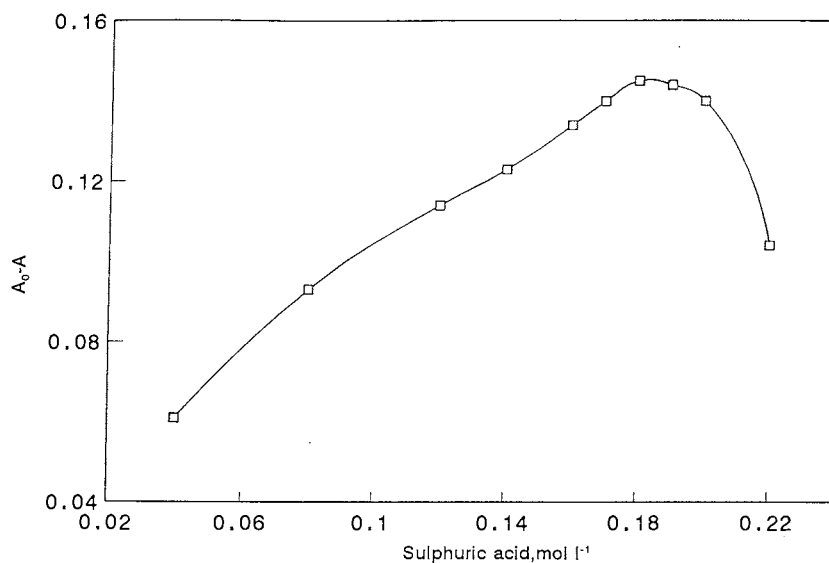


Fig. 3. Effect of sulphuric acid concentration on the reaction rate, conditions: carminic acid, 1.0×10^{-4} mol l⁻¹; bromate, 4.0×10^{-3} mol l⁻¹; nitrite, 10.0 ng ml⁻¹; temperature, 30°C; reaction time, 3.0 min.

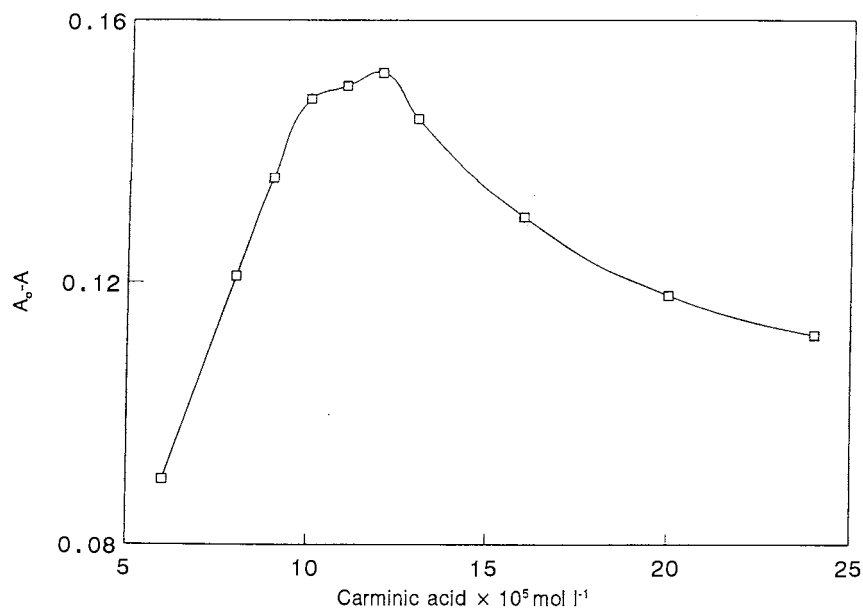


Fig. 4. Effect of carminic acid concentration on the reaction rate, conditions: sulphuric acid, 1.8×10^{-1} mol l⁻¹; bromate, 4.0×10^{-3} mol l⁻¹; nitrite, 10.0 ng ml⁻¹; temperature, 30°C; reaction time, 3.0 min.

3. Results and discussion

Some oxidants such as bromate could oxidize carminic acid irreversibly in acidic media at a

slow rate. This oxidation is increased in the presence of ultra-trace amounts of nitrite. This process was monitored by measuring the decrease in absorbance at 490 nm. Fig. 2 shows absorption

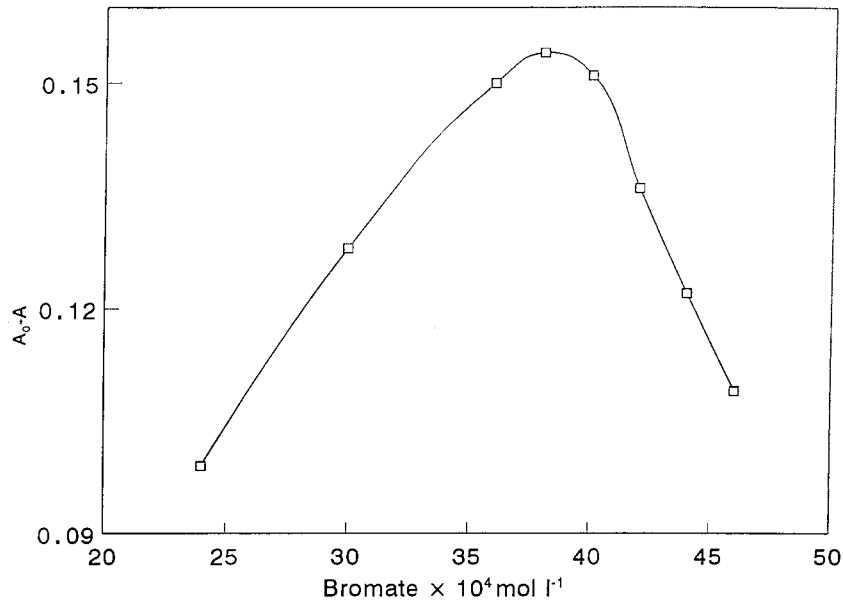


Fig. 5. Effect of bromate concentration on the reaction rate, conditions: sulphuric acid, $1.8 \times 10^{-1} \text{ mol l}^{-1}$; carminic acid, $1.2 \times 10^{-4} \text{ mol l}^{-1}$; nitrite, 10.0 ng ml^{-1} ; temperature, 30°C ; reaction time, 3.0 min.

spectra of carminic acid at different times. As shown in this figure, the change in absorbance at 490 nm with time can be used for the study.

Several acidic media including sulphuric, hydrochloric, nitric and phosphoric acids were investigated for the carminic acid–bromate system. The results indicated that among these four acids, sulphuric acid is the best due to its acidity strength relative to other acids at equimolar concentrations.

3.1. Effect of variables

The effect of sulphuric acid concentration on the rate of the reaction with and without nitrite was studied. The optimum concentration of sulphuric acid is $1.8 \times 10^{-1} \text{ mol l}^{-1}$ as shown in Fig. 3.

Fig. 4 shows the effect of carminic acid concentration on the catalysed and uncatalysed reaction. The results show that the sensitivity increased up to $1.2 \times 10^{-4} \text{ mol l}^{-1}$ carminic acid, whereas a higher concentration of the reagent caused a decrease in the reaction rate. This effect may be due to the change of mechanism of the reac-

tion or deviation from Beer's law. Thus $1.2 \times 10^{-4} \text{ mol l}^{-1}$ carminic acid was used for the study.

The effect of bromate concentration on obtaining maximum sensitivity was investigated. Fig. 5 shows that sensitivity increases up to $3.8 \times 10^{-3} \text{ mol l}^{-1} \text{ BrO}_3^-$. At higher concentrations, the sensitivity decreases, owing to the decrease of A_0 . Thus $3.8 \times 10^{-3} \text{ mol l}^{-1}$ bromate concentration was selected for use.

The effect of the reaction temperature was studied in the range $5\text{--}40^\circ\text{C}$ at optimum conditions. Fig. 6 shows that by increasing the temperature to 30°C , $A_0 - A$ increases with temperature, while at higher temperatures it decreases. This effect is due to the fact that at higher temperatures, the rate of the uncatalysed reaction increases with temperature to a greater extent than the catalysed reaction and the difference between the rates of the catalysed and uncatalysed reactions diminishes. A temperature of 30°C , which gives high sensitivity, was selected.

A chemical inhibitor or rapid cooling is sometimes used to stop the catalytic reaction in practical applications of the fixed time method. It was

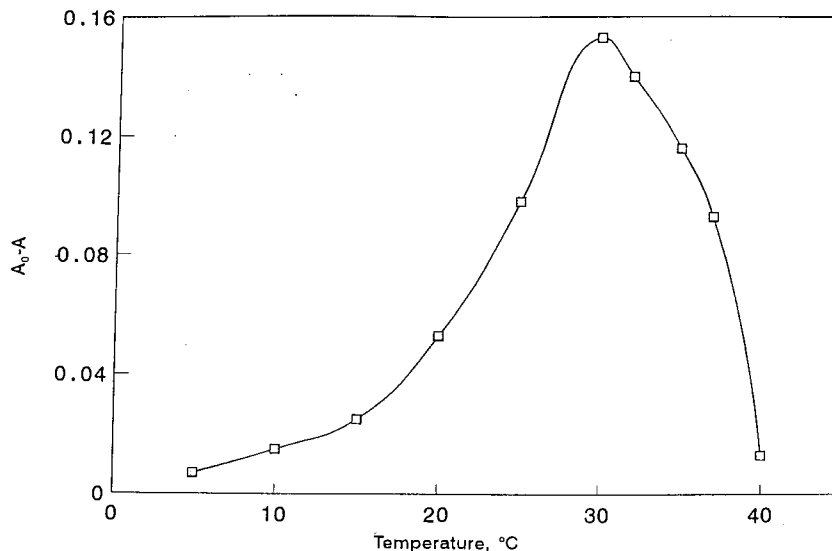


Fig. 6. Effect of temperature on the reaction rate, conditions: sulphuric acid, $1.8 \times 10^{-1} \text{ mol l}^{-1}$; carminic acid, $1.2 \times 10^{-4} \text{ mol l}^{-1}$; bromate, $3.8 \times 10^{-3} \text{ mol l}^{-1}$; nitrite, 10.0 ng ml^{-1} ; temperature, 30°C ; reaction time, 3.0 min.

found that urea is a good inhibitor which decomposes nitrite rapidly. In this study urea was used to stop the catalytic reaction. 0.1 g Solid urea suffices for 10 ml of solution and simultaneously quenches the catalysed reaction. The absorbance of the solution remains constant for a few minutes in the presence of urea.

The effect of ionic strength on the rate of reaction was investigated by using NaNO_3 (2 mol l^{-1}). The reaction rate increases very slightly up to $0.5 \text{ mol l}^{-1} \text{ NaNO}_3$.

The effect of measuring time on the rate of the reaction was studied at the optimum concentra-

tions of the reagents at 30°C . The results show that 3.0 min yields the best sensitivity. Thus, a fixed reaction time of 3 min was chosen for this study.

3.2. Calibration, precision and detection limit

Under the conditions chosen, in the concentration range $0.2\text{--}14 \text{ ng ml}^{-1}$ of nitrite the following regression equation was obtained:

$$\log(A_0/A) = 1.6 \times 10^{-3} + 0.011C \quad (r = 0.9995)$$

where C is the ng ml^{-1} of nitrite. The R.S.D. for six replicate determinations is 1.7% for 6.0 ng ml^{-1} nitrite. The experimental limit of detection is 0.04 ng ml^{-1} , which was calculated as three times the S.D. of the blank (3s criterion).

3.3. Interference

The effects of possible interfering species, which commonly accompany nitrite in natural waters, were studied in the determination of 10 ng ml^{-1} of nitrite following the recommended procedure. A foreign ion was considered to interfere seriously when it gave a determination error of more than 5%. The tolerance limit of foreign ions are sum-

Table 1
Tolerance limits of foreign ions in the determination of 10 ng ml^{-1} of nitrite following the recommended procedure

Tolerance limit ($\mu\text{g ml}^{-1}$)	Foreign ion
100	NO_3^- , F^- , SO_4^{2-} , CO_3^{2-} , ClO_3^- , PO_4^{3-} , Cl^- , acetate, tartarate, NH_4^+ , Na^+ , K^+ , Mg^{2+} , Ca^{2+} , Cu^{2+} , Zn^{2+} , Ni^{2+} , La^{3+} , U (VI)
50	Citrate, Cd^{2+} , Co^{2+} , Mn^{2+} , Cr^{3+} , Al^{3+}
10	CN^- , EDTA, Ag^+ , Pb^{2+}
1	$\text{C}_2\text{O}_4^{2-}$, Hg^{2+} , Ba^{2+} , Mo(VI), W(VI)
0.2	IO_3^- , CrO_4^{2-} , $\text{S}_2\text{O}_3^{2-}$, Bi^{3+} , Fe^{3+}

Table 2
Analytical results and recoveries for rain and river water samples

Sample ^a	Nitrite (ng)		Recovery (%)	Content of nitrite in sample (ng ml ⁻¹)		R.S.D. (%)
	Added	In reaction solution ^b		This method	Standard method	
River	0.0	33.6		16.8	16.9	2.6
	50.0	82.1	97.0			1.4
	80.0	111.4	97.2			0.8
Rain	0.0	55.2		27.6	26.4	1.6
	30.0	84.8	98.7			1.0
	50.0	104.2	98.0			1.2

^a Collected at Iran; the river water was collected from the Talkheroud river on 28 April 1997; the rain water was collected on the roof of the Chemistry building of Tabriz University on 29 April 1997.

^b A sample of 2 ml was used for one measurement. Each result is the average of five determinations.

marized in Table 1. Large amounts of nitrate and ammonium ions have little effect. Thus, the determination of trace amounts of nitrite in nitrate or ammonium salt is possible.

3.4. Determination of nitrite in rain and river water

A freshly collected water sample was filtered through a membrane filter of 0.45 μm pore size into a poly(propylene) bottle, kept in a refrigerator at about 4°C and analysed by recommended procedure within 12 h of collection.

Since the concentration of common pollutants in natural water is generally far below the tolerance levels shown in Table 1, the method was applied directly to the determination of nitrite in rain and river water.

As shown in Table 2, the results obtained with the proposed method agree well with those obtained by the standard method [31]. The reliability of the method to analyse real samples was also checked by recovery experiments. The results show that the method gives good recoveries of added nitrite.

The simplicity, high sensitivity and its freedom from interference effects are significant advantages of the proposed method. The method could be applied to drinking water after removing the chlorine. Furthermore, with the proposed method it is also possible to combine the nitrate and nitrite analysis. This could be feasible by reduc-

tion of nitrate to nitrite by using a copper cadmium reduction column [17] and measuring the sum. Nitrite is determined directly by the proposed method and nitrate can be determined by the difference.

References

- [1] I.A. Wolff, A.E. Wasserman, *Science* 177 (1972) 15.
- [2] K.K. Chio, K.W. Fung, *Analyst* 105 (1980) 241.
- [3] M. Nakamura, T. Mazuka, M. Yamashita, *Anal. Chem.* 56 (1984) 2242.
- [4] E. Szekely, *Talanta* 15 (1968) 795.
- [5] G. Norwitz, P.N. Keliher, *Analyst* 110 (1985) 689.
- [6] P.K. Tarafder, D.P.S. Rathore, *Analyst* 113 (1988) 1073.
- [7] A. Chaube, A.K. Baveja, V.K. Gupta, *Talanta* 31 (1984) 391.
- [8] S. Motomizu, M. Hiroshi, *Talanta* 33 (1986) 792.
- [9] P. Damiani, G. Burini, *Talanta* 33 (1986) 649.
- [10] R.D. Cox, *Anal. Chem.* 52 (1980) 332.
- [11] R.S. Braman, S.A. Hendrix, *Anal. Chem.* 61 (1989) 2715.
- [12] Z. Iskandarani, D.J. Pietrzyk, *Anal. Chem.* 54 (1982) 2601.
- [13] S.H. Lee, L.R. Field, *Anal. Chem.* 56 (1984) 2647.
- [14] Z. Gao, G. Wang, Z. Zhao, *Anal. Chim. Acta* 230 (1990) 105.
- [15] S. Sabharwal, *Analyst* 115 (1990) 1305.
- [16] M.J. Ahmed, C.D. Stalikas, S.M. Tzouwara-Karayanni, M.I. Karayannis, *Talanta* 43 (1996) 1009.
- [17] J.F. Van Staden, A.E. Joubert, H.R. Van Vliet, *Fresenius Z. Anal. Chem.* 325 (1986) 150.
- [18] I.M.P.L.V.O. Ferreira, J.L.F.C. Lima, M.C.B.S.M. Montenegro, R. Perez Olmos, A. Rios, *Analyst* 121 (1996) 1393.

- [19] M. Jiang, F. Jiang, J. Duan, X. Tang, Z. Zhao, *Anal. Chim. Acta* 234 (1990) 403.
- [20] A.A. Ensafi, M. Samimifar, *Talanta* 40 (1993) 1375.
- [21] A.A. Mohamed, M.F. El-shahat, T. Fukasawa, M. Iwatsuki, *Analyst* 121 (1996) 89.
- [22] A.A. Ensafi, B. Rezaii, *Microchem. J.* 50 (1994) 169.
- [23] J. Zhi-Liang, Q. Hai-Cuo, W. Da-Qiang, *Talanta* 39 (1992) 1239.
- [24] R. Montes, J.J. Laserna, *Talanta* 34 (1987) 1021.
- [25] C. Xingguo, W. Ketai, H. Zhide, Z. Zhengfeng, *Anal. Lett.* 29 (1996) 2015.
- [26] A.A. Ensafi, M.S. Kolagar, *Anal. Lett.* 28 (1995) 1245.
- [27] C. Sanchez-Pedreno, M.T. Sierra, M.I. Sierra, A. Sanz, *Analyst* 112 (1987) 837.
- [28] B. Liang, M. Iwatsuki, T. Fukasawa, *Analyst* 119 (1994) 2113.
- [29] Z. Zhang, G. Zhang, *Fenxi Huaxue* 18 (1990) 929.
- [30] T.G. Pecev, S.S. Mitic, *J. Serb. Chem. Soc.* 59 (1994) 195.
- [31] F.J. Welcher (ed.), *Standard Methods of Chemical Analysis*, vol. 2, part B, Van Nostrand, New York, 1963, pp. 2448.

Determination of Fe(II), Cu(II) and Ag(I) by using silica gel loaded with 1,10-phenanthroline

O. Zaporozhets *, O. Gawer, V. Sukhan

Taras Shevchenko Kyiv University, 64 Volodymirska Street, Kyiv 252033, Ukraine

Received 8 August 1997; received in revised form 4 December 1997; accepted 8 December 1997

Abstract

The modified silica gel with 1,10-phenanthroline adsorbed was obtained. The adsorption from aqueous solutions onto loaded silica gel of Fe(II), Cu(II) and Ag(I) and their complexes was studied. The loaded silica gel was applied to Fe(II), Cu(II) and Ag(I) reflectance spectroscopy determinations in water (detection limits 0.08, 0.03 and 0.01 ppm respectively). Visual test scales for Fe, Cu and Ag ion determinations in water were worked out. © 1998 Elsevier Science B.V. All rights reserved.

Keywords: 1,10-Phenanthroline; Adsorption; Loaded silica gel; Fe(II III) determination; Cu(II) determination; Ag(I) determination

1. Introduction

Sorption reflectance spectroscopic methods are known as effective methods to combine metal ions preconcentration and their determination on the surface [1]. Numerous methods for Fe(II), Cu(II) and Ag(I) determination have been based on sorption of metal ions on disks made of polyacrylonitrile fibers filled with KU-2 ion exchanger with detection in the sorbent phase by Rhodasol X, thiocyanate and sodium diethyldithiocarbamate correspondingly [2,3]. The sorbents modified with analytical reagents are the most promising solid phase reagents [4]. Silica gels modified with *p*-dimethylaminobenzylidenerhodanine, in partic-

ular, has been used for Ag(I) preconcentration [5]. 1,10-Phenanthroline (Phen) is known to be one of the effective chelating reagent for some metal ions determination [6]. The possibility of Phen fixation on silica gel in a chemical way was shown in [7]. Adsorption of reagents is a more simple and reliable method of sorbent modification, silica gel (SG) in particular [8]. As far as we know no modification of silica gel by Phen adsorption has been reported.

It is known that the maximum adsorption of metal ions can be obtained during complex with ratio reagent:metal ion = 1:1 forming on a surface of modified sorbent [1]. Ag(I) forms a complex with Phen with a ratio of Ag:Phen = 1:1 in acidic solution [9]. This complex is colourless but with a xanthine dye of the sulfophthalein group it forms a coloured heteroligand complex [9]. Cu(II) also

* Corresponding author. Tel.: + 380 44 2210211; fax: + 380 44 2244188; e-mail: ZUBENKO@analit.chem.univ.kiev.ua

forms a heteroligand complex with ratio Cu:Phen = 1:1 [9]. Fe(II) forms some coloured complexes with Phen in solution and the most stable complex is Fe(Phen)_3^{2+} [10].

In the present work we have studied the possibility of application of silica gel with adsorbed Phen to Fe(II), Cu(II) and Ag(I) determination in water.

2. Experimental

2.1. Reagents

Water was purified according to [11]. Standard Fe(II), Ag(I) and Cu(II) solutions were prepared by dissolving salts $\text{FeSO}_4 \cdot 7\text{H}_2\text{O}$, AgNO_3 and $\text{CuSO}_4 \cdot 5\text{H}_2\text{O}$. Potassium citrate (K_3Cit) (0.3 M), ammonium chloride (1 M), urotropin (17%), 1,10-phenanthroline (1×10^{-3} M), bromopyrogallol red (BPR) (1×10^{-4} M), and ascorbic acid water solutions were prepared by dissolving appropriate substances. The standard solutions of metal salts were acidified with sulfuric or nitric acid and further diluted as required. A saturated solution of ascorbic acid (H_2Asc) was used. Acetate citrate buffer solution (pH 5.5) was prepared according to [12]. Ammonium buffer solution (pH 8.8) was prepared by mixing a 1 M solution of ammonium hydroxide and a 1 M solution of ammonium chloride. Hexane was purified by flowing over metallic sodium. A solution of Phen in hexane (1×10^{-3} M) was obtained by dissolving the appropriate amount of substance. All chemicals were of analytical reagent grade. Silica gel L 100/250 for chromatography (Chemapol, Prague, Czech Republic) was digested in hydrochloric acid, washed with purified water and dried at 80°C for 8 h.

2.2. Apparatus

The spectra of solutions and reflectance spectra of sorbents were registered with a UV/Vis spectrophotometer Specord M-40 (Carl Zeiss Jena, Germany). Atomic absorption measurements were recorded on a model Saturn atomic absorption spectrometer (Severodonetsk) equipped with

a standard burner for use with an air–propane–butane flame. Standard hollow-cathode lamps were used as a line source for all elements.

A potentiometer model EV-74 with a glass electrode (Gomel, Belarus) was used for pH measurements.

2.3. Procedures

The batch technique has been used for the research of Phen adsorption onto unloaded silica gel (SG) and metal ion adsorption onto SG and loaded silica gel (Phen–SG).

2.3.1. Adsorption of Phen from hexane solution

SG (0.01 g) was stirred with 5 ml of 0.05–1 mM Phen solution in hexane for 1–60 min. The Phen residue in hexane was controlled spectrophotometrically by the absorbance of the complex Phen with Fe(II) [13].

2.3.2. Adsorption of Fe(II) and Fe(III) onto Phen–SG

This was realized from 3.0 mM K_3Cit . Fe(Phen)_3^{2+} and Fe(Phen)_3^{3+} were adsorbed onto SG from 1.5 mM Phen. All these solutions were buffered to pH 5.5 with acetate citrate buffer. Fe(II) residue in the solution was controlled spectrophotometrically by the colour of the complex ($\lambda = 510$ nm) and Fe(III) residue was controlled spectrophotometrically by the absorbance of Fe(Phen)_3^{2+} after Fe(III) reduction by ascorbic acid.

2.3.3. Adsorption of Cu(II) onto SG and Phen–SG

This was adsorbed from the solution buffered to pH 8.8 with ammonium buffer.

2.3.4. Adsorption of Ag(I) onto Phen–SG

This was done from 0.02 mM BPR and 1.7% urotropin solutions. The Cu(II) and Ag(I) residues were controlled by atomic absorption measurements.

Sorbents with metal ions adsorbed were dried at room temperature for 24 h and analyzed by using reflectance spectroscopy.

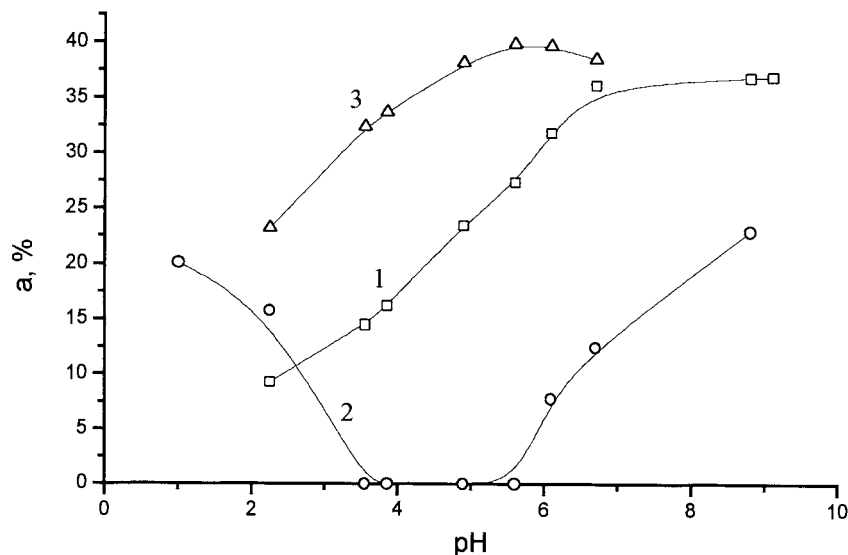


Fig. 1. Adsorption of Fe(II) onto Phen-SG (1) and SG (2), and adsorption of Fe(Phen)_3^{2+} onto SG (3) as functions of pH. Initial concentration, $10^{-3} \text{ mol l}^{-1}$: Fe (II), 0.02; Phen, 1.5 (3); Cit, 3.0 (1–2); $V = 10 \text{ ml}$; pH 5.5; $m = 0.15 \text{ g}$; $t = 5$ (1, 2), 10 min (3).

3. Results and discussion

Modification of SG with Phen has been carried out from hexane solution [13]. Phen-SG containing 0.1 and 0.2 mmol g^{-1} Phen were used.

3.1. Fe(II) and Fe(III) adsorption onto Phen-SG

It is well known that Fe(II) forms a coloured complex with Phen in solution at pH 2.5–9.0 [14]. The pH dependences of Fe(II) adsorption from aqueous solution onto Phen-SG and SG are compared in Fig. 1 (curves 1 and 2) and the optimum pH is 5.5. Fe(II) adsorption onto Phen-SG under these conditions was found to be quick. The maximum adsorption was reached in 5 min. The dependence of maximum adsorption on concentration of Fe(II) is shown in Fig. 2 (curve 5) and Table 1. The chelating capacity of Phen-SG is 0.1 mmol g^{-1} Fe(II) for 0.1 mmol g^{-1} Phen. Spectrophotometrically it was proved that Fe(Phen)_2^{2+} had been formed on the surface under these conditions. Fe(III) forms a colourless complex with Phen but in the presence of citrate

ions it is not adsorbed onto the Phen-SG.

3.2. Fe(Phen)_3^{2+} and Fe(Phen)_3^{3+} adsorption onto SG

Dependence of Fe(Phen)_3^{2+} adsorption on pH is shown in Fig. 1 (curve 3). The maximum adsorption was arrived at pH 5.0–6.3 under optimum conditions for Fe(Phen)_3^{2+} formation [14]. Equilibrium of this complex adsorption onto SG was reached in 10 min.

Adsorption of Fe(Phen)_3^{3+} was found to be quick and quantitative on these conditions, too.

The isotherm of Fe(Phen)_3^{2+} adsorption (Fig. 2, curve 2) can be formally described by a Langmuir equation and linearized in the coordinates $[C]/a - [C]$ with the coefficient of correlation $r = 0.993$. The results of such a description are shown in Table 1. The dependences of Fe(Phen)_3^{2+} adsorption ($y, \%$) onto SG on mass (m, g) of the sorbent and volume (V, ml) of solution can be described by the following equation: $y = a + b \cdot m - c \cdot m^2$ and $y = a + b/V$. The values of a, b and c are shown in Table 2.

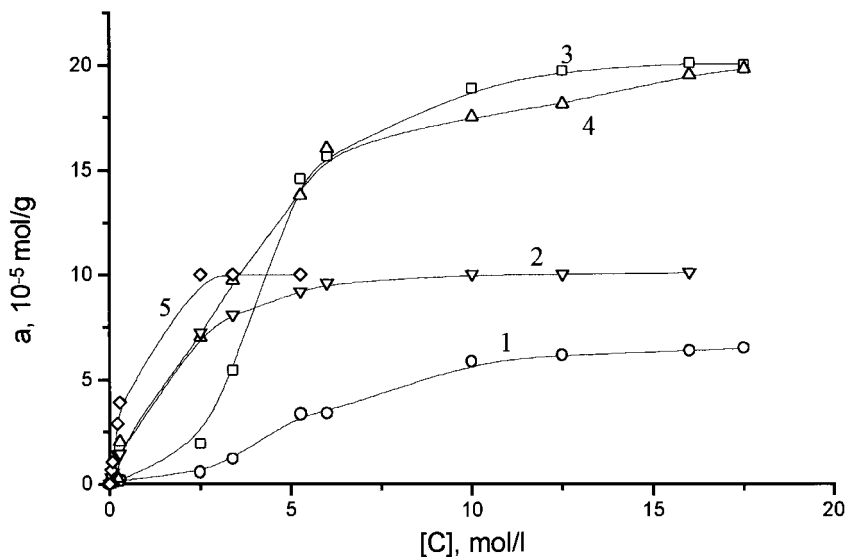


Fig. 2. Isotherms of Cu(II) (1) and Fe(Phen) $_3^{2+}$ (2) adsorption onto SG; and isotherms of Cu(II) (3) and Ag(I) (4) adsorption onto Phen-SG, and dependence of Fe(II) adsorption onto Phen-SG on the concentration of Fe(II) (5). Initial concentration, mol l $^{-1}$: Phen, 1.5×10^{-3} (2); NH $_3$, 0.2 (1, 3); BPR, 2.10^{-5} (4); Cit, 3.10^{-3} (5); equilibrium concentration [C], mol l $^{-1}$: 10^{-5} (1–3), 10^{-4} (4), 10^{-3} (5); $a_{\text{Phen}} = 0.1$ (5), 0.2 mmol g $^{-1}$ (3, 4); $V = 10$ (2, 4, 5), 20 (1, 3) ml; pH 6.5 (4), 5.5 (2, 5), 8.8 (1, 3); $m = 0.02$ (1–3, 5), 0.01 g (4); $t = 10$ (1–4), 5 min (5).

Table 1

The characteristics of dependencies of metal ions adsorption onto sorbents

Compound	Sorbent	Type of the isotherm	a_{max} (mmol g $^{-1}$)	Conditional constant (10^4 l mol $^{-1}$)
Phen	SG	H	0.52	2.7
Fe $^{2+}$	Phen-SG	—	0.1	—
Fe(Phen) $_3^{2+}$	SG	L	0.016	2.9
Cu $^{2+}$	Phen-SG	S	0.19	—
	SG	S	0.063	—
Ag $^+$	Phen-SG	L	0.23	2.4

a_{Phen} (mmol g $^{-1}$): 0.1 (Fe), 0.2 (Cu, Ag).

3.3. Cu(II) adsorption onto Phen-SG and SG

Cu(II) was not adsorbed from aqueous solution onto Phen-SG. So the adsorption of Cu(II) from ammonia solution was studied. Ammonia was chosen because it has a small radius (it escapes steric hindrance) and its complexes with Cu(II) are coloured. To avoid difficulties with soluble hydroxide of Cu(II) conformation at pH 8–9 a concentration of ammonium ions was calculated from the solubility product and stability constant

of Cu(II) ammonia complexes [15,16]. Optimum concentration of ammonium ions was 0.2 M.

Kinetics experiment of Cu(II) adsorption onto Phen-SG and SG showed that the time taken for maximum Cu(II) adsorption was 10 min in both cases.

Isotherms of Cu(II) adsorption onto SG and Phen-SG are shown in Fig. 2 (curves 1 and 3) and Table 1. The maximum Cu(II) adsorption onto Phen-SG is 3 times more than the complex full adsorption onto SG. The chelating capacity of

Table 2

The dependencies of metal ions adsorption on mass of sorbent and volume of solution

Ion	Coefficients of equation for dependencies on					Optimal		Coefficient of preconcentration
	<i>m</i>			<i>V</i>		<i>V</i> (ml)	<i>m</i> (g)	
	<i>a</i>	<i>b</i>	<i>c</i>	<i>a</i>	<i>b</i>			
Fe(Phen) ₃ ²⁺	19.3	564	1350	1.24	211	50	0.15	500
Cu ²⁺	21.9	323	581	114	0.87	50	0.10	333
Ag ⁺	43.3	858	2660	87.8	0.26	40	0.20	200

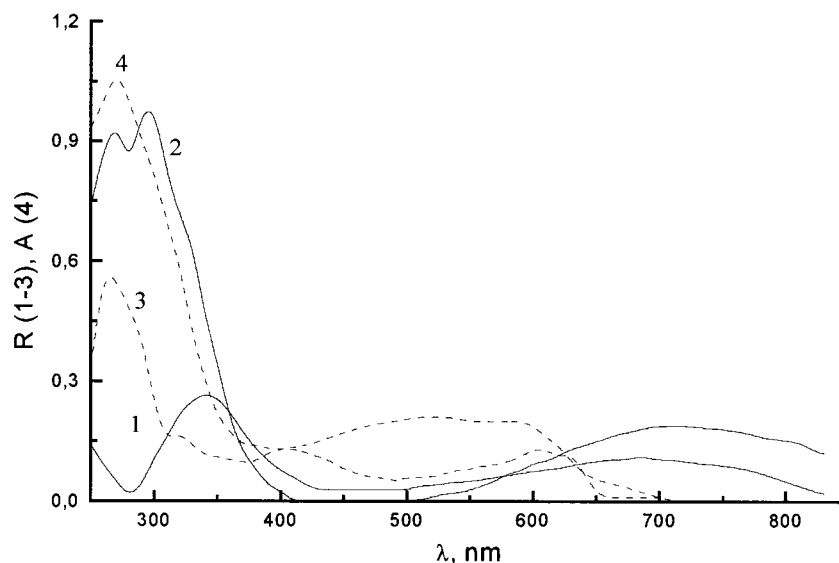


Fig. 3. The reflectance spectra of SG (1), Phen-SG (2) with Cu(II) adsorbed, Phen-SG with Ag(I) adsorbed (3) and the optical absorbance spectrum of an aqueous solution of Ag(Phen)⁺ (4).

Phen-SG (Fig. 2, curve 3) and the reflectance spectra of Phen-SG with Cu(II) adsorbed (Fig. 3) show that Phen on the surface had taken part in forming a complex with Cu(II).

The dependencies of Cu(II) adsorption onto SG on the mass of the sorbent and the volume of solution can be described by the equations: $y = a + b \cdot m - c \cdot m^2$ and $y = a - b \cdot V$. The values of *a*, *b* and *c* are shown in Table 2.

3.4. Ag(I) adsorption onto Phen-SG

Ag(I) is adsorbed onto Phen-SG from aqueous solution at pH 2. But such a complex is colourless so the adsorption of Ag(I) was studied from an

aqueous solution in the presence of BPR at pH 6.5 according to [17]. For comparison an attempt to adsorb Ag(I) onto unloaded silica gel was done but there was no effect.

The Ag(I) adsorption equilibrium was reached in 10 min. The isotherm shown in Fig. 2 (curve 4) can be formally described by a Langmuir equation and linearized with $r = 0.999$. The results of such description are shown in Table 1. It is known that in solution Ag(I) with Phen and BPR forms a heteroligand complex with the ratio Ag:Phen = 1:2 [17]. Spectra (Fig. 3) showed that the complex of Ag(I) on the surface differed from the complex in solution. The chelating capacity of Phen-SG is 0.2 mmol g^{-1} Ag(I) for 0.2 mmol g^{-1} Phen. So it

Table 3
Results of Fe(II), Cu(II) and Ag(I) determination in model solutions (1–3), natural (4) and mineral water “Cylyushcha” (5)

Metal ion	Type of sample	Added (ppm)	Found (ppm)			
			Phen–SG	S_r	SG	S_r
Fe ²⁺	1	2.8	2.8 ± 0.2	0.07	2.8 ± 0.3	0.11
	1	5.8	5.8 ± 0.1	0.02	5.8 ± 0.1	0.02
	4	—	2.0 ± 0.1	0.05	2.0 ± 0.1	0.05
Cu ²⁺	2	3.2	3.2 ± 0.6	0.02	3.2 ± 0.4	0.01
	2	16	16 ± 1	0.06	16 ± 3	0.19
	4	—	1.7 ± 0.6	0.03	1.6 ± 0.8	0.04
Ag ⁺	3	1	1.0 ± 0.3	0.30	—	—
	3	5	4.9 ± ± 0.1	0.02	—	—
	5	—	(5.0 > 0.6) · 10 ⁻³	0.12	—	—

Concentration (ppm): Fe(III), 22.4 (1); Fe(II), 560 (3); 1.8 (4); Co(II), Ni(II), 5.9 (2); Cu(II), 64 (3); 2.0 (4); Ag(I), 0.005 (5).
 $P = 95\%$, $n = 5$.

can proved that the complex with the ratio Ag:Phen = 1:1 is formed on the surface of Phen–SG.

The dependencies of Ag(I) adsorption onto Phen–SG on the mass of the sorbent and the volume of solution can be described by following equations: $y = a + b \cdot m - c \cdot m^2$ and $y = a - b \cdot V$. The values of a , b and c are shown in Table 2.

3.5. Application of modified and unmodified SG for Fe, Cu and Ag ion determinations

The possibility of SG and Phen–SG application to Fe, Cu and Ag ion determination in water has been studied.

3.5.1. Fe(II) determination

The concentration of Fe(III) in natural water is > 100 times more than that of Fe(II) [14]. Our investigation has shown that both Fe(Phen)₃³⁺ and Fe(Phen)₂²⁺ have been adsorbed onto SG simultaneously. So Fe(III) interfered with Fe(II) detection. Unloaded SG can be used to the sum concentration of Fe ions determination in water after reduction of Fe(III) to Fe(II) with ascorbic acid.

Phen–SG adsorbed only Fe(II) in the presence of citrate ions. So this sorbent has been applied to Fe(II) detection in the presence of Fe(III).

The colour scale on the base of Phen–SG for visual test determination of Fe(II) in the range of 3–50 µg per sample was obtained. It was prepared by Fe(II) adsorption onto loaded SG from distilled water contained 0, 6, 10, 30 and 50 µg Fe. The scale has been stable for more than 4 months. This sorbent can also be used for visual detection of the sum concentration of Fe ions in solution (when citrate ions are absent) after reduction of Fe(III) with ascorbic acid.

The adsorption reflectance spectrophotometric methods for this purpose were developed, too.

3.5.2. The sum concentration of Fe ion determination in water by using SG

The calibration graph was linear in the range 0.02–10 ppm. The calibration equation was: $R = 0.33 + 1.5 \cdot 10^{-2} C_{\text{Fe}^{2+}}$, (µg per sample), $r = 0.975$. The detection limit was 0.012 ppm (100 ml of the sample solution).

The sample of natural water (100 ml) with the addition of 1 ml saturated solution of ascorbic acid, 10 ml 15 mM Phen, 10 ml buffer solution (pH 5.5) was been stirred with 0.2 g SG for 10 min.

3.5.3. The Fe(II) determination in water by using Phen–SG

The calibration graph was linear in the range 0.1–15 ppm, calibration equation was: $R =$

$0.31 + 1.3 \cdot 10^{-2} C_{\text{Fe}^{2+}}$, (μg per sample), $r = 0.985$. The detection limit was 0.08 ppm (20 ml sample solution). It was shown that 100 times the quantity of Fe(III) in the presence of citrate ions does not interfere with the Fe(II) determination.

The sample of natural water (20 ml) with the addition of 0.2 ml 0.3 M K_3Cit and 0.2 ml buffer solution (pH 5.5) was been stirred with 0.2 g of Phen-SG mechanically for 10 min.

In both cases the sorbents were filtered, dried at room temperature and the sum of the concentration of Fe was determined by diffusion reflectance spectroscopy ($\lambda = 514$ nm).

The results of Fe(II) determination in the model solutions and natural water are shown in Table 3. The content of Fe ions in natural water was controlled by the spectrophotometric method with Phen [14]. It was found that Fe(II) content was 1.8 ± 0.6 ppm.

3.5.4. Cu(II) determination

The colour scale for the Cu(II) visual test determination in the range 15–320 μg per sample was developed. It was prepared by adsorption of Cu(II) onto Phen-SG from 0.2 M ammonium solution contained 0, 30, 50, 200 and 320 μg Cu. The scale has been stable for more than 4 months.

3.5.5. Cu(II) determination in water by using Phen-SG, SG and diffusion reflectance spectroscopy

The calibration graphs were linear in the range 0.04–32 ppm (SG) and 0.03–16 ppm (Phen-SG). The calibration equations were: $R = 0.03 + 0.25 \cdot 10^{-2} C_{\text{Cu}^{2+}}$, (μg per sample), (SG, $r = 0.993$); $R = 0.01 + 0.56 \cdot 10^{-2} C_{\text{Cu}^{2+}}$, (μg per sample), (Phen-SG, $r = 0.995$). The detection limit was 0.04 ppm (200 ml sample solution) using SG and 0.03 ppm (100 ml sample solution) using Phen-SG.

It is known [10] that Ni(II) and Co(II) form complexes with ammonia and can be adsorbed onto SG and Phen-SG. So their influence on the Cu determination was studied. It was shown that Ni(II) and Co(II) do not influence the

Cu(II) determination at a concentration of $\leq 10^{-4}$ mol l^{-1} (Phen-SG) and $\leq 3 \times 10^{-5}$ mol l^{-1} (SG).

The sample of natural water (100–200 ml) buffered to pH 8.8 with ammonium buffer was been stirred with 0.5 g of SG or Phen-SG mechanically for 10 min. In both cases the sorbents were filtered, dried at room temperature and than content of Cu was determined by diffusion reflectance spectroscopy at 685 nm (SG) and 715 nm (Phen-SG).

The results of Cu(II) determination in different types of water are shown in Table 3. The content of Cu(II) in natural water was determined by the atomic absorption method was 2.0 ppm [18].

3.5.6. Ag(I) determination

The colour scale for the visual test determination of Ag(I) in water in the range 0.5–50 μg per sample was developed. It was prepared by adsorption of Ag(I) from 0.02 mM BPR solution (pH 2) contained 0, 1, 5, 25, 50 μg of Ag. The scale has been stable for more than 4 months.

The diffusion reflectance spectroscopic method for Ag(I) determination was developed. The calibration graph was linear in the range 0.05–1.1 ppm. The calibration equation was: $R = 0.2 + 3.24 \cdot 10^{-2} C_{\text{Ag}^+}$, (μg per sample), ($r = 0.998$). The detection limit was 0.003 ppm (200 ml sample solution). The 10 times Cu(II) and 100 times Fe(III) quantities do not interfere with Ag(I) adsorption in presence of EDTA. This method was applied for Ag(I) determination in mineral water.

The samples of mineral water (200 ml) was mixed with 10 ml 0.1 mM BPR, 5 ml 0.25 mM EDTA, 5 ml 17% urotropin, and 0–5 ml 0.04 mM Ag(I) and stirred mechanically with 0.5 g Phen-SG for 10 min. Sorbents were dried at room temperature for 24 h. Ag(I) content in water was determined by use diffusion reflectance spectroscopy ($\lambda = 560$ nm). The results of Ag(I) determination in the model solutions and the mineral water “Cylushcha” are shown in Table 3. The content of Ag(I) in the mineral water determined by the atomic absorption method was 0.005 ppm [18].

References

- [1] G.D. Brykina, D.O. Marchenko, O.A. Shpygun, Zh. Anal. Khim. 50 (1995) 484 (in Russian).
- [2] R.F. Gur'eva, S.B. Savvin, Zh. Anal. Khim. 52 (1997) 247 (in Russian).
- [3] O.P. Shvoeva, V.P. Dedkova, A.G. Gitlits, S.B. Savvin, Zh. Anal. Khim. 52 (1997) 89 (in Russian).
- [4] S.B. Savvin, A.V. Mikhaylova, Zh. Anal. Khim. 51 (1996) 49 (in Russian).
- [5] K. Terada, K. Morimoto, T. Kiba, Anal. Chim. Acta 116 (1980) 127.
- [6] J.W. O'Laughlin, Anal. Chem. 54 (1982) 178.
- [7] V.N. Zaytsev, A.K. Trofimchuk, Ukr. Khim. Zh. 50 (1984) 1126 (in Russian).
- [8] O.A. Zaporozhets, O.M. Gawer, V.V. Sukhan, Uspekhi Khim. 66 (1997) 702 (in Russian).
- [9] E. Jungreis, Spot Test Analysis, Chemical, Environmental, Forensic, and Geochemical Applications, Wiley, New York, 1985.
- [10] R.M. Smith, A.E. Marthell (Eds.), Crystal Stability Constants, vol.2, Amines, Plenum, New York, 1975, p. 251.
- [11] Methods of Analysis of Pure Chemical Reagents, Chemistry, Moscow, 1984.
- [12] O.M. Petrukhin (Ed.), Handbook of Electrode Technology Orion Research, Mir, Moscow, 1986, 231 p. (in Russian).
- [13] O. Zaporozhets, O. Gawer, V. Sukhan, Conf. Papers, Int. Congr. on Analytical Chemistry, vol. 2, Moscow, Russia, 15–21 June 1997, p. N68.
- [14] G.S. Fomin, Water, Inspection of Chemical, Bacteriological and Radiation Safety according to International Standards, Encyclopedical Handbook, Protector, Moscow, 1995 (in Russian).
- [15] J. Inczedy, Analytical Applications of Complex Equilibria, Akademiai Kiado, Budapest, 1976.
- [16] G.A. Makharadze, G.M. Varshal, G.D. Sulatashvili, Izv. Akad. Nauk GSSR Khimia, 9 (1983) 316 (in Russian).
- [17] B.W. Bailey, R.M. Dagnall, T.S. West, Talanta 15 (1968) 107.
- [18] Yu. Yu. Lur'e, Analytical Chemistry of Industrial Waste Water Khimia, Moscow, 1984 (in Russian).

Microcoated wire sensors for the determination of anticancer drugs cyclophosphamide and ifosphamide in the presence of their degradates

Saad S. Hassan ^a, Mohamed M. Amer ^{b,*}, Soheir A. Abd El-Fatah ^b,
Amira M. El-Kosasy ^b

^a Chemistry Department, Faculty of Science, Ain Shams University, Ain Shams, Egypt

^b Analytical Chemistry Department, Faculty of Pharmacy, Cairo University, P.O. Box 11562, Kasrel Aini Cairo, Egypt

Received 25 August 1997; received in revised form 4 December 1997; accepted 8 December 1997

Abstract

The construction and electrochemical response characteristics of poly (vinyl chloride) and poly (vinyl chloride) carboxylate membrane sensors for the determination of cyclophosphamide and ifosphamide are described. Based on the formation of an ion-pair complex between the drug cation and sodium tetraphenylborate, two poly (vinyl chloride) sensors, namely a cyclophosphamide membrane sensor and ifosphamide membrane sensor were fabricated. They show a linear response for both drugs over the concentration range 10^{-2} – 10^{-4} M with cationic slopes of 56 and 54.6 mV per concentration decade, for sensor 1 and sensor 2, respectively. Based on the interaction between the drug solution and the dissociated COOH groups in the poly (vinyl chloride) carboxylate, sensor 3 was fabricated. It shows a linear response for both drugs over the concentration range 10^{-3} – 10^{-5} M with a cationic slope of 49.7 mV per concentration decade. The direct potentiometric determination of cyclophosphamide and ifosphamide in their pharmaceutical preparations using the proposed sensors gave average recoveries of 101.3 ± 0.6 , 100.8 ± 10.7 and $102.0 \pm 11.0\%$ for the sensors 1, 2 and 3, respectively, which compares reasonably well with the data obtained using the British Pharmacopoeial method (1993). Sensors 1 and 2 were also used to follow up the stability of the drugs studied in the presence of their degradates. These degradation products have no diverse effect on the responses of sensors 1 and 2. © 1998 Elsevier Science B.V. All rights reserved.

Keywords: Cyclophosphamide; Ifosphamide coated wire sensor; PVC matrices; PVC-COOH matrices

1. Introduction

Cyclophosphamide (bis-(2-chloroethyl) amino perhydro-2H-1,3,2-oxazaphosphorine-2-oxide) and its isomer ifosphamide (3-(2-chloroethyl) 2-

chloroethylamino perhydro-2H-1,3,2-oxazaphosphorine-2-oxide) have been used clinically as useful anticancer drugs for more than 30 years [1].

The British [2], Indian [3] and Egyptian [4] pharmacopoeia methods for the determination of cyclophosphamide are based on the monitoring of its phosphorus content via titrimetric procedures.

* Corresponding author. Fax: +20 2 3624105.

The USP [5] recommended assays based on liquid and gas chromatographic techniques for determination of cyclophosphamide and ifosphamide, respectively.

A variety of methods have been also reported for the determination of the two drugs studied and their metabolites. Original studies used nitrobenzylpyridine for the spectrophotometric determination of cyclophosphamide [6]. Other spectrophotometric methods based on the formation of chromogenic species with benzidine [7], cobalt thiocyanate [8] and nitrous acid [9] have been suggested. Infra red [10], nuclear magnetic resonance [11], mass spectrometry [12], polarography [13], flow injection [14], fluorimetry [15,16], analysis via its chloride [17] and phosphorus content [18,19], thin layer chromatography [20,21], gas chromatography [22–24] and high pressure liquid chromatography [25,26] have been also recommended. Only one potentiometric procedure [27] has been reported for the determination of cyclophosphamide using a chloride ion-selective electrode.

Tetraphenylborate was reported as a famous ion exchanger [28] and as a direct titrant [29] for about 17 basic drugs. It has been used in the formation of many sensors [30]. In the present study, it has been found that both cyclophosphamide and ifosphamide react with tetraphenylborate with the formation of water insoluble ion association complexes. The high lipophilicity and remarkable stability of these complexes suggested their use as electroactive materials in PVC matrix membrane sensors for the determination of the two drugs studied, selectively, in the presence of their nine degradation products. The major degradates have been shown to be *N*-(2-hydroxyethyl)-*N*-(3 hydroxypropyl) ethylenediamine, phosphorylated ammonium ion, bis(2-chloroethyl) ammonium chloride, chloride ion and phosphate ion [21,25,31,32].

Another simple and inexpensive procedure for the fabrication of coated wire microelectrodes has been developed using PVC-COOH and plasticizer in the ratio 70:30% as the electroactive membrane.

The advantages of potentiometric sensors is their simplicity, low cost, fast response, wide pH range and applicability to turbid and coloured

solutions, combined with the wide medical use of microsized coated wire design, to form the three investigated potentiometric sensors that offer highly sensitive, selective and a convenient technique for the determination of cyclophosphamide and ifosphamide in their pharmaceutical preparations as well as in the presence of their related substances and degradation products.

2. Experimental

2.1. Apparatus

Potentiometric measurements were made with an Orion Digital ion analyser (model 720A) and an Orion 90–02 Ag/AgCl double junction reference electrode containing 10% w/v KNO₃ in the outer compartment. pH adjustment was made with an Orion 91–20 combination glass electrode. A platinum wire of 1.0 mm diameter was used for the ion selective electrodes.

2.2. Reagents

All chemicals were of analytical reagent grade and bidistilled deionized water was used throughout. Cyclophosphamide and ifosphamide were obtained from Asta Pharma, with a purity of not less than 98% and assayed by the BP (1993) pharmacopoeia method to contain 99.6 ± 1 and

Table 1
Response characteristics for the cyclophosphamide-TPB, PVC membrane sensor (sensor 1), Ifosphamide-TPB, PVC membrane sensor (sensor 2) and PVC-COOH membrane sensor (sensor 3)

Parameter	Sensor 1	Sensor 2	Sensor 3
Slope (mV per decade)	56.0	54.6	49.7
Response time (min)	0.5–1	0.5–1	1–2
Working pH range	4–7	4–7	4–7
Concentration range (M)	10 ⁻² –10 ⁻⁴	10 ⁻² –10 ⁻⁴	10 ⁻³ –10 ⁻⁵
Stability (days)	12	12	10
Average recovery ^a (%)	101.31	100.84	101.64
R.S.D. ^a	0.62	0.65	1.43

^a Results of five determinations.

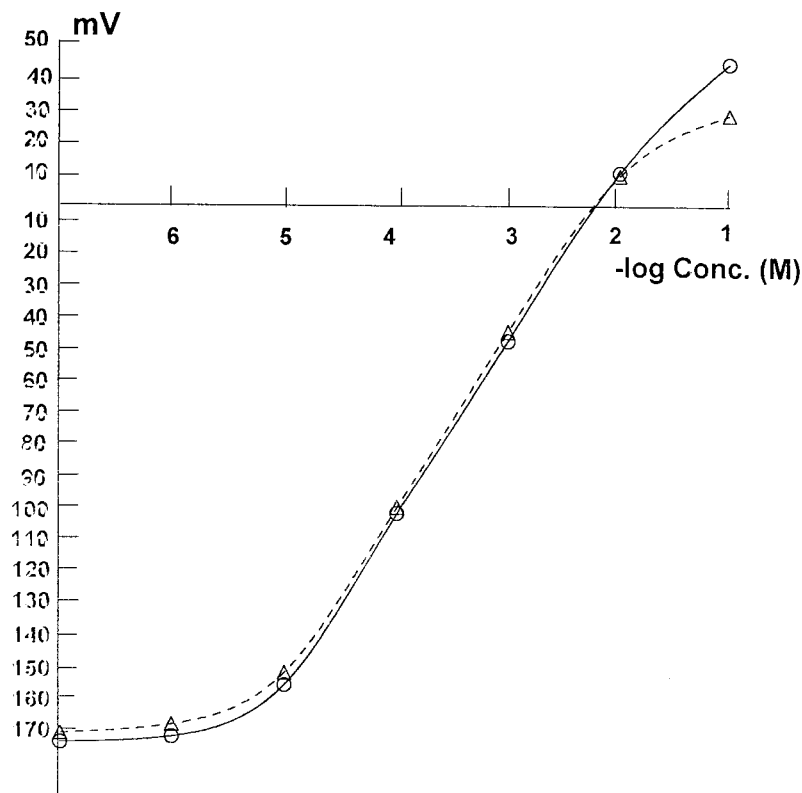


Fig. 1. Profile of the potential in mV to the $-\log$ concentrations of cyclophosphamide sensor 1 (○—○) and ifosphamide using sensor 2 (△---△).

99.6 + 0.9% cyclophosphamide and ifosphamide, respectively.

Aqueous 10^{-3} – 10^{-5} M of the drug solutions were freshly prepared by accurate dilutions of a standard 10^{-2} M stock drug solution. Poly (vinyl chloride) (PVC) (molecular weight \cong 1000, poly (vinyl chloride) carboxylate (PVC-COOH), sodium tetraphenylborate (TPB), tetrahydrofuran (THF), a solvent with a purity of 99%, dioctylphthalate (DOP) and nitrophenyl octyl ether (NPOE), plasticizers with a purity of 99%, 1 M hydrochloric acid.

2.3. Procedures

2.3.1. PVC membrane sensors 1 and 2

We acidified 5 ml 10^{-2} M aqueous drug solution with two drops of 1 M hydrochloric acid and mixed them with the saturated aqueous solution

of TPB. We filtered the resultant precipitate, washed it with cold water, dried it at room temperature and ground it to a fine powder, forming the ion-pair complex. Elemental analysis and infrared data confirmed the formation of 1:1 complexes.

In a glass Petri dish (5 cm diameter), we thoroughly mixed 10 mg of the ion-pair complex with 0.35 ml dioctylphthalate and then added 0.19 g PVC. The mixture was dissolved in 5 ml THF, then the Petri dish was covered with a filter paper and left to stand for 1 h to allow slow evaporation of the solvent, producing the master thick PVC solution.

We removed the cover for a length of about one cm at both ends of an insulated platinum wire. One end of the wire was immersed in the previously prepared PVC solution and was left to stand for 10 min to allow complete air drying,

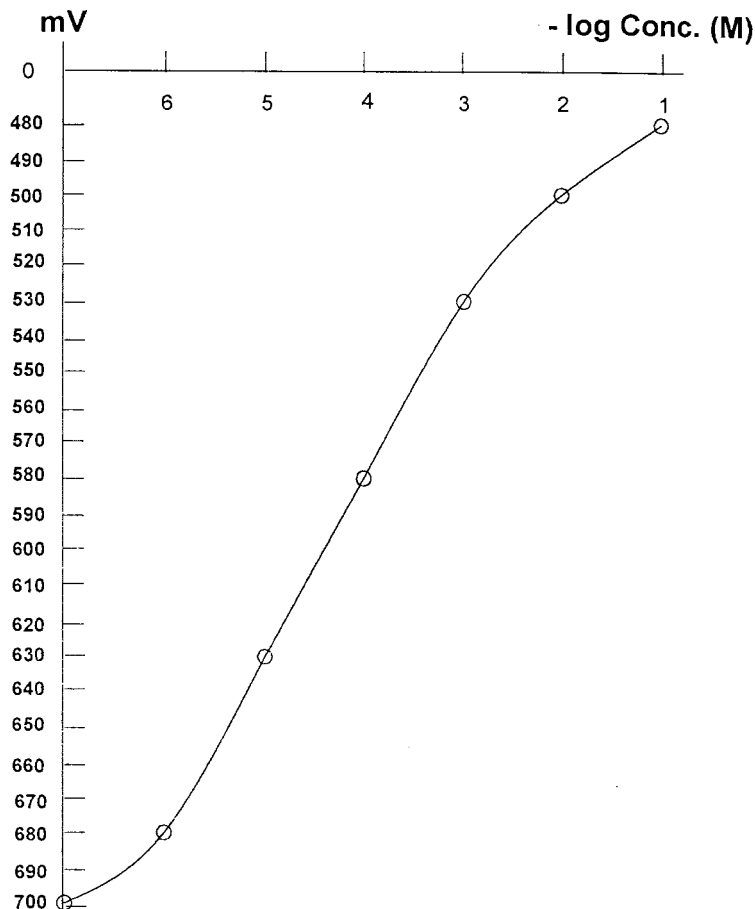


Fig. 2. Profile of the potential in mV to the $-\log$ concentrations of either cyclophosphamide or ifosphamide using sensor 3.

forming a thin membrane around the wire end. We repeated the immersing and air drying until we obtained a globular membrane of about 3 mm diameter around the wire end. The resultant coated wire membrane sensor had to be conditioned by soaking in 10^{-2} M drug solution for 3 h and had to be stored in the same solution when not in use.

2.3.2. PVC-COOH sensor 3

In a glass Petri dish, we thoroughly mixed 0.2 g PVC-COOH with 0.09 ml NPOE then dissolved the mixture in 1.65 ml THF. The Petri dish was covered with a filter paper and left to stand for 10 min to allow slow evaporation of the solvent, producing a thick solution. We constructed a

globular membrane of about 3 mm diameter around the platinum wire end as described above. The resultant coated wire membrane had to be conditioned by soaking in 10^{-2} M drug solution for 24 h and had to be stored in the same solution when not in use.

2.3.3. Sensors calibration

We calibrated the conditioned sensors with aqueous drug solutions in the range from 10^{-2} to 10^{-6} M by immersing the coated wire membrane sensor and the Orion double junction Ag/AgCl reference electrode in the drug solution, allowing them to equilibrate whilst stirring and recording the emf readings within ± 1 mV. We stored the membrane sensor in deionized bidistilled water

between measurements. We plotted the mV–concentration profile.

2.3.4. Potentiometric titration of phosphamides

We transferred 2, 4, 6, 8 and 10 ml aliquots of 10^{-3} M drug to 50 ml beakers. The sensor to be investigated, in conjunction with the Ag/AgCl reference electrode, were immersed in the solution and titrated with 10^{-3} M standard tetraphenyl borate solution. We recorded the mV readings after each addition of the titrant.

2.3.5. Application to pharmaceutical formulations

2.3.5.1. Endoxan vial and Holoxan vial. The contents of 10 vials were mixed and a quantity of the mixed contents corresponding to about 0.279 g were transferred to a 100 ml volumetric flask and filled to the mark with water to prepare a 10^{-2} M aqueous solution of cyclophosphamide or ifosphamide in the case of Endoxan and Holoxan vial, respectively. They were finished as in Section 2.3.3.

2.3.5.2. Endoxan tablet. We mixed and powdered 20 tablets and calculated the average weight of one tablet. A quantity corresponding to about 0.279 g was transferred to a 100 ml volumetric

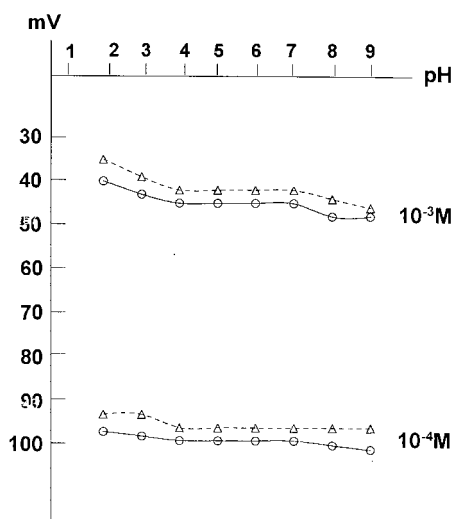


Fig. 3. Effect of pH on the responses of sensor 1 (○—○) and sensor 2 (△---△).

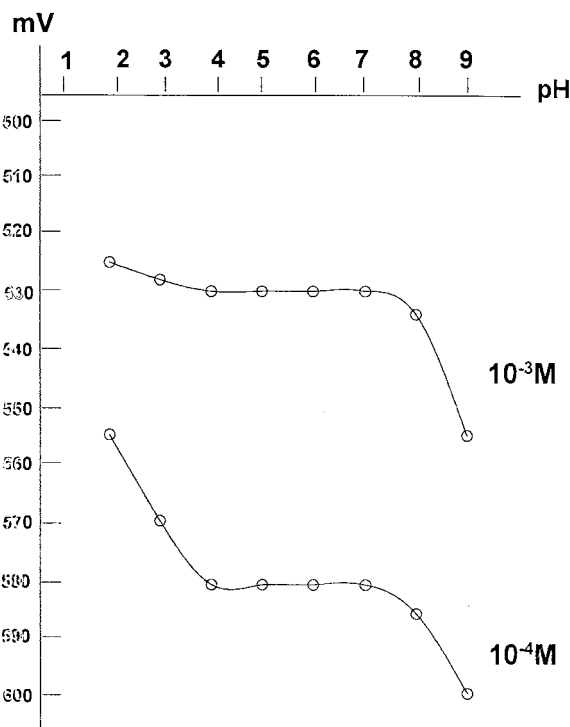


Fig. 4. Effect of pH on the response of sensor 3.

flask and filled to the mark with water to prepare a 10^{-2} aqueous solution of cyclophosphamide. It was finished as in Section 2.3.3.

2.3.5.3. Stability study. Degraded samples of 10^{-3} M cyclophosphamide and ifosphamide solutions were prepared by refluxing an aqueous solution for 6 and 10 h, respectively, followed by cooling. A 10^{-3} M standard drug solution was mixed with its degraded sample in different ratios. The emf of these laboratory prepared mixtures were measured and the recorded results were compared with the calibration plots.

3. Results and discussion

The increasing importance of chemotherapeutic drugs in cancer treatment makes the manufacture of microzised sensors an area of interest. The advantages they offer over conventional electrodes are well known [33], their reduced diffusion

Table 2

Determination of cyclophosphamide (CP) and ifosphamide (IF) in some pharmaceutical preparations using the three proposed sensors

Trade Name and source	Active ingredi-ent	Drug recovery ^a (%)			
		Sensor 1	Sensor 2	Sensor 3	B.P. (1993)
Endoxan vial Asta Pharma, Batch No. 082071	100mg CP/vial	100.2 ± 0.46		101.3 ± 0.87	99.2 ± 0.60
Endoxan tablet, Asta Pharma, Batch No. 099732	50 mg CP/ tablet	100.5 ± 0.55		100.5 ± 0.86	99.1 ± 0.70
Holoxan vial, Asta Pharma, Batch No. 092164	2 g IF/vial		100.7 ± 0.61	100.7 ± 0.73	99.5 ± 0.35

^a Average of five measurements.

Table 3

Recoveries of cyclophosphamide and Ifosphamide in sysathetic mixtures with their degraded samples

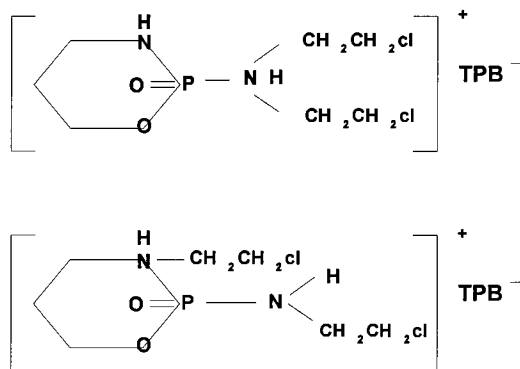
Ratio drug:degraded sample ^a	Drug recovery ^b (%)			
	Sensor 1	Sensor 2	Sensor 3	USP 1995 HPLC method
100:0	100.0	100.0	100.0	100.0
90:10	101.3	100.4	99.8	101.2
80:20	100.5	101.1	100.2	101.3
70:30	100.8	100.4	104.1	99.9
60:40	101.0	99.6	114.1	100.7
50:50	100.7	100.0	115.3	100.6
40:60	108.5	109.8	119.6	101.2
30:70	108.1	109.8	149.8	100.7
20:80	108.2	109.8	183.2	98.9
10:90	110.0	109.8	186.6	100.4

^a The drug solutions were always 10^{-3} M, aqueous.

^b It is a mean of five determinations. Maximum deviation from it is 1.11.

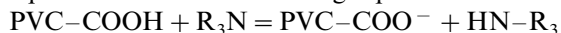
layer allows fast response, their small currents lead to low susceptibility to ohmic loss and thus, enable their use in highly resistive biological media and their small physical size allows exploitation of microscopic domains.

In the present work, the microsized coated wire membrane sensors were fabricated with either PVC or PVC-COOH as a polymer matrix. In the PVC sensors fabrication, it was found that both cyclophosphamide and ifosphamide which contain a tertiary amino group, behave as cations in acidic media. This fact suggests the use of anionic type of ion exchangers, tetraphenylborate with its low solubility product and suitable grain size was found to be the optimum for the formation of 1:1 hydrophobic ion association complexes with the two studied drugs of the type shown below.



In the PVC-COOH sensor fabrication, it was found that the tertiary amino groups in the two drug solutions studied undergo some acid–basic interactions with the dissociated carboxylic

groups of the PVC-COOH till reaching chemical equilibria as in the following equation:



Making use of the two recommended properties of PVC-COOH, that is the partial dissociation and the high adhesion, the proposed sensor 3 was simply fabricated without need of ion association complex formation.

Both PVC and PVC-COOH act as regular support matrices for the membrane and reproducible traps for the ions sensed, but their use creates a need for a mediator [34]. In the present investigation, DOP was found to be the optimum available mediator for the PVC membrane sensors. It plasticizes the membrane, dissolves the ion- association complexes and adjusts both of the membranes permittivity and ion-exchanger sites mobility to give the highest possible selectivity and sensitivity. Except for nitroaromatic mediators which had the same effects as DOP, other mediators such as dibutylsebacate, tricresylphosphate and castor oil gave noisy responses with little discrimination for concentration changes (slopes 42, 28 and 8 mV per decade drug concentration, respectively). On the other hand, NPOE, was found to be the optimum available mediator for the PVC-COOH membrane sensor. The use of nonpolar mediators such as DOP leads to insufficient selectivity differences in the sensor response towards foreign cations. The quantity of the mediator used was found to be a critical factor for the reproducibility and life time of sensor 3; increasing the mediator ratio more than 30% led to a decrease in the highly adhesive property of the PVC-COOH polymer giving the membrane limited life time and nonreproducible results.

Electrochemical performance characteristics of the proposed sensors were systemically evaluated according to IUPAC standards [35].

Table 1 shows the results obtained over a period of three months for 10 different assemblies of each sensor. Typical calibration plots are shown in Figs. 1 and 2. The sensors displayed constant potential readings within ± 1 mV from day to day and the calibration slopes did not change by more than 1 mV per decade over a period of 12 and 10 days for the PVC and PVC-COOH sensors, respectively.

In measurements with the three investigated sensors, the experimental conditions were studied to reach the optimum. A pH value within the range 4–7 was found optimum from the point of view of both sensor function and the chemical form of the test solution, i.e. cyclophosphamide and ifosphamide being in the cationic form in acidic media. Figs. 3 and 4 shows the potential pH profiles for 10^{-3} and 10^{-4} M drug solutions. Above pH 8, the potentials displayed by the sensors sharply decreases due to formation of non-protonated cyclophosphamide and ifosphamide. Below pH 4, the potentials displayed by the sensors were noisy and unbalanced due to sensor shocking. It is apparent that the sensors responses are fairly constant in acetate buffer solutions of pH 4–7.

Although the three suggested sensors exhibit a slight gradual increase in their potentials as the temperature increases in the range 25–45°C, the limit of detection and response time do not significantly vary due to change of temperature, indicating reasonable thermal stability of the PVC and PVC-COOH membranes up to 35°C.

It is clear that both PVC and PVC-COOH polymers were affected similarly by pH and temperature.

Although, the investigated coated wire sensors consist of membranes of either PVC/sensing system/mediator or PVC-COOH/mediator in ratios 34:2:64 or 70:30%, respectively, i.e. without an internal reference system, there is a confident view that the coated wire sensors have an inbuilt reference system which is attributed to the permeability of PVC and PVC-COOH to both water and oxygen and, thus, setting up an oxygen electrode at the wire membrane interface to function as an internal reference system [33].

The reliability of the proposed membrane sensors for the quantification of cyclophosphamide and ifosphamide was assessed by determining 10^2 – 10^{-4} M on using sensors 1 and 2 and 10^{-3} – 10^{-5} M on using sensor 3 on the pure powder of the drugs using both the calibration graph and the standard additions method. The results showed average recoveries of 101.3 ± 0.6 , 100.8 ± 0.7 and $102.0 \pm 1\%$, respectively. Typical S-shape titration curves were obtained using sen-

sors 1 and 2, the equivalence points are reproducible. The excellent agreement between the results obtained for the determination of a series of vials and tablets by both the proposed potentiometric procedures and the B.P. (1993) method (Table 2), suggests the successful application of the proposed methods for the pharmaceutical formulations.

Although, the sensors investigated failed in the differentiation between cyclophosphamide and ifosphamide, they succeeded in the quantification of either drug in presence of their degradates and related substances.

The potentiometric selectivity coefficients of the proposed sensors were calculated in presence of the nine recommended degradates of either drug [21,25,29] and also in presence of some organic and inorganic related substances, using separate technique [36]. The results revealed that PVC membrane sensors 1 and 2 displayed higher selectivity and lower response for the potentially interfering species than the PVC-COOH sensor. Sensors 1 and 2 were at least 10–100 times more selective than sensor 3.

It was reported that cyclophosphamide completely disappeared on exposing it to 0.1 M unbuffered aqueous solution to refluxing for 6 h. Ifosphamide was reported to have a slower disappearance rate; it needs refluxing for 10 h to completely disappear, however, its degradation products are similar to that derived from cyclophosphamide [32].

Table 3 shows the results obtained with synthetic mixtures containing different ratios of drug with its degraded sample. The results show that the proposed sensors 1 and 2 can be successfully used for the determination of intact cyclophosphamide and ifosphamide in the presence of up to 50% of their degradates.

References

- [1] J. Moore, *Clin. Pharmacokinet.* 20 (1991) 194–208.
- [2] The British Pharmacopoeia, HMSO, London, 1993.
- [3] The Indian Pharmacopoeia, 3rd ed., Controller of Publications, Delhi, 1984, p. 144.
- [4] The Egyptian Pharmacopoeia, 3rd ed., General Organization for Government Printing Office, 1984.
- [5] The United States Pharmacopoeia, 22nd ed., United States Pharmacopoeial Convention, Rockvill, MD, 1995.
- [6] C.M. Bagley, F.W. Bostick, V.D. De Vita, *Cancer Res.* 33 (1973) 226–235.
- [7] I.V. Kozolv, N.E. Bernshtein, B.N. Aktual, *Vop. Farm.* 6 (1970) 61–65.
- [8] M. Hirata, H. Kagaua, M. Baba, *Shiongi Res. Lab.* 17 (1967) 107–112.
- [9] Z.H. Mohamed, S.M. Amer, A.M. Al-Kousasy, *J. Pharmaceut. Biomed. Anal.* 12 (9) (1994) 1131–1136.
- [10] N.E. Kozolv, V.G. Shezhnera, *Farmatsiya (Moscow)*, 29(1) (1979) 33–34; through *Chem. Abst.* 92 (1980) 185982n.
- [11] A. Swanson, T. Alm, *Arial Univ. Microfilms Int.*, Order no. DA8615138, 1985, p. 120; through *Chem. Abst.* 106 (1986) 101986a.
- [12] A. Fox, J. Lirely, J. Liq, *Chromatogr. Relat. Technol.* 19 (7) (1996) 1047–1059.
- [13] F.M. El-Tarras, M.M. Elliathy, N.B. Tadros, M.M. Amer, *J. Drug Res.* 14 (12) (1983) 79–88.
- [14] S. Masao, N. Tamoko, T. Shoji, *Lyakuhin Kenkyu* 18 (5) (1987) 749–752.
- [15] S. Akira, A. Yashihiro, M. Takitani, *Shajl. Bunsek Kagaku* 32 (4) (1983) 93–100.
- [16] Z.H. Mohamed, S.M. Amer, A.M. El-Kousasy, M.M. Amer, *Anal. Lett.* 28 (4) (1995) 635–647.
- [17] V. Egerts, N. Ozolens, M. Shimanskaya, A. Cebere, *Sinteza, Sb. Statei* (1965) 13–17; through *Chem. Abst.* 64 (1966) 10404a.
- [18] Z.G. Kalugina, L.P. Filippora, L.B. Kristaleva, *Farmatsiya* 26 (5) (1977) 72–74.
- [19] M.M. Amer, Z.H. Mohamed, S.M. Amer, A.M. El-Kousasy, *Egypt. J. Anal. Chem.* 4 (1995) 115–128.
- [20] S. Al Rawithi, A. El-Yazigi, P. Nicholls, *Pharm. Sci.* 1 (4) (1995) 201–203.
- [21] A. Barbara, N. Mering, *Acta Pol. Pharm.* 26 (3) (1972) 263–269.
- [22] G. Momerency, K. Van Cauwenberghe, E. de Bruifin, A. Van Oosterom, S. Highley, P. Harper, *J. High Resolut. Chromatogr.* 17 (9) (1994) 655–661.
- [23] F. Bohnstengel, S. Johnson, U. Hofmann, M. Eichehaum, *J. Chromatogr. Biomed.* 672 (2) (1995) 271–276.
- [24] T. Steger-Hartmann, K. Kuemmerur, J. Scheck, *J. Chromatogr.* 726 (12) (1996) 179–184.
- [25] S. Hill, J. Aexiou, P. Koranagh, E. Livingstone, P. Shaliker, A. Sosic, *Anal. Commun.* 33 (7) (1996) 235–237.
- [26] A. Ichida, T. Okamoto, I. Yuki, Y. Toga, *Chromatographia* 19 (1984) 280–284.
- [27] Z. Jiyuan, H. Qiu, Yaowu Fenxi Zazhi 3 (2) (1983) 105–107.
- [28] P. Kissinger, *Laboratory Techniques in Electroanalytical Chemistry*, chap. 4, Marcel Dekker, New York, 1991.
- [29] A. EI seabi, Y. Beltagey, S. Rida, *J. Drug Res. Egypt* 4 (1972) 61–69.
- [30] G. Moody, J. Thomas, *Selective Ion Sensitive Electrodes*, chap. 1, Merrow Technical Librery, New York, 1971.

- [31] M. Friedman, B. Shlomo, K. Chakrabarti, *J. Am. Chem. Soc.* 87 (21) (1965) 4978–4979.
- [32] G. Zon, S. Ludeman, W. Egan, *J. Am. Chem. Soc.* 99 (17) (1977) 5786–5795.
- [33] G. Moody, J. Thomas, *Ion-Sel. Electrode Rev.* 1 (1) (1979) 8–10.
- [34] H. Freisar, *Ion-Sel. Electrode Anal. Chem.* 1 (1978) 8.
- [35] AUPAC, Analytical Chemistry Division, Commission on Analytical Nomenclature, *Pure Appl. Chem.* 48 (1976) 129.
- [36] International Union of Pure and Applied Chemistry, 67 (3) (1995) 507–518.

Screen-printed voltammetric sensor for TNT

Joseph Wang ^{a,*}, Fang Lu ^a, Douglas MacDonald ^a, Jianmin Lu ^a,
Mehmet E.S. Ozsoz ^a, Kim R. Rogers ^b

^a Department of Chemistry and Biochemistry, New Mexico State University, Las Cruces, NM 88003, USA

^b US Environmental Protection Agency, National Exposure Research Laboratory, Characterization Research Division,
P.O. Box 93478, Las Vegas, NV 89193-3478, USA

Received 6 October 1997; received in revised form 8 December 1997; accepted 9 December 1997

Abstract

Screen-printed carbon electrodes have been developed as disposable voltammetric sensors for 2,4,6-trinitrotoluene (TNT). Thick-film electrodes based on various conventional and modified inks have been compared for this task. The operation is based on placing the selected thick-film carbon sensor in the non-deaerated/quiescent sample and using a fast (< 1 s) and sensitive square-wave voltammetric scan. Different experimental variables have been optimized to yield a detection limit of 200 ppb TNT and a wide linear range. The high selectivity, demonstrated in assays of various untreated environmental samples, is attributed to the facts that the reducible nitro group is rare in nature and that most electroactive organic compounds require higher potentials. The new single-use sensor strips should facilitate the on-site environmental screening of TNT. © 1998 Elsevier Science B.V. All rights reserved.

Keywords: Electrochemical sensor; Explosive detection; Screen-printed electrode; Square-wave voltammetry; TNT

1. Introduction

Because of upsurge in terrorist and criminal activity, there are urgent needs for reliable methods for the detection of explosives such as 2,4,6-trinitrotoluene (TNT) [1]. In addition to forensic or security considerations, such methods should address the environmental and toxicological significance of various explosives. In particular, with the end of the Cold War, the environmental community is confronted with problems of water and

soil on military sites contaminated with explosives.

Cumbersome and expensive instruments based on X-ray imaging or thermal neutral analysis have been introduced recently for the detection of hidden explosives [1,2]. In addition, bench-top instruments based primarily on chromatographic techniques are commonly used for laboratory measurements of explosives in water samples [3,4]. More compact low-cost instruments, coupled to smaller sensing probes, are highly desired for facilitating the task of on-site monitoring of explosives. Although sniffing dogs can provide high portability and selectivity, they are unpredictable

* Corresponding author. Tel.: +1 505 6462505; fax: +1 505 6462649; e-mail: joewang@nmsu.edu

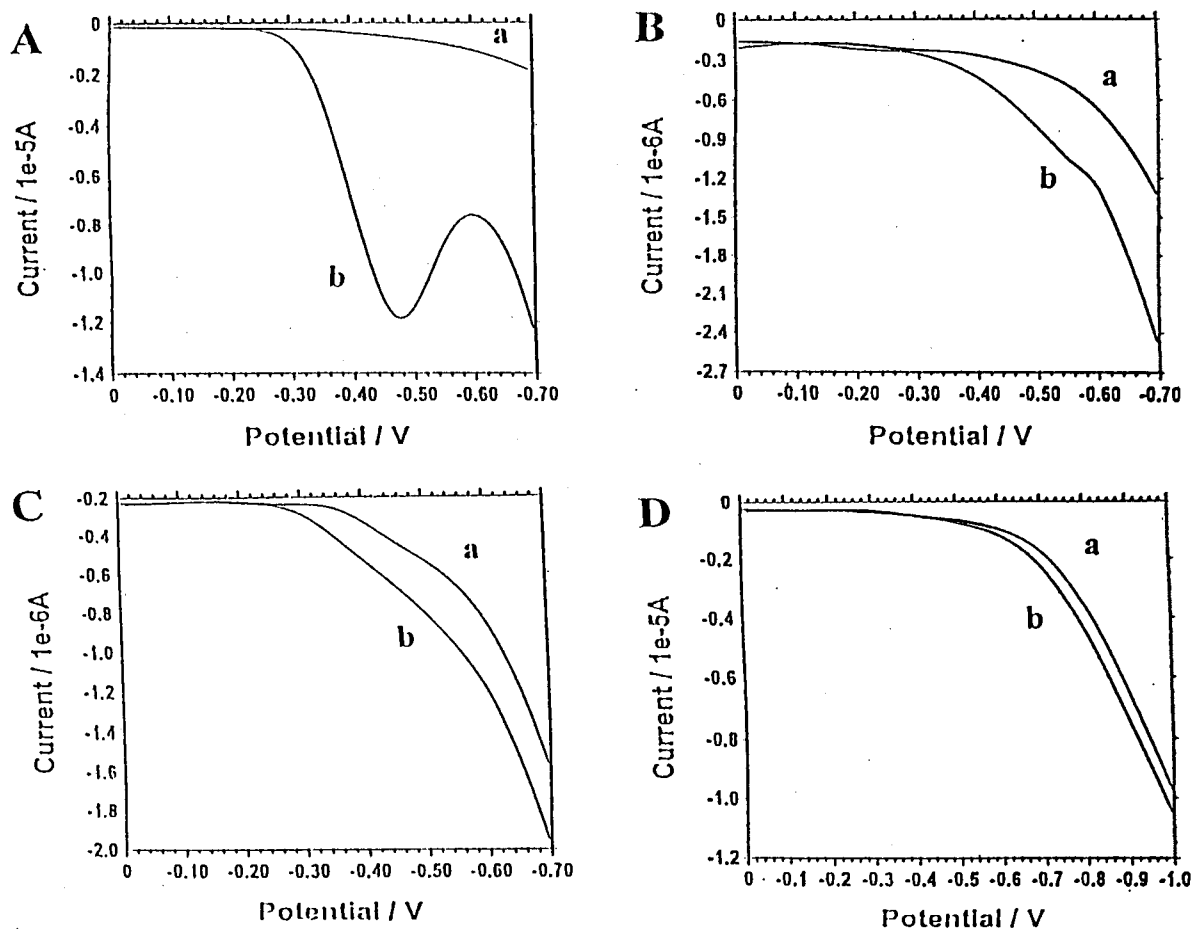


Fig. 1. SWV response for 1 ppm TNT (b), along with blank voltammograms (a) at different screen printed electrodes: carbon (A), gold (B), iridium-dispersed carbon (C) and Ru-dispersed carbon (D). Conditions: amplitude, 25 mV; frequency, 50 Hz; step, 4 mV; quiet time, 2 s; electrolyte, 0.05 M phosphate buffer (pH 6.5).

and require special training. Recent activity at the US Naval Research Laboratory resulted in a portable fiber-optic competitive immunosensor for rapid on-site detection of TNT [5]. Surprisingly, little attention has been given to electrochemical sensing of nitroaromatic explosives, despite their inherent redox activity [4] and the compact nature of electrochemical instruments.

In this paper we describe the characterization and performance of a disposable sensor strip for on-site electrochemical measurements of TNT. The screen-printing (thick-film) technology represents an ideal route for large-scale fabrication of highly reproducible and yet inexpensive electrochemical sensors [6]. While most of

the commercial activity in this direction has focused on 'one-shot' glucose sensors [7], screen-printed electrodes have been shown to be useful for the amperometric biosensing of other metabolites [8] or toxic enzyme inhibitors [9], for decentralized stripping measurements of trace metals [10], or for the specific detection of DNA sequences [11].

In the following sections we will compare various conventional and modified thick-film electrodes for on-site screening of TNT, and will demonstrate the attractive analytical performance accrued from the coupling of disposable carbon strips with rapid square-wave voltammetric (SWV) detection of this important explosive.

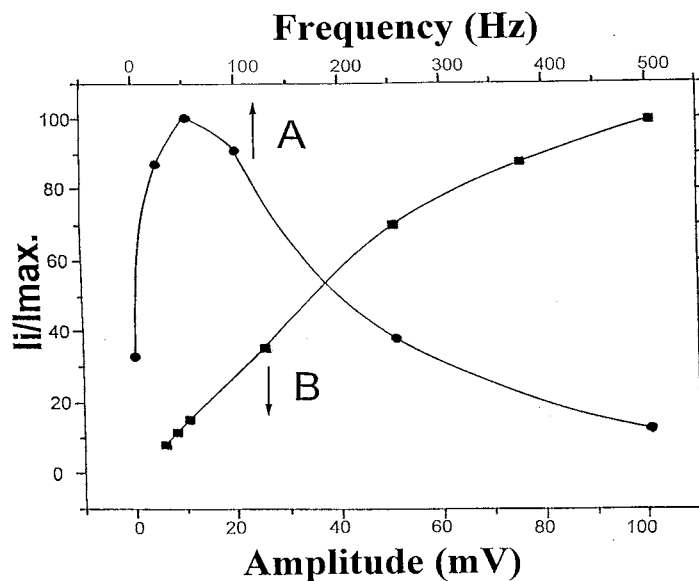


Fig. 2. Effect of the SWV frequency (A) and the amplitude (B) upon the voltammetric response of 10 ppm TNT at the screen-printed carbon electrode. Other conditions as in Fig. 1A.

2. Experimental

2.1. Apparatus

Most experiments were performed using a microprocessor-controlled electrochemical analyzer (Model 620; CH Instruments), interfaced with an IBM personal computer. The AutoLab electrochemical system (Eco Chemie) was used for obtaining the background-corrected voltammograms. SWV measurements were carried out in a 5-ml electrochemical cell (Model VC-2; BAS). The screen-printed electrode, the reference electrode (Ag/AgCl (3 M NaCl), Model RE-1; BAS), and platinum wire auxiliary electrode joined the cell through its Teflon cover.

2.2. Ink preparation

Four different inks were used and compared. These included unmodified carbon or gold inks from Ercon (Ercon G-449 (I) and Exp 44281, respectively), and metal-dispersed carbon inks. These were prepared by thoroughly mixing (for 30 min with a spatula) 1.9 g of carbon ink (Ercon, G-449 (I)) with 100 mg iridium powder (Alfa, 325

mesh, 99.9%) or ruthenium powder (Alfa, 325 mesh, 99.95%) to give a 5%wt. metal loading.

2.3. Screen-printed electrode fabrication

A semi-automatic screen printer (Model TF 100; MPM, Franklin, MA) was used for printing the working electrodes. The inks were printed through a patterned stencil onto 10 cm × 10 cm alumina ceramic plates containing 30 strips (of 3.33 cm × 1.00 cm, as defined by a laser pre/semi cut). The resulting 1 mm × 30 mm printed carbon structures were cured for 30 min at 100°C; the gold ink was cured at 150°C for the same period. An insulating ink (Ercon R-488c1, Green) was subsequently printed on a portion of the plate, to leave 1 mm × 5 mm sections on both ends for defining the working electrode and electrical contact. The insulating layer was cured at 100°C for 30 min.

2.4. Reagents and procedure

All solutions were prepared daily with double-distilled water using reagent-grade chemicals. The TNT stock solution (100 ppm in water) was a gift

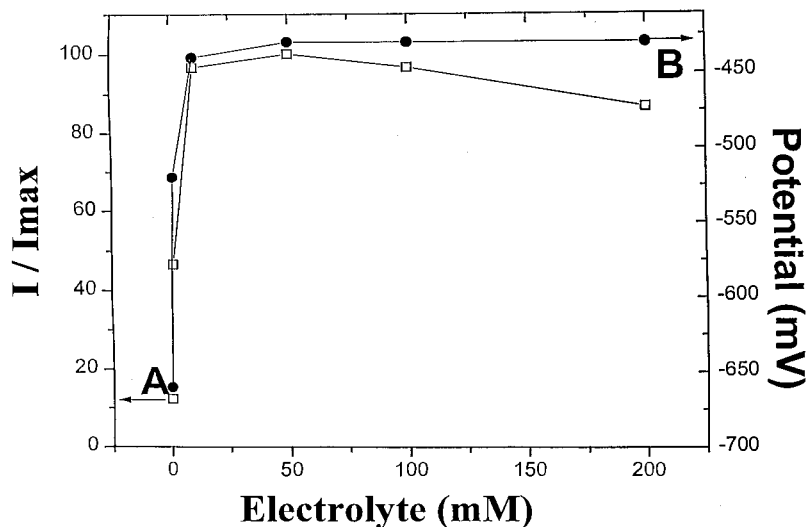


Fig. 3. Effect of the ionic strength upon the SWV response (peak current (A) and potential (B)) of the carbon strip electrode towards 10 ppm TNT. Other conditions as in Fig. 1A.

from Sandia NL. Potassium phosphates (monobasic and anhydrous) were obtained from Sigma, hydrochloric acid from J.T. Baker and acetic acid (glacial) from Fisher Scientific. A potassium phosphate buffer solution (0.05 M, pH 6.5) was employed in most experiments. The river water (Rio Grande) and groundwater samples were collected at Las Cruces (NM) and the Hanford Site (Richland, A), respectively.

All measurements were performed at room temperature, using non-deaerated quiescent solutions and a rapid Osteryoung SWV scan from 0.0 to -0.70V .

3. Results and discussion

Polynitroaromatic compounds, such as TNT, are readily reduced, particularly at various mercury electrodes. Such compounds undergo stepwise reduction processes, involving initial reduction of the nitro groups to a hydroxylamine, followed by conversion to an amine group. While mercury drop [12] or film [4] electrodes have been traditionally used for laboratory measurements of reducible explosive substances, solid-state 'mercury-free' devices should be more attractive for

single-use field-screening applications. Accordingly, we evaluated various conventional and modified screen-printed electrodes as disposable TNT sensors.

Fig. 1b compares square-wave voltammograms for trace (1 ppm) TNT at carbon (A), gold (B), iridium-dispersed carbon (C) and ruthenium-dispersed carbon (D) screen-printed electrodes. All strip electrodes display a single voltammetric peak (at ca. -0.45V), corresponding to the formation of the hydroxylamine moiety. However, only the unmodified carbon strip results in a well-defined response, suitable for such trace measurements. With the other sensors the peak appears as a shoulder on a rising background current (associated with the reduction of dissolved oxygen). Apparently, the metal-dispersed (Ru and Ir) catalytic centers have a more profound effect on the oxygen background than upon the target TNT signal. In view of its favorable signal-to-background characteristics, the screen-printed carbon electrode was used for all subsequent analytical work. The very low oxygen background current of this sensor eliminates the need for a time-consuming deoxygenation step and hence further simplifies practical field operations. Additional reduction peaks were observed at the carbon strip electrode

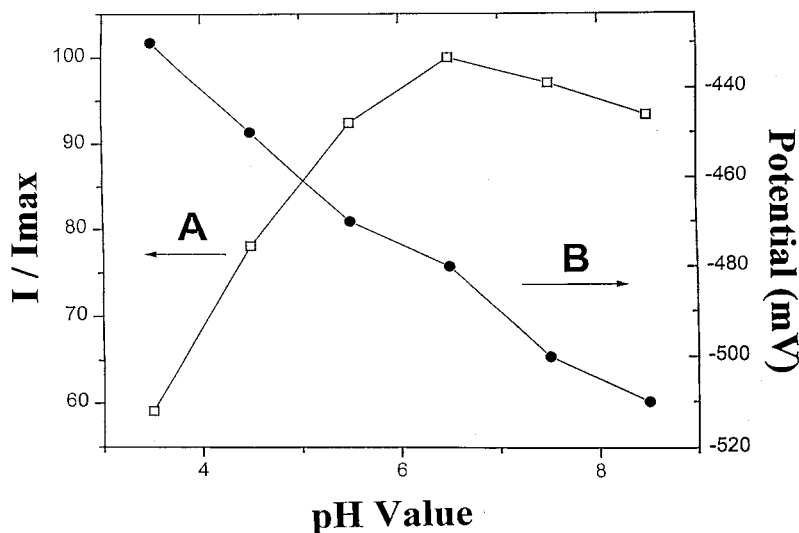


Fig. 4. Effect of solution pH upon the SWV response (peak current (A) and potential (B)) of the carbon strip electrode towards 10 ppm TNT. Other conditions as in Fig. 1A.

upon scanning to more negative potentials (up to -1.1 V). However, due to the high background at these negative potentials all analytical work was focused on the first reduction process at -0.45 V.

The data of Fig. 1 indicate that the combination of carbon strip electrodes with rapid SWV yields an attractive analytical behavior. Besides its high sensitivity and speed, SWV offers higher information content compared to the chronoamperometric measurements commonly employed in connection with screen-printed sensors. The effect of different variables of the SWV waveform was explored for further optimization. Fig. 2A examines the influence of the square-wave frequency upon the response to 10 ppm TNT. The peak current rises sharply with the frequency at first up to 50 Hz, and then decays gradually. The effect of the SWV amplitude (height of square-wave component) is shown in Fig. 2B. The TNT signal increases nearly linearly upon raising the amplitude between 5 and 50 mV, and then more slowly. All subsequent work was thus carried out using an amplitude of 25 mV, a frequency of 50 Hz, and a staircase step height of 4 mV (i.e., less than 5 s for the entire scan). We also attempted to increase the sensitivity by employing a preceding adsorp-

tive accumulation of TNT (i.e., an adsorptive stripping operation). However, only a slight (15%) signal enhancement was observed in connection with a 3 min preconcentration at 0.0 V. Such a stripping approach was abandoned considering also its very slow response time.

Field-screening applications will greatly benefit from the minimization of sample pretreatment. Reduced dependence upon solution variables (such as pH or ionic strength) would assure a minimal sample pretreatment and simplified field operations. Fig. 3 displays the dependence of the SWV response upon the solution ionic strength. As desired, the sensor displays a broad ionic strength independence, with minimal changes in the peak current (A) or potential (B) for phosphate buffer concentrations ranging from 10 to 200 mM. As might be expected, a sharp decrease in the current response and large potential shift are observed without any electrolyte. Environmental water samples commonly contain sufficient natural electrolyte, and hence permit convenient and direct monitoring of TNT (see following sections).

Fig. 4 examines the effect of the pH upon the SWV TNT response. The peak current increases nearly linearly with the pH over the 3.5–5.5

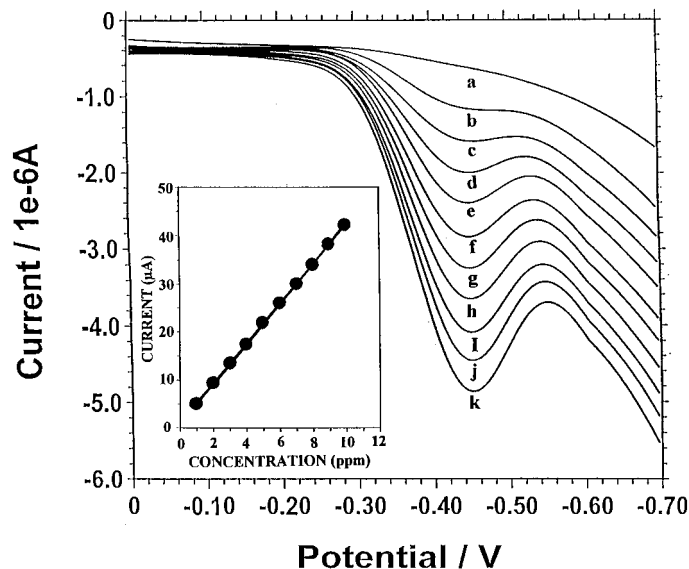


Fig. 5. SWV response of the thick-film carbon sensor to TNT solutions of increasing concentration from 1 ppm to 10 ppm (b–k), along with the background voltammogram (a). Other conditions as in Fig. 1A.

range, and then it starts to level off (A). The nearly pH independence over the 5.5–8.5 range indicates great promise for numerous natural water matrices (with quantitation based on calibration in the given matrix). As expected from the

involvement of protons in the redox reaction, the peak potential shifts negatively (in a nearly linear fashion) upon raising the pH from 3.5 to 8.5 (B).

Fig. 5 displays SW voltammograms for increasing levels of TNT in 1 ppm steps (b–k), along

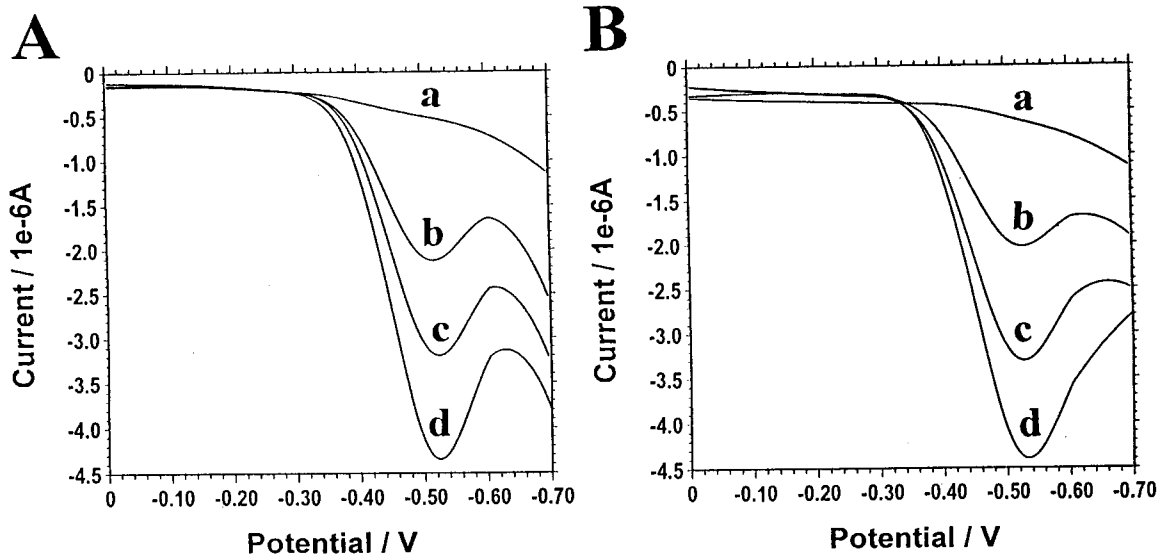


Fig. 6. Assays of untreated river water (A) and groundwater (B) samples. Response to the sample (a), as well as subsequent concentration increments of 3 ppm TNT (b–d). Other conditions as in Fig. 1A.

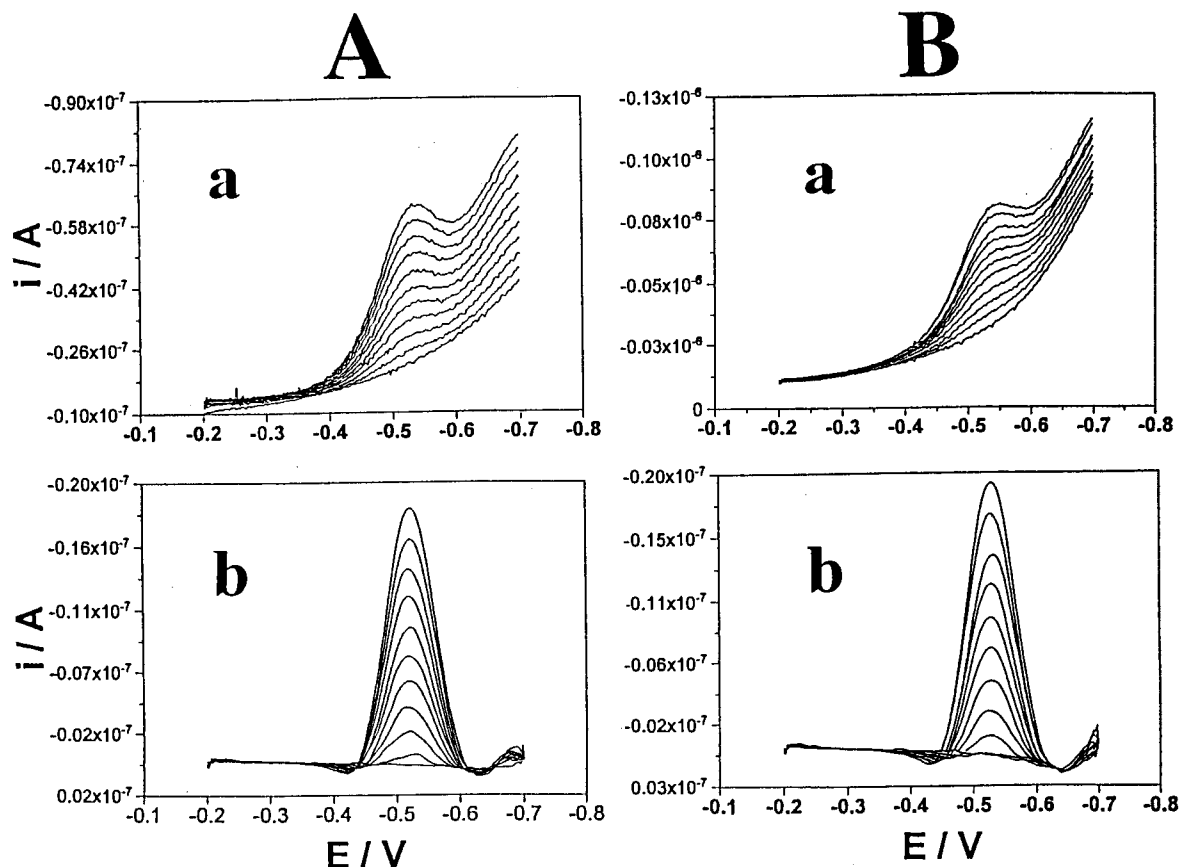


Fig. 7. Conventional (a) and background-corrected (b) square-wave voltammograms for untreated tap water (A) and river water (B) samples containing increasing levels of TNT in 200 ppb steps, along with the sample blank voltammogram. Amplitude, 10 mV; frequency, 30 Hz; step, 2 mV.

with the blank voltammogram (a). Well-defined peaks, proportional to the explosive concentration, are observed, along with the low background response. The resulting calibration plot (also shown) is highly linear (slope, 4.144 $\mu\text{A/ppm}$; correlation coefficient, 0.999). Besides their promise for single-use field applications, the screen-printed electrodes can be used as reusable TNT detecting devices. For example, a prolonged series of 16 repetitive measurements of 10 ppm TNT using the same carbon strip resulted in a highly stable peak current, with a relative standard deviation of 0.6% (not shown).

High selectivity is expected in environmental samples because the nitro group is rare in nature and few other organic compounds are as easily reduced [13]. The screen-printed carbon electrodes

thus holds great promise for direct analysis of relevant water samples, without any prior separation or pretreatment. Fig. 6 displays typical SW voltammograms, illustrating such assays of untreated river water (A) and groundwater (B) samples. A low (nearly flat) baseline is observed for both samples (a), indicating the absence of interfering electroactive species. Three subsequent additions of 3 ppm TNT resulted in well-defined peaks, proportional to the explosive concentration, and similar to those common in synthetic samples. Note again that neither pH nor ionic strength adjustments were required to obtain these high-quality voltammetric data. We also tested the effect of potential organic, inorganic and surface-active interfering materials. The response for 5 ppm TNT was not affected by the presence of 50 ppm of the

similar nitroaromatic compounds nitrophenol and nitrobenzene, by the presence of 1000 ppm of nitrite or nitrate ions, by 1 ppm of the reducible copper, iron(III), lead or zinc ions, or the presence of 10 ppm Triton X-100 or sodium dodecyl sulphate. Yet, it is strongly recommended to employ the new screen-printed voltammetric electrodes as early screening/warning devices (in connection to a high-resolution laboratory confirmation technique). It should be pointed out that even the use of antibodies for imparting selectivity into TNT sensing suffers from cross-reactivity interferences from structurally similar nitroaromatic compounds [5].

Extremely low detection limits can be achieved in connection with a computerized background-correction operation. Fig. 7 compares conventional (a) and background-subtracted (b) square-wave voltammograms for untreated tap (A) and river (B) water samples, containing increasing levels of TNT in 200 ppb steps (along with the blank voltammogram). Such a background-correction operation offers a detection limit of about 100 ppb. Note again the absence of electroactive interferences in these untreated water samples, and the well-defined concentration dependence.

In conclusion, the results presented above demonstrate that the coupling of rapid SWV with screen-printed electrodes results in effective disposable sensors for TNT. As desired for field operations, such coupling leads to a fast, sensitive, simple and low-cost detection of TNT. Although the present work deals with the measurement of TNT, other nitro-containing explosives (e.g. RDX, HMX, picric acid) may be similarly detected on the basis of differences in their peak potentials [4], and in connection with chemometric or on-chip separation schemes. The coupling of these single-use devices with hand-held, battery-operated, instruments should facilitate on-site

environmental screening of TNT.

Remote (submersible) electrochemical sensors, based on the rapid SWV strategy, can also be envisioned for continuous real-time monitoring applications.

Acknowledgements

This work was partially supported by a contract from Sandia National Laboratories. Sandia is a multiprogram laboratory operated by Sandia Corporation, a Lockheed Martin Company, for the US Department of Energy under Contract DE-AC04-94AL85000. K.R. acknowledges EPA support for an IPA assignment at NMSU. Discussions with C. Renschler (Sandia NL) are acknowledged.

References

- [1] P. Kolla, *Angew Chem. Int. Ed. Engl.* 36 (1997) 801.
- [2] A. Fainberg, *Science* 255 (1992) 1531.
- [3] T. Jenkins, D. Leggett, C. Grant, C. Bauer, *Anal. Chem.* 58 (1986) 170.
- [4] K. Bratin, P.T. Kissinger, R. Briner, C. Bruntlett, *Anal. Chim. Acta* 130 (1981) 295.
- [5] L. Shriver-Lake, K. Brestin, P. Charles, D. Conrad, J. Golden, F.S. Ligner, *Anal. Chem.* 67 (1995) 2431.
- [6] J. Hart, S. Wring, *Electroanalysis* 6 (1994) 617.
- [7] M. Green, P. Hilditch, *Anal. Proc.* 28 (1991) 374.
- [8] I. Rohm, M. Gengrich, W. Collier, U. Bilitewski, *Analyst* 121 (1996) 877.
- [9] J. Wang, V. Nascimento, S. Kane, K. Rogers, M. Smyth, L. Angnes, *Talanta* 43 (1996) 1903.
- [10] J. Wang, *Analyst* 119 (1994) 763.
- [11] J. Wang, G. Rivas, X. Cai, *Electroanalysis* 9 (1997) 95.
- [12] K. Conley, W. Mikucki, Migration of explosives and chlorinated pesticide in a simulated sanitary landfill, Technical Report N-8, US Army Construction Engineering Research Laboratory, Champaign, IL.
- [13] P. Kissinger and W. Heineman (Eds.), *Laboratory Techniques in Electroanalytical Chemistry*, 2nd ed., Dekker, New York, 1996, p. 842.

Spectral characterization of a novel near-infrared cyanine dye: a study of its complexation with metal ions

Leila Tarazi, Abraham George, Gabor Patonay *, Lucjan Strekowski

Department of Chemistry, Georgia State University, University Plaza, Atlanta, GA 30303, USA

Received 29 April 1997; received in revised form 4 December 1997; accepted 15 December 1997

Abstract

The spectral features of the near-infrared (NIR) dye TG-170 in different solutions and its complexation with several metal ions were investigated. The absorbance maxima of the dye are at $\lambda = 819, 805,$ and 791 nm in dimethyl sulfoxide (DMSO), methanol, and a buffer of pH 5.9, respectively. These values match the output of a commercially available laser diode (780 nm), thus making use of such a source practical for excitation. The emission wavelengths of the dye are at $\lambda_{em} = 822, 812,$ and 803 nm in DMSO, methanol, and the buffer, respectively. The molar absorptivity and fluorescence quantum yield increase accordingly. The addition of either an Al(III) ion or Be(II) ion resulted in fluorescence quenching of the dye. The Stern–Volmer quenching constant, K_{SV} , was calculated from the Stern–Volmer plot to be $K_{SV} = 3.11 \times 10^5 \text{ M}^{-1}$ for the Al(III) ion and $K_{SV} = 1.17 \times 10^6 \text{ M}^{-1}$ for the Be(II) ion. The molar ratio of the metal to the dye was established to be 1:1 for both metal ions. The stability constant, K_S , of the metal–dye complex was calculated to be $4.37 \times 10^4 \text{ M}^{-1}$ for the Al–dye complex and $1.94 \times 10^6 \text{ M}^{-1}$ for the Be–dye complex. © 1998 Elsevier Science B.V. All rights reserved.

Keywords: Aluminum; Beryllium; Fluorescence; Metal ions; Near-infrared; Quenching

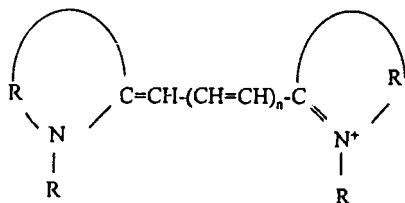
1. Introduction

Fluorescence spectroscopy has long been established as a versatile, sensitive, and easy-to-use analytical technique [1] for a large variety of applications, including chromatography [2], immunoassay [3], and detection of metals [4–6]. Most of the work reported in the literature related to detection of metals by means of fluorescence

techniques used UV-Vis fluorophores such as rhodamine, fluorescein, 8-hydroxyquinoline, and their derivatives [5,7–9]. Unfortunately, spectral interference is significant in this region. The use of near infrared dyes (NIRDs) absorbing in the region from 700 to 1000 nm is a better alternative because this region exhibits low interference [10–13]. Thus, NIR dyes have great potential for the development of chemical sensors for the detection of metal ions.

We have focused our attention on cyanine dyes, a general structure of which is shown below.

* Corresponding author. Tel.: +1 404 6513856; fax: +1 404 6511416; e-mail: cheggp@panther.gsu.edu



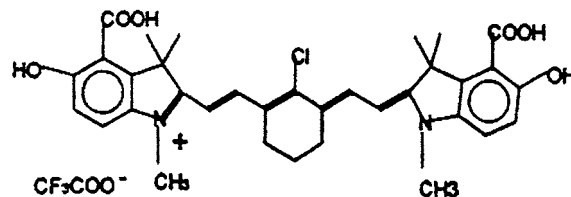
Structure of a typical cyanine dye.

A dye of this class is composed of two heterocyclic systems linked by a polymethine chain, and all three moieties contribute to spectral properties of the chromophore. In particular, the absorption maximum undergoes a bathochromic shift of about 100 nm with elongation of the polymethine chain by one vinyl (CH=CH) group [14]. The heptamethine and higher cyanines absorb in the NIR region with an unusually high molar absorptivity of up to $300\,000\text{ M}^{-1}\text{ cm}^{-1}$. The fluorescence quantum yield is from 0.1 to 0.3 and is structure dependent [15]. Of major concern is the relatively low light fastness of certain cyanines. Indolium derivatives, however, exhibit good light stability that additionally can be improved by incorporating a ring structure into the polymethine chain [16].

The use of semiconductor lasers for excitation further enhances the advantage of the NIR spectral region. The absorbance maxima of most of the NIR dyes are compatible with the output of commercially available laser diodes. The use of laser diodes

for excitation provides a highly powerful monochromatic excitation, which makes detection at extremely low limits possible [13,17].

Recently we have reported synthesis [18] of a heptamethine cyanine dye, 4-carboxy-2-[4'-chloro-7'-(4''-carboxy-5''-hydroxy-1''',3''',3'''-trimethylindolin-2''-ylidene)-3'-5'-(propane-1''',3'''-diyl)-1',3',5'-heptatrien-1'-yl]-5-hydroxy-1,3,3-trimethyl-3H-indolium trifluoroacetate, abbreviated as TG-170. The molecular structure of TG-170 is shown below.



TG 170

This dye is an indolium derivative and contains a six-membered ring in the chromophore for improved light fastness, as discussed. The ortho hydroxy-carboxy functionality, a known selective complexon for Al(III) and Be(II) ions, was incorporated into the molecule for potential use of TG-170 as a sensor for these metal ions. It was reasoned that metal ion complexation would affect spectral properties of the dye chromophore. The results of the complexation studies are presented in this paper.

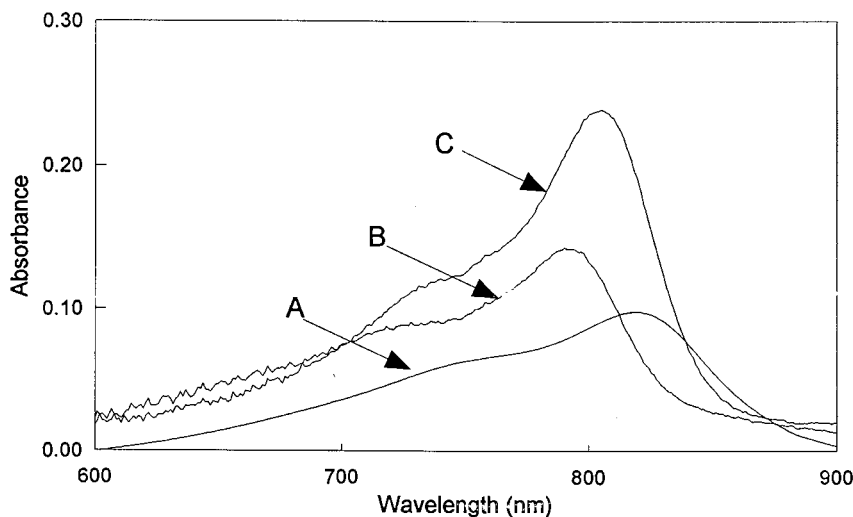


Fig. 1. Absorption spectrum of TG-170 in: (A) DMSO, (B) methanol, (C) buffer, pH 5.9.

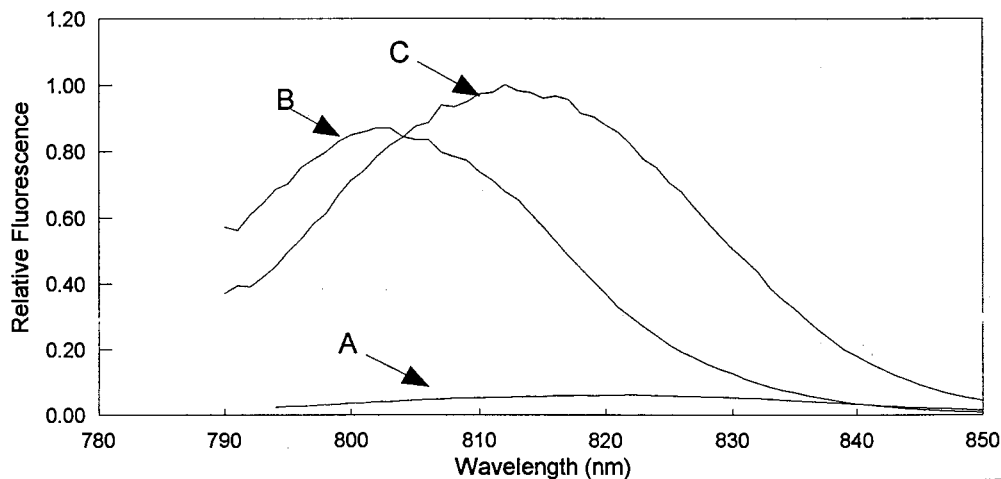


Fig. 2. Emission spectrum of TG-170 in: (A) DMSO, (B) methanol, (C) buffer, pH 5.9.

2. Experimental section

2.1. Reagents and solvents

TG-170 (F.W. 717.12) was synthesized and purified as described previously [18]. Aluminum nitrate, $\text{Al}(\text{NO}_3)_3 \cdot 9\text{H}_2\text{O}$, glacial acetic acid (HPLC Grade), and ammonium hydroxide (certified A.C.S. Plus) were used as received from Fisher (Fair Lawn, NJ). Methanol and dimethyl sulfoxide (DMSO) were obtained from Aldrich (Milwaukee, WI). Distilled water was purified with a NANOpure ultrapure water system (Barstead).

2.2. Apparatus

Absorption measurements were done on a Perkin-Elmer Lambda 2 UV/VIS/near-IR spectrophotometer interfaced to a Zenith 386 computer. Fluorescence measurements were done on an ISS K2 spectrofluorometer (ISS, Champaign, IL). Quartz cuvettes of 1 cm path length were used for absorbance and fluorescence measure-

ments. A commercial GaAlAs laser diode (Laser Max, Rochester, NY) was used as the excitation source (780 nm output, 50 mW). The data acquisition and control of the instrument were done with a Gateway 2000 computer equipped with an ISS software program. The slit width was 2 mm and the integration time was 1 s. A PHOM-10 pH meter (Omega Technologies, Broughton Astley, UK) was used for pH measurements. Micropipetters (Rainin, Woburn, MA) were used to prepare the dilutions.

2.3. Stock solutions

A stock solution of 1.00×10^{-3} M Al(III) was prepared by dissolving $\text{Al}(\text{NO}_3)_3 \cdot 9\text{H}_2\text{O}$ in purified water. A stock solution of 1.00×10^{-3} M TG-170 was prepared by dissolving the dye in DMSO. All stock solutions were kept in Nalgene containers and were stored at 4°C in the dark for a maximum of one month. Stock solutions were brought to room temperature prior to preparation of the required dilutions. Successive

Table 1
Spectroscopic characteristics of TG-170

Solvent	λ_{max} (nm)	λ_{em} (nm)	Φ_{f} (%)	$\text{Log } \epsilon$ ($1 \text{ M}^{-1} \text{ cm}^{-1}$)
DMSO	819	822	0.167	4.96
Methanol	805	812	1.30	5.40
Buffer (pH 5.9)	791	803	2.48	5.99

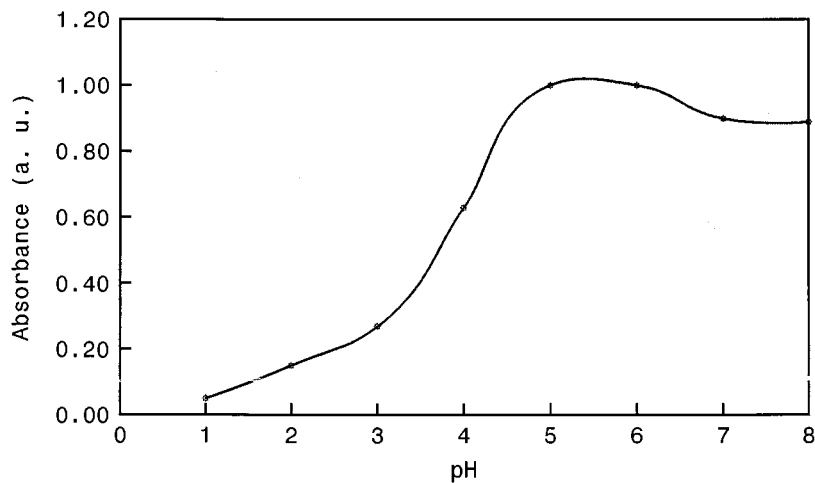


Fig. 3. Variation with pH of the absorption of TG-170.

dilutions of working solutions were made fresh before each experiment.

2.4. Buffer solutions

To 800 ml of distilled water 40 ml of glacial acetic acid was added. Samples of 40 ml each were taken from the above solution and enough ammonium hydroxide was added to adjust the pH of each sample to the desired value.

3. Results and discussion

3.1. Spectral characteristics

The excitation and emission spectra of TG-170 in DMSO, methanol, and aqueous buffer (pH 5.9) are shown in Figs. 1 and 2, respectively. The various spectral properties of TG-170 that have been investigated are summarized in Table 1. The fluorescence quantum yields (Φ_F)

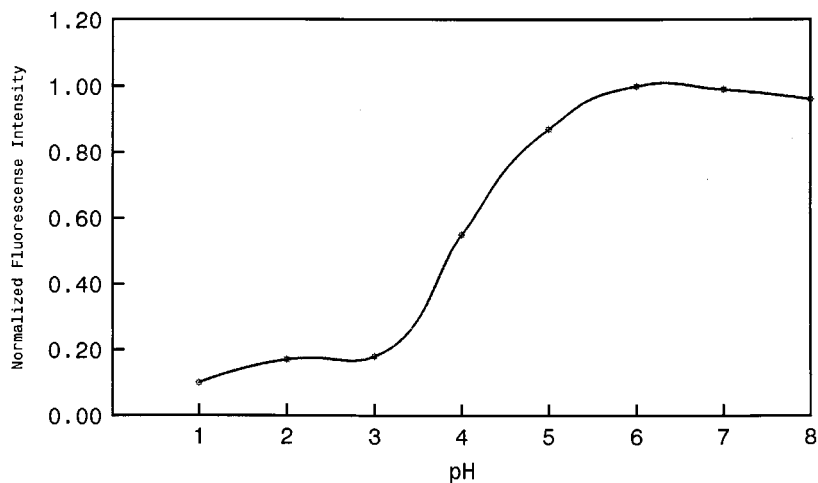


Fig. 4. Variation with pH of the fluorescence intensity of TG-170.

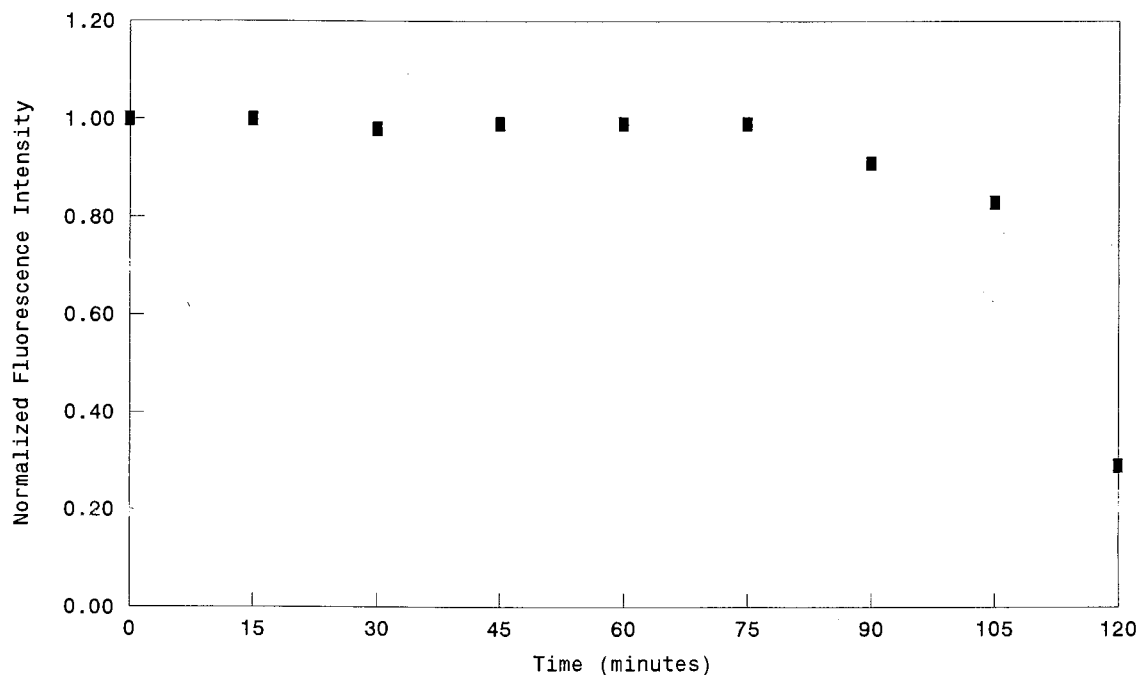


Fig. 5. Variation with time of the fluorescence intensity of TG-170.

were calculated relative to IR-125, $\Phi_F = 0.13$ in DMSO [19].

As can be seen, both the absorption and emission maxima of TG-170 are solvent dependent and, apparently, are a complex function of solvent polarity and hydrogen-bonding ability. Related observations have been noted [20].

3.2. Influence of pH on the absorption and emission spectra of TG-170

Variations of the absorption and emission spectra of TG-170 with pH are shown in Figs. 3 and 4, respectively. The dye reaches its highest values of absorptivity and fluorescence efficiency at pH 5.9. Titration of TG-170 with standardized sodium hydroxide solution on a Schott TR 600 automated titrating system showed one end point only, also at pH 5.9. At this pH one COOH group of the molecule of TG-170 is deprotonated. Varying the pH of the dye solution did not result in any appreciable shift in the λ_{\max} of absorption and fluorescence.

3.3. Determination of pK_a for TG-170

The pK_a of TG-170 was determined from Fig. 4 by interpolation. When the relative fluorescence intensity was 0.50, the corresponding pH was about 3.82. At this pH value the protonated form of the dye and the form in which one proton has been removed from the molecule are present in equal molar concentrations. This pH value corresponds to the pK_a of the dye. The pK_a of 2-naphthoic acid is 4.17 [21]. The pK_a of 3-hydroxy-2-naphthoic acid, computed using the Hammett equation, is 4.00. This is consistent with the pK_a value for TG-170 determined experimentally. The fact that the pK_a of TG-170 is slightly lower than the pK_a of 3-hydroxy-2-naphthoic acid, a related molecule, can be attributed to the positive charge on the nitrogen atom of TG-170. This charge stabilizes the deprotonated form of the molecule and lowers its pK_a .

3.4. Effect of time on the fluorescence intensity of the dye

The fluorescence intensity of 1.00×10^{-6} M of

Table 2
Effect of temperature on the fluorescence intensity of the metal–dye complex

Temperature (°C)	F_i (dye)	ΔF_i (%)	F_i (dye+Al)	ΔF_i (%)	F_i (dye+Be)	ΔF_i (%)
25	1576		1384		760	
40	1508	(−4.31)	1272	(−8.09)	808	(+6.32)
50	1484	(−5.84)	1091	(−21.2)	1104	(+45.3)

TG-170 kept in a buffer of pH 5.9 in the dark at room temperature was found to be steady over a period of 75 min. However, the fluorescence intensity dropped sharply after a period of 2 h (Fig. 5), indicating the need for fresh solutions for each experiment.

3.5. Effect of metal ions on the fluorescence intensity of TG-170

The spectral properties of TG-170 were investigated in the presence of each of the following metal ions: Na, K, Be(II), Cd(II), Co(II), Fe(II), Ni(II), Mg(II), Zn(II), Al(III), and B(III). To a 9.10×10^{-6} M solution of TG-170 each of the above mentioned metal ions under investigation was added, respectively, in concentrations ranging from 0 to 10-fold that of the dye concentration. The final concentration of the dye was kept constant by adding enough buffer to maintain a constant final volume. Only the presence of Al(III) ion or Be(II) ion affected the fluorescence intensity of TG-170, resulting in both cases in quenching of the fluorescence. Metal ions are known to quench fluorophores in a process which probably involves transfer of electron density from the fluorophore to the metal ion to form a charge-transfer complex. This transfer of charge perturbs the conjugated structure of the dye chromophore and results in quenching of its fluorescence. The Stern–Volmer plot represented by equation (1)

$$F_0/F = 1 + K_{SV}[Q] \quad (1)$$

relates F_0 and F , the fluorescence intensities in the absence and presence of the quencher Q , respectively, to K_{SV} , the Stern–Volmer quenching constant, and to the concentration of the quencher.

3.6. Determination of the Stern–Volmer quenching constants

In the presence of Al(III) ion, a plot of F_0/F versus the concentration of Al(III) ion gave a straight line and a correlation coefficient of 0.989. The slope K_{SV} of this line was $3.11 \times 10^5 \text{ M}^{-1}$. In the presence of Be(II) ion, a plot of F_0/F versus the concentration of Be(II) ion gave a straight line and a correlation coefficient of 0.990. The slope K_{SV} of this line was $1.16 \times 10^6 \text{ M}^{-1}$. The nature of the quenching was established by measuring the fluorescence intensity F at different temperatures. It was observed that increasing the temperature resulted in a decrease in the fluorescence intensity of the dye–Al complex and an increase in the fluorescence intensity of the dye–Be complex (Table 2). These results suggest that quenching by Al(III) ion is dynamic (diffusion dependent), and quenching by Be(II) ion is static. In the case of dynamic quenching, higher temperatures result in larger diffusion coefficients and in an increase in the bimolecular quenching constant k_q , thus causing further decrease in the fluorescence intensity. In the case of static quenching, an increase in temperature may result in dissociation of the ground state complex and, consequently, in an increase in the fluorescence intensity [22].

In dynamic quenching the diffusion-controlled bimolecular rate constant k_0 is calculated using the Smoluchovski equation

$$k_0 = 4\pi RDN/1000 \quad (2)$$

where R is the collision radius, D is the sum of the diffusion coefficients of the fluorophore and the quencher, N is the number of molecules. The term $N/1000$ converts molarity to molecules cm^{-3} . The bimolecular quenching constant k_q is related to k_0 by the quenching efficiency γ :

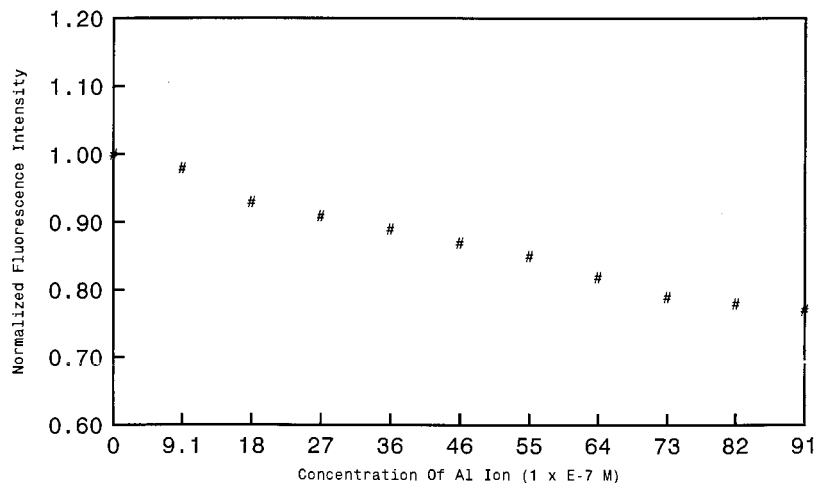


Fig. 6. Variation with Al(III) concentration of the fluorescence intensity of TG-170.

$$k_q = \gamma k_0 = 4\gamma\pi RDN/1000 \quad (3)$$

Eq. (3) suggests that dynamic quenching at such low concentrations of Al(III) used in this study requires unrealistically high diffusion coefficients and thus, rules out the possibility of dynamic quenching by aluminum ion.

3.7. Detection limits

A plot of the fluorescence intensity of TG-170 versus [Al(III)] was linear in the range 1.82×10^{-6} – 6.40×10^{-6} M, i.e. for amounts ranging from 49.1 to 172 ppb (Fig. 6). Also, a linear

relationship between the fluorescence intensity and the concentration of Be(II) existed for $[\text{Be}^{2+}]$ in the range 2.73×10^{-6} – 9.10×10^{-6} M, i.e. for amounts ranging from 24.6 to 82.0 ppb (Fig. 7). The calculated detection limit, at 3 times the S.D. of the blank, was 1.64×10^{-6} M (or 44.3 ppb) for the Al(III) ion and 3.05×10^{-7} M (or 24.6 ppb) for the Be(II) ion.

3.8. Determination of the molar ratio of the dye to the metal in the metal–dye complex.

The molar ratio of TG-170 to the metal in the

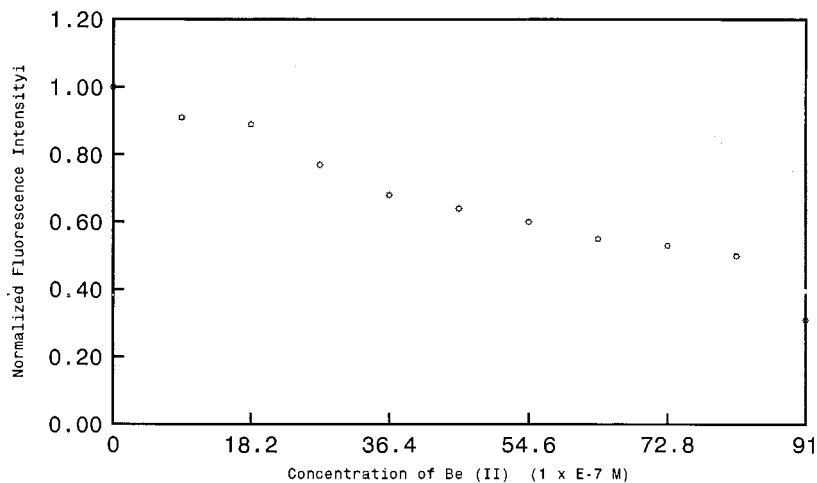


Fig. 7. Variation with Be(II) concentration of the fluorescence intensity of TG-170.

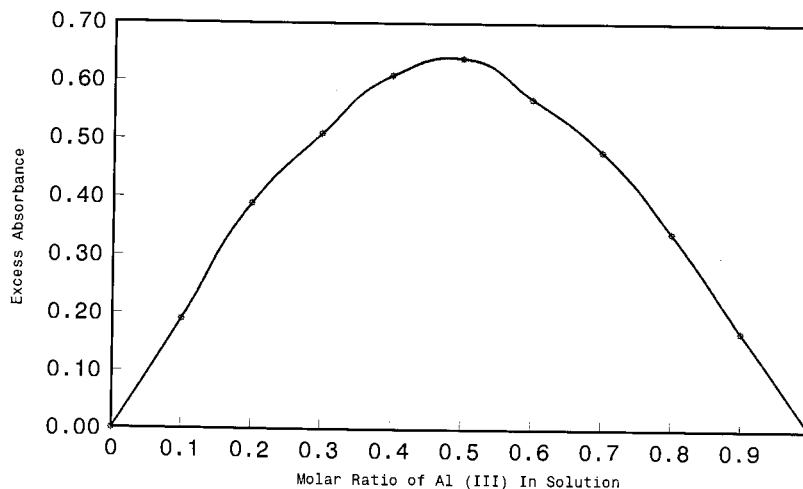


Fig. 8. Job's plot for the Al-dye complex.

dye-metal complex was established by the method of continuous variation. Equimolar solutions of the dye and of the metal ion (9.10×10^{-6} M) were prepared in buffer. At each step the dye and metal ion were mixed such that their initial concentrations varied in such a way that the sum of their concentrations remained constant, after which the mixture was subjected to spectroscopic measurements. A plot of the absolute value of excess absorbance (excess absorbance is equivalent to the total absorbance of the sample solution minus the absorbance of an identical hypothetical solution of the dye and metal ion, except it con-

tains no complex [23]) versus the molar ratio (Job's plot) for the Al ion and the Be ion is shown in Figs. 8 and 9, respectively. The Job's plot for the dye-Al complex showed a 1:1 molar ratio. The Job's plot for the dye-Be complex also showed a 1:1 molar ratio. Fluorescence techniques failed to provide these ratios using the method of continuous variation. However, when plotting the fluorescence intensity against the metal concentration, a monotonous dependence was observed. This indicated a constant 1:1 stoichiometry in the investigated range of concentrations [24]. Since the molecule of TG-170 possesses two hydroxy-

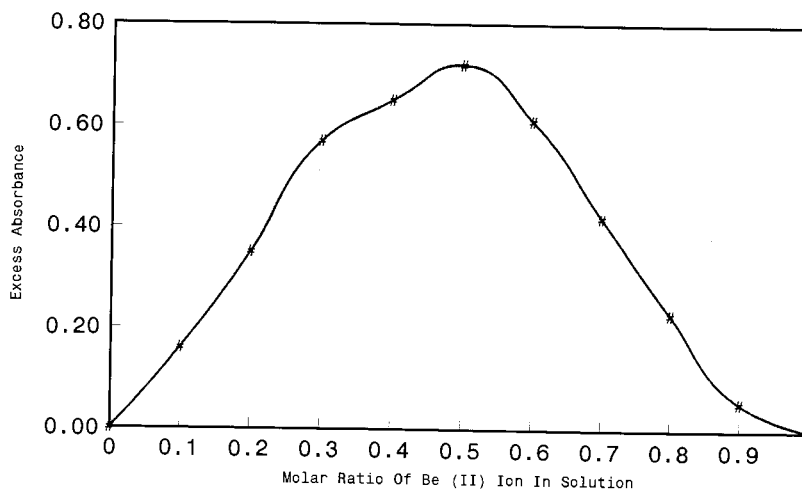


Fig. 9. Job's plot for the Be-dye complex.

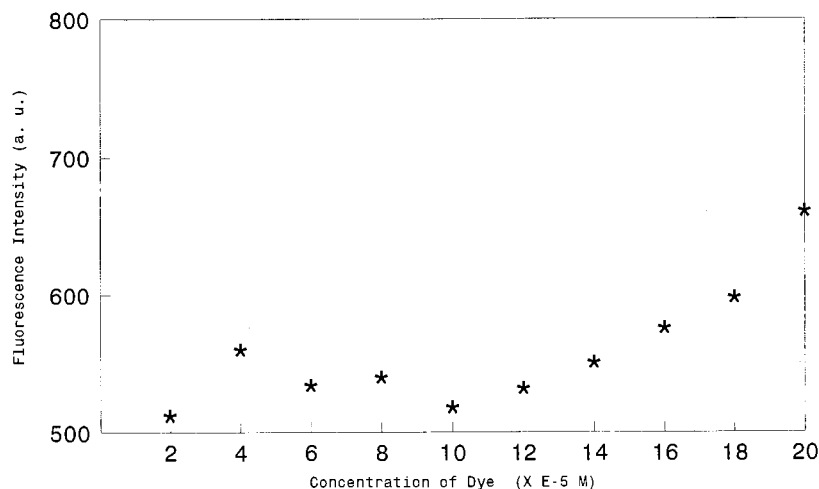


Fig. 10. Variation with Al(III) concentration of the fluorescence intensity of TG-170, Al(III) in large excess.

carboxy functions at each end of the molecule, the expected molar ratio of metal to dye in the complex is 2:1. Apparently, the complexation of a metal ion on one end of the molecule impedes the complexation at the second end of the molecule by electronic features [20].

The reaction between the dye and the metal ion (Al or Be) can be represented by the following reaction expressed by Eq. (4)



where D, M, and DM represent the dye, metal ion, and dye–metal complex, respectively. The stability constant of the complex, K_s , is expressed by Eq. (5)

$$K_s = \frac{[DM]}{[D][M]} \quad (5)$$

where the quantities in the square brackets represent molar concentrations at equilibrium.

3.9. Determination of the stability constant of the dye–metal complex

The stability constant of the dye–metal complex was measured by using Eq. (6) [25]

$$\frac{1}{F} = \frac{1}{kD_T} + \frac{1}{kD_T K_s} \times \frac{1}{[M]} \quad (6)$$

where F is the intensity of fluorescence measured,

k is a constant that depends on the quantum efficiency of the fluorescent process and on the instrument, D_T is the total concentration of the dye, and $[M]$ is the concentration of the metal ion. Keeping the total concentration of the dye in each sample constant, 9.1×10^{-6} M, and varying the metal ion concentration from 9.10×10^{-7} to 9.10×10^{-6} M, a plot of $1/F$ versus $1/[M]$ produces a straight line. The stability constant K_s is the quotient of the intercept divided by the slope. The stability constant for the Al complex is $4.37 \times 10^4 \text{ M}^{-1}$. The stability constant of the Be complex is $1.24 \times 10^6 \text{ M}^{-1}$.

The stability constant K_s was also established from the linear portion of the calibration curve obtained by plotting the fluorescence intensity versus the concentration of the dye, with the concentration of the metal ion constant and in large excess. For each metal ion the concentration of the dye was varied from 2.00×10^{-5} to 20×10^{-5} M. The concentration of the metal ion was 2.00×10^{-3} M. A plot of the fluorescence intensity versus the concentration of Al(III) is shown in Fig. 10. A plot of the fluorescence intensity versus the concentration of Be(II) is shown in Fig. 11.

The stability constant K_s can be derived from Eq. (3) by rewriting it as

$$K_s = \frac{[D]_T - [D]}{[D][M]_T - [DM]} \quad (7)$$

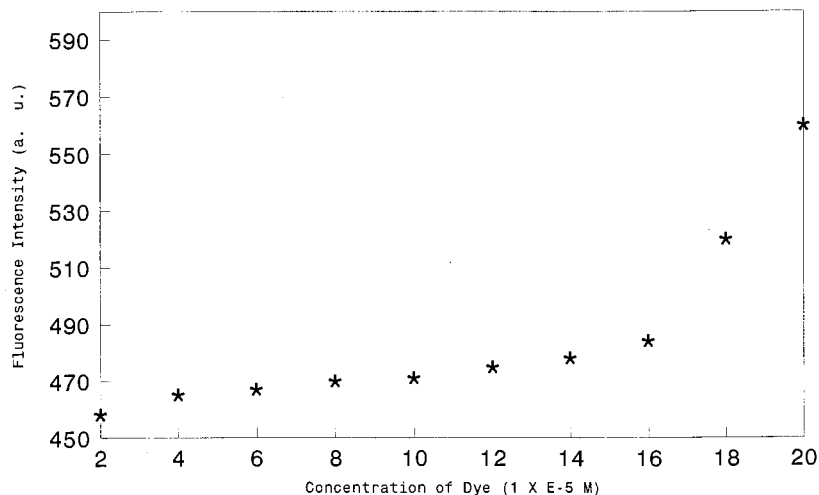


Fig. 11. Variation with Be(II) concentration of the fluorescence intensity of TG-170, Be(II) in large excess.

Since $[M]_T$ is in large excess, Eq. (7) can be written as

$$K_s = \frac{[D]_T - [D]}{[D][M]_T} \quad (8)$$

By definition, the fluorescence intensity F is

$$F = k'I_0\Phi_f\epsilon d[D] \quad (9)$$

where k' is an instrumental constant, I_0 is the intensity of the source, Φ_f is fluorescence quantum yield of the dye, ϵ is its molar absorptivity, and d , the thickness of the cuvette, is 1 cm. Since the

parameters I_0 , Φ_f , ϵ , and d are constant, the product $k'I_0$ can be substituted for by K and the product $\Phi_f\epsilon d$ by K' . Substituting the value of $[D]$ from Eq. (7) into Eq. (9) and rearranging:

$$F = \frac{KK'[D]_T}{K_s[M]_T + 1} \quad (10)$$

which can be rewritten as:

$$F = \frac{KK'[D]_T}{K_s[M]_T} \quad (11)$$

K has been established for the ISS K2 spec-

Table 3
Effect of foreign metal ions on the detection of Al or Be ions

Foreign Ion	Limiting molar ratio for the Al method	Limiting molar ratio for the Be method	% Error in fluorescence for Al	% Error in fluorescence for Be
Na	10			
K	10	20	-13	-17
Ba	10	20	-49	-20
B	10	10	-20	-13
Cd	10	20	-32	-44
Co	10		-28	
Eu	10	20	-69	-45
Fe(II)	20	10	-80	-61
Fe(III)	2	5	-87	-64
Pb	10	10	-76	-61
Mg	10	10	-40	-21
Ni	10	20	-37	-11
Zn	10	10	-75	-25

trofluorometer to be 1.24×10^4 and K' was calculated from the data in Table 1. A plot of F versus $[D]_T$ is a straight line. The stability constant K_s is the quotient of the slope divided by the product KK' . K_s for the Al–dye complex, calculated from the slope of the linear part of Fig. 10, is $2.24 \times 10^5 \text{ M}^{-1}$. K_s for the Be–dye complex, calculated from the linear part of Fig. 11, is $1.20 \times 10^6 \text{ M}^{-1}$.

3.10. Interference by other metal ions

The effect of foreign metal cations on the determination of each of aluminum and of beryllium was investigated. These foreign metal ions were Na^+ , K^+ , Ba^{2+} , B^{3+} , Cd^{2+} , Co^{2+} , Eu^{3+} , Fe^{2+} , Fe^{3+} , Pb^{2+} , Mg^{2+} , Ni^{2+} , and Zn^{2+} . Mixtures of interferents and 44.3 ppb of Al(III) were evaluated to determine the effect of an ion on the formation of Al–dye complex. Mixtures of interferents and 24.6 ppb of Be(II) were evaluated to determine the effect of the ion on the formation of the Be–dye complex. A 100-fold molar excess of each foreign ion over the Al or Be ion was used. Where the buffer capacity of the ammonia–acetic acid buffer was insufficient, the pH was adjusted to 5.9 using dilute ammonia or dilute acetic acid. When a foreign ion was found to interfere, it was further investigated at a lower molar ratio. The limiting value of the molar ratio of a foreign ion to that of Al or Be was taken as that which caused an error of $\pm 10\%$ in the determination of Al(III) or Be(II). Cationic interferences are noted in Table 3.

A 10-fold molar excess of EDTA with respect to Al(III) was enough to restore the original signal of the dye. When EDTA was added in an amount equal to its tolerance limit in the presence of an interfering foreign ion, it was effective in masking the foreign ion in the Al method. The presence of EDTA did not affect the Be complex. However, at low concentrations of Be EDTA prevented the formation of the TG-170–Be complex. Addition of excess Ca(II), a noninterfering cation, was effective in masking the excess EDTA. Addition of a 100-fold molar excess of EDTA to the beryllium complex and a 125-fold molar excess of Ca(II) was effective in preventing the interference of the foreign cation without affecting the fluorescence signal of the Be complex.

Interference by Fe(III) was not tolerated at the 2-fold level in the Al method and at the 5-fold level in the Be method. When Fe(III) was reduced to Fe(II) by the addition of the required amount of ascorbic acid, the interference by Fe(III) was reduced to approximately -81% and -58% in the aluminum and beryllium method, respectively.

4. Concluding remarks

The NIR dye, TG-170, described in this paper, undergoes fluorescence quenching upon binding with either aluminum or beryllium ion in a large range of concentrations. This outcome can be a result of a charge transfer from the ligand to the metal. Such ligand-to-metal charge transfer disturbs the resonance structure of the conjugated NIRD and results in its quenching [26].

The pH of formation of the complex was found to be 5.9, which is higher than the pH at which aluminum hydroxide precipitates (approximately pH 4.1). Since no precipitate was observed, it appears that the reagent inhibits the formation of insoluble hydroxide species. This can occur by means of a mechanism whereby chemical combination of the ligand through replacement of a hydroxyl group in the hydrated alumina unit terminates the possibility of further aggregation [27].

The two values of the stability constant K_s (1.20×10^6 and $1.24 \times 10^6 \text{ M}^{-1}$) obtained from Eqs. (6) and (11), respectively, for the Be–dye complex agree with each other and match the value of the Stern–Volmer quenching constant K_{SV} ($1.16 \times 10^6 \text{ M}^{-1}$) for the Be method. This, as well as the data from Table 3, confirms that the quenching by Be(II) is static and is connected with the capacity of the ground-state complex formation. On the other hand, the two values of the stability constant K_s (4.37×10^4 and $2.24 \times 10^5 \text{ M}^{-1}$) established from Eqs. (6) and (11), respectively, for the Al–dye complex are not in agreement with each other and neither value matches the value of the Stern–Volmer quenching constant K_{SV} ($3.11 \times 10^5 \text{ M}^{-1}$) for the Al method. This excludes the possibility of static quenching. On the other hand, dynamic quenching by aluminum is ruled out for the reason given previ-

ously. It can be concluded that the mechanism of the quenching of TG-170 by aluminum ion is not fully understood. It could be that both dynamic as well as static quenching is a contributing factor in the aluminum method.

The data presented in this study demonstrate the use of fluorescence quenching measurements for studying NIR fluorophores. Since such fluorophores have found an increasing application as labeling agents in various fields of chemical analysis, it is important to study the effect of different quenchers.

References

- [1] E.L. Wehry, *Modern Fluorescence Spectroscopy*, Plenum, New York, 1976.
- [2] E.S. Yeung, M. Speniak, *J. Anal. Chem.* 52 (1980) 1465A.
- [3] C.M. O'Donnel, S.C. Suffin, *Anal. Chem.* 51 (1979) 33A.
- [4] R. Schmidt, W. Weis, V. Klingmuller, H. Standinger, *Z. Klin. Chem. Klin. Biochem.* 5 (1967) 304.
- [5] S.A. Linda, W.R. Seitz, *Anal. Chem.* 55 (1983) 667.
- [6] O.S. Wolbfeis, *Fresenius Z. Anal. Chem.* 337 (1993) 522.
- [7] Z. Zhujun, W.R. Seitz, *Anal. Chim. Acta* 171 (1985) 252.
- [8] Y. Kawabata, R. Tahara, T. Kamishika, T. Imasaka, N. Ishibashi, *Anal. Chem.* 62 (1990) 2054.
- [9] K.S. Litwiler, P.M. Kluczynski, F.V. Bright, *Anal. Chem.* 63 (1991) 797.
- [10] N. Ishibashi, T. Kamikubo, Y. Kawabata, *Anal. Chim. Acta* 153 (1983) 261.
- [11] J. Hicks, G. Patonay, *Anal. Instrum.* 18 (1989) 213.
- [12] E. Unger, G. Patonay, *Anal. Chem.* 61 (1989) 1425.
- [13] J. Hicks, D. Andrews-Wilberforce, G. Patonay, *Anal. Instrum.* 19 (1990) 29.
- [14] J. Fabian, H. Nakazumi, M. Matsuoka, *Chem. Rev.* 92 (1992) 11976.
- [15] J. Hicks, G. Patonay, *Anal. Chem.* 62 (1990) 1543.
- [16] M. Matsuoka, in: M. Matsuoka (Ed.), *Infrared Absorbing Dyes*, Plenum, New York, 1994.
- [17] G. Patonay, M. Antoine, S. Devanathan, L. Strekowski, *Appl. Spectrosc.* 45 (1991) 457.
- [18] T. Górecki, G. Patonay, L. Strekowski, R. Chin, N. Salazar, *J. Heterocycl. Chem.* 33 (1996) 1871.
- [19] S.A. Soper, Q.L. Mattingly, *J. Am. Chem. Soc.* 119 (1994) 3744.
- [20] R. Schulman, in: Pesce, Amadeo (Ed.), *Fluorescence Spectroscopy*, Marcel Dekker, New York, 1977.
- [21] J.A. Dean, *Lange's Handbook of Chemistry*, 14th ed., McGraw-Hill, New York, 1992.
- [22] M. Eftink, in: J. Lakowicz (Ed.), *Topics in Fluorescence Spectroscopy*, vol. 2, Plenum, New York, 1991.
- [23] W.A. McBryde, *Talanta* 21 (1974) 979.
- [24] S. Fery-Forgues, M. Le Bris, J. Guetté, B. Valeur, *J. Phys. Chem.* 92 (1988) 6233.
- [25] G.A. Casay, D.B. Shealy, G. Patonay, in: J. Lakowicz (Ed.), *Topics in Fluorescence Spectroscopy*, Plenum, New York, 1994.
- [26] A.M. De La Peña, in: S. Schulman (Ed.), *Molecular Luminescence Spectroscopy*, Wiley, New York, 1985.
- [27] R.M. Dagnall, R. Smith, T.S. West, *Talanta* 13 (1966) 6092.

Benzeneacetaldehyde-4-hydroxy- α -oxo-aldoxime as a new analytical reagent for the spectrophotometric determination of cobalt

Sanjeev B. Jadhav, Shilpa S. Utekar, Abhijit J. Kulkarni, Anand Varadarajan, Sheela P. Malve *

Faculty of Chemistry, Institute of Science, 15, Madam Cama Road, Mumbai 400032, India

Received 23 June 1997; received in revised form 8 December 1997; accepted 15 December 1997

Abstract

Benzeneacetaldehyde-4-hydroxy- α -oxo-aldoxime is proposed as a new sensitive and selective reagent for the spectrophotometric determination of cobalt. The reagent reacts with cobalt in the pH range 8.6–9.4 to form a yellow colored 1:3 chelate which is very well extracted in chloroform. Beer's law is obeyed in the concentration range 0.05–1.3 $\mu\text{g ml}^{-1}$ cobalt. The molar absorptivity of the extracted species is $2.746 \times 10^4 \text{ l mol}^{-1} \text{ cm}^{-1}$ at 390 nm. The proposed method is highly sensitive, selective, simple, rapid, accurate and has been satisfactorily applied for the determination of cobalt in synthetic mixtures, pharmaceutical samples, biological samples and alloys. © 1998 Elsevier Science B.V. All rights reserved.

Keywords: Benzeneacetaldehyde-4-hydroxy- α -oxo-aldoxime; Cobalt; Spectrophotometric determination

1. Introduction

The significance of cobalt as a transition metal lies in its wide spectrum of applications covering many frontier areas of study, particularly in medicine. Even though cobalt is not considered to be as toxic as most of the heavy metals, it is an equally harmful element. Hence owing to the significance of cobalt, its determination from associated elements by extractive spectrophotometry has been of considerable importance [1]. A

wide variety of chelating agents like thenoyl trifluoroacetone [2], isonitroso-4 methyl-2-pentanone[3], isonitrosomalondianilide [4], 3-(4-phenyl-2-pyridyl)-1,2,4-triazine [5], 5-nitrosalicylaldehyde - 4 - phenyl - 3 - thiosemicarbazone [6], phenyl azobenzaldoxime[7], cyanex-272[8], tetrazolium violet [9], *m*-(mercaptoacetamido) phenol [10], nitrosochromotropic acid [11], 2-(8-quinolyazo)-5-*N,N*'-dimethyl-aminobenzoic acid [12], trifluoroacetylacetone [13], malachite green [14], 2-nitroso-1-naphthol-4-sulfonic acid [21], 2-(5-bromo-2-pyridylazo)-5-diethylaminophenol [22], 2-(2-benzothiazolylazo)-2-*p*-cresol [15], isonitroso-propiofenone [16] and *p*-nitroisonitrosoace-

* Corresponding author. Tel.: +91 22 5165566; fax: +91 22 5425866; e-mail: parthesh@giasbma.vsnl.net.in

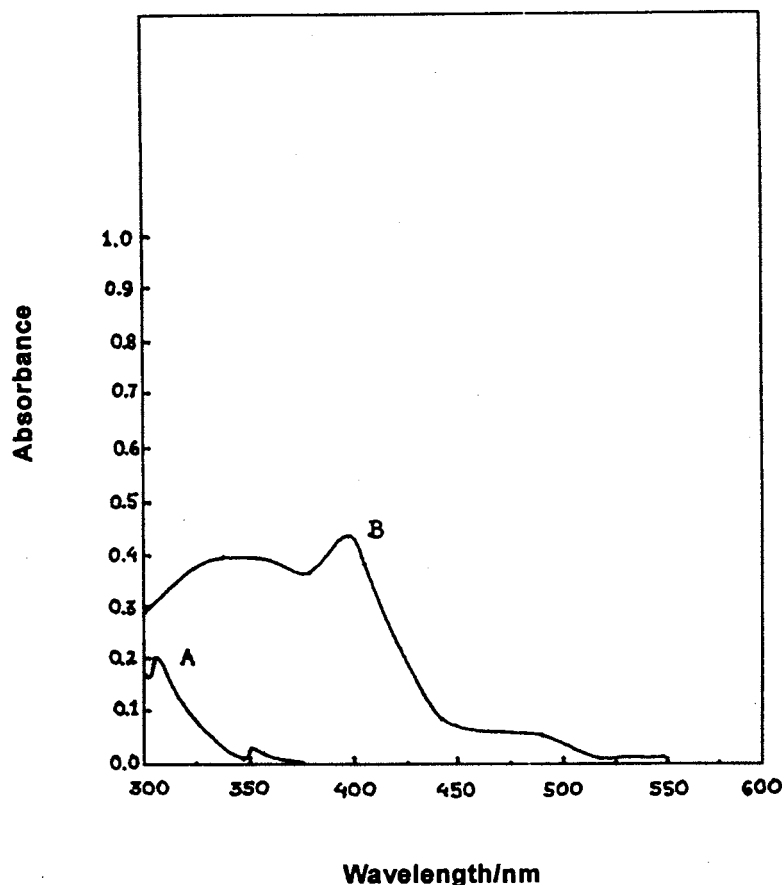


Fig. 1. Absorption spectra of BAHA and its cobalt complex extracted in chloroform.

tophenone [17], etc. have been reported for the spectrophotometric determination of cobalt.

However these methods suffer from limitations such as critical pH [2,11,13], long extraction time [6], long color development time [22] and interference from some ions [2–8,11,13–17,21,22] etc. A method, far superior in sensitivity and selectivity to those reported in the literature [3,5,7–10,12,16,17,21], is developed for the extractive spectrophotometric determination of cobalt with benzeneacetaldehyde-4-hydroxy- α -oxo-aldoxime (*p*-hydroxy isonitrosoacetophenone or BAHA). A close literature survey indicates that BAHA has so far not been employed for either coordination or analytical studies. It forms intensely colored complexes with Fe(III),

Co(III), Cu(II), Ni(II), Pd(II), Pt(IV), Ru(III) and Pb(II) which are extractable in organic solvents under different experimental conditions. The proposed method is free from many limitations.

2. Experimental

2.1. Apparatus

A Shimadzu-140-02 UV-visible spectrophotometer with 10 mm matched cells and a digital ELICO pH meter (model LI-120) with a combined glass electrode assembly were used for the absorbance and pH measurements respectively.

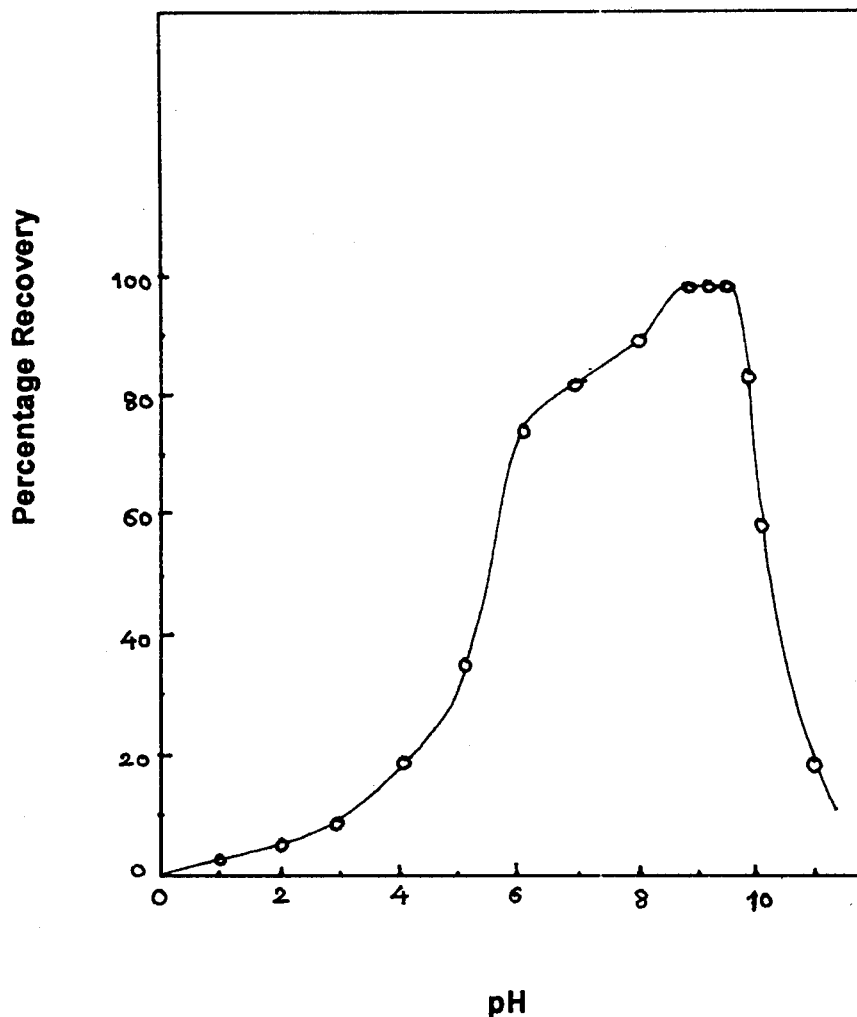


Fig. 2. The effect of pH on the extraction of cobalt with BAHA in chloroform.

2.2. Reagents

All chemicals used were of analytical grade unless otherwise indicated. De-ionised, doubly distilled water was used throughout the experiment.

2.3. BAHA

The ligand was synthesized by the reaction of *n*-amyl nitrite on 4-hydroxy acetophenone (Aldrich), as per the method previously described in the literature [18] using HCl gas. A stock

solution (5 mg ml^{-1}) of BAHA was prepared by dissolving 0.5 g of the reagent in 100 ml absolute alcohol to give a 0.5% reagent solution of BAHA.

2.4. Cobalt(II) solution

A stock solution of cobalt ($10000 \mu\text{g ml}^{-1}$) was prepared by dissolving an accurately weighed amount of Merck cobaltous chloride hexahydrate (10.0930 g) in 250 ml double-distilled water with a few drops of concentrated hydrochloric acid and standardized by a known method [19].

2.5. Buffer solution (pH 9.0)

The pH of aqueous (1.1) NH₃ solution was adjusted to the required pH with 4 N HCl using a pH meter.

2.6. Recommended procedure

To an aliquot of solution containing 1–100 µg cobalt(II) in a separating funnel add 0.4 ml 0.5% alcoholic reagent solution (BAHA) and 1 ml pH 9.0 buffer. Dilute the mixture to 10 ml with double-distilled water and equilibrate the aqueous medium with 10 ml chloroform for 1.5 min. Allow the two layers to separate and measure the absorbance of the organic extract containing the complex at 390 nm against a reagent blank.

3. Results and discussion

3.1. Absorption spectra

The absorption spectrum of the yellow colored cobalt–BAHA complex against a reagent blank in chloroform under optimum condition showed a maximum at 387–391 nm (Fig. 1, curve B). The spectrum of reagent blank against pure solvent 'chloroform' indicates that the ligand practically does not absorb above 380 nm (Fig. 1, curve A). Hence all absorption measurements were carried out at 390 nm against a reagent blank.

Table 1
Precision and accuracy in the determination of cobalt

Concentration cobalt (µg)		S.D.	R.S.D. (%)
Taken	Found ^a		
0.50	0.501	0.0028	0.56
0.75	0.750	0.0033	0.44
1.00	0.998	0.0050	0.51
1.25	1.250	0.0047	0.38
1.50	1.502	0.0052	0.35

^a Average of five determinations.

3.2. Extraction conditions

A preliminary study showed that the formation of an extractable cobalt–BAHA complex is affected by the hydrogen ion concentration. The optimum pH range for the absorbance was studied by means of the standard procedure. The results are shown in Fig. 2. The final pH of each aqueous solution was measured after extraction. A maximum and constant absorbance was obtained over the pH range 8.6–9.4. Hence all extractions were carried out at pH 9.0.

The effect of BAHA concentration on the extraction of cobalt complex was examined. It was found that a 0.02% alcoholic solution of BAHA sufficed for quantitative extraction of 10 µg cobalt. Hence 0.4 ml of 0.5% BAHA solution was used for the extraction of 10 µg cobalt in further studies.

The shaking time for the extraction was varied from 0.1 to 2 min. The minimum shaking time for complete extraction of 10 µg cobalt with chloroform was found to be 1.5 min at room temperature. A longer extraction time had no adverse effect.

The cobalt–BAHA complex was found to be stable for 3 h. Addition of salting agents like NaCl, LiCl, NH₄Cl etc were found to have no significant effect on the absorbance. Extractions at higher temperatures in the range 30–70°C were found to have no adverse effect.

3.3. Effect of solvents

The effect of various solvents such as chloroform, toluene, benzene, carbon tetrachloride, amyl acetate, benzyl acetate, ethyl acetate, butyl acetate, xylene and monochlorobenzene on the extraction of cobalt with BAHA was studied. Chloroform (99.5%) was selected as the optimum solvent for its convenience and sensitivity. The other solvents in sequence gave only 98.1–84.1% extraction of cobalt.

3.4. Beer's law and sensitivity

Under optimum conditions, the cobalt–BAHA complex complied with Beer's law, the calibration

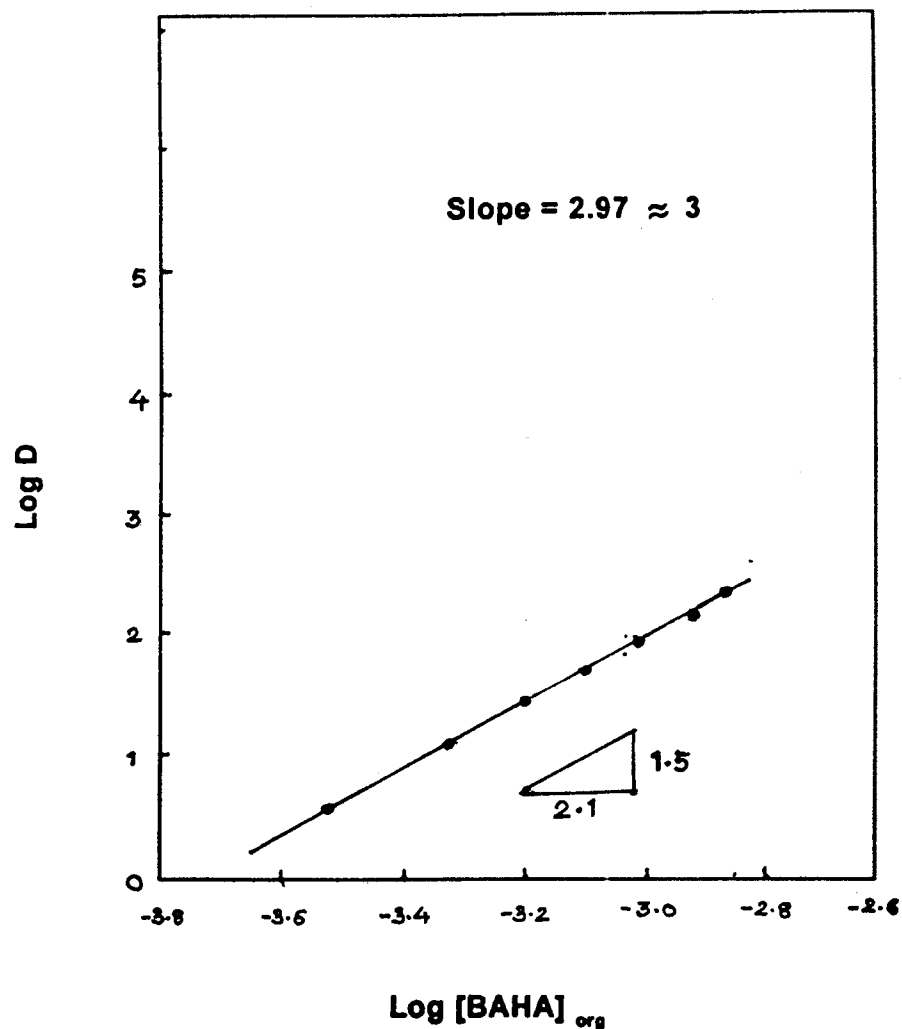


Fig. 3. Logarithmic plot of the distribution of cobalt vs. concentration of BAHA.

graph being linear over the range $0.05\text{--}1.3\ \mu\text{g ml}^{-1}$ cobalt in chloroform. The molar absorptivity of the system was found to be $2.746 \times 10^4\ \text{l mol}^{-1}\ \text{cm}^{-1}$ in Ringbom's [20] optimum working range of $0.42\text{--}1.05\ \mu\text{g ml}^{-1}$. The minimum detectable limit for an absorbance of 0.001 was $2.191\ \text{ng ml}^{-1}$ of cobalt at 390 nm.

3.5. Precision and accuracy

The precision and accuracy of the method were studied by analysing a series of solutions containing known amounts of cobalt(II). The results

presented in Table 1 show that the R.S.D. for pure cobalt solution is about 0.5%.

3.6. Composition of the extracted species

The composition of the complex was determined by the slope–ratio method, a plot of $\log D$ against $\log [\text{BAHA}]_{\text{org}}$ at a fixed pH where D denotes the distribution ratio of cobalt between the two phases and $[\text{BAHA}]_{\text{org}}$ is the equilibration concentration of BAHA in the organic phase. As shown in Fig. 3, a straight line graph with a slope of about 3 indicates a metal to ligand ratio of 1:3.

Table 2
Effect of foreign ions on the extraction of 10 µg cobalt with 0.02% BAHA in chloroform

Ion added	Tolerance limit (mg)	Ion added	Tolerance limit (mg)
Li ⁺	10	Hg ²⁺	0.5
Na ⁺	10	Sn ²⁺	10
K ⁺	10	Pb ²⁺	10
Ca ²⁺	10	Bi ³⁺	10
Mg ²⁺	10	Te ⁴⁺	10
V ⁴⁺	5	Se ⁴⁺	10
Mn ²⁺	5	W ⁶⁺	10
Al ³⁺	10	Cd ²⁺	0.5
Ti ³⁺	10	Fluoride	20
Cr ³⁺	1	Chloride	20
Ni ²⁺	0.5	Bromide	20
Cu ²⁺	0.2	Iodide	20
Ru ³⁺	0.2	Nitrate	20
Pd ²⁺	1	Acetate	20
Pt ⁴⁺	1	Tartrate	20
Zn ²⁺	5	Citrate	11
Mo ⁶⁺	10	Urea	20
U ⁶⁺	0.2	Thiourea	20
Au ³⁺	0.2	Cyanide	2
Rh ³⁺	0.05	Thiocyanate	20
Fe ^{3+a}	0.05	Sulfate	9
Ag ^{+b}	0.1	Sulfite	9
		EDTA	0.250

^a Masked with fluoride.

^b Masked with iodide.

3.7. Effect of foreign ions

Different amounts of diverse ions were added to 10 µg cobalt and were extracted according to the present procedure. The tolerance limit of an ion was taken as the maximum amount (mg)

causing an error not greater than $\pm 2\%$ in the absorbance value of the organic extract. Most of the ions associated with cobalt do not interfere, except Fe³⁺ and Ag⁺. The interference from large amounts of Ag⁺ can be overcome by masking with iodide. Attempts to suppress the interference of Fe³⁺ using citrate were partially successful. Fe³⁺ can be easily masked with fluoride ions. The results are shown in Table 2.

3.8. Preconcentration of cobalt

10 µg cobalt from different volumes of aqueous phase containing 0.4 ml 0.5% alcoholic BAHA was extracted in 10 ml chloroform by the recommended procedure. It was observed that the absorbance of the organic extract was found to remain constant when the aqueous phase taken was up to 70 ml indicating that the preconcentration of cobalt can be achieved up 7.0 times.

3.9. Application to the determination of cobalt in synthetic mixtures

The present method was applied to the determination of cobalt (10 µg) in various synthetic mixtures. The results are shown in Table 3.

3.10. Application to the determination of cobalt in pharmaceutical samples

The proposed method was applied to the determination of cobalt in injectables, liquid formulations and tablets obtained from available sources.

Table 3
Analysis of synthetic mixtures

Synthetic mixture composition ^a	Amount found ^b	S.D.	R.S.D. (%)
Co (10), Zn (200), Pb (500), V (1000)	9.98	0.404	0.441
Co (10), Fe (40), Hg (200), Mo (500)	10.00	0.045	0.450
Co (10), Cr (200), Ni (100), Se (200)	9.95	0.042	0.422
Co (10), Cd (300), Mn (400), Zn (400)	9.98	0.023	0.230
Co (10), Cu (100), Pd (300), Pt (500)	9.97	0.052	0.521
Co (10), Te (1000), Ag (80), Ti (500)	9.91	0.068	0.666

^a Values in parenthesis are in microgram amount of the metals.

^b Average of five determinations.

Table 4
Analysis of real samples

Sample	Concentration of cobalt ^a		S.D.	R.S.D. (%)
	Certified value	Amount found ^b		
Pharmaceutical samples				
Injectables				
Glaxo	4.35	4.347	0.0265	0.610
Merck	8.70	8.701	0.0503	0.578
Merind	8.76	8.760	0.0380	0.434
Liquid formulation				
B-G Prot elixir tonic (Merind)	0.163	0.159	0.0013	0.846
Tablets/capsules				
Surbex-T tablet (Abott)	0.326	0.321	0.0023	0.741
Fe-rich capsules (Maneesh Pharmaceuticals)	0.126	0.122	0.0097	0.794
Biological samples				
SRM ray flour (International Atomic Energy)	3.100	3.102	0.0168	0.543
High speed steel samples				
H.S.S.-3082	9.64	9.632	0.0400	0.416
H.S.S.-3083	10.16	10.164	0.0609	0.600
H.S.S.-3084	9.56	9.522	0.0542	0.568

^a Values in parenthesis are in microgram amounts of the metal.

^b Average of five determinations.

3.10.1. Sample dissolution

To 2 ml of injectable solution, 45 ml of liquid formulation or a tablet/capsule, concentrated sulfuric and nitric acids were added and evaporated until nearly dry. It was treated with hydrogen peroxide (5 ml, 30 V) every time, until the solution became colorless. Finally it was treated with dilute HCl and the solution was evaporated until nearly dry. The residue was dissolved in 10 ml double-distilled water and a suitable aliquot of this solution was used for cobalt analysis by the developed method. The results are shown in Table 4.

3.11. Application to the determination of cobalt in biological samples

The proposed method was applied to the determination of cobalt SRM ray flour (standard reference material supplied by International Atomic Energy) sample.

3.11.1. Sample dissolution

To a 10 g SRM ray flour sample was added distilled 70% nitric and concentrated HCl acids

and evaporated until nearly dry and the residue was extracted in 20 ml distilled water and a suitable aliquot taken of this solution for cobalt analysis by the developed method. The results are shown in Table 4.

3.12. Application to analysis of alloys

The proposed method was applied to the determination of cobalt in high speed steel samples.

3.12.1. Dissolution of high speed steel samples

About 0.2 g of an oven dried (110°C) high speed steel sample was dissolved in 15 ml of aqua regia. It was heated until nearly dry and nitrate expelled from the residue using 5 ml concentrated HCl. The residue was extracted in 20 ml distilled water and a suitable aliquot of this solution was used for cobalt analysis by the developed method. The results are shown in Table 4.

3.12.2. Determination of cobalt in samples

To a suitable aliquot of the above solutions containing cobalt in a separating funnel add 0.5 ml 0.5% alcoholic reagent solution (BAHA) and 1

ml pH 9.0 buffer. To this mixture add 2 ml of a saturated solution of sodium fluoride to mask the interfering ions. Dilute the mixture to 10 ml with double-distilled water and equilibrate the aqueous medium with 10 ml chloroform for 1.5 min. Allow the two layers to separate and measure the absorbance of organic extract containing the complex at 390 nm against a reagent blank.

4. Conclusion

The proposed method is more highly sensitive and selective than the reported methods for the spectrophotometric determination of microgram amounts of cobalt. It offers advantages like reliability and reproducibility in addition to its simplicity, instant color development and suffers from less interference. It has been successfully applied to the determination of cobalt at trace level in synthetic mixtures, pharmaceutical samples, biological samples and alloys. An R.S.D. of about 0.5% for sample analysis underlines the versatility of the developed method.

Acknowledgements

The authors wish to sincerely express their deep gratitude to the Director, Institute of Science for extending facilities to carry out this work and Mr S. Varadarajan for typing this manuscript.

References

- [1] Pathare, M.N., PhD Thesis, University of Mumbai, India, 1996.
- [2] J. Da Silva, W. Martins, *Talanta* 39 (10) (1992) 1307.
- [3] P.S. More, A.D. Sawant, *Indian J. Chem.* 31A (12) (1992) 984.
- [4] R.A. Chaudhari, A.D. Sawant, *Asian J. Chem.* 5 (1) (1993) 1.
- [5] M.I. Toval, P. Richer, L. Silva, S. Andrea, *Microchem. J.* 48 (2) (1993) 221.
- [6] Yamaguchi, Shigercku, Uesugi, Katsuya and Kumagai, *Tetsu Kenkyu Hokoku—Himeji Kogyo Daigaku Kogakubu*, 45 (1992) 8.
- [7] K.C. Kalika, A. Kumar, P. Rajeev, S. Rajeev, *Asian J. Chem.* 5 (3) (1993) 559.
- [8] B.R. Reddy, P.V.R. Sarma, ?. Bhaskara, *Talanta* 41 (8) (1994) 1335.
- [9] M. Kamburova, A. Alexandrov, K. Trifonov, *Chem. Anal.* 39 (5) (1994) 639.
- [10] C. Appadoo, V.W. Bhagwat, *Talanta* 6 (3) (1994) 703.
- [11] V. Maheshwari, N. Balasubramanian, *Fresenius Z. Anal. Chem.* 351 (2–3) (1995) 333.
- [12] H. Shen, Y. Tang, X. Xio, S. Zhang, R. Liu, *Analyst* 120 (5) (1995) 1599.
- [13] V.D. Pillai, V.M. Shinde, *Indian J. Chem.* 34A (5) (1995) 407.
- [14] Y. Yan, R. Su, Q. Wang, Y. Sang, Y. Ma, L. Hong, *Fenxi Shiyanshi* 14 (6) (1995) 36.
- [15] M.S. Carvalho, I.C.S. Fraga, K.C. Mateus, S. Nato, E.Q. Filho, *Talanta* 43 (1996) 1675.
- [16] R. Sharma, D.P. Dave, *Indian J. Chem.* 36A (7) (1997) 629.
- [17] A.M. Khambekar, A.D. Sawant, *Indian J. Chem.* 36A (5) (1997) 459.
- [18] H. Muller, H.V.J. Pechmann, *Chem. Soc.* 58 (1890) 51.
- [19] Vogel, A.I., *Textbook of Quantitative Inorganic Analysis*, 3rd ed., English Language Book Society, London, 1975.
- [20] A. Ringbom, *Z. Anal. Chem.* 115 (1938) 332.
- [21] M.A. Taher, B.K. Puri, *Analyst* 120 (1995) 1589.
- [22] S.L.C. Ferreira, D.S. De Jesus, *J. Braz. Chem. Soc.* 7 (2) (1996) 109.

Second derivative spectrophotometric determination of partition coefficients of phenothiazine derivatives between human erythrocyte ghost membranes and water

Keisuke Kitamura *, Takashi Goto, Tatsuya Kitade

Kyoto Pharmaceutical University, 5 Nakauchicho, Misasagi, Yamashina-ku, Kyoto 607, Japan

Received 23 June 1997; received in revised form 15 December 1997; accepted 17 December 1997

Abstract

The absorption spectra of six phenothiazine derivatives, chlorpromazine, triflupromazine, promazine, promethazine, trifluoperazine and prochlorperazine, measured in the solutions containing various amounts of human erythrocyte ghosts (HEG) showed bathochromic shifts according to the amount of HEG. Due to the strong background signals caused by HEG, the baseline compensation was incomplete, even though the sample and the reference solutions contained the same amount of HEG, hence further spectral information could not be obtained. The second derivative spectra of these absorption spectra clearly showed the derivative isosbestic points, indicating that the residual background signal effects were entirely eliminated. The derivative intensity differences of the phenothiazines (ΔD values) before and after the addition of HEG were measured at a specific wavelength. Using the ΔD values, the partition coefficients (K_p) of these drugs were calculated and obtained with R.S.D. of below 10 %. The fractions of partitioned phenothiazines calculated from the K_p values agreed well with the experimental values. The results indicate that the derivative method can be applicable to the determination of partition coefficients of drugs to HEG without any separation procedures. © 1998 Elsevier Science B.V. All rights reserved.

Keywords: Absorption spectra; Human erythrocyte ghosts; Phenothiazine derivatives; Derivative spectrophotometry

1. Introduction

Partition of drugs between an aqueous phase and biomembranes has been an important subject for study [1–7] since it concerns the drug absorption and/or the direct actions of drugs to biomembranes. Determination of partition coefficients of

drugs to biomembranes has usually been accompanied by separation procedures such as centrifugation or filtration to measure the concentrations of free drugs or the amounts of bound drugs [1–6]. However, the separation procedures are troublesome and may disturb the equilibrium states of sample solutions and also lead to errors due to the possibilities of residue of membrane fragments in the supernatants of sample solutions or nonspecific adsorption of drugs onto filter membranes.

* Corresponding author. Fax: +81 75 5954760; e-mail: kitamura@mb.kyoto-phu.ac.jp

It has been recognized that derivative spectrophotometry can eliminate the effect of background signals and hence does not require optically clear sample solutions [8,9]. We previously applied the second derivative spectrophotometry [10] to the determination of partition coefficients of chlorpromazine and promazine between model membranes (lecithin vesicles) and water (buffer). In this study, we attempt to determine partition coefficients of six phenothiazine drugs between human erythrocyte ghosts (HEG) and water by the second derivative spectrophotometry. The results will show usefulness of the derivative method for the determination of partition coefficients of drugs to HEG. The effect of structural difference of six phenothiazines on their affinity to HEG is also discussed.

2. Theory

The molar partition coefficient of phenothiazine between lipid bilayer of HEG and water is defined as [10],

$$K_p = \frac{([P_m]/[P_t])/[M]}{([P_w]/[P_t])/[W]} \quad (1)$$

where $[P_m]$ and $[P_w]$ represent the concentrations of phenothiazine in the lipid bilayer of HEG membranes and water, respectively, and $[P_t]$ equals to the total amount of phenothiazine added ($[P_t] = [P_m] + [P_w]$), and $[M]$ and $[W]$ are molar concentrations of lipid in HEG membranes and water (55.5 M), respectively.

If the effect of background signal caused by HEG can be entirely eliminated in the derivative spectrum, the derivative intensity (denoted as D) of a phenothiazine at a specific wavelength is represented as follows,

$$D = E_m[P_m] + E_w[P_w]$$

where, E_m and E_w are the molar derivative intensities for $[P_m]$ and $[P_w]$, respectively. With a definition, $E = E_m - E_w$, D can be written as

$$D = E_w[P_t] + E[P_m] \quad (2)$$

A new variable ΔD is introduced to represent the difference between D and $E_w[P_t]$ as below,

$$\Delta D = D - E_w[P_t] \quad (3)$$

From Eq. (2),

$$\Delta D = E[P_m] \quad (4)$$

Thus the ΔD value is proportional to the concentration of phenothiazine in HEG membranes.

Finally, from Eqs. (1) and (4), we can get,

$$\Delta D = \frac{K_p \Delta D_{\max} [M]}{[W] + K_p [M]} \quad (6)$$

where $\Delta D_{\max} = E[Pt]$. The values of K_p and ΔD_{\max} are calculated from the experimental values of $[M]$ and ΔD by applying a non-linear least-squares calculation to Eq. (6) [10].

3. Experimental

3.1. Reagents, materials and apparatus

Chlorpromazine hydrochloride (CPZ), trifluorpromazine hydrochloride (TFZ), promazine hydrochloride (PZ), promethazine hydrochloride (PMZ), trifluoperazine hydrochloride (TFPZ) and prochlorperazine dimaleate (PCPZ) were purchased from Sigma (USA). All other chemicals were reagent grade. Absorption spectra were measured by a spectrophotometer (Hitachi U-3210) equipped with a temperature regulated cell holder. Calculations of second derivative spectra and values of K_p and ΔD_{\max} were performed using BASIC programs on a pc (NEC PC-9801 VX) [10,11].

3.2. Human erythrocyte ghosts

Human erythrocytes were washed three times with 20 volumes of a phosphate buffer (PBS; 10 mM phosphate, 140.5 mM NaCl, pH 7.4) and each time the buffy coat was removed after centrifuged at $900 \times g$ for 5 min. The erythrocytes were suspended in PBS to make 40–50% haematocrit values. HEG were prepared according to the method of Dodge et al. [12]; one volume of the erythrocyte suspension was dissolved in 10 volumes of PBS. Then the obtained suspension was centrifuged at $20000 \times g$ for 20 min, and

hemoglobin and non-sedimentary erythrocytes in the supernatant were removed. These procedures were repeated three times. The HEG obtained were suspended in PBS to make about 1 mM of phosphorous.

3.3. Determination of lipid concentration of HEG

Phospholipid concentration in HEG suspensions was determined from phosphate analysis [13]. Lipid concentration of HEG suspensions was considered to be a sum of the concentrations of phospholipid and sterol assuming that HEG contains 0.90 mol of sterol mol⁻¹ of phospholipid [4]. The other minor lipid contents were ignored.

3.4. Procedure

To each of several 2 ml volumetric flasks, an appropriate amount of a phenothiazine stock solution was added so that the final drug concentration in the sample solutions became 15 μM. Then suitable amounts of HEG suspension were added to the flasks, and the PBS was further added to make up to volume. Each flask was shaken for a short time and incubated at 37°C for 60 min. The sample solution was added in a black micro quartz cuvette having a 1 cm light-pass length and 0.5 cm width and the sample cuvette was set in the cell holder which was maintained at 37°C. After 10 min, the absorption spectrum was recorded against the reference buffer solution containing the same amount of HEG as the sample solution with a band path of 2 nm, wavelength interval of 0.1 nm and a scan speed of 15 nm min⁻¹.

4. Results and discussion

4.1. Absorption and second derivative spectra

The absorption spectra of CPZ and PCPZ in the sample solutions containing various amounts of HEG are shown in Fig. 1A and B, respectively, as the examples of six phenothiazine derivatives studied. The absorption maxima of both drugs

show bathochromic shifts according to the increase in the HEG amounts of the sample solutions, indicating the partition of CPZ and PCPZ into the lipid bilayer of HEG membranes [4]. But, even though the solutions in the sample and reference cuvettes contain the same amount of HEG, the counterbalance of the sample and reference beams is incomplete as seen in Fig. 1. It is usually difficult to cancel the background signal effects completely when the background signal level is very high. Thus, further spectrophotometric data

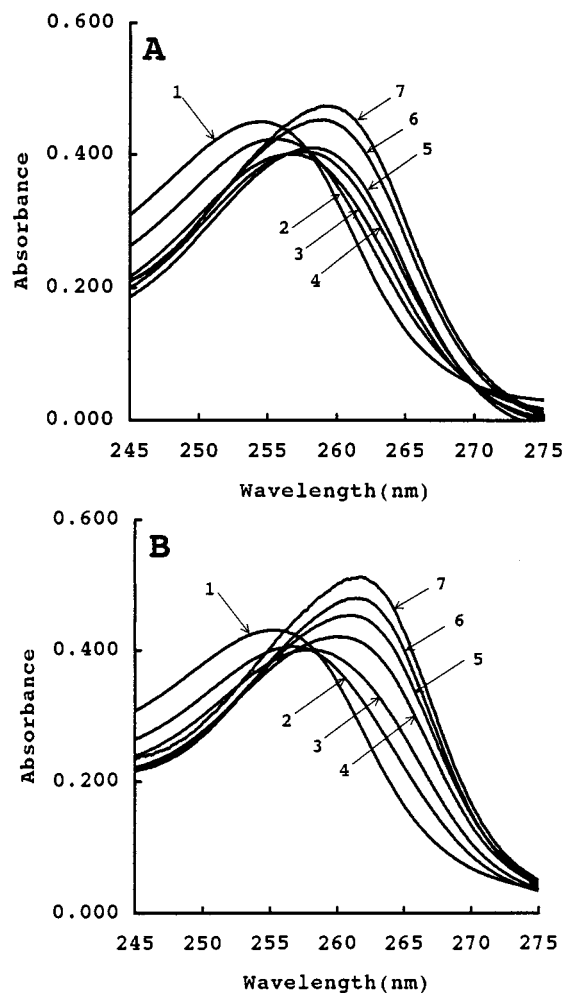


Fig. 1. Absorption spectra of 15 μM chlorpromazine (A) and prochlorperazine (B) in phosphate buffer solutions (pH 7.4, 37°C) containing various amounts of HEG. HEG concentration (mM): 0 (1), 0.060 (2), 0.120 (3), 0.180 (4), 0.240 (5), 0.360 (6), and 0.600 (7).

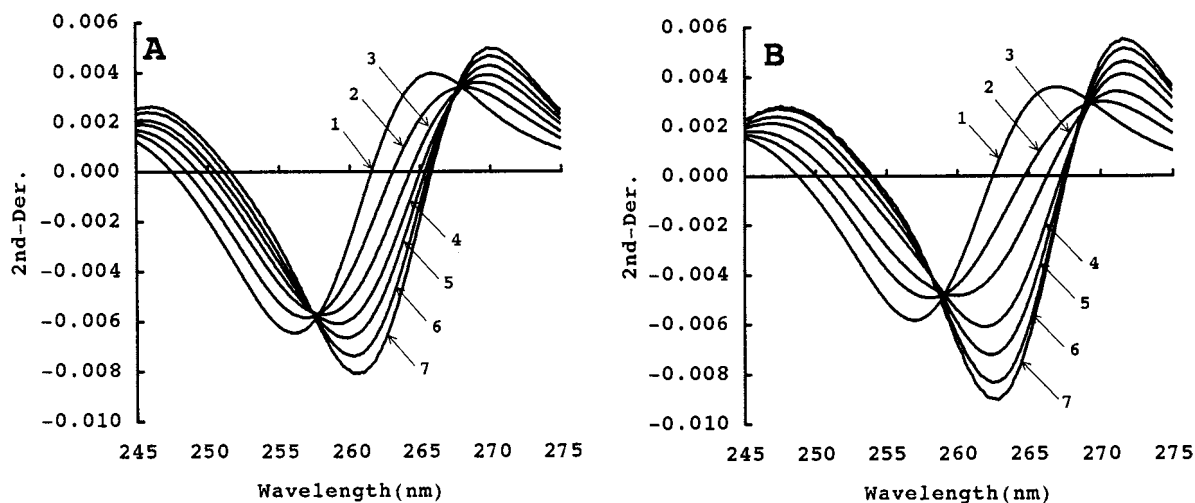


Fig. 2. Second derivative spectra of chlorpromazine (A) and prochlorperazine (B) calculated from the absorption spectra of Fig. 1A and B, respectively. The numbers in the figures are the same as in Fig. 1.

can not be drawn from these absorption spectra. The absorption spectra of the rest of the phenothiazine derivatives showed similar features.

To eliminate the residual background signal effects, the second derivative spectra were obtained from the absorption spectra. It has been known that in the calculation of second derivative spectra too small $\Delta\lambda$ values (the wavelength interval) enhance the noise in the second derivative spectra, and too large $\Delta\lambda$ values cause signal distortions [10]. As the background signal intensities of HEG suspensions are much higher than those of the lecithin vesicle solutions, a larger $\Delta\lambda$ value of 0.8 nm than the value of 0.5 nm for the lecithin vesicle solutions [10] was employed to suppress the generation of noises in the second derivative spectra.

The second derivative spectra obtained from the absorption spectra in Fig. 1A and B are shown in Fig. 2A and B, respectively. Similarly to Fig. 1, bathochromic shifts are observed with the increase in the amounts of HEG in the sample solutions. A noteworthy difference from the original absorption spectra is that the derivative isosbestic points are clearly observed at the wavelengths near 258 and 268 nm for CPZ in Fig. 2A and 259 and 269 nm for PCPZ in Fig. 2B, respectively. The second derivative spectra of the

sample solutions of the another phenothiazine derivatives studied also showed the derivative isosbestic points. The existence of the derivative isosbestic points indicates that the influences of the residual background signal of HEG are entirely eliminated in the second derivative spectra, and that each phenothiazine exists in two states, [14], i.e. in polar bulk water and non-polar lipid membranes of HEG.

4.2. Calculation of K_p and ΔD_{max}

The ΔD values for CPZ or PCPZ were obtained as the differences of the derivative values between the spectrum 1 and spectra 2–7 in Fig. 2A or B at the wavelength of 262 or 263 nm, respectively, since large ΔD values could be obtained at these wavelengths as seen in Fig. 2. It has been already confirmed that the wavelength at which ΔD values are measured do not largely affect the calculated K_p and ΔD_{max} values and large ΔD values will result in a good precision for the K_p values [10]. The wavelengths at which the ΔD values of the rest of the phenothiazine derivatives were measured are given in Table 1.

Using the experimentally obtained ΔD values, the K_p and ΔD_{max} values were calculated. As summarized in Table 1, the K_p values of six

phenothiazine derivatives were obtained with R.S.D. of below 10 %. The results indicate a good precision of the derivative method.

The K_p value of CPZ (10 μM) obtained by difference spectrometry [4] has been reported to be 6.5×10^5 . The partition coefficient based on the HEG membrane volume has been also obtained for CPZ by filtration [1] and centrifugation [6] methods. The reported values are converted to K_p values according to [4], yielding 4.0 and 2.6×10^5 , respectively. The K_p value of CPZ in Table 1 is within these values.

The K_p values of CPZ and PZ between egg yolk lecithin vesicles and water are reported to be 2.93 and 1.15×10^5 , respectively [10]. It seems interesting that these values show a resemblance to the corresponding results in Table 1.

As the K_p values of six phenothiazine derivatives are obtained with good precision, the effect of the structural difference of these compounds on their affinity to HEG membranes is considered. The phenothiazine derivatives studied can be divided into two types with respect to the polar side chain group: one having a *N*-dimethylaminopropyl group (TFZ, CPZ, PMZ and PZ), and the other is having an *N*-methylpiperazinylpropyl group (TFPZ and PCPZ).

In the former type, the K_p values show that the introduction of halogen atom(s) to phenothiazine rings increased the affinity of the drugs to HEG membranes, according to the order of $\text{CF}_3 > \text{Cl} > \text{H}$. The result is consistent with those obtained from the shape changes of human erythrocytes [2], and a microcalorimetric study [7].

Table 1
 K_p values of phenothiazine derivatives

Compound	Wavelength (nm)	$K_p^a (\times 10^{-5})$
CPZ	262 ^b	3.1 ± 0.2 (6)
TFZ	264 ^b	3.7 ± 0.2 (4)
PZ	259 ^b	1.6 ± 0.1 (4)
PMZ	257 ^b	1.5 ± 0.1 (5)
TFPZ	265 ^b	4.6 ± 0.1 (4)
PCPZ	263 ^b	4.5 ± 0.3 (4)

^a Mean \pm S.D. (number of determination).

^b Wavelength (nm) at which ΔD values were measured.

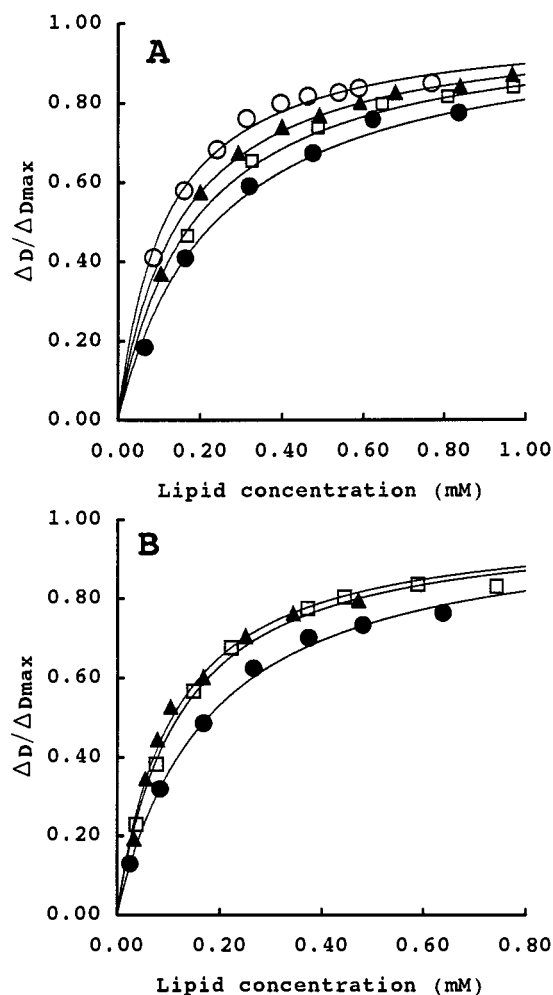


Fig. 3. Fraction ($\Delta D/\Delta D_{\text{max}}$) of phenothiazine derivatives in HEG membranes at various HEG concentrations. The solid lines show the theoretical curves calculated from Eq. (6) using the K_p obtained and ΔD_{max} values. The symbols are the experimental values: CPZ (○), TFZ (●), PZ (△), PMZ (▲), TFPZ (□), and PCPZ (■).

Since the K_p values of the latter type are larger than those of the former type, the partition of the phenothiazine to HEG membranes seems to be affected also by the polar side chain groups. From the results and discussion above it can be seen that not only the hydrophobic interactions of the phenothiazine rings with the acyl chains of the membrane lipids but also the effects of a polar side chain group might contribute to the interac-

tions of the phenothiazine derivatives with HEG membranes.

In Fig. 3, the fractions of six phenothiazine derivatives partitioned in HEG are shown as a plot of the $\Delta D/\Delta D_{\max}$ values versus the lipid concentration of HEG. Solid lines represent theoretical curves calculated from the K_p and ΔD_{\max} values according to Eq. (6). The all curves are well fitted to the experimental data.

Conclusively, it can be emphasized that, when the drugs of interest show spectral changes according to their partition to HEG membranes, the derivative spectrophotometry will be applicable to the determination of their partition coefficients between HEG membranes and water without separation procedures.

Acknowledgements

The authors are indebted to Professor T. Sato for his support in preparation of human erythrocyte ghosts and to Yumiko Kimura for her technical assistance.

References

- [1] B. Bondy, J. Remien, *Life Sci.* 28 (1981) 441.
- [2] Y. Kanaho, T. Sato, T. Fujii, *Mol. Pharmacol.* 20 (1981) 704.
- [3] M.R. Lieber, Y. Lange, R.S. Weinstein, T.L. Steck, *J. Biol. Chem.* 259 (1984) 9225.
- [4] R. Welti, L.J. Mullin, T. Yoshimura, G.M. Helmkamp Jr., *Biochem.* 23 (1984) 6086.
- [5] M. Luxnat, H.-J. Galla, *Biochim. Biophys. Acta* 856 (1986) 274.
- [6] A. Zachowsky, P. Durand, *Biochim. Biophys. Acta* 937 (1988) 411.
- [7] H. Aki, M. Yamamoto, *J. Pharm. Pharmacol.* 42 (1990) 637.
- [8] G. Talsky, L. Mayring, H. Kreuzer, *Angew. Chem. Int. Ed. Engl.* 17 (1978) 785.
- [9] F.S. Rojas, C.B. Ojeda, J.M.C. Pavon, *Talanta* 35 (1988) 753.
- [10] K. Kitamura, N. Imayoshi, T. Goto, H. Shiro, T. Mano, Y. Nakai, *Anal. Chim. Acta* 304 (1995) 101.
- [11] K. Kitamura, K. Hozumi, *Anal. Chim. Acta* 172 (1985) 111.
- [12] J.T. Dodge, C. Mitchel, D.J. Hanahan, *Arch. Biochem. Biophys.* 100 (1963) 119.
- [13] A.J. Christopher, T.R.F.W. Fennell, *Microchem. J.* 12 (1967) 593.
- [14] K.A. Connors, *Binding Constants*, Wiley, New York, 1987, p. 142.

Determination of pK_a 's for thymol blue in aqueous medium: evidence of dimer formation.

Patricia Balderas-Hernández^{a,b}, M.Teresa Ramírez^{a,*}, Alberto Rojas-Hernández^a, Atilano Gutiérrez^a

^a Departamento de Química, Universidad Autónoma Metropolitana-Iztapalapa, Apdo. Postal 55-534, C.P. 09340, México D.F., Mexico

^b Facultad de Estudios Superiores Cuautitlán, U.N.A.M., Sección de Química Analítica, Av. Quetzalcóatl s/n Cuautitlán Izcalli, Estado de México, C.P. 54740, Mexico

Received 26 June 1997; received in revised form 15 December 1997; accepted 17 December 1997

Abstract

Formation constants for recrystallized thymol blue were determined in water, using the SQUAD and SUPERQUAD programs. The best model correlating spectrophotometric, potentiometric and conductimetric data was fitted with the dissociation of $HL^- = L^{2-} + H^+ - \log K = 8.918 \pm 0.070$ and $H_3L_2^- = 2L^{2-} + 3H^+ - \log K = 29.806 \pm 0.133$ with the SUPERQUAD program at variable low ionic strength (1.5×10^{-4} – 3.0×10^{-4} M); and $HL = L^{2-} + H^+ - \log K = 8.9 \pm 0.000$, $H_3L_2^- = 2L^{2-} + 3H^+ - \log K = 30.730 \pm 0.032$, $H_4L_2 = 2L^{2-} + 4H^+ - \log K = 32.106 \pm 0.033$ with SQUAD at 1.1 M ionic strength. © 1998 Elsevier Science B.V. All rights reserved.

Keywords: Aqueous medium; Formation constants; Recrystallized thymol blue

1. Introduction

Determination of equilibrium constants for acid–base indicators has long been a concern in analytical chemistry. Thermodynamic information associated with these constants is mainly useful for determining the end point in acid–base reactions. Because of their binding properties, the applications of indicators have recently been ex-

tended to include their use in the spectrophotometric determination of cations. Therefore, accurate determination of equilibrium constants of the best possible certainty, is of crucial importance.

The sulfonephthalein family of indicators are currently used extensively. Several publications have reported equilibrium constants for the thymol blue family members in aqueous medium: (a) Kolthoff et al. [1–3] determined pK_a values using the limit law of Debye–Hückel, 1.65 and 9.2; (b) Nørgaard [4] reported pK_a values for EFA (evolving factor analysis, 8.87) and for PLS (partial

* Corresponding author. Tel.: +52 5 7244670; fax: +52 5 7244666; e-mail: mtrs218@xanum.uam.mx

least-squares regression, 8.76 and 8.73); and (c) Casula et al. [5] a spectrophotometric method based on the SPECFIT program, reported a pK_a value of 8.47. However at least two pK_a values are reported and in most of the cases the indicator was not purified prior to use.

Kolthoff's studies determined pK_a values for thymol blue in water, in methanol [1], ethanol [2], dimethylsulfoxide [6], *N,N*-dimethylformamide [7], and acetonitrile [3]. Kolthoff proposed a model with three pK_a values in acetonitrile medium. In an attempt to refute or reinforce Kolthoff's model in water, we applied spectrophotometric, conductimetric and potentiometric methods and executed, SQUAD, SUPERQUAD, and SIBYLA (see below for the description of these programs) to determine the equilibrium constant values for purified thymol blue in water over the widest possible pH range.

2. Methods

2.1. Purification

As indicators are not generally of high purity, it is necessary to purify and verify them prior testing because impurities can affect the experimental determinations and the final results. In previously published reports on acidity constants [5] for thymol blue, only Kolthoff [1–3] purified the indicator. In the present study, purification was completed prior to any quantitative experimentation to avoid deviations due to impurities. Thymol blue supplied by Merck was purified and recrystallized in 30% (v/v) acetic acid solution. Purity was assessed by determining the melting point using the Fisher method in a Sybron Powerstat (Thermoline) by the Thiel's Tube method. The IR absorption spectra were obtained for the recrystallized solid in a TF-IR 1600, Perkin-Elmer spectrophotometer, and it was compared with the one reported in the FT-IR spectra catalog [8]. Table 1 shows that the melting point of recrystallized thymol blue agrees with that reported in [8], whereas that of the crude substance does not. The recrystallized thymol blue was then used in its purified form for all experiments.

2.2. Spectrophotometric determination

2.2.1. Absorbance versus time studies

To demonstrate absorbance on time independence during the measurements, absorbance was monitored for 7 days for 2.5×10^{-5} M thymol blue solutions at pH 0.00, 4.84 and 13.00. A maximum variation of 2.7% was observed over this period.

2.2.2. Spectrophotometric data

Two aqueous solutions of 2.50×10^{-5} M thymol blue were prepared, one at pH 0.0 (adjusted with HCl) and the other at pH 13.0 (adjusted with NaOH), each with an ionic strength of 1.1 M NaCl. The experiment was carried out in two steps:

1. The thymol blue 13.0 pH solution was added to the 0.0 pH thymol blue solution until the pH reached 7.0.
2. The thymol blue 0.0 pH solution was added to the 13.0 pH thymol blue solution until the pH reached 7.0.

Absorbance was recorded every 0.25 pH units in a UV-Vis Beckman DU-65 spectrophotometer and pH values were monitored using a Corning model 250 pH-meter equipped with a combined (glass–AgCl/Ag) electrode. These values were corrected for cell efficiency. Constant temperature was kept at $25 \pm 0.1^\circ\text{C}$ with a Lauda temperature controller water bath model T-1.

2.3. Nuclear magnetic resonance (NMR)

Thymol blue NMR spectra were acquired on a Bruker DMX500 NMR spectrometer at a constant temperature (25°C) in CD_3OD (Aldrich),

Table 1
Fusion points for thymol blue using the Thiel tube and Fisher methods

Thymol blue	Fusion point ($^\circ\text{C}$)		
	Reported	Thiel tube	Fisher
As supplied	221	207–208	208–210
Recrystallized		221–222	220–222

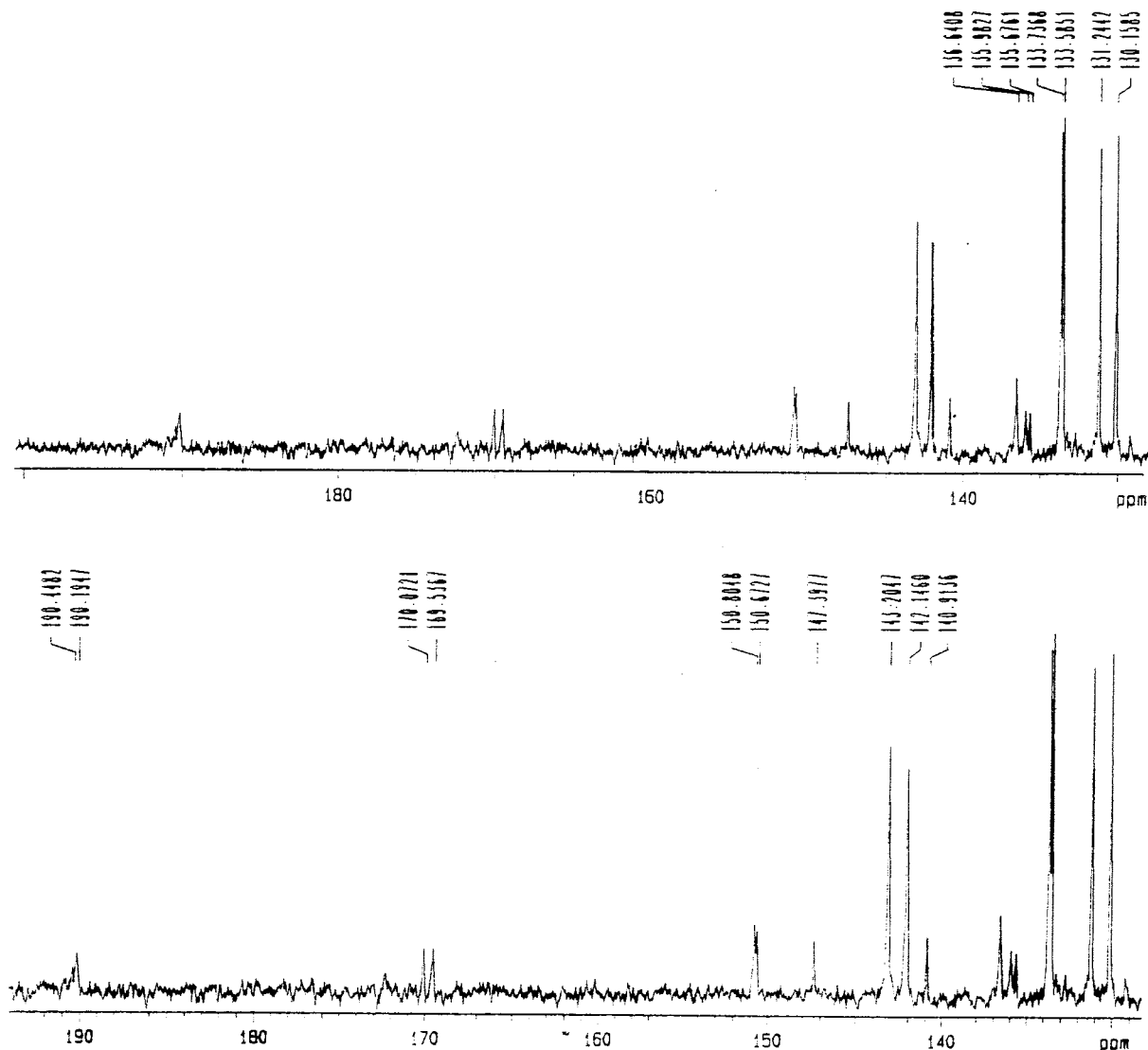


Fig. 1. Thymol blue ^{13}C NMR spectrum in acid medium at 25°C (only the low field part is shown).

using a 5 mm inverse Z-gradient probe. The pH was adjusted by KOH (Merck) or HCl (Mallinckrodt) addition.

2.4. Potentiometric and conductimetric determinations

The titrations of 5.0×10^{-5} , 1.0×10^{-4} or 2.5×10^{-4} M thymol blue solutions were performed under a nitrogen gas inert atmosphere

(Linde Suprapur), with 1.0×10^{-3} or 2.0×10^{-3} M NaOH (Sigma) as the added solutions, at a constant temperature of $25 \pm 0.1^\circ\text{C}$ with a Cole Parmer temperature controller model 12101-10.

The potentiometric response was followed using a Radiometer-Tacussel TTP2 automatic titrator and BX3 automatic burette, or Radiometer-Tacussel LPH430T potentiometer ($\text{pH} \pm 0.001$) equipped with a combined (glass–AgCl/Ag) electrode with inbuilt temperature probe and a Pyrex

burette (10 ± 0.01 ml). Simultaneous spectrophotometric measurements were conducted at some added volumes during these titrations using a Perkin-Elmer Lambda 17 UV-Vis spectrophotometer. Cell potentials were corrected for cell efficiency [9].

The conductimetric response was registered using a Cole Parmer model 19101-00 digital conductivity meter ($\pm 0.1 \text{ m}\Omega^{-1}$) equipped with a dip gold cell and a Pyrex burette (10 ± 0.01 ml).

2.5. Computational programs

SQUAD [10,11] was designed to calculate the best value for stability constants in a proposed model by minimizing the sum of residual squares for absorbance. The program can refine stability constants for complexes such as $M^pM^qL^rL'sH_j$, where $p, q, r, s = 0$ and j is positive (for protons), negative (for hydroxide ions) or zero. For this reason the program is often chosen for acid base equilibria studies in which the species can be weak acids or bases.

SUPERQUAD [11,12] refines equilibrium constant values by minimizing the sum of residual squares for cell potentials. The program also calculates other statistical parameters as χ^2 and the total S.D. (s).

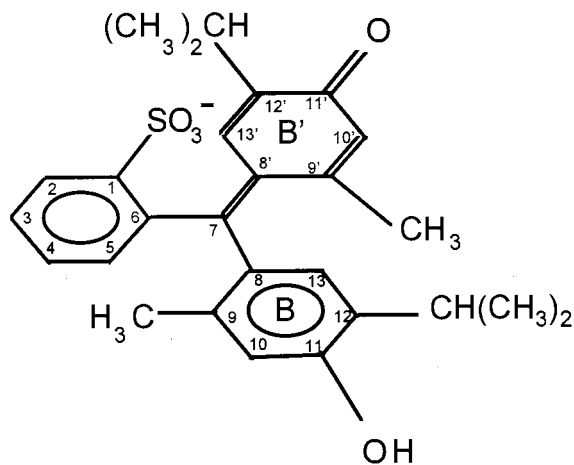


Fig. 2. Thymol blue structure. The carbon atoms in the aromatic rings are labelled.

SIBYLA [13] applies the analysis factor algorithm and Fourier convolution theorem. Principal component analysis (PCA) is the basic multivariate statistical technique of factor analysis. The PCA and factor analysis (FA) techniques involve the analyses of an $m \times n$ data matrix. These can be m spectra (or any others observations) each containing values for n channels (variables). Each 'spectrum' can be represented as a point in a multidimensional space. The FA and PCA techniques are used to find a p -dimensional subspace ($p < n$) in which the spectrum can be approximately represented.

It is important to note that the best model for the programs that use the least squares algorithm (e.g. SQUAD and SUPERQUAD) is the one that reports the smallest value for the sum of square residuals (U). The residuals are the differences between the determined and calculated values of a physicochemical property.

3. Results and discussion

3.1. ^1H NMR and ^{13}C NMR analysis

On the ^{13}C NMR spectrum of thymol blue at $\text{pH} < 2$ (Fig. 1), the broad signal centered at 190.19 ppm was assigned to C-7 (Fig. 2). This low field shift agrees with a carbon having carbocation character. Assignment of C-7 was confirmed by an inverse detection C- H_n long range correlation experiment. The corresponding 2D spectrum (Fig. 3) clearly shows C- H_n correlations between C7-H5 and C7-H13. These data agree with the proposed structure H_3L^+ (Fig. 4 (V)), as proposed by Kolthoff [3]. Nevertheless, the NMR spectra also could be assigned to H_4L_2 species because the techniques used can not distinguish between monomeric or dimeric species.

On the other hand, the ^{13}C NMR spectrum of thymol blue, acquired under alkaline conditions ($\text{pH} > 13$) (Fig. 5), has signals which appear at 180.42 and 179.63 ppm. These were assigned to C-11 and C-11' based on their respective C- H_n long range correlations. Its corresponding ^1H

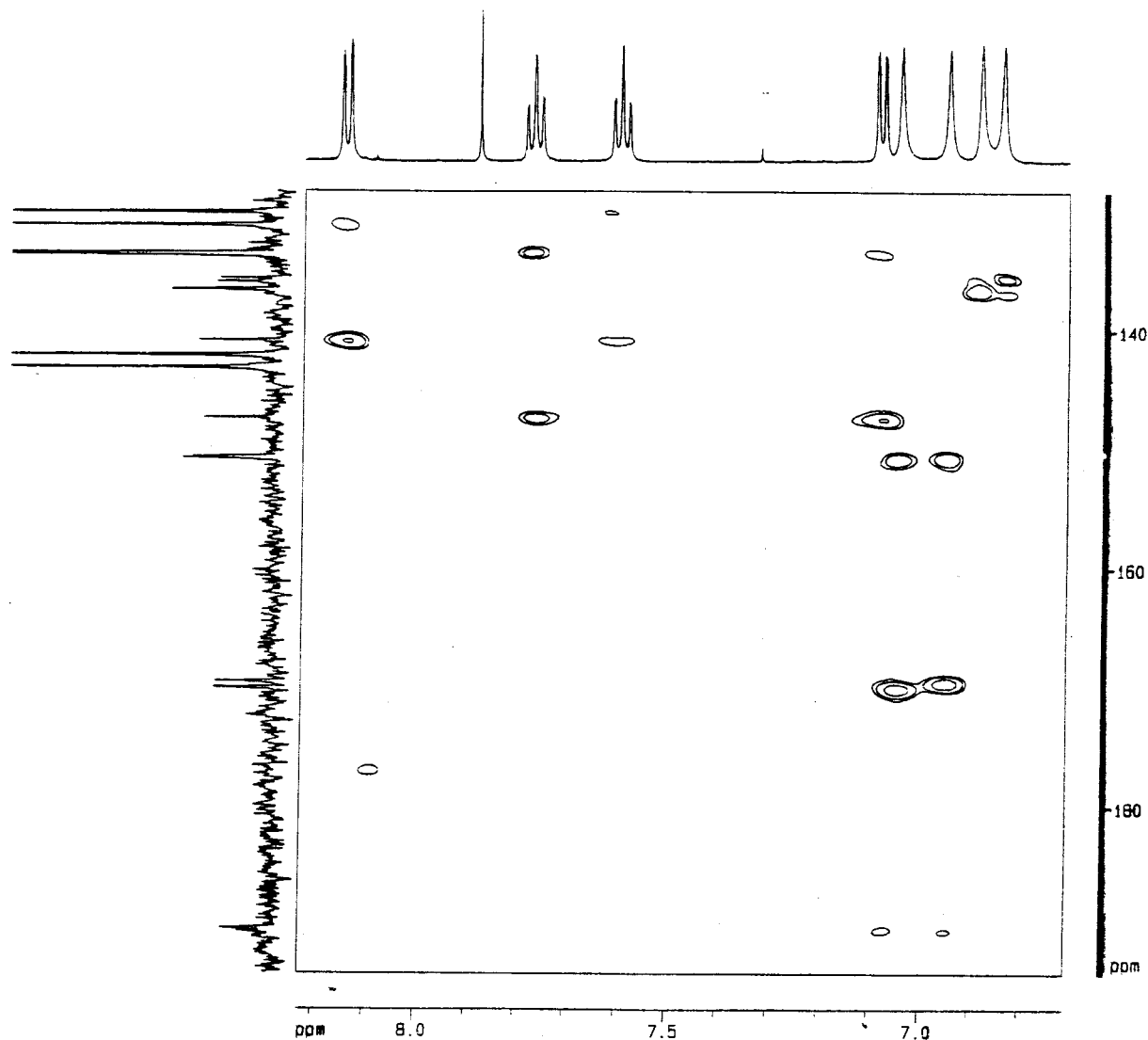


Fig. 3. Thymol blue 2D inverse detection C-H_n long range correlation spectrum in acid medium at 25°C (only part of the plot is shown).

NMR spectrum (Fig. 6) shows evidence for the presence of tautomeric species. There is a pair of signals for the methyls directly attached to the B and B' rings and for the H-10, H-10', H-13 and H-13' hydrogens. This strongly suggests a structure which is in accordance with L²⁻ (Fig. 4, I).

The NMR studies also confirm the high purity of the recrystallized thymol blue, used in the titrations.

3.2. pH variation of thymol blue—spectrophotometric study

Fig. 7a shows typical absorption spectra behavior for a 2.50×10^{-5} M thymol blue solution as a function of pH. At $\text{pH} \leq 1.22$, two absorption bands appear at 390 and at 545 nm. For pH between 2 and 7.5, absorption bands are observed at 430 and 545 nm, and for pH 8.0, the bands are

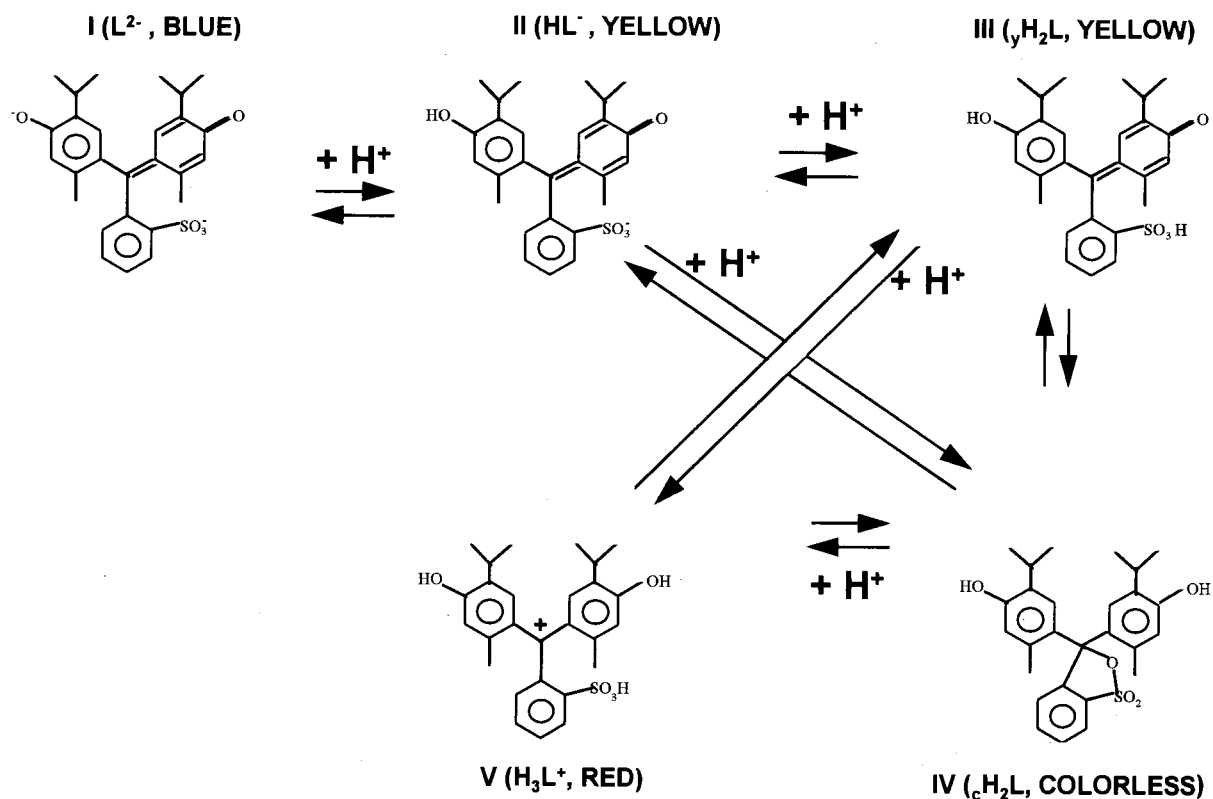


Fig. 4. Model proposed by Kolthoff [3] of three acid–base equilibria. ${}_yH_2L$ and ${}_cH_2L$ correspond to two different chemical species.

present at 390 and 600 nm. Fig. 7b shows identical behavior for a 2.5×10^{-4} M thymol blue solution.

3.3. Determination of the number of absorbing species

In order to determine the number of absorbing species, the absorbance matrices were analyzed at different pH and wavelengths values using SIBYLA for the two different concentrations. The program indicated that the absorbance data must have resulted from 3 or 4 different experimental factors. This implies the presence of at least 3 or 4 absorbing species over the pH interval studied. This is consistent with the Kolthoff model [3] (Fig. 4) which proposed three acid–base equilibria.

3.4. Acid–base titrations

Fig. 8 shows the typical behavior of thymol blue titrations with NaOH followed potentiometrically. It can be seen that in the concentration range studied only the first of the titration reaction is quantitative, because the second one has a low equilibrium constant value. In the same way Fig. 9 shows this same typical titrations but followed conductimetrically. In this case both titration reactions are observed. Results for both methods can be compared successfully.

3.5. Chemical models

As the solutions titrated were prepared from neutral species and following the scheme pro-

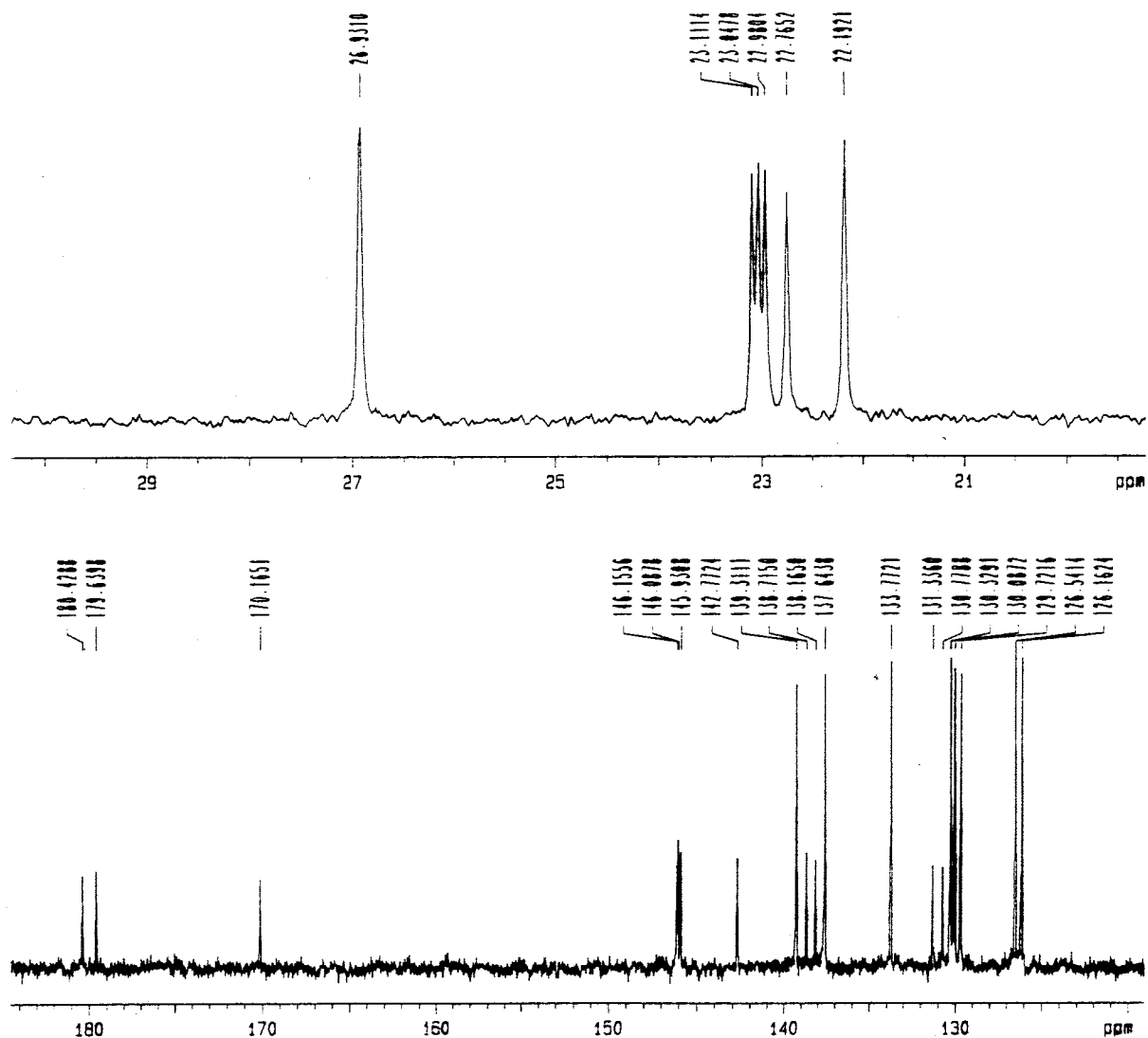
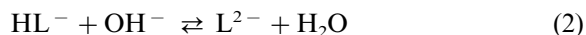
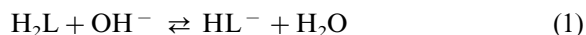


Fig. 5. Thymol blue ^{13}C NMR spectrum in alkaline medium at 25°C .

posed by Kolthoff [3], the titration reactions should be:



The visible or apparent equivalence point could be assigned to the first titration reaction in Eq. (1). However, the calculated end point differs from the experimental value by a factor of 2 ($v_{\text{ep}}(\text{calculated}) = 2v_{\text{ep}}(\text{experimental})$). A dimerization of the neutral and negatively monocharged

species is proposed to explain this 2-fold factor.

It was then, necessary to consider both possibilities in the refining procedure of the equilibrium constants by the SQUAD and SUPERQUAD.

3.6. Equilibrium constants determination by computational methods

The results for SQUAD and SUPERQUAD for the best refining obtained with several models are reported in Table 2. This information allows us to

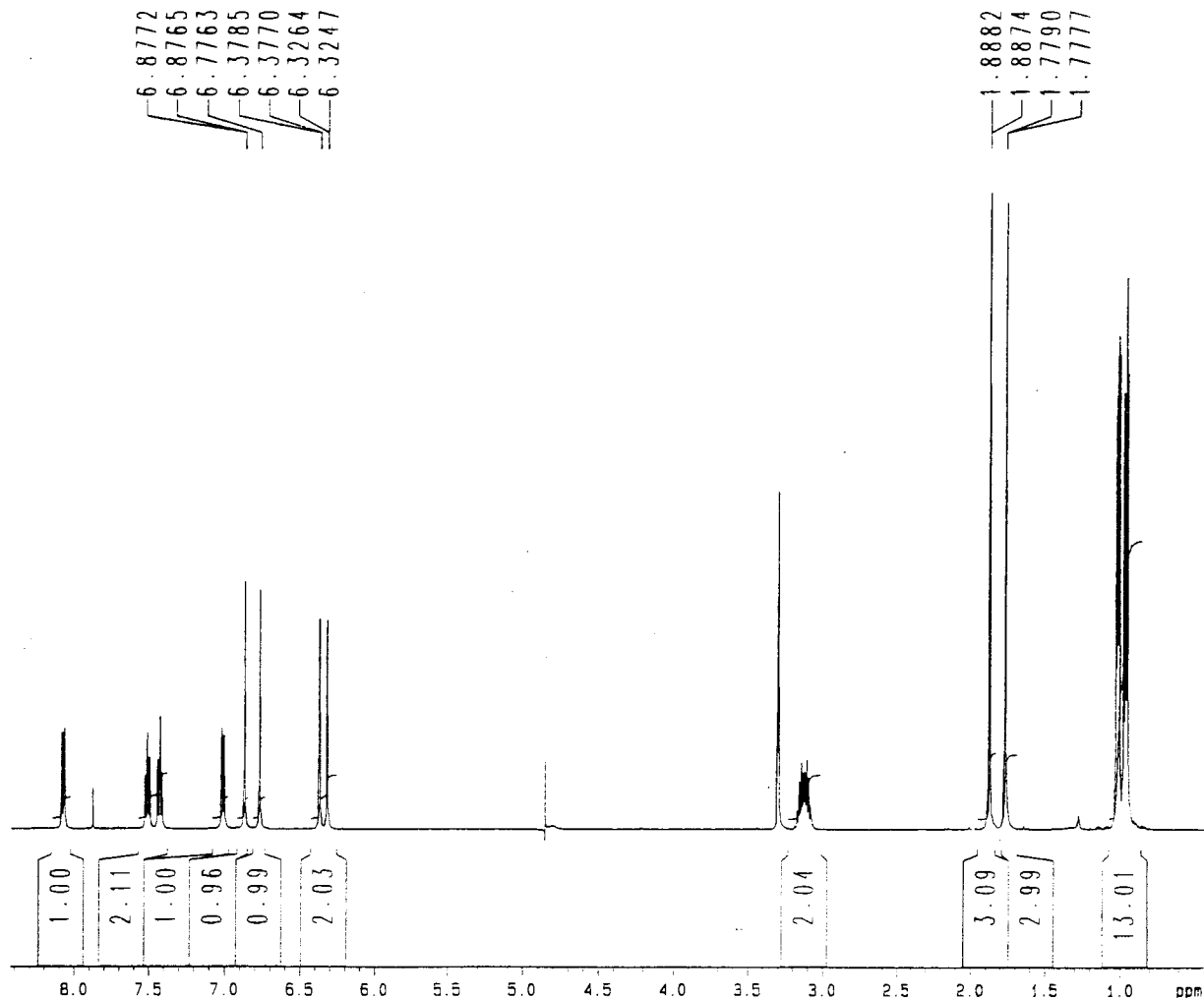


Fig. 6. Thymol blue ^1H NMR spectrum in alkaline medium at 25°C .

conclude that models II and III could be considered as statistically equivalent.

It was then necessary to simulate the data obtained by different analytical methods in the present work (spectrophotometric, potentiometric and conductimetric) with the Excel 6.0, using the values refined with SQUAD and SUPERQUAD.

3.7. Simulations

3.7.1. Potentiometric and conductimetric titrations

Fig. 8 shows overlapped experimental and simulated potentiometric curves. Fig. 8a shows the

simulation obtained using the Kolthoff model. The first part of the simulated curve does not predict the experimental behavior, but after the first equivalence point, the simulation agrees very well with the experimental results.

Fig. 8b considers the model with dimeric species. It shows excellent agreement between simulated and experimental data for all titrations.

The same conclusion can be obtained from the conductimetric data, shown in Fig. 9.

The simulated curves reported in Fig. 8b and Fig. 9b, corresponding to the model III of Table 2, consider the acid dissociation of a dimeric

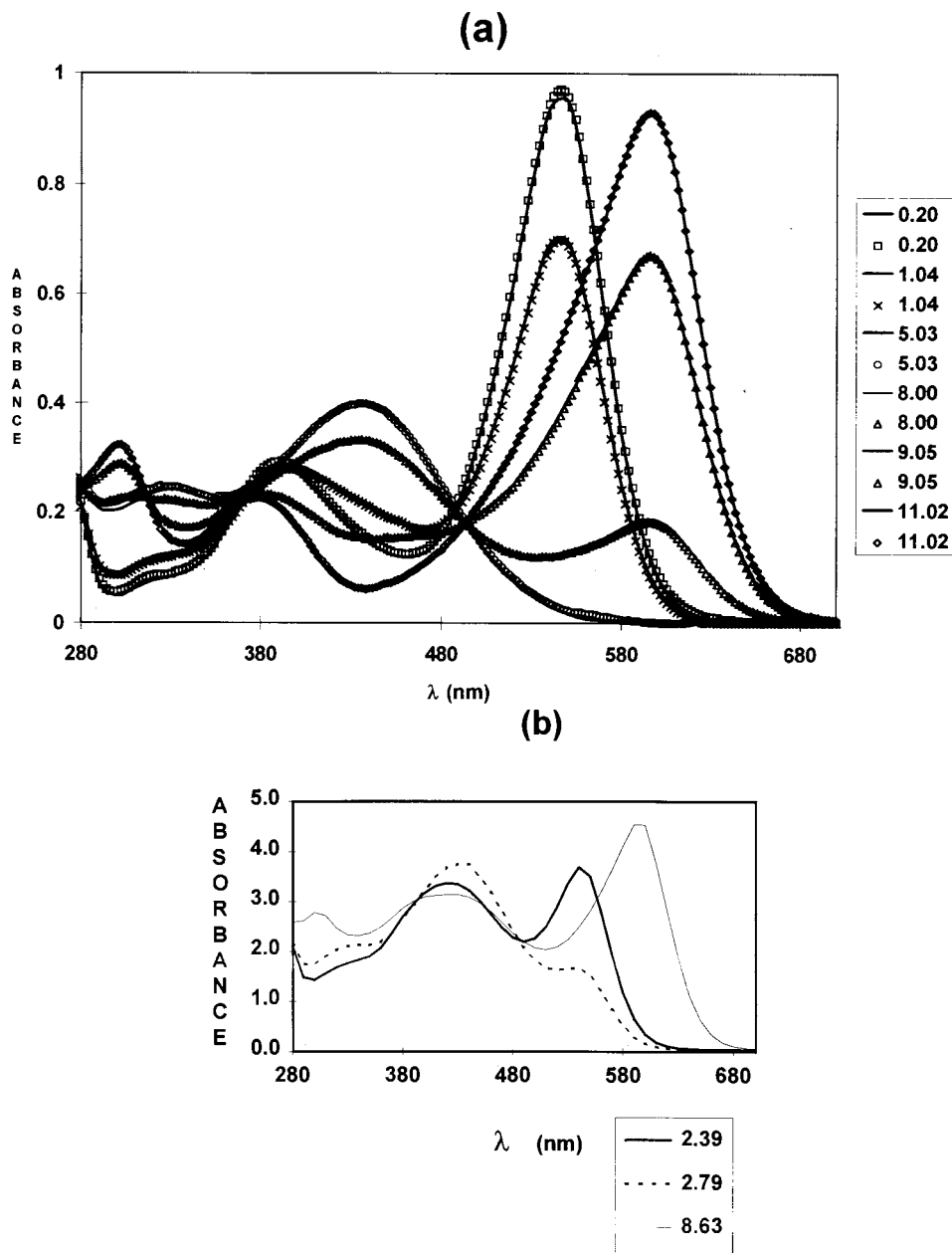


Fig. 7. (a) Absorption spectra simulated and experimental for different values of pH. (b) Absorption spectra for thymol blue at different pH values, the pH values are indicated in the figure, the total concentration of the thymol blue is 2.5×10^{-4} M. (c) Molar absorptivity coefficients calculated for SQUAD program for the thymol blue species.

neutral species in the beginning of the titration, as represented by the equilibrium in Eq. (3).



This first dissociation is strong for the concentrations used in the experimental part of this work. Then, the first titration reaction corresponds to the proton neutralization in Eq. (4):

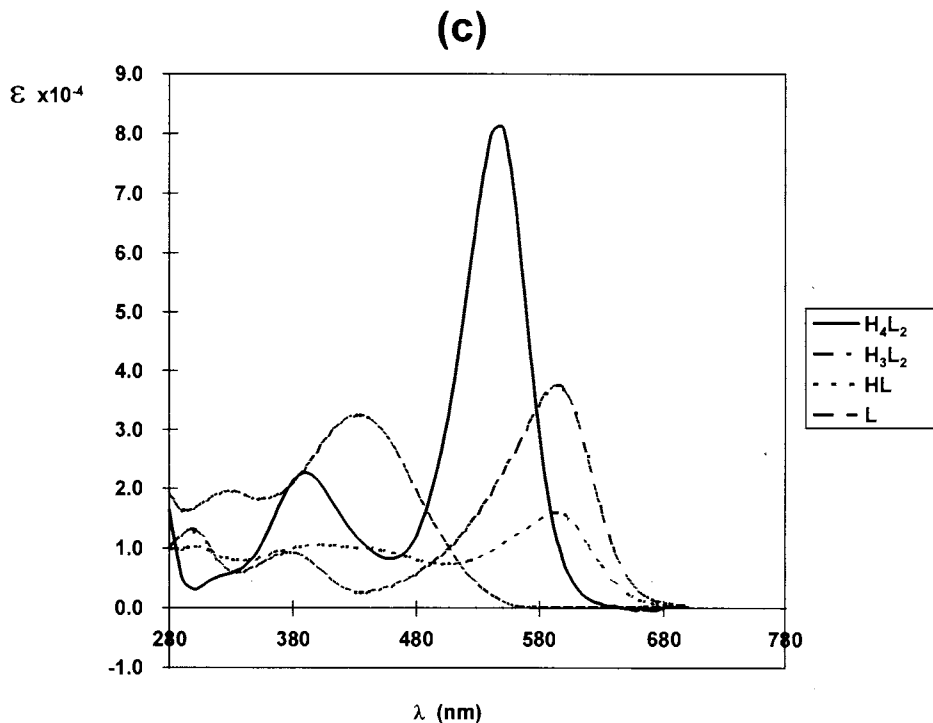
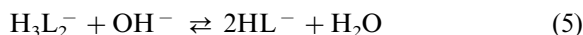


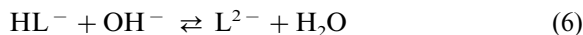
Fig. 7. (Continued)



After the first equivalence point, the reaction of the dimeric charged species H_3L_2^- with NaOH produces the monomeric species HL^- , in agreement with the reaction in Eq. (5):



Finally, the third titration reaction would be the same that is proposed in the Kolthoff model (the reaction in Eq. (6)):



This third reaction could explain why both models fit well the experimental data in the last part of the potentiometric and conductimetric titration curves.

It is interesting to remember that this kind of dimerization–acidic equilibria have been previously suggested [14]. It is known as ‘homoconjugation equilibria’. However, it has been proposed for other reagents in aprotic solvents. The pres-

ence of this equilibria in water for thymol blue could be induced by the big methyl and isopropyl groups residing on the phenyl rings.

3.7.2. Absorption spectra

The best model (III) that can simulate the potentiometric and conductimetric titrations, can be used in order to fit experimental absorption spectra (Fig. 7a).

Fig. 7c shows the absorptivity coefficients calculated with the program SQUAD for each one of the species used in the dimerization model. It is important to note the maximum value for the absorptivity coefficient of H_4L_2 species is achieved at 550 nm, and this fact agrees well with the experimental band observed for a $\text{pH} \leq 1.2$. For the H_3L_2^- species the maximum is achieved at 430 nm this maximum represents well the experimental band observed at $\text{pH} 5.0$. In the same way HL^- shows the maximum wavelength at 590 nm at $\text{pH} 8.0$ and the L^{2-} species at 600 nm at $\text{pH} > 9.0$.

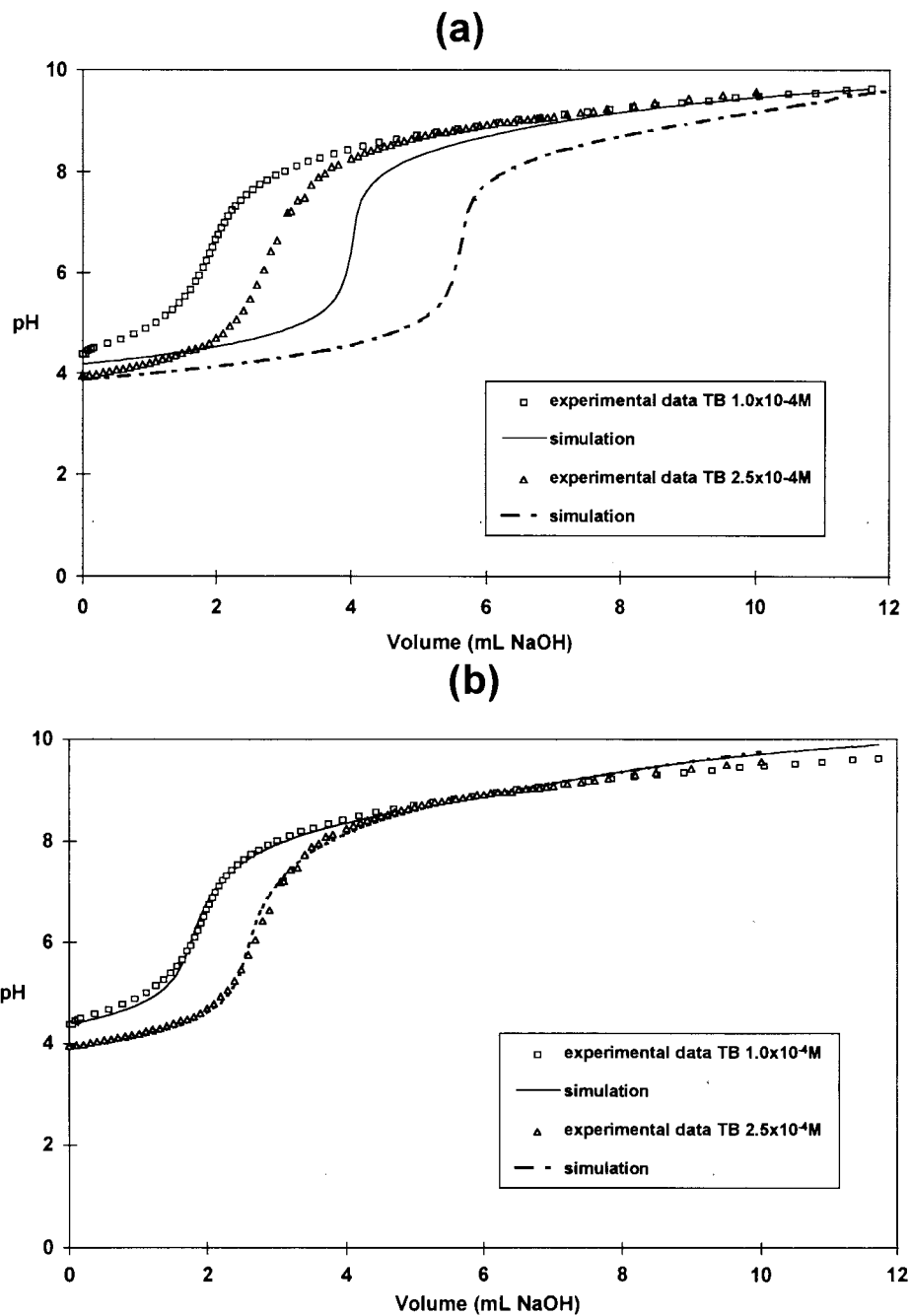


Fig. 8. (a) Simulated and experimental potentiometric curves for two different concentrations of thymol blue, utilizing a model of three acid–base equilibria. (b) Simulated and experimental potentiometric curves for two different concentrations of thymol blue, utilizing a dimeric species model.

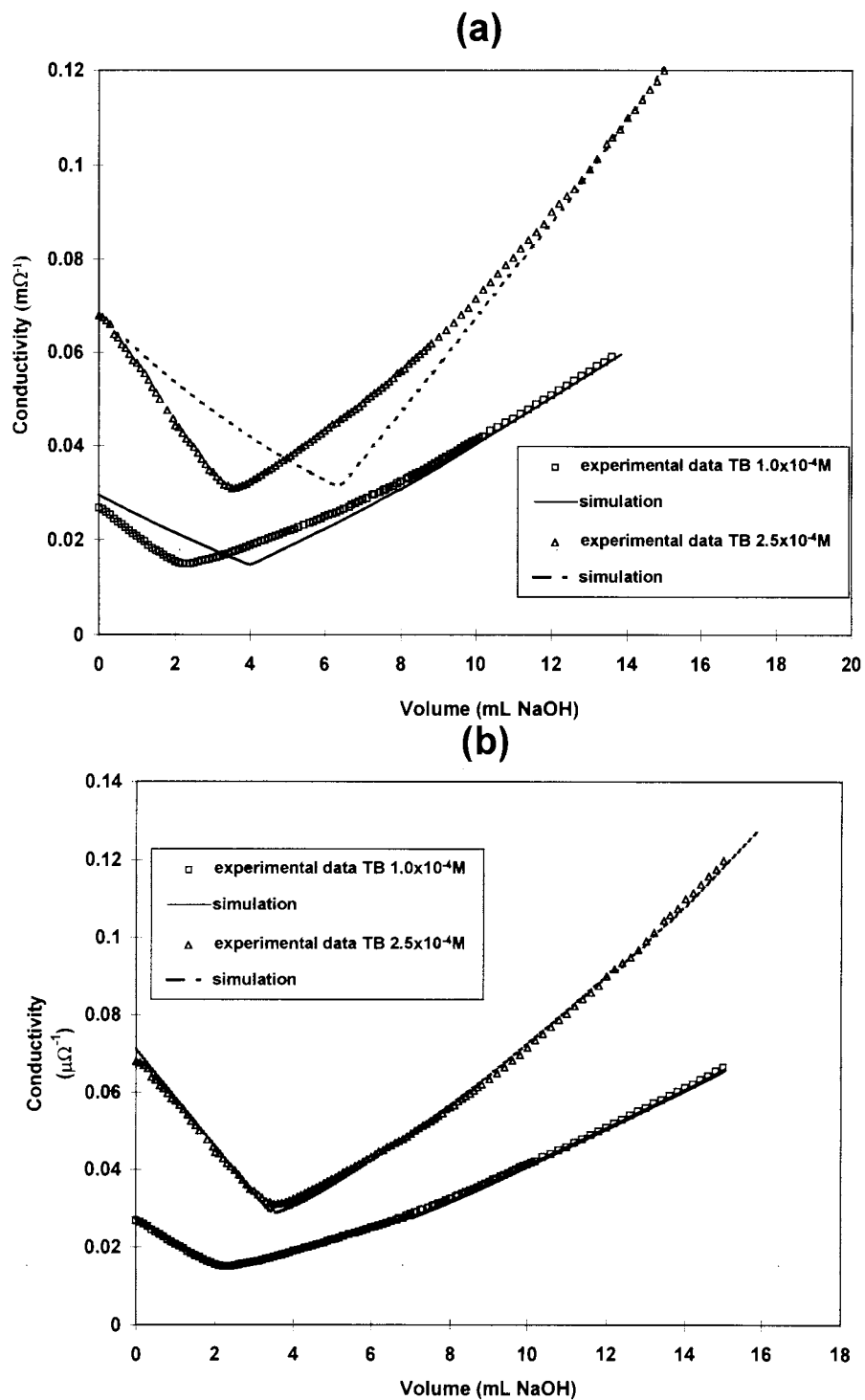


Fig. 9. (a) Simulated curve and experimental conductimetric data for the model of three acid–base equilibria. (b) Simulated curve and experimental conductimetric data for the dimeric species model.

Table 2
SQUAD and SUPERQUAD best results for three different models proposed for the thymol blue

Model	Equilibrium	SQUAD			SUPERQUAD			Ref
		$-\text{Log } K \pm \sigma^a$	U^b	σ_{λ}^c	$-\text{Log } K \pm \sigma$	U^a	χ^2	
I	$\text{HL} \leftrightarrow \text{H}^+ + \text{L}$	8.766 ± 0.055^d	7.8080	9.09×10^{-2}	8.288 ± 0.0054^d	1.560×10^2	37.360	[4–6]
II	$\text{HL} \leftrightarrow \text{H}^+ + \text{L}$	8.621 ± 0.002^d	1.130×10^{-2}	3.631×10^{-3}	8.287 ± 0.026^d	3.655×10^1	26.840	[3]
	$\text{H}_2\text{L} \leftrightarrow \text{HL} + \text{H}^+$	4.050 ± 0.109^d			3.924 ± 0.058^d			
III	$\text{H}_3\text{L} \leftrightarrow \text{H}_2\text{L} + \text{H}^+$	1.358 ± 0.110^d						This work
	$\text{HL} \leftrightarrow \text{H}^+ + \text{L}$	8.900*	3.5382×10^{-2}	7.18×10^{-3}	8.918 ± 0.070^d	3.8580×10^1	27.37	
	$\text{H}_3\text{L}_2 \leftrightarrow 2\text{L}$	30.730 ± 0.032^e			29.806 ± 0.133^e			
	$\text{H}_4\text{L}_2 \leftrightarrow 2\text{L} + 3\text{H}^+$	32.106 ± 0.033^f						
	$+ 4\text{H}^+$							

^a S.D.; ^b minimization of residual squares; ^c absorbance S.D.; ^d equilibrium constant units mol l^{-1} ; ^e equilibrium constant units $(\text{mol l}^{-1})^4$; ^f equilibrium constant units $(\text{mol l}^{-1})^5$ (the equilibrium constants considers concentrations expressed in mol l^{-1}); * fixed during refinement.

Fig. 7a shows the excellent agreement between the simulated and experimental absorption spectra.

4. Conclusions

The $\text{p}K_a$ values determined for thymol blue for a model of three acid–base equilibria (proposed by Kolthoff), statistically corresponded with the best model better than the two acid–base equilibria models proposed in other papers [4–6]. However, this model does not describe all the experimental information. Therefore, a new model considering dimers has been proposed with equilibrium constants ($\text{HL } \log K = 8.918 \pm 0.070$ and $\text{H}_3\text{L}_2 \log K = 29.806 \pm 0.133$ calculated with the SUPERQUAD program at variable low ionic strength (1.5×10^{-4} to 3.0×10^{-4} M); and $\text{HL } \log K = 8.9 \pm 0.000$, $\text{H}_3\text{L}_2 \log K = 30.730 \pm 0.032$ and $\text{H}_4\text{L}_2 \log K = 32.106 \pm 0.033$ calculated with SQUAD program at 1.1 M ionic strength). There is an excellent agreement with this dimerization–acidic scheme and experimental spectrophotometric, potentiometric and conductimetric data.

Acknowledgements

This work was financially supported by CONACYT through Project No. 400200-5-4264PA and the fellowship given to PB-H. We acknowledge Professor A. Vacca for the copy of the SUPERQUAD program and Professor Josef Havel for the copy of the SIBYLA program.

References

- [1] I.M. Kolthoff, L.S. Guss, J. Am. Chem. Soc. 60 (1938) 2516.
- [2] L.S. Guss, I.M. Kolthoff, J. Am. Chem. Soc. 62 (1940) 249.
- [3] I.M. Kolthoff, L.S. Guss, Anal. Chem. 39 (1967) 315.
- [4] L. Nørgaard, Anal. Chem. Acta 255 (1991) 143.
- [5] R. Casula, G. Crisponi, F. Cristiani, V. Nurchi, Talanta 40 (1983) 1781.
- [6] I.M. Kolthoff, M.K. Chantooni, L.S. Guss, J. Am. Chem. Soc. 90 (1968) 23.
- [7] A.J. Libbey, J.T. Sctok, Anal. Chem. 42 (1970) 526.
- [8] Ch. Pouchert, The Aldrich Library of FT-IR Spectra, vol. 2, Aldrich Chemical Company, Milwaukee, WI, 1985.
- [9] C.C. Westcott, pH Measurements, Academic Press, New York, 1978.

- [10] M. Meloun, L. Havel, *Computation of Solution Equilibria. A Guide to Methods in Potentiometry, Extraction, and Spectrophotometry*, Ellis Horwood, Chichester, UK, 1988.
- [11] D. Leggett, *Computational Methods for the Determination of Formation Constants*, Plenum, New York, 1985.
- [12] P. Gans, A. Sabatini, A. Vacca, *J. Chem. Soc. Dalton Trans.* (1985) 1195.
- [13] J. Havel, L. Jancár, *Scripta* 20 (1990) 295.
- [14] O. Popovych, R. Tomkins, *Nonaqueous Solution Chemistry*, Wiley, New York, 1981, p. 40.

Novel PVC-based membrane sensors selective for vanadyl ions

Ajay K. Jain *, Vinod K. Gupta, Lok P. Singh, Upendra Khurana

Department of Chemistry, University of Roorkee, Roorkee-247 667 (U.P.), India

Received 4 August 1997; received in revised form 15 December 1997; accepted 17 December 1997

Abstract

Poly(vinyl chloride) based membranes of di-(2-ethylhexyl)phosphoric acid (DEHPA) and dibutyl-(butyl)phosphonate (DBBP) have been prepared and investigated as VO^{2+} -selective sensors. The membranes containing DEHPA/DBBP and sodium tetraphenylborate, an anion excluder, show near-Nernstian/Nernstian response in the concentration range $\sim 10^{-5}$ – 10^{-1} M. The sensors exhibit a fast response time and good selectivity for VO^{2+} over a number of other cations. Quantitative determination of vanadium in waste V_2O_5 catalyst has been achieved by these sensors and they have also been used as indicator electrodes for the determination of the end point in the potentiometric titration of VO^{2+} against EDTA. © 1998 Elsevier Science B.V. All rights reserved.

Keywords: Di-(2-ethylhexyl)phosphoric acid; Dibutyl(butyl)phosphonate; VO^{2+} -selective sensors

1. Introduction

In spite of widespread activity in the field of ion-selective electrodes during the last two decades, the efforts to make suitable commercially available sensors for heavy metals have not been successful. This appears to be due to the non availability of suitable sensor materials. As heavy metals are present in most samples, it is desirable to have sensors for their quick determination. This may become possible with the increasing availability of new materials showing selectivity for different metals. Vanadyl (VO^{2+}) and uranyl (UO_2^{2+}) are the most well recognized oxometal species and of the two, vanadyl is more stable. It

is seen from the literature that the solutions of VO^{2+} in medium and strongly acidic solutions are stable for many months [1]. Vanadium is an important constituent of steel, petroleum and alloy industries and is also used as a catalyst. Its determination is, therefore, important. A number of electrodes [2–5] have been developed for the determination of vanadium which sense it as vanadate (VO_3^-). However, there is no report of an electrode developed for vanadyl ions. A survey of the literature further revealed that di-(2-ethylhexyl)phosphoric acid (DEHPA) and dibutyl butylphosphonate (DBBP) have good affinity for vanadium and have been used for its extraction from the ores containing vanadium [6,7]. These two extractants can thus be the materials of choice to be used as electroactive material for the fabrication of ion-selective electrodes for vanadyl

* Corresponding author. Tel.: +91 1332 72349; fax: +91 1332 73560.

Table 1

Composition of PVC based membranes (numbered 1–4) and response characteristics of VO²⁺ sensors based on them

Electrode/membrane No.	Component in membranes (% w/w)				Working concentration range (M)	Slope (mV/decade of activity)	Response time (s)
	DEHPA	DBBP	NaTB	PVC			
1	11	—	—	89	2.2×10^{-5} – 3.2×10^{-3}	25.2	60
2	—	11	—	89	7.1×10^{-5} – 2.2×10^{-2}	23.3	55
3	10	—	7	83	1.4×10^{-5} – 1.0×10^{-1}	27.7	25
4	—	10	7	83	7.9×10^{-6} – 1.0×10^{-1}	29.1	15

ions. Therefore, in continuation of our work on the development of ion sensors for oxometal species [8,9], we thought it desirable to investigate poly(vinyl chloride) (PVC) based membranes of the two extractants as vanadyl selective sensors. Our efforts have been successful and the results are reported in the present communication.

2. Experimental

2.1. Reagents

Di-(2-ethylhexyl) phosphoric acid and dibutyl-(butyl) phosphonate were obtained from Mobil, USA. High molecular weight poly(vinyl chloride), sodium tetraphenylborate (NaTB) and vanadyl sulphate were BDH, UK, products. All other reagents used were of analytical grade and the solutions were prepared in doubly distilled water.

2.2. Potential measurements

The potential measurements of the solutions, prepared in the concentration range 1.0×10^{-6} – 1.0×10^{-1} M VO²⁺ ions, were carried out at $25 \pm 0.1^\circ\text{C}$ with a PH 5662 digital pH/millivoltmeter (ECIL, India) and on a CVM 301 Century digital microvoltmeter (Century Instruments, India). Saturated calomel electrodes (SCE) were employed as reference electrodes and potentials were measured by setting up the following cell assembly:

Internal reference electrode (SCE)	Internal solution (0.1MVO ²⁺)	Membrane	Test solutions	External reference electrode (SCE)
------------------------------------	---	----------	----------------	------------------------------------

2.3. Preparation of Membranes

The method reported by Craggs et al. [10] was adopted for the fabrication of membranes. Varying amounts (20–100 mg) of the sensor material (DEHPA or DBBP) and PVC were dissolved in 20 ml tetrahydrofuran. Anion excluder, NaTB, was also added to the membranes in some compositions. The homogeneous mixture was poured into glass rings placed on smooth glass plates and the solvent was allowed to evaporate overnight, yielding a membrane of about 0.5 mm thickness and 10 mm diameter. A number of membranes of different compositions were prepared and only those which gave reproducible and stable potentials were selected for further studies. The composition of these membranes is reported in Table 1. The membranes were fixed to one end of a Pyrex glass tube with Araldite (Ciba Giegy, India) and equilibrated with 0.5 M VO²⁺ solution for three days.

2.4. Dissolution of waste V₂O₅ catalyst sample

1 g of the powdered sample of waste V₂O₅ catalyst was repeatedly digested (four times) with aqua regia. The residue was treated with 10 ml concentrated hydrochloric acid and filtered. The filtrate was boiled with HCl, cooled and made up to 100 ml. The boiling with HCl converted all vanadium(V) to vanadium(IV) [11]. A portion of this solution was further diluted 20 times keeping the overall pH at 2.0. In order to get a representa-

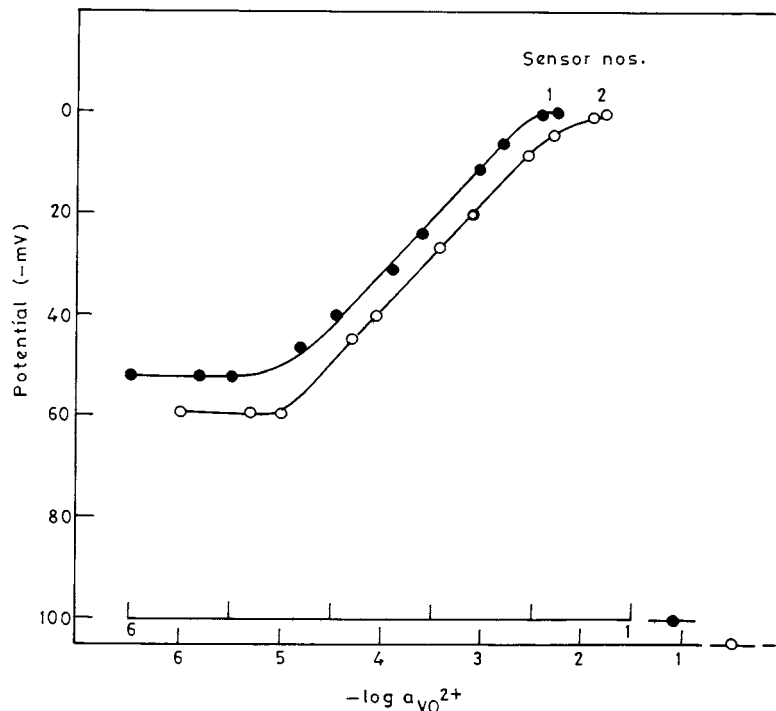


Fig. 1. Variation of potential with VO^{2+} activity for membranes 1 and 2.

tive value, five separate samples of the waste catalyst were dissolved and processed. The solutions were analysed on an ICP-AES (Plasma Lab-tam, Australia, model 8440).

3. Results and discussion

3.1. Working concentration range and slope

The potential response of all the four electrodes using membranes of DEHPA and DBBP of different composition was investigated by varying the concentration of the test solution from 1.0×10^{-6} – 1.0×10^{-1} M and the results obtained are given in Table 1 and shown in Figs. 1 and 2. It is seen from Fig. 1 that the electrodes nos. 1 and 2 having membranes of DEHPA and DBBP exhibit linear potential response in the concentration range 2.2×10^{-5} – 3.2×10^{-3} and 7.1×10^{-5} – 2.2×10^{-2} M with a near-Nernstian slope of 25.2

and 23.3 mV per decade of activity, respectively. Both the electrodes showed high response time of 1 min. The addition of anion excluder, NaTB, to the membranes (electrodes nos. 3 and 4) not only improved the working concentration range to 1.4×10^{-5} – 1.0×10^{-1} and 7.9×10^{-6} – 1.0×10^{-1} M but also the slope to 27.7 and 29.1 mV per decade of activity and response time to 25 and 15 s, respectively. It is important to mention that the addition of plasticizers did not improve the performance of the membranes. This observation may be ascribed to the fact that DEHPA and DBBP themselves act as plasticizers and have been used earlier for this purpose also [12,13]. As the electrodes 3 and 4 are better, they have been studied in detail. The membrane electrodes could be used over a period of six months without showing any significant change in the value of slope or working range. The membranes were stored in 0.1 M VO^{2+} solution when not in use and were re-equilibrated with 0.5 M VO^{2+} solu-

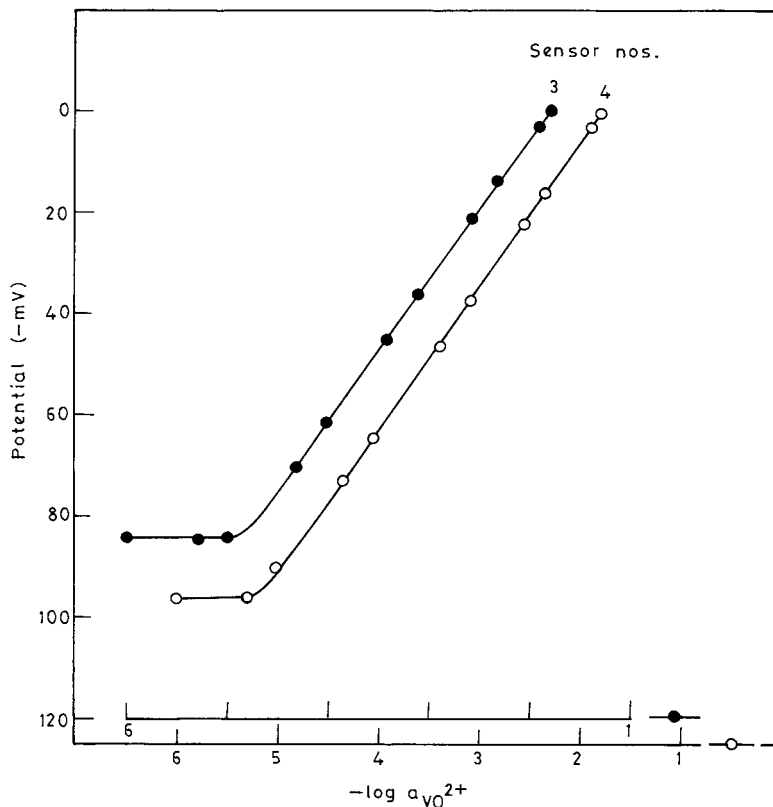


Fig. 2. Variation of potential with VO^{2+} activity for membranes 3 and 4.

tion whenever any drift in potentials was observed. Repeated monitoring of potentials (20 measurements) at 1.0×10^{-3} M VO^{2+} concentration gave a standard deviation of 0.5 mV for both the electrodes.

3.2. Effect of pH and non-aqueous medium

The pH dependence of both the membrane electrodes was investigated at 1.0×10^{-3} M VO^{2+} concentration in the pH range 1.0–4.0 by adjusting the pH of the solution with H_2SO_4 and ammonia. It was observed that the potentials remain constant in the pH range 1.8–2.5 and the same was taken as the working pH range of the electrodes. The functioning of the electrodes was also investigated in partially non-aqueous media using ethanol–water and methanol–water mixtures and the results obtained are presented in

Table 2. It is observed that in the presence of both ethanol and methanol, the slope as well as working concentration range is reduced. The effect is drastic in methanol–water mixture where the slope is considerably decreased even in 10% (v/v) methanol. Therefore, the electrodes are not suitable for estimation in methanol–water mixtures. However, in ethanol–water mixture, up to 10% (v/v) ethanolic content, there is only a small decrease in slope and working concentration range and hence both the electrodes can be satisfactorily used in presence of 10% (v/v) ethanol in water.

3.3. Potentiometric selectivity pattern

The selectivity of the electrodes in presence of various cations was evaluated by the fixed interference method as suggested by Viteri and Dia-

Table 2
Performance of DEHPA-NaTB (N0. 3) and DBBP-NaTB (No. 4) membrane sensors in partially non-aqueous medium

Non-aqueous content (% v/v)	Electrode No. 3		Electrode No. 4	
	Slope (mV/decade of activity)	Working concentration range (M)	Slope (mV/decade of activity)	Working concentration range (M)
Nil	27.7	1.4×10^{-5} – 1.0×10^{-1}	29.1	7.9×10^{-6} – 1.0×10^{-1}
Ethanol				
10	25.1	2.0×10^{-5} – 1.0×10^{-1}	27.0	9.1×10^{-6} – 1.0×10^{-1}
25	19.3	1.6×10^{-4} – 1.0×10^{-1}	25.1	1.2×10^{-5} – 1.0×10^{-1}
50	13.4	5.0×10^{-4} – 1.0×10^{-1}	20.4	1.6×10^{-4} – 1.0×10^{-1}
Methanol				
10	12.5	1.0×10^{-4} – 1.0×10^{-1}	20.2	1.0×10^{-5} – 1.0×10^{-1}
25	11.7	1.0×10^{-4} – 1.0×10^{-1}	19.7	5.0×10^{-5} – 1.0×10^{-1}
50	11.0	3.2×10^{-4} – 1.0×10^{-1}	19.0	1.4×10^{-4} – 1.0×10^{-1}

mond [14] at 1.0×10^{-2} M concentration of interfering ions. A perusal of selectivity coefficient data presented in Table 3 indicates that the electrodes are sufficiently selective over a large number of cations except Ni^{2+} for electrode no. 3 and

Table 3
Potentiometric selectivity values for DEHPA-NaTB (N0. 3) and DBBP-NaTB (N0. 4) membrane sensors for VO^{2+} ions in the presence of 1.0×10^{-2} M concentration of interfering ions

Interfering ion (B)	Selectivity coefficient $K_{\text{VO}^{2+},\text{B}}^{\text{Pot}}$	
	DEHPA-NaTB	DBBP-NaTB
Li^+	8.9×10^{-2}	7.4×10^{-2}
K^+	7.9×10^{-2}	7.9×10^{-2}
Na^+	8.0×10^{-2}	7.4×10^{-2}
NH_4^+	7.9×10^{-2}	3.5×10^{-1}
Ni^{2+}	3.2×10^{-1}	2.5×10^{-2}
Co^{2+}	2.5×10^{-2}	1.6×10^{-2}
Cu^{2+}	1.3×10^{-2}	1.0×10^{-2}
Sr^{2+}	1.0×10^{-2}	1.0×10^{-2}
Ba^{2+}	1.6×10^{-2}	1.0×10^{-2}
Ca^{2+}	4.5×10^{-2}	1.5×10^{-2}
Pb^{2+}	4.0×10^{-2}	2.5×10^{-2}
Zn^{2+}	2.5×10^{-2}	1.0×10^{-2}
Mg^{2+}	4.5×10^{-2}	1.0×10^{-2}
Cd^{2+}	1.0×10^{-2}	1.0×10^{-2}
UO_2^{2+}	6.3×10^{-2}	5.0×10^{-2}
Cr^{3+}	2.0×10^{-2}	3.2×10^{-2}
Al^{3+}	1.4×10^{-2}	1.0×10^{-2}
Fe^{3+}	4.5×10^{-2}	2.2×10^{-2}

NH_4^+ for electrode no. 4. This behaviour may be due to the selective uptake of vanadyl by DEHPA and DBBP in comparison to the other species listed in Table 3. It is worth mentioning that the observed selectivity coefficient values for Ni^{2+} and NH_4^+ are due to the characteristics of the membranes caused by difference in the extraction properties of DEHPA and DBBP. Hence, the electrodes can be used for the estimation of VO^{2+} in presence of equal or less concentration of these ions. However, in view of moderate selectivity of the electrodes, Ni^{2+} and NH_4^+ would cause considerable interference for electrodes 3 and 4, respectively, even if present in comparative amounts. Therefore, in order to realize the level of interference caused by these two ions in the performance of the electrodes, mixed run studies were carried out [8,15–19]. Fig. 3 shows the variation of potentials with VO^{2+} ion concentration in presence of different concentrations of Ni^{2+} . It is observed that the presence of Ni^{2+} ions up to 5.0×10^{-5} M would not cause any interference while determining VO^{2+} with this membrane sensor as no divergence from the potential versus VO^{2+} concentration plot is observed. However, higher concentrations of Ni^{2+} ions cause interference and can not be tolerated over the whole working concentration range of VO^{2+} ions. Thus, in presence of 1.0×10^{-4} and 5.0×10^{-4} M Ni^{2+} ,

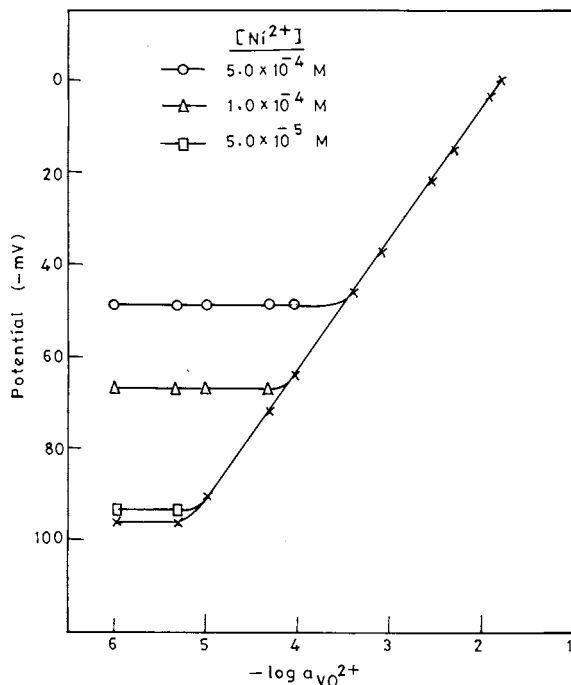


Fig. 3. Effect of different concentrations of Ni^{2+} ions on the variation of potential for membrane 3.

VO^{2+} can be determined over the reduced concentration range of 7.1×10^{-5} – 1.0×10^{-1} and 3.2×10^{-4} – 1.0×10^{-1} M, respectively. Similar mixed run studies were carried out for electrode no. 4 for which NH_4^+ causes maximum interference. Plots of potential versus VO^{2+} concentration in the presence of different concentration levels of NH_4^+ are shown in Fig. 4, which indicate that 5.0×10^{-4} M NH_4^+ ions can be tolerated over the whole working concentration range of VO^{2+} ions, while in the presence of 1.0×10^{-3} and 5.0×10^{-3} M NH_4^+ ions the electrode would be effective over the reduced concentration ranges 3.2×10^{-5} – 1.0×10^{-1} and 1.4×10^{-4} – 1.0×10^{-1} M, respectively. Further, among the two electrode assemblies the DBBP–NaTB membrane (electrode no. 4) is more selective as the $K_{\text{VO}^{2+}, \text{B}}^{\text{Pot}}$ values for this electrode are lower than the DEHPA–NaTB membrane (electrode no.3).

4. Analytical applications

4.1. Analysis of waste V_2O_5 catalyst sample

The utility of the membrane electrodes was checked by using them for the quantitative determination of vanadium in a sample of waste V_2O_5 catalyst and comparing the results with those obtained with ICP-AES. The data shown in Table 4 clearly shows that both the electrodes perform exceptionally well and the results obtained are in concurrence with those obtained with ICP-AES.

4.2. Potentiometric titration

Both the membrane electrodes have also been successfully used as indicator electrodes in the potentiometric titrations of VO^{2+} (1.0×10^{-3} M, 10 ml) with EDTA (1.0×10^{-2} M) at pH 2.3. The addition of EDTA to VO^{2+} solution causes the formation of VO–EDTA complex, resulting in the reduction of VO^{2+} concentration and thereby a decrease in cell potential. The plots (Fig. 5)

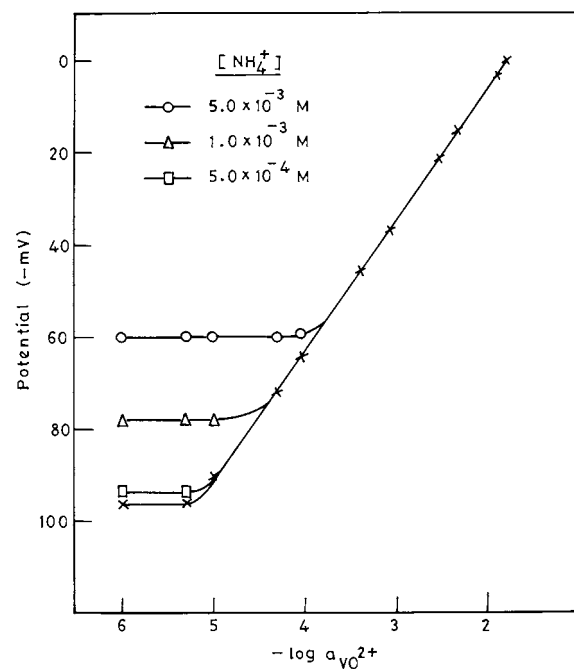


Fig. 4. Effect of different concentrations of NH_4^+ ions on the variation of potential for membrane 4.

Table 4

Analytical data of V_2O_5 waste catalyst sample and vanadium content as determined with the membrane sensors 3 and 4

Element	Concentration as determined by ICP-AES (ppm)	Concentration of V as determined by electrode 3 (ppm)	Concentration of V as determined by electrode 4 (ppm)
Ti	1.00 ± 0.02	—	—
Al	7.50 ± 0.08	—	—
Fe	3.50 ± 0.05	—	—
V	14.4 ± 0.20	13.9 ± 0.4	14.0 ± 0.4

obtained are, however, not of sigmoid shape due to some interference caused by the ions being made available on the addition of the titrant. The combined effect of interference by added ions and change in concentration of VO^{2+} during the course of titration happens to yield linear change in potential as observed by us. This behaviour is commonly met with titration plots obtained by using moderately selective electrodes [15,19]. The titration may be useful if the break points of the plots corresponds to the stoichiometry of the complex. In the present case, the break point

obtained is sufficiently sharp and corresponds to the stoichiometry of $VO-EDTA$ complex. Thus the electrodes can be used to determine VO^{2+} by potentiometric titrations.

5. Conclusion

Among the four PVC-based membranes of the extractants prepared and tried as VO^{2+} sensors, the ones having anion excluder NaTB exhibited good performance with regard to the working

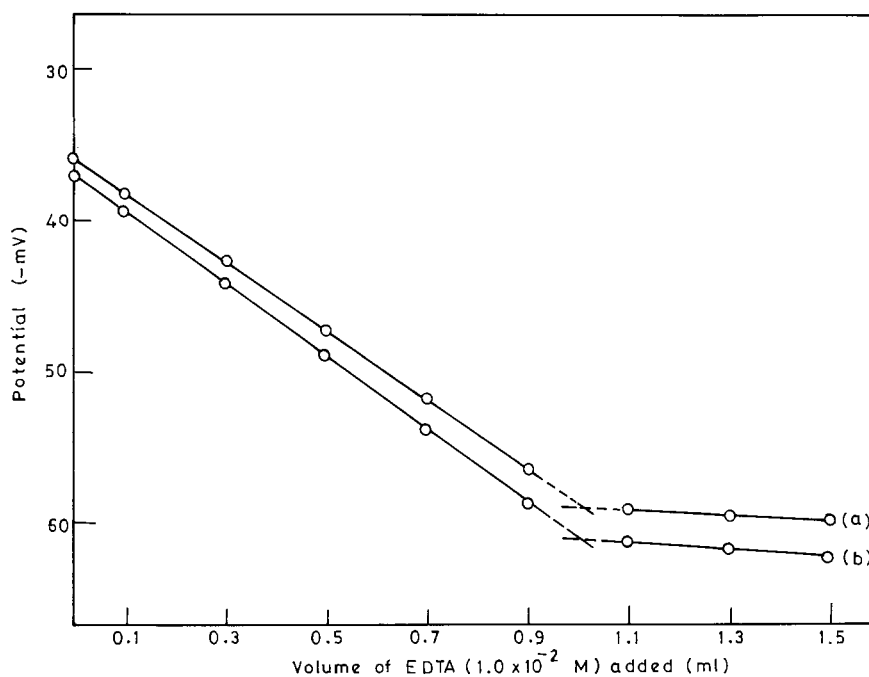


Fig. 5. Potentiometric titration curve of VO^{2+} (1.0×10^{-3} M, 10 ml) versus EDTA (1.0×10^{-2} M). (a) Electrode no. 3 and (b) electrode no. 4.

concentration range and selectivity. They have been successfully used for the quantification of vanadium in a sample of waste V_2O_5 catalyst. The DBBP–NaTB membrane gives the best results as it exhibits a wider working concentration range, 7.9×10^{-6} – 1.0×10^{-1} M and better selectivity. The electrodes have a fast response time and perform satisfactorily in the pH range 1.8–2.5 and in partially non-aqueous medium up to 10% (v/v) alcohol content. They give reproducible results and have a life time of more than six months.

Acknowledgements

We thank Dr A.B. Ghatag, Superintendent, Projects and Development India Ltd. (PDIL) for providing the sample of V_2O_5 waste catalyst. LPS and UK are thankful to the Council for Scientific and Industrial Research (CSIR), India, for providing financial assistance.

References

- [1] R.J.H. Clark, *The Chemistry of Titanium and Vanadium*, Elsevier, Amsterdam, 1968.
- [2] V.A. Luginin, V.I. Komava, A.L. Grekovich, T.I. Pal'niKova, *Vestn. Leningr. Univ. Ser. 4: Fiz. Khim.* 1 (1987) 95.
- [3] V.A. Luginin, V.I. Komova, A.L. Grekovich, *Zh. Prikl. Khim.* 60 (1987) 189.
- [4] V.L. Volkov, M.V. Kruchinia, *Zh. Anal. Khim.* 98 (1993) 1644.
- [5] S.K. Srivastava, V.K. Tewari, H. Vardhan, *Sens. Actuators B* 28 (1995) 21.
- [6] G.M. Ritcey, A.W. Ashbrook, *Solvent Extraction, Part II*, Elsevier, Amsterdam, 1979.
- [7] H. Goldwhite, *Introduction to Phosphorus Chemistry*, Cambridge University Press, Cambridge, 1981.
- [8] A.K. Jain, V.K. Gupta, L.P. Singh, *Anal. Proc.* 32 (1995) 263.
- [9] A.K. Jain, V.K. Gupta, U. Khurana, L.P. Singh, *Electroanalysis* 9 (1997) 857.
- [10] A. Craggs, G.J. Moody, J.D.R. Thomas, *J. Chem. Edu.* 54 (1974) 541.
- [11] F.A. Cotton, G. Wilkinson, *Advanced Inorganic Chemistry*, Wiley, New York, 1988, p. 668.
- [12] W.H. Chan, P.X. Cai, X.H. Gu, *Analyst* 119 (1994) 1853.
- [13] S.P. Awasthi, V.T. Kulkarni, M. Sundaresan, *J. Electrochem. Soc. India* 37 (1988) 309.
- [14] F.I. Sa'ez de Viteri, D. Diamond, *Analyst* 119 (1994) 749.
- [15] A.K. Jain, V.K. Gupta, B.B. Sahoo, L.P. Singh, *Anal. Proc.* 32 (1995) 99.
- [16] A.K. Jain, L.P. Singh, P.K. Jain, *Sens. Actuators B* 25 (1995) 729.
- [17] S.K. Srivastava, V.K. Gupta, S. Jain, *Analyst* 120 (1995) 495.
- [18] S.K. Srivastava, V.K. Gupta, S. Jain, *Anal. Chem.* 68 (1996) 1272.
- [19] A.K. Jain, V.K. Gupta, R.D. Singh, U. Khurana, L.P. Singh, *Sens. Actuators B* 40 (1997) 15.

Synthesis and properties of new chelating resin with a spacer containing α -nitroso- β -naphthol as the functional group

V.G. Akerkar, N.B. Karalkar, R.K. Sharma, M.M. Salunkhe *

Department of Chemistry, The Institute of Science, 15, Madam Cama Road, Mumbai-400032, India

Received 19 August 1997; received in revised form 15 December 1997; accepted 17 December 1997

Abstract

A new chelating ion-exchange resin with a spacer $\text{CH}_2\text{-NH-C}_6\text{H}_4\text{-}$ based on a microreticular chloromethylated styrene-divinylbenzene copolymer containing α -nitroso- β -naphthol as a functional group has been synthesized. The sorption characteristics for manganese(II), iron(III), cobalt(II), nickel(II), copper(II), and zinc(II) have been investigated over the pH range 1.0–7.0. The resin is highly stable in acidic and alkaline medium. Iron(III) and cobalt(II); copper(II) and iron(III) are separated very effectively in a column operation by stepwise elution. © 1998 Elsevier Science B.V. All rights reserved.

Keywords: α -Nitroso- β -naphthol; Column operation; Stepwise elution

1. Introduction

Historically, the development of complexing resins started in 1939, with the work of Erlenmeyer and Dahn [1], leading later on to the suggestion of Meinhard [2] that the complexing agents would be fixed on a supporting solid for work of this kind. α -Nitroso- β -naphthol was the first used for the separation of cobalt from nickel by Ilinski and Von knorre [3]. It was one of the first organic analytical reagents and forms chelate complexes with a number of metal ions in addition to cobalt like copper(II),

iron(III), nickel(II), palladium(II) and uranium(VI) [4–6]. The incorporation of this reagent in a matrix should be of interest in the connection with concentration and separation of heavy metal ions [7]. The preparation and properties of a chelating resin containing α -nitroso- β -naphthol as a functional group has been investigated and the exchange capacity of the resin for Cu(II), Fe(III), Co(II), Ni(II), Pd(II) and U(VI) has been examined as a function of pH [8].

The present paper describes the preparation and characterisation of a microreticular chloromethylated resin with a spacer containing α -nitroso- β -naphthol for Mn (II), Fe (III), Co (II), Ni (II), Cu (II) and Zn (II).

* Corresponding author. Tel.: +91 22 2047962.

Table 1
Separation of Fe(III)–Cu(II)

No.	Metal ion	Amount loaded (ppm)	Amount recovered			Eluent volume	Error (mean)	S.D.
			a	b	c			
1	Fe(III)	50	47.9	47.7	47.8	30	2.20	0.10
	Cu(II)	50	48.6	48.8	48.4	30	1.20	0.20
2	Fe(III)	25	23.7	23.6	23.9	20	1.26	0.15
	Cu(II)	50	48.6	48.9	48.7	20	1.26	0.15
3	Fe(III)	50	47.7	48.0	47.7	20	2.20	0.17
	Cu(II)	25	24.1	23.7	23.9	20	1.10	0.20

2. Experimental

2.1. Apparatus and reagents

IR spectra (KBr disks) were recorded with an FTIR (Perkin Elmer). The stock metal ion solutions were prepared by dissolving reagent grade chlorides in water or in buffer solutions. Buffer solutions were prepared with 0.2 M hydrochloric acid and 0.2 M sodium acetate. The chloromethylated styrene-divinylbenzene copolymer, 2 and 8% divinylbenzene was from the Ion-Exchange, India.

2.2. Preparation of resin

2.2.1. Resin II

To 50 g of resin I 200 ml dioxan was added. The pre-swollen chloromethylated polystyrene resin was refluxed with ortho-phenylenediamine in pyridine for 24 h. The product resin II was washed with cold water and then extracted in a

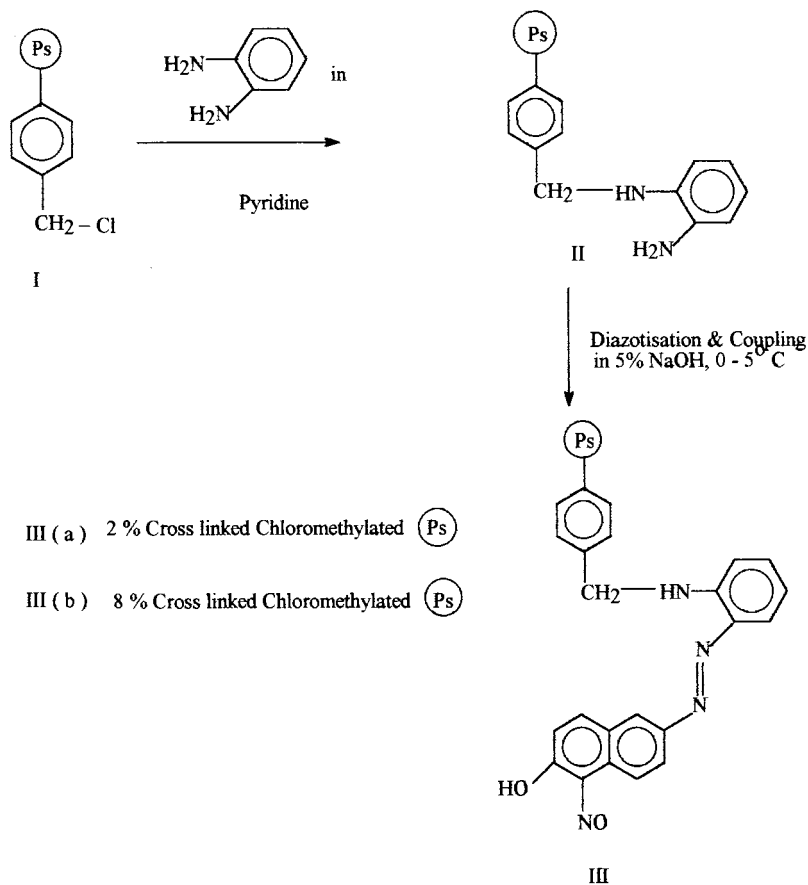
Soxhlet extractor with methanol for two days and dried in a vacuum oven.

2.2.2. Resin III

Resin II was diazotised according to the procedure described by Davies et al. [9]. The diazotised product was rapidly filtered off, washed with cold distilled water until free from acid and then coupled at 0–50°C with a solution of α -nitroso- β -naphthol in 5% aqueous NaOH solution, over a period of 7 days. The resin was then filtered off and thoroughly washed with distilled water until free from alkali. It was then extracted in a Soxhlet extractor with methanol for 3 days. Finally it was washed with dilute hydrochloric acid and then with demineralised water until free from acid. The product was dried under vacuum to get Resin III. The same procedure was carried out for 2 and 8% resin to obtain IIIa and IIIb resin, respectively. The particle size of the resin is 500–800 and 400–800 μm for IIIa and IIIb, respectively.

Table 2
Separation of Fe(III)–Co(II)

No.	Metal ion	Amount loaded (ppm)	Amount recovered			Eluent volume	Error (mean)	S.D.
			a	b	c			
1	Fe(III)	50	48.7	48.4	48.4	30	1.50	0.17
	Co(II)	25	23.9	23.7	23.7	15	1.24	0.14
2	Fe(III)	25	23.7	23.6	23.7	15	1.37	0.07
	Co(II)	50	48.4	48.2	48.4	30	1.67	0.01
3	Fe(III)	20	18.2	18.1	18.1	12	1.80	0.17
	Co(II)	20	18.2	18.3	18.2	12	1.77	0.07



Scheme 1.

2.3. Stability of the resin

Dry resin IIIa/IIIb 0.5 g was shaken with 25 ml acid or alkaline solutions of various concentrations for 3 days, and then filtered and washed successively with water, 0.05 M NaOH solution and water. After drying, the nitrogen content and sorption capacity for Fe(III) and Cu(II) were determined which remained unaffected in acidic and alkaline solutions indicating that resin IIIa and IIIb are stable in acidic and alkaline medium.

2.4. Water regain

A sample of 0.5 g dry resin IIIa and IIIb were immersed in water for 48 h. The resins were then filtered by suction and pressing between filter

papers to remove the surface moisture. Weighed amounts of the swollen resins were dried at 110°C for 48 h to determine water regain values. Water regain for resin IIIa and IIIb was 0.63 and 0.49 respectively.

$$\text{EWC} = \frac{\text{Wt of the wet resin} - \text{Wt of the dry resin}}{\text{Wt of the dry resin}}$$

2.5. Estimation of nitrogen and the amino group

The nitrogen content of fully dried samples of amino and the chelating resin was determined by the sodium fusion test and estimated by the Kjeldhal method. The nitrogen content of aminated polystyrene and the chelating resin was found to be 7.5 and 9.5%, respectively. Amino capacity was determined by using Crystal violet indicator [10].

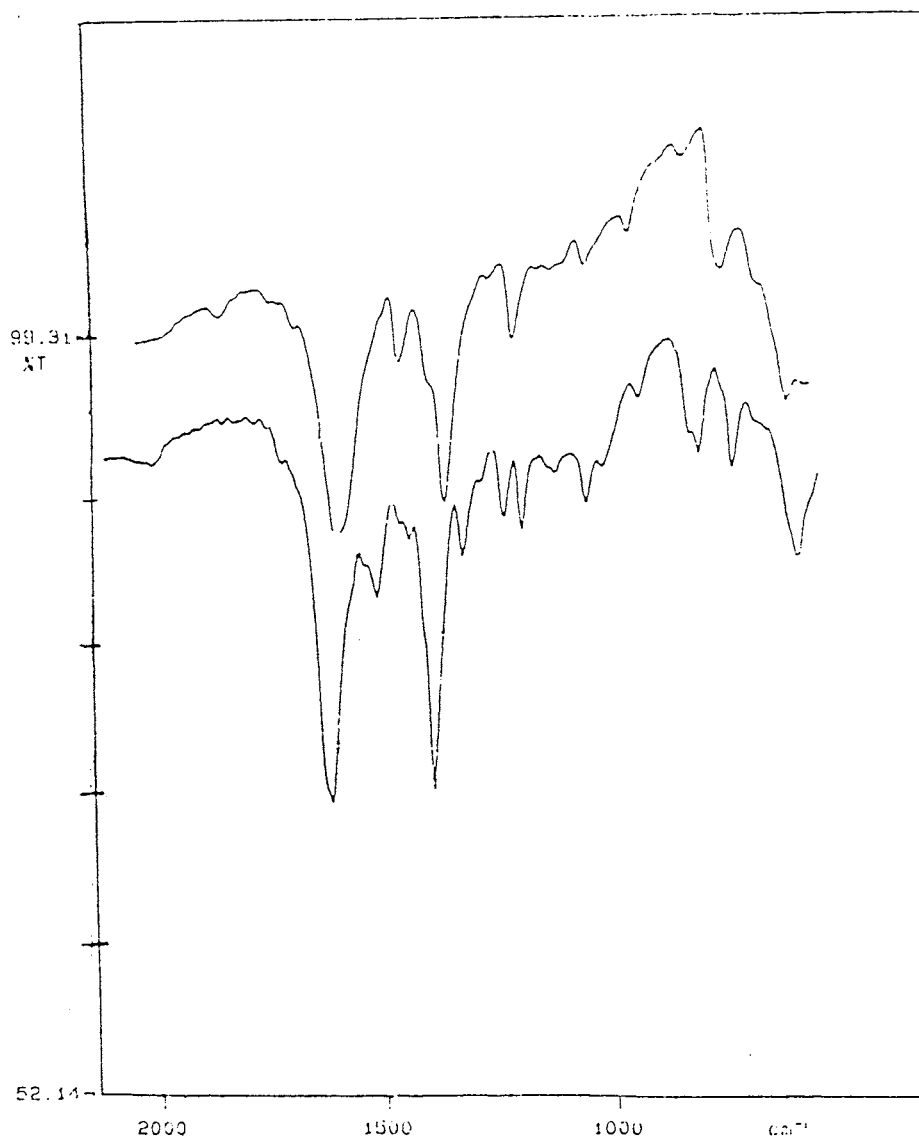


Fig. 1. IR spectra of resin II and III.

2.6. Column operations

A glass column 32 cm long with a 5 mm bore was used. 5 g Air-dried resin (IIIa) was immersed in demineralised water and allowed to swell for 24 h. The column was then packed with the fully swollen beads. The bed was thoroughly washed with 0.1 M HCl acid, then with

demineralised water until free from acid. The attaining equilibrium was 7 min. for column operations. A long column is used to accommodate most of the eluent at one time so that constant flow can be maintained without disturbing the polymeric bed. This precaution was taken as some metals require large quantity of eluent.

Effect of pH on sorption of metal ions

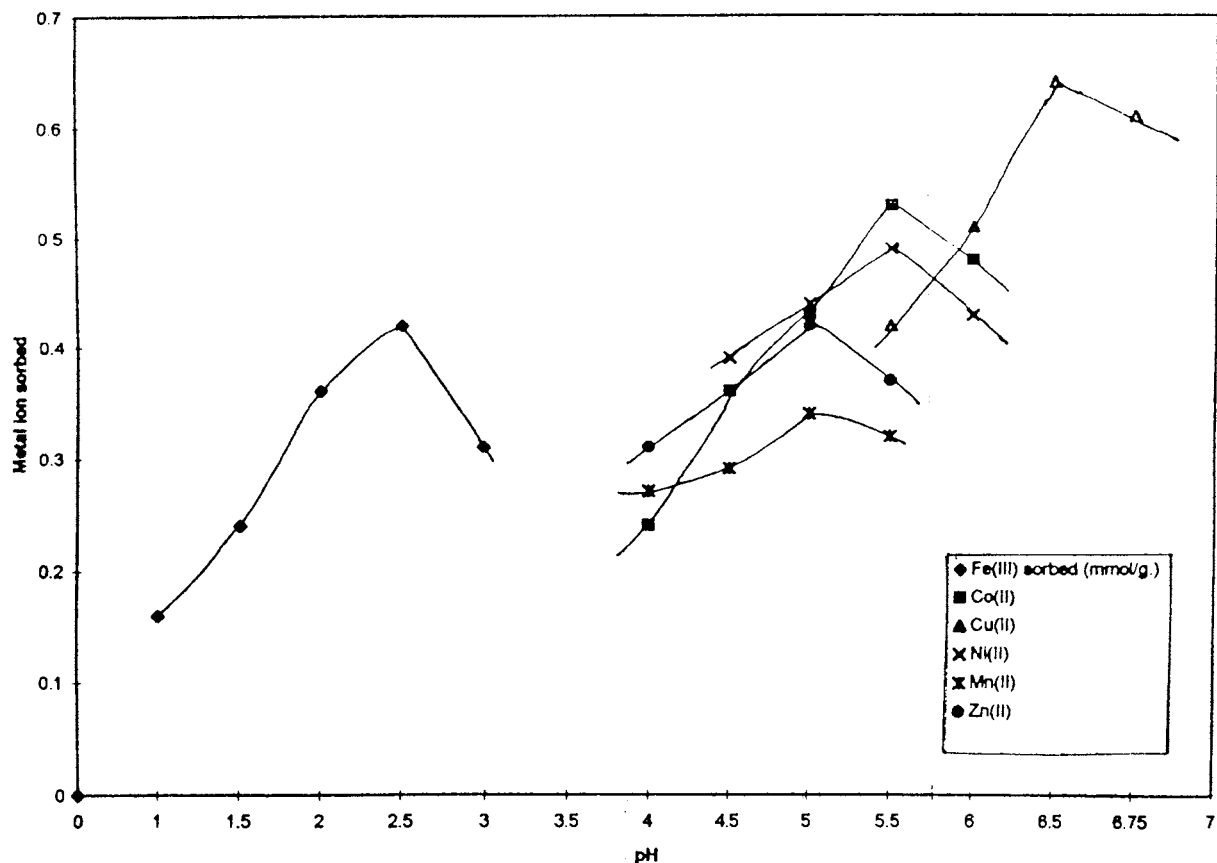


Fig. 2. Sorption behaviour of six metal ions between pH range 1.0–7.0.

2.6.1. Separation of metal ions by using column technique

1. Cu(II)–Fe(III) separation: mixtures of Cu(II) and Fe(III) of various proportions were prepared. The column was preconditioned with 0.01 M HCl. An aliquot of 5 ml of the mixture was introduced at the top of the column. The flow rate was maintained at 0.5 ml min⁻¹. Cu(II) solution was eluted using a 3 M HCl solution while Fe(III) solution was eluted using 2 M HCl at same flow rate and analysed spectrometrically as shown in Table 1.

2. Fe(III)–Co(II) separation: mixtures of Fe(III) and Co(II) of various proportions were prepared. The column was pre-conditioned with 0.01 M HCl. An aliquot of 5 ml of the mixture

was introduced at the top of the column. The flow rate was maintained at 0.5 ml min⁻¹. The Fe(III) solution was eluted using 2 M HCl while the Co(II) solution was eluted using 1 M HCl. The fractions were collected in 5 ml fractions and the concentration of the metal ion determined spectrometrically as shown in Table 2.

2.7. Exchange-capacity determinations

The exchange-capacity of six metal ions Mn(II), Fe(II), Co(II), Ni(II), Cu(II), and Zn(II) were determined in the pH range 1.0–7.0. The 0.25 g of air-dried resins were equilibrated with a buffer and enough metal ion solution adjusted to same pH was added to give the appropriate metal ion

Table 3
Influence of the extent of the crosslinking on metal ion intake by the resin

Crosslinking density	Metal ions (mequi g ⁻¹)					
	Fe(III)	Co(II)	Ni(II)	Cu(II)	Zn(II)	Mn(II)
2%	2.80	2.20	2.40	2.24	1.84	1.73
8%	1.92	1.52	1.95	1.76	1.12	1.05

solution. After shaking for 24 h, the mixture was filtered and the resin was thoroughly washed with buffer until free from the metal ion. The eluted metal ions were determined spectrometrically (Fig. 2).

3. Results and discussion

3.1. Synthesis and characterisation of chelating resin

The resin III presented in this study was synthesized from chloromethylated styrene-divinylbenzene beads (dvb 2 and 8%) through the reaction steps shown in Scheme 1. Fig. 1 shows the IR spectra of resin II and III. The whole characteristic feature in the IR spectrum are the bands due to the nitroso group at 1350, 1410, and 1510 cm⁻¹, a band between 1600–1700 cm⁻¹ due to the tautomeric oxime group and a band at 3150 cm⁻¹ due to O–H stretching frequency of the phenol group.

3.2. Analytical properties of the chelating resin

The high selectivity of resin III towards Cu(II) is shown in Fig. 2, which shows the sorption behaviour of six metal ions at different pH on

resin IIIa and IIIb. An absence of nitroso group shows no significant sorption of metal ions. Equilibrium studies with Cu(II) shows that the time required by the resin III for 50% uptake is 50 min. Therefore Resin III is suitable for column operations if the flow-rate is low.

3.2.1. Influence of the extent of the crosslinking on metal ion intake by resin IIIa and IIIb

The metal ion intake of the resin was studied as a function of pH to determine the optimum pH for maximum complexation. The extent of crosslinking agent in polymeric matrix influence the reactivity and therefore extent of the complexation of polymeric ligand with metal ions is shown in Table 3.

3.2.2. Influence of equilibrium pH on metal ion complexation and their percent recovery by resin III

In order to investigate the optimum pH for maximum complexation, batch studies were carried out at varying pH. The pH dependence of complexation was studied for the regions below and above the natural pH of dipositive metal–salt solutions in aqueous medium. The variation in the amount of the metal ion complexed by the resin III at different pH values are shown in Table 4.

Table 4
Influence of equilibrium pH on metal ion complexation metal ion recovery by resin IIIa

Metal ions	Fe(III) →				Co(II) →				Cu(II)			
	3.5	3.0	2.5	2.0	4.0	4.5	5.0	5.5	5.5	6.0	6.5	6.75
Equilibrium pH	3.5	3.0	2.5	2.0	4.0	4.5	5.0	5.5	5.5	6.0	6.5	6.75
Amount of metal complexed	2.39	2.64	2.78	2.69	1.82	2.01	2.16	2.24	1.93	2.08	2.21	2.03
Recovery (%) of metal ions	86	93	99	97	81	89	95	99	87	94	100	92

Table 5
Recovery of Cu(II) by batch extraction

Recovery of Copper (II)	Molar concentration (M)				
	0.01	0.1	1.0	2.0	3.0
HCl concentration	0.01	0.1	1.0	2.0	3.0
Recovery (%)	12	73	84	94	99

3.2.3. Recovery of Cu(II) by batch operation

Besides the high performance in the adsorption of metal ions, the adsorbed metal ions should be eluted rapidly and quantitatively, from a practical point of view. Various experiments on recovery of Cu(II) from resin III were carried out by batch operation. The results shown in Table 5 indicates that copper can be recovered with HCl by using different concentrations. When the acid concentration is higher than 1.0 M the adsorbed Cu(II) is eluted quantitatively.

In conclusion, the new chelating resin with $\text{CH}_2\text{-NH-C}_6\text{H}_4$ as a spacer containing α -nitroso- β -naphthol as a functional group has been found to be stable in acidic and alkaline medium. It is useful in the separation of Fe(III), Co(II) and Cu(II) and Fe(III). The stability of the chelating functional group in the resin is quite good. The exchange capacity of the resin remains unaltered after quite a number of cycles. The water regain of the resin is satisfactory. The results presented above suggests that resin III can be applied to the concentration and separation of Cu(II) effectively and repeatedly. A decrease in the metal ion capacity at higher crosslinking is due reduced accessibility of the reactive site for complexation. A highly crosslinked system restricts the diffusion of the reducing species into the matrix [11]. The variation in the amount of metal ion complexed even for a highly crosslinked system shows that polymer matrix has a definite influence in the complexation of the different metal ions. In the complexation of polymeric ligands with metal ions, the macromolecular chains coil more tightly

by crosslinking with metal ions. The reduction of EWC is higher in low crosslinked systems. In tightly crosslinked systems, the polymer chain can undergo extensive swelling from the increased diffusion of water molecules into loose networks.

Acknowledgements

The authors are thankful to the Ion-Exchange Co. Ltd. (India) for supplying us with the chloromethylated polystyrene resin and to Dr P.P. Wadgaonkar for thoughtful discussion. We are also thankful to the Polymer Division, National Chemical Laboratory, Pune, India, for determining the particle size of the resins.

References

- [1] H. Erlenmeyer, H. Dahn, *Helv. Chim. Acta* 22 (1939) 1369.
- [2] J.E. Meinhardt, *Science* 110 (1948) 347.
- [3] M. Ilinski, G.V. Knorre, *Berichte der Deutschen Chemischen Gesellschaft* 18 (1885) 699.
- [4] E. Cogan, *Anal. Chem.* 32 (1960) 973.
- [5] I.T. Talahashi, R.J. Robinson, *Anal. Chim. Acta* 32 (1960) 1350.
- [6] F.D. Snell and C.T. Snell, *Colourimetric Methods of Analysis*, vol. 2, Van Nostrand, Reinhold, New York, 1959, p. 290.
- [7] A. Suggi, N. Ogawa, *Talanta* 26 (1981) 274.
- [8] J.P. Ghosh, H.R. Das, *Talanta* 28 (1981) 274.
- [9] R.V. Davies, J. Kennedy, E.S. Lane, J.L. Williams, *J. Appl. Chem.* 9 (1959) 368.
- [10] G.E. Ficken, E.S. Lane, *Anal. Chim. Acta* 16 (1957) 207.
- [11] B. Mathew, V.N.R. Pillai, *Polym. Bull.* 26 (1991) 603.

Effect of ionic strength on the formal potential of the glass electrode in various saline media

Isabel Brandariz ^a, Teresa Vilariño ^a, Pablo Alonso ^a, Roberto Herrero ^a, Sarah Fiol ^b,
Manuel E. Sastre de Vicente ^{a,*}

^a *Departamento de Química Fundamental e Industrial, Facultad de Ciencias, Universidad de La Coruña, Campus da Zapateira s/n, E-15701 La Coruña, Spain*

^b *Departamento de Química Física, Facultad de Química, Universidad de Santiago de Compostela, E-15706 Santiago de Compostela, Spain*

Received 27 May 1997; received in revised form 21 October 1997; accepted 19 December 1997

Abstract

We examined the variation with ionic strength (I , adjusted with KCl, KNO₃, KBr, NaCl or NaClO₄) of the formal potential (E_{const}) for glass electrodes exhibiting a Nernstian response (i.e. $E_{\text{cell}} = E_{\text{const}} - s \log [\text{H}^+]$). For this purpose, we investigated the different factors included in the formal potential, so we obtained reported values for the liquid junction potential as a function of ionic strength and determined the logarithm of the activity coefficient for the proton in various saline media, using Pitzer equations. © 1998 Elsevier Science B.V. All rights reserved.

Keywords: Ionic strength; Formal potential; Glass electrode; Potentiometry

1. Theoretical background

Potentiometry with a commercially available H⁺ ion-sensitive glass electrode, also referred to as ‘pH-metry’, is a powerful tool for determining equilibrium constants [1]. IUPAC recommends calibrating glass electrodes in terms of the proton concentration at a constant ionic strength prior to the determination proper [2]. Glass electrodes exhibit a Nernstian response; consequently, the resulting electromotive force at constant ionic strength will be given by [3]

$$E_{\text{cell}} = E_{\text{const}}(I) + s \log [\text{H}^+] \quad (1)$$

where

$$E_{\text{const}} = E_r + E_1 + E_g^o + s \log \gamma_{\text{H}^+} \quad (2)$$

and s denotes the Nernstian slope, the value of which at 25°C is

$$s = \ln 10 \ RT/F = 59.16 \text{ mV} \quad (3)$$

In Eq. (2), E_g^o is the potential across the glass membrane at unity proton activity; E_r is the combination of the external and internal reference potentials and will thus be independent of the ionic strength of the unknown solution—unlike the liquid junction potential (E_1) and, obviously,

* Corresponding author. Tel.: +34 81 167050; fax: +34 81 167065; e-mail: eman@udc.es

the activity coefficient for the proton ($\log \gamma_{\text{H}^+}$). According to the Stockholm school [4], E_1 varies with acidity; however, several authors have shown that it can be assumed not to vary, within experimental errors, with small acidity changes (e.g. over the $-\log [\text{H}^+]$ ranges 2.3–2.9 and 10.8–11.3). In addition, fulfillment of Eq. (1) has been experimentally confirmed [3,5].

Parameter E_g^0 encompasses the asymmetry potential, resulting from differences between the inner and outer leached layers and potentially arising from composition differences introduced during the electrode's manufacturing process, a differential history for both leached layers or the adsorption of given substances by either [6].

Although formal potentials, E_{const} , are commonly used to determine equilibrium constants, virtually none of the studies involving calibration of glass electrodes in terms of the proton concentration [7–12] has reported on the variation of E_{const} with ionic strength [$E_{\text{const}} = f(I)$]. One interesting exception is the study of Pezza et al. [13], who used various ion-selective electrodes to determine the activity coefficients for the ions sensed by each electrode. In this work, we used commercially available H^+ ion-sensitive glass electrodes to compare the variation of the formal potential with ionic strength in five different electrolytes that are commonly used to adjust the latter parameter (NaCl, KCl, KBr, KNO_3 and NaClO_4).

2. Experimental

Calibrations were done in an acid medium¹ as described elsewhere [5]: variable volumes v of a strong acid of concentration c were successively added to an initial volume V_0 of inert electrolyte solution. The proton concentration was thus given by

$$[\text{H}^+] = \frac{cv}{V_0 + v} \quad (4)$$

¹ If calibration was performed by adding a base to an acid solution, then the combination of relatively small errors in the concentration of both resulted in the slope of the fitted curve deviating from the Nernstian value, as previously noted elsewhere [3,5].

where $2.3 < -\log [\text{H}^+] < 2.9$ [3]. We used an initial volume $V_0 = 40.0$ ml to which 0.04 ml aliquots of 0.1000 M HCl were successively added. Only those points included in the above-mentioned range were used to fit E_{cell} versus $\log [\text{H}^+]$ curves.

We carried out experiments at a variable ionic strength adjusted with NaCl, KBr, KNO_3 , KCl and NaClO_4 (all Merck p.a. reagents). The water used to prepare every solution was purified by passage through a Millipore Milli-Q system. All experiments were performed in a dual-wall cell through which water thermostated at $25.0 \pm 0.1^\circ\text{C}$ was circulated. Nitrogen of 99.999% purity was bubbled through the cell to remove CO_2 and stir the solution. A Crison microBU 2030 autoburette furnished with a 2.5 ml syringe for dispensing the titrant was used. The burette was controlled via a computer that afforded reading the emf of a Crison micropH 2002 pH-meter connected to a Radiometer GK2401C electrode. This last was a glass electrode combined with an Ag/AgCl reference electrode where the liquid junction was established by a salt bridge consisting of a plug of porous ceramics.

3. Results and discussion

Fig. 1 shows a typical calibration curve, of intercept $E_{\text{const}} = 378.9 \pm 0.1$ mV and slope

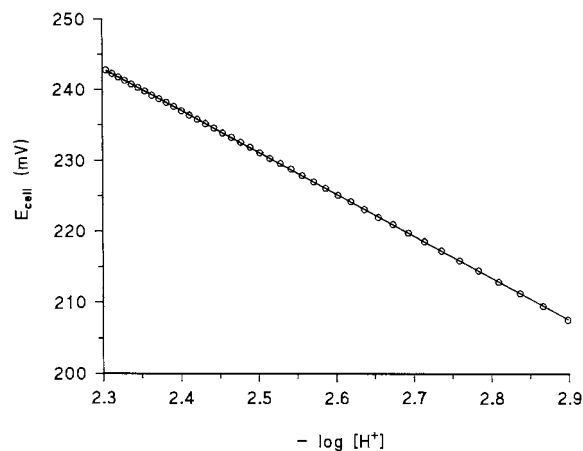


Fig. 1. Calibration curve of equation $E = 378.9 (\pm 0.1) - 59.1 (\pm 0.1) \text{p}[\text{H}^+]$ in 0.6 M KBr.

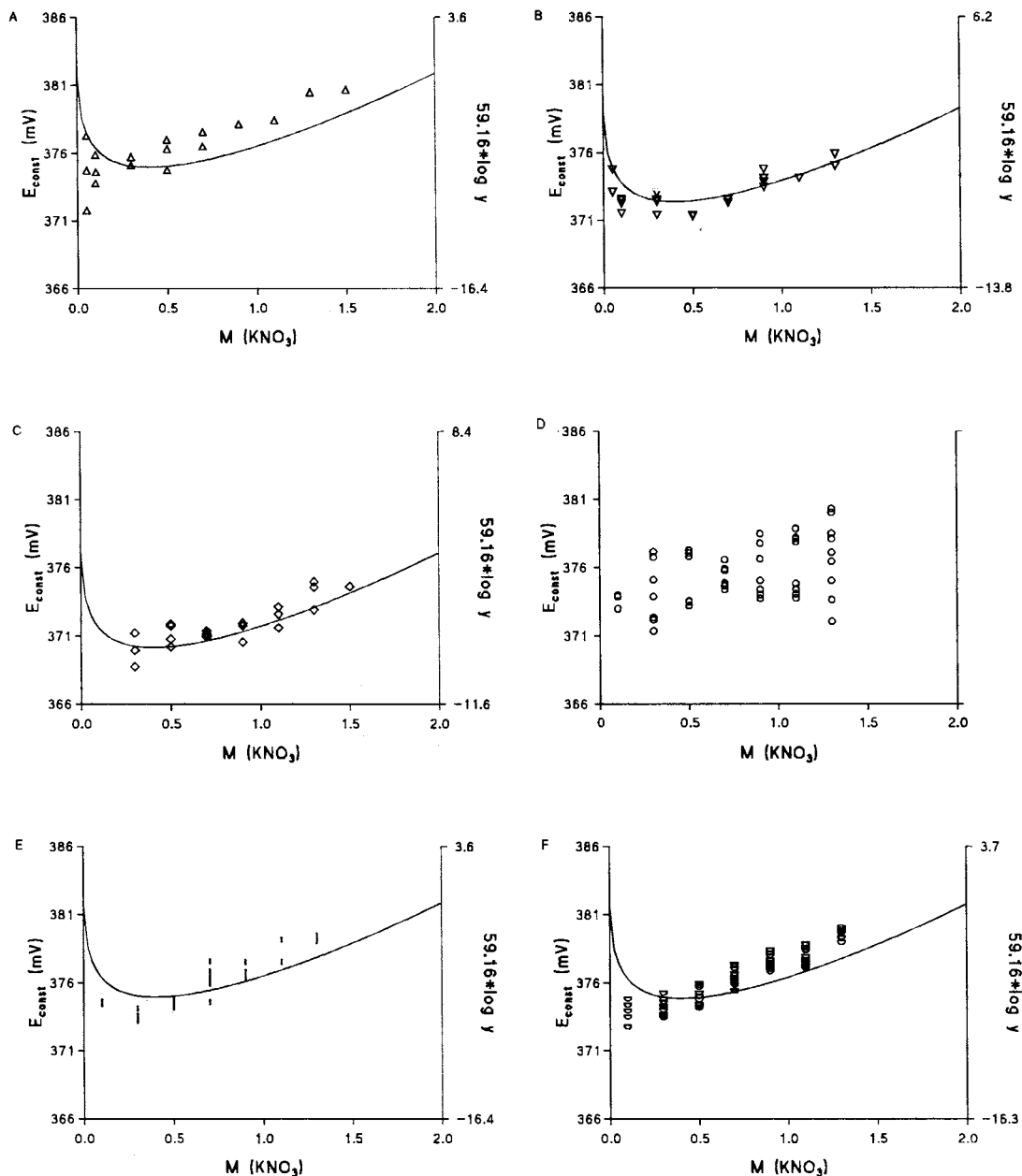


Fig. 2. Variation of E_{const} with I in KNO_3 . Data obtained with the same Radiometer GK2401C electrode on the following time frames: (A) May–June, 1992, (B) April, 1993, (C) January–April, 1994, (D) October, 1994, (E) December, 1994, and (F) February–March, 1995. The solid line represents the variation of $s \log \gamma_{\text{H}^+}$ with I according to the Pitzer equations.

59.1 ± 0.1 mV. The E_{const} values obtained from similar fitted curves for the different electrolytes are shown in Figs. 2, 4 and 5. By way of example, Fig. 3 shows the slopes of the calibration curves

obtained in KNO_3 ; as can be seen, there were no significant deviations from 59.2 mV at 25°C—the largest error was 2%—, which testifies to the Nernstian behaviour of the electrode. Similar re-

sults were obtained regarding the slopes of the fitted curves for the other electrolytes. On the other hand, careful examination of Fig. 2 reveals increased dispersion of formal potentials in graph D. The difference arose from the fact that, except in series 1D, the glass electrode was stored in a slightly acidic solution (about 0.05 M) while not in use in order to improve its response relative to storage in water or a neutral buffer [14]. During the calibrations of Fig. 2D, the electrode was kept in distilled water while not in use—an identical behaviour was observed if it was stored in a neutral buffer.

As can also be seen from Fig. 2, experimental points in the E_{const} versus I graphs followed the same pattern, albeit shifted to lower or higher potentials—note that the same scale was used in all graphs.

In order to account for the behaviour of these E_{const} versus I curves in Figs. 2, 4 and 5 one must break down E_{const} into the factors included in Eq. (2). As noted earlier, both the liquid junction potential, E_l , and the activity coefficient for the proton, vary with ionic strength.

There are few reported liquid junction potentials. By exception, Bagg [15] has reported the potentials for the junction or free diffusion between a 4 M KCl solution and NaCl or KBr solutions at a variable ionic strength (Fig. 6). The results of Bagg [15] for the liquid junction residual potential in dual-junction cells are comparable,

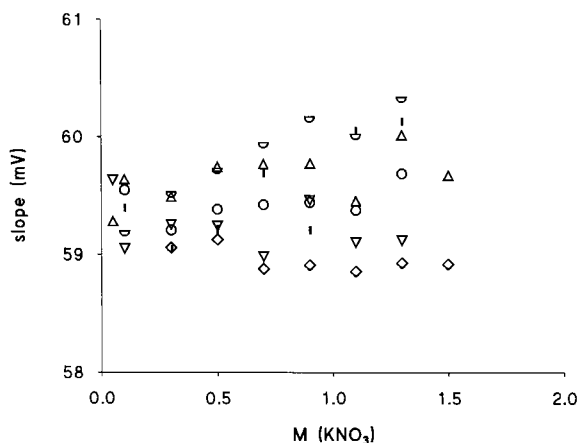


Fig. 3. Mean of the slopes of the calibration curves in Fig. 2.

within experimental error for this type of measurement, with those experimentally—derived in almost every system studied so far. As noted by Bagg himself, ‘this agreement is particularly satisfactory in view of (a) the probable differences of the junctions, sleeve-type and frit, used in the cells from the idealized model of junction used in the calculation, and (b) the extrapolation of some transference numbers beyond the range of concentration in which they are determined.’

The sole constraint to the use of the previous data [15] is that the ionic strength values used do not coincide with those of our experiments, so E_l must be interpolated to the desired I values. For this purpose, we used a polynomial ratio proposed elsewhere [16] as the interpolation function. We used this type of function because it fits the experimental behaviour more closely than does a simple polynomial or a cubic spline interpolation function [16].

Provided the liquid junction potential is known, Eq. (2) can be rewritten as

$$E_{\text{const}} - E_l = E_r + E_g^0 + s \log \gamma_{\text{H}^+} \quad (5)$$

If the only term that depends on ionic strength on the right-hand side of this equation is the activity coefficient for the proton, then, the plots of $(E_{\text{const}} - E_l)$ versus I and $(s \log [\text{H}^+])$ versus I should exhibit the same trend except for the shift due to the $(E_r + E_g^0)$ term. In order to confirm this assumption, we superimposed the $(s \log \gamma_{\text{H}^+})$ versus I curve and shifted it to overlap the previous one, obviously, at the same scale amplitude (20 mV) in both cases (Fig. 5B,D).

The activity coefficient for the proton was calculated in the light of Pitzer’s formalism. The pertinent equations are given in Appendix A and the curves obtained in the different electrolytes studied are shown in Fig. 7. As can be seen, every curve exhibits a minimum at a different ionic strength for each electrode, beyond which the curve is virtually linear. The similar behaviour of the $(s \log \gamma_{\text{H}^+})$ versus I curves and the $(E_{\text{const}} - E_l)$ versus I curves is apparent in Fig. 5B,D for KBr and NaCl, respectively. One quantitative way of comparing the experimental results with the curve derived from the Pitzer equations is by fitting experimental E_{const} versus I data points and

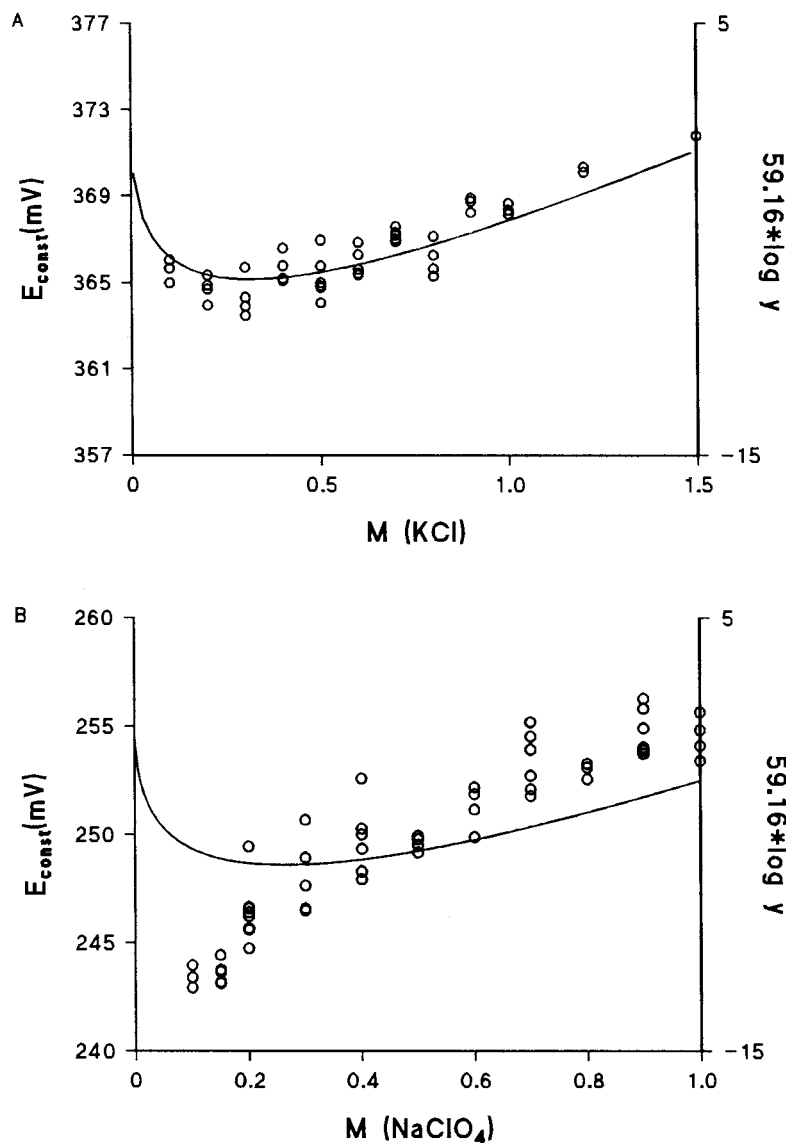


Fig. 4. Variation of E_{const} with I in the following electrolytes: (A) KCl and (B) NaClO₄. The solid line represents the variation of $s \log \gamma_{\text{H}^+}$ with I according to the Pitzer equations.

those in the $(s \log \gamma_{\text{H}^+})$ versus I curve obtained from the Pitzer equations—obviously in the virtually linear zone (Fig. 7)—to a straight line. Table 1 gives the results obtained and the ionic strength range used in each fitting. As can be seen, consistency between data is quite good for KBr (Fig. 5B) but not quite for NaCl (Fig. 5D) as the likely result of Na⁺ ion influencing the behaviour of the

glass electrode. Unfortunately, there seems to be no reported liquid junction potentials for the other systems studied, so we chose to plot E_{const} versus I and $(s \log \gamma_{\text{H}^+})$ versus I in the same graphs.

As can be seen from both Table 1 and Fig. 5A, the results in KBr were still similar, which was to be expected since E_1 remained virtually constant

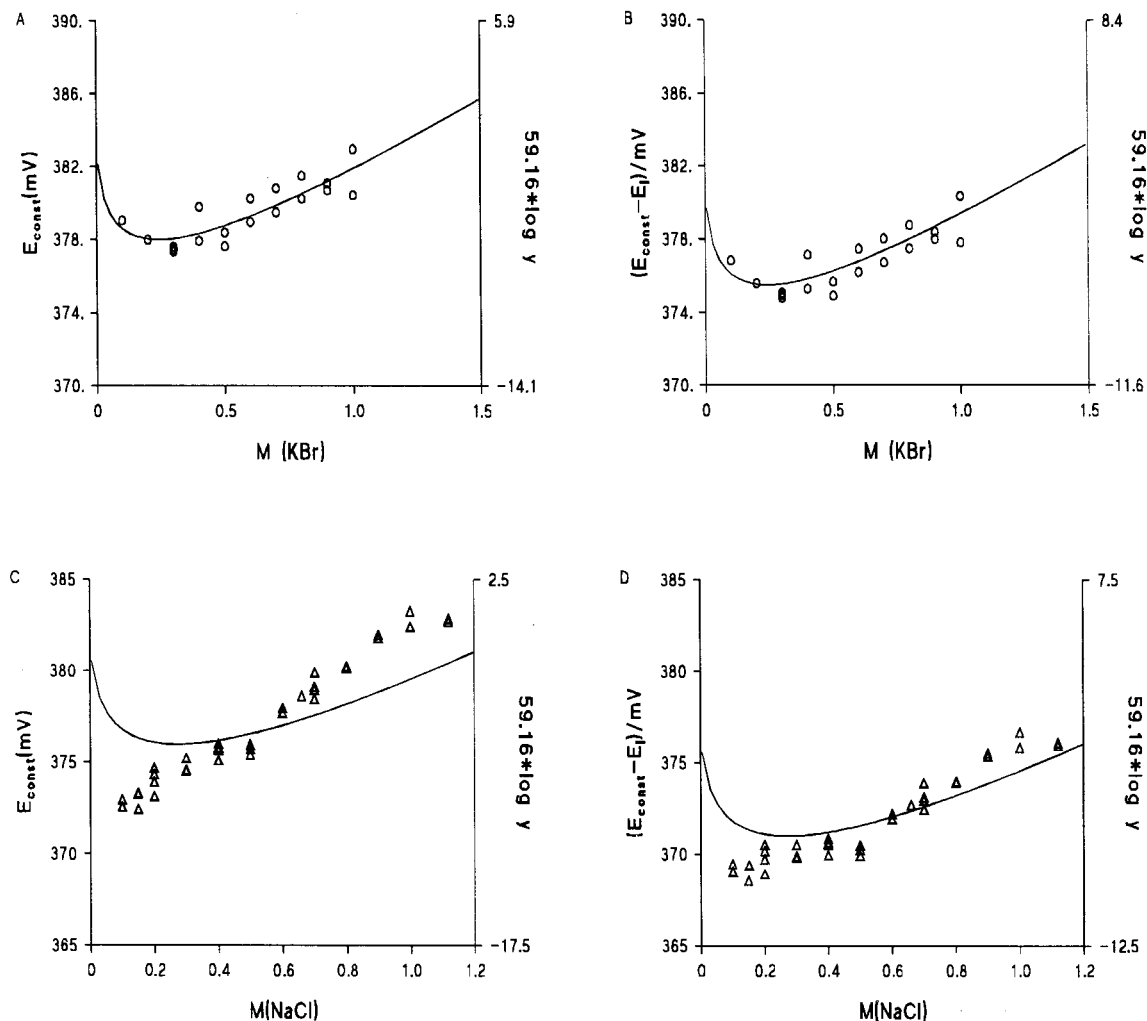


Fig. 5. Variation of (A) E_{const} with I in KBr, (B) $E_{\text{const}} - E_1$ with I in KBr, (C) E_{const} with I in NaCl, and (D) $E_{\text{const}} - E_1$ with I in NaCl. The solid line represents the variation of $s \log \gamma_{\text{H}^+}$ with I according to the Pitzer equations.

throughout the ionic strength range studied. Similar consistency was observed in KCl and KNO_3 (Table 1, Figs. 2 and 4A), which suggests that E_1 remains virtually constant over the ionic strength range where the formal potential was determined. Fig. 2 also shows six data series for the formal potential; while all exhibit a similar trend, the potential is displaced to a greater or lesser extent between one another. Based on Eq. (5), this can be ascribed to change in the $(E_r + E_g^0)$ term because, if the electrodes were theoretically im-

mersed in the same solutions, E_r should have remained constant and the change be due to a variation in the asymmetry potential with time typical of changes at the electrode surface layer.

The E_{const} versus I plot in sodium perchlorate exhibited a much greater slope than that obtained from the Pitzer fitting as the likely result of (a) the influence of sodium ion on glass membranes and/or (b) a major change in the liquid junction potential relative to potassium salts over the ionic strength range studied.

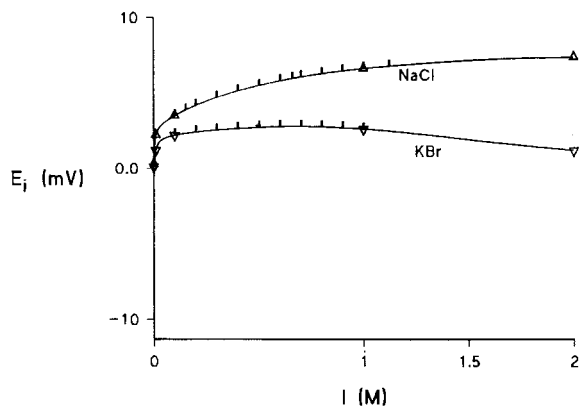


Fig. 6. Variation of E_i with I in NaCl and KBr. Triangles represent data from an earlier reference [15] and ticks the points where E_i was extrapolated.

Appendix A

The relationship of $\log \gamma_{H^+}$ to I was studied in the light of the Pitzer equations [17], which have frequently been used to describe the influence of ionic strength on the activity coefficients for strong electrolytes at moderate to high concentrations and a high electrolyte concentration. Our group has used them to interpret the variation with ionic strength of the acidity constants for some organic molecules [18–26].

Based on Pitzer's formalism, the activity coefficient for H^+ ion in the presence of excess electrolyte is given by

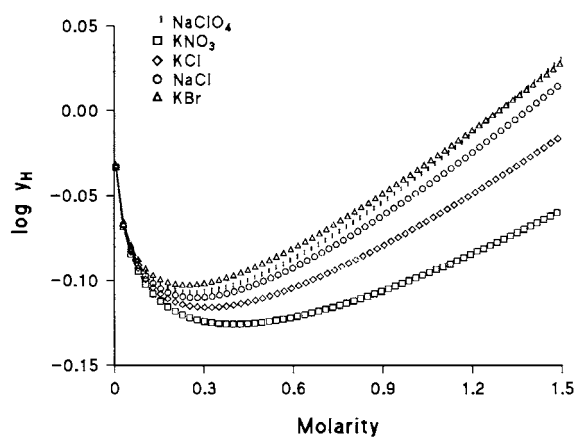


Fig. 7. Variation of $\log \gamma_{H^+}$ with I (on the molar scale) in $NaClO_4$, KNO_3 , KCl , $NaCl$ and KBr .

$$\ln \gamma_{H^+} = f^\gamma + 2I(B_{XH} + IC_{XH}) + I^2(B'_{XK} + C_{XK}) + I(2\theta_{HK} + I\psi_{HXK}) \quad (A.1)$$

where the ionic strength is determined from the salt concentration since the salt is in a large excess relative to the proton. f^γ , B and B' depend on I , as can be seen in the following equations:

$$f^\gamma = -A_\phi \left[\frac{\sqrt{I}}{1 + 1.2\sqrt{I}} + \frac{2}{1.2} \ln(1 + 1.2\sqrt{I}) \right] \quad (A.2)$$

$$B_{XK} = \beta_{XK}^{(0)} + \frac{\beta_{XK}^{(1)}}{2I} [1 - (1 + 1.2\sqrt{I}) \exp(-2\sqrt{I})] \quad (A.3)$$

$$\beta'_{XK} = \beta_{XK}^{(0)} + \frac{\beta_{XK}^{(1)}}{2I} [-1 + (1 + 1.2\sqrt{I} + 2I) \exp(-2\sqrt{I})] \quad (A.4)$$

Substituting B and B' in the expression for the logarithm of the activity coefficient of H^+ ion yields

$$\ln \gamma_{H^+} = f^\gamma + PI + QI^2 + RI e^{-2\sqrt{I}} + T[1 - (1 + 1.2\sqrt{I}) e^{-2\sqrt{I}}] \quad (A.5)$$

where

$$P = 2(\beta_{HX}^{(0)} + \theta_{HK})$$

$$Q = C_{HX}^\phi + \frac{C_{KX}^\phi}{2} + \psi_{HXK}$$

$$R = \beta_{KX}^{(1)}$$

$$T = \beta_{HX}^{(1)} - \frac{\beta_{KX}^{(1)}}{2} \quad (A.6)$$

P , Q , R and T are thus constants that depend on the particular inert electrolyte (see Table 2). The Pitzer parameters used to calculate them were taken from an earlier reference [17].

The activity coefficients in Eq. (A.5) are expressed on the molal scale, so they must be converted into molar units since E_{const} was determined from molar $[H^+]$ values. We used the following equation for this purpose [27]:

$$y = \gamma \frac{\rho_w}{\rho} \left(1 + \sum_i m_i M_i \right) \quad (A.7)$$

Table 1

Slopes of the linear fits of E_{const} versus I , $(E_{\text{const}} - E_1)$ versus I and $\text{slog } \gamma_{\text{H}^+}$ versus I plots in each of the electrolytes studied

Electrolyte	$59.16 \times \log y^a$ (Pitzer eq.)	Slope of E_{const} vs. I	Slope of $E_{\text{const}} - E_1$ vs. I	I range	Fig.
KNO ₃	4.0 ± 0.1	4.8 ± 0.7		0.5–1.5	2a
	4.0 ± 0.1	5.1 ± 0.6		0.5–1.5	2b
	4.0 ± 0.1	3.7 ± 0.6		0.5–1.5	2c
	4.0 ± 0.1	5.7 ± 0.8		0.5–1.5	2e
	4.0 ± 0.1	5.0 ± 0.3		0.5–1.5	2f
KCl	6.2 ± 0.1	6.7 ± 0.6		0.5–1.5	4a
NaClO ₄	6.5 ± 0.1	9.9 ± 1.4		0.5–1.0	4b
KBr	6.3 ± 0.1	6.6 ± 1.5	6.8 ± 1.4	0.5–1.0	5a,b
NaCl	6.0 ± 0.1	11.4 ± 0.5	9.0 ± 0.5	0.4–1.1	5c,d

^a Obtained from those points in Fig. 7 that lay within the stated ionic strength range for each electrolyte.

Table 2

Pitzer Parameters used in Eq. (A.5) for each of the electrolytes studied

Electrolyte	P	Q	R	T
KNO ₃	0.2338	0.0043	0.0494	0.2959
KCl	0.3650	−0.0062	0.2122	0.1884
KBr	0.4020	−0.01363	0.2212	0.2458
NaCl	0.4270	−0.0026	0.2664	0.1613
NaClO ₄	0.4214	−0.00899	0.2755	0.15535

where y and γ denote the activity coefficients on the molar and molal scale, respectively; ρ is the solution density; ρ_w is water density at the working temperature; i denotes any ion in solution; and M_i is the molar mass of ion i , m_i is molality and c_i its molarity.

By way of example, substituting water density at 25°C and the molecular mass of NaCl into Eq. (A.7) yields

$$y_{\text{NaCl}} = \frac{\gamma_{\text{NaCl}}}{\rho_{\text{NaCl}}} (0.997075 + 0.05827m_{\text{NaCl}}) \quad (\text{A.8})$$

Also, molality can be converted into molarity by using the following expression:

$$\frac{c}{m} = \frac{\rho_{\text{NaCl}}}{1 + \sum_i m_i M_i} \quad (\text{A.9})$$

which, for NaCl, becomes

$$c_{\text{NaCl}} = \frac{\rho_{\text{NaCl}} m_{\text{NaCl}}}{1 + 0.10110m_{\text{NaCl}}} \quad (\text{A.10})$$

The dependence of density on the ionic strength can be determined by fitting ρ versus m data pairs to a polynomial expression of m based on reported values [28,29].

References

- [1] E.P. Serjeant, Potentiometry and Potentiometric Titrations, Wiley, New York, 1984.
- [2] A. Braibanti, G. Ostaroli, P. Paoletti, D. Petit, S. Sammaritano, Pure Appl. Chem. 59 (12) (1987) 1721.
- [3] P.M. May, D.R. Williams, P.W. Linder, R.G. Torrington, Talanta 29 (1982) 249.
- [4] P.W. Linder, R.G. Torrington, D.R. Williams, Analysis using Glass Electrodes, Ch. 4, Open University Press, Oxford, 1984.
- [5] S. Fiol, F. Arce, X.L. Armesto, F. Penedo, M. Sastre de Vicente, Fresenius J. Anal. Chem. 343 (1992) 469.
- [6] H. Galster, pH Measurement, VCH, New York, 1991.
- [7] W.A.E. McBryde, Analyst, 96 (1971) p. 739; 94 (1969) p. 337.
- [8] H.S. Dunsmore, D. Midley, Anal. Chim. Acta 61 (1972) 115.
- [9] M.T.S.D. Vasconcelos, A.S.C. Machado, Rev. Port. Quim. 28 (1986) 120.
- [10] E.W. Baumann, Anal. Chim. Acta 64 (1973) 284.
- [11] H.M. Irving, M.G. Miles, L.D. Petit, Anal. Chim. Acta 38 (1967) 475.
- [12] G.R. Hedwig, H.K.J. Powell, Anal. Chem. 43 (10) (1971) 1206.
- [13] L. Pezza, M. Molina, M. de Moraes, C.B. Melios, J.O. Tognolli, Talanta 43 (1996) 1689.
- [14] W.H. Beck, J. Caudle, A.K. Covington, W.F.K. Wynne-Jones, Proc. Chem. Soc., (1963) 110.
- [15] J. Bagg, Electrochim. Acta 35 (2) (1990) 361–367.
- [16] W.H. Press, S.A. Teukolsky, W.T. Vetterling, B.P. Flannery, Numerical Recipes in Fortran Ch., 3, 2nd ed., Cambridge University Press, Cambridge, 1992.

- [17] K.S. Pitzer, Theory: ion interaction approach, in: K.S. Pitzer (Ed.), *Activity Coefficients in Electrolyte Solutions*, 2, CRC Press, Boca Raton, Fl., 1991, p. 75.
- [18] R. Herrero, X.L. Armesto, F. Arce, M. Sastre de Vicente, *J. Solution Chem.* 21 (11) (1992) 1185.
- [19] I. Brandariz, F. Arce, X.L. Armesto, F.J. Penedo, M. Sastre de Vicente, *Monatsh. Chem.* 124 (1993) 249.
- [20] R. Herrero, I. Brandariz, M. Sastre de Vicente, *Ber. Bunsenges. Phys. Chem.* 97 (1) (1993) 59.
- [21] I. Brandariz, R. Herrero, M. Sastre de Vicente, *J. Chim. Phys.* 90 (1993) 63.
- [22] H. Herrero, I. Brandariz, S. Fiol, M. Sastre de Vicente, *Collect. Czech. Chem. Commun.* 58 (1993) 1269.
- [23] S. Fiol, I. Brandariz, X.L. Armesto, F. Arce, M. Sastre de Vicente, *Ann. Chim. (Rome)* 83 (1993) 175.
- [24] I. Brandariz, S. Fiol, R. Herrero, T. Vilariño, M. Sastre de Vicente, *J. Chem. Eng. Data* 38 (1993) 531.
- [25] S. Fiol, I. Brandariz, R. Herrero, T. Vilariño, M. Sastre de Vicente, *Ber. Bunsenges. Phys. Chem.* 98 (1994) 164.
- [26] R. Herrero, I. Brandariz, S. Fiol, T. Vilariño, M. Sastre de Vicente, *An. Quím.* 89 (5) (1993) 602.
- [27] F. Macintyre, *Mar. Chem.* 4 (1970) 205.
- [28] R.C. Weast (ed.), *C.R.C. Handbook of Chemistry and Physics*, C.R.C. Press, Boca Raton, Florida, 1986.
- [29] J.F. Chem, G.R. Choppin, *J. Solution Chem.* 24 (5) (1995) 46.

Column preconcentration of organotin with tropolone-immobilized and their determination by electrothermal atomization absorption spectrometry

P. Bermejo-Barrera *, G. González-Campos, M. Ferrón-Novais, A. Bermejo-Barrera

Department of Analytical Chemistry, Nutrition and Bromatology, Faculty of Chemistry, University of Santiago de Compostela, 15706 Santiago de Compostela, Spain

Received 23 January 1997; received in revised form 02 June 1997; accepted 22 December 1997

Abstract

A method for the determination of total organic tin from marine water samples by electrothermal atomization absorption spectrometry (ETAAS) is described. Samples are previously preconcentrated with a chelating molecule (tropolone) impregnated on a macroporous polymer (Amberlite XAD-2). The graphite furnace programme and preconcentration parameters were optimized. Calibration and addition graphs were performed. Sensitivity obtained with this procedure was 13 ng l^{-1} . Relative standard deviation was always $> 10\%$ and analytical recovery were satisfactory, $\sim 100\%$. Some possible interferences were investigated, having no problems with this factor. This procedure allows the distinction between organotin compounds and inorganic tin IV, since the latter is not retained on the column. © 1998 Elsevier Science B.V. All rights reserved.

Keywords: Organic tin; Tropolone; Amberlite XAD-2; ETAAS

1. Introduction

Interest in the determination of tin and their organic compounds at trace levels in the environment has increased in recent years because of the growing use of organotin compounds over the past 30 years [1–3], due to the great number of industrial applications discovered for these compounds. Organotin toxicity is determined by its own nature and by the number of organic groups

bonded to tin. It has been found teratogenic and genotoxic effects in some organisms [4,5].

The principal use of TBT was in antifouling paints for ships because they are effective biocides against marine fouling organisms, however, they are non-specific and extremely toxic to non-target animal and plant species. Then, this use was restricted in some countries. The first actions were adopted in France in 1982 [6], followed by UK in 1985 [7,8]. France banned the use of TBT-based paints on boats $< 25 \text{ m}$ length. UK regulation restricted the sale of TBT paints containing more than 7.5% total tin in copolymers or 2.5% total tin as free tin.

* Corresponding author. Tel.: +34 981 591079; fax: +34 981 595012; e-mail: qn1956@usc.es

Due to this, marine waters can contain important levels of these compounds that increase in areas with restricted water circulation and significant recreational boating activity, a great number of techniques have been proposed for the measurement of these compounds. One of the methods widely used to determine total tin is ETAAS and although its detection power is high, it cannot be routinely used for the direct trace element analysis of many water samples. Thus, a preconcentration method is necessary to increase the detection limit, to remove interferences and to improve precision and accuracy of the results. Extraction is the most widely used preconcentration technique (liquid–liquid, liquid–solid, ion-exchange,...) over the last few years, but column preconcentration is a good option to obtain an easy, faster and reproducible method. Chelating resins (chelating molecule adsorbed on a polymeric matrix) are used in column preconcentration because of their high selectivity for transition elements, and they combine two very important analytical processes: ionic change and formation of chelates complexes [9]. These resins must contain functional groups with one or more donor atoms (N, O, P, S, As). Once a chelating molecule is adsorbed on the polymeric matrix, it must form stable complex with analytes to be separated. Polymeric matrices must have chemical stability for being no altered in the process and have spherical structure to keep forming complexes once chelating molecule have been adsorbed on it.

Nowadays, a great number of these resins are known, due to the great number of polymeric matrices and chelates available.

The use of Amberlite resins with different complexing groups has been studied by different authors. Lee et al. [10] used the Amberlite XAD-2, -4 and -7 with 8-hydroxyquinoline to separate metals in aqueous solutions. Van Berckel and Maessen [11] introduced the analyte loaded resin into the plasma through graphite furnace electrothermal vaporization. Horward and Danilova-Mirzaian [12] used the Amberlite XAD-4 with thioglycolate groups to preconcentrate Sn, Cd, Pb and Ni and Blain et al. [13] used Amberlite XAD-4 and XAD-7 with lipophilic tetraazo-

macrocycles that have high selectivity for transition metals over alkali and alkaline earth metal ions. Porta et al. [14] used the Amberlite XAD-2 and XAD-7 with ammonium pyrrolidine dithiocarbamate (APDC) and performed the preconcentration of Cd, Cu, Pb, Ni, Co and Fe of Antarctic sea water on line with atomic absorption spectroscopy with graphite furnace using the Zeeman effect background correction. The preconcentration on line also has been developed by Azeredo et al. [15] using a silica-immobilized 8-hydroxyquinoline preconcentration system, eluting trace metals (Cd, Cu, Fe, Mn, Ni, Pb and Zn in sea water) directly in graphite furnace with acid.

The polystyrene support with phosphonic acid [16], a macroreticular support and PVC polymer [17] and the resins Dowex 1X8, Lewaitit MP5080 impregnated with 8-hydroxyquinoline [18] has been also applied in this type of determinations.

The molecule tropolone has been used in previous works for the preconcentration of TBT, DBT and MBT by extraction with chloroform [19] or benzene [20] obtaining good results.

In this paper, the use of tropolone physisorbed on Amberlite XAD-2 is proposed for preconcentration of organic tin (TBT, DBT, MBT) and posterior determination by atomic absorption spectroscopy with electrothermal atomization.

2. Experimental

2.1. Apparatus

A Perkin–Elmer 1100B atomic absorption spectrometer with a deuterium-arc background corrector and a hollow-cathode lamp operating at 35 mA and with a slit width of 0.7 nm was employed to carry out the area of the absorbance peak. The wavelength was 224.6 nm. A Perkin–Elmer Model HGA-400 graphite furnace atomizer with graphite tubes coated with zirconium [21], with L’Vov platform were used. A volume of 20 μ l of sample was injected by an Auto Sampler AS-70. Glass chromatographic columns (30 \times 1.5 cm i.d.) with a glass filter and a Teflon key (Afora).

Table 1
Optimized furnace programme

Step	Temperature (°C)	Hold time(s)	Ramp time (s)	Gas Flow (ml min ⁻¹)
Dry	150	15	10	300
Pyrolysis	1000	15	5	300
Atomization	1900	3	0	0
Clean	2400	4	1	300

2.2. Reagents

Tributyltin solution in methanol, containing 1000 mg l⁻¹ of tin, prepared with tributyltin chloride at 97% of Fluka (Buchs, Switzerland). Dibutyltin solution, containing 1000 mg l⁻¹ of tin, prepared with dibutyltin dichloride at 97% of Aldrich (Milwaukee). Monobutyltin solution in methanol, with 1000 mg l⁻¹ of tin, prepared with monobutyltin trichloride at 95% of Aldrich. Tin stock standard solution, 1.000 mg l⁻¹ of BDH (Poole, UK). Tropolone (2-hydroxy-2,4,6-cycloheptatrienone) at 98% of Aldrich. Isobutylmethylketone at 99%, Analar of BDH (Poole, UK). Methanol, grade HPLC, of Scharlau (Barcelona, Spain). Nitric acid Aristar of BDH. Hydrochloric acid at 37% of Merck (Darmstadt, Germany). Amberlite XAD-2, 20–60 mesh of Aldrich Chemie (Steinheim, Germany).

2.3. Procedure

For preconcentration: 200 ml of sample with 10% HCl was passed through the column and 1 ml of MIBK in two steps (collected in the same tube) was employed to elute the retained compounds. For calibration: 20 µl of eluted sample containing 10, 20, 30, 40 µg l⁻¹ of Sn were introduced into the graphite furnace. The graphite furnace programme (Table 1) was followed and the peak absorbance noted. For the standard addition graph the same procedure than in calibration was applied but using low salinity synthetic marine water, prepared following Baxter and Frech recommendation [22].

3. Results and Discussion

3.1. Optimization of the column preconcentration

The optimum conditions to carry out preconcentration in column were determined. First, Amberlite XAD-2 was purified to avoid contamination problems in the samples. The polymer was shaken for half an hour with a magnetic stirrer with Milli-Q water, HCl 6M and NaOH 2M, respectively, and filtered off in each step, after being rinsed with Milli-Q water until neutrality of pH was obtained. Then, Amberlite XAD-2 was conditioned with 0.01% aqueous tropolone solution for an hour with a magnetic stirrer. Then the conditioned resin (1 g) was introduced in each column, to carry out the preconcentration with a preconcentration factor of 100.

Different eluents as: methanol–acetic acid (HAc) (5–30%), methanol–HCl (0.025–20%), HCl 2M, acetone and MIBK were studied. Optimum was established passing an aqueous standard solution containing 0.15 µg l⁻¹ of organic tin through the column and eluting with mentioned eluents. Then, comparing standards absorbance signals without preconcentration and eluates absorbance signals, it concludes that MIBK is the best eluent in these conditions (Fig. 1).

The addition of hydrochloric acid to eluents produce a better elution because of the good solubility of chlorides in the eluent, and the regeneration of the tropolone molecule with acid proton. Optimum concentration of hydrochloric acid in samples was determined, and it was 10% HCl, as it shows in Fig. 2.

Experiments with tin aqueous standard solution containing 0–40 µg l⁻¹ of Sn were realized and

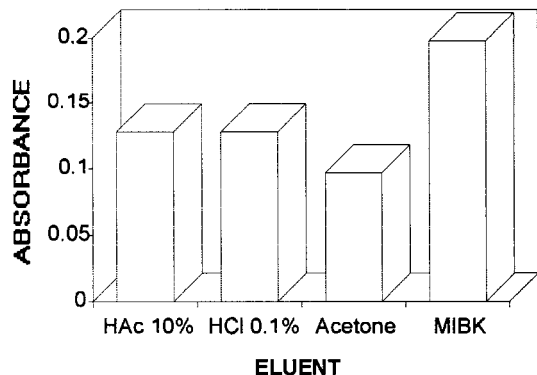


Fig. 1. Eluent optimization.

integrated absorbance signals by ETAAS were about 0.002 Au while signals of tin aqueous solution are the same before or after elution (0.001–0.129 Au). Thus, it appears that inorganic tin is not retained.

The resin capacity was determined passing a standard solution of 0.3 mg l⁻¹ of organic Sn through the conditioned resin and eluting with 2 ml of MIBK. Then, eluates were measured by FAAS and the resin capacity was 600 µg g⁻¹.

Preconcentration factor was 100.

3.2. Optimization of the graphite furnace programme

Graphite tubes coated with zirconium were utilized [21]. Optimum temperatures and times for drying, pyrolysis and atomization were studied (Table 1). Pyrolysis and atomization graphs were

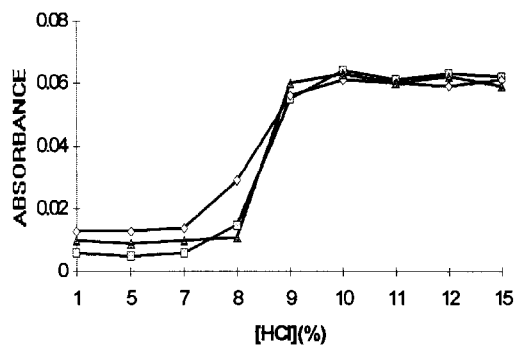


Fig. 2. Optimization of hydrochloric acid concentration for MBT (□), DBT (◇), TBT (△).

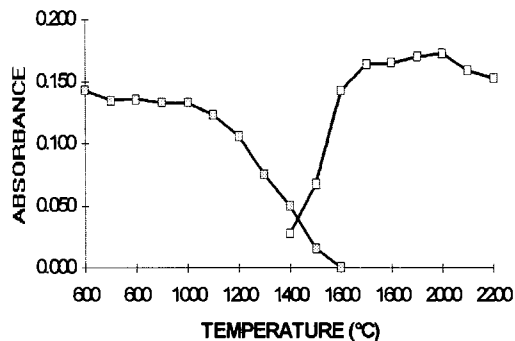


Fig. 3. Optimization of pyrolysis (left) and atomization (right) temperatures.

constructed with a column preconcentrated sample with the procedure described before, containing 40 µg l⁻¹ of tin. The optimum pyrolysis temperature found was 1000°C for 10 s with a ramp time of 5 s and internal gas flow at the maximum rate of 300 ml min⁻¹. The optimum atomization temperature was 1900°C for 3 s without ramp time and internal gas flow (Fig. 3). The tube was cleaned at 2400°C for 4 s with a ramp time of 1 s with the internal gas flow at 300 ml min⁻¹.

3.3. Calibration

Column preconcentrated samples containing 0–40 µg l⁻¹ of Sn were utilized to carry out calibration graph. For the standard addition method, the same concentrations of Sn were utilized, but dissolved in marine water.

Different calibration and addition graphs were performed for MBT, DBT and TBT and for a mixture of MBT, DBT and TBT.

The equations obtained are shown in Table 2: in all cases there are not important differences between the slopes of addition and calibration graphs, then we consider that there are not matrix effects in all cases.

3.4. Sensitivity

The limit of detection (LOD) is calculated as 3 SD m⁻¹ with SD being the within-run standard deviation of a series of blank determination, and

Table 2
Calibration and addition graphs

Compound	Calibration	Addition
MBT	$A_i = 3.2 \cdot 10^{-3} + 2.8 \cdot 10^{-3}[\text{Sn}]$ $r = 0.998$	$A_i = 2.6 \cdot 10^{-3} + 2.8 \cdot 10^{-3}[\text{Sn}]$ $r = 0.998$
DBT	$A_i = 4.2 \cdot 10^{-3} + 2.8 \cdot 10^{-3}[\text{Sn}]$ $r = 0.998$	$A_i = 5.6 \cdot 10^{-3} + 2.8 \cdot 10^{-3}[\text{Sn}]$ $r = 0.997$
TBT	$A_i = 2.2 \cdot 10^{-3} + 2.8 \cdot 10^{-3}[\text{Sn}]$ $r = 0.997$	$A_i = 1.2 \cdot 10^{-3} + 2.9 \cdot 10^{-3}[\text{Sn}]$ $r = 0.997$
MBT + DBT + TBT	$A_i = 5.2 \cdot 10^{-3} + 2.8 \cdot 10^{-3}[\text{Sn}]$ $r = 0.991$	$A_i = 5.4 \cdot 10^{-3} + 2.9 \cdot 10^{-3}[\text{Sn}]$ $r = 0.990$

A_i means integrated absorbance and [Sn] units are in $\mu\text{g l}^{-1}$. Slope units: Au per $\mu\text{g l}^{-1}$.

m is the slope of the calibration curve (99.7% confidence level). The value obtained was 13 ng l^{-1} of tin.

The limit of quantification (LOQ) has been found to be 45 ng l^{-1} .

The characteristic mass (m_0) defined as:

$$m_0 = \frac{(\mu\text{l injected})_{\text{sample}} * (\mu\text{g l}^{-1})_{\text{sample}} * 0.0044}{\text{Abs}_{\text{sample}} - \text{Abs}_{\text{blank}}}$$

was 28.15 pg for a mixture of three studied compounds.

3.5. Precision and accuracy

The within-batch precision of the method was studied with sample spiked with 0.1, 0.2, 0.3, 0.4 $\mu\text{g l}^{-1}$ of total tin as MBT, DBT, TBT and a mixture of three compounds, five replicates each.

Table 3
Precision (five replicate analysis were performed); accuracy

[Sn] ($\mu\text{g l}^{-1}$)	RSD (%)			
	MBT	DBT	TBT	MBT + DBT + TBT
0.1	5.9	7.3	5.0	4.1
0.2	1.8	0.9	2.6	1.5
0.3	0.8	1.0	1.7	1.4
0.4	0.7	0.4	1.6	1.9
Analytical Recovery(%)	98.7	101.3	99.4	101.1

Table 4
Interferences

Metal	Maximum concentration ($\mu\text{g l}^{-1}$)	Absorbance variation (%)
Mg	$1 \cdot 10^5$	21.1
Al	5	17.3
Ca	$1 \cdot 10^5$	-18.8
Ni	$5 \cdot 10^{-3}$	-8.3
Zn	$5 \cdot 10^{-3}$	-4.1
As	$1 \cdot 10^{-2}$	1.0
Sr	$1 \cdot 10^2$	30.2
Ba	$3 \cdot 10^{-2}$	-9.1

The relative standard deviations (RSD) are shown in Table 3.

The accuracy of the method was determined by measuring the analytical recovery of samples containing 0.1, 0.2, 0.3 and 0.4 $\mu\text{g l}^{-1}$ of total tin. Results of analytical recovery are shown in Table 3.

3.6. Interferences

The behaviour of several cations typically present in natural water samples on the retention of butyltin compounds was studied because of their possible effects on the analyte metal preconcentration. A cation is considered as interferent if a variation of $\pm 10\%$ in the measurement of absorbance is observed. The cations studied and absorbance variation were showed in Table 4. The levels of cations necessary to produce an interference are bigger than the levels in the waters.

An effect of high background signal was observed with 1000 mg l^{-1} of Mg and over 300 mg l^{-1} of calcium.

Table 5
Applications

Sample	[Sn] ($\mu\text{g l}^{-1}$)	R.S.D. (%) ($n = 5$)
1	0.18	1
2	0.15	1
3	0.11	3
4	0.13	2
5	0.16	5
6	0.14	5
7	0.15	4

Calibration graph
 $A_i = -4.68 \cdot 10^{-3} + 1.41 \cdot 10^{-3}[\text{Sn}]$
 $r = 0.997$

A_i means integrated absorbance and [Sn] units are in $\mu\text{g l}^{-1}$. Slope units: Au per $\mu\text{g l}^{-1}$.

On the other hand, in the tin determination by ETAAS, principal anion interferences are sulphate and chloride because Sn can form volatile compounds with these anions [23]. These interferences are avoided by use of zirconium-coated graphite tubes [21] perhaps due to the formation of tin–zirconium compounds [24] or because zirconium competes with Sn for chlorine [23].

3.7. Applications

The proposed method was applied to different marine water samples of several ports of Galicia.

In all samples tin from the studied compounds was found. The obtained results, expressed as $\mu\text{g l}^{-1}$ of Sn and showed in Table 5, represent only the organic tin.

3.8. Conclusions

A preconcentration method of organotin compounds in column with an adsorbent resin conditioned with an aqueous solution of tropolone was optimized. In these conditions inorganic tin was not retained. A graphite furnace programme was optimized with the preconcentrated compounds. The tendency of the tin to form volatile compounds and its interaction with graphite surface was avoided by using zirconium coated graphite tubes. Optimum temperatures of pyrolysis and atomization were 1000 and 1900°C, respectively. Calibration and

standard addition graphs slopes were the same, so there are not matrix effects. It has been found that the measurement of these preconcentrated compounds is sensitive, accurate and precise and it does not exhibit important interferences.

References

- [1] R.F. Bennet, *Ind. Chem. Bull.* 2 (1982) 171–176.
- [2] C.J. Evans, *Tin Its Uses* 101 (1974) 12–15.
- [3] S.J. Blunden, A. Chapman, in: P.J. Craig (Ed.), *Organometallic Compounds in the Environment*, Wiley, New York, 1986, pp. 110–159.
- [4] J. Kuballa, R.-D. Wilken, E. Jantzen, K.K. Kwan, Y.K. Chau, *Analyst* 120 (1995) 667–673.
- [5] J.S. Weis, J. Perlmutter, *Estuaries* 10 (1987) 342–346.
- [6] C.D. Alzieu, R. Dalley, *Proc. Oceans '86 Organotin Symp.*, vol. 4, IEEE, Washington, DC, 1986, pp. 1130–1134.
- [7] R. Abel, B. Agius, J. Gyulai, *Proc. Oceans '86 Organotin Symp.*, 4, IEEE, Washington, DC, 1986, pp. 1314–1323.
- [8] J.L. Vossier, *Antifouling Paints New Release*, Department of Environment, London, 1987.
- [9] X. Chang, G. Zhan, X. Luo, Z. Su, *Mikrochim. Acta* 112 (1994) 245.
- [10] D.W. Lee, C.H. Eum, I.H. Lee, S.J. Jeon, *Anal. Sci.* 4 (1988) 505.
- [11] W.W. Van Berkel, F.J.M.J. Maessen, *Spectrochim. Acta* 43B (1988) 1337.
- [12] A.G. Horward, R. Danilova-Mirzaians, *Anal. Lett.* 22 (1989) 257.
- [13] S. Blain, P. Appriou, H. Handel, *Analyst* 116 (8) (1991) 815–820.
- [14] V. Porta, O. Abollino, E. Mentasti, C. Sazarnini, *J. Anal. Atom. Spect.* 6 (2) (1991) 119–122.
- [15] L.C. Azeredo, R.E. Sturgeon, A.J. Curtius, *Spectrochim. Acta B* 48B (1) (1993) 91–98.
- [16] S.D. Alexandratos, M.E. Bates, *Macromolecules* 21 (1988) 2905.
- [17] X. Chang, Y. Li, G. Zhan, Z. Su, J. Gao, *Anal. Chim. Acta* 245 (1991) 13.
- [18] P. Burba, *Fresenius J. Anal. Chem.* 431 (1991) 709.
- [19] P. Bermejo-Barrera, M.C. Tubío-Franco, J.M. Aguiar-Paz, R.M. Soto-Ferreiro, A. Bermejo-Barrera, *Microchem. J.* 53 (1996) 395–403.
- [20] Y.K. Chau, P.T.S. Wong, G.A. Bengert, *Anal. Chem.* 54 (1982) 246–249.
- [21] P. Bermejo-Barrera, R.M. Soto-Ferreiro, M. Aboal-Somoza, A. Bermejo-Barrera, *Quím. Anal.* 13 (1994) 15–18.
- [22] D.C. Baxter, W. Frech, *Anal. Chim. Acta* 225 (1989) 175–183.
- [23] E. Lundberg, B. Begmark, W. Frech, *Anal. Chim. Acta* 143 (1982) 129–142.
- [24] I.J. McColm, R. Steadman, C.O. Dimbylow, *J. Solid State Chem.* 14 (1975) 185.

Cesium-selective optode membrane based on the lipophilic calix[4]biscrown in the 1,3-alternate conformation

Huihui Zeng, Bernard Dureault *

DCC/DESD/SESD/LIRE, Centre d'Etudes de Saclay, Commissariat a l'Energie Atomique, 91191 Gif sur Yvette, France

Received 29 July 1997; received in revised form 8 December 1997; accepted 22 December 1997

Abstract

One type of lipophilic calix[4]biscrowns in the 1,3-alternate conformation which are highly selective complexant for cesium has been used to construct cesium poly(vinyl chloride) (PVC) membrane optode. The reversible sensing system has been formed by incorporating the lipophilic neutral H^+ —selective chromoionophore ETH5294 in the plasticized PVC membrane with 1,3-calix[4]bisnaphthyl-crown-6. The measuring range of cesium ions can be conditioned by buffering different pH in the cesium solutions. At pH 7.0, the measuring range of the optode membrane for cesium ions is from 1×10^{-6} to 1×10^{-2} M. The response behavior of optode membrane including response time, selectivity, reproducibility and lifetime, has been described in detail. © 1998 Elsevier Science B.V. All rights reserved.

Keywords: Optode membrane; 1,3-calix[4]bisnaphthyl-crown-6; Cesium

1. Introduction

Calixarene-based ionophores have been widely studied due to their structural and electronic features [1–3]. They have two principal advantages which make them in the use of constructing ion-selective electrodes and optodes [4–8]. The first advantage is that they allow a tridimensional control of metal ion complexation, so the electrodes and optodes usually show a high efficiency and good selectivity [9,10]. The second one is that there are alkyl group at the upper rim (aromatic nuclei) of the calix make it possible to modulate the lipophilicity of the ligands. Many studies on

the use of calixarene in ion-selective electrodes and optodes for determining lithium [11], sodium [12–15], potassium [16,17], cesium [18,19], silver [20] and amine [21,22] have been successfully carried out.

Recently, a new class of macropolycyclic crown compounds with two opposite OH groups in *p-tert*-butylcalix[4]arene bridged by a poly(oxyethylene) chains has been synthesized [23,24]. The metal cation complexation properties of so-called ‘calixcrown’ compounds has been studied in detail. Due to the presence of a glycol chain in their structure, calixcrowns have been used to complex with alkali and alkaline-earth metal cations. The selectivity of the complexation depends on the conformation (cone, partial cone, 1,2-alternate, 1,3-alternate) adopted by the rigi-

* Corresponding author. Tel.: + 33 01 69083251; fax: + 33 01 69083242.

dified calix[4]arene unit. The lipophilic calix[4]biscrowns in the 1,3-alternate conformation have been shown to be a new family of selective carriers for cesium [25].

In this paper, we report the new optical chemical sensor for the determination of cesium ion based on the use of lipophilic calix[4]biscrown, 1,3-calix[4]bisnaphthyl-crown-6. The developed optical sensing system provides a highly sensitive and selective methods for cesium determination.

2. Experimental

2.1. Reagents

The cesium selective ionophore 1,3-calix[4]bisnaphthyl-crown-6 was provided by the team of J-F. Dozol from SEP/SEATN Centre d'Etudes de Cadarache, Commissariat a l'Energie Atomique. The lipophilic pH indicator ETH5294(9-(diethylamino)-5-(octadecanoylimino)-5H-benzo[a]phenoxazine), ortho-nitrophenyl octyl ether (*o*-NPOE), dioctyl phthalate (DOP), bis(2-ethylhexyl)sebacate(DOS), sodium tetraphenylborate(NaTPB), sodium tetrakis(3,5-bis(trifluoromethyl) phenyl)borate (NaTFPB), high-molecular-weight (HMW) PVC, tetrahydrofuran (THF), tris(hydroxymethyl)aminomethane hydrochloride (Tris-HCl) were purchased from Fluka, cesium standard solution were made from cesium chloride (Fluka). All solutions were made with deionized water.

2.2. Optode membrane preparation

The optode membranes were prepared by the spin-on technique as follows: a mixture of 2.4 mg (0.004 mmol) of ETH5294, 10.2 mg (0.01 mmol) of calix[4]biscrown, 8.9 mg (0.01 mmol) of NaTFPB, 50 mg of PVC, 100 mg of *o*-NPOE was dissolved in 2 ml THF. An aliquot of 0.1 ml of this solution was pipetted onto a circular 35 mm diameter quartz plate which was fixed in a rotating (850 rpm) aluminum alloy rod under a THF-saturated atmosphere. After

about 5 s. the quartz plate with sensing membrane was removed and dried in ambient air for 10 min.

2.3. Experimental measurements

Two identical membranes both on their respective quartz plates were mounted in a flow-through measuring cell [26]. The cell was introduced into a UV-vis-NIR scanning spectrophotometer (Shimadzu UV-3101PC). Sample solutions were pipetted through the flow-through cell containing the sensing membranes by a syringe and absorbances were recorded at 665 nm. Before measurements, the new membranes should be put in pH buffer solution (used for the measurements: tris aminomethane hydrochloride buffer substance pH 7: 0.05M, Fluka Ref. 93368) for 1 h. The limiting absorbance values A_1 and A_0 were determined with the optode membranes contacting with 0.1M HCl and 0.1M NaOH solutions, respectively. For the selectivity measurements, the separate solution method (SSM) for optical sensors was used. Selectivity factors were determined by using different concentrations of cation in pH 7.0 Tris-HCl buffer solution. The selectivity coefficients were evaluated by comparing the concentration-dependent differences on the optical response functions at a common basis of $\alpha = 0.5$ [27]. The response of cesium ion was used as the standard.

3. Results and discussion

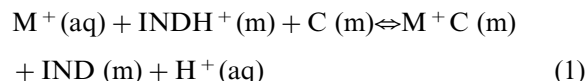
The structure of the cesium selective ionophore is shown in Fig. 1. It has been successfully applied in supported liquid membranes for the removal of cesium in the presence of sodium [24]. Its high selectivity for cesium can be explained by the preorganization of the ligand and by the fact that the less polar 1,3-alternate conformation prefers to bind the 'softer' cesium ion over the 'hard' sodium ion [28]. Moreover, the 1,3-alternate conformation allows interaction of the cesium ion with the p-electrons of two aromatic rings.

3.1. Experimental principle

In the optode membrane, there are neutral calixarene ionophore (C) as the selective host for cesium ion (M^+) and a chromo-ionophore ETH5294 (indicator (IND)) selective for the hydrogen ion. When calixarene in the membrane is complexed with cesium ions in the solution, cesium ions go into the membrane. In order to keep the electroneutrality of the membrane, the hydrogen ions of the chromo-ionophore ETH5294 go out of the membrane. Therefore, the absorption spectra of the membrane change. Fig. 2 shows the absorption spectra of the optode membrane incorporating calixarene and ETH5294, as obtained after equilibrium with pH7.0 Tris–HCl buffer solution containing different concentrations of cesium ion. It can be seen that the formation of the calixarene–cesium complex induced a reduction in the absorption band of $INDH^+$ at 615 and 665 nm. At the same time, an increase in the absorption band of IND at 545 nm was also observed.

If the complex equilibrium between calixarene in the plasticized PVC membrane phase (m) and

cesium ion in the aqueous sample solution (aq) will form an 1:1 complex [24], the over-all equilibrium can be described as follows:



The equilibrium constant K_{exch} depends on the stability constant of the calixarene–cesium complex and can be expressed as:

$$K_{\text{exch}} = \frac{[M^+C][IND][H^+]}{[M^+][INDH^+][C]} \quad (2)$$

where the concentration terms refer to the concentration of each species expressed in Eq. (1).

If α may be defined as the ratio of the concentration of unprotonated chromo-ionophore, [IND], in relation to the total amount present in the membrane, $[IND]_T$, thus,

$$\alpha = \frac{[IND]}{[IND]_T}; (1 - \alpha) = \frac{[INDH^+]}{[IND]_T} \quad (3)$$

In fact the measured absorbance A is directly related to the membrane response α , if the optode membrane obeys Beer's Law:

$$\alpha = \frac{A_1 - A}{A_1 - A_0} \quad (4)$$

where A_1 and A_0 are the limiting absorbance values for fully protonated and deprotonated chromo-ionophore, respectively.

For reasons of electroneutrality, the sum of the concentrations of the two cations must be equal to the total concentration of the accessible anionic sites $[R^-]_T$, which is the concentration of TFPB⁻ anion in the membrane,

$$[R^-]_T = [M^+C] + [INDH^+] \quad (5)$$

If $[C]_T$ and $[IND]_T$ are the respective total concentrations of calixarene and ETH5294 in the membrane, a response function for cesium ion can be derived as follows:

$$\begin{aligned} & \frac{[Cs^+]}{[H^+]} \times K_{\text{exch}} \\ &= \frac{([R^-]_T - (1 - \alpha)[IND]_T)}{[C]_T - [R^-]_T + (1 - \alpha)[IND]_T} \times \frac{\alpha}{(1 - \alpha)} \quad (6) \end{aligned}$$

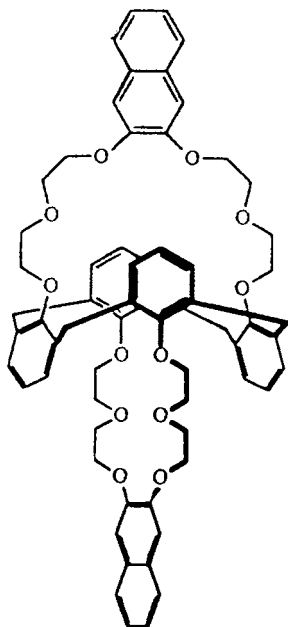


Fig. 1. Structure of the cesium ionophore 1,3-calix[4]bisnaphthyl-crown-6.

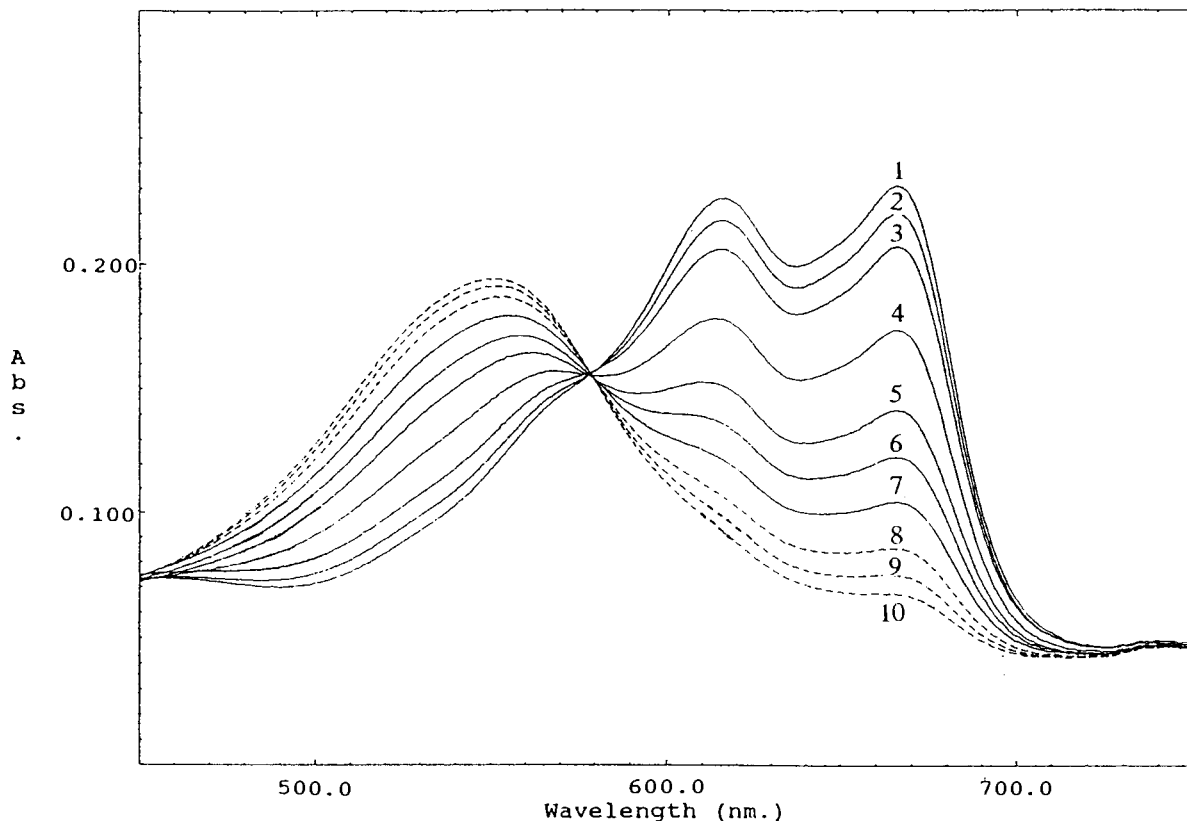


Fig. 2. Absorption spectra of two optode membranes (M2) after equilibration with pH 7.0 Tris-HCl buffer solutions containing different concentrations of Cs^+ : (1) buffer solution; (2) 1.0×10^{-6} M; (3) 5×10^{-6} M; (4) 1×10^{-5} M; (5) 2.5×10^{-5} M; (6) 5.0×10^{-5} M; (7) 1.0×10^{-4} M; (8) 2.5×10^{-4} M; (9) 1.0×10^{-3} M; (10) 5.0×10^{-3} M.

For cesium-selective optode membrane, the chosen concentrations of active materials follow the relationship:

$$[R]_{\text{T}} = [C]_{\text{T}} = \frac{5}{2} [\text{IND}]_{\text{T}} \quad (7)$$

this Eq. (6) can be simplified to:

$$\frac{[\text{Cs}^+]}{[\text{H}^+]} \times K_{\text{exch}} = \frac{(1.5 + \alpha)\alpha}{(1 - \alpha)^2} \quad (8)$$

With a series of standard cesium solutions, the α values can be measured by experiments; the calibration curve can be obtained by fitting the experimental points, and also the value of K_{exch} can be obtained. For the cesium sample solution with a fixed pH, the concentration of cesium can be determined from the calibration curve by measuring the α value.

3.2. Optimization of membrane composition

The cesium-selective optode membranes containing different amounts of active materials, which is summarized in Table 1, have been subjected to response studies. The optode membranes M1–M3 contain different amounts of indicator ETH5294 in the membranes. The measuring range of optode membrane M1 for cesium ions is from 1×10^{-5} to 1×10^{-3} M, while the measuring range of optode membranes M2, M3 for cesium ions are from 1×10^{-6} to 1×10^{-2} M. It can be seen that the amount of indicator ETH5294 affects the measuring range of cesium ions. When the amount of ETH5294 in the membrane is too low, the measuring range of cesium ion is also low and narrow. Indeed, the hydrogen ions, which are

Table 1
Composition of optode membranes (in 2 ml THF)

No.	ETH5294 (mol)	NaTPB (mol)	NaTFPB (mol)	Calixarene (mol)	<i>o</i> -NPOE (mg)	DOP (mg)	DOS (mg)	PVC (mg)
M1	2×10^{-6}	1×10^{-5}	—	1×10^{-5}	100	—	—	50
M2	4×10^{-6}	1×10^{-5}	—	1×10^{-5}	100	—	—	50
M3	6×10^{-6}	1×10^{-5}	—	1×10^{-5}	100	—	—	50
M4	4×10^{-6}	1×10^{-5}	—	1×10^{-5}	—	100	—	50
M5	4×10^{-6}	1×10^{-5}	—	1×10^{-5}	—	—	100	50
M6	4×10^{-6}	—	1×10^{-5}	1×10^{-5}	100	—	—	50

used for keeping membrane electroneutrality when the cesium ions are complexed with calixarene in the membrane comes from the dissociation of ETH5294. Moreover, the initial absorbance of the membrane decreases; when the amount of ETH5294 in the membrane is larger than 1.5×10^{-5} mol, it seems the dimerization of the indicator occurs. So in this paper, 4×10^{-6} mol of indicator has been chosen in the cesium-selective optode membrane. Also, the use of different types of plasticizer has some effect on the response behavior of the optode membrane. The membranes M2, M4, M5 containing three types of plasticizer including *o*-NPOE, DOP, DOS have been studied. The sensitivity and the reversibility of the membrane M2 containing the plasticizer *o*-NPOE is also the best. This can be explained by the fact that *o*-NPOE has high dielectric constant which makes the ionic site and the indicator in the membrane more easily to be dissociated ($\epsilon_{\text{mem}} = 14$) [29]. In contrast, dissociation is hindered in the membranes containing DOS ($\epsilon_{\text{mem}} = 4.8$). So the sensitivity and reversibility of the membrane M2 are improved by the easier dissociation of the ionic site and the indicator in the membrane compared with the membrane M4, M5. As for the anionic site NaTPB and NaTFPB (M2, M6), there is no significant difference in the response behavior of membrane. According to the literature [30], the chemical stability of tetraphenylborate [TPB⁻] is limited due to the decomposition of tetraphenylborate under acidic condition, and this decomposition can be decreased by substituting the phenyl rings with electron-withdrawing groups in para or meta positions. Therefore, in this paper NaTFPB has been chosen as the anionic site in the membrane.

3.3. Measuring range

In Fig. 3, the membrane responses, α , at a wavelength of 665 nm are given as a function of $\log[\text{Cs}^+]$ for three different pH values. The curves fitting the experimental points were calculated from Eq. (8) with $K_{\text{exch}} = 3.5 \times 10^{-4}$. The good correlation of the measured data with theory confirms the validity of the assumption made in Eq. (8). It also can prove that the composition of the complex between calixarene ionophore and cesium ion is 1:1. The measuring range of cesium ion is dependent on the pH value of the solution, the detection limit is decreased with the increase of pH value of the solution. At pH 7.0, the measuring range of the optode membrane for cesium ion is from 1×10^{-6} to 1×10^{-2} M. The precision of the measurement would be poor near either end of the range. At pH 9.0, a higher sensitive optical method for the determination of cesium ion has been established, with a detection limit of 5×10^{-8} M.

3.4. Selectivity

It has been reported that calixarenes with six oxygen atoms in the glycol chain are much more selective toward cesium over sodium [24]. The selectivity data obtained with the optode membrane containing 1,3-calix[4]bisnaphthyl-crown-6 described in this paper are summarized in Table 2. Separate calibration curves has been determined for the analyte ion and the interfering ion *J* at pH 7. The selectivity coefficients has been then calcu-

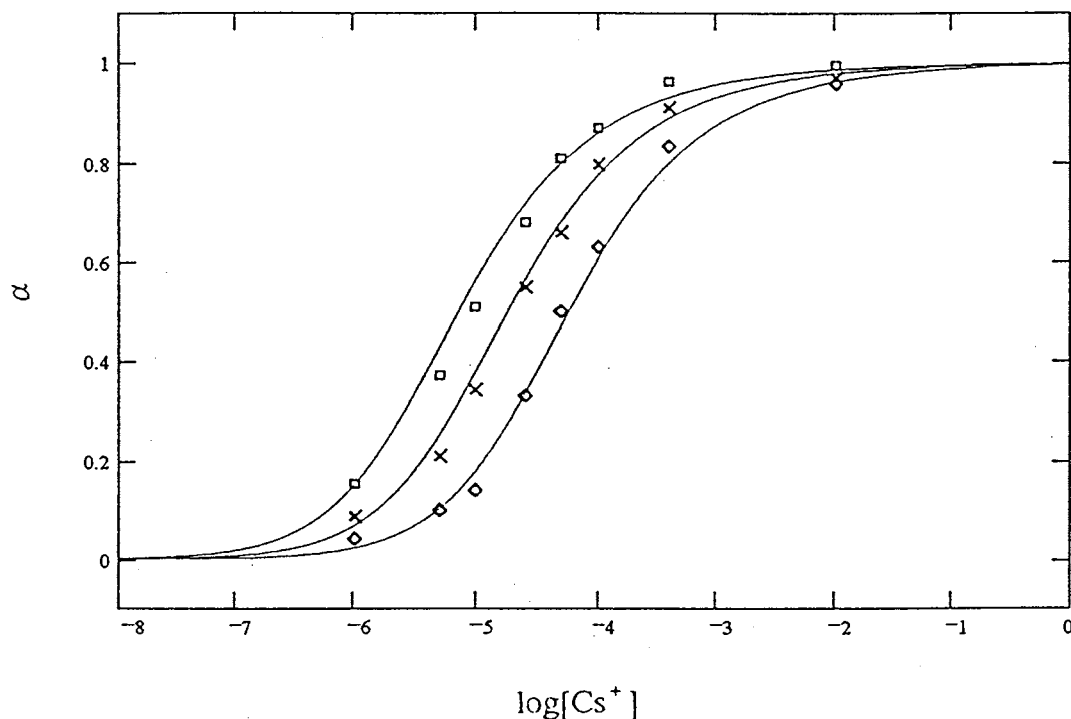


Fig. 3. Membranes response of cesium-selective optode membrane M2 at: \diamond pH 7.0; \times pH 8.0; \square pH 9.0.

lated from the activity ratios for both calibration curves at identical α values as follow:

$$K_{ij}^{\text{opt}}(\text{ssm}) = \frac{a_i}{a_j}$$

Reasonably good selectivity over sodium is evident.

3.5. Response time

It takes 5 min for the membrane to reach the t_{95} value after the concentration step changes from 5×10^{-5} to 5×10^{-4} M cesium ion, as illustrated in Fig. 4. An attempt to improve the response

time by decreasing the thickness of the membrane is unsuccessful. It proves that the response time of the optode membrane is not mainly governed by a diffusion process in the bulk of the membrane. Instead, the rate of the complex formation might play a vital one.

3.6. Reproducibility and short-term stability

The reproducibility of the optical signals was evaluated by repeating changing between two samples of 5×10^{-5} and 5×10^{-4} M cesium ion in Tris-HCl buffer solution at pH 7.0. The mean absorbance values at 665 nm and their standard deviations were obtained from five measurements and were found to be reproducible to $0.122 \pm 1.80\%$ (5×10^{-5} M cesium ion) and $0.075 \pm 1.58\%$ (5×10^{-4} M cesium ion). In defining the short-term stability of the system, the membrane was immersed in a solution of 5×10^{-4} M cesium ion at pH 7.0 for 8 h and the absorbance at 665 nm was determined at hourly intervals. The short-

Table 2

Selectivity coefficients ($\log K_{ij}^{\text{opt}}$) for the optode membrane incorporating 1,3-calix[4]bisnaphthyl-crown-6

Na ⁺	Li ⁺	K ⁺	Rb ⁺	NH ₄ ⁺	Ca ²⁺	Mg ²⁺
-2.1	-3.2	-2.3	-1.8	-2.0	-2.5	-2.8

$\log K_{ij}^{\text{opt}}$, $i = \text{Cs}^+$

term stability was found to be $0.122 \pm 1.9\%$ (in average of nine measurements).

3.7. Lifetime

After several hundreds of measurements, the absorbance value of the optode membrane in contact with 0.1 M HCl solution has been measured at 665 nm. Compared with the absorbance value obtained from a freshly prepared optode membrane under the same conditions, about a 10% decrease in absorbance was observed. It can be seen that the indicator incorporating in the membrane is not seriously washed out by normal measurements.

References

- [1] C.D. Gutsche, Calixarenes, in: F.J. Stoddard (Ed.), *Supramolecular Chemistry*, Royal Society of Chemistry, Cambridge, UK, 1989.
- [2] J. Viens, V. Bohmer (Eds.), *Calixarenes, a Versatile Class of Macrocyclic Compounds*, Kluwer, Dordrecht, The Netherlands, 1990.
- [3] J. Viens, Z. Asfari, J. McB. Harrowfield, *Calixarene 50th Anniversary: Commemorative Volume*, Kluwer, Dordrecht Holland, 1994.
- [4] K. Kimura, T. Matsuba, Y. Tsusjimura, M. Yokoyama, *Anal. Chem.* 64 (1992) 2508.
- [5] Z. Brzozka, B. Lammerink, D.N. Reinhoudt, R.J. Ungaro, *J. Chem. Soc. Perkin. Trans. 2* (1993) 1037.
- [6] D. Diamond, A. Cadogan, T. Mckittrick, T. Grady, S.J. Harris, M.A. Mckervey, *Anal. Proc.* 32 (1995) 137.
- [7] M. McCarrick, S.J. Harris, D. Diamond, *Analyst* 118 (1993) 1127.
- [8] H. Shimizu, K. Iwamoto, K. Fujimoto, S. Shinlai, *Chem. Lett.* (1991) 2147.
- [9] J.A.J. Brunink, J.R. Haak, J.G. Bomer, M.A. Mckervey, S.J. Harris, D.N. Reinhoudt, *Anal. Chim. Acta* 254 (1995) 137.
- [10] D. Diamond, G. Svehla, E.M. Seward, M.A. Mckervey, *Anal. Chim. Acta* 204 (1988) 223.
- [11] D.J. Cram, R.A. Carmack, R.C. Helgeson, *J. Am. Chem. Soc.* 110 (1988) 571.
- [12] M. Careri, A. Casnati, A. Guarinoni, A. Mangia, G. Mori, A. Pochini, R. Ungaro, *Anal. Chem.* 65 (1993) 3156.
- [13] W.H. Chan, A.W.M. Lee, C.M. Lee, K.W. Yau, K. Wang, *Analyst* 120 (1995) 1963.
- [14] S. Walsh, F.J. Saez de Vireri, D. Diamond, *Anal. Proc.* 32 (1995) 365.
- [15] K.M. O'Connor, M. Cherry, G. Svehla, S.J. Harris, M.A. Mckervey, *Talanta* 41 (1994) 1207.
- [16] A. Cadogan, D. Diamond, S. Cremin, M.A. Mckervey, S.J. Harris, *Anal. Proc.* 28 (1991) 13.
- [17] E. Ghidini, F. Ugozzoli, R. Ungaro, S. Harkema, A.A. El-Fadl, D.N. Reinhoudt, *J. Am. Chem. Soc.* 112 (1990) 6979.
- [18] R.J.W. Lugtenberg, Z. Brzozka, A. Casnati, R. Ungaro, J.F.J. Engbersen, D.W. Reinhoudt, *Anal. Chim. Acta* 310 (1995) 263.
- [19] C. Bocchi, M. Careri, A. Casnati, G. Mori, *Anal. Chem.* 67 (1995) 4234.
- [20] P.L.H.M. Cobben, R.J.M. Egberink, J.G. Bomer, P. Bergfeld, D.N. Reinhoudt, *J. Am. Chem. Soc.* 114 (1992) 10573.
- [21] W.H. Chan, A.W.M. Lee, K. Wang, *Analyst* 119 (1994) 2809.
- [22] K. Odashima, K. Yagi, K. Tohda, Y. Umezama, *Anal. Chem.* 65 (1993) 1074.
- [23] C. Alfieri, E. Dradi, A. Pochini, R. Ungaro, G.N. Andreotti, *J. Chem. Soc. Chem Commun.*, (1983) 1075.
- [24] Z. Asfari, Bressot, J. Viens, C. Hill, J.-F. Dozol, H. Rouquette, S. Eymard, V. Lamare, B. Tournois, *Anal. Chem.* 67 (1995) 3133.
- [25] R. Ungaro, A. Casnati, F. Ugozzoli, A. Pochini, J.-F. Dozol, C. Hill, H. Rouquette, *Angew. Chem Int. Ed. Engl.* 33 (1994) 1506.
- [26] H. Zeng, K. Wang, D. Li, R. Yu, *Talanta* 41 (1994) 969.
- [27] W.E. Morf, K. Seiler, B. Rusterholz, W. Simon, *Anal. Chem.* 62 (1990) 738.
- [28] R.G. Pearson, *J. Am. Chem. Soc.* 85 (1963) 3533.
- [29] U. Schaller, E. Bakker, E. Pretsch, *Anal. Chem.* 67 (1995) 3123.
- [30] T. Rosatzin, E. Bakker, K. Suzuki, W. Simon, *Anal. Chim. Acta* 280 (1993) 1970.

An optimization procedure for determination of indomethacin and acemethacin by differential pulse adsorptive stripping voltammetry. Application on urine samples

Celia Reguera, M. Julia Arcos *, M. Cruz Ortiz

Departamento de Química (Area de Química Analítica), Facultad de Ciencias, Universidad de Burgos, Pza. Misael Bañuelos, 09001 Burgos, Spain

Received 08 September 1997; received in revised form 10 December 1997; accepted 22 December 1997

Abstract

Procedures for the determination of indomethacin and acemethacin by differential pulse adsorptive stripping voltammetry with a mercury electrode have been described and optimised. The selection and optimization of the experimental parameters was done using factorial and central composite designs. Indomethacin and acemethacin in urine were determined by this method with good results and without the need for tedious prior separation. For routine calibration and calculation of the 'capacity to detect', the robust regression method least median squares (LMS) has been proposed. © 1998 Elsevier Science B.V. All rights reserved.

Keywords: Experimental design; Differential pulse adsorptive stripping voltammetry; Indomethacin determination; Acemethacin determination

1. Introduction

The acid 1-(4-chlorobenzoyl)-5-methoxy-2-methyl-1-indole-3-acetic known familiarly as indomethacin and the acemethacin, obtained from the esterification of indomethacin by the action of hydroxyacetic acid, are two molecules that form the basis of numerous commercialised pharmaceutical products in the field of anti-inflammatory drugs. Metabolization of the drugs by the organism is an indicator of their therapeutic activity

and the determination of the drugs in body fluids may be used to follow this activity. Human urine is composed of numerous organic substances and frequently the methods described to determine drugs involve tedious separations and previous reactions [1]. A number of analytical procedures for the quantitative determination of these drugs have been proposed. High-performance liquid chromatography [1–3] and UV-visible spectroscopy [4] are commonly used. Electrochemical techniques have been used only by few authors despite the high sensitivity of some of them.

The quantities required to demonstrate the therapeutic effect of indomethacin and

* Corresponding author. Tel: +34 947 258818; fax: +34 947 258831; e-mail: jarcos@cid.cid.ubu.es

acemethacin are very small which makes it essential to optimise sensitive methods for their determination. As is known, many molecules of an organic nature tend to be adsorbed on the surfaces of many electrodes [5]. The improvement in the analytical signal obtained as a result of the preconcentration process allows stripping voltammetry to be considered one of the most accurate techniques in trace analysis. In the indomethacin and acemethacin cases the polarographic reduction of these drugs has been described [6–8] but a study of their adsorption at mercury electrodes was not.

In this work a procedure is reported for the determination of indomethacin and acemethacin by differential pulse adsorptive stripping voltammetry (DPAdSV) based on the adsorption of the molecules at mercury electrode in aqueous media and in urine, without the need for any prior separation steps. With the aim of guaranteeing the maximum analytical signal an optimization procedure using experimental design was carried out in which factors relevant to DPAdSV technique intervene.

Special importance was given to the calibration stage, where robust regression techniques were used to guarantee that outlying experimental points would not influence the calibration parameters.

2. Experimental

2.1. Reagents and equipment

Indomethacin (analytical grade) was kindly provided by Merck Sharp and Dome. Acemethacin (drug standard grade) was kindly supplied by Europharma. Britton–Robinson solutions obtained by adding NaOH 0.2 M to a mixture of boric, phosphoric and acetic acids 0.04 M each were used as buffers. Quantities between 5 and 20 ml of Britton–Robinson buffer are added to the voltammetric cell. The percentage of buffer in the cell thus varies from 25 to 100%. This solution was prepared with deionized water obtained with a Barnstead NANO pure II system and acted as a supporting electrolyte. The stock

solutions (5×10^{-3} M) of indomethacin and acemethacin were prepared in analytically pure grade acetonitrile. The solutions analysed in the procedures of optimization and calibration both in aqueous media and in urine samples were prepared by dilution of stock solutions (5×10^{-3} M) in deionized water.

Urine samples were obtained from fasting and healthy subjects in the morning and diluted 25.0-fold in water. The analysis of indomethacin and acemethacin was made by adding the suitable quantity of each drug separately to the urine sample until the required concentration was obtained.

Voltammetric measurements were carried out using a Metrohm 646 VA Processor (minimum detectable current 3.75 pA) and a 647 VA Electrode Stand with a multimode electrode (MME) operating in the HMDE mode. An Ag/AgCl/KCl (3 M) reference electrode and a platinum wire auxiliary electrode were used.

2.2. Software and hardware

Data analysis was achieved with Statgraphics [9] for the experimental design, Progress [10] for the robust regression and Detarchi [11] for determination of capacity to detect.

2.3. Experimental procedure

In the optimization stages the voltammetric measurements were taken using the following procedure: once the solution (percentage of buffer and pH suitable in each case) had been deoxygenated, the stirrer was connected and deposition began according to a time and potential determined for each experiment. When the time had elapsed, the stirrer was switched off and the solution left to settle for an equilibrium time of 10 s. The voltammogram was then recorded by making a negative sweep from the deposition potential (initial potential) to -1.6 V (final potential). The response analysed for each point of the designs made was the ratio of the intensities, $i_p/i_{p\text{blank}}$, obtained in two electrochemical sweeps: one with analyte and the other without analyte (blank). The following values were used for the rest of the

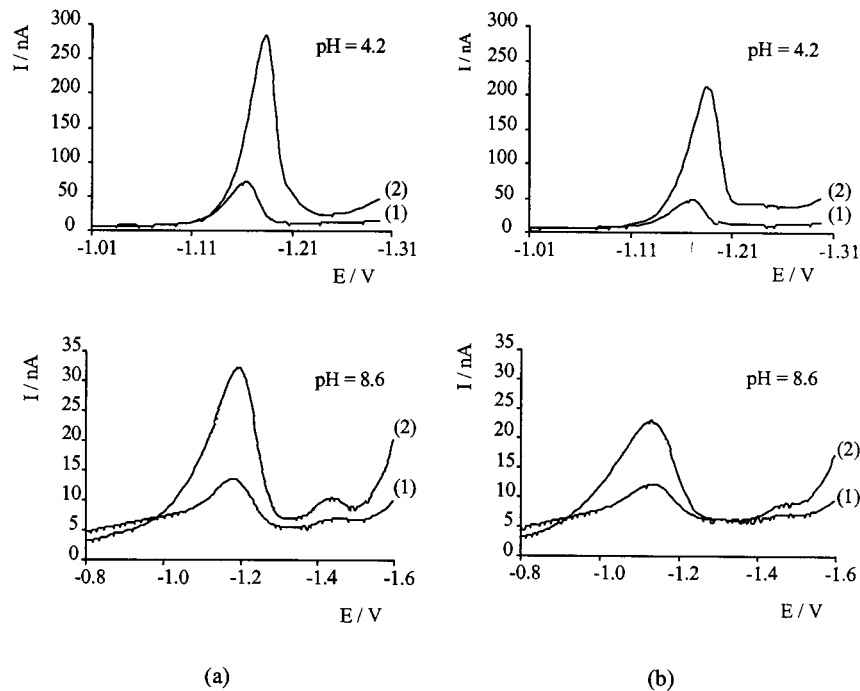


Fig. 1. Differential pulse adsorptive stripping voltammograms for (a) acemethacin 7.5×10^{-7} M and (b) indomethacin 7.5×10^{-7} M in Britton–Robinson buffer (50%) and $E_{\text{dep}} = -0.8$ V. (1) $t_{\text{dep}} = 0$ s; (2) $t_{\text{dep}} = 60$ s.

instrumental settings: mercury drop size, 0.40 mm^2 ; stirring rate in the accumulation period, $1290 \text{ rev min}^{-1}$; sweep rate, 10 mV s^{-1} ; the size and duration of the pulse -50 mV and 5 ms , respectively [12].

3. Results and discussion

3.1. Optimization of the variables in the aqueous media

A few previous electrochemical studies [6–8] on these compounds show that both substances undergo an electrochemical reduction at mercury electrode so being suited to analysis by voltammetric techniques. For acidic solutions $\text{pH} < 6$, the electrode reduction is essentially a two electron process and one voltammetric peak is obtained. For pH values > 6 , indomethacin and acemethacin exhibit two voltammetric reduction peaks. The first peak, which decreases with in-

creasing pH values, can be attributed to the reduction of protonated molecules and the second is caused by the reduction of non protonated molecules. Indomethacin and acemethacin adsorption at the HMDE was ascertained by repetitive cyclic voltammograms recorded after accumulation. A high, well-defined cathodic peak can be observed at the first scan. Later scans show a great decrease in the cathodic peak, pointing to a quick desorption from the surface. Voltammograms obtained with accumulation are always significantly higher than non accumulation ones in similar conditions. Fig. 1 shows the differential pulse adsorptive stripping voltammetric peaks for indomethacin and acemethacin, with and without accumulation, for two different pH .

The voltammetric analysis of trace elements normally involves very small current response. This explains the importance of optimising all those parameters which may have an influence on the measured current. The experimental design has been used as a tool for the optimization. In

this case, in a first step, a 2^4 factorial design was applied with replications in the central point in order to estimate the residual error. In the DPAdSV technique the peak obtained for indomethacin and acemethacin is influenced by a large number of variables. In order to optimize the response, $i_p/i_{p\text{blank}}$, the variables pH of solution, percentage of buffer in the electrochemical cell ($\%_{\text{buffer}}$), deposition potential (E_{dep}) and deposition time (t_{dep}) were chosen as experimental factors. In a first stage and by means of a factorial design the relative influence of these variables will be analysed, the most influential being selected. These factorial designs do not allow one to explore exhaustively a wide range of the experimental space, but they indicate with minimum experimental effort the possible direction that future experiments should take. In a second stage one determines by a central composite design the optimum values of the factors selected by adjustment of the corresponding response surface.

The values of the other parameters which also influence the response such as modulation amplitude, pulse repetition time, sweep rate, mercury drop size, etc. characteristics of the voltammetric technique used was made bearing in mind previous experience in the treatment of similar problems, according to which the optimum reproducibility is achieved under the experimental conditions described above [12,13]. In the first stage the 2^4 factorial design with three replications in the central point involves 19 basic experiments undertaken in random order in separate solutions of indomethacin and acemethacin concentration 5×10^{-8} M. The values corresponding to the high (+) and low (-) levels and to the central point (0) for each factor were chosen taking into account that pH values < 3 and > 9 alter the stability of the drugs, $\%_{\text{buffer}}$ values $< 25\%$ are not sufficient to adjust the solution pH, the E_{dep} values selected are very close to the experimental barriers for this variable (oxidation of mercury electrode and reduction of analyte) and t_{dep} values < 10 s are not sufficient to permit the adsorption of the analyte and values

> 120 s increase too the experimental time. The values for each factor were as follows:

$$\begin{array}{lll} \text{pH (+)} = 9.0 & \text{pH (-)} = 3.0 & \text{pH (0)} = 6.0 \\ \%_{\text{buffer (+)}} = 100.0 & \%_{\text{buffer (-)}} = 25.0 & \%_{\text{buffer (0)}} = 62.5 \\ E_{\text{dep (+)}} = -1.0 \text{ V} & E_{\text{dep (-)}} = -0.2 \text{ V} & E_{\text{dep (0)}} = -0.6 \text{ V} \\ t_{\text{dep (+)}} = 120 \text{ s} & t_{\text{dep (-)}} = 10 \text{ s} & t_{\text{dep (0)}} = 65 \text{ s} \end{array}$$

In each of the experiments carried out, five voltammetrics scans have been realised both for the blank and the analyte. The mean peak current experimental values from this design can be seen in Table 1 for indomethacin and acemethacin. Fig. 2 shows the Pareto chart done with data of Table 1 for indomethacin and acemethacin, respectively. In this figure it can be seen that the more influential experimental factors for both drugs are the pH, percentage of buffer and the deposition time, likewise the interactions $\text{pH}-\%_{\text{buffer}}$ and $\text{pH}-t_{\text{dep}}$ for indomethacin and the interactions $\text{pH}-E_{\text{dep}}$ and $\text{pH}-t_{\text{dep}}$ for acemethacin, while deposition potential and the other interactions are less influential. The directions towards which the variables move in order to maximize the response were obtained considering the vertex of the hypercube with best response.

Deposition potential is the factor that produces least variation in the response, although this increases slightly with it for indomethacin. On the other hand, the choice of this parameter is conditioned by limitations due to the reduction peak itself to potential values of -1.2 V which is why this factor was set at -1.0 V for future experiences.

In the second stage a central composite design was carried out with the variables selected above in the experimental area to which the first factorial design leads in each case. That is, the new experimental conditions of experimental design will move towards low levels of pH and $\%_{\text{buffer}}$ and slightly higher deposition times:

$$\begin{array}{lll} \text{pH (+)} = 6.0 & \text{pH (-)} = 4.0 & \text{pH (0)} = 5.0 \\ \%_{\text{buffer (+)}} = 45.0 & \%_{\text{buffer (-)}} = 25.0 & \%_{\text{buffer (0)}} = 35.0 \\ t_{\text{dep (+)}} = 200 \text{ s} & t_{\text{dep (-)}} = 90 \text{ s} & t_{\text{dep (0)}} = 145 \text{ s} \end{array}$$

Table 1
Results of the 2⁴ experimental design for indomethacin and acemethacin

Experimental factors				Indomethacin			Acemethacin		
pH	% _{buffer}	E_{dep} (V)	t_{dep} (s)	i_{p} (nA)	i_{pblank} (nA)	$i_{\text{p}}/i_{\text{pblank}}$	i_{p} (nA)	i_{pblank} (nA)	$i_{\text{p}}/i_{\text{pblank}}$
9.0	100.0	-1.0	120	10.17	10.10	1.01	16.43	16.84	0.98
9.0	100.0	-1.0	10	8.22	7.52	1.09	8.85	8.38	1.06
9.0	100.0	-0.2	120	14.21	14.07	1.01	33.21	18.13	1.83
9.0	100.0	-0.2	10	15.56	17.44	0.89	21.68	17.96	1.21
9.0	25.0	-1.0	120	10.21	7.66	1.33	10.05	7.25	1.39
9.0	25.0	-1.0	10	6.72	5.41	1.24	6.44	5.63	1.14
9.0	25.0	-0.2	120	14.84	13.56	1.09	13.92	9.11	1.53
9.0	25.0	-0.2	10	7.83	7.19	1.09	6.95	4.29	1.62
3.0	100.0	-1.0	120	53.42	17.80	3.00	29.20	13.05	2.24
3.0	100.0	-1.0	10	14.20	8.07	1.76	10.61	6.12	1.73
3.0	100.0	-0.2	120	97.13	52.44	1.85	82.60	42.40	1.95
3.0	100.0	-0.2	10	26.48	13.69	1.93	19.15	13.12	1.46
3.0	25.0	-1.0	120	70.02	14.39	4.87	32.84	9.06	3.62
3.0	25.0	-1.0	10	14.32	5.40	2.65	8.61	4.21	2.04
3.0	25.0	-0.2	120	96.33	24.54	3.92	49.11	18.88	2.60
3.0	25.0	-0.2	10	24.38	7.74	3.15	15.06	7.39	2.04
6.0	62.5	-0.6	65	16.53	11.34	1.46	19.91	12.34	1.61
6.0	62.5	-0.6	65	15.55	12.08	1.29	19.57	11.49	1.70
6.0	62.5	-0.6	65	14.86	10.43	1.42	19.57	10.91	1.79

The results of this design for both indomethacin and acemethacin can be seen in Table 2. The ANOVA shows that the variables that have an influence in the case of indomethacin are the pH, pH² and t_{dep}^2 ($P_{\text{level}} < 0.05$).

The ANOVA done with the data from Table 2 for acemethacin indicates that for a confidence level of 96% both pH and deposition time continue to have a marked influence while the buffer percentage exerts a smaller influence on the response.

The degree of adjustment of the response surfaces for both indomethacin and acemethacin is acceptable as can be seen from the values of R^2 , 0.92 for indomethacin and 0.90 for acemethacin, and P_{level} for the lack-of-fit 0.08 and 0.04, respectively.

The isoresponse lines (Figs. 3 and 4) for indomethacin and acemethacin allowed one to obtain the optimum values of the variables studied. The equation of the adjusted model, for each drug, appears in the legend of Figs. 3 and 4, respectively.

In accordance with these results, the following experimental conditions were chosen:

Indomethacin	Acemethacin
pH = 4.2	pH = 4.4
% _{buffer} = 35.0	% _{buffer} = 25.0
E_{dep} = -1.0 V	E_{dep} = -1.0 V
t_{dep} = 150 s	t_{dep} = 240 s

Under these conditions the peak current is improved approximately nine times for indomethacin and four times for acemethacin, in comparison with the signal obtained under the conditions of the first design.

3.2. Calibration and detection limit with specified assurance probabilities

Once the optimum parameters for the analysis have been chosen a calibration can be made. In this case three calibrations were made for each drug separately. In all cases the calibrations were carried out with successive additions of 5×10^{-7} M stock solution of indomethacin or

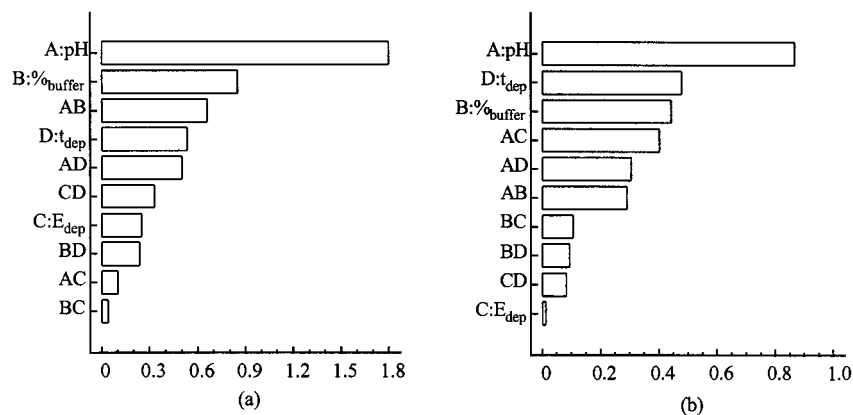


Fig. 2. Pareto chart with the data in Table 1. (a) indomethacin, (b) acemethacin.

acemethacin. To guarantee that erroneous experimental points would not influence the calibration parameters (sensitivity, linear range, detection limit) a robust regression method (LMS) was used [10,14]. Robust regression in LMS has already been applied successfully to calibration problems [15,16]. The experimental data together with the standardized residuals (SR) are shown in Table 3 for both drugs. When the SR was > 2.5 the point was considered as ‘outlier-leverage’ [10] and eliminated and a new regression based on the least

squares (LS) criterion was done with the rest of the experimental data. The fact that in both calibrations the last points are outliers, deviating from the linearity always in the same negative direction, raises considerations about problems of saturation of electrode surfaces (to concentrations $> 8 \times 10^{-8}$ M) since indomethacin or acemethacin are voluminous molecules.

In the evaluation of the detection limit the possibility of false negative (beta value) has been quantified according to the Clayton et al. proce-

Table 2

Results of the 2^3 experimental central composite design for indomethacin and acemethacin

Experimental factors			Indomethacin			Acemethacin		
Ph	% _{buffer}	t_{dep} (s)	i_p (nA)	i_{pblank} (nA)	i_p/i_{pblank}	i_p (nA)	i_{pblank} (nA)	i_p/i_{pblank}
6.0	45.0	200	13.76	10.00	1.38	21.26	9.86	2.16
6.0	45.0	90	12.74	9.26	1.38	13.41	8.07	1.66
6.0	25.0	200	14.43	6.95	2.08	18.48	9.32	1.98
6.0	25.0	90	10.10	5.32	1.90	12.24	7.80	1.57
4.0	45.0	200	65.79	8.74	7.53	40.84	13.35	3.06
4.0	45.0	90	35.92	8.58	4.18	24.05	9.00	2.67
4.0	25.0	200	69.35	19.08	3.63	55.72	13.20	4.22
4.0	25.0	90	42.19	9.34	4.52	33.96	10.76	3.16
6.7	35.0	145	11.25	5.08	2.21	13.50	8.11	1.66
3.3	35.0	145	48.62	6.66	7.30	31.18	12.35	2.52
5.0	51.8	145	48.09	9.03	5.32	34.42	11.06	3.11
5.0	18.2	145	47.72	5.78	8.25	36.41	10.94	3.33
5.0	35.0	237	20.77	24.95	0.83	47.75	11.95	4.00
5.0	35.0	52	11.00	11.25	0.98	20.40	8.18	2.49
5.0	35.0	145	52.19	7.05	7.40	37.05	10.87	3.41
5.0	35.0	145	41.82	5.45	7.67	29.23	8.13	3.59
5.0	35.0	145	42.19	6.12	6.90	42.72	12.30	3.47

Table 3
Experimental data and standardized residuals (SR) for determining the linear range with LMS regression

Add.	$C_{\text{acc}} \times 10^8 \text{ M}$	Indomethacin											
		Acemethacin				Indomethacin				Indomethacin			
		Calibration I		Calibration II		Calibration III		Calibration I		Calibration II		Calibration III	
$i_{p,1}$ (nA)	SR_1	$i_{p,2}$ (nA)	SR_2	$i_{p,3}$ (nA)	SR_3	$C_{\text{ind}} \times 10^8 \text{ M}$	$i_{p,1}$ (nA)	SR_1	$i_{p,2}$ (nA)	SR_2	$i_{p,3}$ (nA)	SR_3	
0	0.0	6.44	-1.56	7.30	-0.82	0.0	12.86	0.11	12.28	-0.85	12.14	-1.49	
1	0.46	11.09	-0.13	10.54	-1.34	0.49	14.81	-1.48	15.69	-0.27	16.18	0.21	
2	0.90	15.95	1.82	15.87	0.82	0.98	18.45	-0.46	18.21	-0.78	18.84	-0.21	
3	1.77	22.50	0.30	21.83	-0.43	1.92	24.95	0.67	25.25	1.01	25.13	0.79	
4	2.60	29.72	0.51	29.42	0.67	2.82	30.62	0.90	30.70	1.02	30.85	1.18	
5	3.41	35.84	-0.79	36.14	1.00	3.69	36.48	1.70	35.09	-0.07	35.47	0.17	
6	4.18	42.53	-0.61	42.12	0.70	4.53	40.58	0.18	40.95	0.99	41.10	1.07	
7	4.93	49.48	0.49	48.09	0.67	5.34	45.16	-0.35	45.39	0.42	45.12	-0.31	
8	5.65	55.64	0.55	53.88	0.66	6.12	49.41	-1.12	50.01	0.32	49.07	-1.54	
9	6.34	60.94	-0.59	58.72	-0.25	6.88	54.67	-0.15	52.90	-1.80	54.67	0.13	
10	7.67	68.27	-7.77 ^a	68.19	-1.68	8.31	58.95	-6.76 ^a	58.65	-5.52 ^a	58.01	-8.36 ^a	
11	8.90	74.80	-15.08 ^a	75.39	-5.05 ^a	9.65	64.89	-10.09 ^a	65.71	-6.82 ^a	64.32	-11.21 ^a	
12	10.06	80.49	-22.73 ^a	81.68	-8.80 ^a	10.91	69.51	-14.61 ^a	68.98	-12.38 ^a	69.24	-15.48 ^a	
13	11.15	83.81	-33.62 ^a	73.30	-29.96 ^a	12.09	72.81	-20.39 ^a	74.44	-14.50 ^a	72.44	-21.76 ^a	
14	12.18	87.25	-43.30 ^a	88.08	-21.87 ^a								
15	13.14	88.91	-55.33 ^a	89.02	-30.30 ^a								

^a Outliers points.

Table 4
 Calibrations parameters, detection limits and detection signals obtained from the different calibrations for indomethacin and acemethacin

	Indomethacin																			
	Acemethacin						Indomethacin						Indomethacin							
	Calibration I			Calibration II			Calibration III			Calibration I			Calibration II			Calibration III				
LS	LMS	LS with-out outliers	LS	LMS	LS with-out outliers	LS	LMS	LS with-out outliers	LS	LMS	LS with-out outliers	LS	LMS	LS with-out outliers	LS	LMS	LS with-out outliers	LS	LMS	LS with-out outliers
Number of data	16	16	10	16	16	11	16	16	16	16	10	14	14	14	10	14	14	14	14	10
Sensitivity $\times 10^{-8}$ (nA M ⁻¹)	5.012	0.626	0.545	5.497	0.941	0.809	4.707	0.745	0.363	2.622	0.679	0.674	2.288	1.118	0.771	2.570	0.699	0.625		
Intercept (nA)	12.90	7.00	7.29	12.87	7.40	7.96	12.26	8.02	7.75	15.39	12.82	12.79	15.16	12.62	12.93	15.66	13.37	13.07		
Coeff. Of de-termination (R ²)	0.9708	0.9998	0.9993	0.9636	0.9993	0.9986	0.9749	0.9997	0.9997	0.9845	0.9994	0.9982	0.9884	0.9982	0.9975	0.9847	0.9993	0.9984		
Linear range (M)	0.0–6.35 $\times 10^{-8}$			0.0–7.67 $\times 10^{-8}$			0.0–7.67 $\times 10^{-8}$			0.0–6.88 $\times 10^{-8}$			0.0–6.88 $\times 10^{-8}$			0.0–6.88 $\times 10^{-8}$				
Detection limit (M)	1.32 $\times 10^{-9a}$	2.65 $\times 10^{-9b}$	2.02 $\times 10^{-9a}$	4.07 $\times 10^{-9b}$	9.15 $\times 10^{-10a}$	1.84 $\times 10^{-9b}$	2.27 $\times 10^{-9a}$	4.56 $\times 10^{-9b}$	1.46 $\times 10^{-9a}$	5.29 $\times 10^{-9b}$	2.13 $\times 10^{-9a}$	4.27 $\times 10^{-9b}$	14.57			14.39				
Detection current (nA)	8.45	9.64			8.51					14.22										

^a $\beta = 0.5$; ^b $\beta = 0.05$.

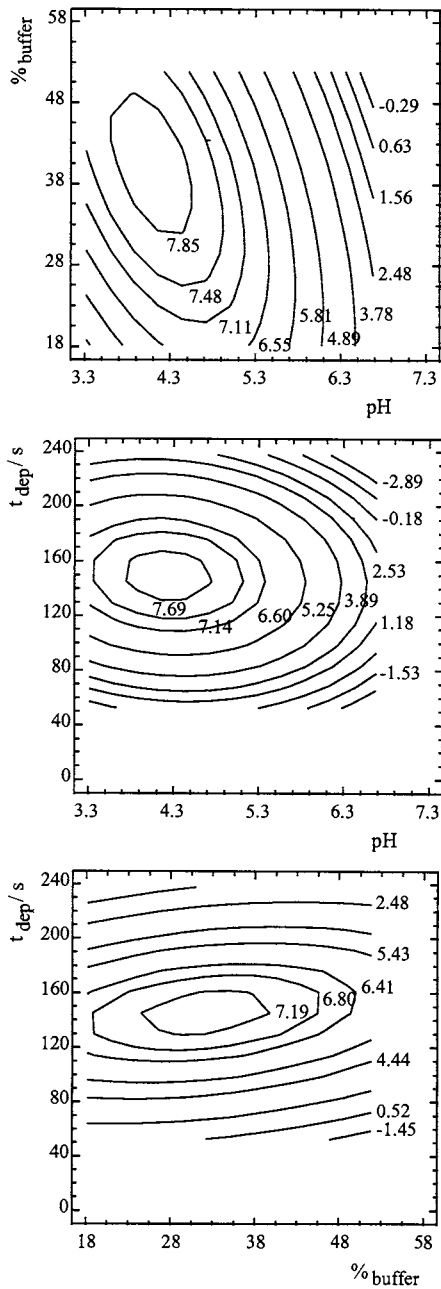


Fig. 3. Isoresponse lines from the data in Table 2 for indomethacin. The equation of the fitted model for indomethacin is: $i_p/i_{pblank} = -41.05 + 11.74A + 1.89B + 0.23C - 0.30AB - 5.19E - 3AC + 4.60E - 3BC - 1.05A^2 - 8.24E - 2B^2 - 7.97E - 4C^2$. A: pH; B: %buffer; C: t_{dep} .

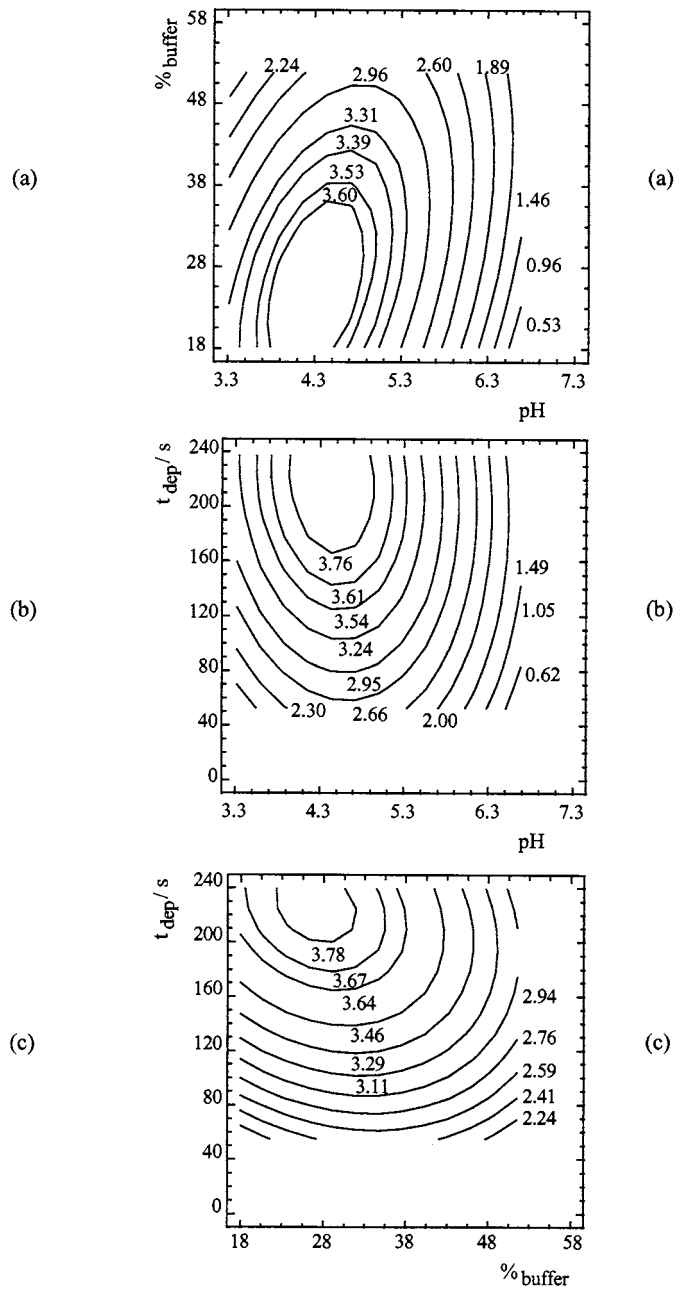


Fig. 4. Isoresponse lines from the data in Table 2 for acemethacin. The equation of the fitted model for acemethacin is: $i_p/i_{pblank} = -8.40 + 4.32A - 2.72E - 2B + 3.12E - 2C + 0.12AB - 1.23E - 3AC - 6.77E - 4BC - 0.55A^2 - 3.81E - 2B^2 - 4.75E - 5C^2$. A: pH; B: %buffer; C: t_{dep} .

Table 5

Results of the 2⁴ experimental design in optimization of experimental variables for acemethacin and indomethacin in urine sample

Experimental factors				Indomethacin			Acemethacin		
pH	% _{buffer}	E_{dep} (V)	t_{dep} (s)	i_p (nA)	i_{pblank} (nA)	i_p/i_{pblank}	i_p (nA)	i_{pblank} (nA)	i_p/i_{pblank}
5.0	50.0	-1.0	30	293.85	32.95	8.92	48.73	34.14	1.43
5.0	50.0	-1.0	10	326.33	20.48	15.94	63.48	32.36	1.96
5.0	50.0	-0.6	30	346.73	67.09	5.17	65.75	42.68	1.54
5.0	50.0	-0.6	10	352.77	39.07	9.03	75.63	37.70	2.01
5.0	25.0	-1.0	30	277.99	27.68	10.04	47.26	44.15	1.07
5.0	25.0	-1.0	10	303.42	18.55	16.35	57.12	40.49	1.41
5.0	25.0	-0.6	30	309.21	49.83	6.20	60.11	59.12	1.02
5.0	25.0	-0.6	10	315.76	33.21	9.51	62.52	53.84	1.16
3.0	50.0	-1.0	30	294.98	55.81	5.29	148.14	107.64	1.38
3.0	50.0	-1.0	10	254.95	37.37	6.82	178.56	143.99	1.24
3.0	50.0	-0.6	30	332.00	82.74	4.01	192.34	130.22	1.44
3.0	50.0	-0.6	10	309.09	53.45	5.78	202.19	110.01	1.84
3.0	25.0	-1.0	30	123.11	57.27	2.15	119.17	62.74	1.90
3.0	25.0	-1.0	10	122.77	37.83	3.24	153.83	54.70	2.81
3.0	25.0	-0.6	30	186.94	75.47	2.48	161.85	72.27	2.24
3.0	25.0	-0.6	10	194.92	52.29	3.73	174.85	70.03	2.50
4.0	37.5	-0.8	20	331.24	52.64	6.29	123.84	85.51	1.45
4.0	37.5	-0.8	20	328.22	50.27	6.53	122.41	83.57	1.46
4.0	37.5	-0.8	20	318.78	52.30	6.09	111.86	61.98	1.80

ture [17] with the Detarchi programme [11], which provides the capacity to detect of the analytical method by evaluating the probability of false positive (α) and false negative (β) as against the probability of false positive normally employed when using the criterion of the IUPAC [18]. It should be pointed out in the rough copy of the already existing ISO norms [19] the false negative is considered in the evaluation of the detection limit. Calibrations parameters, detection limits and detection signal obtained from the different calibrations are summarized in Table 4. In all cases a probability of false positive ($\alpha = 0.05$) and a number of replications ($r = 1$) were taken for different values of probability of false negative ($\beta = 0.5$ and 0.05).

3.3. Determination of indomethacin and acemethacin in urine samples

In the voltammetric determination of indomethacin and acemethacin in urine samples, the response was affected by the same variables, percentage of buffer in the electrochemical cell

(%_{buffer}), pH of solution, deposition potential (E_{dep}) and deposition time (t_{dep}) considered before. However, their influence is not necessarily the same, since the matrix is more complicated, the background is greater and it is necessary to use higher concentrations of analyte to obtain appreciable signals. This is why a new optimization procedure was carried out for these variables by a factorial experimental design 2⁴.

Previous experiences indicate that deposition time values > 100 s favour the adsorption of the other components of the urine preventing the deposition of the drugs. Also pH values and %_{buffer} > 6 and 50%, respectively, exert a decrease of the electrochemical response. Taking into account these facts the initial experimental area is smaller and the values for the high levels (+) and low levels (-) for the variables were:

pH (+) = 5.0	pH (-) = 3.0	pH (0) = 4.0
% _{buffer} (+) = 50.0	% _{buffer} (-) = 25.0	% _{buffer} (0) = 37.5
E_{dep} (+) = -1.0 V	E_{dep} (-) = -0.6 V	E_{dep} (0) = -0.8 V
t_{dep} (+) = 30 s	t_{dep} (-) = 10 s	t_{dep} (0) = 20 s

Table 6
Calibrations parameters obtained from the different calibrations for indomethacin and acemethacin in urine samples

	Indomethacin																				
	Calibration I			Calibration II			Calibration III			Calibration I			Calibration II			Calibration III					
	LS	LMS	LS with-out outliers	LS	LMS	LS with-out outliers	LS	LMS	LS with-out outliers	LS	LMS	LS with-out outliers	LS	LMS	LS with-out outliers	LS	LMS	LS with-out outliers			
Number of data	11	11	9	11	11	11	11	11	11	10	10	10	10	10	10	10	10	10	9		
Sensitivity (nA M ⁻¹) × 10 ⁻⁶	2.110	0.998	0.806	3.057	0.496	0.475	2.255	0.667	0.651	1.139	0.073	0.071	1.289	0.261	0.234	0.958	0.375	0.259	0.259		
Intercept (nA)	68.46	71.67	71.29	68.91	70.95	70.79	68.56	70.92	71.10	19.57	20.03	20.00	19.91	19.64	19.71	19.88	19.67	19.41	19.41		
Coeff. Of determination (R ²)	0.9905	0.9975	0.9982	0.9791	0.9993	0.9992	0.9892	0.9990	0.9988	0.9385	0.9998	0.9994	0.9080	0.9975	0.9960	0.9575	0.9946	0.9963	0.9963		
Linear range (M)	1.97 × 10 ⁻⁶ –10.03 × 10 ⁻⁶			1.97 × 10 ⁻⁶ –8.71 × 10 ⁻⁶			1.97 × 10 ⁻⁶ –10.03 × 10 ⁻⁶			0.50 × 10 ⁻⁷ –2.98 × 10 ⁻⁷			0.50 × 10 ⁻⁷ –3.97 × 10 ⁻⁷			0.0–3.97 × 10 ⁻⁷					

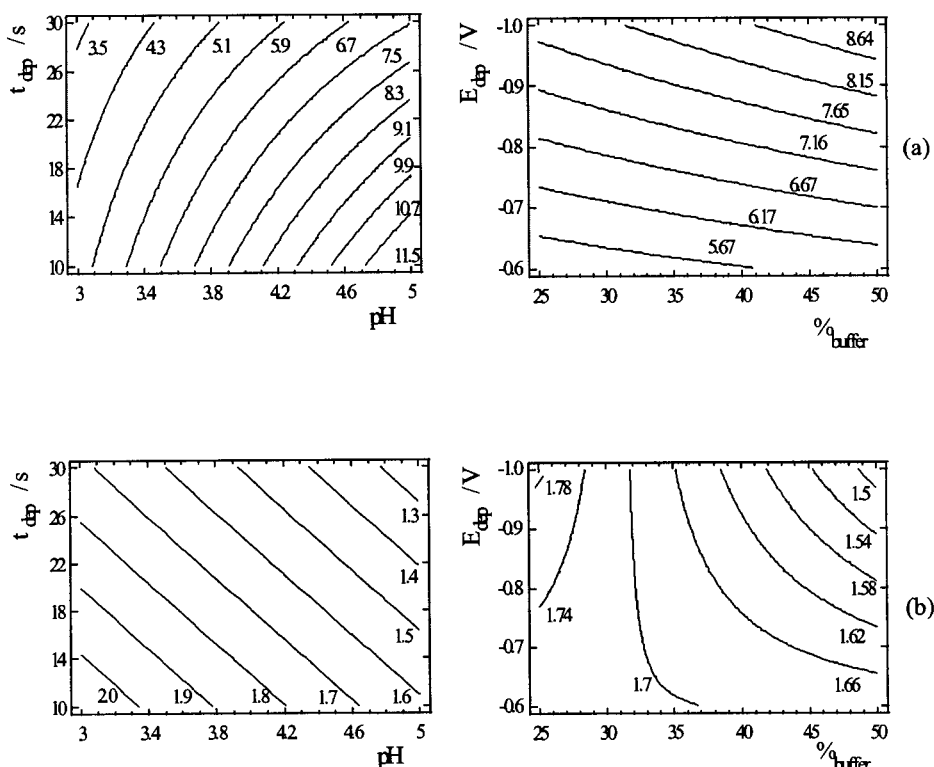


Fig. 5. Isoresponse lines corresponding to the interactions $\text{pH} - t_{\text{dep}}$ and $\%_{\text{buffer}} - E_{\text{dep}}$ for both drugs. (a) The equation of the fitted model for indomethacin is: $i_p/i_{\text{pblank}} = -7.69 + 2.38A + 0.26B - 16.95C + 0.39D - 6.68E - 2AB + 6.20AC - 9.27E - 2AD + 7.74E - 2BC - 1.11E - 3BD - 0.18CD$. A: pH; B: $\%_{\text{buffer}}$; C: E_{dep} ; D: t_{dep} . (b) The equation of the fitted model for acemethacin is: $i_p/i_{\text{pblank}} = 7.65 - 1.53A - 0.11B + 6.07E - 2C - 1.48E - 2D + 2.92E - 2AB + 0.26AC - 3.03E - 4AD - 2.73E - 2BC + 1.94E - 4BD - 1.19E - 2CD$. A: pH; B: $\%_{\text{buffer}}$; C: E_{dep} ; D: t_{dep} .

The results obtained in the 16 basic experiments carried out in random order and those of the three central points are shown in Table 5. The urine samples analysed were spiked 5×10^{-6} M in drug. From the ANOVA with the data of acemethacin it can be deduced that only the pH factor and the interaction $\text{pH} - \%_{\text{buffer}}$ are significant ($P_{\text{level}} < 0.05$). For indomethacin the standardized effects show that all the factors are significant ($P_{\text{level}} < 0.05$) with the exception of the interactions $\%_{\text{buffer}} - E_{\text{dep}}$ and $\%_{\text{buffer}} - t_{\text{dep}}$.

Under the improved conditions of the factorial design the response was improved by a factor of 7 for indomethacin (from 2.15 to 16.35 for the relation i_p/i_{pblank}). This increase in the response is satisfactory and it is not considered necessary to make another new design. For

acemethacin there was not a great increase in the response analysed (from 1.02 to 2.81 for the relation i_p/i_{pblank}) and we could make a new design moving in the direction of the influential effects. However, it has already been pointed out that in this design there are very extreme values for pH and $\%_{\text{buffer}}$. Indeed percentages of buffer $< 25\%$ in the solution are not sufficient to adjust the solution pH. Furthermore, for pH values < 2.5 one can see the precipitation of the drugs.

Fig. 5 shows the isoresponse lines of the interactions $\text{pH} - t_{\text{dep}}$ and $\%_{\text{buffer}} - E_{\text{dep}}$ for indomethacin and acemethacin. Likewise, the equation of the adjusted model for each drug with the 2^4 factorial designs done is shown in the legend of Fig. 5.

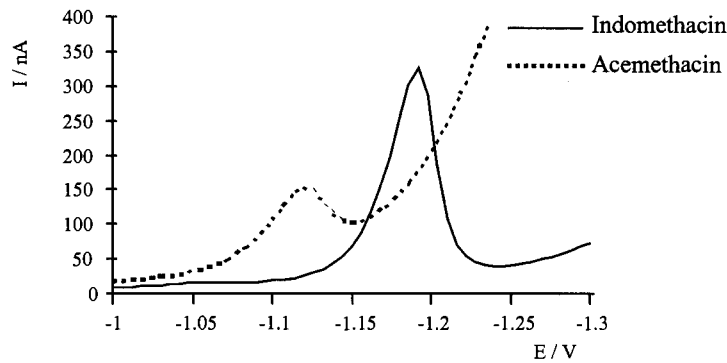


Fig. 6. Differential pulse adsorptive stripping voltammograms obtained for indomethacin and acemethacin in urine sample in Britton–Robinson buffer. — indomethacin 5×10^{-6} M. pH = 5, %_{buffer} = 50, $E_{\text{dep}} = -1.0$ V, $t_{\text{dep}} = 10$ s acemethacin 5×10^{-6} M. pH = 3, %_{buffer} = 25, $E_{\text{dep}} = -1.0$ V, $t_{\text{dep}} = 10$ s.

Thus, to provide optimum conditions for the later calibration in urine samples with DPAdSV, the following were used:

Indomethacin	Acemethacin
pH = 5.0	pH = 3.0
% _{buffer} = 50.0	% _{buffer} = 25.0
$E_{\text{dep}} = -1.0$ V	$E_{\text{dep}} = -1.0$ V
$t_{\text{dep}} = 10$ s	$t_{\text{dep}} = 10$ s

To carry out the determination of indomethacin and acemethacin in urine samples, additions of 20 μl of 5×10^{-5} M indomethacin or acemethacin were made to a urine sample diluted 25.0-fold in water. When obtaining the calibration lines, the criterion of the LMS was taken into account to detect anomalous points whether they be 'outlier or leverage'. Calibration parameters for three replicate calibrations for each drug are summarised in Table 6. The differential pulse adsorptive stripping voltammograms of urine samples from 20 healthy subjects of both sexes, aged between 16 and 60 years, were compared, the qualitative aspect being virtually constant (Fig. 6). The detection limits calculated for the 20 samples analysed, an α value 0.05, a β value 0.05 and a replication oscillate from 1.64×10^{-7} to 7.35×10^{-7} M for acemethacin and from 1.23×10^{-8} to 7.61×10^{-8} M for indomethacin.

References

- [1] T. Hirai, S. Matsumoto, I. Kishi, *J. Chromatogr. B* 692 (1997) 375.
- [2] T.B. Vree, M. Van den Biggelaamarte, *J. Chromatogr. Biomed. App.* 616 (1993) 271.
- [3] G. Gonzalez, R. Ventura, A.K. Smith, R. de la Torre, J. Segura, *J. Chromatogr. A* 719 (1996) 251.
- [4] M.J. Arcos, M.C. Ortiz, B. Villahoz, L.A. Sarabia, *Anal. Chim. Acta* 339 (1997) 63.
- [5] J. Wang, *Stripping Analysis Principles, Instrumentation and Applications*, VCH, Deer Field Beach, FL, 1985.
- [6] J. Lopez Palacios, J. Arcos, P. Sanchez Batanero, *J. Pharm. Biomed. Anal.* 6 (1988) 963.
- [7] J. Arcos, J. Lopez Palacios, P. Sanchez Batanero, *Electroanalysis* 1 (1989) 279.
- [8] J. Arcos, J. Lopez Palacios, J.M. Leal, P. Sanchez Batanero, F. Mata, *Bull. Soc. Chim. Fr.* 128 (1991) 314.
- [9] Statgraphics, Version 5. STSC, Rockville, MD, 1991.
- [10] P.J. Rouseeuw, A.M. Leroy, *Regression Robust and Outlier Detection*, Wiley, New York, 1989.
- [11] L.A. Sarabia, M.C. Ortiz, *Trend Anal. Chem.* 13 (1994) 1.
- [12] S. Sanllorente, M.C. Ortiz, J. Arcos, J. Lopez Palacios, *Electroanalysis* 8 (1996) 285.
- [13] A. Herrero, M.C. Ortiz, J. Arcos, J. Lopez Palacios, *Analyst* 119 (1994) 1585.
- [14] N.R. Draper, H. Smith, *Applied Regression Analysis*, 2nd ed., Wiley, New York, 1981.
- [15] M.C. Ortiz, M.J. Arcos, J.V. Juarros, J. Lopez Palacios, L.A. Sarabia, *Anal. Chem.* 65 (1993) 678.
- [16] M.C. Ortiz, J. Lopez Palacios, L.A. Sarabia, M.G. Piangerelli, D. Cingolani, *Electroanalysis* 8 (1996) 927.
- [17] C.A. Clayton, J.W. Hines, P.D. Elkins, *Anal. Chem.* 59 (1987) 2506.
- [18] IUPAC, *Spectrochem. Acta* 33B (1978) 242.
- [19] ISO/DIS 11843-1, Decision limit, Detection limit, capability terms and definition, Ginebra (1995).

A consideration of electrode polishing prior to application of pulsed amperometric detection

Ayano Inoue, Rosa L. Earley, Mark W. Lehmann, Lawrence E. Welch *

Department of Chemistry, Knox College, Galesburg, IL 61401 USA

Received 28 July 1997; received in revised form 24 December 1997; accepted 29 December 1997

Abstract

An examination was made of the effect of electrode polishing on the direct pulsed amperometric detection (PAD) and indirect PAD response to penicillin G. The polishing procedure produced a temporary loss of sensitivity for both types of PAD, which over time relaxed back to higher levels. A temporary increase in the electrode kinetics can be observed as well, particularly for a PAD waveform in the crossover region between direct and indirect PAD. In extreme cases, the penicillin G response can undergo a complete polarity reversal. By observing post-polish equilibration times, it was recommended that the direct and indirect PAD user observe 3 and 5 h delay times, respectively, to insure stable electrode response following an electrode polish. © 1998 Elsevier Science B.V. All rights reserved.

Keywords: Electrode polishing; PAD; Electrode response

1. Introduction

In his classic text on solid electrode electrochemistry, Adams [1] stated, 'Probably the most serious problem in solid electrode methodology is associated with understanding the true electrode surface conditions and their possible effect on the electrode process.' He went on to describe 'filming', a phenomena that led to a loss of electrode activity, hampering voltammetric studies of amines, phenols, and sulfur compounds. Many other sources have noted the importance of working electrode 'cleanness', and the deleterious ef-

fects of adsorption, electropolymerization, fouling, or poisoning of the working electrode [2–4]. Despite the broad swath of phenomena covered by these descriptions, all essentially involve an accumulation of foreign material on the surface of a working electrode, and the concomitant loss of electrode activity. Completely cleaning the foreign material from the electrode may be nearly impossible, but various techniques alone or in combination have been developed to rejuvenate working electrode activity, such as chemical treatments, potential excursions, and mechanical polishing [1].

Pulsed amperometric detection (PAD), developed by Johnson, Hughes and Polta [5,6], utilized a regular waveform incorporating potential excursions

* Corresponding author. Tel: +1 309 341 7333; fax: +1 309 341 7718; e-mail LWelch@Knox.edu

sions to produce a fresh electrocatalytic electrode surface prior to each current measurement. This methodology allowed amperometric determinations of many organic species that had resisted prior efforts due to loss of electrode activity from fouling [7,8]. Despite adapting one rejuvenating process into the PAD waveform, the practice of polishing the working electrode, at least on an occasional basis, did not disappear. It is interesting to note that in some laboratories using PAD [9–14], the practice of electrode polishing has been incorporated as a part of a regular electrode conditioning ritual prior to experimentation, presumably to fight against fouling from sources that were not completely eliminated via potential excursions. Mechanical polishing is known to temporarily alter the response of a working electrode, often requiring 60–90 min before a stable baseline can be attained following the procedure. However, recent work in this laboratory [15] has suggested that the post-polish instability might extend for a considerably longer period. Some evidence of kinetic alteration was observed after polishing as well. Without suggesting that electrode polishing not be done, as it has proven its value, this study sought to examine the prudence of electrode polishing as a commonplace PAD

pre-experimental ritual. In particular an evaluation was to be made of the signal stability of PAD using a common electrode and a common analyte system following an abrasive polish.

2. Experimental

Penicillin G was purchased from Sigma Chemical (St. Louis, MO). Methanol and acetonitrile were reagent grade from Fisher (Pittsburgh, PA). All other solutions were made from reagent grade chemicals from Aldrich (Milwaukee, WI), Baker (Phillipsburg, NJ), Fisher, or Sigma. Water was distilled and deionized before use as a solvent.

Flow injection analysis trials were done with a Waters 625 LC system (Milford, MA) and a Waters 464 pulsed electrochemical detector. A 75- μ l sample injection loop was employed for all. Injected penicillin solutions were all solvent matched to avoid having a system peak overlapping with the analytical peak. To improve the flow stability during flow injection analysis, an Upchurch (Oak Harbor, WA) U-469 back pressure regulator was placed in-line following the pump. All solvents were vacuum filtered through an Alltech (Deerfield, IL) 0.20- μ m nylon filter. The solvent mixtures were degassed further using a 30 ml min⁻¹ helium sparge during the flow injection trials.

Flowing stream work utilized a thin-layer cell with a single gold working electrode having a diameter of 2.5 mm. The counter electrode was a stainless steel block mounted opposing the thin-layer cell, with the flow channel created by a teflon spacer between the two. The reference electrode was a Ag/AgCl. The BAS MF-2060 polishing kit was used to polish the working electrode at noted intervals. The working electrode was polished using a Buehler (Lake Bluff, IL) Microcloth and Buehler Gamma Micropolish Alumina, no. 3, having a particle size of 0.05 μ m.

Current integration was always during the final 16.7 ms of the detection step, as required by the detector. Detector signal polarity was inverted so that increased anodic response would produce peaks rather than troughs on the output plots. Output data was collected by a PC using LabCalc

Table 1
PAD Waveforms

	Potential (mV)	Time (s)
A	Variable	0.333
	1600	0.333
	-300	0.416
B	1600	0.333
	1700	0.167
	-100	0.249
C	1050	0.167
	1600	0.167
	-100	0.333
D	1300	0.333
	1600	0.333
	-300	0.416
E	1100	0.333
	1600	0.333
	-300	0.416

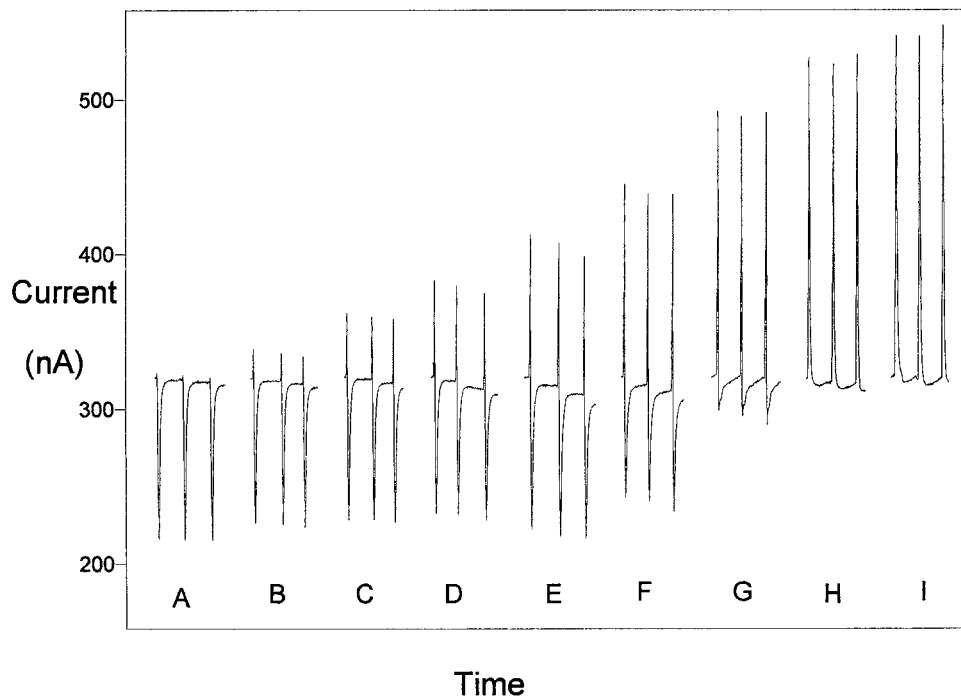


Fig. 1. The crossover region between indirect and direct PAD. Flow injection analysis. Solvent: 12% methanol/8% acetonitrile/80% 0.2 M acetate buffer (pH 4.7) (v/v), 1.0 ml/min. Injections: 1.00×10^{-3} M penicillin G. PAD waveform: given in Table 1A, except for E_1 which was varied for each trace. Traces: (A) $E_1 = 1100$ mV, (B) $E_1 = 1150$ mV, (C) $E_1 = 1200$ mV, (D) $E_1 = 1250$ mV, (E) $E_1 = 1300$ mV, (F) $E_1 = 1350$ mV, (G) $E_1 = 1400$ mV, (H) $E_1 = 1450$ mV, (I) $E_1 = 1500$ mV.

software (Galactic, Salem, NH). The collection interval was synchronized with the potentiostat, such that a single data point was collected per PAD cycle.

3. Results and discussion

The analyte chosen for study was penicillin G, which was observed in acetate buffer solvent containing portions of organic modifier. This system was advantageous in that it had been well characterized by previous studies [13–18], and that it can support both direct and indirect PAD by proper waveform selection. Either of these methods could be used to monitor sensitivity to penicillin G following an electrode polish. For this study, it was decided to operate in or near the crossover region between direct and indirect PAD [13,15,18]. Direct PAD represents an anodic oxidation of the penicillin G following its adsorption

onto the working electrode. Although the adsorption causes an attenuation of electrode surface oxidation, the loss in anodic current is more than offset by electrocatalytic oxidation of the penicillin, causing a net increase in anodic signal. With indirect PAD the penicillin still adsorbs to the working electrode, but the kinetics of the electrocatalytic oxidation of the penicillin have slowed to the point that the anodic current produced from this process is minimal, failing to offset the loss of current from surface oxidation and yielding a net decrease in anodic signal. The crossover region represents the transition zone between using direct and indirect PAD. Response in this region is often bidirectional, yielding both an oxidative and suppressive component. Practical PAD procedures can use either direct or indirect PAD, although for optimum S/N response one would like to avoid the crossover region where the signal from the oxidized penicillin is nearly equal to the suppressed signal from forma-

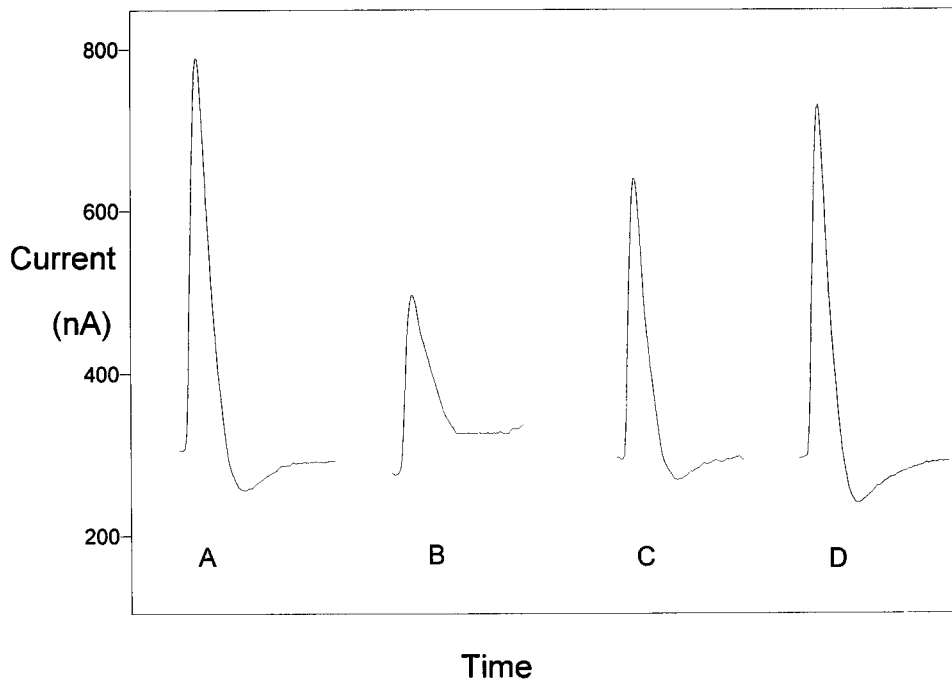


Fig. 2. Direct PAD response to penicillin G following electrode polishing. Flow injection analysis. Solvent: 12% methanol/8% acetonitrile/80% 0.2 M acetate buffer (pH 4.7) (v/v), 1.0 ml/min. Injections: 1.00×10^{-3} M penicillin G. PAD waveform: given in Table 1B. Traces: (A) typical pre-polish response, (B) 5 min after polishing, (C) 58 min after polishing, (D) 184 min after polishing.

tion of residual oxide. For $I-E$ curves that help illustrate the crossover phenomena, direct PAD, and indirect PAD, see Ref. [13].

The crossover region for penicillin G in 12% methanol/8% acetonitrile/80% 0.2 M acetate buffer (pH 4.7) (v/v) (12/8/80), is shown in -3 M penicillin G. PAD waveform: given in Fig. 1. At the initial E_1 (detection) potential value of 1100 mV, very little of the penicillin is oxidized. By shifting the E_1 more positive one can provide additional overpotential to enhance the efficiency of the penicillin oxidation, enabling the conversion from indirect to direct PAD. While this crossover region might be a poor region to perform sensitive detection of penicillin G, it is useful for the study at hand. In particular, peak size in the crossover region is a function of both the amount of adsorbed penicillin G and the particular reaction kinetics for the penicillin oxidation. By monitoring in this region, one can observe kinetic changes in addition to gauging the stability and sensitivity of the detector.

For each different waveform, initial stable output response for repetitive penicillin G injections was obtained. The cell was then disabled, the gold working electrode removed and polished as noted in the experimental section, then the cell reassembled and response to the same penicillin G solution measured as a function of time after reassembling the cell. A plot of the response using a direct PAD waveform is shown in Fig. 2. Looking at the pre-polish trace (A), one can note the 'dip' following the peak. This is typical behavior for a direct PAD waveform that is right on the edge of the crossover region, still containing a trace of the suppressive effect prevalent with indirect PAD. The same effect can be seen in traces (H) and (I) from Fig. 1. After polishing, it can be seen that the sensitivity to penicillin is diminished, but returns gradually over time. Kinetic information can be gathered by observing the relative magnitude of the oxidative and suppressive peak components. Since the changes are subtle in Fig. 2, the ratio produced by dividing the peak height

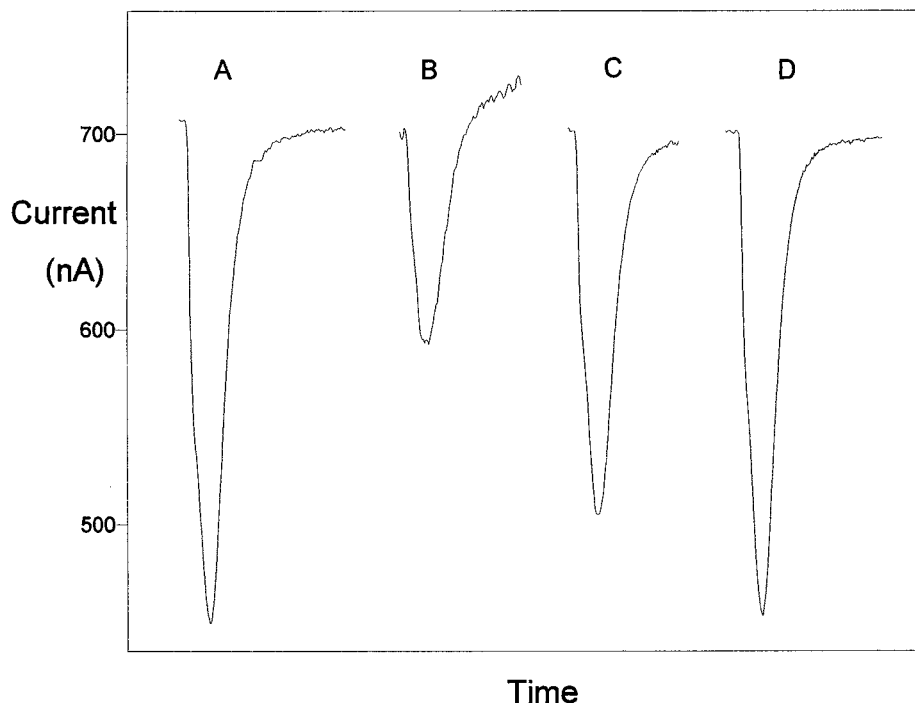


Fig. 3. Indirect PAD response to penicillin G following electrode polishing. Flow injection analysis. Solvent: 12% methanol/8% acetonitrile/80% 0.2 M acetate buffer (pH 4.7) (v/v), 1.0 ml/min. Injections: 1.00×10^{-3} M penicillin G. PAD waveform: given in Table 1C. Traces: (A) typical pre-polish response, (B) 4 min after polishing, (C) 56 min after polishing, (D) 182 min after polishing.

of the positive peak component by that of the negative was calculated. This ratio goes from 9.76 in (A) to 13.9 in (C) to 7.76 for (D). Trace (B) has no negative component at all. This indicates that there is an increase in the rate of penicillin G oxidation following the polish, as the peaks show a shift out of the crossover region toward direct PAD, with relaxation back into the crossover region with sufficient time. The ratio typically will relax back to a similar value as that seen with the pre-polish set, or, in some cases, to a smaller value. This parallels the peak height relaxation, which also end up of similar height to the pre-polish or slightly larger. The disparity arises because of the uncertainty of the electrode surface condition while collecting the pre-polish set.

A plot of the response using an indirect PAD waveform is shown in Fig. 3. The behavior here is similar in regard to the initial loss of sensitivity followed by a gradual regeneration in the wake of the electrode polish. The indirect PAD conditions

in use are remote enough from the crossover region such that there is no positive component to the pre-polish response, nor is there any positive component produced in the aftermath of polishing. It is possible that an increase in oxidation kinetics may be occurring as seen in Fig. 2, but if so it is at most causing a small area reduction of the suppression peak, which could not be isolated from the area change due to sensitivity loss. In any case the degree of penicillin oxidation is very small under these conditions, and a rate increase might not cause an observable change. Other indirect PAD waveforms slightly closer to the crossover region show the generation of a temporary direct PAD component immediately after polishing.

The most dramatic effect takes place when a waveform in the middle of the crossover region for penicillin G was chosen, as shown in Fig. 4. Despite keeping all other experimental conditions exactly the same, one can produce an inversion in

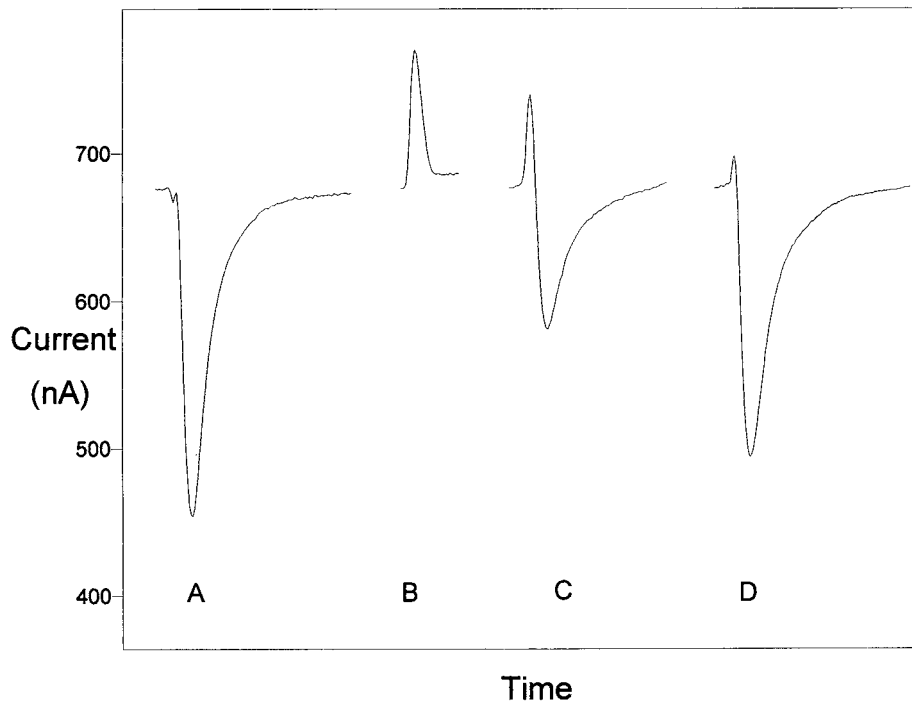


Fig. 4. PAD response to penicillin G in the crossover region after electrode polishing. Flow injection analysis. Solvent: 12% methanol/8% acetonitrile/80% 0.2 M acetate buffer (pH 4.7) (v/v), 1.0 ml/min. Injections: 1.00×10^{-3} M penicillin G. PAD waveform: given in Table 1D. Traces: (A) typical pre-polish response, (B) 4 min after polishing, (C) 57 min after polishing, (D) 178 min after polishing.

response, albeit temporary, simply by polishing the working electrode. This figure very clearly illustrates the increase in oxidation rate, and thus the shift from indirect toward direct PAD caused by polishing. The change in sensitivity is also clear.

For all waveform types, peak heights were reduced upon polishing. This is representative of the process reducing the active surface area of the working electrode. Penicillin detection via either direct or indirect PAD relies on adsorption of the penicillin to the gold surface [13]. When viewed microscopically, the seemingly planar surface of the working electrode actually is quite rough, with active electrode surface ranging over a significant depth. Abrasive polishing will flatten this rough surface, producing something closer to planar which ultimately has much less surface area. Consequently, adsorption dependent detection of penicillins is suppressed after the abrasive proce-

dure. However, as the PAD waveform is reapplied to the electrode and it is allowed to equilibrate, the surface will begin to 'erode' back, eventually producing a rough surface approximating the one observed pre-polish. This would explain the sensitivity change observed for both direct and indirect PAD, as output current depends on the amount of adsorbed analyte for each.

Although not obvious in Fig. 3, it is likely that the oxidation rate kinetics are increased under all circumstances following a polish. The rate change can be observed throughout the crossover region. Prior work has suggested that electrode polishing causes an increase in the oxidation rate for penicillin with PAD, based on an analysis of peak symmetry characteristics [15]. The proposed electrocatalytic oxidation of the penicillins is postulated to occur via an oxygen transfer from a surface oxide site to the sulfide group on the penicillin. This can only occur when the penicillin

is adsorbed to the electrode surface at the sulfide moiety, and if there is nearby oxide to affect the transfer. The mature 'rough' electrode surface appears to have a number of sites which geometrically are hindered from completing the oxygen transfer, thus slowing the overall rate of oxidation. After polishing, the flatter, less tortuous electrode surface is less likely to provide surface geometries hindering the oxygen transfer process, thus leading to more rapid and more efficient penicillin oxidation. As the surface regains its original 'roughness', the oxidation rate reverts back to its original range.

Although waveforms in the crossover region will be a poor choice in terms of sensitivity to penicillins, the change in sensitivity upon polishing extends beyond the crossover region and throughout the PAD detection range for these molecules. This is likely the case for all PAD analytes that involve oxide-catalyzed detection. Given this finding, it would seem imperative to not collect quantitative information until the detector sensitivity has stabilized following an electrode polish. It is important to note that the time required for this stabilization is much greater than

the time required to obtain a stable baseline. Whether or not electrode polishing is done on a regular basis, it would seem a safe assumption that occasional polishing of PAD working electrodes is unavoidable. If so, and given that baseline stability is a poor indicator of the analyte sensitivity of the detector, this begs the question as to how long one should wait before collecting quantitative data following a polish. Numerous studies examining the peak stability following a polish were run for a variety of waveforms. Typical response can be seen in Fig. 5 for both direct and indirect PAD. The direct PAD stabilized somewhat faster, which seems reasonable given the higher current density and faster electrode kinetics. Three hours seemed to be a good minimum waiting period following a polish for this type of waveform, while indirect PAD requires a more lengthy wait: 5 h as a minimum would be recommended. Although they are of less practical utility, waveforms in the middle of the crossover region also required a minimum of 5 h for stabilization.

4. Conclusion

Abrasive polishing of a working electrode should be undertaken with caution as it will require 3–5 h delay before a stable peak response can be obtained. Given this, polishing as part of a regular pre-experimental ritual should not be undertaken unless a long period is available for equilibrating. It might be best to polish the day before an experiment, with overnight equilibration of the detector prior to the quantitative PAD trials.

Acknowledgements

Support for RLE and MWL was from a Ford Undergraduate Research Fellowship from Knox College, partially supported by The Ford Foundation. Additional support came from Knox College via the Faculty Research Program and the College Honors Program. The generous donation of equipment from the Waters Chromatography

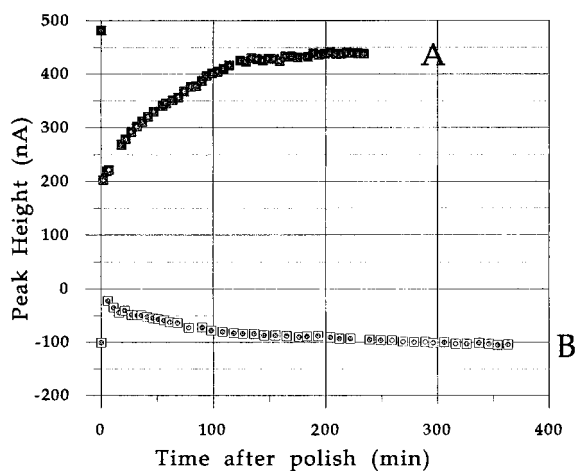


Fig. 5. The equilibration of the anodic response to penicillin G as a function of time following an electrode polish. Flow injection analysis. Solvent: 12% methanol/8% acetonitrile/80% 0.2 M acetate buffer (pH 4.7) (v/v), 1.0 ml/min. Injections: 1.00×10^{-3} M penicillin G. Traces: (A) direct PAD, waveform given in Table 1B, (B) indirect PAD, waveform given in Table 1E.

Division of the Millipore Corporation is acknowledged with gratitude.

References

- [1] R.N. Adams, *Electrochemistry at Solid Electrodes*, Marcel Dekker, New York, 1969.
- [2] J.M. Bobbitt, Anodic electroorganic chemistry and natural products, in: J.T. Stock, M.V. Orna (Eds.), *Electrochemistry, Past and Present*, ACS Symp. Series 390, Ch. 14, American Chemical Society, Washington, DC, 1989.
- [3] B.R. Shaw, Modification of solid electrodes in electroanalytical chemistry 1978–1988, in: J.T. Stock, M.V. Orna (Eds.), *Electrochemistry, Past and Present*, ACS Symp. Series 390, Ch. 22, American Chemical Society, DC, Washington, DC, 1989.
- [4] A.J. Bard, L.R. Faulkner, *Electrochemical Methods*, Wiley, New York, 1976.
- [5] S. Hughes, P.L. Meschi, D.C. Johnson, *Anal. Chim. Acta.* 132 (1981) 1.
- [6] S. Hughes, D.C. Johnson, *Anal. Chim. Acta.* 132 (1981) 11.
- [7] J.A. Polta, D.C. Johnson, *J. Liq. Chromatogr.* 6 (1983) 1727.
- [8] D.C. Johnson, W.R. LaCourse, *Anal. Chem.* 62 (1990) 589A.
- [9] R. Roberts, D.C. Johnson, *Electroanalysis.* 4 (1992) 741.
- [10] R. Roberts, D.C. Johnson, *Electroanalysis* 6 (1994) 269.
- [11] R.M. Ianniello, *J. Liq. Chromatogr.* 15 (17) (1992) 3045.
- [12] W. Lu, R.M. Cassidy, *Anal. Chem.* 65 (1993) 2878.
- [13] L. Koprowski, E. Kirchmann, L.E. Welch, *Electroanalysis* 5 (1993) 473.
- [14] S. Altunata, R.L. Earley, D.M. Mossman, L.E. Welch, *Talanta* 42 (1995) 17.
- [15] M.W. Lehmann, M.R. Fahr, L.E. Welch, *Talanta* 44 (1997) 1231.
- [16] E. Kirchmann, L.E. Welch, *J. Chromatogr.* 633 (1993) 111.
- [17] E. Kirchmann, R.L. Earley, L.E. Welch, *J. Liq. Chromatogr.* 17 (1994) 1755.
- [18] R.L. Earley, J.S. Miller, L.E. Welch, *Talanta* 45 (1998) 1259.

Spectrophotometric determination of trace amounts of cobalt with 2-hydroxybenzaldehyde-5-nitro-pyridylhydrazone in presence of surfactant after separation with Amberlite IRC-718 resin

Chan-Il Park¹, Ki-Won Cha^{*}

Department of Chemistry, Inha University, Incheon 402–751, South Korea

Received 18 September 1997; received in revised form 22 December 1997; accepted 2 January 1998

Abstract

2-Hydroxybenzaldehyde-5-nitro-pyridylhydrazone (2HB-5NPH) was synthesized and its application in the spectrophotometric determination of metal ions was studied in the presence of surfactants. A separation procedure, using a short column filled with Amberlite IRC 718, is proposed for the spectrophotometric determination of traces of cobalt. The influence of several ions, as interference, was discussed. The procedure was applied to determination of cobalt in mixture sample with satisfactory results (\geq recovery 96%; relative error \leq 2%; relative standard deviation \leq 1.2% in the concentration range of 0.02–2.0 mg l⁻¹; detection limit, 0.01 mg l⁻¹ in solution). Control of the pH during the column operation is essential because the adsorption capacities are very sensitive to change in pH. Their separation was carried out in 0.005 M Malic acid, 1.5 M HCl, 2.0 M HNO₃ media. © 1998 Elsevier Science B.V. All rights reserved.

Keywords: Co(II); 2HB-5NPH; Amberlite IRC-718; Spectrophotometric determination

1. Introduction

Hydrazones (characterized by the grouping —C=N—N—, and related to Schiff's base), have been used as photometric [1–5] and fluorimetric [6–10] analytical reagents for the determination of

metal ions. In analytical chemistry, hydrazones have been used for detection, determination and isolation of compounds containing the carbonyl group [11] and hydrazones act as multidentate ligands with metal ions (usually from the transition elements), forming colored chelates [12]. These chelates are then used in selective and sensitive determination of the metal ions. And, with the addition of certain surfactant reagents can increase the stability and solubility of many organic compounds and metal complexes [13–17].

^{*} Corresponding author. Fax: +82 32 8722520; e-mail: kwcha@dragon.inha.ac.kr

¹ IA postdoctoral fellow (1997–1998) by a grant from Inha University.

Table 1
Data of melting point, yields and infrared spectra of synthesized hydrazone

Hydrazone	M.P. (°C)	Yield (%)	IR Spectral Data (cm ⁻¹)		
			$\nu_{\text{C=N}}$	$\nu_{\text{C-N}}$	$\nu_{\text{N-H}}$
5-N-2-PH	200	92.5	—	1420	1290
2HB-5NPH	244	71.6	1600	—	1292

The metal complexes formed in micellar media are generally more stable than those formed in the absence of micelles. These organized molecular assemblies are used in spectroscopic measurements due to their possible effects on the system of interest. In the field of metal ion complexation, at concentrations above the CMC, micelles form a ternary complex with advantageous properties, such as hyperchromic and bathochromic displacements, that can modify sensitivity and selectivity of the method by affecting the interferences and matrix effect [18,19]. The ability of micellar systems to solubilize slightly insoluble or even very insoluble complexes and/or ligands has been used to enhance the analytical merit of given methods [19,20].

In a previous work [21], the author synthesized 2-pyridinecarbaldehyde-5-nitro-pyridyl hydrazone (2PC-5NPH) and showed it to be a sensitive reagent for Fe(III). In this work, the analytical possibilities of a new reagent, 2-hydroxybenzaldehyde-5-nitropyridyl hydrazone (2HB-5NPH) are reported. This paper describes the spectrophotometric determination of Co(II) by 2HB-5NPH with separation of Co(II) using Amberlite IRC-718 resin. One of the few commercial chelating ion exchange resins available is Amberlite IRC-718 for which the chelating ability is attributed to iminodiacetic acid groups. Very little evaluation has been performed on this exchanger. The present paper gives the adsorption capacities for Co(II) and some metal ions between Amberlite IRC-718 resin and inorganic acid solutions and applies the results to quantitative separation of metal ions. The present method is highly sensitive and simple for separation and spectrophotometric determination of Co(II).

2. Experimental

2.1. Apparatus

Absorption spectra and absorbances were measured with recording spectrophotometer, Perkin-Elmer Model 555S, with 1 cm quartz cells. Shimadzu AA-670 atomic absorption spectrometer was used for metal ions determination. All pH measurements were made with a NOVA-310 pH meter. The resin used in the column was Amberlite IRC-718, 16–50 mesh. The resin was washed successively with 6 M HCl, water, 1 M NaOH, water, 1 M HCl and water in order to remove organic and inorganic contaminants.

2.2. Reagent

Analytical-reagent grade chemicals and distilled, deionized water were used throughout. Cobalt(II) stock solution (100 mg l⁻¹) was prepared by dissolving appropriate amounts of analytical grade Co(NO₃)₂·6H₂O in doubly distilled water and was standardized with EDTA. Working solutions were prepared by suitable dilutions of the stock solution with water. Surfactants were from Sigma and all were used without further purification. Surfactant solutions (1 × 10⁻³M) were prepared by dissolving suitable amounts of surfactants in water with gentle heating.

2.3. Procedure

2.3.1. Synthesis of 2-hydroxybenzaldehyde-5-nitro-pyridylhydrazone

2HB-5NPH was prepared as follows. An ethanolic solution of equimolar quantities (0.1M) of 2-hydroxybenzaldehyde and 5-nitro-2-pyridyl-

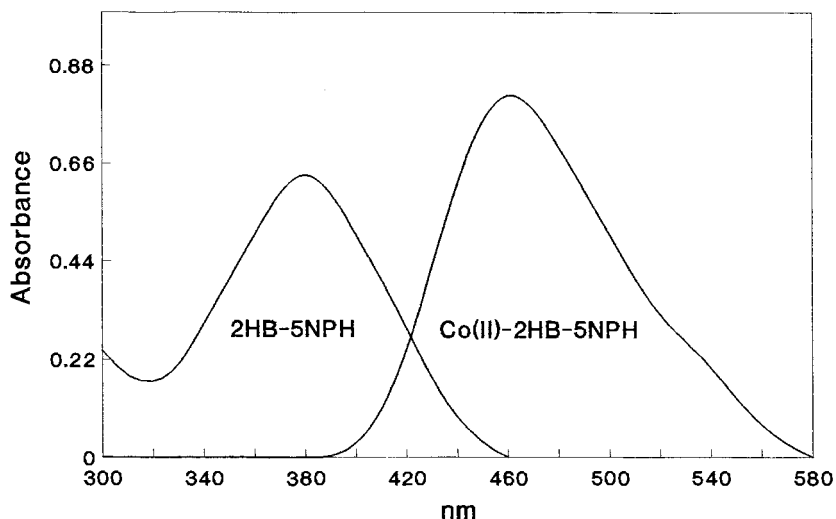


Fig. 1. Absorption spectra of 2HB-5NPH and Co(II)-2HB-5NPH. Co(II): 1.0 mg l^{-1} , 2HB-5NPH: $6.0 \times 10^{-5} \text{ M}$.

hydrazine (Aldrich) was refluxed for 3 h. The product (light yellow needles, m.p. $243.5\text{--}244.1^\circ\text{C}$) was separated after cooling and recrystallized from ethanol. A $1.0 \times 10^{-3} \text{ M}$ solution of the reagent was prepared by dissolving 0.243 g of 2HB-5NPH in 1000 ml of methanol. This solution is stable for several months when kept in an amber glass bottle.

2.3.2. Spectrophotometric determination

An aliquot of metal standard solution was transferred to a 50 ml volumetric flask, and 5.0 ml of $1 \times 10^{-3} \text{ M}$ 2HB-5NPH methanol solution, 3.0 ml of pH 6.5 hexamethylenetetramine (HTM) buffer solution and 7.5 ml of $1.5 \times 10^{-4} \text{ M}$ surfactant solution were added sequentially. The solution was made up to the mark with methanol. The absorbance of the solution was measured at 470 nm against a reagent blank as a reference.

2.3.3. Separation

2.3.3.1. Column separation. A glass column ($25 \times 150 \text{ mm}$) having a stopcock was packed with 15 g of the resin. The resin was regenerated with 6.0 M HCl and a large volume of water.

2.3.3.2. Batch procedure. Resin (1.0 g) and 50 ml solution of Co(II), Cr(III), Ni(II), Zn(II), Cu(II) and Pb(II) in a 100 ml beaker were stirred moderately for 24 h at room temperature. After equilibrium, the solution was filtered through Whatman #2 filter paper. The filtrate was diluted with water and the concentration of metal ions was determined by AAS.

2.3.3.3. Column procedure. Separation of metal ions in the column system was carried out under the following conditions. A fixed volume of aqueous solution of the metal ions was adjusted to a suitable pH and percolated through the column at a flow rate of $1.0 \pm 0.2 \text{ ml min}^{-1}$. Cr(III) and Co(II) was eluted with 0.25 M HCl, Ni(II) with 1.5 M HCl and Cu(II) and Pb(II) with 2.0 M HNO_3 . Co(II) was analysed spectrophotometrically.

3. Result and Discussion

3.1. Identification of hydrazones

2HB-5NPH is yellowish solid which is slightly solution in water but can be easily dissolved in methanol. Identification of the synthesized hydra-

Table 2
Absorption characteristics of Co(II)-2HB-5NPH complex by addition of surfactants

Surfactants	Concentration (M)	λ_{\max} (nm)	Abs	E.F.
Without surfactant	—	462.0	0.74	1.0
CTMAB	1×10^{-4}	470	0.92	1.24
DTMAB	1×10^{-4}	476	0.83	1.12
Triton X-100	1×10^{-4}	467	0.74	1.00
Brij 52	1×10^{-4}	465	0.62	0.84
SDS	1×10^{-4}	470	0.75	1.01

Co(II): 1 mg l^{-1} ; 2HB-5NPH: $1 \times 10^{-4} \text{ M}$.

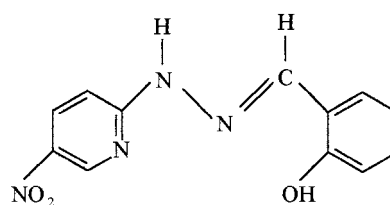
E.F.: enhancement factor.

zones was carried out by Infrared (IR) spectroscopy. The IR spectra of the synthesized hydrazones were measured with potassium bromide pellet in order to confirm their structures. The spectra had absorption peaks assigned to the stretching vibration of an azomethine bond ($-\text{N}=\text{C}$) around 1600 cm^{-1} . The melting point, yield and IR spectral data of the synthesized hydrazones are shown in Table 1.

Table 3
Effects of interfering ions on determination of 1 mg l^{-1} of Co(II)

Foreign ion	Tolerance (mg l^{-1})
Ni(II)	0.5
Cr(III)	2
Cd(II)	15
Cu(II)	0.1
Al(III)	50
Zn(II)	10
Mg(II)	500
Zr(IV)	80
Pt(II)	4.0
Pb(II)	1.5
U(II)	4.5
Na(I)	800
Pd(II)	0.3
Malic Acid	100
Tartaric Acid	50
EDTA	1
Chloride	600

3.2. Spectrophotometric determination



2HB-5NPH [I]

2HB-5NPH is a light yellow crystalline material soluble in most organic solvents. The reagent forms intensely colored complexes with a number of transition metal ions. In these complexes, 2HB-5NPH acts as a tridentate ligand. Complexation is accompanied by elimination of the labile proton of the ligand in most of the chelate systems.

The absorption spectra of the binary and ternary complexes and the reagent blanks are shown in Fig. 1. The Co(II)-2HB-5NPH complex has a strong absorbance at 470–475 nm and that of the reagent blank is at 375–385 nm; the spectra do not overlap. On addition of cetyltrimethylammonium bromide (CTMAB), the absorption band remained unchanged except for a slight increase in peak absorption. Maxima and constant absorbance is obtained for 1.0 mg l^{-1} of Co(II) with 3.0 ml of $1.0 \times 10^{-3} \text{ M}$ 2HB-5NPH solution per 50 ml, so 5.0 ml of this 2HB-5NPH solution is selected as optimal.

The effect of pH on the Co(II)-2HB-5NPH-CTMAB complex formation was studied over the

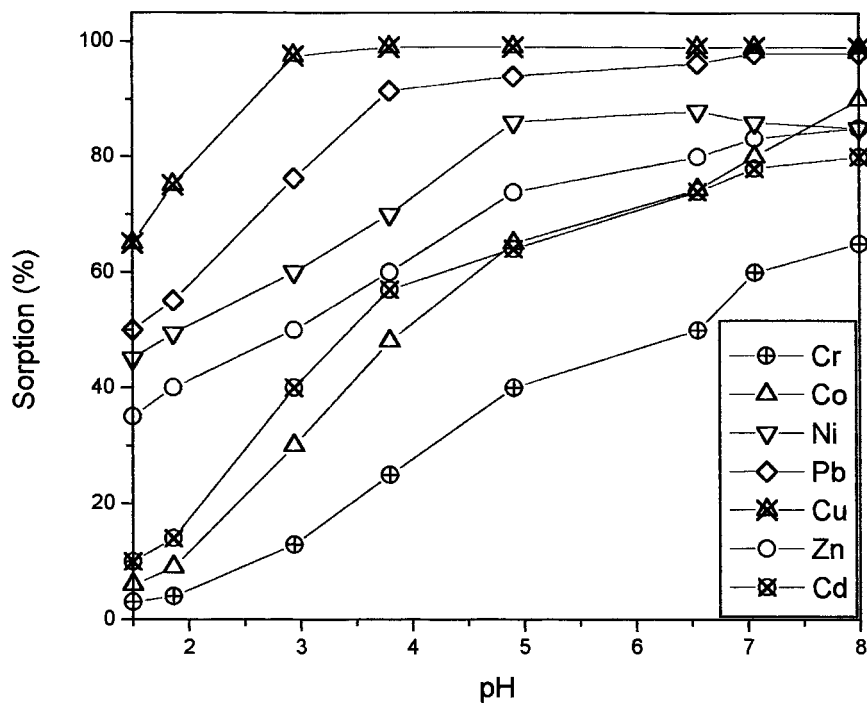


Fig. 2. Sorption capacities of metal ion on Amberlite IRC-718 chelating resin according to pH change. Metal solution: $2.5 \text{ mg } 50 \text{ ml}^{-1}$; resin taken: 1 g; shaking time: 24 h.

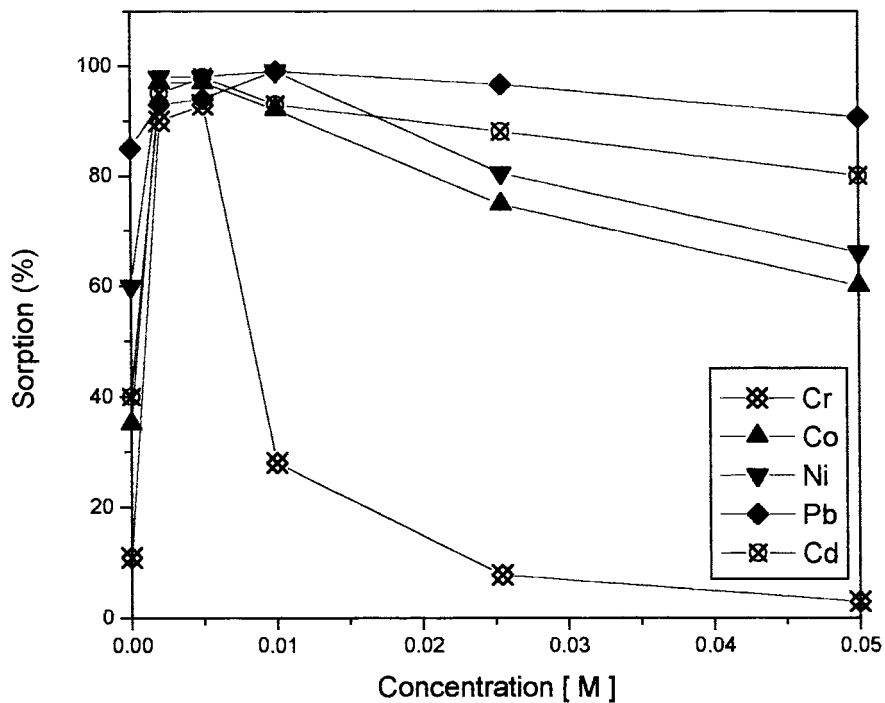


Fig. 3. Sorption capacities of metal ion on Amberlite IRC-718 chelating resin according to Malic acid concentration. Metal solution: $2.5 \text{ mg } 50 \text{ ml}^{-1}$; resin taken: 1 g; shaking time: 24 h, pH: 3.5.

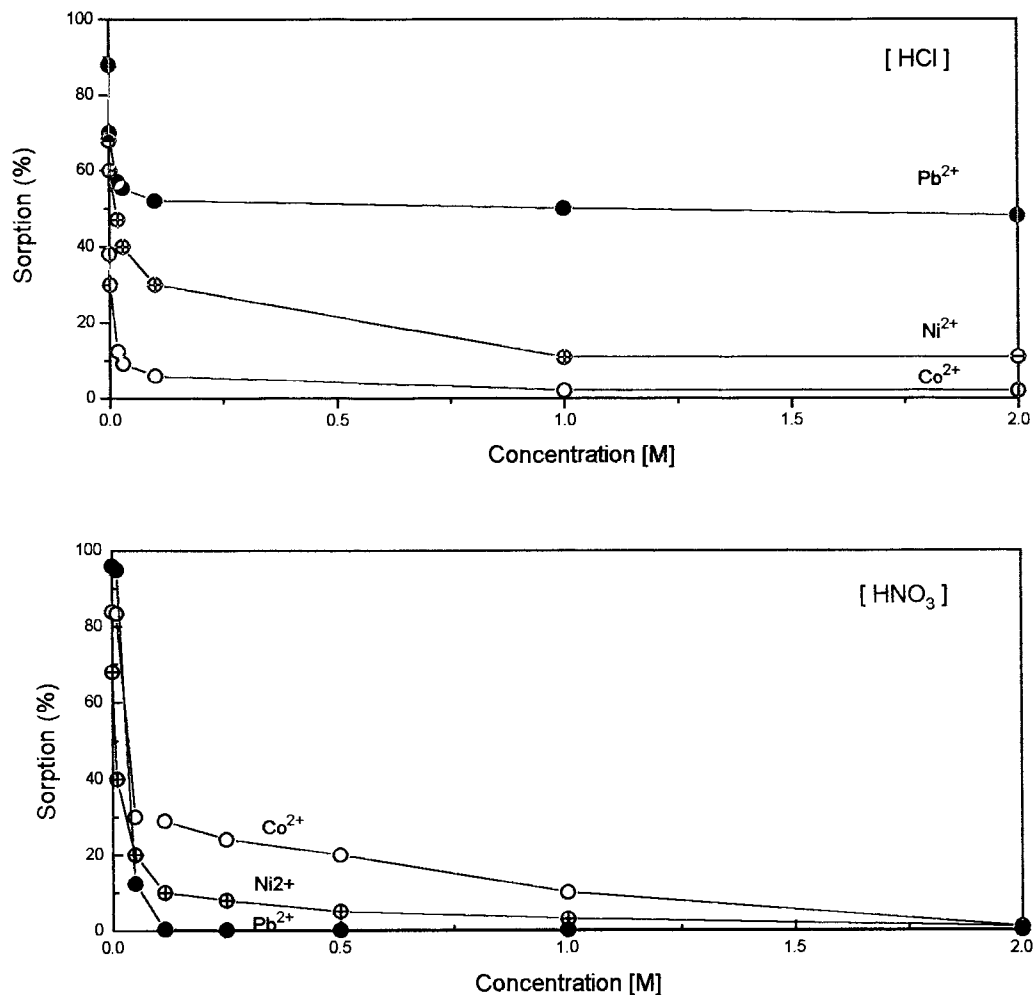


Fig. 4. Sorption capacities of metal ion on Amberlite IRC-718 chelating resin according to HCl and HNO₃ concentration. Metal solution: 2.5 mg 50 ml⁻¹; resin taken: 1 g; shaking time: 24 h.

pH range 3–11. No absorbance was observed with any of the reagents in acidic solutions (< pH 4.5). The optimal pH range for formation of the complex is 6.6–7.2. The solution pH was adjusted with hexamine buffer solution and hydrochloric acid or sodium hydroxide was used to maintain the optimum pH. It does not affect the intensity but improves the stability of the color of the complex.

The effect of nonionic surfactants [Brij 52, Triton X-100], cationic surfactants [cetyltrimethylammonium bromide (CTMAB), dodecyltrimethylammonium bromide (DTMAB)] and anionic

surfactant [sodium dodecyl sulfate (SDS)] were studied. As shown in Table 2, the cationic surfactants had a increase of absorbance but in the anionic and nonionic surfactants showed no effect or diminished on the absorption spectra of the Co(II)-2HB-5NPH complex. The absorbance increased with a increase of CTMAB concentration until 1.5×10^{-4} M, but the absorbance diminished with further increase of CTMAB. As can be seen, CTMAB showed the best enhancement effects and so was selected for further investigations.

We measured the mole ratio of Co(II) and 2HB-5NPH in Co(II)-2HB-5NPH complex with

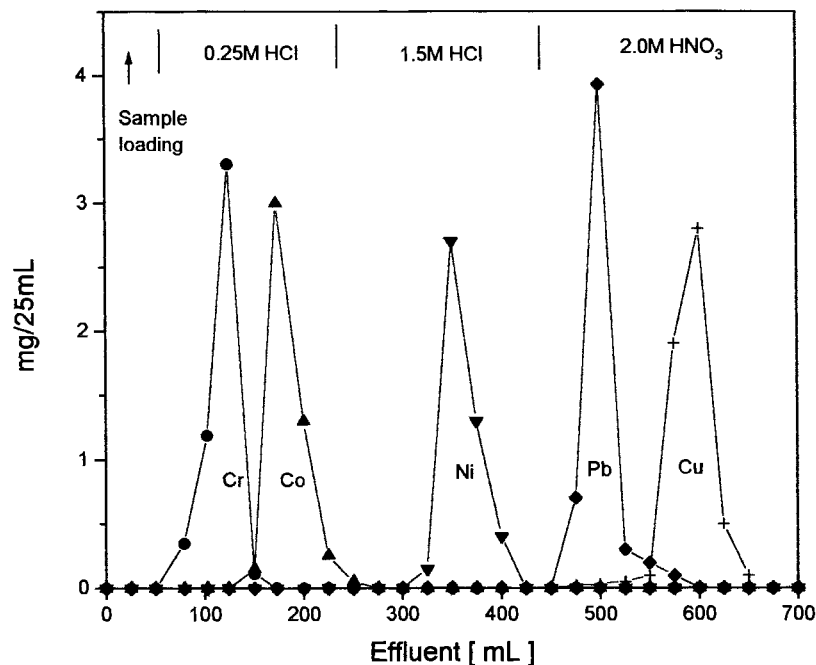


Fig. 5. Elution curve of Cu(II), Cr(III), Co(II), Ni(II) and Pb(II). Loading: 5 mg of Cu(II), Cr(II), Co(II), Ni(II), Pb(II) + 0.005 M Malic acid in 100 ml, pH 3.5. Elution: H₂O, 0.25 M HCl, 1.5 M HCl and 2.0 M HNO₃ solution.

and without CTMAB. The results indicate the formation of a 1:2 complex between Co(II) and 2HB-5NPH with or without CTMAB. An improvement in detection limit achieved upon the addition of CTMAB. The addition of CTMAB to the Co(II)-2HB-5NPH system results in a 1.24-fold improvement in the detection limit of the technique.

The molar absorptivities in presence of CTMAB found by least-squares analysis of 10 measurements, was $6.5 \times 10^4 \text{ mol}^{-1} \text{ cm}^{-1}$. Under the optimal conditions explained above, a

linear calibration curve obtained over the range $0.02\text{--}2.0 \text{ mg ml}^{-1}$ of Co(II) ions. The detection limit ($s/n=2$) was found to be 0.01 mg l^{-1} . The relative standard deviation for 0.5 mg l^{-1} of Co(II) was 1.2% ($n=5$).

The selectivity in the proposed method was investigated by determining 1.0 mg l^{-1} of Co(II) in the presence of various other ions. Interference was regarded as significant when it produced a difference of more than 3% in absorbance from that found with Co(II) ion alone. The results are given in Table 3. The results indicated that the

Table 4
Sensitivities of reagents for the spectrophotometric determination of Co(II)

Method	Detection limit ($\mu\text{g ml}^{-1}$)	λ_{max} (nm)	Reference
Dithizone	0.07	550	[22]
Nitroso-R-salt	0.0019	420	[23]
	0.0042	520	[23]
<i>o</i> -Nitroso-resorcinol	0.0025	430	[23]
Benzyl-2-pyridylketone-2-pyridyl-hydrazone	0.0016	510	[24]
2HB-5NPH	0.01	472	Present method

concentration range of 1.0–0.1 g ml⁻¹ for Pb²⁺, Ni²⁺, Cu²⁺ and Pd²⁺ are upper limits for interference. Therefore, it can be understood that the separation of Co(II) from the matrix is necessary prior to spectrophotometric determination. For this purpose, a column separation method was investigated.

3.3. Column separation method

The adsorption capacity to pH (Amberlite IRC-718 resin) profiles for Co(II), Zn(II), Ni(II) and Pb(II) are given in Fig. 2. Fig. 2 shows that adsorption depends apparently on the pH of the solution due to the competing protonation and complexation reactions of the functional group (iminodiacetic acid) of resin. The order for metal ion's adsorption capacity, as shown by adsorption percent at pH 3.5 (Fig. 2), is as follows: Cr(III) < Co(II) < Cd(II) < Zn(II) < Ni(II) < Pb(II) < Cu(II). The metal ions were found to be adsorbed into malic acid over the concentration range of 0.0025–0.0075 M (Fig. 3). The adsorption capacities of the resin toward metal ions were found to depend on the HCl and HNO₃ concentration of the sample solutions (Fig. 4). For Co(II) ion the capacity decreased gradually with increasing the HCl concentration from 0.1 to 0.5 M. In particular, adsorption capacity of Pb(II) ion did not change over the range 0.25–2.0 M HCl. However, the capacity for Pb(II), Zn(II) ion decreased with increasing HNO₃ concentration (Fig. 4).

The effect of flow rate of the sample loading through the column was studied over the range 0.5–2.0 ml min⁻¹. The adsorption of metal ions remains almost unchanged regardless of any change in the flow rate. In subsequent experiments a flow rate of 1.0 ± 0.2 ml min⁻¹ was maintained for both adsorption and elution. From the results presented in Figs. 3 and 4, HCl and HNO₃ solutions have been considered as an eluent for the separation of the synthetic metal solution. The column was equilibrated with acetic acid buffer of pH 3.5. 50 ml of a 0.05 M malic acid containing 5.0 mg of each metal ion was loaded onto the column (Fig. 5). Co(II) was eluted with 200 ml of 0.25 M HCl after loading

with 50 ml of sample solution. Then 200 ml of 1.5 M HCl and 300 ml of HNO₃ were used to elute Ni(II), Pb(II) and Cu(II).

The effluent of 150 ml of 0.25 M HCl was used directly for the spectrophotometric determination of Co(II) as the 2HB-5NPH complex at 473 nm and Cd(II), Cr(III), Ni(II), Pb(II) and Cu(II) concentration were analysed by atomic absorption spectrophotometry.

3.4. Comparison with some other reagent

2HB-5NPH compares well with the most sensitive and widely used reagents for the spectrophotometric determination of Co(II). The sensitivities of the various reagents are compared in Table 4.

4. Conclusion

The spectrophotometric determination method of Co(II) has been investigated after separation of Co(II) from the mixed ions using Amberlite IRC-718 resin. The complex between 2HB-5NPH and Co(II) in the presence of CTMAB is very stable and more sensitive than that in the absence of surfactant. The Co(II)-2HB-5NPH complex in CTMAB has an absorption maximum at 473 nm and obeys the Beer's law in the range of 0.02–1.5 mg l⁻¹. Molar absorptivity is 6.5 × 10⁴ mol⁻¹ cm⁻¹ l. Co(II) was separated as run 200 ml of 0.25 M HCl after loading with 50 ml of sample solution.

References

- [1] A. Sanz Medel, J.I. Garcia Alonso, *Anal. Chem.* 57 (1985) 1681.
- [2] W.L. Hinze, H.N. Singh, Y. Baba, N.G. Harvey, *Trends Anal. Chem.* 3 (1984) 193.
- [3] G.F. Yan, G.R. Shi, Y.M. Liu, *Anal. Chim. Acta* 264 (1992) 121.
- [4] I. Mori, Y. Fujita, K. Ikuta, Y. Nakahashi, K. Kato, N. Niwa, *Anal. Lett.* 22 (1989) 1969.
- [5] M. Falcon, J. Guiteras, D. Prat, *Talanta* 40 (1993) 17.
- [6] M. Katyal, Y. Dutt, *Talanta* 22 (1975) 151.
- [7] P. Jain, R.P. Singh, *Talanta* 29 (1982) 77.
- [8] Y.X. Fan, Y.X. Zheng, *Anal. Chim. Acta* 281 (1993) 359.

- [9] A. Afonso, J.J. Santana, F.G. Montelongo, *Analyst* 111 (1986) 327.
- [10] H. Yang, G. Zhang, L. Zhang, G. Liu, Z. Zhang, *Talanta* 43 (1996) 747.
- [11] V.A. Terente'v, R.K. Andreeva, *Zh. Analit. Khim.* 23 (1968) 1089.
- [12] G.S. Vasilikiotis, J. Stratis, *Anal. Chim. Acta* 75 (1975) 227.
- [13] M.P. San Andres, M.L. Marina, S. Vera, *Talanta* 41 (1994) 179.
- [14] M.A. Sanz, M.F. Fernandez, *Anal. Chem.* 58 (1986) 2161.
- [15] Y. Jinghe, W. Naixing, W. Yingjie, L. Weian, Z. Jie, *Spectrochim. Acta* 51A (1995) 177.
- [16] H.C. Gin, L. Hong, P.J. Mai, *Talanta* 41 (1994) 1357.
- [17] M. Tarek, M. Zaki, *Talanta* 37 (1990) 1091.
- [18] G.L. McIntire, *Crit. Rev. Anal. Chem.* 21 (1990) 257.
- [19] E. Pelizzetti, E. Pramauro, *Anal. Chim. Acta* 56 (1984) 1132.
- [20] M. Aihara, M. Arai, T. Taketatsu, *Analyst* 111 (1986) 641.
- [21] K.W. Cha, C.I. Park, *Talanta* 43 (1996) 1335.
- [22] M.V. Dawson, S.J. Lyle, *Talanta* 37 (1990) 443.
- [23] E.B. Sandell, *Colorimetric Determination of Trace Metals*, 3rd ed., Interscience, New York, 1965, p. 414.
- [24] R.B. Singh, H.L. Ray, B.S. Garg, R.P. Singh, *Talanta* 26 (1979) 898.

Quantitative separation of zinc traces from cadmium matrices by solid-phase extraction with polyurethane foam

Djane Santiago de Jesus ^a, Marcelo Souza de Carvalho ^b,
Antônio Celso Spínola Costa ^c, Sérgio Luis Costa Ferreira ^{c,*}

^a Centro Federal de Educação Tecnológica da Bahia, SSA-Bahia, Brazil

^b Instituto de Engenharia Nuclear, CNEN-Rio de Janeiro, Brazil

^c Universidade Federal da Bahia, Instituto de Química, 40170-290 Salvador Bahia, Brazil

Received 22 September 1997; received in revised form 22 December 1997; accepted 2 January 1998

Abstract

A system for separation of zinc traces from large amounts of cadmium is proposed in this paper. It is based on the solid-phase extraction of the zinc in the form of thiocyanate complexes by the polyurethane foam. The following parameters were studied: effect of pH and of the thiocyanate concentration on the zinc extraction, shaking time required for quantitative extraction, amount of PU foam necessary for complete extraction, conditions for the separation of zinc from cadmium, influence of other cations and anions on the zinc sorption by PU foam, and required conditions for back extraction of zinc from the PU foam. The results show that zinc traces can be separated from large amounts of cadmium at pH 3.0 ± 0.50 , with the range of thiocyanate concentration from 0.15 to 0.20 mol l⁻¹, and the shaking time of 5 min. The back extraction of zinc can be done by shaking it with water for 10 min. Calcium, barium, strontium, magnesium, aluminum, nickel and iron(II) are efficiently separated. Iron(III), copper(II) and cobalt(II) are extracted simultaneously with zinc, but the iron reduction with ascorbic acid and the use of citrate to mask copper(II) and cobalt(II) increase the selectivity of the zinc extraction. The anions nitrate, chloride, sulfate, acetate, thiosulphate, tartarate, oxalate, fluoride, citrate, and carbonate do not affect the zinc extraction. Phosphate and EDTA must be absent. The method proposed was applied to determine zinc in cadmium salts using 4-(2-pyridylazo)-resorcinol (PAR) as a spectrophotometric reagent. The result achieved did not show significant difference in the accuracy and precision (95% confidence level) with those obtained by ICP–AES analysis. © 1998 Elsevier Science B.V. All rights reserved.

Keywords: Zinc separation; Solid-phase extraction; Polyurethane foam; Cadmium matrices

1. Introduction

Zinc is frequently present at trace level in cadmium and their compounds. However, the spec-

* Corresponding author. Tel.: +55 71 2375784; fax: +55 71 2355166; e-mail:slcf@ufba.br

trophotometric determination of this element in these matrices is troublesome because many of the chromogenic reagents proposed also react with cadmium.

Numerous methods have been published for such determination. However, they are not simple and usually require extensive and laborious steps for the separation of zinc from cadmium, using procedures which involve: liquid–liquid extraction [1–6] of zinc or cadmium, ion exchange [7,8], and precipitation [9].

This paper proposes a method for the separation and determination of zinc in cadmium matrices based on solid-phase extraction (SPE) of zinc in the form of thiocyanate complexes by the polyurethane foam (PU foam).

The PU foam has been used as a solid sorbent on a wide variety of inorganic and organic compounds from different media. It was first proposed by Bowen [10] in 1970. Braun [11–13] and Palagyi [14] have described reviews about the use of PU foam in procedures of separation and preconcentration.

The use of PU foam for zinc extraction has been proposed by several authors [15–18]. The extraction mechanism of the zinc by the PU foam in the form of thiocyanate complexes has been studied by Moody et al. [15]. Maloney et al. [16] have proposed a procedure for simultaneous extraction of zinc, cobalt(II), iron(III) and cadmium(II) from thiocyanate medium by PU foam. Nickel is not extracted. Braun and Abbas [17] have proved that zinc, mercury and indium are extracted quantitatively by PU foam in the form of thiocyanates complexes. Hamza et al. [18] have used PU foam treated with dithizone for the extraction of zinc and bismuth.

Zinc(II) reacts instantaneously with 4-(2-pyridylazo)-resorcinol (PAR) [19,20] in the range of pH from 9.0 to 10.0, forming a complex with maximum absorption at 496 nm and molar absorptivity of $8.30 \times 10^4 \text{ l mol}^{-1} \text{ cm}^{-1}$. Cadmium(II) also reacts with PAR, forming a complex with absorption maximum at 510 nm and molar absorptivity of $8.12 \times 10^4 \text{ l mol}^{-1} \text{ cm}^{-1}$.

2. Experimental

2.1. Apparatus

Spectrophotometric measurements were made using a Varian Cary 1E spectrophotometer with matched 1.00-cm quartz cells.

An Applied Research Laboratories model 3410 minitorch sequential inductively coupled plasma spectrometer with an IBM PC-AT computer was used for ICP-AES analysis.

A Rigaku-B3 wavelength dispersive X-ray fluorescence spectrometer, with a rhodium tube operated at 40 kV and 30 mA, a LiF crystal, and a scintillation counter was used.

A 300 Analyser pH meter was used to measure the pH values.

A VKS-100 mechanical shaker, 100 cpm was used for shaking of the solutions.

2.2. Reagents

All reagents were of analytical-reagent grade unless otherwise stated. Doubly distilled water was used to prepare the solutions. The nitric acid and hydrochloric acid were of Suprapur quality (Merck). The laboratory glassware was kept overnight in a 5% nitric acid solution. Before being used the glassware was washed with doubly distilled water and dried in a dust-free environment.

Zinc solution ($10.00 \mu\text{g ml}^{-1}$) was prepared by diluting a $1000.00 \mu\text{g ml}^{-1}$ zinc solution (atomic absorption Aldrich) using a 5% hydrochloric acid solution.

Potassium thiocyanate solution (1.0 mol l^{-1}) was prepared by dissolving the reagent (Carlo Erba) in doubly distilled water.

Masking solution containing citrate and acid ascorbic (1.6%) was prepared by dissolving its sodium salts (Merck) in doubly distilled water.

4-(2-Pyridylazo)resorcinol solution (0.05% m/v) was prepared by dissolving a monosodium reagent (Merck) in doubly distilled water.

Buffer solution (pH 10.0) was prepared by mixing 42.0 g of di-sodium hydrogen carbonate and 53.0 g of sodium carbonate in 1 l of doubly distilled water.

Polyurethane foam: a commercial, open cell, polyether-type PUF (Vulcan of Brazil, VCON 202, 42% resilience and 10–12 cells/linear cm) was broken into small particles in a blender with doubly distilled water and used as described by Carvalho [21–23].

2.3. Separation procedure

It was added into a polypropylene flask the following reagents: 10.00 ml of zinc(II) cation solution in the mass range of 1.0–60.0 μg , 5.00 ml of 1.0 mol l^{-1} thiocyanate solution and 10.00 ml buffer solution. It was mixed and added the mass of 60 mg of comminuted PU foam (previously treated with 0.20 mol l^{-1} thiocyanate solution). Then the system was stoppered and mechanically shaken for 5 min. The PU foam was collected by vacuum filtration (filter paper $\phi = 2.0$ cm), washed with 0.2 mol l^{-1} KSCN solution, transferred to another polypropylene flask where zinc was, then, back extracted with 10.00 ml of doubly distilled water, after shaking for 10 min.

2.4. Spectrophotometric determination of zinc using PAR reagent

The following reagents were added into a volumetric standard flask of 10 ml: zinc(II) solution in the mass range of 0.40–10.0 μg , 2.50 ml of carbonate buffer and, 1.00 ml of PAR solution. Then, it was filled up with doubly distilled water and its absorbancy was measure at 496 nm.

3. Results and discussion

3.1. Effect of pH on the zinc sorption

The pH effect on the zinc sorption was studied. The results show that the extraction was maximum and constant in the range of pH from 2.0 to 10.0 as it can be seen in Fig. 1. The pH control was done using acetate buffer with pH 3.75–5.75, borate buffer pH 8.0 and carbonate buffer with pH 10.0. For pH 2.0, 3.0, and 12.0, solutions of hydrochloric acid and sodium hydroxide were used, respectively. The procedure proposed rec-

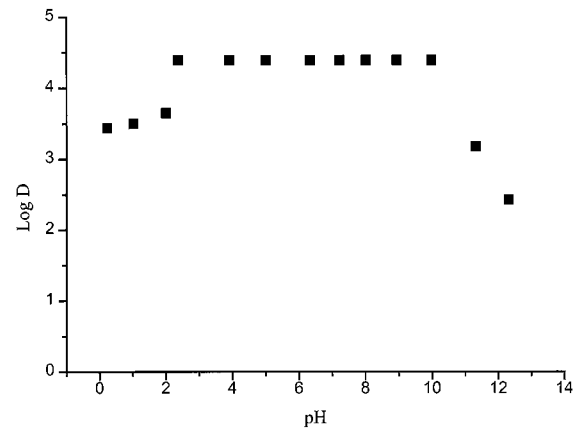


Fig. 1. Effect of pH on the zinc extraction.

ommends the extraction with the pH solution at 3.0 ± 0.5 because in such pH, cadmium is not extracted by the PU foam. At pH higher than 5.0, cadmium can also be extracted by the PU foam in the form of thiocyanate complexes.

3.2. Effect of the thiocyanate concentration on the zinc extraction

In order to test the thiocyanate concentration required for a quantitative extraction, 10.00 μg of zinc was extracted by PU foam changing the thiocyanate concentration from 0.02 to 2.00 mol l^{-1} . The results in Fig. 2 show that the extraction efficiency increases when the thiocyanate concen-

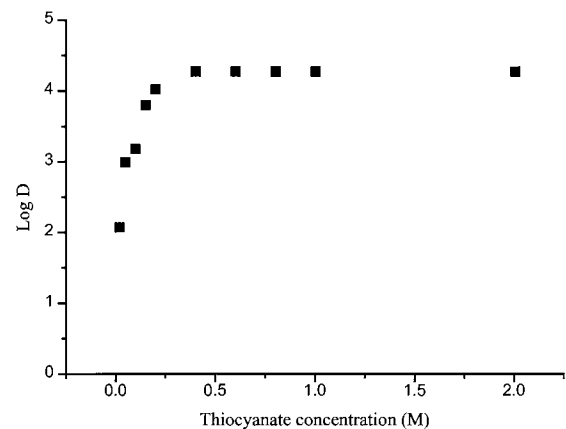


Fig. 2. Effect of thiocyanate concentration on the zinc extraction.

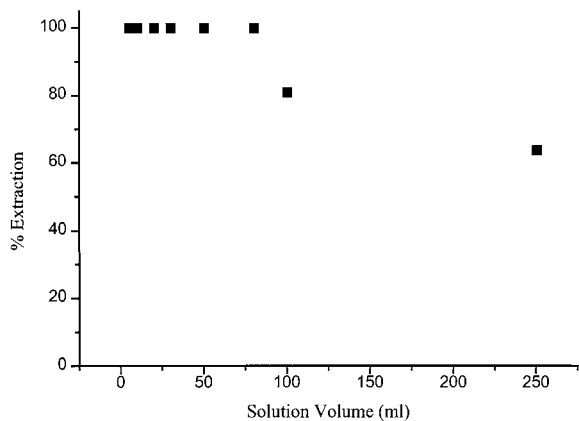


Fig. 3. Effect of the solution volume on the zinc extraction.

tration reaches a constant value over 0.15 mol l^{-1} KSCN, in which the system has the highest distribution coefficient ($D \geq 10^4$).

3.3. Effect of the solution volume on the zinc extraction

In order to evaluate the effect of the solution volume on the efficiency of zinc extraction were prepared several solutions with variable volumes of (5, 10, 25, 50, 80, 100, and 250 ml). All of them contained a fixed mass of $10.00 \mu\text{g}$ of zinc and the thiocyanate concentration of 0.20 mol l^{-1} . Then, zinc was extracted by using 55 mg of PU foam. The system was shaken for 10 min. The results show that the extraction was constant and quantitative for solutions in the range of volume from 5 to 80 ml. It can be seen in Fig. 3.

3.4. Effect of shaking time

The effect of the shaking time on the extraction efficiency was studied. The results show that 3 min are enough for a quantitative extraction of $10.00 \mu\text{g}$ of zinc and the thiocyanate concentration of 0.20 mol l^{-1} . In the procedure proposed, 5 min is recommended to guarantee a maximal extraction.

3.5. Amount of PU foam necessary for complete extraction

The effect of the amount of PU foam on the zinc extraction was also evaluated. It was found that 55 mg of PU foam is required as the minimal mass for a quantitative extraction of $60.00 \mu\text{g}$ of zinc.

Thus, PU foam in the range of mass from 55 to 65 mg is recommended to guarantee a complete extraction. This test was done using PU foam with a sorption capacity of 0.016 mmol of zinc/g of PU foam determined by the sorption isotherm [23].

3.6. Back extraction of zinc

Several solutions were tested for zinc back extraction by PU foam. The results show that zinc can efficiently be recovered using 10 ml of doubly distilled water, or 10 ml of ethanol solution (10% v/v), or 10 ml of nitric acid solution 0.10 mol l^{-1} , or 10 ml hydrochloric acid solution 0.10 mol l^{-1} . The back extraction with water was chosen because it was more convenient for spectrophotometric measurements. The carbonate buffer showed a poor result. Cadmium complexes are not back extracted with water and, in this case, a nitric acid solution must be used.

3.7. Zinc separation from cadmium

Zinc can be separated from large amounts of cadmium. However, at pH higher than 5.0 and the thiocyanate concentration up to 0.30 mol l^{-1} , cadmium in the form of thiocyanate complexes can also be extracted by the PU foam. Thus, the pH recommended for the separation of zinc from cadmium, is at 3.0 ± 0.50 and thiocyanate must be in the range of concentration from 0.15 to 0.20 mol l^{-1} . Table 1 show the pH effect on the separation of zinc from cadmium.

In order to test the separation procedure efficiency for spectrophotometric determination of zinc with PAR reagent, several amounts of zinc (2.00, 4.00, 8.00, 12.00, and $16.00 \mu\text{g}$) were mixed with $1000.00 \mu\text{g}$ of cadmium(II) and the procedure proposed in Section 2 was applied. The

Table 1
Separation of zinc (10.00 µg) in the presence of several amounts of cadmium

Cadmium present (µg)	Zinc extracted at pH 3.00	Cadmium extracted at pH 3.00	Zinc extracted at pH 5.0	Cadmium extracted at pH 5.0 (µg)
200.00	99%	<LD	99%	45.88 (22.94%)
500.00	98%	<LD	98%	72.39 (14.48%)
1000.00	99%	<LD	98%	199.0 (19.90%)
2000.00	98%	6.66 (0.33%)	90%	315.50 (15.78%)
3000.00	94%	11.59 (0.38%)	87%	358.10 (11.94%)
5000.00	90%	31.29 (0.63%)	85%	870.00 (17.40%)

LD, detection limit. PU foam amount: 60 mg [SCN⁻]: 0.20 mol l⁻¹.

Zn and Cd were back extracted with nitric acid solution and determined by ICP–AES.

amount of zinc recovered was plotted on the *y*-axis and the amount of zinc added on the *x*-axis. The linear equation resulted in the followings data: the angular coefficient was 1.022 ± 0.033 and the linear and correlation coefficient were 0.044 ± 0.125 and 0.9997, respectively. These data show the separation efficiency of the method proposed.

3.8. Separation of zinc from other elements

Solutions containing 10.00 µg of zinc(II) and different amounts of several cations were prepared and the efficiency of the separation procedure was tested. The results show that at pH 3.0 and thiocyanate concentration of 0.20 mol l⁻¹, 10 µg of zinc can be perfectly separated from 5.0 mg of the followings ions: aluminum(III), calcium(II), magnesium(II), strontium(II), iron(II), nickel(II), and barium(II). Iron(III), copper(II), cobalt(II), and zinc(II) are extracted simultaneously. However, the iron(III) reduction with ascorbic acid and the use of citrate to mask copper(II) and cobalt(II) increase the selectivity of the zinc separation. Mercury(II), gallium(III) and lead(II) ions are also extracted by the PU foam in this medium. Nevertheless, these ions are not back extracted with water. The anions nitrate, chloride, sulfate, acetate, tartarate, thiosulphate, oxalate, fluoride, citrate, and carbonate do not affect the zinc extraction by the PU foam. Phosphate and EDTA must be absent. In this experiment all determinations of those elements were done using ICP–

AES analysis and/or X-ray fluorescence spectrometry to measure directly metal thiocyanate complexes on the PU foam.

3.9. Application

The analytical curves for the zinc(II)–PAR system was done according to the procedure described in Section 2. The system showed a calibration sensitivity [24] of 1.355 ml µg⁻¹ for a dynamic interval of application from 60 ng ml⁻¹ to 1.00 µg ml⁻¹, detection limit of 20 ng ml⁻¹ and a variation coefficient of 0.84%.

The analytical characteristics of the separation procedure are summarized in the Table 2. They were done based on the zinc extraction from 0.20 mol l⁻¹ thiocyanate solutions at pH 3.0.

The method proposed was applied to zinc determination in several cadmium salts. The accuracy and precision achieved were not significantly different from 95% confidence level those obtained by ICP–AES analysis (Table 3).

Table 2
Analytical characteristics of the system Zn(II)–0.2 M KSCN–PU foam

Distribution coefficient	1.04×10^4 (l Kg ⁻¹)
Shaking time for extraction	5 min
Time for back extraction (water)	10 min
Sorption capacity of the PU foam	0.016 (mmols g ⁻¹)
Recovery range	98–101%
Coefficient of variation	1.35%

Table 3
Zinc determination in cadmium salts

Samples	Zn found (mg g ⁻¹ salt)	
	Proposed method	ICP method
CdSO ₄ ·8/3H ₂ O	1.96 ± 0.01	2.05 ± 0.02
CdSO ₄ ·8/3H ₂ O	3.90 ± 0.02	4.09 ± 0.04
Cd(H ₃ CCOO) ₂ ·2H ₂ O	5.57 ± 0.01	5.63 ± 0.09

4. Conclusions

Zinc can be easily extracted by the PU foam in a wide range of pH and large thiocyanate concentration. However, for the separation of zinc from cadmium the pH and the thiocyanate concentration are critical.

The zinc recovered from PU foam with water is ideal for application of the analytical technique of determination used.

The pH and thiocyanate concentration control as well as the use of masking agents allowed an efficient and simple zinc separation procedure from many others elements.

The solid-phase extraction has two typical advantages over the solvent extraction: avoiding the manipulation of organic solvents, which are frequently toxic and eliminating common problem of emulsions. The PU foam is also commercially available at low price.

The separation method proposed is opportune, considering that the spectrophotometric determination of zinc traces in cadmium matrices is troublesome, could be also applied for determination of zinc by other analytical methods.

Acknowledgements

The authors acknowledge the financial support of the CNPq, FINEP, FAPERJ and CAPES.

References

- [1] I.G. Shafran, T.K. Zelenova, V.I. Kazhdan, Sb. Statei, Vses. Nauchn.-Issled. Inst., Khim. ReaKt. Osobo Chist. Khim. Veshchestv., 24 (1961) 210. Chem. Abstr. 57 (1961) 1543h.
- [2] R. Wess, H. Flaschka, Microchem. J. 14 (1969) 318.
- [3] P.V. Marchenko, A.I. Veronina, Ukr. Khim. Zh. 35 (1969) 652.
- [4] C.W. McDonald, T. Rhodes, Anal. Chem. 46 (1974) 300.
- [5] A. Aleksandrov, M. Kamburova, Mikrochim. Acta II 1/2 (1976) 61.
- [6] T.F. Rudometkina, V.M. Ivanov, A.I. Busev, Zh. Anal. Khim., 31 (1976) 1945. Chem. Abstr. 85 (1976) 164748b
- [7] E.R. Baggott, R.C.W. Willcocks, Analyst 80 (1955) 53.
- [8] Z. Marczenko, Spectrophotometric Determination of Elements, Ellis Horwood, Chichester, 1976, pp. 601.
- [9] V.T. Chuiko, N.P. D'yachenko, Zh. Neorgan. Khim., 7 (1962) 903. Chem. Abstr. 57 (1962) 136b
- [10] H.J.M. Bowen, J. Chem. Soc. 1 (1970) 1082.
- [11] T. Braun, J.D. Navratil, A.B. Farag, Polyurethane Foam Sorbents in Separation Science, CRC Press, Boca Raton, FL, 1985.
- [12] T. Braun, A.B. Farag, Talanta 22 (1975) 699.
- [13] T. Braun, A.B. Farag, Anal. Chim. Acta 99 (1978) 1.
- [14] S. Palágyi, T. Braun, Separation and preconcentration of trace elements and inorganic species on solid polyurethane foam sorbents, in: Z.B. Alfassi, C.M. Wai (Eds.), Preconcentration Techniques for Trace Elements, CRC Press, Boca Raton, FL, 1992.
- [15] G.J. Moody, J.D.R. Thomas, M.A. Yarmo, Anal. Proc. 20 (1983) 132.
- [16] M.P. Maloney, G.J. Moody, J.D.R. Thomas, Analyst 105 (1980) 1087.
- [17] T. Braun, M.N. Abbas, Anal. Chim. Acta 134 (1982) 321.
- [18] G.A. Hamza, A.B. Farag, A. Amierh, Anal. Sci. 6 (1990) 889.
- [19] K. Mitsugu, J. Ueda, J. Chem. Soc. Jpn. Pure Chem. Sect. 91 (1970) 983.
- [20] S. Ahrland, R.G. Herman, Anal. Chem. 47 (1975) 2422.
- [21] M.S. Carvalho, DSc thesis, Pontificia Universidade Católica, Rio de Janeiro, Brazil, 1993.
- [22] M.S. Carvalho, J.A. Medeiros, A.W. Nóbrega, J.L. Mantovano, V.P.A. Rocha, Talanta 42 (1995) 45.
- [23] M.S. Carvalho, I.C.S. Fraga, K.C. Mateus Neto, E.Q. Silva Filho, Talanta 43 (1996) 1675.
- [24] J. Medinilla, F. Ales, F.G. Sanchez, Talanta 33 (1988) 329.

Adsorptive stripping voltammetric determination of antimony

Chang-li Zhou ^a, Yan Lu ^{b,*}, Xiu-ling Li ^b, Chuan-Nan Luo ^b, Zhen-wei Zhang ^b,
Jin-mao You ^a

^a Lanzhou Institute of Chemical Physics, Chinese Academy of Sciences, Lanzhou, 730000, China

^b Department of Applied Chemistry, Shandong Institute of Building Materials, Jinan, 250022, China

Received 27 August 1997; received in revised form 30 December 1997; accepted 5 January 1998

Abstract

A new method is described for the determination of antimony based on the cathodic adsorptive stripping of Sb(III) complexed with 2',3,4',5,7-pentahydroxyflavone(morin) at a static mercury drop electrode (SMDE). The reduction current of the adsorbed antimony complex was measured by 1.5th-order derivative linear-sweep adsorption voltammetry. The peak potential is at -0.51 V (vs. SCE). The effects of various parameters on the response are discussed. The optimized analytical conditions were found to be: supporting electrolyte, chloroacetic acid (0.04 mol/l, pH 2.3); concentration of morin, 5×10^{-6} mol/l; accumulation potential, -0.25 V (vs. SCE); scan rate, 100 mV/s. The limit of detection and the linear range were 7×10^{-10} mol/l and $1.0 \times 10^{-9} \sim 3.0 \times 10^{-7}$ mol/l Sb(III) for a 2-min accumulation time, respectively. This method has been applied to the determination of Sb(III) in steel and brass samples and satisfactory results were obtained. The adsorptive voltammetric characteristics and composition of the Sb(III)–morin complex were studied. © 1998 Elsevier Science B.V. All rights reserved.

Keywords: Voltammetry; 2',3,4',5,7-Pentahydroxyflavone(morin); Antimony; Steel; Brass

1. Introduction

The content of antimony in alloys has certain influences on its corrodibility, conductivity and tenacity, etc. Sensitive analytical methods to determine trace Sb(III) in alloys are needed for the study of materials sciences. Many methods for determining trace Sb are available, including spectrometry, fluorometry, etc. [1–3]. Electrochemically, antimony can be detected by polarography. In hydrochloric acid, the Sb(III) reduction wave is

located at -0.15 V, whereas in 1 mol/l sodium hydroxide it is at -1.25 V [4]. Hua and Gao [5] observed the Sb-hydrogen catalytic wave in an aqueous $\text{Na}_2\text{SO}_4\text{--CoSO}_4\text{--}(\text{C}_4\text{H}_9)_4\text{NBr}$ medium. This method may be used to determine Sb(III) in semiconductor materials at a level of 2.0×10^{-7} mol/l. In succinic acid buffer solution (pH 4), a complex polarographic wave which is formed by Sb(III) and cupferron was observed by Donoso. The detection limit of this AC polarographic method is 2.0×10^{-6} mol/l Sb(III) [6].

The development of adsorptive cathodic stripping voltammetry (ACSV) has allowed the determination of many trace metals including those

* Corresponding author.

that could not be determined by conventional anodic stripping voltammetry (ASV) [7–14]. ACSV has received increasing attention in recent years [15]. Apart from extending the scope of ASV, ACSV offers improved schemes for determination of metals which suffer from difficulties such as extreme redox potentials or poor selectivity. The first step in ACSV is the formation of the metal–ligand complex, followed by controlled interfacial accumulation of the complex onto the electrode during the depositing step and the reduction of the adsorbed metal complex by application of a negative going potential scan. The reduction current generated is a sensitive measure of the concentration of the metal. Thus, ligands that may be used for ACSV must form complexes with the metals of interest, the complexes thus formed must adsorb on the electrode and must be reducible. Several ligands including 8-hydroxyquinoline [7], *p*-dimethylaminophenyl-fluorone (*p*-DMPF) [8], gallic acid [9], and catechol [10] have been used to accumulate antimony as complexes by adsorption on the mercury electrode surface. It has been shown that antimony can be determined successfully in hair [8] and seawater [10] using one of these, but the sensitivity is not great and accurate analyses would require a deposition time of several minutes.

In our laboratory we have been investigating various preadsorptive voltammetric techniques utilizing a variety of organic complexing agents for trace and ultratrace metal determinations which both maximize sensitivity and selectivity [11,16,17]. We report here the trace determination of antimony by adsorptive cathodic stripping voltammetry (ACSV) using the complexing agent 2',3,4',5,7-pentahydroxyflavone (morin) [13]. We have found this technique to be both highly sensitive (detection limit of 7×10^{-10} mol/l with 2 min of accumulation time) and relatively unaffected by a variety of commonly interfering substances. The adsorptive voltammetric characteristics at a static mercury drop electrode (SMDE) were studied. This method has been applied to the determination of antimony in steel samples and satisfactory results were obtained.

2. Experimental

2.1. Apparatus

A model SDP-1 0.5th-order derivative polarograph (Jintan Analytical Instrument Factory) modified according to Ref. [18] (in order to add the 1.5th-order derivative technique mode) was used. It was coupled with a model LZ3-104 X–Y recorder (Shanghai Dahua Instrument Factory). The three-electrode system consisted of a model SH-84 SMDE (Department of Chemistry, Shandong University) as the working electrode, a platinum plate as the counter electrode and a SCE as the reference electrode. A model UV-3000 UV–visible spectrophotometer (Shimadzu) was used for spectrophotometry.

2.2. Reagents and solutions

A 1×10^{-2} mol/l stock solution of morin was prepared by dissolving an appropriate amount of morin (analytical-reagent grade) in ethanol (guarantee reagent). Solutions of other concentration for experiments were obtained by diluting the stock solution with ethanol. A 1×10^{-2} mol/l stock of antimony(III) was prepared by dissolving an appropriate amount of Sb_2O_3 (high purity

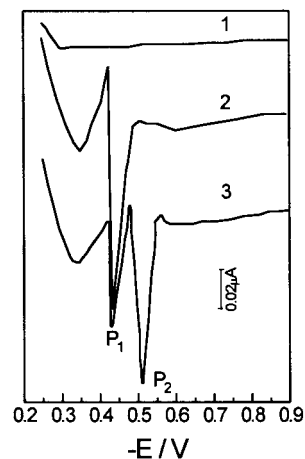


Fig. 1. 1.5th-order derivative plot: 0.4 mol/l chloroacetic acid–0.01 mol/l NaOH (pH = 2.3); $E_a = -0.25$ V; $t_a = 120$ s; $t_r = 30$ s; $v = 100$ mV/s; (1): 1×10^{-7} mol/l Sb(III); (2): 5×10^{-6} mol/l morin; (3): (1) + (2).

reagent) in a small amount of HCl and diluting with 1 mol/l of HCl solution. Standard solutions were obtained by diluting the stock solution with 1 mol/l HCl solution. Chloroacetic acid and NaOH were of analytical-reagent grade. All solutions were prepared using doubly distilled water.

2.3. Procedure

The supporting electrolyte was 0.04 mol/l chloroacetic acid–0.01 mol/l NaOH. The solution containing Sb(III) and morin was deaerated for 10 min with pure nitrogen. The measurements were carried out after a preconcentration step, in which the solution was stirred during an accumulation time, t_a of 2 min at an accumulation potential E_a . After a rest period of 30 s, the response curve was recorded by scanning the potential in the negative direction with the 1.5th-order derivative technique. Each measurement was performed with a fresh drop with an area of the SMDE of 2.23 mm². All potentials were measured against the SCE.

3. Results and discussion

3.1. Adsorptive voltammetric characteristics of the Sb(III) complex with morin

In a solution of 0.04 mol/l chloroacetic acid–0.01 mol/l NaOH (pH 2.30), no peak of 1×10^{-7} mol/l Sb(III) appears (Fig. 1(1)), but a peak (p_1) appears in the linear-sweep voltammogram of morin for $E_a = -0.25$ V at $t_a = 2$ min (Fig. 1(2)). The peak potential, E_{p1} , is -0.43 V. When a micro amount of Sb(III) is added to the solution containing morin, a new peak, p_2 , appears at a potential of -0.51 V (Fig. 1(3)). It seems reasonable to assume that the new peak results from the Sb(III) complex with morin. The peak-to-peak value of the 1.5th-order derivative plot, e'_{pp} , for p_2 is more sensitive than the peak current on the voltammogram of the reduction of the complex, i_p , so that all the measurements were performed using the 1.5th-order derivative technique. e'_{pp} of p_2 increases with the concentrations of Sb(III) and the e'_{pp} of p_1 decreases. When the concentration of

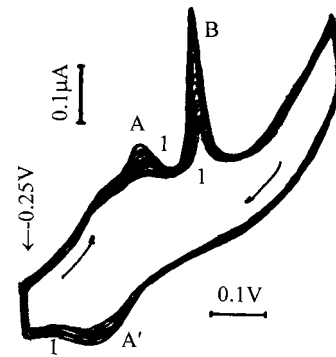


Fig. 2. Repetitive cyclic voltammograms for 8×10^{-6} mol/l morin (A,A') with 1×10^{-6} mol/l Sb(III) (B) in unstirred 0.04 mol/l chloroacetic acid–0.01 mol/l NaOH (pH 2.3) solution. Conditions: scan rate, 100 mV/s; equilibrium, 30 s. The first scan is indicated by the number 1. Total time for the successive scans is 5 min.

Sb(III) is over 4×10^{-7} mol/l, the peak of morin, p_1 disappears. This means that the property of the free morin is not same as the morin in the Sb–morin complex; the latter is not reduced at potential of -0.43 V.

Fig. 2 shows cyclic voltammograms for 5×10^{-6} mol/l morin recorded in the presence of 1×10^{-6} mol/l Sb(III) in an unstirred 0.04 mol/l chloroacetic acid–0.01 mol/l NaOH (pH 2.3) buffer solution. The cathodic peak current of the Sb–morin complex (peak B) at -0.51 V gradually increases with repetitive scans while the current of the free ligand morin (peak A) at -0.43 V simultaneously decreases. Since e'_{pp} values of different concentrations are not the same for long accumulation time, the complex on the surface of electrode should not reach saturation in this case. A peak is observed in the anodic branch. The peak A' which has correspondence to the ligand peak A at -0.31 V was observed to decrease with repetitive scans. The anodic peak of Sb–morin complex is not observed. This means the interfacial electrochemical reduction of the complex is an irreversible process.

The effect of e'_{pp} with accumulation time is shown in Fig. 3A for two different Sb(III) concentrations. Both curves show initially linear behaviour, with the curve of higher concentration showing saturation more rapidly. The i_p and e'_{pp}

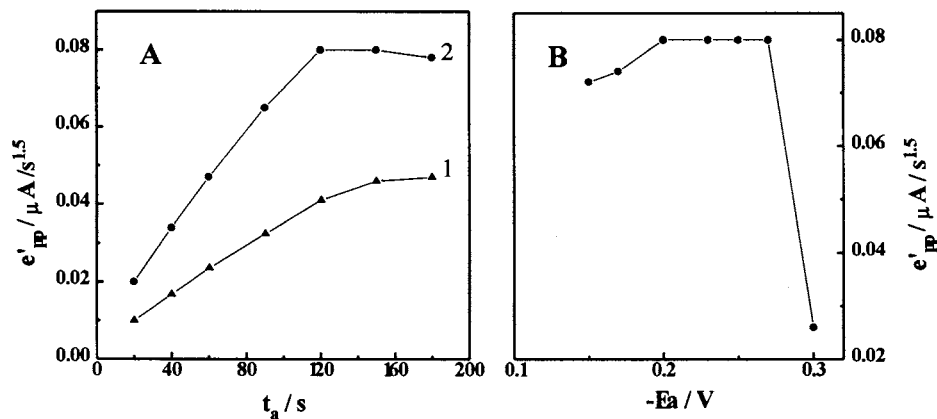


Fig. 3. The effect of accumulation time (A) and potential (B) on the e'_{pp} of the Sb(III)–morin complex. A, 1, 5×10^{-8} mol/l Sb(III); A, 2, 1×10^{-7} mol/l Sb(III). Other conditions as in Fig. 1.

are proportional to the potential scan rate, v , and $v^{2.5}$, respectively. These results are characteristic of the reaction of adsorbed reactants on the electrode [19–21].

Fig. 4 shows the drop-time curves of the supporting electrolyte and that of solutions of morin and its complex with Sb(III). When morin is added to the supporting electrolyte, the drop-time decreases in the potential range from +0.1 to –1.1 V. In the presence of both morin and Sb(III), the shape of the drop-time curve is similar

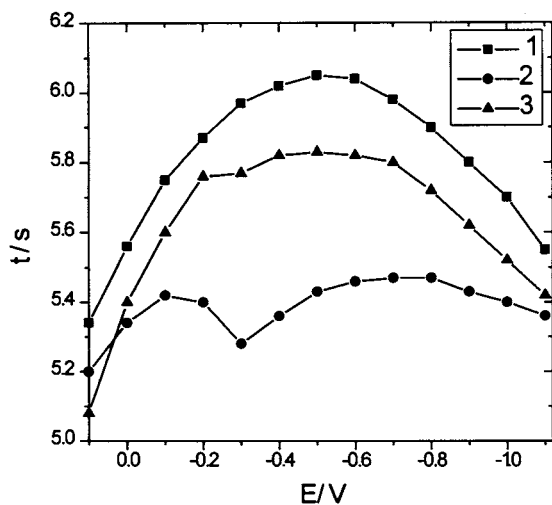


Fig. 4. Drop-time curves. (1): 0.04 mol/l chloroacetic acid–0.01 mol/l NaOH; (2): (1) + 1×10^{-4} mol/l morin; (3): (2) + 1×10^{-4} mol/l Sb(III).

to that of morin alone, but the curve is higher in the potential range from 0.0 to –1.1 V. These phenomena demonstrate the adsorptivity of morin and Sb(III) complex with morin.

3.2. The composition of Sb–morin complex

The absorbance maxima of morin are located at 250 and 340 nm for absorption spectra in 0.04 mol/l chloroacetic acid–0.01 mol/l NaOH. When Sb(III) is added to the solution, a new absorbance peak at 420 nm appears and its intensity increases with concentration of Sb(III) until the maximum absorbance is reached at a ratio of 1:3 Sb(III) to morin (L). This is evidence for the formation of the complex of 1:3 composition, viz, SbL_3 . The value of e'_{pp} for the reduction of the complex adsorbed also has a maximum, when the ratio of the concentration of Sb(III) to that of morin is 1:3. This means that the complex in the bulk of the solution and the complex adsorbed on the surface of the electrode have the same composition.

3.3. Parameters affecting the adsorptive stripping behaviour

To check the applicability of the adsorption preconcentration behaviour of the Sb–morin complex at the SMDE for the determination of Sb(III) by ACSV, different parameters were investigated.

Table 1

Results of the determination of antimony in samples and recoveries of Sb(III) added to the brass samples

Sample	Antimony content ($\mu\text{g/g}$)			Relative standard deviation	Recovery (%)
	Standard	Found	Mean		
Steel-231	13.0	12.8, 13.2 14.1, 13.8 12.6, 12.9	13.3	5.8	
Steel-224B	25.0	23.8, 24.7 23.6, 24.5 24.9, 23.8	24.2	4.1	
Brass		32.5, 31.6 33.2, 31.9 31.8, 32.4	32.2	1.8	97.3

The dependence of e'_{pp} on the accumulation time, t_a , was examined for samples containing 5×10^{-8} mol/l (Fig. 3A,1) and 1×10^{-7} mol/l (Fig. 3A,2) Sb(III) in the range 0 ~ 180 s. The maximum peak height was observed at 120 s and 160 s for 1×10^{-7} mol/l and 5×10^{-8} mol/l Sb(III), respectively. Fig. 3B shows the effect of accumulation potential E_a on the e'_{pp} of the peak of the Sb–morin complex. The largest peak current was obtained in the range of $-0.2 \sim -0.27$ V and the e'_{pp} decreased at more negative potentials. The effects of pH on the e'_{pp} and E_{p2} of the Sb–morin complex were studied. Maximum peak current was reached in the pH range 2.2–2.4. The peak potential, E_{p2} , of Sb–morin complex was observed to shift linearly to more negative potential with increasing pH. The relationship of E_{p2} with pH is $E_{p2} = -0.39 - 0.05\text{pH}$. The morin concentration had a pronounced effect on the adsorptive stripping response. e'_{pp} increases linearly with the morin concentration at a concentration of less than 3×10^{-6} mol/l. The e'_{pp} tended to remain constant at a concentration of more than 3×10^{-6} mol/l.

3.4. Analytical application

It was found experimentally that the optimum composition of the supporting electrolyte is 0.04 mol/l chloroacetic acid–0.01 mol/l NaOH (pH 2.30); the optimum concentration of morin is

5×10^{-6} mol/l and the optimum accumulation potential is -0.25 V. Under these conditions, the linear range and the detection limit of 1.5th-order derivative linear-sweep adsorption voltammetry are $1.0 \times 10^{-9} \sim 3.0 \times 10^{-7}$ mol/l and 7.0×10^{-10} mol/l, respectively, when the accumulation time was 120 s. Reproducibility tests on 11 results at 1×10^{-7} mol/l Sb(III) showed a relative standard deviation of 3.2%.

Solutions containing 5×10^{-8} mol/l antimony and various amounts of foreign ions were prepared and measured according to the above procedure. The experimental results show that a 1000-fold excess of Ca^{2+} , Mg^{2+} , Co^{2+} , Ni^{2+} , Mn^{2+} , Ge^{4+} , Fe^{3+} , Fe^{2+} , Al^{3+} , a 600-fold excess of Zn^{2+} , Cd^{2+} , Cu^{2+} , a 120-fold excess of Cr^{3+} , V^{5+} , Sn^{4+} , a 30-fold excess of Bi^{3+} , a 10-fold excess of Ti^{4+} , a 2-fold excess of Pb^{2+} did not interfere with the determination of Sb(III) under the experimental conditions.

Standard steel samples (ca. 0.4 g) were dissolved with 20 ml of HCl (1 + 1) in a beaker [22,23], then 15 ml of HCl (5 + 1), 10 ml of 5% manganese sulfate solution and 150 ml of water were added. After boiling, 16 ml of 4% potassium permanganate solution was added and boiled for 2 min. The solution was allowed to settle for 5 min and filtered using quantitative filter paper. The precipitate was washed with hot water four times and dissolved with a solution of 8 ml HCl and 2 ml 30% H_2O_2 in a beaker. The solution

obtained by dissolving the precipitate was heated slowly until a large number of bubbles appeared, then the solution was boiled for 1 min. After cooling, the solution was diluted with hydrochloric acid (5 + 1) to 50 ml in a 50-ml volumetric flask and mixed thoroughly.

Samples of brass (ca. 0.4 g) were dissolved with 5 ml of nitric acid (1 + 1) in a beaker. When 10 ml of 8 mol/l sulfuric acid was added to the beaker, the solution was heated to dispossess nitrate radical and boiled to a paste. The same steps as above were followed.

A suitable volume was taken from the flask and transferred into a cell, and the pH of the solution adjusted with sodium hydroxide; the 1.5th-order derivative plot of current was recorded using the above procedure. 1.5th-order derivative plots of current were also recorded for the solution after adding a standard solution of Sb(III) to the sample solution under the same conditions. The amount of antimony in the sample solution can thus be determined from the resulting standard addition plot. Typical results obtained were summarized in Table 1.

References

- [1] H.R. Hovind, *Analyst* 100 (1975) 769.
- [2] V. Stara, *Talanta* 18 (1971) 228.

- [3] R.D. Jee, *Analyst* 113 (1988) 1321.
- [4] I.M. Kolthof, J.J. Ligane, *Polarography*, Interscience, London, 1952, p. 545.
- [5] H.Z. Hua, W. Yun, X.X. Gao, *Scientia Sinica (China)* 12 (1963) 1588.
- [6] G. Donoso N., M.A. Santa Ana V., I. Chadwick W., *Anal. Chim. Acta* 42 (1968) 109.
- [7] X.Y. Wei, *Mtall. Anal. (China)* 2 (1984) 24.
- [8] X.L. Zhang, C.S. Ma, L.Z. Wang, J.G. Zhang, *Talanta* 42 (1995) 897.
- [9] Y.H. Li, W.K. Yao, S.L. Tang, *Chem. J. Chin. Univ.* 5 (1991) 607.
- [10] A. Kumar, R.S. Agarwal, M. Jain, *Chim. Acta Turc.* 18 (1990) 493.
- [11] L.J. Qu, W.R. Jin, *Anal. Chim. Acta* 274 (1993) 65.
- [12] P.A.M. Farias, A.K. Ohara, *Electroanalysis* 3 (1991) 985.
- [13] P.A.M. Farias, C.M.L. Martins, A.K. Ohara, J.S. Gold, *Anal. Chim. Acta* 293 (1994) 29.
- [14] J. Wang, J. Mahmoud, J. Zadeiz, *Electroanalysis* 1 (1989) 229.
- [15] M.D. Ryan, E.F. Bowden, J.Q. Chambers, *Anal. Chem.* 66 (1994) 369R.
- [16] C.L. Zhou, T.Y. Gao, L.J. Qu, *Fenxi Shiyanshi* 4 (1992) 13.
- [17] C.L. Zhou, J.M. You, J.X. Su, *Fenxi Huaxue* 11 (1997) 1337.
- [18] G.J. Lin, W.R. Jin, *Fenxi Shiyanshi* 2 (1990) 56.
- [19] E. Laviron, *J. Electroanal. Chem.* 52 (1974) 355.
- [20] A.P. Brown, F.C. Anson, *Anal. Chem.* 49 (1977) 1589.
- [21] W.R. Jin, H. Cui, L.X. Zhu, S.R. Wang, *J. Electroanal. Chem.* 309 (1991) 37.
- [22] L.S. Shao, *Separation and Complex Compounds Analysis*, Higher Education Publishing House, China, 1984, p. 74.
- [23] S.G. Lin, *Metallurgy Chemical Analysis*, Metallurgical Industry Publishing House, China, 1981, p. 563.

Development and validation of a reversed phase HPLC method for quantitative analysis of bis-isoxazolylnaphthoquinone

Cristina S. Ortiz, María M. de Bertorello *

Departamento de Farmacia, Facultad de Ciencias Químicas, Universidad Nacional de Córdoba A.P. 4, C.C. 61-5000 Córdoba, Argentina

Received 8 September 1997; received in revised form 5 January 1998; accepted 6 January 1998

Abstract

The goal of this study was to determine the kinetic parameters involved in the decomposition of 2-(5-methyl-4-isoxazolylamino)-*N*-(5-methyl-4-isoxazolyl)-1,4-naphthoquinone-4-imine (**1**) in aqueous solution and to identify the main degradation products. An isocratic HPLC assay was used to study the degradation rate of **1**. The products of hydrolysis were identified by comparison of their retention times with those of authentic samples. The amount of **1** and the two degradation products resulting from storage of **1** in various buffer solutions was followed in function of time by a reversed-phase HPLC stability-indicating method. The observed degradation rates followed pseudo-first-order kinetics at constant pH, temperature and ionic strength. The log *k*–pH-profile was constructed at 35°C from the first-order rate constants obtained from studies at pH values ranging from 0.88 to 10.80 ($\mu = 0.5$ M). Hydrolysis in the acidic and alkaline media resulted in the formation of two degradation products in each case. The pH-rate profile of **1** in buffer solution was adequately described using a four-term rate equation. The obtained pH-rate profile indicated specific acid–base catalysis with a region of maximum stability between pH 6.40 and 7.40 which can be adequate for formulations of **1**. © 1998 Elsevier Science B.V. All rights reserved.

Keywords: Isoxazolylnaphthoquinone; Degradation; Stability; Kinetics; pH-Profile

1. Introduction

The isoxazolylnaphthoquinones are a family of compounds that show important biological properties [1–6]. The preliminary results obtained with 4-aminoisoxazolyl-naphthoquinones against *Sta-*

phylococcus aureus [7] were so excellent that we focused our interest on 2-(5-methyl-4-isoxazolylamino)-*N*-(5-methyl-4-isoxazolyl)-1,4-naphthoquinone-4-imine (**1**), a derivative with 4-aminoisoxazol in positions 2 and 4 of the naphthoquinone ring.

Previous studies [8–10] have demonstrated that isoxazolylnaphthoquinones with the amino group in the 4-position of the isoxazole ring decompose in aqueous solution to give degradation products

* Corresponding author. Tel.: + 54 51 334163; fax: + 54 51 334174; e-mail: marcor@dgo.uncor.edu

with very similar structures, which required selective methods of analysis as HPLC.

Stability indicating analytical methods are of fundamental importance in stability studies. One part of the analytical method development is validation; once the method has been selected it is necessary to evaluate it under the conditions expected for real samples before being used for a specific purpose. It is essential to use well-characterized and fully validated analytical methods which yield reliable results that can be satisfactorily interpreted.

The objective of the present study was to determine the stability of **1** in aqueous solutions by HPLC. These data are necessary in the pharmaceutical field, since knowledge of solvent, pH, temperature, or a combination of these parameters under which drug substances are unstable, help to avoid degradation in drug formulation, storage, and some analytical conditions.

2. Experimental

2.1. Materials

The derivatives [2-(5-methyl-4-isoxazolylamino)-*N*-(5-methyl-4-isoxazolyl)-1,4-naphthoquinone-4-imine] (**1**), [*N*-(5-methyl-4-isoxazolyl)-4-amino-1,2-naphthoquinone] (**2**), and [2-hydroxy-*N*-(5-methyl-4-isoxazolyl)-1,4-naphthoquinone-4-imine] (**4**), were synthesized and purified according to a method previously reported [11,12]. The 9,10-anthraquinone (**5**) was purchased from E. Merck and

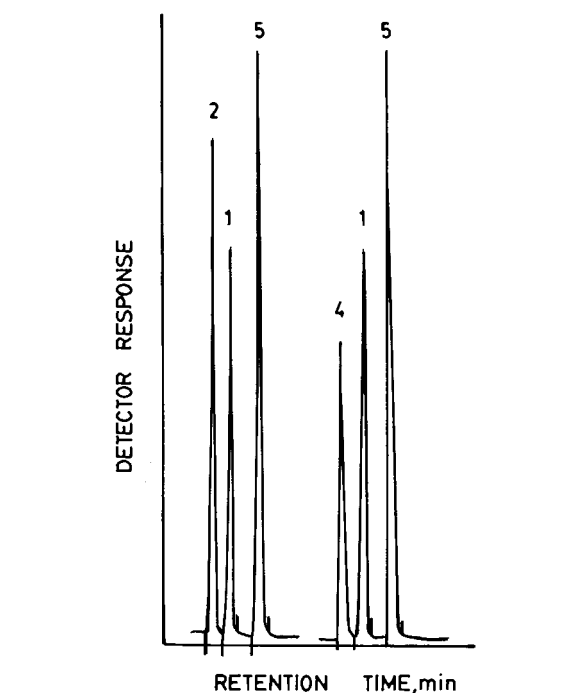


Fig. 1. HPLC chromatograms showing the separation of degradation products **2** and **4** from the peaks **1** and **5**.

purified by successive sublimation [13]. All the other chemicals, including buffer components, were of analytical-reagent grade. Hydrochloric acid, citric acid, sodium hydrogen phosphate, potassium dehydrogen phosphate, sodium hydroxide and sodium hydrogen carbonate buffer solution with varying pH were used in all experiments [14]. These solutions were adjusted to a total ionic strength (μ) of 0.5 M with sodium chloride [15].

Table 1
Statistical analyses from calibration data at 241 nm in methanol for compounds **1**, **2** and **4**

	Slope (SD) $\times 10^{+2}$	Intercept $\times 10^{+3}$	r^a	LOD $\times 10^{+2}$ ($\mu\text{g ml}^{-1}$) ^b	LOQ $\times 10^{-2}$ ($\mu\text{g ml}^{-1}$) ^c
1	8.30 (0.02)	4.7	0.9999	2.2	6.3
2	5.42 (0.04)	7.9	0.9998	3.0	8.2
4	7.97 (0.09)	-18	0.9996	6.3	17

^a Correlation coefficient.

^b Detection limit.

^c Quantification limit.

Table 2
Average recovery of compound **1**

1 ($\mu\text{g ml}^{-1}$)	Recovery ^a (%)	\pm CV
3.1	103.8	1.7
6.1	106.0	1.2
12.2	103.2	1.2
18.4	102.45	0.48

^a Mean of five determinations.

Methanol of HPLC-grade was supplied by Sintorgan[®] (Buenos Aires, Argentina). Distilled-deionized water with a Milli Rho Milli-Q System was used for the preparation of all the solutions and the mobile phase.

2.2. HPLC system

The HPLC system consisted of a solvent delivery pump (Konik 500G), a 150×4 mm column packed with $5.0 \mu\text{m}$ octadecylsilane (MicroPak MCH-5-Varian), an UV detector (UVIS-200 variable-wavelength) and a Konik model SP-4290 Integrator.

A flow-rate of 0.9 ml min^{-1} was maintained and the effluent was monitored at 241 nm with a detector sensitivity of 0.02 AUFS.

The mobile phase consisted of methanol:water (75:25 v/v), and the mixture was filtered through a $0.45 \mu\text{m}$ pore nylon membrane (Schleicher and Schuell) and deaerated under reduced pressure. All the analyses were performed under isocratic conditions at room temperature.

The sample volume was $20 \mu\text{l}$ (Rheodyne Model 7125 injector fitted with a $20 \mu\text{l}$ loop).

2.3. Other instruments

All analytical weighings were performed with an Electrobalance model G with a sensitivity of 2×10^{-4} mg (Cahn Instrument, CA). A pH meter (Orion Model SA 520) fitted with combination electrodes was used for all pH measurements. The pH meter was standardized with the combination of standard buffer solutions at room temperature.

For the kinetic measurements, a constant tem-

perature bath was regulated by a Haake F₃ thermostat with $\pm 0.1^\circ\text{C}$ precision.

2.4. Kinetic method

Sample solutions were prepared by dissolving **1** in suitable amounts of methanol and adjusting to volume (25 ml) with the appropriate buffer, sonicated until completely dissolved, and then 1.8 ml aliquots of these solutions were transferred to 14 tightly closed snap test-tubes. The reaction flasks were immediately placed in a water bath maintained at $35 \pm 0.1^\circ\text{C}$ for up to 7 h. At appropriate time intervals, two flasks were removed from the water bath and 1 ml aliquots of the reaction mixture were added to the volumetric flask containing the internal standard stock solution and immediately brought to a known volume with these solutions in order that the analytical concentration were within the linear range of detection. A fixed volume ($20 \mu\text{l}$) of these samples was injected onto a reversed-phase column at room temperature. Concentration of **1** was determined in duplicate by a stability indicating HPLC method.

2.5. Ionic strength effect studies

The effect of the ionic strength on the hydrolysis of **1** was determined by keeping the pH, buffer concentration, drug concentration and temperature constant, and varying only the ionic strength by addition of different amounts of sodium chloride.

3. Results and discussion

3.1. Analytical results-chromatograms

The 9,10-anthraquinone (**5**) was used as an internal standard for quantification purposes; a stock solution ($3.70 \times 10^{-5}\text{M}$) was prepared in methanol and stored at $+4^\circ\text{C}$ for a maximum period of 24 h. The use of internal standard reduces the variability due to transient changes in the detector sensitivity as well as HPLC column

Table 3
Average recovery of **1** in the presence of degradation products **2** and **4**

Compound	($\mu\text{g ml}^{-1}$)			Recovery ^a % (CV)		
	1	2	4	1	2	4
	3.1	8.2	—	102.49 (0.90)	105.9 (1.7)	—
	3.1	—	8.5	103.94 (0.76)	—	99.5 (1.2)
	6.1	8.2	—	106.52 (0.92)	105.53 (0.83)	—
	6.1	—	8.5	104.80 (0.63)	—	98.4 (1.6)
	12.2	8.2	—	103.60 (0.59)	105.64 (0.74)	—
	12.2	—	8.5	107.2 (1.8)	—	98.5 (1.7)
	18.4	8.2	—	101.80(0.90)	103.6 (1.3)	—
	18.4	—	8.5	106.8 (1.0)	—	96.4 (1.7)

^a Mean of five determinations.

performance since both the internal standard and analytes will exhibit parallel responses at the same time.

The choice of **5** as internal standard for chromatography was based on the fact that it is

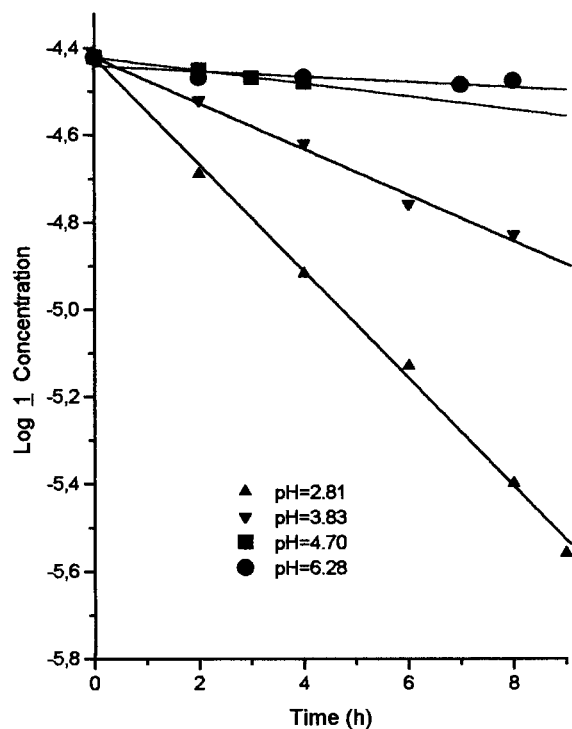


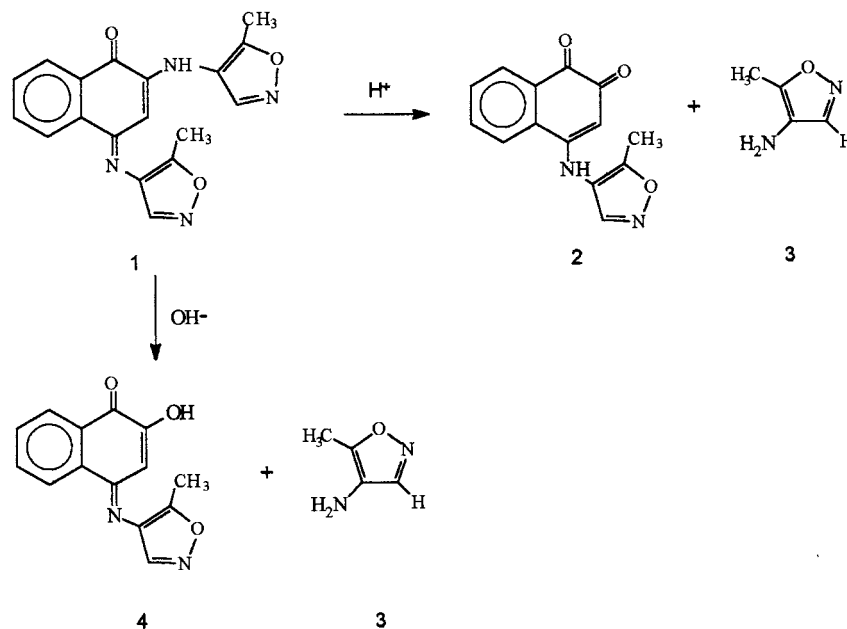
Fig. 2. Pseudo-first-order degradation of **1** at various pH values, 35°C and $\mu = 0.5$.

structurally similar to the compound of interest, elutes close and after the retention time to the peak drug of **1** and its degradation products, and is stable in methanol.

Fig. 1 shows a typical chromatogram obtained using authentic samples under the described analytical conditions. The chromatograms show the separation of the degradation products peaks and the drug peak with an excellent selectivity and peak shape for compounds **1** (peak 1; retention

Table 4
Buffer systems, observed rate constant, t_{90} and $t_{1/2}$ for the degradation of **1**

pH	Buffer system	$10 k_{\text{obs}}$ ($\text{h}^{-1} \pm \text{SD}$)	t_{90} (h)	$t_{1/2}$ (h)
0.88	C1H:C1K	2.52 ± 0.003	0.42	2.75
1.14	C1H:C1K	2.45 ± 0.004	0.43	2.83
1.48	C1H:C1K	2.76 ± 0.002	0.38	2.51
2.81	Ac·Cit:Na ₂ HPO ₄	2.85 ± 0.003	0.37	2.43
3.88	Ac·Cit:Na ₂ HPO ₄	1.22 ± 0.003	0.86	5.68
4.70	Ac·Cit:Na ₂ HPO ₄	0.40 ± 0.001	2.63	17.32
5.48	Ac·Cit:Na ₂ HPO ₄	0.10 ± 0.001	10.50	69.30
6.28	Ac·Cit:Na ₂ HPO ₄	0.07 ± 0.001	15.00	99.00
6.85	Ac·Cit:Na ₂ HPO ₄₀	0.08 ± 0.001	13.13	86.63
7.10	NaOH:KH ₂ PO ₄	0.09 ± 0.002	11.67	77.00
7.40	NaOH:KH ₂ PO ₄	0.07 ± 0.001	15.00	99.00
8.15	NaOH:KH ₂ PO ₄	0.09 ± 0.002	11.67	77.00
8.97	NaOH:NaHCO ₃	0.59 ± 0.003	1.78	11.75
9.66	NaOH:NaHCO ₃	0.89 ± 0.009	1.18	7.79
10.30	NaOH:NaHCO ₃	8.65 ± 0.001	0.12	0.80
10.80	NaOH:NaHCO ₃	9.05 ± 0.004	0.12	0.77



Scheme 1.

time, 4.61 min.), **2** (peak 2; retention time, 2.69 min), **4** (peak 4; retention time, 2.03 min.) and internal standard **5** (peak 5; retention time, 7.75 min). These results permitted the analysis of intact **1** in the presence of its hydrolytic degradation products.

The identity of **2** and **4** was verified by comparison of their retention time with that of authentic samples.

A total chromatographic time of 15 min, including post-run-re-equilibration time, was needed.

3.2. Method validation

The essential parameters to ensure the acceptability of the performance of an analytical method are sensitivity, repeatability, reproducibility, precision, percent recoveries, minimum detectable quantity, minimum detectable concentration, limit of detection and limit of quantitation [16–21].

The linearity of the analytical method was determined by mathematical treatment of the results obtained by analysis of eight standard solutions with varying concentrations of analyte. The regression line was calculated by the least-squares

method of peak area ratio versus analyte concentrations. The regression equations derived from the least-squares method, the correlation coefficients, limits of detection (LOD) and limits of quantification (LOQ) are shown in Table 1. The statistical data evidences the negligible scatter of the experimental points with respect to the regression line. Relative response factors were calculated from the slopes of the corresponding calibration curves. Triplicate samples were run for each concentration.

The range of the analytical method for compounds **1**, **2** and **4** was determined and expressed as 0.8–28.4 $\mu\text{g ml}^{-1}$.

The sensitivity of the method was calculated for each derivative as the slope of the calibration line; the results obtained were 8.3×10^{-2} , 5.42×10^{-2} and 7.97×10^{-2} $\mu\text{g ml}^{-1}$ for **1**, **2** and **4** respectively. These results demonstrate the suitability of the method to measure small decreases in the active ingredient.

The repeatability of the chromatographic procedure was assessed within short intervals of time at a concentration of 12.00 $\mu\text{g ml}^{-1}$. The CV using peak area concentration measurement was $\sim 1.8\%$ (nine injections). Under these condi-

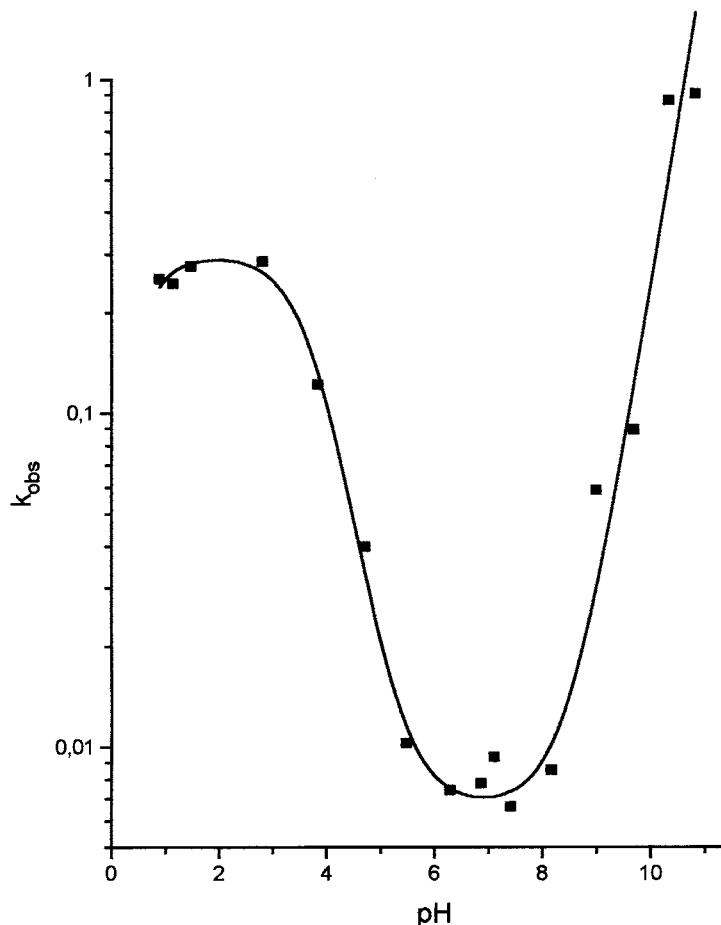


Fig. 3. pH-Rate profile degradation kinetics of **1** at various pH values, 35°C. The points are experimental values, and the solid line is the theoretical curve calculated from Eq. (1).

tions the average retention time (t_R) for **1** was 4.89 min, and the deviation in t_R for each injection was < 2%.

The reproducibility of the assay method for **1** was evaluated at two different concentrations (9.04 and 12.05 $\mu\text{g ml}^{-1}$), six times within one day at time intervals of 1 h. The values obtained within day were $9.37 \pm 0.04 \mu\text{g ml}^{-1}$ ($n = 6$, CV 0.47%) and $12.68 \pm 0.08 \mu\text{g ml}^{-1}$ ($n = 6$, CV 0.61%).

The precision of the analytical procedure was determined by making five consecutive injections of derivative **1** at two different concentrations (6.21 and 11.8 $\mu\text{g ml}^{-1}$). The results indicate excellent precision with CVs < 1.2%.

The analytical recovery of the method was determined using four different concentrations for **1** and synthetic mixtures of **1** with its decomposition products. The average recovery was calculated as the percent of observed concentration divided by the known concentration. Determinations were performed in quintuplicate and by direct comparison with the internal standard sample (**5**). The concentrations of **1** were in the range 3.1–18.4 $\mu\text{g ml}^{-1}$. Table 2 shows the results obtained for intact **1**, which indicates the effectiveness of the analytical method with relative standard deviations < 1.8%. The mean recovery of **1** was found to be $103.9 \pm 1.1\%$ ($n = 20$).

Table 5
Rate constants for compound **1**

Compound	k_1 (h ⁻¹)	k_H (M ⁻¹ h ⁻¹)	k_O (h ⁻¹)	k_{OH} (M ⁻¹ h ⁻¹)	pK _a
1	0.292	0.445	6.7×10^{-3}	2500	3.70

The recovery experiments for four synthetic mixtures of **1**, and its decomposition products were performed by adding varied amounts of authentic drug **1** to a constant concentration of degradation products **2** and **4** Table 3. The percentage mean recovery for **1** in mixtures with **2** was 103.60 ± 0.83 ($n = 20$) and in combination with compound **4** was 105.7 ± 1.0 ($n = 20$). In both cases the recovery of **1** scarcely varied with concentration, in presence of the degradation products.

Minimum detectable quantity and minimum detectable concentration for derivative **1** were 94

ng and $0.12 \mu\text{g ml}^{-1}$ respectively. These results are the mean value of five determinations.

3.3. Reaction order and observed rate constants

The kinetics of the degradation of **1** was studied by following the disappearance of the unchanged compound as a function of time. The results indicated that in aqueous solutions it follows pseudo-first-order kinetics under the constant conditions of pH, temperature, and ionic strength.

Typical first-order plots are shown in Fig. 2 at different pH values. The rates of hydrolysis were determined from the slopes of logarithmic residual concentration of **1** and storage time plots by a least-squares regression analysis. For all the buffer solutions studied for the degradation of **1**, the regression lines were linear with $r > 0.99$.

The buffer systems employed, the observed rate constants and the t_{90} and $t_{1/2}$ values are given in Table 4. The results obtained show that compound **1** reacts according to Scheme 1. At acidic and neutral pH, **1** gives the products **2** and protonated 4-amino-5-methylisoxazole (**3**). In basic pH, **1** undergoes hydrolysis to generate compounds **3** and **4**.

3.4. pH-rate profile

The pH-rate profile of **1** was obtained by plotting the logarithm of k_{obs} versus the pH of solutions at constant μ of 0.5 and at 35°C. The pH dependence of the pseudo-first-order rate constant for degradation of **1** over the pH range 0.88–10.80 is illustrated in Fig. 3. The shape of the curve indicates that in pH < 2.5 solutions, the degradation of **1** is pH independent. The inflection point in the region of pH 3.00–4.00 is due to the dissociation equilibria of **1** with a pK_a of 3.70 which was obtained as the fitted parameters Table

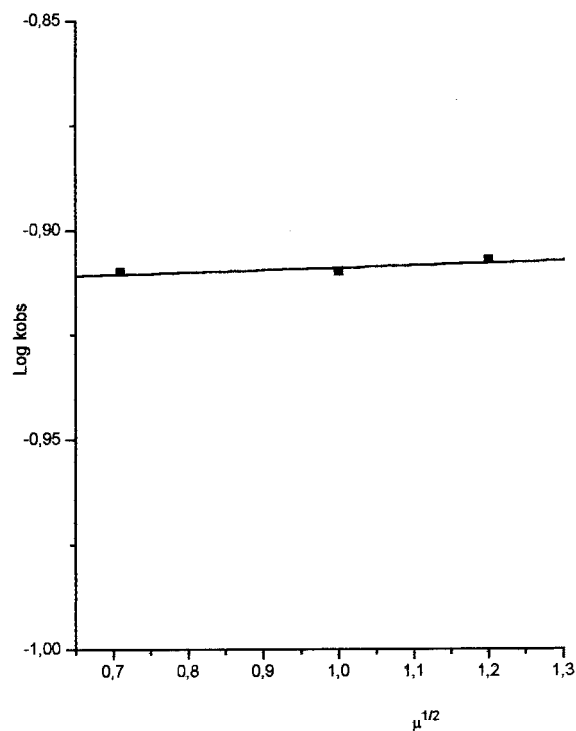


Fig. 4. Plots of $\log k_{\text{obs}}$ vs. the square root of ionic strength for the hydrolysis of **1** at pH 3.86 and 35°C.

5. At pH values < 5.5, specific acid catalysis occurs. In the range of pH 6.00–8.00, **1** was more stable than in other pH regions and the degradation was mainly due to the effect of spontaneous or water catalysis. The optimal stability observed was at a pH of ~ 6.95. At higher values, only the specific base catalysis was significant and in consequence the pH-rate profile exhibited both specific acid and specific base catalysis with neutral pH values optimum for stability. The overall rate equation for the degradation of **1** is:

$$k_{obs} = k_1 \frac{[H^+]}{[H^+] + K_a} + k_H [H^+] + k_o + k_{OH} [OH^-] \quad (1)$$

In Eq. (1) k_1 is the rate constant for water addition to the protonated imine, $[H^+]/[H^+] + K_a$ is the fraction of the compound in the protonated form, k_H is a second-order rate constant for the hydrogen ion catalyzed degradation, k_o represents the rate constant for the uncatalyzed reaction and k_{OH} is the specific basic catalysis rate constant.

The solid curve drawn in Fig. 3 was constructed from the apparent rate constants summarized in Table 5 Eq. (1). The excellent agreement observed between the experimental results and those calculated from this figure indicates that Eq. (1) adequately describes the observed pH effect on the degradation kinetics of **1**.

3.5. Salt effect

The effect of μ on the degradation of **1** was studied at pH 3.86 (citric acid–sodium hydrogen phosphate buffer) at $35.0 \pm 0.1^\circ\text{C}$. The value of μ was varied by addition of sodium chloride. At μ values of 0.5, 1.0 and 1.5 the k_{obs} values were 0.123, 0.123 and 0.124 h^{-1} . The plot of $\log k_{obs}$ versus $\mu^{1/2}$ Fig. 4 indicates that no kinetic salt effect was observed at pH 3.86 for the degradation of **1** [22].

4. Conclusions

The HPLC method developed in this study has proved to be simple, accurate, precise and offers adequate sensitivity and selectivity for the analysis of derivative **1** in presence of its degradation

products. The validation procedure was carried out using compound **1** in a high degree of purity and synthetic mixtures of the intact drug with its degradation products.

The pH-rate profile indicated that the maximum chemical stability of **1** is in the range of 6.40–7.40. The t_{90} value calculated from the pH-rate profile in the valley region was 14.8 h.

The quality parameters here determined support the suitability of the method as a stability-indicating assay.

Acknowledgements

This research project was supported by Consejo Nacional de Investigaciones Científicas y Técnicas (CONICET) de la República Argentina, Consejo de Investigaciones Científicas y Tecnológicas de la Provincia de Córdoba (CONICOR) and Secretaría de Ciencia y Técnica de la Universidad Nacional de Córdoba (SECyT).

References

- [1] P. Amuchástegui, E. Moretti, B. Basso, N. Sperandeo, M.M. de Bertorello, M. Briñón. Isoxazolyl-naphthoquinone activity on the growth of *Trypanosoma cruzi*. J. Protozool. (37) (1990) 15 A/89
- [2] P. Amuchástegui, E. Moretti, B. Basso, N. Sperandeo, M.M. de Bertorello, Isoxazolyl-naphthoquinone effect on the growth of *Trypanosoma cruzi*, Rev. Argent. Microbiol. 22 (1990) 199.
- [3] M. Schwarcz de Tarlovsky, S. Goijman, M. Molina Portela, A.O. Stoppani, Effects of isoxazolyl-naphthoquinoneimines on growth and oxygen radical production in *Trypanosoma*, Experientia 46 (1990) 502.
- [4] P. Bogdanov, I. Albesa, N. Sperandeo, M.M. de Bertorello, Actividad antibacteriana in vitro de isoxazolil-naftoquinonas I, Rev. Argent. Microbiol. 25 (1993) 119.
- [5] I. Albesa, P. Bogdanov, A. Eraso, N. Sperandeo, M.M. de Bertorello, Antibiotic activity of isoxazolyl-naphthoquinone imines on mice infected with *Staphylococcus aureus*, J. Appl. Bacteriol. 78 (1995) 373.
- [6] P. Bogdanov, I. Albesa, N. Sperandeo, C. Luna, M.M. de Bertorello, Antibacterial effect of 2-hydroxy-N-(3,4-dimethyl-5-isoxazolyl)-1,4-naphthoquinone-4-imine on *Staphylococcus aureus*, Experientia 52 (1996) 600–604.
- [7] P. Bogdanov, C. Ortiz, M. M. de Bertorello, I. Albesa, Posible Alternativa en la Terapia Anti-stafilococcica: Isoxazolil-naftoquinoniminas, VII Congreso Argentino de

- Farmacia y Bioquímica Industrial. Buenos Aires, Argentina, 1996.
- [8] C. Ortiz, M.M. de Bertorello, Isoxazoles 9: degradation kinetics of 4-(isoxazolylamino)-1,2-naphthoquinone in acidic aqueous solution., *J. Pharm. Sci.* 83 (10) (1994) 1457.
- [9] C. Ortiz, M.M. de Bertorello, Isoxazoles 10: degradation and enolization kinetics of 4-aminoisoxazolyl-1,2-naphthoquinone in basic aqueous solution, *J. Pharm. Sci.* 84 (6) (1995) 783.
- [10] C. Ortiz, M.M. de Bertorello, Applicability of an HPLC system in stability studies of a 4-isoxazolylamino-1,2-naphthoquinone., *Drug Stability* 1 (2) (1996) 123.
- [11] C. Ortiz, M. Longhi, M.M. de Bertorello, M. Briñón, Synthesis of bis-isoxazolynaphthoquinones, *Org. Prep. Proced. Int.* 23 (2) (1991) 181.
- [12] C. Ortiz, M.M. de Bertorello, HPLC separation of tautomeric compounds of 4-aminoisoxazolyl-1,2-naphthoquinone. III., *J. Liq. Chromatogr.* 14 (19) (1991) 3483.
- [13] The Merck Index, Eleventh Edition, Merck, Rahway, N.J., 1989.
- [14] Lide D.R., *Handbook of Chemistry and Physics*, 72 ed., CRD Press, 1991–1992, pp. 8–30.
- [15] H.A. Laitinen, *Chemical Analysis*, Ch. 2, 2 ed., McGraw-Hill, New York, 1975, p. 2.
- [16] D. Jenke, Chromatographic method validation: a review of current practices and procedures. III. Ruggedness, revalidation and system suitability., *J. Liq. Chromatogr. Rel.* 19 (12) (1996) 1873.
- [17] USP 23 *Validation of Compendial Methods*, 1982 (1995).
- [18] A.C. Metha, The Validation criteria for analytical methods used in pharmacy practice research, *J. Clin. Pharm. Therap.* 14 (1989) 465.
- [19] C. Hartmann, D. L. Massart, R.D. McDowall, An analysis of the Washington Conference Report on bioanalytical method validation, *J. Pharm. Biomed. Anal.* 12 (11) (1994) 1337–1343.
- [20] *Aspects of the Validation of Analytical Methods (Memorandum/Conclusions)*, European Organization for Quality, Interpharm Press, 1991.
- [21] WHO Expert Committee on Specifications for Pharmaceutical Preparations, World Health Organization, Geneva, 1992.
- [22] J.T. Carstensen, *Drug Stability Principles and Practices*, Marcel Dekker, New York, 1990.

A novel thin-layer amperometric detector based on chemically modified ring-disc electrode and its application for simultaneous measurements of nitric oxide and nitrite in rat brain combined with in vivo microdialysis

Lanqun Mao ^a, Guoyue Shi ^a, Yu Tian ^a, Haiying Liu ^a, Litong Jin ^{a,*},
Katsunobu Yamamoto ^b, Shuguang Tao ^b, Jiye Jin ^b

^a Department of Chemistry, East China Normal University, 200062 Shanghai, People's Republic of China

^b BAS Co. Ltd., No. 36-4, 1-Chome, Oshiage, Sumida-Ku, 131 Tokyo, Japan

Received 22 September 1997; received in revised form 06 January 1998; accepted 08 January 1998

Abstract

A novel thin-layer amperometric detector (TLAD) based on chemically modified ring-disc electrode and its application for simultaneous measurements of nitric oxide (NO) and nitrite (NO₂⁻) in rat brain were demonstrated in this work. The ring-disc electrode was simultaneously sensitive to nitric oxide (NO) and nitrite (NO₂⁻) by modifying its inner disc with electropolymerized film of cobalt(II) tetraaminophthalocyanine (polyCoTAPc)/Nafion and its outer ring with poly(vinylpyridine) (PVP), respectively. The ring-disc electrode was used to constitute a novel TLAD in radial flow cell for simultaneous measurements of NO and NO₂⁻ in rat brain combined with techniques of high performance liquid chromatography (HPLC) and in vivo microdialysis. It was found that the basal concentration of NO in the caudate nucleus of rat brain is lower than 1.0×10^{-7} mol l⁻¹, NO₂⁻ concentration is 5.0×10^{-7} mol l⁻¹ and NO exists in brain maybe mainly in the form of its decomposed product. © 1998 Elsevier Science B.V. All rights reserved.

Keywords: Cobalt(II) tetraaminophthalocyanine; Poly(vinylpyridine); Nitric oxide; Nitrite; Thin-layer amperometric detector; In vivo microdialysis

1. Introduction

Nitric oxide has received extensive attention due to its important and mysterious physiological

roles [1–3]. It has been identified as an endothelium-derived relaxing factor [EDRF] in the vascular system [4], a neurotransmitter in the nervous systems [5] and a cytotoxic factor in the immune systems [6]. Moreover, it has been believed to be related to some tissue damage such as ischaemia/reperfusion tissue damage [7] and excitatory neuronal death [8].

* Corresponding author. Fax: +86 21 62451876; e-mail: Ltjin@ch.ecnu.edu.cn

There is an extensive growth in the studies of NO in the fields of life science and its related subjects [9,10]. Many techniques have been developed for the evaluation of NO levels in biological materials. These include spectroscopic and electrochemical methods [11–16]. Also, some indirect methods have been used for this purpose based on NO synthesis processes and its related physiological effects such as measurements of L-citrulline or nitrite [17] or bioassay of the relaxation of blood vessels [18], stimulation of guanylate cyclase [19] and inhibition of platelet aggregation [20]. NO, similar to some other neurotransmitters coexisting with their related metabolites [21], exists in biological systems not only in the form of itself but also its decomposed products, of which NO_2^- is the dominate [22]. Consequently, effectively simultaneous measurements of NO_2^- and NO would not only offer a better approach to evaluate NO levels in biological system but also provide an effective means to investigate NO physiological reactions and roles. However, in most cases, NO_2^- , the main decomposed product of NO, interferes with NO detection, and vice versa. Therefore, it is difficult to determine NO sensitively in presence of NO_2^- and vice versa. To our knowledge, little effort has been made to circumvent this problem up to now. The novel amperometric detector based on chemically modified ring-disc electrode in the radial flow cell is in the equivalent to series daul electrode in a thin-layer cross flow cell. However, the high collection efficiency with the ring-disc electrode makes it possible to achieve high selectivity such as the determination of an analyte in the presence of an interferent and then can meet the requirements mentioned above.

Metal phythalyocyanines (MPc) such as CoPc, NiPc and CuPc have received a great deal attention due to their catalytic behaviors based on the redox centre in the polymer [23–25]. A greatly reduced oxidation potential can be obtained for a variety of organic compounds such as cysteine, mercaptosuccinic acid, glutathione, oxalic acid and catechol at the electrode modified with MPc [26,27]. Also, they can be used as an electron transfer mediator in the enzyme-based biosensors [28]. However, little has been studied on the deter-

mination of NO with the electrode based on the electropolymeric film of CoTAPc.

This work demonstrated a novel TLAD in the radial flow cell simultaneously sensitive to NO and NO_2^- based on a chemically modified ring-disc electrode with polyCoTAPc/Nafion and PVP. The TLAD was employed for simultaneous measurements of NO and NO_2^- in rat brain combined with the techniques of in vivo microdialysis and high performance liquid chromatography (denoted microdialysis/HPLC–TLAD). This combined technique provide an effective means to assay the levels of NO and its main decomposed product, NO_2^- , in rat brain simultaneously.

2. Experimental

2.1. Chemicals

NO saturated solution was prepared by bubbling NO gas through deoxygenated distilled water for 30 min and its saturation concentration is 1.9 mmol l^{-1} [29]. NO serial standard solutions were obtained by diluting NO saturated solution. NO standard solutions could also be obtained by NO producing systems developed in our laboratory [30]. The prepared solutions were kept in a glass flask with rubber septum, stored in a light-free place and could assure to be stable for 3 h.

Cobalt(II)-4,9,16,23-tetraaminophthalocyanine monomer ($\text{C}_{32}\text{H}_{20}\text{N}_{12}\text{Co}$) was synthesized according to the procedure described by Achar et al. [31] and characterized by FT-IR. The structure of CoTAPc was given in Fig. 1. Its FT-IR spectra are (KBr, cm^{-1}): 3281, 3183, ($\gamma_{-\text{NH}_2}$), 1345, 1258, 1060, 1090, ($\gamma_{\text{C}-\text{N}}$), 826, 868 (δ_{Ar}), 735, 752, 950, 1607 ($\delta_{\text{N}-\text{H}}$). PVP was prepared by mixing vinyl pyridine and 1% dimethylbenzoyl peroxide in a little tube. After reacted for 12 h at 80°C , PVP solid was obtained, and its solution was obtained by dissolving PVP solid in methanol. Tetra-*n*-butylammonium perchlorate (TBAP) was prepared by the reaction of tetra-*n*-butylammonium bromide with sodium perchlorate. Artificial cerebrospinal fluid (ACSF) containing 140 mmol l^{-1} NaCl, 2.4 mmol l^{-1} KCl, 1.0 mmol l^{-1} MgCl_2 , 1.0 mmol l^{-1} CaCl_2 ,

5.0 mmol l⁻¹ NaHCO₃ and 0.6 mmol l⁻¹ ascorbic acid was prepared. Phosphate buffer solution consisting of 0.01 mol l⁻¹ Na₂HPO₄ and 0.02 mol l⁻¹ KH₂PO₄ was prepared and was adjusted to pH 5.0. Nafion (5% solution in ethanol) was purchased from Aldrich, Sodium nitrite was obtained from Shanghai First Chemical Factory, its solution was prepared daily. Other chemicals were of at least reagent grade quality and used as received. The aqueous solutions were prepared with doubly distilled water.

2.2. Apparatus

Electrochemical experiments were performed with an Electrochemical Analyzer (CHI832) from USA in conjunction with a computer in which data and voltammograms were recorded and stored. A platinum disc ultra microelectrode was fabricated by sealing a platinum wire (15 μm) into a glass pipe and used as a working electrode while investigating the mechanism of the responses of NO and NO₂⁻ at the modified electrodes. Prior to experiments, the fabricated ultra microelectrode was polished with diamond paste and rinsed thoroughly with acetone and water. Its electrochemical pretreatment was carried out by scanning the potential from -0.30 to +1.30 V for ten cycles

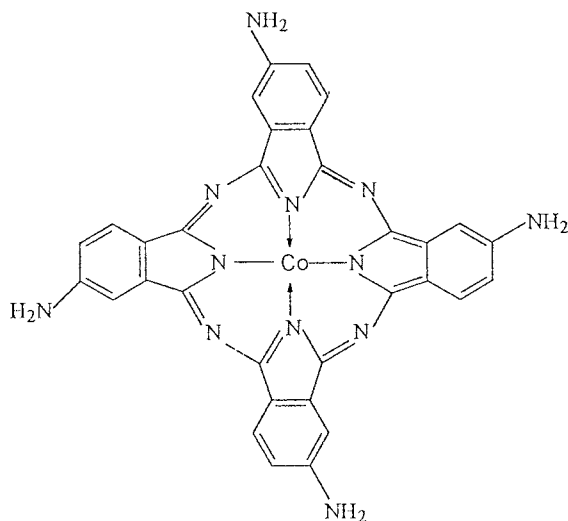


Fig. 1. Structure of CoTAPc

in a 0.5 mol l⁻¹ sulfuric acid solution. A platinum wire was used as counter electrode and potential was referenced to a Ag/AgCl (saturated KCl) electrode. A TLAD, as shown schematically in Fig. 2, was composed of a three-electrode system, Teflon cell body and Teflon pad. A ring-disc electrode from Bioanalytical Systems (BAS) in Japan consisting of dual electrodes (inner disc and outer ring) was used as dual working electrodes, stainless steel was served as counter electrode, and potentials applied with Biosensing Unit (BS-1, BAS, Japan) were referenced to a Ag/AgCl electrode. Microdialysis was accomplished using a CMA 101 microdialysis pump and a microdialysis probe (CMA12, dialysis length, 3 mm; diameter, 0.24 mm; all gifted from BAS, Japan). The collected dialysate was separated with liquid chromatograph (HP1090, USA) coupled with a Synchronpak SAX-300 column from USA.

2.3. Electrode modification

The ultramicroelectrode was allowed to air-dry and then placed into a dimethyl sulfoxide (DMSO) solution containing 5.0×10^{-3} mol l⁻¹ CoTAPc monomer and 0.1 mol l⁻¹ TBAP employed as the supporting electrolyte. Cycling potential between -0.20 and +0.90 V was applied to the working electrode at a scan rate of 100 mV s⁻¹ until a stable voltammetric response was obtained. The electrode was then rinsed with acetone and distilled water and allowed to air-dry. The polyCoTAPc modified ultramicroelectrode was further coated twice with a thin film of Nafion by depositing 1 μl of a 1% Nafion solution on the electrode surface each time and allowing ethanol to air dry.

A PVP coated ultramicroelectrode was constructed by placing 2 μl of 0.1% PVP solution on the surface of a dried ultramicroelectrode and allowing the solvent to evaporate.

2.4. Voltammetric responses of NO and NO₂⁻ at the modified ultramicroelectrodes

Prior to NO measurements, the polyCoTAPc/Nafion modified ultramicroelectrode was placed in a phosphate buffer solution (pH 5.0) and cyclic

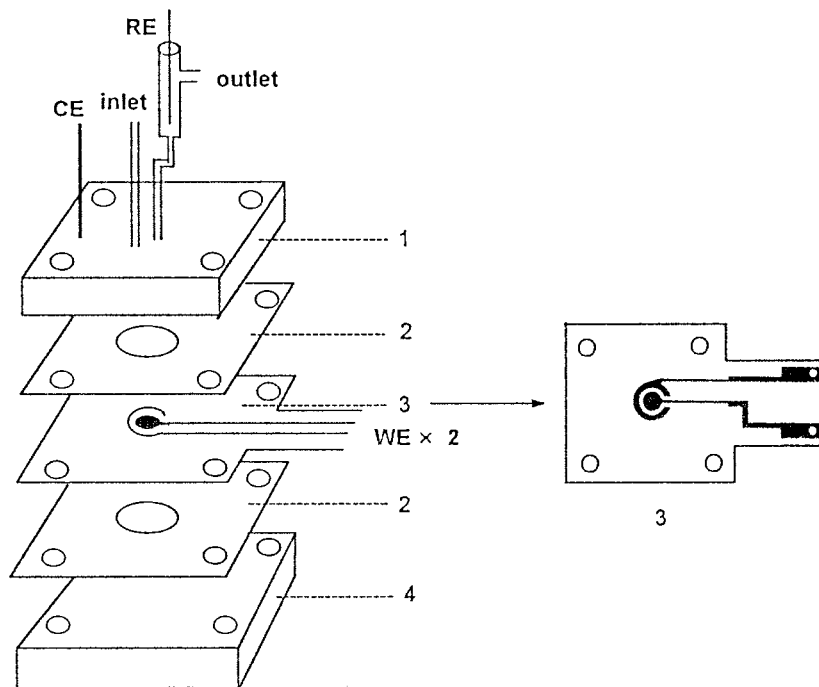


Fig. 2. Schematic diagram of a TLAD

voltammetry was performed in the potential range 0.00 to +1.00 V until a steady-state cyclic voltammetric and differential pulse voltammetric (DPV) responses were obtained. The response of NO at the CoTAPc/Nafion modified ultramicroelectrode were carried out using DPV method, a sensitive and highly distinguished technique, in a hermetic deoxygenated phosphate buffer solution. DPV was performed at a scan rate of 5 mV s^{-1} and 5 pulses per s (pulse height 50 mV, pulse width 60 ms). The response of NO_2^- at a PVP coated ultramicroelectrode was studied by using cyclic voltammetric technique in a phosphate buffer solution.

2.5. Modification of the ring-disc electrode

The inner disc of the ring-disc electrode was modified with polyCoTAPc and Nafion in the same fashion mentioned in Section 2.3. After modified with polyCoTAPc, the inner disc was further coated with Nafion by placing $15 \mu\text{l}$ of 1% Nafion on the electrode surface and allowing the

solvent to evaporate. Prior to coating PVP on the outer ring, it was necessary to rinse it thoroughly and carefully with acetone and distilled water so that the remains such as CoTAPc monomer would be washed away. The outer ring was modified with $5 \mu\text{l}$ of 0.1% PVP solution in the mode mentioned in Section 2.3. The chemically modified ring-disc electrode was served as the dual working electrodes of the TLAD.

2.6. Responses of the system to NO and NO_2^-

Prior to injunction with HPLC, the responses of NO and NO_2^- at the TLAD were evaluated by using a technique of flow injection analysis (FIA). The operating potentials of the outer ring and inner disc were applied at +0.80 and +0.75 V, respectively. A deoxygenated phosphate buffer solution containing 0.1 mmol l^{-1} EDTA was served as a mobile phase. In order to estimate the in vivo concentrations of NO and NO_2^- , it was necessary to determine the in vitro recovery of the microdialysis probe which was performed as described in

the literature [32,33] and the linearity of the microdialysis/HPLC-TLAD. This was accomplished by placing the microdialysis probe in a known concentration of NO or NO_2^- solution and perfusing at a rate of $1.0 \mu\text{l min}^{-1}$. The collected dialysate was injected into the HPLC-TLAD system and served for analysis. The *in vitro* relative recovery could be determined by comparing the results of this experiment with those of an experiment run under similar conditions except that the standard solutions were not perfused with the microdialysis probe. The system linearity was tested in the same mode by using serial different concentrations of NO and NO_2^- .

2.7. *In vivo* brain microdialysis

Experiments were carried out in adult and male Sprague–Dawley rats (280–320 g) that were anesthetized with 125 mg g^{-1} urethane and fixed in a Koff stereotaxic frame. The microdialysis probe was stereotaxically implanted into the nucleus caudatus and then was perfused with ACSF solution at a constant flow rate of $1.0 \mu\text{l min}^{-1}$ using a microdialysis pump. Following 50 min equilibration period, the dialysate were collected every 25 min, and served for the measurements of NO_2^- and NO. At the end of this experiment the positions of the microdialysis probe and the carbon fiber microelectrode, with which *in vivo* voltammetry was carried out, were verified by standard histological procedure. The results were expressed to an average value.

3. Results and discussion

3.1. DPV responses of NO at a polyCoTAPc/Nafion modified ultramicroelectrode

Fig. 3 depicts the DPV responses of NO at a polyCoTAPc/Nafion modified and an unmodified ultramicroelectrode. As can be seen that NO could be oxidized at nearly $+0.70\text{V}$ and a higher response could be obtained at the polyCoTAPc/Nafion modified ultramicroelectrode compared with that at the unmodified ultrami-

croelectrode. This indicated that the polyCoTAPc/Nafion modified ultramicroelectrode shows a sensitive response to NO measurement.

CoPc was demonstrated to show a high catalytic activity for the oxidation of some organic compounds mentioned above based on the redox centre of $\text{Co}^{\text{III}}/\text{Co}^{\text{II}}$ in the polymer which facilitate the electron transfer between the electrode and the analyte. It has been reported that metal complexes could interact with simple diatomic molecules such as O_2 , CO and NO resulting in the formation of their adducts [10,34,35]. For example, the interaction between O_2 and ion(II) metal porphyrin has received extensive studies to elucidate the biological functions of haemoglobin and myoglobin *in vivo* [36]. Metallophthalocyanine complexes, similar to metalloporphyrin and metal salen complexes which are served to model

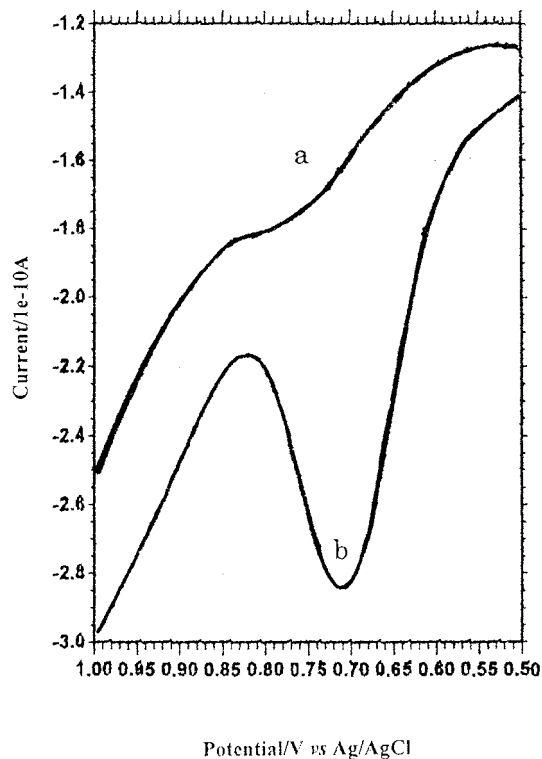


Fig. 3. DPV responses of NO at an unmodified (a) and a polyCoTAPc/Nafion modified ultramicroelectrode (b) in a deoxygenated phosphate buffer solution, NO concentration is $2.0 \times 10^{-6} \text{ mol l}^{-1}$.

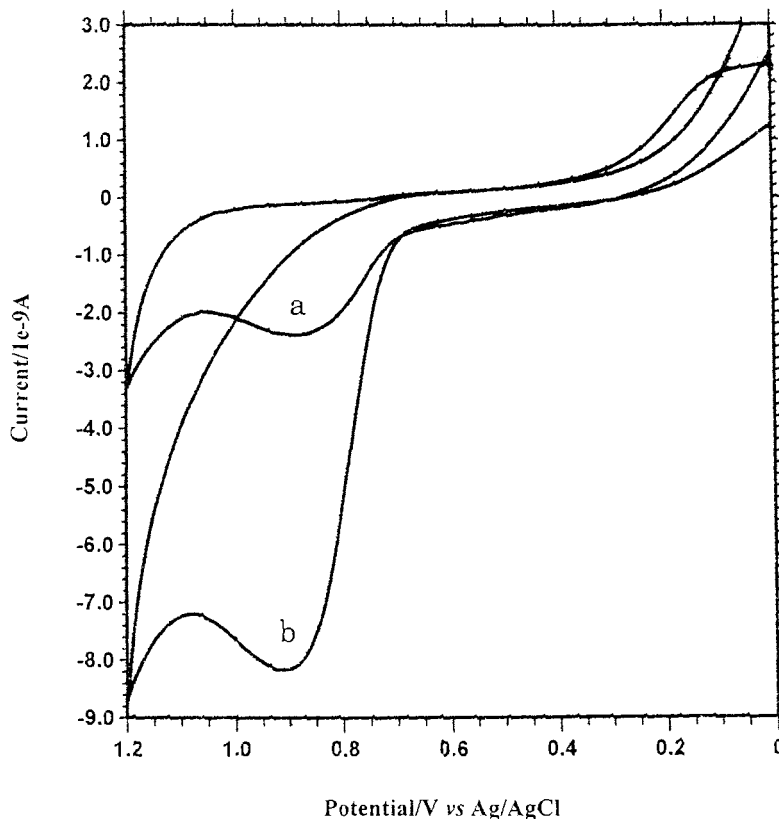
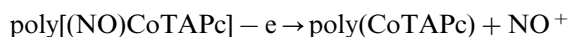
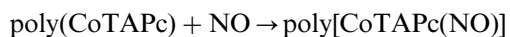


Fig. 4. Cyclic voltammograms of $1.0 \times 10^{-4} \text{ mol l}^{-1} \text{ NO}_2^-$ at an unmodified (a) and a PVP modified ultramicroelectrode at a scan rate of 100 mV s^{-1} in a phosphate buffer solution.

enzyme sites, especially for enzymes of cytochrome P-450 families [37], could also interact with simple molecules [38]. In this work, the electrode process could be expressed as following:

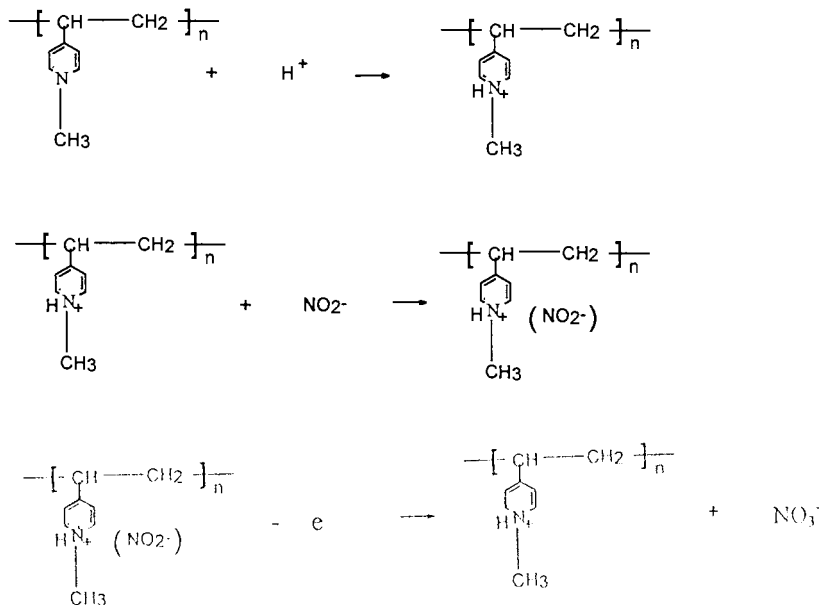


NO, a highly active gas, could penetrate through Nafion film and form its adduct with CoTAPc. The formed adduct, poly[CoTAPc(NO)] could be oxidized easily resulting in a high current response at the electrode. The product of the electrochemical reaction, NO^+ can be fixed in Nafion film and not be further oxidized to produce NO_2^- .

3.2. Voltammetric response of NO_2^- at a PVP coated ultramicroelectrode

Fig. 4 shows the typical voltammetric responses of NO_2^- at a PVP modified and an unmodified ultramicroelectrode. The PVP coated ultramicroelectrode exhibits a sensitive response to NO_2^- compared with that at the unmodified ultramicroelectrode. The response of NO_2^- at a PVP coated ultramicroelectrode is about four times as that at the unmodified one.

PVP is a positively charged polymer due to protonation at its pyridine while in presence of acidic solution. The protonated PVP film attracts negatively charged ions such as NO_2^- resulting in a high response of NO_2^- at the PVP coated ultramicroelectrode. The processes of protonation and electrochemical reaction could be expressed as following:



3.3. Responses of the TLAD to NO and NO_2^-

Responses of the TLAD to NO and NO_2^- were studied by using FIA technique. Prior to the injection of the mixture of NO and NO_2^- solution, NO and NO_2^- solutions were injected separately to study the response of the TLAD to NO and NO_2^- , respectively. Fig. 5 depicts the FIA responses of the TLAD to $1.0 \times 10^{-6} \text{ mol l}^{-1} \text{ NO}_2^-$. As shown in Fig. 5, the inner disc shows no response to NO_2^- while the outer ring displays a good response, indicating that Nafion coated at the inner disc serves as an effective barrier to discriminate against NO_2^- . On injecting $1.0 \times 10^{-6} \text{ mol l}^{-1} \text{ NO}$ solution into the system, a high peak at the inner disc was observed attributed to NO oxidation while the outer ring shows no responses ($\text{S/N} > 3$). This suggests that a high response of NO could be obtained at the polyCo-TAPc/Nafion modified inner disc, and that NO oxidation product, NO^+ was effectively entrapped in Nafion film, not be further oxidized to produce NO_2^- , which can diffuse away from the inner disc and be oxidized at the PVP coated outer ring. It has been reported that NO could be oxidized at the electrodes modified with various gas-permeability films [12,13]. We also found in

this work that the PVP coated outer ring shows response to NO while NO concentration was higher than $1.0 \times 10^{-5} \text{ mol l}^{-1}$. This indicates NO can penetrate through PVP film and be oxidized at the outer ring. Therefore, in this case the response of the outer ring should be ascribed to the oxidation of NO_2^- and NO while injecting the mixture of NO and NO_2^- into the system. How-

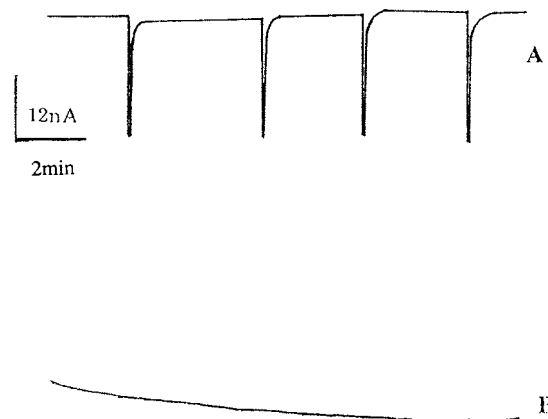


Fig. 5. FIA responses of the TLAD to $1.0 \times 10^{-6} \text{ mol l}^{-1} \text{ NO}_2^-$. A and B are corresponding to the outer ring and inner disc of the ring-disc electrode, respectively. Phosphate buffer solution containing $0.1 \text{ mmol l}^{-1} \text{ EDTA}$ was served as a mobile phase with a flow rate of 1.0 ml min^{-1} .

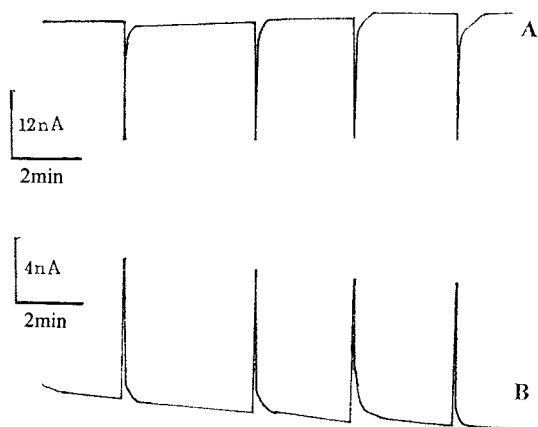


Fig. 6. FIA responses of the TLAD to the mixture of $1.0 \times 10^{-6} \text{ mol l}^{-1} \text{ NO}_2^-$ and $1.0 \times 10^{-6} \text{ mol l}^{-1} \text{ NO}$. The mobile phase was deoxygenated thoroughly. Other conditions were the same as above.

ever, the sensitivity of the outer ring to NO is much lower than that to NO_2^- , and NO shows no observed response at the PVP coated outer ring when its concentration was lower than $5.0 \times 10^{-6} \text{ mol l}^{-1}$. Consequently, the current response at the outer ring could be ascribed to the oxidation of NO_2^- only in this work. Fig. 6 shows the responses of the TLAD to NO and NO_2^- mixture. In comparison with Fig. 5, we could find that NO at the concentration of $1.0 \times 10^{-6} \text{ mol l}^{-1}$ indeed shows no observed response at the PVP coated outer ring. Also, we could find that in Fig. 6, high responses at the inner disc and the outer ring were obtained due to the oxidation of NO and NO_2^- , respectively. This indicates that the TLAD based on chemically modified ring-disc electrode were simultaneously sensitive to NO and NO_2^- and could be employed for the simultaneously sensitive measurements of NO and NO_2^- .

3.4. Simultaneous measurements of NO and NO_2^- in the dialysate

The in vitro relative recovery of a microdialysis probe which is necessary to assess NO and NO_2^- real concentration in rat brain was determined by dialysis rate. Generally, the higher dialysis rate, the lower relative recovery. Also, the lower dialysis rate would cause the collected dialysate fouled

due to the longer collected time. The effect of the dialysis rate was investigated and found that the optimum dialysis rate is $1.0 \mu\text{l min}^{-1}$ in this work. The in vitro relative recovery of NO and NO_2^- , based on $1.0 \times 10^{-6} \text{ mol l}^{-1}$ NO and NO_2^- were determined to be an average of 25 and 30% ($n = 6$) at a dialysis rate of $1.0 \mu\text{l min}^{-1}$, respectively. Prior to the injection of the dialysate, standards of NO and NO_2^- were injected into the assay system for calibration and it was found that the system was linear with NO and NO_2^- concentrations ranging from 2.0×10^{-7} to $4.1 \times 10^{-6} \text{ mol l}^{-1}$ and 2.5×10^{-7} to $7.5 \times 10^{-4} \text{ mol l}^{-1}$ with correlation coefficients of 0.994 ($n = 12$) and 0.996 ($n = 10$), respectively. The calculated detection limits, at a signal-to-noise ratio of 3, of NO and NO_2^- were 1.0×10^{-7} and $1.2 \times 10^{-7} \text{ mol l}^{-1}$, respectively. Fig. 7 shows a typical chromatograms of the dialysate from the caudate nucleus. As can be seen no obvious peak attributed to NO oxidation was observed at the inner disc, indicating that the concentration of NO maybe lower than the detection limit of the system. To testify this result further, in vivo voltammetry was carried out with a carbon fiber microelectrode (CFME) which shows a high response to NO based on the polyCoTAPc and Nafion (whose detection limit is $5.0 \times 10^{-8} \text{ mol l}^{-1}$). The modified CFME also shows no obvious response to NO, indicating that NO concentration in the

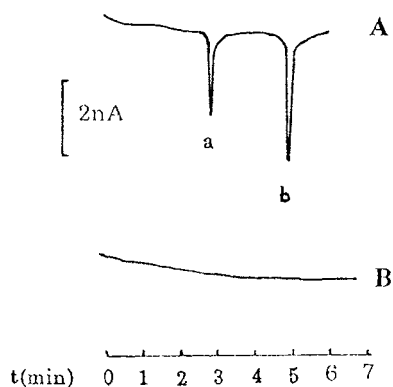


Fig. 7. Typical chromatograms of the dialysate from the nucleus Caudatus of rat brain. The dialysate was separated using a Synchropak SAX-300. Other conditions were the same as above. (a): ascorbate, (b): nitrite.

nucleus caudatus is lower than its detection limit. Bedioui and other groups [39–41] have determined basal NO production by washed platelets with carbon microfibers coated with tetrakis(3-methoxy-4-hydroxyphenyl) nickel porphyrin and Nafion films as described previously [11] and they found that the basal NO level was not detectable due to its low concentration. Our present work also shows that the basal concentration of NO in the nucleus caudatus of rat brain, like in other biological tissues such as platelets and *Rhodobacter sphaeroides* [42] could not be detected either. The two peaks of the outer ring are ascribed to NO_2^- and ascorbate, respectively, and the concentration of NO_2^- is determined to be at an average of $5.0 \times 10^{-7} \text{ mol l}^{-1}$ ($n = 4$), which is in agreement with references [43,44].

4. Conclusion

TLAD, a novel detector in radial flow cell, was developed based on chemically modified a ring-disc electrode with polyCoTAPc/Nafion and PVP, which are sensitive to NO and NO_2^- , respectively. A new effective approach for simultaneous in vivo measurements of NO and NO_2^- was established by combining the TLAD with in vivo microdialysis and HPLC. This combined technique was employed for simultaneous and sensitive measurements of NO and NO_2^- in rat brain. It was found that the basal concentration of NO in the nucleus caudatus of rat brain is lower than $1.0 \times 10^{-7} \text{ mol l}^{-1}$, and NO_2^- concentration is $5.0 \times 10^{-7} \text{ mol l}^{-1}$. These results suggest that NO, a highly active free radical, exists in the region of rat brain maybe mainly in the form of NO_2^- , its main decomposed product. Although the combined technique developed in this work specifically for simultaneous measurements of NO and NO_2^- , it can potentially be applied to some other biochemicals such as neurotransmitters and their related metabolites in the biological materials. We will carry out detailed studies of NO release induced by ischaemia/reperfusion and other biochemicals determinations based on this combined technique, and these results will be reported soon.

Acknowledgements

This work is supported by The Natural Science Foundation of Shanghai Science and Technology Committee and The Open Electroanalytical Chemistry Laboratory of Changchun Institute of Applied Chemistry, Chinese Academy of Sciences.

References

- [1] S. Moncada, R.M.J. Palmer, E.A. Higgs, *Pharmacol. Rev.* 43 (1991) 109.
- [2] R.F. Furchgott, J.V. Zawadzki, *Nature* 288 (1980) 373–376.
- [3] R.F. Schuman, D.V. Madison, *Science* 254 (1991) 1503.
- [4] R.M.J. Palmer, A.G. Ferrige, S. Moncada, *Nature* 327 (1987) 526.
- [5] T.J. O'Dell, R.D. Hawkins, E.R. Kandel, O. Arancio, *Proc. Natl. Acad. Sci. USA* 88 (1991) 11285.
- [6] M.W. Radomski, R.M.J. Palmer, S. Moncada, *Proc. Natl. Acad. Sci. USA* 87 (1990) 5193.
- [7] D. Moncada, D. Lekieffre, B. Arvin, B. Meddrum, *Neuro Rep.* 343 (1992) 530.
- [8] S.A. Lipton, Y.-B. Choi, Z.-H. Pan, S.Z. Lei, H.-S.V. Chen, N.J. Sucher, J. Loscalzo, J. Singel, J.S. Stamler, *Nature* 364 (1993) 626.
- [9] T. Malinski, M.W. Radomski, Z. Taha, S. Moncada, *Biochem. Biophys. Res. Commun.* 194 (1993) 960965.
- [10] M. Hoshino, R. Konishi, N. Tezuka, I. Ueno, H. Seki, *J. Phys. Chem.* 100 (1996) 13569.
- [11] T. Malinski, Z. Taha, *Nature* 358 (1992) 676.
- [12] M.N. Friedemann, S.W. Robinson, G.A. Gerhardt, *Anal. Chem.* 68 (1996) 2621–2628.
- [13] F. Lantoiné, S. Trevin, F. Bedioui, J. Devynck, *J. Electroanal. Chem.* 392 (1995) 85–89.
- [14] M. Maskus, F. Pariente, Q. Wu, A. Toffanin, J.P. Shapleigh, D. Abruna, *Anal. Chem.* 68 (1996) 3128–3134.
- [15] S. Trevin, F. Bedioui, J. Devynck, *Talanta* 43 (1996) 303–311.
- [16] K. Shibuki, *Neurosci. Res.* 9 (1990) 69.
- [17] S. Archer, *J. FASEB* 7 (1993) 349–360.
- [18] R.M.J. Palmer, D.S. Ashlon, S. Moncada, *Nature* 333 (1988) 664.
- [19] R.G. Knowles, M. Palacios, R.M.J. Palmer, S. Moncada, *Proc. Natl. Acad. Sci. USA* 86 (1989) 5159.
- [20] D. Salvemini, G. De Nucci, R.J. Grylewski, J.R. Vane, *Proc. Natl. Acad. Sci. USA* 86 (1989) 6328.
- [21] P.A. Garris, R.M. Wightman, *Voltammetric methods in brain systems*, in: A. Boulton, G. Baker, R.U. Adams (Eds.), *Neuromethods* vol. 27, Humana Press, 1995.
- [22] J.S. Stamler, D.J. Singel, J. Loscalzo, *Science* 258 (1992) 1898.
- [23] F. Xu, H. Li, S.J. Cross, T.F. Guarr, *J. Electroanal. Chem.* 368 (1994) 221.

- [24] H. Li, T.F. Guarr, *J. Electroanal. Chem.* 317 (1991) 189.
- [25] C.M. Lieber, N.S. Lewis, *J. Am. Chem. Soc.* 106 (1984) 5033.
- [26] H. Li, T.F. Guarr, *Synth. Met.* 23 (1990) 243.
- [27] X. Qi, R.P. Baldwin, H. Li, T.F. Guarr, *Electroanalysis* 3 (1991) 119.
- [28] Z. Sun, H. Tachikawa, *Anal. Chem.* 64 (1992) 1112.
- [29] W.F. Linke, *Insolubilities, Inorganic and Metal Organic Compounds*, vol. II, 4th ed., ACS, Washington, DC, 1965.
- [30] L.Q. Mao, Y. Tian, Y.Z. Xian, Q. Xu, L.T. Jin, *NO Producing Systems*, Chinese Patent (No. 97206334).
- [31] B.N. Achar, G.M. Fohlen, J.A. Parker, J. Keshavayya *Polyhedron* 6 (1987) 1463.
- [32] M.O.M. Berners, M.G. Boutelle, M. Fillenz, *Anal. Chem.* 66 (1994) 2017.
- [33] H.L. Wan, P.J. Tsai, M.J. Chiang, J.P. Wu, L. Liu, W.J. Tsai, J.S. Kuo, *Redox Rep.* 2 (1996) 267.
- [34] B.B. Wayland, A.R. Newman, *J. Am. Chem. Soc.* 101 (1979) 6472.
- [35] D.C. Detschman, S.G. Utterback, *J. Am. Chem. Soc.* 103 (1981) 2847.
- [36] W.S. Bringar, C.K. Chang, *J. Am. Chem. Soc.* 96 (1974) 5595.
- [37] D. Mansuy, P.B. Battoni, in: J. Reedijk (Ed.), *Bioinorganic Catalysis*, Marcel Dekker, New York, 1993, p. 395.
- [38] J. Zagal, C. Fierro, R. Rozas, *J. Electroanal. Chem.* 119 (1981) 403.
- [39] F. Lantoine, A. Brunet, F. Bedioui, J. Devynck, M.A. Devynck, *Biochem. Biophys. Res. Comm.* 215 (1995) 842.
- [40] M.W. Radomski, S. Moncada, in: K.S. Authi et al. (Eds.), *Mechanisms of Platelet Activation and Control*, Plenum Press, New York, 1995, pp. 251–264.
- [41] T. Malinski, M.W. Radomski, Z. Taha, S. Moncada, *Biochem. Biophys. Res. Comm.* 194 (1993) 960.
- [42] M. Maskus, F. Pariente, Q. Wu, A. Toffanin, J.P. Shapleigh, H.D. Abruna, *Anal. Chem.* 68 (1996) 3128.
- [43] L.C. Green, D.A. Wagner, J. Glogowski, P.L. Skipper, J.S. Wishnok, S.R. Tannenbanm, *Anal. Biochem.* 126 (1982) 131–138.
- [44] K. Ohta, N. Araki, M. Shibata, J. Hamada, S. Komatsumoto, K. Shimazu, Y. Fukuuchi, *Neurosci. Lett.* 176 (1994) 165–168.

Determination of heavy metal concentration in feed and permeate streams of polymer enhanced ultrafiltration process

Jale Müslehiddinoğlu, Yusuf Uludağ, Hilmi Önder Özbelge, Levent Yılmaz *

Department of Chemical Engineering, Middle East Technical University, 06531 Ankara, Turkey

Received 14 July 1997; received in revised form 6 January 1998; accepted 9 January 1998

Abstract

Polymer enhanced ultrafiltration (PEUF) is a newly developed method for the removal of heavy metals from aqueous solutions. This method was applied for the removal of mercury and cadmium with the presence of polyethyleneimine (PEI) as a water soluble polymer. After ultrafiltration experiments for metal–polymer mixtures, two separate streams, namely, retentate and permeate, former of which contains mainly metal–polymer complex and free polymer molecules while latter of which mainly contains free metal ions, were obtained. At the end of PEUF experiments, performance of operation was determined by concentration analyses which was achieved by atomic absorption spectroscopy (AAS) applied in a different way for permeate and retentate streams considering the effect of presence of polymer. For mercury analysis, cold vapor AAS was applied. It was observed that the presence of PEI did not affect the atomic absorption signal when 10% HCl was added to the sample solutions. For calcium and cadmium, flame AAS was used. It was observed that change in PEI concentration results in change in measured concentration of calcium and cadmium. Therefore, two new approaches were developed for accurate measurement of concentrations of calcium and cadmium. It was also observed that presence of other metals did not affect the accuracy of the measurement of a particular metal in the concentration range studied. © 1998 Elsevier Science B.V. All rights reserved.

Keywords: Polymer enhanced ultrafiltration; Heavy metal ions; Atomic absorption spectrometry; Data treatment

1. Introduction

During the past two decades, increasing attention has been focused on pollution of the natural environment. The threat of pollution of the environment by heavy metals is well known by now

[1]. Thus, stringent quality standards for waste water containing heavy metals have been enacted. With these more stringent standards, industries which previously discharged their effluent with minimal pretreatment are now being required to remove heavy metals down to very low concentrations. One promising method which may meet this requirement is Polymer Enhanced Ultrafiltration (PEUF) described previously in detail [2,3]. This

* Corresponding author. Tel.: +90 312 2102607; fax: +90 312 2101264; e-mail: lyilmaz@rorqual.cc.metu.edu.tr

method includes the addition of water soluble polymer which is followed by the ultrafiltration operation. The water soluble polymer are used to bind metals to form macromolecular complexes. This large molecule will be retained by the membrane in the retentate stream, while the non-complexed ions pass through the membrane to the permeate stream. In most of the previous studies, batch or semi batch ultrafiltration systems were employed to remove metals from aqueous solutions (almost all single metal solutions) using various polymers [4–14]. In our previous studies [2,3], continuous PEUF was applied for removal of mercury and cadmium, which are among the most toxic heavy metals, from single and binary metal containing solutions using polyethyleneimine (PEI) as a water soluble polymer and very high retentions of heavy metals were obtained by adjusting pH and loading ratio (i.e. metal/polymer ratio) values. In our previous study [2], it was also proved that retention is mainly dependent on metal/polymer ratio in the feed rather than their individual concentrations. The water used in industry may contain an excess amount of calcium and magnesium ions (i.e. hard water). Therefore, in many heavy metal containing waste streams, these ions may also exist in abundance. Since calcium and magnesium are Class A metals and have similar properties; one of them, calcium, was selected to investigate the possibility of complex formation with PEI, and the effect of calcium on mercury–PEI complex.

In feed and permeate streams of PEUF process, metal ions and polymeric ligand were present at varying concentrations. Accurate determination of heavy metal concentrations in these streams are very important for the evaluation of the performance of this method which was mainly determined calculating the retention of metal defined as:

$$R_i = 1 - \frac{C_{pi}}{C_{fi}}$$

where i is the metal ion, C_{pi} is the concentration of metal i in the permeate stream and C_{fi} is the concentration of metal i in the feed stream. Atomic absorption spectroscopy (AAS) has been one of the Environmental Protection Agency

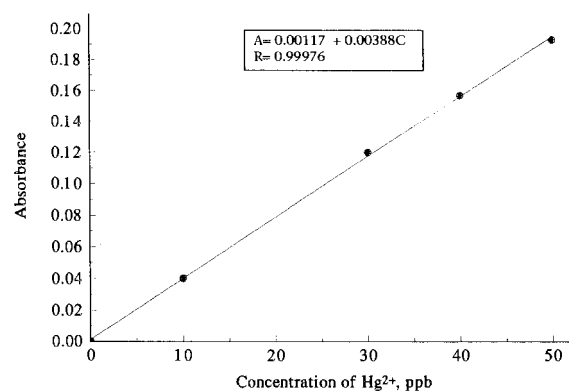


Fig. 1. Results and calibration measurements.

(EPA) method of choice, for the elemental analysis of aqueous samples because of its utility, sensitivity and accuracy [15,16]. This method can rapidly determine metals in trace amounts. In the previous studies on the development of PEUF process for heavy metal removal [4–14], generally AAS was employed for the metal analyses. In these studies, effect of existence of other constituents such as polymeric ligands, surfactants and low molecular weight organics on the measured metal concentrations were hardly discussed. Various complexation enhanced ultrafiltration methods, including PEUF, were also employed as a preconcentration step for determination of trace heavy metals by AAS. In some of these studies, effect of complexation agents were mentioned. In one of these studies, it was found that no interferences due to the presence of dissolved surfactant i.e. Triton X-100 host micelles and 1-(2-pyridyl-

Table 1
CV-AAS measurements of 30 $\mu\text{g l}^{-1}$ mercury at various HCl and PEI concentrations

% HCl	% PEI (w/v)	Hg ²⁺ ($\mu\text{g l}^{-1}$) found
5.0	0.2	33.0
5.0	5.0	30.7
10	0.2	30.0
10	5.0	30.0
15	0.2	28.8
15	5.0	29.8
20	0.2	27.7
20	5.0	28.9

Table 2
CV-AAS measurements of mercury at 10% HCl and different concentrations of mercury and polymer

% PEI (w/v)	Hg ²⁺ ($\mu\text{g l}^{-1}$)	
	Added	Found
0.2	10.0	9.7
2.0	10.0	9.7
0.2	30.0	28.6
2.0	30.0	29.1
0.2	40.0	37.8
2.0	40.0	38.8
0.2	50.0	48.0
2.0	50.0	51.6

lazo)-2-naphthol, were observed during the analyses after applying micellar ultrafiltration method for removal of nickel, cobalt, copper, magnesium and zinc [17]. For determination of Cr(III) and total Cr, a chelating ion exchanger, polyamino phosphonic acid, was used for speciation and preconcentration of the sample and retention of Cr(III) [18]; optimization of process variables were performed to have accurate analyses results by flame atomic absorption spectroscopy and no interferences were observed during the analyses due to the existence of other metals such as calcium, cadmium, lead, zinc. In a study [19], which employs PEUF as preconcentration step, the conditions for the flame atomic absorption spectroscopy were investigated for the determination of metal ions. In this study, polyethyleneimine (PEI) and its thiourea derivatives were used as polymeric ligands. It was found that the presence of polymer affected the analyses of copper, cadmium, zinc and magnesium. As the polymer concentration increased in the range of 1–4%, decrease in absorbance was observed. To eliminate this effect, standard solutions were prepared under the same conditions with the sample solutions which contain polymer. In that study, no attempt was made to obtain true metal concentrations using data evaluation methods.

In the present work, it would be attempted to find suitable analyses conditions for determination of concentrations of mercury, calcium and cadmium using atomic absorption spectroscopy

after PEUF experiments which were performed for removal of mercury and cadmium from aqueous solutions. Effect of various sample preparation parameters were investigated. Effect of presence of polymer at various concentrations on measured metal concentrations were evaluated in detail. To compensate for the presence of polymer, modifications in application of the AAS method and in the data evaluation were attempted. Therefore, we may state that our aim is to widen applicability and accuracy of atomic absorption spectrometric techniques in determination of heavy metal ion concentrations especially for solutions which may contain water soluble complexing polymers and binary metal mixtures.

2. Experimental

2.1. Materials

In the ultrafiltration (UF) experiments and concentration analyses, polyethyleneimine with average molecular weight 50000 Da (Sigma), mercury nitrate ($\text{Hg}(\text{NO}_3)_2 \cdot \text{H}_2\text{O}$, Merck), cadmium nitrate ($\text{Cd}(\text{NO}_3)_2 \cdot 4\text{H}_2\text{O}$, Merck), calcium nitrate ($\text{Ca}(\text{NO}_3)_2 \cdot 4\text{H}_2\text{O}$, Merck), sodium hydroxide (Merck), nitric acid (Merck), hydrochloric acid (Merck) and sodium tetraborohydrate (Merck) were used. Demineralized water of $18.2 \text{ M}\Omega \text{ cm}^{-1}$ obtained from water purification system (Millipore) used for dilution and preparation of feed solution. For the laboratory scale and pilot scale systems, different types of membranes were used. For the former, the membrane was Osmonics flat sheet (HG01) type having effective area of 0.0155 m^2 molecular weight cut-off (MWCO) 5000 Da; for the latter, it was Amicon spiral wound (S10Y10) type having effective area of 0.93 m^2 and MWCO 10000 Da.

2.2. Apparatus

The laboratory scale Osmonics SEPA UF cell and the pilot scale Amicon SP20 UF systems were employed for PEUF experiments which are described previously [2,3]. Philips 9200X AAS were used for analyses of metals used in PEUF experi-

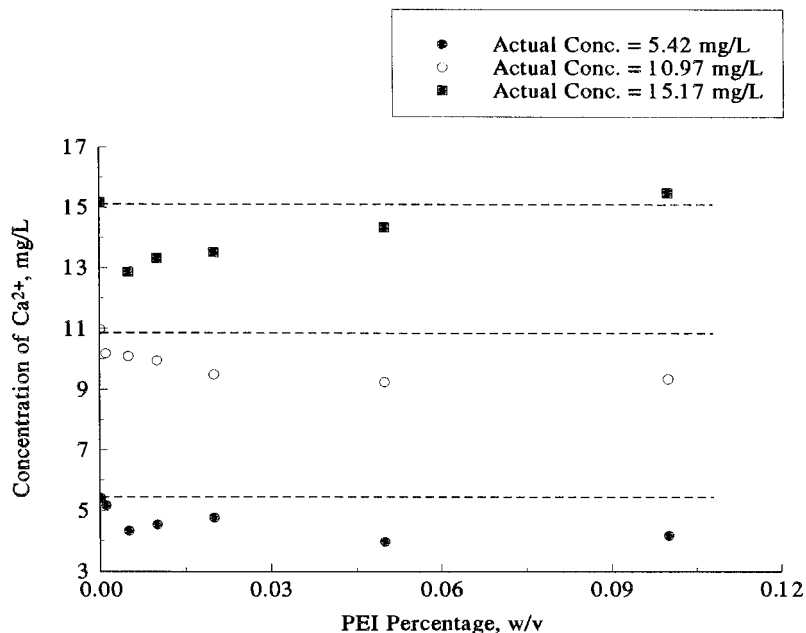


Fig. 2. Effect of change in PEI concentration on determination of concentration of calcium by FAAS.

ments. Cold vapor atomic absorption spectroscopy (CVAAS) was applied for mercury analysis using Philips 9360X cold vapor system.

2.3. Methodology

Feed solutions at desired metal and PEI concentrations were prepared and stirred at 250–300 rpm for 2 h prior to UF experiments. For mercury experiments, studied PEI and mercury concentrations were in the range of 0.003–0.5% and 10–1000 mg l⁻¹, respectively, while, for cadmium and calcium experiments, those were 0.003–0.1 and 10–300 mg l⁻¹, respectively. In mercury and cadmium studies, it was observed that retention of metals was around 0.98 before the critical loading (g metal per g PEI) ratio at which decrease in retention starts [2,3]. Therefore, in permeate streams mercury and cadmium concentrations can be as low as 0.3 mg l⁻¹. On the other hand, as calcium did not form a complex with PEI, almost all calcium ions pass through the membrane [3]. Since molecular weight of polymer is much higher relative to MWCO point of membranes, it is expected that no polymer passes to the permeate

stream. Details of operation of PEUF process was given elsewhere [2,3]. Feed solutions at desired metal and polymer concentrations were prepared and stirred at 250–300 rpm for 2 h prior to ultrafiltration experiments and its pH was adjusted. During the ultrafiltration experiments; pH, temperature, feed flow rate and pressure difference was kept constant and monitored continuously. During an ultrafiltration run feed solution was circulated by means of the pump, then passed through the membrane. Separate retentate and permeate streams were returned to the feed solution tank to keep the feed concentrations constant. At certain time intervals, samples from both permeate and feed were taken to determine the metal concentration. Although feed solution was prepared for certain metal concentration, there were deviations from the prepared concentrations due to evaporation and/or taking samples from feed and permeate streams. Therefore, feed streams should also be analyzed.

Suitable concentration range detected in AAS for each metal varies and can be listed as follows according to the used systems i.e. CVAAS for mercury and air–acetylene for calcium and cad-

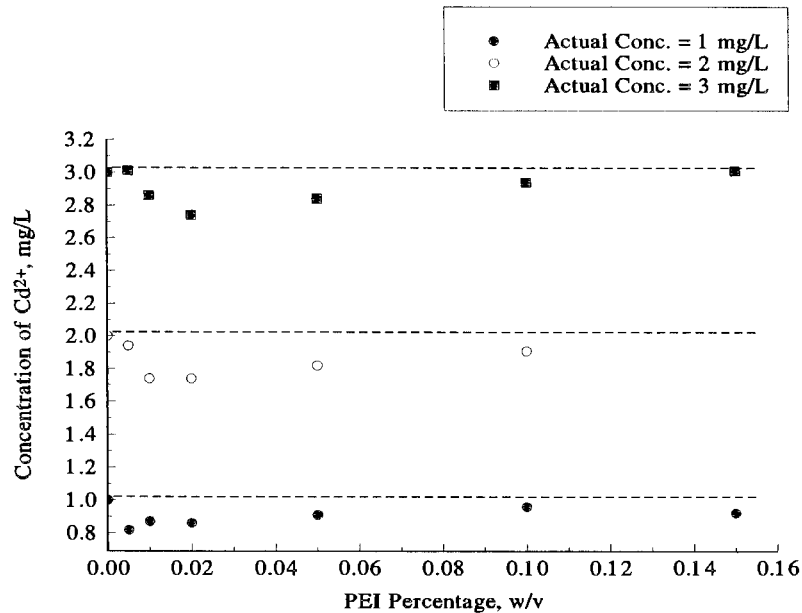


Fig. 3. Effect of change in PEI concentration on determination of concentration of cadmium by FAAS.

mium: mercury $0.01\text{--}50\ \mu\text{g l}^{-1}$, cadmium $0.05\text{--}3\ \text{mg l}^{-1}$ and calcium $0.2\text{--}20\ \text{mg l}^{-1}$ [20]. Exceeding these concentrations, calibration plot usually deviates from linearity. Therefore, sample solutions should be diluted before AAS analyses so that concentration of metal in the solutions is reduced to fall into these range.

For the determination of mercury concentration, CVAAS was employed as it is mentioned,

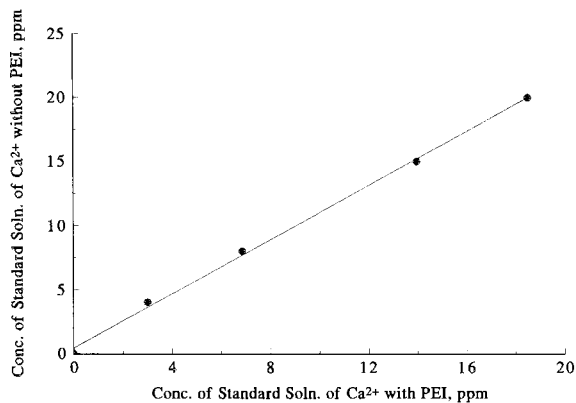


Fig. 4. Calibration curve for standard solutions of cadmium containing PEI.

since mercury is unique among the metallic elements due to its significant vapor pressure at room temperature ($0.16\ \text{kPa}$ at $293\ \text{K}$). Before employing CVAAS, various concentrations of HCl, such as 10% HCl (i.e. concentrated HCl was diluted ten times) added to sample solutions during the dilution to reduce all the forms of mercury in the solution to Hg^{2+} form. NaBH_4 solution was prepared by dissolving NaBH_4 and NaOH in demineralized water with concentrations of 1 and 0.1% w/v, respectively. The function of NaOH was to prevent the hydration reaction between NaBH_4 and water. Containing $10, 30, 40, 50\ \mu\text{g l}^{-1}$ mercury and the same amount HCl as in the diluted sample solutions, standard solutions were prepared. Then, calibration curve was determined by using these standard solutions and blank which includes demineralized water and HCl. In CVAAS method, mercuric ions in the samples can be reduced by NaBH_4 solution to elemental mercury. Mercury is swept out of the solution by N_2 (inert gas) to a long-path glass absorption cell where the atomic absorption of the mercury is measured at $253.7\ \text{nm}$.

For the cadmium and calcium analyses, acetylene–air flame AAS (FAAS) was used: For

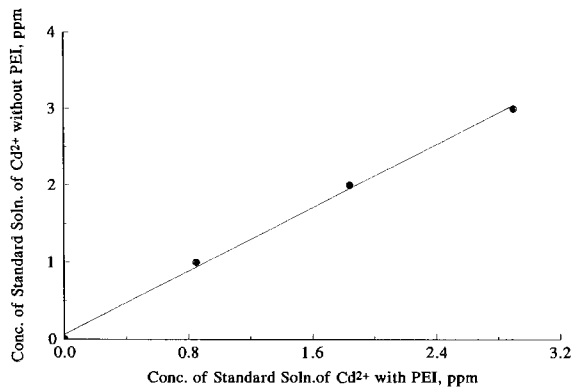


Fig. 5. Calibration curve for standard solutions of cadmium containing PEI.

some cases, there was no need for dilution of sample solutions since the studied concentration was in the range of concentrations of standard solutions. For cadmium, concentrations of standard solutions are 1, 2, 3 mg l^{-1} , while for calcium, those are 4, 8, 15, 20 mg l^{-1} . Like mercury analyses, calibration curves were determined. Wavelengths of most sensitive absorption lines 422.7 nm and 228.8 nm for calcium and cadmium, respectively were employed.

Background correction was achieved by means of deuterium lamp.

3. Results and discussions

Since CVAAS and FAAS were employed for the metal analyses, the best analyses conditions were determined for both techniques and different metals.

3.1. Analysis of solutions without polymer

As it is mentioned, at the beginning of the analyses, calibration of spectrophotometer was performed using standard solutions and blank. Concentrations of standard solutions and their absorbance measurements are plotted in Fig. 1 for mercury. There is a linear relationship between absorbance and concentration which indicates that Beer's Law is valid within the concentration range used ($10\text{--}50 \mu\text{g l}^{-1}$). Linearity was also

proven by means of given equation which is $A = 0.00117 + 0.00388C$, where A is the absorbance, C is the concentration of mercury in terms of $\mu\text{g l}^{-1}$, with a regression coefficient 0.99976.

Similar calibrations were also carried out for calcium and cadmium and linear curves were obtained.

Therefore, it can be concluded that both CVAAS applied for mercury and FAAS applied for cadmium and calcium are suitable to analyze permeate stream which contains almost no PEI.

For each sample, three measurements were taken to see deviations in the signal taken from AAS. It was observed that variations between these measurements did not exceed 1%.

3.2. Analysis of solutions containing polymer

3.2.1. Cold vapor atomic absorption spectroscopy

Before mercury analysis in CVAAS, samples were acidified with HCl to dissociate mercury–PEI complex. However, the amount of acid added to the sample is crucial to eliminate the effect of the presence of PEI in the solution. Thus, experiments were carried out with the solutions of $30 \mu\text{g l}^{-1}$ mercury at different PEI concentrations and HCl concentrations (Table 1). In the range of 10–15% HCl, the errors were acceptable. These observations may be explained as follows: At lower HCl concentrations, the reduction of all mercury forms to Hg^{2+} form may not be achieved, whereas at higher HCl concentration, excess amount of HCl may cause sudden release of hydrogen gas which may result in the dilution of analyte plug. It may be concluded that in 10–15% HCl solutions, PEI was denatured or mercury–PEI complexes were broken completely. Based on these observations, further studies to investigate the effect of polymer presence, at varying mercury and PEI concentrations were carried out at fixed HCl concentration of 10%. Results were reported at Table 2; no significant change in atomic absorption signal was observed in the presence of PEI. There was one study [19] in literature which reports similar findings.

The effect of existence of PEI was also further eliminated by means of dilution from mg l^{-1} to $\mu\text{g l}^{-1}$ ranges after PEUF experiments which

Table 3
Corrected concentration results for solutions containing 0.01% PEI in Fig. 2

Concentration without correction (mg l ⁻¹)	Corrected concentrations (mg l ⁻¹) (with correction I)	Actual concentrations (mg l ⁻¹)
4.54	5.25	5.42
9.95	10.97	10.97
13.33	14.74	15.17

Table 4
Corrected concentration results for solutions containing nearly 0.01% PEI in Fig. 3

Concentration without correction (mg l ⁻¹)	Corrected concentrations (mg l ⁻¹) (with correction I)	Actual concentrations (mg l ⁻¹)
0.87	1.00	1.00
1.74	1.92	2.00
2.86	2.96	3.00

provides decreasing PEI concentrations in the sample solutions. In diluted samples, maximum PEI concentration was around 0.05%.

Since binary studies were carried out with mercury–calcium and mercury–cadmium pairs, the effect of one metal on analysis of other metal was also investigated. No interference was observed in the concentration range studied for all metals.

3.2.2. Flame atomic absorption spectroscopy

Since the presence of PEI in the solution may affect the some properties of the solutions, e.g. the viscosity, surface tension [19] and/or cause some interference in the absorption signals, the influence of PEI concentration on the analysis of calcium and cadmium was investigated: As it is seen in Figs. 2 and 3, increase in PEI concentration causes decrease in measured calcium, cadmium concentrations, respectively, then it gives a minimum value at certain PEI concentration and starts to increase slightly within the studied PEI concentration range. In a previous study [19], it was also found that the existence of PEI affected the analyses of cadmium, copper, nickel and zinc. However, linear decrease was observed in the metal concentrations, as polymer concentration increased. This is due to the difference in the studied PEI concentration ranges, 1–4% in that

study, while 0.005–0.1% in this study. This effect of PEI on atomic absorption signal has special importance for the feed stream in PEUF which mainly contains free PEI and/or metal–PEI complex. For permeate stream, this effect is not considerable because it was found that permeate stream contains almost no PEI from the viscosity measurements which gave that viscosity of the solution taken from permeate streams was approximately equal to that of water.

Therefore, it can be concluded that during the analysis of samples taken from the feed stream, the effect of PEI should be eliminated: at the end of the UF experiments, sample solutions were diluted to acceptable limits for detection of metals by AAS. Although their PEI concentration became smaller, PEI may still affect the analysis results. Therefore, two different approaches were applied to make a correction. First, standard solutions containing PEI the same amount as in the diluted samples and containing no PEI were prepared, separately. According to the first approach, the standard solutions containing PEI were used for the calibration, then, samples were analyzed. For the second approach, standard solutions of each metal containing no PEI were prepared and calibrated by plotting the absorbance versus concentration graphs. Concentrations of samples taken from feed streams and apparent concentra-

Table 5

Corrected concentration results for the PEUF experiment at 0.05% PEI and g Ca²⁺ per g PEI ratio = 0.11 (feed solution was diluted five times)

Number of feed sample	Time (min)	Added Ca ²⁺ (mg l ⁻¹) (without correction)	Found Ca ²⁺ (mg l ⁻¹) (with correction I)	Found Ca ²⁺ (mg l ⁻¹) (with correction II)
F1	0	10.11	11.2	11.4
F2	60	10.12	11.22	11.41
F3	150	10.27	11.35	11.60
F4	150	10.29	11.37	11.63
F5	195	10.75	11.85	12.00

Table 6

Corrected concentration results for the PEUF experiment at 0.09% PEI and g Cd²⁺ per g PEI ratio = 0.017 (feed solution was diluted ten times)

Number of feed sample	Time (min)	Added Cd ²⁺ (mg l ⁻¹) (without correction)	Found Cd ²⁺ (mg l ⁻¹) (with correction I)	Found Cd ²⁺ (mg l ⁻¹) (with correction II)
F1	0	1.49	1.65	1.60
F2	210	1.52	1.68	1.63
F3	230	1.51	1.67	1.62
F4	250	1.54	1.70	1.65
F5	275	1.54	1.70	1.65

tions of standard solutions containing PEI were determined by means of these graphs. Calibration curves were obtained plotting apparent concentrations of standard solutions containing PEI versus concentrations of standard solutions containing no PEI. Linear relationships were observed. Therefore, these relations were used for corrections for sample solutions containing PEI.

To check the accuracy of the second approach, same procedure was applied for solutions with known metal concentrations containing same amount of PEI, approximately 0.01%, as in the curves plotted in Figs. 4 and 5. As it is seen in Tables 3 and 4, actual concentration values and corrected concentration results found with second approach are nearly the same. This means that corrections made by this approach are good enough to eliminate the presence of PEI in the solution and to have accurate concentration results.

To show the applicability of these two approaches to PEUF systems, samples taken from feed stream at certain time intervals during PEUF experiments were analyzed using these methods

(Tables 5 and 6). As mentioned before, exact concentrations of metal in the feed stream were not known and may vary with time. For the second approach, same calibration curves, Figs. 4 and 5, for calcium and cadmium, respectively, were employed, since concentration of PEI in the diluted samples were the same as in the standard solutions containing PEI plotted in Figs. 4 and 5. As it is seen, concentration results obtained from two different approaches were approximately the same. This means that preparing calibration curves for different PEI concentrations like Figs. 4 and 5, analyses can be performed without using standard solutions containing PEI at each experiment. As it is seen in Tables 5 and 6, there was greater than 10% difference between corrected and uncorrected concentration results. Therefore, correction with these methods should be required to evaluate the real performance of UF system.

4. Conclusions

Recently, PEUF method has gained importance from the environmental point of view. Since per-

formance of PEUF mainly depends on the retention of metals, analysis methods are very important to determine the metal concentrations in permeate and feed streams correctly. AAS can be used successfully to determine the concentrations of mercury, calcium and cadmium at the end of PEUF experiments.

It was found that existence of one metal did not affect the analysis of other in binary metal solutions. Also, permeate streams contain almost no PEI therefore they cause no deviation from the correct atomic absorption signal. Therefore, there is no difficulty in determining the concentration in the permeate streams. However, for the samples taken from the retentate streams, the existence of PEI affects the analysis results. This effect can be eliminated by means of adding certain amount of HCl to the sample solutions for the mercury analysis in CVAAS. For cadmium and calcium analyses in FAAS, two approaches using standard solutions containing PEI and no PEI were applied to have corrected concentration results.

Acknowledgements

The authors acknowledge the financial support of Turkish Scientific and Research Council (TÜBİTAK) through grant KTÇAG-122. The authors also thank Professor Dr Yavuz Ataman for his valuable comments.

References

- [1] C. Vandecasteele, C.B. Block, *Modern Methods for Trace Element Determination*, Wiley, New York, 1993, pp. 100.
- [2] Y. Uludağ, H.Ö. Özbelge, L. Yılmaz, *J. Membr. Sci.* 129 (1997) 93.
- [3] J. Müslehiddinoğlu, Y. Uludağ, H.Ö. Özbelge, L. Yılmaz, *J. Membr. Sci.* 40 (1998) 251.
- [4] K. E. Geckeler, E. Bayer, B.Y. Spivakov, V.M. Shkinev, G.A. Vorob'eva, *Anal. Chim. Acta* 189 (1986) 285.
- [5] E. Bayer, B.Y. Spivakov, K.E. Geckeler, *Polym. Bull.* 13 (1985) 307.
- [6] K.E. Geckeler, V.M. Shkinev, B.Y. Spivakov, *Die Angew. Makromol. Chem.* 155 (1987) 151.
- [7] K. E. Geckeler, E. Bayer, G.A. Vorob'eva, B.Y. Spivakov, *Anal. Chim. Acta* 230 (1990) 171.
- [8] P. Masse, T.B. Choe, A. Verdier, *Annali di Chimica* 77 (1987) 925.
- [9] V. Mavrov, I. Petrova, K. Davarsky, S. Manolov, *Desalination* 83 (1991) 289.
- [10] B.Y. Spivakov, K.E. Geckeler, E. Bayer, *Nature* 315 (1985) 313.
- [11] S.D. Mundkur, J.C. Watters, *Sep. Sci. Technol.* 28 (1993) 1157.
- [12] R.S. Juang, M.N. Chen, *J. Membr. Sci.* 119 (1996) 25.
- [13] K. Volchek, L. Keller, D. Velicogna, H. Whittaker, *Desalination* 89 (1993) 247.
- [14] A. P. Novikov, V.M. Shkinev, B.Y. Spivakov, B.F. Myasoev, K.E. Geckeler, E. Bayer, *Radiochim. Acta* 46 (1989) 35.
- [15] S.M. Pyle, J.M. Nocerino, *Environ. Sci. Technol.* 30 (1996) 204.
- [16] J.C. Latino, Z.A. Grosser, *Atom. Spectrosc.* 17 (1996) 215.
- [17] E. Pramauro, A.B. Prevot, V. Zelano, W.L. Hinze, G. Viscardi, P. Savarino, *Talanta* 41 (1994) 1261.
- [18] R.M. Cespon-Romero, M.C. Yebra-Biurrun, M.P. Bermejo-Barrera, *Anal. Chim. Acta* 37 (1996) 327.
- [19] V.M. Shkinev, V.N. Gomolitskii, B.Y. Spivakov, K.E. Geckeler, E. Bayer, *Talanta* 36 (1989) 861.
- [20] A.D. Eaton, L.S. Clesceri, A.E. Greenberg, *Standard Methods for the Examination of Water and Wastewater*, vol 3, 1995, p. 13.

Determination of iron(III) with salicylic acid by the fluorescence quenching method

Ki-Won Cha *, Kwang-Won Park

Department of Chemistry, Inha University, Incheon 402-751, South Korea

Received 18 August 1997; received in revised form 7 January 1998; accepted 13 January 1998

Abstract

The spectrofluorimetric determination of Fe^{3+} using salicylic acid as an emission reagent has been investigated by measuring the decrease of fluorescence intensity of salicylic acid due to the complexation of Fe^{3+} –salicylic acid. An emission peak of salicylic acid, which is decreased linearly by addition of Fe^{3+} , occurs at 409 nm in aqueous solution with excitation at 299 nm. The determination of the ferric ion is in the range 1×10^{-6} – 10×10^{-6} M Fe^{3+} (0.0558–0.558 $\mu\text{g}/\text{ml}$) and the detection limit is 5×10^{-8} M. The quenching effect of Fe^{3+} on the fluorescence intensity of salicylic acid may be considered on the basis of complexation between salicylic acid and Fe^{3+} . The effects of foreign ions were investigated. © 1998 Elsevier Science B.V. All rights reserved.

Keywords: Fluorescence quenching; Stern–Volmer equation; Salicylic acid; Fe^{3+}

1. Introduction

Spectrofluorimetry has been widely applied to determine many anions and cations. However, few spectrofluorimetric methods have been investigated for the determination of Fe^{3+} . This is probably due to the character of its paramagnetism or heavy atomic ion [1]. Some fluorimetric methods have been based on quenching phenomena. For example, one method reported the reduction of Fe^{3+} with hydroxylamine and the addition of fluorescent 2,2',2''-terpyridyl to form a chelate [2]. Iron, copper and cobalt ions, having unfilled d sublevels, and do not usually form

fluorescent chelates but can quench the fluorescence of chelates of aluminium, etc. and can be measured indirectly. Thus the quenching of aluminium 8-hydroxyquinoline can be used to measure clinically important ions, such as Fe^{3+} , Cu^{2+} and Co^{2+} [3].

Mori et al. proposed a sensitive and convenient fluorimetric procedure for the determination of iron using *o*-hydroxyhydroquinonephthalein as the fluorogenic reagent in the presence of Brij-58. Unfortunately, cations such as Al^{3+} , Cu^{2+} and Sn^{4+} interfered [4].

Recently, the use of 5-(4-methylphenylazo)-8-aminoquinoline for the fluorimetric determination of iron was reported [5]. Cha and Park reported spectrofluorimetric determination with 2-pyridine-carbaldehyde-5-nitro-ridyl-hydrazone in the pres-

* Corresponding author. Fax: +82 32 8722520; e-mail: kwcha@dragon.inha.ac.kr

ence of hexadecyltrimethylammonium bromide surfactant [6].

In this work, the fluorescence intensity of salicylic acid in the presence of Fe^{3+} was investigated. The change of fluorescence intensity of salicylic acid due to the interaction of Fe^{3+} –salicylic acid in an aqueous medium was measured. This phenomenon provided a sensitive and very simple determination method of Fe^{3+} in the absence of Fe^{2+} .

2. Experimental

2.1. Apparatus and reagents

All fluorescence measurements were made with a JOBIN YVON SPECTRO JY3-D spectrofluorometer using 1 cm quartz cells. The band passes were at 4 nm for both excitation and emission monochromators. The light source was a 150 W Xenon lamp.

Fe^{3+} and Fe^{2+} stock solutions (1.0×10^{-3} M Fe^{3+} and Fe^{2+}) were prepared by dissolving $\text{FeNH}_4(\text{SO}_4)_2 \cdot 12\text{H}_2\text{O}$ and $\text{Fe}(\text{NH}_4)_2(\text{SO}_4)_2 \cdot 6\text{H}_2\text{O}$ with water. Salicylic acid solution (1.0×10^{-3} M) was prepared by dissolving salicylic acid (Sigma reagent) with 30% ethanol.

pH 8.5 buffer solution was prepared as follows: ammonium chloride (5.35 g of 0.1 M) was added to 1.2 ml of 14.8 M ammonium hydroxide solution, then diluted to 1000 ml with water. Analytical reagent grade chemicals and water obtained from a Millipore Milli-Q water purification system were used throughout.

2.2. Procedure

Salicylic acid solution (4 ml of 1.0×10^{-4} M) was added to a 100 ml volumetric flask, containing an appropriate volume of Fe^{3+} solution and 2 ml of pH 8.5 buffer solution, then diluted to the mark with water. The fluorescence intensity of the solution was measured at 409 nm, with excitation at 299 nm. The duration of each measurement is ca. 10 min. All fluorescence intensity measurements were corrected with blank solution. All experiments were performed at room temperature (22°C). The

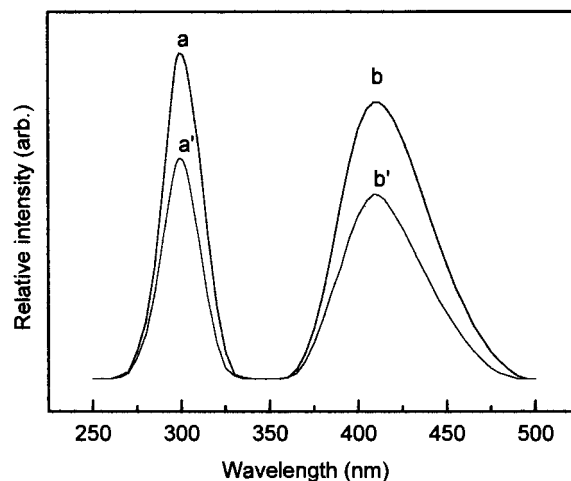


Fig. 1. Fluorescence excitation (a) and emission (b) spectra; a,b: salicylic acid 4.0×10^{-6} M; a',b', adding 1.0×10^{-6} M of Fe^{3+} to the 4.0×10^{-6} M salicylic acid.

quenching effect of oxygen was removed by passing nitrogen gas through the sample solution.

3. Results and discussion

3.1. Excitation and emission spectra of salicylic acid

The excitation and emission spectra of the sali-

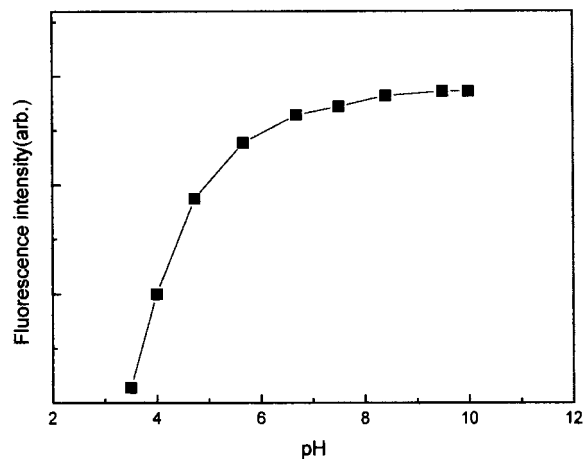


Fig. 2. pH effect of solution on the fluorescence intensity of Fe^{3+} -salicylic acid. Fe^{3+} : 4.0×10^{-6} M; salicylic acid: 4.0×10^{-6} M.

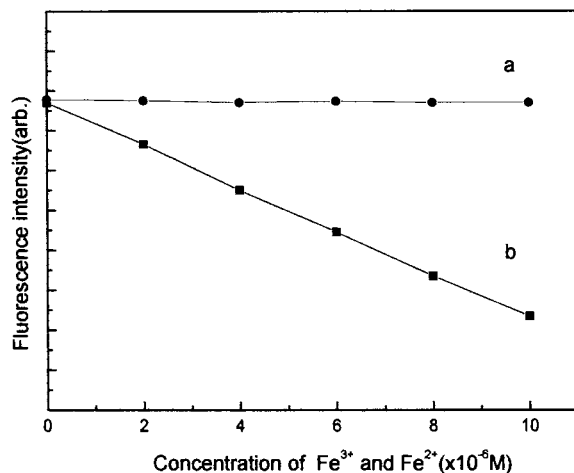


Fig. 3. Calibration curves of Fe^{2+} (a) and Fe^{3+} (b); salicylic acid: 4.0×10^{-6} M.

cylic acid in the presence of Fe^{3+} and of the reagent alone were obtained with a pH 8.5 buffer solution and are shown in Fig. 1. The excitation and emission peaks of the salicylic acid appeared at 299 nm and 409 nm, respectively. As can be seen in Fig. 1, a decrease of the fluorescence intensity in the maximum emission peak (409 nm) can be observed in the presence of Fe^{3+} . Therefore, E_x 299 nm and E_m 409 nm were selected as operating wavelengths during all laboratory work.

3.2. Effect of pH

The pH effect of the test solution on the fluorescence intensity of Fe^{3+} –salicylic acid was studied in the above procedure. The result is shown in Fig. 2. The maximum fluorescence intensity occurred at pH higher than pH 8.0. Thus pH 8.5 is recommended for further studies.

3.3. Effect of salicylic acid concentration

The difference fluorescence intensity (ΔF) of Fe^{3+} solution (4×10^{-6} M) had a linear relationship with a concentration of 1×10^{-6} – 10×10^{-6} M salicylic acid.

Hence, 4×10^{-6} M salicylic acid was chosen as optimum for further studies.

3.4. Calibration curve of Fe^{3+}

Fig. 3 shows the calibration curve of Fe^{3+} in 4×10^{-6} M salicylic acid. In order to determine Fe^{3+} using the decrease of fluorescence intensity of salicylic acid according to Fe^{3+} concentration, the fluorescence decreases of salicylic acid containing various Fe^{3+} concentrations were measured at 409 nm, with excitation at 299 nm (Fig. 3b). In Fig. 3b, the fluorescence intensity of salicylic acid was decreased linearly with increasing Fe^{3+} concentration in the range of 1×10^{-6} – 10×10^{-6} M and the detection limit ($S/N=2$) is 5×10^{-8} M. Also, in order to determine Fe^{2+} , the above described procedure was applied to Fe^{2+} instead of Fe^{3+} . In Fig. 3a, the fluorescence intensities of the salicylic acid solution were approximately constant with increasing Fe^{2+} concentration (1×10^{-6} – 10×10^{-6} M).

3.5. Quenching by Fe^{3+}

The efficiency of quenching of a fluorescent species by a quenching species follows the Stern–Volmer relationship [7], if the fluorophore and quencher concentrations are in the appropriate range:

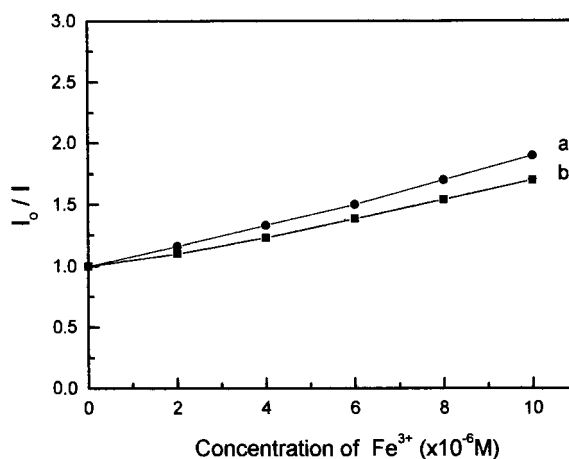


Fig. 4. Stern–Volmer plots for the quenching of salicylic acid fluorescence by Fe^{3+} . (a) 22°C (b) 40°C; salicylic acid: 4.0×10^{-6} M.

Table 1
Tolerance limits for the determination of Fe³⁺

Foreign ions	Tolerance, (M)
Cu ²⁺	4 × 10 ⁻⁵
Cr ³⁺	2 × 10 ⁻⁵
Ni ²⁺	1 × 10 ⁻⁴
Fe ²⁺	7 × 10 ⁻⁶
Mg ²⁺	1 × 10 ⁻⁴
Co ²⁺	1 × 10 ⁻⁵
Zn ²⁺	—
Ba ²⁺	7 × 10 ⁻⁵
Pb ²⁺	2 × 10 ⁻⁵
Al ²⁺	5 × 10 ⁻³
Ca ²⁺	—
Li ⁺	—
Mn ²⁺	5 × 10 ⁻³
Cd ²⁺	5 × 10 ⁻⁵
Sr ²⁺	—
La ³⁺	3 × 10 ⁻⁵
Sm ³⁺	1 × 10 ⁻⁵
Y ³⁺	1 × 10 ⁻⁵
SO ₄ ²⁻	—
Br ⁻	—
SCN ⁻	—
CO ₃ ⁻	—
NO ₃ ⁻	1 × 10 ⁻⁴

Concentration: Fe³⁺ = 1.0 × 10⁻⁶ M, salicylic acid = 4.0 × 10⁻⁶ M.

—, no interference.

$$I_o/I = 1 + K_{sv}[Q]$$

where I_o and I are the fluorescence intensity in the absence and presence of the quencher, respectively. K_{sv} is the Stern–Volmer quenching constant and $[Q]$ is the concentration of the quencher. If a system obeys the Stern–Volmer equation, a plot of I_o/I versus $[Q]$ will give a straight line with a slope of K_{sv} and a y -axis intercept of 1.

Fig. 4 is the Stern–Volmer plot of the Fe³⁺–salicylic acid system. In Fig. 4, I_o/I term linearly increased with increasing the Fe³⁺, $[Q]$. The effect of static quenching according to temperature is lower at higher temperature (Fig. 4b). In the case of dynamic (collisional) quenching, quenching efficiency increases with increasing temperature. Therefore it may be concluded from the consideration of Fig. 4 and Ref. [8] that the quenching mechanism is static quenching (formation of complex between salicylic acid and Fe³⁺).

3.6. Effect of foreign ions

The effect of foreign ions on the fluorescence intensity of the Fe³⁺–salicylic acid system was studied on 1.0 × 10⁻⁶ M Fe³⁺. The tolerance limit was calculated as the concentration of a species which resulted in less than 5% deviation in the fluorescence of Fe³⁺. The results are summarized in Table 1. Most anion and cation species are tolerated in relatively high concentration or did not interfere and Zn²⁺, Ca²⁺, Li⁺, Mn²⁺ and Sr²⁺ ions did not interfere in concentrations 10⁴-fold greater than Fe³⁺ concentration. Fe²⁺, Co²⁺, Sm³⁺ and Y³⁺ ions cause interference.

3.7. Application

The method was applied to the determination of iron ion in tap water and natural water samples. In order to determine the total amount of iron ion in the sample, 1–2 drops of 0.01 M KMnO₄ were added to the sample solution to oxidize Fe²⁺ to Fe³⁺. The sample solution was analyzed for iron without a preconcentration process. The results shown in Table 2 are in good agreement with those obtained by inductively coupled atomic emission spectrometry (ICP–AES) performed for comparison.

In conclusion, this method is worthy of use as an alternative spectrofluorimetric determination of Fe³⁺ at sub-ppm levels at concentrations lower than 7 × 10⁻⁶ M Fe²⁺.

Table 2
Determination of iron ion in tap and natural water

Sample	Found (μg/ml)			
	This method		ICP–AES ^a	
Tap water	0.12		0.13	
(Incheon city)	0.12		0.13	
	0.13	0.12 (mean)	0.13	0.13 (mean)
Natural water	0.19		0.19	
(Munhak Mt.)	0.18		0.19	
	0.19	0.19 (mean)	0.19	0.19 (mean)

^aAnalytical line: 238.04 nm (Labtam 8440 spectrometer).

References

- [1] S.G. Schulman, *Molecular Luminescence Spectroscopy: Methods and Applications, Part 1*, Wiley, New York, 1985, Ch. 4.
- [2] D. Fink, J. Pivnichny, W. Ohnesorge, *Anal. Chem.* 41 (1969) 833.
- [3] S.G. Schulman, *Molecular Luminescence Spectroscopy: Methods and Applications, Part 3*, Wiley, New York, 1993, p. 309.
- [4] I. Mori, Y. Fujita, Y. Nakashi, K. Kato, N. Niwa, *Anal. Lett.* 22 (1989) 1969.
- [5] G.F. Yan, G.R. Shi, Y.M. Liu, *Anal. Chim. Acta* 264 (1992) 121.
- [6] K.W. Cha, C.I. Park, *Talanta* 43 (1996) 1335.
- [7] O.S. Wolfbeis, *Fluorescence Spectroscopy: New Methods and Applications*, Springer, Berlin, 1993, p. 80.
- [8] K.W. Cha, K.W. Park, *J. Korean Soc. Anal. Sci.* 8 (1995) 305.

Detection and spectrophotometric determination of EDTA with cobalt(II) and phosphomolybdic acid in urine and detergents

Ram Parkash *, Reeta Bansal, S.K. Rehani, Seema Dixit

Department of Chemistry, Panjab University, Chandigarh-160014, India

Received 9 October 1997; received in revised form 5 January 1998; accepted 13 January 1998

Abstract

A simple, rapid, sensitive and selective method for the microgram detection and spectrophotometric determination of EDTA in water, human urine and detergents, based on its reaction with Co(II) and phosphomolybdic acid at pH 0.5–2.0 is reported. Absorbance is measured against Co(II)–phosphomolybdic acid reference solution at 750 nm. The effect of time, temperature, pH and Co(II) or phosphomolybdic acid concentration is studied, and optimum operating conditions are established. Beer's law is applicable in the concentration range 0.3–1.9 $\mu\text{g ml}^{-1}$ of 10^{-5}M EDTA. Its detection limit is 0.14 μg in the solution phase and 0.03 μg in the resin phase. The relative standard deviation is $\pm 0.13 \mu\text{g}$. Ag(I), Zn(II), Cu(II), Ni(II), Pb(II), Cd(II), Ca(II), Mg(II), Fe(III), Cr(III), U(VI), chloride, nitrite, phosphate, oxalate, borate and amino acids do not interfere. © 1998 Elsevier Science B.V. All rights reserved.

Keywords: Spectrophotometry; EDTA; Co(II); Phosphomolybdic acid

1. Introduction

EDTA was determined using iron(III) thiocyanate [1], iron(II) complex of 2,4,6-tripyridyl *s*-triazine [2] and ferric alum solution in sulphuric acid [3] at 475 μm , 593 μm and 305 nm, respectively. Yamaguchi et al. [4] determined its traces using a cupric oxide-loaded cation exchanger. The Cu–EDTA complex formed in percolate was determined by reaction with sodium diethyldithiocarbamate in sodium borate buffer (pH

9.3)–NaCl medium. 4-Aminoantipyrine [5] was used as reagent for spectrophotometric determination of EDTA at pH 4. Nemcova et al. [6] proposed an indirect spectrophotometric method for its determination with bromopyrogallol red in the presence of tensides. EDTA has been back titrated with Pb^{2+} using a.c. oscillopolarographic detection of end point [7]. Recently, Sheppard and Henion [8] determined EDTA as nickel chelate in environmental water by solid-phase extraction and capillary electrophoresis/tandem mass spectrometry. In the present communication, a procedure is reported for the detection and spectrophotometric determination of microgram

* Corresponding author. Tel.: +91 172 541435; fax: +91 172 541409.

Table 1
Spectrophotometric determination of EDTA in different samples

Sample	EDTA (μg)		% Recovery	Relative standard deviation (%)	Found by reference procedure, mean recovery (%)
	Added	Found			
Distilled water	13.0	12.9	99.3	0.62	98.9
Tap water	13.0	13.1	100.7	0.97	99.2
Human urine	3.7	3.8	102.7	0.78	99.2
General purpose cleanser	14.8	14.7	99.2	1.30	101.3
Dish washing by hand	14.8	14.9	100.6	0.92	99.8
Clothes washing by hand	14.8	14.8	100.0	1.02	99.6
Delicate clothes washing	14.8	14.7	99.3	1.72	101.2
Machine clothes washing	14.8	14.8	100.0	0.88	98.0

quantities of EDTA based on its colour reaction with Co(II) and phosphomolybdic acid at pH 0.5–2. The method is extended to its determination in water, urine and commonly available Indian detergents.

2. Experimental

2.1. Reagents

Analytical-grade reagents and doubly distilled water were used throughout. Strongly basic anion-exchange resin Amberlite IRA 400 (standard grade, B.D.H.) was used in OH^- form after proper conversion and thorough washing with demineralized water. Solutions of Co(II) (10^{-1} M), EDTA (10^{-1} M) and phosphomolybdic acid (4%) were prepared in demineralized water. More dilute solutions of EDTA were prepared from the stock solution.

2.2. Apparatus

A Hitachi Model 330 double-beam recording spectrophotometer with 10-mm cells was used for absorbance measurements.

2.3. Detection

About 5 to 10 resin beads (OH^- form) are placed on a white spot plate and blotted dry with

filter paper. One drop of test solution is added, followed by one drop each of Co(II) and phosphomolybdic acid solution. A royal blue colour develops instantaneously on the bead surface if the test solution contains EDTA.

2.4. Determination

EDTA (1.0 ml containing 0.3–1.9 μg), Co(II) (2.0 ml of 10^{-1} M solution) and phosphomolybdic acid (2.0 ml of 4% solution) is shaken for a few seconds. The volume is made up to 10 ml with water. The pH is maintained in the range 0.5–2.0. The absorbance is measured at 750 nm against a blank solution at room temperature (25–30°).

Varying amounts of EDTA (3.7–13.0 μg) are added to the tap water, distilled water and human urine samples (5.0 ml), and the EDTA is then determined by the above method (Table 1).

Known amounts of metal ions Zn(II), Cu(II), Pb(II), Cd(II), Ca(II), Mg(II) or Fe(III) (1.0 μg) are added to a normal urine sample (5.0 ml) together with excess EDTA (10.0 μg). EDTA not complexed by the metal, is then determined using the above procedure.

About 500 mg of liquid or powdered detergent is dissolved in distilled water (~20 ml). Any insoluble matter persisting, even after slight warming, is discarded after centrifuging the solution. A blue colour develops on adding Co(II) and phosphomolybdic acid (2 ml each) to the solution. The absorbance is measured at 750 nm (Table 1).

3. Results and discussion

The redox reaction of Co(II)–EDTA complex with phosphomolybdic acid, which forms a royal blue colour, is used for a selective and sensitive detection and spectrophotometric determination of EDTA.

Two types of ion-exchange resin, Amberlite IR 120 (H⁺ form) and Amberlite IRA 400 (OH⁻ form) were added in two different microtest tubes containing the coloured complex formed by the recommended procedure. The negatively charged resin beads turn royal blue, indicating that the complex formed is negatively charged.

The plot of absorbance of the royal blue complex as a function of wavelengths shows a plateau with a maximum absorbance at 750 nm. Beer's law is obeyed for solutions containing 0.3–1.9 µg ml⁻¹ of 10⁻⁵ M EDTA under the optimum conditions.

The effect of time, Co(II) or phosphomolybdic acid concentration and variation in pH on the absorption of the royal blue complex was examined. The royal blue colour developed instantaneously, is stable for 48 h at room temperature (25–30°C), and is also thermally stable up to 50°C. It was revealed that 2.0 ml each of 10⁻¹ M Co(II) and 4% phosphomolybdic acid are the most suitable. The absorbance decreases if the amount of Co(II) is increased further. The absorbance remains constant if the amount of phosphomolybdic acid is more than 2.0 ml of 4% solution. The absorbance was maximum and constant in the pH range 0.5–2.0 at 750 nm. On increasing the pH, the absorbance of the royal blue complex decreases.

The identification limit of EDTA at room temperature (25–30°C) is 0.14 µg in solution phase and 0.03 µg in resin phase, with a minimum concentration of 10⁻⁶ M. Aminocarboxylic acids (NTA, CyDTA, EGTA) interfere with the test in solution phase (if present at more than 50 times excess), but not in the bead test. Ion-exchange beads, thus, act as catalyst and detection medium to improve the selectivity and sensitivity of the test.

Up to 0.3 µg of EDTA is determined quantitatively by this method in the presence of certain ions such as Ag(I), Zn(II), Cu(II), Pb(II), Cd(II), Ca(II), Mg(II), Ni(II), Fe(III), Cr(III), U(VI), chloride, nitrite, phosphate, oxalate and borate, common amino acids (alanine, aspartic acid, glutamic acid, leucine, serine, phenylalanine, lysine and valine) and some other organic compounds (iminodiacetic acid, citric acid, oxalic acid, glycine, gluconic acid), even if present at 100 times excess.

The reproducibility of results was checked by 10 replicate determinations with 9.26 µg EDTA. The accuracy of the method was checked by five unknown determinations. The average error and standard deviation were found to be 0.30 and ± 0.13 µg, respectively. Recovery of EDTA is 98%. In the absence of determination error, the true value fell within 9.17–9.35 µg with a confidence interval of 95%.

The present procedure is suitable for detection and determination of EDTA in natural water, human urine (with or without adding frequently present metal ions such as Zn(II), Cu(II), Pb(II), Cd(II), Ca(II), Mg(II) or Fe(III)) and commercially available detergent samples, without interference from organic compounds and common ions that are known to be present in these samples (Table 1). The recovery of EDTA is satisfactory in each case. For all the samples tested, the method is simple, rapid, precise, accurate and reproducible.

The present method is better than that of Bhattacharya and Kundu [3], as the Fe–EDTA complex is photosensitive [2,9] and undergoes decomposition in sunlight. That the presence of Ca²⁺ and Mg²⁺ does not interfere in the present determination is significant, because the usual titrimetric methods of employing alkali solutions for microdetermination of EDTA are frustrated in the presence of these ions in the sample. The method proposed by Sheppard and Henion [8] is tedious and time consuming.

The results obtained by this procedure agree satisfactorily with those obtained by the method reported in literature [10].

Acknowledgements

One of the authors (Reeta Bansal) is thankful to the U.G.C., New Delhi, India for financial assistance.

References

- [1] C.J. Parker Jr., *Anal. Chem.* 36 (1964) 236.
- [2] B. Kratochvil, M.C. White, *Anal. Chem.* 37 (1965) 111.
- [3] S.N. Bhattacharyya, K.P. Kundu, *Talanta* 18 (1971) 446.
- [4] A. Yamaguchi, K. Ohzeki, T. Kambara, *Z. Anal. Chem.* 310 (1/2) (1982) 30.
- [5] S.Z. Qureshi, R. Bansal, *Z. Anal. Chem.* 308 (1) (1981) 32.
- [6] I. Nemcova, H. Pesinova, V. Suk, *Microchem. J.* 30 (1) (1984) 27.
- [7] B. Mu, J. Sun, *Yejin Fenxi* 15 (2) (1995) 49.
- [8] R.L. Sheppard, J. Henion, *Electrophoresis* 18 (2) (1997) 287.
- [9] S.S. Jones, F.A. Long, *J. Phys. Chem.* 56 (1952) 25.
- [10] F.D. Snell, C.T. Snell, *Colorimetric Methods of Analysis*, vol. IIIA, Van Nostrand, Princeton, 1961, pp. 370–371.

Reversed-phase HPLC method for the estimation of acetaminophen, ibuprofen and chlorzoxazone in formulations

S. Ravisankar *, M. Vasudevan, M. Gandhimathi, B. Suresh

Department of Pharmaceutical Analysis & Drugs Testing Laboratory, J.S.S. College of Pharmacy, Ootacamund, Tamilnadu, India

Received 21 October 1997; received in revised form 12 January 1998; accepted 13 January 1998

Abstract

A simple, precise and rapid reversed-phase HPLC method was developed for the simultaneous estimation of acetaminophen, ibuprofen and chlorzoxazone in formulations. The method was carried out on a Kromasil[®] C₈ column using a mixture of 0.2% triethylamine:acetonitrile (adjusted to pH 3.2 using dilute orthophosphoric acid), and detection was carried out at 215 nm using ketoprofen as internal standard. All these drugs showed linearity in the range of 2–10 µg ml⁻¹, and limits of quantification was found to be 10, 50 and 20 ng ml⁻¹ for acetaminophen, ibuprofen and chlorzoxazone, respectively. © 1998 Elsevier Science B.V. All rights reserved.

Keywords: Acetaminophen; Ibuprofen; Chlorzoxazone; Simultaneous estimation; Reversed-phase HPLC

1. Introduction

Acetaminophen, [1–3] chemically known as *N*-acetyl-*p*-aminophenol is used widely as non-steroidal antiinflammatory and antipyretic agent. Chlorzoxazone [3] is a muscle relaxant and chemically is 5-chloro-2-hydroxy benzoxazole. Ibuprofen [1–3], an aryl acetic acid derivative, chemically is (*RS*)-2-(4-isobutyl phenyl) propionic acid and is used as a non-steroidal antiinflammatory drug. A combination of 325 mg of acetaminophen, 400 mg of ibuprofen and 250 mg of chlorzoxazone is commercially available in tablet form.

A literature survey [4–10] revealed that there are a number of methods available for their individual determination, or for any two of these three drugs in combinations. However, there is no simultaneous method reported for their simultaneous estimation. Hence the present work describes a reversed-phase HPLC method for the estimation of these three drugs in combined dosage form.

2. Experimental

2.1. Reagents and chemicals

Acetonitrile, HPLC grade, orthophosphoric acid, AR grade, and triethylamine, AR grade, were supplied by SD Fine Chemicals Ltd., India,

* Corresponding author. Tel.: +91 423 43393; fax: +91 423 42937.

Water, HPLC grade, was from a Millipore system. Reference standards were obtained from Indoco Remedies, Mumbai, India.

2.2. Chromatographic conditions

A Waters® HPLC system was used for the analysis. The column used was Kromasil® C₈, (5 µm, 25 cm × 4.6 mm ID). A mixture of acetonitrile:0.2% triethylamine (adjusted to pH 3.2 using orthophosphoric acid) (50:50, v/v) was used as mobile phase at a flow rate of 1.5 ml min⁻¹ with an operating pressure of 3000 psi. A Rheodyne® 7125 injector with a 20-µl loop was used for the injection of samples. Detection was done at 215 nm, with a sensitivity of 0.05 AUFS. The mobile phase was filtered through 0.45-µm membrane filter and degassed. The separation was carried out at room temperature, 20 ± 1°C.

2.3. Preparation of standard solutions

Standard stock solutions of acetaminophen, ibuprofen and chlorzoxazone, each of 1 mg ml⁻¹ concentration, were prepared separately in the mobile phase. A stock solution of 100 µg ml⁻¹ of ketoprofen (internal standard) was prepared in the mobile phase. From the standard solutions, suitably diluted mixed standard solutions were prepared to contain 2, 4, 6, 8 and 10 µg ml⁻¹ of acetaminophen, ibuprofen, and chlorzoxazone, containing 10 µg ml⁻¹ of ketoprofen as internal standard.

2.4. Extraction of drugs from the formulations

Twenty tablets, each containing 325 mg of acetaminophen, 250 mg of chlorzoxazone and 400 mg of ibuprofen were weighed and finely powdered. A quantity of powder, equivalent to 32.5 mg of acetaminophen, 25 mg of chlorzoxazone and 40 mg of ibuprofen, was weighed accurately and transferred to a sintered glass crucible and extracted with two quantities, each of 25 ml, of acetonitrile. The combined extracts were made up to 100 ml with the mobile phase. The resulting solution (2.5 ml) was diluted with mobile phase to 25 ml in a standard flask. From this a 2-ml

aliquot was mixed with 1 ml of the internal standard solution (which contains 100 µg ml⁻¹ of ketoprofen) and made up to 10 ml in a standard flask with the mobile phase.

2.5. Procedure

Each 20 µl of mixed standard solutions, containing internal standard, were injected and the chromatograms were recorded (Fig. 1). The retention times of acetaminophen, chlorzoxazone, ketoprofen (Internal standard) and ibuprofen were found to be 1.93, 3.91, 5.65 and 12.50 min, respectively. This was followed by injecting the sample solution obtained from the formulation along with the internal standard. Acetaminophen, ibuprofen, and chlorzoxazone showed linearity in the range of 2–10 µg ml⁻¹. Calibration curves were plotted (Fig. 2) using peak ratios of the standard peak areas and internal standard peak area (response factor). The peak areas of the sample chromatograms were compared, and the amounts of acetaminophen, ibuprofen and chlorzoxazone were calculated, and are shown in Table 1.

3. Recovery studies

To study the reliability and suitability of the above method, recovery experiments were carried out. To 5-ml aliquots of the sample solution obtained from the formulation, 5 ml of the standard solution, which contained 8 µg ml⁻¹ of acetaminophen, ibuprofen and chlorzoxazone, containing 10 µg ml⁻¹ of ketoprofen as internal standard, were added. The contents of acetaminophen, ibuprofen and chlorzoxazone were once again determined by the proposed method by recording the chromatogram. From the amount of the drug present, percentage recovery was calculated using the following formula:

$$\% \text{Recovery} = \left[\frac{b - a}{c} \right] \times 100$$

where, a = amount found before addition, b = amount found after addition and c = amount of standard drug added.

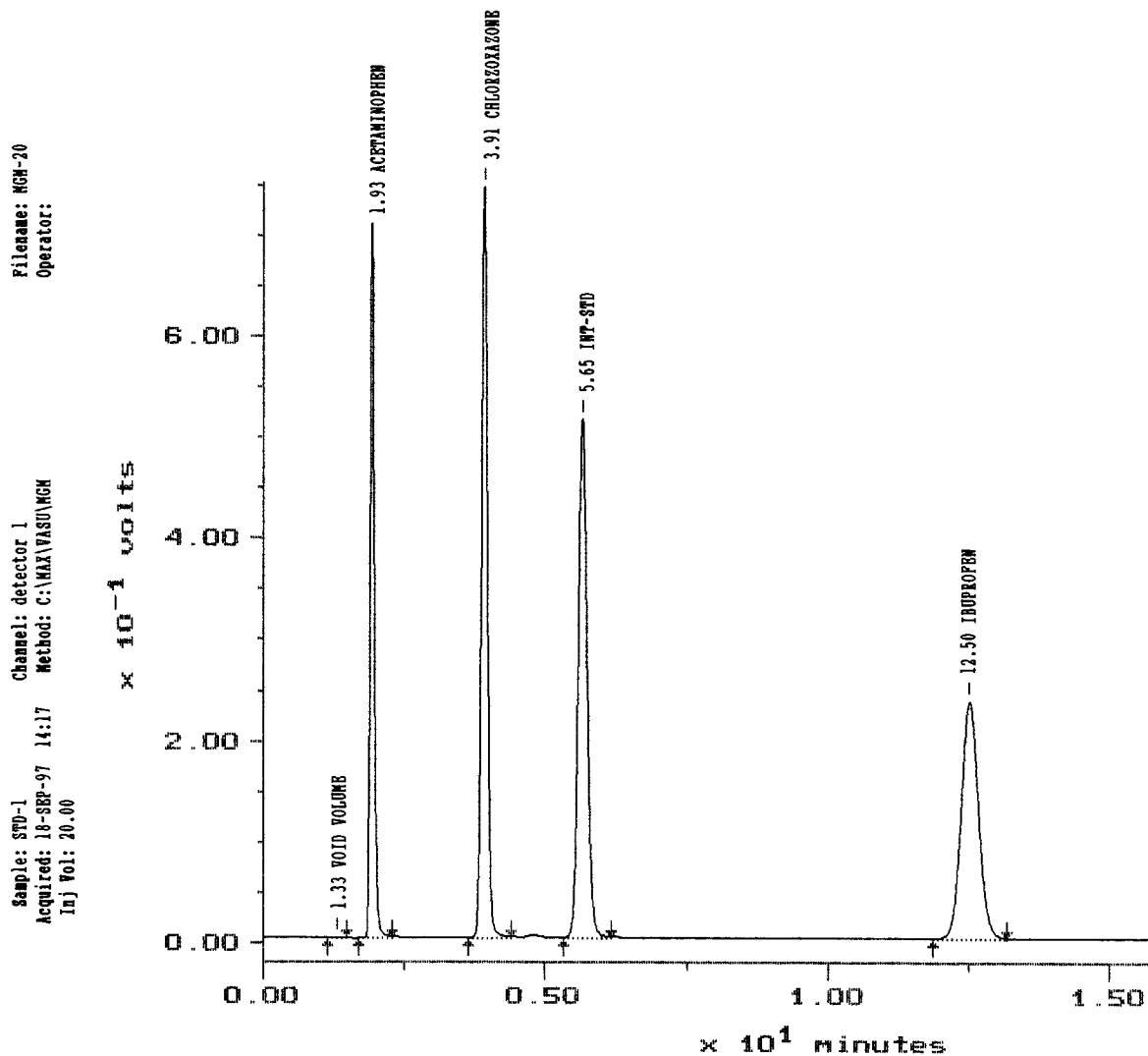


Fig. 1. Chromatogram of acetaminophen, ibuprofen and chlorzoxazone, with ketoprofen as internal standard.

4. Results and discussion

Chromatograms of mixed standard solutions which contained acetaminophen, ibuprofen and chlorzoxazone along with internal standard (ketoprofen) were recorded. A computer-controlled data station with Baseline 810 software was used to plot the peak area vs. concentration in $\mu\text{g ml}^{-1}$. Calibration curves were obtained by using peak area ratios of standard and internal standard vs. concentration. All three drugs showed linearity

in the range of 2–10 $\mu\text{g ml}^{-1}$. The limits of quantification (LOQ) for acetaminophen, ibuprofen and chlorzoxazone were found to be 10, 50 and 20 ng ml^{-1} , respectively. Precision of the method was studied by making five injections of the same standard, with concentrations close to the expected concentrations in samples, and the standard deviation was determined.

From the marketed formulation, sample solutions were made and spiked with internal standard (ketoprofen), and the response factor was

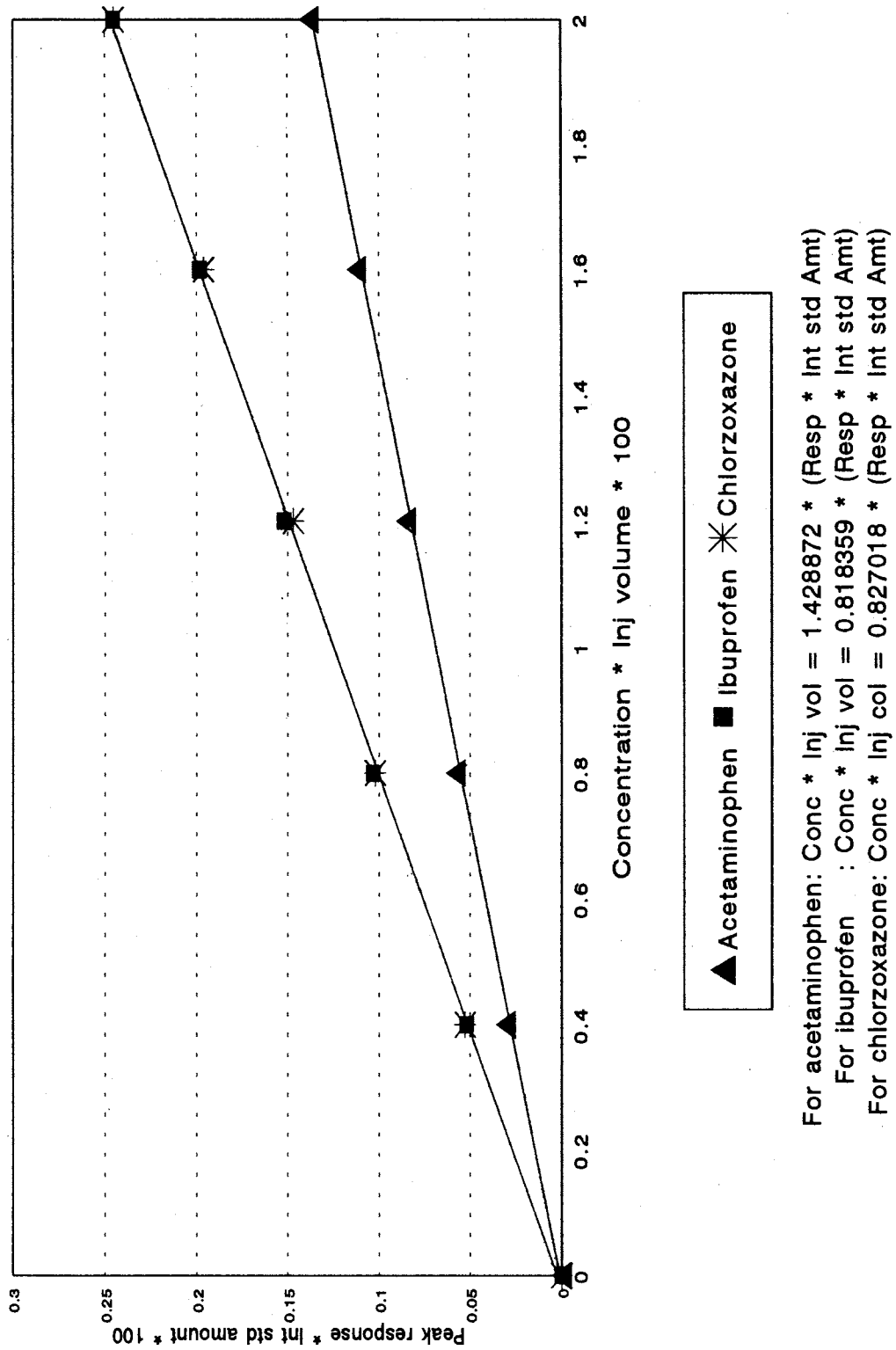


Fig. 2. Calibration curve of acetaminophen, ibuprofen and chlorzoxazone.

Table 1
Analysis of formulations and recovery studies

Drug	Amount (mg tablet ⁻¹)		% label claim ^a	% recovery ^a
	Labeled	Found ^a		
Acetaminophen	325	321.48 ± 3.44	98.96 ± 1.83	99.26 ± 0.52
Chlorzoxazone	250	246.58 ± 2.78	98.63 ± 1.52	100.53 ± 0.84
Ibuprofen	400	406.37 ± 3.21	101.59 ± 0.96	98.62 ± 0.48

^a Mean ± S.D. of five determinations.

used to calculate the concentration of each drug. From the concentration, the amounts of each drug present in tablets were calculated. The reliability and suitability of the method could be seen from the recovery values. Further, there is no interference due to excipients. The proposed HPLC method for the simultaneous estimation of acetaminophen, ibuprofen and chlorzoxazone is simple, rapid and accurate. Thus, the present HPLC method is suitable for the quality control of raw materials, formulations and dissolution studies.

Acknowledgements

The authors are thankful to His Holiness Jagadguru Sri Sri Shivarathri Deshikendra Mahaswamigalavaru of Sri Suttur Mutt for providing facilities for research work.

References

- [1] Indian Pharmacopoeia, vol. I, The Controller of Publications, New Delhi, 1996, pp. 387, 554.
- [2] British Pharmacopoeia, General Medical Council Pharmaceuticals Press, London, vol. I, 1993, pp. 349, 483.
- [3] United States Pharmacopoeia, United States Pharmacopoeia Convention Inc., vol. 16, 1995, pp. 364, 785.
- [4] B.G. Sinder, L.J. Beaubien, D.J. Sears, P.D. Rahn, J. Pharm. Sci. 70 (1981) 1347.
- [5] K.S. Albert, A. Raabe, M. Garry, E.J. Antel, W.R.A. Gillespie, J. Pharm. Sci. 73 (1984) 1487.
- [6] J. Askholt, F.N. Kudsk, Acta Pharmacol. Toxicol. 59 (1986) 382.
- [7] A. Avqerios, A.J. Hutt, J. Chromatogr. 415 (1987) 75.
- [8] P.E. Minkler, C.L. Hoppel, J. Chromatogr. 428 (1988) 388.
- [9] D. Lucas, F. Berthou, C. Girre, F. Poitrenaud, J.F. Manez, J. Chromatogr. Biomed. Appl. 133 (1993) 79.
- [10] M.K.S. El-Din, M.A. Abuirjeie, M.H. Abdel, Anal. Lett. 24 (1991) 2187.

Glutathione oxidase-like activity of glass beads, silica gel and anion-exchange resin modified with cobalt(III)–tetrakis(4-carboxyphenyl)porphine

Masaki Mifune ^a, Rumiko Harada ^a, Akimasa Iwado ^b, Noriko Motohashi ^c,
Yutaka Saito ^{a,*}

^a Faculty of Pharmaceutical Sciences, Okayama University, Tsushima-Naka, Okayama 700, Japan

^b The Graduate School of Natural Science and Technology, Okayama University, Tsushima-Naka, Okayama 700, Japan

^c Kobe Pharmaceutical University, Motoyamakita-Machi, Higashinada-Ku, Kobe 658, Japan

Received 10 November 1997; received in revised form 5 January 1998; accepted 13 January 1998

Abstract

Silica gel and glass beads were modified by using acid chloride of metal–tetrakis(4-carboxyphenyl)porphine (M–TCPP) through a peptide bond, and an anion-exchange resin with M–TCPP by ion-exchange reaction and physical adsorption. The carriers modified with Co³⁺–TCPP proved to accelerate the redox reaction which is catalyzed by glutathione oxidase (GSHOx), while those modified with Mn³⁺–TCPP exhibited no activity. Formation of GS-SG and hydrogen peroxide was confirmed by means of mass spectroscopy and colored reaction, respectively. The silica gel modified with Co³⁺–TCPP exhibited the strongest activity among the tested carriers, and was expected to be useful practically as a solid catalyst for the determination of glutathione. © 1998 Elsevier Science B.V. All rights reserved.

Keywords: Glutathione oxidase-like activity; Oxidation of glutathione; Hydrogen peroxide; Carriers modified with Co³⁺–tetra-(4-carboxyphenyl)porphine

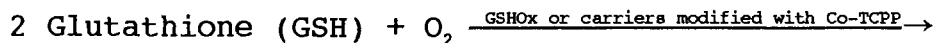
1. Introduction

Previously, we studied the glutathione peroxidase (GSHPx)-like activity of ion-exchange resins modified with metalloporphyrins, which revealed that an anion-exchange resin modified with Mn³⁺–tetrakis(sulfophenyl)porphine exhibited potent

GSHPx-like activity [1]. In the previous study, we suggested that an anion-exchange resin modified with Co³⁺–tetrakis(sulfophenyl)porphine (Co-TSPP_r) and tetrakis(4-carboxyphenyl)porphine (Co-TCPP_r) catalyzed the oxidative reaction of glutathione (GSH) without requiring any peroxide, which is catalyzed by glutathione oxidase [2]. In that time, the modified anion-exchange resins were revealed to have a disadvantageous feature, i.e. adsorption of glutathione with ionic interac-

* Corresponding author. Tel.: +81 86 2517951; fax: +81 86 2517953; e-mail: saito@pheasant.pharm.okayama-u.ac.jp

tion between GSH and the anion-exchange resin. To avoid the adsorption, we had selected, as a carrier, silica gel and glass beads, specifically to aminopropyl silica gel and aminoacyl glass beads to which acid chloride derivative of Co-TCPP may be easily bound. In the present paper, we studied the glutathione oxidase (GSHOx)-like activity of the glass beads and the silica gel modified with Co-TCPP as well as the anion-exchange resin modified with Co-TCPP. Consequently, it has revealed that the carriers modified with Co-TCPP catalyzed the following redox reaction (1).



In addition, hydrogen peroxide in the reaction mixture was determined, and the resulting hydrogen peroxide was revealed to be related to a fixed rate of GSH. This result suggested that GSH can be determined spectrophotometrically based on the amount of hydrogen peroxide released from the reaction (1) catalyzed by the silica gel modified with Co-TCPP.

2. Experimental

2.1. Materials and reagents

Reagent-grade tetrakis(4-carboxyphenyl)porphine ($\text{H}_2\text{-TCPP}$) and tetrakis(4-methylpyridyl)porphine ($\text{H}_2\text{-TMPyP}$) were purchased from Wako Junyaku and used without any purification. Amberlite IRA 900 was selected as a mother anion-exchange resin and Dowex MSC-1 as a mother cation-exchange resin. They were washed with 1 mol l^{-1} HCl and NaOH solutions, and with water and acetone, successively, and dried up. Aminoacyl controlled-pore glass beads (particle size, 200–400 mesh) and aminopropyl silica gel (Licrosorb-NH₂; particle size, 10 μm) were purchased from CPG Inc. and Merck AG, respectively, as mother carriers. Aqueous solutions of glutathione were prepared in requirement from glutathione (reduced form, Sigma and

Aldrich). Peroxidase (Type I, from horseradish) for the determination of hydrogen peroxide was purchased from Sigma and Aldrich. Other reagents and chemicals were of analytical or reagent grade.

2.2. Preparation of ion-exchange resins modified with M-P

$\text{H}_2\text{-TCPP}$ was converted into Co^{3+} and Mn^{3+} complexes (Co- and Mn-TCPP) and $\text{H}_2\text{-}$

TMPyP into Fe^{3+} -TMPyP by the methods described in the literature [3,4]. The modified resins (M-P_r, M-P 25 $\mu\text{mol g}^{-1}$ dry resin) were prepared from aqueous solutions of the metal-porphyrins and ion-exchange resins (Amberlite IRA 900 and Dowex MSC-1), according to the method reported previously [5–9].

2.3. Preparation of glass beads and silica gel modified with Co-TCPP

Co^{3+} - and Mn^{3+} -tetrakis(4-chloroformylphenyl)porphine (M-TCPPCl, M = Co^{3+} and Mn^{3+} , see Fig. 1), acid chloride of M-TCPP, was prepared from M-TCPP and thionyl chloride in dioxane at 70°C by the conventional method. Excess thionyl chloride and dioxane was removed under vacuum, and solid M-TCPPCl was washed with dioxane and dried under vacuum. For linking M-TCPP to carriers, a mixture of M-TCPPCl and silica gel or glass beads in dioxane were refluxed until the mixture becomes clear. Silica gel or glass beads modified with M-TCPP (M-TCPP_s and M-TCPP_g, M-TCPP 25 $\mu\text{mol g}^{-1}$ dry carrier) were filtered, washed with water and acetone, and dried under vacuum.

2.4. Apparatus

Absorption spectra and absorbances were measured on Shimadzu UV-180 and UV-160 spec-

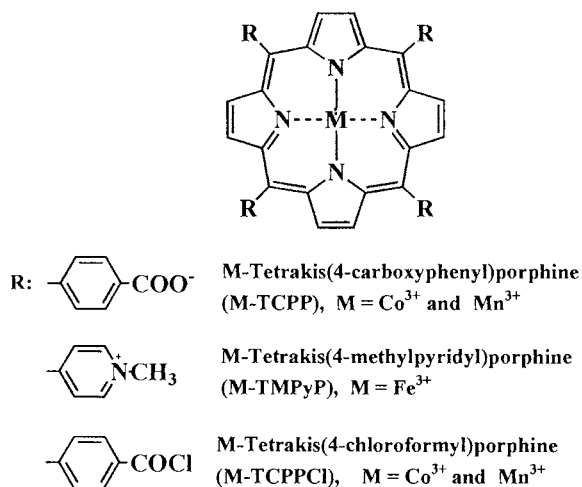


Fig. 1. Structures of metalloporphyrins.

trophotometers with 10-mm fused-silica cells. Mass spectra between 70 and 800 amu were obtained by the electrospray ionization method on a Micromass AutoSpec-OA-Tof mass spectrometer.

2.5. Evaluation of the GSHOx-like activity

A modified carrier (50 mg) was added to a mixture of GSH (10 mmol l⁻¹, 1.0 ml) and 0.05 mol l⁻¹ borate buffer (pH 6.0, 4.0 ml) solutions, and the mixture was incubated at 35°C for 20 min. For the determination of unchanged GSH, 0.1 ml of the supernatant was added to 5.0 ml of the Ellman's reagent solution (a 1:4 mixture of 0.5 mg ml⁻¹ 5,5'-dithiobis(2-nitrobenzoic acid) and 0.05 mol l⁻¹ phosphate buffer (pH 7.2) solutions). An absorbance of the mixture at 412 nm was measured against the reagent blank after standing for 10 min. The control was the supernatant that was obtained in the same manner using IRA 900 in the place of the M-TCPP_r, and the reagent blank for M-TCPP_g and -TCPP_s. The activity of the modified carrier was evaluated on the basis of the decrease in the absorbance against the control.

2.6. Determinations of hydrogen peroxide released from GSH

A sample solution (0.2 ml, containing less than

4 μmol of GSH) was mixed with 0.05 mol l⁻¹ borate buffer (pH 7.0, 2.0 ml) solution. After addition of carrier modified with Co-TCPP (25 mg), the mixture was incubated at 35°C for 20 min, when GSH was oxidized to GS-SG while producing hydrogen peroxide. A supernatant (0.5 ml) of the mixture was added to 4.0 ml of a 4:1:1 mixture of 0.05 mol l⁻¹ borate buffer (pH 7.5), 7.0 mg ml⁻¹ phenol, 0.5 mg ml⁻¹ 4-aminoantipyrine and 10 Unit ml⁻¹ peroxidase (from horseradish) solutions, and the absorbance of the resulting quinoid dye in the mixture was measured at 505 nm against the reagent blank.

2.7. Procedure of determination of GSH

The procedure was essentially the same as that of determination of hydrogen peroxide described in the above section. A calibration curve of GSH against the absorbance was drawn, and GSH should be indirectly determined by referring to the curve.

3. Results and discussion

3.1. Metalloporphyrins

The metalloporphyrins used in this study are shown in Fig. 1. All of them except M-TCPPCl are water soluble. They were immobilized easily and firmly on the ion-exchange resins, as described previously [5–9], by electrostatic and physical interactions. M-TCPPCl, which was an acid chloride of M-TCPP and was easily prepared from M-TCPP, was firmly linked to aminopropyl-silica gel and aminoacyl-glass beads through peptide bonds. All of the modified carriers were stable to temperature, in moisture and storage, and M-TCPP on the carriers was hardly eluted with water and organic solvents.

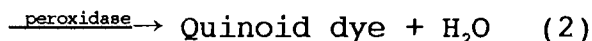
3.2. Reactions

The redox reaction (1) is catalyzed by glutathione oxidase (GSHOx). To confirm the pro-

gress of reaction (1), the formation of GS-SG was investigated by using Co-TCPP_r. To detect GS-SG, the mass spectrum of the supernatant of the reaction mixture was measured using electrospray ionization. As a result, two strong peaks at 307 and 613 amu, attributed to fragment and quasi-molecular ions of GS-SG, were observed. These two peaks, however, were not detectable (less than 1% of intensity) in the mass spectrum of GSH aqueous solution. These results indicated that GSH was oxidized to GS-SG by oxygen in the presence of Co-TCPP_r.

Formation of hydrogen peroxide was also confirmed by using the following color reaction (2).

Hydrogen peroxide + 4-aminoantipyrine (AAP) + phenol



As a result, a considerable amount of hydrogen peroxide was detected in the supernatant of the reaction mixture as discussed in the following section.

Since the higher the GSHOx-like activity of the modified carrier, the more the GSH decreases and the more the hydrogen peroxide generates, quantities of the unchanged GSH and the generated hydrogen peroxide should be a reliable indication of the activity.

3.3. Reaction conditions for examination of GSHOx activity

The anion-exchange resin, IRA 900, adsorbs a considerable amount of GSH. Accordingly, the control by the use of IRA 900 should be referred to in each examination. However, in the cases of M-TCPP_g and -TCPP_s, the reagent blank was used as a reference because glass beads or silica gel do not absorb GSH.

To evaluate the GSHOx-like activity of the modified carriers, unchanged GSH was determined by the Ellman's color reaction with 5,5'-dithiobis(2-nitrobenzoic acid) (DTNB) [10].

The following examinations were carried out to obtain optimum conditions.

3.4. Effect of pH and the GSHOx activity

The amounts of unchanged GSH (%) against pH are presented in Fig. 2; compared to the unchanged GSH at pH 6.0, GSH was nearly zero after treatment with the carriers modified with Co-TCPP, while most of GSH remained unchanged in the case of Mn-TCPP_g and -TCPP_r. This result indicates that the carriers modified with Co-TCPP can exhibit strong GSHOx-like activity in contrast with the no activity of Mn-TCPP_g and -TCPP_r. It is of interest that Mn-TCPP fixed on carriers, having

strong GSH peroxidase-like activity [1], did not show any GSHOx-like activity at pH 6.0. This difference in activity may be caused by the affinity of oxygen and/or GSH to metal ions.

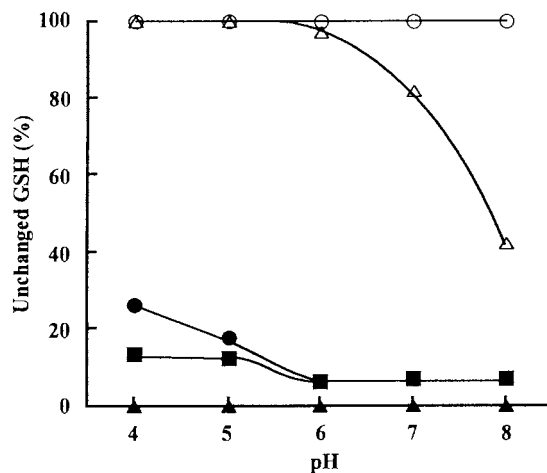


Fig. 2. Effect of pH. Co-TCPP_g (●), Co-TCPP_s (■), Co-TCPP_r (▲), Mn-TCPP_g (○) and Mn-TCPP_r (△). Modified carrier, 50 mg; incubated for 20 min at 35°C.

Within the tested pH region, Mn-TCPP_g had no activity. Even though Mn-TCPP_r exhibited a weak activity in the higher pH region of more than 7.0, the rate of unchanged GSH was more than 40%, as can be seen in Fig. 2. On the contrary, Co-TCPP_r, -TCPP_s and -TCPP_g strongly catalyzed reaction (1) in the tested pH region. However, the activity of Co-TCPP_g was a little weaker than that of Co-TCPP_r and -TCPP_s at pH 5 or below. These results indicated that the activity depends not only on the central metal but also on the carrier.

In the present study, we decided to examine the carrier modified with Co-TCPP in the region between pH 6.0 and 7.0 in detail, as this was the region in which they showed strong activity.

3.5. Time course

Fig. 3 shows the time course of reaction (1). Initially, we presumed that Co-TCPP_r would give more rapid equilibrium of reaction (1) than other two, because a considerable quantity of GSH could be decreased by adsorption on Co-TCPP_r. Contrary to our presumption, 5-min incubation with Co-TCPP_g and -TCPP_s gave equilibrium of reaction (1), but Co-TCPP_r re-

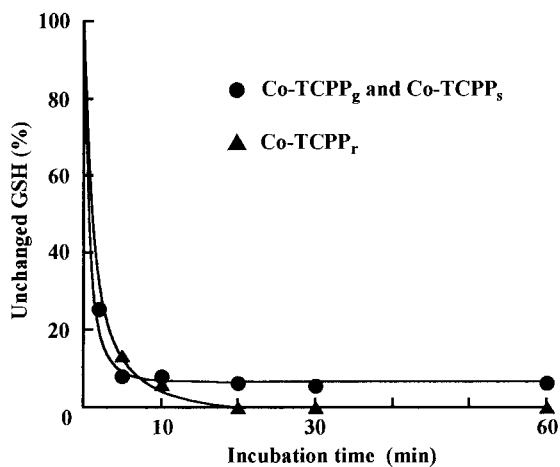


Fig. 3. Time courses. Co-TCPP_g and Co-TCPP_s (●); and Co-TCPP_r (▲). Modified carrier, 50 mg; pH 6.0; incubated at 35°C.

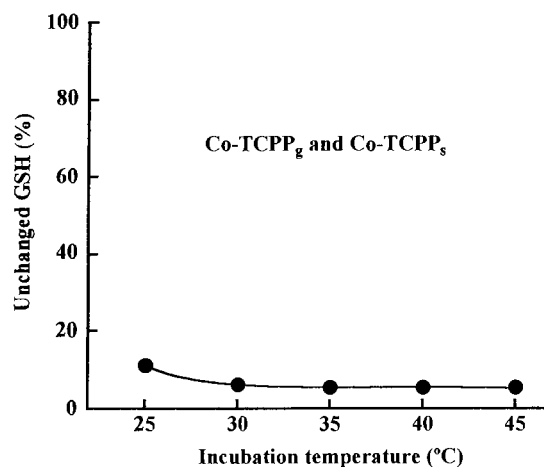


Fig. 4. Effect of incubating temperature. Co-TCPP_g and Co-TCPP_s (●). Modified carrier, 50 mg; pH 6.0; incubated for 20 min.

quired about 15 min incubation before equilibrium as seen (Fig. 3). Co-TCPP_g and -TCPP_s accelerated reaction (1) to a greater extent than Co-TCPP_r, and were suggested to be superior to Co-TCPP_r as a catalyst. For the present examination, we selected Co-TCPP_g and -TCPP_s as catalysts to be used in the further examinations, and we judged incubation for 20 min to be enough for the evolution of the activity, taking time to spare into consideration.

3.6. Effect of incubating temperature

The effect of the incubating temperature on the unchanged GSH (%) was examined between 25 and 45°C by using Co-TCPP_g and -TCPP_s. Most of GSH disappeared between 30 and 45°C. Unchanged GSH was close to zero, except at 25°C, where around 10% of GSH remained unchanged (see Fig. 4). As the standard incubating temperature, we selected the region around 35°C, where, in general, most enzyme reactions take place. One of advantageous features of Co-TCPP_g and -TCPP_s is that their activity is not affected seriously by the incubating temperature, in contrast to most of enzymes.

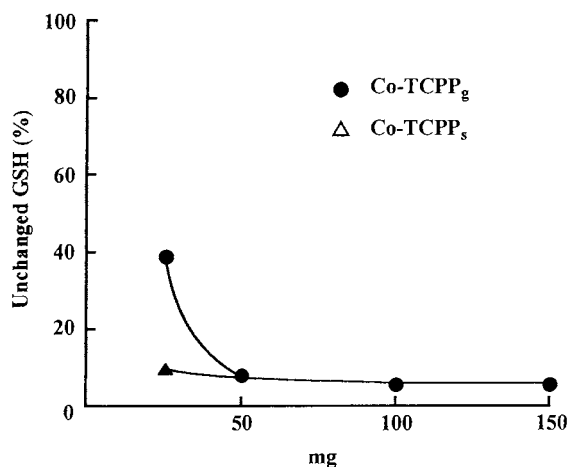


Fig. 5. Effect of amount of the modified carriers. Co-TCPP_g (●) and Co-TCPP_s (▲). pH 6.0; incubated at 35°C for 20 min.

3.7. Effect of amount of Co-TCPP_g and -TCPP_s

Since the amount of catalyst was expected to affect the rate of reactions, we checked the relationships between the amount of the modified carriers and unchanged GSH. Reaction (1) attained equilibrium when more than 50 mg of the carriers were added (see Fig. 5). In addition to 25 mg of carriers, Co-TCPP_s gave about 10% of unchanged GSH, while Co-TCPP_g gave about 40%, indicating that Co-TCPP_s exhibited stronger activity than Co-TCPP_g when a small amount of carrier is used. This result suggested that Co-TCPP_s is more effective than Co-TCPP_g. Thus, in the present study, we concluded that Co-TCPP_s was the best catalyst among the three kinds of modified carriers tested, and that the addition of 50 mg of Co-TCPP_s was significant to examine the activity in more detail.

3.8. Repeated uses

To confirm that Co-TCPP_s acts as a catalyst in the oxidative reaction of GSH, repeated uses of

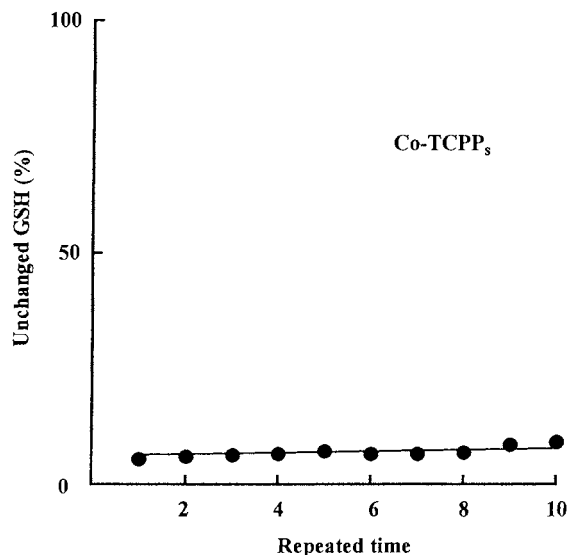


Fig. 6. Repeated uses of Co-TCPP_s. Co-TCPP_s and Fe-TMPyP_r, 50 mg; pH 6.0; incubated at 35°C for 20 min.

Co-TCPP_s were checked. In that time, Fe-TMPyP_r (50 mg), which was reported to have a strong catalase-like activity [8], was added to the reaction mixture to decompose the resulting hydrogen peroxide, which can interfere with reaction (1). After being used 10 times, Co-TCPP_s held enough GSHOx-like activity, although it had decreased by about 5% (see Fig. 6). Thus, we concluded that Co-TCPP_s serves as a catalyst in reaction (1).

3.9. Proposed reaction scheme

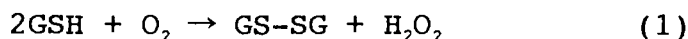
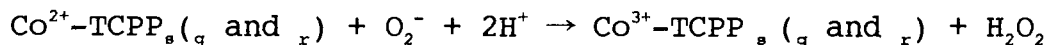
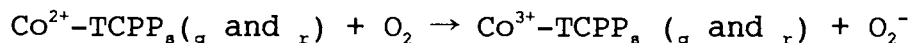
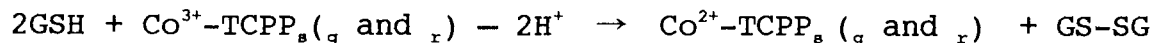
Previously, we studied the uricase-like activity of an anion-exchange resin modified with Mn³⁺ -

Table 1
Resulting hydrogen peroxide when GSH was oxidized

Solid catalysis	Hydrogen peroxide determined ^a (μmol)
Co-TCPP _s	1.2
Co-TCPP _g	1.2
Co-TCPP _r	0.7

^a 4.0 μmol of GSH were used.

tetrakis(sulfophenyl)porphine (Mn-TSPP_r) and demonstrated, from a resonance Raman study, that the activity was due to a redox cycle reaction of manganese ion, as described in the literature [11,12]. By analogy with the above scheme of uricase-like activity, we propose the following reaction scheme, wherein the GSHox-like activity of Co-TCPP on the carriers is involved.



3.10. Quantity of the resulting hydrogen peroxide

According to the above reaction scheme, 1 mol of hydrogen peroxide should be formed from 2 mol of GSH. To check this point, the quantity of hydrogen peroxide was determined by following

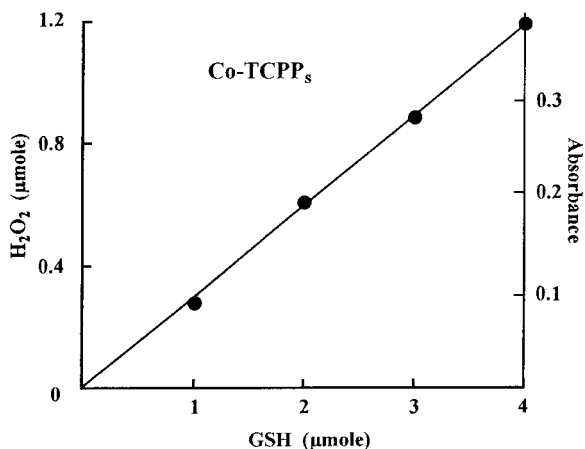


Fig. 7. Plot of amount of GSH against absorbance due to the resulting hydrogen peroxide. Co-TCPP_s, 50 mg; pH 7.0; incubated at 35°C for 20 min.

the procedures described above. The determination was carried out at pH 7.0, which is the optimum pH of peroxidase for determining hydrogen peroxide. As a result, the use of Co-TCPP_g and -TCPP_s gave only 1.2 μmol of hydrogen peroxide from 4.0 μmol of GSH, as shown in Table 1. The lower yield of hydrogen peroxide than that expected was attributed to the

fact that hydrogen peroxide was partially decomposed by Co-TCPP on the carrier, which had been previously reported to exhibit weak catalase-and/or GSHPx-like activities. We, therefore, concluded that this result supported the above scheme.

In the case of Co-TCPP_r, the resulting hydrogen peroxide was 0.7 μmol less than that observed in the case of Co-TCPP_s. Since an anion-exchange resin adsorbs considerable quantity of GSH, and the adsorbed GSH is expected not to take part in the reaction (1), this result again would not contradict the above scheme.

To confirm that hydrogen peroxide is formed from GSH with a fixed rate of the GSH, the resulting hydrogen peroxide from GSH at different concentrations, 1–4 μmol, was determined in the presence of Co-TCPP_s. A plot of GSH quantity against absorbance, that is quantity of hydrogen peroxide, gave a good straight line sufficient to be used as a calibration curve of GSH (Fig. 7). This line indicated that the resulting hydrogen peroxide was proportional to GSH quantity, which was revealed to be the fixed rate of GSH.

3.11. Analytical application

As mentioned above, since the plot of GSH against absorbance was regarded as a calibration curve of GSH where Beer's law was applicable in the range between from 1.0 to 4.0 μmol , we could determine GSH by using the curve. From this point of view, Co–TCPP_s having the strongest activity among the tested carriers, was promising for the determinations of GSH as a solid catalyst.

4. Conclusion

The carriers modified with Co–TCPP exhibited GSHOx-like activity. Particularly, Co–TCPP_s was regarded as a good mimetic of GSHOx, and is expected to be practically applicable to the determination of GSH as a solid catalyst.

Acknowledgements

The authors thank Miss Chizuko Kodama for her technical support of the measurement of the mass spectra. This work was supported in part by a Grant-in-Aid for Scientific Research from Ministry of Education, Science and Culture, Japan.

References

- [1] A. Iwado, M. Mifune, R. Harada, T. Mukuno, N. Motohashi, Y. Saito, *Anal. Sci.* 14 (1998) accepted.
- [2] K. Ormstad, T. Lastbom, S. Orrenius, *FEBS Lett.* 130 (1989) 239.
- [3] R.F. Pasternack, L. Francesconi, D. Raff, E. Spiro, *Inorg. Chem.* 12 (1973) 2606.
- [4] A. Harriman, G. Porter, *J. Chem. Soc., Faraday Trans. II* 75 (1979) 1532.
- [5] Y. Saito, M. Mifune, S. Nakashima, J. Odo, Y. Tanaka, M. Chikuma, H. Tanaka, *Talanta* 34 (1987) 667.
- [6] Y. Saito, M. Mifune, S. Nakashima, J. Odo, Y. Tanaka, M. Chikuma, H. Tanaka, *Anal. Sci.* 3 (1987) 171.
- [7] Y. Saito, M. Mifune, S. Nakashima, Y. Tanaka, M. Chikuma, H. Tanaka, *Chem. Pharm. Bull.* 34 (1986) 5016.
- [8] Y. Saito, M. Mifune, T. Kawaguchi, Y. Tanaka, M. Chikuma, H. Tanaka, *Chem. Pharm. Bull.* 34 (1986) 2885.
- [9] M. Mifune, J. Odo, N. Motohashi, Y. Saito, A. Iwado, Y. Tanaka, M. Chikuma, H. Tanaka, *Anal. Sci.* 7 (1991) 277.
- [10] G.L. Ellman, *Anal. Biochem. Biophys.* 32 (1959) 70.
- [11] M. Mifune, J. Odo, A. Iwado, Y. Saito, *Talanta* 38 (1991) 779.
- [12] J. Odo, M. Mifune, A. Iwado, T. Karasudani, H. Hashimoto, N. Motohashi, Y. Tanaka, Y. Saito, *Anal. Sci.* 7 (1991) 555.

Determination of chloride ion in aqueous samples by isotope-dilution Fourier-transform flame infrared emission (ID-FIRE) spectrometry

Kenneth W. Busch ^{a,*}, Arvie J. Kuehn ^a, Marianna A. Busch ^a, Sandra Yescas ^a,
Ilse Y. Guzman Jimenez ^b, Christine M. Algozo ^c

^a Department of Chemistry, Baylor University, P.O. Box 97348, Waco, TX 76798-7348, USA

^b Instituto Tecnológico y de Estudios Superiores de Monterrey, Monterrey, Mexico

^c Mount Holyoke College, South Hadley, MA, USA

Received 5 September 1997; received in revised form 13 January 1998; accepted 14 January 1998

Abstract

An isotope dilution method for the determination of chloride ion in aqueous samples is described. The method makes use of the isotopic shift in the rotational lines of the 1–0 band of HCl emitted in the near infrared region of the spectrum by vibrationally excited HCl molecules present in a hydrogen/entrained air flame. Chloride ion in the sample is converted to chlorine gas by electrolysis and swept into a hydrogen/entrained air flame where it is converted into HCl. Because isotope dilution is an absolute method of analysis, matrix effects are minimized, and the chlorine generation step need not be quantitative. With the system described in this paper, samples must contain at least 9 mg of chloride ion per ml, and a 2-ml sample is required. Over the range from 10 to 30 mg Cl⁻ ml⁻¹, the average error was -0.96%, and the average relative standard deviation was 3.3% for seven samples using seven of the more intense lines in the P branch. Compared with standard silver nitrate titrations, the isotope dilution procedure was not affected by such common interferences as bromide ion and iodide ion. The technique was applied to several seawater samples from different regions. © 1998 Elsevier Science B.V. All rights reserved.

Keywords: Isotope dilution; Fourier-transform infrared emission; Chloride analysis; Flame spectrometry; Seawater

1. Introduction

The element chlorine occurs widely in nature, primarily as chloride ion, and is generally found combined with sodium, potassium, and magnesium. In minerals, it is found in halite (NaCl),

sylvine (KCl), and carnallite (KCl·MgCl₂·6H₂O), among others [1,2]. Dissolved in water, chloride ion is found in ground water, seawater, mineral springs, and salt brines. Salt brines, which frequently contain large amounts of dissolved chloride ion, are an important source of chemicals throughout the world [2]. While the oceans remain the largest sources of brine, brines are also found in terminal lakes such as the Dead Sea in

* Corresponding author.

Israel and Jordan and the Great Salt Lake in Utah, and in underground deposits formed after evaporation of ancient terminal lakes. In the chloro-alkali process for the production of chlorine and caustic soda (the eighth and ninth largest volume chemicals produced in the United States), solution-mined brines or solar-evaporated solid salt are used as feedstocks [3]. In oceanographic work, chloride ion is used as a reference standard, and its determination in seawater is complicated by the complex nature of the sample matrix [4]. Because of the widespread occurrence of chloride ion naturally, and its importance in many chemical processes, methods for the determination of chloride ion in aqueous samples are of general interest.

Previous work [5] has shown that chloride ion in aqueous samples can be determined by flame infrared emission (FIRE) spectrometry [6,7]. In this procedure, chloride ion was converted to molecular chlorine (Cl_2) by reaction with a saturated solution of potassium permanganate in the presence of concentrated sulfuric acid. The molecular chlorine generated by the strong oxidizing conditions was subsequently purged from solution with a stream of He, and introduced into a hydrogen/entrained-air flame, where a portion of the HCl emission intensity at $3150\text{--}2425\text{ cm}^{-1}$ was monitored with a simple radiometer, equipped with a lead selenide detector and a narrow-band optical band pass filter with a maximum transmission at $3.8\text{ }\mu\text{m}$. Calibration curves were prepared by plotting the peak height of the emission intensity profiles versus the concentration of sodium chloride standard solutions.

While the early FIRE method was generally satisfactory, it was subject to matrix interferences. For example, for a 5 mM Cl^- solution, the presence of 0.595 mM Br^- suppressed the HCl emission signal by as much as 39%, and resulted in large negative analytical errors [5]. While the depressive effect of bromide ion could be prevented by the addition of iodate ion to the sample [5], such measures are frequently inconvenient for complex samples where a number of potential interferences may be present.

To avoid matrix effects in complex samples, isotope dilution analysis is frequently used [8]. Since the technique was introduced in 1931 by Hevesy and Hobbie [9], a variety of techniques based on isotope dilution have been developed. While the method originally employed radioactive isotopes, the availability of mass spectrometry soon led to the use of stable isotopes. In direct-dilution classical isotope dilution [8], a pair of isotopes is selected from among those that make up the analyte, and the isotopic ratio in the unknown sample is determined by some means, such as mass spectrometry. A known aliquot, enriched in one of the selected isotopes of the analyte (the spike), is then added to a known amount of sample. After the isotopes have equilibrated, a portion of the analyte is separated from the sample matrix, purified to eliminate interferences, and the isotopic ratio of the spiked sample is determined. From a knowledge of the amount of sample and spike and the initial and final isotopic ratios, the concentration of the sample can be calculated.

Mass spectrometry is the most frequently used means of determining isotopic ratios with stable isotope dilution. In the case of chlorine [10], the chloride ion is first precipitated as AgCl and filtered with $0.45\text{ }\mu\text{m}$ polytetrafluoroethylene filters. Vaporization of a $1\text{--}10\text{-}\mu\text{g}$ sample of the precipitate from a rhenium double filament at $1600\text{--}1800^\circ\text{C}$ results in the formation of thermal Cl^- ions, which are analyzed by the mass spectrometer. While isotope dilution mass spectrometry is quite good, the technique requires a mass spectrometer and a relatively skilled operator.

Because it should be possible to resolve the rotational lines of H^{35}Cl and H^{37}Cl emitted from a hydrogen flame using a relatively modest Fourier-transform infrared spectrometer, it seemed worthwhile to investigate the use of Fourier-transform flame infrared emission (FT-FIRE) spectroscopy [11] as a means of determining isotopic ratios in the isotope dilution analysis of aqueous samples containing chloride ion. This paper presents the results obtained with isotope-dilution flame infrared emission (ID-FIRE) spectrometry.

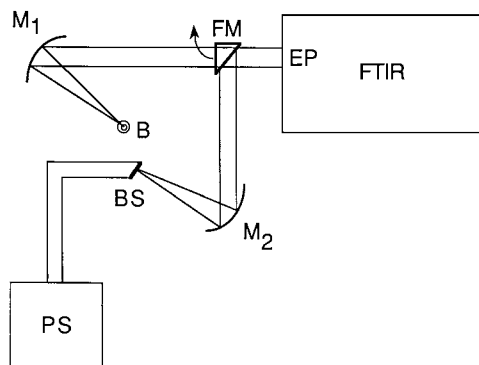


Fig. 1. Scheme of the optical layout used for the isotope-dilution flame infrared emission determination of chloride ion. M_1 , M_2 , spherical mirrors; FM, folding mirror that swings out of the optical path when not needed; B, burner; BS, blackbody source; PS, power supply; EP, emission port of FTIR; FTIR, Fourier-transform infrared spectrometer.

2. Experimental

2.1. Apparatus

Fig. 1 shows a schematic diagram of the ID-FIRE apparatus, which consists of five major sections: (a) the blackbody source, (b) the electrolysis cell, (c) the burner, (d) the FTIR spectrometer, and (e) the exhaust system. Table 1 gives the experimental parameters used in this study.

Table 1
Spectral emission lines used for isotope dilution

P-branch transition: $v1, J^a \rightarrow v'0, J'^b$	Wavenumber (cm^{-1}) ^c	
	H^{35}Cl	H^{37}Cl
$v1, J6 \rightarrow v'0, J'7$	2727.64	2725.76
$v1, J7 \rightarrow v'0, J'8$	2702.86	2701.12
$v1, J8 \rightarrow v'0, J'9$	2677.57	2675.94
$v1, J9 \rightarrow v'0, J'10$	2651.77	2650.70
$v1, J10 \rightarrow v'0, J'11$	2625.57	2624.04
$v1, J11 \rightarrow v'0, J'12$	2598.89	2597.35
$v1, J12 \rightarrow v'0, J'13$	2571.72	2570.27

^a Initial rotational state in the upper vibrational level, $v1$.

^b P-notation (i.e. P(7)). Final rotational state in the lower vibrational level, $v'0$.

^c Measured by FTIR.

2.1.1. FTIR spectrometer

A Mattson Galaxy Series 5000 spectrometer (Model GL-5020, Mattson Instruments, Madison, WI), equipped with a deuterated triglycine sulfate (DTGS) detector, was modified for flame infrared emission measurements by disconnecting the original, internal blackbody source and substituting an external blackbody source located outside the instrument. The FTIR spectrometer was interfaced to a 486/33-MHz computer, and spectral data were collected and processed with WinFirst[®], an FTIR software program from Mattson. Each spectrum was accumulated for 20 scans (2.08 min total time), and the gain of the instrument was set for the maximum of 20. Spectra were acquired with a 0.75-cm^{-1} resolution with 1×0 fill and triangular apodization. The optical axis of the spectrometer was 10 mm above the burner tip.

2.1.2. Blackbody source

The external blackbody source consisted of a coil of nichrome heating wire wound around a ceramic tube (6 mm OD \times 50 mm long) and connected to a 110-V variable transformer. This external source was used only when the spectrometer was first turned on and undergoing an automatic internal systems check. Unless the signal from the detector was above a certain level during this check, the internal software assumed that the blackbody source was not functioning, and the instrument would not initialize.

To circumvent the internal software, radiation from the hot external blackbody source was collimated by M_1 , a front-surfaced spherical mirror (Part Number 34-9845, Ealing Electro-Optics, Holliston, MA) with a 30-cm focal length. The collimated beam was subsequently directed into the emission port of the FTIR by a $5 \times 5\text{-cm}$, plane front-surfaced mirror (Part Number 23-4203, Ealing Electro-Optics) placed 57 cm from M_1 . The plane mirror (FM) was mounted on the side of a triangular aluminum block with a rod through one corner to allow it to swing out of the light path between the burner and the FTIR. Once the initial systems check had been completed, the external blackbody source was turned off, and the plane mirror was rotated out of the light path between the burner and the emission port of the FTIR.

2.1.3. Burner

In previous FIRE studies in this laboratory, different microburner designs have been evaluated [7,12,13]. The microburner used in this study was a modification of a concentric two-tube burner described previously [13]. The stainless steel tubing in the earlier burner [13] could not withstand the corrosive action of the large amount of hydrogen chloride gas present at the flame temperature for more than a few hours. As a result, other materials more inert to the burning of chlorine gas in the flame were investigated.

While burners fabricated from fused silica were satisfactory, the best material investigated to date was ceramic, composed of 99% Al_2O_3 (Omegatite 450, Omega, Stamford, CT). The inner tube had an outer diameter of 3.2 mm and an inner diameter of 1.6 mm (Cat. # ORA11618-6, Omega). The outer tube had an outer diameter of 6.4 mm and an inner diameter of 4.0 mm (Cat. # ORX1814, Omega). Glass wool was packed between the inner and outer ceramic tubes to stabilize the inner tube and diffuse the gas flow in the outer tube. Burners fabricated from these components were found to be unaffected by the corrosive gases present in the flame. A special exhaust system was constructed to prevent the release of toxic and corrosive electrolysis and flame combustion products into the laboratory environment.

Gas flow to the burner was controlled with standard laboratory rotameters (Cole-Palmer, Chicago, IL). The hydrogen flow rate was 175 ml min^{-1} .

2.1.4. Electrolysis cell

An electrolysis cell was used to generate chlorine gas from aqueous chloride solutions. Fig. 2 shows a schematic diagram of the electrolysis cell that was fabricated from Pyrex glass tubing. The body of the cell was 2 cm in diameter and 6.5 cm long. A side arm, 2 cm long with an outside diameter of 6 mm, was positioned 4 cm from the bottom of the cell. A Teflon[®] stopper was machined and fitted with an O-ring to seal the top of the electrolysis cell. Holes in the Teflon[®] stopper for the electrodes and gas dispersion tube were drilled to provide a gas-tight fit. A gas dispersion tube (Cat. # 9435-D, Ace Glass, Louisville, KY)

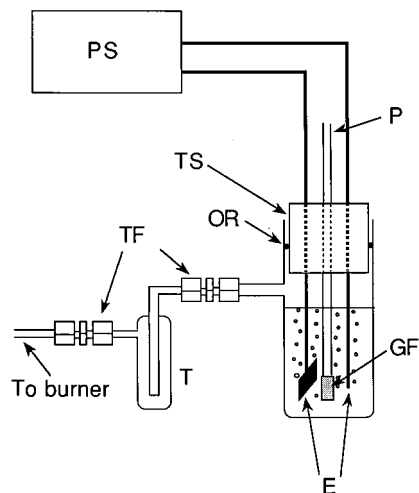


Fig. 2. Scheme of the electrolysis cell. PS, power supply; P, hydrogen purge gas; TS, Teflon[®] stopper; OR, O-ring; GF, glass frit; E, Pt electrodes; TF, Teflon[®] fittings; T, glass trap.

with a porosity of 10–20 μm was used to bubble hydrogen through the aqueous sample. A hydrogen flow rate of 10 ml min^{-1} was used to purge electrolytically generated chlorine gas from the cell and into the flame. The electrodes were made of Pt/20% Ir (Nobel-Met, Roanoke, VA) and were 1.6 mm in diameter and 10 cm long. A d.c. power supply (Model # 3002A, Electro Industries, Chicago, IL) provided a current of 2 A at 5 V to the electrodes.

The purge gases from the electrolysis cell were first passed through a glass trap to prevent spray collecting in the transfer line. The outlet of the spray trap was connected to the burner with Teflon[®] tubing (3.2 mm outside diameter, 1.6 mm inside diameter). All gas connections were made with Teflon[®] Swagelok[®] fittings and ferrules (Texas Valve and Fittings, Irving, TX).

2.2. Reagents and solutions

All chemicals were ACS reagent grade and used without further purification. Standard NaCl solutions were prepared by drying ACS reagent-grade NaCl at 120°C for 24 h and dissolving weighed samples in 3 M H_2SO_4 . The 3 M H_2SO_4 solution was prepared by diluting concentrated sulfuric acid with deionized water.

A stock solution of isotopically enriched NaCl was prepared by dissolving a weighed sample of Na³⁷Cl in 3 M H₂SO₄. Isotopically enriched NaCl with a known isotopic composition (Lot I-2608, 94.97% ³⁷Cl; Lot I-3009, 94.15% ³⁷Cl) was obtained from Cambridge Isotopes, Cambridge, MA, and was dried at 120°C for 24 h before use.

2.3. Procedure

A 2.000-ml aliquot of the aqueous NaCl solution to be analyzed was transferred to the electrolysis cell using a Class A glass pipet. The stopper on the electrolysis cell was replaced, and the hydrogen flow to the burner and the purge tube was turned on. Following activation of the exhaust system, the hydrogen/entrained air flame was ignited. While the flame and the sample introduction system were stabilizing, the plane mirror (FM, Fig. 1) was rotated into position so that radiation from the external blackbody source would be directed into the emission port of the FTIR spectrometer. Once the external blackbody source had been turned on, it was allowed to heat until it glowed red, whereupon the FTIR and computer were turned on. After the FTIR was initialized and ready to collect data, the external blackbody source was turned off, and the mirror (FM) was rotated out of the optical path between the burner and the FTIR. Finally, the power supply to the platinum electrodes was turned on, and the ro-vibrational infrared emission spectrum of HCl was collected between 3200 and 2400 cm⁻¹ with the FTIR spectrometer.

For each analysis, spectra from unspiked and spiked samples were collected. Spectra from unspiked samples were used to determine the ratio of ³⁷Cl/³⁵Cl in the original sample. Once the spectrum of the unspiked sample was collected, the power to the electrodes was turned off, the Teflon[®] stopper was removed from the electrolysis cell, and the waste solution was discarded. The cell was rinsed with deionized water and dried using a tissue. A second 2.000-ml aliquot of the NaCl solution to be analyzed was then added to the electrolysis cell as before, and spiked with 0.500 ml of the isotopically enriched NaCl standard using a 500- μ l Oxford P-7000 Sampler Sys-

tem pipet (Monojet Scientific, St. Louis, MO). After adding the spike, the hydrogen purge was allowed to run for several minutes so that the bubbling action would completely mix the sample and the spike. Finally, the HCl spectrum of the spiked sample was collected as described previously. The ceramic burner tube was changed each time a new sample was run to minimize problems with sample carry-over.

3. Results and discussion

3.1. Sample introduction system

ID-FIRE determination of chloride ion in aqueous media must fulfill two primary requirements: (1) it must deliver analyte to the flame in a steady, continuous manner during the time period over which the FTIR collects spectral data; and (2) the volume should be as small as possible to minimize the size of the spike needed to produce a measurable change in the ³⁷Cl/³⁵Cl intensity ratio. The electrolysis cell shown in Fig. 2 fulfills both of these requirements.

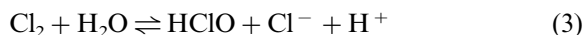
The first requirement arises from the inherent nature of Fourier-transform spectroscopy—namely, that the variations in the intensity of radiation striking the detector are assumed to arise solely from the mirror movement in the Michelson interferometer, and are not due to other external factors such as variations in source intensity and/or the rate of sample introduction. The second requirement arises from the expense associated with isotopically enriched Na³⁷Cl (\$600 per 0.5 g). For the seawater analyses reported in this paper, a 0.500-ml spike of NaCl containing 0.01270 g Cl⁻ ml⁻¹ of isotopically enriched ³⁷Cl (95%) was sufficient to alter the ³⁷Cl/³⁵Cl intensity ratio of a 2.000-ml sample of seawater so that an isotope dilution determination could be conducted. Under these conditions, approximately 50 determinations of chloride ion in seawater could be conducted with a 0.5-g sample of Na³⁷Cl, making the cost per determination approximately \$12.

When the power supply (5 V) is activated and an aqueous sample containing chloride ion is

present in the electrolysis cell, hydrogen is generated at the cathode and chlorine is generated at the anode, according to the following half cells,



If the acidity of the solution in the electrolysis cell is controlled by the addition of 3 M H_2SO_4 , the hydrolysis of Cl_2 to hypochlorous acid can be prevented by the law of mass action, since the reaction



is readily reversible. With this arrangement, the chlorine gas generated by electrolysis can be sparged from solution using a gas dispersion tube and a stream of hydrogen gas. When the mixture of H_2 and Cl_2 enters the hydrogen flame maintained on the microburner, it combusts to HCl according to the reaction,



Once in the flame, the HCl is excited and emits the ro-vibrational 1–0 band at 3.46 μm in the near infrared.

The sample introduction system shown in Fig. 2 accomplishes the following objectives in an extremely convenient manner. (1) It converts the chloride ion in aqueous samples directly into gaseous HCl in a continuous manner compatible with the requirements of the FTIR. (2) The conversion of chloride ion into gaseous HCl occurs automatically and does not require sample handling or collection on the part of the operator. (3) The electrolysis step separates the analyte from most other constituents in the aqueous sample, thereby reducing potential interferences. (4) The HCl produced in the flame is automatically excited vibrationally at the temperature of the flame and emits the ro-vibrational spectrum of HCl at 3.46 μm . (5) The sample volume is small and minimizes the size of the spike needed for seawater analysis.

Finally, it should be stressed that, because of the nature of isotope dilution analysis, it is not necessary to convert all of the chloride ion in the sample to chlorine gas by electrolysis. Nor is it

necessary to purge all of the chlorine gas from solution into the flame and convert it to HCl. It is only necessary that the sample introduction system for ID-FIRE produce sufficient HCl in the flame for the FTIR to collect a spectrum.

3.2. Spectral considerations

Fig. 3 shows a typical infrared emission spectrum from 3200 to 2400 cm^{-1} , obtained by electrolyzing a 2.000-ml aqueous sample containing naturally occurring NaCl, using the sample introduction system described previously. The spectrum in Fig. 3, which clearly shows the P- and R-branches of the 1–0 band of HCl, was obtained by co-adding 20 mirror scans over a period of 2.08 min at a spectral resolution of 0.75 cm^{-1} using triangular apodization and 1×0 filling.

Fig. 4A shows an expanded portion of the HCl spectrum over the wavenumber interval from 2800 to 2500 cm^{-1} . Each rotational line in the HCl infrared emission spectrum is clearly split into a doublet. The smaller intensity component, due to H^{37}Cl , is located on the long wavelength side of the more intense H^{35}Cl line. For the 1–0 band of HCl, the constant separation between the components of the doublets [14,15] is about 2 cm^{-1} , a value that is easily resolved with modern FTIR instruments. For the naturally occurring NaCl sample shown in Fig. 4A, the intensity ratio of the H^{35}Cl component is about three times that of the H^{37}Cl component. This is in line with the expected natural abundance ratio of the two isotopes (75.77% ^{35}Cl and 24.23% ^{37}Cl) [16].

Fig. 4B shows an expanded portion of the HCl spectrum from 2800 to 2500 cm^{-1} for a sample of NaCl that has been spiked with an aliquot of isotopically enriched Na^{37}Cl . Compared with the spectrum in Fig. 4A, the intensity of the H^{37}Cl emission (I^{37}) in Fig. 4B is clearly increased, while the intensity of the H^{35}Cl emission (I^{35}) is clearly reduced.

In contrast to mass spectrometric measurements, where only a single pair of isotopic lines is available (corresponding to the masses of $^{35}\text{Cl}^-$ and $^{37}\text{Cl}^-$) [10], a single spectrum in ID-FIRE produces a large number of rotational pairs in the 1–0 band of HCl, each of which can be used to

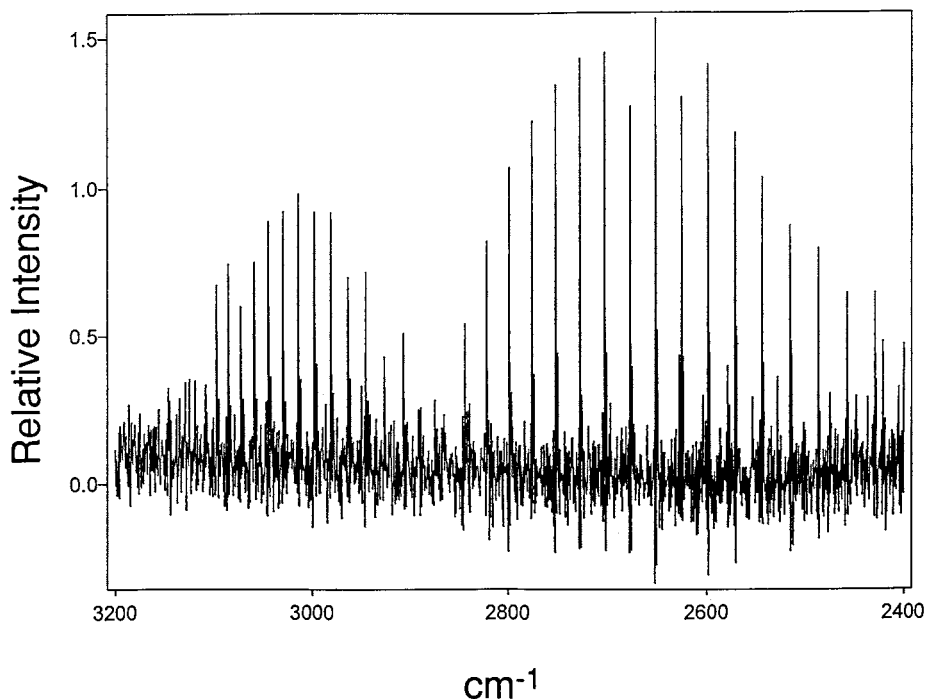


Fig. 3. Flame infrared emission spectrum of HCl from 3200 to 2400 cm^{-1} at 0.75 cm^{-1} resolution showing the P- and R-branches.

determine the relative isotopic abundance of the two stable isotopes of chlorine. In this paper, rotational pairs refer to emission lines from H^{37}Cl and H^{35}Cl which start from the same initial J value and end at the same final J' value. Of the possible lines available in the HCl spectrum, Table 1 lists the pairs which were found to be the most satisfactory for isotope dilution work. Not surprisingly, these lines are the more intense components of the ro-vibrational spectrum and are located in the P-branch.

3.3. Isotope dilution

The concentration of chloride ion in an unknown aqueous sample can be determined by isotope dilution from Eq. (5),

$$\text{Cl}_s = \left[\frac{\text{Cl}_{\text{sp}} V_{\text{sp}}}{V_s} \right] \left[\frac{M_{\text{nat}}}{M_{\text{sp}}} \right] \left[\frac{\phi_{\text{sp}}^{37} - R_m \phi_{\text{sp}}^{35}}{R_m \phi_s^{35} - \phi_s^{37}} \right] \quad (5)$$

where Cl_s is the concentration (g ml^{-1}) of chloride ion in the unknown sample, Cl_{sp} is the known

concentration (g ml^{-1}) of chloride ion in the spike solution, V_s is the volume of the unknown sample, V_{sp} is the volume of the spike added, M_{nat} is the molar mass (g mol^{-1}) of naturally occurring chloride ion, M_{sp} is the molar mass (g mol^{-1}) of isotopically enriched chloride ion in the spike, ϕ_s^{37} is the natural abundance fraction of ^{37}Cl in the unknown sample prior to spiking, ϕ_s^{35} is the natural abundance fraction of ^{35}Cl in the unknown sample prior to spiking, ϕ_{sp}^{37} is the fractional abundance of ^{37}Cl in the spike solution, ϕ_{sp}^{35} is the fractional abundance of ^{35}Cl in the spike solution, and R_m is the measured ratio of $^{37}\text{Cl}/^{35}\text{Cl}$ in the sample after spiking. If R_s is the measured ratio of $^{37}\text{Cl}/^{35}\text{Cl}$ in the sample before spiking, the natural abundance fractions of ^{37}Cl and ^{35}Cl in the unspiked sample are given by Eq. (6) and Eq. (7), respectively.

$$\phi_s^{37} = \frac{R_s}{1 + R_s} \quad (6)$$

$$\phi_s^{35} = (1 - \phi_s^{37}) \quad (7)$$

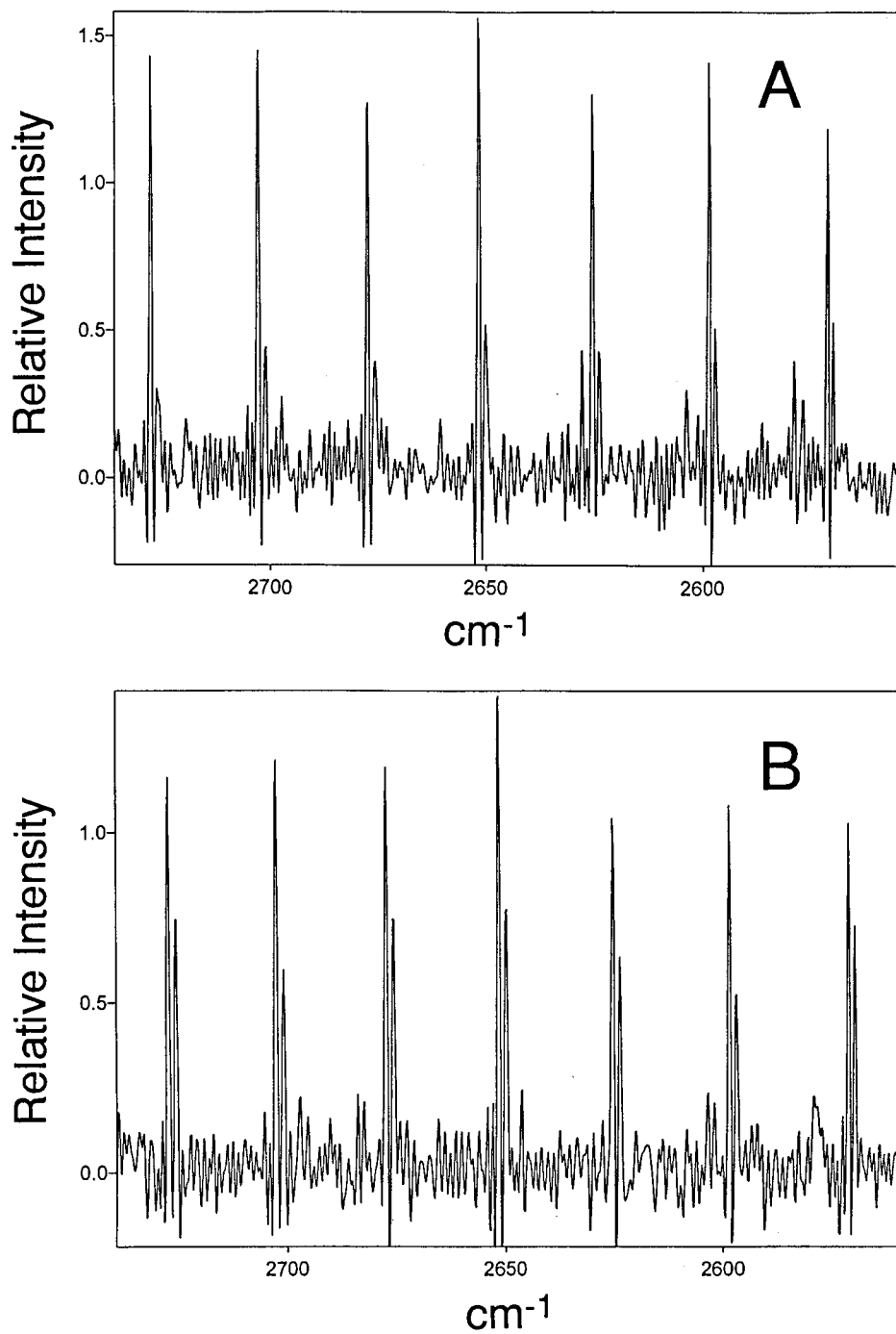


Fig. 4. Flame infrared emission spectrum showing a portion of the P-branch of the HCl spectrum from 2750 to 2550 cm^{-1} at 0.75 cm^{-1} resolution. (A) Sample with the natural isotopic abundance of chlorine. (B) Sample spiked with Na^{37}Cl .

In ID-FIRE spectroscopy, R_s is taken as the ratio of the intensity of the $H^{37}Cl$ line to that of the corresponding $H^{35}Cl$ line for a given rotational transition (Table 1) before the sample is spiked. Likewise, R_m is taken as the ratio of the intensity of the $H^{37}Cl$ line to that of the corresponding $H^{35}Cl$ line for a given rotational transition (Table 1) after the sample is spiked.

3.4. Analytical validation

To validate ID-FIRE as an analytical method for the determination of chloride ion in aqueous samples, a series of analytical studies was conducted using synthetically prepared solutions containing known amounts of NaCl. The first step in the validation was to determine the optimum analytical procedure.

3.4.1. Line selection

As mentioned previously, the 1–0 vibrational band of HCl provides many pairs of transitions whose intensity ratios could be used to determine R_s and R_m . The best results were obtained using the average intensity ratio obtained from the seven line pairs of the P-branch of the HCl spectrum listed in Table 1. Analytical determinations using more than these seven line pairs did not improve the results. As a result, R_s and R_m values in Eq. (5) and Eq. (6) were calculated as the average intensity ratio of the seven line pairs listed in Table 1.

Table 2 gives the measured values of R_s obtained by averaging the ratios of the seven line pairs in Table 1 for 10 trials, each trial involving the coaddition of 20 spectral scans using the FTIR. The average R_s calculated from this spectral data and presented in Table 2 is within 1.2% of the value expected from the tabulated abundances of ^{37}Cl and ^{35}Cl (24.23 and 75.77%, respectively) [16]. The relative standard deviation of the ten trials is 2.60%.

It must be noted that great care was required in performing these experiments to avoid sample carry-over. Although the ceramic material used to fabricate the burner was quite satisfactory with respect to thermal stability and corrosion, it was easily contaminated. It was observed early in the

validation process that, after a spiked sample had been run through the instrument, the R_s values obtained on subsequent samples were noticeably increased. At first, the higher value for R_s was attributed to isotope carry-over in the electrolysis cell (in particular, the fritted glass purge tube) or in other portions of the transfer line. While careful cleaning of the electrolysis cell between samples proved to be important, the major contamination problem was traced to the ceramic tubing used to fabricate the burner. Contamination problems were avoided by carefully cleaning the electrolysis cell and replacing the ceramic tubing of the burner prior to running each new sample.

3.4.2. Limit of quantitation

A precise limit of detection is somewhat difficult to define for the ID-FIRE technique, since the procedure depends more on the determination of an accurate ratio of intensities rather than on the detection of an intensity in the presence of background noise. Thus, even though a weak HCl spectrum may be obtained for a dilute sample (clearly indicating the presence of chloride ion in the sample), the quantitative results obtained from the intensity ratios may be totally inadequate from an analytical standpoint. A limit

Table 2
Precision of R_s measurements

Trial	Measured value of R_s^a
1	0.3134
2	0.3141
3	0.3260
4	0.3341
5	0.3306
6	0.3255
7	0.3149
8	0.3174
9	0.3363
10	0.3238
Average	0.3236
Standard deviation	0.0084
Relative standard deviation (%)	2.60

^a Average of the intensity ratios of seven line pairs (Table 1) for a single acquisition of spectral data (i.e. 20 co-added scans of the FTIR).

Table 3
Accuracy of analytical results

Standard solution (g Cl ⁻ l ⁻¹)	ID-FIRE results (g Cl ⁻ l ⁻¹) ^a	% error	Titration results (g Cl ⁻ l ⁻¹)	% error
10.86	10.85	-0.09	10.96	+0.92
11.83	11.23	-5.07	11.91	+0.68
19.40	18.80	-3.09	19.49	+0.46
24.02	22.97	-4.37	24.16	-0.58
30.49	29.07	-4.66	30.40	-0.30

^a Based on the average of three determinations where R_s was determined 4 times and R_m was determined once.

of quantification, defined as that concentration of Cl⁻ in the sample below which the ro-vibrational spectrum of HCl is no longer intense enough to give reliable ratios, was determined to be about 9 mg Cl⁻ ml⁻¹ (18 mg of chloride ion present in the 2-ml sample in the electrolysis cell).

3.4.3. Accuracy and precision

Table 3 compares the ID-FIRE results with a standard argentometric titration procedure [17] for the determination of chloride ion in a series of five standard solutions containing only aqueous NaCl. Each standard solution was analyzed four times by argentometric titration, and the average of each of the four separate determinations is shown in Table 3. For each ID-FIRE determination, the value of R_s for the sample was measured 4 times with separate aliquots of sample using the average intensity ratio from the seven line pairs in Table 1. The values of these four R_s measurements were then averaged and used in Eq. (5) and Eq. (6). To conserve the enriched Na³⁷Cl spike solution, the value of R_m was measured only once. Each standard NaCl solution was analyzed three times by ID-FIRE spectrometry, and the average of each of the three determinations is shown in Table 3.

The data in Table 3 show an average bias of -3.46% for the ID-FIRE method. Since the analytical results should depend only on the measured values of R_s and R_m , the negative bias must arise from errors associated with the measurement of the intensity ratio for the two isotopic components. One possible correction to the measured intensity ratio could involve differences in the values for the rotational constants for H³⁵Cl and H³⁷Cl.

For H³⁵Cl, the intensity I^{35} of any given rotational line in the infrared emission spectrum will be proportional to N_J^{35} , the number density of H³⁵Cl molecules in the flame in the upper vibrational level, with the rotational quantum number J . The number density, N_J^{35} , is given by [18],

$$N_J^{35} = \frac{N^{35}hcB^{35}}{kT} (2J+1) \exp\left[\frac{-B^{35}J(J+1)hc}{kT}\right] \quad (8)$$

where h is Planck's constant, c is the speed of light, k is Boltzmann's constant, B^{35} is the rotational constant of H³⁵Cl, T is the absolute temperature, and J is the rotational quantum number for the molecule in the upper vibrational state. Since an analogous equation describes the number density of H³⁷Cl molecules in the flame in the upper vibrational level with the rotational quantum number J , it is obvious that the intensity ratio I^{37}/I^{35} for any pair of isotopic rotational lines (emission lines from H³⁷Cl and H³⁵Cl starting from the same J value and ending at the same J' value) will depend on the ratio of the concentrations of these isotopic molecules in the flame and on the ratio of two terms which contain the rotational constants for H³⁵Cl and H³⁷Cl.

Rotational constants for the first vibrational excited state were determined [19] by an analysis of nine line positions in Fig. 3 and found to be 10.09 cm⁻¹ (10.1 cm⁻¹ in Ref. [19]) and 10.08 cm⁻¹ for H³⁵Cl and H³⁷Cl, respectively. This difference is not sufficiently significant to account for the negative bias shown in Table 3.

Another possible source of error in the measured intensity ratio for the two isotopic molecules is the effect of finite mirror retardation on instrumental line shape. Because the distance

Table 4
Accuracy and precision with a single measurement of R_s and R_m

Actual Cl^- concentration ($\text{g Cl}^- \text{ l}^{-1}$) ^a	ID-FIRE ($\text{g Cl}^- \text{ l}^{-1}$) ^b	ID-FIRE ($\text{g Cl}^- \text{ l}^{-1}$) ^c	% error ^d	Relative standard deviation (%) ^b
10.86	10.40	10.63	−2.15	0.85
11.83	11.43	11.72	−0.93	2.0
15.56	15.28	15.81	+1.60	6.0
19.40	18.33	19.05	−1.80	1.8
24.02	23.54	24.59	+2.36	3.1
24.38	22.68	23.67	−2.92	5.9
30.49	28.27	29.61	−2.88	3.4

^a Calculated from the known mass of naturally occurring NaCl dissolved in solution.

^b Based on the average of three determinations for each sample using Eq. (5).

^c Values in column 2 corrected using Eq. (9).

^d Based on data in column 3.

traveled by the mirror in the interferometer is finite, the instrumental line shape obtained by Fourier transformation follows a sinc function [20]. In the ID-FIRE experiments, the side lobes of the sinc function were suppressed using a triangular apodization function. However, the presence of residual negative side lobes adjacent to the large ^{35}Cl peaks is clearly evident in Fig. 4A and Fig. 4B. These side lobes, when blended into nearby peaks, affect both line intensity and peak positions. The effect is most pronounced when one peak is more intense than another and the separation between adjacent peaks is small, i.e. the instrument is being used to monitor lines which are only just resolvable.

The effect of side lobes on the measured $^{37}\text{I}/^{35}\text{I}$ ratio is difficult to predict and will vary with the separation between the pair of isotopic rotational lines. While other apodization functions might be used to reduce side lobes, there will be a corresponding increase in linewidth and reduction in peak height. Clearly the best solution to this problem is to use an instrument with the highest possible resolution so that the ^{37}Cl and ^{35}Cl lines are more widely separated.

Since an increase in resolution or change in apodization function was not possible with the instrument used in these studies, an instrument calibration procedure was employed to minimize the negative bias observed for the ID-FIRE method. When the actual chloride ion concentrations in Table 3 (column 1) were plotted against

the ID-FIRE results, a least-squared linear relationship was obtained,

$$\text{corrected Cl}_s = 1.0622\text{Cl}_s - 0.4209 \quad (9)$$

with a correlation coefficient of 0.9997 for the regression line. As this instrumental correction factor must be empirically determined, Eq. (9) applies strictly to the instrument used in these experiments with the resolution conditions, apodization function and rotational line pairs described for this analysis.

Table 4 gives the results obtained with ID-FIRE using a single measurement of R_s and R_m for each determination. Column 2 gives the values obtained directly from Eq. (5); column 3 shows the results obtained by applying the instrumental correction factor given in Eq. (9). Each value in columns 2 and 3 represents an average of three determinations. From the data in Table 4, the average error was found to be -0.96% for the seven samples, and the average relative standard deviation for the seven samples was 3.3% .

3.4.4. Matrix effects

To assess the accuracy of the ID-FIRE technique in the presence of interferences, a series of synthetic NaCl solutions was prepared containing known amounts of bromide and iodide, two important potential interferences. Table 5 gives the results obtained for the determination of these solutions using ID-FIRE and a standard argentometric titration procedure [17]. The titrations were

Table 5
Effect of Interferences

Solution ^a	Actual Cl ⁻ conc. (g Cl ⁻ l ⁻¹) ^b	ID-FIRE conc. (g Cl ⁻ l ⁻¹) ^c	% error	Titration Conc. (g Cl ⁻ l ⁻¹) ^d	% error
17.1085 g NaCl/12.4151 g NaBr	20.7569	20.55	-1.0	29.29	+41.0
16.0745 g NaCl/1.0230 g NaI	19.5024	19.04	-2.4	20.29	+4.1

^a Mass of solute in 500 ml of solution.

^b Calculated from mass of naturally occurring NaCl.

^c Average of three determinations using Eq. (9).

^d Average of four determinations.

carried out using an autotitrator (DL 70, Mettler Instrument, Hightstown, NJ) equipped with a silver/silver chloride indicator electrode. Table 5 gives the concentration of chloride ion, in g l⁻¹, calculated from the known weight of primary standard NaCl in the solution. The results for ID-FIRE are the average of three determinations, and the results for the silver nitrate titration represent the average of four determinations.

It is clear from the data in Table 5 that the accuracy of the ID-FIRE determination of chloride ion is quite good even in the presence of relatively large amounts of bromide and iodide ions, both of which can be seen to cause substantial systematic errors in the silver nitrate determination. The accuracy obtained with the ID-FIRE determination of chloride ion in the presence of bromide ion, in particular, demonstrates the ability of isotope dilution to eliminate the effects of matrix interferences. In a previous FIRE spectrometry study [5] to determine chloride ion in aqueous media, a calibration curve, based on the intensity of the 1–0 band of HCl, was prepared using calibration standards. In this earlier FIRE study, the presence of bromide ion in the sample was found to significantly reduce the intensity of HCl emission from the flame, leading to large negative systematic errors in the determination of chloride ion.

In the ID-FIRE study, the presence of matrix components that affect the intensity of the HCl emission produced by the flame does not lead to analytical errors as long as the I^{37}/I^{35} intensity ratios of the 1–0 HCl band are unaffected. For

samples containing bromide ion and iodine ion, electrolysis of the sample produces Br₂ and I₂ along with Cl₂. However, when Br₂ and I₂ are introduced into the hydrogen/entrained air flame, they do not produce measurable emission from HBr and HI. They do, however, depress the overall intensity of the HCl emission signal, perhaps by the formation of interhalogen compounds which are known to form with several stoichiometries [21].

The depression of the HCl signal was more severe for the case of iodide ion than for bromide ion. This did not affect the analytical results obtained by ID-FIRE as long as the ro-vibrational spectrum of HCl was strong enough to allow the intensity ratios of ³⁵Cl and ³⁷Cl to be measured. If too much iodide ion was present, however, the emission intensity of the HCl band became too low to measure the intensity ratios.

3.5. Determination of chloride ion in seawater

Seawater was used to demonstrate the utility of ID-FIRE with a complex, real sample. Seawater provides an almost ideal sample for the ID-FIRE chloride ion determination because the concentration of chloride ion is typically about 20 mg Cl⁻ ml⁻¹ (well above the limit of quantification), and because argentometric titrations commonly used for the determination of chlorinity [17] are potentially subject to interference by other ions present in the sample, such as bromide ion and iodide ion.

Table 6 compares the results obtained by argentometric titration [17] and ID-FIRE for four sea-

Table 6
Chloride ion in seawater

Water source	Titration conc. (g Cl ⁻ l ⁻¹) ^a	ID-FIRE conc. (g Cl ⁻ l ⁻¹) ^b	Relative difference (%)
Port Isabel, Texas, Gulf of Mexico	20.44 ^c	19.06	-6.75 ^d -2.21 ^e
Port Isabel, Texas, Laguna Madre Bay	20.83 ^f	20.40	-2.06 ^d -0.63 ^e
Hanauma Bay, Oahu, Hawaii	20.04	20.27	+1.15
Whale Cove, Grand Manan Island, Bay of Fundy	18.86	19.76	+4.77

^a Based on four argentometric titrations using an automatic titrator.

^b Based on three determinations using ID-FTIR and Eq. (9).

^c 19.49 g Cl⁻ l⁻¹ by manual AgNO₃ titration using chromate indicator.

^d Difference relative to result obtained using the automatic titrator.

^e Difference relative to manual AgNO₃ titration using chromate indicator.

^f 20.53 g Cl⁻ l⁻¹ by manual AgNO₃ titration using chromate indicator.

water samples collected from different regions. Each sample was analyzed four times by titration and three times by ID-FIRE using the correction factor in Eq. (9). As shown in Table 6, the values obtained by the two techniques are in good agreement.

4. Conclusion

The ID-FIRE determination of chloride ion in aqueous samples has several important advantages. (1) Because the procedure is based on isotope dilution, sample introduction need not be quantitative, and matrix effects are minimized. (2) The conversion from chloride ion to HCl is handled automatically by the sample introduction system. Consequently, no sample pretreatment and minimal sample handling are required. (3) Compared with silver nitrate titrations, only a relatively small sample size is needed (2 ml). This may be of importance in the analysis of such samples as interstitial water from sediments (i.e. pore water analysis) where sample size is limited. (4) The method is rapid. Only 2 min are required to collect the spectral data.

A small negative bias, believed to be an artifact of the instrumental line profile, could be minimized by application of an empirically determined correction factor. Finally, the accuracy and preci-

sion obtainable with the ID-FIRE procedure depend on the amount of time, effort and expense warranted by the sample. In this paper, effort and expense was reduced by limiting the number of replicate samples and the number of FTIR scans collected for a given determination. It is clear, however, that these parameters can be increased if warranted by the analytical situation.

References

- [1] N.H. Furman (Ed.), Standard Methods of Chemical Analysis, vol. 1, 6th ed., Van Nostrand, Princeton, NJ, 1962, p. 324.
- [2] D. Butts, Chemicals from brine, in: M.H. Grant (Ed.), Encyclopedia of Chemical Technology, 4th ed., vol. 5, Wiley-Interscience, NY, 1993, pp. 817–833.
- [3] L.C. Curlin, T.V. Bommaraju, C.B. Hansson, Alkali and chlorine products, in: M.H. Grant (Ed.), Encyclopedia of Chemical Technology, 4th ed., vol. 1, Wiley-Interscience, NY, 1991, pp. 938–1025.
- [4] H.U. Sverdrup, M.W. Johnson, R.H. Fleming, The Oceans, Prentice-Hall, Englewood Cliffs, NJ, 1942, p. 175.
- [5] S.W. Kubala, D.C. Tilotta, M.A. Busch, K.W. Busch, Anal. Chem. 61 (1989) 2785–2791.
- [6] K.W. Busch, M.A. Busch, Flame and furnace infrared emission spectrometry, in: A. Townshend (Ed.), Encyclopedia of Analytical Science, vol. 2, Academic Press, London, 1995, pp. 1289–1298.
- [7] M.A. Busch, K.W. Busch, Spectrochim. Acta Rev. 14 (1991) 303–336.

- [8] H. Yoshioka, Isotope dilution analysis, in: A. Townshend (Ed.), *Encyclopedia of Analytical Science*, vol. 4, Academic Press, London, 1995, pp. 2399–2409.
- [9] G. Hevesy, R. Hobbie, *Nature* 129 (1931) 1083.
- [10] P. Pekka, L.H.J. Lajunen, P. Perämäki, Chlorine, in: A. Townshend (Ed.), *Encyclopedia of Analytical Science*, vol. 2, Academic Press, London, 1995, pp. 687–693.
- [11] D.C. Tilotta, K.W. Busch, M.A. Busch, *Appl. Spectrosc.* 43 (1989) 704–709.
- [12] K.W. Busch, M.A. Busch, D.C. Tilotta, S.W. Kubala, C.K.Y. Lam, R. Srinivasan, *Spectroscopy* 4 (8) (1989) 22.
- [13] Y. Zhang, K.W. Busch, M.A. Busch, *Appl. Spectrosc.* 46 (1992) 930–939.
- [14] G. Herzberg, *Molecular Spectra and Molecular Structure I. Spectra of Diatomic Molecules*, Van Nostrand, New York, 1950, pp. 56–57.
- [15] G. Herzberg, *Molecular Spectra and Molecular Structure I. Spectra of Diatomic Molecules*, Van Nostrand, New York, 1950, p. 142.
- [16] N.N. Greenwood, A. Earnshaw, *Chemistry of the Elements*, Pergamon Press, Oxford, 1984, p. 935.
- [17] K. Grasshoff, M. Ehrhardt, K. Kremling (Eds.), *Methods of Seawater Analysis*, Verlag Chemie, Weinheim, 1983, pp. 38–45.
- [18] G. Herzberg, *Molecular Spectra and Molecular Structure I. Spectra of Diatomic Molecules*, Van Nostrand, New York, 1950, p. 125.
- [19] E.A. Guggenheim, J.E. Prue, *Physicochemical Calculations*, Interscience, New York, 1956, p. 78.
- [20] K.W. Busch, M.A. Busch, *Multielement Detection Systems for Spectrochemical Analysis*, Wiley-Interscience, New York, 1990, pp. 309–312.
- [21] N.N. Greenwood, A. Earnshaw, *Chemistry of the Elements*, Pergamon Press, Oxford, 1984, pp. 964–966.

Short communication

Transport and separation of Ag^+ and Zn^{2+} by donnan dialysis through a monovalent cation selective membrane

Ahmed Toufik Cherif^a, Claude Gavach^a, Jean Molenat^{a,*}, Azzedine Elmidaoui^b

^a *Laboratoire des Matériaux et Procédés Membranaires CNRS, 1919 route de Mende, F34293, Montpellier, Cedex 5, France*

^b *Faculté des Sciences de Kénitra, Kénitra, Morocco*

Received 17 March 1997; received in revised form 7 November 1997; accepted 12 November 1997

Abstract

Donnan Dialysis of Ag^+ and Zn^{2+} was investigated through a cation exchange membrane (CMS Neosepta) when a proton concentration difference was maintained between the two sides of the membrane. Developed for the production of brine from sea water, CMS Neosepta showed a higher permeability to monovalent than to bivalent cations. Several physico-chemical parameters have been determined (electrical resistance, membrane potential, sorption of electrolytes, Zn^{2+} and Ag^+ diffusion coefficients). The flux of Ag^+ and the diffusion potential in the membrane increase with HNO_3 concentrations. Ag^+ and Zn^{2+} can be separated because of the preferential membrane transfer for Ag^+ . © 1998 Elsevier Science B.V. All rights reserved.

Keywords: Transport; Separation; Ag^+ ; Zn^{2+} ; Donnan dialysis; Monovalent cation selective membrane

1. Introduction

Among various techniques [1–7] that have been used for separation and concentration of cations mixtures, separation by Donnan dialysis is one of the simplest and most economical process.

The purpose of this work is to study Donnan dialysis in order to separate Ag^+ monovalent from Zn^{2+} bivalent cations. A CMS cation exchange membrane separates the salt mixture solutions from the acid solutions. Salts and acid have

the same common anion. Cations and protons move in opposite directions toward a final state corresponding to the equality of the electrochemical potentials for each cation in the two compartments. Previous experiments [8,9] have shown that the permeability of this CMS membrane was greater for sodium than for bivalent cations because a layer of positive charges has been fixed on one side of the membrane. This layer will induce a stronger electrostatic repulsion to bivalent than to monovalent ions.

First, several physico-chemical parameters of the membrane were determined when it was equilibrated with the electrolyte solutions. Then the

* Corresponding author.

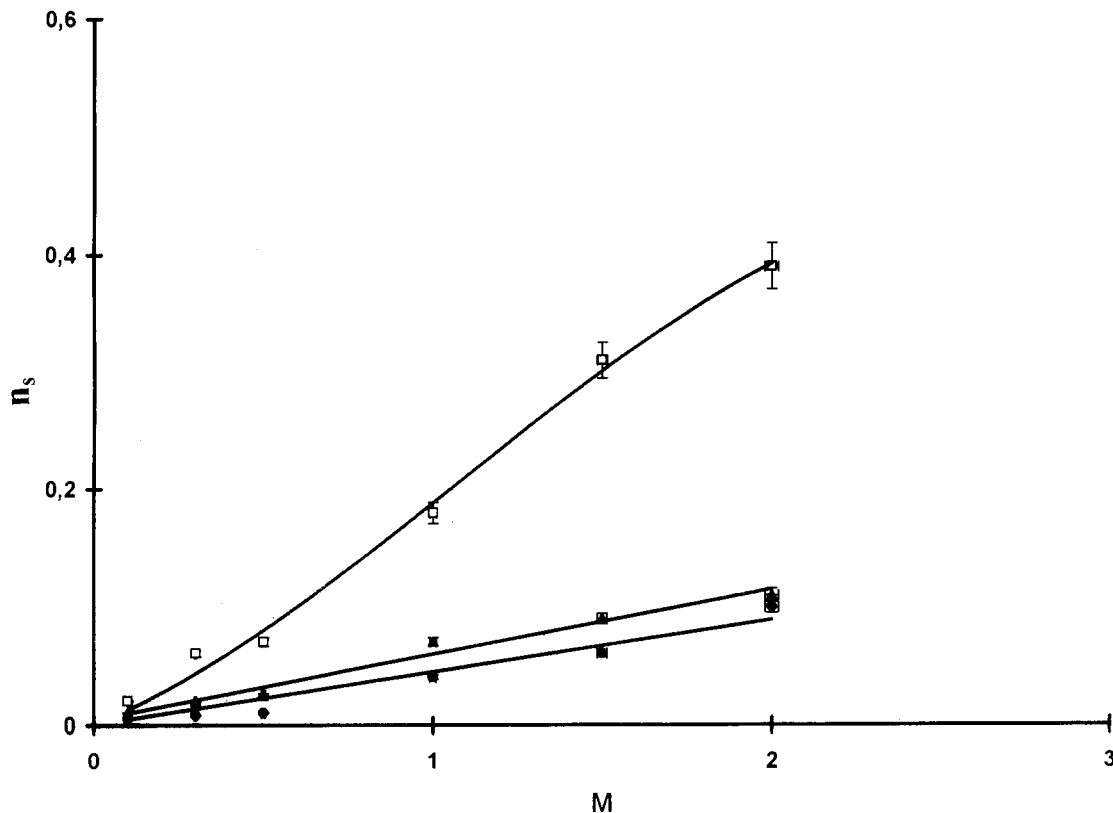


Fig. 1. Moles of sorbed electrolyte (n_s) per cation exchange sites vs the external concentration of electrolyte in the solution. (□) HNO_3 ; (▲) AgNO_3 ; (●) $\text{Zn(NO}_3)_2$.

ionic fluxes as well as the potential difference between the two aqueous sides of the membrane (membrane potential) were measured and analysed for different systems.

2. Experimental

The CMS Neosepta membrane used for the experiments was manufactured by Tokuyama Soda. Its thickness was 150 μm and its exchange capacity 2.3 meq per gram of dry membrane. The working area was 7 cm^2 . Different systems with the following compositions were investigated:

$(10^{-2} \text{ M})\text{AgNO}_3$ and/or

$(10^{-2} \text{ M})\text{Zn(NO}_3)_2$ | CEM | $(x \text{ M})\text{HNO}_3$

In the stripping solution, the HNO_3 concentra-

tions range between 0.25 and 1 M. The salt solutions were in contact with the positive charge layer of the membrane.

The electrical resistance of the membrane, the amounts of sorbed electrolyte and the exchange capacity were determined by previously described methods [10].

The volume of the solutions on both sides of the membrane was 40 ml. The solutions were thoroughly stirred and the temperature maintained at 25°C. The flux of Ag^+ and/or Zn^{2+} arriving into the acid solution was measured by titrating these ions at regular intervals of time.

The membrane potential was measured under the same conditions by introducing two electrodes. These electrodes were connected to a millivoltmeter (Tacussel MINISIS 8000). When the feed solution contained only Zn^{2+} ions, the mem-

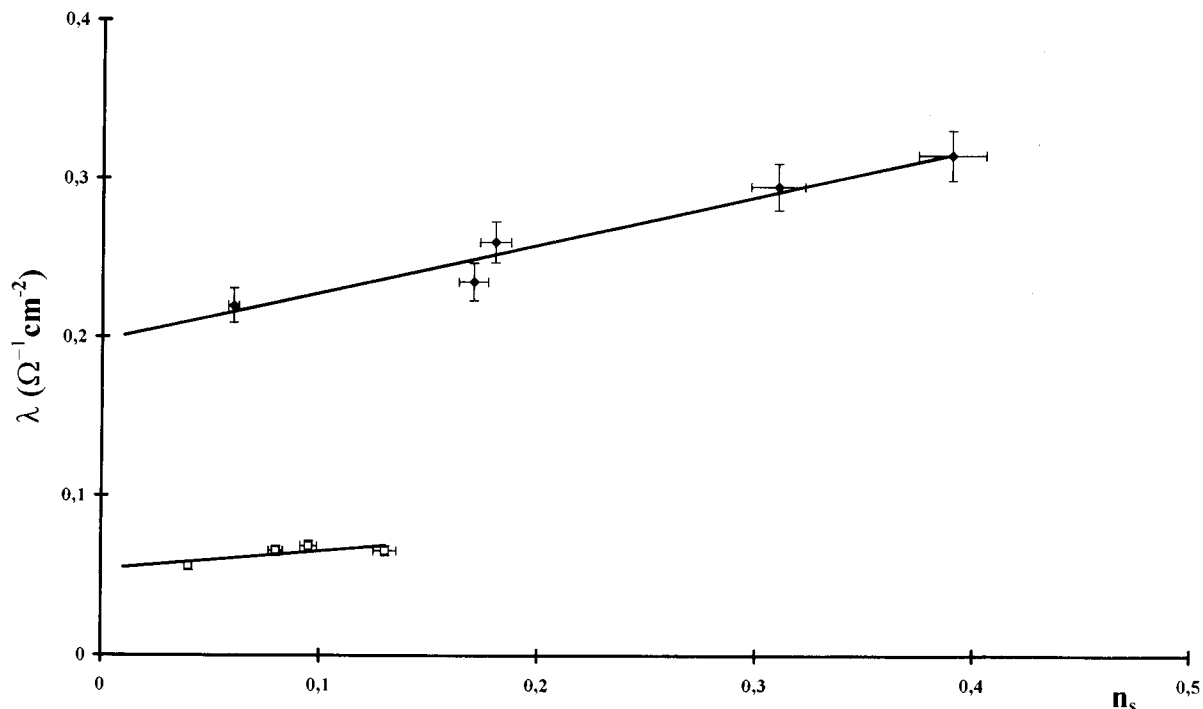


Fig. 2. Conductance (λ) of the membrane versus (n_s), the ratio of the moles of sorbed electrolyte over the exchange capacity. (◆) AgNO_3 ; (□) $\text{Zn}(\text{NO}_3)_2$.

brane potential was directly measured using a pair of KCl saturated calomel electrodes. In the presence of Ag^+ , the membrane potential was measured using a silver or a calomel electrode in the feed solution and a calomel electrode in the acid solution. The value of the membrane potential was deduced from the measured potential, taking into consideration the silver electrode and the calomel electrode standard potentials with the silver ion activity in the feed solution.

3. Results and discussion

3.1. Determination of diffusion coefficients

Fig. 1, shows the amount of sorbed moles per fixed site in the membrane at equilibrium with each electrolyte solution for different concentrations. From these data, it is possible to calculate the cation over anion concentration ratios in the membrane phase. The high values of these ratios

in the considered concentration range show a high rejection of nitrate co-ions, allowing to neglect the amount of nitrate anions in the membrane with respect to that of cations. The error on sorbed moles is $\pm 4\%$.

Figs. 2 and 3 show the variations of the membrane conductance λ ($\Omega^{-1} \text{ cm}^{-2}$) when equilibrated with HNO_3 , AgNO_3 and $\text{Zn}(\text{NO}_3)_2$ solutions as a function of the number of moles of sorbed electrolyte (n_s) present inside the membrane. The λ values were determined with an error lower than $\pm 5\%$. The extrapolated value of λ at $n_s = 0$ gives the value of the conductance when only counter-ions Ag^+ or Zn^{2+} [11] are bound to the fixed sites.

By applying the Nernst–Einstein equation to the extrapolated values of the membrane conductance, and taking into account that the membrane phase density is 1.04, one can deduce the values of the three different diffusion coefficients: 17.8, 3.47 and $0.46 \times 10^{-7} \text{ cm}^2 \text{ s}^{-1}$ for H^+ , Ag^+ and Zn^{2+} respectively.

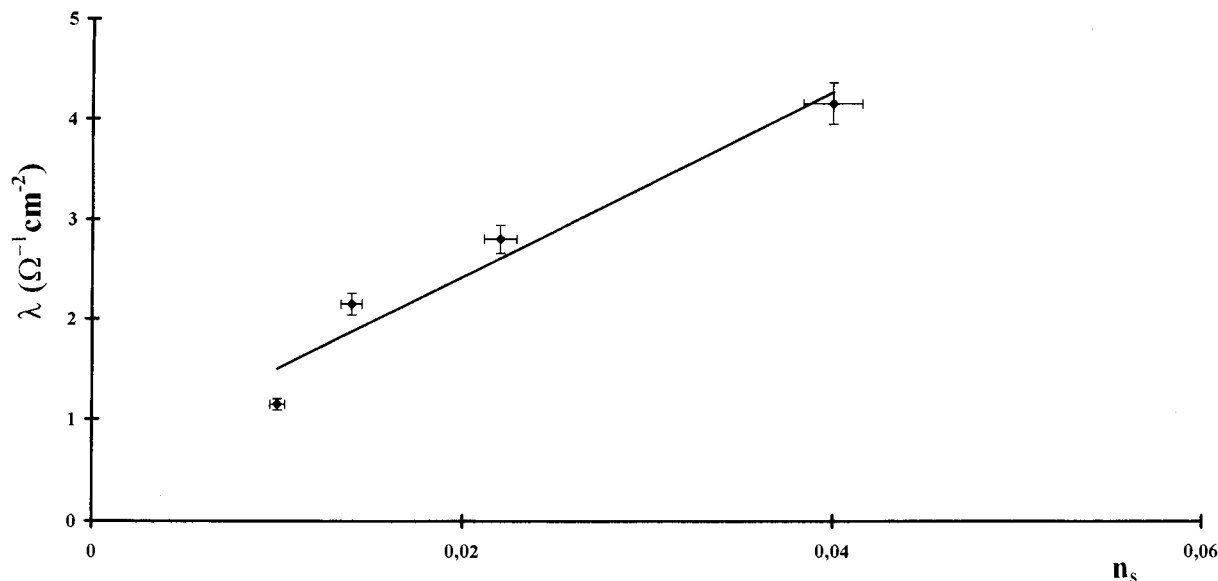


Fig. 3. Conductance (λ) of the membrane versus (n_s), the ratio of the moles of sorbed electrolyte over the exchange capacity. Electrolyte = HNO_3 .

As expected protons give the highest mobility. But these results also show a higher mobility of Ag^+ ions with respect to Zn^{2+} ions and consequently explain the higher permeability of the membrane to Ag^+ .

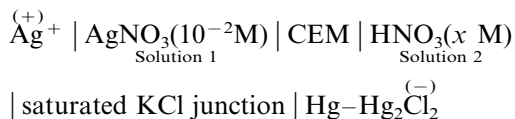
3.2. Dialysis of silver ions

The system AgNO_3 (10^{-2} M)–membrane– HNO_3 (x M) was investigated for several concentrations of HNO_3 .

Table 1 gives the values of the flux of Ag^+ ions (J_{Ag^+}), crossing the membrane, the measured e.m.f. (E_M) of the electrochemical cell and the calculated diffusion potential inside the membrane.

The flux of Ag^+ and the diffusion potential increase with the increasing HNO_3 concentration in compartment 2. These results show that the transfer of protons is a rate determining step.

To determine membrane potentials, the following electrochemical cell was built up:



The measured e.m.f. (E_M) is the sum of all the potentials: electrode E_{Ag} , and $E_{\text{Hg-Hg}_2\text{Cl}_2}$, junction E_j , Donnan E'_i and E''_i and diffusion potentials E_D [12]:

$$E_M = E_{\text{Ag}} + E'_i + E_D - E''_i + [E_j](\text{KCl-HNO}_3) - E_{\text{Hg-Hg}_2\text{Cl}_2} \quad (1)$$

The following equation can be used to calculate the difference of the Donnan potentials, [13–15].

$$E'_i - E''_i = \frac{RT}{F} \ln \frac{(a'_{\text{Ag}^+})_1 (a_{\text{H}^+})_2}{(a_{\text{Ag}^+})_1 (a''_{\text{H}^+})_2} \quad (2)$$

where a' and a'' are the individual ion activities in the layers of the membrane phase in contact with the aqueous solutions and a_{H^+} and a_{Ag^+} the activities in the bulk aqueous solutions, subscripts 1 and 2 refer to the two solutions.

The junction potential $[E_j](\text{KCl-HNO}_3)$ can be calculated by applying the Henderson equation [16].

Eq. (1) can then be used to determine E_D from experimental values of E_M . But several assumptions are required:

1. The continuity of the electrochemical potential of the cations at each membrane–solution interface.

Table 1

Values of J_{Ag^+} , E_{M} , E_{J} and E_{D} for different concentrations of HNO_3 : System: AgNO_3 (10^{-2} M)–membrane– HNO_3 (x M)

HNO_3 (M)	$J_{\text{Ag}^+} \times 10^{10}$ (mol cm $^{-2}$ s $^{-1}$)	E_{M} (mV)	$[E_{\text{J}}]$ (KCl– HNO_3) (mV)	E_{D} (mV)
0.25	$80 \pm 2\%$	582	7	72.5 ± 1.5
0.50	$98 \pm 2\%$	610	10	87.0 ± 1.5
1.00	$123 \pm 2\%$	635	14	95.0 ± 1.5

Table 2

Values of $J_{\text{Zn}^{2+}}$, E_{M} , E_{J} and E_{D} for different concentrations of HNO_3 system: $\text{Zn}(\text{NO}_3)_2$ (10^{-2} M)–membrane– HNO_3 (x M)

HNO_3 (M)	$J_{\text{Zn}^{2+}} \times 10^{10}$ (mol cm $^{-2}$ s $^{-1}$)	E_{M} (mV)	$[E_{\text{J}}]$ $\text{Zn}(\text{NO}_3)_2$ –KCl (mV)	$[E_{\text{J}}]$ KCl– NO_3 (mV)	E_{D} (mV)
0.25	$7.3 \pm 2\%$	120	2	7	141 ± 2
0.50	$14.2 \pm 2\%$	153	2	10	150 ± 2
1.00	$18.0 \pm 2\%$	172	2	14	203 ± 2

- The amount of H^+ in the membrane layer of the (') interface is negligible with respect to the amount of Ag^+ . In the (") interface layer, the amount of Ag^+ is negligible with respect to the amount of protons.
- The activity coefficients of the cations in the membrane are equal to unity.
- The compositions of the aqueous phases are not significantly changed by the transmembrane transport of ions.

3.3. Dialysis of zinc ions

Comparing Tables 1 and 2 shows that Zn^{2+} ions provide lower fluxes than those obtained with Ag^+ ions.

The same type of equations as with Ag^+ is used to obtain the junction potentials and the same assumptions are applied for the calculation of E_{D} using Eqs. (1) and (2). Moreover, the following approximations have been used:

$$(a'_{\text{Zn}^{2+}}) = \frac{X}{2} \quad (3)$$

and

$$(a''_{\text{H}^+}) = X \quad (4)$$

X is the concentration of the fixed sites in the membrane phase.

3.4. Dialysis of silver and zinc ions

Table 3 shows that the Zn^{2+} flux remains always much lower than that of Ag^+ . The fluxes of these two ions increase with the increasing diffusion potential. The same electrochemical cell was used and an Ag^+ electrode has been used again.

The difference between the interfacial Donnan potentials $E'_i - E''_i$ is calculated using as previously the equality of electrochemical potentials of an ion in the solution and inside the membrane. In solutions containing several ions, potential calculations can be performed from the activities of any of these ions. In the present case, it is no longer the Ag^+ ion concentration which is supposed equal to the concentration of the fixed site in the membrane layer adjoining the interface but the sum of Ag^+ and Zn^{2+} concentrations.

$$(C_{\text{Ag}^+})' + 2(C_{\text{Zn}^{2+}})' = X = 2.2 \times 10^{-3} \text{ mol cm}^{-3} \quad (5)$$

These two concentrations were determined by measuring the amount of Zn^{2+} and Ag^+ ions in a membrane sample after being equilibrated in an aqueous solution of (10^{-2} M) AgNO_3 + (10^{-2} M) $\text{Zn}(\text{NO}_3)_2$:

$$(C_{\text{Ag}^+})' = 0.48 \times 10^{-3} \text{ mol cm}^{-3}$$

$$(C_{\text{Zn}^{2+}})' = 0.86 \times 10^{-3} \text{ mol cm}^{-3}.$$

Table 3

Values of J_{Ag^+} , $J_{\text{Zn}^{2+}}$, E_{M} , and E_{D} for different concentrations of HNO_3 System: AgNO_3 (10^{-2} M) + $\text{Zn}(\text{NO}_3)_2$ (10^{-2} M)–membrane– HNO_3 (x M)

HNO_3 (M)	$J_{\text{Ag}^+} \times 10^{10}$ (mol cm $^{-2}$ s $^{-1}$)	$J_{\text{Zn}^{2+}} \times 10^{10}$ (mol cm $^{-2}$ s $^{-1}$)	E_{M} (mV)	$[E_j]$ (KCl– HNO_3) (mV)	E_{D} (mV)
0.25	$80 \pm 2\%$	$10.2 \pm 2\%$	598	7	126.5 ± 1.5
0.50	$120 \pm 2\%$	$11.5 \pm 2\%$	615	10	129.0 ± 1.5
1.00	$132 \pm 2\%$	$12.6 \pm 2\%$	634	14	134.5 ± 1.5

Table 4

Separation of silver from zinc with CMS membrane after one hour dialysis Initial concentration in compartment (1): AgNO_3 (10^{-2} M) + $\text{Zn}(\text{NO}_3)_2$ (10^{-2} M)

Initial [HNO_3] (M) compartment (2)	Compartment composition (2)		Extractions factors	
	[Ag^+] 10^3 M	[Zn^{2+}] 10^3 M	Ag^+	Zn^{2+}
0.25	5.4	0.7	1.17	0.075
1.5	7.6	0.7	3.17	0.075
1	8.4	0.7	5.25	0.075

In classical exchange membranes, cations of different charges can be separated because of the preferential transfer of low charged cations. An extraction factor K_1^2 , is defined for every cation between two solutions (Table 4):

$$K_1^2 = \frac{C_2}{C_1} \quad (6)$$

where C is the concentration of the cation after 1 h dialysis; subscripts 1 and 2 refer to the solutions in compartments (1) and (2).

If $K_1^2 > 1$ or < 1 , most of the cations will be recovered in compartment 2 or in compartment 1 respectively.

Equimolecular amounts of silver and zinc in the feed solution were separated into two fractions, one enriched in silver and the other enriched in zinc. Results show that cations can be separated from each other with this membrane (Table 4).

4. Conclusion

The CMS Neosepta membrane previously used to separate sodium from calcium in sea water can also be used to separate other cations such as

Ag^+ from Zn^{2+} . Our results show that the extraction coefficients were higher than 1 for Ag^+ and lower than 1 for Zn^{2+} (Table 4).

The efficiency of this separation, (i.e. the Ag^+ over Zn^{2+} extraction coefficients ratio) is increasing when HNO_3 concentration and diffusion potential are increasing.

References

- [1] N. Lakshminarayanaiah, Transport phenomena in membranes, Academic Press, New York, 1969.
- [2] J.A. Cox, K.H. Cheng, Anal. Chem. 50 (4) (1978) 601–602.
- [3] P.K. Ng', D.D. Synder, J. Membrane Sci. 13 (1983) 327–336.
- [4] J.E. Dinunzo, M. Jubara, Anal. Chem. 55 (1983) 1013–1016.
- [5] P.K. Ng', D.D. Synder, J. Electrochem. Soc. 128 (8) (1981) 1714–1719.
- [6] R.M. Wallace, Eng. Chem. Process. Des. Dev. 6 (4) (1967) 423–434.
- [7] A. Lindheimer, J. Molénat, C. Gavach, J. Electroanal. Chem. 216 (1987) 71.
- [8] Y. Mizutani, J. Membrane Sci. 54 (1990) 233–257.
- [9] Z. Ogumi, Y. Uchimoto, J. Membrane Sci. 54 (1990) 164–175.
- [10] B. Auclair, private communication, Paris, 1983.

- [11] G. Pourcelly, C. Gavach, J. Electroanal. Chem. 259 (1989) 113–125.
- [12] B.T. Fan, C. Gavach, Biochim. Biophys. Acta 900 (1987) 183–190.
- [13] P. Meares, 4th European Summer School in Membrane Science, Chester College, 13, 1987.
- [14] N. Lakshminarayanaiah, Membrane Electrodes, Academic press, New York, 1976.
- [15] A. Elmidaoui, J. Molénat, C. Gavach, J. Membrane Sci. 55 (1991) 79–98.
- [16] J. Bard, R. Faulkner, Electrochemistry—Principle, methods and applications, Masson, Paris, 1983.

Short communication

The extraction equilibria of the ion associate of periodate with 1-(3,5-diamino-6-chloropyrazinecarboxyl) guanidine

S.M. Aldhaferi *

Department of Chemistry, Faculty of Science, UAE University, P.O. Box 17551, Al-Ain, United Arab Emirates

Received 7 July 1997; received in revised form 30 October 1997; accepted 13 November 1997

Abstract

The extraction equilibrium of the ion-associate of periodate with 1-(3,5-diamino-6-chloropyrazinecarboxyl) guanidine hydrochloride (DPG^+Cl^-) was investigated spectrophotometrically. The optimum conditions for the extraction of the ion associate $\text{DPG}^+ \cdot \text{IO}_4^-$ with cyclohexanone have been established. The ion association constants, β , K_D and K_{ex} and the molar absorptivity of the formed ion associate were determined. These values enable a convenient application of the investigated system for the extraction spectrophotometric determination of periodate ions in the aqueous media. The molar ratio of the ion associate was found to be 1:1 of periodate to the reagent DPG^+Cl^- at pH 4–5. © 1998 Elsevier Science B.V. All rights reserved.

Keywords: Extraction equilibrium; Periodate; DPG^+Cl^- ; Ion-associate

1. Introduction

The oxoanions are amongst the latest studies groups of species from which form liquid–liquid extractable ion associates with onium cations [1–6]. In previous articles, El-Shahawi et al. [4–6] reported the formation and extraction of perruthenate bismuthate and periodate with some onium cations.

The compound 1-(3,5-diamino-6-chloropyrazinecarboxyl) guanidine hydrochloride (DPG^+

Cl^-), also called amiloride hydrochloride (Fig. 1), has been successfully applied as analytical reagent [7–9]. A number of selective and sensitive spectrophotometric and spectrofluorometric methods were developed for the determination of perchlorate, perrhenate and periodate employing this reagent. In these articles, it was shown that the extraction systems of reagent associates formed with oxoanions proceeds rapidly with a high recovery factor. In the connection with the development of new selective analytical methods using amiloride or amiloride derivatives, a deeper understanding of the extraction mechanism is required. Thus, the present communication reports

* Permanent address: Federal Environmental Agency, P.O. Box 5951, Abu Dhabi, United Arab Emirates. Tel.: +971 2 777363; fax: +971 2 770501.

the extraction equilibrium of the reagent associate formed with periodate in aqueous solution with a view to achieve better association and complete extraction of the produced associate into organic phase.

2. Experimental

2.1. Apparatus

A Shimadzu double beam UV-visible spectrophotometer model UV-2101 PC with 1 cm stoppered quartz cells and Shimadzu FTIR 8101 Fourier transform infrared spectrophotometer were used. A Philips 9418 digital pH-meter with a glass and saturated calomel electrodes were used for the pH measurements.

2.2. Reagents and solutions

All chemicals used were of analytical reagent grade. Britton–Robinson buffer was prepared from boric, acetic and phosphoric acids and sodium (chloropyrazinecarboxyl) guanidine hydrochloride dihydrate (Merck) was used without further purification. A 0.01 M solution of the reagent DPG^+Cl^- hydrochloride was made by dissolving 0.3021 g of the reagent in 100 ml of distilled water-hydrochloric acid (1:1 v/v).

2.3. Procedure

Transfer aliquot portions (2 ml) containing various amounts of the reagent DPG^+Cl^- (1.2×10^{-5} – 40×10^{-5} M) to 50 ml of potassium periodate solution to cover the concentration range 1 – 6.5×10^{-6} M KIO_4 at pH 4. Extract twice with 10 ml (2×5) of cyclohexanone and shake the funnels on a shaking machine for 10 min. After separation of the two layers, the aqueous phase was transferred through a filter paper and the periodate in the aqueous phase was then determined iodometrically with 1×10 M sodium thiosulphate or spectrophotometry as triiodate after addition of KI. The concentration of the periodate in the parallel samples containing the same amount of the reagent DPG^+Cl^- was

measured without extraction with cyclohexanone. The amount of periodate in the organic phase was then calculated by the difference and distribution coefficient was calculated by Eq. (11) (see the text below). Collect the organic layer and filter it through a filter paper impregnated with cyclohexanone into 10 mm quartz cell. Measure the absorbance at 354 nm against a reagent blank.

3. Results and discussion

3.1. Examination of the main experimental variables

The extraction of the reaction product of periodate ions and the reagent DPG^+Cl^- was examined in a variety of solvents with a range of functional group types, e.g. ketones, esters, ethers and chlorinated and aromatic hydrocarbons. Cyclohexanone was found the most efficient extraction with a low blank in the absence of periodate ions. Similarly [7,8] with perchlorate and perrhenate, the mechanism of the extraction is presumed to be based on the formation of an ion-associate complex. In cyclohexanone the produced ion-associate gave the highest absorbance and apparent molar absorptivity at 354 nm at pH 4–6 of the aqueous phase. This behaviour is considered to be due to the weak proton-accepting properties of the periodate ion of the ion pair of the donor accepting properties of the ion pair and the solvent respectively [10]. Therefore, cyclohexanone was selected as a proper solvent for these reasons and because its lower density allows a better separation of layers. The extraction of the ion-associate in cyclohexanone was rapid and the absorbance of the extracted species was found to be

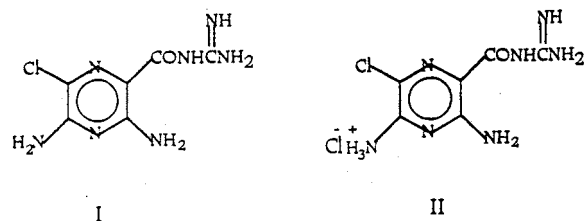


Fig. 1. Structure of amiloride hydrochloride.

Table 1

Results on the extraction of $\text{DPG}^+\text{IO}_4^-$ ion-associate into cyclohexanone at pH 4*

$[\text{DPG}^+ \cdot \text{Cl}^-] \times 10^{-5}$	$[\text{IO}_4^-]_{\text{aq.}} \times 10^{-6}$	$[\text{IO}_4^-]_{\text{org.}} \times 10^{-6}$	$D_{\text{IO}_4^-}$	$\log D_{\text{IO}_4^-}$
39.35	0.56	5.94	10.25	1.01
33.85	0.55	5.95	10.80	1.03
29.45	0.68	5.82	8.56	0.93
18.60	0.74	5.76	7.78	0.98
13.60	0.72	5.78	8.03	0.90
9.45	1.12	5.38	4.80	0.68
7.25	1.52	4.98	4.45	0.64
4.37	2.30	4.20	1.83	0.26
2.41	2.90	3.60	1.24	0.09
5.50	3.60	2.90	0.81	-0.09

*Aqueous solution 10 ml, organic phase 10 ml and $[\text{IO}_4^-] = 6.50 \times 10^{-6}$ M.

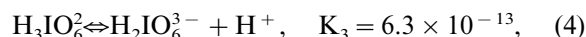
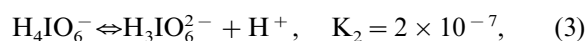
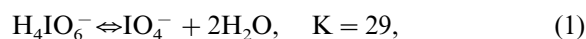
constant up to 2 h standing time for sampling containing $1-6.5 \times 10^{-6}$ M KIO_4 .

The influence of the pH of the aqueous phase was critically investigated by mixing 2 ml of aliquot (10 ppm periodate) solution with 2 ml of 0.01 M amiloride hydrochloride and 5 ml Britton–Robinson buffer (pH 2.2–11). The organic phase was separated, shaken with anhydrous sodium sulfate (0.2 g) and filtered to remove water and the absorbance of the organic extract was measured at $\lambda = 354$ nm against the reagent blank. The absorbance was found high and almost constant in the pH range 4–6 and decreasing outside this limit. Thus, in the subsequent work, the aqueous phase was buffered at pH 4–6. The absorbance of the formed associate was found constant over 5–15 ml of buffer. Thus, 5 ml buffer solution were used in the subsequent work.

The composition of the extracted ion-associate in cyclohexanone was determined by the continuous variation method [11]. Equimolar solutions of potassium periodate and the reagent DPG^+Cl^- (0.001 M) were mixed in complementary proportions to a fixed total volume at pH 5 with 10 ml of cyclohexanone and were allowed to equilibrate for 10 min for completion of the reaction. The absorbance of the produced ion-associate was measured against a reagent blank. A plot of the absorbance of the extracted ion-associate in the organic phase versus $[\text{IO}_4^-]([\text{IO}_4^-] + [\text{DPG}^+\text{Cl}^-])$ produced a graph that indicate the formation of

an ion-associate having a periodate to a reagent ratio 1:1. The molar absorptivity of the produced ion-associate was found to be $4.0 \pm 0.3 \text{ mol l}^{-1} \text{ cm}^{-1}$.

In aqueous acid media periodate ion has complex equilibria and resembles tellurates in their stoichiometries. The main equilibria in acid solutions are as follows [12]:



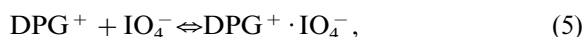
Thus, the produced ion-associate was isolated in the solid state by evaporation of the organic solvent under reduced pressure and was characterized by elemental analysis (Calculated, C = 17.81, H = 2.22, Cl = 8.85, N = 24.23 found, C = 17.92, H = 2.34, Cl = 9.26 and N = 24.66) and visible spectra. The electronic spectrum of the isolated associated dissolved in cyclohexanone was found identical with that of the organic phase obtained by the extraction of the periodate with the reagent DPG^+Cl^- at pH 5 indicating that the extracted and isolated species are identical. The IR spectrum of the isolated solid ion-associate in KBr disc was also compared with those of KIO_4 and the reagent DPG^+Cl^- recorded separately in KBr discs and as a mechanical mixture of KIO_4 and the amiloride hydrochloride with some differences ascribed to the formation of the respective

ion-associate of chemical formula $C_6H_9ION_7^-$ IO_4^- . Thus, the predominant species in the aqueous phase under the used experimental conditions is the IO_4^- species.

3.2. Extraction equilibria

To calculate the equilibrium constants K_{ex} , K_D and β , the extraction equilibrium was critically investigated according to the previously reported model [13]. The following equilibria were considered:

(i) Formation of an ion-associate in the aqueous phase according to the reaction:



with an equilibrium constant (ion-association constant, β)

$$\beta = [DPG^+ \cdot IO_4^-] / [DPG^+ + IO_4^-]. \quad (6)$$

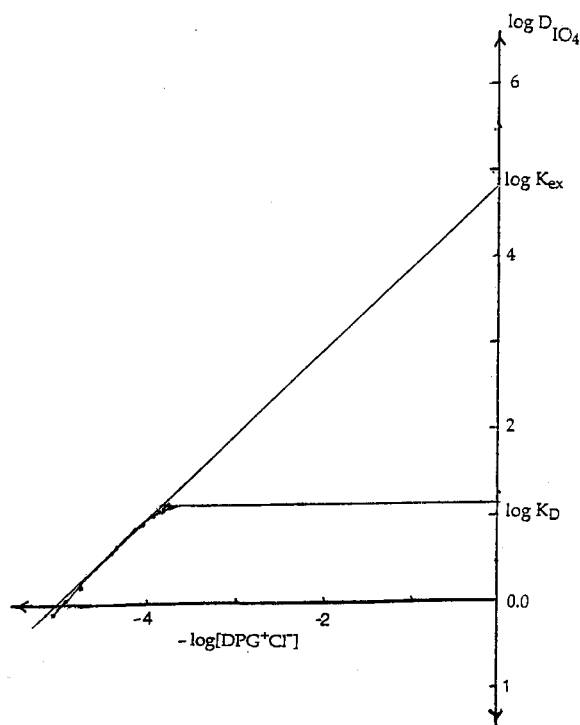


Fig. 2. The plot of $\log [DPG^+ Cl^-]$ vs. $\log D_{IO_4^-}$ ($C_{IO_4^-} = 1.9 \times 10^{-6}$ M).

Table 2

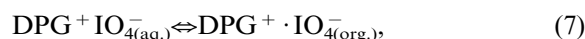
Values of K_{ex} , K_D and β for the extraction system of equilibrium constants of the produced ion-associate in cyclohexanone*

$\log K_{ex} = 4.8 \pm 0.2$	$K_{ex} = 6.3 \times 10^4 \pm 1.7$	$n = 8$
$\log K_{ex}^* = 4.2 \pm 0.3$	$K_{ex}^* = 1.6 \times 10^4 \pm 2.1$	$n = 4$
$\log K_D = 1.2 \pm 0.2$	$K_D = 15.8 \pm 1.4$	$n = 7$
$\log \beta = 3.7 \pm 0.2$	$\beta = 4.8 \times 10^3 \pm 1.61$	$n = 8$

*Values obtained by the Likussar and Boltz method [14].

**Conditions: Extraction from 50 ml of aqueous solution of KIO_4 ($1-6.5 \times 10^{-4}$ M) at pH 4 mixed with 2 ml of the reagent $DPG^+ \cdot Cl^-$ ($1.2 \times 10^{-5}-40.0 \times 10^{-5}$ M) with 10 ml (2×5) cyclohexanone.

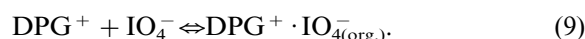
(ii) Distribution of the ion-association complex between the aqueous and the organic phase:



with a distribution constant, K_D

$$K_D = [DPG^+ \cdot IO_{4(org)}^-] / [DPG^+ + IO_{4(aq)}^-]. \quad (8)$$

The overall extraction process is described by the equation



With the corresponding extraction constant K_{ex} .

$$K_{ex} = [DPG^+ \cdot IO_{4(org)}^-] / [DPG^+] \cdot [IO_{4(aq)}^-] = K_D \beta. \quad (10)$$

Hence, assuming one equilibrium species (IO) of periodate (Eq. (1)) is the only predominant at a given pH 4–6, the distribution ratio $D_{IO_4^-}$ was determined at a constant initial IO_4^- concentration in the aqueous phase and various concentrations of $[DPG^+ Cl^-]$ according to the formula:

$$D_{IO_4^-} = [DPG^+ \cdot IO_{4(org)}^-] / [DPG^+ \cdot IO_{4(aq)}^- + [IO_{4(aq)}^-]]. \quad (11)$$

At low concentrations of $DPG^+ Cl^-$, Eq. (11) transforms into the following [13]:

$$D_{IO_4^-} = [DPG^+ \cdot IO_{4(org)}^-] / [IO_{4(aq)}^-]. \quad (12)$$

After substituting Eq. (12) into Eq. (10) and taking the logarithms, the following equation is obtained:

$$\log D_{IO_4^-} = \log K_D \beta + \log [DPG^+]_f. \quad (13)$$

Table 3

A comparison on the values of the molar extinction coefficient ($\log \varepsilon$) of the ion-associates of some spectrophotometric procedures on the determination of periodate ions

Method	λ_{\max} (nm)	$\log \varepsilon$ (mol l ⁻¹ cm ⁻¹)	Reference
Amiloride hydrochloride-IO ₄ ⁻ *	354	4.6	Present work
Trimethylammonium iodide-IO ₄ ⁻ **	509	4.8	[5]
Amiloride hydrochloride-IO ₄ ⁻	354	4.6	[9]
Tiphenyltetrazolium chloride-IO ₄ ⁻	295	5.0	[15]

*Solvent = 4-Methyl-2-pentenone.

**Solvent = Cyclohexanone.

The results obtained at pH 4 are presented in Table 1. The mass balance equation is given by

$$[\text{IO}_4^-]_{\text{aq.}} V_{\text{aq.}} + [\text{IO}_4^-]_{\text{org.}} V_{\text{org.}} = [\text{IO}_4^-]_{\text{aq. initial}} V_{\text{aq.}} \quad (14)$$

where $V_{\text{aq.}} = 10$ ml and $V_{\text{org.}} = 10$ ml. The β , K_{ex} and K_{D} values were then determined graphically from the experimental data (Table 1) of the distribution ratio, $\log D_{\text{IO}_4^-}$ vs. $\log[\text{DPG}^+ \text{Cl}^-]$. The equilibrium concentration of $[\text{DPG}^+]_{\text{f}}$ was calculated employing the equation

$$\begin{aligned} [\text{DPG}^+ \text{Cl}^-]_{\text{initial}} &= [\text{DPG}^+ \text{IO}_4^-]_{\text{org.}} V_{\text{org.}} \\ &= [\text{DPG}^+ \text{IO}_4^-]_{\text{aq.}} V_{\text{aq.}} \end{aligned} \quad (15)$$

The results are summarized in Fig. 2. The values of K_{ex} and K_{D} are read from the plot (Fig. 1) and the β calculated from $\beta = K_{\text{ex}}/K_{\text{D}}$. Table 2 summarizes the values of equilibrium constants of the produced ion-association complex in cyclohexanone. The composition of the extracted species was also obtained from the slope of Fig. 2 and confirmed the composition of the extraction ion-associate to be $\text{DPG}^+:\text{IO}_4^- = 1:1$. The values of K_{ex} (Table 2) was also obtained employing the method of Likussar and Boltz [14] with equimolar solution of periodate and the reagent $\text{DPG}^+ \text{Cl}^-$ in a concentration ($C_{\text{DPG}^+} + C_{\text{IO}_4^-} = 1.1 \times 10^{-4}$ M) and a constant volume of solutions (or extracts) against the proper blank solution containing the $\text{DPG}^+ \text{Cl}^-$ in the same concentration. The values confirmed data obtained according to the chemical model reported by Alexandrov et al. [13].

4. Conclusion

The present article demonstrates that the liquid–liquid extraction procedure involving the formation of the ion-association complex $\text{DPG}^+ \cdot \text{IO}_4^-$ is applicable for periodate determination. The extracted ion-associate has a moderate stability, $\beta = (1.2 \pm 0.28) \times 10^{-4}$. The molar absorptivity of the produced ion-associate $\varepsilon = (4.02 \pm 0.29) \times 10^{-4}$ mol l⁻¹ cm⁻¹ competes favorably with the molar absorptivities of most ion-associates on spectrophotometric determination of periodate (Table 3).

Acknowledgements

The author would like to thank Professor A.S. Al-Sharhan, Dean of the Faculty of Science, UAE University, for the facilities provided, and also thanks to Mrs. Mozza A. Rashid and Miss Raghad H. El-Mahdy for their conscientious help during carrying out their research projects (1 and 2).

References

- [1] D.T. Burns, S.A. Barakat, M. Hariott, M.S. El-Shahawi, Anal. Chim. Acta 270 (1992) 213.
- [2] D.T. Burns, S.A. Barakat, M.S. El-Shahawi, M. Hariott, Z. Fresenius, Anal. Chem. 344 (1992) 131.
- [3] D.T. Burns, M. Harriott, S.A. Barakat, Anal. Chim. Acta 259 (1993) 135.
- [4] M.S. El-Shahawi, A.Z. Abu-Zuhr, S.M. Aldhaheeri, Fresenius J. Anal. Chem. 350 (1994) 674.

- [5] M.S. El-Shahawi, F.A. Al-Hashimi, *Talanta* 43 (1996) 2037.
- [6] M.S. El-Shahawi, S.M. Aldhaheer, *Fresenius J. Anal. Chem.* 354 (1996) 200.
- [7] D.T. Burns, P. Hanprasopwattana, *Anal. Chim. Acta* 118 (1980) 185.
- [8] D.T. Burns, M.S. El-Shahawi, M.J. Kerrigan, P.M.T. Smyth, *Anal. Chim. Acta* 322 (1996) 107.
- [9] M.S. El-Shahawi, *Anal. Chim. Acta* (1994) in press.
- [10] R. Modin, G. Schill, *Talanta* 22 (1975) 1017.
- [11] J. Job, *Ann. Chim. (Paris)* 9 (1928) 113.
- [12] F.A. Cotton, G. Wilkinson, P.L. Gaus, *Basic Inorganic Chemistry*, 3rd ed., John Wiley, 1995, p. 473.
- [13] A. Alexandrov, O. Budevsky, A. Dimitrov, *J. Radioanal. Chem.* 29 (1976) 243.
- [14] W. Likussar, D. Boltz, *Anal. Chem.* 43 (1971) 1265.
- [15] S.M. Kamurova, *Talanta* 39 (1992) 997.

Short communication

Some aspects of the use of heteropoly anions in elemental analysis by simple potentiometric ion-pair formation-based titration

K. Vytřas *, J. Ježková, J. Skořepa

Department of Analytical Chemistry, Faculty of Chemical Technology, University of Pardubice, CZ-532 10 Pardubice, Czech Republic

Received 15 July 1997; received in revised form 8 January 1998; accepted 9 January 1998

Abstract

The possibility of the use of heteropoly anions formed by addition of phosphate to the solutions of either molybdate or tungstate in the determination of phosphorus by the simple method of potentiometric titration was studied. The heteropoly anions are titrated on the ion-pairing principle using a titrant containing a lipophilic counter-ion, i.e. 1-(ethoxycarbonyl)pentadecyltrimethylammonium bromide (Septonex), the titration being monitored by carbon paste electrode, although other liquid membrane-based electrodes can also be used. Calibration plots of the titrant end-point consumption vs. concentration are not linear, but allow one to evaluate the content of phosphorus. Similar procedures, when optimized, should be elaborated for determination of numerous other elements forming heteropoly anions. © 1998 Elsevier Science B.V. All rights reserved.

Keywords: Potentiometric titrations; Ion-pairing reaction; Heteropoly anions; Carbon paste ion-selective electrodes

1. Introduction

Many salts are known having complex anions which contain either molybdenum or tungsten atoms, oxygen atoms, and a much smaller proportion of atoms of another acid-forming, relatively small element, such as P(V), As(V), Si(IV), etc.; the 12-heteropoly anions of general formula

$[X^{n+}M_{12}O_{40}]^{(8-n)-}$ [where X^{n+} is a central cation and M represents either Mo(VI) or W(VI)] are the most common examples [1,2]. Molybdoheteropoly anions of this type are of some importance in analytical chemistry of many elements. For example, the reaction in which the canary-coloured precipitate is obtained in the cold by adding a solution of a phosphate to a solution of ammonium molybdate containing nitric acid and the formula of which is $(NH_4)_3[PMo_{12}O_{40}] \cdot 2HNO_3 \cdot H_2O$, serves for a qual-

* Corresponding author. Tel: +420 40 6037512; fax: +420 40 6037068; e-mail: karel.vytras@hlb.upce.cz

itative detection of phosphate [3]. Spectrophotometric measurements of yellow solutions of molybdoheteropoly anions (or, after their reduction, of so-called molybdenum blue) are often used for quantitative analysis of phosphorus, arsenic and silicon [4]. Recently, a method of spectrophotometric determination of yttrium by reaction with molybdate (in which a heteropoly anion is formed) and Rhodamine B (forming an ion-pair with this heteropoly anion) was reported [5].

In potentiometry, salts of some heteropoly anions (mostly 12-tungstophosphates) can be incorporated as electroactive ion-exchangers into membranes of ion-selective electrodes used in direct potentiometric determination of various cations and, in addition, the solutions of these salts can also be used as anionic titrants in potentiometric ion-pair formation-based titrations. Applications have been described for determination of salts of various alkaloids, antibiotics, vitamins, cationic and non-ionic surfactants, etc. [6–17]. A reverse procedure in which 12-molybdophosphate was titrated with cetylpyridinium chloride and monitored using a cathodically polarized platinum indicator electrode has been described by Selig [18,19]; the method involving the conversion of the orthophosphate first to the molybdophosphate followed by precipitation of it as the tris(cetylpyridinium) 12-molybdophosphate has also been studied.

In this report, we have investigated the new possibilities of monitoring the titrations of heteropoly anions using carbon paste electrodes as potentiometric indicators.

2. Experimental

2.1. Apparatus

Potentiometric titrations were performed using an OP-208/1 pH meter (Radelkis, Budapest) in manual mode, or ATI Orion 960 Autochemistry System (Orion Research, Boston, MA) connected to an HW 486DX2 80 personal computer if auto-

mated mode was used. Sensing electrode was the carbon paste electrode [20], with paste prepared by intimate mixing of 1.0 g graphite powder (CR 5, Tesla, Lanškroun) and 0.4 cm³ of tricresylphosphate (p.a. grade, Lachema, Brno). An RCE-102 calomel electrode (Crytur, Turnov) of double-junction construction, filled with saturated potassium chloride (inner compartment) and 0.1 M sodium nitrate (outer compartment) was used as a reference half-cell.

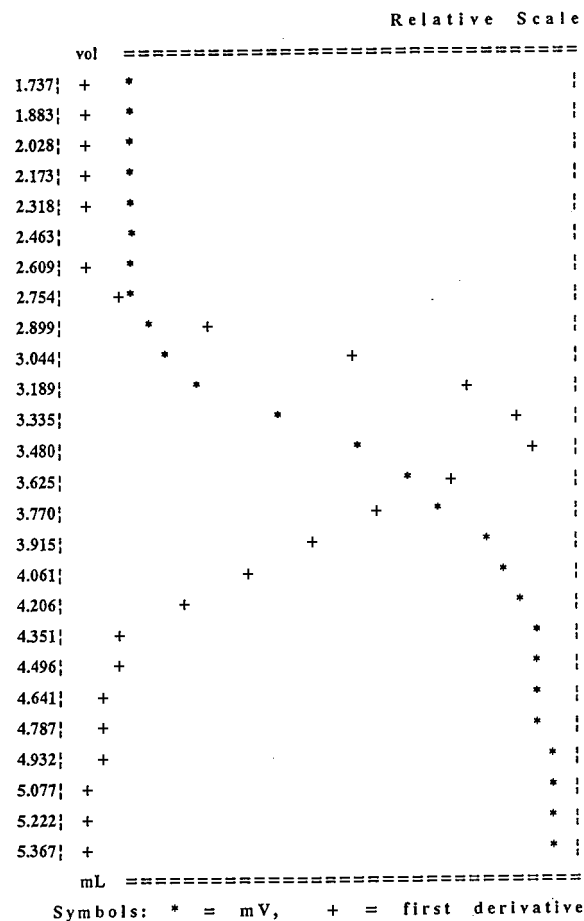


Fig. 1. Automated potentiometric titration of phosphate (10 $\mu\text{mol}/50 \text{ cm}^3$) with 0.01 M Septonex in the presence of 0.12 mmol Na_2WO_4 and 9.6 mmol HCl. Output of the ATI Orion 960 Autochemistry System; end-point titrant consumption, 3.400 cm³.

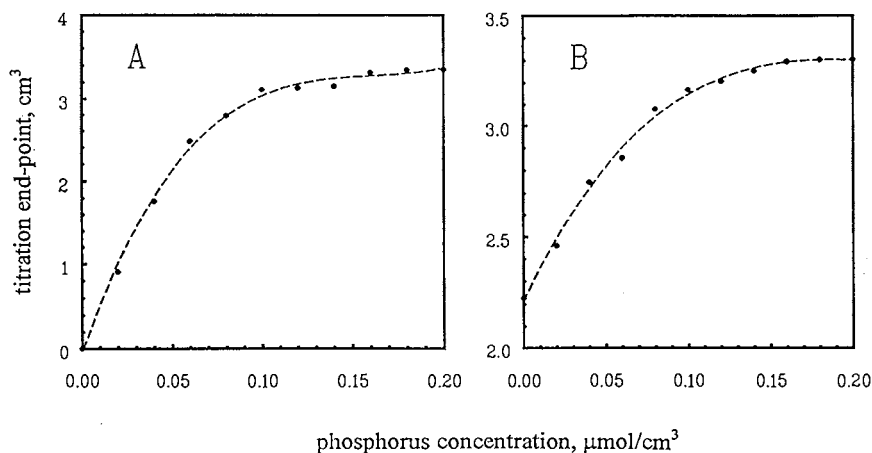


Fig. 2. Calibration dependences for determination of phosphorus forming (A) molybdophosphates; (B) tungstophosphates.

2.2. Titrant and other solutions

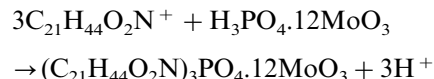
1 - (Ethoxycarbonyl)pentadecyltrimethylammonium bromide (Septonex, Slovakofarma, Hlohovec) as a 0.01 M aqueous solution was used as the titrant. Stock solutions of $\text{Na}_3\text{PO}_4 \cdot 12\text{H}_2\text{O}$, Na_2WO_4 and $(\text{NH}_4)_6\text{Mo}_7\text{O}_{24} \cdot 4\text{H}_2\text{O}$ as well as all other solutions were prepared from analytical grade chemicals; deionized and distilled water was used throughout.

3. Results and discussion

As confirmed by titrations of phosphate mixed with either molybdate or tungstate in various ratios, heteropoly anions of different composition (or mixtures of them) were obtained during such conversions. Although the shape of the potentiometric titration curves was always convenient for evaluation of the end-point (see Fig. 1), the titration stoichiometry did not remain constant, thus not allowing suggestion of a general procedure. It should be noted that the results presented in previous papers [18,19] also did not bring unequivocal conclusions and some corrections based on an empirical logarithmic relationship between the amount of phosphorus present and the optimum Mo/P ratio had to be used (perhaps this was also a reason why no similar study appeared since the papers were published). Finally, it seemed that

such an evaluation must be used which allows determination of the content of phosphorus using calibration dependences.

In the procedure using molybdate, a constant amount of $(\text{NH}_4)_6\text{Mo}_7\text{O}_{24}$ (2 cm³ of 0.009 M solution) was measured into a 100-cm³ beaker, and volumes of 0.0, 0.1, 0.2, ... 1.0 cm³ of 0.01 M Na_3PO_4 were pipetted, water was added to ca. 50 cm³, pH adjusted by addition of 1 cm³ conc. hydrochloric acid, and the solution was titrated with 0.01 M Septonex. In the second procedure, a constant amount of Na_2WO_4 (1 cm³ of 0.12 M solution) was measured into a beaker, and the same portions as given above of other components were added before the titration started. The end-points were evaluated and plotted against the concentration of phosphorus. As seen in Fig. 2, the dependences, although not linear, could be used to determine the content of phosphorus up to ca. 0.1 μmol cm⁻³ concentration in the sample. For lower contents of phosphorus where the calibration curve is nearly linear, it is expected that the determination proceeded via the reaction



i.e. with the stoichiometric 1:3 P/titrant ratio. However, as quite different heteropoly anions may be formed in dependence on the P/Mo (P/W) ratios, the pH value to which solutions are adjusted, sequence of the reagents added, etc.

[23], both calibration curves follow non-linear dependences.

4. Conclusions

Although much work must be done to optimize the procedures (finding the optimum pH value, minimizing the blank when using tungstate, studies at lower concentration levels, etc.), it could be concluded that the formation of heteropoly anions of molybdate and tungstate with other species like PO_4^{3-} , AsO_4^{3-} , BO_3^{3-} , SiO_4^{4-} , IO_4^- , etc. [21,22] offers some new possibilities to determine quite a lot of elements and perhaps also to contribute to their speciation studies by simple potentiometric methods. This preliminary communication is believed to be the first of some systematic research achieved in this field.

Acknowledgements

Financial support from both the Grant Agency of the Czech Republic (project No. 203/96/0124) and the Ministry of Education, Youth and Sports (project No. VS-96058) are gratefully acknowledged.

References

- [1] J.E. Huheey, E.A. Keiher, R.L. Keiher, *Inorganic Chemistry: Principles of Structure and Reactivity*, 4th ed.,

- Harper Collins, New York, 1993, p. 760.
 [2] T.J.R. Weakley, *Struct. Bonding* 18 (1974) 131.
 [3] A. Okáč, *Qualitative Analytical Chemistry* (in Czech), Nakladatelství ČSAV, Prague, 1961.
 [4] M. Malát, *Absorption Inorganic Photometry* (in Czech), Academia, Prague, 1973.
 [5] G.-X. Cheng, Z.-B. Li, J.-L. Wang, Q.-H. Xu, *Yejin Fenxi* 16(5) (1996) 4; *Chem. Abstr.* 126 (1997) 271517s.
 [6] K. Vytřas, *Ion-Sel. Electrode Rev.* 7 (1985) 77.
 [7] Yu.Ya. Vinnikov, L.A. Kostareva, *Zh. Anal. Khim.* 35 (1980) 547.
 [8] V.N. Ivanov, Yu.S. Pravshin, N.I. Bavykina, *Zh. Anal. Khim.* 43 (1988) 1313.
 [9] A.F. Shoukry, S.S. Badawy, R.A. Farghalli, *Anal. Chem.* 60 (1988) 2399.
 [10] D.A. Löwy, A. Patrut, M.A. Walter, *Process Control Quality* 4 (1993) 125.
 [11] A.F. Shoukry, Y.M. Issa, M.S. Rizk, M.M. Abdel-Aal, *Electroanalysis* 6 (1994) 1.
 [12] M.S. Rizk, Y.M. Issa, A.F. Shoukry, M.M. Abdel-Aal, *Anal. Lett.* 27 (1994) 1055.
 [13] Y.M. Issa, M.S. Rizk, A.F. Shoukry, R. Abdel-Aziz, H.M. Abdel-Fattah, E.M. Atia, *Talanta* 41 (1994) 135.
 [14] A. Campiglio, *Analyst* 119 (1994) 2209.
 [15] A.F. Shoukry, *Sci. Pap. Univ. Pardubice, Ser. A* 1 (1995) 5.
 [16] M.S. Rizk, *Electroanalysis* 7 (1995) 687.
 [17] Y.M. Issa, M.S. Rizk, A.F. Shoukry, R.M. El-Nashar, *Electroanalysis* 9 (1997) 74.
 [18] W. Selig, *Talanta* 30 (1983) 695.
 [19] W.S. Selig, *Mikrochim. Acta II* (1984) 133.
 [20] I. Švancara, K. Vytřas, *Chem. Listy* 88 (1994) 138.
 [21] *Gmelins Handbuch der Anorganischen Chemie: Molybdän*, System No. 53, Verlag Chemie, Weinheim, 1933.
 [22] *Gmelins Handbuch der Anorganischen Chemie: Wolfram*, System No. 54, Verlag Chemie, Weinheim, 1933.
 [23] B. Grüttner, G. Jander, *Iso- und Heteropolysäuren und ihre Salze*, in: G. Brauer (Ed.), *Handbuch der Präparativen Anorganische Chemie*, 2nd ed., Vol. 2, F. Enke, Stuttgart, 1962, p. 1473.

Book reviews

Molecular Genetics and Evolution of Pesticide Resistance. T.M. Brown (editor), ACS, Washington, DC, 1996. xiii + 265pp. US\$ 97.95. ISBN 0-8412-3453-1

This volume is compiled from two dozen papers given at a special conference on Molecular Genetics and Ecology of Pesticide Resistance. Although the discussion of pesticide resistance is not new, the investigation of its genetic aspect is a currently expanding field. Papers have been carefully selected to provide coverage of the most important findings in the all relevant areas of pesticides and pests. This must have been a particularly daunting task for the committee since the pests under investigation vary greatly and include species of bacteria, fungi, plants (weeds) and insects, although it is only at the molecular level that some of the similarities in resistance mechanisms become apparent. The similarities between antibiotic and pesticide resistance are also discussed with a chapter specifically set aside to review this issue. This in fact is one of the most interesting chapters as it highlights, in a condensed form, the different molecular and subsequent biochemical modifications which result in resistance.

The text is divided into four sections. Firstly, molecular genetics, which clearly demonstrates how important it is to investigate this aspect of resistance if we are to make any progress in developing novel pesticides that do not quickly become redundant due to further resistance. Secondly, a selection of papers under the topic of evolution and population genetics includes discussion of the use of genetic monitoring to detect the incidence of resistance. The section on resistance management strategies is brief but informative,

giving excellent insight through practical experience. Finally, ecology, transgenesis and regulatory issues are discussed and demonstrate some of the really problematic issues in this field, namely the transfer of resistance throughout a population and between species. The monitoring of the movement of genetic resistance between plants is particularly important with the advent of genetically engineered crops that are resistant to herbicides or pests. This aspect is concisely reviewed in one of the chapter in this section. The book is rounded off with a chapter which considers the role of regulatory organizations (US EPA) in the control of pesticide resistance.

On the whole this is a very informative book which addresses many of the important aspects of pesticide resistance, an area that will certainly gain importance in coming years. This is a relatively specialized text that will not be immediately accessible to those outwith the field. However, I believe that readers from widely differing scientific backgrounds will find something of interest if they take the time to browse through this text.

L.A. Lawton

PII S0039-9140(97)00416-5

Environmental Immunochemical Methods by J.M. Van Emon, C.L. Gerlach and J.C. Johnson (Eds.), ACS, Washington, DC, 1996. x + 342 pp. US\$109.95. ISBN 0-8412-3454-X.

This book provides an excellent cross-section of the many and often widely differing environmental applications of immunochemical detection. In recent years environmental immunochemistry has

gained increasing recognition as an inexpensive but reliable analytical technique with a number of procedures now validated for regulatory purposes. This volume presents almost 30 papers which, between them, encompass aspects of research and development, application of methods, data interpretation, and evaluation. As may be expected a number of the applications focus on the detection of pesticides in the environment, however this fact does not lead to repetition, instead it highlights the many different formats which can be used to exploit immunological interactions. This indeed is one of the real strengths of this text, illustrating, by the diversity of papers, the very many and varied ways the technique can be employed. For example, Van Emom and Lopez-Avila demonstrate how immunoaffinity can be utilised as a preliminary extraction for target analytes with subsequent detection by LC-MS. This application provides a solution to the extraction of pollutants from complex matrices and the added advantage of being adapted to on-line processing. Other methods presented adopt the more traditional methods such as ELISA, but include a number of alternative modifications which customise their application to suit specific analytes.

This publication not only provides papers covering the practical aspects of immunochemistry but also addresses the issue of accessible communication, namely through a focal Web site dedicated to this field. Discussion of this issue is clearly presented, including prototype pages and defined guidelines regarding how this project will be implemented, which once initiated will provide an excellent resource. Importantly, quality assurance and the calibration of assays are dealt with in their own right, providing useful guidelines for researchers setting out to evaluate their immunoassay.

It can be concluded that this book provides a very useful resource to anyone involved in the development, evaluation or use of environmental immunochemistry. The nature of this text is such that it is easily accessible to those new to this field, an aspect which is enhanced by the extensive use of explanatory diagrams, while also providing an exciting collection of papers that will be of interest to those with many years experience in this area.

L.A. Lawton

PII S0039-9140(97)00417-7

Author Index

Volume 46 (1998)

- Aaron, J.-J., 815
Abdalla, N.A., 491
Abd El-Fatah, S.A., 1395
Abdennabi, A.M., 639
Abel, J., 355
Abizanda, A.I., 75
Adams, F., 395
Addleman, R.S., 573
Agrawal, O., 501
Agrawal, Y.K., 1041
Akerkar, V.G., 1461
Aldhaheri, S.M., 1613
Algozo, C.M., 1591
Ali, I., 197
Alonso, P., 1469
Alsberg, T., 423
Aly, F.A., 83
Amer, M.M., 1395
Amrallah, A.H., 491
Andersen, R.A., 291
Angulo, R., 63
Ansary-Fard, A.H., 607
Anuse, M.A., 163
Anzano, J.M., 1265
Apostolova, M., 325
Arakawa, J., 1293
Arcos, M.J., 1493
Arıca, M.Y., 551
Argekar, A.P., 221
- Baeyens, W.R., 961
Balaji, B.K., 1299
Balderas-Hernández, P., 1439
Bamdad, F., 875
Bandekar, S.V., 1181
Bansal, R., 1573
Bantan, T., 227
Barna, R., 375
Bartocci, V., 977
Basavaiah, K., 665
Beattie, J.H., 255
Bebiano, M.J., 301
- Bedair, M.M., 9
Belal, F., 83
Belarra, M.A., 1265
Belategui, I., 1265
Bennett, J., 573
Bermejo-Barrera, A., 1479
Bermejo-Barrera, P., 1479
Bernard Serpaud, 999
Bertotti, M., 149
Berzas Nevado, J.J., 933
Bobbitt, D.R., 565, 907
Bollinger, J.-C., 999
Bontchev, P.R., 325
Bordin, G., 315
Bottari, E., 91
Brandariz, I., 1469
Budnikov, H.C., 465
Bueno, M.I., 1371
Bunde, R.L., 1223
Busch, K.W., 1591
Busch, M.A., 1591
Butler, I.S., 145
- Cabredo, S., 631
Calokerinos, A.C., 961
Campanella, L., 595
Campillo, N., 615
Cañada Rudner, P., 1095
Canning, A., 23
Cano Pavón, J.M., 1095
Castillo, J.R., 1265
Ceulemans, M., 395
Cha, K.-W., 1515, 1567
Chang, S.-C., 861
Chappell, J., 23
Chassaigne, H., 271
Chavan, M.B., 163
Chen, M., 527
Chen, S.-j., 757
Chen, Y., 727, 751
Cherif, A.T., 1605
Chiswell, B., 23
- Chow, A., 507
Coly, A., 815
Contento Salcedo, A., 933
Cornejo-Ponce, L., 1371
Costa, A.C., 1279
Costa Ferreira, S.L., 1525
Costa Lima, J.L., 1131
Cruz Ortiz, M., 1493
Čundeva, K., 1321
- da Cruz Vieira, I., 559
Daniela Piazzese, 1079
Das, J.V., 501
Daus, B., 867
Davis, D.M., 1169
de Andrade, J.B., 1279
de Bertorello, M.M., 1537
De Bièvre, P., 1031
Dehzoei, A.M., 1107
Delanghe, J., 961
Delerue-Matos, C.M., 1131
De Ley, M., 315
Deluchat, V., 999
Denizli, A., 551, 1205
De Robertis, A., 1085
De Stefano, C., 1079, 1085
Dhadke, P.M., 1181
Dixit, S., 1573
Dojozan, D., 123
Donard, O.F., 407
Dubey, R.K., 655
Dureault, B., 1485
Durst, R.A., 851
- Earley, R.L., 1507
Economou, A., 1137
Edkins, T.J., 907
Elçi, L., 1305
El-Enany, N.M., 83
El-Haty, E.Y., 491
El-Kosasy, A.M., 1395
Elmidaoui, A., 1605

- Elshani, S., 573
 Epperlein, U., 743
 Evmiridis, N.P., 179
 Evtugyn, G.A., 465

 Fábíán, R., 1273
 Fällman, A.-M., 365
 Fan, J., 1285
 Fatibello-Filho, O., 559
 Favero, G., 595
 Feng, Y.-L., 1155
 Ferreira, S.L., 1279
 Ferrón-Novais, M., 1479
 Festa, M.R., 91
 Fielden, P.R., 1137
 Finch, J.A., 145
 Fiol, S., 1469
 Fojta, M., 155
 Fraga, J.M., 75
 Fuh, M.-R.S., 861
 Fu, X., 751

 Galbán, J., 631
 Gandhimathi, M., 1577
 Gan, L.M., 1019
 Gao, J.-z., 527
 García-Garrido, J.A., 969
 Garcia de Torres, A., 1095
 Garrido Frenich, A., 1329
 Gass, H.J., 145
 Gauthier, A., 407
 Gavach, C., 1605
 Gawer, O., 1387
 Ghasemi, J., 875
 Ghiasvand, A.R., 1011
 Gholivand, M.B., 875
 Gianguzza, A., 1079, 1085
 Gil García, M.D., 1329
 Giovannetti, R., 977
 Gleichmann, H., 355
 González, A.G., 1259
 González-Campos, G., 1479
 Goto, T., 1433
 Gowda, N.M., 39
 Grudpan, K., 1245
 Guiberteau Cabanillas, C., 933
 Guo, J.-Z., 927
 Guo-Li, S., 943
 Gupta, M.K., 655
 Gupta, V.K., 197, 501, 1453
 Gutiérrez, A., 1439
 Gutiérrez, A.M., 1115
 Gutiérrez Navarro, P., 101
 Gu, W., 1019
 Guzman Jimenez, I.Y., 1591
 Gu, Z.-N., 993

 Habib, I.H., 1195
 Haggag, R.S., 9
 Haji-Shabani, A.M., 1379
 Halmos, P., 1273
 Han, F., 735
 Harada, R., 1583
 Harrington, P.B., 1169
 Hashemi, P., 1051
 Hasirci, V., 551
 Hassan, H.N., 1195
 Hassan, S.S., 1395
 Hassouna, M.E., 1195
 Heidenstam, O., 423
 Hellemans, G., 315
 Hendrickson, H.P., 565
 Hernández-Córdoba, M., 615
 Hernández, L., 985
 Hernández, P., 985
 Herrero, A., 129
 Herrero, R., 1469
 Hjelm, O., 365
 Horita, K., 671
 Hsu, C.-T., 1363
 Huang, X., 215
 Hui-Ping, L., 1
 Huitink, G.M., 1065

 Īnam, R., 1347
 Inoue, A., 1507
 Ismail Mohamed, A.E., 951
 Itoh, S.-i., 139
 Iwado, A., 1583

 Jackson, W.A., 565
 Jadhav, S.B., 1425
 Jahanshahi, A.R., 1011
 Jain, A.K., 1453
 Jakmunee, J., 1245
 Jarvi, E.J., 1223
 Jeřková, J., 1619
 Jie, N., 215, 1163
 Jin, J., 1547
 Jin, L., 1547
 Jin-Lan, H., 1
 Jørgensen, K., 423

 Kabziński, A.K., 335
 Kaise, T., 541
 Kalevi, K., 423
 Kamburova, M., 1073
 Kaneco, S., 139
 Kang, J.-w., 527
 Kapadia, S.U., 221
 Karalkar, N.B., 1461
 Karstensen, K.H., 365, 423
 Kato, H., 717
 Kavakh, C., 1205

 Kehaiov, I., 325
 Kesenci, K., 551
 Khalil, M.M., 53
 Khandwe, R.M., 521
 Khopkar, S.M., 521
 Khuhawar, M.Y., 485
 Khurana, U., 1453
 Kipp, S., 385
 Kitade, T., 1433
 Kitamura, K., 1433
 Kleiböhmer, W., 385
 Koken, M.E., 639
 Koleva, M., 325
 Komaba, S., 1293
 Koppenhoefer, B., 743
 Korany, M.A., 9
 Korn, M.G., 1279
 Koscielniak, P., 155
 Kotsis, I., 1273
 Krishnamurthy, G., 665
 Kubo, K., 347
 Kubota, T., 1311
 Kuehn, A.J., 1591
 Kulkarni, A.J., 1425
 Kureshiro, H., 717
 Kusano, T., 703

 Lacour, S., 999
 Langston, W.J., 301
 Lanjwani, S.N., 485
 Lavilla, I., 1265
 Le Coustumer, P., 407
 Lee, M., 851
 Le Floch, F., 1123
 Lehmann, M.W., 1507
 León, J.J., 75
 Li, B., 203
 Li, L., 1147
 Li, M.-X., 993
 Lin, B., 735, 743
 Li, N.-Q., 993
 Lin, T.-Y., 861
 Li, Q.-M., 927
 Liu, H., 1547
 Liu, J.-W., 757
 Liu, Q., 927
 Liu, S.-x., 527
 Liu, W.-H., 679
 Li, X.-l., 1531
 Lobinski, R., 271
 Locatelli, C., 623
 Lodevico, R.G., 907
 Lokhande, T.N., 163
 López-Cueto, G., 63
 López-García, I., 615
 Lu, F., 1405
 Lu, J., 751, 1405

- Luo, C.-N., 1531
 Luque de Castro, M.D., 969
 Lu, Y., 1531
- MacDonald, D., 1405
 Malve, S.P., 1425
 Maniaci, R., 1079
 Manuela Garrido, E., 1131
 Manzoori, J.L., 1379
 Mao, L., 1547
 Maria Oliveira Brett, A., 1131
 Márquez García, A., 101
 Martín, R., 1115
 Martínez de las Parras, P.J., 101
 Martínez Galera, M., 1329
 Martínez Vidal, J.L., 1329
 Martín, M.J., 1259
 Masuda, Y., 203
 Matsubara, C., 541
 Maung, U.A., 1245
 McGrath, D., 439
 Meguro, Y., 689
 Méhu, J., 375
 Mendes Martins, B., 149
 Menon, S.K., 1041
 Mífune, M., 1583
 Milačić, R., 227
 Minami, T., 347
 Minggui, X., 45
 Min, Y., 943
 Mishra, G., 1299
 Mitáš, J., 155
 Mizuno, T., 139
 Molenat, J., 1605
 Moreno, F.J., 75
 Moszkowicz, P., 375
 Motelica-Heino, M., 407
 Motohashi, N., 1583
 Mousavi, M.F., 1011
 Muñoz de la Peña, A., 1329
 Murakami, S., 1187
 Muromatsu, A., 1187
 Murthy, K.C., 39
 Murugesan, P., 1299
 Müslehiddinoğlu, J., 1557
- Nachev, C., 325
 Nagaosa, Y., 647
 Nagaraja, P., 39
 Naidu, P.Y., 1357
 Nakamura, S., 1293
 Nan, Z., 1237
 Narasaki, H., 1155
 Nie, L., 171
 Nieto, O., 315
 Nikolskaya, E.B., 465
 Nishimoto, J., 703
- Nordberg, M., 243
 Noresson, B., 1051
 Nylund, K., 423
- Ogawa, J., 139
 Ohly, P., 355
 Ohta, K., 139
 Ohyama, T., 541
 Okabe, N., 347
 Okazaki, Y., 347
 Okutani, T., 1311
 Ólafsdóttir, K., 423
 Olin, Á., 1051
 Olsvik, P.A., 291
 Örnemark, U., 1031
 Ortiz, C.S., 1537
 Ortiz, M.C., 129
 Osaka, T., 1293
 Ou, Q.-y., 527
 Ouyang, J., 961
 Özbelge, H.Ö., 1557
 Ozsoz, M.E., 1405
- Pablos, F., 1259
 Pal, A., 583
 Paleček, E., 155
 Pancras, J.P., 1107
 Parkash, R., 1573
 Park, C.-I., 1515
 Park, K.-W., 1567
 Patón, F., 985
 Peralta-Zamora, P., 1371
 Peyrer, H., 385
 Pihlar, B., 227
 Pişkin, E., 1205
 Pişkin, E., 551
 Polese, L., 915
 Pournaghi-Azar, M.H., 123, 607
 Prasada Rao, T., 765
 Puri, B.K., 655, 1107
 Puri, S., 655
- Qiao, Z., 697
 Quevauviller, P., 457
 Quiles-Zafra, R., 969
- Radalla, A.M., 53
 Raj, S.V., 221
 Ramalingom Pillai, A., 765
 Ramanaiah, G.V., 533
 Ram Rao, S., 145
 Ramirez, M.T., 1439
 Rangappa, K.S., 39
 Rauret, G., 449
 Ravisankar, S., 1577
 Reddy, M.L., 765
 Reguera, C., 1493
- Rehani, S.K., 1573
 Reis, J.O., 1279
 Reza Ganjali, M., 1341
 Ribeiro, M.L., 915
 Ringstad, O., 423
 Rizk, M., 83
 Rodríguez, A.R., 315
 Rodríguez Flores, J., 933
 Rogers, K.R., 1405
 Rojas-Hernández, A., 1439
 Ríos, A., 1123
 Rosentreter, J.J., 1223
 Rouhollahi, A., 1341
 Ruo, Y., 943
 Ru-Qin, Y., 943
 Rustad, I., 423
 Rzeszutek, K., 507
- Saitoh, T., 541
 Saito, K., 1187
 Saito, Y., 1583
 Sakata, K., 647
 Sakurai, T., 541
 Saleh, G.A., 111
 Saleh, M.B., 885
 Salih, B., 551, 1205
 Salinas, F., 1329
 Salunkhe, M.M., 1461
 Sammartano, S., 1079, 1085
 Sammartino, M.P., 595
 Sanchez, D.M., 1115
 Sanchez, F., 375
 Sánchez, I., 985
 Sanchez Rojas, F., 1095
 Sandhya, D., 921
 Santiago de Jesus, D., 1525
 Sanyal, M., 1041
 Sanz, J., 631
 Saraçoğlu, S., 1305
 Saravanakumar, G., 1299
 Sarudi, I., 589
 Sasaki, T., 689
 Sastre de Vicente, M.E., 1469
 Sastry, C.S., 1357
 Satake, M., 671
 Satoh, I., 1293
 Sato, M., 717
 Say, R., 1205
 Seyama, M., 1293
 Shamsipur, M., 1341
 Sharma, R.K., 1461
 Sheibani, A., 1107
 Shen, G.-L., 679
 Shen, J., 15
 Shi, G., 1547

- Shrivastav, P., 1041
 Singh, L.P., 1453
 Skořepa, J., 1619
 Slaets, S., 395
 Solberg, H., 423
 Somer, G., 1347
 Song, X.-M., 365
 Song, Z., 1163
 Sooksamiti, P., 1245
 Sorouraddin, M.H., 1379
 Souza de Carvalho, M., 1525
 Spínola Costa, A.C., 1525
 Stafilov, T., 1321
 Staňková, V., 155
 Subramanian, M.S., 921
 Sukhan, V., 1387
 Sultan, S.M., 897
 Sun, C., 15
 Sun, Y., 15
 Sun, Y.-L., 993
 Suresh, B., 1577
 Suzuki, Y., 541
 Sveinsdottir, E.L., 365
 Szpunar, J., 271

 Tabata, M., 703
 Taher, M.A., 1107
 Takagi, N., 717
 Takamura, K., 541
 Tanaka, M., 347
 Tang, J.-H., 679
 Tan, H., 171
 Taninaka, I., 1187
 Tao, S., 1547
 Taylor, P.D., 1031
 Teigen, S.W., 291
 Teixeira, L.S., 1279
 Tena, M.T., 1123
 Teng, X.-l., 527
 Thanasoulas, N.K., 179
 Thomassin, J.H., 407
 Tian, Y., 1547
 Tomassetti, M., 595
 Tong, A., 1147
 Torsi, G., 623
 Toutounchi-Asr, J., 123
 Tsuchiya, H., 717
 Tweedy, S.H., 573

 Ubide, C., 63
 Uludağ, Y., 1557
 Utekar, S.S., 1425

 Valcárcel, M., 1123
 Van der weken, G., 961
 Vaneesorn, Y., 1245
 Varadarajan, A., 1425
 Vasudevan, M., 1577
 Velasco-Arjona, A., 969
 Vilariño, T., 1469
 Villaseñor Llerena, M.J., 933
 Viñas, P., 615
 Visi-Varga, É., 589
 Vlessidis, A.G., 179
 Vyřas, K., 1619

 Wahlström, M., 365
 Wai, C.M., 573
 Walmsley, A.D., 897
 Wan, C., 1169
 Wang, G.F., 671
 Wang, J., 1285, 1405
 Wang, R., 171
 Wang, Y., 679
 Wang, Z., 355
 Watanesk, S., 1245
 Weiß, H., 867
 Wei, W., 697
 Wei, X.-J., 927
 Welch, L.E., 1507
 Wennrich, R., 867
 Wilhelmsen, T.W., 291
 Wolff, J.-C., 1031
 Wong, M.K., 1019
 Wong, R.B., 851
 Wuerthner, S., 743
 Wu, Y., 1147
 Wu, Y.-Q., 993

 Xiao-Ge, L., 1
 Xiaotian, Q., 45
 Xia, X., 845
 Xue, J., 735
 Xu, H., 15
 Xu, Z., 145

 Yamaguchi, T., 1311
 Yamamoto, K., 1547

 Yan, C., 203
 Yang, B., 845
 Yang, D., 1163
 Yang, J., 215, 1163
 Yang, W., 527
 Yang, X., 697
 Yao, B., 711
 Yao, S., 171, 697
 Ye, C., 1285
 Yescas, S., 1591
 Ying, T., 45
 Yilmaz, L., 1557
 Yongchang, Z., 45
 Yoshida, Z., 689
 Yoshita, C., 347
 You, J.-m., 1531
 You-Qun, S., 943
 Yuan, L., 527
 Yu, G., 845
 Yu, R.-Q., 679

 Zaide, Z., 45
 Zaporozhets, O., 1387
 Zeng, H., 1485
 Zen, J.-M., 1363
 Zha, H., 711
 Zhang, C., 711
 Zhang, H., 171
 Zhang, M.-E., 757
 Zhang, Q., 215, 1163
 Zhang, Q.-F., 927
 Zhang, W., 711
 Zhang, X., 15
 Zhang, Y., 203
 Zhang, Z.-w., 1531
 Zhao, J., 15
 Zhao, S., 845
 Zhao, Y., 1147
 Zhi-Qiang, L., 943
 Zhong, S., 711
 Zhou, C.-l., 1531
 Zhou, C.Y., 1019
 Zhou, X., 711
 Zhou, X.-H., 993
 Zhou, X.-M., 757
 Zhu, X., 743
 Zimány, P., 1273

Subject Index

Volume 46 (1998)

- Absorption spectra 1433
Acemethacin determination 1493
Acetaminophen 1577
Acid–base equilibria in montmorillonite suspensions 951
Acid dissociation constant 1285
Activated carbon 1311
Adrenaline 985
Adsorption 1387
Adsorptive cathodic stripping voltammetry 1137
Ag⁺ 1605
Ag(I) determination 1387
Al–EDTA 227
Aliquat-336 921
Alkali Blue 6B 551
Al–oxalate 227
Amberlite IRC-718 1515
Amberlite XAD-2 1479
Amines and amino acids 565
Amino acids 491
Amperometric detection 149, 711
Ampicillin 101
Analysis 815
Analysis of alloy 521
Anilino-(1,3-dioxo-2-indanylidene) acetonitrile 885
Anion coordination chemistry 1079, 1085
Anion exchange chromatography 291
Anion-exchange FPLC–ICP–AES 227
Anodic stripping voltammetry 607
Antimony 1531
Antimony screening 1265
Application studies 45
Aqueous 145
Aqueous medium 1439
Arsenic 867, 1311
Atomic absorption spectrometry 541, 615, 1557
Atomic emission spectrometry 395
Autoprotolysis constant 1285
Azo dyes 491
- Background current 129
Ba(IO₃)₂ 149
Barbiturates and phenytoin 111
- Base dissociation constant 1285
Bentazon 1131
Benzeneacetaldehyde-4-hydroxy- α -oxo-aldoxime 1425
Benzoxainone derivative 573
Berberine 679
Binary and ternary complexes 53
Biogenic amines 1079, 1085
Biological fluids 83
Biological samples 501, 1107
Biosensor 1223
2,2'-bipyridyl 1285
1,4-bis(naphth[2,1-d]oxazole-2-yl)benzene 679
Blood 1347
Borate complex 717
Bovine serum albumin 171
Brass 1531
Bromoacetone 589
5-Br-PADAP 1107
BTEX 1169
Bulk acoustic wave 171
- Cadmium 101, 301
Cadmium(II) 551
Cadmium(II)–taurine complexes 91
Cadmium matrices 1525
Calcium 1245
Calibration transfer 129
Calixarene hydroxamic acid 1041
1,3-calix[4]bisnaphthyl-crown-6 1485
Capillary electrophoresis 255, 565, 735, 743
Capillary gradient gel electrophoresis 727
Capillary zone electrophoresis 1, 291, 347
Captopril 75
Carbon fiber ultramicroelectrode 985
Carbon paste electrode 1363
Carbon paste ion-selective electrodes 1619
Carboxylic ligands 1079
Carminic acid–bromate redox reaction 1379
Carriers modified with Co³⁺–tetra-(4-carboxyphenyl)porphine 1583
Catalyse 595
Catalytic 1011

- Catalytic–photometric method 1299
Catalytic spectrophotometric method 1379
Catechins 717
C₆₀- γ -cyclodextrin 993
Cd(II), In(III), Tl(I), Pb(II) 1195
Central composite design 897
Cerium(IV) 897
Cerium (IV) 961
Certified reference materials 449
Cesium 1485
Cesium ion-selective electrodes 885
Charge-transfer complexes 111
CH-B-15-C-5 45
Chemical analysis 423
Chemical characterization 1273
Chemically modified electrode 993
Chemiluminescence 961
Chemiluminescence (CL)-emission 179
Chemiluminescent detection 565
Chiral drugs 743
Chloride 1299
Chloride analysis 1591
Chloride and iodide detection 639
Chloride–nitrite–nitrate 969
Chloroform 123, 607
5-Chloro-8-quinolinol 647
Chlorzoxazone 1577
Chromatographic resolution 907
Chromium(V) 23
Cobalt 1137, 1425
Cobalt determination 1107
Cobalt(II) 977
Cobalt(II) tetraaminophthalocyanine 1547
Coffee 1259
Co(II) 1515, 1573
Column operation 1461
Competitive ELISA 325
Complexation 999
Complexation of alkaline earth aluminum ions 875
Complexes 491, 765
Complexing reagent 485
Concentration 145, 541
Contaminated soil 423, 449
Continuous flow 969
Copper 615
Copper-base alloys 1279
Copper(II) 1187
Coprecipitation 1305
Coproporphyrin-1 977
Cough syrup 221
Coupled techniques 271
Covalent affinity chromatography 335
Cromatographic determination 485
Cross-sections 1329
Crown ethers 9
Cryogenic preconcentration 631
Cu(II) determination 1387
 β -Cyclodextrin 743
Cyclophosphamide 1395
Cytochrome *c* 993
Data treatment 1557
Degradation 1537
Density 689
Derivative spectrophotometry 933, 1107, 1433
Determination 1299, 1321
Diabetes 355
Dialysis concentrate 1305
Diazepam 951
Diazotization-coupling reaction 671
Dibutyl(butyl)phosphonate 1453
Diethylenetriamine 145
Di-(2-ethylhexyl)phosphoric acid 1453
Differential electrolytic potentiometry 639
Differential pulse adsorptive stripping voltammetry 1493
Differential pulse polarography 123, 655, 1347
Dilute acid 1019
Diphenhydramine hydrochloride 221
Direct analysis 1265
Direct detection of unlabelled polysaccharides 727
Disease 243
5,5'-Dithiobis-(2-nitrobenzoic acid) 1341
Dithizone 1205
Divalent heavy metals 573
DNA biosensor 171
DNA damage 155
DNA-modified electrode 155
DNA separation 735
Donnan dialysis 1605
Dopamine 559
Dopamine hydrochloride 39
DPG + Cl⁻ 1613
Drug analysis 1245
Drug–clay interactions 951
EDTA 1573
Electrocatalysis 993
Electrochemical 465
Electrochemical biosensor 155
Electrochemical quartz crystal microbalance 711
Electrochemical sensor 1405
Electrode polishing 1507
Electrodeposition 139
Electrode response 1507
Electron paramagnetic spectroscopy 23
Electrophoresis 197
Electrothermal atomic absorption spectrometry 139, 1321
Enantiomeric mixtures 907
Enantiomer separation 743
Environment 23
Environmental analysis 155
Enzyme immunoassay (EIA) 385
Enzyme sensors 465
Epinephrine 985

- ETAAS 1479
Europium determination 527
Experimental design 897, 1493
Explosive detection 1405
Extraction 507, 1187
Extraction equilibrium 1613
Extraction procedures 449
Extraction-spectrophotometry 9, 1073
- Fe³⁺ 1567
Fe(II III) determination 1387
Field analysis 385
Flame spectrometry 1591
Flow injection 149, 845, 897, 1011, 1245
Flow injection analysis 1137, 1293
Flow-injection analysis 961
Flow injection analysis 639
Flow-injection liposome immunoanalysis (FILIA) 851
Fluorapatite 1273
Fluorescence quenching 1567
Fluorimetry 527, 815
Fluorometry 1163
Formal potential 1469
Formation constants 1439
Fourier-transform infrared emission 1591
Free concentration taurine measurement 91
Fruit samples 671
Fulvic acid 23
- Gas chromatography 45, 221, 395, 589, 861
Gas oil 607
Gasoline 607
Gas phase molecular absorption spectrometry 631
GC-ECD 915
Gender 243
Geological materials 533
Glass electrode 1469
Glutathione oxidase-like activity 1583
GOD 595
Gold complex 583
Graphite furnace atomic absorption spectrometric (GFAAS) 1041
Graphite furnace atomic absorption spectrometry 1311
Graphite-furnace atomic absorption spectrometry 1265
Gravimetric determination 1237
- 2HB-5NPH 1515
Heavy metal 335
Heavy metal ions 1557
Heavy metal removal 551
Heavy metal removal, cadmium, mercury, chromium and lead 1205
Heavy metals 423, 439, 449
Heparin 757
2-heptanone 861
Herbicide 851
Herbicides 1131
- Heteropoly anions 1619
Hexachlorobenzene 915
Hexacyanomanganate(IV) 63
High-performance capillary electrophoresis 757
High-performance liquid chromatography 717
High resolution separation technique 271
HPLC-DAD 1329
Human erythrocyte ghosts 1433
Human urine 697
Hydrides 631
Hydrochlorothiazide 961
Hydrogen peroxide 63, 1583
Hydroxylamine hydrochloride 39
Hypertension 325
- I⁻ 711
Ibuprofen 1577
ICP 1115
ICP/AES 1279
ICP-MS 407
Ifosphamide coated wire sensor 1395
Imazethapyr 851
Iminodiacetate adsorbent 1051
Immobilization 171
Immunoassay 851
IMS 1169
Indicators 1065
Indirected UV detection 1
Indomethacin determination 1493
Inductively coupled plasma atomic emission spectrometry 533, 1095
Inductively coupled plasma mass spectrometry 1155
Inhibitor determination 465
Inorganic ligands 1085
Inosine 53
Interface 1169
Interlaboratory studies 457
In vivo microdialysis 1547
Iodide ion 15
Iodine in alkaline medium 1357
Ion-associate 1613
Ion chromatography 697
Ion-exchange 1095
Ionic strength 1469
Ion-pairing reaction 1619
Ions 927
Ion selective electrode 1293
Iron 845
Iron (III) 521
Isoform 347
Isoform separation 255
Isoniazid 39, 1357
Isoproturon 501
Isotope dilution 1591
(Isotopic) Reference Materials 1031
Isoxazolylnaphthoquinone 1537

- Kinetics 63, 101, 1537
- β -lactam 101
- Lad(II) benzoylacetate 607
- Lanthanides 203
- Laser ablation 407
- Lauric acid 203
- L-dopa 1163
- Leaching test 365
- Leaching tests 375
- Lead(II) 551
- Lead ion selective electrode 1341
- Levodopa 39
- Liposomes 851
- Liquid chromatography 647
- Liquid-liquid extraction 1041
- Liquid scintillation counting 921
- Lithium porphyrin 703
- Loaded silica gel 1387
- Low background polyacrylamide gradient gel-filled capillaries 727
- Low capacity 1051
- Magnesium hydroxide 1305
- MALDI-TOFMS 255
- Manganese determination 1073
- Mannitol 735
- Matrix elimination 1051
- Meat 969
- MECC 255
- Mechanism 927
- Mercury 1019, 1095
- Mercury(II) 977
- Metabolism 243
- Metal analysis 1237
- Metal chelate 541
- Metal ions 647
- Metallofluorescent 1065
- Metallothionein 243, 255, 301, 325, 335, 347, 355
- Metallothionein isoforms 291
- Metallothioneins 271
- Metals 243
- Method development 457
- Methyldopa 39, 559
- Metol 1357
- Mg-W cell 139
- Micellar electrokinetic capillary chromatography 751
- Microelectrode 711
- Microwave digestion 439, 1019
- Milk 589, 615
- Mineral and pharmaceutical samples 521
- Mixed complexes 875
- Molluscs 301
- Molybdenum and vanadium determination 655
- Molybdoarsenate 1311
- Monaza-15-crown-5 573
- Monolithic material 365
- Monovalent cation selective membrane 1605
- Morpholine-4-carbodithioate 655
- Multianalyte determination 129
- Multilayer films 15
- Multivariate anodic stripping voltammetry 1195
- Murexide 1245
- Nafion® 1363
- Nafion 993
- Naphthalene 1107
- Naphthalene column preconcentration 671
- Naphthalene derivatives 1147
- Natural water 1311, 1379
- N*-Bromosuccinimide 39
- Neutral carrier 943
- Nickel 697, 1137
- Nitrate and nitrite determination 671
- Nitric oxide 1547
- Nitrite 1031, 1547
- Nitrite determination 1379
- α -Nitroso- β -naphthol 1461
- N,N'*-dinaphthyl-*N,N'*-diphenyl-3,6-dioxacanediamide 527
- N-n*-Octylaniline 163
- Nordic laboratories 423
- NP-RTP 1147
- Ofloxacin 83
- \cdot OH radicals 155
- Olive leaves 1123
- OPEEs 595
- Optical fiber sensor 679
- Optode membrane 1485
- Ores analysis 1245
- Organic tin 1479
- Organotin 395
- Orthogonal array design 1019
- Overlapping signals 129
- Oxidants 179
- Oxidation of glutathione 1583
- Oxidised ketone bodies 589
- Oxine 123
- PAD 1507
- Palladium 163
- p*-Aminoacetophenone 501
- Pancreatic islets 355
- Paracetamol 1163
- Partial least squares regression 129
- Pattern recognition 1259
- Penicillamine 197
- Pentachlorophenol 915
- Pentacoordinate organotin complex 943
- 2',3,4',5,7-Pentahydroxyflavone(morin) 1531
- Pentoxifylline 1357
- Periodate 1613
- Perphenazine 897
- Pesticides 815, 1329

- Pharmaceutical analysis 83, 111, 961
Pharmaceutical formulations 559, 1357
Pharmaceutical preparations 665
Pharmaceuticals 39
Phase behavior 689
pH-dependent spectral behavior 1065
1,10-Phenanthroline 1387
Phenol 1123
Phenols 507
Phenothiazine derivatives 665, 1433
Phenytoin 9
pH-metric 491
Phosphomolybdic acid 1573
Phosphonic acid 1181
Phosphonic acids 999
Photoinitiated gold sol 583
pH-Profile 1537
pH-selectivity 179
Piezoelectric quartz crystal 1223
Plasma 717, 757
Polarimetric detection 907
Polarography 75, 83
Pollutant leaching 375
Polyacrylamide-coated tube 347
Polyacrylamide gel electrophoresis 291
Polyamino acids 727
Polycyclic aromatic hydrocarbons 751
Polycyclic aromatic hydrocarbons (PAHs) 385
Poly(EGDMA-HEMA) microbeads 1205
Poly(HEMA) films 551
Polymer enhanced ultrafiltration 1557
Polymorphism 243
Poly(*N*-isopropylacrylamide) 541
Polyphenol oxidase 559
Polyurethane foam 1525
Polyurethane membrane 507
Poly(vinylpyridine) 1547
Ponceau 4R 933
Porphyrin 15
Potassium 1293
Potassium periodate 1163
Potassium permanganate 9
Potential fluorophore 1065
Potentiometric and conductometric studies 53
Potentiometric titrations 1619
Potentiometry 15, 885, 1341, 1469
Prazepam 951
Precipitate flotation 1321
Pre-concentration 1371
Preconcentration 139, 655, 1051, 1095
Pre-normative research 457
Preparation 1273
Pretreatment 717
Principal component regression 75
Prospects for analytical applications 179
Prostaglandins 1
Protein 243
Pseudoephedrine hydrochloride 221
Pulse polarography 607
Purification 1031
PVC-COOH matrices 1395
PVC matrices 1395
PVC membrane 1341
Pyrocatechol 39
Pyrogallol oxidation 179
Quality control 457
Quantification 243
Quantitative analysis 23
8-quinolinol 541
Rare earth elements 533
Rare earths 1371
Recrystallized thymol blue 1439
Reproducibility 423
Response surface 897
Reversed-phase HPLC 1577
Review 1223
Rhodamine 6G 961
Rhodium 139
Robotic 969
Ru(bpy)₃³⁺ 565
Salicylate-selective PVC membrane electrode 943
Salicylic acid 1567
Saliva 717
Salting-out extraction 647
Samarium iodide 861
Scandium 533
Screen-printed electrode 1405
Seawater 1591
Sea water 703
Seawater 123
Sediment 449, 1115
Sediments 623
Selectivity 465
Selenium 1011
Selenium and lead determination 1347
Sensitivity 465
Sensor 15
Separation 521, 1181, 1605
Separation of Al-citrate 227
Separation of aromatic compounds 751
Sequential extraction 867, 1115
Series bulk acoustic wave 697
Serum 703
Silver electrode 91
Silver(I) 1187
Silver(I)-taurine complexes 91
Silver surface 171
Simplex optimization 897
Simultaneous determination 221, 623, 631, 845
Simultaneous estimation 1577
SM&T programme 457

- Sodium 1-naphthol-4-sulfonate 671
Sodium nitroprusside 39
Soil 385, 915, 1019
Soils 439, 1073
Solidified 365
Solidified wastes 375
Solid-phase extraction 1525
Solid phase extraction 123
Solid samples 1265
Solubility 689
Solubility product 149
Solvent extraction 163, 485, 1181
Solvent extraction calix(6)arene 521
SPE-CE 255
Speciation 395, 867, 999, 1115
Speciation of Al 227
Speciation of biological fluids 1079, 1085
Spectrochromatograms 1329
Spectrofluorimetric 765
Spectrophotometric determination 1515
Spectrophotometric 765
Spectrophotometric determination 1041, 1425
Spectrophotometric method 665
Spectrophotometry 39, 111, 501, 521, 671, 689, 703, 977, 1011, 1245, 1357, 1573
Square-wave voltammetry 1405
Square wave voltammetry 1131
Stability 1031, 1537
Stability constant 203
Stability constants 197
Standard alloys 1107
Standard alloys and environmental samples 655
Stationary phase 45
Steel 1531
Steels 1073
Stepwise elution 1461
Stern–Volmer equation 1567
Streptozotocin 355
Stripping agent 1181
Stripping voltammetry 129
Strongly basic anion exchanger 1155
Structure and texture 407
Substituent group 1147
Substituted quinolones 1065
Substoichiometric isotope dilution analysis 921
Sulfadimidine 671
Sulfamethizole 671
Sulfanilamide 671
Sulphide 1011
Sunset Yellow 933
Supercoiled DNA 155
Supercritical carbon dioxide 689
Supercritical fluid extraction 1123
Superheated water extraction 385
Sweet potato (*Ipomoea batatas* (L.) Lam.) 559
Synergistic extraction 203
Synthetic mixture analysis 583
Tartrazine 933
1,4,10,13-Tetrathia-7,16-diazacyclooctadecane 203
Thallium 1321
Thenoyltrifluoroacetone 527
Thiacrown ether carboxylic acid 1187
Thin-layer amperometric detector 1547
Thionine 1011
Tin 1155, 1237
Tin(IV) 1181
TNT 1405
Toxic metals 623
TPB 1107
Trace analysis 123
Trace metal 1011
Trace metals 407
Transport 927, 1605
Tributylphosphate 689
Trivalent cations 999
Tropolone 1479
Tubular silicone membrane 1169
Turnover 301
Tyrosinase 595
Uranium 123
Uranium(VI) 689
Uric acid 1363
Vanadium 1299
Vanadium catalytic determination 63
Vitrified wastes 407
Voltammetry 623, 1531
VO²⁺-selective sensors 1453
Waste analysis 457
Water 139, 671, 1321
Water + alcohol mixed solvent 1285
Western blotting 325
Wool fast blue BL 1357
X-ray fluorescence 1371
Xylenol orange 875
Yttrium 533
Zinc 615, 845, 1279
Zinc determination 921
Zinc(II) 551
Zinc separation 1525
Zirconium(IV) 1041
Zn²⁺ 1605